ANGEWANDTE CHEMIE
INTERNATIONAL EDITION
A Journal of the Gesellschaft Deutscher Chemiker
2002
41/10
Pages 1629 – 1808

COVER PICTURE

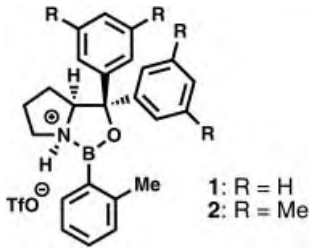
The cover picture shows portraits of Otto Diels (top left) and Kurt Alder together with the original Diels–Alder reaction between cyclopentadiene and *p*-quinone. Also illustrated are the key Diels–Alder reactions that enabled the total synthesis of prostaglandins and taxol as they were carried out by the research groups of Corey and Nicolaou, respectively. This year marks the centennial anniversary of Alder's birth—and this date will be celebrated at Alder's University, the Universität Köln, by a symposium on the 27th May—while last year was the 125th anniversary of the birth of Diels and next year will signify the 75th anniversary of the first publication of Diels and Alder on the reaction of 1,3-dienes with olefins. The Diels–Alder reaction, as it has become known, is without doubt one of the most important reaction of organic syntheses, and thus it is a bonanza that Corey and Nicolaou et al. have written appropriate reviews, which can be found on pp. 1650 – 1667 and 1668 – 1698, respectively.



REVIEWS

Contents

One century after the birth of Kurt Alder and 75 years after the discovery of his famous reaction, research on the Diels – Alder process continues to surprise, excite, and delight the chemical community. The reader is taken on an exciting journey into how chiral Lewis acids, including the new cationic Lewis acids **1** and **2**, have transformed the Diels – Alder reaction into a highly enantioselective process.



Angew. Chem. **2002**, *114*, 1724 – 1741

E. J. Corey* ..... 1650 – 1667

Catalytic Enantioselective Diels – Alder Reactions: Methods, Mechanistic Fundamentals, Pathways, and Applications

Keywords: asymmetric catalysis · chiral ligands · cycloaddition · Lewis acids · transition states

 © WILEY-VCH Verlag GmbH, 69451 Weinheim, Germany, 2002 1433-7851/02/4110-1631 $ 20.00+.50/0

On the occasion of the 100th anniversary of Alder's birth, the authors tell, in a didactic style and through a series of stunning examples of natural-product syntheses, including some from their own laboratories, the thrilling story of how the venerable Diels–Alder reaction enabled and shaped the art and science of total synthesis (see scheme) in the last half century.



Angew. Chem. **2002**, *114*, 1742–1773

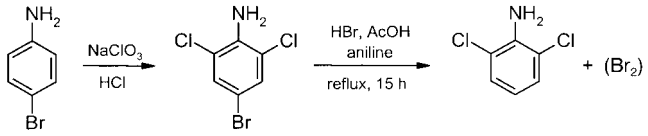
K. C. Nicolaou,* S. A. Snyder, T. Montagnon, G. E. Vassilikogiannakis 1668–1698

The Diels–Alder Reaction in Total Synthesis

Keywords: biomimetic synthesis · cascade reaction · cycloaddition · Diels–Alder reaction · total synthesis

HIGHLIGHTS

The reversibility of electrophilic bromination of aromatic compounds has been known for a long time, but the possibility of using bromine as a protecting group in aromatic or heterocyclic chemistry has now been shown for the first time (see scheme for an example). Compared with typical protective groups (SO_3H, COOH, NH_2, $CHMe_2$, CMe_3) bromine offers many advantages; a decisive aspect for its successful application is the choice of optimized reaction conditions which are predictable from the reaction mechanism.



Angew. Chem. **2002**, *114*, 1775–1776

F. Effenberger* 1699–1700

How Attractive is Bromine as a Protecting Group in Aromatic Chemistry?

Keywords: arenes · bromine · electrophilic subsitution · protecting groups · reversibility

VIPs

The following communications are "Very Important Papers" in the opinion of two referees. They will be published shortly (those marked with a diamond will be published in the next issue). Short summaries of these articles can be found on the *Angewandte Chemie* homepage at the address http://www.angewandte.com

The First Method for Achieving Palladium-Catalyzed Cross-Couplings of Simple Alkyl Chlorides: Suzuki Reactions Catalyzed by $[Pd_2(dba)_3]/PCy_3$ — J. H. Kirchhoff, C. Dai, G. C. Fu* ◆

Catalytic Activity and Poisoning of Specific Sites on Supported Metal Nanoparticles — J. Hoffmann, V. Johánek, J. Hartmann, J. Libuda,* H.-J. Freund

Understanding Zeolite Catalysis: Inverse Shape Selectivity Revised — M. Schenk, S. Calero, T. L. M. Maesen, L. L. van Benthem, M. G. Verbeek, B. Smit*

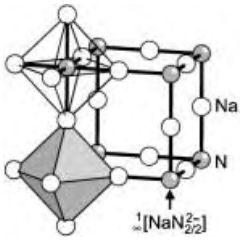
Highly Selective Transport of Organic Compounds by Using Supported Liquid Membranes Based on Ionic Liquids — L. C. Branco, J. G. Crespo, C. A. M. Afonso*

Atom-Transfer Tandem Radical Cyclization Reactions Promoted by Lewis Acids — D. Yang,* S. Gu, H.-W. Zhao, N.-Y. Zhu

 © WILEY-VCH Verlag GmbH, 69451 Weinheim, Germany, 2002 1433-7851/02/4110-1633 $ 20.00+.50/0

The game of hide and seek is over: The existence of a binary sodium nitride Na_3N (see structure) has been the subject of speculation for a long time. Recently, through a novel experimental method, the synthesis and structural characterization of this compound has been successful. The compound crystallizes in the unexpected anti-Re_3O structure type.

Angew. Chem. **2002**, *114*, 1777 – 1778



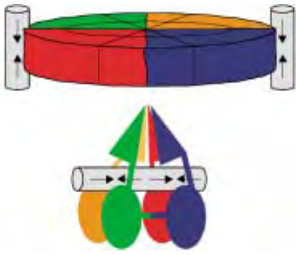
R. Niewa* ..... 1701 – 1702

Na_3N—An Original Synthetic Route for a Long Sought After Binary Nitride

Keywords: alkali metals · nitrides · solid-state reactions · structure elucidation

Despite the high pharmaceutical relevance of the important tumor-suppressor protein p53, its mechanism of activation is still unclear. A recent paper now sheds light on some of the structural features associated with the activation of p53 and its binding to DNA. On the basis of these results, a "sandwich" model for the interaction of p53 with DNA was proposed (top) to replace the long-favored "clamp model" (bottom).

Angew. Chem. **2002**, *114*, 1778 – 1780



P. Chene, W. Jahnke* ..... 1702 – 1704

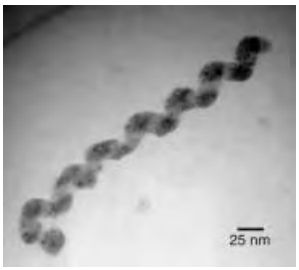
Oligomerization of p53 upon Cooperative DNA Binding: Towards a Structural Understanding of p53 Function

Keywords: DNA recognition · NMR spectroscopy · protein – protein interactions · tumor suppression

COMMUNICATIONS

Helices on helices: Nanohelices of polycrystalline cadmium sulfide (see transmission electron micrograph) have been made by the mineralization of helical self-assembled objects shaped like twisted ribbons. The coiled morphology of the inorganic helices apparently results from growth on only one face of the organic ribbon template.

Angew. Chem. **2002**, *114*, 1781 – 1785

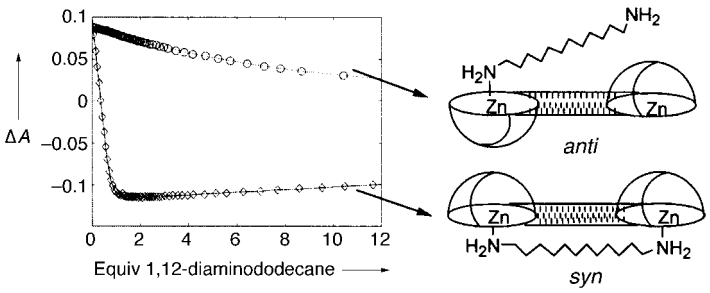


E. D. Sone, E. R. Zubarev, S. I. Stupp* ..... 1705 – 1709

Semiconductor Nanohelices Templated by Supramolecular Ribbons

Keywords: cadmium sulfide · mineralization · nanostructures · self-assembly · template synthesis

The power of supramolecular chemistry to solve problems in structural chemistry where conventional techniques such as NMR, UV, and IR spectroscopy failed is demonstrated in the differentiation of the *syn*- and *anti*-bis(capped porphyrin) isomers (obtained after condensation of a capped porphyrin monomer) by simple UV/Vis binding studies using bidentate ligands that act as "molecular rulers" (see picture).



Angew. Chem. **2002**, *114*, 1785 – 1788

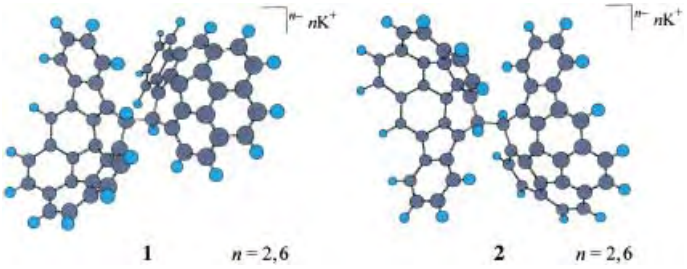
M. J. Crossley,* P. Thordarson ..... 1709 – 1712

Assignment of Stereochemistry of Facially Protected Bis-porphyrins by Use of a "Molecular Ruler"

Keywords: bridging ligands · capped porphyrins · configuration determination · molecular recognition · porphyrinoids

 © WILEY-VCH Verlag GmbH, 69451 Weinheim, Germany, 2002 1433-7851/02/4110-1634 $ 20.00+.50/0

A reduction cascade: The reduction of indenocorannulene by potassium leads to the formation of the diastereomeric dimers **1** and/or **2**; this is the first case of reductive dimerization of a large nonplanar polycyclic aromatic hydrocarbon. The twofold formation of these dimers, and their dissociation to the monomeric species, was monitored by NMR spectroscopic methods.



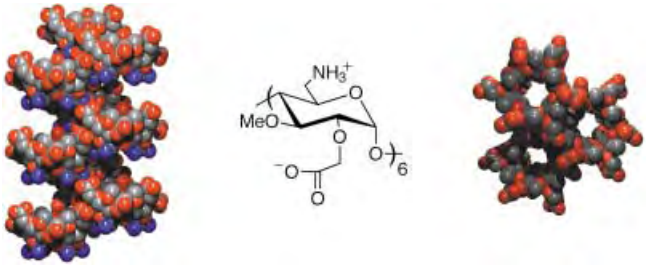
Angew. Chem. **2002**, *114*, 1788 – 1791

I. Aprahamian, R. E. Hoffman, T. Sheradsky, D. V. Preda, M. Bancu, L. T. Scott, M. Rabinovitz* 1712 – 1715

A Four-Step Alternating Reductive Dimerization/Bond Cleavage of Indenocorannulene

Keywords: dimerization · NMR spectroscopy · polyanions · polycycles · reduction

A zwitterionic α-cyclodextrin amino acid (picture, middle) undergoes solid-state self-assembly to give a novel helical column architecture (left), which is cross-linked by hydrogen bonds into an array of parallel straight channels (right). Surprisingly, no hydrogen bonds are formed between proximate cyclodextrin units in the individual channels.



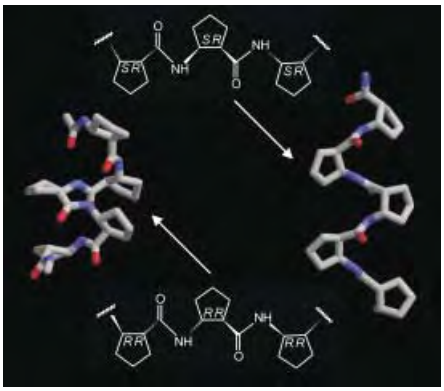
Angew. Chem. **2002**, *114*, 1791 – 1793

T. Kraus,* M. Buděšínský, I. Císařová, J. Závada* ..... 1715 – 1717

Per(6-amino-2-*O*-carboxymethyl-6-deoxy-3-*O*-methyl)-α-cyclodextrin: Helical Self-Assembly of a Polyionic Amino Acid into Nanotubes

Keywords: amino acids · cyclodextrins · helical structures · hydrogen bonds · self-assembly

Rational control over helix and strand secondary structures is possible when conformationally restricted cyclic β-amino acid residues are incorporated in the β-peptides. Inversion of the relative configuration of these residues enables the preferred periodic structure to be switched from a helix to a single nonpolar strand (see picture).



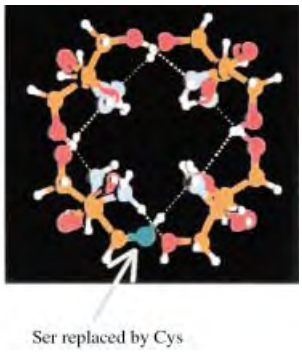
Angew. Chem. **2002**, *114*, 1794 – 1797

T. A. Martinek, G. K. Tóth, E. Vass, M. Hollósi, F. Fülöp* ..... 1718 – 1721

cis-2-Aminocyclopentanecarboxylic Acid Oligomers Adopt a Sheetlike Structure: Switch from Helix to Nonpolar Strand

Keywords: amino acids · chirality · conformation analysis · NMR spectroscopy · peptides

Chiral exchange: Substitution of cysteine for serine in the homochiral serine octamer (see calculated structure) occurs in a chirally dependent fashion and may represent an example of transfer of chirality between primitive biological molecules. The findings are supported by HF/6-31G calculations.



Angew. Chem. **2002**, *114*, 1797 – 1800

K. J. Koch, F. C. Gozzo, S. C. Nanita, Z. Takats, M. N. Eberlin, R. G. Cooks* ..... 1721 – 1724

Chiral Transmission between Amino Acids: Chirally Selective Amino Acid Substitution in the Serine Octamer as a Possible Step in Homochirogenesis

Keywords: amino acids · chirality · mass spectrometry · molecular evolution · supramolecular chemistry

 © WILEY-VCH Verlag GmbH, 69451 Weinheim, Germany, 2002 1433-7851/02/4110-1635 $ 20.00+.50/0

Like spiral staircases connecting the floors of a building, twisted chiral organic "pillars" link hydrogen-bonded guanidinium sulfonate sheets and produce extended supramolecular helices (see picture) that wind through crystals with predictable three-dimensional architectures.



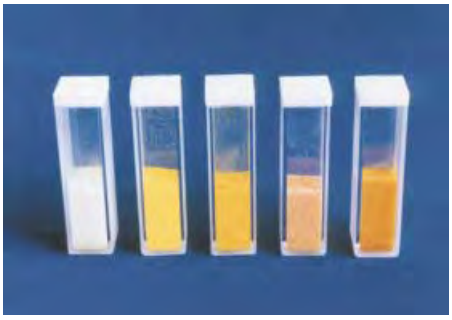
Angew. Chem. **2002**, *114*, 1800 – 1804

R. Custelcean, M. D. Ward* 1724 – 1728

Hydrogen-Bonded Helices in Crystals with Prescribed Organization

Keywords: crystal engineering · helical structures · hydrogen bonds · inclusion compounds · self-assembly

A combination of nucleophilic aromatic substitution of fluorine by amino groups with a sol – gel process leads to the synthesis of organic-functionalized hybrid gels by a one-pot method based on silicates. The sol – gel reaction is catalyzed by hydrofluoric acid formed after addition of ethanol and water. The picture shows a selection of the dried gels.



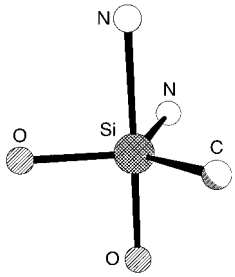
Angew. Chem. **2002**, *114*, 1805 – 1808

S. Spange,* A. Seifert, H. Müller, S. Hesse, C. Jäger ..... 1729 – 1732

A One-Pot Synthesis of Chromophoric Silicate-Based Xerogels

Keywords: fluoroarenes · nucleophilic substitution · silicates · sol – gel processes · synthetic methods

Ligands with enamine structures can be surprisingly well stabilized in pentacoordinate silicon complexes. These novel coordination complexes contain a central Si atom in a trigonal-bipyramidal coordination environment, surrounded by a threefold-deprotonated salen ligand ($2 \times N$, $2 \times O$, see structure). The complexes are starting materials for the synthesis of novel compounds containing hexacoordinate Si atoms by acid-addition reactions.



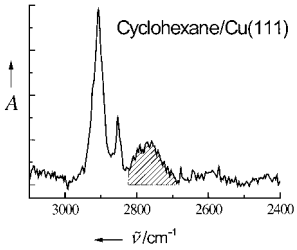
Angew. Chem. **2002**, *114*, 1825 – 1827

J. Wagler, U. Böhme, G. Roewer* ..... 1732 – 1734

Silicon – Enamine Complexes: Pentacoordinate Silicon Compounds

Keywords: chelates · hypervalent compounds · N,O ligands · Schiff bases · silicon

On contact with transition metals, saturated hydrocarbons reveal pronounced red shifts in the C–H stretching region in their IR spectra (shaded region in picture), which are discussed in connection with C–H activation. Detailed ab initio calculations for cyclopropane and cyclohexane on a Cu surface suggest that this anomaly is caused by an unexpected chemical interaction.



Angew. Chem. **2002**, *114*, 1811 – 1814

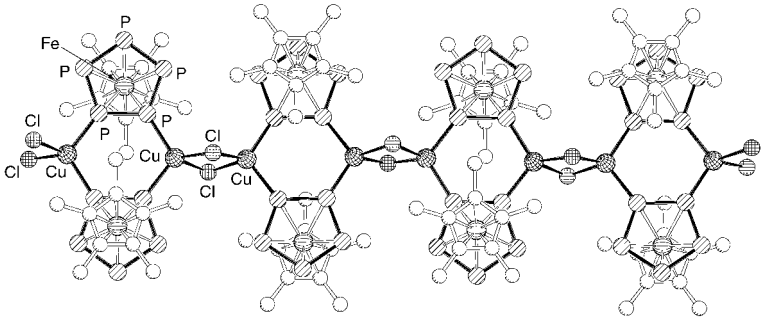
K. A. Fosser, R. G. Nuzzo, P. S. Bagus, C. Wöll* ..... 1735 – 1737

The Adsorption of Cyclopropane and Cyclohexane on Cu(111): An Experimental and Theoretical Investigation on the Nature of the CH–Metal Interaction

Keywords: ab initio calculations · adsorption · alkanes · IR spectroscopy · surface chemistry

 © WILEY-VCH Verlag GmbH, 69451 Weinheim, Germany, 2002 1433-7851/02/4110-1636 $ 20.00+.50/0

Different copper halide, different copper product: The *cyclo*-P_5-ligand complex $[Cp^*Fe(\eta^5\text{-}P_5)]$ (**1**; $Cp^* = C_5Me_5$) reacts with CuBr and CuI to give two-dimensional networks in which **1** is the linking unit. However, a novel one-dimensional-chain coordination polymer (see picture) is formed with CuCl.



Angew. Chem. **2002**, *114*, 1808 – 1811

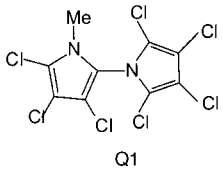
J. Bai, A. V. Virovets, M. Scheer* ..... 1737 – 1740

Pentaphosphaferrocene as a Linking Unit for the Formation of One- and Two-Dimensional Polymers

Keywords: coordination polymers · copper · iron · phosphorus · P ligands

---

Which organism produces it? The natural product Q1 is 64 % chlorine and every third atom is a halogen, but the source of Q1 is unknown. Synthetic Q1, made for the first time, has identical chromatographic and spectroscopic properties to those of Q1 extracted from environmental samples.



Q1

Angew. Chem. **2002**, *114*, 1814 – 1817

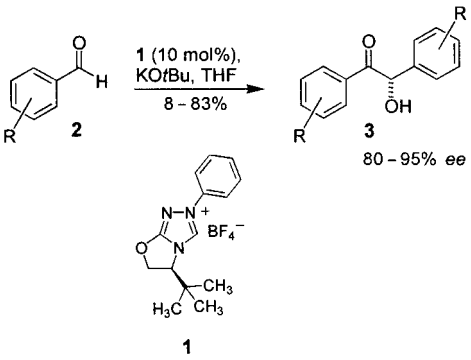
J. Wu, W. Vetter,* G. W. Gribble,* J. S. Schneekloth, Jr., D. H. Blank, H. Görls ..... 1740 – 1743

Structure and Synthesis of the Natural Heptachloro-1′-methyl-1,2′-bipyrrole (Q1)

Keywords: chlorine · halogenation · natural products · nitrogen heterocycles · structure elucidation

---

The chiral bicyclic triazolium salt 1 is currently the most efficient pre-catalyst for the asymmetric benzoin condensation. The substituted acyloins **3** are obtained in moderate to good yields and with very good enantiomeric excesses from the corresponding aldehydes **2**. The high asymmetric induction is presumably based on the conformational rigidity of the bicyclic nucleophilic carbene catalyst and on the steric hindrance of the *tert*-butyl group in the Breslow intermediate.



Angew. Chem. **2002**, *114*, 1822 – 1824

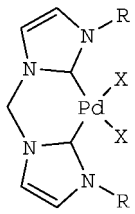
D. Enders,* U. Kallfass ..... 1743 – 1745

An Efficient Nucleophilic Carbene Catalyst for the Asymmetric Benzoin Condensation

Keywords: acyloins · asymmetric catalysis · benzoin condensation · carbenes · triazolium salts

---

Palladium complexes with N-heterocyclic carbenes, such as in the biscarbene chelate ligands shown (R = *t*Bu, Me; X = Br, I), have proved to be stable in strongly acidic media and were tested in the catalytic conversion of methane into methanol. The prominent influence of the halogenide ligand is shown since, in contrast to the bromo complex, the iodo complex does not catalyze the reaction. The steric bulk of the substituents R also influences the catalytic activity.



Angew. Chem. **2002**, *114*, 1817 – 1819

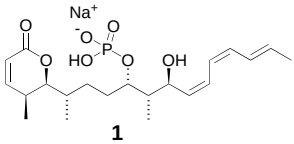
M. Muehlhofer, T. Strassner,* W. A. Herrmann ..... 1745 – 1747

New Catalyst Systems for the Catalytic Conversion of Methane into Methanol

Keywords: alkanes · carbenes · C–H activation · homogeneous catalysis · oxidation

 © WILEY-VCH Verlag GmbH, 69451 Weinheim, Germany, 2002 1433-7851/02/4110-1637 $ 20.00+.50/0

Reagent-controlled reactions are key to the introduction of the stereocenters in the total synthesis of the cytostatin isomer **1**. The stereochemical flexibility of the synthesis allows efficient and convenient access to other isomers.



1

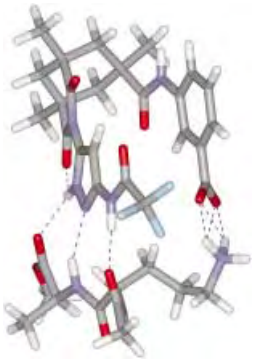
Angew. Chem. **2002**, *114*, 1819 – 1822

L. Bialy, H. Waldmann* .... 1748 – 1751

Synthesis of the Protein Phosphatase 2A Inhibitor (4*S*,5*S*,6*S*,10*S*,11*S*,12*S*)-Cytostatin

Keywords: inhibitors · natural products · phosphorylation · total synthesis

A toolkit of tailor-made peptide receptors contains building blocks for polar, aromatic, and cationic amino acids. Dipeptides are stabilized in the β-sheet conformation by complexation with an aminopyrazole which carries a U-shaped substituent with a properly placed binding site at its tip (see picture). The additional interaction with the amino acid side chain leads to a tenfold increase in the association constant.



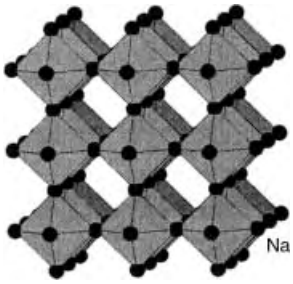
Angew. Chem. **2002**, *114*, 1827 – 1831

M. Wehner, T. Schrader* ... 1751 – 1754

Modular Building Blocks for Amino Acid Recognition in Peptides

Keywords: amino acids · host – guest systems · molecular recognition · peptides · receptors

After a long search the elusive compound Na_3N (see structure) has been synthesized for the first time, starting from the elements dispersed on an atomic level, by a solid-state reaction at extremely low temperatures. The metastable compound crystallizes in the anti-ReO_3 structure type and decomposes into the elements at 360 K.



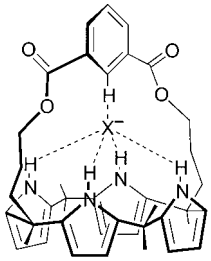
Angew. Chem. **2002**, *114*, 1831 – 1833

D. Fischer, M. Jansen* ..... 1755 – 1756

Synthesis and Structure of Na_3N

Keywords: alkali metals · nitrides · solid-state reactions · structure elucidation

Enhanced affinity and selectivity for halide anions is seen for the strapped calix[4]pyrrole (see picture, $X^- = F^-$, Cl^-) relative to normal calix[4]pyrroles. The encapsulated binding site differentiates the anions on the basis of size, and the existence of hydrogen-bonding interactions between the aromatic proton and halide anions has been verified by ^1H NMR spectroscopy. A binding constant of approximately 3.87×10^6 M was found for the fluoride complex.



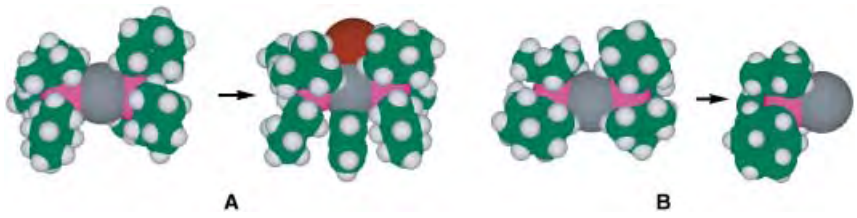
Angew. Chem. **2002**, *114*, 1835 – 1837

D.-W. Yoon, H. Hwang, C.-H. Lee* ..... 1757 – 1759

Synthesis of a Strapped Calix[4]pyrrole: Structure and Anion Binding Properties

Keywords: anions · calixpyrroles · hydrogen bonds · macrocycles · molecular recognition

The steric bulk of the phosphane ligand determines the mechanism of the ArX addition to zero-valent $[PdL_2]$ complexes. This effect has been studied by variation of ligands (catalyst: $[Pd(PCx_ntBu_{3-n})_2]$; $n = 0-3$, Cx = cyclohexyl) in Pd couplings of unsaturated electrophiles, and different reaction pathways (A = associative, B = dissociative) identified, depending on the size of the ligand.



Angew. Chem. **2002**, *114*, 1838 – 1841

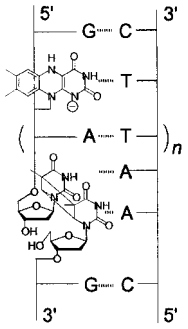
E. Galardon, S. Ramdeehul, J. M. Brown,* A. Cowley, K. K. (Mimi) Hii, A. Jutand 1760 – 1763

Profound Steric Control of Reactivity in Aryl Halide Addition to Bisphosphane Palladium(0) Complexes

Keywords: cross-coupling · palladium · phosphane ligands · reaction mechanisms · steric hindrance

 © WILEY-VCH Verlag GmbH, 69451 Weinheim, Germany, 2002 1433-7851/02/4110-1638 $ 20.00+.50/0

Remote reductive repair of thymine dimers in a DNA duplex by transfer of excess electrons over a distance of up to roughly 24 Å ($n = 7$) has been attributed to thermally activated hopping (see scheme). Possible consequences for humans: the harmful effect of UV irradiation responsible for the development of skin cancer could potentially be reduced by compounds that bind to DNA and trigger long-range electron transport.



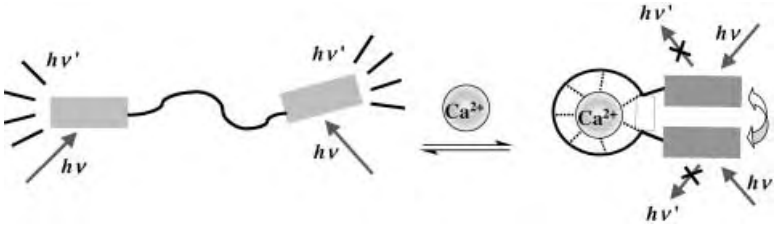
Angew. Chem. **2002**, *114*, 1841 – 1844

C. Behrens, L. T. Burgdorf, A. Schwögler, T. Carell* ..... 1763 – 1766

Weak Distance Dependence of Excess Electron Transfer in DNA

Keywords: bioorganic chemistry · DNA repair · electron transfer · photolyase

Selective, sensitive cation capture: A bichromophoric "H"-foldamer (rigid-flexible-rigid) demonstrates a cation-steered exciton interaction (see figure; the interaction is denoted by the double-headed arrow) and thereby allows the selective signaling of Ca^{2+}-ion binding among Na^+, K^+, and Mg^{2+} ions. The binding can be observed with the naked eye, as well as by absorption, emission, and ^1H NMR spectral changes. An analogous monochromophore (flexible-rigid-flexible) failed to signal any of the binding events.



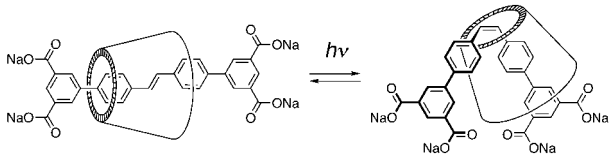
Angew. Chem. **2002**, *114*, 1844 – 1847

A. Ajayaghosh,* E. Arunkumar, J. Daub ..... 1766 – 1769

A Highly Specific Ca^{2+}-Ion Sensor: Signaling by Exciton Interaction in a Rigid – Flexible – Rigid Bichromophoric "H" Foldamer

Keywords: aggregation · calcium · chromophores · host – guest systems · sensors

Up and down the dumbbell: Photoisomerization of a stilbene rotaxane results in relocation of the cyclodextrin macrocycle in just one direction (see scheme). This behavior, and that of related rotaxanes, sheds light on the mechanism of shuttling in molecular machines.



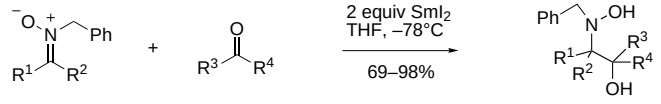
Angew. Chem. **2002**, *114*, 1847 – 1850

C. A. Stanier, S. J. Alderman, T. D. W. Claridge, H. L. Anderson* ..... 1769 – 1772

Unidirectional Photoinduced Shuttling in a Rotaxane with a Symmetric Stilbene Dumbbell

Keywords: cyclodextrins · molecular devices · photoisomerization · rotaxanes · stilbene

Highly substituted amino alcohols or *N*-hydroxyamino alcohols can be prepared in good yield through a novel reductive cross-coupling of nitrones with aldehydes or ketones (see scheme). The reactions are fast and highly chemoselective, that is, no homocoupling or reduction products are formed.



Angew. Chem. **2002**, *114*, 1850 – 1853

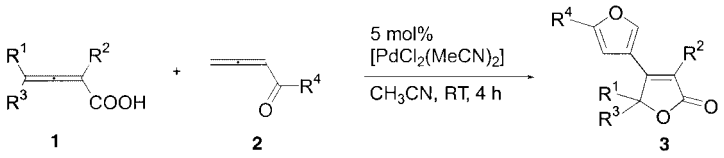
G. Masson, S. Py,* Y. Vallée* 1772 – 1775

Samarium Diiodide-Induced Reductive Cross-Coupling of Nitrones with Aldehydes and Ketones

Keywords: amino alcohols · C–C coupling · cross-coupling · nitrones · samarium

 © WILEY-VCH Verlag GmbH, 69451 Weinheim, Germany, 2002 1433-7851/02/4110-1639 $ 20.00+.50/0

The active Pd^{II} catalyst in the efficient oxidative cyclization/dimerization reaction between 2,3-allenoic acids **1** and 1,2-allenyl ketones **2** to give 4-(3′-furanyl)-butenolide derivatives **3** may be regenerated from Pd^0 after a cyclometalation/protonolysis step in the catalytic cycle.



1 2 3

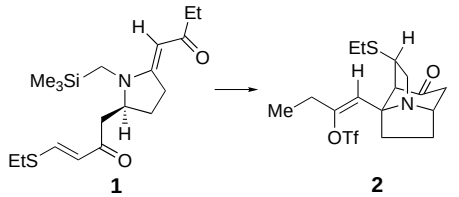
Angew. Chem. **2002**, *114*, 1853 – 1856

S. Ma,* Z. Yu ..... 1775 – 1778

Oxidative Cyclization – Dimerization Reaction of 2,3-Allenoic Acids and 1,2-Allenyl Ketones: An Efficient Synthesis of 4-(3′-Furanyl)butenolide Derivatives

Keywords: allenes · butenolides · carboxylic acids · cyclization · dimerization

An important precursor to the bridged pyrrolizidine core **2** of asparagamine A is vinylogous amide **1**. The key reaction in the synthesis of **2** is an intramolecular 1,3-dipolar cycloaddition of an azomethine ylide derived from the sulfonylation of **1**. A variety of highly functionalized pyrrolidines, pyrrolizidines, and indolizidines can be prepared from vinylogous amides such as **1**. Tf = trifluoromethanesulfonyl.



1 2

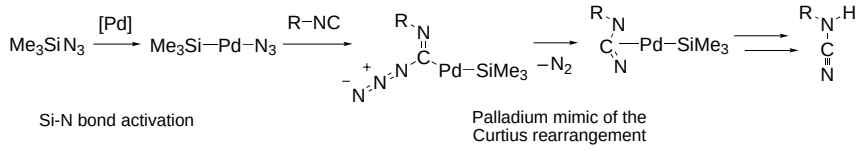
Angew. Chem. **2002**, *114*, 1856 – 1858

M. T. Epperson, D. Y. Gin* 1778 – 1780

Enantiospecific Synthesis of the Bridged Pyrrolizidine Core of Asparagamine A: Dipolar Cycloadditions of Azomethine Ylides Derived from the Sulfonylation of Vinylogous Amides

Keywords: amides · azomethine ylides · cycloaddition · natural products · synthetic methods

A palladium mimic of the Curtius rearrangement and a palladium-catalyzed geminal addition of a Si–N bond occurs in the high-yielding synthesis of cyanamides from isocyanides and trimethylsilyl azide in the presence of a palladium catalyst (see scheme). A wide range of functional groups are tolerated in the reaction.



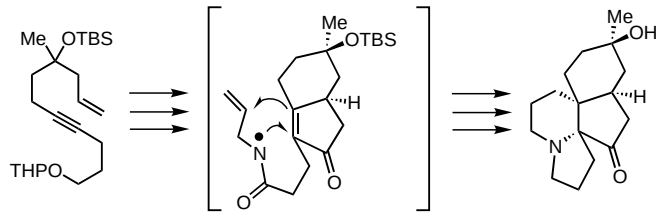
Angew. Chem. **2002**, *114*, 1858 – 1860

S. Kamijo, T. Jin, Y. Yamamoto* ..... 1780 – 1782

Cyanamide Synthesis by the Palladium-Catalyzed Cleavage of a Si–N Bond

Keywords: cyanamides · homogeneous catalysis · isocyanides · palladium · rearrangement

A short and efficient total synthesis of (±)-13-deoxyserratine (**3**) features a highly stereoselective intramolecular Pauson – Khand reaction of **1** and a cascade of radical cyclizations starting with the amidyl radical **2**. The desired alkaloid **3** was thus obtained in ten steps in an overall yield of 12%. THP = tetrahydropyranyl, TBS = *tert*-butyldimethylsilyl.



1 2 3

Angew. Chem. **2002**, *114*, 1861 – 1863

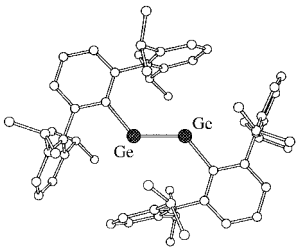
J. Cassayre, F. Gagosz, S. Z. Zard* ..... 1783 – 1785

A Short Synthesis of (±)-13-Deoxyserratine

Keywords: alkaloids · indolizidines · Pauson – Khand reaction · radical reactions · total synthesis

 © WILEY-VCH Verlag GmbH, 69451 Weinheim, Germany, 2002 1433-7851/02/4110-1640 $ 20.00+.50/0 *Angew. Chem. Int. Ed.* **2002**, *41*, No. 10

Multiple Ge–Ge bonds: The title compound, which has a *trans*-bent structure (see structure; Ge-Ge-C = 128.67(8)°) and a short Ge–Ge bond (2.2850(5) Å), is the first stable digermanium analogue of an alkyne.



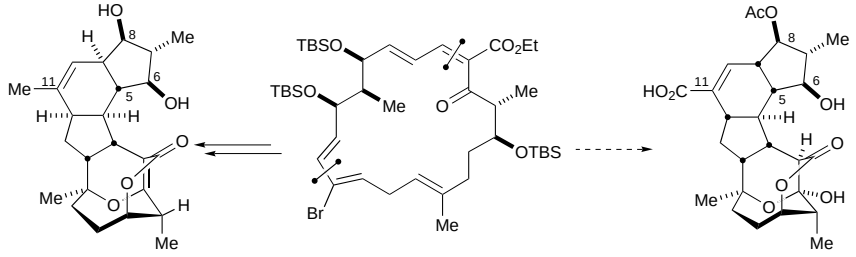
Angew. Chem. **2002**, *114*, 1863 – 1865

M. Stender, A. D. Phillips, R. J. Wright, P. P. Power* ..... 1785 – 1787

Synthesis and Characterization of a Digermanium Analogue of an Alkyne

Keywords: alkynes · digermyne · germanium · multiple bonds · structure elucidation

A tandem transannular [4+2] cycloaddition strategy is presented for the synthesis of the class of natural products containing FR182877 (**1**) and hexacyclinic acid (**2**). As part of this program, a tandem transannular [4+2] cycloaddition reaction has been employed in the enantioselective synthesis of (−)-FR182877 (**1**) via the macrocyclic precursor (**3**).



1 **3** **2**

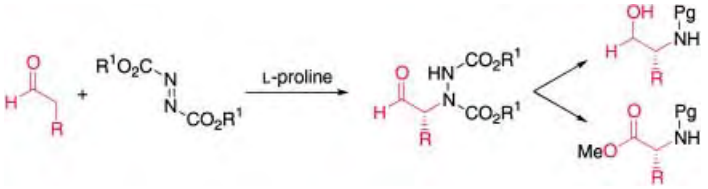
Angew. Chem. **2002**, *114*, 1865 – 1868

D. A. Evans,* J. T. Starr ..... 1787 – 1790

A Cascade Cycloaddition Strategy Leading to the Total Synthesis of (−)-FR182877

Keywords: asymmetric synthesis · cycloaddition · macrocycles · natural products

L-Proline as the catalyst: The first direct asymmetric α-amination of aldehydes using L-proline as the catalyst is presented (see scheme; Pg = protecting group). This new reaction gives easy access to optically active α-amino aldehydes, α-amino alcohols, and α-amino acids from simple and easily available starting materials and catalysts. The reactions proceed in high yields and excellent enantioselectivities with as little as 2 mol % of the catalyst.



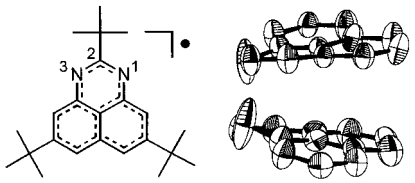
Angew. Chem. **2002**, *114*, 1868 – 1871

A. Bøgevig, K. Juhl, N. Kumaragurubaran, W. Zhuang, K. A. Jørgensen* ..... 1790 – 1793

Direct Organo-Catalytic Asymmetric α-Amination of Aldehydes—A Simple Approach to Optically Active α-Amino Aldehydes, α-Amino Alcohols, and α-Amino Acids

Keywords: aldehydes · amino acids · amino alcohols · amino aldehydes · asymmetric catalysis

Stable gable radical: 1,3-Diazaphenalenyl radical, a typical example of an isoelectronic mode of modification for phenalenyl, has been isolated for the first time as a crystalline solid by introducing bulky substituents (see picture, *tert*-butyl groups are omitted from the crystal structure). The gable *syn* dimer with a column motif shows an extremely strong antiferromagnetic exchange coupling of $2J/k_B = -4.19(2) \times 10^3$ K.



Angew. Chem. **2002**, *114*, 1871 – 1874

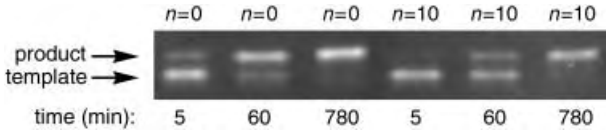
Y. Morita,* T. Aoki, K. Fukui, S. Nakazawa, K. Tamaki, S. Suzuki, A. Fuyuhiro, K. Yamamoto, K. Sato, D. Shiomi, A. Naito, T. Takui,* K. Nakasuji* ..... 1793 – 1796

A New Trend in Phenalenyl Chemistry: A Persistent Neutral Radical, 2,5,8-Tri-*tert*-butyl-1,3-diazaphenalenyl, and the Excited Triplet State of the Gable *syn*-Dimer in the Crystal of Column Motif

Keywords: dimerization · magnetic properties · nitrogen heterocycles · radicals · steric hindrance

 © WILEY-VCH Verlag GmbH, 69451 Weinheim, Germany, 2002 1433-7851/02/4110-1641 $ 20.00+.50/0

Powerful reactions such as Wittig olefinations, nitro-aldol additions, dipolar cycloadditions, and Heck coupling reactions can be mediated by DNA templates. The yields of several DNA-templated reaction products are independent of the number of bases ($n = 0$ or 10) separating the annealed reactive groups (as an example, the denaturing polyacrylamide gel electrophoresis of a DNA-templated Wittig reaction is shown).



Z. J. Gartner, M. W. Kanan, D. R. Liu* ..... 1796 – 1800

Expanding the Reaction Scope of DNA-Templated Synthesis

Angew. Chem. **2002**, *114*, 1874 – 1878

Keywords: coupling reactions · DNA · molecular evolution · synthetic methods · template synthesis

Supporting information on the WWW (see article for access details).

* Author to whom correspondence should be addressed

Accelerated publications

The cover picture was designed by Robbyn Echon and Scott Snyder.

BOOKS

Molecular Switches — Ben L. Feringa — *D. Blunk* 1801

Alkoxo and Aryloxo Derivatives of Metals — D. C. Bradley, R. C. Mehrotra, I. P. Rothwell, A. Singh — *R. Anwander* 1802

The Transuranium People: The Inside Story — Darleane C. Hoffman, Albert Ghiorso, Glen T. Seaborg — *G. B. Kauffman, L. M. Kauffman* 1803

WEB SITES

http://www.biomat.net — The World of Bodybuilding Materials — *E. Bäuerlein* 1805

SERVICE

- **VIPs** 1633
- ***Angewandte's* Sister-Journals** 1643 – 1645
- **Keywords** 1806
- **Authors** 1807
- **Preview** 1808

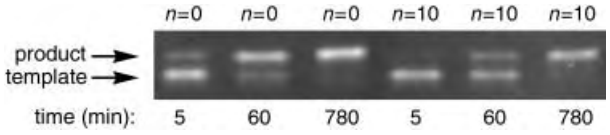
Don't forget all the Tables of Contents from 1998 onwards may be still found on the WWW under: http://www.angewandte.com

CORRIGENDUM

Note from the Editors: unfortunately the results reported in the communication "The Stable Pentamethylcyclopentadienyl Cation" by Joseph B. Lambert et al. in issue 8/2002 (pp. 1429 – 1431) must be corrected. Guy Bertrand et al. quickly discovered that not the pentamethylcyclopentadienyl cation but the pentamethylcyclopentenyl cation was prepared and characterized (the corresponding communication will be published in issue 13, and will appear earlier on the *Angewandte Chemie* homepage).

 © WILEY-VCH Verlag GmbH, 69451 Weinheim, Germany, 2002 1433-7851/02/4110-1642 $ 20.00+.50/0

Powerful reactions such as Wittig olefinations, nitro-aldol additions, dipolar cycloadditions, and Heck coupling reactions can be mediated by DNA templates. The yields of several DNA-templated reaction products are independent of the number of bases ($n = 0$ or 10) separating the annealed reactive groups (as an example, the denaturing polyacrylamide gel electrophoresis of a DNA-templated Wittig reaction is shown).



Z. J. Gartner, M. W. Kanan, D. R. Liu* ..... 1796 – 1800

Expanding the Reaction Scope of DNA-Templated Synthesis

Angew. Chem. **2002**, *114*, 1874 – 1878

Keywords: coupling reactions · DNA · molecular evolution · synthetic methods · template synthesis

Supporting information on the WWW (see article for access details).

* Author to whom correspondence should be addressed

Accelerated publications

The cover picture was designed by Robbyn Echon and Scott Snyder.

BOOKS

Molecular Switches — Ben L. Feringa — *D. Blunk* 1801

Alkoxo and Aryloxo Derivatives of Metals — D. C. Bradley, R. C. Mehrotra, I. P. Rothwell, A. Singh — *R. Anwander* 1802

The Transuranium People: The Inside Story — Darleane C. Hoffman, Albert Ghiorso, Glen T. Seaborg — *G. B. Kauffman, L. M. Kauffman* 1803

WEB SITES

http://www.biomat.net — The World of Bodybuilding Materials — *E. Bäuerlein* 1805

SERVICE

- **VIPs** 1633
- ***Angewandte's* Sister-Journals** 1643 – 1645
- **Keywords** 1806
- **Authors** 1807
- **Preview** 1808

Don't forget all the Tables of Contents from 1998 onwards may be still found on the WWW under: http://www.angewandte.com

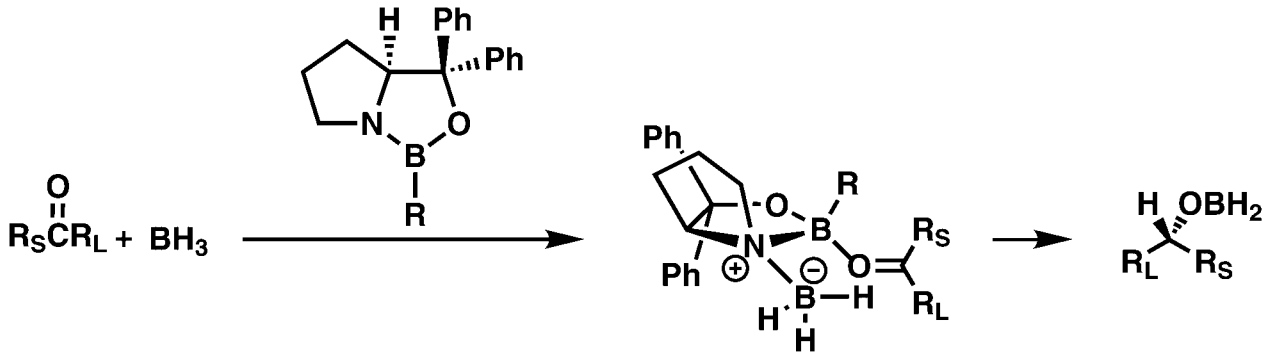
CORRIGENDUM

Note from the Editors: unfortunately the results reported in the communication "The Stable Pentamethylcyclopentadienyl Cation" by Joseph B. Lambert et al. in issue 8/2002 (pp. 1429 – 1431) must be corrected. Guy Bertrand et al. quickly discovered that not the pentamethylcyclopentadienyl cation but the pentamethylcyclopentenyl cation was prepared and characterized (the corresponding communication will be published in issue 13, and will appear earlier on the *Angewandte Chemie* homepage).

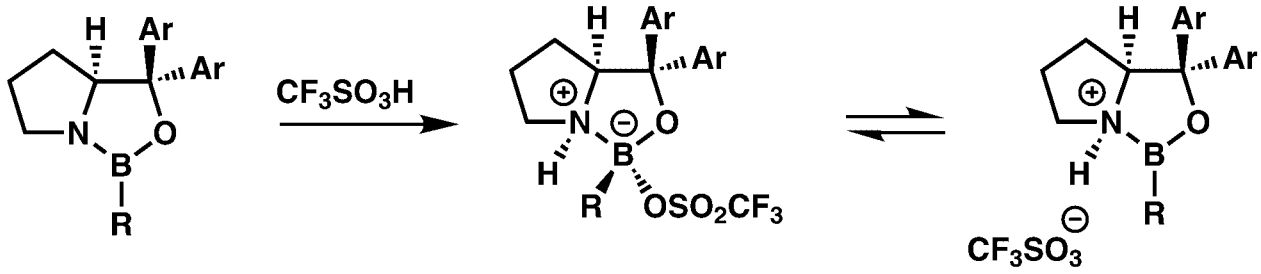
 © WILEY-VCH Verlag GmbH, 69451 Weinheim, Germany, 2002 1433-7851/02/4110-1642 $ 20.00+.50/0

Enantioselective Diels-Alder-Reactions

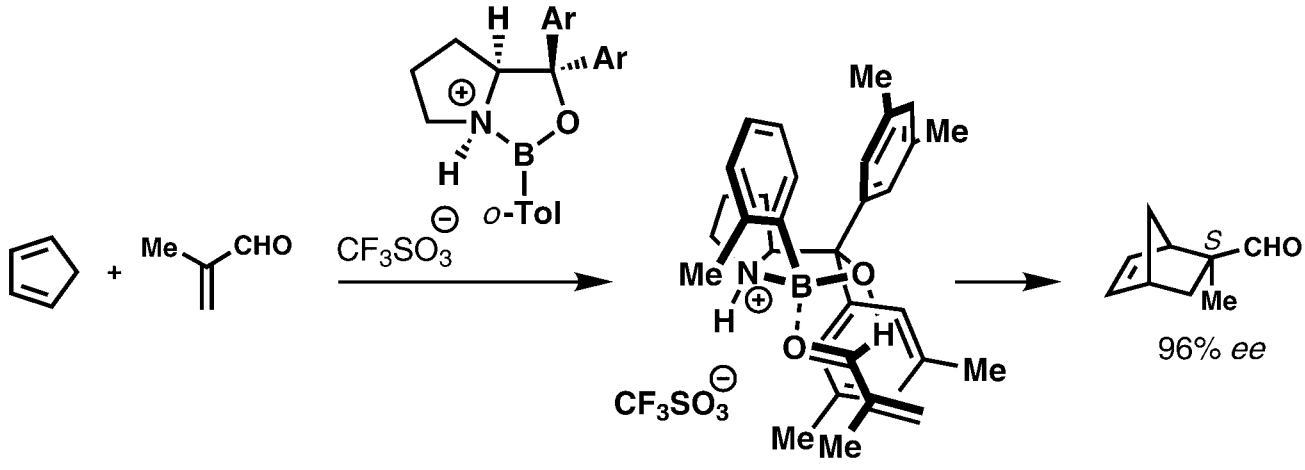
Oxazaborolidines are excellent catalysts for the highly enantioselective reduction of ketones:



The oxazaborolidines are converted by protonation into potent cationic chiral Lewis acids:



These chiral cationic Lewis acids are extraordinarily effective catalysts for enantioselective Diels–Alder reactions, for example:



96% *ee*

ANGEWANDTE CHEMIE
© WILEY-VCH

Catalytic Enantioselective Diels–Alder Reactions: Methods, Mechanistic Fundamentals, Pathways, and Applications

E. J. Corey*

Dedicated to the Memory of Kurt Alder

One hundred years after the birth of Kurt Alder and seventy-five years after the discovery of his famous reaction, one of the most important and fascinating transformations in chemistry, research on that process continues to surprise, excite, delight, and inform the chemical community. This article is based on presentations given first at the University of Cologne, Germany (Kurt Alder lecture, 1992), then at the Roger Adams Award Symposium (1993), and later at the Bürgenstock Conference of 2001, and describes research by our group on the development and understanding of enantioselective versions of the Diels–Alder reactions. The elements of this review include 1) development of new chiral Lewis acid catalysts for highly enantioselective (>25:1) [4+2] cycloadditions; 2) the fine mechanistic details and pre-transition-state assemblies of these reactions; 3) the fundamental understanding of catalytic activity and enantioselectivity for highly enantioselective Diels–Alder processes; and 4) applications to the synthesis of complex molecules. The range and power of the Diels–Alder reaction have steadily increased over seven decades. The end of this remarkable development is not in sight, a high compliment to this field of Science and to its great inventor.

Keywords: asymmetric catalysis · chiral ligands · cycloaddition · Lewis acids · transition states

1. Introduction

This year marks the centennial of the birth of Kurt Alder (1902–1958), one of the twentieth century's great organic chemists. His discovery with Otto Diels[1] and the subsequent development of the Diels–Alder reaction were transforming events in chemistry, as recognized by the award of the Nobel Prize in Chemistry in 1950 to this teacher–student pair. The impact of the Diels–Alder reaction on synthetic chemistry was so great just 15 years after its discovery that Alder wrote in a long review in 1943, "Any attempt at a systematic treatment of the diene synthesis (as he modestly called his reaction) must be strictly limited in its scope."[2] Yet, the true power and effectiveness of the Diels–Alder reaction only began to be realized in the 1950s and 1960s with the elegant applications of the process to the total synthesis of many complex natural products.[3] The development continued with no let up in pace. Many different versions of the Diels–Alder reaction were elaborated, including intramolecular [4+2] cycloadditions, hetero Diels–Alder reactions, pressure-accelerated Diels–Alder reactions, and Lewis acid accelerated Diels–Alder reactions.[4] If one chemical reaction had to be selected from all those in the repertoire of synthetic organic chemists as the most useful and powerful synthetic construction, it was clear by 1970 that the Diels–Alder reaction would be the logical choice. Its application not only leads to a strong increase in molecular complexity (molecular size, topology, stereochemistry, functionality, and appendages), but also can result in structures that lend themselves to additional amplification of complexity by the use of other powerful synthetic reactions. Yet, further advances in scope and utility of this Grand Old Reaction of synthesis were to come. This article summarizes a program of research that has been carried out in our laboratories at Harvard University over the past three decades with the objective of extending the reach of the Diels–Alder reaction to new domains, especially in terms of control of absolute stereochemistry, and to a much deeper understanding of the fine mechanistic details and pathways of Lewis acid accelerated Diels–Alder additions. It must be emphasized at the outset that many other research groups have been active in the field of stereocontrol and enantioselective synthesis during this period. Also, the science of organic synthesis has benefited greatly from the development of new reagents and catalysts for other types of enantiose-

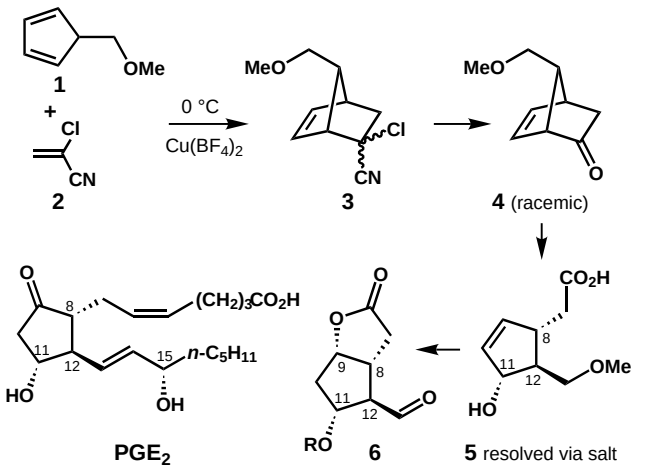
[*] Prof. E. J. Corey
Department of Chemistry and Chemical Biology, Harvard University
12 Oxford Street, Cambridge, Massachusetts, 02138 (USA)
Fax: (+1) 617-495-0376
E-mail: corey@chemistry.harvard.edu

 © WILEY-VCH Verlag GmbH, 69451 Weinheim, Germany, 2002 1433-7851/02/4110-1651 $ 20.00+.50/0

lective reactions, currently one of the most dynamic aspects of chemistry.[5–6]

2. Early Studies

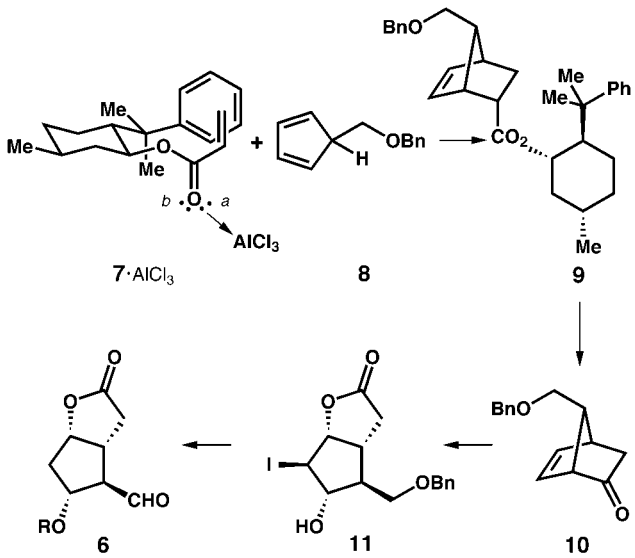
Three decades ago, a general synthesis of prostaglandins was demonstrated which provided access to biologically important prostaglandins (PGs) of all three known families from a common intermediate; for example, PGE_2 (a member of the second family) from lactone aldehyde **6** in Scheme 1.[7–9] The



Scheme 1. Synopsis of a general route for the synthesis of members of each of the three prostaglandin families from a common synthetic intermediate.

first step of the synthetic sequence was the cupric fluoroborate catalyzed Diels–Alder reaction of diene **1** with 2-chloroacrylonitrile (**2**) to form a mixture of the two diastereomeric α-chloronitriles **3**, base treatment of which afforded the racemic bicyclic ketone **4** efficiently. This example constituted the first use of a reactive Cu^{II} salt as a Lewis acid for accelerating the Diels–Alder addition, a demonstration of 2-chloroacrylonitrile as a ketene equivalent, and the first example of a catalytic Diels–Alder reaction in the synthesis of complex natural products. Baeyer–Villiger oxidation of the ketone **4** followed by lactone hydrolysis and resolution of the resulting racemic acid with ephedrine provided the chiral hydroxy acid **5**. Lactone aldehyde **6** was readily obtained from **5** and was transformed into the various PGs of the first, second, and third families. This synthesis proved to be so effective that it was used in many laboratories to prepare many PGs and PG analogues. However, it was apparent to us that the process could, in principle, be improved by eliminating the resolution step and the associated loss of material. This realization and subsequent research led to the development of the first highly enantioselective version of the Diels–Alder reaction.

This enantioselective synthesis of PGs via the key prostaglandin intermediate **6** (Scheme 2) used the dextrorotatory acrylate ester of 8-phenylmenthol (**7**) as a chiral ketene equivalent for the $AlCl_3$-catalyzed Diels–Alder reaction with



Scheme 2. Enantioselective synthesis of **6** by using 8-phenylmenthol as a chiral controller.

the achiral diene **8**.[10, 11] Cycloaddition occurred smoothly at $-55\,^{\circ}C$ in CH_2Cl_2 for 1 hour to give the *endo* adduct **9** in 89% yield with 97:3 diastereoselectivity. An oxidative C–C cleavage protocol converted **9** into the bicyclo[2.2.1]heptenone **10** with recovery of the 8-phenylmenthol controller. Ketone **10** was transformed by known procedures into the iodolactone **11** (100% *ee* after one recrystallization) and thence into the lactone aldehyde **6**.[7, 8]



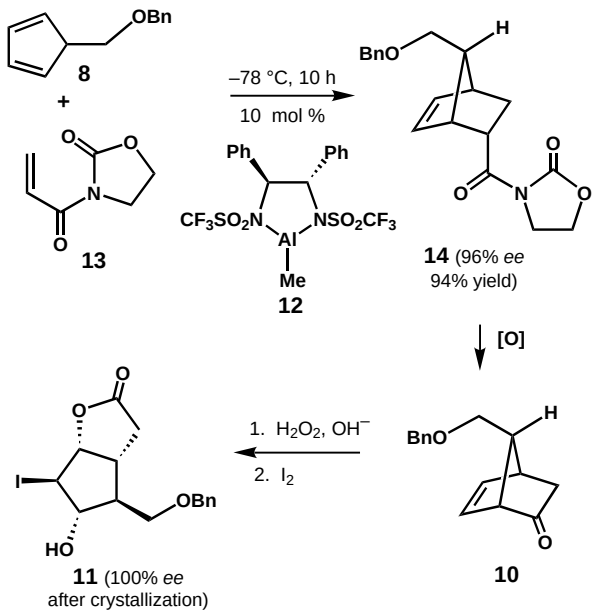
Elias J. Corey, born in 1928 in Methuen, 30 miles north of Boston, studied chemistry from 1945–1950 at the Massachusetts Institute of Technology, where he gained his doctorate for work on synthetic penicillins under the supervision of John C. Sheehan. In January 1951 he joined the University of Illinois at Urbana-Champaign as an Instructor in Chemistry and was promoted in 1956 to full Professor. Since 1959 he has been at Harvard University. For as long as he can remember he has enjoyed study, adventure, and discovery.

The mechanistic insights which guided the selection of the 8-phenylmenthol as chiral controller and the development of this enantioselective route to PGs can be summarized as follows. The activation of the acrylate dienophile **7** by $AlCl_3$ was expected to occur by coordination to the sterically more accessible lone pair *a* on the carbonyl oxygen atom (Scheme 2). In that complex the antiperiplanar (*s-trans*) arrangement of the vinyl and carbonyl subunits of the acrylate is clearly much more stable than the synperiplanar (*s-cis*) form because of strong steric repulsion in the latter. In the complex $\mathbf{7}\cdot AlCl_3$, the phenyl group is situated so as to allow an attractive interaction between the cationic acrylyl group and the π-basic benzenoid ring, which is well positioned with the electron-deficient carbonyl carbon atom lying just over the *ortho* carbon atom of the phenyl substituent at the optimum π–π spacing of approximately 3.5 Å. Thus, the phenyl group of the controller can block the [4+2] cycloaddition of **8** to the rear face α,β-acrylyl olefin (i.e. the *Si* face of C_α) and thereby favor the formation of **9** by forcing the diene to add to the front face (*Re* face of C_α).[12] As expected on the basis of this argument, the stereoselectivity of the reaction of diene **8** with menthyl acrylate is relatively poor under the same conditions employed for the formation of adduct **9**. One more important point must be made here in regard to the transition state for the proposed reaction pathway. In that transition state, that is, as the diene **8** is adding to the α,β-double bond of $\mathbf{7}\cdot AlCl_3$, the carbonyl carbon atom of the acrylate remains highly electron-deficient and hence a strong attractive interaction is maintained between the neighboring π-electron-rich phenyl group and that carbonyl carbon atom. Thus, the phenyl group of the controller directly favors the transition state that leads to the dominant Diels–Alder product **9**.[13]

3. Enantioselective Diels–Alder Reactions with Chiral Diazaaluminolidines as Catalysts

The idea that π-electron-rich aromatic groups could be used both to stabilize specific transition-state geometries and to provide stereoselectivity through facial screening served as a promising heuristic for the development of enantioselective catalysts for Diels–Alder reactions. Guided in part by this idea, a new type of catalytic enantioselective Diels–Alder reaction was discovered, one example of which is shown in Scheme 3. The bistrifluoromethanesulfonamide of (*S*,*S*)-1,2-diphenyl-1,2-diaminoethane reacts with trimethylaluminum in 1,2-dichloroethane to form the diazaaluminolidine catalytic system **12**. The reaction of **8** with 3-acryloyl-1,3-oxazolidin-2-one (**13**) in the presence of **12** (10 mol%) produces efficiently the chiral Diels–Alder adduct **14** (96% *ee*) shown in Scheme 3.[14–16] The bistriflamide ligand is readily recovered for reuse and consequently only 10 mol% of the inexpensive trimethylaluminum is consumed in this process, which provides an excellent route to PGs via the usual intermediates **10** and **11**.

The fine mechanistic details of the Diels–Alder reaction **8** + **13** → **14** are of great interest because of its high efficiency and novelty. In the solid state, the diazaaluminolidine exists as a dimer whose structure was determined by X-ray crystallography to be that shown in Figure 1 A.[17] The ^1H, ^{13}C and ^{19}F NMR spectra of this diazaaluminolidine show that it also exists as a dimer in CH_2Cl_2 solution.[17] However, in the presence of one or more equivalents of 3-acryloyl-1,3-oxazolidin-2-one, the Diels–Alder catalyst forms a 1:1 complex whose preferred geometry was revealed by low-temperature ^1H and ^{13}C NMR spectroscopic analysis (including NOE) to be that shown in Figure 1 B. It is of interest that this geometry of the 1:1 complex places the metal-complexed carbonyl group and an aromatic ring in proximity and leads to the possible transition-state assembly shown in Figure 2 A,



Scheme 3. Catalytic enantioselective Diels–Alder reaction for the general synthesis of prostaglandins.

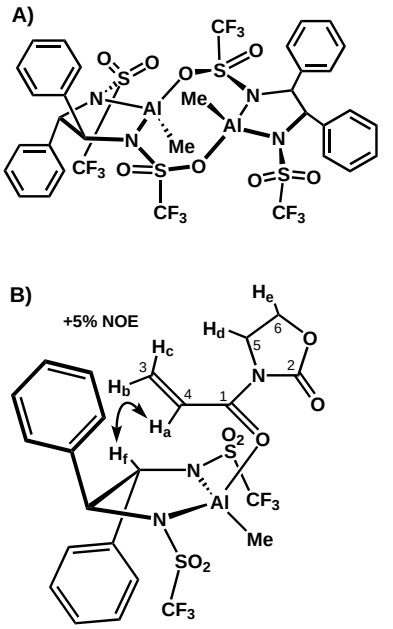


Figure 1. A) X-ray solid-state and solution structure of catalyst **12**. B) Complex of **12** with **13** as revealed by low-temperature ^1H NMR spectroscopic analysis.

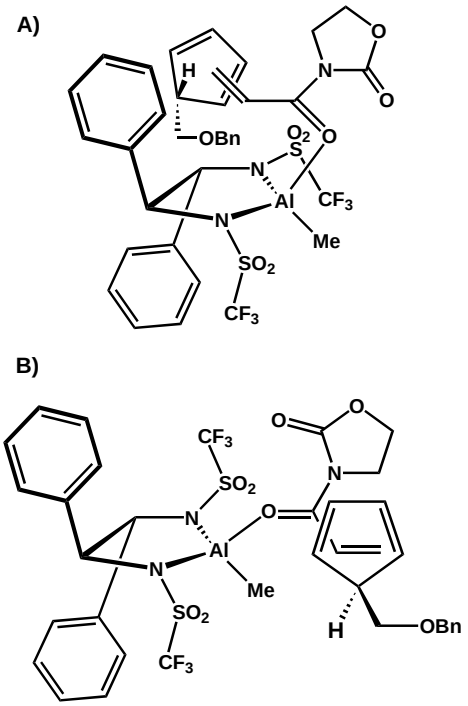
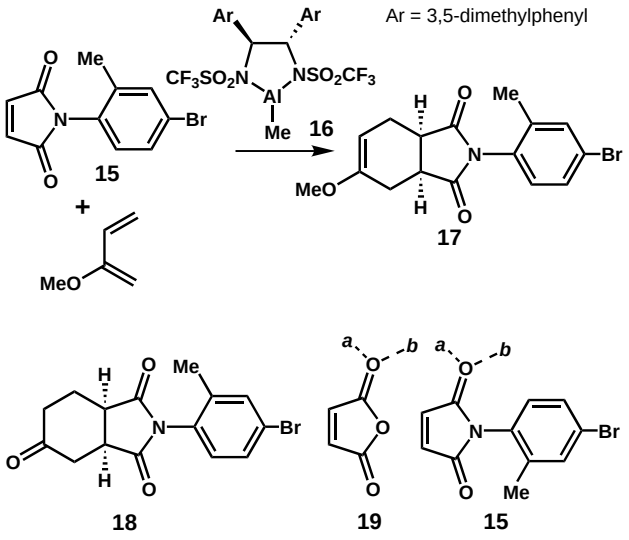


Figure 2. A) Favored pre-transition-state assembly for the formation of **14**. B) Less favored alternative.

which is consistent with the observed enantioselectivity.[17] An alternative transition-state assembly, which cannot be excluded, is shown in Figure 2B. Despite the NMR spectroscopic evidence indicating the geometry of Figure 2A to be favored, it is entirely possible that the main reaction course involves a minor component of the system such as that in Figure 2B. This sort of issue invariably recurs in the analysis of mechanistic pathways for enantioselective reactions, and, indeed, is a central problem in the design of new enantioselective catalysts and reagents. It is one of the most interesting problems in the field of mechanistic chemistry. Further evidence in favor of the transition-state assembly in Figure 2A is the fact that the replacement of the two phenyl groups of the catalyst by cyclohexyl groups results in a catalytic reaction that is not enantioselective. Furthermore, replacement of the two phenyl groups by the more electron-rich 3,5-dimethylphenyl group leads to a catalyst that gives rise to even higher enantioselectivities in various Diels–Alder reactions such as those with *N*-arylmaleimides as dienophiles.

The Diels–Alder reaction of 2-methoxybutadiene with the *N*-arylmaleimide **15** in the presence of catalyst **16** (20 mol%) in toluene at $-78\,^{\circ}C$ affords the adduct **17** in 96% yield with >97% *ee* (Scheme 4), the absolute configuration of which was shown by acidic hydrolysis to the crystalline ketone **18** and X-ray diffraction analysis.[18] *Ortho* substitution on the *N*-aryl group in the maleimide is essential for optimal enantioselectivity, which suggests that steric shielding to prevent complexing of the catalyst to lone pair *b* is crucial. In contrast, the use of maleic anhydride (**19**) instead of **15** in the reaction led to the formation of an adduct with a very low *ee* value (<20%), possibly because of coordination of catalyst **16** with



Scheme 4. Enantioselective synthesis of **17** and **18** through catalyst coordination to electron pair a of **15**.

19 at lone pair *b* or, alternatively, because of a blend of pathways that involves both *a* and *b* coordination.

Low-temperature 2D ^{1}H NMR spectroscopic analysis of the 1:1 complex of the dienophile *N*-(2-*tert*-butylphenyl)maleimide and **16** in CD_2Cl_2 solution at $-73\,^{\circ}C$ revealed the NOE enhancements that are summarized in Figure 3 and led

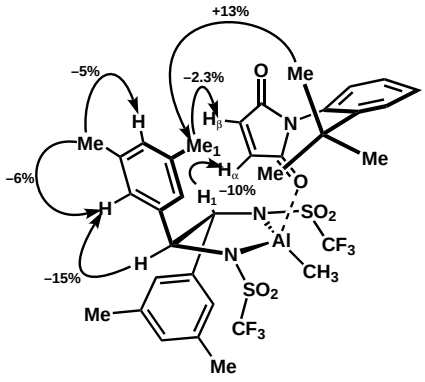


Figure 3. Observed NOE enhancements in the 1:1 complex of **16** with *N*-(2-*tert*-butylphenyl)maleimide.

to the implication of the structure shown in the Diels–Alder pathway.[18] That structure allows optimal $\pi-\pi$ interaction between the Al-coordinated carbonyl group and C2 of the nearby 3,5-dimethylphenyl group. Figure 4A shows the pre-transition-state assembly that leads from this complex as pictured in Figure 3 to the experimentally observed product (e.g. **17**, Scheme 4). Shown in Figure 4B is an alternative pre-transition-state assembly that might also produce a compound such as **17**, but involves severe repulsions and is, therefore, unlikely to be significant.[18]

The utility of the enantioselective Diels–Alder reactions of achiral *N*-arylmaleimides with the chiral catalyst **16** has been demonstrated by an enantioselective total synthesis of gracilins B and C, a pair of structurally novel marine natural products (Scheme 5).[19] The key step is the initial Diels–

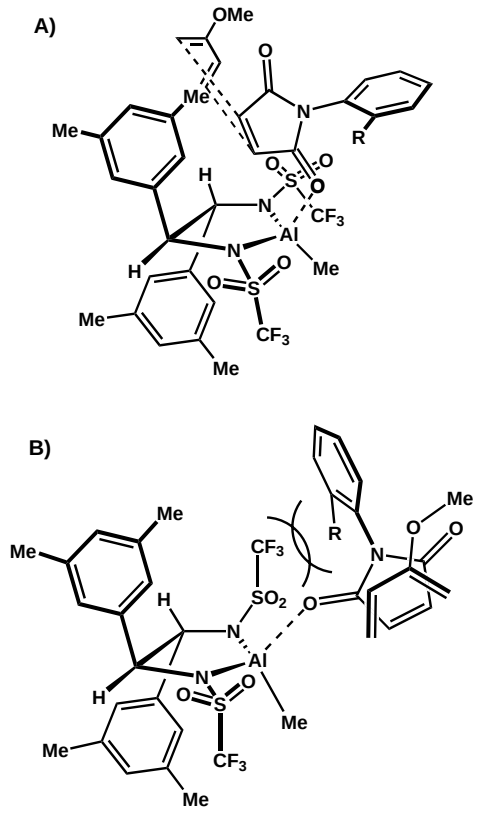
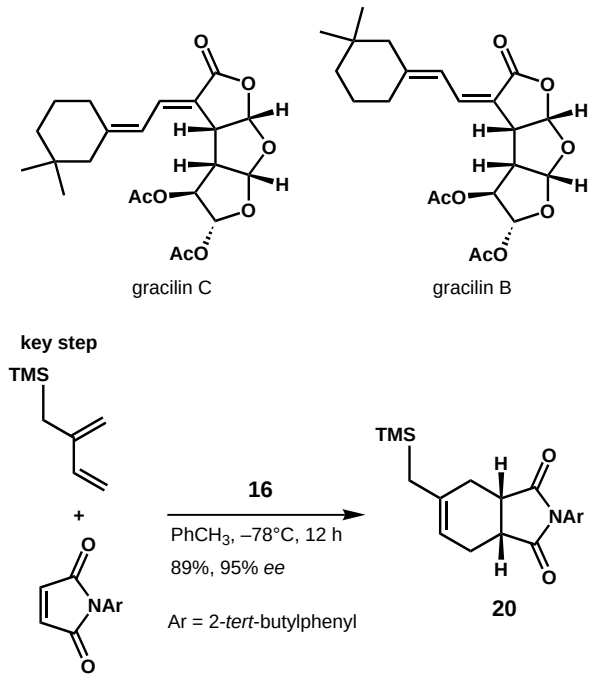


Figure 4. A) Favored and B) disfavored pre-transition-state assemblies for the reaction of 2-methoxybutadiene with **15** and catalyst **16** to form **17**.

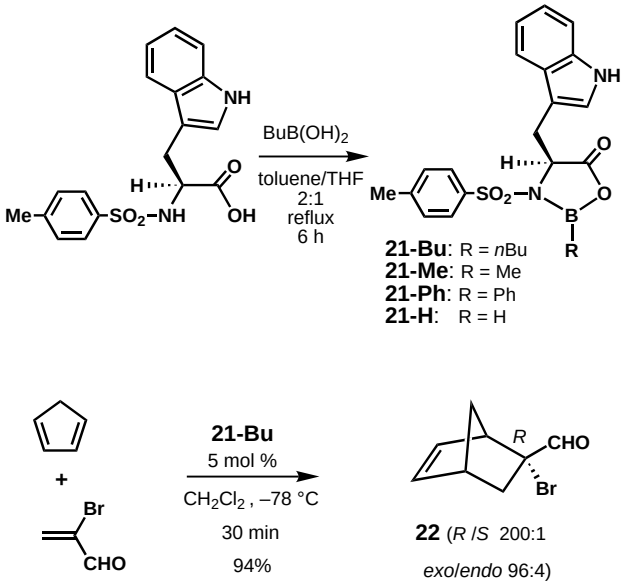


Scheme 5. Establishment of a structural platform (**20**) for the synthesis of gracilins B and C by catalytic enantioselective Diels–Alder reaction. TMS = trimethylsilyl.

Alder reaction using catalyst **16**, which directs the reaction of 2-trimethylsilylmethylbutadiene and *N*-(2-*tert*-butylphenyl)-maleimide to form the chiral adduct **20** (89% yield, 95% *ee*). In the synthesis, the maleimide carbon atoms of **20** become the central tetrahydrofuran subunit of gracilins B and C, and the cyclohexene moiety provides the carbon atoms for the two five-membered rings fused to it. As with the PG syntheses outlined in Schemes 1–3, the six-membered ring formed in the key Diels–Alder step does not remain as such in the final target structure. This is an interesting and now not uncommon "strategic look-ahead" feature of retrosynthetically planned syntheses of complex structures that depends on the remarkable power of the Diels–Alder reaction to create versatile intermediates that can be radically modified en route to the final target.

4. Oxazaborolidines as Chiral Catalysts

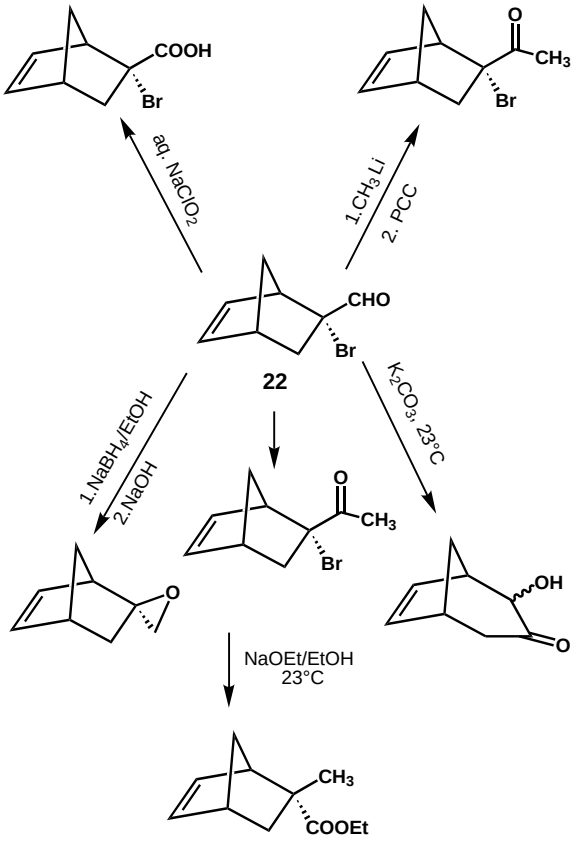
The use of chiral oxazaborolidines as catalysts for the enantioselective reduction of ketones by various boranes has proven to be a valuable synthetic method.[20] The oxazaborolidine system also appeared to have considerable potential for application to other reactions. Our experience with the role of neighboring π-electron-rich aromatic groups to channel Diels–Alder reactions along a specific stereochemical pathway led to a study of *N*-arylsulfonyl tryptophan derivatives as ligands for enantioselective Diels–Alder reactions because of the high π-electron-donating character of the indole ring. (*S*)-*N*-*p*-Toluenesulfonyltryptophan could be converted into the *B*-*n*-butyloxazaborolidine **21-Bu** (Scheme 6).[21] The *B*-methyl (**21-Me**) and *B*-phenyl (**21-Ph**) analogues can be prepared similarly. Furthermore, oxazaborolidine **21-H** · THF is available by reaction of *N*-*p*-toluenesulfonyltryptophan with a solution of BH_3 in THF followed by removal of solvent in vacuo. Just 5 mol% of catalyst **21-Bu** suffices for the acceleration and control of the reaction of cyclopentadiene and 2-bromoacrolein at –78 °C in CH_2Cl_2 to form enantioselectively (ca. 200:1) the 2*R* adduct **22** in high



Scheme 6. Generation of oxazaborolidines from (*S*)-*N*-*p*-toluenesulfonyltryptophan and application to a highly enantioselective Diels–Alder reaction.

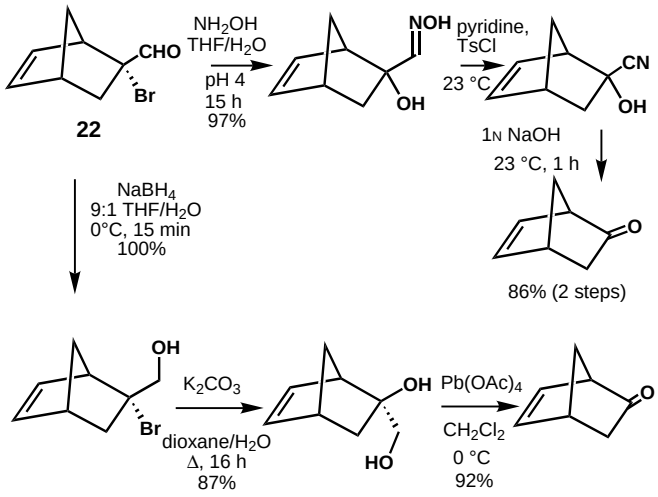
yield.[21] Equally good results are obtained with 2-chloroacrolein. The reaction of 2-methyl- or 2-ethylacrolein with cyclopentadiene affords the 2*R* adduct with 98:2 selectivity. In each of these reactions, the adduct with the *exo* orientation of the formyl group is obtained with high selectivity, for steric reasons. In contrast, the corresponding reaction of cyclopentadiene with acrolein forms the *endo* formyl adduct with opposite and low enantiofacial selectivity (30:70) with respect to the enal under the same conditions.[21] The mechanistic reasons for this difference are discussed below.

The catalytic Diels–Alder process outlined in Scheme 6 is synthetically very useful. The small amount of the diastereomeric *endo* aldehyde that contaminates **22** is easily removed by stirring at room temperature with the equivalent amount of aqueous silver nitrate because it is much more reactive than **22** (owing to the *exo* orientation of the bromine atom) and affords water-soluble products. The bromoaldehyde **22** is a very versatile intermediate as it can be converted into a wide variety of useful products (Scheme 7).



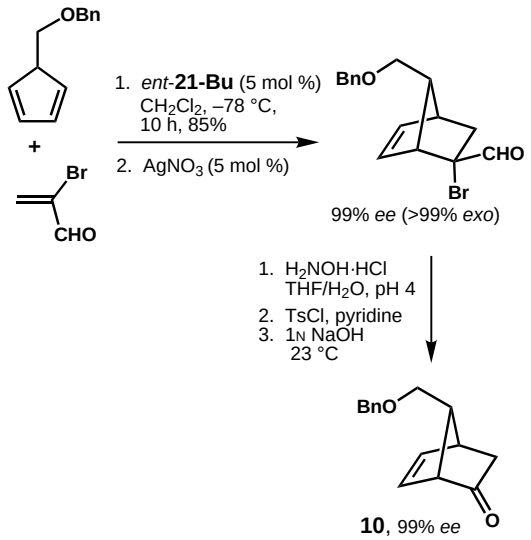
Scheme 7. Some transformations of Diels–Alder adduct **22**. PCC = pyridinium chlorochromate.

Two very efficient methods have been developed for the transformation of **22** into bicyclo[2.2.1]hepten-2-one with high (>99%) enantiomeric purity (Scheme 8). Catalyst **21-Bu** (Scheme 6) is also useful for the promotion of highly enantioselective Diels–Alder reactions of 2-chloro- or 2-bromoacrolein with furan, 2-methylbutadiene, or 2-triisopropylsilyloxybutadiene.[21–24] The application of catalyst *ent*-**21-Bu** to the catalytic enantioselective synthesis of prostaglandins is



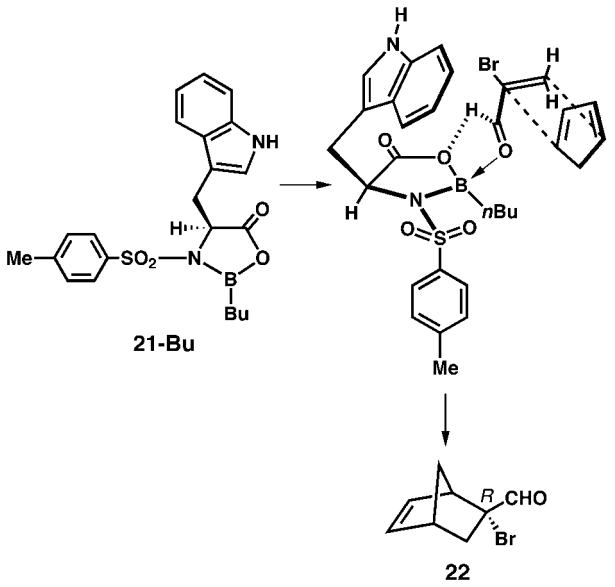
Scheme 8. Efficient syntheses of chiral bicyclo[2.2.1]hepten-2-one. Ts = *p*-toluenesulfonyl.

summarized in Scheme 9.[24] Because of the simplicity and efficiency of this approach it is well suited for large-scale production. The catalyst precursor, (*R*)-*N*-*p*-tosyltryptophan, is cheap and easily recovered for reuse.



Scheme 9. Catalytic enantioselective synthesis of the key prostaglandin intermediate **10**.

The concept that led to the discovery of the enantioselective Diels–Alder catalyst **21** can be summarized as follows: If the dienophilic α,β-enal coordinates to the face of the boron atom in **21** that is *cis* to the 3-indolylmethyl substituent, the π-basic indole unit can stabilize the π-acidic coordinated dienophile through internal π-complexation (Scheme 10). In the complex, the indole and α,β-enal moieties can assume a parallel orientation at the ideal separation (ca. 3.5 Å) for π-interaction. Steric screening by the indole ring would serve to block one face of the α,β-enal from attack by the diene. The pre-transition-state assembly for the reaction of the *s-cis*-α,β-enal complex with cyclopentadiene successfully predicts the correct absolute configuration of the product **22**.



Scheme 10. Proposed pre-transition-state assembly for the enantioselective addition of 2-bromoacrolein and cyclopentadiene catalyzed by **21-Bu**.

Some support for this model is provided by the following experimental results:[24] 1) Addition of 2-bromoacrolein to catalyst **21-Bu** in CH_2Cl_2 at $-78\,^{\circ}C$ results in an immediate orange-red coloration (similar to that of the indole-1,3,5-trinitrobenzene mixture in CH_2Cl_2), thus indicating a π-acceptor/donor interaction. 2) Catalysts in which the 3-indolylmethyl group of **21-Bu** is replaced by phenyl or isopropyl groups are effective in catalyzing the Diels–Alder reaction, but are only weakly enantioselective and actually favor the *enantiomer* of **22**. 3) The catalyst **23-Bu** (Figure 5), which is

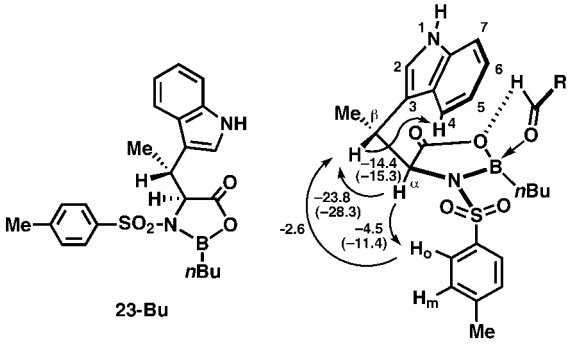


Figure 5. NOE data on the complex of catalyst **23-Bu** with 2-methylacrolein.

analogous to **21-Bu** and is obtained from *N*-tosyl-($\alpha S,\beta R$)-β-methyltryptophan is as effective as **21-Bu** in accelerating and controlling the formation of adduct **22**, as expected for the transition-state assembly shown in Scheme 10. It is even somewhat more enantioselective than **21-Bu** as a catalyst for the reaction of cyclopentadiene and 2-methylacrolein. The geometry of the complex of **23-Bu** with 2-methylacrolein has been probed by NMR spectroscopic studies, especially low-temperature ^{1}H 2D NOESY measurements.[24] The NMR spectral data demonstrate that the catalyst–aldehyde complex is conformationally fairly rigid and that the preferred molecular geometry approximates that depicted in Figure 5 (ca. 55° $HC_\alpha C_\beta H$ dihedral angle). The aldehyde complexation is rapidly reversible on the NMR timescale at 210 K, as indicated by the chemical shifts for the aldehyde moiety (e.g. as compared to the static methylacrolein–BF_3 complex) and its sharp spectrum. The fact that 2-methylacrolein is complexed to the face of the boron atom that is proximate to the indole ring is indicated by the bright orange-red color of the complex at 210 K, which fades upon warming to 250 K and reappears on cooling. This color, which corresponds to a broad absorption band in the 400—600-nm region, indicates π-complexation between the π-donor indole ring and the coordinated aldehyde, consistent with the sort of arrangement shown in Figure 5 and with approximately 3.5-Å spacing between donor and acceptor elements. Further evidence for the proximity of the coordinated aldehyde and indole subunits in the complex derives from the fact that the ^{1}H NMR peak assigned to the CH_3 group of 2-methylacrolein in the 1:1 mixture with **23-Bu** moves *upfield* with decreasing temperature (from $\delta = 1.79$ at 262 K to $\delta = 1.46$ at 188 K in CD_2Cl_2) in contrast to the *downfield* shift of the signal for the CH_3 group in a 1:1 mixture of 2-methylacrolein and BF_3 with decreasing temperature.

Since the NMR spectral data indicate that the association of α,β-enal and catalyst is rapidly reversible on the NMR timescale, it is clear that complexes of both *s-cis* and *s-trans* forms of the α,β-enal are in rapid equilibrium, and that enantioselectivity arises from a faster reaction of the *s-cis* complex **24a** than of the *s-trans* complex **24b** (Figure 6). One

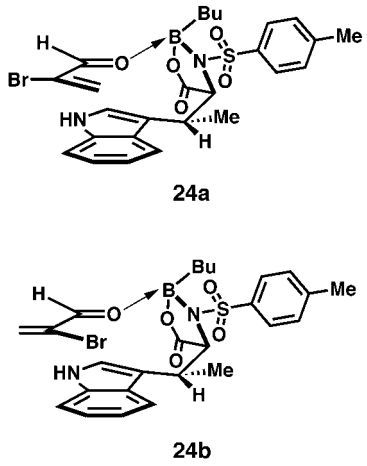


Figure 6. *s-cis* (**24a**) and s-*trans* (**24b**) Complexes of 2-bromoacrolein with Diels–Alder catalyst **23-Bu**.

apparent reason for a preferred pathway via **24a** is that the transition state for the addition of cyclopentadiene involves less steric repulsion than that from **24b**. Specifically, the $sp^2 \rightarrow sp^3$ transformation of the α and β carbon atoms in the transition state from **24b** entails serious repulsion between the α-bromine substituent and the indole ring, which maintains proximity because of the attraction with the electron-deficient formyl carbon atom in the transition state. The transition state from **24a** is free from this repulsion of the bromine atom. The nearest indole atom neighbor of the formyl carbon atom in

complex **24a** or **24b** is the nitrogen atom, a geometry which corresponds electronically (in the HOMO – LUMO sense) to that observed in the crystalline indole – 1,3,5-trinitrobenzene complex,[25] and which is therefore ideal for maintaining proximity between the formyl and indole subunits. In summary, the *s-cis* complex **24a** and the *s-trans* complex **24b** expose opposite faces of the dienophile to attack by the diene, and the enantioselectivity of the reaction is a consequence of the considerable difference in transition-state energies, with that corresponding to reaction from the *s-cis* complex **24a** being the lower. It is of considerable interest in connection with these ideas that, as we have shown for the solid state (by X-ray diffraction analysis) and for solution in CH_2Cl_2 (by low-temperature ^{13}C and ^1H NMR spectroscopic studies), the only observed form of the BF_3 – 2-methylacrolein complex is that with *s-trans* geometry.[26] The fact that the **21-Bu**- or **23-Bu**-catalyzed reaction of cyclopentadiene and acrolein is not very enantioselective is consistent with this analysis for **24a** and **24b** pathways of Figure 6.

Another insight into the fine details of the enantioselective Diels – Alder reactions of α,β-enals with dienes in the presence of the chiral catalysts **21** and **23** emerged from the X-ray crystallographic studies of BF_3 complexes with various formyl compounds, including 2-methylacrolein (see above).[27] These investigations revealed a new kind of hydrogen bond, exemplified generally by structures **25** and **26** (Figure 7).[27b]



25 **26**

Figure 7. Examples of formyl C–H···F and C–H···O hydrogen bonds.

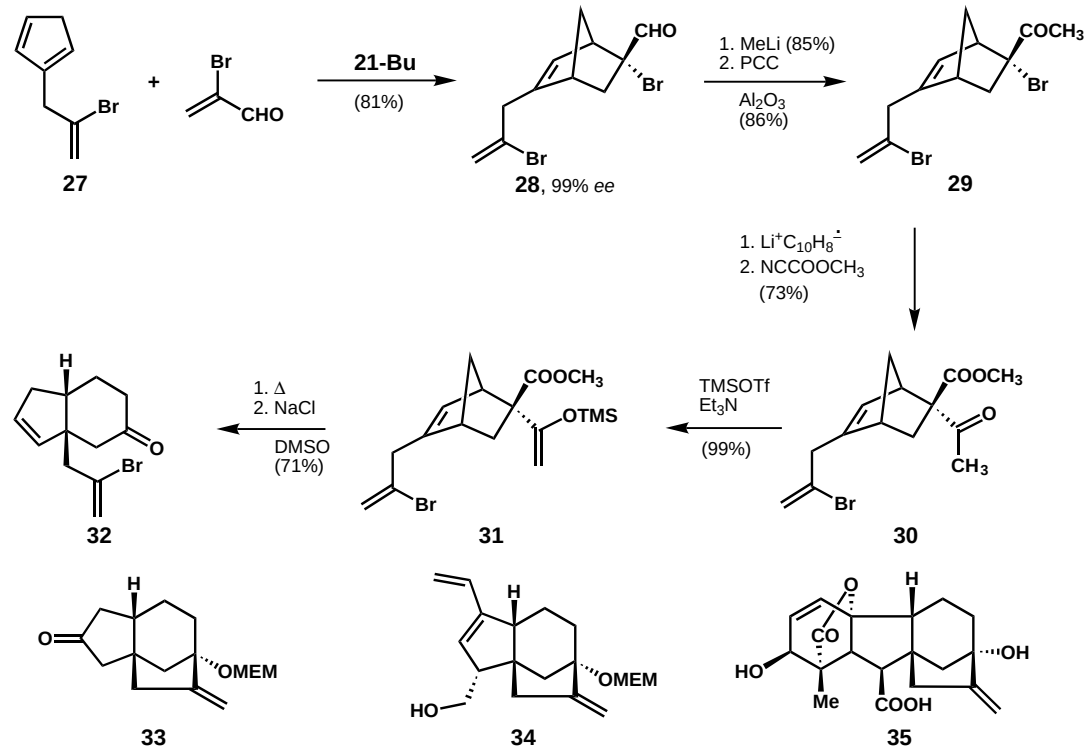
Specifically, the X-ray crystal structures of BF_3 complexes with benzaldehyde, 2-methylacrolein, 2,3-methylenedioxybenzaldehyde, and *N*,*N*-dimethylformamide show a preference for a geometry in which the formyl group and one B–F bond are coplanar (eclipsed) as shown in **25**. The H···F distances in these complexes are 2.35 – 2.36 Å, which is smaller than the sum of the van der Waals radii of the H and F atoms (2.67 Å).[28] The formyl C–H···O hydrogen bonding indicated in **26** has been observed in several different X-ray crystal structures, including that of the complex of catecholboron bromide with *N*,*N*-dimethylformamide.[27b] The formyl C–H···O distances in such complexes range from 2.41 – 2.59 Å and are well below the sum of the van der Waals radii of 2.72 Å.[28] These formyl C–H···F and C–H···O bonds can be thought of as induced or cooperative hydrogen bonds, since coordination of a formyl group at the boron atom simultaneously causes the formyl proton to become more positive and an electronegative atom bonded to the boron atom to become more negative.[29, 30] The formyl C–H···X hydrogen bond appears to be an important organizing factor in many types of Lewis acid catalyzed enantioselective reactions.[29, 30] The pre-transition-state assemblies for oxazaborolidine-catalyzed Diels – Alder reactions of 2-bromoacrolein, which are depicted in Scheme 10 and Figure 5, incorporate the formyl C–H···O hydrogen bond as a key organizing factor in addition to the factors discussed above. The application of the formyl C–H···O hydrogen-bonding idea to the formulation of 3D transition-state structures has led to a clearer understanding of the fundamental reasons for the enantioselectivity of many different catalytic reactions,[30] a fact that adds confidence in its validity and predictive value.

5. Applications of Chiral Oxazaborolidines to Multistep Syntheses

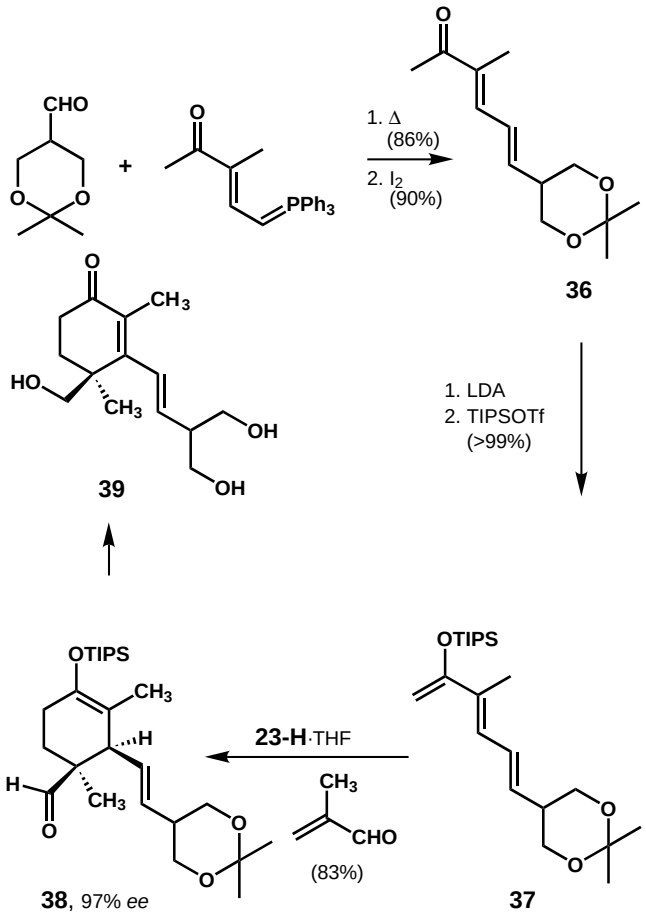
The utility of oxazaborolidine catalysts **21** and **23** in synthesis has been demonstrated by various applications to target-oriented syntheses, three of which are summarized herein. A very effective enantioselective synthesis of the plant hormone gibberellic acid (**35**) is outlined in Scheme 11. The Diels – Alder reaction of diene **27** and 2-bromoacrolein in the presence of catalyst **21-Bu** at $-78\,^\circ C$ provided adduct **28** with 99 % *ee*.[23] α-Bromoaldehyde **28** was converted into the corresponding α-bromo methyl ketone **29**, which underwent reductive methoxycarbonylation to form the *exo* methyl ester **30**. The keto ester **30** was transformed into the enol trimethylsilyl ether **31**. Thermolysis of **31** led to Cope rearrangement to form a β-keto ester, which gave the hydrindanone **32** upon demethoxycarbonylation by heating with NaCl in dimethyl sulfoxide. The transformation of **32** via tricyclic ketone **33** and tricyclic diene **34** to gibberellic acid (**35**) followed the route developed earlier.[31–33]

The key steps in a short enantioselective total synthesis of cassiol (**39**), a scarce and potent antiulcer agent, are depicted in Scheme 12.[23] The diene **37** was produced from the corresponding dienone **36**, which was prepared by the Wittig coupling shown. Diels – Alder reaction of **37** with 2-methylacrolein in the presence of **23-H** · THF as catalyst gave adduct **38** with 97 % *ee* in CH_2Cl_2 at $-78\,^\circ C$. Cassiol (**39**) was accessed from **38** by a simple four-step sequence. The process outlined in Scheme 12 can be used to prepare gram quantities of cassiol conveniently with ordinary laboratory glassware. As predicted from the mechanistic model for the Diels – Alder reaction (Scheme 10), the use of catalyst **21-Bu** produces the adduct with poorer enantioselectivity owing to repulsions between the B–Bu substituent and the terminal substituent on the 1,3-diene subunit. Further, the catalyst **21-H** leads to a somewhat lower *ee* value than does **23-H** (94 vs 97 % *ee*).[23] Finally, the use of the *tert*-butyldimethylsilyloxy analogue of the triisopropylsiloxy triene **37** in the Diels – Alder reaction leads to considerably lower enantioselectivity.[23]

The successful enantioselective synthesis of cassiol (**39**) encouraged us to undertake the more challenging synthesis of eunicenone A (**51**) which is outlined in Scheme 13.[34] The 1,4-disubstituted diene **44** was prepared by starting with geranylgeranylacetylene (**40**). This preparation employed a new silyllithium reagent, 2-anisyldimethylsilyllithium, which was generated from disilane **43**. As in the case of the synthesis of cassiol (Scheme 12), it was necessary to employ the catalyst **23-H** to obtain high enantioselectivity in the Diels – Alder



Scheme 11. Enantioselective total synthesis of gibberellic acid (**35**). DMSO = dimethyl sulfoxide; MEM = methoxyethoxymethyl.

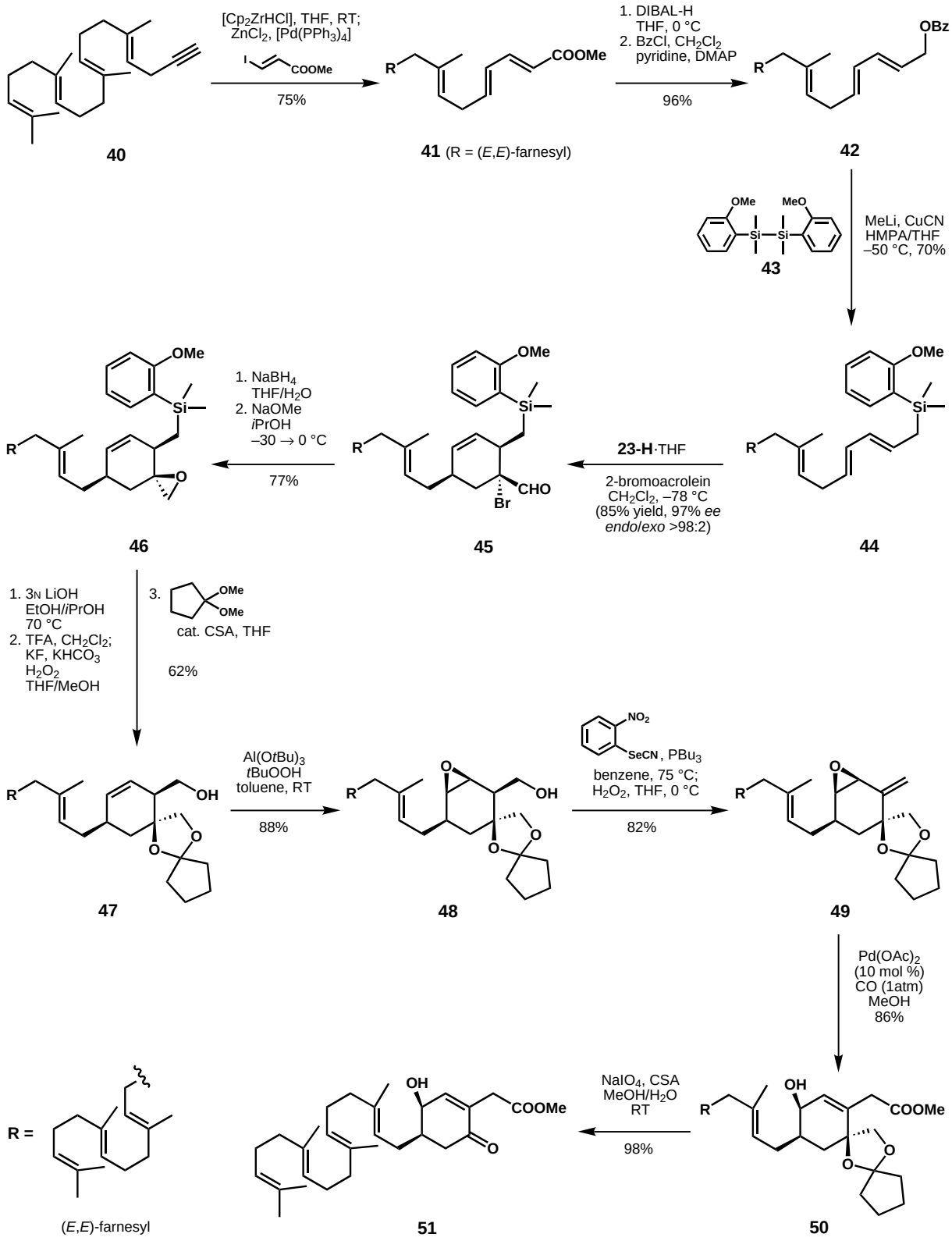


Scheme 12. Enantioselective total synthesis of cassiol (**39**). TIPS = triisopropylsilyl.

reaction of the 1,4-disubstituted diene **44** with 2-bromoacrolein. With this catalyst, in CH_2Cl_2 solution at $-78\,^{\circ}C$, the desired adduct **45** was obtained regiospecifically (as a result of the strong electron-donating effect of the silyl substituent) in 85% yield and 97% *ee*. The α-bromoaldehyde **45** was converted into the epoxide **46** and thence into the hydroxy ketal **47** (Scheme 13). The use of the 2-anisyldimethylsilyl group in the synthesis was beneficial with regard to the yield and enantioselectivity of the Diels–Alder addition and also crucial in the conversion of **46** into **47** because it permitted hydroxydesilylation to be carried out under mild conditions which did not cause unwanted changes in other parts of the substrate.[34] The completion of the synthesis of **51** necessitated the selective epoxidation (**47**→**48**), dehydration (**48**→**49**), catalytic methoxycarbonylation (**49**→**50**) and hydrolytic glycol cleavage (**50**→**51**), all of which are of special note (Scheme 13).

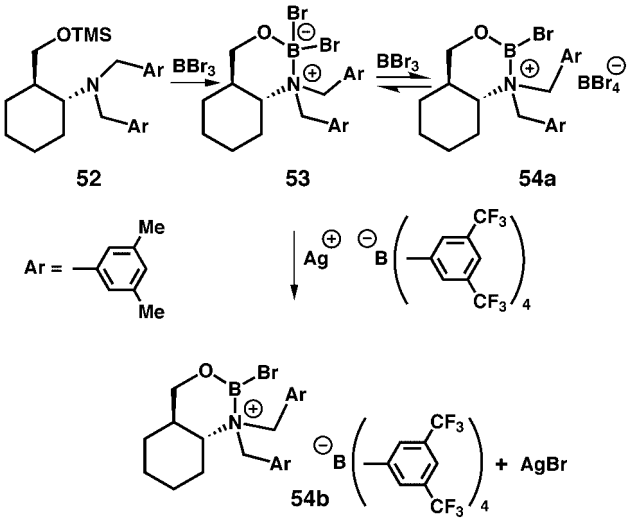
6. Enhancement of Acidity in Chiral Lewis Acids

Attachment of bidentate or higher coordination chiral ligands to a Lewis acidic metal normally reduces the Lewis acidity, since additional electron density generally is transferred from ligand to metal. The development of chirally coordinated Lewis acids of undiminished acidity requires an approach different from that described in the foregoing sections of this review. A successful method for the generation of chiral superreactive Lewis acids has recently been devised (Scheme 14).[35] A key element of this research was the idea that the cationic complex $\mathbf{54}^{+}BBr_4^{-}$ would be a very strong

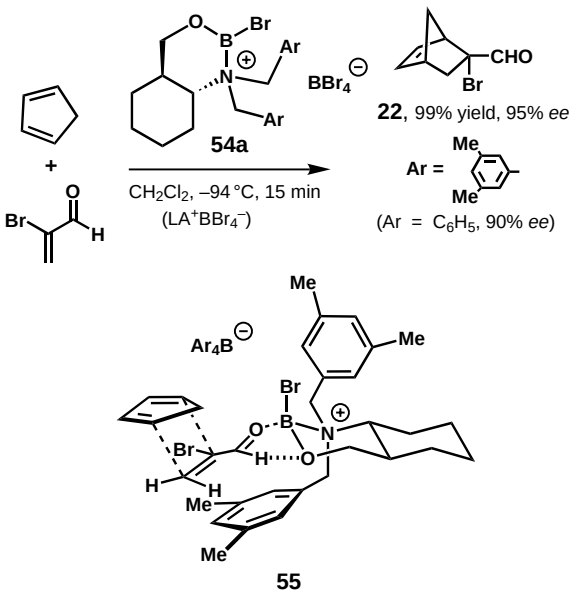


Scheme 13. Enantioselective total synthesis of eunicenone A (**51**). DIBAL-H = diisobutylaluminum hydride; Bz = benzoyl; DMAP = 4-dimethylaminopyridine; HMPA = hexamethyl phosphoramide; CSA = camphorsulfonic acid.

Lewis acid (in the order of acidity of BF_3), even though it carries a bidentate ligand. Reaction of the tertiary amine trimethylsilyl ether **52** with BBr_3 (1 – 1.6 equiv) in CH_2Cl_2 at $-78\,^{\circ}C$ gave bromotrimethylsilane and an equilibrating mixture of the two cyclic oxazaborinanes **53** and **54a**. Treatment of the mixture with a silver tetraarylboronate produced the corresponding tetraarylboronate **54b**. When **54a** or **54b** (10 mol %) is used, cyclopentadiene and a variety of α,β-enals



Scheme 14. Synthesis of cationic Lewis acid **54**.

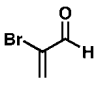
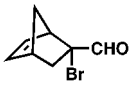
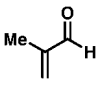
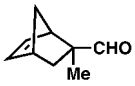
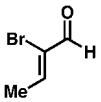
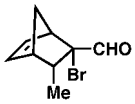
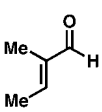
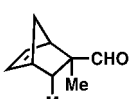
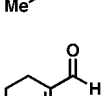
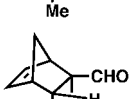


Scheme 15. Enantioselective Diels–Alder reaction of cyclopentadiene and 2-bromoacrolein to form **22**, possibly via pre-transition-state assembly **55**. LA = Lewis acid.[35]

react in CH_2Cl_2, even at $-94\,^{\circ}C$, to form Diels–Alder adducts in very good yield and enantioselectivity (Table 1).

The absolute stereochemical course of the reaction and a likely pre-transition-state assembly **55** are shown in Scheme 15. The conformation of the cationic moiety of **55** corresponds to that determined by X-ray crystallography for the internally hydrogen-bonded hydrobromide of the amino alcohol corresponding to **52** (Scheme 14).[35] The coordinated *s-trans* α,β-enal is oriented for optimal formyl C–H···O hydrogen bonding and π-electron interaction between the formyl carbon atom and the neighboring aromatic donor group. Approach of the diene to the sterically accessible face of the α,β-enal leads to the predominant enantiomer **22**. By the use of catalyst **54b** (but not **54a**) even relatively unreactive dienes such of 1,3-butadiene and 1,3-cyclohexadiene can be converted into Diels–Alder adducts with 2-bromoacrolein in high yield (99%) and with excellent enantioselectivity (93–98% *ee*).[35]

Table 1. Enantioselective Diels–Alder reaction of 1,3-cyclopentadiene with α,β-unsaturated aldehydes[a] catalyzed by **54**.[35]

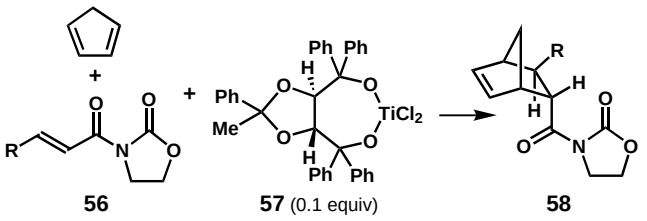
Dienophile	Catalyst	*exo*/*endo*	Yield [%]	*ee* [%] (Configuration)	Product
	**54a**	94:6	99	95 (2*R*)	
	54b	91:9	99	98 (2*R*)	
	**54a**	88:12	99	90 (2*S*)	
	54b	89:11	98	87 (2*S*)	
	**54a**	>98:2	99	91	
	54b	>98:2	99	96	
	**54a**	>98:2	88	89	
	54b	>98:2	97	89	
	**54a**	>98:2	99	96	
	54b	>98:2	97	82	

[a] Reaction conditions: CH_2Cl_2, $-94\,^{\circ}C$, 2 h.

7. Catalytic Enantioselective Diels–Alder Reactions with Bidentate Dienophiles

In principle, another strategy for increasing the reactivity of a catalyst dienophile complex to a degree that allows reaction with unreactive dienes is to replace a monodentate dienophile by a bidentate equivalent. This type of catalytic enantioselective Diels–Alder reaction was demonstrated by the pioneering research of Prof. K. Narasaka and co-workers.[36] A few examples of the Narasaka catalytic enantioselective Diels–Alder process are shown in Scheme 16. Unlike the

The mechanistic and stereochemical ideas that led to the development of the cationic catalyst **54** are valuable, not only because they lead to a rational comprehension of the reasons for enantioselectivity in catalytic Diels–Alder reactions, but also because their predictive power allows the design of new types of effective catalysts. For example, the idea of π-electron-rich aromatic rings for the selective stabilization of specific Diels–Alder transition states led to the selection of the 3,5-dimethylphenyl group for catalyst **54**. It was verified experimentally that **54** is, in fact, a considerably more selective catalyst than the phenyl analogue, in accordance with our guiding principles. One can safely state that at present the discovery of new catalysts is limited more by the time required for experimental testing and execution than by the design process itself. In this sense, the recent advances in catalytic enantioselective reactions are truly revolutionary. Kurt Alder could not possibly have imagined such a level of sophistication for his "diene synthesis."



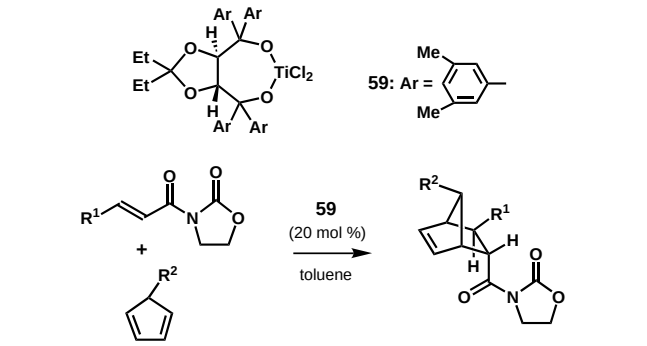
56a: R = H, (93% yield, 96:4 *endo* / *exo*, 64% *ee* (*endo*))
56b: R = Me, (87% yield, 92:8 *endo* / *exo*, 91% *ee* (*endo*))
56c: R = Ph, (72% yield, 88:12 *endo* / *exo*, 64% *ee* (*endo*))

Scheme 16. The catalytic Diels–Alder process of K. Narasaka et al.[36]

Diels–Alder reaction of *N*-acrylyloxazolidinones referred to in Scheme 3 and Figure 3, the Narasaka system involves bidentate coordination of the *N*-acrylyloxazolidinones **56** with catalyst **57** on the pathway to the adducts **58**.[36] Even though the Lewis acid catalyst **57** is not very strong, the bidentate nature of the coordinating dienophile **56** allows sufficient complexation and activation to afford reasonable rates of Diels–Alder reaction at -10 to $-50\,^{\circ}C$. The structure of the catalyst **57**, which is supported by ^1H NMR spectral data,[36] and the bidentate nature of the dienophile **56** strongly suggest that the catalytic process involves the addition of the diene to an octahedral complex of the two.

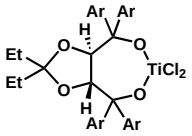
Since there are *ten* possible diastereomeric octahedral complexes, and twice as many if both *s-cis* and *s-trans* conformers of the dienophile are considered, it is quite remarkable that even modest enantioselectivity was observed. Because of the importance of understanding the mechanistic/structural basis for such enantioselectivity, and our interest in the theory of catalytic enantioselective Diels–Alder processes, we extended our investigations to the Narasaka system, with interesting results.[37] As is indicated in Table 2, the replacement of the phenyl group in the Narasaka catalyst by 3,5-dimethylphenyl, which is more π-basic, produced a superior catalyst, **59**, which afforded greatly improved enantioselectivities. The importance of π-basicity in the aryl substituent is further indicated by the results summarized in Table 3 with a series of catalysts in which the aryl group was varied.[37] The superiority of catalyst **59** (Ar = 3,5-dimethylphenyl) over **60** (Ar = 3,5-bis(trifluoromethyl)phenyl or 3,5-dichlorophenyl) provides convincing experimental evidence that the aryl group enhances enantioselectivity as a neighboring π-electron-rich substituent, which simultaneously serves a stabilizing and steric screening function in the transition state. One attractive formulation of the pre-transition-state assembly for the enantioselective pathway in the Narasaka system is depicted in Figure 8.[37]

Table 2. Improved catalyst **59** for the Narasaka Diels–Alder process.



R^1	R^1	T [°C]	t [h]	Yield [%]	*endo*/*exo*	*ee* [%] (*endo*)
H	H	−40	12	80	95:5	94
H	$BnOCH_2$	−30	12	83	>99:1	95
Me	H	−10	8	92	93:7	93
COOEt	H	−30	8	90	81:19	91

Table 3. Enantioselectivity of the reaction of *N*-acrylyloxazolidinone with cyclopentadiene as a function of the Ar group in catalyst **60**.



Ar	T [°C]	t [h]	Yield [%]	*endo*/*exo*	*ee* [%] (*endo*)
Ph[a]	−50	12	70	93:7	73
β-Naphth[a]	−50	36	86	93:7	68
6-MeO-β-Naphth[a]	−50	40	76	90:10	82
3,5-Me_2Ph (**59**)[a]	−40	12	80	95:5	94
3,5-$(CF_3)_2$Ph[b]	−50	20	81	92:8	68
3,5-Cl_2Ph[b]	−50	18	75	93:7	44

[a] Catalyst preparation: 1) diol + $Ti(OiPr)_4$; 2) $SiCl_4$. [b] Catalyst preparation: diol and $TiCl_4$ in diethyl ether, removal of solvent in vacuo, addition of toluene, and evaporation. Naphth = naphthalene.

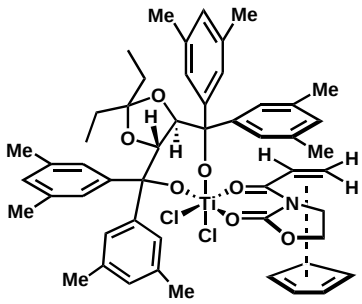


Figure 8. Possible pre-transition-state assembly for the $(RO)_2TiCl_2$-catalyzed Diels–Alder reaction in the Narasaka system.

Another effective catalyst for enantioselective Diels–Alder reactions has been developed for *N*-acrylyloxazolidinones as dienophiles. This catalyst is based on the readily available chiral bisoxazolines **61** and **62** (Figure 9).[38, 39] Metal complexes of these rigid ligands provide catalysts of well-

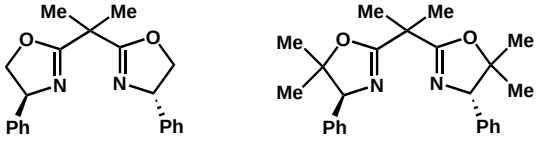
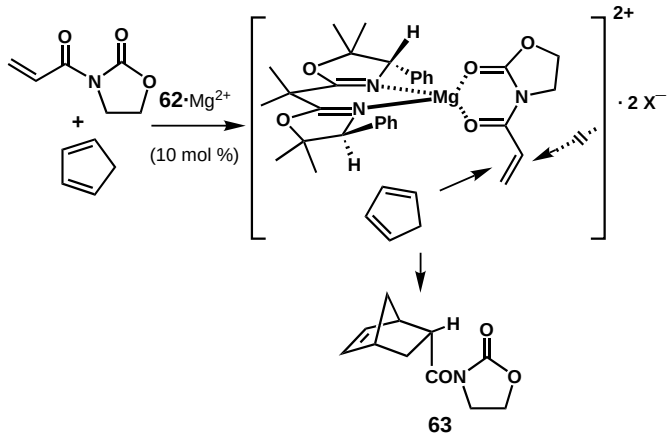


Figure 9. Chiral bisoxazoline ligands for enantioselective metal catalysis.

defined molecular geometry which are very promising for a number of important reactions. The complex of **62** with magnesium iodide or magnesium tetraphenylborate catalyzes the reaction of cyclopentadiene with *N*-acryloyloxazolidinone in CH_2Cl_2 at $-50\,^{\circ}C$ to form the adduct **63** (Scheme 17) with



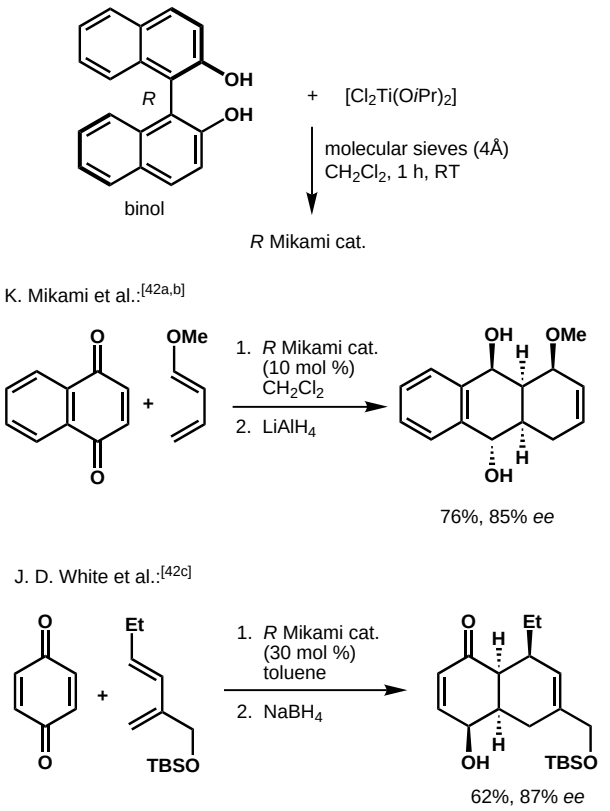
Scheme 17. An enantioselective Diels–Alder reaction catalyzed by the cationic magnesium complex of **62**.[39]

95.5:4.5 enantioselectivity and 98:2 *endo*/*exo* selectivity (84% yield).[39] The absolute stereochemistry of this reaction product agrees with the expectation of the favored pre-transition-state assembly shown in Scheme 17 in which tetrahedral magnesium binds and activates the bidentate dienophile and phenyl screening provides the basis for face-selective addition to the *s-cis* form of the dienophile.[39] The use of the complex of **62** with Cu^{II} to catalyze the same reaction leads to the selective formation of the *enantiomer* of **63**, as expected for a process via the square-planar complex of **61** · Cu^{II} with the dienophile.[40] The complex of **61** with ferric iodide is also an effective catalyst for the synthesis of **63** probably via the octahedral cationic complex [**61** · FeI_2 · *N*-acryloyloxazolidinone]$^+$.[38] An interesting feature of these three catalyst systems is that a cationic form of the metal complex is required to accelerate the reaction. Neutral species are clearly not sufficiently Lewis acidic because of the electron-donating nature of the bidentate bisoxazoline ligand. These findings emphasize the important influence of ligand and charge on catalytic effectiveness.

8. Enantioselective Diels–Alder Reactions with Quinone Monoketals

For more than six decades, the Diels–Alder reaction subtype with quinones as dienophiles has provided a powerful construction for functionalized *cis*-fused decalin systems. Many syntheses of complex natural products have been recorded in which the quinone Diels–Alder reaction has been used to set in place an initial arrangement of rings and stereocenters that paves the way for elaboration of the final target structure by a subsequent series of selective reactions. Examples include some of the most notable achievements in complicated synthetic chemistry, for instance: steroids, reserpine, ibogamine, dendrobine, gibberellic acid, trichodermol, and euonyminol.[41]

In each of these cases, the initial Diels–Alder reaction generated a racemic adduct from which the synthesis of chiral natural product was possible only with an intervening resolution step and the usual loss of material (>50%). For many years, no methods were available for conducting the key quinone Diels–Alder reactions for these syntheses so as to lead enantioselectively to chiral adducts. This gap in methodology is just starting to be filled.[42, 43] Some recent developments, which involve Mikami's catalyst (a red Ti^{IV}–binol complex of unknown structure), are summarized in Scheme 18.[42] The Mikami catalyst appears to be chloride-free and to involve μ-oxo bridges between at least two Ti units. The minimal structure would appear to be the μ_2-bridged possibility binol–Ti(μ_2O,μ_2O)Ti–binol.



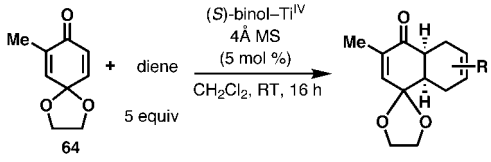
Scheme 18. Preparation of Mikami's catalyst and application to enantioselective quinone Diels–Alder reactions. TBS = *tert*-butyldimethylsilyl.

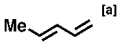
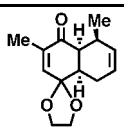
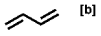
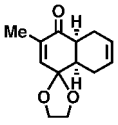
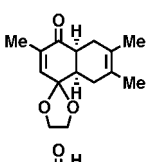
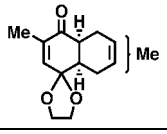
Recent investigations in our laboratories have focused on the use of 1,4-quinone monoketals (which are essentially 1,4-quinone equivalents) rather than the corresponding quinones, for reasons which include the following: 1) the monoketals are expected to be more Lewis basic; 2) the monoketals would provide adducts that do not undergo facile aromatization, in contrast to the 1,4-quinone adducts, which are known to aromatize readily and to be difficult to handle (unless at least one of the 6,6-fusion substituents is a non-hydrogen angular group); 3) the monoketals lead to adducts in which one of the two carbonyl groups of the 1,4-quinone is already protected, thus simplifying the task of further selective transformations;

and 4) the monoketals are accessible synthetically either from oxidative *p*-ketalization of phenols or from transketalization starting from 4,4-dimethoxy-2,5-cyclohexadienones.[44] The 4,4-dimethoxy-2,5-cyclohexadienones themselves did not serve as useful dienophiles. Much better results were obtained with ethylene monoketals (e.g. **64** (Table 4)) and 3,3-dimethyl-1,3-diol-derived (neopentyl) ketals (e.g. **65** (Table 5)) with the binol–Ti^{IV}-based catalyst in the presence of molecular sieves.[45] Very good yields, enantioselectivities, and *endo/exo* selectivities were obtained. The use of 4-Å molecular sieves that contain water was critical, in accordance with previous observations for catalytic ene reactions.[42, 46, 47] In the absence of molecular sieves or in the presence of molecular sieves that had been desiccated by heating to 150 °C under vacuum, the reactions were slower and less efficient. The results for ethylene ketal **64** are summarized in Table 4 for the *S* Mikami catalyst (5 mol %) in CH_2Cl_2 at 23 °C. Enantioselectivities (81–84 % *ee*) were somewhat lower for butadiene and 2,3-dimethylbutadiene than for (*E*)-1,3-pentadiene (98 %). Even better results were obtained with neopentyl monoketal **65** than for ethylene ketal **64** (Table 5).

The quinone monoketal Diels–Alder adducts are more useful in synthesis than the corresponding quinone adducts because they are more stable and already monoprotected so as to differentiate the two carbonyl functions. Thus, adduct **66** is simply and selectively converted into the *trans*-fused isomer **67** and into the bridged iodo ether **68**; these operations are not feasible for the quinone adduct corresponding to **66** (Scheme 19).[44] The advances described herein on the enantioselective Diels–Alder reactions of dienes with quinone monoketals by using the Mikami catalyst provide great incentive to develop other catalysts for these and related systems, for example simple α,β-enones, which present a unique standing challenge.

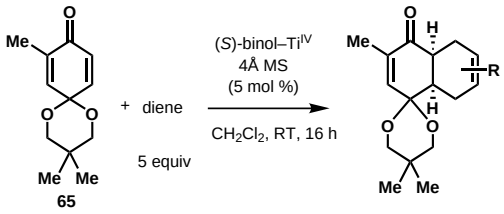
Table 4. Enantioselective Diels–Alder reactions of quinone monoketal **64** with various dienes.

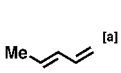
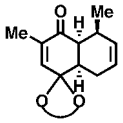
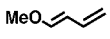
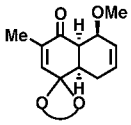
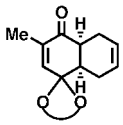
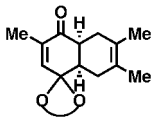
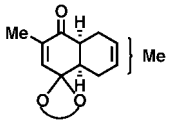


Diene	Product	Yield [%]	*ee* [%]
 [a]		97	98
 [b]		91	81
		88	84
		91	84, 72[c]

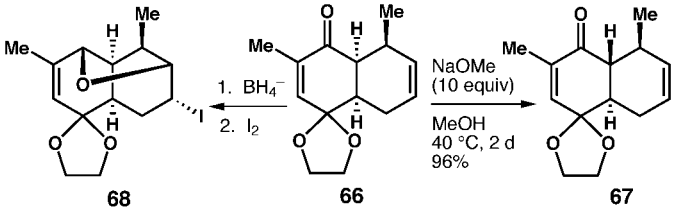
[a] *endo/exo* >98:2. [b] Reaction at −20 °C for 72 h. [c] Mixture of regioisomers (53:47).

Table 5. Enantioselective Diels–Alder reactions of quinone monoketal **65** with various dienes.



Diene	Product	Yield [%]	*ee* [%]
 [a]		90	99
		90	99
 [b]		95	95
		95	90
		91	96, 91[c]

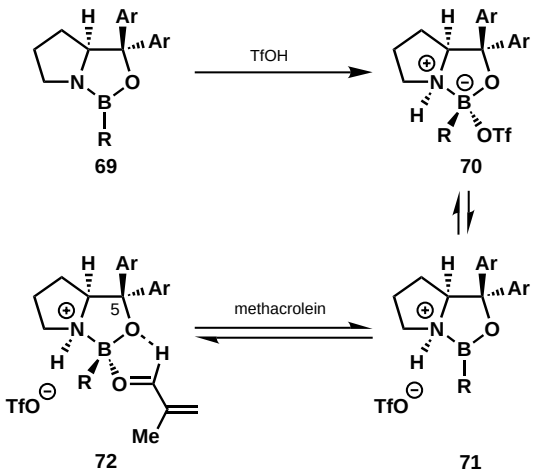
[a] *endo/exo* >99:1. [b] Reaction at −20 °C for 72 h. [c] Mixture of regioisomers (56:44).



Scheme 19. Some transformations of chiral quinone monoketal adduct **66**.

9. Asymmetric Diels–Alder Reactions Catalyzed by a Triflic Acid Activated Chiral Oxazaborolidine

Chiral oxazaborolidines **69** (Scheme 20) are very useful catalysts (e.g. with R = H, Me, *n*Bu, or Ar) for the enantioselective reduction of ketones by using $BH_3 \cdot THF$ or catecholborane as stoichiometric reductants, a reaction that is of interest because of its wide scope and the extraordinary



Scheme 20. Transformation of the chiral oxazaborolidine **69** to the chiral cationic Lewis acid **71**. TfOH = triflic acid = trifluoromethanesulfonic acid.

predictive power of the underlying mechanistic pathway.[20, 48] We have recently devised a new type of catalytic enantioselective Diels–Alder reaction, which was inspired by this process and which employs a proline-derived oxazaborolidine of type **69** as a precatalyst and triflic acid as an activator to generate a potent cationic Lewis acid.[49] In essence, a very strong protic acid is used to create a very strong Lewis acid, the reverse of the formation of a proton superacid from a Lewis acid, for example, $HF + BF_3 \rightarrow H^+BF_4^-$.

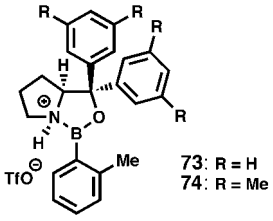
The reaction of the oxazaborolidine **69** (R = Me, Ar = C_6H_5) with anhydrous triflic acid (ratio 1:1) in CH_2Cl_2 (or CD_2Cl_2) results in the formation of an equilibrium mixture of two N-protonated species **70** and **71** (Scheme 20) as indicated by low-temperature (−80 °C) ^{1}H NMR spectroscopic analysis. No appreciable amount of triflic acid appears to be present with these 1:1 mixtures of **69** and triflic acid. The ratio **70**/**71** in CD_2Cl_2 at −80 °C is approximately 1.5:1. The interconversion of **70** and **71** is slow on the ^{1}H NMR timescale, but becomes rapid at 0 °C, the coalescence temperature.

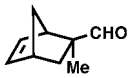
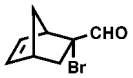
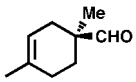
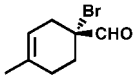
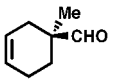
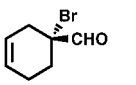
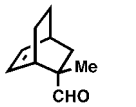
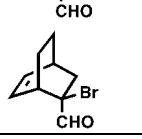
The Lewis acidity of **71** was expected to be high because of its cationic character[35] and because its formation requires the very strong triflic acid (methanesulfonic acid generates relatively weak catalytic activity from **69**). These findings place **71** and triflic acid near one another on an effective acidity scale. In fact, our results on catalysis of Diels–Alder reactions show that triflic acid and **71** lead to similar reaction rates at −94 °C.

The rationale for the application of **71** to the enantioselective catalysis of Diels–Alder reactions of α,β-unsaturated aldehydes is derived from previous research on Lewis superacids and catalytic enantioselective reaction pathways.[30, 35] Coordination of the α,β-enal (e.g. methacrolein) to **71** was expected to lead to an organized formyl C–H···O hydrogen-bonded complex **72** (Scheme 20).[30, 35] The electron-deficient α,β-enal subunit in complex **72** can attract the *cis* Ar group on C5 of the oxazaborolidine ring by a π–π donor–acceptor interaction (see below). This attractive interaction will persist in the Diels–Alder transition state since the formyl carbon atom maintains its strong positive charge all along the reaction pathway.

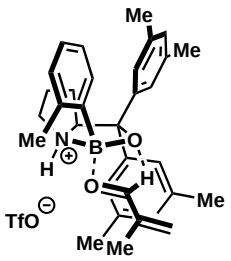
It was determined from studies to optimize the structure of the catalyst **71** that the best results were obtained for **73** (R = *o*-tolyl, Ar = phenyl) and **74** (R = *o*-tolyl, Ar = 3,5-dimethylphenyl) (Table 6). Most Diels–Alder reactions were fast, even at −95 °C in CH_2Cl_2 as solvent with 6 mol% of catalyst and 2-methyl- or 2-bromoacrolein as test dienophiles. As indicated in Table 6, very good yields and enantioselectivities were found with catalysts **73** or **74** in 14 cases, and even unreactive dienes such as 1,3-butadiene and 1,3-cyclohexadiene gave satisfactory results.

Table 6. Diels–Alder reactions of 1,3-dienes with 2-methacrolein or 2-bromoacrolein (CH_2Cl_2) catalyzed by **73** or **74**.



Diene	Product	Catalyst (mol%)	T [°C], t [h]	yield [%] (*exo*/*endo*)	*ee* [%]
		**73** (6) **74** (6)	−95, 1 −95, 1	99 (91:9) 97 (91:9)	91 96
		**73** (6) **74** (6)	−95, 1 −95, 1	99 (91:9) 97 (91:9)	92 96
		**74** (6)	−78, 13	96	97
		**73** (6) **74** (6)	−95, 1 −95, 1	98 98	97 97
		**74** (20)	−78, 24	85	94
		**73** (6) **74** (6)	−95, 2 −95, 2	95 97	96 96
		**73** (20) **74** (20)	−78, 24 −78, 24	91 (5:95) 58 (6:94)	92 92
		**73** (6) **74** (6)	−95, 2 −95, 2	81 (6:94) 85 (7:93)	92 92

The absolute stereochemical course of the Diels–Alder reactions represented in Table 6 can be understood in terms of the type of catalyst–aldehyde complex shown in **73** and the pre-transition-state assembly depicted in **75**. In **75** the formyl carbon atom is situated above C2 of the nearby 3,5-dimethylphenyl group, which effectively screens the rear face of the complexed *s*-



trans α,β-enal from attack by the diene component. Addition of the diene to the *Re* (front) face of the α,β double bond leads to the enantiomers shown in Table 6.

10. Conclusions

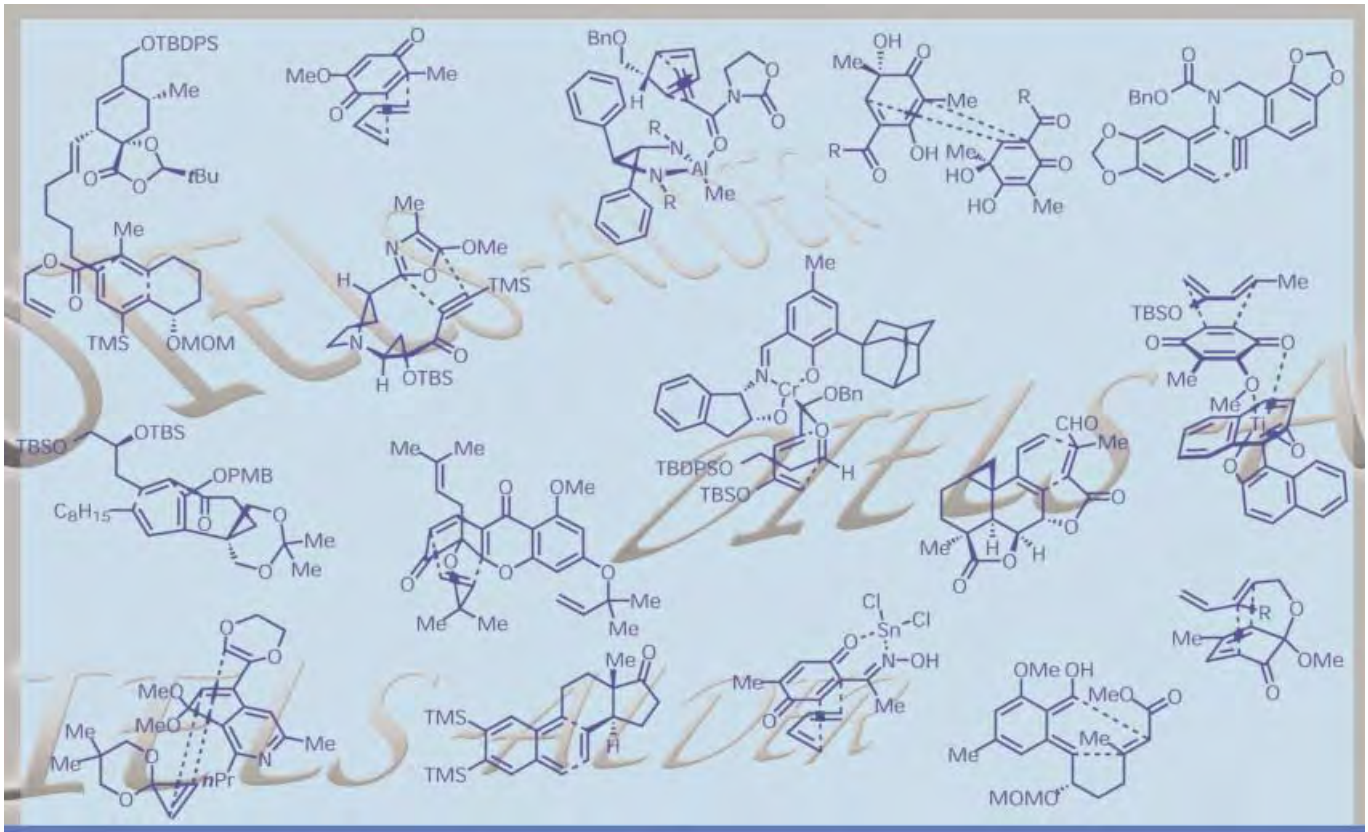
In recent years, the power of the Diels – Alder reaction has been greatly increased as a result of the development of catalytic enantioselective versions, as described herein. Yet, it is likely that there is much more to learn with regard to new catalysts, further extensions to the many types of Diels – Alder partners, and the determination of the fine mechanistic details of these highly intricate processes. The ultimate goal is clear: to control the enantioselectivity of any Diels – Alder reaction that generates a chiral product from achiral diene and dienophile precursors. The realization of all of these objectives would be a tremendous accomplishment and an eloquent testimony to the intellectual prowess of the community of synthetic chemists.

It is a great pleasure to thank the many wonderful coworkers who have accompanied me on the scientific journey that is retraced herein. Their names appear in the references cited. However, special mention needs be made to the following stalwart members of the Corey research family: Harry Ensley, Yi Bin Xiang, Stanislas Pikul, Sephar Sarshar, Michael Letavic, Teck-Peng Loh, Angel Guzman-Perez, Mihai Azimioara, Jeffrey Rohde, Yujiro Hayashi, Noboyuki Imai, Thomas Lee, Matthius Bruening, and Takanori Shibata. I am also grateful to Pfizer Inc. for generous financial support over the years.

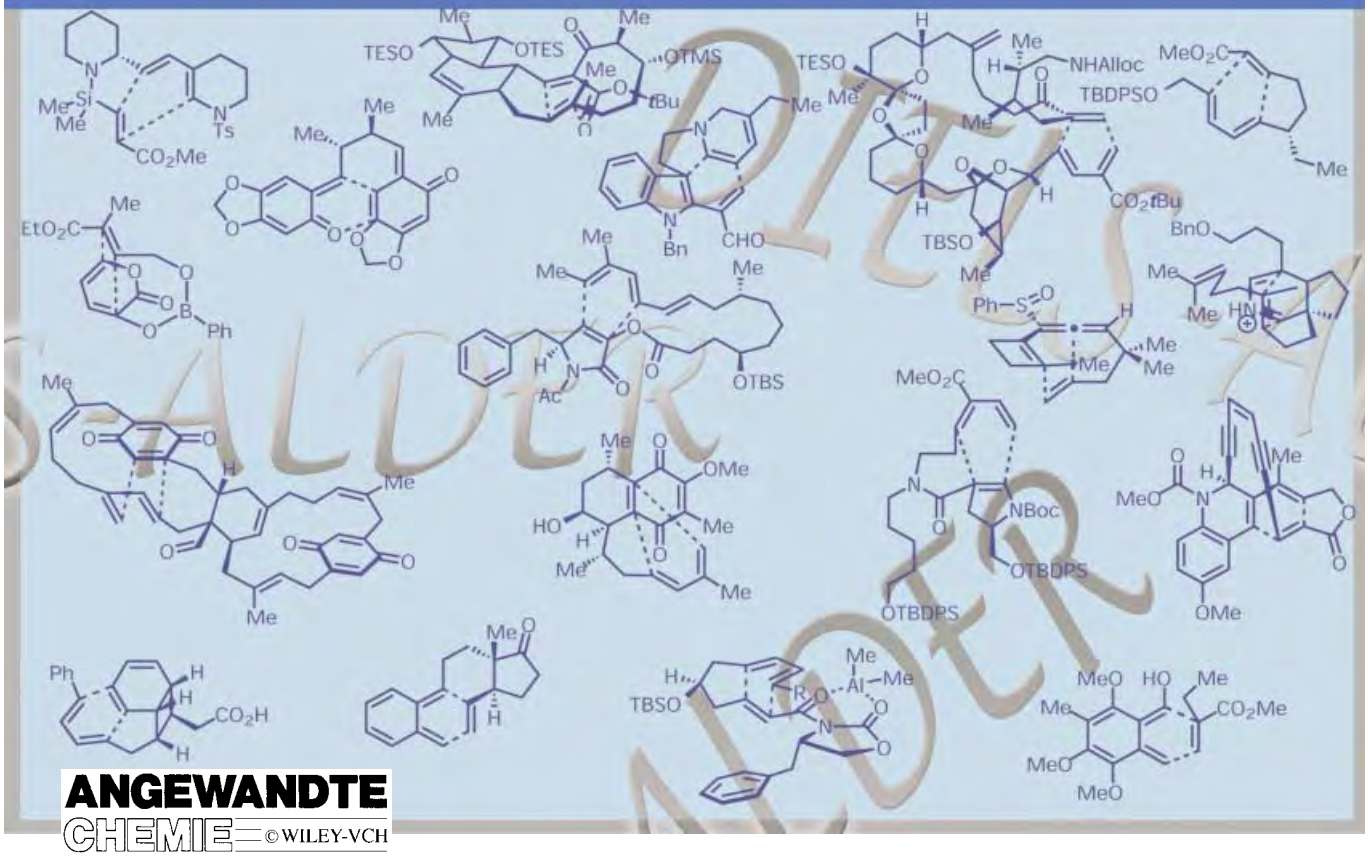
Received: January 30, 2002 [A 513]

[1] O. Diels, K. Alder, *Justus Liebigs Ann. Chem.* **1926**, *450*, 237 – 254; O. Diels, K. Alder, *Justus Liebigs Ann. Chem.* **1927**, *460*, 98 – 122.
[2] K. Alder in *Newer Methods of Preparative Organic Chemistry*, Interscience, New York, **1948**.
[3] N. Anand, J. S. Bindra, S. Ranganathan, *Art in Organic Synthesis*, Holden-Day, San Francisco, **1970**.
[4] W. Carruthers, *Cycloaddition Reactions in Organic Synthesis*, Pergamon, Oxford, **1990**.
[5] R. Noyori, *Asymmetric Catalysis in Organic Synthesis*, Wiley, New York, **1994**; *Catalytic Asymmetric Synthesis* (Ed.: I. Ojima), Wiley-VCH, New York, **2000**.
[6] For reviews specifically on enantioselective Diels – Alder reactions, see a) W. Oppolzer, *Angew. Chem.* **1984**, *96*, 840 – 864; *Angew. Chem. Int. Ed. Engl.* **1984**, *23*, 876 – 889; b) H. Kagan, O. Riant, *Chem. Rev.* **1992**, *92*, 1007 – 1019; c) E. J. Corey, A. Guzman-Perez, *Angew. Chem.* **1998**, *110*, 402 – 415; *Angew. Chem. Int. Ed.* **1998**, *37*, 488 – 501; d) L. C. Diaz, *J. Braz. Chem. Soc.* **1997**, *8*, 289 – 332; e) D. A. Evans, J. S. Johnson in *Comprehensive Asymmetric Catalysis*, *Vol. 3* (Eds.: E. N. Jacobsen, A. Pfaltz, H. Yamamoto), Springer, Berlin, **1999**, pp. 1177 – 1235.
[7] E. J. Corey, N. M. Weinschenker, T. K. Schaaf, W. Huber, *J. Am. Chem. Soc.* **1969**, *91*, 5675 – 5677.
[8] E. J. Corey, T. K. Schaaf, W. Huber, U. Koelliker, N. M. Weinschenker, *J. Am. Chem. Soc.* **1970**, *92*, 397 – 398.
[9] E. J. Corey, *Ann. N. Y. Acad. Sci.* **1971**, *180*, 24 – 37.
[10] E. J. Corey, H. E. Ensley, *J. Am. Chem. Soc.* **1975**, *97*, 6908 – 6909.
[11] E. J. Corey, H. E. Ensley, J. W. Suggs, *J. Org. Chem.* **1976**, *41*, 380 – 381.
[12] Clearly, the face of the diene **8** that undergoes cycloaddition of **7**·$AlCl_3$ is the sterically less shielded one opposite to the benzyloxymethyl group.
[13] For an earlier example of the application of neighboring benzenoid groups to otherwise difficult cases of stereocontrol, see: E. J. Corey, K. B. Becker, R. K. Varma, *J. Am. Chem. Soc.* **1972**, *94*, 8616 – 8617.
[14] S. Pikul, E. J. Corey, *Org. Synth.* **1991**, *71*, 22 – 38.
[15] E. J. Corey, R. Imwinkelried, S. Pikul, Y. B. Xiang, *J. Am. Chem. Soc.* **1989**, *111*, 5493 – 5495.
[16] E. J. Corey, N. Imai, S. Pikul, *Tetrahedron Lett.* **1991**, *32*, 7517 – 7520.
[17] E. J. Corey, S. Sarshar, J. Bordner, *J. Am. Chem. Soc.* **1992**, *114*, 7938 – 7939.
[18] E. J. Corey, S. Sarshar, D.-H. Lee, *J. Am. Chem. Soc.* **1994**, *116*, 12089 – 12090.
[19] E. J. Corey, M. A. Letavic, *J. Am. Chem. Soc.* **1995**, *117*, 9616 – 9617.
[20] E. J. Corey, C. J. Helal, *Angew. Chem.* **1998**, *110*, 2092 – 2118; *Angew. Chem. Int. Ed.* **1998**, *37*, 1986 – 2012.
[21] E. J. Corey, T.-P. Loh, *J. Am. Chem. Soc.* **1991**, *113*, 8966 – 8967.
[22] E. J. Corey, T.-P. Loh, *Tetrahedron Lett.* **1993**, *34*, 2979 – 2982.
[23] E. J. Corey, A. Guzman-Perez, T.-P. Loh, *J. Am. Chem. Soc.* **1994**, *116*, 3611 – 3612.
[24] E. J. Corey, T.-P. Loh, T. D. Roper, M. D. Azimioara, M. C. Noe, *J. Am. Chem. Soc.* **1992**, *114*, 8290 – 8291.
[25] A. W. Hanson, *Acta Crystallogr.* **1964**, *17*, 559 – 568.
[26] E. J. Corey, T.-P. Loh, S. Sarshar, M. Azimioara, *Tetrahedron Lett.* **1992**, *33*, 6945 – 6948.
[27] a) M. T. Reetz, M. Hullmann, W. Massa, S. Berger, P. Rademacher, P. Heymanns, *J. Am. Chem. Soc.* **1986**, *108*, 2405 – 2408; b) E. J. Corey, J. J. Rohde, A. Fischer, M. D. Azimioara, *Tetrahedron Lett.* **1997**, *38*, 33 – 36; for other variants of this formyl hydrogen bonding interaction, see: c) E. P. Kündig, C. M. Saudan, G. Gernardinelli, *Angew. Chem.* **1999**, *111*, 1298 – 1301; *Angew. Chem. Int. Ed.* **1999**, *38*, 1220 – 1223; d) D. J. Parks, W. E. Piers, M. Parvez, R. Atencio, M. J. Zaworotko, *Organometallics* **1998**, *17*, 1369 – 1377.
[28] A. Bondi, *J. Phys. Chem.* **1964**, *68*, 441 – 451.
[29] E. J. Corey, J. J. Rohde, *Tetrahedron Lett.* **1997**, *38*, 37 – 40.
[30] For a review, see: E. J. Corey, T. W. Lee, *Chem. Commun.* **2001**, 1321 – 1329.
[31] E. J. Corey, J. G. Smith, *J. Am. Chem. Soc.* **1979**, *101*, 1038 – 1039.
[32] E. J. Corey, J. E. Monroe, *J. Am. Chem. Soc.* **1982**, *104*, 6129 – 6130.
[33] E. J. Corey, R. L. Danheiser, S. Chandrasekaran, G. E. Keck, B. Gopalan, S. D. Larsen, P. Siret, J.-L. Gras, *J. Am. Chem. Soc.* **1978**, *100*, 8034 – 8036.
[34] T. W. Lee, E. J. Corey, *J. Am. Chem. Soc.* **2001**, *123*, 1872 – 1873.
[35] Y. Hayashi, J. J. Rohde, E. J. Corey, *J. Am. Chem. Soc.* **1996**, *118*, 5502 – 5503.
[36] a) K. Narasaka, H. Tanaka, F. Kanai, *Bull. Chem. Soc. Jpn.* **1991**, *64*, 387 – 391; b) K. Narasaka, N. Iwasawa, M. Inoue, T. Yamada, M. Nakashima, J. Sugimore, *J. Am. Chem. Soc.* **1989**, *111*, 5340 – 5345; c) K. Narasaka, M. Inoue, T. Yamada, *Chem. Lett.* **1986**, 1967 – 1970.
[37] E. J. Corey, Y. Matsumura, *Tetrahedron Lett.* **1991**, *32*, 6289 – 6292.
[38] E. J. Corey, N. Imai, H.-Y. Zhang, *J. Am. Chem. Soc.* **1991**, *113*, 728 – 729.
[39] E. J. Corey, K. Ishihara, *Tetrahedron Lett.* **1992**, *33*, 6807 – 6810.
[40] E. J. Corey, *Abstracts of the 33rd National Organic Chemistry Symposium*, American Chemical Society, June **1993**, pp. 30 – 46.
[41] a) R. B. Woodward, F. Sondheimer, D. Taub, *J. Am. Chem. Soc.* **1952**, *74*, 4223 – 4225; b) R. B. Woodward, R. E. Bader, H. Bickel, A. J. Frey, R. W. Kierstead, *Tetrahedron* **1958**, *2*, 1 – 52; c) S. I. Salley, *J. Am. Chem. Soc.* **1967**, *89*, 6762 – 6764; d) A. S. Kende, T. J. Bently, R. A. Mader, D. Ridge, *J. Am. Chem. Soc.* **1974**, *96*, 4332 – 4334; e) E. J. Corey, R. L. Danheiser, S. Chandrasekaran, P. Siret, G. E. Keck, J.-L. Gras, *J. Am. Chem. Soc.* **1978**, *100*, 8031 – 8033; f) W. C. Still, M. Y. Tsai, *J. Am. Chem. Soc.* **1980**, *102*, 3654 – 3655; g) J. D. White, N. S. Cutshall, T. S. Kim, H. Shin, *J. Am. Chem. Soc.* **1995**, *117*, 9780 – 9781.
[42] a) K. Mikami, M. Terada, Y. Motoyama, T. Nakai, *Tetrahedron: Asymmetry* **1991**, *2*, 643 – 646; b) K. Mikami, Y. Motoyama, M. Terada, *J. Am. Chem. Soc.* **1994**, *116*, 2812 – 2820; c) J. D. White, Y. Choi, *Org. Lett.* **2000**, *2*, 2373 – 2376.
[43] a) T. A. Engler, M. A. Letavic, K. O. Lynch, Jr., F. Takusagawa, *J. Org. Chem.* **1994**, *59*, 1179 – 1183; b) T. A. Engler, M. A. Letavic, F. Takusagawa, *Tetrahedron Lett.* **1992**, *33*, 6731 – 6734.

[44] M. Breuning, E. J. Corey, *Org. Lett.* **2001**, *3*, 1559–1562.
[45] General procedure for the Diels–Alder reactions shown in Tables 4 and 5: A solution of (*S*)-2,2′-dihydroxy-1,1′-binaphthyl (binol) in CH_2Cl_2 (0.02 M, 500 μL, 2.9 mg, 10 μmol) and a solution of $Cl_2Ti(OiPr)_2$ in toluene (0.30 M, 33 μL, 10 μmol) were added to molecular sieves (4 Å, 5–6 % H_2O, Aldrich, 2–3 μ particle size, used as supplied) at room temperature. The red-brown reaction mixture was stirred for 1 h. A solution of the 1,4-quinone monoketal in CH_2Cl_2 (0.50 M, 400 μL, 200 μmol) was added. After 10 min at 23 °C, the diene (5 equiv) was added, and the reaction was stirred until TLC analysis (deactivated silica gel (NEt_3), hexane/Et_2O 1:2) showed complete conversion (ca. 16 h). Column chromatography (deactivated silica gel (5 % NEt_3), hexane/Et_2O 5:1 →1:2) gave the analytically pure Diels–Alder adducts. Enantioselectivities were determined by HPLC analysis with an (*R*,*R*)-Whelk O1 column with hexane/*i*PrOH (99:1) for elution.
[46] a) K. Mikami, M. Terada, Y. Matsumoto, M. Tanaka, Y. Nakamura, *Microporous Mesoporous Mater.* **1998**, *21*, 461–466; b) M. Terada, Y. Matsumoto, Y. Nakamura, K. Mikami, *J. Mol. Catal. A* **1998**, *132*, 165–169.
[47] G. H. Posner, H. Dai, D. S. Bull, J.-K. Lee, F. Eydoux, Y. Ishihara, W. Welsh, N. Pryor, S. Petr, *J. Org. Chem.* **1996**, *61*, 671–676.
[48] a) E. J. Corey, R. K. Bakshi, S. Shibata, *J. Am. Chem. Soc.* **1987**, *109*, 5551–5553; b) E. J. Corey, R. K. Bakshi, S. Shibata, C.-P. Chen, V. K. Singh, *J. Am. Chem. Soc.* **1987**, *109*, 7925–7926.
[49] E. J. Corey, T. Shibata, T. W. Lee, *J. Am. Chem. Soc.* **2002**, *124*, 3808–3809.



The *Diels-Alder* Reaction in Action



ANGEWANDTE CHEMIE
© WILEY-VCH

The Diels–Alder Reaction in Total Synthesis

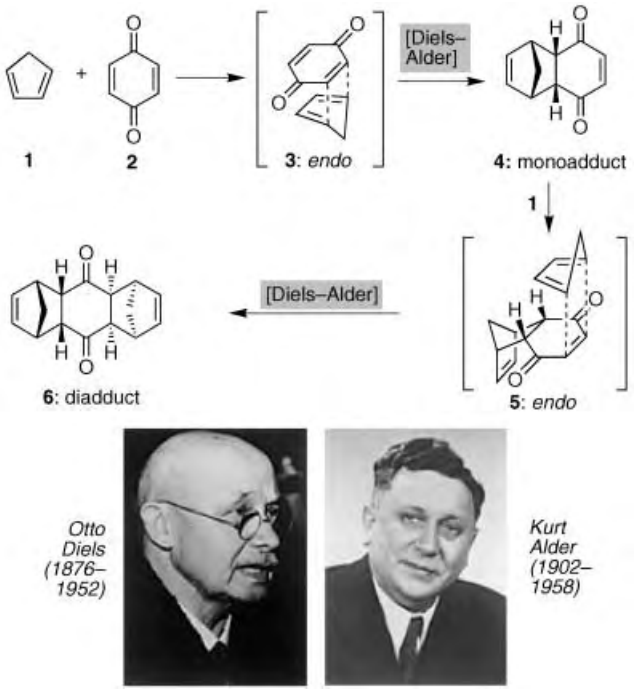
K. C. Nicolaou,* Scott A. Snyder, Tamsyn Montagnon, and Georgios Vassilikogiannakis

The Diels–Alder reaction has both enabled and shaped the art and science of total synthesis over the last few decades to an extent which, arguably, has yet to be eclipsed by any other transformation in the current synthetic repertoire. With myriad applications of this magnificent pericyclic reaction, often as a crucial element in elegant and programmed cascade sequences facilitating complex molecule construction, the Diels–Alder cycloaddition has afforded numerous and unparalleled solutions to a diverse range of synthetic puzzles provided by nature in the form of natural products. In celebration of the 100th anniversary of Alder's birth, selected examples of the awesome power of the reaction he helped to discover are discussed in this review in the context of total synthesis to illustrate its overall versatility and underscore its vast potential which has yet to be fully realized.

Keywords: biomimetic synthesis · cycloaddition · Diels–Alder reaction · molecular diversity · total synthesis

1. Introduction

After numerous near-discoveries of the [4+2] cycloaddition reaction by several luminaries in the field of organic chemistry during the early part of the 20th century,[1, 2] the keen insight of Professor Otto Diels[3] and his student, Kurt Alder,[4] in properly identifying the products (**4** and **6**, Scheme 1) arising from the reaction of cyclopentadiene (**1**) with quinone (**2**) denotes a historic event in the field of chemistry for which these two individuals were rewarded with a reaction that would henceforth bear their names.[5] With prophetic foresight, Diels and Alder clearly anticipated the importance of this discovery in their landmark 1928 paper, particularly as applied to natural product synthesis, through the following remark: "Thus it appears to us that the possibility of synthesis of complex compounds related to or identical with natural products such as terpenes, sesquiterpenes, perhaps even alkaloids, has been moved to the near prospect." However, in an intriguing moment of scientific territoriality, which might appear slightly off-color or even amusing to a contemporary audience, the authors issued the following ominous warning to those researchers interested in applying their discovery to total synthesis: "We explicitly reserve for ourselves the application of the reaction developed by us to the solution of such problems."[2]



Scheme 1. The discovery of the Diels–Alder reaction in 1928, a reaction for which the namesakes would receive the Nobel Prize in Chemistry in 1950: Diels the professor, Alder the student.[5]

[*] Prof. Dr. K. C. Nicolaou, S. A. Snyder, Dr. T. Montagnon, Dr. G. Vassilikogiannakis
Department of Chemistry
and The Skaggs Institute for Chemical Biology
The Scripps Research Institute
10550 North Torrey Pines Road, La Jolla, CA 92037 (USA)
Fax: (+1) 858-784-2469
E-mail: kcn@scripps.edu
and
Department of Chemistry and Biochemistry
University of California San Diego
9500 Gilman Drive, La Jolla, CA 92093 (USA)

 © WILEY-VCH Verlag GmbH, 69451 Weinheim, Germany, 2002 1433-7851/02/4110-1669 $ 20.00+.50/0

Up to the time of their receipt of the Nobel Prize in 1950 it seems that, for the most part, the synthetic community heeded the demand of Diels and Alder, as their cycloaddition reaction did not feature prominently in any total synthesis prior to the stereocontrolled generation of cantharidin[6] by Stork et al. in 1951, or the first synthesis of morphine[7] reported a few months later in which Gates and Tschudi employed the pericyclic process. The apparent delay in applying the Diels–Alder reaction, or "diene synthesis" as it was known at the time, to total synthesis was likely the consequence of a variety of factors. First, with few exceptions, total synthesis during that period played a role inclined more towards structure verification than as its own unique vehicle to advance the field of organic synthesis, as it is practiced today. As such, in a discipline defined by converting known materials by existing methods into other compounds, practitioners would not likely have regarded being the "first" to employ a particular transformation in a synthesis as an important contribution, and the number of compounds in which the Diels–Alder reaction had been demonstrated was limiting in terms of potential synthetic targets. Moreover, the founders of the reaction, while they certainly made significant forays in the


K. C. Nicolaou


S. A. Snyder


T. Montagnon


G. E. Vassilikogiannakis

Professor K. C. Nicolaou, born in Cyprus and educated in England and the US, is currently Chairman of the Department of Chemistry at The Scripps Research Institute, where he holds the Darlene Shiley Chair in Chemistry and the Aline W. and L. S. Skaggs Professorship in Chemical Biology, as well as Professor of Chemistry at the University of California, San Diego. His impact on chemistry, biology, and medicine flows from his works in chemical synthesis and chemical biology described in over 500 publications and 70 patents and his dedication to chemical education, as evidenced by his training of more than 400 graduate students and postdoctoral fellows. His recent book titled Classics in Total Synthesis, *which he co-authored with Erik J. Sorensen, is used around the world as a teaching tool and source of inspiration for students and practitioners of organic synthesis.*

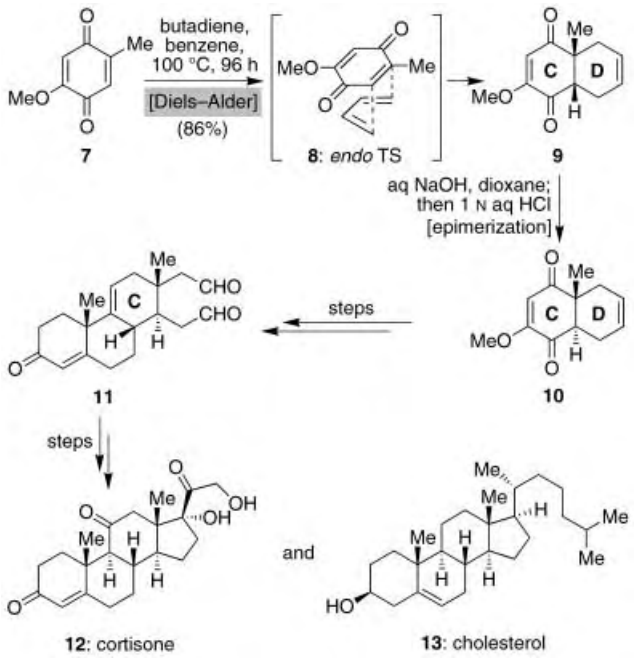
Scott A. Snyder, born in Palo Alto, California in 1976, spent his formative years in the suburbs of Buffalo, New York. He received his B.A. in Chemistry (summa cum laude) from Williams College, Williamstown, Massachusetts, in 1999, where he explored the hetero-Diels–Alder reaction with Prof. J. Hodge Markgraf. He then began graduate studies with Prof. K. C. Nicolaou, where he has devoted his attention to the chemistry and biology of the marine-derived antitumor agent diazonamide A. He is the recipient of a Barry M. Goldwater Fellowship in Science and Engineering, a National Science Foundation Predoctoral Fellowship, and a Graduate Fellowship from Pfizer, Inc. His research interests include complex natural product synthesis, reaction mechanism and design, and application of these fields to chemical biology.

Tamsyn Montagnon was born in Hong Kong in 1975. She received her B.Sc. in Chemistry with Medicinal Chemistry from the University of Leeds, UK, which was followed by a move to the University of Sussex where she obtained a D.Phil in 2000 for research conducted under the supervision of Professor P. J. Parsons, towards the synthesis of complex natural products, including the squalestatins and triptoquinone C. She was awarded a GlaxoWellcome post-doctoral fellowship and joined Professor K. C. Nicolaou's group in January 2001. Her research interests include natural product synthesis, medicinal chemistry, and reaction methods and mechanisms.

Georgios E. Vassilikogiannakis was born in Iraklion, Crete, Greece in 1970. He received his B.Sc. in Chemistry in 1993 and his Ph.D. in 1998 from the University of Crete under the guidance of Professor Michael Orfanopoulos exploring the mechanisms of the electrophilic additions of singlet oxygen, tetracyanoethylene, triazolinediones, and fullerenes to alkenes and dienes. He joined Professor K. C. Nicolaou's group in 1999, and was involved in the total syntheses of bisorbicillinol, bisorbibutenolide, trichodimerol, and colombiasin A. He was recently appointed Assistant Professor of chemistry at the University of Crete, Greece. His primary research interests involve the synthesis of natural products as an enabling endeavor for the discovery of new chemical knowledge and its application to chemical biology.

area of terpene synthesis,[8] became diverted by other research concerns of greater interest to them, particularly in regard to understanding the mechanistic underpinnings of the reaction they had discovered.[9] Significantly, these efforts ultimately resulted in such important advances as the Alder *endo* rule that governs the stereochemical outcome of the typical Diels – Alder reaction.[10] The most dominant reason for the delay in the incorporation of the Diels – Alder cycloaddition into total synthesis, however, might be attributed to World War II and its aftermath, a period for which no analysis can properly estimate the challenges to conducting research in organic synthesis, particularly in Germany.

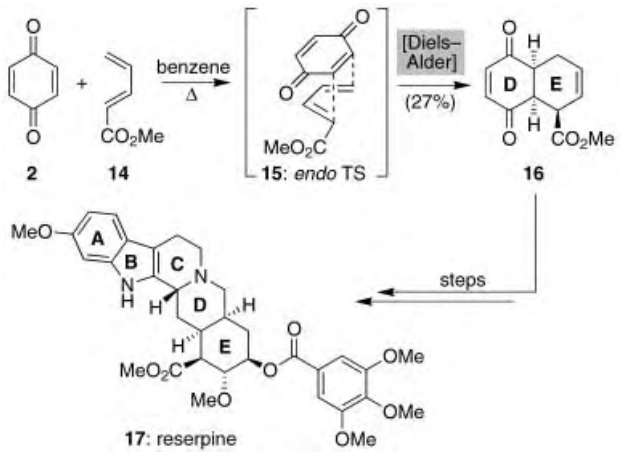
As such, the truly visionary application of the Diels – Alder reaction to total synthesis would have to await the imagination of chemical artists such as R. B. Woodward, who would apply new levels of creativity to the reaction at hand through some highly elegant and instructive syntheses. In 1952, Woodward et al. disclosed their historic routes to the steroids cortisone and cholesterol (**12** and **13**, respectively, Scheme 2)



Scheme 2. The pioneering adoption of a quinone-based Diels – Alder reaction by Woodward et al. in 1952 as the key step in the total synthesis of the steroid hormones cortisone (**12**) and cholesterol (**13**).[11]

where, in the initial step, reaction of quinone **7** with butadiene in benzene at 100 °C for 96 hours effected a smooth Diels – Alder cycloaddition to form bicyclic adduct **9** via the intermediacy of *endo* transition state **8**.[11] Several features of this particular [4+2] cycloaddition reaction are of note. First, Woodward recognized that by using a differentiated quinone nucleus it would be possible to effect regioselective control of the intermolecular Diels – Alder union, as the more electron-rich methoxy-substituted olefin would be less dienophilic than its methyl-substituted counterpart. An equally insightful design element was the anticipation that even though a *cis*-fused adduct would arise from the Diels – Alder reaction, conversion into the requisite thermodynamically more stable *trans*-fused system present in the targeted natural products would be relatively simple to achieve. Thus, in the next synthetic operation, base-induced epimerization readily provided the coveted *trans*-fused ring system (**10**), thus setting the stage for an eventual ring-contraction process that would allow completion of this region of the steroid nucleus.[12]

Similar levels of synthetic ingenuity are reflected in the total synthesis of reserpine (**17**, Scheme 3) by Woodward et al. in 1956,[13] where again an opening Diels – Alder reaction forged the critical bicyclic system (**16**) that would serve as the



Scheme 3. Application of the Diels – Alder reaction in the total synthesis of reserpine (**17**) by Woodward et al. in 1956.[13]

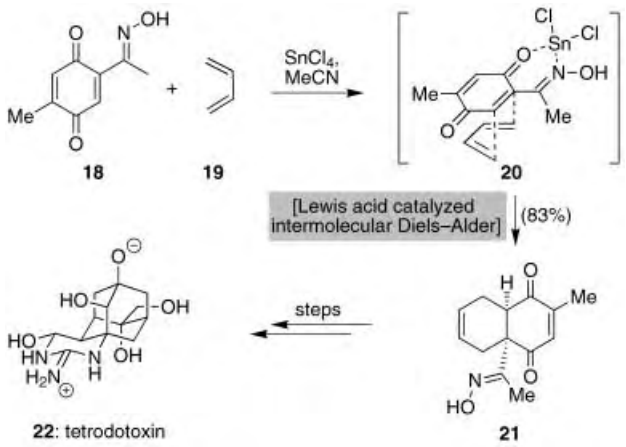
scaffold for the ensuing synthetic sequence.[14] This use of a Diels – Alder strategy to form an initial array of rings and stereocenters, elements which pave the way for subsequent stereocontrolled elaboration to the final target molecule, represents a distinctive hallmark of Woodward's synthetic acumen. Moreover, these two examples from Woodward's research group are illustrative of a new school of thought that emerged in the 1950s which involved approaching the synthesis of complex molecules by rational synthetic strategies, and they admirably demonstrated the inherent strength of the Diels – Alder reaction to solve challenging synthetic puzzles which might otherwise have remained hopelessly complex.

In this review, we hope to highlight didactic exemplars of the Diels – Alder reaction in the context of natural product total synthesis representing work which has decisively advanced both the power and scope of this pericyclic process beyond the pioneering applications of Woodward. In selecting our case studies, we accepted the fact that any review of such a widely used reaction with nearly three-quarters of a century of history could not possibly be comprehensive. Our aspiration is that the delineated examples will sufficiently cover the various areas in which Diels – Alder methodology represents an indispensable tool for the art of total synthesis, and will reflect key paradigm shifts in the field through novel and inventive approaches to this classic reaction. We hope that these discussions will inspire you not only to further explore the literature in terms of syntheses not expounded upon here, but also to create even more fantastic applications of the Diels – Alder reaction in your own research.

2. Regiocontrol and Beyond: Achieving Stereoselection

The early total syntheses by Woodward described above amply illustrate the ability of the Diels–Alder reaction to create molecular complexity. Not only is a cyclohexene ring generated through the formation of two new σ bonds, but up to four contiguous stereocenters are also concomitantly fashioned in the process. Fortunately, as a result of the regio- and stereospecific nature of the Diels–Alder reaction (always a *cis* addition) and the diastereoselectivity of the union based on the Alder *endo* rule[10] (where a more sterically crowded and seemingly less thermodynamically stable transition state results when the dienophile possesses a suitable conjugating substituent), the formation of these chiral elements is often predictable in a relative sense. However, new principles and approaches to the Diels–Alder reaction would be needed beyond those delineated in the syntheses of reserpine and cholesterol if absolute control of stereochemistry is required. In addition, although Woodward's Diels–Alder reactions elegantly achieved regioselectivity, results which can be rationalized successfully on the basis of frontier molecular orbital theory,[15] these examples do not reflect the challenges faced in attempting to achieve such control in certain contexts where particular unsymmetrical diene and/or dienophile units having specific steric and electronic properties are employed. As such, general solutions would be required to address the problem of selectively incorporating useful sets of diverse functionality in Diels–Alder cycloaddition products. In this section, we highlight some answers to the issues of regio- and stereoselectivity which have been developed by leading synthetic chemists to provide a qualitative measure of the current state of the art in Diels–Alder technology.

A classical method to enhance regioselectivity is based on the use of Lewis acid catalysts. Upon complexation of such species to the dienophile, the normal demand Diels–Alder reaction is promoted since the energy gap between the lowest unoccupied molecular orbital (LUMO) of the dienophile and the highest occupied molecular orbital (HOMO) of the diene is reduced, thus decreasing the activation energy required to achieve the cycloaddition. Moreover, as this stabilization is greater for the *endo* transition state, as a result of beneficial enhancement of secondary orbital overlap that is unobtainable in an *exo* mode of reaction, the use of Lewis acids favors an increased ratio of *endo*:*exo* products. More valuable synthetically, however, is the fact that Lewis acids can often reverse the regiochemical course of a Diels–Alder addition and generate products that would not otherwise be observed in a simple, thermally induced reaction.[16] An early and elegant example of this concept is provided by the total synthesis of tetrodotoxin (**22**, Scheme 4) by Kishi et al.[17] As in the Woodward paradigm, an initial Diels–Alder union between quinone **18** and butadiene (**19**) was employed to generate a preliminary set of rings and stereocenters for subsequent elaboration. However, the intriguing feature of this example is that the use of $SnCl_4$ in the Diels–Alder reaction proved critical for the chemoselective engagement of butadiene with the oxime-bound dienophile to form **20**; in the absence of the Lewis acid, the other olefinic bond of quinone

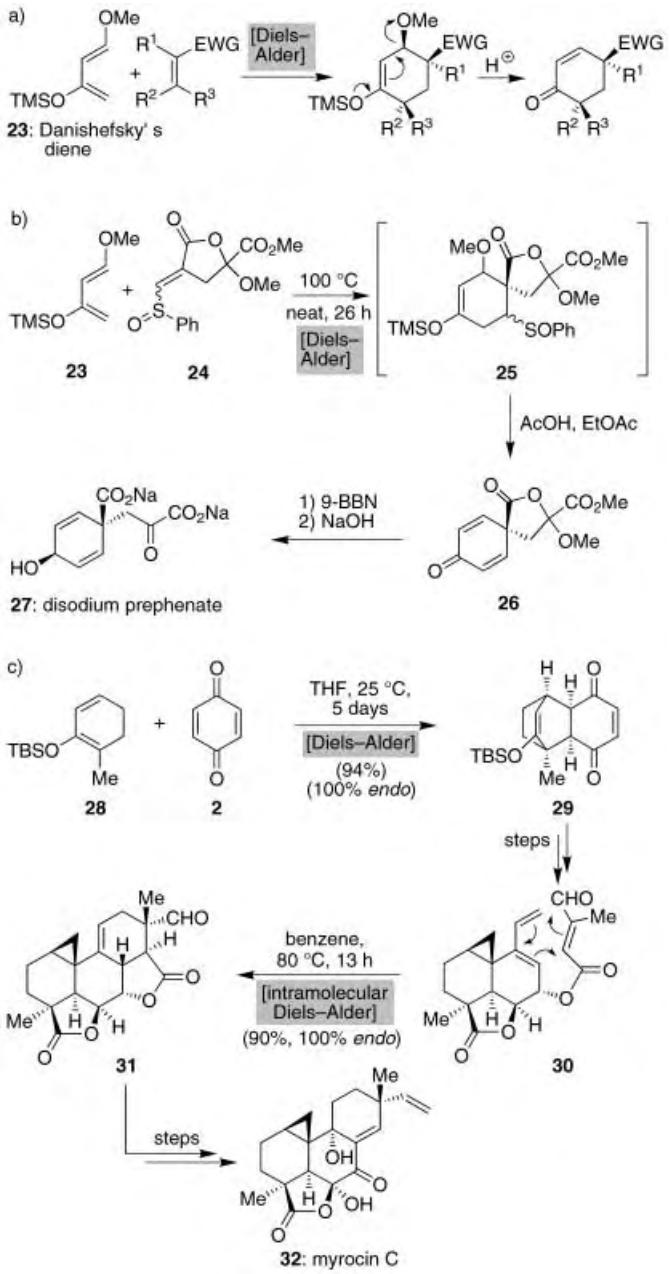


Scheme 4. Use of Lewis acid catalysis by Kishi et al. (1972) to achieve chemoselective control in the formation of key intermediate **21** leading to tetrodotoxin (**22**).[17]

18 reacted exclusively. Although oximes normally behave mesomerically as electron-donating substituents, thus deactivating the neighboring olefin for Diels–Alder reaction, coordination of the Lewis acid reverses this behavior by drawing electron density away from this group, which leads to an adjacent highly competent electron-deficient dienophile.[18] Thus, Lewis acid activation nicely effected regiochemical control in the employed [4+2] cycloaddition that could not have been achieved otherwise.

Among other methods introduced to achieve excellent regioselectivity, as well as to incorporate useful functional groups, Danishefsky's widely applicable diene system (**23**, Scheme 5a) represents one of the most important advances in this regard within the past quarter century.[19] Initially developed as part of a method to selectively generate pyran rings upon reaction with aldehyde dienophiles,[20] the power of the prototype diene **23** rests in the synergistic effects of the two incorporated oxygen groups, which provide mutually reinforcing electronic contributions to the diene system such that regiospecific formation of a lone *endo* adduct results upon reaction with most dienophiles. In addition, upon treatment with mild acid after the Diels–Alder reaction, cleavage of the silyl protecting group residing within the product and the strategic location of the methoxy leaving group enables an ensuing cascade sequence that results in the formation of an α,β-unsaturated system. An early demonstration of this strategy in total synthesis can be found in the route used by Danishefsky et al. to form disodium prephenate (**27**, Scheme 5b),[21] where, although the target may not seem to possess great molecular complexity, application of this designed diene technology provided a highly elegant and concise solution to the synthetic problem at hand. As illustrated, after regioselective formation of Diels–Alder product **25**, in situ treatment of this compound with acetic acid formed the desired α,β-unsaturated system which concurrently eliminated phenyl sulfoxide to provide **26**, a product which was easily elaborated to the target structure.

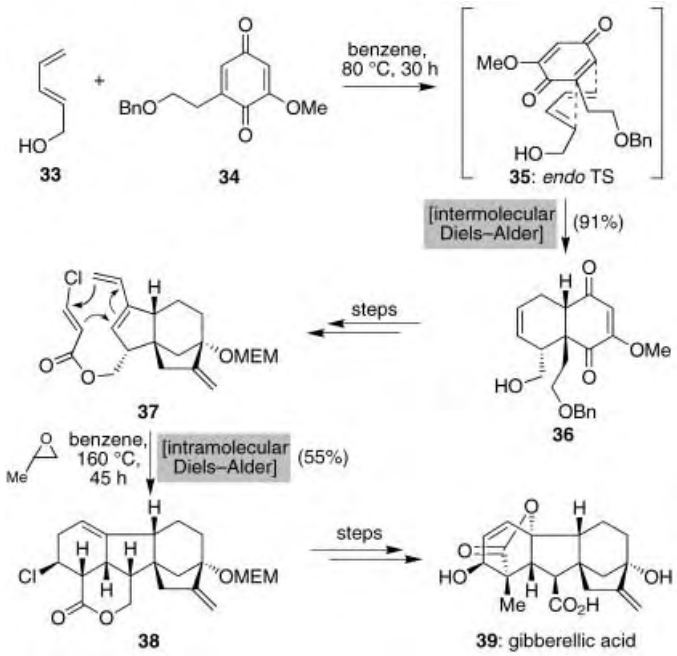
The versatility of this particular technology is underscored by the wide variety of such dienes that can be employed.[22] For example, use of a Danishefsky-type diene (**28**, Scheme 5c)



Scheme 5. Danishefsky's diene (**23**) and its use in organic synthesis: a) generalized stereochemical outcome of Diels–Alder reactions in this paradigm; b) use of **23** as part of the total synthesis of disodium prephenate (**27**; 1979);[21] c) employment of a Danishefsky-type diene (**28**) in the total synthesis of myrocin C (**32**) featuring two Diels–Alder reactions (1994).[23]

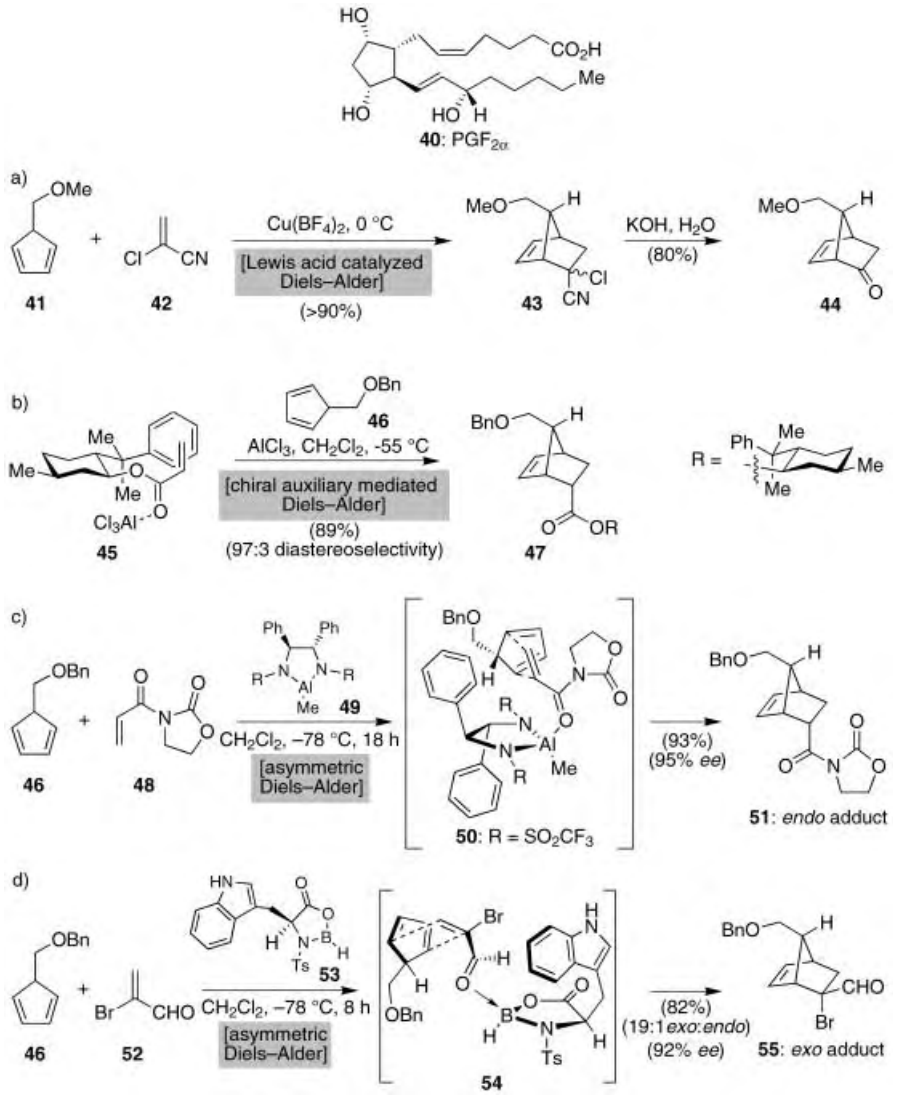
provided an impressive entry into the total synthesis of myrocin C (**32**),[23] even though in this particular case achieving regioselective addition to quinone **2** was clearly not a critical feature of the designed route. The second Diels–Alder reaction in Danishefsky and co-workers elegant sequence to myrocin C (**30** → **31**) is also significant as it reflects an additional means of controlling relative stereochemistry of the process, pertinent only in intramolecular cases, on the basis of substrate control. As illustrated in this example, the stereocenter proximal to the dienophile governed the addition of this unit to only one diastereotopic face of the 1,3-diene system, thus setting the resultant stereochemistry of the product (**31**) in a relative sense.

The power of such strategies to exert stereochemical control is similarly reflected in the brilliant total synthesis of gibberellic acid (**39**, Scheme 6) by Corey et al.,[24] where an initial chemo- and regioselective Diels–Alder union between diene **33** and quinone **34** forged the relative stereochemistry in **36**, and subsequent elaboration to **37** enabled a substrate-controlled intramolecular Diels–Alder reaction which proceeded with selective formation of the expected product (**38**).[25] Overall, one should note that the outcome of the Diels–Alder reaction in these intramolecular instances is generally predictable based on the stereochemical requirements of the resident set of functionalities.



Scheme 6. Use of both inter- and intramolecular Diels–Alder reactions in the stereocontrolled synthesis of gibberellic acid (**39**) by Corey et al. (1978).[24]

Despite these remarkable early advances in developing methods to achieve relative stereochemistry, the issue of controlling the absolute stereochemistry of the Diels–Alder reaction was not successfully addressed until more recent times. An instructive entry into the several elegantly conceived solutions to this problem is afforded by following the progression of the numerous total syntheses of prostaglandin $F_{2\alpha}$ ($PGF_{2\alpha}$, **40**, Scheme 7) and its relatives by Corey et al.[26] The overall challenge of governing the absolute stereochemistry of Diels–Alder products in contexts pertinent to the synthesis of these secondary metabolites is demonstrated in the initial total synthesis of $PGF_{2\alpha}$, first disclosed in 1969 by Corey et al.[26c] In this approach (Scheme 7a), a Lewis acid catalyzed Diels–Alder union between diene **41** and 2-chloroacrylonitrile (**42**) afforded a racemic mixture of Diels–Alder adducts (**43**), as would be expected since the enantiotopic faces of **41** are not differentiated. The random stereochemistry at the carbon center



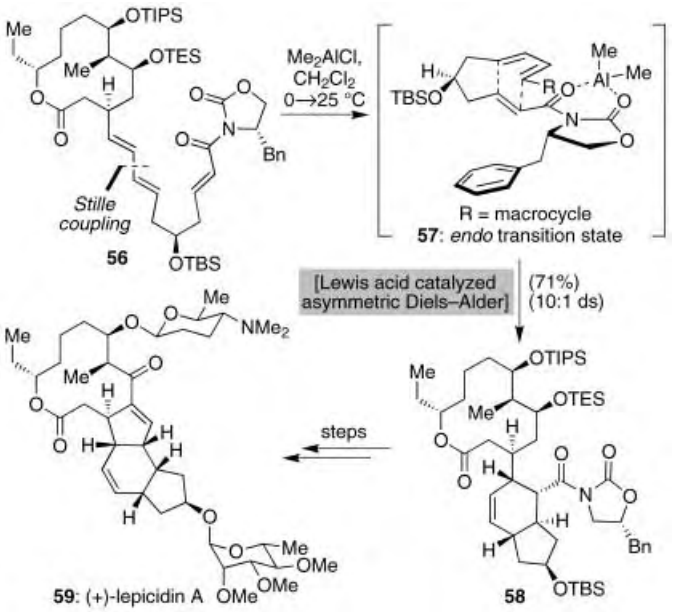
Scheme 7. Creative and didactic applications of the Diels–Alder reaction by Corey et al. to the total synthesis of prostaglandin $F_{2\alpha}$ (**40**): a) original approach using a ketene equivalent (1969);[26c] b) application of a chiral auxiliary to orchestrate the enantioselectivity of the Diels–Alder union (1975);[26f] c) asymmetric catalysis of the Diels–Alder reaction to afford the *endo* adduct in high enantiomeric excess (1989);[26g] d) reversal of selectivity to near-complete *exo* topicity by using chelation with a chiral oxazaborolidinone catalyst (1992).[26h]

bearing the chloro and cyano substituents was of no consequence since it was destroyed in a subsequent hydrolysis event to reveal ketone **44**. As such, an asymmetric synthesis of prostaglandin $F_{2\alpha}$ (**40**) would demand a controlled facial interaction between the diene and dienophile units in the initial Diels–Alder reaction transition state. Ingenious designs and years of research would be required before Corey and his research group would reach the desired goal, despite the simply stated nature of the problem.[26, 27]

The first successfully identified solution involved attachment of the dienophile to a homochiral cyclohexane ring system, that of menthol, to effect the near-exclusive enantioselective formation of *endo* adduct **47** in 98% *ee* (Scheme 7b).[26f] Presumably, this product was the result of closely controlled presentation of the dienophile, achieved through minimization of steric repulsion between the $AlCl_3$-chelated carbonyl group and the menthol-derived phenyl ring and aided by π stacking, with approach of the diene occurring from the more exposed side of the dienophile. Overall, this Diels–Alder strategy represents one of the earliest examples of this mode of asymmetric synthesis, and reflects the value of the induction of asymmetry by a chiral auxiliary[28]—a process in which a temporarily implanted element of stereochemistry in the reacting molecule dictates the stereochemical outcome of the reaction. Although certainly useful, the general strategy is not without drawbacks. Not only must the auxiliary eventually be excised, but the chiral element also has to be placed in proximity to the reacting center (pertinent only to the dienophile component, as such directing groups on the diene portion would likely be too distal to achieve any control). Perhaps the more significant concern, however, is that the chiral auxiliary often needs to be retailored to achieve the opposite stereoselection.

As such, the Corey research group did not remain content with this single solution, but instead sought, through rational design, suitable systems in which they could control the induction of asymmetry through catalysis. The first successful reagent developed in this regard was the C_2-symmetric aluminum catalyst **49** (Scheme 7c), which accomplished the asymmetric union of diene **46** and dienophile **48** to provide *endo* adduct **51** in 95% ee.[26g, 27a,b] The observed induction of asymmetry can be rationalized readily through the presumed transition state **50**, in which the aluminum center acts as a Lewis acid that activates **48** for facile reaction under mild conditions, thereby enhancing the opportunity to achieve high levels of enantiomeric excess. Significantly, the chiral ligand could be recovered from the reaction mixture and subsequently converted back to the initial catalyst system. In an additional demonstration of asymmetric virtuosity, the use of the chiral oxaborolidinone system **53** (Scheme 7d) induced formation of the *exo* product **55** in equally impressive levels of enantiomeric excess.[26h, 27c] Indeed, these latter catalytic approaches persist today as preeminent solutions to asymmetrically controlling topicity in Diels–Alder reactions. Moreover, subtle alteration of these catalysts has enabled their widespread application[29] in numerous other types of reactions where they admirably regulate asymmetric induction. In the ensuing schemes of this section, a number of other elegant and unique expressions of the same general principles in the asymmetric total synthesis of complex natural products are delineated.

Although homochiral auxiliaries often lack broad generality, as mentioned earlier, one glaring exception to this trend resides in the chiral oxazolidinone systems of Evans et al. which have found extensive applications in numerous reactions of prominence in organic synthesis.[30] Within the Diels–Alder paradigm, a wonderful illustration of the power of this class of chiral auxiliary is found in the asymmetric synthesis of (+)-lepicidin A (**59**, Scheme 8), achieved in 1993 by Black and

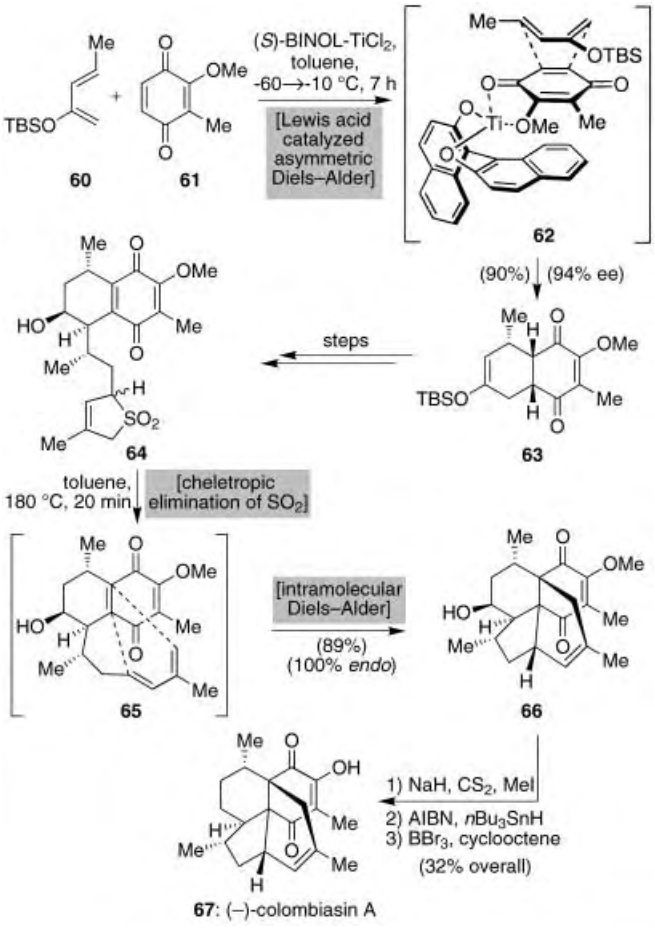


Scheme 8. Use of Evans' chiral auxiliary in a Lewis acid mediated Diels–Alder reaction as part of a stereocontrolled route to (+)-lepicidin A (**59**; Evans and Black, 1993).[31]

Evans.[31] After formation of **56**, in which a Stille coupling reaction was employed to prepare the diene system, exposure of this compound to catalytic amounts of Me_2AlCl effected the stereocontrolled generation of *endo* adduct **58** by an intramolecular [4+2] cycloaddition. In the event, concurrent coordination of the aluminum center to the two carbonyl groups on the dienophile segment framed a rigid six-membered ring system (**57**) in which the lowest energy conformation strategically positioned the benzyl group, thus ensuring approach of the diene moiety exclusively from the opposite face of the activated dienophile to furnish the desired *endo* adduct **58** in high diastereoselectivity (about 10:1). When an achiral imide auxiliary was used in the same reaction, however, the Diels–Alder reaction led to a 6:1 mixture of *endo*:*exo* isomers, except that in the conversion of **57** into **58** the opposite sense of induction resulted than was observed in the case shown! Clearly, the power of the chiral oxazolidinone auxiliary to overcome the latent internal bias of the Diels–Alder cycloaddition represents a remarkable strength of the approach. As an additional beneficial feature, the chiral auxiliary was smoothly recovered from the product, and, although not illustrated in this particular synthesis, can be cleaved in several different ways to leave unique functionality for subsequent elaboration. In terms of advancing this technique beyond substrate control, the Evans research group has recently introduced several exogenous catalytic variants using a copper(II) center,[32] catalysts which have already demonstrated their usefulness in several total syntheses, including selective asymmetric routes to *ent*-shikimic acid and isopulo'upone.[33]

Despite the aforementioned advances, however, a universally applicable catalyst system for all types of Diels–Alder reactions remains elusive. Until recently, for example, no disclosed catalyst proved adequate to induce asymmetry in synthetically useful levels of enantiomeric excess for the [4+2] cycloaddition reaction of quinones, arguably one of the most important dienophiles for total synthesis purposes from both a historical perspective as well as a practical standpoint. Despite long-standing failures in this endeavor, an initial proof-of-principle in the context of total synthesis was achieved in 2000 by White and Choi in their disclosed route to (−)-ibogamine,[34] in which Mikami's catalyst system (formed in situ through reaction of either (*S*)- or (*R*)-BINOL with $[(iPrO)_2TiCl_2]$) provided excellent enantioselectivity in a quinone-based Diels–Alder event.[35]

More recently, the Nicolaou group extended the versatility of this catalyst in their total synthesis of the unique terpenoid (−)-colombiasin A (**67**, Scheme 9).[36] In an early step, the Danishefsky-type diene **60** and quinone **61** were successfully combined in a selective asymmetric Diels–Alder reaction by

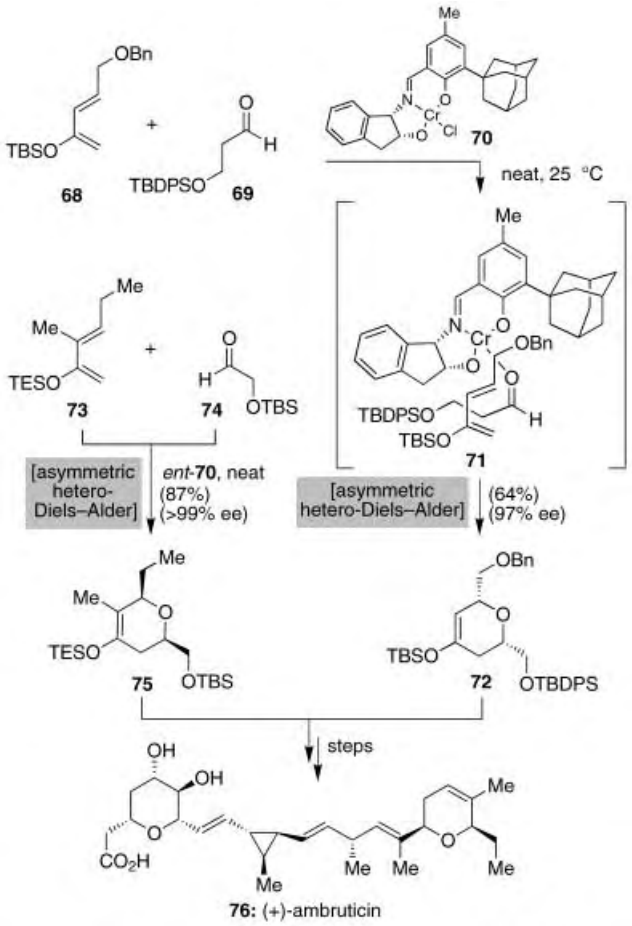


Scheme 9. Reiterative quinone-based Diels–Alder reactions incorporating the use of a sulfone-masked diene in the asymmetric total synthesis of (−)-colombiasin A (**67**; Nicolaou et al., 2001).[36]

using the Mikami catalyst (30 mol %) to orchestrate the event. Although a 5:1 mixture of **63** and its corresponding regioisomer were isolated, significantly **63** was generated in greater than 94 % *ee*. As shown in transition state **62**, this high level of asymmetric induction was anticipated as the inherent chirality of the coordinated (*S*)-BINOL molecule, effectively presented through the formation of $\pi-\pi$ interactions between **61** and one of the naphthol rings of the catalyst, blocked the lower face of the quinone and guided the approach of diene **60** preferentially from the top face onto the reactive olefin of dienophile **61**. Although the catalyst system achieved a stable bidentate mode of chelation in this transition state, the observed mixture of regioisomers was likely the product of partial coordination of the catalyst to the other carbonyl group of **61**, an event which results in less-favored monodentate chelation. Such complexation is conceivable, however, as a consequence of the much higher Lewis basicity of this oxygen atom resulting from it being part of a vinylogous ester. Finally, one should note that the use of a relatively high level of catalyst loading proved critical in achieving sufficient asymmetric induction, as the uncatalyzed background Diels–Alder union proceeded readily, thus eroding enantioselectivity in the presence of less catalyst. After elaboration of adduct **63** to precursor **64** (an entity with a sulfone-masked diene system), thermal extrusion of SO_2 followed by a second, this time intramolecular, Diels–Alder reaction with the regenerated quinone system completed the architectural skeleton of the target molecule. This latter *endo*-stereospecific Diels–Alder event, which remarkably installed two adjacent quaternary centers and formed two new rings using exactly the same carbon atoms for the dienophile component as in the initial Diels–Alder reaction, will be revisited in greater detail in Section 4.

A recent elegant application of a novel asymmetric catalyst to solve a long-standing synthetic problem is found in the synthesis of (+)-ambruticin (**76**, Scheme 10) by Liu and Jacobsen,[37a] in which use of the salen-type catalyst **70**[37b] and its enantiomer smoothly directed the asymmetric syntheses of pyran ring systems **72** and **75** in exceptional yield and exceedingly high enantiomeric excess. This catalyst system reflects the first-known method capable of controlling the induction of asymmetry in Diels–Alder reactions between unactivated carbonyl compounds and dienes that are less-activated than the Danishefsky-type possessing two oxygen substituents.[38] Although the mechanistic rationale for the selectivity observed in these unions has not been explicitly defined, it is reasonable to assume that Lewis acid activation of the aldehyde, with the orientation of the alkyl side chain directed by the bulky adamantyl group and eventual approach of the dienophile dictated by the stereochemistry of the indanone skeleton, is the controlling pathway to the observed enantiospecificity. It is worth noting that the erosion in enantioselectivity obtained in related systems with aldehydes possessing less steric bulk than either **69** or **74** is in agreement with this hypothesis.[37b]

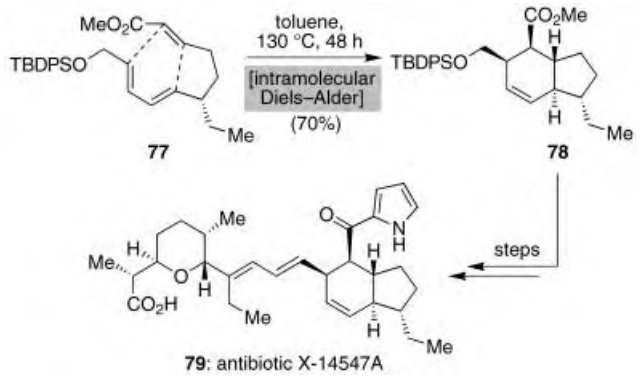
In the absence of homochiral catalysts or auxiliaries, however, the only viable method for achieving absolute stereocontrol in Diels–Alder fusions relies on the presence of homochirality in the starting substrate which then governs the



Scheme 10. Use of a novel chromium-catalyzed hetero-Diels–Alder reaction by Jacobsen and co-workers to fashion the two terminal pyran systems in an asymmetric total synthesis of (+)-ambruticin (**76**; 2001).[37]

resultant stereochemistry of the [4+2] cycloaddition product. This substrate-controlled approach is the direct extension of the concepts discussed earlier in the intramolecular Diels–Alder reactions of myrocin C[23] and gibberellic acid,[24] except that nonracemic starting material is employed in the pericyclic reaction. Within the large group of total syntheses that demonstrate such substrate-controlled diastereoselectivity, an early example includes the conversion of triene **77** into bicyclic system **78** as part of the asymmetric synthesis of the antibiotic X-14547A (**79**, Scheme 11) by Nicolaou et al.[39] Although the outcome of this Diels–Alder process was anticipated, the achieved attachment of a *trans*-fused five-membered ring onto a cyclohexene template is rather remarkable, as this molecular motif would be challenging to construct by means other than a Diels–Alder reaction.[40]

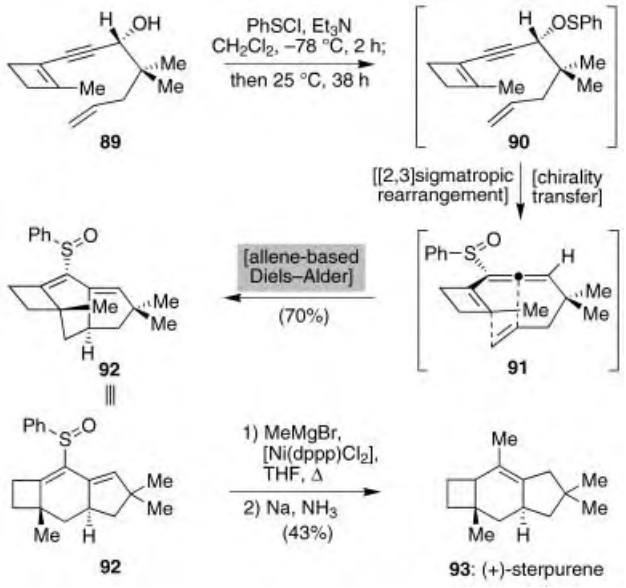
As a further example illustrative of such Diels–Alder reactions in the context of generating polycyclic systems, we turn to the CP molecules (**84** and **85**, Scheme 12), natural products that combine fascinating and complex molecular architectures with interesting biological properties. In successful approaches to these naturally occurring substances, the research groups of both Nicolaou[41] and Fukuyama[42] employed an intramolecular Diels–Alder reaction to fashion the carbogenic core possessing the *anti*-Bredt bridgehead ole-



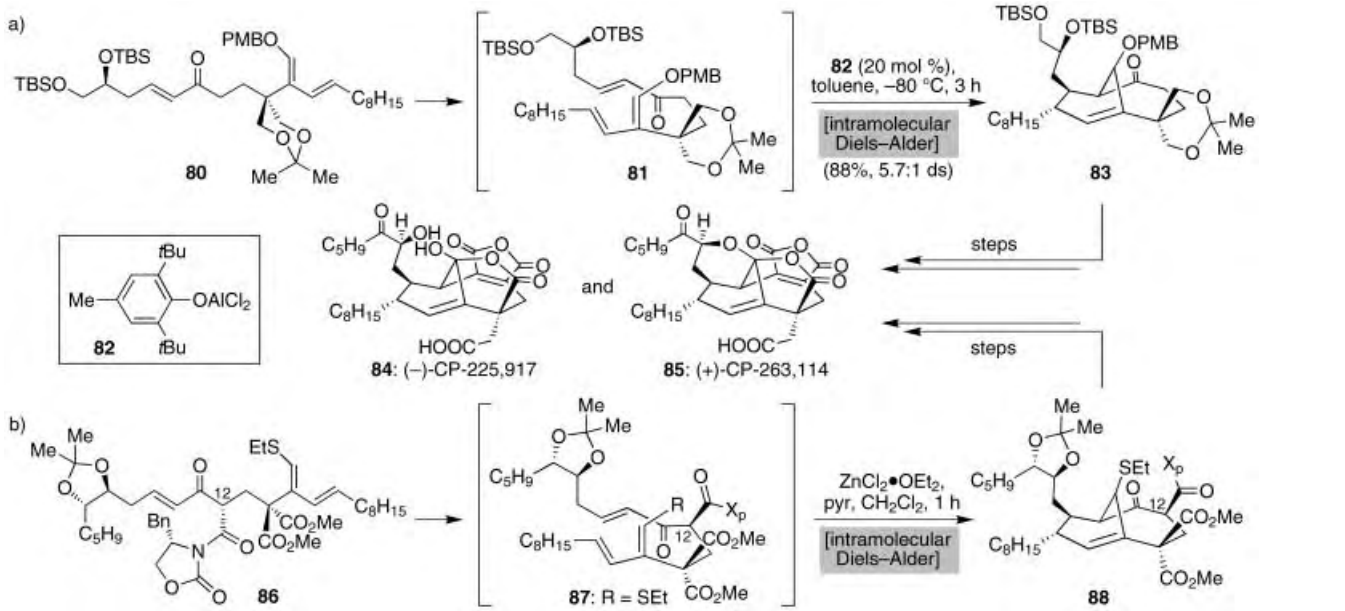
Scheme 11. Asymmetric total synthesis of antibiotic X-14547A (**79**) featuring an intramolecular Diels–Alder reaction to fashion the bicyclic core (Nicolaou et al., 1985).[39]

fin.[43] Besides demonstrating the power of the Diels–Alder cycloaddition as an expedient avenue to fashion such congested and strained structures, each of these syntheses utilized unique substrate-controlled methods to induce diastereoselectivity within the same Diels–Alder-based retrosynthetic blueprint. In the synthesis by Nicolaou et al., the use of a homochiral starting material incorporating a lone, distal stereocenter on the alkyl chain (**80**) in conjunction with the bulky Lewis acid catalyst **82** created a sufficiently controlled chiral environment (**81**) to effect a diastereoselective intramolecular Diels–Alder reaction to provide **83** along with a small amount of its diastereomer (5.7:1). Significantly, attempts to achieve superior induction in this reaction with a number of other chiral Lewis acids failed. In the paradigm of Fukuyama and co-workers, attachment of an Evans' chiral auxiliary on the carbon atom α to the central enone in **86** led to stereoselective formation of *endo* adduct **88** upon activation with $ZnCl_2$. Interestingly, in this scenario the auxiliary did not mediate the selectivity in the same fashion as in the earlier example by Evans and Black (Scheme 8). Instead, the oxazolidinone served solely as a bulky group capable of sufficiently inducing formation of the desired diastereomer, since the C_{12} center had already been installed in a stereochemically pure form.

Along related lines, a striking example of an intramolecular Diels–Alder reaction accompanied by chirality transfer was provided by Okamura and co-workers in 1988.[44] In this elegant synthesis of (+)-sterpurene (**93**, Scheme 13), the controlled generation of a single allene isomer directed the orientation of the diene and dienophile units in such a way as

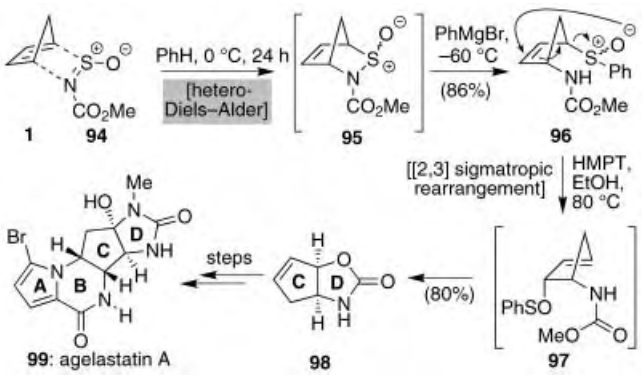


Scheme 13. Asymmetric total synthesis of (+)-sterpurene (**93**) by Okamura and co-workers based on a [2,3] sigmatropic rearrangement accompanied by chirality transfer to an allene and subsequent intramolecular Diels–Alder reaction (1988).[44]



Scheme 12. Applications of the Diels–Alder reaction to form the bicyclic system of the CP molecules, a novel, naturally occurring architecture violating Bredt's rule: a) the approach used by Nicolaou et al. that utilizes a substrate-controlled Lewis acid catalyzed Diels–Alder reaction (1999);[41] b) employment of an Evans' chiral auxiliary by Fukuyama et al. to achieve a diastereoselective union (2000).[42]

to allow entrance into only one of the two possible Diels–Alder pathways, thereby leading to a single product. In the event, attachment of a thiophenyl group to the homochiral alcohol in **89** provided intermediate **90**, a species poised for a [2,3] sigmatropic rearrangement. With the preexisting chiral center in **90** transferred as an axial chiral element in **91**, the smooth formation of **92** was achieved as a single enantiomer in 70% yield. As such, this synthesis reflects a highly creative approach to the stereocontrolled construction of **93**.[45] Finally, we should note that a particularly interesting advance in methodology involving the use of allenes in intramolecular Diels–Alder reactions was recently described by the Wender research group: application of rhodium and nickel catalyst systems engendered the selective reaction of either of the allene olefinic units as the 2π-electron component.[46]



Scheme 14. Total synthesis of agelastatin A (**99**) by Weinreb and co-workers in which an *N*-methylcarbamate was employed as a dienophile in a hetero-Diels–Alder reaction (1999).[50]

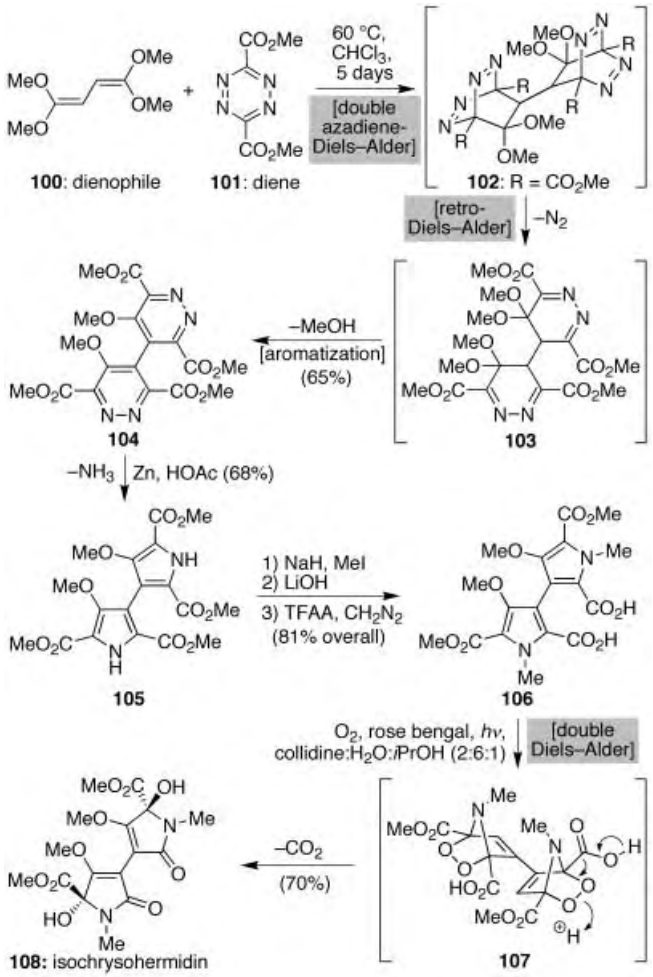
3. Hetero-Diels–Alder Reactions

With the lone exception of the total synthesis of (+)-ambruticin (Scheme 10) by Liu and Jacobsen,[37a] all of the examples discussed thus far involve the formation of solely carbogenic products arising from Diels–Alder cycloaddition reactions. However, the ability to incorporate various heteroatoms at any of the six possible positions in the diene and dienophile components of the reaction constitutes a challenge which has occupied the hearts and minds of synthetic chemists since the discovery of the Diels–Alder reaction.[47] In fact, one of the first examples of a hetero-Diels–Alder reaction was disclosed by Alder himself in 1943 when he discovered, purely by serendipity, that an imine tautomer could engage appropriate dienes in a productive [4+2] cycloaddition.[48] Limited by the confines of space, what we hope to accomplish in this section is to appropriately whet the appetite of the reader with a few, select examples from the vast smorgasbord of total syntheses in which this type of process is employed. In the schemes that follow we illustrate the broad themes that have guided synthetic approaches along these lines, with particular emphasis on cascade-based syntheses and non-obvious retrosynthetic disconnections.

As a first example of the powerful hetero-Diels–Alder reaction we highlight a case where two heteroatoms are present in the dienophilic unit. Despite a report in the 1950s that describes the ability of *N*-sulfinylaniline to undergo reaction with 1,3-dienes in Diels–Alder fashion,[49] this particular variant of the Diels–Alder cycloaddition remained, for the most part, an obscure entry in the literature until extensive studies much later honed this mode of reaction into a sharp synthetic tool. The overall power of this hetero-Diels–Alder-based methodology is beautifully illustrated in the total synthesis of agelastatin A (**99**, Scheme 14) by Weinreb and co-workers,[50] the climax of extensive mechanistic studies and several creative syntheses achieved in this arena by this research group.[51] In the initial step of this synthesis, *N*-sulfinylmethylcarbamate (**94**) smoothly engaged in a hetero-Diels–Alder union with cyclopentadiene (**1**) at 0 °C to provide adduct **95**. One should note that, in general, the addition process with this class of hetero dienophile is particularly reversible, and, as such, the observed products often do not reflect the kinetics of the initial addition. Additionally, the resultant sulfoxide stereochemistry in the Diels–Alder products is often difficult to predict or control. In this instance, however, the latter issue was of no consequence, as a subsequent rearrangement destroyed this element of chirality. Since **95** was prone to retro-Diels–Alder reaction at ambient temperature, the compound was treated immediately upon formation with phenylmagnesium bromide and furnished **96** as a result of nucleophilic attack on the sulfur atom and concurrent lysis of the S–N bond. Heating a solution of this compound in HMPT and Et_3N induced the anticipated conversion into sulfenate ester **97** by a [2,3] sigmatropic rearrangement (an event which is the reverse of the conversion discussed in Scheme 13). Subsequent attack by the resulting nucleophilic oxygen atom on the pendant ester then led to carbamate formation and afforded **98**. As such, the net transformation accomplished by this programmed hetero-Diels–Alder/rearrangement sequence was the regioselective *syn* addition of an oxygen and a nitrogen atom across one of the double bonds of cyclopentadiene to provide a 1,2-amino-alcohol, a motif which is found in numerous natural products besides agelastatin A (**99**).[52] Finally, we should mention that among the relatively limited class of dienophiles possessing two heteroatoms, nitroso compounds (RN=O) are equally valuable participants in hetero-Diels–Alder reactions directed towards natural product total synthesis.[53]

The recognition that the reversal of the electronic properties of the typical Diels–Alder diene/dienophile partners could still enable [4+2] cycloaddition reactions through $LUMO_{diene}$/$HOMO_{dienophile}$-controlled processes represents a significant advance in the field of organic synthesis.[54] While such reactions are highly challenging to achieve in an all-carbon context, extensive studies in this area by several researchers have established the particular fertility of the approach in the hetero-Diels–Alder landscape.[55] Thus, the development of complementary heteroatom-based diene/dienophile partners in such an inverse electron demand Diels–Alder paradigm has encouraged the application of these reactions to total synthesis endeavours with spectacular results.[56] As one highly illustrative example of this approach, we include here the use of heteroaromatic azadienes as the 4π-electron component in [4+2] cycloaddition reactions, a

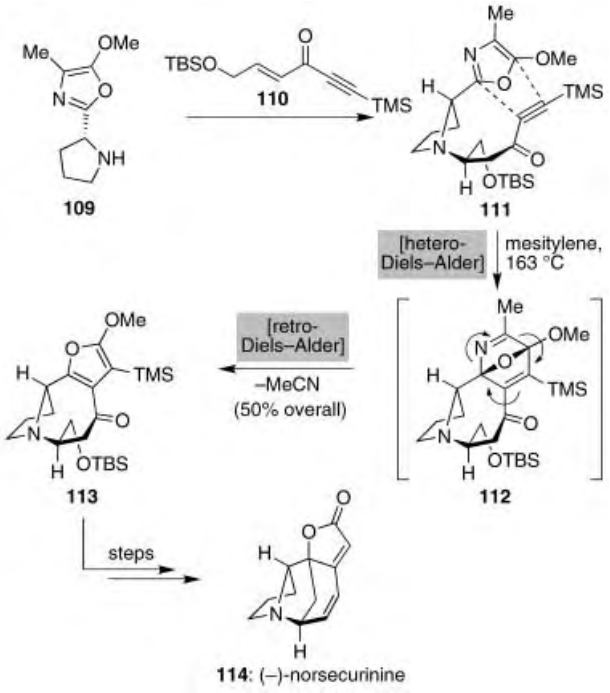
concept particularly championed and mastered by Boger and his group. Their synthesis of isochrysohermidin (**108**, Scheme 15), an effective DNA cross-linking agent, represents a beautiful and instructive case study.[57] Commencing with a



Scheme 15. The elegant total synthesis of isochrysohermidin (**108**) by Boger and co-workers involving a double azadiene inverse electron demand Diels–Alder reaction/nitrogen extrusion cascade and a singlet oxygen [4+2] cycloaddition/decarboxylation sequence (1993).[57]

tandem azadiene Diels–Alder reaction between the electron-rich dienophile **100** and electron-deficient diene **101**, initial formation of the desired cycloadduct **102** was followed by a double retro-Diels–Alder extrusion of nitrogen to give intermediate **103**. The latter species eventually aromatized through loss of methanol, a transformation made possible by the strategic incorporation of methoxy groups flanking the central C–C bond. Use of molecular sieves to remove this alcohol by-product was critical for the success of the one-pot cascade that led to **104** in 65% yield, as the final aromatization otherwise proved sluggish. With admirable synthetic insight, subsequent exposure of **104** to zinc in hot acetic acid readily effected a double reductive ring contraction to bis-pyrrole derivative **105** through loss of two molecules of ammonia. N-methylation and selective deprotection of two of the four methyl esters achieved over three synthetic operations, then set the stage for the final hetero-Diels–Alder reaction with singlet oxygen (generated from molecular oxygen with rose bengal and light). This successful pericyclic union led to intermediate **107**, which immediately collapsed in tandem fashion by the indicated endoperoxide decarboxylation/fragmentation pathway to the targeted natural product **108** in approximately 70% yield (40% *dl*-**108**, 30% *meso*-**108**) from **106**. As such, this sequence encompassing eight synthetic operations, including two different double hetero-Diels–Alder reactions, amounts to a beautiful total synthesis of extraordinary symmetry and appeal. Moreover, it exemplifies the power of this hetero-Diels–Alder approach to prepare highly substituted pyrrole and diazine ring systems, particularly in biaryl contexts.[58]

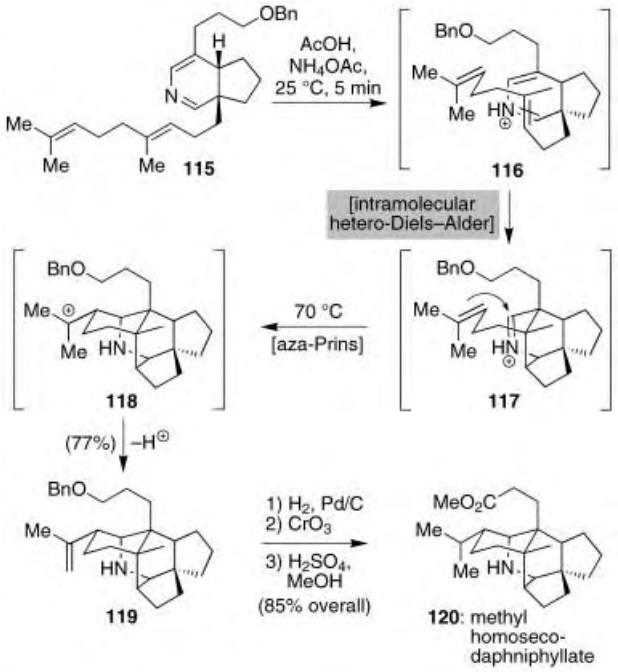
As illustrated above, the programming of hetero-Diels–Alder reactions in tandem with retro-Diels–Alder processes affords a highly effective strategy for the generation of novel heterocycles and molecular motifs which would otherwise be difficult to reach. A further notable example of this concept is the use of methyl-substituted oxazoles in a hetero [4+2] cycloaddition reaction with subsequent thermal extrusion of acetonitrile by a retro-Diels–Alder process to give substituted furan derivatives.[59] In a highly elegant synthesis of norsecurinine (**114**, Scheme 16), Jacobi and co-workers both developed and utilized this strategem.[60] Initial Michael addition of **109** to α,β-unsaturated system **110** afforded acetylenic ketone **111**, which upon heating in refluxing mesitylene provided furan adduct **113** in 50% overall yield through the intermediacy of Diels–Alder adduct **112**. The programmed incorporation of the methoxy group on the furan system in this particular example enabled the facile conversion of this moiety into the desired butenolide of the natural product upon subsequent deprotection and hydrolysis.[61]



Scheme 16. The elegant use of a hetero-Diels–Alder/retro-Diels–Alder cascade sequence by Jacobi and co-workers to fashion the molecular framework of (–)-norsecurinine (**114**; 1989).[60]

Parenthetically, the construction of such highly substituted furans and butenolides is otherwise quite challenging and, significantly, this method has been extended to thiazole systems, thus enabling the formation of thiophenes through Diels – Alder-based technology.[62]

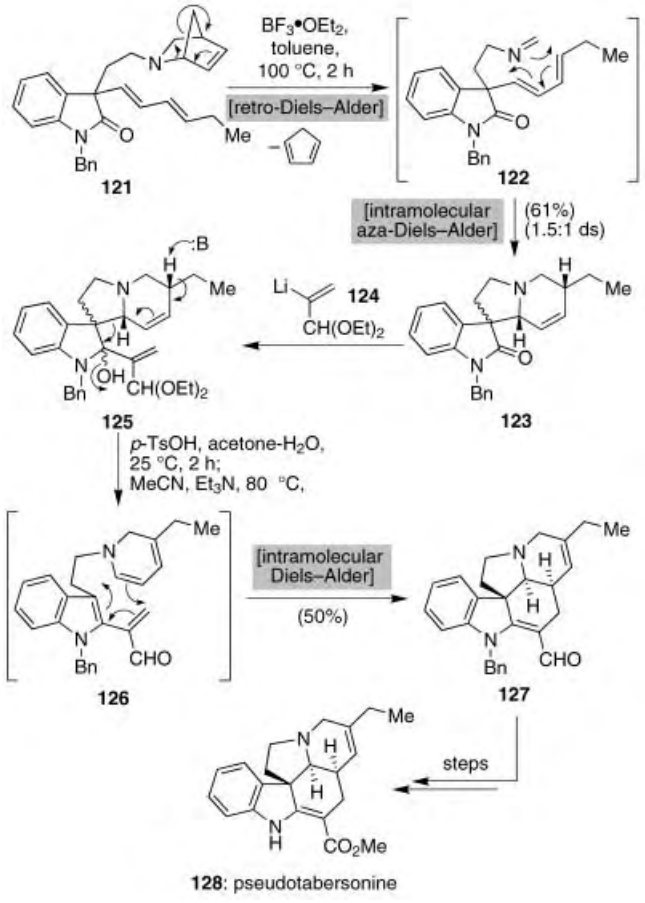
To achieve hetero-Diels – Alder reactions with some azadienes, however, protonation of the nitrogen atom is often required to sufficiently activate the species for facile reaction. A striking example of this process is illustrated in the highly concise and insightful synthesis of methyl homosecodaphniphyllate (**120**, Scheme 17) by Heathcock and co-workers.[63]



Scheme 17. The elegant Diels – Alder/aza – Prins cyclization cascade by Heathcock and co-workers leading to the core molecular architecture of the tetracyclic natural product methyl homosecodaphniphyllate (**120**; 1988).[63]

Protonation of the azadiene system of **115** by exposure to ammonium acetate in acetic acid at ambient temperature was followed by rapid intramolecular Diels – Alder cycloaddition to **117**, a relatively stable intermediate which upon heating at 70 °C participated in an intramolecular aza-Prins cyclization reaction to afford **119** in 77 % yield from **115** through the intermediacy of the stabilized cation **118**. In contrast, under neutral conditions the initial cycloaddition reaction required several hours in refluxing toluene to achieve 50 % conversion and the second, cationic process was precluded. With the entire molecular framework of methyl homosecodaphniphyllate assembled through this elegant, although putative, biomimetic cascade approach, the remaining sequence to complete the synthesis of this intriguing natural product comprised only three relatively routine steps.[63] We should note, however, that in addition to protonation serving to activate dienes or dienophiles, similar enhancements can also be achieved using neighboring heteroatom-stabilized cations (such as oxallyl cations). These achievements represent a critical advance in Diels – Alder methodology within the general class of ionic and radical cation-based pericyclic processes.[64]

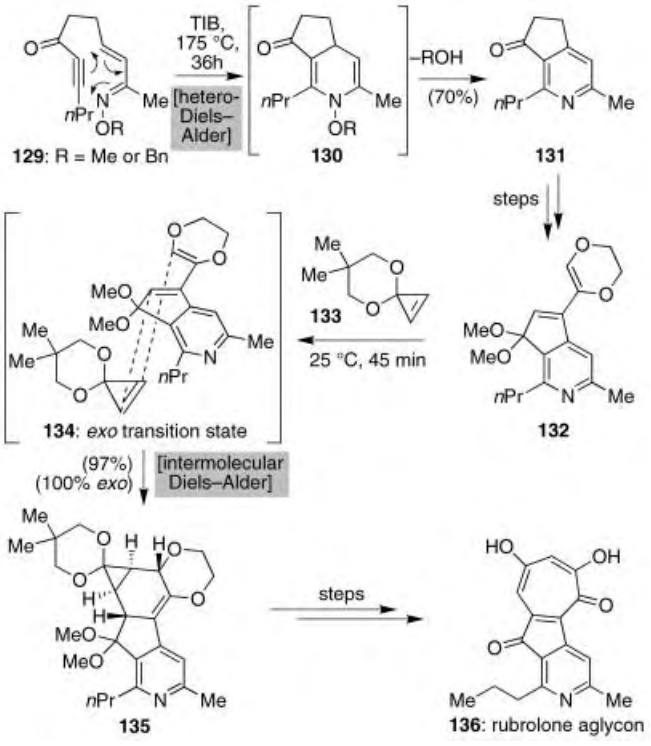
Attempts to switch the location of the nitrogen atom to the 2π-electron component in the form of an imine, although certainly possible in hetero-Diels – Alder reactions, as mentioned in the opening of this section, can often pose challenges in practice.[54a] For example, electron-deficient imines and iminium salts are typically unstable (since they can readily be hydrolyzed in the presence of the merest trace of water) and, as such, require in situ generation prior to trapping in Diels – Alder reactions. Moreover, imines can undergo a variety of other reactions with alkenes; acyl imines can, in fact, participate as dienes in Diels – Alder reactions. As such, synthetic strategies unveiling the requisite imino dienophile in the vicinity of a 1,3-diene system, particularly in an intramolecular setting, should serve to coax the reaction along the desired Diels – Alder pathway. A didactic example of this approach to create molecular complexity is found in the total synthesis of pseudotabersonine (**128**, Scheme 18) by Carroll and Grieco.[65] After preparation of intermediate **121**, application of methodology originally developed by the Grieco research group enabled the formation of imino dienophile **122** through a $BF_3 \cdot OEt_2$-induced retro-Diels – Alder reaction that effected expulsion of cyclopentadiene.[66] With a diene system appended from the same carbon atom of the indole skeleton



Scheme 18. Use of a cloaked imino dienophile, unveiled by a retro-Diels – Alder reaction, followed by an aza-Diels – Alder union and a subsequent intramolecular Diels – Alder reaction as part of an elegant total synthesis of pseudoptabersonine (**128**) by Carroll and Grieco (1993).[65]

in proximity, a facile intramolecular aza-Diels–Alder reaction ensued to form **123** as a 1.5:1 mixture of diastereomers. The anticipated poor diastereoselectivity in this process was of no consequence, however, as all of the newly formed stereocenters were later destroyed, thus enabling each of the obtained Diels–Alder adducts to eventually be converted into the target molecule through the designed sequence. After addition of 2-lithio-1,1-diethoxyprop-2-ene (**124**) to form oxindole derivative **125**, the stage was set to trigger a second Diels–Alder reaction through initial acid-induced deprotection of the ketal, followed by a base-catalyzed rearrangement to the fleeting **126** upon heating at 80 °C. This cascade generated the complete pentacyclic framework of the natural product as expressed in **127** which served as a convenient staging area from which to reach **128**. The elegant strategy used by Carroll and Grieco to generate pseudotabersonine (**128**) not only illustrates an inventive solution to the generation of imino dienophiles, but also provides a plausible strategy (possibly biomimetic) for the construction of several members of the *Aspidosperma* family of alkaloid natural products. We should note at this juncture that imino-based Diels–Alder reactions are prolific in the literature, and in particular we acknowledge the numerous elegant applications of imino-type hetero-Diels–Alder unions in various total syntheses developed by the Weinreb research group.[54a]

As a final entry to this section we present the total synthesis of rubrolone aglycon (**136**, Scheme 19) by Boger et al.[67] which employed an oxime ether as a competent 4π-electron component in an aza-Diels–Alder reaction to access a heavily



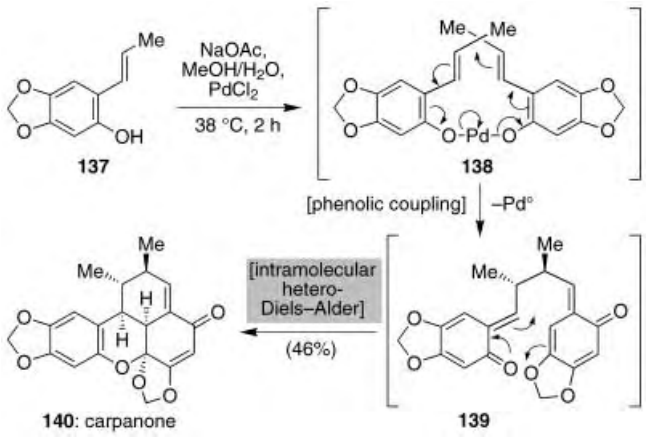
Scheme 19. The beautiful total synthesis by Boger et al. of rubrolone aglycon (**136**) featuring an intramolecular hetero-Diels–Alder reaction of an oxime-containing diene and an intermolecular Diels–Alder cycloaddition involving a highly strained cyclopropene as a dienophile (2000).[67]

substituted pyridine.[68] Unlike the inverse electron demand approaches discussed earlier in an aza-Diels–Alder context (Scheme 15),[57] attachment of an oxime ether onto the nitrogen atom was expected to inject sufficient electron density into the diene portion such that it could enter into Diels–Alder reactions with typical electron-deficient dienophiles under appropriate thermal and/or Lewis acid conditions. Thus, in an early transformation in the synthesis, prolonged heating of either the benzyl or methyl ether (**129**) in 1,3,5-triisopropylbenzene at 175 °C afforded the intermediate aza-Diels–Alder adduct **130** which aromatized in situ to the desired pyridine system **131** through loss of either methanol or benzyl alcohol. After elaboration of the latter intermediate to **132**, a second Diels–Alder reaction with cyclopropenone ketal **133**[69] was smoothly achieved at ambient temperature and provided the single *exo* adduct **135** in 97 % yield. Presumably, the facile combination of these two partners into **135** is most likely a result of the mutually reinforcing facets of the electron-rich diene system bearing two adjacent oxygen atoms, and the relief of ring strain resulting in the conversion of the cyclopropene into a cyclopropane unit upon cycloaddition. Interestingly, despite the normal preference for the *endo* cycloadduct, this process proceeded exclusively through an *exo* pathway; presumably, the absence of any conjugating orbitals on the dienophile enabled the sterically less-congested *exo* transition state to dominate completely.

4. Diels–Alder Reactions in Disguise: Cloaked Dienes and Dienophiles

In the majority of applications of the Diels–Alder reaction in total synthesis the diene and dienophile moieties represent inherent parts of the molecular scaffold, readily visible to the naked eye throughout the synthetic sequence. An often more intriguing strategy, however, is the masking of such units until the key juncture in the synthesis, at which time they are uncloaked for the desired Diels–Alder reaction. Significantly, such approaches often constitute the only feasible method for realizing the desired Diels–Alder union when one or both components are fleeting intermediates or highly reactive species. Such was the case in the generation of an in situ imino dienophile (Scheme 18) by Carroll and Grieco discussed above.[65] The same concept resides in the total synthesis of colombiasin A (Scheme 9) by Nicolaou et al.,[36] where the exposed diene portion intended for the second Diels–Alder reaction caused significant synthetic challenges in the step preceding the key Diels–Alder cycloaddition unless it was masked as a sulfone prior to its unraveling and eventual pericyclic reaction.

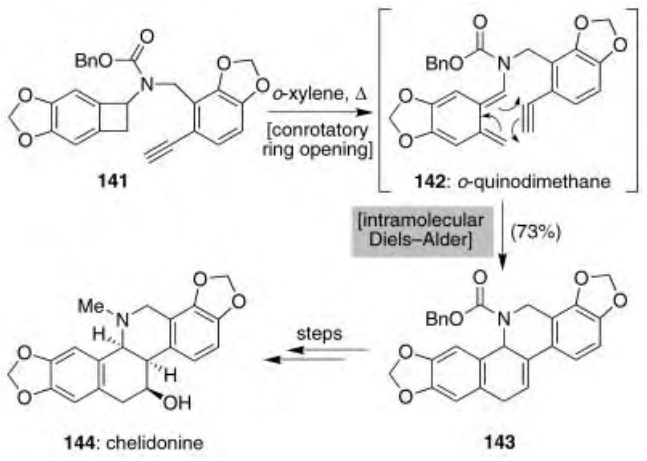
The group of cascade-based total syntheses in which the generation of a highly reactive Diels–Alder component sets the stage for a subsequent immediate [4+2] cycloaddition reaction includes the classic biomimetic synthesis of carpanone (**140**, Scheme 20) in 1971 by Chapman et al.[70] In this example, exposure of monomeric phenol **137** to $PdCl_2$ in basic media effected a phenolic dimerization to **139** via reactive intermediate **138**. This product (**139**), however, proved short-



Scheme 20. The classic biomimetic synthesis by Chapman et al. of carpanone (**140**) featuring a sequential Pd-mediated phenolic coupling and an intramolecular Diels – Alder cycloaddition involving an *o*-oxoquinodimethane (1971).[70]

lived as the highly reactive *o*-oxoquinodimethane which had been unveiled entered spontaneously into an intramolecular hetero Diels – Alder reaction with the resident dienophile in proximity to provide the targeted natural product (**140**) stereoselectively in 46 % overall yield in a single operation from **137**. Of perhaps greater significance than the inherent beauty and concise nature of this total synthesis is the confidence it inspired in using related *o*-quinodimethanes in the context of complex molecule total synthesis.[71]

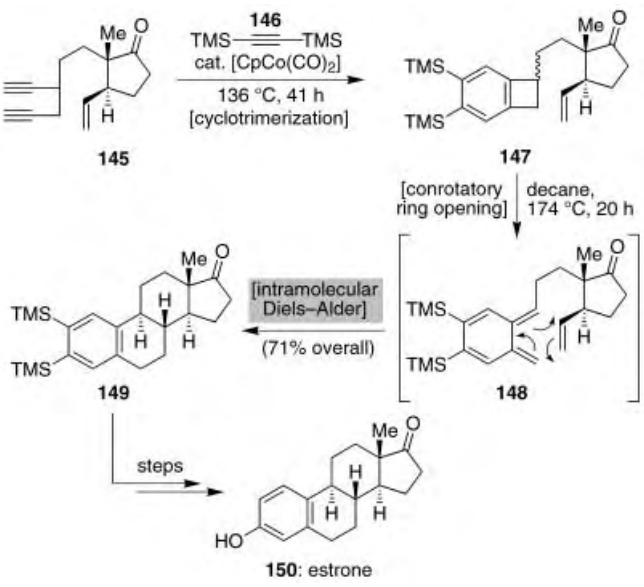
An equally inspirational and instructive approach incorporating *o*-quinodimethanes in a Diels – Alder context was pioneered through the landmark 1971 total synthesis of chelidonine (**144**, Scheme 21) by Oppolzer et al.,[72] where it was anticipated that the desired reactive intermediate could be obtained through electrocyclic ring opening of a strained cyclobutene system. Upon heating **141** in refluxing *o*-xylene, reversible conrotatory ring opening indeed furnished a highly reactive *o*-quinodimethane (**142**) that immediately engaged the pendent alkyne moiety in a productive Diels – Alder union to afford polycyclic system **143** in 73 % overall yield which served as the progenitor of the targeted natural



Scheme 21. The pioneering use of *o*-quinodimethanes generated through electrocyclic ring opening of a benzocyclobutene in the total synthesis of chelidonine (**144**) by Oppolzer and co-workers (1971).[72]

product. Significantly, Oppolzer and Robbiani optimized this cyclobutene-opening methodology[72b] to achieve greatly enhanced yields of **143**. They also further extended this insightful Diels – Alder approach to heterocyclic systems by using tethered imines as substrates, thus paving the way for a plethora of subsequent applications.[73]

A related and equally spectacular application of the intramolecular Diels – Alder reaction of benzocyclobutene-generated *o*-quinodimethanes is demonstrated in the total synthesis of estrone (**150**, Scheme 22)[74] during the conversion of **147** into the steroidal skeleton **149** by Vollhardt and co-workers.[75] Apart from this particular transformation, however, this elegant synthesis includes an additional tantalizing

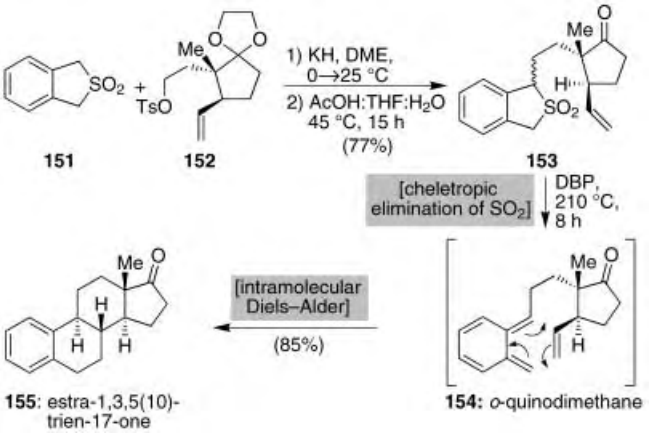


Scheme 22. The brilliant total synthesis of estrone (**150**) by a tandem ring opening/Diels – Alder sequence based on cobalt cyclotrimerization of acetylenic substrates by Vollhardt and co-workers (1979).[74]

feature in its initial stages, namely the reaction of bis-(trimethylsilylacetylene) (**146**) with bisacetylene **145**, orchestrated by catalytic amounts of $[CpCo(CO)_2]$. In this [2+2+2] cycloaddition, as in the Diels – Alder reaction, the ultimate product reflects the direct summation of all the reacting pieces, thus providing an additional set of conversions with atom economy equal to the venerable reaction of Diels and Alder. We should note in passing that the benzocyclobutene technology adopted both in this and the preceding example was also championed and greatly extended by Kametani et al. in numerous complex molecular contexts, including steroids.[76]

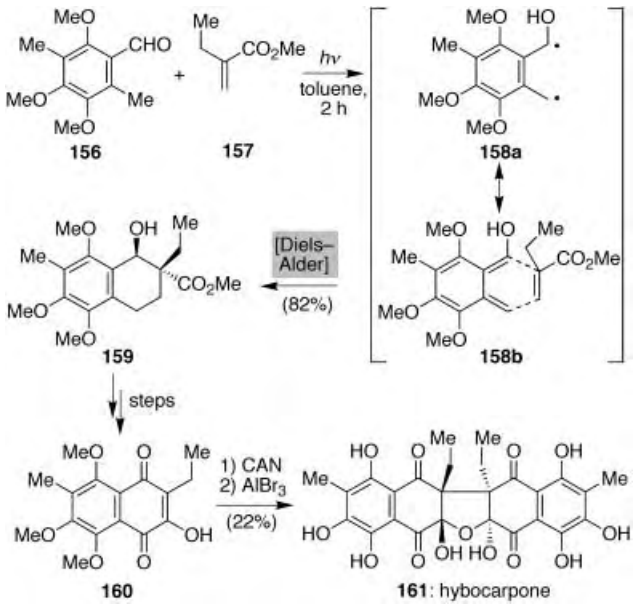
Complementary to the benzocyclobutene approach for *o*-quinodimethane generation is a method which relies on the use of a cyclic sulfone, a chemical entity encountered in the colombiasin A synthesis presented in Section 2 (Scheme 9).[36] Since the pioneering work of Staudinger in the early part of the last century,[77] it has been amply documented that sulfur dioxide can add cleanly to a diene system to provide an adduct that can be reverted back to the original starting material through a thermally induced retro-Diels – Alder reaction in

which SO_2 is extruded.[78] Although sulfones were utilized in Diels–Alder reactions prior to 1950, the methodology was greatly extended through the pioneering work of Cava et al. which established that highly reactive *o*-quinodimethanes could be thermally generated from sulfones appended to aromatic systems.[79] The first application of this strategy in total synthesis, which also represents the first instance in which it was employed in an intramolecular context, was in the synthesis of the steroid estra-1,3,5(10)-trien-17-one (**155**, Scheme 23) by Nicolaou and Barnette.[80] Cheletropic elimination of SO_2 from sulfone **153** was readily effected under thermal conditions and led to the unveiling and trapping of *o*-quinodimethane **154** to form the targeted compound **155**. Both this example and the total synthesis of colombiasin A (Scheme 9) demonstrate the versatility of the sulfone group in facilitating synthetic operations while concurrently remaining inert to a diverse set of reaction conditions. As such, this moiety reflects one of the few effective protecting devices for dienes.



Scheme 23. Tandem cheletropic elimination of SO_2 and intramolecular Diels–Alder reaction in an expedient total synthesis of estra-1,3,5(10)-trien-17-one (**155**; Nicolaou and Barnette, 1979).[80]

As a final set of entries demonstrating the power of *o*-quinodimethanes in total synthesis, we have chosen to highlight a recent series of achievements in a methods-based approach to total synthesis derived from the photochemical generation and trapping of these fleeting intermediates (Scheme 24).[81] Although scant reports of this process have been reported in the chemical literature on simple precursors, the sequence has been virtually ignored in total synthesis endeavors. Enticed by the structurally unique and cytotoxic natural product hybocarpone (**161**, Scheme 24) possessing an aesthetically pleasing C_2-symmetric molecular architecture, Nicolaou and Gray envisioned a plausible biosynthetic origin of this compound to be a dimerization of a percursor naphtharazin, initiated by a single-electron transfer (SET) process, followed by a hydration event.[82] Although this biogenetic hypothesis had no empirical foundation, it nevertheless served as inspiration for the synthetic design. To prepare the dimerization precursor **160**, it was anticipated, and realized, that a photochemically generated hydroxy-*o*-quinodimethane from aromatic aldehyde **156** could engage



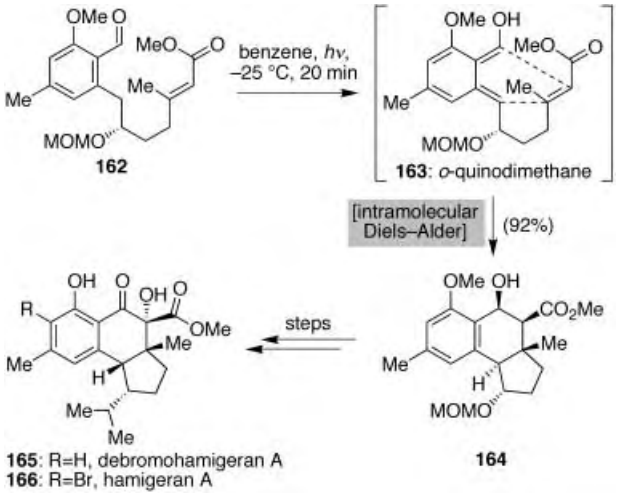
Scheme 24. Total synthesis of hybocarpone (**161**) featuring an intramolecular Diels–Alder trapping of a photolytically generated hydroxy-*o*-quinodimethane (Nicolaou and Gray, 2001).[82]

methyl 2-ethylacrylate (**157**) in a Diels–Alder reaction to regioselectively form the desired bicyclic system **159**. One should note that in the event, initial excitation of the carbonyl group followed by 1,5-hydride abstraction provided diradical **158a**, whose canonical form is hydroxy-*o*-quinodimethane **158b**. The Diels–Alder reaction proceeded with admirable success in this initial testing ground, and as such, the reaction conditions were further optimized for both intra- and intermolecular cycloadditions in even more complex contexts with a variety of aromatic aldehydes and dienophiles.[83a] Significantly, the developed intramolecular technology engendered facile construction of complex polycyclic scaffolds present in a myriad of natural products. As an initial demonstration of the utility of the approach, the Nicolaou group efficiently synthesized two members of the hamigeran family of natural products (**165** and **166**, Scheme 25).[83b]

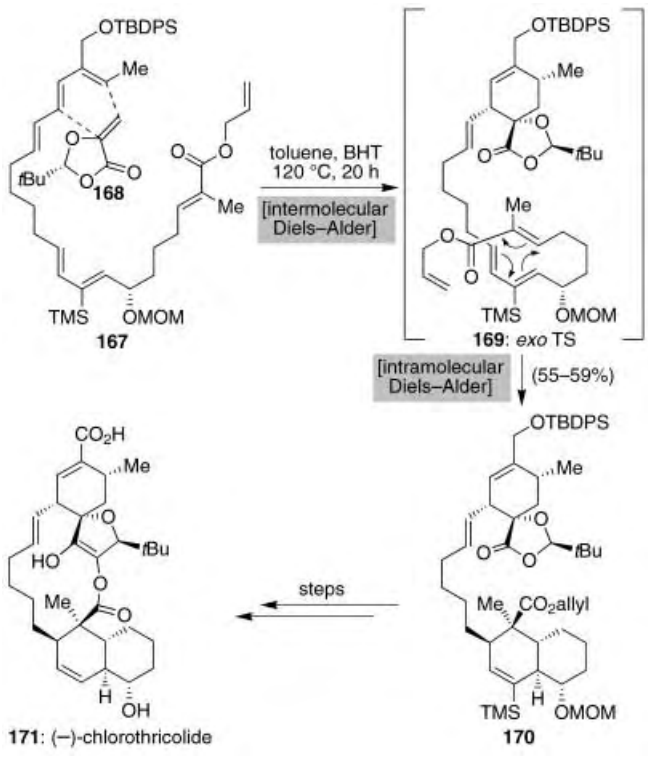
Before ending this section, one should note that the masking devices highlighted in the above schemes do not, by any means, represent the entire range of possibilities for unleashing reactive species for Diels–Alder interception. Other approaches are indeed viable,[84, 85] and some will be encountered in the next section.

5. Diels–Alder Reactions as Part of Cascade Sequences

Among possible synthetic routes, cascade sequences offer an unparalleled ability to efficiently construct molecular complexity. Indeed, as most students of organic chemistry will recognize, the principle of cascade reactions in organic synthesis has a long and enviable history whose roots can be traced forward to the present day from such landmark achievements as Robinson's elegant biomimetic preparation



Scheme 25. Total synthesis of the hamigerans featuring an intramolecular Diels – Alder trapping of a photochemically generated hydroxy-*o*-quinodimethane (Nicolaou et al., 2001).[83b]

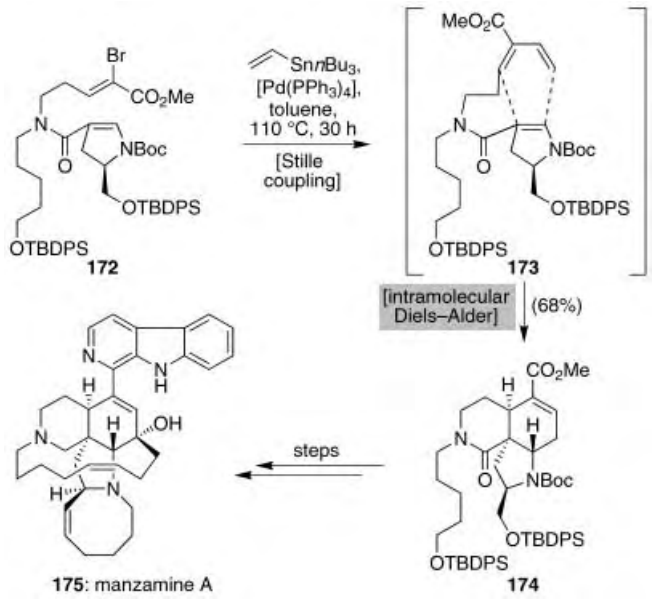


Scheme 26. Beautiful enantioselective total synthesis by Roush and Sciotti of (–)-chlorothricolide (**171**) featuring a tandem inter-/intramolecular Diels – Alder cascade. Note that these processes could certainly occur in the reverse order from that shown here (1994).[90]

of tropinone in 1917,[86] and the total synthesis of progesterone by Johnson et al. in 1971 that was based on a series of cation – π cyclizations.[87] With mounting pressure to rapidly construct molecular complexity through efficient and atom-economical[88] processes with high degrees of selectivity, programmed cascade sequences will inevitably become increasingly utilized in total synthesis. In this section, we outline several examples of cascade processes incorporating the Diels – Alder reaction which have been employed in the total synthesis of naturally occurring substances as a sampling of the types of wondrous reaction sequences we might expect in the future.[89]

The highly concise and elegant enantioselective total synthesis of the antibiotic (–)-chlorothricolide (**171**, Scheme 26) by Roush and Sciotti certainly serves as an outstanding starting point.[90] The key feature of this synthesis resides in a tandem inter-/intramolecular Diels – Alder sequence to simultaneously construct a pentasubstituted cyclohexene ring as well as a *trans*-fused decalin system, events which resulted in the formation of seven new asymmetric centers in a single operation. Critical to the success of the designed cascade, which was brought about through prolonged heating in toluene at 120 °C in the presence of BHT, was the high level of diastereofacial and regiospecific control achieved in the intermolecular *exo* Diels – Alder reaction between the more reactive diene system of **167** and dienophile **168**, a feature which had been soundly established by Roush and co-workers in several model studies.[91] Similarly, the strategically placed trimethylsilyl group on the remaining diene segment enabled the other, intramolecular Diels – Alder reaction to proceed with high selectivity and led to the predominant formation of the anticipated product (**170**) at the expense of other potential Diels – Alder adducts possessing alternative stereochemistries. Indeed, there are 96 distinct Diels – Alder products that could have been formed from all of the possible *endo*, *exo*, diastereofacial, and regiochemical outcomes. The experimental execution of this amazing cascade process elicits further admiration in that the final yield (55 – 59 %) of **170** reflects not only carefully optimized conditions, but also a recycling of the by-product that formed in a deviation from the desired route. This latter compound was the result of successful intramolecular Diels – Alder reaction in the lower half of the molecule, but where reaction of the upper diene with **168** failed because of isomerization of the triene portion to an *E*,*E*,*E* system. After extensive studies, a method to convert this material into the desired adduct was found through additional treatment with **168**, this time in trichloroethylene.[92]

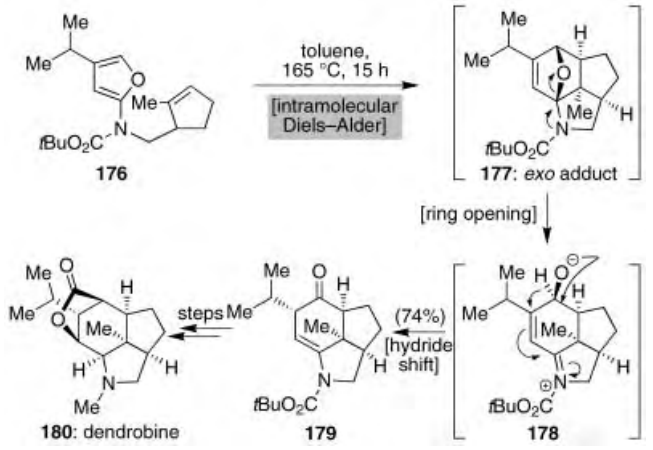
The recent total synthesis of manzamine A (**175**, Scheme 27) by Martin et al. represents another brilliant set of tandem reactions that provides a highly elegant solution to a challenging synthetic problem.[93] Following a synthetic strategy which projected olefin metathesis reactions to forge both the 8- and 13-membered rings of the target molecule, an efficient synthesis of the tricyclic core was defined as the initial prerequisite. Thus, having reached intermediate **172**, exposure of this vinyl bromide to tri-*n*-butylvinylstannane in the presence of catalytic amounts of $[Pd(PPh_3)_4]$ in refluxing toluene initiated a tandem Stille coupling/Diels – Alder cascade sequence that led to **174** in 68 % yield. Although the concept of combining these two reactions in domino fashion was not without precedent,[94] the complexity of the obtained polycyclic system is particularly stunning. Other particularly remarkable features of the Diels – Alder step are the exclusive *endo* topicity (with respect to the five-membered ring) arising from the *E* olefin in the diene and the diastereofacial selectivity arising from the influence the lone distal stereocenter present in **172** which lead to the controlled installation of three new chiral centers, including a quaternary carbon



Scheme 27. Elegant use of a domino Stille coupling/Diels–Alder sequence by Martin et al. to construct stereospecifically three adjacent chiral centers and three of the five rings in a total synthesis of manzamine A (**175**; 1999).[93]

atom. Indeed, such diene geometries are relatively rare participants in Diels–Alder reactions, particularly in intramolecular contexts, because of the overall strain of the system necessary to achieve proper orbital alignment for successful [4+2] cycloaddition.

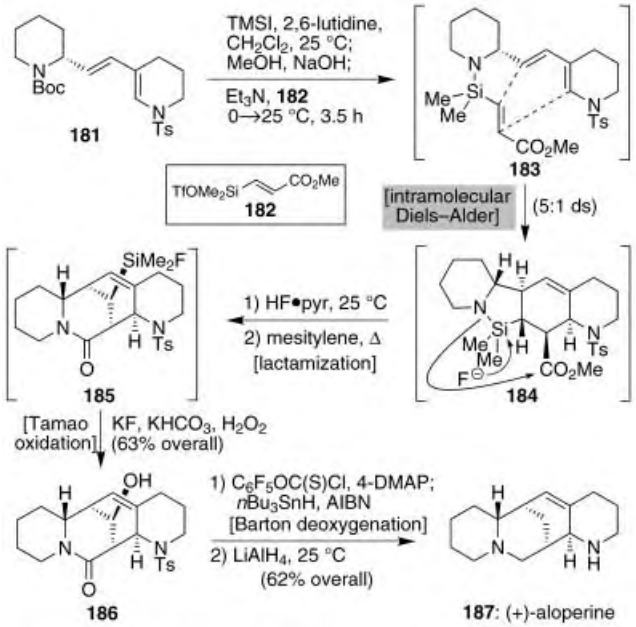
An additional recent example of a highly insightful cascade strategy based on strategic incorporation of functionality is featured in the total synthesis of dendrobine (**180**, Scheme 28) by Padwa et al.[95] First, an initial *exo*-selective Diels–Alder reaction between the unactivated dienophile moiety with the tethered electron-rich furan system, both residing within **176**, provided **177**. The *exo* selectivity in this transformation arose from the fact that there is no conjugating π system on the dienophile to provide a secondary orbital interaction, thereby disfavoring an *endo* transition state. With this intermediate in hand, the placement of a nitrogen atom α to the bridged



Scheme 28. Elegant use of a tethered furan-based Diels–Alder reaction by Padwa et al. to fashion a precursor en route to the total synthesis of dendrobine (**180**; 2001).[95]

system in **177** induced a spontaneous ring-opening reaction, with a subsequent hydride shift providing the functionalized tricyclic core of the natural product (**179**) in 74% overall yield. Among the numerous total syntheses of this substance based on Diels–Alder routes,[96] this sequence certainly represents one of the most concise and beautiful solutions to the challenges posed by its molecular architecture, thus demonstrating, once again, a highly inventive use of the Diels–Alder reaction within a tandem reaction sequence.

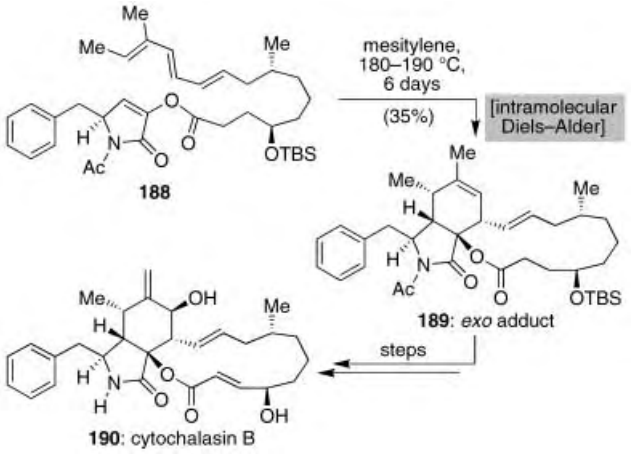
It is perhaps appropriate to close this section with the recently achieved total synthesis of (+)-aloperine (**187**, Scheme 29) by Overman and co-workers which featured a



Scheme 29. The elegant total synthesis of (+)-aloperine (**187**) by Overman and co-workers featuring a cascade sequence involving a silicon-tethered Diels–Alder reaction and a Tamao oxidation (1999).[97]

temporarily tethered dienophile.[97] Although aloperine is a relatively small molecule compared to some of the other targets reached by Diels–Alder technology, it took profound insight and skill to both design and execute the Diels–Alder-based cascade strategy which opened an entry to its skeleton. The approach is based on developing a temporary tether of the dienophile to the diene in the form of an *N*-silyl system (**183**), a concept which had not been previously demonstrated in a Diels–Alder context. However, success in controlling diastereoselectivity through such a strategy was anticipated on the basis of successful intramolecular Diels–Alder reactions in related systems by Gschwend,[98] with the selection of an *N*-silyl-linked tether inspired by the pioneering studies of the research groups of Nishiyama and Stork who had employed *O*-silyl linkages to effect several intramolecular transformations.[99] Starting with **181**, a series of protecting-group manipulations were performed in a one-pot operation that culminated in the attachment of fragment **182** and the transient generation of **183**, a species which rapidly converted into the desired product **184** at ambient temperature by an intramolecular Diels–Alder reaction in 67% de Since this

Diels – Alder product proved labile upon aqueous work-up, it was instead directly exposed to anhydrous HF · pyr and heated in mesitylene, conditions which impressively effected both cleavage of the N–Si bond and an ensuing lactamization to afford **185**. Finally, a subsequent Tamao-type oxidation smoothly completed the conversion of **181** into **186** in 63% overall yield, thus extruding the remnants of the original silicon tether and establishing a beachhead for the completion of the total synthesis of the coveted natural product **187**. This particular set of transformations, in which no intervening purifications were performed, certainly sets a high standard for future approaches to this class of natural products and confirms the status of *N*-silyl tethers as temporary devices to control stereoselectivity through intramolecular Diels – Alder reactions.[100] We shall encounter an additional example of a temporary tether as a means to facilitate an intramolecular Diels – Alder reaction in the upcoming section.



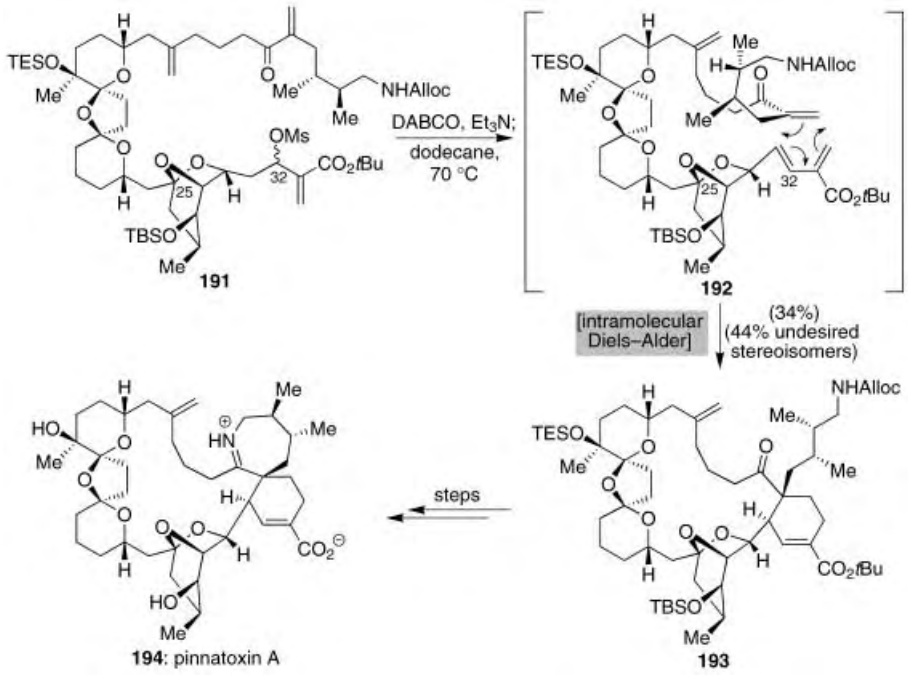
Scheme 30. Use of a bold intramolecular Diels – Alder reaction by Stork and Nakamura in the total synthesis of cytochalasin B (**190**; 1983).[102]

6. Daring Applications of the Diels – Alder Reaction in Total Synthesis

The chemical literature is adorned with many striking examples of the use of the Diels – Alder reaction in total syntheses which are derived from special and unique strategies. This situation renders these particular cases hard to classify under any of the other sections in this review. As such, a few of these instructive archetypes are discussed under this heading. To be sure, however, the elegant nature of all of the exemplars cited in this article certainly could have easily qualified for inclusion in this "daring" category.

Although the power of intramolecular Diels – Alder reactions to forge a five- or six-membered ring in either a fused or bridged fashion across the characteristic cyclohexene product has been amply demonstrated with the above examples, the utilization of this process to concurrently form medium-sized or macrocyclic rings remains to be discussed. First demonstrated as a viable option by Corey and Petrzilka in 1975,[101] one of the earliest and most striking applications of this macrocyclization strategy in total synthesis was achieved by Stork and Nakamura in their 1982 synthesis of cytochalasins F and B (**190**, Scheme 30).[102] In the key step, after achieving a homochiral synthesis of **188**, collapse of this polyunsaturated precursor to the desired tetracyclic system **189** was accomplished in 35% yield as a 4:1 mixture of *endo*:*exo* products upon heating in mesitylene at 180 – 190 °C for nearly a week. This process is remarkable not only because of the concomitant formation of the isoindolone and the highly strained 14-membered macrocyclic ring system, but also because of the fact that the diene system was coaxed to undergo a Diels – Alder reaction with a dienophile that is not particularly electron deficient. Since Stork and Nakamura's landmark synthesis of **190**, numerous other syntheses of members of the cytochalasin family of natural products through Diels – Alder reactions have appeared in the literature.[103]

An equally impressive paragon of macrocyclization through an intramolecular Diels – Alder reaction resides in the bold total synthesis by Kishi and co-workers of pinnatoxin (**194**, Scheme 31), a marine-derived calcium-channel activator with a novel molecular architecture.[104] After generation of advanced key intermediate **191**, subsequent displacement of the allylic mesylate with DABCO followed by Et_3N-induced elimination furnished the requisite diene system necessary for Diels – Alder reaction with the remote dienophile. Since this

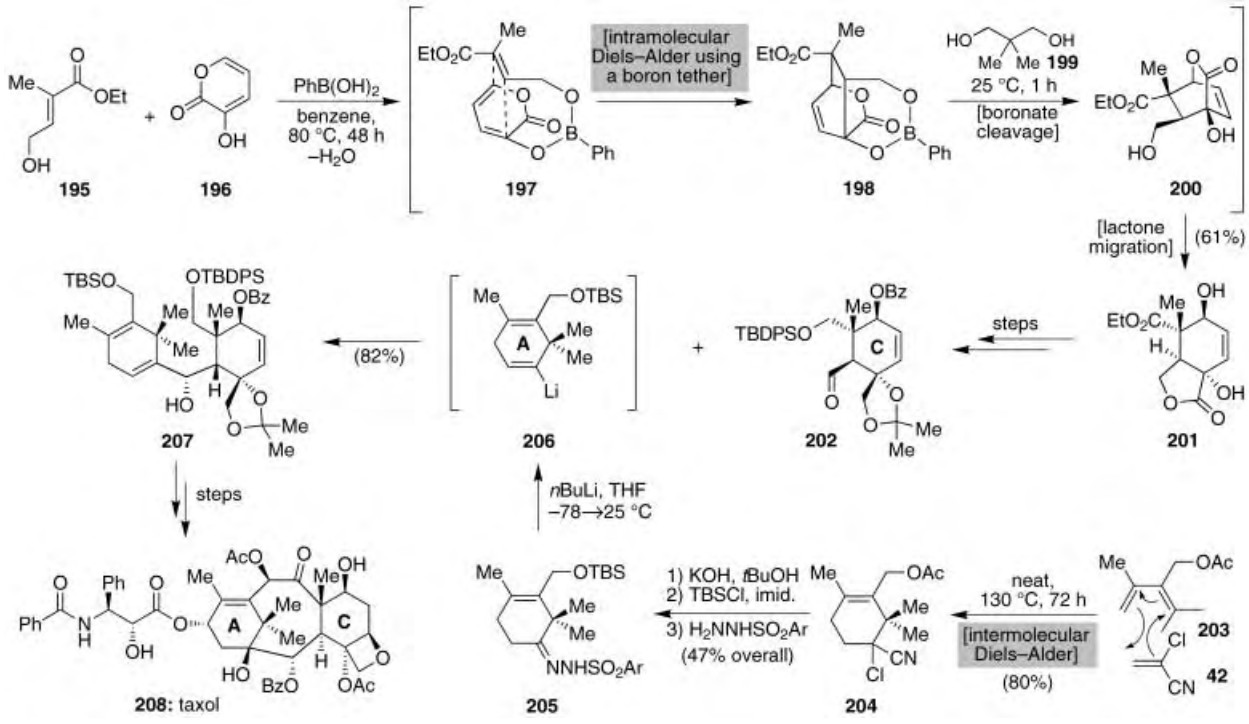


Scheme 31. The impressive adoption of an *exo*-selective Diels – Alder reaction by Kishi and co-workers to effect macrocyclization in the total synthesis of pinnatoxin A (**194**; 1998).[104]

diene underwent intermolecular [4+2] dimerization upon attempted concentration, it was instead directly heated at 70 °C after formation in dodecane. The expected [4+2] fusion was effected to produce the desired *exo* adduct **193** in 34% yield, along with another *exo* product and a minor *endo* congener (in the ratio 1.0:0.9:0.4), all possessing the desired regiochemistry. This result, in which the product corresponding to the target molecule is favored, is remarkable if one considers that a total of eight intramolecular Diels–Alder adducts are possible in this reaction. Although it would be challenging to predict the success of this approach in stereochemical terms on the basis of first principles, experimentation with other intermediates established that the facial selectivity of this Diels–Alder collapse depended critically upon the arrangement of functional groups along the C25–C32 chain. Interestingly, alteration of either the solvent or the temperature had profound effects on the ratios of the three products formed.

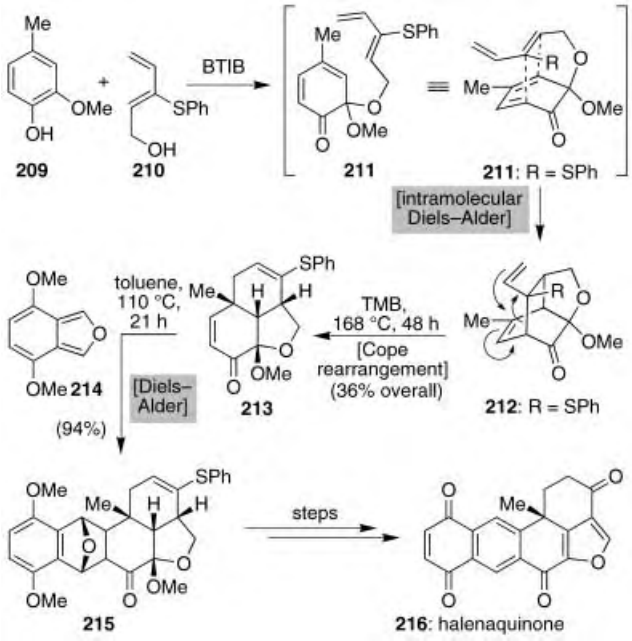
Another well-celebrated application of the Diels–Alder reaction in the context of natural products synthesis is found in the first published total synthesis of taxol (**208**, Scheme 32), in which Nicolaou et al. employed two different [4+2] cycloadditions to construct each of the two six-membered rings of the target molecule.[105] Initial efforts to effect a fusion between the Diels–Alder partners **195** and **196** failed, both in terms of yield and regioselectivity. Fortunately, however, joining the two components through a boron tether according to the procedure developed by Narasaka et al.[106] provided an excellent solution to this regiochemical problem with concurrent enhancement of yield. In the event, treatment of a mixture of **195** and **196** with phenyl boronic acid led to intermediate **197**, by the loss of two molecules of water, thus affording a template in which the diene and dienophile reactants were brought together in a rigorously controlled manner, and hence enabling complete regioselective fidelity in the enforced Diels–Alder transition state leading to *endo* adduct **198**. The boron tether was cleaved upon work-up with diol **199** to liberate bicyclic system **200** which rapidly rearranged through lactone migration to the isolated product **201** in 61% yield.[107] Impressively, two polyfunctional rings and four contiguous stereocenters were arrayed successfully in a relative sense during this cascade sequence. Construction of the other six-membered ring of taxol commenced with a Diels–Alder union of diene **203** with 2-chloroacrylonitrile (**42**) and led exclusively to adduct **204** in 80% yield. Although the regiochemistry of the cycloaddition product was anticipated on the basis of the substitution pattern in the diene system, there was concern that potentially destabilizing steric congestion in the requisite transition state could thwart its formation.[108] Nonetheless, the conversion proved regiospecific, and upon subsequent elaboration this fragment was smoothly joined with **202** in a Shapiro coupling reaction with eventual conversion into the final target molecule **208**. An additional feature of the latter Diels–Alder reaction worth noting is that 2-chloroacrylonitrile (**42**) represents the synthetic equivalent of ketene, as after cycloaddition had been achieved, hydrolysis with base afforded a ketone product (a concept first demonstrated in the total synthesis of the prostaglandins (Scheme 7a) by Corey et al.). Since ketenes cannot be employed directly in Diels–Alder reactions because of preferential [2+2] cycloaddition with one of the olefins of the 1,3-diene system, the development of ketene replacements such as **42** constitutes a highly established field and an objective of continuing interest.[109]

In addition to ketenes, however, as a general precept, Diels–Alder reactions of simple *o*-benzoquinones are similarly highly challenging to achieve, not only because these highly reactive substances undergo facile polymerization



Scheme 32. The synthesis of taxol (**208**) by Nicolaou et al. featuring two Diels–Alder reactions to fashion the molecule's six-membered rings (1994).[105]

through Diels–Alder processes, but also because the pericyclic process is typified by a lack of regiochemical control when successful. An elegant strategy which addresses these issues is found in an intramolecular version of the reaction, beautifully formulated in the elegant total synthesis of halenaquinone (**216**, Scheme 33) by Rodrigo and co-workers.[110a] Thus, oxidative ketalization of 2-methoxy-4-methylphenol (**209**) with diene alcohol **210** in the presence of BTIB



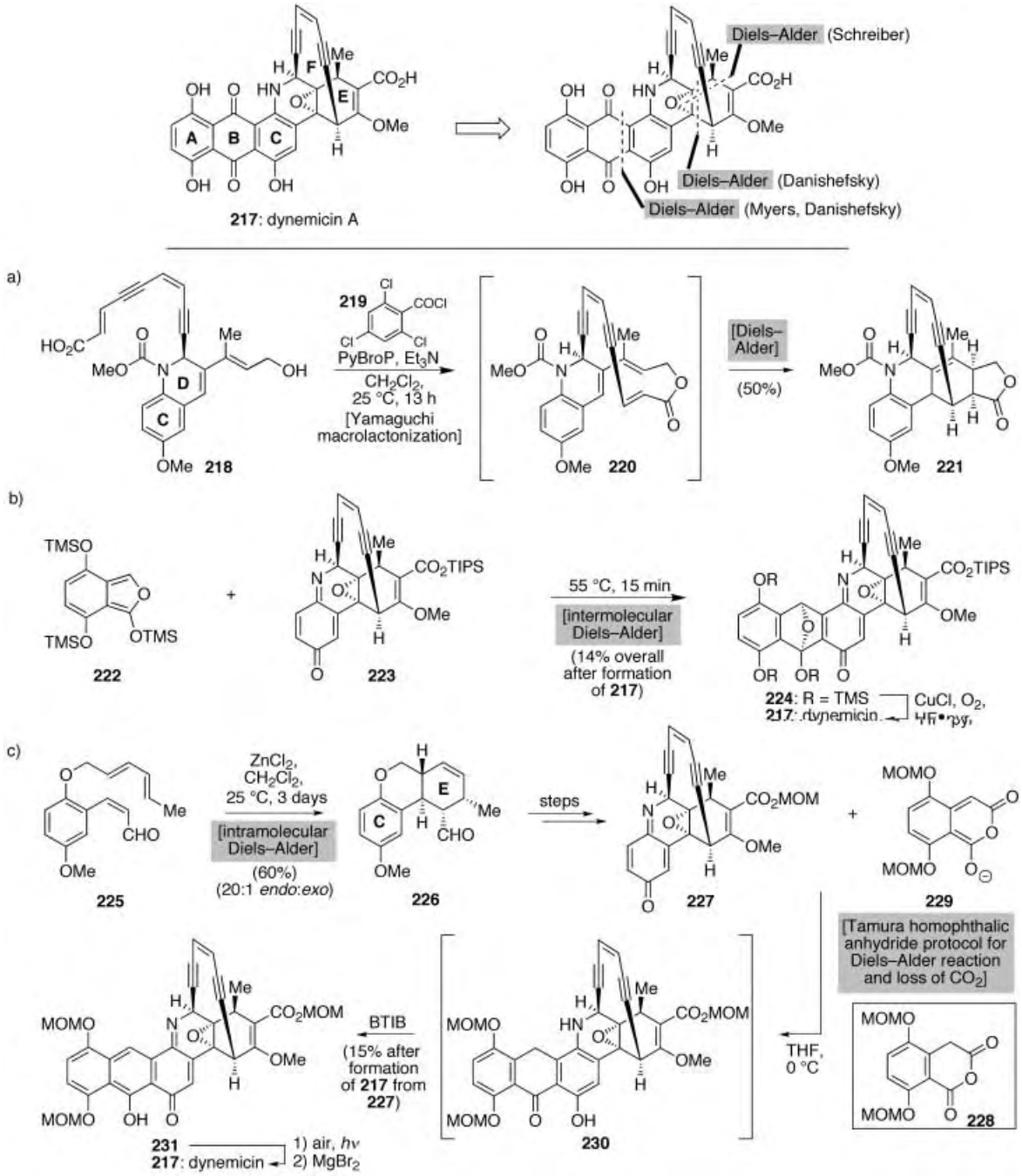
Scheme 33. The elegant approach used by Rodrigo et al. to synthesize halenaquinone (**216**) using a tandem annulation strategy based on oxidative ketalization, a Diels–Alder reaction, and a Cope rearrangement to construct a substrate serving as a dienophile for a second Diels–Alder cycloaddition (2001).[110]

led to the formation of an *o*-quinone monoketal **211**,[110b] an intermediate which smoothly underwent an intramolecular Diels–Alder reaction to provide both adduct **212** and tricyclic system **213** (the product of a Cope rearrangement of **212**). Rather than purify the melange at this juncture, the mixture of **212** and **213** was heated in 1,2,4-trimethylbenzene which resulted in complete conversion into **213**, a product which was isolated in a final yield of 36% from **209**. One should note that the thiophenyl moiety was incorporated as part of this sequence not so much to enhance the electron-richness of the diene, as might be expected, but rather to provide a functional handle for use later on in the sequence. In the next operation, a second Diels–Alder reaction with naphthofuranone **214** was realized in refluxing toluene and produced the expected bridged product **215** in a remarkable 94% yield.[111] Parenthetically, naphthofuranones are particularly competent dienes in Diels–Alder reactions, as the resultant products restore aromaticity to the benzene-type ring. Conversely, although simple furans are excellent diene partners in [4+2] cycloadditions, as first demonstrated by Alder himself,[112] the loss of aromaticity often leads to retro-Diels–Alder processes, which typically result in the ultimate formation of the thermodynamically favored *exo* product. On the other hand, thiophene and pyrrole, furan's close cousins, are rarely employed with success as dienes in Diels–Alder reactions.[113]

As a final example in this section, we turn to the rigorous testing ground for Diels–Alder chemistry provided by the challenging structure of dynemicin A (**217**, Scheme 34), a potent enediyne antitumor antibiotic bearing a complex heterocyclic skeleton and a network of sensitive functional groups. Three different research groups successfully applied [4+2] cycloadditions in their elegant and divergent strategies to reach the target molecule. In the first disclosed synthesis of tri-*O*-methyl dynemicin A methyl ester,[114] Schreiber and co-workers accessed key elements of this striking molecular architecture (namely **221**) through use of a tandem Yamaguchi macrolactonization/Diels–Alder sequence (Scheme 34a). In the event, initial formation of **220** upon reaction of **218** with acid chloride **219** set the stage for a programmed transannular Diels–Alder reaction, which was achieved at ambient temperature to provide **221** in 50% yield. The remarkable facility with which this key Diels–Alder step was realized is likely the result of the inferred excellent proximity and alignment of the diene in relation to the macrocyclic dienophile, enforced by the unique structural characteristics of the enediyne motif, thereby allowing the Diels–Alder reaction to proceed with a relatively low activation energy. Significantly, attempted Diels–Alder cycloadditions with acyclic **218** failed under various scenarios examined, with decomposition observed upon heating at temperatures in excess of 180 °C. As such, transannular activation, as achieved by initial macrocycle formation, clearly represented a crucial element to the success of this conversion.[115]

The use of a late-stage Diels–Alder cycloaddition between two highly functionalized segments in the wholly unique approach to this target (Scheme 34b) by Myers et al. was designed not only from the standpoint of convergency, but also as a vehicle to explore structure–activity relationships, since facile entry into structural variations of dynemicin A would be expected through such a route.[116] In the penultimate step, diene **222**, generated in situ from a protected phthalan derivative precursor, successfully added in Diels–Alder fashion to dienophile **223** to afford the complete hexacyclic framework of the goal structure **224**. This intermediate adduct was then directly converted into the natural product **217** upon application of an oxidation/deprotection protocol using CuCl and O_2 in the presence of HF·pyr.

The instructive synthesis of dynemicin A (Scheme 34c) by Danishefsky and co-workers relied on a similar late-stage Diels–Alder retrosynthetic disconnection as that discussed in the above route, but employed a different protocol to achieve the reaction in the actual forward synthesis.[117] Before reaching this stage, however, Danishefsky and co-workers applied an initial $ZnCl_2$-induced Diels–Alder cycloaddition to form adduct **226** from precursor **225**, a process which proceeded with near-exclusive *endo* stereoselectivity. Adduct **226** was then advanced to intermediate **227**, in anticipation of the second and crucial intermolecular Diels–Alder union with **229**. One of the most versatile and general methods to deliver such naphthoquinone ring systems for Diels–Alder reactions derives from methodology developed by Tamura



Scheme 34. The Diels–Alder reaction in the total synthesis of dynemicin A (**217**): a) use of a tandem Yamaguchi macrolactonization/Diels–Alder sequence by Schreiber and co-workers (1993);[114] b) the Diels–Alder approach used by Myers et al. to form the B ring (1995);[116] c) the strategy used by Danishefsky and co-workers featuring two Diels–Alder cycloadditions (1996).[117]

et al. using compounds of type **228**.[118] When treated with base, these homophthalic anhydrides are deprotonated at the reactive methylene site, which leads to the formation of diene systems such as **229**. In this example, the action of LiHMDS on **228** at 0 °C, followed by the addition of **227**, effected a smooth intermolecular Diels–Alder reaction with concomitant loss of carbon dioxide to afford polycycle **230**, a highly reactive intermediate which was immediately oxidized with BTIB to furnish anthracenol **231**. Taken cohesively, these three separate but similarly effective approaches to the dynemicin A architecture clearly demonstrate the broad scope of the Diels–Alder reaction when incorporated in ingenious schemes toward challenging molecular structures.

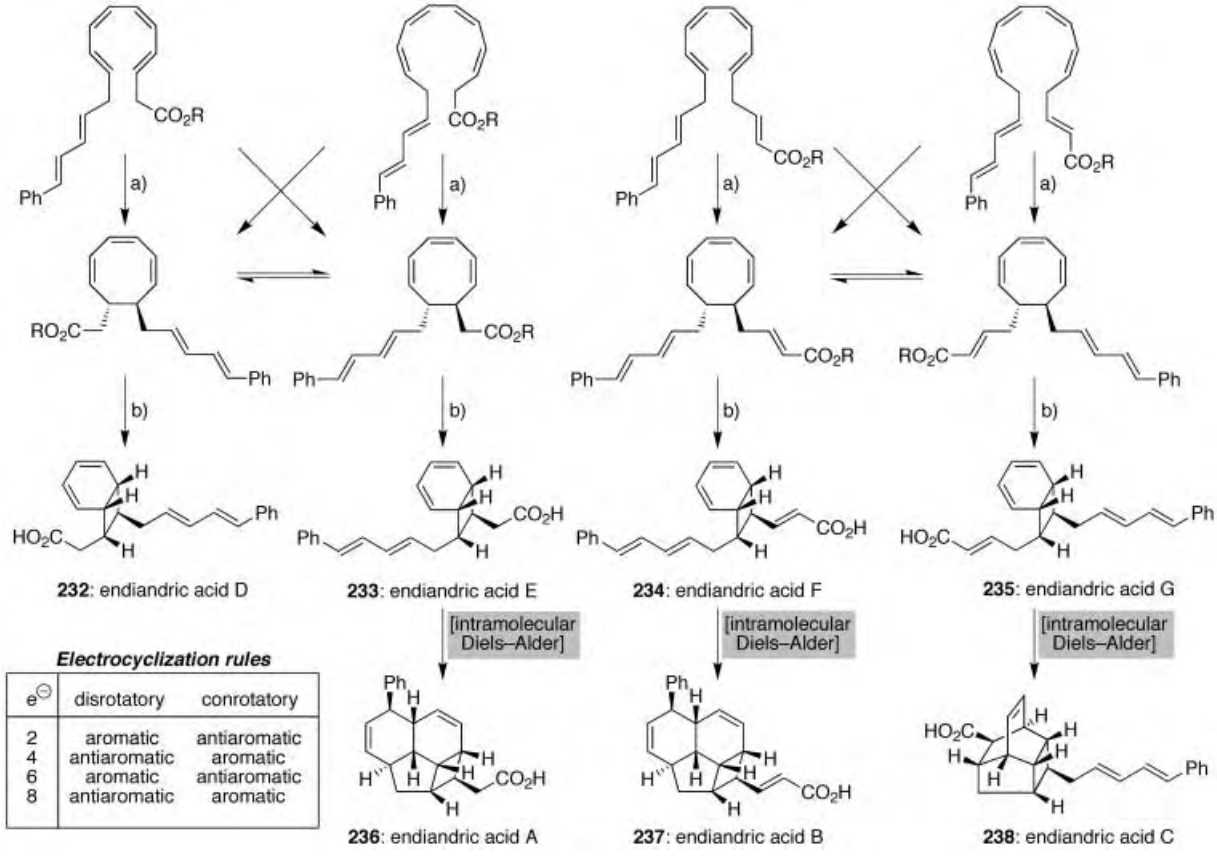
7. The Diels–Alder Reaction in Nature(?)

The numerous total syntheses delineated above appropriately define the awesome power of the Diels–Alder reaction to construct daunting molecular architectures. An issue not yet addressed is whether or not nature deploys [4+2] cyclo-

additions as a weapon in her arsenal to fashion molecular complexity. It is perhaps fair to state at the outset that despite the fact that the Diels–Alder reaction has proven to be a popular tool in the hands of synthetic chemists, its role in the biosynthesis of natural products, although often assumed, remains in question.[119]

At present, several investigators have conclusively established that biological macromolecules such as catalytic antibodies[120] and metal-binding RNA fragments[121] are indeed competent catalysts for the Diels–Alder reaction. Each of these elegant and insightful cases, however, is the product of chemical manipulation as synthetic haptens are required for antibody production and the active RNA molecules are artificial. In an effort to address the question at hand from an absolutely pure biological perspective, considerable effort has been expended in searching for enzymes capable of effecting a Diels–Alder reaction. Although little evidence currently exists for authentic "Diels–Alderases" (entities whose sole and specific purpose is to engender a Diels–Alder reaction),[122] mounting data indicate that enzymes which perform other functions, such as oxidations, are capable of activating bound substrates for in situ intramolecular Diels–Alder reactions in certain circumstances.[119, 123] Such cycloadditions are likely driven by the relative proximity of the diene and dienophile partners enforced within the enzyme's tertiary structure once the primary enzymatic function has been accomplished. As such, it would seem reasonable, despite the absence of confirmed Diels–Alderases, to assume that nature does indeed employ the Diels–Alder reaction as a key C–C bond forming reaction, even if such reactions proceed only by virtue of activating encapsulation. In this section, we will highlight several instructive total syntheses guided by biosynthetic hypotheses that invoke the Diels–Alder reaction as a critical process with or without the aid of enzymes. Each example was selected on the basis of a context where the participation of the pericyclic reaction seems inevitable for the formation of the observed natural product; the sheer elegance of the chemistry involved was another selection criterion.

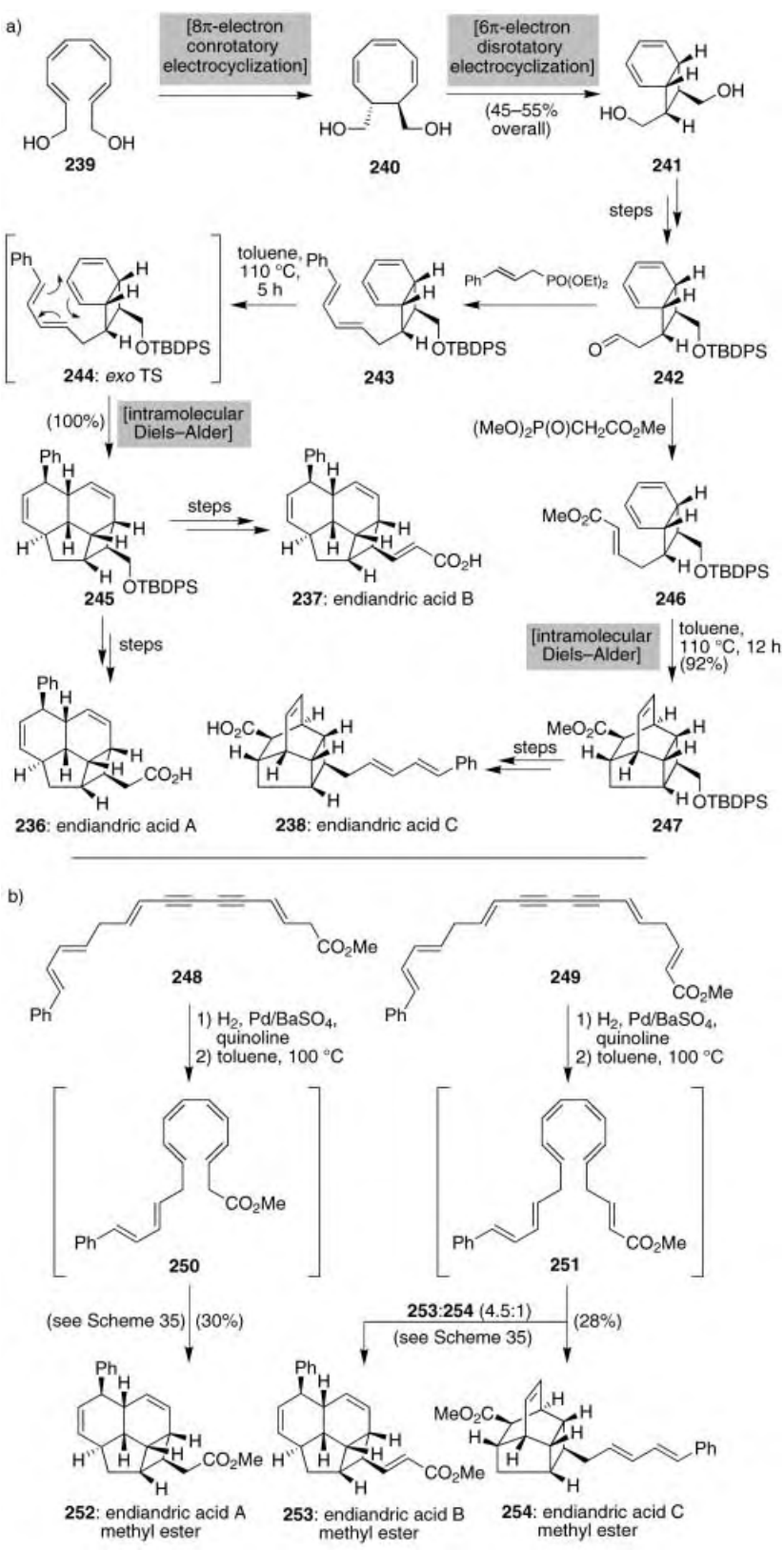
As an initial foray into this fascinating area, we offer the endiandric acids (**232**–**238**, Scheme 35) for closer analysis. This family of natural products, first isolated in 1980 from the Australian plant *Endiandra introrsa* by Black and co-workers, displays striking molecular architectures and unique structural interrelationships.[124] Despite possessing eight chiral centers, the endiandric acids exist in nature as racemates, a highly unusual phenomenon for natural products bearing stereochemical elements, which suggests that these compounds are assembled in nature from prochiral precursors through non-enzymatic reactions. On the basis of this curious observation, Black advanced an intriguing biosynthetic hypothesis in which a series of electrocyclizations from achiral polyenes were postulated to form endiandric acids D–G (**232**–**235**), with a terminating Diels–Alder cycloaddition completing the sequence to endiandric acids A–C (**236**–**238**).[124] As such, although the starting materials lack stereo-



Scheme 35. The biosynthetic endiandric acid cascade proposed by Black and co-workers (R = Me, H): a) conrotatory 8π electrocyclization; b) disrotatory 6π electrocyclization (1980).[124]

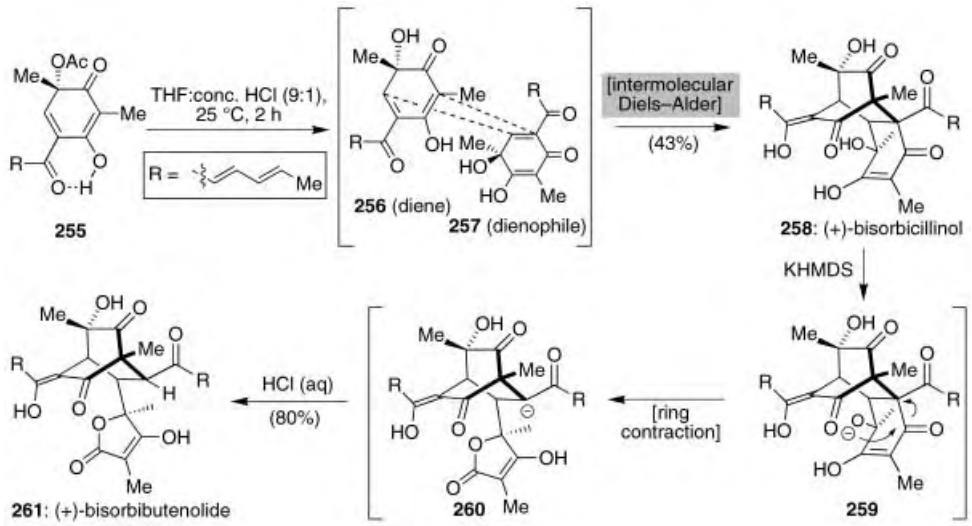
genic centers, the remarkable stereospecificity of the events in the proposed cascade sequence is subtly encoded within the geometry of the olefinic bonds in the postulated precursors. Inspired by this highly intriguing proposal, in 1982 Nicolaou et al. developed both stepwise and biomimetic synthetic routes to all of the endiandric acids (Scheme 36).[125] Significantly, not only did these successful efforts define the first use of 8π and 6π electrocyclizations in natural product total synthesis, they also provided support for the veracity of the non-enzymatic hypothesis proposed by Black and co-workers for the origin of the endiandric acids. Indeed, the one-pot construction of **252** – **254** is particularly remarkable, as no less than eight stereocenters and four rings within each and every natural product were formed concomitantly. Significantly, one should note that endiandric acid methyl esters D – F (Scheme 35) were also observed as products of the biomimetic cascade sequence directly after hydrogenation, prior to heating. However, upon exposure to elevated temperatures, these compounds underwent reversible isomerization processes, eventually being funnelled into the pathways leading to endiandric acids A – C.

A more recent example of a Diels – Alder reaction as a critical component of a presumed biosynthetic pathway includes the dodecaketide (+)-bisorbicillinol (**258**, Scheme 37), a member of the bisorbicillinoid family of natural products possessing potent inhibitory activity against lipopolysaccharide-induced production of tumor necrosis factor α. Careful examination of this group of natural products has led to several biosynthetic hypotheses being advanced by the research groups of both Abe[126] and Nicolaou[127] which uniformly implicate a highly reactive quinol intermediate (tautomers **256** and **257**, masked as an acetate in **255**) as the key building block leading to the biosynthesis of all members of this family of compounds. In 1999, the Nicolaou group was the first to achieve experimental verification of this hypothesis when exposure of homochiral acetate **255** to a solution of base, or even better, concentrated HCl in THF, led to the Diels – Alder adduct **258** ((+)-bisorbicillinol) in 43 % yield with complete regio- and diastereocontrol.[127] The observed selectivity was rationalized on the basis of the anticipated *endo* selectivity (with respect to the six-membered ring) of the postulated transition state in the Diels – Alder union. NMR spectroscopic analysis confirmed the course of the reaction as deacetylation followed by formation of a quinolate system containing the rapidly equilibrating mixture of diene (**256**) and dienophile (**257**) units; these monomers then united in Diels – Alder fashion to form tricyclic skeleton **258** with concurrent installation of four chiral centers, two of which are quaternary.



Scheme 36. The total synthesis of endiandric acids A – C (**236** – **238**) by stepwise (a) and biomimetic (b) routes featuring intramolecular Diels – Alder reactions (Nicolaou et al., 1982).[125]

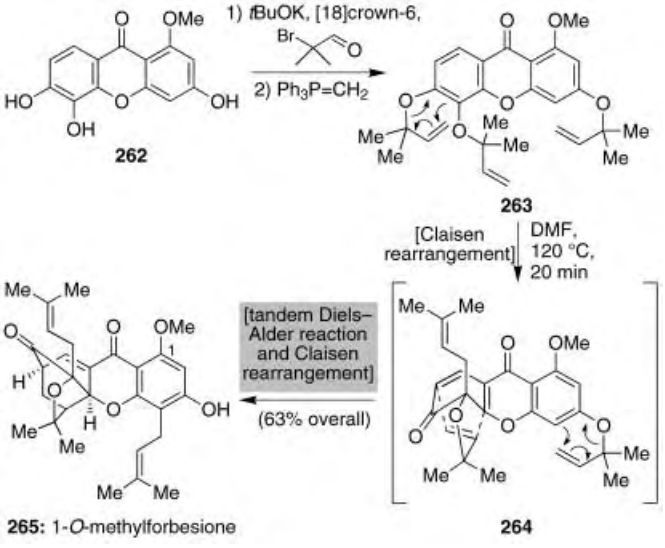
With **258** in hand, subsequent exposure to KHMDS in THF at ambient temperature followed by acidic work-up smoothly led to the formation of (+)-bisorbibutenolide (**261**) in 80 %



Scheme 37. Biomimetic total synthesis of (+)-bisorbicillinol (**258**) and (+)-bisorbibutenolide (**261**) featuring a [4+2] dimerization of a quinol intermediate (Nicolaou et al., 1999).[127]

yield, presumably through the delineated ring-contraction mechanism. Significantly, after the completion of these synthetic efforts, Abe et al. confirmed this biosynthetic hypothesis through careful isolation of the quinol monomer from natural sources.[128]

Along related lines, Nicolaou and Li also recently confirmed[129] a biosynthetic hypothesis first advanced over thirty years ago by Quillinan and Scheinmann[130] in which a series of Claisen rearrangements followed by an intramolecular Diels–Alder reaction was postulated for the formation of the 4-oxatricyclo[4.3.1.0]decan-2-one ring system of numerous secondary metabolites, particularly those isolated from the *guttiferae* family of plants. As a test subject for the proposed cascade sequence the natural product forbesione (the C-1 phenol analogue of **265**, Scheme 38) was targeted: an expedient synthesis of triprenylated derivative **263** was

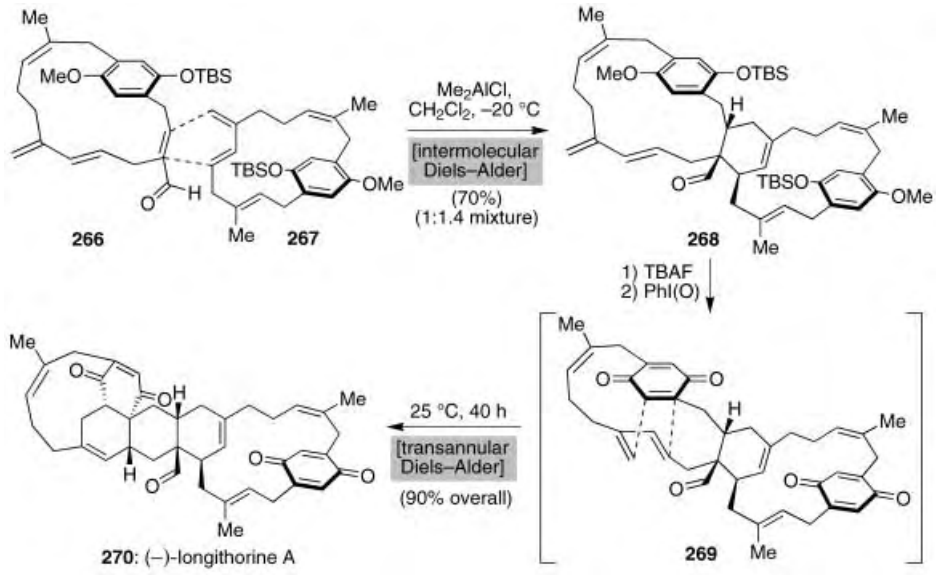


Scheme 38. Putative biomimetic total synthesis of 1-*O*-methylforbesione (**265**) by a cascade sequence featuring tandem Claisen rearrangements and an intramolecular Diels–Alder reaction (Nicolaou and Li, 2001).[129]

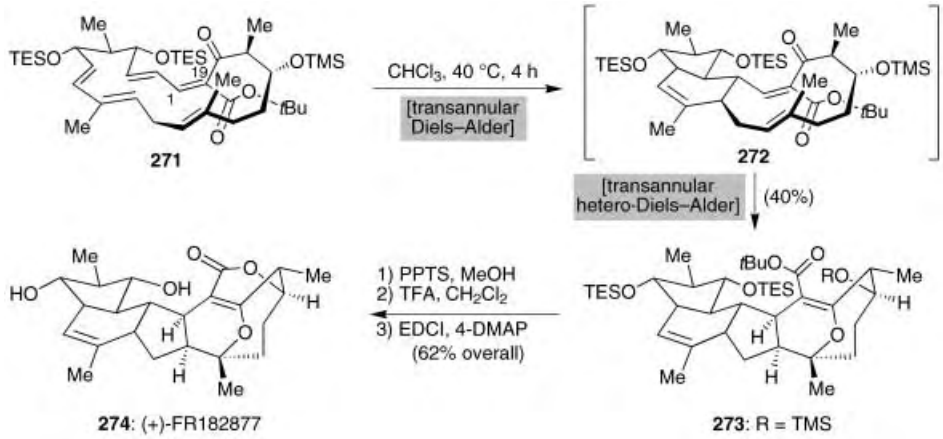
followed by heating the latter compound in DMF at 120 °C for 20 minutes to furnish 1-*O*-methylforbesione (**265**) in 63% yield. Presumably, the final adduct was the result of the anticipated biosynthetic route involving a double Claisen rearrangement/Diels–Alder sequence, via intermediate **264**. The successful development of this technology bodes well for the future construction of the entire functionalized skeleton of other members of this constantly expanding class of important natural products.

Recently, an admirable and highly elegant total synthesis of the marine-derived natural product (−)-longithorone A (**270**, Scheme 39) was achieved by Shair and co-workers[131] based on a biosynthetic hypothesis first proposed by Schmitz and co-workers[132] in which an intermolecular Diels–Alder union of two [12]cyclophanes of type **266** and **267**, followed by an intramolecular transannular Diels–Alder cycloaddition is proposed to concurrently fashion three new rings and completed the target molecule. Thus, in the synthesis by Shair and co-workers, following construction of compounds **266** and **267** by routes which each employed ene-yne metathesis for the macrocyclization step, the merger of these fragments in a Diels–Alder reaction was achieved regioselectively upon exposure to Me_2AlCl to afford a 1:1.4 mixture of diastereomers favoring the undesired adduct. Since careful scrutiny of **266** and **267** reveals no extenuating features which would lead one to expect a diastereoselective [4+2] union, the observed existence of a lone diastereomer of longithorone A in nature may imply an enzyme-mediated fusion of these two pieces, if the proposed biosynthetic pathway is accurate. With **268** in hand, deprotection and quinone formation using iodosylbenzene provided an intermediate (**269**) suitable for the anticipated transannular Diels–Alder reaction, an impressive cycloaddition which was ultimately realized in a remarkable 90% yield upon prolonged reaction at ambient temperature.

As a final entry for discussion in this review, we have selected the very recently achieved biomimetic total synthesis of (+)-FR182877 (**274**, Scheme 40) by Sorensen and co-workers.[133] This example perhaps represents one of the ultimate expressions of the transannular Diels–Alder reaction.[115] The synthesis of key precursor **271** was completed after a 16-step sequence starting with readily available building blocks, in which macrocyclization was brought about through a palladium-mediated Tsuji–Trost reaction. Warming **271** in chloroform at 40 °C then induced an unprecedented domino sequence of transannular Diels–Alder reactions and forged **273** stereoselectively as a lone diastereomer in the absence of any external asymmetric catalyst, with the overall process generating a pentacycle displaying a contiguous array



Scheme 39. The elegant dual Diels–Alder-based strategy of Shair and co-workers for the biomimetic total synthesis of (−)-longithorone A (**270**; 2002).[131]



Scheme 40. The beautiful total synthesis of (+)-FR182877 (**274**) by Sorensen and co-workers featuring a novel double transannular Diels–Alder cascade to fashion the molecule's polycyclic scaffold (2002).[133]

of seven stereocenters in 40% yield. One should note that this overall yield reflects the fact that **271** was taken into the reaction as a 1:1 mixture of *E* and *Z* isomers at the C1−C19 olefin, with approximately 80% of the *E* isomer successfully converting into the desired product. Importantly, the diastereoselectivity of the process, in combination with the observation that the tandem Diels–Alder reactions also proceeded smoothly at ambient temperature (albeit more slowly), are features suggestive of the plausibility of the cascade similarly occurring in nature. As such, this example provides a novel biosynthetic approach to the complete carbogenic framework of (+)-FR182877 (**274**) and, more significantly, represents the first realization of a double transannular Diels–Alder process in organic synthesis, an event conceivable only from a macrocyclic precursor composed of a minimum of 18 atoms. As such, this synthesis highlights the utility of transannular Diels–Alder reactions both in terms of the atom economy as well as the versatility of the process. Clearly, entropic and enthalpic activation in the macrocyclic environment, with the overall geometry governed by transannular steric repulsion and electronic interactions, dictated the facility of the achieved cascade sequence.[115]

Before closing this section, we should note that several of the total syntheses highlighted in the preceding segments of this review similarly employed Diels–Alder unions based on biosynthetic hypotheses, but were mentioned earlier for other overriding reasons. Furthermore, in no way should the present set of examples serve as a complete expression of the power of biomimetic approaches to total synthesis by the Diels–Alder reaction. As such, we refer the reader to several additional and enriching examples in the chemical literature.[134]

8. Conclusions and Future Perspectives

The discussion of the Diels–Alder reaction in the preceding pages speaks volumes of the power of this reaction in total synthesis. As much as one should in general avoid speculation about the future, its application in the assembly of complex molecules is likely to be secured for a long time to come on the grounds of its efficiency, versatility, and scope.[135] With little doubt, both nature and man are the guarantors of its continuing prosperity in the art of total synthesis. Thus, the constantly expanding collection of constructs isolated from nature's library of molecular diversity is bound to contain myriad structures amenable to retrosynthetic analysis based on Diels–Alder transforms. Equally eager to contribute to the reaction's longevity, if not immortality, will be the sustained desire of synthetic chemists to adopt it in their total synthesis endeavors.

Of course, the employment of the Diels–Alder reaction in the total synthesis of naturally occurring substances, although telling, does not reveal the entire story of its widespread utility and enormous potential. Applications in the fabrication of designed molecules, which reflect structures of theoretical interest or chemical entities desired for biological investigations and for material science purposes, may prove even more important in future investigations than natural products. The vast literature pertaining to such examples is testimony to the faith synthetic chemists have placed in the Diels–Alder reaction as an assembly process for tailor-made compounds.

To be sure, this trend will only expand in the future as the demand for new compound libraries increases. Particularly attractive is the concept of incorporating the Diels–Alder reaction within powerful cascade sequences as a means of rapidly assembling molecular complexity and diversity. Such domino reactions are clearly highly desirable and also have the potential to contribute to our efforts for green chemistry.

Finally, we offer the conjecture that Diels and Alder would be enormously pleased to know of the many important and elegant applications of their reaction in total synthesis as seen from 2002. Indeed, they might even derive a considerable measure of satisfaction from the knowledge that their warning against the use of their reaction in total synthesis, a right they reserved for themselves alone, was not heeded by subsequent generations of chemists. What we dare not project, however, are the beautiful examples of Diels–Alder-based molecular constructions which might be included in a review on the subject on the bicentennial anniversary of Alder's birthday.

Abbreviations

Ac	acetyl
AIBN	2,2′-azobisisobutyronitrile
Alloc	allyloxycarbonyl
BBN	borabicyclo[3.3.1]nonane
BHT	*tert*-butylhydroxytoluene
BINOL	2,2′-dihydroxy-1,1′-binapthyl
Bn	benzyl
Boc	*tert*-butoxycarbonyl
BTIB	[bis(trifluoroacetoxy)iodo]benzene
Bz	benzoyl
CAN	ceric ammonium nitrate
Cp	cyclopentadienyl
DABCO	1,4-diazabicyclo[2.2.2]octane
DBP	di-*n*-butyl phthalate
DMAP	4-dimethylaminopyridine
DME	ethylene glycol dimethyl ether
DMF	*N*,*N*-dimethylformamide
dppp	1,3-bis(diphenylphosphanyl)propane
EDC	3-(3-dimethylaminopropyl)-1-ethylcarbodiimide
EWG	electron withdrawing group
HMDS	1,1,1,3,3,3-hexamethyldisilazane
HMPT	hexamethylphosphourous triamide
imid.	imidazole
MEM	(2-methoxyethoxy)methyl
MOM	methoxymethyl
PGF	prostaglandin F
PMB	*p*-methoxybenzyl
PPTS	pyridinium *p*-toluenesulfonate
PyBroP	bromo-tris(pyrrolidino)phosphonium hexafluorophosphate
pyr	pyridine
TBAF	tetra-*n*-butylammonium fluoride
TBDPS	*tert*-butyldiphenylsilyl
TBS	*tert*-butyldimethylsilyl
TES	triethylsilyl
Tf	trifluoromethanesulfonyl
TFA	trifluoroacetic acid
TFAA	trifluoroacetic acid anhydride
THF	tetrahydrofuran
TIB	1,3,5-triisopropylbenzene
TIPS	triisopropylsilyl
TMB	1,2,4-trimethylbenzene
TMS	trimethylsilyl
TS	transition state
Ts	*p*-toluenesulfonyl
p-TsOH	*p*-toluenesulfonic acid
X_p	Evans' chiral auxilliary

It is with enormous pride and pleasure that we wish to thank our collaborators whose names appear in the references, and whose contributions made the described work possible and enjoyable. We gratefully acknowledge the National Institutes of Health (USA), Merck & Co., DuPont, Schering Plough, Hoffmann–La Roche, GlaxoWellcome, Rhone–Poulenc Rorer, Amgen, Novartis, Abbott Laboratories, Bristol Myers Squibb, Boehringer Ingelheim, Zeneca, CaPCURE, the George E. Hewitt Foundation, the Skaggs Institute for Chemical Biology, Pfizer (fellowship to S.A.S.), and the National Science Foundation (fellowship to S.A.S.) for supporting our research programs.

Received: February 21, 2002 [A 521]

[1] a) T. Zincke, H. Günther, *Justus Liebigs Ann. Chem.* **1892**, *272*, 243–270; b) T. Zincke, F. Bergmann, B. Francke, W. Prenntzell, *Justus Liebigs Ann. Chem.* **1897**, *296*, 135–158; c) T. Zincke, K. H. Meyer, *Justus Liebigs Ann. Chem.* **1909**, *367*, 1–13; d) T. Zincke, W. Pfaffendorf, *Justus Liebigs Ann. Chem.* **1913**, *394*, 3–22; e) W. Albrecht, *Justus Liebigs Ann. Chem.* **1906**, *348*, 31–49; f) H. Wieland, *Ber. Dtsch. Chem. Ges.* **1906**, *39*, 1492–1499; g) S. V. Lebedev, *J. Russ. Phys. Chem. Soc.* **1910**, *42*, 949–952; h) H. Staudinger, *Ber. Dtsch. Chem. Ges.* **1911**, *44*, 524–533; i) H. von Euler, K. O. Josephson, *Ber. Dtsch. Chem. Ges. B* **1920**, *53*, 822–826.

[2] For engaging accounts of the early history of the Diels–Alder reaction, see a) J. A. Berson, *Tetrahedron* **1992**, *48*, 3–17; b) J. A. Berson, *Chemical Creativity*, Wiley-VCH, Weinheim, **1999**, pp. 9–32.

[3] For biographies of Otto Diels, see a) S. Olsen, *Chem. Ber.* **1962**, *95*, v–xlvi; b) L. R. Walters in *Nobel Laureates in Chemistry 1901–1992* (Ed.: L. K. James), American Chemical Society, Rahway, **1994**, pp. 332–337. We should note that last year marked the 125th anniversary of Diels' birth, and next year will celebrate the 75th anniversary of the disclosure of the Diels–Alder reaction (see ref. [5]).

[4] For biographies of Kurt Alder, see a) F. Feher, *Chem. Ber.* **1970**, *103*, 1–10; b) J. Sauer, *Chem. Ber.* **1970**, *103*, 11–39.

[5] O. Diels, K. Alder, *Justus Liebigs Ann. Chem.* **1928**, *460*, 98–122.

[6] a) G. Stork, E. E. Van Tamalen, L. J. Friedman, A. W. Burgstahler, *J. Am. Chem. Soc.* **1951**, *73*, 4501; b) G. Stork, E. E. Van Tamalen, L. J. Friedman, A. W. Burgstahler, *J. Am. Chem. Soc.* **1953**, *75*, 384–392.

[7] a) M. Gates, G. Tschudi, *J. Am. Chem. Soc.* **1952**, *74*, 1109–1110; b) M. Gates, G. Tschudi, *J. Am. Chem. Soc.* **1956**, *78*, 1380–1393; c) M. Gates, *J. Am. Chem. Soc.* **1950**, *72*, 228–234.

[8] K. Alder, H. F. Rickert, *Ber. Dtsch. Chem. Ges. B* **1937**, *70*, 1364–1369.

[9] a) O. Diels, *Ber. Dtsch. Chem. Ges. B* **1942**, *75*, 1452–1467; b) K. Alder, W. Gunzl, K. Wolff, *Chem. Ber.* **1960**, *93*, 809–825.

[10] a) K. Alder, G. Stein, F. von Budedenbrock, W. Eckardt, W. Frercks, S. Schneider, *Justus Liebigs Ann. Chem.* **1934**, *514*, 1–33; b) K. Alder, G. Stein, M. Liebmann, E. Rolland, *Justus Liebigs Ann. Chem.* **1934**, *514*, 197–211; c) K. Alder, G. Stein, E. Rolland, G. Schulze, *Justus Liebigs Ann. Chem.* **1934**, *514*, 211–227.

[11] R. B. Woodward, F. Sondheimer, D. Taub, K. Heusler, W. M. McLamore, *J. Am. Chem. Soc*. **1952**, *74*, 4223 – 4251.
[12] Another total synthesis of cortisone by using a Diels – Alder strategy was disclosed a few months after that of Woodward et al.: L. H. Sarett, G. E. Arth, R. M. Lukes, R. E. Beyler, G. I. Poos, W. F. Johns, J. M. Constantin, *J. Am. Chem. Soc*. **1952**, *74*, 4974 – 4976.
[13] a) R. B. Woodward, F. E. Bader, H. Bickel, A. J. Frey, R. W. Kierstead, *Tetrahedron* **1958**, *2*, 1 – 57; b) R. B. Woodward, F. E. Bader, H. Bickel, A. J. Frey, R. W. Kierstead, *J. Am. Chem. Soc.* **1956**, *78*, 2023 – 2025; c) R. B. Woodward, F. E. Bader, H. Bickel, A. J. Frey, R. W. Kierstead, *J. Am. Chem. Soc*. **1956**, *78*, 2657.
[14] For other total syntheses of reserpine using Diels – Alder reactions, see a) P. A. Wender, J. M. Schaus, A. W. White, *J. Am. Chem. Soc.* **1980**, *102*, 6159 – 6161; b) S. F. Martin, S. Grzejszczak, H. Rüeger, S. A. Williamson, *J. Am. Chem. Soc.* **1985**, *107*, 4072 – 4074.
[15] I. Fleming in *Frontier Orbitals and Organic Chemical Reactions*, Wiley, Chichester, **1978**, pp. 87 – 181.
[16] For the first example of a Lewis acid catalyzed Diels – Alder reaction, which clearly demonstrates the principle of reaction acceleration and enhanced *endo* selectivity, see P. Yates, P. Eaton, *J. Am. Chem. Soc.* **1960**, *82*, 4436 – 4437. For an excellent primer in Lewis acid catalysis of the Diels – Alder reaction, see W. Oppolzer in *Comprehensive Organic Synthesis*, *Vol. 5* (Eds.: B. M. Trost, I. Flemming, L. A. Paquette), Pergamon, Oxford, **1991**, chap. 4.1.4, pp. 339 – 345. For representative references in switching the regioselectivity relative to that of a non-Lewis acid catalyzed Diels – Alder reaction, see a) W. Kreiser, W. Haumesser, A. F. Thomas, *Helv. Chim. Acta* **1974**, *57*, 164 – 167; b) T. A. Engler, R. Iyengar, *J. Org. Chem*. **1998**, *63*, 1929 – 1934.
[17] a) Y. Kishi, M. Aratani, T. Fukuyama, F. Nakatsubo, T. Goto, S. Inoue, S. Sugiura, H. Kakoi, *J. Am. Chem. Soc.* **1972**, *94*, 9217 – 9219; b) Y. Kishi, T. Fukuyama, M. Aratani, F. Nakatsubo, T. Goto, S. Inoue, S. Sugiura, H. Kakoi, *J. Am. Chem. Soc.* **1972**, *94*, 9219 – 9221.
[18] a) Y. Kishi, F. Nakatsubo, M. Aratani, T. Goto, S. Inoue, H. Tanino, H. Kakoi, S. Sugiura, *Tetrahedron Lett.* **1970**, *59*, 5127 – 5128; b) Y. Kishi, F. Nakatsubo, M. Aratani, T. Goto, S. Inoue, H. Tanino, H. Kakoi, *Tetrahedron Lett.* **1970**, *59*, 5129 – 5132.
[19] Danishefsky's diene was introduced in the following seminal paper: S. J. Danishefsky, T. Kitahara, *J. Am. Chem. Soc.* **1974**, *96*, 7807 – 7808. The further development of this diene motif is chartered in the following reviews: a) S. Danishefsky, *Acc. Chem. Res.* **1981**, *14*, 400 – 406; b) S. J. Danishefsky, *Aldrichimica Acta* **1986**, 59 – 69.
[20] a) S. J. Danishefsky, J. F. Kerwin, S. Kobayashi, *J. Am. Chem. Soc.* **1982**, *104*, 358 – 360; b) S. Danishefsky, N. Kato, D. Askin, J. F. Kerwin, *J. Am. Chem. Soc.* **1982**, *104*, 360 – 362.
[21] S. J. Danishefsky, M. Hirama, N. Fritsch, J. Clardy, *J. Am. Chem. Soc.* **1979**, *101*, 7013 – 7018.
[22] For selected, further examples of Danishefsky's diene in Diels – Alder reactions reported by his group, see a) S. J. Danishefsky, C. Maring, *J. Am. Chem. Soc.* **1985**, *107*, 7762 – 7764; b) D. C. Myles, S. J. Danishefsky, G. Schulte, *J. Org. Chem.* **1990**, *55*, 1636 – 1648.
[23] a) M. Y. Chu-Moyer, S. J. Danishefsky, *J. Am. Chem. Soc.* **1992**, *114*, 8333 – 8334; b) M. Y. Chu-Moyer, S. J. Danishefsky, G. K. Schulte, *J. Am. Chem. Soc.* **1994**, *116*, 11213 – 11228.
[24] a) E. J. Corey, R. L. Danheiser, S. Chandrasekaran, P. Siret, G. E. Keck, J.-L. Gras, *J. Am. Chem. Soc.* **1978**, *100*, 8031 – 8034; b) E. J. Corey, R. L. Danheiser, S. Chandrasekaran, G. E. Keck, B. Gopalan, S. D. Larsen, P. Siret, J.-L. Gras, *J. Am. Chem. Soc.* **1978**, *100*, 8034 – 8036. For an enantioselective total synthesis of gibberellic acid using a Diels – Alder reaction by the same research group, see E. J. Corey, A. Guzman-Perez, T.-P. Loh, *J. Am. Chem. Soc.* **1994**, *116*, 3611 – 3612.
[25] For other total syntheses of gibberellic acid using a Diels – Alder strategy, see a) H. Nagaoka, M. Shimano, Y. Yamada, *Tetrahedron Lett*. **1989**, *30*, 971 – 974; b) F. Nuyttens, J. Hoflack, G. Appendino, P. J. DeClercq, *Synlett* **1995**, 105 – 107; c) M. Toyota, T. Odashima, T. Wada, M. Ihara, *J. Am. Chem. Soc.* **2000**, *122*, 9036 – 9037.
[26] a) E. J. Corey, N. H. Anderson, R. M. Carlson, J. Paust, E. Vedejs, I. Vlattas, R. E. K. Winter, *J. Am. Chem. Soc.* **1968**, *90*, 3245 – 3247; b) E. J. Corey, I. Vlattas, N. H. Anderson, K. Harding, *J. Am. Chem. Soc.* **1968**, *90*, 3247 – 3248; c) E. J. Corey, N. M. Weinshenker, T. K. Schaaf, W. Huber, *J. Am. Chem. Soc.* **1969**, *91*, 5675 – 5677; d) E. J. Corey, T. K. Schaaf, W. Huber, U. Koelliker, N. M. Weinshenker, *J. Am. Chem. Soc.* **1970**, *92*, 397 – 398; e) E. J. Corey, R. Noyori, T. K. Schaaf, *J. Am. Chem. Soc.* **1970**, *92*, 2586 – 2587; f) E. J. Corey, H. E. Ensley, *J. Am. Chem. Soc.* **1975**, *97*, 6908 – 6909; g) E. J. Corey, R. Imwinkelried, S. Pikul, Y. B. Xiang, *J. Am. Chem. Soc.* **1989**, *111*, 5493 – 5495; h) E. J. Corey, T.-P. Loh, T. D. Roper, M. D. Azimioara, M. C. Noe, *J. Am. Chem. Soc.* **1992**, *114*, 8290 – 8292.
[27] For Corey's further work on catalysts for the Diels – Alder reaction, see a) E. J. Corey, N. Imai, S. Pikul, *Tetrahedron Lett.* **1991**, *32*, 7517 – 7521; b) E. J. Corey, S. Sarshar, J. Bordner, *J. Am. Chem. Soc.* **1992**, *114*, 7938 – 7939; c) E. J. Corey, T.-P. Loh, *J. Am. Chem. Soc.* **1991**, *113*, 8966 – 8967; d) E. J. Corey, N. Imai, H.-Y. Zhang, *J. Am. Chem. Soc.* **1991**, *113*, 728 – 729; e) E. J. Corey, D. Barnes-Seeman, T. W. Lee, *Tetrahedron Lett.* **1997**, *38*, 4351 – 4354.
[28] For an introduction to the use of chiral auxiliaries in Diels – Alder reactions, see W. Oppolzer in *Comprehensive Organic Synthesis*, *Vol. 5* (Eds.: B. M. Trost, I. Flemming, L. A. Paquette), Pergamon, Oxford, **1991**, chap. 4.1.6, pp. 352 – 377.
[29] For a general review of Corey's work developing chiral catalyst systems, see E. J. Corey, *Pure Appl. Chem.* **1990**, *62*, 1209 – 1216.
[30] For an early discussion of Evans' oxazolidinone chiral auxiliaries, see D. A. Evans, J. V. Nelson, T. R. Taber, *Top. Stereochem*. **1982**, *13*, 1 – 115. For applications in Diels – Alder cycloadditions, see D. A. Evans, K. T. Chapman, J. Bisaha, *J. Am. Chem. Soc.* **1988**, *110*, 1238 – 1256.
[31] D. A. Evans, W. C. Black, *J. Am. Chem. Soc.* **1993**, *115*, 4497 – 4513.
[32] For leading references, see a) D. A. Evans, S. J. Miller, T. Lectka, P. von Matt, *J. Am. Chem. Soc.* **1999**, *121*, 7559 – 7573; b) J. S. Johnson, D. A. Evans, *Acc. Chem. Res.* **2000**, *33*, 325 – 335.
[33] D. A. Evans, D. M. Barnes, J. S. Johnson, T. Lectka, P. von Matt, S. J. Miller, J. A. Murry, R. D. Norcross, E. A. Shaughnessy, K. R. Campos, *J. Am. Chem. Soc.* **1999**, *121*, 7582 – 7594.
[34] J. D. White, Y. Choi, *Org. Lett.* **2000**, *2*, 2373 – 2376.
[35] K. Mikami, M. Terada, Y. Motoyama, T. Nakai, *Tetrahedron: Asymmetry* **1991**, *2*, 643 – 646; b) K. Mikami, Y. Motoyama, M. Terada, *J. Am. Chem. Soc.* **1994**, *116*, 2812 – 2820.
[36] a) K. C. Nicolaou, G. Vassilikogiannakis, W. Mägerlein, R. Kranich, *Angew. Chem.* **2001**, *113*, 2543 – 2547; *Angew. Chem. Int. Ed.* **2001**, *40*, 2482 – 2486; b) K. C. Nicolaou, G. Vassilikogiannakis, W. Mägerlein, R. Kranich, *Chem. Eur. J.* **2001**, *7*, 5359 – 5371.
[37] a) P. Liu, E. N. Jacobsen, *J. Am. Chem. Soc.* **2001**, *123*, 10772 – 10773; b) A. G. Dossetter, T. F. Jamison, E. N. Jacobsen, *Angew. Chem.* **1999**, *111*, 2549 – 2552; *Angew. Chem. Int. Ed.* **1999**, *38*, 2398 – 2400. For another total synthesis of ambruticin using a Diels – Alder reaction, see A. S. Kende, J. S. Mendoza, Y. Fujii, *Tetrahedron* **1993**, *49*, 8015 – 8038.
[38] For another catalyst system capable of achieving such hetero-Diels – Alder reactions, see D. A. Evans, E. J. Olhava, J. S. Johnson, J. M. Janey, *Angew. Chem.* **1998**, *110*, 3554 – 3557; *Angew. Chem. Int. Ed.* **1998**, *37*, 3372 – 3375.
[39] K. C. Nicolaou, D. P. Papahatjis, D. A. Claremon, R. L. Magolda, R. E. Dolle, *J. Org. Chem.* **1985**, *50*, 1440 – 1456.
[40] For other total syntheses of X-14547A using a Diels – Alder reaction, see a) M. P. Edwards, S. V. Ley, S. G. Lister, B. D. Palmer, D. J. Williams, *J. Org. Chem*. **1984**, *49*, 3503 – 3516; b) R. K. Boeckman, E. J. Enholm, D. M. Demko, A. B. Charette, *J. Org. Chem.* **1986**, *51*, 4743 – 4745; c) S. D. Burke, A. D. Piscopio, M. E. Kort, M. A. Matulenko, M. H. Parker, D. M. Armistead, K. Shankaran, *J. Org. Chem.* **1994**, *59*, 332 – 347; d) W. R. Roush, S. M. Peseckis, A. E. Walts, *J. Org. Chem.* **1984**, *49*, 3429 – 3432.
[41] For the initial synthesis of the CP molecules, in which the Diels – Alder reaction provided racemic material, see a) K. C. Nicolaou, P. S. Baran, Y.-L. Zhong, H.-S. Choi, W. H. Yoon, Y. He, K. C. Fong, *Angew. Chem.* **1999**, *111*, 1774 – 1781; *Angew. Chem. Int. Ed.* **1999**, *38*, 1669 – 1675; b) K. C. Nicolaou, P. S. Baran, Y.-L. Zhong, K. C. Fong, Y. He, W. H. Yoon, H-S. Choi, *Angew. Chem.* **1999**, *111*, 1781 – 1784; *Angew. Chem. Int. Ed.* **1999**, *38*, 1676 – 1678; for later efforts based on an asymmetric Diels – Alder approach, see c) K. C. Nicolaou, J.-K. Jung, W. H. Yoon, Y. He, Y.-L. Zhong, P. S. Baran, *Angew. Chem.* **2000**, *112*, 1899 – 1902; *Angew. Chem. Int. Ed.* **2000**,

39, 1829 – 1832; d) K. C. Nicolaou, J. Jung, W. H. Yoon, K. C. Fong, H.-S. Choi, Y. He, Y.-L. Zhong, P. S. Baran, *J. Am. Chem. Soc.* **2002**, *124*, 2183 – 2189; e) K. C. Nicolaou, P. S. Baran, Y.-L. Zhong, K. C. Fong, H.-S. Choi, *J. Am. Chem. Soc.* **2002**, *124*, 2190 – 2201; f) K. C. Nicolaou, Y.-L. Zhong, P. S. Baran, J. Jung, H.-S. Choi, W. H. Yoon, *J. Am. Chem. Soc.* **2002**, *124*, 2202 – 2211.

[42] N. Waizumi, T. Itoh, T. Fukuyama, *J. Am. Chem. Soc.* **2000**, *122*, 7825 – 7826.

[43] B. R. Bear, S. M. Sparks, K. J. Shea, *Angew. Chem.* **2001**, *113*, 864 – 894; *Angew. Chem. Int. Ed.* **2001**, *40*, 820 – 849.

[44] a) R. A. Gibbs, W. H. Okamura, *J. Am. Chem. Soc.* **1988**, *110*, 4062 – 4063; b) R. A. Gibbs, K. Bartels, R. W. K. Lee, W. H. Okamura, *J. Am. Chem. Soc.* **1989**, *111*, 3717 – 3725.

[45] For other approaches to sterpurene using Diels – Alder cycloadditions, see a) L. A. Paquette, H.-S. Lin, B. P. Gunn, M. J. Coghlan, *J. Am. Chem. Soc.* **1988**, *110*, 5818 – 5826; b) N. Krause, *Liebigs Ann. Chem.* **1993**, 521 – 525.

[46] P. A. Wender, T. E. Jenkins, S. Suzuki, *J. Am. Chem. Soc.* **1995**, *117*, 1843 – 1844.

[47] For an excellent introduction to heterodienophiles, see S. M. Weinreb in *Comprehensive Organic Synthesis*, *Vol. 5* (Ed.: B. M. Trost, I. Flemming, L. A. Paquette), Pergamon, Oxford, **1991**, chap. 4.2, pp. 401 – 449. For an overview of heterodiene Diels – Alder partners, see D. L. Boger in *Comprehensive Organic Synthesis*, *Vol. 5* (Eds.: B. M. Trost, I. Flemming, L. A. Paquette), Pergamon, Oxford, **1991**, chap. 4.3, pp. 451 – 512.

[48] K. Alder in *Neuere Methoden der Praparativen Organischen Chemie*, Verlag Chemie, Berlin, **1943**, pp. 251 – 412.

[49] O. Wichterle, J. Rocek, *Chem. Listy* **1953**, *47*, 1768 – 1780.

[50] D. Stein, G. T. Anderson, C. E. Chase, Y. Koh, S. M. Weinreb, *J. Am. Chem. Soc.* **1999**, *121*, 9574 – 9579.

[51] For a review on N=S dienophiles, see S. M. Weinreb, *Acc. Chem. Res.* **1988**, *21*, 313 – 318. For a leading reference on the further use of this dienophile, see R. S. Garigipati, A. J. Freyer, R. R. Whittle, S. M. Weinreb, *J. Am. Chem. Soc.* **1984**, *106*, 7861 – 7867.

[52] For selected reviews on the synthesis and applications of 1,2-aminoalcohols, see a) T. Kunieda, T. Ishizuka in *Studies in Natural Products Chemistry*, *Vol. 12* (Ed.: Atta-ur-Rahman), Elsevier, New York, **1993**, p. 411; b) A. Golebiowski, J. Jurczak, *Synlett* **1993**, 241 – 245; c) Y. Ohfune, *Acc. Chem. Res.* **1992**, *25*, 360 – 366; d) T. Yokomatsu, Y. Yuasa, S. Shibuya, *Heterocycles* **1992**, 33, 1051 – 1078; e) M. T. Reetz, *Angew. Chem.* **1991**, *103*, 1559 – 1573; *Angew. Chem. Int. Ed. Engl.* **1991**, *30*, 1531 – 1545.

[53] For review articles on this valuable dienophile in Diels – Alder reactions, see a) J. Streith, A. Defoin, *Synthesis* **1994**, 1107 – 1117; b) J. Streith, A. Defoin, *Synlett* **1996**, 189 – 200.

[54] a) S. M. Weinreb, *Acc. Chem. Res.* **1985**, *18*, 16 – 21; b) D. L. Boger, *Chemtracts: Org. Chem.* **1996**, 149 – 189.

[55] For selected reviews, see a) D. L. Boger, *J. Heterocycl. Chem.* **1996**, *33*, 1519 – 1531; b) D. L. Boger, *Chem. Rev.* **1986**, *86*, 781 – 793; c) D. L. Boger, *Tetrahedron* **1983**, *39*, 2869 – 2939.

[56] For some more recent reviews of azadiene chemistry, see a) S. Jayakumar, M. P. S. Ishar, M. P. Mahajan, *Tetrahedron* **2002**, *58*, 379 – 471; b) M. Behforouz, M. Ahmadian, *Tetrahedron* **2000**, *56*, 5259 – 5288.

[57] a) D. L. Boger, C. M. Baldino, *J. Am. Chem. Soc.* **1993**, *115*, 11418 – 11425; b) H. H. Wasserman, R. W. DeSimone, D. L. Boger, C. M. Baldino, *J. Am. Chem. Soc.* **1993**, *115*, 8457 – 8458.

[58] For selected further examples of azadienes in total synthesis by the Boger group, see a) D. L. Boger, J. S. Panek, *J. Am. Chem. Soc.* **1985**, *107*, 5745 – 5754; b) D. L. Boger, J. Hong, *J. Am. Chem. Soc.* **2001**, *123*, 8515 – 8519.

[59] For other selected total syntheses of furans using this Diels – Alder-based methodology, see a) P. A. Jacobi, K. Lee, *J. Am. Chem. Soc.* **2000**, *122*, 4295 – 4303; b) P. A. Jacobi, C. S. R. Kaczmarek, U. E. Udodong, *Tetrahedron* **1987**, *43*, 5475 – 5488; c) P. A. Jacobi, D. G. Walker, *J. Am. Chem. Soc.* **1981**, *103*, 4611 – 4613.

[60] P. A. Jacobi, C. A. Blum, R. W. DeSimone, U. E. S. Udodong, *Tetrahedron Lett.* **1989**, *30*, 7173 – 7176.

[61] For another synthesis of norsecurinine by using a key Diels – Alder reaction, see G. Han, M. G. LaPorte, J. J. Folmer, K. M. Werner, S. M. Weinreb, *J. Org. Chem.* **2000**, *65*, 6293 – 6300.

[62] For application of this methodology to generate thiophenes, see P. A. Jacobi, M. Egbertson, R. F. Frechette, C. K. Miao, K. T. Weiss, *Tetrahedron* **1988**, *44*, 3327 – 3338.

[63] a) R. B. Ruggeri, M. M. Hansen, C. H. Heathcock, *J. Am. Chem. Soc.* **1988**, *110*, 8734 – 8736. b) C. H. Heathcock, M. M. Hansen, R. B. Ruggeri, J. C. Kath, *J. Org. Chem.* **1992**, *57*, 2544 – 2553; for some interesting reviews on this total synthesis, see c) C. H. Heathcock, *Angew. Chem.* **1992**, *104*, 675 – 814; *Angew. Chem. Int. Ed. Engl.* **1992**, *31*, 665 – 804; d) C. H. Heathcock, *Proc. Natl. Acad. Sci. USA* **1996**, *93*, 14323 – 14327.

[64] For instructive examples in total synthesis efforts, see a) P. A. Grieco, Y. Dai, *J. Am. Chem. Soc.* **1998**, *120*, 5128 – 5129, and references therein; b) S. R. Magnuson, L. Sepp-Lorenzino, N. Rosen, S. J. Danishefsky, *J. Am. Chem. Soc.* **1998**, *120*, 1615 – 1616, and references therein. As an aside, the field of carbocation- and radical-cation-catalyzed Diels – Alder reaction was pioneered by Gassman, though not in the context of total synthesis endeavors. See P. G. Gassman, D. A. Singleton, *J. Am. Chem. Soc.* **1984**, *106*, 6085 – 6086, and references therein as an entry into the start of this field.

[65] W. A. Carroll, P. A. Grieco, *J. Am. Chem. Soc.* **1993**, *115*, 1164 – 1165.

[66] P. A. Grieco, A. Bahsas, *J. Org. Chem.* **1987**, *52*, 5746 – 5749.

[67] D. L. Boger, S. Ichikawa, H. Jiang, *J. Am. Chem. Soc.* **2000**, *122*, 12169 – 12173.

[68] For a further example of a challenging pyridine synthesis by the Boger group, see D. L. Boger, J. Hong, M. Hikota, M. Ishida, *J. Am. Chem. Soc.* **1999**, *121*, 2471 – 2477.

[69] D. L. Boger, K. Takahashi, *J. Am. Chem. Soc.* **1995**, *117*, 12452 – 12459.

[70] O. L. Chapman, M. R. Engel, J. P. Springer, J. C. Clardy, *J. Am. Chem. Soc.* **1971**, *93*, 6696 – 6698.

[71] For other total syntheses of carpanone by using an *o*-quinodimethane/Diels – Alder approach, see a) M. Matsumoto, K. Kuroda, *Tetrahedron Lett.* **1981**, *22*, 4437 – 4440; b) C. W. Lindsley, L. K. Chan, B. C. Goess, R. Joseph, M. D. Shair, *J. Am. Chem. Soc.* **2000**, *122*, 422 – 423.

[72] a) W. Oppolzer, K. Keller, *J. Am. Chem. Soc.* **1971**, *93*, 3836 – 3837; b) W. Oppolzer, C. Robbiani, *Helv. Chim. Acta* **1983**, *66*, 1119 – 1128.

[73] W. Oppolzer, E. Francotte, K. Bättig, *Helv. Chim. Acta* **1981**, *64*, 478 – 481.

[74] a) W. G. L. Aalbersberg, A. J. Barkovich, R. L. Funk, R. L. Hillard, K. P. C. Vollhardt, *J. Am. Chem. Soc.* **1975**, *97*, 5600 – 5602; b) R. L. Funk, K. P. C. Vollhardt, *J. Am. Chem. Soc.* **1979**, *100*, 215 – 217; R. L. Funk, K. P. C. Vollhardt, *J. Am. Chem. Soc.* **1980**, *102*, 5253 – 5261.

[75] For other total syntheses of estrone using a Diels – Alder reaction, see a) J. Das, R. Kubela, G. A. MacAlpine, Z. Stojanac, Z. Valenta, *Can. J. Chem.* **1979**, *57*, 3308 – 3319; b) H. Nemoto, M. Nagai, M. Moizumi, K. Kohzuki, K. Fukumoto, T. Kametani, *J. Chem. Soc. Perkin Trans. 1* **1989**, 1639 – 1645; c) T. Doi, K. Shimizu, T. Takahashi, J. Tsuji, K. Yamamoto, *Tetrahedron Lett.* **1990**, *31*, 3313 – 3316; d) G. S. R. Subba Rao, D. K. Banerjee, L. U. Devi, U. Sheriff, *Aust. J. Chem.* **1992**, *45*, 187 – 203; e) S. Takano, M. Moriya, K. Ogasawara, *Tetrahedron Lett.* **1992**, *33*, 1909 – 1910; f) G. Quinkert, M. Del-Grosso, A. Doering, W. Doering, R. I. Schenkel, M. Bauch, G. T. Dambacher, J. W. Bats, G. Zimmerman, G. Duerner, *Helv. Chim. Acta.* **1995**, *78*, 1345 – 1391; M. E. Jung, K. M. Halweg, *Tetrahedron Lett.* **1984**, *25*, 2121 – 2124.

[76] For representative examples of *o*-quinodimethane chemistry from the Kametani group in the context of total synthesis, see a) T. Kametani, Y. Hirai, F. Satoh, K. Fukumoto, *J. Chem. Soc.* **1977**, 16 – 18; b) T. Kametani, M. Aizawa, H. Nemoto, *J. Chem. Soc. Perkin Trans. 1* **1980**, 2793 – 2796; c) T. Kametani, M. Tsubuki, H. Nemoto, K. Suzuki, *J. Am. Chem. Soc.* **1981**, *103*, 1256 – 1258; d) T. Kametani, T. Toya, K. Ueda, M. Tsubuki, T. Honda, *J. Chem. Soc. Perkin Trans. 1* **1988**, 2433 – 2438.

[77] a) H. Staudinger, German Patent 506,839; [*Chem. Abstr.* **1913**, *25*, 522]; b) H. Staudinger, B. Ritzenthaler, *Chem. Ber.* **1935**, *68B*, 455 – 471.

[78] For a review including dienes masked as sulfones in Diels – Alder reactions applied to natural product total synthesis, see A. Ichihara, *Synthesis* **1987**, 207 – 222.

[79] a) M. P. Cava, A. A. Deana, *J. Am. Chem. Soc.* **1959**, *81*, 4266 – 4268; b) M. P. Cava, M. J. Mitchell, A. A. Deana, *J. Org. Chem.* **1960**, *25*, 1481 – 1484.

[80] a) K. C. Nicolaou, W. E. Barnette, *J. Chem. Soc. Chem. Commun.* **1979**, 1119 – 1120; b) K. C. Nicolaou, W. E. Barnette, P. Ma, *J. Org. Chem.* **1980**, *45*, 1463 – 1470.

[81] For early work in this field, see N. C. Yang, C. Rivas, *J. Am. Chem. Soc.* **1961**, *83*, 2213.

[82] K. C. Nicolaou, D. Gray, *Angew. Chem.* **2001**, *113*, 783 – 785; *Angew. Chem. Int. Ed.* **2001**, *40*, 761 – 763.

[83] a) K. C. Nicolaou, D. Gray, J. Tae, *Angew. Chem.* **2001**, *113*, 3787 – 3790; *Angew. Chem. Int. Ed.* **2001**, *40*, 3675 – 3678; b) K. C. Nicolaou, D. Gray, J. Tae, *Angew. Chem.* **2001**, *113*, 3791 – 3795; *Angew. Chem. Int. Ed.* **2001**, *40*, 3679 – 3683.

[84] For further examples where either the diene or the dienophile is unveiled in situ, see a) H. Miyaoka, Y. Kajiwara, Y. Hara, Y. Yamada, *J. Org. Chem.* **2001**, *66*, 1429 – 1435; b) T. K. M. Shing, Q. Jiang, *J. Org. Chem.* **2000**, *65*, 7059 – 7069; c) E. Vedejs, R. J. Galante, P. G. Goekjian, *J. Am. Chem. Soc.* **1998**, *120*, 3613 – 3622.

[85] The Diels – Alder reaction can also be used as a vehicle to protect olefins over the course of several synthetic operations. For an illustrative example of this concept in total synthesis endeavors, using cyclopentadiene to protect a benzoquinone olefin, see P. Wipf, J.-K. Jung, *J. Org. Chem.* **2000**, *65*, 6319 – 6339.

[86] R. Robinson, *J. Chem. Soc.* **1917**, 762 – 768.

[87] a) W. S. Johnson, M. B. Gravestock, R. J. Parry, R. F. Myers, T. A. Bryson, D. H. Miles, *J. Am. Chem. Soc.* **1971**, *93*, 4330 – 4332; b) W. S. Johnson, M. B. Gravestock, B. E. McCarry, *J. Am. Chem. Soc.* **1971**, *93*, 4332 – 4334; c) M. B. Gravestock, W. S. Johnson, B. E. McCarry, R. J. Parry, B. E. Ratcliffe, *J. Am. Chem. Soc.* **1978**, *100*, 4274 – 4282.

[88] B. M. Trost, *Science* **1991**, *254*, 1471 – 1477.

[89] For a review of cascade-based sequences, including those incorporating the Diels – Alder reaction, see R. A. Bunce, *Tetrahedron* **1995**, *51*, 13103 – 13159.

[90] a) W. R. Roush, R. J. Sciotti, *J. Am. Chem. Soc.* **1994**, *116*, 6457 – 6458; b) W. R. Roush, R. J. Sciotti, *J. Am. Chem. Soc.* **1998**, *120*, 7411 – 7419.

[91] a) W. R. Roush, S. E. Hall, *J. Am. Chem. Soc.* **1981**, *103*, 5200 – 5211; b) W. R. Roush, M. Kageyama, R. Riva, B. B. Brown, J. S. Warmus, K. J. Moriarty, *J. Org. Chem.* **1991**, *56*, 1192 – 1210; c) W. R. Roush, R. J. Sciotti, *Tetrahedron Lett.* **1992**, *33*, 4691 – 4694.

[92] For another total synthesis of chlorothricolide using a Diels – Alder reaction, see K. Takedo, Y. Igarashi, K. Okazaki, E. Yoshii, K. Yamaguchi, *J. Org. Chem.* **1990**, *55*, 3431 – 3434.

[93] S. F. Martin, J. M. Humphrey, A. Ali, M. C. Hillier, *J. Am. Chem. Soc.* **1999**, *121*, 866 – 867. For earlier model studies by the Martin group toward manzamine A, see a) S. F. Martin, Y. Liao, Y. Wong, T. Rein, *Tetrahedron Lett.* **1994**, *35*, 691 – 694; b) S. F. Martin, H.-J. Chen, A. K. Courtney, Y. Liao, M. Patzel, M. N. Ramser, A. S. Wagman, *Tetrahedron* **1996**, *52*, 7251 – 7264.

[94] For another use of a tandem Stille/Diels – Alder strategy, see R. Skoda-Foeldes, G. Jeges, L. Kollar, J. Horvath, Z. Tuba, *J. Org. Chem.* **1997**, *62*, 1326 – 1332.

[95] A. Padwa, M. A. Brodney, M. Dimitroff, B. Liu, T. Wu, *J. Org. Chem.* **2001**, *66*, 3119 – 3123. For earlier studies, see A. Padwa, M. A. Brodney, M. Dimitroff, *J. Org. Chem.* **1998**, *63*, 5304 – 5305.

[96] For other total syntheses of dendrobine using a Diels – Alder reaction, see a) A. S. Kende, J. T. Bentley, R. A. Mader, D. Ridge, *J. Am. Chem. Soc.* **1974**, *96*, 4333 – 4334; b) W. R. Roush, *J. Am. Chem. Soc.* **1980**, *102*, 1390 – 1404; c) S. F. Martin, W. Li, *J. Org. Chem.* **1991**, *56*, 642 – 650.

[97] A. D. Brosius, L. E. Overman, L. Schwink, *J. Am. Chem. Soc.* **1999**, *121*, 700 – 709.

[98] a) H. W. Gschwend, *Helv. Chim. Acta* **1973**, *56*, 1763 – 1775; b) H. W. Gschwend, A. O. Lee, H.-P. Meier, *J. Org. Chem.* **1973**, *38*, 2169 – 2175.

[99] a) H. Nishiyama, T. Kitajima, M. Matsumoto, K. Itoh, *J. Org. Chem.* **1984**, *49*, 2298 – 2300; b) G. Stork, M. Kahn, *J. Am. Chem. Soc.* **1985**, *107*, 500 – 501.

[100] For reviews on the use of silicon tethers for intramolecular reactions, see a) D. Gauthier, K. S. Zandi, K. J. Shea, *Tetrahedron* **1998**, *54*, 2289 – 2338; b) L. Fensterbank, M. Malacria, S. M. Sieburth, *Synthesis* **1997**, 813 – 854; c) M. Bols, T. Skrydstrup, *Chem. Rev.* **1995**, *95*, 1253 – 1277.

[101] E. J. Corey, M. Petrzilka, *Tetrahedron Lett.* **1975**, *16*, 2537 – 2540.

[102] G. Stork, E. Nakamura, *J. Am. Chem. Soc.* **1983**, *105*, 5510 – 5512.

[103] For a review of cytochalasin syntheses, see E. J. Thomas, *Acc. Chem. Res.* **1991**, *24*, 229 – 235. For representative total syntheses using a Diels – Alder reaction, see a) E. Vedejs, J. G. Reid, *J. Am. Chem. Soc.* **1984**, *106*, 4617 – 4618; b) E. J. Thomas, J. W. F. Whitehead, *J. Chem. Soc. Perkin Trans. 1* **1989**, 507 – 518; c) M. Y. Kim, J. E. Starrett, S. M. Weinreb, *J. Org. Chem.* **1981**, *46*, 5383 – 5389.

[104] J. A. McCauley, K. Nagasawa, P. A. Lander, S. G. Mischke, M. A. Semones, Y. Kishi, *J. Am. Chem. Soc.* **1998**, *120*, 7647 – 7648.

[105] a) K. C. Nicolaou, Z. Yang, J.-J. Liu, H. Ueno, P. G. Nantermet, R. K. Guy, C. F. Claiborne, J. Renaud, E. A. Couladouros, K. Paulvannan, E. J. Sorensen, *Nature* **1994**, *367*, 630 – 634; b) K. C. Nicolaou, P. G. Nantermet, H. Ueno, R. K. Guy, E. A. Couladouros, E. J. Sorensen, *J. Am. Chem. Soc.* **1995**, *117*, 624 – 633; c) K. C. Nicolaou, J.-J. Liu, Z. Yang, H. Ueno, E. J. Sorensen, C. F. Claiborne, R. K. Guy, C.-K. Hwang, M. Nakada, P. G. Nantermet, *J. Am. Chem. Soc.* **1995**, *117*, 634 – 644; d) K. C. Nicolaou, Z. Yang, J.-J. Liu, P. G. Nantermet, C. F. Claiborne, J. Renaud, R. K. Guy, K. Shibayama, *J. Am. Chem. Soc.* **1995**, *117*, 645 – 652; e) K. C. Nicolaou, H. Ueno, J.-J. Liu, P. G. Nantermet, Z. Yang, J. Renaud, K. Paulvannan, R. Chadha, *J. Am. Chem. Soc.* **1995**, *117*, 653 – 659.

[106] K. Narasaka, S. Shimada, K. Osoda, N. Iwasawa, *Synthesis* **1991**, 1171 – 1172.

[107] K. C. Nicolaou, J. J. Liu, C.-K. Hwang, W.-M. Dai, R. K. Guy, *J. Chem. Soc. Chem. Commun.* **1992**, 1118 – 1120.

[108] K. C. Nicolaou, C.-K. Hwang, E. J. Sorensen, C. F. Claiborne, *J. Chem. Soc. Chem. Commun.* **1992**, 1117 – 1118.

[109] For a review of ketene equivalents in [4+2] cycloadditions, see V. K. Aggarwal, A. Amjad, M. P. Coogan, *Tetrahedron* **1999**, *55*, 293 – 312.

[110] a) H. S. Sutherland, F. E. S. Souza, R. G. A. Rodrigo, *J. Org. Chem.* **2001**, *66*, 3639 – 3641; b) R. Carlini, K. Higgs, C. Older, S. Randhawa, R. Rodrigo, *J. Org. Chem.* **1997**, *62*, 2330 – 2331.

[111] For another total synthesis of halenaquinone using a Diels – Alder reaction, see N. Harada, T. Sugioka, Y. Ando, H. Uda, T. Kuriki, *J. Am. Chem. Soc.* **1988**, *110*, 8483 – 8487.

[112] O. Diels, K. Alder, E. Naujoks, *Ber. Dtsch. Chem. Ges. B* **1929**, *62*, 554 – 562.

[113] For a general commentary on these issues, see a) T. L. Gilchrist, *Heterocyclic Chemistry*, 3rd ed., Longman, London, **1992**, pp. 193 – 230; b) J. A. Joule, K. Mills, *Heterocyclic Chemistry*, 4th ed., Blackwell Science, Oxford, **2000**, pp. 233 – 314.

[114] J. Taunton, J. L. Wood, S. L. Schreiber, *J. Am. Chem. Soc.* **1993**, *115*, 10378 – 10379, and references cited therein.

[115] For a recent review of transannular Diels – Alder reactions, see E. Marsault, A. Toro, P. Nowak, P. Deslongchamps, *Tetrahedron* **2001**, *57*, 4243 – 4260.

[116] A. G. Myers, M. E. Fraley, N. J. Tom, S. B. Cohen, D. J. Madar, *Chem. Biol.* **1995**, *2*, 33 – 43.

[117] M. D. Shair, T. Y. Yoon, K. K. Mosny, T. C. Chou, S. J. Danishefsky, *J. Am. Chem. Soc.* **1996**, *118*, 9509 – 9525.

[118] Y. Tamura, F. Fukata, M. Sasho, T. Tsugoshi, Y. Kita, *J. Org. Chem.* **1985**, *50*, 2273 – 2277.

[119] For insightful reviews on this subject, see a) G. Pohnert, *ChemBioChem* **2001**, *2*, 873 – 875; b) S. Laschat, *Angew. Chem.* **1996**, *108*, 313 – 315; *Angew. Chem. Int. Ed. Engl.* **1996**, *35*, 289 – 291.

[120] a) D. Hilvert, K. W. Hill, K. D. Nared, M. T. M. Auditor, *J. Am. Chem. Soc.* **1989**, *111*, 9261 – 9262; b) V. E. Governeur, K. N. Houk, B. de Pascual-Teresa, B. Beno, K. D. Janda, R. A. Lerner, *Science* **1993**, *262*, 204 – 208; c) J. T. Yli-Kauhaluoma, J. A. Ashley, C.-H. Lo, L. Tucker, M. M. Wolfe, K. D. Janda, *J. Am. Chem. Soc.* **1995**, *117*, 7041 – 7047; d) F. E. Romesberg, B. Spiller, P. G. Schultz, R. C. Stevens, *Science* **1998**, *279*, 1929 – 1933; e) A. Heine, E. A. Stura, J. T. Yli-Kauhaluoma, C. Gao, Q. Deng, B. R. Beno, K. N. Houk, K. D. Janda, I. A. Wilson, *Science* **1998**, *279*, 1934 – 1940; f) J. Xu, Q. Deng, J. Chen, K. N. Houk, J. Bartek, D. Hilvert, I. A. Wilson, *Science* **1999**, *286*, 2345 – 2348.

[121] a) K. N. Morris, T. M. Tarasow, C. M. Julin, S. L. Simons, D. Hilvert, L. Gold, *Proc. Natl. Acad. Sci. USA* **1994**, *91*, 13028 – 13032; b) B.

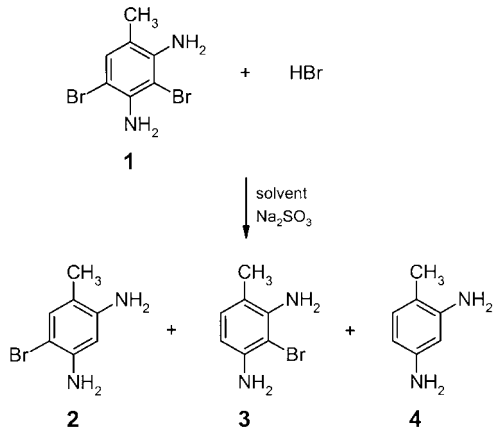
Seelig, A. Jäschke, *Chem. Biol.* **1999**, *6*, 167 – 176; c) T. M. Tarasow, S. L. Tarasow, B. E. Eaton, *J. Am. Chem. Soc.* **2000**, *122*, 1015 – 1021.
[122] For a persuasive report on the isolation of a true Diels – Alderase, see K. Auclair, A. Sutherland, J. Kennedy, D. J. Witter, J. P. Van den Heever, C. R. Hutchinson, J. C. Vederas, *J. Am. Chem. Soc.* **2000**, *122*, 11519 – 11520.
[123] For an example of this concept, see H. Oikawa, T. Kobayashi, K. Katayama, Y. Suzuki, A. Ichihara, *J. Org. Chem.* **1998**, *63*, 8748 – 8756.
[124] a) W. M. Bandaranayake, J. E. Banfield, D. St. C. Black, G. D. Fallon, B. M. Gatehouse, *J. Chem. Soc. Chem. Commun.* **1980**, 162 – 163; b) W. M. Bandaranayake, J. E. Banfield, D. St. C. Black, *J. Chem. Soc. Chem. Commun.* **1980**, 902 – 903; c) W. M. Bandaranayake, J. E. Banfield, D. St. C. Black, G. D. Fallon, B. M. Gatehouse, *Aust. J. Chem*. **1981**, *34*, 1655 – 1667; d) c) W. M. Bandaranayake, J. E. Banfield, D. St. C. Black, *Aust. J. Chem.* **1982**, *35*, 557 – 565; e) c) W. M. Bandaranayake, J. E. Banfield, D. St. C. Black, G. D. Fallon, B. M. Gatehouse, *Aust. J. Chem.* **1982**, *35*, 567 – 579; f) J. E. Banfield, D. St. C. Black, S. R. Johns, R. I. Williams, *Aust. J. Chem.* **1982**, *35*, 2247 – 2256.
[125] a) K. C. Nicolaou, R. E. Zipkin, N. A. Petasis, J. Uenishi, *J. Am. Chem. Soc.* **1982**, *104*, 5555 – 5557; b) K. C. Nicolaou, N. A. Petasis, J. Uenishi, R. E. Zipkin, *J. Am. Chem. Soc.* **1982**, *104*, 5557 – 5558; c) K. C. Nicolaou, N. A. Petasis, R. E. Zipkin, *J. Am. Chem. Soc.* **1982**, *104*, 5558 – 5560; d) K. C. Nicolaou, N. A. Petasis, R. E. Zipkin, *J. Am. Chem. Soc.* **1982**, *104*, 5560 – 5562.
[126] N. Abe, T. Murata, A. Hirota, *Biosci. Biotechnol. Biochem.* **1998**, *62*, 2120 – 2126.
[127] a) K. C. Nicolaou, K. B. Simonsen, G. Vassilikogiannakis, P. S. Baran, V. P. Vidali, E. N. Pitsinos, E. A. Couladouros, *Angew. Chem.* **1999**, *111*, 3762 – 3766; *Angew. Chem. Int. Ed.* **1999**, *38*, 3555 – 3559; b) K. C. Nicolaou, G. Vassilikogiannakis, K. B. Simonsen, P. S. Baran, Y.-L. Zhong, V. P. Vidali, E. N. Pitsinos, E. A. Couladouros, *J. Am. Chem. Soc.* **2000**, *122*, 3071 – 3079.
[128] N. Abe, O. Sugimoto, K. Tanji, A. Hirota, *J. Am. Chem. Soc.* **2000**, *122*, 12606 – 12607.
[129] K. C. Nicolaou, J. Li, *Angew. Chem.* **2001**, *113*, 4394 – 4398; *Angew. Chem. Int. Ed.* **2001**, *40*, 4264 – 4268.
[130] A. J. Quillinan, F. Scheinmann, *J. Chem. Soc. (D)* **1971**, 966 – 967.
[131] M. E. Layton, C. A. Morales, M. D. Shair, *J. Am. Chem. Soc.* **2002**, *124*, 773 – 775.
[132] a) X. Fu, M. B. Hossain, F. J. Schmitz, D. van der Helm, *J. Org. Chem.* **1997**, *62*, 3810 – 3819; b) X. Fu, M. B. Hossain, D. van der Helm, F. J. Schmitz, *J. Am. Chem. Soc.* **1994**, *116*, 12125 – 12126.
[133] D. A. Vosburg, C. D. Vanderwal, E. J. Sorensen, *J. Am. Chem. Soc.* **2002**, *124*, ASAP.
[134] For additional excellent examples of biomimetic syntheses based on Diels – Alder reactions, see a) L. F. Tietze, J. Bachmann, J. Wichmann, O. Burkhardt, *Synthesis* **1994**, 1185 – 1194; b) N. Kato, X. Wu, H. Nishikawa, K. Nakanishi, H. Takeshita, *J. Chem. Soc. Perkin Trans. 1* **1994**, 1047 – 1053; c) S. F. Martin, C. W. Clark, M. Ito, M. Mortimore, *J. Am. Chem. Soc.* **1996**, *118*, 9804 – 9805; d) R. M. Williams, J. F. Sanz-Cervera, F. Sancenón, J. A. Marco, K. Halligan, *J. Am. Chem. Soc.* **1998**, *120*, 1090 – 1091; e) J. E. Baldwin, T. D. W. Claridge, A. J. Culshaw, F. A. Heupel, V. Lee, D. R. Spring, R. C. Whitehead, *Chem. Eur. J.* **1999**, *5*, 3154 – 3161; f) C. Li, E. Lobkovsky, J. A. Porco, *J. Am. Chem. Soc.* **2000**, *122*, 10484 – 10485.
[135] *The Diels – Alder Reaction: Selected Practical Methods* (Eds.: F. Fringuelli, A. Taticchi), Wiley, New York, **2002**.

How Attractive is Bromine as a Protecting Group in Aromatic Chemistry?

Franz Effenberger*

The bromination of aromatic systems belongs to the best investigated reactions in organic chemistry. Kekulé had already concluded from the bromination of bromobenzene, which yielded only three and not four isomeric dibromobenzenes, that fast fluctuating double bonds were present in benzene rings. The bromination of aromatic compounds in both the laboratory and industry is straightforward: the bromoarenes expected from substitution rules can be readily obtained in good yields under common bromination conditions. Hence bromination is regarded as being irreversible. Similar investigations that previously confirmed that alkylation and sulfonation are reversible have attracted little attention up to now regarding the reversibility of the halogenation[1] and acylation[2] of aromatic compounds.

In a recent publication[3] Choi and Chi reported on interesting synthetic applications based on the reversibility of arene bromination. The authors describe in particular two aspects of the reversibility in an application: first, the possibility of a selective protodebromination in the presence of a "scavenger" of bromine, for example, sodium sulfite (Scheme 1), and second, the utilization of bromine as a protecting group in reactions of aromatic compounds (Scheme 2).

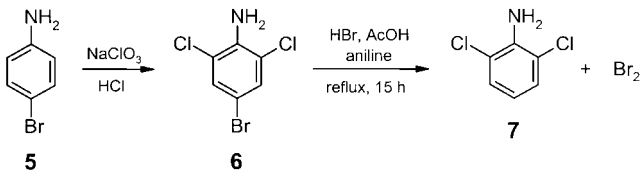


Scheme 1. Protodebromination of aromatic systems using HBr in the presence of Na_2SO_3 as a scavenger of bromine.

The protodebromination of **1**, for example, which proceeds with total yields of greater than 90%, gives the completely dehalogenated compound **4** at longer reaction times. Of the primarily formed monobrominated products **2** and **3** which are obtained at shorter reaction times, **3** reacts more rapidly than **2** to give **4**. Thus, compound **2**, as well as the already formed **4**, is selectively accessible.

The stabilities of the intermediate σ complexes are decisive in the rates of bromine elimination in these protodebrominations, which represent the back reaction of the electrophilic aromatic bromination; that is, the known rules of electrophilic aromatic substitution are also valid for the selectivity of bromine elimination. Thus, as expected, 2,3,4,6-tetrabromoaniline was protodebrominated exclusively to yield 3-bromoaniline as a stable end product.[3]

A prerequisite for the application of bromine as a protecting group in arene reactions as proposed by Choi and Chi[3] is the removal of cationic bromine from the primarily formed σ complexes. An example of bromine being used as a protecting group is given by the preparation of 2,6-dichloroaniline (Scheme 2),[3] which is generally synthesized from



Scheme 2. Utilization of bromine as a protecting group in the selective preparation of substituted aromatic compounds.

4-aminobenzoic acid by dichlorination followed by decarboxylation.[4] It would be particularly advantageous for the application of bromine as a protecting group if the eliminated bromine could be transferred to the scavenger to reform the starting compound, for example, **5**. This possibility is not mentioned by the authors.

The use of bromine as a protecting group in arene chemistry instead of SO_3H, NO_2, COOH, or *tert*-butyl is an interesting alternative for the selective preparation of specially substituted aromatic compounds. The advantages of bromine as a protecting group are:

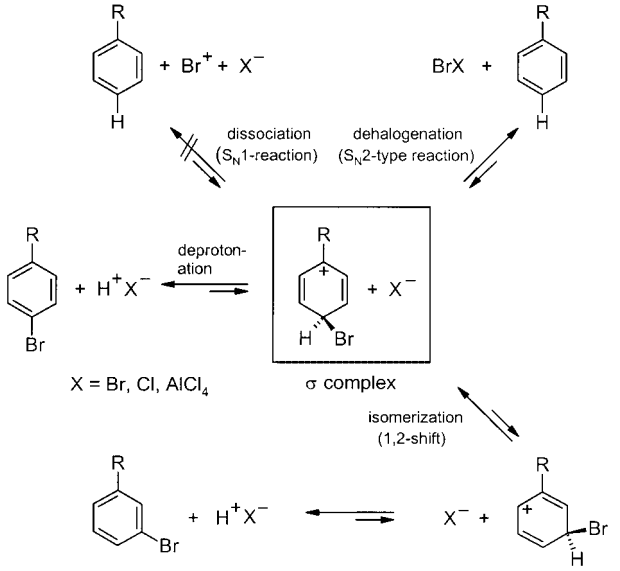
- One or more bromo substituents can be introduced in aromatic compounds without problems.

[*] Prof. Dr. F. Effenberger
Institut für Organische Chemie
Universität Stuttgart
Pfaffenwaldring 55, 70569 Stuttgart (Germany)
Fax: (+49) 711-685-4269
E-mail: franz.effenberger@po.uni-stuttgart.de

 © WILEY-VCH Verlag GmbH, 69451 Weinheim, Germany, 2002 1433-7851/02/4110-1699 $ 20.00+.50/0

- The lower deactivating effect of bromine in contrast to other typically used protecting groups (SO_3H, NO_2, COOH) enables the more facile electrophilic introduction of additional substituents.
- Debromination occurs under typical electrophilic conditions, and hence it is also applicable in the presence of acceptor groups, which is not the case in the commonly applied reductive debrominations.

The reversibility of electrophilic arene bromination has been reported in earlier publications,[5, 6] however, the application of bromine as a protecting group was not indicated in these papers. In the following text, all the important experimental results[3, 5, 6] obtained using bromine as a protecting group in aromatic chemistry are interpreted mechanistically (Scheme 3).



Scheme 3. Possible follow-up reactions of aromatic bromo–σ complexes.

In the examples described so far, reversibility was only observed in the bromination of activated aromatic compounds such as phenols (R = OH) or aminobenzenes (R = NH_2). Hence, the bromoarene must be as electron-rich as these compounds since protonation of the σ complex occurs to a sufficient extent. Consequently, bromine is removed selectively in the position *ortho* or *para*, respectively, to the electron-donating groups OH or NH_2, whereas bromine in a *meta* position is unaffected (see the preparation of 3-bromoaniline from tetrabromoaniline).[3]

While the influence of the substituent R on the protonation step is generally known, this is not the case for the decisive influence the anion X^- has on follow-up reactions of the bromo–σ complexes. Besides deprotonation, an aromatic σ complex can in principle react by 1) dissociation by a S_N1 reaction, 2) nucleophilic removal of the introduced electrophile by anion attack ("S_N2-type"), and 3) isomerization (Scheme 3).

Whereas a dissociation (S_N1-type) can be excluded for bromo–σ complexes because of the instability of bromo cations, the elimination of isopropyl, *tert*-butyl, or sulfonic acid protecting groups follows this mechanism. An elimination of bromine by nucleophiles (S_N2-type reaction) strongly depends on the nucleophilicity of the anion X^- ($Br^- > Cl^- \gg AlCl_4^-$). Therefore, removal of bromine is either not observed[3] or markedly suppressed[5, 6] by replacing HBr by HCl. Bromine is not removed at all with extremely weak nucleophiles (for example, $AlCl_4^-$), but an intramolecular 1,2-shift (isomerization) occurs. Although isomerization of halogenated aromatic and heteroaromatic compounds, via cationic σ complexes could be of great synthetic potential, very little is known about this reaction. On the contrary, the isomerization of methyl–σ complexes is not only well-known but is also applied in a technical process. Thus, the methylation of toluene with $AlCl_3$ as a catalyst ($X^- = AlCl_4^-$) at lower temperature affords mainly *ortho*- and *para*-xylene, at higher temperature the kinetically more stable *meta*-xylene is formed exclusively.

The potential of bromine as a versatile protecting group in aromatic chemistry can impressively be demonstrated, for example, in the preparation of 3-bromothiophene, an important building block for many pharmaceuticals. The synthesis of 3-bromothiophene is almost exclusively described by reductive dehalogenation of 2,3,5-tribromothiophene. A very efficient alternative route to 3-bromothiophene described recently is by an isomerization (Scheme 3) of the readily available 2-bromothiophene by means of Fe^{III}-covered zeolites.[7] The protodebromination developed by Choi and Chi should prove to be an interesting alternative to the reductive dehalogenation.

This short overview on the fundamentals of the reversibility of electrophilic aromatic bromination achieves its objective if it motivates researchers to apply this very useful method to a greater extent in preparative aromatic chemistry.

[1] a) R. O. C. Norman, R. Taylor, *Electrophilic Substitution in Benzenoid Compounds*, Elsevier, Amsterdam, **1965**, p. 57; b) H. J. Shine, *Aromatic Rearrangements*, Elsevier, Amsterdam, **1967**, p. 32; c) Y. G. Erykalov, A. P. Belokurova, I. S. Isaev, V. A. Koptyug, *Zh. Org. Khim.* **1973**, *9*, 343–347 [*Chem. Abstr.* **1973**, *78*, 124161h].

[2] a) D. E. Pearson, C. A. Buehler, *Synthesis* **1971**, 455–477; b) P. H. Gore, *Chem. Ind. (London)* **1974**, 727–731; c) F. Effenberger, H. Klenk, P. L. Reiter, *Angew. Chem.* **1973**, *85*, 819–820; *Angew. Chem. Int. Ed. Engl.* **1973**, *12*, 775–776.

[3] H. Y. Choi, D. Y. Chi, *J. Am. Chem. Soc.* **2001**, *123*, 9202–9203.

[4] a) S. Yasui, K. Nakamura, M. Fujii, A. Ohno, *J. Org. Chem.* **1985**, *50*, 3283–3287; b) A. Zask, P. Helquist, *J. Org. Chem.* **1978**, *43*, 1619–1620; c) D. Bryce-Smith, B. J. Wakefield, *Org. Synth. Coll. Vol.* **1973**, *5*, 998–1001.

[5] E. J. O'Bara, R. B. Balsley, I. Starer, *J. Org. Chem.* **1970**, *35*, 16–19.

[6] a) F. Effenberger, P. Menzel, *Angew. Chem.* **1971**, *83*, 535–536; *Angew. Chem. Int. Ed. Engl.* **1971**, *10*, 493–494; b) F. Effenberger, P. Menzel, *Chem. Ber.* **1977**, *110*, 1342–1355.

[7] a) U. Dettmeier, K. Eichler, K. Kühlein, E. I. Leupold, H. Litterer, *Angew. Chem.* **1987**, *99*, 470–471; *Angew. Chem. Int. Ed. Engl.* **1987**, *26*, 468–469; b) H. M. Gilow, D. E. Burton, *J. Org. Chem.* **1981**, *46*, 2221–2225.

 © WILEY-VCH Verlag GmbH, 69451 Weinheim, Germany, 2002 1433-7851/02/4110-1700 $ 20.00+.50/0

Na_3N—An Original Synthetic Route for a Long Sought After Binary Nitride

Rainer Niewa*

Binary compounds and the binary phase diagrams of metals and nonmetals have been investigated thoroughly since the infancy of modern chemistry, metallography, and materials science. Still, in the last couple of years, a number of new binary compounds were reported, these new phases being mainly compounds of nitrogen. A common feature of these binary nitrides is that all were prepared using new or so far seldom used synthetic techniques. For example, the compound FeN was introduced into the iron–nitrogen phase diagram only few years ago. FeN was prepared by reactive sputtering of iron in an Ar/N_2 atmosphere.[1] Sn_3N_4 forms from SnI_4 with KNH_2 in liquid ammonia, followed by careful annealing at 300 °C.[2] The pressure-homologues rule connects the spinel with the recently reported high-pressure phases γ-Si_3N_4[3] and γ-Ge_3N_4,[4] produced by high-pressure high-temperature syntheses in laser-heated diamond anvil cells or multi-anvil arrangements. Binary nitrides of phosphorus have been known since the 19th Century,[5] but only in the middle of the 1990s were α- and β-P_3N_5 prepared (from a molecular precusor) in crystalline form and structurally characterized.[6] A high-pressure phase γ-P_3N_5 was prepared from a high-pressure high-temperature synthesis in a multi-anvil arrangement.[7] The diazenides (or pernitrides) $SrN{=}Sr_4[N]_2[N_2]$, $Sr[N_2]$,[8] and $Ba[N_2]$[9] were obtained for the first time under high nitrogen-gas-pressures of 400 bar to 5500 bar, while the barium compound apparently also can be prepared under low pressure by careful decomposition of barium azide. The diazenides can be considered as analogues of the peroxides and thus, together with the long-known azide ions, link the series to the polynitrogen compounds and ions, such as N_4[10] and N_5^+ (which was stabilized with the anion of a super acid, $N_5^+AsF_6^-$).[11]

From the alkali-metal nitrides only Li_3N was well characterized. Even at room temperature, Li_3N slowly forms from the elements and was studied intensively as a result of its potential application as a fast lithium ionic conductor.[12] The crystal structure of α-Li_3N was described as early as 1935:[13] it consists of parallel infinite chains $^1_\infty[LiN_{2/2}{}^{2-}]$, arranged in a hexagonal-rod packing motif. These chains are connected by further lithium atoms, which leads to a hexagonal-bipyramidal coordination of the nitrogen atoms (Figure 1a). This arrangement results in a low space filling and thus, it is not surprising, that two high-pressure polymorphs were described to date.[14]

The previous reports on the binary nitrides of the heavier alkali metals, on the other hand, seem doubtful. First hints of the formation of K_3N from the thermal decomposition of KNH_2 date back to the classical work on the isolation of alkali metals by Davy as well as Gay-Lussac and Thénard, performed at the beginning of the 19th Century.[15] Zehnder reported the formation of compounds from sodium and nitrogen after the activation of the elements by electric discharge, however, he suspected that the product obtained was sodium azide rather than sodium nitride.[16] In the following decades of the beginning 20th Century a lengthy dispute started, as to whether the obtained moisture-sensitive products contain a binary nitride. Most of the experimentalists tried to activate the nitrogen with electric discharges, but also reactions in the presence of iron as a catalyst, the decomposition of the azides, or the reaction of alkali-metal amalgams with nitrogen were investigated.[17] Typically, the argument for a successful formation of the nitride was the reaction of aqueous solutions of the reaction products with Neßlers reagent, but the possibility of a reduction of azide ions by hydrogen (from excess alkali metal and water) to ammonia could not be completely excluded. In summary, the reports of the successful preparation of binary nitrides of the heavier alkali metals Na, K, and Cs by any of these ways could never be reproduced without any doubt.

In this issue of *Angewandte Chemie* Fischer and Jansen finally report the successful preparation of Na_3N by an original synthetic route:[18] within a vacuum chamber the elements were transferred to the gas phase in an atomic state. The components were simultaneously deposited on a cooled substrate. In this way an optimal mixing of the components in the solid state was obtained. On heating to room temperature, apparently crystalline Na_3N formed, which is extremely moisture sensitive. The derived crystal structure of the anti-ReO_3 type has a surprisingly low space filling (Figure 1b). The seemingly unusual linear coordination of sodium by nitrogen can be found analogously in the crystal structure of α-Li_3N, in which one third of the lithium atoms are linearly coordinated by nitrogen atoms. The decreasing coordination number of nitrogen from eight in α-Li_3N to six in Na_3N in the anti-ReO_3 type is reasonable, since sodium has a larger radius than lithium.

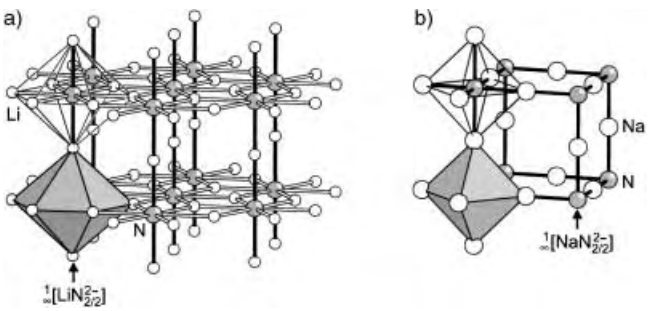


Figure 1. Sections of the crystal structures of a) α-Li_3N with parallel, one-dimensional infinite chains $^1_\infty[LiN_{2/2}{}^{2-}]$ and nitrogen atoms in hexagonal-bipyramidal coordination and b) Na_3N (anti-ReO_3 structure type) with nitrogen atoms in octahedral coordination and one-dimensional infinite chains $^1_\infty[NaN_{2/2}{}^{2-}]$ in all three directions.

[*] Dr. R. Niewa
Max-Planck-Institut für Chemische Physik fester Stoffe
Nöthnitzer Strasse 40
01187 Dresden (Germany)
Fax: (+49) 351-4646-3002
E-mail: niewa@cpfs.mpg.de

 © WILEY-VCH Verlag GmbH, 69451 Weinheim, Germany, 2002 1433-7851/02/4110-1701 $ 20.00+.50/0

Jansen and co-workers have been involved in the prediction of the crystal structures of the binary alkali-metal nitrides for some time.[19] Interestingly, in the course of these studies the anti-ReO_3 type for the nitrides of Na, K, Rb, and Cs was not considered. From that fact it can be taken, that this structure type was not to be expected for Na_3N. Taking the synthetic conditions into account, one has to assume metastability for the obtained form of Na_3N. Since Na_3N was prepared only as a film on a sapphire substrate and since it is extremely moisture sensitive, no physical properties were determined so far. Surely, interesting results are to be expected.

With the synthetic technique presented by Fischer and Jansen it might be feasible to prepare the binary nitrides of K, Rb, and Cs, too. With the development of new synthetic routes further new (especially metastable) compounds of nitrogen might be expected in the near future. Such new compounds will inevitably have surprising structural chemistry and physical properties and, thus, provide new impulses in solid-state chemistry.

[1] K. Suzuki, H. Morita, T. Kaneko, H. Yoshida, H. Fujimori, *J. Alloys Compd.* **1993**, *201*, 11 – 16.
[2] N. Scotti, W. Kockelmann, J. Senker, S. Traßel, H. Jacobs, *Z. Anorg. Allg. Chem*. **1999**, *625*, 1435 – 1439.
[3] A. Zerr, G. Miehe, G. Serghiou, M. Schwarz, E. Kroke, R. Riedel, H. Fueß, P. Kroll, R. Boehler, *Nature* **1999**, *400*, 340 – 342.
[4] K. Leinenweber, M. O'Keeffe, M. Somayazulu, H. Hubert, P. F. McMillan, G. H. Wolf, *Chem. Eur. J.* **1999**, *5*, 3067 – 3078.
[5] F. Briegleb, A. Geuther, *Liebigs Ann.* **1862**, *123*, 228 – 241.
[6] W. Schnick, J. Lücke, F. Krumeich, *Chem. Mater*. **1996**, *8*, 281 – 286.
[7] K. Landskron, H. Huppertz, J. Senker, W. Schnick, *Angew. Chem*. **2001**, *113*, 2713 – 2716; *Angew. Chem. Int. Ed.* **2001**, *40*, 2643 – 2645.
[8] G. Auffermann, Yu. Prots, R. Kniep, *Angew. Chem*. **2001**, *113*, 565 – 567; *Angew. Chem. Int. Ed.* **2001**, *40*, 547 – 549.
[9] G. V. Vajenine, G. Auffermann, Yu. Prots, W. Schnelle, R. K. Kremer, A. Simon, R. Kniep, *Inorg. Chem.* **2001**, *40*, 4866 – 4870.
[10] F. Cacace, G. de Petris, A. Troiani, *Science* **2002**, *295*, 480 – 481.
[11] K. O. Christe, W. Wilson, J. A. Sheehy, J. A. Boatz, *Angew. Chem*. **1999**, *111*, 2112 – 2118; *Angew. Chem. Int. Ed.* **1999**, *38*, 2004 – 2009.
[12] A. Rabenau, *Solid State Ionics* **1982**, *6*, 277 – 293.
[13] E. Zintl, G. Brauer, *Z. Elektrochem*. **1935**, *41*, 102 – 107; A. Rabenau, H. Schulz, *J. Less-Common Met*. **1976**, *50*, 155 – 159.
[14] H. J. Beister, S. Haag, R. Kniep, K. Strößner, K. Syassen, *Angew. Chem*. **1988**, *100*, 1116 – 1118; *Angew. Chem. Int. Ed. Engl.* **1988**, *27*, 1101 – 1103.
[15] H. Davy, *Philos. Trans. R. Soc. London* **1809**, *40*, 150 – 157; J. L. Gay-Lussac, L.-J. Thénard, *Rech. Phys. Chim.* **1811**, *I*, 337 – 342.
[16] L. Zehnder, *Ann. Phys.* **1894**, *52*, 56 – 66.
[17] F. Fischer, F. Schröter, *Chem. Ber.* **1910**, *43*, 1465 – 1480; R. J. Strutt, *Proc. R. Soc. London Ser. A* **1913**, *88*, 539 – 549; R. Suhrmann, K. Clusius, *Z. Anorg. Allg. Chem*. **1926**, *152*, 52 – 58; W. Moldenhauer, H. Möttig, *Chem. Ber*. **1929**, *62*, 1954 – 1959; H. Wattenberg, *Ber. Dtsch. Chem. Ges.* **1930**, *63*, 1667 – 1672; E. Tiede, H.-G. Knoblauch, *Chem. Ber*. **1935**, *68*, 1149 – 1154.
[18] D. Fischer, M. Jansen, *Angew. Chem*. **2002**, *114*, 1831 – 1833; *Angew. Chem. Int. Ed.* **2002**, *41*, 1755 – 1756.
[19] M. Jansen, J. C. Schön, *Z. Anorg. Allg. Chem*. **1998**, *624*, 533 – 540; J. C. Schön, M. A. C. Wevers, M. Jansen, *J. Mater. Chem*. **2001**, *11*, 69 – 77.

Oligomerization of p53 upon Cooperative DNA Binding: Towards a Structural Understanding of p53 Function

Patrick Chene and Wolfgang Jahnke*

P53 is one of the most important gene products involved in cancer suppression, and has concomitantly been an interesting target for oncology research.[1] Despite its high pharmaceutical relevance, one of the basic biological principles of p53, its activation from a latent state to an active DNA-binding state, is still unclear. A recent paper now sheds light on some of the structural features associated with p53 activation and DNA binding.[2] The p53 protein is present in nonstressed cells in a latent form and at very low concentration. However, under different stress conditions—such as DNA damage, oncogene activation, hypoxia, or ribonucleotide depletion—it accumulates in the cell and is activated.[3] The activation of the p53 protein leads either to arrest of the cell cycle or to apoptosis.[4] The outcome of p53 activation, which is cell-type and/or stress dependent, prevents the damaged cells from dividing: p53 is a tumour-suppressor gene. Several lines of evidence show that the deletion or the mutation of the p53 gene favors development of cancer: mice homozygotes with inactivated p53 allele are highly sensitive to tumors,[5] p53 is mutated in about 50% of the human cancers,[6] and p53 germline mutations are associated with the Li – Fraumeni syndrome.[7]

Although part of the p53 activity is mediated by protein – protein interactions, much of it is linked to its ability to bind to DNA and to regulate the transcription of several genes. P53 is a transcription factor and, like other transcription factors, contains several domains: a transactivation and proline-rich domain (residues 1 – 43 and 61 – 94, respectively) at the N-terminus; a DNA-binding domain in the middle of the protein (residues 110 – 286); and a tetramerization domain (residues 326 – 355) and a regulatory region (residues 363 – 393) at the C-terminus of the protein. While no structure of full-length p53 is known, structures have been determined for the individual domains by X-ray structure analysis or NMR spectroscopy (Figure 1). In particular, the determination of

[*] Dr. W. Jahnke, Dr. P. Chene
Novartis Pharma AG
Lichtstrasse, 4002 Basel (Switzerland)
Fax: (+41) 61-324-2686
E-mail: wolfgang.jahnke@pharma.novartis.com

 © WILEY-VCH Verlag GmbH, 69451 Weinheim, Germany, 2002 1433-7851/02/4110-1702 $ 20.00+.50/0

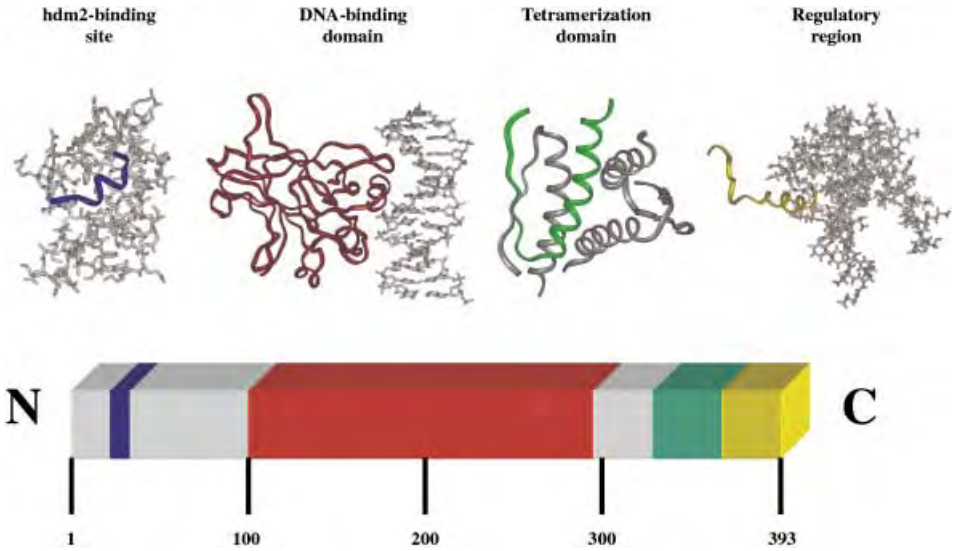


Figure 1. The domains of p53 and sketches of the experimental structures available for the individual domains. The structures of the binding partners are displayed in gray.

the three-dimensional structure of a p53–DNA complex has been a key step in the understanding of the interaction between p53 and DNA.[8] P53 binds to DNA through its central DNA binding domain to consensus DNA-binding sequences, which contain two copies of the 10-base pair motif 5′-Pu · Pu · Pu · C · (A/T) · (T/A) · G · Py · Py · Py-3′ (Pu = A/G, Py = T/C), which can be separated by up to 13 bases.[9] The internal symmetry of each ten-base pair motif made up of two oppositely oriented half-sites suggests that p53 binds to DNA as a tetramer, and indeed p53 exists as a tetramer in solution. The vast majority of p53 mutations occur in the DNA-binding domain.[6] The knowledge of its structure at least in the monomeric form together with an analysis of the thermodynamic stability of different p53 mutants[10] provide a framework for understanding the effect of these mutations on p53 activity. The mutations target either residues involved in the maintenance of the structure of the DNA-binding domain and/or residues that directly contact DNA. In all cases these mutations abolish DNA binding and therefore inactivate the p53 protein.

Two burning questions remain to understand the function of p53 on a molecular level: How is p53 activated from a latent to an active state, and what is the molecular arrangement of individual p53 subunits and p53 domains in the full-length tetrameric p53–DNA complex? Several lines of evidence have shown that the p53 protein exists in a latent conformation where it does not bind to DNA in a sequence-specific manner and in an active conformation where it does.[11] The finding that the shift between both conformations is mediated by activators acting either at its N- or its C-terminus led to the concept of an allosteric regulation of p53 activity.[12] This model assumes the hypothesis that in the latent conformation an interaction between the DNA-binding domain and another region of the protein (most likely its C-terminal 30 amino acids) would prevent DNA binding. The discovery that small peptides mimicking the p53 C-terminus activate the wild-type protein and some of its mutated forms for DNA binding supported this model and suggested that the allosteric activation could be utilized to design new anticancer agents.[13] However, in a recent NMR study researchers of Novaspin and Roche investigated the interaction between the p53 DNA-binding domain and various C- and N-terminal peptides by a variety of NMR methods, such as chemical shift perturbation, diffusion measurements, and saturation transfer difference spectroscopy, and showed that these peptides do not interact with the DNA-binding domain.[2] Therefore these results, which are in agreement with independent recent work[14] and other new findings,[15] show that the allosteric model is not valid for explaining p53 regulation. Instead, some form of competitive binding model is now favored to explain the experimental data.[16] Indeed, a weak (and probably unspecific) interaction between the C-terminal peptide and DNA was reported.[2]

It has long been demonstrated that p53 DNA-binding domains can cooperatively bind to DNA in solution.[17, 18] However, an exact understanding of the structural basis of this cooperative effect is limited because the structure of the (tetrameric) full-length p53 molecule in the complex with DNA is not known. Klein et al.[2] now present additional NMR structural data about the origin of the cooperative binding of the DNA-binding domains to DNA. By titrating unlabeled consensus DNA to ^{15}N-labeled p53 DNA-binding domain, it was possible to selectively observe changes in the chemical shift of the DNA-binding domain, with a spatial resolution at the level of individual amino acid residues. These changes in chemical shift reflect changes in the local environment of the respective amino acids, which is either caused by direct interactions with DNA or another p53 monomer, or by local conformational changes.[19] Chemical-shift peturbations are confined to distinct regions of the p53 DNA-binding domain. This observation indicates that its conformation is not drastically changed upon interaction with DNA, and confirms the site of interaction with DNA.[8] Most importantly, however, it defines the part of the p53 surface that is involved in the interaction between two p53 DNA-binding domains, and therefore provides experimental data for the generation of a model for the p53 tetramer bound to consensus DNA. As already suggested by Cho et al.,[8] the oligomerization interface includes the small helix H1, which spans residues proline-177 to cysteine-182. Very interestingly, some of the p53 mutations that were found in cancer cells are located in this H1 helix region. The involvement of the helix in the oligomerization of p53 explains the presence of these "hot spots" in and around a p53 region that is not in direct contact with DNA. It would be very interesting to determine whether these mutations indeed affect the assembly of the

 © WILEY-VCH Verlag GmbH, 69451 Weinheim, Germany, 2002 1433-7851/02/4110-1703 $ 20.00+.50/0

DNA-binding domains. In other words, can single mutations in the helix H1 prevent assembly of p53 and abolish DNA binding as some mutations in the tetramerization domain do?[20]

What is the structural organization of the complex between tetrameric full-length p53 and DNA? In the "clamp model"[21] (Figure 2A) the consensus DNA is surrounded by one p53 dimer on each side, so that the tetramer binds DNA as a pair

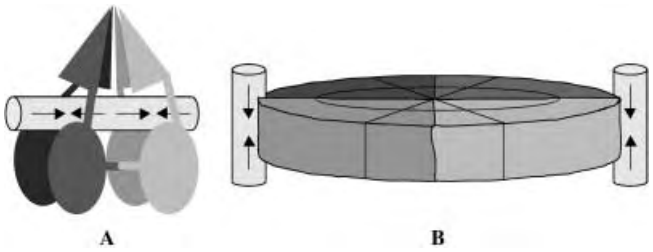


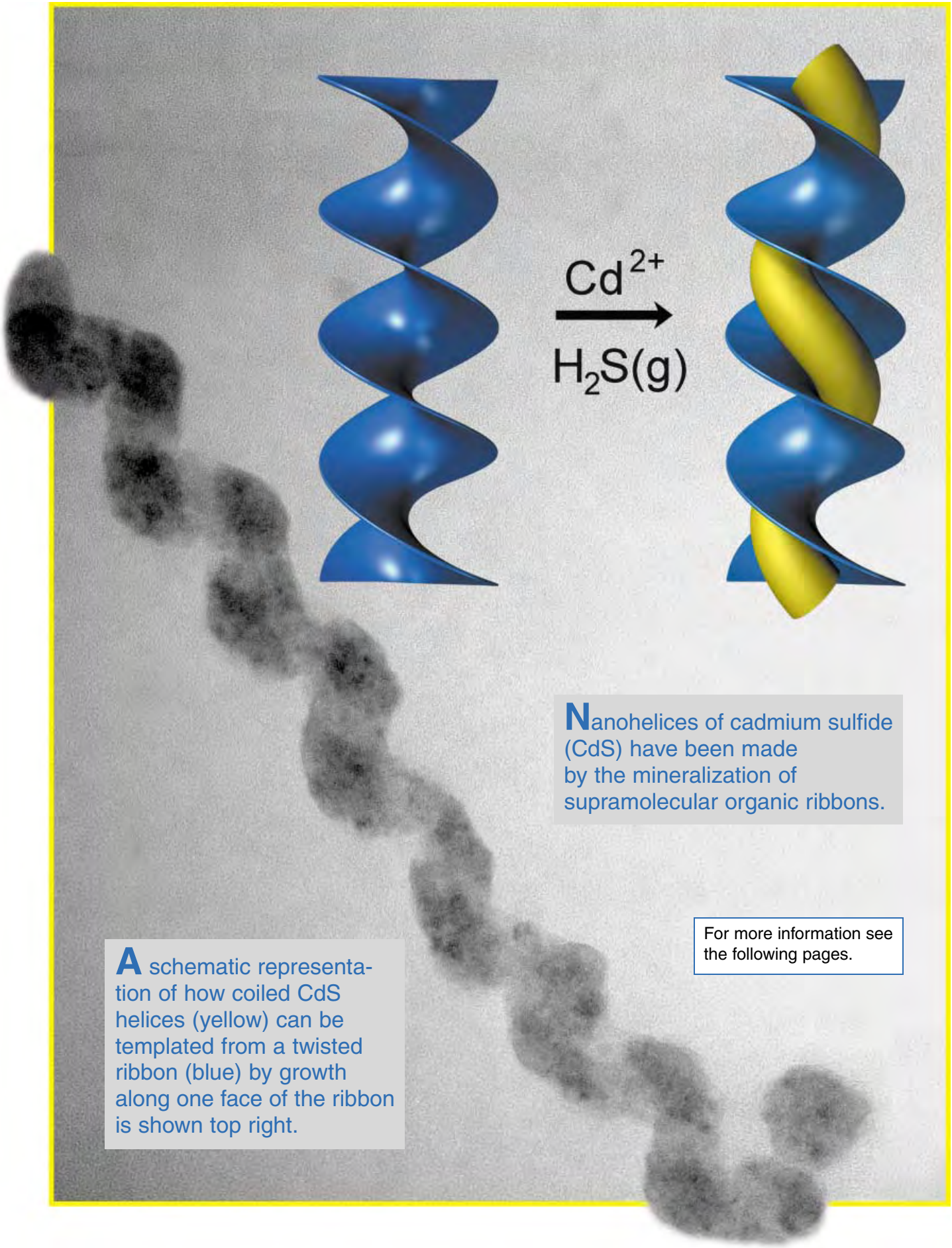
Figure 2. Models for the structures of the complex formed between full-length tetrameric p53 and DNA: A) "clamp model",[21] B) "sandwich model" as proposed by Klein et al.[2] Each p53 monomer is shown by a different shading, DNA is shown by tubes, and the orientation of the respective quarter-sites is indicated with arrows.

of clamps. On the basis of the reported data and on symmetry considerations, Klein et al. now propose a "sandwich model" for the p53–DNA interaction.[2] In this model, it is assumed that p53 tetramers link two separated, juxtaposed DNA consensus sites (Figure 2B). The tetramerization domains form the central part of the disc-shaped tetramer, while DNA-binding domains and transactivation domains are at the outside, with the DNA-binding domains contacting consensus DNA. This model is not only consistent with a D_2 symmetry of the complex and identical conformations of each p53 monomer, but is also supported by electron microscopy studies, which show that p53 can bridge two DNA consensus sites.[22]

Another aspect becomes clear from the work of Klein et al.: Dynamics play an integral role in understanding the p53–DNA interaction. The NMR signals of certain p53 residues broaden significantly after DNA binding. Since the authors provide evidence that the complex is tight enough to exclude chemical exchange as its source, the observed line broadening is likely the result of conformational exchange, that is, conformational flexibility of p53 residues when bound to DNA. This conformational exchange reduced the quality of the NMR spectra and precluded a more detailed NMR structural analysis—however, it is also interesting to note that it adds to the experimental evidence that molecular flexibility is a key driving force in protein–DNA interactions.[23, 24] Analysis of the thermodynamics of the formation of the p53–DNA complex may provide further insight into the function and activation of p53.

[1] P. Chene, *Expert Opin. Ther. Pat.* **2001**, *11*, 923–935.
[2] C. Klein, E. Planker, T. Diercks, H. Kessler, K. P. Kunkele, K. Lang, S. Hansen, M. Schwaiger, *J. Biol. Chem.* **2001**, *276*, 49020–49027.
[3] E. E. Balint, K. H. Vousden, *Br. J. Cancer* **2001**, *85*, 1813–1823.
[4] K. H. Vousden, *Cell* **2000**, *103*, 691–694.
[5] L. A. Donehower, M. Harvey, B. L. Slagle, M. J. McArthur, C. A. Montgomery, J. S. Butel, A. Bradley, *Nature* **1992**, *356*, 215–221.
[6] T. Soussi, K. Dehouche, C. Beroud, *Hum. Mutat.* **2000**, *15*, 105–113.
[7] J. M. Varley, D. G. R. Evans, J. M. Birch, *Br. J. Cancer* **1997**, *76*, 1–14.
[8] Y. Cho, S. Gorina, P. D. Jeffrey, N. P. Pavletich, *Science* **1994**, *265*, 346–355.
[9] W. S. El-Deiry, S. E. Kern, J. A. Pietenpol, K. W. Kinzler, B. Vogelstein, *Nat. Genet.* **1992**, *1*, 45–49.
[10] A. N. Bullock, J. Henckel, B. S. DeDecker, C. M. Jonhson, P. V. Nikolova, M. R. Proctor, D. P. Lane, A. R. Fersht, *Proc. Natl. Acad. Sci. USA* **1997**, *94*, 14338–14432.
[11] T. R. Hupp, D. W. Meek, C. A. Midgley, D. P. Lane, *Cell* **1992**, *71*, 875–886.
[12] T. R. Hupp, D. P. Lane, *Curr. Biol.* **1994**, *4*, 865–875.
[13] G. Selivanova, T. Kawasaki, L. Ryabchenko, K. G. Wiman, *Semin. Cancer Biol.* **1998**, *8*, 369–378.
[14] A. Ayed, F. A. Mulder, G. S. Yi, Y. Lu, L. E. Kay, C. H. Arrowsmith, *Nat. Struct. Biol.* **2001**, *8*, 756–760.
[15] M. D. Kaeser, R. D. Iggo, *Proc. Natl. Acad. Sci. USA* **2002**, *99*, 95–100.
[16] M. E. Anderson, B. Woelker, M. Reed, P. Wang, P. Tegtmeyer, *Mol. Cell. Biol.* **1997**, *17*, 6255–6264.
[17] P. Balagurumoorthy, H. Sakamoto, M. S. Lewis, N. Zambrano, G. M. Clore, A. M. Gronenborn, E. Appella, H. E. Harrington, *Proc. Natl. Acad. Sci. USA* **1995**, *92*, 8591–8595.
[18] Y. Wang, J. F. Schwedes, D. Parks, K. Mann, P. Tegtmeyer, *Mol. Cell. Biol.* **1995**, *15*, 2157–2165.
[19] M. P. Foster, D. S. Wuttke, K. R. Clemens, W. Jahnke, I. Radhakrishnan, L. Tennant, M. Reymond, J. Chung, P. E. Wright, *J. Biomol. NMR* **1998**, *12*, 51–71.
[20] P. Chene, *Oncogene* **2001**, *20*, 2611–2617.
[21] K. G. McLure, P. W. K. Lee, *EMBO J.* **1998**, *17*, 3342–3350.
[22] J. E. Stenger, P. Tegtmeyer, G. A. Mayr, M. Reed, Y. Wang, P. Wang, P. V. Hough, I. A. Mastrangelo, *EMBO J.* **1994**, *13*, 6011–6020.
[23] N. Pastor, H. Weinstein, *Theor. Comput. Chem.* **2001**, *9*, 377–407.
[24] P. G. A. van Tilburg, F. A. A. Mulder, M. M. E. de Backer, M. Nair, E. C. van Heerde, G. Folkers, P. T. van der Saag, Y. Karimi-Nejad, R. Boelens, R. Kaptein, *Biochemistry* **1999**, *38*, 1951–1956.

 © WILEY-VCH Verlag GmbH, 69451 Weinheim, Germany, 2002 1433-7851/02/4110-1704 $ 20.00+.50/0



Nanohelices of cadmium sulfide (CdS) have been made by the mineralization of supramolecular organic ribbons.

A schematic representation of how coiled CdS helices (yellow) can be templated from a twisted ribbon (blue) by growth along one face of the ribbon is shown top right.

For more information see the following pages.

 © WILEY-VCH Verlag GmbH, 69451 Weinheim, Germany, 2002 1433-7851/02/4110-1705 $ 20.00+.50/0

Semiconductor Nanohelices Templated by Supramolecular Ribbons**

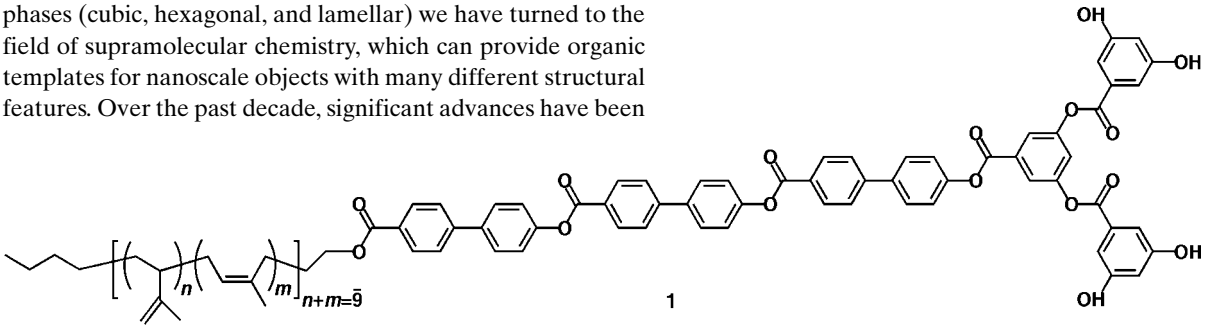
Eli D. Sone, Eugene R. Zubarev, and Samuel I. Stupp*

The synthesis of inorganic nanoobjects[1–15] and materials with nanoscale features[16–23] that are inaccessible by conventional synthetic or lithographic techniques is an important goal for chemistry. The ability to control the morphology of inorganic compounds on the nanoscale could provide systems for the study of quantum-confined behavior and may also have profound implications for a wide variety of technologies.[4, 24] Thus far, aside from extensive work on quantum dots[4, 5] and nanowires,[3, 8, 9, 24] progress has been greater for oxides than for non-oxides, with the latter including many semiconductors of interest for optoelectronic applications. For cadmium sulfide (CdS), for example, a semiconductor potentially suited for photovoltaic applications,[25] the nanoscale morphologies accessible so far have been largely limited to fairly basic shapes.[5–12] Here we report on the use of a self-assembled organic object to template the first example of a nanoscale helical morphology of cadmium sulfide. The CdS helices grow on supramolecular nanoribbons that are themselves found to be helical. The inorganic nanostructures have a coiled morphology with a pitch of 40 – 60 nm, which can be rationalized in terms of the period of the twisted organic ribbons.

Organic molecules that self-assemble into nanostructures have great potential as templates for the growth of inorganic materials.[14, 16–20, 22, 23] In the last few years, we have developed a methodology for the synthesis of nanostructured CdS in which lyotropic liquid crystals act as direct templates for the mineral phase by confining the precursor ions to the hydrophilic regions of the mesophase.[22, 23] In order to progress beyond the morphologies obtainable through typical lyotropic phases (cubic, hexagonal, and lamellar) we have turned to the field of supramolecular chemistry, which can provide organic templates for nanoscale objects with many different structural features. Over the past decade, significant advances have been made on how to organize molecules into new shapes through noncovalent bonds.[26–33] We have recently reported on molecules with a triblock architecture termed "dendron rodcoils" (DRC, **1**).[32, 33]

The DRC molecules (**1**) investigated can hydrogen bond in head-to-head fashion through dendron segments and self-assemble into nanoribbons, thus causing the gelation of various organic solvents. From crystallographic studies on model compounds it can be inferred that each ribbon is held together by hydrogen bonds between hydroxy and carbonyl groups of the hydrophilic dendron segments and $\pi-\pi$ stacking interactions of the aromatic rod segments.[32] We reported previously that the DRC nanoribbons tend to be flat in dichloromethane, with a consistent width of 10 nm and a thickness of 2 nm.[32]

We have investigated the formation of nanoribbons in other solvents and found that in some cases they were not flat. Transmission electron microscopy (TEM) studies on a sample prepared from a DRC gel in ethyl methacrylate (EMA) reveals that the self-assembled ribbons adopt a helical structure in this solvent (Figure 1 a). Most of the ribbons in the micrograph show dark parallel bands across the width of the structure, spaced 15 – 25 nm apart. This pattern is consistent with the density projection of a twisted ribbon, as opposed to a coiled structure (Figure 1 a, inset). One would expect to see a zigzag pattern in projection for a coiled structure. Furthermore, the width of the parallel stripes in the TEM image is approximately 3 nm, which corresponds more closely to the thickness rather than to the width of the flat ribbons in CH_2Cl_2. As expected, both right-handed and left-handed helices are observed. The ribbons which do not show parallel stripes may represent flat structures, as had been observed in CH_2Cl_2, or they may be more tightly twisted helices in which there is not enough density contrast along the length of the ribbon to be visible by TEM. The helical nature



1

of the ribbons remains intact after the addition of a cadmium nitrate ($Cd(NO_3)_2 \cdot 4H_2O$) solution in THF as a precursor to CdS mineralization (Figure 1 b). In other solvents, such as 2-ethylhexyl methacrylate (EHMA), we also found TEM evidence for some helical nanoribbons with similar pitch to those formed in EMA, although the striped pattern was not visible for all of the ribbons (see Supporting Information).

We investigated the possibility of producing novel inorganic structures by mineralizing nanoribbons in both EHMA and EMA. Figure 2 shows TEM images of CdS which was isolated from a 1 wt. % gel of the DRC in EHMA to which a solution of cadmium nitrate in THF had been added prior to exposure to hydrogen sulfide gas. The structure in Figure 2 a shows the

[*] Prof. S. I. Stupp, E. D. Sone, Dr. E. R. Zubarev
Department of Materials Science and Engineering
Department of Chemistry, and Medical School
Northwestern University
Evanston, IL 60208-3108 (USA)
Fax: (+1) 847-491-3010
E-mail: s-stupp@northwestern.edu

[**] This work made use of the Electron Probe Instrumentation Center (EPIC) at Northwestern University and was supported by the U.S. Department of Energy, the U.S. Army Research Office, and the National Science Foundation. E.D.S. is grateful to the Natural Sciences and Engineering Research Council of Canada for a postgraduate scholarship (2000 – 2002).

Supporting information for this article is available on the WWW under http://www.angewandte.com or from the author.

 © WILEY-VCH Verlag GmbH, 69451 Weinheim, Germany, 2002 1433-7851/02/4110-1706 $ 20.00+.50/0

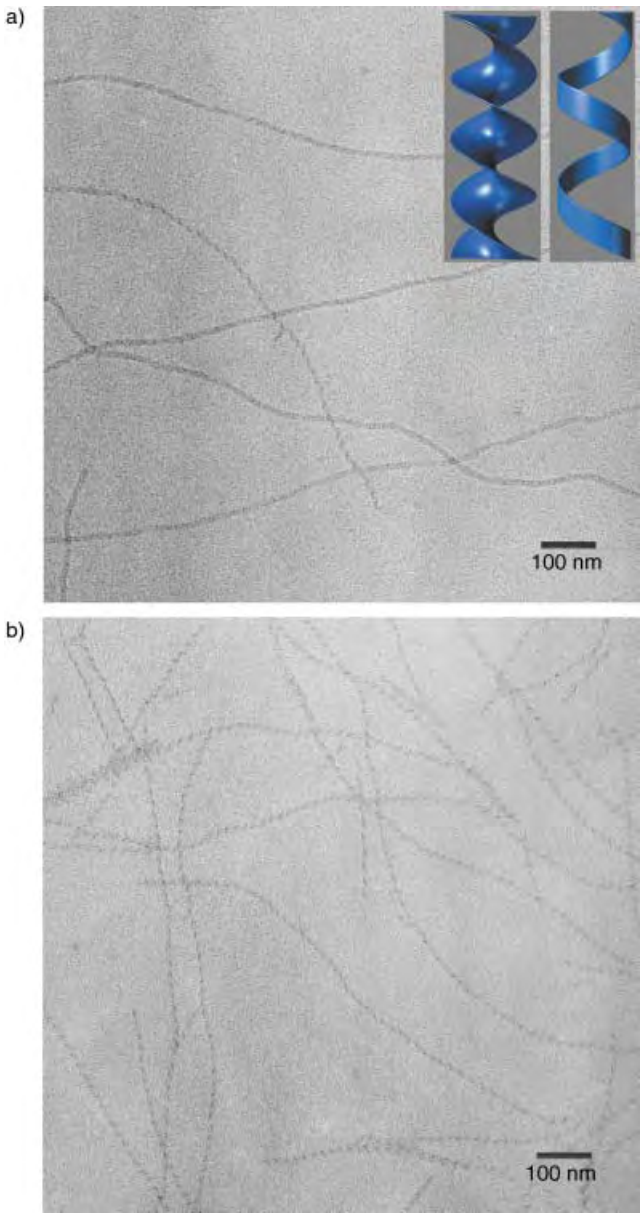


Figure 1. Bright-field TEM micrographs of DRC nanoribbons formed in EMA: a) unstained sample prepared from a 5 wt.% gel of the DRC in EMA; b) helical nanoribbons after addition of mineralization precursor (1.5 wt.% of a 0.2 M solution of $Cd(NO_3)_2 \cdot 4H_2O$ in THF). The inset shows schematic representations of twisted (left) and coiled (right) helical morphologies.

zigzag pattern one would expect from a 2D density projection of a coiled helix (Figure 1a, inset), with a pitch of approximately 40–50 nm. Furthermore, the peaks and valleys of the periodic pattern are darker than the rest of the material. This pattern is consistent with what one would expect to see for the coiled form of a helix, since the strand loops below itself at the turns of the helix. These turns would show up as regions of higher electron density in a TEM image, and thus appear darker, as is observed here. Thicker helical structures, with widths ranging from 35–100 nm and lengths of up to two microns were also found (Figure 2b). The period of these structures is also 40–50 nm, which suggests that they result when structures such as the one shown in Figure 2a mineralize further. Electron diffraction studies (Figure 2b, inset)

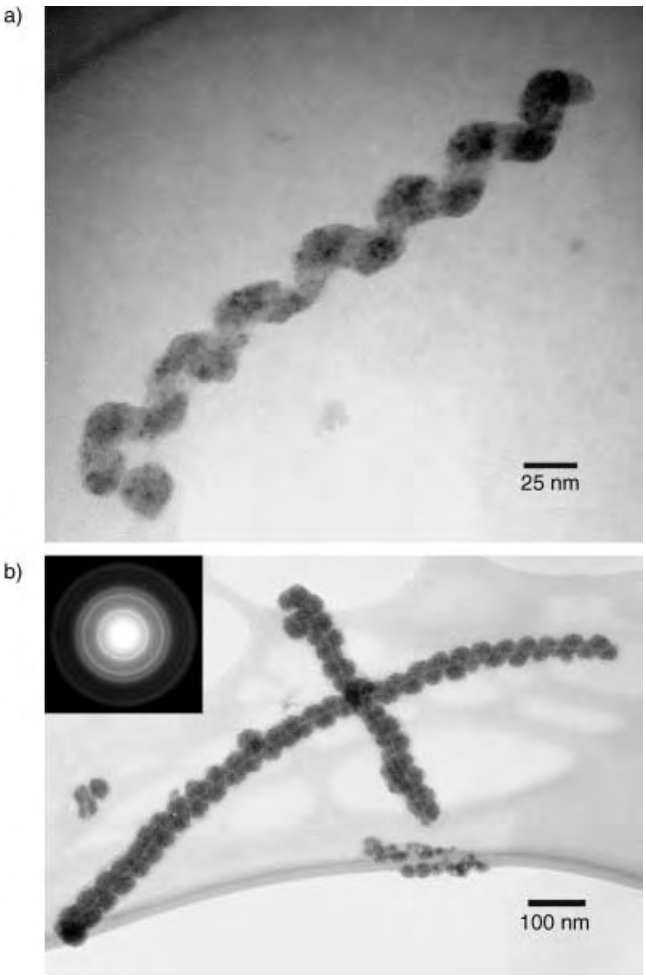


Figure 2. TEM micrographs of CdS precipitated in gels of the DRC in EHMA: a) helical nanostructure of CdS with a pitch of 40–50 nm; b) thicker helical structures with approximately the same pitch as the helix in Figure 2a. The inset shows the electron diffraction pattern corresponding to the CdS zinc blende structure. The lighter stripe visible along the axis of these helices may be the result of the lower contrast generated by the core of the helix.

confirmed that the mineral is CdS with the zinc blende structure, as characterized by rings corresponding to the {111}, {220}, and {311} reflections. High resolution TEM studies (see Supporting Information) revealed that the polycrystalline CdS is made up of small domains with grain sizes of about 4–8 nm. We note that not all of the CdS isolated from the EHMA gels was helical in morphology; there was a significant amount of material which appeared to be untemplated, probably as a result of some nucleation and growth in the bulk solvent, or from single DRC molecules not part of ribbons.

We found that nanoribbons did not need to be in the gelled state to produce helical nanostructures of CdS when mineralized. EMA gels containing 3 or 5 wt.% DRC could be diluted in additional EMA to form a suspension of nanoribbons. Cadmium nitrate in THF was then added to this suspension and the sample was exposed to $H_2S(g)$. This method allowed TEM observation of a drop deposited directly from the suspension onto a holey carbon grid (after exposure to gas). By eliminating the work-up in THF, which was necessary for the gel-mineralized samples, we were able

 © WILEY-VCH Verlag GmbH, 69451 Weinheim, Germany, 2002 1433-7851/02/4110-1707 $ 20.00+.50/0

to simultaneously observe the CdS and the organic ribbons in the suspension-mineralized samples. Furthermore, the early stages of mineralization were more readily observed. Figure 3a shows a CdS helix at an early stage of its growth on a DRC nanoribbon in EMA. The pitch of this helix is about 60 nm. As is evident in the inset, there are gaps between sections of the growing mineral in which the organic ribbon is visible (indicated by the arrow). A lower magnification micrograph in which a number of helical structures are visible is shown in Figure 3b.

We propose that the ribbons act as templates for the CdS because of the likely preferred affinity of Cd^{2+} ions (solvated in THF) for the hydrophilic region of the ribbon (the hydroxy-containing dendron portion) over the relatively hydrophobic solvent. This would produce a local supersaturation of ions around the DRC ribbon, which would lead to nucleation and growth of CdS crystals localized at the ribbon after exposure to $H_2S(g)$. The existence of gaps between sections of the mineral at the early stages of its growth (Figure 3a) suggest that there are many nucleation sites along the length of the ribbon. These nuclei grow until they eventually join to form a continuous solid, rather than the entire structure emanating from a single nucleation event on the ribbon.

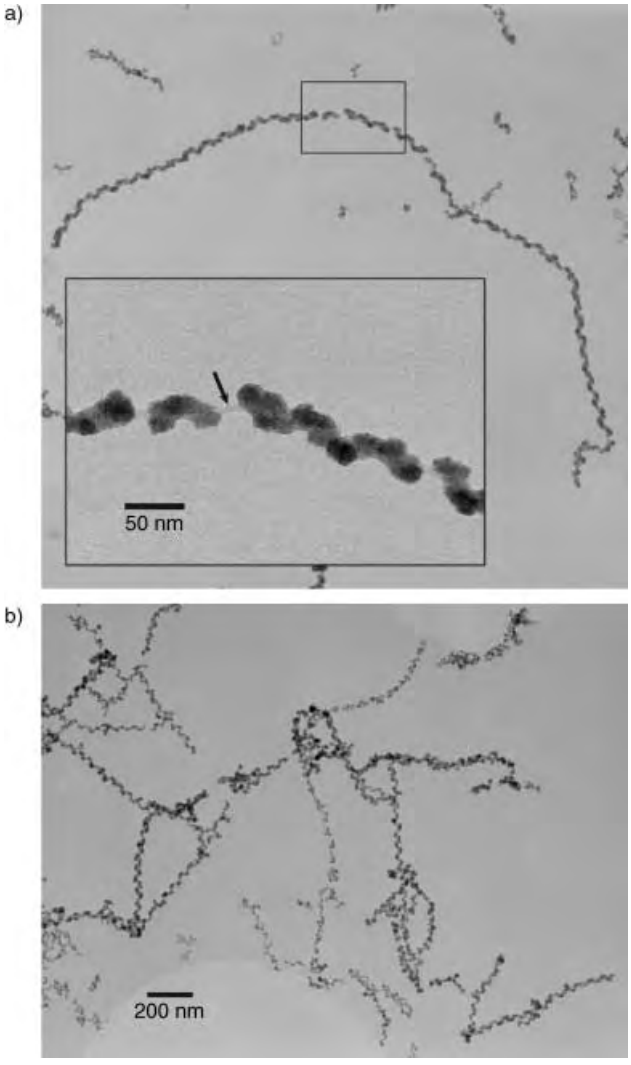


Figure 3. TEM micrographs of CdS precipitated in a suspension of DRC nanoribbons in EMA: a) CdS helix at an early stage of growth. The inset shows an enlargement of the boxed section and highlights the visibility of the organic ribbon in between sections of CdS (indicated by arrow); b) Lower magnification view showing a number of CdS helices.

We note that while the DRC ribbons have a twisted form, the CdS which is templated by these ribbons has a coiled helical structure. This apparent inconsistency could be explained by a templating scheme in which the CdS grows along only one face of the twisted ribbon template (Figure 4). The result would be a coiled helix of CdS with a pitch twice that of the twisted ribbons; in our case the pitch of the CdS (about 50 nm) is a little more than twice the pitch of the twisted ribbons (about 20 nm). The slightly larger than expected pitch of the CdS helices could result from distortions of the nanoribbon structure during mineralization. If the CdS helices are indeed produced by the templating scheme shown in Figure 4, it would suggest that the two faces of the DRC ribbons are not equivalent in terms of their ability to nucleate CdS, since nucleation and growth would have to be favored on one face to produce coiled structures. Twisted ribbons with a slightly coiled axis would have one face that was more exposed to the solvent, thus making it more favorable for mineral nucleation and growth. Alternatively, a nucleation event on one face of the ribbon could distort the ribbon in such a way as to make the two faces inequivalent. We note that while most of the CdS helices are single coils, we do observe some objects that appear to be double coils, which might result from mineralization along both faces of a ribbon. More details of the DRC nanoribbon structure need to be elucidated to gain further insight into the templating mechanism.

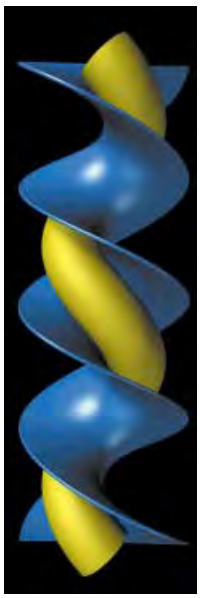


Figure 4. Schematic representation of a possible templating mechanism in which a coiled CdS helix is produced from a twisted helical template through growth along one face of the template. The resulting yellow mineral (shown at an early stage of growth so as not to obscure ribbon) would have a pitch twice that of the ribbon template (blue).

The semiconductor helical structures reported possess a unique morphology for CdS that may have interesting electronic or photonic properties. Perhaps more importantly, the structures represent a step towards the goal of harnessing the power of supramolecular organic chemistry to build inorganic structures for nanotechnology, beyond what has been accomplished with liquid crystals. Our results suggest that by using extremely uniform, stable, nonaggregated supramolecular objects as templates one can achieve good control over the morphology of the templated product.

Experimental Section

EMA gels were prepared by dissolving the DRC (30–50 mg) in EMA (1 g) through sonication, and heating in a sealed vial to about 75 °C for 5 minutes. Gels typically formed overnight. TEM samples of the gels were prepared by suspending a portion of the gel in EMA, casting it onto a holey carbon-

 © WILEY-VCH Verlag GmbH, 69451 Weinheim, Germany, 2002 1433-7851/02/4110-1708 $ 20.00+.50/0

coated Cu grid, and wicking away the excess. TEM was performed on a Hitachi H-8100 microscope operating at 100 kV.

Mineralized gels in EHMA were prepared by placing the DRC (10 mg) and EHMA (1 g, in some cases containing 1 mg mL^{-1} of divinylbenzene) in a sealed vial and heating to about 75 °C to dissolve the DRC. A 0.2 M solution (20 mg) $Cd(NO_3)_2 \cdot 4H_2O$ in THF was then added to the solution, and the vial was capped and allowed to cool to room temperature and gel. We note that some of cadmium nitrate precipitated and settled to the bottom of the vial prior to gelation, thus reducing the actual concentration of available cadmium ions. This precipitate was avoided when working up the gels after exposure to H_2S(g). Gels were aged for approximately one week prior to exposure to H_2S(g) for 30 min, after which time the gas had diffused through most of the gel, as evidenced by a change to a yellow color. After aging the samples again (typically one week). TEM samples were prepared by removing excess organic material by dissolution of the gel in THF (the DRC is soluble in THF) and isolation of the inorganic product by centrifugation. The CdS was resuspended in THF, cast onto a TEM grid, and imaged at 200 kV.

DRC ribbons from EMA gels were mineralized from a suspension of a 3 or 5 wt.% gel (about 100 mg) in EMA (2 g). A 0.2 M solution (20 mg) of $Cd(NO_3)_2 \cdot 4H_2O$ in THF was added to this suspension, and after one hour the sample was exposed to H_2S(g) for 15 min. TEM samples were prepared 5 min after exposure by depositing a drop of the suspension onto a holey carbon grid and wicking away the excess.

Received: December 21, 2001 [Z18427]

[1] S. Iijima, *Nature* **1991**, *354*, 56.
[2] R. Tenne, L. Margulis, M. Genut, G. Hodes, *Nature* **1992**, *360*, 444.
[3] J. T. Hu, O. Y. Min, P. D. Yang, C. M. Lieber, *Nature* **1999**, *399*, 48.
[4] A. P. Alivisatos, *Science* **1996**, *271*, 933.
[5] A. D. Yoffe, *Adv. Phys.* **2001**, *50*, 1.
[6] P. V. Braun, S. I. Stupp, *Mater. Res. Bull.* **1999**, *34*, 463.
[7] J. Huang, Y. Xie, B. Li, Y. Liu, Y. Qian, S. Zhang, *Adv. Mater.* **2000**, *12*, 808.
[8] D. Routkevitch, T. Bigioni, M. Moskovits, J. M. Xu, *J. Phys. Chem.* **1996**, *100*, 14037.
[9] Y. Li, J. H. Wan, Z. N. Gu, *Acta Phys. Chim. Sin.* **1999**, *15*, 1.
[10] C.-C. Chen, J.-J. Lin, *Adv. Mater.* **2001**, *13*, 136.
[11] J. H. Adair, E. Suvaci, *Curr. Opin. Colloid Interface Sci.* **2000**, *5*, 160.
[12] N. Pinna, K. Weiss, J. Urban, M.-P. Pileni, *Adv. Mater.* **2001**, *13*, 261.
[13] L. Manna, E. C. Scher, A. P. Alivisatos, *J. Am. Chem. Soc.* **2000**, *122*, 12700.
[14] J. H. Jung, Y. Ono, K. Hanabusa, S. Shinkai, *J. Am. Chem. Soc.* **2000**, *122*, 5008.
[15] R. C. Jin, Y. W. Cao, C. A. Mirkin, K. L. Kelly, G. C. Schatz, J. G. Zheng, *Science* **2001**, *294*, 1901.
[16] C. T. Kresge, M. E. Leonowicz, W. J. Roth, J. C. Vartuli, J. S. Beck, *Nature* **1992**, *359*, 710.
[17] S. Mann, G. A. Ozin, *Nature* **1996**, *382*, 313.
[18] H. Yang, N. Coombs, G. A. Ozin, *Nature* **1997**, *386*, 692.
[19] P. D. Yang, D. Y. Zhao, D. I. Margolese, B. F. Chmelka, G. D. Stucky, *Nature* **1998**, *396*, 152.
[20] M. E. Raimondi, J. M. Seddon, *Liq. Cryst.* **1999**, *26*, 305.
[21] C. B. Murray, C. R. Kagan, M. G. Bawendi, *Science* **1995**, *270*, 1335.
[22] P. V. Braun, P. Osenar, S. I. Stupp, *Nature* **1996**, *380*, 325.
[23] P. V. Braun, P. Osenar, V. Tohver, S. B. Kennedy, S. I. Stupp, *J. Am. Chem. Soc.* **1999**, *121*, 7302.
[24] C. M. Lieber, *Solid State Commun.* **1998**, *107*, 607.
[25] O. Savadogo, *Sol. Energy Mater. Sol. Cells* **1998**, *52*, 361.
[26] G. M. Whitesides, J. P. Mathias, C. T. Seto, *Science* **1991**, *254*, 1312.
[27] J.-M. Lehn, *Supramolecular Chemistry*, VCH, New York, **1995**.
[28] S. I. Stupp, Y. LeBonheur, K. Walker, L. S. Li, K. E. Huggins, M. Keser, A. Amstutz, *Science* **1997**, *276*, 384.
[29] E. R. Zubarev, M. U. Pralle, L. Li, S. I. Stupp, *Science* **1999**, *283*, 523.
[30] J. S. Moore (Ed.), *MRS Bull.* **2000**, *25*, special issue.
[31] G. N. Tew, M. U. Pralle, S. I. Stupp, *J. Am. Chem. Soc.* **1999**, *121*, 9852.
[32] E. R. Zubarev, M. U. Pralle, E. D. Sone, S. I. Stupp, *J. Am. Chem. Soc.* **2001**, *123*, 4105.
[33] E. R. Zubarev, M. U. Pralle, E. D. Sòne, S. I. Stupp, *Adv. Mater.* **2002**, *14*, 198.

Assignment of Stereochemistry of Facially Protected Bis-porphyrins by Use of a "Molecular Ruler"**

Maxwell J. Crossley* and Pall Thordarson

Herein we introduce a "molecular ruler" concept that can be used to unambiguously assign two stereoisomers of dizinc(II) bis(C_2-capped porphyrins) that could not otherwise be assigned by conventional techniques such as ^{1}H NMR spectroscopy. In essence the molecular ruler concept involves measurement of the distance between binding sites in a ditopic host molecule by determination of the binding of bidentate guest molecules in which the recognition groups are separated by spacers of different length. In a relatively rigid host molecule, the bidentate guest molecule that best fits the host should be most tightly bound. If the bidentate guest molecule is too short to span the binding sites, an energy penalty will have to be paid to distort either the host or the guest to achieve binding at both sites. The energy penalty will appear as a lower association constant. Similarly, when a host is too long it will have to distort itself to bind at both ends. Again this is at an energy cost.

In the present case we use a rigid dizinc(II) bis-porphyrin system and measure the distance between the zinc atoms by examining the molecular recognition of α,ω-diaminoalkanes. The molecular ruler concept is used here to discriminate between two structural isomers of a facially protected bis-porphyrin. Discrimination is possible because although the zinc(II)$\cdots$zinc(II) distance is the same in each case, the distances between the sites of complexation are very different. In the *syn* isomer **4** the capping superstructure of both porphyrin units lie on the same face of the conjugated bis-porphyrin skeleton (C_{2v} symmetry) and hence the sites of complexation of the bidentate ligand both lie on the other unprotected face. In the *anti* isomer **5** (C_{2h} symmetry), the capping superstructures lie on opposite faces of the conjugated bis-porphyrin skeleton, and, therefore, so do the diagonally opposed binding sites.

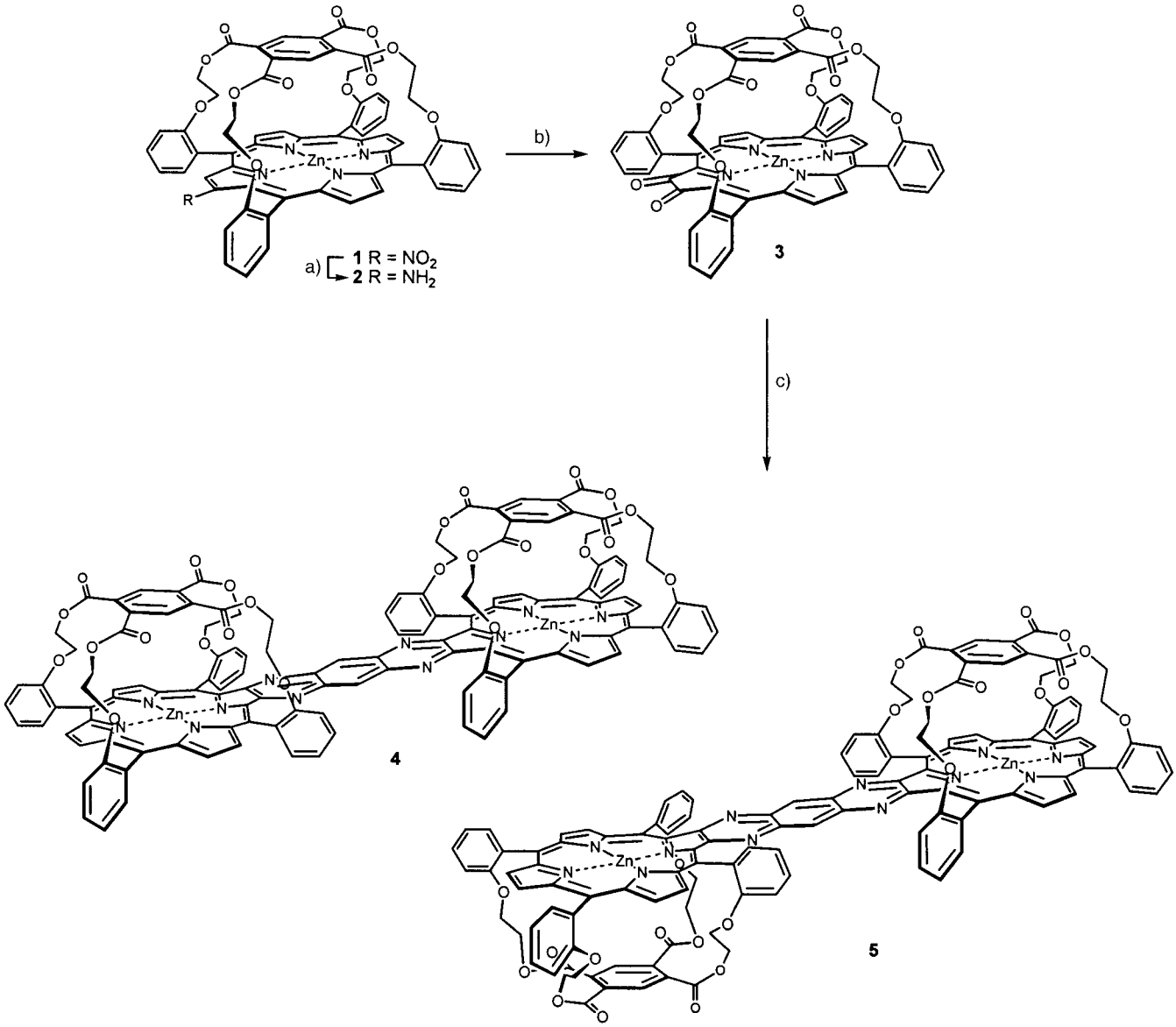
We sought the dizinc(II) *syn*- and *anti*-bis(7,8-C_2-capped porphyrins), **4** and **5**, respectively, for our studies towards self-replication of **4**. These stereoisomers were prepared by the sequence outlined in Scheme 1. The zinc(II) 7-nitro-C_2-capped porphyrin[1, 2] **1** prepared by Baldwin et al. was readily available from the unsubstituted C_2-capped porphyrin[3, 4] by our modified method for porphyrin synthesis.[5] Hydrogenation using sodium borohydride and palladium on active carbon[1, 2] gave the unstable zinc(II) 7-amino-C_2-capped porphyrin **2** that was immediately photooxidized following our methodology[6] to give the zinc(II) 7,8-C_2-capped porphy-

[*] Prof. Dr. M. J. Crossley, Dr. P. Thordarson
School of Chemistry
The University of Sydney
NSW 2006 (Australia)
Fax: (+61) 2-9351-3329
E-mail: m.crossley@chem.usyd.edu.au

[**] We thank the Australian Research Council for financial support.

Supporting information for this article is available on the WWW under http://www.angewandte.com or from the author.

 © WILEY-VCH Verlag GmbH, 69451 Weinheim, Germany, 2002 1433-7851/02/4110-1709 $ 20.00+.50/0



Scheme 1. Conditions: a) $NaBH_4$, $Pd/C/CH_2Cl_2$ and MeOH; not isolated; b) *hν*, O_2/CH_2Cl_2; 36% yield from **1**; c) 1,2,4,5-benzenetetramine tetrahydrochloride/refluxing pyridine, preparative HPLC; 21% and 19% yield, respectively, for **4** and **5** from **3**.

rindione **3** in 36% yield from **1**. Following the method of Crossley and Burn,[7] condensation of two equivalents of **3** and one equivalent of 1,2,4,5-benzenetetramine in refluxing pyridine for two days, gave a 1:1 mixture of **4** and **5** in 42% yield. The two isomers where separated efficiently by preparative HPLC into the more polar compound **4** and the less polar compound **5** (Scheme 1).

All spectroscopic data for **4** and **5** were fully consistent with the expected structures of these compounds but unambiguous assignment of the stereochemistry (*syn* or *anti*) of the two fractions could not be made because the two compounds displayed very similar spectra. The largest difference in the chemical shifts between corresponding signals from the two compounds is only 0.09 ppm.

Molecular modeling (HyperChem,[8] MM+ force field modified for porphyrins[9–11]) of **4** and **5** indicated that the zinc(II)···zinc(II) distance for both compounds was essentially the same, 15.3 Å. Therefore, a ligand which is just long enough to span the two zinc(II) binding sites (15.3 Å) will form a strong intramolecular complex with the *syn* isomer **4** only (Figure 1). Clearly the same ligand would be too short to wind

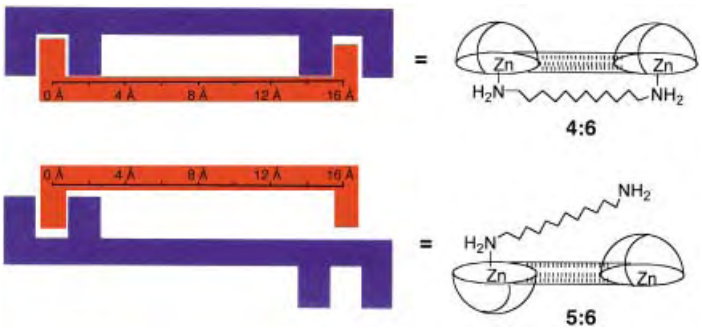
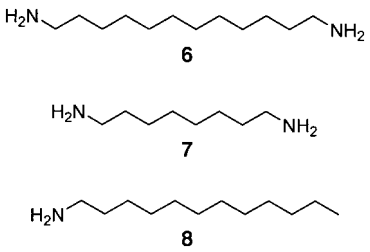


Figure 1. Schematic representation of the expected complexation between *syn* and *anti* isomers of dizinc(II) bis(C_2-capped porphyrins) and a α,ω-diaminoalkane ligand (for example, **6**) acting as a molecular ruler.

 © WILEY-VCH Verlag GmbH, 69451 Weinheim, Germany, 2002 1433-7851/02/4110-1710 $ 20.00+.50/0

itself around the *anti* isomer **5** and form such a intramolecular complex involving both faces. Binding to the second zinc(II) center by threading the ligand through the superstructure of the cap requires substantial steric interactions and distortions, and has not been observed with 7,8-capped porphyrins.

The bidentate ligands 1,12-diaminododecane (**6**) and 1,8-diaminooctane (**7**) and the monodentate ligand, 1-aminododecane (**8**), were used. Ligand **6** (span 16.4 Å[8]) can easily bind between the two binding sites of the *syn* isomer **4** whereas **7** can only span 11.3 Å[8], which is too short to bind between the binding sites of **4**.



UV/Vis and ^{1}H NMR binding studies (see Supporting Information) confirmed this. Drastic differences were seen in the binding isotherms (by UV/Vis titration) of the two fractions obtained from preparative HPLC with **6** (Figure 2). On the basis of this result, the more polar fraction was

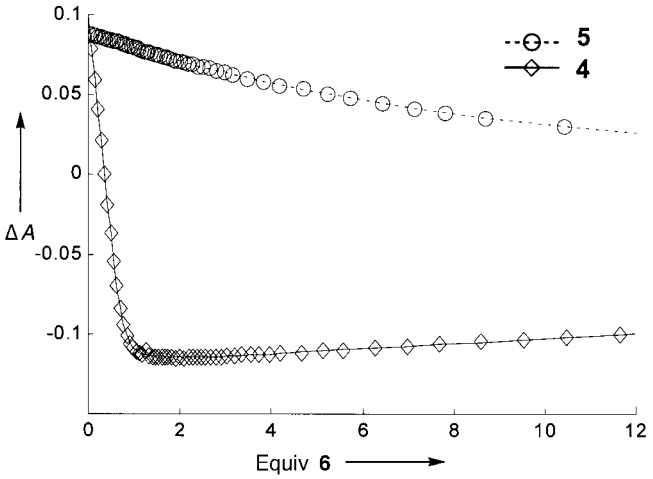


Figure 2. UV/Vis (from the Soret region, in toluene at 25 °C) binding isotherms showing the effect of titration of dizinc(II) s*yn*- and *anti*-bis(7,8-C_2-capped porphyrins), **4** and **5**, respectively, with **6**. The lines drawn between the experimental points are the calculated isotherms for the 1:1 binding model.

assigned as the *syn* isomer **4** and the less polar fraction as the *anti* isomer **5**. The 1:1 (empirical) binding constants for the complexation of the ligands **6**, **7**, and **8** to hosts **4** and **5** further highlight these differences (Table 1). Ligand **6** binds to isomer **4** approximately 2100 times more strongly than it does to isomer **5**. This is in contrast with the binding of **4** and **5** to the monotopic ligand, **8**, the binding constants of which are very similar in magnitude. The approximately fourfold stronger binding of **7** to host **4** compared to its binding to host **5** can be explained by the apparent formation of a 1:2:1 "sandwich"

Table 1. Calculated 1:1 (empirical) binding constants for the complexation of hosts **4** and **5** and the ligands **6**–**8** as measured by UV/Vis titration in $CH_3C_6H_5$ at 298 K.

Host	**6** K [M^{-1}]	**7** K [M^{-1}]	**8** K [M^{-1}]
4	$7.2 \times 10^7 \pm 18\,\%$	$1.7 \times 10^5 \pm 6\,\%$	$4.1 \times 10^4 \pm 6\,\%$ [a]
5	$3.4 \times 10^4 \pm 9\,\%$	$3.8 \times 10^4 \pm 7\,\%$	$3.3 \times 10^4 \pm 33\,\%$ [b]

[a] ^{1}H NMR titration in $CDCl_3$ at 300 K gave $K = 1.7 \times 10^4$ M^{-1}. [b] ^{1}H NMR titration in $CDCl_3$ at 300 K gave $K = 2.5 \times 10^4$ M^{-1}.

complex between **4** and **7**, similar to those reported by Anderson and Taylor,[12, 13] which, because of geometric restraints, isomer **5** cannot form.

^{1}H NMR titrations of hosts **4** and **5** with **6** further highlighted the difference between these two hosts. The formation of the complex **4**:**6** is accompanied by large upfield shifts (up to 6.2 ppm) for the ligand signals. In the much weaker **5**:**6** complex, the ligand signals were in fast exchange between the bound and unbound species and the maximum observed upfield shifts for the ligand were therefore much smaller (2.4 ppm). The much slower exchange in the complex

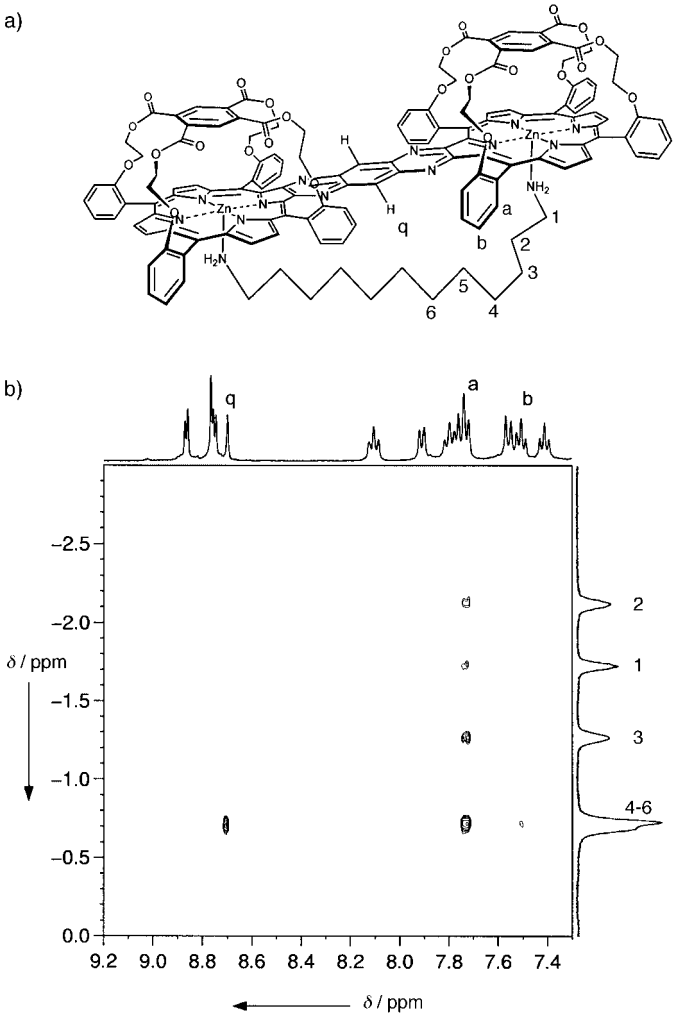


Figure 3. a) Schematic representation, with labels, of the complex formed between **4** and **6**. b) The two-dimensional ROESY ^{1}H NMR (400 MHz, $CDCl_3$) spectrum of the **4**:**6** (1:1) complex mixture. Only the peaks corresponding to the NOE cross peaks are labeled.

 © WILEY-VCH Verlag GmbH, 69451 Weinheim, Germany, 2002 1433-7851/02/4110-1711 $ 20.00+.50/0

4:**6** allowed two-dimensional COSY and ROESY ^{1}H NMR spectroscopy to be carried out at 260 K (uncorrected temperature) and the spectra obtained were fully consistent with the expected structure and symmetry of the complex. Most importantly, the ROESY spectra (see Figure 3b) showed clear NOE cross peaks between the ligand and the host. In particular, the bridging protons (q in Figure 3a) showed NOE peaks to the central portion of the ligand (CH_2 nos. 4–6, Figure 3b). Moreover, the calculated interproton distances (see Supporting Information) obtained from integration of the cross peaks in the ROESY spectra are only consistent with the structure **4**:**6**.

In conclusion, a combination of UV/Vis and ^{1}H NMR binding studies using a simple bidenate ligand as a molecular ruler have unambiguously demonstrated the structural difference between the hosts **4** and **5**: only one (*syn* isomer **4**) could form strong intramolecular complexes with **6**. In other words, molecular recognition studies were used for the structural determination of **4** and **5**, something that could not be achieved with conventional spectroscopic techniques on the compounds themselves. In other work,[14] we have shown that the molecular ruler concept can be used also for determination of the cavity size in ditopic chiral porphyrin-appended Tröger's bases.[15]

Received: November 2, 2001
Revised: March 7, 2002 [Z18142]

[1] J. E. Baldwin, J. F. DeBernardis, *J. Org. Chem.* **1977**, *42*, 3986.
[2] J. E. Baldwin, M. J. Crossley, J. DeBernardis, *Tetrahedron* **1982**, *38*, 685.
[3] J. Almog, J. E. Baldwin, R. L. Pyer, M. Peters, *J. Am. Chem. Soc.* **1975**, *97*, 226.
[4] J. Almog, J. E. Baldwin, M. J. Crossley, J. F. DeBernardis, R. L. Dyer, J. R. Huff, M. K. Peters, *Tetrahedron* **1981**, *37*, 3589.
[5] M. J. Crossley, P. Thordarson, J. P. Bannerman, P. J. Maynard, *J. Porphyrins Phthalocyanines* **1998**, *2*, 511.
[6] M. J. Crossley, L. G. King, *J. Chem. Soc. Chem. Commun.* **1984**, 920.
[7] M. J. Crossley, P. L. Burn, *J. Chem. Soc. Chem. Commun.* **1987**, 39.
[8] Calculated by molecular modeling studies using Hyperchem (PM3): *Hyperchem 6.01*, Hypercube Inc., Gainesville, FL, **2000**.
[9] O. Q. Munro, J. C. Bradley, R. D. Hancock, H. M. Marques, F. Marsicano, P. W. Wade, *J. Am. Chem. Soc.* **1992**, *114*, 7218.
[10] O. Q. Munro, H. M. Marques, P. G. Debrunner, K. Mohanrao, W. R. Scheidt, *J. Am. Chem. Soc.* **1995**, *117*, 935.
[11] H. M. Marques, O. Q. Munro, N. E. Grimmer, D. C. Levendis, F. Marsicano, G. Pattrick, T. Markoulides, *J. Chem. Soc. Faraday Trans.* **1995**, *91*, 1741.
[12] H. L. Anderson, *Inorg. Chem.* **1994**, *33*, 972.
[13] P. N. Taylor, H. L. Anderson, *J. Am. Chem. Soc.* **1999**, *121*, 11538.
[14] M. J. Crossley, L. G. Mackay, J. N. H. Reek, A. C. Try, R. A.-S. Wu, unpublished results.
[15] M. J. Crossley, T. W. Hambley, L. G. Mackay, A. C. Try, R. Walton, *J. Chem. Soc. Chem. Commun.* **1995**, 1077.

A Four-Step Alternating Reductive Dimerization/Bond Cleavage of Indenocorannulene**

Ivan Aprahamian, Roy E. Hoffman, Tuvia Sheradsky, Dorin V. Preda, Mihail Bancu, Lawrence T. Scott, and Mordecai Rabinovitz*

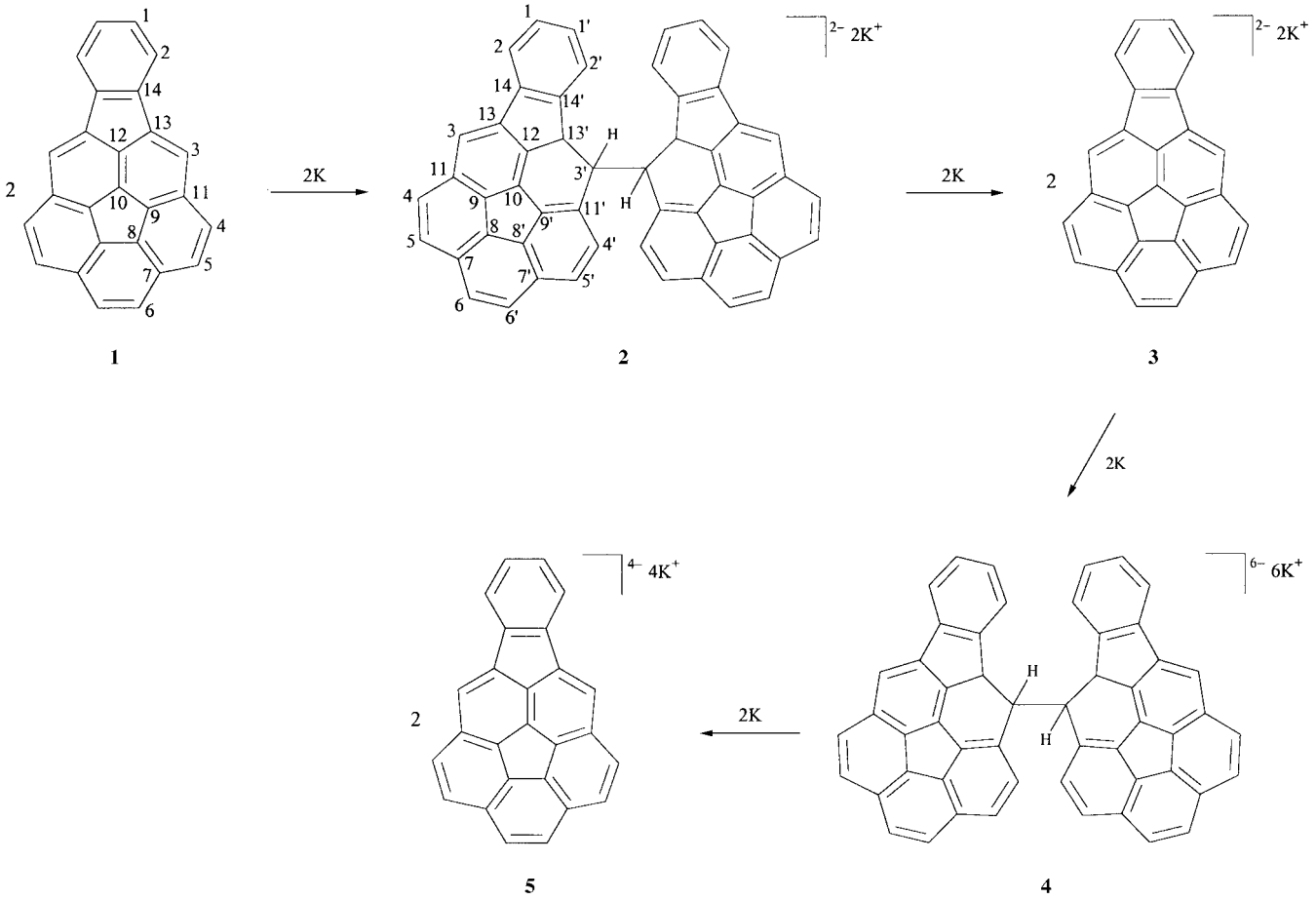
The reduction of polycyclic aromatic hydrocarbons (PAHs) with alkali metals yields negatively charged π-conjugated molecules,[1] which may undergo structural changes, from structural distortions[2] and aggregation,[3] to the formation of new chemical bonds.[4] An anionic dimer is produced when a new σ bond forms between two identical units.[5] Such a reductive dimerization process, that is, radical anion coupling, was observed in the reduction of azulene[6] and in the reductions of certain benzofulvene derivatives.[7] In the former case, further reduction dissociates the newly formed σ bond to afford the azulene dianion and, to our knowledge, this sequence was the first reductive dimerization/bond-cleavage process ever observed.[6] The formation of aggregates upon reduction of PAHs has been observed with the lithium salt of the corannulene tetraanion,[3a] which is the smallest curved subunit of a fullerene. However, aggregation was not observed in the reductions of corannulene derivatives with extended π frameworks, towards fullerenes.[8] Here we report that a curved polycycle, indenocorannulene (**1**), undergoes an unprecedented, alternating, four-step dimerization/bond-cleavage process upon reduction with potassium.

Reduction of **1** with potassium, by successive one-electron transfers, produces four diamagnetic reduction states. Each reduction stage was visually apparent from the change in color and this was monitored by NMR spectroscopy. The first and third stages of reduction give ions **2** (dianion, dark brown) and **4** (hexaanion, green), respectively (Scheme 1), which exhibit doubling of all the NMR resonance signals (Figure 1). The second and fourth stages of reduction give ions **3** (dianion, purple) and **5** (tetraanion, violet), respectively, which have the same simple resonance pattern as the neutral **1** (Figure 1), and their ^{13}C NMR spectra (Table 1) indicate the presence of only sp^2-hybridized carbon atoms. The ^{1}H NMR spectra of **2** and **4** did not show the presence of any dynamic processes over a wide range of temperatures; their ^{13}C NMR spectra (Table 1) each show an extremely upfield signal at $\delta = 56.5$ and 47.6 ppm, respectively (assigned to C3′, see Scheme 1). The

[*] Prof. M. Rabinovitz, I. Aprahamian, Dr. R. E. Hoffman, Prof. T. Sheradsky
Department of Organic Chemistry and
The Lise Meitner-Minerva Center for Computational Quantum Chemistry
The Hebrew University of Jerusalem, Jerusalem 91904 (Israel)
Fax: (+972) 2-652-7547
E-mail: mordecai@vms.huji.ac.il
Dr. D. V. Preda, M. Bancu, Prof. L. T. Scott
Merkert Chemistry Center, Boston College
Chestnut Hill, Massachusetts, 02467-3860 (USA)

[**] We would like to thank Prof. K. Müllen for fruitful discussions. This research was supported by the Israel Science Foundation (Grant No. 147100; M.R. and L.T.S.) and the U.S. Department of Energy (L.T.S.).

 © WILEY-VCH Verlag GmbH, 69451 Weinheim, Germany, 2002 1433-7851/02/4110-1712 $ 20.00+.50/0



Scheme 1. The stepwise reduction process of **1** with potassium.

long-range $^{13}C-^{1}H$ correlation experiments (HMBC) conducted on species **2** and **4** exhibited an unexpected $^{13}C-^{1}H$ correlation, in addition to the three-bond interactions that helped in the full assignment of the carbon spectra. The unexpected interaction was a long-range correlation between C3′ and H3′, which is attached to carbon atom C3′. In addition to the expected one-bond couplings ($^{1}J_{C3',H3'} = 131.7$ and 124.6 Hz, respectively, for **2** and **4**), long-range couplings between H3′ and its symmetrical equivalent were observed from the ^{13}C NMR satellite signals ($^{3}J_{H3',*H3'} = 10.0$ and 10.5 Hz, respectively, for **2** and **4**) in the short-range $^{13}C-^{1}H$ correlation experiments (HSQC).

Oxygen-quench experiments conducted on all the reduced species afforded the neutral species **1**, which indicates that the reduction process might be reversible and that the carbon framework does not degrade.

The process depicted in Scheme 1 is based on the results attained from the ^{1}H NMR, ^{13}C NMR, and 2D NMR spectroscopic measurements. The alternate doubling of signals in the NMR spectra, both in the ^{13}C NMR and in the ^{1}H NMR spectra, indicates that the reduction with potassium affords species of different molecular structures, depending on the degree of reduction. The upfield resonance signal of carbon atom C3′ in species **2** and **4**, and the magnitude of its $^{1}J_{C,H}$ coupling constant, are compatible with an sp^3-hybridized carbon atom. The extra interaction observed in the HMBC experiments on species **2** and **4** indicates that a reaction has taken place between two identical C3 carbon atoms, which thus forms the sp^3-hybridized carbon atoms. All these observations suggest that the alternating duplication of both ^{1}H NMR and ^{13}C NMR spectra is a result of a σ-bond formation between the C3 carbon atoms of two units of **1**, which lowers the symmetry of each component in the system.

Further evidence for the dimerization process can be gained from calculations of the atomic-orbital coefficients of both the LUMO and the LUMO + 1 of **1**. DFT calculations (B3LYP/6-311G**),[9–11] predict a high spin density for the odd electron in the monoanion radical and the trianion radical of **1** at C3, which supports the hypothesis of a radical coupling at this carbon atom. The upfield chemical shift of the NMR resonance signals of all the C3 carbon atoms also lends strength to our conclusions. The presence of a dibenzofulvene moiety in **1**, and its dimerization when reduced to an anion radical (Scheme 2), is reminiscent of the behavior of the parent dibenzofulvene.[5, 7]

The bowl shape of **1**, which does not undergo a dynamic process on the NMR spectroscopy timescale, imparts chirality to each half of the dimer. This property leads to the interesting possibility of multiple diastereomeric reduced species, depending on the position of the connection. Even if one assumes that the new σ bond forms on the less hindered *exo* faces of both indenocorannulenes in each dimer, two possible isomers still remain (Figure 2). The NMR spectra of dimers **2** and **4**, however, contain only one major set of signals,

 © WILEY-VCH Verlag GmbH, 69451 Weinheim, Germany, 2002 1433-7851/02/4110-1713 $ 20.00+.50/0

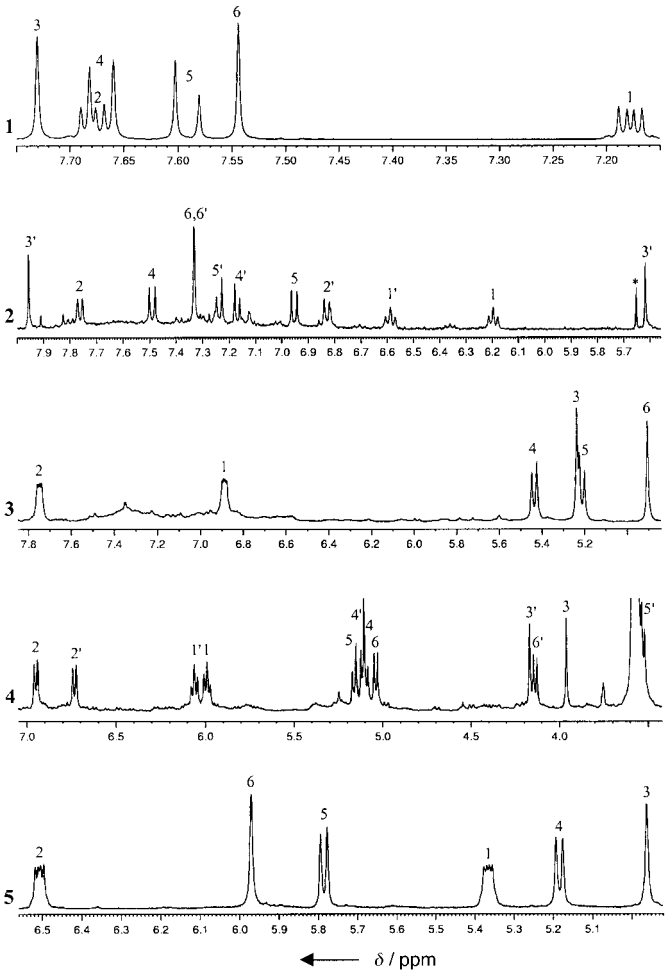
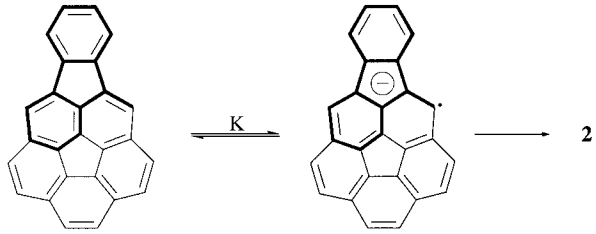


Figure 1. The ^{1}H NMR (400 MHz) spectra of **1**–**5** in [D$_8$]THF. The signal assigned to hydrogen atoms 6 and 6′ in spectrum **2** appears to be a singlet because their chemical shifts are coincident. The ∗ in **2** denotes the signal of an impurity.

Table 1. The ^{13}C NMR (100 MHz) chemical shifts (δ) of **1**–**5** in [D$_8$]THF.

Compound	δ [ppm]
1	145.54 (C12), 142.35 (C13), 140.74 (C14), 140.43 (C10), 139.27 (C9), 138.87 (C11), 138.60 (C8), 131.26 (C7), 129.25 (C1), 129.19 (C4), 127.95 (C6), 127.73 (C5), 123.01 (C3), 122.52 (C2)
2	148.41(C14′), 145.99 (C9′), 143.15 (C12), 142.29 (C9), 138.88 (C8), 136.22 (C8′), 133.08 (C13), 132.94 (C14), 132.50 (C11′), 131.85 (C4′ + C7′), 130.37 (C10), 129.75 (C4), 129.69 (C7), 128.81 (C11), 126.27 (C6), 125.30 (C6′), 124.36 (C3), 123.42 (C1′), 121.91 (C5′), 121.57 (C2), 118.04 (C5), 113.56 (C2′), 108.69 (C1), 95.88 (C13′), 56.56 (C3′, $^1J_{C,H}$ = 131.7 Hz, $^3J_{H,*H}$ = 10.0 Hz)
3	163.22 (C10), 156.73 (C8), 140.48 (C9), 138.43 (C12), 133.14 (C14), 132.28 (C11), 132.02 (C7), 131.77 (C4), 126.81 (C5), 118.98 (C2), 113.79 (C6), 113.58 (C13), 110.44 (C1), 107.72 (C3)
4	146.14 (C8′), 145.79 (C9), 145.48 (C7′), 142.31 (C8), 141.65 (C11), 141.04 (C9′), 139.39 (C12′), 131.92 (C10, C11′), 125.96 (C14′), 125.38 (C6), 123.79 (C5), 119.35 (C4′), 118.71 (C7), 118.27 (C14), 118.18 (C4), 114.44 (C2), 112.97 (C2′), 109.93 (C1′), 107.94 (C1), 106.28 (C13′), 104.48 (C13), 103.87 (C6′), 92.87 (C5′), 87.52 (C3), 47.59 (C3′, $^1J_{C,H}$ = 124.6 Hz, $^3J_{H,*H}$ = 10.5 Hz)
5	143.12 (C11), 124.74 (C8), 123.69 (C9), 123.21 (C12), 122.51 (C13), 119.92(C7), 117.58 (C10), 115.22 (C2), 114.12 (C14), 113.46 (C6), 111.03 (C5), 109.82 (C1), 96.96 (C4), 82.62 (C3)



Scheme 2. The dibenzofulvene-like behavior of the radical anion of **1**.

so one species clearly dominates in each case.[12] Presumably the various stereoisomeric dimers interconvert on the time-scale of the experiment, either by dissociation–recombination, or by slow bowl-to-bowl inversion, or both, and the equilibration is driven by thermodynamic considerations. From the data available, unfortunately, it is not possible to assign fully the stereochemistry of dimers **2** and **4**, although it is apparent from the $^3J_{H,*H}$ coupling constant mentioned above that they adopt an *anti* conformation.

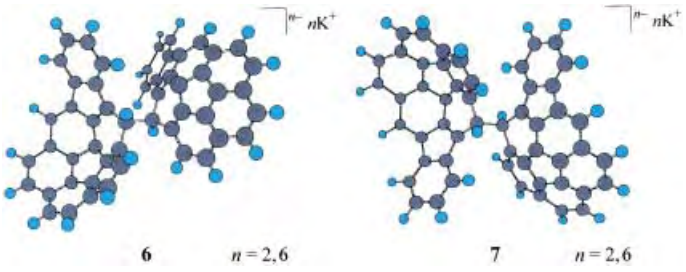


Figure 2. Proposed structures for the observed dimer. Structure **6** depicts the chiral diastereomeric dimer (racemic) and structure **7** depicts the *meso* dimer.

This is the first time that a large nonplanar PAH has demonstrated such a fascinating repetitive dimerization/bond-cleavage process upon reduction. It is also the first time that such a process has been extended beyond a single dimerization/bond-cleavage stage. The ability of **1** to exhibit a second round of this behavior is presumably a consequence of its relatively large size, which allows it to accommodate a high degree of charge, in addition to its electronic structure, which makes the radical coupling possible.[13]

Received: December 7, 2001 [Z 18352]

[1] a) K. Müllen, *Chem. Rev.* **1984**, *84*, 603–646, and references therein; b) M. Rabinovitz, *Top. Curr. Chem.* **1988**, *146*, 99–169, and references therein; c) R. Benshafrut, E. Shabtai, M. Rabinovitz, L. T. Scott, *Eur. J. Org. Chem.* **2000**, 1091–1106, and references therein.
[2] For example: L. Eshdat, A. Ayalon, R. Beust, R. Shenhar, M. Rabinovitz, *J. Am. Chem. Soc.* **2000**, *122*, 12637–12645.
[3] a) A. Ayalon, A. Sygula, P.-C. Cheng, M. Rabinovitz, P. W. Rabideau, L. T. Scott, *Science* **1994**, *265*, 1065–1067; b) R. Shenhar, H. Wang, R. E. Hoffman, L. Frish, L. Avram, I. Willner, A. Rajca, M. Rabinovitz, *J. Am. Chem. Soc.* **2002**, in press.
[4] For example: H. Bock, Z. Havlas, K. Gharagozloo-Hubmann, M. Sievert, *Angew. Chem.* **1999**, *111*, 2379–2382; *Angew. Chem. Int. Ed.* **1999**, *38*, 2240–2243.
[5] M. Baumgarten, K. Müllen, *Top. Curr. Chem.* **1994**, *169*, 1–103, and references therein.
[6] U. Edlund, B. Eliasson, *J. Chem. Soc. Chem. Commun.* **1982**, 950–952.
[7] E. D. Bergmann, *Chem. Rev.* **1968**, *68*, 41–84, and references therein.

 © WILEY-VCH Verlag GmbH, 69451 Weinheim, Germany, 2002 1433-7851/02/4110-1714 $ 20.00+.50/0

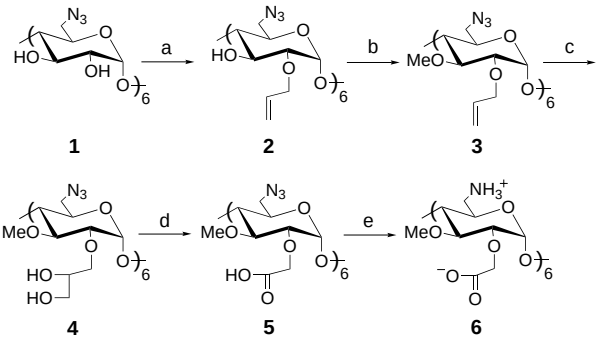
[8] A. Weitz, E. Shabtai, M. Rabinovitz, M. S. Bratcher, C. C. McComas, M. D. Best, L. T. Scott, *Chem. Eur. J.* **1998**, *4*, 234 – 239.
[9] Gaussian 98 (Revision A.7), M. J. Frisch, G. W. Trucks, H. B. Schlegel, G. E. Scuseria, M. A. Robb, J. R. Cheeseman, V. G. Zakrzewski, J. A. Montgomery, R. E. Stratmann, J. C. Burant, S. Dapprich, J. M. Millam, A. D. Daniels, K. N. Kudin, M. C. Strain, O. Farkas, J. Tomasi, V. Barone, M. Cossi, R. Cammi, B. Mennucci, C. Pomelli, C. Adamo, S. Clifford, J. Ochterski, G. A. Petersson, P. Y. Ayala, Q. Cui, K. Morokuma, D. K. Malick, A. D. Rabuck, K. Raghavachari, J. B. Foresman, J. Cioslowski, J. V. Ortiz, B. B. Stefanov, G. Liu, A. Liashenko, P. Piskorz, I. Komaromi, R. Gomperts, R. L. Martin, D. J. Fox, T. Keith, M. A. Al-Laham, C. Y. Peng, A. Nanayakkara, C. Gonzalez, M. Challacombe, P. M. W. Gill, B. G. Johnson, W. Chen, M. W. Wong, J. L. Andres, M. Head-Gordon, E. S. Replogle, J. A. Pople, Gaussian, Inc., Pittsburgh, PA, **1998**.
[10] a) A. D. Becke, *J. Chem. Phys.* **1993**, *98*, 5648 – 5652; b) A. D. Becke, *Phys. Rev. A* **1988**, *38*, 3098 – 3100; c) C. Lee, W. Yang, R. G. Parr, *Phys. Rev. B* **1988**, *37*, 785 – 789; d) H. Vosko, L. Wilk, M. Nusair, *Can. J. Phys.* **1980**, *58*, 1200 – 1211.
[11] a) W. J. Hehre, R. Ditchfield, J. A. Pople, *J. Chem. Phys.* **1972**, *56*, 2257 – 2261; b) P. C. Hariharan, J. A. Pople, *Theor. Chim. Acta* **1973**, *28*, 213 – 222; c) R. Krishnan, J. S. Binkley, R. Seeger, J. A. Pople, *J. Chem. Phys.* **1980**, *72*, 650 – 654.
[12] A duplication pattern of a minor component is observed in the ^{1}H NMR spectrum of **3**, which is in a ratio of 1:5 to the major component.
[13] The ability to accommodate a high degree of charge is not the only factor required for the repetition of the process. Azulenes with extended π-conjugation afforded only a single coupling/bond-cleavage process upon reduction, whereas their trianion radicals did not dimerize. For example: a) M. Baier, J. Daub, A. Hasenhündl, A. Merz, K. M. Rapp, *Angew. Chem.* **1981**, *93*, 196 – 197; *Angew. Chem. Int. Ed. Engl.* **1981**, *20*, 198 – 199; b) J. Daub, J. Salbeck, *Chem. Ber.* **1989**, *122*, 727 – 735; c) J. Salbeck, J. Daub, *Chem. Ber.* **1989**, *122*, 1681 – 1690.

Per(6-amino-2-*O*-carboxymethyl-6-deoxy-3-*O*-methyl)-α-cyclodextrin: Helical Self-Assembly of a Polyionic Amino Acid into Nanotubes**

Tomáš Kraus,* Miloš Buděšínský, Ivana Císařová, and Jiří Závada*

Designed macrocyclic oligopeptides[1] and oligosaccharides[2] serve as versatile building units (tectons) for supramolecular self-assembly of nanotubes.[3] In this respect, cyclodextrin derivatives possessing a hollow, chiral, truncated-cone interior with a variable diameter deserve particular interest. The two rims of cyclodextrin, respectively bearing primary and secondary hydroxy groups, can be selectively modified to create complementary binding sites. Cyclodextrins monofacially persubstituted at the primary rim with carboxy groups were already shown[4] to self-assemble in nonpolar solvents into dimeric head-to-head hydrogen-bonded aggregates. Analogous amino-persubstituted cyclodextrins associate, on treatment with the corresponding monofacially carboxymethyl-persubstituted derivatives, by means of ionic hydrogen bonds into head-to-head heterodimers, which persist even in aqueous solutions.[5, 6] This strongly suggests that hermaphroditic cyclodextrins bearing complementary donor and acceptor groups on the opposite rims might self-assemble into infinite head-to-tail chiral nanotubes. We designed hexakis(6-amino-2-*O*-carboxymethyl-6-deoxy-3-*O*-methyl)-α-cyclodextrin (**6**) as a model for such investigation. Here we report on its synthesis and its unique architecture in the solid state.

The persubstituted amino acid **6** is an elusive target because of the array of incompletely substituted derivatives that can arise and persist in the course of synthesis.[7] To obtain a chemically uniform persubstituted product, which is indispensable for X-ray diffraction analysis, we employed a novel procedure[8] for the facial percarboxymethylation of cyclodextrins. Starting from the easily accessible[9] hexakis(6-azido-6-deoxy)-α-cyclodextrin (**1**; Scheme 1), all secondary hydroxy groups at C2 were selectively allylated, and the pure hexaallyl derivative **2** was isolated by chromatography in 52% yield. Subsequent methylation of the free hydroxy groups at C3 furnished the peralkylated compound **3** in a quantitative yield. The allylic groups of **3** were catalytically dihydroxylated with osmium tetroxide and 4-methylmorpholine *N*-oxide as auxiliary oxidant, and the resulting mixture of diastereoisomers **4** was isolated by reversed-phase chromatography in 71% yield. The diol groups were cleaved with sodium periodate and, in the same pot, the intermediate polyaldehyde was oxidized to the carboxymethyl derivative **5** with TEMPO/NaClO/KBr in an overall yield of 91%. Customary reduction of per-6-azidocyclodextrins with triphenylphosphane surprisingly failed. However, an excellent alternative for the reduction



Scheme 1. a) Allyl bromide, $Ba(OH)_2 \cdot H_2O$, BaO, DMF, 25 °C, 24 h, 52%; b) MeI, NaH, DMF, 25 °C, 3.5 h, 99%; c) OsO_4, 4-methylmorpholine *N*-oxide, acetone/water, 25 °C, 24 h, 71%; d) 1. $NaIO_4$, H_2O, 25 °C, 2.5 h; 2. TEMPO, NaBr, NaClO, 25 °C, 2.5 h, 91%; e) H_2S, pyridine/water, 25 °C, 72 h, 90%. TEMPO = 2,2,6,6-tetramethyl-1-piperidineoxyl.

[*] Dr. T. Kraus, Dr. J. Závada, Dr. M. Buděšínský
Institute of Organic Chemistry and Biochemistry
Academy of Sciences of the Czech Republic
Flemingovo nám. 2, 166 10 Prague 6 (Czech Republic)
Fax: (+420) 2-33331-733
E-mail: kraus@uochb.cas.cz, zavada@uochb.cas.cz
Dr. I. Císařová
Department of Inorganic Chemistry, Charles University
Hlavova 2030, 128 40 Prague 2 (Czech Republic)

[**] This work was supported by the Grant Agency of the Czech Republic (203/01/D082, 203/00/137). I.C. is grateful for an instrument-providing grant (203/99/M037) and for access to the CSD (203/02/0436).

Supporting information for this article is available on the WWW under http://www.angewandte.com or from the author.

 © WILEY-VCH Verlag GmbH, 69451 Weinheim, Germany, 2002 1433-7851/02/4110-1715 $ 20.00+.50/0

of **5** was devised by using hydrogen sulfide[10] in pyridine/water, which allowed isolation of the pure amino acid **6** in nearly quantitative yield.

At neutral pH, the zwitterionic **6** is insoluble in both protic (water, methanol, ethanol) and dipolar aprotic solvents (dimethyl sulfoxide) at ambient temperature and at the boiling point. However, it dissolves readily in water on addition of an acid (HCl) or a base (NaOH, NH_4OH). Structural identity and homogeneity of the product were proved by ^1H and ^{13}C NMR spectra of the water-soluble hydrochloride salt of **6** which confirmed the expected symmetry of the molecule. Single crystals of the free amino acid **6** could be obtained by slow evaporation of a solution in aqueous ammonia.

Cyclodextrins and their derivatives and inclusion complexes crystallize in three arrangements:[11] cage, channel, and layer types. In the crystal structure of **6** we have identified[12] a highly symmetrical arrangement (space group *R*3) unique in the family of cyclodextrins. Individual cyclodextrin tectons recline on helical (staircase) trajectories (Figures 1 and 2) along the crystallographic *c* axis so that the *i*th and $(i+3)$th tectons always occupy eclipsed positions (e.g., units A and D in Figure 1a). An infinite array of parallel columns thus results in which each column is shifted by $\pm 1/3$ of the cell parameter *c* with respect to its neighbors.

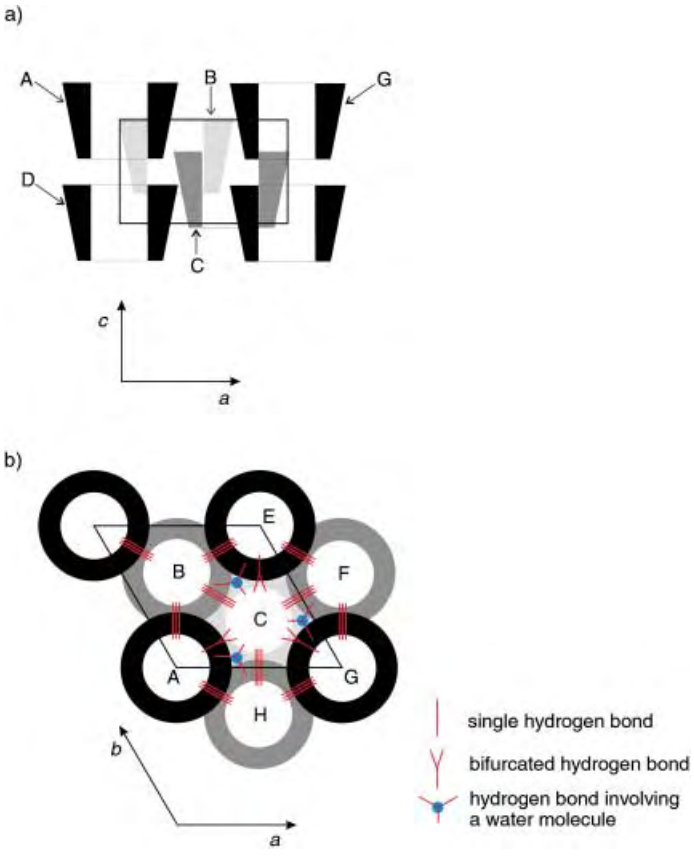


Figure 1. Schematic representation of packing of **6** in the unit cell; a) view along the *b* axis; b) view along the *c* axis with hydrogen bonds depicted as red lines (tectons F and H are added to the unit cell to describe the complete bonding pattern). The degree of shading reflects the relative distance of CD units from the observer (black represents the nearest macrocycles).

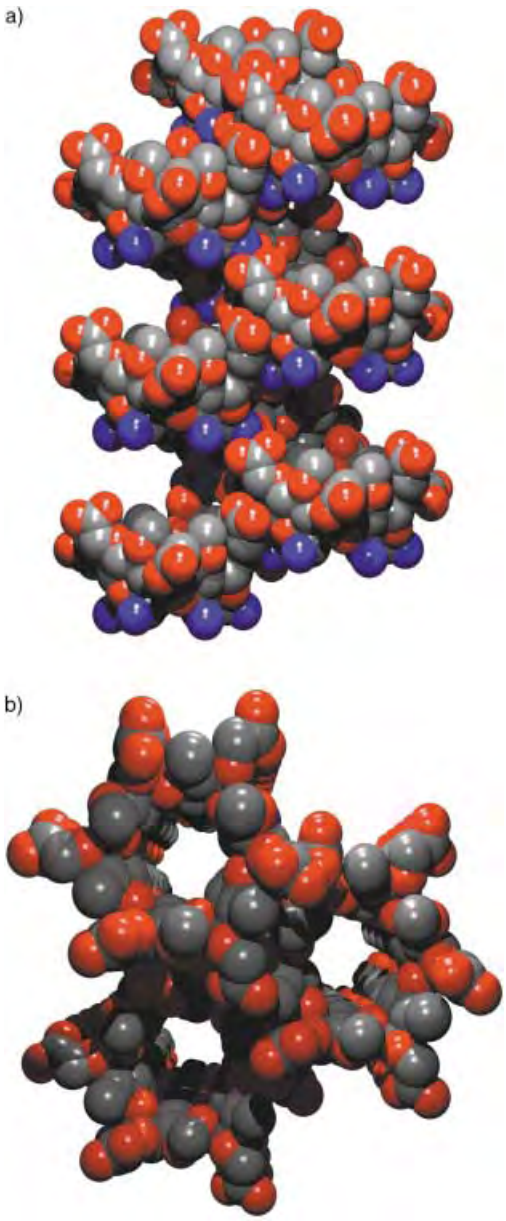


Figure 2. Space-filling representation of the crystal structure of **6**; a) helical arrangement viewed along the *b* axis and b) open channels viewed along the *c* axis. Hydrogen atoms and water molecules are omitted for clarity.

A closer analysis reveals that the helical framework is held together by hydrogen bonds (red lines in Figure 1b). A complete proton transfer from carboxy to amino groups occurs in the crystal. The overall hydrogen-bonding pattern is nonetheless complex; each cyclodextrin unit is anchored to its neighbors by 30 hydrogen bonds. Each pair of neighboring cyclodextrins is bonded by three intermolecular hydrogen bonds; two bonds are formed between ammonium cations of A and carboxylate anions of B, while the third involves an ammonium group of A and a methoxy group of B. In addition, a bifurcated hydrogen bond connects an ammonium group of molecule A and a carboxylate moiety of another proximate cyclodextrin C. One of the five water molecules (in fully occupied positions[13]) contributes to the overall stability of the helix by accepting two free hydrogen atoms from

 © WILEY-VCH Verlag GmbH, 69451 Weinheim, Germany, 2002 1433-7851/02/4110-1716 $ 20.00+.50/0

ammonium cations, one from macrocycle A and the other from macrocycle H; at the same time, it acts as a donor for two hydrogen bonds to the oxygen atom of one carboxy group of C and a neighboring water molecule (for the detailed description of hydrogen bonds and an ORTEP plot, see Supporting Information).

Each of the three glucose pairs of the cyclodextrin macrocycle respectively acts as a donor and acceptor of hydrogen bonds in two helices that differ in the sense of twist. Thus, each cyclodextrin unit represents a nodal point of six intersecting helices with alternating handedness (e.g., ABC, EBC, EFC, GFC, GHC, and AHC, as depicted for the central macrocycle C in Figure 1b).[14] In this way, a strong hydrogen-bonded network is formed that cross-links the parallel columns, but the surprising feature is the complete absence of hydrogen bonds between the proximate heads and tails of the eclipsed tectons in the individual columns. This differs from the customary[11] cyclodextrin channel architecture, in which hydrogen-bonding interactions bind together the tectons stacked in the individual columns, whereas weak van der Waals interactions govern the packing along the remaining directions.

Although the distance between the faces of the eclipsed cyclodextrin units is 4 Å in the crystal of **6**, the staircase arrangement of cyclodextrin units in the neighboring columns effectively shields these "holes" and gives rise to a system of separate straight channels. Thus, the helical self-assembly of the C_3-symmetrical α-cyclodextrin tectons **6** gives rise to a highly cross-linked, densely packed nanotubular material; the higher (β- and γ-) homologues, which are now on our agenda, are envisaged to open access to other chiral tubular superstructures, with different porosity and other physicochemical properties (e.g., solubility).

Experimental Section

^{1}H and ^{13}C spectra were assigned by using 2D COSY and ^{1}H-^{13}C 2D-HMQC experiments; hard copies of the spectra of the hexahydrochloride of **6** can be found in the Supporting Information.

Hexakis(6-amino-2-*O*-carboxymethyl-6-deoxy-3-*O*-methyl)-α-cyclodextrin hexahydrochloride: Compound **6** (20 mg, 12.6 μmol) was dispersed in water (1 mL), and aqueous hydrochloric acid (0.10 N, 0.130 mL, 13 μmol) was added. The solution was lyophilized to give a white foam (22.4 mg, 99 %, calculated for nonahydrate). ^{1}H NMR (D_2O, 500 MHz, 50 °C): δ = 3.69 (dd, $J(6',6)$ = 13.8, $J(6',5)$ = 5.4 Hz, 6H, H-6′), 3.79 (dd, $J(6,6')$ = 13.8, $J(6,5)$ = 3.8 Hz, 6H, H-6), 3.90 (dd, $J(2,1)$ = 3.3, $J(2,3)$ = 9.8 Hz, 6H, H-2), 3.97 (s, 18H, OCH_3), 4.04 (dd, $J(4,3)$ = 8.1, $J(4,5)$ = 9.2 Hz, 6H, H-4), 4.20 (dd, $J(3,2)$ = 9.8, $J(3,4)$ = 8.1 Hz, 6H, H-3), 4.57 (m, $J(5,4)$ = 9.2, $J(5,6)$ = 3.8, $J(5,6')$ = 5.4 Hz, 6H, H-5), 4.72 (s, 12H, OCH_2COO), 5.64 (d, $J(1,2)$ = 3.3 Hz, 6H, H-1); ^{13}C NMR (D_2O, 125.7 MHz, 50 °C): δ = 43.42 (C-6), 63.89 (OCH_3), 71.24 (C-5), 71.25 (OCH_2COOH), 82.16 (C-2), 83.68 (C-4), 83.71 (C-3), 102.15 (C-1), 177.15 (OCH_2COOH); ESI-MS: *m*/*z*: 1399.4 (30 %) $[M+H]^+$, 700.4 (100 %) $[M+2H]^{2+}$; elemental analysis (%) calcd for $C_{54}H_{96}Cl_6N_6O_{36}\cdot 9H_2O$: C 36.43, H 6.45, N 4.72; found: C 36.44, H 6.25, N 4.55.

Received: October 29, 2001
Revised: February 26, 2002 [Z18128]

[1] a) M. R. Ghadiri, J. R. Granja, R. A. Milligan, D. E. McRee, N. Khazanovich, *Nature* **1993**, *366*, 324–327; b) J. D. Hartgerink, J. R. Granja, R. A. Milligan, M. R. Ghadiri, *J. Am. Chem. Soc.* **1996**, *118*, 43–50; c) J. Sánchez-Quesada, H. Sun Kim, M. R. Ghadiri, *Angew. Chem.* **2001**, *113*, 2571–2574; *Angew. Chem. Int. Ed.* **2001**, *40*, 2503–2506.

[2] a) G. Gattuso, S. Menzer, S. A. Nepogodiev, J. F. Stoddart, D. J. Williams, *Angew. Chem.* **1997**, *109*, 1615–1617; *Angew. Chem. Int. Ed. Engl.* **1997**, *36*, 1451–1454; b) P. R. Ashton, S. J. Cantrill, G. Gattuso, S. Menzer, S. A. Nepogodiev, A. N. Shipway, J. F. Stoddart, D. J. Williams, *Chem. Eur. J.* **1997**, *3*, 1299–1314.

[3] D. T. Bong, T. D. Clark, J. R. Granja, M. R. Ghadiri, *Angew. Chem.* **2001**, *113*, 1016–1041; *Angew. Chem. Int. Ed.* **2001**, *40*, 988–1011.

[4] T. Kraus, M. Buděšínský, J. Závada, *Eur. J. Org. Chem.* **2000**, 3133–3137.

[5] L. Jullien, H. Cottet, B. Hamelin, A. Jardy, *J. Phys. Chem. B* **1999**, *103*, 10866–10875.

[6] B. Hamelin, L. Jullien, C. Derouet, C. H. du Penhoat, P. Berthault, *J. Am. Chem. Soc.* **1998**, *120*, 8438–8447.

[7] B. J. Ravoo, R. Darcy, A. Mazzaglia, D. Nolan, K. Gaffney, *Chem. Commun.* **2001**, 827–828.

[8] T. Kraus, M. Buděšínský, J. Závada, *J. Org. Chem.* **2001**, *66*, 4595–4600.

[9] T. Kraus, M. Buděšínský, J. Závada, *Collect. Czech. Chem. Commun.* **1998**, *63*, 534–540.

[10] S. Kusumuto, K. Sakai, T. Shiba, *Bull. Chem. Soc. Jpn.* **1986**, *59*, 1296–1298.

[11] K. Harata, *Chem. Rev.* **1998**, *98*, 1803–1827.

[12] Crystallographic data for **6**: Prismatic crystals were grown from a solution of **6** in aqueous ammonia; $C_{54}H_{126}N_6O_{54}$, M_r = 1723.61, ρ_{calcd} = 1.279 g cm^{-3}, crystal dimensions 0.3 × 0.25 × 0.1 mm, trigonal, space group *R*3 (No. 146), a = 23.2901(4), c = 14.2681(3) Å, Z = 3. Data collection: Nonius Kappa CCD diffractometer, $Mo_{K\alpha}$ radiation (λ = 0.71073 Å, graphite monochromator) at 150(2) K. A total of 36549 reflections were collected, 6747 were unique (R_{int} = 0.040), and 6091 observed ($I > 2\sigma(I)$). The structure was solved by direct methods (SIR 97[15a]) and refined by full-matrix least-squares technique on F^2 (SHELXL97[15b]). The hydrogen atoms were located on the difference Fourier map, except those on partially occupied water molecules; however, some of them behaved erroneously during refinement, and therefore all hydrogen atoms of the cyclodextrin moiety were recalculated in idealized positions (riding model) and assigned temperature factors $H_{iso}(H) = 1.2\,U_{eq}$ (pivot atom), multiplied by 1.5 for the methyl group. Final *R* factors: R_1 = 0.049 (observed data) and 0.057 (all data); wR_2 = 0.134, S = 1.057, 365 parameters. Residual peaks on final difference map were $\Delta\rho_{max}$ = 0.760 and −0.296 e Å^{-3}. CCDC 171795 contains the supplementary crystallographic data for this paper. These data can be obtained free of charge via www.ccdc.cam.ac.uk/conts/retrieving.html (or from the Cambridge Crystallographic Data Centre, 12, Union Road, Cambridge CB2 1EZ, UK; fax: (+44) 1223-336-033; or deposit@ccdc.cam.ac.uk).

[13] Aside from the five molecules of water (per asymmetric unit, i.e., one glucose pair of the cyclodextrin macrocycle) fully occupying positions in the intercolumnar space, there are disordered water molecules that partially occupy two distinguishable positions; one is located above the secondary rim of the cavity, while the other is situated in the mean plane defined by the methoxy groups, so that the space inside the cyclodextrin cavity is essentially left empty (see Supporting Information).

[14] All cyclodextrin units in the crystal lattice are equivalent; the arbitrary denotations A–H are only used to describe the bonding pattern.

[15] a) A. Altomare, M. C. Burla, M. Camalli, G. L. Cascarano, C. Giacovazzo, A. Guagliardi, A. G. G. Moliterni, G. Polidori, R. Spagna, *J. Appl. Crystallogr.* **1999**, *32*, 115–119; b) G. M. Sheldrick, SHELXL97, Program for crystal structure refinement from diffraction data, University of Gottingen, Göttingen, **1997**.

 © WILEY-VCH Verlag GmbH, 69451 Weinheim, Germany, 2002 1433-7851/02/4110-1717 $ 20.00+.50/0

cis-2-Aminocyclopentanecarboxylic Acid Oligomers Adopt a Sheetlike Structure: Switch from Helix to Nonpolar Strand**

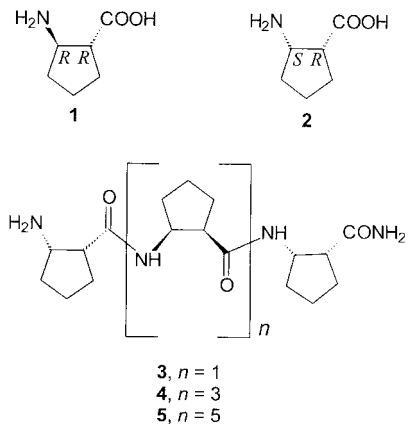
Tamás A. Martinek, Gábor K. Tóth, Elemér Vass, Miklós Hollósi, and Ferenc Fülöp*

It is now well known that biological molecules (peptides and RNA) are not alone in forming periodic secondary structures.[1] The extremely rapidly growing area of nonnatural foldamers has provided a number of examples of synthetic molecular chains, and especially β-peptides, which adopt well-defined three-dimensional structures.[2–4] Interest has recently turned towards the residue-based control of secondary structure formation, and it was demonstrated that the substituent pattern and the stereochemistry do indeed exert certain effects on the β-peptide folding.[5] The conformational control over the secondary structure continues to attract considerable interest,[6, 7] and the induced switch between a stable helix and a stable nonpolar strand with a propensity to form a pleated sheet remains an unresolved problem. Here we show that, by inversion of the relative configuration of conformationally restricted cyclic β-amino acid residues, the preferred periodic structure can be switched from a helix to a single nonpolar strand. These results may furnish a general tool for foldamer designers, thereby promoting the synthesis of future tertiary structures of β-peptides.

β-Oligopeptides consisting of *trans*-2-aminocyclohexanecarboxylic acid and *trans*-2-aminocyclopentanecarboxylic acid (*trans*-ACPC, **1**) monomers (*anti*-disubstituted in the aldol convention) have been reported to exhibit an especially high propensity to form helical structures[8] and the rational residue-based control of helix shape could be achieved by the application of these fascinating molecules. After the first successes, the natural question emerged of whether the 1*R*,2*S*-disubstitution of the cyclic β-amino acid monomers leads to a stable secondary structure or to a random coil conformation.

We used homo-oligomers composed of *(1R,2S)*-2-aminocyclopentanecarboxylic acid/(1*R*,2*S*)-*cis*-ACPC **2** as a model system to test the effect of the inversion of the relative configuration. The generally accepted rules of thumb for the effects of the stereochemistry of the β-amino acid residues would anticipate an extended polar strand for 1*R*,2*S*-disubstitution;[9] however, the NH-C$^{\beta}$-C$^{\alpha}$-CO torsion in *cis*-ACPC is restrained in the *gauche* position, which facilitates either the helix or nonpolar strand conformation. Our preliminary modeling results do not allow the possible helix structures to be excluded from the analysis since the inter-residue steric repulsion[10] is not a real issue in the modeled helices of the *cis*-ACPC oligomers. This therefore facilitates study of the general effects of the stereochemistry on the preferences for the periodic structure formation of β-peptides with cyclic monomers.

Enantiomerically pure *(1R,2S)-cis*-ACPC oligomers **3**–**5** (Scheme 1) were prepared by solid-phase synthesis techniques, with *tert*-butoxycarbonyl chemistry.[11] The couplings were performed with *N*,*N*′-dicyclohexylcarbodiimide (DCC) without difficulty. The crude peptides were purified by reversed-phase HPLC and the compounds were characterized by mass spectrometry.



Scheme 1. Chemical structures of *trans*- and *cis*-ACPC, and the studied oligomers.

High-resolution three-dimensional structure analysis was performed in the solution phase by utilizing NMR cross-relaxation data. All NH, C$^{\alpha}$H, and C$^{\beta}$H resonances were assigned for pentamer **4** by means of standard NMR methods (TOCSY[12] and ROESY[13]). The linewidths and chemical shifts seen in the NMR spectra as well as the ROESY cross-peak pattern of **4** were identical for 1 mM and 8 mM samples, thus demonstrating the absence of any uncontrolled aggregation in [D$_6$]DMSO. The studied compounds, **4** and **5**, displayed very similar ROESY cross-peak patterns, but the unsatisfactory chemical shift resolution for the heptamer led to the high-resolution conformational analysis being carried out for the pentamer only.

The low-intensity ROESY cross-peaks defining four long-range NH$_i$–C$^{\beta}$H$_{i+1}$ and NH$_i$–C$^{\beta}$H$_{i-1}$ interactions could readily be assigned in terms of monomers with $i = 1$, 2, and 3 (Figure 1a). The low chemical shift resolution of the C$^{\beta}$H$_i$ protons for monomers with $i = 3$, 4, and 5 did not allow direct assignment and integration of the expected signals, but the multiplet pattern and the increased intensity of the short-range NH$_i$–C$^{\beta}$H$_i$ cross-peaks forecast the presence of further valuable long-range NH$_i$–C$^{\beta}$H$_j$ NOE interactions as signal overlaps. To obtain direct experimental evidence, a series of

[*] Prof. Dr. F. Fülöp, Dr. T. A. Martinek
Institute of Pharmaceutical Chemistry
University of Szeged
Eötvös 6, 6720 Szeged (Hungary)
Fax: (+36) 62-545-564
E-mail: fulop@pharma.szote.u-szeged.hu
Dr. G. K. Tóth
Department of Medical Chemistry
University of Szeged
Dóm tér 10, 6720 Szeged (Hungary)
Dr. E. Vass, Prof. Dr. M. Hollósi
Department of Organic Chemistry
Eötvös Loránd University
Pázmány P. 11/17, 1117 Budapest (Hungary)

[**] We thank the Hungarian Research Foundation (OTKA) for financial support.

Supporting information for this article is available on the WWW under http://www.angewandte.com or from the author.

 © WILEY-VCH Verlag GmbH, 69451 Weinheim, Germany, 2002 1433-7851/02/4110-1718 $ 20.00+.50/0

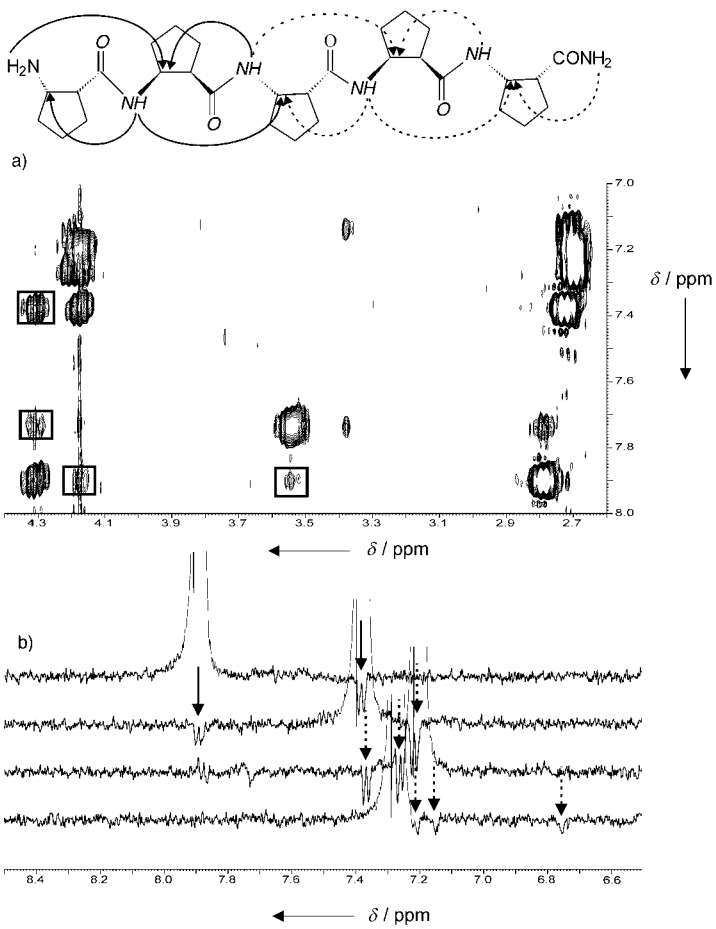


Figure 1. Spectra used for the assignment of the long-range NOE interactions: a) 2D ROESY experiment, b) selective 1D TOCSY (30 ms)/ ROESY (400 ms) experiments. The solid lines show the assignments resulting from spectrum shown in (a), while the dashed lines designate the interactions proved by the series of spectra shown in (b).

selective 1D experiments was performed (Figure 1b), which involved selective excitation of the amide proton signals, subsequent short (30 ms) homonuclear Hartmann–Hahn mixing, and a final ROESY spin-lock (400 ms). The magnetization exclusively transferred by the cross-relaxation between the NH_i and $C^{\beta}H_j$ protons could be detected as a negative phase signal in the amide region, since no direct interaction is observed between the amide protons. As a result, we obtained the full periodic pattern of the long-range $NH_i-C^{\beta}H_{i+1}$ and $NH_i-C^{\beta}H_{i-1}$ NOE interactions, which rules out any helical or random-coil conformation, and can thus be assigned to a predominantly populated strandlike secondary structure. The analysis of the corrected short-range $NH_i-C^{\beta}H_i$ and $NH_i-C^{\alpha}H_{i-1}$ cross-peak intensities provided further evidence of the highly ordered strand conformation.

To retain as much quantitative information as possible from the cross-peak integrals we calculated the intensity ratio from Equation (1), where I designates the integrated and offset-compensated ROESY cross-peak intensities. The intensity

$$R = I_{NOE}(NH_i-C^{\alpha}H_{i-1})/I_{NOE}(NH_i-C^{\beta}H_i) \quad (1)$$

ratios were compared with those calculated from the structures obtained by using the molecular mechanical force-field,[14] literature data on torsions of accessible periodic conformations, and H-bond restraints. We applied the isolated spin-pair approximation for the calculation.[15] The R value is unique for each possible secondary structure; it is in the proximity of the theoretical maximum for the six-strand conformation (Figure 2). The experimental values ($R = 5.6$, 5.9, 5.2, and 6.2 for $i = 2$, 3, 4, and 5, respectively) clearly point to the predominance of the six-strand conformation.

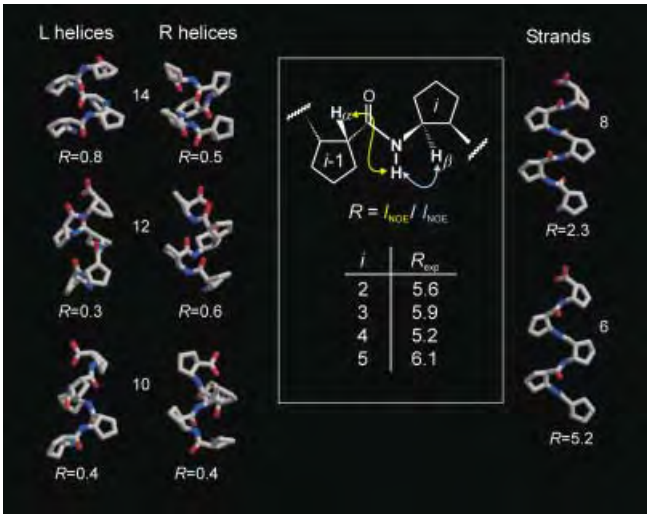


Figure 2. Calculated R values for the theoretically possible periodic conformations and the experimental values. The estimated value of R for a random-coil conformation is 2.1. See the text for the details of the calculations.

We carried out a standard restrained simulated annealing conformational search protocol by using the internuclear distances estimated from the 2D ROESY spectrum and selective ROESY experiments to reinforce our results. Each final low-energy structure displayed a mean restraint violation of less than 0.03 Å and a highest restraint violation of 0.06 Å (Figure 3). The conformational family obtained has a strand-like structure stabilized by the intra-residue electrostatic attraction between amide oxygen atoms and protons, which may form weak H-bonds in an appropriate solvent and lead to six-membered H-bonded rings. Within experimental error, the measured coupling constants $^3J(NH_i-C^{\beta}H_i)$ are uniformly 8.2 Hz, which likewise points to the presence of a periodically ordered structure and supports the result of the conformation selection protocol applied.

The test for the possible weak H-bonds stabilizing the strand was carried out by using infrared spectroscopy in the intramolecular H-bond-promoting solvent CH_2Cl_2 (Figure 4) and in the H-bond-breaking solvent DMSO at a concentration of 2 mg ml^{-1}. The strongest band in the amide I region of the FTIR spectra of *cis*-ACPC oligomers **3**–**5** in CH_2Cl_2 appears at about 1645 cm^{-1}. In CH_2Cl_2, this band is missing only from the spectrum of trimer **3**; instead, a shoulder is seen at about 1653 cm^{-1}. In DMSO, the band at approximately 1645 cm^{-1} in the spectrum of pentamer **4** is replaced by a shoulder at about 1653 cm^{-1}, and in the spectrum of heptamer **5** it appears with a decreased relative intensity. The strongest band occurs at approximately 1670 cm^{-1} in the FTIR spectra of the pentamer

 © WILEY-VCH Verlag GmbH, 69451 Weinheim, Germany, 2002 1433-7851/02/4110-1719 $ 20.00+.50/0

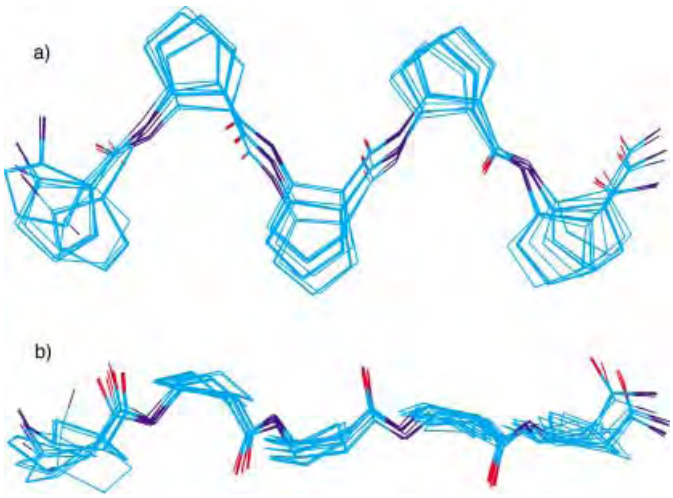


Figure 3. Superposition of the 30 lowest energy structures of pentamer **4** determined by NMR distance restraints and molecular mechanics: a) top view, b) side view. Molecular mechanics simulations were carried out on a SGI Origin 2000 using Accelrys' CDiscover in an Insight 2000 environment. For the energy calculations, the CVFF force field was used, with a 12-Å cutoff for van der Waals and Coulomb interactions. Before the restrained simulated annealing (RSA), a random structure set of 100 molecules was generated by saving the conformations during a 100-ps dynamics simulation at 1000 K in every 1000 steps. The RSA was performed for each structure with an exponential temperature profile in 75 steps and a total duration of 25 ps. Minimization was applied after every RSA in a cascade manner.

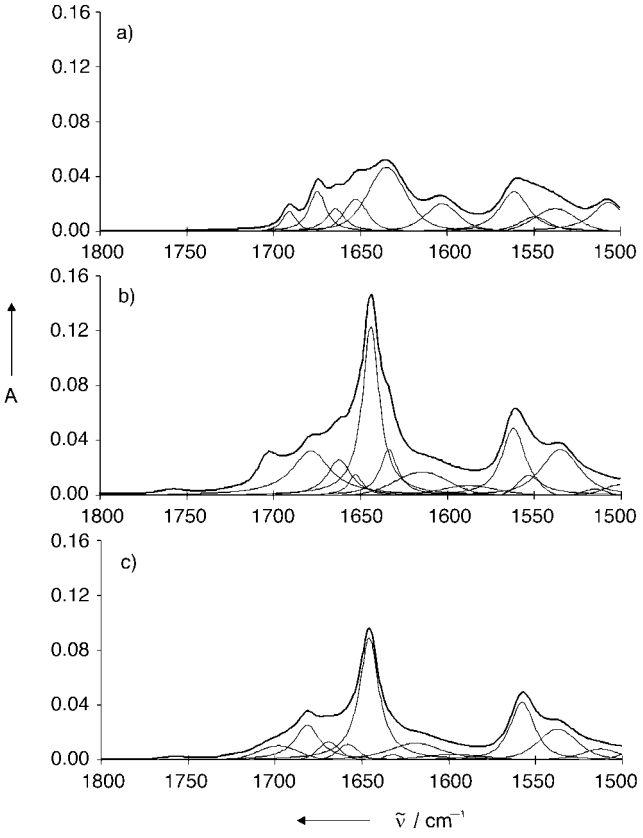


Figure 4. Comparison of the IR spectra of *cis*-ACPC oligomers recorded in CH_2Cl_2: a) trimer, b) pentamer, c) heptamer. The thick curve represents the measured data, while the thin curves show the component bands obtained from nonlinear fitting.

and heptamer in DMSO. Shoulders or weak bands are present near or above 1680 cm^{-1} in the spectra measured in CH_2Cl_2 or DMSO. DMSO is a solvent which is well known to destroy weak intramolecular H-bonds. On the basis of its absence or decreased intensity in the FTIR spectra measured in DMSO, the band at about 1645 cm^{-1} can be assigned to repeats of C_6 intramolecular H-bonds. The high-frequency (>1660 cm^{-1}) component bands in the curve-fitted spectra, which in many cases appear as shoulders in the experimental spectra obtained in CH_2Cl_2 or DMSO, belong to amide CO groups not involved as acceptors in H-bonding. In DMSO, the NH part of these amides probably forms a H-bond with the acceptor SO group of DMSO. Bands (or component bands) near or below 1635 cm^{-1} are indicative of the presence of strong intermolecular H-bonds. In agreement with this assignment, the band at 1635 cm^{-1} is most intense in the opaque solution of trimer **3** in CH_2Cl_2, and it is replaced only by a weak shoulder (at 1637 cm^{-1}) in DMSO, which is known to dissolve aggregates.

Our conclusion from the IR measurements is that pentamer **4** and heptamer **5** display the same characteristic features in regard to the H-bonding pattern, which reinforces the results obtained from the comparison of the ROESY cross-peak patterns. The component bands with decreased relative intensity for the heptamer point to a more stable strand conformation; however, we expected the same spectral features to be present in the CD spectra of both compounds. The CD spectra were recorded both in methanol and in trifluoroethanol (TFE) at a concentration of 1 mM. The curves obtained in methanol and normalized for the residue concentration (Figure 5) point to the same spectroscopic behavior of both compounds, except for the higher intensity of the

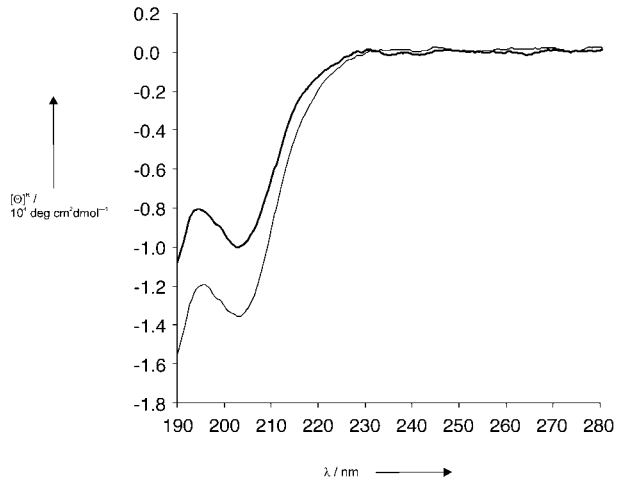


Figure 5. Circular dichroism spectra of **4** and **5** in methanol. The thick curve corresponds to the pentamer and the thin curve to the heptamer. The mean residue ellipticity is displayed.

negative band at 203 nm in the spectrum of the heptamer. The IR results obtained in TFE exhibit the same characteristics as those obtained in methanol. These observations suggest stabilization of the strand conformation in the heptamer as a result of the longer chain and the smaller relative contribution of the less-fixed terminal residues.

 © WILEY-VCH Verlag GmbH, 69451 Weinheim, Germany, 2002 1433-7851/02/4110-1720 $ 20.00+.50/0

The results of CD spectroscopy accord well with the amide proton/deuterium exchange NMR measurements performed in [D_4]methanol, where **4** lost its amide signal intensity in 15 minutes, while the amide protons of **5** survived for more than 1 hour. The lower exchange rate for heptamer **5**, together with the IR and CD results, supports the view that the folding occurs in a cooperative manner as the chain length increases.

Herein we have shown that the 1*R*,2*S*-ACPC pentamer and heptamer adopt a self-stabilizing six-strand secondary structure in the solution phase. From earlier results, we know that the model system composed of (1*R*,2*R*)-*trans*-ACPC monomers adopts the highly stable 12-helix conformation[16] (Figure 6). The change in the relative configuration of the ACPC residues in these models provides an efficient control over the secondary structures of the helix and strand. The application of the 2-aminocycloalkanecarboxylic acids as a general backbone in the controlled design of β-peptide foldamers is supported by the relatively easy synthetic availability of this family of compounds.[17] This type of chirality-based selection between regular secondary structures may become a general tool in the design of β-peptide foldamers and may facilitate the construction of stable tertiary structures.

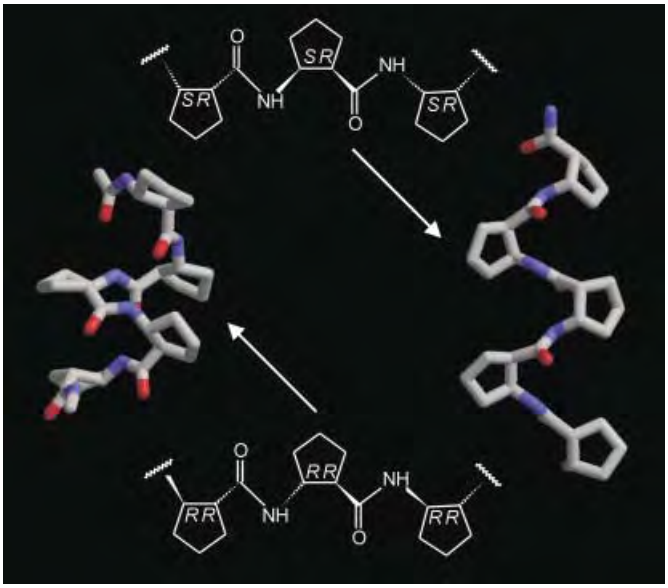


Figure 6. Comparison of the secondary structures induced by the different relative configurations of the ACPC residues.

Received: January 10, 2002
Revised: March 4, 2002 [Z18510]

[1] a) D. J. Hill, M. J. Mio, R. B. Prince, T. S. Hughes, J. S. Moore, *Chem. Rev.* **2001**, *101*, 3893 – 4011; b) E. A. Archer, H. Gong, M. J. Krische, *Tetrahedron* **2001**, *57*, 1139 – 1159.
[2] D. Seebach, J. L. Matthews, *Chem. Commun.* **1997**, 2015 – 2022.
[3] S. H. Gellman, *Acc. Chem. Res.* **1998**, *31*, 173 – 180.
[4] a) R. Günther, H. Hofmann, K. Kuczera, *J. Phys. Chem. B* **2001**, *105*, 5559 – 5567; b) W. F. DeGrado, J. P. Schneider, Y. Hamuro, *J. Pept. Res.* **1999**, *54*, 206 – 217.
[5] a) D. Seebach, S. Abele, K. Gademann, B. Jaun, *Angew. Chem.* **1999**, *111*, 1700 – 1703; *Angew. Chem. Int. Ed.* **1999**, *38*, 1595 – 1597; b) X. Daura, K. Gademann, B. Jaun, D. Seebach, W. F. van Gunsteren, A. E. Mark, *Angew. Chem.* **1999**, *111*, 249 – 253; *Angew. Chem. Int. Ed.* **1999**, *38*, 236 – 240.
[6] D. H. Appella, L. A. Christianson, D. A. Klein, D. R. Powell, X. Huang, J. J. Barchi, S. H. Gellman, *Nature* **1997**, *387*, 381 – 384.
[7] a) D. Seebach, T. Sifferlen, P. A. Mathieu, A. M. Häne, C. M. Krell, J. D. Bierbaum, S. Abele, *Helv. Chim. Acta.* **2000**, *83*, 2849 – 2863; b) D. Seebach, S. Abele, K. Gademann, G. Guichard, T. Hintermann, B. Jaun, J. L. Matthews, J. V. Schreiber, *Helv. Chim. Acta.* **1998**, *81*, 932 – 982.
[8] D. Appella, L. A. Christianson, I. L. Karle, D. R. Powell, S. H Gellman, *J. Am. Chem. Soc.* **1999**, *121*, 6206 – 6212.
[9] R. P. Cheng, S. H. Gellman, W. F. DeGrado, *Chem. Rev.* **2001**, *101*, 3219 – 3232.
[10] D. Seebach, M. Overhand, F. N. M. Kühnle, B. Martinoni, L. Oberer, H. Ulrich, H. Widmer, *Helv. Chim. Acta.* **1996**, *79*, 913 – 941.
[11] R. B. Merrifield, *J. Am. Chem. Soc.* **1963**, *85*, 2149 – 2154.
[12] L. Braunschweiler, R. R. Ernst, *J. Magn. Reson.* **1983**, *53*, 521 – 528.
[13] A. A. Bothner-By, R. L. Stephens, J. Lee, C. D. Warren, R. W. Jeanloz, *J. Am. Chem. Soc.* **1984**, *106*, 811 – 813.
[14] N. L. Allinger, Y. H. Yuh, J. J. Lii, *J. Am. Chem. Soc.* **1989**, *111*, 8551 – 9556.
[15] B. A. Borgias, M. Gochin, D. J. Kerwood, T. L. James, *Prog. Nucl. Magn. Reson. Spectrosc.* **1990**, *22*, 83 – 100.
[16] D. H. Appella, L. A. Christianson, D. A. Klein, M. R. Richards, D. R. Powell, S. H. Gellman, *J. Am. Chem. Soc.* **1999**, *121*, 7574 – 7581.
[17] F. Fülöp, *Chem. Rev.* **2001**, *101*, 2181 – 2204.

Chiral Transmission between Amino Acids: Chirally Selective Amino Acid Substitution in the Serine Octamer as a Possible Step in Homochirogenesis**

Kim J. Koch, Fabio C. Gozzo, Sergio C. Nanita, Z. Takats, Marcos N. Eberlin, and R. Graham Cooks*

Pasteur's discovery[1] that tartaric acid can occur in two enantomeric forms raised still unanswered questions[2–6] concerning the origin of chirality in biological systems (homochirality). Homochirogenesis, the set of events leading to the almost exclusive preference for one enantiomeric form over the other in the suite of biological compounds that make up living organisms, can be considered to have involved three steps: 1) symmetry breaking, 2) chiral enrichment, and 3) chiral transmission.

[*] Prof. R. G. Cooks, K. J. Koch, S. C. Nanita, Z. Takats
Purdue University
Department of Chemistry
1393 Brown Laboratory
West Lafayette, IN 47907 (USA)
Fax: (+1) 765-494-9421
E-mail: cooks@purdue.edu
F. C. Gozzo, Prof. M. N. Eberlin
Institute of Chemistry
State University of Campinas
CP6154 Campinas (Brazil)

[**] This work was supported by the US Department of Energy, Office of Basic Energy Sciences, and by the National Science Foundation (Grant CHE 97-32670). F.C.G. and M.N.E. thank the Research Support Foundation of the State of São Paulo (FAPESP) and the Brazilian National Research Council (CNPq), respectively, for financial support. We thank Zheng Ouyang for helpful comments.

 © WILEY-VCH Verlag GmbH, 69451 Weinheim, Germany, 2002 1433-7851/02/4110-1721 $ 20.00+.50/0

Symmetry breaking requires a chemical, physical, or merely statistical process that favors one chiral form over the other. As a case in point, an intrinsic energy difference is predicted between enantiomeric molecules as a result of a parity violation in the weak nuclear force.[7, 8] Symmetry breaking might also arise in appropriate circumstances from external chiral agents, such as circularly polarized light,[9–12] vortex motion,[13] and magnetic forces.[14, 15] Chiral enrichment, the second step, involves the build-up of large enantiomeric excesses in biologically relevant compounds. Mechanisms that have been considered include chirally directed ("majority rules"[16]) polymerization, polycondensation in particular cases (such as leucine) where the chirally pure polymer has significantly enhanced stability,[17] autocatalytical processes including those catalyzed by enantiomorphous crystal faces such as that of quartz,[18] asymmetric synthesis,[19] and self-replication by such biomolecules as peptides.[20] We hypothesize that chiral accumulation occurred in one or just a few compounds during terrestrial homochirogenesis, thus underlining the importance of the third step of the overall process, chiral transmission—the transfer of chirality from one molecule (or molecular assembly) to another. We consider here the transfer of chirality from serine, a presumed primitive amino acid, to other biomolecules. Serine attracts attention because it is known that molecular clusters with strong chiral preferences[21–23] can be extracted from aqueous solutions by electrospray ionization mass spectrometry (ESI-MS). We now report that chiral transmission from serine to other amino acids occurs under these same conditions. The formation of clusters presumably occurs during the evaporation of highly concentrated microdroplets.

The transmission of chirality from serine to other amino acids occurs by substitution of the amino acids in the recently discovered homochiral serine octamer.[21–23] Addition of cysteine to a solution of serine followed by electrospray ionization of the mixture yields the homochiral octamer and the products in which substitution of one or two cysteine molecules of matching chirality into the cluster has occurred. In contrast, cysteine alone forms a singly protonated, hexameric magic number cluster, without regard to chiral composition. All the other amino acids investigated (aspartic acid, asparagine, leucine, and methionine) are also incorporated into the serine octamer (by either mono- or disubstitution) provided they have the same chirality as serine; much less incorporation of the wrong enantiomer was observed. The net result is the transmission of the chiral choice made in the serine octamer to the amino acid that is substituted into the cluster. We argue that this chirally selective incorporation represents a method of chiral transmission and that it might have had a role in this phenomenon as it occurred on the primitive earth. At the very least, this case represents a striking display of homochiral selectivity in an elementary biomolecule of great importance.

The positive-ion ESI mass spectrum of cysteine, chosen since it is the sulfur analogue of serine, exhibits a magic number cluster m/z 727 (corresponding to the singly charged hexamer and doubly charged dodecamer). Figure 1a shows the ESI mass spectrum of a 0.01M solution of L-Cys; note that only the singly charged monomer, dimer, and hexamer are

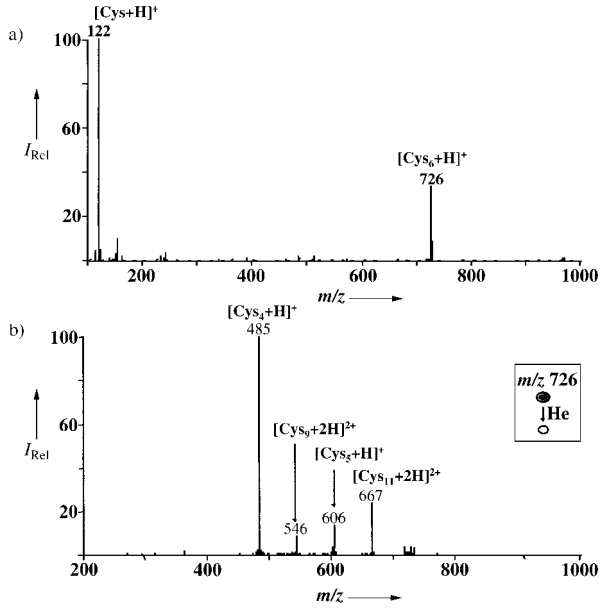


Figure 1. a) The positive-ion ESI mass spectrum of a 0.01M solution of L-cysteine in aqueous methanol. b) Tandem mass spectrum showing products of the collision-induced dissociation of $[Cys_6+H]^+$ m/z 727.

sufficiently stable to be isolated using an isolation window of $m/z = 20$. A series of D:L mixtures (100:0, 80:20, 50:50, 20:80, 0:100) showed absolute and relative ion abundances that were reproducible within $\pm 5\,\%$ in their mass spectra as well as in their tandem (MS^2) spectra when examining the products of collision-induced dissociation of the m/z 727 ion, the protonated hexamer. These observations indicate that, unlike the case of serine, there is no chiral preference for clustering. Collision-induced dissociation (CID) of the hexamer (Figure 1b) yielded both singly and doubly charged fragments, an indication of the presence of the doubly charged dodecamer.[24]

Ab initio calculations were performed using the GAMESS program[25] at the Hartree–Fock (HF) level using the 6-31G double-zeta basis set. The calculated geometries were assembled using the Spartan program. The maximum and root-mean square gradient values for the octamers were set to 0.0003 and 0.0001, respectively. For all the other calculated systems, the default values were used (0.0001 and 0.00003). The final structures were checked using the MOLDEN program.[26] The electronic energies associated with each optimized structure are reported in Table 1. Ab initio calculations on the Cys hexamer show the lowest energy structure to be a trimer of neutral dimers (Figure 2). The hexamer is composed of three Cys dimers, bound to each other by hydrogen bonding through the amino groups. Note that the

Table 1. Electronic energies obtained using Hartree–Fock level calculations.

Calculated structure	Electronic energies (Hartree)
$[L\text{-}Ser_8+H]^+$	−3172.87005
$[L\text{-}Ser_7+L\text{-}Cys+H]^+$	−3495.52063
$[L\text{-}Ser_7+D\text{-}Cys+H]^+$	−3495.51662
$[Cys_2+H]^+$	−1438.40273
[Ser+Cys]	−1115.75135

 © WILEY-VCH Verlag GmbH, 69451 Weinheim, Germany, 2002 1433-7851/02/4110-1722 $ 20.00+.50/0

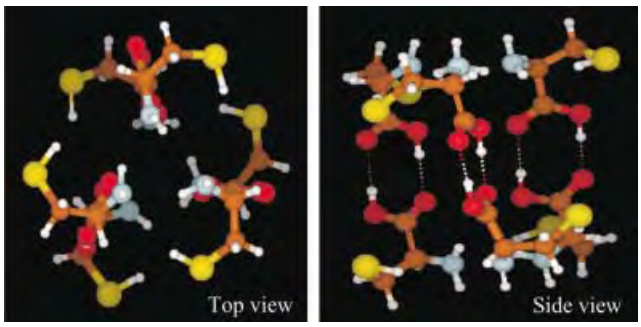


Figure 2. The calculated structure of the cysteine hexamer shown to be assembled from three Cys dimers bound together by interactions between the amino groups.

weak hydrogen-bonding character of the SH group of cysteine, unlike the strong hydrogen-bonding character provided by the OH group in serine, rationalizes the diminished abundance of the cluster and the lack of chiral dependence.

The characteristic homochiral clustering of serine is observed in the mixed clusters generated from a mixture of cysteine and serine. The mass spectrum of a mixture of 0.01M solutions each of L-Ser and L-Cys (Figure 3a) shows the

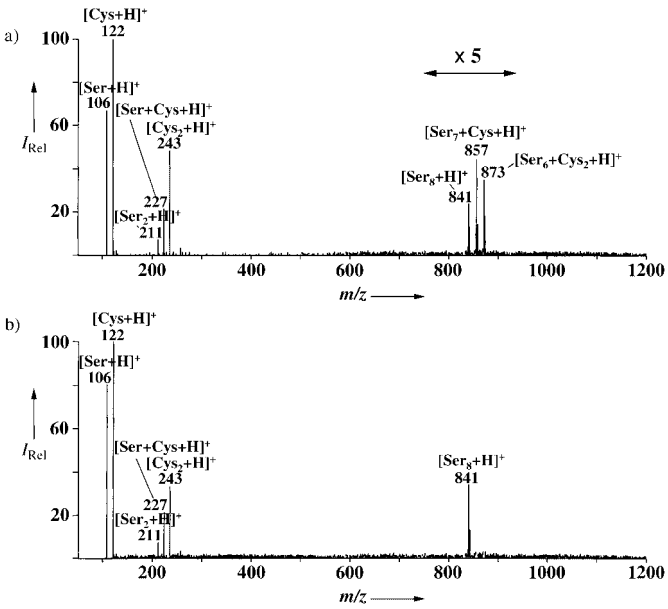


Figure 3. a) ESI mass spectrum of a mixture of L-serine (0.01M) and L-cysteine (0.01M) showing the formation of singly and doubly substituted serine octamers. b) ESI mass spectrum of a mixture of L-serine (0.01M) and D-cysteine (0.01M) showing the lack of formation of mixed octamers.

formation of the singly and doubly substituted serine octamers.[27] A series of Ser:Cys mixtures (100:1, 20:1, 10:1, 4:1, 1:1, 1:4, 1:10, 1:20, 1:100) demonstrates that a maximum of two serine molecules can be substituted by cysteine. The resulting structure has been calculated at the HF/6-31G level and the results indicate that one serine residue in each of the two faces of the serine octamer is replaced by cysteine and results in destabilization of the octamer by 0.5 kcal mol^{-1}. The octamer ions $[Ser_8+H]^+$, $[Ser_6+Cys_2+H]^+$, and $[Ser_7+Cys+H]^+$ fragment by preferential loss of neutral serine dimers.

The mass spectrum of a 0.01M solution of D-Ser mixed with a 0.01M solution of L-Cys (Figure 3b) stands in dramatic contrast to that of the homochiral mixture. The serine octamer is observed in approximately its original abundance, but few substituted octamers are generated.[28] The contrast between the two mass spectra clearly indicates that the chirality of cysteine plays a critical role in its incorporation into the serine octamer. Ab initio calculations reveal a destabilization energy of 2.5 kcal mol^{-1} associated with the incorporation of the wrong enantiomer. By contrast, the cost in terms of energy of incorporating the "wrong" amino acid but with the "right" chirality is only 0.5 kcal mol^{-1} per incorporation!

Preliminary data have been obtained for the formation of singly and doubly substituted serine octamers with a set of amino acids, including aspartic acid, asparagine, leucine, methionine, and phenylalanine, selected as representative of amino acids with acidic, amide, aliphatic, aromatic, and sulfur-containing side chains. When examined in the presence of serine, up to two amino acids with the correct chirality are incorporated into the serine octamer in each case. Figure 4a shows that one or two asparagine molecules of the correct

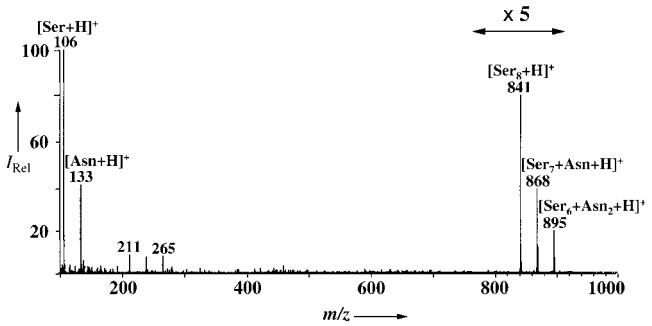


Figure 4. ESI mass spectrum of a mixture of L-serine (0.01M) and L-asparagine (0.01M) showing the formation of singly and doubly substituted serine octamers.

chirality are readily incorporated into the serine octamer; the following data, given as the relative abundance ratios (serine octamer):(singly substituted serine octamer):(doubly substituted serine octamer), summarize the relative extent of formation of the various substituted L-serine clusters: L-Asp (6:2:1), L-Asn (4:2:1), L-Leu (3:4:3), L-Met (1:2:1), L-Phe (2:1:1). Octamer substitution appears to be a function of the size and functional groups of the amino acid side chain. The absence of incorporation of the wrong enantiomer (Figure 4b) clearly shows the effects of chirality in the asparagine case. Chiral transmission from serine to the other amino acids—through their incorporation into the homochiral octameric cluster—represents a novel possibility for the transmission of chirality between amino acids. Chiral transmission is clearly demonstrated by the fact that cysteine itself clusters in a chirally independent fashion, but in the presence of serine one enantiomer is strongly favored for substitution into the homochiral cluster. The possible role of this process in primitive earth is the subject of ongoing enquiry.[29]

Received: November 19, 2001
Revised: February 19, 2002 [Z18245]

 © WILEY-VCH Verlag GmbH, 69451 Weinheim, Germany, 2002 1433-7851/02/4110-1723 $ 20.00+.50/0

[1] M. L. Pasteur, *Ann. Chim. Phys.* **1848**, *24*, 442.
[2] W. A. Bonner, *Origins Life Evol. Biosphere* **1995**, *25*, 175.
[3] S. Mason, *Trends Pharmacol. Sci.* **1986**, *7*, 20.
[4] M. Avalos, R. Babiano, P. Cintas, J. L. Jimenez, J. C. Palacios, L. D. Barron, *Chem. Rev.* **1998**, *98*, 2391.
[5] J. Podlech, *Angew. Chem.* **1999**, *111*, 501; *Angew. Chem. Int. Ed.* **1999**, *38*, 477.
[6] J. Podlech, *Cell. Mol. Life Sci.* **2001**, *58*, 44.
[7] R. Berger, M. Quack, G. S. Tschumper, *Helv. Chim. Acta* **2000**, *83*, 1919.
[8] A. Bakasov, T. K. Ha, M. Quack, *J. Chem. Phys.* **1998**, *109*, 7263.
[9] J. H. Hough, J. A. Bailey, A. Chrysostomou, T. M. Gledhill, P. W. Lucas, M. Tamura, S. Clark, J. Yates, F. Menard, *Adv. Space Res.* **2001**, *27*, 313.
[10] J. Bailey, *Origins Life Evol. Biosphere* **2001**, *31*, 167.
[11] K. S. Burnham, G. B. Schuster, *J. Am. Chem. Soc.* **1999**, *121*, 10245.
[12] V. I. Gol'danskii, *Khim. Fiz.* **1999**, *18*, 3 [*Chem. Abstr.* **1999**, *131*, 358023e, 1276].
[13] R. M. Ribo, J. Crusats, F. Sagues, J. Claret, R. Rubires, *Science* **2001**, *292*, 2063.
[14] G. L. J. A. Rikken, E. Raupach, *Nature* **2000**, *405*, 932.
[15] L. Van Wullen, *ChemPhysChem* **2001**, *2*, 107.
[16] M. M. Green, K.-S. Cheon, S.-Y. Yang, J.-W. Park, S. Swansburg, W. Liu, *Acc. Chem. Res.* **2001**, *34*, 672.
[17] N. E. Blair, W. A. Bonner, *Origins Life* **1980**, *10*, 255.
[18] K. Soai, S. Osanai, K. Kadowaki, S. Yonekubo, T. Shibata, I. Sato, *J. Am. Chem. Soc.* **1999**, *121*, 11235.
[19] B. L. Feringa, R. A. Van Delden, *Angew. Chem.* **1999**, *38*, 3419.
[20] A. Saghatelian, Y. Yokobayashi, K. Soltani, M. R. Ghadiri, *Nature* **2001**, *409*, 797.
[21] R. G. Cooks, D. Zhang, K. J. Koch, F. C. Gozzo, M. N. Eberlin, *Anal. Chem.* **2001**, *73*, 3646.
[22] A. E. Counterman, D. E. Clemmer, *J. Phys. Chem. B* **2001**, *105*, 8092.
[23] R. Hodyss, R. R. Julian, J. L. Beauchamp, *Chirality* **2001**, *13*, 703.
[24] CID was achieved by isolation of the ion of interest in the ion trap, then applying 0.1 – 1.0 V AC resonance excitation at the secular frequency of the ion and allowing it to collide with helium gas.
[25] M. W. Schmidt, K. K. Baldridge, J. A. Boatz, S. T. Elbert, M. S. Gordon, J. H. Jensen, S. Koseki, N. Matsunaga, K. A. Nguyen, S. J. Su, T. L. Windus, M. Dupuis, J. A. Montgomery, *J. Comput. Chem.* **1993**, *14*, 1347.
[26] G. Schaftenaar, J. H. Noordik, *J. Comput. Aided Mol. Design* **2000**, *14*, 123.
[27] In this experiment, the cysteine solution was injected into a flowing stream of the serine solution. The degree of incorporation is always limited to two molecules but relative abundances are strongly dependent on the ESI operating conditions.
[28] The chiral effect is sensitive to the precise conditions used, which include the solution pH, the solution flow rate, and the ESI temperature. Under some operating conditions, especially gentle conditions that favor clustering, the discrimination between the homo- and heterochiral systems can be much less pronounced.
[29] Amino acid substitution into homochiral serine clusters is also reported in R. R. Julian, R. Hodyss, B. Kinnear, M. F. Jarrold, J. L. Beauchamp, *J. Phys. Chem. B* **2002**, *106*, 1219, but the chiral selectivity of the process is not discussed.

Hydrogen-Bonded Helices in Crystals with Prescribed Organization**

Radu Custelcean and Michael D. Ward*

Self-assembled molecular helices are ubiquitous in nature and can be found in many biologically important macromolecules. It is therefore not surprising that chemists have made significant efforts to introduce helicity in many artificial systems.[1] The inherent chirality present in such spiral structures is generally associated with enantioselectivity[2] or interesting optoelectronic properties.[3] Theoretical[4] and experimental[5] studies have indicated that helical supramolecular networks can affect chiral ordering in crystal lattices.

Molecular helicity can be programmed by judicious selection of elements that are encoded with structural and conformational information designed to enforce intramolecular self-organization in a spiral arrangement. Examples such as helicenes,[6] poly(*m*-phenylene),[7] polyheterocyclic strands,[8] *m*-phenylacetylene oligomers,[9] β-peptides,[10] polyisocyanates,[11] and oligoarylamides[12] elegantly illustrate this concept. The generation of supramolecular helices requires an additional design element, namely, a reliable noncovalent motif that can provide the desired connectivity of the building blocks in a predictable manner. Hydrogen bonds,[13] metal coordination,[14] and $\pi-\pi$ stacking interactions[15] are often utilized in this regard. These design strategies, however, are generally limited to one dimension, coinciding with the helix direction, while the assembly and structure along the remaining two crystal dimensions are difficult to control. The rational construction of new materials with tailored functions and properties, however, requires control of crystal architecture in all three dimensions. Here we report the formation of hydrogen-bonded helices with predictable three-dimensional (3D) organization in the solid state. This study represents a key first step towards the rational design of crystalline, hydrogen-bonded chiral networks with potential applications in enantioselective separation.[16]

We are actively involved in the design of molecular crystals based on the self-assembly of complementary guanidinium and organosulfonate ions, which typically crystallize in a quasihexagonal hydrogen-bonded network (Figure 1a).[17] These 2D layers can be described as consisting of 1D ribbons along a_1. The S···S distance along this axis is nominally identical for all these compounds (7.5 ± 0.2 Å). The ribbons themselves aggregate by hydrogen bonding along the orthogonal direction b_1. The magnitude of b_1 can vary significantly (7.3 – 13 Å) as a result of puckering of the sheet about the hydrogen bonds that connect the ribbons.

[*] Prof. M. D. Ward, Dr. R. Custelcean
Department of Chemical Engineering and Materials Science
University of Minnesota
Minneapolis, MN 55455 (USA)
Fax: (+1) 612-626-7805
E-mail: wardx004@tc.umn.edu

[**] This work was supported by National Science Foundation, Grant DMR-9908627.

 © WILEY-VCH Verlag GmbH, 69451 Weinheim, Germany, 2002 1433-7851/02/4110-1724 $ 20.00+.50/0

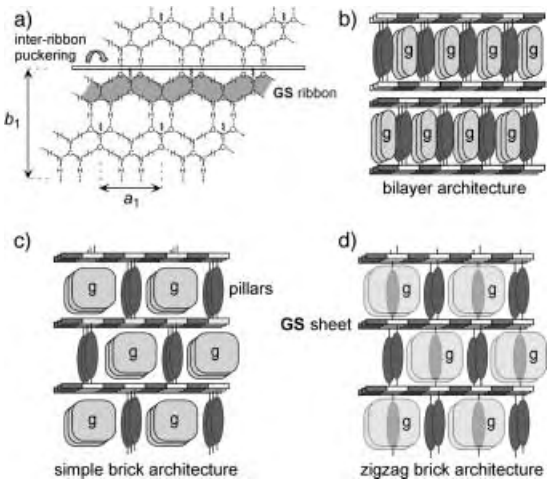
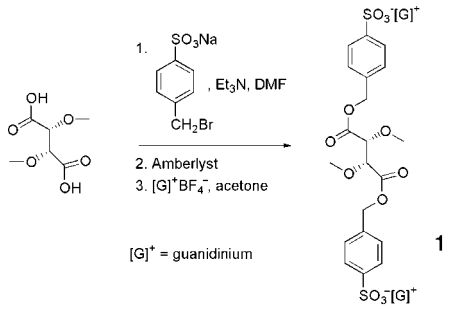


Figure 1. a) Quasihexagonal guanidinium–sulfonate hydrogen-bonding motif of one-dimensional ribbons running along the a_1 direction. The ribbons are linked to each other by hydrogen bonding along b_1 (a_1 and b_1 here represent generic lattice constants). The magnitude of b_1 can vary substantially through inter-ribbon puckering. b) Bilayer architecture. c) Simple brick architecture. d) Zigzag brick architecture. All three architectures contain inclusion cavities that can be occupied by guest molecules (g).

The persistence of the 2D guanidinium–sulfonate (**GS**) motif, observed in over 200 compounds synthesized in our laboratory, simplifies the engineering of these "lamellar" crystals by allowing convenient manipulation of the structure in the third dimension through the choice of the organic substituent. Organodisulfonates can be employed to link the hydrogen-bonded sheets and thereby act as molecular "pillars" that support the formation of either discrete bilayers, in which all the organic groups project from the same side of each sheet (Figure 1b), or continuous "brick" architectures, in which the organic substituents alternate up and down in each sheet (Figure 1c and d). Because of the low density enforced by the quasihexagonal hydrogen-bonding motif, these topologies can produce inclusion cavities that are occupied by guest molecules. The flexibility of the **GS** hydrogen-bonded networks, through puckering and conformational freedom of the pillars, allows self-optimization of host–guest interactions and efficient packing needed for crystallization.

The ability to modify the pillars with retention of the overall crystal architecture facilitates the rational design of functional materials. In this regard, the employment of chiral pillars could afford asymmetric cavities capable of including chiral guests, which in turn could serve as a basis for enantioselective separations. Flexible pillars may be ideal in this regard, as this characteristic would permit the host to mold to a chiral guest while maintaining the persistent lamellar architecture. These concepts prompted us to synthesize the chiral guanidinium disulfonate **1**, starting from the readily accessible, optically pure *O*,*O*′-dimethyl-L-tartaric acid (Scheme 1).

Tartrates have been successfully employed for the synthesis of liquid-crystalline[18] and oligomeric helical materials.[19] Moreover, a search of the Cambridge Structural Database revealed that simple, optically pure tartaric acid derivatives have a propensity to crystallize in the space groups $P2_1$ and $P2_12_12_1$. These compounds contain at least one twofold screw



Scheme 1. Synthesis of **1**.

axis, a symmetry element that favors helical organization. Most of them, however, do not possess functional groups that provide the supramolecular connectivity required for the formation of a continuous helix. Those that do exhibit unpredictable hydrogen-bonding patterns, and this limits their potential for rational assembly.

Molecular modeling[20] indicated that the disulfonate dianion in **1** is extremely flexible, with more than 100 low-energy conformations within 10 kcal mol^{-1}. The most stable conformation (Figure 2a), optimized by DFT at the B3LYP/6-31G* level,[21] has an S···S separation of 18.8 Å and a dihedral angle between the two S–C terminal bonds of 54.4°. This conformational twist, which originates from the two chiral centers in the pillar, provides the structural encoding for helical organization in **1**.

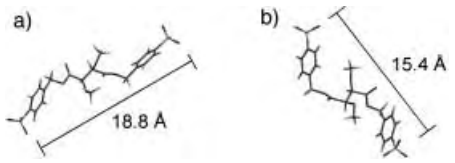


Figure 2. a) Calculated structure (B3LYP/6-31G*) of the organodisulfonate pillar in **1**. b) Structure of the same pillar in the crystalline state.

Crystallization of **1** from methanol/1,4-dioxane afforded single crystals suitable for X-ray diffraction,[22] which revealed the existence of the simple brick architecture (Figure 3c). We surmise that formation of a bilayer framework is prevented by the steric bulk of the pillars which thereby promotes the lower density brick framework. The steric bulk is further reflected by the intermolecular S···S distance along the ribbon direction, which at 8.03 Å is the largest observed value to date for a_1 in guanidinium sulfonates. The **GS** sheets actually display a shifted-ribbon hydrogen-bonding motif, which is a slight variation of the quasihexagonal arrangement that was observed in some other guanidinium mono- and disulfonates.[17]

The pillars in **1** are strongly twisted, with an S–C···C–S dihedral angle of 53.7°, in agreement with the theoretical calculations. Compared to the gas-phase calculated geometry, however, the pillars are significantly more folded in the crystal which results in a shorter S···S separation of 15.4 Å (Figure 2b). This structural "collapse" apparently reflects the tendency for dense packing and a preference to fill the void space of the framework by conformational distortion of the pillars instead of guest inclusion. Hydrogen bonds between

 © WILEY-VCH Verlag GmbH, 69451 Weinheim, Germany, 2002 1433-7851/02/4110-1725 $ 20.00+.50/0

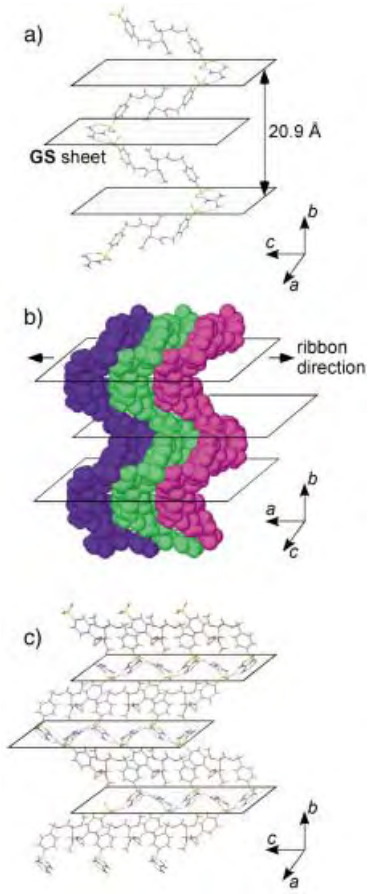
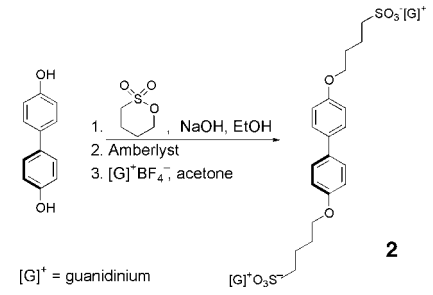


Figure 3. X-ray crystal structure of **1**. a) Self-assembly into the hydrogen-bonded helix. b) Association of helices along the **GS** ribbon (crystallographic *a* direction). c) Formation of the "brick" architecture by hydrogen bonding of helices along the crystallographic *c* direction.

the sulfonate and guanidinium ions generate extended right-handed helices about the twofold crystallographic *b* axis, with a pitch of 20.9 Å (Figure 3a). The intramolecular S–C···C–S twist is augmented by an intermolecular C–S···S–C torsion angle of 97.7° through guanidinium–sulfonate hydrogen bonds. When combined with the flexible backbone of the pillar, the result is a smoothly curved, supramolecular spiral. The helices further associate along the crystallographic *a* direction to generate the typical **GS** ribbons (Figure 3b), and then orthogonally, along the *c* direction, to complete the **GS** sheets and form the familiar 3D brick architecture (Figure 3c). The twisted organic pillars, winding through the crystal and connecting the **GS** sheets, are reminiscent of spiral staircases connecting the floors of a building. It is remarkable that despite the significant conformational twist and flexibility of the pillars, this compound still self-assembles in the brick topology, a crystal architecture found for numerous rigid pillars in this class of molecular materials.

The ability of the **GS** system to generate helical networks was further explored with the guanidinium disulfonate **2** (Scheme 2). Although this compound is not inherently chiral, it can assume chiral conformations upon twisting about the C(Ph)–C(Ph) bond. The flexible butoxy chains were introduced to amplify this conformational twist and promote helical self-organization.



Scheme 2. Synthesis of **2**.

Single-crystal X-ray diffraction[22] on **2** (from MeOH/AcOEt) revealed the formation of supramolecular helices that self-assemble into a "zigzag brick" architecture[17b] (Figure 4). The twist of the biphenyl core induces a S–C···C–S dihedral angle of 49.8° in the 19.3-Å-long pillar, which in combination with the intermolecular C–S···S–C torsion angle of of 21.0° (by hydrogen bonding to guanidinium cations) results in the formation of a helix about the crystallographic *b* axis with a pitch of 18.1 Å. Helices of the

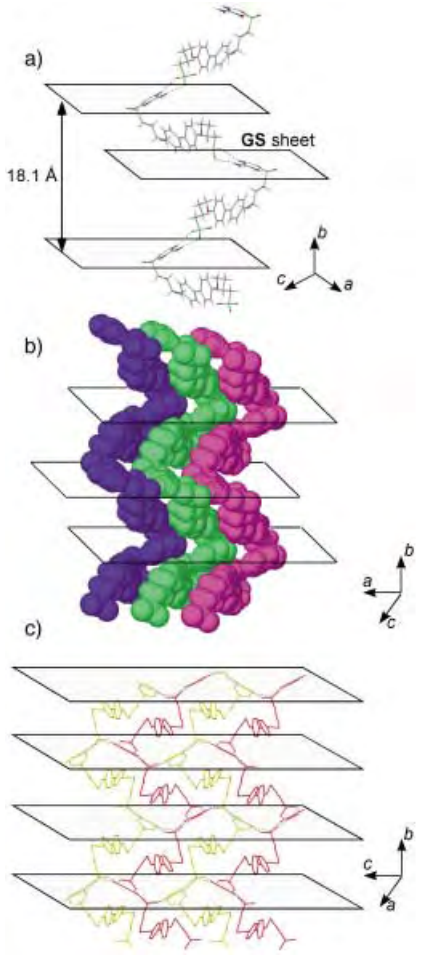


Figure 4. X-ray crystal structure of **2**. a) Self-assembly into the hydrogen-bonded helix. b) Homochiral association of helices along the *a*-axis. c) Formation of the "zigzag brick" architecture by hydrogen bonding of helices along the *c*-axis. Left- (red) and right-handed (yellow) helical domains alternate along *c*, producing a racemic crystal.

 © WILEY-VCH Verlag GmbH, 69451 Weinheim, Germany, 2002 1433-7851/02/4110-1726 $ 20.00+.50/0

same handedness aggregate through guanidinium–sulfonate hydrogen bonds along the crystallographic *a* axis to generate homochiral domains, as illustrated in Figure 4b. Further association of helical domains with opposite chirality, by hydrogen bonding along *c* (Figure 4c), generates the "zigzag brick" architecture (Figure 1d), in which the pillars alternate up and down along both the *a* and *c* axes that delineate the **GS** sheets.

We have illustrated here a rational approach towards hydrogen-bonded helices with predictable three-dimensional organization in the crystalline state. While other strategies for encoding helicity in self-assembled materials have been reported, this approach offers advanced control of the overall crystal architecture. Though no guests are included in the frameworks described here, the pronounced folding and tilt of the pillars, together with the substantial puckering of the **GS** sheets, suggest the potential for guest inclusion upon conformational expansion of these networks, and the prospect of inclusion-based enantioselective separation.

Experimental Section

1: *O*,*O*′-dimethyl-L-tartaric acid[23] (0.178 g, 1 mmol) was dissolved in anhydrous DMF (1 mL). The resulting solution was cooled in ice, and triethylamine (0.212 g, 2.1 mmol) was added dropwise with stirring under an inert atmosphere. A solution of sodium *p*-bromomethylbenzene sulfonate[24] (0.546 g, 2 mmol) in anhydrous DMF (8 mL) was then added dropwise while stirring the reaction mixture under ice. The solution was warmed to room temperature, and stirred for 3 d under an inert atmosphere. It was subsequently poured over 75 mL of 2-propanol, and the resulting precipitate was collected by filtration, washed well with 2-propanol, then dissolved in 5 mL of deionized water, and passed over Amberlyst 36 ion-exchange resin (Aldrich). After the removal of water in vacuo at 40 °C, the resulting oil was extracted with acetone (10–15 mL) and poured over a solution of 0.3 g guanidinium tetrafluoroborate in 5 mL acetone. The resulting precipitate was filtered and washed with acetone. Yield 0.06 g. ^{1}H NMR (300 MHz, [D$_6$]DMSO, 25 °C): $\delta = 3.26$ (s, 6H), 4.40 (s, 2H), 5.12 (d, J(H,H) = 12.9 Hz, 2H), 5.25 (d, J(H,H) = 12.6 Hz, 2H), 6.94 (s, 12H), 7.35 (d, J(H,H) = 8.1 Hz, 4H), 7.60 (d, J(H,H) = 8.1, 4H).

2: 4,4′-Biphenol (0.93 g, 5 mmol) and NaOH (0.4 g, 10 mmol) were dissolved in EtOH (40 mL). The resulting solution was added dropwise over 90 min to a vigorously stirred solution of 1,4-butanesultone (2.72 g, 20 mmol) in refluxing EtOH (10 mL). The mixture was refluxed for 44 h with stirring. The resulting precipitate was filtered from the hot solution, washed with EtOH, then with 50 mL of hot MeOH. The obtained white powder was dissolved in minimum amount of deionized water and passed over Amberlyst 36 ion-exchange resin. After the removal of water in vacuo, the resulting solid was dissolved in 85 mL acetone, and a solution of 1.46 g guanidinium tetrafluoroborate in 10 mL acetone was subsequently added. The resulting precipitate was collected by filtration and washed with acetone. Yield 1.4 g. ^{1}H NMR (300 MHz, [D$_6$]DMSO, 25 °C): $\delta = 1.78$ (m, 8H), 2.61 (t, J(H,H) = 7.2 Hz, 4H), 3.98 (t, J(H,H) = 6.0 Hz, 4H), 6.97 (d, J(H,H) = 6.9 Hz, 4H), 7.06 (s, 12H), 7.51 (d, J(H,H) = 6.9 Hz, 4H).

Received: December 27, 2001 [Z18439]

[1] Recent reviews: a) T. J. Katz, *Angew. Chem.* **2000**, *112*, 1997; *Angew. Chem. Int. Ed.* **2000**, *39*, 1921; b) A. E. Rowan, R. J. M. Nolte, *Angew. Chem.* **1998**, *110*, 65; *Angew. Chem. Int. Ed.* **1998**, *37*, 63; c) C. Piguet, G. Bernardinelli, G. Hopfgartner, *Chem. Rev.* **1997**, *97*, 2005.

[2] a) I. Sato, R. Yamashima, K. Kadowaki, J. Yamamoto, T. Shibata, K. Soai, *Angew. Chem.* **2001**, *113*, 1130; *Angew. Chem. Int. Ed.* **2001**, *40*, 1096; b) S. D. Dreher, T. J. Katz, K. C. Lam, A. L. Rheingold, *J. Org. Chem.* **2000**, *65*, 815; c) M. T. Reetz, S. Sostmann, *Tetrahedron* **2001**, *57*, 2515; d) E. Yashima, Y. Maeda, Y. Okamoto, *Polym. J.* **1999**, *31*, 1033; e) K. S. Broo, H. Nilsson, J. Nillson, L. Baltzer, *J. Am. Chem. Soc.* **1998**, *120*, 10287.

[3] a) J. Nishida, T. Suzuki, M. Ohkita, T. Tsuji, *Angew. Chem.* **2001**, *113*, 3351; *Angew. Chem. Int. Ed.* **2001**, *40*, 3251; b) P. Gangopadhyay, T. P. Radhakrishnan, *Angew. Chem.* **2001**, *113*, 2517; *Angew. Chem. Int. Ed.* **2001**, *40*, 2451; c) B. Busson, M. Kauranen, C. Nuckolls, T. J. Katz, *Phys. Rev. Lett.* **2000**, *84*, 79; d) T. Verbiest, S. Van Elshocht, M. Kauranen, L. Hellemans, J. Snauwaert, C. Nuckolls, T. J. Katz, A. Persoons, *Science* **1998**, *282*, 913; e) D. S. Hermann, *Mol. Cryst. Liq. Cryst.* **2001**, *358*, 167; f) G. Treboux, P. Lapstun, Z. H. Wu, K. Silverbrook, *Chem. Phys. Lett.* **1999**, *301*, 493; g) R. A. van Delden, B. L. Feringa, *Angew. Chem.* **2001**, *113*, 3298; *Angew. Chem. Int. Ed.* **2001**, *40*, 3198.

[4] D. P. Craig, P. E. Schipper, *Chem. Phys. Lett.* **1974**, *25*, 476.

[5] K. Biradha, C. Seward, M. J. Zaworotko, *Angew. Chem.* **1999**, *111*, 584; *Angew. Chem. Int. Ed.* **1999**, *38*, 492.

[6] a) K. P. Meurer, F. Vögtle, *Top. Curr. Chem.* **1985**, *127*, 1; b) W. H. Laarhoven, W. J. C. Prinsen, *Top. Curr. Chem.* **1984**, *125*, 63; c) C. Nuckolls, T. J. Katz, G. Katz, P. J. Collings, L. Castellanos, *J. Am. Chem. Soc.* **1999**, *121*, 79.

[7] D. J. Williams, H. M. Colquhoun, C. A. O'Mahoney, *J. Chem. Soc. Chem. Commun.* **1994**, 1643.

[8] M. Ohkita, J.-M. Lehn, G. Baum, D. Fenske, *Chem. Eur. J.* **1999**, *5*, 3471.

[9] J. C. Nelson, J. G. Saven, J. S. Moore, P. G. Wolynes, *Science* **1997**, *277*, 1793.

[10] a) D. H. Appella, L. A. Christianson, D. A. Klein, D. R. Powell, X. L. Huang, J. J. Barchi, S. H. Gellman, *Nature* **1997**, *387*, 381; b) D. Seebach, K. Gademann, J. V. Schreiber, J. L. Matthews, T. Hintermann, B. Jaun, L. Oberer, U. Hommel, H. Widmer, *Helv. Chim. Acta* **1997**, *80*, 2033.

[11] a) D. B. Amabilino, E. Ramos, J. L. Serrano, J. Veciana, *Adv. Mater.* **1998**, *10*, 1001; b) K. S. Cheon, J. V. Selinger, M. M. Green, *Angew. Chem.* **2000**, *112*, 1542; *Angew. Chem. Int. Ed.* **2000**, *39*, 1482.

[12] B. Gong, *Chem. Eur. J.* **2001**, *7*, 4336.

[13] a) Y. Hamuro, S. J. Geib, A. D. Hamilton, *J. Am. Chem. Soc.* **1997**, *119*, 10587; b) W. E. Allen, C. J. Fowler, V. M. Lynch, J. L. Sessler, *Chem. Eur. J.* **2001**, *7*, 721; c) J. H. K. K. Hirschberg, L. Brunsveld, A. Ramzi, J. A. J. M. Vekemans, R. P. Sijbesma, E. W. Meijer, *Nature* **2000**, *407*, 6801; d) M. Mazik, D. Bläser, R. Boese, *Tetrahedron Lett.* **1999**, *40*, 4783; e) W. Yue, R. Bishop, D. C. Craig, M. L. Scuder, *Tetrahedron* **2000**, *56*, 6667; f) T. B. Norsten, R. McDonald, N. R. Branda, *Chem. Commun.* **1999**, 719; g) M. J. Hardie, P. D. Godfrey, C. L. Raston, *Chem. Eur. J.* **1999**, *5*, 1828; h) S. Hanessian, R. Saladino, R. Margarita, M. Simard, *Chem. Eur. J.* **1999**, *5*, 2169.

[14] a) M. Albrecht, *Chem. Rev.* **2001**, *101*, 3457; b) F. M. Tabellion, S. R. Seidel, A. M. Arif, P. J. Stang, *Angew. Chem.* **2001**, *113*, 1577; *Angew. Chem. Int. Ed.* **2001**, *40*, 1529; c) G. Baum, E. C. Constable, D. Fenske, C. E. Housecroft, T. Kulke, *Chem. Eur. J.* **1999**, *5*, 1862; d) M. Meyer, B. Kersting, R. E. Powers, K. N. Raymond, *Inorg. Chem.* **1997**, *36*, 5179; e) M. J. Hannon, C. L. Painting, N. W. Alcock, *Chem. Commun.* **1999**, 2023; f) O. Mamula, A. von Zelewsky, T. Bark, G. Bernardinelli, *Angew. Chem.* **1999**, *111*, 3129; *Angew. Chem. Int. Ed.* **1999**, *38*, 2945; g) C. Kaes, M. W. Hosseini, C. E. F. Rickard, B. W. Skelton, A. H. White, *Angew. Chem.* **1998**, *110*, 970; *Angew. Chem. Int. Ed.* **1998**, *37*, 920; h) D. A. McMorran, P. J. Steel, *Angew. Chem.* **1998**, *110*, 3495; *Angew. Chem. Int. Ed.* **1998**, *37*, 3295; i) J. D. Ranford, J. J. Vittal, D. Wu, X. Yang, *Angew. Chem.* **1999**, *111*, 3707; *Angew. Chem. Int. Ed.* **1999**, *38*, 3498; j) T. Ezuhara, K. Endo, Y. Aoyama, *J. Am. Chem. Soc.* **1999**, *121*, 3279.

[15] a) L. A. Cuccia, J.-M. Lehn, J.-C. Homo, M. Schmutz, *Angew. Chem.* **2000**, *112*, 239; *Angew. Chem. Int. Ed.* **2000**, *39*, 233; b) L. Brunsveld, E. W. Meijer, R. B. Prince, J. S. Moore, *J. Am. Chem. Soc.* **2001**, *123*, 7978; c) H. Engelkamp, S. Middelbeek, R. J. M. Nolte, *Science* **1999**, *284*, 785.

[16] a) O. R. Evans, H. L. Ngo, W. Lin, *J. Am. Chem. Soc.* **2001**, *123*, 10395; b) J. S. Seo, D. Whang, H. Lee, S. I. Jun, J. Oh, Y. J. Jeon, K. Kim, *Nature* **2000**, *404*, 982; c) C. J. Kepert, T. J. Prior, M. J. Rosseinsky, *J. Am. Chem. Soc.* **2000**, *122*, 5158; d) M. Czugler, P. P. Korkas, P. Bombicz, W. Seichter, E. Webber, *Chirality* **1997**, *9*, 203; e) M. E. Garcia, J. L. Naffin, N. Deng, T. E. Mallouk, *Chem. Mater.* **1995**, *7*, 1968; f) F. Toda, *Top. Curr. Chem.* **1987**, *140*, 43.

[17] a) K. T. Holman, A. M. Pivovar, J. A. Swift, M. D. Ward, *Acc. Chem. Res.* **2000**, *34*, 107; b) K. T. Holman, S. M. Martin, D. P. Parker, M. D. Ward, *J. Am. Chem. Soc.* **2001**, *123*, 4421.

[18] a) A. Singh, Y, Lvov, S. B. Qadri, *Chem. Mater.* **1999**, *11*, 3196; b) T. G. Krzywicki, C. Fouquey, J.-M. Lehn, *Proc. Natl. Acad. Sci. USA* **1993**, *90*, 163.

[19] M. S. Gin, J. S. Moore, *Org. Lett.* **2000**, *2*, 135.

[20] MMFF94 force field (Titan, Wavefunction, Inc.). T. A. Halgren, *J. Comput. Chem.* **1996**, *17*, 490.

[21] A. D. Becke, *J. Chem. Phys.* **1993**, *98*, 5648.

[22] A Siemens SMART CCD diffractometer with $Mo_{K\alpha}$ radiation ($\lambda = 0.71073$) was used for single-crystal X-ray diffraction studies. The structures were solved by direct methods and refined by full-matrix least-squares methods on F^2 with the SHELXTL package (Structure Analysis Program 5.1, Brucker AXS, Inc., Madison, WI, **1997**). Absorption corrections were applied with SADABS. All non-hydrogen atoms were refined anisotropically. Hydrogen atoms were calculated and placed in idealized positions. Crystal data for **1**: crystal dimensions $0.39 \times 0.22 \times 0.17$ mm; $T = 173$ K; monoclinic, space group $P2_1$; $a = 8.029(2)$ Å, $b = 20.895(5)$ Å, $c = 9.033(3)$ Å, $\beta = 98.312(5)^\circ$, $V = 1499.4(7)$ Å^3, $Z = 2$; $\rho_{calcd} = 1.410$ g cm^{-3}; $2\theta_{max} = 54.0^\circ$; 5805 reflections collected, 2711 unique reflections; 381 parameters; $R_1 = 0.0463$, $wR_2 = 0.0938$ for $I > 2\sigma(I)$; residual electron density: 0.28 e Å^{-3}. Crystal data for **2**: crystal dimensions: $0.39 \times 0.25 \times 0.08$ mm; $T = 173$ K; monoclinic, space group $P2_1/c$; $a = 12.8032(17)$ Å, $b = 18.092(2)$ Å, $c = 12.8969(18)$ Å, $\beta = 91.646(3)^\circ$, $V = 2986.1(7)$ Å^3, $Z = 4$; $\rho_{calcd} = 1.283$ g cm^{-3}; $2\theta_{max} = 54.0^\circ$; 6513 reflections collected, 4120 unique reflections; 343 parameters; $R_1 = 0.0662$, $wR_2 = 0.1269$ for $I > 2\sigma(I)$; residual electron density: 0.55 e Å^{-3}. CCDC-175036 (**1**) and CCDC-175037 (**2**) contain the supplementary crystallographic data for this paper. These data can be obtained free of charge via www.ccdc.cam.ac.uk/conts/retrieving.html (or from the Cambridge Crystallographic Data Centre, 12, Union Road, Cambridge CB2 1EZ, UK; fax: (+44) 1223-336-033; or deposit @ccdc.cam.ac.uk).

[23] J. J. Bou, A. Rodriguez-Galán, S. Muñoz-Guerra, *Macromolecules* **1993**, *26*, 5664.

[24] A. Hubbuch, R. Bindewald, J. Föhles, V. K. Naithani, H. Zahn, *Angew. Chem.* **1980**, *92*, 394; *Angew. Chem. Int. Ed. Engl.* **1980**, *19*, 394.

 © WILEY-VCH Verlag GmbH, 69451 Weinheim, Germany, 2002 1433-7851/02/4110-1728 $ 20.00+.50/0

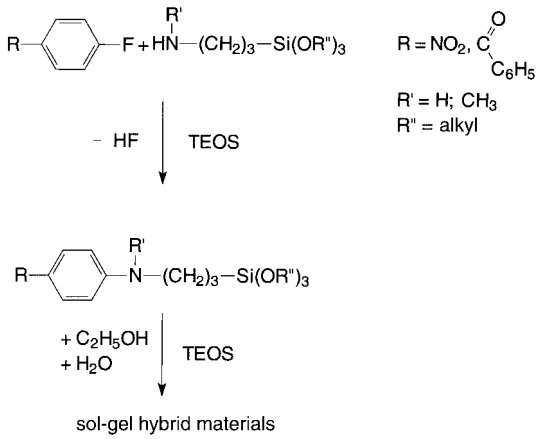
A One-Pot Synthesis of Chromophoric Silicate-Based Xerogels**

Stefan Spange,* Andreas Seifert, Hardy Müller, Stephanie Hesse, and Christian Jäger

The development of the sol–gel process has had a significant impact on materials science and catalysis research during the last 15 years, and has opened up completely new perspectives in the planning of the synthesis and structure of complex hybrid materials.[1–5] One area of this field, the synthesis of hydro- and xero-hybrid gels, has a wide variety of applications, such as nonlinear-optical (NLO) materials, semiconductors, or for use in sensors.[6–13]

The first step of the synthesis involves the covalent modification of a trialkoxysilane with an organic (e.g. chromophoric) group. This functionalized trialkoxysilane (ormosile) is converted into an organically modified silica gel (hydrogel or xerogel) by addition of tetraalkoxysilane in a sol–gel process. Class 2 xerogels are obtained in this way.[9, 14] The direct encapsulation of, for example, dissolved dyes during the sol–gel process leads to class 1 xerogels.[9, 14] This procedure is often not effective, because in most cases the dye is only physically bound. The encapsulated components are thus frequently extracted by organic solvents, and phase separation between the organic components and the inorganic matrix can also occur.

We now present a new procedure for the synthesis of organofunctionalized class 2 silicate-based xerogels, in which the sol–gel process is carried out immediately after the one-pot synthesis of the chromophoric trialkoxysilane components in tetraethoxysilane (TEOS). The key step of the procedure is the nucleophilic substitution of a fluorine atom in an electron-deficient activated aromatic system (such as $-NO_2$ or -COR substituted aromatic groups) by a primary or secondary amine that is bonded by an alkyl chain to a trialkoxysilane group (Scheme 1). One of these aminoalkylalkoxysilanes, which are widely commercially available, is 3-aminopropyltrimethoxysilane (APS).[15] Although the nucleophilic substitution of fluorine in activated aromatics by amino groups is an often used synthetic method,[16, 17] it has only recently been used in the preparation of ormosiles and organofunctionalized silicates.[18, 19] One particular advantage of the reaction is that it can be carried out in TEOS (or another tetraalkoxysilane) as solvent (see Experimental Section).



Scheme 1. One-pot synthesis of chromophoric sol–gel hybrid materials.

The combined procedure was tested on a series of structurally different aromatic fluorine compounds (Table 1, 4,4′-difluorobenzophenone (**6**), 4-fluoronitrobenzene, 4,4′-difluorobenzil (**7**), and 1,5-difluoro-2,4-dinitrobenzene (**8**) are not shown). Surprisingly, in the case of fluorine compounds with additional C=C bonds, such as **5**, no Michael addition was observed but only nucleophilic substitution, which lead to the formation of the chromophoric xerogel. However, the yields of the nucleophilic substitution were low, we are currently working on an optimized synthesis which involves, in particular, enhancement of the nucleophilicity of the amino nitrogen atom by the introduction of an activating group (e.g. $Si(CH_3)_3$), or by the addition of base (e.g. NaH). Activation with sodium hydride has given promising results in preliminary experiments.

In the UV/Vis spectrum of the xerogel, the corresponding absorption band (or bands) of the chromophoric group can be detected easily (Table 1). Because of the high polarity of the silicate matrix, bathochromic shifts of the UV/Vis absorption bands are sometimes observed, as the chromophoric groups used are all positively solvatochromic.[23, 24] The intense colors of the new xerogels can be seen in Figure 1. The materials contain up to 20% of the organofunctionalized silane components and thus are also suitable for use as pigments.

When 4-nitroaniline derivatives (starting from **2**) are incorporated into the silicate matrix, uniformly spherical particles with a narrow size-distribution in the μm region are formed in the sol–gel process, as the scanning electron micrograph of a $4\text{-}O_2NC_6H_4NH(CH_2)_3SiO_{1.5}(SiO_2)_x$ material (Figure 2) demonstrates.

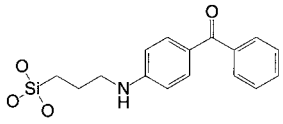
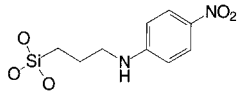
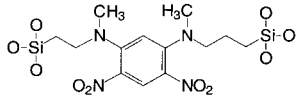
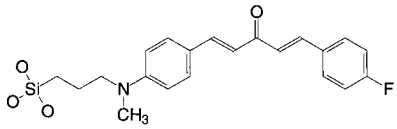
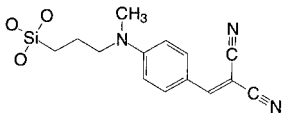
Light-scattering experiments[25] indicate that the polar nitroaniline derivative forms micellelike aggregates in TEOS, which also has a structure-determining effect during the sol–gel process. The polar push–pull-substituted aromatic ring in $4\text{-}O_2NC_6H_4NH(CH_2)_3Si(OC_2H_5)_3$ seems to be responsible for the structure formation. Through this simultaneous formation of the catalyst (HF) and the structure-forming agent, there is synergy between the two reactions (nucleophilic aromatic substitution and the sol–gel process). The ratio of ormosile to

[*] Prof. Dr. S. Spange, Dipl.-Chem. A. Seifert, Dr. H. Müller
Institut für Chemie
Fakultät für Naturwissenschaften
Technischen Universität Chemnitz
Strasse der Nationen 62, 09111 Chemnitz (Germany)
Fax: (+49) 371-531-1642
E-mail: stefan.spange@chemie.tu-chemnitz.de
Dipl.-Phys. S. Hesse, Prof. Dr. C. Jäger
Institut für Physik
Friedrich-Schiller-Universität Jena
Max-Wien-Platz 1, 07743 Jena (Germany)

[**] This work was part of an undergraduate and a diploma project and was financially supported by the state of Saxony. We thank A. Oehlke and M. Plettig for the experimental work, Prof. M. Hietschold (Institute of Physics, TU Chemnitz) for the scanning electron micrographs, and Dr T. Hellweg (TU Berlin) for help with the light-scattering measurements. We thank the Fonds der Chemischen Industrie for financial support.

 © WILEY-VCH Verlag GmbH, 69451 Weinheim, Germany, 2002 1433-7851/02/4110-1729 $ 20.00+.50/0

Table 1. Chromophore groups of the xerogels prepared from fluoroaromatics **1**–**5** and aminosilanes, and their UV/Vis absorption bands.

Components[a]	Molar ratio [b]	Chromophore group	λ_{max} [nm]
4-fluorobenzophenone **1**:APS[c]	1:1:10		355 nm
4-fluoronitrobenzene **2**:APS[c]	1:2.5:4.6		350 nm, 443 nm
1,5-difluoro-2,4-dinitrobenzene **3**:MAPS[d]	1:4:10		350 nm, 398 nm
7,7′-difluorodibenzylidenacetone **4**:MAPS[d]	1:2:10		445 nm
1,1-dicyano-2-(4-fluorophenyl)ethene **5**:MAPS[d]	1:1:10		358 nm, 425 nm

[a] Solvent:TEOS. [b] Fluoroarene:aminosilane:solvent. [c] 3-Aminopropyltrimethoxysilane = APS. [d] *N*-methylaminopropyltrimethoxysilane = MAPS.

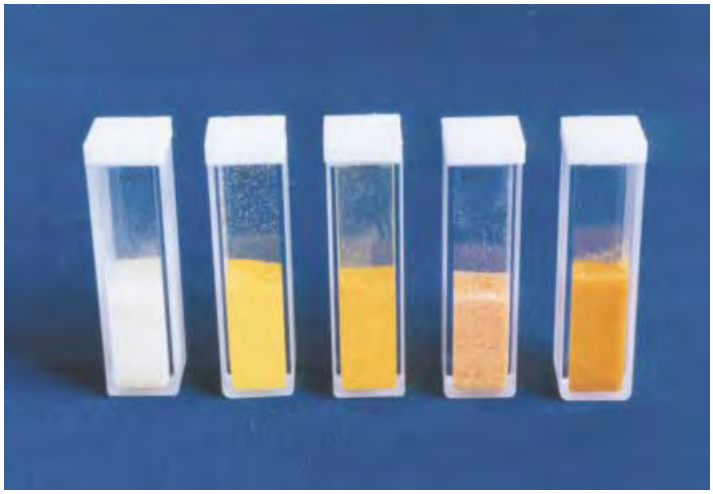


Figure 1. Photograph of the xerogels prepared from fluoroaromatics **1**–**5** (from left to right) and APS or MAPS in TEOS (see Table 1).

TEOS seems to be the morphology-controlling factor that determines the particle size of the 4-nitroaniline-functionalized xerogels.[26a]

A solid-state cross-polarization magic-angle spinning (CPMAS) {^{1}H}-^{29}Si NMR spectrum of the ormosile prepared from **2** and APS in TEOS shows only three signals. The signal at $\delta = -68.9$ ppm (T^3-signal) arises from the trialkoxysilane components which are completely incorporated into the silicate matrix, and the signals at $\delta = -101.6$ (Q^3) and $\delta = -111.9$ ppm (Q^4) are assigned to the silanol groups and the siloxane bridges of the silicate matrix.[20, 21]

The use of bifunctional fluoroaromatic molecules, for example **3** or **6**, could give rise to disubstituted products. In the case of **3**, which because of the two nitro groups is highly activated towards nucleophilic aromatic substitution, after two hours stirring at 130 °C, complete disubstitution was observed; half an hour of stirring at 50 °C lead to the monosubstituted product (see Figure 3). In the case of the less activated **6**, even at a reaction temperature of 210 °C complete disubstitution does not occur, and a mixture of mono- and disubstituted products was obtained. The xerogels were synthesized in TEOS with molar ratios of **3** to *N*-methylaminopropyltrimethoxysilane (MAPS) of 1:1 for monosubstitution and 1:4 for disubstitution (**3**:TEOS 1:10). The assignment of the ^{13}C NMR spectrum signals is shown in Figure 3. The disubstituted product is characterized by a higher symmetry than that of the monosubstituted one and gives rise to fewer signals in the NMR spectrum.

At room temperature and a 1:1 molar ratio of **3**:MAPS, only one fluorine atom is replaced (Figure 3). This monofunctionalized xerogel can be further functionalized with primary or secondary amino compounds. This offers an elegant possibility for the covalent immobilization of water-soluble polymers containing amino groups (such as proteins or polyvinylamines) on chromophoric xerogels.[22]

Several degradation steps are seen in the thermogravimetric analysis of the xerogels. For example, the xerogel synthesized by disubstitution of **3** with MAPS shows two degradation steps. The first arises from the physically bound water and is as expected at 100 °C. The second appears between 300 and 350 °C and arises from degradation of the organic component. Preliminary Brunauer–Emmett–Teller (BET) measurements on the compounds described here show the possibility of formation of both relatively compact and also porous materials, depending on the reaction conditions.[26a,b]

Experimental Section

Reaction of **1** with APS in TEOS: **1** (2.14 g, 10.5 mmol) was dissolved in TEOS (23.5 mL, 105 mmol) with stirring. APS (1.9 mL, 1.88 g, 10.5 mmol)

 © WILEY-VCH Verlag GmbH, 69451 Weinheim, Germany, 2002 1433-7851/02/4110-1730 $ 20.00+.50/0

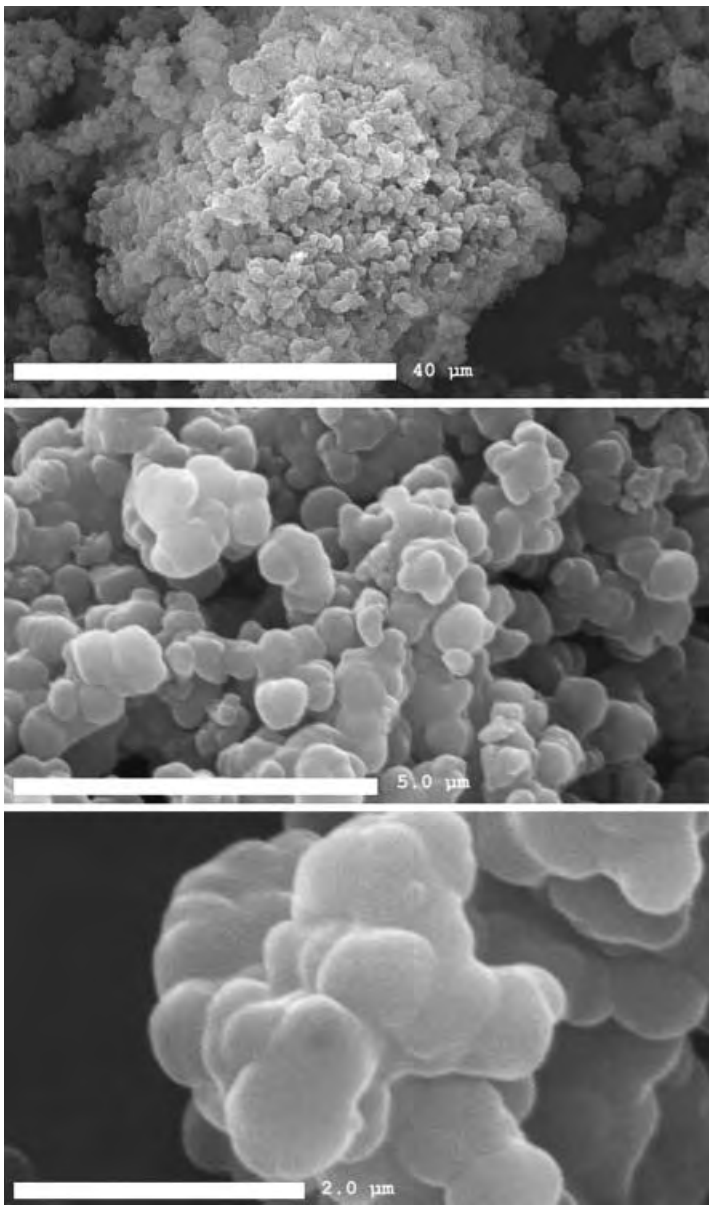


Figure 2. Scanning electron micrograph of the xerogel which was prepared from **2** and APS in TEOS (also see Figure 1 and Table 1).

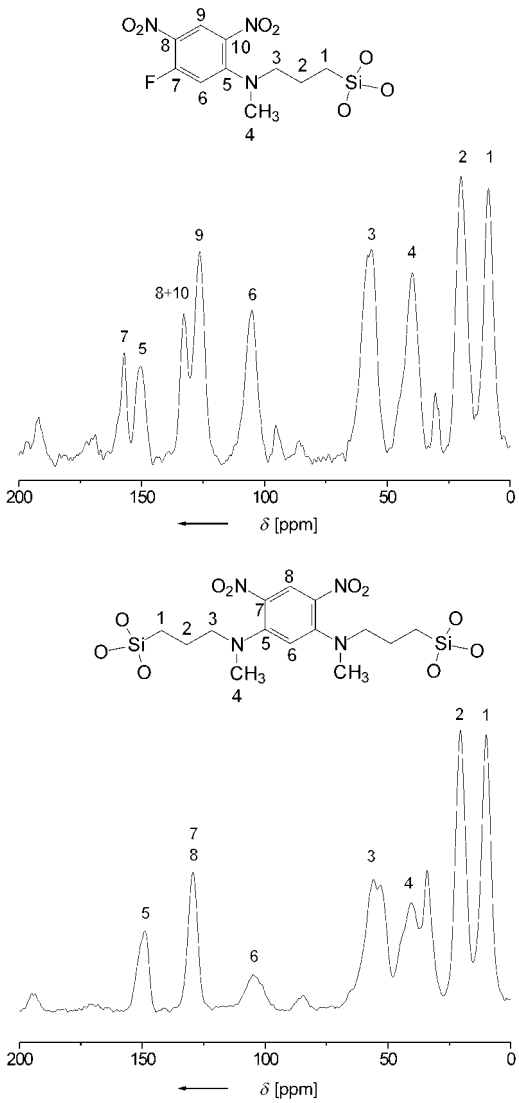


Figure 3. Solid-state $^{13}C\{^1H\}$-CPMAS-NMR spectrum of xerogels prepared from **3** and MAPS in TEOS. A molar ratio of 1:1:10 (**3**:MAPS:TEOS) and a reaction temperature of 50 °C (30 min) leads to monosubstitution (top spectrum). Disubstitution (bottom spectrum) can be achieved by a molar ratio of 1:4:10 at 130 °C (2 h). The ^{13}C resonance signals between $\delta = 8-60$ ppm are assigned to the CH_2 groups of the MAPS. Unlabelled signals arise from unreacted MAPS, or are rotational side-bands.

and *N*,*N*-dimethyloctylamine (2.2 mL, 1.65 g, 10.5 mmol) were then added. The mixture was heated to reflux 14 h (b.p. TEOS: 166–169 °C). An intense yellow coloration developed and a nonviscous yellow solution formed. After cooling to room temperature (25 °C), the dark yellow solution was treated first with ethanol (30 mL) and then with distilled water (8.2 mL, 0.45 mol). After a few seconds or minutes, gel formation began. When the gel was solid, it was dried at 25 °C in vacuo and then unreacted **1** was removed by Soxhlet extraction with acetone. The xerogel was then redried in vacuo. $HOSi^{Q3}O_{1.5}(Si^{Q4}O_{1.5})_xO_{1.5}Si^{T3}C^aH_2C^bH_2C^cH_2NHC_6H_4$-$COC_6H_5$: $^{13}C\{^1H\}$-CPMAS-NMR: $\delta = 10$ (C^a), 23 (C^b), 43 (C^c), 115, 128–133 (br. s), 158 (br. s). ^{29}Si NMR: $\delta = 68.9$ (T^3), 101.6 (Q^3), 111.9 ppm(Q^4).

The reaction of **2** with APS in TEOS was carried out analogously but at 140 °C. No gel formation occurred after the addition of water, but a homogeneous yellow powder precipitated (Figure 2). $HOSi^{Q3}O_2(Si^{Q4}O_2)_x$-$O_2Si^{T3}C^aH_2C^bH_2C^cH_2NHC_6H_4NO_2$: $^{13}C\{^1H\}$-CPMAS-NMR: $\delta = 10.1$ (C^a), 22.1 (C^b), 42.9 (C^c), 111.2 (C1 aromatic), 127.0 (C2 aromatic), 136.4 (C3 aromatic), 155.4 (C4 aromatic).

The $^{13}C\{^1H\}$-CPMAS-NMR spectra were measured on a Bruker AMX 400 and the $^{29}Si\{^1H\}$-CPMAS-NMR spectra with a Tecmag spectrometer. Chemical shifts were measured relative to adamantane for the ^{13}C NMR spectra, and hexamethyldisiloxane (HMDS) for the ^{29}Si NMR signals, respectively. The UV/Vis spectra were measured using a MCS 400 (Carl Zeiss Jena) UV/Vis spectrometer with a special reflection instrument. The scanning electron micrographs were recorded in the electron-microscope laboratory of the Institute of Physics at the Technical University of Chemnitz, on a Philips SEM 515. Before the photographs were taken, gold was evaporated onto the samples to render them electrically conductive.

Received: October 25, 2001 [Z18121]

[1] G. Philipp, H. Schmidt, *J. Non-Cryst. Solids* **1984**, *63*, 283.
[2] C. J. Brinker, G. W. Scherer, *Sol-Gel Science*, Academic Press, New York, **1989**.
[3] B. Boury, R. J. P. Corriu, *Adv. Mater.* **2000**, *12*, 989.
[4] R. J. P. Corriu, *Angew. Chem.* **2000**, *112*, 1433; *Angew. Chem. Int. Ed.* **2000**, *39*, 1376.
[5] B. M. Novak, *Adv. Mater.* **1993**, *5*, 422.

 © WILEY-VCH Verlag GmbH, 69451 Weinheim, Germany, 2002 1433-7851/02/4110-1731 $ 20.00+.50/0

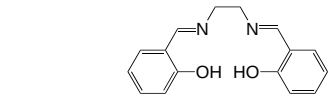
[6] C. Rottman, M. Ottolenghi, R. Zusman, O. Lev, M. Smitz, G. Gong, M. L. Kagan, D. Avnir, *Mater. Lett.* **1992**, *13*, 293.
[7] Z. Yang, C. Xu, B. Wu, L. R. Dalton, S. Kalluri, W. H. Steier, Y. Shi, J. H. Bechtel, *Chem. Mater.* **1994**, *6*, 1899.
[8] *Sol-Gel Optics, Processing and Applications* (Ed.: S. C. Klein), Kluwer Academic, Boston, **1994**.
[9] C. Sanchez, F. Ribot, *New J. Chem.* **1994**, *18*, 1007.
[10] D. Avnir, *Acc. Chem. Res.* **1995**, *28*, 330.
[11] K. Yagi, S. Shibata, T. Yano, A. Yasumor, M. Yamane, B. Dunn, *J. Sol-Gel Sci. Technol.* **1995**, *4*, 67.
[12] C. Sanchez, B. Lebeau, *Pure Appl. Opt.* **1996**, *5*, 689.
[13] H. Jiang, A. K. Kakkar, *J. Am. Chem. Soc.* **1999**, *121*, 3657.
[14] S. Pandey, G. A. Baker, M. A. Kane, N. J. Bonzagni, F. V. Bright, *Chem. Mater*. **2000**, *12*, 3547.
[15] a) B. Arkles, *CHEMTECH* **1977**, *7*, 766; b) Gelest catalogue (Tullytown, PA), **2000**, p. 16, and references therein.
[16] J. F. Bunnett, R. E. Zahler, *Chem. Rev.* **1951**, *49*, 273.
[17] J. Sauer, R. Huisgen, *Angew. Chem.* **1960**, *72*, 294.
[18] K. Neimann, R. Neumann, *Chem. Commun*. **2001**, 487.
[19] A. G. S. Prado, C. Airoldi, *J. Colloid Interface Sci*. **2001**, *236*, 161.
[20] D. Hoebbel, M. Nacken, H. Schmidt, *J. Sol-Gel Sci. Technol*. **1998**, *12*, 169.
[21] C. Wies, K. Meise-Gresch, W. Müller-Warmuth, W. Beier, A. A. Göktas, G. H. Frischat, *Ber. Bunsen-Ges.* **1988**, *92*, 689.
[22] Poly(vinyl amine)s ($M_n = 60000\ g\,mol^{-1}$) react directly with $(SiO_2)_x$-$SiO(CH_2)_3NHC_6H_2F(NO_2)_2$ in aqueous suspension. I. Roth, A. Seifert, S. Spange, unpublished results.
[23] S. Spange, Y. Zimmermann, A. Gräser, *Chem. Mater.* **1999**, *11*, 3245, and references therein.
[24] C. Reichardt, *Chem. Rev.* **1994**, *94*, 2319.
[25] We were able to detect aggregate formation of 4-nitroaniline-functionalized trialkoxysilanes in TEOS using light scattering. A. Seifert, T. Hellweg, S. Spange, unpublished results.
[26] a) A. Seifert, S. Spange, H. Müller, M. Hietschold, J. Schulze, *Chem. Mater.* **2002**, submitted; b) A. Seifert, Diplomarbeit, TU Chemnitz, **2001**; c) A. Seifert, H. Müller, S. Spange, S. Hesse, C. Jäger, *J. Sol-Gel Sci. Technol.* **2002**, submitted.

Silicon – Enamine Complexes: Pentacoordinate Silicon Compounds**

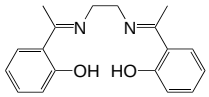
Jörg Wagler, Uwe Böhme, and Gerhard Roewer*

Organosilicon compounds with hypercoordinate Si atoms are interesting both because of their structural features as well as their use in syntheses and as catalytically active intermediates.[1] Their chemical reactivity is controllable by ligand variation. In addition polysilanes which contain hypercoordinate Si atoms in their skeleton display unique electronic and optical properties.[2] Although there are a large number of compounds with penta- or hexacoordinate Si atoms, to date, the principles for a deliberate "switch" between the penta- and hexacoordination are not known. Nevertheless, recently some examples have been described in which the coordination number of a silicon atom can be controlled by the variation of temperature, solvent, and stoichiometry, or by UV irradiation.[3]

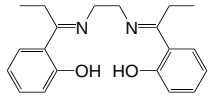
The dianions of the compounds **1** and **2** of the type (sal^{2-}) are well established in transition-metal-complex chemistry. We have shown that their tetradentate donor-atom system $^-O\frown N\frown N\frown O^-$ enables the synthesis of highly coordinated



1

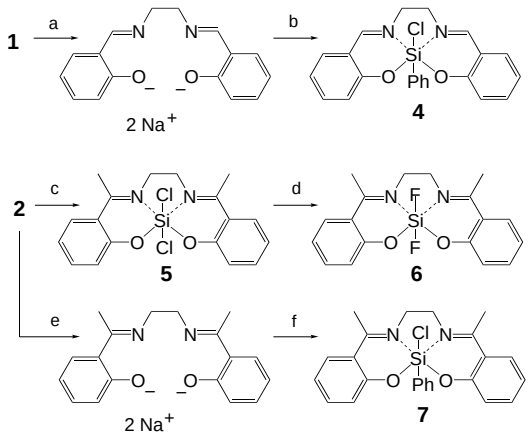


2



3

Si complexes, such as **4**, **5**, and **7**.[4] The remaining Si-bound chlorine atoms in **5** can be exchanged for fluorine atoms, for example, by reaction with ZnF_2, (→**6**; Scheme 1). The hexacoordination in **6** is demonstrated by X-ray crystal-structure analysis.[4]



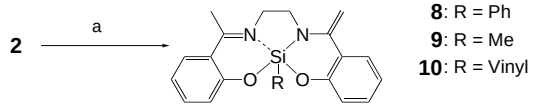
Scheme 1. Syntheses of hexacoordinate silicon – salene complexes. a) NaO*i*Pr/*i*PrOH; b) $PhSiCl_3$/*i*PrOH/88 °C; c) $SiCl_4$/THF/65 °C/2 h; d) ZnF_2/THF/65 °C/1 h; e) 1) NaOMe/THF/MeOH 2) hexane; f) $PhSiCl_3$/THF/30 min.

In contrast to H_2salene (**1**; ethylene-*N*,*N*-bissalicylideniimine), in the methyl- and ethyl-substituted compounds **2** and **3** there is the possibility of imine – enamine tautomerism. However, in complexes with transition-metal ions the enamine structures of **2** and **3** have not yet been observed. To our surprise we found this type of arrangement in the pentacoordinate silicon complexes **8** – **10** (Scheme 2). The synthesis of this new class of enamine complexes can be easily performed by the addition of diethylamine as a base in the reaction of the chlorosilanes $PhSiCl_3$, $MeSiCl_3$, or $vinylSiCl_3$ with the ligands **2** and **3**. The driving force for this unusual HCl elimination, which is clearly promoted by the hypercoordinate silicon atom, arises from both the high basicity of amine used as well

[*] Prof. Dr. G. Roewer, Dipl.-Chem. J. Wagler, Dr. U. Böhme
Institut für Anorganische Chemie
Technische Universität Bergakademie Freiberg
Leipziger Strasse 29, 09596 Freiberg (Germany)
Fax: (+49) 3731-39-4058
E-mail: gerhard.roewer@chemie.tu-freiberg.de

[**] This work has been supported by the Fonds der Chemischen Industrie.

 © WILEY-VCH Verlag GmbH, 69451 Weinheim, Germany, 2002 1433-7851/02/4110-1732 $ 20.00+.50/0



Scheme 2. Synthesis of pentacoordinate silicon complexes with enamine-functionalized salene ligands. a) $RSiCl_3/HNEt_2/THF/65\,^{\circ}C/2.5$ h.

as from the very low solubility of the precipitated ammonium salt $[NH_2Et_2]Cl$.

The X-ray structure analyses of the complexes **8** and **9**[5] reveal the presence of the enamine structure. The structures of both compounds are similar, despite the differences in the conformation of the molecules, which are caused by different substituents at the silicon atom. Therefore, only the structure of the compound **9** will be described (Figure 1). In **9** there is a

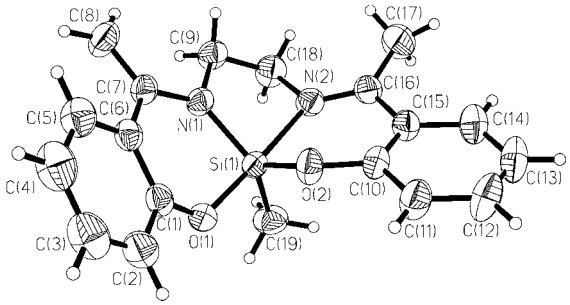


Figure 1. Molecular structure of compound **9** (thermal ellipsoids set at the 50% level); selected bond lengths [Å] and angles [°]: Si(1)-O(2) 1.683(2), Si(1)-O(1) 1.713(2), Si(1)-N(1) 1.756(2), Si(1)-C(19) 1.858(3), Si(1)-N(2) 2.017(2), O(1)-C(1) 1.341(3), O(2)-C(10) 1.349(3), N(1)-C(7) 1.394(3), N(1)-C(9) 1.466(3), N(2)-C(16) 1.284(4), N(2)-C(18) 1.459(3),C(7)-C(8) 1.343(4), C(16)-C(17) 1.509(4); O(2)-Si(1)-O(1) 91.59(9), O(2)-Si(1)-N(1) 120.1(1), O(1)-Si(1)-N(1) 95.2(1), O(2)-Si(1)-C(19) 114.7(1), O(1)-Si(1)-C(19) 94.2(1), N(1)-Si(1)-C(19) 124.0(1), O(2)-Si(1)-N(2) 88.2(1), O(1)-Si(1)-N(2) 176.64(9), N(1)-Si(1)-N(2) 82.0(1), C(19)-Si(1)-N(2) 88.9(1).

pentacoordinate silicon atom surrounded by the threefold deprotonated salene ligand **2**. The silicon atom is in a distorted trigonal-bipyramidal coordination environment. The atoms O(1) and N(2) form the axis of the bipyramid with an O(1)-Si(1)-N(2) angle of 176.64(9)°. The atoms N(1), O(2), and C(19) are in the equatorial plane of the bipyramid. The sum of the bonding angles at both the nitrogen atoms is 360°. Thus the atoms N(1) and N(2) are sp^2-hybridized. The C(7)–C(8) bond (1.343(4) Å) is remarkably shortened in comparison with that between C(16)–C(17) (1.509(4) Å) and falls unambiguously within the range of a C–C double bond. Besides both the O atoms of the ligand also the carbon atom C(8) is deprotonated leading to the formation of a silicon-stabilized enamine. This situation has consequences for the shape of the whole molecule: The C(7)–N(1) bond (1.394(3) Å) of the enamine is longer than that of the imine group C(16)–N(2) (1.284(4) Å). The Si(1)–N(2) bond is elongated by 0.26 Å in comparison with the Si(1)–N(1) bond. The chiral molecule crystallizes in the noncentrosymmetric space group $P2_1$. During crystallization conglomerate formation occurs, that is, the crystal investigated consists of only one enantiomer of the compound. The absolute configuration of this molecule has been determined.[6]

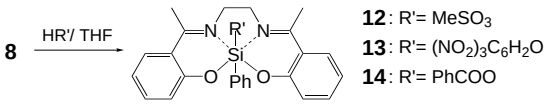
The chemical shifts from the solution ^{29}Si NMR spectra of complexes **8**–**10** are given in Table 1 and clearly indicate the pentacoordination of the Si atoms. In the complexes with the

Table 1. Yields, melting points, and ^{29}Si NMR spectroscopic data of pentacoordinate Si complexes.

	Yield [%]	M.p. [°C][a]	^{29}Si NMR[b]
8	71	250	–115.8
9	73	189	–103.2
10	85	140	–117.0

[a] The melting points of the hydrolysis-sensitive compounds **8**–**10** were determined under Ar atmosphere in a closed glass capillary. [b] $CDCl_3$ was used as solvent; tetramethylsilane (TMS) as internal standard.

ligand **3**, the C atom, in the α position to the imine group, has different substituents. The resulting complexes, which are analogous to the compounds **8**–**10**, form *E*/*Z*-diastereomeres, as we have demonstrated by ^1H NMR and ^{13}C NMR spectroscopy. Formally, the pentacoordinate silicon complexes with enamine structure could originate by 1,4-elimination of hydrogen chloride from initially formed compounds with a hexacoordinate Si atom. The compound **8** could also be prepared by HCl elimination from **7** with Et_2NH or Et_3N. The reverse of this process should be possible: to convert penta- into new hexacoordinate silicon complexes by adding H-acidic molecules, that is, pentacoordinate Si compounds can be used synthetically as precursors for hexacoordinate ones. The driving force for these Brønsted acid addition reactions should be determined by the acidity of the HR′ component (R′=$MeSO_3$, $(NO_2)_3C_6H_2O$, PhCOO). The use of OH acidic molecules leads to a significant energy effect by the formation of additional energetically favorable Si–O bonds. Indeed, the pentacoordinate silicon complexes react with the picric acid, methane sulphonic acid, and benzoic acid by 1,4-addition. With **8** as educt the complexes **12**–**14** were formed, which are almost insoluble in THF (Scheme 3).



Scheme 3. Synthesis of hexacoordinate silicon–salene complexes.

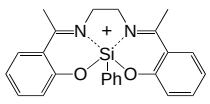
The resulting hexacoordination of the Si atoms in the solid state is clearly demonstrated by the upfield shift of the signals in the ^{29}Si cross-polarization magic-angle spinning (CPMAS) NMR spectrum, (see Table 2). The assumption, that the

Table 2. Yields, THF content, and ^{29}Si CPMAS NMR spectroscopic data of hexacoordinate Si complexes.

Compound	THF content[a] [equivalents]	Yield [%]	^{29}Si CPMAS NMR $\delta(^{29}Si)$ [ppm]
12	0.5	89	–174.3
13	2	72	–173.5
14	1	65	–186.5

[a] The THF content of isolated products was determined by ^1H NMR spectroscopy and is compatible with the elemental analyses of these compounds.

 © WILEY-VCH Verlag GmbH, 69451 Weinheim, Germany, 2002 1433-7851/02/4110-1733 $ 20.00+.50/0



11

addition of an acid initially causes a protonization of the ligands, is supported by the result of the analysis with ESI-MS (compound **8** in THF, formic acid, cation mode), this indicates the formation of the cation **11** (*m*/*z* 398). In principle, acid addition is fast and with high yields. Therefore, this general route seems to be a more favorable synthetic pathway to these hexacoordinate Si compounds than the alternative introduction of the respective acid anions to obtain the complexes **12**–**14** by nucleophilic substitution.

Experimental Section

The syntheses of **2** and **3** were by literature methods.[7]

8: $PhSiCl_3$ (7.5 g, 35.5 mmol) was rapidly added dropwise to a stirred solution of **2** (10.0 g, 33.8 mmol) and diethylamine (13.0 g, 178.1 mmol) in dry THF (400 mL) at room temperature. $NHEt_2 \cdot HCl$ started to precipitate immediately. After 2.5 hours stirring under reflux the mixture was cooled to room temperature and stored overnight in the refrigerator (about 8 °C). Afterwards $NHEt_2 \cdot HCl$ was removed by filtration and the clear yellow solution concentrated. Compound **8** precipitated at room temperature as bright yellow crystals; crystallization took several days. The product was collected by filtration over a G3 frit, washed with a small amount of THF, and dried in vacuo; yield: 9.5 g (23.9 mmol, 71 %); m.p. 250 °C; ^{29}Si NMR (80 mHz): $\delta = -115.8$ ppm ($CDCl_3$); $\delta = -117.1$ ppm ([D$_6$]DMSO); ^{29}Si CPMAS NMR (60 mHz): $\delta = -116.1$ ppm; ^{1}H NMR (400 mHz, $CDCl_3$): $\delta = 2.42$ (s, 3H, CH_3), 3.38–4.03 (3m, 2H, 1H, 1H, CH_2CH_2), 4.16 (s, 1H, (*Z*)-C=CH_2), 4.63 (s, 1H, (*E*)-C=CH_2), 6.75–7.60 ppm (m, 13H, aromatic protons); ^{13}C NMR (101 mHz, $CDCl_3$): $\delta = 17.1$ (CH_3), 45.8, 46.4 (CH_2CH_2), 85.5 (=CH_2), 119.1, 119.7, 119.8, 120.5, 122.7, 125.7, 126.0, 128.4, 128.9, 135.2, 151.7, 154.4 (salene aromatic carbon atoms), 158.4 (=C–N), 168.8 (C=N), 127.3, 128.2, 131.9, 141.5 (C_6H_5); IR (KBr): $\tilde{\nu} = 1620$ cm^{-1} (C=N).

9 and **10** were synthesized analogously to **8**. The products were obtained as solids by crystallization induced by the addition of *n*-hexane to the concentrated filtrate (**9**) or precipitation with *n*-hexane (**10**). **9**: ^{29}Si NMR ($CDCl_3$): $\delta = -103.2$ ppm; ^{1}H NMR ($CDCl_3$): $\delta = 0.03$ (s, 3H, $SiCH_3$), 2.46 (s, 3H, CCH_3), 3.35–4.05 (3m, 2H, 1H, 1H, CH_2CH_2), 4.10 (s, 1H, (*Z*)-C=CH_2), 4.56 (s, 1H, (*E*)-C=CH_2), 6.75–7.60 ppm (m, 8H, aromatic protons); ^{13}C NMR ($CDCl_3$): $\delta = 1.6$ ($SiCH_3$), 17.0 (CCH_3), 46.2 (CH_2CH_2), 85.8 (=CH_2), 119.1, 119.6, 119.8, 120.4, 122.8, 125.8, 126.9, 128.3, 128.8, 134.9, 151.8, 154.2 (salene aromatic carbon atoms), 158.1 (=C–N), 167.6 (C=N); elemental analysis calcd (%) for $C_{19}H_{20}N_2O_2Si$: C 67.83, H 5.99, N 8.33; found: C 67.69, H 6.30, N 8.07; **10**: ^{29}Si NMR ($CDCl_3$): $\delta = -117.0$; ^{1}H NMR ($CDCl_3$): $\delta = 2.51$ (s, 3H, CH_3), 3.35–4.03 (3m, 2H, 1H, 1H, CH_2CH_2), 4.13 (s, 1H, (*Z*)-C=CH_2), 4.60 (s, 1H, (*E*)-C=CH_2), 6.75–7.60 (m, 8H, aromatic protons), 5.60–5.75 (m, 3H, CH=CH_2); ^{13}C NMR ($CDCl_3$): $\delta = 17.1$(CH_3), 46.3, 46.7 (CH_2CH_2), 86.1 (=CH_2), 119.1, 119.7, 120.3, 120.4, 122.6, 125.8, 126.4, 128.3, 128.8, 135.0, 151.7, 154.4, (salene aromatic carbon atoms), 158.1 (=C–N), 168.7 (C=N), 132.7, 138.4 (CH=CH_2); elemental analysis calcd (%) for $C_{20}H_{20}N_2O_2Si$: C 68.93, H 5.78, N 8.04; found: C 67.85, H 6.41, N 6.99.

12–**14**: The stoichiometric amount of the acid (CH_3SO_3H, $(NO_2)_3C_6H_2OH$, C_6H_5COOH) dissolved in a small amount of THF was added dropwise to a stirred solution of **8** (about 1 g) in THF (about 40 mL) at about 30 °C. The compounds **12**–**14** precipitated as solids and could be collected by filtration over a G3 frit, washed with a small amount of THF, and dried in vacuo.

Compounds **12** and **14** melt above 200 °C with partial decomposition (turn brown) or decompose without melting. Compound **13** melts at 106 °C; **12**: elemental analysis calcd (%) for $C_{27}H_{30}N_2O_{5,5}SiS$: C 61.11, H 5.70, N 5.28; found: C 59.80, H 5.76, N 5.66; ^{13}C NMR ([D$_6$]DMSO): $\delta = 19.0$ (CH_3), 46.0 (CH_2CH_2), 174.7, 159.2, 150.3, 136.0, 133.0, 130.4, 126.4, 126.2, 120.9, 119.5, 119.2 ppm; **13**: elemental analysis calcd (%) for $C_{38}H_{41}N_5O_{11}Si$: C 59.13, H 5.35, N 9.07; found: C 59.12, H 5.24, N 9.03; ^{13}C NMR ([D$_6$]DMSO): $\delta =$ 19.1 (CH_3), 46.0 (CH_2CH_2), 174.7, 160.7, 159.2, 150.4, 141.8, 136.1, 133.0, 130.4, 126.4, 126.2, 125.1, 124.1, 120.9, 119.6, 119.2 ppm; **14**: elemental analysis calcd (%) for $C_{35}H_{36}N_2O_5Si$: C 70.92, H 6.12, N 4.73; found: C 71.52, H 5.65, N 5.38; ^{13}C NMR ([D$_6$]DMSO): $\delta = 18.3$ (CH_3), 45.6 (CH_2CH_2) 172.0, 161.1, 158.2, 134.7, 133.4, 129.7, 127.1, 126.4, 125.2, 120.6, 120.1, 117.5 ppm.

Received: November 7, 2001 [Z 18181]

[1] R. Tacke, M. Mallak, R. Willeke, *Angew. Chem.* **2001**, *113*, 2401–2403; *Angew. Chem. Int. Ed.* **2001**, *40*, 2339–2341; R. Tacke, M. Pülm, B. Wagner, *Adv. Organomet. Chem.* **1999**, *44*, 221–273; I. S. Ignatyev, H. F. Schäfer III, *Organometallics* **2001**, *20*, 3113–3121; R. J. P. Corriu, J. C. Young in *The chemistry of organic silicon compounds*, *Vol. 1* (Eds.: S. Patai, Z. Rappoport), Wiley, **1989**, pp. 1241–1288; D. Kost, I. Kalikhman in *The chemistry of organic silicon compounds*, *Vol. 2* (Eds.: Z. Rappoport, Y. Apeloig), Wiley, **1998**, pp. 1339–1446.

[2] C. Chuit, R. J. P. Corriu, C. Reye, J. C. Young, *Chem. Rev.* **1993**, *93*, 1371–1448; I. El-Sayed, Y. Hatanaka, S. Onozawa, M. Tanaka, *J. Am. Chem. Soc.* **2001**, *123*, 3597–3598.

[3] I. Kalikhman, S. Krivonos, L. Lameyer, D. Stalke, D. Kost, *Organometallics* **2001**, *20*, 1053–1055; V. Kingston, B. Gostevski, I. Kalikhman, D. Kost, *Chem. Commun.* **2001**, 1272–1273; I. Kalikhman, O. Girshberg, L. Lameyer, D. Stalke, D. Kost, *J. Am. Chem. Soc.* **2001**, *123*, 4709–4716; N. Kano, F. Komatsu, T. Kawashima, *J. Am. Chem. Soc.* **2001**, *123*, 10778–10779.

[4] F. Mucha, J. Haberecht, U. Böhme, G. Roewer, *Monatsh. Chem.* **1999**, *130*, 117–132; F. Mucha, U. Böhme, G. Roewer, *Chem. Commun.* **1998**, 1289–1290; M. S. Singh, P. K. Singh, *Main Group Met. Chem.* **2000**, *23*, 183–188.

[5] X-ray structure analyses: The measurements were carried out with an ENRAF-NONIUS-CAD4 diffractometer. The structures were solved by direct methods, all non-hydrogen atoms were refined anisotropically. The hydrogen atoms were placed in idealized positions and were refined by the riding model. The structures were solved and refined on F^2 by full-matrix least-square methods with the programs SHELXS-86 (G. M. Sheldrick, Universität Göttingen, **1986**) and SHELXL-97 (G. M. Sheldrick, Universität Göttingen, **1997**). Compound **9**: $C_{19}H_{20}N_2O_2Si$, $M_r = 336.46$, yellow prism, $0.4 \times 0.3 \times 0.3$ mm, monoclinic, space group $P2_1$, $a = 6.734(1)$, $b = 11.540(6)$, $c = 11.051(5)$ Å, $\beta = 98.77(1)^\circ$, $V = 848.7(6)$ Å^3, $\rho_{calcd} = 1.317$ g cm^{-3}, $F(000) = 356$, $\mu = 1.330$ mm^{-1}, no absorption correction, $Z = 2$, $\lambda = 1.54178$ Å, $T = 293$ K, $\omega/2\theta$-scans, 6769 measured reflections ($-8 \le h \le 7$, $-14 \le k \le 14$, $-13 \le l \le 13$), 3508 independent and 3182 observed reflections with $I > 2\sigma(I)$, 219 parameters, $R = 0.0596$, $wR_2 = 0.1280$ (all reflections), residual electron density 0.529 and -0.303 e Å^{-3}, Flack parameter 0.00(3). Compound **8**: $C_{24}H_{22}N_2O_2Si$, $M_r = 398.53$, pale-yellow crystal, $0.6 \times 0.4 \times 0.4$ mm, monoclinic, space group $P2_1$; $a = 8.795(1)$, $b = 11.491(1)$, $c = 10.739(1)$ Å, $\beta = 112.90(2)^\circ$, $V = 999.8(2)$ Å^3, $\rho_{calcd} = 1.324$ g cm^{-3}, $F(000) = 420$, $\mu = 1.219$ mm^{-1}, no absorption correction, $Z = 2$, $\lambda = 1.54178$ Å, $T = 293$ K, $\omega/2\theta$-scans, 5022 measured reflections ($-11 \le h \le 11$, $-6 \le k \le 14$, $-13 \le l \le 13$), 2517 independent and 2108 observed reflections with $I > 4\sigma(I)$, 271 parameters, $R = 0.0533$, $wR_2 = 0.1013$ (all reflections), residual electron density 0.348 and -0.231 e Å^{-3}, Flack parameter $-0.04(4)$. CCDC-171307 (**9**) and CCDC-165814 (**8**) contains the supplementary crystallographic data for this paper. These data can be obtained free of charge via www.ccdc.cam.ac.uk/conts/retrieving.html (or from the Cambridge Crystallographic Data Centre, 12, Union Road, Cambridge CB2 1EZ, UK; fax: (+44) 1223-336-033; or deposit@ccdc.cam.ac.uk).

[6] The measurement has been performed with $Cu_{K\alpha}$ radiation, 1661 Friedel pairs were measured (89.9 %), Flack parameter 0.00(3).

[7] P. Pfeiffer, E. Breit, E. Lübbe, T. Tsumaki, *Liebigs Ann. Chem.* **1933**, *503*, 127.

 © WILEY-VCH Verlag GmbH, 69451 Weinheim, Germany, 2002 1433-7851/02/4110-1734 $ 20.00+.50/0

The Adsorption of Cyclopropane and Cyclohexane on Cu(111): An Experimental and Theoretical Investigation on the Nature of the CH–Metal Interaction**

Kari A. Fosser, Ralph G. Nuzzo, Paul S. Bagus, and Christof Wöll*

The nature of the interactions of molecules with surfaces is a topic of considerable importance in technology. For example, the chemical properties and dynamics of adsorbate systems directly underlie the reactivity patterns seen in heterogeneous catalysis.[1, 2] Related adsorption phenomena are also of relevance for many other areas, such as adhesion, wetting, lubrication, and corrosion inhibition.[3] For simple diatomic molecules such as CO bound to metal surfaces significant progress has been made in the past few years in moving from the early simple but valuable picture developed by Blyholder[4] to more recent, advanced descriptions.[5, 6] For the detailed understanding of interactions between hydrocarbons and metals, comparable approaches are just beginning to emerge. The adsorption of simple unsaturated hydrocarbons such as ethylene, acetylene, and benzene on Cu surfaces[7–10] are relatively well understood, and the early Dewar–Chatt–Duncanson model of these interactions[11, 12] has been improved significantly.

For saturated hydrocarbon adsorbates, the situation is less satisfying. In fact there are several properties of adsorbed alkanes on metals that are incompatible with the occurrence of simple physical interactions only. The most disturbing experimental observation is the now well-established occurrence of vibrational mode softening that results from metal–CH contacts, which was first reported by Demuth et al. 25 years ago for cyclohexane adsorbed on Ni(111) and Pt(111).[13] Similar observations have been reported since then for a variety of alkane adsorbates bound to many other substrates.[14, 15] A satisfying theoretical analysis of these unusual soft vibrational modes has been lacking—a surprising omission given the obvious relevance of such effects to the mechanisms of catalytic C–H bond activation. We have addressed this fundamental problem by a combined experimental and theoretical investigation of the binding of the small, highly symmetric saturated hydrocarbons cyclopropane and cyclohexane to Cu(111).

The reflection absorption infrared spectra (RAIRS) recorded for submonolayers of cyclopropane adsorbed on Cu(111) reveal only one C–H vibration at 3074 cm^{-1} (Figure 1, top). The observation of only one mode is expected from the surface selection rule[16] applied to a planar cyclopropane adsorption geometry (Figure 1, insert). Soft modes in the frequency range between 2700 and 2900 cm^{-1}, which are commonly observed for saturated hydrocarbons adsorbed on copper surfaces, were not detected.[14, 17] Thus this is the first example for the adsorption of a saturated hydrocarbon on a Cu(111) surface, for which no soft modes occur.

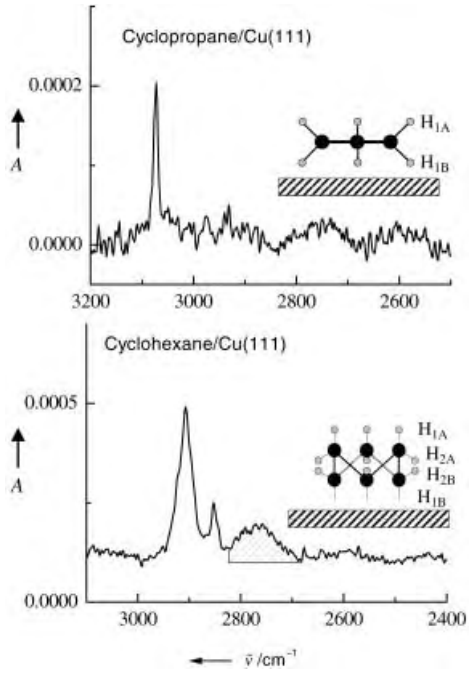


Figure 1. RAIR spectra recorded for a submonolayer of cyclopropane (top) and cyclohexane (bottom) adsorbed on Cu(111) at a surface temperature of 100 K. The two insets show the adsorption geometry for the two molecules. The hatched area shows the soft C–H stretch modes seen for adsorbed cyclohexane.

The RAIR spectra for cyclohexane adsorbed on the Cu(111) surface (Figure 1, bottom) is very similar to that reported previously.[14, 17] In addition to the vibrations at 2907 and 2852 cm^{-1} expected for cyclohexane in a planar adsorption geometry with a chair conformation, pronounced soft modes, centered at 2770 cm^{-1}, with a half-width of 60 cm^{-1} and an integrated intensity of 50% of that of the dominant mode at 2907 cm^{-1} are clearly visible.

A comparison between the calculated ab initio frequencies provided in Table 1 and the experimental values strongly suggests that the soft modes seen for cyclohexane on the Cu(111) surface are in fact derived from the totally symmetric ν_2 mode (symmetric CH_2 stretch). That the adsorption-induced reduction of the molecular symmetry from D_{3h} to C_{3v} in principle makes the observation of this mode possible had been realized earlier.[14] No connection to the soft modes

[*] Prof. Dr. C. Wöll
Lehrstuhl für Physikalische Chemie I
Ruhr-Universität Bochum
44780 Bochum (Germany)
Fax: (+49) 234-32-14182
K. A. Fosser, Prof. R. G. Nuzzo
School of Chemical Sciences and
Frederick Seitz Materials Research Laboratory
University of Illinois at Urbana-Champaign
Urbana, IL 61801 (USA)
Prof. P. S. Bagus
Department of Chemistry
Texas A&M University
College Station, TX 77842-3012 (USA)
E-mail: woell@pc.ruhr-uni-bochum.de

[**] This work was supported by the National Science Foundation (Grant CHE 9626871) and the Department of Energy through the University of Illinois at Urbana-Champaign Frederick Seitz Materials Research Laboratory (Grant DEFG02-91ER45439). The workstation used for the computations is operated in Bochum under a grant from the Deutsche Forschungsgemeinschaft (SFB 558).

 © WILEY-VCH Verlag GmbH, 69451 Weinheim, Germany, 2002 1433-7851/02/4110-1735 $ 20.00+.50/0

Table 1. Experimental and calculated frequencies for the free cyclohexane molecule (gp) and cyclohexane adsorbed in a planar geometry on a Cu(111) surface.

Mode[a]	Experimental			Calculated[b]		
	gp[c] [cm^{-1}]	Cu(111) [cm^{-1}]	Δ gp [cm^{-1}]	gp [cm^{-1}]	Cu(111) [cm^{-1}]	Δ gp [cm^{-1}]
ν_{25} EU CH_2 a-str	2933	–	–	3025 (123)	3010 (ia)[d]	15
ν_{26} EU CH_2 s-str	2863	–	–	2966 (37)	2959 (ia)[d]	7
ν_{12} a2u CH_2 a-str	2915	2907	8	3039 (156)	3024 (304)	15
ν_{13} a2u CH_2 s-str	2860	2852	8	2969 (87)	2959 (102)	10
ν_2 a1g CH_2 s-str	2852 (ia)	$\approx$2770	$\approx$80	2967 (ia)	2948 (50)	19

[a] The modes are labeled by the corresponding symmetry for the free molecule. Note that for the species adsorbed on the surface the symmetry will be lower. [b] The numbers in parentheses give the excitation probability; "ia" denotes IR-inactive. [c] Ref. [23]. [d] IR inactive because of surface selection rule (see text).

has yet been made, since the corresponding dynamic dipole moment, although finite, is expected to be very small for the ν_2 mode. This is nicely illustrated by the results of calculations for cyclopropane (Table 2), where the corresponding ν_1 mode is lower in intensity by about a factor of 40 with regard to the most intense vibration ν_6 of the adsorbed cyclopropane molecule. This small dynamic dipole moment explains why this mode is mot observed experimentally.

Inspection of the theoretical results for cyclohexane reveals, perhaps unexpectedly from an analogy made to the cyclopropane results, that the intensity of the symmetric CH_2-stretching ν_2 mode for adsorbed cyclohexane is of the same order of magnitude as that of the most intense ν_{12} mode (Table 1). This result suggests that for adsorbed cyclohexane a new mechanism comes into play. In fact a detailed analysis of the calculated data reveals that there is a significant transfer of charge from the Cu substrate into the adsorbed cyclohexane molecules.[18] Since this charge transfer depends very strongly on the distance of the molecule (in particular the proximal hydrogen atoms H_{1B}; Figure 1) from the surface, the dynamic dipole moment, $d\mu/dr$, for the cyclohexane ν_2 mode becomes significant and, accordingly, makes the ν_2 mode very intense. The strongly distance-dependent charge transfer thus provides a well-supported explanation as to why the ν_2 mode is so intense for the adsorbed cyclohexane molecule. Although the calculated frequency shift relative to the gas-phase, $-19\,cm^{-1}$, is by far the largest seen for any of the cyclohexane modes characterized here, the absolute shift does not agree in a quantitative way with that seen in the experiment ($\approx -80\,cm^{-1}$). This latter discrepancy most likely results from systematic errors associated with the finite size of the Cu cluster used and is expected to decrease in magnitude with an increasing cluster size.

From a chemical point of view, the occurrence of significant (and specific forms) of charge transfer is very important for understanding the reactivity of hydrocarbons adsorbed on metal surfaces and is of relevance for developing an understanding of the relationship between structure and rate of reaction in C–H bond activation processes on solid surfaces. The results of the theoretical analysis for the different contributions to the interactions occurring between the adsorbate and substrate[18] suggest that a heretofore unappreciated mechanism exists that leads to a charge transfer into empty molecular orbitals with predominantly Rydberg character. Such a transfer can be considered a form of back-donation, since it is one that passes from the substrate into the molecule. We note that this charge transfer bears no similarity to a Blyholder donation/back-donation model such as might describe the binding of CO on metal surfaces[4–6] or a Dewar–Chatt–Duncanson type donation/back-donation scheme[11, 12] that defines aspects of the interactions of unsaturated hydrocarbons with metal substrates.

The driving force for the charge transfer into the cyclohexane molecule is the dispersion forces pulling the hydrocarbon towards the metal states. This attraction is eventually compensated by the Pauli repulsion between the HOMOs of the cyclohexane and the metal states. If the attraction is sufficiently strong, as appears to be the case for cyclohexane, some degree of the metal charge will flow into the molecule. This charge flow dominates the perturbations of the spectroscopy noted above. That the charge is back-donated into Rydberg orbitals and not into orbitals of C–C σ^* or C–H σ^* character also explains why the changes in the adsorbate intramolecular geometry are at best only minor. For the case of a back-donation into, for example, CH σ^* orbitals one would expect a significant increase of the C–H bond length.

Calculations should help to explain why the charge transfer is so much smaller for cyclopropane than for cyclohexane. As noted above, a detailed investigation revealed a strong dependence of the extent of charge transfer on the distance between the surface and molecule. The optimized adsorption geometry for cyclohexane yields a distance of 2.75 Å between

Table 2. Experimental and calculated frequencies for the free cyclopropane molecule (gp) and cyclopropane adsorbed in a planar geometry on a Cu(111) surface.

Mode[a]	Experimental			Calculated[b]		
	gp[c] [cm^{-1}]	Cu(111) [cm^{-1}]	Δ(gp) [cm^{-1}]	gp [cm^{-1}]	Cu(111) [cm^{-1}]	Δ(gp) [cm^{-1}]
ν_6 A_2'' CH_2 as-str	3103	3074	29	3238 (41)	3218 (69)	20
ν_8 E′ CH_2 s-str	3038	–	–	3120 (21)	3101 (ia)[d]	19
ν_1 A_1 CH_2 s-str	3025 (ia)	–	–	3136 (ia)	3110 (1.2)	26

[a] The modes are labeled by the corresponding symmetry for the free molecule. Note that for the species adsorbed on the surface the symmetry will be lower. [b] The numbers in parentheses give the excitation probability; "ia" denotes IR inactive. See text for details on calculations. [c] Ref. [23]. [d] IR inactive because of surface selection rule (see text).

 © WILEY-VCH Verlag GmbH, 69451 Weinheim, Germany, 2002 1433-7851/02/4110-1736 $ 20.00+.50/0 *Angew. Chem. Int. Ed.* **2002**, *41*, No. 10

the H_{1B} atoms and the Cu surface. The corresponding distance between the H_{1B} atoms of cyclopropane and the surface is 3.0 Å. It thus appears that the dispersion forces for cyclopropane are not quite strong enough to push the molecule as deeply into the surface, which results in a lesser degree of charge transfer into the molecule than occurs for cyclohexane.

Experimental Section

The UHV chamber used in these experiments was operated at a base pressure of $< 3.0 \times 10^{-10}$ Torr and has been described previously.[19, 20] The RAIRS data were collected with a Digilab FTS 60A spectrometer with a liquid nitrogen cooled wide-band MCT detector in conjunction with external reflection optics, maximized for single grazing angle reflection. The crystal temperature was monitored by a chromel-alumel thermocouple lodged in a hole on the side of the crystal. The crystal could be cooled and heated within the temperature range of 100 – 950 K. The crystal was cleaned by sputtering with 1 keV Ar^+ ions for 30 min at 850 K and then annealed for 15 min at 850 K. The adsorbates were introduced into the chamber by using an effusive molecular beam doser located approximately 5 cm from the crystal. Cyclopropane (> 99 %) was obtained from Aldrich and used as received. Cyclohexane (> 99 %) was obtained from EM Science and degassed by freeze-pump-thaw cycles before introduction into the chamber. The pressure during dosing varied between 1×10^{-9} and 5×10^{-7} Torr. Exposures, reported in Langmuirs (1×10^{-6} Torr), are not corrected for the ion gauge sensitivity.

Ab initio calculations: The calculations for cyclopropane and cyclohexane adsorbed on Cu(111) closely follow an approach described previously.[21] Briefly, high-quality ab initio Hartree – Fock calculations were carried out for a (7,3)-cluster exhibiting C_{3v} symmetry modeling a Cu(111) surface with a Cu lattice constant of 2.54 Å using a commercial software package (Gaussian 98[22]). Correlation effects were included at the MP2 level. For the Cu atoms a 28-electron pseudopotential (see reference [21] and [23] for a detailed discussion) together with an extensive basis set for the remaining electrons was used together with a 6-311 ++ basis set for the C and the H atoms. This basis set has been demonstrated to be sufficiently large to account for the details of the alkane electronic structure seen in X-ray absorption spectroscopy[24] and to the corresponding adsorption-induced changes in those data.[21] Previous work has shown that this theoretical approach provides a very reasonable potential for the cyclopropane/Cu(111) interaction, giving good agreement with experimental quantities such as the binding energy and the curvature of the surface – molecule potential.[21] All results reported here were obtained for the electronic ground state of the Cu(7,3)-cluster, which is a triplet state.

Received: August 22, 2001
Revised: December 27, 2001 [Z17775]

[1] G. Ertl, H. J. Freund, *Phys. Today* **1999**, *52*, 32 – 38.
[2] W. M. H. Sachtler, *Ber. Bunsen-Ges.* **1995**, *99*, 1295 – 1305.
[3] G. A. Somorjai, *Introduction to Surface Chemistry and Catalysis*, Wiley, New York, **1994**.
[4] G. Blyholder, *J. Phys. Chem.* **1964**, *68*, 2772.
[5] P. S. Bagus, K. Hermann, W. Müller, C. J. Nelin, *Phys. Rev. Lett.* **1986**, *57*, 1496.
[6] A. Fohlisch, M. Nyberg, J. Hasselstrom, O. Karis, L. G. M. Pettersson, A. Nilsson, *Phys. Rev. Lett.* **2000**, *85*, 3309 – 3312.
[7] K. Hermann, M. Witko, *Surf. Sci.* **1995**, *337*, 205.
[8] L. Pettersson, H. Agren, Y. Luo, L. Triguero, *Surf. Sci.* **1998**, *408*, 1 – 20.
[9] L. Triguero, L. G. M. Petterson, B. Minaev, H. Agren, *J. Chem. Phys.* **1998**, *108*, 1193 – 1205.
[10] L. Triguero, A. Fohlisch, P. Väterlein, J. Hasselstrom, M. Weinelt, L. G. M. Pettersson, Y. Luo, H. Agren, A. Nilsson, *J. Am. Chem. Soc.* **2000**, *122*, 12310 – 12316.
[11] J. Chatt, L. A. Duncanson, *J. Chem. Soc.* **1953**, 2939.
[12] M. J. S. Dewar, *Bull. Soc. Chim. Fr.* **1951**, *18*, C79.
[13] J. E. Demuth, H. Ibach, S. Lehwald, *Phys. Rev. Lett.* **1978**, *40*, 1044.
[14] R. Raval, M. A. Chesters, *Surf. Sci.* **1989**, *219*, L505 – L514.
[15] M. J. Hostetler, W. L. Manner, R. G. Nuzzo, G. S. Girolami, *J. Phys. Chem.* **1995**, *69*, 15269.
[16] Y. J. Chabal, *Surf. Sci. Rep.* **1988**, *8*, 211 – 357.
[17] A. V. Teplyakov, B. E. Bent, J. Eng, J. G. Chen, *Surf. Sci.* **1998**, *399*, L342 – L350.
[18] K. A. Fosser, R. G. Nuzzo, P. S. Bagus, C. Wöll, unpublished results.
[19] B. C. Wiegand, S. P. Lohokare, R. G. Nuzzo, *J. Phys. Chem.* **1993**, *97*, 11553.
[20] M. J. Hostetler, R. G. Nuzzo, G. S. Girolami, L. H. Dubois, *J. Phys. Chem.* **1994**, *98*, 2952.
[21] C. Wöll, K.Weiss, P. S. Bagus, *Chem. Phys. Lett.* **2000**, *332*, 553 – 561.
[22] Gaussian 98 (Revision A.7), M. J. Frisch, G. W. Trucks, H. B. Schlegel, G. E. Scuseria, M. A. Robb, J. R. Cheeseman, V. G. Zakrzewski, J. A. Montgomery, R. E. Stratmann, J. C. Burant, S. Dapprich, J. M. Millam, A. D. Daniels, K. N. Kudin, M. C. Strain, O. Farkas, J. Tomasi, V. Barone, M. Cossi, R. Cammi, B. Mennucci, C. Pomelli, C. Adamo, S. Clifford, J. Ochterski, G. A. Petersson, P. Y. Ayala, Q. Cui, K. Morokuma, D. K. Malick, A. D. Rabuck, K. Raghavachari, J. B. Foresman, J. Cioslowski, J. V. Ortiz, B. B. Stefanov, G. Liu, A. Liashenko, P. Piskorz, I. Komaromi, R. Gomperts, R. L. Martin, D. J. Fox, T. Keith, M. A. Al-Laham, C. Y. Peng, A. Nanayakkara, C. Gonzalez, M. Challacombe, P. M. W. Gill, B. G. Johnson, W. Chen, M. W. Wong, J. L. Andres, M. Head-Gordon, E. S. Replogle, J. A. Pople, Gaussian, Inc., Pittsburgh, PA, **1998**.
[23] B. C. Laskowski, P. S. Bagus, *Surf. Sci.* **1984**, *138*, 1142.
[24] P. S. Bagus, K. Weiss, A. Schertel, C. Wöll, W. Braun, C. Hellwig, C. Jung, *Chem. Phys. Lett.* **1996**, *248*, 129 – 135.

Pentaphosphaferrocene as a Linking Unit for the Formation of One- and Two-Dimensional Polymers**

Junfeng Bai, Alexander V. Virovets, and Manfred Scheer*

Dedicated to Professor Joachim Strähle on occasion of his 65th birthday

Common approaches in the field of self-organization of discrete supramolecular[1] aggregates, networks, and coordination polymers[2] make use of N-donor containing ligands and N-heterocycles to connect different metal centers together. In contrast, however, our goal in this field has been the use of P_n-ligand complexes as linking moieties between metal cations to form well-oriented assemblies as well as one-dimensional (1D) and two-dimensional (2D) polymers.

The coordination chemistry of P_n-ligand complexes[3] towards cationic metal centers (excluding cationic organometallic complex moieties[4]) has so far been limited to the use of *cyclo*-P_3-ligand complexes, such as [(triphos)M(η^3-P_3)] (M = Co, Rh, or Ir; triphos = 1,1,1-tris(diphenylphosphanylmethyl)ethane), which usually form metal-bridged dimers.[5]

[*] Prof. Dr. M. Scheer, Dr. J. Bai, Dr. A. V. Virovets
Institut für Anorganische Chemie der Universität Karlsruhe
Engesserstrasse, Geb. 30.45
76128 Karlsruhe (Germany)
Fax: (+49) 721-608-7021
E-mail: mascheer@chemie.uni-karlsruhe.de

[**] This work was supported by the Deutsche Forschungsgemeinschaft and the Fonds der Chemischen Industrie.

In the reactions of the Co complex with CuBr, a multidecker Co complex containing a $(CuBr)_6$ middle deck was obtained,[6] whereas for the Ir complex, the cationic product $[\{(triphos)IrP_3\}_3Cu_5Br_4]^+$ was formed.[7] However, recently we were able to show that $[\{CpMo(CO)_2\}_2(\mu,\eta^2\text{-}P_2)]$ ($Cp = C_5H_5$) can be used as a building block to connect Cu^I and Ag^I centers to form 1D polymers such as the complexes **1** and **2**.[8] Further, we have tried to incorporate compound **3** ($Cp^* = C_5Me_5$)[9] into these investigations. In the past few years, the reaction behavior of **3** has been intensively examined by the group of O. J. Scherer.[3f]

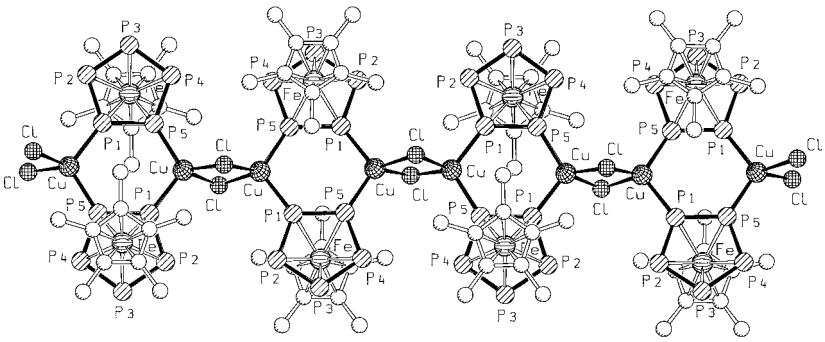


Figure 1. View of the 1D chain structure of complex **4** (H atoms are omitted for clarity). Selected bond lengths [Å] and angles [°]: P1-P5 2.109(2), P1-P2 2.119(1), P2-P3 2.124(2), P3-P4 2.123(2), P4-P5 2.121(1), Cu-P1 2.286(1), Cu-P5 2.272(1), Cu-Cl 2.356(1), Cu-Cl′ 2.342(1); P5-Cu-P1′ 111.02(5), P5-P1-Cu 126.19(5), Cu′-Cl-Cu 83.94(4), Cl-Cu-Cl′ 95.43(4).

$[Ag_2\{Cp_2Mo_2(CO)_4(\mu,\eta^2\text{:}\eta^1\text{:}\eta^1\text{-}P_2)\}_3(\mu,\eta^1\text{:}\eta^1\text{-}NO_3)]_\infty[NO_3]_n$ **1**

$[Cu(\mu\text{-}Br)\{Cp_2Mo_2(CO)_4(\mu,\eta^2\text{:}\eta^1\text{:}\eta^1\text{-}P_2)\}]_\infty$ **2**

$[Cp^*Fe(\eta^5\text{-}P_5)]$ **3**

Besides its capacity to form cationic triple-decker complexes[10] or undergo P_5-transfer reactions,[11] there are reactions known in which the *cyclo*-P_5 ring remains more or less intact, or is cleaved with formation of a P_5 chain, or P_4/P_1, P_3/P_2, or P_2 fragments.[3f, 10–12] In the case where the *cyclo*-P_5 ring remains intact, $\eta^5\text{:}\eta^1$, $\eta^5\text{:}\eta^2$, and $\eta^5\text{:}\eta^2\text{:}\eta^2\text{:}\eta^1$ coordination modes to organometallic fragments have been found,[13] which are accompanied by a significant lengthening of the P–P bonds. Herein we report the first use of the *cyclo*-P_5 ligand complex **3** to form novel 1D and 2D polymers by the hitherto unknown 1,2-ligation and 1,3,4-ligation, respectively, to different Cu^I ions.

Complexes **4**–**6** were obtained by the reaction of **3** with CuX (X = Cl, Br, I) in solvent mixtures of CH_3CN and CH_2Cl_2

$[CuCl\{Cp^*Fe(\eta^5\text{:}\eta^1\text{:}\eta^1\text{-}P_5)\}]_\infty$ **4**

$[CuBr\{Cp^*Fe(\eta^5\text{:}\eta^1\text{:}\eta^1\text{:}\eta^1\text{-}P_5)\}]_\infty$ **5**

$[CuI\{Cp^*Fe(\eta^5\text{:}\eta^1\text{:}\eta^1\text{:}\eta^1\text{-}P_5)\}]_\infty$ **6**

at ambient temperature. The yellow-brown crystals of the products are stable under nitrogen and in common solvents are insoluble without decomposition.[14] All the products have been characterized by X-ray diffraction analysis.[15]

In Figure 1 the linear 1D chain structure of **4** is depicted, it consists of planar six-membered Cu_2P_4 and four-membered Cu_2Cl_2 rings, alternately arranged in an orthogonal manner. The planar *cyclo*-P_5 rings are coplanar with the six-membered Cu_2P_4 units, and the coordination geometry around the Cu^I center is tetrahedral. Furthermore, the 1,2 coordination of the *cyclo*-P_5 ring to two different metal centers has not been observed before. The structure of **4** is reminiscent of the 1D polymeric structure of the Mo_2P_2-containing complex **2**, with the difference that, aside of the different P_n ligand used, the Cu_2Cl_2 moieties in **4** are bent along the Cl–Cl axis, and the Cu^I atoms are nonsymmetrically bound to the P (2.272(1) and 2.286(1) Å) and Cl atoms (2.356(1) and 2.342(1) Å). Interestingly, the P–P bond between the coordinating atoms P1 and P5 is slightly shorter (2.109(2) Å) than the remaining P–P bonds of the *cyclo*-P_5 ring (2.119(1)–2.124(1) Å), whereas the latter are nearly consistent with those of the uncoordinated molecule **3** (2.117(4) Å), as determined by electron diffraction.[16] However, compared to the P–P bonds in the related complex $[Cp^xFe(\mu,\eta^5\text{-}P_5)]$ (**7**; $Cp^x = \eta^5\text{-}C_5Me_4Et$; 2.088(3)–2.108(3) Å), determined by single-crystal X-ray structure analysis, the P–P bonds of **4** are slightly lengthened.[17] Nevertheless, this coordination behavior of the *cyclo*-P_5 moiety in **4** is in contrast to the previously observed lengthening of the P–P bonds on the coordination of organometallic fragments to the *cyclo*-P_5 ring.[13] For example, the additional side-on coordination of an organometallic fragment at the *cyclo*-P_5 ring in $[Cp^*Fe(\mu,\eta^5\text{:}\eta^2\text{-}P_5)Cp^*Ir(CO)]$ leads to a lengthening of the corresponding P–P bond to 2.359(2) Å.[13b] Furthermore, η^1 coordination of the $[\{Cp^*Ir(CO)\}_2]$ unit in $[Cp^*Fe(\mu,\eta^5\text{:}\eta^1\text{-}P_5)(Cp^*IrCO)_2]$[13a] leads to P–P bond lengths about the coordinating P atom of 2.166(3) and 2.170(3) Å as well as a significant bending of the *cyclo*-P_5 ring, which results in a P_4/P_1 arrangement. In contrast, therefore, the *cyclo*-P_5 units in the polymers **4**–**6** are still essentially planar.[18]

In the crystal lattice of both **5** and **6** the distorted tetrahedrally coordinated Cu^I atoms are surrounded by one halogen atom and three P atoms each coming from three different $[Cp^*Fe(\eta^5\text{-}P_5)]$ fragments (Figure 2). Thus, a new $\eta^5\text{:}\eta^1\text{:}\eta^1\text{:}\eta^1$ coordination mode is obtained which result in a novel 1,3,4 substitution pattern at the *cyclo*-P_5 ring. In contrast to the structure of **4**, and as a result of the additional third coordination of the Cu^IX moiety at the *cyclo*-P_5 rings in **5** and **6**, novel 2D coordination polymers are formed where the layers are separated by the Cp*Fe moieties (Figure 3). The structure of **6** (space group $P\bar{4}2_1c$) is similar to that of **5** (space group $P\bar{4}2_1m$) except that the latter possesses no symmetry plane within the crystallographic *c* axis, which leads to a mirror plane within the Cp^*FeP_5 moieties of **6**. Within the layers of **5** and **6** (Figure 4) there is an alternating array of six-membered Cu_2P_4 rings and novel Cu_4P_{12} rings. The Cu_2P_4 rings are in a boatlike conformation, unlike the previously reported planar Cu_2P_4 rings in the 1D polymer of **2**. The P–P distances within the nearly planar[18] *cyclo*-P_5 moieties of **5** (2.099(2)–2.108(2) Å) and **6** (2.114(3)–2.120(3) Å), are comparable to

 © WILEY-VCH Verlag GmbH, 69451 Weinheim, Germany, 2002 1433-7851/02/4110-1738 $ 20.00+.50/0 *Angew. Chem. Int. Ed.* **2002**, *41*, No. 10

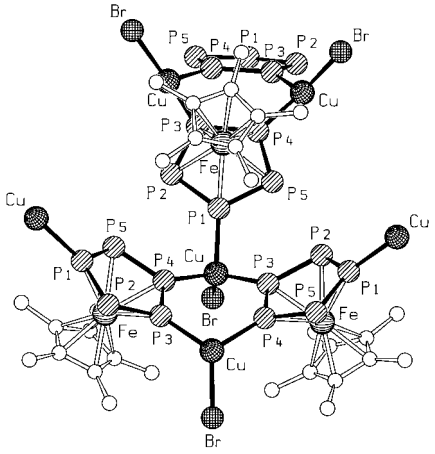


Figure 2. View of the coordination geometry around a Cu atom within the polymeric structure of complex **5** (H atoms are omitted for clarity). Selected bond lengths [Å] and angles [°]: P1-P5 2.106(2), P1-P2 2.108(2), P2-P3 2.104(2), P3-P4 2.101(2), P4-P5 2.099(2), Cu-P1 2.320(1), Cu-P3 2.278(1), Cu-P4 2.281(1), Cu-Br 2.343(1); P1-Cu-P3 103.01(5), P1-Cu-P4 103.98(5), P3-Cu-P4 104.48(5), P1-Cu-Br 101.24(4), P3-Cu-Br 122.27(5), P4-Cu-Br 119.03(4).

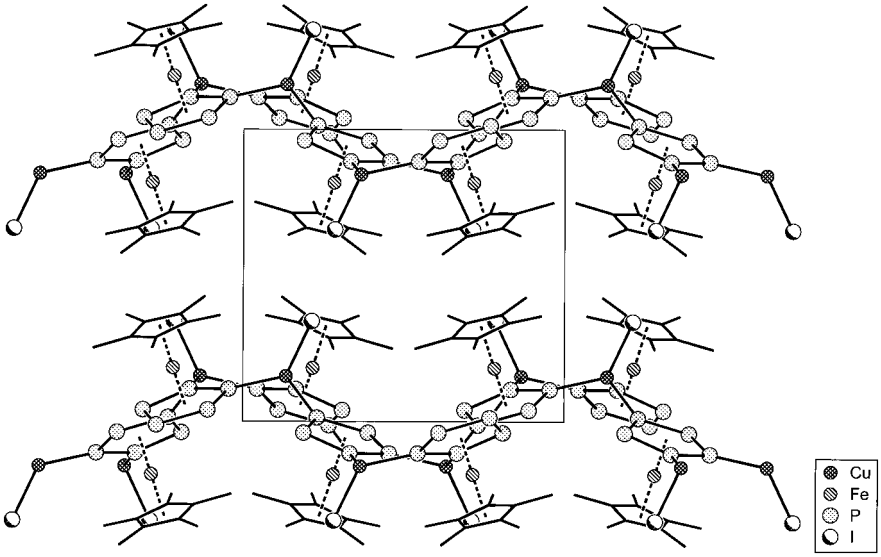


Figure 3. View of the zigzag 2D layer structure of complex **6** along the *b* axis (H atoms are omitted for clarity). Selected bond lengths [Å] and angles [°]: P1-P2 2.114(3), P1-P1′ 2.116(4), P2-P3 2.120(3), P3-P2′ 2.120(3), Cu-P1 2.296(2), Cu-P1′ 2.296(2), Cu-P3 2.332(3), Cu-I 2.549(2); P1-Cu-P1′ 106.59(12), P1-Cu-P3 105.15(9), P1′-Cu-P3′ 105.14(9), P1-Cu-I 119.28(7).

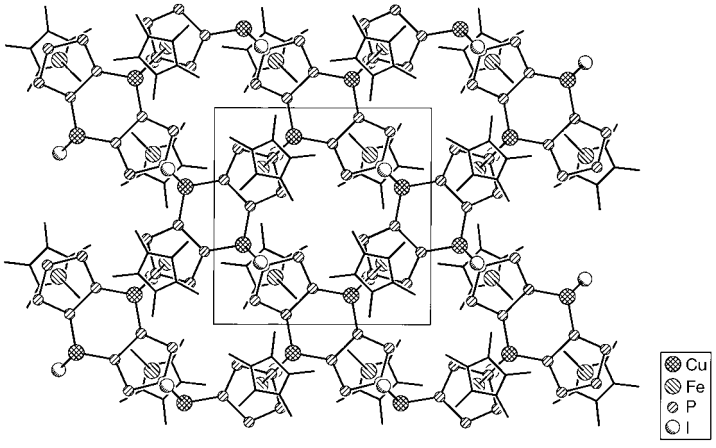


Figure 4. View of layer of the 2D structure of complex **6** orthogonal to the *a*,*b* plane (H atoms are omitted for clarity).

the distances within **4** and are slightly shorter than those of the uncoordinated **3** (2.117(4) Å)[16] but slightly elongated in comparison to the related complex **7** (2.088(3)–2.108(3) Å).[17] Thus, as already discussed for **4**, the coordination of Cu^{I} halides in **5** and **6** does not influence the corresponding P–P bond lengths.

The tendency for the reaction of **3** with CuCl on the one hand and CuBr/CuI on the other to yield products with disparate structures is surprising and difficult to explain. Whereas within the CuCl product **4** the linear chains are separated from each other by π stacking between Cp* and *cyclo*-P_5 moieties of different chains, **5** and **6** form 2D networks through additional metal coordination to the *cyclo*-P_5 rings rather than π stacking.

In summary, the results have shown that in addition to $[\{CpMo(CO)_2\}_2(\mu,\eta^2\text{-}P_2)]$, the complex $[Cp^*Fe(\eta^5\text{-}P_5)]$ (**3**) can also be successfully used as a linking unit for coordination polymers, which opens perspectives to generate novel well-defined assemblies and networks. In contrast to previously reported reactivity studies of **3** with organometallic complexes, where the P–P bond lengths of the products have been significantly lengthened and the *cyclo*-P_5 ring is partially distorted, the P–P bonds of the planar *cyclo*-P_5 ring in the new coordination polymers **4**–**6** do not differ significantly to those of **3**.

Experimental Section

4–**6**: A solution of CuX (0.15 mmol; X = Cl (15 mg), Br (21 mg), I (28 mg)) in CH_3CN (3 mL) and CH_2Cl_2 (2 mL) was added to a solution of **3** (52 mg, 0.15 mmol) in CH_2Cl_2 (5 mL) at room temperature. This mixture was allowed to stand for two days, and yellow-brown crystals of **4** (33 mg, 0.067 mmol, 49%), **5** (65 mg, 0.13 mmol, 89%), and **6** (78 mg, 0.14 mmol, 93%), respectively, were formed. The products were collected by filtration and washed with 2 mL each of CH_2Cl_2 and CH_3CN, and then dried under vacuum; **4**·$0.5\,CH_2Cl_2$: elemental analysis (%) calcd for $C_{10.5}H_{16}Cl_2CuFeP_5$ (487.37): C 25.88, H 3.28; found: C 26.03, H 3.22; **5**: elemental analysis (%) calcd for $C_{10}H_{15}BrCuFeP_5$ (489.39): C 24.54, H 3.09; found C 24.64 H, 3.15; **6**: elemental analysis (%) calcd for $C_{10}H_{15}ICuFeP_5$ (536.40): C 22.39, H 2.82; found C 22.30, H 2.96.

Received: December 18, 2001 [Z18411]

[1] Recent review articles: a) P. J. Stang, B. Olenyuk, *Acc. Chem. Res.* **1997**, *30*, 502–518; b) D. Braga, F. Grepioni, G. R. Desiraju, *Chem. Rev.* **1998**, *98*, 1375–1405; c) O. M. Yaghi, H. Li, C. Davis, D. Richardson, T. L. Groy, *Acc. Chem. Res.* **1998**, *31*, 474–484; d) P. F. H. Schwab, M. D. Levin, J. Michl, *Chem. Rev.* **1999**, *99*, 1863–1933; e) S. Leininger, B. Olenyuk, P. J. Stang, *Chem. Rev.* **2000**, *100*, 853–908.

[2] Selected review articles: a) M. J. Zaworotko, *Chem. Commun.* **2001**, 1–9; b) I. Manners, *Angew. Chem.* **1996**, *108*, 1712–1731; *Angew.*

 © WILEY-VCH Verlag GmbH, 69451 Weinheim, Germany, 2002 1433-7851/02/4110-1739 $ 20.00+.50/0

Chem. Int. Ed. Engl. **1996**, *35*, 1602 – 1621; c) M. O'Keeffe, M. Eddaoudi, H. Li, T. Reineke, O. M.Yaghi, *J. Solid. State Chem.* **2000**, *152*, 3 – 20.

[3] a) M. Scheer, E. Herrmann, *Z. Chem.* **1990**, *29*, 41 – 55; b) O. J. Scherer, *Angew. Chem.* **1990**, *102*, 1137 – 1155; *Angew. Chem. Int. Ed. Engl.* **1990**, *29*, 1104 – 1122; c) M. Di Vaira, P. Stoppioni, *Coord. Chem. Rev.* **1992**, *120*, 259 – 279; d) M. Di Vaira, M. Peruzzini, P. Stoppioni, *Polyhedron* **1987**, *3*, 351 – 382; e) K. H. Whitmire, *Adv. Organomet. Chem.* **1998**, *42*, 1 – 42; f) O. J. Scherer, *Acc. Chem. Res.* **1999**, *32*, 751 – 762; g) M. Ehses, A. Romerosa, M. Peruzzini, *Top. Curr. Chem.* **2002**, *220*, 107 – 140.

[4] In the reaction with $MeHg^+$, $[(triphos)CoP_3HgMe]PF_6$ was obtained: M. Di Vaira, D. Rovai, P. Stoppioni, *Polyhedron* **1990**, *20*, 2477 – 2481. For the use of bifunctional phosphinidene clusters, such as $[Fe_3(CO)_9(\mu_3\text{-}PH)]$, to build up 1D oligomers see: C. C. Borg-Breen, M. T. Bautista, C. K. Schauer, P. S. White, *J. Am. Chem. Soc.* **2000**, *122*, 3952 – 3962.

[5] a) M. Di Vaira, M. P. Ehses, M. Peruzzini, P. Stoppioni, *Polyhedron* **1999**, *18*, 2331 – 2336; b) M. Di Vaira, P. Stoppioni, M. Peruzzini, *J. Chem. Soc. Dalton Trans.* **1990**, 109 – 113.

[6] M. F. Cecconi, C. A. Ghilardi, S. Midollini, A. Orlandini, *J. Chem. Soc. Chem. Commun.* **1982**, 229 – 230.

[7] F. Cecconi, C. A. Ghilardi, S. Midollini, A. Orlandini, *Angew. Chem.* **1983**, *95*, 554 – 555; *Angew. Chem. Int. Ed. Engl.* **1983**, *22*, 554 – 555.

[8] J. Bai, E. Leiner, M. Scheer, *Angew. Chem.* **2002**, *114*, 820 – 823; *Angew. Chem. Int. Ed.* **2002**, *41*, 783 – 786.

[9] O. J. Scherer, T. Brück, *Angew. Chem.* **1987**, *99*, 59 – 61; *Angew. Chem. Int. Ed. Engl.* **1987**, *26*, 59 – 61.

[10] O. J. Scherer, T. Brück, G. Wolmershäuser, *Chem. Ber.* **1989**, *122*, 2049 – 2054.

[11] B. Rink, O. J. Scherer, G. Wolmershäuser, *Chem. Ber.* **1995**, *128*, 71 – 74.

[12] a) O. J. Scherer, T. Mohr, G. Wolmershäuser, *J. Organomet. Chem.* **1997**, *529*, 379 – 385; b) C. Hoffmann, O. J. Scherer, G. Wolmershäuser, *J. Organomet. Chem.* **1998**, *559*, 219 – 222; c) B. Koch, O. J. Scherer, G. Wolmershäuser, *Z. Anorg. Allg. Chem.* **2000**, *626*, 1797 – 1802.

[13] a) M. Detzel , T. Mohr, O. J. Scherer, G. Wolmershäuser, *Angew. Chem.* **1994**, *106*, 1142 – 1144; *Angew. Chem. Int. Ed. Engl.* **1994**, *33*, 1110 – 1112; b) M. Detzel, G. Friedrich, O. J. Scherer, G. Wolmershäuser, *Angew. Chem.* **1995**, *107*, 1454 – 1456; *Angew. Chem. Int. Ed. Engl.* **1995**, *34*, 1321 – 1223; for NMR spectroscopic evidence for $\eta^5{:}\eta^2{:}\eta^1$ coordination of **3** see: c) G. Friedrich, Dissertation, Universität Kaiserslautern, **1995**; M. Detzel, Dissertation, Universität Kaiserslautern, **1995**; d) O. J. Scherer, S. Weigel, G. Wolmershäuser, *Chem. Eur. J.* **1998**, *4*, 1910 – 1916.

[14] Because to their insolubility, no NMR spectroscopic investigation could be carried out. Solid-state NMR investigations are in progress.

[15] Crystal structure analyses of **4** – **6** were performed on STOE IPDS diffractometers with $Mo_{K\alpha}$ radiation ($\lambda = 0.71073$ Å) for **5** and $Ag_{K\alpha}$ radiation ($\lambda = 0.56087$ Å) for **4** and **6**. The structures were solved by direct methods with the program SHELXS-97,[19a] and full-matrix least-squares refinement on F^2 in SHELXL-97[19b] was performed with anisotropic displacements for non-hydrogen atoms. Hydrogen atoms were located in idealized positions and refined isotropically according to the riding model. **4**·0.5 CH_2Cl_2: $C_{10.5}H_{16}Cl_2CuFeP_5$, $M_r = 487.37$, crystal dimensions $0.20 \times 0.14 \times 0.04$ mm^3, monoclinic, space group $C2/c$ (No. 15), $a = 20.184(4)$, $b = 16.885(3)$, $c = 13.860(3)$ Å, $\beta = 129.33(3)^\circ$, $T = 203(2)$ K, $Z = 8$, $V = 3653.7(13)$ Å^3, $\rho_{calcd} = 1.772$ Mg m^{-3}, $\mu = 1.382$ mm^{-1}, 3831 independent reflexes ($R_{int} = 0.0365$, $2\theta_{max} = 42^\circ$), 3128 observed with $F_o = 4\sigma(F_o)$, 190 parameters, $R_1 = 0.0370$, $wR_2 = 0.0974$. **5**: $C_{10}H_{15}BrCuFeP_5$, $M = 489.37$, crystal dimensions $0.20 \times 0.20 \times 0.01$ mm^3, tetragonal, space group $P\bar{4}2_1c$ (No. 114), $a = b = 12.147(2)$, $c = 21.859(4)$ Å, $T = 200(1)$ K, $Z = 8$, $V = 3225.2(9)$ Å^3, $\rho_{calcd} = 2.016$ Mg m^{-3}, $\mu = 5.170$ mm^{-1}, 3152 independent reflexes ($R_{int} = 0.0777$, $2\theta_{max} = 52^\circ$), 2681 observed with $F_o = 4\sigma(F_o)$, 168 parameters, $R_1 = 0.0345$, $wR_2 = 0.0809$. **6**: $C_{10}H_{15}CuFeIP_5$, $M_r = 536.36$, crystal dimensions $0.10 \times 0.10 \times 0.10$ mm^3, tetragonal, space group $P\bar{4}2_1m$ (No. 113); $a = b = 12.372(2)$, $c = 11.241(2)$ Å, $T = 203(1)$ K, $Z = 4$, $V = 1720.6(5)$ Å^3, $\rho_{calcd} = 2.071$ Mg m^{-3}, $\mu = 2.258$ mm^{-1}, 8297 independent reflexes ($R_{int} = 0.1663$, $2\theta_{max} = 40^\circ$), 1475 observed with $F_o = 4\sigma(F_o)$; 94 parameters, $R_1 = 0.0496$, $wR_2 = 0.1312$. CCDC 175139 – 175141 contain the supplementary crystallographic data for this paper. These data can be obtained free of charge via www.ccdc.cam.ac.uk/conts/retrieving.html (or from the Cambridge Crystallographic Data Center, 12, Union Road, Cambridge CB21EZ, UK; fax: (+44) 1223-336-033; or deposit@ccdc.cam.ac.uk).

[16] R. Blom, T. Brück, O. J. Scherer, *Acta Chem. Scand.* **1989**, *43*, 458 – 462.

[17] O. J. Scherer, T. Brück, G. Wolmershäuser, *Chem. Ber.* **1988**, *121*, 935 – 938.

[18] Mean deviation from planarity: 0.0098(6) Å (**4**), 0.0293(9) Å (**5**), 0.0350 (20) Å (**6**).

[19] a) G. M. Sheldrick, SHELXS-97, University of Göttingen, **1998**; b) G. M. Sheldrick, SHELXL-97, University of Göttingen, **1997**.

Structure and Synthesis of the Natural Heptachloro-1′-methyl-1,2′-bipyrrole (Q1)

Jun Wu, Walter Vetter,* Gordon W. Gribble,* John S. Schneekloth, Jr., David H. Blank, and Helmar Görls

A number of anthropogenic organohalogen compounds such as polychlorinated biphenyls (PCBs), polychlorinated dibenzo-*p*-dioxins (PCDDs), and chlorinated pesticides (DDT, toxaphene, lindane, and others) are recognized as persistent, bioaccumulative, and toxic chemicals.[1] The majority of these substance classes are ubiquitously distributed in the environment, and long-term exposure is one of the major threats to humans and wildlife from these substances.[2] The scientific interest in anthropogenic halogenated compounds is reflected in the fate of these contaminants and related compounds in the environment, which was reported on in more than 1000 publications in the past 40 years.

More than 3600 naturally occurring organohalogens have been identified to date.[3] The total amount of these compounds is not known, but is probably higher than currently known.[4] It was thought that these natural products are neither persistent nor lipophilic, and thus do not accumulate in the lipids of higher organisms. This hypothesis is currently under reconsideration, as recent work has resulted in the detection of a series of unknown halogenated compounds that

[*] Priv.-Doz. Dr. W. Vetter, Dr. J. Wu
Lehrbereich Lebensmittelchemie
Friedrich-Schiller-Universität Jena
Dornburger Strasse 25, 07743 Jena (Germany)
Fax: (+49) 3641-949-652
E-mail: walter.vetter@uni-jena.de

Prof. Dr. G. W. Gribble, J. S. Schneekloth, Jr., Dr. D. H. Blank
Department of Chemistry, 6128 Burke Laboratory
Dartmouth College
Hanover, NH 03755 (USA)
Fax: (+1) 603-646-3946
E-mail: gordon.w.gribble@dartmouth.edu

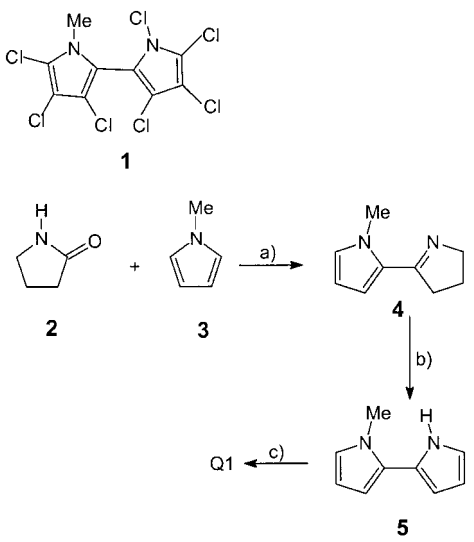
Priv.-Doz. Dr. H. Görls
Institut für Anorganische und Analytische Chemie
Friedrich-Schiller-Universität Jena
Lessingstrasse 8, 07743 Jena (Germany)

 © WILEY-VCH Verlag GmbH, 69451 Weinheim, Germany, 2002 1433-7851/02/4110-1740 $ 20.00+.50/0

can reach significant levels in organisms. Some of these compounds were supposed to be natural compounds because of the lack of a plausible anthropogenic source.[5–8]

One of these potential natural organohalogens is the heptachloro compound Q1, which was previously detected in over 100 environmental samples from virtually all over the world and in matrices, such as Antarctic air, human milk, eggs of seabirds, and the blubber of marine mammals.[7, 9, 10] The highest concentrations of Q1 found in wildlife reported to date exceed 9 mg kg^{-1} lipid content.[7] GC, in combination with high resolution MS, revealed that the molecular formula of Q1 is $C_9H_3Cl_7N_2$.[6] No stable compound with this chemical composition has been synthesized to date.[6] Furthermore, GC–MS analysis suggested that Q1 is a heptachlorobipyrrole derivative.[9] Synthesis of Q1 was attempted independently in two laboratories, and the results are reported together herein.

The naturally occurring 3,3′,4,4′,5,5′-hexabromo-2,2′-bipyrrole as well as 3,3′,4,4′-tetrabromo-5,5′-dichloro-1,1′-dimethyl-2,2′-bipyrrole and analogues have been identified in marine bacteria and seabird eggs.[5, 11, 12] This occurrence suggested that the structure of Q1 may be heptachloro-1-methyl-2,2′-bipyrrole (**1**; Scheme 1). The presence of such a structural variant would be surprising in view of the proposed N–Cl bond, but on the basis of the structurally similar 2,2′-bipyrrole derivatives mentioned above, **1** could not be generally ruled out.

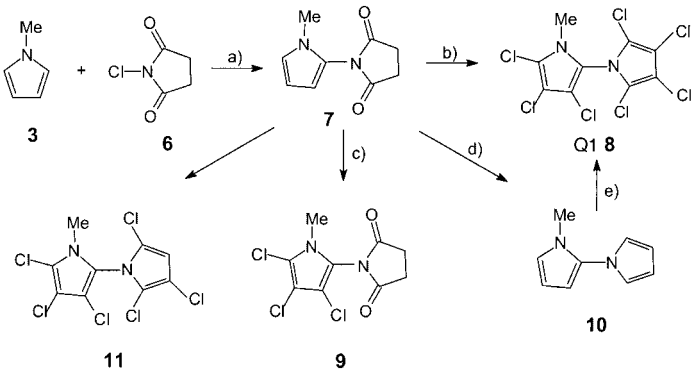


Scheme 1. Reagents and conditions: a) $POCl_3$, Et_2O, RT, 2 h (43 %); b) Ar, Pd/C 10 %, xylene, 138 °C, 4 h (51 %); c) SO_2Cl_2, RT, 6 h (< 0.1 %).

Preparation of the precursor 1-methyl-2-(pyrrol-2-yl)pyrrole (**5**) (also known as 1-methyl-2,2′-bipyrrole) was synthesized by dehydrogenation of 1-methyl-2-(4,5-dihydropyrrol-2-yl)pyrrole (**4**) over Pd/C; compound **4** was prepared from pyrrolidin-2-one and 1-methylpyrrole.[13, 14] Reaction of **5** with sulfuryl chloride (in a molar ratio of 1:10) should produce Q1. However, none of the major products was as nonpolar as expected for Q1 ($\log K_{OW} \approx 6$[9]), so the analytical method we employed for the analysis of the environmental samples[10] (extraction into *n*-hexane, followed by chromatography on 8 g activated silica, 16 h, 130 °C) was applied to the reaction solution. This method allowed us to obtain μg amounts of pure Q1 for ^{13}C NMR spectroscopic investigation. Compound **5** is susceptible to oxidation and polymerization in acid solution.

The ^{13}C NMR spectrum of Q1 shows only six singlets arising from pyrrole carbon atoms, two of which have an intensity that is double that of the others. This is contrary to the proposed structure **1**, which should have eight individual signals of bipyrrole carbons in the ^{13}C NMR spectrum. Rearrangement of the basic 2,2′-bipyrrole framework to a 1,2′-bipyrrole framework during the chlorination of **5** is a possibility; this is supported by the identification of several pyrrole derivatives as cleavage products of the bipyrrole. Thus, synthesis of the heptachloro-1′-methyl-1,2′-bipyrrole **8** was attempted.

The Dartmouth group synthesized the known compound *N*-(1-methyl-1*H*-pyrrol-2-yl)succinimide (**7**) from 1-methylpyrrole and *N*-chlorosuccinimide[15] in 51 % yield, according to the procedure of Rosa et al. Reduction of **7** with triethoxysilane and titanium tetraisopropoxide[16] gave 1′-methyl-1,2′-bipyrrole (**10**) in 30 % yield. Chlorination of **10** with sulfuryl chloride gave Q1 (**8**) in 16 % yield (Scheme 2).



Scheme 2. Reagents and conditions: a) $NaHCO_3$, CH_2Cl_2, reaction in the dark, RT, 4 h (49 %); b) $PCl_5/POCl_3$, 100 °C, 6 h (7.2 %); c) PCl_5, $CHCl_3$, 55 °C, 3 h (61 %); d) $HSi(OEt)_3$, $Ti(OiPr)_4$, THF, 65 °C, 12 h (30 %); e) SO_2Cl_2, Et_2O, RT, 3 h (16 %).

The Jena group also produced **7** according to the method of Rosa et al.;[15] this was then directly chlorinated. Treatment of **7** with phosphorus pentachloride at 55 °C gave *N*-(3,4,5-trichloro-1-methyl-1*H*-pyrrol-2-yl)succinimide (**9**; Scheme 2). Treatment of **7** with a mixture of phosphorus pentachloride and phosphorus oxychloride at 100 °C provided Q1 in a yield of 7 %, while the use of sulfuryl chloride in the chlorination of **7** gave less Q1.

Spectroscopic investigation confirmed that both groups had synthesized the heptachloro-1′-methyl-1,2′-bipyrrole (**8**; Figure 1). Solutions of **8** and the Q1 isolated from the environmental samples had matching retention times on three GC capillary columns of different polarity. Furthermore, the mass-spectral fragmentation patterns and the relative abundances of the molecular ion and fragment ions also agreed. The synthetic compound and the Q1 isolated from marine creatures also showed the same chromatographic behavior. Therefore, it is clear that Q1 is identical to **8**.

 © WILEY-VCH Verlag GmbH, 69451 Weinheim, Germany, 2002 1433-7851/02/4110-1741 $ 20.00+.50/0

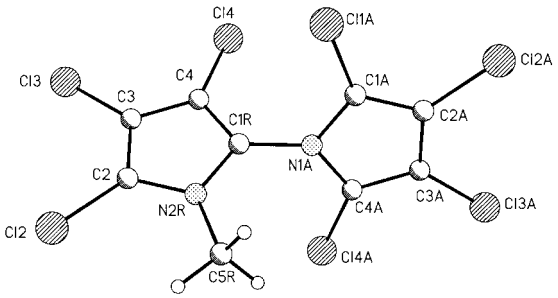


Figure 1. Molecular structure of Q1 (**8**). Selected bond lengths [Å] and bond angles [°]: C1R-N1A 1.409(4), C1R-N2R 1.376(3), N2R-C5R 1.501(4), N2R-C2 1.367(3), C2-C3 1.396(3), C2-Cl2 1.695(2), C3-C4 1.384(3), C3-Cl3 1.702(2), C4-C1R 1.380(3), C4-Cl4 1.688(2), N1A-C4A 1.380(3), N1A-C1A 1.376(3), C1A-Cl1A 1.676(4); C1R-N1A-C1A 127.1(2), C1R-N1A-C4A 124.1(2), C1R-N2R-C5R 124.3(2), N1A-C1A-Cl1A 124.3(2). Torsional angle N2R-C1R-N1A-C4A 71.5. Symmetry transformations used to generate equivalent atoms: A $-X+2$, Y, $-Z+3/2$.

Furthermore, a hexachloro congener of **8** was obtained as a by-product. According to the ^{1}H NMR spectroscopic data, the additional proton is in the β position as it gives rise to a resonance signal with the expected chemical shift of $\delta =$ 6.2 ppm (while α protons give signals at $\delta = 6.8$ ppm[13]). Because of the fast formation of **9**, the β proton is probably attached to the nonmethylated ring, which results in the chiral compound **11**. In the case of hindered rotation about the C–N bond, stable atropisomers may be separated by GC with a chiral stationary phase.

Halogenated 1,2′-bipyrroles have not been reported and, because of the cumbersome synthesis (yield $< 3.5\%$), we can exclude the possibility of an anthropogenic source of Q1, which is found in high concentrations in marine samples from all over the world. However, natural halogen-free 1,2′-bipyrroles have also not been discussed by natural-product chemists, which makes the source of Q1 a phenomenon. It will thus be highly interesting to elucidate the biochemical pathway/system that produces this molecule with 64% chlorine by weight, in which every third atom is a halogen.

Figure 2 shows the GC/NCI-MS (NCI = negative chemical ionization) chromatogram of the blubber extract of an Australian melon-headed whale (*Peponocephala electra*). Compound Q1 accounted for $> 50\%$ of all halogenated compounds present in this sample. This example illustrates that Q1 is of environmental concern, even though its toxic potential has not been established. The present synthesis of the compound may thus open up various possibilities for determination of the environmental impact of this natural halogenated compound.

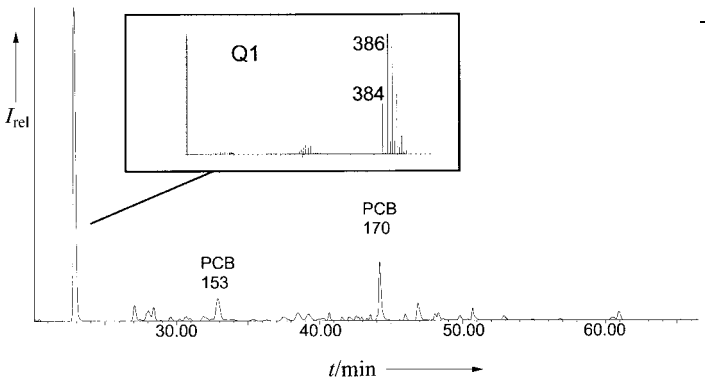


Figure 2. GC-MS-CNI chromatogram of a blubber extract of an Australian melon-headed whale (*Peponocephala electra*).

Experimental Section

9: m.p. 137–139 °C; ^{1}H NMR (250 MHz, $CDCl_3$): $\delta =$ 3.40 (3H, s, NCH_3), 3.01 ppm (4H, s, $COCH_2CH_2CO$); GC-MS (EI 70 eV): m/z (%) 280 (88), 217 (100).

8: m.p. 154–155.5 °C; ^{1}H NMR (500 MHz, $CDCl_3$): $\delta = 3.33$ ppm (3H, s, NCH_3); ^{13}C NMR (250 MHz, $CDCl_3$): $\delta = 116.6$, 115.6, 115.1, 111.2, 111.1, 108.3, 31.3 ppm; GC-MS (NCI, 70 eV): m/z 384 ($[M^-]$); GC-MS (EI, 70 eV): m/z 314 ($[M^+ - 2\,Cl]$, 349 $[M^+ - Cl]$, 384 $[M^+]$.

Crystal Structure Determination: The intensity data for Q1 were collected on a Nonius Kappa CCD diffractometer, with graphite-monochromated $Mo_{K\alpha}$ radiation. Data were corrected for Lorentz and polarization effects, but not for absorption.[17, 18] The structure was solved by direct methods (SHELXS[19]) and refined by full-matrix least-squares techniques against F_o^2. Compound Q1 crystallized in the centro-symmetric space group *Pbcn* on a special position with a two-fold axis passing through the atoms C1R and N1A. Therefore, the atoms C1R, N2R, and C5R are superimposed on the atoms N1A, C1A, and Cl1A, respectively. The superposition was solved by refining the pairs C1R/N1A and N2R/C1A at the same positions and with identical thermal parameters. Only the C5R atom of the methyl group and the chloride atom Cl1A were refined without such restraints (SHELXL-97[20]). The hydrogen atoms of the C5R methyl group were included at geometrically idealized positions with fixed thermal parameters (1.5-fold isotropic temperature factor). The non-hydrogen atoms (except for the methyl group C5R) were refined anisotropically.[20] XP (SIEMENS Analytical X-ray Instruments, Inc.) was used for structure representations.

Crystal data:[21] $C_9H_3Cl_7N_2$, $M_r = 387.28$ g mol^{-1}, colorless prism, size $0.10 \times 0.10 \times 0.08$ mm^3, orthorhombic, space group *Pbcn*, $a = 12.1617(6)$, $b = 8.7043(3)$, $c = 12.9576(4)$ Å, $V = 1371.68(9)$ Å^3, $T = -90$ °C, $Z = 4$, $\rho_{calcd} = 1.875$ g cm^{-3}, $\mu(Mo_{K\alpha}) = 14.26$ cm^{-1}, $F(000) = 760$, 9217 reflections in $h(-10/15)$, $k(-10/11)$, $l(-16/16)$, measured in the range $2.88° \le \Theta \le 27.46°$, completeness $\Theta_{max} = 99.2\%$, 1562 independent reflections, $R_{int} = 0.029$, 1410 reflections with $F_o > 4\sigma(F_o)$, 86 parameters, no restraints, $R1_{obs} = 0.0367$, $wR2_{obs} = 0.105$, $R1_{all} = 0.040$, $wR2_{all} = 0.1086$, GOF = 1.053, largest difference peak and hole: 0.394/ −0.480 e Å^{-3}.

Sample origin and preparation: The blubber sample of melon-headed whale came from a creature that was found dead in Queensland (Australia). The sample preparation was described elsewhere.[7] The GC-MS (NCI) spectrum was recorded in full scan mode (m/z 50–550) after a solvent delay of 20 min, all the other parameters have been published in detail.[6]

Received: November 13, 2001 [Z18211]

[1] a) B. Jansson, R. L. Lipnick, D. Mackay, M. Petreas, *ACS Symp. Ser.* **2001**, *773*, 1–13; b) *The Handbook of Environmental Chemistry*, *Vol. 3*, Part K (Ed.: J. Paasivirta), Springer, Berlin, **2000**; c) *Chlorinated Organic Compounds in the Environment: Regulatory and Monitoring Assessment* (Eds.: S. Ramamoorthy, S. Ramamoorthy), Lewis, Boca Raton, **1998**.

[2] C. Bernes, *Persistent Organic Pollutants. A Swedish view of an international problem*, Swedish Environmental Agency, Monitor 16, **1998**.

[3] G. W. Gribble, *Acc. Chem. Res.* **1998**, *31*, 141–152; G. W. Gribble, unpublished results.

[4] K. Naumann, *Chem. Unserer Zeit* **1993**, *27*, 33–41.

[5] S. A. Tittlemier, M. Simon, W. M. Jarman, J. E. Elliott, R. J. Norstrom, *Environ. Sci. Technol.* **1999**, *33*, 26–33.

[6] W. Vetter, L. Alder, R. Palavinskas, *Rapid Commun. Mass Spectrom.* **1999**, *13*, 2118–2124.

 © WILEY-VCH Verlag GmbH, 69451 Weinheim, Germany, 2002 1433-7851/02/4110-1742 $ 20.00+.50/0

[7] W. Vetter, E. Scholz, C. Gaus, J. F. Müller, D. Haynes, *Arch. Environ. Toxicol. Chem.* **2001**, *41*, 221 – 231.
[8] W. Vetter, J. Hiebl, N. J. Oldham, *Environ. Sci. Technol.* **2001**, *35*, 4157 – 4162.
[9] W. Vetter, *ACS Symp. Ser.* **2001**, *773*, 243 – 259.
[10] W. Vetter, L. Alder, R. Kallenborn, M. Schlabach, *Environ. Poll.* **2000**, *110*, 401 – 409.
[11] D. J. Faulkner, *The Handbook of Environmental Chemistry*, *Vol. 1*, Part A, Springer, Berlin, **1980**, pp. 229 – 254.
[12] G. W. Gribble, D. H. Blank, J. P. Jasinski, *Chem. Commun.* **1999**, 2195 – 2196.
[13] D. Brown, D. Griffiths, M. E. Rider, R. C. Smith, *J. Chem. Soc. Perkin Trans. 1*, **1986**, 455 – 464.
[14] P. H. Daniels, J. L. Wong, J. L. Atwood, L. G. Canada, R. D. Rogers, *J. Org. Chem.* **1980**, *45*, 435 – 440.
[15] M. D. Rosa, G. C. Nieto, F. F. Gago, *J. Org. Chem.* **1989**, *54*, 5347 – 5350.
[16] S. L. Buchwald, A. Gutierrez, S. Berk, K. Kreutzer, US Patent 5220020, **1993**.
[17] COLLECT, Data Collection Software, B. V. Nonius, Netherlands, **1998**.
[18] Z. Otwinowski, W. Minor, *Methods Enzymol.* **1997**, *276*, 307 – 326.
[19] G. M. Sheldrick, *Acta Crystallogr. Sect. A* **1990**, *46*, 467 – 473.
[20] G. M. Sheldrick, SHELXL-97 (Release 97-2), Universität Göttingen, Germany, **1997**.
[21] CCDC-173675 contains the supplementary crystallographic data for this paper. These data can be obtained free of charge via www.ccdc.cam.ac.uk/conts/retrieving.html (or from the Cambridge Crystallographic Data Centre, 12, Union Road, Cambridge CB2 1EZ, UK; fax: (+44) 1223-336-033; or deposit@ccdc.cam.ac.uk).

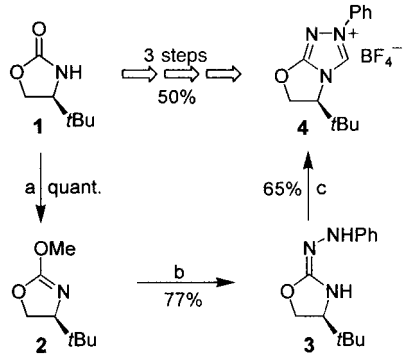
An Efficient Nucleophilic Carbene Catalyst for the Asymmetric Benzoin Condensation**

Dieter Enders* and Ulrike Kallfass

Since the early work of Ugai et al.[1] and Breslow et al.[2] it is known that thiazolium salts, such as 3-ethylthiazolium bromide or the naturally occurring thiamine (vitamin B_1), catalyze the condensation of benzaldehyde to benzoin under basic conditions. In 1966 Sheehan et al.[3–4] reported the first investigations into an asymmetric variant of the benzoin condensation by using (*S*)-4-methyl-3-(1-naphthyl)-ethylthiazolium bromide[4] as a precatalyst; the 52% *ee* obtained was remarkable for that time. In the following years, a great number of differently substituted chiral thiazolium salts were synthesized and tested in the asymmetric benzoin condensation.[5–10] However, the enantiomeric excesses hardly increased (1 – 57%).

A true breakthrough in which 1,2,4-triazolium salts[11–12] were employed was described in 1995 by our group in cooperation with Teles et al. (BASF)[13]. We reported the first efficient chiral system of this class of compounds, (4*S*,5*S*)-4-(2,2-dimethyl-4-phenyl-1,3-dioxan-5-yl)-1-phenyl-4*H*-1,2,4-triazol-1-ium perchlorate, in 1996[11] (yield of benzoin 66%, 75% *ee*, 1.25 mol% cat.). These results allowed the enantioselective benzoin condensation to be extended for the first time to a variety of aromatic aldehydes (yields 22 – 72%, 20 – 86% *ee*). Later, comparable enantioselectivities were found with chiral bicyclic triazolium salts developed by Knight and Leeper (20 – 82.5% *ee*).[12]

We report herein the synthesis of a novel enantiopure bicyclic triazolium salt **4** and its application as an efficient chiral catalyst in the form of the corresponding Wanzlick carbene in the asymmetric variant of the benzoin condensation. We used a modification of the Knight and Leeper synthesis[12] for the three-step conversion of the oxazolidin-2-one **1**[14] into the triazolium salt **4**, which was isolated as a crystalline solid (Scheme 1). Methylation of **1** with Meerwein's reagent yielded iminoether **2**, which was transformed into phenylhydrazone **3**. Final cyclization with trimethylorthoformate gave **4** (50% yield over three steps). The structure of the salt **4** was confirmed by X-ray crystallographic analysis.



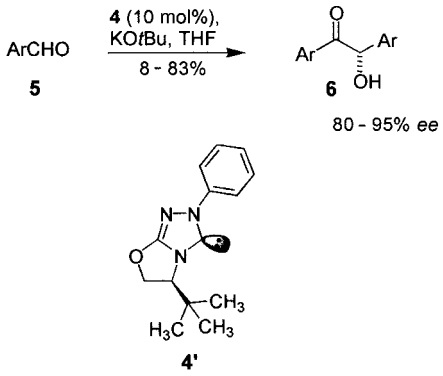
Scheme 1. Synthesis of triazolium salt **4**. a) Me_3OBF_4 (1.2 equiv), CH_2Cl_2, room temperature, 15 h; b) $PhNHNH_2$ (1 equiv), NEt_3 (1 equiv), THF, 80 °C, 7 d; c) HBF_4 (1 equiv) in diethyl ether, CH_2Cl_2, room temperature; $HC(OMe)_3$ (20 equiv), MeOH, 80 °C, 12 h.

Bicyclic chiral triazolium salt **4** (10 mol%) was used as a precatalyst in the asymmetric benzoin condensation; benzoin was obtained in very good yields (83%) and with the highest enantioselectivities ever reported (90% *ee*). The condensation of different substituted aromatic aldehydes **5** led to the corresponding α-hydoxyketones **6** in moderate to good yields and with excellent enantiomeric excesses of up to 95% (Scheme 2). The active catalyst is actually the corresponding nucleophilic Wanzlick carbene **4′**, which is formed in situ by deprotonation of **4** with KO*t*Bu in the presence of the aldehyde **5**. This nucleophilic carbene **4′** then enters the catalytic cycle of the thiazolium-catalyzed acyloin condensation, which was first proposed by Breslow more than 40 years ago.[2, 13]

After aqueous work-up and column chromatography, the acyloins **6a – j** were isolated in 6 – 100% yield and with enantiomeric excesses of 53 – 95% (Tables 1 and 2). As shown in Table 2, an increase in the amount of catalyst led to higher yields. The higher concentration of base or triazol-5-ylidene

[*] Prof. Dr. D. Enders, Dipl.-Chem. U. Kallfass
Institut für Organische Chemie, RWTH Aachen
Professor-Pirlet-Strasse 1, 52074 Aachen (Germany)
Fax: (+49) 241-8092-127
E-mail: enders@rwth-aachen.de

[**] This work was supported by the Fonds der Chemischen Industrie. We are grateful to Degussa AG, BASF AG, and Bayer AG for donations of chemicals.



Scheme 2. The asymmetric variant of the benzoin condensation, catalyzed by triazol-5-ylidene **4′**.

Table 1. Acyloins (*S*)-**6a–j**,[a] prepared by asymmetric benzoin condensation in the presence of precatalyst **4**.[b]

6	Ar	*T* [°C]	Yield [%]	*ee* [%][c]	$[\alpha]_D^{20}$[d]
a	Ph	18	83	90	+146.5
b	4-FC_6H_4	18	81	83	
b′	4-FC_6H_4	0	61	91	+117.5
c	4-ClC_6H_4	18	80	64	
c′	4-ClC_6H_4	0	44	89	+39.5
d	4-BrC_6H_4	18	82	53	
d′	4-BrC_6H_4	0	59	91	+9.6
e	3-ClC_6H_4	18	92	62	
e′	3-ClC_6H_4	0	85	86	+62.2
f	4-MeC_6H_4	18	16	93	+129.8
g	3-MeC_6H_4	18	70	86	
g′	3-MeC_6H_4	0	36	91	+138.1
h	4-$MeOC_6H_4$	18	8	95	+70.0
i	2-furyl[e]	0	100	64	
i′	2-furyl	−78	41	88	+57.4
j	2-naphthyl	18	69	80	−42.9

[a] Determined by polarimetry;[15] the absolute configurations of the products **6** were then assigned based on a uniform reaction mechanism. [b] General reaction conditions: aldehyde (10 mmol), **4** (10 mol%), KO*t*Bu (10 mol%), absolute THF (11 mL), 16 h. [c] Determined by HPLC with chiral stationary phases (Daicel AD2, Daicel OD3, (*S*,*S*)-Whelk-01). [d] $c = 1$ in MeOH. [e] Reaction time: 45 min.

Table 2. Influence of the reaction conditions on the yield and enantiomeric excess in the synthesis of benzoin (**6a**, Ar = Ph).[a]

4 [mol%]	KO*t*Bu [mol%]	Yield [%]	*ee* [%][b]
2.5	2.5	33	99
5.0	5.0	46	93
10.0	10.0	83	90

[a] General reaction conditions: aldehyde (10 mmol), absolute THF (11 mL), 18 °C, 16 h. [b] Determined by HPLC with chiral stationary phases (Daicel AD2, Daicel OD3, (*S*,*S*)-Whelk-01).

intermediate **4′**, which also has basic properties, led to a partial racemization (Table 2).

Generally, electron-rich aromatic aldehydes **6f–h** showed better asymmetric induction at room temperature than electron-deficient and therefore activated aromatic aldehydes **6b–e**. Nevertheless, the +I/+M substituents in the *para* position led to a distinct decrease in the TTN (total turnover number) of catalyst **4′** (see **6f**,**h**). To enhance the asymmetric induction for activated aldehydes, they were allowed to react at 0 °C (**6b′–e′**). When the highly reactive furane-2-carbaldehyde was employed, the reaction mixture was cooled to −78 °C; furoin (**6i′**) was isolated with a very good enantiomeric excess of 88%.

The enantiomeric excesses were determined by HPLC with chiral stationary phases. The absolute configuration of benzoin (**6a**) was found to be *S* by correlation of the optical rotation with that reported in the literature.[15] The absolute configurations of the acyloins **6** were then assigned as *S*, assuming a uniform reaction mechanism. The absolute configuration of the resulting acyloins can be explained by the relative topicity shown in Figure 1. The *tert*-butyl group

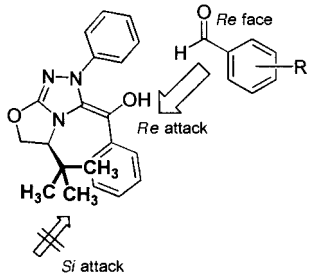


Figure 1. Postulated transition-state model (Breslow intermediate) to explain the facial selectivity in the asymmetric benzoin condensation in the presence of precatalyst **4**.

shields the *Si* face of the Breslow intermediate, which is formed during the catalytic cycle.[2] Therefore the attack of the incoming second aldehyde molecule occurs from the less-hindered *Re* face. Furthermore, the phenyl substituent on the N atom causes a preorientation of the attacking second aldehyde. It favorably approaches the Breslow intermediate with its *Re* face, thus leading to an *S* configuration at the newly formed stereogenic center.

The triazolium salt **4** is currently the most efficient precatalyst for the asymmetric variant of the benzoin condensation. The acyloins are obtained throughout in moderate to good yields and with very good enantiomeric excesses. The high asymmetric inductions are a result of the conformational rigidity of the bicyclic nucleophilic carbene catalyst **4′** and the shielding of the Breslow intermediate by the sterically demanding *tert*-butyl group.

Experimental Section

Synthesis of **2**: A dry, argon-flushed Schlenk tube was charged with a suspension of trimethyloxonium tetrafluoroborate (1.2 equiv) absolute dichloromethane (3 mL mmol^{-1}). A solution of **1** (1 equiv) in absolute dichloromethane (3 mL mmol^{-1}) was added, and the mixture was stirred for 15 h at room temperature. The mixture was then diluted with dichloromethane and washed with ice-cold saturated aqueous sodium hydrogen carbonate (3 × 3 mL per mmol^{-1} of oxazolidinone). The solution was dried over anhydrous magnesium sulfate and concentrated in vacuo to afford **2** as a colorless liquid in quantitative yield. The product was used in the next step without further purification.

Synthesis of **3**: A dry, argon-flushed Schlenk tube equipped with a reflux condenser was charged with iminoether **2** in absolute THF (1.5 mL mmol^{-1}) and with phenylhydrazine (1 equiv). Triethylamine (1 equiv) was then added, and the reaction mixture was heated at 80 °C for 7 d. The solution was cooled to room temperature and concentrated in vacuo. The crude product was purified by washing it several times with petroleum ether/diethyl ether (4:1, 5 mL mmol^{-1}). After drying under high vacuum, **3** was obtained as a pink solid in 77% yield.

 © WILEY-VCH Verlag GmbH, 69451 Weinheim, Germany, 2002 1433-7851/02/4110-1744 $ 20.00+.50/0 *Angew. Chem. Int. Ed.* **2002**, *41*, No. 10

Synthesis of **4**: A dry, argon-flushed Schlenk tube was charged with phenylhydrazone **3** (1.0 equiv) in absolute dichloromethane (10 mL mmol^{-1}) and with tetrafluoroboronic acid (1 equiv) in absolute diethyl ether (54 wt %). The solution was stirred for 30 minutes at room temperature, and then evaporated under reduced pressure. The highly hygroscopic salt was dissolved in orthoformate:methanol (2:1, 20 equiv) and transferred under argon into a pyrex tube; the sealed tube was then heated in a sand bath at 80 °C for 12 h. The mixture was cooled to room temperature and concentrated in vacuo. The crude product was dried under high vacuum for 2 h. The residue was recrystallized from methanol to give the triazolium salt **4** as an ochre crystalline solid in 65 % yield.

Synthesis of **6** (general procedure): The aromatic aldehyde (10 mmol) was added to a solution of **4** (331 mg, 1 mmol, 10 mol %) in absolute THF (0.7 mL mmol^{-1}) of at room temperature. The reaction mixture was tempered for 5 min, then KO*t*Bu (112 mg, 1 mmol, 10 mol %) in absolute THF (0.4 mL mmol^{-1}) was added dropwise. The reaction mixture was stirred for 16 h, poured into water, extracted twice with dichloromethane, and dried ($MgSO_4$). The solvent was evaporated and the residue was purified by column chromatography (silica gel, diethyl ether:pentane 1:1) or by crystallization to give the aromatic acyloins as colorless crystalline solids or pale yellow oils.

Received: December 5, 2001 [Z18335]

[1] T. Ugai, S. Tanaka, S. Dokawa, *J. Pharm. Soc. Jpn.* **1943**, *63*, 269 – 300; [*Chem. Abstr.* **1951**, *45*, 5148e].
[2] a) R. Breslow, *J. Am. Chem. Soc.* **1958**, *80*, 3719 – 3726; b) R. Breslow, R. Kim, *Tetrahedron Lett.* **1994**, *35*, 699 – 702.
[3] J. Sheehan, D. H. Hunneman, *J. Am. Chem. Soc.* **1966**, *88*, 3666 – 3667.
[4] J. Sheehan, T. Hara, *J. Org. Chem.* **1974**, *39*, 1196 – 1199.
[5] W. Tagaki, Y. Tamura, Y. Yano, *Bull. Chem. Soc. Jpn.* **1980**, *53*, 478 – 480.
[6] C. Zhao, S. Chen, P. Wu, Z. Wen, *Huaxue Xuebao* **1988**, *46*, 784 – 790.
[7] J. Marti, J. Castells, F. López-Calahorra, *Tetrahedron Lett.* **1993**, *34*, 521 – 524.
[8] R. L. Knight, F. J. Leeper, *Tetrahedron Lett.* **1997**, *38*, 3611 – 3614.
[9] A. U. Gerhard, F. J. Leeper, *Tetrahedron Lett.* **1997**, *38*, 3615 – 3618.
[10] C. A. Dvorak, V. H. Rawal, *Tetrahedron Lett.* **1998**, *39*, 2925 – 2928.
[11] a) D. Enders, K. Breuer, J. H. Teles, *Helv. Chim. Acta* **1996**, *79*, 1217 – 1221; b) D. Enders, K. Breuer, *Comprehensive Asymmetric Catalysis*, *Vol. 3*, Springer, Heidelberg, **1999**, pp. 1093 – 1102.
[12] R. L. Knight, F. J. Leeper, *J. Chem. Soc. Perkin. Trans. 1* **1998**, 1891 – 1893.
[13] a) D. Enders, K. Breuer, G. Raabe, J. Runsink, J. H. Teles, J.-P. Melder, K. Ebel, S. Brode, *Angew. Chem.* **1995**, *107*, 1119 – 1122; *Angew. Chem. Int. Ed. Engl.* **1995**, *34*, 1021 – 1024; b) J. H. Teles, J.-P. Melder, K. Ebel, R. Schneider, E. Gehrer, W. Harder, S. Brode, D. Enders, K. Breuer, G. Raabe, *Helv. Chim. Acta* **1996**, *79*, 61 – 83.
[14] For the synthesis from L-*tert*-leucine by reduction (a) and cyclization (b), see: a) D. A. Dickman, A. I. Meyers, G. A. Smith, R. E. Ganley, *Org. Synth.* **1990**, *Coll. Vol. 7*, 530 – 533; b) M. S. Newman, A. Kutner, *J. Am. Chem. Soc.* **1951**, *73*, 4199 – 4204.
[15] H. G. Rule, J. Crawford, *J. Chem. Soc.* **1937**, 138 – 145.

New Catalyst Systems for the Catalytic Conversion of Methane into Methanol**

Michael Muehlhofer, Thomas Strassner,* and Wolfgang A. Herrmann

The catalytic conversion of methane into methanol is one of the major challanges for chemists. Methane, as the major part of natural gas, is currently the cheapest source for hydrocarbons, and the need for methanol will increase in the near future. Catalytic homogeneous oxidation at low temperatures is economically interesting, but also very difficult to achieve as a result of the high stability of C–H bonds. Metal centers which allow a direct oxidative addition are probably needed for this approach to succeed.

Palladium and platinum compounds have been successfully used for the functionalization of alkanes and arenes.[1, 2] After the pioneering work of Shilov and Shteinman,[3] Periana et al.[2] and Fujiwara et al.,[1] in particular, reported interesting results. Some of the ligands which have been used in C–H activation are shown in Figure 1.

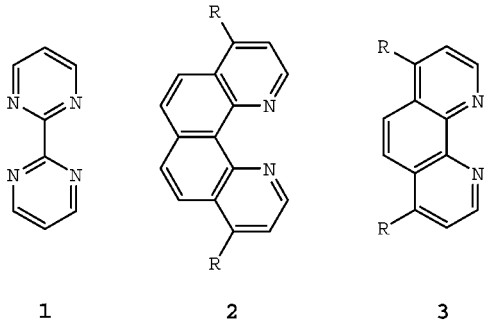


Figure 1. Ligands which have been successfully used in C–H activation reactions.

Up to now the catalytic system described by Periana and coworkers, a platinum complex with the bipyrimidine ligand **1**, has proven to be the most efficient and highly selective system providing methanol in yields of up to 72 %.[4] The major drawback of the system is the reaction medium: oleum leads to a large amount of diluted sulfuric acid when the formed ester is hydrolized. Very recently an even higher activity was reported for palladium and platinum complexes of ligand **3**.[5] This structural motif can also be found in other ligands, such as **2**, which are derived from 1,10-phenanthroline (Figure 1).[6] In general, however, only a small number of systems which are capable of functionalizing methane catalytically has been

[*] Dr. T. Strassner, M. Muehlhofer, Prof. Dr. W. A. Herrmann
Technische Universität München
Anorganisch-chemisches Institut
Lichtenbergstrasse 4, 85747 Garching (Germany)
Fax: (+49) 89-289-13473
E-mail: thomas.strassner@ch.tum.de

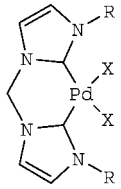
[**] C–H activation by N-heterocyclic carbenes, Part 1. This work was supported by Süd-Chemie AG.

Supporting information for this article is available on the WWW under http://www.angewandte.com or from the author.

 © WILEY-VCH Verlag GmbH, 69451 Weinheim, Germany, 2002 1433-7851/02/4110-1745 $ 20.00+.50/0

published,[7–10] with many of them dealing with the direct carbonylation to form acetic acid.[1, 11–16]

We now report for the first time the use of N-heterocyclic carbene (NHC) complexes for the catalytic activation of methane. We found that solutions of palladium(II) complexes of NHCs in carboxylic acids catalyze the conversion of methane into the corresponding methyl esters. High thermal stability of palladium(II)–carbene complexes was shown, for example by **4a** (Figure 2),[17] but an extraordinary feature is



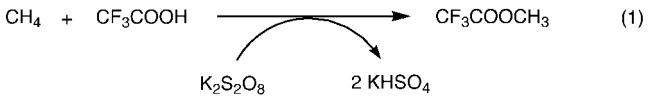
4a: R = *t*Bu, X = Br
4b: R = *t*Bu, X = I
4c: R = Me, X = Br
4d: R = Me, X = I

4

Figure 2. Palladium(II) complexes with chelating biscarbene ligands.

the unprecedented resistance of the NHC complexes under the acidic conditions which are necessary for C–H activation.

A suspension of potassium peroxodisulfate in a mixture of trifluoroacetic acid and trifluoroacetic acid anhydride at a methane pressure of 20–30 bar and 80–100 °C in the presence of catalytic amounts of **4** leads to the formation of trifluoroacetic acid methyl ester. Equation (1) shows the oxidative character of the reaction which formally can be described as $CH_4 \rightarrow [CH_3]^+ + H^+ + 2e^-$.



(1)

The analogous platinum complexes[18] can not be used as catalysts, since they immediately decompose in trifluoroacetic acid to platinum black, whereas compounds **4a**–**4d** form clear yellow solutions in the same solvents, which do not show signs of decomposition (NMR) even after 20 hours. The characteristic pattern of the ^{1}H NMR signals for the bridging methylene groups does not change, thus a reprotonation of the carbene ligands to the corresponding bisimidazolium salts can be excluded. The complexes are also stable against the addition of strong oxidants and no precipitation of palladium(II) salts was observed.

Therefore palladium–NHC complexes fulfill the requirements for catalysts which are suitable for C–H activation: a strong acid can be used as the reaction medium to protect the formed alcohols against overoxidation by forming an ester;[8] the NHC ligands stabilize the strong Lewis acidic metal centers, which can bind the methyl species formed by activation of a C–H bond in methane; and the extraordinary thermal and chemical stability allows reactions to be performed at higher temperatures in the presence of strong oxidants.

For the catalytic functionalization of methane a suspension of **4a** (0.21 mmol) and $K_2S_2O_8$ (100 equiv) in a mixture of trifluoroacetic acid (60 mL) and trifluoroacetic acid anhydride (10 mL) were transferred into an autoclave. The only product formed with an initial methane pressure of 20 bar and a temperature of 80 °C was trifluoroacetic acid methyl ester. The conversion is greater than 500 % relative to palladium.

The choice of the counterion has a significant influence on the activity of the catalyst, since according to GC-MS analysis no methyl ester is produced by compound **4b**. The quantum chemically optimized structure of compound **4c** shows that the six-membered ring formed by the palladium center and the chelating biscarbene ligand has a strained boat conformation (Figure 3).[19] Besides the negative influence of the

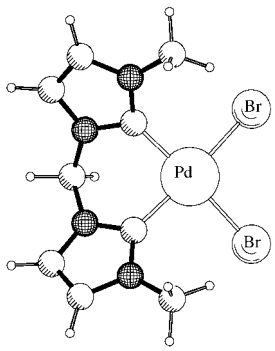


Figure 3. Pluton[20] plot of the quantum-chemically optimized structure (B3LYP/6-31G*)[21–24] of complex **4c**.

sterically more demanding *tert*-butyl groups of **4b**, the relatively low basicity of the iodide ligands compared to the bromide ligands enhances the difficulties in creating a free coordination site by protonation of the halogen ligands. According to this rationalization, the use of compound **4c**, where the steric demand of the ligands R (methyl) is significantly lower, approximately doubles the yield (980 % relative to palladium), while **4d** does not produce any ester at all.

Control experimentes with palladium(II) acetate and similar salts show, that the NHC ligands have a significant effect on the activation (Table 1). Under these conditions the system of Sheldon and co-workers $[Pd(L)(OAc)_2]$ (L = 4,7-diphenyl-1,10-phenanthrolinedisulfuric acid disodium salt),[6] the system of Periana and co-workers $[Pt(bpym)Cl_2]$ (bpym = bipyridinium), $[Pd(phen)Cl_2]$ (phen = 1,10-phenanthroline), or a reaction without catalyst at all did not yield traceable

Table 1. Catalytic conversion of methane into methanol.

Entry	Catalyst	Yield[a] [%]
1	**4a**	510
2	**4b**	0
3	**4c**	980
4	**4d**	0
5	$Pd(OAc)_2$	380
6	Sheldon system	0
7	Periana system	0
8	none	0
9	**4c**	3000[b]

[a] By GC analysis, relative to palladium. [b] $T = 90$ °C, $t = 14$ h, $p(CH_4) = 30$ bar.

 © WILEY-VCH Verlag GmbH, 69451 Weinheim, Germany, 2002 1433-7851/02/4110-1746 $ 20.00+.50/0 *Angew. Chem. Int. Ed.* **2002**, *41*, No. 10

amounts of ester. Additional reactions under different conditions show that the limit of the palladium system has not yet been reached. A yield of 3000% relative to palladium (TON = 30) could be reached in 14 hours with **4c** at 90 °C and an initial methane pressure of 30 bar.

The use of trifluoroacetic acid has the additional advantage that the formed ester can easily be removed from the reaction mixture by destilation, hydrolized, and the recovered acid together with remaining methane can be transferred back. Therefore, it is possible to run it as a cyclic process.

In summary a new field for the application of NHC complexes has opened up with C–H activation. Up to now they have been mainly used for olefin metathesis,[25–29] hydroformylation,[30, 31] or C–C coupling reactions.[32–34] The unexpected high stability in strong acids and under oxidative conditions allows the use of the compounds described here for catalytic C–H activation of methane. In view of the significantly lower bond energies of higher alkanes and arenes there is a multitute of other applications, which are currently under investigation.

Experimental Section

Catalytic oxidation of methane: Catalyst **4** (0.21 mmol) was dissolved in a mixture of trifluoroacetic acid (60 mL) and trifluoroacetic acid anhydride (10 mL) in a 200-ml autoclave. Potassium peroxodisulfate (5.70 g, 21 mmol) was then suspended in the solution and the autoclave closed and flushed three times with methane (20 bar). Under stirring of the solution, the autoclave was pressurized with methane (20 atm) and heated to 80 °C. After 24 h the autoclave was cooled to −10 °C and the pressure slowly reduced. The cold, liquid reaction mixture was isolated and characterized by GC analysis.

Received: December 7, 2001 [Z18342]

[1] Y. Fujiwara, T. Jintoku, Y. Uchida, *New J. Chem.* **1989**, *13*, 649 – 650.
[2] R. A. Periana, D. J. Taube, S. Gamble, H. Taube, T. Satoh, H. Fujii, *Science* **1998**, *280*, 560 – 564.
[3] A. E. Shilov, A. A. Shteinman, *Kinet. Katal.* **1977**, *18*, 1129 – 1145.
[4] H. Arakawa, M. Aresta, J. N. Armor, M. A. Barteau, E. J. Beckman, A. T. Bell, J. E. Bercaw, C. Creutz, E. Dinjus, D. A. Dixon, K. Domen, D. L. DuBois, J. Eckert, E. Fujita, D. H. Gibson, W. A. Goddard, D. W. Goodman, J. Keller, G. J. Kubas, H. H. Kung, J. E. Lyons, L. E. Manzer, T. J. Marks, K. Morokuma, K. M. Nicholas, R. Periana, L. Que, J. Rostrup-Nielson, W. M. H. Sachtler, L. D. Schmidt, A. Sen, G. A. Somorjai, P. C. Stair, B. R. Stults, W. Tumas, *Chem. Rev.* **2001**, *101*, 953 – 996.
[5] H.-U. Wüstefeld, F. Schüth, W. C. Kaska, G. D. Stucky, GdCh Annual Conference, Wuerzburg, **2001**.
[6] G.-J. ten Brink, I. W. C. E. Arends, R. A. Sheldon, *Science* **2000**, *287*, 1636 – 1639.
[7] S. Stahl, J. A. Labinger, J. E. Bercaw, *Angew. Chem.* **1998**, *110*, 2298 – 2311; *Angew. Chem. Int. Ed.* **1998**, *37*, 2181 – 2192.
[8] D. Wolf, *Angew. Chem.* **1998**, *110*, 3545 – 3547; *Angew. Chem. Int. Ed.* **1998**, *38*, 3351 – 3353.
[9] R. H. Crabtree, *Chem. Rev.* **1995**, *95*, 987 – 1007.
[10] R. H. Crabtree, *Chem. Rev.* **1995**, *95*, 2599.
[11] K. Nakata, Y. Yamaoka, T. Miyata, Y. Taniguchi, K. Takaki, Y. Fujiwara, *J. Organomet. Chem.* **1994**, *473*, 329 – 334.
[12] M. Kurioka, K. Nakata, T. Jintoku, Y. Taniguchi, K. Takaki, Y. Fujiwara, *Chem. Lett.* **1995**, 244.
[13] Y. Taniguchi, T. Hayashida, H. Shibasaki, D. Piao, T. Kitamura, T. Yamaji, Y. Fujiwara, *Org. Lett.* **1999**, *1*, 557 – 559.
[14] M. Asadullah, T. Kitamura, Y. Fujiwara, *Angew. Chem.* **2000**, *111*, 2609 – 2612; *Angew. Chem. Int. Ed.* **2000**, *39*, 2475 – 2478.
[15] M. Lin, A. Sen, *Nature* **1994**, *368*, 613 – 615.
[16] M. Lin, T. E. Hogan, A. Sen, *J. Am. Chem. Soc.* **1996**, *118*, 4574 – 4580.
[17] J. Schwarz, V. P. W. Bohm, M. G. Gardiner, M. Grosche, W. A. Herrmann, W. Hieringer, G. Raudaschl-Sieber, *Chem. Eur. J.* **2000**, *6*, 1773 – 1780.
[18] T. Strassner, M. Muehlhofer, W. A. Herrmann, unpublished results, **2001**.
[19] T. Strassner, unpublished results, **2001**.
[20] A. L. Spek, PLUTON, Utrecht University, Utrecht, The Netherlands, **2001**.
[21] C. Lee, W. Yang, R. G. Parr, *Phys. Rev. B* **1988**, *37*, 785 – 789.
[22] A. D. Becke, *J. Chem. Phys.* **1992**, *97*, 9173 – 9177.
[23] A. D. Becke, *J. Chem. Phys.* **1993**, *98*, 5648 – 5652.
[24] Gaussian 98 (Revision A.7), M. J. Frisch, G. W. Trucks, H. B. Schlegel, G. E. Scuseria, M. A. Robb, J. R. Cheeseman, V. G. Zakrzewski, J. A. Montgomery, R. E. Stratmann, J. C. Burant, S. Dapprich, J. M. Millam, A. D. Daniels, K. N. Kudin, M. C. Strain, O. Farkas, J. Tomasi, V. Barone, M. Cossi, R. Cammi, B. Mennucci, C. Pomelli, C. Adamo, S. Clifford, J. Ochterski, G. A. Petersson, P. Y. Ayala, Q. Cui, K. Morokuma, D. K. Malick, A. D. Rabuck, K. Raghavachari, J. B. Foresman, J. Cioslowski, J. V. Ortiz, A. G. Baboul, B. B. Stefanov, G. Liu, A. Liashenko, P. Piskorz, I. Komaromi, R. Gomperts, R. L. Martin, D. J. Fox, T. Keith, M. A. Al-Laham, C. Y. Peng, A. Nanayakkara, C. Gonzalez, M. Challacombe, P. M. W. Gill, B. G. Johnson, W. Chen, M. W. Wong, J. L. Andres, M. Head-Gordon, E. S. Replogle, J. A. Pople, Gaussian, Inc., Pittsburgh, PA, **1998**.
[25] T. Weskamp, W. C. Schattenmann, M. Spiegler, W. A. Herrmann, *Angew. Chem.* **1998**, *110*, 2631 – 2633; *Angew. Chem. Int. Ed.* **1998**, *37*, 2490 – 2493.
[26] T. Weskamp, F. J. Kohl, W. Hieringer, D. Gleich, W. A. Herrmann, *Angew. Chem.* **1999**, *111*, 2573 – 2576; *Angew. Chem. Int. Ed.* **1999**, *38*, 2416 – 2419.
[27] M. S. Sanford, J. A. Love, R. H. Grubbs, *J. Am. Chem. Soc.* **2001**, *123*, 6543 – 6554.
[28] A. Fuerstner, O. R. Thiel, L. Ackermann, H.-J. Schanz, S. P. Nolan, *J. Org. Chem.* **2000**, *65*, 2204 – 2207.
[29] M. Scholl, S. Ding, C. W. Lee, R. H. Grubbs, *Org. Lett.* **1999**, *1*, 953 – 956.
[30] W. A. Herrmann, C. W. Kohlpaintner, *Angew. Chem.* **1993**, *105*, 1588 – 1609; *Angew. Chem. Int. Ed. Engl.* **1993**, *32*, 1524 – 1544.
[31] W. A. Herrmann, J. A. Kulpe, W. Konkol, H. Bahrmann, *J. Organomet. Chem.* **1990**, *389*, 85 – 101.
[32] V. P. W. Bohm, T. Weskamp, C. W. K. Gstottmayr, W. A. Herrmann, *Angew. Chem.* **2000**, *112*, 1672 – 1674; *Angew. Chem. Int. Ed.* **2000**, *39*, 1602 – 1604.
[33] W. A. Herrmann, M. Elison, J. Fischer, C. Koecher, G. R. J. Artus, *Angew. Chem.* **1995**, *107*, 2602 – 2605; *Angew. Chem. Int. Ed. Engl.* **1995**, *34*, 2371 – 2374.
[34] S. Caddick, F. G. N. Cloke, G. K. B. Clentsmith, P. B. Hitchcock, D. McKerrecher, L. R. Titcomb, M. R. V. Williams, *J. Organomet. Chem.* **2001**, *617 – 618*, 635 – 639.

 © WILEY-VCH Verlag GmbH, 69451 Weinheim, Germany, 2002 1433-7851/02/4110-1747 $ 20.00+.50/0

Synthesis of the Protein Phosphatase 2A Inhibitor (4*S*,5*S*,6*S*,10*S*,11*S*,12*S*)-Cytostatin**

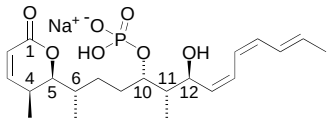
Laurent Bialy and Herbert Waldmann*

Dedicated to Professor Lutz F. Tietze on the occasion of his 60th birthday

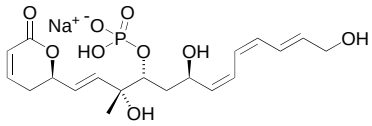
The reversible phosphorylation of proteins is employed by living organisms for the regulation of innumerable cellular processes, and aberrant protein phosphorylation contributes to the development of many human diseases, including cancer and diabetes.[1] Protein kinases (PKs) catalyze protein phosphorylation, whereas protein phosphatases (PPs) are responsible for dephosphorylation. PKs are established targets for drug discovery.[2] However, the development of small-molecule inhibitors of PPs is emerging only very recently[3] as a very rapidly growing area of investigation in clinical biology and medicinal chemistry.[4] Naturally occurring PP inhibitors have been used widely to antagonize PP action in biology experiments.[5] Thus, natural products with PP-inhibitory activity can serve as invaluable starting points in structural space for the development of potent and selective PP inhibitors. This was recently demonstrated by the successful solid-phase synthesis and biological investigation of analogues of the Cdc25 phosphatase inhibitor dysidiolide.[6]

The naturally occurring PP2A inhibitor cytostatin **1** (IC_{50} = 210 nM[7a]), which was isolated from a *Streptomyces* strain by Ishizuka and co-workers,[7b] inhibits the adhesion of B16 melanoma cells to laminin and collagen, displays antimetastatic and cytotoxic activity,[7c] and induces apoptosis of B16 melanoma cells[7d] at submicromolar concentrations. Herein we disclose the synthesis of the 4*S*,5*S*,6*S*,10*S*,11*S*,12*S* isomer of cytostatin.

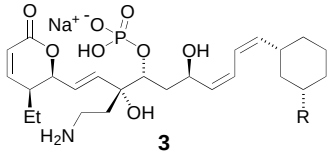
Ishizuka et al. determined the constitution of cytostatin, but not its relative and absolute configuration.[7e] Therefore, in planning the synthesis, we drew from the structurally related natural products fostriecin **2**[8] and the phoslactomycins **3**.[9] Given that the biosynthesis of these natural products might follow similar pathways and/or use identical starting materials and biocatalysts, the configurations of stereocenters 4, 5, 10, and 12 were chosen by analogy. The configuration of stereocenter 6 was assigned arbitrarily. The unknown absolute configuration of cytostatin prompted us to design the synthesis with a high degree of flexibility to allow rapid and reliable variation of absolute and relative configuration if desired. This was ensured by employing the asymmetric Evans aldol condensation (which gives access to *syn* and *anti* aldol products in both enantiomeric forms[10]), the asymmetric Evans alkylation, and the enantioselective reduction of an acetylenic ketone (for which efficient reagent-controlled processes that give rise to both possible stereoisomers are known).[11]



(4*S*,5*S*,6*S*,10*S*,11*S*,12*S*) –**1**

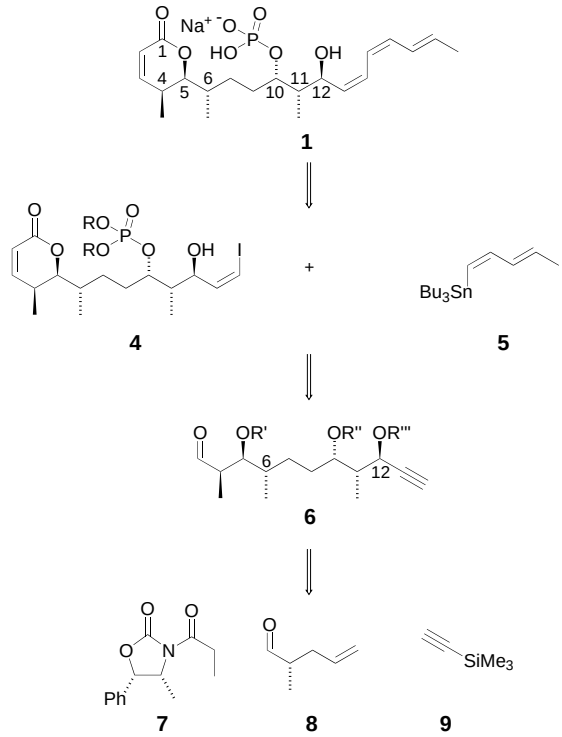


2



3

Retrosynthetic analysis of cytostatin (**1**) led to vinyl iodide **4** and dienylstannane **5** (retro Stille coupling). In this strategy, the labile triene unit is generated in a late step of the synthesis, which allows convenient and efficient access to more stable analogues (Scheme 1).[12] The α,β-unsaturated lactone incorporated in **4** was traced back to β-hydroxyaldehyde **6** from which it should be accessible by a Still – Gennari olefination[13] and subsequent lactonization. It was planned to generate both *syn* diols (corresponding to C5/C6 and C10/C11 in the natural product) by means of an asymmetric aldol reaction with *N*-



Scheme 1. Retrosynthetic analysis of (4*S*,5*S*,6*S*,10*S*,11*S*,12*S*)-cytostatin.

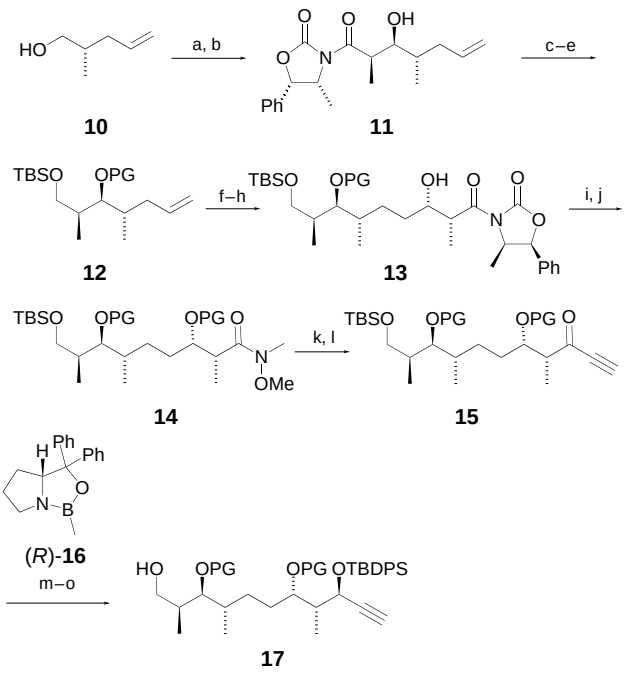
[*] Prof. Dr. H. Waldmann, Dipl.-Chem. L. Bialy
Max-Planck-Institut für molekulare Physiologie
Abteilung Chemische Biologie
Otto-Hahn-Strasse 11, 44227 Dortmund (Germany)
Fax: (+49) 231-133-2499
and
Fachbereich 3, Organische Chemie, Universität Dortmund
44221 Dortmund (Germany)
Fax: (+49) 231-133-2499
E-mail: herbert.waldmann@mpi-dortmund.mpg.de

[**] This research was supported by the Fonds der Chemischen Industrie.

 © WILEY-VCH Verlag GmbH, 69451 Weinheim, Germany, 2002 1433-7851/02/4110-1748 $ 20.00+.50/0

propionyloxazolidinone **7** as nucleophile.[14] The chiral aldehyde **8**, which is accessible by means of an asymmetric alkylation of the same acyloxazolidinone **7**,[15] should serve as electrophile. After conversion of the double bond into an aldehyde group, a second aldol reaction would be carried out. Elaboration of the resulting *N*-acyl group into an alkynyl ketone by using trimethylsilylacetylene (**9**) as nucleophile and subsequent reduction would yield **6**, the precursor to vinyl iodide **4**.

Chiral alcohol **10** was synthesized as described by Evans et al.[15] and subjected to Swern oxidation to yield the corresponding aldehyde. The volatile aldehyde was employed in an asymmetric aldol reaction with the dibutylboron enolate derived from acyloxazolidinone **7** (Scheme 2). Crystalline aldol adduct **11** was obtained in high yield and with very high stereoselectivity. Only traces of undesired diastereomers were detected and were readily separated by crystallization. Protection of the hydroxy group as the methoxymethyl (MOM) ether, reductive removal of the chiral auxiliary with "$LiBH_3OH$"[16] (generated in situ), and masking of the primary alcohol as the *tert*-butyldimethylsilyl (TBS) ether



Scheme 2. Synthesis of intermediate **17**, which incorporates all stereogenic centers. a) $(COCl)_2$, DMSO, NEt_3, CH_2Cl_2, $-78\,^\circ C \rightarrow RT$; b) **7**, Bu_2BOTf, DIPEA, CH_2Cl_2, $-78\,^\circ C \rightarrow RT$, then H_2O_2, pH 7, $0\,^\circ C \rightarrow RT$, 68% over two steps; c) MOMCl, DIPEA, CH_2Cl_2, room temperature, 97%; d) $LiBH_4$, H_2O, Et_2O, $0\,^\circ C \rightarrow RT$, 78%; e) TBSCl, imidazole, DMF, room temperature, 97%; f) 9-BBN, THF, room temperature, then H_2O_2, NaOH, 83%; g) $(COCl)_2$, DMSO, NEt_3, CH_2Cl_2, $-78\,^\circ C \rightarrow RT$; h) **7**, Bu_2BOTf, DIPEA, CH_2Cl_2, $-78\,^\circ C \rightarrow RT$, then H_2O_2, pH 7, $0\,^\circ C \rightarrow RT$; TBSCl, NEt_3, DMAP, CH_2Cl_2, room temperature, 86% over two steps; i) Me_3Al, $(H_2NMeOMe)^+Cl^-$, THF, $-10\,^\circ C \rightarrow 0\,^\circ C$, 84%; j) MOMCl, DIPEA, CH_2Cl_2, room temperature, 92%; k) **9**, BuLi, $-78\,^\circ C$; THF, $-78\,^\circ C \rightarrow -10\,^\circ C$; l) borax, methanol, H_2O, $-10\,^\circ C \rightarrow RT$, 95% over two steps; m) (*R*)-**16**, $BH_3 \cdot Me_2S$, THF, $-30\,^\circ C$, 96%; n) TBDPSCl, imidazole, DMF, room temperature; o) HF/pyridine, THF, room temperature, 40 min, 88% over two steps. DMSO = dimethyl sulfoxide, Tf = trifluoromethanesulfonyl, DIPEA = diisopropylethylamine, DMF = *N*,*N*-dimethylformamide, 9-BBN = borabicyclo[3.3.1]nonane, DMAP = 4-dimethylaminopyridine, PG = protecting group = MOM = methoxymethyl.

yielded olefin **12** with high overall efficiency. Hydroboration of the double bond by using 9-BBN, oxidative workup, and subsequent Swern oxidation of the resulting primary alcohol delivered the desired aldehyde intermediate. As expected, a second asymmetric *syn* aldol reaction with the boron enolate formed from acyloxazolidinone **7** gave β-hydroxyamide **13** with high overall yield and high stereoselectivity (only one diastereomer could be detected by ^1H NMR spectroscopic analysis). The absolute configuration of aldol adduct **13** was assigned based on the assumption that the aldol reaction proceeds in a reagent-controlled fashion with *syn* selectivity, as described for various other cases.[14] In the course of the aldol reaction the TBS group was cleaved, but the primary alcohol was readily resilylated.

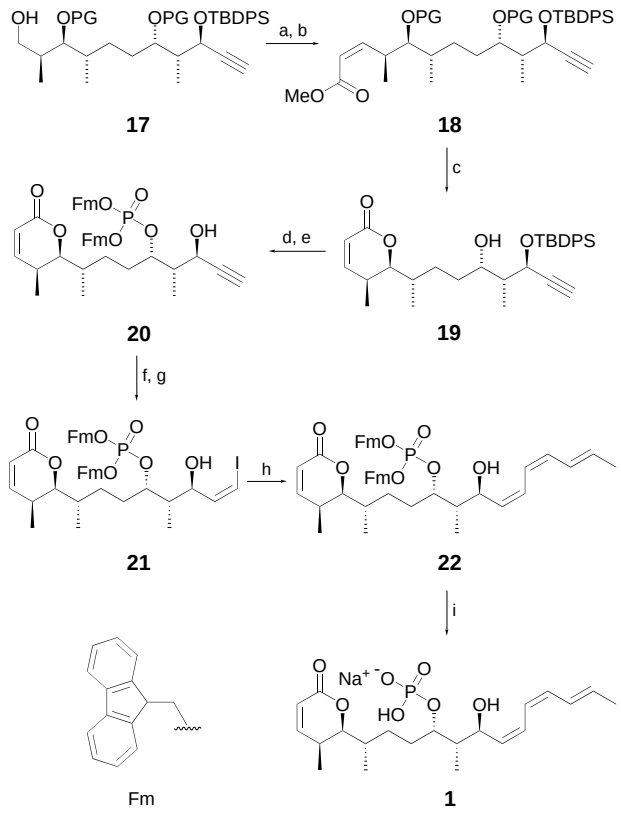
To generate the last stereocenter, an alkynyl ketone was required. This ketone was obtained by conversion of acyloxazolidinone **13** into the fully protected Weinreb amide **14**, which was treated with lithium trimethylsilylacetylide. After removal of the TMS group by treatment with catalytic amounts of borax in methanol, alkynyl ketone **15** was obtained in high overall yield. The stereoselective reduction of the keto group was attempted with different reagents, including Alpine borane[11a] and borane in the presence of a phenylglycine-derived oxazaborolidine.[11e] The highest yields were obtained with borane in the presence of oxazaborolidine (*R*)-**16** (2 equiv).[11c,d] The desired secondary alcohol was formed in nearly quantitative yield, and a second diastereomer could not be detected by means of ^1H NMR spectroscopic analysis. The protection of the propargylic alcohol required a blocking group that is stable under the conditions of the planned Still–Gennari olefination and the subsequent acid-mediated lactonization. Furthermore, it had to survive the removal of the TBS ether. After substantial experimentation, it was found that the *tert*-butyldiphenylsilyl (TBDPS) group fulfils these criteria, and the protecting group pattern was arranged accordingly. Primary alcohol **17** was selectively formed by removal of the TBS group with HF/pyridine.

Alcohol **17** was oxidized to the corresponding aldehyde with DMP,[17] and the carbonyl compound was converted into *Z*-olefin **18** under Still–Gennari conditions (Scheme 3). Subsequently, the MOM protecting groups were removed by treatment with CBr_4 in 2-propanol. Under these conditions (HBr is probably formed in situ),[18] lactone **19** was formed simultaneously.

To develop a reaction sequence that would give flexible access to different phosphorylated analogues of the natural product, it was planned to introduce the phosphate group at this stage of the synthesis. The correct choice of phosphate-protecting group proved to be crucial. Initial experiments with the methoxybenzyl group, which was successfully applied in the synthesis of fostriecin,[8b] were not successful. Similarly, the cyanoethyl ester was not suitable because only one cyanoethyl group could be removed in the final deprotection step without destroying the entire molecule. Finally, the use of the fluorenylmethyl ester[19] allowed the successful cleavage of the protecting group.

The phosphate was formed by phosphitylation and subsequent oxidation. After selective cleavage of the TBDPS ether, the desired alkyne **20** was obtained in high yield. Conversion

 © WILEY-VCH Verlag GmbH, 69451 Weinheim, Germany, 2002 1433-7851/02/4110-1749 $ 20.00+.50/0



Scheme 3. Synthesis of **1**. a) DMP, CH_2Cl_2, $NaHCO_3$, 93%; b) $(CF_3CH_2O)_2P(O)CH_2CO_2Me$, [18]crown-6, KHMDS, THF, −78°C, 92%; c) CBr_4, 2-propanol, 82°C, 83%; d) $(FmO)_2PNiPr_2$, tetrazole, CH_2Cl_2/CH_3CN, 0°C→RT, then I_2, pyridine, H_2O, THF; 95%; e) HF/pyridine, THF, room temperature, 28 h, 82%; f) NIS, $AgNO_3$, DMF, room temperature, quant.; g) $K^+{}^-OOC{-}N{=}N{-}COO^-K^+$, HOAc, 2-propanol/dioxane, 63%; h) **5**, $[PdCl_2(CH_3CN)_2]$ (cat.), DMF/THF, 62%; i) NEt_3:CH_3CN 1:5, room temperature, then Na^+-Dowex resin, 85%. DMP = Dess—Martin periodinane, HMDS = hexamethyldisilazane, NIS *N*-iodosuccinimide; PG = MOM.

of **20** into vinyl iodide (*Z*)-**21** proved to be problematic. After substantial experimentation, **21** was obtained by conversion of the alkyne into the corresponding alkynyl iodide in the presence of silver nitrate followed by reduction of the triple bond with diimide.[20] All attempts to reduce the triple bond with different reagents gave undesired side reactions, in particular, the reduction of the α,β-unsaturated lactone and ring opening. However, when diimide was generated in situ in 2-propanol, these side reactions were largely suppressed and vinyl iodide (*Z*)-**21** was obtained in 63% yield (Scheme 3). This advanced intermediate was then subjected to Stille coupling with *Z*,*E*-dienylstannane **5** with $[PdCl_2(CH_3CN)_2]$ as catalyst and without additional phosphane.[12] Under these conditions, sensitive (*Z*,*Z*,*E*)-**22** was formed in a satisfactory yield (62%). Dienylstannane **5** was synthesized from crotonaldehyde: the latter was converted into the dibromoolefin with CBr_4 and PPh_3 treated with *n*BuLi followed by Bu_3SnCl to give an enyne stannane, and subsequently subjected to hydrozirconation (not shown). Finally, the phosphate was unmasked. Upon treatment of phosphoric acid triester **22** with excess triethylamine, both fluorenylmethyl groups were cleaved in a β-elimination reaction, and the 4*S*,5*S*,6*S*,10*S*,11*S*,12*S* isomer of cytostatin **1** was isolated in 85% yield.

Synthetic **1** displays a specific rotation of $[\alpha]_D^{20} = +50$ (c = 0.114 in $[D_4]$MeOH). Unfortunately, this value can not be employed to ascertain the absolute configuration of the natural product because Ishizuka and co-workers did not report the specific rotation of the isolated sample.[7e]

The phosphatase-inhibiting activity of synthetic **1** was investigated with *p*-nitrophenyl phosphate as substrate.[7d] Isomer **1** inhibited PP2A (IC_{50} = 33 nM). This value is one order of magnitude lower than that of the natural product. This finding suggests that our assumption about the absolute configuration of the natural product may be correct, at least for most of the stereogenic centers.

In conclusion we have developed an asymmetric synthesis of the 4*S*,5*S*,6*S*,10*S*,11*S*,12*S* of the PP2A inhibitor cytostatin. The synthesis is stereochemically flexible and employs only reagent-controlled transformations, thus allowing access to each desired isomer of cytostatin in a reliable and efficient manner. This successful synthesis now opens up new opportunities for the development of new tools for biological studies and of new cancer drugs.

Received: January 31, 2002 [Z18620]

[1] T. Hunter, *Cell* **2000**, *100*, 113–127.
[2] For a review, see: A. J. Bridges, *Chem. Rev.* **2001**, *101*, 2541–2572.
[3] Z.-Y. Zhang, *Curr. Opin. Chem. Biol.* **2001**, *5*, 416–423.
[4] For example, see: J. S. Lazo, D. C. Aslan, E. C. Southwick, K. A. Cooley, A. P. Ducruet, B. Joo, A. Vogt, P. Wipf, *J. Med. Chem.* **2001**, *44*, 4042–4049; R. A. Urbanek, S. J. Suchard, G. B. Steelman, K. S. Knappenberger, L. A. Sygowski, C. A. Veale, M. J. Chapdelaine, *J. Med. Chem.* **2001**, *44*, 1777–1793.
[5] a) K. Hinterding, D. Alonzo-Díaz, H. Waldmann, *Angew. Chem.* **1998**, *110*, 716–780; *Angew. Chem. Int. Ed.* **1998**, *37*, 668–749; b) J. E. Sheppeck II, C.-M. Gauss, A. R. Chamberlin, *Bioorg. Med. Chem.* **1997**, *5*, 1739–1750.
[6] a) D. Brohm, S. Metzger, A. Bhargava, O. Müller, F. Lieb, H. Waldmann, *Angew. Chem.* **2002**, *114*, 319–323; *Angew. Chem. Int. Ed.* **2002**, *41*, 307–311; b) J. L. Blanchard, D. M. Epstein, M. D. Boisclair, J. Rudolph, K. Pal, *Biorg. Med. Chem. Lett.* **1999**, *9*, 2537-2538; c) M. Takahashi, K. Dodo, Y. Sugimoto, Y. Aoyagi, Y. Yamada, Y. Hashimoto, R. Shirai, *Biorg. Med. Chem. Lett.* **2000**, *10*, 2571-2574.
[7] a) M. Kawada, M. Amemiya, M. Ishizuka, T. Takeuchi, *Biochim. Biophys. Acta* **1999**, *1452*, 209–217; b) M. Amemiya, M. Ueno, M. Osono, T. Masuda, N. Kinoshita, C. Nishida, M. Hamada, M. Ishizuka, T. Takeuchi, *J. Antibiot.* **1994**, *47*, 536–540; c) T. Masuda, S.-I. Watanabe, M. Amemiya, M. Ishizuka, T. Takeuchi, *J. Antibiot.* **1995**, *48*, 528–529; d) M. Kawada, M. Amemiya, M. Ishizuka, T. Takeuchi, *Jpn. J. Cancer Res.* **1999**, *90*, 219–225; e) M. Amemiya, T. Someno, R. Sawa, H. Naganawa, M. Ishizuka, T. Takeuchi, *J. Antibiot.* **1994**, *47*, 541–544.
[8] a) Structure determination: G. C. Hokanson, J. C. French, *J. Org. Chem.* **1985**, *50*, 462–466; D. L. Boger, M. Hikota, B. M. Lewis, *J. Org. Chem.* **1997**, *62*, 1748–1753; b) Synthesis: D. L. Boger, S. Ichikawa, W. Zhong, *J. Am. Chem. Soc.* **2001**, *123*, 4161–4167; D. E. Chavez, E. N. Jacobsen, *Angew. Chem.* **2001**, *113*, 3779–3782; *Angew. Chem. Int. Ed.* **2001**, *40*, 3667–3670.
[9] Structure determination: T. Kohama, T. Nakamura, T. Kinoshita, I. Kaneko, A. Shiraishi, *J. Antibiot.* **1993**, *46*, 1512–1519; T. Shibata, S. Kurihara, K. Yoda, H. Haruyama, *Tetrahedron* **1995**, *51*, 11999–12012.
[10] M. Braun, *Methoden Org. Chem. (Houben-Weyl) 4th Ed. 1952–*, *Vol. E21b*, **1995**, pp. 1612–1712.
[11] a) M. M. Midland, D. C. McDowell, R. L. Hatch, A. Tramontano, *J. Am. Chem. Soc.* **1980**, *102*, 867–869; b) P. V. Ramachandran, A. V.

 © WILEY-VCH Verlag GmbH, 69451 Weinheim, Germany, 2002 1433-7851/02/4110-1750 $ 20.00+.50/0

Teodorovic, M. V. Rangaishenvi, H. C. Brown, *J. Org. Chem.* **1992**, *57*, 2379 – 2386; c) K. A. Parker, M. W. Ledeboer, *J. Org. Chem.* **1996**, *61*, 3214 – 3217; d) E. J. Corey, R. K. Bakshi, S. Shibata, *J. Am. Chem. Soc.* **1987**, *109*, 5551 – 5553; e) J. Bach, R. Berenguer, J. Garcia, T. Loscertales, J. Vilarrasa, *J. Org. Chem.* **1996**, *61*, 9021 – 9025; f) K. Matsumura, S. Hashiguchi, T. Ikariya, R. Noyori, *J. Am. Chem. Soc.* **1997**, *119*, 8738 – 8739.
[12] J. K. Stille, B. L. Groh, *J. Am. Chem. Soc.* **1987**, *109*, 813 – 817.
[13] W. C. Still, C. Gennari, *Tetrahedron Lett.* **1983**, *24*, 4405 – 4408.
[14] D. A. Evans, J. A. Bartroli, T. L. Shih, *J. Am. Chem. Soc.* **1981**, *103*, 2127 – 2129.
[15] D. A. Evans, S. L. Bender, J. Morris, *J. Am. Chem. Soc.* **1988**, *110*, 2506 – 2526.
[16] T. D. Penning, S. D. Djuric, R. A. Haack, V. J. Kalish, J. M. Myashiro, B. W. Rowell, S. S. Yu, *Synth. Commun.* **1990**, *20*, 307 – 312.
[17] D. B. Dess, J. C. Martin, *J. Am. Chem. Soc.* **1991**, *113*, 7277 – 7287.
[18] A. S.-Y. Lee, Y.-J. Hu, S.-F. Chu, *Tetrahedron* **2001**, *57*, 2121 – 2126.
[19] Y. Watanabe, T. Nakamura, H. Mitsumoto, *Tetrahedron Lett.* **1997**, *38*, 7407 – 7410.
[20] For example, see: J.-M. Duffault, J. Einhorn, A. Alexakis, *Tetrahedron Lett.* **1991**, *32*, 3701 – 3704.

Modular Building Blocks for Amino Acid Recognition in Peptides

Mark Wehner and Thomas Schrader*

The selective recognition of short peptide sequences is a key concept in many natural regulatory processes. Thus, the natural antibiotic vancomycin binds tightly to the C-terminal D-Ala-D-Ala fragment in peptides, which is used for the construction for bacterial cell walls.[1] Numerous cell – cell recognition events rely on the recognition of the specific Arg-Gly-Asp sequence.[2]

The first attempts to mimic Nature's potent peptide hosts with artificial structures, confined the conformational freedom of a host molecule by creating a cleft (Rebek and co-workers), a macrocycle (Still and co-workers), or even a cavity (Still and co-workers); the specific binding sites were often taken from (non)natural amino acids.[3] Several groups have created receptor molecules for important secondary structures found in peptides and proteins. Thus, α-helical[4] and β-sheet[5] portions of polypeptides can be recognized by synthetic ligands with a complementary hydrogen-bond-donor and acceptor pattern. In recent years, considerable progress has been achieved with a combinatorial approach.[6]

Various site-specific proteases, such as thrombin, trypsin, and many others provide a shallow groove for the efficient recognition of the backbone of the peptide to be cleaved, in its extended conformation. This array is combined with a specific binding pocket for the side chains of the target amino acid, and thus defines the cleavage site. We asked ourselves if such a rational design could also be used for artificial peptide recognition. Is it possible to create a set of modules, each of which recognizes a certain amino acid in a peptidic environment or, even better, a short peptide sequence?

We recently reported the stabilization of small peptides in their β-sheet conformation by external ligands.[7] N-acylated 3-aminopyrazoles were shown to interact with every hydrogen-bond-donor (D) and acceptor (A) available at the top face of a dipeptide. Two consecutive amino acids can be clamped together with one of these heterocycles, which causes the formation of three almost-linear hydrogen bonds in a DAD sequence (Figure 1). This recognition process simultaneously fixes the peptide in the thermodynamically favorable β-sheet conformation. Thus, small soluble models of this important secondary structure have been prepared.

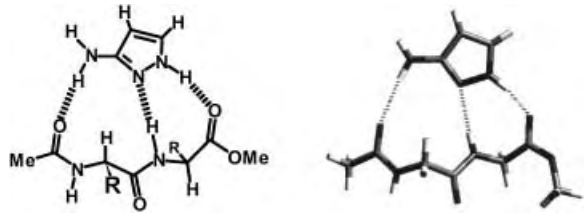


Figure 1. β-Sheet stabilization with aminopyrazoles—three-point binding of the top face of a dipeptide by the DAD binding sites of the aminopyrazole; left: Lewis structure; right: results of molecular-mechanics calculation (Cerius², Molecular Simulations, Dreiding 2.21).

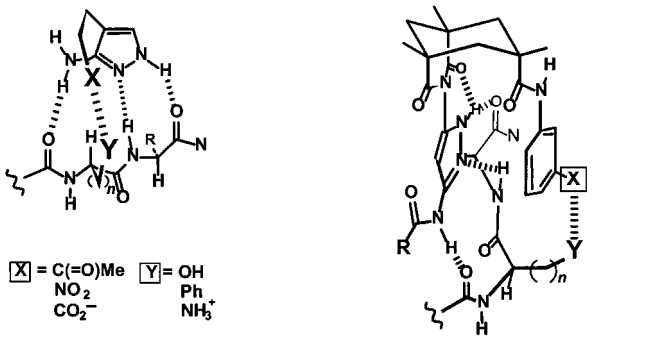
In a β sheet, the N–H and C=O bonds of the backbone point up and down, whereas the amino acid residues (R) are extended horizontally away from the peptide in a well-defined geometry. This preorganized arrangement was our starting point for a new modular concept of peptide receptors: If it were possible to attach to the aminopyrazole a rigid U-shaped substituent with a properly placed binding site at its tip, this could reach down to the side chain of the respective amino acid and lead to an additional, specific noncovalent interaction. With an interchangeable tip, various binding sites could be introduced into the basic peptide receptor, which would lead to a modular set of building blocks, selective for the typical classes of amino acids. To our knowledge, no example of such a rationally designed set of peptide receptors exists to date.

For the U-shaped spacer, we chose the framework of Kemp's triacid, because it is exceptionally rigid and its chemistry is well developed.[8] Two acid groups were designated to carry the monoacylated 3,5-diaminopyrazole unit by way of an imide functionality, while the third could be coupled to an aniline derivative with the correct binding site in the *m*-position. Scheme 1 shows the general structure of the building blocks: both the imide and the neighboring aminopyrazole unit are in the same plane, locked together by an intramolecular hydrogen bond.

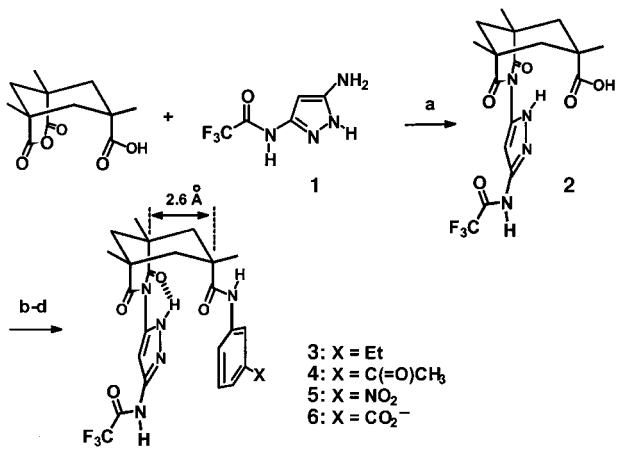
During the synthesis, care must be taken to chemoselectively address the three amino functionalities of 3,5-diaminopyrazole, without an extensive use of protecting groups. We begin with imide formation between mono(trifluoroacetylated) diaminopyrazole **1** and Kemp's acid anhydride (Scheme 2). The imide intermediate **2** must be *N*-Boc pro-

[*] Prof. Dr. T. Schrader, M. Wehner
Fachbereich Chemie der Universität
Hans Meerwein Strasse
35032 Marburg (Germany)
Fax: (+49) 6421-28-28917
E-mail: schradet@mailer.uni-marburg.de

 © WILEY-VCH Verlag GmbH, 69451 Weinheim, Germany, 2002 1433-7851/02/4110-1751 $ 20.00+.50/0



Scheme 1. Representation of the modular building blocks for peptide recognition; right: the U-turn formed by Kemp's triacid brings the receptor tip X close to the characteristic group Y of the amino acid in the peptide.



Scheme 2. Synthesis of hosts **3**–**6**; a) toluene, 110 °C (−H_2O); b) Boc_2O, 90 °C; c) *m*-aminobenzene derivative, PyCloP, 50 °C, $CHCl_3$; d) silica gel, (−Boc); a)–d) 17–22 % overall yield, Boc = *tert*-butoxycarbonyl, PyCloP = chlorotris(pyrrolidin-1-yl)phosphonium hexafluorophosphate.

tected for the subsequent attachment of the aniline derivative. The most critical step involves introduction of the aniline derivative carrying the binding site. Although this only requires formation of an amide bond, the product of this coupling reaction contains two aromatic rings at a distance of 2.6 Å and less. We were successful with PyCloP, but only at 50 °C in chloroform. The Boc group was removed during the subsequent chromatographic purification, which leads directly to the desired products **3**–**6**.

Following this synthetic method, *m*-ethylaniline, *m*-aminoacetophenone, *m*-aminobenzoic acid benzyl ester, and even *m*-aminonitrobenzene could be coupled to the imide intermediate **2**. The benzyl ester was finally removed by hydrogenolysis, and the resulting free acid converted into the tetrabutylammonium benzoate **6**—the binding site for basic, cationic amino acid residues. The *m*-aminoacetophenone derivative **4** is a host molecule for OH- and SH-containing amino acids, *m*-aminonitrobenzene **5** should recognize electron-rich aromatic amino acids, and *m*-ethylaniline **3** serves as a reference compound with a comparable steric demand, but which is suitable only for recognition of the peptide backbone.

Compounds **3**–**6** are some of the first Kemp's triacid derivatives with a double aromatic substitution.[9] As both aromatic moieties are unsymmetrical, two conformers may exist, which should, in principle, differ in their spectroscopic properties. However, in the ^1H and the ^{13}C NMR spectra of **3**–**6**, only one set of resonance signals is seen. NOESY spectra of **4** reveal numerous contacts between the alkyl substituents of the cyclohexyl skeleton, but only one between the two aromatic planes, which should be in close contact with each other. Correspondingly, in the productive conformation only one H–H separation is calculated to be less than 4.5 Å, which is exactly the one observed in the NOESY experiment (3.2 Å, Figure 2).

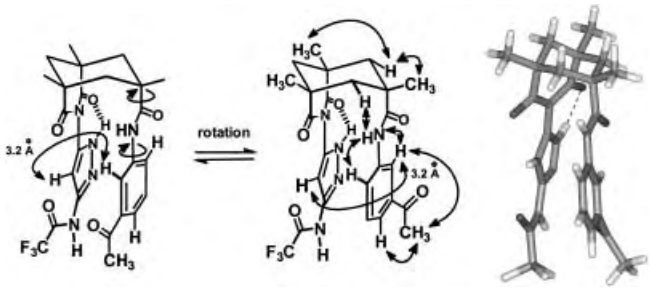


Figure 2. NOE contacts in host **4** and possible rotation around the *trans* amide bond. The productive conformation is on the right; double arrows indicate reciprocal NOE cross peaks. The two conformers shown are by far the lowest-energy structures of all the geometries found during the conformational search.[15]

A self-association experiment with **4** was conducted in chloroform in the concentration range between 10^{-2} M and 10^{-3} M. In this range, which was later used for the NMR spectroscopic titrations, no complexation-induced shifts could be observed for any of the signals arising from the host protons. Clearly the sterically demanding U-turn effectively prevents dimerization of the receptor molecules.

From the simple acylated aminopyrazoles, we knew that preformed dipeptides in an extended conformation gave the highest association constants. However, contrary to all previous experiments, our new reference compound **3** produced no complexation-induced shift after it had been added to N/C-protected divaline (Ac-Val-Val-OMe). It seems that two of the valine isopropyl groups are sterically too demanding to allow complexation with the aminopyrazole-modified Kemp's acid. This view is also supported by force-field calculations.

Pleasingly, exchange of valine for alanine restored the expected downfield shift of the signal arising from the top-face NH proton of the peptide. A Job plot[10] (Figure 3) confirmed the desired 1:1 stoichiometry, and NMR spectroscopic titrations in $CDCl_3$ furnished association constants below 100 M^{-1} (Ac-Ala-Ala-OMe/Ac-Phe-Ala-OMe).[11] These numbers are relatively small, but they must be lower than those for valine-containing dipeptides, as alanine has a much higher tendency to adopt an α-helix conformation than to form a β sheet. For comparison, we titrated the two alanine-containing dipeptides mentioned above with the best β-sheet ligands developed previously by us, and obtained identical values (Table 1).

In molecular-mechanics calculations (MacroModel 7.0, OPLS-AA force-field), the backbone of a serine-containing

 © WILEY-VCH Verlag GmbH, 69451 Weinheim, Germany, 2002 1433-7851/02/4110-1752 $ 20.00+.50/0 *Angew. Chem. Int. Ed.* **2002**, *41*, No. 10

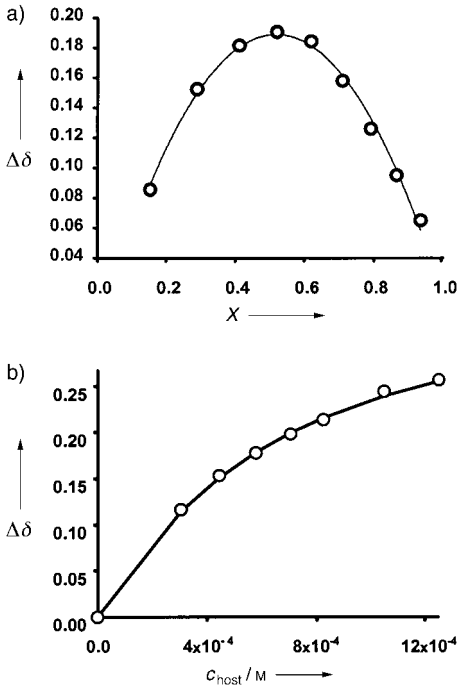


Figure 3. a) Job plot for complex formation between **6** and Ac-Orn-Ala-OMe. b) NMR spectroscopy titration curve for complex formation between **6** and Ac-Orn-Ala-OMe.

Table 1. Association constants K_a [M^{-1}] for complex formation between hosts **3**–**6** and various dipeptides.[a]

Host	Standard	Selective binding	Special cases
triflAMP[b]	Ala – Ala: 50[c]	–	Phe – Ala: 40
reference **3**	Orn – Ala: 280	Ala – Ala: 70	Phe – Ala: $\leq$ 40
XH-binder **4**	Ala – Ala: 80	Ser – Ala: 900	Ser – Val: no shifts
arene-binder **5**	–	Phe – Ala: 350	Ala – Phe: no shifts
cation-binder **6**	Propylamine: 490	Orn – Ala: 2360	–

[a] The association constants were determined by NMR spectroscopic titrations in $CDCl_3$. All dipeptides were protected as *N*-acetyl methyl esters. Stoichiometries were always 1:1, unless otherwise stated. [b] TriflAMP = 3-trifluoroacetylamino-5-methylpyrazole. [c] Errors were determined as standard deviations from the nonlinear regressions; they usually varied between 10% and 40% (exceptions: very weak binding).

dipeptide forms a complex with the trifluoroacetylated aminopyrazole by three-point binding (Figure 4). The serine hydroxy group comes close to the acetophenone C=O group, and a relatively strong, new hydrogen bond is formed.

First we tested our receptor module for serine: NMR spectroscopic titration with dialanine gave a K_a value of $80\,M^{-1}$, in good agreement with the reference compound. When Ac-Ser-Ala-OMe was bound by **4**, however, a 11-fold increase in K_a to $900\,M^{-1}$ was observed. A Job plot confirmed that a 1:1 complex was indeed formed.[12] In conclusion, the introduction of an additional hydrogen-bond acceptor in the rigid framework of the receptor module resulted in a substantial increase in free binding enthalpy for a serine-containing dipeptide, but not for dialanine.

As a representative example of electron-rich, aromatic amino acids, we tested phenylalanine in a peptidic environment. With reference compound **3** and Ac-Phe-Ala-OMe a K_a value of $\leq 40\,M^{-1}$ was measured, which again indicates

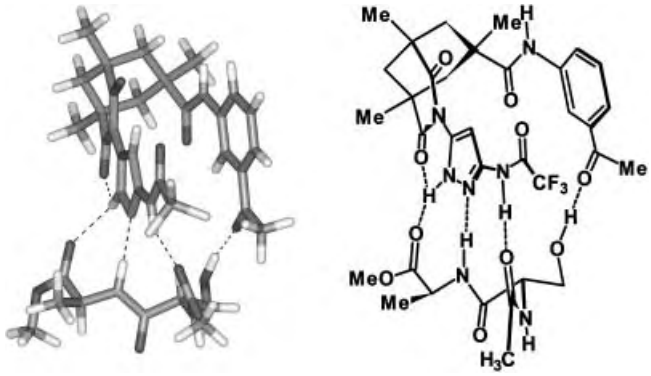


Figure 4. Result of the Monte Carlo simulation of the productive complex geometry in sequence-selective binding of serinyl – alanine-containing dipeptides by **4**.

steric repulsion of the benzyl group by the Kemp's acid derivative. When our *m*-nitroaniline-based receptor module for aromatic amino acids **5** was titrated with Ac-Phe-Ala-OMe, the nonlinear regression of binding curves for several proton signals unanimously converged at a K_a value of $350\,M^{-1}$. Again, the complex stoichiometry was calculated to be 1:1, by means of a Job plot. This time, the ninefold increase in K_a value was accompanied by marked upfield shifts for the signals arising from the aromatic protons of host and guest, which indicates π-stacking interactions. We could thus show that a nitroarene in the correct place in the rigid receptor considerably strengthened the complex of **5** with a dipeptide containing phenylalanine.

In protein recognition, basic amino acids often form ion pairs with carboxylate groups, for example, with aspartates or glutamates. These interactions are generally much stronger in apolar media than simple hydrogen bonds. To avoid the possibility that such an ion pair could override the backbone recognition by the aminopyrazole, we chose a counterion for the basic amino acid which itself forms a strong ion-pair-reinforced hydrogen bond with the alkylammonium ion. Therefore, the short, basic amino acid, ornithine, was incorporated as the acetate salt into the alanine-containing dipeptide Ac-Orn-Ala-OMe.[13] The benzoate group in **6** thus had to compete with the acetate (Ac) counterion of ornithine in the dipeptide. During the NMR spectroscopic titration, an unusually high number of proton signals shifted by $\Delta\delta_{sat}$ values of up to 1 ppm (Figure 5). The broad ammonium group signal and the signal arising from its neighboring methylene group, as well as those from both *ortho* protons next to the host benzoate anion, showed pronounced complexation-induced shifts, which indicates the formation of the new ion pair. Interesting enough, the signal for the top-face NH proton of the peptide also shifted drastically, by about 1 ppm. The nonlinear regression of various binding curves of host and guest signals gave association constants around $2400\,M^{-1}$; 1:1 stoichiometry was again proven by a Job plot (Figure 3). As a control experiment, we titrated **6** with *n*-propylammonium acetate and found a K_a value of $490\,M^{-1}$ for the formation of the salt bridge. The difference between these two numbers must come from the backbone recognition of the peptide by **6**, and provides experimental evidence that both

 © WILEY-VCH Verlag GmbH, 69451 Weinheim, Germany, 2002 1433-7851/02/4110-1753 $ 20.00+.50/0

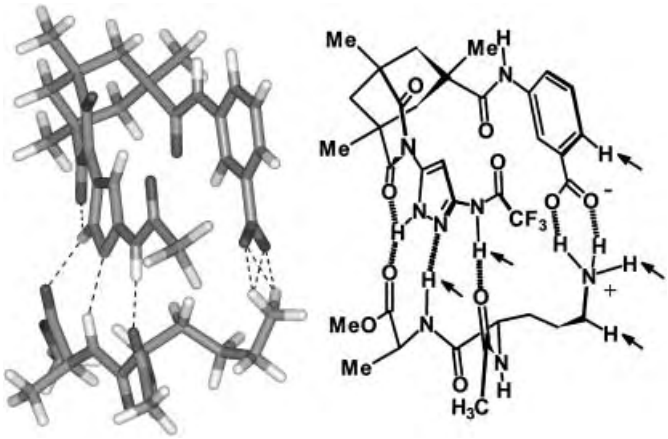


Figure 5. Left: Monte Carlo optimized structure of **6**@Ac-Orn-Ala-OMe in chloroform (1000 steps). Right: arrows indicate the atoms in host and guest for which complexation-induced shifts of proton signals are observed during the titration.

recognition processes operate simultaneously in the aggregate formation between **6** and Ac-Orn-Ala-OMe. This peptide was also titrated with reference compound **3**, which furnished a relatively low binding constant of about $280\,\text{M}^{-1}$. In this case, however, it is not clear if the aminopyrazole reacts with the backbone of the peptide or with the alkylammonium acetate ion pair. In any case, a preference of $\approx 9{:}1$ was established for the selective recognition of ornithine by the anionic receptor module **6**. Thus, introduction of a properly placed benzoate anion into the rigid receptor module led to an additional ion-pair-reinforced hydrogen bond with a representative basic amino acid.

Direct information about the peptide conformation can be drawn from Karplus analyses of the H(N),H(α-C) coupling constants, which correlate with the characteristic torsion angle θ.[14] We examined complexes of the three hosts with additional binding sites, with their best peptide-binding partners. Addition of hosts **3**–**6** to the peptide solution invariably leads to sharper resonance signals and, in most cases, increased ^3J values by comparison to the free peptides, which approach the calculated values for the pure complexes.

To conclude, we have shown that peptide receptors can be developed by rational design; these receptors are selective for some of the main classes of amino acids in a peptidic environment. We are currently working on the selective recognition of acidic and apolar amino acids in peptides. In some cases, complex formation is so sensitive towards steric factors that the same receptor module completely rejects the same dipeptide with an inverted sequence. Thus, Ac-Ala-Phe-OMe is not complexed at all. Modeling studies indicate that only one mutual orientation of the binding partners is productive, the other one seems to be sterically hindered. The sequence selectivity of the new receptor modules is currently under investigation. For a better comparison, we kept the other amino acid as an alanine in most cases. It will be interesting to find out if larger groups than the small methyl group are tolerated at all. The titration of Ac-Ser-Val-OMe with our serine binder **4** gives an initial indication of this. No complexation-induced shifts are produced, although the same dipeptide with a C-terminal alanine was bound with a high association constant of $900\,\text{M}^{-1}$.

In the future, we will combine two or more of these fragments by specific covalent linkers, to achieve sequence-selective binding of tetra- and pentapeptides in polar solution. With these receptor modules, it should be possible to dock onto specific essential-recognition motifs in peptides and proteins. This approach could ultimatively be used for protein tagging, protection, or allosteric inhibition of enzymes.

Received: December 4, 2001 [Z18326]

[1] D. H. Williams, B. Bardsley, *Angew. Chem.* **1999**, *111*, 1264–1286; *Angew. Chem. Int. Ed.* **1999**, *38*, 1172–1193.

[2] R. Haubner, D. Finsinger, H. Kessler, *Angew. Chem.* **1997**, *109*, 1440–1456; *Angew. Chem. Int. Ed. Engl.* **1997**, *36*, 1374–1389.

[3] a) M. Famulok, K.-S. Jong, G. Deslongchamps, J. Rebek, Jr., A*ngew. Chem.* **1991**, *103*, 880–882; *Angew. Chem. Int. Ed. Engl.* **1991**, *30*, 858–860; b) S. S. Yoon, W. C. Still, *J. Am. Chem. Soc.* **1993**, *115*, 823–824; c) C.-T. Chen, H. Wagner, W. C. Still, *Science* **1997**, *279*, 851–853; d) M. A. Hossain, H. J. Schneider, *J. Am. Chem. Soc.* **1998**, *120*, 11208–11209.

[4] Review: J. P. Schneider, J. W. Kelly, *Chem. Rev.* **1995**, *95*, 2169–2187; a) D. S. Kemp, T. P. Curran, J. G. Boyd, T. J. Allen, *J. Org. Chem.* **1991**, *56*, 6683–6697; b) M. W. Peczuh, A. D. Hamilton, *J. Am. Chem. Soc.* **1997**, *119*, 9327–9328; c) Y. Mito-Oka, S. Tsukiji, T. Hiraoka, N. Kasagi, S. Shinkai, I. Hamachi, *Tetrahedron Lett.* **2001**, *42*, 7059–7062.

[5] Overview: J. S. Nowick, *Acc. Chem. Res.* **1999**, *32*, 287–296; H. L. Schenck, S. H. Gellman, *J. Am. Chem. Soc.* **1998**, *120*, 4869–4870.

[6] a) W. C. Still, *Acc. Chem. Res.* **1996**, *29*, 155–163; b) H. Wennemers, M. Conza, M. Nold, P. Krattiger, *Chem. Eur. J.* **2001**, *7*, 3342–3347; c) T. Braxmeier, M. Demarcus, T. Fessmann, S. McAteer, J. D. Kilburn, *Chem. Eur. J.* **2001**, *7*, 1889–1898.

[7] C. Kirsten, T. Schrader, *J. Am. Chem. Soc.* **1997**, *119*, 12061–12068.

[8] J. Rebek, Jr., *Angew. Chem.* **1990**, *102*, 261–272; *Angew. Chem. Int. Ed. Engl.* **1990**, *29*, 245–255.

[9] S. Shinoda, H. Tsukube, Y. Nishimura, I. Yamazaki, A. Osuka, *J. Org. Chem.* **1999**, *64*, 3757–3762.

[10] a) P. Job, *C. R. Hebd. Seances Acad. Sci.* **1925**, *180*, 928; b) M. T. Blanda, J. H. Horner, M. Newcomb, *J. Org. Chem.* **1989**, *54*, 4626.

[11] a) H. J. Schneider, R. Kramer, S. Simova, U. Schneider, *J. Am. Chem. Soc.* **1988**, *110*, 6442; b) C. S. Wilcox in *Frontiers in Supramolecular Chemistry* (Ed.: H. J. Schneider), Verlag Chemie, Weinheim, **1991**, p. 123.

[12] Unfortunately, the NMR signal for the hydroxy proton remained extremely broad throughout the entire titration, so that no direct evidence for this additional hydrogen bond could be obtained.

[13] The short side chain of ornithine can be reached more easily by the benzoate unit of the host than that of lysine (Figure 5).

[14] a) M. Delepierre, C. M. Dobson, F. M. Poulsen, *Biochemistry* **1982**, *21*, 4756; b) V. F. Bystrov, *Prog. Nucl. Magn. Reson. Spectrosc.* **1976**, *10*, 41.

[15] MacroModel 7.0, Schrödinger Inc., 2000. Force field: Amber* and OPLS-AA.

 © WILEY-VCH Verlag GmbH, 69451 Weinheim, Germany, 2002 1433-7851/02/4110-1754 $ 20.00+.50/0

Synthesis and Structure of Na_3N

Dieter Fischer and Martin Jansen*

One of the most pronounced violations of the homology principle in the periodic table is found in the binary nitrides of the alkali metals. While Li_3N forms spontaneously from the elements at room temperature,[1] the synthesis of the homologues Na_3N and K_3N has failed so far in spite of a multitude of attempts over many decades, and early claims of success reported in the literature have turned out to be irreproducible.[2]

To date, the methods employed for the synthesis of Na_3N or K_3N have been based either on a selective decomposition of the azides (in ammonia) or on a reaction of finely dispersed metal particles with nitrogen in an electrical discharge.[2–4] In particular, the latter route constitutes an attempt to perform the chemical reactions with already activated elements. Following this line of reasoning, one realizes that the highest possible activation is reached if single atoms of the elements are mixed on an atomic scale, in the desired ratio, before the reaction takes place. It is exactly this approach which we have chosen for the successful synthesis of Na_3N reported herein.

In a vacuum chamber atomic gas-phase species of the various components (here Na and N_2) are generated separately. The resulting atomic beams are codeposited onto a cooled substrate resulting in a statistical mixture of the atoms on the substrate. Subsequently, the samples are heated to room temperature (within 3 h for Na_3N) and analyzed by X-ray diffraction. After this short time, the X-ray powder diffraction patterns show remarkably well-resolved Bragg reflections with a very low background (Figure 1). Upon further heating, Na_3N decomposes above 360 K releasing nitrogen.

The diffraction patterns of Na_3N can be indexed according to a primitive cubic unit cell, with a refined lattice constant $a = 473.25(2)$ pm. The structure refinement, using the Rietveld profile-fitting method, clearly reveals the anti-ReO_3 structure type for Na_3N (Figure 1).[5] Thus, the structure of Na_3N consists of corner-sharing NNa_6 octahedra with an Na–N bond of 236.6 pm. This distance is in the expected range and compares well to those observed in the binary oxides and nitrides of Na and Li. The Na–Na and N–N separations are 334.6 and 473.3 pm, respectively. In Na_3N the coordination number of the nitrogen atom is lower (six) because of the higher effective radius of the alkali metal, than in Li_3N, in which eight Li atoms surround the nitrogen atom to form a hexagonal bipyramide (Li–N distances 194/211 pm).[1] As a result of the structure type the space filling in Na_3N is low, similar to ReO_3, WO_3, or Cu_3N. The calculated diffraction patterns of alternative structure models containing additional sodium or nitrogen atoms, which fill the vacancy in the center of the unit cell, show a considerably reduced intensity of the first Bragg reflection (100). However, all the measured powder patterns of Na_3N show (100) as the strongest reflection, even if texture-dependent intensity deviations are considered. Thus, we can conclude that no significant occupation of this position occurs. Similarly, a possible contamination with hydrogen can be excluded because no release of hydrogen was detected by mass spectrometry during the decomposition of Na_3N.

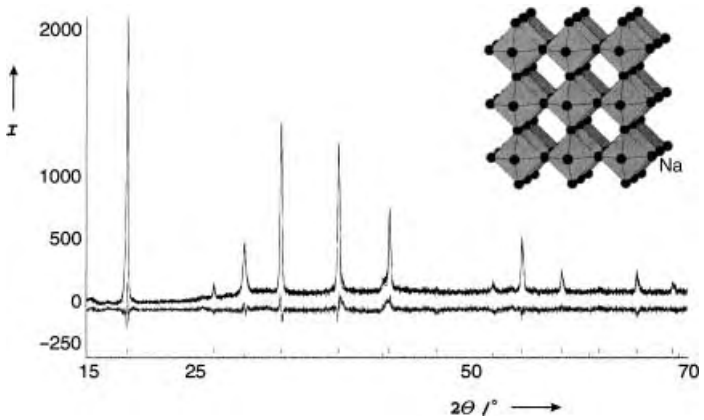


Figure 1. X-ray powder diffraction pattern (298 K) and crystal structure of Na_3N, measured (●), calculated (——), difference plot (gray), line diagram: top Na_3N and bottom Na.

In our new and versatile preparative approach,[8] the desired elements are deposited as an atomic-level dispersion resulting in an amorphous solid at liquid-nitrogen temperature. Upon heating ordered structures evolve, the order of appearance of which seems to follow Ostwald's rule, that is, at supersaturated conditions the low-density polymorphs crystallize first. Thus, the obtained polymorph of Na_3N is a metastable one and additional, denser modifications of Na_3N are expected to exist. This assumption is consistent with the results of the computational predictions of structure candidates for the alkali-metal nitrides.[6] A large number of (meta)stable structure candidates for Na_3N have been identified using global optimization and the energy-lid method. Ab initio calculations reveal the Li_3P-type to be the most stable modification followed by the Li_3N- and the anti-ReO_3-type (Figure 2), which differ only slightly in energy. However, out of these the anti-ReO_3 structure type possesses the lowest density, and thus this modification was not further considered at the time. According to these results, a phase transformation of Na_3N (anti-ReO_3 type) into the Li_3P- or Li_3N-type seems to be possible.

Temperature-dependent X-ray diffraction under high-vacuum conditions indicates that Na_3N (dispersed educt mixture) is amorphous at 77 K, orders at around 200 K into the anti-ReO_3 type, and is stable until 360 K with no further phase transformation (Figure 3).[7] Above 360 K Na_3N decomposes into Na and N_2 (demonstrated by mass spectrometry). Thus, increasing the temperature does not induce a phase transformation. Experiments to achieve a phase transformation through applying high pressure have not yet been performed.

In conclusion, with the aid of a novel and complex synthesis method the elusive compound Na_3N has been prepared for the first time. The crucial advantage of this new approach is the use of educts dispersed on an atomic scale. Thus, the

[*] Prof. Dr. M. Jansen, Dr. D. Fischer
Max-Planck-Institut for Solid-State Research
Heisenbergstrasse 1
70569 Stuttgart (Germany)
Fax: (+49) 711-689-1502
E-mail: martin.jansen@fkf.mpg.de

 © WILEY-VCH Verlag GmbH, 69451 Weinheim, Germany, 2002 1433-7851/02/4110-1755 $ 20.00+.50/0

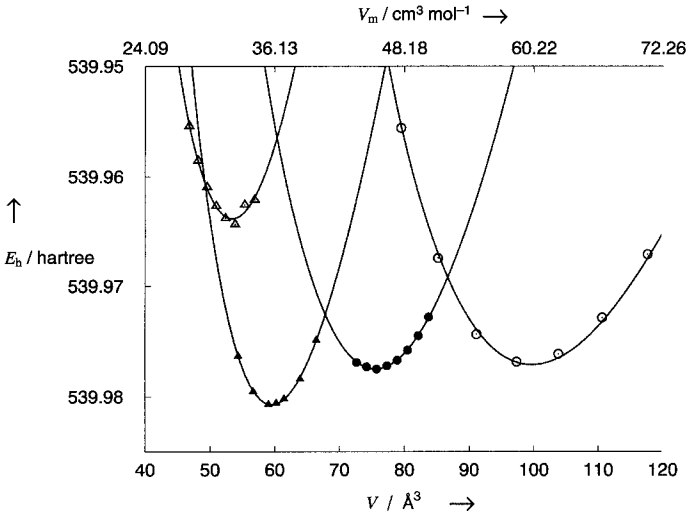


Figure 2. Energy of the structure candidates in the system Na_3N as a function of the volume (△ Li_3Bi type, ▲ Li_3P type, ● Li_3N type, ○ ReO_3 type).[9]

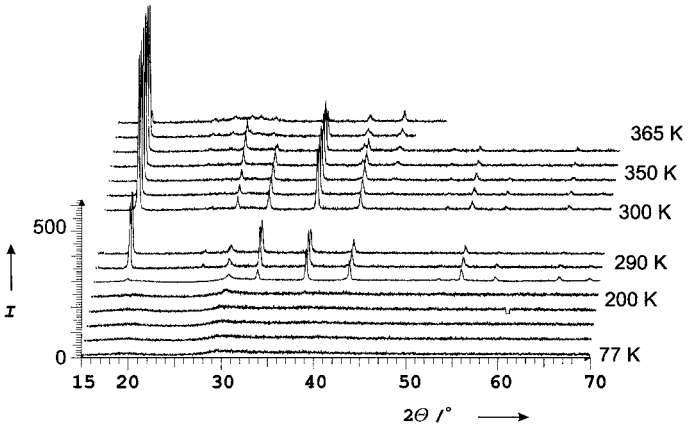


Figure 3. Temperature-dependent X-ray diffraction measurements of Na_3N under high vacuum. The sample is amorphous in the range from 77 – 200 K, Bragg reflections of Na_3N are present between 200 – 360 K, and Na_3N decomposes into Na and N_2 above 360 K. Two different samples are used (sample of the high-temperature study shows texture-dependent intensity deviations). The temperatures of the single scans are: (from bottom to top) 77, 110, 140, 170, 200, 200 – 273, 290, 295, 300, 320, 330, 350, 360, 365, 370 K.

transport distances during the subsequent solid-state reactions are reduced to atomic scales, and crystalline products are formed at unrivaled low temperatures and within extremely short times.[8] Besides its conceptual singularity, a particular advantage of this synthesis method is its ability to allow the synthesis of extremely labile or metastable solids. This feature is convincingly demonstrated by the synthesis of Na_3N, the decomposition of which at 360 K almost certainly precludes a preparation by classical solid-state reactions.

Experimental Section

Na_3N was prepared using an evaporation system consisting of an ultra-high-vacuum (UHV) chamber, for further details see ref. [8]. Segregated sodium was evaporated from a PBN crucible using an effusion cell, at 473 K. Nitrogen (purity 5.0; Westfalen, Münster) mass flow was controlled to 1.6 $cm^3 min^{-1}$ and the stream into the chamber passed through a microwave plasma source (2.45 GHz, 80 mA). Sodium and nitrogen (100-fold excess) were codeposited for a period of 3 – 9 h onto sapphire substrates (0001) both sides of which were epitaxial-polished; TBL-Kelpin, Neuhausen) in the temperature range 77 – 300 K (process pressure: 5×10^{-5} mbar).

The samples obtained at 77 K have a reflecting, metallic appearance. At room temperature all the samples are red-brown. Samples of Na_3N are very hygroscopic, and after storage in a glove box (Ar, $H_2O < 0.04$ ppm) for 14 days, the X-ray diffraction patterns indicate a considerable decomposition to NaOH. Even freshly prepared samples sometimes exhibit small amounts of NaOH. However, most samples contain metallic sodium as an impurity, which presumably was formed by partial decomposition of Na_3N during the preparation process.

Received: December 21, 2001 [Z18431]

[1] A. Rabenau, H. Schulz, *J. Less-Common Met.* **1976**, *50*, 155 – 9.
[2] H. Wattenberg, *Ber. Dtsch. Chem. Ges.* **1930**, *63*, 1667.
[3] E. Tiede, H.-G. Knoblauch, *Ber.* **1935**, *68*, 1153.
[4] R. Suhrmann, K. Clusius, *Z. Anorg. Allg. Chem.* **1926**, *152*, 56.
[5] Crystallographic data of Na_3N at 298 K (X-ray powder diffraction analysis): cubic, space group $Pm\bar{3}m$ (No. 221) $a = 473.25(2)$ pm, $Z = 1$, Na in (3d), N in (1a), $R_p = 8.0\,\%$ $R_{wp} = 10.3\,\%$, $R_{Bragg} = 5.3\,\%$, $B_{eq} = 4.5$, 11 reflections. The program Topas (Bruker AXS, Karlsruhe) was used for the refinement of the lattice constant and of the structure (Rietveld). Further details on the crystal structure investigation(s) may be obtained from the Fachinformationszentrum Karlsruhe, 76344 Eggenstein-Leopoldshafen, Germany (fax: (+49) 7247-808-666; e-mail: crysdata@fiz-karlsruhe.de), on quoting the depository number (number CSD-412313).
[6] M. Jansen, J. C. Schön, *Z. Anorg. Allg. Chem.* **1998**, *624*, 533 – 40.
[7] X-ray investigations: All powder diffraction patterns were measured on a theta/theta D8-Advance powder diffractometer (Bruker AXS) with parallel beam (Göbelmirror, $Cu_{K\alpha}$) in an X-ray chamber under high vacuum (5×10^{-7} mbar) with incidence angles of 2 to 10°, step 0.02°. The temperature of the samples was controlled by the sample holder. The residual gas was recorded by a mass spectrometer (C-100M, Leybold-Inficon).
[8] D. Fischer, M. Jansen, *J. Am. Chem. Soc.* in press.
[9] Z. Cancarevic, J. C. Schön, M. Jansen, unpublished results.

 © WILEY-VCH Verlag GmbH, 69451 Weinheim, Germany, 2002 1433-7851/02/4110-1756 $ 20.00+.50/0

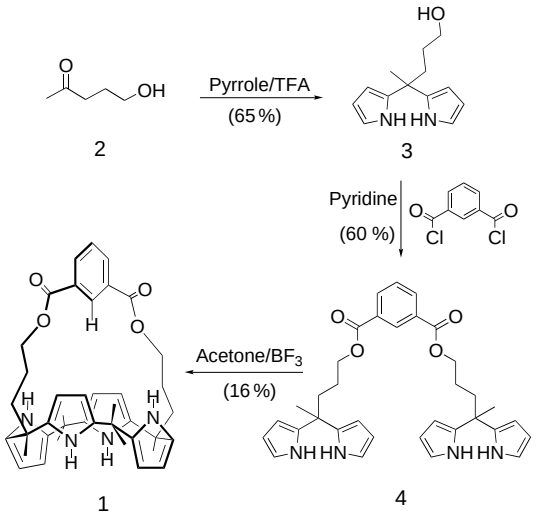
Synthesis of a Strapped Calix[4]pyrrole: Structure and Anion Binding Properties**

Dae-Wi Yoon, Hoon Hwang, and Chang-Hee Lee*

Anion binding chemistry using neutral host molecules has been extensively studied as a result of its potential biological applications, and has emerged as one of the key areas in the field of molecular recognition.[1] The application of anion receptors to molecular devices, such as ion-selective electrodes, fluorescence sensors, and electrochemical signaling devices has received particular attention.[2] The development of newer and more specifically functionalized receptors with enhanced selectivity requires maximized interactions with guest molecules, and this remains a critical goal in the synthesis of neutral receptors for anions. Anion recognition is often affected by hydrogen-bonding interactions; such interactions are weak and this is one of the reasons that anion recognition is more challenging to achieve than cation complexation.[3, 4] Among the various neutral anion receptors described in the literature, calix[4]pyrroles, which are readily accessible from pyrrole and acetone, have been identified as one of the more attractive hosts for the binding of halide anions, especially for fluoride ions.[5] A number of new homologues have been synthesized recently by Sessler and coworkers and subsequently applied in anion sensing[5] and separation.[6] In most cases, the design is based on the modification of either the β-pyrrolic positions or the *meso* substituents.[7–10] A three-dimensional cyclic oligopyrrole unit as well as expanded calixpyrroles have also been reported as part of the efforts to tune the binding abilities of the receptors.[6] However, the synthesis of calix[4]pyrrole receptors bearing preorganized and adjustable binding domains has not been attempted, although the idea has been documented,[4] and encapsulated calixpyrroles prepared by template-based methods have been reported.[10, 11]

Herein we report the first example of a new class of calix[4]pyrroles bearing *trans*-substituted straps on one side of the molecule. We also report the solid-state structure and chloride and fluoride anion binding behavior of this prototypical system. In the design of the receptor (**1**) a flexible strap was used to enable isolation and encapsulation of the binding site. The strap was expected to provide additional hydrogen-bonding sites and allow specific modulation of the inherent anion affinities. Furthermore, it was anticipated that further modifications in affinities could be engendered by using different sizes of straps or by introducing various functional groups into the straps. Ultimately, different kinds of straps could be used to probe the relationships between structure, guest size, and binding affinity.

The synthesis of host (**1**) was accomplished in three steps (Scheme 1). The condensation of 5-hydroxy-2-pentanone (**2**) with pyrrole in the presence of an acid catalyst afforded



Scheme 1. Synthesis of the strapped calix[4]pyrrole **1**. TFA = trifluoroacetic acid.

dipyrromethane **3**.[12] The reaction of isophthaloyl dichloride with two equivalent of **3** in the presence of pyridine gave **4**. The acid-catalyzed condensation of **4** in the presence of excess acetone afforded the desired receptor **1** in 16% yield. The separation of the desired product was straightforward and purification by column chromatography on silica gel (single column) gave a sample of analytical purity. A crystallographic analysis of **1** (Figure 1) reveals that the compound is surprisingly asymmetric at least in the solid state. The overall

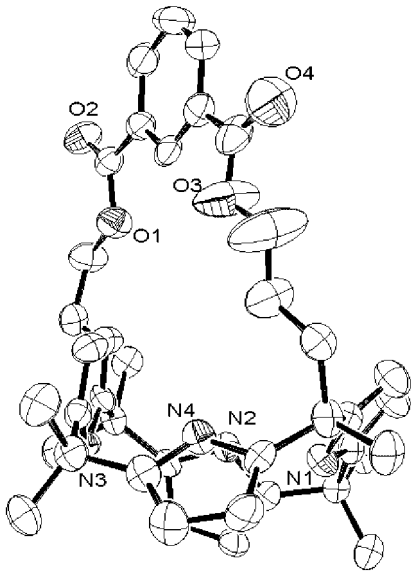


Figure 1. ORTEP view of the molecular structure of **1**. Four pyrrole rings are distorted and form an irregular 1,3-alternating conformation.

[*] Prof. C.-H. Lee, D.-W. Yoon, Prof. H. Hwang
Department of Chemistry
Kangwon National University
Chun-Chon 200-701 (Korea)
Fax: (+82) 33-253-7582
E-mail: chhlee@kangwon.ac.kr

[**] This work was supported by the Basic research program of the Korea Science and Engineering Foundation (grant no. 2000-1-12300-007-3). A grant from VSRC at Kangwon National University is also gratefully acknowledged. The author thanks Prof. K. Ahn (POSTECH) and Prof. J. Sessler (University of Texas at Austin) for helpful discussions.

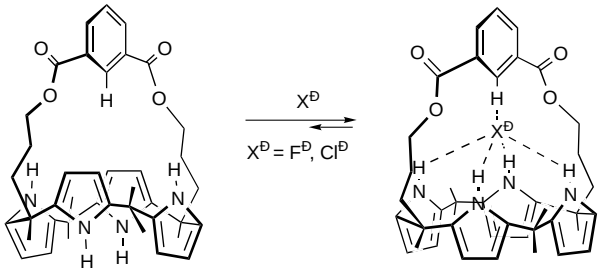
Supporting information for this article is available on the WWW under http://www.angewandte.com or from the author.

 © WILEY-VCH Verlag GmbH, 69451 Weinheim, Germany, 2002 1433-7851/02/4110-1757 $ 20.00+.50/0

conformation is close to the cyclic 1,3-alternate form seen in other calix[4]pyrroles. However, all four pyrrole rings are tilted at different angles.[13] The two pyrrolic nitrogen atoms (N2 and N4) point toward the strap while the other two (N1 and N3) point downward. The N3 pyrrolic proton points almost outward and is nearly parallel with the N1 pyrrole ring. Close inspection of the 3D-packing structure indicates that the N3 pyrrolic proton is involved in intermolecular hydrogen bonding with one of the carbonyl groups in the neighboring molecule. The observed distance between N3 and O2′ atoms is 3.008 Å. The strap also adopts a slight tilt to compensate for the steric interactions incurred by this intermolecular hydrogen-bonding interaction. These latter features contrast those of other reported calix[4]pyrroles, which, as a general rule, display completely symmetric conformations.[14]

In spite of the asymmetric nature of the solid-state structure, the ^{1}H NMR spectra of **1** recorded in [D_6]DMSO displayed a single NH resonance as a sharp singlet at $\delta = 9.39$ and two distinctive β-pyrrolic resonances at $\delta = 5.76$ and 5.74. ^{1}H NMR spectroscopy was also used to study the anion binding behavior of host **1** in [D_6]DMSO. The extremely slow nature of the binding/release equilibrium has enabled the direct observation of the complexation phenomenon. Quantitative binding titrations with fluoride and chloride ions reveal distinctive resonances for all the proton signals, as well as dramatic shifts in the NH resonances. The singlet for the NH resonance at $\delta = 9.39$ was split into two distinctive singlets and shifted to $\delta = 13.03$ and 13.07 on addition of fluoride anions. The splitting of the pyrrole NH resonance is thought to reflect a coupling of the bound fluoride anion with the NH protons.[15] The β-pyrrolic resonance originally appearing as two doublets at $\delta = 5.76$ and 5.74 ($J = 2.5$ Hz) was also shifted to $\delta = 5.40$. The integrals of the new resonance signals observed were proportional to the concentration to the amount of added fluoride anions (see Supporting Information). The inner aromatic proton located between the two carbonyl groups on the strap originally resonating at $\delta = 8.65$ was shifted to $\delta = 9.06$ upon addition of fluoride anions while those of the other aromatic protons remained almost unchanged. This large downfield shift is consistent with the presence of a hydrogen-bonding interaction between the inner aromatic proton and fluoride anion in addition to the expected normal strong hydrogen-bonding interaction between the pyrrolic NH protons and the fluoride anion found in simple calix[4]pyrroles. The binding of a fluoride ion to the pocket locks the calixpyrrole into the cone conformation (Scheme 2).

The inner aromatic proton located between the two carbonyl groups in **1** showed an even larger downfield shift (to $\delta = 9.52$) upon addition of chloride anions. The other ring protons were shifted to higher field ($\delta = 7.54$ and 8.00). The pyrrolic NH resonance was also shifted to $\delta = 11.33$ and appeared as a broad singlet in the presence of chloride anions. These results provide support for the contention that chloride anions form a stronger hydrogen-binding interaction than fluoride anions with the inner aromatic proton. Such a conclusion is rationalized in terms of a better match of the size between the chloride ion and the binding site defined by the presence of the strap. The smaller fluoride anion sits snuggly within the cavity generated by the four pyrrolic NH protons and, accordingly, the bound fluoride anion must be further away from the aromatic proton than the chloride anion is. The slow equilibrium exchange seen in the strapped system is also noteworthy (this is not seen in the unstrapped calix[4]pyrroles) and provides a further indication that the use of a flexible strap bearing potential hydrogen bonding elements may allow for the generic design of optimized anion receptors.



Scheme 2. Controlling the conformation of the strapped calix[4]pyrrole **1**.

Qualitative assessments of anion binding affinity were made by following the chemical shift changes or integrated intensity changes of the corresponding resonance signals as a function of anion concentration in the evolving ^{1}H NMR spectra. These binding studies clearly indicate that one fluoride (or one chloride) anion binds with one host molecule,[16] even though the two discrete binding sites (upper and lower part) may have different affinities towards anionic substrates. The ^{1}H NMR spectra indicate that the smaller fluoride anion binds more tightly with the pyrrolic NH proton and thus forms a loose hydrogen bond with the inner aromatic proton. On the other hand, the relatively large chloride anion interacts less well with the pyrrolic NH proton but forms a stronger hydrogen bond with the inner aromatic proton. No appreciable binding interaction is observed with bromide, iodide, sulfate, and phosphate anions. The 1:1 binding stoichiometry for both the fluoride and chloride anions was confirmed by Job plots. The encapsulated binding site in **1** should modulate the inherent affinity of calixpyrroles towards specific anions by differentiating them on the basis of their size. The cavity generated in the presence of the strap may not have enough room to accommodate larger anions.

Unfortunately, the association constants for host **1** with fluoride and chloride anions proved too large to determine accurately from the titration curves obtained by ^{1}H NMR spectroscopy.[10, 16, 17] Thus, we attempted to obtain accurate binding constant by using isothermal titration calorimetry (ITC). Here, DMSO was chosen as the solvent because of the limited solubility of the host compound in other solvents. It was also thought that the high dielectric constant of DMSO combined with the low concentrations of the guest and host required for these experiments would eliminate aggregation effects. The calorimetric traces in DMSO for fluoride anion did not show constant baseline and heat pulses. However, the calorimetric traces measured for chloride anions (Bu_4NCl) revealed progressive changes in the heat pulses, and a K_a value of $1.01 \times 10^5 (\pm 1.01 \times 10^4)$ M for the formation of the 1:1 complex [(**1**)Cl^-] was calculated.

Since accurate determination of the binding constant for a fluoride anion proved to be problematic by ITC, we per-

 © WILEY-VCH Verlag GmbH, 69451 Weinheim, Germany, 2002 1433-7851/02/4110-1758 $ 20.00+.50/0 *Angew. Chem. Int. Ed.* **2002**, *41*, No. 10

formed a competition experiment by using ^{1}H NMR spectroscopy. Specifically, an equimolar amount of fluoride anions was added to a premixed [(**1**)Cl$^-$] complex (1:1 molar ratio) in [D$_6$]DMSO. The spectra obtained indicated the rapid replacement of the precomplexed chloride anion by a fluoride anion. Integration of the spectra at equilibrium gave a ratio of 6.3:1 for the two complexes ([(**1**)F$^-$]/[(**1**)Cl$^-$]). A binding constant of approximately $3.87 \times 10^6\,\text{M}^{-1}$ for the formation of [(**1**)F$^-$] was calculated from the observed ratio and assuming that a negligible amount of free host **1** was present in the final equilibrium mixture.[9a] This assumption is reasonable because the measured association constant for the chloride anion is large and the competition experiment indicates that the affinity constant for a fluoride anion is even larger. In both cases the derived association constants in DMSO are larger than those reported for normal calix[4]pyrroles, as well as for various deep cavities or chromophore-functionalized calix[4]-pyrroles measured in acetonitrile.[9b, 17, 18]

Given the above findings and cognizant of the dangers of comparing K_a values in different solvents, we elected to measure the binding constant of unstrapped calix[4]pyrrole with chloride anions in DMSO by using ITC. We obtained a value of $1.270 \times 10^3\,\text{M}^{-1}$ for the binding of a chloride anion, a value that agrees well with that ($K_a = 1.025 \times 10^3\,\text{M}^{-1}$) determined by NMR titration in [D$_6$]DMSO.[18a] The concordance between these old and new values, measured by different methods, lends credence to the argument that strapping the calixpyrrole increases its anion binding affinity significantly, at least for chloride anions where good values for comparison are available. Apparently, encapsulation of the binding domain and the introduction of straps with weak hydrogen-bonding donors acts to reduce the matrix–host interaction and enhance the host–guest interaction. Less well determined at the present time is whether the inherent selectivity of the calixpyrrole system is being modulated. Further studies of this issue using a range of other strapped calixpyrroles bearing various chromophores and different length of strap are in progress.

In conclusion, we have succeeded in synthesizing a strapped calix[4]pyrrole for the first time. The current results support the use of super-structured elements to generate calix[4]pyrrole systems with affinities and selectivities that are modified relative to normal calix[4]pyrroles. As such, the approach detailed here could provide a new and useful complement to other affinity modulations currently being pursued in the context of calixpyrrole chemistry.

Received: June 20, 2001
Revised: February 4, 2002 [Z17326]

[1] a) F. P. Schmidtchen, M. Berger, *Chem. Rev.* **1997**, *97*, 1609–1646; b) P. D. Beer, J. Cadman, *Coord. Chem. Rev.* **2000**, *205*, 131–155; c) P. D. Beer, *Chem. Commun.* **1996**, 689–696; d) P. D. Beer, P. A. Gale, *Angew. Chem.* **2001**, *113*, 502–532; *Angew. Chem. Int. Ed.* **2001**, *40*, 486–516; e) F. P. Schmidtchen, *Org. Lett.* **2002**, 431–434.

[2] a) A. P. de Silva, H. Q. N. Guanarante, T. Gunnlaugson, A. J. M. Huxley, C. P. McCoy, J. T. Rademacher, T. E. Rice, *Chem. Rev.* **1997**, *97*, 1515–1566; b) J. L. Sessler, *CHEMTECH*, **1999**, *29*, 16–24.

[3] J. L. Sessler, A. Gebauer, P. A. Gale, *Gazz. Chim. Ital.* **1997**, *127*, 723.

[4] J. L. Sessler, P. Anzenbacher, Jr., K. Jursikova, H. Miyaji, J. W. Genge, N. A. Tvermoes, W. E. Allen, J. A. Shriver, *Pure Appl. Chem.* **1998**, *70*, 2401–2408.

[5] a) P. A. Gale, P. Anzenbacher, Jr., J. L. Sessler, *Coord. Chem. Rev.* **2001**, *222*, 57–102; b) J. L. Sessler, P. A. Gale in *The Porphyrin Handbook*, *Vol. 6* (Eds.: K. M. Kadish, K. M. Smith, R. Guilard) Academic Press, San Diego, **2000**, chap. 45; c) J. L. Sessler, P. Anzenbacher, Jr., H. Miyaji, K. Jursikova, E. R. Bleasdale, P. A. Gale, *Ind. Eng. Chem. Res.* **2000**, *39*, 3471–3478.

[6] a) J. L. Sessler, P. A. Gale, J. W. Genge, *Chem. Eur. J.* **1998**, *4*, 1095–1099; b) J. L. Sessler, J. W. Genge, P. A. Gale, V. Kral, *ACS Symp. Ser.* **2000**, *757*, 238–254; c) C. Bucher, R. S. Zimmerman, V. Lynch, J. L. Sessler, *J. Am. Chem. Soc.* **2001**, *123*, 9716–9717.

[7] a) H. Miyaji, W. Sato, J. L. Sessler, *Angew. Chem. Int. Ed.* **2000**, *39*, 1777–1779; b) P. Anzenbacher, Jr., K. Jursikova, J. A. Shriver, H. Miyaji, V. M. Lynch, J. L. Sessler, P. A. Gale, *J. Org. Chem.* **2000**, *65*, 7641–7645.

[8] P. A. Gale, L. J. Twyman, C. T. Handlin, J. L. Sessler, *Chem. Commun.* **1999**, 1851–1852.

[9] a) Attempts are currently underway to verify this value by more sensitive methods (for example, by UV/Vis spectroscopy, fluorescence quenching); b) P. Anzenbacher, Jr., K. Jursikova, J. L. Sessler, *J. Am. Chem. Soc.* **2000**, *122*, 9350–9351.

[10] a) P. A. Gale, J. L. Sessler, V. Lynch, P. I. Sansom, *Tetrahedron Lett.* **1996**, *37*, 7881–7884; b) P. A. Gale, J. W. Genge, V. Kral, M. A. McKervey, J. L. Sessler, A. Walker, *Tetrahedron Lett.* **1997**, *38*, 8443–8444.

[11] H. Miyaji, P. Anzenbacher, Jr., J. L. Sessler, E. R. Bleasdale, P. A. Gale, *Chem. Commun.* **1999**, 1723–1724.

[12] a) J. W. Ka, C. H. Lee, *Tetrahedron Lett.* **2000**, *41*, 4609–4613; b) C. H. Lee, J. Y. Park, K. T. Oh, J. W. Ka, *Bull. Korean Chem. Soc.* **1997**, *17*, 222–224; c) C. H. Lee, J. S. Lindsey, *Tetrahedron* **1994**, *50*, 11427–11440.

[13] X-ray data of a crystal with dimensions of $0.3 \times 0.3 \times 0.4$ mm were collected on a Nonius CAD4 mach 3 diffractometer equipped with graphite-monochromated $Mo_{K\alpha}$ radiation ($\lambda = 0.71373$ Å) at room temperature. The unit cell was determined to be monoclinic, $P2_{1/n}$ (No. 14), $a = 10.335(2)$, $b = 16.519(3)$, $c = 20.329(3)$ Å, $\beta = 95.297(14)$, $V = 3455.9(9)$ Å^3, $\rho_{calcd} = 1.243$ g cm^{-3} $Z = 4$, on the basis of 25 reflections. A total of 7467 reflections were measured, 6990 unique ($R_{int} = 0.0646$). The structure was refined on F^2 to $R_w = 0.3248$, $R = 0.1013$ (3162 reflections with $F_o > 4\sigma F_o$), and GOF = 1.125 for 433 refined parameters. The data were collected by using the ω-2θ scan technique in the range $2.14 < \theta < 26.29^\circ$. No absorption corrections were applied. The structure was solved by direct methods and refined by full-matrix least-squares calculation with SHELXL-97. Anisotropic thermal parameters were used for all non-hydrogen atoms.

[14] P. A. Gale, J. L. Sessler, V. Kral, V. M. Lynch, *J. Am. Chem. Soc.* **1996**, *118*, 5140–5141.

[15] W. Sato, H. Miyaji, J. L. Sessler, *Tetrahedron Lett.* **2000**, *41*, 6731–6736.

[16] The stoichiometries were determined from continuous variation (Job plot); see the Supporting Information.

[17] P. Anzenbacher, Jr., K. Jursikova, V. M. Lynch, P. A. Gale, J. L. Sessler, *J. Am. Chem. Soc.* **1999**, *121*, 11020–11021.

[18] a) S. Camiolo, P. A. Gale, *Chem. Commun.* **2000**, 1129–1130; b) P. A. Gale, J. L. Sessler, W. E. Allen, N. A. Tvermoes, V. M. Lynch, *Chem. Commun.* **1997**, 665–666.

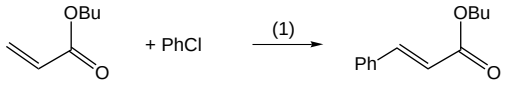
 © WILEY-VCH Verlag GmbH, 69451 Weinheim, Germany, 2002 1433-7851/02/4110-1759 $ 20.00+.50/0

Profound Steric Control of Reactivity in Aryl Halide Addition to Bisphosphane Palladium(0) Complexes**

Erwan Galardon, Shailesh Ramdeehul, John M. Brown,* Andrew Cowley, King Kuok (Mimi) Hii, and Anny Jutand

The application of bulky electron-rich phosphanes typified by P*t*Bu$_3$ has permitted significant new advances in palladium-catalyzed cross-couplings and aminations.[1] Recent work by Roy and Hartwig indicates that the enhanced reactivity may be associated with a change in mechanism of the oxidative-addition step compared to, for example, PPh$_3$ complexes; the intervention of monoligated [PdP*t*Bu$_3$] species is strongly implicated by studies of the reverse ArX elimination, observed indirectly.[2] Notably, the successful palladium-catalyzed coupling of alkyl boranes with alkyl halides without competing β-elimination requires the less bulky PCx$_3$ (Cx = cyclohexyl), and P*t*Bu$_3$ is ineffective.[3]

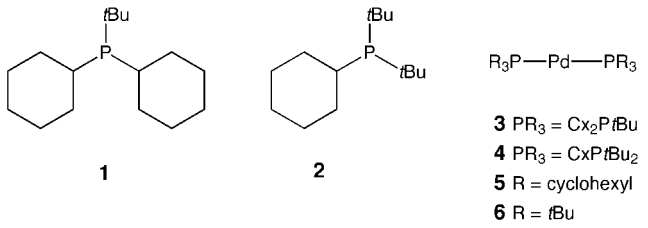
We report here that the mechanism of the ArX addition step to zerovalent [PdL$_2$] complexes is highly sensitive to the bulk of the ligand L, by study of the series of complexes [Pd(PCx$_n$*t*Bu$_{3-n}$)$_2$]; $n = 0-3$. The ligands PCx$_2$*t*Bu **1** and PCx*t*Bu$_2$ **2** were prepared from known compounds Cx$_2$PCl and CxPCl$_2$, by reaction with *t*BuLi at $-78\,^{\circ}$C,[4] and converted into the corresponding complexes [Pd(PCx$_2$*t*Bu)$_2$] (**3**) and [Pd(PCx*t*Bu$_2$)$_2$] (**4**), by reaction with [C$_5$H$_5$PdC$_3$H$_5$].[5] Complexes [Pd(PCx$_3$)$_2$] (**5**) and [Pd(P*t*Bu$_3$)$_2$] (**6**) have already been described; both are commercially available. Attempted Heck reaction between *n*-butyl acrylate and chlorobenzene as previously described,[6] indicated the clear distinction between complexes **3** or **5** which were ineffective, and **4** or **6** which were comparably effective (Scheme 1). This points to crucial differences between the ligands with one and two *tert*-butyl groups.



Ligand	PCx$_3$	**1**	**2**	P*t*Bu$_3$
Yield [%]	0	7	53	58

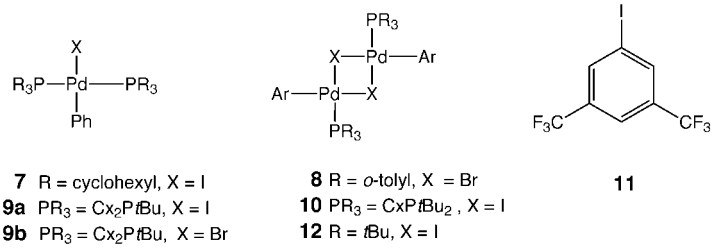
Scheme 1. 1) 1.5 mol% [Pd$_2$(dba)$_3$], 6% ligand, Cs$_2$CO$_3$ (1.1 equiv), 120 °C, 40 h; C$_{13}$H$_{28}$ as GC internal standard. dba = *trans*,*trans*-dibenzylideneacetone

The addition of PhI to complex **5** in THF occurs very rapidly; tenfold excess of added ligand did not cause any evident inhibition and the sole product is the *trans* bisphosphane complex **7**. The reaction with PhOTf (Tf = triflate), which is slower by a factor of about sixty, was studied in detail by electrochemical techniques at 25 °C. Under these conditions, the reaction follows an associative mechanism, as the rate is unaffected by the addition of excess PCx$_3$, within experimental error (Figure 1a). These observations contrast with the known mechanism of ArBr addition to [Pd(P(*o*-tolyl)$_3$)$_2$],[7] where dissociation of one phosphane ligand precedes addition of the electrophile and the product is the halide-bridged dimer **8**.[8]



1 **2**

3 PR$_3$ = Cx$_2$P*t*Bu
4 PR$_3$ = CxP*t*Bu$_2$
5 R = cyclohexyl
6 R = *t*Bu



7 R = cyclohexyl, X = I
9a PR$_3$ = Cx$_2$P*t*Bu, X = I
9b PR$_3$ = Cx$_2$P*t*Bu, X = Br

8 R = *o*-tolyl, X = Br
10 PR$_3$ = CxP*t*Bu$_2$, X = I
12 R = *t*Bu, X = I

11

The more slowly reacting complex **3** proved to be too air-sensitive for electrochemical studies under these conditions. By monitoring its reaction with PhI by ^{1}H NMR spectroscopy, we established that an associative mechanism was again followed, albeit around 10^3 times slower than in the case of complex **5**, and again without inhibition by excess ligand (Figure 1b). The ^{1}H NMR spectrum of the product **9a** showed the characteristic virtual coupling in the *t*Bu resonance signal, associated with *trans*-L$_2$M geometry (M = metal center).[9] When the initial reaction was carried out with PhBr, the product **9b** could be isolated and characterized by X-ray crystallography, which demonstrates the lack of steric distortion of the coordination sphere, although some van der Waals strain is apparent. The Ph group is sandwiched between opposing cyclohexyl rings (Figure 2).[10]

[*] Dr. J. M. Brown, Dr. E. Galardon, Dr. S. Ramdeehul
Dyson Perrins Laboratory
South Parks Road, Oxford, OX1 3QY (UK)
Fax: (+44) 1865-275642
E-mail: bjm@herald.ox.ac.uk.
Dr. A. Cowley
Chemical Crystallography Laboratory
Parks Road, Oxford, OX1 3QZ (UK)
Dr. K. K. (Mimi) Hii
Department of Chemistry, King's College
Strand, London, WC2R 2LS (UK)
Dr. A. Jutand
Ecole Normale Superieure, Departement de Chimie
CNRS UMR 8640, 24 Rue Lhomond 75231 Paris Cedex 5 (France)

[**] We thank the EPSRC for support (PDRA posts for E.G. and S.R., purchase of diffractometer) and Johnson-Matthey for the loan of Pd salts. Dr. R. T. Aplin was very helpful in the acquisition of electrospray MS.

Supporting information for this article is available on the WWW under http://www.angewandte.com or from the author.

 © WILEY-VCH Verlag GmbH, 69451 Weinheim, Germany, 2002 1433-7851/02/4110-1760 $ 20.00+.50/0

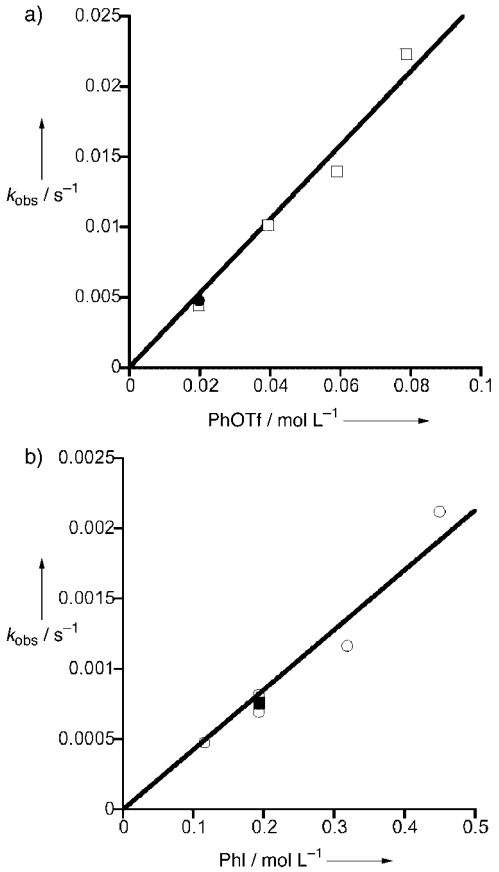


Figure 1. a) Reaction of PhOTf with complex **5**, monitored by amperometry in THF at 25 °C; k_{obs}/[PhOTf] = 0.26 $M^{-1} s^{-1}$; b) Reaction of PhI with complex **3** at 22 °C monitored by ^1H NMR spectroscopy in C_6D_6; k_{obs}/[PhI] = 0.0045 $M^{-1} s^{-1}$. Runs with □ or ○ were carried out with equimolar complex and electrophile, ● in (a) with 30-fold excess PCx_3; ■ in (b) with tenfold excess PCx_2tBu. In (a), the reaction with PhI is about sixty times faster and is unaffected by excess PCx_3.

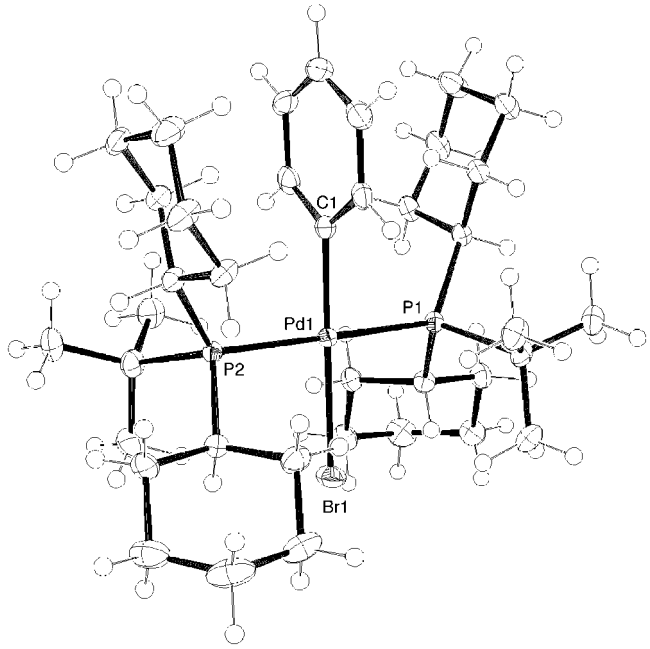
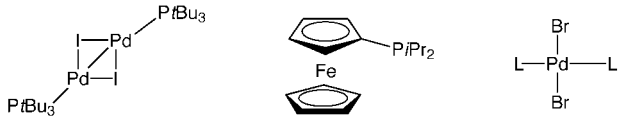


Figure 2. Molecular structure of **9b**. Selected bond lengths [Å] and angles [°]: Pd1-P1 2.3963(7), Pd1-P2 2.4020(7), Pd1-Br1 2.5596(3), Pd1-C1 1.997(3); Br1-Pd1-P1 89.624(18), P1-Pd1-P2 178.81(2), Br1-Pd1-C1 178.93(8), P1-Pd1-C1 90.66(7), P2-Pd1-C1 88.99(7).

Treatment of **4** with PhBr lead to the slow generation of a monophosphane palladium complex and an equivalent of free phosphane. With the more strongly electrophilic halide **11**, it was shown that doubling the concentration of excess phosphane inhibited the rate by a factor of two, in C_6D_6 at 22 °C. This places the reaction in the same mechanistic class as that of [Pd(P(*o*-tolyl)$_3$)$_2$], described above, with reversible phosphane dissociation preceding the addition of electrophile to a monoligated species [PdL]. The ^{31}P NMR spectrum of product **10**, from the addition of PhI, indicates complex temperature-dependent equilibria. In parallel experiments, very slow addition of PhI to the tBu_3P-derived complex **6** was detected and, after 4 days at RT, the solution contained one equivalent of free phosphane and one equivalent of dimer **12**, characterized by NMR spectroscopy. On redissolution, **12** was readily converted into biphenyl and the known Pd–Pd dimer **13**.[11] This behavior was not observed for the related complex **10** described above.



13 **14** **15** L = **14**

The presence of distinct reaction pathways of oxidative addition for the two closely related complexes **3** and **4** indicates an extreme sensitivity to steric environment, as does the gross difference in reactivity between **3** and **5**, which react by the same mechanism. This was elaborated by semiempirical calculations of the optimum energy and geometry for the sequence of [Pd(X)L_2Ph] complexes (X = Cl, Br, I), and their [PdL_2] precursors; the [Pd(I)L_2Ph] complexes are shown in Figure 3.[12] The evident increase in steric crowding demonstrates that *sec*-alkyl substituents on phosphorus ligands permit the formation of the square-planar *trans* bisphosphane-addition complexes more easily, with a substantial enthalpy penalty arising from each additional *tert*-alkyl group.

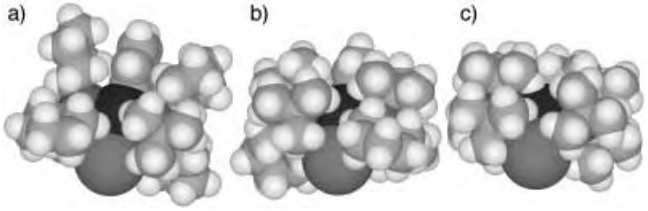
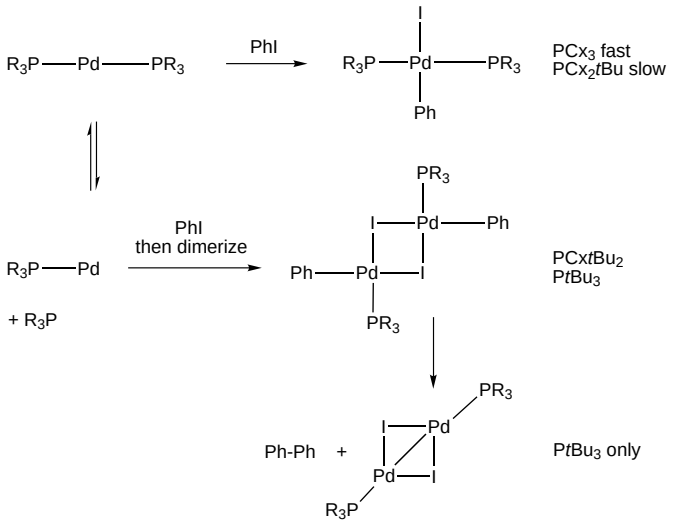


Figure 3. PM3-derived space-filling models of complexes a) [Pd(I)-(Cx_2tBuP)$_2$Ph] (**9a**); b) [Pd(I)($CxtBu_2P$)$_2$Ph]; c) [Pd(I)(tBu_3P)$_2$Ph], which demonstrates the progressive increase in crowding in the region of the Ph and I units.

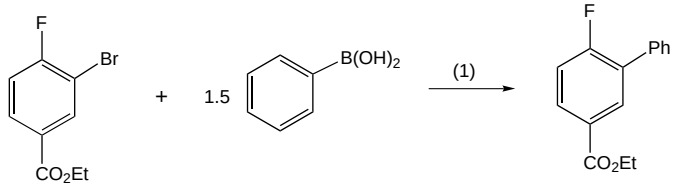
The results summarized in Scheme 2 support the general conclusion that the less bulky ligands **1** and PCx_3 initiate coupling reactions through the initial formation of *trans*-[Pd(X)L_2R], whilst the bulkier ligands **2** and $PtBu_3$ generate

 © WILEY-VCH Verlag GmbH, 69451 Weinheim, Germany, 2002 1433-7851/02/4110-1761 $ 20.00+.50/0



Scheme 2. Summary of the reactivities and reaction pathways for the oxidative additions of PhI to the Pd^0 complexes described.

[{Pd(X)LR}$_2$] species from a monoligated reactant. Easy access to the former structure can sometimes provide significant disadvantages for coupling chemistry. For example, the electron-rich but less bulky ligand **14** is effective in the reaction outlined in Scheme 3, but only for about 40 turnovers with about 15% of both biaryl and C–Br reduction product formed in side-reactions.[13] The loss of activity correlates well with the observed formation of the X-ray characterized complex **15**,[10] which quite rapidly becomes the sole Pd-containing species in the reaction when followed by NMR spectroscopy. It was separately confirmed that complex **15** is noncatalytic in this procedure.



Scheme 3. 1) 1 mol% $Pd(OAc)_2$, 2 mol% ligand **14**, Cs_2CO_3 (2 equiv), toluene, RT.

In conclusion, the effectiveness of P*t*Bu$_3$ and ligand **4** in Pd couplings of unsaturated electrophiles is associated with a propensity to form monophosphane complexes, either as, or en route to, the true catalytic species. Steric inhibition of the formation of [Pd(X)L$_2$Ar] and [Pd(X)$_2$L$_2$] *trans* diphosphane complexes must play an important role here. In alkyl–alkyl couplings,[3] the accessibility of stable *trans*-[L$_2$Pd(X)R] and *trans*-[L$_2$PdRR′] complexes is likely to be important in directing the reaction from β-elimination towards C–C bond formation after the initial RX addition step. Hence, it is to be expected that different palladium-catalyzed reactions will respond to different ligation states, but in a potentially predictable way.

Experimental Section

NMR studies: Kinetic experiments were performed at 22 °C with 0.013 M solutions of palladium complex in C_6D_6 for **3** and 0.015 M for **4**. After addition of the aryl iodide, spectra were then recorded at regular time intervals until the conversion reached about 50%. The data were acquired by following the disappearance of one of the cyclohexyl signals (δ = 2.44 ppm for **3**, δ = 2.70 ppm for **4**) and/or the *t*Bu signal (δ = 1.51 ppm for **3** and δ = 1.48 ppm for **4**).

Electrochemical studies: Kinetic experiments were performed at 25 °C with 0.0016 M solutions of [Pd(PCx$_3$)$_2$] in THF. The data were acquired by following the disappearance of the oxidation current of [Pd(PCy$_3$)$_2$] at a rotating gold disk electrode polarized at +0.3 V versus saturated calomel electrode (SCE). The electrochemical procedure has been described.[14]

Oxidative addition products:

9a: ^{1}H NMR (250 MHz, C_6D_6): δ = 1.25–2.09 (m, 44H, Cx), 1.69 (t, 18H, ^3J + ^5J = 12.4 Hz, *t*Bu), 6.93–7.05 (m, 3H, Ar), 7.69 ppm (m, 2H, Ar); ^{31}P NMR (101 MHz, C_6D_6): δ = 32.6 ppm (br).

10: ^{1}H NMR (250 MHz, C_6D_6): δ = 0.97–1.92 (m, 11H, Cx), 1.45 (d, 18H, 12.6 Hz, *t*Bu), 6.90 (t, 1H, 7.2 Hz, Ar), 7.07 (t, 2H, 7.8 Hz, Ar), 7.86 ppm (d, 2H, 7.8 Hz, Ar); ^{31}P NMR (101 MHz, C_6D_6): δ = 64.4 ppm (s).

12: ^{1}H NMR (250 MHz, C_6D_6): δ = 1.09 (d, 27H, 12.5 Hz, *t*Bu), 6.87 (m, 3H, Ph), 7.47 ppm (m, 2H, Ph); ^{31}P NMR (101 MHz, C_6D_6) δ = 57.9 ppm (s).

Synthetic procedures are recorded in the Supporting Information.[15]

Received: November 12, 2001 [Z18197]

[1] A. F. Littke, G. C. Fu, *J. Org. Chem.* **1999**, *64*, 10–12; A. F. Littke, C. Dai, G. C. Fu, *J. Am. Chem. Soc.* **2000**, *122*, 4020–4028; S. Lee, M. Jorgensen, J. F. Hartwig, *Org. Lett.* **2001**, *3*, 2729–2732; C. Dai, G. C. Fu, *J. Am. Chem. Soc.* **2001**, *123*, 2719–2724; S. Lee, M. Jorgensen, J. F. Hartwig, *Org. Lett.* **2001**, *3*, 2729–2732; for the original work on this ligand see: T. Yoshida, S. Otsuka, *Inorg. Synth.* **1990**, *28*, 113–119; T. Yoshida, S. Otsuka, *J. Am. Chem. Soc.* **1977**, *99*, 2134–2140; S. Otsuka, T. Yoshida, M. Matsumoto, K. Nakatsu, *J. Am. Chem. Soc.* **1976**, *98*, 5850–5858.

[2] A. H. Roy, J. F. Hartwig, *J. Am. Chem. Soc.* **2001**, *123*, 1232–1233.

[3] M. R. Netherton, C. Dai, K. Neuschütz, G. C. Fu, *J. Am. Chem. Soc.* **2001**, *123*, 10099–10100.

[4] For example, E. Niecke, M. Leuer, M. Nieger, *Chem. Ber.* **1989**, *122*, 453–461; for a recent preparation of compound **3** see: D. Jan, L. Delaude, F. Simal, A. Demonceau, A. F. Noels, *J. Organomet. Chem.* **2000**, *606*, 55–64.

[5] T. Yoshida, S. Otsuka, *Inorg. Synth.* **1985**, *28*, 113–119.

[6] F. Ozawa, N. Kawasaki, H. Okamoto, T. Yamamoto, A. Yamamoto, *Organometallics* **1987**, *6*, 1640–1651.

[7] F. Paul, J. Patt, J. F. Hartwig, *Organometallics* **1995**, *14*, 3030–3039; J. F. Hartwig, F. Paul, *J. Am. Chem. Soc.* **1995**, *117*, 5373–5374.

[8] For related X-ray structures see: A. L. Rheingold, W. C. Fultz, *Organometallics* **1984**, *3*, 1414–1417; V. V. Grushin, H. Alper, *Organometallics*, **1993**, *12*, 1890–1901.

[9] G. M. Whitesides, J. F. Gaasch, *J. Organomet. Chem.* **1971**, *33*, 241–246; J. P. Fackler, Jr., J. A. Fetchin, J. Mayhew, W. C. Seidel, T. J. Swift, M. Weeks, *J. Am. Chem. Soc.* **1969**, *91*, 1941–1947, and references therein.

[10] Crystal structure data for **9b**: $C_{38}H_{67}BrP_2Pd$, M_r = 772.20, monoclinic, space group $P2_1/c$, a = 12.4106(1), b = 10.0836(1), c = 30.0611(3) Å, α = 90, β = 91.1483(4), γ = 90°, cell volume = 3761.2 Å^3, Z = 4, R = 0.0297. The crystal structure of **15** is given in the Supporting Information and the full details of crystal structures are deposited with the Cambridge Crystallographic Data Centre. CCDC-173949 (**9b**) and CCDC-173948 (**15**) contain the supplementary crystallographic data for this paper. These data can be obtained free of charge via www.ccdc.cam.ac.uk/conts/retrieving.html (or from the Cambridge Crystallographic Data Centre, 12, Union Road, Cambridge CB2 1EZ, UK; fax: (+44) 1223-336-033; or deposit@ccdc.cam.ac.uk).

 © WILEY-VCH Verlag GmbH, 69451 Weinheim, Germany, 2002 1433-7851/02/4110-1762 $ 20.00+.50/0

[11] V. Dura-Vila, M. P. D. Mingos, R. Vilar, A. J. P. White, D. J. Williams, *J. Organomet. Chem.* **2000**, *600*, 198–205, and references therein.
[12] Calculations at the PM3 level (MacSpartan Pro) on the complete series of complexes [Pd(X){tBu$_n$$iPr_{3-n}$)P}$_2$Ph]; X = Cl, Br, I and the [PdL$_2$] parents, reveal that a progressive increase in strain occurs in both the linear complexes and their PhX addition products with increasing tBu substitution. For the reaction in Equation (1), ΔH_r is 0, 7.8, 15.6, and 39.8 Kcal mol^{-1} for PiPr$_3$ (standard), P(iPr)$_2$$tBu, Pi$Pr($t$Bu)$_2$, and P$tBu_3$. These trends were confirmed when ligands **1** and **2** were employed in the calculations.

$$[PdL_2] + PhI \rightarrow [Pd(I)L_2(Ph)] + \Delta H_r \quad (1)$$

[13] W. R. Cullen, S. J. Rettig, T. C. Zheng *Organometallics* **1992**, *11*, 3434–3439.
[14] A. Jutand, K. K. Hii, M. Thornton-Pett, J. M. Brown, *Organometallics* **1999**, *18*, 5367–5374.
[15] Experimental details are recorded in the Supporting Information.

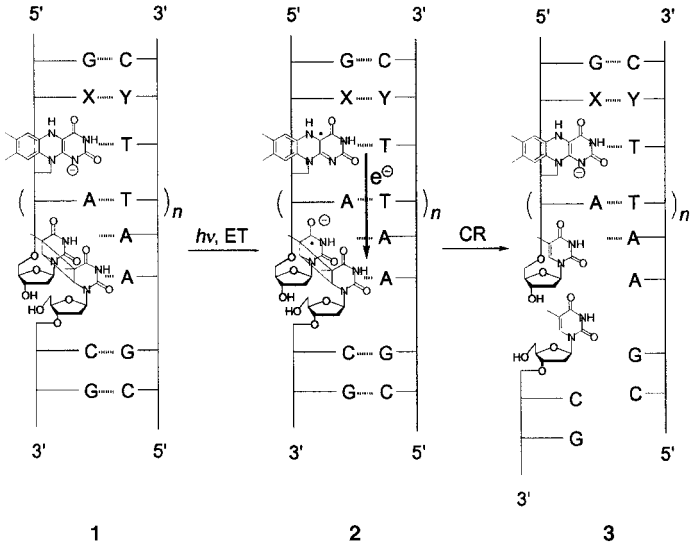
Weak Distance Dependence of Excess Electron Transfer in DNA**

Christoph Behrens, Lars T. Burgdorf, Anja Schwögler, and Thomas Carell*

Electron transfer phenomena in DNA are of fundamental importance for DNA damage[1] and DNA repair.[2] In this context, the movement of a positive charge (hole) through DNA has been studied intensively over the past few years.[3–6] After a controversial debate about the "hole conductivity" of double-stranded DNA,[7, 8] it is now accepted that a positive charge can move through DNA over significant distances.[9] Two mechanisms, namely coherent superexchange for small transfer distances[10, 11] and hole[4] or polaron hopping[6] for long-range transfer are evoked to describe this phenomenon. Experimentally, it is becoming clear that long-range hole transfer requires intermediate guanines and to a lesser extent also adenines to function as temporarily oxidizable "stepping stones".[12] Whether long-range hole transfer has biological consequences is unclear, but there are speculations that the process might define the genome sites damaged during oxidative stress.[13]

In contrast to hole transfer, little is known about the transport of excess electrons (negative charges) through a DNA duplex.[14, 15] Such an excess electron transfer, however, is important in biology because DNA photolyase enzymes[16–18] repair UV-induced cyclobutane pyrimidine dimer lesions in the DNA duplex by an electron transfer from a reduced and deprotonated FADH$^-$ cofactor to the dimer lesion.[19] The cytotoxic and mutagenic dimer lesions undergo rapid cycloreversion after one-electron reduction, which rescues cells from UV-induced cell death.[20] Recently γ-radiolysis together with electron paramagnetic resonance (EPR) studies provided initial evidence that excess electrons might also move through the DNA duplex by thermally activated hopping.[21–24] In the reductive regime, however, thymines and cytosines are predicted to function as "stepping stones" because they are the most easily reduced nucleobases.[25, 26]

We report here on the distance dependence of an excess electron transfer in a defined donor–DNA–acceptor system recently introduced by us as a photolyase mimic.[27, 28] In DNA double strands like **1** (Scheme 1), the electron flows from a photoexcited reduced flavin electron donor to a thymine dimer acceptor, separated by adenine:thymine bridges (A:T)$_n$ of various lengths. The electron injection is initiated by irradiation of the DNA double strand at 360 nm which causes excitation of the reduced and deprotonated flavin donor. The injected electron can either recombine with the resulting neutral flavin radical or it can move until it reduces the thymine dimer **1**→**2**. The negative charge captured by the dimer subsequently triggers a cycloreversion **2**→**3**. To allow rapid quantification of this dimer reversal step, we introduced a special dimer into the DNA strand, which lacks the connecting phosphodiester unit between the 3′- and 5′-



Scheme 1. Depiction of the DNA double strands containing the reduced flavin electron injector and the dimer electron acceptor. Photoexcitation ($h\nu$) initiates charge injection and transfer of the negative charge (ET) to the dimer unit (**1**→**2**). This causes cycloreversion (CR) of the dimer, which is accompanied by a strand break (**2**→**3**). Photolysis was performed in a fluorimeter (JASCO) equipped with a 150-W xenon lamp and a monochromator (10-nm band path) at 360 nm and at pH 9 (Tris buffer). Irradiations were carried out after reduction of the flavin in the DNA duplex by addition of sodium dithionite solution in the absence of oxygen at 10 °C.

[*] Prof. Dr. T. Carell, Dipl.-Chem. C. Behrens, Dipl.-Chem. L. T. Burgdorf, Dr. A. Schwögler
Fachbereich Chemie
Philipps-Universität Marburg
Hans-Meerwein-Straße, 35032 Marburg (Germany)
Fax: (+49) 6421-282-2189
E-mail: carell@mailer.uni-marburg.de

[**] We thank B. Giese, F. Hensel, and M. E. Michel-Beyerle for intensive discussions and two referees for providing valuable insights into the photochemistry of the reaction. This work was supported by the Volkswagenstiftung, the Fonds der Chemischen Industrie, and the Boehringer Ingelheim Fonds (predoctoral fellowship to L.T.B.).

 © WILEY-VCH Verlag GmbH, 69451 Weinheim, Germany, 2002 1433-7851/02/4110-1763 $ 20.00+.50/0

hydroxy groups.[29] Cycloreversion of this "backbone-opened" dimer induces a strand break, which is easily detectable by HPLC.[30]

The distance dependence of the reductive charge transfer was investigated with the DNA double-strand series **1a–e** (see Figure 2a). The double strands were dissolved in buffer (10^{-5} M), and the solutions were transferred to UV cuvettes sealed with rubber septa. The cuvettes were purged with nitrogen for 20 min to establish anaerobic conditions, then a sodium dithionite solution was added to reduce the flavin. These solutions were stirred and irradiated under exactly identical conditions in a fluorimeter with the same light intensity. During the irradiation small samples (10 μL) were removed with a microsyringe, immediatly reoxidized by shaking them exposed to air, and analyzed for the amount of cleaved product by reversed-phase HPLC.[31, 32]

The HPLC analysis of an irradition reaction performed with **1a** is depicted in Figure 1. Clearly evident is the clean photoinduced cleavage of **1a** ($t_{ret} = 13$ min) to give the flavin-containing shorter product strand ($t_{ret} = 11$ min). All DNA

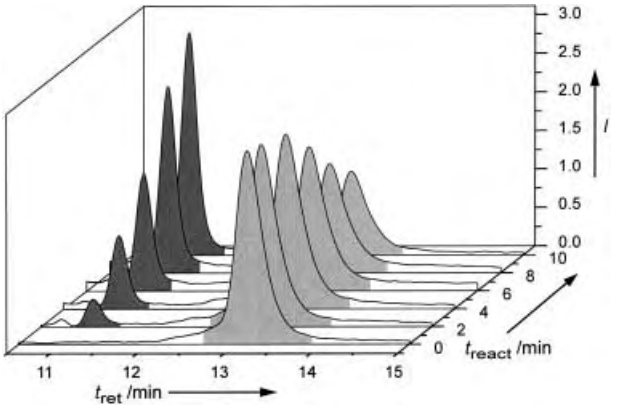


Figure 1. Time-dependent HPLC analysis of the electron transfer driven cycloreversion of **1a**. During the irradiation experiment small aliquots (10 μL) were removed from the assay solution. These samples were shaken rigorously in the presence of air in the dark to reoxidize the flavin. Analysis of these samples by ion-exchange chromatography with a Nucleogen DEAE column (125 mm × 4 mm, 60 Å/7 μm) and a KCl gradient (0 M KCl → 1.0 M KCl, 20 mM sodium acetate buffer pH 6) enabled detection at 360 nm of the flavin-containing starting DNA (retention time = 13 min) and the "flavin-tagged" product strand (retention time = 11 min). Integration of the peak areas was performed with standard software. t_{ret} = retention time, t_{react} = irradiation time.

duplexes investigated (**1a–e**) gave such clean cycloreversions and no degradation products were observed. Plots of the yield of cleaved DNA versus the irradiation time (Figure 2b) gave straight lines approximately up to 20% conversion. The data was analyzed in this regime by linear approximation. We finally determined the quantum yield of the cleavage reaction in **1a**. A value of $\Phi = 10^{-3}$ was determined, which is among the highest reported for photochemistry in DNA.[33]

Two further experiments were performed to prove the intramolecularity of the repair reaction. 1) Concentration-dependent studies show that the repair rate does not change even after the DNA concentration is decreased by a factor of five or ten. 2) When a noncomplementary dimer-containing single strand was added to a solution of double-stranded

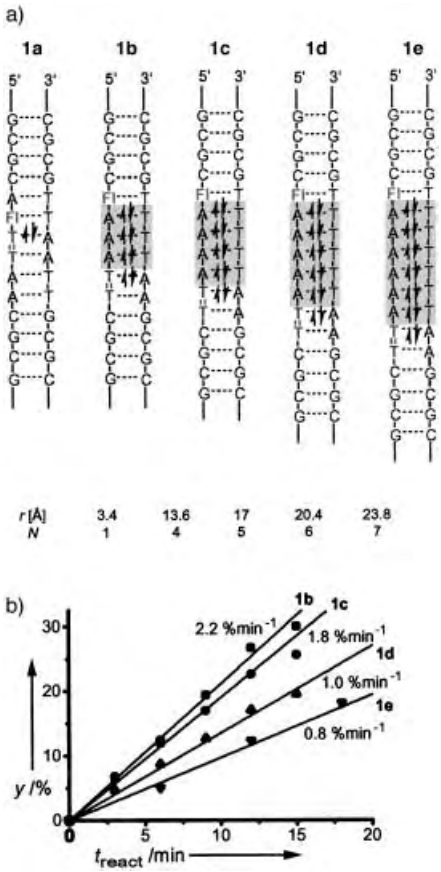


Figure 2. a) Depiction of the oligonucleotides **1a–e** containing a thymine dimer and a flavin at increasing distances. b) A plot of the observed yields versus the irradiation time. The data up to 20% conversion were fitted linearly. ■ = **1b**, ● = **1c**, ▲ = **1d**, ▼ = **1e**. For the determination of the quantum yield, the number of photons emitted onto the cuvette were determined with a two-channel optometer from United Detector Technology. The value $\varepsilon = 4900\ L\,mol^{-1}\,cm^{-1}$ was used as the extinction coefficient of the reduced flavin at 366 nm. y/% = amount of cleaved DNA in percent.

DNA, the double strand was repaired but not the added single strand.

In the double-strand series **1b–e** the flavin donor and the dimer acceptor are separated by a minimum of three A:T base pairs. This ensures that the duplex can adopt a B-conformation between the potentially duplex-disturbing chromophores. Because conformation and stacking might influence the efficiency of excess electron transfer[34] we investigated the structure of the DNA duplexes **1b–e** by circular dichroism (CD) spectroscopy and performed UV-melting studies. All DNA duplexes adopt a B-duplex conformation based on their CD spectra, which show a maximum at 280 nm and a minimum at 250 nm. Thermal denaturing of the duplexes provided in all cases two melting points.[35] One melting point at approximately 25 °C was observed at 260 nm and 460 nm and hence attributed to local melting of the duplex around the flavin. This melting point was confirmed by fluorescence melting studies that showed sigmoidal increase of the flavin fluorescence at the same temperature. This suggests flavin destacking. The second melting point was observed only at 260 nm and hence was attributed to full denaturing of the duplexes. All oligonucleotides **1b–e** show sharp melting

 © WILEY-VCH Verlag GmbH, 69451 Weinheim, Germany, 2002 1433-7851/02/4110-1764 $ 20.00+.50/0 *Angew. Chem. Int. Ed.* **2002**, *41*, No. 10

behaviors and no hysteresis. These initial data suggest that the flavin donor is intercalated into the duplex. For the thymine dimer, stacking inside the duplex caused only small structural perturbations, confirmed by NMR spectroscopy.[36–39] We assume that our DNA duplexes exist in a B-like conformation below the first melting point at about 20 °C. All electron transfer studies were in consequence performed at 10 °C. Analysis of the cleavage efficiency in **1b**–**e** shows that the observed yield decreases from 2.2 % after 1 min of irradiation of **1b** to 0.8 % after 1 min of irradiation of **1e** (Figure 2b). The cleavage yield hence decreases only by about 30 % with every additional A:T base pair between the donor and the acceptor.

If we assume that the negative charge is transferred directly from the donor (D) to the acceptor (A) by coherent superexchange, then the distance dependence of the charge transfer rate k_{CT} would be described by Equation (1).

$$k_{CT} = A\,e^{-\beta' \Delta r} \quad (1)$$

If we assume electron hopping, in which the thymines act as discrete charge carriers, the distance dependence of the charge transfer would be shallow and described in the simplest case by Equation (2), where N is the number of hopping steps and η a proportionality factor, which in the ideal case of a random walk has the value of $\eta = 2$.

$$\ln(k_{CT}) = -\eta \ln(N) \quad (2)$$

As a result of the constant irradiation conditions and under the assumption that the electron injection efficiency is the same in all DNA strands, the observed differences in yield reflect directly differences in the efficiency of the electron transfer from the flavin donor to the dimer acceptor.

A plot of our observed yields as ln(yield per minute) against the distance as Δr (Å) between the flavin donor and the dimer acceptor, assuming the duplex is in the B-conformation, is depicted in Figure 3a. We obtain a straight line and a rather small β' value of just 0.1 Å^{-1}. Such small β' values were determined for long-range hole transfer as well.[40] Our data show that excess electron transfer proceeds with similar efficiency. Plotting our yield data according to the hopping model ln(yield per minute) against ln(N) by assuming that every thymine between the flavin donor and the dimer acceptor can function as a discrete charge carrier, gives a straight line as well (Figure 3b) and a plausible η-value of close to 2.[21–23]

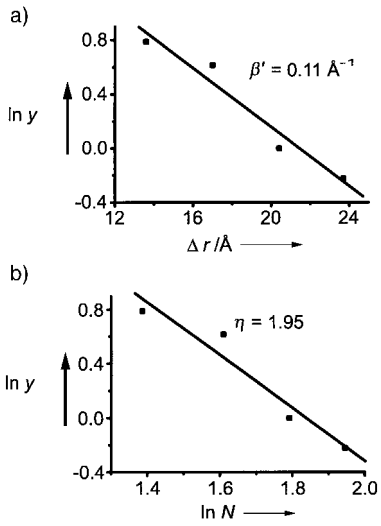


Figure 3. a) A plot of $\ln y = \ln$(yield per minute) against the distance Δr (in Å) between the flavin and the dimer in **1b**–**e**. b) A plot of $\ln y$ against $\ln(N)$, where N is the number of putative electron hopping steps defined by the number of thymines between the flavin and the thymine dimer.

Today, small β' values are generally taken as an indication that the charge transfer proceeds by hopping. In fact, hole-transfer studies with DNA duplexes, in which hopping is not possible, provided β' values between 0.7 Å[41] and 1.4 Å.[42, 43] Our small β' value of 0.1 furnishes therefore evidence that excess electron transfer in DNA might involve thermally activated hopping. This view is supported by thermodynamic considerations. The free energy for the electron transfer steps involved in such an excess electron hopping can be estimated from the singlet energy of the reduced flavin ($E_s = -2.8$ V, vs SCE)[44] and the reduction potentials of thymine ($E_{red} = -2.1$ V, vs SCE in CH_3CN)[44] and of the thymine dimer ($E_{red} = -2.2$ V, vs SCE in CH_3CN).[44] Electron transfer from the reduced flavin to thymine and to the dimer is exergonic. Electron transfer from the thymine radical anion to the thymine dimer should be approximately thermoneutral.

The fact that a single electron can move through a DNA duplex with a rather weak distance dependence—which allowed for the first time remote reductive repair of thymine dimers over a distance of about 24 Å—has important consequences in biology. For example, the harmful effect of UV irradiation responsible for the development of skin cancer in humans[45, 46] could be reduced by compounds that bind to DNA and trigger long-range electron transport.

Received: November 21, 2001 [Z18253]

[1] J. P. Pouget, T. Douki, M. J. Richard, J. Cadet, *Chem. Res. Toxicol.* **2000**, *13*, 541–549.
[2] E. C. Friedberg, G. C. Walker, W. Siede, *DNA Repair and Mutagenesis*, ASM Press, Washington, DC, USA, **1995**.
[3] R. E. Holmlin, P. J. Dandliker, J. K. Barton, *Angew. Chem.* **1997**, *109*, 2830–2848; *Angew. Chem. Int. Ed. Engl.* **1997**, *36*, 2715–2730.
[4] B. Giese, *Acc. Chem. Res.* **2000**, *33*, 631–636.
[5] F. D. Lewis, R. L. Letsinger, M. R. Wasielewski, *Acc. Chem. Res.* **2001**, *34*, 159–170.
[6] G. B. Schuster, *Acc. Chem. Res.* **2000**, *33*, 253–260.
[7] D. N. Beratan, S. Priyadarshy, S. M. Risser, *Chem. Biol.* **1997**, *4*, 3–8.
[8] U. Diederichsen, *Angew. Chem.* **1997**, *109*, 2411–2413; *Angew. Chem. Int. Ed. Engl.* **1997**, *36*, 2317–2319.
[9] B. Giese, *ChemPhysChem* **2000**, *1*, 195–198.
[10] S. O. Kelly, R. E. Holmlin, E. D. A. Stemp, J. K. Barton, *J. Am. Chem. Soc.* **1997**, *119*, 9861–9870.
[11] J. Jortner, M. Bixon, T. Langenbacher, M. E. Michel-Beyerle, *Proc. Natl. Acad. Sci. USA* **1998**, *95*, 12759–12765.
[12] B. Giese, J. Amaudrut, A.-K. Köhler, M. Spormann, S. Wessely, *Nature* **2001**, *4112*, 318–320.
[13] A. Heller, *Faraday Discuss.* **2000**, *116*, 1–13.
[14] F. D. Lewis, X. Liu, Y. Wu, S. E. Miller, M. R. Wasielewski, R. L. Letsinger, R. Sanishvili, A. Joachimiak, V. Tereshko, M. Egli, *J. Am. Chem. Soc.* **1999**, *121*, 9905–9906.
[15] B. Giese, S. Wessely, M. Sporman, U. Lindemann, E. Meggers, M. E. Michel-Beyerle, *Angew. Chem.* **1999**, *111*, 1050–1052; *Angew. Chem. Int. Ed.* **1999**, *38*, 996–998.
[16] A. Sancar, *Biochemistry* **1994**, *33*, 2–9.

 © WILEY-VCH Verlag GmbH, 69451 Weinheim, Germany, 2002 1433-7851/02/4110-1765 $ 20.00+.50/0

[17] T. Carell, *Angew. Chem.* **1995**, *107*, 2697 – 2700; *Angew. Chem. Int. Ed. Engl.* **1995**, *34*, 2491 – 2494.
[18] G. B. Sancar, M. S. Jorns, G. Payne, D. J. Fluke, C. S. Rupert, A. Sancar, *J. Biol. Chem.* **1987**, *262*, 492 – 498.
[19] T. Carell, L. T. Burgdorf, L. M. Kundu, M. K. Cichon, *Curr. Opin. Chem. Biol.* **2001**, 491 – 498.
[20] J.-S. Taylor, *Acc. Chem. Res.* **1994**, *27*, 76 – 82.
[21] M. G. Debije, M. T. Milano, W. A. Bernhard, *Angew. Chem.* **1999**, *111*, 2926 – 2930; *Angew. Chem. Int. Ed.* **1999**, *38*, 2752 – 2755.
[22] A. Pezeshk, M. C. R. Symons, J. D. McClymont, *J. Phys. Chem.* **1996**, *100*, 18562 – 18566.
[23] A. Messer, K. Carpenter, K. Forzley, J. Buchanan, S. Yang, Y. Razskazovskii, Z. Cai, M. D. Sevilla, *J. Phys. Chem. B* **2000**, *104*, 1128 – 1136.
[24] Z. Cai, Z. Gu, M. D. Sevilla, *J. Phys. Chem. B* **2000**, *104*, 10406 – 10411.
[25] C. A. M. Seidel, A. Schulz, M. H. M. Sauer, *J. Phys. Chem.* **1996**, *100*, 5541 – 5553.
[26] S. Steenken, J. P. Telo, H. M. Novais, L. P. Candeias, *J. Am. Chem. Soc.* **1992**, *114*, 4701 – 4709.
[27] A. Schwögler, L. T. Burgdorf, T. Carell, *Angew. Chem.* **2000**, *112*, 4082 – 4085; *Angew. Chem. Int. Ed.* **2000**, *39*, 3918 – 3920.
[28] A. Schwögler, T. Carell, *Org. Lett.* **2000**, *2*, 1415 – 1418.
[29] S. Nadji, C.-I. Wang, J.-S. Taylor, *J. Am. Chem. Soc.* **1992**, *114*, 9266 – 9269.
[30] D. A. Vivic, D. T. Odom, M. E. Nunez, D. A. Gianolio, L. W. McLaughlin, J. K. Barton, *J. Am. Chem. Soc.* **2000**, *122*, 8603 – 8611.
[31] R. Epple, E.-U. Wallenborn, T. Carell, *J. Am. Chem. Soc.* **1997**, *119*, 7440 – 7451.
[32] R. Epple, T. Carell, *J. Am. Chem. Soc.* **1999**, *121*, 7318 – 7329.
[33] D. Ly, Y. Kan, B. Armitage, G. B. Schuster, *J. Am. Chem. Soc.* **1996**, *118*, 8747 – 8748.
[34] P. K. Bhattacharya, J. K. Barton, *J. Am. Chem. Soc.* **2001**, *123*, 8649 – 8656.
[35] K. J. Breslauer, *Methods Enzymol.* **1987**, *259*.
[36] J. Kemmink, R. Boelens, T. Koning, G. A. van der Marel, G. A. van Boom, R. Kaptein, *Nucleic Acids Res.* **1987**, *15*, 4645 – 4653.
[37] K. McAteer, Y. Jing, J. Kao, J.-S. Taylor, M. A. Kennedy, *J. Mol. Biol.* **1998**, *282*, 1013 – 1032.
[38] J.-S. Taylor, D. S. Garrett, I. A. Brockie, D. L. Svoboda, J. Tesler, *Biochemistry* **1990**, *29*, 8858 – 8866.
[39] J.-K. Kim, D. Patel, B.-S. Choi, *Photochem. Photobiol.* **1995**, *62*, 44 – 50.
[40] D. B. Hall, R. E. Holmlin, J. K. Barton, *Nature* **1996**, *382*, 731 – 735.
[41] E. Meggers, M. E. Michel-Beyerle, B. Giese, *J. Am. Chem. Soc.* **1998**, *120*, 12950 – 12955.
[42] K. Fukui, K. Tanaka, *Angew. Chem.* **1998**, *110*, 167 – 170; *Angew. Chem. Int. Ed.* **1998**, *37*, 157 – 161.
[43] S. Hess, M. Götz, W. B. Davis, M. E. Michel-Beyerle, *J. Am. Chem. Soc.* **2001**, *123*.
[44] M. P. Scannel, D. J. Fenick, S.-R. Yeh, D. E. Falvey, *J. Am. Chem. Soc.* **1997**, *119*, 1971 – 1977.
[45] H. Slaper, G. J. M. Velders, J. S. Daniel, F. R. deGruijl, J. C. van den Leun, *Nature* **1996**, *384*, 256 – 258.
[46] J.-S. Taylor, *J. Chem. Educ.* **1990**, *67*, 835 – 841.

A Highly Specific Ca^{2+}-Ion Sensor: Signaling by Exciton Interaction in a Rigid – Flexible – Rigid Bichromophoric "H" Foldamer**

Ayyappanpillai Ajayaghosh,* Easwaran Arunkumar, and Jörg Daub

The design of chemosensors which are specific for the detection of biologically relevant cations, such as Na^+, K^+, Mg^{2+}, and Ca^{2+}, is a topic of considerable interest.[1] Selective detection of one of these cations in the presence of others, particularly the sensing of Ca^{2+} ions in the presence of Na^+, K^+, and Mg^{2+} ions, is a challenging task. Crown-ether based binding sites, which are integrated into the signaling units of organic chromophores, are the usual configuration of a chemosensor.[1b] A recognition event is signaled by perturbation in the absorption or emission properties of the chromophore, which are highly sensitive and easy to detect.[2] Even though a variety of crown-ether and related macrocycle-based chemosensors are known, the corresponding acyclic-polyether- (podand-) based sensors are relatively rare.[3] In most of the latter systems, the binding of a metal ion forces the attached donor and the acceptor moieties to come close enough to interact, thereby triggering either a charge-transfer, electron-transfer, or energy-transfer process, except in a recent report where conformational restrictions and charge transfer are invoked for a dual signaling of cation binding.[3h]

Herein we describe a different approach to the design of a highly specific Ca^{2+} ion sensor, which exploits the principle of a metal-ion induced conformational folding of a rigid – flexible – rigid bichromophore **3** (Scheme 1) to form an "H" foldamer,[4] thereby leading to dramatic perturbations in the optical properties as a result of exciton interactions. To our knowledge, this is the first report of a cation sensor based on the exciton interaction of a Ca^{2+} foldamer, in which the tethered chromophores are positioned akin to the "H" aggregate of an organic dye.

The rationale behind the design of the new sensor is based on the formation of "H" and "J" aggregates of cyanines and squaraines, which show distinctly different optical properties under appropriate conditions.[5, 6] According to the exciton theory of Kasha, the excited-state energy level of a monomeric dye splits into two upon aggregation, one level being lower and the other higher in energy than the monomer excited states.[7] Studies related to the aggregation of squar-

[*] Dr. A. Ajayaghosh, E. Arunkumar
Photochemistry Research Unit
Regional Research Laboratory, CSIR
Trivandrum-695019 (India)
Fax: (+91) 471-490-186
E-mail: aajayaghosh@rediffmail.com
Prof. Dr. J. Daub
Institut für Organische Chemie
Universität Regensburg, 93040 Regensburg (Germany)

[**] This work was supported through a Swarnajayanti Grant (DST/SF/C6/99-2000) from the Department of Science and Technology, Government of India and DST-DAAD-PP Program. This is contribution number RRLT-PRU-147.

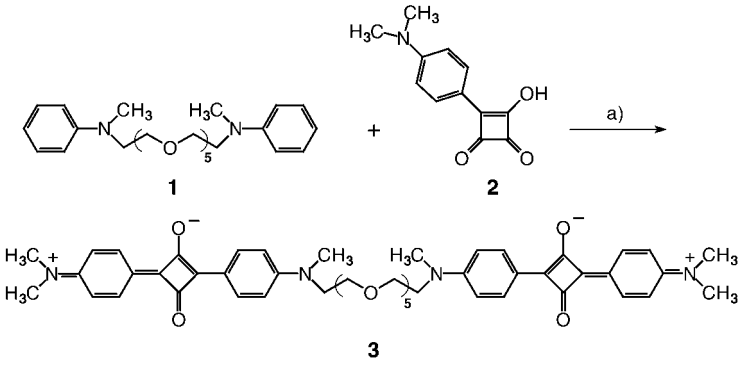
Supporting information for this article is available on the WWW under http://www.angewandte.com or from the author.

 © WILEY-VCH Verlag GmbH, 69451 Weinheim, Germany, 2002 1433-7851/02/4110-1766 $ 20.00+.50/0

aine dyes show that they prefer to form "H" aggregates in the appropriate solvents.[6] In this context, Liang et al. have reported the exciton interaction in tethered squaraine dyes.[8] However, this property has never before been exploited in the design of sensors for the selective detection of metal ions. Although squaraine-dye-based fluoroionophores have been reported, none of them show any selectivity towards Ca^{2+} ions in the presence of Na^+, K^+, or Mg^{2+} ions.[9, 10]

A rigid–flexible–rigid bichromophore **3**, which contains a squaraine dye as the rigid signaling unit and an oxyethylene chain as the flexible recognition moiety, was chosen as the sensor (see Scheme 1 for synthetic procedure). The bisaniline derivative **1** was prepared according to standard procedures starting from *N*-methylaniline. The 3-cyclobuten-1,2-dione **2** was obtained by heating *N*,*N*-dimethylaniline under reflux with squaryl chloride.[11] Reaction of **1** and **2** in 2-propanol, in the presence of tributylorthoformate, gave the bichromophore **3** in 24% yield, which was characterized by spectral analyses.

In acetonitrile, the bichromophore **3** showed an absorption maximum at 630 nm with a weak shoulder around 570 nm (Figure 1a), and an emission maximum at 652 nm (Figure 1b). Interestingly, addition of Na^+ and K^+ ions did not alter the absorption or emission properties of **3**. In contrast, addition of Ca^{2+} ions to the acetonitrile solution of **3** (1.7×10^{-5} M) showed a color change visible to the naked eye, from light blue ($\lambda_{max} = 630$ nm) to an intense purple-blue ($\lambda_{max} = 552$ nm). The intensity of the absorption maximum at 630 nm decreased with the concomitant growth of a hypsochromically shifted band at 552 nm, through an isosbestic point at 580 nm. Apart from these changes, the fluorescence emission of **3**, when excited at 580 nm ($\lambda_{max} = 652$ nm, 1.7×10^{-5} M in CH_3CN, $\Phi_f = 0.03$), underwent considerable quenching upon



Scheme 1. Synthesis of the foldamer **3**; a) 2-propanol, tributylorthoformate, 80 °C, 24%.

addition of Ca^{2+} ions ($\Phi_f = 0.008$; Figure 1b). The Benesi–Hildebrand plot (not shown) was in agreement with a 1:1 complexation between **3** and Ca^{2+} ions. A stability constant (K_s) of $1.9 \times 10^4\,M^{-1}$ was estimated from this plot, which is reasonably high for an acyclic polyether. Addition of other metal ions, such as Mg^{2+}, Sr^{2+}, and Ba^{2+} showed only marginal changes to the absorption and emission of **3** when compared to those with Ca^{2+} ions. In a separate experiment, a mixture of a threefold excess each of Na^+ and K^+ ions was added to a

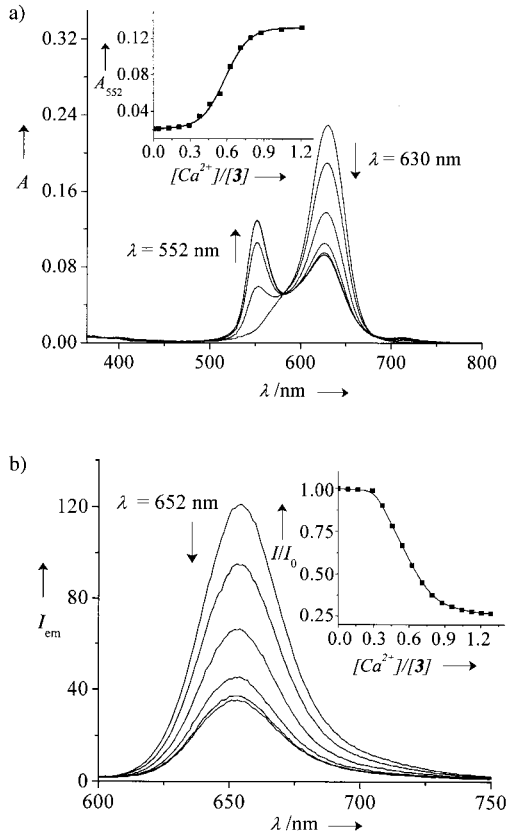


Figure 1. Changes in a) the absorption and b) emission ($\lambda_{ex} = 580$ nm) spectra of **3** upon addition of Ca^{2+} ions. Arrows indicate the changes that result from progressively increasing the concentration of Ca^{2+} ions relative to **3** in acetonitrile (**3**: Ca^{2+}; 1:0, 1:0.48, 1:0.65, 1:0.83, 1:1, 1:1.2). Insets: a) Variation of absorbance at 552 nm and b) fluorescence intensity of **3** with increasing Ca^{2+}-ion concentration.

solution of **3** in CH_3CN, which did not change its absorption or emission properties. Addition of Ca^{2+} ions to this solution caused the same kind of changes in the absorption and emission behavior as shown in Figure 1a and 1b, respectively. These observations show the unique ability of **3** to detect Ca^{2+} ions selectively, which is evident from Figure 2.

The observed changes in the absorption and emission behavior of **3** in the presence of Ca^{2+} ions can be

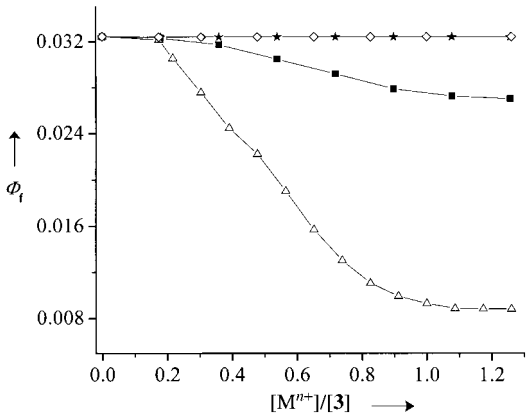


Figure 2. Plot of Φ_f versus the ratio metal ion:**3**, which illustrates the selectivity for Ca^{2+} ions over Na^+, K^+, and Mg^{2+} ions: Na^+ (*), K^+ (◇), Mg^{2+} (■), Ca^{2+} (△).

 © WILEY-VCH Verlag GmbH, 69451 Weinheim, Germany, 2002 1433-7851/02/4110-1767 $ 20.00+.50/0

rationalized on the basis of the metal-ion-induced folding of the chromophore to form a face-to-face stacked foldamer **4**, which is analogous to the "H" aggregates of squaraine dyes (Figure 3). The blue-shifted band of **4** matches the absorption spectra of the "H" aggregates of *N*,*N*-dialkylaniline derived squaraine dyes.[12] The fluorescence of **4** is weaker than that of the unfolded **3**, because the internal conversion from an upper excited state into a lower one occurs immediately, and the emission from a lower excited state is theoretically forbidden (inset, Figure 3). Changes in the ^{1}H NMR spectrum of **3** before and after the addition of Ca^{2+} ions support the proposed folded conformation **4** (see Supporting Information). On the other hand, addition of Na^+ or K^+ ions did not cause any considerable change in the ^{1}H NMR spectrum of **3**. Unlike in macrocyclic crown ethers, the ionic size of the cations does not play a crucial role when they bind to noncyclic polyethers. The binding in such cases will depend mainly upon the charge density and the coordination number of the cation, which may be the reasons for the specific binding of Ca^{2+} ions with **3**.[3d]

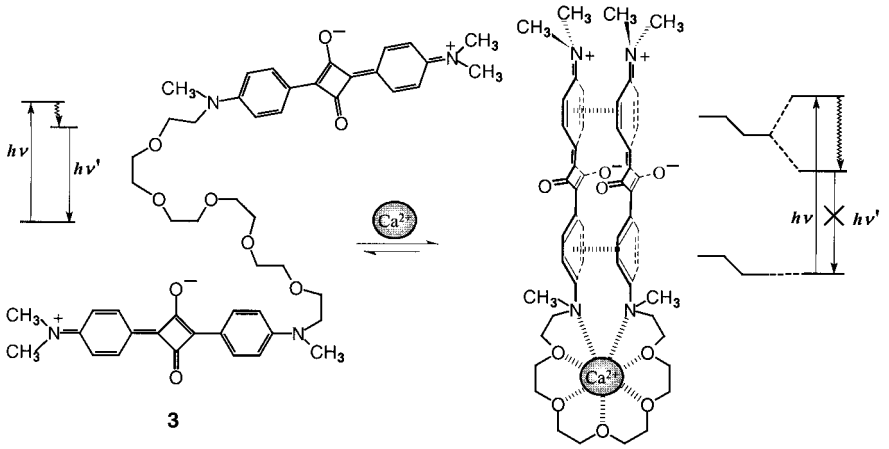
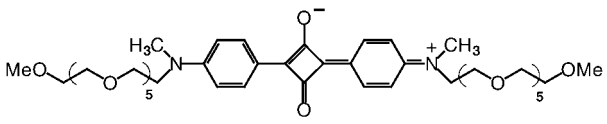


Figure 3. Ca^{2+}-ion-induced folding of **3** to the "H" foldamer **4**. Insets show the corresponding allowed and forbidden transitions in the two conformations.

To confirm the involvement of a folded conformation of the bichromophore **3** upon Ca^{2+}-ion binding, a monochromophore **5** of the flexible–rigid–flexible type was synthesized and mixed with various metal ions. None of the metal ions could produce any change to the absorption or emission properties of **5**.



5

In conclusion, a Ca^{2+}-ion selective rigid–flexible–rigid type bichromophoric sensor is described, which works on the principle of Ca^{2+}-ion-steered folding, and the consequent exciton coupled signal transduction.

Experimental Section

Fluorescence quantum yields were determined in spectroscopic grade CH_3CN, by use of optically matching solutions of bis[4-(dimethylamino)-phenyl]squaraine in chloroform ($\Phi_f = 0.70$) as a standard, at an excitation wavelength of 580 nm. Metal-ion titrations were carried out by adding small volumes (1–5 μL) of the metal solutions (10^{-5} M in CH_3CN, 4 mL) in a quartz cuvette. The stability constant K_s was determined from absorption spectral changes using Equation (1), where ε_L and ε_{ML} are the molar extinction coefficients of the ligand and the complex, respectively. The quantity $A_0/(A_0 - A)$ is plotted versus $[M^{-1}]$, and the stability constant is then given by the ratio intercept:slope. K_s was also determined from the emission-spectral changes using Equation (2), where ϕ_L and ϕ_{ML} are the fluorescence quantum yields of the ligand and the complex, respectively. The quantity $I_F^0/(I_F^0 - I_F)$ is plotted versus $[M^{-1}]$, and the stability constant is then given by the ratio intercept:slope.

$$\frac{A_0}{A_0 - A} = \frac{\varepsilon_L}{\varepsilon_L - \varepsilon_{ML}}\left(\frac{1}{K_s[M]} + 1\right) \quad (1)$$

$$\frac{I_F^0}{I_F^0 - I_F} = \frac{\varepsilon_L \phi_L}{\varepsilon_L \phi_L - \varepsilon_{ML} \phi_{ML}}\left(\frac{1}{K[M]} + 1\right) \quad (2)$$

Bichromophore **3**: *N*,*N*-(dimethylaminophenyl)-4-hydroxy-3-cyclobuten-1,2-dione (**2**; 117 mg, 0.54 mmol) and tributylorthoformate (1 mL) were added to a 100-mL round-bottomed flask containing isopropanol (50 mL) and **1** (100 mg, 0.22 mmol). The reaction mixture was then heated to reflux for 20 h. The hot reaction mixture was filtered and the solid was washed with isopropanol until the filtrate was almost colorless. Column chromatography (chloroform:-methanol 9:1) of the crude product on neutral alumina gave pure **3** (45 mg, 24%) as a green powder. M.p. 225–227 °C; FTIR (KBr): $\tilde{\nu} = 1593$, 1401, 1367, 1182, 1122, 937, 830, 784.5 cm^{-1}; ^{1}H NMR (300 MHz, $CDCl_3$, TMS): $\delta = 3.18$ (s, 18H, -NCH_3), 3.59–3.69 (m, 24H, -NCH_2 and -OCH_2), 6.74–6.79 (dd, 8H, $J = 1.2$, 9.2 Hz, aromatic), 8.33–8.38 ppm (dd, 8H, $J = 2.8$, 9.1 MHz, aromatic). MS (ESI, 4 kV): 859.7 [MH^+].

Received: January 23, 2002 [Z 18570]

[1] a) G. W. Gokel, *Crown Ethers and Cryptands*, CRC Press LLC, Boca Raton, **1991**, pp. 99–128; b) B. Valeur in *Topics in Fluorescence Spectroscopy, Vol. 4* (Ed.: J. R. Lakowicz), Plenum Press, New York, **1994**, pp. 21–48.

[2] a) L. Fabbrizzi, A. Poggi, *Chem. Soc. Rev.* **1995**, 197–202; b) A. P. de Silva, H. Q. N. Gunaratne, T. Gunnlaugsson, A. J. M. Huxley, C. P. McCoy, J. T. Rademacher, T. E. Rice, *Chem. Rev.* **1997**, *97*, 1515–1566; c) D. T. McQuade, A. E. Pullen, T. M. Swager, *Chem. Rev.* **2000**, *100*, 2537–2574; d) B. Valeur, I. Leray, *Coord. Chem. Rev.* **2000**, *205*, 3–40; e) A. P. de Silva, D. B. Fox, A. J. M. Huxley, T. S. Moody, *Coord. Chem. Rev.* **2000**, *205*, 41–57.

[3] a) J. P. Dix, F. Vögtle, *Chem. Ber.* **1980**, *113*, 457–470; b) H.-G. Löhr, F. Vögtle, *Chem. Ber.* **1985**, *118*, 914–921; c) Y. Kakizawa, T. Akita, H. Nakamura, *Chem. Lett.* **1993**, 1671–1674; d) Y. Suzuki, T. Morozumi, H. Nakamura, M. Shimomura, T. Hayashita, R. A. Bartsh, *J. Phys. Chem. B* **1998**, *102*, 7910–7917; e) T. Morozumi, T. Anada, H. Nakamura, *J. Phys. Chem. B* **2001**, *105*, 2923–2931; f) B. Valeur, J. Pouget, J. Bourson, M. Kaschke, N. P. Ernsting, *J. Phys. Chem.* **1992**, *96*, 6545–6549; g) F. Vögtle, E. Webber, *Angew. Chem.* **1979**, *91*, 813–837; *Angew. Chem. Int. Ed. Engl.* **1979**, *18*, 753–776; h) J. V. Mello, N. S. Finney, *Angew. Chem.* **2001**, *113*, 1584–1586; *Angew. Chem. Int. Ed.* **2001**, *40*, 1536–1538.

[4] Foldamers are molecules designed to utilize noncovalent interactions to stabilize a well-defined conformation in solution. a) S. H. Gellman,

 © WILEY-VCH Verlag GmbH, 69451 Weinheim, Germany, 2002 1433-7851/02/4110-1768 $ 20.00+.50/0

Acc. Chem. Res. **1998**, *31*, 173 – 180; b) In the present context, we use the term H foldamer to describe the folded conformation of a dimerlike bichromophore, the optical properties of which are analogous to the H aggregates of an organic dye.

[5] a) T. Katoh, Y. Inagaki, R. Okazaki, *J. Am. Chem. Soc.* **1998**, *120*, 3623 – 3628; b) L. Lu, R. J. Lachicotte, T. L. Penner, J. Perlstein, D. G. Whitten, *J. Am. Chem. Soc.* **1999**, *121*, 8146 – 8156; c) E. N. Ushakov, S. P. Gromov, O. A. Fedorova, Y. V. Pershina, M. V. Alfimov, F. Barigelletti, L. Flamigni, V. Balzani, *J. Phys. Chem. A* **1999**, *103*, 11188 – 11193; d) F. Würthner, S. Yao, *Angew. Chem.* **2000**, *112*, 2054 – 2057; *Angew. Chem. Int. Ed.* **2000**, *39*, 1978 – 1981; e) S. Zeena, K. G. Thomas, *J. Am. Chem. Soc.* **2001**, *123*, 7859 – 7865.

[6] a) K. Liang, K.-Y. Law, D. G. Whitten, *J. Phys. Chem.* **1994**, *98*, 13379 – 13384; b) H. Chen, M. S. Farahat, K.-Y. Law, D. G. Whitten, *J. Am. Chem. Soc.* **1996**, *118*, 2584 – 2594; c) E. Buncel, A. J. McKerrow, P. M. Kazmaier, *J. Chem. Soc. Chem. Commun.* **1992**, 1242 – 1243; d) S. Das, T. L. Thanulingam, K. G. Thomas, P. V. Kamat, M. V. George, *J. Phys. Chem.* **1993**, *97*, 13620 – 13624; e) S. Das, K. G. Thomas, K. J. Thomas, V. Madhavan, D. Liu, P. V. Kamat, M. V. George, *J. Phys. Chem.* **1996**, *100*, 17310 – 17315.

[7] The allowed and the forbidden transitions to the excitons are governed by the tilt angle (α) of the transition moments, with respect to the line of centers. When α is less than 54°, transition to the lowest excited level is allowed, which results in a bathochromically shifted absorption caused by head-to-tail J aggregates. If α is greater than 54°, transition to the highest excited level is favored, which leads to hypsochromically shifted absorption corresponding to the head-to-head H aggregates. M. Kasha, H. R. Rawls, M. A. El-Bayoumi, *Pure Appl. Chem.* **1965**, *11*, 371 – 392.

[8] K. Liang, M. S. Farahat, J. Perlstein, K.-Y. Law, D. G. Whitten, *J. Am. Chem. Soc.* **1997**, *119*, 830 – 831.

[9] a) S. Das, K. G. Thomas, K. J. Thomas, P. V. Kamat, M. V. George, *J. Phys. Chem.* **1994**, *98*, 9291 – 9296; b) K. G. Thomas, K. J. Thomas, S. Das, M. V. George, *Chem. Commun.* **1997**, 597 – 598; c) C. R. Chenthamarakshan, A. Ajayaghosh, *Tetrahedron Lett.* **1998**, *39*, 1795 – 1798; d) C. R. Chenthamarakshan, J. Eldo, A. Ajayaghosh, *Macromolecules*, **1999**, *32*, 5846 – 5851.

[10] a) U. Oguz, E. U. Akkaya, *Tetrahedron Lett.* **1997**, *38*, 4509 – 4512; b) U. Oguz, E. U. Akkaya, *Tetrahedron Lett.* **1998**, *39*, 5857 – 5860.

[11] D. Keil, H. Hartmann, *Dyes Pigm.* **2001**, *49*, 161 – 179.

[12] The aggregation of *N,N*-dialkylaniline-based squaraine dyes is well-documented. They form blue-shifted H aggregates around 520 – 570 nm (ref. [6]).

Unidirectional Photoinduced Shuttling in a Rotaxane with a Symmetric Stilbene Dumbbell**

Carol A. Stanier, Sara J. Alderman, Tim D. W. Claridge, and Harry L. Anderson*

Dedicated to Professor Fraser Stoddart on the occasion of his 60th birthday

A molecular machine is a molecular or supramolecular structure in which the components can be forced to move past each other, to achieve a functional outcome.[1–3] New insights into biological molecular motors[1] have stimulated a surge of activity towards the construction of artificial molecular machines.[2–11] Rotaxanes feature prominently among these prototypes, because they offer the possibility of long-range translational motion of a threaded macrocycle "shuttle" along the length of a dumbbell "rail track".[3–11] This shuttling motion can be driven chemically,[4] electrochemically,[5] or photochemically.[6–11] Use of light as the external stimulus or power source is particularly appealing because it can lead to a fast response without forming by-products. Light-driven translational motion has been achieved in rotaxanes using photoinduced electron transfer,[5, 6] excited-state changes in hydrogen-bonding,[7] and *E*/*Z* photoisomerization of azobenzene dumbbells.[8–11] Here we report the photochemical behavior of the azobenzene and stilbene rotaxanes shown in Scheme 1.[12] One of the stilbene rotaxanes (**3** ⊂ α-CD) exhibits unprecedented unidirectional shuttling, with the asymmetry of the cyclodextrin macrocycle determining its direction of motion on a symmetric dumbbell. Comparison of the *E*/*Z* photoisomerization of all four rotaxanes provides some general insights into the workings of a rudimentary molecular machine.

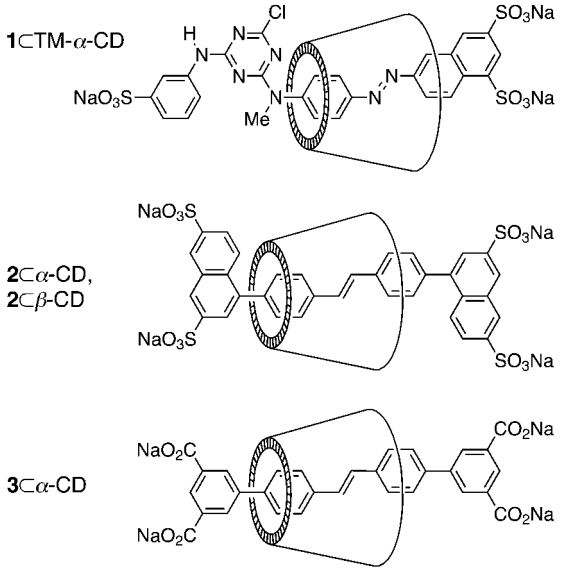
The *E*/*Z* photoisomerism of azobenzene rotaxane **1** ⊂ TM-α-CD, and its dumbbell analogue **1**, were investigated by monitoring the change in absorption during irradiation of the *E* isomers at 361 nm.[13] The dumbbell compound *E*-**1** underwent rapid photoisomerization to give a photostationary *E*/*Z* mixture characterized by the rise of a new absorption maximum at 255 nm, and a decrease in absorption at 361 nm; the photostationary equilibrium can be shifted back towards the *E* isomer by irradiation at 255 nm and displays excellent reversibility. In contrast, irradiation of rotaxane *E*-**1** ⊂ TM-α-CD under identical conditions results in no change in absorption. The cyclodextrin completely prevents $E \rightarrow Z$ photoisomerization. This may seem surprising, as

[*] Dr. H. L. Anderson, C. A. Stanier, S. J. Alderman, Dr. T. D. W. Claridge
University of Oxford
Department of Chemistry, Dyson Perrins Laboratory
South Parks Road, Oxford OX1 3QY (UK)
Fax: (+44) 1865-275674
E-mail: harry.anderson@chem.ox.ac.uk

[**] This work was supported by the Engineering and Physical Sciences Research Council, Avecia Ltd., and DyStar UK Ltd. We are grateful to Dr. M. R. Craig for providing samples of **1** ⊂ TM-α-CD and **1**.

Supporting information for this article is available on the WWW under http://www.angewandte.com or from the author.

 © WILEY-VCH Verlag GmbH, 69451 Weinheim, Germany, 2002 1433-7851/02/4110-1769 $ 20.00+.50/0



Scheme 1. Structures of rotaxanes studied. α-CD = α-cyclodextrin, β-CD = β-cyclodextrin, and TM-α-CD = hexakis(2,3,6-tri-*O*-methyl)-α-cyclodextrin. The cyclodextrins are drawn with a wide 2,3-rim and a narrow 6-rim; **1** ⊂ TM-α-CD is a single isomer. Compounds **1**, **2**, and **3** are the free dumbbells.[12]

azobenzene is known to photoisomerize in its α-CD inclusion complex,[14] and in Nakashima's rotaxane,[8] but these systems provide more freedom for translational motion and allow the azobenzene to move partly out of the cavity prior to photoisomerization, whereas in *E*-**1** ⊂ TM-α-CD it is difficult for the cyclodextrin to move away from the azo unit.

Next we turned our attention to the stilbene-based rotaxanes. The photochemistry of stilbenes is well studied,[15] but, as far as we know, there is no work on the photochemistry of stilbene rotaxanes.[16] Compounds **2** ⊂ β-CD, **3** ⊂ α-CD, **2**, and **3** all undergo reversible *E*/*Z* photoisomerization.[13] Irradiation at 340 nm generates the *Z* isomer, which leads to a decrease in absorption at around 340 nm and an increase in the absorption at 265 nm; irradiation at 265 nm shifts the system back towards the *E* isomer, as illustrated in Figure 1. No photoisomerization was detected with *E*-**2** ⊂ α-CD, which reflects the fact that it is the most tightly constrained of these three rotaxanes: the smaller endgroups in **3** ⊂ α-CD allow the cyclodextrin to shift away from the center of the stilbene unit, and the larger cyclodextrin in **2** ⊂ β-CD also gives the stilbene unit more space to move.[17] Prolonged irradiation leads eventually to irreversible degradation. NMR and mass spectrometric analysis of the products from prolonged irradiation of **3** showed the presence of the expected cyclobutane, as well as the hydrated stilbene unit.[18] Under the same conditions the rotaxane **3** ⊂ α-CD does not form any cyclobutane, and photohydration is about five times slower than with the dumbbell **3**, but gives a mixture of diastereomers.[19] Thus encapsulation enhances the fatigue-resistance of the chromophore.

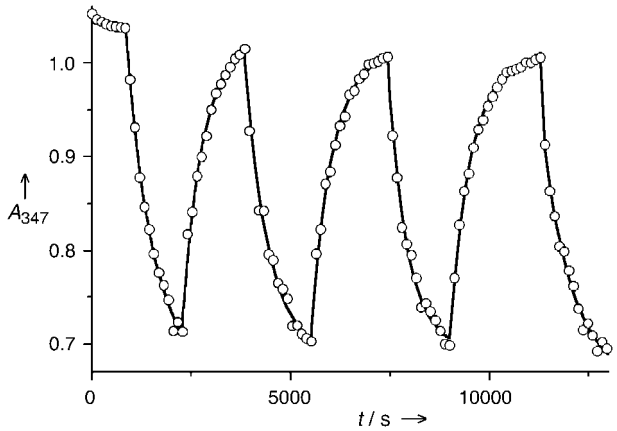
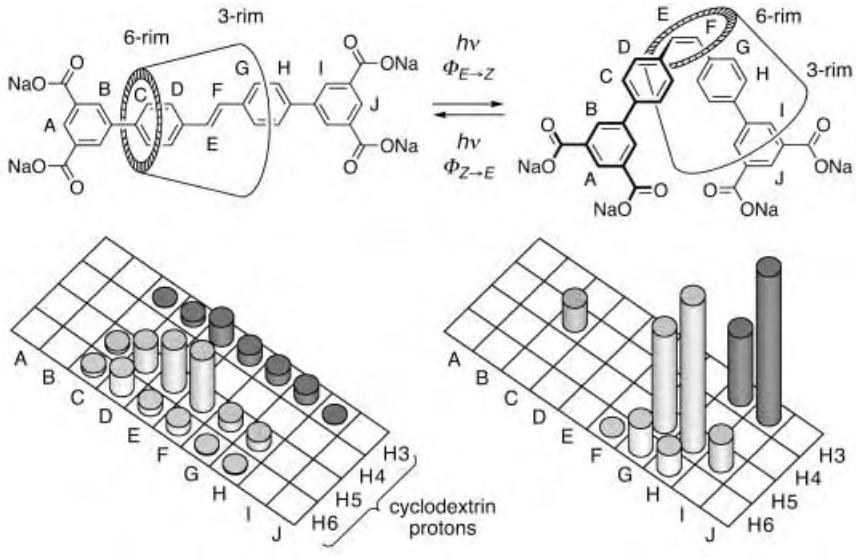


Figure 1. Plot of absorption at 347 nm versus time during alternating irradiation of an aqueous solution of **3** ⊂ α-CD at λ = 265 nm and λ = 347 nm.

The shuttling motion accompanying *E*/*Z* isomerization of **3** ⊂ α-CD is revealed by the pattern of NOEs for each isomer (Scheme 2).[20] Each rotaxane gives ten ^{1}H NMR resonance signals (arising from $H_A - H_J$) in the aromatic region, because of the asymmetry of the cyclodextrin.[12b] In the *E* isomer, many NOEs are observed from protons $H_C - H_I$ on the dumbbell to the internal protons H3, H5, and H6 of the cyclodextrin. This set of NOEs is not consistent with any single static geometry, and shows that the cyclodextrin rapidly glides up and down the dumbbell. A completely different pattern of NOEs is observed in the *Z* isomer; here the NOEs are much stronger and more selective. Only one end of the dumbbell ($H_G - H_I$) makes contact with the internal surface of



Scheme 2. Photoisomerization of *E*-**3** ⊂ α-CD to *Z*-**3** ⊂ α-CD, and key NOEs observed in these two isomers between $H_A - H_J$ of the dumbbell and H3 – H6 of the cyclodextrin; H3 and H5 are internal protons near the wide and narrow rim, respectively, H4 is on the external surface and H6 is on the narrow rim. The height of each column indicates the strength of the NOE (determined from the integrated NOE intensities, see Supporting Information).

 © WILEY-VCH Verlag GmbH, 69451 Weinheim, Germany, 2002 1433-7851/02/4110-1770 $ 20.00+.50/0 *Angew. Chem. Int. Ed.* **2002**, *41*, No. 10

the cyclodextrin. An NOE is also observed between H_C, on the other end of the dumbbell, and H4, on the external surface of the cyclodextrin. All these NOEs are consistent with the geometry of the *Z* isomer shown in Scheme 2, with the *cis* alkene unit near the 6-rim of the cyclodextrin. Strong support for this geometry comes from the observation of NOEs from H_F to H6 (but not to H3), and from H_I to H3 (but not to H6). The alternative co-conformer, with the 6-rim of the cyclodextrin near an endgroup, is not detected. Although we do not yet know the origin of this remarkable directionality, we believe it could be useful in the construction of molecular machines; for example, it might enable cyclodextrins to be propelled in one direction along a polymer thread.

The kinetics of photoisomerization of **3** $\subset$ α-CD and **3** were investigated to determine the quantum yields for $E \rightarrow Z$ and $Z \rightarrow E$ photoisomerization, $\Phi_{E\rightarrow Z}$ and $\Phi_{Z\rightarrow E}$ (Table 1).[21, 22]

Table 1. Photoisomerization and fluorescence quantum yields.[a]

Compound	$\Phi_{E\rightarrow Z}$	$\Phi_{Z\rightarrow E}$	$\Phi_{E,f}$
3 $\subset$ α-CD	0.06	0.71	0.94
3	0.17	0.79	0.67

[a] In N_2-saturated aqueous solutions (concentration $< 10\ \mu M$). $\Phi_{E,f}$ is the fluorescence quantum yield of the *E* isomer ($\pm 10\%$).[12b] The estimated uncertainty in these photoisomerization quantum yields is $\pm 20\%$.[21]

The presence of the cyclodextrin reduces $\Phi_{E\rightarrow Z}$ in the rotaxane to about a third of the value in the free dumbbell, while having no significant effect on $\Phi_{Z\rightarrow E}$. This result indicates that in the *E* isomer, the mobile cyclodextrin spends a third of its time sufficiently far from the center of the stilbene unit to permit *E*/*Z* photoisomerization. It appears that when the cyclodextrin sits directly over the alkene, it blocks photoisomerization by increasing the barrier for conversion of the initially formed S_1 state into the twisted p state.[23] Thus the decrease in $\Phi_{E\rightarrow Z}$ is accompanied by an increase in the fluorescence quantum yield $\Phi_{E,f}$ (Table 1). An even larger increase in $\Phi_{E,f}$ occurs in *E*-**2** $\subset$ α-CD, where $\Phi_{E\rightarrow Z}$ becomes negligible.[12b]

Two mechanisms for photoinduced shuttling in a photoisomerizable rotaxane are shown in Figure 2. In this model, the macrocycle prefers to sit on the photoactive unit in the *E* isomer (A is lower in energy than C), but it prefers to sit near one end in the *Z* isomer (D is lower in energy than B). In route 1 (A $\rightarrow$ B $\rightarrow$ D) photoisomerization occurs while the cyclodextrin is sitting round the photoactive unit, which forces it to relocate, like the piston of an engine. In route 2 (A $\rightarrow$ C $\rightarrow$ D), the photoactive unit waits until thermal motion has relocated the macrocycle, then photoisomerizes to block its return. Both mechanisms might sometimes apply, but our results indicate that photoisomerizable rotaxanes, such as **3** $\subset$ α-CD and Nakashima's rotaxane,[8] operate by route 2 rather than route 1. This mechanism illustrates how molecular machines can differ from their macroscopic analogues by utilizing random thermal motion.[1b]

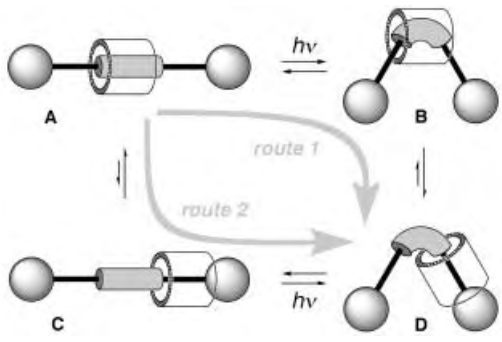


Figure 2. Two mechanisms for rotaxane photoisomerization. See text for details.

Received: January 17, 2002 [Z18537]

[1] a) R. D. Vale, R. A. Milligan, *Science* **2000**, *288*, 88–95; b) C. Bustamante, D. Keller, G. Oster, *Acc. Chem. Res.* **2001**, *34*, 412–420.

[2] V. Balzani, A. Credi, F. M. Raymo, J. F. Stoddart, *Angew. Chem.* **2000**, *112*, 3484–3530; *Angew. Chem. Int. Ed.* **2000**, *39*, 3348–3391; A. R. Pease, J. O. Jeppesen, J. F. Stoddart, Y. Luo, C. P. Collier, J. R. Heath, *Acc. Chem. Res.* **2001**, *34*, 433–444; R. Ballardini, V. Balzani, A. Credi, M. T. Gandolfi, M. Venturi, *Acc. Chem. Res.* **2001**, *34*, 444–455; J.-P. Collin, C. Dietrich-Buchecker, P. Gaviña, M. C. Jimenez-Molero, J.-P. Sauvage, *Acc. Chem. Res.* **2001**, *34*, 477–487; B. L. Feringa, *Acc. Chem. Res.* **2001**, *34*, 504–513; T. R. Kelly, *Acc. Chem. Res.* **2001**, *34*, 514–522.

[3] C. A. Schalley, K. Beizai, F. Vögtle, *Acc. Chem. Res.* **2001**, *34*, 465–476.

[4] P. R. Ashton, R. Ballardini, V. Balzani, I. Baxter, A. Credi, M. C. T. Fyfe, M. T. Gandolfi, M. Gómez-López, M.-V. Martínez-Díaz, A. Piersanti, N. Spencer, J. F. Stoddart, M. Venturi, A. J. P. White, D. J. Williams, *J. Am. Chem. Soc.* **1998**, *120*, 11932–11942.

[5] N. Armaroli, V. Balzani, J.-P. Collin, P. Gaviña, J.-P. Sauvage, B. Ventura, *J. Am. Chem. Soc.* **1999**, *121*, 4397–4408; R. Ballardini, V. Balzani, W. Dehaen, A. E. Dell'Erba, F. M. Raymo, J. F. Stoddart, M. Venturi, *Eur. J. Org. Chem.* **2000**, 591–602; C. P. Collier, J. O. Jeppesen, Y. Luo, J. Perkins, E. W. Wong, J. R. Heath, J. F. Stoddart, *J. Am. Chem. Soc.* **2001**, *123*, 12632–12641.

[6] P. R. Ashton, R. Ballardini, V. Balzani, A. Credi, K. R. Dress, E. Ishow, C. J. Kleverlaan, O. Kocian, J. A. Preece, N. Spencer, J. F. Stoddart, M. Venturi, S. Wenger, *Chem. Eur. J.* **2000**, *6*, 3558–3574; A. M. Brouwer, C. Frochot, F. G. Gatti, D. A. Leigh, L. Mottier, F. Paolucci, S. Roffia, G. W. H. Wurpel, *Science* **2001**, *291*, 2124–2128.

[7] G. W. H. Wurpel, A. M. Brouwer, I. H. M. van Stokkum, A. Farran, D. A. Leigh, *J. Am. Chem. Soc.* **2001**, *123*, 11327–11328.

[8] H. Murakami, A. Kawabuchi, K. Kotoo, M. Kunitake, N. Nakashima, *J. Am. Chem. Soc.* **1997**, *119*, 7605–7606.

[9] M. Asakawa, P. R. Ashton, V. Balzani, C. L. Brown, A. Credi, O. A. Matthews, S. P. Newton, F. M. Raymo, A. N. Shipway, N. Spencer, A. Quick, J. F. Stoddart, A. J. P. White, D. J. Williams, *Chem. Eur. J.* **1999**, *5*, 860–875.

[10] C. Kauffmann, W. M. Müller, F. Vögtle, S. Weinman, S. Abramson, B. Fuchs, *Synthesis* **1999**, 849–853.

[11] I. Willner, V. Pardo-Yissar, E. Katz, K. T. Ranjit, *J. Electroanal. Chem.* **2001**, *497*, 172–177.

[12] a) M. R. Craig, M. G. Hutchings, T. D. W. Claridge, H. L. Anderson, *Angew. Chem.* **2001**, *113*, 1105–1108; *Angew. Chem. Int. Ed.* **2001**, *40*, 1071–1074; b) C. A. Stanier, M. J. O'Connell, W. Clegg, H. L. Anderson, *Chem. Commun.* **2001**, 493–494 and C. A. Stanier, M. J. O'Connell, W. Clegg, H. L. Anderson, *Chem. Commun.* **2001**, 787.

[13] Irradiations were performed in N_2-saturated aqueous solution; see the Supporting Information.

[14] P. Bortolus, S. Monti, *J. Phys. Chem.* **1987**, *91*, 5046–5050; T. Fujimoto, A. Nakamura, Y. Inoue, Y. Sakata, T. Kaneda, *Tetrahedron Lett.* **2001**, *42*, 7987–7989.

[15] H. Meier, *Angew. Chem.* **2001**, *113*, 1903–1905; *Angew. Chem. Int. Ed.* **2001**, *40*, 1851–1853; H. Meier, *Angew. Chem.* **1992**, *104*, 1425–1446; *Angew. Chem. Int. Ed. Engl.* **1992**, *31*, 1399–1420; H. Görner, H. J. Kuhn, *Adv. Photochem.* **1995**, *19*, 1–117.

 © WILEY-VCH Verlag GmbH, 69451 Weinheim, Germany, 2002 1433-7851/02/4110-1771 $ 20.00+.50/0

[16] M. Kunitake, K. Kotoo, O. Manabe, T. Muramatsu, N. Nakashima, *Chem. Lett.* **1993**, 1033 – 1036; C. J. Easton, S. F. Lincoln, A. G. Meyer, H. Onagi, *J. Chem. Soc. Perkin Trans. 1* **1999**, 2501 – 2506; C. Heim, A. Affeld, M. Nieger, F. Vögtle, *Helv. Chim. Acta* **1999**, *82*, 746 – 759; A. H. Parham, B. Windisch, F. Vögtle, *Eur. J. Org. Chem.* **1999**, 1233 – 1238.

[17] Nonrotaxane α-CD and β-CD – stilbene complexes photoisomerize in aqueous solution (W. Herrmann, S. Wehrle, G. Wenz, *Chem. Commun.* **1997**, 1709 – 1710) but not in the solid β-CD complex; M. S. Syamala, S. Devanathan, V. Ramamurthy, *J. Photochem.* **1986**, *34*, 219 – 229.

[18] J. W. Happ, M. T. McCall, D. G. Whitten, *J. Am. Chem. Soc.* **1971**, *93*, 5496 – 5501.

[19] We have not detected phenanthrene formation from **3** or **3** $\subset \alpha$-CD, even after irradiation in the presence of iodine.

[20] We have been unable to separate the *E* and *Z* isomers of **3** $\subset \alpha$-CD. NOE measurements were carried out on a photogenerated mixture of both isomers, of known composition, which facilitates comparison of the strengths of NOEs in the two isomers; see Supporting Information.

[21] The ratios $\Phi_{E\rightarrow Z}/\Phi_{Z\rightarrow E}$ for **3** and **3** $\subset \alpha$-CD were evaluated from the *E*/*Z* ratios of their photostationary states. Values of $\Phi_{E\rightarrow Z}$ were obtained by comparing the initial rates of photoisomerization with that of *E*-stilbene in cyclohexane ($\Phi_{E\rightarrow Z} = 0.50$; S. Malkin, E. Fischer, *J. Phys. Chem.* **1964**, *68*, 1153 – 1163) during irradiation under identical conditions; see Supporting Information.

[22] The $\Phi_{E\rightarrow Z}$ in compounds **3** and **3** $\subset \alpha$-CD is lower than that in simple stilbene because of the 4,4′-diaryl substitution; see: G. Gauglitz, R. Goes, W. Stooss, R. Raue, *Z. Naturforsch. A* **1985**, *40*, 317 – 323.

[23] A similar reduction in $\Phi_{E\rightarrow Z}$ was reported in a cationic azobenzene rotaxane, compared to the free dumbbell, but in that case it was attributed to radiationless decay by charge-transfer states, rather than to steric hindrance.[9]

Samarium Diiodide-Induced Reductive Cross-Coupling of Nitrones with Aldehydes and Ketones**

Géraldine Masson, Sandrine Py,* and Yannick Vallée*

The use of nitrones as free-radical traps (spin traps) is well known. Nitrones have been designed to react with oxygen radicals to lengthen their half-lives and allow their detection in EPR studies.[1] They have also been used as in vivo protective agents against radicals generated by oxidative stress.[2] Surprisingly, nitrones have seldom been involved in radical reactions aimed to create C–C bonds,[3, 4] even though the addition of radicals to other C=N bonds is known.[5] We decided to explore the possibility of reductive cross-coupling between nitrones and carbonyl compounds, promoted by samarium diiodide, to produce vicinal amino alcohols. Vicinal amino alcohol fragments are common in natural products, and a preparation of these compounds by C–C bond formation (similar to the pinacol coupling reaction) is highly desirable.

The intramolecular reductive coupling of aldehydes or ketones with oximes,[6] hydrazones,[7] and imines[8] is well documented. These couplings have been accomplished with different degrees of stereoselectivity and generally yield the *trans* α-amino alcohol derivatives as the major products. The mechanism of this reaction is generally assumed to involve the initial formation of a ketyl radical by a single electron tranfer (SET) from the reducing agent, followed by its addition to the C=N double bond.

The intermolecular cross-coupling of C=O and C=N groups, on the other hand, has been far less successful in the past because of competitive homocoupling or formation of reduction products. Pedersen and Roskamp[9] used $NbCl_3 \cdot$ DME as a two-electron reducing agent to synthesize efficiently a variety of amino alcohols from the corresponding aldimines and ketones or aldehydes. The method was less efficient with aliphatic imines, and it failed with sterically hindered substrates. Electroreductive methods have also been employed to couple carbonyl compounds with aromatic aldimines, aliphatic aldoximes and ketoximes, and nitrones.[10] Samarium(II) diiodide (SmI_2) is another reducing agent which has been used with varying degrees of success in reductive cross-couplings involving carbonyl compounds and imine derivatives. It was initially reported to give poor selectivity in reductive couplings involving imines,[11, 12] the main side reaction being reduction to the corresponding amines. SmI_2 was employed for the aminomethylation of aliphatic aldehydes and ketones with *O*-benzylformaldoxime in the presence of hexamethylphosphoramide (HMPA) and an alcohol (2 equiv), but this reaction could not be extended to other oximes.[13] The cross-coupling of aromatic aldimines with nonaromatic ketones could be induced by SmI_2 under mild conditions, provided that NiI_2 was used as an additive in the reaction mixture.[14] Recently, Taniguchi and Uemura showed that SmI_2-promoted reductive coupling of aromatic aldehydes and imine derivatives was an efficient and selective way to prepare vicinal amino alcohols, provided that the imine derivatives were aromatic *N*-sulfonylimines, as these substrates exhibit a suitable redox potential for selective cross-coupling.[15]

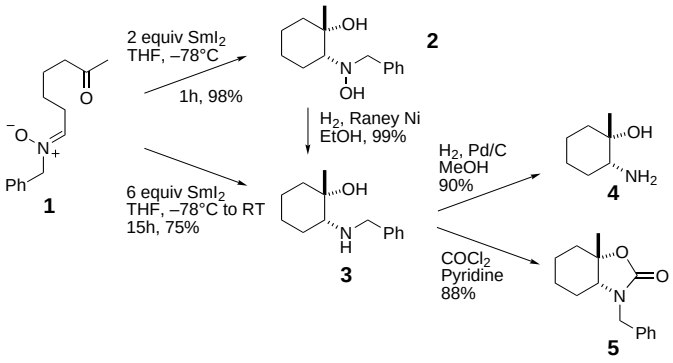
Here we disclose our preliminary results on SmI_2-induced cross-coupling of nitrones with aldehydes or ketones. Because of its good oxophilicity, samarium(II) diiodide was chosen as the SET reagent to mediate the reductive coupling of nitrones with carbonyl compounds. It was supposed that coordination of a samarium(III) ketyl radical to the oxygen atom of the nitrone and of the C=O group would favor the reaction and might induce good stereoselectivities in the coupling reactions.

To verify these assumptions we first conducted an intramolecular reaction by treating a 0.04 M solution of ketonitrone **1**[16] in THF with 2 equiv of SmI_2 at $-78\,^{\circ}C$ (Scheme 1). Cyclization proceeded rapidly (1 h) to yield 2-[benzyl(hydroxy)amino]-1-methylcyclohexanol (**2**) as a single diastereoisomer in almost quantitative yield. Moreover, treatment

[*] Dr. S. Py, Prof. Y. Vallée, G. Masson
LEDSS, UMR 5616
Université Joseph Fourier - CNRS
BP53; 38041 Grenoble Cedex 9 (France)
Fax: (+33) 476-51-43-82
E-mail: Sandrine.Py@ujf-grenoble.fr
Yannick.Vallee@ujf-grenoble.fr

[**] We thank the Centre National de la Recherche Scientifique (CNRS) and the Université Joseph Fourier for financial support. G.M. is grateful to the French Ministry of Education, Research and Technology (MENRT) for a doctoral fellowship.

 © WILEY-VCH Verlag GmbH, 69451 Weinheim, Germany, 2002 1433-7851/02/4110-1772 $ 20.00+.50/0

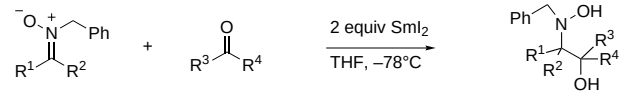


Scheme 1. Synthesis of cyclic α-*N*-hydroxyamino and α-amino alcohols by intramolecular coupling of ketonitrone **1**.

of **1** with 6 equiv of SmI_2 at room temperature[17] directly afforded the amine **3**, albeit in lower yield.

This pinacol-like reductive coupling took place under very mild conditions, with no need for additives such as alcohols or the toxic co-solvent HMPA, which was essential for the coupling of oximes and hydrazones to carbonyl compounds. It is noteworthy that in this case the product has a *cis* configuration,[18] which suggests that the reaction pathway is different from that generally assumed for other imine derivatives.

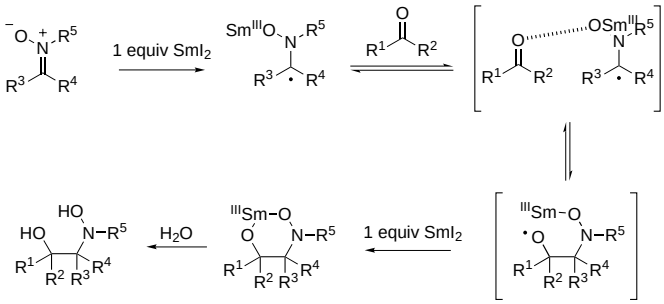
Encouraged by this result, we turned our efforts to the more challenging intermolecular cross-coupling of nitrones with a variety of carbonyl compounds (Scheme 2, Table 1). We found that both aromatic and aliphatic nitrones are effective



Scheme 2. Intermolecular reductive cross-coupling of nitrones and carbonyl compounds.

substrates for efficient and selective cross-coupling, not only with ketones, but also with aldehydes. When prochiral substrates were used, a mixture of diastereoisomers was obtained. The reactions are fast and highly chemoselective: no side products such as homocoupling or reduction products were isolated in any case. When both aldehyde and ketone functionalities were present in the substrate, coupling occurred selectively with the aldehyde (entries 14 and 15). Reactions with aromatic nitrones were faster. No limitations on the nature of substrates were revealed in this study, and even "bis-quaternary" amino alcohols could be prepared efficiently (entries 12 and 13). Interestingly, the presence of a proton source such as a remote hydroxy group in substrates does not impair the progress of this reaction (entry 10). The coupling can even be conducted in the presence of *tert*-butyl alcohol (entry 8, see footnote).

Based on the stability of the aminoxyl radical possibly formed by addition of R$^\bullet$ to the nitrone group and on the good electrophilicity of nitrones compared to that of imines, oximes, or hydrazones, we initially postulated a mechanism in which the first step is the formation of a ketyl radical from the carbonyl compound, followed by addition to the nitrone, and reduction of the resulting aminoxyl radical. However, several experiments indicate that the initial SET occurs at the nitrone group (Scheme 3). First, when benzylbenzylidene



Scheme 3. Proposed mechanism for the reductive cross-coupling of nitrones and carbonyl compounds.

amine *N*-oxide was treated under the described conditions in the absence of carbonyl compound its dimerization product was isolated in 73% yield. Second, reactions involving an α-cyclopropylketone as the carbonyl substrate yielded the expected cross-coupling products with no trace of ring opening, which suggests that the mechanism does not involve a ketyl radical (entries 4, 5, and 9). Finally when a 1,6-dicarbonyl substrate was treated with a nitrone (entries 14 and 15), only the α-*N*-hydroxyamino alcohols resulting from the coupling of the nitrone with the aldehyde were isolated (80–84% yied), and no intramolecular pinacol coupling occurred.

In conclusion, we have demonstrated that nitrones are the substrates of choice for the reaction with a variety of aldehydes and ketones under SmI_2-promoted reductive coupling conditions. This reaction provides a new method to prepare highly substituted and unsymmetrical vicinal *N*-hydroxyamino and amino alcohols. Its mechanism involves chemoselective SET from SmI_2 to the nitrone group, followed by addition of the resulting species to aldehydes or ketones. We are currently studying the scope and limitations of this reaction in the field of asymmetric synthesis. This process should be of interest both in the synthesis of natural products and in the design of new diversely substituted chiral ligands.

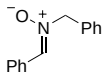
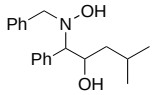
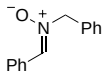
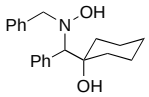
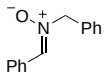
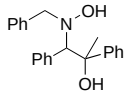
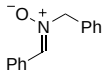
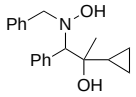
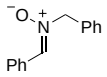
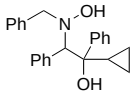
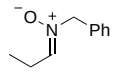
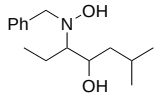
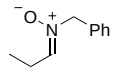
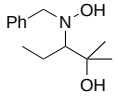
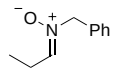
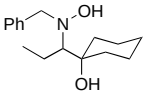
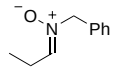
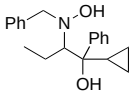
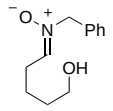
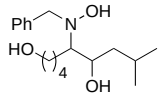
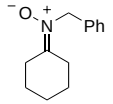
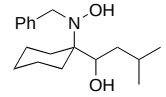
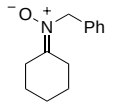
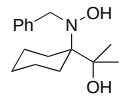
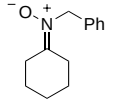
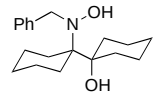
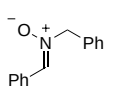
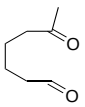
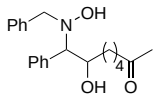
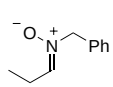
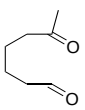
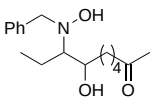
Experimental Section

A stirred and carefully deoxygenated solution of nitrone (*N*-alkylidenebenzylamine *N*-oxide, 0.5 mmol) in dry THF (10 mL) was cooled to $-78\,^\circ C$ under argon. Then the carbonyl compound (0.5 mmol) and a solution of SmI_2 (0.1 mol L^{-1}, 10 mL, 1 mmol) in THF were added. The temperature was kept at $-78\,^\circ C$ until the reaction was judged to be complete by TLC, and then saturated aqueous solutions of $Na_2S_2O_3$ (20 mL) and $NaHCO_3$ (20 mL) were added. The yellow mixture was extracted with AcOEt (3×50 mL), and the combined layers were washed with a saturated aqueous solution of NaCl and dried over $MgSO_4$. Filtration, concentration in vacuo and purification by chromatography on silica gel afforded the expected α-*N*-hydroxyamino alcohol(s) as single products (or as mixtures of diastereomers). All new compounds gave spectroscopic and analytical data in agreement with the assigned structures.

Received: December 27, 2001 [Z 18440]

 © WILEY-VCH Verlag GmbH, 69451 Weinheim, Germany, 2002 1433-7851/02/4110-1773 $ 20.00+.50/0

Table 1. Preparation of α-*N*-hydroxyamino alcohols by selective cross-coupling of nitrones with carbonyl compounds.

Entry	Nitrone	Carbonyl Compound	*N*-Hydroxyamino alcohol	Time	Yield	d.r.[a]
1				1 h	75 %	1:1
2				1 h	80 %	–
3				1 h	91 %	7:3
4				5 min	93 %	1:1
5				20 min	99 %	3:2
6				2 h	92 %	1:1
7				1 h	69 %	–
8[b]				2 h30	74 %	–
9				2 h	79 %	3:2
10				2 h	83 %	1:1
11				2 h	98 %	–
12				2 h	98 %	–
13				2 h	77 %	–
14				5 min	80 %	1:1
15				3 h	84 %	3:2

[a] According to ^{1}H NMR analysis of the crude materials. [b] The same result was obtained when *t*BuOH (2 equiv) was added to the reaction mixture before addition of SmI_2.

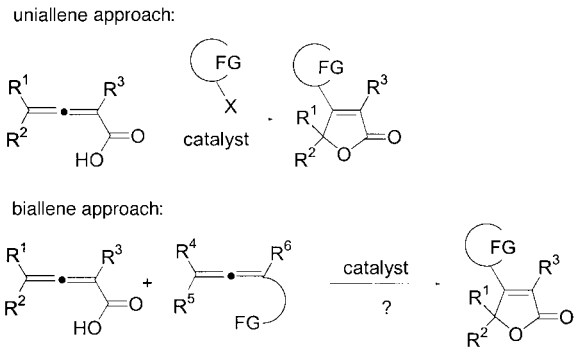
 © WILEY-VCH Verlag GmbH, 69451 Weinheim, Germany, 2002 1433-7851/02/4110-1774 $ 20.00+.50/0

[1] E. G. Janzen, D. E. Nutter, Jr., E. R. Davis, B. J. Blackburn, J. L. Poyer, P. B. McCay, *Can. J. Chem.* **1978**, *56*, 2237.
[2] a) R. A. Floyd, K. Hensley, *Ann. N.Y. Acad. Sci.* **2000**, *899*, 222; b) R. A. Floyd, *Adv. Pharmacol.* **1997**, *38*, 361.
[3] H. Miyabe, M. Ueda, T. Naito, *J. Org. Chem.* **2000**, *65*, 5043.
[4] A. Jeevanandam, C. Cartwright, Y. C. Ling, *Synth. Commun.* **2000**, *30*, 3153.
[5] G. K. Friestad, *Tetrahedron* **2001**, *57*, 5461.
[6] a) E. J. Corey, S. G. Pyne, *Tetrahedron Lett.* **1983**, *24*, 2821; b) T. Kiguchi, K. Tajiri, I. Ninomiya, T. Naito, H. Hiramatsu, *Tetrahedron Lett.* **1995**, *36*, 253; c) T. Naito, K. Nakagawa, T. Nakamura, A. Kasei, I. Ninomiya, T. Kiguchi, *J. Org. Chem.* **1999**, *64*, 2003; d) J. Tormo, D. S. Hays, G. C. Fu, *J. Org. Chem.* **1998**, *63*, 201; e) J. Marco-Contelles, P. Gallego, M. Rodriguez-Fernandez, N. Khiar, C. Destabel, M. Bernabe, A. Martinez-Grau, J. L. Chiara, *J. Org. Chem.* **1997**, *62*, 7397; f) H. Miyabe, S. Kanehira, K. Kume, H. Kandori, T. Naito, *Tetrahedron* **1998**, *54*, 5883; g) H. Miyabe, M. Torieda, K. Inoue, K. Tajiri, T. Kiguchi, T. Naito, *J. Org. Chem.* **1998**, *63*, 4397; h) A. Boiron, P. Zillig, D. Faber, B. Giese, *J. Org. Chem.* **1998**, *63*, 5877; i) I. Storch de Gracia, H. Dietrich, S. Bobo, J. L. Chiara, *J. Org. Chem.* **1998**, *63*, 5883; j) I. S. de Gracia, S. Bobo, M. D. Martin Ortega, J. L. Chiara, *Org. Lett.* **1999**, *1*, 1705; k) K. C. Nicolaou, X. Huang, N. Giuseppone, P. B. Rao, M. Bella, M. V. Reddy, S. A. Snyder, *Angew. Chem.* **2001**, *113*, 4841 – 4845; *Angew. Chem. Int. Ed.* **2001**, *40*, 4705.
[7] a) C. F. Sturino, A. G. Fallis, *J. Am. Chem. Soc.* **1994**, *116*, 7447; b) C. F. Sturino, A. G. Fallis, *J. Org. Chem.* **1994**, *59*, 6514; c) P. Tauh, A. G. Fallis, *J. Org. Chem.* **1999**, *64*, 6960; d) D. Riber, R. Hazell, T. Skrydstrup, *J. Org. Chem.* **2000**, *65*, 5382.
[8] N. Taniguchi, T. Hata, M. Uemura, *Angew. Chem.* **1999**, *111*, 1311; *Angew. Chem. Int. Ed.* **1999**, *38*, 1232.
[9] E. J. Roskamp, S. F. Pedersen, *J. Am. Chem. Soc.* **1987**, *109*, 6551.
[10] a) T. Shono, N. Kise, T. Fujimoto, *Tetrahedron Lett.* **1991**, *32*, 525; b) T. Shono, N. Kise, N. Kunimi, R. Nomura, *Chem. Lett.* **1991**, 2191; c) T. Shono, N. Kise, T. Fujimoto, A. Yamanami, R. Nomura, *J. Org. Chem.* **1994**, *59*, 1730.
[11] T. Imamoto, S. Nishimura, *Chem. Lett.* **1990**, 1141.
[12] E. J. Enholm, D. C. Forbes, D. P. Holub, *Synth. Commun.* **1990**, *20*, 981.
[13] T. Hanamoto, J. Inanaga, *Tetrahedron Lett.* **1991**, *32*, 3555.
[14] F. Machrouhi, J.-L. Namy, *Tetrahedron Lett.* **1999**, *40*, 1315.
[15] N. Taniguchi, M. Uemura, *J. Am. Chem. Soc.* **2000**, *122*, 8301.
[16] Nitrones were prepared according to literature procedures: a) A. Dondoni, S. Franco, F. Junquera, P. Merino, T. Tejero, *Synth. Commun.* **1994**, *24*, 2537; S. Franco, F. L. Merchan, P. Merino, T. Tejero, *Synth. Commun.* **1995**, *25*, 2275.
[17] A. S. Kende, J. S. Mendoza, *Tetrahedron Lett.* **1991**, *32*, 1699.
[18] As indicated by the formation of the cyclic carbamate **5** on treating the amino alcohol **3** with phosgene in pyridine, and by comparison of **3** with a sample of the isomeric *trans* amino alcohol.

Oxidative Cyclization – Dimerization Reaction of 2,3-Allenoic Acids and 1,2-Allenyl Ketones: An Efficient Synthesis of 4-(3′-Furanyl)butenolide Derivatives**

Shengming Ma* and Zhanqian Yu

Allenes are a class of compounds with interesting reactivities owing to the presence of two cumulative carbon-carbon double bonds.[1] As a result of the axial chirality as well as the substituent-loading capability, allenes show great potential in organic synthesis in terms of chirality transfer[2] and diversity. Recently, we[3–5] and others[6–14] established the cycloisomerization of functionalized allenes and the coupling – cyclization of functionalized allenes with organic halides for the synthesis of carbo- and heterocyclic compounds based on transition-metal-catalyzed or mediated cyclization of functionalized allenes.[14] However, to the best of our knowledge, no protocol has been established in the area of cyclization – dimerization reactions between two different classes of functionalized allenes to give interesting cyclic compounds in a single step (Scheme 1). The formidable *challenge* is to match the reactivities of two different classes of allenes.



Scheme 1. Cyclization – dimerization reactions of functionalized allenes to give butenolide derivatives.

With this idea in mind, we screened different combinations of several functionalized allenes, for example, 2,3-allenoic acids,[3] 2,3-allenols,[4a,b] 2,3-allenamides,[4c] and 1,2-allenyl ketones.[5] Fortunately, after numerous trial and error reactions, we observed the $[PdCl_2(MeCN)_2]$-catalyzed (5 mol %)

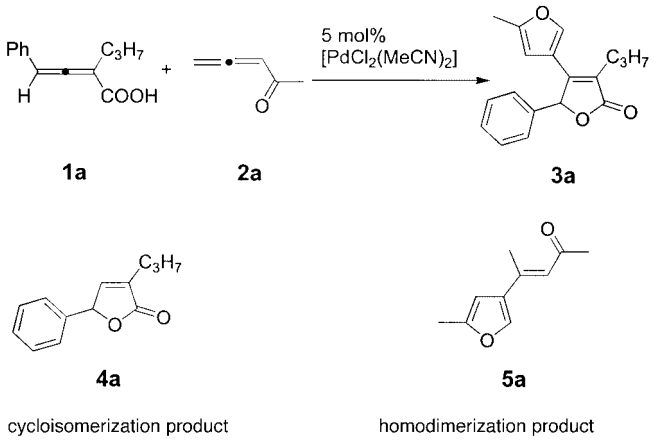
[*] Prof. S. Ma, Z. Yu
State Key Laboratory of Organometallic Chemistry
Shanghai Institute of Organic Chemistry, Chinese Academy of Sciences
354 Fenglin Lu, Shanghai 200032 (P. R. China)
Fax: (+86) 21-6416-6128
E-mail: masm@pub.sioc.ac.cn

[**] Financial support from the National Science Foundation of China, the Major State Basic Research Development Program (Grant No. G2000077500), the Chinese Acadamy of Sciences, and the Shanghai Municipal Committee of Science and Technology are greatly appreciated. S.M. is the recipient of the 1999 Qiu Shi Award for Young Scientific Workers issued by the Hong Kong Qiu Shi Foundation of Science and Technology (1999-2003).

Supporting information for this article is available on the WWW under http://www.angewandte.com or from the author.

 © WILEY-VCH Verlag GmbH, 69451 Weinheim, Germany, 2002 1433-7851/02/4110-1775 $ 20.00+.50/0

cyclization – dimerization reaction of allenoic acid **1a** with ketone **2a** in THF, which afforded furanone **3a** in 14% yield (Scheme 2; Table 1, entry 2). The reaction can also be carried out in methanol, CH_2Cl_2, acetone, toluene, DMA (N,N-dimethylacetamide), and acetonitrile. In CH_2Cl_2 or toluene, the major by-product is the cycloisomerization[3d, 7] product of **1a**, that is, furanone **4a** (Scheme 2; Table 1, entries 1 and 6). The reaction in DMA afforded **3a** exclusively in 76% yield (Table 1, entry 4). The best results were obtained in MeCN (Table 1, entry 11) with 5 equivalents of **2a**. Hashmi and coworkers established the Pd^{II}- and Au^{III}-catalyzed cyclization – homodimerization reaction of 1,2-allenyl ketones which led to 3-(3′-oxo-1′-alkenyl)furans and 2-(3′-oxo-1′-alkenyl)- or 2-(3′-oxo-1′-alkanyl)furans, respectively.[15, 16] In this case, **5a** (the homodimerization product of **2a**) was formed in 13% yield (based on the initial amount of **2a** used (Scheme 2)). With smaller amounts of **2a**, the reaction in acetonitrile also afforded **4a** as the by-product (Table 1, entries 7 – 10).



Scheme 2. Cyclization – dimerization reaction of allenoic acid **1a** with ketone **2a**

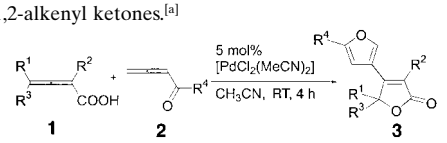
Table 1. Cyclization – dimerization reaction of **1a** and **2a**.[a]

Entry	**2a** [equiv]	Solvent	Time [h]	Yield (**3a**) [%]	Yield (**4a**) [%]
1	5	CH_2Cl_2	11	23	14
2	5	THF	11	14	0
3	5	acetone	11	40	0
4	5	DMA	17.5	76	0
5	5	methanol	12	30	trace
6	5	toluene	16.5	13	18
7	1	CH_3CN	10	27	30
8	2	CH_3CN	22	42	30
9	3	CH_3CN	11.5	57	12
10	4	CH_3CN	11	69	6
11	5	CH_3CN	4	90	0

[a] The reaction of **1a** (0.25 mmol), **2a** (1.25 mmol), and $[PdCl_2(MeCN)_2]$ (5 mol%) was carried out in the solvent (3 mL).

Some typical results are summarized in Table 2: 1) these are the first examples of sequential cyclization – dimerization reactions of two different functionalized allenes; 2) various substituents are tolerated and mono-, di-, and trisubstituted 2,3-allenoic acids can be used; 3) the reaction can occur under mild conditions (room temperature, 4 h) and the yields range from moderate to fairly good.

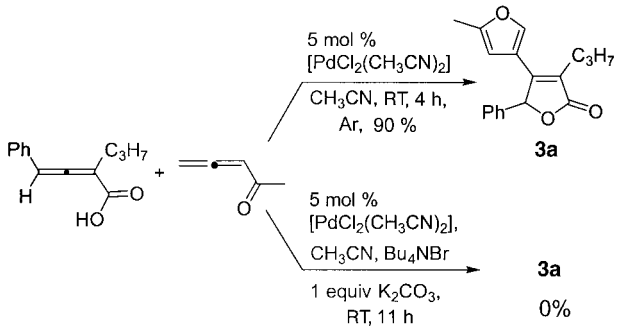
Table 2. Pd^{II}-catalyzed cyclization – dimerization reaction of 2,3-allenoic acids and 1,2-alkenyl ketones.[a]



Entry	**1**		**2**		Yield (**3**) [%]
	R^1	R^2	R^3	R^4	
1	Ph	n-C_3H_7	H (**1a**)	CH_3 (**2a**)	90 (**3a**)
2	Ph	$PhCH_2$	H (**1b**)	CH_3 (**2a**)	92 (**3b**)
3	Ph	CH_3	Et (**1c**)	CH_3 (**2a**)	85 (**3c**)
4	Ph	Allyl	H (**1d**)	CH_3 (**2a**)	61 (**3d**)
5	α-naphthyl	n-C_3H_7	H (**1e**)	CH_3 (**2a**)	86 (**3e**)
6	CH_3	$PhCH_2$	H (**1f**)	CH_3 (**2a**)	90 (**3f**)
7	n-C_7H_{15}	H	H (**1g**)	CH_3 (**2a**)	69 (**3g**)
8	Ph	n-C_3H_7	H (**1a**)	n-C_4H_9 (**2b**)	84 (**3h**)
9	Ph	CH_3	Et (**1c**)	n-C_4H_9 (**2b**)	86 (**3i**)
10	n-C_7H_{15}	H	H (**1g**)	n-C_4H_9 (**2b**)	69 (**3j**)
11	Ph	n-C_3H_7	H (**1a**)	$PhCH_2$ (**2c**)	74 (**3k**)
12	Ph	CH_3	Et (**1c**)	$PhCH_2$ (**2c**)	84 (**3l**)
13	n-C_7H_{15}	H	H (**1g**)	$PhCH_2$ (**2c**)	71 (**3m**)

[a] The reaction of **1** (0.25 mmol), **2** (1.25 mmol), and $[PdCl_2(MeCN)_2]$ (5 mol%) was carried out in CH_3CN (3 mL).

To clarify the mechanism of this reaction, two control experiments were conducted (Scheme 3): Under an argon atmosphere, the reaction occurs smoothly to afford **3a** in 90% yield, which indicates that air does not participate in the catalytic cycle. However, the reaction does not yield **3a** in the presence of K_2CO_3 (1 equiv), which indicates that HCl may be formed by the loss of two protons from both starting materials and play an important role in this reaction.

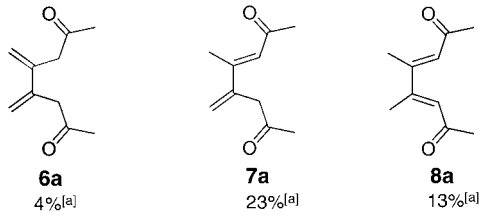


Scheme 3. The reaction does not occur in the presence of K_2CO_3 (1 equiv), which indicates that HCl may be formed by the loss of two protons from both starting materials.

A further study shows that the reaction also affords 4,5-dimethyleneocta-2,7-dione (**6a**) and its C=C double-bond isomers **7a** and **8a** as by-products (Scheme 4). Based on these facts, a plausible mechanism was proposed for this reaction: the Pd^0 species generated after the reductive elimination of **9a** reacts with penta-3,4-dienone (2 equiv) to form the cyclic Pd intermediate **10a**, which can be protonated with the HCl (2 equiv, generated in situ) to form **6a**, **7a**, and **8a**. The $[PdL_nCl_2]$ is regenerated and can reenter the catalytic cycle (Scheme 5).[17]

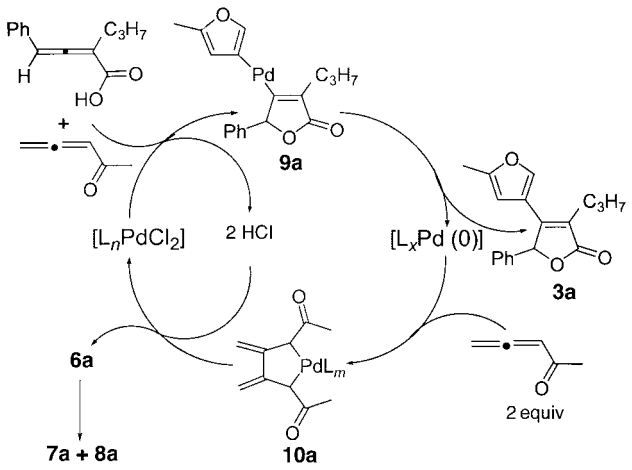
In conclusion, an oxidative cyclization – dimerization reaction between two different allenes provides an efficient route to polysubstituted 4-(3′-furanyl)-2(5*H*)-furanones **3**, which

 © WILEY-VCH Verlag GmbH, 69451 Weinheim, Germany, 2002 1433-7851/02/4110-1776 $ 20.00+.50/0 *Angew. Chem. Int. Ed.* **2002**, *41*, No. 10



[a] Yields are calculated based on penta-3,4-dienone used.

Scheme 4. 4,5-Dimethyleneocta-2,7-dione (**6a**) and its C=C double-bond isomers **7a** and **8a** are by-products in the reaction of **1a** and **2a**. [a] Yields are calculated based on **2a**.



Scheme 5. Proposed catalytic cycle for the cyclization–dimerization reaction.

are not readily available. Further studies into the scope, mechanism, and synthetic applications of this reaction are being carried out in our laboratory.

Experimental Section

Typical procedure: $[PdCl_2(MeCN)_2]$ (3 mg, 5 mol%) was added to a mixture of **1a** (50 mg, 0.248 mmol) and **2a** (103 mg, 1.26 mmol) in CH_3CN (3 mL), and the mixture was stirred at room temperature for 4 h. Evaporation and chromatography on silica gel (petroleum ether/diethyl ether 3:1) afforded pure **3a** (63 mg, 90%) as a white solid. M.p. 84–85 °C (ethyl acetate/hexane); ^{1}H NMR ($CDCl_3$, 300 MHz): $\delta = 7.41-7.21$ (m, 5H), 7.18 (s, 1H), 6.04 (s, 1H), 5.89 (s, 1H), 2.62-2.50 (m, 2H), 2.24 (s, 3H), 1.78–1.63 (m, 2H), 1.06 ppm (t, $J = 7.33$ Hz, 3H); ^{13}C NMR ($CDCl_3$, 75.4 MHz): $\delta = 13.30$, 14.14, 21.39, 26.51, 82.99, 104.77, 118.09, 126.24, 127.86, 129.04, 129.55, 135.85, 141.42, 150.37, 153.82, 174.30 ppm; MS (70 eV): *m*/*z* (%): 283 (28.39) [M^++1], 282 (100) [M^+]; IR (neat): $\tilde{\nu} = 2960$, 2920, 2869, 1732, 1654, 1603 cm^{-1}; elemental analysis: calcd for $C_{18}H_{18}O_3$ (%): C 76.57, H 6.43; found C 76.46, H 6.45.

Received: January 4, 2002 [Z18480]

[1] a) H. F. Schuster, G. M. Coppola, *Allenes in Organic Synthesis*, Wiley, New York, **1984**; b) S. Patai, *The Chemistry of Ketenes, Allenes, and Related Compounds, Part 1*, Wiley, New York, **1980**.

[2] For some typical examples of axial chirality transfer, see: a) G. Kresze, L. Kloimstein, W. Runge, *Justus Liebigs Ann. Chem.* **1976**, *64*, 979; b) S. Musierowicz, A. E. Wroblewski, *Tetrahedron* **1978**, *34*, 461; c) J. A. Marshall, M. A. Wolf, E. M. Wallace, *J. Org. Chem.* **1997**, *62*, 367; d) S. Ma, S. Wu, *Chem. Commun.* **2001**, 441.

[3] For the synthesis of butenolides from 2,3-allenoic acids, see: a) S. Ma, Z. Shi, *J. Org. Chem.* **1998**, *63*, 6387; b) S. Ma, Z. Shi, S. Wu, *Tetrahedron: Asymmetry* **2001**, *12*, 193; c) S. Ma, S. Wu, *J. Org. Chem.* **1999**, *64*, 9314; d) S. Ma, Z. Yu, S. Wu, *Tetrahedron* **2001**, *57*, 1585.

[4] a) For the stereoselective synthesis of epoxides, see: S. Ma, S. Zhao, *J. Am. Chem. Soc.* **1999**, *121*, 7943; b) For the synthesis of 2,5-dihydrofurans, see: S. Ma, W. Gao, *Tetrahedron Lett.* **2000**, *41*, 8933; c) for the synthesis of 4-halopyrrol-2(5*H*)-ones, see: S. Ma, H. Xie, *Org. Lett.* **2000**, *2*, 3801; d) for the synthesis of carbocycles, see: S. Ma, S. Zhao, *Org. Lett.* **2000**, *2*, 2495.

[5] For the synthesis of polysubstituted furans from 1,2-allenyl ketones, see: a) S. Ma, Z. Zhang, *Chem. Commun.* **2000**, 117; b) S. Ma, L. Li, *Org. Lett.* **2000**, *2*, 941.

[6] For catalytic cycloisomerization of allenols, see: a) J. A. Marshall, X. Wang, *J. Org. Chem.* **1990**, *55*, 2995; b) J. A. Marshall, X. Wang, *J. Org. Chem.* **1991**, *56*, 960; c) L. I. Olsson, A. Claesson, *Synthesis* **1979**, 743; d) S. S. Nikam, K. H. Chu, K. K. Wang, *J. Org. Chem.* **1986**, *51*, 745; e) R. Gelin, S. Gelin, M. Albrand, *Bull. Soc. Chim. Fr.* **1972**, 1946; f) J. A. Marshall, C. A. Sehon, *J. Org. Chem.* **1995**, *60*, 5966; g) J. A. Marshall, R. H. Yu, J. F. Perkins, *J. Org. Chem.* **1995**, *60*, 5550; h) A. Hoffmann-Roder, N. Krause, *Org. Lett.* **2001**, *3*, 2537.

[7] For catalytic cycloisomerization of 2,3-allenoic acids, see: J. A. Marshall, G. S. Bartley, E. M. Wallace, *J. Org. Chem.* **1996**, *61*, 5729.

[8] For the Pd^0-catalyzed coupling–cyclization reaction of allenols with aryl or vinyl halides, see: a) K. Uemura, D. Shiraishi, M. Noziri, Y. Inoue, *Bull. Chem. Soc. Jpn.* **1999**, 1063; b) S.-K. Kang, T.-G. Baik, A. N. Kulak, *Synlett* **1999**, 324; c) S.-K. Kang, T. Yamaguchi, S.-J. Pyun, Y.-T. Lee, T.-G. Baik, *Tetrahedron Lett.* **1998**, *39*, 2127; d) R. D. Walkup, L. Guan, Y. S. Kim, S. W. Kim, *Tetrahedron Lett.* **1995**, *36*, 3805; e) R. D. Walkup, L. Guan, M. D. Mosher, S. W. Kim, Y. S. Kim, *Synlett* **1993**, 88.

[9] a) For the Ru-catalyzed reaction of allenols in the presence of CO, see: E. Yoneda, T. Kaneko, S.-W. Zhang, K. Onitsuka, S. Takahashi, *Org. Lett.* **2000**, *2*, 441; b) for the Ru-catalyzed cyclization of allenols with α,β-unsaturated enones, see: B. M. Trost, A. B. Prinkerton, *J. Am. Chem. Soc.* **1999**, *121*, 10842.

[10] For the Pd^0-catalyzed coupling–cyclization reaction of allenic amides with aryl or vinyl halides, see: a) H. Ohno, M. Anzai, A. Toda, S. Ohishi, N. Fujii, T. Tanaka, Y. Takemoto, T. Ibuka, *J. Org. Chem.* **2001**, *66*, 4904; b) S.-K. Kang, K.-J. Kim, *Org. Lett.* **2001**, *3*, 511; c) M. Anzai, A. Toda, H. Ohno, Y. Takemoto, N. Fujii, T. Ibuka, *Tetrahedron Lett.* **1999**, *40*, 7393; d) F. P. J. T. Rutjes, K. C. M. F. Tjen, L. B. Wolf, W. F. J. Karstens, H. E. Schoemaker, H. Hiemstra, *Org. Lett.* **1999**, *1*, 717; e) H. Ohno, A. Toda, Y. Miwa, T. Taga, E. Osawa, Y. Yamaoka, N. Fuji, T. Ibuka, *J. Org. Chem.* **1999**, *64*, 2992; f) W. F. J. Karstens, M. Stol, F. P. J. T. Rutjes, H. Hiemstra, *Synlett* **1998**, 1126; g) W. F. J. Karstens, F. P. J. T. Rutjes, H. Hiemstra, *Tetrahedron Lett.* **1997**, 6275; h) I. W. Davies, D. I. C. Scopes, T. Gallagher, *Synlett* **1993**, 85.

[11] For the Pd-catalyzed coupling–cyclization reaction of allenic amides with allylic halides, see: a) W. F. J. Karstens, D. Klomp, F. P. J. T. Rutjes, H. Hiemstra, *Tetrahedron* **2001**, *57*, 5123; b) M. Kimura, S. Tanaka, Y. Tamaru, *J. Org. Chem.* **1995**, *60*, 3764; c) M. Kimura, K. Fugami, S. Tanaka, Y. Tamaru, *J. Org. Chem.* **1992**, *57*, 6377; d) J. S. Prasad, L. S. Liebeskind, *Tetrahedron Lett.* **1988**, *29*, 4257.

[12] For Ag^+-catalyzed cycloisomerization of amino allenes, see: a) M. O. Amombo, A. Hausherr, H.-U. Reissig, *Synlett* **1999**, 1871; b) I. W. Davies, T. Gallagher, R. B. Lamont, D. I. C. Scopes, *J. Chem. Soc. Chem. Commun.* **1992**, 335; c) D. N. A. Fox, D. Lathbury, M. F. Mahon, K. C. Molloy, T. Gallagher, *J. Chem. Soc. Chem. Commun.* **1989**, 1073; d) J. S. Prasad, L. S. Liebeskind, *Tetrahedron Lett.* **1988**, *29*, 4253; e) R. Kinsman, D. Lathbury, P. Vernon, T. Gallagher, *J. Chem. Soc. Chem. Commun.* **1987**, 243.

[13] a) For Pd-catalyzed cycloisomerization of 2-(allenyl)malonates, see: S. Kamijo, Y. Yamamoto, *Tetrahedron Lett.* **1999**, *40*, 1747; M. Meguro, Y. Yamamoto, *J. Org. Chem.* **1999**, *64*, 694; M. Meguro, S. Kamijo, Y. Yamamoto, *Tetrahedron Lett.* **1996**, *37*, 7453; b) for Pd-catalyzed coupling–cyclization of 2-(allenyl)malonates with organic halides, see: L. Besson, J. Bazin, J. Gore, B. Cazes, *Tetrahedron Lett.* **1994**, *35*, 2881; M. Ahmar, B. Cazes, J. Gore, *Tetrahedron Lett.* **1985**, *26*, 3795.

[14] For a review on the palladium-catalyzed chemistry of allenes, see: R. Zimmer, C. U. Dinesh, E. Nandanan, F. A. Khan, *Chem. Rev.* **2000**, *100*, 3067.

 © WILEY-VCH Verlag GmbH, 69451 Weinheim, Germany, 2002 1433-7851/02/4110-1777 $ 20.00+.50/0

[15] For dimerization of 1,2-allenyl ketones, see: a) A. S. K. Hashmi, J. -H. Choi, J. W. Bats, *J. Prakt. Chem.* **1999**, *341*, 342; b) A. S. K. Hashmi, T. L. Ruppert, T. Knöfel, J. W. Bats, *J. Org. Chem.* **1997**, *62*, 7295; c) A. S. K. Hashmi, *Angew. Chem.* **1995**, *105*, 1749; *Angew. Chem. Int. Ed. Engl.* **1995**, *34*, 1581; d) A. S. K. Hashmi, L. Schwarz, J.-H. Choi, T. M. Frost, *Angew. Chem.* **2000**, *112*, 2382; *Angew. Chem. Int. Ed.* **2000**, *39*, 2285.

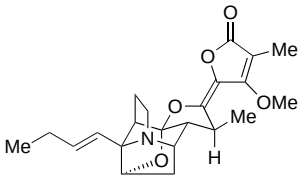
[16] For a recent highlight, see: A. S. K. Hashmi, *Angew. Chem.* **2000**, *112*, 3737; *Angew. Chem. Int. Ed.* **2000**, *39*, 3590.

[17] For protonolysis of Pd enolate to regenerate divalent palladium, see: Z. Wang, X. Lu, *J. Org. Chem.* **1996**, *61*, 2254.

Enantiospecific Synthesis of the Bridged Pyrrolizidine Core of Asparagamine A: Dipolar Cycloadditions of Azomethine Ylides Derived from the Sulfonylation of Vinylogous Amides.**

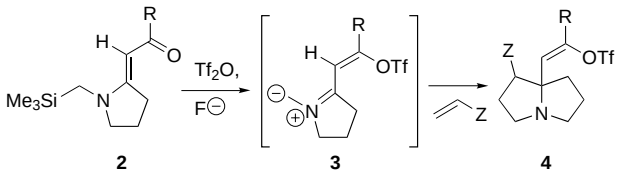
Matthew T. Epperson and David Y. Gin*

The efficient construction of highly functionalized pyrrolizidines is regarded as an important synthetic challenge owing to the diverse array of complex alkaloids that possess the necine skeleton. Asparagamine A (**1**) is a bridged pyrrolizidine alkaloid isolated from *Asparagus racemosus* that incorporates an intricate and rigid pentacyclic core[1] akin to the insecticidal stemofoline alkaloids,[2] natural products that have garnered considerable synthetic interest.[3] In vivo biological assays of **1** revealed potent antioxytocin activity,[4] despite its lack of structural homology with known oxytocin receptor antagonists.[5] We report herein an enantiospecific synthesis of the bridged pyrrolizidine skeleton of **1** that utilizes a complex intramolecular 1,3-dipolar cycloaddition as the key transformation.[6]



1

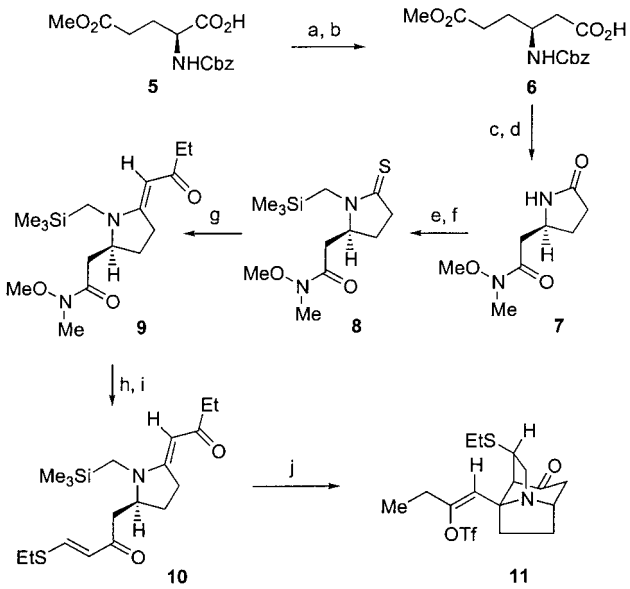
In the context of the synthesis of five-membered N heterocycles, azomethine ylides have proven to be valuable intermediates in a variety of 1,3-dipolar cycloadditions. A plethora of methods for the generation of these reactive intermediates exists and includes deprotonation, desilylation, or destannylation of imine or iminium salts, as well as the thermolysis or photolysis of aziridines.[7] However, in surveying the known procedures and substrates in the context of constructing the pyrrolizidine cage of **1**, a key challenge in this synthetic approach involves the direct installation of the angular C8 *E*-1-butenyl substituent during the cycloaddition reaction. As a result, vinylogous amides such as **2** (Scheme 1) were examined as potential precursors to azomethine ylides such as **3** through sequential O-sulfonylation[8] and desilylation.[9, 10] A 1,3-dipolar cycloaddition of **3** with a suitable dipolarophile would presumably lead to a pyrrolizidine that incorporates an enol triflate moiety at the angular position of **4**, a structure that maps directly onto the framework of **1**.



2 **3** **4**

Scheme 1. Vinylogous amides (e.g. **2**) are suitable precursors to azomethine ylides (e.g. **3**).

Application of this strategy to the synthesis of **1** would necessitate an intramolecular mode of the cycloaddition to access the bridged azatricyclo[5.3.0.0^{4,8}]decane core of the alkaloid. *N*-Benzyloxycarbonyl-L-glutamic acid-5-methyl ester (**5**)[11] was employed as a readily available starting material whose sole stereogenic center dictates the enantiospecific course of the synthesis (Scheme 2). Arndt–Eistert reaction of



Scheme 2. Reagents and conditions: a) EtOCOCl, Et_3N, THF, 0 °C; CH_2N_2, Et_2O, 87%; b) AgOAc, 1,4-dioxane, H_2O, 23 °C, 86%; c) EDCl, MeONHMe, Et_3N, $CHCl_3$, 23 °C, 89%; d) H_2, 10% Pd/C, MeOH, 23 °C, atmospheric pressure, 99%; e) NaH, $TMSCH_2Cl$, DMF, 23 °C, 49%; f) Lawesson's reagent (0.51 equiv), PhMe, 23 °C, 88%; g) $BrCH_2COEt$, then PPh_3, Et_3N, MeCN, 23 °C, 92%; h) CH≡CMgCl, THF, 0 °C; i) EtSH, Et_3N, CH_2Cl_2, 23 °C, 75%; j) Tf_2O (1.1 equiv), $CHCl_3$, 23 °C; TBAT (1.1 equiv), 65 °C, 24 h, 51%. EDCl = 1-(3-dimethylaminopropyl)-3-ethylcarbodiimide hydrochloride, TMS = trimethylsilyl, DMF = *N*,*N*-dimethylformamide, Tf = trifluoromethanesulfonyl, TBAT = tetrabutylammonium triphenyldifluorosilicate.

[*] Prof. D. Y. Gin, M. T. Epperson
Department of Chemistry, University of Illinois
Urbana, IL 61801 (USA)
Fax: (+1) 217-244-8024
E-mail: gin@scs.uiuc.edu

[**] This research was supported by generous gifts from Pfizer Inc., Glaxo Wellcome, Merck, Eli Lilly, Abbott, and Johnson & Johnson. Support from the Arnold and Mabel Beckman Foundation (BYI), the Alfred P. Sloan Foundation, and the Camille and Henry Dreyfus Foundation are gratefully acknowledged. M.T.E. thanks the NSF and AstraZeneca for predoctoral fellowships.

Supporting information for this article is available on the WWW under http://www.angewandte.com or from the author.

 © WILEY-VCH Verlag GmbH, 69451 Weinheim, Germany, 2002 1433-7851/02/4110-1778 $ 20.00+.50/0

the carboxylic acid functionality within **5** proceeded smoothly and provided the homologous glutamic acid **6**. Coupling of **6** with *N*,*O*-dimethylhydroxylamine in the presence of EDCl afforded the corresponding Weinreb amide in 89% yield. Subsequent hydrogenolysis of the benzyl carbamate and concomitant spontaneous lactamization led to the formation of the 2-pyrrolidinone intermediate **7**. N-Alkylation of lactam **7** with chloromethyltrimethylsilane, followed by chemoselective thionation with Lawesson's reagent gave thiolactam **8** in 88% yield. S-Alkylation of **8** with 1-bromo-2-butanone followed by Eschenmoser sulfide contraction afforded the vinylogous amide (*E*)-**9** as a single stereoisomer in 92% yield. The configuration of the trisubstituted double bond was established through NOE enhancement (9.5%) of the methylene protons adjacent to the trimethylsilyl group upon irradiation of the vinyl proton. Addition of ethynylmagnesium chloride to the Weinreb amide, followed by hydrolysis and conjugate addition of ethanethiol provided the cycloaddition substrate **10** in 75% yield as a 6:1 mixture of *E* and *Z* isomers.

The azomethine ylide intermediate was generated by treatment of **10** with Tf_2O in chloroform at room temperature followed by the addition of TBAT[12] at room temperature. After heating the reaction at 65 °C for 24 h, the bridged pyrrolizidine **11** was isolated in 51% yield as a single regio- and stereoisomer. The constitution and configuration of **11** were unambiguously established by single-crystal X-ray diffraction (Figure 1). The formation of the *Z* enol triflate is consistent with the initial sulfonylation step, which proceeds via the *s-cis* conformer and ultimately provides the desired precursor to the *E*-1-butenyl substituent in **1**. Moreover, the intramolecular cycloaddition process occurred with complete regiochemical control. When the reaction was carried out in CD_3CN with cesium fluoride (1.1 equiv) as the silicon scavenger and monitored by ^1H NMR spectroscopy, the only product detected was **11**.

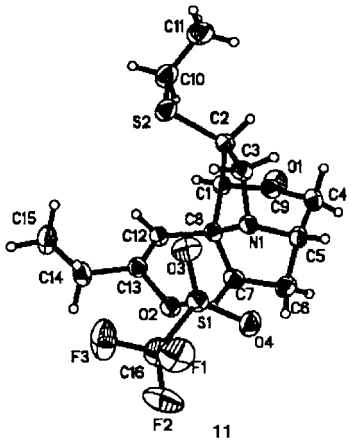
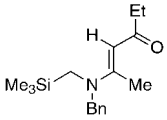
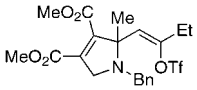
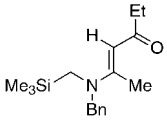
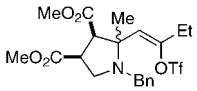
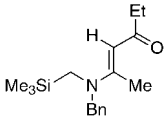
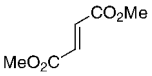
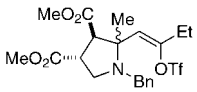
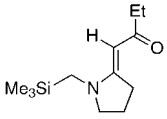
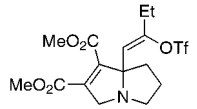
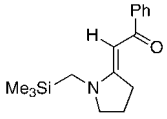
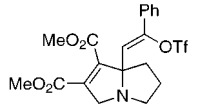
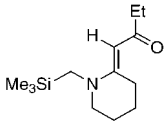
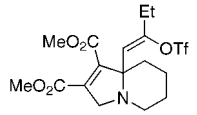
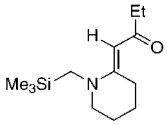
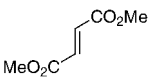
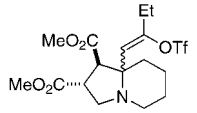
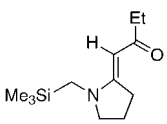
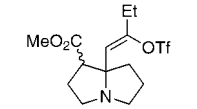


Figure 1. ORTEP diagram of **11**.

Table 1.

Entry	Substrate	Dipolarophile[a]	Product	Yield	*endo*/*exo*
1		DMAD		68%	
2				62%	1:1
3				71%	1:1
4		DMAD		70%	
5		DMAD		75%	
6		DMAD		63%	
7				63%	1:1
8				69%	2.9:1

[a] DMAD = dimethylacetylene dicarboxylate.

 © WILEY-VCH Verlag GmbH, 69451 Weinheim, Germany, 2002 1433-7851/02/4110-1779 $ 20.00+.50/0

Neither the cycloadduct derived from the *Z* isomer nor the azatricyclo[5.2.1.0^{4,8}]decane regioisomer was observed in the reaction mixture.

The success of the dipolar cycloaddition reaction with a relatively complex substrate **10** to form **11** prompted an investigation into the utility of the sulfonylation of vinylogous amides as azomethine ylide precursors for the synthesis of functionalized *N*-heterocycles in general. Thus, a series of intermolecular cycloadditions were performed with DMAD, dimethyl maleate, or dimethyl fumarate as the dipolarophile and a variety of vinylogous amides to serve as 1,3-dipole precursors. Acyclic vinylogous amides (see Table 1, entries 1–3) undergo the transformation efficiently, generating highly substituted pyrrolidines. As seen in the synthesis of **11**, vinylogous amides derived from 2-pyrrolidinones (Table 1, entries 4 and 5) provide facile access to pyrrolizidines. Furthermore, highly functionalized indolizidines can be prepared from vinylogous amides derived from 2-piperidinones (Table 1, entries 6 and 7).

In summary, the first enantiospecific synthesis of the bridged pyrrolizidine core of asparagamine A has been accomplished. The synthetic approach highlights an intramolecular 1,3-dipolar cycloaddition of an azomethine ylide derived from the sulfonylation of a vinylogous amide. This strategy allows concomitant installation of the angular *E*-1-butenyl side chain during the assembly of the azatricyclo-[5.3.0.0^{4,8}]decane skeleton of **1**. The use of vinylogous amides in this capacity can be extended to the preparation of a variety of highly functionalized pyrrolidines, pyrrolizidines, and indolizidines.

Received: February 7, 2002 [Z18668]

[1] T. Sekine, N. Fukasawa, Y. Kashiwagi, N. Ruangrungsi, I. Murakoshi, *Chem. Pharm. Bull.* **1994**, *42*, 1360–1362.

[2] H. Irie, N. Masaki, K. Ohno, K. Osaki, T. Taga, S. Uyeo, *J. Chem. Soc. Chem. Commun.* **1970**, 1066.

[3] For racemic syntheses of the pyrrolizidine core of stemofoline, see: a) R. L. Beddoes, M. P. H. Davies, E. J. Thomas, *J. Chem. Soc. Chem. Commun.* **1992**, 538–540; b) T. Kercher, T. Livinghouse, *J. Am. Chem. Soc.* **1996**, *118*, 4200–4201; for a synthesis of (±)-isostemofoline, see: c) A. S. Kende, T. L., Smalley, Jr., H. Huang, *J. Am. Chem. Soc.* **1999**, *121*, 7431–7432.

[4] a) S. Tip-Pyang, P. Tangpraprutgul, N. Wiboonpun, G. Veerachato, P. Phuwapraisirisan, B. Sup-Udompol, *ACGC Chem. Res. Commun.* **2000**, *12*, 31–35; b) T. Sekine, F. Ikegami, N. Fukasawa, Y. Kashiwagi, T. Aizawa, Y. Fujii, N. Ruangrungsi, I. Murakoshi, *J. Chem. Soc. Perkin Trans. 1* **1995**, 391–393.

[5] a) P. D. Williams, D. J. Pettibone, *Curr. Pharm. Des.* **1996**, *2*, 41–58; b) T. M. Goodwin, A. Zograbyan, *Clin. Perinatol.* **1998**, *25*, 859–871.

[6] The absolute configuration of **1** has not been established.

[7] Reviews: a) J. W. Lown in *1,3-Dipolar Cycloaddition Chemistry*, *Vol. 1* (Ed.: A. Padwa), Wiley, New York, **1984**, p 663; b) E. Vedejs, F. G. West, *Chem. Rev.* **1986**, *86*, 941–955; c) Y. Terao, M. Aono, K. Achiwa, *Heterocycles* **1988**, *27*, 981–1008; d) R. Grigg, *Chem. Soc. Rev.* **1987**, *16*, 89–121; e) K. V. Gothelf, K. A. Jorgensen, *Chem. Rev.* **1998**, *98*, 863–909; f) O. Tsuge, S. Kanemasa, *Adv. Heterocycl. Chem.* **1989**, *45*, 231–349; g) E. Vedejs in *Advances in Cycloaddition*, *Vol. 1* (Ed.: D. P. Curran), JAI, Greenwich, **1988**, pp. 33–51; h) A. Padwa in *Comprehensive Organic Synthesis*, *Vol. 4*, (Eds.: B. M. Trost, I. Fleming, M. F. Semmelhack), Pergamon, Oxford, **1991**, pp. 1069–1109; i) P. A. Wade in *Comprehensive Organic Synthesis*, *Vol. 4* (Eds.: B. M. Trost, I. Fleming, M. F. Semmelhack), Pergamon, Oxford, **1991**, pp. 1111–1168; for related 2-azaallylanion cycloadditions, see: j) W. H. Pearson, Y. Mi, I. Y. Lee, P. Stoy, *J. Am. Chem. Soc.* **2001**, *123*, 6724–6725, and references therein.

[8] For a recent review on the activation of amides and vinylogous amides with triflic anhydride, see: a) I. L. Baraznenok, V. G. Nenajdenko, E. S. Balenkova, *Tetrahedron* **2000**, *56*, 3077—3119, and references therein; for the activation of *O*-silylhydroxamic acids with triflic anhydride to generate nitrile oxides, see: b) D. Muri, J. W. Bode, E. M. Carreira, *Org. Lett.* **2000**, *2*, 539–541.

[9] For an example of the generation of azomethine ylides from the N-alkylation of vinylogous imidates, see: A. Padwa, G. Haffmanns, M. Tomas, *Tetrahedron Lett.* **1983**, *24*, 4303–4306.

[10] For the use of amides and thioamides as azomethine ylide precursors, see: a) E. Vedejs, G. R. Martinez, *J. Am. Chem. Soc.* **1980**, *102*, 7993–7994; b) F. G. West, E. Vedejs, *J. Org. Chem.* **1983**, *48*, 4773–4774, and references therein.

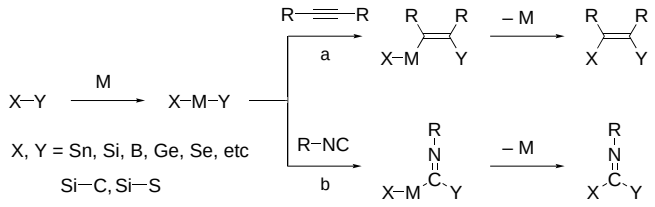
[11] a) X. Feng, E. D. Edstrom, *Tetrahedron: Asymmetry* **1999**, *10*, 99–105; b) commercially available from Bachem.

[12] A. S. Pilcher, H. L. Ammon, P. DeShong, *J. Am. Chem. Soc.* **1995**, *117*, 5166–5167.

Cyanamide Synthesis by the Palladium-Catalyzed Cleavage of a Si–N Bond**

Shin Kamijo, Tienan Jin, and Yoshinori Yamamoto*

Studies on the transition-metal-catalyzed reaction of main-group-element–element bonds with unsaturated bonds have spread widely and extensively because of the synthetic utilities of the resulting products.[1] Various element–element bonds (X–Y) add to unsaturated C–C bonds, such as alkynes, 1,3-dienes, and allenes, in the presence of a transition-metal catalyst (route a in Scheme 1, vicinal addition). Among the bismetallic compounds, perhaps the most well-studied



Scheme 1. Transition-metal-catalyzed addition of X–Y bonds to unsaturated bonds.

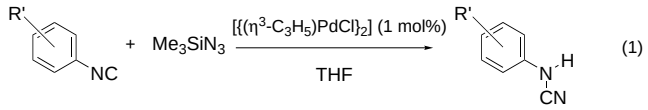
[*] Prof. Dr. Y. Yamamoto, S. Kamijo, T. Jin
Department of Chemistry
Graduate School of Science, Tohoku University
Sendai 980-8578 (Japan)
Fax: (+81) 22-217-6784
E-mail: yoshi@yamamoto1.chem.tohoku.ac.jp

[**] We thank collaborators at the Instrumental Analysis Center, Department of Chemistry at Tohoku University, for measurements of mass spectra and elemental analyses. S.K. is also thankful for a fellowship from the Japan Society of Promotion of Science for Young Scientists.

Supporting information for this article is available on the WWW under http://www.angewandte.com or from the author.

 © WILEY-VCH Verlag GmbH, 69451 Weinheim, Germany, 2002 1433-7851/02/4110-1780 $ 20.00+.50/0

metal–metal bond is found in silicon-containing derivatives such as Si–Si, Si–Sn, Si–B, Si–Se.[2, 3] The geminal addition of Si–Sn,[4] Si–Si,[5] and Si–B[6] to isocyanides is also known (route b in Scheme 1). However, only limited studies on the transition-metal-catalyzed addition of a Si–R bond (R = organic group) have been done.[7–12] The vicinal addition (route a) of Si–C[7–9] and Si–S[10] bonds is known. Quite recently, we have found that the geminal addition (route b) of the C–N bond takes place in the presence of a palladium catalyst.[13] However, the metal-catalyzed addition of a Si–N bond, either in a vicinal or in geminal mode, is not known. We now report the first example of the catalytic geminal addition of a $Si–N_3$ bond to isocyanides **1**. The reaction of **1** with Me_3SiN_3 (**2**) in the presence of $[\{(\eta^3\text{-}C_3H_5)PdCl\}_2]$ as a catalyst gave cyanamides **3** [Eq. (1)], possibly through the proposed intermediate **B** (see Scheme 2) formed through the geminal addition mode (route b, Scheme 1).



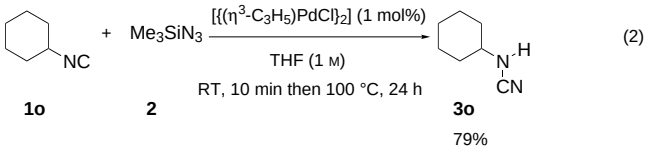
The results are summarized in Table 1. Trimethylsilyl azide (**2**) was added to a solution of 4-methoxyisocyanobenzene (**1a**) and $[\{(\eta^3\text{-}C_3H_5)PdCl\}_2]$ (1 mol%)[14] in THF. The mixture was stirred at room temperature for 10 min and then at 60 °C for 6 h to give (4-methoxyphenyl)cyanamide (**3a**) in 85% yield (entry 1).[15] We carried out reactions with the isocyanides **1b** and **1c** which have an electron-donating group on the aromatic ring. The corresponding aryl cyanamides **3b** and **3c** were obtained in high yields (entries 2 and 3). The reaction of isocyanobenzene **1d** was complete in only 2 h to afford phenylcyanamide (**3d**) in high yield (entry 4). We next carried out the reactions with the isocyanides **1e–g** having an electron-withdrawing group at the *para* position. All these reactions were complete within 3 h to give the corresponding cyanamides **3e–g** in high yields (entries 5–7). The reactions of isocyanides **1e–g** with an electron-withdrawing group proceeded faster than those (**1a–c**) with an electron-donating group. The isocyanides **1h–j** conjugated with an alkynyl group afforded the corresponding cyanamides **3h–j** in good to high yields (entries 8–10). The above results indicate that the cyanamide-forming reaction tolerates a wide range of functional groups and proceeds well, irrespective of the position of the substituents. Even the disubstituted isocyanobenzenes **1k** and **1l** afforded the corresponding cyanamides **3k** and **3l** in good to high yields (entries 11 and 12). The reaction of dimethoxyisocyanobenzene **1m** and trimethoxyisocyanobenzene **1n** afforded the corresponding cyanamides **3m** and **3n** in high yields, although elevated temperature was needed (entries 13 and 14).

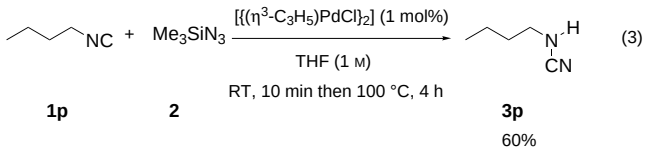
Table 1. Palladium-catalyzed formation of cyanamides.[a]

Entry	1	R′	Time [h]	3	Yield [%][b]
1	**1a**	4-MeO	6	**3a**	85
2	**1b**	4-*i*Pr	5	**3b**	84
3	**1c**	4-morpholino	8	**3c**	87
4	**1d**	H	2	**3d**	84
5	**1e**	4-CO_2Me	3	**3e**	80
6	**1f**	4-CN	2	**3f**	81
7	**1g**	4-Cl	3	**3g**	81
8	**1h**	4-Me_3SiCC	2	**3h**	65
9	**1i**	3-Me_3SiCC	2	**3i**	83
10	**1j**	2-Me_3SiCC	3	**3j**	58
11	**1k**	2,6-dimethyl	13	**3k**	79
12	**1l**	2,4-dichloro	1.5	**3l**	79
13	**1m**	2,4-dimethoxy[c]	2	**3m**	94
14	**1n**	3,4,5-trimethoxy[c]	2	**3n**	88

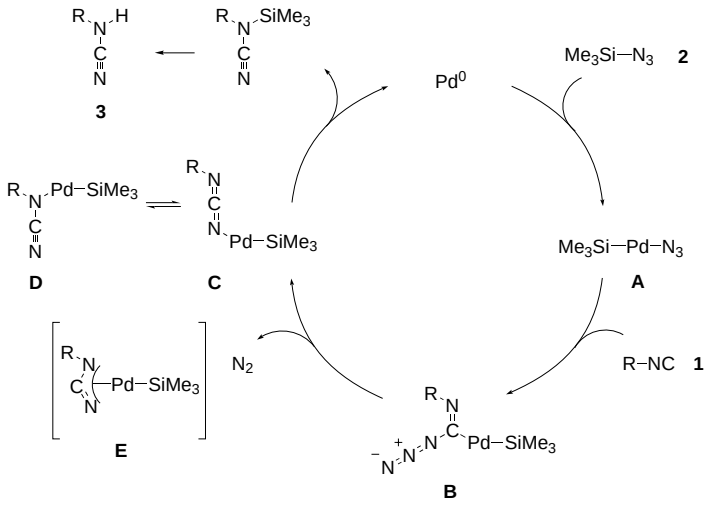
[a] A solution of **2** (1.2 equiv) in THF (1M) was added to a mixture of **1** and $[\{(\eta^3\text{-}C_3H_5)PdCl\}_2]$ (1 mol%). The mixture was stirred at RT for 10 min and then at 60 °C for the period shown in Table 1. [b] Isolated. [c] The reaction was conducted at 100 °C.

We next investigated the reactivity of alkyl isocyanides.[16] The reaction of cyclohexyl isocyanide (**1o**) at 100 °C for 24 h gave the corresponding cyanamide **3o** in 79% yield [Eq. (2)]. When the reaction was conducted at 60 °C, the yield was lowered and a longer reaction time was needed. The reaction of butyl isocyanide (**1p**) under similar conditions gave butylcyanamide **3p** in 60% yield [Eq. (3)].





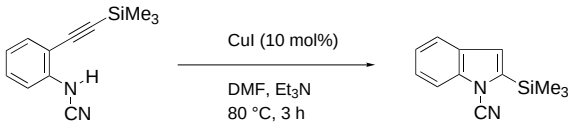
Scheme 2 shows the most probable mechanism for the present transformation. First, oxidative addition of Pd^0 to trimethylsilyl azide (**2**) produces the $Me_3Si\text{-}Pd\text{-}N_3$ complex (**A**). Then, the insertion of isocyanide **1** in the $Pd–N_3$ bond of complex **A** gives the intermediate **B**. The 1,2-migration of the



Scheme 2. Proposed mechanism for the formation of cyanamides.

Me_3Si–Pd group from the carbon atom to the α nitrogen atom followed by concomitant elimination of N_2 affords the palladium–carbodiimide complex **C** (the Me_3Si-Pd mimic of the Curtius rearrangement).[13, 17] The palladium–carbodiimide complex **C** could be in equilibrium with the palladium–cyanamide complex **D**, or, more probably, could be represented as **E**. Reductive elimination of Pd^0 from the palladium intermediates **C**–**E** gives the corresponding trimethylsilyl-protected cyanamide, which is converted into **3** during chromatographic separation on silica gel.

An application of a cyanamide obtained by the above procedure to indole synthesis is shown in Equation (4). The reaction of (2-alkynylphenyl)cyanamide (**3j**) in the presence of catalytic amounts of CuI gave the corresponding indole **4** in 76% yield.[18]



3j **4** 76% (4)

We are now in a position to synthesize aryl and alkyl cyanamides **3** with a wide range of substituents in very high to good yields through the palladium-catalyzed reaction between isocyanides **1** and trimethylsilyl azide (**2**). This is the first example of Si–N bond cleavage catalyzed by Pd^0 and of the geminal addition of a Si–N bond to isocyanides. In addition, we have shown that a Me_3Si–Pd mimic of the Curtius rearrangement could intervene in the catalytic cycle. Further studies on the synthetic application of this novel reaction and on the mechanistic detail are in progress.

Experimental Section

Trimethylsilyl azide (80 µL, 0.6 mmol) was added under an argon atmosphere to a solution (0.5 mL) of **1a** (66.6 mg, 0.5 mmol) and $[\{\eta^3\text{-}(C_3H_5)PdCl\}_2]$ (1.8 mg, 0.005 mmol) in THF. The solution was stirred at room temperature for 10 minutes and then at 60 °C for 6 h. The reaction mixture was cooled to room temperature and filtered through a short Florisil pad and concentrated. The residue was purified by column chromatography (silica gel, hexane/ether 10/1 →1/3) to afford **3a** in 85% yield (63.0 mg).

Received: December 28, 2001 [Z18456]

[1] For reviews on bimetallic compounds, see a) I. Beletskaya, C. Moberg, *Chem. Rev.* **1999**, *99*, 3456–3461 and references therein; b) L.-B. Han, M. Tanaka, *Chem. Commun.* **1999**, 395–402; c) G. J. Irvine, M. J. G. Lesley, T. B. Marder, N. C. Norman, C. R. Tice, E. G. Robins, W. R. Roper, G. R. Whittell, L. J. Wright, *Chem. Rev.* **1998**, *98*, 2685–2722; d) T. B. Marder, N. C. Norman, *Top. Catal.* **1998**, *5*, 63–67; e) T. Ishiyama, N. Miyaura, *J. Organomet. Chem.* **2000**, *611*, 392–402.

[2] For reviews on silicon-containing compounds, see a) M. Suginome, Y. Ito, *Chem. Rev.* **2000**, *100*, 3221–3256 and references therein; b) K. A. Horn, *Chem. Rev.* **1995**, *95*, 1317–1350; c) H. K. Sharma, K. H. Pannell, *Chem. Rev.* **1995**, *95*, 1351–1374.

[3] For Si–Se and Si–Ge addition, see a) A. Ogawa, H. Kuniyasu, M. Takeba, T. Ikeda, N. Sonoda, T. Hirao, *J. Organomet. Chem.* **1998**, *564*, 1–4; for Si–Ge addition (stoichiometric), see b) M. Suginome, H. Oike, P. H. Shuff, Y. Ito, *J. Organomet. Chem.* **1996**, *521*, 405–408; for Si–Te addition (stoichiometric), see c) L.-B. Han, S. Shimada, M. Tanaka, *J. Am. Chem. Soc.* **1997**, *119*, 8133–8134.

[4] For Si–Sn addition, see Y. Ito, T. Bando, T. Matsuura, M. Ishikawa, *J. Chem. Soc. Chem. Commun.* **1986**, 980–981.

[5] For Si–Si addition, see a) Y. Ito, S. Nishimura, M. Ishikawa, *Tetrahedron Lett.* **1987**, *28*, 1293–1294; b) Y. Ito, T. Matsuura, M. Murakami, *J. Am. Chem. Soc.* **1988**, *110*, 3693–3695; c) Y. Ito, M. Suginome, T. Matsuura, M. Murakami, *J. Am. Chem. Soc.* **1991**, *113*, 8899–8908.

[6] For Si–B addition without the use of a transition metal, see M. Suginome, T. Fukuda, H. Nakamura, Y. Ito, *Organometallics* **2000**, *19*, 719–721.

[7] For Si–C (strained) addition, see a) H. Sakurai, T. Imai, *Chem. Lett.* **1975**, 891–894; b) H. Saso, W. Ando, *Chem. Lett.* **1988**, 1567–1570; c) Y. Takeyama, K. Nozaki, K. Matsumoto, K. Oshima, K. Utimoto, *Bull. Chem. Soc. Jpn.* **1991**, *64*, 1461–1466.

[8] For Si–CN addition, see a) N. Chatani, T. Hanafusa, *J. Chem. Soc. Chem. Commun.* **1985**, 838–839; b) N. Chatani, T. Takeyasu, N. Horiuchi, T. Hanafusa, *J. Org. Chem.* **1988**, *53*, 3539–3548; c) N. Chatani, T. Takeyasu, T. Hanafusa, *Tetrahedron Lett.* **1986**, *27*, 1841–1844; d) N. Chatani, T. Takeyasu, T. Hanafusa, *Tetrahedron Lett.* **1988**, *29*, 3979–3982; e) M. Suginome, H. Kinugasa, Y. Ito, *Tetrahedron Lett.* **1994**, *35*, 8635–8638.

[9] For related carbosilylation catalyzed by Lewis acids, see a) N. Asao, Y. Yamamoto, *Bull Chem. Soc. Jpn.* **2000**, *73*, 1071–1087; b) I. N. Jung, B. R. Yoo, *Synlett* **1999**, 519–528.

[10] For Si–S addition, see L.-B. Han, M. Tanaka, *J. Am. Chem. Soc.* **1998**, *120*, 8249–8250.

[11] For Si–H, see a) T. Hiyama, T. Kusumoto in *Comprehensive Organic Synthesis*, *Vol. 8* (Eds.: B. M. Trost, I. Fleming), Pergamon, Oxford, **1991**, pp. 763–792; b) ref. [2b].

[12] For reactions involving the activation of a Si–halogen bond, see a) N. Chatani, N. Amishiro, S. Murai, *J. Am. Chem. Soc.* **1991**, *113*, 7778–7780; b) N. Chatani, N. Amishiro, T. Morii, T. Yamashita, S. Murai, *J. Org. Chem.* **1995**, *60*, 1843–1840; c) H. Yamashita, T. Kobayashi, T. Hayashi, M. Tanaka, *Chem. Lett.* **1991**, 761–762.

[13] S. Kamijo, T. Jin, Y. Yamamoto, *J. Am. Chem. Soc.* **2001**, *123*, 9453–9454 (the utilities of cyanamides are mentioned in this paper).

[14] $[\{\eta^3\text{-}(C_3H_5)PdCl\}_2]$ showed the best catalytic activities among the palladium catalysts we tested. Other palladium catalysts such as $[Pd_2(dba)_3\cdot CHCl_3]$, $[Pd(PPh_3)_4]$, $[PdCl_2(PPh_3)_2]$, $[Pd(OAc)_2]$, $[Pd(acac)_2]$, and $PdCl_2$ were less active. dba = *trans*,*trans*-dibenzylideneacetone, acac = acetylacetonate.

[15] The reaction of isocyanobenzene **1a** and trimethylsilyl azide (**2**) without a palladium catalyst did not give the cyanamide **3** at all, and **1a** was recovered.

[16] Tertiary isocyanide did not give the desired cyanamide.

[17] For the stoichiometric reaction of palladium–azido complexes with isocyanides, see a) Y.-S. Kim, Y.-S. Kwak, S.-W. Lee, *J. Organomet. Chem.* **2000**, *603*, 152–160; b) W. Beck, K. Burger, W. P. Fehlhammer, *Chem. Ber.* **1971**, *104*, 1816–1825.

[18] A similar cyclization of 2-alkynylanilines is reported, see a) T. Sakamoto, Y. Kondo, S. Iwashita, T. Nagano, H. Yamanaka, *Chem. Pharm. Bull.* **1988**, *36*, 1305–1308; b) C. E. Castro, E. J. Gaughan, D. C. Owsley, *J. Org. Chem.* **1966**, *31*, 4071–4078.

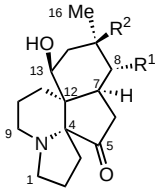
 © WILEY-VCH Verlag GmbH, 69451 Weinheim, Germany, 2002 1433-7851/02/4110-1782 $ 20.00+.50/0

A Short Synthesis of (±)-13-Deoxyserratine**

Jérome Cassayre, Fabien Gagosz, and Samir Z. Zard*

Dedicated to Professor Pierre Potier

Lycopodium alkaloids[1] exhibit a fascinating structural complexity and have emerged as challenging synthetic targets in recent years. In the serratinane subgroup, with the exception of (±)-serratinine (**1a**)[2] and the corresponding 8-deoxy derivative,[3] both of which have been synthesized previously by a long and low-yielding route, not much attention has been paid to other alkaloids of this structural family. So far, only one approach to serratine (**1b**)[1, 4] has been reported by Livinghouse and Luedtke.[5]



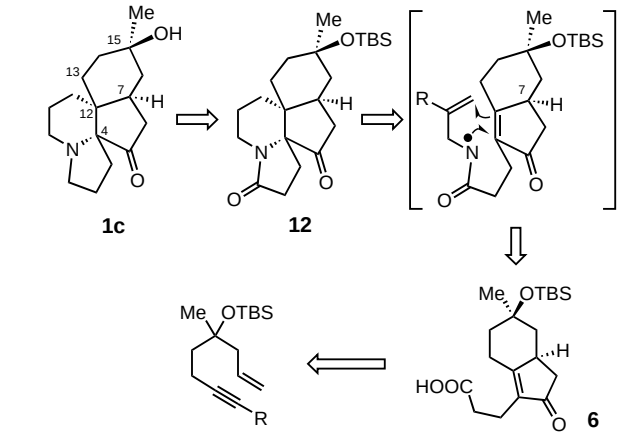
1a: R^1=OH, R^2=H

1b: R^1=H, R^2=OH

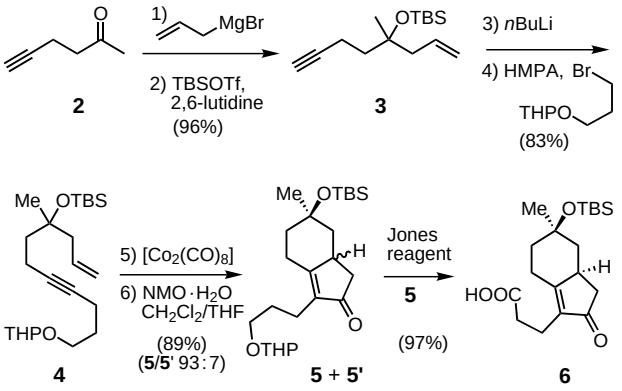
We recently developed several processes for generating various types of nitrogen-centered radicals, which can be captured by internal olefins to give a variety of nitrogen-containing heterocycles.[6, 7, 8] Our interest in the synthesis of (±)-serratine (**1b**) was therefore stimulated by the possibility that the indolizidine framework could be introduced by using a cascade of radical cyclizations starting with an amidyl radical. We report herein the successful implementation of this strategy to the synthesis of (±)-13-deoxyserratine (**1c**).

As shown in Scheme 1, our synthetic plan hinges on two key steps that allow the stereocontrolled introduction of the four stereogenic centers at C4, C7, C12, and C15. A diastereoselective Pauson–Khand[9] reaction would allow easy access to the key bicyclo[4.3.0]nonenone intermediate **6**. The concave shape of this molecule will then control the stereochemistry in the cascade sequence to give **1c**.

The synthesis started with the alkylation of 5-hexyn-2-one (**2**) allylmagnesium bromide. The resulting tertiary alcohol was treated with TBSOTf to afford the protected alcohol **3** in 96% yield. Subsequent deprotonation with *n*BuLi followed by alkylation with THP-protected 3-bromopropanol furnished precursor **4** for the Pauson–Khand reaction. Treatment of the [alkyne–$Co_2(CO)_6$] complex derived from **4** with NMO·H_2O[10] resulted in a rapid conversion into the desired bicyclo[4.3.0]nonenone as a 93:7 mixture of diastereoisomers **5** and **5′** in 89% yield. The major isomer **5** was submitted to Jones oxidation to give the key intermediate acid **6** (64% from 2) (Scheme 2).



Scheme 1. Retrosynthetic analysis of (±)-13-deoxyserratine (**1c**).



Scheme 2. Synthesis of key intermediate acid **6**. TBSOTf = *tert*-butyldimethylsilyl trifluoromethanesulfonate, HMPA = hexamethyl phosphoramide, THP = tetrahydropyran, NMO = 4-methylmorpholine *N*-oxide.

The high diastereoselectivity (93:7)[11] observed in the Pauson–Khand reaction may be explained by considering the relative stability of the intermediates that lead to **5** and **5′**.[12] The preferred conformers of the [alkyne–$Co_2(CO)_6$] complex can be regarded as **A** and **B** in which the TBSO group lies in a pseudo-equatorial position. A weaker repulsion between H7 and the pseudo-axial methyl group in **A** than that between H6 and the axial-like methyl group in **B** favors cyclization through the conformer **A** (Scheme 3).

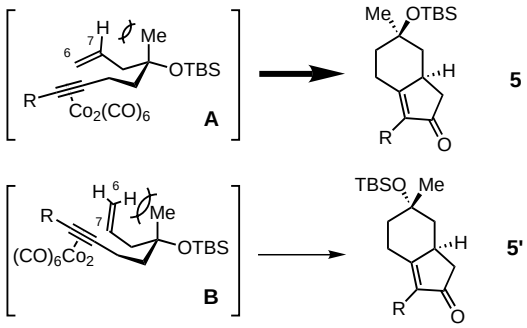
O-Benzoyl-*N*-allylhydroxamine **7** was chosen as a suitable precursor for the crucial radical cyclization, since the addition of tributylstannyl radical to the oxygen atom of the benzoate group would induce cleavage of the weak N–O bond and formation of the desired radical **8** (Scheme 5).[7] Successive treatment of **6** with isobutylchloroformate, *N*-allylhydroxylamine,[13] and benzoyl chloride led to the precursor **7** in 78% yield; the intermediates were not isolated (Scheme 4). We

[*] Prof. S. Z. Zard, F. Gagosz
Laboratoire de Synthèse Organique associé au CNRS
École Polytechnique
91128 Palaiseau (France)
Fax: (+33) 1-6933-3010
E-mail: zard@poly.polytechnique.fr
Dr. J. Cassayre
Present address: Syngenta, 4002 Basel (Switzerland)

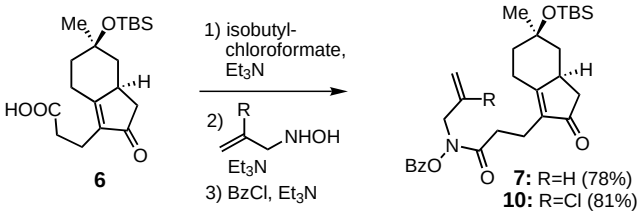
[**] We wish to thank M. Levart for numerous GC/MS spectra, which speeded up our work considerably, as well as A.-C. Callier-Dublanchet and B. Quiclet-Sire for preliminary studies and Patrick Schmizt for the scaling-up of numerous steps.

Supporting information for this article is available on the WWW under http://www.angewandte.com or from the author.

 © WILEY-VCH Verlag GmbH, 69451 Weinheim, Germany, 2002 1433-7851/02/4110-1783 $ 20.00+.50/0

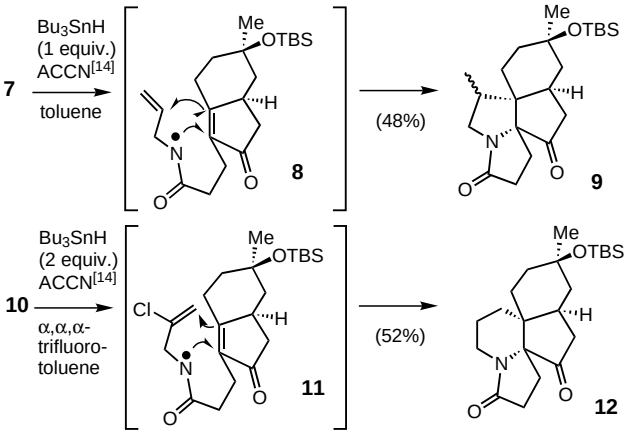


Scheme 3. Conformations of the intermediates in the Pauson–Khand reaction.



Scheme 4. Synthesis of radical precursors **7** and **10**.

were delighted that a cyclization cascade occurred upon slow addition of Bu_3SnH and ACCN[14] to a refluxing solution of **7** in toluene. However, the product was identified as pyrrolidine **9**, which resulted from a 5-*exo*/5-*exo* cyclization mode (48%), despite our expectation that 5-*exo*/6-*endo* mode should have been favored by considering steric factors in the intermediate carbon-centered radical (Scheme 5).

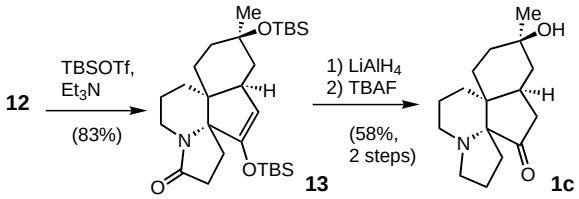


Scheme 5. Synthesis of pyrrolidine **9** and indolizidine **12**.

Clearly, as is usually the case with radical cyclizations, closure of the intermediate amidyl radical occurred from the least hindered convex face of the molecule, thus fixing the relative stereochemistry of **9**. Even though the 13-deoxyserratine skeleton could not be constructed by using **7** as a precursor, amidyl radical **8** proved to be a powerful intermediate since two bonds and two adjacent quaternary centers were created in a stereoselective manner.

To overcome the formation of the second five-membered ring, a small structural modification was performed, inspired by the earlier work of Knapp et al and Smith and coworkers.[15] A chlorine atom was thus placed on the olefinic trap to discourage a 5-*exo* closure without hindering the desired 6-*endo* mode. The new radical precursor **10**, obtained by using *N*-(2-chloroallyl)hydroxylamine instead of *N*-allylhydroxylamine (81%) (Scheme 4), was therefore treated with Bu_3SnH (2 equiv) in α,α,α-trifluorotoluene.[16]

A second equivalent of Bu_3SnH was necessary to reductively remove the chlorine atom in situ after the cascade process. As expected, indolizidine **12**,[17] which contains the correct skeleton of compound **1c**, was isolated as the major product (52%) (Scheme 5). Finally, protection of **12** as the *tert*-butyldimethylsilyl enol ether followed by reduction of the lactam moiety with $LiAlH_4$[18] and deprotection of the alcohol with TBAF completed the synthesis of (±)-13-deoxyserratine (**1c**) in 48% yield over the last three steps (Scheme 6).



Scheme 6. Synthesis of 13-deoxyserratine (**1c**).

In summary, we have in hand a concise (10 steps) and efficient (12% overall yield) synthesis of (±)-13-deoxyserratine (**1c**). The use of an amidyl radical intermediate allowed us to create the two adjacent quaternary centers at C4 and C12 in *one* step, with the correct relative stereochemistry. The presence of these centers in the serratine skeleton has considerably hampered previous approaches. Moreover, the radical cascade can be directed at will to produce either an indolizidine or a pyrrolizidine framework, both of which are found in a large number of alkaloids.

Received: February 27, 2002 [Z 18786]

[1] a) W. A. Ayer, *Nat. Prod. Rep.* **1990**, *8*, 455–463; b) W. A. Ayer, *The Alkaloids*, *Vol. 45*, Academic Press, New York, **1994**, pp. 233–266.

[2] a) T. Harayama, M. Ohtani, M. Oki, Y. Inubushi, *Chem. Pharm. Bull.* **1975**, *23*, 1511; b) T. Harayama, M. Ohtani, M. Oki, Y. Inubushi, *J. Chem. Soc. Chem. Commun.* **1974**, 827–828.

[3] a) T. Harayama, M. Takatani, Y. Inubushi, *Chem. Pharm. Bull.* **1980**, *28*, 1276–1286; b) T. Harayama, M. Takatani, Y. Inubushi, *Tetrahedron. Lett.* **1979**, *20*, 4307–4310.

[4] Y. Inubushi, H. Ishii, T. Harayama, *Chem. Pharm. Bull.* **1967**, *15*, 250.

[5] G. Luedtke, T. Livinghouse *J. Chem. Soc. Perkin Trans. 1* **1995**, 2369–2370.

[6] For reviews of cyclizations of nitrogen-centered radicals, see: a) A. G. Fallis, I. M. Brinza, *Tetrahedron* **1997**, *53*, 17543–17594; b) S. Z. Zard, *Synlett* **1996**, 1148–1158.

[7] a) A.-C. Callier-Dublanchet, B. Quiclet-Sire, S. Z. Zard, *Tetrahedron Lett.* **1994**, *35*, 6109–6112; b) J. Boivin, A.-C. Callier-Dublanchet, B. Quiclet-Sire, S. Z. Zard, *Tetrahedron* **1995**, *51*, 6517–6528; c) A.-C. Callier-Dublanchet, B. Quiclet-Sire, S. Z. Zard, *Tetrahedron Lett.* **1995**, *36*, 8791–8794.

[8] We recently completed a short synthesis of (±)-γ-lycorane which involved a cascade process that started with a nitrogen-centered radical: X. Hoang-Cong, B. Quiclet-Sire, S. Z. Zard, *Tetrahedron Lett.* **1999**, *39*, 2125–2126.

 © WILEY-VCH Verlag GmbH, 69451 Weinheim, Germany, 2002 1433-7851/02/4110-1784 $ 20.00+.50/0

[9] For reviews on the Pauson–Khand reaction, see: a) K. M. Brummond, J. L. Kent, *Tetrahedron* **2000**, *56*, 3263–3283; b) N. E. Schore, *Org. React.* **1991**, *40*, 1–90; c) N. E. Schore in *Comprehensive Organic Synthesis*, *Vol. 5* (Eds.: B. M. Trost, I. Fleming, L. A. Paquette), Pergamon, Oxford, **1991**, pp. 1037–1064.
[10] For acceleration of Pauson–Khand reactions with tertiary amine *N*-oxides, see: a) S. Shambayati, W. E. Crowe, S. L. Schreiber, *Tetrahedron Lett.* **1990**, *31*, 5289–5292; b) N. Jeong, Y. K. Chung, B. Y. Lee, H. L. Lee, S. E. Yoo, *Synlett* **1991**, 204–206.
[11] Determined on the basis of ^{1}H NMR spectroscopic analysis.
[12] C. Mukai, J. S. Kim, H. Sonobe, M. Hanaoka, *J. Org. Chem.* **1999**, *64*, 6822–6832, and references therein.
[13] For the synthesis of *N*-alkylhydroxylamines, see: S. L. Mellor, W. C. Chan, *Chem. Commun.* **1997**, *20*, 2005–2006.
[14] ACCN = 1,1′-azobis(cyclohexanecarbonitrile), VAZO catalyst 88, used as a thermal initiator.
[15] a) S. Knapp, F. S. Gibson, Y. H. Choe, *Tetrahedron Lett.* **1990**, *31*, 5397–5400; b) P. F. Keusenkothen, M. B. Smith, *Tetrahedron* **1992**, *48*, 2977–2992.
[16] The use of α,α,α-trifluorotoluene instead of toluene increased the yield of the reaction (33% →52%); we assume that a possible reduction of the nitrogen-centered radical by abstraction of a benzylic hydrogen atom may occur in toluene.
[17] Structure confirmed on the basis of ^{1}H, ^{13}C, COSY, HMBC, HMQC and NOESY NMR experiments.
[18] Attempts to reduce the lactam moiety selectively in the presence of the ketone failed. For a recent use of a similar procedure to reduce selectively an amide in the presence of a ketone, see: R. Iyengar, K. Schildknegt, J. Aubé, *Org. Lett.* **2000**, *11*, 1625–1627.

Synthesis and Characterization of a Digermanium Analogue of an Alkyne**

Matthias Stender, Andrew D. Phillips, Robert J. Wright, and Philip P. Power*

The heavier Group 14 element analogues of alkynes, in which one or both carbon atoms of the triple bond are replaced by silicon, germanium, tin, or lead, are a unique compound class that has attracted considerable discussion and interest.[1, 2] Over the last decade, a rapidly growing series of computational papers[3–26] have predicted a *trans*-bent structure[27] for heavier-element analogues that carry organic substituents.[16–26] With the exception of the lead compound 2,6-Trip$_2$H$_3$C$_6$PbPbC$_6$H$_3$-2,6-Trip$_2$ (Trip = C$_6$H$_2$-2,4,6-*i*Pr$_3$),[28] which has a planar, *trans*-bent CPbPbC core (Pb-Pb-C = 94.26(4)° and a long, essentially single Pb–Pb bond (Pb–Pb = 3.1881(1) Å),[14, 28] no stable Group 14–Group 14 heavier analogues of alkynes have been described. Various experiments[29–34] have indicated the existence of alkyne-like transient species but none of these has been isolated and no structural details are available. The synthesis, structural characterization, and reaction chemistry of such compounds would provide valuable bonding information, especially in view of the current debate on the nature of multiple bonds between heavier main group elements.[35–39] An additional feature of interest is that these potentially triple-bonded systems have been described as "a final challenge" in the area of main-group multiple bonding.[2] The isolation and structural characterization of a germanium alkyne analogue 2,6-Dipp$_2$H$_3$C$_6$GeGeC$_6$H$_3$-2,6-Dipp$_2$ (**1**; Dipp = C$_6$H$_3$-2,6-*i*Pr$_2$) are now described.

2,6-Dipp$_2$H$_3$C$_6$GeGeC$_6$H$_3$-2,6-Dipp$_2$ **1**

Compound **1** was synthesized by the reaction of Ge(Cl)C$_6$H$_3$-2,6-Dipp$_2$ with potassium in THF or benzene. It was isolated as orange-red crystals which were characterized by ^{1}H and ^{13}C NMR, IR, and UV/Vis spectroscopy and by single-crystal X-ray crystallography.[40] The UV/Vis spectrum displays three relatively intense absorptions at 280, 371, and 501 nm which may be the result of $\pi-\pi^*$ and $n-\pi^*$ transitions. The X-ray structure revealed a centrosymmetric molecule (Figure 1) that has a planar *trans*-bent C1-Ge1-Ge1A-C1A core array as required by symmetry. The

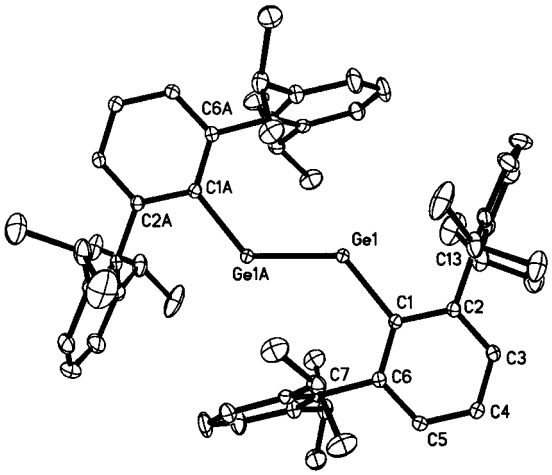


Figure 1. ORTEP plot of **1**, thermal ellipsoids set at 30% probability, H atoms are not shown. Selected bond lengths [Å] and angles [°]. Ge1-Ge1A 2.2850(6), Ge1-C1 1.996(3), C1-C2 1.412(4), C1-C6 1.408(4); Ge1A-Ge1-C1 128.67(8), Ge1-C1-C2 116.9(2), Ge1-C1-C6 124.6(2), C1-C2-C6 118.5(3).

Ge1–Ge1A and Ge1–C1 bond lengths are 2.2850(6) and 1.996(3) Å, and the Ge1-Ge1A-C1A angle is 128.67(8)°. The central aryl ring of the terphenyl ligand is essentially coplanar (torsion angle 0.4°) with the C1-Ge1-Ge1A-C1A array, and the planes of the flanking aryl rings are oriented at approximately 82° with respect to the central aryl ring. The Ge1-C1-C2 and Ge1-C1-C6 angles differ by 7.7° and there is a 4.0° angle between the Ge1-C1 bond and the C1···C4 vector. A cyclic voltammogram of the compound in THF solution displays a reduction wave at −1.38 V and an oxidation at +0.7 V versus the saturated calomel electrode (SCE).

Compound **1** is a stable digermanium analogue of an alkyne. The Ge–Ge distance is considerably shorter than a normal Ge–Ge single bond (ca. 2.44 Å)[41] and indicates the presence of considerable multiple-bonding character. The

[*] Prof. P. P. Power, Dr. M. Stender, Dr. A. D. Phillips, R. J. Wright
Department of Chemistry
University of California
One Shields Avenue, Davis, CA 95616 (USA)
Fax: (+1) 530-752-8995
E-mail: pppower@ucdavis.edu

[**] This work was supported by the National Science Foundation Grant No. 0094913.

 © WILEY-VCH Verlag GmbH, 69451 Weinheim, Germany, 2002 1433-7851/02/4110-1785 $ 20.00+.50/0

Ge–Ge distance is in the shorter half of the known range (2.21 – 2.46 Å) for digermenes—the digermanium analogues of alkenes.[42, 43] The most sterically related digermene is the compound 2,6-$Trip_2H_3C_6$(Me)GeGe(Me)C_6H_3-2,6-$Trip_2$[43] which has Ge–Ge and Ge–C (aryl) distances of 2.3173(3) Å and 1.971(2) Å. On this basis it could be argued that the Ge–Ge bond order in **1** is approximately two—a conclusion that receives support from some calculations.[7] The bending is a consequence of an accumulation of nonbonding electron density at the germanium atoms that is indicative of incipient lone-pair formation.[27] As a result, the Ge–Ge bond strength and order is decreased from idealized triple bonding.[44] Nonetheless, models of RGeGeR species have been described as "digermynes" and as being triply bonded.[5, 10, 45] The chemistry of **1** should reflect the decreased Ge–Ge bond strength and the lone-pair character at the germanium centers.[46]

The structure of **1** may also be compared with those calculated[10] for the closely related, but structurally uncharacterized, derivative **2** which differs only in that it possesses *para-i*Pr substituents on the flanking aryl rings and for the simpler aryl species PhGeGePh.[13]

2,6-$Trip_2H_3C_6$GeGeC_6H_3-2,6-$Trip_2$ **2**

The calculations for **2** afforded an optimized structure with a Ge–Ge distance of 2.277 Å whereas a shorter Ge–Ge bond length of 2.25 Å was calculated for PhGeGePh. These values are in reasonable agreement with the experimentally observed 2.2850(6) Å in **1**. In contrast, the calculated Ge-Ge-C *trans*-bending angle of 123.2° and torsion angle of 22.4° between the germanium coordination planes in **2** differ from the measured values in **1**. In addition, the central aryl rings of the terphenyl groups of the optimized structure of **2** were calculated to be almost perpendicular to the CGeGeC core. The differences between the observed structure of **1** and the calculated structure of **2** underline the important effects of *para-i*Pr substituents of the flanking rings. The coplanarity of the central aryl rings with the CGeGeC array in **1** suggests conjugation between the Ge–Ge multiple bond and the arene. However, the Ge–C distance in **1**, 1.996(3) Å, lies in the range found for terphenyl substituted digermenes (1.971(2) – 2.00(6) Å) where conjugation is precluded by high torsion angles.[43] The structure of **1** emphasizes the large effects that substituents on the periphery of the molecule can have on the molecular configuration. This effect is the key to the successful characterization of a "digermyne". Although the name "digermyne" suggests Ge–Ge triple bonding, a triple bond is present only in the linear, less stable configuration.[7] The bond order in **1** is lower than three owing to the *trans*-bending and the length of the Ge–Ge bond. Bond-order calculations for the *trans*-bent ground-state structures of the model compounds afford the bond order and bond length values: MeGeGeMe (2.097, Ge–Ge = 2.197 Å;[10] 2.10, Ge–Ge = 2.24 Å[15]), PhGeGePh (1.74, Ge–Ge = 2.24 Å[15]).

Experimental Section

Under anaerobic and anhydrous conditions an orange solution of Ge(Cl)C_6H_3-2,6-$Dipp_2$[47] (0.79 g, 1.57 mmol) in THF (10 mL) was added to finely divided potassium (0.064 g, 1.65 mmol; ca. 5% excess) in THF (30 mL) at ambient temperature under vigorous stirring. After around 2 h the reaction mixture began to turn red, and upon stirring for 24 h the solution had become deep red. The THF was removed under reduced pressure and the red solid residue was redissolved in hexane (30 mL). The potassium chloride precipitate and any remaining potassium was allowed to settle and the supernatant solution was removed by decantation. The deep red solution was then concentrated to incipient crystallization (ca. 15 mL). Storage at 5 °C for 12 h yielded the product **1** as carmine red-orange crystals. Yield: 0.28 g, 38%; m.p. 214 – 216 °C (turns dark red/black after melting); Correct C, H analysis; ^{1}H NMR (C_6D_6, 399.77 MHz, 25 °C): δ = 1.05 (d, $^3J_{H,H}$ = 6.8 Hz, 24H; *o*-CH(CH_3)$_2$), 1.30 (d, $^3J_{H,H}$ = 6.8 Hz, 24H; *o*-CH(CH_3)$_2$), 2.72 (sept, $^3J_{H,H}$ = 6.8 Hz, 8H; *o*-C*H*(CH_3)$_2$), 6.91 (d, $^3J_{H,H}$ = 7.2 Hz, 4H; *m*-C_6H_3), 7.09 (d, $^3J_{H,H}$ = 8.0 Hz, 8H; *m*-Dipp), 7.18 (t, $^3J_{H,H}$ = 7.2 Hz, 2H; *p*-C_6H_3), 7.29 ppm (t, $^3J_{H,H}$ = 8.0 Hz, 4H; *p*-Dipp); ^{13}C {^{1}H} NMR (C_6D_6, 100.59 MHz, 25 °C): δ = 25.59 (*o*-CH(*C*H$_3$)$_2$), 26.06 (*o*-CH(*C*H$_3$)$_2$), 31.59 (*o*-*C*H(CH$_3$)$_2$), 124.58 (*m*-Dipp), 127.28 (*p*-C_6H_3), 130.024 (*m*-C_6H_3), 141.36 (*p*-Dipp), 145.67 (*i*-Dipp), 146.81 (*i*-C_6H_3), 147.29 (*o*-Dipp), 158.76 ppm (*o*-C_6H_3); IR (nujol): $\tilde{\nu}$ = 1925(w), 1885(w), 1590(w), 1570(2), 1550(w), 1325(sh), 1055(m), 750(m), 450(w), 320(w) cm^{-1}; UV/Vis (hexanes): λ_{max}, ε(L mol^{-1} cm^{-1}): 501 (7,500), 371 (34,000), 280 nm (28,000).

Received: February 28, 2002 [Z 18790]

[1] The absence of stable examples of such compounds has been discussed for many years. See for example: W. E. Dasent, *Non Existent Compounds*, Marcel Dekker, New York, **1965**; M. J. Taylor, *Metal-to-Metal Bonded States*, Academic, New York, **1975**.

[2] For a short discussion of prospective developments see: P. Jutzi, *Angew. Chem.* **2000**, *112*, 3953; *Angew. Chem. Int. Ed.* **2000**, *39*, 3797.

[3] H. Lischka, H. J. Köhler, *J. Am. Chem. Soc.* **1985**, *105*, 6646.

[4] B. S. Thies, R. S. Grev, H. F. Schaeffer, *Chem. Phys. Lett.* **1987**, *140*, 355; B. T. Colegrove, H. F. Schaeffer, *J. Am. Chem. Soc.* **1991**, *113*, 1557.

[5] R. S. Grev, *Adv. Organomet. Chem.* **1991**, *33*, 125.

[6] K. Kobayashi, S. Nagase, *Organometallics* **1997**, *16*, 2489.

[7] T. L. Allen, W. H. Fink, P. P. Power, *Dalton Trans.* **2000**, 407.

[8] S. Nagase, K. Kobayashi, N. Takagi, *J. Organomet. Chem.* **2000**, *611*, 264.

[9] K. Kobayashi, N. Takagi, S. Nagase, *Organometallics* **2001**, *20*, 234.

[10] N. Takagi, S. Nagase, *Organometallics* **2001**, *20*, 5498.

[11] N. Takagi, S. Nagase, *Chem. Lett.* **2001**, 966.

[12] D. Danovich, F. Ogliaro, M. Karni, Y. Apeloig, D. L. Cooper, S. Shaik, *Angew. Chem.* **2001**, *113*, 4146; *Angew. Chem. Int. Ed.* **2001**, *40*, 4023.

[13] J. Grunenberg, *Angew. Chem.* **2001**, *113*, 4150; *Angew. Chem. Int. Ed.* **2001**, *40*, 4027.

[14] Y. Chen, M. Hartmann, M. Diedenhofen, G. Frenking, *Angew. Chem.* **2001**, *113*, 4146; *Angew. Chem. Int. Ed.* **2001**, *40*, 2051.

[15] A. J. Bridgeman, L. R. Ireland, *Polyhedron* **2001**, *20*, 2841.

[16] For hydrogen-substituted species, E_2H_2 (E = Si, Ge, Sn, or Pb), a hydrogen-bridged structure is often the lowest energy configuration. See refs. [3, 17 – 26].

[17] G. Trinquier, J.-P. Malrieu, *J. Am. Chem. Soc.* **1987**, *109*, 5303.

[18] R. S. Grev, B. L. Deleeuw, H. F. Schaeffer, *Chem. Phys. Lett.* **1990**, *165*, 257.

[19] M. Bogey, H. Bolvin, C. Demuynck, J.-L. Destombes, *Phys. Rev. Lett.* **1991**, *66*, 413.

[20] M. Cordonnier, C. Demuynck, J.-L. Destombes, *J. Chem. Phys.* **1992**, *97*, 7984.

[21] R. S. Grev, H. F. Schaeffer, *J. Chem. Phys.* **1992**, *97*, 7990.

[22] Z. Palagyi, H. F. Schaeffer, E. Kapuy, *J. Am. Chem. Soc.* **1993**, *115*, 6901.

[23] M. T. Nguyen, D. Sengupta, L. G. Vanquickenborne, *Chem. Phys. Lett.* **1995**, *115*, 6901.

[24] R. Stegmann, G. Frenking, *J. Comput. Chem.* **1996**, *17*, 781.

[25] Y. Apeloig, M. Karni, *Organometallics* **1997**, *16*, 310.

[26] S. M. Stogner, R. S. Grev, *J. Chem. Phys.* **1998**, *108*, 5458.

[27] The *trans*-bending in such molecules results from the lower tendency of heavier main-group elements to involve s electrons in bonding.

 © WILEY-VCH Verlag GmbH, 69451 Weinheim, Germany, 2002 1433-7851/02/4110-1786 $ 20.00+.50/0

Alternatively, it can be regarded as a second-order Jahn–Teller distortion arising from mixing of σ* and π levels which are closer in energy in heavier element compounds. For further discussion see: ref. [5] and W. Kutzelnigg, *Angew. Chem.* **1984**, *96*, 262; *Angew. Chem. Int. Ed.* **1984**, *23*, 272.

[28] L. Pu, B. Twamley, P. P. Power, *J. Am. Chem. Soc.* **2000**, *122*, 3524.

[29] A. Sekiguchi, S. S. Zigler, R. West, J. Michl, *J. Am. Chem. Soc.* **1986**, *108*, 4241.

[30] N. Wiberg, C. M. M. Finger, K. Polborn, *Angew. Chem.* **1993**, *105*, 1140; *Angew. Chem. Int. Ed.* **1993**, *32*, 1054.

[31] M. Karni, Y. Apeloig, D. Schröder, W. Zummack, R. Rabezzana, H. Schwarz, *Angew. Chem.* **1998**, *111*, 344; *Angew. Chem. Int. Ed.* **1999**, *38*, 332.

[32] R. Pietschnig, R. West, D. R. Powell, *Organometallics* **2000**, *19*, 2724.

[33] N. Wiberg, W. Niedermayer, H. Nöth, M. Warchold, *Z. Anorg. Allg. Chem.* **2001**, *627*, 1717.

[34] C. Bibal, S. Mazières, H. Gornitzka, C. Couret, *Angew. Chem.* **2001**, *113*, 978; *Angew. Chem. Int. Ed.* **2001**, *40*, 952.

[35] K. W. Klinkhammer, *Angew. Chem.* **1997**, *109*, 2414; *Angew. Chem. Int. Ed.* **1997**, *36*, 2320.

[36] P. P. Power, *Dalton Trans.* **1998**, 2939.

[37] G. H. Robinson, *Acc. Chem. Res.* **1999**, *32*, 773.

[38] A. J. Downs, *Coord. Chem. Rev.* **1999**, *189*, 59.

[39] H. Grützmacher, T. Fässler, *Chem. Eur. J.* **2000**, *6*, 2317.

[40] Crystallographic data for **1** at 90 K with $Mo_{K\alpha}$ ($\lambda = 0.71073$ Å) radiation: $a = 15.991(12)$, $b = 20.514(2)$, $c = 15.927(1)$ Å, orthorhombic, space group *Pccn*, $Z = 4$, $R1 = 0.043$ for 3616 ($I > 2\sigma(I)$) data. CCDC-180660 (**1**) contains the supplementary crystallographic data for this paper. These data can be obtained free of charge via www.ccdc.cam.ac.uk/conts/retrieving.html (or from the Cambridge Crystallographic Data Centre, 12, Union Road, Cambridge CB2 1EZ, UK; fax: (+44) 1223-336-033; or deposit@ccdc.cam.ac.uk).

[41] A. F. Wells, *Structural Inorganic Chemistry*, 5th ed., Oxford, **1984**, p. 1279.

[42] J. Escudié, C. Couret, H. Ranaivonjatovo, J. Satgé, *Coord. Chem. Rev.* **1994**, *130*, 427; P. Rivière, M. Rivière-Baudet, J. Satgé, *Comprehensive Organometallic Chemistry II*, *Vol. 2* (Eds.: E. W. Abel, F. G. A. Stone, G. Wilkinson, A. G. Davies), Pergamon, Oxford, **1995**, chap. 5; K. M. Mackay, *The Chemistry of Organic Germanium, Tin, and Lead Compounds* (Ed.: S. Patai), Wiley, Chichester, **1995**, chap. 2; K. M. Baines, W. G. Stibbs, *Adv. Organomet. Chem.* **1996**, *39*, 275; J. Escudié, C. Couret, H. Ranaivonjatovo, *Coord. Chem. Rev.* **1998**, *178–180*, 565; M. Rivière-Baudet, *Main Group Met. Chem.* **1995**, *118*, 353; J. Escudié, H. Ranaivonjatovo, *Adv. Organomet. Chem.* **1999**, *44*, 113; M. Weidenbruch, *Eur. J. Chem.* **1999**, 373; P. P. Power, *Chem. Rev.* **1999**, *99*, 3463.

[43] M. Stender, L. Pu, P. P. Power, *Organometallics* **2001**, *20*, 1820.

[44] Compounds with triple bonds between almost linearly coordinated germanium and transition-metal centers have been characterized, see: R. S. Simons, P. P. Power, *J. Am. Chem. Soc.* **1996**, *118*, 11966; A. C. Filippou, A. I. Philippopoulos, P. Portius, D. Neumann, *Angew. Chem.* **2000**, *112*, 2881; *Angew. Chem. Int. Ed.* **2000**, *39*, 2778.

[45] It should be noted that the neutral **1** electronically resembles the putative $[(GaC_6H_3\text{-}2,6\text{-}Trip_2)_2]^{2-}$ ion in the controversial compound $Na_2(GaC_6H_3\text{-}2,6\text{-}Trip_2)_2$.[45a] However, such a dianion has not been shown capable of existence as a solvent-separated species, and the core Na_2Ga_2 unit in $Na_2(GaC_6H_3\text{-}2,6\text{-}Trip_2)_2$ has been described as an Na_2Ga_2 cluster with weak Ga–Ga bonding.[45b] a) J. Su, X.-W. Li, C. Crittendon, G. H. Robinson, *J. Am. Chem. Soc.* **1997**, *119*, 5471; b) N. Takagi, M. W. Schmidt, S. Nagase, *Organometallics* **2001**, *20*, 1646.

[46] The reactions of **1** and of its singly and doubly reduced congeners are under investigation. For the structure of the doubly reduced $Na_2(GeC_6H_3\text{-}2,6\text{-}Trip_2)_2$, see: L. Pu, M. O. Senge, M. M. Olmstead, P. P. Power, *J. Am. Chem. Soc.* **1998**, *120*, 12682.

[47] This compound was synthesized in an identical manner to its $\text{-}C_6H_3\text{-}2,6\text{-}Trip_2$ substituted analogue[43] by the reaction of $GeCl_2 \cdot$ dioxane with $LiC_6H_3\text{-}2,6\text{-}Dipp_2$.[48]

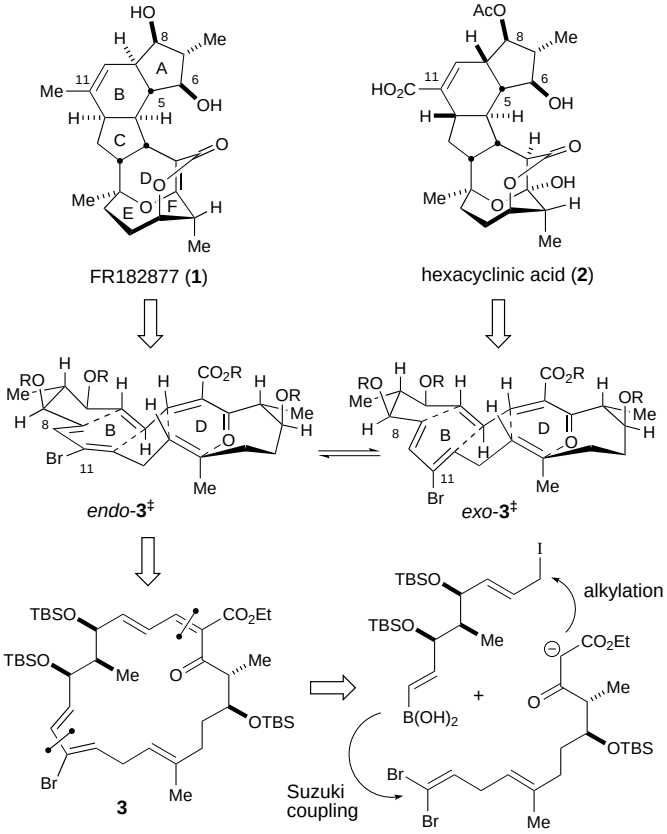
[48] B. Schiemenz, P. P. Power, *Angew. Chem.* **1996**, *108*, 2288; *Angew. Chem. Int. Ed.* **1996**, *35*, 2150.

A Cascade Cycloaddition Strategy Leading to the Total Synthesis of (−)-FR182877**

David A. Evans* and Jeremy T. Starr

Herein we outline a general strategy for the synthesis of the closely related natural products FR182877 (**1**)[1] and hexacyclinic acid (**2**)[2] from a common macrocyclic precursor (**3**) by a sequence of transannular [4+2] cycloadditions (Scheme 1).[3, 4] This approach has been validated by its successful application to the enantioselective synthesis of (−)-FR182877, and provided confirmation of its assigned absolute configuration.

The cytotoxic substance FR182877 (**1**) was isolated from *Streptomyces* sp. No. 9885 in 1998, and at that time was reported as the enantiomer to the illustrated structure (Scheme 1).[1a] FR182877 exhibits microtubule stabilizing



Scheme 1. FR182877 and hexacyclinic acid retrosynthesis.

[*] Prof. D. A. Evans, Dr. J. T. Starr
Department of Chemistry and Chemical Biology
Harvard University
Cambridge, MA 02138 (USA)
Fax: (+1) 617-495-1460
E-mail: evans@chemistry.harvard.edu

[**] Financial support was provided by the NIH (GM-33327). A postdoctoral fellowship from the NIH (J.T.S.) is gratefully acknowledged. Dr. Bunji Sato and Dr. Seiji Yoshimura of Fujisawa Pharmaceutical Corp. are gratefully acknowledged for providing helpful advice and spectra of natural FR182877 and its derivatives.

Supporting information for this article is available on the WWW under http://www.angewandte.com or from the author.

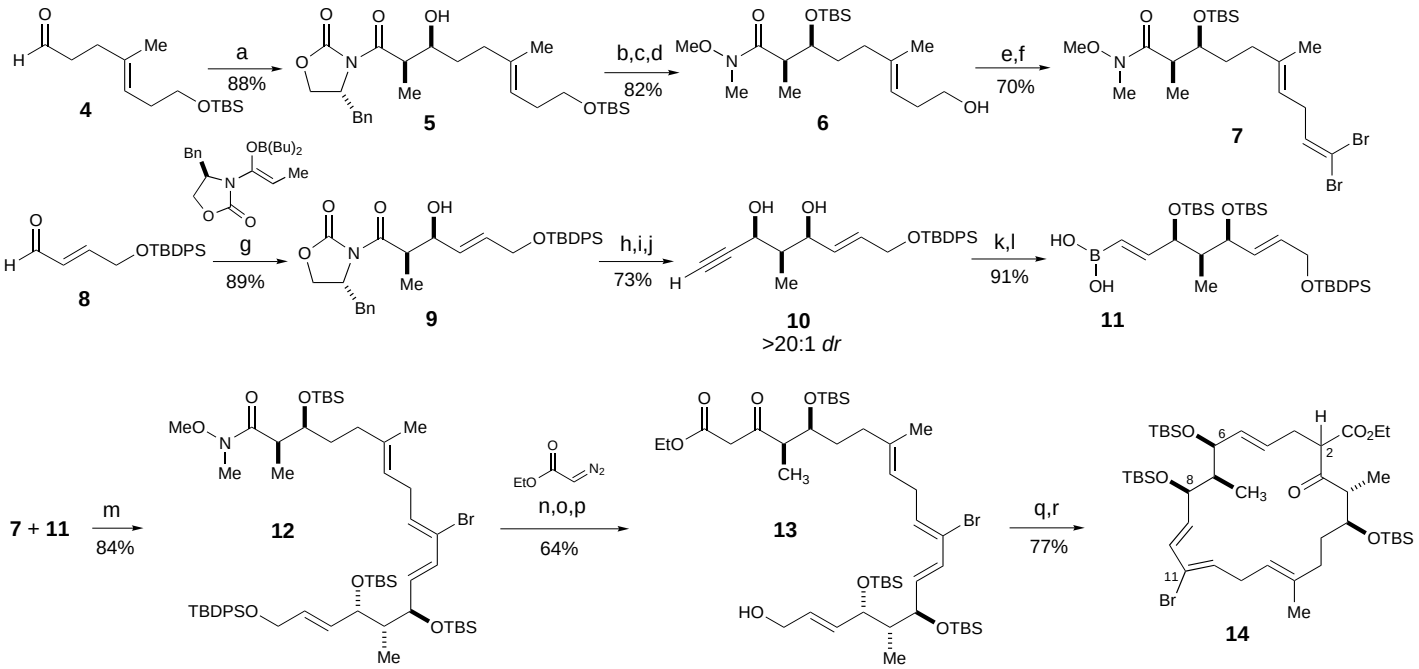
activity similar to the mode of action of paclitaxel and shows potent cytotoxicity towards multiple tumor cell lines.[1b, 1c] The hexacyclic structure includes a bridgehead enol ether and an embedded cyclohexene ring which suggest it originates biosynthetically from a sequence of intramolecular [4+2] cycloaddition events.[1d]

The recently reported hexacyclinic acid (**2**) bears a strong resemblance to **1** and is probably biosynthetically related.[2] FR182877 and hexacyclinic acid have common relative and absolute configurations of the C6–C8 substituents as well as of the entire lower DEF ring system. The only important stereochemical difference between **1** and **2** is in the relationships of the ring fusions in the ABC ring system.

The gross structures and relative stereochemistries of **1** and **2** were established by X-ray crystallographic analysis, and the absolute configurations were determined in each case by the Mosher ester method.[5] However, on the basis of our own analysis of the reported data for the FR182877 Mosher esters, we suspected its absolute configuration may be opposite to the published assignment and instead be in agreement with the hexacyclinic acid assignment. This suspicion was later confirmed by the recent publication of the structure illustrated in Scheme 1.[1e]

The suspected stereochemical relationship between FR182877 and hexacyclinic acid led us to target macrocycle **3** as a precursor common to both natural products. The pivotal transformations associated with both syntheses are the sequential transannular Diels–Alder (TADA)[3a–c] and hetero-Diels–Alder[3d–g] cycloadditions (Scheme 1). Given the assumption that the transannular Diels–Alder reaction would be the initiating cycloaddition, the *endo*-**3** transition state should afford the FR182877 skeleton while the diastereomeric *exo*-**3** transition state should afford the hexacyclinic acid ring system. Since we did not know, a priori, the stereochemical outcome of the postulated cyclization events, we designed **3** with a bromine substituent at C11 so that it could serve as a common intermediate for the synthesis of either natural product.

The convergent synthesis of **3** began with the syntheses of two principal fragments **7** and **11** of comparable complexity (Scheme 2). Synthesis of **7** began with an aldol addition of (*R*)-4-benzyl-*N*-propionyl-2-oxazolidinone to **4** mediated by dibutylboron triflate to give *syn* aldol adduct **5** in 88% yield.[6] Conversion of **5** into the Weinreb amide (Me_3Al, $MeNH_2O$-MeCl, 96%),[7] silylation of the secondary hydroxyl group (TBSCl, 96%), then desilylation of the primary hydroxyl group (1:4 TsOH:nBu_4NHSO_4, MeOH, 89%) gave primary alcohol **6**. Oxidation (DMP, 94%)[8] and Corey–Fuchs olefination (CBr_4, PPh_3, 74%)[9] gave the desired vinyldibromide fragment **7**. The synthesis of **11** began with the same boron-enolate-mediated aldol addition described above to aldehyde **8** to give the expected *syn* aldol adduct **9** in 89% yield. The conversion of **9** into the Weinreb amide (Me_3Al, $MeNH_2OMeCl$, 97%), was followed by alkynone formation (HCCMgBr, 77%),[10] and diastereoselective *syn* reduction by using Kiyooka's method (DIBAL, THF, *dr* > 20:1, 98%),[11] to give diol **10**. Double silylation (TBSCl, 94%) was then followed by hydroboration (catecholborane, cat. Cy_2BH) and saponification (1N NaOH, 97%) to give the desired boronic acid fragment **11**.[12]

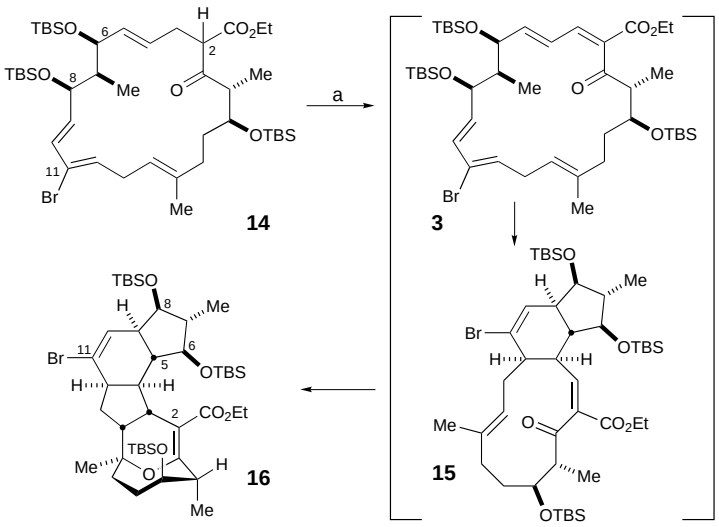


Scheme 2. Reagents and conditions: a) (*R*)-4-benzyl-*N*-propionyl-2-oxazolidinone, Bu_2BOTf, TEA, 88%; b) MeNHOMe/HCl, Me_3Al, THF, 96%; c) TBSCl, imid., 96%; d) TsOH:nBu_4NHSO_4 (1:4), MeOH, 89%; e) DMP, 94%; f) CBr_4, PPh_3, 74%; g) (*R*)-4-benzyl-*N*-propionyl-2-oxazolidinone, Bu_2BOTf, TEA, 89%; h) MeNHOMe/HCl, Me_3Al, THF, 97%; i) HCCMgBr, THF, 77%; j) DIBAL, THF, *dr* > 20:1, 98%; k) TBSCl, imid., 94%; l) cat. Cy_2BH, catecholborane then 1N NaOH, 97% (crude); m) $Pd(PPh_3)_4$, Tl_2CO_3, 84%; n) DIBAL, THF; o) ethyl diazoacetate, cat. $SnCl_2$, 70% (2 steps); p) nBu_4NF, AcOH, 92%; q) I_2, PPh_3; r) Cs_2CO_3, 77% two diastereomers (1:1); TBS = *tert*-butyldimethylsilyl; Bn = benzyl; TBDPS = *tert*-butyldiphenylsilyl; DIBAL = diisobutylaluminum hydride; TsOH = *p*-toluenesulfonic acid; DMP = Dess–Martin Periodinane; TEA = triethylamine; Tf = trifluoromethanesulfonyl; imid. = imidazole; Cy_2BH = dicyclohexylborane.

 © WILEY-VCH Verlag GmbH, 69451 Weinheim, Germany, 2002 1433-7851/02/4110-1788 $ 20.00+.50/0 *Angew. Chem. Int. Ed.* **2002**, *41*, No. 10

Suzuki coupling of **7** and **11** (Tl_2CO_3, $Pd(PPh_3)_4$, 84%) gave, regioselectively, bromodiene **12**.[13] Reduction to the corresponding aldehyde (DIBAL) was followed by a two carbon homologation (ethyl diazoacetate, $SnCl_2$, 70%, 2 steps)[14] and selective removal of the TBDPS group (nBu$_4$NF hydrate, HOAc, DMF, 92%) to provide **13**.[15] Iodination of **13** (I_2, PPh_3) gave a sensitive allyl iodide that was immediately submitted to macrocyclization conditions (Cs_2CO_3, THF, RT, 77%, 2 steps) to give **14** as a 1:1 mixture of diastereomers, epimeric at C2.[16] It was correctly anticipated that this intermediate, lacking the C2–C3 double bond, would not engage in a transannular Diels–Alder reaction.

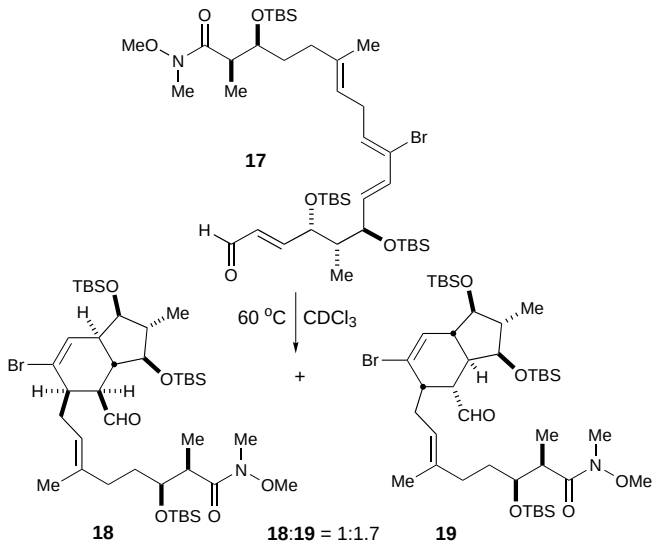
Oxidation of **14** ($Ph_2Se_2O_3$, TEA, THF, RT then 50 °C)[17] initiated a sequence of transannular cycloadditions (**3** → **15** → **16**) culminating in the formation of **16** as a single diastereomer and the only isolable product (63% yield; Scheme 3). The macrocyclic conformation of **3** appears to



Scheme 3. Reagents and conditions: a) $Ph_2Se_2O_3$, SO_3/pyridine, TEA, THF, RT (2 h) then 50 °C (6 h), 63%.

predispose the reacting olefin/carbonyl faces to a single orientation, and the resulting high stereoselectivity of the cycloaddition sequence stands in stark contrast to the results obtained by us and Sorensen and co-workers in similar acyclic systems.[18] We observed excellent *endo* selectivity in a related acyclic intramolecular Diels–Alder cycloaddition (IMDA) study (Scheme 4), but only 1:1.7 diastereoface selectivity was realized. Sorensen and co-workers observed 1.6:1 diastereoface selectivity in a similar system leading to an analogous pair of *endo* diastereomers.[18b]

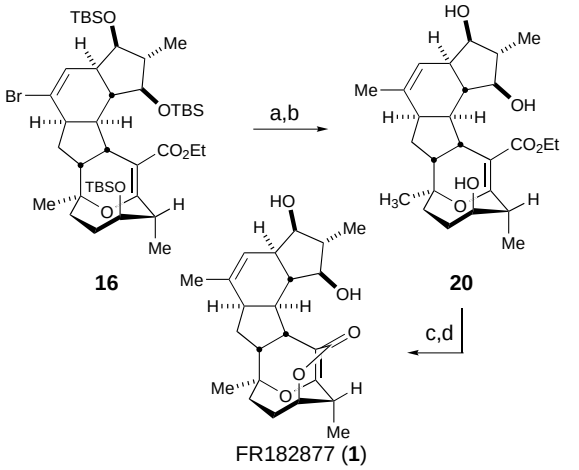
COSY and NOESY studies established the C5 center of **16** as having the desired configuration relative to the C6–C8 triad, but lacked a suitably diagnostic NOESY crosspeak to assign the C9 and C12 stereocenters unambiguously. Since **1** and **2** have the C5 stereocenter in common, we could only surmise that **16** must correspond to one of the natural product configurations for the ABC system, but the question of which one remained unanswered at this stage. Comparison of the coupling patterns for the C5–C9 protons in the ^{1}H NMR spectrum of **16** to the corresponding signals in the ^{1}H NMR of spectrum of aldehyde **18** obtained in our IMDA study



Scheme 4. Open-chain intramolecular Diels–Alder results.

provided qualitative evidence that the substituents at C5 and C9 were *trans* in **16** and corresponded to the ring system of FR182877. This similarity encouraged us to proceed on the premise that a successful synthesis of **1** from **16** would confirm the structure assignment of **16**.

Scheme 5 illustrates the final steps in the synthesis of **1**. Global desilylation of **16** (HF/CH_3CN, 89%) was followed by Suzuki methylation by using the recently reported procedure of Gray et al. ($Me_3B_3O_3$, $[Pd(dppf)Cl_2]$, Cs_2CO_3, 71%) to give **20**.[19] Saponification of the ethyl ester (TMSOK, THF)[20] and lactonization (1-methyl-2-chloropyridinium iodide, $NaHCO_3$, 62%, 2 steps)[21] afforded a white solid whose ^{1}H NMR and ^{13}C NMR spectra as well as mass spectral characteristics were identical to those published for the natural product.[22] In addition, synthetic **1** exhibited an optical rotation of $[\alpha]_D^{23} = -5^\circ$ while that reported for the natural sample was $[\alpha]_D^{23} = -3.5^\circ$. This observation led us to conclude that synthetic **1** was of the same absolute stereochemistry as natural (−)-FR182877, therefore confirming the corrected structure.



Scheme 5. Reagents and conditions: a) HF/CH_3CN 5:95; 89%; b) trimethylboroxine, Cs_2CO_3, $[Pd(dppf)Cl_2]$, DMF, 80 °C, 71%; c) TMSOK, THF; d) Mukaiyama's reagent, $NaHCO_3$, 62% (2 steps). dppf = 1,1′-bis(diphenylphosphanyl)ferrocene; TMS = trimethylsilyl.

 © WILEY-VCH Verlag GmbH, 69451 Weinheim, Germany, 2002 1433-7851/02/4110-1789 $ 20.00+.50/0

Efforts are underway to access the alternate transannular [4+2] cycloaddition pathway leading to the hexacyclinic acid framework, and will be reported in due course.

Received: March 15, 2002 [Z18907]

[1] a) H. Muramatsu, M. Miyauchi, B. Sato, S. Yoshimura, *40th Symposium on the Chemistry of Natural Products* (Fukuoka, Japan), **1998**, Paper 83, p. 487; b) B. Sato, H. Muramatsu, M. Miyauchi, Y. Hori, S. Takese, M. Mino, S. Hashimoto, H. Terano, *J. Antibiot.* **2000**, *53*, 123. Susceptible cell lines were : MCF-7 ($IC_{50}=27\ ng\,mL^{-1}$), A549 ($IC_{50}=73 ng\,mL^{-1}$), HT-29 ($IC_{50}=73\ ng\,mL^{-1}$), Jurkat ($IC_{50}=33\ ng\,mL^{-1}$), P388 ($IC_{50}=21\ ng\,mL^{-1}$), and B16 ($IC_{50}=67\ ng\,mL^{-1}$); c) B. Sato, H. Makajima, Y. Hori, M. Hino, S. Hashimoto, H. Terano, *J. Antibiot.* **2000**, *53*, 204; d) S. Yoshimura, B. Sato, T. Kinoshita, S. Takese, H. Terano, *J. Antibiot.* **2000**, *53*, 615; e) S. Yoshimura, B. Sato, T. Kinoshita, S. Takese, H. Terano, *J. Antibiot.* **2002**, *55*, C-1.

[2] R. Höfs, M. Walker, A. Zeeck, *Angew. Chem.* **2000**, *39*, 3400; *Angew. Chem. Int. Ed.* **2000**, *39*, 3258.

[3] a) For a review of TADA reactions, see E. Marsault, A. Toro, P. Nowak, P. Deslongchamps, *Tetrahedron* **2001**, *57*, 4243; b) for a recent example in synthesis, see also longithorone A: M. E. Layton, C. A. Morales, M. D. Shair, *J. Am. Chem. Soc.* **2002**, *124*, 773; c) for the use of a bromodiene in a TADA reaction, see W. R. Roush, K. Koyama, M. L. Curtin, K. J. Moriarty, *J. Am. Chem. Soc.* **1996**, *118*, 7502; d) for this type of hetero-[4+2] cycloaddition, see K. Shin, M. Moriya, K. Ogasawara, *Tetrahedron Lett.* **1998**, *39*, 3765; e) S. Takano, S. Satoh, K. Ogasawara, *J. Chem. Soc. Chem. Commun.* **1988**, 59; f) S. Takano, S. Satoh, K. Ogasawara, K. Aoe, *Heterocycles* **1990**, *30*, 583; g) M. Yamauchi, S. Katayama, O. Baba, T. Watanabe, *J. Chem. Soc. Chem. Commun.* **1983**, 281.

[4] Sorensen and co-workers have recently completed a synthesis of FR182877 through an approach that is closely related to the route described in this Communication: D. A. Vosburg, C. D. Vanderwal, E. J. Sorenson, *J. Am. Chem. Soc.* **2002**, *ASAP*.

[5] I. Ohtani, T. Kusumi, Y. Kashman, H. Kakisawa, *J. Am. Chem. Soc.* **1991**, *113*, 4092. See also ref. [1d] for analytical data on the Mosher esters of FR182877.

[6] J. R. Gage, D. A. Evans, *Org. Synth.* **1990**, *68*, 77.

[7] H. Ishiwata, H. Sone, H. Kigoshi, K. Yamada, *J. Org. Chem.* **1994**, *59*, 4712.

[8] D. B. Dess, J. C. Martin, *J. Am. Chem. Soc.* **1991**, *113*, 7277.

[9] E. J. Corey, P. L. Fuchs, *Tetrahedron Lett.* **1972**, 3769.

[10] M. A. Brodney, J. P. O'Leary, J. A. Hansen, R. J. Giguere, *Synth. Commun.* **1995**, *25*, 521.

[11] S.-i. Kiyooka, H. Kuroda, Y. Shimasaki, *Tetrahedron Lett.* **1986**, *27*, 3009.

[12] A. Arase, M. Hoshi, A. Mijin, K. Nishi, *Syn. Commun.* **1995**, *25*, 1957.

[13] a) For a review, see N. Miyaura, A. Suzuki, *Chem. Rev.* **1995**, *95*, 2457; b) for the use of TlOH, see J. Uenishi, J. M. Beau, R. W. Armstrong, Y. Kishi, *J. Am. Chem. Soc.* **1987**, *109*, 4756; c) for the use of TlOEt, see S. A. Frank, H. Chen, R. K. Kunz, M. J. Schnaderbeck, W. R. Roush, *Org. Lett.* **2000**, *2*, 2691; d) for the use of Tl_2CO_3, see I. E. Marko, F. Murphy, S. Dolan, *Tetrahedron Lett.* **1996**, *37*, 2507; e) for the first Suzuki coupling with vinyldibromide, see W. R. Roush, R. Riva, *J. Org. Chem.* **1988**, *53*, 710.

[14] C. R. Holmquist, E. J. Roskamp, *J. Org. Chem.* **1989**, *54*, 3258.

[15] S. Higashibayashi, K. Shinko, T. Ishizu, K. Hashimoto, H. Shirahama, M. Nakata, *Synlett* **2000**, 1306.

[16] For a Cs_2CO_3-mediated macrocarbocyclization, see S. Phoenix, E. Bourque, P. Deslongchamps, *Org. Lett.* **2000**, *2*, 4149.

[17] L. Ouellet, P. Langlois, P. Deslongchamps, *Synlett* **1997**, 689, and references therein.

[18] a) C. D. Vanderwal, D. A. Vosberg, S. Weiler, E. J. Sorensen, *Org. Lett.* **1999**, *1*, 645; b) C. D. Vanderwal, D. A. Vosberg, E. J. Sorensen, *Org. Lett.* **2001**, *3*, 4307.

[19] M. Gray, I. P. Andrews, D. F. Hook, J. Kitteringham, M. Voyle, *Tetrahedron Lett.* **2000**, *41*, 6237.

[20] E. D. Laganis, B. L. Chenard, *Tetrahedron Lett.* **1984**, *25*, 5831.

[21] T. Mukaiyama, M. Usui, K. Saigo, *Chem. Lett.* **1976**, 49.

[22] A sample of natural FR182877 was not available for direct comparison.

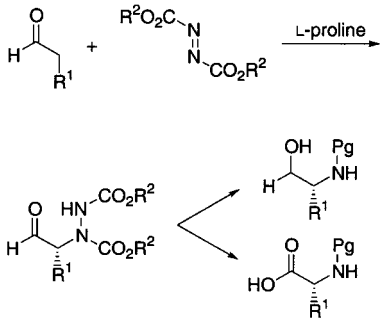
Direct Organo-Catalytic Asymmetric α-Amination of Aldehydes—A Simple Approach to Optically Active α-Amino Aldehydes, α-Amino Alcohols, and α-Amino Acids**

Anders Bøgevig, Karsten Juhl, Nagaswamy Kumaragurubaran, Wei Zhuang, and Karl Anker Jørgensen*

One of the ultimate goals and challenges in chemistry is to develop stereoselective transformations for the creation of functionalized optically active molecules with structural diversity from simple and easily available starting materials. Several procedures to generate optically active molecules are known and among these asymmetric catalysis plays an important role.

The importance of optically active α-amino acids, α-amino aldehydes, and α-amino alcohols, formed by asymmetric catalysis,[1] has stimulated an enormous development in synthetic strategies, and two different catalytic, enantioselective approaches are attractive: the C–C and the C–N bond-forming reactions. The catalytic enantioselective C–C bond-forming reactions include the addition to imines, such as the Strecker[2] and Mannich[3] reactions.

The catalytic, enantioselective, direct C–N bond-forming reaction using aldehydes and a nitrogen source, such as azodicarboxylates, would constitute one of the simplest procedures for the construction of a stereogenic carbon center attached to a nitrogen atom (Scheme 1). Recently, we presented the first direct, enantioselective α-amination of 2-keto esters catalyzed by chiral copper(II)–bisoxazoline complexes.[4, 5] This development led to a simple synthetic approach to optically active *syn*-β-amino-α-hydroxy esters.



Scheme 1. Pg = protecting group.

[*] Prof. Dr. K. A. Jørgensen, Dr. A. Bøgevig, Dr. K. Juhl, Dr. N. Kumaragurubaran, W. Zhuang
Center for Catalysis
Department of Chemistry
Aarhus University
8000 Aarhus C (Denmark)
Fax: (+45) 8919-6199
E-mail: kaj@chem.au.dk

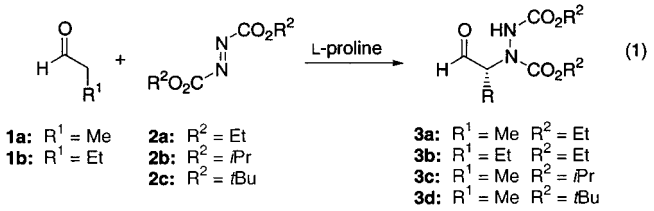
[**] This work was made possible by a grant from The Danish National Research Foundation.

Supporting information for this article is available on the WWW under http://www.angewandte.com or from the author.

 © WILEY-VCH Verlag GmbH, 69451 Weinheim, Germany, 2002 1433-7851/02/4110-1790 $ 20.00+.50/0

Herein we present the first catalytic, enantioselective, direct α-amination of aldehydes, that is, the successful and unprecedented use of unmodified aldehydes for the stereoselective creation of C–N bonds using L-proline[3c,d, 6, 7] as the catalyst (Scheme 1). These reactions give an easy and simple access to many classes of optically active molecules with high structural diversity. The molecules include α-amino aldehydes, α-amino alcohols, and α-amino acids, all key chiral elements in many natural products as well as in medicinal chemistry.

The results for the direct α-amination of some representative aldehydes **1a**, **b** with different azodicarboxylates **2a**–**c** catalyzed by L-proline [Eq. (1)] under various reaction conditions are presented in Table 1.



(1)

1a: R^1 = Me
1b: R^1 = Et

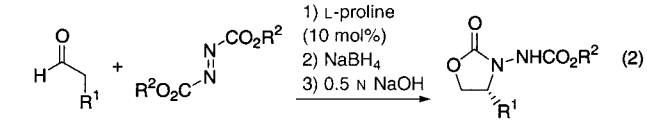
2a: R^2 = Et
2b: R^2 = *i*Pr
2c: R^2 = *t*Bu

3a: R^1 = Me R^2 = Et
3b: R^1 = Et R^2 = Et
3c: R^1 = Me R^2 = *i*Pr
3d: R^1 = Me R^2 = *t*Bu

Propanal **1a** reacts with diethyl azodicarboxylate (DEAD) **2a** catalyzed by L-proline at room temperature under ambient conditions in CH_2Cl_2 and the α-aminated product **3a** is formed in 93% yield and with 92% *ee* (Table 1, entry 1). The procedure for the isolation of the α-aminated product is remarkable: addition of H_2O and extraction with Et_2O followed by evaporation of the excess aldehyde and the solvent gives pure **3a**. At 0 °C the enantioselectivity of the reaction is not significantly improved (93% *ee*). However, the reaction also proceeds with lower catalyst loadings (Table 1, entries 2–4) and a highly enantioselective reaction takes place using only 2 mol% of L-proline as the catalyst. A variety of other solvents can also be applied with success for the catalytic, enantioselective, direct α-amination reaction (Table 1, entries 5–9). Butanal **1b** is α-aminated, in good yield, and high enantioselectivity using DEAD **2a** to give **3b** in 77% yield and 90% *ee* (Table 1, entry 10). The direct α-amination of **1a** was also investigated for the azodicarboxylates **2b**, **c** (Table 1, entries 11 and 12) to introduce more useful *N*-protecting groups (see below).

Further attractive features of the L-proline-catalyzed direct α-amination reactions are: 1) the neat reaction proceeds smoothly in, for example, propanal with only a slight decrease in enantioselectivity,[8] and 2) the reaction can also be performed in gram scale with the same high yield and enantioselectivity (e.g. propanal reacts with DEAD (10 mmol scale) to give the α-aminated product **3a** in 98% yield and 92% *ee*).

The enantiomeric excesses of the products formed by the direct α-amination of aldehydes decrease slowly because of the acidity of the α-position next to the carbonyl group. This problem can easily be solved by the in situ reduction of the aldehyde group of the α-aminated aldehydes. This approach leads to a simple, catalytic, enantioselective procedure for the formation of valuable α-amino alcohols [Eq. (2)]. To simplify the isolation and analytical procedures the α-amino alcohols were converted into the *N*-amino oxazolidinones **4**. The results are presented in Table 2.



(2)

1a: R^1 = Me
1b: R^1 = Et
1c: R^1 = *i*Pr
1d: R^1 = *t*Bu
1e: R^1 = allyl
1f: R^1 = Bn

2a: R^2 = Et
2d: R^2 = Bn

4a: R^1 = Me R^2 = Et
4b: R^1 = Et R^2 = Et
4c: R^1 = *i*Pr R^2 = Et
4d: R^1 = *t*Bu R^2 = Et
4e: R^1 = allyl R^2 = Et
4f: R^1 = Bn R^2 = Et
4g: R^1 = *i*Pr R^2 = Bn

The various aldehydes **1a**–**f** all react with azodicarboxylates affording the α-aminated aldehydes in high yields and enantioselectivities in the presence of L-proline (10 mol%) as the catalyst. Further transformations give the *N*-amino oxazolidinones **4**. The results given in Table 2, entries 1 and

Table 1. Catalytic, enantioselective, direct α-amination of aldehydes **1a**, **b** using the azodicarboxylates **2a**–**c** catalyzed by L-proline under various reaction conditions.[a]

Entry	Aldehyde	Azodicarboxylate	Solvent	Cat. Load [%]	Reaction time [min]	Yield [%][b]	*ee* [%][c]
1	R^1 = Me (**1a**)	R^2 = Et (**2a**)	CH_2Cl_2	50	45	**3a**–93	92
2	R^1 = Me (**1a**)	R^2 = Et (**2a**)	CH_2Cl_2	20	55	**3a**–82	92
3	R^1 = Me (**1a**)	R^2 = Et (**2a**)	CH_2Cl_2	5	105	**3a**–87	91
4	R^1 = Me (**1a**)	R^2 = Et (**2a**)	CH_2Cl_2	2	300	**3a**–92	84
5	R^1 = Me (**1a**)	R^2 = Et (**2a**)	$ClCH_2CH_2Cl$	50	120	**3a**–87	89
6	R^1 = Me (**1a**)	R^2 = Et (**2a**)	MeCN	50	30	**3a**–70	91
7	R^1 = Me (**1a**)	R^2 = Et (**2a**)	EtOAc	50	300	**3a**–77	81
8	R^1 = Me (**1a**)	R^2 = Et (**2a**)	toluene	50	450	**3a**–81	86
9	R^1 = Me (**1a**)	R^2 = Et (**2a**)	dioxane	50	50	**3a**–86	68
10	R^1 = Et (**1b**)	R^2 = Et (**2a**)	CH_2Cl_2	10	120	**3b**–77	90
11	R^1 = Me (**1a**)	R^2 = *i*Pr (**2b**)	CH_2Cl_2	10	105	**3c**–91	88
12	R^1 = Me (**1a**)	R^2 = *t*Bu (**2c**)	CH_2Cl_2	10	205	**3d**–99	89

[a] Experimental conditions: L-proline was added to a stirred solution of the azodicarboxylate (1.0 mmol) and aldehyde (1.5 mmol) in the solvent (3 mL) at room temperature. The reaction mixture was quenched with H_2O (5 mL), extracted with Et_2O, and dried over anhydrous Na_2SO_4. The solvent and the excess aldehyde were removed by evaporation (see Supporting Information). [b] Yield of isolated product. [c] Enantiomeric excesses determined by GC using a chiral Chrompack CP Chiralsil-Dex Cβ column.

 © WILEY-VCH Verlag GmbH, 69451 Weinheim, Germany, 2002 1433-7851/02/4110-1791 $ 20.00+.50/0

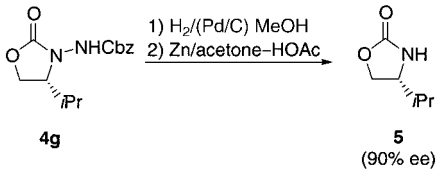
Table 2. Catalytic, enantioselective, direct α-amination of aldehydes **1a–f** with azodicarboxylates **2a**, **d** catalyzed by L-proline (10 mol%) at room temperature in CH_2Cl_2 [Eq. (2)].[a]

Entry	Aldehyde	Azodicarboxylate	Yield [%][b]	*ee* [%][c]
1	R^1 = Me (**1a**)	R^2 = Et (**2a**)	**4a** – 67	93
2	R^1 = Et (**1b**)	R^2 = Et (**2a**)	**4b** – 77	95
3	R^1 = *i*Pr (**1c**)	R^2 = Et (**2a**)	**4c** – 83	93
4	R^1 = *t*Bu (**1d**)	R^2 = Et (**2a**)	**4d** – 57	91
5	R^1 = allyl (**1e**)	R^2 = Et (**2a**)	**4e** – 92	93
6	R^1 = Bn (**1f**)	R^2 = Et (**2a**)	**4f** – 68	89
7	R^1 = *i*Pr (**1c**)	R^2 = Bn (**2d**)	**4g** – 70	91

[a] Experimental conditions: L-proline (11.5 mg, 0.10 mmol) was suspended in CH_2Cl_2 (2.5 mL) followed by the addition of the aldehyde (1.50 mmol) and the azodicarboxylate (1.00 mmol). The reaction mixture was stirred at room temperature until the yellow color of the azodicarboxylate disappeared. MeOH (2.5 mL) was added followed by careful addition of $NaBH_4$ (50 mg). After 20 min, NaOH (0.5 N, 2.5 mL) was added and after 2 h the organic solvents were removed in vacuo. The aqueous phase was diluted and extracted with EtOAc and the organic phase dried over anhydrous $MgSO_4$ and concentrated in vacuo to give pure *N*-amino oxazolidinones (see Supporting Information). [b] Yield of isolated product. [c] *ee* values determined by GC using a chiral Chrompack CP Chiralsil-Dex Cβ column or by chiral HPLC.

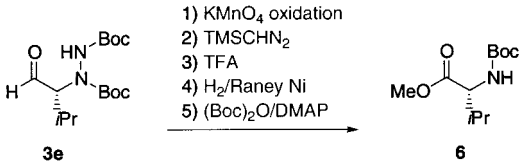
2 show that the masked α-amino alcohols are obtained with excellent enantioselectivity and that a slightly higher enantioselectivity is obtained when the aldehyde is reduced to the alcohol prior to workup. The other aldehydes **1c–f** are directly α aminated in a highly enantioselective fashion with DEAD **2a** in the presence of L-proline as the catalyst to give, after reduction and cyclization, the corresponding oxazolidinones in high yields and very high enantioselectivities (Table 2, entries 3–6, 89% to 93% *ee*). To expand the scope of the reaction we also treated **1c** with dibenzyl azodicarboxylate **2d** in the presence of L-proline (10 mol%) as the catalyst. The *N*-Cbz protected (Cbz = phenylmethoxycarbonyl) *N*-amino oxazolidinone **4g** was isolated in 70% yield and 91% *ee* (Table 2, entry 7) thus showing that a readily removable protecting group can be introduced.

The *N*-protecting group and the N–N bond in the *N*-amino oxazolidinone **4g** can be removed and cleaved, respectively. The α-aminated product **4g** is first treated with H_2/(Pd/C), followed by reaction with Zn/acetone in acetic acid to afford oxazolidinone **5** in 31% overall yield based on **2d** [Eq. (3)]. The absolute configuration of **5** has been assigned as *R*.[9] Hydrolysis of the oxazolidinones at this point would give the α-amino alcohols.[10]



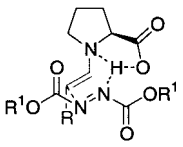
4g **5** (90% ee) (3)

A very important aspect of the direct α-amination reaction is the easy and attractive access it gives to optically active nonproteogenic α-amino acids. Reaction of 3-methyl butanal (**1c**) with di-*tert*-butyl azodicarboxylate (**2c**) catalyzed by L-proline (10 mol%, CH_2Cl_2, 4 h, RT) gives the α-hydrazino aldehyde **3e** (>90% yield). Oxidation of the aldehyde by $KMnO_4$ to the carboxylic acid and esterification followed by hydrolysis of the Boc groups (Boc = *tert*-butoxycarbonyl), reduction, and finally a *N*-Boc protection gives the *N*-Boc-protected valine methyl ester **6** [Eq. (4); TMS = trimethylsilyl, TFA = trifluoroacetic acid, DMAP = 4-dimethylaminopyridine] maintaining the enantiomeric excess obtained in the enantioselective amination step (90% *ee*). The absolute configuration of the chiral carbon center in **6** was assigned as *R*.[11]



3e **6** (4)

Based on the absolute configuration of the α-aminated products, we propose the transition-state model **7** for the reaction. The approach of the azodicarboxylate might be directed by interaction of the incoming nitrogen atom with the proton of the carboxylic acid of the L-proline–enamine intermediate.



7

In conclusion, we have demonstrated the first organo-catalytic, direct, asymmetric α-amination of aldehydes with azodicarboxylates as the nitrogen source and L-proline as the catalyst. The new reaction provides easy access to optically active α-amino aldehydes, α-amino alcohols, and α-amino acids from simple and easily available starting materials and catalyst. Aldehydes react with azodicarboxylates and the corresponding optically active α-aminated adducts are formed in high yields and enantiomeric excesses, with as little as 2 mol% of L-proline. It is also demonstrated that masked α-amino alcohols are formed in high yields and excellent enantioselectivities (up to 95% *ee*). Furthermore, the formation of oxazolidinones and α-amino acids is demonstrated. This direct α-amination reaction uses readily available and inexpensive achiral starting materials, and can be carried out under environmentally friendly and operationally simple reaction conditions.

Received: March 1, 2002 [Z18800]

[1] See for example a) R. M. Williams, *Synthesis of Optically Active α-Amino* Acids, Pergamon, Oxford, **1989**; b) R. M. Williams, J. A. Hendrix, *Chem. Rev.* **1992**, *92*, 889; c) M. Arend, *Angew. Chem.* **1999**, *111*, 3047; *Angew. Chem. Int. Ed.* **1999**, *38*, 2873; d) L. Yet, *Angew. Chem.* **2001**, *113*, 900; *Angew. Chem. Int. Ed.* **2001**, *40*, 875; e) R. O. Duthaler, *Tetrahedron* **1994**, *50*, 1539; f) S. C. Bergmeier, *Tetrahedron* **2000**, *56*, 2561; g) K. L. Reddy, K. B. Sharpless, *J. Am. Chem. Soc.* **1998**, *120*, 1207, and references therein.

[2] See for example: a) M. S. Sigman, E. N. Jacobsen, *J. Am. Chem. Soc.* **1998**, *120*, 5315; b) M. S. Sigman, P. Vachal, E. N. Jacobsen, *Angew. Chem.* **2000**, *112*, 1336; *Angew. Chem. Int. Ed.* **2000**, *39*, 1279; c) M. S. Sigman, E. N. Jacobsen, *J. Am. Chem. Soc.* **1998**, *120*, 4901; d) C. A. Krueger, K. W. Kuntz, C. D. Dzierba, W. G. Wirschun, J. D. Gleason,

 © WILEY-VCH Verlag GmbH, 69451 Weinheim, Germany, 2002 1433-7851/02/4110-1792 $ 20.00+.50/0

M. L. Snapper, A. H. Hoveyda, *J. Am. Chem. Soc.* **1999**, *121*, 4284; e) M. Takamura, Y. Hamashima, H. Usuda, M. Kanai, M. Shibasaki, *Angew. Chem.* **2000**, *112*, 1716; *Angew. Chem. Int. Ed.* **2000**, *39*, 1650; f) E. J. Corey, M. J. Grogan, *Org. Lett.* **1999**, *1*, 157; g) H. Ishitani, S. Komiyama, S. Kobayashi, *Angew. Chem.* **1998**, *110*, 3369; *Angew. Chem. Int. Ed.* **1998**, *37*, 3186; f) H. Ishitani, S. Komiyama, Y. Hasegawa, S. Kobayashi, *J. Am. Chem. Soc*. **2000**, *122*, 762.

[3] Catalytic enantioselective direct Mannich reactions: a) S. Yamasaki, T. Iida, M. Shibasaki, *Tetrahedron* **1999**, *55*, 8857; b) K. Juhl, N. Gathergood, K. A. Jørgensen, *Angew. Chem.* **2001**, *113*, 3083; *Angew. Chem. Int. Ed.* **2001**, *40*, 2995; c) A. Córdova, S.-I. Watanabe, F. Tanaka, W. Notz, C. F. Barbas III, *J. Am. Chem. Soc.* **2002**, *124*, 1842; d) A. Córdova, W. Notz, G. Zhong, J. M. Betancort, C. F. Barbas III, *J. Am. Chem. Soc.* **2002**, *124*, 1866.

[4] K. Juhl, K. A. Jørgensen, *J. Am. Chem. Soc.* **2002**, *124*, 2420.

[5] For an review on asymmetric α-amination reactions see J.-P. Genet, C. Greck, D. Lavergne, *Modern Amination Methods* (Ed.: A. Ricci), Wiley-VCH, Weinheim, **2000**, chap. 3.

[6] D. A. Evans, S. G. Nelson, *J. Am. Chem. Soc.* **1997**, *119*, 6542.

[7] For the use of proline and other chiral amines as catalysts see for example, a) P. I. Dalko, L. Moisan, *Angew. Chem.* **2001**, *113*, 3840; *Angew. Chem. Int. Ed.* **2001**, *40*, 3726; b) A. Córdova, W. Notz, C. F. Barbas III, *J. Org. Chem.* **2002**, *67*, 301; c) K. Sakthivel, W. Notz, T. Bui, C. F. Barbas III, *J. Am. Chem. Soc.* **2001**, *123*, 5260; d) B. List, R. A. Lerner, C. F. Barbas III, *J. Am. Chem. Soc.* **2000**, *122*, 2395; e) J. F. Austin, D. W. C. MacMillan, *J. Am. Chem. Soc.* **2002**, *124*, 1172; f) A. B. Northrup, D. W. C. MacMillan, *J. Am. Chem. Soc.* **2002**, *124*, 2458; g) N. A. Paras, D. W. C. MacMillan, *J. Am. Chem. Soc.* **2001**, *123*, 4370; h) W. S. Jen, J. J. M. Wiener, D. W. C. MacMillan, *J. Am. Chem. Soc.* **2000**, *122*, 9874; i) K. A. Ahrendt, C. J. Borths, D. W. C. MacMillan, *J. Am. Chem. Soc.* **2000**, *122*, 4243; j) A. Bøgevig, N. Kumaragurubaran, K. A. Jørgensen, *Chem. Commun*. **2002**, 620.

[8] The enantiomeric excess was 77% and full conversion was obtained after only 2 min reaction time!

[9] Absolute configuration of **5**: W. A. Kleschick, M. W. Reed, J. Bordner, *J. Org. Chem.* **1987**, *52*, 3168.

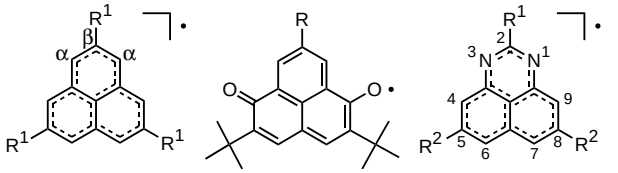
[10] S. J. Katz, S. C. Bergmeier, *Tetrahedron Lett.* **2002**, *43*, 557.

[11] Absolute configuration of **6**: M. J. Burk, J. G. Allen, *J. Org. Chem.* **1997**, *62*, 7054.

A New Trend in Phenalenyl Chemistry: A Persistent Neutral Radical, 2,5,8-Tri-*tert*-butyl-1,3-diazaphenalenyl, and the Excited Triplet State of the Gable *syn*-Dimer in the Crystal of Column Motif**

Yasushi Morita,* Takashi Aoki, Kozo Fukui, Shigeaki Nakazawa, Koichi Tamaki, Shuichi Suzuki, Akira Fuyuhiro, Kagetoshi Yamamoto, Kazunobu Sato, Daisuke Shiomi, Akira Naito, Takeji Takui,* and Kazuhiro Nakasuji*

Phenalenyl (**1**) is a highly symmetric (D_{3h}) odd alternating-hydrocarbon π radical, found as early as 1956,[1] and it still plays an important role as a building block for spin-mediated molecular functions in organic molecule-based magnets,[2] and organic metal and conducting materials.[3] Recent progress in phenalenyl chemistry has been made in the isolation of the radical itself in the crystalline state by employing bulky substituents (**2**[4a] and perchlorophenalenyl[4b]), with the exploration of amphoteric redox systems[5] which have intriguing potential applications, such as organic molecular batteries,[6] and with the synthesis of novel phenalenyls with extended conjugation, such as compound **3**.[7] 1,3-Diazaphenalenyl (**4**) is a typical example of the isoelectronic mode of heteroatomic modification for phenalenyl. Successful isolation of **2**[4] aided by the steric hindrance induced by the bulky



1 R^1 = H
2 R^1 = *t*Bu

3

4 $R^1 = R^2$ = H
5 R^1 = *t*Bu, R^2 = H
6 $R^1 = R^2$ = *t*Bu

[*] Prof. Dr. Y. Morita, Prof. Dr. K. Nakasuji, T. Aoki, Dr. K. Tamaki, S. Suzuki, Prof. Dr. A. Fuyuhiro, Prof. Dr. K. Yamamoto
Department of Chemistry, Graduate School of Science
Osaka University
Toyonaka, Osaka 560-0043 (Japan)
Fax: (+81) 6-6850-5395
E-mail: nakasuji@chem.sci.osaka-u.ac.jp

Prof. Dr. T. Takui, Dr. K. Fukui, Dr. S. Nakazawa, Prof. Dr. K. Sato, Prof. Dr. D. Shiomi
Departments of Chemistry and Materials Science
Graduate School of Science
Osaka City University
Sumiyoshi-ku, Osaka 558-8585 (Japan)
Fax: (+81) 6-6605-3137
E-mail: takui@sci.osaka-cu.ac.jp

Prof. Dr. A. Naito
Faculty of Engineering, Yokohama National University
Hodogaya-ku, Yokohama 240-0085 (Japan)

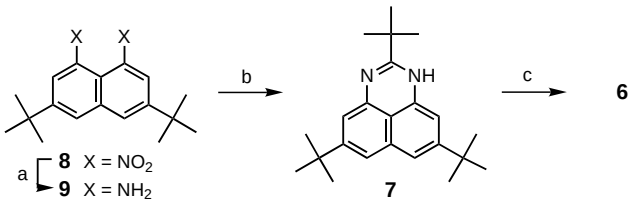
[**] This work has been supported by Grants-in-Aid for General Scientific Research and Scientific Research on Priority Area "Delocalized π-Electronic Systems (No. 297)" from the Ministry of Education, Culture, Sports, Science, and Technology, Japan.

Supporting information for this article is available on the WWW under http://www.angewandte.com or from the author.

 © WILEY-VCH Verlag GmbH, 69451 Weinheim, Germany, 2002 1433-7851/02/4110-1793 $ 20.00+.50/0

groups at the β-positions (2-, 5-, and 8-positions) has encouraged us to synthesize 2,5,8-tri-*tert*-butyl-1,3-diazaphenalenyl (**6**), which has led to the isolation of such a radical as crystalline solid for the first time, in contrast to a pioneering attempt by Sabanov et al. for compound **5**.[8] The synthesis, electronic structure, and a gable *syn*-dimerization of **6** in the crystal structure, which has a column motif, are reported here. Interestingly, the column structure motif is a counterpart of the herringbone one of homoatomic phenalenyl **2**.

The precursor, 2,5,8-tri-*tert*-butyl-1,3-diazaphenalene (**7**; Scheme 1), was prepared from *tert*-butylated dinitronaphthalene **8**[9] in two steps: 1) reduction with Sn, $SnCl_2 \cdot 2H_2O$ under acidic conditions, 2) condensation with *t*BuCHO followed by the dehydrogenation with Pd/C catalyst.[10] Treatment of **7** with active PbO_2 and recrystallization gave **6** as green crystals (Scheme 1).[11] The radical **6** in the crystal is stable in the absence of air. In air the radical decomposes slowly, but most of it remains unchanged for weeks, thus showing higher stability than **2**.[4a] The increased stability resulting from the heteroatomic modification in the π conjugation is contrary to the claim by Sabanov et al. for **5**.[8]



Scheme 1. Synthetic route for **6**. Reagents and conditions: a) Sn (4.3 equiv), $SnCl_2 \cdot 2H_2O$ (7.9 equiv), conc. HCl:AcOH (1:1), 100 °C, 5 h, 82 %; b) *t*BuCHO (1.3 equiv), 3 mol % Pd/C, xylene, reflux, 3.5 h, 77 %; c) PbO_2 (5 equiv), degassed benzene, RT, 1.5 h, recrystallized from hexane, 42 %.

To clarify the bulk magnetic properties of the crystalline state of **6**, the magnetic susceptibility χ_p of a polycrystalline sample was measured from 1.8 to 350 K at 0.1 T.[12] Below 250 K **6** exhibits a weak paramagnetism from impurity radicals (ca. 0.1 %) presumably arising from lattice defects. The result shows that molecular assemblies of **6** in the crystal are in the spin-singlet state, thus revealing the dimerization of **6**. Dissolution of this solid sample in organic solvents gave the strong ESR signals characteristic of **6**, confirming that **6** remains stable and unchanged in the crystal under inert atmosphere. On raising the temperature to 350 K, a small but significant increase in $\chi_p T$ was observed, which suggests the possible existence of thermally accessible paramagnetic states.

To identify such a thermally activated paramagnetic state, cw-ESR (cw = continuous wave) spectra were measured for the solid sample of **6** (Figure 1 a). In addition to the central intense signal from the monoradical impurities, fine-structure triplet-state ESR signals ($\Delta M_S = \pm 1$ allowed transitions) with axial symmetry are clearly seen. The spectral simulation yielded spin-Hamiltonian parameters $S = 1$, $g = 2.004$, $|D|/hc = 0.0173\ cm^{-1}$, and $|E|/hc < 10^{-3}\ cm^{-1}$. The temperature dependence of the triplet signal intensity was best described by a singlet–triplet model[13] with an energy gap of $2J/k_B = -4.19(2) \times 10^3$ K (Figure 1 b). The results seemingly resemble

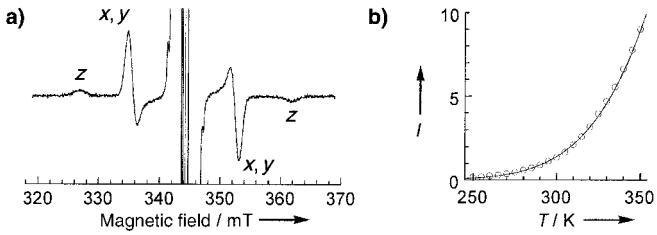


Figure 1. a) Observed triplet-state ESR spectrum of the powder sample of **6** at 350 K. The *x*, *y*, and *z* denote the canonical absorption peaks. The microwave frequency used is 9.638615 GHz. b) Temperature dependence of the triplet signal intensity ○ = observed, —— = calculated; $2J/k_B = -4.19 \times 10^3$ K.

those for **2** ($S = 1$, $g = 2.003$, $|D|/hc = 0.0167\ cm^{-1}$, $|E|/hc < 10^{-3}\ cm^{-1}$, and $2J/k_B = -3.34(3) \times 10^3$ K), but the values for **6** are larger than those for **2**. The comparison suggests that **6** also forms a dimer structure with a face-to-face staggered arrangement. Such an arrangement ensures minimum steric repulsion between the *tert*-butyl groups, but the bonding character of the dimerization of **6** is different from that in **2**.

The X-ray crystal-structure analysis[14] gives a rationale for the difference in the D and $2J/k_B$ values between **2** and **6**. Figure 2 a and b show ORTEP views of the *syn*-dimer of **6** with a gable structure. In the gable *syn*-dimer the shortest distance between the α-carbon sites is 0.215 nm and the longest one

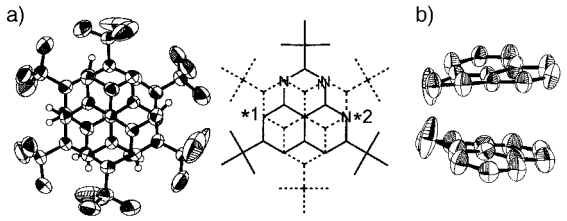


Figure 2. ORTEP views of the gable *syn*-dimer of **6**. a) Top view and a schematic representation; the nitrogen sites are located in terms of the most probable face-to-face arrangement; *1: the shortest C–C distance and *2: the longest distance between the α-carbon and nitrogen sites (see text). b) Side view; the *tert*-butyl groups are omitted for clarity.

between the α-carbon and the nitrogen sites is 0.379 nm, in contrast to the pancake-type stacking of symmetric pure π-dimerization for **2** (0.320–0.332 nm).[4a] The gable *syn*-dimer structure for **6** and asymmetric bonding nature formed in the dimer are induced by the symmetry-breaking incorporation of nitrogen atoms at the 1- and 3-positions. The dimer packing mode is a column structure for **6** (see Supporting Information), which is important in organic metals and conducting materials,[3a,b] whereas the herringbone structure for **2** does not give properties that are relevant for these areas.[4a]

The observed very low E value ($|E|/hc < 10^{-3}\ cm^{-1}$) for **6** reflects axially symmetric nature of the dipolar spin–spin interaction in the excited triplet state of the dimer. The assumed dimer structure, however, does not straightforwardly lead to the electronic structure with a threefold or greater axial symmetry because of the symmetry lowering caused by the incorporated nitrogen atoms. Indeed, ^{13}C cross-polarization magic-angle spinning (CPMAS) solid-state NMR measurements of the molecular crystal at room temperature

 © WILEY-VCH Verlag GmbH, 69451 Weinheim, Germany, 2002 1433-7851/02/4110-1794 $ 20.00+.50/0 *Angew. Chem. Int. Ed.* **2002**, *41*, No. 10

indicated the lower symmetric (C_1) dimerization of **6** in the singlet ground state. A rationale for the low E value is that the dipolar spin–spin interaction within the *syn*-dimer molecule undergoes averaging and smearing out of a small amount of the departure from the axial symmetry as a result of inhomogeneous hyperfine broadening in the fine-structure spectra, which gives rise to an apparent high symmetry with a more than threefold rotation axis.

To evaluate the heteroatomic effects of **6** induced by a pair of nitrogen atoms, the π-spin-density distribution of **6** was determined by liquid-phase ESR and ENDOR/TRIPLE spectroscopy. Under inert atmosphere, **6** in a toluene solution was extremely stable in contrast to **5**.[8] The ESR spectrum is interpreted by ^{1}H-, ^{14}N-, and ^{13}C (1.1 %) hyperfine couplings as summarized in Table 1. The π-spin densities on the nitrogen and carbon sites were determined by the observed couplings with the help of McConnell and Heller–McConnell equations, respectively. To determine the π-spin densities on the other carbon sites without protons, the Fraenkel–Karplus equation was applied. Such an empirical treatment gave all the π-spin densities, as depicted in Figure 3. It appears that a robust π-spin polarization similar to the parent phenalenyl radical **1** is maintained in **6** in spite of the heteroatomic modification, which gives rise to the alternation of the signs of the π spin densities between the neighboring sites. By comparing the spin densities of **6** with those of **2**,[4a] it appears that the spin densities of the 1- and 3-positions decrease appreciably, while those of the 4-, 6-, 7-, and 9-positions increase, that is, these four sites become more "active" following the heteroatomic perturbation. Nevertheless, the presence of the bulky substituents at the 5- and 8-positions contributes to the chemical stabilization of the 1,3-diazaphenalenyl π system.

Table 1. Hyperfine coupling constants (hfccs) of ^{1}H, ^{13}C, and ^{14}N nuclei, and g value.[a]

a^H [mT]				a^N [mT]		g Value
4, 9	6, 7	2-*t*Bu	5, 8-*t*Bu	1, 3		2.0033
−0.638	−0.715	+0.006	+0.021	+0.292		
			a^C [mT]			
2	4, 9	5, 8	6, 7	10, 11	12	13
−0.550	+0.880	−0.820	+1.087	−0.654	−0.885	+0.081

[a] Assignments of hfccs were based on DFT calculation by using Gaussian 94 with SVWN/6–31G*//SVWN/6-31G* method.

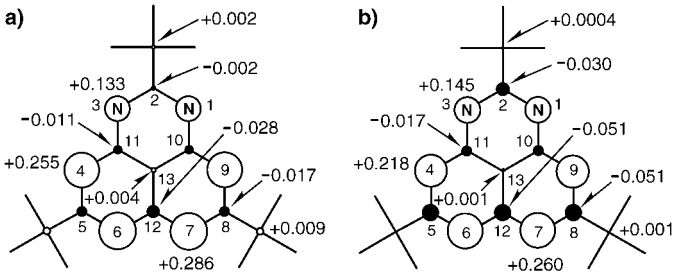


Figure 3. π-spin-density distribution of **6** a) experimentally determined and b) calculated by DFT method using Gaussian 94 (SVWN/6–31G*//SVWN/6-31G*). Open and filled circles denote positive and negative spin densities, respectively.

The spin structure of **6** is in harmony with such a gabled face-to-face arrangement of the *syn*-dimer in the crystal. In such an arrangement maximum orbital overlaps occur between the α-carbon sites with largest and next-largest spin densities, which causes a strong bonding interaction ($2J/k_B = -4.19(2) \times 10^3$ K) between the radicals in the *syn*-dimer of **6**. The reflection spectroscopy and the refined X-ray crystal-structural analysis of **6** and other azaphenalenyls are underway. To our knowledge, the *syn*-dimer of **6** is not only the first example that exhibits a column crystal-structure motif with pseudo π dimerization between neutral organic radicals,[15] but also diverse potentials, such as those of organic conducting materials. In contrast to the herringbone motif for the pure π-dimer **2**, the finding of the gable *syn*-dimer with the column motif for **6** derived by the heteroatomic modification should be of interest in crystal engineering and organic materials science.

Received: February 25, 2002 [Z18760]

[1] a) D. H. Reid, *Chem. Ind. (London)* **1956**, 1504–1505; b) P. B. Sogo, M. Nakazaki, M. Calvin, *J. Chem. Phys.* **1957**, *26*, 1343–1345.

[2] For a recent overview, see: a) *Molecular Magnetism* (Eds.: K. Itoh, M. Kinoshita), Kodansha, and Gordon and Breach Science Publishers, **2000**, pp. 1–347; b) *Magnetic Properties of Organic Materials* (Ed.: P. M. Lahti), Marcel Dekker, New York, **1999**, pp. 1–728.

[3] a) R. C. Haddon, *Nature* **1975**, *256*, 394–396; b) R. C. Haddon, *Aust. J. Chem.* **1975**, *28*, 2343–2351; c) X. Chi, M. E. Itkis, B. O. Patrick, T. M. Barclay, R. W. Reed, R. T. Oakley, A. W. Cordes, R. C. Haddon, *J. Am. Chem. Soc.* **1999**, *121*, 10395–10402; d) K. Tamaki, Y. Morita, J. Toyoda, H. Yamochi, G. Saito, K. Nakasuji, *Tetrahedron Lett.* **1997**, *38*, 4583–4586.

[4] a) K. Goto, T. Kubo, K. Yamamoto, K. Nakasuji, K. Sato, D. Shiomi, T. Takui, M. Kubota, T. Kobayashi, K. Yakushi, J. Ouyang, *J. Am. Chem. Soc.* **1999**, *121*, 1619–1620; b) P. A. Koutentis, Y. Chen, Y. Cao, T. P. Best, M. E. Itkis, L. Beer, R. T. Oakley, A. W. Cordes, C. P. Brock, R. C. Haddon, *J. Am Chem. Soc.* **2001**, *123*, 3864–3871.

[5] T. Kubo, K. Yamamoto, K. Nakasuji, T. Takui, I. Murata, *Bull. Chem. Soc. Jpn.* **2001**, *74*, 1999–2009.

[6] Y. Morita, S. Nishida, J. Kawai, K. Fukui, S. Nakazawa, K. Sato, D. Shiomi, T. Takui, K. Nakasuji, *Org. Lett. in press.*

[7] Y. Morita, T. Ohba, N. Haneda, S. Maki, J. Kawai, K. Hatanaka, K. Sato, D. Shiomi, T. Takui, K. Nakasuji, *J. Am. Chem. Soc.* **2000**, *122*, 4825–4826.

[8] V. Kh. Sabanov, E. S. Klimov, I. V. Bogdanova, E. P. Trub, N. T. Berberova, O. Yu. Okhlobistin, *Khim. Geterotsikl. Soedin.* **1986**, 970–972. They reported that **5** was unstable because of an increase in spin density at the nitrogen sites.

[9] K.-H. Koch, K. Müllen, *Chem. Ber.* **1991**, *124*, 2091–2100.

[10] Selected physical data: **7**, m.p. 267–268 °C; ^{1}H NMR ($CDCl_3$/CF_3COOH; 270 mHz): $\delta = 1.29$ (s, 18), 1.49 (s, 9), 6.93 (d, $J =$ 1.2 Hz), 7.27 ppm (d, $J = 1.2$ Hz); IR (KBr): $\tilde{\nu} = 3320$ cm^{-1}; EI-MS, m/z 336 (M^+, 100 %); elemental analysis calcd (%) for $C_{23}H_{32}N_2$: C 82.09, H 9.59, N 8.33; found: C 82.30, H 9.65, N 8.17.

[11] Selected physical data: **6**, m.p. 164–166 °C; TLC $R_f = 0.62$ (5:1 hexane:ethyl acetate); TLC (alumina) $R_f = 0.58$ (10:1 hexane:ethyl acetate); elemental analysis calcd (%) for $C_{23}H_{31}N_2$: C 82.33, H 9.31, N 8.35, found: C 82.04, H 9.42, N 8.23.

[12] The diamagnetic susceptibility χ_{dia}: -219.7×10^{-6} emu mol^{-1}.

[13] B. Bleaney, K. D. Bowers, *Proc. R. Soc. London Ser. A* **1952**, *214*, 451–465.

[14] The X-ray structure analysis was performed for **6** with an isotopic enrichment of ^{15}N at room temperature: $C_{46}H_{62}{}^{15}N_4$, $M_r = 675.00$, crystal dimensions $0.20 \times 0.10 \times 0.08$ mm^3, pale green, Rigaku/MSC

Mercury CCD diffractometer, $Mo_{K\alpha}$ radiation, $T = 23.0\,^{\circ}C$, monoclinic, space group $P2_1/n$ (No. 14), $a = 12.783(1)$, $b = 21.697(2)$, $c = 15.441(2)$ Å, $\beta = 105.957(4)^{\circ}$, $V = 4117.7(7)$ Å^3, $Z = 4$, $\rho_{calcd} = 1.082\,g\,cm^{-3}$, 28321 reflections collected, 4934 unique intensities reflections observed $[I > 4.00\sigma(I)]$, $2\theta_{max} = 55.0^{\circ}$, structure solution with direct methods (SIR92) and refinement on F with 483 parameters, R (R_w) = 0.153 (0.396), S (GOF) = 2.23. CCDC-183912 (**6**) contains the supplementary crystallographic data for this paper. These data can be obtained free of charge via www.ccdc.cam.ac.uk/conts/retrieving.html (or from the Cambridge Crystallographic Data Centre, 12, Union Road, Cambridge CB2 1EZ, UK; fax: (+44) 1223-336-033; or deposit@ccdc.cam.ac.uk).

[15] For pure π dimerization, see: a) M. R. Gleiter, B. Kanellakopulos, C. Krieger, F. A. Neugebauer, *Liebigs Ann.* **1997**, 473–483, and references therein; b) P. A. Capiomont, B. Chion, J. Lajzérowicz, *Acta Crystallogr. Sect. B* **1971**, *27*, 322–326.

Expanding the Reaction Scope of DNA-Templated Synthesis**

Zev J. Gartner, Matthew W. Kanan, and David R. Liu*

The translation of amplifiable information into chemical structure is a key component of nature's approach to generating functional molecules. The ribosome accomplishes this feat by catalyzing the translation of RNA sequences into proteins. Developing general methods to translate amplifiable information carriers into synthetic molecules may enable chemists to evolve non-natural molecules in a manner analogous to the cycles of translation, selection, amplification, and diversification currently used by nature to evolve proteins. As an initial step towards this goal, we recently examined the generality of DNA-templated synthetic chemistry.[1, 2] We demonstrated the ability of DNA-templated synthesis to direct a modest collection of chemical reactions without requiring the precise alignment of reactive groups into DNA-like conformations. Indeed, the distance independence and sequence fidelity of DNA-templated synthesis allowed the simultaneous, one-pot translation of a model library of more than 1000 templates into the corresponding thioether products, one of which was enriched by in vitro selection for binding to the protein streptavidin and amplified by the polymerase chain reaction (PCR).

The range of reactions known to be supported by DNA-templated synthesis,[2] however, remains a tiny fraction of those used either by synthetic chemists or by nature to generate molecules with desired properties. Many reactions central to the construction of natural or synthetic molecules have yet to be developed in a DNA-templated format despite their known compatibility with water.[3] We describe here the development of several useful DNA-templated reactions, including the first reported DNA-templated organometallic couplings and carbon–carbon bond forming reactions other than pyrimidine photodimerization.[4, 5] Collectively, these reactions represent an important additional step towards the in vitro evolution of non-natural synthetic molecules by enabling the DNA-templated construction of a much more diverse set of structures than has been previously achieved.

We first investigated the ability of DNA-templated synthesis to direct reactions that require a non-DNA-linked activator, catalyst, or other reagent in addition to the principal reactants. To test the ability of DNA-templated synthesis to mediate such reactions without requiring structural mimicry of the DNA backbone, we performed DNA-templated reductive aminations between amine-linked template **1** and benzaldehyde- or glyoxal-linked reagents (**2** and **3**) with millimolar concentrations of $NaBH_3CN$ at room temperature in aqueous solutions. Products formed efficiently when the template and reagent sequences were complementary. In contrast, control reactions in which the sequence of the reagent did not complement that of the template, or in which $NaBH_3CN$ was omitted, yielded no significant product (Table 1 and Figure 1). While DNA-templated reductive aminations to generate products closely mimicking the structure of double-stranded DNA have been previously reported,[6, 7] the above results demonstrate that reductive amination to generate structures unrelated to the phosphoribose backbone can take place efficiently and sequence specifically. We also performed DNA-templated amide bond formations[8, 9] between amine-linked templates **4** and **5** and carboxylate-linked reagents **6**–**9** mediated by 1-(3-dimethylaminopropyl)-3-ethylcarbodiimide (EDC) and *N*-hydroxysulfosuccinimide (sulfo-NHS) to generate amide products in good yields at pH 6.0 and 25 °C (Table 2). Product formation was sequence specific, dependent on the presence of EDC, and surprisingly insensitive to the steric encumbrance of the amine or carboxylate group. Efficient DNA-templated amide formation was also mediated by the water-stable activator 4-(4,6-dimethoxy-1,3,5-triazin-2-yl)-4-methylmorpholinium

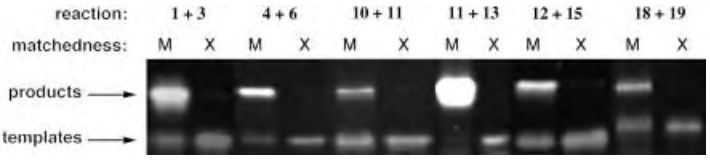


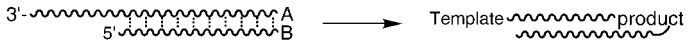
Figure 1. Analysis by denaturing polyacrylamide gel electrophoresis of representative DNA-templated reactions listed in Tables 1 and 2. The structures of reagents and templates correspond to the numbering in Tables 1 and 2. Lanes 1, 3, 5, 7, 9, and 11: reaction of matched (complementary) reagents and templates under the conditions listed in Tables 1 and 2 (the reaction of **4** and **6** was mediated by DMT-MM). Lanes 2, 4, 6, 8, 10, and 12: reaction of mismatched (noncomplementary) reagents and templates under conditions identical to those used in lanes 1, 3, 5, 7, 9, and 11, respectively.

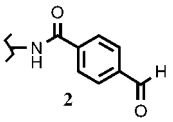
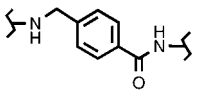
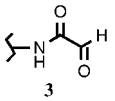
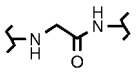
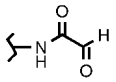
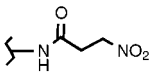
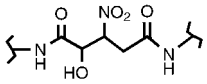
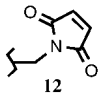
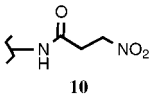
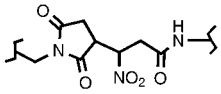
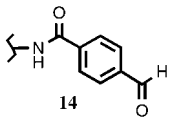
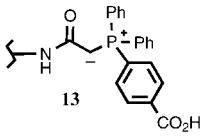
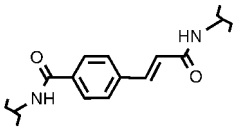
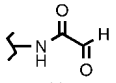
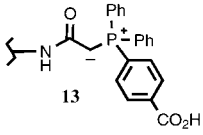
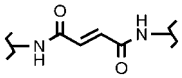
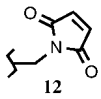
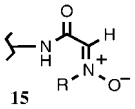
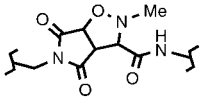
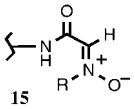
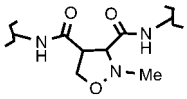
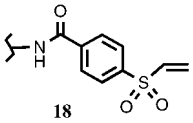
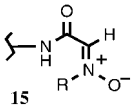
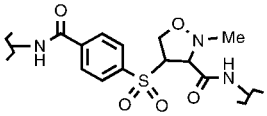
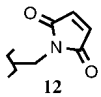
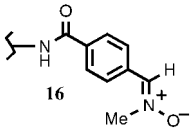
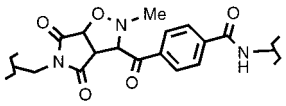
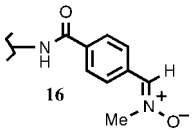
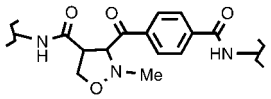
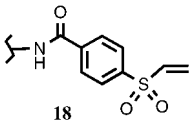
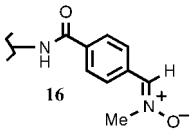
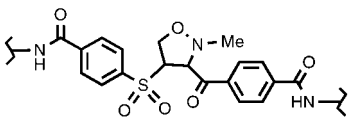
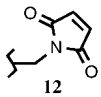
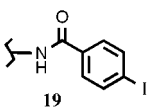
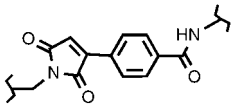
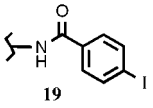
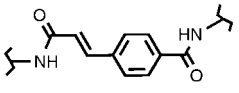
[*] Prof. D. R. Liu, Z. J. Gartner, M. W. Kanan
Department of Chemistry and Chemical Biology
Havard University
12 Oxford Street, Cambridge, MA 02138 (USA)
Fax: (+1) 617-496-5688
E-mail: drliu@fas.harvard.edu

[**] Funding was generously provided by the Searle Scholars Program (00-C-101), an Office of Naval Research Young Investigator Award (N0014-00-1-0596), a Research Corporation Research Innovation Award, and Harvard University. Z.J.G. and M.W.K are supported by NSF Graduate Research Fellowships.

 © WILEY-VCH Verlag GmbH, 69451 Weinheim, Germany, 2002 1433-7851/02/4110-1796 $ 20.00+.50/0

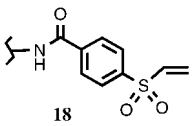
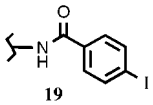
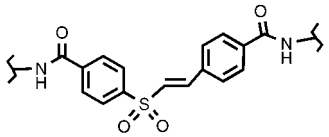
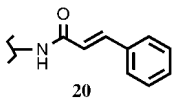
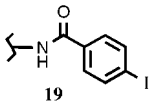
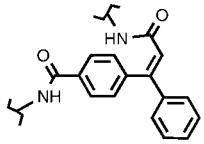
Table 1. Product yields of the various reactions.[a]



A	B	Conditions	Product	Yield [%]
 **1**	 **2**	a		81
 **1**	 **3**	a		70
 **11**	 **10**	b		45
 **12**	 **10**	b		42
 **14**	 **13**	c		93
 **11**	 **13**	c		>97
 **12**	 **15**	d		53 (R = Me) 42 (R = Bn)
 **17**	 **15**	d		54
 **18**	 **15**	d		47
 **12**	 **16**	d		41
 **17**	 **16**	d		15
 **18**	 **16**	d		44
 **12**	 **19**	e		54
 **17**	 **19**	f		26

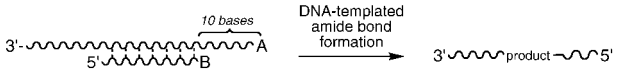
 © WILEY-VCH Verlag GmbH, 69451 Weinheim, Germany, 2002 1433-7851/02/4110-1797 $ 20.00+.50/0

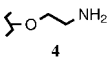
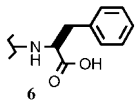
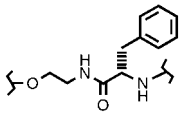
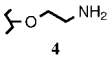
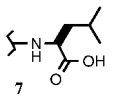
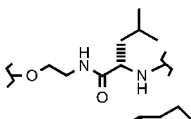
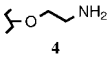
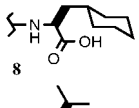
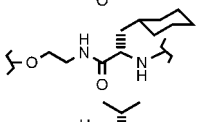
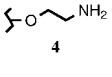
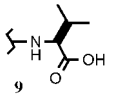
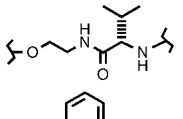
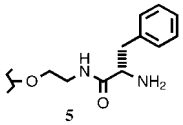
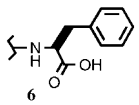
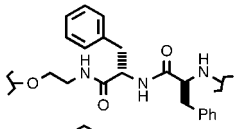
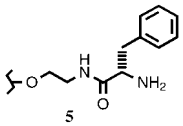
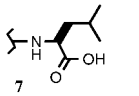
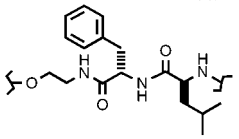
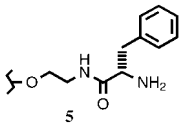
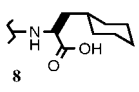
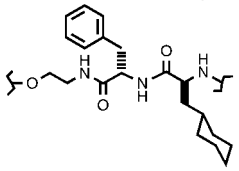
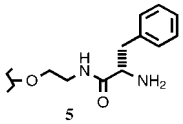
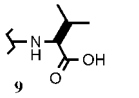
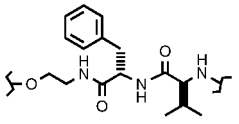
Table 1. (Continued)

A	B	Conditions	Product	Yield [%]
 **18**	 **19**	f		51
 **20**	 **19**	f		31

[a] Product yields of all reactions with matched template and reagent sequences under the specified conditions were greater than 20-fold higher than that of control reactions with scrambled reagent sequences. Reactions were conducted at 25 °C with one equivalent each of template and reagent at 60 nM final concentration unless otherwise specified. Conditions: a) 3 mM $NaBH_3CN$, 0.1 M 2-[*N*-morpholino]ethanesulfonic acid (MES) buffer pH 6.0, 0.5 M NaCl, 1.5 h; b) 0.1 M [2-hydroxy-1,1-bis(hydroxymethyl)ethyl]amino-1-propanesulfonic acid (TAPS) buffer pH 8.5, 300 mM NaCl, 12 h; c) 0.1 M pH 8.0 TAPS buffer, 1 M NaCl, 55 °C, 1.5 h; d) 50 mM 3-[*N*-morpholino]propanesulfonic acid (MOPS) buffer pH 7.5, 2.8 M NaCl, 22 h; e) 120 nM **19**, 1.4 mM Na_2PdCl_4, 0.5 M NaOAc buffer pH 5.0, 18 h; f) premix Na_2PdCl_4 with two equivalents of $P(p\text{-}SO_3C_6H_4)_3$ in water 15 min, then add to reactants in 0.5 M NaOAc buffer pH 5.0, 75 mM NaCl, 2 h (final [Pd] = 0.3 mM, [**19**] = 120 nM). The olefin geometry of products from **13** and the regiochemistries of cycloaddition products from **15** and **16** are presumed, but not verified.

Table 2. DNA-templated amide bond formation mediated by EDC and sulfo-NHS or by DMT-MM for a variety of substituted carboxylic acids and amines.[a]



A	B	Product	Yield [%]
 **4**	 **6**		79, 59
 **4**	 **7**		73, 54
 **4**	 **8**		81, 62
 **4**	 **9**		79, 46
 **5**	 **6**		58, 66
 **5**	 **7**		47, 64
 **5**	 **8**		56, 71
 **5**	 **9**		58, 53

[a] In each row, the yields of DMT-MM-mediated reactions between reagents and templates complementary in sequence are followed by yields of EDC and sulfo-NHS-mediated reactions. Conditions: 60 nM template, 120 nM reagent, 50 mM DMT-MM in 0.1 M MOPS buffer pH 7.0, 1 M NaCl, 16 h, 25 °C; or 60 nM template, 120 nM reagent, 20 mM EDC, 15 mM sulfo-NHS, 0.1 M MES buffer pH 6.0, 1 M NaCl, 16 h, 25 °C. In all cases, control reactions with mismatched reagent sequences yielded little or no detectable product.

 © WILEY-VCH Verlag GmbH, 69451 Weinheim, Germany, 2002 1433-7851/02/4110-1798 $ 20.00+.50/0

chloride (DMT-MM)[10] instead of EDC and sulfo-NHS (Table 2 and Figure 1). The efficiency and generality of DNA-templated amide bond formation under these conditions, together with the large number of commercially available chiral amines and carboxylic acids, make this reaction an attractive candidate in future DNA-templated syntheses of structurally diverse small-molecule libraries.

As a result of the importance of carbon–carbon bond forming reactions in both chemical and biological synthesis, we explored several such reactions in a DNA-templated format. Both the reaction of nitroalkane-linked reagent **10** with aldehyde-linked template **11** (nitro-aldol or Henry reaction) and the conjugate addition of **10** to maleimide-linked template **12** (nitro-Michael addition) proceed efficiently and with high sequence specificity at pH 7.5–8.5 and 25 °C (Table 1). In addition, the sequence-specific DNA-templated Wittig reaction between stabilized phosphorus ylide reagent **13** and aldehyde-linked templates **14** or **11** provided the corresponding olefin products in excellent yields at pH 6.0–8.0 and 25 °C (Figure 2). Finally, the DNA-templated 1,3-dipolar cycloaddition between nitrone-linked reagents **15** and **16** and olefin-linked templates **12**, **17**, or **18** also afforded products sequence specifically at pH 7.5 and 25 °C (Table 1). While these cycloadditions in general proceeded efficiently with maleimides, vinyl sulfones, and acrylamides, unactivated alkenes provided products in much lower yield (< 10 %).

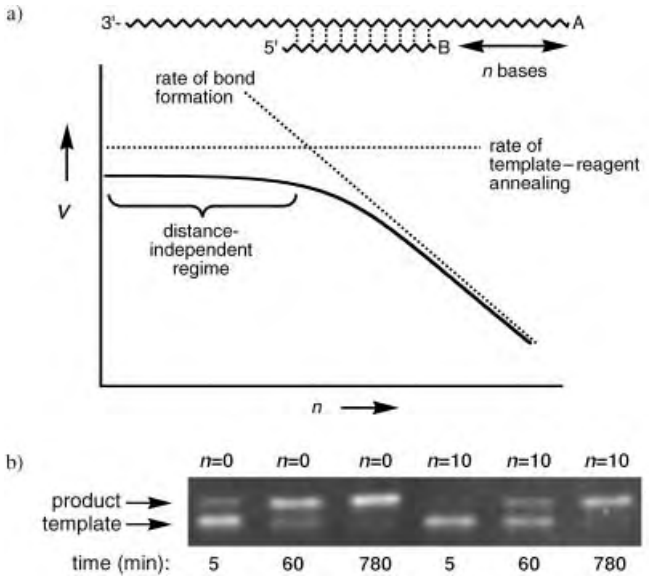


Figure 2. a) Conceptual model for distance-independent DNA-templated synthesis. As the distance between the reactive groups of an annealed reagent and template (n) is increased, the rate of bond formation (V) is presumed to decrease. For those values of n in which the rate of bond formation is significantly higher than the rate of template–reagent annealing, the rate of product formation (solid line) remains constant. In this regime, the DNA-templated reaction shows distance independence. b) Denaturing polyacrylamide gel electrophoresis of a DNA-templated Wittig olefination between complementary **11** and **13** with either zero bases (lanes 1–3) or ten bases (lanes 4–6) separating annealed reactants. Although the apparent second order rate constants for the $n = 0$ and $n = 10$ reactions differ by threefold ($k_{app}(n = 0) = 9.9 \times 10^3\,M^{-1}s^{-1}$ while $k_{app}(n = 10) = 3.5 \times 10^3\,M^{-1}s^{-1}$), product yields after 13 h at both distances are nearly quantitative. Control reactions containing sequence mismatches yielded no detectable product (not shown).

Organometallic couplings constitute a powerful class of complexity-building synthetic reactions. We performed DNA-templated Heck couplings in the presence of water-soluble Pd precatalysts to test the ability of DNA templates to direct organometallic reactions in aqueous solution. In the presence of 170 μM Na_2PdCl_4, aryl iodide reagent **19** and a variety of olefin-linked templates including maleimide **12**, acrylamide **17**, vinyl sulfone **18**, or cinnamamide **20** provided Heck coupling products in modest yields at pH 5.0 and 25 °C (Table 1). Adding two equivalents of $P(p\text{-}SO_3C_6H_4)_3$ per equivalent of Pd prior to template and reagent addition typically increased overall yields twofold for the coupling with olefins **17**, **18**, and **20**. Control reactions containing sequence mismatches or lacking the Pd precatalyst yielded no product. To the best of our knowledge the above DNA-templated nitro-aldol addition, nitro-Michael addition, Wittig olefination, dipolar cycloaddition, and Heck coupling represent the first reported nucleic acid-templated organometallic reactions and carbon–carbon bond forming reactions other than pyrimidine photodimerization.[4, 5]

We previously discovered[1] that some DNA-templated reactions demonstrate distance independence—the ability to form product at a rate independent of the number of intervening bases between the annealed reactants. We hypothesized (Figure 2a) that distance independence arises when the rate of bond formation in the DNA-templated reaction is greater than the rate of template–reagent annealing. Although only a subset of chemical reactions fall into this category, any DNA-templated reaction that affords comparable product yields when the reagent is annealed at various distances from the reactive end of the template is of special interest because it can be encoded at a variety of template positions. To evaluate the ability of the DNA-templated reactions developed above to take place efficiently when reactants are separated by distances relevant to library encoding, we compared the yields of reductive amination, amide formation, nitro-aldol addition, nitro-Michael addition, Wittig olefination (Figure 2b), dipolar cycloaddition, and Heck coupling when zero or ten bases separated annealed reactive groups (Figure 2a, $n = 0$ versus $n = 10$). Among the reactions described above or in our previous work,[1] amide bond formation, nitro-aldol addition, Wittig olefination, Heck coupling, conjugate addition of thiols to maleimides, and S_N2 reactions between thiols and α-iodo amides demonstrate comparable product formation when reactive groups are separated by zero or ten bases. Our findings indicate that these reactions can be encoded during synthesis by nucleotides that are distal from the reactive end of the template without significantly impairing product formation.

Taken together, these results expand considerably the reaction scope of DNA-templated synthesis. A wide variety of reactions proceed efficiently and selectively only when the corresponding reactants are programmed with complementary sequences. By augmenting the repertoire of known DNA-templated reactions to now include carbon–carbon bond forming and organometallic reactions (nitro-aldol additions, nitro-Michael additions, Wittig olefinations, dipolar cycloadditions, and Heck couplings) in addition to previously reported amide bond formation,[8, 9] imine formation,[11]

 © WILEY-VCH Verlag GmbH, 69451 Weinheim, Germany, 2002 1433-7851/02/4110-1799 $ 20.00+.50/0

reductive amination,[6, 7] S_N2 reactions,[1, 12, 13] conjugate additions of thiols,[1] and phosphoester or phosphonamide formation,[14, 15] these results may enable the sequence-specific translation of libraries of DNA into libraries of structurally and functionally diverse synthetic products. Since minute quantities of templates encoding desired molecules can be amplified by PCR,[1] the yields of DNA-templated reactions are arguably less critical than the yields of traditional synthetic transformations. Nevertheless, many of the reactions developed above proceed efficiently. In addition, by demonstrating that DNA-templated synthesis in the absence of proteins can direct a large diversity of chemical reactions, our findings support previously proposed hypotheses[16–18] that nucleic-acid-templated synthesis may have translated replicable information into some of the earliest functional molecules such as polyketides, terpenes, and polypeptides prior to the evolution of protein-based enzymes. The diversity of chemistry shown here to be controllable simply by bringing reactants into proximity using DNA hybridization without any apparent structural requirements provides an experimental basis for these possibilities. The translation of amplifiable information into a wide range of structures is a key requirement of our ongoing efforts to apply nature's molecular evolution approach to the discovery of non-natural molecules with new functions.

Experimental Section

Functionalized templates and reagents were typically prepared by treating 5′-NH_2-terminated oligonucleotides (for template **1**), 5′-NH_2-$(CH_2O)_2$-terminated oligonucleotides (for all other templates) or 3′-OPO_3-$CH_2CH(CH_2OH)(CH_2)_4NH_2$-terminated oligonucleotides (for all reagents) with the appropriate NHS esters (0.1 volumes of a 20 mg mL^{-1} solution in DMF) in 0.2 M sodium phosphate buffer at pH 7.2 and 25 °C for 1 h to provide the template and reagent structures shown in Tables 1 and 2. For amino-acid-linked reagents **6**–**9**, 3′-OPO_3-$CH_2CH(CH_2OH)$-$(CH_2)_4NH_2$-terminated oligonucleotides in 0.2 M sodium phosphate buffer at pH 7.2 were treated with 0.1 volumes of a 100 mM bis[2-(succinimidyloxycarbonyloxy)-ethyl]sulfone (BSOCOES, Pierce) solution in DMF for 10 min at 25 °C, followed by 0.3 mL of a 300 mM solution of amino acid in 300 mM NaOH for 30 min at 25 °C.

Functionalized templates and reagents were purified by gel filtration using Sephadex G-25 followed by reverse-phase HPLC (0.1 M triethylammonium acetate/acetonitrile gradient) and characterized by MALDI mass spectrometry. DNA-templated reactions were conducted under the conditions described in Tables 1 and 2, and products were characterized by denaturing polyacrylamide gel electrophoresis and MALDI mass spectrometry.

The sequences of oligonucleotide templates and reagents are as follows (5′ to 3′ direction, *n* refers the number of bases between reactive groups when template and reagent are annealed as shown in Figure 2): **1**: TGGTACGAATTCGACTCGGG; **2** and **3** matched: GAGTCGAATTCGTACC; **2** and **3** mismatched: GGGCTCAGCTTCCCCA; **4** and **5**: GGTACGAATTCGACTCGGGAATACCACCTT; **6**–**9** matched ($n = 10$): TCCCGAGTCG; **6** matched ($n = 0$): AATTCGTACC; **6**–**9** mismatched: TCACCTAGCA; **11**, **12**, **14**, **17**, **18**, **20**: GGTACGAATTCGACTCGGGA; **10**, **13**, **16**, **19** matched: TCCCGAGTCGAATTCGTACC; **10**, **13**, **16**, **19** mismatched: GGGCTCAGCTTCCCCATAAT; **15** matched: AATTCGTACC; **15** mismatched: TCGTATTCCA; template for $n = 10$ versus $n = 0$ comparison: TAGCGATTACGGTACGAATTCGACTCGGGA

Reaction yields were quantitated by denaturing polyacrylamide gel electrophoresis followed by staining with ethidium bromide, UV visualization, and CCD-based densitometry of the product and template starting material bands. Calculations of the yields assumed that the templates and products stained with equal intensity per base; for those cases in which products are partially double stranded during quantitation, changes in staining intensity may result in higher apparent yields.

Received: March 1, 2002 [Z 18798]

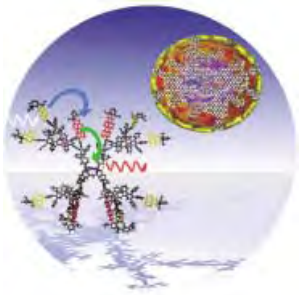
[1] Z. J. Gartner, D. R. Liu, *J. Am. Chem. Soc* **2001**, *123*, 6961.
[2] D. Summerer, A. Marx, *Angew. Chem.* **2002**, *114*, 93; *Angew. Chem. Int. Ed.* **2002**, *41*, 89.
[3] C.-J. Li, T.-H. Chan, *Organic reactions in aqueous media*, Wiley, New York, **1997**.
[4] J. Liu, J. S. Taylor, *Nucleic Acids Res.* **1998**, *26*, 3300.
[5] K. Fujimoto, S. Matsuda, N. Takahashi, I. Saito, *J. Am. Chem. Soc.* **2000**, *122*, 5646.
[6] X. Li, Z. Y. Zhan, R. Knipe, D. G. Lynn, *J. Am. Chem. Soc.* **2002**, *124*, 746.
[7] Y. Gat, D. G. Lynn, *Biopolymers* **1998**, *48*, 19.
[8] J. G. Schmidt, L. Christensen, P. E. Nielsen, L. E. Orgel, *Nucleic Acids Res.* **1997**, *25*, 4792.
[9] R. K. Bruick, P. E. Dawson, S. B. H. Kent, N. Usman, G. F. Joyce, *Chem. Biol.* **1996**, *3*, 49.
[10] M. Kunishima, C. Kawachi, K. Hioki, K. Terao, S. Tani, *Tetrahedron* **2001**, *57*, 1551.
[11] J. L. Czlapinski, T. L. Sheppard, *J. Am. Chem. Soc.* **2001**, *123*, 8618.
[12] Y. Xu, N. B. Karalkar, E. T. Kool, *Nat. Biotechnol.* **2001**, *19*, 148.
[13] M. K. Herrlein, J. S. Nelson, R. L. Letsinger, *J. Am. Chem. Soc.* **1995**, *117*, 10151.
[14] L. E. Orgel, *Acc. Chem. Res.* **1995**, *28*, 109.
[15] A. Luther, R. Brandsch, G. von Kiedrowski, *Nature* **1998**, *396*, 245.
[16] A. I. Scott, *Tetrahedron Lett.* **1997**, *38*, 4961.
[17] T. Li, K. C. Nicolaou, *Nature* **1994**, *369*, 218.
[18] K. Tamura, P. Schimmel, *Proc. Natl. Acad. Sci. USA* **2001**, *98*, 1393.

 © WILEY-VCH Verlag GmbH, 69451 Weinheim, Germany, 2002 1433-7851/02/4110-1800 $ 20.00+.50/0

ANGEWANDTE CHEMIE
INTERNATIONAL EDITION
A Journal of the Gesellschaft Deutscher Chemiker
2002
41/11
Pages 1809 – 1972

COVER PICTURE

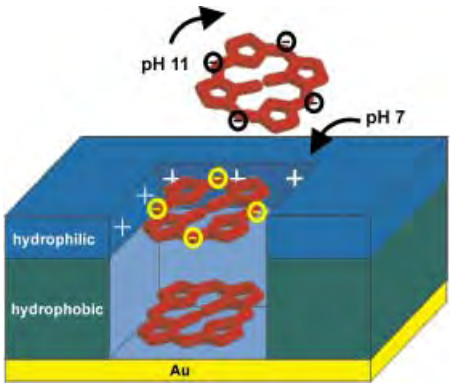
The cover picture shows the calculated energy-minimized 3D-structure of a polyphenylene dendrimer, which was prepared in a multistep synthesis. The nanoparticle carries three different types of chromophores, located in the center (terrylene), within the scaffold (perylene), and at the periphery (naphthalene). This multichromophoric triad absorbs over the whole range of the visible spectrum and shows, as shown in the picture, a stepwise vectorial energy transfer over a distance of 30 Å from the surface to the core. There is more about polyphenylene chromophores in the communication from Müllen et al. on p. 1904 ff.



REVIEW

Contents

Hydrogen-bond chains and stiff segments rigidify spherical lipid membranes in bulk water and molecular monolayers on carrier systems. Reactive components can be anchored within them at any desired separation on the Ångström scale. Reactive nanometer-sized hills and clefts are thus accessible and should be useful in the construction of complex reaction systems, including redox-active dyes (see picture).



G. Li, W. Fudickar, M. Skupin, A. Klyszcz, C. Draeger, M. Lauer, J.-H. Fuhrhop* ..... 1828 – 1852

Rigid Lipid Membranes and Nanometer Clefts: Motifs for the Creation of Molecular Landscapes

Angew. Chem. **2002**, *114*, 1906 – 1931

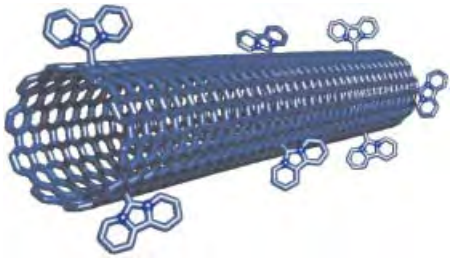
Keywords: membranes · molecular landscapes · nanostructures · self-assembly · synkinesis

 © WILEY-VCH Verlag GmbH, 69451 Weinheim, Germany, 2002 1433-7851/02/4111-1811 $ 20.00+.50/0

MINIREVIEW

Contents

Soluble carbon nanotubes can be obtained by chemical derivatization, such as functionalization of defects, covalent sidewall functionalization (see picture), and noncovalent formation of adducts with surfactants or polymers. This new nanochemistry not only provides a combination of the unprecedented materials properties of nanotubes with those of other compound classes, but also forms the basis for the processibility of these systems.



A. Hirsch* ..... 1853 – 1859

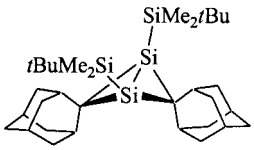
Functionalization of Single-Walled Carbon Nanotubes

Angew. Chem. **2002**, *114*, 1933 – 1939

Keywords: addition · carbon allotropes · electronic components · host – guest systems · nanotubes

HIGHLIGHTS

Si bond-stretch isomers? Different Si–Si separations are proposed for the bond-stretch isomers of tetrasilabicyclobutane compounds. With **1**, the existence of an isomer with a longer bond between the bridge-head Si atoms could be demonstrated. Thus the Si compound **1** has been obtained even before the corresponding carbon homologue. With regard to the great advances in the chemistry of small Si rings, other ring systems are discussed.



1

R. Koch, M. Weidenbruch* 1861 – 1863

A Spiropentasiladiene and Other Strained Silicon-Containing Rings

Angew. Chem. **2002**, *114*, 1941 – 1943

Keywords: bond-stretch isomers · silicon · small-ring systems · solid-state structures · spiro compounds

"Definitely not" is the answer to the question posed in the title: New experiments, which allow a comparison between microwave reaction conditions and conventional reaction conditions for the first time, support this statement. However, it has not yet been clarified whether or not there are special microwave effects in the selectivity of chemical reactions.

N. Kuhnert* ..... 1863 – 1866

Microwave-Assisted Reactions in Organic Synthesis —Are There Any Nonthermal Microwave Effects?

Angew. Chem. **2002**, *114*, 1943 – 1946

Keywords: microwave chemistry · solid-phase synthesis · solvent effects · synthetic methods

VIPs

The following communications are "Very Important Papers" in the opinion of two referees. They will be published shortly. Short summaries of these articles can be found on the *Angewandte Chemie* homepage at the address http://www.angewandte.com

Catalytic Activity and Poisoning of Specific Sites on Supported Metal Nanoparticles — J. Hoffmann, V. Johánek, J. Hartmann, J. Libuda,* H.-J. Freund

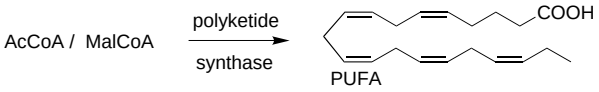
Understanding Zeolite Catalysis: Inverse Shape Selectivity Revised — M. Schenk, S. Calero, T. L. M. Maesen, L. L. van Benthem, M. G. Verbeek, B. Smit*

Highly Selective Transport of Organic Compounds by Using Supported Liquid Membranes Based on Ionic Liquids — L. C. Branco, J. G. Crespo, C. A. M. Afonso*

Atom-Transfer Tandem Radical Cyclization Reactions Promoted by Lewis Acids — D. Yang,* S. Gu, H.-W. Zhao, N.-Y. Zhu

 © WILEY-VCH Verlag GmbH, 69451 Weinheim, Germany, 2002 1433-7851/02/4111-1812 $ 20.00+.50/0

Psychrophilic marine bacteria can produce polyunsaturated fatty acids (PUFAs; see scheme). Until recently, PUFAs were known as important metabolites exclusively produced by eukaryotes with oxygen-dependent desaturases. Surprisingly, functional analysis of a PUFA biosynthetic gene cluster from *Shewanella* sp. strain SCRC2738 points towards a unique mixed pathway involving a polyketide synthase.



Angew. Chem. **2002**, *114*, 1947 – 1950

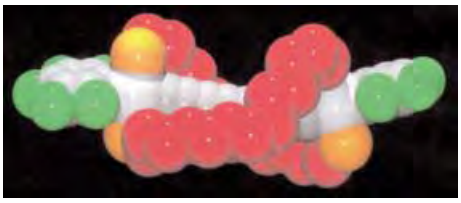
U. Kaulmann, C. Hertweck* 1866 – 1869

Biosynthesis of Polyunsaturated Fatty Acids by Polyketide Synthases

Keywords: biosynthesis · biotechnology · fatty acids · marine bacteria · polyketides

COMMUNICATIONS

Neither bonding interactions between the strands nor covalent bonds to metal templates dispersed throughout the strands are needed for the molecules presented here to adopt double-helical structures (see picture). The molecules consist of rigid $(C{\equiv}C)_m$ chains that bridge two platinum atoms, which are in turn bridged by two diphosphane ligands of the formula $Ar_2P(CH_2)_nPAr_2$.



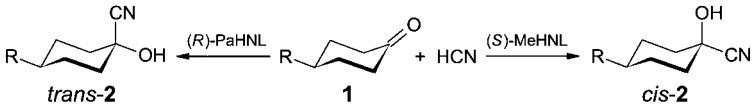
Angew. Chem. **2002**, *114*, 1951 – 1957

J. Stahl, J. C. Bohling, E. B. Bauer, T. B. Peters, W. Mohr, J. M. Martín-Alvarez, F. Hampel, J. A. Gladysz* ..... 1871 – 1876

sp Carbon Chains Surrounded by sp^3 Carbon Double Helices: A Class of Molecules that are Accessible by Self-Assembly and Models for "Insulated" Molecular-Scale Devices

Keywords: Helical structures · Metathesis · Molecular devices · Platinum · Self-assembly

The choice of enzyme is decisive: for the enzyme-catalyzed addition of HCN to 4-substituted cyclohexanones **1**, highly selective biocatalysts are available that allow control to yield the *cis* or the *trans* addition product **2**. Modeling of the *S* enzyme – substrate complex reveals remarkable parallels with the Prelog/Ringold model of the LADH-catalyzed hydrogenation of cyclohexanones.



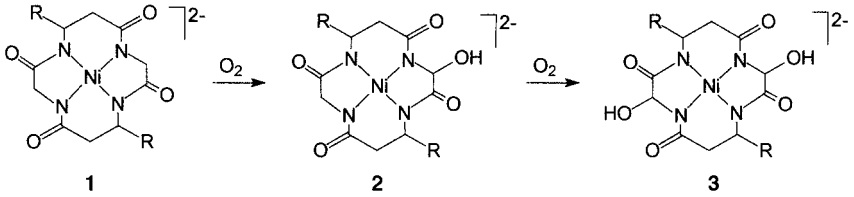
Angew. Chem. **2002**, *114*, 1957 – 1959

F. Effenberger,* J. Roos, C. Kobler ..... 1876 – 1879

cis – *trans* Selectivity of Enzyme-Catalyzed Additions to 4-Substituted Cyclohexanones—Correlation with the Prelog/Ringold Model of Enzymatic Hydrogenation

Keywords: cyanohydrins · enzyme catalysis · ketones · lyases · molecular modeling

Hydroxy groups added consecutively: the reaction of Ni^{II} cyclotetrapeptide complexes **1** with oxygen affords selective and stepwise α-C hydroxylation of the two ligand glycine units (formation of **2** and **3**). The mechanism of these reactions, which occur via Ni^{III} intermediates, is related to the function of the copper-containing enzyme peptidylglycine α-hydroxylating monooxygenase (PHM).



Angew. Chem. **2002**, *114*, 1969 – 1972

K. Haas, H. Dialer, H. Piotrowski, J. Schapp, W. Beck* ..... 1879 – 1881

Selective α-Carbon Hydroxylation of Glycine in Nickel(II) – Cyclotetrapeptide Complexes by Oxygen

Keywords: amino acids · cyclopeptides · hydroxylation · nickel · N ligands

 © WILEY-VCH Verlag GmbH, 69451 Weinheim, Germany, 2002 1433-7851/02/4111-1813 $ 20.00+.50/0

A nanostructured phase: this is how the Ga_{22} unit in the $[Ga_{12}(GaR)_{10}]^{2-}$ cluster (see picture), which exhibits a structure distinctly different from the one reported for other Ga_{22} units, can be interpreted. In this cluster 11 Ga atoms (black spheres) are grouped around a central Ga atom, this Ga_{12} core is then stabilized by ten GaR units.



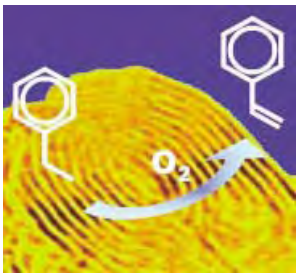
Angew. Chem. **2002**, *114*, 1959 – 1962

A. Schnepf,* G. Stösser, H. Schnöckel* ..... 1882 – 1884

$[Ga_{22}\{N(SiMe_3)_2\}_{10}]^{2-}$: A Metalloid Cluster Compound with a Variation of the Ga_{22} Framework

Keywords: cluster compounds · gallium · metal – metal interactions · subvalent compounds

The microstructure is appealing: Onion-like carbon forms are used for the first time in the field of catalysis and thus open new routes for the potential applications of nonplanar carbon materials. An example is given with the oxidative dehydrogenation of ethylbenzene to styrene (see scheme).



Angew. Chem. **2002**, *114*, 1962 – 1966

N. Keller, N. I. Maksimova, V. V. Roddatis, M. Schur, G. Mestl,* Y. V. Butenko, V. L. Kuznetsov, R. Schlögl* ..... 1885 – 1888

The Catalytic Use of Onion-Like Carbon Materials for Styrene Synthesis by Oxidative Dehydrogenation of Ethylbenzene

Keywords: carbon allotropes · dehydrogenation · heterogeneous catalysis · surface chemistry

The cyclic stannylenes I which are accessible by transamination from $[Sn(NSiMe_3)_2]$ and α-amino aldimines undergo easy cheletropic decomposition and may formally transfer a "naked" tin atom to a diazadiene. Computational studies suggest an electronic polarization in the form of the chelated atom canonical structure **I′** as the reason for this behavior.



I **I'**

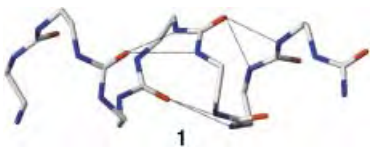
Angew. Chem. **2002**, *114*, 1966 – 1969

T. Gans-Eichler, D. Gudat,* M. Nieger ..... 1888 – 1891

Tin Analogues of "Arduengo Carbenes": Synthesis of 1,3,2λ^2-Diazastannoles and Transfer of Sn Atoms between a 1,3,2λ^2-Diazastannole and a Diazadiene

Keywords: carbene homologues · cheletropic reaction · cycloaddition · oxidative addition · tin

Closely related to the (*P*)2.6$_{14}$ helix of γ-peptides: Heptamer **1** bearing side chains of Ala, Val, and Tyr adopts a stable 2.5-helical secondary structure in solution that is characterized by a pitch of approximately 5.1 Å and by the simultaneous presence of 12- and 14-membered hydrogen-bonded rings. Thus *N*,*N*′-linked oligoureas belong to the growing family of non-natural non-peptide oligomers with defined and predictable secondary structure.



1

Angew. Chem. **2002**, *114*, 1973 – 1975

V. Semetey, D. Rognan, C. Hemmerlin, R. Graff, J.-P. Briand, M. Marraud, G. Guichard* ..... 1893 – 1895

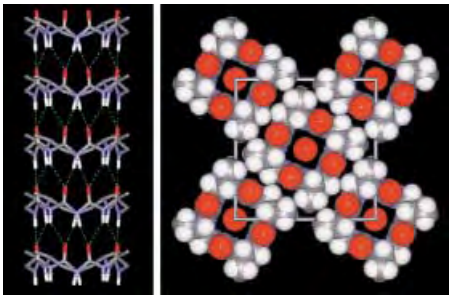
Stable Helical Secondary Structure in Short-Chain N,N′-Linked Oligoureas Bearing Proteinogenic Side Chains

Keywords: molecular modeling · NMR spectroscopy · oligoureas · peptidomimetics · structure elucidation

 © WILEY-VCH Verlag GmbH, 69451 Weinheim, Germany, 2002 1433-7851/02/4111-1814 $ 20.00+.50/0

Square-shaped hydrogen-bonded polar nanotubes are formed when the C_4-symmetrical *all-S* cyclotetraurea bearing side chains of alanine self-assembles in the solid state (see picture). The four urea fragments in the macrocyle present an *all-trans* planar conformation with an unidirectional alignment of all the carbonyl groups. The anisotropy is further maintained in the crystal as neighboring tubes are all arranged in the same direction.

Angew. Chem. **2002**, *114*, 1975 – 1978



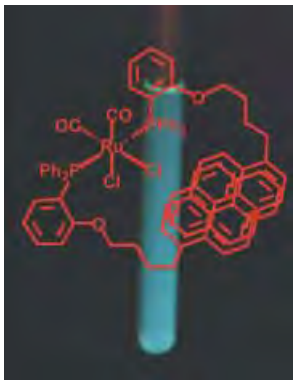
V. Semetey, C. Didierjean, J.-P. Briand, A. Aubry, G. Guichard* .... 1895 – 1898

Self-Assembling Organic Nanotubes from Enantiopure Cyclo-*N*,*N*′-Linked Oligoureas: Design, Synthesis, and Crystal Structure

Keywords: macrocycles · nanotubes · peptidomimetics · self-assembly · solid-state structures

From weak blue to intense blue-green: this change in emission results when $[RuCl_2(POC4Pyr\text{-}P,O)_2]$ reacts with carbon monoxide. The reason is the formation of the dicarbonyl complex shown (see picture), in which CO has replaced the labile coordinating site of the hemilabile ligand POC4-Pyr. The increased flexibility in the tethered pyrenyl groups allows the formation of inter- and intramolecular excimers in this complex. POC4Pyr = 4-{2-(diphenylphosphanyl)phenoxy}-butylpyrene.

Angew. Chem. **2002**, *114*, 1978 – 1980



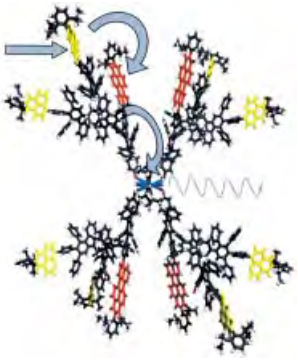
C. W. Rogers, M. O. Wolf* 1898 – 1900

Drastic Luminescence Response to Carbon Monoxide from a Ru^{II} Complex Containing a Hemilabile Phosphane Pyrene Ether

Keywords: fluorescence · hemilabile ligands · ruthenium · sensors

Dendritic multichromophores based on a rigid polyphenylene scaffold contain up to three different types of rylene chromophores incorporated at the focal point, the scaffold, and the periphery of the dendrimer. An energy gradient between the periphery and the core is thus generated and allows an efficient transfer of excitation energy (see picture).

Angew. Chem. **2002**, *114*, 1980 – 1984



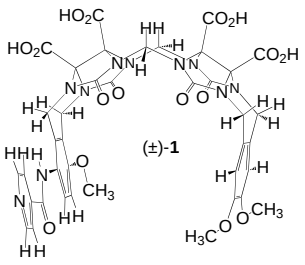
T. Weil, E. Reuther, K. Müllen* ..... 1900 – 1904

Shape-Persistent, Fluorescent Polyphenylene Dyads and a Triad for Efficient Vectorial Transduction of Excitation Energy

Keywords: chromophores · dendrimers · dyes/pigments · energy transfer · light harvesting

Enantiomeric self-recognition is triggered by addition of $[Pd(ONO_2)(en)]$ (**2**; en = 1,2-ethylenediamine) to a solution of (±)-**1** in water, a process that results in a 2:2 aggregate ($\mathbf{1}_2 \cdot \mathbf{2}_2$ and (*ent*-**1**)$_2 \cdot \mathbf{2}_2$) of well-defined geometry. The use of analytical ultracentrifugation as a tool for the elucidation of molecular weight and stoichiometry in synthetic self-assembly studies is highlighted.

Angew. Chem. **2002**, *114*, 1985 – 1987



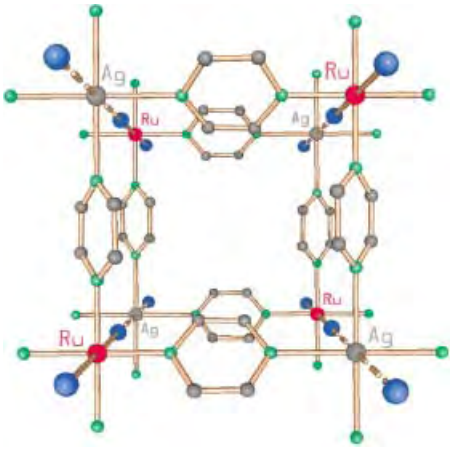
L. Isaacs,* D. Witt ..... 1905 – 1907

Enantiomeric Self-Recognition of a Facial Amphiphile Triggered by $[\{Pd(ONO_2)(en)\}_2]$

Keywords: amphiphiles · hydrophobic effect · palladium · pi interactions · glycoluril · self-assembly

 © WILEY-VCH Verlag GmbH, 69451 Weinheim, Germany, 2002 1433-7851/02/4111-1815 $ 20.00+.50/0

Three structural motifs have been obtained by using the novel building block *trans*-[$RuCl_2(pyz)_4$] with different silver salts: A two-dimensional network with an unprecedented double-honeycomb topology, a three-dimensional array with the rutile (6,3) structure, and an interesting tetragonal network with both Ru and Ag in octahedral environments, which can be related to the rock-salt topology (see picture).



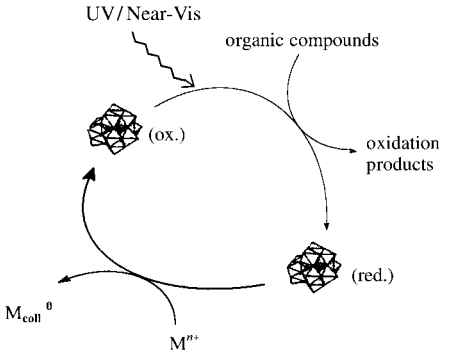
Angew. Chem. **2002**, *114*, 1987 – 1991

L. Carlucci, G. Ciani,* F. Porta, D. M. Proserpio, L. Santagostini ..... 1907 – 1911

Crystal Engineering of Mixed-Metal Ru – Ag Coordination Networks by Using the *trans*-[$RuCl_2(pyz)_4$] (pyz = pyrazine) Building Block

Keywords: coordination polymers · N ligands · ruthenium · silver

Fine metal nanoparticles of Ag, Au, Pd, and Pt were obtained at room temperature, by simple mixing of the corresponding metal ions with reduced polyoxometalates (POMs) that serve both as photocatalysts and stabilizers, according to the cycle shown.



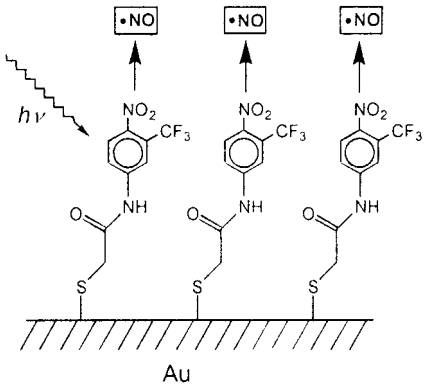
Angew. Chem. **2002**, *114*, 1991 – 1994

A. Troupis,* A. Hiskia, E. Papaconstantinou* ..... 1911 – 1914

Synthesis of Metal Nanoparticles by Using Polyoxometalates as Photocatalysts and Stabilizers

Keywords: homogeneous catalysis · nanostructures · photochemistry · polyoxometalates

Quantitative release of NO is exclusively controlled by light excitation in a self-assembled monolayer of an NO donor on a gold surface (see picture). The low excitation energy required, the absence of noxious side effects, the thermal stability under physiological conditions, and the ease of preparation are additional advantages offered by the monolayer-modified gold plate.



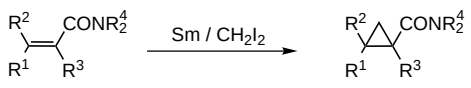
Angew. Chem. **2002**, *114*, 1994 – 1997

S. Sortino,* S. Petralia, G. Compagnini, S. Conoci, G. Condorelli .... 1914 – 1917

Light-Controlled Nitric Oxide Generation from a Novel Self-Assembled Monolayer on a Gold Surface

Keywords: nitrogen oxides · photochemistry · monolayers

Samarium learns another trick: Complete stereospecific cyclopropanation of α,β-unsaturated amides, in which the double bond is di-, tri-, or tetrasubstituted is promoted by Sm/CH_2I_2 [Eq. (1)]. The reaction is high yielding and unaffected by the bulk of the substituents $R^1 - R^4$.



(1)

complete stereospecificity

Angew. Chem. **2002**, *114*, 1997 – 1999

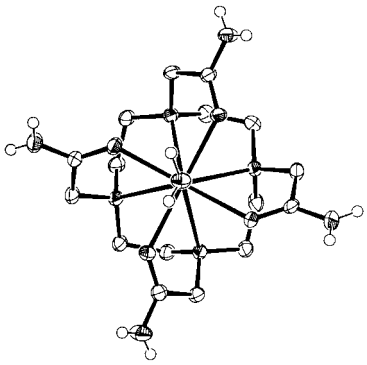
J. M. Concellón,* H. Rodríguez-Solla, C. Gómez ..... 1917 – 1919

Complete Stereospecific Cyclopropanation of α,β-Unsaturated Amides Promoted by Sm/CH_2I_2

Keywords: carbenoids · cyclopropanations · samarium · stereospecificity

 © WILEY-VCH Verlag GmbH, 69451 Weinheim, Germany, 2002 1433-7851/02/4111-1816 $ 20.00+.50/0

Contrast agent for magnetic resonance imaging: The exchangeable amide protons in the Yb^{3+} complex of 1,4,7,10-tetraazacyclododecane-1,4,7,10-tetraacetamide (see crystal structure) act as efficient antennae for transfer of saturated spins to bulk water. Saturation of all eight protons in a 5 mM solution of this complex results in a 38% decrease in the signal intensity of bulk water. The compound thus has promise as a magnetization-transfer contrast agent for magnetic resonance imaging.



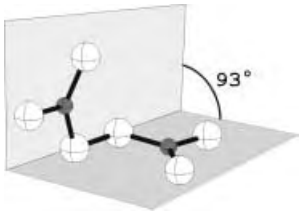
S. Zhang, L. Michaudet, S. Burgess, A. D. Sherry* ..... 1919 – 1921

The Amide Protons of an Ytterbium(III) dota Tetraamide Complex Act as Efficient Antennae for Transfer of Magnetization to Bulk Water

Angew. Chem. **2002**, *114*, 1999 – 2001

Keywords: amides · imaging agents · lanthanides · macrocycles · NMR spectroscopy

By using high-resolution X-ray powder diffraction, we have determined the first crystal structure of a peroxodicarbonate compound, synthesized by electrocrystallization at −20°C. The constitution of the peroxodicarbonate anion was established and all structural details, including its conformation (see picture), can be understood qualitatively in terms of classical concepts of the chemical bond.



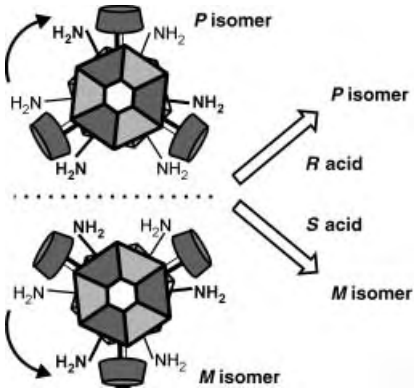
R. E. Dinnebier, S. Vensky, P. W. Stephens, M. Jansen* 1922 – 1924

Crystal Structure of $K_2[C_2O_6]$—First Proof of Existence and Constitution of a Peroxodicarbonate Ion

Angew. Chem. **2002**, *114*, 2002 – 2004

Keywords: electrocrystallization · peroxodicarbonate · solid-state structures · structure eluciation · X-ray powder diffraction

Stereospecific recognition of substrate molecules for certain chiral carboxylic acids is achieved by a noncovalent receptor system based on acid – base interactions of amino groups in the host system with the carboxylic acids. Enantioselectivity in the binding process is caused by secondary interactions with a chiral platform that preorganizes the amino functionalities (see scheme).



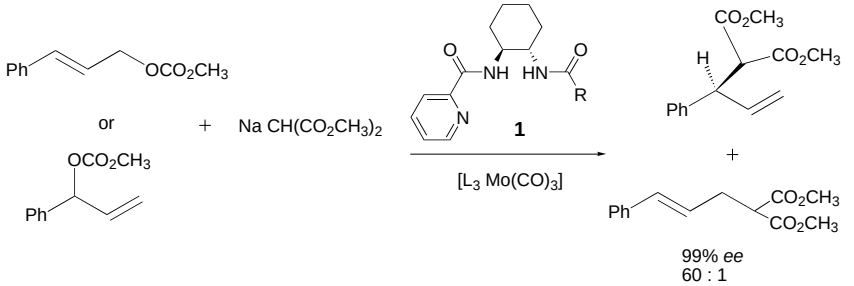
T. Ishi-i, M. Crego-Calama, P. Timmerman,* D. N. Reinhoudt,* S. Shinkai ..... 1924 – 1929

Self-Assembled Receptors for Enantioselective Recognition of Chiral Carboxylic Acids in a Highly Cooperative Manner

Angew. Chem. **2002**, *114*, 2004 – 2009

Keywords: acid – base complexation · chirality · host – guest systems · hydrogen bonds · noncovalent interactions · supramolecular chemistry

Unusual coordination in the asymmetric allylic alkylation catalyzed by molybdenum (see scheme) was revealed by a study on several ligands, for example, **1**. Unexpectedly, only the nitrogen atom of one picolinamide group coordinates to Mo, while the other amide group rigidifies the system. Based on the effectiveness of the bisdeprotonated ligand, the observed reaction can be rationalized and new ligands can be designed for asymmetric induction in allylic alkylations.



B. M. Trost,* K. Dogra, I. Hachiya, T. Emura, D. L. Hughes,* S. Krska, R. A. Reamer, M. Palucki, N. Yasuda, P. J. Reider ..... 1929 – 1932

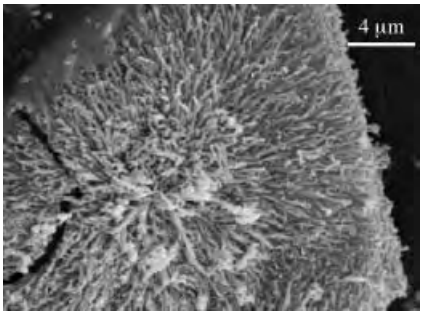
Designed Ligands as Probes for the Catalytic Binding Mode in Mo-Catalyzed Asymmetric Allylic Alkylation

Angew. Chem. **2002**, *114*, 2009 – 2012

Keywords: allylic compounds · asymmetric catalysis · ligand design · molybdenum · regioselectivity

 © WILEY-VCH Verlag GmbH, 69451 Weinheim, Germany, 2002 1433-7851/02/4111-1817 $ 20.00+.50/0

A simple mixture of thiourea and $AgNO_3$ in alkaline solution without any template or substrate, allowed to stand at room temperature, forms a unique self-supported pattern of Ag_2S nanorods. The picture shows a scanning electron micrograph of a typical product: a flake of polycrystalline Ag_2S with Ag_2S nanorods that radiate from a central point.



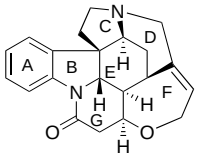
Angew. Chem. **2002**, *114*, 2012 – 2014

Q. Lu, F. Gao, D. Zhao* .... 1932 – 1934

Creation of a Unique Self-Supported Pattern of Radially Aligned Semiconductor Ag_2S Nanorods

Keywords: nanostructures · self-assembly · silver · sulfur

The power of palladium catalysts is shown in a total synthesis of (−)-strychnine (**A**). The construction of all the rings of this challenging molecule relied on Pd^0- or Pd^{II}-catalyzed reactions. The final step in this efficient synthesis involved the reduction of (+)-isostrychnine by a known method to form (−)-strychnine.



A

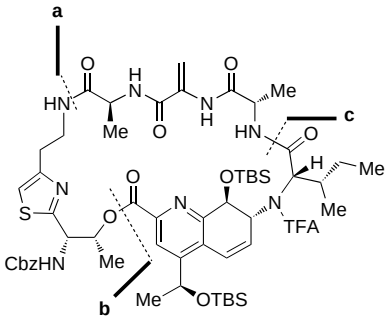
Angew. Chem. **2002**, *114*, 2014 – 2016

M. Nakanishi, M. Mori* .... 1934 – 1936

Total Synthesis of (−)-Strychnine

Keywords: alkaloids · allylic compounds · Heck reaction · palladium · total synthesis

An efficient construction of the quinaldic acid macrocycle (see picture) of the antibiotic thiostrepton is based on state-of-the-art asymmetric synthesis. The 27-membered macrocycle includes a quinaldic acid moiety, a thiazole ring, and a dehydroalanine unit. The key steps in the convergent assembly included: a) amide bond formation, b) esterification, and c) macrolactamization.



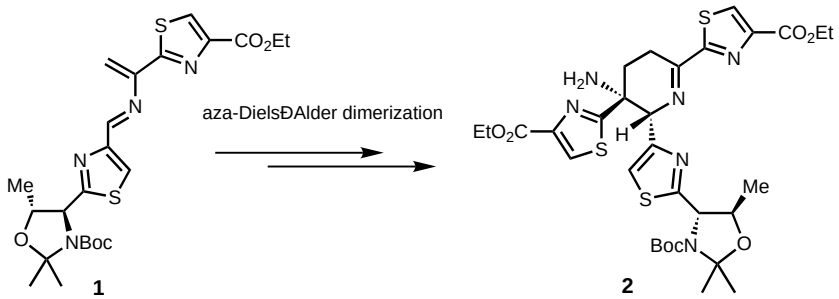
Angew. Chem. **2002**, *114*, 2017 – 2020

K. C. Nicolaou,* B. S. Safina, C. Funke, M. Zak, F. J. Zécri ..... 1937 – 1940

Stereocontrolled Synthesis of the Quinaldic Acid Macrocyclic System of Thiostrepton

Keywords: antibiotics · asymmetric synthesis · macrocycles · natural products · total synthesis

The key step in the dimerization of the azadiene **1** is a hetero-Diels – Alder reaction. The product **2** constitutes the dehydropiperidine core of the antibiotic thiostrepton.



1 **2**

Angew. Chem. **2002**, *114*, 2021 – 2025

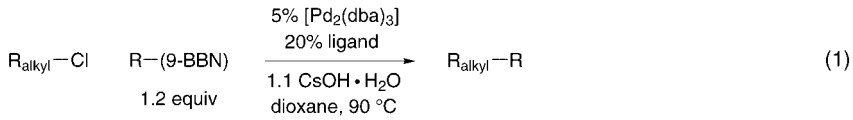
K. C. Nicolaou,* M. Nevalainen, B. S. Safina, M. Zak, S. Bulat 1941 – 1945

A Biomimetically Inspired Synthesis of the Dehydropiperidine Domain of Thiostrepton

Keywords: antibiotics · asymmetric synthesis · cycloaddition · natural products · total synthesis

 © WILEY-VCH Verlag GmbH, 69451 Weinheim, Germany, 2002 1433-7851/02/4111-1818 $ 20.00+.50/0

The window of reactivity is relatively narrow in the first Suzuki cross-coupling of alkyl chlorides with alkyl 9-borabicyclo[3.3.1]nonane (9-BBN) derivatives catalyzed by $[Pd_2(dba)_3]$ [Eq. (1); dba = (*E*,*E*)-dibenzylideneacetone]: whereas good yields are obtained with the ligand tricyclohexylphosphane for ligands that are appreciably larger or smaller, essentially no coupling is observed. As the conditions are compatible with a variety of functional groups, this method introduces a new class of substrates into the family of potential partners in palladium-catalyzed cross-coupling reactions.



(1)

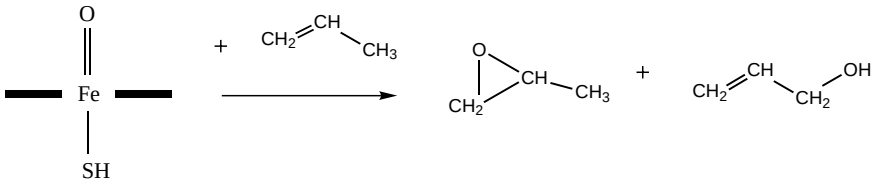
Angew. Chem. **2002**, *114*, 2025 – 2027

J. H. Kirchhoff, C. Dai, G. C. Fu* ..... 1945 – 1947

A Method for Palladium-Catalyzed Cross-Couplings of Simple Alkyl Chlorides: Suzuki Reactions Catalyzed by $[Pd_2(dba)_3]/PCy_3$

Keywords: alkyl chlorides · cross-coupling · homogeneous catalysis · palladium · P ligands

Changes of two orders of magnitude or more in the epoxidation to hydroxylation ratio of propene by the iron-oxo species **1**, the primary active species of cytochrome P450 (see scheme) occur when the molecular species is subject to NH ··· S hydrogen bonding and electronic polarization as in the protein pocket.



1

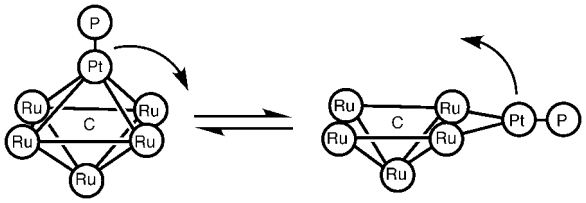
Angew. Chem. **2002**, *114*, 2027 – 2031

S. P. de Visser, F. Ogliaro, P. K. Sharma, S. Shaik* ..... 1947 – 1951

Hydrogen Bonding Modulates the Selectivity of Enzymatic Oxidation by P450: Chameleon Oxidant Behavior by Compound I

Keywords: density functional calculations · enzyme catalysis · epoxidation · hydroxylation · solvent effects

Metal in motion: The reaction of $[Ru_5(CO)_{15}(\mu_5\text{-}C)]$ with $[Pt(PtBu_3)_2]$ yields $[Ru_5Pt(PtBu_3)(CO)_{15}(C)]$. The product exists as two isomers, an open and a closed form, which interconvert rapidly on the NMR timescale by a process that resembles the diffusion of metal adatoms across a metal surface (see scheme; at 20 °C the rate = 24000 s^{-1}).



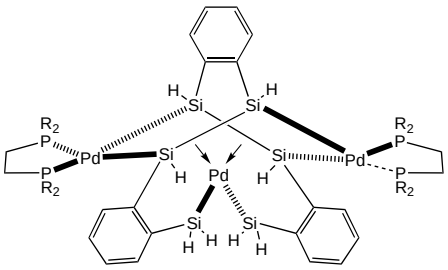
Angew. Chem. **2002**, *114*, 2031 – 2033

R. D. Adams,* B. Captain, W. Fu, P. J. Pellechia, M. D. Smith 1951 – 1953

A Dynamic Rearrangement of a Metal Cluster in a Process that Closely Resembles the Hopping Mechanism of Adatom Diffusion on Metal Surfaces

Keywords: cluster compounds · platinum · rearrangements · ruthenium

Pd^{II} not Pd^{VI}: Electronic structure calculations indicate that the central palladium atom in the trinuclear Pd compound (see picture) is bonded to two SiH_2R groups and two Si—Si σ bonds, consistent with an oxidation state of Pd^{II}, not Pd^{VI}, as might otherwise be inferred from the structural data.



Angew. Chem. **2002**, *114*, 2033 – 2036

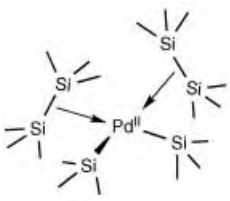
E. C. Sherer, C. R. Kinsinger, B. L. Kormos, J. D. Thompson, C. J. Cramer* ..... 1953 – 1956

Electronic Structure and Bonding in Hexacoordinate Silyl – Palladium Complexes

Keywords: bond theory · density functional calculations · electronic structure · palladium · Si ligands

 © WILEY-VCH Verlag GmbH, 69451 Weinheim, Germany, 2002 1433-7851/02/4111-1819 $ 20.00+.50/0

Side-bound Si–Si single bonds: A theoretical study indicates that in a recently reported compound, two Si–Si bonds are side-on coordinated to a square-planar Pd^{II} ion (see picture).





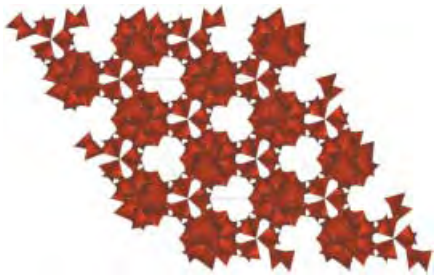
Angew. Chem. **2002**, *114*, 2036 – 2039

G. Aullón, A. Lledós, S. Alvarez* ..... 1956 – 1959

Hexakis(silyl)palladium(VI) or Palladium(II) with η^2-Disilane Ligands?

Keywords: agostic interactions · density functional calculations · electronic structure · palladium · Si ligands

Fine-tuning structures: A family of noncluster-based 3D open-framework indium chalcogenides are reported. The framework composition is highly flexible and controllable. Such a compositional diversity makes it feasible to tune structural, electronic, and optical properties. The structure shows a polyhedral view of 3D cross-linking in an In – Te compound.



Angew. Chem. **2002**, *114*, 2039 – 2041

C. Wang, X. Bu, N. Zheng, P. Feng* ..... 1959 – 1961

A 3D Open-Framework Indium Telluride and Its Selenide and Sulfide Analogues

Keywords: chalcogens · indium · microporous materials · self-assembly

Supporting information on the WWW (see article for access details).

Accelerated publications

* Author to whom correspondence should be addressed

BOOKS

Biopolymers	Alexander Steinbüchel, Martin Hofrichter	*O. Faix* 1963
Magnetism, Vol. I – III	Joel S. Miller, Marc Drillon	*W. Plass* 1964
Understanding Chemistry	C. N. R. Rao	*J. D. Dunitz* 1965
The Biological Chemistry of the Elements	J. J. R. Frausto da Silva, R. J. P. Williams	*G. C. Dismukes* 1966
Heme, Chlorophyll, and Bilins	Alison G. Smith, Michael Witty	*R. Neier* 1966
Fundamentals of Quantum Chemistry	Michael Mueller	*N. L. Doltsinis* 1968

WEB SITES

http://www.quantum-physics.polytechnique.fr, http://phys.educ.ksu.edu/	Interactive Quantum Mechanics	*R. Berger* 1969

 © WILEY-VCH Verlag GmbH, 69451 Weinheim, Germany, 2002 1433-7851/02/4111-1820 $ 20.00+.50/0

SERVICE

- **VIPs** 1812
- ***Angewandte's* Sister-Journals** 1823 – 1825
- **Sources** A49
- **Keywords** 1970
- **Authors** 1971
- **Preview** 1972

Don't forget all the Tables of Contents from 1998 onwards may be still found on the WWW under: http://www.angewandte.com

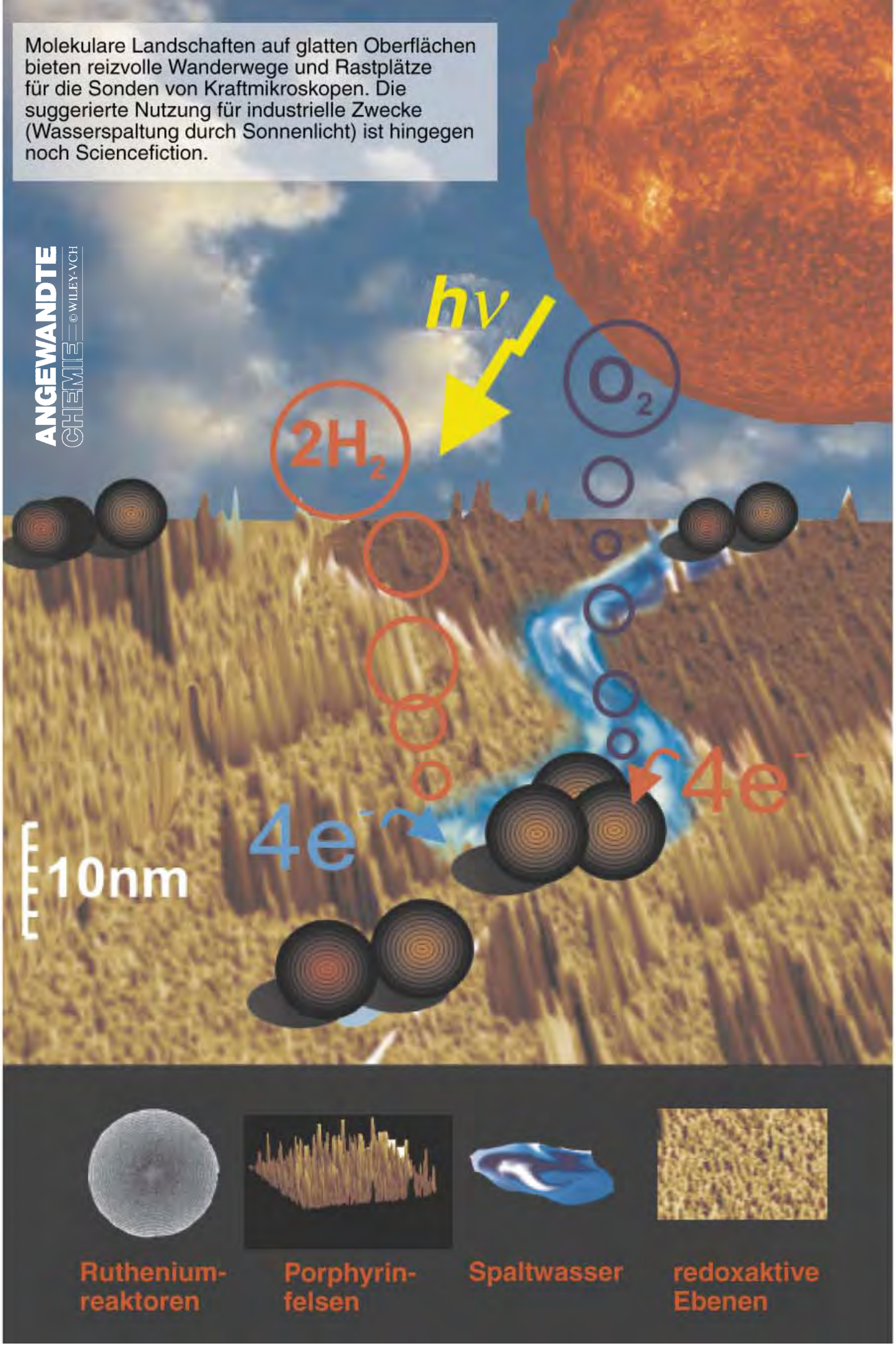
Issue 9, 2002 was published online on May 2.
Issue 10, 2002 was published online on May 15.

CORRIGENDUM

In the review by **L. Que, Jr.** and **W. B. Tolman** (*Angew. Chem. Int. Ed.* **2002**, *41*, 1114 – 1137) it was incorrectly stated that the $Fe^{III}Fe^{IV}$ complex reported by Lee et al. in ref. [54] has a bis(μ-oxo)diiron structure. In fact, in ref. [54] it is made clear that from the experimental data for the complex the mode of ligation could not be specified. The authors apologize for this mistake.

© WILEY-VCH Verlag GmbH, 69451 Weinheim, Germany, 2002

1433-7851/02/4111-1821 $ 20.00+.50/0


Molekulare Landschaften auf glatten Oberflächen bieten reizvolle Wanderwege und Rastplätze für die Sonden von Kraftmikroskopen. Die suggerierte Nutzung für industrielle Zwecke (Wasserspaltung durch Sonnenlicht) ist hingegen noch Sciencefiction.
ANGEWANDTE CHEMIE © WILEY-VCH
hν
2H2
O2
4e-
4e-
10nm
Ruthenium-reaktoren
Porphyrin-felsen
Spaltwasser
redoxaktive Ebenen

Rigid Lipid Membranes and Nanometer Clefts: Motifs for the Creation of Molecular Landscapes

Guangtao Li, Werner Fudickar, Marc Skupin, Andreas Klyszcz, Christian Draeger, Matthias Lauer, and Jürgen-Hinrich Fuhrhop*

Amphiphilic lipids associate in water spontaneously to form micelles, vesicles, monolayers, or biological membranes. These aggregates are soft and their shape can be changed easily. They behave like complex fluids because they are merely held together by weak, nondirected forces. The most important characteristic of these monolayers is their ability to dissolve hydrophobic molecules in the form of freely movable monomers. The fluid molecular layers are not suitable to anchor the components of chain reactions. However, if the alkyl chains are replaced by rigid skeletons or if the head groups are connected through intermolecular interactions, the aggregates become rigid and their fluid solvent character is lost. The construction of chiral surfaces by synkinesis (synthesis of noncovalent compounds) and of enzyme-type surface clefts of defined size can now be carried out by using rigid lipid membranes. Monolayers and nanometer pores on solid substrates attain sharp edges, and upright nanometer columns on smooth surfaces no longer dissipate. Five examples illustrate the advantages of using rigid molecular assemblies: 1) Cationic domains of rigid edge amphiphiles in fluid membranes act as manipulable ion channels. 2) Spherical micelles, micellar helical fibers, and vesicular tubes can be dried and stored as stable material. Molecular landscapes form on smooth surfaces. 3) α,ω-Diamide bolaamphiphiles form rigid nanometer-thick walls on smooth surfaces and these barriers cannot be penetrated by amines. Around steroids and porphyrins, they form rigid nanometer clefts whose walls and water-filled centers can be functionalized. 4) The structure of rigid oligophenylene- and quinone monolayers on electrodes can be changed drastically and reversibly by changing the potential. 5) 10^{10} Porphyrin cones on a 1-cm^2 gold electrode can be controlled individually by AFM- and STM-tips and investigated by electrochemical, photochemical, and mechanical means. In summary, rigid monolayers and bilayers allow the formation of a great variety of membrane structures that cannot be obtained from classical fluid alkyl amphiphiles.

Keywords: membranes · molecular landscapes · nanostructures · self-assembly · synkinesis

1. Introduction

The spontaneous self-assembly of amphiphilic lipids in aqueous solution leads to small molecular aggregates such as micelles, planar molecular bilayers (Myelin figures), vesicles, or biological membranes. Such aggregates are soft and flexible and behave like fluids. This is still valid at higher concentrations when lipid aggregates associate to micellar tubes (hexagonal or cubic phases) or when they are attached to solid substrates (Langmuir—Blodgett (LB) layers). The fluid character is a consequence of the fact that only weak undirected forces (van der Waals forces, hydrophobic effects) hold the lipid aggregates together and keep the head groups apart.[1]

Nevertheless, the spherical and rodlike micelles and vesicles in water as well as the planar lipid monolayers on solid surfaces are structurally well-defined. The effect of these ultrathin lipid membranes is, however, limited to the solubilization of hydrophobic organic molecules in water, the modification of the surface properties of water and of solids, and the separation of trapped volumes of water from bulk water. The fluidity of the alkyl chains of ordinary amphiphiles and detergents gives rise to their ability to dissolve hydrophobic isolated molecules. At the same time, this fluidity hinders the construction of rigid molecular cavities, which would correspond to enzyme clefts. Chain reactions, which, for example, would allow photolysis of water by sunlight, cannot be realized with fluid membranes.[2, 3] The organic chemist who wants to create stable molecular landscapes,

[*] Prof. Dr. J.-H. Fuhrhop, Dr. G. Li, Dr. W. Fudickar, Dr. M. Skupin, Dr. A. Klyszcz, Dr. C. Draeger, Dipl.-Chem. M. Lauer
Institut für Chemie/Organische Chemie, Freie Universität Berlin
Takustrasse 3, 14195 Berlin (Germany)
Fax: (+49) 30-838-55589
E-mail: fuhrhop@chemie.fu-berlin.de

 © WILEY-VCH Verlag GmbH, 69451 Weinheim, Germany, 2002 1433-7851/02/4111-1829 $ 20.00+.50/0

architectures, and machines by combining synkinesis (e.g. of heterodimers with defined molecular distances)[2, 3] with self-assembly,[1] should avoid fluid components. Instead, nature should be imitated as closely as possible: form and function are established by rigid proteins, which incorporate extremely complex reaction centers for biological processes.

To incorporate effective reaction centers within the easily accessible molecular mono- and bilayers of amphiphilic lipids, the properties of fluid membranes have to be modified. One should prevent micellar spheres of flexible amphiphiles from decomposing into planar bilayers within milliseconds of their removal from water. Boundaries between different motifs (plain, hill, valley, pond) should not be smeared out beyond recognition by molecules in the border region. Form-stable modules, which arrange in a defined order to allow a directed sequence of events, are needed for the construction of molecular machines. Rigid molecules based on amphiphiles will only be possible if the repulsive hydration forces are overcompensated by directed binding interactions between the membrane-forming amphiphiles or if the flexible alkyl chains are replaced by rigid polyenes, arenes, or steroids. Rigid membrane structures on solid surfaces or colloids can then be arranged around functional molecules that lie flat on the substrate. The membrane structures can then combine the function of proteins (to anchor reactive centers) with the matrix function of the membrane. Water remains the bulk solvent. However, the self-assembly properties of the ultrathin fluid lipid membranes must be retained. Figure 1 summarizes some typical characteristics of fluid and rigid lipid membranes: a) if the repulsive interactions between the small head groups of the amphiphiles are replaced by (weak) hydrogen bonds of bulky head groups, the micelles will no longer decompose upon drying; b) vesicle membranes on solid surfaces will no longer collapse upon drying, if fluid hydrophobic chains are replaced by rigid polyenes; c) micellar and vesicular fibers will survive in a highly diluted solution and on solid substrates if they are stabilized by two parallel hydrogen-bond chains between secondary amide groups; and d) the nanometer clefts in monolayers on solid substrates are also stabilized by hydrogen-bond chains.

The binding forces between the head groups may cause the curved rigid membrane systems (Figure 1) to crystallize quickly in bulk water.[1] Only those nanometer clefts in anchored surface layers (Figure 1 d), which resemble the edges of microcrystals, have a chance to survive. Herein we describe methods to isolate highly curved dry micelles and vesicles, as well as first attempts to integrate redox-active molecular modules into rigid membranes through noncovalent interactions. We focus on systems with the following characteristics: 1) easily prepared; 2) the components and their distances can be modified; 3) analyzable with routine methods; and 4) producible in large quantities. These requirements are best fulfilled by using water as solvent in combination with self-assembling polymer or lipid systems. We limit this Review to rigid lipid systems, but occasionally mention parallel developments with amphiphilic block polymers and multiple layers of polyelectrolytes.

2. Formation of Domains

The smallest rigid membrane structures, the domains, are generated by polar binding interactions between dissolved guest molecules in the center of fluid lipid bilayers. Ordinary micelles are too small to serve as hosts for large domains, and they usually dissolve molecules as monomers.[4] Exceptions are nucleic bases with short alkyl chains which agglomerate to give heterodimeric base pairs as a solid core in the fluid environment of the micelle (Figure 2 a).[5] Micelles also proved to be suitable for the synthesis of macrocycles, for



Back: G. Li, C. Draeger, M. Lauer, J.-H. Fuhrhop; front: W. Fudickar, M. Skupin, A. Klyszcz (from left to right)

Prof. Jürgen Fuhrhop has been instructing at the Institute of Organic Chemistry of the Freie Universität Berlin since 1977. His scientific work covers metalloporphyrin radicals und their diamagnetic π,π′-dimers, the ring opening of metalloporphyrins with molecular oxygen to form formylbiliverdins, ultrathin vesicle membranes of unsymmetrical and chiral bolaamphiphiles, and the transformation of helical fiber aggregates into sheetlike structures by the addition of enantiomers (chiral bilayer effect). Among other publications, his work has been summarized in two monographs.[2]

Dr. Guangtao Li, Dr. Werner Fudickar, Dr. Marc Skupin, Dr. Andreas Klyszcz, and Dr. Christian Draeger are current co-workers. They produced and characterized the form-stable nanometer pores (Fudickar, Li, Skupin), porphyrin towers (Klyszcz, Lauer), and micelles (Draeger) discussed in this Review.

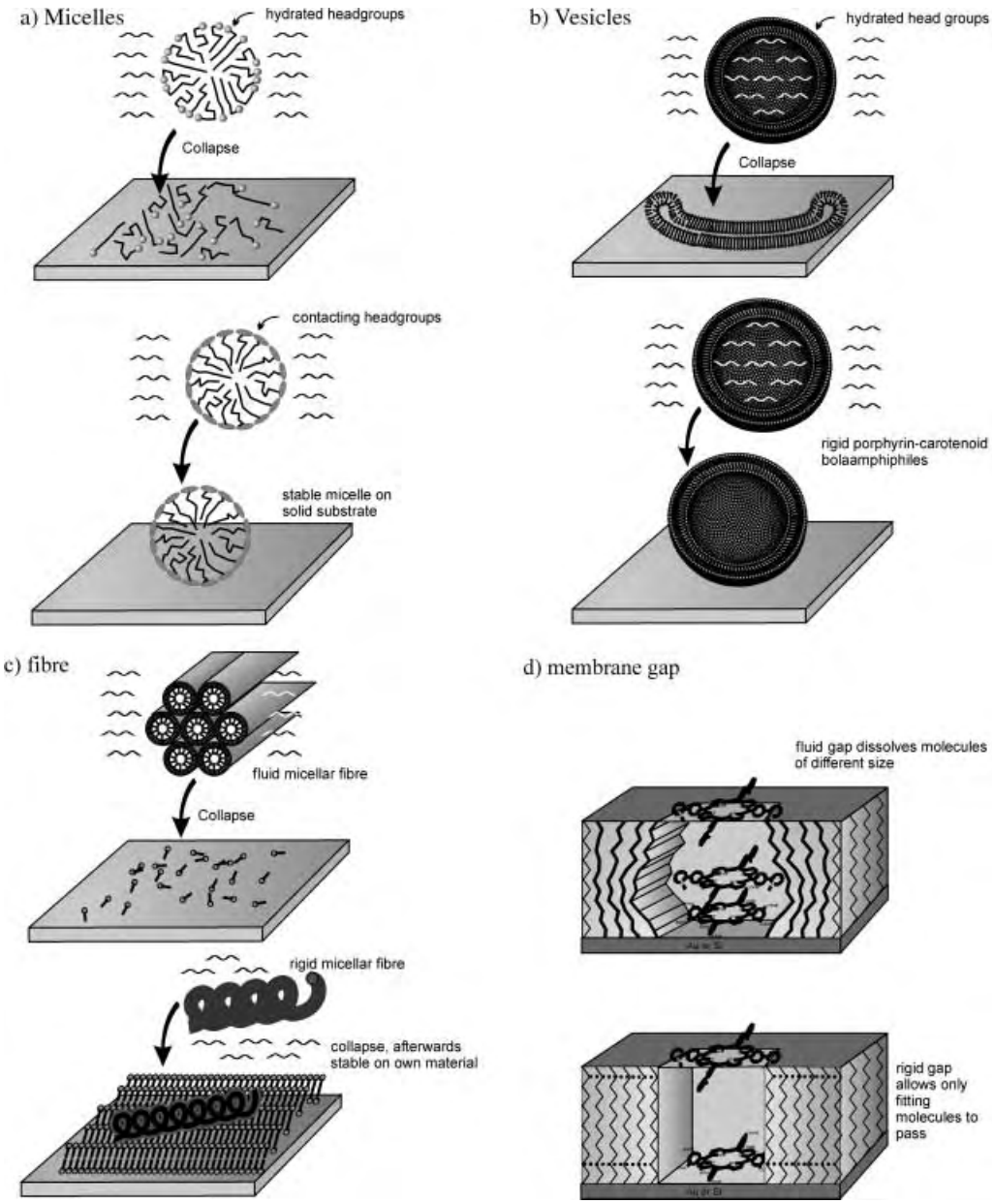


Figure 1. Comparison of fluid and rigid amphiphiles in a) micelles, b) vesicles, c) micellar fibers, and d) monolayers with nanometer clefts on smooth, solid substrates. Micelles and micellar fibers with a rigid head group area can be isolated. Fluid clefts in monolayers act as solvent, and rigid clefts act as filters and matrices.

example, porphyrinogens. Hydrophobic aromatic aldehydes and pyrrole form small aggregates that dissolve in micelles (Figure 2b). The shape of the micelle prevents the formation of large linear oligomers in the subsequent acid-catalyzed condensation. Instead, only small copolymers are formed. As soon as a cyclic porphyrinogen is formed, the reaction is interrupted. Oxidation with air leads to porphyrins; the average yield is 5–10 times higher than in homogeneous solutions.[6]

Polypeptide ion channels in biological cell membranes and synkinetic vesicle membranes occasionally consist of cavities in rigid protein helices (e.g. gramicidin S, Figure 3b), but mostly they consist of domains made of helical or linear edge amphiphiles (e.g. melittin, Figure 3a; see also Figures 4 and 5). The hydrophobic edge of these molecules dissolves in the membrane, the polar edges aggregate, attract water, and form pores. Positive electric charges at the hydrophilic edge seem to be essential to keep the edge amphiphiles at a distance, thus allowing ion transport.[7, 8] The alignment of the helices controls the ion flow: an inward-directed, negative membrane potential of 100–200 mV causes a higher cationic current when the dipole of the helix bundle is aligned in such a way that its positive end points to the outside. The bee poison melittin thus behaves like an adjustable edge amphiphile. First, it associates to the vesicle surface with its hydrophobic side and forms a helix with a strong dipole moment. Upon application of a membrane potential, it is integrated into the membrane.[7, 8] The hydrophilic surfaces are positively charged and form a broad ion channel (Figure 3a).[7]

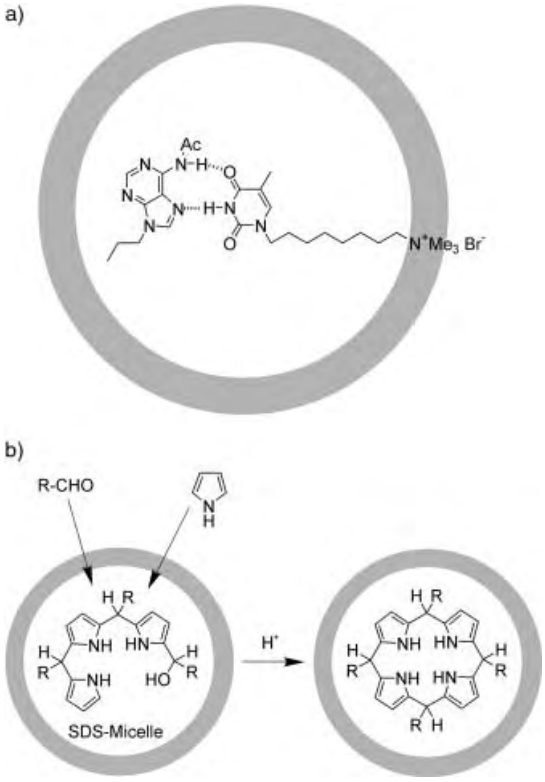


Figure 2. Fluid micelles are suitable a) to accumulate rigid hydrogen-bonded dimers, and b) as a trap for water-insoluble intermediates. In general, one only finds monomers in micelles. SDS = sodium dodecylsulfate.

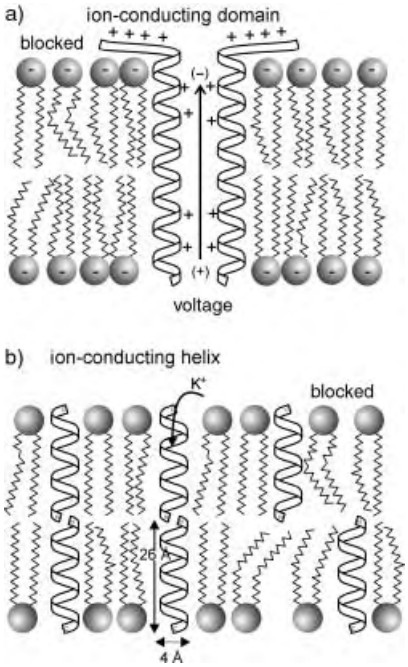


Figure 3. a) Domain formation of the helical edge amphiphile melittin leads to natural peptide channels in fluid lipid membranes. b) Alignment of two gramicidin helices in both halves of a lipid bilayer also produces rigid ion channels.

Helical protein edge amphiphiles occasionally also act as monomers or linear dimers without building domains. Gramicidin contains a hydrophilic cavity, whose diameter is large enough for the transport of potassium ions.[9–12] The gramicidin tube penetrates either the total double layer membrane by contracting it, or only half of an intact lipid bilayer. In the latter case, two gramicidin tubes must associate at their ends to allow an ion flow (Figure 3b). The relative mobility of two gramicidin helices towards each other is then necessary for the formation of the ion channel. If the inner and outer gramicidin helices are individually anchored by covalent bonds to a solid substrate, an ion current will no longer flow.[12] If, however, both helices are connected to each other covalently at the ends, the pore will be opened permanently.[11] In any case, the rigid membrane helix always migrates parallel to the alkyl chains of the membrane-forming amphiphiles. As the valine and leucine side chains fit perfectly within the fluid membrane structure, the helix does not leave the membrane nor does it form any domains that could disturb the fluidity and the impermeability towards ions.[9–11]

Not only water-conducting pores allow ions to penetrate through lipid membranes. Ill-defined edges of incorporated crystallites have a similar, though uncontrollable, effect. It was shown, for example, that a fluid vesicle membrane completely lost its osmotic activity, when carotenoid bolaamphiphiles had been incorporated. Borohydride and dithionite ions permeate the membrane within a few seconds along the edges of the hydrophobic crystallites, whereas the fluid membrane without crystallites constitutes a perfect barrier against ion transport.[13]

Real channel formation within defined domains or spacious helices can hardly be distinguished from membrane disturbances by current measurements with the patch–clamp method. Each pore should rather be defined as such by its ability to open and close reversibly. This can be effected by molecular plugs, light signals, modification of the pH-value, or other similar methods. Water runlets at the edges of crystallites would not give an "all or nothing" response to such a stimulus. With respect to artificial pores, reversible opening and closing procedures have so far only been demonstrated with oligoamine pores with carboxylate end groups. At pH 7, ethylenediaminetetraacetic acid (EDTA) acted as a plug. At pH 3, after neutralizing the terminal carboxy groups, it dissolved again in the bulk water, and the pore allowed the transport of ferrous ions (Figure 4). The positive charges of the ammonium groups on the hydrophilic surfaces of these edge amphiphiles clearly interacted with the carboxylate groups of the EDTA.[14]

Rigid tubes of cyclopeptide stacks were arranged vertically on gold electrodes (Figure 5), as proved by using small-angle FTIR spectroscopy ($I_{\perp} \gg I_{\parallel}$).[15, 16] The ability of the pore to be closed reversibly by plugs, has, however, not been demonstrated yet. Permeable boundaries between fluid membranes and crystallites or individual stacks could perhaps explain the permeability for ferricyanide ions just as well as the proposed ion channels made of domains of parallel peptide cylinders. Cyclic voltammetric studies of ferricyanide ions in bulk water did also not allow the determination of the exact mechanism of ion transport.[17] Patch–clamp measurements of the potassium transport through lecithin membranes showed considerable increases and decreases in conductivity; from these results one could deduce that opening and closing

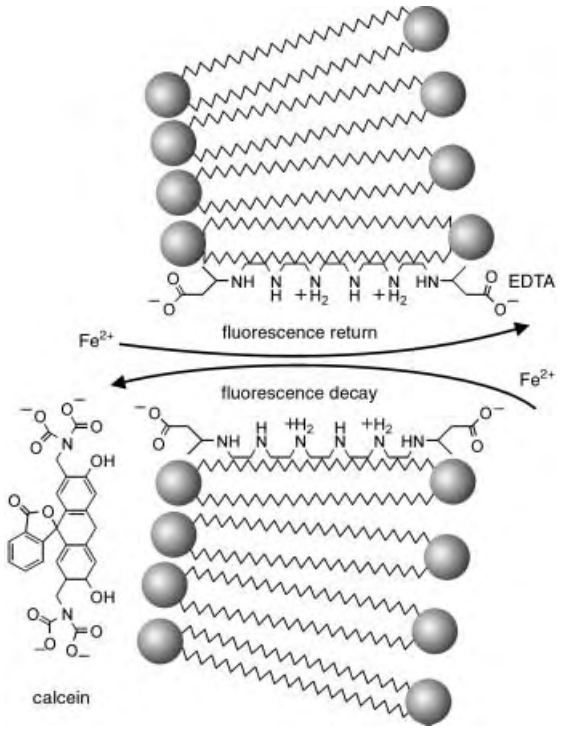


Figure 4. Closing and opening of a pore-forming domain by associating EDTA to a synthetic oligoamine edge amphiphile with terminal carboxylate groups. The penetrating ferrous ion extinguishes the fluorescence of the chromophore entrapped within the vesicle. EDTA in the bulk water withdraws the ferrous ions again.

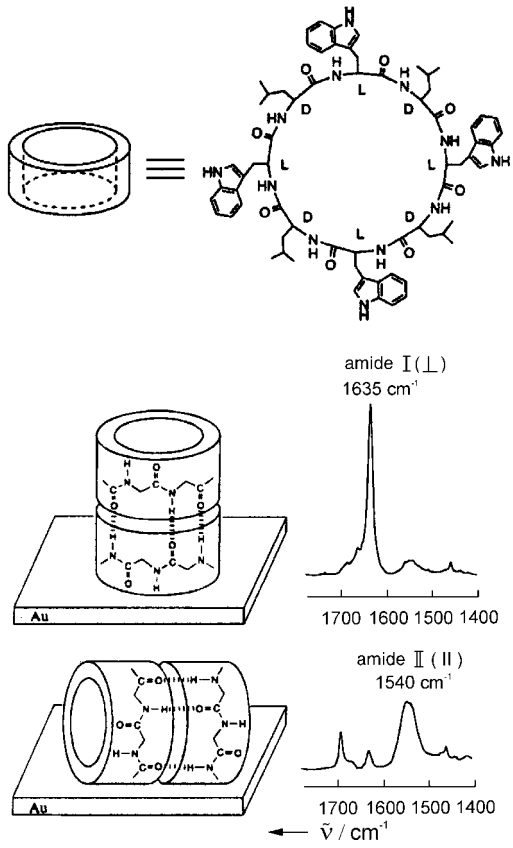


Figure 5. Cyclopeptide tubules can be arranged vertically or lie flat on a planar gold surface. Both positions can clearly be differentiated by FTIR spectra because the dipole directions of the functional groups drastically differ from each other in rigid aggregates.

operations are probably triggered by reversible dissociation of the staples.[18] Moreover, atomic force microscopy (AFM) measurements demonstrated that flat-lying cyclopeptide stacks arranged themselves vertically on glass when a lipid matrix was built up around them.[17]

The relative solubilities of amphiphiles either in the form of domains in fluid membranes or as micelles in bulk water are difficult to predict. Furthermore, edge amphiphiles tend to form complexes with metal ions. In general, rod-like polyol– or crown ether–oligomer edge amphiphiles do not directly transport metal ions through membranes, but accelerate potassium transport through valinomycin or proton transport along hydrogen-bond chains. It is remarkable that all these highly water-soluble compounds associate to lecithin membranes without any problem and presumably also span them.[8, 19, 20]

This applies similarly to the so-called electronic conductors or "molecular wires" made of the membrane-spanning polyene caroviologen, a carotene with a viologen head group.[19] Clear evidence of electronic conductivity through polyene molecules has only been obtained electrochemically, by two methods:[21a,b] 1) a gold-supported monolayer of β-carotene with thiol end groups produced a 10^6-fold higher conductivity to a tunnel microscope tip than an equally thick monolayer of alkyl sulfides, but its conductivity was, nevertheless, 10^4-fold lower than that of solid-phase polyacetylene;[20a] 2) the rate constants (k_{obs}) for the electron transfer from gold to ferrocene were measured as a function of the bridge lengths (in Å) of the alkane and phenylethynyl bridges.[21b] For the conjugated aromatic systems, a β value (β = linear inclination of $\ln k_{obs}/l$) of $-0.9\,\text{Å}^{-1}$ was measured, and for alkyl chains a value of only $-0.36\,\text{Å}^{-1}$ was found. A distance of $l = 20$ Å thus corresponds to an electron-transfer rate that is 10^{10}-fold faster in conjugated systems. The chemical Michael addition analogy of electrons "adding" to polyenes with carboxylate or pyridinium end groups and subsequent electron movement along the rigid "wire" is a plausible mechanism, but has presumably never been realized.

In one case it was clearly shown that ion transport through vesicle membranes occurred by translocation of ions along the "polyene wires" and not by electron conductivity.[14] Such proof will be possible, if the electron acceptor that is trapped within the vesicle, for example, an indigo dye, forms different products with different reductants: reduction with electrons should lead to a single product, regardless of the electron source.

3. Isolable Micelles and Vesicles

Micelles are molecular assemblies with the smallest possible diameter, that is, with the highest curvature of a molecular bilayer of alkyl chains.[1–4] This curvature occurs because the fluid alkyl chains, which have many *gauche* bends, are broader than the head groups and consequently push them wide apart. The head groups then bind a considerable amount of hydration water and are isolated from each other by repulsive hydration forces.[3, 4] If, however, the bulky head groups occupy the total spherical surface of the alkyl droplets and

if the cohesion of neighboring head groups are enforced by intermolecular hydrogen bonds, the hydrated water will partially be dislocated, the critical micellar concentration (CMC) will drop sharply, and the fluid micelles will become isolable as dry material.

The easiest way to enable contact between the head groups on a highly curved surface is to make them large. Bulky cationic head groups, especially those of trialkyl ammonium groups combined with large soft anions, lead to cationic micelles, which could be deposited on solid substrates with a negatively charged surface, for example on amorphous silica gel. Under water, 7-nm micelles or the corresponding cylindrical micelles were found by AFM.[22a,b] With even larger head groups, which have binding interactions with each other, spherical micelles were found that could even be isolated in the dry state. Kanamycin, a trisaccharide-like tuberculosis remedy with four amino groups, proved to be a suitable head group for this purpose. The surface of a sphere of 100 fluid octadecyl chains should measure about 12000 Å^2. The surface of a kanamycin molecule amounts to 75 Å^2. Consequently 150 head groups are sufficient to cover the surface of the micelle completely. Moreover, intermolecular hydrogen bonds between amino-, ammonium-, and hydroxy groups can displace most of the hydration sphere. Indeed, upon simple shaking, a C_{18} amide of kanamycin gave an aqueous micellar solution with a CMC of $< 10^{-5}$ M. A solution of these micelles (10^{-3} M) was applied to a carbon foil; transmission electron microscopy (TEM) showed the expected stable micelles with a diameter of about 6 nm (Figure 6a). AFM images of the same micelles on mica showed them as well-ordered stripes on the crystal planes of the substrate. The height of 5 nm corresponded to a molecular bilayer (Figure 6b). After applying a dilute solution (100 ×), the micelles did not lie side by side, but were isolated from each other, and dissipated over a molecular bilayer to semi-micelles. Both the densely packed micelles and the isolated semi-micelles

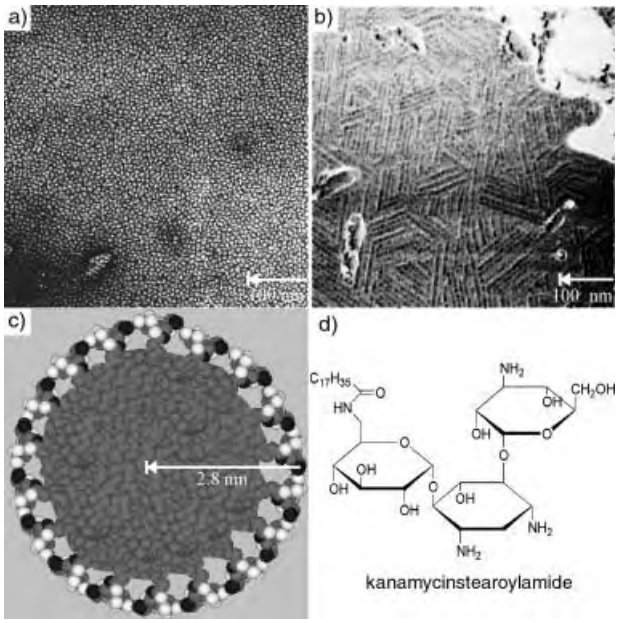


Figure 6. a) TEM and b) AFM pictures as well as the model of c) a kanamycin – stearylamide micelle.

remained stable for hours on solid surfaces in the dry state. In aqueous solution they behaved like fluid micelles and formed monomolecular solutions of metalloporphyrins.[23]

The concept of using large, interconnected head groups to make isolable micelles was also successful with metal complexes with two oligomethylene chains. Tris(bipyridinium) complexes of ruthenium with two C_{18} or C_{16} chains dissolved in water to form multishell micelles upon sonication (Figure 7).[24] However, these are micelles and not vesicles

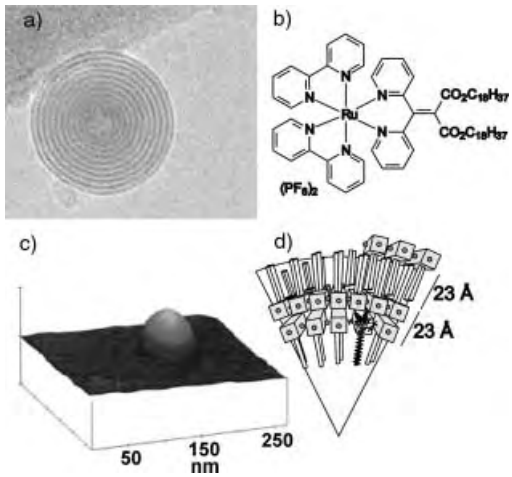


Figure 7. a) TEM pictures and b) structure of the monomeric tris(bipyridine)ruthenium hexafluorophosphate, c) AFM pictures of a micelle, d) model of a micellar fragment.

because no volumes of water are included by their membranes. The oligomethylene chains of the amphiphile form the core of the aggregate. The following forces are involved in the formation of micelles: 1) strong bonds between the ruthenium bipyridine dications and the hexafluorophosphate counterions; 2) van der Waals forces between interdigitated alkyl chains; and 3) (so far unique to micelles) back-to-back van der Waals forces between the head groups. The result is an assembly of spherical shells made of interdigitated double combs or herringbone patterns (Figure 7). The micelle can be isolated in the dry state and does not spontaneously associate as crystals of planar double layers, because the two highly organized, interdigitating oligomethylene chains do not allow reorientation of the head groups. These ruthenium micelles fluoresce and are photochemically active. If the rigid order of the double layers is disturbed, the fluorescence disappears. The corresponding palladium analogues form homogeneous micelles in water and have been utilized to catalyze Heck reactions.[25] AFM analysis has shown the $(C_{18})_2$–Ru compound in the form of undistorted micelles on gold and mica surfaces (Figure 7c). On graphite, however, the micelles were torn apart to form planar bilayers of flat amphiphiles.[24]

The C_{16} homologues are stable only on alkane layers. On graphite, mica, silica, and gold they spontaneously form three different configurations of planar double layers (flat-upright; head-to-head; head-to-tail; Figure 8). The most extensive decomposition of the micellar bilayer always takes place on graphite, because it strongly interacts with both the hydrophobic tails and the hydrophilic head groups. On mica, gold

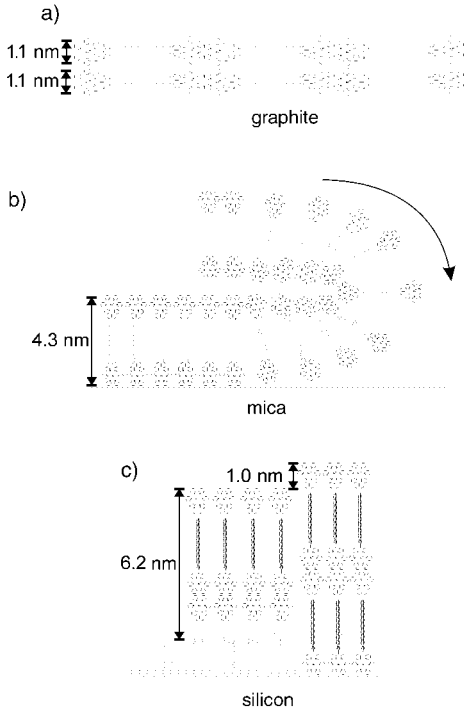


Figure 8. Model of the molecular configuration of bilayers, as they are formed on different planar substrates after the micelle has burst (see Figure 7).

and silica surfaces, the original interdigitated bilayer is maintained, only the curvature is lost.[26]

Spherical aggregates, which can be dried and stored, can thus be maintained by reversibly connecting head groups with a large surface area. The dominance of repulsive hydration forces does not necessarily lead to crystal planes upon drying. Water-free bi- and multilayered micelles are now available as isolable material, and it should be possible to load them with any monomer.

Isolable vesicles can generally only be obtained as covalent polymers. The first solvent-resistant polymeric vesicles with bilayered membranes were produced from vinyl groups in the head group region or at the end of the alkyl chains. However, nothing is known about the stability of these vesicles on solid substrates.[27–33] A large number of block polymers made of hydrophobic and hydrophilic subunits were synthesized; these block polymers formed spherical particles with an undefined membrane thickness and diameters of about 10–100 nm.[31–33] Those vesicles were loaded, for example, with colloidal palladium or rhodium and then used to catalyze Heck or hydroformylation reactions.[31a,b] Other polymer vesicles were used in toluene to optimize cryoelectron microscopy methodology.[33] Vesicles of noncovalently bonded cationic amphiphiles, which were solidified by cholesterol (50 mol%), proved to be stable on a cationic substrate and were characterized by AFM.[34] However, they remained stable only for a few minutes, before converting into planar bilayers.

Mono- or bilayered lipid vesicles without an included volume of water appear impossible at first sight: a free-standing 5-nm thick membrane should immediately collapse upon drying. Only one exception is known and is a result of the rigidity of the polyene amphiphile used, whose inner end had to be anchored to a rigid porphyrin carrier: eight α,ω-dicarboxycarotenoids (bixin) were attached on a porphyrin skeleton in such a way that four carboxy groups both above and below the macrocycle produced a bolaamphiphile with a large surface. The rigid polyene rods were arranged parallel to each other, and the porphyrins formed a rigid center. Spheres (40 nm, with 5-nm-thick walls) then formed in water and remained stable upon drying and on solid surfaces, even without covalent polymerization (Figure 9). The membrane is permeable to ions and therefore osmotically inactive and completely resistant to the addition of electrolytes.[35] After radiation with visible light, the polyene polymerized and the rigid vesicle became totally inert to organic solvents.

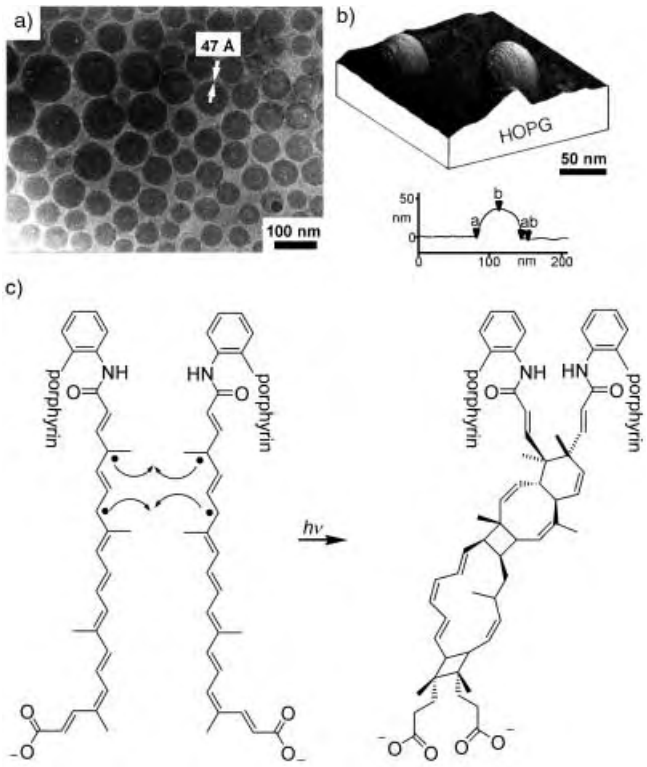


Figure 9. a) TEM and b) AFM pictures of the porphyrin–octabixin ester sphere with 4-nm thick walls; c) model of the light-induced polymerization. HOPG = highly orientated pyrolytic graphite.

An octabixinatoporphyrin is certainly not a useful amphiphile for general use. Thick-walled polyelectrolyte vesicles are also not promising transport systems for active substances in the human body. These rigid spheres can thus not compete with fluid vesicles (cyclodextrins and polymer microcapsules), which have proved to be effective transport systems.

4. Micellar and Vesicular Fibers

Amphiphiles with chiral head groups (glycon, amino acids) and secondary amide groups in the hydrophobic skeleton also form fluid, spherical micelles in water at temperatures above 80 °C. Upon rapid cooling of the aqueous solution, the

amphiphiles agglomerate to give extraordinarily form-stable, noncovalent fibrous micelles, which are frequently helical and can be isolated in the dry state. Quadruple helices, twisted ribbons, or tubular helices have been observed by TEM. The fibers are often very similar in appearance to protein fibers, which have been discussed in detail in a previous review.[36]

D-Gluconamides form isolable quadruple helices in water (Figure 10a, c), which convert into sheetlike structures and precipitate upon the addition of the L enantiomers (Figure 10b). This effect is of general importance for the stability of bioorganic gel and is called the chiral bilayer effect (Figure 10d).[37] This effect occurs in numerous amphiphiles with chiral head groups (for example, glycon,[37–39] glutamic acid,[40] and tartaric acid[41]) or with a chiral hydrophobic skeleton[42, 43] as well as for the helical polymer homopolylysine.[44] The pure enantiomers always form chiral fibers and stable gels in water. Upon the addition of the opposite enantiomer to the gel, crystallites precipitate and the gel is totally liquefied. In the case of gluconamide quadruple helices, which were isolated in the dry state and studied by solid-state ^{13}C NMR spectroscopy, the conformation of the head group was completely analyzed by comparing spectra of crystals of related open-chain carbohydrates, whose crystal structure was known (Figure 10e).[45, 46] A *gauche* bend near the outer end ($_2G^-$ conformation) of the head group was found in the fibers. This *gauche* bend is stabilized by a cyclic arrangement of hydrogen bonds and is responsible for the curvature of the fiber, because it makes room for hydration water, which enlarges the head group and promotes the curvature. Here, the formation of planar bilayers is prevented by directed hydrogen bonds and not by repulsive hydration forces. Recent experiments show that these well-ordered aggregates can be isolated as a dry material and preserved for years. Upon contact with solid surfaces they rearrange spontaneously to planar bilayers. The remaining fibers can then be deposited without any rearrangement onto the bilayers. AFM analysis shows them as "crests" on the plane. The solid substrate, for example graphite or gold, is located 5 nm below (Figure 10f).[47]

Other chiral amphiphiles form nonhelical bilayers, which roll up to multilayered tubes. Examples are D-mannonamide and D-galactonamide,[39] chiral alcohols from pine needles,[43] and bolaamphiphilic diamides with a lysine head group.[48] Lipid tubules made of bolaamphiphiles with an amino acid head group (e.g. lysine) and an amino head group are particularly easy to produce and handle. A slight variation of pH values produces homogeneous tubules of spherical vesicles and micelles (Figure 11).[48] The mannonamide fibers gave rise to hard, completely insoluble polymer rods when the diacetylene groups in the center of the bilayer were irradiated with ultraviolet light.[49] The gluconamide quadruple helices with their extremely high curvature disintegrated under identical polymerization conditions to ill-defined single strands.

Micellar fibers are consistently formed upon contact with solid substrates, for example, in the case of achiral 2-octadecyl-*p*-quinone-5-sulfonate, which is used in photographic layers. The amphiphile forms a stable monolayer on water; upon transfer to mica, the planar layer rearranges to form a lattice of micellar fibers, which are ordered side by side and have been resolved laterally by atomic force microscopy (Figure 12).[50] A strong interaction between the mica substrate and the quinone head group seems to be responsible for this fiber formation and not for its destruction. Although this

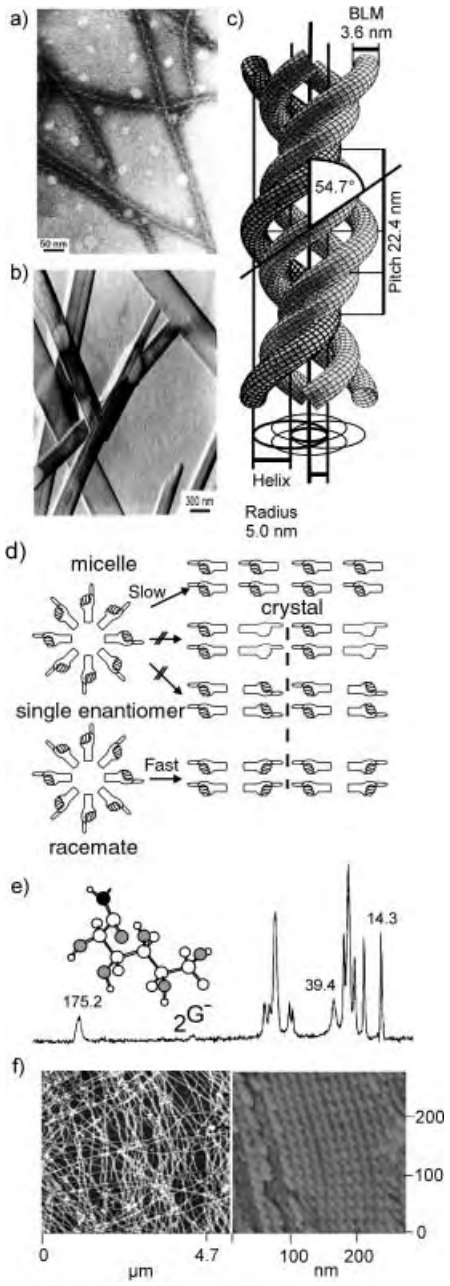


Figure 10. a) TEM of the micellar quadruple helix of *N*-D-octylgluconamide and b) of the racemate of both enantiomers. c) Model of the cross-section of a quadruple helix of a chiral amphiphile (BLM = bilayer micelle) and d) of the three corresponding crystal planes. Top: the head-to-tail arrangement corresponds to the most stable 3D crystal. Middle and bottom: two bilayers, in which the right- and left-handed chiral head groups are arranged differently. Such crystals are unstable and can usually not be isolated. The formation of the stable crystal (head-to-tail) needs a reorientation of the micellar bilayer and is therefore very slow in water. The micellar fiber remains stable for a long time. However, a spherical micelle from a racemate crystallizes rapidly upon cooling as a symmetrical bilayer. The micellar fiber is therefore short-lived. e) solid-state ^{13}C NMR spectrum of the fiber. f) AFM of the solid fibers.

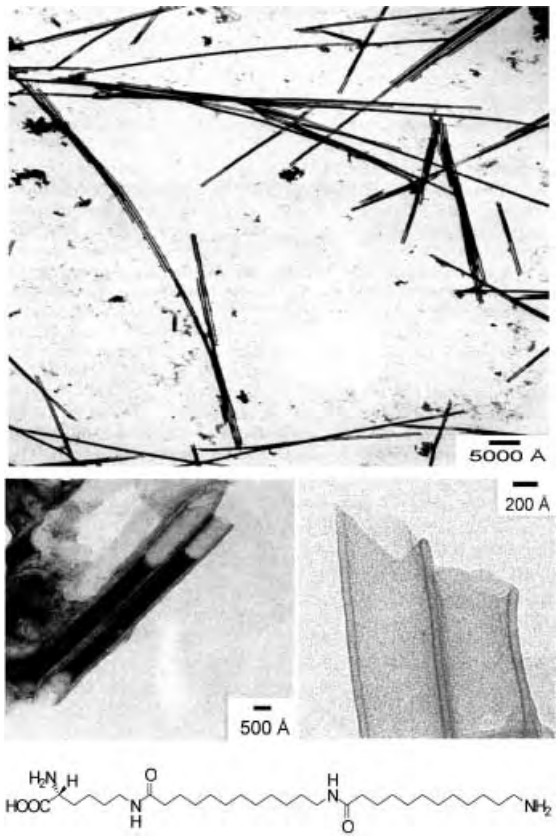


Figure 11. Vesicular tubules of a α-lysine-ω-aminobolaamphiphile.

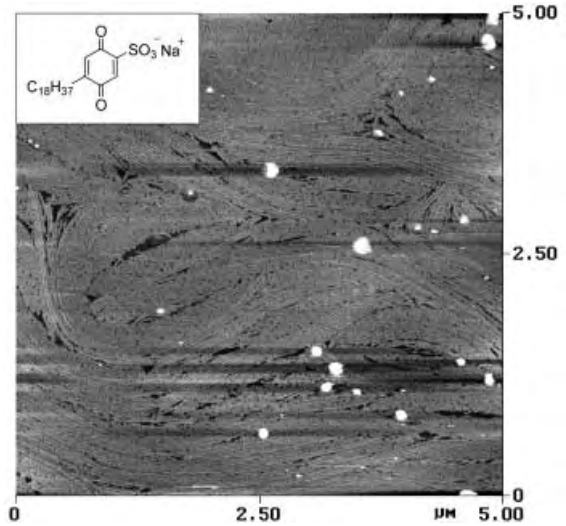


Figure 12. TEM of micellar 5-octadecyl-*p*-quinone-2-sulfonate fibers on mica.

phenomenon has not yet been explained, it is likely that the quinone sulfonate group plunges vertically into the water surface, but lies flat on the mica surface. The highly enlarged molecular surface of the monolayer promotes the transformation into a bilayer. In the present case, the repulsion between nonhydrated negatively charged sulfonic acid groups favor micellar fibers instead of planar interdigitated bilayers.

The flexible oligomethylene chain of the fiber-forming amphiphiles can be replaced by rigid porphyrins.[51–54] A suitable crystal of the amphiphilic protoporphyrin IX for structural analysis has not yet been obtained, although about 1600 porphyrin crystal structures are known, for example, that of the protoporphyrin dimethyl ester. Protoporphyrin itself is not among them because it forms fibers in water and other polar solvents, but not well-defined crystals. We suggest that this behavior applies to almost all natural products that appear in biological organisms in larger quantities: hardly any of the water-insoluble amphoteric natural products (e.g. fatty acids, carotenoid acids, biogenic amines, membrane proteins) crystallize spontaneously. Crystals are avoided, because they may clog capillaries and destroy the osmotic activity and fluidity of membranes. Cholesterol is an exception: it crystallizes from lipid fractions (this property gave steroids their name: stereos = solid) and is responsible for the damage caused by cholesterol in blood vessels.

Fibers with many different head groups were obtained from amphiphilic protoporphyrin derivatives. In the case of chiral head groups[52] or chiral axial ligands[53] their optical spectra showed very strong circular dichroism (CD) effects, whereas exciton effects and aggregate-specific fluorescence bands were not observed. This contrasts sharply to planar porphyrin platelets[55, 56] and fibers of amphiphilic polymethine dyes[57] (Figure 13), all of which fluoresce strongly. Some of the

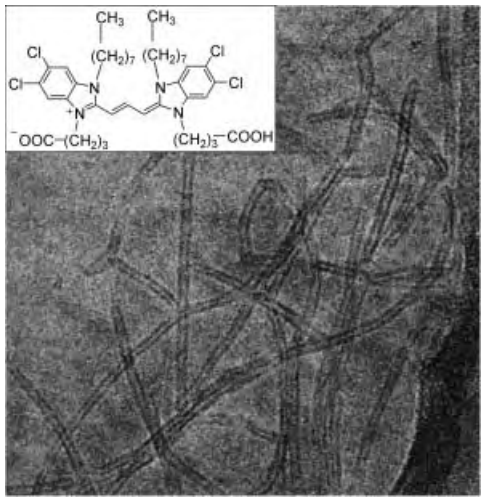


Figure 13. TEM of an energy-conducting fiber of the indicated methine dye.

polymethine dye fibers are stable in solvents as well as on solid surfaces. The thickness of their layers corresponds to a molecular bilayer, whose inner cavity has a diameter of about 1 nm. These assemblages were detected first by Scheibe[58] and Jelley[59] because of their extremely sharp fluorescence band, which is not common with monomers. Furthermore, these fibers and many monolayered porphyrin platelets show very large exciton effects, that is, the main optical absorption bands split up into two bands because of dipolar interactions in the excited states of the dyes. Typical wavelength differences between the two absorption maxima range from 30 to 120 nm. The polymethine dye fibers are used as "sensitizers" in commercial photographic layers and help transfer light energy to silver chloride particles. The extremely high photosensitiv-

ity of today's photographic films is partly a result of these fluorescent fiber aggregates.[60] The structural reasons for the sharp fluorescence band and the extreme exciton splitting of the aggregates, which seems to be necessary for an efficient energy transfer, was rationalized in theory,[61] but structural analysis of the molecular structures of the assemblies is still incomplete. TEM pictures of the fibers and platelets as well as the relative yields of fluorescence and exciton splitting merely suggest a positive correlation between the rigidity of the aggregates and their effective energy transfer. Optimization of the molecular interactions, which lead to energy-conducting material, remains an empirical venture.

5. Rigid Monolayers and Form-Stable Nanometer Clefts on Smooth Substrates

In the following section we limit the expression "molecular landscapes" to profiles on smooth surfaces of solids in the height range from 0.5 to 20 nm. In general, only the usual classic smooth solids are used in scanning force microscopy (SFM), namely graphite, gold and similar precious soft metals, as well as mica, quartz, silicon, and polymer films. On rougher substrates, <5-nm landscapes are hardly visible by STM or SFM. Since metal surfaces are the materials best suited for electrodes, gold (Au(111) surface) is most frequently used as substrate. Even quartz balances are first modified by covering the oscillating quartz with a thin gold layer and afterwards with receptor-active lipid monolayers.[62]

We start with polar molecules, which are deposited parallel to smooth surfaces. The classic example is guanine, which forms 3-Å thick monolayers on graphite upon self-assembly in 3×10^{-5} M aqueous solutions (0.1 M NaCl). When the surface potential is adjusted to $+80$ mV,[63] the guanine lies flat on the graphite grid and forms hydrogen-bonded aggregates. The guanine film between the positively charged electrode and a layer of chloride counterions remained unchanged at a voltage of 0 V. As the hydrated organic layer was then only a few Ångstroms thick, the electric field in the molecular plate condenser could be varied from -10^7 to $+10^7$ V cm^{-1} before electrolysis began. Such large variations in the field strength have an influence on the structure of the guanine monolayer. At a negative potential of -330 mV, the monolayer dissolved, whereas it formed again at $+420$ mV (Figure 14). At surface potentials of 80, 280, and 480 mV, rearrangements of the monolayer without detachment were observed by AFM. Although the formation, dissolution, and shape of the ultrathin 3-Å layer can be modified in many ways, it is totally stable at a given potential in the presence of bulk water.

Stable monolayers of flat-lying molecules were also obtained by the self-assembly of porphyrins. The simplest example is the *meso*-tetrakis(3,5-dicarboxyphenyl)porphyrin, which dissolves in water at pH 12 but nevertheless forms a stable monolayer on gold from such an aqueous solution. Presumably the carboxy groups interlock in subnanometer clefts on the gold surface, which form upon routine treatment with nitric acid, and are thus protected from deprotonation and hydration. After washing with potassium hydroxide

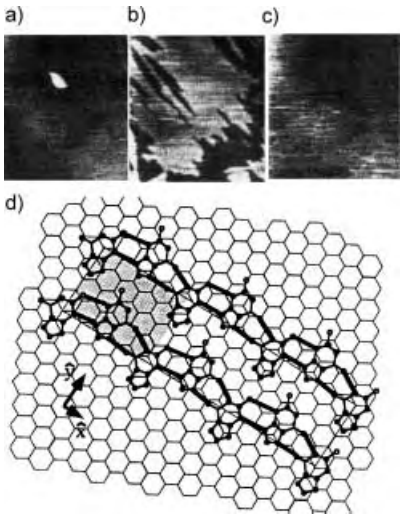


Figure 14. a)–c) AFM pictures and d) model of a guanine monolayer lying flat on graphite; a) the AFM picture at 0 and 420 mV shows a closed monolayer, which b) dissolves at -320 mV and c) re-forms at $+450$ mV.

solution, a porous monolayer remains in which the porphyrins adopt a Monte-Carlo arrangement (Figure 15; see also Figures 24 and 25). This implies that each porphyrin is bound in the place and orientation in which it arrives at the gold surface, that is subsequent rearrangements do not take place.

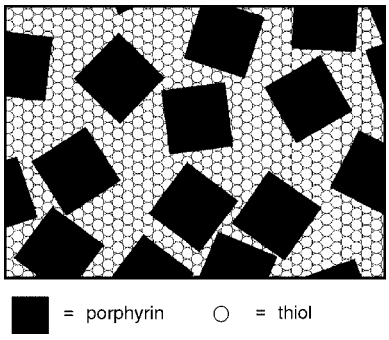


Figure 15. Model of the Monte Carlo arrangement of porphyrin molecules bound to gold after complete self-assembly. In a second step, a long-chain thiol is added to close the clefts (see also Figures 24 and 25).

The fluorescence yield of the porphyrin on such slightly rough gold surfaces is about 4–8% of that of the porphyrin on nonmetallic polyethylene surfaces. The addition of cationic porphyrin counterions with paramagnetic central ions quenched this fluorescence quantitatively and porphyrin heterodimers were observed on the gold surface. On a totally smooth gold surfaces ("mica gold"), the fluorescence was completely quenched, and the porphyrin carboxylates were not bound very strongly.[64]

Simple self-assembly from *n*-octylbenzene solutions allowed porphyrins with long alkyl substituents to be anchored in a flat and crystalline arrangement on graphite.[65] Such porphyrin monomers were still mobile after their adsorption to graphite. It is not clear yet whether this behavior is a result of the substrate smoothness or of the lack of polarity of the porphyrin. STM micrographs produced a perfect lateral resolution of the four pyrrole units and alkyl chains (Fig-

ure 16). Graphite surfaces bind equally strongly to polar head groups, aromatic compounds, and linear alkyl chains. As a result one usually finds only layers of flat-lying molecules (compare Figure 8). This behavior was not found on the amorphous carbon films used in TEM. In the latter case, most bilayers transferred from aqueous solutions survive without rearrangement.

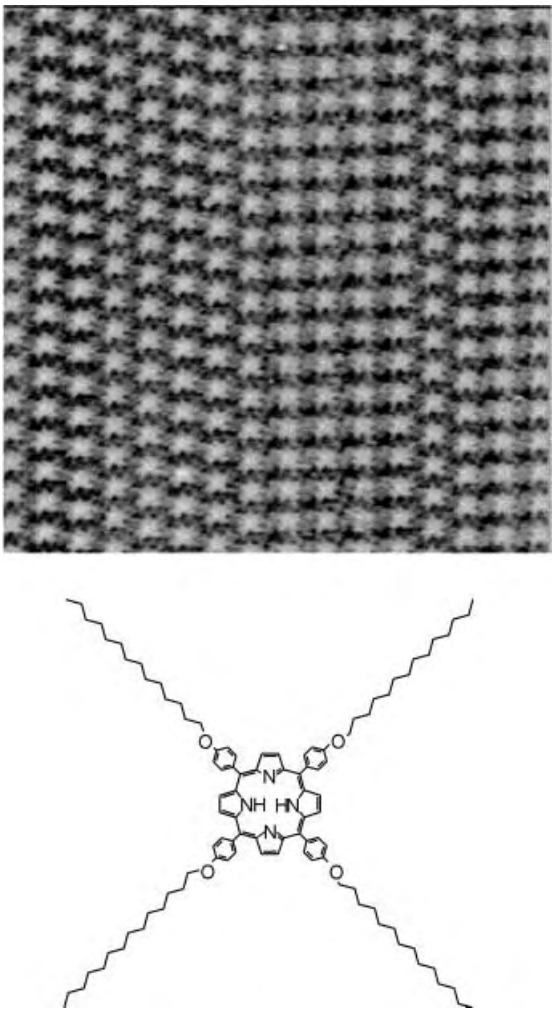


Figure 16. Perfectly resolved STM picture of a flat-lying crystalline layer made of long-chain (C_{14}) tetraalkyl porphyrins on graphite.

Steroids also bind in a flat orientation on gold when the binding thiol group appears in an axial position in the center of the sterol. The covalent Au – S bond forces the steroid into a position parallel to the gold surface. A suitable steroid for such flat monolayers is 7α-spironolactone. After self-assembly until saturation, about 50 % of the gold surface was occupied by steroids in a Monte Carlo arrangement; the remaining 50 % of the gold atoms remained unoccupied, as in the case of the octacarboxylatoporphyrin.[66] However, when 3β-thiocholesterol with a terminal equatorial SH group was used, the steroid molecules arranged themselves on the gold surface in a tilted, vertical orientation. The surface was covered quantitatively (Figure 17).[67] When ferricyanide was added to the bulk water, the electron current flowed freely through the flat-lying, porous membrane, whereas the vertically

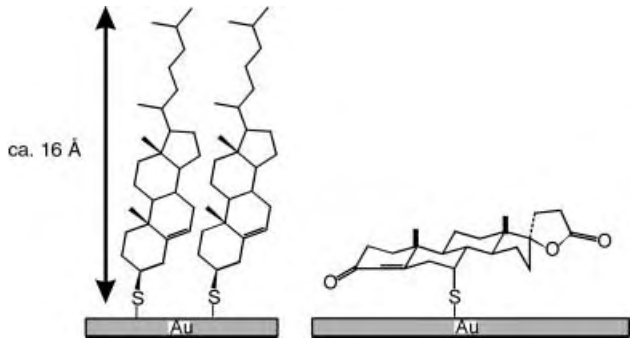


Figure 17. 3β-Thiocholesterol forms closed monolayers of vertically arranged molecules on gold; in contrast, 7α-thiospironolactone lies flat on the surface in a Monte Carlo fashion (see Figure 15).

arranged molecules produced a perfectly insulating 2-nm thick layer.

Thiocholesterol was our first example of a rigid amphiphile that forms impermeable, well-arranged monolayers on gold. Monolayers with fluid alkyl chains are arranged equally well in aqueous media. Their IR spectra show almost undisturbed *all-trans* conformations of the oligomethylene chains. As an example, cadmium arachidate monolayers are perfect insulators for ion currents and give rise to sharp Bragg reflections in neutron diffraction,[68] which means that the fluidity is lost in the 2D crystal, especially when bivalent cadmium ions solidify the basis. However, the oligomethylene monolayers become fluid upon contact with solvents, and their ordering is thus lost. Rigid rods, on the other hand, remain well-ordered, and the substrate thus remains "passivated" against attack from the surrounding bulk water.

Form-stable nanometer clefts as they are found on the surface of globular proteins do not occur in fluid membranes in water. A crystalline order only appears in the interior of the monolayers, not at the boundaries. This was shown in Sagiv's early experiments with dyes adsorbed to glass and surrounded by fluid monolayers.[69, 70] The dyes could be removed reversibly and introduced again; adsorptions and desorptions took place within seconds. Large dye molecules were also adsorbed, and size selectivity only determined the speed at which the adsorption took place.

Monolayers with cavities can also be created by the microwave-induced condensation of long-chained primary amines with surface-bound carboxylic anhydrides. The intermolecular cavities could be filled with alkanes (e.g. hexadecane or 1-octadecene). The IR spectra then indicated only *all-trans* chains. Weak dispersion forces between a fluid template and a fluid host clearly force the formation of a homogeneous *all-trans* conformation of the alkyl chains in aqueous media (Figure 18).[71] If the crystallinity of the alkyl chains in the hydrophobic areas is disturbed by inserting polar and/or large substituents (oxygen atoms, methyl groups) or slim rigid alkynes, the latter rearrange to form domains. Border regions are always amorphous. This is qualitatively valid for all mixed monolayers that contain rigidifying parts in the alkyl chain, for example, diacetylene[72] or sulfone dipoles.[73]

Several redox-active sulfides with rigid cycloalkane spacers are arranged vertically on the gold surface and allow charge transfer from the electrode to a distant electron acceptor and

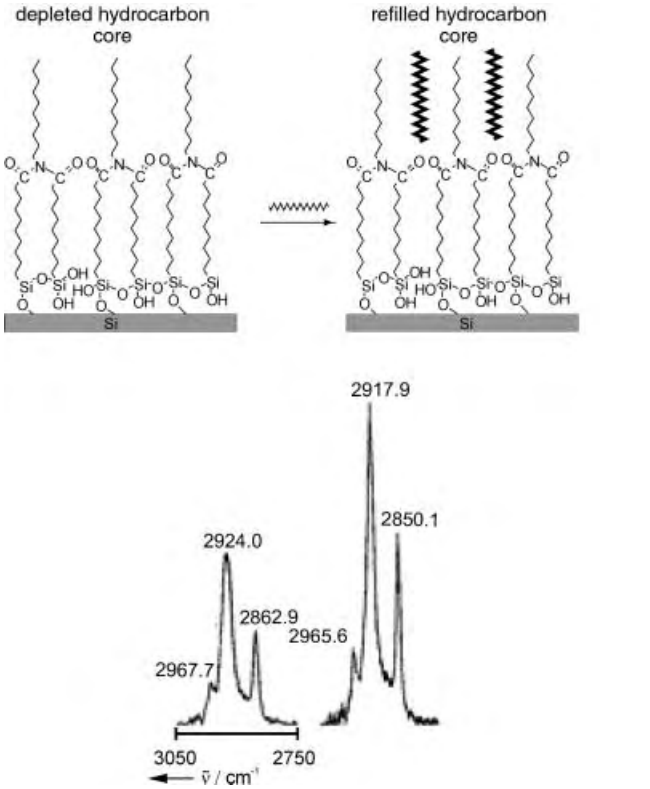


Figure 18. Rigidification of a porous fluid monolayer by adding equally fluid water-insoluble hydrocarbons such that the clefts are closed. IR spectra indicate flexible (left) and exclusively *all-trans* chains (right). For clarity, the alkyl chains have been shortened.

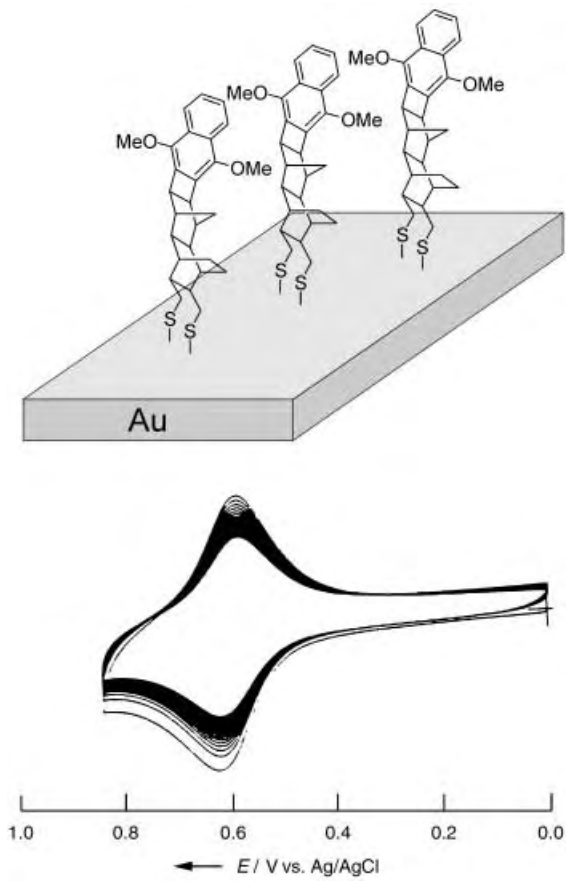


Figure 19. *O*,*O*-Dimethylnaphthoquinone, vertically bound on gold electrodes by a rigid skeleton, undergoes many redox cycles without being detached from the gold substrate. The sensitive Au–S binding is probably cleaved several times, but the reaction is reversed because the insoluble rigid molecule does not leave the surface of the electrode.

from an electron donor to the electrode. Dimethoxynaphthalene monolayers with a thioacetal substituent located far away from the quinone redox center were subjected several times to redox cycles of cyclic voltammetry. After 25 cycles, half of the original monolayer was still present[74] (Figure 19). The oxidation of the gold surface and the oxidative or reductive cleavage of the gold sulfide bond were essentially blocked. This is also true for multilayers of oligoimides (polymeric imides of naphthalene-1,4,5,8-tetracarboxyl anhydride)[75, 76] or staffane derivatives (oligomers of equally rigid bicyclo[1.1.1]pentanes)[77] with ruthenium(II) complexes located far away from the gold surface. An electron transfer across the Au–S bond was possible without reductive or oxidative cleavage of the Au–S bond, that is, the monolayer survived the redox cycles undamaged.

Complex but easily manipulable rigid membranes are accessible from amphiphiles whose hydrophobic portions are firmly connected to each other by hydrogen-bond chains. Secondary diamides are mostly used in analogy to protein sheets. Completely different end groups were anchored to gold surfaces by means of alkyl thiols ($RNHCOCH_2SH$). However, the monoamides do not offer a clear advantage over oligomethylene chains without functional groups.[8, 79] Rigidity only arises when two amide hydrogen bond chains run parallel to each other,[80] and both amide groups are located near the α and ω positions of a longer alkyl chain. Two neighboring amide groups do not induce rigidifying.[81] Well-insulating 2-nm layers were also obtained from combinations of monoamides with perfluorated end groups. The fluorine-substituted hydrocarbons not only act as perfect diffusion barriers and lubricants, but also keep the surface free from organic pollution (Figure 20)[82, 83]. Such monolayers are very efficient in protecting the Au–S bond.

The development of rigid monolayers that contain form-stable nanometer pores began with experiments on reactive diazido bolaamphiphiles on polyacrylamide (PAN). It was observed that two parallel chains of amide hydrogen bonds

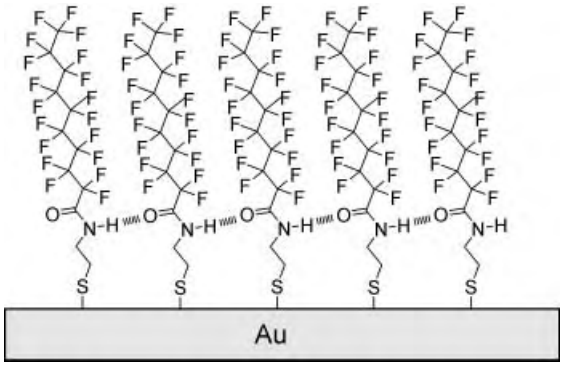


Figure 20. Double diffusion barriers made up of chains of amide hydrogen bonds and hydrophobic fluorocarbons protects the gold–sulfur bond from corrosion.

made the monolayer totally impermeable to methylamine, which is highly soluble in fluid membranes. The outer azido group reacted quickly, whereas the inner group was unreactive, even after several hours (Figure 21, left). A single amide group in the hydrophobic chain did not have any rigidifying effect.[80] On the other hand, two parallel chains of amide hydrogen bonds rendered the 15-nm monolayer impermeable, and an important odd–even effect was observed. This effect results from the angle of the alkyl chains with the substrate; parallel hydrogen-bond chains are possible if both amide groups form the same angle with the substrate (Figure 21, right).[84] This is only possible when there is an even number of connecting links between both amide groups. In the case of an odd number, there are nonpolar methylene groups located on both sides of one of the amide groups (not shown).[84]

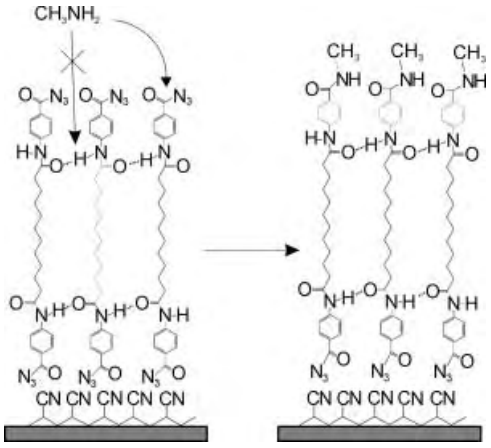


Figure 21. Left: a 15-nm lipid monolayer is totally impermeable to methylamine if two parallel amide hydrogen bond chains rigidify the monolayer; azide groups on the inside do not react with methylamine. Right: tilted monolayers of diamides remain fluid if the connecting carbon chain has an odd number of links; the monolayer is rigid with an even number of links.

A second method to solidify monolayers is to replace the alkyl chains by oligoarene derivatives, which also serve as light-harvesting antennae and as electron conductors. The simplest of this kind of layer gold consists of 4-methylthiophenol and is not thick enough to passivate the gold surface. Nevertheless, it protects the gold surface well from corrosion.[85–87] In contrast to toluene- or biphenyl homologues, phenylthiol hardly has any inhibiting effect on the transport of ferricyanide ions from the bulk water to the gold surface. Presumably, the unsubstituted phenyl rings are partly vertically orientated to each other, similar to benzene crystals, thus preventing the formation of insulating monolayers. Ferricyanide and ruthenium(II) salts in bulk water therefore produce almost undisturbed cyclovoltammograms (CVs). Substituted biphenylthiols are good insulators in most cases, but quickly decompose electrochemically or on exposure to oxidants. The self-assembly of a mixture of 4-nitrobiphenyl and 4-dimethylaminobiphenyl leads to an interesting selectivity: in the resulting monolayer the two components mixed spontaneously in a constant molar ratio of 3:2. With this ratio, the total dipole moment is reduced to zero, that is, the growing rigid monolayer rejects invading molecules if they polarize the monolayer too strongly.[88] STM micrographs of monolayers of substituted 4-thiobiphenyls showed ordered domains whose periodicity corresponded to the herringbone pattern of the crystal surface of biphenyl (Figure 22).[89] Terphenylthiol monolayers on gold were destroyed only very slowly by electrochemical and chemical oxidation. The rigid terphenyl layer acts as a good and stable insulator against the transport of ferricyanide ions to the electrode.[89]

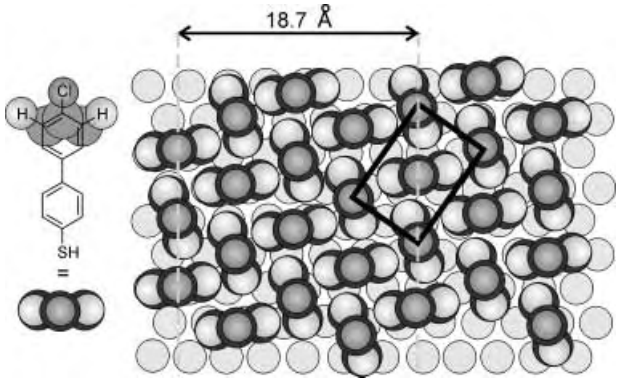


Figure 22. The herringbone pattern found in the crystal structures of biphenyl compounds is reflected in their molecular monolayers.

Rigid molecular arenethiol rods with connecting acetylene units gave heterogeneous, patchlike monolayers on gold,[90] whose clefts could only be closed by fluid thiols. In a second self-assembly step, hexadecanethiol partly substituted the rigid amphiphiles, closed the gaps, and led to perfect passivating monolayers. IR spectroscopic analysis revealed showed that the rigid rods still formed the main part of the membrane at the end of the self-assembly process. It is clear that isolated assemblies of rigid amphiphiles or small soluble domains are quickly substituted, whereas large blocklike domains remain upright.

The oligophenylene films on gold should conduct energy-rich electrons in cases in which they can produce anion radicals. A corresponding electrical conductor was actually characterized in mixed layers of acetylene-connected terphenylthiol and dodecanethiol monomers by means of STM. Each time the tip went over the 5-Å elevations of the rigid electron-rich domains on the dodecyl layer, tunnel current peaks of up to 40 Å were observed (Figure 23).[91] The effect here is much more distinctive than in the case of polyenes.[20]

The domains of rigid molecules in fluid membranes, of isolable micelles, vesicles, and fibers that have been discussed so far resemble those found in covalent polymers. However, they do not have covalent bonds, which survive drastic changes in external conditions such as rises in temperature, changes in pH, and attack from solvents. Proteins and nucleic acids, to name the best-known polymers that appear as micelles and fibers, also change their shape according to their environmental conditions, but they do not simply release their monomers. The molecular aggregates lack the robustness of the primary structure. In spite of this, will it be possible to mill clefts into the membrane structure, which correspond to the clefts in protein enzyme or to the grooves of nucleic acids? In principle, yes, if two rigid aggregates of different height are anchored successively onto a solid substrate. Conditions must

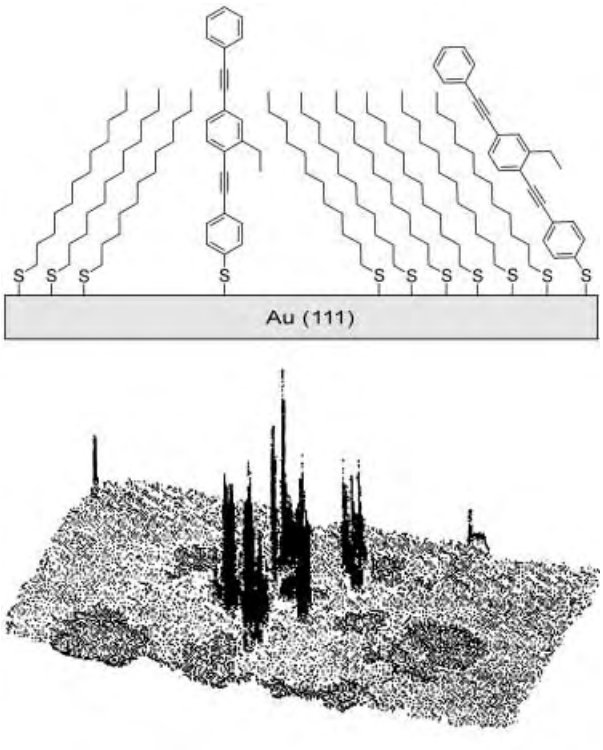


Figure 23. Scheme of a mixed monolayer of fluid dodecanethiol and rigid acetylene-linked terphenylthiol monomers; the latter act as electron conductors (1 V voltage of the electrode at 3-pA tunnel current); this leads to local current peaks (≈40 Å).

be chosen so that the substance applied first will not be substituted by the second, and that only unoccupied areas on the substrate will be occupied in the second step. At present, a two-step self-assembly of thiols on gold is the best procedure. The first substrate should shield its Au–S bonds efficiently and/or should be anchored by several Au–S bonds, which will probably not all be broken at the same time and will form again under mildly reductive conditions.

Porphyrin monolayers lying flat over about 50 % of the gold surface in a Monte-Carlo arrangement (see Figure 15) were surrounded with vertically arranged diamide bolaamphiphiles. Form-stable 2-nm pores formed around the porphyrin. A paramagnetic metalloporphyrin tetracation, which fitted perfectly into such a pore, extinguished the fluorescence of the porphyrin located at the bottom of 2-nm well within 30 min. A 10-Å broader porphyrin did not fit into and did not extinguish the fluorescence. This selectivity proves the desired rigidity of the pore walls. When a fluid membrane without amide hydrogen bonds was treated in the same way, no significant difference was found between large and small porphyrins (Figure 24).[64] Not only the size selectivity of the rigid cleft is remarkable but also its inaccessibility: the fluorescence in the fluid cleft is extinguished within a few seconds, whereas quenching requires 30 min in the rigid membrane. The relatively quick response in the adaptable cleft shows that the fluid membrane acts as solvent for the porphyrin cation. On the other hand, rigid tunnels allow heterodimerization only in the case of suitable porphyrins if the guest porphyrin diffuses spontaneously into the narrow tunnel. There is no long-distance driving force between positively and negatively charged porphyrins because the well is too deep to allow attracting ion–ion interactions between the upper opening and the bottom of the well.

Comparable diffusion processes are found in porous minerals, but rarely in biopolymers or biomembranes as the clefts and pores (enzyme clefts, DNA grooves etc.) are never deeper than a few Ångströms. Furthermore, the diffusion of metal ions through water-filled membrane pores along a concentration gradient has little in common with the diffusion of individual molecules in monolayer clefts.

Hydrophilic groups can be introduced on the rigid walls of the well without destabilizing them. C=C double bonds that are incorporated in the alkyl chains of diamide amphiphiles can be aminated by amines that migrate into the water-filled cleft. At pH values under 7, a cyclic arrangement of ammonium groups is formed at which a second anionic porphyrin can be anchored at a distance of 20 Å (amine formation the edge of the well) or 8 Å (amine formation in the interior of the wall; Figure 25).[92]

Porphyrin heterodimers with an intermolecular distance of 8 Å are promising systems for studying light-induced charge separation between electron donors (e.g. zinc porphyrinates) and electron acceptors (e.g. tin(IV) porphyrinates). Anionic quinones, flavins, and other redox partners can also be anchored to the ammonium rings by reversible salt formation. Addition of a base neutralizes the amino groups so that the anchored anionic electron acceptor is released into the bulk water. Fresh acceptor molecules can then be reinserted into the cleft, which means that bleached dye molecules are regenerated. The built-up charge can be neutralized by oxidants on the water side or by the electrode on the metal side. Connected systems may thus be established which split water with the aid of sunlight to hydrogen and oxygen.

6. Molecular Plateaus and Towers

The nanometer clefts in lipid monolayers described above are not suitable for electrochemical experiments with AFM or STM tips, as the clefts are too small to be detected by the tips. Noncovalent synthesis, synkinesis, can be used to construct towers of redox-active molecules on smooth substrates. Such objects are attractive, because they can be controlled individually by the AFM or STM tip and because they provide a great variety of objects for analysis. If, for example, only 10 tower-like nanometer-sized objects are anchored on an area of 100×100 nm^2, then ten billion towers will be present on an area of 1 cm^2. Each individual object may allow experiments concerning photochemical conductivity, destruction by photochemical oxidation, recognition experiments with coated tips, etc.

The most important method to build up elevated objects on flat substrates is contact-printing with polymer stamps. This technique has a resolution of about 100 nm,[93] which is far above the dimensions discussed in this paper. Nevertheless we

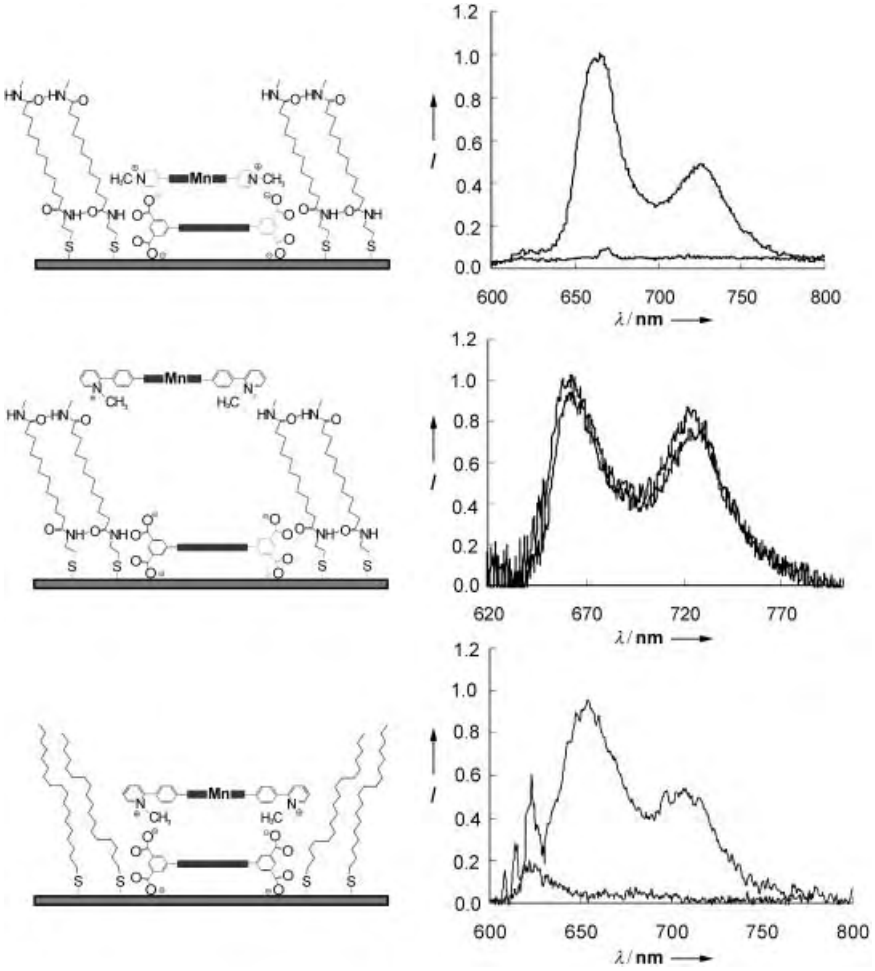


Figure 24. Porphyrins (20 Å wide) form close heterodimers in rigid membrane clefts, as indicated by the quenching the fluorescence (top). Porphyrins (30 Å wide) cannot penetrate into the rigid cleft (middle), but can do so into a fluid cleft (bottom). I = fluorescence signal, normalized for $I_{max} = 1.0$.

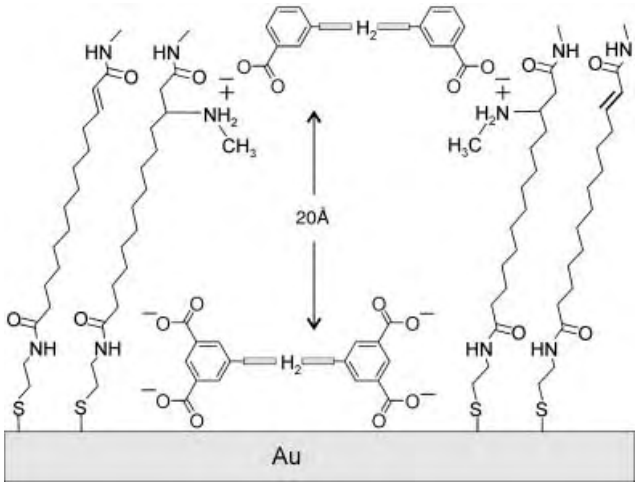


Figure 25. Noncovalent heterodimers of porphyrins that are anchored in a 2-nm-wide membrane cleft by functional groups at the walls at a defined distance (here: 20 Å).

discuss briefly the "inks" applied. For example, if alkane thiols are used on gold, the ink molecules will diffuse the edges are smeared. Palladium complexes and proteins, however, hardly move on the gold surface and therefore produce pictures of the stamp pattern that are accurate to a few nanometers.[94] Again we are clearly dealing with rigid objects and consequently an unmovable link between monolayer and substrate.

Rigid domains within a fluid molecular monolayer were produced from β-pyridinium-β-ethylporphyrin sheets and eicosanoic acid by using the LB technique. The porphyrin aggregated both in bulk water and on the water surface to form monomolecular sheets, which were characterized by a strong exciton splitting of the Soret band (λ_{max} 405 nm $\rightarrow$350 and 450 nm) and by intensive fluorescence bands (λ_{max} 620 and 730 nm).[55, 56] AFM images of these monolayers taken in the tapping mode showed, at first, closely ordered inclined eicosanoic acid molecules (h = 24 Å) as well as upright porphyrin molecules (h = 18 Å). Upon further tapping of the mixed monolayer with the AFM tip, a large number of the fatty acid molecules became vertically orientated to give 30-Å high peaks (singularities) in the 24-Å plane of sloping molecules (Figure 26). These singularities were long-lived (>7 days) even though they were located in the fluid part of the monolayer.[95]

It is rather easy to produce well-defined porphyrin multilayers from tetracationic and tetraanionic porphyrins. A particularly homogenous multilayer of this kind is composed of *meso*- tetrapyridylporphyrins with four peripheral ruthenium(II) complexes and *meso*-tetraphenylsulfonatoporphyrin.[96] The stepwise construction of isolated porphyrin towers suited for SFM experiments, however proved to be more difficult. A promising method involved the use of bifunctional axial ligands to bind the porphyrin metal centers. In the case of zinc – pyrazine or zinc – 4,4′-bipyridine complexes, only large aggregates were obtained, because the binding constants were too small ($K_1 \approx 10^3\,\text{M}^{-1}$; $K_2 = 0.1\,\text{M}^{-1}$) to enforce rigid edges.[97] In linear copolymers of zink porphyrinate and phenylene ethyne units, which form complexes with gold-supported bipyridine molecules, better results were obtained. Netlike structures up to a height of 60 nm were produced in six steps in the self-assembly of porphyrinate polymers with bis(pyridyl)ethylene ligands and characterized by AFM. (Figure 27).[98] Analogous interdigitations in monomolecular fibrous structures have also been obtained by means of covalent oxygen bridges between the phosphorus centers.[99] Isolated porphyrin towers or rocks did not form.

Experiments with porphyrin octaphosphonates and zirconium(IV) salts on silicon wafers were more successful. At first, phosphonate groups were anchored to the silicon surface, and their polarity was then reversed with Zr^{4+} ions. Subsequently, a layer of porphyrin was deposited, their polarity was again

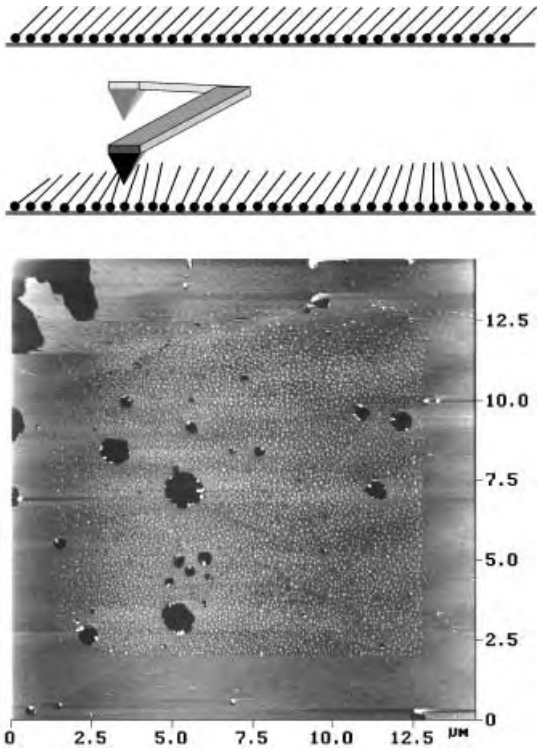


Figure 26. Model and AFM picture of long-lived waves (singularities; white areas) vertically arranged on a fluid membrane besides rigid porphyrin domains (black areas). The singularities are formed by AFM measurements in the tapping mode.

reversed with Zr^{4+}, and the procedure was repeated (Figure 28). This procedure is based on the finding by Alberti[100] that α,ω-bisphosphonate bolaamphiphiles with zirconium salts produce perfect single crystals as well as on the report by Mallouk and co-workers[101] on the self-assembly of regular layers of phosphonate amphiphiles on Cabosil colloids. Indeed, after establishing an appropriate capping procedure with the complex-forming Alizarin S, a landscape of isolated porphyrin towers with a maximum height of about 20 nm and a width of 4–6 nm was produced.[102] Alizarin derivatives, which are known to grow in the form of crystalline monolayers on smooth surfaces,[103] proved to be much better capping reagents than isolated single molecules, for example, *tert*-butylphosphonate. No slim towers were formed, but hard broadened cones were abundant (Figure 28); these were hard enough to be moved with an AFM tip without disturbing neighboring cones.

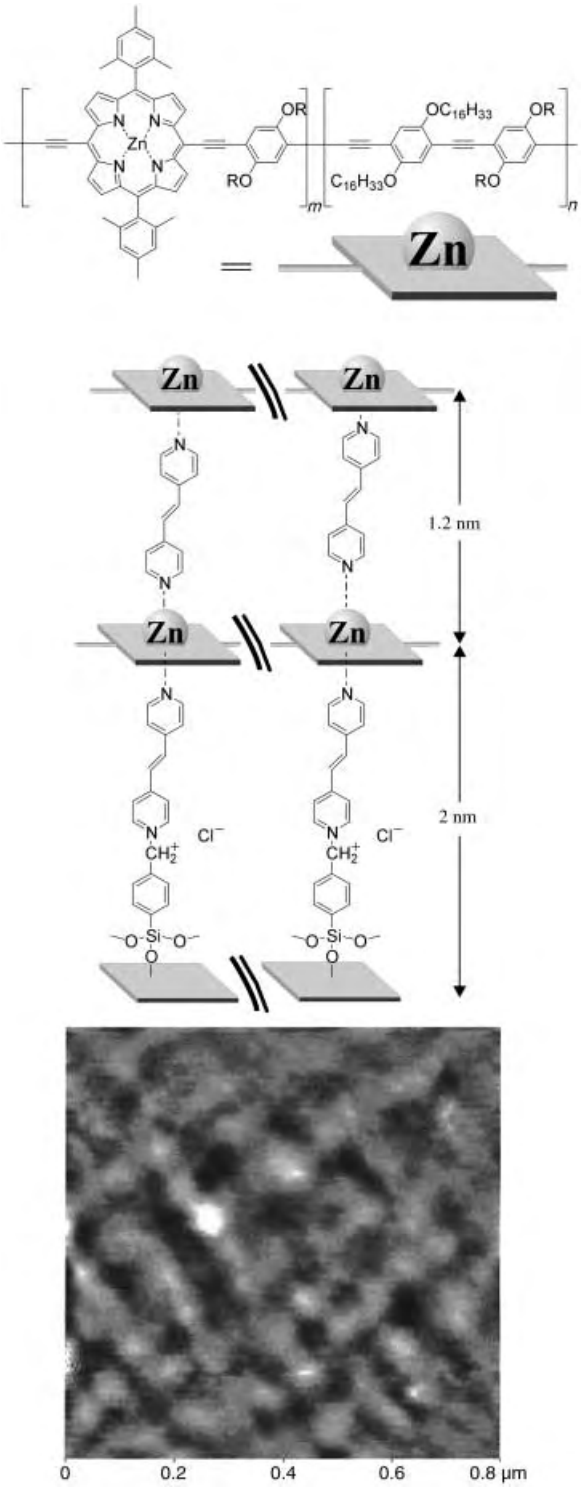


Figure 27. Model and AFM picture of the netlike, rigid zinc porphyrinate polymer, which is linked to multilayers by axial ligands.

7. Unmovable, Aqueous Molecules at Interfaces

Neither in ice nor in liquid water is the orientation of the water molecules such that hydrogen bonds connect only two specific oxygen atoms. Relocations of protons (i.e. nonlinear networks) frequently occur. In each case only one hydrogen atom lies on every oxygen–oxygen axis, but many configurations are possible and none are particularly preferred.[104, 105] Two borderline structures of ice define the possible configurations: 1) in the usual ice XI (or I_c) configuration the oxygen atoms form chairlike hexagonal rings similar to the diamond structure with the hydrogen atoms lying preferentially on the connecting lines between the oxygen atoms; 2) in the pentagonal ice arrangement, the oxygen atoms are positioned at the corners of planar pentagonal rings and assemble into dodecahedral $(H_2O)_{20}$ units. Such structures have been observed in gas hydrates[105, 106] (Figure 29). Between these two extremes lie many other hydrate structures, which consist of 5^n and 6^n polyhedra. The transformation from

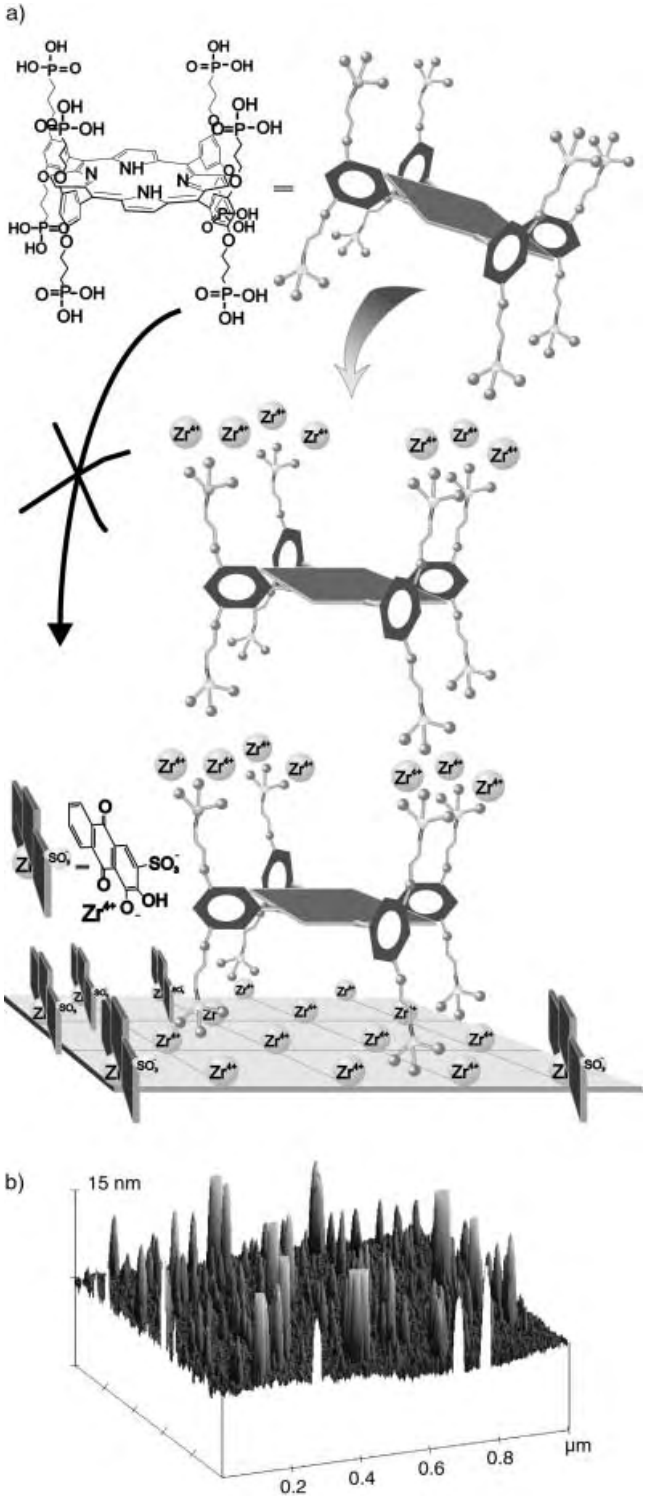


Figure 28. a) Model of the construction of pophyrin rocks on zirconium(IV)-covered silicon surfaces by stepwise self-assembly. Capping with Alizarin S restricts the number of conelike rocks. b) AFM picture of porphyrin cones on silicon (without capping).

amorphous ice to hexagonal ice is catalyzed by the incorporation of KOH (0.06 M). It seems to be effective, because it decreases the number of freely movable protons drastically. Single crystals of ice for neutron diffraction were thus obtained and allowed the localization of protons by neutron diffraction.[107]

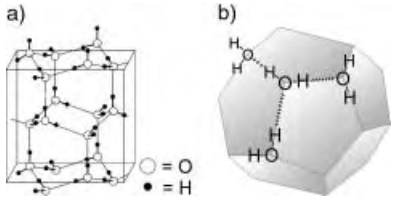


Figure 29. Crystal structures of a) hexagonal water in ice XI and b) of pentagonal water in clathrates and hydrophobic surfaces.

Water in hydrophobic clefts is immobile and can be used as a functional part of a landscape. It must, however, be stabilized by dissolved molecules (solutes), which are integrate into the water structure and aid the freezing process (Figure 30). Little is known about the kinetic inertness of thin aqueous films on hydrophobic surfaces in contact with bulk water. It has, for example, been demonstrated that motions within micrometer-thick layers of ice on metallic ruthenium at $-130\,^{\circ}C$ were much faster than the desorption of the molecules in the outer layer. Diffusion measurements of $H_2{}^{18}O$ bilayers, which were evaporated from $H_2{}^{16}O$ layers of ice lying underneath, showed that the desorption and lateral mobility of the uppermost layers of water were extremely slow (hours),[108a] whereas mixing with the $H_2{}^{16}O$ layer of ice underneath was much faster. It was also found that water layers became stable only when they consisted of at least three bilayers, at which point they can incorporate nonpolar gas molecules such as N_2.[108b]

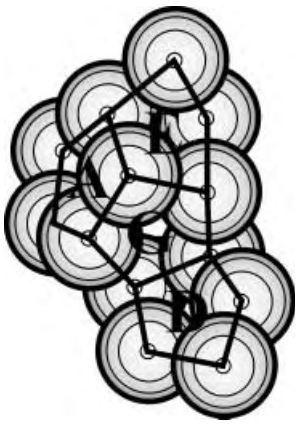


Figure 30. The water structure on the hydrophobic surface of the crambin protein. The concentric circles symbolize the height of the oxygen atoms (ring B is hidden).

Surface water on hydrophobic material mostly consists of the same clusters that can be found in liquid water or in the diamond-like orthorhombic ice XI (Figure 29a). At low temperatures ($<37\,^{\circ}C$) surface water is more ordered than bulk water. Surface ice, on the other hand, melts at low temperatures. However, in clathrate water (hydration water of crystalline inclusion compounds of hydrophobic organic compounds) pentagonal arrangements of water have been found as well as fullerene-like combinations of pentagonal and hexagonal rings.[105, 108] Furthermore, the interaction with hydrophobic surfaces compresses the structure of the water.[105, 106, 109]

Ordered hydrate coatings have been observed on hydrophobic surfaces of proteins. The highest resolution of the crystal structure of surface water was found for the protein crambin, in which a hydrophobic patch is covered by four water pentagons with a common peak (Figure 30, resolution 0.88 Å).[105, 110] In enzymes such water-binding areas function as active centers. In protease A of *S. griseus*, a water cluster is displaced from the protein, when it forms a complex with an

analogous substrate. Water clusters consisting of pentagons and occasionally of hexagons will only be well ordered if the protein offers anchor groups in suitable positions. In the case of crambin, the pentagons A and D are bound to the protein by hydrogen bonds, whereas B, C, and E are only bound by water–water interactions. A well ordered aqueous monolayer is thus formed on the hydrophobic surface; the monolayer consists of only 16 water molecules and is retained during crystallization. Such clathrate-analogous surface water could be bound equally tightly if the protein was surrounded by bulk water; an exchange of water molecules does not take place. Similar pentagonal structures have also been found on insulin, again on a hydrophobic protein surface around a hydrophilic tip.[105] In polar inorganic surroundings, the water decamer of ordinary ice seems to occur more frequently.[111]

Computer simulations of the water structure on planar walls showed that three or four molecular water layers formed a very stable ice-like structure.[109, 112] The water molecules next to the wall orientated their oxygen atoms towards the hydrophobic wall. However, these simulations did not disclose to what extent the ice-like water exchanges with the surrounding bulk water.

Charged molecules, which are anchored to the water surface by long alkyl chains, bind to counterions of appropriate size in bulk water about a thousand times stronger than the same molecules dissolved in bulk water. Hydrogen bonds formed in interfacial regions are also much stronger than those in the bulk water. This has been established, for example, for guanidinium-, calixarene-, and cyclic triazine diamine in ordered surface layers, which selectively bind to 10^{-4} M nucleotide and carbohydrate solutions in the water phase. The particular stability of the binding of the dissolved molecules to monolayers at the surface was related to a large decrease in the dielectric constant from 80 (water) to 2 (alkyl chains) at a distance of a few Ångströms. The quantum-mechanical reaction-field theory then shows a large enhancement of binding energy.[113]

Hydrophobic clefts with a width of 1–2 nm in lipid monolayers on smooth surfaces are filled with water when the electrodes are plunged into water. Neither hydrophobic repulsion nor formation of air bubbles occurs. Ferricyanide ions penetrate into the water-filled pores from the surrounding bulk water and produce simple CVs. The measured strength of the electric current through 0.6–2-nm membrane clefts does not change with rigid or fluid walls[64, 92, 114] (see Figure 24). Nonporous membranes show an almost perfect insulating effect.

The electron transport of ferricyanide ions through the water-filled membrane clefts was completely blocked when the electrode was first plunged for one hour into a 0.1M aqueous solution of 1,2-*trans*-cyclohexanediol, ascorbic acid, cellobiose, or tyrosine, then washed in water, and finally again plunged into the ferricyanide–KCl solution, which did not contain any organic solutes. The blocking effect lasted for several hours, in most cases even for months and ended only when HCl (pH 3)[114] or ethanol was added. Presumably the solutes formed three-dimensional hydrogen bond nets with surface water within the nanometer pores. HCl destroys the net by making the fluctuation of the protons easier (see crystallization in the presence of KOH; Figure 29a) and ethanol destroys the crystallinity of immovable water, because it can only build one hydrogen bond. CV investigations showed that dimethyl viologen worked as a "molecular stirring rod" and opened the pores.[115] Neither open-chained compounds, nor flexible cyclopentanediols, *cis*-1,2-cyclohexanediol or maltose had any blocking effect. It seems that the solutes fit into a pentagonal (ascorbic acid) or hexagonal (cellobiose) water structure thus strengthening it considerably. The model shown in Figure 31 suggests the formation of

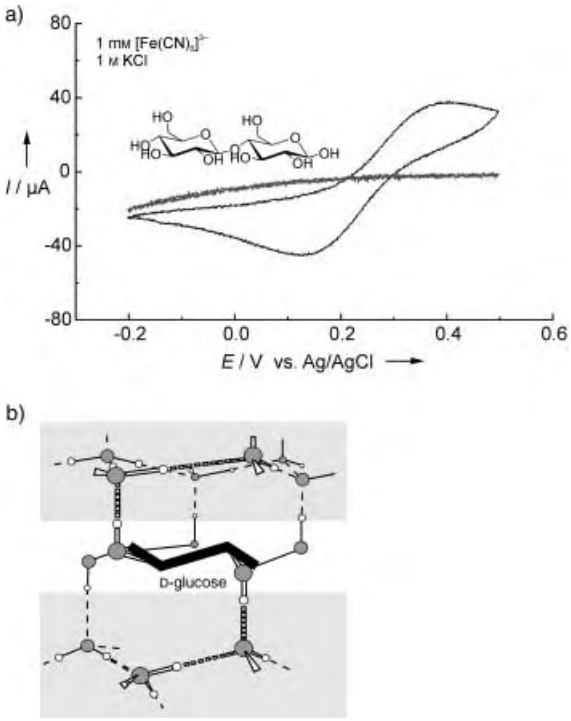


Figure 31. a) Cyclovoltammogram of ferricyanide at a porous octadecylsulfide membrane before (open curve) and after (closed curve) treatment with cellobiose, b) model of the ice plug with a glucose unit.

ice-like plugs induced by the rigid solute. The plugs are tightly connected to the hydrophobic walls of the membrane cleft. This tight structure does not allow diffusion of ferricyanide ions into the nanometer cleft and the slow electron transport from ions in bulk water by tunneling does not occur. The model does not explain the longevity of the "ice plug" positioned in direct contact with the bulk water. A dilution experiment provided a clue: the addition of 1% of maltose to the cellobiose totally eliminated its blocking effect. The entrapment of cellobiose in the cleft may thus be compared with that of a slow crystallization of already immobile surface water. Foreign molecules disturb this process.[115]

Similarly immovable water molecules have also been found in polar surroundings, that is, as large hydration spheres of potassium ions in layered thiophosphates. After replacing a bivalent cadmium ion by two hydrated potassium ions, the preformed layer system becomes associated in interlamellar regions in the form of monolayer water domains. On one side there was enough room for a unilateral hydration of

potassium ions, whereas the other side was occupied by hydrophobic sulfide ions of the thiophosphate grid. ^{1}H NMR Pake spectra of the pulverized thiophosphates showed movable and immovable water molecules side by side. The movable water could be removed in vacuum, whereas the immovable water could not (Figure 32). The position and splitting of the Pake doublets did not change with temperature. The exchange between the mobile and tightly-bound water molecules was at least 10^6 times slower than in bulk water. The rigid surrounding of the water monolayers clearly did not allow a widening of the hydrate cover and thus slowed down exchange reactions.[116]

Thin water layers on membrane surfaces serve as a medium for recognition processes between signal substances in surrounding bulk water and biological cell surfaces and hence further investigations are warranted.[117a–d] Cell-specific recognition processes between glycoproteins of differentiated cells and hormones can certainly not be attributed to high binding constants, which are unlikely in the case of carbohydrates in aqueous media, but rather to the kinetics of surface reactions. Water clusters that are immobilized and structurally defined by adequate carbohydrates may provide a perfect scenario for molecular trapping, for example, of a steroid hormone from the surface of its carrier protein in blood.

8. Colloidal Carrier Systems

The previously described membrane systems with form-stable clefts and hills can be characterized and then optimized on solid metal surfaces with the aid of fluorescence measurements, cyclic voltammetry, FTIR-spectroscopy, and scanning electron microscopy. The monolayers cannot be used on solid electrodes for NMR spectroscopic examinations of entrapped volumes of water, for photolysis experiments (charge separation and water splitting), and as catalysts in bulk water as the area (a few cm^2) of the large monolayers do not contain enough material ($\approx 10^{-10}-10^{-9}$ mol). The surface of membrane systems has to be enlarged and transferred into volume water to carry out flash photolysis experiments and solid-state NMR spectroscopy.

Spherical citrate gold particles (15–30 nm diameter; formed by the reduction of $AuCl_4^-$ with sodium citrate at 100) were found to be most suitable for experiments with closed membrane systems and form-stable nanometer clefts.[118–120] The smooth surface and curvature of citrate (citric acid gives rise to crystallites) largely corresponds to those of lipid vesicles. The curvature does not noticeably impair lateral interactions and the formation of closed lipid membranes. Smaller gold particles that contain many edges between crystal planes (e.g. Brust gold obtained from reduction with sodium borohydride)[121] do not allow the deposition of closed monolayers (Figure 33).

The use of citrate gold gives rise to some problems: 1) the particles are very heavy and sedimentation can occur during lengthy experiments; 2) the lipid membrane/gold mass ratio is very low ($\approx 1{:}10^3$); 3) the colloidal gold surfaces extinguish the fluorescence of directly applied dyes to a much greater extent than the rougher gold electrodes; 4) the flash photolysis of deposited dyes is difficult with strongly absorbing gold particles; 5) gold particles would be a prohibitively expensive system for the commercial production of hydrogen from water. Citrate gold is therefore only suitable for establishing synkinetic methods to produce well defined curved surfaces

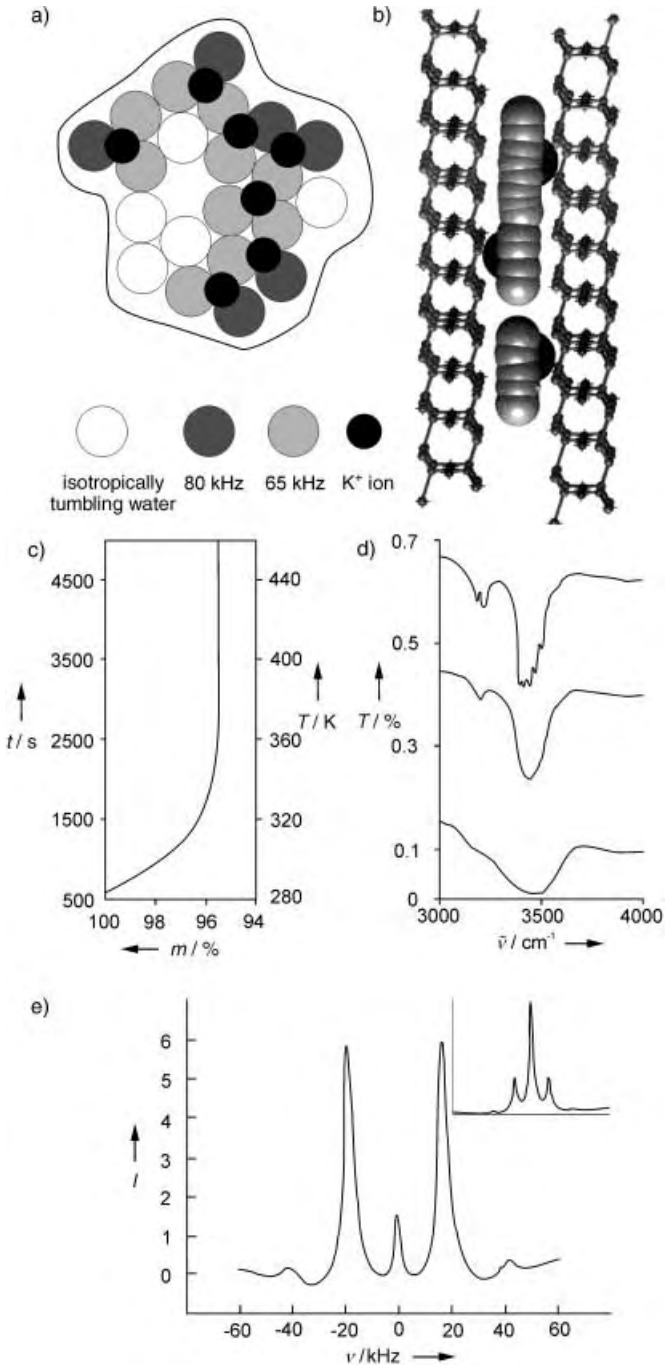


Figure 32. Trapped water in molecular cadmium–potassium thiophosphate layers. a, b) model of the three types of water between the crystal layers before (left) and after (right) vacuum drying. c) Isothermal weight loss in vacuo. d) IR spectra before (top), during (middle), and after (bottom) drying. e) PAKE ^{1}H NMR spectra before (insert) and after drying. The coupling constant of the remaining water (85 KHz) indicates immobile water molecules that surround the potassium ions; the isotropically movable water (a) produced doublets with a coupling constant of 65 KHz.

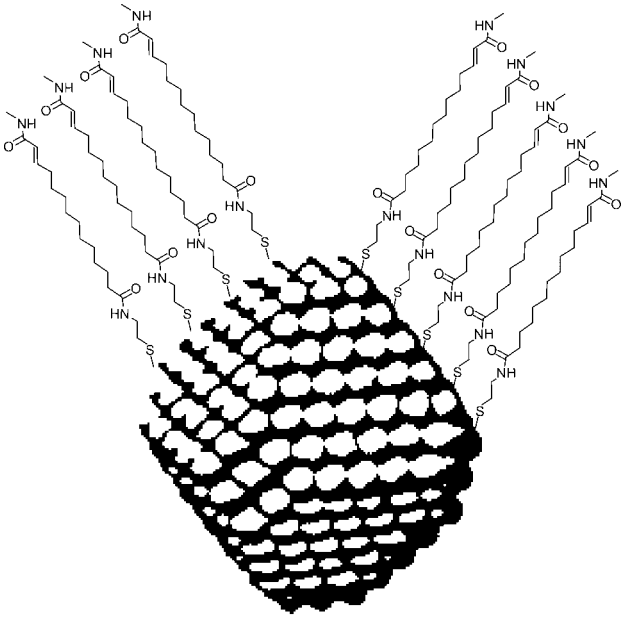


Figure 33. Typical disordered arrangement of membrane fragments on the crystal planes of 2–5-nm gold particles.

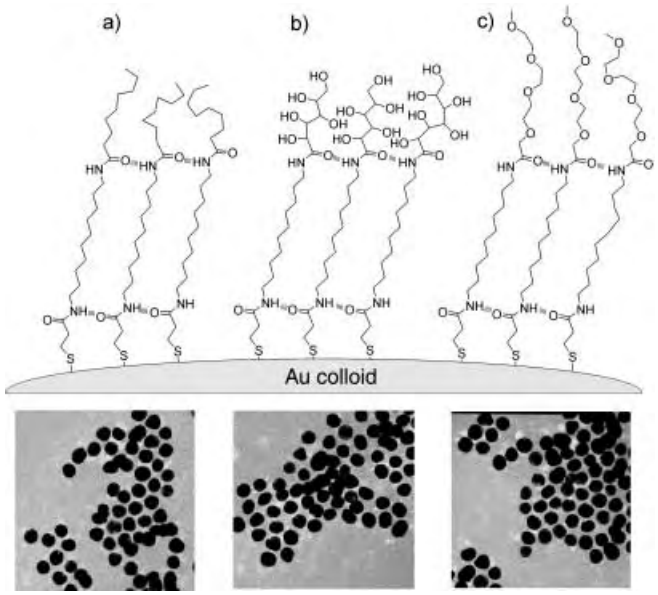


Figure 34. TEM pictures and models of solvatable gold colloids with a rigid, functional membrane core. a) soluble in toluene, b) soluble in water, c) soluble in toluene and water.

for characterization by electron microscopy and for electrochemical experiments. For photolytic processes such as the splitting of water, the reaction systems obtained have to be transferred to colloids, which do not absorb visible light.

The problem of sedimentation with 30 nm gold particles was solved by simple swelling and solvation of the outermost layer of the membrane coating. Introduction of a flexible 1–2 nm layer was sufficient. The inner part of the membranes is applied by self-assembly, can be rigid, and shows as many pores as are needed. The outer part can consist of loosely packed alkyl chains (for organic solvents) or open-chain gluconamide (for water). Oligoethylene glycol end groups stabilize the colloid in organic solvents as well as in water (Figure 34).[115]

The functional membrane/gold mass ratio can only be enhanced by flattening the spherical particles, not by shrinking them (see Figure 33). However, 5-nm thick gold platelets in aqueous solution would be a much better carrier system for solid-state NMR experiments. References to colloidal platelets can actually be found in earlier publications on "acetone gold".[118, 122] Own work along this line (reduction of gold chloride with citric acid and/or acetone in aqueous solution) produced thin crystalline platelets, which were characterized by TEM and a broad plasmon absorption (650 nm).

Reliable conservation of porphyrin fluorescence was more difficult. In the case of simple physical or chemical adsorption, at least 99% of the fluorescence of the porphyrins was quenched.[123] Roughening the surface of the gold, which had been helpful in the case of rigid gold electrodes, did not increase the fluorescence. Even when the chromophore was shielded from the gold surface by nonmetallic material, the problem of the plasmon absorption and fluorescence persisted.

Colloidal citrate gold was also bound to aminated indium/tin oxide (ITO) electrodes and then used as a basis for anchoring viologen catenanes. The viologen catenanes on the citrate film act as electron acceptors for tris(bipyridine)ruthenium in the excited state[123] and produce a photocurrent when irradiated with 434 nm light and with the support of a prepotential at the ITO-electrode. At 0.0 V all redox pairs produced a current and at < -0.6 V the viologen units were reduced and the photocurrent was blocked. A direct Ru* $\rightarrow$gold electron transport did not occur; the viologen transferred the electron to the metal. This corresponds to the classic Green–Shilov system in which a chemically reduced molecule reacts with platinum colloids and releases molecular hydrogen.[124, 125] The quantum yield of photoelectron formation was very low (10^{-4}); that of the Ru* $\rightarrow$Bipy electron transfer amounted to 5%.

Gold and silver particles in aqueous media were also dimerized by means of phenyl acetylene bridges of variable length. Dimers of 30-nm silver particles connected by short bridges showed the splitting and displacements of plasmon absorption bands typical for the electronic coupling of both particles[126] (Figure 35). Electron donor–acceptor systems with very large surface areas for charge separation may become accessible from such membrane-covered heterodimers.

Citrate gold was also entrapped in the form of linear chains within the pores of aluminum oxide membranes. Pyrrole polymerization within these pores produced a connective mantle. Afterwards the aluminum oxide was dissolved with KOH, and a one-dimensional chain of gold particles linked to polypyrrole was obtained. Since the polypyrrole has conductive properties, "electron hopping" between the gold clusters should be possible, similar to that observed in radical-containing acetylene or DNA polymers.[127] The rigidity of the pyrrole polymers allowed AFM manipulations of this system (Figure 36). Complementary DNA branches were also used successfully to interlink membrane-covered gold colloid

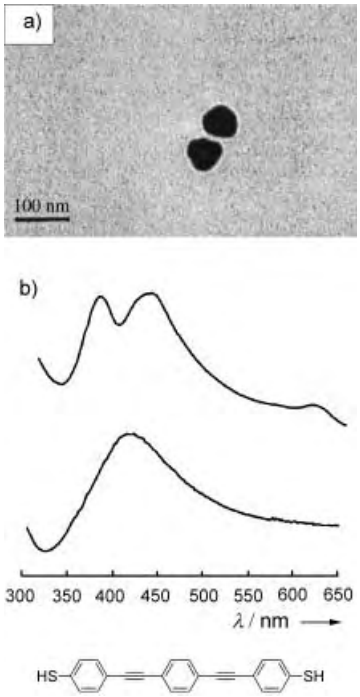


Figure 35. a) SEM pictures of a silver–colloid dimer bound by a rigid α,ω-disulfide. The distance is $\approx$20 nm. b) Plasmon spectrum of the monomeric silver colloid (bottom) and of the dimer (top).

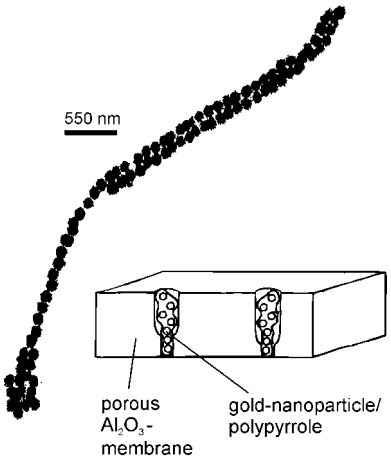


Figure 36. TEM picture of linear gold colloid wires with polypyrrole connections, which can be released from aluminum oxide pores.

particles, which melted sharply as is typical for DNA duplexes.[128]

ITO electrodes that are coated with a cationic 3-aminopropylsiloxane layer and are thus positively charged connect citrate gold particles as a porous monolayer. This layer absorbed at 520 nm and at 650 nm when packed more closely which corresponds to the absorption of gold foils. The same band shifting occurred when spherical gold particles were converted into platelets by treatment of citrate gold with acetone as mentioned above. Negatively charged citrate gold particles were also connected to a zinc porphyrinate through a spacer. Viologen was used as an anchor and electron acceptor. Upon irradiation with visible light, the energy-rich electrons of the porphyrin were transferred to the electrode and a

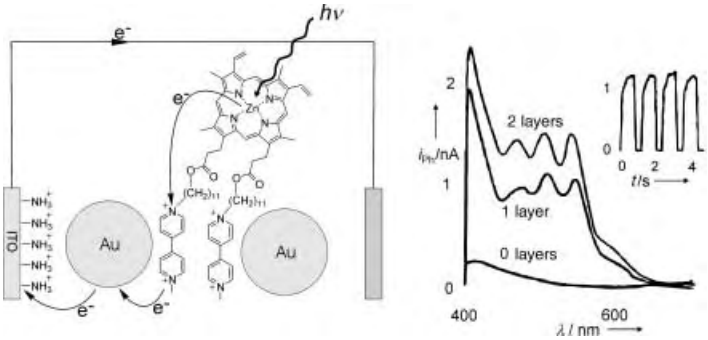


Figure 37. Positive charges of viologen substituents on porphyrin molecules connect gold colloids and gold electrodes. A layer consists of a combination of a citrate gold layer with a layer of porphyrin counterions (the left picture shows 1.5 layers). When the system is irradiated in the presence of weak reductants, photoelectric currents flow after about one second. The wave dependence of this photoelectric current corresponds to the absorption spectrum of the porphyrin.

photoelectric current of several nanoampere was measured (Figure 37).[129]

Spherical gold particles are also soft enough to penetrate into clefts on the surface of globular proteins. It has for example been found that cytochrome with naked ITO electrodes did not produce any electric contact, but did so when gold colloids were deposited between the proteins and the electrode. Many electrochemical chain reaction can thus be established by combining gold-colloids with proteins.[130] Furthermore, 4–5 nm gold particles that are only partly covered by octadecanethiol move together so closely by interdigitation of the incomplete monolayer surface that 2-nm long aryldithiols connect the gold particles and allow a current to flow. Monolayers of colloids then also conduct currents when anchored to a nonconducting substrate.

Mesoscopic polyelectrolyte films with alternating charges compete with the rigid monolayers described herein. They are also accessible by applying dip and wash procedures and can also be loaded with cationic and anionic dyes.[131, 132]

9. Summary and Outlook

Rigid molecular assemblies in bulk water and in landscapes on support systems allow complex arrangements of reactive components. This Review described domains, micelles, vesicles, and fibers in bulk water as well as in the dry state, followed by monolayers on gold, immobile volumes of water in membrane clefts on solid surfaces, and finally rigid lipid membranes on gold colloids in solution. This sequence is only logical under the aspect of systematically building up chain reactions by means of synkinesis.

The structures of the systems produced so far have been visualized be means of AFM, STM, and TEM, and were characterized indirectly by fluorescence quenching and cyclic voltammetry. The determination of the changes in molecular conformation by solid-state ^{13}C NMR spectroscopy in the transition from 3D crystals to noncovalent fibers was only possible with glyconamide. This structural analysis was successful because the fibers were isolated in the solid state

in gram quantities and because their solid-state NMR spectra could be correlated with those of many 3D crystals whose structure had already been determined by X-ray crystallographic analysis. Molecular structures on solid supports, in particular at membrane edges and in immobile water volumes, and the utilization of the chemical reactivity of the components (catalysis, light-induced charge separation) has been investigated indirectly only on gold electrodes. Colloids present new problems: Appropriately-sized gold colloids absorb light and are therefore not suitable for flash photolysis experiments. Silicates, on the other hand, tend to produce pores with a high curvature and with different depths which renders the construction of closed membranes and clefts virtually impossible. Poreless CaBosil particles were unstable in self-assembly processes: they tended to swell and to formed threads. Semiconductor colloids are notoriously sensitive to oxygen, acids, and bases and little is known about the stability of smooth surfaces. What matters in synkineses is the production of colloid particles whose surfaces remain both reactive and smooth in several self-assembly steps and which do not disturb photochemical and electrochemical experiments.

The Review answers the frequently asked question: why is the term "synkinesis"[2] necessary in supramolecular chemistry? Why do the terms self-assembly and supramolecular synthesis not suffice? There is no "self" in complex systems (e.g., see Figures 25, 26 and 29) as every single component of molecular systems has to be optimized with regard to size, charge, counterion, solubility, adhesion to surfaces, redox potential, fluorescence, etc. The synkinetic chemist combines molecules that fit with each other. The synthesis of these synkinons need careful plans. New syntheses will be necessary if anything does not fit or stick tightly to the system. Finally, if the required system has been obtained in quantitative yields (systems cannot be cleaned!), it would be the result of planning, successful experiments, and optimization. Synkinesis is consequently analogous to a successful synthesis. After all, a Grignard reaction is not a "self-assembly" simply because negatively and positively charged carbon atoms reacted together "by themselves".

A cursory comparison of the figures in books on self-assembly[1, 68, 133] and synkinesis[2] reveals the difference between physical and organic chemistry of the membrane. Structural formula, stereochemistry, optimized yields in multistage synkinesis, and complex synkinons are only made in laboratories active in organic chemistry. Physical chemists describe molecules and their fragments as spheres, cones, cylinders, and wavy lines that are assembled according to the laws of elementary geometry and thermodynamics. In this respect it is justified, but not very helpful as a basis for the construction of complex systems.

Synkinesis is the creation of well defined and isolable molecular assemblies in the same rational way that cyclic, helical, branched, rigid, or flexible polymers are synthesized. In this case too one speaks of synthesis and not of self-assembly. The term synkinesis refers directly to a multistage process in which all reactions are completely reversible. In many cases, heating or changing the pH value is sufficient for a complete dissolution into monomers or a reconstitution of high-molecular-weight systems. The term "supramolecular synthesis" would also be applicable, but is no longer appropriate as most "supramolecular" molecules currently produced consist of interlocked rings or of several molecular subunits connected by covalent bonds.

What can be expected of rigid mono- and bilayers and of molecular landscapes? The application of fluid membranes to organize chain reaction mostly fails because the components are too flexible and neither distances nor orientations can be fixed. Rigid and reactive membrane systems on nanoparticles hopefully behave more like biosystems anchored by membrane proteins. A 1-cm^2 area of a gold electrode or of a silicon microchip may carry 10^{10} separate landscape motifs, which can all be oxidized, reduced, shifted, eroded, enlarged, and coated separately and offer an almost infinite number of possibilities for manipulation. In restricted areas it should be possible to interconnect valleys, hills in vectorial chain reactions.

Financial support by the Deutsche Forschungsgemeinschaft (SFB 312 "Vectorial Membrane Processes" and SFB 448 "Mesoscopic Systems"), the European TMR-networks "Artificial Photosynthesis" and "Carbohydrate Recognition", by the Fonds der Deutschen Chemischen Industrie, and by the Förderkomission der Freien Universität Berlin is gratefully acknowledged. We thank Dr. Laurent Ruhlmann and Dr. Jörg Zimmermann for their major contributions to the characterization of nanometer pores. Dr. Marie-Françoise Gouzy developed the kanamycin micelles. Dr. Christoph Böttcher and Dr. Christian Messerschmidt worked as pioneers in AFM, STM, and TEM of molecular landscapes. We also thank the referees of our manuscript for their helpful and constructive reviews.

Received: May 7, 2001 [A 472]

[1] J. N. Israelachvili, *Intermolecular and Surface Forces*, Academic Press, London, **1985**.
[2] a) J.-H. Fuhrhop, J. Köning in *Monographs in Supramolecular Chemistry; Molecular Assemblies and Membranes: The Synkinetic Approach* (Ed.: J. F. Stoddart), Royal Society of Chemistry, London, **1994**, pp. i-xiii; b) J. H. Fuhrhop, C. Endisch, *Molecular and Supramolecular Chemistry of Natural Products and Model Compounds*, Marcel Dekker, New York, **2000**.
[3] a) J.-H. Fuhrhop, *Angew. Chem.* **1974**, *86*, 363; *Angew. Chem. Int. Ed. Engl.* **1974**, *13*, 321; b) J.-H. Fuhrhop, *Angew. Chem.* **1976**, *88*, 704; *Angew. Chem. Int. Ed. Engl.* **1976**, *15*, 648; c) J.-H. Fuhrhop, J. Mathieu, *Angew. Chem.* **1984**, *96*, 124; *Angew. Chem. Int. Ed. Engl.* **1984**, *23*, 100.
[4] F. M. Menger, *Acc. Chem. Res.* **1979**, *12*, 111.
[5] J. S. Nowick, J. S. Chen, G. Noronha, *J. Am. Chem. Soc.* **1993**, *115*, 7636.
[6] R. P. Bonar-Law, *J. Org. Chem*. **1996**, *61*, 3623.
[7] P. Juvvadi, S. Vunnam, R. B. Merrifield, *J. Am. Chem. Soc*. **1996**, *118*, 8989.
[8] N. Sakai, D. Gerard, S. Matile, *J. Am. Chem. Soc.* **2001**, *123*, 2517.
[9] O. S. Andersen, *J. Phys. Chem*. **2001**, *100*, 4622.
[10] R. R. Ketchem, W. Hu, T. A. Cross, *Science* **1993**, *261*, 1457.
[11] O. S. Andersen, R. E. Koeppe II, *Physiol. Rev.* **1992**, *72*, 89.
[12] B. A. Cornell, V. L. B. Braach-Maskvytis, L. G. King, P. D. J. Osman, B. Raguse, L. Wieczorek, R. J. Pace, *Nature* **1997**, *387*, 580.
[13] J.-H. Fuhrhop, M. Krull, A. Schulz, D. Möbius, *Langmuir* **1990**, *6*, 497.

[14] J.-H. Fuhrhop, U. Liman, V. Koesling, *J. Am. Chem. Soc.* **1988**, *110*, 6840.
[15] J. D. Hartgerink, J. R. Granja, R. A. Milligan, M. R. Ghadiri, *J. Am. Chem. Soc.* **1996**, *118*, 43.
[16] H. S. Kim, J. D. Hartgerink, M. R. Ghadiri, *J. Am. Chem. Soc.* **1998**, *120*, 4417.
[17] K. Motesharei, R. Ghadiri, *J. Am. Chem. Soc.* **1997**, *119*, 11312.
[18] T. D. Clark, L. K. Buehler, M. R. Ghadiri, *J. Am. Chem. Soc.* **1998**, *120*, 651.
[19] T. S. Arrhenius, M. Blanchard-Desce, M. Dvolaitzky, J.-M. Lehn, J. Malthete, *Proc. Natl. Acad. Sci. USA* **1986**, *83*, 5355.
[20] a) G. W. Gokel, O. Murillo, *Acc. Chem. Res.* **1996**, *29*, 425; b) L. A. Weiss, N. Sakai, B. Ghebremariam, C. Ni, S. Matile, *J. Am. Chem. Soc.* **1997**, *119*, 12142.
[21] a) G. Leatherman, E. N. Durantini, D. Gust, T. A. Moore, S. Stone, Z. Zhou, P. Rez, Y. Z. Liu, S. M. Lindsay, *J. Phys. Chem. B* **1999**, *103*, 4006; b) S. Creager, C. J. Yu, C. Bamdad, S. O'Connor, T. MacLean, E. Lam, Y. Chong, G. T. Olsen, J. Luo, M. Gozin, J. F. Kayyem, *J. Am. Chem. Soc.* **1999**, *121*, 1059.
[22] a) V. Subramanian, W. A. Ducker, *Langmuir* **2000**, *16*, 4447; b) V. Subramanian, W. A. Ducker, *J. Phys. Chem. B* **2001**, *105*, 1389.
[23] M. Gouzy, F. Gonzaga, M. Lauer, A. Schulz, C. Boettcher, J.-H. Fuhrhop, *Langmuir*, submitted.
[24] C. Draeger, C. Boettcher, C. Messerschmidt, L. Ruhlmann, J.-H. Fuhrhop, U. Siggel, L. Hammerström, *Langmuir* **2000**, *16*, 2068.
[25] B. Klarewicz, C. Draeger, K. Jansen, J.-H. Fuhrhop, unpublished results.
[26] C. Messerschmidt, C. Draeger, A. Schulz, J. P. Rabe, J.-H. Fuhrhop, *Langmuir* **2001**, *17*, 3526.
[27] M. F. Roks, H. G. J. Visser, J. W. Zwikker, A. J. Verkley, R. J. M. Nolte, *J. Am. Chem. Soc.* **1983**, *105*, 4507.
[28] H. Ohno, S. Takeoka, E. Tsuchida, *Polymer Bull.* **1985**, *14*, 487.
[29] H. Ringsdorf, B. Schlarb, J. Venzmer, *Angew. Chem.* **1988**, *100*, 117; *Angew. Chem. Int. Ed. Engl.* **1988**, *27*, 113.
[30] L. Zhang, A. Eisenberg, *J. Am. Chem. Soc.* **1996**, *118*, 3168.
[31] a) S. Klingelhöfer, W. Heitz, A. Greiner, S. Oestreich, S. K. Förster, M. Antonietti, *J. Am. Chem. Soc.* **1997**, *119*, 10116; b) M. Schreuder Goedheijt, B. E. Hanson, J. N. H. Reek, P. C. J. Kramer, P. W. N. M. van Leeuwen, *J. Am. Chem. Soc.* **2000**, *122*, 1650.
[32] a) S. A. Jenekhe, X. L. Chen, *Science* **1998**, *279*, 1903; b) B. M. Discher, Y. Y. Won, D. S. Ege, J. C. M. Lee, F. S. Bates, D. E. Discher, D. A. Hammer, *Science* **1999**, *284*, 1143.
[33] G. T. Oostergetel, F. J. Esselink, G. Hadziioannou, *Langmuir* **1995**, *11*, 3721.
[34] N. H. Thomson, I. Collin, M. C. Davies, K. Palin, D. Parkins, C. J. Roberts, S. J. B. Tendler, P. M. Williams, *Langmuir* **2000**, *16*, 4813.
[35] T. Komatsu, E. Tsuchida, C. Boettcher, D. Donner, C. Messerschmidt, U. Siggel, W. Stocker, J. P. Rabe, J.-H. Fuhrhop, *J. Am. Chem. Soc.* **1997**, *119*, 11660.
[36] J.-H. Fuhrhop, W. Helfrich, *Chem. Rev.* **1993**, *93*, 1565.
[37] J. H. Fuhrhop, P. Schnieder, J. Rosenberg, E. Boekema, *J. Am. Chem. Soc.* **1987**, *109*, 3387.
[38] J. Köning, C. Boettcher, H. Winkler, E. Zeitler, Y. Talmon, J.-H. Fuhrhop, *J. Am. Chem. Soc.* **1993**, *115*, 693.
[39] J.-H. Fuhrhop, C. Boettcher, *J. Am. Chem. Soc* **1990**, *112*, 1768.
[40] T. Kunitake, Y. Okahata, M. Shimomura, S. Yasunami, K. Takarabe, *J. Am. Chem. Soc.* **1985**, *107*, 509.
[41] J.-H. Fuhrhop, C. Demoulin, J. Rosenberg, C. Boettcher, *J. Am. Chem. Soc.* **1990**, *112*, 2827.
[42] T. Tachibana, T. Yoshizumi, K. Hori, *Bull. Chem. Soc. Jpn.* **1979**, *52*, 34.
[43] J.-H. Fuhrhop, T. Bedurke, A. Hahn, S. Grund, J. Gatzmann, M. Riederer, *Angew. Chem.* **1994**, *106*, 351; *Angew. Chem. Int. Ed. Engl.* **1994**, *33*, 350.
[44] J.-H. Fuhrhop, M. Krull, G. Büldt, *Angew. Chem.* **1987**, *99*, 707; *Angew. Chem. Int. Ed. Engl.* **1987**, *26*, 699.
[45] S. Svenson, B. Kirste, J.-H. Fuhrhop, *J. Am. Chem. Soc.* **1994**, *116*, 11969.
[46] I. Sack, S. Macholl, J.-H. Fuhrhop, G. Buntkowsky, *Phys. Chem. Chem. Phys.* **2000**, *2*, 1781.
[47] C. Messerschmidt, S. Svenson, W. Stocker, J.-H. Fuhrhop, *Langmuir* **2000**, *16*, 7445.
[48] J.-H. Fuhrhop, D. Spiroski, C. Boettcher, *J. Am. Chem. Soc.* **1993**, *115*, 1600.
[49] J.-H. Fuhrhop, P. Blumtritt, C. Lehmann, P. Luger, *J. Am. Chem. Soc.* **1991**, *113*, 7437.
[50] C. Messerschmidt, A. Schulz, J. Zimmermann, J.-H. Fuhrhop, *Langmuir* **2000**, *16*, 5790.
[51] I. Inamura, K. Uchida, *Bull. Chem. Soc. Jpn.* **1991**, *64*, 2005.
[52] a) J.-H. Fuhrhop, C. Demoulin, C. Boettcher, J. Köning, U. Siggel, *J. Am. Chem. Soc.* **1992**, *114*, 4159; b) J.-H. Fuhrhop, U. Bindig, U. Siggel, *J. Chem. Soc. Chem. Commun.* **1994**, 1583.
[53] B. Rosengarten, C. Böttcher, A. Schulz, J.-H. Fuhrhop, U. Siggel, *J. Porphyrins Phthalocyanines* **1998**, *2*, 273.
[54] J.-H. Fuhrhop, U. Bindig, U. Siggel, *J. Am. Chem. Soc.* **1993**, *115*, 11036.
[55] C. Endisch, C. Böttcher, J.-H. Fuhrhop, *J. Am. Chem. Soc.* **1995**, *117*, 8273.
[56] D. Donner, C. Böttcher, C. Messerschmidt, U. Siggel, J.-H. Fuhrhop, *Langmuir* **1999**, *15*, 5029.
[57] H. von Berlepsch, C. Böttcher, A. Quart, M. Regenbrecht, S. Akari, U. Keiderling, H. Schnablegger, S. Dähne, S. Kirstein, *Langmuir* **2000**, *16*, 5908.
[58] G. Scheibe, *Angew. Chem.* **1936**, *49*, 563; G. Scheibe, *Angew. Chem.* **1937**, *50*, 51.
[59] E. E. Jelley, *Nature* **1936**, *138*, 1009; E. E. Jelley, *Nature* **1937**, *139*, 631.
[60] S. Daehne, *Photogr. Sci. Eng.* **1979**, *23*, 219.
[61] V. Czikklely, H. D. Försterling, H. Kuhn, *Chem. Phys. Lett.* **1970**, *6*, 207.
[62] M. T. Cygan, G. E. Collins, T. D. Dunbar, D. L. Allara, C. G. Gibbs, C. D. Gutsche, *Anal. Chem.* **1999**, *71*, 142.
[63] N. J. Tao, Z. Shi, *J. Phys. Chem.* **1994**, *98*, 1464.
[64] W. Fudickar, J. Zimmermann, L. Ruhlmann, B. Roeder, U. Siggel, J.-H. Fuhrhop, *J. Am. Chem. Soc.* **1999**, *121*, 9539.
[65] X. Qiu, C. Wang, Q. Zeng, B. Xu, S. Yin, H. Wang, *J. Am. Chem. Soc.* **2000**, *122*, 5550.
[66] J.-H. Fuhrhop, T. Bedurke, M. Gnade, J. Schneider, K. Doblhofer, *Langmuir* **1997**, *13*, 455.
[67] Z. P. Yang, I. Engquist, J.-M. Kauffmann, B. Liedberg, *Langmuir* **1996**, *12*, 1704.
[68] A. Ulman, *Ultrathin Organic Films*, Academic Press, New York, **1991**.
[69] J. Sagiv, *J. Am. Chem. Soc.* **1980**, *102*, 92.
[70] J. Sagiv, *Isr. J. Chem.* **1979**, *18*, 346.
[71] R. Maoz, H. Cohen, J. Sagiv, *Langmuir* **1998**, *14*, 5988.
[72] D. N. Batchelder, S. D. Evans, T. L. Freeman, L. Häussling, H. Ringsdorf, H. Wolf, *J. Am. Chem. Soc.* **1994**, *116*, 1050.
[73] S. D. Evans, K. E. Goppert-Berarducci, E. Urankar, L. J. Gerenser, A. Ulman, *Langmuir* **1991**, *7*, 2700.
[74] A. J. Black, T. T. Wooster, W. E. Geiger, M. N. Paddon-Row, *J. Am. Chem. Soc.* **1993**, *115*, 7924.
[75] W. S. V. Kwan, L. Atanaoska, L. L. Miller, *Langmuir* **1991**, *7*, 1419.
[76] W. S. V. Kwan, V. Cammarate, L. L. Miller, M. G. Hill, K. R. Mann, *Langmuir* **1992**, *8*, 3003.
[77] Y. S. Obeng, M. E. Laing, A. C. Friedli, H. C. Yang, D. Wang, E. W. Thulstrup, A. J. Bard, J. Michl, *J. Am. Chem. Soc.* **1992**, *114*, 9943.
[78] S.-W. Tam-Chang, H. A. Biebuyck, G. M. Whitesides, N. Jeon, R. G. Nuzzo, *Langmuir* **1995**, *11*, 4371.
[79] R. S. Clegg, J. E. Hutchison, *Langmuir* **1996**, *12*, 5239.
[80] P. Böhme, H.-G. Hicke, C. Böttcher, J.-H. Fuhrhop, *J. Am. Chem. Soc.* **1995**, *117*, 5824.
[81] R. S. Clegg, S. M. Reed, R. K. Smith, B. L. Barron, J. A. Rear, J. E. Hutchison, *Langmuir* **1999**, *15*, 8876.
[82] M.-W. Tsao, C. L. Hoffmann, J. F. Rabolt, H. E. Johnson, D. G. Castner, C. Erdelen, H. Ringsdorf, *Langmuir* **1997**, *13*, 4317.
[83] T. J. Lenk, V. M. Hallmark, C. L. Hoffmann, J. F. Rabolt, *Langmuir* **1994**, *10*, 4610.
[84] J. Schneider, C. Messerschmidt, A. Schulz, M. Gnade, B. Schade, P. Luger, P. Bombicz, V. Hubert, J.-H. Fuhrhop, *Langmuir* **2000**, *16*, 8575.
[85] O. Chailapakul, R. M. Crooks, *Langmuir* **1993**, *9*, 884.

[86] V. Chechik, R. M. Crooks, C. J. M. Stirling, *Adv. Mater.* **2000**, *12*, 1161.
[87] E. Sabatani, J. Cohen-Boulakia, M. Bruening, I. Rubinstein, *Langmuir* **1993**, *9*, 2974.
[88] J. F. Kang, A. Ulman, S. Liao, R. Jordan, *Langmuir* **1999**, *15*, 2095.
[89] J. F. Kang, A. Ulman, S. Liao, R. Jordan, G. Yand, G.-Y. Liu, *Langmuir* **2001**, *17*, 95.
[90] R. W. Zehner, L. R. Sita, *Langmuir* **1997**, *13*, 2973.
[91] M. T. Cygan, T. D. Dunbar, J. J. Arnold, L. A. Bumm, N. F. Shedlock, T. P. Burgin, L. Jones II, D. L. Allara, J. M. Tour, P. S. Weis, *J. Am. Chem. Soc.* **1998**, *120*, 2721.
[92] M. Skupin, G. Li, W. Fudickar, J. Zimmermann, B. Röder, J.-H. Fuhrhop, *J. Am. Chem. Soc.* **2001**, *123*, 3454.
[93] Y. Xia, G. M. Whitesides, *Angew. Chem.* **1998**, *110*, 568; *Angew. Chem. Int. Ed.* **1998**, *37*, 550.
[94] M. Geissler, A. Bernard, A. Bietsch, H. Schmidt, B. Michel, E. Delamarche, *J. Am. Chem. Soc.* **2000**, *122*, 6303.
[95] C. Messerschmidt, A. Schulz, J. P. Rabe, A. Simon, J.-H. Fuhrhop, *Langmuir* **2000**, *16*, 1299.
[96] K. Araki, M. J. Wagner, M. S. Wrighton, *Langmuir* **1996**, *12*, 5393.
[97] D. A. Offord, S. B. Sachs, M. S. Ennis, T. A. Eberspacher, J. H. Griffin, C. E. D. Chidsey, J. P. Collman, *J. Am. Chem. Soc.* **1998**, *120*, 4478.
[98] D. M. Sarno, B. Jiang, D. Grosfeld, J. O. Afriyie, L. J. Matienzo, W. E. Jones, Jr., *Langmuir* **2000**, *16*, 6191.
[99] M. S. Boeckl, A. L. Bramblett, K. D. Hauch, T. Sasaki, B. D. Ratner, J. W. Rogers, Jr., *Langmuir* **2000**, *16*, 5644.
[100] A. Alberti in *Comprehensive Supramolecular Chemistry*, *Vol. 7* (Ed.: J.-M. Lehn), Pergamon, Oxford, **1996**, p. 151.
[101] M. Fang, D. M. Kaschak, A. C. Sutorik, T. E. Mallouk, *J. Am. Chem. Soc.* **1997**, *119*, 12184.
[102] A. Klyszcz, M. Lauer, J.-H. Fuhrhop, unpublished results.
[103] A. Neuhaus, *Fortschr. Mineral.* **1950/51**, *29/30*, 138.
[104] L. Pauling, *J. Am. Chem. Soc.* **1935**, *57*, 2680.
[105] G. A. Jeffrey, W. Saenger, *Hydrogen Bonding in Biological Structures*, Springer, Heidelberg, **1991**, p. 425.
[106] P. T. Beurskens, G. A. Jeffrey, *J. Chem. Phys.* **1964**, *40*, 2800.
[107] S. M. Jackson, V. M. Nield, R. W. Whitworth, M. Oguro, C. C. Wilson, *J. Phys. Chem. B* **1997**, *101*, 6142.
[108] a) D. E. Brown, S. M. George, *J. Phys. Chem.* **1996**, *100*, 15460; b) Y. Lilach, L. Romm, T. Livnch, M. Asscher, *J. Phys. Chem. B* **2001**, *105*, 2736.
[109] K. A. T. Silverstein, A. D. J. Haymet, K. A. Dill, *J. Am. Chem. Soc.* **1998**, *120*, 3166.
[110] M. M. Teeter, S. M. Roe, N. H. Heo, *J. Mol. Biol.* **1993**, *230*, 292.
[111] L. J. Barbour, G. W. Orr, J. L. Atwood, *Nature* **1998**, *393*, 671.
[112] M. Vossen, F. Forstmann, *J. Chem. Phys.* **1994**, *101*, 2379.
[113] K. Ariga, T. Kunitake, *Acc. Chem. Res.* **1998**, *31*, 371.
[114] J.-H. Fuhrhop, T. Bedurke, M. Gnade, J. Schneider, K. Doblhofer, *Langmuir* **1997**, *13*, 455.
[115] G. Li, J.-H. Fuhrhop, *Angew. Chem.*, in press.
[116] N. Arun, S. Vasudevan, K. V. Ramanathan, *J. Am. Chem. Soc.* **2000**, *122*, 6028.
[117] a) H. S. Frank, W. M. Evans, *J. Chem. Phys.* **1945**, *13*, 507; b) J. Israelachvili, H. Wennerstroem, *Nature* **1996**, *379*, 219; c) R. U. Lemieux, *Acc. Chem. Res.* **1996**, *29*, 373; d) B. Kirchner, D. J. Searles, A. J. Dyson, P. S. Vogt, H. Huber, *J. Am. Chem. Soc.* **2000**, *122*, 5379.
[118] J. Turkevich, P. C. Stevenson, J. Hillier, *Faraday Discuss.* **1951**, *11*, 55.
[119] S. Biggs, P. Mulvaney, C. F. Zukoski, F. Grieser, *J. Am. Chem. Soc.* **1994**, *116*, 9150.
[120] K. C. Grabar, R. G. Freeman, M. B. Hommer, M. J. Natan, *Anal. Chem.* **1995**, *67*, 735.
[121] A. C. Templeton, W. P. Wuelfing, R. W. Murray, *Acc. Chem. Res.* **2000**, *33*, 27.
[122] J. Davies, *J. Phys. Chem.* **1929**, *33*, 276.
[123] M. Lahav, V. Heleg-Shabtai, J. Wasserman, E. Katz, I. Willner, H. Dürr, Y.-Z. Hu, S. H. Bossmann, *J. Am. Chem. Soc.* **2000**, *122*, 11480.
[124] D. E. Green, L. H. Stickland, *Biochem. J.* **1934**, *28*, 898.
[125] B. V. Koryakin, T. S. Dzhabier, A. E. Shilov, *Dokl. Akad. Nauk SSSR* **1977**, *233*, 620.
[126] W. P. McConnell, J. P. Novak, L. C. Brousseau III, R. R. Fuierer, R. C. Tenent, D. L. Feldheim, *J. Phys. Chem. B* **2000**, *104*, 8925.
[127] S. M. Marinakos, D. A. Shultz, D. L. Feldheim, *Adv. Mater.* **1999**, *11*, 34.
[128] C. A. Mirkin, R. L. Letsinger, R. C. Mucic, J. J. Storkoff, *Nature* **1996**, *382*, 607.
[129] A. N. Shipway, M. Lahav, I. Willner, *Adv. Mater.* **2000**, *12*, 993.
[130] a) K. R. Brown, A. P. Fox, M. J. Natan, *J. Am. Chem. Soc.* **1996**, *118*, 1154; b) K. C. Grabar, K. J. Allison, B. E. Baker, R. M. Bright, K. R. Brown, R. G. Freeman, A. P. Fox, C. D. Keating, M. D. Musick, M. J. Natan, *Langmuir* **1996**, *12*, 2353; c) A. Gole, C. Dash, V. Ramakrishnan, S. R. Sainkar, A. B. Mandale, M. Rao, M. Sastry, *Langmuir* **2001**, *17*, 1674.
[131] G. Decher in *Comprehensive Supramolecular Chemistry*, *Vol. 9* (Ed.: J.-M. Lehn), Pergamon, Oxford, **1996**, p. 507.
[132] C. Tedeschi, H. Möhwald, S. Kirstein, *J. Am. Chem. Soc.* **2001**, *123*, 954.
[133] J. H. Fendler, *Membrane Mimetic Chemistry*, Wiley, New York, **1982**.

Functionalization of Single-Walled Carbon Nanotubes

Andreas Hirsch*

Abstract: Through chemical functionalization of single-walled carbon nanotubes, the prerequisites for possible applications of such nanostructures are established. The derivatized tubes differ from the crude materials in their good solubility, which enables both a more extensive characterization and subsequent chemical reactivity. Current derivatization methods include defect and covalent sidewall functionalization, as well as noncovalent exo- and endohedral functionalization. In this way, for example, a range of nanotubes can be prepared: with sidewall substituents, wrapped with polymers, or with guest molecules included. The current state of the literature is presented in this Minireview.

1. Introduction

Research into carbon nanotubes has, in the past, mainly concentrated on the investigation of their physical properties.[1–4] The size of these macromolecular carbon allotropes and the continuous development of the fields of scanning tunneling microscopy and electron spectroscopy has made it possible to conduct precise investigations of individual molecules. Thus it was demonstrated that carbon nanotubes possess an array of unprecedented structural, mechanical, and electronic properties. For example, carbon nanotubes can exhibit metallic conductivity at the same time as: a) chemical and thermal stability, b) extremely high tensile strength and elasticity, c) the ability to absorb gas molecules as nanocapillaries, d) solubility when treated with surfactants, and e) the potential of further chemical functionalization. Uniquely, these are stable organic molecules that require no additional doping to become metallic conductors. Once this property profile was known, the question of technological applications quickly arose. In reaching this goal, however, it is necessary that not only single molecules, but also large ensembles, of the most pure and uniform nanotubes possible can be manipulated and investigated by analytical methods. This goal is currently a great challenge for chemists and materials scientists. In this context, chemical functionalization is an especially attractive target, as it can improve solubility[5] and processibility and allows the unique properties of single-walled nanotubes (SWNTs) to be coupled to those of other types of materials. Carbon nanotubes can be divided into SWNTs and multi-walled nanotubes (MWNTs). In this Minireview, the focus is on SWNTs, as their monomolecular character and the related simpler structure, and easier handling for chemical functionalization make them especially interesting (Figure 1).

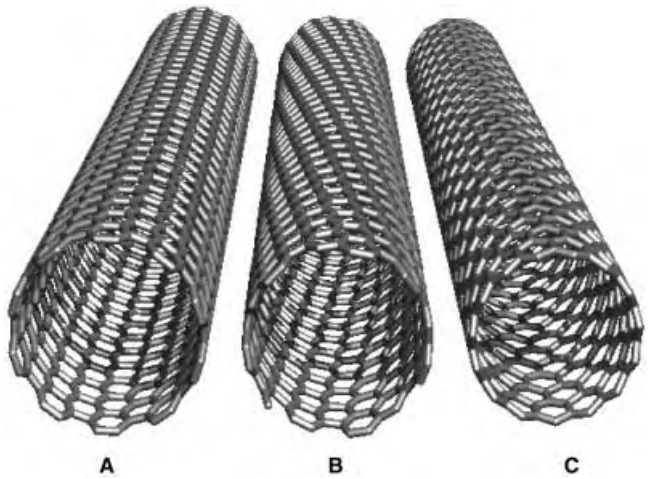


Figure 1. Idealized representation of defect-free (*n*,*m*) SWNTs with open ends. A) A metallic conducting (10,10) tube ("armchair"), B) a chiral, semiconducting (12,7) tube, and C) a conducting (15,0) tube ("zigzag"). The armchair (A) and zigzag (C) tubes are achiral. All the (*n*,*n*) armchair tubes are metallic, whilst this is only the case with chiral or zigzag tubes if $(n-m)/3$ is a whole number, otherwise, they are semiconductors.[1–4]

2. Synthesis and Purification of SWNTs

Several methods are known for the synthesis of SWNTs.[4] The first synthesis proceeded by arc discharge of graphite in the presence of metal catalysts (e.g. Fe, Co, Ni)[4]. Alternative routes are based on the laser vaporization of graphite–Ni–Co mixtures or chemical vapor deposition (CVD), in which carbon sources such as acetylene, metallocenes, $Fe(CO)_5$/C_2H_2, and CO can be used.[4] With one particular method, in which CO serves as the carbon source, very thin nanotubes

[*] Prof. Dr. A. Hirsch
Institut für Organische Chemie
der Universität Erlangen-Nürnberg
Henkestrasse 42, 91054 Erlangen (Germany)
Fax: (+49) 9131-852-68-64
E-mail: Hirsch@organik.uni-erlangen.de

 © WILEY-VCH Verlag GmbH, 69451 Weinheim, Germany, 2002 1433-7851/02/4111-1853 $ 20.00+.50/0

(HiPCO tubes) can be produced.[6] Milligram to gram quantities can currently be manufactured by using such routes, within a matter of hours. The raw material that results contains up to 70% SWNTs by weight. The contaminants are mainly amorphous carbon and catalyst particles, which can be removed by treatment with oxidizing acids,[1–7] microfiltration,[8] or chromatographic procedures.[9, 10]

3. Structural and Physical Properties

What do the nanotubes we obtain look like? Are they well-defined molecules, as is the case with the fullerenes, or polydisperse mixtures? It appears that the situation is much more complicated than with other macromolecular systems because a) the SWNTs preferentially aggregate into bundles of different diameters (Figure 2), b) the nanotubes vary

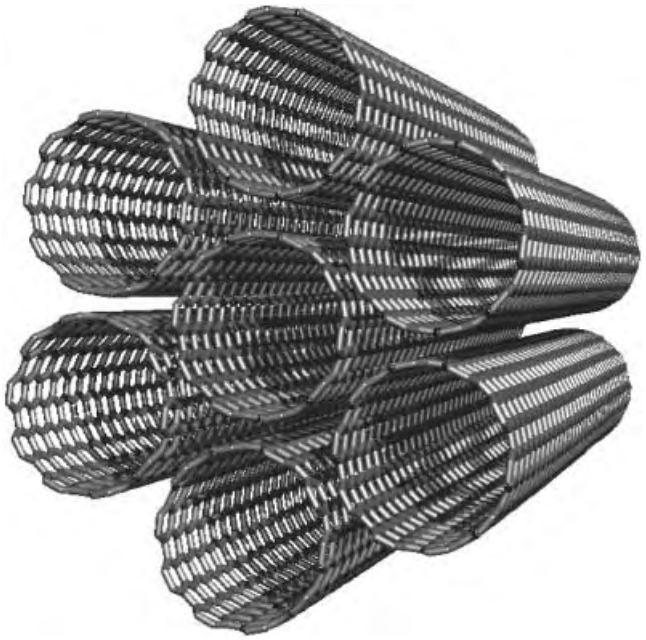


Figure 2. An idealized bundle of (10,10) nanotubes. In such bundles individual tubes are held together with strong $\pi-\pi$-stacking interactions. Almost all the tubes are organized in bundles in a typical sample.

greatly in length, c) the diameters of the nanotubes themselves can vary, d) the nanotubes possess a range of helicities, and e) defects occur, both at the tube ends and on the sidewalls (Figure 3).[11] The probability of finding a pair of identical tubes in a normal macroscopic sample of SWNTs is extremely small.

This multitude of possibilities highlights the difficulties that occur in the structural characterization of the resulting mixtures. Enrichment of particular structural forms by use of classical separation techniques (for example, separation according to length, by use of centrifugation) is only possible within narrow limits. The spectroscopic characteristics of subsequently derivativatized nanotubes will always give the average of a polydisperse mixture. Past a certain length, the electronic properties of nanotubes are independent of their

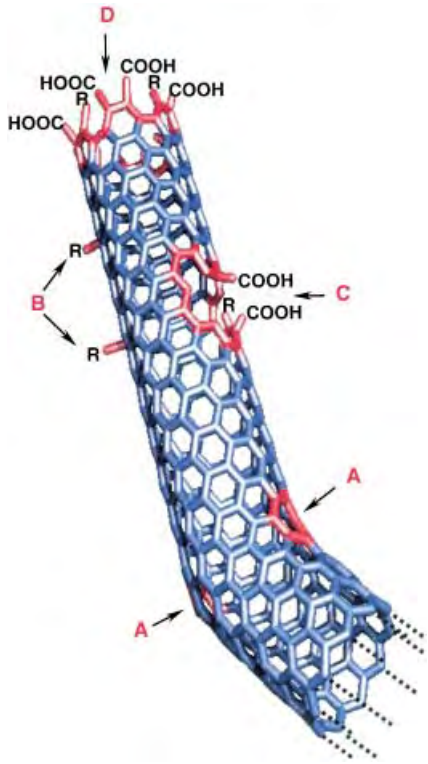


Figure 3. Typical defects in a SWNT: A) five- or seven-membered rings in the C framework, instead of the normal six-membered ring, leads to a bend in the tube, B) sp^3-hybridized defects (R = H and OH), C) C framework damaged by oxidative conditions, which leaves a hole lined with -COOH groups, and D) open end of the SWNT, terminated with -COOH groups. Besides carboxy termini, the existence of which has been unambigously demonstrated, other terminal groups such as $-NO_2$, OH, H, and =O are possible.

length.[11] Therefore, only diameter, helicity, and defects will be considered in the following section, which contains an analysis of structure–property relationships.

3.1. Diameter and Helicity

The electronic properties of carbon nanotubes depend primarily on the roll-up vector $C_h = n a_1 + m a_2$ (Figure 4)[11] and thus on the diameter and helicity. The rolling-up of a 2D graphite sheet to a quasi-1D nanotube causes the formation of so-called van Hove singularities, which are energy levels with a significantly high density of states. Only in some cases, such as (10,10) or (15,0) tubes, does a finite density of states occur at the Fermi level, which results in metallic conductivity. In a typical sample of SWNTs, there is a continuous distribution of tubes with different roll-up vectors.[11] The diameter of the SWNTs lies typically in the range 1–2 nm.[1, 4] In contrast, the diameter of HiPCO tubes is about 0.7 nm.[6]

3.2. Defects

Some defects of the six-membered-ring carbon structure of the nanotubes, such as the inclusion of five- or seven-membered rings in the carbon network, stem from the initial

 © WILEY-VCH Verlag GmbH, 69451 Weinheim, Germany, 2002 1433-7851/02/4111-1854 $ 20.00+.50/0

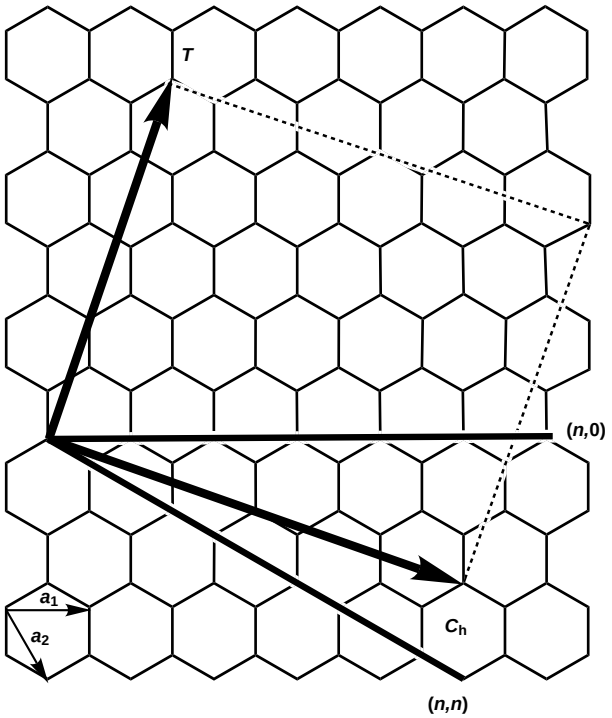


Figure 4. Schematic representation of a 2D graphite layer with the lattice vectors a_1 and a_2 and the roll-up vector $C_h = n a_1 + m a_2$. Achiral tubes exhibit roll-up vectors derived from $(n,0)$ (zigzag) or (n,n) (armchair). The translation vector T is parallel to the tube axis and defines the 1D unit cell. The rectangle represents an unrolled unit cell, defined by T and C_h. In this example, $(n,m) = (4,2)$.[1–4]

formation of the tubes (Figure 3A). No intact endcaps which, like fullerenes, possess a curvature enforced by the presence of five-membered rings, have been observed. The open ends of the tubes are often closed by particles of catalyst in the crude material. These catalyst particles can be removed by oxidative workup with, for example, HNO_3, which results in ends largely decorated with carboxy groups (Figure 3B).[7, 12–16] However, defects in the sidewalls can also be introduced under such drastic conditions. The appearance of carboxy groups in these positions[12, 13] can only be explained by the tube structure breaking open. Defects in SWNTs are important in the covalent chemistry of the tubes because they can either serve as anchor groups for further functionalization, or be created by the covalent attachment of further groups. The evidence collected to date indicates that nanotubes can tolerate a limited number of defects before a macroscopic sample loses its special electronic and mechanical properties.[15, 17, 18] Defects are therefore a promising starting point for the development of the covalent chemistry of SWNTs.

In recent years, several approaches to the functionalization of SWNTs have been developed, in both molecular and supramolecular chemistry. These approaches include defect functionalization, covalent functionalization of the sidewalls, noncovalent exohedral functionalization, for example, formation of supramolecular adducts with surfactants or polymers, and endohedral functionalization (Figure 5).

4. Defect-Group Chemistry

As mentioned in Section 2, the purification of SWNTs involves the removal of metal particles or amorphous carbon from the crude material by oxidative methods. Under harsh conditions, the SWNTs themselves are also attacked, which results in the formation of very short tubes (pipes) of lengths 100–300 nm.[7] These small nanotubes, 300 nm long and with a diameter of 1.4 nm, contain around 50000 C atoms in about 25000 benzene rings, which corresponds to a molecular weight of about 600000. These properties are similar to those of high-molecular-weight polymers. It was shown that defects are present in the sidewalls of these pipes, as well as at the open ends.[12, 13, 16] An analysis in which the evolution of CO or CO_2 upon heating the tubes was measured, demonstrated that about 5% of the C atoms in a pipe are localized at defects.[13] Reactive groups, suitable for further functionalization of the tubes, lie at these defect positions. Thus, long-chain alkylamines were coupled to carboxy groups activated with $SOCl_2$ (Scheme 1).[14, 15]

The functionalized tubes are more soluble in organic solvents than the starting material, so their spectroscopic characterization in the liquid phase is possible. The bundles of pipes are broken up into smaller bundles or individual tubes during the functionalization. The space available within most of the tubes is sufficient to allow the uptake of solvent molecules.[15] An IR spectroscopic estimate of the degree of

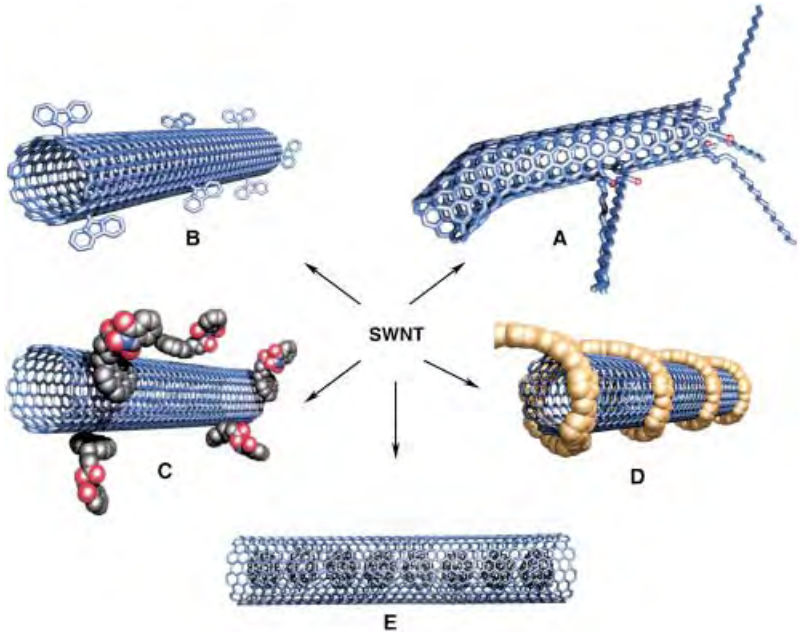
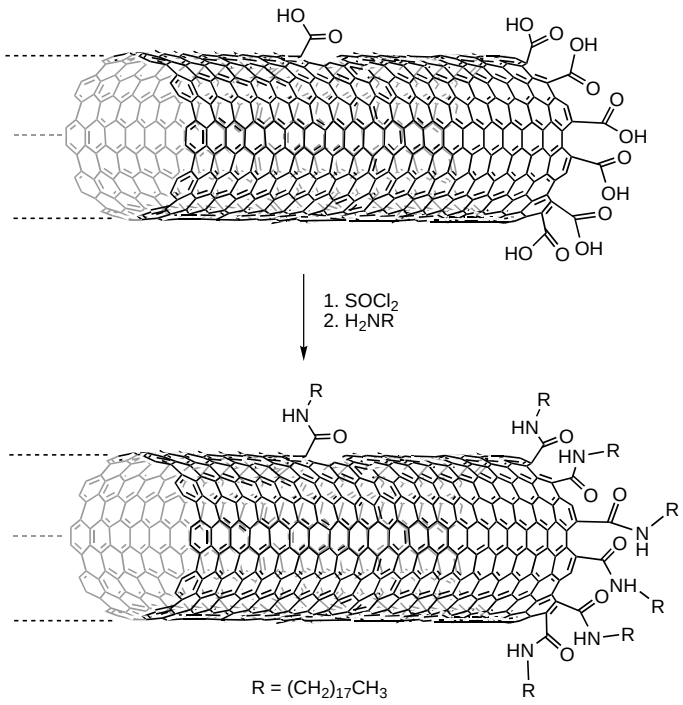


Figure 5. Functionalization possibilities for SWNTs: A) defect-group functionalization, B) covalent sidewall functionalization, C) noncovalent exohedral functionalization with surfactants, D) noncovalent exohedral functionalization with polymers, and E) endohedral functionalization with, for example, C_{60}. For methods B–E, the tubes are drawn in idealized fashion, but defects are found in real situations.

 © WILEY-VCH Verlag GmbH, 69451 Weinheim, Germany, 2002 1433-7851/02/4111-1855 $ 20.00+.50/0



Scheme 1. Defect-group functionalization of SWNTs with octadecylamine.[14]

functionalization of pipes that had been amidated with octadecylamine gave an mass percentage of $55 \pm 10\,\%$ for the added groups; this is a mole fraction of 6 %.[12] This high degree of functionalization suggests that a large proportion of the defect sites are located on the sidewalls. Polymers and dendrimers with terminal amino or hydroxy groups were coupled to activated tubes to give amides or esters.[19–23] Monolayers of SWNTs were deposited on surface-modified silicon wafers.[24] Moreover, functionalized SWNTs have been employed as tips for atomic-force microscopy by use of this technique.[25] When the unactivated carboxy groups of the tubes are treated with amines, ammonium salts result, which are also quite soluble in organic solvents.[15, 18] This reaction was also successful with uncut nanotubes, of lengths of over 1 μm.[18] In this case, the tubes were heated in molten long-chain amines. The electronic properties of the tubes remain essentially unaltered after functionalization. The yields of such ionic derivatives are around 30 %, which are considerably higher than those of the covalently functionalized amide systems (approximately 5 %).

5. Covalent Sidewall Functionalization

The systematic development of fullerene chemistry has shown that their reactivity in addition reactions depends very strongly on the curvature of the fullerene.[26] An increase of the curvature of the carbon framework leads to a more pronounced pyramidalization of the sp^2-hybridized C atoms and therefore an increased tendency to undergo addition reactions. This effect is clear in the case of C_{70}, in which the [6,6] bonds at the poles are much more reactive than those around the flatter equatorial region. Efficient addition at the equator takes place only with very reactive species, such as arynes, carbenes, or halogens. Normally, SWNTs bear no caps at their poles, and consist instead of graphitic sidewalls, usually with defects. Thus, there are no strongly curved regions that could serve as reactive targets for direct additions. As the typical diameter of a SWNT (1 – 2 nm) is larger than that of a fullerene, its relative reactivity is even less than that of the flat regions in fullerenes. Further problems in reactions with SWNTs are their low solubility or dispersability, and their occurrence in bundles. Therefore, functionalization of the sidewalls by covalent-bond formation will only be successful if a highly reactive reagent is used. It has not been possible to make quantitative assessments of whether such additions take place preferentially on intact regions of the sidewalls or at pre-existing defect sites.

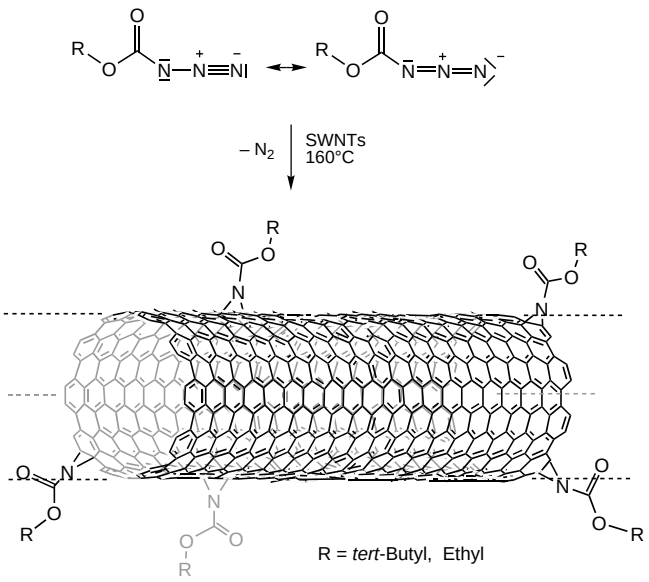
As discussed in Section 3, the sidewalls of freshly prepared SWNTs are partially attacked under oxidative workup.[12, 13, 16] This attack generates defect sites saturated, for example, with COOH groups. Because SWNT sidewalls are expected to be inert, fluorination was chosen for initial studies as it was described in the chemical transformation of graphite.[27] Highly pure SWNTs[28] were treated with elemental fluorine between 150 °C – 600 °C. For products synthesized at 600 °C, the degree of fluorination was 0.1 – 1. The covalent bond with fluorine was confirmed by IR spectroscopy, through the C–F valence vibration at 1220 – 1250 cm^{-1}. The fluorination of SWNTs has the consequence that their electronic properties change drastically. Whilst untreated samples of SWNTs exhibit high electrical conductivity, tubes fluorinated above 250 °C are insulators. Treatment of these tubes with hydrazine at room temperature causes defluorination. Raman spectroscopy of the defluorinated tubes showed that fluorination at higher temperatures is accompanied by partial fluorolysis of the carbon framework. Molecular modeling results from (10,0) tubes[29] suggested that the formation of a C–F bond is exothermic. The energy of a second C–F bond is highest when the bond forms adjacent to the first. The bond energy of a C–F bond on a tube is, however, lower than that of a C–F bond on an sp^3-hybridized C atom in an unstrained molecule. STM investigations of SWNTs with a fluorination degree of around 0.5 show that the fluorine atoms are grouped into very regular bandlike arrays.

The fluorinated SWNTs can be dissolved in alcohols by ultrasonication[30, 31] and hence become available for transformations using wet chemistry. In this way, the fluorine atoms in fluorinated SWNTs can be substituted for alkyl groups by treatment with alkyl lithium or Grignard compounds.[32] The resulting derivatized nanotubes are soluble, for example, in chloroform (0.6 $mg\,mL^{-1}$) and exhibit a degree of alkylation of about 0.1.

The direct sidewall functionalization of SWNTs with organic groups is possible by reactive species such as nitrenes, carbenes, and radicals.[14, 33] For example, the thermal reaction of azidoformiates leads to N_2 extrusion and to aziridino-SWNTs (Scheme 2), which dissolve in organic solvents such as DMSO to give black solutions.[33]

Especially stable solutions of functionalized SWNTs are formed from the addition of nucleophilic carbenes.[33] In this case, no cyclopropanation occurs, rather, each added group is

 © WILEY-VCH Verlag GmbH, 69451 Weinheim, Germany, 2002 1433-7851/02/4111-1856 $ 20.00+.50/0



Scheme 2. Sidewall functionalization of SWNTs with alkyl azidoformiates.[33]

bound through just one covalent bond to the tube and is positively charged. One negative charge per added group is transferred to the nanotube framework, as in the analogous reactions with C_{60}. The high solubility of the carbene adducts can be explained through mutual, electrostatic repulsion of the tubes.

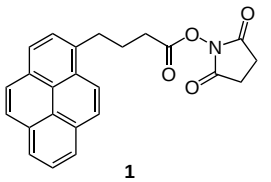
The reaction products of direct sidewall functionalizations can be characterized in solution, for example, by NMR and absorption spectroscopy. Atomic-force micropscopy shows that the original bundles of SWNTs are broken up in the course of adduct formation.[33]

In a similar fashion, SWNTs were functionalized by reaction with azomethinylides.[34] The degree of functionalization of the resulting pyrrolidines is very high, which causes a high solubility in organic solvents.

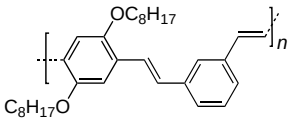
In one other example of sidewall functionalization, the electrical conductivity of SWNTs was exploited.[35] A solid film of SWNTs (bucky paper) served as the electrode for the electrochemical reduction of aryl diazonium salts. Here, aryl radicals were formed by the extrusion of N_2; these radicals then reacted with the tube walls. Addition degrees of up to 0.05 were recorded, that is, one in 20 C atoms in each nanotube bore an aryl substituent. As with other organonanotubes,[32] the added species could be removed by thermal treatment and the starting materials recovered.

6. Noncovalent Exohedral Functionalization

The formation of noncovalent aggregates with surfactants or wrapping with polymers have shown themselves to be suitable methods for the synthesis of functional SWNTs (Figure 5C, D). In the search for nondestructive purification methods, it has been shown that nanotubes can be transferred to the aqueous phase in the presence of surface-active molecules such as sodium dodecylsulfate (SDS) or benzylalkonium chloride.[8, 9, 36] It is believed that the nanotubes are in the hydrophobic interiors of the corresponding micelles, which results in stable dispersions. When the hydrophobic part of the amphiphile contains an aromatic group, an especially strong interaction results, because effective $\pi-\pi$-stacking interactions can then form with the graphitic sidewalls of the SWNTs. This effect was demonstrated in the aggregation with *N*-succinimidyl-1-pyrenebutanoate (**1**).[37] In these aggregates, the succinimidyl group could be substituted with amino groups from proteins such as ferritin or streptavidin, which caused immobilization of the biopolymers on the tubes. This effect could be interesting for the development of biosensors, because the electronic properties of the tubes can be combined with the recognition properties of the immobilized biosystems.



1



2

Direct, nonsurfactant-mediated immobilization of metallothionein proteins[38–40] and streptavidin[41] has also been carried out on MWNTs. The hydrophobic regions of the proteins are probably important for adsorption. A monoclonal antibody, specific for C_{60} fullerenes, could also be bound directly to SWNTs.[42] It was thus shown that the binding site of this IgG antibody is a domain of hydrophobic amino acids. Pronounced noncovalent interactions were also found between SWNTs and anilines[43] or amines.[44] This interaction was detected, for example, by the alteration of the electrical conductivity of SWNTs upon adsorption of primary amines, and through their very high solubility (up to 8 mg mL^{-1}) in anilines. Presumably, as in the case of C_{60} fullerenes,[45] donor–acceptor complexes are formed, as the curvature present in both classes of materials lends acceptor character to the corresponding molecular or macromolecular carbon networks.[46] The stable aniline solutions of SWNTs can be diluted with other organic solvents such as acetone, DMF, or THF, without causing precipitation of the tubes.

Polymers have also been used in the formation of supramolecular complexes of SWNTs. Thus, the suspension of purified tubes in the presence of polymers such as poly(*m*-phenylene-*co*-2,5-dioctoxy-*p*-phenylenevinylene) (PmPV, **2**), in organic solvents such as $CHCl_3$, leads to the polymer wrapping around the tubes (Figure 5D).[47–49] The properties of these supramolecular compounds are markedly different from those of the individual components. For example, the SWNT/PmPV complex exhibits a conductivity eight-times higher than that of the pure polymer, without any restriction of its luminescence properties. The stable solutions of the SWNT/PmPV complex can be characterized by UV/Vis and NMR spectroscopy. Atomic-force microscopy shows that the polymer coats the tubes uniformly. The small average diameter of the complexes (of around 7.1 nm) suggests that the bundles are mostly broken up on complex formation. The promising optoelectronic properties of the SWNT/PmPV

complexes have been used in the manufacture of photovoltaic devices.[48]

The wrapping of SWNTs with polymers that bear polar side-chains, such as polyvinylpyrrolidone (PVP) or polystyrenesulfonate (PSS), leads to stable solutions of the corresponding SWNT/polymer complexes in water.[50] The bundles are again broken up by complex formation in this case. The thermodynamic driving force for complex formation is the need to avoid unfavorable interactions between the apolar tube walls and the solvent water. A range of other, mostly ionic polymers, such as bovine serum albumin, are capable of coating SWNTs. Polymers such as poly(ethylene glycol) and poly(vinyl alcohol) are ineffective in this respect. It is thought that multi-helical wrapping of the tubes with the polymers is most favorable for reasons of strain. Changing to a less polar solvent such as THF causes the polymer complexes to dissociate once more. The SWNT/PVP complexes exhibit liquid-crystalline properties.

7. Endohedral Functionalization

The inner cavity of SWNTs offers space for the storage of guest molecules (Figure 5E). To date, the uptake and the endohedral chemistry of metals and metal salts have been intensively investigated.[51–56] For example, gold and platinum nanothreads have been created in the capillaries of the tubes, by treating the SWNTs with the corresponding perchlorometallic acids at high temperatures. In some cases, the resulting nanothreads are single crystals. The incorporation of fullerenes such as C_{60}[57, 58] (Figure 5) or metallofullerenes such as $Sm@C_{82}$[59] are especially impressive examples of the endohedral chemistry of SWNTs. This incorporation is executed at defect sites localized at the ends or in the sidewalls. The encapsulated fullerenes tend to form chains that are coupled by van der Waals forces. Such arrays are sometimes called "bucky peapods". Upon annealing, the encapsulated fullerenes coalesce in the interior of the SWNTs, which results in new, concentric, endohedral tubes, with a diameter of 0.7 nm. The progress of such reactions inside the tubes could be monitored in real time by use of high-resolution electron microscopy.[59]

8. Concluding remarks

The examples described of the functionalization of single-walled carbon nanotubes demonstrate that the chemistry of this new class of molecules is just beginning. The basis for the exploitation of macroscopic quantities of this carbon allotrope has been laid. The unique properties of SWNTs can now be coupled with those of other classes of material. For the successful future development of this research area, however, it is important to improve the quality of the nanotube raw material, with particular emphasis on the uniformity of the samples. Furthermore, comparative studies on individual nanotubes before and after functionalization are necessary, so that both the dependence of reactivity on electronic structure and the effect of chemical modification on the electrical and mechanical properties can be determined.

This work was supported by the European Union under the 5th Framework Programme 1999, HPRNT 1999-00011 FUNCARS.

Received: December 5, 2001 [M1535]

[1] P. M. Ajayan, *Chem. Rev.* **1999**, *99*, 1787 – 1799.
[2] S. S. Xie, B. H. Chang, W. Z. Li, Z. W. Pan, L. F. Sun, J. M. Mao, X. H. Chen, L. X. Qian, W. Y. Zhou, *Adv. Mater.* **1999**, *11*, 1135 – 1138.
[3] L. Dai, A. W. H. Mau, *Adv. Mater.* **2001**, *13*, 899 – 913.
[4] C. N. R. Rao, B. C. Satishkumar, A. Govindaraj, M. Nath, *ChemPhysChem* **2001**, *2*, 78 – 105.
[5] J. L. Bahr, E. T. Mickelson, M. J. Bronikowski, R. E. Smalley, J. M. Tour, *Chem. Commun.* **2001**, 193 – 194.
[6] P. Nikolaev, M. J. Bronikowski, R. K. Bradley, F. Rohmund, D. T. Colbert, K. A. Smith, R. E. Smalley, *Chem. Phys. Lett.* **1999**, *313*, 91 – 97.
[7] J. Liu, A. G. Rinzler, H. Dai, J. H. Hafner, R. K. Bradley, P. J. Boul, A. Lu, T. Iverson, K. Shelimov, C. B. Huffman, F. Rodriguez-Macias, Y.-S. Shon, T. R. Lee, D. T. Colbert, R. E. Smalley, *Science* **1998**, *280*, 1253 – 1256.
[8] S. Bandow, A. M. Rao, K. A. Williams, A. Thess, R. E. Smalley, P. C. Eklund, *J. Phys. Chem. B* **1997**, *101*, 8839 – 8842.
[9] G. S. Duesberg, M. Burghard, J. Muster, G. Philipp, S. Roth, *Chem. Commun.* **1998**, 435 – 436.
[10] M. Holzinger, A. Hirsch, P. Bernier, G. S. Duesberg, M. Burghard, *Appl. Phys. A* **2000**, *70*, 599 – 602.
[11] T. W. Odom, J.-L. Huang, P. Kim, C. M. Lieber, *J. Phys. Chem. B* **2000**, *104*, 2794 – 2809.
[12] M. A. Hamon, H. Hu, P. Bhowmik, S. Niyogi, B. Zhao, M. E. Itkis, R. C. Haddon, *Chem. Phys. Lett.* **2001**, *347*, 8 – 12.
[13] D. B. Mawhinney, V. Naumenko, A. Kuznetsova, J. T. Yates, J. Liu, R. E. Smalley, *Chem. Phys. Lett.* **2000**, *324*, 213 – 216.
[14] J. Chen, M. A. Hamon, H. Hu, Y. Chen, A. M. Rao, P. C. Eklund, R. C. Haddon, *Science* **1998**, *282*, 95 – 98.
[15] M. A. Hamon, J. Chen, H. Hu, Y. Chen, M. E. Itkis, A. M. Rao, P. C. Eklund, R. C. Haddon, *Adv. Mater.* **1999**, *11*, 834 – 840.
[16] M. Monthioux, B. W. Smith, B. Burteaux, A. Claye, J. E. Fischer, D. E. Luzzi, *Carbon* **2001**, *39*, 1251 – 1272.
[17] A. Kukovecz, C. Kramberger, M. Mannsberger, H. Kuzmany, M. Holzinger, A. Hirsch, *J. Phys. Chem. B*, in press.
[18] J. Chen, A. M. Rao, S. Lyuksyutov, M. E. Itkis, M. A. Hamon, H. Hu, R. W. Cohn, P. C. Eklund, D. T. Colbert, R. E. Smalley, R. C. Haddon, *J. Phys. Chem. B* **2001**, *105*, 2525 – 2528.
[19] J. E. Riggs, Z. Guo, D. L. Carroll, Y.-P. Sun, *J. Am. Chem. Soc.* **2000**, *122*, 5879 – 5880.
[20] Y.-P. Sun, W. Huang, Y. Lin, K. Fu, A. Kitaygorodskiy, L. A. Riddle, Y. J. Yu, D. L. Carroll, *Chem. Mater.* **2001**, *13*, 2864 – 2869.
[21] K. Fu, W. Huang, Y. Lin, L. A. Riddle, D. L. Carroll, Y.-P. Sun, *Nano Lett.* **2001**, *1*, 439 – 441.
[22] M. Sano, A. Kamino, J. Okamura, S. Shinkai, *Langmuir* **2001**, *17*, 5125 – 5128.
[23] "Electronic Properties of Novel Materials—Molecular Nanostructures": M. Holzinger, A. Hirsch, P. Bernier, G. S. Duesberg, M. Burghard, *AIP Conf. Proc.* **2000**, *544*, 246 – 249.
[24] D. Chattopadhyay, I. Galeska, F. Papadimitrakopoulos, *J. Am. Chem. Soc.* **2001**, *123*, 9451 – 9452.
[25] S. S. Wong, A. T. Woolley, E. Joselevich, C. L. Cheung, C. M. Lieber, *J. Am. Chem. Soc.* **1998**, *120*, 8557 – 8558.
[26] A. Hirsch, *Top. Curr. Chem.* **1999**, *199*, 1 – 65.
[27] E. T. Mickelson, C. B. Huffman, A. G. Rinzler, R. E. Smalley, R. H. Hauge, J. L. Margrave, *Chem. Phys. Lett.* **1998**, *296*, 188 – 194.
[28] A. Thess, R. Lee, P. Nikolaev, H. Dai, P. Petit, J. Robert, C. Xu, Y. H. Lee, S. G. Kim, *Science* **1996**, *273*, 483 – 487.
[29] C. W. Bauschlicher, *Chem. Phys. Lett.* **2000**, *322*, 237 – 241.
[30] K. F. Kelly, I. W. Chiang, E. T. Mickelson, R. H. Hauge, J. L. Margrave, X. Wang, G. E. Scuseria, C. Radloff, N. J. Halas, *Chem. Phys. Lett.* **1999**, *313*, 445 – 450.

 © WILEY-VCH Verlag GmbH, 69451 Weinheim, Germany, 2002 1433-7851/02/4111-1858 $ 20.00+.50/0

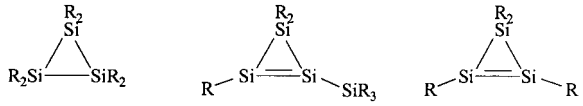
[31] E. T. Mickelson, I. W. Chiang, J. L. Zimmerman, P. J. Boul, J. Lozano, J. Liu, R. E. Smalley, R. H. Hauge, J. L. Margrave, *J. Phys. Chem. B* **1999**, *103*, 4318 – 4322.
[32] P. J. Boul, J. Liu, E. T. Mickelson, C. B. Huffman, L. M. Ericson, I. W. Chiang, K. A. Smith, D. T. Colbert, R. H. Hauge, J. L. Margrave, R. E. Smalley, *Chem. Phys. Lett.* **1999**, *310*, 367 – 372.
[33] M. Holzinger, O. Vostrowsky, A. Hirsch, F. Hennrich, M. Kappes, R. Weiss, F. Jellen, *Angew. Chem.* **2001**, *113*, 4132 – 4136; *Angew. Chem. Int. Ed.* **2001**, *40*, 4002 – 4005.
[34] V. Georgakilas, K. Kordatos, M. Prato, D. M. Guldi, M. Holzinger, A. Hirsch, *J. Am. Chem. Soc.* **2002**, *124*, 760 – 761.
[35] J. L. Bahr, J. Yang, D. V. Kosynkin, M. J. Bronikowski, R. E. Smalley, J. M. Tour, *J. Am. Chem. Soc.* **2001**, *123*, 6536 – 6542.
[36] V. Krstic, G. S. Duesberg, J. Muster, M. Burghard, S. Roth, *Chem. Mater.* **1998**, *10*, 2338 – 2340.
[37] R. J. Chen, Y. Zhang, D. Wang, H. Dai, *J. Am. Chem. Soc.* **2001**, *123*, 3838 – 3839.
[38] S. C. Tsang, J. J. Davis, M. L. H. Green, H. A. O. Hill, Y. C. Leung, P. J. Sadler, *J. Chem. Soc. Chem. Commun.* **1995**, 2579.
[39] S. C. Tsang, Z. Guo, Y. K. Chen, M. L. H. Green, H. A. O. Hill, T. W. Hambley, P. J. Sadler, *Angew. Chem.* **1997**, *109*, 2292 – 2294; *Angew. Chem. Int. Ed. Engl.* **1997**, *36*, 2198 – 2200.
[40] Z. Guo, P. J. Sadler, S. C. Tsang, *Adv. Mater.* **1998**, *10*, 701 – 703.
[41] F. Balavoine, P. Schultz, C. Richard, V. Mallouh, T. W. Ebbesen, C. Mioskowski, *Angew. Chem.* **1999**, *111*, 2036 – 2039; *Angew. Chem. Int. Ed.* **1999**, *38*, 1912 – 1915.
[42] B. F. Erlanger, B.-X. Chen, M. Zhu, L. Brus, *Nano Lett.* **2001**, *1*, 465 – 467.
[43] Y. Sun, S. R. Wilson, D. I. Schuster, *J. Am. Chem. Soc.* **2001**, *123*, 5348 – 5349.
[44] J. Kong, H. Dai, *J. Phys. Chem. B* **2001**, *105*, 2890 – 2893.
[45] A. Hirsch, *Chemistry of the Fullerenes*, Thieme, New York, **1994**.
[46] M. A. Hamon, M. E. Itkis, S. Niyogi, T. Alvaraez, C. Kuper, M. Menon, R. C. Haddon, *J. Am. Chem. Soc.* **2001**, *123*, 11292 – 11293.
[47] S. A. Curran, P. M. Ajayan, W. J. Blau, D. L. Carroll, J. N. Coleman, A. B. Dalton, A. P. Davey, A. Drury, B. McCarthy, S. Maier, A. Strevens, *Adv. Mater.* **1998**, *10*, 1091 – 1093.
[48] A. Star, J. F. Stoddart, D. Steuerman, M. Diehl, A. Boukai, E. W. Wong, X. Yang, S.-W. Chung, H. Choi, J. R. Heath, *Angew. Chem.* **2001**, *113*, 1771 – 1775; *Angew. Chem. Int. Ed.* **2001**, *40*, 1721 – 1725.
[49] J. N. Coleman, A. B. Dalton, S. Curran, A. Rubio, A. P. Davey, A. Drury, B. McCarthy, B. Lahr, P. M. Ajayan, S. Roth, R. C. Barklie, W. J. Blau, *Adv. Mater.* **2000**, *12*, 213 – 216.
[50] M. J. O'Connell, P. Boul, L. M. Ericson, C. Huffman, Y. Wang, E. Haroz, C. Kuper, J. Tour, K. D. Ausman, R. E. Smalley, *Chem. Phys. Lett.* **2001**, *342*, 265 – 271.
[51] W. Han, S. Fan, Q. Li, Y. Hu, *Science* **1997**, *277*, 1287 – 1289.
[52] J. Sloan, J. Hammer, M. Zwiefka-Sibley, M. L. H. Green, *Chem. Commun.* **1998**, 347 – 348.
[53] E. Dujardin, T. W. Ebbesen, A. Krishnan, M. M. J. Treacy, *Adv. Mater.* **1998**, *10*, 1472 – 1475.
[54] K. Matsui, B. K. Pradhan, T. Kyotani, A. Tomita, *J. Phys. Chem. B* **2001**, *105*, 5682 – 5688.
[55] A. Govindaraj, B. C. Satishkumar, M. Nath, C. N. R. Rao, *Chem. Mater.* **2000**, *12*, 202 – 205.
[56] M. Wilson, P. A. Madden, *J. Am. Chem. Soc.* **2001**, *123*, 2101 – 2102.
[57] B. W. Smith, M. Monthioux, D. E. Luzzi, *Chem. Phys. Lett.* **1999**, *315*, 31 – 36.
[58] B. W. Smith, D. E. Luzzi, *Chem. Phys. Lett.* **2000**, *321*, 169 – 174.
[59] T. Okazaki, K. Suenaga, K. Hirahara, S. Bandow, S. Iijima, H. Shinohara, *J. Am. Chem. Soc.* **2001**, *123*, 9673 – 9674.

 © WILEY-VCH Verlag GmbH, 69451 Weinheim, Germany, 2002 1433-7851/02/4111-1859 $ 20.00+.50/0

A Spiropentasiladiene and Other Strained Silicon-Containing Rings

Rainer Koch and Manfred Weidenbruch*

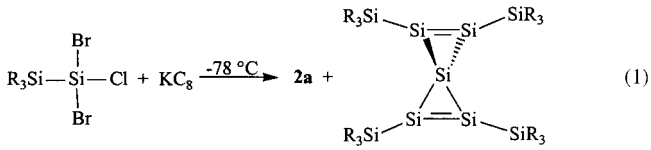
Although the chemistry of unsaturated silicon compounds and small rings containing silicon atoms has experienced a rapid development over the past 25 years, silicon chemistry is still far removed from the broad chemistry of its homologue carbon. Whereas cyclopropanes and cyclopropenes represent well known classes of compounds, the synthesis of the first cyclotrisilane **1a** did not succeed until 1982. Masamune et al. prepared this compound from the reductive elimination of halogen from a diaryldichlorosilane.[1] The reason for the relatively late synthesis of cyclotrisilanes is the greater ring strain compared to that of the carbon analogues. This strain manifests itself in the facile light-induced cleavage of two Si–Si bonds under formation of disilenes $R_2Si{=}SiR_2$ and silylenes $R_2Si{:}$; the latter dimerize to afford further disilene. An exception is the highly strained cyclotrisilane **1b**, which under photolytical conditions decomposes into a disilene and a silylene, both of which could be characterized by numerous trapping reactions.[3, 4]



1a R = 2,6-$Me_2C_6H_3$ **2a** R = *t*$BuMe_2Si$ **2b** R = *t*Bu_2MeSi
1b R = *t*Bu

Very little is known about the chemical behavior of the first cyclotrisilenes **2a** and **b**, which were only recently synthesized by Kira et al. and Sekiguchi et al., **2b** was structurally characterized.[5, 6] A more detailed investigation of the dehalogenation of the oligosilane **3** revealed a surprising result; in addition to the main product **2a**, red crystals of the spiro pentasiladiene **4** could be isolated in 3.5% yield [Eq. (1)].[7]

Compound **4** is the first thermally stable spiropentadiene comprising Group 14 elements. Even though the analogous carbon spiro compound C_5H_4, as well as the 1,1′-dichloro derivative could indeed be generated, both molecules decompose in solution within minutes, even at temperatures below $-100\,^{\circ}C$.[8, 9] The most striking feature of the structure of **4** is

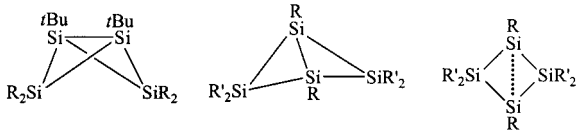


3 R = *t*$BuMe_2Si$ **4** (1)

the twisting of the two halves of the molecule by 78.26°. This arrangement allows through-space interactions between the π orbitals as well as the π* orbitals of both double bonds and leads to the breaking of the degeneracy of these orbitals. The energy values calculated for the interactions between the π as well as the π* orbitals of the parent compound Si_5H_4 with D_2 symmetry are reflected by the electronic spectrum, where the longest wavelength absorptions of **4** at 560 nm and 500 nm are shifted bathochromically compared to the cyclotrisilenes **2a** (482 nm) and **2b** (466 nm).[10]

A further achievement of the Kira group is the preliminary solution to another problem of silicon chemistry: the bond-stretch isomerism in tetrasilabicyclo[1.1.0]butanes. A number of theoretical investigations had predicted the existence of two bond-stretch isomers of these compounds, in which the bond lengths between the bridge-head atoms differ. The molecule containing a short "central" bond was considered to be a classical molecule with closed shells, with the length of the bridge bond in the range typical for Si–Si single bonds. On the other hand, this bond was expected to be markedly stretched in the second isomer, where the central bond was predicted to exhibit a noticeable singlet biradical character.[11, 12] The substituents at the bridge-head atoms are expected to have a significant influence over the bond length. In this context, medium sized groups, such as the methyl group, should be suitable candidates for the observation of bond-stretch isomerism in substituted tetrasilabicyclo[1.1.0]-butane compounds.[11g]

The as yet only structurally confirmed tetrasilabicyclo-[1.1.0]butane **5** exhibits a transanular Si–Si separation of merely 237.3 pm, apparently a result of the bulky *tert*-butyl groups at the bridge-head atoms, and is thus classified as an

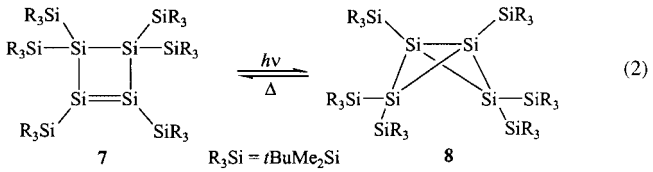


5 R = 2,6-$Et_2C_6H_3$ **6a** **6b**

[*] Prof. Dr. M. Weidenbruch, Dr. R. Koch
Fachbereich Chemie der Universität
Carl-von-Ossietzky-Strasse 9–11, 26111 Oldenburg (Germany)
Fax: (+49) 441-798-3352
E-mail: manfred.weidenbruch@uni-oldenburg.de

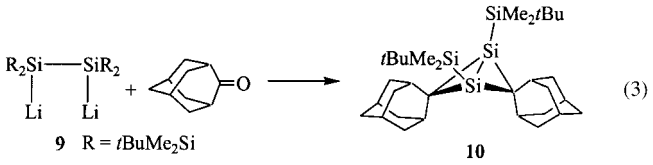
 © WILEY-VCH Verlag GmbH, 69451 Weinheim, Germany, 2002 1433-7851/02/4111-1861 $ 20.00+.50/0

isomer containing a short central bond.[13] According to calculations carried out for the parent compound Si_4H_6, the isomer **6b** with its large transanular Si···Si separation of >280 pm and a dihedral angle of 142° for the Si_4 skeleton, is more stable than the classical isomer **6a**, for which no energy minimum was found.[11h] Another molecule, **8** also containing the bicyclo[1.1.0]butane framework, results from the photolysis of the tetrasilene **7** by a 1,2-silyl shift. However, even at ambient temperature **8** rearranges thermally back to compound **7** [Eq. (2)].[14]



(2)

A strong indication for the existence of a molecule with a long central Si–Si bond was obtained by Kira et al. for the 1,3-disilabicyclo[1.1.0]butane **10**, which was obtained by an as yet unknown mechanism from the treatment of the dilithiated compound **7** with adamantanone [Eq. (3)].[15]



(3)

The distance between the two central silicon atoms of 241 pm is rather long for an Si–Si bond. The dihedral angle between the two Si-C-Si planes is markedly opened with a value of 141.1°, whereas the Si-Si-R angle, which, in spite of the bulky substituents, has a value of 118.1°. DFT calculations for the model compounds **A** and **B** (Figure 1), which contain methyl and silyl groups instead of the adamantyl and *tert*-butyl substituents in **10**, reveal noticeable differences between those structures containing a long, and those containing a short central Si–Si bond. The central separation in **A** amounts to 244.8 pm (**B**: 220.1 pm), the dihedral angle is 141.5° (**B**: 126.7°) and the R-Si-Si angle is 106.9° (**B**: 152.1°). In analogy to calculations for the bicyclo[1.1.0]tetrasilane, the bond-stretch isomer with the larger separation is favored energetically. The newly observed structure of **10** corresponds far more to that of **A**, both in the solid state and in solution. Not only the separation as well as both angles, but also the chemical shifts of the ring atoms of the framework in the ^{13}C and ^{29}Si NMR spectra are in very good agreement with the calculated values.

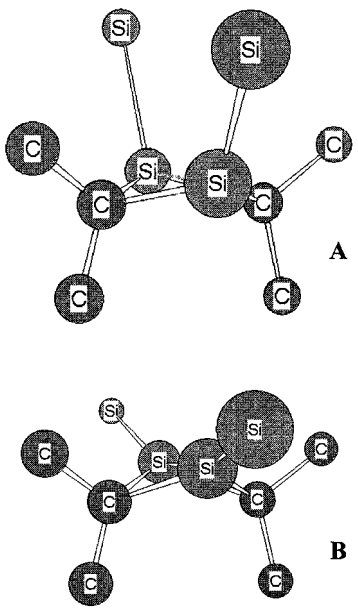
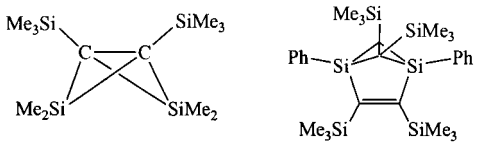


Figure 1. Model compounds **A** (long central Si–Si bond) and **B** (short central Si–Si bond). Hydrogen atoms are omitted.

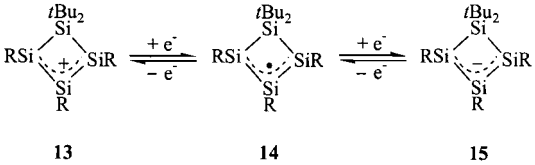
A characteristic feature of all the compounds with long bonds is, according to theoretical investigations, the singlet biradical character of this bond, which was confirmed by multiconfiguration self-consistent field (MCSCF) calculations.[11a] Moreover, low-lying antibonding Si–Si σ* orbitals allow for an efficient interaction with the HOMOs.

Towards the heavier Group 14 elements an increasing tendency to avoid strained three-membered rings in favor of four-membered rings is observed. The s orbitals contract relative to the p orbitals. Consequently only sp hybrid orbitals, which favor orthogonal arrangements, are formed (compare the R-Si-Si angles).[12]

Although bond-stretch isomerism has been considered for the corresponding carbon compounds, it still needs to be demonstrated experimentally.[16] A value of 175 pm was calculated for the isomer with the longer central C–C bond.[11a] This value is in good agreement with the very long C–C bond of 178.1 pm in the 2,4-disilabicyclo[1.1.0]butane derivative **11**.[17] A noticeably elongated C–C bond of 168.0 pm has been observed in the disilabenzvalene **12** which also contains this structural element.[18]



It can be anticipated from the recent work of Sekiguchi et al. that the chemistry of small silicon rings will have further surprises to offer. In addition to the synthesis of the cyclotetrasilylenium ion **13**,[19] they succeeded for the first time in the isolation and complete characterization of the silyl radical **14**.[20] Further one-electron reduction finally resulted in the cyclotetrasilenide ion **15** [Eq. (4)],[21] of which only an analogous germanium compound had been known to exist.[22]



(4)

 © WILEY-VCH Verlag GmbH, 69451 Weinheim, Germany, 2002 1433-7851/02/4111-1862 $ 20.00+.50/0 *Angew. Chem. Int. Ed.* **2002**, *41*, No. 11

[1] S. Masamune, Y. Hanzawa, S. Murakami, T. Bally, J. F. Blount, *J. Am. Chem. Soc.* **1982**, *104*, 1150.
[2] a) A. F. Sax, *Chem. Phys. Lett.* **1986**, *127*, 163; b) A. F. Sax, *Chem. Phys. Lett.* **1986**, *129*, 66.
[3] A. Schäfer, M. Weidenbruch, K. Peters, H. G. von Schnering, *Angew. Chem.* **1984**, *96*, 311; *Angew. Chem. Int. Ed. Engl.* **1984**, *23*, 302.
[4] For recent reviews see: a) T. Tsumuraya, S. A. Batcheller, S. Masamune, *Angew. Chem.* **1991**, *103*, 916; *Angew. Chem. Int. Ed. Engl.* **1991**, *30*, 902; b) M. Weidenbruch, *Chem. Rev.* **1995**, *95*, 1479.
[5] T. Iwamoto, C. Kabuto, M. Kira, *J. Am. Chem. Soc.* **1999**, *121*, 886.
[6] M. Ichinohe, T. Matsumo, A. Sekiguchi, *Angew. Chem.* **1999**, *111*, 2331; *Angew. Chem. Int. Ed.* **1999**, *38*, 2194.
[7] T. Iwamoto, M. Tamura, C. Kabuto, M. Kira, *Science* **2000**, *290*, 504.
[8] W. E. Billups, M. M. Haley, *J. Am. Chem. Soc.* **1991**, *113*, 5084.
[9] R. K. Saini, V. A. Litosh, A. D. Daniels, W. E. Billups, *Tetrahedron Lett.* **1999**, *40*, 6157.
[10] Recent reviews on disilenes: a) R. Okazaki, R. West, *Adv. Organomet. Chem.* **1996**, *39*, 231; b) M. Weidenbruch in *The chemistry of organic silicon compounds*, *Vol. 3* (Eds.: Z. Rappoport, Y. Apeloig), Wiley, Chichester, UK, **2001**, p. 391.
[11] Theoretical investigations of tetrasilabicyclo[1.1.0]butanes: a) P. von R. Schleyer, A. F. Sax, J. Kalcher, R. Janoschek, *Angew. Chem.* **1987**, *89*, 374; *Angew. Chem. Int. Ed. Engl.* **1987**, *26*, 364; b) W. W. Schöller, T. Dabisch, T. Busch, *Inorg. Chem.* **1987**, *26*, 4083; c) S. Nagase, T. Kudo, *J. Chem. Soc. Chem. Commun.* **1988**, 54; d) T. Kudo, S. Nagase, *J. Chem. Phys.* **1989**, *93*, 2888; e) D. B. Kitchen, J. E. Jackson, L. C. Allen, *J. Am. Chem. Soc.* **1990**, *112*, 3407; f) J. A. Boatz, M. S. Gordon, *J. Phys. Chem.* **1992**, *96*, 7331; g) J. A. Boatz, M. S. Gordon, *Organometallics* **1996**, *15*, 2118; h) T. Müller in *Organosilicon Chemistry IV* (Eds.: N. Auner, J. Weis), Wiley-VCH, Weinheim, **2000**, p. 110.
[12] For recent reviews see: a) S. Nagase, *Acc. Chem. Res.* **1995**, *28*, 469; b) M.-M. Rohmer, M. Bénard, *Chem. Soc. Rev.* **2001**, *30*, 340.
[13] a) S. Masamune, Y. Kabe, S. Collins, D. J. Williams, R. Jones, *J. Am. Chem. Soc.* **1985**, *107*, 552; b) R. Jones, D. J. Williams, Y. Kabe, S. Masamune, *Angew. Chem.* **1986**, *98*, 176; *Angew. Chem. Int. Ed. Engl.* **1986**, *25*, 173.
[14] a) M. Kira, T. Iwamoto, C. Kabuto, *J. Am. Chem. Soc.* **1996**, *118*, 10303; b) T. Iwamoto, M. Kira, *Chem. Lett.* **1998**, 277.
[15] T. Iwamoto, D. Yin, C. Kabuto, M. Kira, *J. Am. Chem. Soc.* **2001**, *123*, 12730.
[16] a) W.-D. Stohrer, R. Hoffmann, *J. Am. Chem. Soc.* **1974**, *96*, 779; b) W.-D. Stohrer, R. Hoffmann, *J. Am. Chem. Soc.* **1974**, *96*, 1661; c) M. N. Paddon-Row, L. Radom, A. R. Gregory, *J. Chem. Soc. Chem. Commun.* **1976**, 477; d) A. R. Gregory, M. N. Paddon-Row, L. Radom, W.-D. Stohrer, *Aust. J. Chem.* **1977**, *30*, 473.
[17] G. Fritz, S. Wartenessian, E. Matern, W. Hönle, H. G. von Schnering, *Z. Anorg. Allg. Chem.* **1981**, *475*, 87.
[18] W. Ando, T. Shiba, T. Hidaka, K. Morihashi, O Kikuchi, *J. Am. Chem. Soc.* **1997**, *119*, 3629.
[19] A. Sekiguchi, T. Matsumo, M. Ichinohe, *J. Am. Chem. Soc.* **2000**, *122*, 11250.
[20] A. Sekiguchi, T. Matsumo, M. Ichinohe, *J. Am. Chem. Soc.* **2001**, *123*, 12436.
[21] T. Matsumo, M. Ichinohe, A. Sekiguchi, *Angew. Chem.* **2002**, *114*, 1668; *Angew. Chem. Int. Ed.* **2002**, *41*, 1559.
[22] H. Schäfer, W. Saak, M. Weidenbruch, *Angew. Chem.* **2000**, *112*, 3847; *Angew. Chem. Int. Ed.* **2000**, *39*, 3703.

Microwave-Assisted Reactions in Organic Synthesis—Are There Any Nonthermal Microwave Effects?

Nikolai Kuhnert*

Introduction

The development of resource- and environmentally friendly processes in terms of sustainable chemistry has become a focal point in chemical research in recent years. Of particular importance is a reduction in the amounts of solvents and hazardous substances required, and the more efficient use of energy.[1, 2] Synthetic chemists have neglected alternative sources of heat for chemical reactions, and still rely on isomantles, oil, sand and water baths, or heatguns as heating devices.

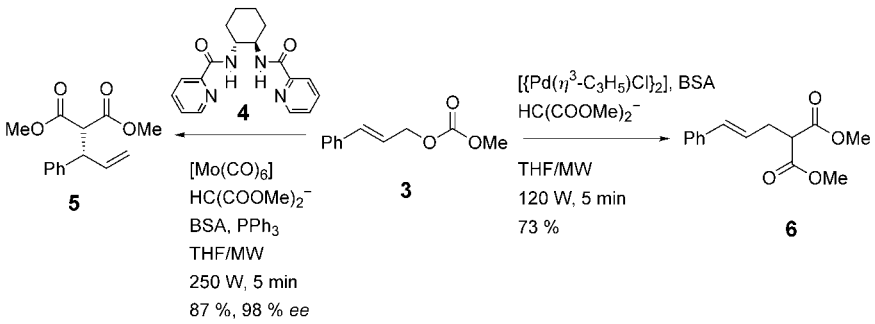
The use of microwave (MW) irradiation as a source of heat in synthetic chemistry offers a promising alternative. Microwaves differ from conventional heat sources, in that the solvents or reactants are directly heated without heating the reaction vessel. By conventional methods, the vessel is heated and this then transfers the heat by convection. Microwave heating is more efficient in terms of the energy used, produces a higher temperature homogeneity, and is considerably more rapid than conventional heat sources. The first application of microwave irradiation in chemical synthesis was published in 1986.[3] It is worth noting that the first commercial household microwave oven was introduced to the market in 1954, and that the transfer of microwave technology into the chemistry laboratory has taken the unusually long time of over three decades. In typical microwave ovens, the magnetrons (microwave generators) produce a microwave wavelength of 12.25 cm, which corresponds to a frequency of 2.45 GHz. The basic theory underlying the interaction of microwaves with macroscopic matter was formulated by von Hippel[4] and, for the basic equations, the reader is referred to this work and to an excellent overview by Mingos.[5]

Over the last decade, microwave-assisted chemistry has matured into a highly useful technique and provides an interesting alternative for heating chemical reactions. The large number of publications clearly indicates the development of this area of chemistry.[6–11]

[*] Dr. N. Kuhnert
Department of Chemistry
The University of Surrey
Guildford, GU2 7XH (UK)
Fax: (+44) 1483-876-851
E-mail: n.kuhnert@surrey.ac.uk

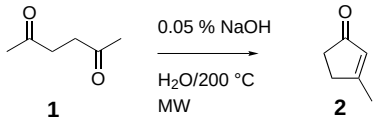
 © WILEY-VCH Verlag GmbH, 69451 Weinheim, Germany, 2002 1433-7851/02/4111-1863 $ 20.00+.50/0

Microwave techniques in synthetic chemistry often elicit a dramatic increase of the reaction rate and yields. An impressive example was reported by Loupy et al., who observed an increase in yield from 2% to 95% under microwave conditions, in the Leuckart reductive amination.[12] These rate and yield enhancements have been suggested by some to be caused by specific, nonthermal microwave effects.[13–15] This article will report the current state of microwave chemistry and highlights the latest experiments, which for the first time allow a direct comparison between the microwave and thermal procedures. This comparison allows the first clear conclusions to be drawn in the discussion about nonthermal microwave effects.



Scheme 2. Transition-metal-catalyzed reactions under microwave conditions. [17] BSA = *N*,*O*-Bis-(trimethylsilyl)acetamide.

Prior to the discussion of special microwave effects, I would like to introduce two representative examples of microwave chemistry that illustrate the confusion caused by an uncritical consideration of published results and lead to an overestimate of the capabilities of the method. Work by the Strauss group has focused on the use of water under microwave conditions.[16] In a high-pressure reactor, water temperatures of 200–300 °C can be reached by rapid microwave heating. Under these high temperatures, the dielectric constant of water changes considerably and water behaves as a "pseudo-organic solvent". The cyclization of the 1,4-diketone **1** in 0.05% NaOH solution at 200 °C yields the 2-cyclopentenone **2** (Scheme 1) within 15 minutes.[16]



Scheme 1. Cyclizations in water under aqueous conditions.[16]

Hallberg and co-workers have shown that a molybdenum-catalyzed allylic substitution of the carbonate **3** and dimethylmalonate can be performed under microwave heating with a shortened reaction time, excellent stereoselectivity, and excellent yield to give the regioisomeric products **5** and **6.** By use of the enantiomerically pure ligand **4**, mostly **5** is formed, but in the presence of palladium catalysts, **6** is the main product (Scheme 2).[17] Careful monitoring of the reaction temperature revealed that the reaction proceeded at 220 °C in THF, far above the boiling point of this solvent under normal pressure. This temperature was achieved by an effect termed "microwave flash heating" by the authors.

Both examples illustrate the differences between the reaction conditions of thermal and microwave conditions, and underline the difficulties in such a comparison. Under microwave conditions, the reactions proceed in closed vessels at considerable pressure, far above the boiling points of the solvents. Any rate acceleration in these cases might be caused by the high reaction temperature and the changes of the physical properties of the solvent. However, as no direct comparison with a thermal procedure under comparable conditions was undertaken, some room remains for speculation about nonthermal microwave effects.

Instrument Design and History

Most microwave chemistry is still performed in multimodal household ovens. For a long time, these instruments have been treated with scepticism and are of limited use. Synthetic chemistry in such commercial household ovens is heavily criticized as it suffers from a low reproducibility.[11] Furthermore, microwave work using household ovens centers around the use of polar solvents such as alcohols, water, DMF, and DMSO, or mixtures of these. As a result, uncontrolled heating of the reaction mixtures occurs, usually accompanied by a considerable build-up of pressure in closed reaction vessels, or rapid evaporation of the solvent in open vessels; these effects often turn microwave synthetic chemistry in these ovens into a hazardous adventure. Recent advances in instrumentation design, in particular the design of dedicated microwave ovens for organic synthesis, have improved the situation enormously. The ovens for organic synthesis use a monomodal cavity and the microwave beam is focused onto the sample using a waveguide. In this way, the interaction between the microwave field and the reaction mixture is well controlled and can easily be optimized. An elegant demonstration of the optimization of reaction conditions with respect to temperature, pressure, reaction time, and solvent in the microwave-assisted Hantzsch dihydropyridine synthesis was recently reported by Öhberg and Westman.[18] Figure 1 illustrates the basic set up of the two alternative microwave ovens.

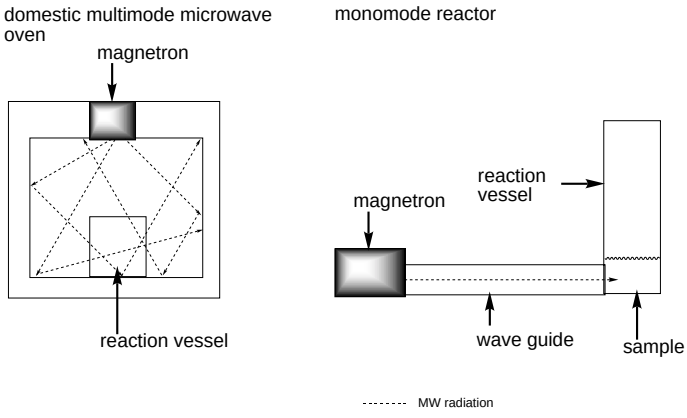


Figure 1. Schematic representation of a household microwave oven and an oven designed for synthesis.

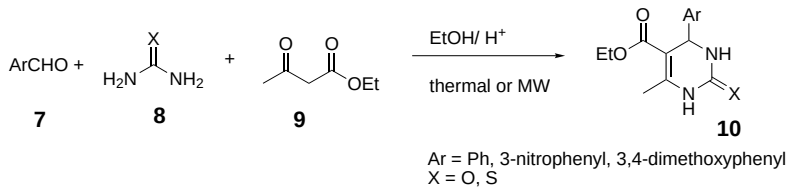
 © WILEY-VCH Verlag GmbH, 69451 Weinheim, Germany, 2002 1433-7851/02/4111-1864 $ 20.00+.50/0

In the microwave oven for synthesis, the reaction temperature can be monitored and controlled using a fiber-optic temperature probe or, alternatively, the surface temperature can be monitored using an IR thermometer, which allows the maintenance of a constant reaction temperature. Pressure can be monitored in sealed systems, and the ovens can be fitted with reflux condensers to realize conventional reflux processes in open vessels. Additionally, mechanical stirring can effectively suppress localized superheating and bumping (delayed boiling). These additional features mean that individual reactions can be easily optimized, are reproducible, have a low energy useage, and result in better chemical yields and faster reactions. Most importantly, the reaction conditions are well defined and allow a direct comparison of microwave heating with conventional thermal heating. This instrumentation is now readily available at affordable prices for routine laboratory use.

Rate Enhancements and Nonthermal Effects

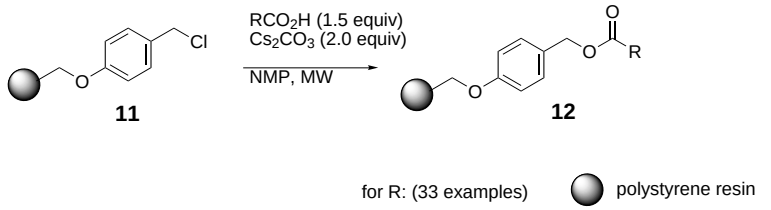
Kappe and Stadler have now for the first time made a direct comparison between microwave heating and thermal heating under almost identical conditions. In their first contribution,[19] they revisited the Bignelli reaction, for which two microwave protocols have been published; these both report increased yields and shorter reaction times.[20, 21] In this three-component coupling reaction, an aromatic aldehyde **7**, a urea or thiourea derivative **8**, and ethylacetoacetate (**9**) condense to form a dihydropyrimidine **10** (Scheme 3).

Careful comparisons of the conventional thermal with the microwave-assisted reaction revealed the following finding: there was no appreciable difference in the reaction rates between reactions carried out under thermal heating or microwave heating at identical temperatures. The differences in rates and yields observed between thermal and microwave heating can be fully attributed to higher reaction temperatures in the microwave methods. The advantages of the microwave method are thus based only on a conventional thermal effect. In sealed vessels, appreciable superheating is observed (e.g. ethanol 180 °C at 20 bar), which leads to the formation of undesired side-products, rather than to an improvement of the reaction in terms of yield and rate. Increased yields are obtained by using a conventional household microwave oven and can be rationalized in terms of increased concentration of the reactants caused by rapid evaporation of the solvent and water, which acts as a driving force in the condensation.



Scheme 3. Bignelli reaction under microwave conditions.[19]

In a second publication, Kappe and Stadler turned their attention to microwave-assisted, solid-supported chemistry.[22] As a model reaction, they investigated the Cs_2CO_3-mediated ester formation with Wang resin-bound benzoyl chloride (**11**; Scheme 4). Again, no appreciable nonthermal effects could be observed by comparing the microwave-heating and thermal-heating reactions at the same temperature. The increased efficiency observed for the microwave method in comparison to procedures published earlier can be attributed to a direct rapid heating and the use of NMP as a high boiling polar solvent, ideally suited to the microwave conditions. However, the authors have discovered one of the most promising niches for microwave chemistry. In the synthesis of combinatorial libraries on solid supports, an increase in reaction rates and efficiency would improve the otherwise rather sluggish and slow reactions. Other drawbacks of thermal solid-supported chemistry, such as degradation of the polymer support caused by long reaction times, are avoided.



Scheme 4. Solid-phase reaction under microwave conditions. [22] NMP = *N*-Methylpyrrolidinone.

Summary and Outlook

Because of the thorough work of Kappe's group, the comparison of thermal- and microwave-heating methods is possible for the first time. It can be cautiously concluded (see below) that all speculation of special and nonthermal effects in microwave heating has no basis. The reported increased reaction rates and yields have lost their magic; they can be rationalized by taking into account increased temperatures caused by superheating or concentration effects. I strongly hope that all future publications in microwave chemistry will follow Kappe's example and thoroughly account for the observed improvements in reaction rates and yields.

Recent work by Jones and co-workers, however, [23] might open up a completely different question in microwave chemistry. Although not explicitly stated, their work on the heterogeneous deuteration of indole derivatives shows that there is a difference in the selectivity for deuterium incorporation between thermal-[24] and microwave-heating methods. Whereas in homogenous reactions under microwave conditions, the selectivity essentially follows the thermal pattern,[25] it seems to be possible to alter the selectivity in heterogeneous reactions. It is left open to interpretation, whether a special microwave effect has to be taken into account in these heterogeneous reactions.

[1] J. H. Clark, *Green Chem.* **1999**, *1*, 1.
[2] J. O. Metzger, *Angew. Chem.* **1998**, *110*, 3145; *Angew. Chem. Int. Ed.* **1998**, *37*, 2975; M. Eissen, J. O. Metzger, E. Schmidt, U. Schneidewind, *Angew. Chem.* **2002**, *114*, 402; *Angew. Chem. Int. Ed.* **2002**, *41*, 414.
[3] R. Gedey, F. Smith, K. Westaway, H. Ali, L. Baldisera, L. Laberge, J. Roussel, *Tetrahedron Lett.* **1986**, *27*, 279.
[4] A. R. von Hippel, *Dielectric Materials and Applications*, MIT Press, Cambridge, MA, **1954**.
[5] C. Gabriel, S. Gabriel, E. H. Grant, B. S. J. Halstead, D. M. P. Mingos, *Chem. Soc. Rev.* **1998**, *27*, 213.
[6] R. S. Varma, *Green Chem.* **1999**, *1*, 43.
[7] S. Chaddick, *Tetrahedron* **1995**, *51*, 10403.
[8] C. R. Strauss, R. W. Trainor, *Aust. J. Chem.* **1995**, *48*, 1665; C. R. Strauss, *Aust. J. Chem.* **1999**, *52*, 83.
[9] N. Elander, J. R. Jones, S.-Y. Lu, S. Stone-Elander, *Chem. Soc. Rev.* **2000**, *29*, 239.
[10] A. Loupy, A. Petit, J. Hamelin, F. Texier-Boullet, P. Jacquault, D. Mathe, *Synthesis* **1998**, *9*, 1213.
[11] N. Kuhnert, *Nachr. Chem.* **2001**, *49*, 306.
[12] A. Loupy, D. Monteux, A. Petit, J. M. Aizpurua, E. Dominguez, C. Palomo, *Tetrahedron Lett.* **1996**, *37*, 8177.
[13] R. Laurent, A. Laportiere, J. Dubac, J. Berlan, S. Lefeuvre, M. Audhuy, *J. Org. Chem.* **1992**, *57*, 7099.
[14] R. N. Gedey, J. B. Wei, *Can. J. Chem.* **1998**, *76*, 525.
[15] P. Goncalo, C. Roussel, J. M. Milot, J. Vebrel, *J. Chem. Soc. Perkin Trans. 2* **1999**, 2111.
[16] I. Bagnell, M. Bliese, T. Cablewski, C. R. Strauss, J. Tsanaktsidis, *Aust. J. Chem.* **1997**, *50*, 921; J. Y. An, I. Bagnell, T. Cablewski, C. R. Strauss, R. W. Trainor, *J. Org. Chem.* **1997**, *62*, 2505.
[17] N.-F. K. Kaiser, U. Bremberg, M. Larhed, C. Moberg, A. Hallberg, *Angew. Chem.* **2000**, *112*, 3741; *Angew. Chem. Int. Ed.* **2000**, *39*, 3595.
[18] L. Öhberg, J. Westman, *Synlett* **2001**, 1296.
[19] A. Stadler, C. O. Kappe, *J. Chem. Soc. Perkin Trans. 2* **2000**, 1363.
[20] R. Gupta, A. K. Gutpa, S. Paul, P. L. Kachroo, *Ind. J. Chem.* **1995**, *34B*, 151.
[21] A. Dandia, M. Saha, H. Taneja, *J. Fluorine Chem.* **1998**, *90*, 17.
[22] A. Stadler, C. O. Kappe, *Eur. J. Org. Chem.* **2001**, 919.
[23] S. Anto, G. S. Gethvoldsen, J. R. Harding, J. R. Jones, S.-Y. Lu, J. C. Russell, *J. Chem. Soc. Perkin Trans. 2* **2000**, 2208.
[24] W.-M. Yau, K. Gawrisch, *J. Labelled Compd. Radiopharm.* **1999**, *42*, 709.
[25] N. Kuhnert, T. N. Danks, *Green Chem.* **2001**, *3*, 68.

Biosynthesis of Polyunsaturated Fatty Acids by Polyketide Synthases

Ursula Kaulmann and Christian Hertweck*

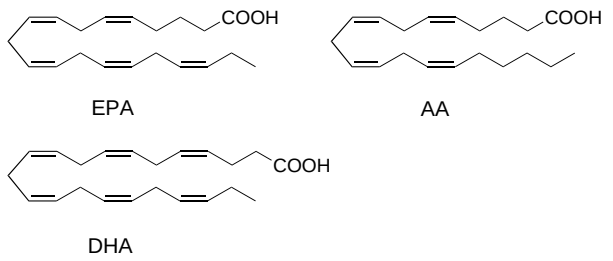
Nature's virtuosity of linking and tailoring simple carboxylic acid monomers to give a huge structural diversity of polyketide and fatty acid metabolites has been a fascinating subject for interdisciplinary research since the early works of Collie at the start of the 20th century.[1] During the past few decades a large body of knowledge has been established by using modern molecular biology methods, from which a deeper insight into the processes employed in fatty acid and polyketide biosynthesis has been gained.[2–4] Both biosynthetic pathways have strong homologies in the chemical mechanisms involved in chain extension and in the common pool of simple precursors (acetyl-CoA, malonyl-CoA),[5, 6] as well as in the character of the enzymes used for chain propagation and processing.[2, 7] In general, polyketides and fatty acids are constructed by repetitive decarboxylative Claisen ester condensations of an acyl-CoA starter unit with (methyl)malonyl-CoA units catalyzed by a β-ketoacyl synthase (KS). This process usually involves a (malonyl)acyl transferase (MAT/AT) and an acyl carrier protein (ACP). In fatty acid biosynthesis, subsequent β-oxo processing by a keto reductase (KR), dehydratase (DH), and an enoyl reductase (ER) generally yields a fully saturated acyl backbone. In contrast to this, the reductive steps in polyketide biosynthesis are partly or fully omitted, thus giving rise to a more complex pattern of functionalization. The elongation/reduction cycles are repeated until a defined chain length is obtained. The thioester-bound substrate is then released from the enzyme complex and may be subjected to further tailoring, such as desaturation (especially fatty acids), oxidation, glycosylation, or methylation (especially polyketides).[8] On the basis of genetic analyses and the architecture of the proteins employed, fatty acid synthases (FASs) and polyketide synthases (PKSs) are both generally classified into two types: type I, in which the active sites are linearly arranged on a large module, and type II, which consists of a dissociable complex of small, discrete monofunctional proteins.[9, 10] Despite remarkable similarities in their setup and functions, PKSs and FASs are clearly distinct in their detailed programming at the amino acid level, and—more importantly—they constitute a branch point between primary and secondary metabolism. It is thus a matter of speculation that both pathways diverged at an early stage during evolution.

In view of this knowledge, a recent discovery that long-chain polyunsaturated fatty acids (PUFAs) can be biosynthesized by bacterial polyketide synthases is ground-breaking news.[11] PUFAs have long been known as essential membrane components in the brain and retina[12, 13] as well as precursors of signaling molecules, such as the prostaglandins, thromboxanes, and leukotrienes,[14, 15] but—until recently—they were believed to be produced exclusively by eukaryotic organisms, not by bacteria. Recently, several research groups have independently identified PUFAs, such as eicosapentaenoic acid (EPA, 20:5n3), docosahexaenoic acid (DHA, 22:6n3), and arachidonic acid (AA, 20:4n6), from various psychro-

[*] Dr. C. Hertweck, Dr. U. Kaulmann
Hans-Knöll-Institut für Naturstoff-Forschung
Beutenbergstrasse 11a, 07745 Jena (Germany)
Fax: (+49) 3641-656-699
E-mail: hertweck@pmail.hki-jena.de

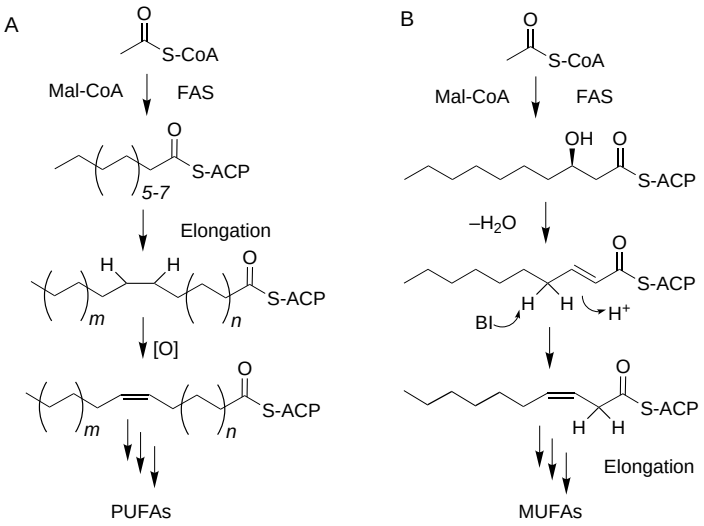
 © WILEY-VCH Verlag GmbH, 69451 Weinheim, Germany, 2002 1433-7851/02/4111-1866 $ 20.00+.50/0

philic bacteria (bacteria thriving at low temperatures), for example, *Shewanella hanedai*, *S. gelidimarina*, and *Colwellia psycherythraea* (Scheme 1).[16–20] As reviewed by Russell and Nichols, a long-existing dogma had thus been refuted, but it remained a mystery as to how these bacterial metabolites can be formed.[16]



Scheme 1. Structures of polyunsaturated fatty acids (PUFAs) found in several psychrophilic marine bacteria and in the protist *Schizochytrium*.

Two major routes are known for the introduction of double bonds into saturated fatty acids. In plants, mammals, and insects, double bonds are inserted by position-specific desaturases using molecular oxygen as a terminal electron acceptor (Scheme 2, route A). Several homoconjugated double



Scheme 2. Biosynthetic pathways (FASs) for unsaturated fatty acids. Route A: aerobic, found in plants and animals. Route B: anaerobic, found in microorganisms.

bonds can be introduced sequentially along this route.[21] In contrast, anaerobic bacteria may form a double bond during an incomplete reductive cycle of the FAS. Subsequently, a specific isomerase activity may catalyze a 2,3-*trans*/*cis* rearrangement (Scheme 2, route B). Unlike the aerobic route, only monounsaturated fatty acids (MUFAs) can be produced by this mechanism.[16] Although anaerobic and aerobic FAS pathways are in fact not mutually exclusive in a single organism,[22] bacterial PUFA biosynthesis remained unclear, since it can function under anaerobic conditions in several marine bacteria. The dilemma was that on the one hand an anaerobic pathway is not capable of introducing more than one double bond per fatty acid, and on the other hand the conventional aerobic pathway had to be excluded.[16] Consequently, it was assumed that another mechanism and/or an electron acceptor other than molecular oxygen had to be present, but it was probably too daring to speculate that methylene-interrupted double-bond patterns could be formed by an entirely different path.

How has this riddle been solved? Clustered genes involved in the synthesis of EPA were isolated for the first time in 1996, thanks to the efforts of Yazawa.[20] He identified five open reading frames (ORFs) from the EPA-producing bacterium *Shewanella* sp. strain SCRC2738, which proved to be necessary and sufficient for EPA production in *Escherichia coli*[23] and in a cyanobacterium (*Synechococcus* sp.).[23, 24] Only recently, the protein products encoded by the EPA cluster have been proposed by researchers of the same research group. Metz et al. identified eleven regions within the five open reading frames as putative enzyme domains.[11] The linear organization of the active site in the ORFs is reminiscent of that in iterative fungal PKSs or type I FASs. Instead of finding genes encoding for fatty acid synthesis, elongation, and aerobic desaturation, as was proposed by others to be involved in bacterial PUFA biosynthesis,[16] it was a great surprise to discover genes that suggest a mixed polyketide/fatty acid biosynthetic pathway exists. In fact, all keto synthases involved in PUFA biosynthesis are homologues of KSs found in bacterial modular type I PKSs, rather than being related to FAS keto synthases.[11] According to Metz et al., ORF5 codes for four PKS-related enzyme domains, which were proposed to function as KS, MAT, ACP (six repeats), and KR. A PKS-related phosphopantetheine transferase and a PKS-related AT are encoded by ORF2 and ORF6, respectively. ORF7 comprises two PKS-related genes (KSs) and two FAS-like genes, which are homologues of the *E. coli* dehydratase FabA. Interestingly, while one KS appears to be fully functional, the second KS lacks a cysteine residue in the active site and is thus assumed to be inactive. This situation is strikingly similar to the iterative type II PKS subunits KS_α and KS_β, the latter also often referred to as the chain length factor (CLF).[25] ORF8 finally codes for a FAS-related putative enoyl reductase.

Actually, genes with a high homology to the *Shewanella* gene cluster have been found in other PUFA-containing marine bacteria which indicates that the novel PKS pathway may be widely distributed in these organisms. In 1999, Tanaka et al. found four ORFs in the DHA-producing bacterium *Moritella marina* strain MP-1 (formerly *Vibrio marinus* strain MP-1), which had high homology with ORFs 5–8 of the EPA biosynthesis cluster.[26, 27] At that time, Tanaka et al. had already exploited information from the databases and compared the organization of both the EPA and DHA gene clusters. They found that the only difference in the latter was two more regions encoding putative KSs, and five instead of six repetitive copies of ACP. Furthermore, an EPA-deficient strain of the deep-sea bacterium *Photobacterium profundum* SS9 was constructed successfully by gene disruption experiments based on the known EPA ORF3/4 gene sequence of *Shewanella* sp. SCRC2738, which provided another indication of the common distribution of the novel PUFA pathway among psychrophilic marine bacteria.[28] Metz et al. have also

 © WILEY-VCH Verlag GmbH, 69451 Weinheim, Germany, 2002 1433-7851/02/4111-1867 $ 20.00+.50/0

shown for a eukaryote, the marine protist *Schizochytrium*, that DPA and DHA biosynthesis does not necessarily involve membrane-bound desaturases or fatty acid elongation enzymes. Sequences that are located on three ORFs exhibited homology to eight of the eleven domains of *Shewanella* (Figure 1). A horizontal gene transfer is likely to have occurred.[11]

What might a mixed PKS/FAS pathway for bacterial PUFA synthesis look like? In this respect it is useful to recall the function of FabA in *E. coli*.[29] FabA is one of the two β-hydroxyacyl-ACP dehydratases involved in the biosynthesis of fatty acids in *E. coli*. After the acyl chain length has reached ten carbon atoms, FabA is responsible for diverting the flow of intermediates into the unsaturated fatty acid branch of the pathway. Besides catalyzing the dehydration, FabA also isomerizes *trans*-2-decenoyl-ACP to *cis*-3-decenoyl-ACP, which by-passes the following reduction step (ER). The unsaturated acyl-ACP is loaded onto FabB (one of the two β-ketoacyl-ACP synthases) to initiate the first cycle of elongation in the unsaturated fatty acid synthesis. Since the *Shewanella* DHs show high homology to FabA, at least some of the double bonds in EPA from *Shewanella* sp. SCRC2738 are probably introduced by a dehydrase/isomerase mechanism. Furthermore, it has been shown by heterologous expression of the cluster in *E. coli* that EPA biosynthesis occurs anaerobically.[11]

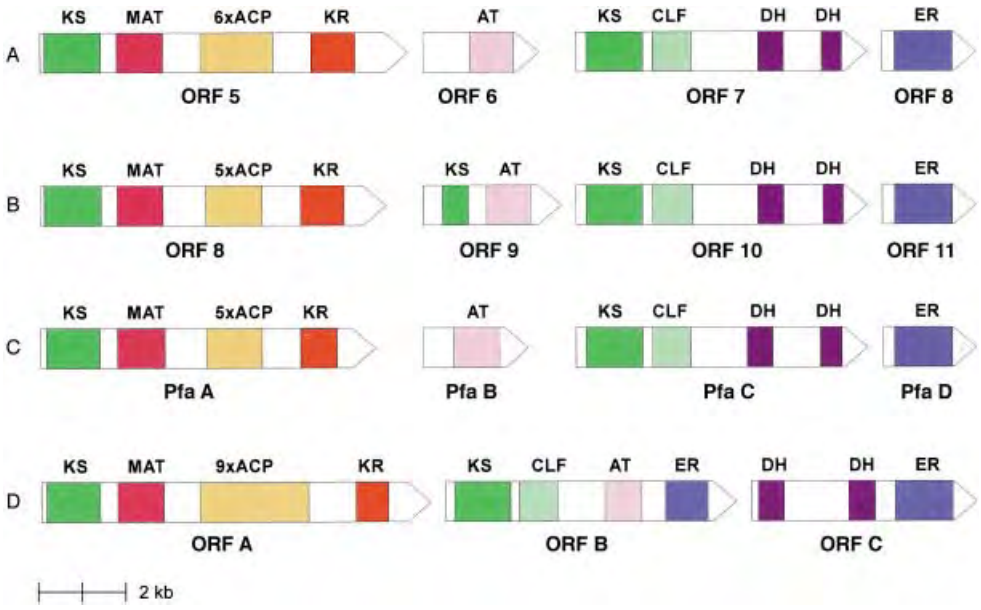
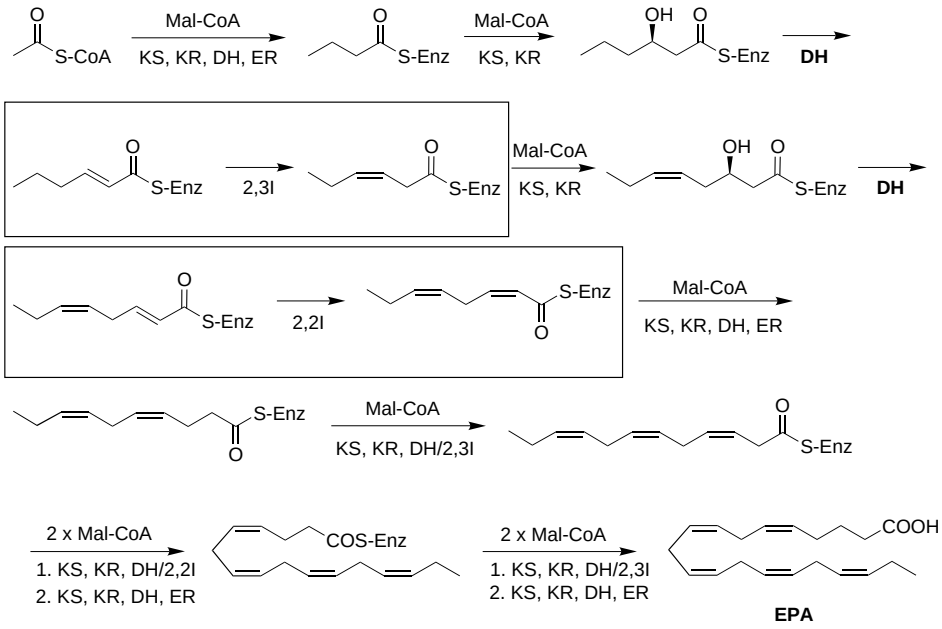


Figure 1. Organization of the core regions of PUFA biosynthetic gene clusters; A: *Shewanella* sp. SCRC-2738 (GenBank accession no.: U73935.1);[11] B: *Moritella marinus* strain MP-1 (GenBank accession no.: AB025342.1);[26, 27] C: *Photobacterium profundum* strain SS9 (GenBank accession no.: AF409100, unpublished data); D: *Schizochytrium* (GenBank accession nos.: AF378327, AF378328, AF378329).[11]



Scheme 3. Proposed biosynthetic pathway of EPA in *Shewanella* sp. with putative intermediates and key catalytic activities employed. Mal-CoA: malonyl-CoA; KS: keto synthase; KR: keto reductase; DH: dehydratase; ER: enoyl reductase; 2,3I: 2,3-isomerase; 2,2I: 2,2-isomerase.

One of the plausible schemes that can be derived from what we know so far was proposed by Metz et al. (Scheme 3): The first elongation step from a putative acetyl-CoA starter molecule and malonyl-CoA as well as a complete cycle of reduction is catalyzed by KS, KR, DH, and ER. The following elongation step occurs by a keto reduction to the β-hydroxy-
ester. The FabA-like bifunctional dehydratase/isomerase would then catalyze dehydration as well as the *trans*-2,3-*cis* rearrangement of the acyl intermediate. In analogy to the requirement of a special β-ketoacyl-ACP synthase in *E. coli* for the elongation of the 3-*cis*-acyl-ACP intermediate, a designated KS might be responsible for chain propagation. After subsequent reduction and dehydration steps, a methylene-interrupted double-bond pattern would require that a *trans*-2,2-*cis* isomerization occurs. A similar reaction is known for the regeneration of 11-*cis*-retinol. For EPA biosynthesis, the same set of reactions is then repeated twice, with the last 2,3-isomerization being followed by an elongation in which a full reductive cycle is employed (Scheme 3). In analogy, the formation of DHA and AA may be explained with only minor modifications. However, the proposed pathway needs to be

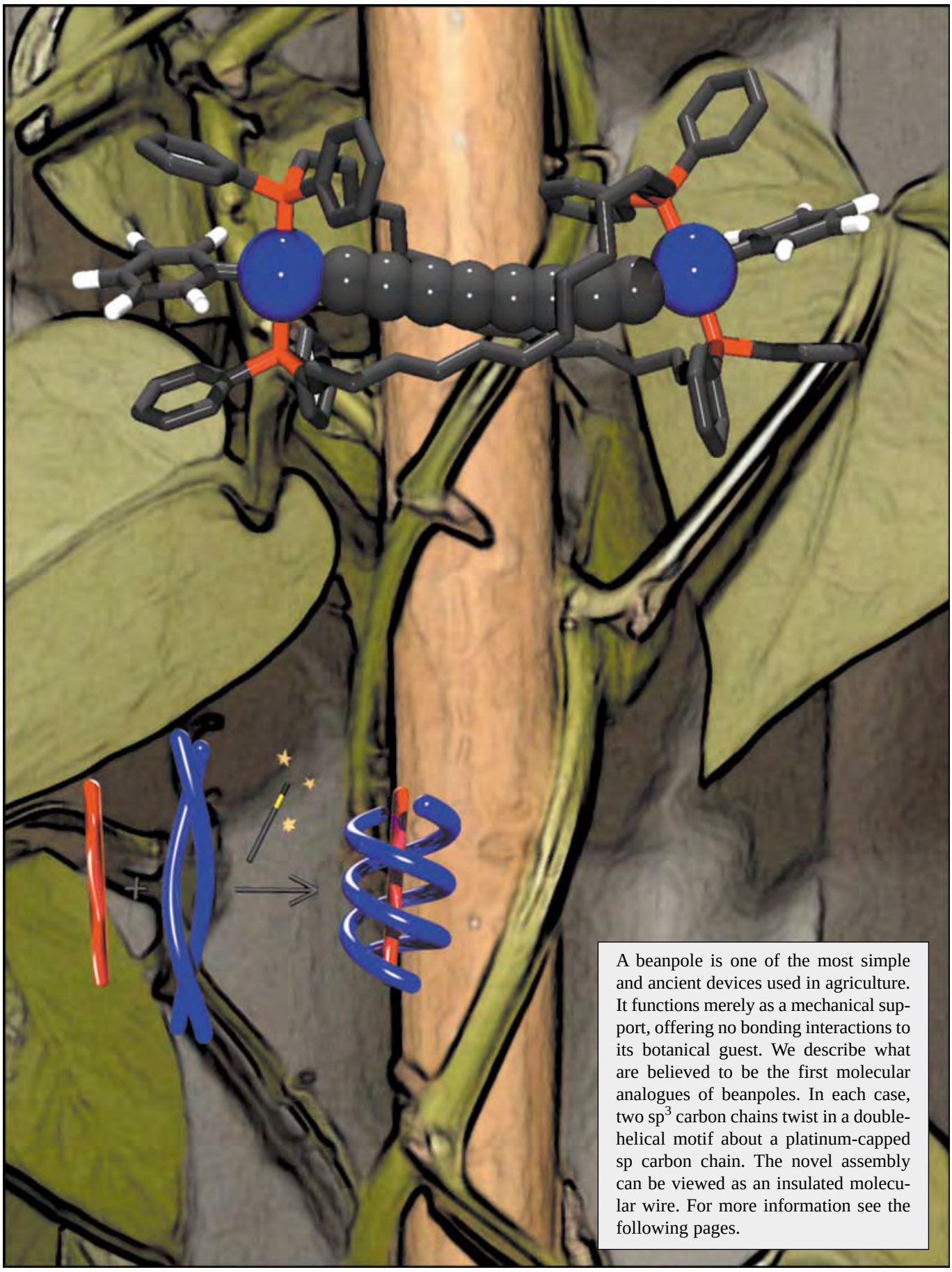
 © WILEY-VCH Verlag GmbH, 69451 Weinheim, Germany, 2002 1433-7851/02/4111-1868 $ 20.00+.50/0

verified and studied in more detail by further biochemical analyses. As for fungal iterative type I PKSs, it is completely unresolved how chain length and degree of reduction is controlled at specific steps. Also, the function of multiple ACPs (5–9 copies!) for PUFA biosynthesis is enigmatic.

What benefit will the discovery of PUFA gene clusters in marine psychrophilic bacteria have for us? The finding and functional analysis of these novel gene clusters is relevant for several reasons: It is advantageous to the biotechnological production of PUFAs from marine bacteria. Since there is medical evidence for the relevance of PUFAs to prevent, for example, artheriosclerosis and heart disease, there is a great demand on such drugs.[16, 30] Psychrophilic bacteria could be used as a primary PUFA-rich feedstock in artificial food chains in the aquaculture industry, thereby protecting natural fish stocks. Gene transfer to industrially relevant producer organisms will be a further solution to the supply of PUFAs.[24] Apart from the commercial aspect, PUFA genes will help in bacterial taxonomy to redefine old classifications, to create new groupings, and to trace-back evolution.[17, 31] New strains with active and silent copies of the PUFA genes can be tracked by using molecular biology tools, and more might be learned about the world-wide distribution of strains with PUFA-biosynthesis gene clusters and their ecological importance.[18, 32] Last, but not least, the genes for PUFA biosynthesis are distinct from previously recognized PKSs in both structure and mechanism as well as the novel putative dehydrases/isomerases, and may thus provide new tools for combinatorial biosynthesis of polyketide antibiotics.[33–35]

[1] R. Bentley, J. W. Bennett, *Annu. Rev. Microbiol.* **1999**, *53*, 411.
[2] J. Staunton, K. J. Weissman, *Nat. Prod. Rev.* **2001**, *18*, 380.
[3] D. O'Hagan, *The Polyketide Metabolites*, Ellis Horwood, Chichester, **1991**.
[4] J. W. Campbell, J. E. J. Cronan, *Annu. Rev. Microbiol.* **2001**, *55*, 305.
[5] B. J. Rawlings, *Nat. Prod. Rep.* **1998**, *15*, 275.
[6] B. S. Moore, C. Hertweck, *Nat. Prod. Rep.* **2002**, *19*, 70.
[7] M. P. Crump, J. Crosby, C. E. Dempsey, J. A. Parkinson, M. Murray, D. A. Hopwood, T. J. Simpson, *Biochemistry* **1997**, *36*, 6000.
[8] C. Khosla, R. S. Gokhale, J. R. Jacobsen, D. E. Cane, *Annu. Rev. Biochem.* **1999**, *68*, 219.
[9] D. A. Hopwood, *Chem. Rev.* **1997**, *97*, 2465.
[10] J. L. Harwood, N. J. Russell, *Lipids in Plants and Microbes*, George Allen and Unwin, London, **1984**.
[11] J. G. Metz, P. Roessler, D. Facciotti, C. Levering, F. Dittrich, M. Lassner, R. Valentine, K. Lardizabal, F. Domergue, A. Yamada, K. Yazawa, V. Knauf, J. Browse, *Science* **2001**, *293*, 290.
[12] L. Lauritzen, H. S. Hansen, M. H. Jorgensen, K. F. Michaelsen, *Prog. Lipid Res.* **2001**, *40*, 1.
[13] M. McConn, J. Browse, *Plant J.* **1998**, *15*, 521.
[14] A. Heller, T. Koch, J. Schmeck, K. van Ackern, *Drugs* **1998**, *55*, 487.
[15] R. A. Creelman, J. E. Mullet, *Annu. Rev. Plant Physiol. Plant Mol. Biol.* **1997**, *48*, 355.
[16] N. J. Russell, D. S. Nichols, *Microbiology* **1999**, *145*, 767.
[17] D. Nichols, J. Bowman, K. Sanderson, C. Mancuso Nichols, T. Lewis, T. McMeekin, P. D. Nichols, *Curr. Opin. Biotechnol.* **1999**, *10*, 240.
[18] F. DeLong, A. A. Yayanos, *Appl. Environ. Microbiol.* **1986**, *51*, 730.
[19] K. Watanabe, C. Ishikawa, I. Ohtsuka, M. Kamata, M. Tomita, K. Yazawa, H. Muramatsu, *Lipids* **1997**, *32*, 975.
[20] K. Yazawa, *Lipids* **1996**, *31*, S297.
[21] H. Sprecher, Q. Chen, *Prostaglandins Leukotrienes Essent. Fatty Acids* **1999**, *60*, 317.
[22] M. Wada, N. Fukunaga, S. Sasaki, *J. Gen. Appl. Microbiol.* **1991**, *37*, 355.
[23] R. Yu, A. Yamada, K. Watanabe, K. Yazawa, H. Takeyama, T. Matsunaga, R. Kurane, *Lipids* **2000**, *35*, 1061.
[24] H. Takeyama, D. Takeda, K. Yazawa, A. Yamada, T. Matsunaga, *Microbiology* **1997**, *143*, 2725.
[25] B. J. Rawlings, *Nat. Prod. Rep.* **1999**, *16*, 425.
[26] M. Tanaka, A. Ueno, K. Kawasaki, I. Yumoto, S. Ohgiya, T. Hoshino, K. Ishizaki, H. Okuyama, N. Morita, *Biotechnol. Lett.* **1999**, *21*, 939.
[27] N. Morita, M. Tanaka, H. Okuyama, *Biochem. Soc. Trans.* **2000**, *28*, 943.
[28] E. E. Allen, D. Facciotti, D. H. Bartlett, *Appl. Environ. Microbiol.* **1999**, *65*, 1710.
[29] R. J. Heath, C. O. Rock, *J. Biol. Chem.* **1996**, *271*, 27795.
[30] R. S. Lees, *Food Sci. Technol.* **1990**, *37*, 1.
[31] D. S. Nichols, P. D. Nichols, N. J. Russell, N. W. Davies, T. A. McMeekin, *Biochim. Biophys. Acta* **1997**, *1347*, 164.
[32] D. S. Nichols, P. Hart, P. D. Nichols, T. A. McMeekin, *Aquaculture* **1996**, *147*, 115.
[33] L. Rohlin, M. K. Oh, J. C. Liao, *Curr. Opin. Microbiol.* **2001**, *4*, 330.
[34] P. F. Leadlay, *Curr. Opin. Chem. Biol.* **1997**, *1*.
[35] M. Chartrain, P. M. Salmon, D. K. Robinson, B. C. Buckland, *Curr. Opin. Biotechnol.* **2000**, *11*, 209.

 © WILEY-VCH Verlag GmbH, 69451 Weinheim, Germany, 2002 1433-7851/02/4111-1869 $ 20.00+.50/0



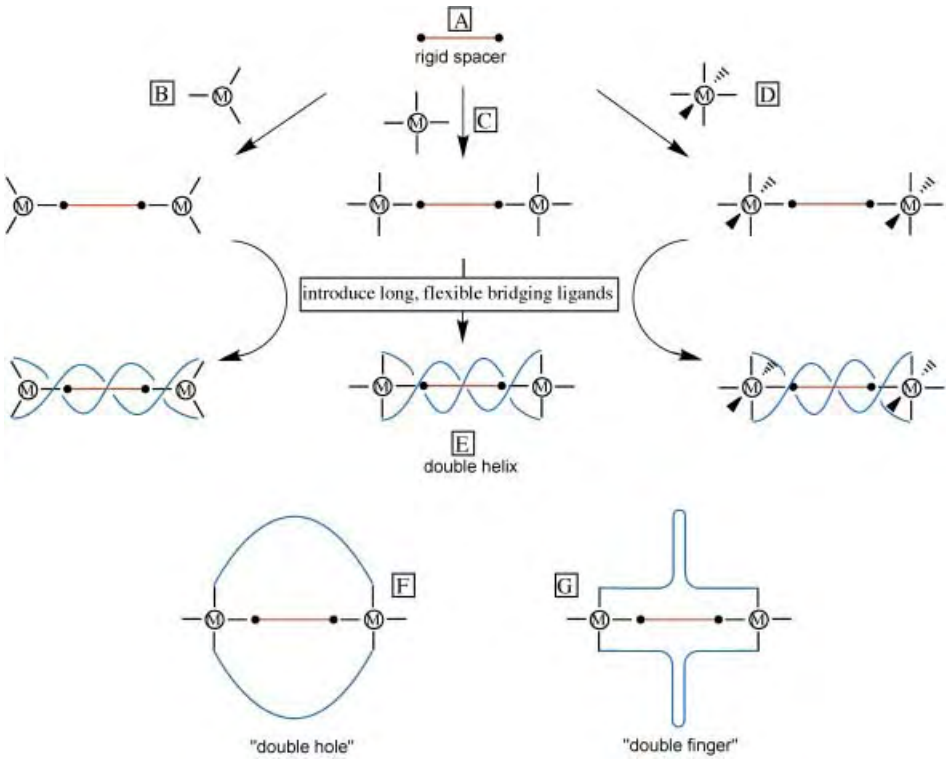
A beanpole is one of the most simple and ancient devices used in agriculture. It functions merely as a mechanical support, offering no bonding interactions to its botanical guest. We describe what are believed to be the first molecular analogues of beanpoles. In each case, two sp^3 carbon chains twist in a double-helical motif about a platinum-capped sp carbon chain. The novel assembly can be viewed as an insulated molecular wire. For more information see the following pages.

 © WILEY-VCH Verlag GmbH, 69451 Weinheim, Germany, 2002 1433-7851/02/4111-1871 $ 20.00+.50/0

sp Carbon Chains Surrounded by sp^3 Carbon Double Helices: A Class of Molecules that are Accessible by Self-Assembly and Models for "Insulated" Molecular-Scale Devices**

Jürgen Stahl, James C. Bohling, Eike B. Bauer, Thomas B. Peters, Wolfgang Mohr, José M. Martín-Alvarez, Frank Hampel, and John A. Gladysz*

DNA was the first chemical substance to be recognized as a double helix. This structural motif, which is capable both of carrying information (e.g., the genetic code) and protecting interior functional domains, has since been engineered into a variety of nonnatural molecules.[1–6] Many of these are coordination compounds, often referred to as "helicates".[3, 4] To our knowledge, all double-helical molecules feature bonding interactions between the helix strands (e.g., hydrogen bonds), or covalent bonds to metal templates dispersed throughout the strands. Factors that promote or enforce complementarity—that is, the programming[1] or "encoding of specific structural and conformational information"[7]—are thought to be required. We wondered whether it might be possible to design double-helical molecules that lack these conventional binding elements or driving forces—in an extreme sense, species that would form double helices because "they felt like it".



Scheme 1. Geometrical analysis: representative endgroups (**B**, **C**, **D**) that can support double-helical motifs of flexible bridging ligands about rigid spacer ligands (**A**).

Our strategy was as follows. Start with a rigid, linear connecting rod, as represented by **A** in Scheme 1. Such building blocks are playing leading roles in the development of molecular-scale devices and nanochemistry.[8, 9] One of the most fundamental and svelte of such blocks would be a chain of sp-hybridized carbon atoms.[10, 11] Attach to each terminus an atom that supports at least two additional bonds, symmetrically disposed with respect to the rod. Transition metals would be obvious candidates, as exemplified by **B**–**D** (Scheme 1). The endgroups could anchor two (and sometimes more) long flexible chains incapable of bonding interactions—for example polymethylene $(CH_2)_n$ or polydifluoromethylene segments $(CF_2)_n$.

Once all covalent bonds are in place, there is the obvious question of conformation. Will the flexible chains twist about the rigid rod to give double helices as in **E** (Scheme 1), or preferentially adopt conformations with "holes" (**F**) or "fingers" (**G**)? Since monocyclic crown ethers and related macrocycles seldom exhibit conformations with holes,[12] we discounted possibility **F**. Space filling molecular models of various target molecules allowed the number of twists in the helical conformer **E** to be estimated. When the flexible chains were too short, twists or finger protrusions became impossible.

Such target structures have potential practical applications that merit note at the outset. Molecules in which unsaturated ligands span two transition metals can often be generated in more than one oxidation state, each of which is capable of exhibiting a variety of charge transfer phenomena, ranging from optical transitions to photoinduced electron transfer, and from hyperpolarizability to electron delocalization in radical ions.[13] Such properties are being exploited in nonlinear optics, various light-harvesting protocols, and many types of molecular-scale devices. With sp carbon bridges, chains as long as 20 carbon atoms, corresponding to metal–metal separations of 3 nm, have been realized.[11e] However, the stabilities of charged and/or radical oxidation states drastically decrease with chain length, precluding many applications of these wirelike assemblies. We thought that

[*] Prof. Dr. J. A. Gladysz, Dipl.-Chem. J. Stahl, Dipl.-Chem. E. B. Bauer, Dipl.-Chem. W. Mohr, Dr. F. Hampel
Institut für Organische Chemie
Friedrich-Alexander-Universität Erlangen-Nürnberg
Henkestrasse 42, 91054 Erlangen (Germany)
Fax: (+49) 9131-85-26865
E-mail: gladysz@organik.uni-erlangen.de
Dr. J. C. Bohling, Dr. T. B. Peters, Dr. J. M. Martín-Alvarez
Department of Chemistry
University of Utah
Salt Lake City, UT 84112 (USA)

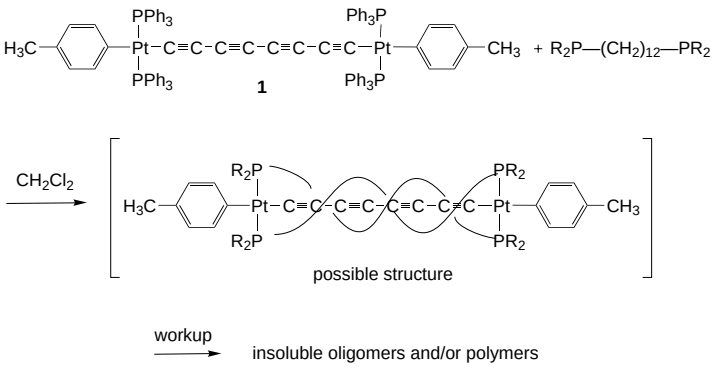
[**] We thank the Deutsche Forschungsgemeinschaft (SFB 583), Johnson Matthey PMC (platinum loan), the Spanish Ministerio de Educación y Ciencia, and the Fulbright Commission (Fellowships, J.M.M.-A.) for support, and Dr. A. M. Arif for assistance with the analysis of one crystal structure.

 © WILEY-VCH Verlag GmbH, 69451 Weinheim, Germany, 2002 1433-7851/02/4111-1872 $ 20.00+.50/0

the double helix of **E** would shield and protect the often sensitive bridge, analogous to the insulation about household electrical wire.[14]

Here we describe successful syntheses of a family of diplatinum sp carbon chain complexes $[Pt(C{\equiv}C)_mPt]$ with the double-helical structure **E**. Two routes are presented. The first involves an unprecedented sequence of high-risk reactions that significantly advances the art of organometallic chemistry with respect to rational, directed syntheses of new materials. The second can be viewed as a coordination-driven "self-assembly" process with potential for operationally simple nanodevice syntheses.

We first utilized the $[Pt(C{\equiv}C)_4Pt]$ complex **1** (Scheme 2),[15] which features an eight-carbon tetrayne bridge and square-planar endgroups. A related [PtC≡CPt] complex had been shown to undergo facile phosphane substitution.[16] Reactions of **1** with diphosphanes, in which the phosphorus atoms were separated by flexible bridges of twelve sp^3 carbon atoms, proceeded rapidly below room temperature. One product formed, as assayed by ^{31}P NMR spectroscopy and thin layer chromatography. However, when the solution was concentrated, an insoluble, presumably oligomeric or polymeric material formed. Only small portions could be induced to redissolve. Several monoplatinum complexes of macrocyclic diphosphanes have also been observed to oligomerize.[17]

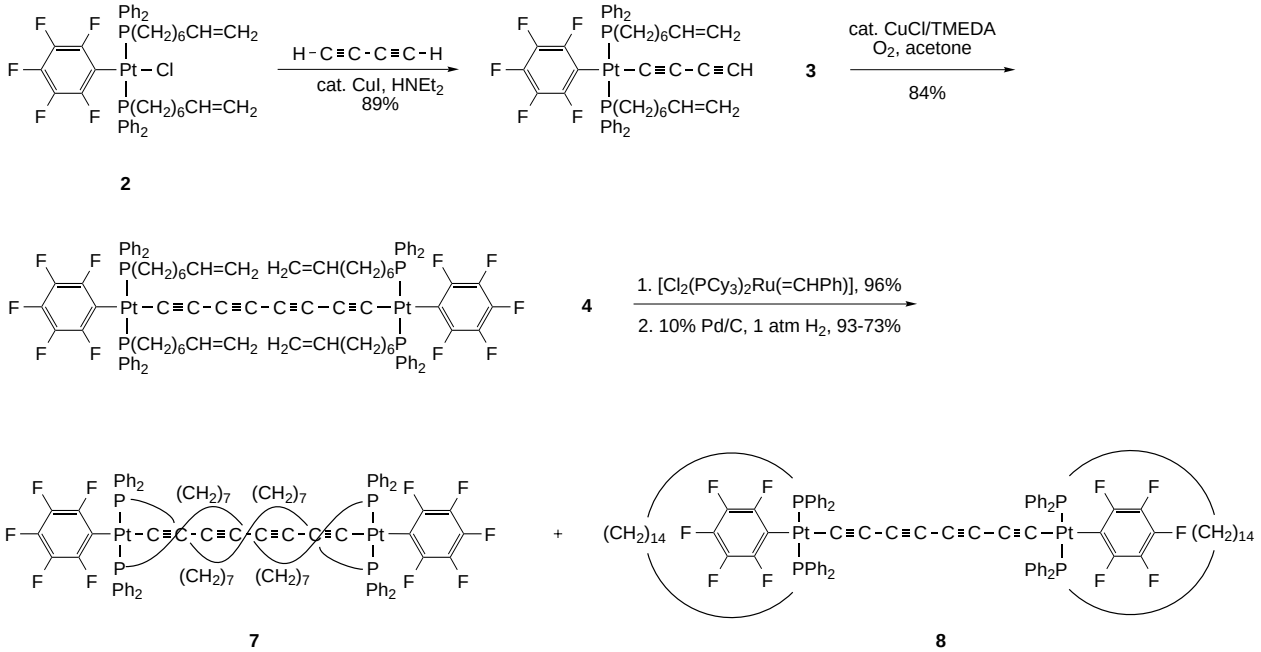


Scheme 2. First synthetic approach to double-helical complexes. R = Ph, *c*-C_6H_9.

A second-generation approach with two new design elements was investigated. First, the *p*-tolyl ligands on platinum were replaced with pentafluorophenyl (C_6F_5) ligands. This was intended to increase the Lewis acidity of platinum and retard phosphane dissociation, the suspected key step in oligomerization. Second, the diphosphane bridges would not be introduced by substitution, but generated within the coordination sphere by linking *functionalized mono*phosphane ligands. Accordingly, the monoplatinum complex **2** (Scheme 3), in which each phosphane ligand contains a hexamethylenevinyl group $(CH_2)_6CH{=}CH_2$, was prepared as previously described.[18]

As shown in Scheme 3, **2** was elaborated to the $[Pt(C{\equiv}C)_4Pt]$ complex **4**. We were concerned that the first step (conditions as used en route to **1**) might be compromised by the vinyl groups in the phosphane ligands. This proved not to be a problem, and the 1,3-butadiynyl complex **3** was isolated in 89% yield. An oxidative coupling was attempted under standard Hay conditions for terminal alkynes. Competing reactions involving vinyl groups were viewed as even more probable here, but **4** was isolated in 84% yield.

We thought that it might be possible to connect the vinyl groups utilizing alkene metathesis, which we have shown can be effected in a variety of metal coordination spheres.[18] However, the mechanism involves a catalyst-bound alkylidene (RCH=M) that is also reactive towards alkynes—as evidenced by the wide use of ene/yne metathesis in organic synthesis.[19] Addition to either the $P(CH_2)_6CH{=}CH_2$ (desired) or $[Pt(C{\equiv}C)_4Pt]$ (undesired) moieties might occur. Furthermore, two isomeric products would be possible: one in which phosphane ligands on opposite platinum atoms are joined (**5**, desired; similar to **7**), and one in which phosphane



Scheme 3. Synthesis of a double-helical complex through C=C metathesis. TMEDA = tetramethylethylenediamine.

 © WILEY-VCH Verlag GmbH, 69451 Weinheim, Germany, 2002 1433-7851/02/4111-1873 $ 20.00+.50/0

ligands on the same platinum atom are joined to give an unusual *trans*-spanning diphosphane (**6**, undesired; similar to **8**). Statistically, the former is twice as probable, but the viability of the latter has been explicitly demonstrated.[18]

The reaction of **4** with Grubbs's ruthenium metathesis catalyst[20] gave a mixture (96%) of *cis*/*trans* C=C isomers of **5** and/or **6** according to physical data. To simplify analysis, we sought to hydrogenate the C=C bonds without affecting the C≡C bonds. We were unaware of precedents for such selectivity, but a standard method gave exclusively C=C hydrogenation (Scheme 3; 93%), as assayed by mass spectrometric and NMR spectroscopic analysis. We view this as evidence for the shielding of the sp carbon chain by the sp^3 carbon chains. As many as five ^{31}P NMR signals were observed, suggesting the presence of higher-order metathesis products not detected in the mass spectrum. Chromatography gave a highly crystalline species, shown below to have the desired structure **7**, in 32% yield. An authentic sample of **8** (Scheme 3), which has *trans*-spanning diphosphane ligands, was independently prepared.[21] NMR analyses of product mixtures showed comparable amounts of **7** and **8**.

The crystal structures of both benzene and toluene sesquisolvates of **7** were determined.[22] Figure 1 offers five views (**H**–**L**) of the striking double-helical motif found in each. The planes of the platinum termini (P-Pt-P/Pt) define angles of 196.5°—more than a half twist. The sp and sp^3 carbon chains entwine with a spacing slightly greater than their van der Waals radii. The shielding of the sp carbon chain is extensive in **K**, but less in **L**, where a line of sight through a protecting rim of peripheral groups remains. The bond lengths and angles, and the slight sp carbon chain curvature in **7**, are unexceptional. They are very close to those of $[(C_6F_5)(p\text{-tol}_3P)_2Pt(C{\equiv}C)_4Pt(Pp\text{-tol}_3)_2(C_6F_5)]$ (**9**),[23] which lacks bridging diphosphanes, and other model compounds.[24]

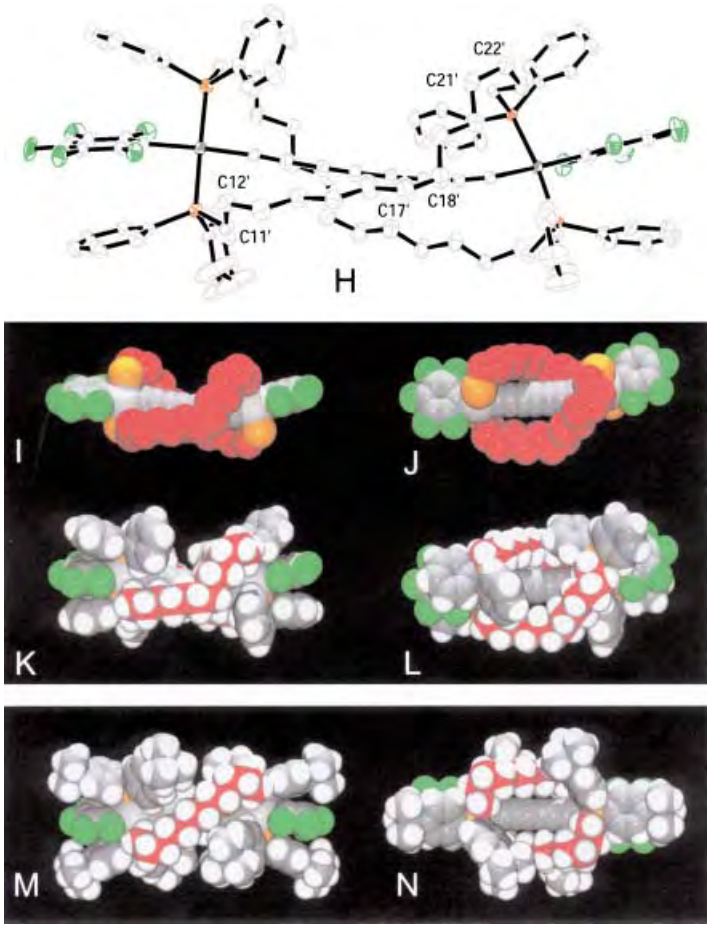
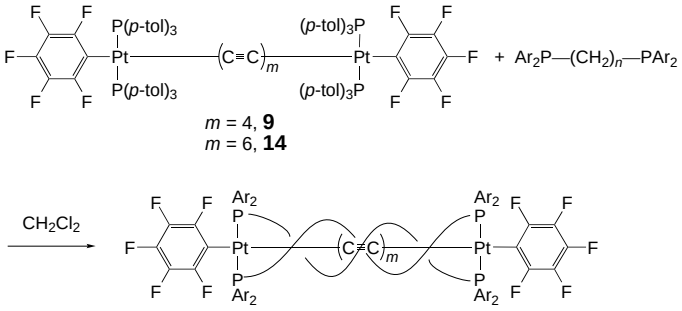


Figure 1. Structures of double-helical $[Pt(C{\equiv}C)_4Pt]$ complexes. **H**: ORTEP diagram of **7**; **I**, **J**: views of **7** parallel and perpendicular, respectively, to the planes of the C_6F_5 ligands with phenyl rings and hydrogen atoms omitted and the other atoms at van der Waals radii; **K**, **L**: analogous views of **7** but with phenyl rings and hydrogen atoms; **M**, **N**: analogous views of **11**.

Double-helical **7** is chiral, and both enantiomers are present in the unit cell. Stereogenesis can be analyzed as follows. One sp^3 carbon chain exhibits four *gauche* $CH_2CH_2CH_2X$ segments (X = CH_2, P) with torsion angles of ca. 60° (see C11′-C12′, C17′-C18′, C21′-C22′, C22′-C23′ in **H**), and the other three. Such segments are inherently chiral. In order for enantiomers of **7** to interconvert, each *gauche* segment must "untwist" to an *anti* conformation (torsion angle 180°), and then continue to a *gauche* segment of the opposite chirality. These motions need not occur in concert. However, each will be coupled to other conformational changes. Together, these provide the bulk of the energy barrier for enantiomer interconversion, a subject we return to below.

With the accessibility and double-helical structure of **7** confirmed, we checked whether detectable quantities might be generated by substitution reactions of the type in Scheme 2. As shown in Scheme 4, the $[Pt(C{\equiv}C)_4Pt]$ complex



Scheme 4. Syntheses of double-helical and nonhelical complexes by substitution at high dilution. For preparative details see Table 1.

9 was treated with the diphosphane $Ph_2P(CH_2)_{14}PPh_2$ under moderately dilute conditions. To our great surprise, **7** could be isolated in 87% yield (Table 1); none of the isomer **8** was detected. Reactions with analogous diphosphanes bearing

Table 1. Experimental details of the reactions shown in Scheme 4.

m	*n*/Ar	*c*(**9**) or *c*(**14**) [mM]	Product	Yield [%]	sp^3/sp ratio	Structure
4	14/Ph	2.5	**7**	87	1.75	helical
4	14/*p*-tol	1.9	**10**	91	1.75	helical
4	14/*p*-C_6H_4tBu	1.5	**11**	77	1.75	helical
4	10/Ph	1.0	**12**	80	1.25	nonhelical[a]
4	11/Ph	1.0	**13**	80	1.38	–[b]
6	18/Ph	0.025	**15**	27	1.50	helical and nonhelical

[a] Helical structure impossible. [b] No crystal structure.

 © WILEY-VCH Verlag GmbH, 69451 Weinheim, Germany, 2002 1433-7851/02/4111-1874 $ 20.00+.50/0 *Angew. Chem. Int. Ed.* **2002**, *41*, No. 11

para-substituted phenyl rings gave the corresponding complexes **10** (*p*-Me) and **11** (*p*-*tert*-butyl) in 91 and 77 % yields, respectively. These also crystallized in double-helical motifs (189.8 and 193.3° twisted). The structure of the latter is shown as **M** and **N** in Figure 1. The sp^3 carbon chains are more symmetrically arrayed than in **7**, with two four-carbon *gauche* segments in every $P(CH_2)_5$ moiety. The *tert*-butyl groups enhance the overall steric protection.

Next we expanded the range of sp^3 and sp carbon chain lengths investigated. As shown in Scheme 4 and Table 1, **9** and the shorter-chain diphosphanes $Ph_2P(CH_2)_nPPh_2$ ($n = 10$, 11) were reacted at higher dilution. Workup gave the corresponding complexes **12** and **13** (80 %), respectively, with sp^3:sp carbon ratios (1.25, 1.38) appreciably lower than for **7**, **10**, and **11** (1.75). Two polymorphs of **12** crystallized (**O**, **P**; Figure 2), which, as expected, showed nonhelical motifs. The sp^3 carbon chains of the first were slightly disordered and laterally shielded the sp carbon chain. The sp^3 carbon chains of the second bowed in similar directions, exposing more of the sp carbon chain. The $[Pt(C{\equiv}C)_6Pt]$ complex **14**[23] was treated at very high dilution with the longer-chain diphosphane $Ph_2P(CH_2)_{18}PPh_2$ (Scheme 4, Table 1). Workup gave the corresponding complex **15** (27 %), with an sp^3:sp carbon ratio of 1.50, as well as oligomeric material. In crystalline **15** two independent molecules are present in the unit cell (**Q**, **R**; Figure 2). The first exhibits a double-helical motif, but less twisted than the others (163.2°). The second is nonhelical. Hence, we currently consider an sp^3:sp carbon ratio of 1.50 as the minimum required for helicity.

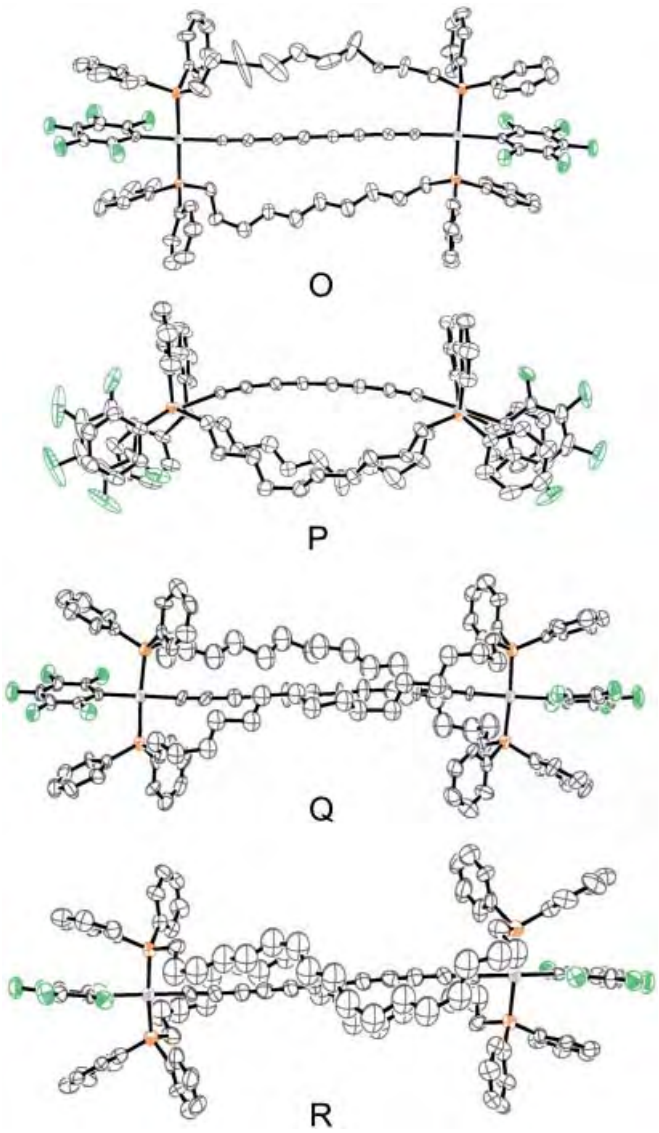


Figure 2. Molecular structures of other complexes (ORTEP diagrams). **O**, **P**: polymorphs of **12**; **Q**, **R**: the helical and nonhelical conformers of **15**.

Each of the synthesized molecules that could reasonably be expected to adopt a double-helical structure crystallizes in this structure. The phenomenon is no isolated occurrence. Thus, it is likely that similar motifs are favored in solution, and not imposed solely by crystal lattices. Helical molecules usually contain diastereotopic groups, such as the *tert*-butyl substituents in **11**. In solution, separate NMR signals are often observed.[7] However, when the helix can "untwist" and invert configuration, exchange occurs, giving a single signal. At the lowest feasible NMR temperatures, we see only one signal for the various diastereotopic groups in **7**, **10**, and **11**.[25] We interpret this as indicating a low barrier, on the order of 12 kcal mol^{-1}, for interconverting enantiomeric double helices. This would involve torsional motions about *gauche* segments as analyzed above, and the possible intermediacy of achiral conformers such as **F** and **G** (see Scheme 1).

The estimated barrier of 12 kcal mol^{-1} represents a measure of sp carbon chain protection—just as electrical wire coatings can be graded for durability under various conditions. We expect such barriers to correlate to the extra activation energy required for attack upon the sp carbon chains in **7**, **10**, and **11**, versus model compounds such as **9** lacking double-helical sheathing. In this regard, the $[Pt(C{\equiv}C)_mPt]$ complexes undergo electrochemical oxidation to labile radical cations. The cyclic voltammogram of **10** indicates a much more reversible oxidation than for **9**, and thus a kinetically more stable radical cation (ratio of cathodic to anodic currents, 0.71 and 0.49, respectively).[26] We are presently attempting to synthesize analogs of **7** with higher barriers. However, from the standpoint of device engineering, the ultimate goal is a portfolio of flexible bridges with a gradation of barriers.

Dynamic issues aside, our molecules are unique in the *absence* of bonding interactions or complementarity along the two helical chains. The sp carbon chain provides a mechanical support, without which the helical motif would not be an energetically competitive conformation. This represents the first molecular analog of a beanpole, an implement known to the most ancient agrarian societies.[27] The double-helical conformation is volumetrically compact, and crystal packing forces may play a role in the solid state. However, van der Waals attractions between the sp^3 and sp carbon chains should also be significant, as evidenced by studies showing that the affinities of single-helical foldamers for rodlike guests depend upon their lengths.[28]

In conclusion, we have discovered a surprising new class of double-helical molecules that can be accessed by directed syntheses (Scheme 3) and simple substitution processes (Scheme 4). The latter holds promise for the self-assembly of molecular-scale devices, whereas the alkene metathesis/hydrogenation sequence in the former can be viewed as an

 © WILEY-VCH Verlag GmbH, 69451 Weinheim, Germany, 2002 1433-7851/02/4111-1875 $ 20.00+.50/0

annealing protocol that cements a target structure in place. It can be expected that these wirelike assemblies, insulated similarly to shrink-wrapped electrical cord, can be extended to a variety of redox-active endgroups with various coordination geometries. This novel family of building blocks is certain to have applications in nanotechnology.

Received: February 28, 2002 [Z18795]

[1] A. E. Rowan, R. J. M. Nolte, *Angew. Chem.* **1998**, *110*, 65; *Angew. Chem. Int. Ed.* **1998**, *37*, 63.

[2] For brevity, the introductory references emphasize double-helical molecules—the theme of this study. A rich literature on relevant single- and triple-helical molecules also exists.

[3] J.-M. Lehn, A. Rigault, J. Siegel, J. Harrowfield, B. Chevrier, D. Moras, *Proc. Natl. Acad. Sci. USA* **1987**, *84*, 2565.

[4] a) C. Piguet, G. Bernardinelli, G. Hopfgartner, *Chem. Rev.* **1997**, *97*, 2005; b) M. Albrecht, *Chem. Rev.* **2001**, *101*, 3457.

[5] a) D. P. Funeriu, J.-M. Lehn, K. M. Fromm, D. Fenske, *Chem. Eur. J.* **2000**, *6*, 2103; b) V. Berl, I. Huc, R. G. Khoury, J.-M. Lehn, *Chem. Eur. J.* **2001**, *7*, 2810.

[6] O. Mamula, A. von Zelewsky, T. Bark, G. Bernardinelli, *Angew. Chem.* **1999**, *111*, 3129; *Angew. Chem. Int. Ed.* **1999**, *38*, 2945.

[7] M. Ohkita, J.-M. Lehn, G. Baum, D. Fenske, *Chem. Eur. J.* **1999**, *5*, 3471.

[8] P. F. H. Schwab, M. D. Levin, J. Michl, *Chem. Rev.* **1999**, *99*, 1863.

[9] a) J. M. Tour, A. M. Rawlett, M. Kozaki, Y. Yao, R. C. Jagessar, S. M. Dirk, D. W. Price, M. A. Reed, C.-W. Zhou, J. Chen, W. Wang, I. Campbell, *Chem. Eur. J.* **2001**, *7*, 5118; b) *Molecular Switches* (Ed.: B. Feringa), Wiley-VCH, Weinheim, **2001**; c) "Molecular Machines": *Acc. Chem. Res.* **2001**, *34*, 409–522 (special issue).

[10] a) M. I. Bruce, *Coord. Chem. Rev.* **1997**, *166*, 91; b) F. Paul, C. Lapinte, *Coord. Chem. Rev.* **1998**, *178–180*, 427; c) G. Schermann, T. Grösser, F. Hampel, A. Hirsch, *Chem. Eur. J.* **1997**, *3*, 1105.

[11] Full papers from our laboratory: a) W. Weng, T. Bartik, M. Brady, B. Bartik, J. A. Ramsden, A. M. Arif, J. A. Gladysz, *J. Am. Chem. Soc.* **1995**, *117*, 11922; b) M. Brady, W. Weng, Y. Zhou, J. W. Seyler, A. J. Amoroso, A. M. Arif, M. Böhme, G. Frenking, J. A. Gladysz, *J. Am. Chem. Soc.* **1997**, *119*, 775; c) S. B. Falloon, S. Szafert, A. M. Arif, J. A. Gladysz, *Chem. Eur. J.* **1998**, *4*, 1033; d) T. Bartik, W. Weng, J. A. Ramsden, S. Szafert, S. B. Falloon, A. M. Arif, J. A. Gladysz, *J. Am. Chem. Soc.* **1998**, *120*, 11071; e) R. Dembinski, T. Bartik, B. Bartik, M. Jaeger, J. A. Gladysz, *J. Am. Chem. Soc.* **2000**, *122*, 810; f) W. E. Meyer, A. J. Amoroso, C. R. Horn, M. Jaeger, J. A. Gladysz, *Organometallics* **2001**, *20*, 1115.

[12] G. W. Gokel, *Crown Ethers and Cryptands*, Royal Society of Chemistry, Cambridge, UK, **1991**, chapter 4.

[13] For excellent recent reviews of these and related themes, see *Electron Transfer in Chemistry*, *Vol. 3*, *Part 2*, *and Vol. 5*, *Part 1* (Ed.: V. Balzani), Wiley-VCH, Weinheim, **2001**.

[14] Others have reported complementary approaches to shielding unsaturated assemblies that connect two electroactive groups: a) S. Anderson, R. T. Aplin, T. D. W. Claridge, T. Goodson III, A. C. Maciel, G. Rumbles, J. F. Ryan, H. L. Anderson, *J. Chem. Soc. Perkin Trans. 1* **1998**, 2383; b) P. N. Taylor, M. J. O'Connell, L. A. McNeill, M. J. Hall, R. T. Aplin, H. L. Anderson, *Angew. Chem.* **2000**, *112*, 3598; *Angew. Chem. Int. Ed.* **2000**, *39*, 3456; c) A. P. H. J. Schenning, J.-D. Arndt, M. Ito, A. Stoddart, M. Schreiber, P. Siemsen, R. E. Martin, C. Boudon, J.-P. Gisselbrecht, M. Gross, V. Gramlich, F. Diederich, *Helv. Chim. Acta* **2001**, *84*, 296; d) J. E. H. Buston, F. Marken, H. L. Anderson, *Chem. Commun.* **2001**, 1046.

[15] T. B. Peters, J. C. Bohling, A. M. Arif, J. A. Gladysz, *Organometallics* **1999**, *18*, 3261.

[16] K. Sünkel, U. Birk, C. Robl, *Organometallics* **1994**, *13*, 1679.

[17] W. E. Hill, D. M. A. Minahan, J. G. Taylor, C. A. McAuliffe, *J. Am. Chem. Soc.* **1982**, *104*, 6001.

[18] J. Ruwwe, J. M. Martín-Alvarez, C. R. Horn, E. B. Bauer, S. Szafert, T. Lis, F. Hampel, P. C. Cagle, J. A. Gladysz, *Chem. Eur. J.* **2001**, *7*, 3931.

[19] a) M. Mori, *Top. Organomet. Chem.* **1998**, *1*, 131; b) for a C≡C addition to $[Cl_2L_2Ru{=}CHPh]$, see T. M. Trnka, M. W. Day, R. H. Grubbs, *Organometallics* **2001**, *20*, 3845.

[20] T. M. Trnka, R. H. Grubbs, *Acc. Chem. Res.* **2001**, *34*, 18.

[21] E. B. Bauer, F. Hampel, J. A. Gladysz, unpublished results.

[22] CCDC-171481–CCDC-171486 contain the supplementary crystallographic data for this paper. These data can be obtained free of charge via www.ccdc.cam.ac.uk/conts/retrieving.html (or from the Cambridge Crystallographic Data Centre, 12, Union Road, Cambridge CB21EZ, UK; fax: (+44) 1223-336-033; or deposit@ccdc.cam.ac.uk).

[23] W. Mohr, J. Stahl, F. Hampel, J. A. Gladysz, *Inorg. Chem.* **2001**, *40*, 3263.

[24] a) T. B. Peters, Q. Zheng, J. Stahl, J. C. Bohling, A. M. Arif, F. Hampel, J. A. Gladysz, *J. Organomet. Chem.* **2002**, *641*, 53; b) W. Mohr, T. B. Peters, J. C. Bohling, F. Hampel, A. M. Arif, J. A. Gladysz, *C. R. Chim.* **2002**, *5*, 111.

[25] **7**: in CD_2Cl_2 (−40 °C, solubility limit), in $[D_8]$toluene (−90 °C, ^{13}C NMR signals *i*/*p* to P); **10**: in $[D_8]$THF (−120 °C, ^{13}C NMR signals *i*/*p* to P, ^1H and ^{13}C NMR signals of CH_3 groups); **11**: in $[D_8]$THF (−120 °C, ^{13}C NMR signals *i*/*p* to P, ^1H and ^{13}C NMR signals of $C(CH_3)_3$ groups).

[26] CH_2Cl_2, 100 mV s^{-1}, E° vs SCE (ferrocene = 0.46 V), **10**/**9**: $E_{p,a}$ 1.259/1.261 V; $E_{p,c}$ 1.168/1.143 V; E° 1.214/1.202 V; ΔE 91/118 mV.

[27] To our knowledge, the closest analogues would be biphenyls in which the *o*/*o* and *o*′/*o*′ positions are bridged by methylene chains. Systems with as many as four methylene groups have been described: K. Müllen, W. Heinz, F.-G. Klärner, W. R. Roth, I. Kindermann, O. Adamczak, M. Wette, J. Lex, *Chem. Ber.* **1990**, *123*, 2349.

[28] a) A. Tanatani, M. J. Mio, J. S. Moore, *J. Am. Chem. Soc.* **2001**, *123*, 1792; b) A. Tanatani, T. S. Hughes, J. S. Moore, *Angew. Chem.* **2002**, *114*, 335; *Angew. Chem. Int. Ed.* **2002**, *41*, 325.

cis–*trans* Selectivity of Enzyme-Catalyzed Additions to 4-Substituted Cyclohexanones—Correlation with the Prelog/Ringold Model of Enzymatic Hydrogenation**

Franz Effenberger,* Jürgen Roos, and Christoph Kobler

Dedicated to Professor Lutz F. Tietze on the occasion of his 60th birthday

V. Prelog and co-workers were the first to use the conformational stability of cyclic ketones and alcohols to make a statement about the topography of the active site of an enzyme.[1] The enzymatic hydrogenation of 4-substituted cyclohexanones using NADH-dependent horse-liver alcohol dehydrogenase (LADH; NADH = nicotinamide adenine dinucleotide, reduced form) was particularly suitable for this

[*] Prof. Dr. F. Effenberger, Dr. J. Roos, Dipl.-Chem. C. Kobler
Institut für Organische Chemie
Universität Stuttgart
Pfaffenwaldring 55, 70569 Stuttgart (Germany)
Fax: (+49) 711-685-4269
E-mail: franz.effenberger@po.uni-stuttgart.de

[**] Enzyme-catalyzed reactions, Part 44. This work was supported by Degussa AG. We thank Dr. B. Miehlich for modeling calculations and Dr. A. Baro for assistance in preparing the manuscript. Part 43: F. Effenberger, S. Oßwald, *Tetrahedron: Asymmetry* **2001**, *12*, 2581–2587.

purpose. Assuming a defined spatial arrangement of the amino acid residues and the NADH for the "hydride ion" transfer in the enzyme–substrate complex, then the different binding modes of the cyclohexanones in the active site must be responsible for the formation of *cis* and *trans* isomers.

Based on this idea, H. J. Ringold and co-workers investigated the influence of substituents in the 3- and 4-positions of cyclohexanone on the stereochemical outcome of the LADH-catalyzed hydrogenation to cyclohexanols.[2] Comprehensive correlations of hydrogenation rates and the stereochemistry of product formation resulted in models for two types of enzyme–substrate complexes, capable of plausibly explaining the stereoselectivity of hydrogenation.[2] "Horizontal" orientation of the cyclohexanone in the active site should give the *cis* isomer, and a "vertical" orientation should give the corresponding *trans* isomer (Figure 1).[2b]

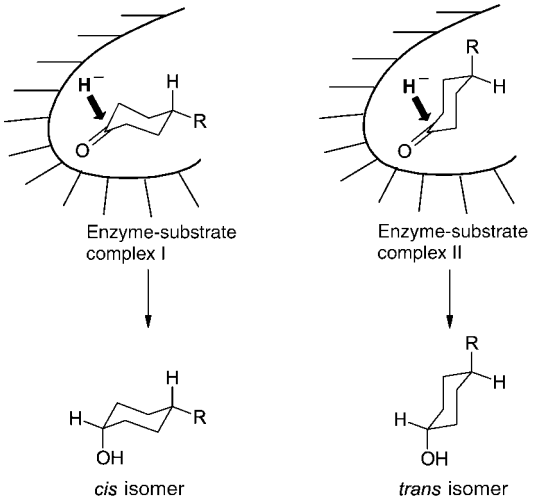


Figure 1. Formation of the *cis* and *trans* alcohol by the LADH-catalyzed hydrogenation of 4-substituted cyclohexanones.[2b]

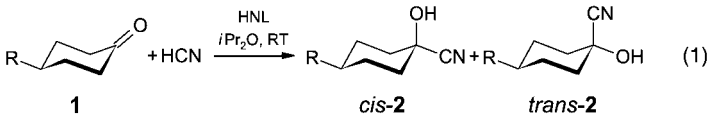
Although X-ray crystal structures of LADH have been published[3a, b] and the structure of ketone–enzyme adducts for drosophila ADH was also solved,[3c] the Prelog/Ringold model based on the stereoselectivity of cyclohexanone hydrogenation has not been confirmed.

The NADH-dependent enzymatic hydrogenation of carbonyl compounds mechanistically resembles the hydroxynitrile-lyase (HNL) catalyzed addition of HCN to carbonyl compounds, which yields cyanohydrins.[4] In both cases, the primary addition of the nucleophile, either hydride or cyanide, determines the stereochemistry of the product formation.

In the past few years, the HNL-catalyzed addition of HCN to prochiral aldehydes and alicyclic ketones, to give optically active cyanohydrins, has been intensively investigated.[5, 6] Herein, we report the corresponding reaction with 4-substituted cyclohexanones. This reaction is of interest in two respects: first, how well the results fit to the Prelog/Ringold model, and second, the stereoselective preparation of 4-substituted cyclohexanone cyanohydrins as starting compounds for, for example, substituted tetronic acids, known to be potent herbicides and insecticides.[7]

The synthesis of very few 4-substituted cyclohexanone cyanohydrins has been described to date.[8–10] In all cases, mixtures of *cis*–*trans* isomers were obtained. For the 4-methyl compound, the *cis*:*trans* ratio is 1:2 and in the case of the 4-*tert*-butyl derivative, the *cis*:*trans* ratio is 1:3. These ratios are the same under base catalysis,[10a] and are therefore assumed to correspond to the thermodynamic equilibria.

In the HNL-catalyzed preparation of the 4-substituted cyclohexanone cyanohydrins **2**, the hydroxynitrile lyases from almonds ((*R*)-PaHNL) and cassava ((*S*)-MeHNL) have been applied. The cyclohexanones **1** are good substrates for both enzymes [Eq. (1)], which exhibit high *cis* and *trans* selectivity,



(1)

respectively (Table 1). The structures of the stereoisomers were assigned by NMR spectroscopy, by comparison with literature data.[11] The (*R*)-PaHNL-catalyzed reaction afforded almost exclusively *trans* isomers with all ketones **1a–g** (Table 1), but (*S*)-MeHNL catalyzes the HCN addition to **1** in favor of the *cis* isomers. Only 4-methylcyclohexanone (**1a**) shows a low stereoselectivity. The reaction rate with (*S*)-MeHNL is considerably faster than that with (*R*)-PaHNL,

Table 1. Preparation of cyclohexanone cyanohydrins **2** by (*S*)-MeHNL- and (*R*)-PaHNL-catalyzed addition of HCN to the 4-substituted cyclohexanones **1** [Eq. (1)] and comparison to the addition without enzyme catalysis.[a]

		(*S*)-MeHNL[b]			(*R*)-PaHNL[b]			Without enzyme[c]	
	R	*t* [h]	conversion [%]	*cis*:*trans* [%]	*t* [h]	conversion [%]	*cis*:*trans* [%]	conversion [%]	*cis*:*trans* [%]
a	Me	2	80	35:65	1.5	99	3:97	4	17:83
b	Et	5	quant	74:26	22	99	2:98	0.5	16:84
c	Pr	5	93	96:4	31	83	2:98	< 1	15:85
d	*i*Pr	5	quant	97:3	22	94	1:99	< 1	13:87
e	*t*Bu	3	82	99:1	216	50	10:90	2	13:87
f	H_2C=CMe	9	99	98:2	24	99	1:99	2.5	11:89
g	Ph	3	95	99:1	264	71	4:96	28	9:91

[a] The support was treated as described previously.[5] [b] Substrates **1** (1 mmol) and HCN (150 μL, 3.9 mmol) were treated in diisopropyl ether (5 mL) with (*S*)-MeHNL (180 U) or (*R*)-PaHNL (200 U), as catalyst. Conversion and isomeric ratios were determined by GC after acetylation. [c] The enzyme solution was replaced by the same volume of sodium citrate buffer (0.02 M, pH 5.4). The reaction times were the same as those of the (*R*)-PaHNL-catalyzed conversions.

 © WILEY-VCH Verlag GmbH, 69451 Weinheim, Germany, 2002 1433-7851/02/4111-1877 $ 20.00+.50/0

even in case of the sterically demanding substrates **1e** and **1f** (Table 1).

The X-ray crystal structure of MeHNL[4] reveals that the active site is accessible by a narrow channel and consists of a smaller (S_1) and a larger binding pocket (S_2). In the acetone–MeHNL complex, the carbonyl group of the substrate is bound by hydrogen bonds from Thr11 and Ser80.[4] Whereas in the LADH hydrogenation, the hydride ion attacks the carbonyl group of cyclohexanone from "above" (Figure 1), the addition of cyanide in the MeHNL-catalyzed reaction occurs from "below",[4] so that, according to the Prelog/Ringold model, the *cis* isomer should be generated from the vertically positioned cyclohexanone ring. Superposition of the catalytically inactive mutant MeHNL–Ser80Ala complexed with acetone cyanohydrin, onto the MeHNL–acetone complex structure, reveals that the cyanohydrin is bound in an analogous manner to the ketone.[12]

Assuming the binding by hydrogen bonding in the active site, and the chair conformation of the cyclohexane ring with a preferentially equatorial *tert*-butyl group,[13] the *cis* selectivity of MeHNL can easily be explained by use of molecular-modeling calculations, as shown for **2e**. The *cis* isomer **2e** in its "vertical" position, bound by hydrogen bonds to Thr11 and Ser80, fits perfectly into the channel and the active site (Figure 2a). The corresponding "horizontally" positioned

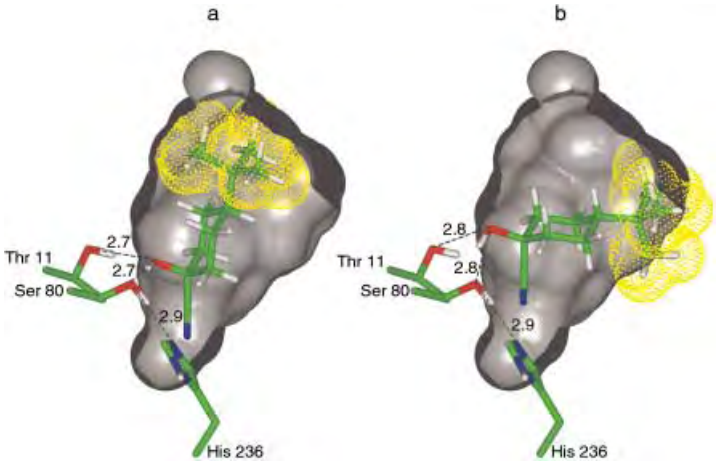


Figure 2. Molecular-modeling representation of the *cis* (a) and *trans* conformation (b) of 4-*tert*-butylcyclohexanone cyanohydrin **2e**, in the active site of (*S*)-MeHNL.

trans isomer **2e**, however, clearly clashes with the channel wall (Figure 2b). This model also explains the low stereoselectivity of the 4-methyl derivative **2a**, in which both the "vertical" and "horizontal" binding modes are sterically possible. Hence, it is not surprising that the *cis*:*trans* ratios for the HCN addition to **1a** vary, and depend, for example, on enzyme activity and reaction conditions.

The major isomer of cyanohydrin **2f**, obtained by MeHNL-catalyzed HCN addition to **1f**, was crystallized as the *p*-nitrobenzoyl derivative. Its X-ray crystal structure[14] (Figure 3) provides clear experimental evidence for the formation of the *cis* isomer (Table 1) and thus supports the modeling calculations for the *tert*-butyl derivative **2e**. The *trans* selectivity of PaHNL cannot yet be explained by structural arguments, because too little is known about the enzyme structure.[15]

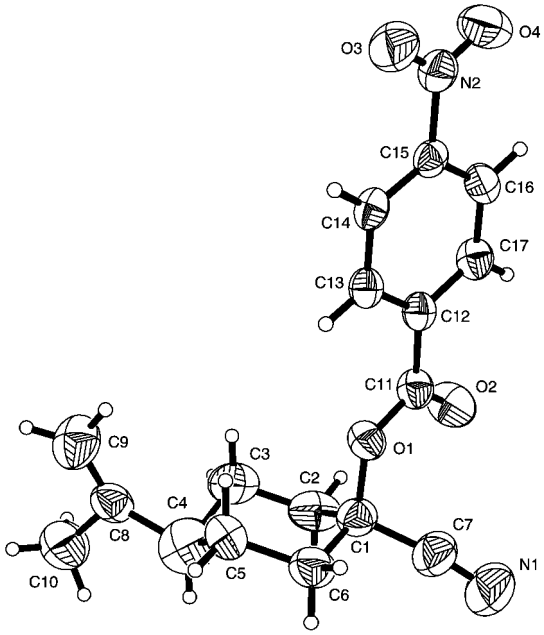


Figure 3. X-ray crystal structure of the *p*-nitrobenzoyl derivative of **2f**.

Received: November 26, 2001 [Z18279]

[1] a) V. Prelog, *Pure Appl. Chem.* **1964**, *9*, 119–130; b) H. Dutler, M. J. Coon, A. Kull, A. Vogel, G. Waldvogel, V. Prelog, *Eur. J. Biochem.* **1971**, *22*, 203–212; c) J. Rétey, J. A. Robinson, *Stereospecificity in Organic Chemistry and Enzymology*, Verlag Chemie, Weinheim, **1982**, pp. 73–82.
[2] a) J. M. H. Graves, A. Clark, H. J. Ringold, *Biochemistry* **1965**, *4*, 2655–2671; b) J. B. Jones in *Applications of Biochemical Systems in Organic Chemistry*, *Part I* (Eds.: J. B. Jones, C. J. Sih, D. Perlman), Wiley, New York, **1976**, pp. 15–18.
[3] a) S. Al-Karadaghi, E. S. Cedergren-Zeppezauer, S. Hövmoller, K. Petratos, H. Terry, K. S. Wilson, *Acta Crystallogr. Sect D* **1994**, *50*, 793–807; b) S. Ramaswamy, H. Eklund, B. V. Plapp, *Biochemistry* **1994**, *33*, 5230–5237; c) J. Benach, S. Atrian, R. Gonzàlez-Duarte, R. Ladenstein, *J. Mol. Biol.* **1999**, *289*, 335–355.
[4] H. Lauble, S. Förster, B. Miehlich, H. Wajant, F. Effenberger, *Acta Crystallogr. Sect D* **2001**, *57*, 194–200.
[5] a) F. Effenberger, *Angew. Chem.* **1994**, *106*, 1609–1619; *Angew. Chem. Int. Ed. Engl.* **1994**, *33*, 1555–1564; b) F. Effenberger in *Stereoselective Biocatalysis* (Ed.: R. N. Patel), Marcel Dekker, New York, **2000**, pp. 321–342.
[6] a) M. Schmidt, H. Griengl, *Top. Curr. Chem.* **1999**, *200*, 193–226; b) R. J. H. Gregory, *Chem. Rev.* **1999**, *99*, 3649–3682.
[7] R. Fischer, B. W. Krüger, H.-J. Santel, M. Dollinger, U. Wachendorff-Neumann, C. Erdelen (Bayer AG), Ger. Offen. DE 4337853, **1995** [*Chem. Abstr.* **1995**, *123*, 32947p].
[8] a) R. D. Desai, R. F. Hunter, G. Khan, G. S. Saharia, *J. Chem. Soc.* **1936**, 416–419; b) G. A. Kraus, K. Frazier, *J. Org. Chem.* **1980**, *45*, 4820–4825.
[9] L. Munday, *J. Chem. Soc.* **1964**, 1413–1416.
[10] a) R. W. Freerksen, D. S. Watt, *Synth. Commun.* **1976**, *6*, 447–451; b) H. Ohno, A. Mori, S. Inoue, *Chem. Lett.* **1993**, 375–378.
[11] M. Mousseron, J.-M. Kamenka, M. R. Darvich, *Bull. Soc. Chim. Fr.* **1970**, 208–211.
[12] H. Lauble, B. Miehlich, S. Förster, H. Wajant, F. Effenberger, *Protein Sci.* **2001**, *10*, 1015–1022.

 © WILEY-VCH Verlag GmbH, 69451 Weinheim, Germany, 2002 1433-7851/02/4111-1878 $ 20.00+.50/0

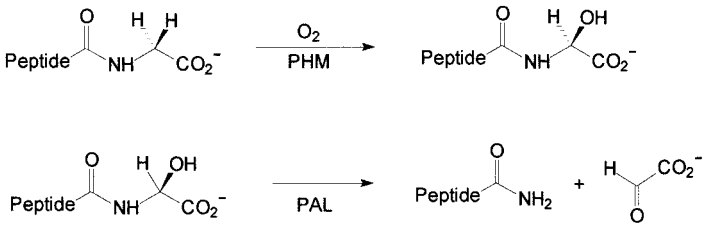
[13] a) J. M. A. Baas, B. van de Graaf, A. van Veen, B. M. Wepster, *Recl. Trav. Chim. Pays-Bas* **1980**, *99*, 228–233; b) E. L. Eliel, N. L. Allinger, S. J. Angyal, G. A. Morrison, *Conformational Analysis*, Interscience, New York, **1965**, pp. 436–443.
[14] CCDC-174989 contains the supplementary crystallographic data for this paper. These data can be obtained free of charge via www.ccdc.cam.ac.uk/conts/retrieving.html (or from the Cambridge Crystallographic Data Centre, 12, Union Road, Cambridge CB2 1EZ, UK; fax: (+44) 1223-336-033; or deposit@ccdc.cam.ac.uk).
[15] I. Dreveny, K. Gruber, A. Glieder, A. Thompson, C. Kratky, *Structure (Cambridge)* **2001**, *9*, 803–815.

Selective α-Carbon Hydroxylation of Glycine in Nickel(II)–Cyclotetrapeptide Complexes by Oxygen**

Katharina Haas, Harald Dialer, Holger Piotrowski, Jan Schapp, and Wolfgang Beck*

Dedicated to Professor Ernst-Ludwig Winnacker on the occasion of his 60th birthday

The copper-containing bifunctional enzyme peptidylglycine α-amidating monooxygenase (PAM) catalyzes the bioactivation of peptide hormones by amidation.[1] In the first step the copper-containing peptidylglycine α-hydroxylating monooxygenase (PHM) catalyzes the stereospecific hydroxylation of the C-terminal glycine to give an α-hydroxyglycine peptide (Scheme 1). A second enzyme, the peptidyl-α-hydroxyglycine

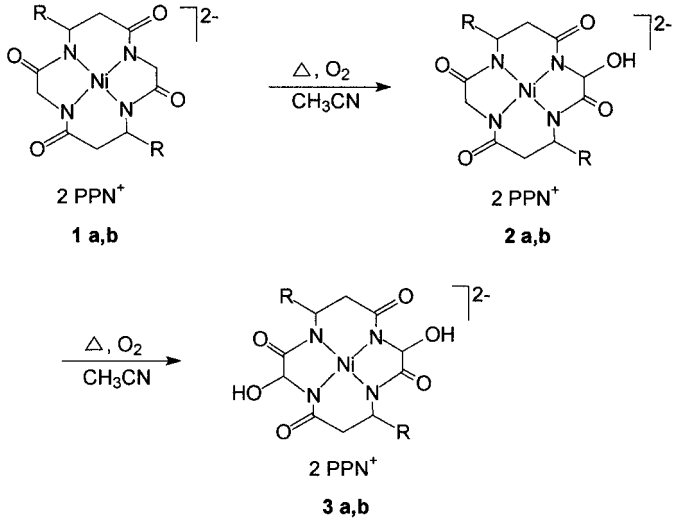


Scheme 1. Steps in the bioactivation of peptide hormones.

α-amidating lyase (PAL) generates the bioactive peptide amide and glyoxylate under α-C–N cleavage. Some reactions which are related to these transformations have been reported:

- The reactions of nickel(II) complexes of open-chain peptides with oxygen occur via nickel(III) intermediates to give oxidative cleavage of the terminal glycine α-C–N bond.[2]
- The nickel(II) complex [Ni^{II}(Gly-Gly-His)] is decarboxylated and α-C hydroxylated by oxygen via a nickel(III) intermediate.[3] This reaction can lead to the formation of DNA adducts.[4]
- α-C hydroxylation of the amino acid component in Ni^{II} Schiff base complexes from salicylaldehyde and α-amino acid esters which is followed by C–N cleavage was observed by Paul Pfeiffer,[5] one of the fathers of coordination chemistry.
- The copper(II)-mediated α-hydroxylation of an *N*-acylglycine,[6] the glycine-specific α-C–N cleavage of a dipeptide by nickel and copper peroxide,[7] and especially the α-hydroxylation of glycine-containing dipeptide ligands in a Co^{III} terpyridine complex by oxygen[8] are models for PAM.

The cyclocondensation of non-activated dipeptide esters at Cu^{II}, Ni^{II}, and Pd^{II} templates is a simple and attractive synthesis of cyclotetrapeptides.[9, 10] Cyclotetrapeptides are of interest for, among others, the formation of optically active, C-substituted cyclams. Following the method which was introduced by Neumann et al.[11] for the reduction of cyclopentapeptides, the carbonyl functions of cyclotetrapeptides can be reduced with $LiAlH_4$.[12] We have now found that α-hydroxylation of the glycine components of the cyclopeptide ligands in the nickel(II) complexes **1a**, **b** occurs stepwise on heating the complexes in acetonitrile in air to give the compounds **2** and **3** (Scheme 2). The monohydroxylated



Scheme 2. α-C hydroxylation of the cyclotetrapeptide complex **1** by atmospheric oxygen. **1a**–**3a**: R = H; **1b**–**3b**: R = CO_2Me.

species **2a**-$(PPN)_2$ (PPN = triphenyl[triphenylphosphoranylidene)amino]phosphonium) precipitates from the solution as orange crystals, which on heating in a saturated acetonitrile solution react with the oxygen in the air to afford the dihydroxylated complex **3a**-$(PPN)_2$. Because of the strong bonding of the cyclotetrapeptide to the Ni^{II} center an α-C–N cleavage does not take place and the rare α-hydroxyglycine unit remains intact.

In the mass spectra (FAB or ESI) of **2** and **3** the ions [M^{2-}] (171, **3a**) and [$M^{2-}+H^+-H_2O$] (M = **2a**, **b**, **3b**) were detected. The transformation of the C_2-symmetric complex **1a** to the

[*] Prof. W. Beck, Dr. K. Haas, Dr. H. Dialer, Dr. H. Piotrowski, Dipl.-Chem. J. Schapp
Department Chemie der Ludwig-Maximilians-Universität
Butenandtstrasse 5–13, 81377 Munich (Germany)
Fax: (+49) 89-2180-7866
E-mail: wbe@cup.uni-muenchen.de

[**] Metal complexes of biologically important ligands, Part 144. For Part 143 see: J. Schapp, W. Beck, *Z. Naturforsch.* **2002**, *576*, 280–284. This work was supported by the Deutsche Forschungsgemeinschaft and Fonds der Chemischen Industrie. We thank Professor Bernard Meunier, Tolouse, for a very valuable comment.

 © WILEY-VCH Verlag GmbH, 69451 Weinheim, Germany, 2002 1433-7851/02/4111-1879 $ 20.00+.50/0

asymmetric compound **2a** can be clearly detected in the ^{1}H and ^{13}C NMR spectra. Thus, for the amide carbon atoms two signals appear for **1a** and four signals for **2a** in the ^{13}C NMR spectra. The characteristic signal of the α-hydroxylated carbon atom appears downfield ($\delta = 90.2$ ppm). In the IR spectra intensive OH absorptions are observed at 3405 cm^{-1}. Because the compounds **2** are formed as enantiomers, the complexes **3** are formed as the corresponding diastereoisomers, as can be seen from the several overlapping sets of signals in the ^{1}H NMR spectra of **3a**.

The X-ray structure determination of **2a**-$(PPN)_2$[13] which was only successful after several attempts confirms the composition of the molecule. The nickel(II) ion is surrounded by the four N atoms of the cyclopeptide in a square-planar fashion. The hydroxy group, which results from the oxidation of the α-C atom, can be clearly detected (Figure 1). The complex anion crystallizes with two PPN counterions and with about 8.5 water molecules from the aqueous methanol solution. The solution of the structure was hampered by a low quality of the crystal and disorder of the complex in the crystal.

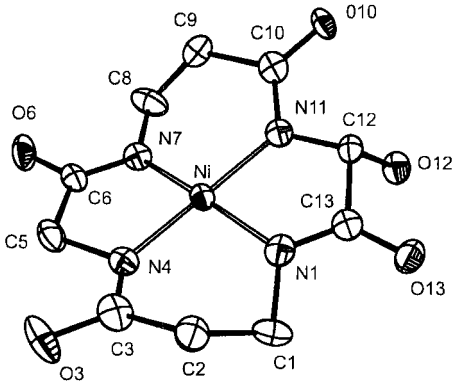
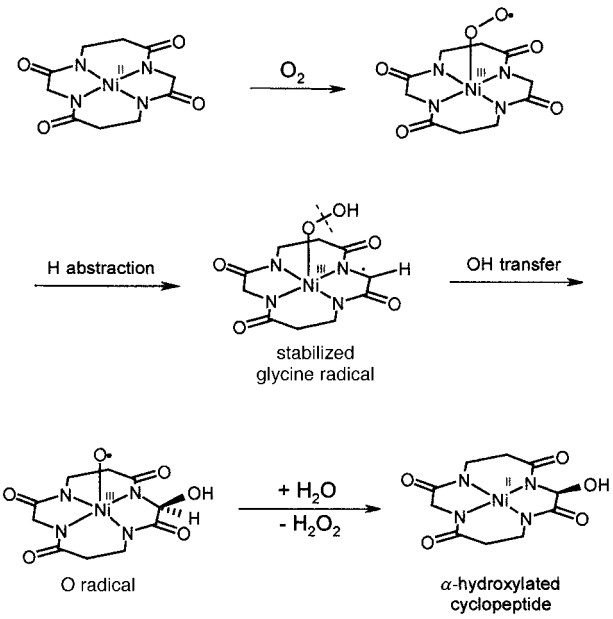


Figure 1. Molecular structure of the complex anion of **2a** (thermal ellipsoids set at 25% probability, hydrogen atoms omitted for clarity). The disordered molecule with the higher site-occupation factor is shown. The hydroxy group generated by oxidation is on C12. Selected bond lengths [pm] and angles [°]: Ni-N1 191.4(12), Ni-N4 188.1(12), Ni-N7 181.1(10), Ni-N11 187.7(12); N1-Ni-N4 94.2(5), N4-Ni-N7 86.6(5), N7-Ni-N11 97.6(5), N11-Ni-N1 82.3(5).

Solutions of **1** in acetonitrile turn deep red on exposure to the air. In the first step nickel(III) complexes are formed (Scheme 3)—confirmed by cyclic voltammetry—as also observed for the oxidation of Ni^{II} complexes with deprotonated open-chain peptide ligands.[14] The cyclic voltammogram of **1a** in acetonitrile shows perfect reversible redox behavior with the Ni^{II}/Ni^{III} event at a normal potential $E^0 = 615$ mV. For the oxidation of Ni^{II} complexes of open-chain peptides E^0 values of 800–850 mV were measured in aqueous solution.[15] For the PHM reaction it was demonstrated by $^{18}O_2$ experiments that the hydroxy groups originate from air oxygen and not from water[1, 16] which could attack an *N*-acyl imine or a glycine α-C cation. Mass spectra of the product of **1a** and $^{18}O_2$ containing air[17] point to a complex of the composition $[Ni(cyclo\text{-}\alpha\text{-OH-Gly-}\alpha\text{-OH-}\beta\text{-Ala} - 4H^+)_2(NCCH_3)_2]^{2-}$ with ^{18}O-containing hydroxy groups. In relation to the suggested mechanism of the PHM transformation[1] we formulate the



Scheme 3. Proposed mechanism for the α-hydroxylation of **1**.

hydroxylation of **1** as shown in Scheme 3 in which a glycine radical functions as an intermediate. Glycine radicals have been frequently observed, for example, in polypeptides.[18] We have found that complex **1** is an active catalyst for the disproportionation of hydrogen peroxide and thus **1** could exhibit superoxide bismutase activity.[19] Unexpectedly hydroxylation of the glycine component of the copper(II) complex $[Cu(cyclo\text{-Gly-}\beta\text{-Ala-Gly-}\beta\text{-Ala} - 4H^+)](PPN)_2$[9] could not be observed.

Experimental Section

2a-$(PPN)_2$: **1a**-$(PPN)_2 \cdot 5H_2O$ (74 mg; 0.5 mmol) was dissolved in CH_3CN (10 mL). The solution was heated in air to 80 °C for 5 min and on cooling to room temperature orange needle-shaped crystals formed. The crystals were collected and recrystallized from methanol/water, washed with water, and dried in vacuo at 60 °C, yield 61%. IR (KBr): $\tilde{\nu} = 3405.7$ (vs, br OH), 1576.7 (vs), 1569.0 (vs), 1539.7 cm^{-1} (vs; amide-I); ^{1}H NMR (400 MHz, CD_2Cl_2): $\delta = 7.70 - 7.47$ (m, 60H, PPN^+), 5.39 (s, 1H, OH), 4.91 (s, 1H, CH), 3.36 (s, 2H, CH_2), 2.79 (m, 2H, CH_2CH_2), 2.70 (m, 2H, CH_2CH_2); 1.96 (m, 2H, CH_2CH_2), 1.91 ppm (m, 2H, CH_2CH_2); ^{13}C NMR (68 MHz, CD_2Cl_2): $\delta =$ 180.2, 179.5, 177.8, 175.9 (CONR), 84.2 (CHOH), 55.1 (CH_2), 38.9, 39.3, 39.5, 39.8 ppm (CH_2CH_2); MS (ESI): *m*/*z* (%): 309 (24) $[M^{2-}+H^+ - H_2O]$, 327 (100), 328 (52), 329 (38) $[M^{2-}+H^+]$; 864, 865, 866 $[M^{2-}+PPN^+]$; elemental analysis calcd (%) for $C_{82}H_{72}N_6O_5P_4Ni \cdot 6H_2O$ (1512.192): C 65.13, H 5.59, N 5.55; found: C 65.08, H 5.56, N 5.54.

3a-$(PPN)_2$: **2a**-$(PPN)_2$ (45 mg, 0.03 mmol) was dissolved in CH_3CN (10 mL). The solution was heated in air to 80 °C for 5 min and on cooling to room temperature an orange, crystalline precipitate formed which was separated, recrystallized from methanol/water, washed with water and dried in vacuo at 60 °C. Orange crystals, yield 61%. IR (KBr): $\tilde{\nu} = 3408$ (vs, br; OH), 1575.8 (vs), 1535.8 cm^{-1} (vs, br, amide-I); ^{1}H NMR (400 MHz, CD_3OD): $\delta = 7.72 - 7.51$ (m, 60H, PPN^+), 5.13 (s, 2H, OH), 5.10 (s, 2H, OH), 3.65 – 3.55 (m, 2H, CHOH), 3.16 – 3.08 (m, 1H, CH_2CH_2), 2.92 – 2.83 (m, 1H, CH_2CH_2), 2.61 – 2.59 (m, 1H, CH_2CH_2), 2.15 – 1.99 ppm (m, 3H, CH_2CH_2); MS (ESI): *m*/*z* (%): 171 (4) $[M^{2-}]$, 325 (35) $[M^{2-}+H^+ - H_2O]$; 343 (100), 344 (67), 345 (51) $[M^{2-}+H^+]$, 880, 881, 882 $[M^{2-}+PPN^+]$; elemental analysis calcd (%) for $C_{82}H_{72}N_6O_6P_4Ni \times 5H_2O$ (1510.175): C 65.21, H 5.47, N 5.56; found: C 65.11, H 5.50, N 5.17.

2b-$(PPN)_2$: **1b**-$(PPN)_2 \cdot 7H_2O$ (20 mg, 0.012 mmol) were dissolved in CH_3CN (5 mL) and the solution heated to reflux several times. Needles

 © WILEY-VCH Verlag GmbH, 69451 Weinheim, Germany, 2002 1433-7851/02/4111-1880 $ 20.00+.50/0 *Angew. Chem. Int. Ed.* **2002**, *41*, No. 11

of **2b** were formed as orange crystals, yield 5%; MS (negative ion FAB): *m/z* (%): 443 (19), 444 (12), 445 (8) [$M^{2-}+H^+$].

3b-$(PPN)_2$: **2b**-$(PPN)_2$ (20 mg, 0.012 mmol) were dissolved in CH_3CN (5 mL) and the solution heated to reflux several times, whereby the orange red solution turns dark red. On cooling the solution crystals of **3b** formed as orange needles, yield 69%; MS (negative ion FAB): *m/z* (%): 459 (100), 460 (31), 461 (9) [$M^{2-}+H^+$].

Labeling experiment: **1a**-$(PPN)_2$ (0.013 mmol, 20 mg) were dissolved in CH_3CN (5 mL) and the solution heated to reflux several times under a $^{16}O_2$/$^{13}O_2$ atmosphere. Orange needlelike crystals were obtained after removal of the solvent. MS (negative ion FAB): *m/z* : 461, 462, 463.

Received: November 14, 2001 [Z18218]

[1] Reviews: S. T. Prigge, R. E. Mains, B. A. Eipper, L. M. Amzel, *Cell. Mol. Life Sci.* **2000**, *57*, 1236 – 1259; E. I. Solomon, P. Chen, M. Metz, S.-K. Lee, A. E. Palmer, *Angew. Chem.* **2001**, *113*, 4702 – 4724; *Angew. Chem. Int. Ed.* **2001**, *40*, 4570 – 4590.

[2] E. B. Paniago, D. C. Weatherburn, D. W. Margerum, *J. Chem. Soc. Chem. Commun.* **1971**, 1427 – 1428; F. P. Bossu, E. B. Paniago, D. W. Margerum, S. T. Kirksey, Jr., J. L. Kurtz, *Inorg. Chem.* **1978**, *17*, 1034 – 1042.

[3] T. Sakurai, A. Nakahara, *Inorg. Chim. Acta* **1979**, *34*, L243 – L244; W. Bal, M. I. Djuran, D. W. Margerum, E. T. Gray, Jr., M. A. Mazid, R. T. Tom, E. Nieboer, P. J. Sadler, *J. Chem. Soc. Chem. Commun.* **1994**, 1889 – 1890.

[4] J. G. Muller, L. A. Kayser, S. J. Paikoff, V. Duarte, N. Tang, R. J. Perez, S. E. Rokita, C. J. Burrows, *Coord. Chem. Rev.* **1999**, *185 – 186*, 761 – 774; R. J. Perez, J. G. Muller, S. E. Rokita, C. J. Burrows, *Pure Appl. Chem.* **1998**, *70*, 275. For oxidative cleavage of DNA and RNA by Ni-peptide-complexes see also: I. J. Brittain, X. Huang, E. C. Long, *Biochemistry* **1998**, *37*, 12 113 – 12 120.

[5] P. Pfeiffer, W. Offermann, H. Werner, *J. Prakt. Chem.* **1942**, *159*, 313. These reports could be confirmed (O. E. Woisetschläger, W. Beck, unpublished results).

[6] P. Capdevielle, M. Maumy, *Tetrahedron Lett.* **1991**, *31*, 3831 – 3834.

[7] C. J. Easton, S. K. Eichinger, M. J. Pitt, *Tetrahedron* **1997**, *53*, 5609 – 5616; S. Nishino, M. Kunita, Y. Kani, S. Ohba, H. Matsushima, T. Kokii, Y. Nishida, *Inorg. Chem. Commun.* **2000**, *3*, 145 – 148.

[8] K. Jitsukawa, T. Irisa, H. Einaga, H. Masuda, *Chem. Lett.* **2001**, 30 – 31.

[9] K. Haas, W. Ponikwar, H. Nöth, W. Beck, *Angew. Chem.* **1998**, *110*, 1200 – 1203; *Angew. Chem. Int. Ed.* **1998**, *37*, 1086 – 1089; K. Haas, E.-M. Ehrenstorfer-Schäfers, K. Polborn, W. Beck, *Eur. J. Inorg. Chem.* **1999**, 465 – 469.

[10] For other cyclooligomerizations of linear peptides and monomeric amino acids see: M. North, G. Pattenden, *Tetrahedron* **1990**, *46*, 8267 – 8290; A. J. Blake, J. S. Hannam, K. A. Joliffe, G. Pattenden, *Synlett* **2000**, 1515 – 1518; J. N. Lambert, J. P. Mitchell, K. D. Roberts, *J. Chem. Soc. Perkin Trans. 1* **2001**, 471 – 484; N. Sokolenko, G. Abbenante, M. J. Scanlon, A. Jones, L. R. Gahan, G. R. Hanson, D. P. Fairlie, *J. Am. Chem. Soc.* **1999**, *121*, 2603 – 2604; L. Zhang, J. P. Tam, *Tetrahedron Lett.* **1997**, *38*, 4375; H. Gerlach, A. Thalmann, *Helv. Chim. Acta* **1974**, *57*, 2661; S. Masamune, S. Kamata, W. Schilling, *J. Am. Chem. Soc.* **1975**, *97*, 3515.

[11] K. W. Aston, S. L. Henke, A. S. Modak, D. P. Riley, K. R. Sample, R. H. Weiss, W. L. Neumann, *Tetrahedron Lett.* **1994**, *35*, 3687 – 3690.

[12] M. A. Lang, W. Beck, unpublished results; M. A. Lang, Dissertation, Universität München, **2001**.

[13] X-ray structure determination **2a**-$(PPN)_2$. Kappa-CCD (Bruker-Nonius), rotating anode, $Mo_{K\alpha}$ (graphite monochromator, $\lambda =$ 71.069 pm), direct methods (SIR97), refinement with full matrix on F^2 (SHELXL), H atoms at C in calculated positions, H atoms at O not considered. Geometrical analysis and graphics with PLATON and ORTEP. **2a**: $[NiC_{10}H_{12}N_4O_5][C_{36}H_{30}NP_2]_2 \cdot 8.5\,H_2O$, $M_r = 1557.18$, crystal size $0.34 \times 0.14 \times 0.02$ mm, triclinic, $P\bar{1}$, $a = 14.3402(2)$, $b =$ 14.7447(2), $c = 19.3789(3)$ Å, $\alpha = 79.0455(5)$, $\beta = 75.3656(6)$, $\gamma =$ 74.7252(5)°, $V = 3790.92(9)$ Å^3, $Z = 2$, $\rho_{calcd} = 1.36423(3)$ g cm^{-3}, $T =$ 200 K, $\mu = 0.410$ mm^{-1}, 49 829 reflections collected, $2\theta_{max} = 45°$, 9877 unique reflections, Lp-correction, $R_{int} = 0.1105$, absorption correction (6 faces, min/max transmission = 0.9116/0.9918), average $\sigma(I)/I =$ 0.0629, 8165 reflections with $I > 2\sigma(I)$, $w^{-1} = \sigma^2(F_o) + (0.0718P)^2 +$ 26.8552*P*, $3P = \max(F_o^2; 0 + 2F_c^2)$, 1 molecule of water disordered, 2 molecules of water with site occupation factors (SOFs) < 1, the complex anion is disordered. The disorder can be described by a rotation of the ligand molecule around an axis through Ni perpendicular to the coordination plane. 986 parameters, no geometrical restraints, $R_1 = 0.1006$, $R_w(F^2) = 0.2311$, $S = 1.082$, max. residual electron density 1.295 e Å^{-3}. The high residual electron density near the second α-C atom presumably originates from traces of the dihydroxylated species.CCDC 179782 contains the supplementary crystallographic data for this paper. These data can be obtained free of charge via www.ccdc.cam.ac.uk/conts/retrieving.html (or from the Cambridge Crystallographic Data Centre, 12, Union Road, Cambridge CB2 1EZ, UK; fax: (+44) 1223-336-033; or deposit@ccdc.cam.ac.uk).

[14] D. W. Margerum, S. L. Anliker in T*he Biochemistry of Nickel* (Ed.: J. R. Lancaster, Jr.), VCH, Weinheim, **1988**, pp. 29 – 51; S. A. Jacobs, D. W. Margerum, *Inorg. Chem.* **1984**, *23*, 1195 – 1201; S. L. Anliker, M. W. Beach, H. D. Lee, D. W. Mangerum, *Inorg. Chem.* **1988**, *27*, 3809 – 3818; A. G. Lappin, C. K. Marray, D. W. Margerum, *Inorg. Chem.* **1978**, *17*, 1630 – 1634; G. E. Kirran, D. W. Margerum, *Inorg. Chem.* **1985**, *24*, 3245 – 3253. An oxo-bridged nickel^{III} complex $[\{Ni(salen)_2\}_2O]$ (salen = *N*,*N*′-bis(salicylidene)ethylenediamine dianion) was recently prepared by reaction of [Ni(salen)] with oxygen (B. Bag, N. Mondal, G. Rosair, S. Mitra, *Chem. Commun.* **2000**, 1729 – 1730).

[15] F. P. Bossu, D. W. Margerum, *J. Am. Chem. Soc.* **1976**, *98*, 4003 – 4004; F. P. Bossu, D. W. Margerum, *Inorg. Chem.* **1977**, *16*, 1210 – 1214.

[16] T. M. Zabriskie, H. Cheng, J. C. Vederas, *J. Chem. Soc. Chem. Commun.* **1991**, 571 – 572; M. Noguchi, H. Seino, H. Kochi, H. Okamoto, T. Tanaka, M. Hirama, *Biochem. J.* **1992**, *283*, 883 – 888.

[17] We thank Professor T. Klapötke for a sample of $^{18}O_2$. In the mass spectra of the product of **1** with air in the presence of a large excess of $^{18}OH_2$ no evidence for the addition of ^{18}O to **2a** was found.

[18] See for example V. A. Burgess, C. J. Easton, M. P. Hay, *J. Am. Chem. Soc.* **1989**, *111*, 1047 – 1052; M. Frey, M. Rothe, A. F. V. Wagner, J. Knappe, *J. Biol. Chem.* **1994**, *269*, 12 432 – 12 437; F. Turecek, F. H. Carpenter, M. J. Polce, C. Wesdemiotis, *J. Am. Chem. Soc.* **1999**, *121*, 7955 – 7956; D. T. Logan, J. Andersson, B.-M. Sjöberg, P. Nordlund, *Science* **1999**, *283*, 1499 – 1504; B. N. Nukuna, M. B. Goshe, V. E. Anderson, *J. Am. Chem.* **2001**, *123*, 1208 – 1214; C. L. Hawkins, M. J. Davies, *J. Chem. Soc. Perkin Trans. 2* **1998**, 2617 – 2622.

[19] See, for example R. P. Bonomo, G. Impellizzeri, G. Pappalardo, R. Purrello, E. Rizzarelli, G. Tabbi, *J. Chem. Soc. Dalton Trans.* **1998**, 3851 – 3857.

$[Ga_{22}\{N(SiMe_3)_2\}_{10}]^{2-}$: A Metalloid Cluster Compound with a Variation of the Ga_{22} Framework**

Andreas Schnepf,* Gregor Stößer, and Hansgeorg Schnöckel*

Dedicated to Professor Walter Siebert on the occasion of his 65th birthday

In recent years the chemistry of the subvalent aluminum and gallium compounds, which display a large variety of Al or Ga frameworks, has developed rapidly.[1–4] Within a short time two Al_{22} clusters[5, 6] and three Ga_{22} clusters[7–9] were prepared by different synthetic methods. In the Al_{22} clusters an icosahedral Al_{12} frame is bound in a unique manner through Al–Al bonds to ten AlX_2 units (X = Cl, Br), and the tips of the Al_{12} icosahedron are saturated with donor molecules, such as THF. In contrast, all the Ga_{22} clusters have a framework of 14 "naked" Ga atoms, in which a central Ga atom is surrounded by 13 Ga atoms in a modified cubo-octahedral form. The eight outer Ga atoms which are bound directly to the ligands R, lie above the eight square faces of the modified cubo-octahedron. The stability of this neutral $[Ga_{22}R_8]$ cluster **1** is attributed, on the one hand, to the Jellium state in the Ga_{22}^{8+} ion (58 electrons)[7] and on the other to the arrangement of the Ga atoms which resembles that of the high-pressure modification of Ga-III.[9] Herein we describe the preparation and structure of $[Ga_{22}\{N(SiMe_3)_2\}_{10}]^{2-}[Li_4Br_2 \cdot 10\,THF]^{2+}$, a compound containing the $[Ga_{22}R_{10}]^{2-}$ cluster **2**, in which the average oxidation state of the Ga atoms corresponds to that found in **1**: +0.36. Thus, the existence of two completely different Ga_{22} frameworks in the clusters of type **1** and **2** is even more astounding.

For the preparation of **2**-$[Li_4Br_2 \cdot 10\,THF]^{2+}$ a GaBr solution[3, 10] in toluene/THF at −78 °C was treated with a toluene solution of $LiN(SiMe_3)_2$ (1.25 equiv). After slowly allowing the reaction solution to warm to room temperature and subsequent warming to 55 °C for 20 hours crystals of the cluster compound $[Ga_{84}\{N(SiMe_3)_2\}_{20}]^{4-}$ (**3**) formed in the solution.[11] Following evaporation of the solution and extraction with pentane, colorless crystals of $Ga[N(SiMe_3)_2]_3$ were obtained from the dark brown pentane extract.[12] After the separation of these crystals from the pentane solution, black crystals with the composition **2**-$[Li_4Br_2 \cdot 10\,THF]^{2+}$ precipitated from the solution over several weeks.

The X-ray structural analysis of the latter black crystals shows an unexpected metal framework of 22 Ga atom in **2**: A central Ga atom is surrounded by 11 Ga atoms at an average distance of 293.0 pm (Figure 1a). These 12 Ga atoms are in turn surrounded by ten $[GaN(SiMe_3)_2]$ units (Figure 1b),

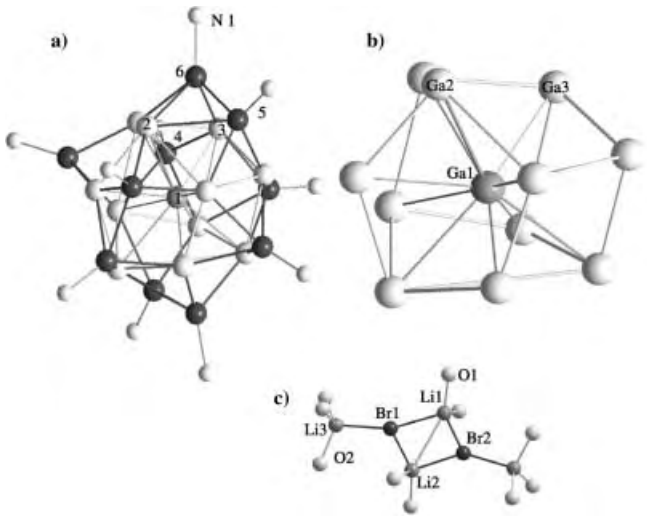


Figure 1. $[Ga_{22}\{N(SiMe_3)_2\}_{10}]^{2-}[Li_4Br_2 \cdot 10\,THF]^{2+}$: a) molecular structure of **2**. For clarity only the N atoms bound to the Ga atoms are shown for the $N(SiMe_3)_2$ ligands. Selected bond lengths [pm]: Ga1-Ga2 297.3, Ga1-Ga3 299.4, Ga2-Ga3 399.7, Ga1-Ga5 380.1, Ga1-Ga4 367.9, Ga3-Ga5 369.5, Ga3-Ga6 256.9, Ga5-Ga6 264.0, Ga4-Ga6 452.0, Ga1-N1 194.9. b) Central Ga_{12} unit from **2**. c) $[Li_4Br_2 \cdot 10\,THF]^{2+}$: Only the O atoms of the THF donor molecules are shown. Selected bond lengths [pm] and angles [°]: Br1-Li1 254.7, Br1-Li2 252.5, Br1-Li3 249.1, Li1-Li2 326.9, Li1-O1 190.8, Li3-O2 193.2; Br1-Li1-Br2 96.7.

where, in each case, the average distance to the nearest Ga atom of the Ga_{12} framework is 265.8 pm. The average distance between the ligand-bearing Ga atoms and the central Ga atom is 382.3 pm. The Ga–N bond lengths (average Ga–N bond = 192.45 pm) are not different from those in other Ga–N clusters (e.g. in **3** the Ga–N bonds are 192.5 pm).[11] The structure of the $[Li_4Br_2 \cdot 10\,THF]^{2+}$ ion is shown in Figure 1c. In the crystal lattice the $[Ga_{22}\{N(SiMe_3)_2\}_{10}]^{2-}$ ions exhibit a distorted hexagonal-primitive arrangement and the cations occupy the trigional-prismatic holes.

The different arrangement of the 22 Ga atoms in **1** and **2** (Figure 2) which have the same average oxidation state of +0.36 suggests the following: if two additional R^- groups were bound to compounds of type **1** the additional bonds would clearly result in a stabilization of the cluster. Through the transfer of charge to the cluster a further stabilization of the cluster unit in the crystal lattice would result from the increase in lattice energy. As the stabilization is linked to the complete enclosure of the Ga_{22} framework by ten ligands, **2** can be seen as the final product of a reaction pathway that is different to that for the formation of the $[Ga_{84}R_{20}]^{2-}$ clusters ($R = N(SiMe_3)_2$) **3**. This stabilization of **2** is possible as the $N(SiMe_3)_2$ ligands are less sterically demanding than the ligands in **1** ($Si(SiMe_3)_3$,[7] $Ge(SiMe_3)_3$,[8] $SitBu_3$[9]). In this way, with ten Ga atoms, a denser surface packing occurs in **2**, than that obtained with eight Ga atoms in **1** (Figure 2), so that in the space-filling model of **2** the ligand-bearing Ga atoms merge together while those in **1** appear as separate entities.

With **1** and **2** it is possible for the first time to compare the total packing density of two structurally different metallic clusters that have the same number of metal atoms. To aid this comparison single-point self-consistent field (SCF) calculations were performed.[13] Volumina were determined for the experimentally determined topology of the Ga atoms in **1** and

[*] Dr. A. Schnepf, Prof. Dr. H. Schnöckel, Dipl.-Chem. G. Stößer
Institut für Anorganische Chemie
Universität Karlsruhe (TH)
Engesserstrasse, Geb. 30.45, 76128 Karlsruhe (Germany)
Fax: (+49) 721-608-4854
E-mail: schnepf@aoc2.uni-karlsruhe.de
hg@achpc9.chemie.uni-karlsruhe.de

[**] This work was supported by the Deutsche Forschungsgemeinschaft and the Fonds der Chemische Industrie.

 © WILEY-VCH Verlag GmbH, 69451 Weinheim, Germany, 2002 1433-7851/02/4111-1882 $ 20.00+.50/0

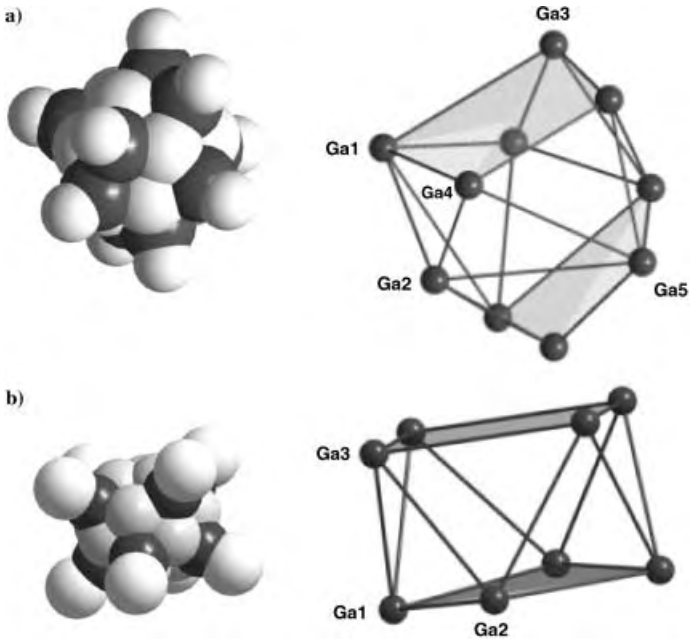


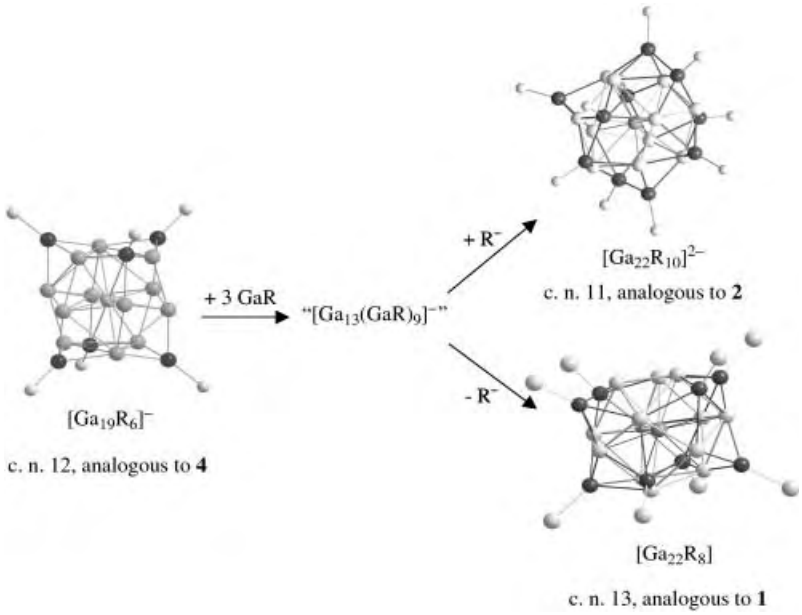
Figure 2. Space-filling model and ball-and-stick representations of the ligand-bearing Ga atoms of the Ga_{22} clusters a) **2** and b) **1**. In the space-filling model only the atoms bound directly to the outer-most (shown in black) eight or ten Ga atoms are shown (that is, the N atoms shown in white in **2** and the Si atoms in **1**). To emphasize the spatial arrangement in the ball-and-stick representations, two Ga_4 faces are highlighted in each case; **2**: selected bond lengths [pm] Ga4-Ga5 493.4, Ga1-Ga2 493.4, Ga2-Ga4 272.1, Ga1-Ga3 510.1; **1**: selected bond lengths [pm] Ga1-Ga2 478.3, Ga1-Ga3 487.0, Ga2-Ga3 457.2.

2, which differ according to the charge, 0 or +8.[14] Independent of the charge the volume of the Ga_{22} framework in **2** is 2% larger than that of **1**. The small, but significant, difference in the volumina, which arises from the arrangement of, and interatomic distances between, the eight or ten ligand-bearing Ga atoms, can be clearly seen in Figure 2. This difference in volume should result almost entirely from the coordination numbers of the central Ga atoms, which in **1** is 13 and thus two larger than that of **2** in which it is 11. As **1** has a topology similar to that of the high-pressure modification of Ga-III (4 + 8 coordination),[9] the coordination sphere of the central Ga atom in **2** must lie between that of Ga-III and β-Ga (2 + 6 coordination).[9] As the macroscopic increase in volume from Ga-III to β-Ga is approximately 5%,[9] the volume difference (ΔV) determined between **1** and **2** does in fact show that based on topology, **2** lies between Ga-III and β-Ga.[15] To demonstrate the similarity between the phase transition from Ga-III to β-Ga and the different arrangements of the Ga_{22} framework of **1** and **2**, we have tried to assign an energy to the volume decrease in the transition from **2** to **1**. Single-point SCF calculations[13] for the Ga_{22} frameworks show large differences which depend upon the given charge distribution. Thus, for the charges +8 and ±0 energy differences of 14.5 and 4.1 kJ mol^{-1}, respectively, are calculated, that is, the Ga_{22} framework of **2** is more stable than that of **1** [Eq (1)].

$$Ga_{22}\text{ framework }\mathbf{2} \longrightarrow Ga_{22}\text{ framework }\mathbf{1} \quad (1)$$
$$\Delta V = -2\%,\ \Delta E = 4.1 \text{ or } 14.5\ \text{kJ mol}^{-1}$$

The volume and energy differences resulting from the transformation of **2** to **1** could, as a first approximation, be interpreted as a phase change of Ga_{22} units—for classical molecules one should really speak of isomers. It has been shown many times,[16] that gallium in the hypothetical cubic-close-packing topology, similar to the (4 + 8) coordination in Ga-III, has a higher energy, by a few kJ, than in β-Ga.[17] Cluster **1** (analogous to Ga-III) has more similarity to "real" metals than **2** (analogous to β-Ga). To make this greater similarity between **1** and "real" metals clearer from an electronic point of view, we have calculated the chemical shifts for the resonance signals of the central Ga atoms in the ^{71}Ga NMR spectrum for the Ga_{22} frameworks of **1** and **2** (Ga_{22}^{8+}).[18] Analogous to similar calculations for metallic Al clusters,[19] the larger downfield shift of the signals from **1** ($\delta = -718$) compared to that of **2** ($\delta = -794$) supports the interpretation,[20] that for **1**, in addition to the topological and energetic factors, the electronic situation is also indicative of a greater similarity to "real" metals than in **2**.

That the greater steric demands of the ligands $Si(SiMe_3)_3$,[7] $Ge(SiMe_3)_3$,[8] $SitBu_3$[9] relative to $N(SiMe)_2$, is responsible for the different arrangements of the Ga_{22} moieties in the clusters **1** and **2**, is also emphasized through the relationship shown in Scheme 1: in the $[Ga_{13}(GaR)_6]^-$ cluster **4** with $C(SiMe_3)_3$ ligands the central Ga atom has the coordination number 12.[10] A hypothetical $[Ga_{13}(GaR)_9]^-$ compound can be



Scheme 1. Influence of the steric demands of ligands on the form of the Ga_n cluster core: starting from a $[Ga_{19}R_6]^-$ species which is analogous to **4**, a hypothetical $[Ga_{13}(GaR)_9]^-$ species is formed by the addition of three (GaR) groups. This species is stabilized by conversion into clusters analogous to **1** or **2** through the elimination (sterically demanding unit) or addition (less demanding unit) of an R^- ligand. The coordination numbers (c.n.) given refer to the central Ga atom.

 © WILEY-VCH Verlag GmbH, 69451 Weinheim, Germany, 2002 1433-7851/02/4111-1883 $ 20.00+.50/0

formed by a cluster expansion in the form of the addition of three (GaR) units. With bulky ligands this cluster is stabilized by the loss of an R^- unit, with less bulky ligands through the addition of an R^- unit to give $[Ga_{22}R_8]$ and $[Ga_{22}R_{10}]^{2-}$ compounds, respectively, in which the coordination number of the central Ga atom increases from 12 to 13 (analogous to **1**) or decreases from 12 to 11 (analogous to **2**).

Experimental Section

$LiN(SiMe_3)_2$ (1.8 g, 10 mmol) was suspended in toluene (30 mL) and cooled to $-78\,^\circ C$. A solution of GaBr (0.3 M; 27 mL, 8.3 mmol) in toluene/THF (3/1) at $-78\,^\circ C$ was slowly added to this suspension through a steel cannula. The stirred mixture was then slowly warmed to room temperature to give an almost black solution. This solution was heated to 55 °C for 20 h. On cooling to room temperature black diamond-shaped crystals of $[Ga_{84}\{N(SiMe_3)_2\}_{20}][Li(thf)_4]_2[Li_2Br(thf)_6]_2\cdot 2$ toluene (220 mg, 0.02 mmol) formed on the glass walls. After collection of the crystals the solution was evaporated to dryness and the residue extracted with pentane. On evaporation of the pentane extract, colorless crystals of $Ga[N(SiMe_3)_2]_3$ (1.45 g, 2.8 mmol) precipitated. The pentane extract was evaporated further and after several weeks black crystals of **2**-$[Li_4Br_2\cdot 10THF]^{2+}$ (10 mg, 0.0025 mmol) formed. Crystal-structure data: $M_r = 4046.40$, crystal dimensions $0.5\times0.5\times0.2$ mm, monoclinc, space group $P2(1)/c$, $a = 16.1376(9)$, $b = 34.7635(15)$, $c = 32.704(2)$ Å, $\beta = 91.616(7)^\circ$, $V = 18339.8(18)$ Å^3, $Z = 4$, $\rho_{calcd} = 1.465$ g cm^{-3}, $\mu_{Mo} = 3.779$ mm^{-1}, $2\theta_{max} = 45^\circ$, 85740 measured reflections, 23667 unique reflections ($R_{(int)} = 0.0890$), absorption correction: numeric (min./max. transmission = 0.1041/0.3439), $R_1 = 0.0597$, w$R_2 = 0.1438$, Stoe-IPDS diffractometer, $Mo_{K\alpha}$ radiation, $\lambda = 0.71073$ Å, 200 K. The structure was solved by direct methods and refined against F^2 for all observed reflections. Programs: SHELXS and SHELXTL (G.M.Sheldrick, Universität Göttingen). CCDC 175035 contains the supplementary crystallographic data for this paper. These data can be obtained free of charge via www.ccdc.cam.ac.uk/conts/retrieving.html (or from the Cambridge Crystallographic Data Centre, 12, Union Road, Cambridge CB21EZ, UK; fax: (+44) 1223-336-033; or deposit@ccdc.cam.ac.uk).

Recieved: December 3, 2001 [Z18324]

[1] H. Schnöckel, A. Schnepf, *Adv. Organomet. Chem.* **2001**, *47*, 235.

[2] W. Uhl, *Angew. Chem.* **1993**, *105*, 1449; *Angew. Chem. Int. Ed. Engl.* **1993**, *32*, 1386.

[3] C. Dohmeier, D. Loos, H. Schnöckel, *Angew. Chem.* **1996**, *108*, 141; *Angew. Chem. Int. Ed. Engl.* **1996**, *35*, 129.

[4] G. Linti, H. Schnöckel, *Coord. Chem. Rev.* **2000**, *206*, 285.

[5] C. Klemp, R. Köppe, E. Weckert, H. Schnöckel, *Angew. Chem.* **1999**, *111*, 1852; *Angew. Chem. Int. Ed.* **1999**, *38*, 1740.

[6] C. Klemp, M. Bruns, J. Gauss, U. Häussermann, G. Stößer, L. van Wüllen, M. Jansen, H. Schnöckel, *J. Am. Chem. Soc.* **2001**, *123*, 9099.

[7] A. Schnepf, E. Weckert, G. Linti, H. Schnöckel, *Angew. Chem.* **1999**, *111*, 3578; *Angew. Chem. Int. Ed.* **1999**, *38*, 3381.

[8] G. Linti, A. Rodig, *Chem. Commun.* **2000**, 127.

[9] A. Donchev, A. Schnepf, G. Stößer, E. Baum, H. Schnöckel, T. Blank, N. Wiberg, *Chem. Eur. J.* **2001**, *7*, 3348.

[10] A. Schnepf, G. Stößer, H. Schnöckel, *J. Am. Chem. Soc.* **2000**, *122*, 9178.

[11] A. Schnepf, H. Schnöckel, *Angew. Chem.* **2001**, *113*, 734; *Angew. Chem. Int. Ed.* **2001**, *40*, 711.

[12] P. J. Brothers, R. J. Wehmschulte, M. M. Olmstead, K. Ruhland-Senge, S. R. Parkin, P. P. Power, *Organometallics*, **1994**, *13*, 2792.

[13] The molecular volumina were determined with the GAUSSIAN 98 program package by SCF calculations with a 3-21G* basis set. For this process single-point calculations based on the experimentally determined geometries of the Ga_{22} cluster frameworks were carried out. Following the IPCM method a surface of uniform electron density (4×10^{-3} e Å^{-3}) was placed around the Ga_{22} unit. The resulting molecular volumina serve as the basis for the discussion in the text. a) IPCM: J. B. Foresmann, T. A. Keith, K. B. Wiberg, J. Snoonian, M. J. Frisch, *J. Phys. Chem.* **1996**, *100*, 16098; b) Gaussian 98, M. J. Frisch, G. W. Trucks, H. B. Schlegel, G. E. Scuseria, M. A. Robb, J. R. Cheeseman, V. G. Zakrzewski, J. A. Montgomery, R. E. Stratmann, J. C. Burant, S. Dapprich, J. M. Millam, A. D. Daniels, K. N. Kudin, M. C. Strain, O. Farkas, J. Tomasi, V. Barone, M. Cossi, R. Cammi, B. Mennucci, C. Pomelli, C. Adamo, S. Clifford, J. Ochterski, G. A. Petersson, P. Y. Ayala, Q. Cui, K. Morokuma, D. K. Malick, A. D. Rabuck, K. Raghavachari, J. B. Foresman, J. Cioslowski, J. V. Ortiz, B. B. Stefanov, G. Liu, A. Liashenko, P. Piskorz, I. Komaromi, R. Gomperts, R. L. Martin, D. J. Fox, T. Keith, M. A. Al-Laham, C. Y. Peng, A. Nanayakkara, C. Gonzalez, M. Challacombe, P. M. W. Gill, B. G. Johnson, W. Chen, M. W. Wong, J. L. Andres, M. Head-Gordon, E. S. Replogle, J. A. Pople, Gaussian, Inc., Pittsburgh, PA, **2001**.

[14] For example, the Ga_{22} framework of **2**: 622 Å^3 (0), 550 Å^3 (+8).

[15] An increase of the coordination number during the transition from crystalline to liquid gallium is also responsible for the unusual melting behavior of this element ($\Delta V = -3.3\,\%$).[21]

[16] H. G. v. Schnering, R. Nesper, *Acta Chem. Scand.* **1991**, 45, 870; U. Häußermann, S. Simak, I. Abrikosov, S. Lidin, *Chem. Eur. J.* **1997**, 3, 904; X. G. Gong, G. Chiarotti, M. Parrinello, E. Tosatti, *Phys. Rev. B* **1991**, *43*, 14277.

[17] A connection to the melting process of elemental gallium seems plausible, as here a reduction of the atomic volume is coupled to an increase in coordination number in the melt, in which the Ga atoms are approximately hexagonal close packed.[21] In the melt the topology of the Ga atoms again indicates a similarity to "real" metals.

[18] The chemical shifts of the signals in the ^{71}Ga NMR spectrum were first determined relative to the calculated shift of the signal from GaCp ($Cp = C_5H_5$) and then set relative to the normal standard ($[Ga(H_2O)_6]^{3+}$). For this process DFT calculations with the MPSHIFT module of the program package TURBOMOLE (BP-86-Funktional) were performed: TURBOMOLE: O. Treutler, R. Ahlrichs, *J. Chem. Phys.* **1995**, *102*, 346; b) BP-86-Funktional: A. D. Becke, *Phys. Rev. A* **1998**, *38*, 3098; J. P. Perdew, *Phys. Rev. B* **1996**, *33*, 8822; c) RIDFT: K. Eichkorn, O. Treutler, H. Öhm, M. Häser, R. Ahlrichs, *Chem. Phys. Lett.* **1995**, *242*, 652; K. Eichkorn,F. Weigend, O. Treutler, R. Ahlrichs, *Theor. Chem. Acc.* **1997**, *97*, 119; d) DFT calculations with the GIAO module: G. Schreckenbach, T. Ziegler, *J. Phys. Chem.* **1995**, *99*, 606; SCF calculations with the GIAO module: M. Häser, R. Ahlrichs, H. P. Baron, P. Weiss, H. Horn, *Theor. Chim. Acta* **1992**, *83*, 455.

[19] H. Köhnlein, G. Stößer, E. Baum, E. Möllhausen, U. Huniar, H. Schnöckel, *Angew. Chem.* **2000**, *112*, 828; *Angew. Chem. Int. Ed.* **2000**, *39*, 799.

[20] While the triplet state of the neutral Ga_{22} unit in **1** is some what more favorable (the energy difference between **2** and **1** is in the region of the margin of error for the calculated results), the corresponding chemical shifts of the ^{71}Ga NMR signals were also calculated for the neutral cluster of **1** (triplet) and of **2** (singulet): $\delta = -491$ for **1**, $\delta = -632$ for **2**.

[21] *Gmelins Handbuch der anorganischen Chemie*, 8th ed., volume 36, VCH, Berlin, **1936**, pp. 18ff.

 © WILEY-VCH Verlag GmbH, 69451 Weinheim, Germany, 2002 1433-7851/02/4111-1884 $ 20.00+.50/0

The Catalytic Use of Onion-Like Carbon Materials for Styrene Synthesis by Oxidative Dehydrogenation of Ethylbenzene

Nicolas Keller, Nadezhda I. Maksimova, Vladimir V. Roddatis, Michael Schur, Gerhard Mestl,* Yurii V. Butenko, Vladimir L. Kuznetsov, and Robert Schlögl*

Since the discovery of fullerenes in 1985,[1] the chemistry of sp^2-hybridized nanostructured carbon has received increasing attention both from a fundamental point of view and for potential applications. A large variety of new fullerene-related materials (giant fullerenes, nanotubes, nanospheres, nanocones, nanofolders, nanobundles, onion-like carbons (OLCs)) have been synthesized.[2] Their unique chemical and physical properties suggest novel applications, which include nanoscale engineering and electronics, optoelectronic sensors, three-dimensional composite materials, microfilters, magnetic materials, and catalysis.[3] Current research on OLCs is confined to the development of synthesis methods and to the description of physical and chemical properties.[4] These closed, spherical, carbon shells, however, could also provide interesting catalytic properties as a result of the almost perfect graphite network with a high degree of curvature.

Direct dehydrogenation of hydrocarbons is used in numerous industrial processes. Because of their endothermic character, such processes are restricted by thermodynamic limitations, thus alternatives are called for. In case of styrene synthesis, one of the ten most important industrial processes, the exothermic oxidative dehydrogenation (ODH) of ethylbenzene is an elegant and promising reaction, for which carbon catalysts have already proved their efficiency.[5, 6] The porosity of carbon catalysts used to date seems to play a negative role by hindering the styrene desorption. This effect limits the ethylbenzene conversion and leads to nonselective, consecutive reactions.[5, 7] Therefore, because of the absence of inner particle porosity OLCs are valuable candidates as catalysts.[8]

Figure 1 displays the catalytic behavior of the OLC material for the ODH of ethylbenzene to styrene with time on stream (t). For comparison, the steady-state yields are also shown, which were obtained over the industrial K–Fe catalyst and other forms of carbon. The OLC catalyst exhibited a minor initial activity developing into conversion levels of 92% after an activation period of about 2 hours on stream. The stable styrene selectivity of 68% allowed high styrene yields of 62%. The performance of OLC in ODH is not restricted as in case of traditional K-promoted iron-oxide systems, for which thermodynamic constraints limit the maximum styrene yield to 50%.[9, 10]

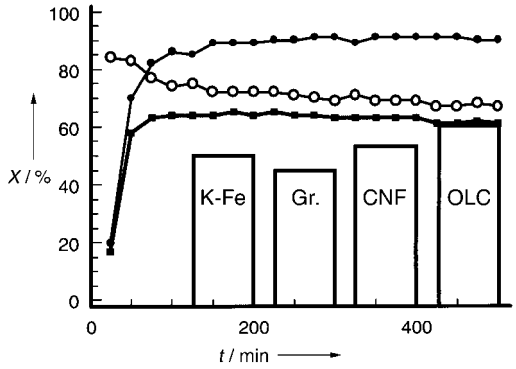


Figure 1. Performance of OLC in the ODH of ethylbenzene at 790 K with time on stream. X = ethylbenzene conversion (●), selectivity to styrene (○), and styrene yield (■). Steady-state styrene yields for graphite (Gr.), carbon nanofilaments (CNF), and the industrial K–Fe catalyst are also given. Data are given relative to the catalyst mass.

Figure 2A displays high-resolution transmission electron micrographs of fresh OLC. The left-hand image of Figure 2A shows clean, multishell particles with an interlayer distance close to 0.35 nm, typical for sp^2-hybridized carbon structures. The inset of Figure 2A shows one example of a well resolved OLC. The contrast variations of this OLC indicate not-intact graphene layers and structurally less-defined areas (indicated by arrows) of the curvature. The right-hand image displays OLC material after 40 h catalysis. The OLC seems to have disintegrated into more or less disorganized carbon.

X-ray diffraction (XRD) was further used to characterize the structure of OLC before and after catalysis. Figure 2B shows the XRD data, the diffractogram of fresh OLC is characteristic for graphite-like material with a high degree of stacking faults. For comparison in Figure 2B, the theoretical pattern of hexagonal graphite is indicated by the vertical lines with the respective indexing. The diffractogram recorded after catalysis (Figure 2B, b) demonstrates the generation of diamond-like-carbon (DLC) material, that is, sp^3-hybridized carbon atoms, during the styrene reaction. The peaks at 43.9 and 75.3° 2Θ coincide with the 111 and 220 reflections of diamond as indicated by the vertical lines. Hence, DLC is part of the ill-defined material formed during catalysis.

Figure 2C shows the Raman spectra obtained from the fresh and used OLC. The deconvolution of these spectra is displayed on the right side of Figure 2C. Spectrum (a) exhibits the Raman bands characteristic for disordered (D: 1318 cm^{-1}, and D′: 1602 cm^{-1}) and ordered (G: 1573 cm^{-1} graphene structures.[11] This Raman spectrum is in agreement with the HR-TEM analysis which revealed intact graphene layers and ill-defined structures at the curvatures of OLC (Figure 2A, left) and the XRD data (Figure 2B, pattern a). The intense Raman signature of the D (1328 cm^{-1}) and D′ (1594 cm^{-1}) bands of the catalyst after reaction, completely overwhelming the G band at 1572 cm^{-1} clearly indicate a pronounced presence of disordered carbon structures after the catalytic run. The intensity increase of the two D and D′ Raman signals was accompanied by a broadening and a slight blue-shift of

[*] Prof. Dr. R. Schlögl, Dr. N. Keller, N. I. Maksimova, Dr. V. V. Roddatis, Dr. M. Schur
Abteilung Anorganische Chemie
Fritz-Haber-Institut der Max-Planck-Gesellschaft
Faradayweg 4–6, 14195 Berlin (Germany)
Fax: (+49) 30-8413-4401
E-mail: Schloegl@fhi-berlin.mpg.de
Dr. G. Mestl
Nanoscape AG
Frankfurter Ring 193A, 80809 Munich (Germany)
Dr. Y. V. Butenko, Dr. V. L. Kuznetsov
Boreskov Institute of Catalysis
Lavrentieva 5, 630090 Novosibirsk (Russian Federation)

 © WILEY-VCH Verlag GmbH, 69451 Weinheim, Germany, 2002 1433-7851/02/4111-1885 $ 20.00+.50/0

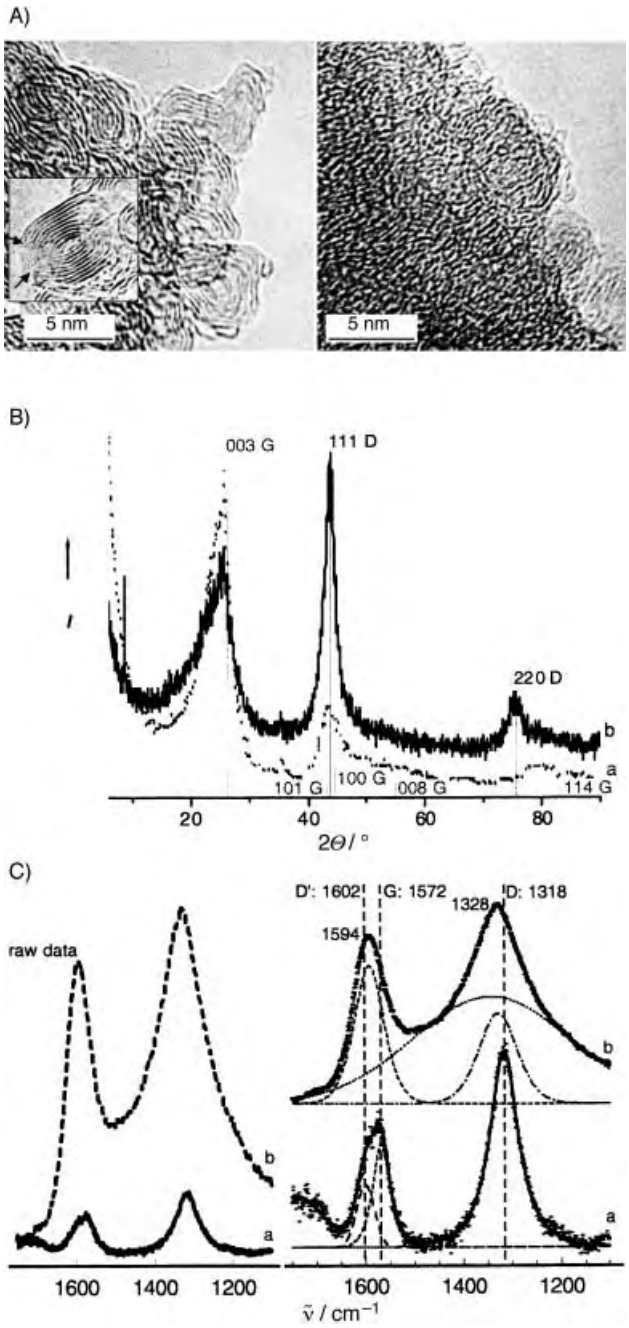


Figure 2. A) High-resolution (HR) TEM images of OLC prior (left) and subsequent to use in the ODH of ethylbenzene (right). The inset shows an enlargement of a single, intact OLC. The arrows indicate the blurred regions with less-ordered structure. B) X-ray diffractograms of the OLC material prior (a) and subsequent to catalysis (b); the calculated positions of the reflections of graphite (G) and diamond (D) are shown. C) Left: original Raman spectra (raw data) of OLC prior (a) and subsequent to use in the ODH of ethylbenzene (b); right: deconvolutions of the Raman spectra prior (a) and subsequent to catalysis (b).

the D band. The deconvolution additionally revealed a very broad background contribution to this band from C–H, C–C deformations.[12] This very broad D band does not exclude the presence of sp^3-hybridized carbon atoms after the reaction, as indicated by XRD (Figure 2B, pattern b).[12] Indeed, IR spectroscopy (spectra not shown) revealed the presence of C–H valence bands at 2920 cm^{-1} after catalysis, together with bands at 1740, 1175, and 1090 cm^{-1} which indicate the presence of basic C=O and C–O groups, respectively.

In addition to Raman spectroscopy and XRD, thermogravimetry temperature-programmed oxidation (TG-TPO) confirmed the presence of these two carbon species (Figure 3). Compared to the fresh, well-organized sp^2-hybridized OLC (Figure 3, curve a), the used catalyst displayed a

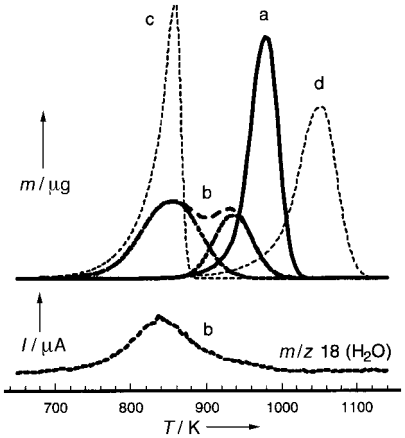


Figure 3. Differential thermal gravimetry of the temperature-programmed combustion of OLC prior (a), subsequent to use in the ODH of ethylbenzene (b), T = temperature, from amorphous carbon (c; Norit A, Aldrich), and graphite (d; SFG6, Timcal AG). Below: mass spectrometer trace of water formed during the combustion of OLC following catalysis.

composite signal (Figure 3, curve b), which indicated disordered sp^2/sp^3-hybridized carbon with a maximum combustion rate at around 850 K, in agreement with the reference sample, amorphous activated charcoal. The contribution to combustion at higher temperatures was assigned to remaining ordered sp^2-carbon structures. The water release, also at 850 K, was detected by mass spectroscopy (Figure 3, bottom) and confirmed the presence of hydrogen atoms (as indicated by IR spectroscopy) in the highly disordered carbon array.

Figure 4 shows the O1s and C1s (X-ray photoemission) XP spectra of fresh and used OLC samples. The almost oxygen-free carbon surface of the fresh OLC (Figure 4A, solid line) was transformed after reaction into an oxygen-containing surface (open circles, Figure 4A). The O1s spectrum after reaction can be deconvoluted into two signals. The first, with a binding energy (B.E.) of 530.9 eV,[13] is similar to spectra reported for other active carbon catalysts[6, 8] and is assigned to chinoidic carbonyl functions. The dehydrogenating power of the catalyst thus seems to be linked to the generation of these strongly basic sites during activation. The second with a B.E. of 533.4 eV arises from water adsorbed during transport through air. Through an increased intensity at the high-energy side of the C1s signal, the C1s spectra (Figure 4B) also indicate the presence of oxidized carbon. The inset of Figure 4B shows the difference spectrum of used OLC (full line) and fresh OLC (dotted line). Its deconvolution confirmed the presence two contributions, at 288.2, indicative for basic, chinoidic surface groups, and 286.0 eV from C–O groups. This XPS finding is in agreement with the IR spectroscopy observations mentioned above. Additionally,

 © WILEY-VCH Verlag GmbH, 69451 Weinheim, Germany, 2002 1433-7851/02/4111-1886 $ 20.00+.50/0

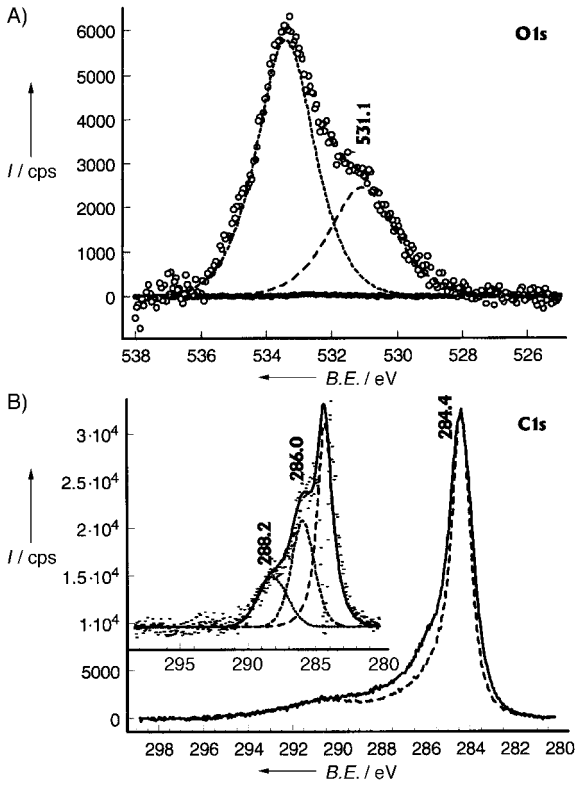


Figure 4. A) O1s XP spectra of the OLC prior (solid line) and subsequent (open circles) to catalysis. The deconvolution into two contributions with B.E. of 531.1 and 533.4 eV is shown. B) C1s XP spectra of OLC prior (dashed line) and subsequent to catalysis (full line). The inset shows the deconvolution of the difference C1s spectrum into three contributions with BE of 288.2, 286.0, and 284.4 eV.

the graphitic C1s line at 284.4 eV was considerably broadened after catalysis demonstrating the presence of structurally ill-defined carbon in line with Raman, XRD, and TG-TPO results

The structural characterization reveals that the function of the OLC as an ODH catalyst is uniquely related to its microstructure. The starting material, intact OLC with a large surface abundance of graphitic (0001) facets combined with a small abundance of edge/kink sites where the bending of the graphene layers occurs (blurred contrast in the TEM, Figure 2), is characterized by the complete absence of surface oxygen functionalities. This material does not show any catalytic activity. Catalytic activity develops with time on stream. The XP spectra indicate the generation of strongly basic, chinoidic surface functionalities on the active carbon catalyst which are responsible for the catalytic activity. These basic, dehydrogenating, surface groups are generated as resonance-stabilized C=O surface terminations of the edge/kink regions of OLC.[7] This oxidation of the edge/kink sites is also seen as being responsible for the disintegration of the OLC during catalysis. The catalytic activity develops with increasing formation of these basic functionalities and accordingly increasing OLC disintegration. Hence, it may be questioned whether OLCs are catalytically active at all. Comparative experiments with ultradispersed diamond (UDD), however, revealed that the DLC material detected by XRD after catalysis can not account for the catalytic activity of OLC (data not shown). UDD are initially also completely inactive, like OLC, but their selectivity, which develops with time, is different from that of OLC; with UDD the main product from the ODH of ethylbenzene is benzene.

That the OLC is superior in its performance to other forms of carbon (Figure 1) indicates that this type of carbon contains a higher number of active sites per unit weight at steady state. This superior performance is also related to the optimized distribution of the oxygen-activating sites (basal planes) and Brønsted basic centers (prismatic planes).[9] The presence of disordered, sp^2- and sp^3-hybridized polymeric carbon resulting from unwanted styrene polymerization is characteristic of all the catalytic systems tested so far.[9, 14] However the large volume and great number of defects in such polymeric (amorphous) species, makes them particularly susceptible to oxidation in situ (see Figure 3). As the formation of coke cannot be completely avoided a large difference in specific reactivity of the soft coke (polymeric species)[15] and the carbon catalyst is a prerequisite for stable operation. Reducing the number of basic sites, which cause polymerization, to the minimum necessary for activating the ethylbenzene substrate, makes the tendency for coke formation on carbon lower than on (potassium-promoted) metal-oxide systems.

The results reveal that a significant potential for catalytic application lies in unpromoted nanocarbon materials if their microstructure can be tailored to support the optimum distribution of electron-donating and C–H-activating functions. The chemical simplicity of carbon and the unique self-cleaning property that deactivated surfaces gasify themselves in ODH reactions, not only makes carbon species well-suited model systems but also allows realistic expectations of an industrial application in heterogeneous catalysis. The difficulties associated with the synthesis of the present OLC model system may be overcome by tailoring other more abundant forms of carbon into the desired target structure by synthetic[16] and post-synthetic thermochemical procedures.

Experimental Section

OLCs were produced by thermal annealing of UDD powder at 2140 K under a 10^{-6} torr vacuum, according to ref. [17]. The reaction was carried out in a tubular quartz reactor of 4 mm inner diameter and 200 mm length. The catalyst (0.04 g) was placed in the isothermal oven zone between quartz wool plugs. He and O_2 were fed by mass-flow controllers (Bronkhorst). Ethylbenzene in a stream of He was provided by a saturator kept at the required temperature (35 °C, corresponding to 2.16 kPa) and mixed with the O_2 flow to obtain the ethylbenzene:O_2 ratio of 1:1. The reaction was conducted at 790 K with an inlet ethylbenzene concentration of 2 vol% and a liquid hourly space velocity (LHSV) of 0.5 h^{-1}. The inlet and outlet gas analysis was carried out online by a gas chromatograph using a packed column (5% SP-1200/1.75% Bentone 34) for hydrocarbons and a capillary column (Carboxen 1010 PLOT) for permanent gases coupled to a flame ionization detector (FID) and a thermal conductivity detector (TCD), respectively.

TEM micrographs were taken on a Phillips CM200-FEG at an acceleration voltage of 200 kV. XP spectra were recorded with a modified Leybold Heraeus spectrometer (LHS12 MCD) with $Mg_{K\alpha}$ radiation (1253.6 eV) at a power of 240 W. The bandpass energy was set to 50 eV. X-ray satellites and Shirley background were subtracted. Thermal gravimetry analysis was performed on a Netzsch STA 449C balance, with a heating rate of 10 K min^{-1} and by using a 20% (v/v) O_2/He mixture, and coupled to a QMS200 mass spectrometer (Thermostar, Pfeiffer Vacuum). Raman spectra were recorded with a LabRam spectrometer (Dilor). The slit width

 © WILEY-VCH Verlag GmbH, 69451 Weinheim, Germany, 2002 1433-7851/02/4111-1887 $ 20.00+.50/0

was set at 500 μm giving a spectral resolution of 5 cm^{-1}. A He/Ne laser at 632.8 nm was used as the excitation source. IR spectra in diffuse reflectance were recorded on a Bruker IFS-66 FT-IR spectrometer. XRD was performed on a Stoe Theta-Theta diffractometer in reflection ($Cu_{K\alpha}$ radiation).

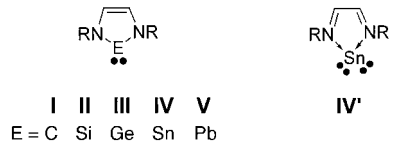
Received: July 23, 2001
Revised: March 5, 2002 [Z17567]

[1] H. W. Kroto, J. R. Heath, S. C. O'Brien, R. F. Curl, R. E. Smalley, *Nature* **1985**, *318*, 162.
[2] a) S. Iijima, *Nature* **1991**, *354*, 56; b) D. Ugarte, *Nature* **1992**, *359*, 670; c) H. O. Pierson, *Handbook of Carbon, Graphite, Diamond and Fullerenes. Properties, Processing and Applications*, Noyes Publications, Park Ridge, **1993**; d) M. Jose-Yacamau, H. Terrones, L. Rendou, J. M. Dominguez, *Carbon* **1995**, *33*, 669; e) *Carbon nanotubes: preparation and properties* (Ed.: T. W. Ebbesen), CRC, Boca Raton, **1997**; f) M. Knupfer, *Surf. Sci. Rep.* **2001**, *42*, 1, and references therein.
[3] a) M. Terrones, W. Kuang Hsu, H. W. Kroto, D. R. M. Walton, *Top. Curr. Chem.* **1999**, *199*, 189, and references therein; b) P. M. Ajayan, O. Z. Zhou *Top. Appl. Phys.* **2001**, *80*, 391.
[4] a) D. Ugarte, *Carbon* **1995**, *33*, 989; b) V. L. Kuznetsov, Yu. V. Butenko, A. L. Chuvilin, A. I. Romanenko, A. V. Okotrub, *Chem. Phys. Lett.* **2001**, *336*, 397.
[5] M. F. R. Pereira, J. J.M Orfao, J. L. Figueiredo, *Appl. Catal. A* **1999**, *184*, 153.
[6] G. Mestl, N. I. Maksimova, N. Keller, V. V. Roddatis, R. Schlögl, *Angew. Chem.* **2001**, *113*, 2122; *Angew. Chem. Int. Ed.* **2001**, *40*, 2066.
[7] a) C. Kuhrs, Y. Arita, W. Weiss, W. Ranke, R. Schlögl, *Top. Catal.* **2001**, *14*, 111; b) J. A. Maciá, D. C. Amorós, A. L. Solano, *Proceedings of the Reunión de la Sociedad Española de Catálisis*, **2001**, pp. 97–98.
[8] a) A more detailed comparison of the performances obtained with different forms of carbon will be given in a coming extended paper; b) storage in air and transfer to the XPS chamber led to a second contribution arising from adsorbed water.
[9] G. Emig, H. Hofmann, *J. Catal.* **1983**, *84*, 15.
[10] F. Cavani, F. Trifiro, *Appl. Catal. A* **1995**, *133*, 219.
[11] a) R. P. Vidano, D. B. Fishbach, L. J. Willis, T. M. Loehr, *Solid State Commun.* **1981**, *39*, 423; b) M. S. Dresselhaus, G. Dresselhaus, *Adv. Phys.* **1981**, *30*, 139; c) Y. Kawashima, G. Katagiri, *Phys. Rev. B* **1995**, *52*, 10053.
[12] D. Espinat, H. Dexpert, E. Freund, G. Martino, M. Couzi, P. Lespade, F. Cruege, *Appl. Catal.* **1985**, *16*, 343.
[13] a) H. Ago, T. Kugler, F. Cacialli, W. R. Salaneck, M. S. P. Shaffer, A. H. Windle, R. H. Friend, *J. Phys. Chem. B* **1999**, *103*, 8116; b) M. Voll, H. P. Boehm, *Carbon* **1971**, *9*, 481.
[14] G. E. Vrieland, *J. Catal.* **1988**, *111*, 14.
[15] R. Schlögl in *Handbook of Heterogeneous Catalysis*, *Vol. 1* (Eds.: G. Ertl, H. Knözinger, J. Weitkamp), Wiley-VCH, Weinheim, **1997**, pp. 138–191.
[16] C. Pham-Huu, N. Keller, V. V. Roddatis, G. Mestl, R. Schlögl, M. J. Ledoux, **2002**, *4*, 514–521.
[17] a) V. L. Kuznetsov, A. L. Chuvilin, Yu. V. Butenko, I. Y. Mal'kov, V. M. Titov, *Chem. Phys. Lett.* **1994**, *222*, 343; b) V. L. Kuznetsov, A. L. Chuvilin, E. M. Moroz, V. N. Kolomiichuk, Sh. K. Shaikhutdinov, Yu. V. Butenko, *Carbon* **1994**, *32(5)*, 873.

Tin Analogues of "Arduengo Carbenes": Synthesis of 1,3,2λ^2-Diazastannoles and Transfer of Sn Atoms between a 1,3,2λ^2-Diazastannole and a Diazadiene**

Timo Gans-Eichler, Dietrich Gudat,* and Martin Nieger

The discovery of persistent and in preparative-scale isolable carbenes launched not only a rapid development of carbene chemistry,[1] but stimulated as well investigations on carbene homologues with heavier Group 14 elements. Utilization of the concept that mesomeric interaction with the π electrons of two nitrogen atoms and a C–C double bond allows efficient electronic stabilization of the divalent carbon atom in imidazoyl ("Arduengo-type") carbenes **I**[2] lead to the isolation of analogous silylenes **II**;[3] and germylenes **III** (Scheme 1).[4] Homologues of **I** with Sn (**IV**) and Pb (**V**) are—apart from a few annellated 1,3,2λ^2-diazastannoles[5]—still unknown, although divalent compounds of these elements should become increasingly more stable descending the group from C to Pb.[6] We report here the preparation and first reaction studies of monocyclic 1,3,2λ^2-diazastannoles **IV** which reveal that the reactivity of these compounds displays some striking dissimilarities when compared to the lighter homologues **I**–**III**.



I **II** **III** **IV** **V** **IV'**
E = C Si Ge Sn Pb

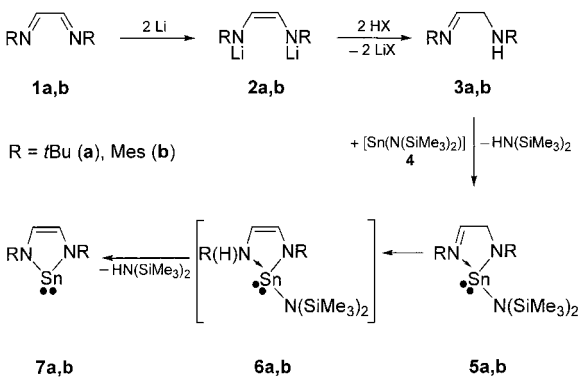
Scheme 1.

λ^2-Diazagermoles **III** and annellated λ^2-diazastannoles can be prepared by metathesis of dilithiated diazadienides or *o*-phenylene diamides with $GeCl_2 \cdot$ dioxane or $SnCl_2$, respectively.[4, 5] Analogous reactions of $SnCl_2$ with the dilithiumdiamides **2a**, **b** (Scheme 2) failed,[7] but the desired monocyclic diazastannoles **7a**,**b** were found to be accessible by transamination of the α-amino aldimines **3a**,**b**[8] with $[Sn(N(SiMe_3)_2)_2]$ (**4**) at 40–45 °C in nonpolar solvents. Mechanistically, the formation of **7a**,**b** can be explained by a multistep sequence (Scheme 2) which involves the initial condensation of **3a**,**b** and **4** to give stannylenes **5**, a subsequent 1,3-H-shift to afford **6**, and finally intramolecular elimination of $HN(SiMe_3)_2$ to produce the final products **7a**,**b** which were isolated after workup as red, air sensitive, and rather thermolabile solids. Experimental support for this

[*] Prof. Dr. D. Gudat, Dipl.-Chem. T. Gans-Eichler, Dr. M. Nieger
Institut für Anorganische Chemie
Universität Bonn
Gerhard-Domagk Strasse 1, 53121 Bonn (Germany)
Fax: (+49) 228-73-5327
E-mail: dgudat@uni-bonn.de

[**] This work was supported by the Deutsche Forschungsgemeinschaft. Parts were presented as a poster at the Jahrestagung Chemie 2001 der GDCH.

 © WILEY-VCH Verlag GmbH, 69451 Weinheim, Germany, 2002 1433-7851/02/4111-1888 $ 20.00+.50/0



Scheme 2.

mechanism comes from detection of the intermediate **5a**[9, 10] by NMR spectroscopy.

The constitution of the λ^2-diazastannoles **7a**,**b** follows unequivocally from their analytic and spectroscopic data. The shielding of the ^{119}Sn NMR signals ($\delta(^{119}\mathrm{Sn}) = 237$ (**7a**), 259 ppm (**7b**)), compared to benzannellated ($\delta(^{119}\mathrm{Sn}) = 269-455$ ppm[5]) and acyclic Sn^{II} amides ($\delta(^{119}\mathrm{Sn}) = \approx 750$ ppm[5]), is remarkable; analogous effects are also known for compounds of type **I** and **II**[1, 3, 11] and diazaphospholenium cations,[12] and originate from the raising of the π^* orbital and the associated blue shift of the n-π^* transition as a consequence of π conjugation.[11, 12] A single-crystal X-ray diffraction study[13] of **7b** (Figure 1) revealed, in contrast to λ^2-benzo-diazastannole, [1,2-$C_6H_4(NCH_2t\mathrm{Bu})_2$Sn] (**8**), the presence of isolated molecules without intermolecular contacts.[5a] The C3/C4 and N2/N5 atoms in the five-membered ring lie in

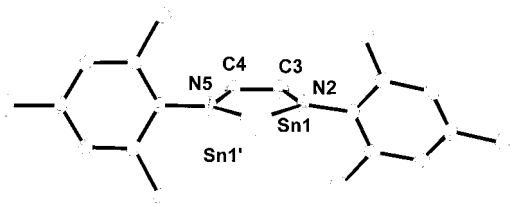
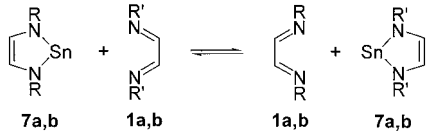


Figure 1. Molecular structure of **7b** (thermal ellipsoids set at 50% probability, H atoms omitted for clarity). The Sn atom is disordered over two positions (relative populations Sn1:Sn1′ 60:40); important distances [Å] and angles [°]: Sn1-N2 2.084(3), Sn1-N5 2.102(3), N2-C3 1.378(5), C3-C4 1.356(6), C4-N5 1.378(5); N2-Sn1-N5 77.63(13).

one plane while the Sn atom is found in a split position and occupies two positions slightly above and below this plane.[14] We interpret this finding by assuming the presence of two superimposed disordered molecules with flat envelope conformations. The C3–N2/C4–N5 (1.378(5) Å) and C3–C4 bonds in the ring (1.356(6) Å) match those in the **II** and **III**[3, 4] and are intermediate between pure single and double bonds. The Sn1–N bonds (2.084(3), 2.102(3) Å) are longer than, and the N-Sn1-N angle (77.63(13)°) is similar to, those in **8** (Sn–N 2.051(5), 2.067(5) Å, N-Sn-N 78.5(2)°[5a]).

Compounds **7a**,**b** are distinguished by a remarkable thermal instability and decompose at 60 °C in a cheletropic reaction to the diazadienes **1a**,**b**, and Sn.[15] In contrast to **I**–**III**, no formation of stannylene complexes occurred with $[Ni(CO)_4]$, $[W(CO)_5(C_8H_{16})]$, or $[Pt(C_2H_4)(PPh_3)_2]$. The observed decrease of the $\delta(^{119}\mathrm{Sn})$ resonance signal ($\Delta\delta(^{119}\mathrm{Sn}) = -26$ ppm (**7b**)) upon addition of excess 4-dimethylamino pyridine (DMAP) suggests the formation of donor–acceptor adducts and implies that **7a**,**b** react like **8**,[5a] as Lewis acids.[16]

A surprising behavior, which is unprecedented for **I**–**III** and **8**, was observed with diazadienes: reactions of **7a** (**7b**) with **1b** (**1a**) did not proceed as in the case of silylenes **II**[17] by oxidative addition, but rather by metathesis to afford the complementary $2\lambda^2$-diazastannoles and diazadienes (Scheme 3) which were identified by NMR spectroscopy.



Scheme 3. Sn-transfer reaction between 1,3,2-λ^2-diazastannoles and diazadienes having different (R = *t*Bu, R′ = Mes) and the same (R = R′ = Mes) substituents; Mes = 2,4,6-trimethylphenyl.

Experimental proof for a direct transfer of an Sn atom from a diazastannole to a diazadiene group in these reactions was obtained by the "degenerate" metathesis between **7b** and **1b**: the appearance of intense exchange cross-peaks in ^{1}H EXSY NMR spectra (Figure 2) certifies that the exchange between both reactants is reversible and proceeds at a considerable rate and without participation of further detectable intermediates even at 30 °C.

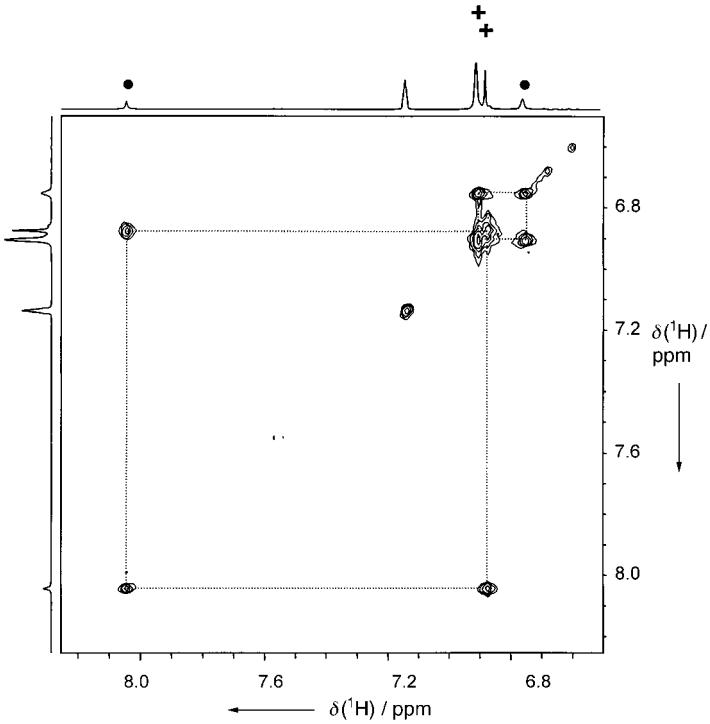


Figure 2. Expansion of a gradient-selected ^{1}H EXSY NMR spectrum (300 MHz, C_6D_6, 30 °C, mixing time 0.5 sec, ^{1}H spectra as projections, only positive contours) of a mixture of **1b** and **7b**. The marked signals are assigned to the NCH and $C_6H_2Me_3$ hydrogen atoms of **1b** (●) and **7b** (+). The visible cross-peaks prove the presence of intermolecular exchange between both reactants.

 © WILEY-VCH Verlag GmbH, 69451 Weinheim, Germany, 2002 1433-7851/02/4111-1889 $ 20.00+.50/0

To understand the unusual reactivity of **7a**,**b**, we carried out quantum-chemical studies on the model compounds **IV**-H (R = H) and **IV**-Ar (R = 2,6-$Me_2C_6H_3$).[18] Energy optimization of the molecular structures afforded planar five-membered rings with similar bond lengths (**IV**-Ar: Sn–N 2.116, N–C 1.382, C–C 1.374 Å) as had been found experimentally for **7b**. Natural bond order (NBO) population analyses[19] of the Kohn–Sham orbitals show a high degree of s character (**IV**-H: 88 %) for the lone pair at the Sn atom, which accounts for the low nucleophilicity observed for **7a**,**b**. The population of the p^{π}(E) orbital perpendicular to the C_2N_2E Ring (**IV**-H: n[p^{π}(Sn)] 0.57) comes close to that in **I** and is larger than in **II** and **III** (n[p^{π}(E)] = 0.62 (**I**), 0.48 (**II**), 0.53 (**III**); R = H), which suggests more efficient π stabilization of the divalent Sn atom in **IV** than of the Si and Ge atoms of **II** and **III**, respectively.[11] Comparison of Wiberg bond indices (WBIs) and the atomic contributions to the localized σ(E–N) orbitals for the series **I**→**IV** reveals a continuous decrease of covalent E–N bond orders and a concomitant increasing polarization of the σ bonds towards nitrogen.[20] Both effects together imply an eventual weakening of E–N σ bonds in the sequence **I**→**IV** and suggest for **IV** an electronic polarization in the form of the "chelated atom" resonance structure **IV′**[21] (Scheme 1) which allows the easy cheletropic fragmentation of **7a**,**b** to be rationalized.

Assuming that transfer of an Sn atom from a diazastannole to a diazadiene group follows an associative mechanism, we modeled the interaction of **IV**-H with HN=CHCH=NH (**VI**-H). Two stationary states on the energy hypersurface were located of which **VIII**-H (ΔE + zpe = +1.6 kcal mol^{-1} relative to **IV**-H + **VI**-H) was assigned by vibrational analysis as a local minimum, and **VII**-H (ΔE + zpe = +5.5 kcal mol^{-1}) as a transition state between **VIII**-H and the separate molecules **IV**-H and **VI**-H (Figure 3). The adduct **VIII**-H is formally the product of oxidative addition of **VI** to **IV** and features an unusual Ψ-trigonal-bipyramidal geometry with different axial (2.269 Å) and equatorial (2.157 Å) Sn–N bonds. The resemblance of this structure to those of Sn^{II} amidinates[22] as well as an NBO analysis suggest a formal description of **VIII**-H as donor-stabilized Sn^{II} amide with a lone-pair on the Sn atom. Computational analysis of the oxidative addition of **VI**-H to the silylene **II** (R = H) revealed that the reaction is in this case strongly exothermic (ΔE + zpe = −56.5 kcal mol^{-1}) and gives, in accord with the experimental findings,[17] a D_{2d}-symmetric Si^{IV} spiro compound with distorted tetrahedral coordination at the silicon center and four equal Si–N bonds(1.724 Å). The strong distortion from tetrahedral coordination at the tin atom in **VIII**-H is for geometric reasons—the small diazadienide "bite angle" forces contraction of endocyclic and concomitant widening of exocyclic N-Sn-N angles—and is considered to be the main reason that the oxidative addition of **VI**-H to **IV**-H is endothermic (and not as for **II** exothermic). Upon introducing 2,6-$Me_2C_6H_3$ substituents to the N atom, the corresponding adduct **VIII**-Ar is further destabilized (ΔE + zpe = 31.9 kcal mol^{-1}), because of the increased steric congestion, and is thus no longer a local minimum, but the transition state of the Sn-transfer reaction.

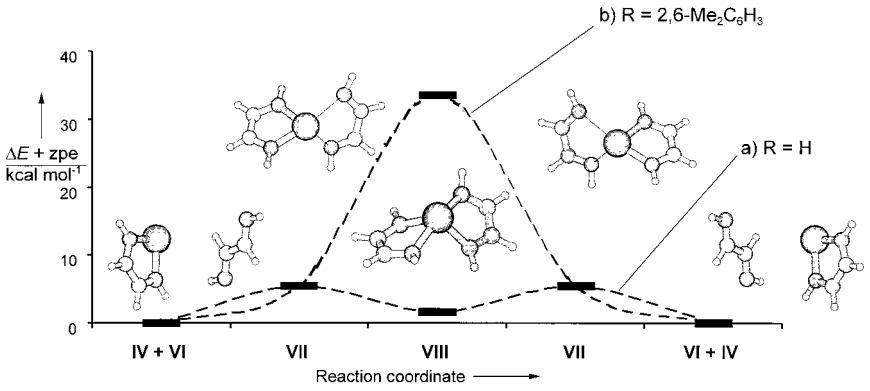


Figure 3. Computed energy profile[15] for the Sn-transfer reaction between a diazadiene (**VI**-H) and a 1,3,2-λ^2-diazastannole (**IV**-H), and MOLDEN plots[23] of the molecular structures of **VII**-H and **VIII**-H. Relative energies of the stationary states: **VII**: 1.1 (R = H), 28.6 kcal mol^{-1} (R = 2,6-$Me_2C_6H_3$); **VIII**: 5.6 (R = H) kcal mol^{-1}.

Experimental Section

3a: Solid Et_3NHCl (0.22 mol) was added to a solution of freshly prepared **2a** (0.11 mol)[3, 17] in THF (250 mL) until complete decolorization occurred. The solvent was evaporated in vacuum, the residue washed with hexane, and dissolved in a small volume of toluene. Filtration and evaporation of the filtrate produced a colorless solid of composition **1a**·LiCl (m.p. 80 °C, yield 30 %) which was used for further reactions. ^{1}H NMR (300 MHz, $CDCl_3$): δ = 1.11 (s, 9H; *t*Bu), 1.17 (s, 9H; *t*Bu), 1.32 (br, 1H; NH), 3.36 (dd, ^3J(H,H) = 3.4 Hz, 7.3 Hz; NCH_2), 7.67 ppm (t, ^3J(H,H) = 3.4 Hz, 1H; N=CH); IR (KBr): $\tilde{\nu}$ = 3230 (NH), 1674 cm^{-1} (C=N).

3b: Absolute EtOH (140 mmol) and a solution of freshly prepared **2a** (70 mmol)[3, 17] in THF (150 mL) and were added simultaneously, dropwise, to a flask containing THF (50 mL). After the reaction was complete, the mixture was evaporated to dryness and the residue dissolved in hexane (50 mL). Precipitated LiOEt was removed by filtration and the product left to crystallize at −2 °C, yield 45 %; ^{1}H NMR (300 MHz, C_6D_6): δ = 2.01 (m, 6H; CH_3), 2.16 (m, 3H; CH_3), 2.19 (m, 3H; CH_3), 2.27 (m, 6H; CH_3), 3.62 (dd, ^3J(H,H) = 2.2 Hz, 5.2 Hz; NCH_2), 4.73 (t, ^3J(H,H) = 5.2 Hz, 1H; NH), 6.78 (m, 1H; Mes-CH), 6.79 (m, 1H; Mes-CH), 7.22 ppm (t, ^3J(H,H) = 2.2 Hz; N=CH); MS (EI, 12 eV): *m*/*z* (%): 294 (90) [M^+]; IR (KBr): $\tilde{\nu}$ = 3350 (NH), 1666 cm^{-1} (C=N).

7a,**b**: A solution of **3a**,**b** (1.7 mmol) in toluene (**3a**; 10 mL) or hexane (**3b**; 10 mL) was combined with a solution of **4** (1.7 mmol) in a small volume of hexane and the mixture stirred for 2 h at 40–45 °C. The resulting red solution was cooled to ambient temperature and evaporated to dryness (**3a**), or concentrated until a dark red solid precipitated (**3b**). The crude products were recrystallized from a small volume of hexane, yield 35 % (**7a**), 50 % (**7b**); satisfactory elemental analyses; **7a**: ^{1}H NMR (C_6D_6): δ = 1.41 (s, 18H; *t*Bu), 7.44 ppm (s, 2H, ^3J(^{119}Sn,H) = 8 Hz; NCH); ^{13}C{^{1}H} NMR: δ = 33.9 (CH_3), 56.7 (NC), 125.5 ppm (NCH); ^{15}N NMR: δ = −111.9 ppm; ^{119}Sn NMR: δ = 237 ppm; **7b**: ^{1}H NMR: δ = 2.22 (m, 6H; CH_3), 2.27 (m, 12H; CH_3), 6.88 (s, 2H, ^3J(^{119}Sn,H) = 10 Hz; NCH), 6.89 ppm (m, 4H; Mes-CH); ^{13}C{^{1}H} NMR: δ = 18.5 (CH_3), 20.9 (CH_3), 128.7 (NCH), 129.2 (*m*-C), 133.3 (*p*-C), 134.3 (*o*-C), 146.1 ppm (*i*-C); ^{15}N NMR: δ = −135.0 ppm; ^{119}Sn NMR: δ = 259 ppm; MS (EI, 16 eV): *m*/*z* (%): 408(20) [M^+].

Received: November 8, 2001 [Z18189]

[1] D. Bourissou, O. Guerret, F. P. Gabbai, G. Bertrand, *Chem. Rev.* **2000**, *100*, 39.
[2] A. J. Arduengo, R. L. Harlow, M. Kline, *J. Am. Chem. Soc.* **1991**, *113*, 361.
[3] M. Denk, R. Lennon, R. Hayashi, R. West, A. V. Belyakov, H. P. Verne, A. Haaland, M. Wagner, N. Metzler, *J. Am. Chem. Soc.* **1994**, *116*, 2691.

 © WILEY-VCH Verlag GmbH, 69451 Weinheim, Germany, 2002 1433-7851/02/4111-1890 $ 20.00+.50/0

[4] a) W. A. Herrmann, M. Denk, J. Behm, W. Scherer, F. R. Klingan, H. Bock, B. Solouki, M. Wagner, *Angew. Chem.* **1992**, *104*, 1489; *Angew. Chem. Int. Ed. Engl.* **1992**, *31*, 1485; b) O. Kühl, P. Lönnecke, J. Heinicke, *Polyhedron* **2001**, *20*, 2215.

[5] a) H. Braunschweig, B. Gehrhus, P. B. Hitchcock, M. F. Lappert, *Z. Anorg. Allg. Chem.* **1995**, *621*, 1922; b) J. Heinicke, A. Oprea, M. K. Kindermann, T. Karpati, L. Nyulaszi, T. Veszpremi, *Chem. Eur. J.* **1998**, *4*, 541.

[6] M. F. Lappert, P. P. Power, A. R. Sanger, R. C. Srivastava, *Metal and Metalloid Amides*, Ellis Horwood, Chichester, **1980**.

[7] The reactions produced mainly insoluble solids which were assigned on the basis of solid-state magic-angle spinning (MAS) NMR spectroscopic studies ($\delta(^{119}Sn)$ −590 ppm (broad); $\delta(^{13}C)$ 164 ppm, CH signal of coordinated CH=N moiety) as polymeric $SnCl_2$–diazadiene adducts.

[8] Compound **3a** has to date only been described as an unstable intermediate: H. tom Dieck, U. Verfürth, K. Diblitz, J. Ehlers, G. Fendesack, *Chem. Ber.* **1989**, *122*, 129.

[9] NMR data (C_6D_6, 30 °C): ^{1}H NMR: $\delta = 0.37$ (s, 18H; $SiMe_3$), 1.06 (s, 9H; *t*Bu), 1.32 (s, 9H; *t*Bu), 3.86 (dd, $^2J(H,H) = 25$ Hz, $^3J(H,H) = 1.2$ Hz, $^3J(^{119}Sn,H) = 22$ Hz, 1H; CH_2), 4.50 (dd, $^2J(H,H) = 25$ Hz, $^3J(H,H) = 1.2$ Hz, $^3J(^{119}Sn,H) = 22$ Hz, 1H; CH_2); 7.43 ppm (t, $^3J(H,H) = 1.2$ Hz, $^3J(^{119}Sn,H) = 25$ Hz, 1H; N=CH); ^{119}Sn NMR: $\delta =$ 118 ppm.

[10] Reaction of **3a** with $[Pb(N(SiMe_3)_2)_2]$ gave, beside $HN(SiMe_3)_2$, a product with a constitution similar to **5a**, which was characterized by NMR spectroscopy (^{1}H NMR: $\delta = 0.38$ (s, 18H; $SiMe_3$), 1.05 (s, 9H; *t*Bu), 1.35 (s, 9H; *t*Bu), 4.51 (d, $^2J(H,H) = 25$ Hz, $^3J(^{207}Pb,H) = 32$ Hz, 1H; CH_2), 5.91 (d, $^2J(H,H) = 25$ Hz, 1H; CH_2), 8.08 ppm (s, $^3J(^{207}Pb,H) = 56$ Hz, 1H; N=CH); ^{207}Pb NMR: $\delta = 2590$ ppm) but decayed to **1a**, $HN(SiMe_3)_2$, and Pb without further detectable intermediates.

[11] R. West, J. J. Buffy, M. Haaf, T. Müller, B. Gehrhus, M. F. Lappert, Y. Apeloig, *J. Am. Chem. Soc.* **1998**, *120*, 1639.

[12] a) D. Gudat, A. Haghverdi, H. Hupfer, M. Nieger, *Chem. Eur. J.* **2000**, *6*, 3414; b) M. K. Denk, S. Gupta, R. Ramachandran, *Eur. J. Inorg. Chem.* **1999**, 41.

[13] Crystal data for **7b**: $C_{20}H_{24}N_2Sn$, dimensions $0.60 \times 0.40 \times 0.20$ mm, $M_r = 411.1$, triclinic, space group $P\bar{1}$ (No. 2), $a = 8.1282(2)$, $b = 10.3477(2)$, $c = 12.4490(3)$ Å, $\alpha = 92.12(1)$, $\beta = 104.45(1)$, $\gamma = 111.76(1)°$, $V = 931.80(4)$ Å^3, $Z = 2$, $Mo_{K\alpha}$ radiation, $\mu(Mo_{K\alpha}) = 1.37$ mm^{-1}, $T = 123(2)$ K, $F(000) = 416$; data collection: Nonius Kappa CCD, 12237 reflections up to $2\theta_{max} = 50°$, 3284 independent reflections, $R_{int} = 0.048$; structure solution (direct methods: G. M. Sheldrick, *Acta Crystallogr. Sect. A* **1990**, *46*, 467) and refinement (on F^2, C,N atoms anisotropically, Sn atom isotropically, H atoms with a riding model; SHELXL-97, G. M. Sheldrick, Universität Göttingen, **1997**): empirical absorption correction, 213 parameters, 14 restraints, $R(I > 2\sigma(I)) = 0.042$, *wR*2 (all data) = 0.105, max./min. residual electron density (near the disordered Sn atoms) 2.96/−1.10 e Å^{-3}. CCDC-172771 contains the supplementary crystallographic data for this paper. These data can be obtained free of charge via www.ccdc.cam.ac.uk/conts/retrieving.html (or from the Cambridge Crystallographic Data Centre, 12, Union Road, Cambridge CB2 1EZ, UK; fax: (+44) 1223-336-033; or deposit@ccdc.cam.ac.uk).

[14] Crystal structure studies on several crystals obtained from different reactions and solvents revealed in all cases identical disorder phenomena.

[15] The observed acceleration of the fragmentation upon addition of Cl^- ions suggested that formation of diazadiene–$SnCl_2$ adducts from **2** and $SnCl_2$ may occur by decomposition of intermediate λ^2-diazastannole species and subsequent reaction of the resulting diazadiene with excess $SnCl_2$.

[16] Spectroscopic data indicate that as for DMAP adducts of diazaphospholenes (cf. ref. [12]) in solution, dynamic equilibria between adducts and separated molecules are present.

[17] M. Haaf, A. Schmiedl, T. A. Schmedake, D. R. Powell, A. J. Millevolte, M. Denk, R. West, *J. Am. Chem. Soc.* **1998**, *120*, 12714.

[18] DFT calculations were performed using the Gaussian suite of programs: Gaussian 98 (Revision A.7), M. J. Frisch, G. W. Trucks, H. B. Schlegel, G. E. Scuseria, M. A. Robb, J. R. Cheeseman, V. G. Zakrzewski, J. A. Montgomery, R. E. Stratmann, J. C. Burant, S. Dapprich, J. M. Millam, A. D. Daniels, K. N. Kudin, M. C. Strain, O. Farkas, J. Tomasi, V. Barone, M. Cossi, R. Cammi, B. Mennucci, C. Pomelli, C. Adamo, S. Clifford, J. Ochterski, G. A. Petersson, P. Y. Ayala, Q. Cui, K. Morokuma, D. K. Malick, A. D. Rabuck, K. Raghavachari, J. B. Foresman, J. Cioslowski, J. V. Ortiz, B. B. Stefanov, G. Liu, A. Liashenko, P. Piskorz, I. Komaromi, R. Gomperts, R. L. Martin, D. J. Fox, T. Keith, M. A. Al-Laham, C. Y. Peng, A. Nanayakkara, C. Gonzalez, M. Challacombe, P. M. W. Gill, B. G. Johnson, W. Chen, M. W. Wong, J. L. Andres, M. Head-Gordon, E. S. Replogle, J. A. Pople, Gaussian, Inc., Pittsburgh, PA, **1998**. Basis sets and methods: B3LYP/SDD with relativistic pseudo potentials at the Sn atom and polarization functions on all heavy atoms for **I**–**III**, **IV**-H–**VII**-H; two-level ONIOM using B3LYP/SDD + d for the bicyclic ring system and MNDO for the aryl groups for **IV**-Ar–**VI**-Ar.

[19] NBO 5.0: E. D. Glendening, J. K. Badenhoop, A. E. Reed, J. E. Carpenter, J. A. Bohmann, C. M. Morales, F. Weinhold, Theoretical Chemistry Institute, Univ. of Wisconsin, Madison, WI, **2001**; http://www.chem.wisc.edu/~nbo5.

[20] WBI(E-N) = 1.27 (**I**), 0.79 (**II**), 0.77 (**III**), 0.70 (**IV**-H); contribution (in %) of E to the σ(E-N) LMO: 32.6 (**I**), 14.8 (**II**), 14.5 (**III**), 11.8 (**IV**-H).

[21] A. J. Arduengo, H. Bock, H. Chen, M. Denk, D. A. Dixon, J. C. Green, W. A. Herrmann, N. L. Jones, M. Wagner, R. West, *J. Am. Chem. Soc.* **1994**, *116*, 6641; the increased importance of canonical structure **IV′** is substantiated by concomitant shifts in bond orders (WBI(N−C/C=C) = 1.12/1.67 (**I**), 1.21/1.57 (**IV**-H)).

[22] b) Y. Zhou, D. S. Richeson, *J. Am. Chem. Soc.* **1996**, *118*, 10850; b) S. R. Foley, Y. Zhou, G. P. A. Yap, D. S. Richeson, *Inorg. Chem.* **2000**, *39*, 924.

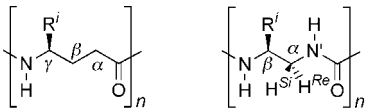
[23] G. Schaftenaar, J. H. Noordik, *J. Comput.-Aided Mol. Des.* **2000**, *14*, 123.

Stable Helical Secondary Structure in Short-Chain *N*,*N*′-Linked Oligoureas Bearing Proteinogenic Side Chains**

Vincent Semetey, Didier Rognan, Christine Hemmerlin, Roland Graff, Jean-Paul Briand, Michel Marraud, and Gilles Guichard*

Dedicated to Professor Dieter Seebach on the occasion of his 65th birthday

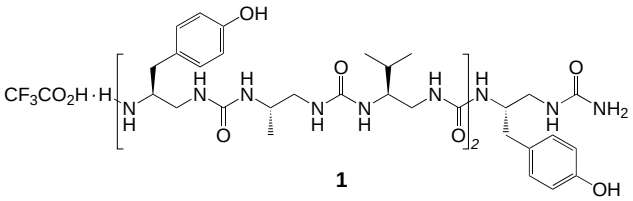
The functional diversity in proteins, although mediated by sophisticated tertiary and quaternary structures, relies on a small set of distinct secondary structural elements: sheets, helices, and turns. Unnatural oligomeric scaffolds designed to reproduce or mimic these essential protein features while retaining the chemical diversity of amino acid side chains have gained considerable interest in recent years, with potential application in drug discovery.[1] Work published by the research groups of Seebach, Gellman, and Hanessian has revealed that short-chain peptides consisting exclusively of enantiopure β- or γ-amino acids with defined substitution patterns can form stable helical or pleated-sheet-type structures in solution and in the solid state.[2–4] In particular, γ-peptides such as **A**, with chirality centers from an L-amino



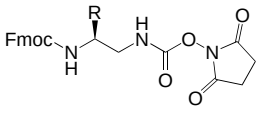
A **B**

acid form a right-handed (*P*)2.6$_{14}$ helix of about 5 Å pitch in which both ethane bonds are in a (+)-synclinal (si) conformation.[4a, 4c] Enantiopure *N*,*N*′-linked oligoureas of general formula **B**, obtained by formal replacement of the $^{\alpha}$C atom of γ-amino acid residues in **A** by a nitrogen atom, were originally described in 1995 by Burgess et al. and used as novel peptide backbone mimetics.[5]

Although *N*,*N*′-linked oligoureas are readily accessible by solid-phase synthesis using appropriate monomers,[5, 6] their conformational preferences and their folding propensities have not been elucidated so far. We reasoned that, subject to an antiperiplanar arrangement of the N′H and $^{\alpha}$CH^{Si} atoms (in **B**), the substitution of NH for the $^{\alpha}$CH$_2$ group of γ-amino acid residues (**A** → **B**), should be sterically compatible with an approximate 2.6-helical backbone. Herein, we report the solution structure of heptaurea **1** bearing side chains of natural amino acids Ala, Val, and Tyr.



1



2

2	R
a	Me
b	*i*Pr
c	Bn(O*t*Bu)

Oligourea **1** was prepared as described previously by solid-phase synthesis using succinimidyl carbamate derivatives **2a–c** (Fmoc = 9-fluorenylmethoxycarbonyl, Bn = benzyl) as activated monomers.[6d] The structure of **1** was investigated by 1D and 2D NMR spectroscopy in [D$_5$]pyridine. This solvent was used because of the larger dispersion of chemical shifts compared to those found in nonaromatic solvents such as CD$_3$OH or (CD$_3$)$_2$SO as a result of the ring current effect in the former. The spin systems of all seven residues were unambiguously identified from DQF-COSY and TOCSY experiments. The sequence was assigned on the basis of ROESY experiments (mixing time = 300 ms) and was deduced from the strong N′H$_i$-NH$_{i+1}$ NOE connectivities observed along the urea backbone. A number of data relevant to the structure determination were extracted from 1D and COSY spectra. The *J*(NH,$^{\beta}$CH) values for residues 2–7 were large ($J > 9$ Hz), which indicates a restricted rotation around the N–$^{\beta}$C bond and a nearly antiperiplanar arrangement of the corresponding protons. Analysis of 1D spectra recorded between 288 and 368 K at 10 K increments revealed that the coupling values are only weakly affected by temperature changes and remain large over the temperature range studied.[7]

Furthermore, the geminal protons at the $^{\alpha}$C atom exhibited significant differences in their chemical shift ($1.3 < \Delta\delta < 1.6$ ppm for central residues 3–6 and $\Delta\delta = 1.0–1.1$ ppm for residues 2 and 7). This chemical shift difference, which reflects a defined and distinct spatial arrangement for both diastereotopic $^{\alpha}$CH protons along the backbone, remained constant over the range 271–368 K. Careful examination of the $^3J(^{\alpha}\mathrm{CH_2},\mathrm{N'H})$ and $^3J(^{\beta}\mathrm{CH},^{\alpha}\mathrm{CH_2})$ values for residue 3[8] at 332 K (Table 1) revealed that the downfield diastereotopic $^{\alpha}$CH proton has a large coupling constant with the N′H proton

[*] Dr. G. Guichard, V. Semetey, Dr. J.-P. Briand
Immunologie et Chimie Thérapeutiques, UPR CNRS 9021
Institut de Biologie Moléculaire et Cellulaire
15, rue Descartes, 67084 Strasbourg (France)
Fax: (+33) 3-88-61-06-80
E-mail: G.Guichard@ibmc.u-strasbg.fr
Dr. D. Rognan
Laboratoire de Pharmacochimie de la Communication Cellulaire, UMR CNRS-ULP 7081
74, route du Rhin - B.P. 24, 67401 Illkirch (France)
Dr. C. Hemmerlin, Dr. M. Marraud
LCPM, UMR CNRS-INPL 7568
ENSIC-INPL, BP 451, 54001 Nancy (France)
Dr. R. Graff
Faculté de Chimie
1 Rue Blaise Pascal, 67008 Strasbourg (France)

[**] Access to both the Bruker ARX 500 facilities of the Service Commun de RMN (Faculté de Chimie, Strasbourg) and the Bruker DRX 600 NMR facilities of the Service Commun de Biophysicochimie des Interactions Moléculaires (Université Henri Poincaré, Nancy I) were deeply appreciated.

Supporting information for this article is available on the WWW under http://www.angewandte.com or from the author.

 © WILEY-VCH Verlag GmbH, 69451 Weinheim, Germany, 2002 1433-7851/02/4111-1893 $ 20.00+.50/0

Table 1. Chemical shifts and coupling constants for backbone protons of residue 3.

Proton	δ	J [Hz]
NH	6.64	$^{3}J(\mathrm{NH},{}^{\beta}\mathrm{CH}) = 10$
$^{\beta}$CH	4.02	$^{3}J({}^{\beta}\mathrm{CH},{}^{\alpha}\mathrm{CH}^{Si}) = 2.5$, $^{3}J({}^{\beta}\mathrm{CH},{}^{\alpha}\mathrm{CH}^{Re}) = 11$
$^{\alpha}$CH^{Re}	2.53	$^{2}J({}^{\alpha}\mathrm{CH}^{Re},{}^{\alpha}\mathrm{CH}^{Si}) = -14$
$^{\alpha}$CH^{Si}	3.96	
N′H	6.66	$^{3}J(\mathrm{N'H},{}^{\alpha}\mathrm{CH}^{Si}) = 10$, $^{3}J(\mathrm{N'H},{}^{\alpha}\mathrm{CH}^{Re}) = 3.5$

(ca. 10 Hz) but a small one with the corresponding $^{\beta}$CH proton (ca. 2.5 Hz), which implies that this $^{\alpha}$CH proton is nearly antiperiplanar to N′H and synclinal to $^{\beta}$CH.[8]

These data strongly suggested that oligourea **1** adopts a well-defined and stable secondary structure in solution. To gain more information about the three-dimensional structure of heptaurea **1** ROESY experiments were acquired at 332 K with a mixing time of 300 ms. A total of 106 NOE interactions were extracted and classified in three distance categories according to their cross-peak volume. Out of the 26 inter-residue NOE interactions, 17 are from residue i to residue $i+2$. Particularly noteworthy were the medium-to-strong NOE interactions observed between $^{\beta}\mathrm{CH}_i$ and NH_{i+2} for $i = 2-5$ and between $^{\beta}\mathrm{CH}_i$ and $\mathrm{N'H}_{i+2}$ for $i = 2-5$. Unambiguous assignment of the diastereotopic $^{\alpha}$CH protons was possible for all residues by direct comparison of intraresidue NOE interactions between the NH and both $^{\alpha}$CH protons. The downfield $^{\alpha}$CH proton displayed a weaker NOE correlation with NH than did the corresponding upfield proton, and could thus be assigned to $^{\alpha}\mathrm{CH}^{Si}$.

The NOE interactions and J values were used as distance and dihedral angle restraints, respectively, in a 100-ps simulated-annealing protocol using the AMBER6 suite of programs.[9] Calculations converged well and yielded a set of 20 structures with no NOE violation greater than 0.3 Å and no dihedral angle violation greater than 5°. A bundle of the best 20 structures chosen to be representative of the structure in solution is depicted in Figure 1.

The secondary structure of heptaurea **1** is a right-handed 2.5 helix with a pitch of approximately 5.1 Å that is well defined for residues 2–6, with residue 1 and, to a lesser extent, residue 7 being flexible. Although the structure shares overall similarity with the helical backbone of γ-peptides, the helix of **1** displays a more complicated intramolecular hydrogen-bonding pattern that is characterized by the simultaneous presence of 12- and 14-membered pseudocycles resulting from $\mathrm{C{=}O}_i \cdots \mathrm{HN'}_{i+2}$ and $\mathrm{C{=}O}_i \cdots \mathrm{HN}_{i+3}$ hydrogen bonds (Figure 2).

However, $\mathrm{C{=}O}_i$ is not equidistant from $\mathrm{N'H}_{i+2}$ and NH_{i+3}, and statistics performed on the calculated 20 structures

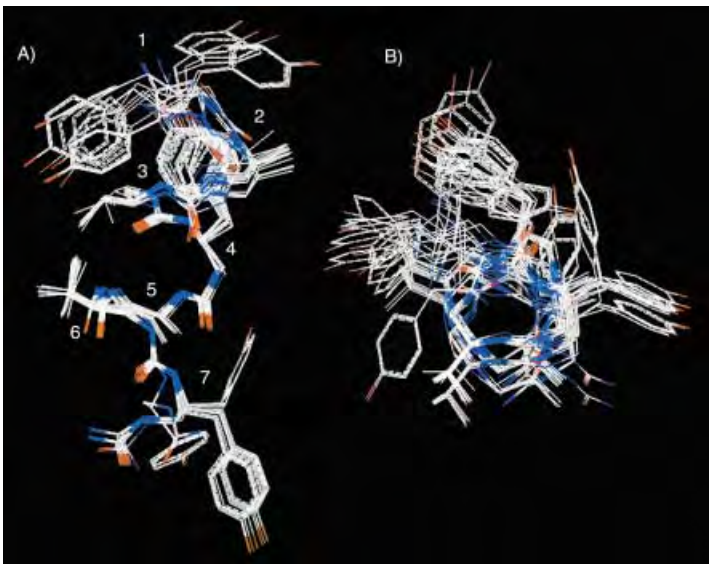


Figure 1. Bundle of the 20 best structures of lowest energy A) viewed along the helix axis, and B) top view. Root-mean-square (rms) differences of bond and angle deviations from ideality were less than 0.02 Å and 3°, respectively. Rms deviations for all heavy backbone atoms from a mean structure were 0.56 ± 0.18 for residues 1–7 and 0.36 ± 0.19 Å for residues 2–7.

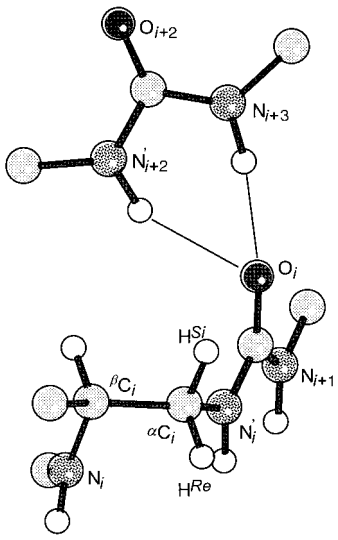


Figure 2. Atom numbering and schematic representation of the hydrogen-bonding pattern as found in the 2.5 helix of oligourea **1**.

(Table 2) suggest that the 14-membered H-bonded rings are more populated than the corresponding 12-membered rings, at least in the inner part of the helix.[10]

Table 2. Estimated $\mathrm{C{=}O}_i \cdots \mathrm{HN'}_{i+2}$ and $\mathrm{C{=}O}_i \cdots \mathrm{HN}_{i+3}$ hydrogen-bonding pattern for $i = 1-4$ based on statistical analysis of the final 20 structures of lowest energy.[a]

	$\mathrm{C{=}O}_i \cdots \mathrm{HN'}_{i+2}$			$\mathrm{C{=}O}_i \cdots \mathrm{HN}_{i+3}$		
	H-bond occurence [%]	Average N-H-O angle	Average d(N-O) [Å]	H-bond occurence [%]	Average N-H-O angle	Average d(N-O) [Å]
$i = 1$	50	142	3.10	55	157	2.98
$i = 2$	35	137	3.41	90	166	3.13
$i = 3$	50	139	3.46	100	160	2.91
$i = 4$	50	156	3.24	100	167	2.98

[a] The geometry of a hydrogen bond is defined by d(N-O) < 3.25 Å and N-H-O angle > 120°.

 © WILEY-VCH Verlag GmbH, 69451 Weinheim, Germany, 2002 1433-7851/02/4111-1894 $ 20.00+.50/0 *Angew. Chem. Int. Ed.* **2002**, *41*, No. 11

In conclusion, by determining the solution structure of **1**, we have demonstrated that *N*,*N*′-linked oligoureas of general formula **B** belong to the growing family of non-natural non-peptide oligomers with defined and predictable secondary structures. Although heptaurea **1** forms a (*P*)2.5 helix of approximately 5.1 Å pitch that is closely related to the $(P)2.6_{14}$ helix of approximately 5 Å pitch of corresponding γ^4-peptides,[4a] it is worth noting that both NH groups within the same urea linkage may participate in intramolecular hydrogen bonding to the same C=O group. The knowledge of the three-dimensional structure of **1** is likely to be useful for the de novo design of oligoureas with controlled shape and defined biological activities.

Received: October 1, 2001 [Z17991]

[1] S. H. Gellman *Acc. Chem. Res.* **1998**, *31*, 173 – 180; K. Kirshenbaum, R. N. Zuckermann, K. A. Dill, *Curr. Opin. Struct. Biol.* **1999**, *9*, 530 – 535.

[2] For representative examples of helical β-peptides, see D. Seebach, M. Overhand, F. N. M. Kühnle, B. Martinoni, L. Oberer, U. Hommel, H. Widmer, *Helv. Chim. Acta* **1996**, *79*, 913 – 941; D. Seebach, S. Abele, K. Gademann, G. Guichard, T. Hintermann, B. Jaun, J. L. Matthews, J. V. Schreiber, L. Oberer, U. Hommel, H. Widmer, *Helv. Chim. Acta* **1998**, *81*, 932 – 982; S. Abele, G. Guichard, D. Seebach, *Helv. Chim. Acta* **1998**, *81*, 2141 – 2156; D. Seebach, T. Sifferlen, P. A. Mathieu, A. M. Häne, C. M. Krell, D. J. Bierbaum, S. Abele, *Helv. Chim. Acta* **2000**, *83*, 2849 – 2864; H. Appella, L. A. Christianson, I. L. Karle, D. R. Powell, S. H. Gellman, *J. Am. Chem. Soc.* **1996**, *118*, 13071 – 13072; D. H. Appella, L. A. Christianson, D. A. Klein, D. R. Powell, X. Huang, J. J. Barchi, Jr, S. H. Gellman, *Nature* **1997**, *387*, 381 – 384; D. H. Appella, J. J. Barchi, Jr, S. R. Durell, S. H. Gellman, *J. Am. Chem. Soc.* **1999**, *121*, 2309 – 2310; X. Wang, J. F. Espinosa, S. H. Gellman, *J. Am. Chem. Soc.* **2000**, *122*, 4821 – 4822.

[3] For representative examples of sheet and turn structures with β-peptides, see a) D. Seebach, S. Abele, K. Gademann, B. Jaun, *Angew. Chem.* **1999**, *111*, 1700 – 1703; *Angew. Chem. Int. Ed.* **1999**, *38*, 1595 – 1597; b) S. Krauthäuser, L. A. Christianson, D. R. Powell, S. H. Gellman, *J. Am. Chem. Soc.* **1997**, *119*, 11719 – 11720; c) Y. J. Chung, R. B. R. Huck, L. A. Christianson, H. E. Stanger, S. Krauthäuser, D. R. Powell, S. H. Gellman, *J. Am. Chem. Soc.* **2000**, *122*, 3995 – 4004.

[4] For leading references on γ-peptides, see a) T. Hintermann, K. Gademann, B. Jaun, D. Seebach, *Helv. Chim. Acta* **1998**, *81*, 983 – 1002; b) D. Seebach, M. Brenner, M. Rueping, B. Schweizer, B. Jaun, *Chem. Commun.* **2001**, 207 – 208; c) S. Hanessian, X. Luo, R. Schaum, S. Michnick, *J. Am. Chem. Soc.* **1998**, *120*, 8569 – 8570; d) S. Hanessian, X. Luo, R. Schaum, *Tetrahedron Lett.* **1999**, *40*, 4925 – 4929.

[5] a) K. Burgess, D. S. Linthicum, H. Shin, *Angew. Chem.* **1995**, *107*, 975 – 977; *Angew. Chem. Int. Ed. Engl.* **1995**, *34*, 907 – 908; b) K. Burgess, J. Ibarzo, D. S. Linthicum, D. H. Russell, H. Shin, A. Shitangkoon, R. Totani, A. J. Zhang, *J. Am. Chem. Soc.* **1997**, *119*, 1556 – 1564.

[6] a) J. M. Kim, Y. Bi, S. Paikoff, P. G. Schultz, *Tetrahedron Lett.* **1996**, *37*, 5305 – 5308; b) A. Boeijen, R. M. J. Liskamp, *Eur. J. Org. Chem.* **1999**, 2127 – 2135; c) G. Guichard, V. Semetey, C. Didierjean, A. Aubry, J. P. Briand, M. Rodriguez, *J. Org. Chem.* **1999**, *64*, 8702 – 8705; d) G. Guichard, V. Semetey, M. Rodriguez, J. P. Briand, *Tetrahedron Lett.* **2000**, *41*, 1553 – 1557.

[7] Similarly, Seebach and co-workers have shown in the case of a β-heptapeptide that $J(\mathrm{NH},{}^{\beta}\mathrm{CH})$ values decrease only slowly upon an increase of the temperature from 298 to 353 K. A decrease of about 0.4 Hz was observed for the central residues (3 – 6) and about 0.7 Hz for the flanking residues 2 and 7: K. Gademann, B. Jaun, D. Seebach, R. Perozzo, L. Scapozza, G. Folkers, *Helv. Chim. Acta* **1999**, *82*, 1 – 11.

[8] In the case of residue 3, $^3J({}^{\alpha}\mathrm{CH}_2,\mathrm{N}'\mathrm{H})$ values were extracted directly from the 1D NMR spectrum, but decoupling experiments were required to access precise $^3J({}^{\beta}\mathrm{CH},{}^{\alpha}\mathrm{CH}_2)$values. Severe overlaps in the ${}^{\alpha}\mathrm{CH}$ region precluded measurement of the $^3J({}^{\beta}\mathrm{CH},{}^{\alpha}\mathrm{CH}_2)$ values for other residues. However, qualitative examination of the COSY spectrum reveals similar vicinal coupling patterns.

[9] D. A. Case, D. A. Pearlman, J. W. Caldwell, D. E. Cheatham III, W. S. Ross, C. L. Simmerling, T. A. Darden, K. M. Merz, R. V. Stanton, A. L. Cheng, J. J. Vincent, M. Crowley, V. Tsui, R. J. Radmer, Y. Duan, J. Pitera, I. Massova, G. L. Seibel, U. C. Singh, P. K. Weiner, P. A. Kollman, AMBER6, University of California, San Francisco, **1999**

[10] Further experimental evidence for $\mathrm{C{=}O}_i\cdots\mathrm{HN}'_{i+2}$ and $\mathrm{C{=}O}_i\cdots\mathrm{HN}_{i+3}$ hydrogen bonds is gained from the determination of temperature coefficients. $\mathrm{N}'\mathrm{H}_{i+2}$ for $i=1-4$ and NH_{i+3} for $i=1-4$ have temperature coefficients with absolute values <4 ppb K^{-1}, which indicates limited solvent accessibility. In addition, temperature coefficients of $\mathrm{N}'\mathrm{H}_{i+2}$ for $i=2-4$ ($3.5\ \mathrm{ppb\,K^{-1}} < -\Delta\delta/\Delta T < 3.8\ \mathrm{ppb\,K^{-1}}$) have higher absolute values than those of NH_{i+3} for $i=2-4$ ($1.5\ \mathrm{ppb\,K^{-1}} < -\Delta\delta/\Delta T < 2.5\ \mathrm{ppb\,K^{-1}}$). This trend could suggest an increased solvent accessibility for $\mathrm{N}'\mathrm{H}_{i+2}$ compared to NH_{i+3}.

Self-Assembling Organic Nanotubes from Enantiopure Cyclo-*N*,*N*′-Linked Oligoureas: Design, Synthesis, and Crystal Structure

Vincent Semetey, Claude Didierjean, Jean-Paul Briand, André Aubry, and Gilles Guichard*

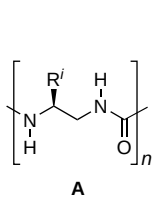
Assembly of self-complementary cyclo-oligomeric subunits through noncovalent processes (for example, hydrogen bonding, aromatic stacking) has emerged as a powerful strategy to generate artificial organic nanotubular structures.[1, 2] Highly functionalized tubular assemblies based on peptides have attracted much interest recently in this area. Ghadiri and co-workers have compellingly demonstrated that 24- and 30-membered-ring cyclo-α-peptides with an even number of alternating D- and L-amino acids stack in an antiparallel β-sheet-like arrangement to form hydrogen-bonded tubular structures, that is, "peptide nanotubes".[2–4] Remarkably, related cyclic peptides consisting exclusively of β-amino acids[5, 6] (16- and 12-membered ring), of alternating α- and β-amino acids[7] (14-membered ring), or of vinylogous δ-amino acids[8] (18-membered ring) also form tubular stacks.

We have shown previously[9] that linear *N*,*N*′-linked oligoureas **A** consisting of homochiral residues adopt a stable 2.5-helical secondary structure in solution. The helix is characterized by the simultaneous presence of 12- and 14-membered hydrogen-bonded rings resulting from the capacity of the urea group to establish self-complementary bidirec-

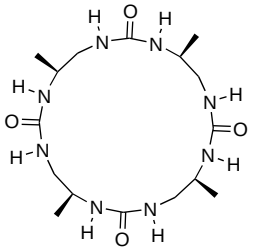
[*] Dr. G. Guichard, V. Semetey, Dr. J.-P. Briand
Immunologie et Chimie Thérapeutiques, UPR CNRS 9021
Institut de Biologie Moléculaire et Cellulaire
15, rue Descartes, 67084 Strasbourg (France)
Fax: (+33) 3-88-61-06-80
E-mail: G.Guichard@ibmc.u-strasbg.fr
Dr. C. Didierjean, Dr. A. Aubry
LCM3B, UMR-CNRS 7036, Groupe Biocristallographie
Université Henri Poincaré
BP 239, 54506 Vandœuvre, France

Supporting information for this article is available on the WWW under http://www.angewandte.com or from the author.

 © WILEY-VCH Verlag GmbH, 69451 Weinheim, Germany, 2002 1433-7851/02/4111-1895 $ 20.00+.50/0



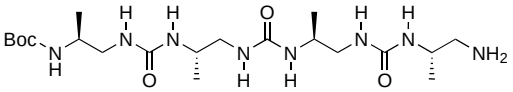
A



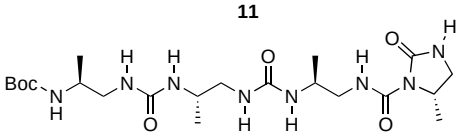
1

tional intermolecular hydrogen bonds. We envisioned that the corresponding macrocyclic derivatives might lead to flat ring structures with a high degree of self-complementarity that would allow self-assembling processes to occur. Herein we report the design and the synthesis of the C_4-symmetric (all-*S*) cyclotetraurea **1** bearing side chains of alanine, and demonstrate by single-crystal X-ray analysis that **1** forms square-shaped nanotubes.

The general stepwise strategy used to synthesize the 20-membered-ring macrocycle **1** is outlined in Scheme 1. Reaction of the succinimidyl carbamate derivative **2**[10] with the monoprotected benzylated diamine **3** yielded the trisubstituted urea **4**. Removal of the Boc group followed by urea formation with **2** gave the bisurea **5**. Repetition of this two-step sequence gave the fully protected triurea **6** in an overall yield of 45% from **3**. Following quantitative removal of the Alloc group, the resulting amine **7** was converted into the key activated linear precursor **8** by treatment with di(*N*-succinimidyl carbonate). At this stage, the temporary protection of the urea with a benzyl group was mandatory. Initial attempts to convert the linear oligotriurea precursor **11** under the same conditions were not successful and led exclusively to the formation of the cyclic biuret derivative **12**.



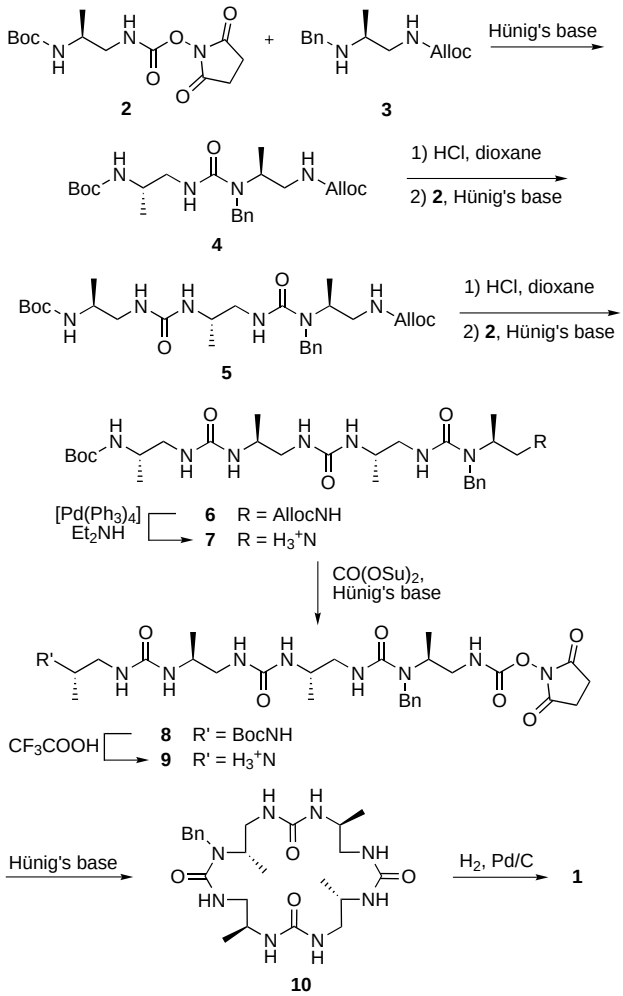
11



12

The Boc protecting group was selectively removed upon treatment of crude **8** with CF_3COOH to give the trifluoroacetate salt **9**. Slow addition of a solution of **9** in MeCN to a dilute solution of Hünig's base in MeCN resulted in the formation of the expected monobenzylated cylic oligotetraurea **10** in a yield of 62% from **7** after HPLC purification (C_{18} column, reversed phase). Cyclotetraurea **1** was obtained in 92% yield from **10** following deprotection of the urea group by hydrogenation in EtOH. Single crystals of **1** suitable for X-ray studies were grown by slow evaporation of the EtOH solution.

X-ray crystallographic analysis[11] revealed that cyclourea **1** adopts a C_4-symmetric conformation in the solid state and stacks to form a hollow tubular structure (Figure 1). The four



Scheme 1. Synthesis of **1**. Alloc = allyloxycarbonyl, Boc = *tert*-butoxycarbonyl, Bn = benzyl, Hünig's base = diisopropylethylamine, Su = succinimidyl.

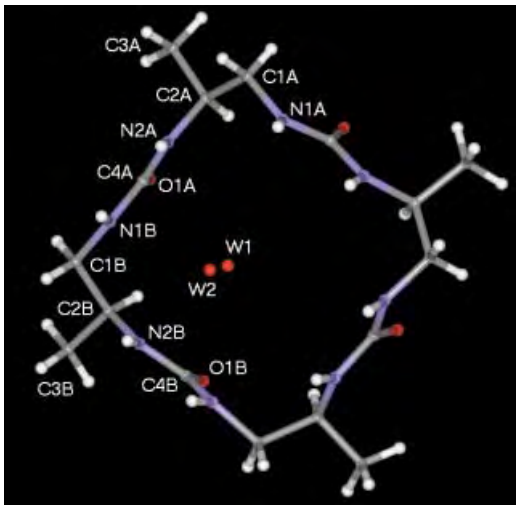


Figure 1. Ball and stick representation of **1** showing the numbering scheme. The torsion angles [°] of the main chain are : N1A-C1A-C2A-N2A 57.9(2), C1A-C2A-N2A-C4A −156.7(2), C2A-N2A-C4A-N1B 177.4(2), N2A-C4A-N1B-C1B 172.6(2), C4A-N1B-C1B-C2B 78.0(3).

 © WILEY-VCH Verlag GmbH, 69451 Weinheim, Germany, 2002 1433-7851/02/4111-1896 $ 20.00+.50/0 *Angew. Chem. Int. Ed.* **2002**, *41*, No. 11

urea fragments in the macrocyle present an all-*trans*, planar conformation with all the urea carbonyl groups pointing down and all the NH groups pointing up (Figure 1). The macrocyle exhibits a square shape with a cross-section of 6.052(7) Å (distance between C1A and C1B).

A difference map analysis revealed the presence of two peaks located on the fourfold symmetry axis. The distance between the two peaks was 1.42 Å. NMR experiments gave no evidence for the presence of any organic solvent molecules in the crystal, thus the two peaks were treated as disordered water molecules W1 and W2. The internal van der Waals diameter (approximately 3.5 Å) of the tubular structure is actually large enough to accommodate such molecules. The distance between the two water molecules is too short to have both sites occupied at the same time. There is no short atomic contact favoring hydrogen bonding between the water molecules W1 and W2 and the macrocyle.

The square-shaped cycloureas stack along the crystallographic fourfold axis of the crystal through backbone–backbone hydrogen-bonding interactions so that the two NH hydrogen atoms of each urea fragment interact with a urea oxygen atom of a neighboring macrocycle (Figure 2).

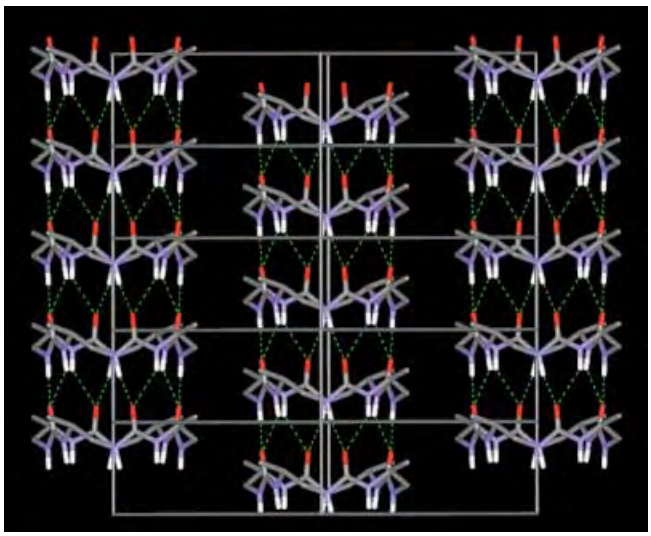


Figure 2. View of the nanotubular organization of **1** along the channel axis. The intermolecular hydrogen bonds are marked as dashed lines. The solvent molecules and H atoms, except those of the NH groups, are omitted for clarity. The edges of the unit cells are represented in gray.

One of the intermolecular N···O distances has standard dimensions (2.798(2) Å), while the other (3.281(2) Å) is just above the limit generally considered for hydrogen-bonding interactions (Figure 2). This stacking of the macrocyles differs from that observed in the crystal structure of cystine-based macrocyclic bisureas that also exhibits a backbone–backbone urea-type hydrogen-bonding interaction.[12] As a consequence of the absence of a local symmetry for the motif C1A–C1B (Figure 1), the urea N–H and C=O bonds in **1** are not parallel to the channel axis and generate two different N···O contacts. Each cyclourea is perpendicular to and centered on the crystallographic quaternary axis in the crystal of **1**. The stacking of the cyclourea units along the crystallographic *c* axis gives rise to an infinite nanotube. The crystal obtained exhibits a body-centered Bravais lattice, and thus the X-ray structure consists of an array of nanotubes in which each tubular stack is surrounded by four close neighbors at a distance of $a\sqrt{2}/2$ Å ($a = 15.333(3)$ Å is one of the unit cell parameters). Neighboring tubes are all arranged in the same direction.[13]

The nanotubes are held together in the crystal by loose van der Waals contacts. The intermolecular distances between equivalent C1A atoms and equivalent C3A atoms are 4.097(7) and 4.218(10) Å, respectively.

In summary, we have reported a versatile approach to the synthesis of 20-membered cyclic oligoureas bearing proteinogenic side chains. The cyclic units consisting of homochiral residues self-assemble in the crystal state to form hydrogen-bonded polar nanotubes. The structure of the tubular stack with all the carbonyl and NH groups pointing, respectively, in the same direction is reminiscent of the nanotubes formed by cyclotetra-β-peptides with homochiral residues.[5a] Particularly noteworthy is the presence of electronic density inside the tubular cavity which was modeled as disordered water molecules at overlapping sites. Further work to explore other tubular arrangements made from cycloureas with different side-chain functionalities and different stereochemistry is on going.

Received: December 18, 2001 [Z18407]

[1] B. König, *Angew. Chem.* **1997**, *109*, 1919–1921; *Angew. Chem. Int. Ed.* **1997**, *36*, 1808–1832.

[2] D. T. Bong, T. D. Clark, J. R. Granja, M. R. Ghadiri, *Angew. Chem.* **2001**, *113*, 1016–1041; *Angew. Chem. Int. Ed.* **2001**, *40*, 988–1011, and references therein.

[3] a) M. R. Ghadiri, J. R. Granja, R. A. Milligan, D. E. McRee, N. Khazanovich, *Nature* **1993**, *366*, 324–327; b) J. R. Granja, R. M. Ghahiri, *J. Am. Chem. Soc.* **1994**, *116*, 10785–10786; c) M. R. Ghadiri, K. Kobayashi, J. R. Granja, R. K. Chadha, *Angew. Chem.* **1995**, *107*, 76–78; *Angew. Chem. Int. Ed.* **1995**, *34*, 93–95.

[4] Cyclo-α-peptides are stable to proteases and hold great promise as antibacterial agents: S. Fernandez-Lopez, S. H. Kim, E. C. Choi, M. Delgado, J. R. Granja, A. Khasanov, K. Kraehenbuehl, G. Long, D. A. Weinberger, K. M. Wilcoxen, M. R. Ghadiri, *Nature* **2001**, *412*, 392–393.

[5] a) The structure and tubular stacking of three stereoisomers of cyclo(β^3-HAla)$_4$ have been determined from powder diffraction data: D. Seebach, J. L. Matthews, A. Meden, T. Wessels, C. Baerlocher, L. B. McCusker, *Helv. Chim. Acta* **1997**, *80*, 173–182; b) the structure of the 12-membered-ring cyclo(β^3-HGlu)$_3$ with *S*,*S*,*S* configuration investigated by NMR spectroscopy in D_2O reveals a C_3-symmetric arrangement with all the carbonyl groups pointing upwards. Modeling experiments suggest that cyclo-β-tripeptides can adopt stacked tubular structures: K. Gademann, D. Seebach, *Helv. Chim. Acta.* **1999**, *82*, 957–962.

[6] T. D. Clarck, L. K. Buehler, M. R. Gadhiri, *J. Am. Chem. Soc.* **1998**, *120*, 651–656.

[7] I. Karle, B. K. Handa, C. H. Hassall, *Acta Crystallogr. B* **1975**, *B31*, 555–560.

[8] D. Gauthier, P. Baillargeon, M. Drouin, Y. L. Dory, *Angew. Chem.* **2001**, *113*, 4765–4768; *Angew. Chem. Int. Ed.* **2001**, *40*, 4635–4638.

[9] V. Semetey, D. Rognan, C. Hemmerlin, R. Graff, J.-P. Briand, M. Marraud, G. Guichard, *Angew. Chem.* **2002**, *114*, 1973–1975; *Angew. Chem. Int. Ed.* **2002**, *41*, 1893–1895.

[10] G. Guichard, V. Semetey, C. Didierjean, A. Aubry, J. P. Briand, M. Rodriguez, *J. Org. Chem.* **1999**, *64*, 8702–8705.

 © WILEY-VCH Verlag GmbH, 69451 Weinheim, Germany, 2002 1433-7851/02/4111-1897 $ 20.00+.50/0

[11] Crystal data: $C_{16}H_{32}N_8O_4$, $M_r = 400.48\ g\,mol^{-1}$, colorless prism, crystal size $0.3 \times 0.1 \times 0.1\ mm^3$, $a = b = 15.333(3)$, $c = 4.724(1)$ Å, $V = 1110.6(4)$ Å^3, $T = 293$ K, tetragonal, space group $I\bar{4}$, $Z = 2$, $\rho_{calcd} = 1.226\ Mg\,m^{-3}$, $\mu = 0.763\ mm^{-1}$. Nonius Mach3 diffractometer, $\lambda = 1.54178$ Å. 4293 measured reflections, 1052 unique ($R_{int} = 0.017$), 953 with $I > 2\sigma(I)$, the structure was solved by direct methods and refined by full-matrix least squares on F^2 for all data to $R_1 = 0.0411$ [$I > 2\sigma(I)$] and $wR_2 = 0.1036$ [$I > 2\sigma(I)$], 93 parameters. CCDC 175843 contains the supplementary crystallographic data for this paper. These data can be obtained free of charge via www.ccdc.cam.ac.uk/conts/retrieving.html (or from the Cambridge Crystallographic Data Centre, 12, Union Road, Cambridge CB2 1EZ, UK; fax: (+44) 1223-336-033; or deposit@ccdc.cam.ac.uk).

[12] Nonsymmetrical macrocyclic bisureas consisting of one cystine unit and one hexamethylenediamine unit bridged together form tubelike hydrogen-bonded aggregates in the solid state. In this case, the carbonyl groups of the two urea units within the same ring point in opposite directions: D. Ranganathan, C. Lakshmi, I. L. Karle, *J. Am. Chem. Soc.* **1999**, *121*, 6103 – 6107.

[13] A different packing is observed in the structure of the β-peptide cyclo(β^3-HAla)$_4$ with *S,S,S,S* configuration. Although all C=O and N–H bonds point, respectively, in the same direction in each tubular stack, neighboring tubes are arranged in opposite directions. See reference [5a].

Drastic Luminescence Response to Carbon Monoxide from a Ru^{II} Complex Containing a Hemilabile Phosphane Pyrene Ether**

Cerrie W. Rogers and Michael O. Wolf*

The rapid, reversible nature of the coordinative bonding between metals and Lewis-basic small molecules makes molecular chemosensors based on this phenomenon quite promising. Indeed, recent reviews contain numerous reports of sensors based on metal – ligand interactions.[1–3] Of particular potential are metal complexes designed such that the analyte-binding event changes the luminescence properties of an intramolecular lumophore. One approach is to use a modular design in which a metal-based analyte receptor is covalently linked to a separate lumophore. The emission of the lumophore is influenced by the binding of the analyte, usually through On – Off switching of energy- or electron-transfer quenching mechanisms.[1, 2, 4] Pyrene, which emits intense indigo-blue fluorescence in dilute solution[5] and blue-green excimer emission in concentrated solution,[5, 6] is a popular lumophore for such molecule-based sensors, particularly those based on photoinduced electron transfer (PET) processes.[2, 7] Switching between pyrene monomer and excimer emission has also been used to obtain a sensor response, whereby the ability of pyrene moieties to interact with one another is influenced by the binding of analyte to the receptor.[2, 8]

We used a [RuCl$_2$(POR-*P,O*)$_2$] complex (where POR is an ether-substituted phosphane) as the basis for a modular molecular sensor. This type of complex reacts rapidly and reversibly with numerous Lewis-basic small molecules, including CO,[9–11] a small-molecule analyte for which effective new sensor materials may be useful, by displacement of the labile ether moiety. Incorporation of a pyrene group in the hemilabile ligand leads to metal-based reactivity towards small molecules and pyrene-based luminescence. Here a Ru^{II} complex containing the hemilabile phosphane ether ligand 4-{2-(diphenylphosphanyl)phenoxy}butylpyrene (POC4Pyr) is described. The complex [RuCl$_2$(POC4Pyr-*P,O*)$_2$] (**1**, see Scheme 1) reacts with carbon monoxide to produce a significant luminescence response in which monomer-to-excimer emission switching is observed. This is the first example of the use of the hemilabile-ligand approach to obtain a molecular sensor with a room-temperature luminescence response, although we have previously reported a Ru bipyridyl complex containing a hemilabile ligand that exhibits small-molecule-dependent luminescence at low temperature.[12]

Complex **1** was prepared by reaction of POC4Pyr with $RuCl_3 \cdot x\,H_2O$ in boiling deaerated ethanol/toluene. The burgundy-pink complex is mildly sensitive to oxidation by air, both in solution and as a solid. The $^{13}C\{^1H\}$ and $^{31}P\{^1H\}$ NMR data of **1** (Tables 1 and 2) are analogous to those of [RuCl$_2$(POMe-*P,O*)$_2$] (POMe = (2-methoxyphenyl)diphenylphosphane), which has been crystallographically characterized[9] and found to contain two *P,O*-coordinated phosphane ether ligands with the phosphane moieties *cis* to each other.

The absorption spectrum of complex **1** is essentially a combination of those of [RuCl$_2$(POMe-*P,O*)$_2$] and the pyrenyl ligand POC4Pyr. The color of the complex is caused by a weak

Table 1. Summary of $^{13}C\{^1H\}$ NMR spectroscopic data[a] for **1** – **3**.

Complex	CO	δ/ppm (multiplicity) [*J*/Hz] *ortho*[b]	*ipso*	*ipso'*
1	–	161.7 (t) [5.2]	134.1 (d) [25.3]	ND[c]
2	197.6 (t) [13.5]	160.5 (t) [2.3]	132.8 (t) [24.4]	118.8 (t) [23.9]
3	193.7 (t) [10.9]	159.0 (t) [2.3]	131.8 (t) [24]	119.3 (t) [23.5]

[a] In CD_2Cl_2. [b] Phenyl C atom bound to oxygen. [c] ND = not determined.

Table 2. Comparison of **1** – **3** with analogous POMe complexes.[a]

Complex	Color	$\delta(^{31}P\{^1H\})$/ppm	$\tilde{\nu}$(C=O)/cm^{-1}
tcc-**1**	red	63.7[b]	–
ttt-**2**	greenish yellow	27.1[b]	2005[c]
cct-**3**	greenish yellow	13.9[b]	2005, 2058[c]
tcc-[RuCl$_2$(POMe-*P,O*)$_2$]	red	62.7[d]	–
ttt-[RuCl$_2$(CO)$_2$(POMe-*P*)$_2$]	yellow	26.7	1962
cct-[RuCl$_2$(CO)$_2$(POMe-*P*)$_2$]	white	10.6	2000, 2060

[a] From ref. [9]; $^{31}P\{^1H\}$ NMR spectra measured in $CDCl_3$ solution; IR spectra measured in mineral-oil mulls. [b] In CD_2Cl_2. [c] In $CHCl_3$. [d] In $CDCl_3$.

[*] Prof. M. O. Wolf, C. W. Rogers
Department of Chemistry, The University of British Columbia
2036 Main Mall, Vancouver, V6T 1Z1 (Canada)
Fax: (+1) 604-822-2847
E-mail: mwolf@chem.ubc.ca

[**] This work was supported by the Natural Sciences and Engineering Research Council (NSERC) of Canada. C.W.R. thanks NSERC and UBC for graduate fellowships.

Supporting information for this article is available on the WWW under http://www.angewandte.com or from the author.

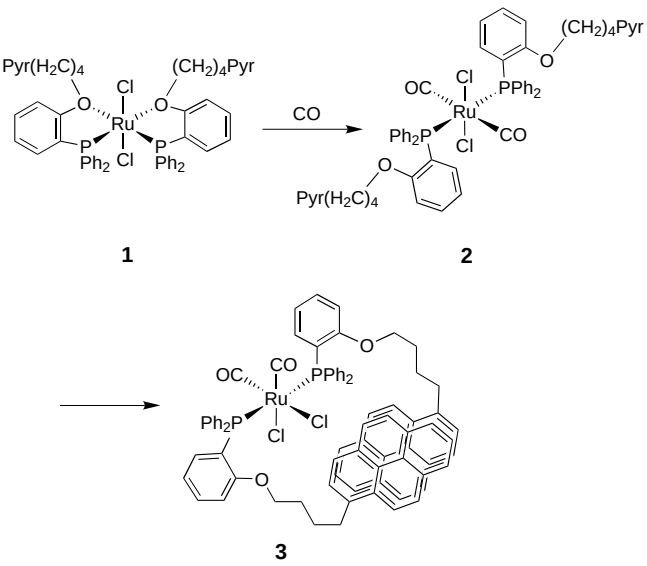
 © WILEY-VCH Verlag GmbH, 69451 Weinheim, Germany, 2002 1433-7851/02/4111-1898 $ 20.00+.50/0

metal-based absorption band ($\varepsilon_{519} = 490\,\text{M}^{-1}\text{cm}^{-1}$ in cyclohexane), similar to that of $[RuCl_2(POMe\text{-}P,O)_2]$ ($\varepsilon_{517} = 550\,\text{M}^{-1}\text{cm}^{-1}$ in $CHCl_3$).[13] The peaks in the emission spectrum of complex **1** (measured in air-saturated solution) appear at energies similar to those of free POC4Pyr. However, the emission from the complex is significantly diminished in intensity, presumably because of some intramolecular quenching of pyrene emission by the metal.

When a solution of **1** is treated with 1 atm of CO, the raspberry-red color changes immediately to greenish yellow, as is typical of $[RuCl_2(POR\text{-}P,O)_2]$ complexes.[9, 10] Analysis of the samples by $^{31}P\{^1H\}$ NMR spectroscopy immediately after the reaction revealed quantitative formation of the new complex **2** ($\delta = 27.1$). Removal of the CO atmosphere from **2** leads to geometric isomerization with formation of **3** ($\delta = 13.9$); samples kept under CO atmosphere are almost entirely inert to this isomerization. The mechanism of this isomerization has not yet been established, but it appears to involve dissociation of CO, as is common for $[RuCl_2(CO)_2(PR_3)_2]$ complexes.[14] The combinations of spectroscopic properties for complexes **1**–**3** (color, NMR chemical shifts, IR bands) are similar to those of the analogous POMe complexes[9] (Table 2).

Complex **2** was identified as a dicarbonyl complex on the basis of the triplet $^{31}P\{^1H\}$ signal of samples prepared with ^{13}CO; furthermore, the triplet carbonyl $^{13}C\{^1H\}$ signal indicates that the two equivalent CO moieties in **2** are coupled to two equivalent ^{31}P nuclei. The magnitude of the $^{13}C,^{31}P$ coupling constant (ca. 13 Hz) is typical of $[RuCl_2(CO)_2(PR_3)_2]$ complexes with phosphanes *cis* to the carbonyl ligands ($^2J_{P,C} < 20$ Hz).[9] From these data and the NMR and IR spectroscopic data listed in Tables 1 and 2, **2** is identified as *trans*,*trans*,*trans*-$[RuCl_2(CO)_2(POC4Pyr\text{-}P)_2]$. Similarly, **3** contains two equivalent phosphane groups, and the ^{13}CO-labeled complex has a triplet ^{31}P NMR signal in accord with the presence of two equivalent carbonyl ligands. The spectroscopic data are consistent with assignment of the thermodynamically favored dicarbonyl complex **3** as *cis*,*cis*,*trans*-$[RuCl_2(CO)_2(POC4Pyr\text{-}P)_2]$. Scheme 1 shows the proposed reaction of **1** with CO and the further isomerization of the kinetic product **2** to the thermodynamically favored isomer **3**.

In the context of chemical sensing, the change in the luminescence properties on reaction of **1** with CO is of greater interest than the color change associated with the reaction because superior detection limits are achievable for measurements based on luminescence than on absorption. When concentrated solutions of **1** (ca. 10^{-2} M) were treated with CO under UV irradiation, the dim blue pyrene emission from **1** switched to strong blue-green excimer emission from **2**. Displacement of the ether from the metal center increases the conformational freedom of the alkylpyrene moiety by further lengthening the tether between the pyrene ring and the metal atom. This increased conformational freedom influences the ability of the pyrene moieties to interact with one another, and these interactions are manifested as excimer emission. It is noteworthy that in dilute solution ($[\mathbf{2}] = 1.8 \times 10^{-6}$ M), a trace of excimer emission persists, as is evident from the spectra in Figure 1. This implies that excimers can also form intramolecularly, since intermolecular excimer emission



Scheme 1. Reaction of **1** with CO and further isomerization of the kinetic product **2** to the thermodynamically favored isomer **3**.

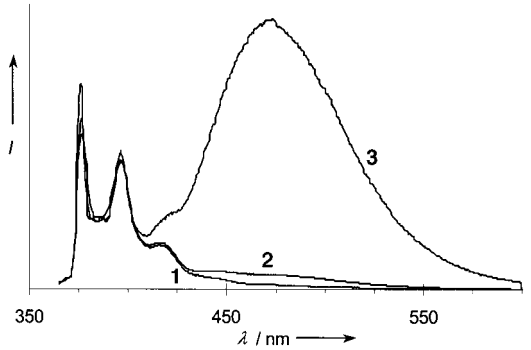


Figure 1. Comparison of the emission from dilute solutions of **1**–**3**. According to excimer band intensity *I*: highest: $[\mathbf{3}] = 3.4 \times 10^{-6}$ M; middle: $[\mathbf{2}] = 1.8 \times 10^{-6}$ M; lowest: $[\mathbf{1}] = 1.4 \times 10^{-6}$ M; in air-saturated CH_2Cl_2 solution at RT; $\lambda_{ex} = 350$ nm; excitation path 10 mm, emission path 2 mm.

from pyrene is typically insignificant for concentrations below about 10^{-3} M.[5]

After isomerization of **2** to **3**, strong excimer emission is observed, even in dilute solution. Thus, the pyrene moieties in the thermodynamically preferred complex **3** must be readily able to interact with each other to form intramolecular excimers. Although both complexes have *trans* phosphane groups, the *cis* disposition of both the carbonyl and chloro ligands in **3** evidently favors π stacking of the pyrene rings. Interactions between the pyrene rings are possibly involved in the isomerization process and stabilize a geometry in the purported five-coordinate intermediate that favors formation of the *cis*,*cis*,*trans* isomer **3**.

The rapid CO-induced switching from weak pyrene monomer fluorescence to strong excimer emission makes **1** an attractive candidate for further study as a molecule-based sensor. The luminescence response to CO occurs within seconds at room temperature, and the response is easily observed by the naked eye in concentrated solutions (ca. 10^{-2} M), as shown in Figure 2; the reaction is also evidenced by a color change that is readily observed under ambient lighting.

 © WILEY-VCH Verlag GmbH, 69451 Weinheim, Germany, 2002 1433-7851/02/4111-1899 $ 20.00+.50/0

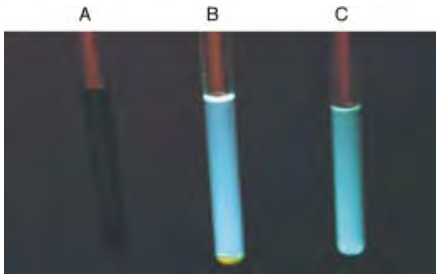


Figure 2. Concentrated solutions (ca. 10^{-2} M) of A) **1**, B) **2** and C) **3** under UV light (366 nm).

Furthermore, exposure of a solution (ca. 10^{-6} M) of **1** to an atmosphere containing 0.05 % (ca. 850 ppm) CO results in a detectable change in emission (not shown), and studies are ongoing to determine the detection range for this sensor complex. Investigations are also underway to determine whether the intensely emissive excimer of **3** can be observed immediately when the reaction with CO occurs at elevated temperature.[14] This would result in a substantial difference in emission intensity from the sensor material before and after CO exposure. Importantly, the drastic difference in behavior of **2** and **3** suggests that luminescence changes may be triggered by subtle changes in the bonding environment at the metal atom. This is significant because it indicates that it may be possible to design sensors based on this approach in which differences in response result not only from selectivity for specific analytes by tuning the reactivity of the metal, but also from steric and electronic considerations which favor or disfavor the formation of pyrene excimers.

Experimental Section

Full experimental and characterization details for POC4Pyr and complexes **1**–**3** are available in the Supporting Information.

Received: November 5, 2001
Revised: March 1, 2002 [Z18161]

[1] L. Fabbrizzi, M. Licchelli, G. Rabaioli, A. Taglietti, *Coord. Chem. Rev.* **2000**, *205*, 85.
[2] A. P. de Silva, H. Q. N. Gunaratne, T. Gunnlaugsson, A. J. M. Huxley, C. P. McCoy, J. T. Rademacher, T. E. Rice, *Chem. Rev.* **1997**, *97*, 1515.
[3] a) D. Parker, *Coord. Chem. Rev.* **2000**, *205*, 109; b) M. H. Keefe, K. D. Benkstein, J. T. Hupp, *Coord. Chem. Rev.* **2000**, *205*, 201; c) J. W. Canary, B. C. Gibb, *Prog. Inorg. Chem.* **1997**, *45*, 1.
[4] a) R. Corradini, A. Dossena, G. Galaverna, R. Marchelli, A. Panagia, G. Sartor, *J. Org. Chem.* **1997**, *62*, 6283; b) R. Bergonzi, L. Fabbrizzi, M. Licchelli, C. Mangano, *Coord. Chem. Rev.* **1998**, *170*, 31; c) L. Fabbrizzi, M. Licchelli, L. Parodi, A. Poggi, A. Taglietti, *Eur. J. Inorg. Chem.* **1999**, 35; d) M. Shionoya, T. Ikeda, E. Kimura, M. Shiro, *J. Am. Chem. Soc.* **1994**, *116*, 3848; e) M. Takeuchi, M. Yamamoto, S. Shinkai, *Chem. Commun.* **1997**, 1731; f) K. J. Franz, N. Singh, B. Spingler, S. J. Lippard, *Inorg. Chem.* **2000**, *39*, 4081.
[5] J. B. Birks, *Photophysics of Aromatic Molecules*, Wiley-Interscience, London, **1970**.
[6] F. M. Winnik, *Chem. Rev.* **1993**, *93*, 587.
[7] a) A. Yamauchi, T. Hayashita, A. Kato, S. Nishizawa, M. Watanabe, N. Teramae, *Anal. Chem.* **2000**, *72*, 5841; b) H.-F. Ji, R. Dabestani, G. M. Brown, R. L. Hettich, *Photochem. Photobiol.* **1999**, *69*, 513.
[8] a) S. Nishizawa, Y. Kato, N. Teramae, *J. Am. Chem. Soc.* **1999**, *121*, 9463; b) B. Bodenant, F. Fages, M.-H. Delville, *J. Am. Chem. Soc.* **1998**, *120*, 7511.
[9] T. B. Rauchfuss, F. T. Patino, D. M. Roundhill, *Inorg. Chem.* **1975**, *14*, 652.
[10] E. Lindner, M. Geprags, K. Gierling, R. Fawzi, M. Steimann, *Inorg. Chem.* **1995**, *34*, 6106.
[11] a) E. Lindner, C. Scheytt, P. Wegner, *Chem. Ber.* **1987**, *120*, 1621; b) E. Lindner, S. Pautz, M. Haustein, *Coord. Chem. Rev.* **1996**, *155*, 145.
[12] C. W. Rogers, M. O. Wolf, *Chem. Commun.* **1999**, 2297.
[13] J. C. Jeffrey, T. B. Rauchfuss, *Inorg. Chem.* **1979**, *18*, 2658.
[14] D. W. Krassowski, J. H. Nelson, K. R. Brower, D. Hauenstein, R. A. Jacobson, *Inorg. Chem.* **1988**, *27*, 4294.

Shape-Persistent, Fluorescent Polyphenylene Dyads and a Triad for Efficient Vectorial Transduction of Excitation Energy**

Tanja Weil, Erik Reuther, and Klaus Müllen*

Plants and some bacteria have the unique ability to convert sunlight into chemically bound energy, thus opening up a nearly unlimited energy source.[1] Since supplies of fossil fuels are expected to become exhausted in the near future, there has been an increasing interest in the synthesis of novel organic and polymeric molecules for the efficient harvesting of solar energy as well as for the conversion of solar radiation into electrical energy.[2a–d] The geometry of linear chain macromolecules is not ideal for efficient energy transfer; in particular, it is difficult to achieve an energy gradient for a vectorial transduction of light energy.[3] Not surprisingly, therefore, dendrimers have received great interest. Their globular shape provides a large surface area that can be decorated with chromophores, which thus results in a large absorption cross section and enables efficient capturing of photons.[4] Balzani et al. have synthesized light-harvesting dendrimers that bear an osmium complex in the center and several ruthenium complexes at the periphery.[5] In the phenylacetylene dendrimers reported by Moore and co-workers, a focal perylene chromophore acts as a light-harvesting antenna and there is an energy gradient from the periphery towards the center.[6] For light-harvesting dendrimers based on a flexible scaffold[7a–d] the investigation of energy transfer is often complicated because conformational mobility leads to undesired chromophore interactions such as aggregation, excimer formation, and dye self-quenching.[8, 9] Other drawbacks are often the very limited photostability[9] and low fluorescence quantum yields of the chosen chromophores.

[*] Prof. Dr. K. Müllen, T. Weil, E. Reuther
Max-Planck-Institut für Polymerforschung
Ackermannweg 10, 55128 Mainz (Germany)
Fax: (+49) 6131-379-350
E-mail: muellen@mpip-mainz.mpg.de

[**] This research was supported by the TMR European Research Program through the SISITOMAS project, the Volkswagen-Stiftung, and the Bundesministerium für Bildung and Forschung. We also thank S. Spang and C. Beer for support in the synthetic work.

 © WILEY-VCH Verlag GmbH, 69451 Weinheim, Germany, 2002 1433-7851/02/4111-1900 $ 20.00+.50/0

The use of a rigid polyphenylene dendrimer[10a, b] should overcome most of the above-mentioned difficulties[11, 12] since no back-folding of the dendritic branches can occur[13] and self-quenching of the chromophores is not observed.[12] Furthermore, energy-transfer processes, including those at the single-molecule level, were investigated by using polyphenylene dendrimers decorated with very photostable perylene dicarboxmonoimide chromophores; collective effects, quite well known in biological systems, have been recognized.[14a, b] Herein, we present structurally well-defined light-harvesting arrays that consist of up to three different types of chromophores for efficient energy transfer with an energy gradient. The design comprises globular polyphenylene dendrimers that bear a terrylene tetracarboxdiimide chromophore (TDI, Figure 1b) in the center and perylene

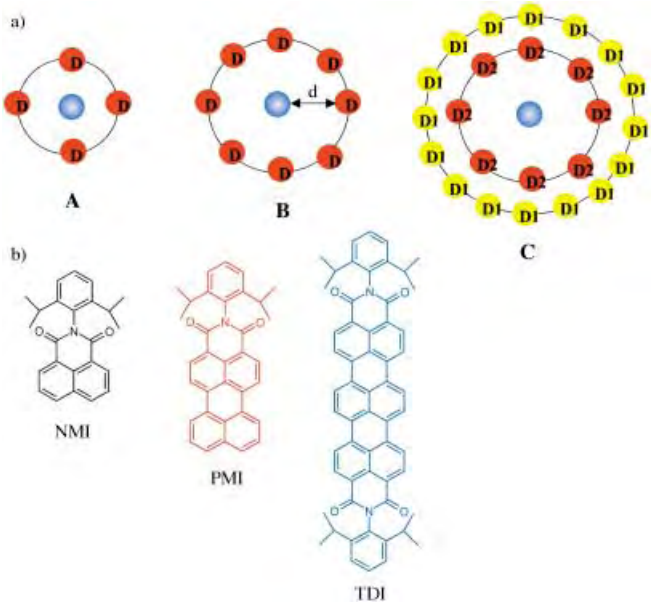
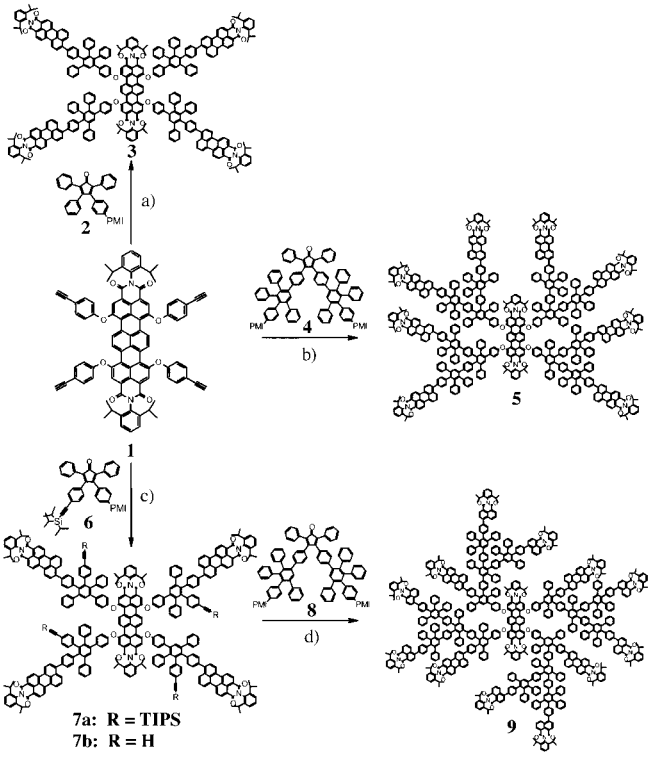


Figure 1. a) Sketch of the synthetic approach. **A** and **B** represent two molecular PMI – TDI dyads, **C** represents an NMI-PMI-TDI triad, and *d* is the distance between one donor and one acceptor chromophore. b) Structures of unsubstituted ryleneimide chromophores: naphthalene dicarboximide (NMI) , perylene dicarboximide (PMI), and terrylene tetracarboxdiimide (TDI).

dicarboxmonoimide (PMI, Figure 1b) as well as naphthalene dicarboxmonoimide chromophores (NMI, Figure 1b) at the periphery (Figure 1a). We have already demonstrated an efficient energy transfer between perylene and terrylene chromophores in two different systems.[11, 15] The combination of chemically very stable, shape-persistent polyphenylene dendrimers and rylene chromophores (e.g. TDI, PMI, NMI, Figure 1b), which possess excellent photostability, high extinction coefficients, and show a fluorescence quantum yield close to unity opens up the design of an outstanding multichromophoric array.[16] Figure 1a shows the envisaged multichromophores: **A** and **B** represent two molecular dyads that have an increasing interchromophoric distance and bear PMI chromophores in the outer sphere as well as a TDI core. **C** represents an NMI-, PMI-, and TDI-containing multichromophore. To clarify the molecular structure, the terms dyad and triad correspond to a multichromophore that bears two and three different types of chromophores, respectively.

The synthesis of the novel multichromophores is based on both a convergent[17] and a divergent[18] approach. A tetraethynyl terrylene tetracarboxydiimide chromophore **1**[19] serves as a core molecule that bears four ethynyl groups and therefore allows further dendrimer growth by repetitive Diels – Alder cycloaddition (Scheme 1). The reaction of the



Scheme 1. Synthesis of **3**, **5**, and **9**. Reagents and conditions: a) **2** (5 equiv), *o*-xylene, 170 °C, 12 h, 92 %; b) **4** (10 equiv), *o*-xylene, 170 °C, 3 d, 83 %; c) 1) **6** (5 equiv), *o*-xylene, 170 °C, 12 h, 90 %; 2) tetrabutylammonium chloride · $3H_2O$ (1 equiv), THF, 4 min, 88 %; d) **8** (16 equiv), *o*-xylene/diphenyl ether (1:1), 195 °C, 3 d, 63 %. TIPS = triisopropylsilyl.

TDI core **1** with a cyclopentadienone **2**, which bears a PMI chromophore, proceeded smoothly with the extrusion of carbon monoxide (170 °C, *o*-xylene, 12 h). Column chromatography on silica with dichloromethane eluant afforded first-generation multichromophore **3**, which bears four PMI substituents at the periphery as a purple solid in excellent yields (92 %). The second-generation multichromophore **5** was formed by reacting the TDI core **1** with 10 equivalents of the PMI-substituted dendron **4** (170 °C, *o*-xylene, 3 d); after chromatography, **5** was obtained as a purple solid in 83 % yield. The use of different dendrimer branches **2** and **4** permitted the study of energy transfer as a function of the interchromophoric distance. The synthesis of the dendritic triad **9** required a complex multistep route using cyclopentadienone **6**, which carries a chromophore as well as a protected ethynyl group. This building unit was prepared by means of a six-step reaction sequence, which will be published separately.[19] The TDI core **1** was treated with five equivalents of the PMI-labeled branching agent **6** (170 °C, 12 h), and column

 © WILEY-VCH Verlag GmbH, 69451 Weinheim, Germany, 2002 1433-7851/02/4111-1901 $ 20.00+.50/0

chromatography with dichloromethane gave **7a** in 90% yield. Multichromophore **7a** has nearly the same chemical structure as **3**, the only difference being the four triisopropylsilyl-protected ethynyl groups situated at the periphery of the dendrimer. After the removal of the protecting groups (1 equivalent tetrabutylammonium chloride, THF, 4 min), quenching with water, and filtration through a short pad of silica gel with dichloromethane, pure **7b** was obtained in nearly quantitative yield. This first-generation polyphenylene dendrimer **7b**, which bears two different types of chromophores, was then treated with dendron **8**, which carries two NMI substituents (*o*-xylene/diphenyl ether (1:1), 195°C, 3 d). In this way, multichromophore **9** was obtained as a dark purple solid in 63% yield.

The structure of all compounds was confirmed by means of NMR spectroscopy and matrix-assisted laser desorption/ionization time-of-flight (MALDI-TOF) spectrometry, with special attention being paid to the complete functionalization of the multichromophores. All MALDI-TOF mass spectra showed only a single peak that corresponded to the molecular mass of the multichromophores **3** (4643 g mol^{-1}), **5** (9606 g mol^{-1}), and **9** (12053 g mol^{-1}). A detailed discussion of the spectra of all the compounds reported herein will be published elsewhere.[19] A key feature of polyphenylene dendrimers as well as of rylene chromophores is their outstanding thermal stability. Thermal gravimetric analysis (TGA) showed decomposition of the multichromophores only at temperatures above 450°C. Molecular-modeling studies[20] of the dendrimers **3**, **5**, and **9** were used to determine the size, the topology of the functional groups, and the average interchromophoric distances of the multichromophores (Table 1). One can clearly see how the diameter of the multichromophores increases for higher generations, and that the average interchromophoric distances between different types of chromophores are in the range of 2 to 3 nm. The 3D structures of **3**, **5**, and **9** are given in Figures 2 and 5 d.

The multichromophores **3**, **5**, and **9** show good solubility in most organic solvents. The color corresponds to the spectral sum of the red PMI and the blue TDI. Dyads **3** and **5** display well-separated absorption envelopes (Figure 2). With increasing dendrimer generation, the extinction coefficients of the multichromophores also increase, and therefore the absolute light intensity harvested by the antenna is dramatically enhanced. Furthermore, no spectral broadening or shifts of the absorption maxima are observed, thus indicating that there is no interaction between the chromophores. An

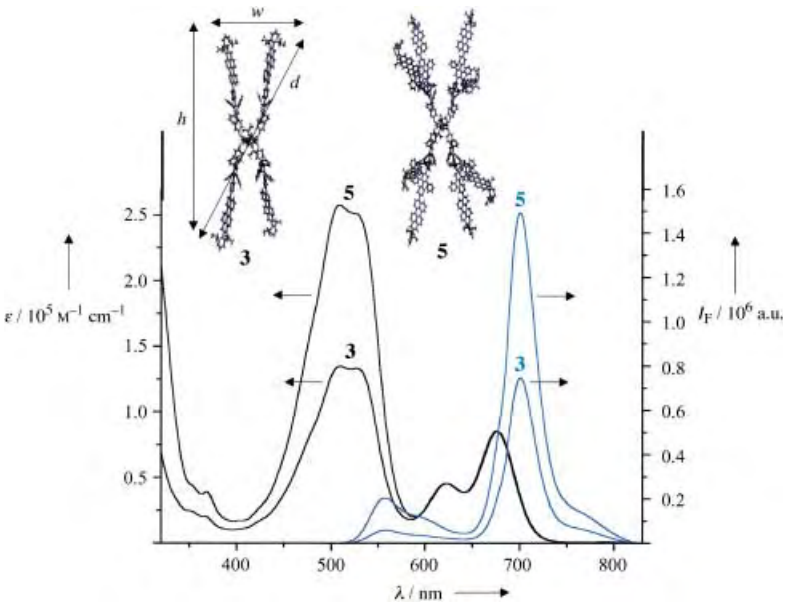


Figure 2. 3D structures of **3** and **5** obtained from molecular-mechanics calculations. UV/Vis absorption (black line, 10^{-5} M) and emission spectra (blue line, $\lambda_{exc.} = 480$ nm, 10^{-6} M) of **3** and **5** in toluene.

overview of the optical properties of all multichromophores is given in Table 2. Energy transfer only takes place if there is a sufficient spectral overlap of the donor emission and the acceptor absorption. Figure 3 shows the absorption and emission spectra of the separated rylene chromophores. One can clearly see that there is a large spectral overlap of the PMI emission and the TDI absorption. Excitation of a dilute solution (10^{-6} M) of dyads **3** and **5** at 480 nm results in a strong emission, predominantly from the TDI-acceptor chromo-

Table 2. Values of $\lambda_{max,abs}$ (ε), $\lambda_{max,em}$, and ϕ_f for **1**, **3**, **5**, and **9**.

	λ_{max} (toluene) [nm]	λ_{max} (chloroform) [nm]	λ_{em} (toluene) [nm]	λ_{em} (chloroform) [nm]	ϕ_f[a]
1	667 (87125)	665 (88865)	698	706	0.98
3	501 (118200)	509 (135016)	559	578	0.04
	526 (111350)	526 (133404)	701	709	(PMI)
	675 (85671)	675 (85635)			
5	500 (227270)	509 (258150)	557	577	0.09
	524 (222680)	526 (251611)	702	709	(PMI)
	674 (89990)	675 (85413)			
9	370 (178854)	371 (182163)	431	438	0.17
	501 (134576)	509 (138112)	555	576	(NMI)
	526 (136565)	527 (141218)	700	710	0.20
	676 (98462)	677 (98578)			(PMI)

[a] ϕ_f values of both separate PMI and TDI chromophores of Figure 3 are 0.98 (PMI) and 0.95 (TDI) in toluene.

Table 1. Size and average distances between separate chromophore units of **3**, **5**, and **9** obtained from the 3D structures after energy minimization.

	Height (h) [nm]	Width (w) [nm]	Diameter (d) [nm]	d(NMI→PMI) [nm]	d(PMI→TDI) [nm]	d(NMI→TDI) [nm]
5	7.37	5.85	7.89	–	2.50	–
3	5.87	2.59	6.11	–	1.89	–
9	5.81	6.91	8.1	2.15	1.83	2.85

 © WILEY-VCH Verlag GmbH, 69451 Weinheim, Germany, 2002 1433-7851/02/4111-1902 $ 20.00+.50/0 *Angew. Chem. Int. Ed.* **2002**, *41*, No. 11

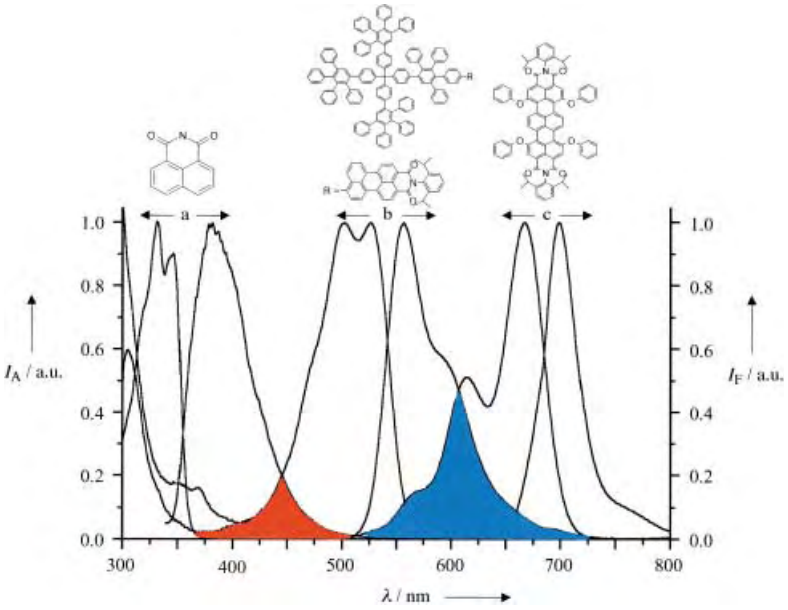


Figure 3. UV/Vis absorption (10^{-5} M) and emission spectra (10^{-6} M) of the separate rylene chromophores in toluene: a) naphthalimide ($\lambda_{exc} = 332$ nm), b) a polyphenylene dendrimer with a single PMI chromophore[11] ($\lambda_{exc} = 480$ nm), and c) a TDI chromophore ($\lambda_{exc.} = 665$ nm).

phore. The almost complete disappearance of the donor emission at 550 nm, which is quenched by about 93% in comparison to the separate PMI chromophore, along with a strong acceptor emission, indicates a very efficient energy transfer from the PMI donor to the TDI acceptor (Figure 2). This efficient and fast energy transfer can be explained by the large Förster interaction radius ($R_0 = 6$ nm),[21] as well as the high spectral overlap of the PMI emission and the TDI absorption.

The multichromophoric triad **9** absorbs over the whole range of the visible spectrum and also shows well-separated absorption envelopes (Figure 4). This feature opens up the possibility of specifically exciting distinct chromophores within the dendrimer, which is crucial for the investigation of vectorial energy transfer. The NMI emission ($\lambda_{max,em} =$ 341 nm) does not coincide with the TDI absorption ($\lambda_{max} = 665$ nm, Figure 3), which is a prerequisite for a well-defined stepwise energy transfer. Excitation of the NMI chromophores of **9** at 370 nm results in weak emissions at 431 nm (NMI) and at 555 nm (PMI), but in a strong acceptor emission at 700 nm (Figure 5a). This finding indicates the existence of an energy gradient and is consistent with a stepwise energy transfer from the periphery *via* the scaffold towards the center of the dendrimer. Although the Förster radius for the dendritic dyads has been calculated to be quite large, there is no spectral overlap of the NMI emission and of the TDI absorption (Figure 3). Consequently, the energy transfer from the NMI towards the TDI is explained as occurring through a stepwise mechanism across the PMI donors.

A relative fluorescence quantum yield (ϕ_f^{apr}) of the energy-transfer steps can be derived from the observed fluorescence intensities of the chromophores according to Equation (1),[22] in which C

$$\phi_f^{apr}(C) = \left(\frac{Em(C)^{obs}}{Em(C)^{max}}\right)\left(\frac{\varepsilon(C)}{\varepsilon_{370}(C)}\right) \quad (1)$$

represents the observed chromophores (NMI, PMI, TDI), $Em(c)^{obs}$ is the observed fluorescence intensity of C excited at the absorption maximum, $Em(c)^{max}$ corresponds to the fluorescence intensity of C in the absence of the energy-donor chromophore, $\varepsilon(C)$ is the extinction coefficient of the chromophore under the present experimental conditions, and $\varepsilon(C)_{370}$ is the extinction coefficient of the NMI donor at 370 nm. This method allows the fluorescence quantum yields of the NMI and the PMI chromophores in the triad **9** to be reduced from a value of nearly one to 0.17 and 0.2, respectively.

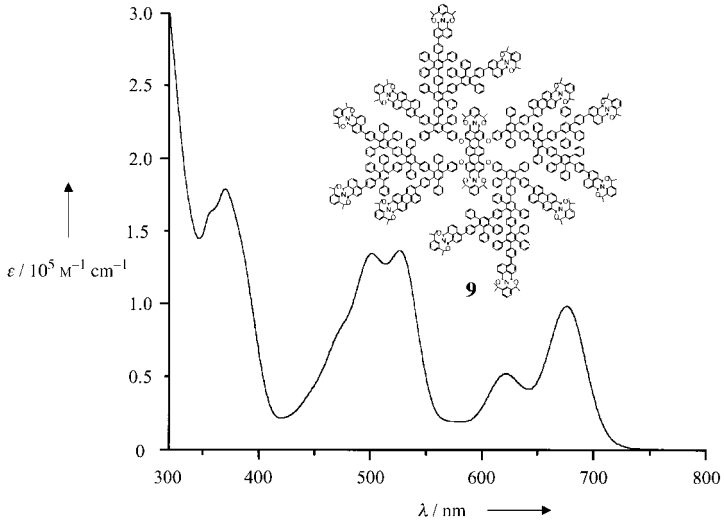


Figure 4. UV/Vis absorption spectrum of **9** in toluene (10^{-5} M).

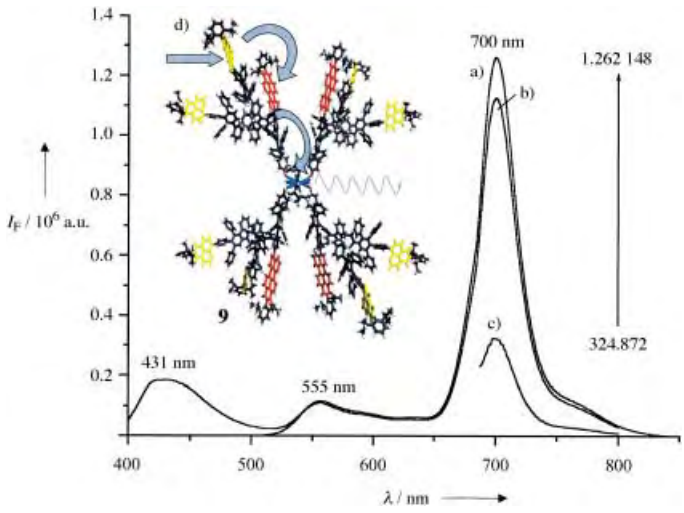


Figure 5. Emission spectra of **9** after excitation of a) the NMI chromophores at the periphery ($\lambda_{exc} = 370$ nm, 10^{-6} M), b) the PMI chromophores in the scaffold ($\lambda_{exc} = 480$ nm, 10^{-6} M), and c) the TDI chromophore in the center ($\lambda_{exc} = 665$ nm, 10^{-6} M). d) 3D structure of **9** obtained from molecular-mechanics calculations and visualization of the vectorial energy transfer from the periphery towards the center.

 © WILEY-VCH Verlag GmbH, 69451 Weinheim, Germany, 2002 1433-7851/02/4111-1903 $ 20.00+.50/0

Figure 5 shows the emission spectra of the dendritic triad **9** when excited at different wavelengths. Upon excitation of the dendrimer periphery at 370 nm, a very strong TDI emission is observed (Figure 5a). By exciting at the absorption maximum of the PMI chromophores at 500 nm, the fluorescence intensity of the core emission is slightly decreased (Figure 5b). When exciting the TDI core at 676 nm, a comparatively low emission of the TDI core is detected (Figure 5c). The intensity of a sensitized emission is stronger than that of a direct-core emission, that is, sensitization of the chromophore by a large light-harvesting antenna is more efficient than direct excitation at the absorption maximum by an external light source. In fact, when the TDI core is excited directly, its emission intensity is reduced by a factor of three. A similar effect has already been described for coumarin-labeled dendrimers[8, 23] as well as for phenylacetylene dendrimers that bear a focal perylene chromophore[6, 24] However, multichromphore **9** represents the first example of a dendritic triad in which the energy transfer as well as the energy gradient are induced by different types of chromophores being located at the periphery, in the scaffold, and in the core of a polyphenylene dendrimer and are thus independent of the dendritic scaffold.

We present a novel synthetic approach towards structurally well-defined polyphenylene multichromophores that bear two or three different types of chromophores at spatially well-defined positions in the core, in the scaffold, and at the periphery of the dendrimer. Different dendritic dyads show an efficient energy transfer from the PMI towards the TDI units. The first example of a dendritic triad **9** covers the whole spectrum of visible light and shows a stepwise energy transfer over a distance of 30 Å from the periphery via the scaffold towards the center of the dendrimer. The high thermal and chemical stability of the novel multichromophores makes them attractive candidates as emissive layers for the design of novel photonic devices as well as for solar-cell applications. Their high photochemical stability further allows single-molecule measurements, which are currently underway. Future work will focus on the combination of these highly emissive macromolecules with artificial reaction centers that convert excitation energy into chemical potential, which is still a challenging task in the design of opto-electronic devices.

Received: November 19, 2001
Revised: February 18, 2002 [Z18242]

[1] D.-P. Häder, *Photosynthese*, Thieme, Stuttgart, **1999**.
[2] a) S. E. Webber, *Chem. Rev.* **1990**, *90*, 1469 – 1482; M. A. Fox, *Acc. Chem. Res.* **1992**, *25*, 569 – 574; b) D. M. Watkins, M. A. Fox, *J. Am. Chem. Soc.* **1994**, *116*, 6441 – 6442; c) D. Gust, T. A. Moore, A. L. Moore, *Acc. Chem. Res.* **1993**, *26*, 198 – 205; d) D. Gust, T. A. Moore, A. L. Moore, *Acc. Chem. Res.* **2001**, *34*, 40 – 48.
[3] P. G. van Patten, A. P. Shreve, J. S. Lindsay, R. J. Donohoe, *J. Phys. Chem. B* **1998**, *102*, 4209 – 4216.
[4] A. Adronov, J. M. J. Frechet, *Chem. Commun.* **2000**, 1701 – 1710.
[5] V. Balzani, S. Capagna, G. Denti, A. Juris, S. Serroni, M. Venturi, *Acc. Chem. Res.* **1998**, *31*, 26 – 34.
[6] C. Devadoss, P. Bharathi, J. S. Moore, *J. Am. Chem. Soc.* **1996**, *118*, 9635 – 9644.
[7] a) S. L. Gilat, A. Adronov, J. M. J. Frechet, *J. Org. Chem.* **1999**, *64*, 7474 – 7484; b) S. L. Gilat, A. Adronov, J. M. J. Frechet, *Angew. Chem.* **1999**, *111*, 1519 – 1524; *Angew. Chem. Int. Ed. Engl.* **1999**, *38*, 1422 – 1427; c) M.-S. Choi, T. Aida, T. Yamazaki, I. Yamazaki, *Angew. Chem.* **2001** *113*, 3294 – 3298; *Angew. Chem. Int. Ed.* **2001**, *40*, 3194 – 3198; d) M. Plevoets, F. Vögtle, L. De Cola, V. Balzani, *New J. Chem.* **1999**, 63 – 69.
[8] A. Adronov, S. L. Gilat, J. M. J. Fréchet, K. Ohta, F. V. R. Neuwahl, G. R. Fleming, *J. Am. Chem. Soc.* **2000**, *122*, 1175 – 1185.
[9] V. R. Neuwahl, R. Righini, A. Adronov, P. R. L. Malenfant, J. M. J. Frechet, *J. Phys. Chem. B* **2001**, *105*, 1307 – 1312.
[10] a) F. Morgenroth, K. Müllen, *Tetrahedron* **1997**, *53*, 15349 – 15366; b) H. Zhang, P. C. M. Grim, P. Foubert, T. Vosch, P. Vanoppen, U. M. Wiesler, A. J. Berresheim, K. Müllen, F. C. D. Schryver, *Langmuir* **2000**, *16*, 9009 – 9014.
[11] T. Weil, U. M. Wiesler, A. Herrmann, R. Bauer, J. Hofkens, F. C. D. Schryver, K. Müllen, *J. Am. Chem. Soc.* **2001**, *123*, 8101 – 8108.
[12] M. Maus, R. De, M. Lor, T. Weil, S. Mitra, U.-M. Wiesler, A. Herrmann, J. Hofkens, T. Vosch, K. Müllen, F. C. D. Schryver, *J. Am. Chem. Soc.* **2001**, *123*, 7668 – 7676.
[13] M. Wind, U.-M. Wiesler, K. Saalwächter, K. Müllen, H. W. Spiess, *Adv. Mater.* **2001**, *13*, 752 – 756.
[14] a) J. Hofkens, M. Maus, T. Gensch, T. Vosch, M. Cotlet, F. Kohn, A. Herrmann, K. Müllen, F. C. D. Schryver, *J. Am. Chem. Soc.* **2000**, *122*, 9278 – 9288; b) T. Vosch, J. Hofkens, M. Cotlet, F. Köhn, H. Fujiwara, R. Gronheid, K. V. D. Best, T. Weil, A. Herrmann, K. Müllen, S. Mukamel, M. V. d. Auweraer, F. C. D. Schryver, *Angew. Chem.* **2001**, *113*, 4779 – 4784; *Angew. Chem. Int. Ed.* **2001**, *40*, 4643 – 4648.
[15] P. Schlichting, B. Duscherer, G. Seisenberger, T. Basche, C. Bräuchle, K. Müllen, *Chem. Eur. J.* **1999**, *5*, 2388 – 2395.
[16] G. Seybold, G. Wagenblast, *Dyes Pigm.* **1989**, *11*, 303 – 317.
[17] U. Wiesler, K. Müllen, *Chem. Commun.* **1999**, *22*, 2293 – 2294.
[18] U. M. Wiesler, A. J. Berresheim, F. Morgenroth, G. Lieser, K. Müllen, *Macromolecules* **2001**, *34*, 187 – 199.
[19] T. Weil, E. Reuther, K. Müllen, *J. Org. Chem.* **2001**, unpublished results.
[20] The minimized structures of the multichromophores have been obtained by applying the MM+ force field and the Conjugate Gradient algorithm implemented in the HyperChem 6.0 program package of Hypercube *Inc.* The 3D structure of the TDI-core molecule was first calculated separately by using the semi-empirical PM3 method, and a global minimum was evaluated. In the next step, the separately minimized dendrimer branches were attached to the core, and the geometry of the complete molecule was calculated with the MM+ force field and the Fletcher Reeves algorithm. Only in the case of the first-generation dyad **3** was a global minimum obtained. The fairly flat hypersurface obtained for higher generation dendrimers means that the three-dimensional structures of **5** (Figure 2) and **9** (Figure 5) represent one of several possible local minima. However, these structures were sufficient to evaluate the dimensions of the molecules as well as the approximate position of the chromophores with respect to each other (Table 1).
[21] R. Gronheid, J. Hofkens, F. Köhn, T. Weil, E. Reuther, K. Müllen, F. C. D. Schryver, *J. Am. Chem. Soc.* **2001**, in print.
[22] S. I. Kawahara, T. Uchimaru, S. Murata, *Chem. Commun.* **1999**, 563 – 564.
[23] A. Adronov, P. R. L. Malenfant, J. M. J. Frechet, *Chem. Mater.* **2000**, *12*, 1463 – 1472.
[24] M. R. Shortreed, S. F. Swallen, Z.-Y. Shi, W. Tan, Z. Xu, C. Devadoss, J. S. Moore, R. Kopelman, *J. Phys. Chem. B* **1997**, *101*, 6318 – 6322.

 © WILEY-VCH Verlag GmbH, 69451 Weinheim, Germany, 2002 1433-7851/02/4111-1904 $ 20.00+.50/0

was between 1:1 and 1:4, which suggests that the relative stoichiometry is $\mathbf{1}_n \cdot \mathbf{2}_n$. This stoichiometry was confirmed by ^{1}H NMR spectral integration of the resonance signals for **1** ($H_a - H_u$) versus **2** (H_v; see Figure 2 for assignments).

A major challenge in self-assembly studies is an accurate determination of absolute stoichiometry. To determine the value of n in aggregate $\mathbf{1}_n \cdot \mathbf{2}_n$, we turned to analytical ultracentrifugation (AUC).[9] AUC is a first-principles analytical technique that allows equilibrium thermodynamic measurements in dilute solution and offers advantages over the techniques commonly used in synthetic self-assembly studies (vapor-pressure osmometry (VPO), gel-permeation chromatography (GPC), and ES–MS). For example, VPO suffers from low sensitivity (±3 mmolal), aggregates often dissociate during GPC experiments, and ES–MS experiments occur in the desolvated gas phase. We performed sedimentation-equilibrium measurements with solutions of $\mathbf{1}_n \cdot \mathbf{2}_n$ (50 μM) containing an excess of **2** (200 μM). In this experiment we were able to selectively monitor $\mathbf{1}_n \cdot \mathbf{2}_n$, as it has an absorption maximum at 278 nm ($\varepsilon = 6700\ M^{-1}\ cm^{-1}$), whereas **2** has an absorption minimum. The results are well explained by a model of a single homogenous species with a molecular weight of 2632 ± 125. Comparison of the measured molecular weight with those calculated for $\mathbf{1}_2 \cdot \mathbf{2}_2$ and $\mathbf{1}_3 \cdot \mathbf{2}_3$ ($[(\mathbf{1}\text{-}4H^+)_2 \cdot (\mathbf{2}\text{-}2NO_3^-)_2] \cdot 4Na^+$: 2214; $[(\mathbf{1}\text{-}4H^+)_3 \cdot (\mathbf{2}\text{-}2NO_3^-)_3] \cdot 6Na^+$: 3322) strongly suggests the absolute stoichiometry $\mathbf{1}_2 \cdot \mathbf{2}_2$. When the standard techniques such as VPO, GPC, and ES–MS do not provide accurate molecular weights, AUC is a powerful alternative that should be considered in synthetic self-assembly studies.[7b, 9]

The observation of a single aggregate by ^{1}H NMR spectroscopy implies that only one of the two possible aggregates is formed, that is, the racemic mixture $\mathbf{1}_2 \cdot \mathbf{2}_2$ and *ent*-$\mathbf{1}_2 \cdot \mathbf{2}_2$ by an enantiomeric self-recognition process, or $(\mathbf{1} \cdot \textit{ent}\text{-}\mathbf{1}) \cdot \mathbf{2}_2$ by a heterochiral recognition process. We assigned most of the resonance signals in the ^{1}H NMR spectrum of $\mathbf{1}_2 \cdot \mathbf{2}_2$ to specific protons by 2D NMR spectroscopic techniques (COSY and ROESY spectra) and chemical-correlation arguments. Geometrical features of the aggregate were deduced, based on intermolecular (intra-aggregate) cross-peaks in the ROESY spectrum and ^{1}H NMR spectroscopic changes in the chemical shift (Figure 3). In particular, the ROESY spectrum shows cross-peaks between signals arising from protons on the pyridyl rings, and those from methylene protons on the convex face of the opposing dimethoxy xylylene ring ($H_a - H_o$; $H_a - H_p$; $H_b - H_o$; $H_b - H_p$), which indicates that these groups form close intermolecular contacts in $\mathbf{1}_2 \cdot \mathbf{2}_2$. A prominent feature in the ^{1}H NMR spectrum is the OCH_3 (t) resonance at 1.7 ppm, which shifts upfield by more than 2 ppm. This large upfield shift strongly suggests that this methoxy group is located in the shielded region, defined by the two xylylene rings of a second molecule. Examination of Corey–Pauling–Koltun (CPK) models reveals that these intermolecular contacts are only possible in the aggregate that is formed by enantiomeric self-recognition, $\mathbf{1}_2 \cdot \mathbf{2}_2$ and *ent*-$\mathbf{1}_2 \cdot \mathbf{2}_2$. The resulting geometry (Figure 3) places the two pyridyl rings in the vicinity of H_o, H_p, and one of the carboxylate solubilizing groups on the convex face of the other molecule of **1**. Simultaneous coordination of these two carboxylate groups to the two palladium centers locks the aggregate into a well-defined geometry.[10] In the hypothetical aggregate based on heterochiral recognition (Figure 1b), only one carboxylate–palladium interaction is possible. The dashed arrow shows the sizable distance between the remaining carboxylate group and the palladium center; the lack of this second carboxylate–palladium interaction drives the enantiomeric self-recognition process.

In conclusion, we have shown that (±)-**1** self-associates in water to form a diastereomeric mixture of aggregates. Upon addition of **2**, an enantiomeric self-recognition process is triggered, which results in the formation of an unexpected 2:2 aggregate, $\mathbf{1}_2 \cdot \mathbf{2}_2$ and *ent*-$\mathbf{1}_2 \cdot \mathbf{2}_2$. This enantiomeric self-recognition process is driven by the presence of an additional coordination interaction between the Pd centers and the carboxylate solubilizing groups, which is not possible in the hypothetical aggregate resulting from heterochiral recognition. This new model system offers the opportunity to study enantiomeric self-recognition processes in water and may provide insights into related biological and catalytic processes.

Received: November 21, 2001
Revised: March 3, 2002 [Z18256]

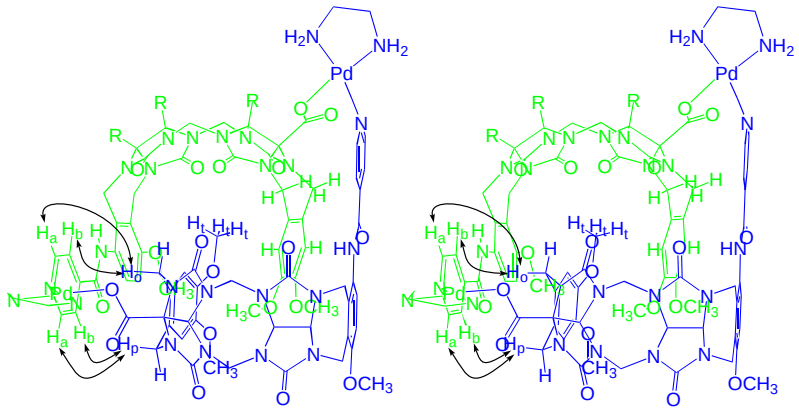


Figure 3. A stereoscopic drawing of the proposed geometry of $\mathbf{1}_2 \cdot \mathbf{2}_2$. The double-headed arrows denote cross-peaks that were observed in the ROESY spectrum.

[1] R. Krämer, J.-M. Lehn, A. Marquis-Rigault, *Proc. Natl. Acad. Sci. USA* **1993**, *90*, 5394–5398; J. M. Rivera, T. Martín, J. Rebek, Jr., *Science* **1998**, *279*, 1021–1023; T. Bark, M. Düggeli, H. Stoeckli-Evans, A. von Zelewsky, *Angew. Chem.* **2001**, *113*, 2924–2927; *Angew. Chem. Int. Ed.* **2001**, *40*, 2848–2851; J. C. Nelson, J. G. Saven, J. S. Moore, P. G. Wolynes, *Science* **1997**, *277*, 1793–1796.

[2] A. R. A. Palmans, J. A. J. M. Vekemans, E. E. Havinga, E. W. Meijer, *Angew. Chem.* **1997**, *109*, 2763–2765; *Angew. Chem. Int. Ed. Engl.* **1997**, *36*, 2648–2651; E. Yashima, K. Maeda, Y. Okamoto, *Nature* **1999**, *399*, 449–451; M. M. Green, N. C. Peterson, T. Sato, A. Teramoto, R. Cook, S. Lifson, *Science* **1995**, *268*, 1860–1866.

[3] E. J. Enemark, T. D. P. Stack, *Angew. Chem.* **1998**, *110*, 977–981; *Angew. Chem. Int. Ed.* **1998**, *37*, 932–935; C. Provent, E. Rivara-Minten, S. Hewage, G. Brunner, A. F. Williams, *Chem. Eur. J.* **1999**, *5*,

 © WILEY-VCH Verlag GmbH, 69451 Weinheim, Germany, 2002 1433-7851/02/4111-1906 $ 20.00+.50/0

3487 – 3494; G. Baum, E. C. Constable, D. Fenske, C. E. Housecroft, T. Kulke, *Chem. Eur. J.* **1999**, *5*, 1862 – 1873; E. E. Simanek, S. Qiao, I. S. Choi, G. M. Whitesides, *J. Org. Chem.* **1997**, *62*, 2619 – 2621; O. Mamula, A. von Zelewsky, G. Bernardinelli, *Angew. Chem.* **1998**, *110*, 302 – 305; *Angew. Chem. Int. Ed.* **1998**, *37*, 289 – 293; R. K. Castellano, C. Nuckolls, J. Rebek, Jr. *J. Am. Chem. Soc.* **1999**, *121*, 11156 – 11163; T. Kondo, K.-I. Oyama, K. Yoshida, *Angew. Chem.* **2001**, *113*, 918 – 922; *Angew. Chem. Int. Ed.* **2001**, *40*, 894 – 897; C. R. Woods, M. Benaglia, F. Cozzi, J. S. Siegel, *Angew. Chem.* **1996**, *108*, 1977 – 1980; *Angew. Chem. Int. Ed. Engl.* **1996**, *35*, 1830 – 1833; L. J. Prins, P. Timmerman, D. N. Reinhoudt, *J. Am. Chem. Soc.* **2001**, *123*, 10153 – 10163.

[4] M. A. Masood, E. J. Enemark, T. D. P. Stack, *Angew. Chem.* **1998**, *110*, 973 – 977; *Angew. Chem. Int. Ed.* **1998**, *37*, 928 – 932; J.-M. Vincent, C. Philouze, I. Pianet, J.-B. Verlhac, *Chem. Eur. J.* **2000**, *6*, 3595 – 3599; X. Shi, J. C. Fettinger, M. Cai, J. T. Davis, *Angew. Chem.* **2000**, *112*, 3254 – 3257; *Angew. Chem. Int. Ed.* **2000**, *39*, 3124 – 3127; X. Shi, J. C. Fettinger, J. T. Davis, *J. Am. Chem. Soc.* **2001**, *123*, 6738 – 6739; L. J. Prins, J. Huskens, F. de Jong, P. Timmerman, D. N. Reinhoudt, *Nature* **1999**, *398*, 498 – 502.

[5] J. N. H. Reek, A. Kros, R. J. M. Nolte, *Chem. Commun.* **1996**, 245 – 247; J. A. A. W. Elemans, R. de Gelder, A. E. Rowan, R. J. M. Nolte, *Chem. Commun.* **1998**, 1553 – 1554; S. J. Holder, J. A. A. W. Elemans, J. J. J. M. Donners, M. J. Boerakker, R. de Gelder, J. Barberá, A. E. Rowan, R. J. M. Nolte, *J. Org. Chem.* **2001**, *66*, 391 – 399.

[6] C. S. Wilcox, L. M. Greer, V. Lynch, *J. Am. Chem. Soc.* **1987**, *109*, 1865 – 1867; S. C. Zimmerman, M. Mrksich, M. Baloga, *J. Am. Chem. Soc.* **1989**, *111*, 8528 – 8530; M. Harmata, C. L. Barnes, S. R. Karra, S. Elahmad, *J. Am. Chem. Soc.* **1994**, *116*, 8392 – 8393; F.-G. Klärner, J. Panitzky, D. Bläser, R. Boese, *Tetrahedron* **2001**, *57*, 3673 – 3687.

[7] a) D. Witt, J. Lagona, F. Damkaci, J. C. Fettinger, L. Isaacs, *Org. Lett.* **2000**, *2*, 755 – 758; b) L. Isaacs, D. Witt, J. Lagona, *Org. Lett.* **2001**, *3*, 3221 – 3224.

[8] Selected references: M. Fujita, J. Yazaki, K. Ogura, *J. Am. Chem. Soc.* **1990**, *112*, 5645 – 5647; M. Fujita, D. Oguro, M. Miyazawa, H. Oka, K. Yamaguchi, K. Ogura, *Nature* **1995**, *378*, 469 – 471; S.-Y. Yu, T. Kusukawa, K. Biradha, M. Fujita, *J. Am. Chem. Soc.* **2000**, *122*, 2665 – 2666; K. Umemoto, K. Yamaguchi, M. Fujita, *J. Am. Chem. Soc.* **2000**, *122*, 7150 – 7151; N. Fujita, K. Biradha, M. Fujita, S. Sakamoto, K. Yamaguchi, *Angew. Chem.* **2001**, *113*, 1768 – 1771; *Angew. Chem. Int. Ed.* **2001**, *40*, 1718 – 1721.

[9] D. Schubert, C. Tziatzios, P. Schuck, U. S. Schubert, *Chem. Eur. J.* **1999**, *5*, 1377 – 1383; T. M. Laue, *Methods Enzymol.* **1995**, *259*, 427 – 452.

[10] Coordination compounds with N and O ligands: L. D. Pettit, M. Bezer *Coord. Chem. Rev.* **1985**, *61*, 97 – 114; K. Matsumoto, H. Moriyama, K. Suzuki *Inorg. Chem.* **1990**, *29*, 2096 – 2100; T. G. Appleton, D. R. Bedgood, Jr., J. R. Hall *Inorg. Chem.* **1994**, *33*, 3834 – 3841.

Crystal Engineering of Mixed-Metal Ru – Ag Coordination Networks by Using the *trans*-$[RuCl_2(pyz)_4]$ (pyz = pyrazine) Building Block**

Lucia Carlucci, Gianfranco Ciani,* Francesca Porta, Davide M. Proserpio, and Laura Santagostini

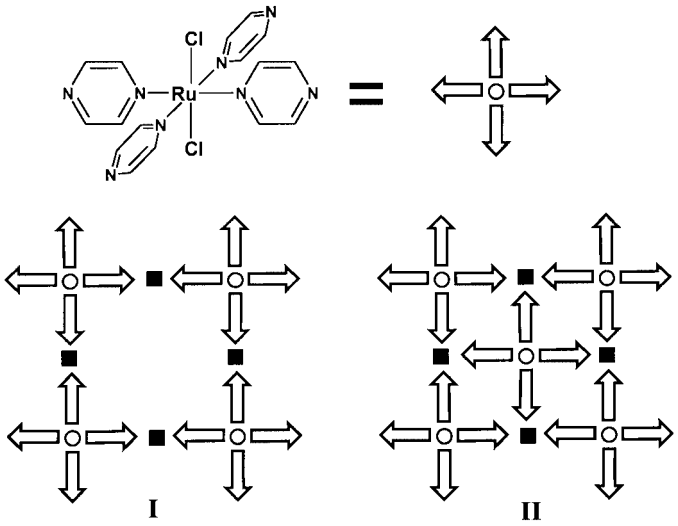
In the rational development of new strategies for the crystal engineering of coordination networks[1] and of metal-based supramolecular architectures[2] the use of predetermined building blocks has assumed an increasing relevance in recent times. For example, molecular corners containing transition metals with programmed coordination angles, such as *cis*-protected Pd^{II} and Pt^{II} square-planar complexes, have been employed for the construction of frameworks and, particularly, of macromolecular polygons or polyhedral cages,[3] of potential utility for molecular recognition. We have recently employed the corner unit $[Cu(2,2'\text{-bpy})]^{2+}$ (2,2′-bpy = 2,2′-bipyridine) for the self-assembly of polymeric species[4] and new architectures.[5] These building blocks generally work as acceptors and can be used with a variety of spacer ligands with different types of donor ends for the assembly of desired arrays. A different type of potentially useful metal-containing unit is represented by complexes containing ligands with *exo*-oriented donor functions. These complexes can be considered as nonconventional "ligands" in which the orientation of the donor groups can be controlled by the nature of the coordinated bases and by the coordination geometry at the metal center. Few examples of such species have been as yet reported, though they can find interesting applications for many purposes, such as the deliberate construction of *homo*- or *hetero*metallic networks with specific topologies, or the assembly of hydrogen-bonded frames, by using suitable (hydrogen-donor) organic molecules as spacers. Square-planar metal-porphyrinate complexes bearing four donor 4-pyridyl substituents on the macrocycle have been used, for instance, for the deliberate assembly of cooperite-like networks[6] and of other types of bimetallic frames.[7] Some other metal-containing "ligands" have been employed,[8] such as the anionic square-planar $[Pt(CN)_4]^{2-}$ [9] and digonal $[M(CN)_2]^-$ (M = Ag, Au)[10] species.

We have prepared as a new building block the neutral complex *trans*-$[RuCl_2(pyz)_4]$ (**1**; pyz = pyrazine): it was obtained by reacting $[RuCl_2(dmso)_4]$ in toluene with a large

[*] Prof. G. Ciani, Dr. D. M. Proserpio
Dipartimento di Chimica Strutturale e Stereochimica Inorganica
Via G. Venezian 21, 20133 Milano (Italy)
Fax: (+39) 02-5031-4454
E-mail: davide@csmtbo.mi.cnr.it
Prof. F. Porta, Dr. L. Santagostini
Dipartimento di Chimica Inorganica, Metallorganica e Analitica, and centro CNR
Via G. Venezian 21, 20133 Milano (Italy)
Dr. L. Carlucci
Dipartimento di Biologia Strutturale e Funzionale
Università dell'Insubria
Via J. H. Dunant 3, 21100 Varese (Italy)

[**] This work was supported by MURST within the project "Solid Supermolecules" 2000 – 2001 and by CSMTBO-CNR Center.

excess (tenfold) of the pyrazine ligand. Complex **1** displays four equatorial pyrazine molecules with free *exo*-oriented N-donor atoms, in square-planar orientation (see Scheme 1).



Scheme 1.

It is a stable species that has many potential applications for the crystal engineering of new polymeric materials, such as bimetallic coordination networks of predictable topology, as well as hydrogen-bonded arrays. The strongly bonded axial chlorides can prevent the self-assembly of **1**, which differs from what occurs with the M^{II}—tetrapyridyl–porphyrinate building blocks.[11] On reacting **1** with digonal metal centers (d^{10} metal ions or metal complexes with two free *trans* sites) one can predict the formation of layers of square grids like **I** in Scheme 1, while square-planar metal centers can give layers such as **II** in Scheme 1. However, the axial chlorides of **1** can also play a noninnocent role, extending the array in the third dimension through interactions with the other metals.

We report here on three new self-assembled networks obtained from **1** with different silver salts ($AgCF_3SO_3$ and $AgNO_3$), that is $[RuCl_2(pyz)_4Ag](SO_3CF_3)$ (**2**), $[RuCl_2(pyz)_4Ag_2(SO_3CF_3)_2]\cdot C_2H_2Cl_4\cdot 0.5\,n\text{-}CH_3(CH_2)_3OH$ (**3**) and $[RuCl_2(pyz)_4Ag]NO_3$ (**4**). The latter two species exhibit interesting mineralomimetic 3D structures[12] that can be related to the prototypical lattices of rutile and rock salt, respectively.

The reactions of **1** with $AgCF_3SO_3$ afford different products depending on the molar ratio of the reagents and on the solvent system. Slow diffusion of a solution of the silver salt in MeOH into a solution of **1** in CH_2Cl_2 (molar ratio 1:1) gave dark red crystals of **2**. On the other hand, when $AgCF_3SO_3$ in *n*-butanol is diffused into a solution of **1** in 1,1,2,2-tetrachloroethane (TCE), using a 2:1 molar ratio of the reagents, brown-red crystals separated, corresponding to compound **3**.

The crystal structures[13] of these species revealed the formation of polymeric bimetallic frames. Compound **2** consists of 2D double layers containing molecular square units with alternate Ru and Ag corners (Figure 1 top; Ru···Ag edges 7.21–7.26 Å). Two of the pyrazine ligands of the original Ru building block act as terminal ligands, while the other two form bridges to two silver atoms (Ru–N in the range 2.06–2.09 Å; Ag–N 2.37–2.38 Å). The squares are joined together through chloride bridges, two per metal corner, that connect the octahedral Ru centers to the distorted tetrahedral Ag corners (Ru···Ag contacts 4.48–4.59 Å). The chloride bridges are asymmetric and markedly bent (mean Ru–Cl 2.40 Å, mean Ag–Cl 2.56 Å, and mean Ag-Cl-Ru 132°). The resulting 2D array is a double layer structure schematically shown in Figure 1 (center) and displays parallel channels running in the [0 1 0] direction, perpendicular to the Ru_2Ag_2 squares (see Figure 1 bottom), that contain half of the triflate anions. The network topology of this double honeycomb[14] layer (4^36^3) is, to our knowledge, unprecedented. The double layers stack in the [1 0 0] direction (with AAA... sequence) and exhibit strong $\pi-\pi$ interlayer interactions involving pairs of dangling pyz ligands (distance 3.33 Å, offset 1.69 Å).[15] The interlayer regions contain the remaining triflate anions.

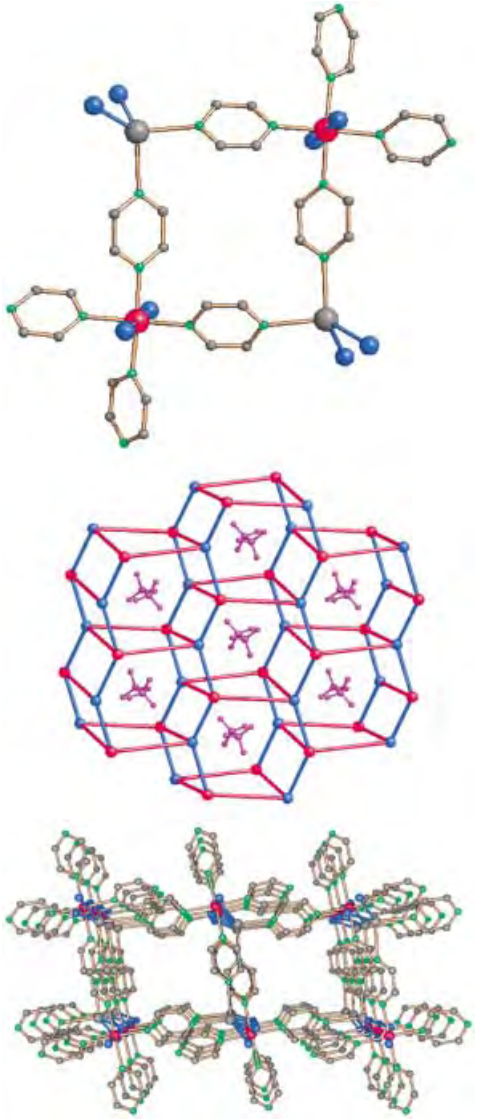


Figure 1. Structure of compound **2**: top: a square Ru_2Ag_2 unit; center: a schematic view of the double honeycomb layer, with the square units in red and the Cl bridges in blue; bottom: a lateral view of the layer showing the channels along the [0 1 0] direction.

 © WILEY-VCH Verlag GmbH, 69451 Weinheim, Germany, 2002 1433-7851/02/4111-1908 $ 20.00+.50/0

The structure of compound **3** consists of a single 3D bimetallic network of alternating six-connected Ru centers and three-connected Ag centers in the ratio 1:2. The Ru complexes use in this case all the pyrazine ligands and the two chloride ions for bridging to six different silver atoms. The structure can be rationalized considering that the Ru building blocks form with the silver atoms simple 2D undulated layers of square meshes (Figure 2, top and center), with Ru-pyz-Ag-pyz-Ru edges (Ru···Ag contacts of 7.17 Å, Ru–N 2.05–2.08 Å, Ag–N 2.29–2.33 Å), similar to those expected (see **I** in Scheme 1). However, these layers are not isolated but interconnected through Ru-Cl-Ag bridges (Ru···Ag 4.44 Å) and superimposed to give the overall 3D network schematically illustrated in Figure 2, bottom. The coordination geometry at the silver atoms is distorted tetrahedral, involving two pyrazine ligands, one bridging chloride, and a terminal O-bonded triflate ligand. As in **2** the chloride bridges are asymmetric and bent (mean Ru–Cl 2.40 Å, mean Ag–Cl 2.51 Å, and Ag-Cl-Ru 134°). The topology of this network, based on six- and three-connected nodes in the ratio 1:2, is the same of the prototypical rutile,[12, 14] with Ru in the place of Ti and Ag in the place of O (see Figure 3, bottom left). Few other examples of coordination networks with this topology have been previously reported.[16] The channels along [101] (Figure 3, top) contain solvated molecules of TCE and butanol (that are lost on heating the bulk samples above 120 °C). It is like that the templating effect of these guest solvents can also prevent interpenetration. Note that the void spaces in the framework, evaluated without the solvated molecules, represent about the 30 % of the cell volume.

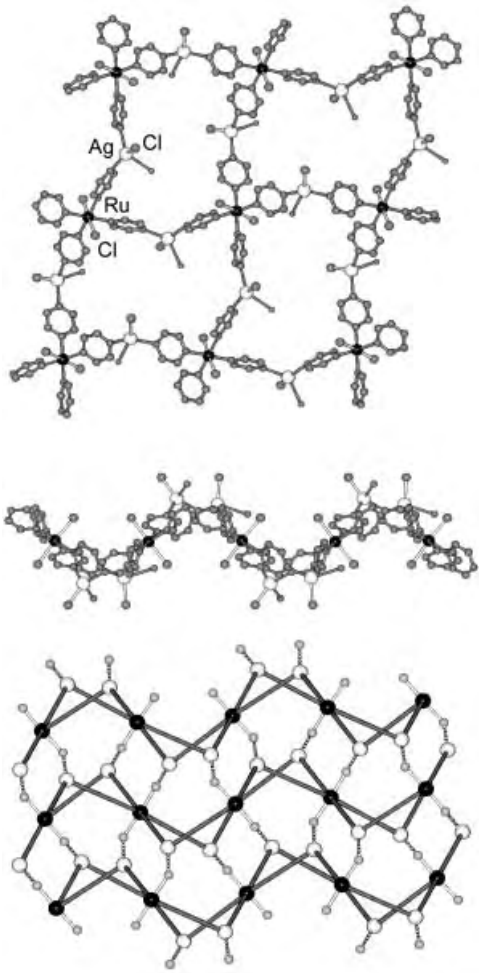


Figure 2. Two views, perpendicular (top) and lateral (center), of the undulated layers of Ru_4Ag_4 meshes contained in the 3D structure of compound **3**. The linkage of these layers (dashed) operated by the Cl bridges is also schematically shown (bottom).

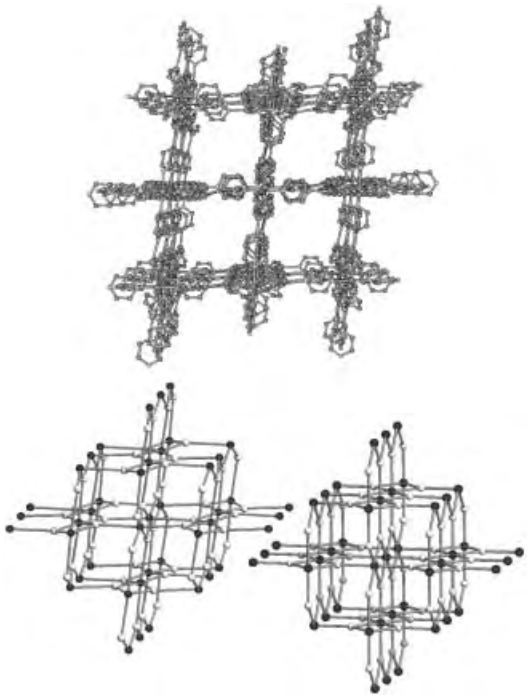


Figure 3. The 3D network in **3** down the [101] direction (top), and its schematic view (bottom left) compared with the structure of rutile (bottom right).

A systematic investigation of the role of the solvents in driving the formation of **2** or **3** has been carried out. Binary combinations of the solvents TCE, *n*-butanol, methanol and CH_2Cl_2 were used for the syntheses of **2** (Ru/Ag = 1/1) and **3** (Ru/Ag = 1/2). The nature of the synthesised bulk products was recognized by superimposing their XRPD spectra with the patterns calculated using the atomic positions of single crystal. It was pointed out that methanol and TCE are essential in driving the formation of the 2D (**2**) and 3D (**3**) species, respectively. In particular it was also observed that solid samples of **3** left in methanol are transformed into **2** after a few hours.

Slow diffusion of $AgNO_3$ dissolved in MeCN into a solution of **1** in CH_2Cl_2 (molar ratio ca. 4:1) produces red crystals of another species, (**4**), that, in spite of the fact that its stoichiometry is similar to that of **2**, shows a quite different structure.[13] This species contains a 3D network with alternate six-connected Ru and Ag octahedral centers. We can describe the structure as comprising 2D layers like **II** in Scheme 1 (Ru···Ag 7.27 Å), that are superimposed with a translation of [½ ½ *z*] (in an *ABAB* stacking sequence) in such a way that the Ru-bonded chlorides can form bridges to the silver atoms of the two adjacent layers (Ru···Ag 5.28 Å, Figure 4, top). Though both metals display octahedral enviroments, these are significantly different (Ru–N 2.06 versus Ag–N 2.40 Å; Ru–Cl 2.40 versus Ag–Cl 2.88 Å). All the bridges (Ru-pyz-

 © WILEY-VCH Verlag GmbH, 69451 Weinheim, Germany, 2002 1433-7851/02/4111-1909 $ 20.00+.50/0

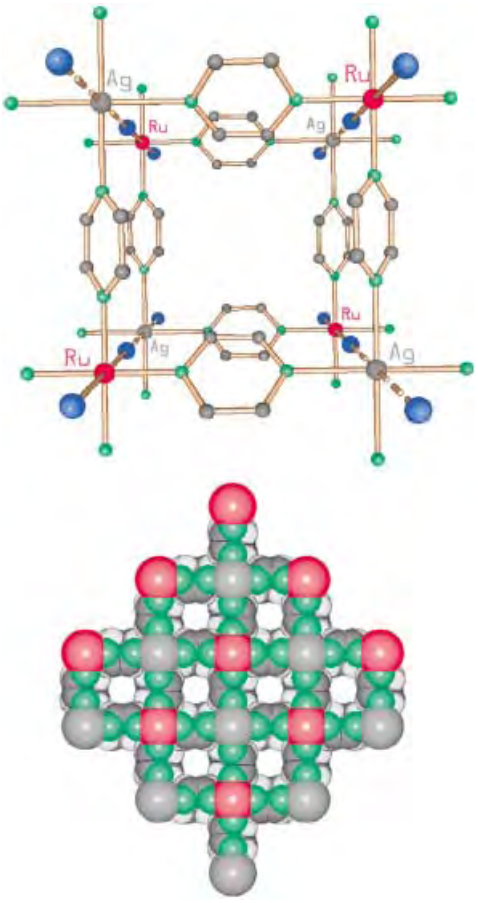


Figure 4. Structure of compound **4**: top: a single cage; bottom: the sphere-packing view of the network down the tetragonal axis.

Ag and Ru-Cl-Ag) in these species (**2**–**4**) are asymmetric, with longer distances to the silver atoms, but the asymmetry of the Ru-Cl-Ag (exactly linear) bridges in **4** is particularly pronounced (also taking into account the increased coordination number of Ag). The Ag–Cl interactions are rather weak and highly ionic in nature (see, for example, the Ag–Cl value of 2.77 Å in AgCl). The octahedral coordination for silver is unusual but we have already described a similar situation in $[Ag(pyz)_3]SbF_6$ that contains an "octahedral" network with the α-polonium topology.[17] Because of the alternation of the two metal atoms in **4** a more proper reference lattice, rather than α-polonium, is NaCl. The centers of the cells (of dimensions $7.27 \times 7.27 \times 5.28$ Å, free internal volume of about 53 Å^3) are all occupied by statistically distributed nitrate anions with half occupancy. A view of the packing in **4**, showing the channels along the tetragonal axis is given in Figure 4, bottom. It is worth noting that the framework of **4** has the same composition as that of **2**. This "network isomerism" is clearly related to the different dimensions of the counterions. While the nitrate anions can be accomodated in the cells of **4** the bulkier triflate anions cannot occupy such cavities, thus determining the different framework topology of **2**, where much larger cells (of dimensions ca. $7.2 \times 7.3 \times 8.4$ Å, free internal volume of ca. 122 Å^3) are present (see Figure 1, center), each containing a triflate anion with full occupancy. We have also obtained the $[RuCl_2(pyz)_4Ag]BF_4$ species, though only as polycrystalline samples. The BF_4^- ions, that are only sligthly bulkier than the nitrates, can still be accomodated inside the smaller cells, as evidenced by the XRPD pattern that is almost the same as that of **4**.

In conclusion, the results here described show that **1** is a useful and stable building block for the construction of networks that exhibit some predictable structural features. In these silver species also the two *trans*-chlorides of the Ru complex are involved in the networking process, but this can be prevented by using other types of metal-based centers. Investigations are in progress on other bimetallic frames based on **1**, with potential electronic properties, and on architectures assembled by joining these building blocks through hydrogen-bond bridges.

Experimental Section

1: A brown solution of pyrazine (1280 mg, 16.0 mmol) and $[RuCl_2(dmso)_4]$ (200 mg, 0.413 mmol) in toluene (20 mL) was refluxed for 3.5 h to give a brown precipitate. This was filtered off, washed with toluene, and dried in vacuo for 2 h. Yield: 190 mg; 90%. M.p. 165–170 °C; elemental analysis calcd (%) for $C_{16}H_{18}Cl_2N_8ORu$: C 37.6, H 3.56, N 22.0, Ru 19.8; found: C 37.1, H 3.50, N 21.5, Ru 19.7.

2: A solution of $AgSO_3CF_3$ (7.50 mg, 0.0290 mmol) in MeOH (9.5 mL) was added dropwise to a red-brown solution of **1** (13.9 mg, 0.0270 mmol) in CH_2Cl_2 (14 mL). After 45 min a precipitate was collected and filtered off. This crude amorphous solid was treated with MeOH (15 mL) under magnetic stirring for 45 min, then filtered off, washed with further MeOH, and dried in vacuo for 3 h, to obtain a microcrystalline brown powder of **2**. Yield: 16 mg, 79%. Elemental analysis calcd (%) for $C_{17}H_{16}AgCl_2F_3N_8O_3RuS$: C 27.2, H 2.15, N 14.9, Ru 13.5, Ag 14.4; found: C 27.3, H 2.70, N 13.6, Ru 13.3, Ag 13.9; IR (KBr): $\tilde{\nu} = 1261$, 1035 $\nu(SO_3)$, 1583 ν(ring), 809, 630 cm^{-1} δ(CH); UV/Vis spectroscopy of a solid sample: $\lambda_{max} \approx 400$ nm, shoulders at 480 and 620 nm. TGA measurements show a weight loss of 22% between 120 and 280 °C, probably due to the loss of two pyrazine molecules (21.4%). A second higher weight loss (about 50%) is observed in the range 310–570 °C corresponding to the complete decomposition of the polymer to give a residue of metallic ruthenium and silver. Dark red crystals were obtained by slow diffusion of a solution of $AgSO_3CF_3$ in MeOH (6.5 mL, 2.8×10^{-3} M) into a brown solution of $[RuCl_2(pyz)_4]$ in CH_2Cl_2 (2 mL, 1.8×10^{-3} M).

3: A solution of $AgSO_3CF_3$ (21.1 mg, 0.0820 mmol) in n-$CH_3(CH_2)_3OH$ (14 mL) was added dropwise to a brown-red solution of **1** (21.0 mg, 0.0410 mmol) in TCE (18.6 mL). The brown-red microcrystalline product was filtered off after 1 h, washed with n-butanol, and dried in vacuo for 3 h. Yield: 44.7 mg, 90%. Elemental analysis calcd (%) for $C_{22}H_{23}Ag_2Cl_6F_6N_8O_{6.5}RuS_2$: C 21.8, H 1.91, N 9.25, Ru 8.34, Ag 17.8; found: C 21.1, H 1.90, N 9.50, Ru 7.70, Ag 18.9; IR (KBr): $\tilde{\nu} = 1261$, 1034 $\nu(SO_3)$, 1585 ν(ring), 810, 638 cm^{-1} δ(CH). UV/Vis spectroscopy of a solid sample: $\lambda_{max} = 380$ nm, shoulders at 500 and 600 nm. TGA measurements confirm the presence of the solvents in the lattice; two weight losses between 120 and 235 °C (calcd (found) [%]: 23.4 (21.0)) due to the losses of ½ n-butanol, 1 tetrachloroethane, and 1 pyrazine per formula unit, and a successive strong weight loss in the broad range 235–600 °C leading to the complete decomposition of the polymer to give a metallic residue (ca. 27%) of ruthenium and silver. Brown-red crystals were obtained by slow diffusion of a solution of $AgSO_3CF_3$ in n-$CH_3(CH_2)_3OH$ (5.5 mL, 5.8×10^{-3} M) into a brown solution of $[RuCl_2(pyz)_4]$ in TCE (4 mL, 1.9×10^{-3} M). An XRPD spectrum of the massive product **3** fit the profile derived from the crystal structure.

4: A solution of $AgNO_3$ (38.4 mg, 0.230 mmol) in MeCN (10 mL) was added under magnetic stirring to a red-brown solution of **1** (30.4 mg, 0.0590 mmol) in CH_2Cl_2 (25 mL). The microcrystalline product was completely precipitated within 30 min, then filtered off, washed with MeCN, and dried in vacuo for 3 h. Yield: 36 mg, 92%. Elemental analysis calcd (%) for $C_{16}H_{16}AgCl_2N_9O_3Ru$: C 29.0, H 2.44, N 19.0, Ru 15.3, Ag 16.3; found: C 28.7, H 2.30, N 19.0, Ru 15.5, Ag 15.6; IR (KBr): $\tilde{\nu} = 1357$ $\nu(NO_3)$, 1583 ν(ring C), 811, 635 cm^{-1} δ(CH). An XPS survey analysis

 © WILEY-VCH Verlag GmbH, 69451 Weinheim, Germany, 2002 1433-7851/02/4111-1910 $ 20.00+.50/0

shows peaks of $Ru_{3p3/2}$, Ag_{3d}, N_{1s}, Cl_{2p} (respectively at the binding energy (BE) values of 461.5, 367.2, 399.2, and 197.1 eV) and elemental molar ratios respectively equal to 1.0:1.07:7.63:2.10, that fit with the experimental elemental analysis. TGA measurements show a weight loss of about 33 % in the range 130 – 270 °C due to the loss of three pyrazine molecules, followed by a two-step demolition (range 270 – 600 °C) leading to the metals (ca. 32 %). An XRPD spectrum of the massive product **4** was found to be identical to a simulated profile achieved from the single-crystal structure. Red crystals were obtained by slow diffusion of a solution of $AgNO_3$ in MeCN (3.5 mL, 7.1×10^{-3} M) into a brown solution of $[RuCl_2(pyz)_4]$ in TCE (3 mL, 1.9×10^{-3} M), by using pure MeCN (1.5 mL) as a spacer between the two solutions.

Received: December 27, 2001 [Z18436]

[1] a) B. F. Hoskins, R. Robson, *J. Am. Chem. Soc.* **1990**, *112*, 1546; b) R. Robson, B. F. Abrahams, S. R. Batten, R. W. Gable, B. F. Hoskins, J. Liu, *Supramolecular Architecture*, American Chemical Society, New York, **1992**, chap. 19; c) C. L. Bowes, G. A. Ozin, *Adv. Mater*. **1996**, *8*, 13; d) M. Eddaoudi, D. B. Moler, H. Li, B. Chen, T. M. Reineke, M. O'Keeffe, O. M. Yaghi, *Acc. Chem. Res.* **2001** *34*, 319; e) M. Munakata, L. P. Wu, T. Kuroda-Sowa, *Adv. Inorg. Chem.* **1999** *46*, 173; f) A. J. Blake, N. R. Champness, P. Hubberstey, W. S. Li, M. A. Withersby M. Schröder, *Coord. Chem. Rev.* **1999**, *183*, 117; g) P. J. Hagrman, D. Hagrman, J. Zubieta, *Angew. Chem.* **1999**, *111*, 2798; *Angew. Chem. Int. Ed.* **1999**, *38*, 2638; h) B. Moulton, M. J. Zaworotko *Chem. Rev.* **2001**, *101*, 1629.

[2] See, for example: S. Leininger, B. Olenyuk P. J. Stang, *Chem. Rev.* **2000**, *100*, 853; M. Fujita, *Acc. Chem. Res.* **1999**, *32*, 53; M. Fujita, K. Umemoto, M. Yoshizawa, N. Fujita, T. Kusukawa, K. Biradha, *Chem. Commun.* **2001**, 509.

[3] a) M. Fujita, J. Yazaki K. Ogura, *J. Am. Chem. Soc.* **1990**, *112*, 5645; b) M. Fujita K. Ogura, *Coord. Chem. Rev.* **1996**, *148*, 249; c) M. Fujita, O. Sasaki, T. Mitsuhashi, T. Fujita, J. Yazaki, K. Yamaguchi K. Ogura, *Chem. Commun.* **1996**, 1535.

[4] L. Carlucci, G. Ciani, A. Gramaccioli, D. M. Proserpio S. Rizzato, *CrystEngComm* **2000**, 29.

[5] L. Carlucci, G. Ciani, D. M. Proserpio S. Rizzato, *Chem. Commun.* **2001**, 1198.

[6] B. F. Abrahams, B. F. Hoskins, D. M. Michail R. Robson, *Nature* **1994**, *369*, 727.

[7] C. V. K. Sharma, G. A. Broker, J. G. Huddleston, J. W. Baldwin, R. M. Metzger R. D. Rogers, *J. Am. Chem. Soc.* **1999**, *121*, 1137.

[8] a) A. Kamiyama, T. Noguchi, T. Kajiwara, T. Ito, *Angew. Chem.* **2000**, *112*, 3260; *Angew. Chem. Int. Ed.* **2000**, *39*, 3130. b) A series of interesting polymers based on M(2-pyrazinecarboxylate)$_2$ building blocks has been recently reported: Y. B. Dong, M. D. Smith, H. C. zur Loye, *Inorg. Chem.* **2000**, *39*, 1943; Y. B. Dong, M. D. Smith, H. C. zur Loye, *Angew. Chem. Int. Ed.* **2000**, *112*, 4441; *Angew. Chem. Int. Ed.* **2000**, *39*, 4271; Y. B. Dong, M. D. Smith, H. C. zur Loye, *Solid State Sci.* **2000**, *2*, 335; Y. B. Dong, M. D. Smith, H. C. zur Loye, *Solid State Sci.* **2000**, *2*, 861; D. M. Ciurtin, M. D. Smith, H. C. zur Loye, *Chem. Commun.* **2002**, 74.

[9] R. W. Gable, B. F. Hoskins R. Robson, *J. Chem. Soc. Chem. Commun.* **1990**, 762.

[10] See, for example: T. Soma, T. Iwamoto, *Angew. Chem.* **1994**, *106*, 1746; *Angew. Chem. Int. Ed. Engl.* **1994**, *33*, 1665; B. F. Hoskins, R. Robson, N. V. Y. Scarlett, *Angew. Chem.* **1995**, *107*, 1317; *Angew. Chem. Int. Ed. Engl.* **1995**, *34*, 1203.

[11] I. Goldberg, *Chem. Eur. J.* **2000**, *6*, 3863.

[12] a) M. Schindler, F. C. Hawthorne, W. H. Baur, *Acta Crystallogr. Sect. B* **1999**, *55*, 811; b) M. O'Keeffe, M. Eddaoudi, Hailian Li, T. Reineke, O. M. Yaghi, *J. Solid State Chem.* **2000**, *152*, 3.

[13] Crystal data for **2**, $C_{17}H_{16}AgCl_2F_3N_8RuS$: monoclinic, space group $P2/c$ (no. 13), $a = 16.7527(12)$, $b = 8.4254(6)$, $c = 17.0204(13)$ Å, $\beta = 97.417(3)°$, $V = 2382.3(3)$ Å^3, $Z = 4$, $\rho_{calcd} = 2.089$ Mg m^{-3}, final *R1* value 0.0662 for 3138 independent reflections ($I > 2\sigma(I)$). Crystal data for **3**, $C_{22}H_{23}Ag_2Cl_6F_6N_8O_{6.5}RuS$: monoclinic, space group $P2_1/c$ (no. 14), $a = 18.837(2)$, $b = 15.021(2)$, $c = 14.950(2)$ Å, $\beta = 109.520(10)°$, $V = 3987.0(9)$ Å^3, $Z = 4$, $\rho_{calcd} = 2.018$ Mg m^{-3}, final *R1* value 0.0655 for 3337 independent reflections ($I > 2\sigma(I)$). Crystal data for **4**, $C_{16}H_{16}AgCl_2N_9O_3Ru$: tetragonal, space group $P4/nnc$ (no. 126), $a = b = 10.2793(4)$, $c = 10.5587(5)$ Å, $V = 1115.67(8)$ Å^3, $Z = 2$, $\rho_{calcd} = 1.971$ Mg m^{-3}, final *R1* value 0.0406 for 574 independent reflections ($I > 2\sigma(I)$). The data collections were performed at room temperature for **2** and **3** and at 193 K for **4** on a Bruker SMART CCD area detector diffractometer, by using $Mo_{K\alpha}$ radiation ($\lambda = 0.71073$ Å), by the ω-scan method, within the limits $1 < \theta < 25°$ for **2**, $1 < \theta < 23°$ for **3**, and $1 < \theta < 30°$ for **4**. Empirical absorption corrections (SADABS) were applied. The structures were solved by direct methods (SIR97) and refined by full-matrix least-squares on F^2 (SHELX-97). Anisotropic thermal factors were assigned to all the non-hydrogen atoms but to the chlatrate *n*-butanol molecules in **3** and the nitrate anion in **4**. Disordered triflate anions were found in **2** and a suitable 50 % – 50 % double model was refined. A similar treatment was applied to the disordered chlatrate *n*-butanol molecule in **3**. The nitrate anions in **4** are statistically distributed on all the *c* Wyckoff positions with half occupancy. All the diagrams were generated by using the SCHAKAL 97 program. CCDC-175850 (**2**), CCDC-175851 (**3**), and CCDC-175852 (**4**) contain the supplementary crystallographic data for this paper. These data can be obtained free of charge via www.ccdc.cam.ac.uk/conts/retrieving.html (or from the Cambridge Crystallographic Data Centre, 12, Union Road, Cambridge CB21EZ, UK; fax: (+44) 1223-336-033; or deposit@ccdc.cam.ac.uk).

[14] M. O'Keeffe, B. G. Hyde, *Crystal Structures I. Patterns and Symmetry*, Mineralogical Society of America, Washington, DC, **1996**.

[15] For a discussion of the $\pi - \pi$ interactions see: C. Janiak, *J. Chem. Soc. Dalton Trans.* **2000**, 3885.

[16] P. Jensen, D. J. Price, S. R. Batten, B. Moubaraki K. S. Murray, *Chem. Eur. J.* **2000**, *6*, 3186, and references therein.

[17] L. Carlucci, G. Ciani, D. M. Proserpio, A. Sironi, *Angew. Chem.* **1995**, *107*, 2037; *Angew. Chem. Int. Ed. Engl.* **1995**, *34*, 1895.

Synthesis of Metal Nanoparticles by Using Polyoxometalates as Photocatalysts and Stabilizers**

Aristidis Troupis,* Anastasia Hiskia, and Elias Papaconstantinou*

Formation of colloidal metal nanoparticles is a topic of great interest from a fundamental and practical point of view.[1–4] Metal nanoparticles have been obtained by thermal,[3, 5] photochemical,[6] radiolytic,[7] electrochemical,[8] or sonochemical methods,[9] by using various reagents.

Polyoxometalates (POMs) are well-defined metal – oxygen cluster anions.[10, 11] Their redox chemistry is characterized by

[*] A. Troupis, Dr. E. Papaconstantinou, Dr. A. Hiskia
Institute of Physical Chemistry
NCSR Demokritos
153 10 Athens (Greece)
Fax: (+30) 16511766
E-mail: atroup@chem.demokritos.gr, epapac@mail.demokritos.gr
A. Troupis
Chemical Engineering Department
National Technical University
157 80 Athens (Greece)

[**] We thank the Ministry of Development, General Secretariat of Research and Technology of Greece, for supporting part of this work. We also thank Dr. A. Travlos for help with the TEM images.

their ability to undergo stepwise, multielectron redox reactions, whilst their structure remains intact. They participate in catalytic redox processes as electron relays. POMs can be reduced in a plethora of ways, for example, photochemically,[12] through $^{60}Co-\gamma$-radiolysis,[13] electrolytically,[10] and with reducing reagents[14] [Eq. (1) S = substrate]. Various oxidants, which include O_2 and H_2O_2, restore reduced POM to the original form, which completes the photocatalytic cycle. Gordeev noticed the ability of radiolytically two-electron-reduced 12-tungstophosphate, $[PW_{12}O_{40}]^{5-}$, to reduce Ag^+ ions into stable silver hydrosols.[15]

$$POM + S \rightarrow POM(e^-) + S_{ox} \quad (1)$$

We have shown[16] that illumination of a deaerated POM/S/M^{n+} solution (POM: $[PW_{12}O_{40}]^{3-}$, $[SiW_{12}O_{40}]^{4-}$; S: propan-2-ol or 2,4-dichlorophenol; M^{n+}: Ag^+, Pd^{2+}, Cu^{2+}) with an ionic strength of 0.1 M, results in formation of large metal particulates (easily retained by a 0.45 μm filter) which rapidly precipitate out. This route has been proposed as a potential process for the removal–recovery of valuable or toxic metals.

We present here a low ionic strength (no addition of $HClO_4$ and $NaClO_4$) photolysis method with near-visible and UV light, which leads to the formation of metal nanoparticles, through a process in which POMs serve both as photocatalysts, reducing reagents, and stabilizers. Specifically, several metal ions (Ag^+, Pd^{2+}, Au^{III}, and Pt^{IV}) can form metal nanoparticles in the presence of photochemically reduced POMs, in aqueous solutions, according to Equation (2); M_{coll} = colloidal metal. This reaction takes place at ambient temperature, within a few seconds, and without the addition of any stabilizer. The diversified redox chemistry of POM and the potential that the reactions in Equations (1) and (2) may be separated in time and space, or occur in a one-pot system, makes these compounds capable of acting as new multifunctional mediators, which show both reducing and stabilizing ability, in the synthesis of metal nanoparticles.

$$POM(e^-) + M^{n+} \rightarrow POM + M^0{}_{coll} \quad (2)$$

A typical experiment in which Equations (1) and (2) proceed separately is presented below. A representative Keggin-structure POM, $[SiW_{12}O_{40}]^{4-}$, was chosen to study the reaction in Equation (2), between the one-equivalent of the photochemically reduced tungstosilicate, $[SiW_{12}O_{40}]^{5-}$, and the metal ions. The $[SiW_{12}O_{40}]^{5-}$ ion was obtained by photolysis of a deaerated propan-2-ol/$[SiW_{12}O_{40}]^{4-}$ aqueous solution with $\lambda > 320$ nm light, in the presence of, for instance, propan-2-ol as a sacrificial reagent[12] [Eq. (3)].[12c]

$$2[SiW_{12}O_{40}]^{4-} + (CH_3)_2CHOH \xrightarrow{h\nu} 2[SiW_{12}O_{40}]^{5-} + (CH_3)_2C{=}O + 2H^+ \quad (3)$$

The photoreduction of 12-tungstosilicate was monitored at 730 nm, the characteristic absorption of the one-electron-reduced, blue POM, $[SiW_{12}O_{40}]^{5-}$ (Figure 1). After irradiation ceased, Ag^+, Pd^{2+}, $PtCl_6^{2-}$ (0.1 mM), or $AuCl_4^-$ (1 mM) ions were added to the photolysed solution. Within a few seconds the absorption at 730 nm disappeared and the solution turned gradually yellow (Ag), pink (Au), or black-brown (Pd, Pt),

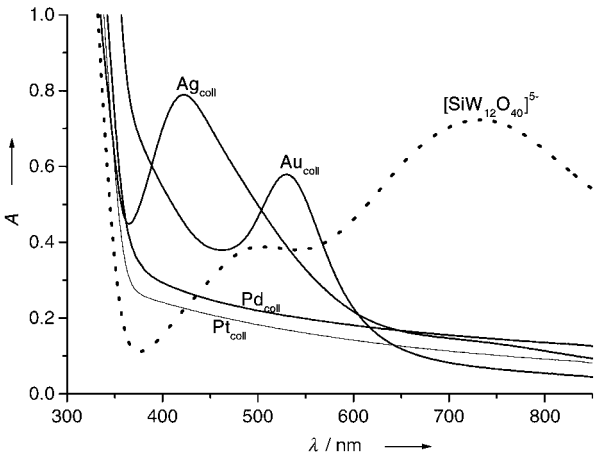


Figure 1. Absorption spectra of metal nanoparticles (Ag, Au, Pd, Pt) in solution, obtained after thermal reaction of photogenerated 1-equivalent-reduced POM, $[SiW_{12}O_{40}]^{5-}$ (about 0.35 mM; spectrum shown), with the corresponding metal ions (Ag^+, Pd^{2+}, $[PtCl_6]^{2-}$ (0.1 mM) or $[AuCl_4]^-$ (1 mM)); pH 5. coll = colloidal.

[Eq. (4)]. The spectra obtained after 2 minutes, assigned to plasmon-resonance absorbance of the corresponding metal nanoparticles, are shown in Figure 1.[17]

$$n[SiW_{12}O_{40}]^{5-} + M^{n+} \rightarrow n[SiW_{12}O_{40}]^{4-} + M^0 \quad (4)$$

Thus, the reaction in Equation (2) proceeds at room temperature within seconds and utilizing a mild reductant, $[SiW_{12}O_{40}]^{5-}$, whereas other reductive methods that proceed promptly at room temperature use rather strong reductants such as BH_4^-, hydrogen atoms, or organic radicals, produced upon radiolysis or sonolysis of aqueous solutions. On the other hand, conventional processes that use mild reducing agents often need heat to enable them to proceed within minutes or days.[5]

Step 2 functions because of: a) the ability of reduced POM to transfer the electrons efficiently to many reagents[14] and b) the lower potential of the one-equivalent-reduced tungstate couple $[SiW_{12}O_{40}]^{4-}/[SiW_{12}O_{40}]^{5-}$ (0.057 V vs. NHE; NHE = normal hydrogen electrode) relative to Ag^+/Ag^0 (0.799 V vs. NHE), $AuCl_4^-/Au^0$ (0.99 V vs. NHE), Pd^{2+}/Pd^0 (0.987 V vs. NHE), or $PtCl_6^{2-}/Pt^0$ (0.725 V vs. NHE).

The TEM pattern of the metal particles indicated in Figures 2–5 verify the formation of metal nanoparticles in the process. The Au (Figure 2) or Ag (Figure 3) particles produced are almost spherical with a diameter of 13.1 ± 3.9 nm (±30%, sample population 197) and 15.3 ± 3.4 nm (±22%, sample population 177), respectively. The palladium particles (Figure 4) obtained were of 5.0 ± 1.1 nm (±22%, sample population 97). In the case of platinum (Figure 5), smaller particles of 2.7 ± 0.6 nm diameter (±24%, sample population 98) were assembled to give larger spheres with an average diameter of 24.0 ± 7.2 nm (±30%). The colloids obtained were stable against aggregation for over two months.

The restriction of the size of the metal particles to the nanometer scale is attributed to the stabilizing role of POM

 © WILEY-VCH Verlag GmbH, 69451 Weinheim, Germany, 2002 1433-7851/02/4111-1912 $ 20.00+.50/0 *Angew. Chem. Int. Ed.* **2002**, *41*, No. 11

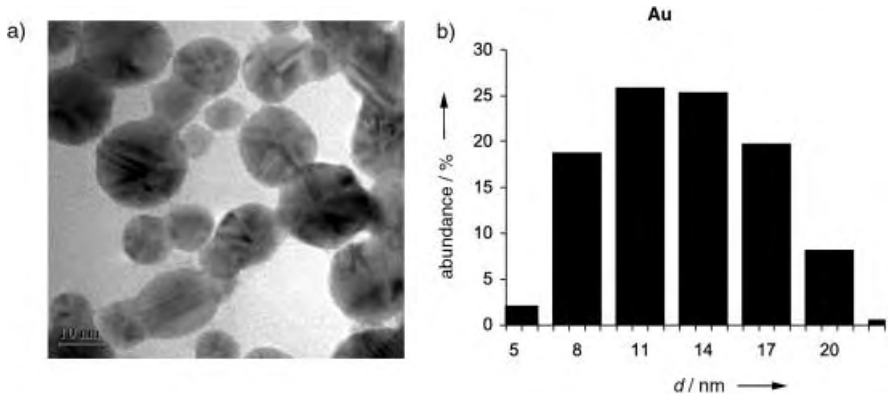


Figure 2. a) Transmission electron micrograph and b) size histogram of the Au particles.

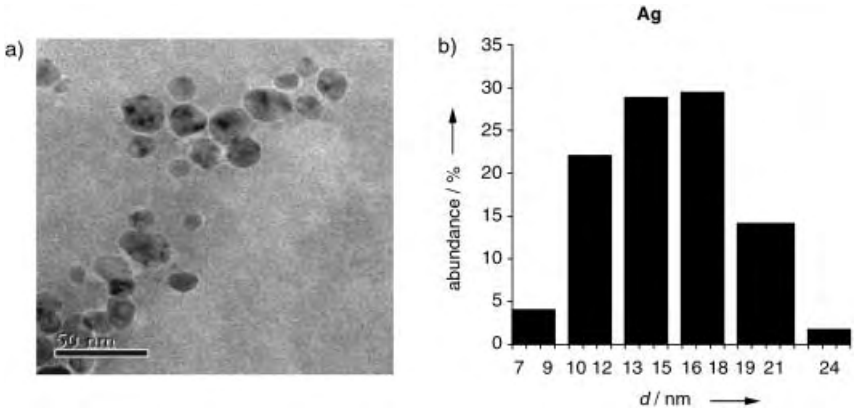


Figure 3. a) Transmission electron micrograph and b) size histogram of the Ag particles.

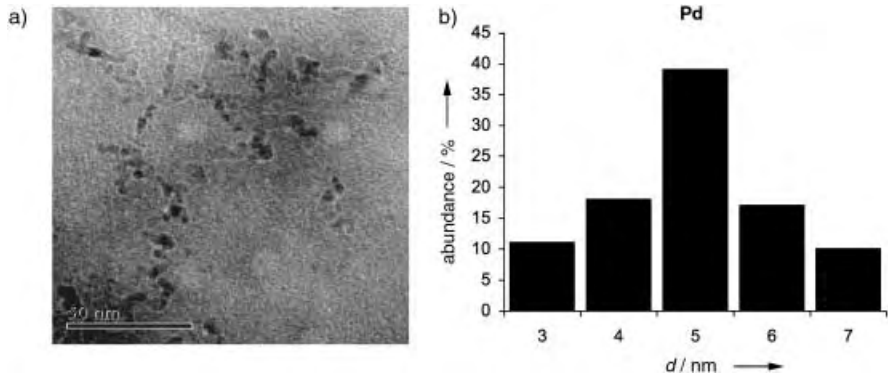


Figure 4. a) Transmission electron micrograph and b) size histogram of the Pd particles.

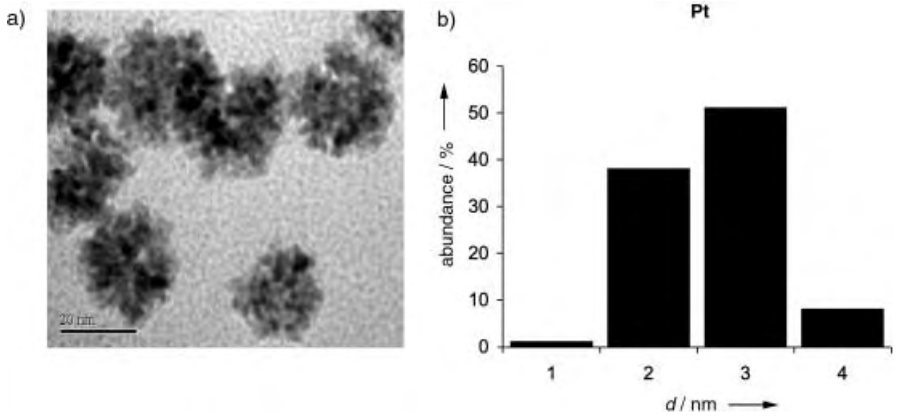


Figure 5. a) Transmission electron micrograph and b) size histogram of the Pt particles.

because: a) the colloidal solution contains no other potential stabilizing reagent but POM, b) the volume of 12-tungstosilicate (considered to be spherical, with a diameter of about 12 Å) and its (4 –) negative charge (the anion is not protonated, even at pH 1[18]) could account for the prevention of agglomeration of the metal particles, as for other POM,[3c] c) the stabilizing role of POM in organic systems (acetone or acetonitrile solutions) has been reported in a process in which H_2 was the reducing agent for Ir or Rh complexes, while the POM $[Bu_4N]_9[P_2W_{15}Nb_3O_{62}]$ functioned solely as a stabilizer. In addition, TEM, ion-exchange, and electrophoresis experiments revealed that POMs attach to the surface of Ir^0 or Rh^0 nanoclusters,[3] and d) the ability of $[SiW_{12}O_{40}]^{4-}$ not only to attach but also to self-assemble onto Ag(111) or Au(111) surfaces has been demonstrated.[19] Addition of $NaClO_4$ 0.1 M into the colloidal solutions leads to immediate precipitation in all cases.

These results have been obtained through the separation of the photochemical reaction from the thermal reaction. However, combination of both in a one-pot system gave satisfactory results with Ag^+ ions. Figure 6 shows the gradual development of the yellow color (410 nm), characteristic of silver-nanoparticle absorbance, upon photolysis of a deaerated $[SiW_{12}O_{40}]^{4-}$/propan-2-ol/Ag^+ aqueous solution. It is noteable that, in all experiments, the POMs remained intact in the process, determined from the stability of the absorbance peak at 263 nm (Figure 6), which is characteristic of the oxidized form of Keggin-structured POMs.

In summary, a novel and facile method has been proposed to synthesize metal nanoparticles directly from aqueous solutions, by use of POMs to serve as reducing reagents, photocatalysts, and stabilizers. As the solubility of POMs can be tuned by altering the counterion, which renders these compounds soluble in many organic solvents without affecting their redox properties, the process could be extended to nonpolar solvents. This prospect is attractive as the solubility of the reducing agent and the stabilizer are limiting factors in the chemical-reductive synthesis of metal nanoparticles.[5]

 © WILEY-VCH Verlag GmbH, 69451 Weinheim, Germany, 2002 1433-7851/02/4111-1913 $ 20.00+.50/0

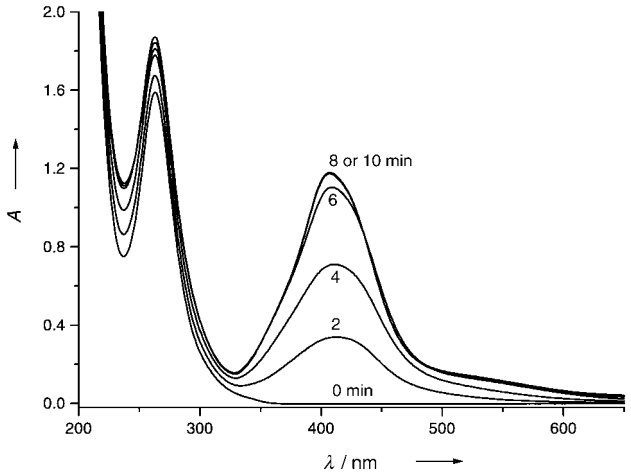


Figure 6. Photolysis profile: the formation of colloidal silver at different illumination times ($\lambda \approx 410$ nm) and the stability of $[SiW_{12}O_{40}]^{4-}$ photocatalyst ($\lambda = 263$ nm). Photolysis of a deaerated solution containing propan-2-ol (0.5 M), $[SiW_{12}O_{40}]^{4-}$ (0.035 mM), Ag^+ (0.1 mM) at pH 5 ($\lambda >$ 320 nm).

Experimental Section

$K_4[SiW_{12}O_{40}]$ was synthesized according to literature methods.[18] The metal ions added to the photolysed solution were aqueous solutions of $AgNO_3$, $PdCl_2$, $HAuCl_4$, or H_2PtCl_6.

In photolysis experiments, an aqueous solution of $SiW_{12}O_{40}^{4-}$ 0.7 mM and propan-2-ol 0.5 M, at pH 5, was put into a spectrophotometer cell (1 cm path length) deaerated with Ar and covered with a cerum cap. Photolysis was performed with a 1000 W Xe arc lamp, the light intensity of which was mechanically reduced by approximately 40%, while cut-off filters (up to 320 nm) were used to avoid direct photolysis of organic substrates. The absorption spectra of metal particles or catalyst were taken with a UV/Vis/NIR Spectrometer (Perkin Elmer Lambda 19), and the degree of reduction of POM in photolyzed, deaerated solutions was calculated from the known extinction coefficient of reduced catalyst, $SiW_{12}O_{40}^{5-}$, at 730 nm ($0.21 \times 10^4\ M^{-1}cm^{-1}$). TEM images were obtained using a Philips 200 kV microscope, and the samples were prepared by placing microdrops of colloid solution on a Formvar/carbon coated copper grid.

Received: October 8, 2001 [Z18024]

[1] *Clusters And Colloids: From Theory To Applications*, (Ed.: G. Schmid), VCH, Weinheim, **1994**.
[2] A. Henglein, *J. Phys. Chem.* **1993**, *97*, 5457 – 5471.
[3] a) J. D. Aiken III, R. G. Finke, *J. Mol. Catal.* **1999**, *145*, 1 – 44, and references therein; b) J. D. Aiken III, Y. Lin, R. G. Finke, *J. Mol. Catal.* **1996**, *114*, 29 – 51; c) Y. Lin and R. G. Finke *J. Am. Chem. Soc.* **1994**, *116*, 8335 – 8353. The polyoxoanion-stabilized nanoclusters studied by Finke and co-workers constitute a modern class of well-defined nanoclusters, which can be isolated and redissolved whilst retaining their catalytic activity and having huge catalytic lifetimes (> 190000 turnovers) in solution.
[4] M. A. El-Sayed, *Acc. Chem. Res.* **2001**, *34*, 257 – 264.
[5] D. V. Goia, E. Matijevic, *New J. Chem.* **1998**, 1203 – 1215.
[6] a) Y. Yonezawa, T. Sato, M. Ohno, H. Hada, *J. Chem. Soc. Faraday Trans.* **1987**, *83*, 1559 – 1567; b) M. R. V. Sahyun, N. Serpone, *Langmuir* **1997**, *13*, 5082 – 5088.
[7] J. Belloni, M. Mostafavi, H. Remita, J.-L. Marignier, M.-O. Delcourt, *New J. Chem.* **1998**, 1239 – 1255.
[8] M. T. Reetz, W. Helbig, *J. Am. Chem. Soc.* **1994**, *116*, 7401 – 7402.
[9] Y. Nagata, Y. Watananabe, S.-I. Fujita, T. Dohmaru, S. Taniguchi, *J. Chem. Soc. Chem. Commun.* **1992**, 1620 – 1622.
[10] M. T. Pope, *Heteropoly and Isopoly Oxometalates* in *Inorganic Chemistry Concepts*, *Vol. 8* (Eds.: C. K. Jorgensen, M. F. Lappert, S. J. Lippard, J. L. Margrave, K. Niedenzu, H. Noth, R. W. Parry, and H. Yamatera), Springer Verlag, Berlin, **1983**.
[11] *Chem. Rev.* **1998**, *98*, 1 – 389, volume dedicated to polyoxometalates.
[12] a) E. Papaconstantinou, *Chem. Soc. Rev.* **1989**, *16*, 1 – 31; b) A. Hiskia, A. Mylonas, E. Papaconstantinou, *Chem. Soc. Rev.* **2001**, *30*, 62 – 69; c) A. Mylonas, A. Hiskia, E. Androulaki, D. Dimotikali, E. Papaconstantinou, *Phys. Chem. Chem. Phys.* **1999**, *1*, 437 – 440.
[13] E. Papaconstantinou, *J. Chem. Soc. Faraday Trans. 1,* **1982**, *78,* 2769 – 2772.
[14] I. A. Weinstock, *Chem. Rev.* **1998**, *98*, 113 – 170.
[15] A. V. Gordeev, B. G. Ershov, *High Energy Chem.* **1999**, *33*, 218 – 223.
[16] a) A. Troupis, A. Hiskia, E. Papaconstantinou, *New J. Chem.* **2001**, *25*, 361 – 363; b) L. Chalkley was the first to observe precipitation of metal ions (Ag^+) by photoreduced $[PW_{12}O_{40}]^{3-}$, *J. Phys. Chem.* **1952**, *56*, 1084 – 1086.
[17] J. A. Creighton, D. G. Eadon, *J. Chem. Soc. Faraday Trans.* **1991**, *87*, 3881 – 3891.
[18] M. T. Pope, G. M. Varga, *Inorg. Chem.* **1966**, *5*, 1249.
[19] W. G. Klemperer, C. G. Wall *Chem. Rev.* **1998**, *98*, 297 – 306.

Light-Controlled Nitric Oxide Generation from a Novel Self-Assembled Monolayer on a Gold Surface**

Salvatore Sortino,* Salvatore Petralia, Giuseppe Compagnini, Sabrina Conoci, and Giuseppe Condorelli

Increasing evidence demonstrates that nitric oxide (NO) plays important roles in numerous physiological processes.[1–8] For instance, it is involved in the bioregulation of functions such as vasodilatation, neurotransmission, and hormone secretion in living bodies. In addition to these effects, NO has also been reported to act as efficient anticancer agent that inhibits key metabolic pathways to block the growth of or to kill cells.[9–13] This has stimulated intense interest in com-

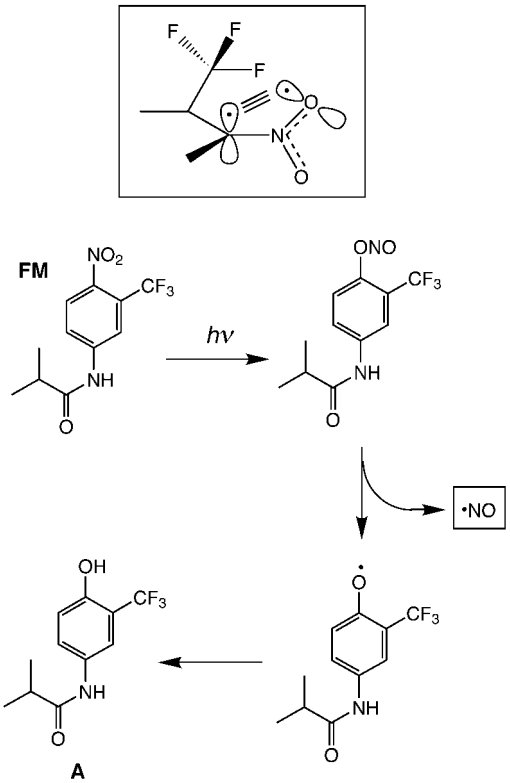
[*] Dr. S. Sortino, Dr. S. Petralia, Prof. G. Condorelli
Dipartimento di Scienze Chimiche
Università di Catania
Viale Andrea Doria 8, 95125 Catania (Italy)
Fax: (+39) 095-580-138
E-mail: ssortino@mbox.unict.it
Dr. G. Compagnini
Dipartimento di Scienze Chimiche
Università di Catania
and
Istituto Nazionale per la Fisica della Materia
Unità di Catania (Italy)
Dr. S. Conoci
Si optoelectronics, bio- and nano-systems Corporate Technology R&D, ST Microelectronics Stradale Primosole 50,
95125 Catania (Italy)

[**] This work was supported by MURST "cofinanziamento di programmi di ricerca di rilevante interesse nazionale" (Project: Mechanisms of Photoinduced Processes in Organized Systems). We also thank Prof. S. Giuffrida for his critical reading of the manuscript, Prof. V. Amico for his useful suggestions, and the referees for constructive comments.

 © WILEY-VCH Verlag GmbH, 69451 Weinheim, Germany, 2002 1433-7851/02/4111-1914 $ 20.00+.50/0

pounds which can deliver NO to a biological target on demand. In this regard, substances of low thermal reactivity that photochemically generate NO, preferentially with localized action, would be appealing photochemotherapeutic agents. Despite the considerable amount of reports on NO photogenerators in solution in the last years,[14–18] the delivery of quantitative amounts of NO at a desired target is still a critical problem for medical applications. A viable strategy for overcoming the site specificity dilemma would be the immobilization of suitable NO photogenerators on solid substrates. In this way, the probe can be driven directly to the area of interest and irradiated by using apposite fiber optic light guides. Such an approach is encouraged by the great variety of self-assembled monolayers (SAMs) of bioactive compounds on different metal electrodes. These systems are successfully applied in the biomedical field by using electrochemical stimuli.[19–24] Here we report on a novel SAM on a gold surface, which to the best of our knowledge is the first SAM that quantitatively releases NO exclusively by light excitation.

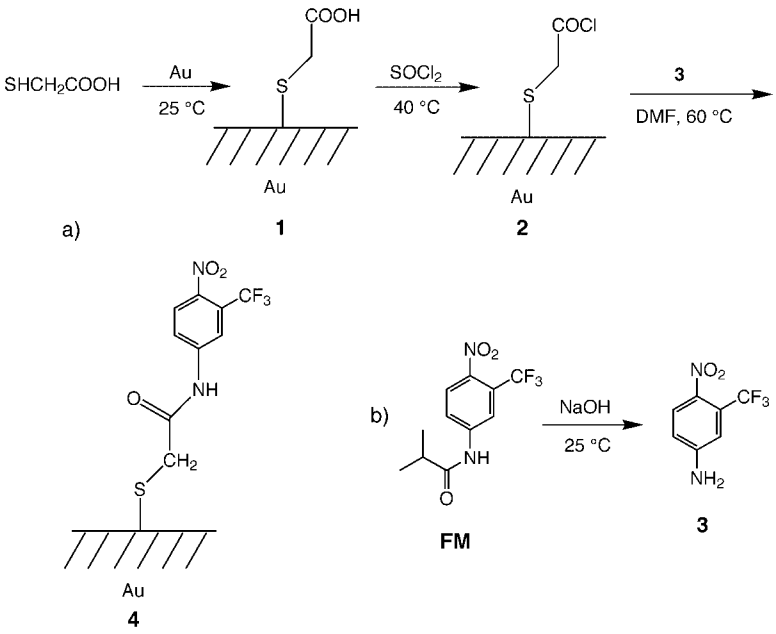
Our recent study on the photoreactivity of the anticancer drug flutamide (FM) was a decisive starting point for this work. We found that in homogeneous solution FM leads to the phenol derivative **A** as the sole stable photoproduct upon light excitation (Scheme 1).[25, 26] Owing to the presence of the CF_3 substituent the nitro group is almost perpendicular to the aromatic plane, with which it is therefore not conjugated. In this "out-of-plane" geometry, the p orbital of the oxygen atom has a constructive overlap with the adjacent p orbital of the aromatic ring in both the ground and excited states. Formation of **A** was rationalized on the basis of the well-known nitro-to-nitrite photorearrangement followed by rupture of the O–N bond to generate a phenoxy radical and NO (Scheme 1).



Scheme 1. Photodegradation of FM in homogeneous solution.

Besides contributing to the general picture of drug photochemistry, these findings stimulated the idea of developing a SAM of a FM-related compound on a gold surface and testing its ability to act as a NO photogenerator. In this regard, it is noteworthy that, apart from the low excitation energy required for NO production by FM photodecomposition (the absorption spectrum extends beyond 400 nm), the insignificant quantum yield of singlet oxygen by photosensitization[25] is an additional advantage in avoiding undesired side photoeffects.

The SAM **4** was prepared (Scheme 2) by first immobilizing sulfanylacetic acid on gold plates (1×1 cm, ca. 800 Å thick) by soaking (12 h at RT) to give SAM **1**, which was heated in refluxing $SOCl_2$ for 3 h to give SAM **2**. X-ray photoelectron spectroscopy (XPS) was used to check the degree of conversion after the reaction on the surface. The chlorine:



Scheme 2. a) Preparation of SAM **4**. b) Preparation of reagent **3**.

sulfur ratio in SAM **2** of 1:1.1 (±0.2) indicated quantitative conversion of **1** to **2**. Finally, SAM **4** was obtained by condensation of **2** with **3** (see Experimental Section for details) in anhydrous dimethylformamide for 12 h.

Again, the XPS analysis provided clear evidence that the reaction occurred efficiently: The signal of the sulfur 2p photoelectrons at 162 eV (binding energy) remained, whereas the signal of the chlorine 2p electrons (199 eV in **2**) completely disappeared and the diagnostically important and unambiguous signals related to fluorine 1s and nitrogen 1s electrons at 688 and 402 eV, respectively, appeared.

To test the suitability of **4** as an NO generator under light excitation, the monolayer-modified gold plate was immersed in phosphate buffer solution and irradiated. The NO photorelease was measured directly in real time with an NO electrode (see Experimental Section). Figure 1 shows that **4**

 © WILEY-VCH Verlag GmbH, 69451 Weinheim, Germany, 2002 1433-7851/02/4111-1915 $ 20.00+.50/0

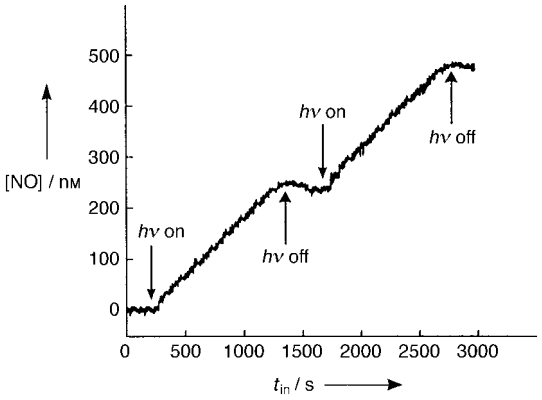
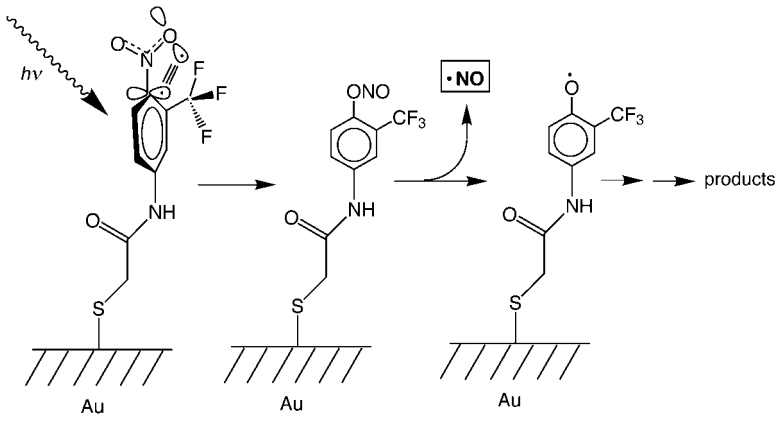


Figure 1. NO released upon photolysis ($\lambda_{exc} > 380$ nm) of SAM **4** immersed in phosphate buffer solution (3 mL, 10 mM, pH 7.4).

was stable to thermal release of NO, as indicated by the line with zero slope prior to irradiation. On excitation, slow and linear generation of NO at nanomolar levels was observed, which stopped when the light was turned off, after which a slight decline in the NO concentration was observed, most likely due to diffusion and oxidation by molecular oxygen in solution. The subsequent illumination of the sample triggered further NO photorelease from **4** until the light was turned off. The linearity observed in the performed experiments indicates that only a small fraction of SAM **4** is photodecomposed after about 50 min of irradiation under our experimental conditions.

On the basis of the electronic and molecular structure there are no reasons to believe that the photochemical behavior of SAM **4** differs from that of FM, and therefore a molecular mechanism for NO photogeneration triggered by the nitro-to-nitrite photorearrangement appears the most likely (Scheme 3).

In summary, the exclusive control of NO release through modulation of the illumination conditions, the relatively low excitation energy required, the absence of noxious side effects such as singlet-oxygen photosensitization, the thermal stability under physiological conditions, and the ease of preparation are remarkable advantages offered by SAM **4**. The coupling of such features with the ability to deliver light in discrete regions through optical fibers makes this compound an appealing candidate in the design of probes for applications where site-directed control of small and quantitative amounts of NO is required. This topic is currently under investigation in our laboratory.



Scheme 3. Proposed mechanism for the NO photogeneration from SAM **4**.

Experimental Section

3 was prepared as shown in Scheme 2b. After the hydrolysis reaction, **3** was purified on a silica gel column (40–63 μm; 1.0 × 20 cm) with dichloromethane:cyclohexane (3:2) as eluent and fully characterized by NMR spectroscopy and mass spectrometry. ^{1}H NMR ($CDCl_3$): $\delta = 4.46$ (br s, 2H, NH_2), 6.78 (dd, J(H6,H5) = 8.8, J(H6,H2) = 2.6 Hz, 1H, H6), 6.98 (d, J(H2,H6) = 2.6 Hz, 1H, H2), 7.97 ppm (d, J(H5,H6) = 8.8 Hz, 1H, H5). ^{19}F NMR ($CDCl_3$): $\delta = 16.34$ ppm (s, CF_3). FAB-MS (+; glycerol as matrix): m/z: 207 $[M+H]^+$. EI-MS (70 eV, 60 °C): m/z (%): 206 $[M]^{\bullet+}$ (25.5), 176 $[M-NO]^{\bullet+}$ (28.9), 167 (18.9), 160 $[M-NO_2^{\bullet}]^+$ (21.1), 125 $[176-CHF_2^{\bullet}]^+$ (20.0), 69 $[CF_3]^+$ (100).

4 was irradiated in a quartz fluorescence cuvette (10 mm pathlength) by using a Rayonet photochemical reactor equipped with eight RPR lamps with an emission in the 380–480 nm range with a maximum at 420 nm. The incident photon flux on the sample was about 5×10^{16} quanta per second.

NO photogenerated by **4** was measured with an amperometric sensor (ISO-NO, World Precision Instruments, Sarasota, FL), equipped with a data-acquisition system, and based on direct electrochemical detection of NO with short response time (< 5 s) and extremely low detection limit (1 nM). The sensor was accurately calibrated by mixing standard solutions of $NaNO_2$ with 0.1M H_2SO_4 and 0.1M KI according to the reaction[27] $4H^+ + 2I^- + 2NO_2^- \rightarrow 2H_2O + 2NO + I_2$.

XPS spectra were obtained on an AXIS HS machine (Kratos Analytical) with $Mg_{K\alpha}$ excitation (1253.6 eV). The binding energies of the collected spectra were calibrated against the Au 4f photoelectron signal originating from the underlying substrate.

Received: November 19, 2001
Revised: February 15, 2002 [Z18247]

[1] R. F. Furchgott, J. V. Zawadzki, *Nature* **1980**, *288*, 373.
[2] E. Culotta, D. E. Koshland, *Science* **1992**, *258*, 1862.
[3] J. M. Fukuto, L. J. Ignarro, *Acc. Chem. Res.* **1997**, *30*, 149.
[4] R. M. Palmer, A. G. Ferrige, S. Moncada, *Nature* **1987**, *327*, 524.
[5] A. R. Butler, D. L. H. Williams, *Chem. Soc. Rev.* **1993**, *22*, 233.
[6] C. T. Gnewuch, G. Sosnowsky, *Chem. Rev.* **1997**, *97*, 829.
[7] S. Pfeiffer, B. Mayer, B. Hemmens, *Angew. Chem.* **1999**, *111*, 1824; *Angew. Chem. Int. Ed.* **1999**, *38*, 1714.
[8] a) F. Murad, *Angew. Chem.* **1999**, *111*, 1976; *Angew. Chem. Int. Ed.* **1999**, *38*, 1856; b) R. F. Furchgott, *Angew. Chem.* **1999**, *111*, 1990; *Angew. Chem. Int. Ed.* **1999**, *38*, 1870; c) L. J. Ignarro, *Angew. Chem.* **1999**, *111*, 2002; *Angew. Chem. Int. Ed.* **1999**, *38*, 1882.
[9] C. M. Maragos, J. M. Wang, J. A. Hrabie, J. J. Oppenheim, L. K. Keefer, *Cancer Res.* **1993**, *53*, 564.
[10] J. B. Mitchell, D. A. Wink, W. DeGraff, J. Gamson, L. K. Keefer, M. C. Krishna, *Cancer Res.* **1993**, *53*, 5845.
[11] L. Li, R. G. Kilbourn, J. Adams, I. J. Fidler, *Cancer Res.* **1991**, *52*, 2531.
[12] R. J. Griffin, C. W. Song, Presented at the 43rd Annual Meeting of the Radiation Research Society, San Jose, CA, **1995**, P15–204.
[13] D. Moncada, D. Lekieffre, B. Arvin, B. Meldrum, *NeuroReport* **1993**, *343*, 530.
[14] J. Baurassa, W. DeGraff, S. Kudo, D. A. Wink, J. B. Mitchell, P. C. Ford, *J. Am. Chem. Soc.* **1997**, *119*, 2853.
[15] K. M. Miranda, X. Bu, I. Lorkovic, P. Ford, *Inorg. Chem.* **1997**, *36*, 4838.
[16] V. R. Zhelyaskov, K. R. Gee, D. W. Godwin, *Photochem. Photobiol.* **1998**, *67*, 282.
[17] L. R. Makings, R. Y. Tsien, *J. Biol. Chem.* **1994**, *269*, 6282.

 © WILEY-VCH Verlag GmbH, 69451 Weinheim, Germany, 2002 1433-7851/02/4111-1916 $ 20.00+.50/0

[18] D. J. Sexton, A. Muruganandam, D. J. McKenney, B. Mutus, *Photochem. Photobiol.* **1994**, *59*, 463.
[19] J. Aizenberg, A. J. Black, G. M. Whitesides, *Nature* **1998**, *394*, 868.
[20] C. M. Ruan, F. Yang, C. H. Lei, J. Q. Deng, *Anal. Chem.* **1998**, *70*, 1721.
[21] G. E. Poirier, *Chem. Rev.* **1997**, *97*, 1117.
[22] L. Jian, A. Glidle, A. Griffith, C. J. McNeil, J. M. Cooper, *Bioelectrochem. Bioenerg.* **1997**, *42*, 15.
[23] A. J. Guiomar, S. D. Evans, J. T. Guthrie, *Supramol. Sci.* **1997**, *4*, 279.
[24] Y. Hou, Y. Chen, N. A. Amro, K. Wadu-Mesthrige, P. R. Andreana, G. Liu, P. G. Wang, *Chem. Commun.* **2000**, 1831.
[25] S. Sortino, S. Giuffrida, G. De Guidi, R. Chillemi, S. Petralia, G. Marconi, G. Condorelli, S. Sciuto, *Photochem. Photobiol.* **2001**, *73*, 6.
[26] S. Sortino, G. Marconi, G. Condorelli, *Chem. Commun.* **2001**, 1226.
[27] D. W. Godwin, D. Che, D. M. O'Malley, Q. Zhou, *J. Neurosci. Methods* **1997**, *73*, 91.

Complete Stereospecific Cyclopropanation of α,β-Unsaturated Amides Promoted by Sm/CH_2I_2**

José M. Concellón,* Humberto Rodríguez-Solla, and Cecilia Gómez

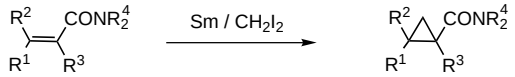
The cyclopropane ring is present in a great number of natural products.[1] In addition, the use of cyclopropanes in mechanistic studies[2] and their utility as synthetic intermediates[3] warrants the interest in these carbocycles from various fields in organic chemistry. The majority of the methodologies developed for the synthesis of cyclopropanes[4] rely on variants of the following reactions: Simmons–Smith cyclopropanation,[5] transition-metal catalyzed cyclopropanation of alkenes with diazomethane[6] or diazoesters,[7] and cyclopropanation of Michael acceptors.[8] However, these methods leave much to be desired: total control of diastereoselectivity in the synthesis of polysubstituted cyclopropanes is beyond reach, some methodologies call for toxic reagents, and in other cases, synthesis of cyclopropanes from unsaturated compounds in which the C=C bond is tri- or tetrasubstituted cannot be carried out.[9]

In particular, and to the best of our knowledge, the cyclopropanation of α,β-unsaturated amides in which the C–C double bond is tri- or tetrasubstituted has not been published. Only the transformation of mono- or disubstituted α,β-unsaturated amides into the corresponding cyclopropanecarboxamides has been described.[10] Consequently new methods for the diastereoselective construction of cyclopropylamides, in which the cyclopropane ring is polysubstituted, are of significant interest.

In their work on the synthetic applications of samarium(II) compounds Molander et al. reported the use of samarium amalgam/diiodomethane to cyclopropanate allylic alcohols with complete stereospecificity with respect to the olefin geometry.[11] Imamoto et al. described the cyclopropanation of lithium enolates derived from ketones by using SmI_2/CH_2I_2.[12] However, to the best of our knowledge, no cyclopropanation of α,β-unsaturated acid derivatives by using Sm/CH_2I_2 has been published.[13]

Recently, we described the SmI_2-promoted highly diastereoselective synthesis of vinyl halides,[14] α,β-unsaturated esters[15] and amides,[16] deuterated β,γ-unsaturated esters,[17] and vinylsilanes.[18] Here we report a new methodology for complete stereospecific cyclopropanation of α,β-unsaturated amides by using samarium and diiodomethane. The stereospecific synthesis of cyclopropylcarboxamides, in which the cyclopropane ring is di-, tri-, or tetrasubstituted, is achieved in high yield.

Treatment of several α,β-unsaturated amides **1** with samarium metal and diiodomethane at room temperature gave, after hydrolysis, the corresponding cyclopropylamides **2**, with complete stereospecificity and in high yield (Eq. (1), Table 1).



1 **2** (1)

These results show that this cyclopropanation reaction: a) takes place in high yield; b) is general and can be carried out starting from aliphatic (linear, branched, or cyclic) or aromatic α,β-unsaturated amides; c) is unaffected by the presence of bulky groups R^3 on the carbonyl amide (entries 3, 10, and 11); d) can be carried out starting from α,β-unsaturated amides **1**, in which the C=C bond is di-, tri-, or tetrasubstituted; e) takes place with complete stereospecificity—*trans*- and *cis*-cyclopropanamides are obtained from (*E*)- and (*Z*)-α,β-unsaturated amides, respectively (entries 1, 2 and 10, 11); f) takes place with very high chemoselectivity—selective cyclopropanation of the C=C bond conjugated with the carbonyl group is achieved in polyunsaturated amides (entry 5).[19]

The diastereoisomeric purity of compounds **2** was determined on the crude reaction products by ^1H NMR spectroscopy (300 MHz) and GC-MS, which showed the presence of a

[*] Dr. J. M. Concellón, H. Rodríguez-Solla
Departamento de Química Orgánica e Inorgánica
Facultad de Química, Universidad de Oviedo
33071 Oviedo (Spain)
Fax: (+34) 98-510-3446
E-mail: jmcg@sauron.quimica.uniovi.es
Dr. C. Gómez
Departamento de Química Orgánica
Facultad de Ciencias, Universidad de Alicante
Apartado 99, 03080 Alicante (Spain)

[**] We acknowledge financial support from II Plan Regional de Investigación del Principado de Asturias (PB-EXP01-11) and Ministerio de Ciencia y Tecnología (BQU2001-3807). We thank Dr. Francisco J. González for valuable discussions and Robin Walker for revising the English manuscript. J.M.C. thanks Carmen Fernández-Flórez for her time. H.R.S. thanks Principado de Asturias for a predoctoral fellowship.

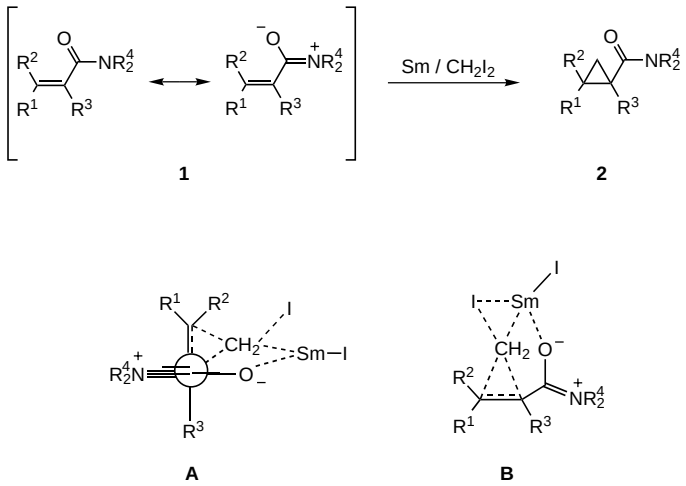
Supporting information for this article is available on the WWW under http://www.angewandte.com or from the author.

 © WILEY-VCH Verlag GmbH, 69451 Weinheim, Germany, 2002 1433-7851/02/4111-1917 $ 20.00+.50/0

Table 1. Synthesis of cyclopropanecarboxamides by using Sm/CH_2I_2.

Entry	2[a]	R^1	R^2	R^3	R^4	Yield [%][b]
1	**2a**	Ph	H	H	Et	79
2	**2b**	H	Ph	H	Et	71
3	**2c**	Ph	H	H	*i*Pr	72
4	**2d**	Me(CH)Ph	H	H	Et	75
5	**2e**	(*E*)-MeCH=CH	H	H	Et	73
6	**2f**	Ph	H	Me	Et	73
7	**2g**	C_7H_{15}	H	Me	Et	69
8	**2h**	Bu	H	Et	Et	66
9	**2i**	cyclohexyl	H	Me	Et	72
10	**2j**	*p*-$MeOC_6H_4$	H	Me	*i*Pr	83
11	**2k**	H	*p*-$MeOC_6H_4$	Me	*i*Pr	85
12	**2l**	Ph	Et	Me	Et	70
13	**2m**	$PhCH_2$	Me	Me	Et	69
14	**2n**	-$(CH_2)_5$-		Me	Et	74

[a] All products were obtained with complete stereospecificity. Diastereoisomeric purity was determined by GC-MS, and ^1H and ^{13}C NMR (300 MHz) analysis of the crude products **2**. [b] Yield after column chromatography based on compound **1**.



Scheme 1. Mechanistic proposal for the conversion of **1** into **2**. **A** and **B** depict the proposed transition state.

single diastereoisomer. The relative *trans* or *cis* configuration of substituents on the cyclopropane ring was established by analysis of ^1H NMR coupling constants between the cyclopropane protons of compounds **2a**–**e**,[20] or by NOE experiments in the case of tri- and tetrasubstituted cyclopropanes (**2j**, **k** and **2l**).

Exposure of the substrate to Sm/CH_2I_2 for extended periods of time appears to have no detrimental effect on either the yield or the diastereoselectivity of the isolated products.[21] When the same reaction conditions were used to obtain cyclopropylesters from α,β-unsaturated esters, no cyclopropanation was observed at room temperature or at reflux.

The formation of products **2** may be explained by assuming the formation of Sm^{II} carbenoids (e.g. $ISmCH_2I$). Such species have been proposed as intermediates in the cyclopropanation of allylic alcohols[11] and in the generation of the SmI_2 from samarium metal and diiodomethane.[22] Our experimental results can be explained using a model similar to the staggered model previously proposed by Houk and co-workers for the addition of carbenoids to olefins,[23] and which was also utilized to explain the cyclopropanation of allylic alcohols (Scheme 1).[11] Tentatively, we propose a transition-state model **A** (similar to the Houk model), in which the coordination of the divalent samarium atom with the oxygen atom of the amide group provides the obtained cyclopropylamide **2**, whilst maintaining the geometry about the C=C bond. Another view of the same transition state is shown in **B**. Indirect support for this mechanism is the non-cyclopropanation of α,β-unsaturated esters, because of the decreased ability of the oxygen atom of the carbonyl group in esters relative to that in amides to coordinate with the Sm^{II} center.

In conclusion, an easy, rapid, and general cyclopropanation of α,β-unsaturated amides with complete stereospecificity by using samarium/diiodomethane has been developed. This cyclopropanation reaction is achieved from α,β-unsaturated amides in which the C=C bond is di-, tri-, or tetrasubstituted. Studies designed to prepare enantiopure cyclopropylcarboxamides are currently in progress.

Experimental Section

To a suspension of Sm (1.4 mmol) in THF (15 mL) was added the α,β-unsaturated amide **1** (0.4 mmol) in THF (2 mL) and diiodomethane (1.4 mmol) at 0 °C. After stirring at room temperature for 2 h the reaction mixture was quenched by the addition of 0.1 M aqueous HCl (5 mL). Standard workup afforded the crude cyclopropanecarboxamides **2**, which were purified by flash column chromatography on silica gel (hexane/EtOAc 5:1).

Received: January 21, 2002 [Z 18547]

[1] a) "Biochemistry of the Cyclopropyl Group": H. W. Liu, C. T. Walsh in *The Chemistry of the Cyclopropyl Group* (Eds.: S. Patai, Z. Rappoport), Wiley, New York, **1987**, chap. 16, pp. 959–1025; b) R. Faust, *Angew. Chem.* **2001**, *113*, 2312–2314; *Angew. Chem. Int. Ed.* **2001**, *40*, 2251–2253; c) W. A. Donaldson, *Tetrahedron* **2001**, *57*, 8589–8627; d) J. Salaün, *Top. Curr. Chem.* **2000**, *207*, 1–67.

[2] a) G. Maier, S. Senger, *Angew. Chem.* **1994**, *106*, 605–606; *Angew. Chem. Int. Ed. Engl.* **1994**, *33*, 558–559; b) L. Dechoux, E. Doris, *Tetrahedron Lett.* **1994**, *35*, 2017–2020; c) R. B. Silverman, Y. Zelechonok, *J. Org. Chem.* **1992**, *57*, 6373–6374.

[3] "Carbocyclic Three- and Four-Membered Ring Systems": *Methods of Organic Chemistry (Houben-Weyl) 4th ed. 1952–, Vol. E* **1997**, p. 17a–f.

[4] For some reviews, see: a) "Preparation of Cyclopropyl Derivatives": T. Tsuji, S. Nishida in *The Chemistry of the Cyclopropyl Group* (Eds.: S. Patai, Z. Rappoport), Wiley, New York, **1987**, pp. 308–373; b) J. Salaün, *Chem. Rev.* **1989**, *89*, 1247–1270.

[5] a) T. Morikawa, H. Sasaki, R. Hanai, A. Shibuya, T. Taguchi, *J. Org. Chem.* **1994**, *59*, 97–103; b) A. B. Charette, J. F. Marcoux, *Synlett* **1995**, 1197–1207; c) A. B. Charette, J. F. Marcoux, *J. Am. Chem. Soc.* **1996**, *118*, 4539–4549.

[6] a) R. Paulissen, A. J. Hubert, P. Teyssie, *Tetrahedron Lett.* **1972**, *13*, 1465–1468; b) M. Suda, *Synthesis* **1981**, 714–714; c) J. E. A. Luithle, J. Pietruszka, *J. Org. Chem.* **1999**, *64*, 8287–8297.

[7] M. P. Doyle, M. A. McKervey, T. Ye, *Modern Catalytic Methods for Organic Synthesis with Diazo Compounds*, Wiley, New York, **1998**, pp. 163–288.

[8] A. H. Li, L. X. Dai, V. K. Aggarwal, *Chem. Rev.* **1997**, *97*, 2341–2372.

[9] E. V. Dehmlow, K. Eulenberg, *Liebigs Ann. Chem.* **1978**, 1112–1115.

[10] For recent reports on the cyclopropanation of α,β-unsaturated amides see: a) S. Goumri-Magnet, T. Kato, H. Gornitzka, A. Baceiredo, G. Bertrand, *J. Am. Chem. Soc.* **2000**, *122*, 4464–4470; b) S. Ye, L. Yuan, Z. Z. Huang, Y. Tang, L. X. Dai, *J. Org. Chem.* **2000**, *65*, 6257–6260; c) A. Mamai, J. S. Madalengoitia, *Tetrahedron Lett.* **2000**, *41*, 9009–9014.

 © WILEY-VCH Verlag GmbH, 69451 Weinheim, Germany, 2002 1433-7851/02/4111-1918 $ 20.00+.50/0

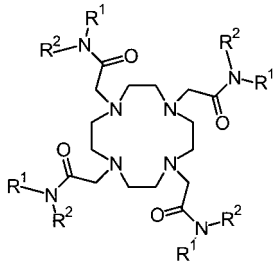
[11] a) G. A. Molander, J. B. Etter, *J. Org. Chem.* **1987**, *52*, 3942 – 3944; b) G. A. Molander, L. S. Harring, *J. Org. Chem.* **1989**, *54*, 3525 – 3532.
[12] T. Imamoto, N. Takiyama, *Tetrahedron Lett.* **1987**, *28*, 1307 – 1308.
[13] Previously, it was indicated that the cyclopropanation promoted by samarium carbenoids takes place exclusively with allylic alcohols, and other functionalized olefinic substrates are inert (see ref. [11b]).
[14] J. M. Concellón, P. L. Bernad, J. A. Pérez-Andrés, *Angew. Chem.* **1999**, *111*, 2528 – 2530; *Angew. Chem. Int. Ed.* **1999**, *38*, 2384 – 2386.
[15] J. M. Concellón, J. A. Pérez-Andrés, H. Rodríguez-Solla, *Angew. Chem.* **2000**, *112*, 2866 – 2868; *Angew. Chem. Int. Ed.* **2000**, *39*, 2773 – 2775.
[16] J. M. Concellón, J. A. Pérez-Andrés, H. Rodríguez-Solla, *Chem. Eur. J.* **2001**, *7*, 3062 – 3068.
[17] J. M. Concellón, P. L. Bernad, H. Rodríguez-Solla, *Angew. Chem.* **2001**, *113*, 4015 – 4017; *Angew. Chem. Int. Ed.* **2001**, *40*, 3897 – 3899.
[18] J. M. Concellón, P. L. Bernad, E. Bardales, *Org. Lett.* **2001**, *3*, 937 – 939.
[19] The product of double cyclopropanation was obtained in 2% yield (GC-MS).
[20] "Nuclear Magnetic Resonance and Infrared Spectra of Cyclopropanes and Cyclopropenes": D. G. Morris in *The Chemistry of the Cyclopropyl Group* (Eds.: S. Patai, Z. Rappoport), Wiley, New York, **1987**, chap. 3, pp. 101 – 172.
[21] When the reaction time is increased, the yield of some Simmon – Smith cyclopropanations decrease: C. D. Poulter, E. C. Fiedrich, S. Winstein, *J. Am. Chem. Soc.* **1969**, *91*, 6892 – 6894.
[22] a) J. L. Namy, P. E. Caro, P. Girard, H. B. Kagan, *Nouv. J. Chim.* **1981**, *5*, 479 – 484; b) T. Imamoto, H. Koto, T. Takeyama, *Tetrahedron Lett.* **1986**, *27*, 3243 – 3246; c) T. Tabuchi, J. Inanaga, M. Yamaguchi, *Tetrahedron Lett.* **1986**, *27*, 3891 – 3894.
[23] a) M. N. Paddon-Row, N. G. Rondan, K. N. Houk, *J. Am. Chem. Soc.* **1982**, *104*, 7162 – 7166; b) J. Mareda, N. G. Rondan, K. N. Houk, *J. Am. Chem. Soc.* **1983**, *105*, 6997 – 6999.

The Amide Protons of an Ytterbium(III) dota Tetraamide Complex Act as Efficient Antennae for Transfer of Magnetization to Bulk Water**

Shanrong Zhang, Lydie Michaudet, Shawn Burgess, and A. Dean Sherry*

Current diagnostic contrast agents (CAs) for magnetic resonance imaging (MRI) are largely based on paramagnetic gadolinium complexes that shorten the relaxation time of bulk-water protons in tissue by rapid exchange of at least one gadolinium-bound inner sphere water molecule with bulk solvent.[1] Recently, Balaban et al.[2] demonstrated that image contrast can be altered by applying a frequency-selective RF pulse at the resonance frequency of an NH or OH group of an intrinsic amino acid, sugar, nucleotide, or other metabolite prior to collection of the imaging data. An advantage of a chemical exchange saturation transfer (CEST) agent over a paramagnetic relaxation agent is that image contrast can be switched on and off at will. A disadvantage is that the amount of CEST agent required to produce significant water contrast is unrealistically high,[3] although a later report demonstrated that the CEST effect can be amplified considerably by using polymers that contain a large number of amide NH groups.[4] As the chemical shifts of diamagnetic NH or OH protons are typically within 5 ppm of that of bulk water, it may ultimately prove difficult to avoid off-resonance direct saturation of the bulk-water signal or indirect saturation via water tightly bound to tissue macromolecules. The latter effect provides the basis of magnetization-transfer (MT) imaging.[5]

We recently reported that the weakly paramagnetic complex $[Eu(\mathbf{2})]^{3+}$, which has a bound-water signal near $\delta =$ 50 ppm with an exchange lifetime of $\tau_M^{298} \approx 350$ μs, acts as an MT contrast agent.[6] Aime et al.[7] also demonstrated that the MT effect can be used to measure pH by using two different exchange sites (OH in $[Eu(\mathbf{3})]^-$ and NH in $[Yb(\mathbf{3})]^-$) to eliminate the concentration dependence. Although paramagnetic systems offer the advantage over diamagnetic systems of having exchangeable protons that are shifted well away from the bulk-water signal,[2, 3] they suffer from a similar lack of sensitivity. One way to increase the sensitivity of a paramagnetic MT agent and thereby make it more practical would be to increase the number of exchangeable protons[4] at a hyperfine-shifted site. Here the Yb^{3+} complex of 1,4,7,10-tetraazacyclododecane-1,4,7,10-tetraacetamide (**1**), which has eight exchangeable, hyperfine-shifted amide protons, is reported as a prototype high-sensitivity MT agent. The eight amide protons of this complex should in principle allow a fourfold reduction in concentration compared to an agent with a single exchangeable bound water molecule.[8]



$R^1 = H_a$, $R^2 = H_b$ **1**
$R^1 = H$, $R^2 = CH_2COOEt$ **2**
$R^1 = H$, $R^2 = CH_2COO^-$ **3**

A crystal of $[Yb(\mathbf{1})(H_2O)](CF_3SO_3^-)_3 \cdot 4H_2O$ was grown from water at room temperature and studied by X-ray diffraction at 153 K (Figure 1).[9] The geometry around the Yb^{3+} ion is a typical square antiprism with average N-C-C-N and N-C-C-O torsion angles of 58.3 and $-22.5°$, respectively. The Yb^{3+} ion is nine-coordinate with average macrocyclic Yb–N and Yb–O bond lengths of 2.608 and 2.301 Å, respectively, and a Yb^{3+}–O_{water} distance of 2.335 Å. The Yb^{3+} – macrocyclic ligand distances are similar to those

[*] Prof. A. D. Sherry, Dr. S. Zhang, Dr. L. Michaudet
Department of Chemistry, University of Texas at Dallas
PO Box 830688, Richardson, TX 75083 (USA)
Fax: (+1) 972-883-2925
E-mail: sherry@utdallas.edu
Prof. A. D. Sherry, Dr. S. Burgess
Department of Radiology, Rogers Magnetic Resonance Center
5801 Forest Park Road, Dallas, TX 75235 (USA)

[**] This work was supported in part by grants from the Robert A. Welch Foundation (AT-584), the National Institutes of Health (CA-84697), and the Division of Research Resources, National Institutes of Health (RR-02584). We thank Professor Silvio Aime for providing a copy of his manuscript prior to publication.

Supporting information for this article is available on the WWW under http://www.angewandte.com or from the author.

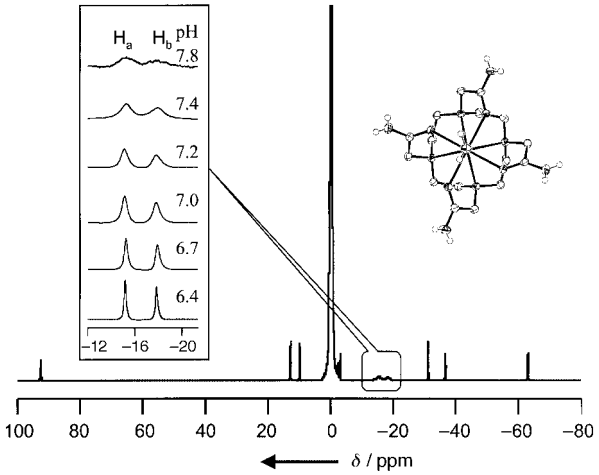


Figure 1. 500 MHz ^{1}H NMR spectrum of a 30 mM aqueous solution of $[Yb(\mathbf{1})]^{3+}$ at pH 7.4 and 25 °C ($\delta_{bulk\,water} = 0$ ppm). The inset shows the signals of H_a and H_b as a function of pH. A top view of the crystal structure of $[Yb(\mathbf{1})]^{3+}$ is also shown. For clarity, four additional water molecules and three triflate anions are omitted.

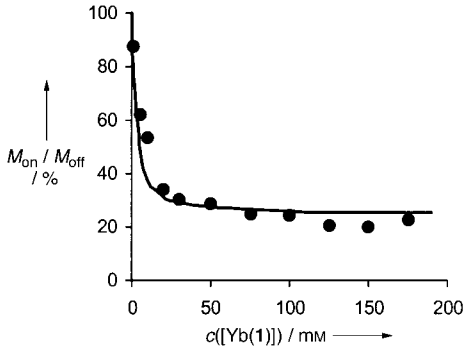


Figure 2. A plot of M_{on}/M_{off} versus concentration of $[Yb(\mathbf{1})]^{3+}$ at 25 °C and pH 7.4. The solid line through the data represents the fit to Equation (1) (see also text). Data were obtained with a Varian Inova-300 NMR spectrometer by simultaneous saturation of both amide protons with a modified water-elimination technique (wet1d pulse sequence, see Varian User Manual). Loops were added to the shaped pulse train (90° e-burp1, typically repeated 0–500 times) at a frequency offset corresponding to the chemical shift of the amide protons to yield a 1500 Hz square bandwidth (pwwet = 3.0 ms and wetpwr = 28 db).

reported for another Yb^{3+} tetraamide complex ($\langle Yb{-}N\rangle$ 2.62 Å and $\langle Yb{-}O\rangle$ 2.28 Å) while the $Yb{-}O_{water}$ distance is significantly shorter ($Yb{-}O_{water}$ 2.44 Å).[10] The high-resolution ^{1}H NMR spectrum of $[Yb(\mathbf{1})]^{3+}$ in solution at pH 7.4 and 25 °C (Figure 1) is consistent with its solid-state structure (see Supporting Information). The spectrum is dominated by one axially symmetric coordination isomer[11] with two magnetically nonequivalent amide protons on each NH_2 group, which appear as two broad peaks at $\delta = -14.5$ and -17.7 ppm. The inset illustrates the different sensitivity of the amide proton linewidths to pH.

Table 1 summarizes the lifetimes τ_M^{298}, as determined by fitting the linewidths at each temperature to standard exchange theory. Interestingly, the exchange lifetimes of the amide protons differed only slightly ($\tau_M^{298}(H_a) \approx 1.3\,\tau_M^{298}(H_b)$). Table 1 shows that both sites meet the slow-exchange condition, $\Delta\omega\,\tau_M^{298} > 1$, at all pH values and should therefore act as efficient antennae for transferring magnetization to bulk water.

Table 1. Amide proton lifetimes τ_M^{298} versus pH for $[Yb(\mathbf{1})]^{3+}$. Experimental values of $\Delta\omega\,\tau_M$ at 7.05 T are also listed.

pH	τ_M^{298} [ms]		$\Delta\omega\,\tau_M^{298}$	
	H_a	H_b	H_a	H_b
6.46	5.00	4.00	139.3	133.7
6.76	2.30	1.78	64.1	59.5
7.06	1.21	0.82	33.6	27.2
7.21	0.92	0.72	25.5	24.2
7.43	0.64	0.52	17.9	17.4
7.84	0.57	0.44	15.9	14.7

A plot of M_{on}/M_{off} (simultaneous saturation at both NH sites) versus concentration at pH 7.4 and 25 °C is shown in Figure 2. Bulk-water magnetization in the presence (M_{on}) or absence (M_{off}) of selective RF irradiation at an exchange site is given by Equation (1),[12] where k_{obs} is the pseudo-first-order

$$\frac{M_{on}}{M_{off}} \approx \left(\frac{1}{1 + k_{obs}\,T_{1sat}}\right) \qquad (1)$$

exchange rate (n[CA]/(110 τ_M^{NH}), where n is the number of exchanging sites),[13] and T_{1sat} is the spin-lattice relaxation time of the bulk-water protons during saturation of the exchanging NH protons; T_{1sat} also depends on the concentration of paramagnetic agent and the exchange lifetime of the amide proton(s) being saturated. If one makes the simplifying assumption that $T_{1sat}^{-1} \approx T_{1obs}^{-1} = r_1[CA] + T_{1dia}^{-1}$ (where r_1 is the water relaxivity ($mM^{-1}s^{-1}$) of $[Yb(\mathbf{1})]^{3+}$ and T_{1dia} is the spin-lattice relaxation time of water in the absence of $[Yb(\mathbf{1})]^{3+}$), then it is easy to show that M_{on}/M_{off} becomes independent of [CA] at high concentrations. This indicates that M_{on}/M_{off} will be dominated by three parameters: the number of exchangeable sites n, the exchange lifetime τ_M, and the paramagnetic relaxivity r_1 when $r_1[CA] \gg T_{1dia}^{-1}$. This is experimentally shown in Figure 2: M_{on}/M_{off} is sensitive to the concentration of $[Yb(\mathbf{1})]^{3+}$ below about 30 mM but nearly independent of concentration above about 50 mM. Fitting this theory to the data of Figure 2 gave $r_1 = 0.04\ mM^{-1}s^{-1}$, $T_{1dia} = 3.0$ s, and $\tau_M^{NH} = 0.58$ ms, with an agreement factor of 0.90. The low r_1 value is consistent with Yb^{3+} having a much lower magnetic moment than Gd^{3+}. The fitted value of τ_M^{NH} is identical to the average value of τ_M^{NH} for the two H_a and H_b sites determined by variable-temperature NMR spectroscopy (Table 1) and similar to those estimated for $[Eu(\mathbf{3})]^{3+}$ ($\tau_M^{NH} \approx 0.1-10$ ms in the pH range 3–9 at 25 °C (unpublished data)) and for other $[Ln(\mathbf{3})]^-$ complexes ($\tau_M^{NH} \approx 0.29-0.40$ ms at 37 °C and pH 8.1, $Ln^{3+} = Ho^{3+}$, Er^{3+}, Tm^{3+}, and Yb^{3+}).[7]

The pH dependence of M_{on}/M_{off} with selective presaturation of either H_a, H_b, or both is shown in Figure 3 for 30 mM $[Yb(\mathbf{1})]^{3+}$. At the minimum of these curves, about 52 and 42% of the bulk-water signal was eliminated upon saturation of H_a or H_b alone, respectively, while about 70% was eliminated upon simultaneous saturation of both NH groups. This compares to about 13 and 38% decrease in the bulk-water signal with 1 and 5 mM $[Yb(\mathbf{1})]^{3+}$, respectively (Figure 2). Large MT effects have been reported for macromolecules: about 43% saturation of bulk water was achieved with 0.1 mM poly-L-lysine (corresponds to 467 mM of NH groups) and 51%

 © WILEY-VCH Verlag GmbH, 69451 Weinheim, Germany, 2002 1433-7851/02/4111-1920 $ 20.00+.50/0

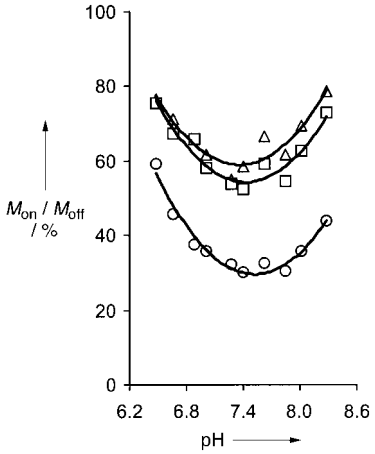


Figure 3. A plot of M_{on}/M_{off} versus pH for $[Yb(\mathbf{1})]^{3+}$ at 30 mM and 25 °C. Data were obtained on the same instrument (see Figure 2 caption), by using a RF bandwidth of 600 Hz for saturating H_a or H_b (pwwet = 7.5 ms and wetpwr = 20 db) and 1500 Hz for saturating both simultaneously. The symbols □, △, and ○ represent data points for saturating H_a, H_b, or both, respectively.

with 1 mM PAPAM dendrimer (256 mM of NH groups),[4] but $[Yb(\mathbf{1})]^{3+}$ appears to exhibit even more efficient MT simply on the basis of these concentration comparisons. The shape of the curves of Figure 3 reflects the sensitivity of the MT effect to proton exchange. This, in combination with the τ_M^{298} values of Table 1, leads to the conclusion that $\Delta\omega\tau_M$ values in the range 15–18 are optimal for this system. To check the general validity of this value, we also measured the pH dependence of τ_M^{298} and M_{on}/M_{off} for $[Eu(\mathbf{3})]^-$, a complex with monosubstituted amido groups containing only four NH protons, with a chemical shift of $\delta = -6$ ppm. Here again, we found that $\Delta\omega\tau_M \approx 15$ was optimal (Figure 4). This was further confirmed by saturating the resonance of the Eu^{3+}-bound water in $[Eu(\mathbf{3})]^-$ at 4.7 T.[14]

In summary, the eight exchangeable amide protons in $[Yb(\mathbf{1})]^{3+}$ appear as two magnetically inequivalent signals at $\delta = -14.5$ and -17.7 ppm. These could be saturated by using selective RF pulses, either separately or simultaneously, to yield an easily measurable MT effect at concentrations similar to that used for other clinical MRI contrast agents. Most importantly, this study revealed in two different paramagnetic complexes, $[Yb(\mathbf{1})]^{3+}$ and $[Eu(\mathbf{3})]^-$, with similar τ_M^{NH} but different $\Delta\omega$ values optimal MT efficiency for $\Delta\omega\tau_M$ values near 15. This provides a useful guideline for developing even more efficient MT agents.

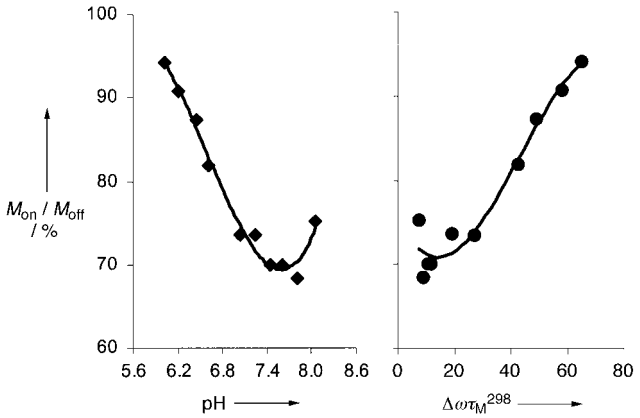


Figure 4. A plot of M_{on}/M_{off} versus pH (left) and versus $\Delta\omega\tau_M^{298}$ (right) for $[Eu(\mathbf{3})]^-$ at 30 mM and 25 °C. Data were obtained on the same instrument (see Figure 2 caption) by using a RF irradiation (with a bandwidth of 300 Hz, pwwet = 15 ms and wetpwr = 16 db) centered at the resonance of four amide protons (single peak at $\delta \approx -6$ ppm). A low saturation power was used to avoid any direct off-resonance saturation.

Received: December 4, 2001 [Z18316]

[1] R. B. Lauffer, *Chem. Rev.* **1987**, *87*, 901–927; b) S. H. Koenig, R. D. Brown III, *Prog. Nucl. Magn. Reson. Spectrosc.* **1990**, *22*, 487–567; c) J. A. Peters, J. Huskens, D. J. Raber, *Prog. Nucl. Magn. Reson. Spectrosc.* **1996**, *28*, 283–350; d) S. Aime, M. Botta, M. Fasano, E. Terreno, *Chem. Soc. Rev.* **1998**, *27*, 19–29; e) P. Caravan, J. J. Ellison, T. J. McMurry, R. B. Lauffer, *Chem. Rev.* **1999**, *99*, 2293–2352.

[2] K. M. Ward, A. H. Aletas, R. S. Balaban, *J. Magn. Reson.* **2000**, *143*, 79–87.

[3] K. M. Ward, R. S. Balaban, *Magn. Reson. Med.* **2000**, *44*, 799–802.

[4] N. Goffeney, J. W. M. Bulte, J. Duyn, L. H. Bryant, Jr., P. C. M. van Zijl, *J. Am. Chem. Soc.* **2001**, *123*, 8628–8629.

[5] R. M. Henkelman, G. J. Stanisz, S. J. Graham, *NMR Biomed.* **2001**, *14*, 57–64.

[6] S. Zhang, P. Winter, K. Wu, A. D. Sherry, *J. Am. Chem. Soc.* **2001**, *123*, 1517–1518; b) A. D. Sherry, S. Zhang, *J. Inorg. Biochem.* **2001**, *86*, 98.

[7] E. Terreno, S. Aime, A. Barge, D. D. Castelli, F. U. Nielsen, *J. Inorg. Biochem.* **2001**, *86*, 452; b) S. Aime, A. Barge, D. D. Castelli, F. Fedeli, A. Mortillaro, F. U. Nielsen, E. Terreno, *Magn. Reson. Med.* **2002**, *47*, 639–648.

[8] $[Eu(\mathbf{2})]^{3+}$ has four exchangeable amide protons but the chemical shift of those protons (−5 ppm upfield of bulk water) offers no advantage over diamagnetic agents.

[9] X-ray data for $[Yb(C_{16}H_{32}H_8O_4)(H_2O)](CF_3SO_3^-)_3 \cdot 4H_2O$: $M = 1110.83$, triclinic, space group $P\bar{1}$, $\rho_{calcd} = 1.879\ Mg\,m^{-3}$, $Z = 2$, $a = 12.8780(2)$, $b = 12.9861(3)$, $c = 13.0747(3)$ Å, $\alpha = 86.483(1)$, $\beta = 64.549(1)$, $\gamma = 84.192(1)°$, $V = 1963.83(7)$ Å^3, $T = 153$ K. Large, colorless prisms grew by slow evaporation of an aqueous solution of the complex. The crystal was cut from a larger crystal and had approximate dimensions $1.4 \times 0.4 \times 0.24$ mm. The data were collected on a Nonius Kappa CCD diffractometer with a graphite monochromator with $Mo_{K\alpha}$ radiation ($\lambda = 0.71073$ Å). The structure was solved by direct methods by using SIR92 and refined by full-matrix least-squares methods on F^2 with anisotropic displacement parameters for the non-hydrogen atoms by using SHELXL-97. The hydrogen atoms on carbon atoms were calculated in ideal positions with displacement parameters set to $1.2\,U_{eq}$ of the attached atom. The hydrogen atoms bound to the amide nitrogen atoms were located in a ΔF map and refined with isotropic displacement parameters. The hydrogen atoms of the water molecules were also located in a ΔF map. Final residual $wR2 = 0.0760$ for all data and $R1 = 0.0326$. CCDC-175397 contains the supplementary crystallographic data for this paper. These data can be obtained free of charge via www.ccdc.cam.ac.uk/conts/retrieving.html (or from the Cambridge Crystallographic Data Centre, 12, Union Road, Cambridge CB2 1EZ, UK; fax: (+44) 1223-336-033; or deposit @ccdc.cam.ac.uk).

[10] A. S. Batsanov, A. Beeby, J. I. Bruce, J. A. K. Howard, A. M. Kenwright, D. Parker, *Chem. Commun.* **1999**, 1011–1012.

[11] $[Eu(\mathbf{1})]^{3+}$ consists of two isomers with a ratio of 4.5 between the square antiprism and the twisted square antiprism. F. A. Dunand, S. Aime, A. E. Merbach, *J. Am. Chem. Soc.* **2000**, *122*, 1506–1512.

[12] S. Forsén, R. A. Hoffman, *J. Chem. Phys.* **1963**, *39*, 2892–2901; b) S. Forsén, R. A. Hoffman, *J. Chem. Phys.* **1964**, *40*, 1189–1196.

[13] R. A. Dwek, *Nuclear Magnetic Resonance (NMR) in Biochemistry*, Oxford University Press, London, **1973**.

[14] S. Zhang, A. D. Sherry in *Proceedings of the International Society for Magnetic Resonance in Medicine, 10th Scientific Meeting and Exhibition* (Hawaii, **2002**), p. 2590.

Crystal Structure of $K_2[C_2O_6]$—First Proof of Existence and Constitution of a Peroxodicarbonate Ion**

Robert E. Dinnebier, Sascha Vensky,
Peter W. Stephens, and Martin Jansen*

The characteristics of homonuclear bonds between second-row elements are predominantly determined by the strong π overlap of 2p-type wave functions. These interactions can, on one hand, cause considerable strengthening through multiple bond formation, and on the other, weakening of the bonds through lone pair/lone pair repulsion, as soon as the number of p electrons involved per atom exceeds three. The general trend is significantly modulated by the nature of the substituents and the conformation across the homonuclear bond. Those substituents lacking lone pairs and exhibiting high electronegativities appear to reinforce the X–X homonuclear single bonds, by increasing the s contribution to the sigma bond, and by removing electron density from the repulsive lone pairs. This is immediately evident upon comparing the O–O bond lengths in O_2F_2, $O_2(SiMe_3)_2$, and O_2^{2-} (in K_2O_2) which cover the impressively wide range from 122 to 150 and 154 pm.[1] Fully in line with these considerations, among the known diperoxo anions, peroxodisulfate is more stable than peroxodiphosphate, and similar anions of Group 14 elements, such as peroxodisilicate, are not known at all.[2] Since their discovery in the 19th century, percarbonates have been studied repeatedly, in order to reveal constitutions and bonding properties, and to inspect their potential for application as bleaching agents in the detergent industry.[3] In spite of these efforts, the extent of reliable insights has remained limited.[4] Major problems arise from the fact that peroxide functions in the structures can also originate from hydrogen peroxide of crystallization,[6] and because of the thermal lability preventing complete removal of water by drying. It has been shown recently by single-crystal X-ray structure analysis that $KHCO_4 \cdot H_2O_2$, and the respective rubidium compound, unambiguously constitute hydrogen-monoperoxocarbonates.[7] For a peroxodicarbonate, however, conclusive evidence for its constitution,[8] and even existence, has been lacking. Therefore we have reinvestigated a material with the bulk composition of $K_2C_2O_6$ which, according to vibrational spectroscopy,[3e] contains peroxide functions. By means of a crystal structure determination using high-resolution X-ray powder diffraction data (Figure 1) we show that this compound is free of water and hydrogen peroxide of crystallization, and contains the fully deprotonated peroxodicarbonate anion.[9]

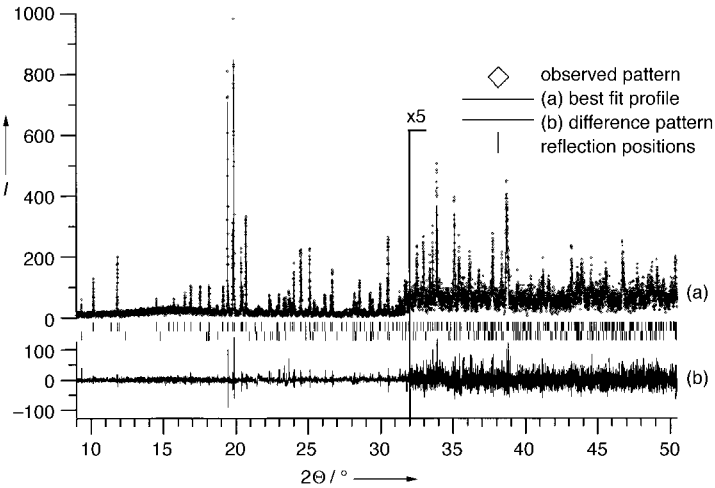


Figure 1. Scattered X-ray intensity for potassium peroxodicarbonate at $T = -123\,^{\circ}C$ as a function of diffraction angle 2Θ. Shown are the observed pattern (diamonds), the best Rietveld-fit profile in $P2_1/c$ (line a), the difference curve between observed and calculated profile (line b), and the reflection markers (vertical bars). The wavelength was $\lambda = 1.12074(2)$ Å. The higher angle part starting at $2\Theta = 32^{\circ}$ is enlarged by a factor of 5.

Potassium peroxodicarbonate was synthesized electrochemically from a saturated aqueous solution of K_2CO_3 at $T = -20\,^{\circ}C$. The samples as obtained are microcrystalline and white, with a faint sky blue color. We have been able to prepare single-phase material; however, most charges contain small amounts of $KHCO_3$, the first decomposition product of $K_2C_2O_6$ in an aqueous environment, as an impurity.

The peroxodicarbonate anion (Figure 2) consists of two carbonate groups that are connected through two of its oxygen atoms to form a peroxo group. The molecular symmetry was found to be C_2 within the limits of experimental error.[13] The carbon atoms are surrounded by oxygen atoms in a near trigonal-planar arrangement and in general, the

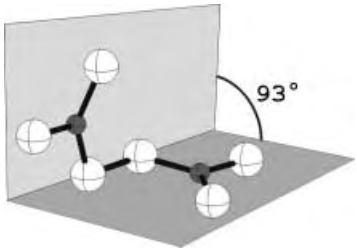


Figure 2. Conformation of the peroxodicabonate anion as found in $K_2C_2O_6$ at $T = -123\,^{\circ}C$. The torsion angle between the two carbonate groups is given.

[*] Prof. Dr. M. Jansen, Priv.-Doz. Dr. R. E. Dinnebier,
Dipl.-Chem. S. Vensky
Max-Planck-Institute for Solid-State Research
Heisenbergstrasse 1, 70569 Stuttgart (Germany)
Fax: (+49) 711-689-1502
E-mail: m.jansen@fkf.mpg.de

Prof. Dr. P. W. Stephens
Department of Physics and Astronomy
State University of New York
Stony Brook, NY 11974-3800 (USA)

[**] This work was supported by the Deutsche Forschungsgemeinschaft (DFG) and the Fonds der Chemischen Industrie. Research was carried out in part at the National Synchrotron Light Source at Brookhaven National Laboratory, which is supported by the U.S. Department of Energy, Division of Materials Sciences and Division of Chemical Sciences. The SUNY X3 beamline at NSLS is supported by the Division of Basic Energy Sciences of the US Department of Energy under Grant No. DE-FG02-86ER45231. Work at Stony Brook was partially supported by the National Science Foundation. We thank Michael Knapp from beamline B2 (Hasylab) for the measurements at Hasylab.

 © WILEY-VCH Verlag GmbH, 69451 Weinheim, Germany, 2002 1433-7851/02/4111-1922 $ 20.00+.50/0

intramolecular bond lengths and angles of the carbonate group are within the typical range found for this class of molecules (Table 1). Remarkably, the bond length between the carbon atom and the peroxo-oxygen atom is only 3% longer than the lengths of the terminal C–O bonds. Therefore, this bond contains some degree of double-bond character. The deviations from planarity for the carbonate groups including the second peroxo-oxygen atom are below the precision of the measurement. The O–O bond length in the peroxo group (147(1) pm) is virtually the same as for the related peroxomonohydrogencarbonate anion (146 pm).[7] The C-O-O-C dihedral angle of 93(1)° corresponds to that for dicyclohexylperoxodicarbonate (90°)[15c] and for solid H_2O_2 (93°).[15a] According to the experimental findings (short bonds, planarity of $OOCO_2$ moiety) the C–O(peroxo) bonds show double-bond character and the peroxo-oxygen atoms can be regarded as sp^2 hybridized which leads to an occupied p_z orbital orthogonal to the O_2C–OO plane. The strong repulsion of these orbitals across the O–O bond favors the staggered conformation of O_2C-O-O-CO_2.

Table 1. Selected bond lengths [pm] and torsion angles [°] for $K_2C_2O_6$ and related molecules.

Substance	Ref.	d(O–O)	d(K–O)	d(C–O)	d(C–O_O)	C-O-O-C
$K_2C_2O_6$		147(1)	263(1) – 290(1)	126(2) – 129(2)	131(1)	93(1)
$KHCO_4 \cdot H_2O_2$	[7a]	146	275 – 283	123 – 125	138	101_{COOH}
H_2O_2	[15a]	146	–	–	–	93_{HOOH}
K_2CO_3	[15b]	–	264 – 286	127 – 129	–	–
$(C_6H_{11})_2C_2O_6$	[15c]	143	–	118 – 132	138	90

There are two inequivalent potassium sites, but every potassium ion is coordinated to seven oxygen atoms, forming irregular KO_7 polyhedra (Figure 3). The polyhedra can be described as strongly distorted trigonal prisms with an additional oxygen atom above one of the rectangular faces, which forms a long bond to the central cation. The bond lengths between the potassium atoms and the oxygen atoms are in the range 2.63 to 2.9 Å, comparable to that of related compounds (Table 1). The potassium ions are connected to seven oxygen atoms of five different peroxodicarbonate dianions. In the case of the $K(1)O_7$ polyhedron, one edge is equivalent to a peroxo bridge, whereas in the case of the $K(2)O_7$ polyhedron, one edge is equivalent to the triangular edge of a carbonate group. In both cases another peroxodicarbonate group is side-on coordinated (carbonate- and peroxo-oxygen atoms).

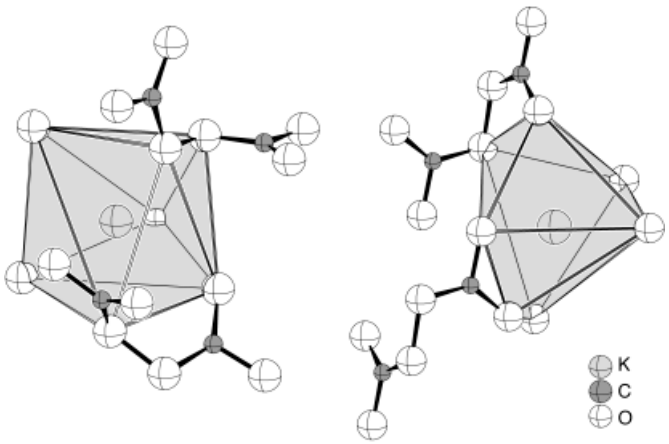


Figure 3. Representation of the two crystallographically distinct KO_7 coordination polyhedra and specially connected peroxodicarbonate groups of potassium peroxodicarbonate at $T = -123$ °C. The other oxygen atoms are carbonate-oxygen atoms of end-on coordinated peroxodicarbonate groups.

The crystal structure of $K_2[C_2O_6]$ is based on a three-dimensional framework of KO_7 polyhedra, interconnected by carbonate groups. For a better understanding, if only the central carbon atoms of the carbonate groups are considered, the crystal structure of $K_2C_2O_6$ can be viewed as a strongly distorted NaCl arrangement with mean KC_6 and CK_6 distances of 350(20) pm (Figure 4).

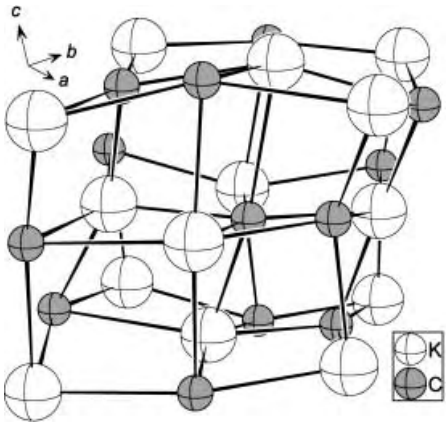


Figure 4. Packing scheme of $K_2C_2O_6$ at $T = -123$ °C in a view perpendicular to the plane spanned by the c axis and the median of a and b axes. The structural relationship to the NaCl type of structure is clearly visible.

Application of peroxodicarbonate as a bleaching component in detergents would liberate harmless carbon dioxide and potassium, besides the desired active oxygen, and would help to maintain favorable pH conditions. Also the onset of rapid decomposition occurs at an appreciably high temperature of 141 °C. Nevertheless all prospects for application in the detergent industry seem to be hindered by its reduced stability during long-term storage.

Experimental Section

$K_2C_2O_6$ was synthesized by anodic oxidation of a saturated aqueous solution of potassium carbonate (p.a., Merck) at $T = -20$ °C. The electrocrystallization was carried out under galvanostatic conditions ($I = 250$ mA, $U > 16$ V) with a potentiostat (EG&G Princeton Applied Research, Type 363). A Pt wire ($\varnothing = 0.5$ mm, $l = 40$ mm) was used as an anode, a Pt mesh ($\varnothing_{cyl.} = 40$ mm, $h = 50$ mm, 20 mesh) as cathode. The anodic part was separated by a glassy membrane. Potassium peroxodicarbonate, obtained as a microcrystalline, light blue powder, was filtered and washed with ethanol and diethyl ether. The peroxide content was determined iodometrically.[16] $K_2C_2O_6$ decomposes rather slowly when stored below -20 °C for several weeks (8% per week).

According to the results of thermal analysis (DTA/TG/MS; Metzsch STA 429; 20 °C – 800 °C; 2 °C min^{-1}) and in agreement with previous experiments,[3e] $K_2C_2O_6$ decomposes at 141 °C by generation of oxygen and carbon dioxide.

Received: January 28, 2002 [Z 18360]

[1] a) J. J. Turner, *Endeavour* **1968**, *27*, 42 – 47; b) D. Königstein, M. Jansen, *Monatsh. Chem.* **1996**, *127*, 1221 – 1227; c) T. Bremm, M. Jansen, *Z. Anorg. Allg. Chem.* **1992**, *610*, 64 – 66.
[2] a) D. Y. Naumov, A. V. Virovets, N. V. Podberezskaya, P. B. Novikov, A. A. Politov, *J. Struct. Chem.* **1997**, *38*, 772 – 778; b) W. P. Griffith, R. D. Powell, A. C. Skapski, *Polyhedron* **1988**, *7*, 1305 – 1310.
[3] a) E. J. Constam, A. von Hansen, *Z. Elektrochem.* **1896**, *7*, 137 – 144; b) A. von Hansen, *Z. Elektrochem.* **1896**, *7*, 445 – 448; c) A. K. Melnikov, T. P. Firsova, A. N. Molodkina, *Russ. J. Inorg. Chem.* **1962**, *7*, 637 – 640; d) P. A. Giguère, D. Lemaire, *Can. J. Chem.* **1972**, *50*, 1472 – 1477; e) D. P. Jones, W. P. Griffith, *J. Chem. Soc. Dalton Trans.* **1980**, 2526 – 2532.
[4] Early X-ray powder diffraction erperiments have been reported, which failed to find the correct unit cell and X-ray density.[5]
[5] V. I. Sokol, V. M. Bakulina, E. Y. Filatov, T. P. Firsova, *Russ. J. Inorg. Chem.* **1968**, *13*, 1211 – 1212.
[6] a) E. H. Riesenfeld, B. Reinhold, *Ber. Dtsch. Chem. Ges.* **1909**, *42*, 4377 – 4383; b) J. M. Adams, R. G. Pritchard, *Acta Crystallogr. Sect. B* **1977**, *33*, 3650 – 3653.
[7] a) A. Adam, M. Mehta, *Angew. Chem.* **1998**, *110*, 1457 – 1459; *Angew. Chem. Int. Ed.* **1998**, *37*, 1387 – 1388; b) A. Adam, M. Mehta, *Z. Kristallogr.* **1998**, *Supplement Issue 15*, 46.
[8] Interpretation of the IR data was based on the wrong molecular symmetry; however, the postulation of a peroxodicarbonate anion was correct.[3e]
[9] a) Crystal structure data of $K_2C_2O_6$: monoclinic, space group $P2_1/c$ (no. 14), $a = 838.05(1)$, $b = 1076.41(2)$, $c = 711.67(1)$ pm, $\beta = 111.24(0)^\circ$ $V = 598.4(2) \times 10^6$ pm^3, $\rho_{calcd} = 2.200$ g cm^{-3}, $\rho_{measured} = 2.14(1)$ g cm^{-3} (He pycnometer, Micrometritics AccuPyc 1330 GB), $Z = 4$, $\mu = 55.04$ cm^{-1}. b) Devices for X-ray diffraction experiments: Suny X3B1 beamline at National Synchroton Light Source, Brookhaven National Laboratory, USA, double Si(111) monochromator, and Ge(111) crystal analyzer, $\lambda = 115.011(2)$ pm, Na(Tl)I scintillation counter with pulse height discriminator, $T = -73\,^\circ$C, $5.0^\circ < 2\Theta < 43.679^\circ$ in steps of $0.003^\circ 2\Theta$, glass capillary of 0.7 mm diameter; due to decomposition even at low temperature, a second measurement for structure refinement was performed at beamline B2 at the Hamburger Synchrotronstrahlungslabor (HASYLAB) immediately after synthesis of the material: Three-circle Huber goniometer, Ge(111) double crystal monochromator, and Ge(111) crystal analyzer, $\lambda = 112.074(2)$ pm, Na(Tl)I scintillation counter, $T = -123\,^\circ$C, $9.0^\circ < 2\Theta < 50.5^\circ$ in steps of $0.003^\circ 2\Theta$, glass capillary of 0.7 mm diameter. c) Structure determination process: Data reduction and background modeling by using the GUFI program,[10] crystal structure solution by global optimization with 15 parameters by using the DASH program package,[11] two phases of Rietveld refinements by employing a model for anisotropic micro-strain with potassium hydrogencarbonate as second phase by using the GSAS program package,[12] $R_p = 0.193$, $R_{wp} = 0.246$, $R_F = 0.080$, $\chi^2 = 0.84$, number of reflections 281, number of variables 35, number of refined atoms 10. The relatively high weighted-profile R factor is due to the statistics of the observed step scan intensities caused by limited time for measurement. d) Further details on the crystal structure investigation may be obtained from the Fachinformationszentrum Karlsruhe, 76344 Eggenstein-Leopoldshafen, Germany (fax: (+49) 7247-808-666; e-mail: crysdata@fiz-karlsruhe.de), on quoting the depository number CSD-412335.
[10] R. Dinnebier, GUFI a program for measurement and evaluation of powder patterns, Version 5.0, Heidelberger Geowiss. Abh. 68, Heidelberg, **1997**.
[11] a) W. I. F. David, K. Shankland, N. Shankland, *Chem. Commun.* **1998**, 931 – 932; b) J. W. Visser, *J. Appl. Crystallogr.* **1969**, *2*, 89 – 95; c) A. Le Bail, H. Duroy, J. L. Fourquet, *Mater. Res. Bull.* **1988**, *23*, 447 – 452; d) J. Rodriguez-Carvajal, *Abstracts of the Satellite Meeting on Powder Diffraction of the XV Congress of the IUCR*, **1990**, p. 127.
[12] a) A. C. Larson, R. B. von Dreele, *GSAS* **1990**, Version Sept. 1997, Los Alamos National Laboratory Report LAUR 86 – 748; b) H. M. Rietveld, *J. Appl. Crystallogr.* **1969**, *2*, 65 – 71; c) P. Thompson, D. E. Cox, J. B. Hastings, *J. Appl. Crystallogr.* **1987**, *20*, 79 – 83; d) L. W. Finger, D. E. Cox, A. P. Jephcoat, *J. Appl. Crystallogr.* **1994**, *27*, 892 – 900; e) P. W. Stephens, *J. Appl. Crystallogr.* **1999**, *281 – 289*.
[13] Molecular calculations (MINDO), in which C_2 symmetry was assumed for the peroxodicarbonate group, failed to correctly postulate the bond lengths and the dihedral angle.[14]
[14] C. Glidewell, *J. Mol. Struct.* **1980**, *67*, 35 – 44.
[15] a) J.-M. Savariault, M. S. Lehmann, *J. Am. Chem. Soc.* **1980**, *102*, 1298 – 1303; b) Y. Idemoto, J. W. jr. Richardson, N. Koura, S. Kohara, C.-K. Loong, *J. Phys. Chem. Solids* **1998**, *59*, 363 – 376; A. Y. Kosnikov, V. L. Antonovsky, S. V. Lindeman, Y. T. Struchkov, I. P. Zyatkov, *Kristallografiya* **1988**, *33*, 875 – 877.
[16] G. Jander, K. F. Jahr, *Maßanalyse*, 15th ed., de Gruyter, Berlin, **1989**, pp. 197 – 198.

Self-Assembled Receptors for Enantioselective Recognition of Chiral Carboxylic Acids in a Highly Cooperative Manner

Tsutomu Ishi-i, Mercedes Crego-Calama, Peter Timmerman,* David N. Reinhoudt,* and Seiji Shinkai

One of the ultimate aims in molecular recognition is to understand fully and mimic the exquisite selectivities so eminently observed in natural receptors, such as antibodies and enzymes. A first approach is to build synthetic receptors by using rigid covalent scaffolds, to which are attached functional groups that can bind their guest molecules by multiple noncovalent interactions, such as hydrogen bonding, $\pi - \pi$ stacking, or metal coordination.[1] However, covalent systems are often too rigid and unable to adapt their shape to that of the guest, which can result in less than optimal binding affinities and selectivities. Another important drawback of covalent receptor molecules is their labor-intensive synthesis, which leaves little potential for structural variations in the scaffold.[2]

A different approach to shaping the binding site of an artificial receptor is to bring together the different components by multiple noncovalent interactions.[3, 4] This approach, which more closely resembles Nature's strategy, is currently being investigated as a potential alternative to covalent receptor molecules. A number of systems based on coordinative metal – ligand interactions[5] or hydrogen-bonding interactions[6] have been investigated, and some show significant structural selectivities.[7] However, in the majority of cases, substrate selectivity is the result of shape complementarity

[*] Dr. P. Timmerman, Prof. Dr. Ir. D. N. Reinhoudt, Dr. T. Ishi-i, Dr. M. Crego-Calama
Laboratory of Supramolecular Chemistry and Technology
MESA$^+$ Research Institute, University of Twente
PO Box 217, 7500 AE Enschede (The Netherlands)
Fax: (+31) 53-4894645
E-mail: d.n.reinhoudt@ct.utwente.nl
Prof. Dr. S. Shinkai
Chemotransfiguration Project
Japan Science and Technology Corporation (Japan)

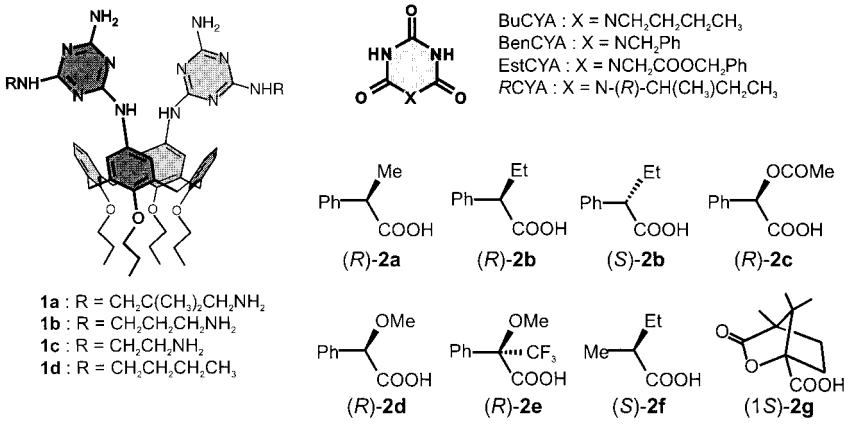
Supporting information for this article is available on the WWW under http://www.angewandte.com or from the author.

 © WILEY-VCH Verlag GmbH, 69451 Weinheim, Germany, 2002 1433-7851/02/4111-1924 $ 20.00+.50/0

rather than specific binding. Strong coordinative metal–ligand interactions have been used for the synthesis of receptors with specific binding of guest molecules.[4] Nevertheless, hydrogen-bonded, self-assembled receptors which bind the guest through functional-group interactions are rare,[8] probably because such functionalities are often not compatible with the noncovalent interactions that hold the receptor together.[3] Here we show that amino functionalities positioned on a chiral noncovalent scaffold stereospecifically recognize carboxylic acids with detailed structural selectivities, both with respect to the substrate and the scaffold. The recognition takes place primarily by use of acid–base (NH_2–HOOC) interactions,[9–12] whereas the observed enantioselectivity is the result of a secondary interaction with the noncovalent platform, which acts in a cooperative manner, similar to the binding of oxygen in hemoglobin.

The core of the self-assembled scaffold consists of a double-rosette hydrogen-bonded assembly $\mathbf{1}_3 \cdot (CYA)_6$ (CYA = cyanuric acid), to which six amino functionalities have been attached; these serve as principal binding sites for guest complexation. The scaffold is composed of nine different components, that is, three calix[4]arene dimelamines **1** and six units of a barbituric or cyanuric acid derivative.[13] A total of 36 cooperative hydrogen bonds hold the components together, so that these structures are fully assembled at $>5\ \mu M$ in benzene or at $>100\ \mu M$ in chloroform.[14] The scaffold can be present in three isomeric forms (D_3, C_s, and C_{3h}), of which the chiral D_3 isomer is formed in most cases.[15] When no chiral centers are present in either one of the components, the D_3 isomer exists as a racemic mixture of the *P* and *M* enantiomers (Figure 1). However, chiral centers present in either **1** or CYA induce the supramolecular chirality of the scaffold, and only one of the two diastereoisomers (*P* or *M*) is formed.[16] Assembly $\mathbf{1}_3 \cdot (CYA)_6$ is strongly circular-dichroism (CD) active because of the dissymmetric arrangement of the many different chromophoric units within the structure.[14]

We studied the complex formation of double-rosette assembly $\mathbf{1a}_3 \cdot (CYA)_6$ (R = 2,2-dimethylpropyl amine)[17] with a variety of chiral carboxylic acids **2**. The assembly $\mathbf{1a}_3 \cdot (CYA)_6$ is used as a platform to organize the six amino functionalities. Typically, six equivalents of **2** were added to a solution of $\mathbf{1a}_3 \cdot (BuCYA)_6$ (1.0 mM) in [D_8]toluene at room temperature (ratio of COOH:NH_2 1:1) and the mixtures were equilibrated for ten hours. The interaction between host and guest becomes apparent from shifts of the signals in the ^1H NMR spectrum (Figure 2). For example, in the case of acid (*S*)-**2b** (6 equiv), the H^k (2.57 ppm) and H^l (2.37 ppm) proton signals shift upfield and downfield $-(0.09-0.18$ ppm) and $+0.32$ ppm, respectively, upon addition of the guest (Figure 3). In addition, signals for the H^b, H^c, H^k, and H^l protons are split, because of the formation of the diastereomeric assemblies (*M*)-$\mathbf{1a}_3 \cdot (BuCYA)_6$/(*S*)-**2b** and (*P*)-$\mathbf{1a}_3 \cdot (BuCYA)_6$/(*S*)-**2b**, which are no longer mirror images (Figure 2 and 3).[18] In contrast, (*S*)-**2b** shows no interaction with assembly $\mathbf{1d}_3 \cdot (BuCYA)_6$, which



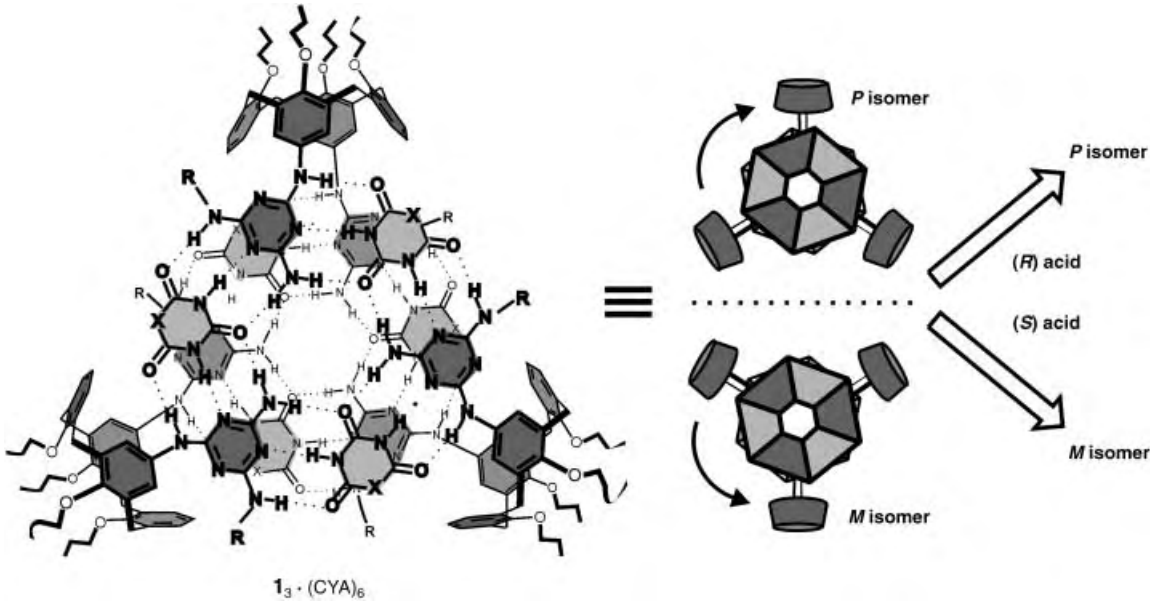


Figure 1. Chiral recognition by D_3-symmetrical rosette assemblies.

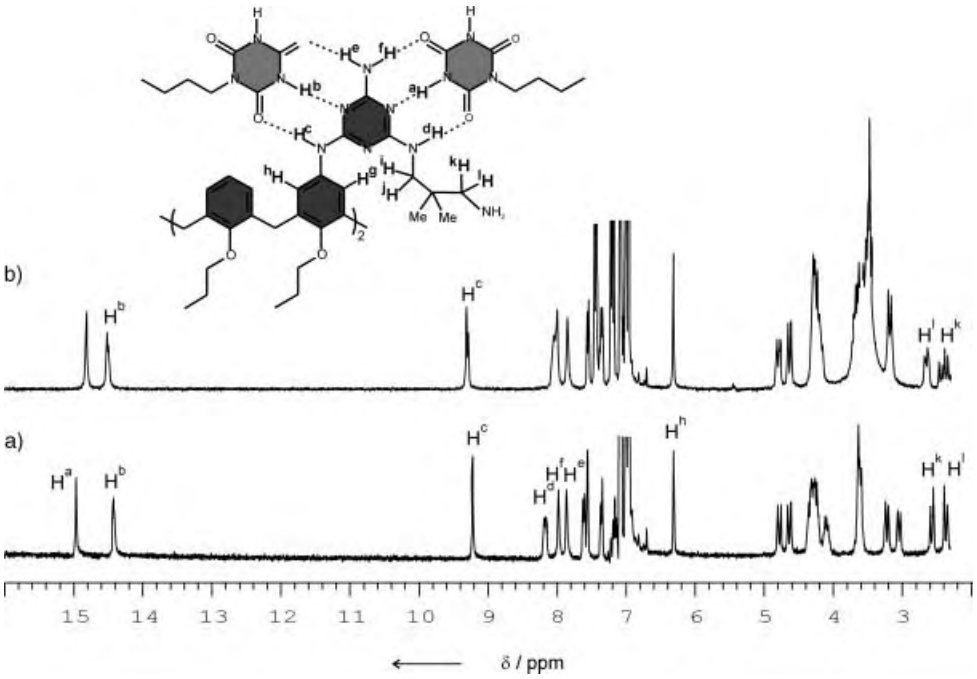


Figure 2. ^{1}H NMR spectra of $\mathbf{1a}_3\cdot(\mathrm{BuCYA})_6$ (1 mM) in [D_8]toluene in the presence of a) none and b) six equivalents of (*S*)-**2b**.

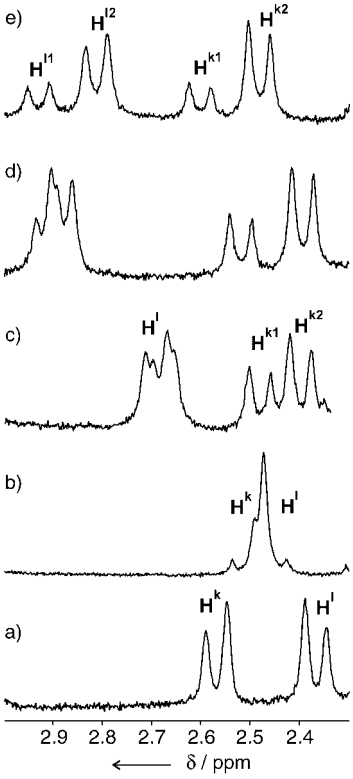


Figure 3. H^k and H^l proton resonance signals in the ^{1}H NMR spectra of $\mathbf{1a}_3\cdot(\mathrm{BuCYA})_6$ in the presence of (*S*)-**2b**: in [D_8]toluene, [$\mathbf{1a}_3\cdot(\mathrm{BuCYA})_6$] = 1 mM: a) 0, b) 1.5, c) 6, d) 12, and e) 60 equivalents of (*S*)-**2b**.

lacks the pendant amino groups. Complexation-induced shifts were not observed in this case, even when (*S*)-**2b** was present in a large excess (≈90 equiv), which clearly indicates that (*S*)-**2b** interacts primarily with the pendant amino group in $\mathbf{1a}_3\cdot(\mathrm{BuCYA})_6$.

The chiral acids (*R*)-**2a**, (*R*)-**2b**, (*S*)-**2b**, (*R*)-**2c**, (*S*)-**2f**, and (1*S*)-**2g** express a clear selectivity in binding towards one of the two enantiomers (*M* or *P*) of assembly $\mathbf{1a}_3\cdot(\mathrm{BuCYA})_6$. As a result, the enantiomer that is bound most strongly is amplified in the mixture, as both enantiomers are in dynamic equilibrium. This increase causes the CD spectrum of assembly $\mathbf{1a}_3\cdot(\mathrm{BuCYA})_6$ to show reliable and reproducible Cotton effects in the presence of these chiral acids (Figure 4). The corresponding *de* values can be determined by measuring the peak intensities for both diastereomeric complexes in the ^{1}H NMR spectrum: for the complexation with (*S*)-**2b** (>12 equiv), the *de* values were directly estimated by integration of the completely split

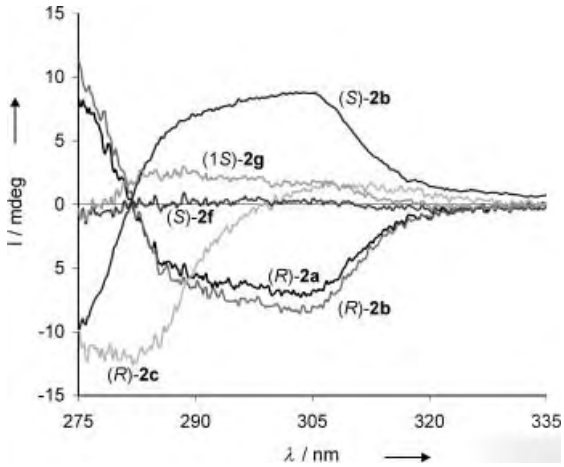


Figure 4. CD spectra of $\mathbf{1a}_3\cdot(\mathrm{BuCYA})_6$ (1 mM) in [D_8]toluene in the presence of (*R*)-**2a**, (*R*)-**2b**, (*S*)-**2b**, (*R*)-**2c**, (*S*)-**2f**, and (1*S*)-**2g** (6 equiv; in 0.01-cm-width cell).

signals arising from H^{k1} and H^{k2} (Figure 3). Under the optimum conditions (60 equivalents of (*S*)-**2b**, Figure 3e) a *de* value of 50% can be achieved. A plot of these values against the CD intensities at 305 nm (see Supporting Information) gives a straight line, from which an ellipticity of ~36 mdeg ($\Delta\varepsilon \sim 110\ \mathrm{cm^2\,mmol^{-1}}$) can be determined at 100% *de*, by extrapolation from the data. This value compares well with CD intensities of diastereomerically pure rosette assemblies.[17] This relationship allows us to calculate *de* values directly from the CD spectra (Table 1), because the *de* values could be obtained directly from ^{1}H NMR titration methods in (*S*)-**2f** and (1*S*)-**2g** systems.

The enantioselectivity differs strongly amongst the various chiral acids **2**. The highest enantioselectivities were observed

 © WILEY-VCH Verlag GmbH, 69451 Weinheim, Germany, 2002 1433-7851/02/4111-1926 $ 20.00+.50/0 *Angew. Chem. Int. Ed.* **2002**, *41*, No. 11

Table 1. Induction of chirality in assembly $\mathbf{1a}_3 \cdot (\mathrm{BuCYA})_6$ as a result of the addition of chiral acids **2a**–**g**.[a]

Entry	**2**	Yield [b] [%]	*de* value [d] [%]	Helicity[f]	CD_{305} [g] [mdeg]
1	–	100	–	–	–
2	(*R*)-**2a**	100	19	*P*	– 6.79
3	(*R*)-**2b**	100	21	*P*	– 7.80
4	(*S*)-**2b**	100	21	*M*	7.73
5	(*R*)-**2c**	54	[e]	–	– 12.6[h]
6	(*R*)-**2d**	[c]	–	–	–
7	(*R*)-**2e**	[c]	–	–	–
8	(*S*)-**2f**	100	1	*M*	0.43
9	(1*S*)-**2g**	55	5	*M*	1.87

[a] Conditions: in [D_8]toluene, $[\mathbf{1a}_3 \cdot (\mathrm{BuCYA})_6] = 1.0$ mM, $[\mathbf{2}]/[\mathbf{1a}_3 \cdot (\mathrm{BuCYA})_6] = 6$, at room temperature. [b] Determined by integration of the $ArCH_2Ar$ and the NH/ArH^h proton signals in the ^1H NMR spectrum. [c] Precipitate was formed upon addition of the acid. [d] Calculated from the CD signal intensity at 305 nm (see Supporting Information). [e] The *de* value could not be checked because of the different CD pattern and lack of splitting in the ^1H NMR spectrum. [f] Helicity of the preferentially formed isomer (*M* or *P*) of assembly $\mathbf{1a}_3 \cdot (\mathrm{BuCYA})_6$, which is assigned on the basis of CD signal sign: see reference [16]. [g] CD signal intensity at 305 nm. [h] CD signal intensity at 282 nm.

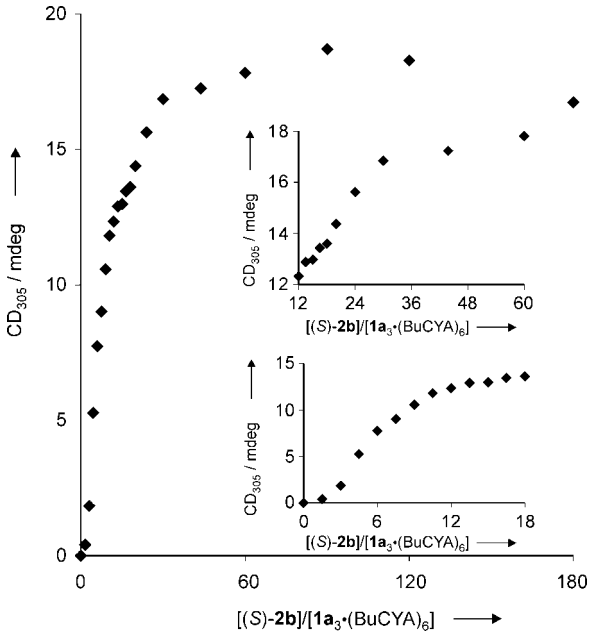


Figure 5. Plot of CD values at 305 nm versus $[(S)\text{-}\mathbf{2b}]/[\mathbf{1a}_3 \cdot (\mathrm{BuCYA})_6]$ for the titration of $\mathbf{1a}_3 \cdot (\mathrm{BuCYA})_6$ by (*S*)-**2b** in [D_8]toluene; $[\mathbf{1a}_3 \cdot (\mathrm{BuCYA})_6] = 1$ mM. The insets show expansions of the main plot.

for acids **2a** and **2b**, that is, 19 and 21 % *de* (6 equiv, entries 2–4 in Table 1). However, a drastic decrease in *de* value (to ≈1 %) was observed upon substitution of the phenyl for a methyl group, as in **2f** (compare entries 3 and 4 with 8 in Table 1), emphasizing the crucial importance of the phenyl group in the chiral recognition process. The acids (*R*)-**2c** and (1*S*)-**2g** seem to break down the scaffold, while complex formation occurs (entries 5 and 9 in Table 1). Interestingly, the CD spectrum in the presence of (*R*)-**2c** is entirely different from the others (Figure 4), which may suggest that the assembly changes structure upon binding to (*R*)-**2c**. On the addition of the acids (*R*)-**2d** and (*R*)-**2e**, a white precipitate was immediately formed (entries 6 and 7 in Table 1), which precludes solution studies on these systems. ^1H NMR spectroscopic analysis ([D_6]DMSO) shows that for (*R*)-**2d**, the hexameric complex $\mathbf{1a}_3 \cdot (\mathrm{BuCYA})_6 \cdot [(R)\text{-}\mathbf{2d}]_6$ precipitates (molar ratio of 1:2:2 for **1a**:BuCYA:(*R*)-**2d**).

Interestingly, the observed CD signals are strongly dependent on the amount of chiral acid **2** present. It is likely that the *de* value will increase with an increasing number of chiral acid units in the complex.[16] Indeed, titration of assembly $\mathbf{1a}_3 \cdot (\mathrm{BuCYA})_6$ against (*S*)-**2b** clearly shows a nonlinear increase in the CD intensity at 305 nm. First, the CD intensity increases by up to 90 times and then slowly decreases upon further addition of (*S*)-**2b** (Figure 5). The observed CD spectrum changes clearly indicate two saturation points around 15 equivalents and 60 equivalents, which suggests a two-step mechanism for the complex formation. An isosbestic point observed in both the first and second complexation indicates that only two species are present in each equilibrium (see Supporting Information). Interestingly, both the first and second CD spectra display sigmoidal curvatures; this curvature is a sign of homotropic positive allosterism, which arises from cooperativity in the complexation process.[10, 19] The cooperativity was analyzed using Equation (1)

$$y = K/([G]^{-n} + K) = \mathrm{CD_{obs}}/\mathrm{CD_{sat}} \quad (1)$$

and the Hill equation [Eq. (2)],[20] where [*G*] is the concentration of the added guest (*S*)-**2b**, *K* the association constant, *n* the Hill coefficient, $\mathrm{CD_{obs}}$ the observed CD intensity, and $\mathrm{CD_{sat}}$ the saturated CD intensity.

$$\log(y/(1-y)) = n \log[G] + \log K \quad (2)$$

From a plot of $\log(y/(1-y))$ against $\log[G]$, values of $\log K = 6.6$ and $n = 2.9$ were calculated for the first sigmoidal CD change (correlation coefficient, 0.996). For the second sigmoidal change, values of $\log K = 4.1$ and $n = 2.1$ (correlation coefficient, 0.995) were obtained (for details see Supporting Information).[21] These *n* values suggest that three molecules of (*S*)-**2b** interact with the three amino groups on one side of assembly $\mathbf{1a}_3 \cdot (\mathrm{BuCYA})_6$, to form the 1:3 complex $\mathbf{1a}_3 \cdot (\mathrm{BuCYA})_6 \cdot [(S)\text{-}\mathbf{2b}]_3$, whereupon three additional molecules of (*S*)-**2b** interact with the remaining three amino groups at the other side to form the 1:6 complex $\mathbf{1a}_3 \cdot (\mathrm{BuCYA})_6 \cdot [(S)\text{-}\mathbf{2b}]_6$.[22] In each step, the three amino groups interact with (*S*)-**2b** in a cooperative way.

The observed selectivity for complexation of chiral acid **2b** is very sensitive to structural changes in the hydrogen-bonded scaffold. For example, replacement of the 2,2-dimethyl-1,3-propylene linkers in **1a** with 1,3-propylene (**1b**) or ethylene (**1c**) spacers completely inhibits complex formation. Instead, the corresponding assemblies $\mathbf{1b}_3 \cdot (\mathrm{BuCYA})_6$ and $\mathbf{1c}_3 \cdot (\mathrm{BuCYA})_6$ are not stable and dissociate in the presence of (*R*)-**2b** (6 equiv). Similarly, the selectivities change dramatically when BuCYA is replaced with BenCYA or EstCYA. Despite the complete stability of the corresponding assemblies $\mathbf{1a}_3 \cdot (\mathrm{BenCYA})_6$ and $\mathbf{1a}_3 \cdot (\mathrm{EstCYA})_6$ in [D_8]toluene in the presence of (*R*)-**2b** (6 equiv), the observed *de* value decreases to 0 %. Most remarkable is the observation that

 © WILEY-VCH Verlag GmbH, 69451 Weinheim, Germany, 2002 1433-7851/02/4111-1927 $ 20.00+.50/0

addition of six equivalents of (*R*)-**2b** to the chiral assembly (*P*)-$\mathbf{1a}_3\cdot(\mathrm{RCYA})_6$, which bears an additional methyl group on the α-carbon of the propyl chain, leads to almost complete loss of optical activity (assembly formation decreased to about 50% and CD intensity at 305 nm decreased to about 10%). These results clearly illustrate how sensitive the observed enantioselectivity is to structural changes, which emphasizes once more the subtle nature of this particular complexation process.

How exactly does **2b** interact with the chiral assembly $\mathbf{1a}_3\cdot(\mathrm{BuCYA})_6$? The interaction is primarily electrostatic in nature, as **2b** transfers a proton to the basic amino group. The tight ion pair is the main species.[23] According to computer simulations of the hexacation $\mathbf{1a}_3\cdot(\mathrm{BuCYA})_6\cdot(\mathrm{H}^+)_6$ (gas phase MM calculation, Quanta 97/CHARMm 24.0; Figure 6), it is possible that the pendant

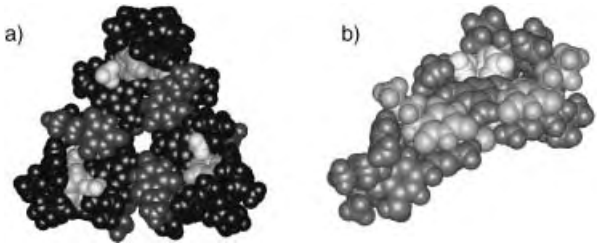


Figure 6. Computer-simulated structure of a) hexacation $\mathbf{1a}_3\cdot(\mathrm{BuCYA})_6\cdot(\mathrm{H}^+)_6$ and b) close-up (only half of the structure is shown for clarity).

NH_3^+ groups interact strongly with the electron-rich aromatic ring in the connecting calix[4]arene moiety, through cation–π interactions (Figure 6).[24, 25] The calculated distances between the NH^+ nitrogen atom and the aromatic carbon atoms (NH^+–ArC; 3.0–3.7 Å) are very close to those of the benzene–ammonia dimer (distance N–benzene plane = 3.59 Å), as measured by spectroscopy.[26] This interaction induces a significant conformational change in the scaffold and removes any rotational freedom within the binding site. The fixed RNH_3^+ functionalities are in a chiral environment and adopt a clearly defined spatial orientation to recognize chiral guests enantioselectively. The strong RNH_3^+–benzene interaction also accounts for the observed cooperativity, because the binding of one molecule of **2** will strongly preorganize and fix the binding site for the second, third, etc. molecules of **2**,[19] as the various binding sites are interconnected by the noncovalent scaffold. It seems likely that attractive guest–guest interactions[27] (for example, face-to-face or edge-to-face π–π stacking) might also contribute to the observed cooperativity, with regards to the drastic decrease in enantioselectivity from **2b** to **2f**.[28]

In conclusion, we have demonstrated that noncovalent hydrogen-bonded assemblies are able to recognize chiral carboxylic acids by a simple acid–base complexation, with considerable structural and stereoselectivities. Cooperativity in the binding process probably plays an important role in the observed selectivities, which are very sensitive to changes in the structure of the host.

Received: February 4, 2002 [Z18639]

[1] *Comprehensive Supramolecular Chemistry* (Eds.: J.-M. Lehn, J. L. Atwood, J. E. D. Davies, D. D. MacNicol, F. Vögtle), Pergamon, Oxford, **1996**.

[2] A. Fürer, T. Marti, F. Diederich, H. Künzer, M. Brehm, *Helv. Chim. Acta* **1999**, *82*, 1843–1859.

[3] a) M. M. Conn, J. Rebek, Jr., *Chem. Rev.* **1997**, *97*, 1647–1668; b) J. Rebek, Jr., *Acc. Chem. Res.* **1999**, *32*, 278–286; c) J. Rebek, Jr., *Chem. Commun*. **2000**, 637–643.

[4] a) M. S. Goodman, V. Jubian, B. Linton, A. D. Hamilton, *J. Am. Chem. Soc*. **1995**, *117*, 11610–11611; b) B. Linton, A. D. Hamilton, *Chem. Rev*. **1997**, *97*, 1669–1680.

[5] a) M. Fujita, *Chem. Soc. Rev*. **1998**, *27*, 417–425; b) D. L. Caulder, K. N. Raymond, *Acc. Chem. Res*. **1999**, *32*, 975–982; c) D. L. Caulder, K. N. Raymond, *J. Chem. Soc. Dalton Trans*. **1999**, 1185–1200; d) M. Fujita, K. Umemoto, M. Yoshizawa, N. Fujita, T. Kusukawa, K. Biradha, *Chem. Commun*. **2001**, 509–518.

[6] T. Heinz, D. M. Rudkevich, J. Rebek, Jr., *Nature* **1998**, *394*, 764–766.

[7] a) J. Kang, J. Rebek, Jr., *Nature* **1997**, *385*, 50–52; b) T. Kusukawa, M. Yoshizawa, M. Fujita, *Angew. Chem*. **2001**, *113*, 1931–1936; *Angew. Chem. Int. Ed*. **2001**, *40*, 1879–1884.

[8] a) Counteranion recognition by cation-templated assemblies: X. Shi, J. C. Fettinger, J. T. Davis, *Angew. Chem*. **2001**, *113*, 2909–2913; *Angew. Chem. Int. Ed*. **2001**, *40*, 2827–2831; b) tripyridine-templated assembly by metal–ligand interaction: M. Crego-Calama, P. Timmerman, D. N. Reinhoudt, *Angew. Chem*. **2000**, *112*, 771–774; *Angew. Chem. Int. Ed*. **2000**, *39*, 755–758.

[9] E. Yashima, K. Maeda, Y. Okamoto, *Nature* **1999**, *399*, 449–451.

[10] a) M. Takeuchi, T. Imada, S. Shinkai, *Angew. Chem*. **1998**, *110*, 2242–2246; *Angew. Chem. Int. Ed*. **1998**, *37*, 2096–2099; b) M. Ikeda, M. Takeuchi, A. Sugasaki, A. Robertson, T. Imada, S. Shinkai, *Supramol. Chem*. **2000**, *12*, 321–345.

[11] Y. Furusho, T. Kimura, Y. Mizuno, T. Aida, *J. Am. Chem. Soc*. **1997**, *119*, 5267–5268.

[12] Y. Inai, K. Tagawa, A. Takasu, T. Hirabayashi, T. Oshikawa, M. Yamashita, *J. Am. Chem. Soc*. **2000**, *122*, 11731–11732.

[13] P. Timmerman, R. H. Vreekamp, R. Hulst, W. Verboom, D. N. Reinhoudt, K. Rissanen, K. A. Udachin, J. Ripmeester, *Chem. Eur. J*. **1997**, *3*, 1823–1832.

[14] L. J. Prins, C. Thalacker, F. Würthner, P. Timmerman, D. N. Reinhoudt, *Proc. Natl. Acad. Sci*. **2001**, *98*, 10042–10045.

[15] L. J. Prins, K. A. Jolliffe, R. Hulst, P. Timmerman, D. N. Reinhoudt, *J. Am. Chem. Soc*. **2000**, *122*, 3617–3627.

[16] L. J. Prins, J. Huskens, F. de Jong, P. Timmerman, D. N. Reinhoudt, *Nature* **1999**, *398*, 498–502.

[17] J. M. C. A. Kerckhoffs, M. Crego-Calama, I. Luyten, P. Timmerman, D. N. Reinhoudt, *Org. Lett*. **2000**, *2*, 4121–4124.

[18] L. J. Prins, R. Hulst, P. Timmerman, D. N. Reinhoudt, *Chem. Eur. J*. **2002**, *8*, 2288–2301.

[19] Similar forms of cooperativity have been observed for covalent host molecules: S. Shinkai, M. Ikeda, A. Sugasaki, M. Takeuchi, *Acc. Chem. Res*. **2001**, *34*, 494–503.

[20] K. A. Connors, *Binding Constants*, Wiley, New York, **1987**.

[21] The observed positive allosterisms were also analyzed by use of the Scatchard plots, in which Hill coefficients (n) are correlated with the maximum values (y_{max}), according to the equation: $n = 1/(1 - y_{max})$, and the positive and negative allosterisms are expressed by the upward and downward curvatures, respectively. From the plots of y versus $y/[(S)\text{-}\mathbf{2b}]$, y_{max} values were observed at 0.6 ($n = 2.5$ for the first CD change) and at 0.51 ($n = 2.0$ for the second CD change) with upward curvatures (see Supporting Information). For the Scatchard plot see: B. Permutter-Hayman, *Acc. Chem. Res*. **1986**, *19*, 90–96.

[22] The two-step mechanism for the complexation was also corroborated by use of a Job plot (see Supporting Information). The plot of CD values at 305 nm against $[\mathbf{1a}_3\cdot(\mathrm{BuCYA})_6]/([\mathbf{1a}_3\cdot(\mathrm{BuCYA})_6]+[(S)\text{-}\mathbf{2b}])$ has a gentle curvature with a maximum around 0.2, which is attributed to the combination of the two maxima at 0.25 (for 1:3 complex) and 0.143 (for 1:6 complex).

[23] Judging from the acidity of benzyl carboxylic acids ($pK_a \approx 4$) and the basicity of aliphatic amines ($pK_a = 10$–11), ion-pair formation ($NH_3^+/{}^-OOC$) can be expected in the complexation of $\mathbf{1a}_3\cdot(\mathrm{BuCYA})_6$ with **2**. See also C. Reichardt, *Solvents and Solvent Effects in Organic Chemistry*, VCH, Weinheim, Germany, **1990** and R. H. Vreekamp, W.

 © WILEY-VCH Verlag GmbH, 69451 Weinheim, Germany, 2002 1433-7851/02/4111-1928 $ 20.00+.50/0

Verboom, D. N. Reinhoudt, *J. Org. Chem.* **1996**, *61*, 4282 – 4288. Furthermore, in nonpolar solvents such as toluene, the tight ion pair can be the main species. See also E. Yashima, T. Matsushima, Y. Okamoto, *J. Am. Chem. Soc.* **1997**, *119*, 6345 – 6359 and E. Yashima, Y. Maeda, Y. Okamoto, *J. Am. Chem. Soc.* **1998**, *120*, 8895 – 8896.

[24] J. C. Ma, D. A. Dougherty, *Chem. Rev.* **1997**, *97*, 1303 – 1324.

[25] C. A. Deakyne, M. Meot-Ner (Mautner), *J. Am. Chem. Soc.* **1985**, *107*, 474 – 479.

[26] D. A. Rodham, S. Suzuki, R. D. Suenram, F. J. Lovas, S. Dasgupta, W. A. Goddard III, G. A. Blake, *Nature* **1993**, *362*, 735 – 737.

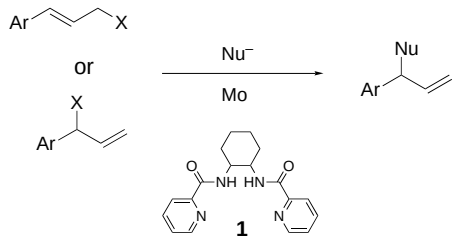
[27] Y. Kikuchi, Y. Tanaka, S. Sutarto, K. Kobayashi, H. Toi, Y. Aoyama, *J. Am. Chem. Soc.* **1992**, *114*, 10302 – 10306.

[28] Additional interaction of an NH_3^+ group with the phenyl group of the neighboring guest moiety by cation – π interactions might also contribute to the observed cooperativity. However, it seems likely that solvent molecules in the first solvation shell play an important role in these interactions, because modeling studies indicate that direct contact between two complexed acid molecules is rather unlikely.

Designed Ligands as Probes for the Catalytic Binding Mode in Mo-Catalyzed Asymmetric Allylic Alkylation**

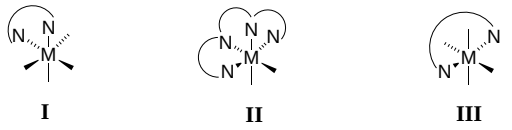
Barry M. Trost,* Kalindi Dogra, Iwao Hachiya, Takashi Emura, David L. Hughes,* Shane Krska, Robert A. Reamer, Michael Palucki, Nobuyoshi Yasuda, and Paul J. Reider

Asymmetric allylic alkylation has been developing significantly over the past several years.[1] Among the metals capable of effecting such reactions are palladium,[2] molybdenum,[3] and tungsten.[4] In contrast to these metals, in which the chirality of some substrates, notably vinylcarbinols of the type shown in Equation (1), is lost, iridium,[5] rhodium,[6] and ruthenium[7] normally retain the optical purity of such starting substrates. In spite of these many studies, very little is known about the structure of the active complex in the catalytic cycle. The case of Mo is quite intriguing. The catalyst system based on ligand **1**[8] has shown extraordinary levels of regio- and enantioselectivity, even at elevated temperatures (80 – 100 °C) [Eq. (1)].[3a] Furthermore, the reactions were qualitatively significantly faster than in the previously reported achiral reactions.[9] How such a seemingly flat system is able to provide such high selectivities has stimulated the development of an understanding of its binding mode. Although the direct characterization of π-allyl – metal complexes is certainly desirable, the relevance of these isolable/observable complexes to the catalytic cycle is not assured. Herein we adopted an indirect probe of the question of the binding of this ligand to Mo during the catalytic cycle which has led to a totally unexpected result.

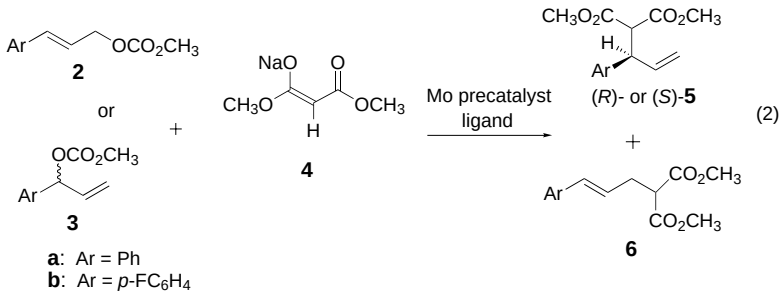


(1)

In the original design, three binding modes **I**—**III** for these octahedral metals were considered. Conceptually, it was postulated that binding mode **I**, while the most common,



would have less probability of inducing high enantiomeric excesses in asymmetric allylic alkylations than **II** and **III**. The reaction depicted in Equation (2) was employed to evaluate



(2)

the ligands. Several ligands were evaluated, and their effectiveness compared with that of **1** as the standard ligand (Table 1, entries 1, 2, and 12).

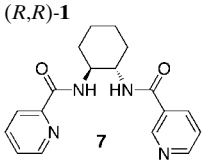
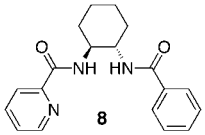
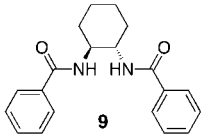
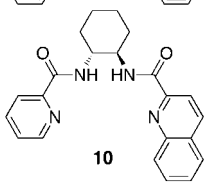
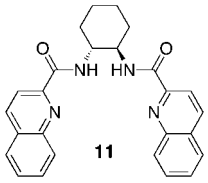
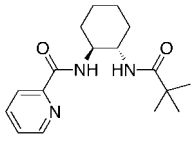
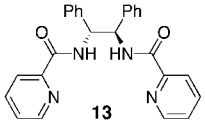
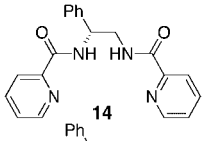
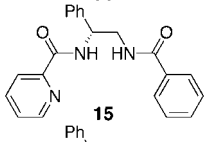
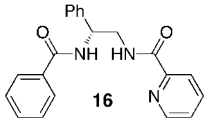
In initial studies, one of the two picolinamide units was replaced with a nicotinamide group (see **7**). Surprisingly, the regio- and enantioselectivities were slightly better than with the standard ligand **1**, although the reactions were slower (Table 1, entry 3). Since it seemed that the nitrogen atom of the nicotinamide group could not participate in the binding, the simple benzamide ligand **8** was examined. In agreement with the above hypothesis, the reaction of ligand **8** with the achiral substrate **2** (Table 1, entry 4) gave the same results as the reaction of ligand **7** with **2** (Table 1, entry 3). Interestingly, better selectivities were obtained in the reaction of ligand **8** with chiral racemic substrate **3** (Table 1, entry 5) than in the

[*] Prof. B. M. Trost, K. Dogra, Dr. I. Hachiya, T. Emura
Department of Chemistry, Stanford University
Stanford, CA 94305 (USA)
Fax: (+1) 650-725-0002
E-mail: bmtrost@stanford.edu
Dr. D. L. Hughes, Dr. S. Krska, Dr. R. A. Reamer, Dr. M. Palucki, Dr. N. Yasuda, Dr. P. J. Reider
Department of Process Research, Merck Research Laboratories
Rahway, NJ 07065 (USA)
Fax: (+1) 732-594-4717
E-mail: dave_hughes@merck.com

[**] We thank the National Science Foundation and the National Institutes of Health for their generous support of the work carried out at Stanford. I.H. thanks the Japan Society for the Promotion of Science for a postdoctoral fellowship. Mass spectra were provided by the Mass Spectrometry Facility at the University of California, San Francisco, which is supported by the NIH Division of Research Resources.

 © WILEY-VCH Verlag GmbH, 69451 Weinheim, Germany, 2002 1433-7851/02/4111-1929 $ 20.00+.50/0

Table 1. Ligand effects in the Mo-catalyzed asymmetric allylic alkylation with sodium dimethyl malonate.

Entry	Ligand	Substrate	Yield	**5/6**	% *ee*
1a	(*S*,*S*)-**1**	**2a**	95	35	97 (*R*)
1b	(*R*,*R*)-**1**	**2a**	90	28	99 (*S*)
2a	(*S*,*S*)-**1**	**3a**	93	25	87 (*R*)
2b[b]	(*R*,*R*)-**1**	**3a**	70	13	92 (*S*)
3	 **7**	**2a**	93	46	99 (*R*)
4	 **8**	**2a**	90	60	99 (*R*)
5		**3a**	90	53	92 (*R*)
6	 **9**	**2a**	35	1	24 (*R*)
7[b]	 **10**	**2a**	29	19	98 (*S*)
8[b]	 **11**	**2a**	traces	–	–
9	 **12**	**2a**	95	30	98 (*R*)
10		**3a**	88	28	88 (*R*)
11	 **13**	**2a**	95	19	99 (*S*)
12	(*R*,*R*)-**1**	**2b**	93	13	96 (*S*)
13		**2b**	84	10	94 (*S*)
14	 **14**	**2b**	92	6	91 (*S*)
15	 **15**	**2b**	43	9	77 (*S*)
16	 **16**	**2b**	72	8	90 (*S*)

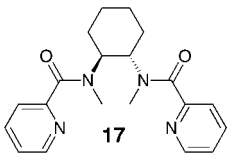
[a] $(C_7H_8)Mo(CO)_3$ was employed as the precatalyst in all reactions, unless otherwise indicated. The reactions were performed by adding sodium hydride (2 equiv) and dimethyl malonate (2.1 equiv) to a solution of allyl substrate (1 equiv) in THF (0.1M). [b] $(CH_3CH_2CN)_3Mo(CO)_3$ was used as precatalyst.

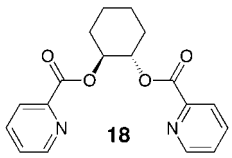
reaction of standard ligand **1** with **3** (Table 1, entry 2). Removal of both pyridine nitrogen atoms (e.g. bisbenzamide **9**) led to a very poor ligand in terms of rate and selectivity (Table 1, entry 6).

Steric factors also play a role in the effectiveness of a ligand. When a picolinamide unit of **1** is replaced by one or two quinoline analogues (**10** (Table 1, entry 7) and **11** (Table 1, entry 8), respectively), much lower reaction rates were observed, although ligand **10** was highly enantioselective. A similar observation was recently reported by Moberg and coworkers who used the methyl-2-picolinamide ligand.[3c,d] When a pivalamide group (see **12**) was used instead of a picolinamide group, good selectivities were still observed (Table 1, entries 9 and 10) but with a further decrease in rate (fourfold slower than the reaction with the standard ligand **1**). A ligand with a different backbone (e.g. stilbenediamine **13**) gave comparable results as **1** (Table 1, entry 11), with a decrease in the branched/linear (**5/6**) ratio.

Substrate **2b** showed similar behavior with the standard ligand **1** (Table 1, entry 12). The stilbenediamine ligand **13** gave slightly poorer selectivity (Table 1, entry 13). Removing the symmetry in the chiral backbone (see **14**) led to a reaction that was twice as fast, but with diminished regio- and enantioselectivity (Table 1, entry 14). The effect of the position of the picolinamide and the benzamide groups in the unsymmetrical ligand was investigated (**15** (Table 1, entry 15) vs. **16** (Table 1, entry 16)). As anticipated, different results in terms of rate, regioselectivity, and enantioselectivity were observed. Interestingly, ligand **16** gave significantly better results than ligand **15**.[10]

The role of the secondary amides was probed by using ligands **17** and **18**. The former generated a catalyst that was 200-fold less active than **1** and gave very poor enantioselectivities; the latter did not lead to any observable reaction.

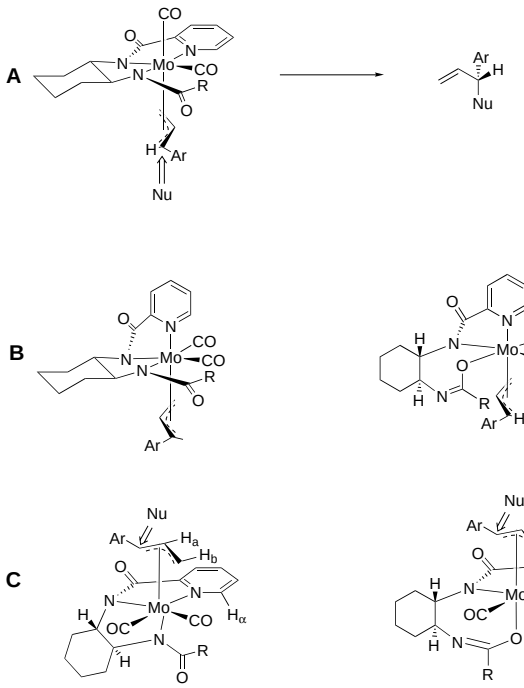

17


18

These observations led us to suspect that the secondary amide ligands were deprotonated under the basic conditions of the reaction. This suspicion was supported by deprotonating the ligand with tritylllithium and then forming the catalyst. The results of the reaction of substrate **2a** were identical to those of Table 1, entry 1 within experimental error.

The ligand study provides the first picture of the type of coordination involved. Contrary to our initial working hypothesis, bidentate coordination of the two pyridine nitrogen atoms of ligand **1** is clearly not involved. This conclusion also contradicts the recent structural studies of bisoxazolidine chiral ligands for Mo.[11] The efficiency of ligands **8** and **12** indicates that only one pyridyl nitrogen atom of ligand **1** is involved. Furthermore, either the dianion or the monoanion of the two secondary amides appears to be involved. Scheme 1 depicts several reasonable potential monoanionic complexes.

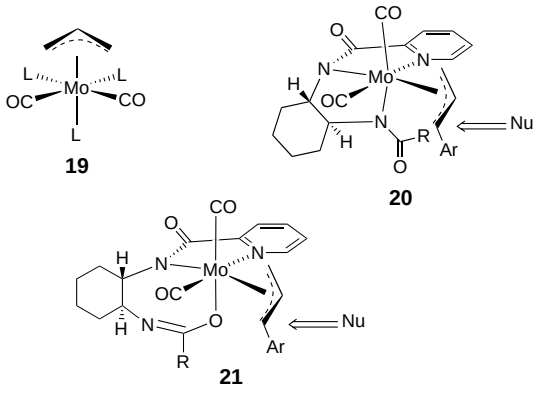
 © WILEY-VCH Verlag GmbH, 69451 Weinheim, Germany, 2002 1433-7851/02/4111-1930 $ 20.00+.50/0



Scheme 1. Possible binding modes of the ligands.

NMR spectroscopic studies of the π-allyl complex formed from ligand **8**, [Mo(CO)$_4$(norbornadiene)], and linear carbonate **2** in [D$_8$]THF reveal a monoanionic complex as the major species in solution. In the ^{15}N NMR spectrum of this complex, the amide nitrogen atoms give rise to signals at $\delta = 130$ and 175 ppm and the pyridine nitrogen atom results in a signal at $\delta = 263$ ppm; for the free ligand, signals are found at $\delta = 118$, 119, and 304 ppm, respectively. The $\delta = 175$ ppm resonance of one of the amide nitrogen atoms, the absence of a signal for one NH proton in the ^{1}H NMR spectrum, as well as proton coupling data clearly indicate that one amide is deprotonated in the complex. The other amide is still protonated, but the downfield shifts of the signal for the nitrogen atom in the ^{15}N NMR spectrum and of the signal for the NH proton in ^{1}H NMR spectrum relative to the uncomplexed ligand suggest that this amide is also involved in coordination to Mo in the complex. The complex shows NOE interactions between H$_a$ and H$_b$ of the allyl moiety (see Scheme 1, **C**), and the picoline hydrogen (H$_\alpha$) at C6, which effectively rules out structures **A** and **B** in Scheme 1 since the π-allyl moiety is too far removed from the pyridine ring in these structures to give rise to NOE interactions. Furthermore, the other two protons of the allyl moiety (not shown for clarity) show NOE interactions with each other and correlations to both CO groups.

Theoretical calculations on allyl (dicarbonyl) molybdenum complexes suggest a strong bias for structures like **19**.[12] Structures **20** and **21** meet this requirement, fit all the other data, and also rationalize the regio- and enantioselectivities. The ligands studied to date reveal that one binding position does involve both nitrogen atoms of a picolinamide unit; the binding of the remote amide then provides the additional rigidification required for the high chiral recognition and reactivity. The presence of good donor ligands (anionic amides) and acceptor ligands (CO) provides a good balance for alkene coordination (which is facilitated by acceptor ligands) and for ionization (which is facilitated by donor ligands). Although further studies are clearly required to establish the structure of the catalytically active species, the current results implicate an unusual coordination mode and reveal that the ligands have much broader potential than originally suggested. Furthermore, monopicolinamide ligands (e.g. **8** and **12**) are the best ligands for maximum regio- and enantioselectivity with the chiral racemic substrates, although at the expense of rate. The ability to design new ligands for octahedral complexes has now been greatly expanded.



Received: January 15, 2002 [Z 18525]

[1] B. M. Trost, D. L. van Vranken, *Chem. Rev.* **1996**, *96*, 395; B. M. Trost, C. B. Lee in *Catalytic Asymmetric Synthesis II* (Ed.: I. Ojima), Wiley-VCH, Weinheim, **2000**, pp. 593–650; T. Hayashi in *Catalytic Asymmetric Synthesis* (Ed.: I. Ojima), Wiley-VCH, Weinheim, **2000**, p. 193; A. Pfaltz, M. Lautens, *Compr. Asymmetric Catal.* **1999**, *2*, 833–884; A. Zampella, M. V. D'Auria, L. Minale, C. Debitus, *Tetrahedron* **1997**, *53*, 3243.

[2] B. M. Trost, *Acc. Chem. Res.* **1996**, *29*, 355; B. M. Trost, *Chem. Pharm. Bull.* **2001**, *49*, in press; C. G. Frost, J. Howarth, J. M. J. Williams, *Tetrahedron:Asymmetry* **1992**, *3*, 1089; G. Helmchen, S. Kudis, P. Sennhenn, H. Steinhagen, *Pure Appl. Chem.* **1997**, *69*, 513; G. Helmchen, A. Pfaltz, *Acc. Chem. Res.* **2000**, *33*, 336.

[3] a) B. M. Trost, I. Hachiya, *J. Am. Chem. Soc.* **1998**, *120*, 1104; b) B. M. Trost, S. Hildbrand, K. Dogra, *J. Am. Chem. Soc.* **1999**, *121*, 10416; Also see c) N.-F. Kaiser, U. Bremberg, M. Larhed, C. Moberg, A. Hallberg, *Angew. Chem.* **2000**, *112*, 33741; *Angew. Chem. Int. Ed.* **2000**, *39*, 3595; d) O. Belda, N.-F. Kaiser, U. Bremberg, M. Larhed, A. Hallberg, C. Moberg, *J. Org. Chem.* **2000**, *65*, 5868; e) A. V. Malkov, P. Spoor, V. Vinader, *Compr. Asymmetric Catal.* **1999**, *2*, 833–884; f) F. Glorius, M. Neuburger, A. Pfaltz, *Helv. Chem. Acta* **2001**, *84*, 3178; g) J. P. Janssen, G. Helmchen, *Tetrahedron Lett.* **1997**, *38*, 8025.

[4] G. C. Lloyd-Jones, A. Pfaltz, *Angew. Chem.* **1995**, *107*, 534; *Angew. Chem. Int. Ed. Engl.* **1995**, *34*, 462.

[5] R. Takeuchi, N. Ue, K. Tanabe, K. Yamashita, N. Shiga, *J. Am. Chem. Soc.* **2001**, *123*, 9525; R. Takeuchi, M. Kashio, *J. Am. Chem. Soc.* **1998**, *120*, 8647; B. Bartels, G. Helmchen, *Chem. Commun.* **1999**, 741.

[6] P. A Evans, L. J. Kennedy, *J. Am. Chem. Soc.* **2001**, *123*, 1234; P. A. Evans, J. D. Nelson, *Tetrahedron Lett.* **1998**, *39*, 1725.

[7] B. M. Trost, P. Fraisse, Z. T. Ball, unpublished results; see also S. W. Zhang, T. Mitsudo, T. Kondo, Y. Watanabe, *J. Organomet. Chem.* **1993**, *450*, 197; S. W. Zhang, T. Mitsudo, T. Kondo, Y. Watanabe, *J. Organomet. Chem.* **1995**, *485*, 55; S.-K. Kang, D.-Y. Kim, R.-K. Hong,

P.-S. Ho, *Synth. Commun.* **1996**, *26*, 3225; Y. Morisaki, T. Kondo, T. A. Mitsudo, *Organomet.* **1999**, *18*, 4742; Y. Matsushima, K. Onitsuka, T. Kondo, T. Mitsudo, S. Takahashi, *J. Am. Chem. Soc.* **2001**, *123*, 10405.
[8] D. J. Barnes, R. L. Chapman, R. S. Vagg, E. C. Watton, *J. Chem. Eng. Data* **1978**, *23*, 349; H. Adolfsson, C. Moberg, *Tetrahedron: Asymmetry* **1995**, *6*, 2023.
[9] B. M. Trost, M. Lautens, *J. Am. Chem. Soc.* **1987**, *109*, 1469.
[10] The results with ligands **14** and **15** mirror those in recent reports: A. V. Malkov, P. Spoor, V. Vinader, P. Kocovsky, *Tetrahedron Lett.* **2001**, *42*, 509–512.
[11] This conclusion contradicts those of Pfaltz and co-workers for related systems; see ref. [3f].
[12] M. D. Curtis, O. Eisenstein, *Organometallics* **1984**, *3*, 887.

Creation of a Unique Self-Supported Pattern of Radially Aligned Semiconductor Ag_2S Nanorods**

Qingyi Lu, Feng Gao, and Dongyuan Zhao*

Novel technologies based on nanoscale machines and devices will bring us a new world.[1] The key to realizing this nanotech world is to devise simple and efficient methods to create patterns of well-arranged nanocrystallites.[2] Recent research on metal and semiconductor nanostructures is expanding rapidly into the assembly of nanoparticles in two- (2D) and three-dimensional (3D) ordered superstructures.[3] A range of methods, including solvent evaporation of hydrophobic colloids,[4] molecular cross-linking in colloidal aggregates,[5] and biotemplate-directed synthesis,[6] have been reported, and they usually require the synthesis of initial nanoparticles with uniform size. One-dimensional (1D) nanostructures are of particular interest because of their potential in fundamental research and industrial applications.[7] The synthesis of nanorod arrays, especially the creation of aligned nanorods with novel patterns on surfaces, is considered to be a definitive step towards the fabrication of advanced electronic and opto-electronic nanodevices.[8] However, due to the anisotropic structure of nanorods, the oriented growth of nanorods on surfaces is difficult and usually requires solid templates, such as porous alumina,[9] polymer nanotubes,[10] and patterned catalysts,[11] to control the directional growth. Mostly substrates such as silicon wafers, Al_2O_3 membranes, and polycrystal glass plates are used to sustain nanorod growth.[12] The development of simple, mild, and effective methods for creating novel assemblies of 1D metal or semiconductor nanostructures on heterogeneous substrates, or even on self-generated homogeneous substrates, is of importance to nanotechnology and remains a key research challenge.

Here we demonstrate a room-temperature solution-growth method to synthesize of a self-supported pattern of radial semiconductor Ag_2S nanorod arrays with only $AgNO_3$, thiourea (Tu), and NaOH as the reagents. To the best of our knowledge, this is the first self-supported growth of Ag_2S nanorods. The reaction between $AgNO_3$ and Tu to form an unstable Ag-Tu complex has been well studied.[13] Our strategy is based on the experimental finding that basic conditions accelerate the decomposition of Tu.[14] We induce the reaction of $AgNO_3$ and Tu under basic conditions to control the decomposition rate of the complex and hence the nucleation and growth rates of crystalline Ag_2S. This synthetic process is very simple and mild, free of any templates (either membranes or surfactants), and provides a novel method for low-temperature homogeneous growth of 1D nanostructures and their simultaneous assembly into patterns.

The formation of the crystalline Ag_2S phase was established from X-ray diffraction (XRD) pattern (Figure 1). All peaks can be indexed to monoclinic Ag_2S with lattice constants comparable to the values of JCPDS card 14-72, and no impurities can be detected in this pattern, which indicates that crystalline Ag_2S is formed from solution at room temperature.

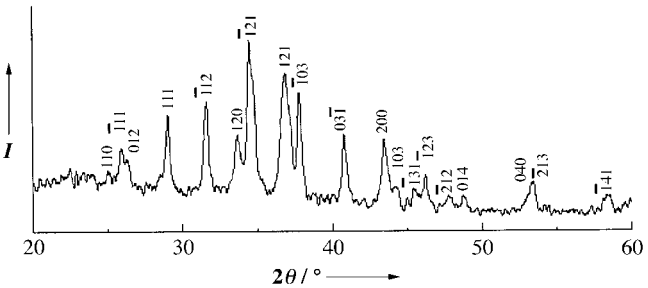


Figure 1. XRD pattern of the Ag_2S nanorod arrays.

The product morphology and chemical composition were determined by scanning electron microscopy (SEM) and energy dispersive spectroscopy (EDS). Figure 2 shows the unusual structure of radially aligned Ag_2S nanorods grown on a flakelike substance. The flakes usually have an irregular morphology with size up to dozens of micrometers, on which a large number of Ag_2S nanorods grow radially from one center. The nanorods have nonuniform diameters in the range of 50 to 200 nm and lengths of up to several micrometers. The Ag_2S nanorods at the radial center are slightly wider and longer than those at the edge. The EDS spectra (not shown) of the Ag_2S nanorods and flakes show strong silver and sulfur signals with Ag:S ratios of 2.00:1.03 and 2.04:1.00, respectively, which indicate stoichiometric relations between Ag and S in both the nanorods and the flakelike material. These results clearly indicate the formation of a distinctive radial pattern of aligned Ag_2S nanorods on self-provided Ag_2S flakes.

[*] Prof. D. Zhao, Dr. Q. Lu, F. Gao
Molecular Catalysis and Innovative Materials Lab
Department of Chemistry
Fudan University
Shanghai 200433 (P.R. China)
Fax: (+86) 21-6564-1740
E-mail: dyzhao@fudan.edu.cn

[**] This work was supported by the National Natural Science Foundation of China (No. 20173012, 29925309, and 20101002), the Education Ministry of China, the Shanghai Science Foundation (0152nm029), the State Key Basic Research Program of PRC (2001CB610505) and the Chinese Post-doc Foundation.

 © WILEY-VCH Verlag GmbH, 69451 Weinheim, Germany, 2002 1433-7851/02/4111-1932 $ 20.00+.50/0

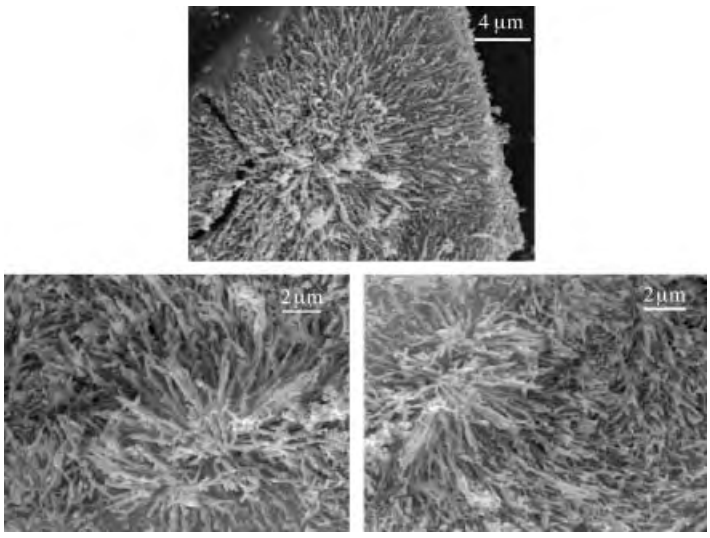


Figure 2. SEM images of the Ag_2S nanorod arrays.

The product was further characterized by high-resolution transmission electron microscopy (TEM), accompanied by EDS and selected-area electron diffraction (SAED). Figure 3a shows a typical TEM image of the product. The diameters of the nanorods are in the range of 30 to 120 nm, slightly less than those determined by SEM. This may be due to the Au cladding sprayed on the sample for SEM observation, which makes the diameters determined from SEM images slightly larger than the true sizes.[15] The high-resolution TEM image of an individual Ag_2S nanorod (inset in Figure 3a) clearly shows that the nanorod is highly crystalline and has a preferred growth direction. The calculated interplanar distance is 2.4 Å for the ($\bar{1}03$) face, consistent with that previously reported.[16] The ($\bar{1}03$) face is parallel to the long axis of the rod, that is, the preferred growth direction is [010]. Figures 3b and c show the SAED pattern and EDS spectrum, respectively, of an individual nanorod. The diffraction spots, indexed in Figure 3b, further suggest that the nanorod has a [010] growth direction. Figures 3d and e show a typical SAED pattern and an EDS spectrum, resectively, of a single flake; they indicate that the flakelike material is polycrystalline Ag_2S. The Cu and Cr signals are attributed to Cu grids for TEM observation. The powder XRD pattern (Figure 1) does not show any distinguishing diffraction peaks, which may be due to the fact that this pattern was measured on the randomly oriented polycrystalline flakes with radial nanorods. The TEM results are consistent with those obtained from SEM observations and further confirm the formation of the unique self-supported pattern of radially aligned Ag_2S nanorods.

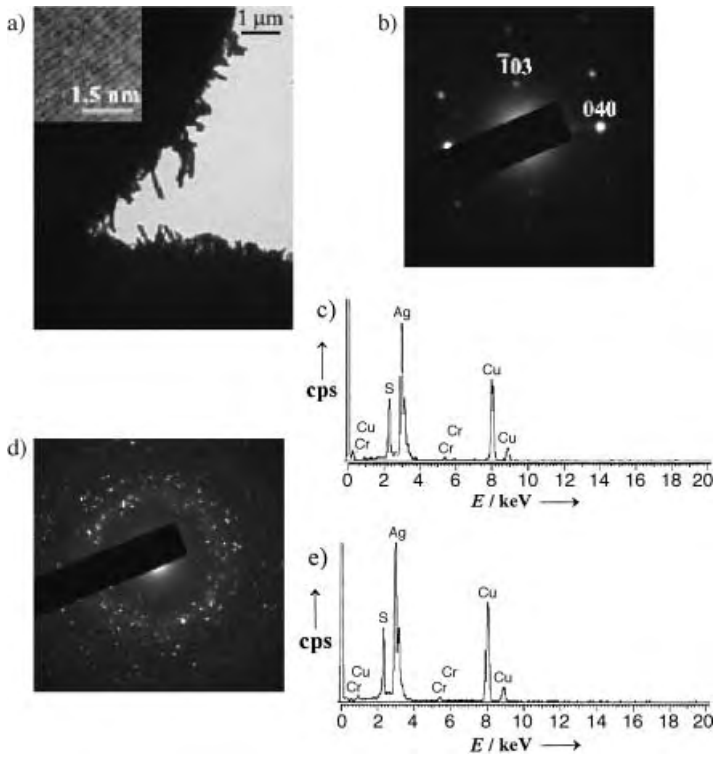


Figure 3. a) TEM image of the Ag_2S nanorod arrays. The inset is a high-resolution TEM image of a nanorod. b) SAED pattern obtained from a nanorod. c) EDS spectrum obtained from a nanorod. d) SAED pattern obtained from a flake. e) EDS spectrum obtained from a flake.

The addition of an appropriate amount of NaOH is undoubtedly vital in the formation of the unique pattern. In our experiments, 0.75 – 1.15 mL of 2 M NaOH solution led to formation of the self-supported pattern of radial Ag_2S nanorod arrays; otherwise, no nanorod arrays were observed. The reaction without NaOH resulted in the formation of Ag_2S microrods due to the strong coordinating ability of Tu. At low concentrations of NaOH (0.50 mL), the decomposition and nucleation rates are very slow, and the gradual transference and aggregation of the substance lead to the formation of flakelike Ag_2S. At high concentrations of NaOH (1.95 mL), decomposition of the Ag-Tu complex is so fast that much Ag_2S nucleates immediately after the two solutions are mixed, and homogeneous Ag_2S nanoparticles are formed.

The structure-directing agent (Tu) is also important for controlling the decomposition of the Ag-Tu complex, and therefore the growth of Ag_2S nanorods. In our experiments, a slight increase in the amount of Tu did not seriously affect the formation of the nanorod arrays, but did lead to a slight decrease in diameter. The reaction temperature is another factor that affects diameter and length. Increasing the reaction temperature from 20 to 40 °C increased the average diameter of the Ag_2S nanorods and decreased the length.

In summary, a simple and mild solution-growth method, free of any templates and substrates, creates a unique self-supported pattern of radial semiconductor Ag_2S nanorod arrays at room temperature, and may provide a new method for directed growth of nanorods and related materials.

Experimental Section

In a typical procedure for the synthesis of self-supported, radially aligned Ag_2S nanorods, 0.95 mL of 2 M NaOH solution was mixed with 10 mL of 0.26 M Tu solution with stirring. Then the mixed solution was slowly added to 5 mL of 0.39 M $AgNO_3$ solution, and the mixture was kept at room temperature for several days. The resulting black precipitate was collected by filtration, washed several times with distilled water and absolute alcohol, and dried at room temperature.

Received: November 27, 2001
Revised: March 4, 2002 [Z 18286]

 © WILEY-VCH Verlag GmbH, 69451 Weinheim, Germany, 2002 1433-7851/02/4111-1933 $ 20.00+.50/0

[1] a) S. K. Haram, B. M. Quinn, A. J. Bard, *J. Am. Chem. Soc.* **2001**, *123*, 8860; b) T. Trindade, P. O'Brein, N. L. Pickett, *Chem. Mater.* **2001**, *13*, 3843; c) C. Feldmann, H. O. Jungk, *Angew. Chem.* **2001**, *113*, 372; *Angew. Chem. Int. Ed.* **2001**, *40*, 359; d) H. Yu, P. C. Gibbons, K. F. Kelton, W. E. Bubro, *J. Am. Chem. Soc.* **2001**, *123*, 9198.

[2] a) M. P. Pileni, *J. Phys. Chem. B* **2001**, *105*, 3358; b) C. B. Murray, C. R. Kagan, M. G. Bawendi, *Science* **1995**, *270*, 1335; c) S. He, J. Yao, P. Jiang, D. Shi, H. Zhang, S. Xie, S. Pang, H. Gao, *Langmuir* **2001**, *17*, 1571; d) J. Lergand, A. T. Ngo, C. Petit, M. P. Pileni, *Adv. Mater.* **2001**, *13*, 58; e) M. A. Firestone, D. E. Williams, S. Seifert, R. Csencsits, *Nano Lett.* **2001**, *1*, 129; f) K. Soulantica, A. Maisonnat, M. C. Fromen, M. J. Casanove, P. Lecante, B. Chaudret, *Angew. Chem.* **2001**, *113*, 462; *Angew. Chem. Int. Ed.* **2001**, *40*, 448.

[3] a) T. Yonezawa, S. Onoue, N. Kimizuka, *Adv. Mater.* **2001**, *13*, 140; b) B. A. Korgel, S. Fullam, S. Connolly, D. Fitzmaurice, *J. Phys. Chem. B* **1998**, *102*, 8379; c) R. Maoz, E. Frydman, S. R. Cohen, J. Sagiv, *Adv. Mater.* **2000**, *12*, 424; d) Z. Y. Pan, X. J. Liu, S. Y. Zhang, G. J. Shen, L. G. Zhang, Z. H. Lu, J. Z. Liu, *J. Phys. Chem. B* **1997**, *101*, 9703; e) T. Vossmeyer, E. DeIonno, J. R. Heath, *Angew. Chem.* **1997**, *109*, 1123; *Angew. Chem. Int. Ed. Engl.* **1997**, *36*, 1080.

[4] a) P. C. Ohara, J. R. Heath, W. M. Gelbart, *Angew. Chem.* **1997**, *109*, 1119; *Angew. Chem. Int. Ed. Engl.* **1996**, *36*, 1078; b) X. M. Liu, H. M. Jaeger, C. M. Sorensen, K. J. Klabunde, *J. Phys. Chem. B* **2001**, *105*, 3353; c) Z. L. Wang, Z. Dai, S. Sun, *Adv. Mater.* **2000**, *12*, 1944.

[5] R. P. Andres, J. D. Bielefeld, J. I. Henderson, D. B. Janes, V. R. Kolagunta, C. P. Kubiak, W. J. Mahoney, R. G. Osifchin, *Science* **1996**, *273*, 1690.

[6] I. Willner, F. Patolsky, J. Wasserman, *Angew. Chem.* **2001**, *113*, 1913; *Angew. Chem. Int. Ed.* **2001**, *40*, 1861.

[7] a) D. Xu, Y. Xu, D. Chen, G. Guo, L. Gui, Y. Tang, *Adv. Mater.* **2000**, *12*, 520; b) Z. L. Wang, *Adv. Mater.* **2000**, *12*, 1295; c) A. M. Morales, C. M. Lieber, *Science* **1998**, *279*, 208; d) J. H. Song, B. Messer, Y. Wu, H. Kind, P. Yang, *J. Am. Chem. Soc.* **2001**, *123*, 9714; e) Z. Zhang, D. Gekhtman, M. S. Dresselhaus, J. Y. Ying, *Chem. Mater.* **1999**, *11*, 1659; f) C. C. Chen, C. Y. Chao, Z. H. Lang, *Chem. Mater.* **2000**, *12*, 1519; g) N. R. Hana, L. Gearheart, C. J. Murphy, *J. Phys. Chem. B* **2001**, *105*, 4065.

[8] a) L. Vayssieres, N. Beermann, S. E. Lindquist, A. Hagfeldt, *Chem. Mater.* **2001**, *13*, 233; b) Z. Zhang, G. Ramanath, P. M. Ajavan, D. Goldberg, Y. Bando, *Adv. Mater.* **2001**, *13*, 197; c) X. Peng, L. Manna, W. Yang, J. Wickham, E. Scher, A. Kadavanich, A. P. Alivisatos, *Nature* **2000**, *404*, 59; d) A. Hatzor, P. S. Weiss, *Science* **2001**, *291*, 1019; e) Z. L. Wang, R. P. Gao, J. L. Gole, J. D. Stout, *Adv. Mater.* **2000**, *12*, 1938; f) M. Li, H. Schnablegger, S. Mann, *Nature* **1999**, *402*, 393; g) J. K. N. Mbindyo, B. D. Reiss, B. R. Martin, C. D. Keating, M. J. Natan, T. E. Mallouk, *Adv. Mater.* **2001**, *13*, 249.

[9] a) H. Masuda, T. Yanagishita, K. Yasui, K. Nishio, I. Yagi, T. N. Rao, A. Fujishima, *Adv. Mater.* **2001**, *13*, 247; b) D. Routkevitch, T. Bigioni, M. Moskovits, J. M. Xu, *J. Phys. Chem.* **1996**, *100*, 14037.

[10] H. Cao, Z. Xu, H. Sang, D. Sheng, C. Tie, *Adv. Mater.* **2001**, *13*, 121.

[11] M. H. Huang, S. Mao, H. Feick, H. Yan, Y. Wu, H. Kind, E. Weber, R. Russo, P. Yang, *Science* **2001**, *292*, 1897.

[12] a) L. T. Canham, *Appl. Phys. Lett.* **1990**, *57*, 1046; b) L. Vayssieres, N. Beermann, S. E. Lindquist, A. Hagfeldt, *Chem. Mater.* **2001**, *13*, 233; c) Z. Zhang, G. Ramanath, P. M. Ajavan, D. Goldberg, Y. Bando, *Adv. Mater.* **2001**, *13*, 197; d) J. K. N. Mbindyo, B. D. Reiss, B. R. Martin, C. D. Keating, M. J. Natan, T. E. Mallouk, *Adv. Mater.* **2001**, *13*, 249.

[13] X. Zhong, W. Xiao, Q. Yuan, R. Lou, S. Xu, Q. Xu, Y. Tian, S. Liu, Y. Lu, W. Wang, S. Liu, Z. Ji, *A Series of Inorganic Chemistry Books (No. 6)*, 1st ed., Kexue Press, Beijing, **1995**.

[14] X. Jiang, Y. Xie, J. Lu, W. He, L. Zhu, Y. Qian, *J. Mater. Chem.* **2000**, *10*, 2193.

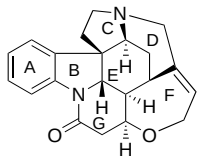
[15] C. H. Liang, G. W. Meng, G. Z. Wang, L. D. Zhang, *Chem. Mater.* **2001**, *13*, 2150.

[16] M. C. Brelle, J. Z. Zhang, L. Nguyen, R. K. Mehra, *J. Phys. Chem. A* **1999**, *103*, 10194.

Total Synthesis of (−)-Strychnine

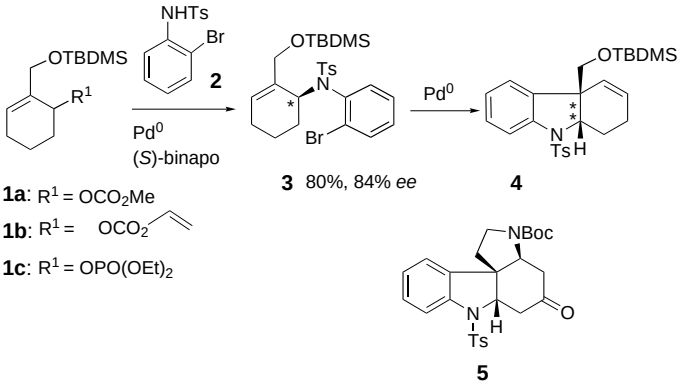
Masato Nakanishi and Miwako Mori*

(−)-Strychnine (**A**),[1] the most famous of the *Strychnos* alkaloids, has seven rings and six stereogenic centers in the molecule and is one of the most complex natural products of its size. Although Woodward et al. succeeded in the total synthesis of (−)-strychnine in 1954,[2] there were no reports of its total synthesis for 40 years. In 1992, Magnus et al. reported the total synthesis of strychnine,[3] and then Overman and coworkers succeeded in the first asymmetric total synthesis of (−)- and (+)-strychnine in 1993.[4] Since then, several groups have reported the total synthesis of (−)- or (±)-strychnine.[5, 6] Very recently, Vollhardt and coworkers completed the total synthesis of (±)-strychnine by using an ingenious cobalt-catalyzed [2+2+2] cycloaddition as a key step.[7]



A

We recently reported a novel method for synthesizing indole derivative **4** by means of palladium-catalyzed cyclization of 2-bromoaniline **3**. The aniline derivative **3** was obtained from cyclohexenol **1** and aniline **2** by using palladium-catalyzed asymmetric allylic substitution (Scheme 1).[8] (−)-Dehydrotubifolin and (−)-tubifolin were synthesized from tetracyclic ketone **5**, which was formed from **10** (Scheme 3; cf. **4**).



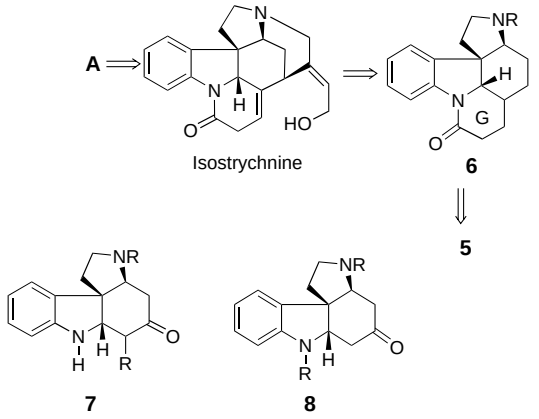
Scheme 1. Palladium-catalyzed asymmetric allylic substitution. Ts = toluene-4-sulfonyl, TBDMS = *tert*-butyldimethylsilyl, binapo = (*S*)-2,2′-bis-(diphenylphosphanoxy)-1,1′-binapthyl, Boc = *tert*-butoxycarbonyl.

These results prompted us to synthesize (−)-strychnine, as tetracyclic ketone **5** is considered to be a very important intermediate in the syntheses of *Strychnos* indole alkaloids. Our retrosynthetic analysis of (−)-strychnine is shown in Scheme 2. The method for the construction of the G ring is

[*] Prof. M. Mori, M. Nakanishi
Graduate School of Pharmaceutical Sciences, Hokkaido University
Sapporo 060-0812 (Japan)
Fax: (+81) 11-706-4982
E-mail: mori@pharm.hokudai.ac.jp

Supporting information for this article is available on the WWW under http://www.angewandte.com or from the author.

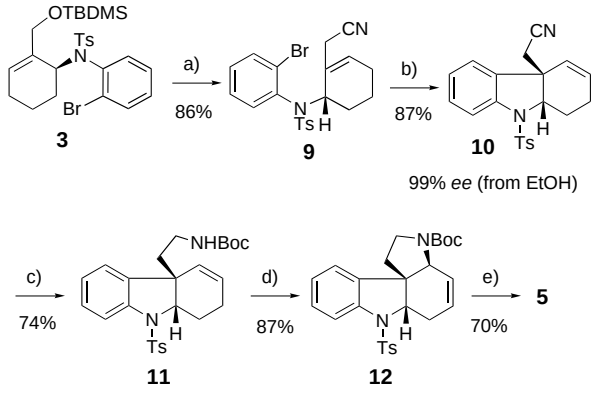
 © WILEY-VCH Verlag GmbH, 69451 Weinheim, Germany, 2002 1433-7851/02/4111-1934 $ 20.00+.50/0



Scheme 2. Retrosynthetic analysis of (−)-strychnine (**A**).

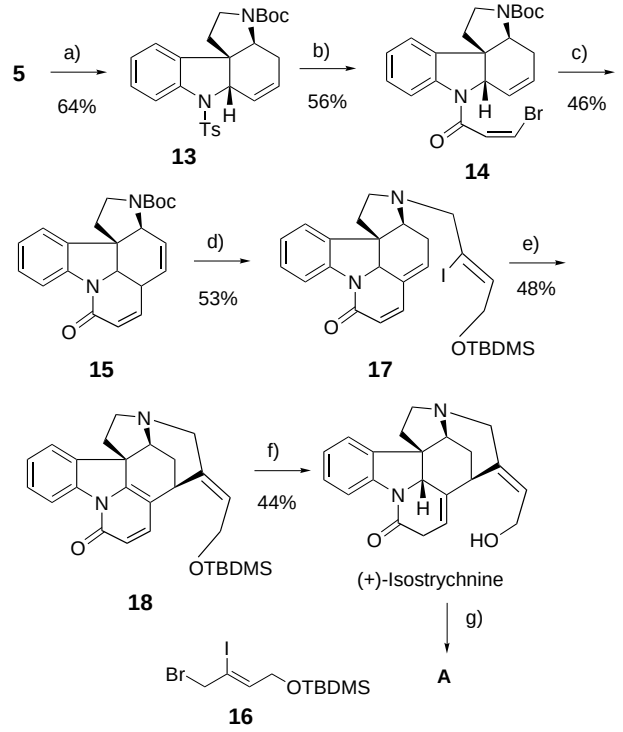
important for the synthesis of (−)-strychnine from **5**. Two pathways should be considered: 1) introduction of an alkyl group at the α position of the carbonyl group to give **7** followed by C–N bond formation to construct the G ring; 2) introduction of an acyl group at the nitrogen atom to form **8** followed by construction of the G ring.

The synthesis of **5** is summarized in Scheme 3. Indoline **10** (84 % *ee*) was recrystallized from EtOH to give the enantiomerically pure form (99 % *ee*, 73 % recovery, $[\alpha]_D^{20} = -46.7$ (*c* 2.16, $CHCl_3$)),[9] The optically pure tetracyclic ketone **5** could then be prepared from **10**.



Scheme 3. Synthesis of **5**. a) 1) HCl; 2) PBr_3; 3) NaCN; b) $Pd(OAc)_2$ (2 mol %), $PPhMe_2$, Ag_2CO_3, DMSO, 90 °C, 17 h; c) 1) $LiAlH_4$; 2) $(Boc)_2O$; d) $Pd(OAc)_2$, benzoquinone, MnO_2, AcOH, 50 °C; e) 1) 9-BBN, then H_2O_2, NaOH; 2) DMSO, $(COCl)_2$, then NEt_3. DMSO = dimethyl sulfoxide, Boc = *tert*-butoxycarbonyl, 9-BBN = 9-borabicyclo[3.3.1]-nonane.

At first we chose the reaction pathway in which an acyl group is introduced at the α position of the carbonyl group in **5**. However, several attempts were unsuccessful as a result of the steric hindrance of the large Ts protecting group on the nitrogen atom. Instead, we tried to introduce an acyl group at the nitrogen atom to form a C–C bond by a Heck-type reaction. Conversion of **5** into **13** was carried out by a known method (Scheme 4). Detosylation followed by treatment with (*Z*)-3-bromoacryloyl chloride gave **14**, which was treated with $Pd(OAc)_2$ (10 mol %) and PPh_3 (20 mol %) in the presence of iPr_2NEt in DMSO at 80 °C for 1.5 h. We were pleased to find



Scheme 4. Synthesis of (−)-strychnine. a) 1. $PhNTf_2$, $KN(TMS)_2$, 2. $Pd(OAc)_2$, PPh_3, HCO_2H, iPr_2NEt; b) 1. $NaC_{10}H_8$, 2. (*Z*)-3-bromoacryloyl chloride, K_2CO_3; c) $Pd(OAc)_2$ (10 mol %), PPh_3 (20 mol %), iPr_2NEt, DMSO, 80 °C, 1.5 h; d) 1. NaO*i*Pr, 2. CF_3CO_2H, 3. **16**, Li_2CO_3, DMF, 40 °C; e) $Pd(OAc)_2$, Bu_4NCl, K_2CO_3, DMF, 70 °C, 0.5 h; f) 1. $LiAlH_4$, 2. HCl; g) KOH, EtOH. TMS = trimethylsilyl, Tf = trifluoromethanesulfonyl, DMF = *N*,*N*-dimethylformamide.

that pentacyclic compound **15** was obtained in 46 % yield after the usual work-up procedure. Isomerization of the double bond of **15** by treatment with NaO*i*Pr in 2-propanol followed by removal of the Boc group and then alkylation with **16** afforded compound **17**, which is an intermediate in the synthesis of (±)-strychnine by Vollhardt and co-workers. By following their procedure, **17** was converted into pentacyclic compound **18** by treatment with $Pd(OAc)_2$, Bu_4NCl, and K_2CO_3 (Scheme 4).

Treatment of **18** with $LiAlH_4$ followed by cleavage of the silyl group gave (+)-isostrychnine, whose spectral data and $[\alpha]_D^{20}$ value (+23.7 (*c* 0.59, EtOH)) agreed with those of (+)-isostrychnine reported by Woodward and co-workers.[2] (+)-Isostrychnine was converted into our final target (−)-strychnine (**A**) by treatment with KOH in EtOH according to a known method.[10]

In summary, palladium catalysis played an important role in our total synthesis of (−)-strychnine: 1) rings A, B, and E were constructed by using by palladium-catalyzed asymmetric allylic substitution of a cyclohexenol derivative followed by palladium-catalyzed cyclization; 2) ring C was formed by means of a palladium-catalyzed allylic oxidation; 3) the synthesis of ring G and then ring F required $Pd(OAc)_2$. The extensive use of Pd^0 or Pd^{II} highlights the importance of palladium catalysts in modern synthetic organic chemistry.

Received: February 11, 2002 [Z 18687]

[1] Isolation: a) P. J. Pelletier, J. B. Caventou, *Ann. Chim. Phys.* **1818**, *8*, 323; structural elucidation: b) L. H. Briggs, H. T. Openshaw, R. Robinson, *J. Chem. Soc.* **1946**, 903; c) R. B. Woodward, W. J. Brehm, *J. Am. Chem. Soc.* **1948**, *70*, 2107.

[2] a) R. B. Woodward, M. P. Cave, W. D. Ollis, A. Hunger, H. U. Daeniker, K. J. Schenker, *J. Am. Chem. Soc.* **1954**, *76*, 4749; b) R. B. Woodward, M. P. Cave, W. D. Ollis, A. Hunger, H. U. Daeniker, K. J. Schenker, *Tetrahedron* **1963**, *19*, 247.

[3] P. Magnus, M. Giles, R. Bonnet, C. S. Kim, L. McQuire, A. Merritt, A. Vicker, *J. Am. Chem. Soc.* **1993**, *115*, 8116.

[4] a) S. D. Knight, L. E. Overman, G. Pairaudeau, *J. Am. Chem. Soc.* **1993**, *115*, 9293; b) S. D. Knight, L. E. Overman, G. Pairaudeau, *J. Am. Chem. Soc.* **1995**, *117*, 5776.

[5] For a review of the total syntheses of strychnine, see: J. Bonjoch, D. Solé, *Chem. Rev.* **2000**, *100*, 3455.

[6] Racemic syntheses: a) G. Stork, reported at the Ischia Advanced School of Organic Chemistry, Ischia Porto, Italy, **1992**; b) M. E. Kuehne, F. Xu, *J. Org. Chem.* **1993**, *58*, 7490; c) V. H. Rawal, S. Iwasa, *J. Org. Chem.* **1994**, *59*, 2685; for enantioselective syntheses, see: d) M. E. Kuehne, F. Xu, *J. Org. Chem.* **1998**, *63*, 9427; e) D. Solé, J. Bonjoch, S. García-Rubio, E. Peidró, J. Bosch, *Angew. Chem.* **1999**, 111, 408; *Angew. Chem. Int. Ed.* **1999**, *38*, 395.

[7] a) M. J. Eichberg, R. L. Dorta, K. Lamottke, K. P. C. Vollhardt, *Org. Lett.* **2000**, *2*, 2479; b) M. J. Eichberg, R. L. Dorta, D. B. Grotjahn, K. Lamottke, M. Schmidt, K. P. C. Vollhardt, *J. Am. Chem. Soc.* **2001**, *123*, 9324.

[8] M. Mori, M. Nakanishi, D. Kajishima, Y. Sato, *Org. Lett.* **2001**, *3*, 1913.

[9] The enantiomeric purity of **4a** was determined by HPLC analysis (DAICEL CHIRALPAK AD, hexane/2-propanol 95:5).

[10] V. Prelog, J. Battegay, W. I. Taylor, *Helv. Chim. Acta* **1948**, *31*, 2244.

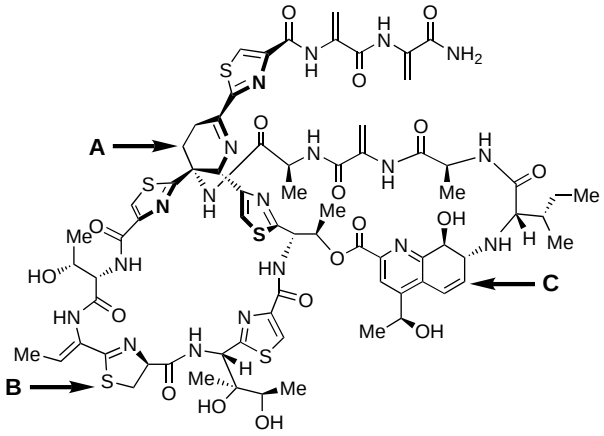
 © WILEY-VCH Verlag GmbH, 69451 Weinheim, Germany, 2002 1433-7851/02/4111-1936 $ 20.00+.50/0

Stereocontrolled Synthesis of the Quinaldic Acid Macrocyclic System of Thiostrepton**

K. C. Nicolaou,* Brian S. Safina, Christian Funke, Mark Zak, and Frédéric J. Zécri

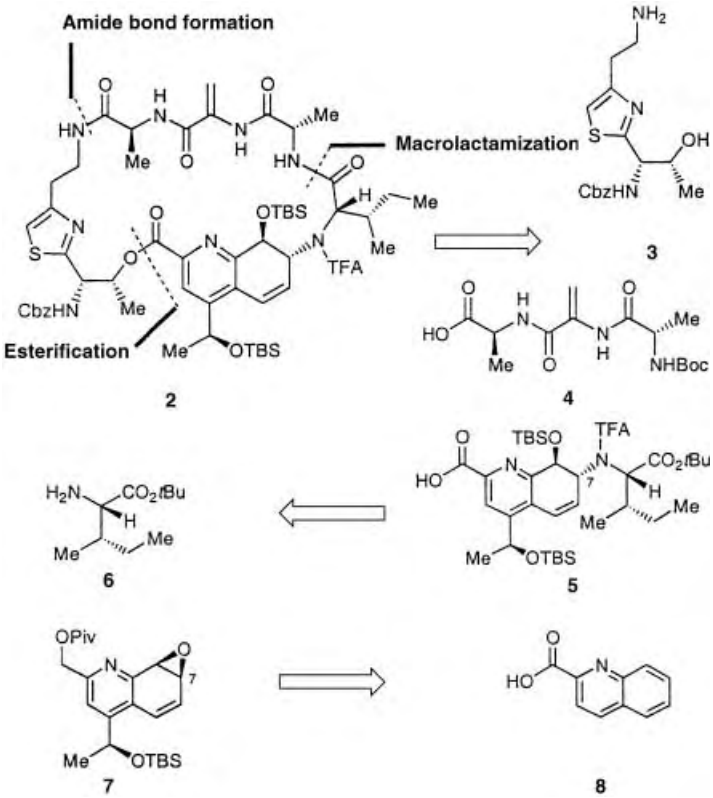
Dedicated to Professor Ralph F. Hirschmann on the occasion of his 80th birthday

Thiostrepton (**1**)[1] is the most complex and best characterized member of the thiopeptide antibiotics whose structure has been secured by X-ray crystallographic,[2] degradative,[3]



1

and spectroscopic techniques.[4] Produced by *Streptomyces azureus* ATCC 14921, *S. hawaiiensis* ATCC 12236, and *S. laurentii* ATCC 31255, this natural product is used as a topical antibiotic in veterinary medicine.[5] Its low solubility in water and poor bioavailability are the main obstacles that prevent its use in humans. This agent is widely used in recombinant DNA research.[6] Thiostrepton (**1**) is active against gram-positive bacteria, and exerts its biological action by binding to the 23S region of ribosomal RNA and ribosomal protein L11, thereby blocking the GTPase-dependent activities of the 50S ribosomal subunit.[7] Furthermore, **1** exhibits antimalarial activity against *Plasmodium falciparum*, which is the parasite responsible for causing over 85% of human malarial infections.[8] Isolated in 1955, thiostrepton itself still remains elusive to total synthesis, although the construction of its dehydropiperidine moiety has recently been reported;[9] simpler members of the thiopeptide family have also been prepared.[10] From a synthetic perspective, thiostrepton presents a considerable challenge, not only because of its highly complex molecular architecture, but also because of several sensitive functionalities. The most impressive features of this target molecule reside within three domains: a) region A includes the dehydropiperidine ring system that bears a quaternary center composed of three carbon atoms and a nitrogen atom and serves as the fulcrum for the molecule's two macrocycles; b) region B includes a thiazoline ring known for its sensitivity towards both acidic and basic conditions; and c) region C carries the novel quinaldic acid moiety with three asymmetric centers. Other notable features of this novel natural product include a contiguous dehydroamino acid tail (a motif which is relatively conserved throughout the thiopeptide family), three dehydroalanine moieties, one dehydrothreonine unit, a dihydroxyisoleucine side chain, and four thiazole rings. Herein we report a stereocontrolled synthesis of a model system **2** (Scheme 1) for the highly functionalized quinaldic acid macrocycle of **1**.



Scheme 1. Retrosynthetic analysis of the thiostrepton quinaldic acid macrocycle **2**.

Retrosynthetic analysis of the targeted quinaldic acid macrocycle model system **2** at two of the three indicated bonds (two amides, one ester) leads to the dehydroalanine tripeptide acid **4**, the simplified dehydropiperidine thiazole equivalent **3**, and the quinaldic acid system **5**. Further discon-

[*] Prof. Dr. K. C. Nicolaou, B. S. Safina, Dr. C. Funke, M. Zak, Dr. F. J. Zécri
Department of Chemistry and The Skaggs Institute for Chemical Biology
The Scripps Research Institute
10550 North Torrey Pines Road, La Jolla, California 92037 (USA)
Fax: (+1) 858-784-2469
E-mail: kcn@scripps.edu
and
Department of Chemistry and Biochemistry
University of California San Diego
9500 Gilman Drive, La Jolla, California 92093 (USA)

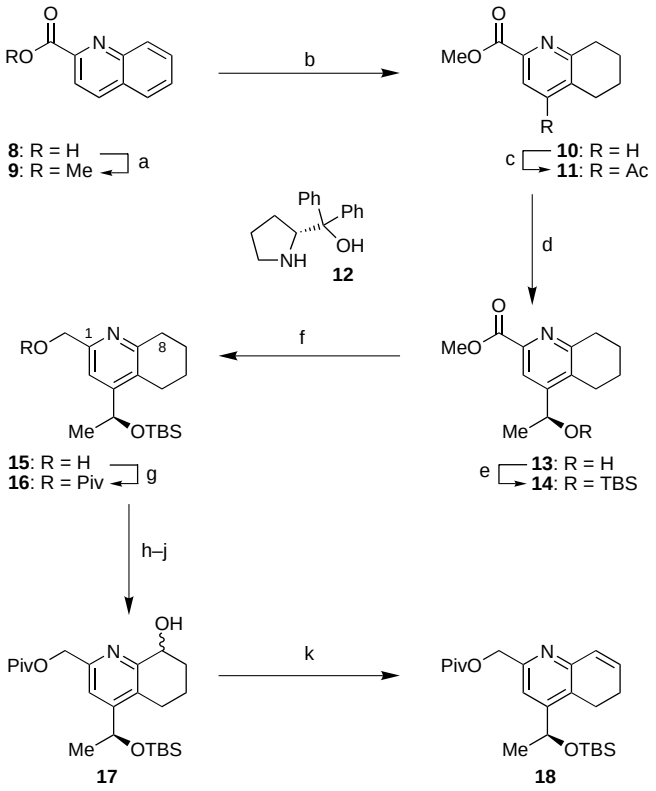
[**] We thank Drs. D. H. Huang and G. Suizdak for NMR spectroscopic and mass spectrometric assistance, respectively, as well as Mike Sertic (University of California, San Diego) for experimental assistance. Financial support for this work was provided by The Skaggs Institute for Chemical Biology, the National Institutes of Health (USA), fellowships from The Skaggs Institute for Research (to M.Z. and F.Z.), and grants from Abbott, Amgen, Array Biopharma, Boehringer-Ingelheim, Glaxo, Hoffmann-LaRoche, DuPont, Merck, Novartis, Pfizer, and Schering Plough.

 © WILEY-VCH Verlag GmbH, 69451 Weinheim, Germany, 2002 1433-7851/02/4111-1937 $ 20.00+.50/0

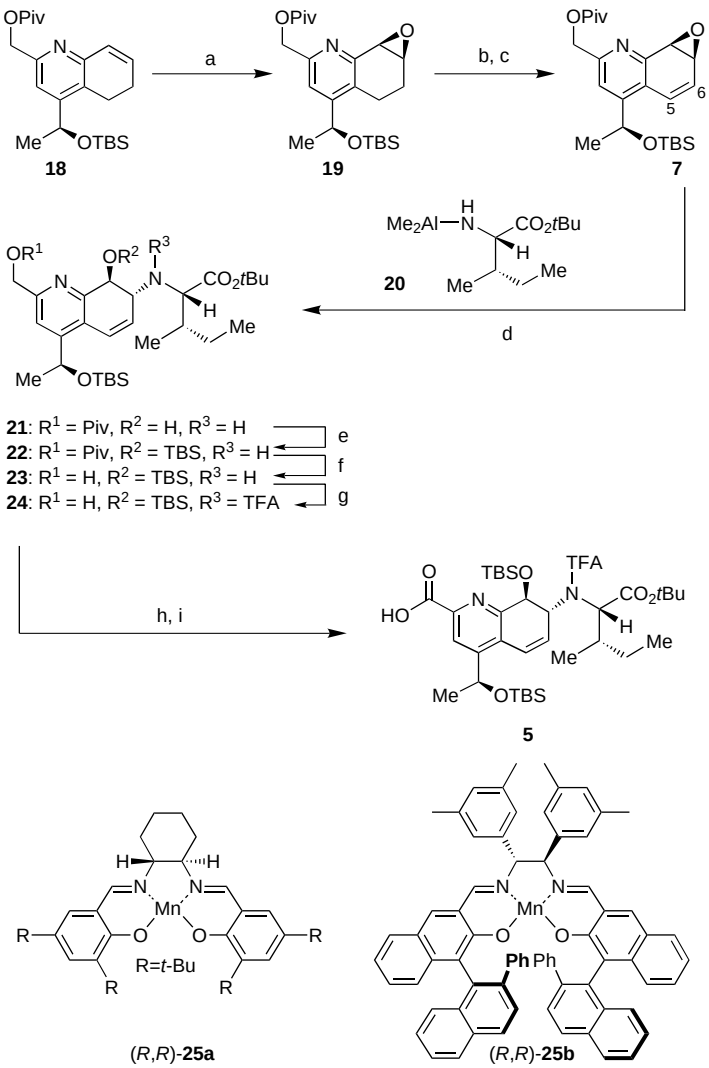
nection of the quinaldic acid fragment **5** reveals isoleucine derivative **6** and vinyl epoxide **7**. Intermediate **7** was traced to the commercially available 2-quinoline carboxylic acid (**8**). Significantly, it was envisioned that the three stereocenters of **5** could arise from an asymmetric reduction of the corresponding methyl ketone and a regioselective nucleophilic opening of the corresponding vinyl epoxide at C7 by using **6**.

Esterification of the commercially available 2-quinolinecarboxylic acid (**8**, Scheme 2) gave **9**. Selective reduction of the quinoline system **9** under catalytic hydrogenation conditions[11] afforded 5,6,7,8-tetrahydro derivative **10**. Nucleophilic addition of an acetyl radical species[12] *para* to the protonated pyridine nitrogen atom proceeded in nearly quantitative yield to generate the prochiral acetyl derivative **11**. To reduce the pyridine-containing methyl ketone **11** asymmetrically, a modified CBS[13] procedure, which required the in situ preparation of *B*-methoxyoxazaborolidine catalyst, was employed.[14] Methyl ketone **11** was reduced by using chiral ligand **12** (4 mol%) and a stoichiometric amount of $BH_3 \cdot SMe_2$ to provide alcohol **13** (95%, 90% *ee*). Following TBS protection (TBSOTf, 2,6-lutidine, 90%), the resulting ester **14** was reduced with $LiAlH_4$ to the primary alcohol **15** (88%) and subsequently protected (PivCl, pyridine, 82%) as pivaloate ester **16**. Pivaloate **16** was oxygenated at C8 by means of a Boekelheide-type cascade sequence (Scheme 2, steps h–j): 1) *m*CPBA-induced oxidation; 2) trifluoroacetylation (TFAA) of the resulting *N*-oxide; and 3) rearrangement and $NaHCO_3$-induced trifluoroacetate cleavage to give a mixture of C8 alcohols **17**[15] in 54% overall yield. Finally, elimination of triflic acid from the triflate of **17** (Tf_2O, 2,6-*t*Bu-4-Me-py) led to the desired olefin **18** in 81% yield.

Epoxidation of olefin **18** was then studied under a variety of conditions (Scheme 3), aiming for optimum diastereoselec-



Scheme 2. Synthesis of **18**. Reagents and conditions: a) MeOH, $SOCl_2$ (3.0 equiv), 60°C, 6 h, 99%; b) PtO_2/H_2, CF_3CO_2H, 25°C, 4 h, 60%; c) MeCHO, H_2O_2 (2.0 equiv), $FeSO_4$ (0.1 equiv), CF_3CO_2H (1.0 equiv), 25°C, 2 h, 99%; d) **12** (4 mol%), $B(OMe)_3$ (0.12 equiv), $BH_3 \cdot SMe_2$ (1.0 equiv), THF, 25°C, 4 h, 95%, 90% *ee*; e) TBSOTf (2.0 equiv), 2,6-lutidine (2.0 equiv), CH_2Cl_2, 0°C, 4 h, 90%; f) $LiAlH_4$ (1.1 equiv), THF, 0°C, 0.5 h, 88%; g) PivCl (3.0 equiv), pyridine (3.0 equiv), CH_2Cl_2, 25°C, 24 h, 82%; h) *m*CPBA (1.0 equiv), CH_2Cl_2, 25°C, 12 h, 99%; i) TFAA (3.0 equiv), CH_2Cl_2, 25°C, 12 h, 73%; j) aqueous $NaHCO_3$ (2M), CH_2Cl_2, 25°C, 8 h, 75%; k) Tf_2O (1.0 equiv), 2,6-*t*Bu-4-Me-pyridine (2.0 equiv), CH_2Cl_2, 25°C, 1 h, 81%. TBSOTf = *tert*-butyldimethylsilyl trifluoromethanesulfonate; *m*CPBA = *m*-chloroperoxybenzoic acid; TFAA = trifluoroacetic anhydride; Tf_2O = trifluoromethanesulfonic anhydride; 2,6-lutidine = 2,6-dimethylpyridine; Piv = pivaloate = trimethylacetate.



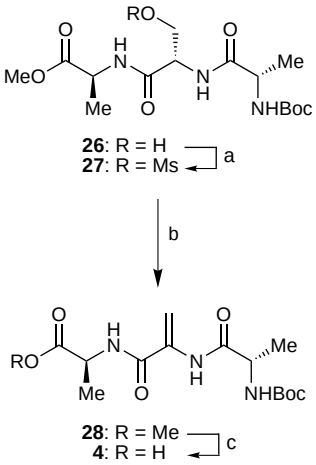
Scheme 3. Synthesis of **5**. Reagents and conditions: a) **25b** (1 mol%), 4-phenylpyridine *N*-oxide, NaOCl, pH 11.5, phosphate buffer, CH_2Cl_2, 25°C, 1 h, 74%, 80% *de*; b) NBS (1.1 equiv), AIBN (10 mol%), CCl_4, 80°C, 1 h, 63%; c) DBU (1.0 equiv), PhMe, 60°C, 2 h, 86%; d) **20** (9.0 equiv), PhMe, 25°C, 36 h, 56%; e) TBSOTf (3.0 equiv), Hünig's base (5.0 equiv), CH_2Cl_2, 0°C, 4 h, 88%; f) K_2CO_3 (1.0 equiv), MeOH, 25°C, 10 h, 99%; g) TFAA (4.0 equiv), pyridine (20 equiv), CH_2Cl_2; then K_2CO_3 (1.0 equiv), MeOH, 25°C, 10 h, 84% over two steps; h) IBX (1.1 equiv), DMSO, 25°C, 4 h, 98%; i) $NaClO_2$ (2.0 equiv), NaH_2PO_4 (4.0 equiv), 2-methyl-2-butene (6.0 equiv), H_2O, *t*BuOH, 25°C, 1 h, 95%. NBS = *N*-bromosuccinimide; AIBN = 2,2′-azobisisobutyronitrile; DBU = 1,8-diazabicyclo[5.4.0]undec-7-ene; IBX = *o*-iodylbenzoic acid; DMSO = dimethyl sulfoxide; Hünig's base = *N*,*N*-diisopropylethylamine.

 © WILEY-VCH Verlag GmbH, 69451 Weinheim, Germany, 2002 1433-7851/02/4111-1938 $ 20.00+.50/0 *Angew. Chem. Int. Ed.* **2002**, *41*, No. 11

tivity. Attempts to epoxidize **18** selectively with the commercially available Jacobsen–Katsuki catalyst **25a**[16] with either NaOCl or *m*CPBA/4-methylmorpholine *N*-oxide[17] as oxidants led to low yields, poor stereoselectivity, and significant C–H oxidation, with subsequent aromatization. In contrast to these results, the more recently disclosed Katsuki catalyst **25b**[18] (1 mol %) in conjunction with NaOCl allowed selective epoxidation of **18** (74 %, 80 % *de*). Introduction of the desired double bond in **19** was then effected by selective benzylic bromination (NBS/AIBN, 63 %), followed by elimination of HBr under basic conditions in toluene at 60 °C to give epoxide **7** (86 %).[19]

The highly sensitive nature of epoxide **7** did not allow introduction of nucleophiles through Brønsted or Lewis acid activation. It was, therefore, necessary to activate the isoleucine nucleophile as its dimethylaluminum derivative **20** through the addition of stoichiometric amounts of $AlMe_3$ before the opening of **7**, which led to amino alcohol **21** regioselectively in 56 % yield.[20] Accompanying the desired product **21** was the corresponding phenol (19 %). Neither the regioisomer of **21** nor its isomer from 1,4 addition to the vinyl epoxide moiety were observed in this reaction. Interestingly, the same nucleophile **20** led to the exclusive opening of the *saturated* (C5/C6) epoxide in the opposite regiochemical sense (at C8). Amino alcohol **21** was then selectively protected as its TBS derivative **22** (TBSOTf, 2,6-lutidine, 88 %), from which the pivaloate group was smoothly removed with K_2CO_3 in MeOH (99 %) to afford intermediate **23**. To trifluoacetylate the secondary amino group, **23** was treated with TFAA in pyridine, and then K_2CO_3 in MeOH was used to cleave the trifluoroacetate selectively from the primary alcohol trifluoroacetate (84 % over two steps). The resulting product **24** was oxidized in a two-step process (IBX; $NaClO_2$) to the desired quinaldic acid fragment **5** in 93 % yield.

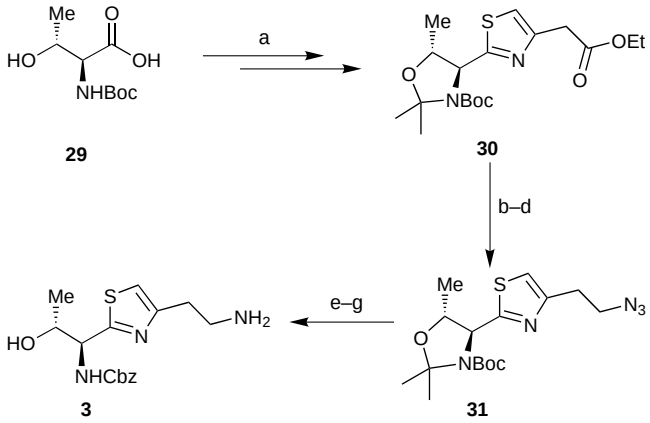
Dehydroalanine tripeptide segment **4** was synthesized from the individual component amino acid derivatives to afford **26** by following standard peptide-coupling protocols (Scheme 4).



Scheme 4. Synthesis of **4**. Reagents and conditions: a) MsCl (1.1 equiv), Et_3N (1.1 equiv), CH_2Cl_2, 0 °C, 13 h, 79 %; b) DBU (1.1 equiv), CH_2Cl_2, 0 °C, 16 h, 81 %; c) LiOH (2.0 equiv), THF, 25 °C, 2 h, 92 %. Ms = methanesulfonyl.

A mesylation/elimination sequence led to dehydroalanine tripeptide ester **28** via mesylate **27**, and, finally, LiOH-induced ester hydrolysis furnished the tripeptide carboxylic acid **4** in 92 % yield.

The required thiazole fragment **3** was derived from L-threonine **29** (Scheme 5). Standard acetonide formation and thiazole generation according to the Hantzsch protocol[21] led to derivative **30**. Reduction of the ester group ($LiBH_4$/LiCl, 88 %) in **30**, iodide formation (PPh_3, I_2, imidazole, 92 %), and displacement with NaN_3 (96 %) led to azide **31**. Acid-induced acetonide cleavage (TFA, 84 %) followed by Cbz protection (83 %) of the resulting amino group and Staudinger reduction (PPh_3/H_2O, 87 %) of the azide moiety then led to the desired thiazole **3**.



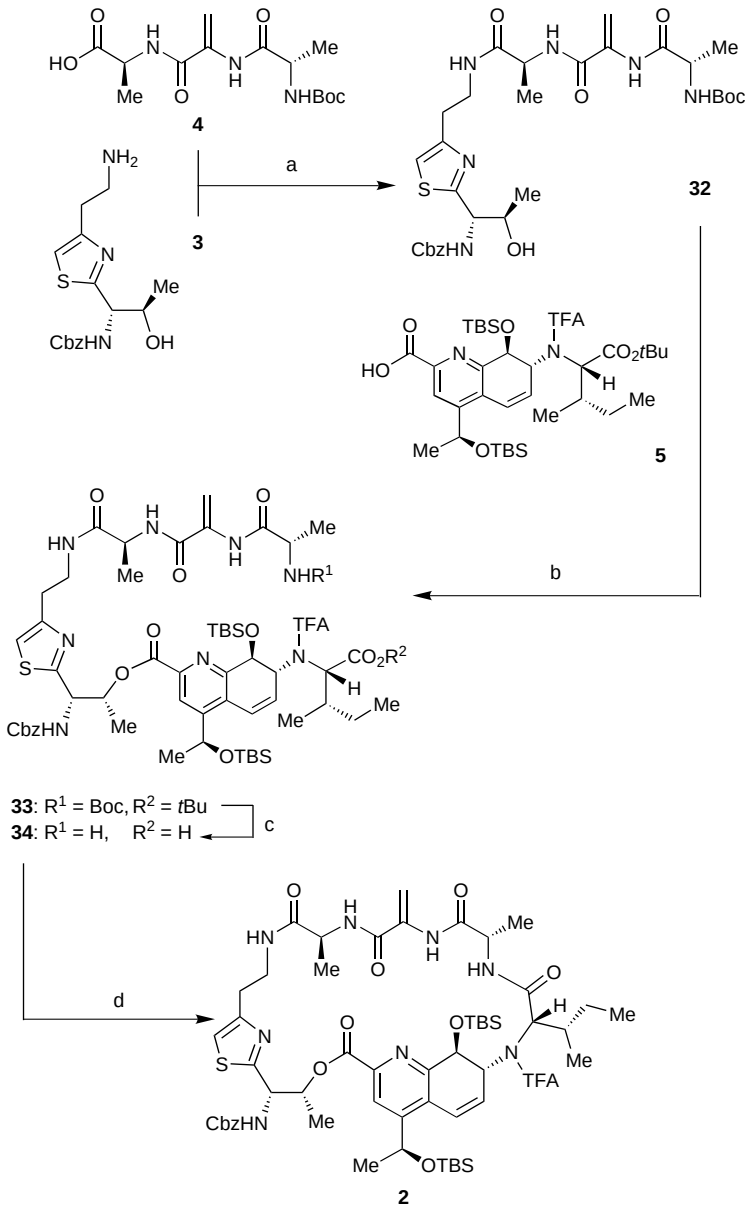
Scheme 5. Synthesis of **3**. Reagents and conditions: a) ref. [21]; b) $LiBH_4$ (3.0 equiv), LiCl (3.0 equiv), THF, 25 °C, 24 h, 88 %; c) PPh_3 (1.3 equiv), imidazole (1.4 equiv), I_2 (1.5 equiv), 25 °C, 1.5 h, 92 %; d) NaN_3 (1.0 equiv), DMF, 25 °C, 14 h, 96 %; e) TFA, CH_2Cl_2, 0 °C, 6 h, 84 %; f) CbzCl (1.0 equiv), $NaHCO_3$, THF/H_2O (1:1), 25 °C, 4 h, 83 %; g) PPh_3 (1.0 equiv), THF, H_2O, 50 °C, 6 h, 87 %. DMF = *N*,*N*-dimethylformamide; TFA = trifluoroacetic acid; Cbz = benzyloxy carbonyl.

The assembly of the quinaldic acid macrocycle **2** began with the coupling of carboxylic acid fragment **4** with amino thiazole derivative **3** under EDC/HOBt conditions, which led to secondary alcohol **32** in 71 % yield (Scheme 6). Quinaldic acid derivative **5** was appended onto fragment **32** by means of a Yamaguchi esterification[22] to furnish advanced intermediate **33** in 71 % yield. The Boc and *t*Bu groups were then removed from **33** by TFA in the presence of triisopropylsilane (to prevent degradation of the dehydroalanine moiety) to afford amino acid **34** (86 %). Ring closure of **34** led to macrocycle **2** in an unoptimized yield of 30 %.

The described chemistry offers methods for the construction of the quinaldic acid system[24] of thiostrepton (**1**) and its incorporation into the macrocycle of the natural product. The following communication describes the construction of the dehydropiperidine domain of this target molecule.[23]

Received: January 2, 2002 [Z 18462]

 © WILEY-VCH Verlag GmbH, 69451 Weinheim, Germany, 2002 1433-7851/02/4111-1939 $ 20.00+.50/0



Scheme 6. Synthesis of **2**. Reagents and conditions: a) EDC (1.1 equiv), HOBt (1.1 equiv), DMF, 0°C, 16 h, 72%; b) 2,4,6-trichlorobenzoyl chloride (1.5 equiv), Et_3N (7.0 equiv), PhMe; then 4-DMAP (2.5 equiv), **5** (1.3 equiv), THF, 25°C, 71%; c) TFA/CH_2Cl_2 (3:1), triisopropylsilane (19 equiv), 25°C, 2.5 h, 86%; d) HATU (3.0 equiv), 2,4,6-collidine (9.0 equiv), MeCN, 0°C, 24 h, 30%. EDC = 1-(3-dimethylaminopropyl)-3-ethylcarbodiimide hydrochloride; HOBt = 1-hydroxybenzotriazole hydrate; 4-DMAP = 4-dimethylaminopyridine; HATU = *O*-(7-azabenzotriazol-1-yl)-*N*,*N*,*N*′,*N*′-tetramethyluronium hexafluorophosphate; 2,4,6-collidine = 2,4,6-trimethylpyridine.

[1] a) J. F. Pagano, M. J. Weinstein, H. A. Stout, R. Donovick, *Antibiot. Annu.* **1955 – 1956**, 554 – 559; b) J. Vandeputte, J. D. Dutcher, *Antibiot. Annu.* **1955 – 1956**, 560 – 561; c) B. A. Steinberg, W. P. Jambor, L. O. Suydam, *Antibiot. Annu.* **1955 – 1956**, 562 – 565.

[2] a) C. S. Bond, M. P. Shaw, M. S. Alphey, W. N. Hunter, *Acta Crystallogr. Sect. D* **2001**, *D57*, 755 – 758; b) B. Anderson, D. C. Hodgkin, M. A. Viswamitra, *Nature* **1970**, *225*, 233 – 235.

[3] M. Bodanszky, J. Fried, J. T. Sheehan, N. J. Williams, J. Alicino, A. I. Cohen; B. T. Keeler, C. A. Birkhimer, *J. Am. Chem. Soc.* **1964**, *86*, 2478 – 2490.

[4] a) U. Mocek, J. M. Beale, H. G. J. Floss, *Antibiot. Chemother.* **1989**, *42*, 1649 – 1652; b) O. D. Hensens, G. J. Albers-Schonberg, *Antibiot. Chemother.* **1983**, *36*, 832 – 845.

[5] S. M. Dennis, T. G. Nagaraja, A. D. Dayton, *Res. Vet. Sci.* **1986**, *41*, 251 – 256.

[6] G. Rosendahl, S. Douthwaite, *Nucleic Acids Res.* **1994**, *22*, 357 – 363.

[7] Y. Xing, D. E. Draper, *Biochemistry* **1996**, *35*, 1581 – 1588.

[8] a) G. A. McConkey, M. J. Rogers, T. F. McCutchan, *J. Biol. Chem.* **1997**, *272*, 2046 – 2049; b) J. G. Hardman, L. E. Limbird, P. B. Molinoff, R. W. A. Ruddon, G. Gilman, *Goodman & Gilman*'s *The Pharmacological Basis of Therapeutics*, 9th ed., The McGraw-Hill, New York, **1996**, pp. 965 – 985.

[9] S. Higashibayashi, K. Hashimoto, M. Nakata, *Tetrahedron Lett.* **2002**, *43*, 105 – 110.

[10] a) M. C. Bagley, K. E. Bashford, C. L. Hesketh, C. J Moody, *J. Am. Chem. Soc.* **2000**, *122*, 3301 – 3313; b) M. A. Ciufolini, Y.-C. Shen, *Org. Lett.* **1999**, *1*, 1843 – 1846; c) K. Okumura, T. Suzuki, Y. Nakamura, C.-G. Shin, *Bull. Chem. Soc. Jpn*. **1999**, *72*, 1561 – 1569; d) K. Okumura, A. Ito, D. Yoshioka, C.-g. Shin, *Heterocycles* **1998**, *48*, 1319 – 1324; e) C. J. Moody, M. C. Bagley, *Chem. Commun*. **1998**, 2049 – 2050; f) C.-G. Shin, K. Okumura, M. Shigekuni, Y. Nakamura, *Chem. Lett*. **1998**, 139 – 140; g) M. A. Ciufolini, Y. C. Shen, *J. Org. Chem*. **1997**, *62*, 3804 – 3805; h) K. Okumura, M. Shigekuni, Y. Nakamura, C.-G. Shin, *Chem. Lett.* **1996**, 1025 – 1026; i) Y. Nakamura, C.-G. Shin, K. Umemura, J. Yoshimura, *Chem. Lett.* **1992**, 1005 – 1008; j) T. R. Kelly, C. T. Jagoe, Z. Gu, *Tetrahedron Lett.* **1991**, *32*, 4263 – 4266.

[11] F. W. Vierhapper, E. L. Eliel, *J. Org. Chem*. **1975**, *40*, 2729 – 2734.

[12] N. G. Priestley, T. M. Smith, P. R. Shipley, H. G. Floss, *Bioorg. Med. Chem.* **1996**, *4*, 1135 – 1147.

[13] For a review, see: E. J. Corey, C. J. Helal, *Angew. Chem.* **1998**, *110*, 2092 – 2118; *Angew. Chem. Int. Ed.* **1998**, *37*, 1986 – 2012.

[14] M. Masui, T. Shioiri, *Synlett* **1997**, 273 – 274.

[15] C. Fontenas, E. Bejan, H. A. Haddou, G. A. Galavoine, *Synth. Commun*. **1995**, *25*, 629 – 633.

[16] a) E. Jacobsen, W. Zhang, A. R. Muci, J. R. Ecker, L. Deng, *J. Am. Chem. Soc.* **1991**, *113*, 7063 – 7064; b) R. Irie, K. Noda, Y. Ito, N. Matsumoto, T. Katsuki, *Tetrahedron Lett*. **1990**, *31*, 7345 – 7348.

[17] M. Palucki, G. J. McCormick, E. N. Jacobsen, *Tetrahedron Lett*. **1995**, *36*, 5457 – 5460.

[18] a) K. Ito, M. Yoshitake, T. Katsuki, *Tetrahedron* **1996**, *52*, 3905 – 3920; b) H. Sasaki, R. Irie, T. Hamada, K. Suzuki, T. Katsuki, *Tetrahedron* **1994**, *50*, 11827 – 11838; c) for a review, see: T. Katsuki, *Curr. Org. Chem.* **2001**, *5*, 663 – 678.

[19] S. K. Agarwal, D. R. Boyd, R. J. H. Davies, L. Hamilton, D. M. Jerina, J. J. McCullough, H. P. Porter, *J. Chem. Soc. Perkin Trans. 1* **1990**, 1969 – 1974.

[20] a) M. F. Lipton, A. Basha, S. M. Weinreb, *Org. Synth.* **1980**, *59*, 49 – 53; b) L. E. Overman, L. A. Flippin, *Tetrahedron Lett.* **1981**, *22*, 195 – 198; c) A. M. Jeffrey, H. J. C. Yeh, D. M. Jerina, R. M. DeMarinis, C. H. Foster, D. E. Piccolo, G. A. Berchtold, *J. Am. Chem. Soc.* **1974**, *96*, 6929 – 6937; d) G. H. Posner, D. Z. Rogers, *J. Am. Chem. Soc.* **1977**, *99*, 8214 – 8218.

[21] K. Okumura, H. Saito, C. Shin, K. Umemura, J. Yoshimura, *J. Bull. Chem. Soc. Jpn.* **1998**, *71*, 1863 – 1870.

[22] K. C. Nicolaou, A. P. Patron, K. Ajito, P. K. Richter, H. Khatuya, P. Bertinato, R. A. Miller, M. J. Tomaszewski, *Chem. Eur. J.* **1996**, *2*, 847 – 868.

[23] K. C. Nicolaou, M. Nevalainen, B. S. Satina, M. Zak, S. Bulat, *Angew. Chem. Int. Ed.* **2002**, *41*, 1941 – 1945.

[24] Note added in proof: For an alterntive approach to a quinaldic acid system, see: S. Higashibayashi, T. Mori, K. Shinko, K. Hashimoto, M. Nakata, *Heterocycles* **2002**, *57*, 111 – 122.

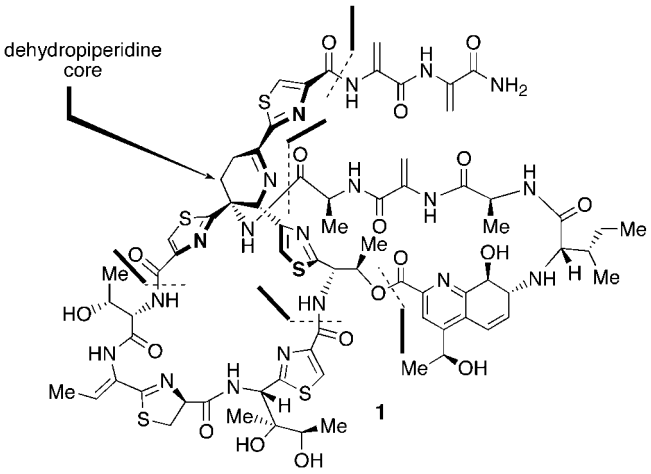
 © WILEY-VCH Verlag GmbH, 69451 Weinheim, Germany, 2002 1433-7851/02/4111-1940 $ 20.00+.50/0

A Biomimetically Inspired Synthesis of the Dehydropiperidine Domain of Thiostrepton**

K. C. Nicolaou,* Marta Nevalainen, Brian S. Safina, Mark Zak, and Stephan Bulat

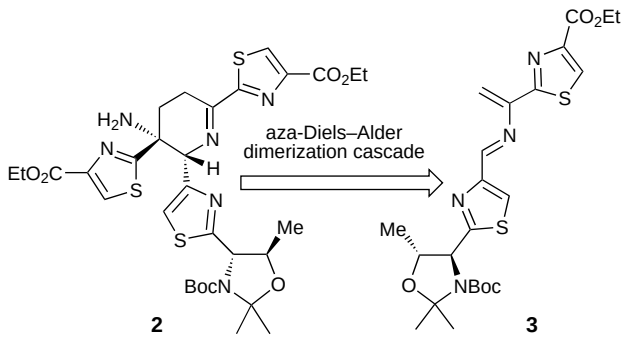
Dedicated to Professor Ralph F. Hirschmann on the occasion of his 80th birthday

In the preceding communication,[1] we described a stereoselective construction of the macrocycle of thiostrepton (**1**)[2] which incorporates the quinaldic acid moiety of the molecule.[3a] Herein we report an expedient synthesis of the

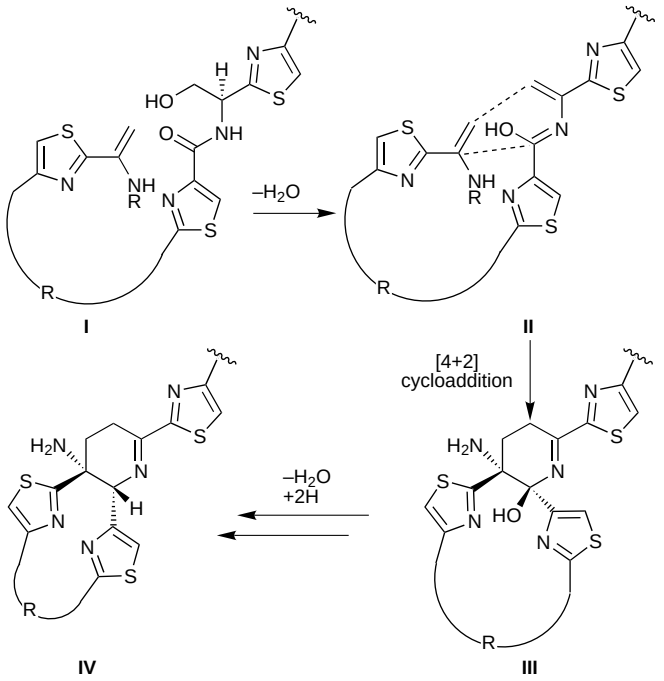


dehydropiperidine domain **2** (Scheme 1)[3b] of this complex antibiotic based on a biomimetic strategy involving a cascade reaction, which features a striking dimerization of a designed azadiene **3**, through a hetero-Diels–Alder reaction,[4] followed by hydrolytic excision of the superfluous thiazole moiety.

Based on some elegant biosynthetic studies, Floss and coworkers[5] suggested a hetero-Diels–Alder reaction (Scheme 2, **II**→**III**) as a key step in the biosynthesis of thiostrepton (**1**). Specifically, it was proposed that a precursor such as **I** (Scheme 2), upon elimination of a water molecule,



Scheme 1. Retrosynthetic analysis of the dehydropiperidine core **2**.



Scheme 2. Postulated biosynthesis of the dehydropiperidine domain of thiostrepton (**1**). R = peptide backbone.

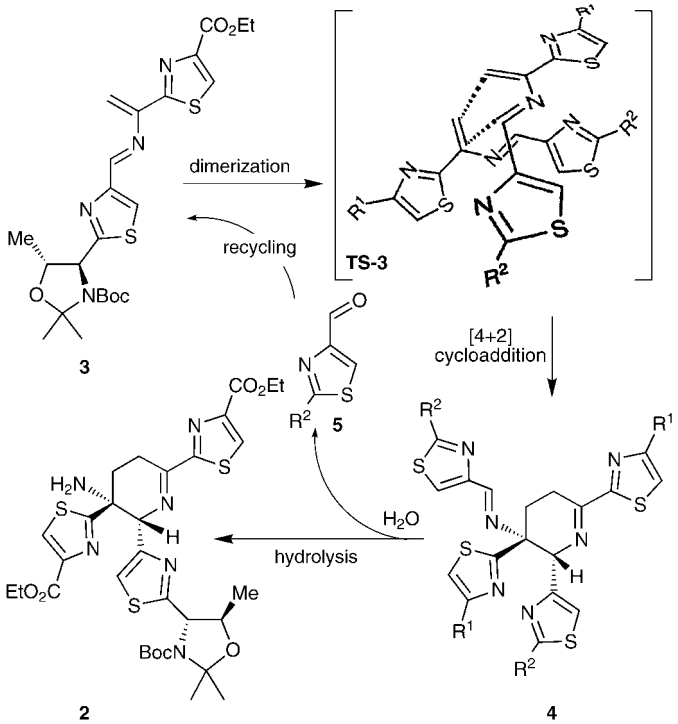
gives rise to the hydroxy azadiene system **II**, which undergoes an intramolecular [4+2] cycloaddition reaction to afford hydroxydehydropiperidine system **III**. Subsequent 1,4 dehydration then furnishes a conjugated azadiene system, whose 1,4 reduction leads to the thiostrepton structure **IV** (Scheme 2).

Inspired by this fascinating hypothesis, we sought to devise a chemical route for the construction of dehydropiperidine moiety **2** of thiostrepton, as shown in Scheme 3. Our proposed strategy involved the design of a cascade sequence whereby a suitable precursor would generate the 2-azadiene **3**,[6] whose dimerization[7] through a hetero-Diels–Alder cyclization would proceed through a pathway in which the conjugated imino-olefin system of one molecule would act as the diene and the olefinic unit of another molecule would serve as the dienophile (Scheme 3, **TS-3**). Although no facial selectivity was anticipated in this process, the *endo* rule was expected to prevail, thus leading to the desired *trans* relationship between the two adjacent thiazole rings in structure **4**. Whether the remote chiral Boc acetonide moiety of **3** would exert any

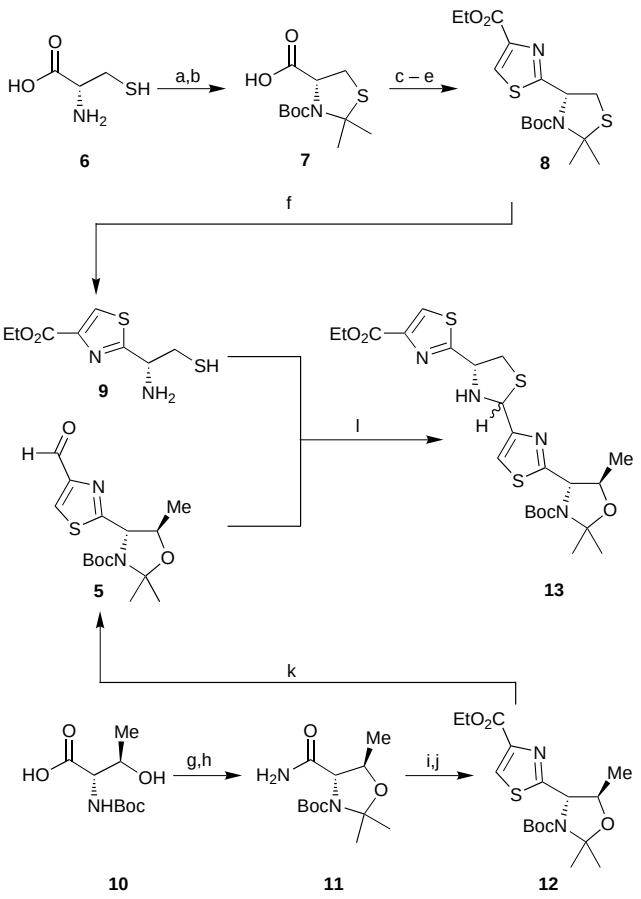
[*] Prof. Dr. K. C. Nicolaou, Dr. M. Nevalainen, B. S. Safina, M. Zak, Dr. S. Bulat
Department of Chemistry and The Skaggs Institute for Chemical Biology
The Scripps Research Institute
10550 North Torrey Pines Road, La Jolla, CA 92037 (USA)
Fax: (+1) 858-784-2469
Department of Chemistry and Biochemistry
University of California, San Diego
9500 Gilman Drive, La Jolla, CA 92093 (USA)
E-mail: kcn@scripps.edu

[**] We thank Drs. D. H. Huang and L. Pasternack, G. Suizdak, and R. Chadja for NMR spectroscopic, mass spectrometric, and X-ray crystallographic assistance, respectively. Financial support for this work was provided by The Skaggs Institute for Chemical Biology, the National Institutes of Health (USA), fellowships from The Academy of Finland (M.N.), The Skaggs Institute for Research (M.Z.), and Bayer AG (S.B.), and grants from Abbott, Amgen, Array Biopharma, Boehringer-Ingelheim, Glaxo, Hoffmann-LaRoche, DuPont, Merck, Novartis, Pfizer, and Schering Plough.

 © WILEY-VCH Verlag GmbH, 69451 Weinheim, Germany, 2002 1433-7851/02/4111-1941 $ 20.00+.50/0



Scheme 3. Proposed biomimetic strategy for the laboratory synthesis of the dehydropiperidine domain **2**. $R_1 = CO_2Et$, R_2 = Boc acetonide threonine side chain. Boc = *tert*-Butoxycarbonyl.



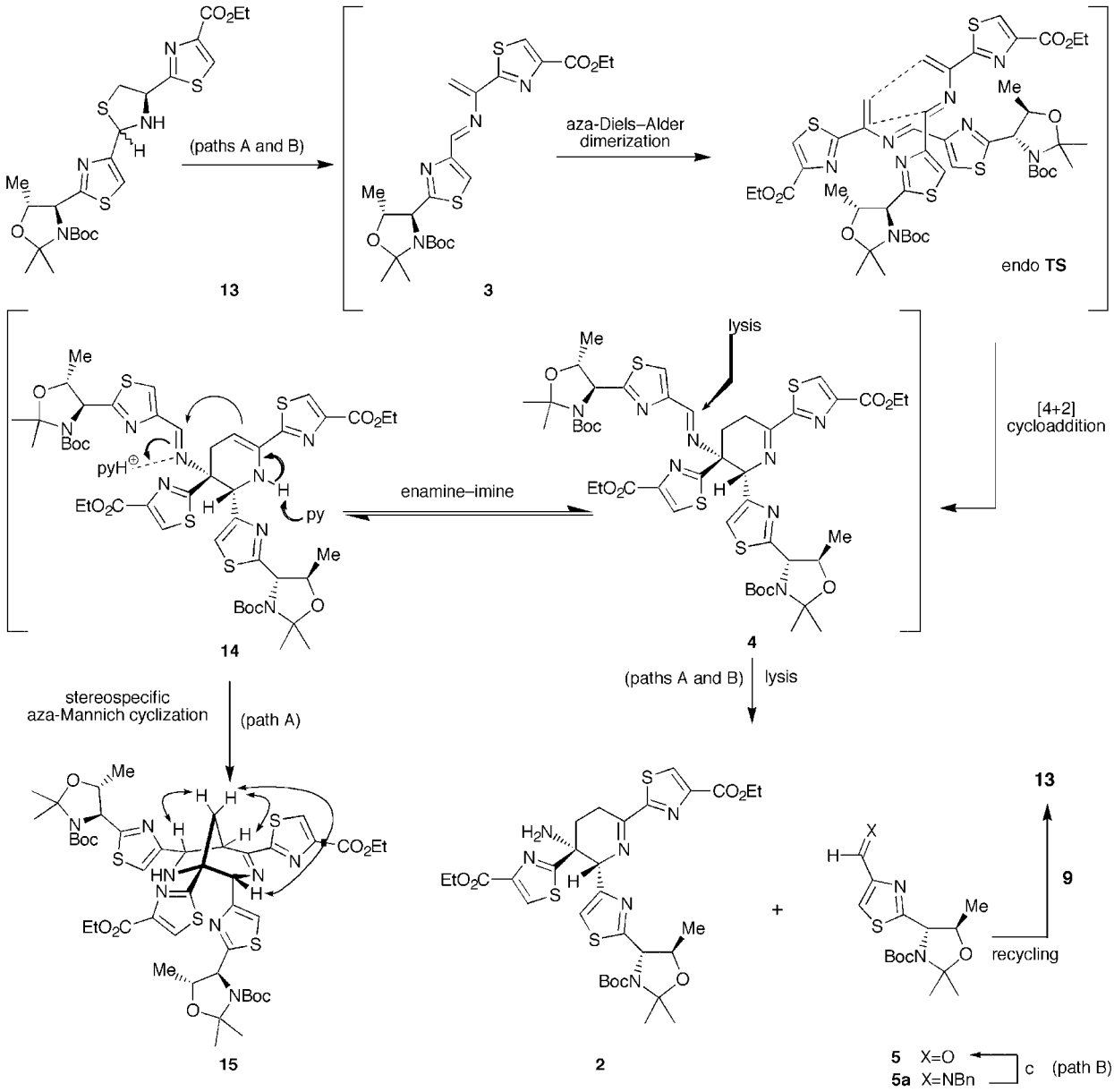
Scheme 4. Synthesis of thiazolidine **13**. Reagents and conditions: a) acetone, 60 °C, 2 h, 99 %; b) Boc_2O (1.2 equiv), *i*Pr_2NEt (1.1 equiv), MeCN, 25 °C, 48 h, 40 %; c) DCC (1.1 equiv), HOSu (1.1 equiv), THF, 0 °C, 3 h; then NH_3 (aqueous, 28 %), 0 °C, 30 min, 65 %; d) Lawesson's reagent (0.6 equiv), DME, 25 °C, 12 h, 85 %; e) $BrCH_2COCO_2Et$ (3.0 equiv), $KHCO_3$ (3.0 equiv), THF, 25 °C, 24 h; then TFAA (1.5 equiv), pyridine (3.0 equiv), 0 °C, 3 h, 90 %; f) TFA/CH_2Cl_2 (3:1), 25 °C, 3 h; then EtOH/H_2O (1:1), 25 °C, concentration in vacuo, 98 %; g) $(MeO)CMe_2$ (22.0 equiv), *p*-TsOH (0.1 equiv), CH_2Cl_2, 25 °C, 24 h, 91 %; h) $ClCO_2Et$ (1.1 equiv), Et_3N (1.1 equiv), THF, 0 °C, 30 min; then NH_3 (aqueous, 28 %), 0 °C, 1.5 h, 78 %; i) Lawesson's reagent (0.6 equiv), benzene, 80 °C, 1 h, 85 %; j) $BrCH_2COCO_2Et$ (3.0 equiv), $NaHCO_3$ (8.0 equiv), DME, 25 °C, 24 h; then TFAA (4.0 equiv), pyridine (9.0 equiv), 0 °C, 1 h, 90 %; k) DIBAL (2.0 equiv), toluene, −78 °C, 2 h, 87 %; l) **9**·TFA (1.0 equiv), **5** (1.0 equiv), $KHCO_3$ (3.0 equiv), EtOH/H_2O (1:1), 25 °C, 12 h, 90 %. Boc = *tert*-butoxycarbonyl; DCC = 1,3-dicyclohexylcarbodiimide; HOSu = *N*-hydroxysuccinimide; DME = dimethoxyethane; TFAA = trifluoroacetic anhydride; TFA = trifluoroacetic acid; *p*-TsOH = *p*-toluenesulfonic acid.

stereochemical control on the expected [4+2] cycloaddition was an open question. Subsequent hydrolysis of the labile exocyclic imine functionality of **4** was then expected to generate the desired dehydropiperidine system **2**, with the concomitant release of thiazole aldehyde **5**. Thiazole **5** would be recycled back into **3** thus, in principle, increasing the efficiency of the overall process.

To implement this strategy we chose thiazolidine compound **13** (Scheme 4) as a suitable precursor for the required 2-azadiene system **3** (Scheme 2). The convergent synthesis of **13** proceeded from L-cysteine (**6**) and L-threonine (**10**), as shown in Scheme 4. Thus, the amino acids **6** and **10** were converted into their Boc acetonide derivatives **7** and **11**, respectively, by known procedures.[8] Acetonides **7** and **11** were then converted into **8** and **12**, respectively, by means of the modified Hantzsch thiazole-forming reaction.[9] Removal of the Boc group from intermediate **8** under acidic conditions (TFA) and subsequent concentration in the presence of EtOH and H_2O led to complete removal of the generated acetone and the isolation of amino thiol **9** in 98 % yield. On the other hand, DIBAL reduction of ethyl ester **12** furnished aldehyde **5** cleanly (87 % yield). Finally, condensation of fragments **9** and **5** in EtOH/H_2O (1:1) in the presence of $KHCO_3$ proceeded smoothly to afford the desired thiazolidine **13** in 90 % yield.

With thiazolidine **13** in hand, we were now in a position to test the hypothesis of the hetero-Diels–Alder reaction proposal as part of the cascade leading to the projected dehydropiperidine system **2**. Indeed, exposure of a solution of **13** in pyridine to Ag_2CO_3 and catalytic amounts of DBU at −15 °C led to the rupture of the thiazolidine moiety and generation of the 2-azadiene system **3**, which underwent spontaneous [4+2] cycloaddition to afford the coveted dehydropiperidine system **4**, apparently as a mixture with its tautomeric form, enamine **14** (Scheme 5, path A).[6c, 7] Upon quenching with water at −15 °C, the desired dehydropiperidine fragment **2** (22 %), aldehyde **5** (20 %), and [3.2.1]-bridged bicycle **15** (63 %, see Table 1 for data) were obtained. Whereas the origin of **2** and **5** can be attributed to a simple imine hydrolysis of imino compound **4**, the formation of **15** must be the result of a stereospecific aza-Mannich cyclization within **14**, as designated by the arrows in Scheme 5. The relative stereochemistry of **15** was established on the basis of NOE studies (Scheme 5), and later confirmed by X-ray

 © WILEY-VCH Verlag GmbH, 69451 Weinheim, Germany, 2002 1433-7851/02/4111-1942 $ 20.00+.50/0 *Angew. Chem. Int. Ed.* **2002**, *41*, No. 11



Scheme 5. Hetero-Diels–Alder dimerization cascade. Reagents and conditions: path A. a) Ag_2CO_3 (1.1 equiv), DBU (0.2 equiv), pyridine, −15 °C, 1 h; b) H_2O, 10 min; products: **15** (63%, ca. 1:1 ratio of diastereomers), **2** (22%, ca. 1:1 ratio of diastereomers), **5** (20%); path B. a) Ag_2CO_3 (1.1 equiv), DBU (0.2 equiv), $PhCH_2NH_2$ (1.0 equiv), pyridine, −15 °C, 1 h; b) H_2O, 10 min; c) silica gel, 25 °C, CH_2Cl_2/AcOEt (1:1); products: **15** (trace); **2** (60%, ca. 1:1 ratio of diastereomers); **5** (68%). DBU = 1,8-diazabicyclo[5.4.0]undec-7-ene.

crystallographic analysis (of **16**, see below). Although the Diels–Alder reaction proceeded both in a regioselective and *endo*-selective manner, it showed no facial selectivity and, therefore, compounds **4**, **14**, **15**, and **2** are mixtures of diastereomers (ca. 1:1) with regards to the relative stereochemistry of the core substituents and those already existing on the remote chiral Boc acetonide moiety.

To further establish the stereochemistry of the [3.2.1]-bridged system **15**, and, therefore, that of its precursors, the rather labile imine **15** was subjected to reduction with $NaCNBH_3$ in the presence of AcOH/EtOH, which led to its more stable amino counterpart **16** (Table 1) in 85% yield (Scheme 6). Compound **16** was chromatographically purified to a single diastereomer and crystallized from hexanes/ethyl acetate. X-ray crystallographic analysis (Figure 1) confirmed its absolute stereochemistry, which was also clear from NOE experiments (see arrows in **16**, Scheme 6).

To improve the yield of the targeted tertiary amine **2**, we chose transimination as a possible means to excise the undesired fragment **5** from the dimerization product **4**, and thus suppress the aza-Mannich reaction that leads to **15**. Indeed, the addition of stoichiometric amounts of benzylamine to the reaction mixture led to **2** (60%), **5** (68%, after hydrolysis of the resulting imine **5a**), and only traces of **15** (see Scheme 5, path B).

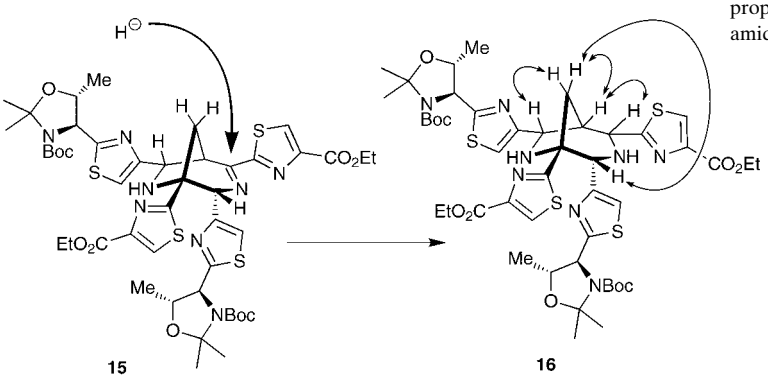
In further experiments (Scheme 7), the imine functionality of **2** (ca. 1:1 mixture of diastereomers) was reduced with $NaCNBH_3$–AcOH in EtOH to afford the corresponding

 © WILEY-VCH Verlag GmbH, 69451 Weinheim, Germany, 2002 1433-7851/02/4111-1943 $ 20.00+.50/0

Table 1. Selected data for compounds **15** and **16**.

15. $R_f = 0.32$ (silica gel, CH_2Cl_2/EtOAc, 1:1); $[\alpha]_D^{20} = -29.8$ ($c = 2.2$, $CHCl_3$); IR (film): $\tilde{\nu}_{max} = 3354$, 3005, 2991, 1702, 1478, 1367, 1208, 1131, 1096, 756 cm^{-1}; ^1H NMR (600 MHz, CD_3CN, 70 °C): $\delta = 8.13$ (s, 1H), 8.02 (s, 1H), 7.55 (s, 1H), 7.42 (s, 1H), 6.02 (s, 1H), 5.04 (m, 1H), 4.58 (d, $J =$ 7.4 Hz, 1H), 4.46 (d, $J = 7.0$ Hz, 1H), 4.40–4.25 (m, 5H), 3.96 (m, 1H), 3.80 (m, 1H), 2.80 (d, $J = 11.4$ Hz, 1H), 2.58 (dd, $J = 11.4$, 3.5 Hz, 1H), 1.59 (s, 3H), 1.59 (s, 3H), 1.55 (s, 3H), 1.55 (s, 3H), 1.51 (s, 3H), 1.40–1.05 ppm (m, 30H); ^{13}C NMR (125 MHz, CD_3CN, 70 °C): $\delta = 178.2$, 171.1, 169.0, 165.2, 161.7, 161.1, 154.1, 153.6, 151.9, 148.2, 148.1, 148.0, 131.6, 131.1, 128.2, 118.9, 116.8, 116.0, 95.1, 95.0, 80.5, 80.3, 78.5, 77.5, 73.0, 72.1, 67.2, 66.0, 65.9, 61.4, 61.2, 45.2, 41.3, 28.1, 27.9, 28.0–27.0 (b), 25.7 (b), 18.2, 17.5, 14.0, 14.0 ppm; HRMS (MALDI): calcd for $C_{46}H_{60}N_8O_{10}S_4$ [M+Na$^+$]: 1035.3214; found: 1035.3293

16. $R_f = 0.24$ (silica gel, CH_2Cl_2/EtOAc, 1:1); $[\alpha]_D^{20} = -39.7$ ($c = 1.6$, $CHCl_3$); IR (film): $\tilde{\nu}_{max} = 3400$, 2979, 1702, 1366, 1210, 1090, 754 cm^{-1}; ^1H NMR (600 MHz, CD_3CN, 70 °C): $\delta = 7.94$ (s, 1H), 7.89 (s, 1H), 7.13 (s, 1H), 7.04 (s, 1H), 4.95 (d, $J = 4.4$ Hz, 1H), 4.89 (s, 1H), 4.82 (br s, 1H), 4.72 (d, $J = 8.0$ Hz, 1H), 4.65 (d, $J = 6.5$ Hz, 1H), 4.64 (s, 1H), 4.36 (q, $J = 7.0$ Hz, 2H), 4.32 (q, $J = 7.0$ Hz, 2H), 4.04 (m, 1H), 3.95 (m, 1H), 3.83 (bs, 1H), 3.47 (t, $J = 4.0$ Hz, 1H), 2.71 (d, $J = 11.4$ Hz, 1H), 2.64 (dd, $J = 11.4$, 4.4 Hz, 1H), 1.63 (s, 6H), 1.56 (s, 3H), 1.55 (s, 3H), 1.40–1.25 ppm (m, 30H); ^{13}C NMR (150 MHz, CD_3CN, 70 °C): $\delta = 173.5$, 171.5, 162.2, 161.9, 154.8, 154.5, 148.4, 147.3, 128.2, 127.9, 117.2, 95.6, 95.6, 78.1, 77.6, 69.8, 66.8, 66.7, 65.5, 62.8, 62.7, 61.5, 61.5, 46.7, 45.9, 28.5, 28.4, 28.0–27.0 (br), 26.5, 26.3, 20.8, 20.2, 19.7, 18.3, 14.4, 14.4 ppm; HRMS (MALDI): calcd for $C_{46}H_{62}N_8O_{10}S_4$ [M+Na$^+$]: 1037.3364; found: 1037.3371



Scheme 6. Stereospecific reduction of the imine functionality in **15** and structural assignment of **16** by NMR spectroscopy (see indicated NOE interactions). Reagents and conditions: $NaCNBH_3$ (2.0 equiv), AcOH/EtOH (1:1), 25 °C, 2 h, 85%.

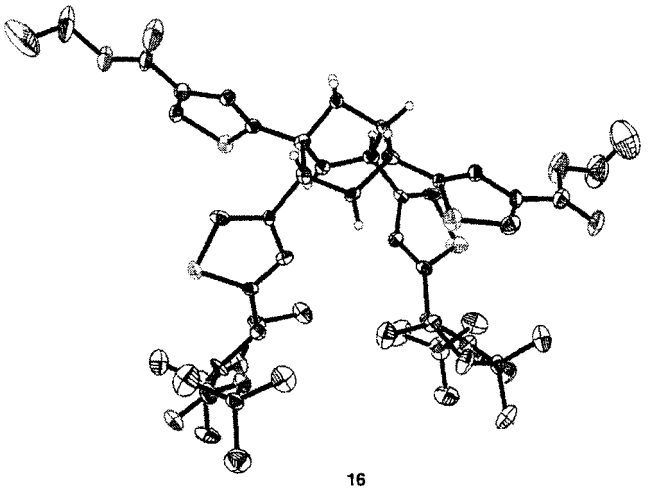
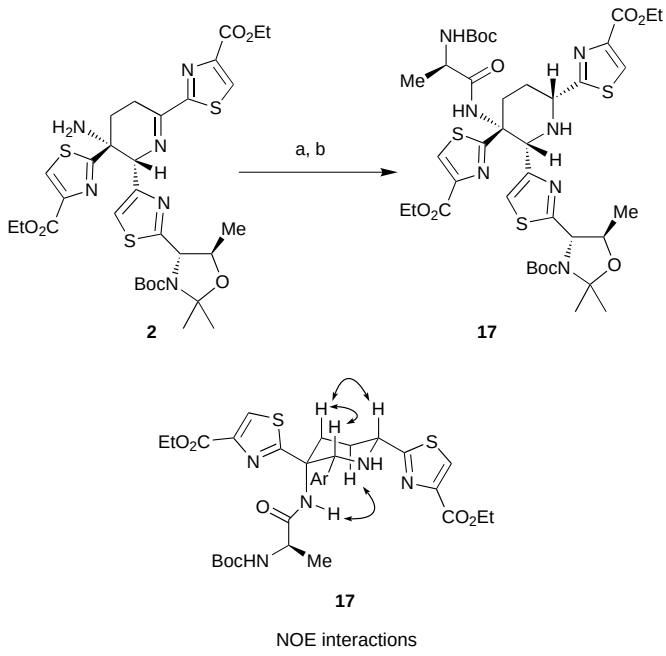


Figure 1. ORTEP diagram of **16**.



Scheme 7. Stereospecific reduction, coupling of **2**, and stereochemical assignment of **17** by NOE studies. Reagents and conditions: a) $NaCNBH_3$ (2.0 equiv), AcOH/EtOH (1:1), 25 °C, 2 h; b) HOAt (1.1 equiv), EDC (1.1 equiv), H-Ala-NBoc (1.1 equiv), DMF, 0 → 25 °C, 19 h, 82% over two steps. HOAt = 1-hydroxy-7-azabenzotriazole; EDC = 1-(3-dimethylaminopropyl)-3-ethylcarbodiimide hydrochloride; DMF = *N*,*N*-dimethylformamide.

diamine, whose selective coupling with H-Ala-NBoc in the presence of EDC–HOAt led to peptide **17** (82% yield, ca. 1:1 mixture of diastereomers).[3b] The stereochemistry of **17** and therefore of **2** became clear from NOE studies, as indicated in Scheme 7 (arrows in **17**).

In conclusion, we devised and experimentally demonstrated a biomimetic approach to the unusual dehydropiperidine domain of thiostrepton (**1**) based on a novel intermolecular hetero-Diels–Alder reaction followed by imine hydrolysis. Refinements of this cascade reaction with regards to efficiency and stereochemical control are anticipated and should facilitate the total synthesis of this challenging target. Furthermore, other modifications of this hetero-Diels–Alder reaction, including heterodimerizations and intramolecular versions, are currently considered as alternative approaches to thiostrepton. The described synthetic technology also appears to be amenable to the construction of a wide range of novel and biologically relevant heterocycles, including complex structures such as the [3.2.1]-bridged systems **15** and **16** for biological screening purposes.

Received: March 15, 2002 [Z18904]

[1] K. C. Nicolaou, B. S. Safina, C. Funke, M. Zak, F. J. Zécri, *Angew. Chem.* **2002**, *114*, 2017–2020; *Angew. Chem. Int. Ed.* **2002**, *41*, 1937–1940, preceding communication.

[2] Isolation: a) J. F. Pagano, M. J. Weinstein, H. A. Stout, R. Donovick, *Antibiot. Ann.* **1955–1956**, 554–559; b) J. Vandeputte, J. D. Dutcher, *Antibiot. Ann.* **1955–1956**, 560–561; c) B. A. Steinberg, W. P. Jambor, L. O. Suydam, *Antibiot. Ann.* **1955–1956**, 562–565; structure determination: d) C. S. Bond, M. P. Shaw, M. S. Alphey, W. N. Hunter, *Acta*

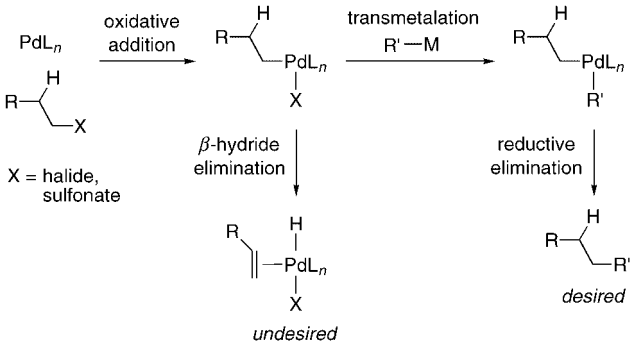
 © WILEY-VCH Verlag GmbH, 69451 Weinheim, Germany, 2002 1433-7851/02/4111-1944 $ 20.00+.50/0

Crystallogr. Sect. D **2001**, *57*, 755 – 758; e) B. Anderson, D. C. Hodgkin, M. A. Viswamitra, *Nature* **1970**, *225*, 233 – 235.
[3] For other related synthetic studies towards thiostrepton, see: a) S. Higashibayashi, T. Mori, K. Shinko, K. Hashimoto, M. Nakata, *Heterocycles* **2002**, *57*, 111 – 122; b) S. Higashibayashi, K. Hashimoto, M. Nakata, *Tetrahedron Lett.* **2002**, *43*, 105 – 110.
[4] For reviews, see: a) "Hetero-Diels – Alder Methodology in Organic Chemistry": D. L. Boger, S. M. Weinreb in *Organic Synthesis*, *Vol. 47*, Academic Press, San Diego, **1987**, p. 386; b) "Stereoselective Heterocyclic Synthesis I": L. F. Tietze, G. Kettschau, *Top. Curr. Chem.* **1997**, *189*, 1 – 120.
[5] U. Mocek, Z. Zeng, D. O'Hagan, P. Zhou, L.-D. G. Fan, J. M. Beale, H. G. Floss, *J. Am. Chem. Soc.* **1993**, *115*, 7992 – 8001.
[6] For some recent examples of Diels – Alder reactions of 2-azadienes, see: a) F. Palacios, E. Herrán, G. Rubiales, J. M. Ezpeleta, *J. Org. Chem.* **2002**, *67*, 2131 – 2135; b) F. Palacios, C. Alonso, P. Amezua, G. Rubiales, *J. Org. Chem.* **2002**, *67*, 1941 – 1946; c) T. M. V. D. Pinho e Melo, R. Fausto, A. M. d'A. Rocha Gonsalves, *J. Org. Chem.* **1998**, *63*, 5350 – 5355, and references therein.
[7] For similar dimerizations, see: a) G. Wulff, H. T. Klinken, *Tetrahedron* **1992**, *48*, 5985 – 5990; b) G. Wulff, H. G. Lindner, H. Bohnke, A. Steigel, H. T. Klinken, *Liebigs Ann. Chem.* **1989**, 527 – 531; c) G. Wulff, H. Böhnke, *Angew. Chem.* **1986**, *98*, 101 – 102; *Angew. Chem. Int. Ed. Engl.* **1986**, *25*, 90 – 92.
[8] a) K. Okumura, Y. Nakamura, C.-g. Shin, *Bull. Chem. Soc. Jpn.* **1999**, *72*, 1561 – 1569; b) D. S. Kemp, R. I. Carey, *J. Org. Chem.* **1989**, *54*, 3640 – 3646; c) K. Okumura, H. Saito, C. Shin, J. Yoshimura, K. Uemura, *Bull. Chem. Soc. Jpn.* **1998**, *71*, 1863 – 1870.
[9] C. Holzapfel, G. J. Pettit, *J. Org. Chem.* **1985**, *50*, 2323 – 2327.

A Method for Palladium-Catalyzed Cross-Couplings of Simple Alkyl Chlorides: Suzuki Reactions Catalyzed by $[Pd_2(dba)_3]/PCy_3$**

Jan H. Kirchhoff, Chaoyang Dai, and Gregory C. Fu*

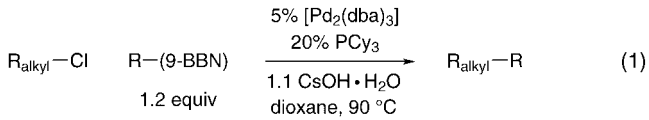
Palladium-catalyzed cross-couplings of organic electrophiles with main-group organometallic compounds serve as straightforward, powerful methods for carbon – carbon bond formation, and such processes are routinely used in fields ranging from materials science to natural product synthesis.[1] The overwhelming majority of studies of metal-catalyzed cross-couplings have employed a halide or sulfonate as the electrophile and a organometallic reagent as the nucleophile in which the carbon atoms to be coupled are all sp^2-hybridized (e.g., for the synthesis of biaryls). In contrast, reports of successful couplings of simple halides/sulfonates bound to sp^3-hybridized carbon atoms are very rare.[2] Two of the likely reasons that have hampered the utilization of these important families of electrophiles are: 1) slow oxidative addition of the alkyl halide/sulfonate to palladium, and 2) if oxidative addition has indeed taken place, β-hydride elimination of the resulting alkyl – palladium complex, in preference to cross-coupling (Scheme 1).



Scheme 1. Palladium-catalyzed cross-coupling of an alkyl halide/sulfonate.

It is critical to point out that three studies in particular have, however, described noteworthy progress in overcoming this considerable limitation in the scope of metal-catalyzed cross-coupling reactions. In a pioneering investigation in 1992, Suzuki et al. discovered that $[Pd(PPh_3)_4]$ can catalyze couplings of alkyl iodides with alkyl boranes at 60 °C in yields as high as 71 %.[3, 4] Furthermore, we established last year that $Pd(OAc)_2/PCy_3$ effects Suzuki reactions of alkyl bromides at room temperature.[5] Finally, in a series of reports beginning in 1995, Knochel et al. have demonstrated that a nickel-based catalyst can promote cross-couplings of alkyl bromides and iodides with organozinc reagents.[6] Although each of these studies represents an important development, even collectively they provide a solution to only a small subset of the coupling processes of interest.

Thus, there is still a very substantial need for the development of catalysts to cross-couple alkyl halides. Since there has been essentially no success to date in any palladium- or nickel-catalyzed coupling of simple alkyl chlorides, in contrast to iodides or bromides, they represent a particularly significant challenge.[2, 7] In view of our recent progress in developing mild conditions for Suzuki reactions of alkyl bromides,[5] we decided to determine if we might also be able to contribute to solving the problem of coupling alkyl chlorides. In this communication, we describe the advances that we have made toward this objective [Eq. (1); 9-BBN = 9-borabicyclo[3.3.1]-nonane].



[*] Prof. Dr. G. C. Fu, Dr. J. H. Kirchhoff, Dr. C. Dai
Department of Chemistry
Massachusetts Institute of Technology
Cambridge, MA 02139 (USA)
Fax: (+1) 617-258-7500
E-mail: gcf@mit.edu

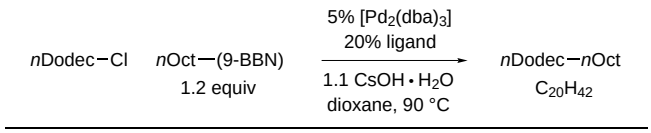
[**] dba = (*E*,*E*)-dibenzylideneacetone, Cy = cyclohexyl. We thank Dr. Matthew R. Netherton for helpful discussions and Johnson Matthey Inc. for supplying palladium compounds. Support has been provided by the Deutsche Akademie der Naturforscher Leopoldina (Leopoldina fellowship to J.H.K., BMBF-LPD 9901/8-48), Bristol-Myers Squibb, the National Institutes of Health (National Institute of General Medical Sciences, R01-GM62871), the Natural Sciences and Engineering Research Council of Canada (postdoctoral fellowship to C.D.), and Novartis. Funding for the MIT Department of Chemistry Instrumentation Facility has been provided in part by NSF CHE-9808061 and NSF DBI-9729592.

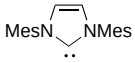
Supporting information for this article is available on the WWW under http://www.angewandte.com or from the author.

 © WILEY-VCH Verlag GmbH, 69451 Weinheim, Germany, 2002 1433-7851/02/4111-1945 $ 20.00+.50/0

Lower reactivity for alkyl chlorides, as compared to bromides or iodides, is of course a recurring observation in organic chemistry that probably originates from the decreased leaving-group ability of the chloride ion[8] and/or the higher strength of the C–Cl bond (C–Cl: ≈79; C–Br: ≈66; C–I: ≈52 kcal mol^{-1}).[9] Not surprisingly, when we subjected an alkyl chloride (1-chlorododecane) to the conditions that have proved useful for the corresponding cross-coupling of an alkyl bromide with an alkyl borane (4% $Pd(OAc)_2$, 8% PCy_3, 1.2 $K_3PO_4 \cdot H_2O$, THF, room temperature), we obtained only very small amounts (<5% yield) of the desired product. However, through optimization and by increasing the reaction temperature, we have been able to perform the targeted coupling in good yield (Table 1, entry 1).

Table 1. Relative efficiency of various ligands in the palladium-catalyzed Suzuki cross-coupling of an alkyl chloride.



Entry	Ligand[a]	Yield of $C_{20}H_{42}$ [%][b]
1	PCy_3	77
2	P(cyclopentyl)$_3$	57
3	P*i*Pr$_3$	53
4	P*t*Bu$_3$	<2
5	P*n*Bu$_3$	5
6[c]	dcpe	<2
7	PPh_3	<2
8	P(*o*-tol)$_3$	<2
9	P(2-furyl)$_3$	4
10[c]	dppf	<2
11[c]	binap	<2
12	$AsPh_3$	<2
13	$P(OPh)_3$	<2
14		8

[a] dcpe = 1,2-bis(dicyclohexylphosphanyl)ethane, tol = tolyl, dppf = 1,1′-bis(diphenylphosphanyl)ferrocene, binap = 2,2′-bis(diphenylphosphanyl)-1,1′-binaphthyl, Mes = mesityl. [b] Determined by GC versus a calibrated internal standard. [c] For bidentate ligands, 10% of the ligand was used.

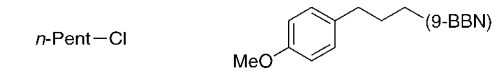
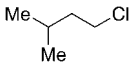
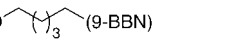
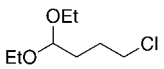
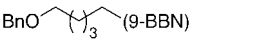
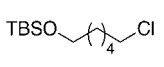
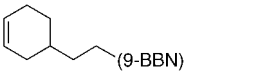
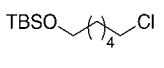
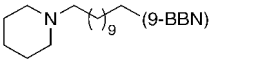
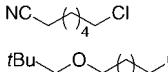
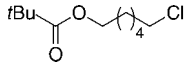
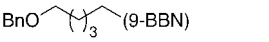
As we had determined for alkyl bromides, the efficiency of the Suzuki cross-coupling of alkyl chlorides is strongly dependent on the structure of the phosphane.[10] P(cyclopentyl)$_3$ and P*i*Pr$_3$, which are sterically and electronically similar to PCy_3, are, however, significantly less effective (Table 1, entries 2 and 3, respectively). For trialkyl phosphanes that are appreciably larger (P*t*Bu$_3$) or smaller (P*n*Bu$_3$) than PCy_3, essentially no coupling is observed (<5%; entries 4 and 5), which illustrates that the window of reactivity is relatively narrow. Furthermore, dcpe, a bidentate analogue of PCy_3, does not furnish the desired product (entry 6).

A wide array of triarylphosphanes, both monodentate (entries 7–9) and bidentate (entries 10 and 11), are also ineffective under these conditions. Finally, arsanes, phosphites, and N-heterocyclic carbenes provide virtually no activity (entries 12–14).

The conditions described in Equation (1) are the best that we have developed to date for Suzuki cross-couplings of alkyl chlorides. Thus, we have determined that a 2:1 phosphane:palladium ratio is optimal[11] and that $[Pd_2(dba)_3]$, $CsOH \cdot H_2O$, and dioxane are the palladium source, the activator, and the solvent of choice, respectively. $Pd(OAc)_2$, $K_3PO_4 \cdot H_2O$, and THF, which we employed in Suzuki reactions of alkyl bromides, furnish markedly lower activity.[12]

By using our optimized reaction conditions, we can perform Suzuki cross-couplings of an array of alkyl chlorides that possess β hydrogen atoms (Table 2). Thus, $[Pd_2(dba)_3]/PCy_3$ couples unfunctionalized substrates in good yield (83%; entry 1). Furthermore, the process is compatible with a variety of functional groups, including aryl, benzyl, and silyl

Table 2. Suzuki cross-couplings of alkyl chlorides [Eq. (1)].

Entry	R_{alkyl}–Cl	R–(9-BBN)[a]	Yield [%][b]
1	*n*-Dodec–Cl	*n*-Oct–(9-BBN)	83
2	*n*-Pent–Cl		82
3			74
4			70
5			72
6[c]			73
7		*n*-Oct–(9-BBN)	73
8[d]			65

[a] Prepared by hydroboration with 9-BBN of the corresponding alkene and used without purification. [b] Yield of isolated product, average of two runs. [c] 1.05 equiv of R–(9-BBN) was used. [d] KOH was used instead of $CsOH \cdot H_2O$.

ethers (entries 2–6), acetals (entry 4), olefins (entry 5), amines (entry 6), nitriles (entry 7), and esters (entry 8).[13] In the case of esters, we employ KOH, rather than $CsOH \cdot H_2O$,[14] to decrease the extent of hydrolysis.[15]

This report has introduced an important new class of substrates into the family of compounds that can be considered as potential partners in metal-catalyzed cross-coupling reactions. Until now, the limited progress that had been achieved in coupling alkyl halides had been restricted to iodides and bromides. In this study, we have described the first catalyst that is effective for reactions of alkyl chlorides; specifically, we have established that $[Pd_2(dba)_3]/PCy_3$ catalyzes the Suzuki cross-coupling of a range of chlorides that contain β hydrogen atoms with an array of alkyl-9-BBN derivatives. The conditions are compatible with a variety of functional groups, including potential ligands such as nitriles and amines. Current investigations are focused on discovering even more active catalysts, expanding the scope of suitable substrates, and developing additional coupling processes.

 © WILEY-VCH Verlag GmbH, 69451 Weinheim, Germany, 2002 1433-7851/02/4111-1946 $ 20.00+.50/0 *Angew. Chem. Int. Ed.* **2002**, *41*, No. 11

Experimental Section

A vial equipped with a septum screw-cap and a stir bar was purged with argon. The olefin (1.20 mmol, 1.20 equiv) and then a solution of 9-BBN (0.50 M in THF; 2.40 mL, 1.20 mmol, 1.20 equiv) were introduced to the vial, and the resulting homogeneous solution was stirred for at least 6 hours at room temperature. After that time, the THF was removed under vacuum and replaced with dioxane (0.9 mL).[16] In air, a stir bar, $[Pd_2(dba)_3]$ (45.8 mg, 0.05 mmol, 5%), PCy_3 (56.0 mg, 0.20 mmol, 20%), and $CsOH \cdot H_2O$ (185 mg, 1.10 mmol, 1.10 equiv) were placed into a second vial, which was then capped with a septum screw-cap and purged with argon for 10 minutes. Dioxane (0.3 mL) was added by syringe, and then the solution of the alkyl-9-BBN was added through a cannula (the alkyl-9-BBN was transfered completely by rinsing the first vial with dioxane (2×0.3 mL)). The alkyl chloride (1.00 mmol, 1.00 equiv) was introduced to this homogeneous brown solution, and the resulting mixture was stirred vigorously under argon for 48 hours at 90 °C. At the conclusion of the coupling, the reaction mixture, which was now heterogeneous, was cooled to room temperature, diluted with Et_2O (5 mL), and filtered through a short plug of silica gel with Et_2O washings (30 mL). The solvent was evaporated, and the resulting yellow residue was purified by flash chromatography.

Received: March 15, 2002 [Z18905]

[1] *Metal-Catalyzed Cross-Coupling Reactions* (Eds.: F. Diederich, P. J. Stang), Wiley-VCH, New York, **1998**.

[2] For reviews, see: a) T.-Y. Luh, M.-K. Leung, K.-T. Wong, *Chem. Rev.* **2000**, *100*, 3187 – 3204; b) D. J. Cárdenas, *Angew. Chem.* **1999**, *111*, 3201 – 3203; *Angew. Chem. Int. Ed.* **1999**, *38*, 3018 – 3020.

[3] T. Ishiyama, S. Abe, N. Miyaura, A. Suzuki, *Chem. Lett.* **1992**, 691 – 694.

[4] For reviews of the Suzuki reaction, see: a) A. Suzuki in *Metal-Catalyzed Cross-Coupling Reactions* (Eds.: F. Diederich, P. J. Stang), Wiley-VCH, New York, **1998**; chap. 2; b) N. Miyaura, A. Suzuki, *Chem. Rev.* **1995**, *95*, 2457 – 2483; c) S. R. Chemler, D. Trauner, S. J. Danishefsky, *Angew. Chem.* **2001**, *113*, 4676 – 4701; *Angew. Chem. Int. Ed.* **2001**, *40*, 4544 – 4568.

[5] Suzuki coupling of alkyl bromides: M. R. Netherton, C. Dai, K. Neuschütz, G. C. Fu, *J. Am. Chem. Soc.* **2001**, *123*, 10099 – 10100.

[6] a) A. Devasagayaraj, T. Stüdemann, P. Knochel, *Angew. Chem.* **1995**, *107*, 2592 – 2594; *Angew. Chem. Int. Ed. Engl.* **1995**, *34*, 2723 – 2725; b) R. Giovannini, T. Stüdemann, G. Dussin, P. Knochel, *Angew. Chem.* **1998**, *110*, 2512 – 2515; *Angew. Chem. Int. Ed.* **1998**, *37*, 2387 – 2390; c) R. Giovannini, T. Stüdemann, A. Devasagayaraj, G. Dussin, P. Knochel, *J. Org. Chem.* **1999**, *64*, 3544 – 3553; d) M. Piber, A. E. Jensen, M. Rottländer, P. Knochel, *Org. Lett.* **1999**, *1*, 1323 – 1326; e) A. E. Jensen, P. Knochel, *J. Org. Chem.* **2002**, *67*, 79 – 85.

[7] After our paper was submitted for publication, Kambe et al. reported one example of a nickel-catalyzed Kumada coupling of a simple alkyl chloride: J. Terao, H. Watanabe, A. Ikumi, H. Kuniyasu, N. Kambe, *J. Am. Chem. Soc.* **2002**, *124*, 4222 – 4223.

[8] For example, see: J. March, *Advanced Organic Chemistry*, Wiley, New York, **1992**, p. 357.

[9] J. March, *Advanced Organic Chemistry*, Wiley, New York, **1992**, p. 24.

[10] If no phosphane is present, no coupling product is detected (< 2%).

[11] With a 1:1 phosphane:palladium ratio, the yield according to GC is ca. 70%; with a 1:2 phosphane:palladium ratio, ca. 60%.

[12] Each change in parameter leads to a change in yield of ≈15 – 25%.

[13] Lower yields are observed for reactions of more hindered substrates. To date, we have not been able to perform couplings of secondary alkyl chlorides or secondary alkyl boranes.

[14] When 1.0 equiv of $CsOH \cdot H_2O$ or KOH is added to *n*-octyl-9-BBN ($\delta(^{11}B) = 89$ ppm) in dioxane at 90 °C, ^{11}B NMR analysis indicates that a soluble [*n*-octyl-9-BBN(OH)]$^-$ "ate" complex is quickly formed ($\delta = -1$ for $CsOH \cdot H_2O$; $\delta = 18$ ppm for KOH (equilibrium between three- and four-coordinate boron; the four-coordinate adduct resonates at $\delta = -2$ ppm)). Presumably, this is the species that transfers the *n*-octyl group to palladium (Scheme 1). For ^{11}B NMR investigations of related systems, see: K. Matos, J. A. Soderquist, *J. Org. Chem.* **1998**, *63*, 461 – 470. See also: R. Köster, G. Seidel, B. Wrackmeyer, *Chem. Ber.* **1992**, *125*, 617 – 625.

[15] Use of a less hindered (methyl) ester leads to a lower yield (≈55%).

[16] If desired, the synthesis of the alkyl-9-BBN can be conducted directly in dioxane by hydroborating the olefin with solid 9-BBN dimer, rather than a solution of 9-BBN in THF (both are commercially available).

Hydrogen Bonding Modulates the Selectivity of Enzymatic Oxidation by P450: Chameleon Oxidant Behavior by Compound I**

Samuël P. de Visser, François Ogliaro, Pankaz K. Sharma, and Sason Shaik*

Two of the important reactions of the enzyme cytochrome P450 are C–H hydroxylation and C=C epoxidation.[1–5] Different P450 isozymes give different ratios of these products with substrates which can undergo both hydroxylation and epoxidation.[1] Furthermore, mutation of a single amino acid away from the reaction center changes the ratio of the two products.[6] What are the factors that determine the oxidation regioselectivity? There may exist many answers[1–5] to this question and it is desirable to begin unraveling them step by step. Here we use model calculations of C–H hydroxylation and C=C epoxidation pathways, which show that the primary active species of the enzyme, compound I (Cpd I), behaves like a chameleon oxidant that changes its reactivity and selectivity patterns under the influence of hydrogen bonding and polarization effects, which mimic the protein environment.

To explore this issue, we used density functional calculations (see Methods Section) of a model Cpd I species that reacts with propene to give both allylic hydroxylation and C=C epoxidation. The reaction profiles were computed under different conditions, including effects of the environment such as polarization effect and NH ··· S hydrogen bonding of the type found in the crystal structures of P450 enzymes.[6, 7] Our model calculations, which focus on the electronic component of the environment, do not involve stereoelectronic effects

[*] Prof. S. Shaik, Dr. S. P. de Visser, Dr. F. Ogliaro, Dr. P. K. Sharma
Department of Organic Chemistry and
The Lise Meitner-Minerva Center
for Computational Quantum Chemistry
Hebrew University
91904 Jerusalem (Israel)
Fax: (+972) 2-658-4680
E-mail: sason@yfaat.ch.huji.ac.il

[**] The research was supported in parts by the Israel Science Foundation (ISF), the German Israeli Binational Foundation (GIF), and by the Ministry of Science, Culture, and Sports. F.O. thanks the European community for a Marie Curie Fellowship.

Supporting information for this article is available on the WWW under http://www.angewandte.com or from the author.

arising from variations in the substrate,[1–5, 8] or effects arising from substrate binding and juxtaposition in the enzyme's pocket.[9, 10]

Figure 1 shows the lowest energy profiles of the two possible reaction pathways for the bare molecules, Cpd I (^{2}**1** and ^{4}**1**) and propene. The compounds exhibit two-state-reactivity (TSR), involving quartet high-spin (HS) and doublet low-spin (LS) processes,[11–13] which have the appearance of stepwise mechanisms. However, while the HS mechanism is truly stepwise with carbon-radical intermediates (^{4}**2** and ^{4}**4**), possessing barriers for the subsequent C–O bond formation steps, the LS radical species (^{2}**2** and ^{2}**4**) behave as shoulders on the potential energy surface, without significant barriers for the C–O bond formation.[11, 12]

A major difference between the epoxidation and hydroxylation processes is that the barriers to bond activation, via ^{4}**TS1** and ^{2}**TS1** as well as ^{4}**TS3** and ^{2}**TS3**, favor epoxidation by 3.1 – 3.8 kcal mol^{-1}. However, as can be seen from Figure 2a, upon inclusion of zero point energies (ZPE), the four transition states, ^{4}**TS1** and ^{2}**TS1** as well as ^{4}**TS3** and ^{2}**TS3**, become almost isoenergetic. The ZPE effect is primarily due to the loss of a high-frequency C–H mode (> 3000 cm^{-1}) that becomes imaginary in the hydroxylation transition states, ^{4}**TS3** and ^{2}**TS3**, and consequently lowers their ZPE compared with those of the epoxidation transition states. Thus, taking into account only the intrinsic reactivities of the bare molecules, it is expected that Cpd I will have a small preference for C=C epoxidation over C–H hydroxylation, and will generate stereoselective epoxidation products but less stereoselective hydroxylation products (due to the differences in the barriers to C–O bond making via ^{4}**TS2** and ^{4}**TS4**).

Figure 2 shows the effects of the environment on the relative energies of the transition states for bond activation, ^{2}**TS1** and ^{4}**TS1** as well as ^{2}**TS3** and ^{4}**TS3.** The environmental effects were chosen[14] to mimic, albeit naively, the interactions of the thiolate ligand (the cysteinate residue) with the protein pocket.[7] Accordingly, Figure 2b shows the energies of the transition states when the thiolate ligand is coordinated by two NH···S hydrogen bonds, while Figure 2c shows the effect of a relatively nonpolar, yet polarizing, environment represented by the dielectric constant $\varepsilon = 5.7$.[14] Finally, Figure 2d shows the combined effects.

It is seen that in the bare system (Figure 2a), the four transition states, ^{4}**TS1** and ^{2}**TS1** as well as ^{4}**TS3** and ^{2}**TS3**, are very close in energy (E + ZPE), whereas the environmental effects (Figure 2b—d) tip the balance in favor of hydroxylation. Thus, with just two hydrogen bonds (Figure 2b) away from the reaction center, the lowest transition state becomes ^{2}**TS3**, the LS species for hydroxylation. When a polarization effect is applied (Figure 2c) the HS hydroxylation species ^{4}**TS3** descends also below the epoxidation species. Finally, when both effects are combined (Figure 2d), the preference for hydroxylation further increases. In fact, the general trend is true without ZPE, as well as when free energies at different temperatures are considered (see Supporting Information). The calculated energy changes correspond to a regioselectivity change of at least two orders of magnitude. Furthermore, the environmental effects prefer the effectively concerted LS process for both reactions. Thus, the present study demonstrates that the stereospecificity and regioselectivity changes are emergent properties that can, in principle, originate in the electronic interaction exerted on the active species of the enzyme by the protein pocket.

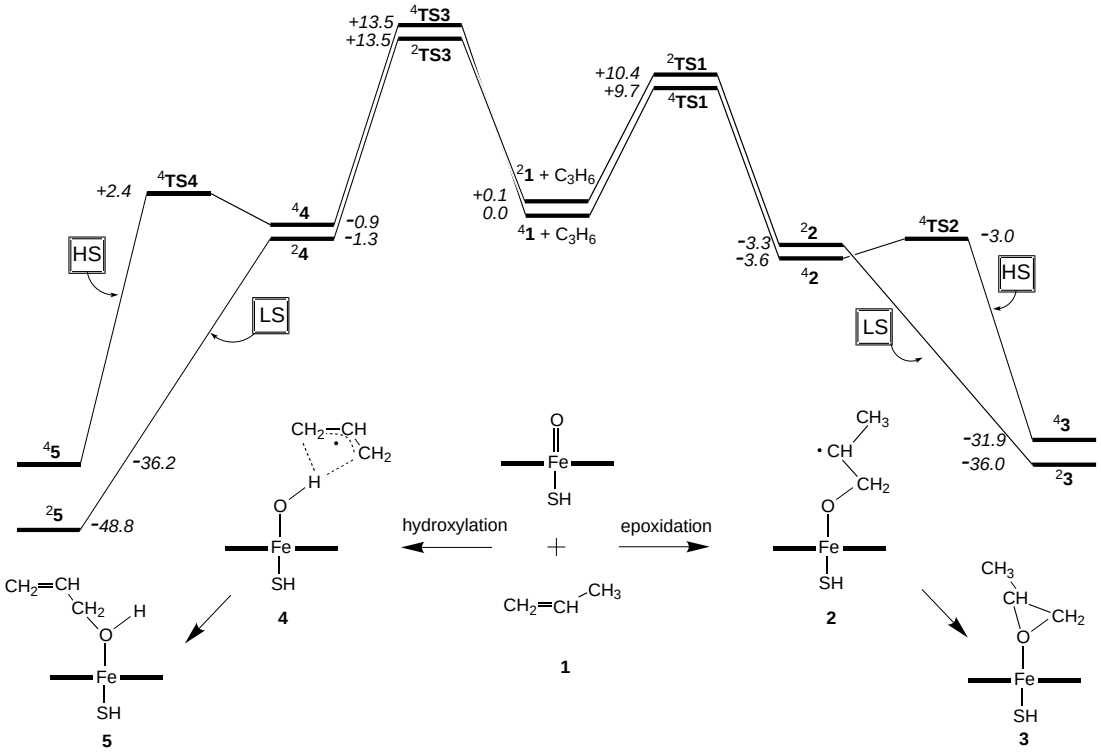


Figure 1. Energy profiles for hydroxylation and epoxidation of propene (energies in kcal mol^{-1}).

 © WILEY-VCH Verlag GmbH, 69451 Weinheim, Germany, 2002 1433-7851/02/4111-1948 $ 20.00+.50/0 *Angew. Chem. Int. Ed.* **2002**, *41*, No. 11

A straightforward comparison with experiment is not possible, since our calculations focus on the electronic component alone. Nevertheless, some general trends can be addressed. The calculated facility of C–H hydroxylation concurs with the opinion that the thiolate ligand enables P450 enzymes to carry out hydroxylations of nonactivated C–H bonds.[3, 15] The calculations show, however, that this function is made more selective by the NH···S bonding machinery and the electric field of the protein. The calculated C=C/C–H ratio is 0.007 – 0.11, and falls within the range of observed values.[6, 8] Moreover, in line with the preference for the LS processes, experimental data show that alkane hydroxylation by P450 isozymes occurs with high degrees of stereoselectivity, albeit incomplete.[1, 3] Similarly, epoxidations of *cis*- and *trans*-butenes by a few P450 isozymes were shown[16] to be stereospecific. An experimental study that addresses the effect of NH···S hydrogen bonding on the ratio of C–H hydroxylation to C=C epoxidation, shows that in $P450_{cam}$,[6] two hydrogen bonds are slightly more favorable for hydroxylation than three. While this is not directly comparable to the results of our calculations, it nevertheless shows that the NH···S hydrogen bonds apply a subtle effect on the reaction center.

Insight into the origins of the computed environmental effects can be gained from Figure 3 and 4. Figure 3 shows the bond activation transition state structures, along with two indicators of their electronic features, the transition state dipole moments (μ) and their polarizabilities (α). For each process, larger dipole moments and polarizabilities are possessed by the LS transition states. Moreover, the hydroxylation transition states are significantly more polarizable than those of the epoxidation species. It seems that the polarizability is the more important factor, and comes into play especially through the localized NH···S hydrogen-bonding interactions. Consequently, the most highly affected species is the most polarizable one, the LS hydroxylation species, ^{2}**TS3**, which becomes the lowest transition state.[17]

To understand the roots of this behavior of the system, consider first Cpd I. As shown recently,[14] the electronic structure of Cpd I can be reconstructed as a hybrid of the resonance structures **a** and **b** (Figure 4 A). In both structures there are three unpaired electrons: two in the π* (d_{xz}, d_{yz}) orbitals of the FeO moiety and the third one is located either in a porphyrin (Por) orbital (a_{2u}) in structure **a**, or in a sulfur hybrid orbital in

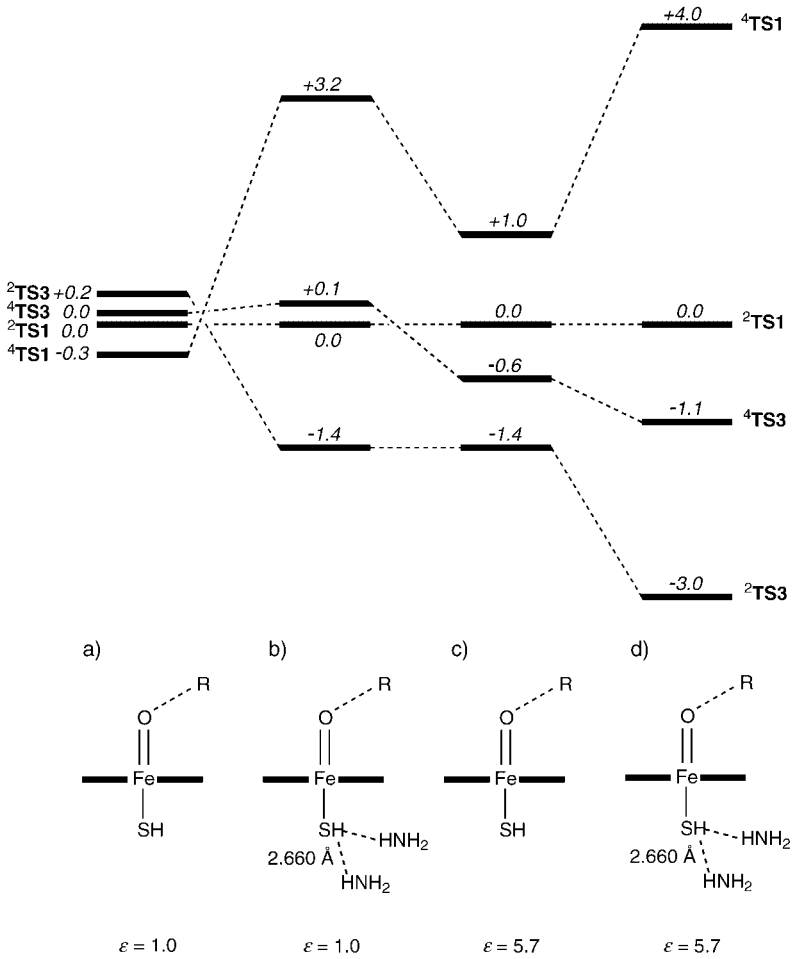


Figure 2. Relative energies (including ZPE) of the bond-activation transition states, ^{4}**TS1** and ^{2}**TS1** as well as ^{4}**TS3** and ^{2}**TS3** (R is the propene moiety); a) $\varepsilon = 1$ refers to the gas-phase situation, b) bare molecules with NH···S hydrogen bonds, c) molecules in a polarizing medium of $\varepsilon = 5.7$, and d) combined effects of b) and c). Energies are in kcal mol^{-1}, relative to ^{2}**TS1**.

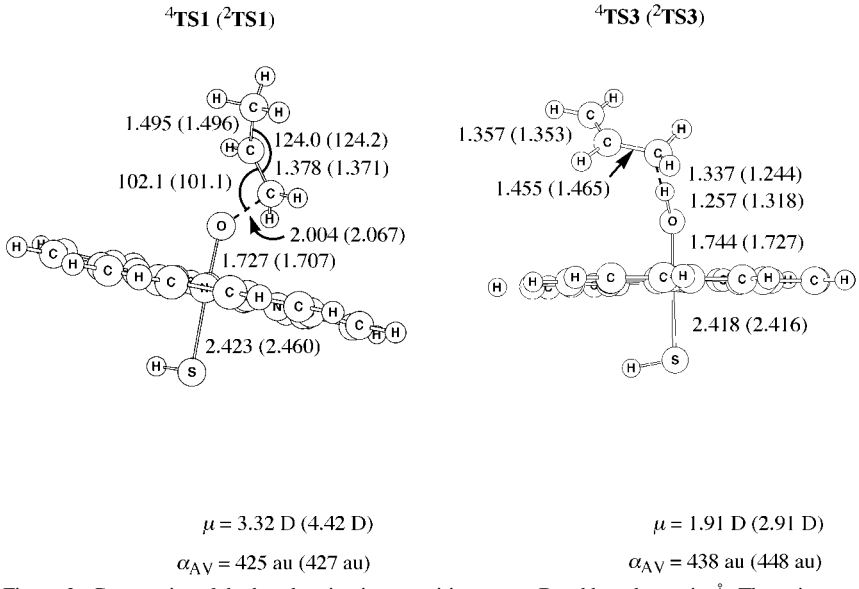
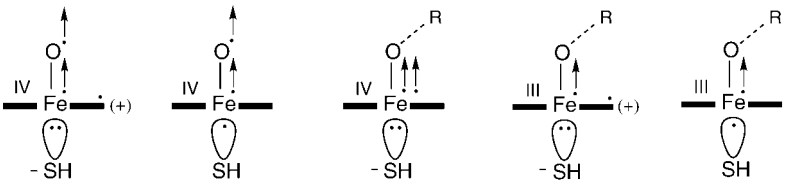


Figure 3. Geometries of the bond-activation transition states. Bond lengths are in Å. The pairs of data refer to the high-spin species and the low-spin species (in parentheses). Below the structures we specify dipole moment (μ) in Debye units, and the average electronic polarizability (α_{AV}) in atomic units.

 © WILEY-VCH Verlag GmbH, 69451 Weinheim, Germany, 2002 1433-7851/02/4111-1949 $ 20.00+.50/0

A)



	a	b	c	d	e
ρ(O)	= 1	1	0	0	0
ρ(Fe)	= 1	1	2	1	1
ρ(Por)	= 1 (-1)	0	0	1 (-1)	0
ρ(SH)	= 0	1 (-1)	0	0	1 (-1)

B)

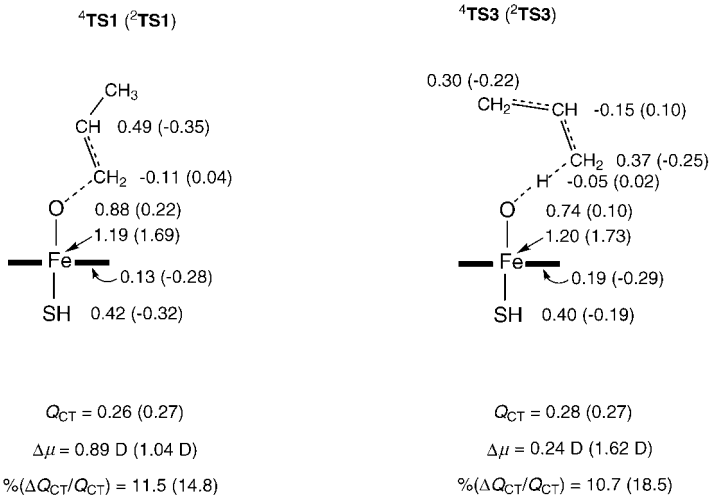


Figure 4. A) Some of the resonance forms that contribute to the chameleonic nature of the transition states (**TS**), and their idealized group spin densities, ρ (ρ values in parentheses correspond to the LS situation). B) Spin densities in ^{2}**TS1** and ^{4}**TS1** as well as ^{2} **TS3** and ^{4}**TS3**, degrees of charge transfer (Q_{CT}) in units of electrons, changes in dipole moments ($\Delta\mu$) and in degree of charge transfer (% $\Delta Q_{CT}/Q_{CT}$), induced by the two NH $\cdots$ S hydrogen bonds. The pairs of data refer to the high-spin species (out of parentheses) and low-spin ones (in parentheses).

structure **b**.[14,18] Whereas the bare system is **b**-like, medium polarization and NH $\cdots$ S hydrogen bonding stabilize structure **a**. The stronger the hydrogen bonding and the polarizing effect, the more **a**-like is Cpd I. Thus, Cpd I, the reactant of the two oxidation processes, behaves as a chameleon state that changes character to fit the environment into which it is accomodated.

Transition states are generally more polarizable than their reactants and products, owing to electronic delocalization in the bonds that are broken and formed during the reaction. However, the transition states of the P450 oxidation are special, since in addition they also possess available orbitals on the iron center, the porphyrin, and the thiolate moieties. These orbitals are not fully occupied and are also close in energy, and can therefore participate in delocalizing the electrons in the transition state, thereby making the transition state very polarizable. A similar idea was articulated by experimentalists.[2–5, 19]

In addition to **a** and **b**, among the many other resonance structures that contribute to electron delocalization in the transition state, three important reference forms are those that represent the flavors of the reaction intermediates (**2** and **4**, Figure 2), and are depicted in **c**–**e** in Figure 4 A.[12] One form is the Fe^{IV} species (**c**) and the other two forms are the singlet and triplet Fe^{III} species shown in **d** and **e**. The computed transition states spin density, on iron, in Figure 4 B is seen to reflect different blends of **c**–**e**. In the HS species, ^{4}**TS3** and ^{4}**TS1**, the spin density on Fe (ca 1.2) is closer to the situation in Fe^{III}, while in ^{2}**TS1** and ^{2}**TS3**, this spin density (ca 1.7) is closer to the situation in Fe^{IV}. In addition to these contributions, there are resonance forms in which the propene transfers an electron to the available low-lying orbitals of the Cpd I moiety. The quantity Q_{CT} in Figure 4 B shows that the degree of charge transfer from the propene is about 0.26–0.28 e^{-}, which in turn means that the charge transfer forms constitute some 26–28 % of the transition state character, and will generally vary with the donor capability of the substrate. Clearly, the transition states are richly blended in terms of closely lying resonance structures, and this rich blend endows them with high polarizability and response to the protein environment.

To summarize the changes imparted by the environment most succinctly, we indicate below the structures in Figure 4 B, the computed changes in the dipole moment and in the percentages of charge transfer, when ^{4}**TS1** and ^{2}**TS1** as well as ^{4}**TS3** and ^{2}**TS3** are subject to NH $\cdots$ S hydrogen bonds. These changes are seen to be larger for the LS species ^{2}**TS1** and ^{2}**TS3** than for the HS counterparts. Especially large changes are apparent in the dipole moments of the LS hydroxylation species, ^{2}**TS3** that changes its dipole by as much as 1.62 D upon hydrogen bonding to the thiolate. Apparently, the variable blend of resonance structures endows the transition states with a chameleonic nature. It follows therefore that not only is Cpd I a chameleon species, it is also a chameleon oxidant that tunes its reactivity and selectivity patterns in response to the protein environment in which it is accommodated.

Our study is a first principle demonstration that, in addition to classical factors (such as active species accessibility, substrate fit, and steric effects[1, 8, 9]), there is a significant electronic component that modulates regioselectivity of oxidation by P450 enzymes. This factor is the chameleonic character of the active species that varies in response to the hydrogen-bonding machinery of the protein pocket and its polarity. Especially notable is the effect of the NH $\cdots$ S hydrogen bonding, which exerts its influence on the Fe=O reaction center from the remote proximal side. Thus, a single oxidant having chameleon character like Cpd I, can in principle exhibit a library of reactivity patterns, depending on the electric and hydrogen-bonding properties of the protein pocket.

 © WILEY-VCH Verlag GmbH, 69451 Weinheim, Germany, 2002 1433-7851/02/4111-1950 $ 20.00+.50/0 *Angew. Chem. Int. Ed.* **2002**, *41*, No. 11

Methods

The calculations were performed with JAGUAR 4.1,[20a] following previously established procedures.[11, 12, 14] The calculations utilized the hybrid B3LYP density functional and the double zeta basis set, LACVP(Fe)/6-31G(C,H,N,O). Geometries were optimized and characterized by frequency calculations. To consider the pure environmental effect, the calculations (with hydrogen bonding and with $\varepsilon = 5.7$) did not involve geometry re-optimization. The ZPEs (calculated with the more accurate Gaussian 98 routine[20b]) of the bare systems were added to the total energies for the different conditions in Figure 2.

Received: March 20, 2002 [Z 18940]

[1] *Cytochrome P450: Structure, Mechanisms and Biochemistry*, 2nd ed. (Ed.: P. R. Ortiz de Montellano), Plenum, New York, **1995**.

[2] J. T. Groves, Y.-Z. Hang in *Cytochrome P450: Structure, Mechanisms and Biochemistry*, 2nd ed. (Ed.: P. R. Ortiz de Montellano), Plenum, New York, **1995**, chap. 1, p. 3.

[3] W.-D. Woggon, *Top. Curr. Chem.* **1996**, *184*, 39 – 95.

[4] M. Sono, M. P. Roach, E. D. Coulter, J. H. Dawson, *Chem. Rev.* **1996**, *96*, 2841 – 2887.

[5] B. Meunier, J. Bernadou, *Struct. Bonding* **2000**, *97*, 3 – 35.

[6] S. Yoshioka, S. Takahashi, K. Ishimori, I. Morishima, *J. Inorg. Biochem.* **2000**, *81*, 141 – 151.

[7] T. L. Poulos, J. C. Vickery, H. Li in *Cytochrome P450: Structure, Mechanisms and Biochemistry*, 2nd ed. (Ed.: P. R. Ortiz de Montellano), Plenum, New York, **1995**, chap. 4, p. 125.

[8] a) R. E. White, J. T. Groves, G. A. McClusky, *Acta Biol. Med. Ger.* **1975**, *38*, 475 – 482; b) R. T. Ruettinger, A. J. Fulco, *J. Biol. Chem.* **1981**, *256*, 5728 – 5734.

[9] E. J. Mueller, P. J. Lioda, S. G. Sligar in *Cytochrome P450: Structure, Mechanisms and Biochemistry*, 2nd ed. (Ed.: P. R. Ortiz de Montellano), Plenum, New York, **1995**, chap. 3, p. 83.

[10] J. J. Devos, O. Sibbeseb, Z. Zhang, P. R. Ortiz de Montellano, *J. Am. Chem. Soc.* **1997**, *119*, 5489 – 5498.

[11] F. Ogliaro, N. Harris, S. Cohen, M. Filatov, S. P. de Visser, S. Shaik, *J. Am. Chem. Soc.* **2000**, *122*, 8977.

[12] S. P. de Visser, F. Ogliaro, N. Harris, S. Shaik, *J. Am. Chem. Soc.* **2001**, *123*, 3037.

[13] S. Shaik, M. Filatov, D. Schröder, H. Schwarz, *Chem. Eur. J.* **1998**, *4*, 193 – 198.

[14] F. Ogliaro, S. Cohen, S. P. de Visser, S. Shaik, *J. Am. Chem. Soc.* **2000**, *122*, 12892.

[15] T. Ohno, N. Suzuki, T. Dokoh, Y. Urano, K. Kikuchi, M. Hirobe, T. Higuchi, T. Nagano, *J. Inorg. Biochem.* **2000**, *82*, 123 – 125.

[16] A. D. N. Vaz, D. F. McGinnity, M. J. Coon, *Proc. Natl. Acad. Sci. USA* **1998**, *95*, 3555 – 3560.

[17] A pioneering study of the effect of the protein electric field on the resting state of P450 is given in: D. Harris, G. Loew, *J. Am. Chem. Soc.* **1993**, *115*, 8775 – 8779.

[18] D. L. Harris, *Curr. Opin. Chem. Biol.* **2001**, *5*, 724 – 735.

[19] R. Weiss, D. Mandon, T. Wolter, A. X. Trautwein, M. Muther, B. Eckhard, A. Gold, K. Jayaray, J. Terner, *J. Biol. Inorg. Chem.* **1996**, *1*, 377.

[20] a) Jaguar 4.1. Portland OR, **1998**; b) Gaussian 98 (Revision A.7), M. J. Frisch, G. W. Trucks, H. B. Schlegel, G. E. Scuseria, M. A. Robb, J. R. Cheeseman, V. G. Zakrzewski, J. A. Montgomery, R. E. Stratmann, J. C. Burant, S. Dapprich, J. M. Millam, A. D. Daniels, K. N. Kudin, M. C. Strain, O. Farkas, J. Tomasi, V. Barone, M. Cossi, R. Cammi, B. Mennucci, C. Pomelli, C. Adamo, S. Clifford, J. Ochterski, G. A. Petersson, P. Y. Ayala, Q. Cui, K. Morokuma, D. K. Malick, A. D. Rabuck, K. Raghavachari, J. B. Foresman, J. Cioslowski, J. V. Ortiz, B. B. Stefanov, G. Liu, A. Liashenko, P. Piskorz, I. Komaromi, R. Gomperts, R. L. Martin, D. J. Fox, T. Keith, M. A. Al-Laham, C. Y. Peng, A. Nanayakkara, C. Gonzalez, M. Challacombe, P. M. W. Gill, B. G. Johnson, W. Chen, M. W. Wong, J. L. Andres, M. Head-Gordon, E. S. Replogle, J. A. Pople, Gaussian, Inc., Pittsburgh, PA, **1998**.

A Dynamic Rearrangement of a Metal Cluster in a Process that Closely Resembles the Hopping Mechanism of Adatom Diffusion on Metal Surfaces**

Richard D. Adams,* Burjor Captain, Wei Fu, Perry J. Pellechia, and Mark D. Smith

It has been over 20 years since Muetterties proposed the widely discussed cluster – surface analogy as a model for understanding surface phenomena on an atomic level.[1–5] Over the years, however, there have been surprisingly few well-characterized experimental confirmations of this concept.[6–8] One important surface process that has been well studied over the years is that known as adatom diffusion.[9–12] Adatom diffusion is important to understanding crystal and thin-film growth, phase transitions, segregation, cluster nucleation, and other surface phenomena. The two most important mechanisms are atom hopping and atom exchange.[9–11]

In the atom hopping mechanism, an adatom moves from one hollow site to another by moving over a pair of atoms via an "edge bridge" twofold transition state, see the fourfold, twofold, fourfold example in Figure 1.

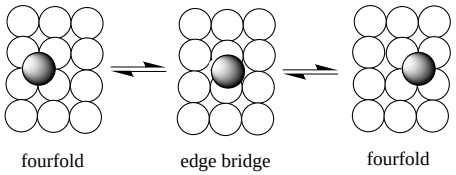


Figure 1. The shaded surface adatom moves from one fourfold site to another via an edge-bridging transition state.

Here we report the synthesis and molecular structures of the compound $[PtRu_5(CO)_{15}(PtBu_3)(C)]$ (**1**) and a study of its unusual molecular dynamics in solution by variable temperature NMR spectroscopy.[13] Compound **1** was obtained in 52% yield from the reaction of $[Ru_5(CO)_{15}(C)]$[14] with $[Pt(PtBu_3)_2]$[15] at 25 °C.[16] The compound crystallizes in three different crystal modifications depending on the solvent that is used. Mixtures of a triclinic form and a monoclinic form **A** were observed to form by crystallization from solutions in benzene/octane solvent mixtures.[17, 18] The molecular structure of the compound is similar in both of these crystal forms and the structure consists of a square-pyramidal cluster of five ruthenium atoms with one platinum atom spanning the square base with significant bonding to the four proximate ruthenium atoms (Figure 2). The four Pt–Ru distances range from

[*] Dr. R. D. Adams, B. Captain, W. Fu, Dr. P. J. Pellechia, Dr. M. D. Smith
Department of Chemistry and Biochemistry and USC Nanocenter
University of South Carolina
Columbia, SC 29208 (USA)
Fax: (+1) 803-777-6781
E-mail: Adams@mail.chem.sc.edu

[**] This work was supported by the Office of Basic Energy Sciences, US Department of Energy.

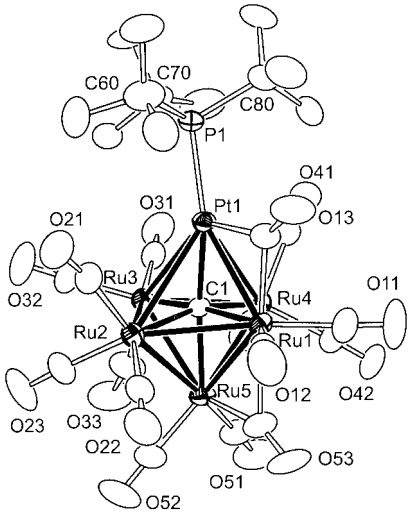


Figure 2. The molecular structure of **1** as found in the triclinic crystal form. Selected bond lengths [Å]: Pt1-Ru1 2.7966(5), Pt1-Ru3 3.1413(5), Pt1-Ru4 3.1463(5), Pt1-Ru2 3.1483(6). Ru1-Ru2 2.9280(7), Ru1-Ru4 2.9297(7), Ru2-Ru3 2.8585(7), Ru3-Ru4 2.8576(7).

2.7966(5) – 3.1483(6) Å. A carbido ligand lies inside the cluster of six metal atoms. The single tri-*tert*-butylphosphane ligand coordinates to the platinum atom.

A second monoclinic form **B** was obtained from crystallization by using diethyl ether as the solvent.[18, 19] In this crystalline form there are two independent complete molecules. Both are structurally similar, and a diagram of the molecular structure of one of these molecules is shown in Figure 3. In this crystalline state the compound has assumed

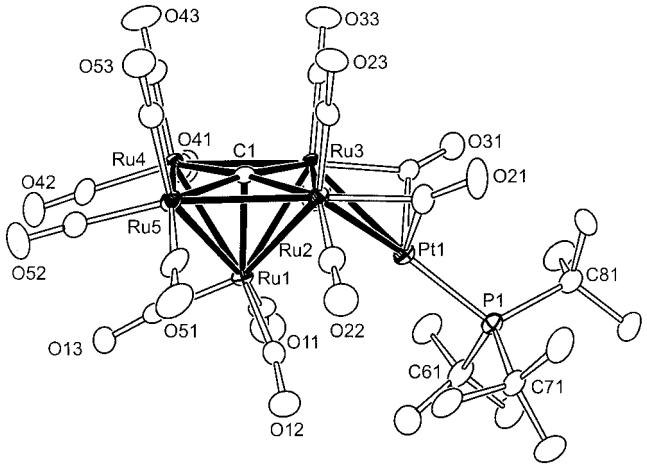


Figure 3. The molecular structure of **1** as found in the monoclinic crystal form **B**. There are two independent molecules in the crystal. Selected interatomic distances [Å] for molecule 1: Pt1-Ru3 2.7894(5), Pt1-Ru2 2.8018(5), Pt1 ··· Ru1 3.3076(5); for molecule 2 (not shown): Pt11-Ru12 2.8213(5), Pt11-Ru13 2.8282(5), Pt11 ··· Ru11 3.1603(5). Ru2-Ru3 2.8928(6), Ru2-Ru5 2.8355(6), Ru3-Ru4 2.8407(7), Ru4-Ru5 2.8726(6).

an isomeric structure in which the platinum atom has moved off the square base to an edge of the cluster of ruthenium atoms (that is, the platinum atom is bonded primarily to only two ruthenium atoms, for molecule 1: Ru3 and Ru2; for molecule 2: Ru12 and Ru13). As indicated by the interatomic distances Pt1 – Ru1 = 3.3076(5) Å and Pt11 – Ru11 = 3.1603(5) Å, there may also be some weak bonding between the platinum atom and the ruthenium atom at the apex of the Ru_5 square pyramid.

Interestingly, the ^{31}P NMR spectrum of **1** in [D_8]toluene solution at $-40\,^{\circ}$C shows two phosphorus resonance signals, $\delta = 118.2$ and 92.7 ppm, both of which exhibit large coupling to platinum (^{195}Pt, 33 % natural abundance), which indicates that both isomers exist in equilibrium in solution and that the phosphorus atom is bonded directly to a platinum atom in each case. The equilibrium is temperature dependent and favors the isomer with the resonance at $\delta = 118.2$ ppm as the temperature is lowered below $-40\,^{\circ}$C. For this equilibrium $\Delta H^{\circ} = -1.4(1)$ kcal mol^{-1}; $\Delta S^{\circ} = -6.1(3)$ cal mol^{-1} K^{-1}. Most interestingly, as the temperature is raised above $-40\,^{\circ}$C, the resonances broaden, coalesce, and average into a single resonance, $\delta = 103.9$ ppm, with appropriate coupling to platinum at $40\,^{\circ}$C. This line broadening indicates that the isomers are interconverting rapidly on the NMR timescale. From computer line-shape simulations it was possible to determine the rates of interconversion at the various temperatures, and in turn, determine the thermodynamic activation parameters: $\Delta H^{\ddagger} = 8.8(5)$ kcal mol^{-1}; $\Delta S^{\ddagger} = -8.4$ cal mol^{-1} K^{-1}, (Figure 4).[20] The mechanism of interconversion involves a

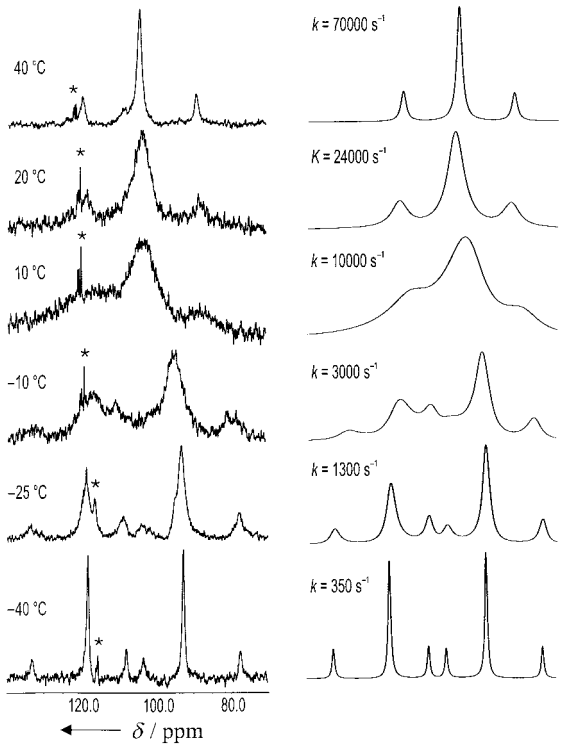


Figure 4. Left: ^{31}P NMR spectra of compound **1** at various temperatures in [D_8]toluene solvent. Signals labeled * are unidentified impurities. Right: computer-simulated spectra at various exchange rates, *k*.

reversible breaking and making of two Pt–Ru bonds with a shift of the platinum – phosphane grouping back and forth between the fourfold Ru_4 site and the twofold edge-bridging Ru_2 site, and it occurs at a rate of 24000 sec^{-1} at $20\,^{\circ}$C (Figure 5).

 © WILEY-VCH Verlag GmbH, 69451 Weinheim, Germany, 2002 1433-7851/02/4111-1952 $ 20.00+.50/0

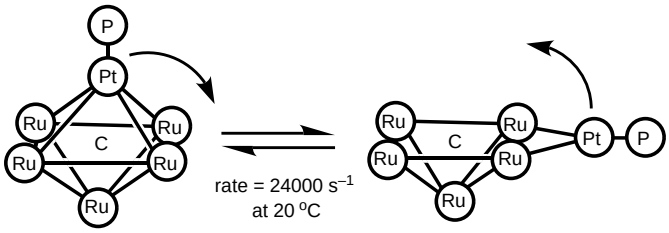


Figure 5. Interconversion of the Pt center between a fourfold and a twofold site.

The great facility of the transformation can be explained by the participation of the CO ligands that help to stabilize the open cluster through their bridging coordination to the platinum atom. Our studies of this molecular cluster model system provide an interesting and unusual new perspective of rearrangements involving the making and breaking of metal–metal bonds in polynuclear metal complexes and by analogy also of the corresponding types of transformations that occur on metal surfaces.

Received: March 11, 2002 [Z18863]

[1] E. L. Muetterties, *Chem. Rev.* **1979**, *79*, 93.
[2] E. L. Muetterties, *Chem. Soc. Rev.* **1982**, *11*, 283.
[3] E. L. Muetterties, *Surv. Prog. Chem.* **1983**, *10*, 61.
[4] M. R. Albert, J. T. Yates, Jr., *The Surface Scientist's Guide to Organometallic Chemistry*, American Chemical Society, Washington, DC, **1987**.
[5] X. Xu, N. Wang, Q. Zhang, *Bull. Chem. Soc. Jpn.* **1996**, *69*, 529.
[6] C. M. Friend, *Chem. Rev.* **1992**, *92*, 491.
[7] S. Brait, S. Deabate, S. A. R. Knox, E. Sappa, *J. Cluster Sci.* **2001**, *12*, 139.
[8] D. B. Brown, B. F. G. Johnson, C. M. Martin, A. E. H. Wheatley, *J. Chem. Soc. Dalton Trans.* **2000**, 2055.
[9] T. T. Tsong, *Prog. Surf. Sci.* **2001**, *67*, 235.
[10] G. L. Kellogg, *Surf. Sci. Rep.* **1994**, *21*, 1.
[11] C. M. Chang, C. M. Wei, J. Hafner, *J. Phys. Condens. Matter* **2001**, *13*, L321.
[12] A. Zangwill, *Physics at Surfaces*, Cambridge University Press, Cambridge, **1988**.
[13] *Dynamic Nuclear Magnetic Resonance Spectroscopy*, (Eds.: L. M. Jackman, F. A. Cotton), Academic Press, New York, **1975**.
[14] P. J. Dyson, *Adv. Organomet. Chem.* **1999**, *43*, 43.
[15] S. Otsuka, T. Yoshida, M. Matsumoto, K. Nakatsu, *J. Am. Chem. Soc.* **1976**, *98*, 5850.
[16] $[Ru_5(CO)_{15}(\mu_6\text{-C})]$ (18.0 mg) was allowed to react with $[Pt(PtBu_3)_2]$ (10.5 mg) in CH_2Cl_2 (15 mL) under a nitrogen atmosphere at room temperature for 30 min. The product was isolated by TLC to yield 13.2 mg (52%) of red crystals of $[Ru_5Pt(CO)_{15}(PtBu_3)(\mu_6\text{-C})]$ (**1**). Spectral data for **1**: IR ν_{CO} (in CH_2Cl_2): $\tilde{\nu}$ = 2087 (m), 2055 (s), 2033 (s), 2028 (s), 1991 (sh), 1822 cm^{-1} (w, br); $^{31}P\{^1H\}$ NMR (−40 °C, [D$_8$]toluene, 202.5 MHz): δ = 118.2 ($^1J_{Pt\text{-}P}$ = 5983 Hz), δ = 92.7 ppm ($^1J_{Pt\text{-}P}$ = 6164 Hz); elemental analysis (%) calcd: C 25.19, H 2.02; found: C 25.28, H 1.92.
[17] Crystal data for **1** in triclinic form: $PtRu_5PO_{15}C_{28}H_{27}$, M_r = 1334.91, space group $P\bar{1}$, a = 9.9510(5), b = 12.1523(6), c = 16.8957(8) Å, α = 79.797(1), β = 87.338(1), γ = 72.9380(10)°, V = 6769.1(9) Å^3, Z = 2, T = 293 K, $Mo_{K\alpha}$ radiation, λ = 0.71073 Å. The final R factor $R1$(F) was 0.0384 for 7697 reflections with $I > 2\sigma(I)$. Crystal data for **1** in the monoclinic form **A**: space group $P2_1/n$, a = 12.4684(10), b = 17.9669(15), c = 17.3482(14) Å, β = 107.613(2)°, V = 3704.1(5) Å^3, Z = 4, T = 190 K, $Mo_{K\alpha}$ radiation, λ = 0.71073 Å. The final R factor $R1(F)$ was 0.0463 for 5594 reflections with $I > 2\sigma(I)$.
[18] CCDC-181108–181110 contains the supplementary crystallographic data for this paper. These data can be obtained free of charge via www.ccdc.cam.ac.uk/conts/retrieving.html (or from the Cambridge Crystallographic Data Centre, 12, Union Road, Cambridge CB21EZ, UK; fax: (+44) 1223-336-033; or deposit@ccdc.cam.ac.uk).
[19] Crystal data for **1** in the monoclinic form **B**: space group $P2_1/c$, a = 14.1957(12), b = 18.0213(15), c = 29.027(2) Å, β = 92.113(2)°, V = 3704.1(5) Å^3, Z = 4, T = 190 K, $Mo_{K\alpha}$ radiation, λ = 0.71073 Å. The final R factor $R1(F)$ was 0.0379 for 14877 reflections with $I > 2\sigma(I)$.
[20] Line-shape simulations of the NMR spectra in the exchange-broadened region were preformed by using the program EXCHANGE written by R. E. D. McClung, Department of Chemistry, University of Alberta, Edmonton, Alberta, Canada.

Electronic Structure and Bonding in Hexacoordinate Silyl–Palladium Complexes**

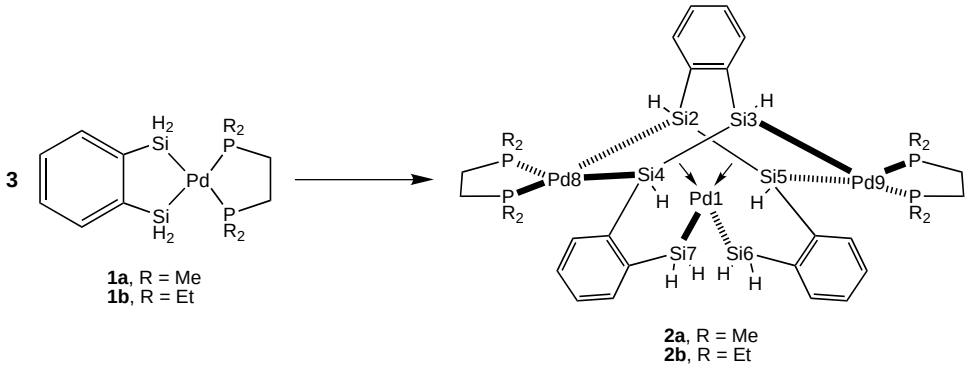
Edward C. Sherer, Christopher R. Kinsinger, Bethany L. Kormos, Jason D. Thompson, and Christopher J. Cramer*

Trimerization of $[Pd^{II}(R_2PCH_2CH_2PR_2)\{1,2\text{-}C_6H_4(SiH_2)_2\}]$ (**1**; where R = Me or Et) has been demonstrated to produce a trinuclear complex **2** where two of the Pd atoms can be readily characterized as Pd^{II} centers but the nature of the third, central Pd atom is less clear (Scheme 1, by-products not shown).[1] While this Pd atom (Pd1) is drawn in Scheme 1 as bonding directly to two Si atoms and further interacting with two Si–Si bonds, the interatomic distances from the X-ray crystal-structure data could also be interpreted to be consistent with an absence of Si–Si bonds and instead six Pd–Si bonds,[1] that is, the central metal would formally be Pd^{VI}. Both structures are without precedent in palladium coordination chemistry,[2, 3] although compounds of Pd[4–7] and Pt[8, 9] *have* been reported for inorganic compounds of the form $[MF_n]$ (M = Pd, Pt; n = 2,4,6), where the extreme electronegativity of fluorine is exploited for the generation of higher oxidation states.[10]

To better understand the nature of the bonding in **2**, we have carried out DFT calculations on **2** and relevant model compounds. With the exception of single-point calculations using the X-ray geometries of **2a** and **2b**, all the structures were fully optimized and verified as minima by analytic frequency calculations. The functional employed was of the hybrid variety[11] and combined exact Hartree–Fock exchange with the gradient-corrected exchange and correlation functionals of Becke[12] and Lee, Yang, and Parr,[13] respec-

[*] Prof. Dr. C. J. Cramer, E. C. Sherer, C. R. Kinsinger, B. L. Kormos, J. D. Thompson
Department of Chemistry and Supercomputing Institute
University of Minnesota
207 Pleasant Street SE, Minneapolis, MN 55455-0431 (USA)
Fax: (+1) 612-626-2006
E-mail: cramer@chem.umn.edu

[**] Support from the National Science Foundation (CHE-9876792) is gratefully acknowledged.



Scheme 1.

tively (B3LYP).[14] Relativistic compact effective core potentials were employed with a split-valence basis set for the Pt, Pd, P, Si, and F centers (CEP-31G);[15] d polarization functions were also included on the P, Si, and F atoms. The minimal STO-3G basis set was used for C and H atoms.[16] All the electronic states were singlets unless otherwise noted. Bond orders between atoms were computed using the method of Mayer,[17] which has been shown to be robust and relatively insensitive to basis-set size.[18–20] All calculations made use of the Gaussian 98 program suite[21] augmented with the MN-GSM package.[22]

To validate the chosen level of theory, we carried out several calculations to compare either to known experimental data or to previously published high-level calculations. In the case of $[PtF_n]$ molecules, we compute triplet ground states for $[PtF_2]$, $[PtF_4]$, and $[PtF_6]$ with Pt–F bond lengths of 1.857 Å for $[PtF_2]$, 1.871 and 1.903 Å for $[PtF_4]$ (which is Jahn–Teller distorted from square planar) and 1.882 and 1.902 Å for $[PtF_6]$ (which is Jahn–Teller distorted from octahedral). These results are in good quantitative agreement with large-basis-set B3LYP and CCSD(T) optimizations of Wesendrup and Schwerdtfeger.[23] However, both sets of calculations predict Pt–F bonds that are somewhat too long in $[PtF_6]$, the only experimentally characterized platinum fluoride compound; gas-phase electron diffraction results provide an average Pt–F length of 1.853 Å.[9] The error may be a result of large relativistic effects that are not fully accounted for in the computed values.

In the case of the more relevant palladium fluorides, experimental structures have been reported from $[PdF_2]$[4] and $[PdF_4]$[5] powder studies, but the instability of $[PdF_6]$ has not yet permitted any structural analysis.[6] These species and other fluorinated Pd^{II} and Pd^{IV} compounds have network-solid characteristics which can significantly affect Pd–F bond lengths in the crystal—in an analysis of 32 such palladium fluorides observed lengths vary from 1.86 to 2.25 Å.[7] In the gas phase, we compute $[PdF_2]$ to have a triplet ground state with a Pd–F bond of 1.902 Å, well within the experimental range although shorter than the only prior calculation of 1.94 Å at the less complete Hartree–Fock theoretical level.[24] We also predict $[PdF_4]$ to have a triplet ground state and a square planar geometry with a Pd–F bond of 1.874 Å, again within the experimental range, although at the low end.

Finally, we compared the optimized structure of **2a** to its X-ray crystal-structure geometry. The theoretical structure has C_2 symmetry, while the crystal structure is slightly distorted from symmetric. The mean difference over all 36 Pd–Pd, Pd–Si, and Si–Si interatomic distances in the two structures is 0.078 Å, while the heavy-atom root-mean-square displacement is 0.441 Å. These differences are reasonably small and entirely consistent with what might be expected from crystal packing effects; in particular, the theoretical interatomic separations are always slightly larger than those found in the crystal structure (see below). Such agreement in geometrical details bodes well for the accuracy of the molecular electronic structure. Insofar as analyses carried out for the two alternative geometries of **2a** as well as the crystal geometry of **2b** provided quantitatively similar bond orders, Kohn–Sham orbitals, etc., we restrict further discussion to the symmetric theoretical structure of **2a** so as to simplify data presentation.

To establish a calibrating scale for our analysis, we first computed optimized geometries and Mayer bond orders for the singlet ground states of $[Pd(SiH_3)_2]$ (**3**), $[Pd(SiH_3)_4]$ (**4**), and $[Pd(SiH_3)_6]$ (**5**; Figure 1). Bonding in **3** is entirely consistent with a formal Pd^{II} oxidation state: the total Pd–Si bond order is 2.00, and the Pd–Si bond lengths are 2.320 Å. Nevertheless, there is a small amount of direct Si–Si bonding, with an interatomic separation of 3.063 Å and a bond order of 0.20. This situation is very similar to that found for monomer **1a**, although in that case the ligating phosphorus atoms additionally make dative bonds to the Pd center—these bonds have bond order 0.71—and this lengthens and very slightly reduces the bond order for the Pd–Si bonds.

In **4**, the situation is rather different. The two pairs of symmetrically related Pd–Si bonds have lengths in excess of 2.45 Å, and two Si–Si distances of 2.720 Å are found. The four Pd–Si bond orders sum to only 2.96, while the interacting Si–Si fragments are predicted to have bond orders of 0.43. Thus, even with only 4 SiH_3 ligands, a tendency toward multicenter delocalized bonding is observed that would tend to argue for a formal oxidation state of less than the total number of ligands.[2] Analysis of **5**, which is found as a local minimum on starting from an octahedral initial geometry, suggests that further oxidation of the Pd center cannot be accomplished by SiH_3 as a ligand. Instead, a disilane molecule (Si–Si bond order of 0.97) is effectively ejected, and a weak complex resembling **4**·disilane is formed. In this case, the disilane molecule breaks the molecular symmetry so that one pair of SiH_3 ligands is nearly as strongly bound as in **3** while the other pair is *less* strongly bound than in **4**, but not completely ejected as disilane (the Si–Si bond order is 0.57). The total Pd–Si bond order in **5** is 3.11. The coordination geometry, where the coordinating fragments are two SiH_3

 © WILEY-VCH Verlag GmbH, 69451 Weinheim, Germany, 2002 1433-7851/02/4111-1954 $ 20.00+.50/0

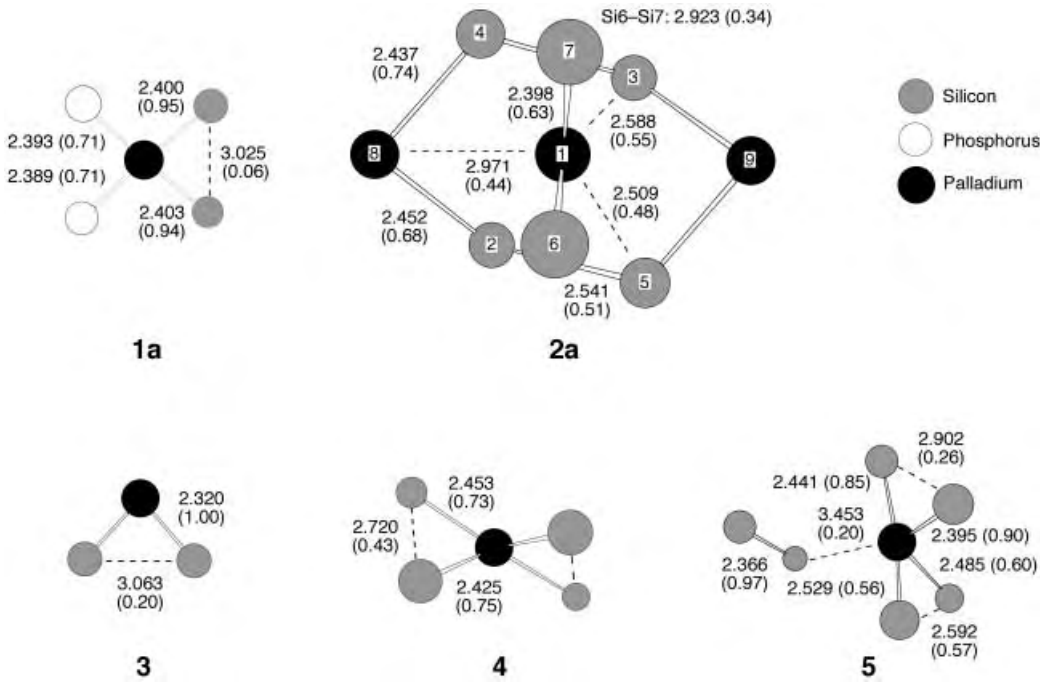


Figure 1. B3LYP optimized bond lengths [Å] and bond orders (in parentheses) for Pd–Pd, Pd–P, Pd–Si, and Si–Si bonds in compounds **1**–**5**. Other atoms have been removed for clarity. Atom numbering for **2a** is consistent with Scheme 1.

groups, one Si–Si σ bond, and one hydrogen atom of disilane, is approximately square planar, which is consistent with a Pd^{II} oxidation state.[25]

Within this context, the bonding in **2a** is readily rationalized. Just as in **5**, there are two Si atoms that are most strongly bound (Si6 and Si7, with Pd–Si bond orders of 0.63) but the overall symmetry of the complete molecule reduces the difference between "bonding" and "non-bonding" interactions. Thus, the remaining Pd–Si bond orders are 0.48 and 0.55, with a total Pd–Si bond order of 3.32. Computed Si–Si bond orders are consistent with these trends: weak between Si6 and Si7 (0.34) and stronger between the other two relevant pairs (0.51). Interestingly, in the trinuclear complex, a bond order of 0.44 is found between the central Pd and each of the other Pd atoms. This suggests some Pd cluster aspects in the overall bonding, and is consistent with Pd–Si bond orders of 0.68 and 0.74 between these outer Pd atoms and the Si atoms to which they are formally bonded, but less strongly so than computed for monomer **1**. All the bond lengths follow the trends expected based on the above analysis of bond orders.

Support for the coordination shown in Scheme 1, as opposed to hexavalent Pd^{VI}, is further offered by the highest occupied molecular orbital (HOMO) for **2a** (Figure 2). The HOMO is dominated by σ bonding between Si3 and Si4 and symmetrically related Si2 and Si5. These σ bonds hybridize in an interesting way with d_{xy} orbitals on the outer Pd atoms and the d_{z^2} orbital of the central Pd atom, but the contribution from the metal orbitals, particularly the central one, is relatively minor.

Thus, the bonding in **2a** is rather similar to that found in **5**, except that structural constraints in the former seem to reduce the total variation over all the Pd–Si bond orders compared to the latter. In that sense, the greater degree of delocalized, multicenter bonding in **2a** resembles that found in **4**. That so many different Pd–Si bond orders are so readily accommodated in **1**–**5** suggests that the ligand environment about a $PdSi_6$ fragment may be quite fluxional, and this is consistent with our interpretation above that crystal packing forces are sufficient to explain the small observed deviation of the C_2-symmetric theoretical structure from the X-ray crystal structure.

As Crabtree has pointed out,[2, 3] in delocalized bonding situations such as that computed for **2** there is no simple way to assign a metal oxidation state. However, it seems clear that assigning the central metal to be Pd^{VI} is *not* warranted for **2**, unless such an assignment is permitted to encompass the ambiguity of multicenter, delocalized bonding, to which it must be noted that silyl groups appear to be particularly apt, with no obvious preference for integer bond orders. As a theoretical model, Mayer bond orders computed from DFT density matrices clearly provide a useful tool for quantifying this phenomenon.

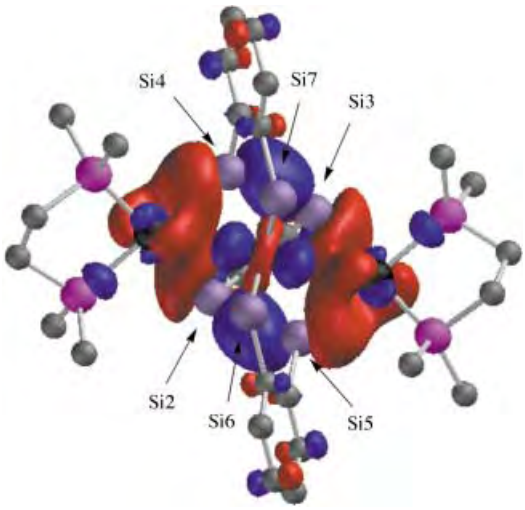


Figure 2. B3LYP HOMO for **2a**. Atom numbering is consistent with Scheme 1 and Figure 1. Hydrogen atoms have been removed for clarity.

Received: February 25, 2002 [Z18773]

[1] W. Chen, S. Shimada, M. Tanaka, *Science* **2002**, *295*, 308.
[2] R. H. Crabtree, *Science* **2002**, *295*, 288.
[3] R. H. Crabtree, *The Organometallic Chemistry of the Transition Metals*, 3rd ed, Wiley, New York, **2001**.

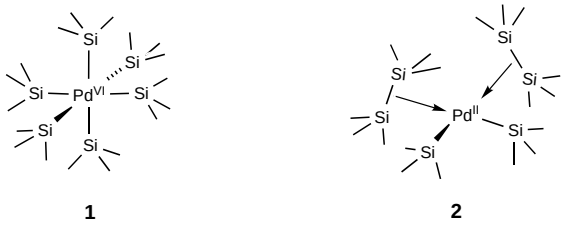
 © WILEY-VCH Verlag GmbH, 69451 Weinheim, Germany, 2002 1433-7851/02/4111-1955 $ 20.00+.50/0

[4] N. Bartlett, R. Maitland, *Acta Crystallogr.* **1958**, *11*, 747.
[5] A. F. Wright, B. E. F. Fender, N. Bartlett, K. Leary, *Inorg. Chem.* **1978**, *17*, 748.
[6] A. A. Timakov, V. N. Prusakov, Y. V. Drobyshevskii, *Russ. J. Inorg. Chem. (Engl. Transl.)* **1982**, *27*, 1704.
[7] V. N. Serezkhin, L. B. Serezkhin, Y. A. Buslaev, *Russ. J. Inorg. Chem. (Engl. Transl.)* **2000**, *45*, 1241.
[8] R. Marx, K. Seppelt, R. M. Ibberson, *J. Chem. Phys.* **1996**, *104*, 7658.
[9] A. D. Richardson, K. Hedberg, G. M. Lucier, *Inorg. Chem.* **2000**, *39*, 2787.
[10] M. Hargittai, *Chem. Rev.* **2000**, *100*, 2233.
[11] A. D. Becke, *J. Chem. Phys.* **1993**, *98*, 5648.
[12] A. D. Becke, *Phys. Rev. A* **1988**, *38*, 3098.
[13] C. Lee, W. Yang, R. G. Parr, *Phys. Rev. B* **1988**, *37*, 785.
[14] P. J. Stephens, F. J. Devlin, C. F. Chabalowski, M. J. Frisch, *J. Phys. Chem.* **1994**, *98*, 11 623.
[15] W. J. Stevens, M. Krauss, H. Basch, P. G. Jasien, *Can. J. Chem.* **1992**, *70*, 612.
[16] W. J. Hehre, R. F. Stewart, J. A. Pople, *J. Chem. Phys.* **1969**, *51*, 2657.
[17] I. Mayer, *Chem. Phys. Lett.* **1983**, *97*, 270.
[18] S. M. Bachrach, in *Reviews in Computational Chemistry*, *Vol. 5* (Eds.: K. B. Lipkowitz, D. B. Boyd), VCH, New York, **1993**, p. 171.
[19] J. Li, T. Zhu, C. J. Cramer, D. G. Truhlar, *J. Phys. Chem. A* **1998**, *102*, 1820.
[20] An alternative bonding analysis would be to employ the atoms-in-molecules method (R. F. W. Bader, *Acc. Chem. Res.* **1985**, *18*, 9). All attempts to do so, however, were foiled by the complexity of the electron density in trinuclear **2**.
[21] Gaussian 98 (Revision A.7), M. J. Frisch, G. W. Trucks, H. B. Schlegel, G. E. Scuseria, M. A. Robb, J. R. Cheeseman, V. G. Zakrzewski, J. A. Montgomery, R. E. Stratmann, J. C. Burant, S. Dapprich, J. M. Millam, A. D. Daniels, K. N. Kudin, M. C. Strain, O. Farkas, J. Tomasi, V. Barone, M. Cossi, R. Cammi, B. Mennucci, C. Pomelli, C. Adamo, S. Clifford, J. Ochterski, G. A. Petersson, P. Y. Ayala, Q. Cui, K. Morokuma, D. K. Malick, A. D. Rabuck, K. Raghavachari, J. B. Foresman, J. Cioslowski, J. V. Ortiz, B. B. Stefanov, G. Liu, A. Liashenko, P. Piskorz, I. Komaromi, R. Gomperts, R. L. Martin, D. J. Fox, T. Keith, M. A. Al-Laham, C. Y. Peng, A. Nanayakkara, C. Gonzalez, M. Challacombe, P. M. W. Gill, B. G. Johnson, W. Chen, M. W. Wong, J. L. Andres, M. Head-Gordon, E. S. Replogle, J. A. Pople, Gaussian, Inc., Pittsburgh, PA, **2000**.
[22] J. D. Xidos, J. Li, J. D. Thompson, G. D. Hawkins, P. D. Winget, T. Zhu, D. Rinaldi, D. A. Liotard, C. J. Cramer, D. G. Truhlar, M. J. Frisch, MN-GSM version 1.8, University of Minnesota, Minneapolis, MN, **2002**.
[23] R. Wesendrup, P. Schwerdtfeger, *Inorg. Chem.* **2001**, *40*, 3351.
[24] P. E. M. Siegbahn, *Theor. Chim. Acta* **1994**, *87*, 441.
[25] G. Aullón, A. Lledós, S. Alvarez, *Angew. Chem.* **2002**, *114*, 2036; *Angew. Chem. Int. Ed.* **2002**, *41*, 1956.

Hexakis(silyl)palladium(VI) or Palladium(II) with η^2-Disilane Ligands?**

Gabriel Aullón, Agustí Lledós, and Santiago Alvarez*

One of those earthquakes that shake from time to time the established chemical concepts has been recently provoked by the report of the thermal condensation product of three molecules of [Pd(L){1,2-$C_6H_4(SiH_2)_2$}], where L = dmpe (bis(dimethylphosphanyl)ethane) or depe (bis(diethylphosphanyl)ethane).[1] The molecular structures of the resulting trinuclear complexes, as determined by X-ray crystallography, have a central Pd atom coordinated by six silyl groups to which the highly unusual Pd^{VI} oxidation state has been assigned, as schematically shown in **1** (Scheme 1). The same



1 **2**

Scheme 1.

authors, however, noted that an alternative interpretation of the bonding would imply a Pd^{II} oxidation state and a side-on coordination of two Si–Si single bonds (**2**; Scheme 1). In either case, the new compound would be the first one in his class, but it is appropriate to wonder whether its formulation as Pd^{VI} or Pd^{II} is a matter of taste, as happens in other transition-metal complexes with non-innocent ligands, or there are clear criteria to decide which is the right oxidation state and coordination mode.

Herein we present several reasons why we strongly favor the formulation of such a compound as a Pd^{II} center with two η^2-coordinated Si–Si single bonds rather than as a Pd^{VI} center with six-coordinate silyl groups:

a) The structural parameters are consistent with the square-planar Pd^{II} center formulation but not with an hexacoordinate Pd^{VI} center.

[*] Prof. S. Alvarez, Dr. G. Aullón
Departament de Química Inorgànica
and Centre de Recerca en Química Teòrica
Universitat de Barcelona
Diagonal 647, 08028 Barcelona (Spain)
Fax: (+34) 93-490-7725
E-mail: santiago.alvarez@qi.ub.es

Prof. A. Lledós
Departament de Química
Universitat Autònoma de Barcelona
08193 Bellaterra (Spain)

[**] This work was supported by the Dirección General de Enseñanza Superior (DGES), grant PB98-1166-C02-01, and the Comissionat per a Universitats i Recerca (Generalitat de Catalunya), grant SGR99-0046. Computing resources at the Centre de Supercomputació de Catalunya (CESCA) and Centre de Paral·lelisme de Barcelona (CEPBA) were made available by the Comissió Interdepartamental per a la Recerca i la Innovació Tecnològica (CIRIT) and the Universitat de Barcelona. The authors are grateful to Prof. C. Tessier (University of Akron, Ohio) for discussions.

 © WILEY-VCH Verlag GmbH, 69451 Weinheim, Germany, 2002 1433-7851/02/4111-1956 $ 20.00+.50/0

b) Continuous symmetry measures confirm that the $PdSi_2(centroid)_2$ core is almost perfect square planar, whereas the $PdSi_6$ group cannot be identified as octahedral, or trigonal prismatic, or any intermediate stereochemistry.

c) Qualitative models of bonding and electronic structure predict a Pd^{VI} complex to be paramagnetic, whereas no experimental evidence of paramagnetism has been presented.

d) DFT calculations on model molecules indicate that the hexacoordinate complex has a triplet ground state and is significantly less stable than alternative structures with a Pd^{II} center and Si–Si bonds.

e) There is evidence for side-on coordination of other main-group-element single bonds.

f) The analogy between $[Pd(SiH_3)_6]$ and $[PdH_6]$ proposed by Crabtree[2] also suggests that formation of η^2-coordinated single bonds is preferred over the formation of a Pd^{VI} complex.

a) *Structural parameters*: The Si–Si distances that should be considered as nonbonding in the Pd^{VI} formulation **1**, but as bonding in the Pd^{II} form **2**, are 2.49 and 2.59 Å. Well established Si–Si bonds in Si_2Ph_6 and $Si_2(tBu)_6$ are up to 2.52[3] and 2.70 Å[4, 5] long, respectively, so it seems reasonable to consider these Si atoms to be bonded. The corresponding Si-Pd-Si angles (69.0 and 58.8°) strongly deviate from the values expected for an octahedral (90°) or a trigonal prismatic (ca. 82°) Pd coordination sphere and can be only justified by a tendency of two Si atoms to bond to each other. In contrast, if we analyze the coordination geometry by considering the centroids of the Si–Si bonds as the coordination sites, we find the following angles: centroid-Pd-centroid 93.4°, Si-Pd-Si 74.2°, centroid-Pd-Si 95.6 and 96.9°, indicative of a perfectly planar (bond angle sum of 360.1°) and nearly square $PdSi_2(centroid)_2$ core as expected for a tetracoordinate Pd^{II} complex.

b) *Continuous symmetry measures*: The continuous symmetry measures[6, 7] provide quantitative estimates of how much the coordination sphere of a given atom deviates from an ideal polyhedron. For the presently studied compound, we find the *distance* of the $PdSi_6$ group to the octahedron to be 13.4, which indicates that it can by no means be considered as octahedral, yet it is also far from being a trigonal prism (distance of 6.5). It has been found[8] that for structures intermediate between the octahedron and the trigonal prism the sum of the square root of these two symmetry measures must be 4.1. The value found for the present case (6.2) clearly indicates a quite anomalous $PdSi_6$ coordination polyhedron which cannot be described as an octahedron or a trigonal prism or an intermediate structure. In contrast, if we consider the centroids of the two Si–Si bonds in the Pd^{II} formulation **2**, the very small distance to the square (0.7) indicates a slightly distorted square-planar coordination sphere, consistent with the discussion on bond angles above.

c) *Spin state and magnetism*: Hexacoordinate transition-metal ions with a d^4 electron configuration may appear in either high- or low-spin states (net spins $S = 2$ and 1, respectively) in the case of first-row transition metals but only in the low-spin state for second- and third-row transition metals. In any case such d^4 configurations are paramagnetic, with the only exception of $[M(bipy)_3]$ (bipy = 2,2′-bipyridine) for M = Ti or Zr.[9] One should therefore expect the silyl – Pd^{VI} form **1** with a d^4 electronic configuration to be paramagnetic. Although the magnetic properties of these compounds have not been reported, there is no evidence of paramagnetic shifts in the published NMR spectra, clearly indicative of a diamagnetic behavior. One may argue, though, that the severe distortion of the coordination sphere from the octahedron could be responsible for a spin-paired ground state, an issue that is worth of a theoretical investigation and will be discussed below.

d) *DFT calculations*: To find out whether side-on coordination of a Si–Si bond is theoretically sound, we have carried out DFT calculations[10] on several simplified model complexes. First, we considered octahedral $[Pd(SiH_3)_6]$, which would correspond to the Pd^{VI} center **1**, and performed a geometry optimization by assuming each pair of *trans* silyl groups to be equivalent. Optimization resulted in a nearly octahedral isomer (Pd–Si bond lengths 2.491 – 2.497 Å and all Si–Si distances larger than 3.52 Å) more stable in its triplet than in its singlet state (by 11 kcal mol^{-1}), as expected for an hexacoordinate d^4 complex.

Next, we consider the singlet state of $[Pd(SiH_3)_2(\eta^2\text{-}Si_2H_6)_2]$ as a model of the square-planar Pd^{II} center **2**, assuming a C_2 symmetry. Such a model is indeed found to be square planar (Figure 1 a), when the centroid of the Si–Si bond is considered as the coordination site of each η^2-bonded group, and much more stable than the octahedral isomer **1** in its triplet state (by 58 kcal mol^{-1}). The interaction energy between the $Pd(SiR_3)_2$ group and two disilane units is calculated to be barely -1.4 kcal mol^{-1}. Similar geometries were obtained for the substituted analogues $[Pd(SiH_3)_2(\eta^2\text{-}Si_2R_6)_2]$, where $R_3 = H_2Me$, HMe_2 or Me_3. An interesting result for these model compounds is that the Pd–Si distances corresponding to the η^2 groups (3.675 Å) are much longer, and the Si–Si distances

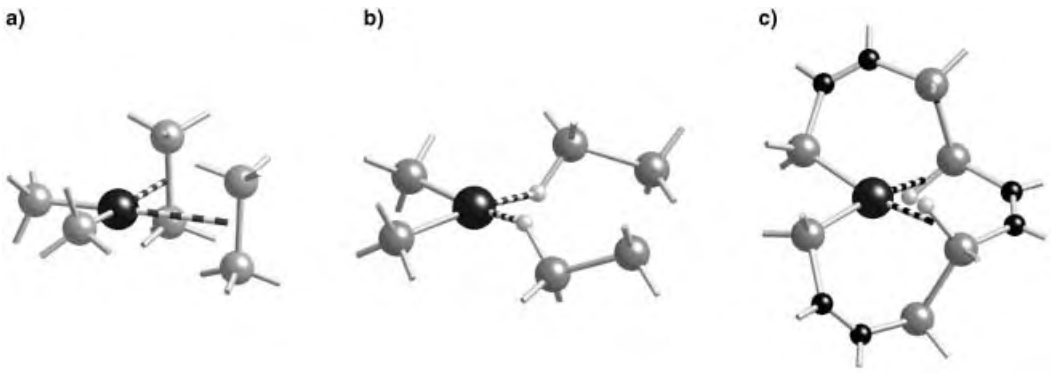
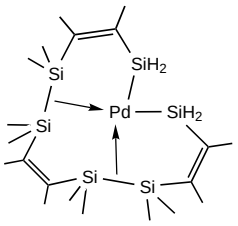


Figure 1. Calculated structures for a) $[Pd(SiH_3)_2(\eta^2\text{-}Si_2H_6)_2]$ with symmetry restrictions, b) the same model without symmetry restrictions, and c) model **3**.

 © WILEY-VCH Verlag GmbH, 69451 Weinheim, Germany, 2002 1433-7851/02/4111-1957 $ 20.00+.50/0

(2.329 Å) significantly shorter, than the experimental values (2.49 – 2.59 and 2.44 – 2.56 Å, respectively); however, when the Si atoms are forced to be closer to the Pd atom, the Si–Si distance is elongated. All these results reveal a quite weak bonding between the disilane molecules and the Pd^{II} center. Full relaxation of the geometry of such a compound results in the coordination of the disilane molecules through one hydrogen atom rather than through the Si–Si bond (Figure 1b, Pd–H 2.02 Å), a structure that is 9 kcal mol^{-1} more stable than that of Figure 1a. The results for the two mononuclear models clearly indicate that the formation of Si–Si bonds combined with a Pd^{II} oxidation state is strongly favored relative to the hexakis(silyl)palladium(VI) situation.



3

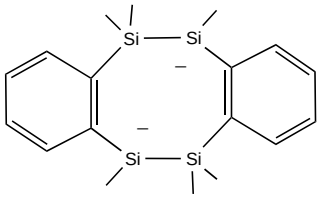
In the third model (**3**) we used the silyl ligands as they appear in the experimental structure rather than independent SiH_3 groups, replacing the benzo groups by HC=CH linkers and saturating the missing bonds from the Si centers to the peripheral Pd atoms with hydrogen atoms. The optimized structure in this case presents σ Si–H bonds coordinated to a square-planar Pd^{II} center (Figure 1c), which seems to be more stabilizing than coordination of a Si–Si bond. It is to be noted that two Si–Si bonds can be clearly identified (Si–Si 2.340 Å). The Si–H-bond coordination is probably an artifact of the model adopted, since these hydrogen atoms are replacing the peripheral Pd atoms of the experimental structure.

Finally, we have optimized the trinuclear complex with each terminal diphosphane ligand substituted by PH_3 and the benzo groups replaced by HC=CH linkers. In the absence of the artificial Si–H bonds used in the previous model, the silylated ligand of **3** is reorganized to allow for Si–Si side-on coordination to the central Pd atom. The calculated Si–Si distances (2.507 Å) as well as the corresponding Pd–Si ones (2.523 and 2.594 Å) are now in excellent agreement with the experimental data (2.538 – 2.554 Å and 2.420 – 2.565 Å, respectively). The Pd–Si bond lengths for the η^1-silyl groups (2.403 Å) are consistent with the experimental ones (2.345 – 2.364 Å), and even the short Pd···Pd contacts are well reproduced (2.893 – 2.912 Å and 2.941 Å in the experimental and calculated structures, respectively). These results clearly show that the interaction between the Pd center and the Si–Si bond is stronger than in the mononuclear model **2** because the multidentate nature of the ligand in **3** keeps them in closer contact.

That the Si–Si distance is elongated when the Pd–Si distance decreases is in agreement with a Dewar – Chatt – Duncanson-like bonding model (as applies to the η^2 coordination of the dihydrogen molecule[11]), in which each σ(Si–Si) molecular orbital donates its two electrons to the metal atom while the σ*(Si–Si) molecular orbitals of the two disilane groups accept back donation from the π-type d_{xz} and d_{yz} orbitals. The existence of two such interactions requires the Si–Si bonds to be nearly perpendicular to the $PdSi_2(centroid)_2$ coordination plane as actually found in the experimental structure and in the trinuclear model (angles of 75 and 69°, respectively).

e) *Precedents of side-on coordination of single bonds*: Although the presence of a lone pair seems a prerequisite for a particular group to act as a ligand towards a transition metal, the bonding electrons of such covalent bonds as H–H or Si–H can also act as donors. Hence, one of the aspects of transition-metal chemistry that has opened new perspectives in recent years is the study and characterization of dihydrogen complexes, in which a H_2 molecule is coordinated in an η^2 mode and is more or less elongated with respect to the free molecule.[11–13] Overwhelming evidence has accumulated in the last few years on the η^2 coordination of Si–H, Ge–H, Sn–H, and B–H bonds.[12–15] Let us quote just two remarkable examples: a C–H bond of a solvation *n*-heptane molecule found at 2.88 Å from the Fe atom in a porphyrinato complex,[16] and the structures of two complexes in which two Si–H bonds of the same molecule are coordinated to *trans* positions of a Ru atom.[17]

Even if there is no clearly established precedent for an η^2-coordinated Si–Si single bond, there is a recent report of such coordination mode for an Si=Si double bond linked to a Pt center.[18] In that compound, the Si–Si bond (2.321 Å) is clearly shorter than, but the M–Si bonds (2.432 Å) practically identical to, those in the compound studied here (2.486 – 2.590 Å, and 2.445 – 2.565 Å, respectively). It must be stressed that similar Si–Si bonds (2.69 Å) are found in a dinuclear Ni complex,[19] although the Si–Si bond was not clearly established by the authors, thus providing a fascinating example of the formation of the heterocyclic ligand **4**, the neutral octamethylated analogue of which is well known.[20] This compound should be probably considered as the first example of η^2 coordination of a Si–Si single bond to a transition metal. A related niobocene derivative also showing a dichotomy between two silyl or disilane coordinated groups has been reported more recently.[21]



4

f) *Similarities between Si and H*: Crabtree[2] has suggested that the bonding situation in the compound[1] studied here should be analogous to that in $[PdH_6]$. Bayse and Hall had actually performed ab initio calculations on $[PdH_6]$ and $[PtH_6]$ and found that the former dissociates into $H_2+Pd(\eta^2\text{-}H_2)_2$, whereas the latter has a square-planar structure with two side-on coordinated dihydrogen molecules and two hydrides.[22] Andrews et al., on the other side, found a trigonal-planar $Pd(\eta^2\text{-}H_2)_3$ structure that seems to be consistent with the infrared spectra in noble-gas matrices.[23] Such studies are therefore in general agreement with the results presented here, in the sense that H–H, Si–H, and Si–Si bonds present similar coordinating abilities toward transition metals.

The assignment of a Pd^{VI} oxidation state within the $PdSi_6$ core in the recently reported compound should be disregarded according to our structural, symmetry, and theoretical analysis.[24] Nevertheless, the alternative structure is no less remarkable since it presents side-on coordination of Si–Si

 © WILEY-VCH Verlag GmbH, 69451 Weinheim, Germany, 2002 1433-7851/02/4111-1958 $ 20.00+.50/0 *Angew. Chem. Int. Ed.* **2002**, *41*, No. 11

single bonds that are formed with a Pd complex as a template, which can now be incorporated to the gallery of other σ bonds that are known to coordinate to transition metals: H–H, C–H, Si–H, Ge–H, Sn–H, and B–H. The present study also suggests that the structure of a related dinuclear Ni complex[19] should be revisited and reinterpreted, and might be considered as the first structurally characterized example of such kind of novel coordination of Si–Si bonds.

Received: April 1, 2002 [Z18962]

[1] W. Chen, S. Shimada, M. Tanaka, *Science* **2002**, *295*, 308.
[2] R. H. Crabtree, *Science* **2002**, *295*, 288.
[3] N. Kleiner, M. Drager, *J. Organomet. Chem.* **1984**, *270*, 151.
[4] N. Wiberg, H. Schuster, A. Simon, K. Peters, *Angew. Chem.* **1986**, *98*, 100; *Angew. Chem. Int. Ed. Engl.* **1986**, *25*, 79.
[5] N. Wiberg, W. Niedenmayer, *Z. Naturforsch. B* **2000**, *55*, 389.
[6] H. Zabrodsky, S. Peleg, D. Avnir, *J. Am. Chem. Soc.* **1992**, *114*, 7843.
[7] H. Zabrodsky, S. Peleg, D. Avnir, *J. Am. Chem. Soc.* **1993**, *115*, 8278 (Erratum: H. Zabrodsky, S. Peleg, D. Avnir, *J. Am. Chem. Soc.* **1994**, *116*, 656).
[8] S. Alvarez, D. Avnir, M. Llunell, M. Pinsky, *New J. Chem.* **2002**, in press.
[9] E. A. Boudreaux, L. N. Mulay, *Theory and Applications of Molecular Paramagnetism*, Wiley, New York, **1976**.
[10] The structures were optimized at the B3LYP level of theory implemented in Gaussian 98 (Revision A.11).[10a] Effective core potentials and their associated double-ζ basis set LANL2DZ were used for Pd, P, and Si atoms, supplemented with polarization functions for Si and P, whereas a 6-31G basis set was used for H and C. The structures shown in Figure 1b–c have been charactrized as energy minima through vibrational frequencies calculations. Interaction energies were corrected for the basis set superposition error by means of the counterpoise method; a) Gaussian 98 (Revision A.11), M. J. Frisch, G. W. Trucks, H. B. Schlegel, G. E. Scuseria, M. A. Robb, J. R. Cheeseman, V. G. Zakrzewski, J. A. Montgomery, R. E. Stratmann, J. C. Burant, S. Dapprich, J. M. Millam, A. D. Daniels, K. N. Kudin, M. C. Strain, O. Farkas, J. Tomasi, V. Barone, M. Cossi, R. Cammi, B. Mennucci, C. Pomelli, C. Adamo, S. Clifford, J. Ochterski, G. A. Petersson, P. Y. Ayala, Q. Cui, K. Morokuma, D. K. Malick, A. D. Rabuck, K. Raghavachari, J. B. Foresman, J. Cioslowski, J. V. Ortiz, B. B. Stefanov, G. Liu, A. Liashenko, P. Piskorz, I. Komaromi, R. Gomperts, R. L. Martin, D. J. Fox, T. Keith, M. A. Al-Laham, C. Y. Peng, A. Nanayakkara, C. Gonzalez, M. Challacombe, P. M. W. Gill, B. G. Johnson, W. Chen, M. W. Wong, J. L. Andres, M. Head-Gordon, E. S. Replogle, J. A. Pople, Gaussian, Inc., Pittsburgh, PA, **1998**.
[11] F. Maseras, A. Lledós, E. Clot, O. Eisenstein, *Chem. Rev.* **2000**, *100*, 601.
[12] G. J. Kubas, *Metal Dihydrogen and σ-Bond Complexes*, Kluwer Academic/Plenum Publishers, New York, **2001**.
[13] G. J. Kubas, *J. Organomet. Chem.* **2001**, *635*, 37.
[14] G. I. Nikonov, *J. Organomet. Chem.* **2001**, *635*, 24.
[15] G. I. Nikonov, *Angew. Chem.* **2001**, *113*, 3457; *Angew. Chem. Int. Ed.* **2001**, *40*, 3353.
[16] D. R. Evans, T. Drovetskaya, R. Bau, C. A. Reed, P. D. W. Boyd, *J. Am. Chem. Soc.* **1997**, *119*, 3633.
[17] F. Delpech, S. Sabo-Etienne, J.-C. Daran, B. Chaudret, K. Hussein, C. J. Marsden, J.-C. Barthelat, *J. Am. Chem. Soc.* **1999**, *121*, 6668.
[18] H. Hashimoto, Y. Sekiguchi, T. Iwamoto, C. Kabuto, M. Kira, *Organometallics* **2002**, *21*, 454.
[19] S. Shimada, M. L. N. Rao, T. Hayashi, M. Tanaka, *Angew. Chem.* **2001**, *113*, 219; *Angew. Chem. Int. Ed.* **2001**, *40*, 213.
[20] T. Kusukawa, Y. Kabe, B. Nestler, W. Ando, *Organometallics* **1995**, *14*, 2556.
[21] G. I. Nikonov, S. F. Vyobishchikov, L. G. Kuzmina, J. A. K. Howard, *Chem. Commun.* **2002**, 568.
[22] C. A. Bayse, M. B. Hall, *J. Am. Chem. Soc.* **1999**, *121*, 1348.
[23] L. Andrews, X. Wang, M. E. Alikhani, L. Manceron, *J. Phys. Chem. A* **2001**, *105*, 3052.
[24] Similar conclusions have been reached independently by Cramer and co-workers E. C. Sherer, C. R. Kinsinger, B. L. Kormos, J. D. Thompson, C. J. Cramer, *Angew. Chem.* **2002**, *114*, 2033; *Angew. Chem. Int. Ed.* **2002**, *41*, 1953.

A 3D Open–Framework Indium Telluride and Its Selenide and Sulfide Analogues**

Cheng Wang, Xianhui Bu, Nanfeng Zheng, and Pingyun Feng*

There has been increasing interest in designing host–guest materials with crystalline conducting frameworks.[1] The combination of porosity and conductivity in the same material is expected to lead to unique properties suitable for electronic applications as well as molecular-sieve type applications. One application that might be envisioned to benefit from the development of host–guest chalcogenide open frameworks is in the area of thermoelectric materials, where there has been interest in developing host–guest order–disorder materials.[2] The disordered portion of the structure is expected to scatter phonons and minimize lattice thermal conductivity while the ordered crystalline framework serves to maintain high electric conductivity.[3] The recent interest in host–guest germanium–silicon clathrates reflects the application of this design strategy.[4, 5]

So far, extensive studies have been made with purely inorganic chalcogenides because of their useful optoelectronic and thermoelectric properties.[6] For example, $CuInSe_2$ is among the most efficient photovoltaic materials and Bi_2Te_3 is one of the best thermoelectric materials. In comparison, very little research has been done on the optical, electronic, and thermoelectric properties of open-framework chalcogenides. This is in part a result of the rarity of host–guest heavy-chalcogenide open frameworks. To our knowledge, no amine-templated 3D open-framework tellurides have been made prior to this work, even though some open-framework sulfides and selenides are already known.[7–11]

In the synthesis of metal-chalcogenide open-framework materials, small clusters are often found to serve as structural building units (SBUs) in extended frameworks. These clusters include supertetrahedral T2 (M_4X_{10}), T3 ($M_{10}X_{20}$), and T4 ($M_{20}X_{35}$), where M is a metal ion and X is a chalcogen anion.[12, 13] While the cluster-based structural-design approach is known to generate large pores,[12, 13] the intercluster connection is typically provided by a single atom. This situation may not represent the best configuration for electronic properties, therefore, it is highly desirable to have open-framework chalcogenides with topological features that extend beyond the cluster-based configurations.

Here we report an amine-directed, chain-based 3D telluride open framework together with its selenide and sulfide analogues. It is also demonstrated here that mixed-chalcoge-

[*] Prof. P. Feng, Dr. C. Wang, N. Zheng
Department of Chemistry
University of California
Riverside, CA 92521 (USA)
Fax: (+1) 909-787-4713
E-mail: pingyun.feng@ucr.edu
Dr. X. Bu
Department of Chemistry
University of California
Santa Barbara, CA 93106 (USA)

[**] We thank UC Riverside, UC Energy Institute, and the donors of The Petroleum Research Fund (administered by the ACS) for funding.

nide open frameworks with various compositions can be made. These open-framework chalcogenides have the same framework connectivity and are collectively called UCR-2 (see Table 1). The smallest integral unit ($In_{33}X_{56}$, X = S, Se, Te, S/Se, and S/Te) in these compounds has 89 atoms and is very large compared to similar units in reported open framework sulfides. These structures are in general more complex than cluster-based frameworks and they offer additional opportunities to study the structure – property correlation in open-framework chalcogenides.

Table 1. A summary of crystallographic data for selected open-framework chalcogenides synthesized in this study.[a]

Name[b]	Framework formula	a [Å]	c [Å]	$R(F)$	$2\theta_{max}$
UCR-2InS-TMDP	$(In_{33}S_{56})^{13-}$	21.650(1)	33.610(2)	5.54	50
UCR-2InSe-DIPA	$(In_{33}Se_{56})^{13-}$	22.455(3)	34.335(6)	5.69	45
UCR-2InSe-TETA	$(In_{33}Se_{56})^{13-}$	22.344(3)	34.100(5)	4.18	45
UCR-2InSe-TAA	$(In_{33}Se_{56})^{13-}$	22.54(1)	34.09(1)		
UCR-2InSe-AEAE	$(In_{33}Se_{56})^{13-}$	22.333(5)	34.397(9)		
UCR-2InSe-DPA	$(In_{33}Se_{56})^{13-}$	22.370(6)	34.355(9)		
UCR-2InSe-TMHD	$(In_{33}Se_{56})^{13-}$	22.476(7)	34.29(1)		
UCR-2InSe-BAPP	$(In_{33}Se_{56})^{13-}$	22.69(1)	34.71(2)		
UCR-2InSe-TOTD	$(In_{33}Se_{56})^{13-}$	22.566(8)	34.701(9)		
UCR-2InSe-HMI	$(In_{33}Se_{56})^{13-}$	22.493(3)	34.281(5)		
UCR-2InSe-DAO	$(In_{33}Se_{56})^{13-}$	22.254(3)	34.144(7)		
UCR-2InSe-DMMP	$(In_{33}Se_{56})^{13-}$	22.256(7)	34.23(2)		
UCR-2InSe-APM	$(In_{33}Se_{56})^{13-}$	22.322(6)	34.46(2)		
UCR-2InTe-TETA	$(In_{33}Te_{56})^{13-}$	23.710(5)	36.076(9)		
UCR-2InTe-APDA	$(In_{33}Te_{56})^{13-}$	23.619(3)	36.370(7)	4.78	45
UCR-2InTe-TAA	$(In_{33}Te_{56})^{13-}$	23.912(4)	35.910(7)	6.40	45
UCR-2InSTe-APDA	$(In_{33}S_{36}Te_{20})^{13-}$	22.653(11)	34.115(23)	7.74	42
UCR-2InSSe-TMDP	$(In_{33}S_{16}Se_{40})^{13-}$	22.037(4)	34.101(9)	6.03	45
UCR-2InSSe-DIPA	$(In_{33}S_6Se_{50})^{13-}$	22.354(4)	34.337(9)	5.51	45

[a] Crystal structures were solved from single-crystal data collected at 298 K on a SMART CCD diffractometer with $Mo_{K\alpha}$. The space group is $R32$ for all structures and $Z = 3$. $R(F) = \Sigma||F_o| - |F_c||/\Sigma|F_o|$ with $F_o > 4.0\sigma(F)$. [b] TMDP = 4,4′-trimethylenedipiperidine, $C_{13}H_{26}N_2$; DIPA = diisopropylamine, $C_6H_{15}N$; APDA = *N*-(2-aminoethyl)-1,3-propanediamine, $C_5H_{15}N_3$; TETA = triethylenetetramine, $C_6H_{18}N_4$; TAA = tris(2-aminoethyl)amine, $C_6H_{18}N_4$; AEAE = 2-(2-aminoethylaminoethanol), $C_4H_{12}N_2O$; DPA = dipropylamine, $C_6H_{15}N$; BAPP = 1,4-bis(3-aminopropyl)piperazine, $C_{10}H_{24}N_4$; TMHD = C,C,C-trimethyl-1,6-hexanediamine, $C_9H_{22}N_2$; TOTD = 4,7,10-trioxa-1,13-tridecanediamine, $O[CH_2CH_2O(CH_2)_3NH_2]_2$; HMI = hexamethyleneimine, $C_6H_{13}N$; DAO = 1,8-diaminooctane, $C_8H_{20}N_2$; DMMP = 2,6-dimethylmorpholine, $C_6H_{13}NO$; APM = *N*-(3-aminopropyl)morpholine, $C_7H_{16}N_2O$.

Unlike the known sulfide open frameworks that contain building units related to admantane clusters, the 3D framework in the UCR-2 family of materials is constructed from the cross-linking of helical chains. Therefore, the synthesis of UCR-2 demonstrates the feasibility of creating open-framework chalcogenides without the use of supertetrahedral clusters.

To prepare crystals of UCR-2InTe-APDA, *N*-(2-aminoethyl)-1,3-propanediamine (APDA) was added to a 23 ml-Teflon-lined stainless steel autoclave containing 3.264 g of water until the pH of the solution was 13.50. Indium metal (84 mg) and tellurium (187 mg) were then added. The vessel was sealed and heated at 200 °C for 10 days. The autoclave was subsequently allowed to cool to room temperature.

With proper choice of the solution pH value and structure-directing agents, both sulfide and selenide analogues (see Table 1) can be synthesized under similar conditions. In addition, mixed chalcogenides with more than one chalcogen type in the inorganic framework (e.g., S/Se, S/Te) have also been synthesized. Crystals are pale yellow, orange-red, and dark red for sulfides, selenides, and tellurides, respectively, demonstrating the variation in their electronic bandgap.

While all the framework atoms can be determined unambiguously in all the structures (Figure 1), guest amine molecules are disordered inside large cavities and can not be located. The presence of organic molecules is verified by

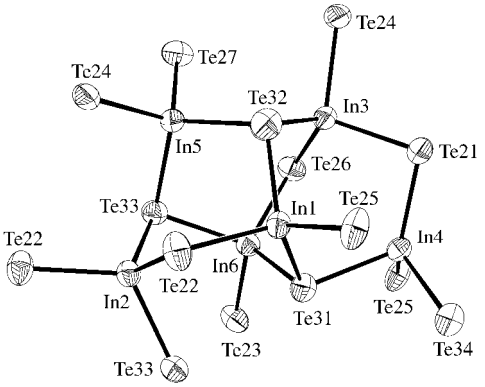


Figure 1. The ORTEP view of coordination environments for In and Te atoms in UCR-2InTe-APDA. (thermal ellipsoids set at the 50 % level).[19]

elemental analysis.[14] The disorder of the amine molecules may be related to the relatively weak host – guest interaction in open-framework chalcogenides. In particular, the hydrogen bonding (i.e. N-H···X, X = S, Se, or Te) is considerably weaker than the N-H···O type of hydrogen bonding that is often responsible for the ordering of guest amine molecules in oxides.[15, 16] When these extra-framework species are not considered, by using the program PLATON[17] the porosity of UCR-2InS-TMDP is calculated to be 50 %.

When divalent metal cations are included in the synthesis mixture for UCR-2InS-TMDP, the formation of UCR-2InS-TMDP is suppressed and another type of framework containing supertetrahedral T4 clusters $(M_4In_{16}S_{33})^{10-}$ (M = Mn, Co, Fe, Zn, Cd, denoted collectively as UCR-1MInS) is formed.[13] The addition of these divalent metal cations, however, does not have an effect on the formation of UCR-2 selenide and telluride analogues. It can be inferred that selenides and tellurides have a stronger tendency to form non-cluster-based open frameworks than sulfides.

Instead of forming a cluster that would resemble a fragment of the cubic ZnS type structure, InX_4 tetrahedra in UCR-2 share corners to form infinite chains (Figure 2 and Figure 3). Chains are cross-linked to give a 3D framework with large cages. Cages are interconnected to form a 3D channel system.

Noteworthy is that the T-X-T angles vary from 96.8– 112.9° for the sulfide, 93.3 – 110.3° for the selenide, and 92.6 – 108.2° for the telluride. This is a range of up to 17°. While this range is small compared to the range of T-O-T angles (T = tetrahedral atom) in zeolites it is considerably greater than the 5° range (i.e., 103 – 108°) of T-S-T angles in some Ge – S compounds.[7] This observation suggests that there could be a richer structural diversity in indium chalcogenides than in

 © WILEY-VCH Verlag GmbH, 69451 Weinheim, Germany, 2002 1433-7851/02/4111-1960 $ 20.00+.50/0

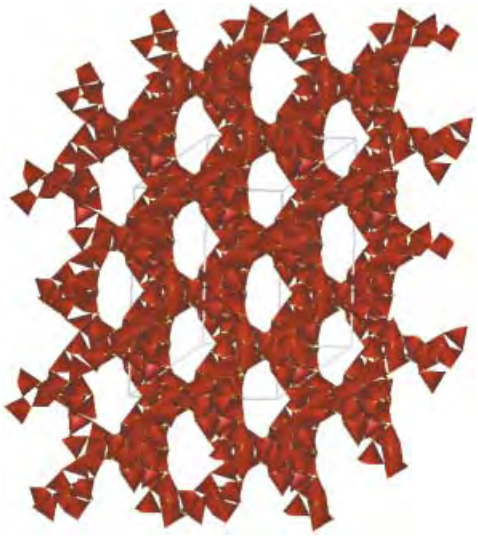


Figure 2. A polyhedral view of the 3D framework of UCR-2InTe-APDA showing the formation of cages by the fusion of chains propagating along the *c* axis.[19]

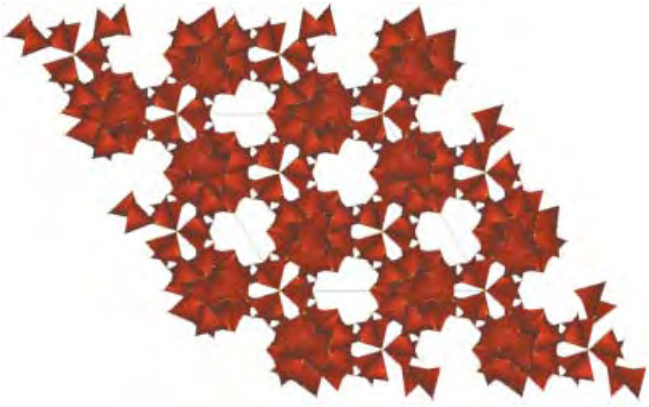


Figure 3. A polyhedral view of the 3D framework of UCR-2InTe-APDA projected down the *c* axis.[19]

other chalcogenides. It is also apparent that the T-X-T angle becomes smaller for heavier chalcogens. However, compared to the significant change in the T-X-T angle from oxides (about 140°) to sulfides (about 106°), the change in the T-X-T angle from sulfides (about 106°) to tellurides (about 100°) is relatively minor. This situation suggests that the structural properties of open-framework sulfides, selenides, and tellurides should be quite similar and are significantly different from those of oxides.

In mixed compounds with more than one type of chalcogen ions, the distribution of different chalcogen ions among crystallographic sites is not random as shown by the refined occupancy factors. For example, in UCR-2InSTe-APDA, the tricoordinate chalcogen sites are occupied by light sulfur atoms. In the bicoordinate chalcogen sites, the refined occupancies show that about 56% of atoms are tellurium ions (the S:Te molar ratio = 1:1 in the synthesis mixture). The overall S:Te atomic ratio of 1.76:1 derived from the occupancy refinement agrees well with the measurement (1.70:1) obtained from the energy-dispersive spectrum collected by scanning electron microscopy.

Fluorescent spectra were measured on a SPEX Fluorolog-3 system equipped with a 450 W xenon lamp. For UCR-2InS-TMDP, a broad emission centered at 520 nm was observed when excited at 470 nm. For UCR-2InSe-BAPP, the emission was centered at 563 nm when excited at 482 nm. Compared to open-framework oxides such as phosphates and germanates with typical absorption and emission maxima at 360 nm and 410 nm, respectively,[18] it is apparent that there is a systematic variation in the spectral characteristics of these open-framework materials. It can be anticipated that by varying the topologies and compositions of open-framework chalcogenides, photoluminescent materials with a wide range of emission characteristics may be developed.

In conclusion, we have shown that a family of chalcogenides, tellurides in particular, have been synthesized and structurally characterized. The framework composition is highly flexible and controllable. The unique host–guest, order–disorder features may make them useful for studies in semiconductor applications, for example, in the development of a new class of semiconducting materials based on heavy-chalcogenide host–guest open-framework materials.

Received: February 13, 2002 [Z18703]

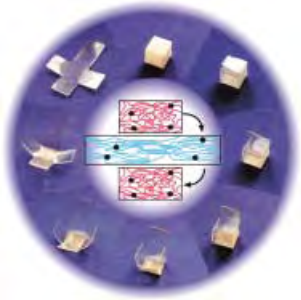
[1] A. K. Cheetham, G. Ferey, T. Loiseau, *Angew. Chem.* **1999**, *111*, 3466; *Angew. Chem. Int. Ed.* **1999**, *38*, 3268.
[2] T. M. Tritt, *Science* **1999**, *283*, 804.
[3] J. L. Cohn, G. S. Nolas, V. Fessatidis, T. H. Metcalf, G. A. Slack, *Phys. Rev. Lett*. **1999**, *82*, 779.
[4] G. S. Nolas, J. J. Cohn, G. A. Slack, S. B. Schuiman, *Appl. Phys. Lett*. **1998**, *73*, 178.
[5] S. Latturner, X. Bu, N. Blake, H. Metiu, G. D. Stucky, *J. Solid State Chem*. **2000**, *151*, 61.
[6] D. Chung, T. Hogan, P. Brazis, M. Rocci-Lane, C. Kannewurf, M. Bastea, C. Uher, M. G. Kanatzidis, *Science* **2000**, *287*, 1024.
[7] R. L. Bedard, S. T. Wilson, L. D. Vail, J. M. Bennett, E. M. Flanigen, in *Zeolites: Facts, Figures, Future. Proceedings of the 8th International Zeolite Conference* (Eds.: P. A. Jacobs, R. A. van Santen), Elsevier, Amsterdam, **1989**, p. 375.
[8] H. Li, J. Kim, T. L. Groy, M. O'Keeffe, O. M. Yaghi, *J. Am. Chem. Soc*. **2001**, *123*, 4867.
[9] C. L. Cahill, Y. Ko, J. B. Parise, *Chem. Mater*. **1998**, *10*, 19.
[10] H. Ahari, A. Garcia, S. Kirby, G. A. Ozin, D. Young, A. J. Lough, *J. Chem. Soc. Dalton Trans.* **1998**, 2023.
[11] H. Ahari, A. Lough, S. Petrov, G. A. Ozin, R. L. Bedard, *J. Mater. Chem*. **1999**, *9*, 1263.
[12] H. Li, A. Laine, M. O'Keeffe, O. M. Yaghi, *Science* **1999**, *283*, 1145.
[13] C. Wang, Y. Li, X. Bu, N. Zheng, O. Zivkovic, C. Yang, P. Feng, *J. Am. Chem. Soc.* **2001**, *123*, 11506.
[14] Elemental analysis (%) calcd for UCR-2InS-TMDP based on the formula $[In_{33}S_{56}](C_{13}H_{26}N_2H_2)_{6.5}$: C 14.57, H 2.63, N 2.61; found: C 14.16, H 2.06, N 2.57; (%) calcd for UCR-2InSe-BAPP based on the formula $[In_{33}Se_{56}](C_{10}H_{24}N_4H_2)_{6.5}$: C 8.19, H 1.79, N 3.82; found: C 9.02, H 1.81, N 3.43; (%) calcd for UCR-2InTe-APDA based on the formula $[In_{33}Te_{56}](C_5H_{15}N_3H_3)(C_5H_{15}N_3H_2)_5$: C 3.09, H 0.95, N 2.16; found: C 2.94, H 0.84, N 1.43.
[15] P. Feng, X. Bu, G. D. Stucky, *Nature* **1997**, *388*, 735.
[16] W. T. A. Harrison, M. L. F. Phillips, T. M. Nenoff, E. J. MacLean, S. J. Teat, R. S. Maxwell, *J. Chem. Soc. Dalton Trans.* **2001**, *5*, 546.
[17] A. L. Spek, *Acta Crystallogr. Sect. A* **1990**, *46*, C34.
[18] P. Feng, *Chem. Commun*. **2001**, 1668.
[19] CCDC-179232–CCDC-179234 contains the supplementary crystallographic data for this paper. These data can be obtained free of charge via www.ccdc.cam.ac.uk/conts/retrieving.html (or from the Cambridge Crystallographic Data Centre, 12, Union Road, Cambridge CB21EZ, UK; fax: (+44) 1223-336-033; or deposit@ccdc.cam.ac.uk).

 © WILEY-VCH Verlag GmbH, 69451 Weinheim, Germany, 2002 1433-7851/02/4111-1961 $ 20.00+.50/0

ANGEWANDTE CHEMIE
INTERNATIONAL EDITION
A Journal of the Gesellschaft Deutscher Chemiker
2002
41/12
Pages 1973 – 2208

COVER PICTURE

The cover picture shows the thermally induced shape-memory effect for a covalently cross-linked polymer network. The polymer in its temporary shape (cube, picture on top) is heated from room temperature up to 70°C. Within 60 seconds the sample recovers its memorized, permanent shape of a nearly planar foil (picture on top left). The visual change of the material from opaque to transparent is caused by the melting of crystallites of the switching segments. The scheme in the center of the picture illustrates the molecular mechanism of the shape-memory effect. The shown polymer network, which is synthesized from poly(ε-caprolactone)dimethacrylate as macromonomer, is one of the first polymer systems that have specifically been developed for applications in the biomedical field. The net points (black) determine the permanent shape while the crystallites (blue) stabilize the temporary shape. More on the current state and the potential of this technology can be found in the review by A. Lendlein and S. Kelch on p. 2034 ff.

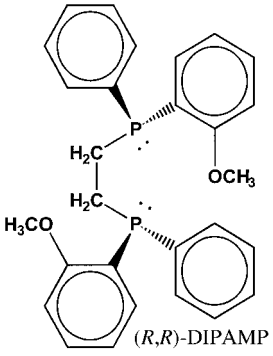


REVIEWS

Contents

Phosphorus is where the action is! Knowles and his co-workers were convinced that only chiral phosphorus ligands such as (*R*,*R*)-DIPAMP (see picture), whose stereogenic center lies directly on the phosphorus atom, would lead to high enantiomeric excesses when used as catalysts in asymmetric hydrogenation reactions. This hypothesis was contradicted by the development of ligands with chiral carbon backbones, and the mystery of how the phosphorus ligands work must still be solved.

Angew. Chem. **2002**, *114*, 2096 – 2107



(*R*,*R*)-DIPAMP

W. S. Knowles* ..... 1998 – 2007

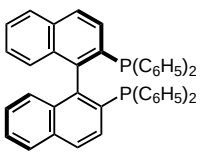
Asymmetric Hydrogenations (Nobel Lecture)

Keywords: asymmetric catalysis · asymmetric hydrogenation · Nobel lecture · phosphane ligands · rhodium

 © WILEY-VCH Verlag GmbH, 69451 Weinheim, Germany, 2002 1433-7851/02/4112-1975 $ 20.00+.50/0

From sub-femtomole to ton scale: Asymmetric catalysis with organometallic complexes plays a major role in all areas of modern synthetic chemistry. The author has worked in this area since the beginning and has been honored for his research with the Nobel prize. Asymmetric hydrogenation with transition-metal complexes of BINAP ligands (see picture) has been an important step in his personal research career.

Angew. Chem. **2002**, *114*, 2108 – 2123



(*R*)-BINAP

R. Noyori* ..... 2008 – 2022

Asymmetric Catalysis: Science and Opportunities (Nobel Lecture)

Keywords: asymmetric catalysis · asymmetric hydrogenation · Nobel lecture · phosphane ligands · ruthenium

Fishing for coelacanths (see picture) is how the author regards his Nobel-prize-winning research on the selective, asymmetric oxidation of alkenes. His procedures for asymmetric epoxidation and dihydroxylation use small, highly selective catalysts that are tolerant of a wide range of substrates.

Angew. Chem. **2002**, *114*, 2126 – 2135



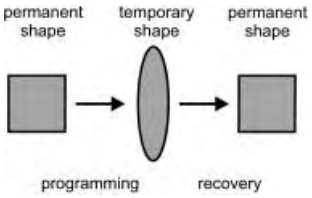
K. B. Sharpless* ..... 2024 – 2032

Searching for New Reactivity (Nobel Lecture)

Keywords: asymmetric catalysis · epoxidation · hydroxylation · Nobel lecture · N ligands

Upon exposure to an external stimulus, shape-memory polymers can change their shape (see scheme). This ability opens up numerous fields of application, such as intelligent, bulky implants, which can be inserted in a compressed, temporary shape into the body through a small incision, or auto bodies, which could be brought back to their original shape after a collision by a simple heat treatment. The current state and the potential of this technology is summarized in the article.

Angew. Chem. **2002**, *114*, 2138 – 2162



A. Lendlein,* S. Kelch ..... 2034 – 2057

Shape-Memory Polymers

Keywords: block copolymers · elastomers · materials science · polymers · shape-memory polymers

VIPs

The following communications are "Very Important Papers" in the opinion of two referees. They will be published shortly (those marked with a diamond will be published in the next issue). Short summaries of these articles can be found on the *Angewandte Chemie* homepage at the address http://www.angewandte.org

Poly(*p*-phenylenephosphaalkene): A π-Conjugated Macromolecule Containing P=C Bonds in the Main Chain — V. A. Wright, D. P. Gates* ◆

Catalytic Activity and Poisoning of Specific Sites on Supported Metal Nanoparticles — S. Schauermann, J. Hoffmann, V. Johánek, J. Hartmann, J. Libuda,* H.-J. Freund

Understanding Zeolite Catalysis: Inverse Shape Selectivity Revised — M. Schenk, S. Calero, T. L. M. Maesen, L. L. van Benthem, M. G. Verbeek, B. Smit*

Highly Selective Transport of Organic Compounds by Using Supported Liquid Membranes Based on Ionic Liquids — L. C. Branco, J. G. Crespo, C. A. M. Afonso*

Atom-Transfer Tandem Radical Cyclization Reactions Promoted by Lewis Acids — D. Yang,* S. Gu, H.-W. Zhao, N.-Y. Zhu

 © WILEY-VCH Verlag GmbH, 69451 Weinheim, Germany, 2002 1433-7851/02/4112-1977 $ 20.00+.50/0

Uncle Tungsten. Memories. In the new book by Oliver Sacks the history of chemistry, encompassing the ancient and the modern subdisciplines, is captured and told retrospectively through the eyes, heart, and voice of a passionate and precocious teenager.

Angew. Chem. **2002**, *114*, 2163 – 2170

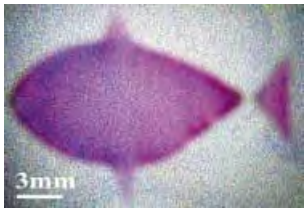
J. M. Thomas* ..... 2059 – 2065

An Omnivorous Curiosity, a Sense of Wonder, and a Taste for the Spectacular

Keywords: Sacks, Oliver · history of chemistry

COMMUNICATIONS

The unique photochemical properties of TiO_2 provides a stepwise approach for the easy and precise patterning of colloidal crystal films. In this approach patterns of hydrophobic and hydrophilic areas are formed on a TiO_2 surface and then a colored film of monodispersed polystyrene spheres is deposited on to the hydrophilic region (fish-shaped pattern in the example shown).



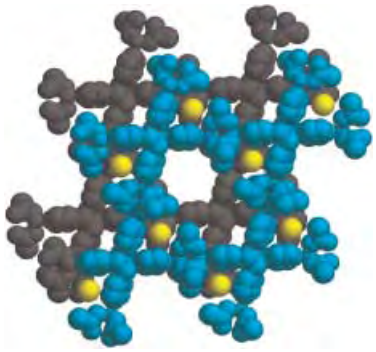
Angew. Chem. **2002**, *114*, 2171 – 2174

Z.-Z. Gu, A. Fujishima, O. Sato* ..... 2067 – 2070

Patterning of a Colloidal Crystal Film on a Modified Hydrophilic and Hydrophobic Surface

Keywords: colloids · surface chemistry · thin films · titanium dioxide · wettability

Gridlock: A porous metal – organic framework with an interior tailored supramolecularly with organic groups is described (see structure; two grids have been differentiated using cyan and gray, while the yellow spheres represent included methyl groups). The approach relies on inverting the role of a secondary building unit (SBU) and an organic linker such that the organic linker serves as a node and the SBU serves as a linear bridge. The organic node used to construct the framework has been obtained by way of a template-directed solid-state organic synthesis.



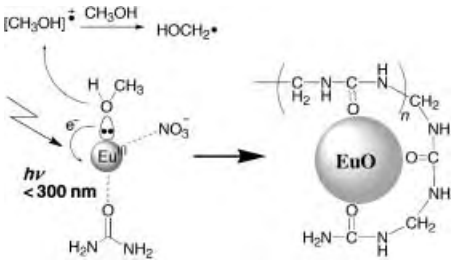
Angew. Chem. **2002**, *114*, 2174 – 2177

G. S. Papaefstathiou, L. R. MacGillivray* ..... 2070 – 2073

An Inverted Metal-Organic Framework with Compartmentalized Cavities Constructed by Using an Organic Bridging Unit Derived from the Solid State

Keywords: copper · cycloaddition · host – guest systems · layered compounds · self-assembly

Photoinduced enhancement of magnetization is exhibited by polyurea-modified EuO nanocrystals, prepared by photolysis of europium(III) nitrate and urea in methanol (see scheme). The nanoparticles, which have an average diameter of 3.4 nm and a narrow size distribution, also exhibit a remarkably high emission quantum yield.



Angew. Chem. **2002**, *114*, 2177 – 2179

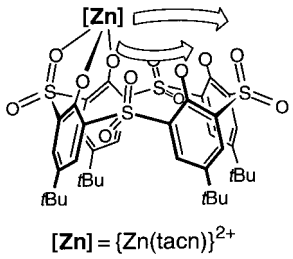
Y. Hasegawa, S. Thongchant, Y. Wada, H. Tanaka, T. Kawai, T. Sakata, H. Mori, S. Yanagida* ..... 2073 – 2075

Enhanced Luminescence and Photomagnetic Properties of Surface-Modified EuO Nanocrystals

Keywords: lanthanides · luminescence · magnetic properties · nanostructures

 © WILEY-VCH Verlag GmbH, 69451 Weinheim, Germany, 2002 1433-7851/02/4112-1978 $ 20.00+.50/0

The Zn^{II} ion slides smoothly over an "O_8" surface on the NMR spectroscopic timescale. The surface is formed by two phenol oxygen atoms, two phenoxy oxygen atoms, and four sulfonyl oxygen atoms of an analogue of *p-tert*-butylcalix[4]arene in a cone conformation in which the bridging methylene groups are replaced by sulfonyl moieties (see scheme). tacn = 1,4,7-triazacyclononane.



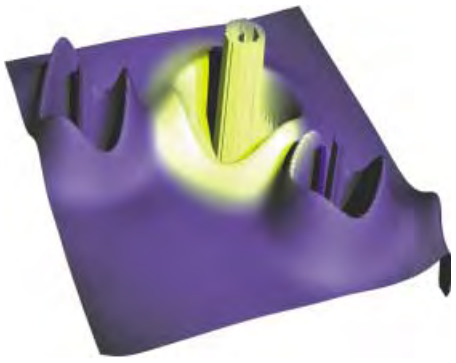
Angew. Chem. **2002**, *114*, 2180 – 2182

T. Kajiwara,* S. Yokozawa, T. Ito,* N. Iki, N. Morohashi, S. Miyano* .. 2076 – 2078

Zinc(II) Slides on a Ligand Surface: The X-Ray Crystal Structure and Dynamic Behavior in Solution of $[Zn(H_2L)(tacn)]$

Keywords: calixarenes · fluxionality · macrocyclic ligands · solid-state structures · zinc

Short bonds explained at long last: The charge-density distribution in the S–N bonds of $H_2C\{S(NtBu)_2(NHtBu)\}_2$, the NR analogue of methane disulfonic acid $H_2C\{S(O)_2(OH)\}_2$, was studied by high-resolution X-ray diffraction and subsequent multipole structure refinement (see picture). This experiment reveals that all three nitrogen atoms at each sulfur atom are sp^3 hybridized. The formal S–N double bonds are shortened by electrostatic reinforcement and not by $p_\pi - d_\pi$ interaction.



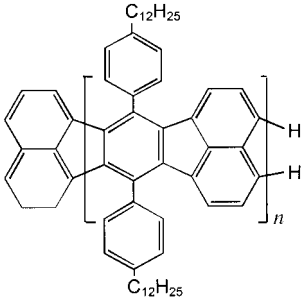
Angew. Chem. **2002**, *114*, 2183 – 2186

D. Leusser, B. Walfort, D. Stalke* ..... 2079 – 2082

Charge-Density Study of Methane Di(triimido)sulfonic Acid $H_2C\{S(NtBu)_2(NHtBu)\}_2$—the NR Analogue of $H_2C\{S(O)_2(OH)\}_2$

Keywords: bond theory · electron-density distribution · nitrogen · structure elucidation · sulfur

Chain length and dimerization, the missing link? The influence of chain length on the dimerization of the extended π-conjugated ladder-type fluoranthenopyracylene oligomers (see picture) during charge transfer is studied by cyclic voltammetry and in situ ESR/UV/Vis-NIR spectroelectrochemistry. The π conjugation in higher extended structures is found to be sufficient for the stabilization of charges in the molecule and disfavors chemical dimerization. This finding is an indication that dimerization in organic conducting polymers may not be a necessary stabilization mechanism of general validity.



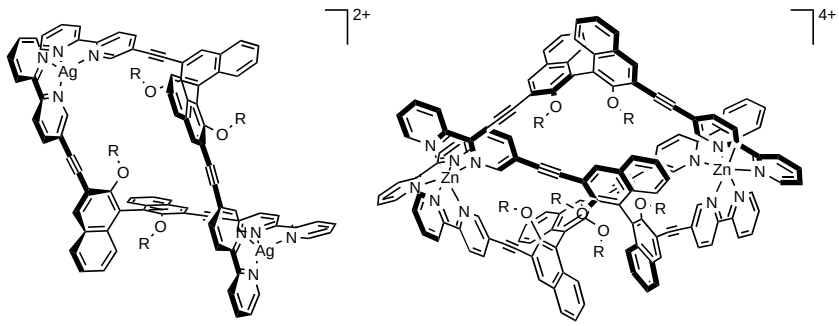
Angew. Chem. **2002**, *114*, 2187 – 2190

L. Dunsch,* P. Rapta, N. Schulte, A. D. Schlüter ..... 2082 – 2086

Structural Dependence of Redox-Induced Dimerization as Studied by In Situ ESR/UV/Vis-NIR Spectroelectrochemistry: The Fluoranthenopyracylene Oligomers

Keywords: conducting materials · conducting polymers · cyclic voltammetry · EPR spectroscopy · spectroelectrochemistry

Chiral cavities with inward-pointing functional groups are afforded by chiral bis(bipyridine) ligands. Upon coordination to suitable transition-metal ions, these self-assemble in a diastereoselective manner to form double- and triple-stranded helicates (left and right pictures, respectively).



Angew. Chem. **2002**, *114*, 2190 – 2194

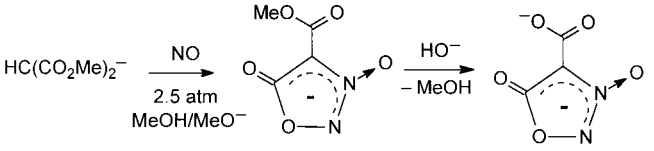
A. Lützen,* M. Hapke, J. Griep-Raming, D. Haase, W. Saak ..... 2086 – 2089

Synthesis and Stereoselective Self-Assembly of Double- and Triple-Stranded Helicates

Keywords: coordination chemistry · diastereoselectivity · helical structures · N ligands · supramolecular chemistry

 © WILEY-VCH Verlag GmbH, 69451 Weinheim, Germany, 2002 1433-7851/02/4112-1979 $ 20.00+.50/0

An unusual heterocycle results from the Traube reaction of dimethyl malonate and nitric oxide (see scheme). This newly characterized *E*-ONNO sydnone is formed preferentially to the condensation product with a *Z* geometry.



Traube's "oxazomalonic" acid

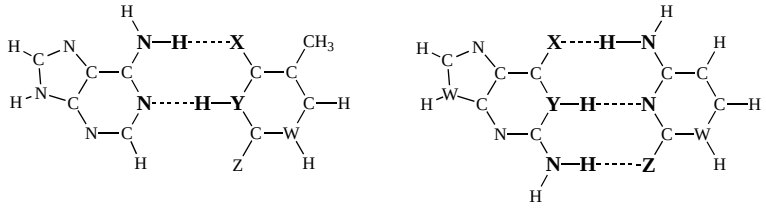
Angew. Chem. **2002**, *114*, 2200 – 2203

N. Arulsamy, D. S. Bohle* 2089 – 2091

Traube's "Oxazomalonic Acid" is a 3-Hydroxysydnone Carboxylate with an *E*-ONNO Geometry

Keywords: condensations · nitrogen heterocycles · nitrogen oxides · reaction mechanisms · structure elucidation

Not only the shape of the bases, but also the orbital interactions in the hydrogen bonds are essential for DNA replication, as follows from quantum-chemical analyses of Watson – Crick pairs and mimics thereof (see Figure: X, Z = O, F, H; W, Y = N, C), in combination with earlier experimental results.



A **$T_{XY'Z}$** **$G_{XY'N'}$** **$C_{N'NZ}$**

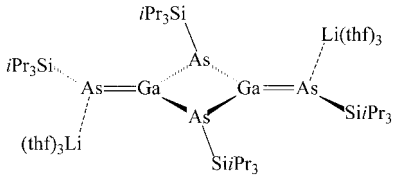
Angew. Chem. **2002**, *114*, 2194 – 2197

C. Fonseca Guerra, F. M. Bickelhaupt* ..... 2092 – 2095

Orbital Interactions in Strong and Weak Hydrogen Bonds are Essential for DNA Replication

Keywords: charge transfer · density functional calculations · DNA replication · hydrogen bonds · orbital interactions

A planar Ga_2As_4 unit is the central structural motive of the title compound (see picture). The compound results from the reaction of $GaCl_3$ with $Li_2AsSiiPr_3$ in a mixture of THF and heptane. It is the first example of a molecule with Ga–As double bonds.



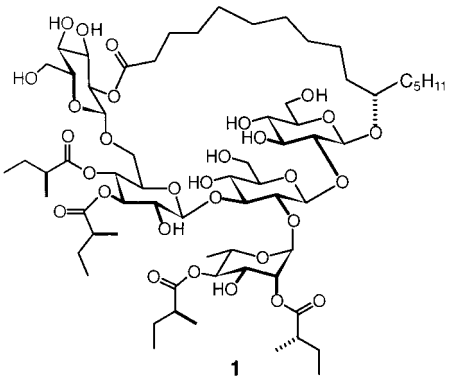
Angew. Chem. **2002**, *114*, 2198 – 2200

C. von Hänisch,* O. Hampe 2095 – 2097

$[\{Li(thf)_3\}_2Ga_2\{As(SiiPr_3)\}_4]$—A Compound with Gallium–Arsenic Double Bonds

Keywords: arsenic · gallium · multiple bonds · Zintl anions

The reliability of ring-closing metathesis, even in complex cases, is highlighted in the first total synthesis of the structurally intriguing resin glycoside woodrosin I (**1**). The synthesis also shows the maturity of the trichloroacetimidate method for glycosylation and features the most advanced application of an orthoester rearrangement for the formation of a β-glycosidic bond.



1

Angew. Chem. **2002**, *114*, 2203 – 2206

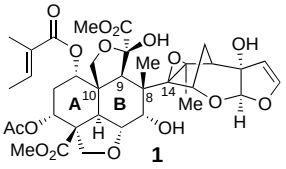
A. Fürstner,* F. Jeanjean, P. Razon ..... 2097 – 2101

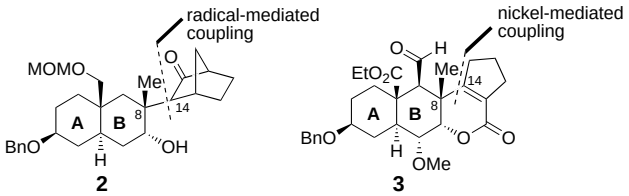
Total Synthesis of Woodrosin I

Keywords: glycosides · macrocycles · metathesis · natural products · ruthenium

 © WILEY-VCH Verlag GmbH, 69451 Weinheim, Germany, 2002 1433-7851/02/4112-1980 $ 20.00+.50/0

Two strategies—one goal: Two novel methodologies for the construction of the crowded C^8–C^{14} bond of azadirachtin (**1**) are described. The first approach to this thorny synthetic hurdle utilizes radical chemistry and furnishes model system **2**, whereas the second foray employs a nickel-mediated coupling reaction and affords model system **3**.





K. C. Nicolaou,* M. Follmann, A. J. Roecker, K. W. Hunt 2103 – 2106

Model Studies Towards Azadirachtin: Part 1. Construction of the Crowded C8–C14 Bond by Radical Chemistry

K. C. Nicolaou,* A. J. Roecker, M. Follmann, R. Baati ..... 2107 – 2110

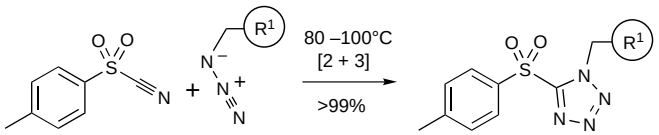
Model Studies Towards Azadirachtin: Part 2. Construction of the Crowded C8–C14 Bond by Transition Metal Chemistry

Angew. Chem. **2002**, *114*, 2207 – 2210

Angew. Chem. **2002**, *114*, 2211 – 2214

Keywords: azadirachtin · cascade reactions · natural products · radical reactions · steric hindrance

Quantitative yields are observed from the reaction of aryl sulfonyl cyanides with unhindered azides by simply heating at 80 – 100°C (see scheme). The reactions are run neat, and there are no by-products, so no workup is necessary. The resulting tetrazoles are activated for rapid functionalization by an S_NAr reaction.



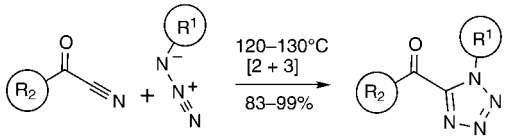
Z. P. Demko, K. B. Sharpless* ..... 2110 – 2113

A Click Chemistry Approach to Tetrazoles by Huisgen 1,3-Dipolar Cycloaddition: Synthesis of 5-Sulfonyl Tetrazoles from Azides and Sulfonyl Cyanides

Angew. Chem. **2002**, *114*, 2214 – 2217

Keywords: azides · cyanides · cycloaddition · nitrogen heterocycles · synthetic methods

Click chemistry: Acyl cyanides react with alkyl azides in high yield by heating at 120 – 130°C (see scheme). The reactions are run neat, and the workup is simple. When *p*-nitrophenyl cyanoformate is used as the dipolarophile, the resulting tetrazoles are activated for rapid functionalization as an activated ester.



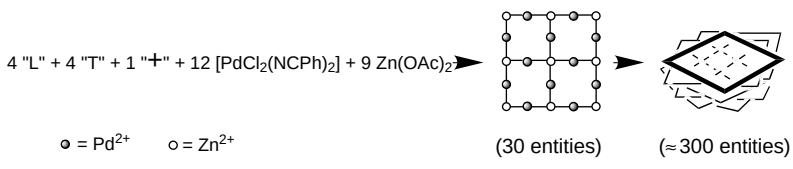
Z. P. Demko, K. B. Sharpless* ..... 2113 – 2116

A Click Chemistry Approach to Tetrazoles by Huisgen 1,3-Dipolar Cycloaddition: Synthesis of 5-Acyltetrazoles from Azides and Acyl Cyanides

Angew. Chem. **2002**, *114*, 2217 – 2220

Keywords: azides · cyanides · cycloaddition · nitrogen heterocycles · synthetic methods

Piles of molecules: Self-assembled nonamer arrays self-organize into 3D aggregates (see scheme: L = "L-shaped" porphyrin (corner piece), T = "T-shaped" porphyrin (side piece), + = "cross-shaped" porphyrin (center)). The size of the nanoscaled material on surfaces can be controlled from 1 nonamer to 50-nm-tall aggregates by chemistry, kinetics, and choice of surface.



T. N. Milic, N. Chi, D. G. Yablon, G. W. Flynn, J. D. Batteas,* C. M. Drain* ..... 2117 – 2119

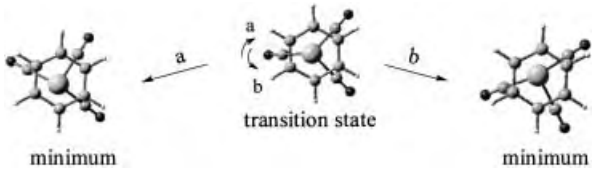
Controlled Hierarchical Self-Assembly and Deposition of Nanoscale Photonic Materials

Angew. Chem. **2002**, *114*, 2221 – 2223

Keywords: nanostructures · palladium · porphyrinoids · self-assembly · zinc

 © WILEY-VCH Verlag GmbH, 69451 Weinheim, Germany, 2002 1433-7851/02/4112-1981 $ 20.00+.50/0

Two of each! In the C_{3v} point group, the 16-electron $[\eta^6$-(benzene)$Nb(CO)_3]^+$ fragment has accessible Jahn–Teller-active singlet and triplet electronic states. Distortion into the C_s point group leads to two low-energy minima and two transition states (see scheme). This finding is shown to have important implications for other unsaturated complexes such as $[\eta^5$-$CpMo(CO)_2Cl]$ and $[\eta^5$-$CpMn(CO)_2]$ (Cp = cyclopentadienyl).



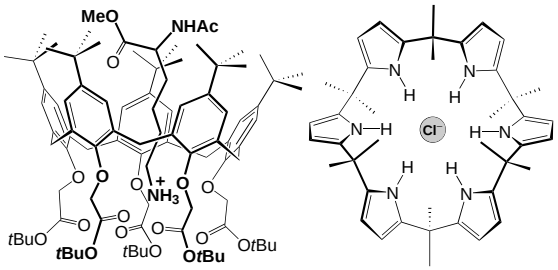
Angew. Chem. **2002**, *114*, 2224–2226

F. Abu-Hasanayn,* P. H.-Y. Cheong, M. Oliff 2120–2122

Identification of Jahn–Teller Effects in both Singlet and Triplet Low-Energy States of $[(\eta^6$-benzene)$Nb(CO)_3]^+$

Keywords: density functional calculations · electron-deficient compounds · Jahn–Teller distortion · transition metals

Confinement of the charged constituents of ion-paired organic salts within the complementary cavities of suitably chosen pairs of cation and anion receptors to form supramolecular systems, as shown for the complexation of N^{α}-Ac-L-Lys-OMe · HCl by a calix[5]arene/calix[6]pyrrole combination, results in a remarkable (up to 10^4-fold) enhancement of the binding ability of the binary host systems compared to that of either receptor taken individually.



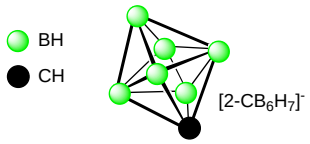
Angew. Chem. **2002**, *114*, 2226–2230

G. Cafeo, G. Gattuso, F. H. Kohnke, A. Notti, S. Occhipinti, S. Pappalardo, M. F. Parisi* 2122–2126

Remarkable Boosting of the Binding of Ion-Paired Organic Salts by Binary Host Systems

Keywords: calixarenes · calixpyrroles · cooperative effects · inclusion compounds · ion-pair recognition

Opening up *closo*-cluster chemistry: The first representative of the seven-vertex *closo* monocarbaborane series, the $[closo$-2-$CB_6H_7]^-$ ion (see structure), was isolated together with the $[closo$-1-$CB_7H_8]^-$ ion from simple reactions between *nido*-1-CB_8H_{12} and Et_3N. Both ions exhibit high stability in air and are potentially useful for weakly coordinating anion chemistry.



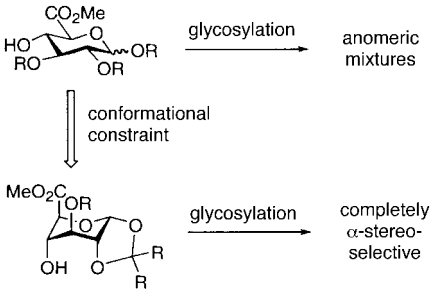
Angew. Chem. **2002**, *114*, 2230–2232

B. Štíbr,* O. L. Tok, W. Milius, M. Bakardjiev, J. Holub, D. Hnyk, B. Wrackmeyer 2126–2128

The $[closo$-2-$CB_6H_7]^-$ Ion: The First Representative of the 7-Vertex Monocarbaborane Series

Keywords: boron · carboranes · structure elucidation

Complete control over the stereoselectivity of key coupling reactions in the synthesis of heparin can be exerted by conformationally locking the uronic acid acceptor (see scheme).



Angew. Chem. **2002**, *114*, 2232–2235

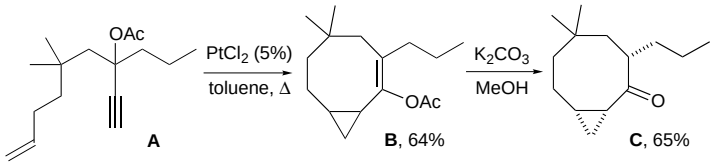
H. A. Orgueira, A. Bartolozzi, P. Schell, P. H. Seeberger* 2128–2131

Conformational Locking of the Glycosyl Acceptor for Stereocontrol in the Key Step in the Synthesis of Heparin

Keywords: carbohydrates · conformation analysis · glycosylation · stereoselectivity

 © WILEY-VCH Verlag GmbH, 69451 Weinheim, Germany, 2002 1433-7851/02/4112-1982 $ 20.00+.50/0

The versatile ketone C can be obtained by hydrolyzing cyclooctene **B**, which is formed in a $PtCl_2$-catalyzed cycloisomerization reaction from the enyne precursor **A**. A carbene platinum complex is invoked in the process, which also represents one of the few efficient syntheses of functionalized cyclooctanes from acyclic precursors.



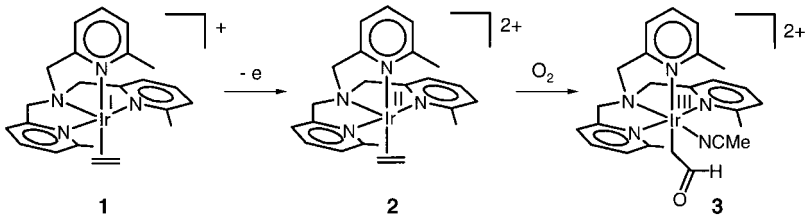
E. Mainetti, V. Mouriès, L. Fensterbank,* M. Malacria,* J. Marco-Contelles* ..... 2132 – 2135

The Effect of a Hydroxy Protecting Group on the $PtCl_2$-Catalyzed Cyclization of Dienynes—A Novel, Efficient, and Selective Synthesis of Carbocycles

Angew. Chem. **2002**, *114*, 2236 – 2239

Keywords: carbenes · carbocations · diastereoselectivity · enynes · platinum

Oxidation induces oxygenation: The first Ir^{II} – ethene complex ever (**2**) was obtained by one-electron oxidation of the corresponding Ir^{I} – ethene complex **1**. Whereas **1** reacts with dioxygen to give an Ir^{III} – peroxo-ethene complex, the Ir^{II} – ethene complex **2** activates dioxygen towards C–O bond formation and gives the Ir^{III} – formylmethyl complex **3**.



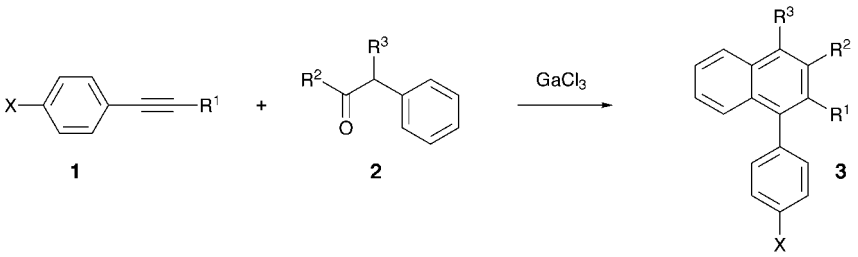
B. de Bruin,* T. P. J. Peters, S. Thewissen, A. N. J. Blok, J. B. M. Wilting, R. de Gelder, J. M. M. Smits, A. W. Gal* ..... 2135 – 2138

Dioxygen Activation by a Mononuclear Ir^{II} – Ethene Complex

Angew. Chem. **2002**, *114*, 2239 – 2242

Keywords: alkenes · iridium · N ligands · O–O activation · oxidation

A convenient synthesis of polysubstituted naphthalenes 3 involves the gallium trichloride catalyzed coupling of aromatic alkynes **1** and phenyl acetaldehydes or ketones **2** in dichloromethane. The reaction is highly regioselective.



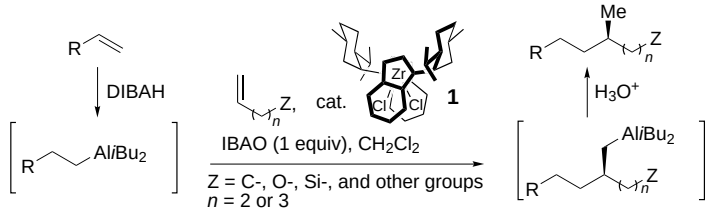
G. S. Viswanathan, M. Wang, C.-J. Li* ..... 2138 – 2141

A Highly Regioselective Synthesis of Polysubstituted Naphthalene Derivatives through Gallium Trichloride Catalyzed Alkyne – Aldehyde Coupling

Angew. Chem. **2002**, *114*, 2242 – 2245

Keywords: aldehydes · alkynes · gallium · naphthalenes · synthetic methods

Methyl-substituted alkanols have been synthesized enantioselectively (90 – 93 % *ee*) in a one-pot hydroalumination/carboalumination tandem process (see scheme). This enantioselectively represents an increase of about 15 % from the previously attainable *ee* values. DIBAH = diisobutylaluminum hydride, IBAO = isobutylaluminoxane.



S. Huo, J.-c. Shi, E.-i. Negishi* ..... 2141 – 2143

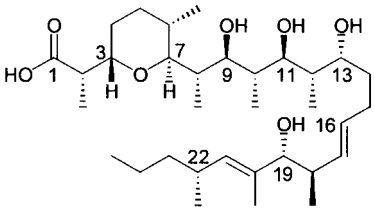
A New Protocol for the Enantioselective Synthesis of Methyl-Substituted Alkanols and Their Derivatives through a Hydroalumination/Zirconium-Catalyzed Alkylalumination Tandem Process

Angew. Chem. **2002**, *114*, 2245 – 2247

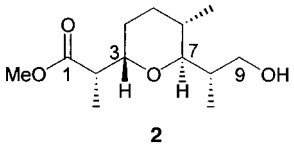
Keywords: alcohols · alkenes · aluminum · asymmetric catalysis · C–C coupling · zirconium

 © WILEY-VCH Verlag GmbH, 69451 Weinheim, Germany, 2002 1433-7851/02/4112-1983 $ 20.00+.50/0

Antibiotics made from cyclopropylmethanols: The C1 – C9 subunit (**2**) of zincophorin (**1**) has been synthesized by using three key steps: a hydroboration of an enantiomerically enriched isopropenylcyclopropane, an aldol reaction, and an intramolecular oxymercuration of a cyclopropylmethanol.



1



2

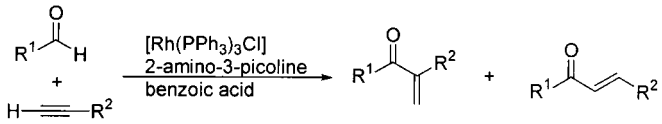
Angew. Chem. **2002**, *114*, 2248 – 2250

J. Cossy,* N. Blanchard, M. Defosseux, C. Meyer* ..... 2144 – 2146

A Synthetic Approach towards the C1 – C9 Subunit of Zincophorin

Keywords: aldol reaction · mercury · natural products · synthesis design · zincophorin

Terminal alkynes successfully undergo chelation-assisted hydroacylation with aldehydes to give branched or linear alkyl α,β-unsaturated ketones (see scheme).



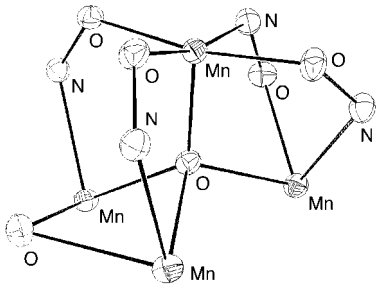
Angew. Chem. **2002**, *114*, 2250 – 2251

C.-H. Jun,* H. Lee, J.-B. Hong, B.-I. Kwon ..... 2146 – 2147

Efficient and Selective Hydroacylation of 1-Alkynes with Aldehydes by a Chelation-Assisted Catalytic System

Keywords: C–H activation · homogeneous catalysis · hydroacylation · ketones · rhodium

A difference of two electrons: A tetranuclear cluster $[Mn^{II}Mn^{II}Mn^{II}Mn^{IV}(O)(pko)_4(3,4\text{-}D)_4]\cdot 2.5\,CH_3OH$ (Hpko = di(2-pyridyl)ketonoxime, H-3,4-D = 3,4-dichlorophenoxy acetic acid) with a $(\mu_4\text{-}O)Mn_4$ bridging moiety is reported (see core structure). This compound is the only example of a manganese cluster with a $2e^-$ difference between the oxidation states of the metal ions and with four metal centers interacting through a μ_4-O bridging atom.



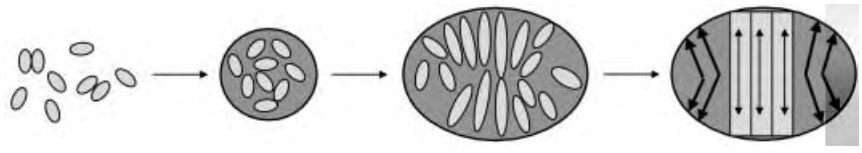
Angew. Chem. **2002**, *114*, 2252 – 2254

T. Afrati, C. Dendrinou-Samara, C. P. Raptopoulou, A. Terzis, V. Tangoulis,* D. P. Kessissoglou* ..... 2148 – 2150

A Tetranuclear Mixed-Valent $Mn^{II}_3Mn^{IV}$ Compound with a $(\mu_4\text{-}O)Mn_4$ Core

Keywords: bioinorganic chemistry · manganese · metal – oxo complexes · mixed-valent compounds · N,O ligands

A controlled quenching process allows the nucleation period to be increased sufficiently, such that high-resolution transmission electron microscopy can be used to reveal the structural and shape transformations during the onset and development of mesophase ordering of the hexagonally ordered silica – surfactant mesophase MCM-41 (see scheme).



Angew. Chem. **2002**, *114*, 2255 – 2257

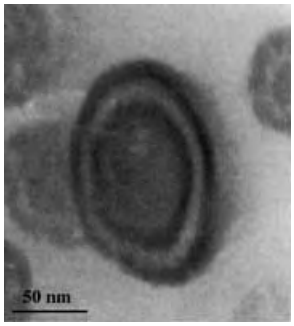
S. Sadasivan, C. E. Fowler, D. Khushalani, S. Mann* ..... 2151 – 2153

Nucleation of MCM-41 Nanoparticles by Internal Reorganization of Disordered and Nematic-Like Silica – Surfactant Clusters

Keywords: mesophases · mesoporous materials · nanostructures · silica · surfactants

 © WILEY-VCH Verlag GmbH, 69451 Weinheim, Germany, 2002 1433-7851/02/4112-1984 $ 20.00+.50/0

A three-layer substructure morphology is found in the vesicular nanostructures formed (see transmission electron micrograph) upon melt blending of polyamide 12 (PA12) with a symmetric polystyrene-*b*-polyisoprene (PS-*b*-PIP) copolymer end-capped by an anhydride group. However, macrophase separation occurs when the diblock is unreactive.



Angew. Chem. **2002**, *114*, 2258 – 2260

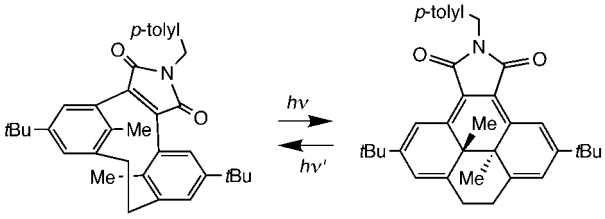
C. Koulic, Z. Yin, C. Pagnoulle, R. Jérôme* ..... 2154 – 2156

Vesicular Nanostructures Prepared by Reactive Melt Blending

Keywords: block copolymers · melt blending · nanostructures · self-assembly · vesicles

---

No racemization occurs in the first reported enantioselective photochromic reaction. Upon irradiation with UV light, a single enantiomer of [2.2]metacyclophane-1-ene **1a** undergoes photocyclization to give a single enantiomer of tetrahydropyrene **1b**. Upon irradiation with visible light, **1b** is converted back cleanly into the initial enantiomer **1a**.



1a **1b**

Angew. Chem. **2002**, *114*, 2260 – 2261

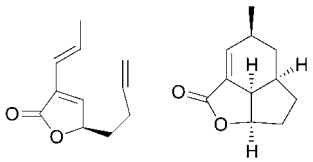
M. Takeshita,* T. Yamato ... 2156 – 2157

Enantioselective Photochromic Reaction of a [2.2]Metacyclophan-1-ene

Keywords: chiral resolution · circular dichroism · cyclophanes · enantioselectivity · photochromism

---

An intramolecular Diels – Alder reaction with inverse electron demand in a polyketide biosynthetic pathway is reported in which the rate of the cyclization is enhanced in vivo. Alive mycelia of the fungus *Galiella rufa* catalyze the cyclization of (−)-pregaliellalactone (**1**) to (+)-desoxygaliellalactone (**2**), while dead mycelia have no effect. No rate increase was observed with the unnatural enantiomer (+)-**1**.



1 **2**

Angew. Chem. **2002**, *114*, 2261 – 2264

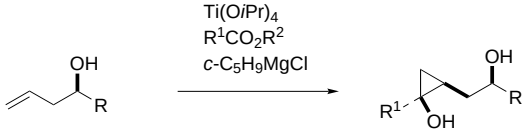
M. Johansson, B. Köpcke, H. Anke, O. Sterner* ..... 2158 – 2160

Cyclization of (−)-Pregaliellalactone in the Fungus *Galiella rufa*

Keywords: biosynthesis · cycloaddition · enzyme catalysis · natural products

---

The hydroxy group regulates the stereoselectivity in a modification of the titanium-mediated Kulinkovich cyclopropanation procedure (see scheme). This method provides a diastereoselective synthesis of *trans*-1,2-dialkylcyclopropanols, which starts with homoallylic alcohols and proceeds via a bicyclic titanacyclopropane intermediate. Enantiopure products may also be obtained if the corresponding chiral alcohols are used.



Angew. Chem. **2002**, *114*, 2264 – 2266

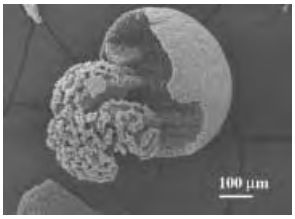
L. G. Quan, S.-H. Kim, J. C. Lee, J. K. Cha* ..... 2160 – 2162

Diastereoselective Synthesis of *trans*-1,2-Dialkylcyclopropanols by the Kulinkovich Hydroxycyclopropanation of Homoallylic Alcohols

Keywords: allylic compounds · cyclization · cyclopropanation · diastereoselectivity · titanium

 © WILEY-VCH Verlag GmbH, 69451 Weinheim, Germany, 2002 1433-7851/02/4112-1985 $ 20.00+.50/0

Spheres without templates: The direct assembly of a complex inorganic polymer with a spherical-shell architecture (see electron microscopy image) was obtained by addition of polyacrylate or polyaspartate during the crystallization of octacalcium phosphate from aqueous solutions. The process does not require the intervention of external templates, and involves the radial growth of dense multilayered spheroids, secondary overgrowth of a porous thin-shell precursor, and anisotropic dissolution of the spheroidal cores.



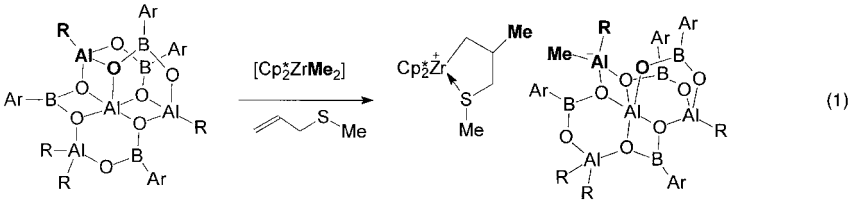
Angew. Chem. **2002**, *114*, 2267 – 2270

A. Bigi,* E. Boanini, D. Walsh, S. Mann ..... 2163 – 2166

Morphosynthesis of Octacalcium Phosphate Hollow Microspheres by Polyelectrolyte-Mediated Crystallization

Keywords: calcium · crystal growth · materials science · microspheres · phosphates

How do alumoxane activators activate? Reaction (1) may help to answer this question. The product of this reaction is a zirconocene alkyl cation (Cp* = C_5Me_5) with its methylated boralumoxane anion. The structure of this compound is in accord with Barron's "latent Lewis acidity" concept for alumoxane activators.



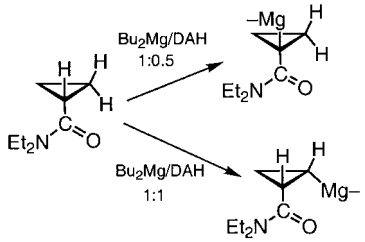
Angew. Chem. **2002**, *114*, 2270 – 2273

B. Richter, A. Meetsma, B. Hessen,* J. H. Teuben ..... 2166 – 2169

Structural Characterization of a Cationic Zirconocene Olefin Polymerization Catalyst with its Methylated Boralumoxane Counterion

Keywords: aluminum · homogeneous catalysis · metallocenes · polymerization · zirconium

Using the irreversible formation of an alkane, the proton-removing ability of a magnesiated amine, and the activating effect of a carboxamido group, weakly acidic CH groups in a variety of systems can be selectively converted into useful amido-Grignard reagents (see scheme; DAH = dehydrated diisopropylamine).



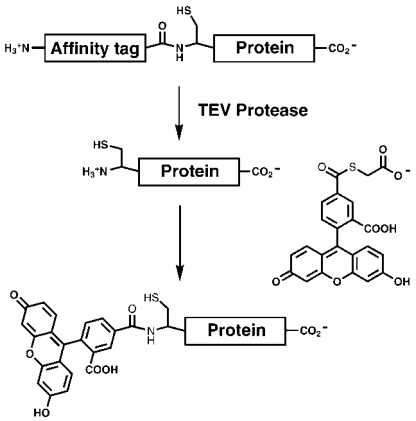
Angew. Chem. **2002**, *114*, 2273 – 2275

M.-X. Zhang, P. E. Eaton* 2169 – 2171

BuMgN*i*Pr_2: A New Base for Stoichiometric, Position-Selective Deprotonation of Cyclopropane Carboxamides and Other Weak CH Acids

Keywords: amides · cyclopropanes · Grignard reagents · magnesiation · metalation

The highly selective tobacco etch virus Nla protease (TEV protease) can be used to remove affinity tags with mutated cleavage sites to produce proteins for site-specific labeling and chemoselective ligations (see scheme). This provides a simple, efficient method for producing proteins with N-terminal cysteines for proteomic applications.



Angew. Chem. **2002**, *114*, 2275 – 2278

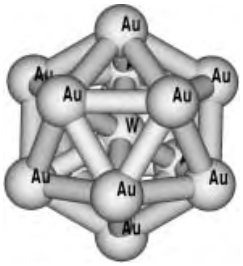
T. J. Tolbert, C.-H. Wong* 2171 – 2174

New Methods for Proteomic Research: Preparation of Proteins with N-Terminal Cysteines for Labeling and Conjugation

Keywords: amino acids · chemoselectivity · nanotechnology · proteins · proteomics

 © WILEY-VCH Verlag GmbH, 69451 Weinheim, Germany, 2002 1433-7851/02/4112-1986 $ 20.00+.50/0

A new class of molecules, WAu_{12} (see picture) and its isoelectronic analogues, has been proposed and theoretically studied. The calculated radial W–Au distance is unusually short, 268 pm at the best level of theory. The frontier orbitals, both HOMO and LUMO, have fivefold degenerate h_g symmetry. The gap between them approaches 3 eV. Possible applications of these isoelectronic clusters are discussed.



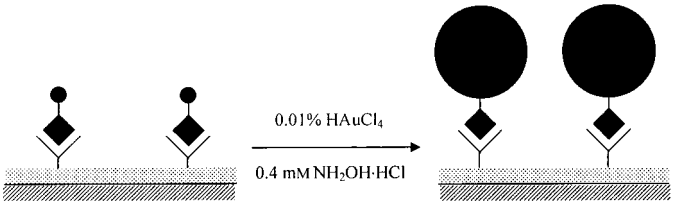
P. Pyykkö,* N. Runeberg .... 2174 – 2176

Icosahedral WAu_{12}: A Predicted Closed-Shell Species, Stabilized by Aurophilic Attraction and Relativity and in Accord with the 18-Electron Rule

Angew. Chem. **2002**, *114*, 2278 – 2280

Keywords: cluster compounds · gold · icosahedral symmetry · nanostructures · tungsten

Growing gold: Human immunoglubulin G (h-IgG) can be detected by the naked eye after enlarging Au nanoparticles in vitro with $HAuCl_4/NH_2OH \cdot HCl$, which immobilizes the Au nanoparticles on the nitrocellulose filter (see scheme; ● = Au nanoparticle, ◆ = anti-h-IgG, Y = h-IgG). The detection limit of approximately 10 pg mL^{-1} rivals the limits of fluorescent, radioactive, and enzyme-colorometric methods.



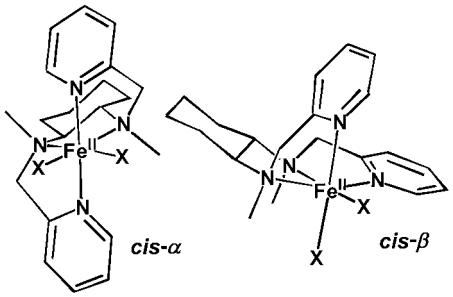
Z. Ma, S.-F. Sui* ..... 2176 – 2179

Naked-Eye Sensitive Detection of Immunoglubulin G by Enlargement of Au Nanoparticles In Vitro

Angew. Chem. **2002**, *114*, 2280 – 2283

Keywords: gold · immunoglobulins · nanoparticles · particle enlargement · sensors

Quite unexpectedly, the topology of the tetradentate ligand in [Fe^{II}(bpmcn)$(OTf)_2$] (bpmcn = *N*,*N*′-bis-(2-pyridylmethyl)-*N*,*N*′-dimethyl-*trans*-1,2-diaminocyclohexane), whether *cis*-α or *cis*-β (see picture), determines the course of catalytic alkane hydroxylation and olefin oxidation reactions with H_2O_2, which afford products with varying stereoselectivity and dramatically different sources of incorporated oxygen. These results demonstrate the exquisite role ligands can play in the fine tuning of the reactivity of an iron catalyst.



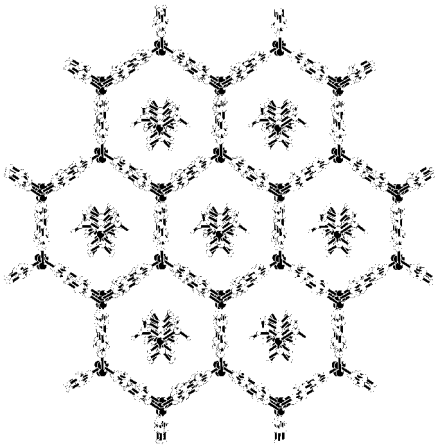
M. Costas, L. Que, Jr.* ..... 2179 – 2181

Ligand Topology Tuning of Iron-Catalyzed Hydrocarbon Oxidations

Angew. Chem. **2002**, *114*, 2283 – 2285

Keywords: homogeneous catalysis · iron · ligand effects · oxidation · reaction mechanisms

Designed bilayer structure: The formation of a bilayer structure is reported, in which two guest molecules are contained within each local segment of tunnel within a layered urea host structure (one layer of which is shown in the picture). One novel feature of this structure is a locally empty region within the urea host tunnel, which arises from a significant van der Waals "gap" between adjacent guest molecules within the bilayer.



S.-O. Lee, B. M. Kariuki, K. D. M. Harris* ..... 2181 – 2184

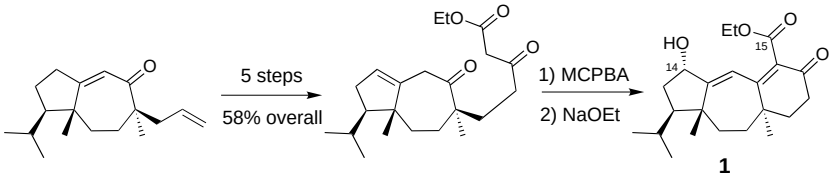
Design of a Bilayer Structure in an Organic Inclusion Compound

Angew. Chem. **2002**, *114*, 2285 – 2288

Keywords: host – guest systems · hydrogen bonds · inclusion compounds · solid-state structures · urea

 © WILEY-VCH Verlag GmbH, 69451 Weinheim, Germany, 2002 1433-7851/02/4112-1987 $ 20.00+.50/0

Some serious and unexpected complications emerged in the key annulation step required to reach **1**, the core of guanacastepene A (see scheme). The solution to these problems concurrently solved the major issues associated with the different oxidation states of C14 and C15. Although the authors have not generalized this type of annulation, it could have broad applications to building incrementally oxygenated polycyclic natural products.



1

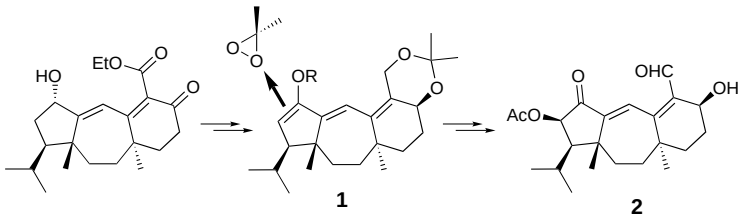
Angew. Chem. **2002**, *114*, 2289 – 2292

D. S. Tan, G. B. Dudley, S. J. Danishefsky* ..... 2185 – 2188

Synthesis of the Functionalized Tricyclic Skeleton of Guanacastepene A: A Tandem Epoxide-Opening β-Elimination/Knoevenagel Cyclization

Keywords: antibiotics · cyclization · natural products · oxidation · total synthesis

An external oxidant approaches *syn* to the isopropyl and methyl substituents on the five-membered ring of **1**. This surprising and selective epoxidation was exploited in the total synthesis of guanacastepene A (**2**).



1 **2**

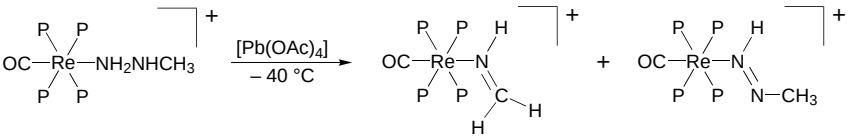
Angew. Chem. **2002**, *114*, 2292 – 2295

S. Lin, G. B. Dudley, D. S. Tan, S. J. Danishefsky* ..... 2188 – 2191

A Stereoselective Route to Guanacastepene A through a Surprising Epoxidation

Keywords: antibiotics · diastereoselectivity · epoxidation · natural products · total synthesis

Unexpectedly, oxidation of the coordinated methylhydrazine group in the $[Re(CH_3NHNH_2)(CO)P_4]BPh_4$ ($P = P(OEt)_3$) complex by $Pb(OAc)_4$ at $-40^\circ C$ affords not only the methyldiazene $[Re(CH_3N{=}NH)(CO)P_4]^+$ ion, but also the methyleneimine $[Re(\eta^1\text{-}NH{=}CH_2)(CO)P_4]^+$ derivative (see scheme), which was isolated and characterized by spectroscopy and X-ray crystallography.



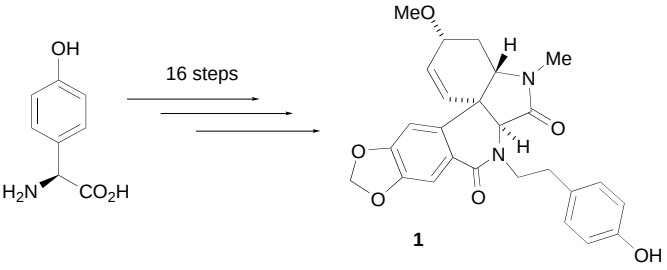
Angew. Chem. **2002**, *114*, 2296 – 2298

G. Albertin,* S. Antoniutti, A. Bacchi, E. Bordignon, M. T. Giorgi, G. Pelizzi ..... 2192 – 2194

Methyleneimine $CH_2{=}NH$ as a Unidentate Ligand in Rhenium Complexes

Keywords: imines · N ligands · oxidation · P ligands · rhenium

A sequence of polymer-supported reagents and scavengers was used to promote the synthetic transformations in the first total synthesis of (+)-plicamine (**1**), a member of the amaryllidaceae alkaloid family, starting from L-4-hydroxyphenylglycine (see scheme).



1

Angew. Chem. **2002**, *114*, 2298 – 2301

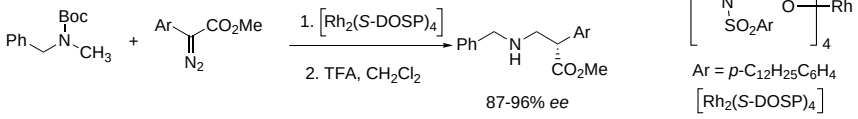
I. R. Baxendale, S. V. Ley,* C. Piutti ..... 2194 – 2197

Total Synthesis of the Amaryllidaceae Alkaloid (+)-Plicamine and Its Unnatural Enantiomer by Using Solid-Supported Reagents and Scavengers in a Multistep Sequence of Reactions

Keywords: alkaloids · scavengers · solid-supported reagents · synthetic methods · total synthesis

 © WILEY-VCH Verlag GmbH, 69451 Weinheim, Germany, 2002 1433-7851/02/4112-1988 $ 20.00+.50/0

A very direct approach for the synthesis of β-amino esters is provided by catalytic asymmetric C–H activation by means of carbenoid-induced C–H insertion (see scheme; Boc = butyloxycarbonyl; TFA = trifluoroacetic acid). The reactions described herein represent the first regioselective intermolecular C–H insertions occurring at a methyl site.



H. M. L. Davies,*
C. Venkataramani ..... 2197 – 2199

Catalytic Enantioselective Synthesis of β^2-Amino Acids

Angew. Chem. **2002**, *114*, 2301 – 2303

Keywords: amino acids · asymmetric catalysis · C–H activation · insertion · rhodium

Supporting information on the WWW (see article for access details).

* Author to whom correspondence should be addressed

Accelerated publications

BOOKS

The 13th Element: The Sordid Tale of Murder, Fire, and Phosphorus — John Emsley — *G. G. Kauffman* 2201

The Nitro Group in Organic Synthesis — Noboru Ono — *Y. Ishii* 2202

Richard Willstätter im Briefwechsel mit Emil Fischer in den Jahren 1901 bis 1918 — Horst Remane, Wolfgang Schweitzer — *R. Huisgen* 2203

Protein-Based Surfactants — Ifendu A. Nnanna, Jiding Xia — *W. von Rybinski* 2204

WEB SITES

http://www.webmo.net/ — Your Web Browser as a Computational Chemistry Frontend — *G. Rauhut* 2205

SERVICE

• **VIPs**	**1977**	• **Keywords**	**2206**
• ***Angewandte's* Sister-Journals**	**1991 – 1993**	• **Authors**	**2207**
• **Vacancies**	**A53**	• **Preview**	**2208**

Issue 11, 2002 was published online on May 28.

Don't forget all the Tables of Contents from 1998 onwards may be still found on the WWW under: http://www.angewandte.org

 © WILEY-VCH Verlag GmbH, 69451 Weinheim, Germany, 2002 1433-7851/02/4112-1989 $ 20.00+.50/0

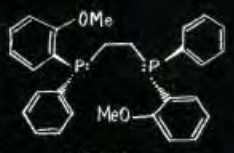
THE NOBEL PRIZE IN CHEMISTRY 2001

© The Royal Swedish Academy of Sciences

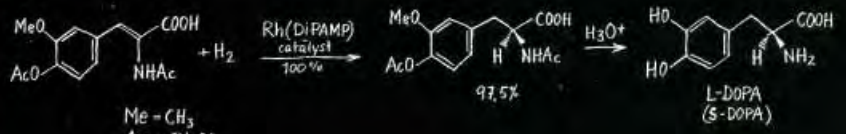
Pioneering work

In 1968 **William S. Knowles** discovered that the metal rhodium can be used in a chiral molecule to catalyze asymmetric *hydrogenation reactions*.

Knowles quickly developed an industrial synthesis of the amino acid L-DOPA, which has proved to be useful in the treatment of Parkinson's disease. This was the first industrial catalytic asymmetric synthesis. It has been followed by many others.



DiPAMP



Me = CH_3
Ac = CH_3CO



Photo: Pressens Bild

William S. Knowles
St Louis, Missouri, USA

General hydrogenations

Ryoji Noyori realized the need for more selective catalysts with broader applications. Among the catalysts he has developed is Ru-BINAP, which is used for the synthesis of (*R*)-1,2-propandiol in the production of an antibiotic, levofloxacin. Noyori's catalysts are widely used for the synthesis of fine chemicals and pharmaceutical products as well as new advanced materials.

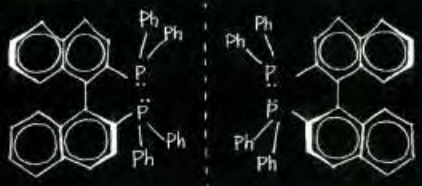


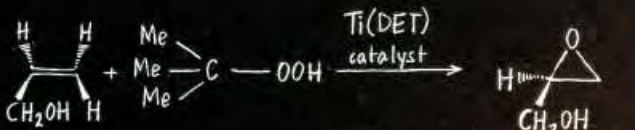


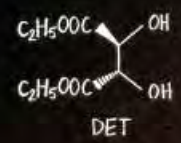
Photo: Mr. Satoshi Oga

Ryoji Noyori
Nagoya University, Chikusa, Nagoya, Japan

Catalytic asymmetric oxidations

Parallel with the advances in catalytic asymmetric hydrogenation reactions, **Barry Sharpless** has developed corresponding chiral catalysts for other important reactions, *oxidation reactions*. He has made several important discoveries, such as for catalytic asymmetric epoxidation, which utilizes titanium in a chiral molecule. Epoxides are useful intermediate products for various types of synthesis, including the production of drugs for reducing blood pressure.





DET



Photo: Pressens Bild

K. Barry Sharpless
The Scripps Research Institute, La Jolla, California, USA



ANGEWANDTE CHEMIE © WILEY-VCH

Asymmetric Hydrogenations (Nobel Lecture)**

William S. Knowles*

The start of the development of catalysts for asymmetric hydrogenation was the concept of replacing the triphenylphosphane ligand of the Wilkinson catalyst with a chiral ligand. With the new catalysts, it should be possible to hydrogenate prochiral olefins. Knowles and his co-workers were convinced that the phosphorus atom played a central role in this selectivity, as only chiral phosphorus ligands such as (*R*,*R*)-DIPAMP, whose stereogenic center lies directly on the phosphorus atom, lead to high enantiomeric excesses when used as catalysts in asymmetric hydrogenation reactions. This hypothesis was disproven by the development of ligands with chiral carbon backbones. Although the exact mechanism of action of the phosphane ligands is not incontrovertibly determined to this day, they provide a simple entry to a large number of chiral compounds.

Keywords: asymmetric catalysis · asymmetric hydrogenation · Nobel lecture · phosphane ligands · rhodium

1. My biography

I was born in Taunton, Massachusetts on June 1, 1917, but I actually grew up in nearby New Bedford. My family background was heavily slanted toward business and seafaring matters. I can't think of any relatives that ever went into science. My family gave me the best in education. To my father, business was the highest calling, but to my mother, medicine was the top profession. She would probably have gone to medical school if she had been born in a more enlightened era.

I went to boarding school at Berkshire in western Massachusetts, definitely the most beautiful part of the state. I'll never forget the fall colors on the Berkshires. In those days I was terrible at athletics and never made a team, but quite easily led my class in academics. I was particularly good at math and science. I also got a good lesson in New England thrift. To get free ice for our physics experiments, we had to wait until it snowed.

On graduating, I was easily admitted to Harvard. In that era, all one had to do was pass the College Board exams. If anyone in my family went to college, that was where he went. My father spent a year there and quit to go into the textile business. At this point I was strongly advised that I was too young socially to go to college, so I took a second senior year at Andover, another boarding school. At that time many students did this. At Andover, I took my first chemistry course from a teacher named Bushy Graham and was fascinated by the subject. I remember him trying to explain Avogadro's number, and his discussion of the dangers of hydrogen and oxygen. At the end of the year, I took a competitive exam and won my first prize, the $50 Boylston Prize in Chemistry.

That summer I took a cruise on a 75-foot schooner with no engine, and sailed from Gloucester, Massachusetts to Norway. We sailed around the Baltic and ended up at Stockholm. I didn't think of it at the time, but we spent most of three weeks on the north Atlantic with no contact at all with the outside world. Today, one is always in touch with home base, even if one goes to the South Pole or the Moon. Memories of this sailing trip have always been vivid. On one instance I was mistakenly arrested in Tallinn, Estonia and got a ride in the paddy-wagon. Later we were released without comment. Little did I think that one day, years later, I would be returning to Stockholm to share the Nobel Prize in Chemistry.

At Harvard I majored in chemistry with a strong inclination for math. I took the minimum of humanities. I was told I'd be a natural for physical chemistry but taking organic with Louis Fieser changed my mind. It was there I got my introduction to optical isomerism and the tetrahedral carbon atom. At Harvard, competition was fierce and I always got a solid B, but not the straight As of many of my class mates. These were the days when most get a gentleman's C.

On graduating in 1939, I was strongly advised to go elsewhere to graduate school. I went to Columbia with Professor Elderfield and worked on making simple analogues of the cardiac aglucones. These were tested at Eli Lilly for

[*] Dr. W. S. Knowles
661 East Monroe Avenue
St. Louis, MO 63122 (USA)
E-mail: wsk9656@aol.com

[**] Copyright© The Nobel Foundation 2002. We thank the Nobel Foundation, Stockholm, for permission to print this lecture.

cardiac activity. Bob Elderfield was at his best when he talked steroids at the Rockefeller Institute. In parallel with Nobel's experience, I too had an explosion. Mine came when distilling diazomethane. No one was hurt, but a bottle of intermediate that I had labored on for months was destroyed.

In those days, Professor Elderfield spent a lot of time away on the antimalarial project in the military, and we were on our own a lot. Professor Nelson Leonard, long at the University of Illinois in Champagne, was in our research group. Later he consulted at Monsanto.

New York was an exciting place to be in those war years, and my draft board forced Columbia to push me out sooner than would ordinarily happen. In those days, industry would hire any chemist that could breathe. In 1942, I started in Dayton, Ohio, at the Thomas and Hock Walt laboratories, which had recently joined Monsanto. Most of my assignments were pretty mundane, such as making super-pure hexamethylenetetramine, to be used for making the explosive cyclonite.

In 1944, I was transferred to St. Louis to work on plasticizers and intermediates. We did make a lot of benzyl benzoate as a mite repellent for soldiers clothing. We later had a DDT project which never got into production until the war was over. More interestingly, we had a synthetic process for vanillin but lost out to lignin as a way to get that desirable molecule. In those days we did get involved with the custom manufacture of the antibiotic Chloramphenicol and made 10 – 15 000 lb before it was taken off the market because a very small percentage of patients developed aplastic anemia. At the time my dog had a fungus on her chest that wouldn't heal and resisted treatment. I made an ointment with our product and it cleared up in two days. She lived to 17 years.

Shortly after the war, the discovery that cortisone might become a large-volume pharmaceutical caused Monsanto to engage Professor Woodward, with the hope of commercializing his synthetic approach. I was selected to join this effort since I had a steroid background. Actually, I got to spend nine months in his lab at Cambridge on this total synthesis. The experience working with the "great man" is one I'll never forget. For the first three months in his lab, he would come in at noon and say, "Let's go to Schraft's". We would spend an hour or more scribbling chemical structures on the menu or place mats. His phenomenal memory was beyond anything I'd ever seen. In those days he never kept a file or wrote a reference. He'd just say "Look on page so-and-so in Beilstein and you'll find something on that". He lost some of this ability as he grew older and it bothered him. He really hoped Monsanto would commercialize his steroid synthesis, but the Mexican yam, with its high content of diosgenin, eventually killed our effort. Our program for cortisone got fairly well along. We made a few milligrams of racemic cortisone and we had resolved an early intermediate, which we intended to carry through to the real thing. It was made too complex to compete with the lowly yam.

Later in the fifties I got involved in kinetic studies, and used my long-forgotten math background. These studies led to improvements in several of our processes by doubling production with little or no additional capital. In those days, industry was hungry for chemicals and much effort was spent to get more out in the same equipment.

Monsanto had developed a separate line of advancement for those who wished to stay in technology, and I rose to the top of that ladder before I even thought of asymmetric hydrogenations. I was one who liked to work with my hands as well as my brain. Chemical research in the lab was ideal for filling this need. The work on the asymmetric project, which started in the mid-1960s, is the subject of my lecture. Obviously, I kept active in this area[1] until I retired in 1986, and continued in a consulting capacity for several years after.

On the home front, we had purchased a cabin in Jackson Hole, Wyoming, 25 years ago, and have spent summers and some winter skiing time there ever since. It is there that our four children and four grand children often meet. On several occasions, Professor Kagan has visited us there and we've been able to talk asymmetric hydrogenations. I have always loved doing things outdoors, such as fly-fishing, hiking, and biking. When things are going wrong, I find splitting wood quite therapeutic.

2. The Development of Chiral Phosphane Ligands

Actually, this account is the story of the genesis of an invention. The inventive process is not clearly understood, but one factor that seems to be important is to have a heavy



Dr. William S. Knowles received an AB from Harvard in 1939 and a Ph.D. from Columbia in 1942, under Professor Robert C. Elderfield, in synthetic organic chemistry. He went to Monsanto in 1942 and did a company-sponsored post-doc with Professor Robert B. Woodward at Harvard in 1951. He has been involved in a variety of synthetic problems, which include the total synthesis of steroids and Chloramphenicol. Later in his career, he became interested in selective hydrogenation reactions. He retired from Monsanto in 1986, after many years as a Distinguished Science Fellow. He now lives in St. Louis, Missouri, in the winter and Jackson Hole, Wyoming, in the summer. Amongst the many awards and prizes that Knowles has received are the IR 100 Awards for Asymmetric Hydrogenation (1974), the St. Louis ACS Section Award (1978), the Monsanto Thomas and Hochwalt Award (1981), the ACS Award for Creative Invention (1982), and The Organic Reactions Catalysis Society-Paul N. Rylander Award (1996). In 2001 he shared the Nobel prize for chemistry with R. Noyori[4] and K. B. Sharpless.[8]

infusion of naivety. That is why, so frequently, it is not the experts that do the inventing, but they are the ones who, once the lead is established, come in and exploit the area. Our work is an excellent illustration of this phenomenon.

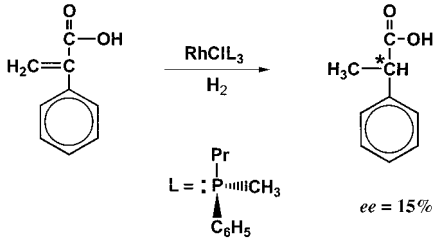
In the study of any of the life sciences, chiral compounds are important. In the past when chiral compounds were needed, chemists have had to use biochemical processes or make racemic mixtures followed by laborious resolutions. In industry the problem is particularly severe, since resolution, with its numerous recycle loops and fractional crystallizations, is an inherently expensive process. Thus, large-volume products such as monosodium L-glutamate, L-lysine, and L-menthol have been made traditionally by biochemical routes, even though efficient procedures are available to make their racemic forms.

In the early 1960s we became aware of this problem when we made a paper evaluation of a monosodium glutamate process. The racemic mixture was easy to obtain, but by the time we had resolved, the projected costs doubled, even though we racemized and recycled back the unwanted D isomer. It looked as though, if one wanted to beat "the bug", it would be necessary to have a catalyst which would direct the reaction to give a predominance of the desired isomer, when an asymmetric center was formed. For this purpose, the 100% efficiency of enzymes would not be needed to have something of real value.

At this point in time I was aware of the extensive studies by Akabori, which started in the mid-1950s, in which heterogeneous catalysts such as Raney nickel and palladium were modified with a chiral agent. The asymmetric bias was always too small to be of preparative interest. All these thoughts remained fallow for several years.

In the interim, I became part of a program for doing exploratory research. I was given a new Ph.D. student to train for a year before going into more pressing things. Industrial labs are always wrestling with the problem of how much undirected research they should do and this was just one of many ways to achieve this goal. I had been through several new employees on a number of projects, when I became aware of Professor Wilkinson's discovery of chlorotris(triphenylphosphane) rhodium, $[RhCl(PPh_3)_3]$, and its amazing properties as a soluble hydrogenation catalyst for unhindered olefins. Homogeneous catalysts had been reported before, but this was the first one that compared in rates with the well-known heterogeneous counterparts.

A second development in the mid-1960s was the development of methods for making chiral phosphanes by Mislow and also by Horner. Phosphorus, like carbon, is tetrahedral and, when four different substituents are attached, can exist in D and L forms. In the case of phosphanes, the lone pair of electrons counts as a substituent. Earlier, it was thought that phosphanes might pyramidally invert like their nitrogen analogues, but Mislow and also Horner showed that they were stable at room temperature. They turned out to have a half-life of a couple of hours at 115°. For our contemplated hydrogenations, this stability would be quite adequate. Then the basic strategy was to replace the triphenylphosphane of Wilkinson's catalyst with a chiral counterpart and hydrogenate a prochiral olefin. This experiment was performed on α-phenylacrylic acid using the known chiral methylpropylphenylphosphane, and gave an enantiomeric excess (*ee*) value of 15% (Scheme 1).

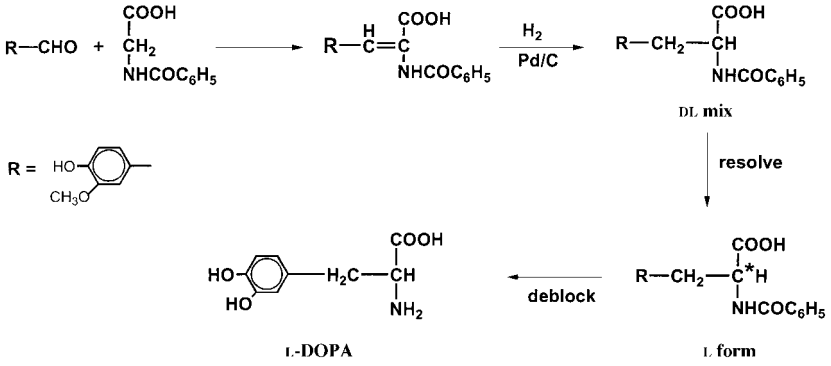


Scheme 1. First use of a chiral ligand in the hydrogenation of an olefin.

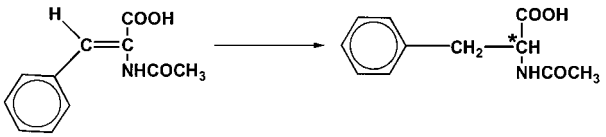
This modest result, of course, was of no preparative value, but it did establish that the hydrogenation technique gave a definite asymmetric bias. In order to achieve this bias, the hydrogen atom, the ligand, and the substrate all had to be on the metal at the same time. Furthermore, we established that the hydrogenation was accomplished in solution and not from some extraneous rhodium plating out in our reactor. The inherent generality of the method offered almost unlimited opportunities for matching substrate and catalyst for moving toward the goal of achieving efficient results.

We were not alone in having this idea, but were the first to report on it. I think it was discussed in the question session after Wilkinson's lecture on his soluble hydrogenation catalyst at a Welch Foundation conference. Horner, shortly after our paper, reported even more modest results with the same methylpropylphenylphosphane on a substituted styrene. There were others using other phosphanes with uninteresting results. Seemingly, we may have been the only ones naive enough to pursue this lead in depth. Actually there was definitely nothing in the literature to encourage us to proceed further. A mechanistic study showed that just two ligands were all that were needed and not the three, as in Wilkinson's structure. α-Phenylacrylic acid worked better as a triethylamine salt, but even so we never got good results with this system.

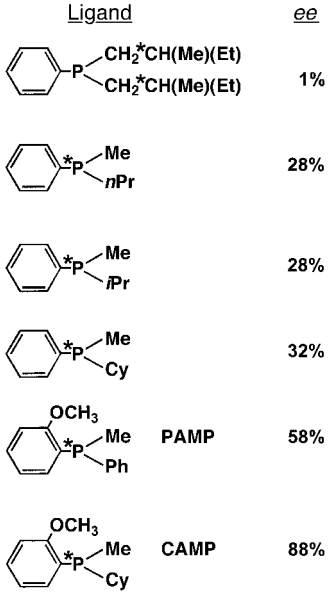
While groping in this area, another seemingly unrelated development appeared, which played an important role in our project. This was the discovery that a fairly massive dose of L-DOPA was useful in treating Parkinson's disease. It created a sizable demand for this rare amino acid. Because of Monsanto's position in vanillin, which provided the 3,4-dihydroxyphenyl moiety, we found that they were custom-manufacturing a racemic intermediate, which Hoffman–LaRoche resolved and deblocked to give L-DOPA. The synthesis, which closely followed the Erlenmeyer azlactone procedure described in *Organic Syntheses*, went by way of a prochiral enamide, which was hydrogenated to give blocked DL-DOPA (Scheme 2). This enamide offered a golden opportunity for commercializing this burgeoning technology. We soon found out that these prochiral enamide precursors of α-amino acids hydrogenated much faster than one would expect for such a highly substituted olefin. Even so, the chiral results were only 28%, but the stage was nicely set to make a structure versus activity study. We had a good test reaction in Scheme 3, in which we used the simple phenylalanine intermediate.



Scheme 2. The Hoffman–LaRoche L-Dopa process.



Scheme 3. Test reaction for the structure–activity-relationship study.



Scheme 4. Phosphane ligands for asymmetric hydrogenation.

We also had a good test for efficiency, since all we had to do was run rotation measurements on a properly diluted reaction mixture. Our job was to find a phosphane of the proper structure. Early on we tried phosphanes with a chiral alkyl side chain, and the asymmetric bias was barely detectable. We felt strongly that, if one wanted to get high *ee* values, the asymmetry would have to be directly on the phosphorus. That is where the action is.

Initially, we varied the alkyl groups on the phosphorus, by converting the normal propyl to the more hindered isopropyl or cyclohexyl, but *ee* values still remained in the range of 28–32%. Our first real variation was to introduce the *o*-anisyl group. This should provide some steric hindrance as well as a possible hydrogen-bonding site. Furthermore, the ether linkage would be stable enough to survive the rigors of a phosphane synthesis. In those days, our small group was in continuous contact and what we decided to do was arrived at by informal consensus. I hate to admit it, but it's much easier to invent in a small, underfunded group. Being lean and hungry is conducive to invention.

We made methylphenyl-*o*-anisylphosphane (PAMP) and got *ee* values, after playing with hydrogenation conditions, up to 58%. Further modification of this molecule gave us methylcyclohexyl-*o*-anisylphosphane (CAMP); this change gave up to 88%. These results are summarized in Scheme 4.

It all seems too easy and simple, but this was the first time ever that anyone had obtained enzymelike selectivity with a man-made catalyst! Never in our wildest imagination did we think a structure versus activity study would converge so quickly to a product with commercial potential. CAMP was our sixth candidate. As I look back from this perspective, I don't think that even we were emotionally equipped to realize what we had done. Here, with this simplest of molecules (CAMP), we had solved one of the toughest synthetic problems. For the past hundred years, it had been almost axiomatic among chemists that only nature's enzymes could ever do this job.

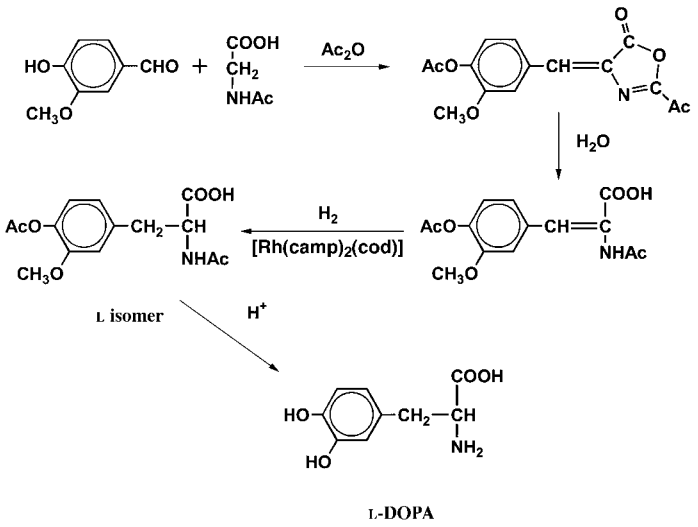
Our patent department always considered our invention was the use of chiral phosphanes with rhodium but, of course, without finding PAMP and CAMP, we would have had only a new way of doing what had been done before. The lawyers felt that this first result wasn't much, but that we could very rapidly come up with an improved embodiment, and in this they were unusually prescient.

We have called these catalysts man-made but this is not strictly true. We have not violated the general principal that, if you want chiral molecules, you will have to get them with the assistance of previously formed natural products. Our asymmetry was obtained from the (−)-menthol used in the chiral phosphane synthesis, but being a catalyst, a small amount of (−)-menthol could lead to a large amount of chiral product. CAMP worked equally well for the L-DOPA precursor (Scheme 2), and it made no difference whether the amine-blocking group was benzoyl or acetyl.

At this point, we were strongly motivated to develop a commercial L-DOPA process. It is a rare thing that the emergence of a substantial demand for a chemical is so closely timed with an invention for a new way of making it. Our management reluctantly increased our manpower but didn't really believe we could do it until the hydrogenation was done on a 50-gallon scale without incident.

Since CAMP was already good enough, we stopped exploring phosphanes and concentrated on converting this unique hydrogenation into large-scale production. This process was helped when another fortuitous event occurred. Monsanto decided to get out of its first product, saccharin, and an idle plant was now available for this kind of fine-chemical manufacture. These things were then put together to give our simplified L-DOPA process, which started with vanillin (Scheme 5).

The chiral hydrogenation was the simplest step in the sequence. We started with a slurry of prochiral olefin in an alcohol–water mix and ended with a slurry of chiral product which could be filtered, to leave the catalyst and residual racemate in the mother liquor. We could use an in situ prepared catalyst, but it was more convenient to use a solid

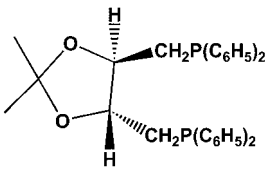


Scheme 5. Monsanto L-DOPA process.

air-stable complex of the type $[Rh(1,5\text{-cod})L_2]^+BF_4^-$ (cod = cyclooctadiene). These catalysts were fast, so that mole ratios of substrate:catalyst were about 20000:1. Thus, even this super-expensive complex was used at close to throwaway levels.

Even in the best case, some racemic product is made and must be separated. This separation is easy or hard, depending on the nature of the racemate. If the racemic modification has a different crystalline form than pure D or L, then separation of the pure excess enantiomer will be inefficient. If one achieves a 90% *ee* value, then it is possible to get out easily only 75–80% pure enantiomer. With lower *ee* values, the losses become prohibitive. For such a system, a catalyst of very high efficiency must be used. Unfortunately, most compounds are of this type; their racemic modifications do not crystallize as pure D or L forms. If, on the other hand, the racemic modification is a conglomerate or an equal mix of D and L crystals, then recovery of the excess L form can be achieved with no losses. Since the L and DL forms are not independently soluble, a 90% *ee* value easily gives a 90% recovery of pure isomer. In our L-DOPA process, the intermediate is such a conglomerate and separations are efficient. This lucky break was most welcome. If one thinks back, ours was the same luck that Pasteur encountered in his classical tartaric acid separations, 150 years ago.

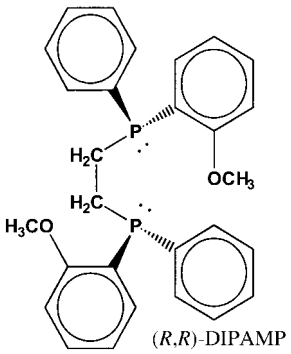
At the time of our initial commercialization, we learned of a new, efficient ligand invented by Kagan et al., which he called DIOP. This was a chelating bisphosphane ligand made from tartaric acid with chirality on the carbon backbone and it gave results comparable to CAMP. We had hypothesized that, to get good results, one needed chirality directly on the phosphorus atom. It made sense, but Kagan showed us to be totally wrong. It is most appropriate that this invention using tartaric acid should have come from a Frenchman in the land of Louis Pasteur, who, of course, was the one who got it all started. Kagan's discovery was the wave of the future for a whole series of bisphosphane ligands with asymmetry on the chiral backbone.[2]



83% *ee*

(*R*,*R*)-DIOP, Kagan

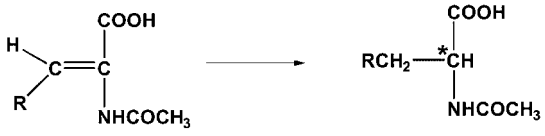
Shortly afterwards, we came up with our own chelating bisphosphane ligand, by dimerizing PAMP by another Mislow procedure. We called it DIPAMP, and chirality resided on the phosphorus atom. DIPAMP worked at about 95% *ee* in our L-DOPA system and we quickly converted our commercial process to use it. Part of our motivation to make a quick change was that DIPAMP was easier to make than CAMP, and, in addition, it was a nice, crystalline air-stable solid.



95% *ee*

(*R*,*R*)-DIPAMP

When we started this work we expected these man-made systems to have a highly specific match between substrate and ligand, just like enzymes. Generally, in our hands and in the hands of those that followed us, a good candidate has been useful for quite a range of applications. This feature has substantially enhanced their value in synthesis. It turned out that these chiral hydrogenations, as applied to enamides, were entirely general, especially with DIPAMP. Here it should be pointed out that these prochiral enamides can exist in both *E* and *Z* forms. The *Z* form hydrogenates efficiently whereas the *E* form hydrogenates less efficiently. Both give the same product. Fortunately for us, the base condensation used in their preparation gives us only the desirable *Z* form (Scheme 6).[3] The R group can be just about anything except



Scheme 6. Generality for *Z* enamides.

-COOH. It's easy to see how our rhodium catalyst could become confused with two carboxy groups so close together. Thus, aspartic acid is best made by an enzymatic process.

However, almost all the known familiar α-amino acids can be prepared this way since, at least in principle, an enamide precursor is possible. Evidently the polar carboxy and amide groups overwhelm any variation in the R group. Also, the carboxy- and the nitrogen-blocking group can be varied

extensively. Once again lady luck was with us, since if we had a choice where the catalyst would be useful, we couldn't have selected a more important area than the α-amino acids, the building blocks of the proteins.

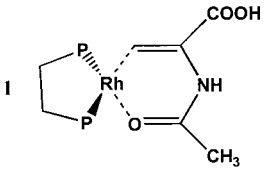
A few of the more important ones are listed in Table 1. Our colleagues at Hoffman LaRoche have added about a dozen more nonaromatic members to this list using DIPAMP. This

Table 1. Important amino acids produced by asymmetric catalysis.

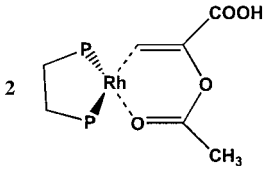
Product	*ee*[a] value [%]
L-DOPA	94
L-phenylalanine	96
L-tryptophan	93
L-alanine	90
L-lysine	85

[a] *ee* = enantiomeric excess.

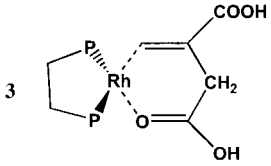
generality can be extended to a variety of enol esters and itaconic acid derivatives. Evidently what is required is the ability to chelate with the metal. Thus, the nitrogen atom can be replaced with an oxygen atom or a methylene group (**1** – **3**).[3]



enamides



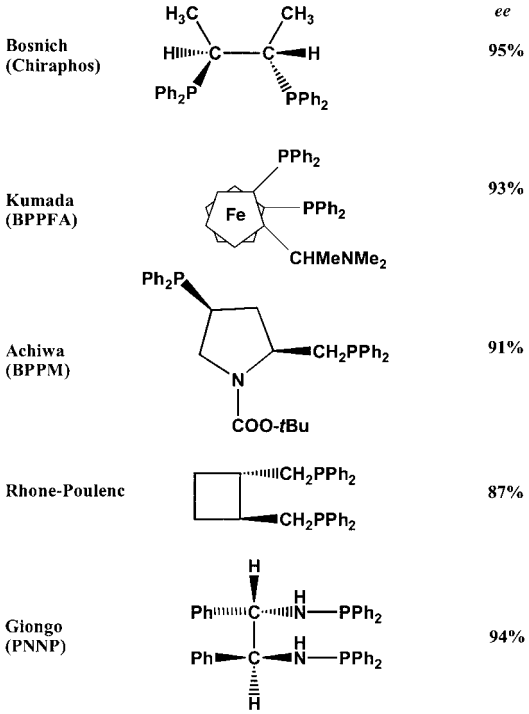
enol esters



carboxylic acids

One compound which did not work well in our system was our original model, α-phenylacrylic acid. A number of these aryl propionic acids have value as nonsteroidal antiarthritics. Here, as is the usual case, only one enantiomer is active and thus a process to make one isomer directly was needed. We tried hard to solve this problem, even using ruthenium – ligand systems, but without success. It took Professor Noyori with his BINAP – ruthenium complex to solve this problem.[4] I'm afraid this is just another example in the history of invention. The one who makes the first discovery seldom makes the second. On a grander stage, this may explain why there are so few Nobel Laureate repeats.

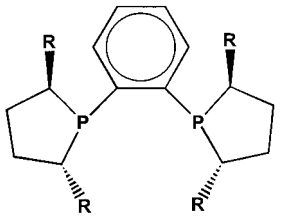
Soon after the appearance of DIOP and DIPAMP, a considerable number of bisphosphane ligands with chiral carbon backbones were found. All of these worked well with the same enamides and on related oxygen analogues. A few of these are shown in Scheme 7.[5]



Scheme 7. Phosphane catalysts used in the catalytic hydrogenation of *Z*-α-acetamidocinnamic acid.

It is interesting, that over the years, we made a lot of chiral phosphanes but never got a good one without our beloved *o*-anisyl group. Others have used it in connection with their bisphosphanes but it gives them no particular advantage. Thus, the choice of suitable structures is still pretty much guesswork.

In our hands, DIPAMP was by far the most versatile ligand, and remained supreme for enamides for many years. Later, in the 1990s, an improved bisphosphane ligand was reported by Burk, then at DuPont, to which he gave the name DuPHOS.[6]



R = Me or Et

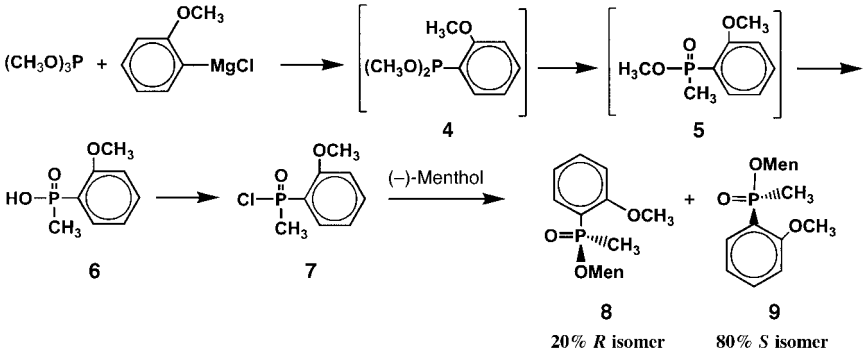
DuPHOS, Burk

This bisphosphane ligand, complexed with rhodium, gave fast hydrogenations of enamides with efficiencies of 99%. Once again, the next invention was made by someone else. These high *ee* values can be important where the racemate is not a conglomerate.

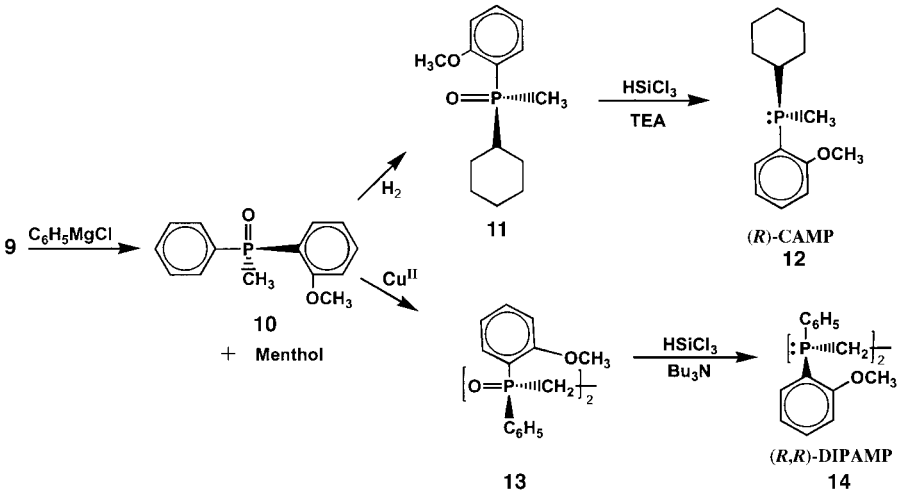
3. Synthesis and Properties of the Phosphanes

The key to asymmetric hydrogenation is the structure of the chiral ligand. The phosphanes are prepared by a multistep route and are quite expensive, but fortunately one mole of

catalyst will make many thousands of moles of product. Even so, the ligand must be made from cheap starting materials. Some economy of scale is achieved by making a ten year supply in a few plant-size batches. At first, CAMP was prepared from phenyldichlorophosphane via Mislow's menthyl ester, by introducing the *o*-anisyl group last. Unfortunately, the desired isomer was produced in minor amounts and, to correct this situation, it was necessary to reverse the order of addition of the aryl groups. The sequence starting with trimethylphosphite is outlined in Scheme 8 and Scheme 9.



Scheme 8. Synthesis and resolution of the menthyl ester. men = menthyl



Scheme 9. Improved synthetic procedure for CAMP and DIPAMP.

A large excess of trimethylphosphite was needed to get good yields of monosubstituted product **4**. In the sequence **4**→**6**, only the nicely crystalline phosphinic acid **6** was isolated. The fact that the acid chloride **7** can be converted to an 80:20 mix of (*S*) and (*R*) isomers means that the menthol preferentially reacts with one form while the other isomer rapidly racemizes. Thus, the catalyst preparation was greatly facilitated by an asymmetric synthesis of its own directed by (−)-menthol.

Another advantage of the sequence in Schemes 8 and 9 was that CAMP and DIPAMP were prepared from a common intermediate (**10**) and no new resolution procedure needed to be worked out. Thus, the change to an improved ligand could be done with minimum dislocation, both at the synthesis and the utilization end. It is a clear advantage of catalytic processes that it is often easy to shift from the old to the new.

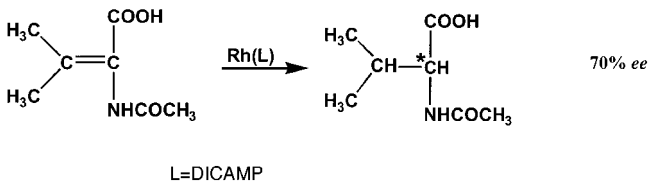
CAMP was prepared by a selective hydrogenation reaction of **10** (Scheme 9) using a rhodium-on-carbon heterogeneous catalyst. It was important to monitor the reaction closely and stop before the anisyl ring started to hydrogenate. Reduction with trichlorosilane and triethylamine (TEA) gave (*R*)-CAMP **12**, with inversion. The (*R*)-menthyl ester **8** could also have been used in this sequence if the last step was run with pure $HSiCl_3$; this modification results in retention of configuration.

In the case of DIPAMP the copper-coupling step, run with lithium diisopropyl amide and $CuCl_2$, did not affect the stereochemistry. However, only the base-promoted reaction with trichlorosilane to give a double inversion was applicable. In this case, an empirical study showed that use of tributylamine minimized formation of the *meso* product.

In principle, the menthol recovered in Scheme 9 could be recycled, which makes the usage of chiral agent derived from nature truly minimal, but in practice it has not been worth the effort. More useful is the recovery by hydrolysis of the phosphinic acid from the (*R*)-menthyl ester (Scheme 8).

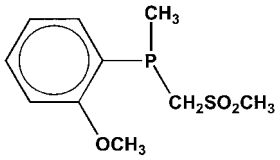
In contrast to CAMP, DIPAMP is a stable solid that melts at 102° C. Heated at 100° C, it has a half-life of 3–5 h. This racemization was somewhat faster than Mislow's phosphanes, which did not invert appreciably until 10–15° C higher. The rate was reasonable, if one considers that inversion at either end destroys chirality. DIPAMP complexed to rhodium must invert much more slowly because efficient, asymmetric hydrogenations have been obtained at 95–100° C. For the sake of convenience, particularly on a large scale, a solid complex was made by reacting two equivalents of phosphane with one equivalent of $[Rh(cod)Cl]_2$ in alcohol. This air-stable orange solid $[Rh(bisligand)(cod)]^+BF_4^-$ made a most suitable catalyst precursor.

We have used the resolved menthyl ester **9** to make a variety of phosphane ligands. The first and most obvious use is to convert DIPAMP into DICAMP. You will recall that, in the monophosphane series, the exchange of a phenyl group for a cyclohexyl group gave an enormous increase in selectivity. Not so with DICAMP, which gave only 60–65 % *ee* in our enamide systems. It was, however, our best candidate for preparing the more hindered amino acid, valine, for which the other systems were very poor (Scheme 10).



Scheme 10. Synthesis of valine by use of the DICAMP ligand.

In the monophosphane series, we only found one ligand that was marginally better than CAMP. This rarity of good monophosphanes shows how lucky we were to find an efficient one on almost the first try. We never found a good candidate without the *o*-anisyl group. This is contrasted with all our colleagues in other labs who never found much benefit from it.



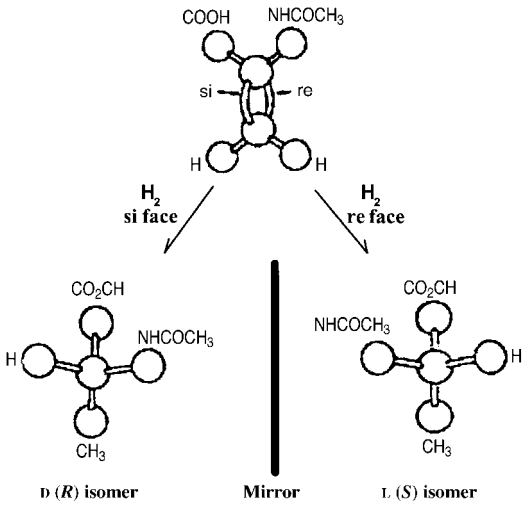
92% *ee*

We could sulfonate DIPAMP and make it water soluble. It worked fine but gave only 85% *ee* which, by current standards, is too low. I winced when I came in one morning and saw our valuable DIPAMPO being treated with concentrated sulfuric acid, but it worked. This exploratory effort suffices to show that, as one might expect, the catalysis continues to be a very sensitive function of ligand structure and that our ability to predict or proceed in a rational manner is severely limited.

4. Mechanism of the Asymmetric Catalysis

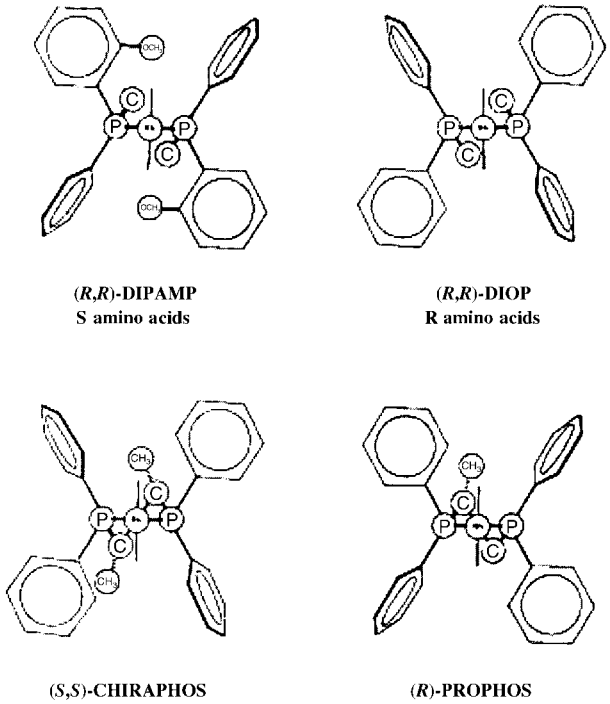
Now that we have these catalysts and have the ability to use them commercially, we would like to know how they work. When we look at energy calculations and realize that, to get 90% *ee*, we are talking about only a 2 kcal difference, and this is just about the same as the rotation barrier in ethane. Thus, the asymmetric bias may be caused by very subtle effects.

Using the ball-and-stick models in Scheme 11 to illustrate a typical prochiral olefin, we can see that attack at the si face gives the D isomer and at the re face the L, which correspond to *R* and *S* isomers in more modern nomenclature. These of course are mirror images and our catalyst must discriminate between them.



Scheme 11. Ball-and-stick models of the prochiral olefin and the resulting isomers.

We examined the X-ray crystal structure of the catalyst precursor $[Rh(cod)(dipamp)]^+BF_4^-$, and we noticed that this system presented an array of four aryl groups arranged in an edge–face manner. The phenyl groups present an edge and the *o*-anisyl group a face. This is depicted in Scheme 12 where,



Scheme 12. Edge–face diagrams.

for clarity's sake, we have omitted the cyclooctadiene ligand and the counterion, as well as oversimplifying the structure. In this picture, we are looking along the phosphorus–rhodium–phosphorus plane. One could speculate that an approaching substrate might prefer to lie on the flat face rather than on the hindered edge. We can more easily show this by a quadrant diagram (Figure 1), in which the shaded quadrants represent

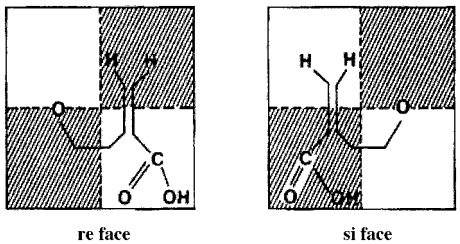


Figure 1. Quadrant diagrams of positioning of the prochiral olefin.

the edge or hindered side. We speculated that a prochiral olefin might prefer to lie in the unhindered quadrant. You will note that all the other bisphosphanes in Scheme 7 also present a similar array of four phenyl groups in their X-ray crystal structures, though not quite as convincingly, but there was always a face-exposed ring next to the skewed methylene group.

It makes no difference whether one attributes the bias to the edge–face configuration, as I prefer, or to the skewed

methylene group. By using this quadrant interpretation, we could predict what the chirality of the product would be, from the chirality of the phosphane. For any single case where there is a 50% chance of being right, such a prediction has no significance, but having predicted correctly for five cases where X-ray crystal structures were available, one gains credibility. We felt pretty good about how things were fitting into place.

Then along came Halpern's studies.[7] He had been able to isolate a more advanced intermediate, in which the enamide substrate actually formed a complex with the metal–ligand system. He got it crystalline, and it was with considerable eagerness we awaited the X-ray crystallograpic analysis results. It turned out that the enamide was lying nicely in the hindered quadrant.

So much for our theory. As so often happens in science, one comes up with an explanation in which everything seems to be fitting in nicely, and someone else shows your whole interpretation may well be wrong. We were stranded with the argument that, at the square-planar stage, Halpern reported that these steric factors may not be important. However, to get asymmetric bias, we know that the hydrogen atom, the ligand, and the substrate must all be on the metal center at the same time. Such a configuration requires an octahedral structure. Perhaps then these quadrant constraints are important. So far as I know, there is no evidence either to support or reject this contention. Our theory, though possibly wrong, does predict correctly.

All this thinking does not explain CAMP, unless we argue that, during the hydrogenation step, this monodentate ligand prefers to occupy adjacent sites on the metal center and acts as a bidentate species.[3b]

In any case this unique catalysis has enabled chemists to study mechanistic details that it was not previously possible to study. When one thinks of it, it is quite remarkable that we are even in a position to debate such subtle features.

5. Concluding Comments

These soluble hydrogenation catalysts have started a new era in catalytic processes. Since we are now dealing with pure complexes, we can design something to do just the job you want. This catalysis will continue to find many uses in industry, whenever an efficient route to the unsaturated precursor is available. These catalytic processes can be a nice alternative but will by no means replace biochemical processes. Here, the problems with dilute solutions and difficult isolations are often less than the problems of a multistep synthesis. One area where these catalysts will reign supreme is in the preparation of D-amino acids or other unnatural isomers. Here, biochemical alternatives will not be available.

Perhaps the most important use of these catalysts will be to provide an easy way to make a large number of chiral compounds. In the past, research chemists have been reluctant to run laborious resolutions and have done so only when necessary. Now they can get chiral compounds for their life-sciences research with very little effort. We can look on these catalysts as a labor-saving device for the laboratory. For this, they will have an impact for as long as chemists run reactions.

For an invention to succeed, Paul Ehrlich, the father of chemotherapy, stated that four Gs are required; Geist, Geld, Geduld and Gluck. The first of these is axiomatic; you have got to have a good idea. The second is essential; one needs financial support, but I would suggest a proper balance; too much or too little is inhibitory. For the third, you must have patience. Things never move as fast as you would have them. Finally, luck is all-important. I suspect that no invention has ever been made without some fortuitous help.

I have pointed out, and will continue to do so, that ours has been very much a joint effort. It would not have been possible without my associates, Jerry Sabacky and Billy Vineyard. In closing, I would like to add a couple of Gs to Ehrlich's list. We are extremely Grateful to have so Great an honor bestowed on us by your committee.

Received: February 1, 2002 [A 514]

[1] W. S. Knowles, *Acc. Chem. Res.* **1983**, *16*, 106, and references therein.
[2] I. V. Komarov, A. Börner, *Angew. Chem.* **2001**, *113*, 1237; *Angew. Chem. Int. Ed.* **2001**, *40*, 1197.
[3] K. E. Koenig in *Asymmetric Synthesis*, *Vol. 5*, *Chiral Catalysis* (Ed.: J. D. Morrison), Academic Press, New York, **1985**, chap. 3: The Applicability of Asymmetric Homogeneous Catalytic Hydrogenation.
[4] R. Noyori, *Angew. Chem.* **2002**, *114*, 2108; *Angew. Chem. Int. Ed.* **2002**, *41*, 2008.
[5] H. B. Kagan in *Asymmetric Synthesis*, *Vol. 5*, *Chiral Catalysis* (Ed.: J. D. Morrison), Academic Press, New York, **1985**, chap. 1: Chiral Ligands for Asymmetric Catalysis.
[6] M. J. Burk, J. E. Feaster, W. A. Nugent, R. L. Harlow, *J. Am. Chem. Soc.* **1993**, *115*, 10125; M. J. Burk, M. F. Gross, J. P. Martinez, *J. Am. Chem. Soc.* **1995**, *117*, 9375.
[7] J. Halpern in *Asymmetric Synthesis*, *Vol. 5*, *Chiral Catalysis* (Ed.: J. D. Morrison), Academic Press, New York, **1985**, chap. 2: Asymmetric Catalytic Hydrogenation: Mechanism and Origin of Enantioselection.
[8] K. B. Sharpless, *Angew. Chem.* **2002**, *114*, 2116; *Angew. Chem. Int. Ed.* **2002**, *41*, 2024.

Asymmetric Catalysis: Science and Opportunities (Nobel Lecture)**

Ryoji Noyori*

Asymmetric catalysis, in its infancy in the 1960s, has dramatically changed the procedures of chemical synthesis, and resulted in an impressive progression to a level that technically approximates or sometimes even exceeds that of natural biological processes. The recent exceptional advances in this area attest to a range of conceptual breakthroughs in chemical sciences in general, and to the practical benefits of organic synthesis, not only in laboratories but also in industry. The growth of this core technology has given rise to enormous economic potential in the manufacture of pharmaceuticals, animal health products, agrochemicals, fungicides, pheromones, flavors, and fragrances. Practical asymmetric catalysis is of growing importance to a sustainable modern society, in which environmental protection is of increasing concern. This subject is an essential component of molecular science and technology in the 21st century. Most importantly, recent progress has spurred various interdisciplinary research efforts directed toward the creation of molecularly engineered novel functions. The origin and progress of my research in this field are discussed.

Keywords: asymmetric catalysis · asymmetric hydrogenation · Nobel lecture · P ligands · ruthenium

1. Prologue

Chirality (handedness; left or right) is an intrinsic universal feature of various levels of matter.[1] Molecular chirality plays a key role in science and technology. In particular, life depends on molecular chirality, in that many biological functions are inherently dissymmetric. Most physiological phenomena arise from highly precise molecular interactions, in which chiral host molecules recognize two enantiomeric guest molecules in different ways. There are numerous examples of enantiomer effects which are frequently dramatic. Enantiomers often smell and taste different. The structural difference between enanatiomers can be serious with respect to the actions of synthetic drugs. Chiral receptor sites in the human body interact only with drug molecules having the proper absolute configuration, which results in marked differences in the pharmacological activities of enantiomers. A compelling example of the relationship between pharmacological activity and molecular chirality was provided by the tragic administration of thalidomide to pregnant women in the 1960s. (*R*)-Thalidomide has desirable sedative properties, while its *S* enantiomer is teratogenic and induces fetal malformations.[2, 3] Such problems arising from inappropriate molecular recognition should be avoided at all costs. Nevertheless, even in the early 1990s, about 90 % of synthetic chiral drugs were still racemic—that is, equimolar mixtures of both enantiomers, which reflects the difficulty in the practical synthesis of single-enantiomeric compounds.[4] In 1992, the Food and Drug Administration in the U.S. introduced a guideline regarding "racemic switches", in order to encourage the commercialization of clinical drugs consisting of single enantiomers.[5] Such marketing regulations for synthetic drugs, coupled with recent progress in stereoselective organic synthesis, resulted in a significant increase in the proportion of single-enantiomer drugs. In 2000, the worldwide sales of single-enantiomer compounds reached 123 billion U.S. dollars.[6] Thus, gaining access to enantiomerically pure compounds in the development of pharmaceuticals, agrochemicals, and flavors is a very significant endeavor.

Discovery of truly efficient methods to achieve this has been a substantial challenge for chemists in both academia and industry. Earlier, enantiomerically pure compounds were obtained by the classical resolution of a racemate or transformation of readily accessible, naturally occurring chiral compounds such as amino acids, tartaric and lactic acids, carbohydrates, terpenes, or alkaloids. Even though stereoselective conversion of a prochiral compound to a chiral product, namely through an asymmetric reaction, is the most attractive approach, practical access to pure enantiomers relied largely on biochemical or biological methods. However,

[*] Prof. Dr. R. Noyori
Department of Chemistry
Nagoya University
Chikusa, Nagoya 464-8602 (Japan)
Fax: (+81) 52-783-4177
E-mail: noyori@chem3.chem.nagoya-u.ac.jp

[**] Copyright© The Nobel Foundation 2002. We thank the Nobel Foundation, Stockholm, for permission to print this lecture.

 © WILEY-VCH Verlag GmbH, 69451 Weinheim, Germany, 2002 1433-7851/02/4112-2008 $ 20.00+.50/0

the scope of such methods using enzymes, cell cultures, or whole microorganisms is limited because of the inherent single-handed, lock-and-key specificity of biocatalysts. On the other hand, a chemical approach allows for the flexible synthesis of a wide array of enantiopure organic substances from achiral precursors. The requirements for practical asymmetric synthesis include high stereoselectivity, high rate and productivity, atom economy, cost efficiency, operational simplicity, environmental friendliness, and low-energy consumption. Traditional asymmetric synthesis using a stoichiometric amount of a chiral compound, though convenient for small to medium-scale reactions, is practical only if the expensive chiral auxiliary deliberately attached to a substrate or reagent is readily recyclable; otherwise it is a wasteful procedure.

Figure 1 illustrates a general principle of asymmetric catalysis which provides an ideal way for multiplying molecular chirality.[7] A small amount of a well-designed chiral

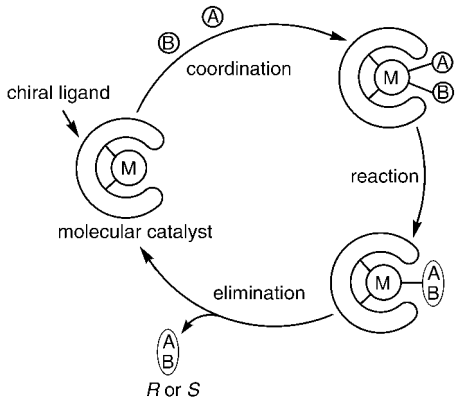


Figure 1. A general principle of asymmetric catalysis with chiral organometallic molecular catalysts. M = metal; A, B = reactant and substrate.

catalyst can combine A and B, which produces the chiral AB compound stereoselectively in a large quantity. Of various possibilities, the use of chiral organometallic molecular catalysts would be the most powerful strategy for this purpose. Asymmetric catalysis is an integrated chemical approach in which the maximum chiral efficiency can be obtained only by a combination of suitable molecular design with proper reaction conditions. The reaction must proceed with a high turnover number (TON) and a high turnover frequency (TOF), while the enantioselectivity ranges from 50:50 (nonselective) to 100:0 (perfectly selective). The chiral ligands that modify intrinsically achiral metal atoms must possess suitable three-dimensional structures and functionality, to generate sufficient reactivity and the desired stereoselectivity. Sometimes the properties of achiral ligands are also important. The chiral catalyst can permit *kinetically* precise discrimination among enantiotopic atoms, groups, or faces in achiral molecules. Similarly, enantiomeric molecules can also be discriminated. Certain well-designed chiral metal catalysts not only accelerate the chemical reactions repeatedly but also differentiate between diastereomeric transition states (TSs) with an accuracy of 10 kJ mol^{-1}. In this way, such compact molecular catalysts with a molecular weight less than 1000, or <20 Å in length or diameter, allow for an ideal method for synthesizing enantiomeric compounds. The diverse catalytic activities of metallic species, as well as the virtually unlimited structural variation of the organic ligand, provides enormous opportunities for asymmetric catalysis.

2. Discovery of Asymmetric Catalysis by Chiral Organometallic Complexes

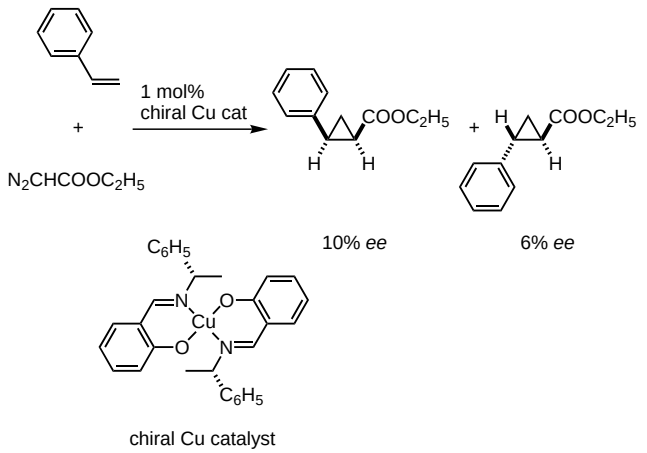
In 1966, when I was in H. Nozaki's (Figure 2) laboratory at Kyoto, we discovered the first example of asymmetric catalysis using a structurally well-defined chiral transition-metal complex.[8] This finding resulted from research done for an entirely different purpose, which was to elucidate the mechanism of carbene reactions. As illustrated in Scheme 1, when a small amount (1 mol %) of a chiral Schiff base – Cu^{II} complex was used as a molecular catalyst in the reaction of styrene and ethyl diazoacetate, the *cis*- and *trans*-cyclopropanecarboxylates were obtained in 10 and 6% enantiomeric excess (*ee*), respectively. We also observed asymmetric induction in carbene insertion to a C–O bond of 2-phenyloxetane, which gave optically active 2,3-substituted tetrahydrofuran derivatives. At that time, the finding was syntheti-



Figure 2. Professor H. Nozaki (1985).

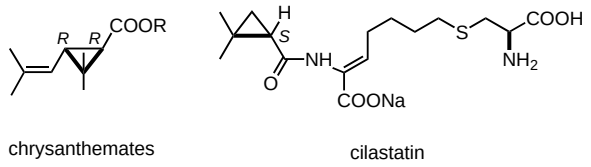


Ryoji Noyori, born in Kobe in 1938, completed his master's degree at Kyoto University and thereafter became an Instructor at the same university. He received his Ph.D. degree in 1967 under the supervision of H. Nozaki. He was appointed Associate Professor at Nagoya University in 1968 and promoted to Professor in 1972. He spent a postdoctoral year in 1969 – 1970 at Harvard University with E. J. Corey. His research has focused on the fundamentals and applications of molecular catalysis, based on organometallic chemistry, particularly asymmetric catalysis. His scientific contributions have been recognized by numerous awards including: the Tetrahedron Prize (1993), the Japan Academy Prize (1995), the Arthur Cope Award (1997), the King Faisal International Prize (1999), the Order of Culture (2000), the Wolf Prize (2001), and the Roger Adams Award (2001). In 2001, he shared the Nobel Prize in Chemistry with W. S. Knowles and K. B. Sharpless.



Scheme 1. Discovery of asymmetric reaction by means of a chiral organometallic molecular catalyst.

cally primitive since the degree of enantioselection was meaningless practically. Later, T. Aratani, a Kyoto student, went to Sumitomo Chemical Co., where he invented an excellent chiral Cu catalyst for asymmetric cyclopropanation, which achieved the industrial synthesis of chrysanthemates (efficient insecticides) and (*S*)-2,2-cyclopropanecarboxylic



acid. The latter compound is a building block of cilastatin, an in vivo stabilizer of the carbapenem antibiotic, imipenem (Merck Co.; Figure 3).[9]



Figure 3. Reaction apparatus for the Sumitomo asymmetric cyclopropanation.

3. Asymmetric Hydrogenation in the Early Days

At present the asymmetric cyclopropanation is important practically, but in the late 1960s, it was just a special reaction in organic synthesis. I decided to pursue hydrogenation, which is a core technology in chemistry. It is the simplest but most powerful way to produce a wide array of important compounds in large quantities using inexpensive, clean hydrogen gas without forming any waste. Hydrogenation was initiated at the end of the 19th century by P. Sabatier (1912 Nobel laureate), who used fine metal particles as heterogeneous catalysts. Some notable achievements that attracted me, before doing research in this area, include: activation of H_2 by a transition-metal complex in the late 1930s (M. Calvin, 1961 Nobel laureate),[10] homogeneous hydrogenation of olefinic substrates with $RuCl_3$ in 1961 (J. Halpern, J. Harrod, and B. R. James),[11] and hydrogenation of olefinic compounds using $[RhCl\{P(C_6H_5)_3\}_3]$ in 1965 (G. Wilkinson, 1973 Nobel laureate).[12] Most importantly, in 1956, S. Akabori at Osaka reported that metallic Pd drawn on silk catalyzes asymmetric (heterogeneous) hydrogenation of oximes and oxazolones.[13] This pioneering work, though not effective synthetically, was already well known throughout Japan. In 1968, two years after our asymmetric cyclopropanation in 1966, W. S. Knowles (fellow Nobel laureate in 2001)[14] and L. Horner[15] independently reported the first homogeneously catalyzed asymmetric hydrogenation of olefins with chiral monodentate tertiary phosphane–Rh complexes, albeit in 3–15% optical yield.[16] H. B. Kagan provided a major breakthrough in this area in 1971, when he devised DIOP, a C_2-chiral diphosphane ligand derived from tartaric acid. He used its Rh complex for asymmetric hydrogenation of dehydro amino acids leading to phenylalanine in about 80% *ee*, then recorded as 72% *ee*.[17] The Knowles group at Monsanto established a method for the industrial synthesis of L-DOPA, a drug for treating Parkinson's disease, which used his DIPAMP–Rh catalyzed asymmetric hydrogenation as a key step.[18] These achievements significantly stimulated the subsequent investigation of this important subject.

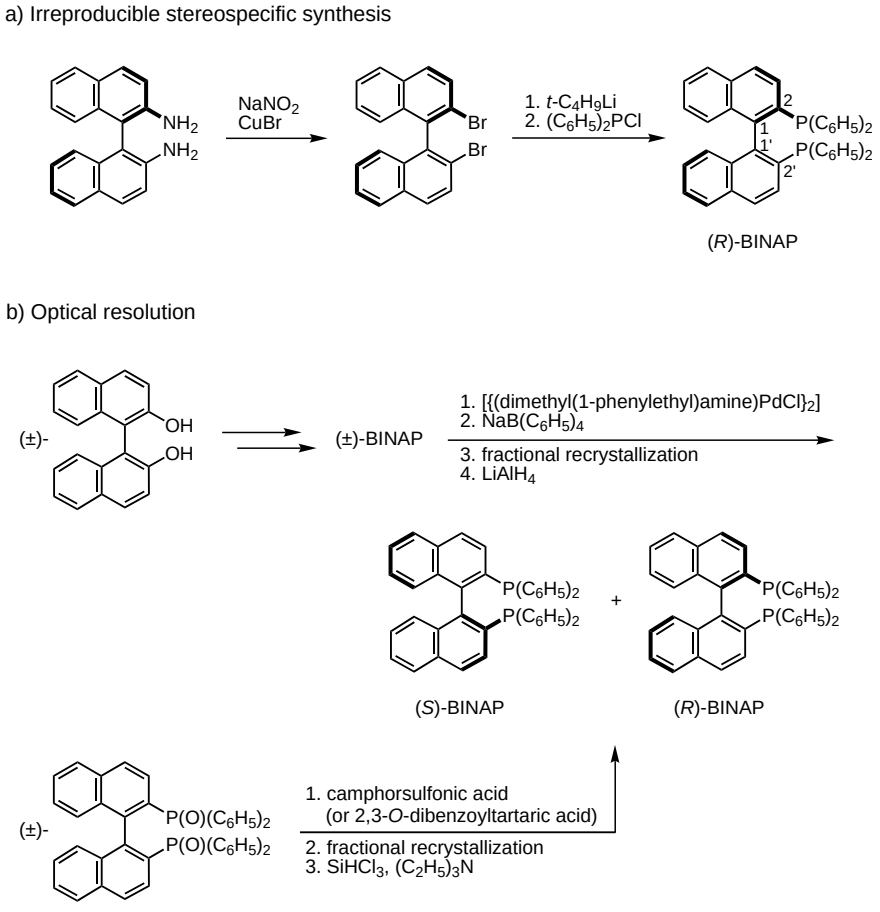
Shortly after moving from Kyoto to Nagoya in 1969–70, I spent a postdoctoral year at Harvard with E. J. Corey (1990 Nobel laureate). He asked me to hydrogenate selectively one of the two C=C bonds in a prostaglandin $F_{2\alpha}$ derivative to give the $F_{1\alpha}$ form having only one C=C bond.[19] This research was helped by K. B. Sharpless (another fellow Nobel laureate in 2001)[102], who was then a postdoctoral fellow with K. Bloch (1964 Nobel laureate in Physiology or Medicine) and who suggested a convenient TLC technique for analyzing the structurally very similar olefinic compounds. In addition to this background, my personal interaction with J. A. Osborn, a former Wilkinson student and co-inventor of $[RhCl\{P(C_6H_5)_3\}_3]$[12] who was then an Assistant Professor at Harvard, greatly enhanced my interest in asymmetric hydrogenation, which later became my life-long research interest. My desire was to develop a truly efficient asymmetric hydrogenation which would have a wide scope of applications. In the early 1970s, chiral phosphane–Rh complexes could hydrogenate satisfactorily only dehydro amino acids but not many other olefins. Asymmetric hydrogenation of ketones was totally unexplored.[20]

4. BINAP, a Beautiful Chiral Molecule

H_2 is the simplest molecule but it has enormous potential from both a scientific and technical point of view. To discover high-performance asymmetric catalysts, the development of an excellent chiral ligand is crucial. Attracted by its molecular beauty,[21] we initiated the synthesis of BINAP (2,2′-bis(diphenylphosphanyl)-1,1′-binaphthyl)[22] in 1974 at Nagoya with the help of H. Takaya, my respected long-term collaborator. BINAP was a new, fully aromatic, axially dissymmetric C_2-chiral diphosphane that would exert strong steric and electronic influences on transition-metal complexes. Its properties could be fine-tuned by substitutions on the aromatic rings. However, synthesis of this optically pure C_2-chiral diphosphane was unexpectedly difficult. In 1976, for the first time, we managed to obtain optically active BINAP starting from optically pure 2,2′-diamino-1,1′-binaphthyl (Scheme 2a). However, this seemingly straightforward synthetic pathway was not reproducible, because of the tendency of the chiral intermediates to cause racemization.[23] In 1978, we found a reliable method for resolving racemic BINAP with an optically active dimethyl(1-phenylethyl)aminopalladium(II) chloride complex,[22] while, later, optically pure BINAP became available more conveniently by resolution of BINAP dioxide with camphorsulfonic acid or 2,3-*O*-dibenzoyltartaric acid (Scheme 2b).[24, 25]

Although the elusive BINAP was available, our goal was still in the distance. Enantioselectivity of BINAP–Rh^I catalyzed asymmetric hydrogenation of α-(acylamino)acrylic acids was highly variable and not satisfactory at that time, *ee* values of the chiral products being at most about 80%. However, we remained patient. In 1980, six years after the start, thanks to the unswerving efforts of my young associates, we published our first work on asymmetric synthesis of amino acids of high enantiomeric purity, up to 100% *ee*, together with the X-ray crystalline structure of a cationic BINAP–Rh(norbornadiene) complex.[22, 26]

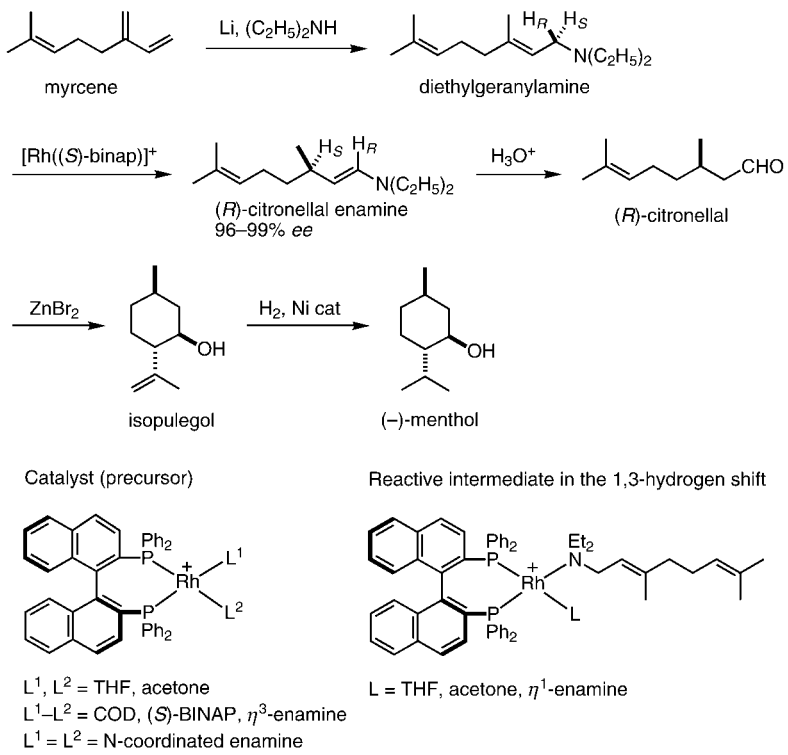
BINAP, a conformationally flexible atropisomeric C_2 diphosphane, can accommodate a range of transition metals by rotating about the binaphthyl C(1)-C(1′) pivot and C(2 or 2′)-P bonds, without seriously increasing torsional strain, while the resulting seven-membered chelate rings containing only sp^2 carbon atoms are in turn skeletally unambiguous. The chirality of BINAP is transmitted to other metal-coordination sites through the chelate structure.[22, 26] The δ or λ geometry is highly skewed and determines the chiral disposition of the *P*-phenyl rings that play a key role in generating outstanding chirality-discriminating ability at the reactive coordination sites. Thus BINAP-based metal complexes were expected to exhibit high chiral-recognition ability in various catalytic reactions, in addition to hydrogenation.



Scheme 2. Access to enantiomerically pure BINAP.

5. Asymmetric Synthesis of Menthol

The cationic BINAP–Rh complex was best used in asymmetric isomerization of allylic amines,[27] which realized an industrial synthesis of (−)-menthol from myrcene (Scheme 3).[28] This resulted from a fruitful academic/industrial collaboration between groups at Osaka University (S. Otsuka and H. Tani),[29] Nagoya University (R. Noyori), Institute for Molecular Science (H. Takaya), Sizuoka University (J. Tanaka and K. Takabe),[30] and Takasago International Co. (Figure 4). The key step was the asymmetric isomerization of geranyldiethylamine, catalyzed by an (*S*)-BINAP–Rh complex in THF and forming (*R*)-citronellal enamine, which upon hydrolysis gives (*R*)-citronellal in 96–99% *ee*. This is far superior to the 80% *ee* of the naturally occurring product available from rose oil. Among various Rh and other catalysts examined, the BINAP-based cationic Rh complex was the most reactive and the most stereoselective. The BINAP–Rh catalyst clearly differentiates between the pro-*S* and pro-*R* hydrogen atoms on the flexible allylic amine skeleton during the 1,3-suprafacial shift that occurs by a nitrogen-triggered mechanism.[31] The asymmetric reaction is performed on a nine-ton scale. The full technical refinements of the position- and stereo-



Scheme 3. Takasago menthol synthesis. COD = 1,5-cyclooctadiene.

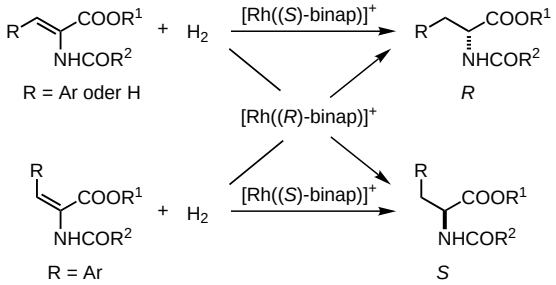


Figure 4. At the Takasago plant for (−)-menthol synthesis (February, 1984). From the left, K. Tani, H. Takaya, R. Noyori, S. Otsuka, S. Akutagawa, and H. Kumobayashi.

selective addition of diethylamine to myrcene, which gives the starting geranylamine, and the $ZnBr_2$-catalyzed intramolecular ene reaction of (*R*)-citronellal, which forms isopulegol with the three correct stereogenic centers, allowed for the production of terpenic substrates totaling about 1500 tons per year at Takasago International Co. Most of the (*R*)-citronellal is converted to 1000 tons per year of (−)-menthol, one-third of the world demand. (*R*)-7-Hydroxydihydrocitronellal thus prepared is a perfumery agent that smells like lily of the valley. Its methyl ether is an intermediate in the synthesis of methoprene, a growth regulator of the yellow-fever mosquito.[28, 29]

6. Asymmetric Hydrogenation of Olefins by BINAP – Ruthenium Complexes

Returning to the topic of asymmetric hydrogenation, our success resulted from the invention of the BINAP ligand[32] and also from the use of Ru, which behaves differently from the conventional Rh.[33, 34] The cationic BINAP – Rh complexes catalyze hydrogenation of α-(acylamino)-acrylic acids or esters to give the corresponding amino acid derivatives in high *ee* values (Scheme 4).[22, 23] However, the reaction is relatively slow, and high enantioselectivity is obtained only under special conditions, probably because of the operation of the unsaturate/dihydride mechanism. J. Halpern[35] and J. M. Brown[36] showed that hydrogenation of enamides in the presence of a C_2-chiral diphosphane – Rh complex proceeds by oxidative addition of H_2 to diastereomeric Rh – substrate chelate complexes, followed by stepwise transfer of the two hydrides to the coordinated olefin. Most significantly, the minor diastereomer of these complexes is the more reactive one.[37] Because of the excellent chiral-recognition ability of BINAP, the reactive species, which leads to the desired hydrogenation



Scheme 4. Asymmetric hydrogenation of α-(acylamino)acrylic acids catalyzed by BINAP – Rh complexes.

product, is present in a very small quantity and is even NMR-invisible in the equilibrium mixture.[23a] Therefore, conditions such as hydrogen pressure, temperature, and concentration must be chosen carefully to obtain high enantioselectivity. Furthermore, asymmetric hydrogenation was limited to the synthesis of amino acids.

A major breakthrough occurred when we devised the BINAP – Ru^{II} dicarboxylate complexes in 1986 (Figure 5).[38, 39] The Ru complexes are excellent catalysts for asymmetric hydrogenation of various functionalized olefins, as summarized in Scheme 5. The reaction proceeds via a Ru monohydride intermediate formed by heterolysis of H_2 by the Ru complex. The Ru center remains in the +2 oxidation state throughout the catalytic cycle,[40] in contrast to the Rh complex, which involves a +1/+3 redox process. Heteroatoms in the functional groups serve as a binding tether to the catalytic Ru center. This hydrogenation has a very wide scope. Hydrogenation of α,β- and β,γ-unsaturated carboxylic acids takes place in alcoholic media, where the sense and degree of

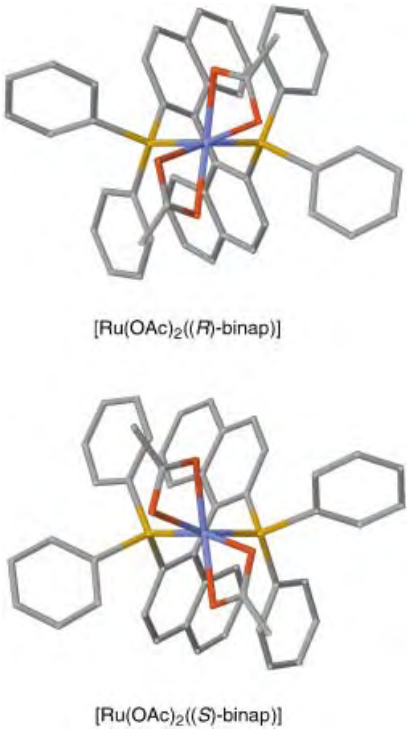
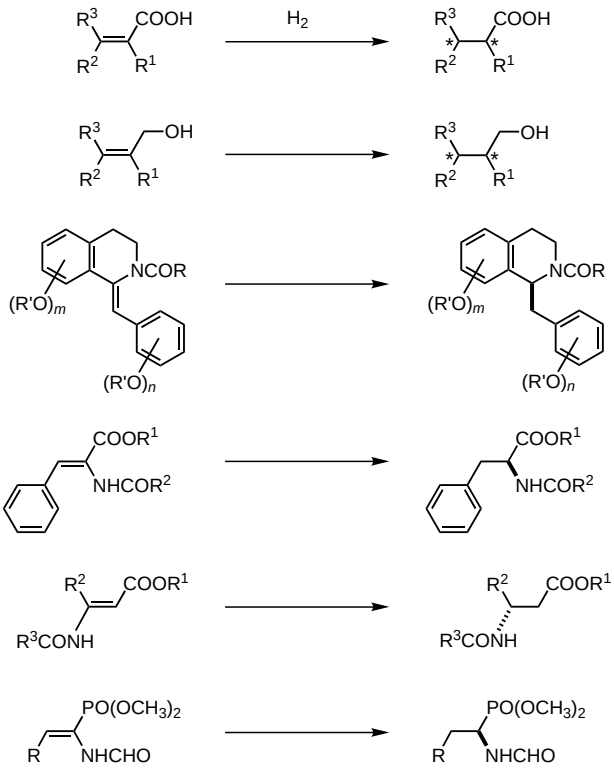


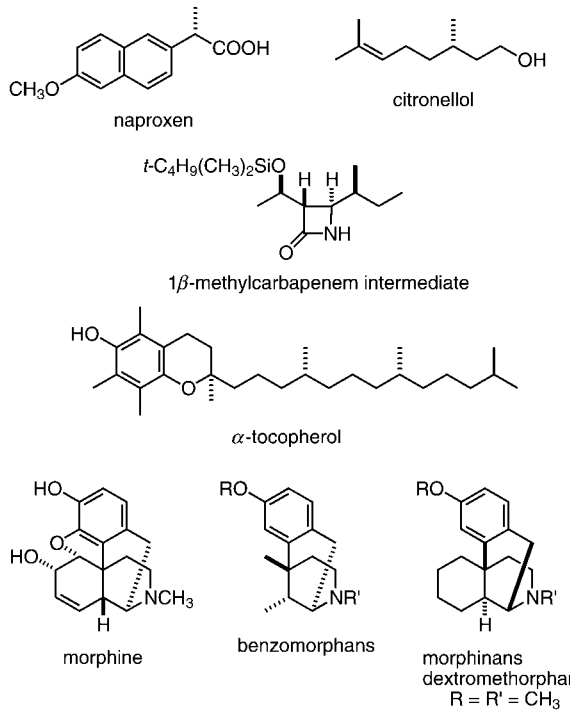
Figure 5. Structures of BINAP–Ru diacetate complexes.



Scheme 5. Asymmetric hydrogenation of functionalized olefins catalyzed by (*S*)-BINAP–Ru dicarboxylates.

the enantioselection are highly dependent on the substitution pattern and hydrogen pressure.[41] Allylic and homoallylic alcohols are also hydrogenated with high enantioselection.[42] Certain racemic allylic alcohols can be resolved by the BINAP–Ru-catalyzed hydrogenation.[43] The chiral Ru complexes effect highly enantioselective hydrogenation of (*Z*)-2-acyl-1-benzylidene-1,2,3,4-tetrahydroisoquinolines.[38, 44] In a similar manner, enantio-enriched α- and β-amino acids,[45] as well as α-amino phosphonic acids,[46] are obtainable from suitably amido-substituted olefins. Notably, the Ru^{II} and Rh^{I} complexes possessing the same BINAP chirality form antipodal amino acids as the predominant products.[47]

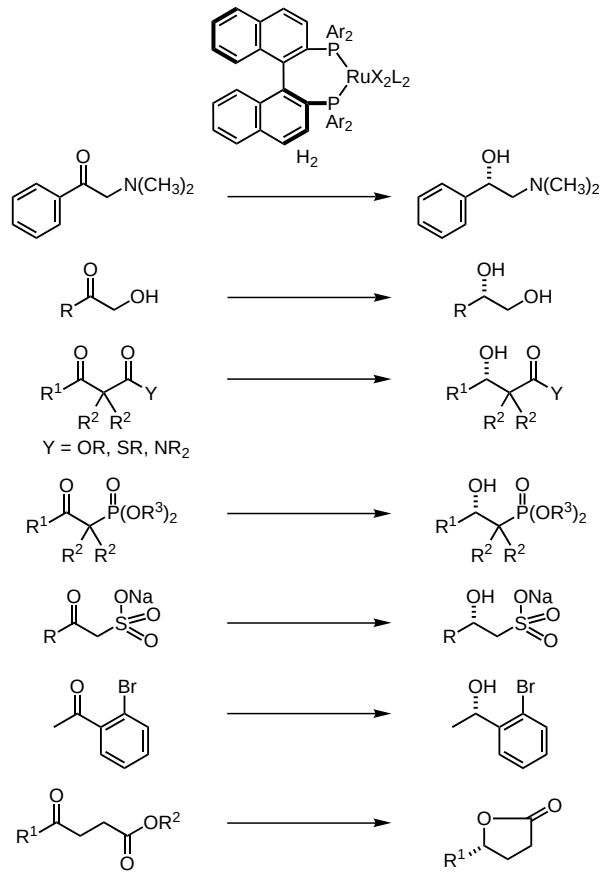
Scheme 6 illustrates some chiral compounds that can be obtained by this asymmetric hydrogenation. An important application is the synthesis of the anti-inflammatory drug, naproxen, in 97% *ee* from an α-aryl-acrylic acid.[41, 46] Natural



Scheme 6. Applications of BINAP–Ru catalyzed hydrogenation of olefins.

and unnatural citronellol with up to 99% *ee* are obtainable from geraniol or nerol without saturation of the C(6)–C(7) double bond, with a high substrate to catalyst (S:C) ratio. The hydrogenation of (*R*,*E*)-6,7,10,11-tetrahydrofarnesol produces (3*R*,7*R*)-hexahydrofarnesol, a C_{15} side-chain of α-tocopherol (vitamin E) and a part of vitamin K_1. The hydrogenation of an allylic alcohol possessing a chiral azetidinone unit gives a 1β-methylcarbapenem synthetic intermediate diastereoselectively.[48] The discovery of this asymmetric hydrogenation made possible the general asymmetric synthesis of isoquinoline alkaloids including morphine, benzomorphans, and morphinans such as the antitussive dextomethorphan.[43, 49]

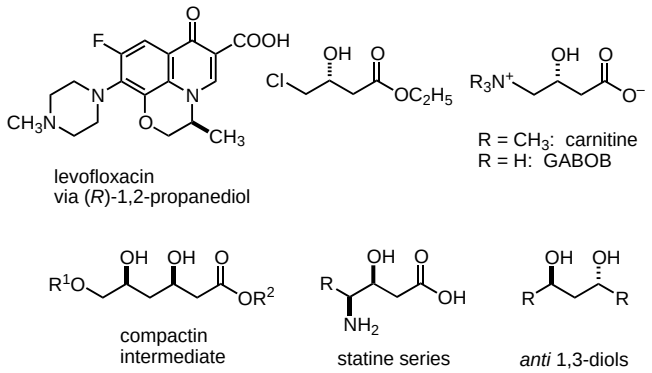
Importantly, the list of substrates can be extended to include various ketones, as generalized in Scheme 7 and Figure 6. The halogen-containing BINAP–Ru^{II} complexes (oligomers),[50] but not the diacetate complexes, are efficient catalysts for the asymmetric hydrogenation of a range of functionalized ketones, wherein coordinative nitrogen, oxygen, and halogen atoms near C=O functions direct the



Scheme 7. Asymmetric hydrogenation of functionalized ketones catalyzed by (*S*)-BINAP–Ru dihalide complexes (X = halogen).



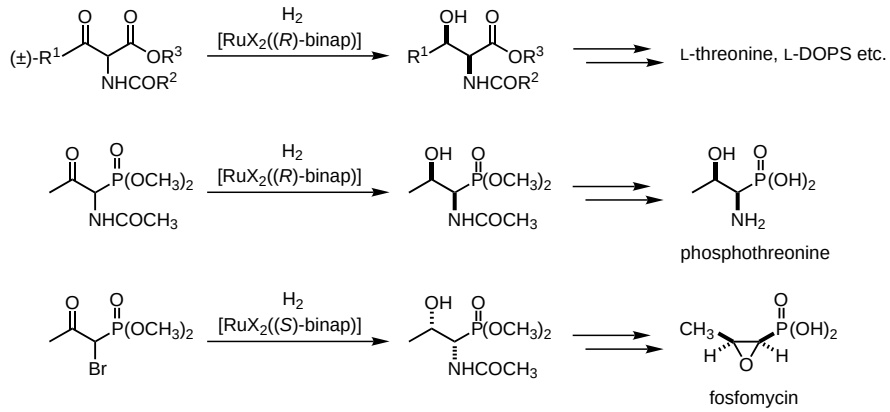
Figure 6. H. Takaya, M. Kitamura, and T. Ohkuma (from the left) made major contributions to the asymmetric hydrogenation of functionalized ketones catalyzed by (*S*)-BINAP–Ru dihalide complexes.



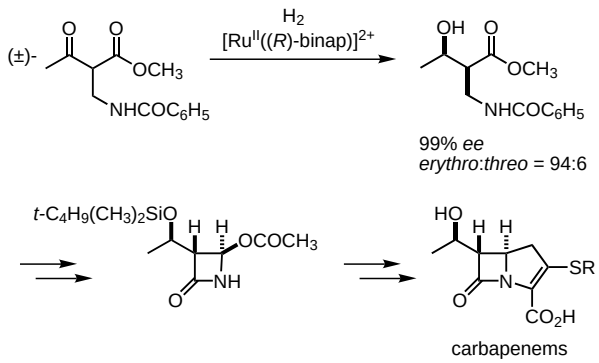
Scheme 8. Applications of BINAP–Ru-catalyzed hydrogenation of ketones.

reactivity and stereochemical outcome in an absolute sense.[51] A wide variety of achiral ketones are hydrogenated enantioselectively to the corresponding chiral alcohols in 90–100% *ee*, in a predictable manner. The reaction can normally be performed in alcohols with up to 50% substrate concentration under 4–100 atm at room temperature with an S:C ratio of up to 10000:1 on any scale, even using >100 kg of the substrate. Scheme 8 shows some synthetic applications of this asymmetric hydrogenation. (*R*)-1,2-Propanediol thus obtained from hydroxyacetone is used for industrial synthesis of the antibacterial levofloxacin (Takasago Co./Daiichi Pharmaceutical Co.). In addition, γ-amino-β-hydroxybutyric acid (GABOB) and a compactin intermediate can be prepared with high enantiomeric purity.[49, 52] Pre-existing stereogenic centers in the ketonic substrate significantly affect the steric course. Statines can be obtained with a high diastereo- and enantioselectivity.[53] The double hydrogenation of 1,3-diones via chiral hydroxy ketones leads to the anti 1,3-diols in close to 100% *ee*.[51a]

Racemic β-keto esters with a configurationally labile α-stereogenic center, by undergoing in situ stereoinversion, can be transformed into a single stereoisomer out of the four stereoisomers, with high stereoselectivity, as illustrated in Scheme 9.[54] This dynamic kinetic resolution[55] has been used for the synthesis of various biologically important compounds such as threonine, (2*S*,3*R*)-3-(3,4-dihydroxyphenyl)serine (L-DOPS),[52] phosphothreonine,[56] and fosfomycin.[57] Its utility was highlighted by the industrial synthesis of carbapenem antibiotics at Takasago International Co. (Scheme 10). The requisite chiral 4-acetoxyazetidinone is prepared by the (*R*)-BINAP–Ru-catalyzed hydrogenation of racemic methyl α-(benzamidomethyl)acetoacetate in dichloromethane, to give the 2*S*,3*R* hydroxy ester with 94:6 *erythro*:*threo* diastereoselectivity[58] and 99.5:0.5 enantioselectivity.[54a] Quantitative analysis[54] indicates that the 2*S* substrate is hydrogenated 15 times faster than the *R* enantiomer, and the slow-reacting *R* isomer is inverted to the 2*S* enantiomer 92 times easier than



Scheme 9. Asymmetric hydrogenation by dynamic kinetic resolution. X = Cl, Br.



Scheme 10. Stereoselective synthesis of carbapenem antibiotics.

it is hydrogenated. The extent of the BINAP catalyst-based asymmetric induction is calculated to be 104:1 in favor of the 3*R* isomer, whereas the substrate-based asymmetric induction is 9:1 in favor of the C(2)/C(3) *erythro* stereochemistry. The volume of the hydrogenation reactor shown in Figure 7 is 13 m^3.



Figure 7. A large-scale BINAP – Ru-catalyzed hydrogenation at Takasago International Co.

β-Keto esters are the best substrates for the Ru catalyzed asymmetric hydrogenation and lead to the β-hydroxy esters in $>98\,\%$ *ee*.[59] Figure 8 illustrates the mechanistic model. The halide ligand in the Ru complex, which generates a strong acid and a RuHCl species by the action of H_2, is important to facilitate the hydride transfer from the Ru center to the carbonyl carbon.[55] In addition, the presence of the ester

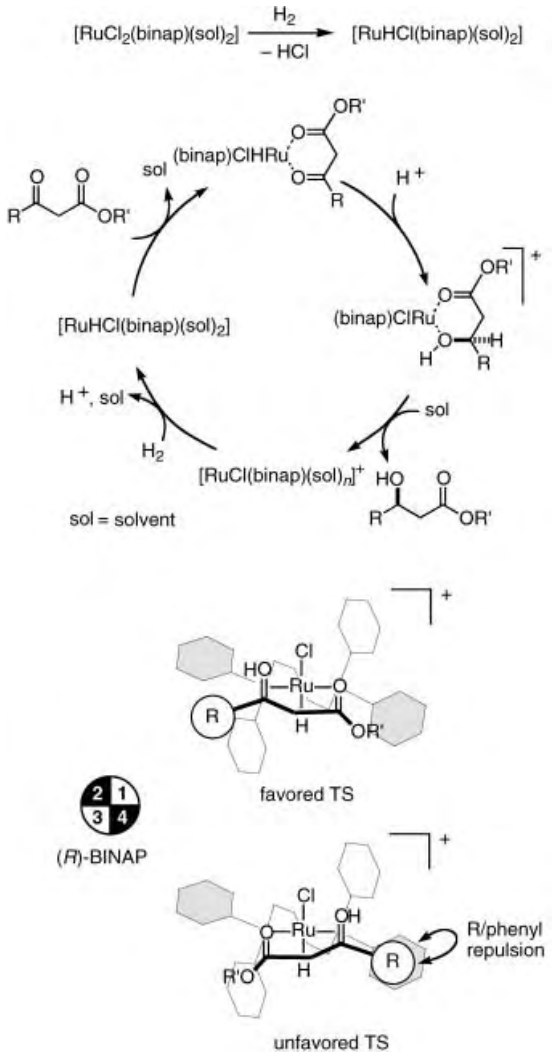


Figure 8. Mechanism of (*R*)-BINAP – Ru catalyzed hydrogenation of β-keto esters.

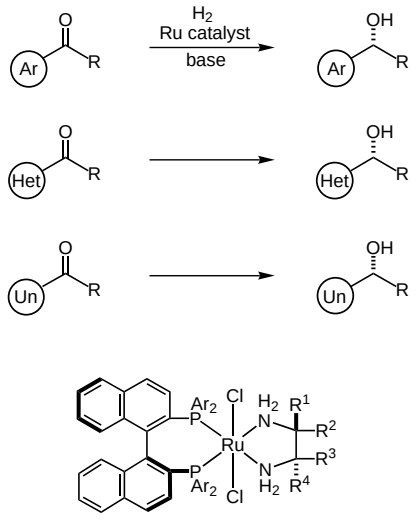
moiety interacting with the Ru center is crucial for both high reactivity and enantioselectivity. Because of the excellent chiral recognition ability of BINAP, the two stereo-determining diastereomeric transition states (TSs) are well differentiated with the assistance of the oxygen – Ru interaction. The *R*-directing TS is highly favored over the *S*-generating diastereomer, which suffers from substantial R/*P*-phenyl repulsive interaction. The oxygen – Ru dative bond (and related interaction in the reactions in Scheme 7) exerts a pivotal function in the acceleration of hydrogenation as well. Thus, β-keto esters are hydrogenated smoothly even in the simplest ketone, acetone, containing a small amount of water. Thus, although BINAP – Ru dihalide catalysts have a very wide scope, they are unable to hydrogenate simple, unfunctionalized ketones.

7. Asymmetric Hydrogenation of Simple Ketones by BINAP/Diamine – Ruthenium Complexes

For more than half a century, selective reduction of simple ketones relied heavily on the metal-hydride chemistry devel-

oped largely by H. C. Brown (1979 Nobel laureate). Chemoselective reduction of a C=O function in the presence of a C=C group has been best effected by the stoichiometric $NaBH_4$ reagent.[60] Diastereoselective reduction of ketones has frequently been achieved by Selectrides.[61] Enantioselective reduction of achiral ketones are effected by chiral stoichiometric reagents including BINAL-H,[62] DIP chloride,[63] and Alpine-borane[64], or by the Corey–Bakshi–Shibata (CBS) method combining B_2H_6 or catecholborane and a chiral oxazaborolidine catalyst.[65] Until very recently, these types of selective C=O reductions were not generally achievable by catalytic hydrogenation.[49d, 66]

In 1995, when I was the director of the ERATO Molecular Catalysis Project, we found that hydrogenation catalyzed by a $[RuCl_2(phosphane)_2(diamine)]$ complex and an alkaline base provided a general solution to this long-standing problem.[67] The use of appropriate chiral diphosphanes and chiral diamines allows asymmetric hydrogenation of simple ketones which lack any Lewis basic functionality capable of interacting with the metal center. The reactivity and stereoselectivity are fine-tuned by changing the steric (bulkiness and chirality) and electronic properties of the auxiliaries. As generalized in Scheme 11, the newly devised BINAP/diamine complex



(*S*)-BINAP/(*S*)-diamine–Ru^{II} catalyst

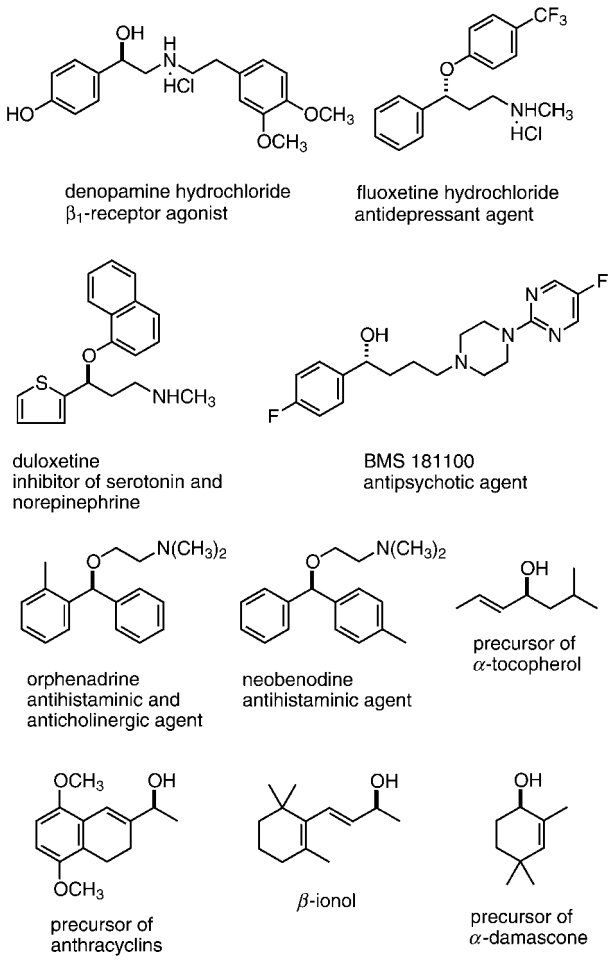
(*S*)-BINAP: Ar = C_6H_5
(*S*)-TolBINAP: Ar = 4-$CH_3C_6H_4$
(*S*)-XylBINAP: Ar = 3,5-$(CH_3)_2C_6H_3$
(*S,S*)-DPEN: $R^1 = R^4 = C_6H_5$; $R^2 = R^3 = H$
(*S*)-DAIPEN: $R^1 = R^2$ = 4-$CH_3OC_6H_4$; $R^3 = H$; $R^4 = (CH_3)_2CH$

Scheme 11. General asymmetric hydrogenation of simple ketones. Ar = aryl, Het = heteroaryl, Un = alkenyl.

catalyzes rapid, productive, and highly enantioselective hydrogenation of a range of aromatic, heteroaromatic, and olefinic ketones in 2-propanol containing *t*BuOK or KOH.[68–70] Among various complexes, $[RuCl_2(xylbinap)(daipen)]$[71] is particularly effective. For example, acetophenone and its derivatives are hydrogenated with S:C of up to 100000:1, to give the secondary alcohols quantitatively in 99% *ee*,[72] although the diamine-free BINAP–Ru complexes are totally ineffective. Normally, C=C bonds are much more reactive than C=O in catalytic hydrogenation, but this system allows for the preferential saturation of a C=O function over a coexisting C=C linkage.[73, 74] Olefinic ketones, either conjugated or nonconjugated, can be converted to olefinic alcohols selectively. The hydrogenation tolerates various functionalities including F, Cl, Br, I, CF_3, OCH_3, $OCH_2C_6H_5$, $COOCH(CH_3)_2$, NO_2, NH_2, and NRCOR. Both electron-rich (furan, thiophene, thiazole, etc.) and -deficient rings (pyridine and pyrimidine) are left intact.[75] The simple $[RuCl_2(PAr_3)_2(NH_2CH_2CH_2NH_2)]$ complex hydrogenates various substituted cyclic and acyclic ketones with high diastereoselectivity, where the RuH intermediate acts as a bulky hydride species.[76] Because of the basic and protic nature of the reaction environment, hydrogenation of configurationally labile ketones allows for the dynamic kinetic discrimination of diastereomers, epimers, and enantiomers,[76–78] which effects a new type of stereoselective reductions of ketones which are not possible with stoichiometric hydride reagents.

This asymmetric hydrogenation shows promise for the practical synthesis of a wide variety of chiral alcohols. The chiral diphosphane/diamine–Ru complexes effect enantioselective hydrogenation of certain amino or amido ketones by a nonchelate mechanism, without interaction between the Ru center and nitrogen or oxygen atoms.[78] This method has been applied to the asymmetric synthesis of various important pharmaceuticals, which includes (*R*)-denopamine, a β_1-receptor agonist, the antidepressant (*R*)-fluoxetine, the antipsychotic BMS 181100, and (*S*)-duloxetine, which is a potent inhibitor of serotonin and norepinephrine uptake carriers (Scheme 12). Benzophenones can be hydrogenated to benzhydrols with an S:C ratio of up to 20000:1 without overreduction.[79] Enantioselective hydrogenation of certain *ortho*-substituted benzophenones leads to the unsymmetrically substituted benzhydrols with high *ee* values, which allows convenient synthesis of the anticholinergic and antihistaminic (*S*)-orphenadrine. The antihistaminic (*R*)-neobenodine can be synthesized by using asymmetric hydrogenation of *o*-bromo-*p*′-methylbenzophenone.

This approach is the first example of general and efficient asymmetric hydrogenation of α,β-unsaturated ketones to chiral allylic alcohols of high enantiomeric purity.[72–74] The selectivity profile is in sharp contrast to that observed with the diamine-free BINAP–Ru complex, and efficiently catalyzes asymmetric hydrogenation of allylic alcohols (Scheme 5). Its utility has been demonstrated by the synthesis of intermediates of an α-tocopherol side-chain and anthracyclines, as well as β-ionol (Scheme 12).[72, 73] The asymmetric hydrogenation shown in Scheme 11 is generally achieved by the combined use of an (*S*)-BINAP ligand and an (*S*)-1,2-diamine (or both *R* enantiomers). This is also the case for the reaction of s-*cis* exocyclic enones, such as (*R*)-pulegone. However, asymmetric hydrogenation of 2,4,4-trimethyl-2-cyclohexenone was effected best with $[RuCl_2\{(S)\text{-tolbinap}\}\{(R,R)\text{-dpen}\}]$.[74, 80] The cyclic allyl alcohol obtained in 96% *ee* (Scheme 12) can be converted into a series of carotenoid-derived odorants and bioactive terpenes, such as α-damascone. The *R* or *S* alcohols with *ee* values as high as 95% can be obtained, even with a



Scheme 12. Application of asymmetric hydrogenation of simple ketones.

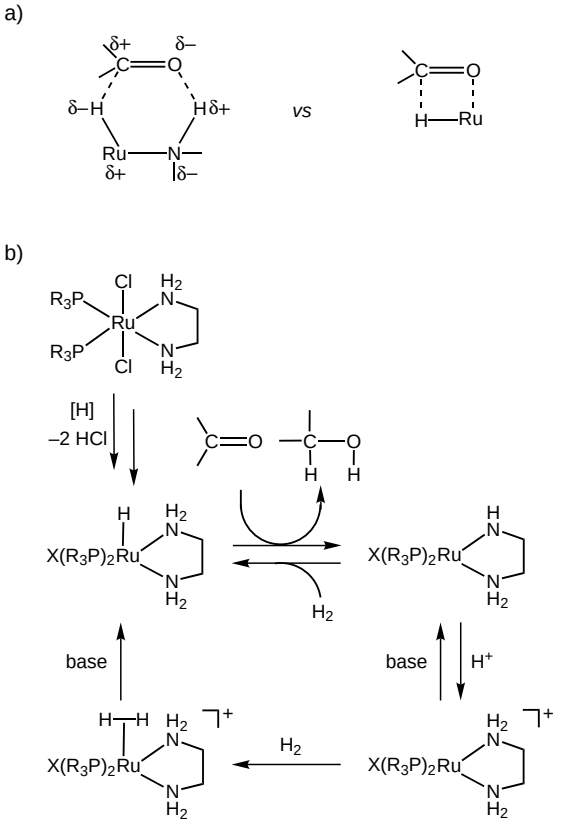


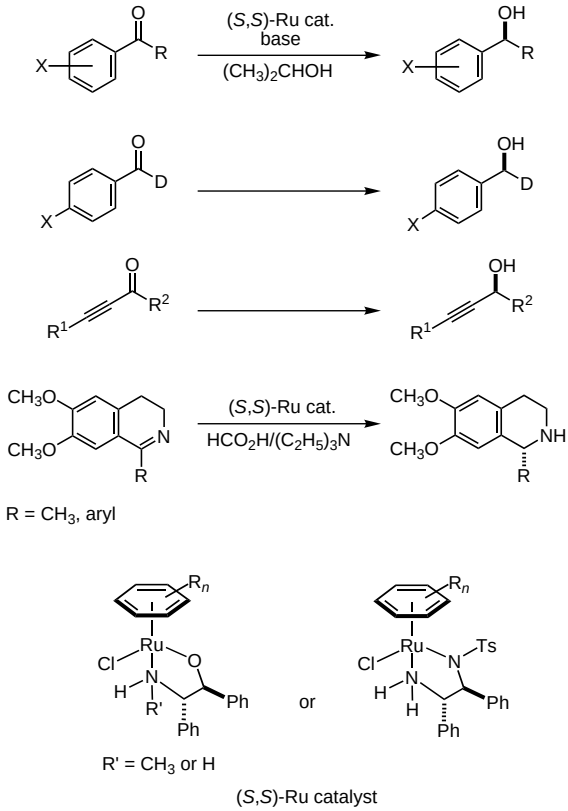
Figure 9. a) Nonclassical metal–ligand bifunctional mechanism and conventional [2+2] mechanism. b) Catalytic cycle of hydrogenation of ketones with a $[RuCl_2(PR_3)_2(NH_2CH_2CH_2NH_2)]$/strong base combined system in 2-propanol. X = H, OR, etc.

racemic TolBINAP–$RuCl_2$ complex in the presence of (*R*,*R*)- or (*S*,*S*)-DPEN by asymmetric activation.[80–82] In this case, the highly enantioselective hydrogenation catalyzed by the *S* diphosphane/*R*,*R* diamine complex (or *R*/*S*,*S* combination) turns over 121 times faster than the less stereoselective reaction promoted by the diastereomeric *S*/*S*,*S* (or *R*/*R*,*R*) complex.[83]

The reaction is rapid and highly productive. For example, when a mixture of acetophenone (601 g), the (*S*)-TolBINAP/(*S*,*S*)-DPEN Ru complex (2.2 mg), and *t*BuOK (5.6 g) in 2-propanol (1.5 L; 30% w/v substrate concentration) was stirred under 45 atm H_2 at 30 °C for 48 h, the *R* alcohol was obtained with 80% *ee* and 100% yield.[71, 84] Under such conditions, the turnover number was greater than 2400000, while the turnover frequency at 30% conversion was 228000 h^{-1} or 63 s^{-1}.

This high rate and chemoselectivity for the C=O function are caused by the nonclassical metal–ligand bifunctional mechanism (Figure 9).[68, 70] The hydrogenation involves a metal-hydride intermediate. Hydride transfer from the metal center to the carbonyl carbon atom has been considered to occur by a [2+2] mechanism. This reaction involves a Ru hydride species possessing an NH_2 ligand, whose hydridic Ru–H and protic N–H are simultaneously transferred to the C=O linkage via a six-membered pericyclic TS, thereby forming an alcoholic product directly, without formation of a metal alkoxide (Figure 9a). In this hydrogenation, the metal and the ligand participate cooperatively in the bond-forming and -breaking processes. A more detailed mechanistic model is given in Figure 9b. The 18-electron-RuH species reduces the ketone substrate by the pericyclic mechanism and the formal 16-electron Ru–amide complex reacts directly with H_2 in a [2+2] manner, or by a stepwise mechanism assisted by an alcohol and a base, to give back the reducing RuH complex.[85] The reducing activity of the RuH species is generated by the hydrogen-bonding NH_2 end in the diamine ligand, which forms a *fac* relationship with the hydride ligand in the octahedral geometry. Neither ketone substrate nor alcoholic product interacts with the metallic center throughout the hydrogenation. The enantiofaces of prochiral ketones are differentiated on the molecular surface of the coordinatively saturated RuH intermediate. This notion is in contrast to the conventional mechanism for hydrogenation of unsaturated bonds that requires the metal–substrate π complexation.

This NH effect is common to the mechanism of Ru-catalyzed asymmetric transfer hydrogenation.[86] Recently we found that $[RuCl\{(S,S)\text{-}YCH(C_6H_5)CH(C_6H_5)NH_2\}(\eta^6\text{-arene})]$ (Y = O, NTs) complexes or their analogues catalyze asymmetric transfer hydrogenation of aromatic and acetylenic carbonyl compounds, by using a 2-propanol/alkaline-base system to give the corresponding *S* chiral alcohols of high enantiomeric purity, as generalized in Scheme 13.[87, 88] A formic acid/triethylamine mixture often serves as a better



Scheme 13. Asymmetric transfer hydrogenation of carbonyl compounds and imines catalyzed by chiral Ru complexes. Ts = 4-toluenesulfonyl.

reducing agent. Certain imines are also reduced enantioselectively by this method. The detailed experimental[89] and theoretical analyses[90] revealed that the transfer hydrogenation of carbonyl compounds with 2-propanol proceeds via a coordinatively saturated 18-electron complex, [RuH{(*S*,*S*)-YCH(C_6H_5)CH(C_6H_5)NH_2}(η^6-arene)], as illustrated in Figure 10. The metal–ligand bifunctional mechanism allows for simultaneous delivery of the Ru–H and N–H to the C=O function via a six-membered pericyclic TS, which gives an *S* alcohol and [Ru{(*S*,*S*)-YCH(C_6H_5)CH(C_6H_5)NH}-(η^6-arene)]. The latter 16-electron Ru–amide complex dehydrogenates 2-propanol to regenerate the Ru-hydride species.[86, 91]

8. Toward Cerebral Molecular Science

The major goals of synthetic chemists and the chemical industry have been the efficient synthesis of known valuable compounds. Another, and perhaps more important, pursuit is the creation of new valuable substances and materials through chemical synthesis. Toward this end, mere chemical knowledge or technology is

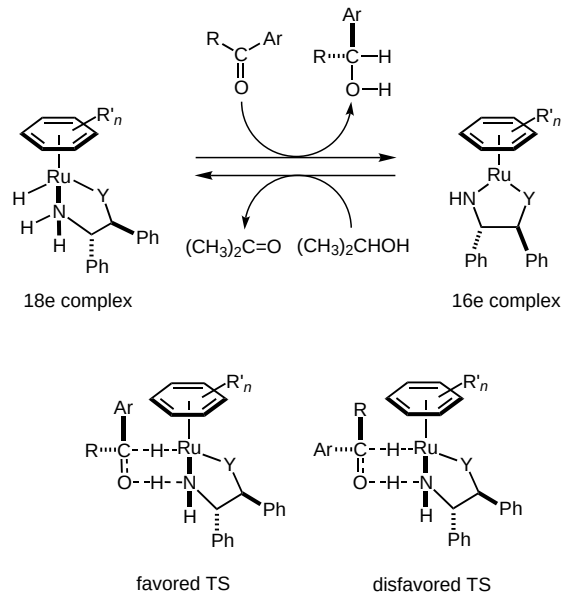
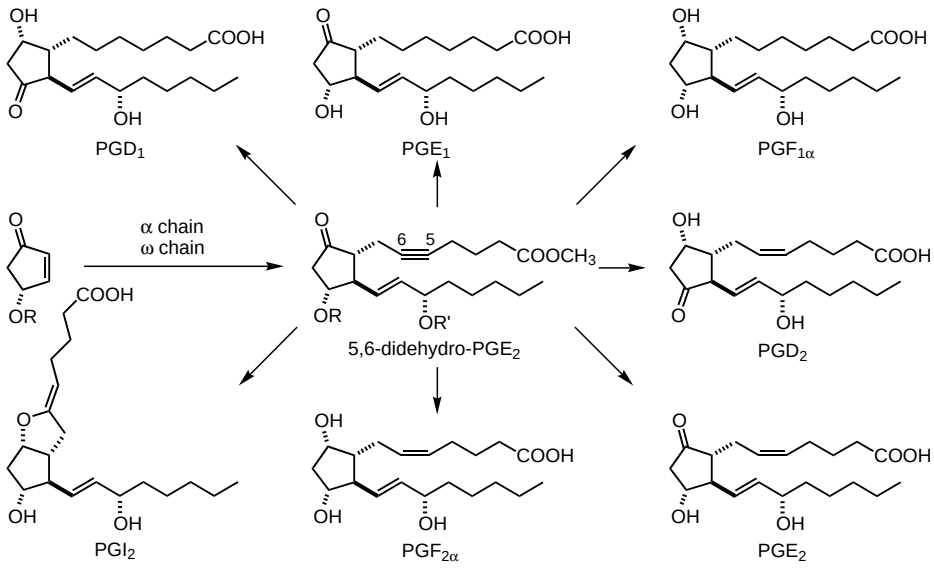


Figure 10. Metal–ligand bifunctional mechanism in asymmetric transfer hydrogenation catalyzed by [RuH{(*S*,*S*)-YCH(C_6H_5)CH(C_6H_5)NH_2}(η^6-arene)]. R = alkyl or D; Y = O or NTs.

often insufficient and basic research through interdisciplinary collaboration with scientists in other fields is needed. The recent progress in asymmetric synthesis has, in fact, spurred such endeavors which are directed toward the creation of molecularly engineered novel functions.

In the mid-1980s, we established the long-sought after three-component coupling synthesis of prostaglandins (PGs) illustrated in Scheme 14.[92] The five-membered unit could be combined with the two C_7 and C_8 side-chain (α and ω side chains) units by organometallic methodologies. Our asymmetric methods play a key role in controlling the C(11) and C(15) OH-bearing stereogenic centers. The requisite (*R*)-4-hydroxy-2-cyclopentenone is conveniently prepared on a multikilogram scale by kinetic resolution of the racemate by



Scheme 14. Three-component synthesis of prostaglandins. α chain = $ICH_2C{\equiv}C(CH_2)_3COOCH_3$; ω chain = (*E*,*S*)-LiCH=CHCH(OR′)$(CH_2)_4CH_3$.

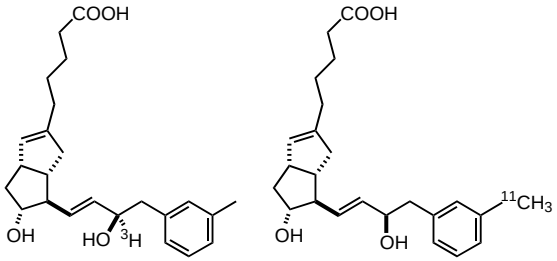
BINAP–Ru-catalyzed hydrogenation.[43] The BINAL-H reagent is useful for asymmetric synthesis of the lower side-chain block.[93, 94] This straightforward procedure is useful for the synthesis of not only naturally occurring PGs but also their artificial analogues.[95]

To explore applications to the science of the human brain, we collaborated with the research groups led by M. Suzuki (my long-term collaborator at Nagoya and now at Gifu University), Y. Watanabe (Osaka City University), and B. Långström (Uppsala University; Figure 11).[96, 97] After a long



Figure 11. The interdisciplinary collaborative team (from the left, M. Suzuki, R. Noyori, Y. Watanabe, and B. Långström) that studied (15*R*)-TIC and the methyl esters, labeled by radioactive nuclides.

investigation, (15*R*)-TIC, a PGI_2-type carboxylic acid, was found to show strong, selective binding in the central nervous system, which thereby identifies the novel IP_2 receptor. Interestingly, this compound has the unnatural 15*R* configuration, although most biologically active PG derivatives have the natural 15*S* configuration. This discovery was made by an in vitro study using frozen sections of rat brain and frozen sections of rat brain and (15*R*)-[^{3}H]TIC as a probe.[98] However, this radioactive probe is not appropriate for studies



(15*R*)-[^{3}H]TIC (15*R*)-[^{11}C]TIC

on living monkey or human brain, since β^- particles emitted from ^{3}H can not penetrate tissues. Incorporation of ^{11}C, a positron emitter with a short half-life of about 20 min and a high specific radioactivity, as a radioactive nuclide is essential for noninvasive studies using positron-emission tomography (PET). Positrons (β^+) interact with free electrons in biological materials, and produce γ rays that can penetrate tissues and are detectable outside the human body. However, this presents a new chemical problem. The $^{11}CH_3$ group must be incorporated in the final step of the synthesis of (15*R*)-TIC methyl ester, and the total time for synthesis, workup, purification, and sterilization should be less than 40 min because of the short half-life time of ^{11}C. A student in my group at Nagoya made a concerted effort to achieve this and, eventually succeeded with a rapid Pd-mediated coupling of methyl iodide and tributyl(aryl)stannane (excess) which is applicable to the synthesis of (15*R*)-[^{11}C]TIC methyl ester.[99]

This technology was then transferred to the PET Center at Uppsala. A very dedicated colleague in our team, M. Suzuki, volunteered to test this new artificial compound on himself. After being carefully examined, (15*R*)- [^{11}C]TIC methyl ester was injected into his right arm. The methyl ester was carried through his blood stream, passed through the blood-brain barrier, reached his brain, and was hydrolyzed to the free carboxylic acid, which was bound to IP_2 receptors in his central nervous system. Figure 12 shows the PET images of horizontal slices of his brain, from the lower to the upper portions. From this trial, a new receptor, IP_2, was found in various important structures of the human brain. Thus, (15*R*)-TIC and its analogues are expected to have effects on the brain and, in fact, do show a unique neuroprotective effect, which may be of clinical benefit. Primary cultured hippocampal neurons exposed to a high oxygen concentration display the morphological features of apoptotic cell death and (15*R*)-TIC effectively protects them against such oxygen

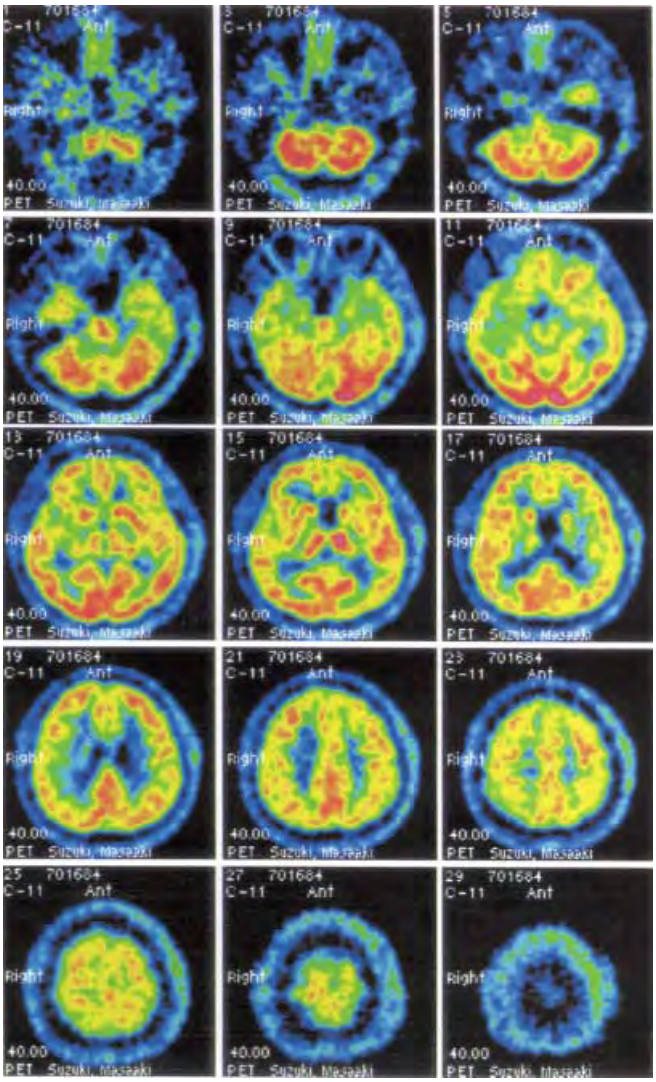


Figure 12. The uptake of (15*R*)-[^{11}C]-TIC in the human brain. The PET images of 18 horizontal slices from the lower to the upper portions of the brain (volunteer: M. Suzuki; June 13, 2000. PET Center of Uppsala University).

toxicity.[100] Similar neuroprotective effects were demonstrated in other in vitro experiments using serum deprivation and in in vivo studies of ischemic insults with gerbils, rats, and monkeys. Thus, the IP_2 receptor is a novel target for developing drugs which may be neuroprotective in brain disorders and neutrodegenerative diseases.

9. Prospects for the future

Studies of molecular chirality have the promise to yield significant clinical, scientific, and industrial benefits in the future. A structurally diverse array of molecular substances exists. All molecules possess common characteristics, namely, fixed elemental composition, definite atomic connectivity, a defined relative and absolute stereochemistry, and some conformation. From such precise nanometer-scale structures, certain significant properties and functions emerge. Chemists can design and synthesize molecules at will, based on accumulated scientific knowledge. The practical synthesis of enantiomers with a defined absolute stereochemistry is one of the most significant areas of research. This endeavor is not only an intellectual pursuit but is also a fertile area for the development of beneficial technologies.[101] Its utility is obvious, and ranges from basic scientific research at a subfemtomole scale, as in the case of brain research described above, to the industrial production of high-value compounds in multithousand tons per annum quantities. Louis Pasteur stated in 1851 that "Dissymmetry is the only and distinct boundary between biological and nonbiological chemistry. Symmetrical physical or chemical force cannot generate molecular dissymmetry". This notion is no longer true. The recent revolutionary development in asymmetric catalysis has totally changed the approach to chemical synthesis. This field is still growing rapidly and I am certain that it will play a pivotal role in the development of the life sciences and nanotechnology in the 21st century.

The highest honor for me is to be recognized with the prestigious 2001 Nobel Prize in Chemistry. This honor must be shared with my research family at Nagoya and with many collaborators at other institutions. Asymmetric hydrogenation has been the life-long focus of my research, and my studies have relied largely on BINAP chemistry, which I initiated with the late Professor Hidemasa Takaya. Subsequently, BINAP chemistry was developed further in our laboratories at Nagoya, where Professors Masato Kitamura and Takeshi Ohkuma made major contributions. Other asymmetric hydrogenation methods were discovered during my directorship of the ERATO Molecular Catalysis Project (1991–1996), which was managed by Professor Takao Ikariya (now Tokyo Institute of Technology) and Dr. Shohei Hashiguchi (Takeda Chemical Industry). Our laboratory at Nagoya is small. To realize the utilization of our scientific achievements, it was important to collaborate with other institutions. In this regard, I appreciate the cooperation of the groups led by Professors Sei Otsuka and Kazuhide Tani (Osaka University), and Professors Masaaki Suzuki (Gifu University), Yasuyoshi Watanabe (Osaka City University), and Bengt Långström (Uppsala University). These are just the names of the leaders of the research groups, although many young associates and students also contributed significantly. I had opportunities to have fruitful collaborations with many other scientists whose names are cited in the references. We have been supported by many companies, particularly Takasago International Corporation and Teijin Company. The generous and consistent support from the Ministry of Education, Culture, Sports, Science and Technology was essential for the success of my research. I am also grateful to the Japan Science and Technology Corporation and many private foundations for their support. Last, but not least, I acknowledge Professor Hitosi Nozaki at Kyoto University, my mentor who first introduced me to this fascinating and rewarding field of research.

Received: January 25, 2002 [A 512]

[1] For example, a) M. Gardner, *The New Ambidextrous Universe*, *3rd ed.*, W. H. Freeman & Co., New York, **1990**; b) E. Heilbronner, J. D. Dunitz, *Reflections on Symmetry*, VHCA, Basel, **1993**; c) R. Hoffmann, *The Same and Not the Same*, Columbia University Press, New York, **1995**; d) H. Brunner. *Rechts oder links in der Natur und anderswo*, Wiley-VCH, Weinheim, **1999**.
[2] G. Blaschke, H. P. Kraft, K. Fickentscher, F. Köhler, *Arzneim.-Forsch.* **1979**, *29*, 1640.
[3] This interpretation must be considered carefully, because the *R* enantiomer racemizes in vivo.
[4] a) *Chem. Eng. News* **1990**, *68*(12), 26; b) S. Borman, *Chem. Eng. News* **1990**, *68*(28), 9.
[5] S. C. Stinson, *Chem. Eng. News* **1992**. *70*(39), 46.
[6] S. C. Stinson, *Chem. Eng. News* **2001**, *79*(20), 45.
[7] R. Noyori, *Asymmetric Catalysis in Organic Synthesis*, Wiley, New York, **1994**.
[8] a) H. Nozaki, S. Moriuti, H. Takaya, R. Noyori, *Tetrahedron Lett.* **1966**, 5239; b) H. Nozaki, H. Takaya, S. Moriuti, R. Noyori, *Tetrahedron* **1968**, *24*, 3655.
[9] a) T. Aratani, *Pure Appl. Chem.* **1985**, *57*, 1839; b) T. Aratani in *Comprehensive Asymmetric Catalysis*, *Vol. 3* (Eds.: E. N. Jacobsen, A. Pfaltz, H. Yamamoto), Springer, Berlin, **1999**, p. 1451.
[10] a) M. Calvin, *Trans. Faraday Soc.* **1938**, *34*, 1181; b) M. Calvin, *J. Am. Chem. Soc.* **1939**, *61*, 2230.
[11] J. Halpern, J. F. Harrod, B. R. James, *J. Am. Chem. Soc.* **1961**, *83*, 753.
[12] J. F. Young, J. A. Osborn, F. H. Jardine, G. Wilkinson, *Chem. Commun.* **1965**, 131.
[13] S. Akabori, S. Sakurai, Y. Izumi, Y. Fujii, *Nature* **1956**, *178*, 323.
[14] a) W. S. Knowles, M. J. Sabacky, *Chem. Commun.* **1968**, 1445; Nobel Lecture: b) W. S. Knowles, *Angew. Chem.* **2002**, *114*, 2096; *Angew. Chem. Int. Ed.* **2002**, *41*, 1998.
[15] L. Horner, H. Siegel, H. Büthe, *Angew. Chem.* **1968**, *80*, 1034; *Angew. Chem. Int. Ed. Engl.* **1968**, *7*, 942.
[16] These achievements were based on the classic work of Mislow and Horner on resolution of chiral tertiary phosphanes: a) O. Korpiun, R. A. Lewis, J. Chickos, K. Mislow, *J. Am. Chem. Soc.* **1968**, *90*, 4842; b) L. Horner, *Pure Appl. Chem.* **1964**, *9*, 225,
[17] T. P. Dang, H. B. Kagan, *J. Chem. Soc. Chem. Commun.* **1971**, 481.
[18] a) W. S. Knowles, M. J. Sabacky, B. D. Vineyard, *J. Chem. Soc. Chem. Commun.* **1972**, 10; b) B. D. Vineyard, W. S. Knowles, M. J. Sabacky, G. L. Bachman, D. J. Weinkauff, *J. Am. Chem. Soc.* **1977**, *99*, 5946; c) W. S. Knowles, *Acc. Chem. Res.* **1983**, *16*, 106; d) J. Crosby in *Chirality in Industry: The Commercial Manufacture and Applications of Optically Active Compounds* (Eds.: A. N. Collins, G. N. Sheldrake, J. Crosby), Wiley, Chichester, **1992**, chap. 1.
[19] E. J. Corey, R. Noyori, T. K. Schaaf, *J. Am. Chem. Soc.* **1970**, *92*, 2586.
[20] One of the early examples of successful asymmetric catalysis was the Ni-catalyzed hydrovinylation of norbornene, see: B. Bogdanović, B. Henc, A. Lösler, B. Meister, H. Pauling, G. Wilke, *Angew. Chem.* **1973**, *85*, 1013; *Angew. Chem. Int. Ed. Engl.* **1973**, *12*, 954.
[21] R. Noyori, H. Takaya, *Chem. Scr.* **1985**, *25*, 83.

[22] A. Miyashita, A. Yasuda, H. Takaya, K. Toriumi, T. Ito, T. Souchi, R. Noyori, *J. Am. Chem. Soc*. **1980**, *102*, 7932.

[23] a) A. Miyashita, H. Takaya, T. Souchi, R. Noyori, *Tetrahedron* **1984**, *40*, 1245; b) K. J. Brown, M. S. Berry, K. C. Waterman, D. Lingenfelter, J. R. Murdoch, *J. Am. Chem. Soc*. **1984**, *106*, 4717.

[24] H. Takaya, K. Mashima, K. Koyano, M. Yagi, H. Kumobayashi, T. Taketomi, S. Akutagawa, R. Noyori, *J. Org. Chem*. **1986**, *51*, 629.

[25] For the more recent stereospecific synthesis by Ni-catalyzed coupling between optically pure binaphthol bis(triflate) and diphenylphosphane, see: D. Cai, J. F. Payack, D. R. Bender, D. L. Hughes, T. R. Verhoeven, P. J. Reider, *Org. Synth*. **1998**, *76*, 6.

[26] K. Toriumi, T. Ito, H. Takaya, T. Souchi, R. Noyori, *Acta Crystallogr. Sect. B* **1982**, *38*, 807.

[27] a) K. Tani, T. Yamagata, S. Otsuka, S. Akutagawa, H. Kumobayashi, T. Taketomi, H. Takaya, A. Miyashita, R. Noyori, *J. Chem. Soc. Chem. Commun*. **1982**, 600; b) K. Tani, T. Yamagata, S. Akutagawa, H. Kumobayashi, T. Taketomi, H. Takaya, A. Miyashita, R. Noyori, S. Otsuka, *J. Am. Chem. Soc*. **1984**, *106*, 5208.

[28] a) S. Akutagawa in *Organic Synthesis in Japan: Past, Present, and Future* (Eds.: R. Noyori, T. Hiraoka, K. Mori, S. Murahashi, T. Onoda, K. Suzuki, O. Yonemitsu), Tokyo Kagaku Dozin, Tokyo, **1992**, p. 75; b) S. Akutagawa in *Chirality in Industry: The Commercial Manufacture and Applications of Optically Active Compounds* (Eds.: A. N. Collins, G. N. Sheldrake, J. Crosby), Wiley, Chichester, **1992**, chap. 16.

[29] a) S. Otsuka, K. Tani in *Asymmetric Synthesis Vol. 5* (Ed.: J. D. Morrison), Academic Press, Orlando, **1985**, chap. 6; b) S. Otsuka, K. Tani, *Synthesis* **1991**, 665; c) S. Otsuka, *Acta Chem. Scand*. **1996**, *50*, 353.

[30] K. Takabe, T. Yamada, T. Katagiri, J. Tanaka, *Org. Synth*. **1989**. *67*, 48.

[31] M. Yamakawa, R. Noyori, *Organomet*. **1992**, *11*, 3167.

[32] a) R. Noyori, *Chem. Soc. Rev*. **1989**, *18*, 187; b) R. Noyori, *Science* **1990**, *248*, 1194; c) R. Noyori, H. Takaya, *Acc. Chem. Res.* **1990**, *23*, 345; d) R. Noyori, *CHEMTECH* **1992**, *22*, 360; e) R. Noyori, *Tetrahedron* **1994**, *50*, 4259; f) R. Noyori in *(IUPAC) Stereocontrolled Organic Synthesis* (Ed.: B. M. Trost), Blackwell, Oxford, **1994**, p. 1; g) R. Noyori, *Acta Chem. Scand*. **1996**, *50*, 380.

[33] An early example of phosphane – Ru-complex-catalyzed hydrogenation: P. S. Hallman, B. R. McGarvey, G. Wilkinson, *J. Chem. Soc. A* **1968**, 3143.

[34] Ru-catalyzed asymmetric hydrogenation of olefins was first achieved using a DIOP – Ru complex: B. R. James, D. K. W. Wang, R. F. Voigt, *J. Chem. Soc. Chem. Commun*. **1975**, 574.

[35] C. R. Landis, J. Halpern, *J. Am. Chem. Soc*. **1987**, *109*, 1746.

[36] J. M. Brown, P. A. Chaloner, *J. Am. Chem. Soc*. **1980**, *102*, 3040.

[37] For an example of a solution to this problem, see: I. D. Gridnev, N. Higashi, K. Asakura, T. Imamoto, *J. Am. Chem. Soc*. **2000**, *122*, 7183.

[38] R. Noyori, M. Ohta, Y. Hsiao, M. Kitamura, T. Ohta, H. Takaya, *J. Am. Chem. Soc*. **1986**, *108*, 7117.

[39] a) T. Ohta, H. Takaya, R. Noyori, *Inorg. Chem*. **1988**, *27*, 566; b) M. Kitamura, M. Tokunaga, R. Noyori, *J. Org. Chem*. **1992**, *57*, 4053; c) H. Takaya, T. Ohta, S. Inoue, M. Tokunaga, M. Kitamura, R. Noyori, *Org. Synth*. **1993**, *72*, 74.

[40] a) T. Ohta, H. Takaya, R. Noyori, *Tetrahedron Lett*. **1990**, *31*, 7189; b) M. T. Ashby, J. Halpern, *J. Am. Chem. Soc*. **1991**, *113*, 589.

[41] T. Ohta, H. Takaya, M. Kitamura, K. Nagai, R. Noyori, *J. Org. Chem*. **1987**, *52*, 3174.

[42] H. Takaya, T. Ohta, N. Sayo, H. Kumobayashi, S. Akutagawa, S. Inoue, I. Kasahara, R. Noyori, *J. Am. Chem. Soc*. **1987**, *109*, 1596; H. Takaya, T. Ohta, N. Sayo, H. Kumobayashi, S. Akutagawa, S. Inoue, I. Kasahara, R. Noyori, *J. Am. Chem. Soc*. **1987**, *109*, 4129.

[43] M. Kitamura, I. Kasahara, K. Manabe, R. Noyori, H. Takaya, *J. Org. Chem*. **1988**, *53*, 708.

[44] a) M. Kitamura, Y. Hsiao, R. Noyori, H. Takaya, *Tetrahedron Lett*. **1987**, *28*, 4829; b) M. Kitamura, Y. Hsiao, M. Ohta, M. Tsukamoto, T. Ohta, H. Takaya, R. Noyori, *J. Org. Chem*. **1994**, *59*, 297.

[45] W. D. Lubell, M. Kitamura, R. Noyori, *Tetrahedron: Asymmetry* **1991**, *2*, 543.

[46] M. Kitamura, M. Yoshimura, M. Tsukamoto, R. Noyori, *Enantiomer* **1996**, *1*, 281.

[47] T. Ikariya, Y. Ishii, H. Kawano, T. Arai, M. Saburi, S. Yoshikawa, S. Akutagawa, *J. Chem. Soc. Chem. Commun*. **1985**, 922. This was the first use of BINAP in Ru-catalyzed asymmetric hydrogenation.

[48] M. Kitamura, K. Nagai, Y. Hsiao, R. Noyori, *Tetrahedron Lett*. **1990**, *31*, 549.

[49] For other synthetic applications, see reviews: a) G. M. Ramos Tombo, G. Belluš, *Angew. Chem.* **1991**, *103*, 1219; *Angew. Chem. Int. Ed. Engl*. **1991**, *30*, 1193; b) A. Börner, J. Holz in *Transition Metals for Organic Synthesis*, *Vol. 2* (Eds.: M. Beller, C. Bolm), Wiley-VCH, Weinheim, **1998**, p. 3; c) J. M. Brown in *Comprehensive Asymmetric Catalysis*, *Vol. 1* (Eds.: E. N. Jacobsen, A. Pfaltz, H. Yamamoto), Springer, Berlin, **1999**, p. 121; d) T. Ohkuma, M. Kitamura, R. Noyori in *Catalytic Asymmetric Synthesis*, *2nd ed.* (Ed.: I. Ojima), Wiley-VCH, New York, **2000**, p. 1.

[50] a) M. Kitamura, M. Tokunaga, T. Ohkuma, R. Noyori, *Tetrahedron Lett*. **1991**, *32*, 4163; b) M. Kitamura, M. Tokunaga, T. Ohkuma, R. Noyori, *Org. Synth*. **1993**, *71*, 1; c) K. Mashima, K. Kusano, N. Sato, Y. Matsumura, K. Nozaki, H. Kumobayashi, N. Sayo, Y. Hori, T. Ishizaki, S. Akutagawa, H. Takaya, *J. Org. Chem*. **1994**, *59*, 3064. The halogen-containing Ru complexes are also effective for asymmetric hydrogenation of various functionalized olefins.

[51] a) M. Kitamura, T. Ohkuma, S. Inoue, N. Sayo, H. Kumobayashi, S. Akutagawa, T. Ohta, H. Takaya, R. Noyori, *J. Am. Chem. Soc*. **1988**, *110*, 629; b) K. Mashima, K. Kusano, T. Ohta, R. Noyori, H. Takaya, *J. Chem. Soc. Chem. Commun*. **1989**, 1208; c) T. Ohkuma, M. Kitamura, R. Noyori, *Tetrahedron Lett*. **1990**, *31*, 5509.

[52] M. Kitamura, T. Ohkuma, H. Takaya, R. Noyori, *Tetrahedron Lett*. **1988**, *29*, 1555.

[53] T. Nishi, M. Kitamura, T. Ohkuma, R. Noyori, *Tetrahedron Lett*. **1988**, *29*, 6327.

[54] a) R. Noyori, T. Ikeda, T. Ohkuma, M. Widhalm, M. Kitamura, H. Takaya, S. Akutagawa, N. Sayo, T. Saito, T. Taketomi, H. Kumobayashi, *J. Am. Chem. Soc*. **1989**, *111*, 9134; b) M. Kitamura, T. Ohkuma, M. Tokunaga, R. Noyori, *Tetrahedron: Asymmetry* **1990**, *1*, 1.

[55] a) M. Kitamura, M. Tokunaga, R. Noyori, *J. Am. Chem. Soc.* **1993**, *115*, 144; b) M. Kitamura, M. Tokunaga, R. Noyori, *Tetrahedron* **1993**, *49*, 1853; c) R. Noyori, M. Tokunaga, M. Kitamura, *Bull. Chem. Soc. Jpn.* **1995**, *68*, 36.

[56] M. Kitamura, M. Tokunaga, T. Pham, W. D. Lubell, R. Noyori, *Tetrahedron Lett*. **1995**, *36*, 5769.

[57] M. Kitamura, M. Tokunaga, R. Noyori, *J. Am. Chem. Soc.* **1995**, *117*, 2931.

[58] For the *threo*/*erythro* nomenclature, see: R. Noyori, I. Nishida, J. Sakata, *J. Am. Chem. Soc.* **1981**, *103*, 2106.

[59] R. Noyori, T. Ohkuma, M. Kitamura, H. Takaya, N. Sayo, H. Kumobayashi, S. Akutagawa, *J. Am. Chem. Soc*. **1987**, *109*, 5856.

[60] a) H. C. Brown, H. I. Schlesinger, I. Sheft, D. M. Ritter, *J. Am. Chem. Soc*. **1953**, *75*, 192; b) H. I. Schlesinger, H. C. Brown, A. E. Finholt, *J. Am. Chem. Soc*. **1953**, *75*, 205. Reviews: c) H. C. Brown, S. Krishnamurthy, *Tetrahedron* **1979**, *35*, 567; d) "Reductions in Organic Synthesis: Recent Advances and Practical Applications": P. V. Ramachandran, H. C. Brown, *ACS Symp. Ser.* **1996**, *641*, 1.

[61] a) H. C. Brown, S. Krishnamurthy, *J. Am. Chem. Soc.* **1972**, *94*, 7159; b) S. Krishnamurthy, H. C. Brown, *J. Am. Chem. Soc.* **1976**, *98*, 3383.

[62] a) R. Noyori, I. Tomino, Y. Tanimoto, M. Nishizawa, *J. Am. Chem. Soc*. **1984**, *106*, 6709; b) R. Noyori, I. Tomino, M. Yamada, M. Nishizawa, *J. Am. Chem. Soc.* **1984**, *106*, 6717.

[63] "Reductions in Organic Synthesis: Recent Advances and Practical Applications": P. V. Ramachandran, H. C. Brown, *ACS Symp. Ser.* **1996**, *641*, 84.

[64] M. M. Midland, *Chem. Rev.* **1989**, *89*, 1553.

[65] E. J. Corey, C. J. Helal, *Angew. Chem*. **1998**, *110*, 2092; *Angew. Chem. Int. Ed*. **1998**, *37*, 1986.

[66] For early efforts, see: a) J. Solodar, *CHEMTECH* **1975**, *5*, 421; b) T. Hayashi, T. Mise, M. Kumada, *Tetrahedron Lett*. **1976**, 4351; c) S. Törös, B. Heil, L. Kollár, L. Markó, *J. Organomet. Chem*. **1980**, *197*, 85; d) J. Bakos, I. Tóth, B. Heil, L. Markó, *J. Organomet. Chem*. **1985**, *279*, 23; e) X. Zhang, T. Taketomi, T. Yoshizumi, H. Kumobayashi, S. Akutagawa, K. Mashima, H. Takaya, *J. Am. Chem. Soc*. **1993**, *115*, 3318. See also: f) F. Robin, F. Mercier, L. Ricard, F. Mathey, M. Spagnol, *Chem. Eur. J.* **1997**, *3*, 1365; g) U. Nagel, C. Roller, *Z.*

Naturforsch. B **1998**, *53*, 267; h) Q. Jiang, Y. Jiang, D. Xiao, P. Cao, X. Zhang, *Angew. Chem.* **1998**, *110*, 1203; *Angew. Chem. Int. Ed.* **1998**, *37*, 1100; i) P. Cao, X. Zhang, *J. Org. Chem*. **1999**, *64*, 2127. Heterogeneous hydrogenation, see: j) T. Osawa, A. Tai, Y. Imachi, S. Takasaki in *Chiral Reactions in Heterogeneous Catalysis* (Eds.: G. Jannes, V. Dubois), Plenum, New York, **1995**, p. 75; k) T. Harada, T. Osawa in *Chiral Reactions in Heterogeneous Catalysis* (Eds.: G. Jannes, V. Dubois), Plenum, New York, **1995**, p. 83.

[67] T. Ohkuma, H. Ooka, S. Hashiguchi, T. Ikariya, R. Noyori, *J. Am. Chem. Soc.* **1995**, *117*, 2675.

[68] R. Noyori, T. Ohkuma, *Angew. Chem.* **2001**, *113*, 41; *Angew. Chem. Int. Ed.* **2001**, *40*, 40.

[69] R. Noyori, T. Ohkuma, *Pure Appl. Chem*. **1999**, *71*, 1493.

[70] R. Noyori, M. Koizumi, D. Ishii, T. Ohkuma, *Pure Appl. Chem*. **2001**, *73*, 227.

[71] Abbreviations: TolBINAP = 2,2′-Bis(di-4-tolylphosphano)-1,1′-binaphthyl. XylBINAP = 2,2′-Bis(di-3,5-xylylphosphano)-1,1′-binaphthyl. DPEN = 1,2-Diphenylethylenediamine. DAIPEN = 1,1-Di-4-anisyl-2-isopropyl-1,2-ethylenediamine.

[72] T. Ohkuma, M. Koizumi, H. Doucet, T. Pham, M. Kozawa, K. Murata, E. Katayama, T. Yokozawa, T. Ikariya, R. Noyori, *J. Am. Chem. Soc*. **1998**, *120*, 13529.

[73] T. Ohkuma, H. Ooka, T. Ikariya, R. Noyori, *J. Am. Chem. Soc.* **1995**, *117*, 10417.

[74] T. Ohkuma, H. Ikehira, T. Ikariya, R. Noyori, *Synlett* **1997**, 467.

[75] T. Ohkuma, M. Koizumi, M. Yoshida, R. Noyori, *Org. Lett*. **2000**, *2*, 1749.

[76] T. Ohkuma, H. Ooka, M. Yamakawa, T. Ikariya, R. Noyori, *J. Org. Chem*. **1996**, *61*, 4872.

[77] T. Matsumoto, T. Murayama, S. Mitsuhashi, T. Miura, *Tetrahedron Lett*. **1999**, *40*, 5043.

[78] T. Ohkuma, D. Ishii, H. Takeno, R. Noyori, *J. Am. Chem. Soc.* **2000**, *122*, 6510.

[79] T. Ohkuma, M. Koizumi, H. Ikehira, T. Yokozawa, R. Noyori, *Org. Lett*. **2000**, *2*, 659.

[80] T. Ohkuma, H. Doucet, T. Pham, K. Mikami, T. Korenaga, M. Terada, R. Noyori, *J. Am. Chem. Soc.* **1998**, *120*, 1086.

[81] T. Ohkuma, H. Takeno, Y. Honda, R. Noyori, *Adv. Synth. Catal*. **2001**, *343*, 369.

[82] Review: K. Mikami, M. Terada, T. Korenaga, Y. Matsumoto, M. Ueki, R. Angelaud, *Angew. Chem.* **2000**, *112*, 3676; *Angew. Chem. Int. Ed*. **2000**, *39*, 3532. See also: K. Mikami, T. Korenaga, M. Terada, T. Ohkuma, T. Pham, R. Noyori, *Angew. Chem.* **1999**, *111*, 517; *Angew. Chem. Int. Ed*. **1999**, *38*, 495; K. Mikami, T. Korenaga, T. Ohkuma, R. Noyori, *Angew. Chem.* **2000**, *112*, 3854; *Angew. Chem. Int. Ed*. **2000**, *39*, 3707.

[83] Nonlinear effects in catalysis should be investigated carefully because of the homochiral and heterochiral interaction of the chiral species present in the catalytic system. For reviews, see: a) R. Noyori, S. Suga, H. Oka, M. Kitamura, *Chem. Rec*. **2001**, *1*, 85; b) C. Girard, H. B. Kagan, *Angew. Chem.* **1998**, *110*, 3088; *Angew. Chem. Int. Ed*. **1998**, *37*, 2922; c) D. R. Fenwick, H. B. Kagan, *Top. Stereochem*. **1999**, *22*, 257.

[84] H. Doucet, T. Ohkuma, K. Murata, T. Yokozawa, M. Kozawa, E. Katayama, A. F. England, T. Ikariya, R. Noyori, *Angew. Chem.* **1998**, *110*, 1792; *Angew. Chem. Int. Ed.* **1998**, *37*, 1703.

[85] The ketone substrate reacts in an outer sphere of the coordinatively saturated 18-electron complex without interaction with the metallic center. Thus the general scheme given in Figure 1 is to be modified to some extent. For other mechanistic investigations, see: a) K. Abdur-Rashid, M. Faatz, A. J. Lough, R. H. Morris, *J. Am. Chem. Soc*. **2001**, *123*, 7473; b) R. Hartmann, P. Chen, *Angew. Chem.* **2001**, *113*, 3693; *Angew. Chem. Int. Ed.* **2001**, *40*, 3581.

[86] R. Noyori, M. Yamakawa, S. Hashiguchi, *J. Org. Chem*. **2001**, *66*, 7931.

[87] R. Noyori, S. Hashiguchi, *Acc. Chem. Res.* **1997**, *30*, 97.

[88] a) K. Matsumura, S. Hashiguchi, T. Ikariya, R. Noyori, *J. Am. Chem. Soc*. **1997**, *119*, 8738; b) I. Yamada, R. Noyori, *Org. Lett*. **2000**, *2*, 3425.

[89] K.-J. Haack, S. Hashiguchi, A. Fujii, T. Ikariya, R. Noyori, *Angew. Chem.* **1997**, *109*, 297; *Angew. Chem. Int. Ed. Engl*. **1997**, *36*, 285.

[90] a) M. Yamakawa, H. Ito, R. Noyori, *J. Am. Chem. Soc.* **2000**, *122*, 1466; b) D. A. Alonso, P. Brandt, S. J. M. Nordin, P. G. Andersson, *J. Am. Chem. Soc*. **1999**, *121*, 9580.

[91] M. Yamakawa, I. Yamada, R. Noyori, *Angew. Chem.* **2001**, *113*, 2900; *Angew. Chem. Int. Ed.* **2001**, *40*, 2818.

[92] a) M. Suzuki, A. Yanagisawa, R. Noyori, *J. Am. Chem. Soc*. **1985**, *107*, 3348; b) M. Suzuki, A. Yanagisawa, R. Noyori, *J. Am. Chem. Soc.* **1988**, *110*, 4718; c) M. Suzuki, Y. Morita, H. Koyano, M. Koga, R. Noyori, *Tetrahedron* **1990**, *46*, 4809.

[93] M. Suzuki, H. Koyano, Y. Morita, R. Noyori, *Synlett* **1989**, 22.

[94] This process has been used at Ono Pharmaceutical Co. for the industrial synthesis of PGs using the Corey method.

[95] a) R. Noyori, M. Suzuki, *Angew. Chem.* **1984**, *96*, 854; *Angew. Chem. Int. Ed. Engl*. **1984**, *23*, 847; b) R. Noyori, M. Suzuki, *Chemtracts: Org. Chem*. **1990**, *3*, 173; c) R. Noyori, M. Suzuki, *Science* **1993**, *259*, 44.

[96] a) M. Suzuki, K. Kato, R. Noyori, Yu. Watanabe, H. Takechi, K. Matsumura, B. Långström, Y. Watanabe, *Angew. Chem.* **1996**, *108*, 366; *Angew. Chem. Int. Ed. Engl*. **1996**, *35*, 334; b) H. Takechi, K. Matsumura, Yu. Watanabe, K. Kato, R. Noyori, M. Suzuki, Y. Watanabe, *J. Biol. Chem*. **1996**, *271*, 5901.

[97] Account: M. Suzuki, R. Noyori, B. Långström, Y. Watanabe, *Bull. Chem. Soc. Jpn*. **2000**, *73*, 1053.

[98] Yu. Watanabe, K. Matsumura, H. Takechi, K. Kato, H. Morii, M. Björkman, B. Långström, R. Noyori, M. Suzuki, Y. Watanabe, *J. Neurochem*. **1999**, *72*, 2583.

[99] a) M. Suzuki, H. Doi, M. Björkman, Y. Andersson, B. Långström, Y. Watanabe, R. Noyori, *Chem. Eur. J.* **1997**, *3*, 2039; b) M. Suzuki, H. Doi, K. Kato, M. Björkman, B. Långström, Y. Watanabe, R. Noyori, *Tetrahedron* **2000**, *56*, 8263.

[100] T. Satoh, Y. Ishikawa, Y. Kataoka, Y. Cui, H. Yanase, K. Kato, Yu. Watanabe, K. Nakadate, K. Matsumura, H. Hatanaka, K. Kataoka, R. Noyori, M. Suzuki, Y. Watanabe, *Eur. J. Neurosci*. **1999**, *11*, 3115.

[101] R. Noyori, S. Hashiguchi, T. Yamano in *Applied Homogeneous Catalysis by Organometallic Complexes, 2nd ed*. (Eds.: B. Cornils, W. A. Hermann), VCH-Wiley, Weinheim, 557.

[102] Nobel lecture: K. B. Sharpless, *Angew. Chem.* **2002**, *114*, 2126; *Angew. Chem. Int. Ed.* **2002**, *41*, 2024.

Searching for New Reactivity (Nobel Lecture)**

K. Barry Sharpless*

The processes for the selective oxidation of olefins have long been among the most useful tools for day-to-day organic synthesis. Herein, the focus is on the asymmetric-epoxidation (AE) and asymmetric-dihydroxylation (AD) reactions developed by Sharpless and co-workers. The reactions have a wide scope, are simple to run, and involve readily available starting materials. Ligand-accelerated catalysis is crucial to these reactions and might be the agent for uncovering more catalytic processes. In addition to the selectivity benefits of catalysis, the phenomenon of turnover (amplification) raises its potential impact. The author and his co-workers developed small, highly enantioselective catalysts that were unfettered by the "lock-and-key" selectivity of Natures enzymes, and tolerant of substrates throughout the entire range of olefin substitution patterns.

Keywords: asymmetric catalysis · epoxidation · hydroxylation · N ligands · Nobel lecture

In 1938, three years before I was born, a live coelacanth was taken from the waters off the eastern coast of South Africa. Previously known only in the fossil record from some hundred million years ago, the coelacanth and the implications of its discovery remained big news for years, and fueled an enthusiasm for "creatures" that persisted for decades. Those of us born in the 1940s grew up on photos of eminent scientists setting off on expeditions, their sunburned faces dwarfed by mountain explorers' garb, or making thumbs-up signs as they entered the water in scuba gear. We shared their confident expectation that the Loch Ness Monster, Sasquatch, the Yeti—even a dinosaur—soon would be taken alive.

I grew up loving the sea and loving fishing in particular, but unlike most fishermen I cared less for the size or quantity of the catch than for its rarity. Nothing could be more exciting than pulling (if not this time, surely the next!) a mysterious and hitherto unknown creature from the water. As a kid, I passionately wanted to be one who caught the next coelacanth, the first to see something that was beyond reasoning, even beyond imagining.

Opening a Nobel Lecture with a fishing expedition may seem frivolous, even indecorous, but I assure you no disrespect is intended. These are the circumstances that shaped my professional life: my first laboratory was New Jersey's Manasquan River, whose astonishingly rich variety addicted me to discovery; a few years later, when I was as comfortable at sea as I'd been on the river, my laboratory became the Atlantic Ocean. Later, when I started doing chemistry, I did it the way I fished—for the excitement, the discovery, the adventure, for going after the most elusive catch imaginable in uncharted seas.

Chemists usually write about their chemical careers in terms of the different areas and the discrete projects in those areas on which they have worked. Essentially all my chemical investigations, however, are in only one area, and I tend to view my research not with respect to projects, but with respect to where I've been driven by two passions which I acquired in graduate school: I am passionate about the Periodic Table (and selenium, titanium, and osmium are absolutely thrilling), and I am passionate about catalysis.

What the ocean was to the child, the Periodic Table is to the chemist; new catalytic reactivity is, of course, my personal coelacanth.

Even though I grew up in Philadelphia, if someone asks me where I'm from, I usually say "the Jersey Shore", because that's where my family spent summers, as well as many weekends and holidays, with my father joining us whenever he

[*] Prof. Dr. K. B. Sharpless
Department of Chemistry
The Scripps Research Institute
10550 North Torrey Pines Road, La Jolla, CA 92037 (USA)
Fax: (+1) 858-784-7562
E-mail: sharples@scripps.edu

[**] Copyright© The Nobel Foundation 2002. We thank the Nobel Foundation, Stockholm, for permission to print this lecture. Adapted with the permission of the editors from "Coelacanths and Catalysis": K. B. Sharpless, *Tetrahedron* **1994**, *50*, 4235.

 © WILEY-VCH Verlag GmbH, 69451 Weinheim, Germany, 2002 1433-7851/02/4112-2024 $ 20.00+.50/0

could. My father had a flourishing one-man general-surgery practice, which meant he was perpetually on call. With him at home so little and practically guaranteed to be called away when he was, my mother liked being near family and friends at the Shore, where her parents had settled and established a fishery after emigrating from Norway. When I was a baby, my parents bought land on a bluff overlooking the Manasquan River, about four miles up from where the river enters the Atlantic.

Like many scientists, I was a very shy child, happier and more confident when on my own, and my interest was totally absorbed by the river. In those days, the incoming tide transformed our part of the river, from a channel flanked by broad mudflats to a quarter-mile basin that exploded with life of myriad variety—about a dozen kinds of fish big enough to make it to the dinner table, plus blue crab, eel, and a bounty of fry and fingerlings that would graduate downstream to the ocean. I was obsessed with finding and observing everything that lived in the river and knowing everyone who worked on it.

My most delicious childhood memory is the excitement I experienced at the instant of awakening on almost every summer morning; the sound I associate with that feeling is the distant whine of my first scientific mentor's outboard motor. That was my wake-up call, and within minutes I was at the river's edge, waiting in the predawn stillness for Elmer Havens and his father Ollie to make their way across the river from Herbertsville to pick me up to "help" them seine for crabs. Amused by my regularly walking along the bank to watch them haul their seine, Elmer eventually installed me in the boat, which he used for transportation as well as for steadying himself as he dragged the seine's deep-water end. Ollie walked one end of the seine along the shore, alarming the crabs gathered at the river's edge, and frightening them toward deeper water, and so into the net's pocket. Chest deep in water and mud, Elmer walked parallel to his father, with one arm clasping the seine, the other hooked over the boat's gunwale. Elmer and I, our heads close together, would speculate about the catch, taking into account all the variables—the weather, the season, the tide. Every hundred yards or so, Elmer doubled ahead toward the shore to draw the purse. I liked it best if a big eel or a snapping turtle got caught up in the net, which made the water boil and the net flop into the air. I always hoped we'd catch something new.

I had a little dinghy, and my realm of exploration expanded in direct proportion to my rowing ability. The same tide that created this abundant estuary also was my nemesis, which forever stranded me upriver in the narrows or perhaps at Chapman's Boat Yard, a mile downstream and on the opposite bank. Since my parents couldn't keep me off the water, they opted for increasing the likelihood of my getting home unaided by giving me a boat with an outboard. It wasn't long before I went down river all the way to the inlet (absolutely forbidden, of course), and, soon after, the prospect of new creatures to pull from the water lured me out through the rock jetty and into the ocean; at the time I was only seven or perhaps eight years old.

By the time I was ten, I ran crab and eel traps and supplied everyone we knew with fish as well; at 14 I started working during the summer as the first (and only) mate on a charter boat. My parents allowed me to go to sea when I was so young and small even for my age because I was offered a job on a relative's boat—little did my parents or I know that Uncle Dink, a cousin actually, offered me the job so he wouldn't have to pay a "full-sized" helper. I so wanted to keep working on the boats that it was years before I dared tell my parents what went on aboard the Teepee, like how the Coast Guard refused assistance to Dink because his boat was in chronic disrepair. (Consequently, some of our adventures at sea were memorable indeed—grappling hooks and guns have their place in the canon—and I mention this trove of Uncle Dink stories because, for years, my MIT colleagues begged me to tell them over and over again).

On a charter boat, the captain pilots the ship and finds the fish the customers reel in. Meanwhile, the mate is over the boat like a dervish, skillfully arraying the water with fishy temptations—adjusting outriggers, finding the perfect combination of lure or bait and tackle, always mindful of the action on nearby boats competing for the same fish[*]. Since my

K. Barry Sharpless and his co-workers have discovered and developed many widely used catalytic oxidation processes, including the first general methods for stereoselective oxidation—the Sharpless reactions for asymmetric epoxidation, dihydroxylation, and aminohydroxylation of olefins. His mentors at Dartmouth College (BA in 1963), Stanford College (PhD in 1968 and postdoctoral research), and Harvard University (further postdoctoral research) were Prof. T. A. Spencer, Prof. E. E. van Tamelen, Prof. J. P. Collman, and Prof. K. Bloch, respectively. Before 1990, when he became W. M. Keck Professor of Chemistry at the Scripps Research Institue, Prof. Sharpless was a member of Faculty at the Massachusetts Institute of Technology (1970–77, 1980–90) and Stanford University (1977–80). Prof. Sharpless's honours include the Chemical Sciences Award of the National Academy of Sciences (of which he is a member), the Roger Adams and Arthur C. Cope Awards from the American Chemical Society, the Tetrahedron Award, the King Faisal Prize, the Prelog Medal, the Wolf Prize, the Nobel Prize (2001), and honorary doctorates from five American and European universities. The Sharpless research group continues to search for new homogeneous oxidation catalysts and for transition-metal-catalyzed asymmetric processes.



friends were all mates, we naturally agreed that enticing fish to bite was the greatest challenge, but I alone felt that getting the strike was the most fun, even more exciting than landing the fish. I worked as a mate almost daily every summer, right up until the day before I set out from New Jersey, headed toward the biggest ocean and graduate school at Stanford University.

That was in 1963. In the spring of that year, my inspiring Dartmouth College chemistry professor and first research director, Tom Spencer, talked me into delaying entering medical school to try a year of graduate school. He sent me to Stanford specifically to work for E. E. van Tamelen, Tom's own mentor at Wisconsin. The appeal of fishing was such that Tom, to my later regret, never succeeded in getting me to spend any summers working in his lab. In fact, even in graduate school, I expressed my ambivalence by continuing to fantasize about finding a boat out of Manasquan to skipper and by failing—this did not please v.T.—to do the simple paperwork required to renew my NSF predoctoral fellowship.

However, toward the end of my first year at Stanford, a serendipitous misunderstanding catalyzed the complete transfer of my passion (some would say my monomania) from one great science to another; from fishing to chemistry. Before leaving for a lengthy European visiting professorship, v.T. sent me to the library to look for reactive inorganic species that might produce interesting transformations of organic compounds. My first projects with v.T. were selective oxidation of polyolefins and titanium-mediated deoxygenative coupling of alcohols, and I was already primed to appreciate useful chemistry employing "strange" elements after selecting the Wittig Reaction from a list of suggested topics for my student seminar. The Wittig Reaction really engaged my enthusiasm, and I ingenuously concluded that finding new reactions other chemists could use looked like a lot of fun.

In any event, upon v.T.'s return, I discovered he had not intended for me to spend all those months immersed in the literature. While I had no research results to report, I did have a notebook filled with ideas and an eagerness to drop my line throughout the vastness of the Periodic Table. I don't think I've gone fishing in the literal sense a dozen times since then!

From van Tamelen, a Gilbert Stork protégé, I inherited enthusiastic disdain for "safe" problems, deep admiration for traditional multistep organic synthesis, and awe before selective biological catalysis: studying the squalene oxide/lanosterol cyclase enzyme left me impressed by enzymic selectivity, but depressed by the difficulty of using enzymes for synthetic transformations. After getting a double dose of him in the classroom, Derek Barton became my model. At Dartmouth, Tom Spencer taught a course on conformational analysis, based on one he took at Wisconsin from William S. Johnson (Tom's uncle, in fact), then I experienced the original at Stanford.[**] Being wet behind the ears, I took conformational analysis for granted; it was Sir Derek's search for new reactivity that electrified me. A postdoc with Jim Collman (the only person, I concede, who gets more excited about chemistry than I do) ignited my interest in using simple metal complexes to develop catalysts (in the Collman lab, incidentally, I had the privilege of many hours at the blackboard with labmate Bob Grubbs). Then, before taking up my job at MIT, a postdoc with Konrad Bloch confirmed my hunch that impatience rendered me incompetent around enzymes. Konrad graciously let me start working on my own ideas when his were much too frustrating for me.

One other part of my background seems to have contributed to my chemistry. The first American Sharpless ("Sharples" then) came to Pennsylvania in the 17th Century, not long after William Penn. My father was a practicing Quaker only as a child, but the values in our home were Quaker values, and I was educated in a Quaker school. The Quakers encourage modesty, thrift, initiative, and enterprise, but the greatest good is being a responsible member of the community—being useful. "Elegant" and "clever" were the chemical accolades of choice when I started doing research, just as "novel" is high praise now. Perhaps the Quakers are responsible for me valuing "useful" most.

So that is my background as a chemist. I've been accused of going too far, when I speculate that chirality fascinates me because I handled my umbilical cord in utero, but I'm quite sincere in proposing that the extraordinary training I received as a young chemist transformed an existing passion for discovering the unknown into the search for new reactivity, and that Quaker utilitarianism made the selective oxidation of olefins so appealing.

With respect to chemical reactions, "useful" implies wide scope, simplicity to run, and an essential transformation of readily available starting materials. Clearly, if useful new reactivity is the goal, the obvious strategy is investigating the

[*] This diversion into fishing as a metaphor for research could go on for pages; consider how, when a boat was hooking tuna—the catch of choice—word spread by radio and the competition converged from every compass point. The hot boat's captain greeted this acknowledgment of his success with some anxiety; while he liked setting the other captains' agendas and pleasurably speculating that the parties on the other boats were considering chartering him next time, the secrets of his success nonetheless required protection, so trolling speeds were lowered to sink the lures and prevent rubberneckers from identifying them, and red herrings (literally, on occasion!) were casually displayed on the fish box.
Isaak Walton and John Hersey devoted whole books to this metaphor, so indulge me for a few more sentences. The handy process versus product dichotomy that applies so neatly to much of human endeavor illuminates this fisherman–chemist comparison, too. Conventional wisdom places fly-fishing at the "process" end of the scale, while a "product" fisherman uses sonar to find a school before he bothers to get his line wet. Process person though I am, only the Manasquan River ran through my fishing days; trolling for the unknown always had more appeal than hooking a trout I already knew was there.

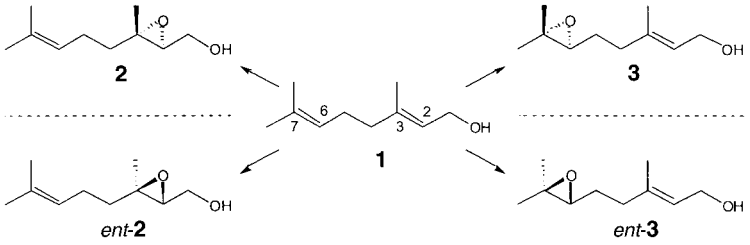
[**] When teaching MIT undergraduates, I always said "The lights came on with conformational analysis", without thinking where I picked up the phrase, but now I know: the previous Tetrahedron Prize article states "Just as chemists of the Robinson generation worked without concern for stereochemical factors so we, in the early days, were working in ignorance of conformational considerations until Derek Barton showed us the light in 1950". The author is, of course, Bill Johnson (see reference [1]).

transformations chemists rely on. The processes for the selective oxidation of olefins have long been among the most useful tools for day-to-day organic synthesis because of these appealing characteristics of olefins:

1) they are among the cheapest functionalized organic starting materials,
2) they can be carried "hidden" through conventional acid/base-catalyzed transformations, then "revealed" at will by adding heteroatoms through selective oxidations,
3) most simple olefins are prochiral, and provide a prominent portal to the chiral world.

The trisubstituted olefin geraniol, in addition to being one of my favorite smells, provides an excellent case study both for laying out the challenges of selective olefin oxidation as well as for noting some benchmarks in meeting those challenges.

As shown in Scheme 1, geraniol (**1**) has two trisubstituted olefinic units, one of which has a hydroxy group in the allylic position. Four monoepoxides are possible: making either racemic **2** or racemic **3** requires regio- or chemoselectivity,



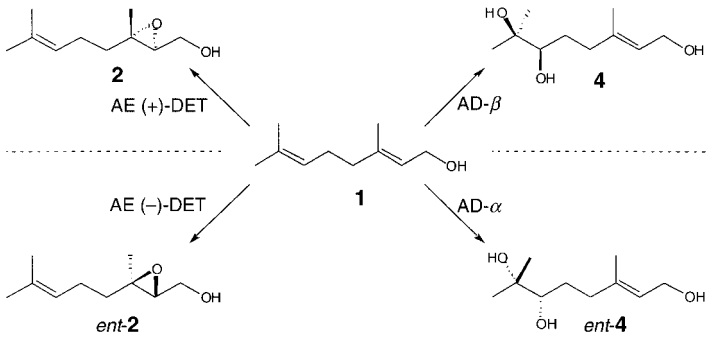
Scheme 1. Regio- and enantioselective monoepoxidations of geraniol.

while making each of the individual enantiomers requires enantioselectivity. When Henbest showed that the electronic deactivation by the oxygen substituent at C-1 causes peracids to prefer the 6,7-double bond (especially on the ester derivatives), making racemic **3** became possible.[2] When I started doing research in the 1960s, neither racemic **2** nor any of the enantiomers could be synthesized directly. Solving the other half of the regioselectivity problem was an obvious challenge, but enantioselectivity was considered well-nigh impossible.

In 1973, Bob Michaelson cracked the other half of the regioselectivity problem presented by geraniol.[3] Since early-transition-metal-catalyzed epoxidations with alkyl hydroperoxides were highly selective for the 2,3-position, racemic **2** could be prepared as well.

In 1980, Tsutomu Katsuki discovered the titanium-catalyzed asymmetric epoxidation (AE); the enantioselective oxidation of olefins bearing allylic hydroxy groups made it possible to make either **2** or *ent*-**2**, which thereby solved one side of the enantioselectivity problem.[4]

The osmium-catalyzed asymmetric dihydroxylation (AD), discovered in 1987, subsequently was improved to the point that either **3** or *ent*-**3** could be made by way of the diol, an



Scheme 2. Asymmetric epoxidation and dihydroxylation reactions of geraniol.

indirect solution to enantioselective epoxidation at the 6,7-position (Scheme 2).[5]

In 1990 came the breakthrough introduction of enantioselectivity into existing manganese–salen ligand catalysts for the epoxidation of isolated olefins.[6] Developed independently by the groups of Jacobsen[6a,10] and Katsuki,[6b] these epoxidation catalysts work best on only a few of the six olefin-substitution classes. Nonetheless, their very existence is tantalizing, and encourages the hope that a general, off-the-shelf solution will be found for the direct asymmetric-epoxidation reaction across the full range of isolated-olefin substitution patterns.

The greater generality of man-made catalysts, such as these catalysts, compared with enzymes was noted first by Knowles[7a,c] and Kagan.[7b] During the lean times in the first decade of my career, their pioneering development of man's first highly enantioselective catalysts (the L-DOPA synthesis that came out of Knowles' Monsanto lab was the asymmetric hydrogenation's first commercial application) sustained my faith that a catalyst for asymmetric oxidation could be found. Jack Halpern's mechanistic studies[7d] on asymmetric-hydrogenation catalysis likewise inspired me. Several Japanese chemists, chief among them Ryoji Noyori,[7e] hugely extended both the scope and application of the asymmetric hydrogenation process.[8]

This focused search has frustrated but never bored me, even after so many years, and the geraniol paradigm illustrates why. My own investigations into the oxidation of olefins commenced at MIT in 1970, but, fittingly, I was back at Stanford on January 18, 1980, for Tsutomu Katsuki's dramatic discovery of the titanium-catalyzed asymmetric epoxidation.[4,9a] Two years later, the most scientifically stimulating and professionally gratifying collaboration of my career, the total syntheses of the eight L-hexoses with my MIT colleague Sat Masamune, capped the AE's discovery.[11] Previous articles[12] in a vein similar to this one describe that chemistry; understanding the AE's significance and putting that understanding to work are the purview here.

After the euphoria of completing the hexose syntheses, three years were spent developing, refining, and finding more applications for the AE. During this time I returned to the

search for new reactivity, but it was clear that my random, scattershot attempts were going nowhere,[*] so I was grateful for the opportunity to spend the first three months of 1987 as a Sherman Fairchild Scholar at Caltech.

Many universities and institutions have handsome Fairchild buildings, but Caltech, ever the bastion of collegiality and camaraderie, used its Fairchild grant to endow a program that brings scientists from many fields to be housed graciously in the sunshine for as long as a year. Since my research group's investigation of the AE had reached the point of diminishing returns, I left for Pasadena hoping to renew my mission.

I love reading journals, and I love mountains, so the Caltech library with its panoramic view of Mount Wilson became my thinking place of choice. Every day Mount Wilson offered new vistas, especially on those occasions when snow fell during the night. One morning, the mountain was completely cloaked (the first time a freezing temperature was recorded in downtown LA, I recall), and the melting snow receded at such a clip that I was sure I saw it happening. Mount Wilson was the perfect backdrop for bringing my own big picture back into focus, and I returned to MIT eager to renew my search for new reactivity. Meditating on the AE yielded this lesson to guide that search: Ligand-accelerated catalysis (the significance of which is documented in M. G. Finn's fine MIT thesis on the mechanism of the AE[13]), is crucial to the AE and not merely a feature of it; despite its rarity, this phenomenon might be the agent for uncovering more catalytic processes.

Of course, the first and best-known example of ligand acceleration is found in Criegee's papers from the 1930s.[14] He observed that pyridine accelerates the reaction in his classic study of osmium tetroxide and olefins. Ironically, the lesson from the AE was directing me back toward Criegee, whose discoveries in olefin oxidation and osmylation were, in large measure, the jumping-off point for my own research career.

I first looked into Criegee's process shortly after becoming an assistant professor at MIT. My attraction to the reaction of OsO_4 with olefins was inevitable. Osmium tetroxide not only accomplishes an important synthetic transformation, but it does so with a scope and reliability unique among reactions used for organic synthesis. It reacts only with olefins and it reacts with all olefins (slight poetic license here). Even R. B. Woodward valued Criegee's stoichiometric transformation so much he was willing to use 100 g of OsO_4 in one shot. Osmium's expense was not compatible with "useful," however and, since the existing catalytic variants were not very effective, I started searching for a reliable catalytic method. In 1975, Kagayasu Akashi found a good process for us, based on a hydroperoxide as an oxidant, *tertiary*-butyl hydroperoxide (TBHP),[15] but the brass ring was ultimately captured that same year with the publication of the famous Upjohn process based on *N*-methyl morpholine-*N*-oxide (NMO).[16]

Throughout the rest of the 1970s, osmium remained our primary tool for looking for new reactivity. We discovered that imido osmium(VIII) species effected stoichiometric *cis*-oxyamination of olefins in direct analogy to the *cis*-dihydroxylation of olefins by osmium tetroxide; even more effective catalytic versions of those transformations came shortly thereafter.

In 1977 I left MIT, where I had been a contented member of a wonderful chemistry faculty since 1970, for Stanford University, where I previously spent six contented years as a graduate student and postdoc, surrounded by a wonderful chemistry faculty. I never made the transition back to contentment at Stanford, probably because my research wasn't churning up much. This frustrated me and scared off potential graduate students who wanted publications, not a fishing expedition. In addition, at Stanford I remained awed by a faculty I worshiped when a graduate student, and I lacked the confidence to stand firm on issues, particularly faculty appointments, that meant a lot to me. In 1979, at about the same time I made the decision to return to MIT, Steve Hentges, who worked in our well-developed osmium imido area and already had the material for a good Ph.D. thesis in hand, decided to take on one more project before writing up.

The notion of an asymmetric ligand for osmium tetroxide had been knocking around the lab for years, and Steve first approached the idea by making several pyridines with chiral substituents at the 2-position; these gave diols with essentially 0% *ee*![17] Pyridine is only a modest ligand for osmium tetroxide, and, as we discovered, any *ortho* substituent is

[*] I have enormous admiration for colleagues who can keep multiple research projects alive and large groups humming, but the "monomania" that prevents me from being able to do that is my long suit as well, making it possible to concentrate—for years, actually—on a single topic. I know some chemists call my approach "intuitive," a term I've always thought underestimates the rigor that frames my method; perhaps "unstructured" or "contemplative" is more accurate. Many of my cohorts are quick and facile and can jump on a few interesting bits of data and start building tentative edifices that get taken apart and reassembled to suit new data. I, on the other hand, am ruminative: my training after all consisted of busily poking and perturbing the Manasquan River, a curriculum both urgent and leisurely, one that permitted exploration without assumptions and without the structure imposed by deadlines or competition, or by knowing too little or too much. Since I was compelled by shyness to learn to do much on my own, there was (and is) no right or wrong way, only many ways, some more or less suited to a given endeavor. The discipline, nonetheless, is exacting; everything that can be observed should be observed, even if it is only recalled as the bland background from which the intriguing bits pop out like Venus in the evening sky. The goal is always finding something new, hopefully unimagined and, better still, hitherto unimaginable. When I became a bench- and desk-bound explorer, the method stayed the same. I try to imagine away the packaging the information arrives in, then let bits and pieces move around lazily, rather like objects tumbling slowly in zero gravity, but eventually, over time, exploring every possible relationship with other information that's previously arrived. Since joining the faculty of The Scripps Research Institute, I've discovered that ocean swimming and running on the beach provide an excellent medium for this kind of activity. However, in any climate, the best catalyst is generous, stimulating conversation. This slow, but endlessly fascinating, method is like an exotic ritual courtship, full of displays of bright feathers or offerings of shiny metal or towers of sticks—what does it all, what does any of it mean? Enormous concentration is required to remember it all in a way that causes little sparks when certain conjunctions appear, making a connection with something noted previously, perhaps decades ago. Sadly, as I grow older, the connections become harder to summon up, so the sparks, though they seem as bright as ever, are less frequent. I describe this process at length because it's not the way most scientists approach their work, nor is it well suited to the demands of funding agencies that are railroaded into answering questions posed for political rather than scientific reasons, nor to the needs of graduate students who require publications to compete for jobs. Academic chemistry is much harder now, and I'm glad I was born when I was.

lethal to binding. But since William Griffith at Imperial College had shown that quinuclidine binds much more strongly to OsO_4, I suggested trying the cinchona alkaloids, essentially substituted quinuclidines.[18] (Many chemists have expressed surprise at how quickly we arrived at what is now the best ligand framework for the AD: anyone with a natural products background and who is also a fan of Hans Wynberg's chemistry recognizes the cinchona alkaloids as the obvious next step.) The results were spectacular, even without taking into account a measurement error (discovered years later) that caused most of the *ee* values to be underreported by 5–15%![17]

Steve had a dramatic story to cap his thesis work, so he started writing; my attention was taken up by the decision to return to MIT. Then, a couple of months later, Katsuki discovered an asymmetric process with ingredients so cheap it made working with osmium look like Rolls-Royce chemistry. Although the AE was only weakly catalytic in the early days,[19] its uniformly high *ee* values and nontoxic, inexpensive reagents were enough to completely divert our attention from its promising but stoichiometric predecessor, the OsO_4/cinchona asymmetric dihydroxylation.

The preceding paragraph has no doubt failed to deflect your attention from the obvious question: Why didn't I try the Hentges ligands in the Upjohn system in 1979? Indeed, why did I propose the experiment in my NIH grant renewal in January, 1984, but not follow up on it? "As for the ligand," I wrote in the proposal, "it is probably best to stay with the cinchona derivatives because the quinuclidine moiety is the best ligand we know of for Os^{VIII} complexes. The substrate will be stilbene…the osmium catalyst will be recycled using an amine *N*-oxide. Ideally, both the osmium and the chiral alkaloid could be used in catalytic quantities. A successful system of this type could be of great practical importance."

Instead of poking and perturbing, the Jersey Shore School of Thinking's cardinal rule, I stuck with the odds logic suggested: ligands accelerate the reaction of OsO_4 with olefins, but they also bind avidly to the resulting osmate ester, and lethally affect catalyst turnover. This ability of ligands, such as pyridine and quinuclidine, to kill turnover in catalytic-osmylation systems had often been observed in my laboratory. What I did not, nor could not, anticipate is the perfect balance cinchona alkaloids achieve in ligating ability; they bind well enough to accelerate the key step, but weakly enough to slip off allowing the hydrolysis/reoxidation steps of the catalytic cycle to proceed. At the time, however, the precedents seemed clear, so the AD languished until 1987.

Unraveling the mechanism of the AE was largely the work of M. G. Finn.[13] His persistent exploration during the early to mid-1980s of the AE's titanium–tartrate-catalyst system exposed a complex mixture of species in dynamic equilibrium with one another.[20] M. G. discovered the main species $[Ti(dipt)(O\text{-}iPr)_2]_2$ (DIPT = diisopropyl tartrate) is substantially more active than the many other species present (significantly, it is five to ten times more active than $Ti(OR)_4$, a catalyst for the formation of racemic epoxy alcohol) and this rate advantage funnels catalysis through the appropriate tartrate-bearing species.

If the tartrate-induced acceleration of the titanium-catalyzed epoxidation reaction came as a surprise, investigating that phenomenon brought even more surprising results. We ultimately found 24 metals other than Ti that catalyze the epoxidation of allylic alcohols by TBHP (Figure 1), but all these systems were strongly inhibited or killed by adding tartrate![21] Ligand-decelerated catalysis was clearly the rule, while ligand acceleration was the extraordinarily valuable exception.

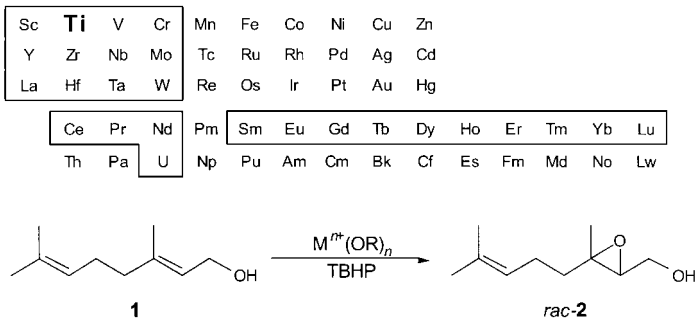
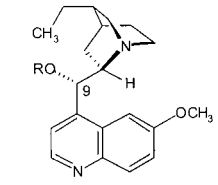
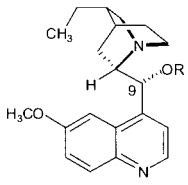


Figure 1. Metals catalyzing the epoxidation of allylic alcohols by TBHP. Adding tartrate ligand always affects reactivity: the titanium system is accelerated.

Shortly before I left for Caltech, Chris Burns, encouraged by Pui Tong Ho, presciently lobbied to resurrect the OsO_4/cinchona asymmetric dihydroxylation, and, without any encouragement from me, I must admit, he embarked on the synthesis of a stoichiometric C_3-symmetric ligand for the AD.[22] A few months later, I too was again committed to osmium, and when Bill Mungall and Georg Schröder reexamined the work from 1979, they uncovered *ee* values even better than previously reported. Meanwhile, Eric Jacobsen attacked the problem from the mechanistic side, and discovered that the ligand-dependent rate accelerations could be enormous.[23]



dihydroquinidine derivatives



dihydroquinine derivatives

With these very encouraging results on the stoichiometric reaction just in, Istvan Markó joined the project. I was traveling at the time, and on his own initiative, unaware of the NIH proposal, he combined Hentges' system[17] with the reliable Upjohn NMO-based catalytic-osmylation system,[16] immediately getting results indicating the reaction was catalytic.[24] However, unlike the dramatic "Eureka!" that accompanied the discovery of the AE, cautious optimism was the response to the catalytic AD and its initially modest *ee* values. Now, however, after years of research since Markó's first experiments in October of 1987, the AD's utility rivals and often surpasses the AE's.[9] Unlike the AE, for which

Katsuki's initial tartrate-ester ligands have yet to be eclipsed, the ligands for the AD have evolved substantially in effectiveness and scope, through substitution at the C-9 hydroxy moiety.

The simple ester derivatives (e.g. the acetate and *para*-chlorobenzoate esters) gave way in 1990 and 1991 to aryl ether derivatives, first proposed by Yun Gao during a late-night group meeting to address the mechanistic question of a possible ligating role of the ester carbonyl. Brent Blackburn made the phenyl ether which, to our surprise, gave good *ee* values, but was too hard to make to be competitive with the then dominant *para*-chlorobenzoate (CLB) ligand.

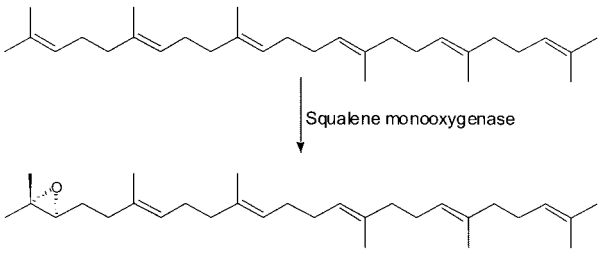
Almost a year later, Declan Gilheany correctly predicted that aryl ethers should be better for aliphatic olefins than the CLB ligand,[25] and these results laid the foundation for a steady expansion of this ligand class, which culminated in the phenanthryl ether ligand.[26] Another big jump in effectiveness came with the dimeric alkaloid ligands having a phthalazine core, first made by Jens Hartung in 1990.[27] Along with the pyrimidine ligands[28] whose development they inspired, they remain the best general ligands for the AD reaction.

The search for better ligands was paralleled by advances in catalyst turnover efficiency:

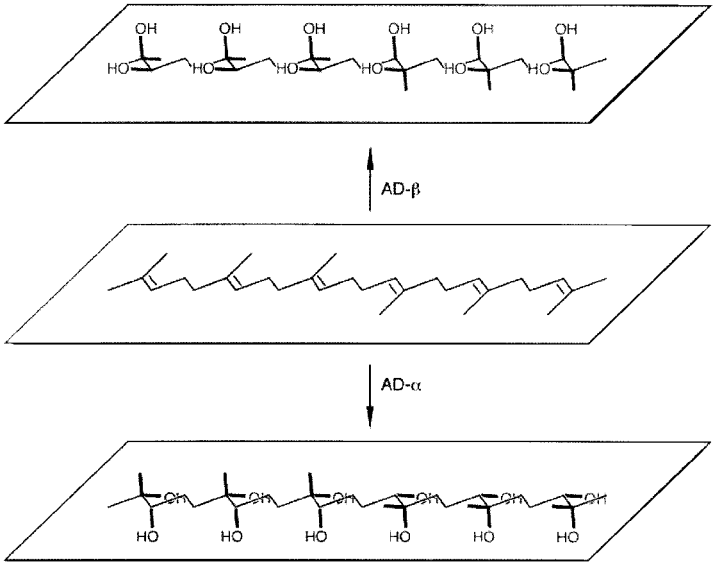
1) John Wai found both the second-catalytic-cycle problem and its partial remedy; slow addition of the olefin.[29]
2) Since ferricyanide in *tert*-butanol/water provides an excellent two-phase system for catalytic osmylation,[30] Hoi-Lun Kwong applied it to the AD, which solved the second-cycle problem and the need for slow addition.[31]
3) Willi Amberg found that adding organic sulfonamides greatly facilitates the rate of catalyst turnover for olefins whose osmate esters resist hydrolysis.[27]

As the practicality (it has been scaled up to run in 4000-liter reactors with no ill effects on yield or *ee* value[32]) and scope of the AD process grew, so did the pressure to understand the origin of its enantioselectivity. Mechanistic studies dating from the 1970s by Alan Teranishi and Jan Bäckvall[33] were rekindled by Eric Jacobsen in 1987 and continued into the mid-1990s.[34]

While a complete and general solution to the geraniol paradigm's final challenge is clearly within reach, comparing selectivity at the bench with selectivity in living systems remains striking. For example, the squalene monooxygenase in our livers unerringly deposits a single oxygen atom on the squalene molecule and, in so doing, further chooses only the si-enantioface of the terminal double bond (Scheme 3).[35] On the other hand, the attempted AD of a single double bond of squalene does give the terminal diol in 96% *ee*. The preference for the terminal double bond is slight, however, and internal diols as well as tetraols also can be isolated from the reaction.[36] Thus, while the AD catalyst cannot match the exquisite selectivity of the enzymic system, this very inability to discriminate between the six trisubstituted double bonds of squalene allows the exhaustive AD of squalene (Scheme 4) in an overall yield of 79.8% for the AD-β reaction.[37]



Scheme 3. Enzymatic epoxidation of squalene.



Scheme 4. Exhaustive, stereoselective dihydroxylations of squalene.

Serial multistep reactions such as these are generally stymied by Bob Ireland's "arithmetic demon"—the geometric fall in yield in sequential chemical reactions. The AD of each double bond is one step in a procession of six dihydroxylations, each with a chemical and an optical yield, twelve yields in all. Thus the average yield of each step is $(0.798)^{1/12}$ or 98%, which translates to 98% for each chemical yield, 96% *ee* for the single enantioselective reaction and 96% *de* for each of the five diastereoselective reactions. The high yield of a single enantiomer from the multiple hydroxylation events required to oxidize squalene completely reflects the reliability and selectivity of the AD process. Joel Hawkins' Berkeley lab kinetically resolved the chiral fullerene C_{76}, which resulted in the first enantiomerically pure allotrope of carbon, the AD's most intriguing use to date.[38]

My decision, nearly 25 years ago, to study the selective oxidation of olefins produced an unexpected bonus, one that gave me an opportunity to investigate uncharted territory on a scale that is more associated with the previous half-century than with our own. Selenium, titanium/alkyl peroxides, and osmium, my three most successful olefin oxidation catalysts, all had phobias associated with them, with the result that much of their chemistry remained terra incognito. Selenium and osmium were considered highly toxic, and the peroxide oxidants used with titanium had a nasty reputation. Rarely did I find myself in another chemist's territory; likewise, few wanted to cast a line in mine.

Tracking these elements offers a rather curious way to view my research. Figure 2a plots the time course of their

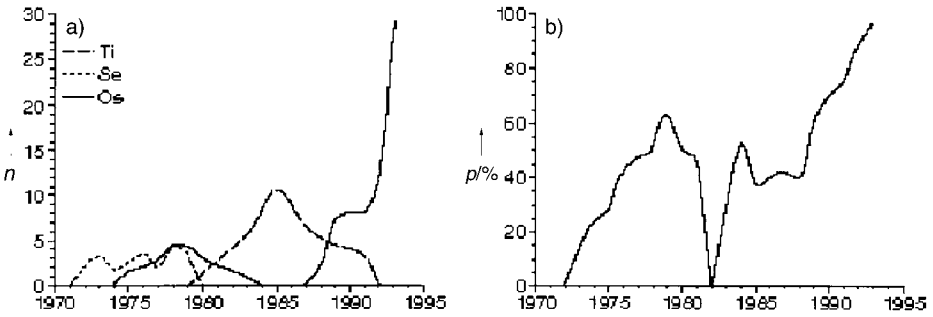


Figure 2. a) Selenium, titanium, and osmium chemistry; note the osmium line's bimodality. b) Growth of catalysis in my laboratory. n = number of publications; P = percentage of publications.

dominance (as measured by publications, for want of a more qualitative ruler) during the years 1970–1993. Selenium came first, flourished, then ended abruptly. Osmium research came next, coexisting with selenium until both were eclipsed by titanium, the descendant of molybdenum and vanadium. Osmium made a strong comeback, knocking off titanium.

Figure 2b, which charts my research with respect to catalytic transformations, looks quite unlike Figure 2a, but relates directly to it. As my involvement with catalysis grew, the largely stoichiometric selenium reagents lost their appeal; titanium fell because the effectiveness of the titanium catalyst for the AE is modest, with about only 20 turnovers per titanium center before all activity is lost. Osmium, despite a bimodal presentation, was never actually out of the picture, merely quiescent until the discovery of the highly catalytic AD (it has been run to completion with as little as 1/50,000 of osmium catalyst).

In Figure 2b, the only real defection from the steady growth of catalysis to dominion in my research was the 1982 trough caused by the hexose synthesis collaboration with Sat Masamune. Stepping out of the realm of catalysis is almost unimaginable to me now.

Because of its unique potential for channeling a reaction sequence along one of myriad possible pathways, selective catalysis lies at the heart of both pure and applied chemistry, not to mention life chemistry. In addition to the selectivity benefits of catalysis, the phenomenon of turnover (which equals amplification), implicit in the definition, highly leverages its potential impact. For all these reasons, catalysis was and continues to be the engine driving my research.

Nature's enzymes made it possible to imagine simpler asymmetric catalysts. What we found, however, was unimaginable on two scores: small, highly enantioselective catalysts that were not only not fettered by nature's "lock-and-key" modus operandi, but tolerant as well of substrates throughout the entire range of olefin substitution patterns. Now, going on four decades later, I am still plumbing the vastness of the Periodic Table in search of new catalytic reactivity. The unpredictability and rarity of what I seek are not deterrents since I am, after all, the product of optimistic times. There are other coelacanths to be found!

Above all I thank and express my deep gratitude to my past and present co-workers at MIT, Stanford and The Scripps Research Institute. Many of you learned to tolerate my style of directing research (an oxymoron perhaps?); indeed, some of you flourished. Others were not well served, and to you I sincerely apologize. I'm exceedingly proud of the MIT undergraduates who got their feet wet in my lab and now hold leading academic and industrial positions: remember you got your opportunities because Tom Spencer gave me mine, and I expect you to do the same. Mentioning Tom brings me back, as so many things do, to E. E. van Tamelen: the bright flashes of his career remain of the first magnitude and still inspire me. And finally, my scientific career would have been unthinkable without the constant support and counsel of my wife, best friend—and ghost writer—Jan.

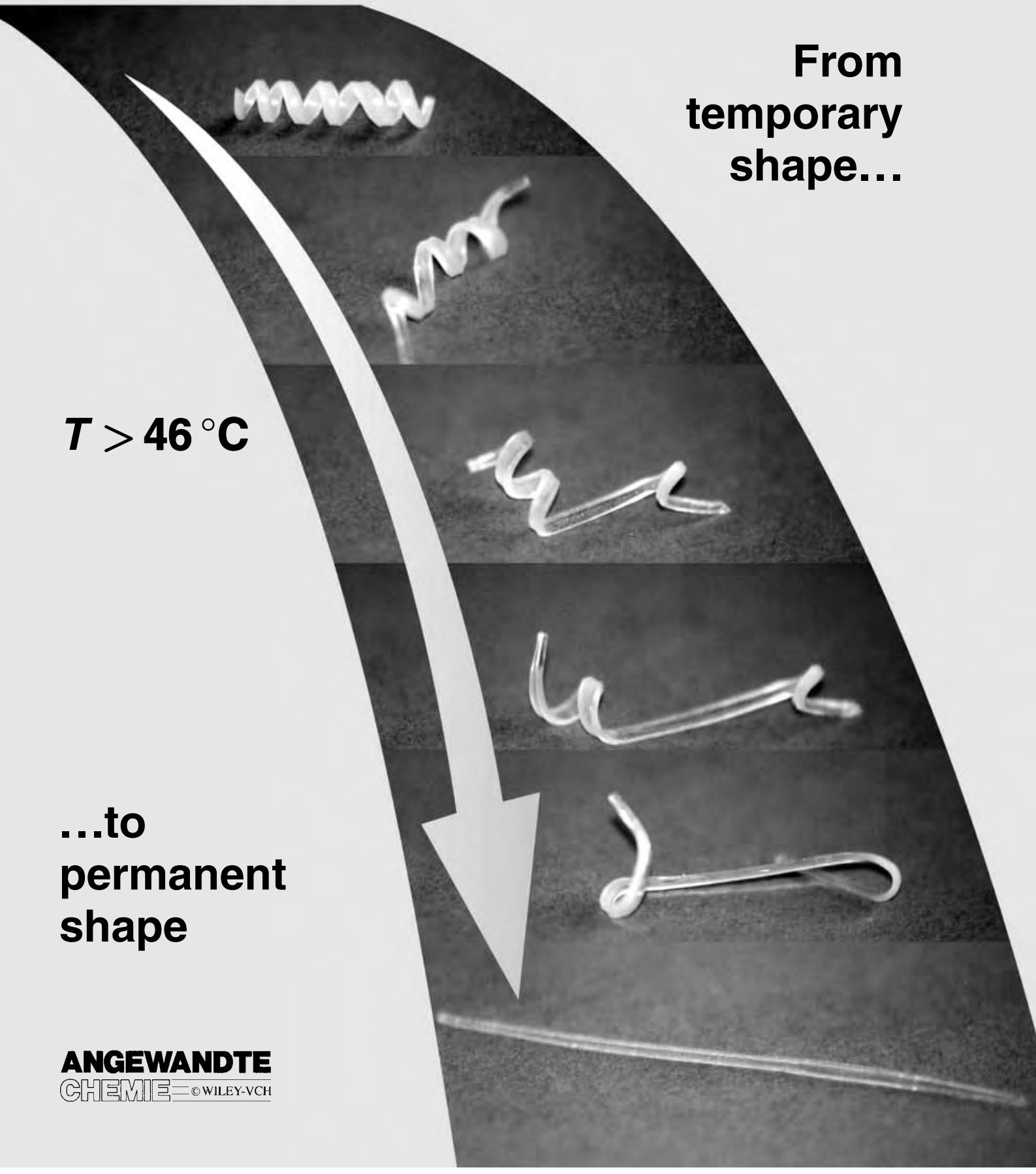
I also thank the National Institute of General Medical Sciences, National Institutes of Health (GM-28384) and the National Science Foundation for their continuous financial support over the past 25 years and, more recently, the W. M. Keck Foundation and the Skaggs Institute for Chemical Biology for helping to make possible my present tenure at The Scripps Research Institute in La Jolla.

Received: March 12, 2002 [A 524]

[1] W. S. Johnson, *Tetrahedron* **1991**, *47*, XI.
[2] H. B. Henbest, R. A. L. Wilson, *J. Chem. Soc.* **1957**, 1958.
[3] K. B. Sharpless, R. C. Michaelson, *J. Am. Chem. Soc.* **1973**, *95*, 6136.
[4] T. Katsuki, K. B. Sharpless, *J. Am. Chem. Soc.* **1980**, *102*, 5974.
[5] a) David Xu synthesized **4** and *ent*-**4** in 1991 during his work on the AD mechanism, from which synthesis of **3** and *ent*-**3** was implicit; two other groups reported this reaction sequence: b) E. J. Corey, M. C. Noe, W. C. Shieh, *Tetrahedron Lett.* **1993**, *34*, 5995; c) G. Vidari, A. Dapiaggi, G. Zanoni, L. Garlaschelli, *Tetrahedron Lett.* **1993**, *34*, 6485; d) G. Vidari, A. Giori, A. Dapiaggi, G. Lanfranchi, *Tetrahedron Lett.* **1993**, *34*, 6925. Gerry Crispino's juvenile hormone III synthesis demonstrates the same conversion: e) G. A. Crispino, K. B. Sharpless, *Synthesis* **1993**, *8*, 777.
[6] a) W. Zhang, J. L. Loebach, S. R. Wilson, E. N. Jacobsen, *J. Am. Chem. Soc.* **1990**, *112*, 2801; b) R. Irie, K. Noda, Y. Ito, N. Matsumoto, T. Katsuki, *Tetrahedron Lett.* **1990**, *31*, 7345.
[7] a) W. S. Knowles, M. J. Sabacky, *J. Chem. Soc. Chem. Commun.* **1968**, 1445; b) T. P. Dang, H. B. Kagan, *J. Chem. Soc. Chem. Commun.* **1971**, 481; c) W. S. Knowles, M. J. Sabacky, B. D. Vineyard, D. J. Weinkauv, *J. Am. Chem. Soc.* **1975**, *97*, 2567; d) See his excellent review: J. Halpern, *Science* **1982**, *217*, 401; e) A. Miyashita, A. Yasuda, H. Takaya, K. Toriumi, T. Ito, T. Souchi, R. Noyori, *J. Am. Chem. Soc.* **1980**, *102*, 7932.
[8] a) H. Takaya, T. Ohta in *Catalytic Asymmetric Synthesis* (Ed.: I. Ojima), VCH, Weinheim, **1993**, p. 1; b) H. Kumobayashi, S. Akutagawa, S. Otsuka, *J. Am. Chem. Soc.* **1978**, 100, 3949; c) S. Akutagawa, K. Tani in *Catalytic Asymmetric Synthesis* (Ed.: I. Ojima,) VCH, Weinheim, **1993**, p. 41. A history and review of the development of the asymmetric hydrogen migration of allylamines can be found in: d) S. Otsuka, K. Tani, *Synthesis* **1991**, 665.
[9] For review chapters on both the AE and AD, written largely by Roy Johnson despite being coauthored by both of us, see: a) R. A. Johnson, K. B. Sharpless, in *Catalytic Asymmetric Synthesis* (Ed.: I. Ojima) VCH, Weinheim, **1993**, p. 101; b) R. A. Johnson, K. B. Sharpless in *Catalytic Asymmetric Synthesis* (Ed.: I. Ojima), VCH, Weinheim, **1993**, p. 227.

[10] E. N. Jacobsen in *Catalytic Asymmetric Synthesis*, (Ed.: I. Ojima), VCH, Weinheim, **1993**, p. 159.
[11] a) S. Y. Ko, A. W. M. Lee, S. Masamune, L. A. Reed, K. B. Sharpless, F. J. Walker, *Science* **1983**, *220*, 949; b) S. Y. Ko, A. W. M. Lee, S. Masamune, L. A. Reed, K. B. Sharpless, F. J. Walker, *Tetrahedron* **1990**, 46, 245.
[12] a) K. B. Sharpless, *CHEMTECH* **1985**, 692; b) K. B. Sharpless, *Chem. Br.* **1986**, *22*, 1.
[13] M. G. Finn's thesis work has appeared in two full papers: a) S. S. Woodard, M. G. Finn, K. B. Sharpless, *J. Am. Chem. Soc*. **1991**, *113*, 106; b) M. G. Finn, K. B. Sharpless, *J. Am. Chem. Soc.* **1991**, *113*, 113.
[14] a) R. Criegee, *Justus Liebigs Ann. Chem.* **1936**, *522*, 75; b) R. Criegee, *Angew. Chem.* **1937**, *50*, 153; c) R. Criegee, *Angew. Chem*. **1938**, *51*, 519; d) R. Criegee, B. Marchand, H. Wannowias, *Justus Liebigs Ann. Chem.* **1942**, *550*, 99.
[15] K. B. Sharpless, K. Akashi, *J. Am. Chem. Soc*. **1976**, *98*, 1986.
[16] V. van Rheenen, R. C. Kelly, P. Y. Cha, *Tetrahedron Lett*. **1976**, 1973.
[17] S. G. Hentges, K. B. Sharpless, *J. Am. Chem. Soc.* **1980**, *102*, 4263.
[18] a) M. J. Cleare, P. C. Hydes, W. P. Griffith, M. J. Wright, *J. Chem. Soc. Dalton Trans.* **1977**, 941; b) W. P. Griffith, A. C. Skapski, K. A. Woode, M. J. Wright, *Inorg. Chim. Acta* **1978**, 31, l413.
[19] Five years later, Bob Hanson made the simple but wonderful discovery that adding molecular sieves to the reaction dramatically increases catalyst turnover, so that the AE process became truly catalytic: R. M. Hanson, K. B. Sharpless, *J. Org. Chem.* **1986**, *51*, 1922.
[20] Steve Pedersen provided invaluable structural results to aid M. G. Finn's studies during this period. Steve's work gave us our first glimpse into the dynamic world of complex mixtures in rapid equilibrium with each other. His contributions are summarized in: K. B. Sharpless, *Chem. Scr.* **1987**, *27*, 521. These studies led to no new catalysts, but they drove home our appreciation for the absolute need for a ligand-acceleration effect in catalyst systems where ligand exchange is rapid.
[21] K. S. Kirshenbaum, Ph. D. Thesis, Massachusetts Institute of Technology, **1985**.
[22] C. J. Burns, Ph. D. Thesis, Massachusetts Institute of Technology, **1989**.
[23] E. N. Jacobsen, E. I. Markó, M. B. France, J. S. Svendsen, K. B. Sharpless, *J. Am. Chem. Soc*. **1989**, *111*, 737.
[24] E. N. Jacobsen, E. I. Markó, W. S. Mungall, G. Schröder, K. B. Sharpless, *J. Am. Chem. Soc.* **1988**, *110*, 1968.
[25] T. Shibata, D. G. Gilheany, B. K. Blackburn, K. B. Sharpless, *Tetrahedron Lett*. **1990**, *31*, 3817.
[26] K. B. Sharpless, W. Amberg, M. Beller, H. Chen, J. Hartung, Y. Kawanami, D. Lübben, E. Manoury, Y. Ogino, T. Shibata, T. Ukita, *J. Org. Chem*. **1991**, *56*, 4585.
[27] K. B. Sharpless, W. Amberg, Y. Bennani, G. Crispino, J. Hartung, K. Jeong, H. Kwong, K. Morikawa, Z. M. Wang, D. Xu, X. L. Zhang, *J. Org. Chem*. **1992**, *57*, 2768.
[28] G. Crispino, K. S. Jeong, H. Kolb, Z. M. Wang, D. Xu, K. B. Sharpless, *J. Org. Chem.* **1993**, *58*, 1958.
[29] J. S. M. Wai, I. Markó, J. S. Svendsen, M. G. Finn, E. N. Jacobsen, K. B. Sharpless, *J. Am. Chem. Soc*. **1989**, *111*, 1123.
[30] M. Minato, K. Yamamoto, J. Tsuji, *J. Org. Chem*. **1990**, *55*, 766.
[31] H. Kwong, C. Sorato, Y. Ogino, H. Chen, K. B. Sharpless, *Tetrahedron Lett*. **1990**, *31*, 2999.
[32] Private communication from Dr. Yun Gao of Sepracor, Inc., Marlborough, MA.
[33] K. B. Sharpless, A. Y. Teranishi, J. E. Bäckvall, *J. Am. Chem. Soc*. **1977**, *99*, 3120.
[34] a) E. N. Jacobsen, E. I. Markó, M. B. France, J. S. Svendsen, K. B. Sharpless, *J. Am. Chem. Soc.* **1989**, *111*, 737; b) T. Göbel, K. B. Sharpless, *Angew. Chem*. **1993**, *105*, 1823; *Angew. Chem. Int. Ed. Engl*. **1993**, *32*, 1329; c) P. O. Norrby, H. Kolb, K. B. Sharpless, *Organometallics* **1994**, *13*, 44 – 47; d) H. C. Kolb, P. G. Andersson, Y. L. Bennani, G. A. Crispino, K. S. Jeong, H. L. Kwong, K. B. Sharpless, *J. Am. Chem. Soc.* **1993**, *115*, 12226 – 12227; e) H. C. Kolb, P. G. Andersen, K. B. Sharpless, *J. Am. Chem. Soc*. **1994**, *116*, 1278 – 1291; f) H. L. Kwong, Ph. D. Thesis, Massachusetts Institute of Technology, **1993**.
[35] a) R. B. Boar, K. Damps, *Tetrahedron Lett*. **1974**, 3731; b) D. H. R. Barton, T. R. Jarman, K. G. Watson, D. A. Widdowson, R. B. Boar, K. Damps, *J. Chem. Soc. Chem. Commun.* **1974**, 861; c) D. H. R. Barton, T. R. Jarman, K. G. Watson, D. A. Widdowson, R. B. Boar, K. Damps, *J. Chem. Soc. Perkin Trans. 1* **1975**, 1134.
[36] G. Crispino, K. B. Sharpless, *Tetrahedron Lett*. **1992**, *33*, 4273.
[37] G. A. Crispino, P. T. Ho, K. B. Sharpless, *Science* **1993**, *259*, 64.
[38] J. M. Hawkins, A. Meyer, *Science* **1993**, *260*, 1918.

Shape-Memory Effect



ANGEWANDTE CHEMIE
©WILEY-VCH

Shape-Memory Polymers

Andreas Lendlein* and Steffen Kelch

Material scientists predict a prominent role in the future for self-repairing and intelligent materials. Throughout the last few years, this concept has found growing interest as a result of the rise of a new class of polymers. These so-called shape-memory polymers by far surpass well-known metallic shape-memory alloys in their shape-memory properties. As a consequence of the relatively easy manufacture and programming of shape-memory polymers, these materials represent a cheap and efficient alternative to well-established shape-memory alloys. In shape-memory polymers, the consequences of an intended or accidental deformation caused by an external force can be ironed out by heating the material above a defined transition temperature. This effect can be achieved because of the given flexibility of the polymer chains. When the importance of polymeric materials in our daily life is taken into consideration, we find a very broad, additional spectrum of possible applications for intelligent polymers that covers an area from minimally invasive surgery, through high-performance textiles, up to self-repairing plastic components in every kind of transportation vehicles.

Keywords: block copolymers · material science · polymers · shape-memory polymers

1. Introduction

Shape-memory materials are stimuli-responsive materials. They have the capability of changing their shape upon application of an external stimulus. A change in shape caused by a change in temperature is called a thermally induced shape-memory effect. The main focus of this review article is on thermoresponsive shape-memory polymers. The shape-memory effect is not related to a specific material property of single polymers; it rather results from a combination of the polymer structure and the polymer morphology together with the applied processing and programming technology. Shape-memory behavior can be observed for several polymers that may differ significantly in their chemical composition. However, only a few shape-memory polymers are described in the literature. The process of programming and recovery of a shape is shown schematically in Figure 1. First, the polymer is conventionally processed to receive its permanent shape. Afterwards, the polymer is deformed and the intended temporary shape is fixed. This process is called programming. The programming process either consists of heating up the sample, deforming, and cooling the sample, or drawing the sample at a low temperature (so called "cold drawing"). The permanent shape is now stored while the sample shows the temporary shape. Heating up the shape-memory polymer above a transition temperature T_{trans} induces the shape-memory effect. As a consequence, the recovery of the stored, permanent shape can be observed. Cooling down the polymer below the transition temperature leads to solidification of the material, however, no recovery of the temporary shape can be observed. The effect described is named as a one-way shape-memory effect. By further programming, including mechanical deformation, the work piece can be brought into a temporary shape again. This new temporary shape does not necessarily match the first temporary shape.

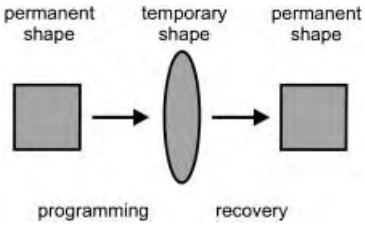


Figure 1. Schematic representation of the thermally induced one-way shape-memory effect. The permanent shape is transferred to the temporary shape by the programming process. Heating the sample to a temperature above the switching transition T_{trans} results in the recovery of the permanent shape.

In Figure 2 a picture sequence demonstrates impressively the performance of shape-memory polymers. The permanent shape of the polymers formed from **1** and **2** is that of a rod,

[*] Dr. A. Lendlein, Dr. S. Kelch
Institut für Chemie
GKSS Forschungszentrum
Kantstrasse 55, 14513 Teltow (Germany)
Fax: (+49) 3328 352 452
E-mail: lendlein@gkss.de

 © WILEY-VCH Verlag GmbH, 69451 Weinheim, Germany, 2002 1433-7851/02/4112-2035 $ 20.00+.50/0

which has been deformed to a spiral (temporary shape) during the programming process. Under the influence of hot air having a temperature of 70 °C the permanent shape is recovered as soon as the switching temperature T_{trans} is reached. The permanent shape is recovered with a precision of more than 99% with appropriately optimized programming conditions. This precision makes these materials suitable for highly demanding applications.[1]

Since the 1960s, polyethylene that is covalently cross-linked by means of ionizing radiation has found broad application as heat-shrinking film or tubing, especially for the insulation of electric wires or as protection against corrosion of pipe lines.[2–7] These materials are marketed under the catchphrase "heat-shrinkable materials". The mechanism of the heat-shrinking process is in analogy with the thermally induced shape-memory effect. Here, the permanent shape is also fixed by covalent cross-links and the switching process is controlled by the melting temperature of the polyethylene crystallites.

More and more reports about linear, phase-segregated multiblock copolymers, mostly polyurethanes, can be found in the literature under the name of the generic term "shape-memory polymers" (see Section 2.4.1). These elastic materials show at least two separated phases. The phase showing the highest thermal transition T_{perm} acts as the physical cross-link and is responsible for the permanent shape. Above this temperature the polymer melts and can be processed by conventional processing techniques such as extrusion or injection molding. A second phase serves as a molecular switch and enables the fixation of the temporary shape. The transition temperature for the fixation of the switching segments can either be a glass transition (T_g) or a melting temperature (T_m). After forming the material above the switching temperature, but below T_{perm}, the temporary shape can be fixed by cooling the polymer below the switching temperature. Heating up the material above T_{trans} again cleaves the physical cross-links in the switching phase. As a result of its entropy elasticity (see Section 2.1.3) the material is forced back to its permanent shape. Polyurethanes with shape-memory properties have found application as, for example, components in auto chokes. In this application it is



A. Lendlein S. Kelch

Andreas Lendlein, born in 1969 in Bendorf (Germany), studied chemistry at the Johannes Gutenberg University of Mainz (1988–1993). In 1993–1996 he did his dissertation with Prof. Dr. Ulrich W. Suter at the material science department of the Swiss Federal Institute of Technology (ETH) in Zurich, Switzerland. In his Ph.D. thesis he dealt with degradable and biocompatible multiblock copolymers with hard segments based on bacterially produced polyesters. In 1996, after a short post-doctoral stay in Zurich, he was awarded the ETH Medal, and in 1997 he moved, as a visiting scientist, to the group of Prof. Dr. Robert Langer at the Massachusetts Institute of Technology (MIT) in Cambridge, USA. Since 1998 he has been head of the department for the Development and Engineering of New Biomaterials, which he established at the German Wool Research Institute at the RWTH Aachen and he habilitated from the Chair of Textile Chemistry and Macromolecular Chemistry at the University of Technology, Aachen. He recently accepted a position as full professor at the University of Potsdam (Germany) and as director of the Institute of Chemistry at the GKSS Research Center in Teltow (Germany). Currently, he is working on the development of intelligent polymers, especially block copolymers and multiphase covalent networks, the processing of these materials, as well as their application in the biomedical field. Besides his academic career, in 1998 he founded, together with Robert Langer, the start-up company mnemoScience GmbH of Aachen, which he runs as managing director. He has received numerous grants, among others, Studienstiftung des deutschen Volkes (1989–1993), Fritz-Ter-Meer Stiftung (1989–1992), Gottlieb Daimler- und Karl Benz-Stiftung (1993–1996), as well as the Liebig Stipendium of the Fonds der Chemischen Industrie (1997–1999). In 1998 he was laureate in the BioFuture Contest of the Ministry for Education and Research (BMBF), in 1999 he was honored by Pinguin Stiftung, in 2000 he received the Hermann-Schnell award of the GDCH, as well as the Innovationspreis of Zenit e. V.

Steffen Kelch, born in 1967 in Mannheim (Germany), studied chemistry from 1989 to 1995 at the University of Karlsruhe (TH) and did his dissertation from 1995–1999 at the Polymer Institute there in the group of Prof. Dr. Matthias Rehahn. In his Ph.D. thesis he dealt with the synthesis and characterization of high molecular weight coordination polymers. In 1996 he worked in the group of PD Dr. Walter Caseri at the Institute of Polymers of the Swiss Federal Institute of Technology in Zurich on the modification of inorganic surfaces. During his doctorate and thereafter as a research associate at the German Plastics Institute (DKI) in Darmstadt he worked on the characterization of polyurethane networks. Since 2000 he has worked as a research scientist in the department for the Development and Engineering of New Biomaterials at the German Wool Research Institute at the University of Technology Aachen.

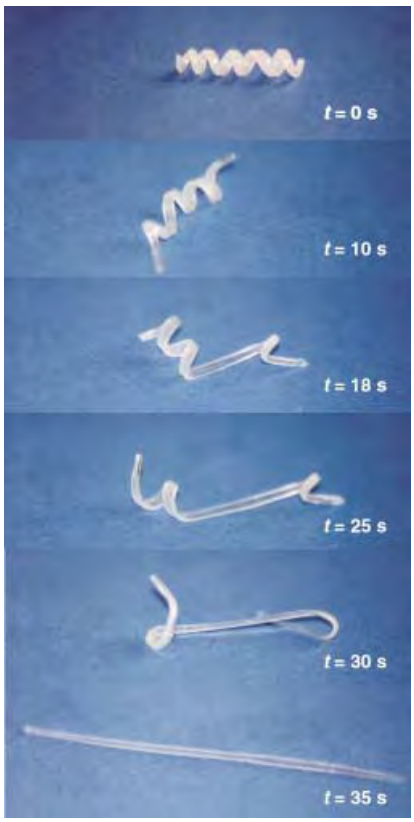
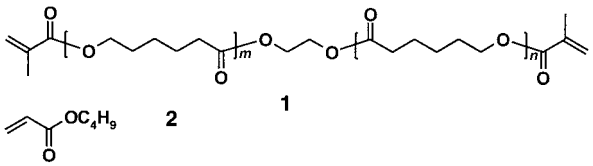


Figure 2. Transition from the temporary shape (spiral) to the permanent shape (rod) for a shape-memory network that has been synthesized from poly(ε-caprolactone) dimethacrylate (**1**) and butylacrylate (**2;** co-monomer content: 50 wt %; see Section 2.6.2). The switching temperature of this polymer is 46 °C. The recovery process takes 35 s after heating to 70 °C.



not the shape-memory effect that is used, but the property of the polymer to soften upon being heated up above the switching temperature.[8–19]

A substantially new development in connection with the design of shape-memory polymers are polymer systems. These are families of polymers in which macroscopic properties (for example, mechanical properties or T_{trans}) can be controlled by a specific variation of molecular parameters. This makes it possible to tailor the specific combination of the properties of the shape-memory polymers that are required for specific applications just by a slight variation of the chemical composition. The shape-memory material presented in Figure 2 belongs to a family of multiphase polymer networks that are biocompatible and biodegradable. Such materials are highly interesting for applications in the field of minimally invasive surgery (see Section 2.6).

There are other classes of materials such as metallic alloys, ceramics, and gels that show thermoresponsive shape-memory properties. A short overview about these other shape-memory materials is given before shape-memory polymers are discussed in detail.

1.1. Metal Alloys

The one-way shape-memory effect as described at the beginning was observed for the first time by Chang and Read in 1951 for a gold–cadmium alloy.[20] In 1963 Buehler et al. described the shape-memory effect of nitinol, an equiatomic nickel–titanium alloy.[21] Here, the shape-memory effect is based on a martensitic phase transition taking place without diffusion (Figure 3). To generate the martensitic phase the

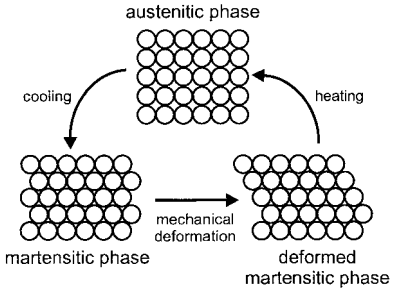


Figure 3. Schematic representation of the mechanism of the shape-memory effect for metallic alloys based on a martensitic phase transformation.

material is cooled from a high temperature or parent phase showing a cubic symmetry (austenitic phase) down to a low temperature phase with lower symmetry (martensitic phase). The formation of the martensitic phase can be controlled by a temperature program which includes heating to temperatures up to 450 °C. The temporary shape of the material can now be produced by deformation of the material in the martensitic phase. The austenitic phase is reached upon heating the sample above the phase transition temperature and a recovery of the original external shape for deformations of up to 8 % can be observed.

Since nitinol is an equiatomic Ni-Ti alloy, possible fluctuations in stoichiometry have a strong influence on the resulting properties of the material. A deviation in the nickel content of 1 atom % can shift the switching temperature up to 100 K. Besides the one-way shape-memory effect, nitinol exhibits so called superelasticity. Superelasticity is based on the phenomenon that the martensitic phase is not stable above a certain temperature in the absence of an external force. Above this temperature an external deformation will spontaneously be recovered.[22a,b,e,f, 23–29]

The Ni-Ti and Cu-Zn-Al alloys all found technical application. Nitinol is widely used for the manufacture of surgical devices and implants because of its biocompatibility.[22h, 30, 31] Cu-Zn-Al alloys are often used for nonmedical applications as a result of their advantageous thermal and electrical conductivity and their better ductility. Cu-Al-Ni as well as iron-based alloys such as Fe-Mn-Si, Fe-Cr-Ni-Si-Co, Fe-Ni-Mn, or Fe-Ni-C alloys have also been investigated in regard to their shape-memory properties. Fe-Mn-Si alloys, in particular, find applications as materials for screwed joints that can be heated after being screwed together to obtain further compression.[22c,d, 23]

Metallic alloys with shape-memory properties can show a two-way shape-memory effect after a certain "thermal train-

ing". In this case the material does not only "remember" the external shape in the parent phase but also the external shape in the martensitic phase. By this, it is possible to produce a defined structure at a defined temperature that has been programmed before.[22a, 27, 30]

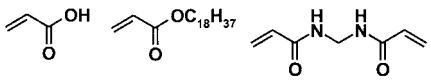
1.2. Ceramics

With certain ZrO_2 ceramics, the transition from a tetragonal to a monoclinic structure occurs as a martensitic phase transition which is induced thermally or by the application of stress. These materials are called martensitic ceramics. The transformation back from the monoclinic to the tetragonal symmetry can occur thermoelastically, which is why martensitic ceramics show a thermoresponsive shape-memory effect.[22g, 23, 24]

1.3. Gels

A remarkable property of polymer gels is their ability to react to changes in the external conditions by considerable volume changes, swelling or shrinkage. The external stimulus is not only limited to temperature changes. Volume changes can also be triggered by a variation in the pH value, the ionic strength, or the quality of the solvent. In addition to this, it is possible to stimulate certain gels by the application of electric fields or light. The crucial point with gels is their poor mechanical stability.[32–45]

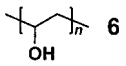
Hydrogels with hydrophobic, crystallizable side chains, and cross-linked poly(vinyl alcohols) show a thermoresponsive one-way shape-memory effect.[32, 33, 37, 39, 40] Hydrogels formed from copolymerized acrylic acid **3** and stearyl acrylate (**4**) cross-linked with methylenebisacrylamide (**5**) show a strong temperature dependence in their mechanical properties.



3 **4** **5**

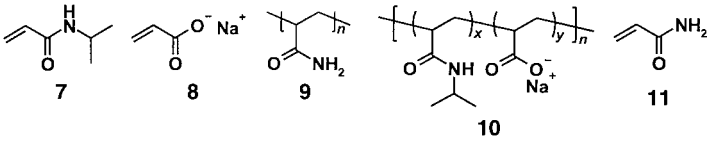
Below 25 °C these polymers behave like tough polymers, while above 50 °C softening enables the materials to be extended up to 50 %. The softening results in a decrease of the elastic modulus by three orders of magnitude. The mechanical stability below 50 °C arises from the crystalline packing of the stearyl side chains. Above this temperature, the aliphatic side chains are amorphous and contribute to the flexibility of the hydrogels. The stretched shape can be maintained by applying the deformation force during the cooling process. When the material is heated up again above the transition temperature the one-way shape-memory effect takes place and the external shape in which the material was produced initially is recovered. The permanent shape is predetermined by the covalent polymer network.[36, 39]

Linear poly(vinyl alcohol) molecules form hydrogels as a result of the formation of physical cross-links through hydrogen bonds and microcrystallites. Above a temperature of 50 °C the physical cross-links melt and results in an increasing loss of stability. Above a temperature of 80 °C the physically cross-linked hydrogels become soluble in water. Chemically cross-linked hydrogels whose permanent shape is stable above 80 °C can be obtained by cross-linking the poly(vinyl alcohol) **6** with glutaraldehyde. After melting the physical cross-links in boiling water, these chemically cross-linked hydrogels can be streched by 200 %. By immersion of the system in methanol, a poor solvent, the elongation, and thus the temporary shape, can be fixed by deswelling and formation of physical cross-links. The permanent shape can be recovered by exposing the gel to boiling water.[32]



6

An example of materials with a thermally induced two-way shape-memory effect are modulated gels. Such gels consist of layers and can perform even more complex shape changes. They contain two types of layers: a thermosensitive control layer (control element) and a substrate layer (substrate element) which is not sensitive to changes in temperature. The control layer consists of an ionic gel made from the copolymer **10** prepared from *N*-isopropylacrylamide (NIPA, **7**) and sodium acrylate (**8**) cross-linked with methylenebisacrylamide (**5**). A tenfold change in volume can be reached as a consequence of a thermally induced abrupt change in the gels microstructure. The gel is swollen below the lower critical



7 **8** **9** **10** **11**

solution temperature (LCST) of 37 °C. Exceeding this temperature causes shrinkage of the gel and the resulting decrease in the thermodynamic quality of the solvent produces a polymer-rich phase. The substrate layer can consist of a gel formed from polyacrylamide (PAAM) cross-linked with **5**. At temperatures above 37 °C, the control layer shrinks drastically while the substrate layer does not undergo any noticeable changes in volume. To connect the two different layers, one side of the control layer, which consists of cross-linked copolymer **10**, is exposed to an aqueous solution of acrylamide (**11**). In this way, the acrylamide solution diffuses into the control layer for a certain time period. The acrylamide is then polymerized by the addition of a radical initiator and **5** to form an interpenetrating network. The bigel strip bends uniformly upon heating to form an arch. A further rolling-up of the gel structure can be realized by an additional increase in temperature or by producing a longer sample. The change in shape is reversible and the system can switch between two defined shapes depending on whether it is below or above the transition temperature. By producing a modulated gel consisting of several alternating layers it is possible to obtain spirally, cylindrically, wavy structures, or any kind of bent, ribbonlike structure.[35, 41]

2. Thermally Induced Shape-Memory Effect in Polymers

Before the molecular mechanism of the thermally induced shape-memory effect is explained in detail, the basic principles of entropy elasticity are discussed. Methods for the quantification of shape-memory properties are presented and the corresponding physical quantities are introduced based on a description of the macroscopic shape-memory effect. A structured overview of thermoplasts and polymer networks that show shape-memory properties will be concluded by a summary of current research work in the field of shape-memory polymers. Polymers developed for biomedical applications in particular will be focused upon.

2.1. Thermodynamic Aspects Significant for the Shape-Memory Effect of Polymers

2.1.1. Chain Conformation of Linear, Amorphous Polymers

In the amorphous state, polymer chains take up a completely random distribution in the matrix, without the restriction that is given by the order of crystallites in semicrystalline polymers. All possible conformations of a polymer chain have the same inner energy. If W expresses the probability of a conformation, a strongly coiled conformation, which is the state of maximum entropy, represents the most probable state for an amorphous linear polymer chain according to the Boltzmann equation [Eq. (1), S = entropy, k = Boltzmann constant].[46]

$$S = k \ln W \tag{1}$$

2.1.2. Transition from the Glassy State to the Rubber-Elastic State

In the glassy state all movements of the polymer segments are frozen. The transition to the rubber-elastic state occurs upon increasing the thermal activation, which means that the rotation around the segment bonds becomes increasingly unimpeded. This situation enables the chains to take up one of the possible, energetically equivalent conformations without disentangling significantly. The majority of the macromolecules will form compact random coils because this conformation is entropically favored and, as a result, much more probable than a stretched conformation (see Section 2.1.1).

In this elastic state a polymer with sufficient molecular weight ($M_n > 20\,000$) stretches in the direction of an applied external force. If the tensile stress is only applied for a short time interval, the entanglement of the polymer chains with their direct neighbors will prevent a large movement of the chain. Consequently, the sample recovers its original length when the external stress is released. In this way, the sample shows a kind of memory for the nonstretched state. This recovery is sometimes called "memory effect", and is based on the sample's tendency to return to its original, most randomly coiled state that represents the most probable state. However, if the external tensile stress is applied for a longer time period, a relaxation process will take place which results in a plastic, irreversible deformation of the sample because of slipping and disentangling of the polymer chains from each other. The tendency of the polymer chains to disentangle and to slip off each other into new positions enables the segments to undergo a relaxation process and to form entropically more favorable random coils.

In a similar way, an increasing rise in temperature above the glass transition temperature favors a higher segment mobility and a decrease in the mechanical stress in the elastic material being stretched by an external force.[47, 48]

2.1.3. Entropy Elasticity

The described slipping or flow of the polymer chains under stress can be stopped almost completely by cross-linking the chains. The cross-linkage points act as anchors or "permanent entanglements" and prevent the chains from slipping from each other. The cross-links can either be chemical and/or physical. Those materials are called elastomers.

Chemically cross-linked polymers form insoluble materials which swell in good solvents. Their shape is fixed during the cross-linking and can not be changed afterwards.

Thermoplastic elastomers contain physical netpoints. A requisite for the formation of the netpoints is the existence of a certain morphology of a phase-separated material, as found for block copolymers containing thermodynamically immiscible components. The highest thermal transition T_{perm} is related to the hard-segment-forming phase. If this thermal transition is not exceeded, these domains will stabilize the permanent shape by acting as physical netpoints in the material. Thermoplastic elastomers are very soluble in suitable solvents and can be processed from the melt.

Besides the netpoints, networks contain flexible components in the form of amorphous chain segments. If the glass transition temperature of these segments is below the working temperature, the networks will be elastic. They show entropy elasticity and can be stretched with a loss of entropy. The distance between netpoints increase during stretching and they become oriented. As soon as the external force is released, the material returns to its original shape and gains back the entropy lost before. As a result, the polymer network is able to maintain the mechanical stress in equilibrium.

Elastomers exhibit some extraordinary properties: they warm up when they are stretched; the elastic modulus increases upon heating; the coefficient of thermal expansion for a stretched elastomer is negative above the glass transition temperature; below the T_g value the sample behaves like a glass and contracts if it is further cooled down (Figure 4). While the coefficient of thermal expansion is negative for a stretched sample, it is positive for an unloaded sample.

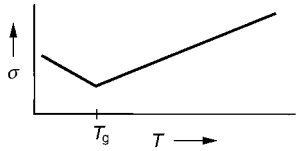


Figure 4. Plot of the stress σ in an elastomer which is stretched and then kept under constant strain over a temperature range above and below the T_g value.

The inner energy of an ideal elastomer will not change if it is stretched. For this reason, the Helmholtz equation for the free energy U is reduced according to

Equation (2). From the stress–strain behavior of a polymer network with a low degree of cross-linking and netpoints that

$$U = -T\Delta S \quad (2)$$

are sufficiently far away from each other, the change in free energy for the stretching of a standard volume is given by Equation (3). N is the number of chain segments between the netpoints and λ_x, λ_y, and λ_z represent the elongation ratios in three dimensions ($\lambda = l/l_0$), where l represents the length of the segments between the netpoints in the stretched state, and l_0 represents the length of the segments in the unloaded state.[46, 47]

$$U = \frac{1}{2}NkT(\lambda_x^2+\lambda_y^2+\lambda_z^2-3) \quad (3)$$

2.2. Molecular Mechanism of the Shape-Memory Effect of Polymers

An elastomer will exhibit a shape-memory functionality if the material can be stabilized in the deformed state in a temperature range that is relevant for the particular application. This can be reached by using the network chains as a kind of molecular switch. For this purpose the flexibility of the segments should be a function of the temperature. One possibility for a switch function is a thermal transition (T_{trans}) of the network chains in the temperature range of interest for the particular application. At temperatures above T_{trans} the chain segments are flexible, whereas the flexibility of the chains below this thermal transition is at least partly limited. In the case of a transition from the rubber-elastic or viscous state to the glassy state, the flexibility of the entire segment is limited. If the thermal transition chosen for the fixation of the temporary shape is a melting point, strain-induced crystallization of the switching segment can be initiated by cooling the material which has been stretched above the T_{trans} value. The crystallization achieved is always incomplete, which means that a certain amount of the chains remains amorphous. The crystallites formed prevent the segments from immediately reforming the coil-like structure and from spontaneously recovering the permanent shape that is defined by the netpoints. The permanent shape of shape-memory networks is stabilized by covalent netpoints, whereas the permanent shape of shape-memory thermoplasts is fixed by the phase with the highest thermal transition at T_{perm}.

The molecular mechanism of programming the temporary form and recovering the permanent shape is demonstrated schematically in Figure 5 for a linear multiblock copolymer, as an example of a thermoplastic shape-memory polymer, as well as for two covalently cross-linked polymer networks.

The "memory effect" mentioned in Section 2.1.2 is not a shape-memory effect. This expression describes the property of an elastomer one would not expect for an amorphous polymer chain. The "memory effect" represents a problem in the processing of non-vulcanized natural rubber. In the case of a quick deformation of the amorphous material by a sudden subsequent decrease or removal (or reduction) of the external force, the polymer re-forms its original shape. Such polymers

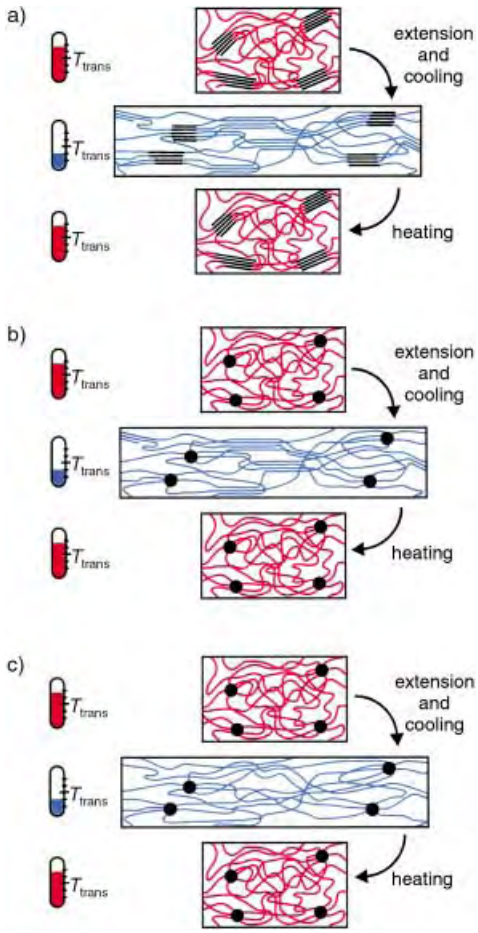


Figure 5. Schematic representation of the molecular mechanism of the thermally induced shape-memory effect for a) a multiblock copolymer with $T_{trans} = T_m$, b) a covalently cross-linked polymer with $T_{trans} = T_m$, and c) a polymer network with $T_{trans} = T_g$. If the increase in temperature is higher than T_{trans} of the switching segments, these segments are flexible (shown in red) and the polymer can be deformed elastically. The temporary shape is fixed by cooling down below T_{trans} (shown in blue). If the polymer is heated up again, the permanent shape is recovered.

will also exhibit a shape-memory effect if a suitable programming technique is applied. In this case, temporary entanglements of the polymer chains which act as physical netpoints can be used for the fixation of the permanent shape. This thermal transition can be used as a switching transition if the glass transition of the amorphous material is in the temperature range that is relevant for a specific application. In Section 2.4.2 this shape-memory mechanism is explained for a high molecular weight, amorphous polynorbornene.

2.3. Macroscopic Shape-Memory Effect and Thermomechanical Characterization

2.3.1. Cyclic, Thermomechanical Characterization

The shape-memory effect can be quantified by cyclic, thermomechanical investigations. The measurements are performed by means of a tensile tester equipped with a thermochamber. In this experiment, different test protocols

are applied that differ, for example, in the programming procedure (cold drawing at $T < T_{trans}$ or temporarily heating up of the test piece to $T > T_{trans}$) or in the control options (stress or strain controlled). A single cycle includes programming the test piece and recovering its permanent shape. A typical test protocol is as follows: first, the test piece is heated up to a temperature T_{high} above the switching temperature T_{trans} and is stretched to the maximum strain ε_m. In the case of thermoplasts it is important not to exceed the highest thermal transition T_{perm} which would cause the polymer sample to melt. The sample is cooled down below the transition temperature T_{trans} under a constant strain ε_m to a temperature T_{low}, thus fixing the temporary shape. Retracting the clamps of the tensile tester to the original distance of 0% strain causes the sample to bend. After heating the sample up to $T_{high} > T_{trans}$, it contracts and the permanent shape is recovered. The cycle then begins again.

The result of such a measurement is usually presented in a $\varepsilon - \sigma$ curve (Figure 6a; σ = tensile stress). This is the reason for this test protocol being called a "two-dimensional measurement". Figure 6 represents schematic curves. Different effects can result in changes to the curve, particularly when the stretched sample is cooled down (position ② in Figure 6a). Among others, the following effects play a role in these changes: differences in the expansion coefficient of the stretched sample at temperatures above and below T_{trans} as a result of entropy elasticity (see Section 2.1.3, Figure 4), as well as volume changes arising from crystallization in the case of T_{trans} being a melting point.

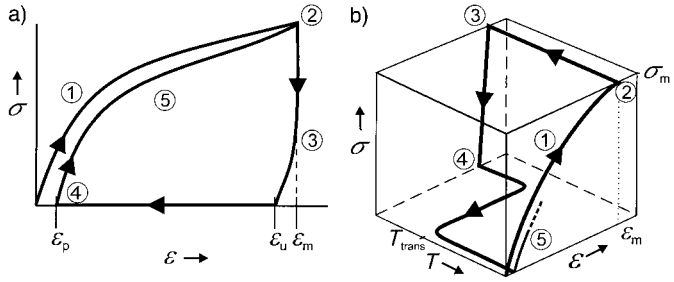


Figure 6. Schematic representation of the results of the cyclic thermomechanical investigations for two different tests: a) ε-σ diagram: ①—stretching to ε_m at T_{high}; ②—cooling to T_{low} while ε_m is kept constant; ③—clamp distance is driven back to original distance; ④—at $\varepsilon = 0\%$ heating up to T_{high}; ⑤—start of the second cycle. b) ε-T-σ diagram: ①—stretching to ε_m at T_{high}; ②—cooling down to T_{low} with cooling rate $k_{cool} = dT/dt$ while σ_m is kept constant; ③—clamp distance is reduced until the stress-free state $\sigma = 0$ MPa is reached; ④—heating up to T_{high} with a heating rate $k_{heat} = dT/dt$ at $\sigma = 0$ MPa; ⑤—start of the second cycle.

In addition to the elastic modulus $E(T_{high})$ at T_{high}, which can be determined from the initial slope in the measurement range ① (Figure 6a), the elastic modulus of the stretched sample at T_{low} can also be determined from the slope of the curve at ③ (Figure 6a). The important quantities to be determined for describing the shape-memory properties of the material at a strain ε_m are the strain recovery rate R_r and the strain fixity rate R_f. Both can be determined according to equations (4), (5), and (6) from cyclic, thermomechanical measurements.

The strain recovery rate R_r quantifies the ability of the material to memorize its permanent shape and is a measure of how far a strain that was applied in the course of the programming $\varepsilon_m - \varepsilon_p(N-1)$ is recovered in the following shape-memory transition. For this purpose the strain that occurs upon programming in the Nth cycle $\varepsilon_m - \varepsilon_p(N-)$ is compared to the change in strain that occurs with the shape-memory effect $\varepsilon_m - \varepsilon_p(N)$ [Eq. (4)]. $\varepsilon_p(N-1)$ and $\varepsilon_p(N)$

$$R_r(N) = \frac{\varepsilon_m - \varepsilon_p(N)}{\varepsilon_m - \varepsilon_p(N-1)} \quad (4)$$

represent the strain of the sample in two successively passed cycles in the stress-free state before yield stress is applied. The total strain recovery rate $R_{r,tot}$ is defined as the strain recovery after N passed cycles based on the original shape of the sample [Eq. (5)]. The strain fixity rate R_f describes the ability

$$R_{r,tot}(N) = \frac{\varepsilon_m - \varepsilon_p(N)}{\varepsilon_m} \quad (5)$$

of the switching segment to fix the mechanical deformation which has been applied during the programming process. It describes how exactly the sample can be fixed in the stretched shape after a deformation to ε_m. The resulting temporary shape always differs from the shape achieved by deformation. The strain fixity rate R_f is given by the ratio of the strain in the stress-free state after the retraction of the tensile stress in the Nth cycle $\varepsilon_u(N)$ and the maximum strain ε_m [Eq. (6)].[1]

$$R_f(N) = \frac{\varepsilon_u(N)}{\varepsilon_m} \quad (6)$$

As indicated in Figure 6, the first few cycles can differ from each other. The curves become more similar with an increasing number of cycles. The process of deformation and recovery of the permanent shape becomes highly reproducible. The changes in the first few cycles are attributed to the history of the sample, thus, processing and storage play an important role. During the first cycles a reorganization of the polymer on the molecular scale takes place which involves deformation in a certain direction. Single polymer chains arrange in a more favorable way in regard to the direction of deformation. Covalent bonds may be broken during this process.

An important variable that can not be determined by a two-dimensional measurement is T_{trans}. In this respect, the three-dimensional test record is interesting, and is shown schematically in Figure 6b. In contrast to the two-dimensional measurement, the sample is cooled down in a controlled way at a strain of ε_m and a constant tensile stress σ_m. The change in strain in this region is influenced by the temperature dependence of the coefficient of thermal expansion of the stretched polymer (see Section 2.1.3) and volume effects based on the thermal transition at T_{trans} (for example, a crystallization process). Having reached T_{low}, the strain is driven back until a stress-free state is reached. The sample is then heated up to T_{high} in a controlled way. In the course of this experiment the tensile stress is kept constant at 0 MPa, which

means that the clamps follow the movement of the test piece. The mechanical movement occurring in the course of the shape-memory effect is recorded as a function of the temperature. Both the temperature interval as well as T_{trans} in which the shape-memory effect takes place can be determined from the interpretation of the ε-T plane of the ε-T-σ diagram.

2.3.2. Bending Test for the Determination of the Shape-Memory Effect

In the course of the bending test a sample is bent at a given angle θ_i at a temperature above the switching transition and is kept in this shape. The so-deformed sample is cooled down to a temperature $T_{low} < T_{trans}$ and the deforming stress is released. Finally, the sample is heated up to the measuring temperature $T_{high} > T_{trans}$ and the recovery of the permanent shape is recorded. The deformation angle θ_f varies as a function of time. The recovery rate R_b is calculated from the ratio of the different angles before and after recovery Θ_f and the deformation angle Θ_i in the temporary shape [Eq. (7)].[18, 19]

$$R_b = \frac{(\theta_i - \theta_f)}{\theta_i} \quad (7)$$

2.3.3. Shrinkage Determination of Heat-Shrinkable Products

The test samples stretched at room temperature are kept under a constant stress of about 0.2 MPa and heated above T_{trans}. In the case of polyethylene cross-linked by means of ionizing rays, the material is heated up above the melting point of the PE crystallites. The shrinkage is then given by the ratio [Eq. (8)], where $\lambda = l_{str}/l_0$, l_{str} is the length of the stretched sample, and l_s the length of the sample after the shrinkage process. Partly, instead of the original length of the sample l_0, the stretching ratio λ, the ratio of the length of the stretched sample l_{str} and l_0, is used. The shrinkage process depends on the temperature T_{high}. Therefore, the shrinkage $l_s(t)$ is often determined as a function of time for a given shrinkage temperature T_{high}.[49, 50]

$$\text{Heat shrinkage [\%]} = \frac{l_{str} - l_s}{l_{str} - l_0}100 = \frac{l_{str} - l_s}{l_{str}(1 - \lambda^{-1})}100 \quad (8)$$

2.4. Physically Cross-Linked Shape-Memory Polymers

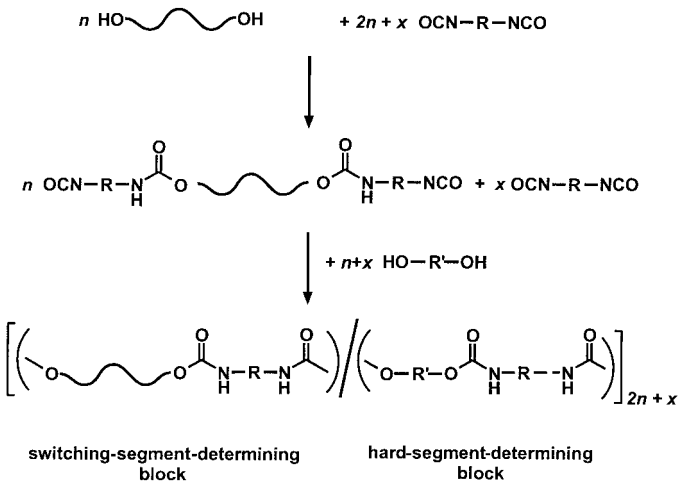
2.4.1. Linear Block Copolymers

In this section shape-memory polymers are presented that form part of the class of linear block copolymers. The mechanism of the thermally induced shape-memory effect of these materials is based on the formation of a phase-segregated morphology, which has been described in Section 2.2, with one phase acting as a molecular switch. Through the formation of physical netpoints, the phase with the highest thermal transition T_{perm} on the one hand provides the mechanical strength of the material, especially at $T < T_{perm}$, and on the other hand is responsible for the fixation that determines the permanent shape. The materials are divided into two categories according to the thermal transition of the particular switching segment on which the shape-memory effect is based. Either the transition temperature T_{trans} is a melting temperature T_m or a glass transition temperature T_g. In the case of a melting temperature, one observes a relatively sharp transition in most cases while glass transitions always extend over a broad temperature range. Mixed glass transition temperatures T_{gmix} between the glass transition of the hard-segment- and the switching-segment-determining blocks may occur in the cases where there is no sufficient phase separation between the hard-segment-determining block (block A) and the switching-segment-determining block (block B). Mixed glass transition temperatures can also act as switching transitions for the thermally induced shape-memory effect. Table 1 gives an overview of the various possible combinations of hard-segment- and switching-segment-determining blocks in linear, thermoplastic shape-memory polymers.

All the linear polyurethane systems presented in the following paragraph are synthesized according to the prepolymer method. Thermoplastic polyurethane elastomers are produced on an industrial scale by means of this technique. In this process, isocyanate-terminated pre-polymers are obtained by reaction of difunctional, hydroxy-terminated oligoesters and -ethers with an excess of a low molecular weight diisocyanate (Scheme 1, 1st reaction step). Low molecular weight diols and diamines are added as so called chain extenders to further couple these prepolymers. Linear, phase-segregated polyurethane- or polyurethane–urea block copolymers are obtained in this way (Scheme 1, 2nd reaction step). Each polymer chain contains segments of high polarity composed of urethane and urea bonds that are linked through

Table 1. Possible combinations of hard-segment- (block A) and switching-segment-determining blocks (block B) in linear, thermoplastic block copolymers with thermally induced shape-memory effects. In the block polymers in category 1 the permanent shape is determined by the thermal transition at melting ($T_{perm} = Tm\,A$), in category 2 at the glass transition ($T_{perm} = T_{gA}$) of the hard-segment-determining block.

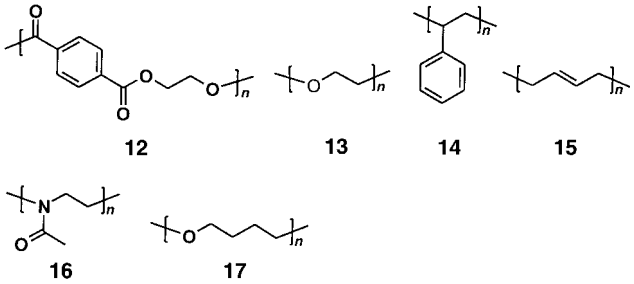
Category	Block A		Block B		Phase-segregated block copolymers	
	highest thermal transition	2nd thermal transition	highest thermal transition	2nd thermal transition	T_{perm}	possible switching transitions T_{trans}
1.1	T_{mA}	T_{gA}	T_{mB}	T_{gB}	T_{mA}	T_{mB}, T_{gA}, T_{gB}
1.2	T_{mA}	T_{gA}	T_{mB}	T_{gB}	T_{mA}	T_{mB}, T_{gmix}
1.3	T_{mA}	T_{gA}	T_{gB}		T_{mA}	T_{gA}, T_{gB}
1.4	T_{mA}	T_{gA}	T_{gB}		T_{mA}	T_{gmix}
2.1	T_{gA}		T_{mB}	T_{gB}	T_{gA}	T_{mB}, T_{gB}
2.2	T_{gA}		T_{mB}	T_{gB}	T_{gA}	T_{mB}, T_{gmix}
2.3	T_{gA}		T_{gB}		T_{gA}	T_{gB}



Scheme 1. Prepolymer method for the synthesis of thermoplastic polyurethanes. R and R′ are short chain groups with two free valences.

chain-extender molecules. As a consequence of their high intermolecular interaction, they form the so called hard segments. Strictly speaking, they represent the hard-segment-forming phase that is embedded in an amorphous elastic matrix. This amorphous matrix, with its low glass transition temperature lying far below the normal operating temperature, forms the so called soft segment. In the case of polyurethanes with shape-memory effects, this segment serves as a switching segment. For this purpose it is modified in such way that the thermal transition is located in a temperature range relevant for the respective application. Hard segment "clusters" with dimensions under 1 μm are formed by the phase-separation process that occurs. These clusters have high T_g or T_m values and act as multifunctional physical netpoints. These so-called plastic domains act as a reinforcing filler. Their ability to deflect mechanical energy by deformation enables the growth of microcracks to be prevented. They also impart cross-breaking strength and impact strength to the material.[51]

In the following paragraph polymer systems are introduced whose shape-memory effect can be triggered by the transition of a melting point. Shape-memory polymers with $T_{trans} = T_m$ are represented by polyurethanes, polyurethanes with ionic or mesogenic components, block copolymers consisting of polyethyleneterephthalate (**12**, PET) and polyethyleneoxide (**13**, PEO), block copolymers containing polystyrene (**14**) and poly(1,4-butadiene) (**15**), and an ABA triblock copolymer made from poly(2-methyl-2-oxazoline) (**16**, A block) and poly(tetrahydrofuran) **17** (B block). Polyurethane systems with



12 **13** **14** **15**

16 **17**

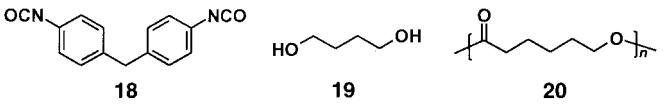
$T_{trans} = T_g$ are then introduced. Table 2 gives an overview of the chemical composition of the linear block copolymers and their respective transition temperatures that resulted in switching transitions, as well as the variability in the switching temperatures.

The thermal transitions of the pure polymer blocks of those shape-memory materials mentioned in paragraph 2.4.1 are listed in Table 3.

2.4.1.1. Multiblock Copolymers with $T_{trans} = T_m$

Polyurethanes with a Poly(ε-caprolactone) Switching Segment

Kim and co-workers synthesized polyesterurethanes (PEUs, Table 2, first entry) with a hard-segment-determining block of methylenebis(4-phenylisocyanate) (**18**, MDI) and 1,4-butanediol (**19**) by using the pre-polymer method.[13, 14, 52] The highest thermal transition T_{perm} corresponding to the



18 **19** **20**

melting temperature of the hard-segment-determining blocks is found in the range between 200 and 240 °C. Poly(ε-caprolactone)diols with a number-average molecular weight (M_n) between 1600 and 8000 form the switching segments. The switching temperature for the shape-memory effect can vary between 44 and 55 °C depending on the weight fraction of the switching segments (variation between 50 and 90 wt %) and the molecular weight of the used poly(ε-caprolactone)-diols. The crystallinity of the switching segment blocks determined by comparision of the partial melt enthalpies with the melt enthalpy of 100 % crystalline poly(ε-caprolactone) (**20**) becomes higher as the weight fraction and the molecular weight of the poly(ε-caprolactone)diols used increases. Hence, the crystallization of the poly(ε-caprolactone) segments is hindered by incorporating them into the multiblock copolymers. The crystallinity observed is between 10 and 40 %. No crystallization can be observed when the poly(ε-caprolactone)diol has a number-average molecular weight below 2000, presumably, because of the low degree of phase separation. In cyclic thermomechanical measurements, an increase of the initial slope with the number of cycles is found. A behavior which is named "cyclic hardening" can be observed during the initial four to five cycles. This effect is caused by a relaxation of the material in the stretched state which results in an increasing orientation and crystallization of the chains. As a consequence, the resistance of the material against the strain grows with the number of cycles. The materials reach constant strain recovery rates after the third cycle. Polyurethanes formed from a high molecular weight poly(ε-caprolactone) and a high weight fraction of hard-segment-determining blocks show the best shape-memory properties: the strain recovery rate increases up to 98 % with strains ε_m of 80 %. Moreover, the shape-memory properties are strongly influenced by the degree of strain applied: the strain recovery rates reached decrease with applied strains of

Table 2. Overview of linear, thermoplastic block copolymers with thermally induced shape-memory effects.

Category according to Table 1	Hard-segment-forming phase	Switching-segment-forming phase	T_{trans} [°C]	Ref.
Multiblock copolymers with $T_{trans} = T_m$				
1.1	MDI/1,4-butanediol	poly(ε-caprolactone) (M_n = 1600, 2000, 4000, 5000, 7000, and 8000)	T_m of poly(ε-caprolactone) crystallites: 44 – 55	[13, 14, 52]
1.1	MDI/1,4-butanediol dimethyloylpropionic acid	poly(ε-caprolactone) (M_n = 2000, 4000, and 8000)	T_m of poly(ε-caprolactone) crystallites: 45 – 55	[17]
1.2 (mesogenic segments cause further transitions)	MDI/BEBP or BHBP	poly(ε-caprolactone) (M_n = 4000)	T_m of poly(ε-caprolactone) crystallites: 41 – 50	[53]
1.2 (mesogenic segments cause further transitions)	HDI/4,4′-dihydroxybiphenyl	poly(ε-caprolactone) (M_n = 4000)	T_m of poly(ε-caprolactone) crystallites: 38 – 59	[54]
1.2 (mixed T_g at −25 – 15 °C)	poly(ethylene terephthalate)	poly(ethylene oxide) (M_n = 4000, 6000, 10000)	T_m of poly(ethylene oxide) crystallites: 40 – 60	[15, 16, 55]
2.1	PS (**14**)	poly(1,4-butadiene) (**15**)	T_m of polybutadiene crystallites: 45 – 65	[56, 95]
2.1 (ABA triblock copolymer)	poly(2-methyl-2-oxazoline)	poly(tetrahydrofuran) (M_n = 4100 – 18800)	T_m of poly(tetrahydrofuran) crystallites: 20 – 40	[57]
Multiblock copolymers with $T_{trans} = T_g$				
1.1 (separate T_g values for poly(tetrahydrofuran) segments with M_n = 1000, 2000, 2900)	MDI/1,4-butanediol	poly(tetrahydrofuran) (M_n = 250, 650, 1000, 2000, 2900)	T_g of poly(tetrahydrofuran) segments or mixed T_g: −56 – 54	[18, 19]
1.2 (mixed T_g for poly(tetrahydrofuran) segments with M_n = 250, 650)				
1.3	MDI/1,4-butanediol	poly(ethylene adipate) (M_n = 300, 600, 1000, 2000)	T_g of poly(ethylene adipate) segments: −5 – 48	[11]
1.2 – 1.4	2,4-TDI or MDI	poly(propylene oxide) (M_n = 400, 700, 1000)	T_g: −45 – 48	[58, 59]
	carbodiimide-modified diisocyanates (MDI and HDI)	poly(butylene adipate) (M_n = 600, 1000, 2000)		
	ethylene glycol or bis(2-hydroxyethyl)hydrochinone	poly(tetrahydrofuran) (M_n = 400, 650, 700, 850, 1000)		
	combination of (2,2′-bis(4-hydroxyphenyl)-propane (bisphenol A) and ethylene oxide	combination of (2,2′-bis(4-hydroxyphenyl)-propane (bisphenol A) and propylene oxide (M_n = 800)		
		poly(ethylene oxide) (M_n = 600)		

250 % from rates of more than 90 % to rates of 80 %. Besides the crystallinity of the switching segments, the decisive factors that influence the recovery properties are the formation and stability of the hard-segment-forming domains, especially in the temperature range above the melting temperature of the switching-segment crystallites. Above a lower limit of the hard-segment-determining blocks of 10 wt %, the hard-segment domains are no longer sufficiently pronounced to function efficiently as physical cross-links. A slight increase in the switching temperature can be observed during the initial three cycles. This behavior is interpreted as the destruction of weak netpoints followed by an increasing formation of an ideal elastic network. Tables 4 and 5 show values determined for the shape recovery and shape fixity rates. The samples were stretched at room temperature after a thermal pretreatment at 80 °C.

Incorporation of Ionic Components into the Hard-Segment-Forming Phase

Several investigations have dealt with the question as to whether the incorporation of ionic or mesogenic moities into the hard-segment-forming phase can influence the mechanical and shape-memory properties through the introduction of additional intermolecular interactions by possibly enhancing the degree of phase separation. For this purpose, polyester urethanes have been synthesized by the pre-polymer method using MDI and 1,4-butanediol as the hard-segment-determining block. Half of the chain-extending 1,4-butanediol in the hard-segment-forming phase was substituted by 2,2-bis(hydroxymethyl)propionic acid (**21**) so as to introduce additional intermolecular interactions.[17] Poly(ε-caprolactone)diols with number-average molecular weights between 2000 and 8000 were used as the switching-segment-forming phase. The weight fraction of the switching segment was around 70 wt % for materials based on poly(ε-caprolactone)diols with number-average molecular weights between 2000 and 8000 and varied between 55 and 90 wt % for poly(ε-caprolactone)diol with a molecular weight of 4000. The switching temperatures for the shape-memory effect were between 44 and 55 °C. A hard-segment phase additionally stabilized by ionic interactions can be formed by neutralization of the propionic acid moities with triethylamine. These multiblock copolymers having polyelectrolyte character are so called "ionomers". As a result of their additional Coulomb



21

Table 3. Thermal properties of the pure polymer blocks.

Polymer block	Block type	T_m [°C]	T_g [°C]
MDI/1,4-butanediol	A	200–240[60]	125[62]
		193–232[61]	100[63]
poly(ε-caprolactone)	B	M_n = 1600: 46.3	−60[67]
		M_n = 4000: 53.5	
		M_n = 7000: 55.9[64]	
		M_n > 10000 (semicristalline): 59–64[65, 66]	
poly(tetrahydrofuran)	B	M_n = 250: −7.9	
		M_n = 250: −95[70]	
		M_n = 650: 20.2	
		M_n = 1000: 23.6	
		M_n = 2000: 27.7	
		M_n = 2900: 45.8[68]	
		57[69]	−84 °C[71]
poly(ethylene adipate)	B		−46[72]
poly(ethylene terephthalate)	A	260 (semicrystalline)[73]	81 (semicrystalline)[75]
		280 (semicrystalline, equilibrium)[74]	125 (semicrystalline and oriented)[76]
poly(ethylene oxide)	B	M_n = 1400–1600: 45–50	
		M_n = 1900–2200: 50–52	
		M_n = 3500–4000: 59–61	
		M_n = 5000–7000: 60–63	
		M_n = 8500–11500: 63–65[77]	
		69[78]	−67[79]
PS(**14**)	A	270[80]	100 (amorphous)[82]
		240[81]	90[83]
poly(1,4-butadiene) (**15**)	B	97 (modification I)	−107[86]
		145 (modification II)[84, 85]	
Polyethylene	A	134 (90% crystalline, linear PE)	−125 to −120 (γ)
		115 (60% crystalline; LDPE)[87]	−80 to −40 (β) [88]
poly(vinyl acetate)	B		31[89]
polyamide-6 (nylon-6)	A	215–220[90]	40[92]
		223[91]	
poly(2-methyl-2-oxazoline)	A		480[93]

Table 4. Dependence of the strain recovery rate after the first cycle ($R_r(1)$ in %) at $\varepsilon_m = 80\%$ on the switching segment content SC [wt%] for different molecular weights M_n of the used poly(ε-caprolactone)diols.[14]

M_n	SC	$R_r(1)$	M_n	SC	$R_r(1)$
4000	81	98	7000	92	60
5000	89	50	7000	88	93
5000	84	96	7000	85	95
5000	80	98	7000	81	98

Table 5. Dependence of the strain recovery rate (R_r) and strain fixity rate (R_f) after the first and fourth cycle on the switching segment content SC [wt%] and the strain ε_m for different molecular weights M_n of the poly(ε-caprolactone)diols used.[13]

M_n	SC	ε_m	$R_r(1)$ [%]	$R_r(4)$ [%]	$R_f(1)$ [%]	$R_f(4)$ [%]
2000	70	200	48	20	95	98
2000	55	200	73	65	58	60
4000	75	600	75	60	85	90
4000	70	200	82	73	92	95
8000	55	200	62	52	88	90

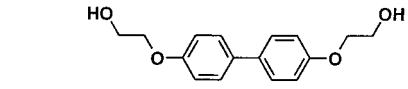
interactions, they exhibit a higher elastic modulus and higher mechanical strength than the systems containing uncharged hard segment blocks. The transition from the uncharged multiblock copolymers to ionomers results in an increase in the elastic moduli to between 24 and 34% at 25 °C, depending on the molecular weight and the weight fraction of the poly(ε-caprolactone)diols used. An increase in the elastic moduli between 38 and 156% is observed at 65 °C. In addition, an increasing hard-segment content increases the mechanical stability of the materials. The charged systems show up to approximately 10% higher strain recovery rates and equal strain fixity rates relative to the uncharged systems. Table 6 displays the strain fixity and strain recovery rates for two materials with and without ionomer, both based on poly(ε-caprolactone)diol with a number-average molecular weight of 4000 and a poly(ε-caprolactone) content of 70 wt%.

Table 6. Comparison of strain recovery rate (R_r) and strain fixity rate (R_f) at $\varepsilon_m = 200\%$ and a switching segment content of 70 wt% for ionomers and the corresponding non-ionomers.[17]

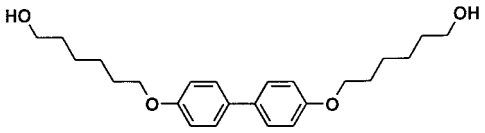
	$R_r(1)$ [%]	$R_r(4)$ [%]	$R_f(1)$ [%]	$R_f(4)$ [%]
ionomer (charged)	66	45	95	95
non-ionomer (uncharged)	62	35	95	95

Incorporation of Mesogenic Components into the Hard-Segment-Forming Phase

In the case of the incorporation of mesogenic diols such as 4,4′-bis(2-hydroxyethoxy)biphenyl (**22**, BEBP) or 4,4′-bis-(2-hydroxyhexoxy)biphenyl (**23**, BHBP) into the hard-segment-determining blocks based on MDI, an increased solubility of these blocks in the switching segment made of poly-(ε-caprolactone) ($M_n = 4000$) is observed.[53] As a consequence, a mixed T_g value of the hard-segment- and switching-segment-forming phase occurs. The strain-induced fixa-



22



23

tion observed is attributed to crystallization of the switching-segment blocks. An increase in the strain fixity rate of more than 20% is observed in the case of the polymers with added BEBP with a switching-segment content increasing from 60 to 80 wt% and a strain ε_m value of 100%. Materials with added BHBP show an increase in the strain fixity rate of 5 to 10% with a strain ε_m of 100 to 300%. Table 7 shows an overview of the recorded shape-memory properties. The strain recovery rates observed at a strain ε_m of 100% correspond to those with a hard-segment-forming phase containing MDI/1,4-butanediol.

Table 7. Dependence of the strain recovery rate ($R_r(4)$) and strain fixity rate ($R_f(4)$) of multiblock copolymers with a hard-segment-forming phase of MDI/1,4-butanediol after the fourth cycle on the switching segment content SC [wt%], the strain ε_m, and the added mesogenic diols.[a]

Additive	SC	ε_m [%]	$R_r(4)$ [%]	$R_f(4)$ [%]
BEBP	80	100	80	98
BEBP	71	100	80	95
BEBP	57	100	85	75
BHBP	80	100	85	85
BHBP	70	100	80	80
BHBP	59	100	85	80
BHBP	80	300	68	95
BHBP	70	300	73	90
BHBP	59	300	63	85

[a] The values are calculated from Figures 2–4 in ref. [53].

*Block Copolymers Made of Polyethylene Terephthalate (**12**) and Polyethylene Oxide (**13**)*

A further example of shape-memory polymers with $T_{trans} = T_m$ are linear, phase-separated block copolymers with a hard-segment-forming phase based on PET and switching-segment blocks of PEO.[15, 16, 55, 94] The highest thermal transition T_{perm} is the melting point of the PET blocks at 260 °C. The thermally induced shape-memory effect is triggered by the melting temperature of the PEO crystallites and can be varied between 40 and 60 °C depending on the molecular mass of the PEO blocks or on the PET content (see Table 2).

The crystalline fraction of the switching segments increases as the molecular weight of the PEO blocks grows. Simultaneously, the melting temperature of the PEO blocks increases as their molecular weight increases. The crystallization of the PEO blocks is more and more hindered as the weight fraction of PET increases. As a consequence, the melting temperature of the switching segment with the same molecular weight decreases in the case of a polymer with an increased content of hard-segment-determining PET blocks. Streching a sample at a temperature near the melting temperature of the PEO segments results in the crystallites of the PEO segments becoming parallelly orientated. They change their shape from spherulitic to fibril-like structures. If these structures are too well developed they hinder the recovery process. This is why a change in the strain recovery rate as a function of the applied strain ε_m is observed depending on the composition of the copolymer or on the developed morphology. To investigate the strain recovery rate the samples were stretched above the melting point of the PEO crystallites at 58 °C, cooled down, and heated up again with a heating rate of 1 K min^{-1}. The shrinkage observed upon heating increases with an increasing molecular weight of the PEO segments up to strains ε_m (up to 100%). After reaching a maximum at a strain of around 150%, the observed shrinkage decreases again. The series of block copolymers investigated here shows improved strain recovery rates if the weight fraction of PET increases. This behavior is explained with the formation of more stable physical bonds in the better aggregated PET blocks. The temperature at which the highest recovery rate can be observed is the so-called recovery temperature T_r. This temperature is found in the range of the melting temperature of the PEO switching segment. Tables 8 and 9 show typical shape-memory properties of PET/PEO block copolymers.

Table 8. Dependence of the strain recovery rate after the first cycle ($Rr(1)$) and the recovery temperature T_r on the switching segment content SC [wt%] and the strain ε_m for different molecular weight M_n poly(ethylene oxide)diols taken from Table 2 in ref. [15].

M_w	SC	T_r [°C]	$R_r(1)$ [%]	ε_m [%]
2000	73	–	–	–
4000	68	43.0	89.8	85
6000	79	48.0	98.7	120
6000	74	47.5	99.1	120
6000	68	46.8	98.9	120
10000	83	54.5	99.5	150
10000	78	53.4	99.7	150

Table 9. Dependence of the strain recovery rate after the first cycle $R_r(1)$ (in%) at $\varepsilon_m = 180\%$ and T_m [°C] on the switching segment content SC [wt%] for different molecular weight M_n poly(ethylene oxide)diols in Table 2 in ref. [16].

M_w	SC	T_m	$R_r(1)$	M_w	SC	T_m	$R_r(1)$
4000	72	45.2	84	6000	74	46.5	92
4000	68	43.9	85	10000	83	54.5	93
6000	79	47.3	90	10000	78	52.7	95

*Block Copolymers Made of Polystyrene (**14**) and Poly(1,4-butadiene) (**15**)*

The poly(1,4-butadiene) blocks in phase-segregated block copolymers consisting of 34 wt% PS and 66 wt% poly(1,4-butadiene) are found to be semicrystalline with a high *trans* ratio.[56, 95] The melting temperature of the poly(1,4-butadiene) crystallites represents the switching temperature for the thermally induced shape-memory effect. The glass transition of the polystyrene is the highest thermal transition T_{perm} and is found at 90 °C. Thus, polystyrene supplies the hard-

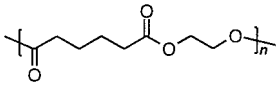
segment-determining blocks. The high glass transition temperature of the polystyrene blocks hinders the polybutadiene chains from slipping off each other upon stretching. The elastic properties, which are not only responsible for the elastic strain but also for the recovery because of the material's entropy relaxation, are attributed to the amorphous areas of the polybutadiene phase. For a material with a poly(1,4-butadiene) content of 86 mol% and a weight-average molecular weight of 70000, the formation of two crystal modifications in the polybutadiene blocks is reported. One of the observed crystal modifications is stable at room temperature. First, the low temperature modification converts into the high temperature modification upon heating up to temperatures higher than 45 °C. Only if a temperature of 65 °C is exceeded does the poly(1,4-butadiene) reach a completely molten, amorphous state. A reversible solid-state transformation is possible between the two crystal modifications. Whereas, a melting point usually guarantees a sharp transition, here, the existance of the two different crystal modifications does not allow an exact tuning of the switching temperature. A high strain recovery rate in the range of 80% is observed ($T = 80$ °C) upon application of a maximum strain ε_m in the range of 100%. R_r still reaches values of around 60% at a maximum strain ε_m of more than 400%. The appearance of the shape-memory effect is explained by the formation of oriented crystallites upon application of high elongations of up to 600%. These oriented crystallites form a fibril-like structure with high regularity over large distances. The single fibrils are linked through amorphous 1,4-polybutadiene chains that are anchored in several crystallites at the same time. The highly ordered morphology described remains stable even after heating above 80 °C.

*ABA Triblock Copolymers Made from Poly(tetrahydrofuran) (**17**) and Poly(2-methyl-2-oxazoline) (**16**)*

ABA triblock copolymers with a central poly(tetrahydrofuran) block (B block) with number-average molecular weights between 4100 and 18800 and equipped with terminal poly(2-methyl-2-oxazoline) blocks (A block) with molecular weights of 1500 are obtained by cationic ring-opening polymerization.[57] The A blocks exhibit glass transition temperatures around 80 °C and represent the hard-segment-forming phase. The poly(tetrahydrofuran) blocks are semicrystalline and exhibit a melting temperature between 20 and 40 °C, depending on their molecular weight. These melting temperatures are used as switching temperatures for a thermally induced shape-memory effect. As the thermal data of the two different segments do not differ significantly from the values of the respective homopolymers, one can assume that the material shows microphase separation. The materials with poly(tetrahydrofuran) blocks having a molecular weight greater than 13000 exhibit very good mechanical strength at room temperature. In contrast to pure poly(tetrahydrofuran), the block copolymer materials show elastic properties and incomplete softening even above the melting temperature of the poly(tetrahydrofuran) segments. This observation is interpreted as the formation of a network with physical cross-links by the poly(2-methyl-2-oxazoline) blocks. These blocks solidify below 80 °C to form a glass. If a sample with a number-average molecular weight of the central poly(tetrahydrofuran) block of 19000 is stretched to 250% elongation at 22 °C, half the elongation will be kept after releasing the external stretching force. A nearly complete recovery takes place upon heating the sample to 40 °C.

2.4.1.2. Multiblock Copolymers with $T_{trans} = T_g$

In phase-segregated block copolymers a glass transition can also be used as the switching transition for the shape-memory effect. A prerequisite is a glass transition that takes place within a narrow temperature range and above the usual operating temperature of this material. In the following paragraph, polymer systems are introduced whose shape-memory effect can be triggered by using a glass transition. All examples are polyurethane systems, in which the hard-segment-forming phase is synthesized from MDI/1,4-butanediol. The switching segment blocks are mostly polyethers such as poly(tetrahydrofuran) but also polyesters such as poly(ethylene adipate) (**24**) are used. In the case of an almost complete phase separation, the glass transition temperature used as the switching transition can origin from the pure switching-segment blocks. In the case of less-separated phases, which can typically be found for short switching-segment blocks, a mixed T_g value from the glass transition temperatures of the hard-segment-forming and the switching-segment-forming phase can occur. This mixed T_g value can be found between the glass transition temperatures of the pure hard-segment- and switching-segment-determining blocks.



24

An example of materials with a mixed T_g value are the systems with poly(tetrahydrofuran) switching-segment blocks having number-average molecular weights of 250 and 650 that have been provided with a hard-segment-forming phase from MDI and 1,4-butanediol by using the pre-polymer method.[18, 19] The highest thermal transition T_{perm} corresponding to the melting temperature of the hard-segment-forming phase can be found between 200 and 240 °C. The phase-segregated block copolymers containing a switching segment with a molecular weight of $M_n = 250$ exhibit a T_g value in the range between 16 and 54 °C, depending on the hard-segment content (hard-segment content between 57 and 95 wt%), a T_g value between -13 and 38 °C for a switching segment with a molecular weight $M_n = 650$ (hard segment content between 32 and 87 wt%), and a T_g value between -36 and 22 °C for a switching segment with a molecular weight of $M_n = 1000$ (content of hard segment determining blocks between 23 and 81 wt%). A mixed T_g value can not be observed if poly(tetrahydrofurans) with a molecular weight of 2000 or 2900 are used because of the good separation of the different blocks. Here, the occurring glass transition temperatures of the poly(tetrahydrofuran) blocks are also dependent on the hard-segment content because the hard segments restrict the mobility of the switching-segment chains.

The shape-memory behavior is determined by means of a bending test (see Section 2.3.2). In the course of the bending

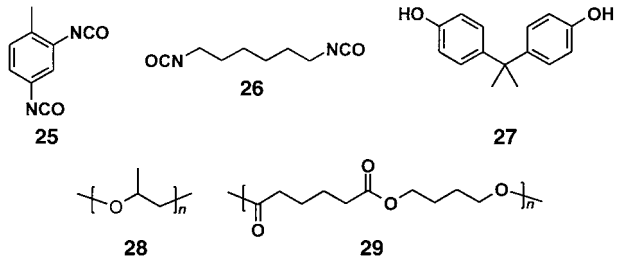
test, the sample is bent at a certain angle θ_i at 80 °C and kept in this deformation. The deformed sample is quickly cooled down to −20 °C and the external force is released. Finally, the sample is brought to the test temperature and its recovery to the original angle is recorded. The deformation recovery rate is calculated from Equation (7). The T_g value increases with increasing amounts of the hard-segment-determining blocks. As a consequence, the temperature at which the shape-memory effect is triggered rises. The deformation recovery rate increases with increasing amounts of the hard segment, and reaches values of up to 99% for the material synthesized from a poly(tetrahydrofuran) with $M_n = 250$ and a hard-segment content of 75 wt%. Complete recovery of materials prepared from a switching segment with $M_n = 650$ is only reached for a hard-segment content of 87% and higher. A constant recovery rate of 95% is reached after approximately 100 repetitions of the bending experiment. If the deformation recovery rate is plotted against the temperature, an increase in the switching temperature with increasing T_g, or increasing hard-segment content, can be found, as expected.

Materials obtained from low molecular weight poly(tetrahydrofurans) but with a high weight fraction of the hard-segment-forming phase show more or less complete deformation recovery. The block copolymers with high amounts of hard segments (between 67 and 95 wt%) show almost complete recovery, independent of the molecular weight of poly(tetrahydrofurans). The deformation recovery rate is higher as the molecular weight of the switching segment decreases. This effect is caused by an increased restriction of the shorter switching-segment chains to coil themselves. A large amount of hard-segment-determining blocks limits the twisting and coiling of the switching segment chains and thus considerably controls the shape-memory properties. In materials with high molecular weight poly(tetrahydrofuran) blocks, the hard-segment-determining blocks can not fulfill this task effectively. Here, the more intense twisting of the chains clearly results in lower recovery rates. This effect can only be compensated for by increasing the proportion of hard-segment-determining blocks.

Block copolymers containing a hard-segment-forming phase of MDI and 1,4-butanediol and a switching segment based on poly(ethylene adipate) (**24**) can be triggered by a glass transition temperature.[11] The glass transition temperature obtained with switching segment blocks with weight-average molecular weights of 300, 600, and 1000 at a constant hard segment content of 75 mol% decreases from 48 to −5 °C with increasing molecular weight of the poly(ethylene adipate)diols used. The T_g value of the switching-segment phase in a block copolymer prepared from poly(ethylene adipate)diol with a molecular weight $M_w = 600$ increases from 13 to 35 °C as the hard-segment content increases (from 75 to 90 mol%). This effect is caused by an increased hindrance in the mobility of the switching-segment chains. Cyclic, thermomechanical tensile tests ($\varepsilon_m = 100\%$) of a material synthesized from a polymer with $M_w = 600$ and a hard segment content of 88 mol% (69 wt%) show that the remaining strain after recovery ε_p increases with the number of cycles. The strain recovery rate decreases from 85% after the first cycle to 70% after the fourth cycle. This behavior is a sign of increased fatigue in the material as the number of cycles increases; this fatigue is caused by an increase in the slippage of the amorphous segments.

Since the 1980s Mitsubishi Heavy Industries have marketed shape-memory polymers that are triggered by means of a glass transition temperature. Hayashi and co-workers have described polyurethane systems with shape-memory properties that exhibit a glass transition temperature in the range between −30 and 30 °C and discussed their application as auto chokes or thermosensitive switching valves.[9, 58] An extension of these polyurethane systems was described in a patent in 1992.[59] Here, materials with glass transition temperatures in the range of −45 to 48 °C are described. This patent refers to the production of fabrics using threads made of polyurethane elastomers showing the shape-memory effect. These are supposed to enhance the crease resistance of the fabrics. Other applications discussed are moisture-permeable membranes in breathable fabrics whose permeability shows a sharp rise above the T_g value because of a higher segment mobility.

Table 2 presents a summary of the possible composition of the hard-segment- and the switching-segment-forming phases prepared at Mitsubishi. The hard-segment-determining blocks can be formed by toluene-2,4-diisocyanate (**25**, 2,4-TDI), MDI (**18**), carbodiimide-modified diisocyanates such as MDI and hexamethylene diisocyanate (**26**, HDI), and chain extenders such as ethylene glycol, bis(2-hydroxyethyl)hydroquinone, or a combination of 2,2′-bis(4-hydroxyphenyl)propane (**27**, bisphenol A) and ethylene oxide. The switching-



segment-determining blocks can be formed by polyethers, for example, PEO (**13**, $M_n = 600$), poly(propylene oxide) (**28**, $M_n = 400$, 700, 1000), poly(tetrahydrofuran) (**17**, $M_n = 400$, 650, 700, 850, 1000), or a combination of bisphenol A and propylene oxide ($M_n = 800$), or oligoesters, for example, poly(butylene adipate) (**29**, $M_n = 600$, 1000, 2000).

The results of cyclic, thermomechanical tensile tests with maximum elongations ε_m of 50 and 100% for two materials differing in E modulus above their T_g values of 45 °C are reported: one material with polyester switching blocks and a relatively high E modulus and another material with polyether switching blocks with a low E modulus. In the course of the cyclic, thermomechanical tensile test, the test pieces were stretched at a temperature T_{high} of 65 °C to the maximum elongation ε_m mentioned above. The samples were then cooled down to a temperature T_{low} of 25 °C and kept for five minutes at this temperature—the deformation was fixed by cooling below the system's glass transition temperature. Subsequently, the external stress was released, the sample

was heated to T_{high}, and the recovery caused by the thermally induced shape-memory effect was recorded. The next cycle was then started. The strain remaining after the materials recovery ε_p increases with a growing number of cycles. The strain recovery rate already decreases during the first 4–5 cycles, which indicates an increasing fatigue of the material or a deterioration of the shape-memory properties. This behavior is interpreted in terms of an irreversible slipping of the chains within the amorphous segments, disentangling of mechanical entanglements, and a partial breakage of the crystalline hard segments especially after the first two cycles. The best strain recovery rates for an applied maximum elongation ε_m of 50 and 100 % are observed for the polyether-based material (Table 10).

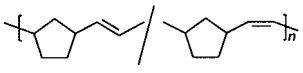
Table 10. Strain recovery rate after the first and fourth cycle. The values are calculated from Figures 6 and 9 in ref. [9].

Switching segment	ε_m [%]	$R_r(1)$ [%]	$R_r(4)$ [%]
polyester	50	80	70
polyester	100	85	80
polyether	50	85	75
polyether	100	90	85

2.4.2. Other Thermoplastic Polymers

Polynorbornene

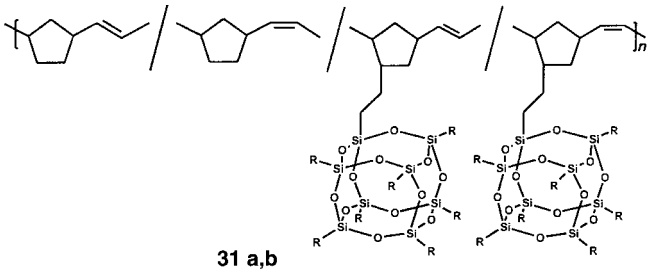
Norsorex is a linear, amorphous polynorbornene **30** developed by the companies CdF Chemie/Nippon Zeon in the late 1970s. The molecular weight of this polynorbornene is about 3×10^6.[8, 96] It is synthesized by a ring-opening metathesis polymerization of norbornene using a tungsten–carbene complex as catalyst. The obtained polynorbornene contains 70 to 80 mol % of *trans*-linked norbornene units and has a glass transition temperature between 35 and 45 °C.[96, 97] The shape-memory effect of this strictly amorphous material is based on the formation of a physically cross-linked network as a result of entanglements of the high molecular weight linear chains, and on the transition from the glassy state to the rubber-elastic state (see Section 2.1.1).[98] The material softens abruptly above the glass transition temperature T_g. If the chains are stretched quickly in this state and the material is rapidly cooled down again below the glass transition temperature the polynorbornene chains can neither slip over each other rapidly enough nor disentangle. It is possible to freeze the induced elastic stress within the material by rapid cooling. Therefore, the sum of the time period for the stretching process $\Delta t_{stretch}$ and the cooling process Δt_{cool} has to be much shorter than the time period it would take the stretched system to relax $\Delta t_{relaxation}$ ($\Delta t_{stretch} + \Delta t_{cool} \ll \Delta t_{relaxation}$). The recovery of the material's original shape can be observed by heating again to a temperature above T_g. This occurs because of the thermally induced shape-memory effect.[98]



30

The norsorex described is not inevitably purely amorphous. Sakurai and Takahashi have reported a high molecular weight polynorbornene with a high proportion of *trans*-linked norbornene units showing a tendency towards strain-induced crystallization.[96, 97] A material that has been stretched four times at 90 °C and has been cooled down rapidly to 0 °C, then exhibits a melting point of 85 °C. Wide-angle X-ray scattering (WAXS) analysis shows X-ray reflections that can be attributed to *cis* and *trans* crystallites. The intensity of these reflections correlates with the content of *cis* and *trans* crystallites. On the basis of this observation, the possibility must not be excluded that crystallites acting as physical netpoints contribute to the shape-memory effect.

Organic–inorganic hybrid polymers consisting of polynorbornene units that are partially substituted by polyhedral, oligomeric silsesquioxanes (POSS, that is, polycyclic silicon–oxygen compounds of the general formula $Si_{2n}H_{2n}O_{3n}$) also form an amorphous polynorbornene material.[99] The hydrogen atoms of the POSS units are either substituted by cyclohexyl or cyclopentyl substituents (**31a**, **b**). A POSS-modified polynorbornene is obtained with a content of 60 to 73 mol % *cis*-linked norbornene units by a ring-opening metathesis polymerization of hybrid-POSS-norbornene monomers and norbornene using a molybdenum catalyst. Up to 8.4 mol % or 50 wt % of the POSS-modified norbornene can be incorporated into the polynorbornene material by using this copolymerization process. The weight-average molecular weights obtained are in the range between 75000 and 740000. The glass transition temperature increases from 52 °C for pure polynorbornene (60 mol % *cis* content) to 81 °C in the case of a polynorbornene with a content of 50 wt % of a POSS norbornene with cyclohexyl substituents.



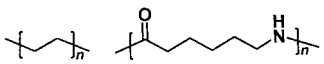
31 a,b
a: R = Cyclopentyl
b: R = Cyclohexyl

The increase in the glass transition temperature of the polynorbornene by incorporation of the POSS modified comonomers results in an improved heat and oxidation resistance. It is the C–C double bond in each repeating unit that makes pure polynorbornene sensitive towards oxidation. It should be possible to obtain better shape-memory properties by increasing the glass transition temperature to additionally slow down the relaxation of the polynorbornyl chains after stretching above T_g. WAXS investigations show that the material with cyclohexyl substituents is amorphous, like pure polynorbornene, whereas the POSS groups aggregate within the material containing cyclopentyl substituents and show phase separation to a certain extent. This arrangement of the side groups provides an additional physical cross-link and hence a stabilization of the material above T_g.

Clearly, better shape-memory properties can be observed relative to pure polynorbornene or the polynorbornene materials with POSS co-monomers bearing cyclohexyl substituents. If a maximum elongation ε_m of 300% is applied, both the pure polynorbornene and the POSS-modified polynorbornene with cyclopentyl substituents show a strain recovery rate of approximately 75% upon heating to a temperature above T_g. If the recovery experiment is performed under a stress of 0.8 MPa for the polynorbornene homopolymer, because of the increased softening at temperatures above T_g after reaching the maximum recovery of 75% at a temperature of 70 °C, again a stretching to over 200% at a temperature of 90 °C can be observed. However, the polynorbornene with a content of 50 wt% POSS-modified norbornene with cyclopentyl substituents retains its shape even at high temperatures (up to 130 °C) because of the stabilization described.

2.4.2.2. Polyethylene/Nylon-6-Graft Copolymer

Polyethylene (**32**, PE) grafted with nylon-6 (**33**) that has been produced in a reactive blending process of PE with nylon-6 by adding maleic anhydride and dicumyl peroxide shows shape-memory properties.[100] The nylon-6 content of



32 **33**

these materials is between 5 and 20 wt%. Nylon-6, which has a high melting temperature of around 220 °C, comprises the hard-segment-forming domains (domain size below 0.3 μm) in a matrix of semicrystalline PE. These domains form stable physical netpoints. The switching temperature for the thermally induced shape-memory effect is given by the melting point of the PE crystallites of 120 °C. The polyethylene crystallites act as molecular switches. Strain fixity rates of around 99% and strain recovery rates between 95 and 97% have been determined for these materials for an elongation ε_m of 100% (see Table 11). For nylon-6 contents between 5 and 20 wt%, no definite influence of the nylon content on the shape-memory properties can be found. The highest recovery rate has been determined to be at 120 °C ± 2 K, which is in the range of the melting temperature of the PE crystallites. The shape-memory properties of PE cross-linked by treatment with ionizing radiation are given in Table 11 for comparison.

Table 11. Dependence of the strain recovery rate (R_r) and strain fixity rate (R_f) on nylon-6 content. The values are taken from Table 3 in ref. [100].

Material	R_r [%]	R_f [%]
LDPE cross-linked with ionizing radiation	94.4	96
PE with 5 wt% nylon-6	95.0	99.8
PE with 10 wt% nylon-6	94.9 – 96.9	99.0 – 99.5
PE with 15 wt% nylon-6	96.0	98.9
PE with 20 wt% nylon-6	96.6	98.6

2.5. Chemically Cross-Linked Shape-Memory Polymers

There are two strategies for the synthesis of polymer networks. Firstly, the polymer network can be synthesized by polymerization, polycondensation, or polyaddition of difunctional monomers and macromonomers by the addition of tri- or higher functional cross-linkers. Figure 7a shows the synthesis of covalently bound networks by treating methacrylate

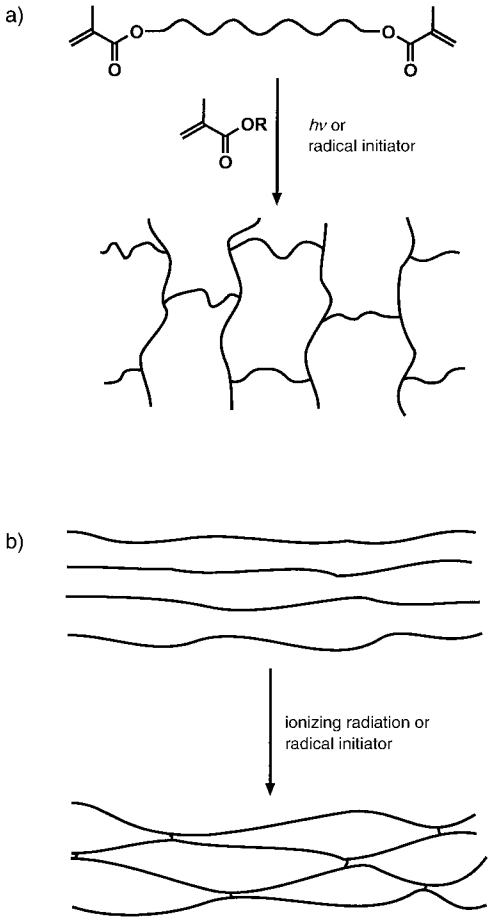


Figure 7. Synthesis strategies for polymer networks a) by polymerization or b) by cross-linking of linear polymers.

monomers with an oligomeric dimethacrylate as a cross-linker. The chemical, thermal, and mechanical properties of the network can be adusted by the choice of monomers, their functionality, and the cross-linker content. The second strategy to obtain polymer networks is the subsequent cross-linking of linear or branched polymers (Figure 7b). In all the methods aimed at subsequent cross-linking of linear polymers the structure of the obtained network is strongly dependent on the reaction conditions and curing times, especially the cross-link density. The cross-linking of linear polymers can take place by a radical mechanism involving ionizing radiation or by the elimination of low molecular weight compounds to generate unsaturated carbon bonds. These have the capability to form chemical cross-links. The addition of radical initiators to linear polymers makes it possible to convert polymer chains into radicals that are able to recombine intermolecularly.

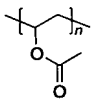
In the following section examples of the synthesis of shape-memory polymer networks for both synthetic strategies are presented. Polymers cross-linked by means of ionizing radiation have particular economic significance.

2.5.1. Network Synthesis by Subsequent Cross-Linking of Linear Polymers

2.5.1.1. Polymers Cross-Linked by Means of Ionizing Radiation

Charlesby was the first to describe the "memory effect" of polyethylene treated with ionizing radiation (γ rays or neutrons).[2] A chemically cross-linked network is formed by application of low doses of irradiation. Polyethylene chains are orientated upon application of mechanical stress above the melting temperature of the polyethylene crystallites, which can be in the range between 60 and 134 °C. Polyethylene crystals are formed by cooling below its crystallization temperature, and these can fix the temporary shape by acting as physical netpoints. Heating the material above the melting temperature of the crystalline domains results in the material returning to its permanent shape, which was fixed during the irradiation process.[2, 101]

This technology has reached high economic significance in the field of heat-shrinkable products. Materials that are most often used for the production of heat-shrinkable polymers are HDPE, LDPE, and copolymers of PE and poly(vinyl acetate) (**34**).[3, 5, 6] After shaping, for example, by extrusion or compression molding, the polymer is covalently cross-linked by means of ionizing radiation, for example, by highly accelerated electrons having energies of 0.5 to 3 MeV. The energy and dose of the radiation have to be adjusted to the geometry of the sample to reach a sufficiently high degree of cross-linking and hence sufficent fixation of the permanent shape. The radiation dose should reach values between 20 and 30 Mrad (200 – 300 kGy). Subsequently, the preformed parts are heated above the melting temperature of the crystallites. At this temperature the material has rubber-elastic or viscoelastic properties. The samples formed in this state and then cooled down keep their temporary shape in the cooled state. The technical term for this process is "expansion". Commercial products have expansion ratios of up to 6:1. Depending on the intended application, heat-shrinkable products made of cross-linked, semicrystalline polymers are delivered either as semifinished products, for example, as heat-shrinkable tubing, or as the final products in the expanded state. These are connected to a substrate by a heat treatment. Areas of applications are, among others, the packing industry, electronic, civil, and process engineering.


34

The influence of the degree of cross-linking of γ-cross-linked PE on the gel content and heat-shrink properties was described for LDPE and HDPE.[102] The gel content increases with the applied radiation dose (0 – 160 kGy). For both materials, the gel point is exceeded by application of radiation doses between 11 and 22 kGy. A higher gel content is reached at the same dose for HDPE. The gel content reaches values of around 60 % for radiation doses of 160 kGy. At a dose of 100 kGy, the heat shrinkage is between 94 and 100 % (T = 130 °C) for LDPE and 100 % (T = 150 °C) for HDPE. Both the applied radiation dose and the shrink temperature chosen have a decisive influence on the heat shrinkage is reached: it increases with increasing radiation dose and temperature.

2.5.1.2. Networks Synthesized by Subsequent Chemical Cross-Linking

Heating poly(vinyl chloride) (**35**, PVC) under a vacuum results in the elimination of hydrogen chloride in a thermal dehydrochlorination reaction. The material can be subsequently cross-linked in an HCl atmosphere. The polymer network obtained shows a shape-memory effect. Skákalová et al. have dehydrochlorinated a non-cross-linked PVC with a number-average molecular weight of about 50 000 and subsequently cross-linked it.[103] The degree of dehydrochlorination varied between 0.6 and 86 %. At the beginning of the dehydrochlorination reaction a strongly cross-linked structure is formed. Afterwards, an increasing degradation of the chains takes place that is accompanied by a loss in the thermal and mechanical stability of the material.


35

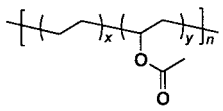
The shape-memory effect of the material was recorded on observing the recovery of a sample, which had been compressed before, with an original volume V_0 upon heating above the glass transition temperature of about 83 °C by means of dilatometry [Eq. (9)]. The highest relative increase

$$\varepsilon(T) = \frac{\Delta V(T)}{V_0} \quad (9)$$

in volume $\Delta V(T)$ with values $\varepsilon(T)$ of 2.0 is reached by samples with a degree of dehydrochlorination of 12.9 and 22.5 % at a temperature of 100 °C. The very weakly dehydrochlorinated sample (degree of dehydrochlorination of 0.6 %) shows almost no recovery. Samples with a degree of dehydrochlorination of 2.6 and 54.4 % exhibit an increase in their relative volume $\varepsilon(T)$ of 1.0.

Polyethylene – Poly(vinyl acetate) Copolymers

Cross-linked poly[ethylene-*co*-(vinyl acetate)] is produced by treating the radical initiator dicumyl peroxide with linear poly[ethylene-*co*-(vinyl acetate)] (**36**) in a thermally induced cross-linking process.[104] Materials with different degrees of cross-linking are obtained depending on the initiator concentration, the cross-linking temperature, and the curing time. The gel content of the obtained cross-linked materials can be used as an estimate of the degree of cross-linking. The co-monomer vinyl acetate, which is randomly incorporated into poly(ethylene-*co*-vinyl acetate) by copolymerization, causes a decrease in the melting temperature of polyethylene crystallites relative to the PE homopolymer. A copolymer having a vinyl acetate content of 28 wt % shows a melting temperature of 70 °C ± 1.5 K for the polyethylene crystallites. The cross-linking does not significantly influence the melting temperature. The values obtained


36

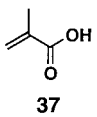
for strain fixity and strain recovery rates at a maximum elongation ε_m of 100% for materials which have been cross-linked at 170 °C are shown in Table 12. To determine these properties, polymer samples were heated up to 80 °C, stretched to $\varepsilon_m = 100\%$, and cooled down quickly to fix the deformation. A strain recovery is observed upon heating the sample up to 90 °C. The strongest recovery effect is found at temperatures just above 60 °C, which is close to the melting point. The strain recovery rate for polymer networks having gel contents lower than 30% already decreases strongly during the first four thermocycles. In contrast, the strain recovery rates of polymer networks which are cross-linked more strongly, with gel contents higher than 30%, stay constant or increase during the first four cycles.

Table 12. Dependence of the strain recovery rate (R_r) and strain fixity rate (R_f) on gel content of poly[ethylene-*co*-(vinyl acetate)] (EVA) as an estimate for the degree of cross-linking. The values are taken from Table 3 in ref. [104].

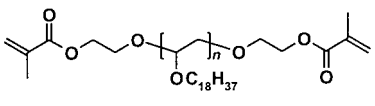
Sample (gel content)	R_r [%]	R_f [%]
EVA non-cross-linked	34.8	99.0
EVA (3.2%)	40.0	98.5
EVA (5.5%)	50.0	97.5
EVA (10.5%)	68.3	97.7
EVA (33.5%)	94.2	96.1
EVA (41.5%)	98.3	95.0

2.5.2. Synthesis of Shape-Memory Networks by Copolymerization of Monofunctional Monomers with Low-Molecular Weight or Oligomeric Cross-Linkers

Covalently cross-linked copolymers made from stearyl acrylate, methacrylate (**37**), and *N*,*N*′-methylenebisacrylamide as a cross-linker exhibit a shape-memory effect. The thermal transition triggering the shape-memory effect is the melting point of the crystalline domains formed by the stearyl side chains. The content of stearyl acrylate varies between 25 and 100 mol%. The melting/switching temperatures T_{trans} for the shape-memory effect are found between 35 °C for a stearyl acrylate content of 25 mol% and 50 °C for pure stearyl acrylate cross-linked by *N*,*N*′-methylenebisacrylamide. The temporary shape is programmed by stretching the sample at 60 °C and then cooling. The permanent shape will be recovered if the polymer sample is heated up above the switching temperature.[105]



37



38

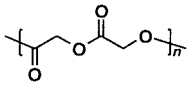
Multiphase copolymer networks are obtained by radical copolymerization of poly(octadecyl vinyl ether)diacrylates (**38**) or -dimethacrylates with butyl acrylate. The octadecyl side chains can crystallize because of the phase separation. The poly(octadecyl vinyl ether)diacrylates used in the synthesis have number-average molecular weights of around 5000. The poly(octadecyl vinyl ether) contents are between 20 and 100 wt%. The melting point of the crystalline domains of 41 to 42 °C is independent of the octadecyl vinyl ether content, which supports the assumption of almost complete phase separation. A strain fixity rate of 83% is reached upon stretching a polymer sample to $\varepsilon_m = 100\%$ at 60 °C and subsequent cooling. A further heating up to 60 °C initiates the shape-memory effect. The materials recovery is described as being complete. However, the strain recovery rate was not quantified more precisely with respect to the composition of the material.[106, 107]

2.6. Biodegradable Shape-Memory Polymer Systems

A very promising field in which shape-memory polymers can be the enabling technology for future applications, is the area of biomedicine.[1, 108, 109] Synthetic, degradable implant materials have led to dramatic progress in a variety of medical treatments. The highly innovative potential of degradable biomaterials is opposed by the time-consuming and cost-intensive procedure for obtaining approval for use in medical devices. In the next section, a short overview about well-established materials used for implants is followed by the introduction of degradable implant materials which exhibit a thermally induced shape-memory effect.

2.6.1. Degradable Implant Materials

Significant progress was made in surgical procedures at the beginning of the 1970s by the introduction of resorbable, synthetic implant materials as suture materials.[110, 111] These materials are polyhydroxycarboxylic acids, such as polyglycolide **39**, or the copolyesters of L-lactic acid and glycolic acid. These aliphatic polyesters are still being used successfully today and have become a well established standard. Only a few other degradable polymers have been commercialized since that time. This fact is caused by the time-consuming and cost-intensive approval procedure for medical devices. An example of a group of materials which were developed in the 1980s are the polyanhydrides.[112] Based on a polyanhydride matrix, the implantable drug-delivery systems gliadel (treatment of brain tumors *glioblastoma multiforme*) and septicin (combat of chronic bone infections) have been developed. Polyanhydrides show surface erosion, while polyhydroxycarboxylic acids are degraded in the bulk.



39

The number of potential applications for degradable implant materials is growing constantly. On the one hand, the growing confidence of clinicians in the concept of degradable implants on the basis of the positive experience gained upon application of established materials have led to this trend. On the other hand, novel therapeutic concepts have been developed using the advantages of degradable biomaterials, for example, tissue reconstruction based on porous scaffolds, which can be cultivated with cells (tissue engineering).[113, 114]

The requirements for an implant material are determined by the specific application. The key properties of degradable biomaterials are their mechanical properties, their degrada-

tion rate, and degradation behavior, as well as biocompatibility and functionality. Each application requires a specific combination of these properties. With the growing number of potential applications, the number of materials needed that show different combinations of these properties is also increasing. However, the properties of the established biomaterials can only be varied in a limited range. Therefore, a new generation of degradable implant materials is needed.

The shape-memory polymers presented in the following section are considered to be promising candidates for the next generation of degradable implant materials. This concept is especially promising for these materials because it is a polymer system, that is, a group of polymers in which different macroscopic properties of the polymer can be varied virtually independently from each other in a wide range by only small changes in the chemical structure.

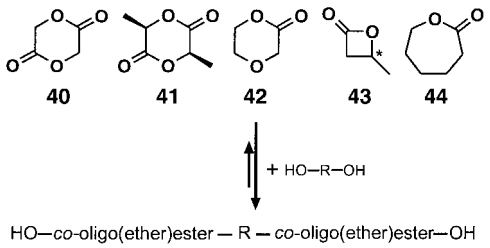
2.6.2. Polymer Systems with Shape-Memory Properties

Stimuli-sensitive implant materials have a high potential for applications in minimally invasive surgery. Degradable implants could be inserted into the human body in a compressed (temporary) shape through a small incision. When they are placed at the correct position, they obtain their application-relevant shape after warming up to body temperature. After a defined time period, the implant is degraded and becomes resorbed. In this case a follow-on surgery to remove the implant is not necessary.

Metallic shape-memory alloys such as nitinol are already used for biomedical applications as cardiovascular stents, guide wires, as well as orthodontic wires.[31] However, the mechanical properties of these alloys can only be varied in a limited range. The deformation between temporary and permanent shape is limited to 8% at best. Furthermore, the programming of these materials is time-consuming and demands temperatures of several hundred degree Celsius.[22e]

Designing degradable shape-memory polymers includes selecting suitable netpoints, which determine the permanent shape, and net chains, which act as switching segments. Furthermore, appropriate synthetic strategies have to be developed. The risk of possible toxic effects of polymers can already be minimized by selecting monomers whose homo- or copolymers have been proven to be biocompatible.

Appropriate switching segments for degradable shape-memory polymers can be found by considering the thermal properties of well-established degradable implant materials. The respective macrodiols, which can be used for the synthesis of shape-memory polymers, can be produced by means of ring-opening polymerization of lactones and cyclic diesters, such as **40** – **44**, with a low molecular weight diol (Scheme 2). The sequence structure of the copolyesters can be influenced by polymerizing with or without catalyst. The molecular weight M_n could be adjusted between 500 and 10000 by the stochiometric ratio of the starting materials.[115] For biomedical applications, a thermal transition of the switching segments in the temperature range between room and body temperature is of special interest. Two possible candidates were identified for use in this temperature range: poly(ε-caprolactone)diols, which exhibit a melting temperature T_m



Scheme 2. Synthesis macrodiols from cyclic of diesters and lactones.

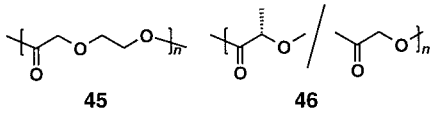
in the range of 46 and 64 °C (see Table 3), as well as amorphous copolyesters of diglycolide **40** and dilactide, which have a glass transition temperature T_g in the range between 35 and 50 °C.[110] However, one has to be aware that the decrease in glass transition temperature of macrodiols with decreasing chain length is attributed to the amount of freely moving chain ends. If the end groups of these telechelics are bonded covalently into a polymer, the decrease in the T_g value can no longer be observed.

The netpoints can either be of physical or chemical nature (see Section 2.1.2). In the following section one example for each case of a thermoplastic elastomer and a covalently cross-linked polymer network are described.

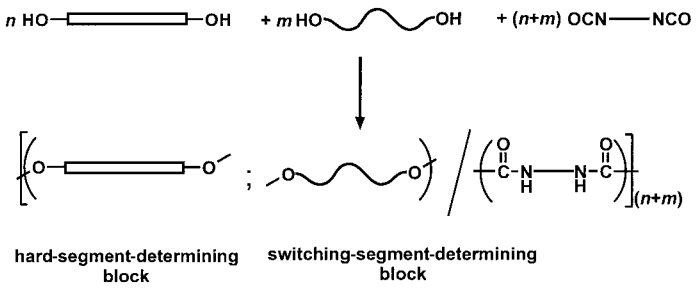
2.6.2.1. Biodegradable Thermoplastic Elastomers with Shape Memory

A series of biocompatible and simultaneously biodegradable multiblock copolymers with shape-memory properties could be synthesized for the first time based on the macrodiols shown in Scheme 2. The thermoplastic elastomers resulting from the synthesis are elastic at room temperature and exhibit high elongation at break ε_R of 650 to 1100% with tensile moduli between 34 and 90 MPa.[116]

On the one hand, these polymers are linear multiblock copolymers that have a crystallizable hard segment (T_m) of poly(*p*-dioxanone) (**45**) and an amorphous switching segment (here, poly[(L-lactide)-*co*-glycolide] (**46**) with a glycolide content of 15 mol%) that exhibits a glass transition temperature T_g. On the other hand, multiblock copolymers have been synthesized whose switching-segment-determining blocks consist of a crystallizable poly(ε-caprolactone) segment.



The thermoplastic elastomers are synthesized by a co-condensation of two different macrodiols by means of a bifunctional coupling agent, for example, diisocyanate, diacid dichloride, or phosgene (Scheme 3). It is necessary to reach high molecular weights with values of M_w in the range of 100000 to obtain the desired mechanical properties. The molecular parameters that determine this polymer system are the molecular weight, the microstructure (sequence), and the co-monomer ratio of the macrodiols as well as the hard-



Scheme 3. Synthesis of multiblock copolymers by the coupling of different macrodioles.

segment content within the multiblock copolymer. The new copolyester urethanes are completely hydrolytically degradable, and the degradation rate can be varied over a wide range (Figure 8). In contrast to the degradation behavior of several polyhydroxycarboxylic acids, mass loss can be observed quite early in the case of the shape-memory polymers under investigation. It is found that they become almost linear with degradation time.

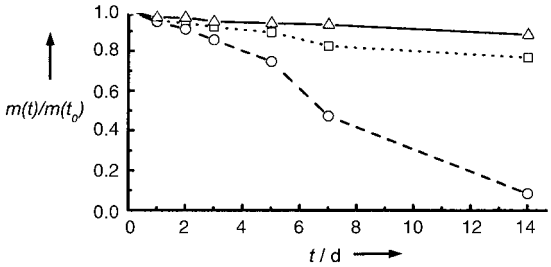


Figure 8. Hydrolytic degradation of different copolyester urethanes in aqueous buffer solution (pH = 7) at 70 °C. System A: Switching segment from poly(L-lactide-*co*-glycolide) with a content of 15 mol% glycolide with 30 wt% (□) and 40 wt% hard segment (○); system B: switching segment from poly(ε-caprolactone) with 30 wt% hard segment (△).

2.6.2.2. Biodegradable Polymer Networks with Shape Memory

A polymer system with an AB polymer network structure has been developed based on oligo(ε-caprolactone)diol as the component that forms a crystallizable switching segment.[1] For that purpose, oligo(ε-caprolactone)diols have been functionalized with methacrylate end groups that can undergo a polymerization reaction. The co-monomer of choice was *n*-butyl acrylate because of the low T_g value of pure poly(*n*-butyl acrylate) (−55 °C) which is supposed to determine the soft segment of the resulting polymer network. The molecular weight of the used oligo(ε-caprolactone)dimethacrylate cross-linker and the co-monomer content of butyl acrylate represent the molecular parameters for controlling crystallinity as well as the switching temperature and mechanical properties. In contrast to the described process for the cross-linking of diacrylates by photopolymerization, in this case the cross-linking is performed without the addition of an initiator.[117] The number-average molecular weights of the oligo(ε-caprolactone)dimethacrylates used were 2000 and 10000. The cross-link density was varied by the addition of 11 to 90 wt% butyl acrylate in the case of the low molecular weight and by addition of 20 to 71 wt% butyl acrylate for the high molecular weight oligo(ε-caprolactone)dimethacrylate. The cross-link density increases with decreasing content of butyl acrylate.

The butyl acrylate content influences the thermal properties of the AB network formed, especially for the oligo(ε-caprolactone)dimethacrylate with a molecular weight of 2000. Here, a melting point of $T_m = 25$ °C can be observed only in the case of a very low content of butyl acrylate of 11 wt%. The corresponding homo-network of oligo(ε-caprolactone)dimethacrylate has a melting point of 32 °C. All the other networks of this series were found to be completely amorphous. For the networks of butyl acrylate and oligo(ε-caprolactone)dimethacrylate having a number-average molecular weight of 10000, the melting point decreases by up to 5 K to 46 °C with increasing butyl acrylate content.

The mechanical properties of both materials containing oligo(ε-caprolactone) segments with number-average molecular weights of 2000 or 10000 change significantly with increasing butyl acrylate content. The values of the elastic modulus, the tensile strength σ_m, and the tensile stress at break σ_R decrease by approximately an order of magnitude. The absolute values are one order of magnitude higher for the series with the oligo(ε-caprolactone) segments having number-average molecular weights of 10000. Strain fixity rates between 95 and 85% as well as strain recovery rates from 98 to 93% could be obtained in cyclic, thermomechanical tensile tests of the network containing the higher molecular weight oligo(ε-caprolactone) segments. All materials reached a constant strain recovery rate of 99% after three thermocycles (Figure 9).

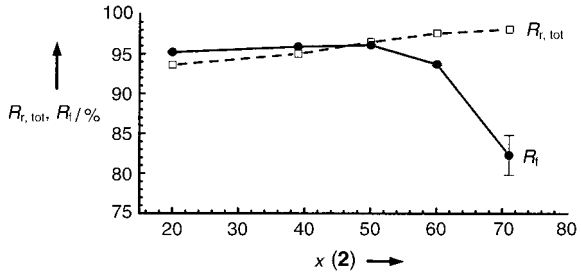


Figure 9. Shape recovery rate $R_{r,tot}$ and shape fixity rate R_f as a function of butyl acrylate (**2**) content x (in wt%).

3. Summary and Outlook

Shape-memory polymers belong to the group of intelligent ("smart") polymers. They have the capability to change their shape on exposure to an external stimulus. This article has given an overview of the state of the art and the future potential of the shape-memory technology for polymers with a thermally induced one-way effect. The polymer switches from its actual, temporary shape to its memorized, permanent shape when it exceeds the switching temperature T_{trans}.

This shape-memory technology consists of two components: on the one hand the polymer architecture or morphology has to fulfill certain structural requirements, and on the other hand a special processing and programming technology is needed. Optimizing these two components includes the application of special characterization techniques. In partic-

ular cyclic, thermomechanical measurements are performed. These methods allow not only quantification of the shape-memory effect but also optimization of programming parameters (T_{low}, T_{high}, heating rates, ε_m, etc.). A detailed knowledge of the molecular mechanism of the shape-memory effect and of the corresponding structure/property relationships is necessary to understand the mutual dependencies of the different macroscopic effects. For example, the strain recovery rate R_r not only depends on the kind of polymer but also on the strain ε_m that describes the maximum deformation during the cyclic thermomechanical tensile test. Only a few data sets concerning the shape-memory properties of the polymers which are comparable to each other and systematically determined are described in the scientific literature. A complete data set comprises, in particular, a comprehensive characterization of the structure and composition of these polymers.

In the broadest sense, shape-memory polymers that show a thermally induced shape-memory effect are networks. The netpoints, which can either have chemical or physical nature, determine the permanent shape. The net chains show a thermal transition in the temperature range in which the shape-memory effect is supposed to be triggered. The temporary shape can be stabilized by the transition T_{trans} which is based on the switching segments. If a polymer contains several different blocks, mixed phases can be formed, to which a single mixed glass transition is attributed. The mixing behavior of the switching segment with other segments has to be considered during the design of the polymer. This is of particular importance if the shape-memory effect is triggered by a glass transition. If T_{trans} is a melting point the crystallization behavior of the switching segment can be influenced by modifying different programming parameters. These parameters include the cooling rate from T_{high} to T_{low}, the temperature T_{low} at which the polymer sample crystallizes, and the time period when the sample is held at T_{low}. Both the deformability from the permanent to the temporary shape and the recovery of the permanent shape can be attributed to entropy elasticity on the molecular scale (see Section 2.1.3).

Thermoplastic elastomers and covalent polymer networks differ not only in their properties but also in the corresponding processing and programming procedures. Certain limitations arise from the molecular structure of both types of materials. Block copolymers with shape-memory properties require a minimum weight fraction of hard-segment-determining blocks to ensure that the respective domains act as physical netpoints. Relaxation and reorganization processes, such as the sliding of chains in single domains, can complicate the programming of these materials. Covalently cross-linked shape-memory polymers can comprise a higher weight fraction of switching-segment-determining blocks compared to thermoplasts. Exceeding the switching transition may, in the case of a very high content of the switching segment, result in the occurrence of high stresses, which may, in an extreme example, cause damage to the sample.

As a result of their different profile qualities, both types of material, thermoplastic elastomers and covalently cross-linked polymer networks, are qualified for different applications. Therefore, both will have relevance for industrial applications in the future.

The handling of high molecular weight, amorphous polymers whose permanent shape is exclusively fixed by entanglements of the polymer chains within a certain time interval are challenging. For example, high precision for the programming as well as for the recovery process is necessary to avoid a flowing of the material. However, long-term storage of samples in their temporary shape is difficult because modification of the permanent shape by any type of relaxation processes may occur. Therefore, a broad range of applications for such materials is unlikely.

A group of implant materials with shape memory that have been developed for biomedical applications was described. These implant materials are not a single polymer with a specific composition but polymer systems which allow variation of different macroscopic properties within a wide range through only small changes in the chemical structure. For this reason a variety of different applications can be realized with tailor-made polymers of the same family. The polymers are mainly synthesized from a few monomers that are already used in the synthesis of established, degradable biomaterials. Both thermoplastic elastomers as well as covalently cross-linked polymer networks have been prepared and investigated. The synthesis of thermoplastic multiblock copolymers could successfully be scaled-up to the production of kilogram amounts in batch processes. Comprehensive in vitro investigations of their tissue compatibility are currently being performed. The first results are promising. In cooperation with physicians and biologists, concrete applications are being developed and tested in preclinical studies.

The thermally induced one-way shape-memory effect is not confined to polymers. It has also been described for other materials, especially for metallic alloys and gels. However, the mechanical properties of shape-memory alloys, such as nitinol, can only be varied over a limited range. Their strongest restriction is the maximum deformation of only 8% between their permanent and temporary shapes. Shape-memory polymers can be deformed to much higher degrees and elongation up to 1100% is possible. Their mechanical properties can be varied over a wide range, particularly in the case of polymer systems. Polymers are cheaper than metallic alloys. Their processing and programming is less complicated. The fast programming process of shape-memory polymers enables an implant to be individually adapted to the need of a patient in the operating theatre. In principle, shape-memory polymers differ from stimuli-sensitive hydrogels in their higher mechanical stability.

Potential applications for shape-memory polymers exist in almost every area of daily life: from self-repairing auto bodies to kitchen utensils, from switches to sensors, from intelligent packing to tools. Only a few of these applications have been implemented to date, since only a few shape-memory polymers have so far been investigated and even less are available on the market. The majority of these polymers have not been designed especially as shape-memory materials. Here, the material design is at its very beginning. Extensive innovations have to be anticipated because of the interesting economical prospects that have already been realized for the

shape-memory technology within a short time period. Besides other stimuli, such as light or electromagnetic fields, the two-way shape-memory effect will play a prominent role in future developments.

An example which illustrates the tremendous potential of the shape-memory technology are polymer systems with shape-memory properties which have specifically been developed for medical applications by applying modern methods of polymer chemistry and biomaterial science. These developments have resulted in available intelligent polymers with tailor-made properties. Degradable shape-memory polymers provide interesting advantages over metal implants. On the one hand a follow-on surgery to remove the implant can be avoided, and on the other hand such medical products can be introduced into the body by minimally invasive procedures through a small incision. In this way, patients benefit from a more gentle treatment and costs in health care can be reduced. In this sense, shape-memory implant materials have the potential to influence decisively the way medicinal products are designed in the future.

4. Abbreviations

2,4-TDI	toluene-2,4-diisocyanate
BEBP	bis(2-hydroxyethoxy)biphenyl
BHBP	bis(2-hydroxyhexoxy)biphenyl
HDI	hexamethylene diisocyanate
HDPE	high density polyethylene
LDPE	low density polyethylene
MDI	methylenebis(phenylisocyanate)
NIPA	*N*-isopropylacrylamide
PAAM	polyacrylamide
PE	polyethylene
PEO	polyethylene oxide
PET	polyethylene terephthalate
PEU	polyester urethane
Poly(THF)	poly(tetrahydrofuran)
POSS	polyhedral, oligomeric silsesquioxane
PS	polystyrene
PVC	poly(vinyl chloride)
R_f	strain fixity rate
R_r	strain recovery rate
SC	switching segment content
T_g	glass transition temperature
T_m	melting temperature
T_{trans}	switching temperature
ε_m	maximum strain in the cyclic thermomechanical test
σ	tensile stress

The authors are grateful to Dr. Karl Kratz and Dr. Werner Grasser for recording the series of pictures. Dr. Werner Grasser is acknowledged for his assistance in graphical presentation. For financial support we would like to thank the German Ministry for Education and Research (BMBF, BioFuture Award project no. 0311867), Fonds der Chemischen Industrie (FCI), and mnemoScience GmbH, Aachen.

Received: June 6, 2001 [A 475]

[1] A. Lendlein, A. M. Schmidt, R. Langer, *Proc. Natl. Acad. Sci. USA* **2001**, *98*, 842 – 847.
[2] A. Charlesby, *Atomic Radiation and Polymers*, Pergamon Press, Oxford, **1960**, pp. 198 – 257.
[3] S. Ota, *Radiat. Phys. Chem.* **1981**, *18*, 81 – 87.
[4] W. Chen, K. Xing, L. Sun, *Radiat. Phys. Chem.* **1983**, *22*, 593 – 601.
[5] G. Kleinhans, W. Starkl, K. Nuffer, *Kunststoffe* **1984**, *74*, 445 – 449.
[6] G. Kleinhans, F. Heidenhain, *Kunststoffe* **1986**, *76*, 1069 – 1073.
[7] S. Machi, *Radiat. Phys. Chem.* **1996**, *47*, 333 – 336.
[8] K. Nakayama, *Int. Polym. Sci. Technol.* **1991**, *18*, T43 – 48.
[9] H. Tobushi, S. Hayashi, S. Kojima, *JSME Int. J. Ser. I* **1992**, *35*, 296 – 302.
[10] S. Hayashi, S. Kondo, C. Giordano, Conference Proceedings of the Annual Technical Conference and Exhibition of Plastic Engineers, **1994**, 1998 – 2001.
[11] T. Takahashi, N. Hayashi, S. Hayashi, *J. Appl. Polym. Sci.* **1996**, *60*, 1061 – 1069.
[12] H. Tobushi, S. Hayashi, A. Ikai, H. Hara, *J. Phys. IV* **1996**, *6*, 377 – 384.
[13] B. K. Kim, S. Y. Lee, M. Xu, *Polymer* **1996**, *37*(26), 5781 – 5793.
[14] F. Li, X. Zhang, J. Hou, M. Xu, X. Luo, D. Ma, B. K. Kim, *J. Appl. Polym. Sci.* **1997**, *64*, 1511 – 1516.
[15] M. Wang, X. Luo, X. Zhang, D. Ma, *Polym. Adv. Technol.* **1997**, *8*, 136 – 139.
[16] X. Luo, X. Zhang, M. Wang, D. Ma, M. Xu, F. Li, *J. Appl. Polym. Sci.* **1997**, *64*, 2433 – 2440.
[17] B. K. Kim, S. Y. Lee, J. S. Lee, S. H. Baek, Y. J. Choi, J. O. Lee, M. Xu, *Polymer* **1998**, *39*, 2803 – 2808.
[18] J. R. Lin, L. W. Chen, *J. Appl. Polym. Sci.* **1998**, *69*, 1563 – 1574.
[19] J. R. Lin, L. W. Chen, *J. Appl. Polym. Sci.* **1998**, *69*, 1575 – 1586.
[20] L. C. Chang, T. A. Read, *Trans. AIME* **1951**, *189*, 47.
[21] W. J. Bühler, J. W. Gilfrich, R. C. Wiley, *J. Appl. Phys.* **1963**, *34*, 1475.
[22] a) *Shape Memory Materials* (Eds.: K. Otsuka, C. M. Wayman), Cambridge University Press, Cambridge, **1998**, ; b) K. Otsuka, C. M. Wayman in ref. [22a], pp. 1 – 48; c) T. Saburi in ref. [22a], pp. 49 – 96; d) T. Tadaki in ref. [22a], pp. 97 – 116; T. Maki in ref. [22a], pp. 117 – 132; e) Y. Suzuki in ref. [22a], pp. 133 – 148; f) J. van Humbeeck, R. Stalmans ref. [22a], pp. 149 – 183; g) K. Uchino in ref. [22a], pp. 184 – 202; h) S. Miyazaki in ref. [22a], pp. 267 – 281.
[23] Z. G. Wei, R. Sandström, S. Miyazaki, *J. Mater. Sci.* **1998**, *33*, 3743 – 3762.
[24] Z. G. Wei, R. Sandström, S. Miyazaki, *J. Mater. Sci.* **1998**, *33*, 3763 – 3783.
[25] J. Van Humbeeck, *Mater. Sci. Eng.* **1999**, *A273 – 275*, 134 – 148.
[26] K. Otsuka, X. Ren, *Intermetallics* **1999**, *7*, 511 – 528.
[27] M. Merkel in *Taschenbuch der Werkstoffe* (Eds.: M. Merkel, K.-H. Thomas), Fachbuchverlag Leipzig im Carl Hanser Verlag, Munich, **2000**, pp. 358 – 368.
[28] K. E. Wilkes, P. K. Liaw, *JOM* **2000**, *10*, 45 – 51.
[29] D. Yang, *Mater. Des.* **2000**, *21*, 503 – 505.
[30] D. Mantovani, *JOM* **2000**, *10*, 36 – 44.
[31] P. Lipscomb, L. D. M. Nokes, *The Application of Shape Memory Alloys in Medicine*, Suffolk, MEP, **1996**.
[32] T. Hirai, H. Maruyama, T. Suzuki, S. Hayashi, *J. Appl. Polym. Sci.* **1992**, *45*, 1449 – 1451.
[33] T. Hirai, H. Maruyama, T. Suzuki, S. Hayashi, *J. Appl. Polym. Sci.* **1992**, *45*, 1849 – 1855.
[34] T. Aoyagi, F. Miyata, Y. J. Nagase, *J. Controlled Release* **1994**, *32*, 87 – 96.
[35] Z. Hu, X. Zhang, Y. Li, *Science* **1995**, *269*, 525 – 526.
[36] Y. Osada, A. Matsuda, *Nature* **1995**, *376*, 219.
[37] M. Uchida, M. Kurosawa, Y. Osada, *Macromolecules* **1995**, *28*, 4583 – 4586.
[38] X. Zhang, Y. Li, Z. Hu, C. L. Littler, *Chem. Phys.* **1995**, *102*, 551 – 555.
[39] X. He, Y. Oishi, A. Takahara, T. Kajiyama, *Polym. J.* **1996**, *28*, 452 – 457.
[40] Y. M. Lee, S. H. Kim, C. S. Cho, *J. Appl. Polym. Sci.* **1996**, *62*, 301 – 311.
[41] Y. Li, Z. Hu, Y. Chen, *J. Appl. Polym. Sci.* **1997**, *63*, 1173 – 1178.
[42] Y. Osada, J.-P. Gong, *Adv. Mater.* **1998**, *10*, 827 – 837.
[43] P. Hron, J. Šlechtová, *Angew. Makromol. Chem.* **1999**, *268*, 29 – 35.
[44] T. Miyata, N. Asami, T. Uragami, *Nature* **1999**, *399*, 766 – 769.

[45] C. Alvarez-Lorenzo, O. Guney, T. Oya, S. Yasuzo, K. Masatoshi, E. Takashi, T. Yukikazu, I. Toru, K. Kenichi, T. Kazunori, W. Guoqiang, A. Y. Grosberg, S. Masamune, T. Tanaka, *Macromolecules* **2000**, *33*, 8693 – 8697.
[46] P. J. Flory, *Principles of Polymer Chemistry*, Cornell University Press, Ithaca, **1969**, pp. 432 – 494.
[47] J. M. G. Cowie, *Chemie und Physik der synthetischen Polymeren*, Vieweg, Braunschweig, **1997**, pp. 278 – 405; J. M. G. Cowie, *Polymers: Chemistry and Physics of Modern Materials 2nd ed.*, Chapman & - Hall, London, **1991**.
[48] *Römpp Lexikon Chemie*, *Vol. 4*, 10th ed. (Eds.: J. Falbe, M. Regitz), Thieme, Stuttgart, **1998**, p. 2586.
[49] G. Capaccio, I. M. Ward, *Colloid Polym. Sci.* **1982**, *260*, 46 – 55.
[50] S. R. Chowdhury, J. K. Mishra, C. K. Das, *Polym. Degrad. Stab.* **2000**, *70*, 199 – 204; S. R. Chowdhury, C. K. Das, *J. Appl. Polym. Sci.* **2000**, *77*, 2088 – 2095.
[51] T. L. Smith, *Polym. Eng. Sci.* **1977**, *17*, 129.
[52] F. Li, J. Hou, W. Zhu, X. Zhang, M. Xu, X. Luo, D. Ma, B. K. Kim, *J. Appl. Polym. Sci.* **1996**, *62*, 631 – 638.
[53] H. M. Jeong, J. B. Lee, S. Y. Lee, B. K. Kim, *J. Mater. Sci.* **2000**, *35*, 279 – 283.
[54] H. M. Jeong, B. K. Kim, Y. J. Choi, *Polymer* **2000**, *41*, 1849 – 1855.
[55] M. Wang, Z. Lide, *J. Polym. Sci. Part B* **1999**, *37*, 101 – 112.
[56] K. Sakurai, Y. Shirakawa, T. Kashiwagi, T. Takahashi, *Polymer* **1994**, *35*, 4238 – 4239.
[57] P. van Caeter, E. J. Goethals, V. Gancheva, R. Velichkova, *Polym. Bull.* **1997**, *39*, 589 – 596.
[58] Y. Shirai, S. Hayashi, *Mitsubishi Tech. Bull.* **1988**, *184*, 1 – 6.
[59] K. Kobayashi, S. Shunichi (Mitsubishi Heavy Industries), US-A 5 128 197, **1992** (see http://www.uspto.gov/patft/).
[60] R. M. Briber, E. L. Thomas, *J. Macromol. Sci. Phys. B* **1983**, *22*, 509.
[61] J. R. Lin, L. W. Chen, *J. Appl. Polym. Sci.* **1998**, *69*, 1575.
[62] C. G. Seefried, J. V. Koleske, F. E. Critchfield, *J. Appl. Polym. Sci.* **1975**, *19*, 2493.
[63] J. R. Lin, L. W. Chen, *J. Appl. Polym. Sci.* **1998**, *69*, 1575.
[64] F. Li, J. Hou, W. Zhu, X. Zhang, M. Xu, X. Luo, D. Ma, B. K. Kim, *J. Appl. Polym. Sci.* **1996**, *62*, 631 – 638.
[65] D. B. Johns, R. W. Lenz, A. Luecke in *Ring Opening Polymerization*, *Vol. 1*, Elsevier, New York, **1984**, pp. 461 – 521.
[66] C. G. Pitt in *Biodegradable Polymers as Drug Delivery Systems*, Marcel Dekker, New York, **1990**, pp. 71 – 120.
[67] F. Li, J. Hou, W. Zhu, X. Zhang, M. Xu, X. Luo, D. Ma, B. K. Kim, *J. Appl. Polym. Sci.* **1996**, *62*, 631 – 638.
[68] J. R. Lin, L. W. Chen, *J. Appl. Polym. Sci.* **1998**, *69*, 1575 – 1586.
[69] U. Gaur, B. Wunderlich, *J. Phys. Chem.* **1981**, *10*, 1023.
[70] J. R. Lin, L. W. Chen, *J. Appl. Polym. Sci.* **1998**, *69*, 1575 – 1586.
[71] Ref. [69].
[72] B. M. Grieveson, *Polymer* **1960**, *1*, 499.
[73] *Römpp Lexikon Chemie*, *Vol. 5*, 10th ed. (Eds.: J. Falbe, M. Regitz), Thieme, Stuttgart, **1998**, p. 3449.
[74] S. Fakirov, E. W. Fisher, G. H. Schmidt, *Makromol. Chem.* **1975**, *176*, 2459.
[75] O. B. Edgar, R. Hill, *J. Polym. Sci.* **1952**, *8*, 1.
[76] D. W. Woods, *Nature* **1954**, *174*, 753.
[77] Laboratory Chemicals 2001/2002, Fluka Chemie GmbH, pp. 1231 – 1234.
[78] U. Gaur, B. Wunderlich, *J. Phys. Chem.* **1981**, *10*, 1010.
[79] H. Suzuki, B. Wunderlich, *J. Polym. Sci. Polym. Phys. Ed.* **1985**, *23*, 1671.
[80] *Römpp Lexikon Chemie*, *Vol. 5*, 10th ed. (Eds.: J. Falbe, M. Regitz), Thieme, Stuttgart, **1998**, p. 3506.
[81] R. Dedeurwaerder, J. F. M. Oth, *J. Chem. Phys.* **1959**, *56*, 940.
[82] T. G. Fox, P. J. Flory, *J. Appl. Phys.* **1950**, *21*, 581.
[83] F. P. Reding, J. A. Faucher, R. D. Whitmann, *J. Polym. Sci.* **1962**, *57*, 483.
[84] M. Berger, D. J. Buckley, *J. Polym. Sci. A* **1963**, *1*, 2945.
[85] G. Nata, *Science* **1965**, *147*, 269.
[86] W. S. Bahary, D. I. Sapper, J. H. Lane, *Rubber Chem. Technol.* **1967**, *40*, 1529.
[87] *Encyclopedia of Polymer Science and Engineering*, *Vol. 6*, Wiley, New York, **1986**, p. 410.
[88] *Encyclopedia of Polymer Science and Engineering*, *Vol. 6*, Wiley, New York, **1986**, p. 411.
[89] U. Gaur, B. B. Wunderlich, B. Wunderlich, *J. Phys. Chem.* **1983**, *12*, 56.
[90] *Römpp Lexikon Chemie*, *Vol. 5*, 10th ed. (Eds.: J. Falbe, M. Regitz), Thieme, Stuttgart, **1998**, p. 3415.
[91] *Encyclopedia of Polymer Science and Engineering*, *Vol. 11*, Wiley, New York, **1986**, p. 366.
[92] *Encyclopedia of Polymer Science and Engineering*, *Vol. 11*, Wiley, New York, **1986**, p. 349.
[93] T. G. Bassari, A. Levy, M. Litt, *J. Polym. Sci. B* **1967**, *5*, 871.
[94] M. Wang, X. Luo, D. Ma, *Eur. Polym. J.* **1998**, *34*, 1 – 5.
[95] K. Sakurai, H. Tanaka, N. Ogawa, T. Takahashi, *J. Macromol. Sci. Phys. B* **1997**, *36*, 703 – 716.
[96] K. Sakurai, T. Takahashi, *J. Appl. Polym. Sci.* **1989**, *38*, 1191 – 1194.
[97] K. Sakurai, T. Kashiwagi, T. Takahashi, *J. Appl. Polym. Sci.* **1993**, *47*, 937 – 940.
[98] P. T. Mather, H. G. Jeon, T. S. Haddad, *Polym. Prepr. Am. Chem. Soc. Div. Polym. Chem.* **2000**, *41*, 528 – 529.
[99] P. T. Mather, H. G. Jeon, A. Romo-Uribe, *Macromolecules* **1999**, *32*, 1194 – 1203.
[100] F. Li, Y. Chen, W. Zhu, X. Zhang, M. Xu, *Polymer* **1998**, *39*, 6929 – 6934.
[101] A. Charlesby, *Proc. R. Soc. London* **1952**, *215*, 187 – 214.
[102] S. Kumar, M. V. Pandya, *J. Appl. Polym. Sci.* **1996**, *64*, 823 – 829.
[103] V. Skákalová, V. Lukeš, M. Breza, *Macromol. Chem. Phys.* **1997**, *198*, 3161 – 3172.
[104] F. Li, W. Zhu, X. Zhang, C. Zhao, M. Xu, *J. Appl. Polym. Sci.* **1999**, *71*, 1063 – 1070.
[105] Y. Kagami, J. P. Gong, Y. Osada, *Macromol. Rapid Commun.* **1996**, *17*, 539 – 543.
[106] E. J.Goethals, W. Reyntjens, S. Lievens, *Macromol. Symp.* **1998**, *132*, 57 – 64.
[107] W. G. Reyntjens, F. E. Du Prez, E. J. Goethals, *Macromol. Rapid Commun.* **1999**, *20*, 251 – 255.
[108] M. Brennan, *Chem. Eng. News* **2001**, *79*(6), 5.
[109] S. Ashley, *Sci. Am.* **2001**, No. 5.
[110] A. Lendlein, *Chem. Unserer Zeit* **1999**, *33*, 279 – 295.
[111] S. W. Shalaby, R. A. Johnson in *Biomedical Polymers* (Ed.: S. W Shalaby), Hanser, München, **1994**.
[112] C. T. Laurencin, I. E. M. Sobrasua, R. S. Langer in *Biomedical Applications of Synthetic Biodegradable Polymers* (Ed.: J. O. Hollinger), CRC Press, Boca Raton, **1995**.
[113] J. D. Bronzino, *The Biomedical Engineering Handbook*, CRC Press, Boca Raton, **1995**.
[114] F. H. Silver, C. Doillon, *Biocompatibility: Interactions of Biological and Implantable Materials*, VCH-Wiley, New York, **1989**.
[115] A. Lendlein, P. Neuenschwander, U. W. Suter, *Macromol. Chem. Phys.* ***2000***, *201*, 1067 – 1076.
[116] A. Lendlein, R. Langer, *Science*, in press; published online on 25 April, 2002 as 10.1126/science.1066102 (Science Express Reports).
[117] A. Nathan, D. Bolikal, N. Vyavahave, S. Zalipsky, J. S. Kohn, *Macromolecules* **1992**, *25*, 4476 – 4484.

An Omnivorous Curiosity, a Sense of Wonder, and a Taste for the Spectacular

Sir John Meurig Thomas*

1. Introduction

We are what we remember. Novelists, philosophers, and neuroscientists all seem to agree that human beings are the sum total of their memories: this is one of the reasons why each individual is unique. Oliver Sacks' memories of his "chemical boyhood" as a teenager growing up in a large family of Russian-Lithuanian-Jewish descent in a London suburb at the close of the Second World War constitutes one of the most riveting, humane, and lyrical biographies that one is ever likely to encounter.[**] Fascinating, pyrotechnic, kaleidoscopic, it is a joy to read; and an extra pleasure to animadvert on its contents and qualities.

The history of chemistry, which encompasses almost all its ancient and modern subdisciplines, is captured here, and told retrospectively (and perhaps with a touch of post-event rationalization) through the eyes, heart, and voice of a passionate and precocious teenager, but with the lapidary, literary skills of this distinguished neurologist, now almost 70 years old. Analytical chemistry, radiation and radiochemistry, spectroscopy (from the X-ray atomic to the molecular), the rudiments of quantum theory, electrochemistry, kinetics, photography, and the phenomenology of luminescence (embracing fluorescence, phosphorescence, thermoluminescence, and (obliquely) crystalloluminescence) are all introduced in a nontechnical, and effortlessly compelling manner. How very different is the entire texture of Sacks' exposition and the impact of his magical story-telling—which succeeds in smoothly weaving many disparate scientific activities into the fabric of chemistry—from the aridly factual and desiccated historical discourses that professional philosophers of science sometimes produce, discourses which expunge and excise the intrinsic romance and excitement from great and subsidiary scientific discoveries alike. The remarkable communicative gifts of Oliver Sacks bring to life the vitality, exuberance, commitment, and genius of so many of the founders of modern chemistry. We are told in a fresh and vivid fashion of the essence and significance of the contributions, lives, and publications of Boyle, Scheele, Lavoisier, Dalton, Davy, Crookes, Mendeleev, Kirchhoff and Bunsen, the Curies, Moseley, Bohr, Langmuir, as well as several other less-well-known investigators.

2. The Author

Until this wonderful book came my way, I knew of Oliver Sacks—largely from what my wife had told me—only as the author of *The Man Who Mistook His Wife for a Hat*, the story of a musician of distinction who genuinely made that mistake, a story that was even converted into an opera. My wife had also described Sacks' perceptive *A Leg To Stand On*, a neuropsychological odyssey about a damaged leg[1] (Sacks') and the nature of selfhood, in which he exposed (as the author and critic Anthony Burgess put it) "*the damnable rift that subsists between doctor and patient. The book's value lies in its willingness to combine the technical and the demonic, to admit poetry and philosophy and the religious impulse*".

Born in July 1933, Sacks was educated in an English Public (that is, private) school, St. Paul's, London, before proceeding to the University of Oxford and then to California. He practices neurology in New York City, where he is also clinical professor of neurology at the New York University School of Medicine. His Internet Web page tells us that just as Nietsche claimed that "*Bizet makes me a better philosopher*", so Sacks asserts that "*Mozart makes me a better neurologist*". He tells us also that he was much influenced by the writings of Charles Dickens and H. G. Wells.

It is quite astonishing, given that his principal preoccupation is neurology, that he has such an encyclopaedic and penetrating grasp of the origins and applicability of chemistry, of its major theoretical constructs and key turning points, as well as of its creative and destructive power, its "musicality in the sphere of thought" (to borrow a phrase used by Einstein to describe Bohr's theory of the atom), and its poetic dimension. It is dazzling to discover from *Uncle Tungsten* the sheer body of connected fact that he knew—what he had read and what he had experimented with—by the time he was a mere 14-year-old. I doubt whether there are many young professors of chemistry in respectable universities and colleges these days who could rival, let alone surpass, his corpus of fundamental chemical knowledge or his remarkable powers of pedagogy and exposition. As for his ratiocinative skills and perspicacity,

[*] Prof. Sir J. M. Thomas
The Royal Institution, London
and The Master's Lodge
Peterhouse, Cambridge, CB2 1QY (UK)
Fax: (+44) 1223-339-200
E-mail: has22@cam.ac.uk

[**] *Uncle Tungsten: Memories of a Chemical Boyhood* By Oliver Sacks, pp. 396 + viii, Picador, **2001**

 © WILEY-VCH Verlag GmbH, 69451 Weinheim, Germany, 2002 1433-7851/02/4112-2059 $ 20.00+.50/0

consider the following (pp. 202–203) when the young teenager argues as follows (more than a decade before Neil Bartlett's momentous discovery of the reactivity of the noble gases):

> *"I think I identified at times with the inert gases, and at other times anthropomorphized them, imagining them lonely, cut off, yearning to bond. Was bonding, bonding with other elements, absolutely impossible for them? Might not fluorine, the most active, the most outrageous of the halogens—so eager to combine that it had defeated efforts to isolate it for more than a century—might not fluorine, if given a chance, at least bond with xenon, the heaviest of the inert gases? I pored over tables of physical constants and decided that such a combination was just, in principle, possible."*

Or, again, his discussions on p. 79:

> *"But the most mysterious and beautiful of all the blues for me was that produced by dissolving alkali metals in liquid ammonia (Uncle Dave showed me this). The fact that metals* could *be dissolved at all was startling at first, but the alkali metals were all soluble in liquid ammonia (some to an astounding degree—cesium would completely dissolve in a third of its weight of ammonia). When the solutions became more concentrated, they suddenly changed character, turning into lustrous bronze-coloured liquids that floated on the blue—and in this state they conducted electricity as well as a liquid metal like mercury. The alkaline earth metals would work as well, and it did not matter whether the solute was sodium or potassium, calcium or barium—the ammoniacal solutions, in every case, were an identical deep blue, suggesting the presence of some substance, some structure, something common to them all. It was like the colour of the azurite in the Geological Museum, the very colour of heaven."*

Such passages not only reveal his depth of knowledge, they celebrate the sheer joy of existence, which, as chemists, we are privileged to experience in a profoundly aesthetic and intellectual way.

The omnivorous Sacks even knew of the relatively obscure Urbain, that pertinacious professor of Mineral Chemistry at the Sorbonne, who "*had done fifteen thousand fractional crystallizations to isolate lutecium*" (p. 295); of the discovery of lithium (p. 217); of the Curies' work on radium and polonium; and of Lockyer's discovery of helium (Figure 1). Of the latter he writes (p. 218):

> *"The wonder of spectral analysis, analysis at a distance, had literary resonances as well. I had read* Our Mutual Friend *(written in 1864 just four years after Bunsen and Kirchhoff had launched spectroscopy) and here Dickens imagined a "moral spectroscopy" whereby the inhabitants of remote galaxies and stars might analyse the light from the Earth to gauge its good and evil, the moral spectrum of its inhabitants."*

The young teenager Sacks started to read some philosophy. Leibnitz, because he spoke of "Divine mathematics", appealed to him for he saw that (p. 308):

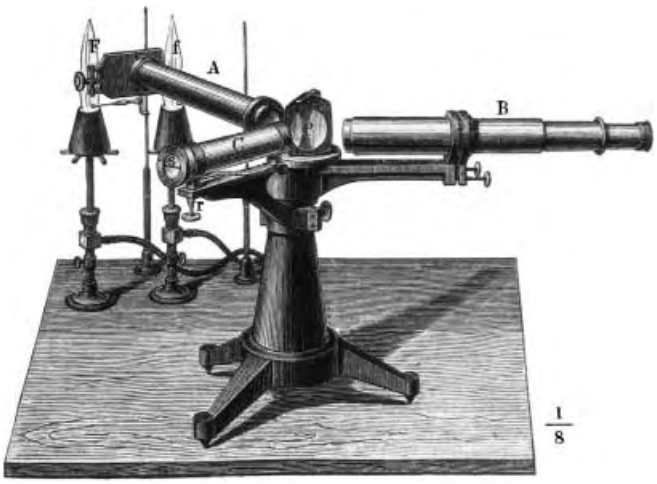


Figure 1. Spectral apparatus designed by R. Bunsen and G. R. Kirchhoff, steel engraving. Photo obtained from the Deutsches Museum, Munich.

> *"…one could create the richest possible reality by the most economical means, and this, it now seemed to me, was everywhere apparent: in the beautiful economy by which millions of compounds could be made from a few dozen elements, and the hundred-odd elements from hydrogen itself; the economy by which the whole range of atoms was composed from two or three particles; and in the way that their stability and identity were guaranteed by the quantal numbers of the atom itself—all this was beautiful enough to be the work of God."*

These philosophical thoughts, and the echoes they carry of Pythagorean and Galilean views of the cosmos, contrast with Sacks' earlier religious feelings (p. 179):

> *"…I myself, traumatized at Braefield,[2] had lost touch with, lost interest in, the religion of my childhood. I regret that I was to lose it so early and as abruptly as I did, and this feeling of sadness or nostalgia was strangely admixed with a raging atheism, a sort of fury with God for not existing, not taking care, not preventing the war, but allowing it, and all its horrors, to occur."*

3. A Concatenation of Influential Circumstances

How come that this youngest of teenagers knew such a wealth of facts and ruminated so deeply on their significance? First, he was a member of a large and gifted family and an even larger extended family: his maternal grandparents (the Landaus) had 18 children, most of whom were imbued with an unquenchable thirst for knowledge that characterizes so many of the families who attended synagogues and yeshivas in that era. His parents—both doctors who met at the Ibsen Society—were bookish people who read extensively and experimented freely. The home library contained many of the books that the juvenile Sacks felt impelled to read (such as his mother's copy of Eve Curie's biography of her mother, Marie,

 © WILEY-VCH Verlag GmbH, 69451 Weinheim, Germany, 2002 1433-7851/02/4112-2060 $ 20.00+.50/0 *Angew. Chem. Int. Ed.* **2002**, *41*, No. 12

given to the boy when he was just ten); and he early formed the habit of taking advantage of his local municipal library.

As a result of his irrepressible sense of wonder and a self-confessed taste for the spectacular, he readily persuaded his parents to convert one of the rooms in their large house into a chemical laboratory, equipped with a fume cupboard. (His parents were comfortably off, financially; there were two Bechstein pianos in their large detached home, and, when very young, Sacks was taken out by a resident nanny to play with other children.) Above all, however, his uncles and aunts were exceptionally gifted intellectually, and many were resourceful entrepreneurs. Each member of the family, it seemed, was animated by the desire to learn the causes of things (Vergil's famous dictum springs to mind: *Felix, qui potuit rerum cognoscere causas*.[*]

They had voracious appetites for all manner of human endeavours; but two of his uncles, in particular, were extraordinarily scholarly and gifted practical scientists with an eye for the commercial exploitation of their knowledge. They had their own laboratories, workshops (one, even an observatory), and a factory dripping with the kind of equipment that captured Oliver's imagination—a spinthariscope, vacuum pumps, induction coils, ultraviolet and infrared lamps, photometers, photoelectric cells, telescopes, microscopes, pocket spectroscopes, an array of inorganic phosphors, radioactive and fluorescent minerals. Moreover, his uncle Abe (15 years his mother's senior), the more physically and mathematically oriented of the two, had a repository of exotic chemicals such as pitch blende, radium bromide, polonium, as well as old X-ray and Crookes' tubes in his possession. Uncle Dave (the "Uncle Tungsten" of the title) was six years his brother Abe's junior, and was Oliver's chemical and mineralogical uncle. He greatly inspired Oliver because he saw all science as a wholly human, no less than an intellectual and technological, enterprise. There was also his Auntie Len, an admirable lady with a social conscience,[3] who delighted in showing her nephew all sorts of botanical, astronomical, and mathematical pleasures. She showed him as an eight-year-old the spiral patterns on the faces of sunflowers in the garden, and suggested that he count the florets in them. As he did so, she pointed out that they were arranged according to a series: 1, 1, 2, 3, 5, 8, 13, 21…, each number being the sum of the two that preceded it, thereby revealing to him the famous Fibonacci series[4] and all its proliferating charm.

His father's family were also exceptionally talented; indeed Alida, his father's sister, a gifted linguist, worked with Chaim Weizmann (a leader of the Zionistic movement in England) and was responsible for translating the famous Balfour Declaration[5] of 1917 into French and Russian. Her son Aubrey later became (as Abba Eban) the first Israeli Ambassador to the U.N., which is further proof of the remarkable pool of genes from which he emerged.

However, there were two other factors over and above these familial and filial relationships that seemed to have influenced greatly the young and growing Oliver. First, his visits to London's National Museums, especially the Science and Geological ones. These were initiated by his mother when he was about six years of age. From the moment she showed him the Landau lamp (a variant of Humphry Davy's miners' safety lamp), invented in the 1870s by her father, he immediately identified Davy in his mind *"as an ancestor of sorts, almost part of the family"*. Davy was and remains one of Oliver Sacks' heroes. Second, his parents, uncles, and aunts drew to his attention and portrayed the trajectory of the lives of many famous scientists, and the magnanimity of the attitudes and pursuits of many of them. Take, for example, what Uncle (Tungsten) Dave told young Oliver about the great Swedish chemist Carl Wilhelm Scheele (Figure 2), after whom the mineral scheelite, $CaWO_4$, is named (p. 44):



Figure 2. Carl Wilhelm Scheele (1742–1786), statue by Börjeson. Photo obtained from the Deutsches Museum, Munich.

"Scheele was one of Uncle Dave's great heroes. Not only had he discovered tungstic acid and molybdic acid (from which the new element molybdenum was made), but hydrofluoric acid, hydrogen sulfide, arsine, and prussic acid, and a dozen organic acids, too. All this, Uncle Dave said, he did by himself, with no assistants, no funds, no university position or salary, but working alone, trying to make ends meet as an apothecary in a small provincial Swedish town. He had discovered oxygen, not by a fluke, but by making it in several different ways; he had discovered chlorine; and he had

[*] Happy is he who is able to understand the cause of things

 © WILEY-VCH Verlag GmbH, 69451 Weinheim, Germany, 2002 1433-7851/02/4112-2061 $ 20.00+.50/0

pointed the way to the discovery of manganese, of barium, of a dozen other things.

Scheele, Uncle Dave would say, was wholly dedicated to his work, caring nothing for fame or money and sharing his knowledge, whatever he had, with anyone and everyone. I was impressed by Scheele's generosity, no less than his resourcefulness, by the way in which (in effect) he gave the actual discovery of elements to his students and friends—the discovery of manganese to Johan Gahn, the discovery of molybdenum to Peter Hjelm, and the discovery of tungsten itself to the d'Elhuyar brothers.

Scheele, it was said, never forgot anything if it had to do with chemistry. He never forgot the look, the feel, the smell of a substance, or the way it was transformed in chemical reactions, never forgot anything he read, or was told, about the phenomena of chemistry. He seemed indifferent, or inattentive, to most things else, being wholly dedicated to his single passion, chemistry. It was this pure and passionate absorption in phenomena—noticing everything, forgetting nothing—that constituted Scheele's special strength.

Scheele epitomized for me the romance of science. There seemed to me an integrity, an essential goodness, about a life in science, a lifelong love affair. I had never given much thought to what I might be when I was "grown up"—growing up was hardly imaginable—but now I knew: I wanted to be a chemist. A chemist like Scheele, an eighteenth-century chemist coming fresh to the field, looking at the whole undiscovered world of natural substances and minerals, analyzing them, plumbing their secrets, finding the wonder of unknown and new metals."

Sacks' remark about the essential goodness of a life in science, was exactly the sentiment that the young Michael Faraday had expressed after listening to the brilliant lecture-demonstrations of Humphry Davy in 1812.[6]

In retrospect, we see that young Oliver was the beneficiary of a concatenation of fortunate circumstances, not the least important of which was the guidance by precept and example, using the life and work of the Curies, Roentgen, Davy, and others, which uncle Dave and uncle Abe provided.

4. The Success and Uniqueness of the Book

Why is this such an inspiring book, commendable to nonscientists and scientists alike? The reasons are many. Apart from the fact that Sacks is a supremely skilful raconteur, brimming with human sympathy, psychological insight, and emotional commitment, he is also the master of introducing the apt aside, usually contained in his teeming footnotes—which, for example, offer a retrospective medical analysis of Henry Cavendish (p. 121) that concludes that he was a unique autistic genius; or that Eve Curie came to one of his lectures, and he got her to sign the copy of her book on Madame Curie acquired by him fifty years earlier; or the unbearable vividness with which, whenever he now hears Schubert's *Nachtgesang*, he recalls the childhood memory of his mother's figure and voice as she leaned over the piano and sang. In his story-telling gifts he combines the qualities of Primo Levi with the vivid recollections of childhood and adolescent thought reminiscent of the poet Dylan Thomas.[7]

Other keys to Sacks' success here lie in his ingenious way of weaving an enchanting story about a specific technique, instrument, or individual, such as his chapters on (photographic) images, a pocket spectroscope, or Mendeleev and Davy, and his brilliant choice of truly memorable quotations (very few of which, unfortunately, carry a reference to source).

Of dramatic still photographs, Sacks said that they *"confirmed—or did they suggest?—my own very early memories!"*. It seemed to him *"wonderful that photographs could capture actual moments, clean cross sections, as it were, of time fixed forever in silver"*. Photographs *"seemed to me like an extension of my own memory and identity, helped to moor me, anchor me in space and time, as an English boy born in the 1930s, born into a London similar to that in which my parents had grown up, a London which would have been recognizable to Wells, Dickens or Conan Doyle…If photography was a metaphor for perception and memory and identity, it was equally a model, a microcosm, of science at work—and a particularly sweet science, since it brought chemistry and optics and perception together into a single, indivisible unity"*.

For his tenth birthday Auntie Len gave Oliver a copy of Sir James Jeans's book *The Stars in their Courses*, in which he read that the sun contained platinum, silver, lead, and most of the elements we have on earth. When he told his Uncle Abe this, he was given a copy of J. Norman Lockyer's *The Spectroscope*, published in 1878; his uncle also gave him a small pocket spectroscope. Very shortly, young Sacks was grappling with the dark lines Fraunhofer had reported in 1814. Did they, he wondered, have any relation to the bright spectral lines, visible in his spectroscope, of flamed elements? Soon he was reading about the brilliant collaborative efforts of Gustav Kirchhoff and Robert Bunsen (Figure 3). These two



Figure 3. Right: Robert Bunsen (1811–1899) and left: Gustav Robert Kirchhoff (1824–1887). Photo obtained from the Deutsches Museum, Munich.

pioneers and others (notably Lockyer and Huggins,[8] who is surprisingly not mentioned in the book) went on to identify 20 other terrestrial elements in the sun, and soon the Fraunhofer mystery—the hundreds of black lines in the solar system—could be rationalized as the absorption spectra of the

 © WILEY-VCH Verlag GmbH, 69451 Weinheim, Germany, 2002 1433-7851/02/4112-2062 $ 20.00+.50/0

elements in the outermost layers of the sun. Exciting accounts are given by Sacks of how Bunsen discovered caesium spectroscopically after concentrating some 44 tons of mineral water rich in sodium and potassium down to a few liters. All this prompted the young Sacks to explore, with his pocket spectroscope, the absorption spectra of blood, leaves, urine, and wine. *"I was fascinated to discover how characteristic the spectrum of blood was even when dried and how small a quantity was needed to analyse in this fashion—one could identify a faint blood-stain more than fifty years old and distinguish it from a rust stain."* (One wonders whether his erudite uncles ever told him that the seminal work of the Nobel Prizewinner, Gowland Hopkins (discoverer of vitamins, Figure 4), who had studied the pigments in butterflies' wings and other chemical physiological problems, was greatly

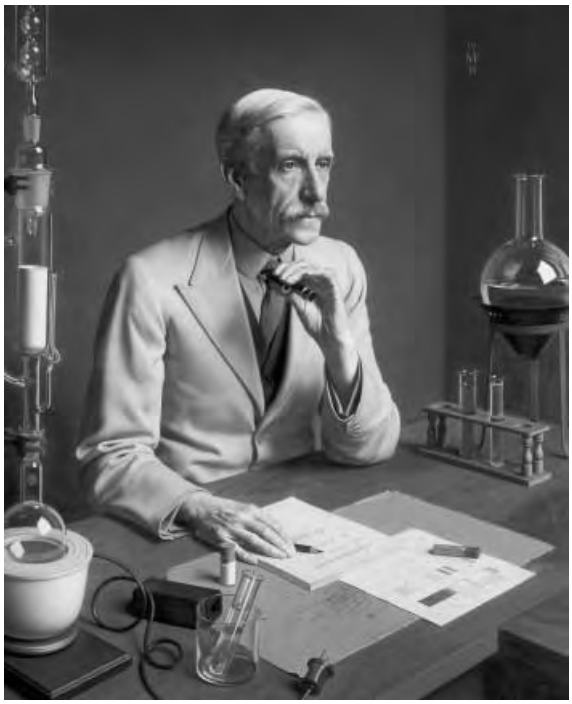


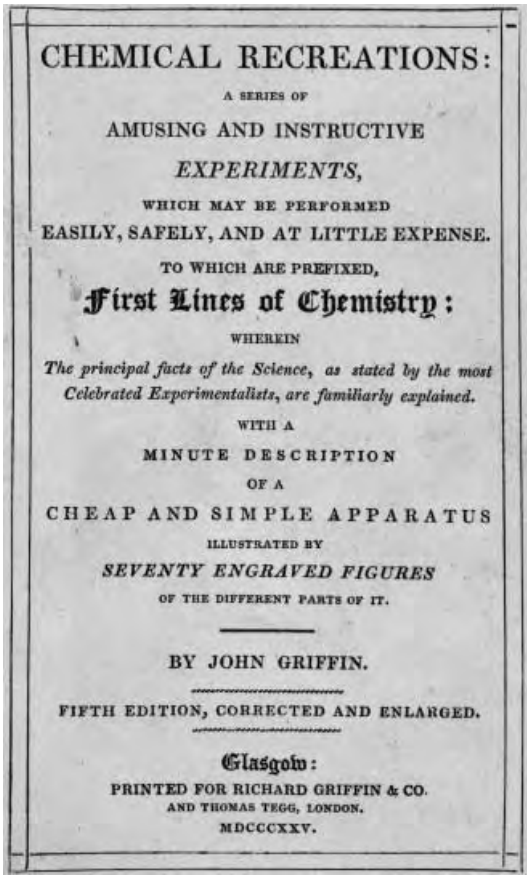
Figure 4. Sir F. Gowland Hopkins (1861–1947) with a pocket spectroscope. Photo obtained from The Royal Society.

aided by a pocket spectroscope.) Sacks recalls going to Piccadilly Circus and Leicester Square, at the heart of neon-lit London, with his pocket spectroscope, and looking at the new sodium lights that were used for street lighting, at the scarlet neon advertisements, and at the other gas-discharge tubes that turned the center of the metropolis into *"a glory of coloured lights after the long blackout of the war"*.

In a marvellously evocative chapter entitled "Chemical Recreations" (Figure 5), Sacks writes:

"My first taste was for the spectacular—the frothings, the incandescences, the stinks and the bangs, which almost defined a first entry into chemistry. One of my guides was J. J. Griffin's Chemical Recreations, *an 1850ish book I had found in a second-hand bookshop. Griffin had an easy, practical, and above all playful style; chemistry was clearly fun for him, and he made it fun for his readers, readers who must often have been, I decided, boys like myself, for he had sections like "Chemistry for the Holidays"—this included the "Volatile Plum Pudding" ("When the cover is removed … it leaves its dish and rises to the ceiling"), "A Fountain of Fire" (using phosphorus—"the operator must take care not to burn himself"), and "Brilliant Deflagration" (here, too, one was warned to "remove your hand instantly"). I was amused by the mention of a special formula (sodium tungstate) to render ladies' dresses and curtains incombustible—were fires that common in Victorian times?—and used it to fire-proof a handkerchief for myself.*

Griffin suggested experiments with bleaching—here I used my mother's bleaching powder in place of the chlorine water he suggested, and with this I bleached litmus paper, cabbage juice, and a red handkerchief of my father's. Griffin also suggested holding a red ose over burning sulfur, so that the sulfur dioxide produced would bleach it. Dipping it into water, miraculously, restored its colour."



CHEMICAL RECREATIONS:

A SERIES OF

AMUSING AND INSTRUCTIVE

EXPERIMENTS,

WHICH MAY BE PERFORMED

EASILY, SAFELY, AND AT LITTLE EXPENSE.

TO WHICH ARE PREFIXED,

First Lines of Chemistry:

WHEREIN

The principal facts of the Science, as stated by the most Celebrated Experimentalists, are familiarly explained.

WITH A

MINUTE DESCRIPTION

OF A

CHEAP AND SIMPLE APPARATUS

ILLUSTRATED BY

SEVENTY ENGRAVED FIGURES

OF THE DIFFERENT PARTS OF IT.

BY JOHN GRIFFIN.

FIFTH EDITION, CORRECTED AND ENLARGED.

Glasgow:

PRINTED FOR RICHARD GRIFFIN & CO.

AND THOMAS TEGG, LONDON.

MDCCCXXV.

Figure 5. Chemical Recreations of J. J. Griffin (1825). Reprinted with permission from Cambridge University Library.

Griffin was himself a remarkable individual: an educator as well as a purveyor of chemical apparatus used throughout Europe. His firm, Griffin & Tatlock[9] was a major supplier to universities until very recently. His skill in capturing a potential audience (and customers) is reflected in the compact and compelling descriptions contained in the cover page of *Chemical Recreations*, fifth edition, Glasgow 1825.

 © WILEY-VCH Verlag GmbH, 69451 Weinheim, Germany, 2002 1433-7851/02/4112-2063 $ 20.00+.50/0

Rhapsodic delight is what the reader senses on reading how Mendeleev's (Figure 6) Periodic Table impressed itself upon Sacks' mind and imagination. Almost every scientist I have ever met admits to succumbing to unqualified admiration and awe when they first encounter the Periodic Table—the exhilarations experienced by C. P. Snow and Freeman Dyson are quoted here—but few, not even Primo Levi, have written



Figure 6. Dimitri Mendeleev (1834–1907). Photo obtained from Bridgeman Art Library.

so eloquently and passionately about Mendeleev's achievement than Oliver Sacks. On seeing it for the first time, the Periodic Table gave him "*for the first time, a sense of the transcendent power of the human mind, and the fact that it might be equipped to discover or decipher secrets of nature, to read the mind of God.*

There was a photograph of Mendeleev next to the periodic table in the museum; he looked like a cross between Fagin and Svengali,[10] *with a huge mass of hair and beard and piercing, hypnotic eyes. A wild, extravagant, barbaric Figure—but as romantic, in his way, as the Byronic Humphry Davy. I needed to know more of him, and to read his famous* Principles, *in which he had first published his periodic table.*

His book, his life, did not disappoint me. He was a man of encyclopaedic interests. He was also a music lover and a close friend of Borodin (who was also a chemist). And he was the author of the most delightful and vivid chemistry text ever published, The Principles of Chemistry.

In his very first footnote, in the preface, Mendeleev spoke of "how contented, free and joyous is life in the realm of science"—and one could see, in every sentence, how true this was for him. The Principles grew like a living thing in Mendeleev's lifetime, each edition larger, fuller, more mature than its predecessors, each filled with exuberating and spreading footnotes (footnotes which became so enormous that in the last editions they filled more pages than the text; indeed, some occupied nine-tenths of the page—I think my own love of footnotes, the excursions they allow, was partly determined by reading the Principles."

An outstanding feature of this book is the rich and appositely chosen quotations that the author incorporates into his text. Almost all of them are worthy of repetition here, but I shall restrict myself to a mere few. Ever since I studied Sir William Crookes's comments on Faraday,[11] I have been aware of the almost hypnotic use of words of which he was capable. Sacks provides (p. 208) an excellent example of Crookes's skills when he quotes the latter's thoughts on the bewildering properties of the rare earth elements:

> *"The rare earths perplex us in our researches, baffle us in our speculations, and haunt us in our very dreams. They stretch like an unknown sea before us, mocking, mystifying, and murmuring strange revelations and possibilities."*

When he describes (p. 266) Madame Curie's (Figure 7) *"outrageous thought (in 1898) that radioactivity might come*



Figure 7. Marie Curie (1867–1934). Photo obtained from the Deutsches Museum, Munich.

from the disintegration of atoms", he recalls the beautiful words of Clerk Maxwell:

> *"Though in the course of ages catastrophes have occurred and may yet occur in the heavens, though ancient systems may be dissolved and new systems evolved out of their ruins, the [atoms] out of which these systems are built—the foundation stones of the material universe—remain unbroken and unworn. They continue to this day as they were created—perfect in number and measure and weight".*

Interestingly, we are reminded that, after her bold thoughts about atomic disintegration, Marie Curie withdrew from the idea and finally concluded, with poetic resonance, "*the cause*

 © WILEY-VCH Verlag GmbH, 69451 Weinheim, Germany, 2002 1433-7851/02/4112-2064 $ 20.00+.50/0 *Angew. Chem. Int. Ed.* **2002**, *41*, No. 12

of this spontaneous radiation remains a mystery…a profound and wonderful enigma."

5. Envoi

Is this book completely without fault? Not quite; there are a few relatively minor errors of fact. It is not correct to say (p. 127) that Davy was the first scientist to be knighted since Sir Isaac Newton: his immediate predecessor as President of the Royal Society, Sir Joseph Banks, was one, and Newton's successor in the same presidency, Sir Hans Sloane, was another. So also was Sir Benjamin Thompson (Count Rumford), who was the first to offer Davy a Professorship, at the Royal Institution, where, incidentally, Davy first experimented with and invented the electric arc (not at Thomas Beddoes' Pneumatic Institute in Bristol, pp. 119–122).

It is also incorrect to say (p. 266) that J. J. Thomson was one of the founders of the British Psychical Society. He certainly showed an interest in such phenomena, but he was always an arch sceptic.[12] It is also not true to assert (p. 167) that before Maxwell's work in the early 1860s *"no-one had suspected any relationship between magnetism and light"*. Michael Faraday, in 1845, discovered what has since become known as the Faraday effect, the rotation of the plane of polarization of light by a magnetic field—effectively the birth of magneto-optics. In nonstoichiometric compounds (p. 148) such as Fe_7S_8 and Fe_8S_9 there is no substitution of iron by sulphur; and the phenomenon of catalysis (p. 130) was not discovered by Davy, the Arabs knew about it as early as the 8th Century.

But even to recite these minor infelicities seems churlish. This is one of the most enjoyable, stimulating, and rewarding books that I have ever read. It is so replete with poetic insight and expression that I wish I had chanced upon it before addressing a joint symposium of the Akademia Leopoldina and the French Academy at Gottingen on "Poetic Suggestion in Chemical Science" in October 2001. The examples that I cited[13] on that occasion would have been enriched by many splendid ones contained in this memorable tome.

[1] When I consulted "A Leg to Stand On", Sacks endeared himself to me by the epigraph of that book taken from Mortaigne's Essays: "*Plato therefore was right in saying that to become a true doctor, a man must have experienced all the illnesses he hopes to cure and all the accidents and circumstances he is to diagnose… Such a man I would trust. For the rest guide us like the person who paints seas, rocks and harbours while sitting at his table and sails his model of a ship in perfect safety. Throw him into the real thing, and he does not know where to begin*."

[2] Braefield is the name of the village in England to which the seven-year-old Oliver was sent as an evacuee from London to the reconstituted preparatory school. His four years there were a misery.

[3] Aunt Len had founded in Cheshire the Jewish Fresh Air School for "delicate children", children from working-class families in Manchester.

[4] Fibonacci, otherwise known as Leonardo of Pisa (ca. 1170–1240) was the most distinguished mathematician of the Middle Ages. He studied calculation with an Arab master while his father was serving as a Consul in Algeria. His best know work is *Liber Abaci* (The Book of the Abacus, published in 1202). In it he made the Arabic numeral system generally available in Europe. The Fibonacci series is said to have arisen from the following problem: A certain man put a pair of rabbits in a place surrounded on all sides by a wall. How many pairs of rabbits can be produced from the pair in a year. If it is supposed that every month each pair begets a new pair which from the second month on becomes productive? The answer is 1, 1, 2, 3, 5, 8, 13… (Fibonacci himself omitted the first term).

[5] The Balfour Declaration (1917), named after A J. Balfour, the British Foreign Secretary in Lloyd George's Government pledged British support for a Jewish national home in Palestine.

[6] John Meurig Thomas in "*Michael Faraday and the Royal Institution: The Genius of Man and Place*", Institute of Physics, Bristol, **1991**. Michael Faraday, while still an apprentice bookbinder aged 21, wrote (in 1812): "*My desire to escape from trade, which I thought vicious and selfish, and to enter into the services of Science, which I imagined made its pursuers amiable and liberal, induced me at last to take the bold and simple step of writing to Sir H. Davy expressing my wishes and a hope that, if an opportunity came in his way, he would favour my views: at the same time I sent the notes I had taken of his lectures."* Faraday began work as Davy's assistant at the Royal Institution on 1 March, 1813.

[7] Some of Sacks' lyrical passages made me think of "*Fern Hill*", the poem written by Dylan Thomas when he was 18 years old: "*And as I was green and carefree, famous among the barns / About the happy yard and singing as the farm was home, / In the sun that is young once only / Time let me play and be / Golden in the mercy of his means…"*

[8] Sir William Huggins (1824–1910), who was President of the Royal Society, 1900–1905, on learning about Kirchhoff's exciting discovery of the chemical composition of the sun from the study of the Fraunhofer line-spectrum, he immediately foresaw that this constituted the key to a novel method of astronomical research to which the remainder of his life was dedicated. One application of stellar spectroscopy to which he turned his attention was that of determining the radial velocity of a star from the displacement of its spectral lines to the red or blue. In a dramatic Friday Evening Discourse[5] given at the Royal Institution on 19 May, 1865, entitled "*On the Physical and Chemical Composition of the Fixed Stars and Nebulal*", Huggins presented spectroscopic proof that the star "Aldebaran" contained hydrogen, sodium, magnesium, calcium, iron, bismuth, tellurium, antimony, and mercury. (W. Huggins, *Proc. R. Inst. G.B.* **1862–1865**, *IV*, 441–449.)

[9] The company is now (and has for some time been) named Griffin & George. The parent company was established in Glasgow in 1826, but it is now part of Fisher Scientific, the world's largest supplier of scientific equipment to industry, education, and governmental contractors in 145 countries.

[10] Fagin is a character in Charles Dickens' novel *Oliver Twist* (1870). The word is now used to denote an adult who instructs others (especially children) in theft and other crimes. Svengali is someone who attempts, usually with sinister motives, to mould another to his will. The name comes from that of a sinister hypnotist in the novel *Trilby* by George Du Maurier (1896).

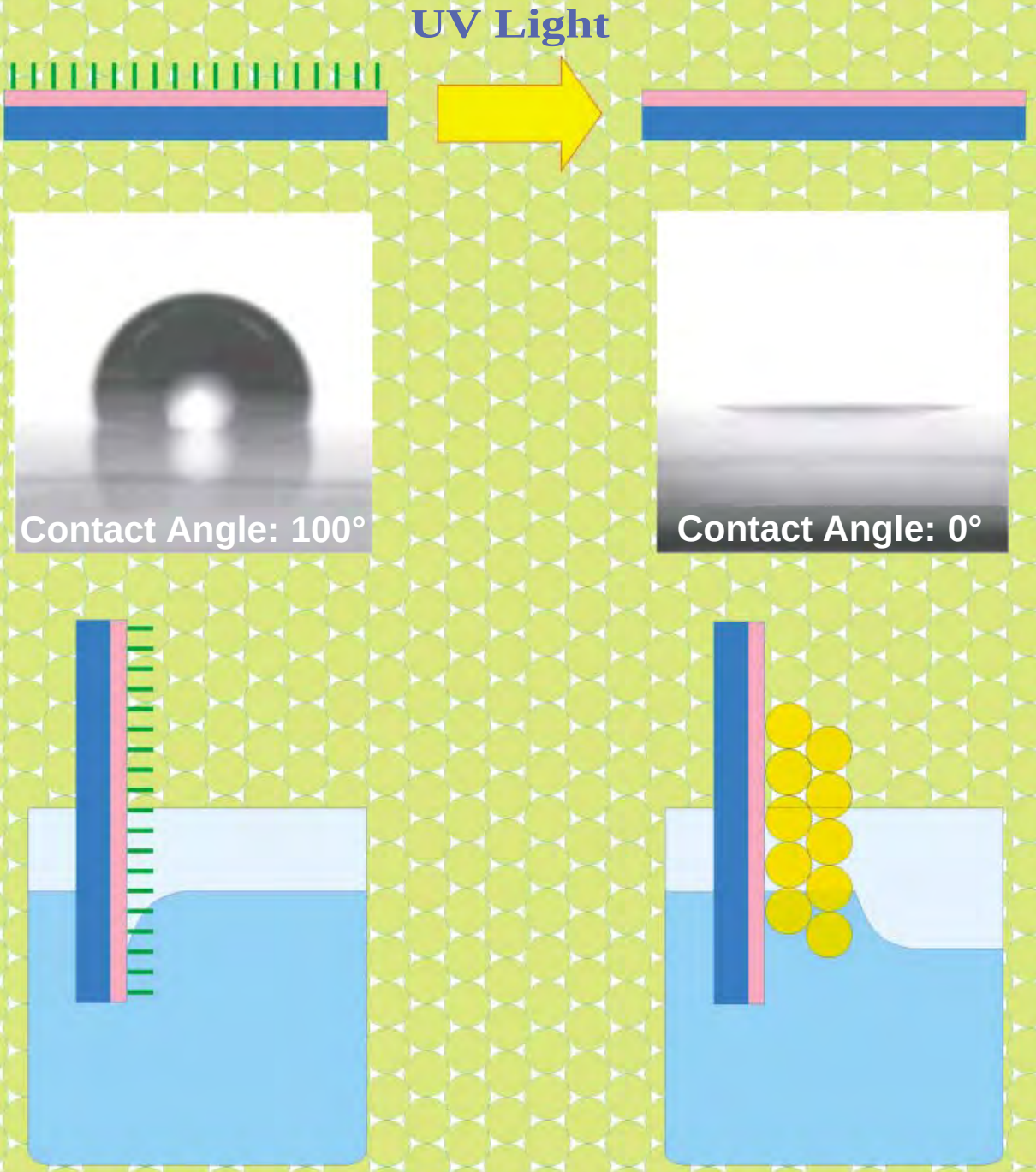
[11] See Ref. [6], pp. 65–69. An example of Crookes's literary skills is contained on p. 195 of this book on Faraday, in the charming manner in which he wrote the Preface to *The Chemical History of a Candle*: "From the primitive pine torch to the paraffin candle, how wide an interval! Between them how vast a contrast! The means adopted by man to illuminate his home at night, stamp at once his position in the scale of civilization…".

[12] See J. J. Thomson, *Recollections and Reflections*, Chap V, G. Bell & Sons, London, **1936**.

[13] "Proceedings of Leopoldina Symposium on Chemistry and Mathematics: Two Scientific Languages of the 21st Century", edited by H. W. Roesky, G. Ourisson, *Nova Acta Leopold.* **2002**, in press.

 © WILEY-VCH Verlag GmbH, 69451 Weinheim, Germany, 2002 1433-7851/02/4112-2065 $ 20.00+.50/0

A new approach is proposed for the patterning of colloidal crystal films by taking advantage of the photocatalytic and photoinduced super-hydrophilic properties of titanium dioxide. The substrate used for the patterning of the colloidal crystal film was glass coated with titanium dioxide which was treated with fluoroalkylsilane to render the surface hydrophobic.



Photoirradiation with ultraviolet light through a photomask transforms the irradiated surface of the substrate from hydrophobic to hydrophilic in character. A subsequent dipping process causes patterns of colloidal crystal films to deposit on the hydrophilic surface of the substrate. For more information see the following pages.

 © WILEY-VCH Verlag GmbH, 69451 Weinheim, Germany, 2002 1433-7851/02/4112-2067 $ 20.00+.50/0

Patterning of a Colloidal Crystal Film on a Modified Hydrophilic and Hydrophobic Surface**

Zhong-Ze Gu, Akira Fujishima, and Osamu Sato*

Structural color-change mechanisms play an important role in the protective and warning coloration of animals.[1] These structural color changes originate from the diffraction and scattering of light by microstructures on the surface of the animal's body, and are therefore very different from coloration phenomena that are brought about by the absorption of dyes. Structural color changes have been extensively investigated recently, since they are not only important for biological systems, but also play a role in the study of photonic crystals.[2] It is important to note that the application of photonic crystals has been proposed for the next generation pigments and optical devices.[3–6] For practical applications of photonic crystals with a three-dimensional microstructure it is essential to be able to fabricate photonic crystal films onto substrates with specific patterns both simply and cheaply, and this is still proving to be a challenge.[7–11] Herein we discuss a new technique for the fabrication of colloidal crystal films on specific areas of substrates that takes advantage of the photocatalytic and photoinduced superhydrophilic properties of TiO_2. We show that this approach makes possible the practical application of colloidal crystals as pigments and optical devices.

A patterned colloidal crystal film was fabricated onto a glass substrate that had been treated by procedures a) and b) in Figure 1. The glass substrate was first coated with a thin film of TiO_2 using the sol–gel method (the coating solutions used are NDH-500A and NDH-510C, which were bought from Nippon Soda, Co. Ltd.). The surface of the TiO_2 film was then modified with fluoroalkylsilane ($CF_3(CF_2)_7$-$CH_2CH_2Si(OCH_3)_3$, made by Toshiba Silicone, Japan) by using a self-assembly method. The surface of the substrate becomes hydrophobic after the treatment with fluoroalkylsilane, and the contact angle of water was measured as 100°. The substrate was irradiated with ultraviolet light through a photomask to make a pattern with different degrees of wettability on different areas. This changed the contact angle of water on the irradiated surface to 0°, while no change occurred for the un-irradiated surface. The change in the contact angle of the irradiated part derives from the photocatalytic and photoinduced superhydrophilic properties of TiO_2. TiO_2 is a unique photocatalyst that does not exhibit irreversible photocorrosion, but which does display photoinduced superhydrophilic properties.[12, 13] When a film of TiO_2 is irradiated with UV light, active oxygen is generated on the surface of the TiO_2 film as a result of a photo redox reaction. These photogenerated chemical species, which have a very strong redox potential, decompose the fluoroalkylsilane that is adsorbed on the TiO_2 surface. In addition, the UV irradiation creates surface oxygen vacancies on the TiO_2, which renders the surface favorable for the adsorption of dissociative water. This in turn causes the surface of the TiO_2 to become superhydrophilic.[12, 14] Consequently, the unique properties of the TiO_2 allow the easy and precise patterning of the surface to give a large contrast in wettability.

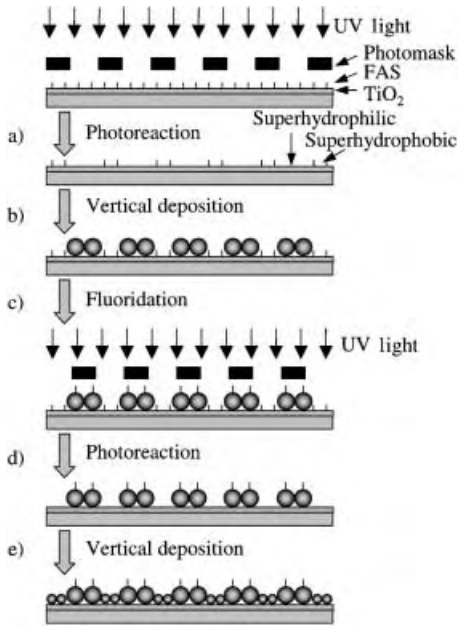


Figure 1. The process of patterning with colloidal crystal films.

The substrate was inserted vertically into an aqueous suspension containing either monodispersed silica spheres or polystyrene to fabricate a pattern consisting of a colloidal crystal film. The liquid surface is concave above the hydrophilic surface, while it is convex over the hydrophobic area. The substrate was then extracted from the liquid at a constant rate, which ranged from 2 to 8 $\mu m\,s^{-1}$. Colloidal crystals form over the hydrophilic areas during the lifting process, whilst no film was observed on the hydrophobic regions. The reason for this selective formation of the film can be explained as follows:[15, 16] The solution forms a meniscus on the hydrophilic surface of the substrate with an angle smaller than 90°. Such a meniscus contributes to the generation of a capillary force, which causes the spheres to assemble on the surface. The slope of the meniscus over the hydrophobic surface increases to an angle of greater than 90°, and the capillary force responsible for the assembly of the spheres disappears.

Figure 2 shows pictures of a colloidal crystal film fabricated on a glass substrate with a fish-shaped hydrophilic pattern.

[*] Dr. O. Sato, Dr. Z.-Z. Gu
Kanagawa Academy of Science and Technology
KSP Bldg., East 412, 3-2-1 Sakado
Takatsu-ku, Kawasaki-shi, Kanagawa 213-0012 (Japan)
Fax: (+81) 44-819-2070
E-mail: sato@fchem.chem.t.u-tokyo.ac.jp
Dr. Z.-Z. Gu
National Laboratory of Molecular and Biomolecular Electronics
Southeast University, Nanjing 210096 (China)
Prof. A. Fujishima
Department of Applied Chemistry
School of Engineering, The University of Tokyo
7-3-1 Hongo Bunkyo-ku, Tokyo 113-8565 (Japan)

[**] This work was supported in part by the Japan Society for the Promotion of Science and the Kanagawa Prefecture Joint-Research Project from the Regional Intensive, Japan Science and Technology Corporation.

 © WILEY-VCH Verlag GmbH, 69451 Weinheim, Germany, 2002 1433-7851/02/4112-2068 $ 20.00+.50/0

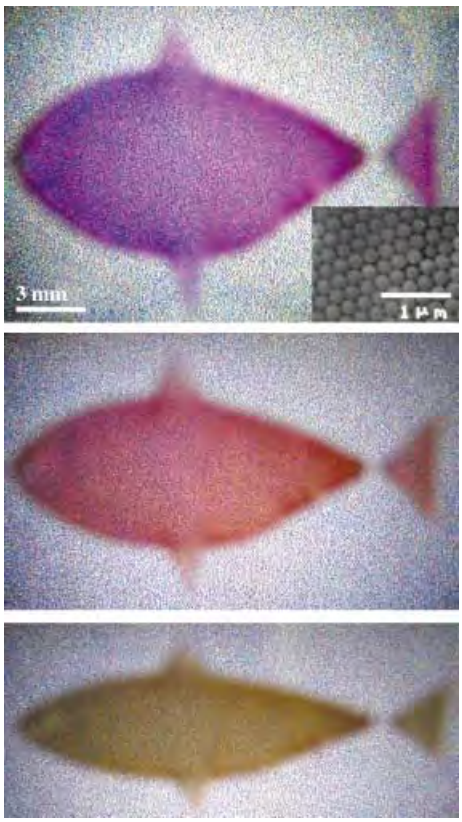


Figure 2. The fish-shaped pattern observed from different angles. The inset shows the arrangement of polystyrene spheres in the film.

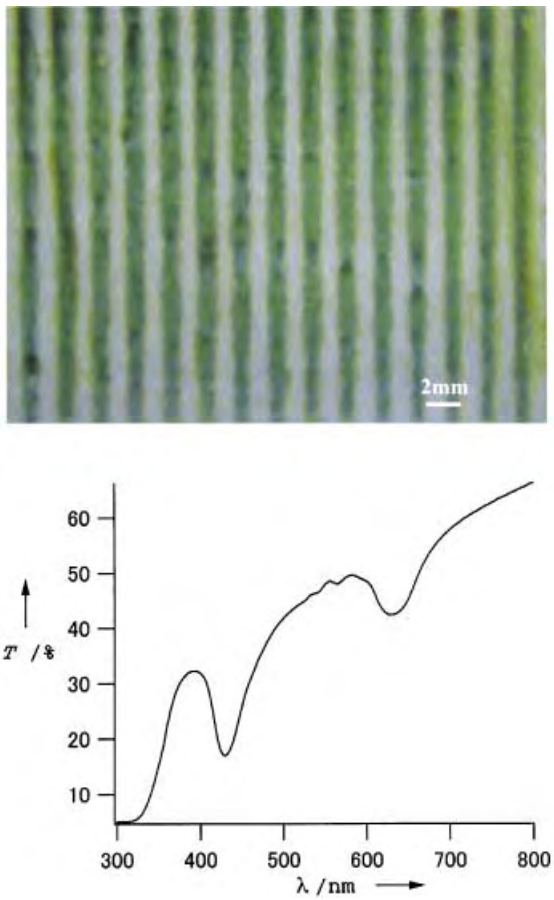


Figure 3. Top: Lines composed of different silica spheres. Bottom: Transmission spectrum of the line pattern. The two peaks can be assigned to lines composed of spheres with diameters of 195 nm and 275 nm, respectively.

Monodispersed polystyrene spheres with a diameter of 230 nm form films on the fish-shaped hydrophilic regions, while no film was observed in the region where the substrate was hydrophobic. Uniform colors can be observed at different glancing angles and are caused by diffraction induced by the ordered monodispersed spheres. A hexagonal arrangement of spheres can be observed over a wide area.

A complex pattern composed of different types of monodispersed spheres can be fabricated by repeating the processes of fluoridation and photodecomposition. Figure 3a shows a pattern of alternate lines composed of two different types of silica spheres. The green lines are films composed of spheres of 275-nm diameter, between which are films composed of spheres with a diameter of 195 nm. The difference in colors comes from the change in the wavelength of the diffraction peaks (Figure 3b). The fabrication details for this sample are outlined in Figure 1 as procedures a) – e). Firstly, a linear colloidal crystal film pattern composed of silica spheres with a diameter of 275 nm was deposited onto a substrate by following the same procedure as described above (procedures a) and b)). Then, the substrate was again modified with fluoroalkylsilane (procedure c)). The subsequent irradiation with UV light decomposes the molecules of fluoroalkylsilane on the surface of the TiO_2, while those on the surface of the silica spheres remained unchanged (procedure d)). Therefore, the surface of the TiO_2 becomes hydrophilic, while the surface of the colloidal crystal, which is composed of silica spheres, is hydrophobic. The final vertical deposition, procedure e), causes the silica spheres with a diameter of 195 nm to form crystals only between the lines of the colloidal crystals composed of 275-nm silica spheres.

In conclusion, a method of controlling wettability has been developed for the patterning of colloidal crystal films. Films composed of different types of spheres can be deposited simply onto the substrate step by step. Since the materials used for patterning are very cheap and readily commercially available and the fabrication process is very simple, it can be anticipated that the approach exhibited here would enable the application of colloidal crystals to a new generation of decorative materials and optical devices. In addition, this method also provides a new approach for the study of the crystallization of colloidal particles onto a surface with modified wettability, which is important in the fields of colloids and biological films.

Received: January 18, 2002 [Z 18543]

[1] H. Kasukawa, N. Oshima, R. Fujii, *Zool. Sci.* **1987**, *4*, 243.
[2] A. R. Parker, R. C. McPhedran, D. R. McKenzie, L. C. Botten, N.-A. P. Nicorovici, *Nature* **2001**, *409*, 36.
[3] S. John, *Phys. Rev. Lett.* **1987**, *58*, 2486.
[4] E. Yablonovitch, *Phys. Rev. Lett.* **1987**, *58*, 2059.
[5] E. Yablonovitch, *Nature* **1999**, *401*, 539.
[6] A. Blanco, E. Chomski, S. Grabtchak, M. Ibisate, S. John, S. W. Leonard, C. Lopez, F. Meseguer, H. Miguez, J. P. Mondia, G. A. Ozin, O. Toader, H. M. van-Driel, *Nature* **2000**, *405*, 437.
[7] Y. D. Yin, Y. Lu, Y. N. Xia, *J. Am. Chem. Soc.* **2001**, *123*, 771.

 © WILEY-VCH Verlag GmbH, 69451 Weinheim, Germany, 2002 1433-7851/02/4112-2069 $ 20.00+.50/0

[8] Y. Yin, Y. Lu, B. Gates, Y. Xia, *J. Am. Chem. Soc.* **2001**, *123*, 8718.
[9] R. C. Hayward, D. A. Saville, I. A. Aksay, *Nature* **2000**, *404*, 56.
[10] O. D. Velev, A. M. Lenhoff, E. W. Kaler, *Science* **2000**, *287*, 2240.
[11] B. A. Ozin, S. M. Yang, *Adv. Funct. Mater.* **2001**, *11*, 95.
[12] A. Fujishima, K. Hashimoto, T. Watanabe, *TiO_2 Photocatalysis: Fundamentals and Applications*, BKC Inc., Tokyo, **1999**.
[13] A. Fujishima, K. Honda, *Nature* **1972**, *238*, 37.
[14] R. Wang, K. Hashimoto, A. Fujishima, M. Chikuni, E. Kojima, A. Kitamura, M. Shimohigoshi, T. Watanabe, *Nature* **1997**, *388*, 431.
[15] Z.-Z. Gu, O. Sato, A. Fujishima, *Chem. Mater.* **2002**, *14*, 760.
[16] M. Yamaki, J. Higo, K. Nagayama, *Langmuir* **1995**, *11*, 2975.

An Inverted Metal-Organic Framework with Compartmentalized Cavities Constructed by Using an Organic Bridging Unit Derived from the Solid State**

Giannis S. Papaefstathiou and
Leonard R. MacGillivray*

Porous crystalline solids that employ metal-organic components as building blocks, where a rigid, linear organic bridge propagates the coordination geometry of a metal node in one-, two-, or three-dimensions, are attracting much interest.[1–3] Such metal–organic frameworks (MOFs) are designed to exhibit properties that mimic, and improve upon, more conventional porous solids, such as zeolites[4] and mesoporous materials (MCMs).[5] Many porous MOFs, however, have fallen short, in contrast to zeolites and MCMs, as robust porous solids.[2, 6] Interpenetration[6] and framework fragility[2] have hampered progress such that host cavities tend to self-include while guest removal often results in a collapse of host structure. Recently, however, such problems of interpenetration and framework fragility have been largely circumvented by using metal clusters, as secondary building units (SBUs), for host design.[7] SBUs (e.g. metal carboxylates) reduce the likelihood of interpenetration owing to their large sizes which can preclude filling of void spaces,[8] producing stable, porous solids able to support inclusion and catalysis.[1a–c]

Although SBUs have been successfully employed for the construction of MOFs with stable pores, it can be difficult, in contrast to MCMs,[5, 9] to line the interiors of such solids with organic groups since an elaborate covalent synthesis of a linear organic bridge is often required to introduce simple (e.g. -Me) and diverse (e.g. chiral) functional groups. With this in mind, it has occurred to us that one way to circumvent this problem may be to invert the structural role[10] of the SBU and linear organic bridge such that the SBU serves as a linear bridge and the organic ligand serves as a node. In this design, the bonds of the SBU that support the framework are minimized (i.e. two) such that the remaining coordination sites of the SBU may be filled with organic ligands that decorate the interior of the framework. Moreover, such an inverted metal-organic framework (IMOF) would enable the second sphere of a SBU to line the walls of a host, in contrast to a covalent synthesis, supramolecularly[11] where convergent[12] terminal groups may be tailored to define structure and recognition properties of the solid.

Herein, we describe initial results of a strategy for the construction of such a porous IMOF that employs a molecule

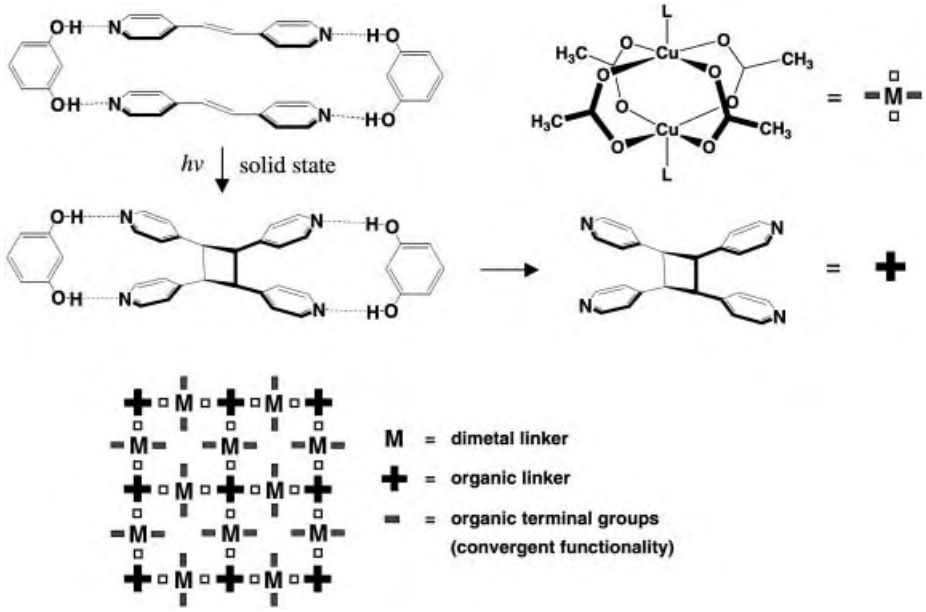


Figure 1. Construction of a porous inverted metal-organic framework (IMOF).

derived from a template-directed[13] solid-state [2+2] photodimerization[14] as the node (Figure 1). Owing to the presence of divergent and multiple Lewis-base functional groups, we anticipated that the product of this solid-state approach, *rctt*-tetrakis (4-pyridyl)cyclobutane[15] (4,4′-tpcb), upon reaction with the Cu paddle-wheel complex $[Cu_2(O_2CR)_4L_2]$,[16] would serve as a 4-connected node, propagating the dimetal complex, as a linear SBU through axial coordination, within a porous 2D IMOF.[17] Moreover, in contrast to a planar organic node (e.g. 4,4′-bipyridine),[18] the ligand derived from the solid-state synthesis was anticipated to produce cavities with deepened interiors owing to enforced twisting of the

[*] Prof. L. R. MacGillivray, G. S. Papaefstathiou
Department of Chemistry
University of Iowa
Iowa City, IA 52242-1294 (USA)
Fax: (+1) 319-335-1270
E-mail: len-macgillivray@uiowa.edu

[**] We are grateful to the National Science Foundation (CAREER Award, L.R.M., DMR-0133138) and the University of Iowa for funding. Acknowledgement is also made to the Donors of The Petroleum Research Fund, administered by the American Chemical Society, for support of this research.

Supporting information for this article is available on the WWW under http://www.angewandte.org or from the author.

 © WILEY-VCH Verlag GmbH, 69451 Weinheim, Germany, 2002 1433-7851/02/4112-2070 $ 20.00+.50/0

pyridyl groups with respect to the cyclobutane rings which would orient the pyridyl groups orthogonal to the plane of the 2D framework (Figure 2). That the R groups of the SBU may be readily modified[19] would provide a ready means to decorate the walls of the deepened cavities with organic functional groups.



Figure 2. The orientation of the pyridyl groups (space-filling representation) orthogonal to the plane of the 2D framework.

When $[Cu(O_2CCH_3)_2(H_2O)_2]$ (0.06 g) and 4,4′-tpcb (0.025 g) in methanol (15 mL) was layered with benzene (25 mL), green crystals of **1**·3 benzene grew within approximately three weeks (yield: 75%). The formulation of **1**·3 benzene was confirmed by single-crystal X-ray diffraction (Figure 3), X-ray powder diffraction, and thermal analysis.

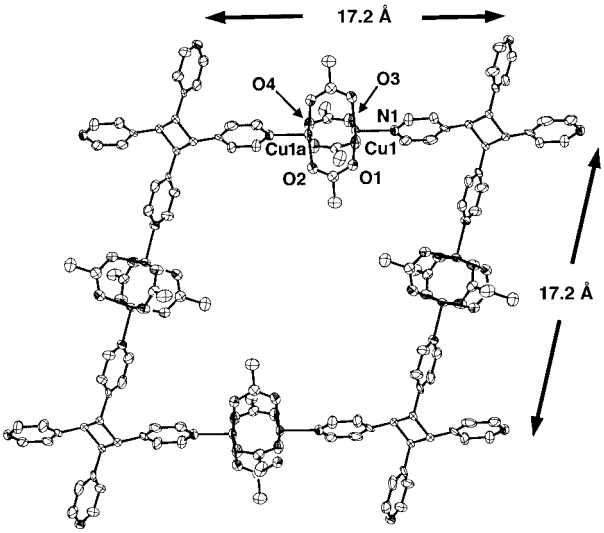


Figure 3. ORTEP perspective of **1**. Selected interatomic distances [Å]: Cu1-N1 2.148(3), Cu1-O1 1.971(3), Cu1-O2 1.980(3), Cu1-O3 1.968(2), Cu1-O4 1.965(2), Cu1 ··· Cu1a 2.600(1).

The components assemble to form a porous 2D IMOF. Each 4,4′-tpcb unit, each of which sits around a crystallographic center of inversion, is surrounded by four paddle-wheel complexes, each of which is bisected by a mirror plane, such that the organic unit serves as a 4-connected vertex. As anticipated, the pyridyl rings are twisted approximately orthogonal with respect to the cyclobutane ring (dihedral angle: 139.8°) such that the pyridyl groups "thicken" the 2D framework.[16, 18] As a consequence of the assembly process, a 2D IMOF with very large rhombic cavities of dimensions of about $17.2 \times 17.2 \times 5.0$ Å and corner angles of about 75° and 105° is formed. Owing to the ability of 4,4′-tpcb to propagate the SBU within a (4,4)-framework, **1** may be regarded a novel inverted analogue of those cavity-containing rhombic- and square-grid frameworks designed by using linear bipyridine groups and transition-metal ions.[17] The cavity of **1** is larger than most metal-(4,4′-bipyridine) rhombic- and square-grid frameworks (dimensions $\sim 12.0 \times 12.0$ Å)[17] and compares favorably with a metal–bipyridine square grid, $[\{Ni(4,4'\text{-bis}(4\text{-pyridyl})\text{biphenyl})_2(NO_3)_2\}_n]$ (dimensions of about 20.0×20.0 Å), with a lengthened linear bridge.[3c]

The cavities of **1**, unlike those metal–bipyridine grids,[17] are decorated with convergent organic functional groups; four methyl groups are directed into the rhombic cavities such that the ligands subdivide each cavity into three compartments (Figure 4). The largest compartment, which defines a large

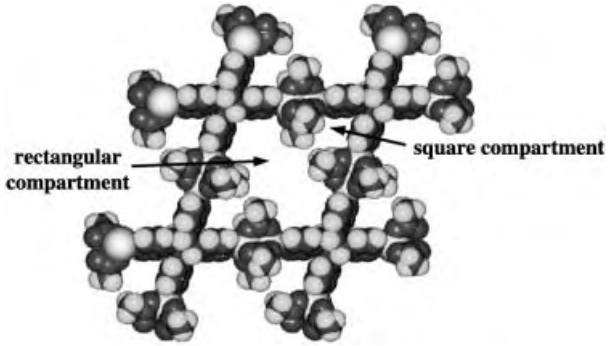


Figure 4. A space-filling view of the rhombic cavity of **1**. The cavity is subdivided by organic functional groups stemming from the SBU to form one rectangular or two square compartments.

rectangular box of dimensions of about $20.0 \times 9.5 \times 5.0$ Å, runs along the diagonal of the obtuse corner angles and is occupied by one ordered and two disordered benzene guests. The two smaller compartments, which define moderately sized[20] square boxes of dimensions of about $7.0 \times 7.0 \times 5.0$ Å, are located in the remaining corners and are filled by methyl groups, directed above and below each cavity, of adjacent grids. As depicted in Figure 5, the inclusion of the methyl groups (Figure 5a) results in oblique stacking of the grids (interlayer separation: 5.7 Å) along the crystallographic *c* axis which, in turn, gives rise to a porous 3D MOF with, in a similar way to MCM-41,[5, 9] isolated 1D channels, of dimensions of about 12×10 Å (Figure 5b). The channels are occupied by ordered (one per cavity) and disordered (two per cavity) benzene solvent molecules, which assemble edge-to-face (Figure 5c), and represent about 40% of the volume of the unit cell.[21] Thus, the organic functional groups of the SBU accommodate the methyl groups as "pegs" in lining up the layers, preorganizing the grids to form the channels. To our knowledge, such molecular compartmentalization within a MOF has not been realized.[22]

Thermogravimetric (TGA) and differential scanning calorimetry (DSC) analysis (see Supporting Information), along with X-ray powder diffraction and optical microscopy, suggest that the structure of **1** is maintained between 27 °C and 180 °C. During this temperature change, the guest is liberated in two mass losses at 27 °C (two guests) and 75 °C (one guest), which may be attributed to the disordered and ordered guests,[3a] respectively, for which DSC and optical microscopy indicate

 © WILEY-VCH Verlag GmbH, 69451 Weinheim, Germany, 2002 1433-7851/02/4112-2071 $ 20.00+.50/0

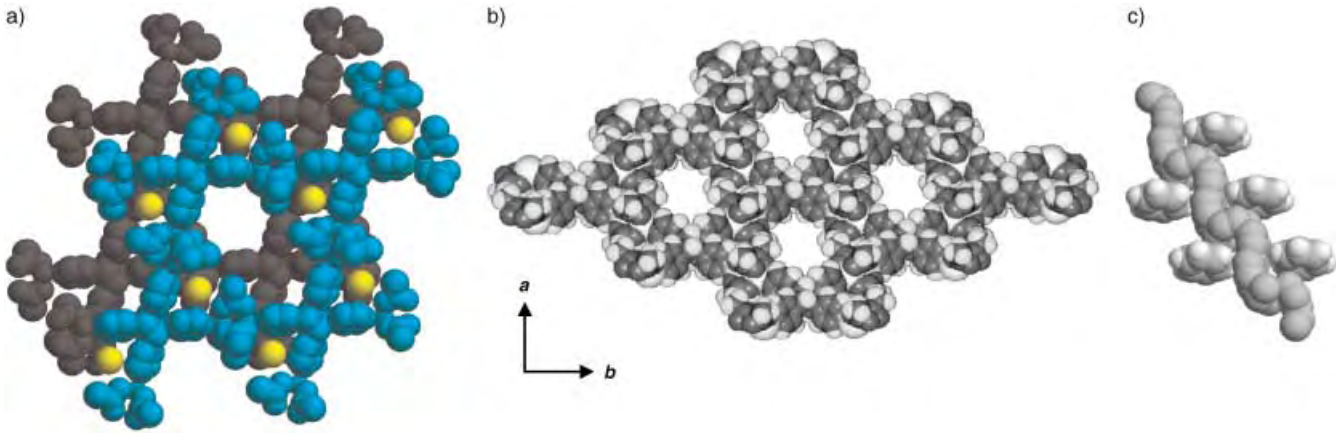


Figure 5. Space-filling views that demonstrate the stacking of the grids of **1** that form 1D channels and enable guest inclusion: a) stacking of two grids showing the inclusion of methyl groups, or "pegs", within the square compartments (hydrogen atoms omitted for clarity; color scheme: two grids have been differentiated using cyan and gray while the yellow spheres represent the included methyl groups), b) the 1D elliptical channels that arise from stacking of the larger compartments, and c) the ordered and disordered benzene guests.

no evidence of a phase change. Moreover, although diffraction-peak broadening is observed with the increase in temperature, single-crystal X-ray analysis performed on a sample after removal of the guest confirms the structure of **1**, the framework being virtually identical to guest-filled **1** save for high thermal motion of the organic components.[23] Indeed, **1** is a rare example of a MOF with single crystals stable to guest removal.[3] Preliminary results reveal that reintroduction of benzene can be achieved by placing **1** in neat benzene and heating the solvent to approximately 70 °C. Notably, guest uptake is accompanied by further diffraction-peak broadening which may be attributed to additional disorder of the organic groups.[24] Heating beyond 180 °C results in decomposition of the solid.

Herein, we have presented a strategy for the construction of porous MOFs that enables the supramolecular decoration of cavities with organic functional groups. Lining of the interior is achieved by using convergent[12] terminal ligands of a linear SBU[7] and a product of a template-directed solid-state organic synthesis.[13] In the present case, the organic functional groups compartmentalize the rhombic cavities of a 2D porous IMOF[22] and preorganize the framework to assemble to form a 3D nanoporous solid. Following these observations, experiments are underway to expand this approach to organic groups of increasing diversity and additional SBUs.[25] That the node has been generated by a template-directed solid-state organic synthesis[13, 14] also suggests that access to MOFs (as in the case of **1**) poorly available,[26, 27] or completely inaccessible, in solution, may now be realized.

Experimental Section

1·3benzene: A solution of $[Cu(O_2CCH_3)_2(H_2O)_2]$ (0.06 g) and 4,4′-tpcb (0.025 g) in methanol (15 mL) was layered with benzene (25 mL) at room temperature. Upon standing, green crystals of **1**·3benzene grew within 3 weeks and were isolated in 75% yield by way of filtration. IR (KBr pellets): $\tilde{\nu} = 1630$ (s), 1610 (s), 1579 (sh, br), 1428 (s, br), 1346 (m), 1223 (m), 1071 (w), 1022 (m), 835 (m), 682 (m), 527 (m), 565 (m) cm^{-1}. Crystal data for **1**·3benzene: monoclinic, $C2/m$, $a = 14.354(3)$, $b = 27.238(5)$, $c = 8.064(2)$ Å, $\beta = 93.56(3)^\circ$, $V = 3147.0(11)$ Å^3, $2\theta = 45^\circ$, $Mo_{K\alpha}$ radiation ($\lambda = 0.71070$ Å) for $Z = 2$ and $R = 0.037$. Crystal data for the heated sample of **1**: triclinic, space group $P\bar{1}$, $a = 8.002(2)$, $b = 13.956(3)$, $c = 15.409(3)$ Å, $\alpha = 64.33(3)^\circ$, $\beta = 88.01(3)^\circ$, $\gamma = 83.39(3)^\circ$, $V = 1540.3(5)$ Å^3, $2\theta = 40^\circ$, $Mo_{K\alpha}$ radiation ($\lambda = 0.71070$ Å) for $Z = 1$ and $R = 0.128$. The crystal data for **1**·3benzene and the heated sample of **1** were measured on a Nonius Kappa CCD single-crystal X-ray diffractometer at 100 K. After anisotropic refinement of all non-hydrogen atoms, aromatic, methyl, and methine hydrogen atoms were placed in idealized positions and allowed to ride on the atom to which they are attached. The cyclobutane moieties in both **1**·3benzene and the heated sample of **1** were observed to lie disordered across two positions. Correspondingly, ring carbon atoms were refined with fixed site occupancies of 0.50/0.50 and 0.55/0.45, respectively. The disordered guest molecules of **1**·3benzene were disordered in a manner consistent with benzene. The atoms were treated as carbon atoms and refined with isotropic thermal parameters and fixed site occupancies. The mosaic nature of the heated sample of **1** made accurate integration of the reflection data difficult, precluding the possibility of an accurate structure with $2\theta > 40^\circ$. All crystallographic calculations were conducted using SHELXL-97[28] locally implemented on an IBM compatible pentium-based PC. CCDC-172946 (**1**·3benzene) and CCDC-172947 (**1**) contains the supplementary crystallographic data for this paper. These data can be obtained free of charge via www.ccdc.cam.ac.uk/conts/retrieving.html (or from the Cambridge Crystallographic Data Centre, 12, Union Road, Cambridge CB2 1EZ, UK; fax: (+44) 1223-336-033; or deposit@ccdc.cam.ac.uk).

Received: October 30, 2001
Revised: January 30, 2002 [Z18135]

[1] Recent representative examples: a) J. S. Seo, D. Whang, H. Lee, S. I. Jun, J. Oh, Y. J. Jeon, K. Kim, *Nature* **2000**, *404*, 982–986; b) S. M.-F. Lo, S. S.-Y. Chui, L.-Y. Shek, Z. Lin, X. X. Zhang, G. Wen, I. D. Williams, *J. Am. Chem. Soc.* **2000**, *122*, 6293–6294; c) H. Li, M. Eddaoudi, M. O'Keeffe, O. M. Yaghi, *Nature* **1999**, *402*, 276–279; d) B. Moulton, C. Seward, M. J. Zaworotko, *Chem. Commun.* **1999**, 1327–1328; e) S. W. Keller, S. Lopez, *J. Am. Chem. Soc.* **1999**, *121*, 6306–6307; f) J. D. Ranford, J. J. Vittal, D. Wu, X. Yang, *Angew. Chem.* **1999**, *111*, 3707–3710; *Angew. Chem. Int. Ed.* **1999**, *38*, 3498–3501; g) L. R. MacGillivray, R. H. Groeneman, J. L. Atwood, *J. Am. Chem. Soc.* **1998**, *120*, 2676–2677.
[2] M. J. Zaworotko, *Angew. Chem.* **2000**, *112*, 3180–3182; *Angew. Chem. Int. Ed.* **2000**, *39*, 3052–3054.
[3] a) D. Venkataraman, G. B. Gardner, S. Lee, J. S. Moore, *J. Am. Chem. Soc.* **1995**, *117*, 11600–11601; b) C. J. Kepert, M. J. Rosseinsky, *Chem. Commun.* **1999**, 375–376; c) K. Biradha, Y. Hongo, M. Fujita, M. *Angew. Chem.* **2000**, *112*, 4001–4003; Angew. *Chem. Int. Ed.* **2000**, *39*, 3843–3845.
[4] J. V. Smith, *Chem. Rev.* **1988**, *88*, 149–182.
[5] P. Selvam, S. K. Bhatia, C. G. Sonwane, *Ind. Eng. Chem. Res.* **2001**, *40*, 3237–3261.

 © WILEY-VCH Verlag GmbH, 69451 Weinheim, Germany, 2002 1433-7851/02/4112-2072 $ 20.00+.50/0

[6] S. R. Batten, R. Robson, *Angew. Chem.* **1998**, *110*, 1558 – 1595; *Angew. Chem. Int. Ed.* **1998**, *37*, 1460 – 1494.
[7] M. Eddoudi, D. B. Moler, H. Li, B. Chen, T. M. Reineke, M. O'Keeffe, O. M. Yaghi, *Acc. Chem. Res.* **2001**, *34*, 319 – 330.
[8] T. M. Reineke, M. Eddaoudi, D. Moler, M. O'Keeffe, O. M. Yaghi, *J. Am. Chem. Soc.* **2000**, *122*, 4843 – 4844.
[9] MCMs are readily functionalized with organic groups by post-synthetic graphting: See: M. H. Lim, C. F. Blanford, A. Stein, *J. Am. Chem. Soc.* **1997**, *119*, 4090 – 4091.
[10] For studies involving metal linkers as linear bridges, see: a) K. S. Min, M. P. Suh, *Chem. Eur. J.* **2001**, *7*, 303 – 313; b) Y.-H. Kiang, G. B. Gardner, S. Lee, Z. Xu, E. B. Lobkovsky, *J. Am. Chem. Soc.* **1999**, *121*, 8204 – 8215; c) L. Carlucci, G. Ciani, D. W. V. Gudenberg, D. M. Proserpio, A. Sironi, *Chem. Commun.* **1997**, 631 – 632; d) M.-L. Tong, S.-L. Zheng, X.-M. Chen, *Chem. Commun.* **1999**, 561 – 562; e) B. F. Abrahams, B. F. Hoskins, R. Robson, *J. Am. Chem. Soc.* **1991**, *113*, 3606 – 3607.
[11] M. C. T. Fyfe, J. F. Stoddart, *Acc. Chem. Res.* **1997**, *30*, 393 – 401.
[12] a) A. R. Renslo, J. Rebek, Jr., *Angew. Chem.* **2000**, *112*, 3419 – 3421; *Angew. Chem. Int. Ed.* **2000**, *39*, 3281 – 3283; b) K. Choi, A. D. Hamilton, *J. Am. Chem. Soc.* **2001**, *123*, 2456 – 2457.
[13] a) L. R. MacGillivray, *Cryst. Eng. Commun.* **2002**, *4*, 37 – 41; b) G. S. Papaefstathiou, A. J. Kipp, L. R. MacGillivray, *Chem. Commun.* **2001**, 2462 – 2463; c) L. R. MacGillivray, J. L. Reid, J. A. Ripmeester, *J. Am. Chem. Soc.* **2000**, *122*, 7817 – 7818;
[14] G. M. J. Schmidt, *Pure Appl. Chem.* **1971**, *27*, 647 – 678.
[15] A. J. Blake, N. R. Champness, S. S. M. Chung, W.-S. Li, M. Schröder, *Chem. Commun.* **1997**, 1675 – 1676.
[16] For recent studies involving paddle-wheel complexes as linear bridges in extended frameworks, see: a) B. Moulton, J. Lu, M. J. Zaworotko, *J. Am. Chem. Soc.* **2001**, *123*, 9224 – 9225; b) F. A. Cotton, C. Lin, C. A. Murillo, *Chem. Commun.* **2001**, 11 – 12; c) S. R. Batten, B. F. Hoskins, B. Moubaraki, K. S. Murray, R. Robson, *Chem. Commun.* **2000**, 1095 – 1096; d) H. Miyasaka, C. S. Campos-Fernández, R. Clérac, K. R. Dunbar, *Angew. Chem.* **2000**, *112*, 3989 – 3993; *Angew. Chem. Int. Ed.* **2000**, *39*, 3831 – 3835; e) J. L. Wesemann, M. H. Chisholm, *Inorg. Chem.* **1997**, *36*, 3258 – 3267, and references therein.
[17] a) B. Moulton, M. J. Zaworotko, *Chem. Rev.* **2001**, *101*, 1629 – 1658; b) P. J. Hagrman, D. Hagrman, J. Zubieta, *Angew. Chem.* **1999**, *111*, 2798 – 2848; *Angew. Chem. Int. Ed.* **1999**, *38*, 2638 – 2684.
[18] 2D frameworks based on paddle-wheel complexes involving multi-topic ligands that bridge by way of axial positions have involved planar linkers (see ref. [10b – e].
[19] F. A. Cotton, R. A. Walton, *Multiple Bonds Between Metal Atoms*, 2nd ed., Oxford University Press, Oxford, UK, **1993**.
[20] The smaller square cavities are comparable in size to the cavities of $[Fe(pyrazine)_2(NCS)_2]$, see: J. A. Real, G. DeMunno, M. C. Munoz, M. Julve, *Inorg. Chem.* **1991**, *30*, 2701 – 2704.
[21] P. van der Sluis, A. L. Spek, *Acta. Crystallogr. Sect. A* **1990**, *46*, 194 – 201.
[22] For a metal – organic cage that has molecular compartments, see: a) P. N. W. Baxter, J.-M. Lehn, A. Decian, J. Fischer, *Angew. Chem.* **1993**, *105*, 92 – 95; *Angew. Chem. Int. Ed. Engl.* **1993**, *32*, 89 – 90; b) P. N. W. Baxter, J.-M. Lehn, G. Baum, D. Fenske, *Chem. Eur. J.* **1999**, *5*, 102 – 112. For an organic cage that has molecular compartments, see: D. M. Rudkevich, W. Verboom, D. N. Reinhoudt, *J. Org. Chem.* **1995**, *60*, 6585 – 6587.
[23] The rhombic cavity of the heated sample of **1** displays cavity dimensions $\sim 17.1 \times 17.1 \times 5.0$ Å and corner angles of $\sim 72^\circ$ and 108°. The slight deformation in shape of the cavities results in a lowering in symmetry of the unit cell to the triclinic setting.
[24] The additional peak broadening following reintroduction of the guest precludes a single-crystal structure determination of **1**. Experiments are underway to determine the effect of guest uptake on the structure of **1** and the range of guests that may be included within the framework.
[25] It is possible to decorate the interior of a similar IMOF with olefins (G. S. Papaefstathiou, L. R. MacGillivray, unpublished results).
[26] Such solid-state reactivity has been referred to as latent chemical behavior, see: E. Cheung, T. Kang, J. R. Scheffer, J. Trotter, *Chem. Commun.* **2000**, 2309 – 2310.
[27] We note that *trans*-1,2-bis(4-pyridyl)ethylene is photostable as a pure solid and produces a mixture of photoproducts upon UV irradiation in solution that may be separated by way of column chromatography (see: J. Vansant, S. Toppet, G. Smets, J. P. Declerq, G. Germain, *J. Org. Chem.* **1980**, *45*, 1565 – 1573). Therefore, **1** may be regarded as a latent MOF (see ref. [25]).
[28] G. M. Sheldrick, SHELXL-97, Program for Refinement of Crystal Structure, University of Göttingen, Göttingen (Germany), **1997**.

Enhanced Luminescence and Photomagnetic Properties of Surface-Modified EuO Nanocrystals**

Yasuchika Hasegawa, Supitcha Thongchant, Yuji Wada, Hidekazu Tanaka, Tomoji Kawai, Takao Sakata, Hirotaro Mori, and Shozo Yanagida*

Europium(II) oxide (EuO) has localized narrow 4f orbitals that exist as the degeneracy levels between the conduction band (5d orbitals of Eu^{II}) and the valence band (2p orbitals of O^{2-}).[1] The 4f – 5d electron transition and spin configuration of EuO lead to unique optical, magnetic, and electronic properties.[2, 3] In fact, the theoretical quantum-confinement model predicts enhanced luminescence and specific magnetic properties for nanosized Eu^{II} semiconductors.[4, 5] Whereas the preparation of bulk EuO by thermal reduction of Eu_2O_3 above 1000 °C was reported in 1965,[6] EuO nanocrystals were only synthesized and isolated recently. We recently prepared spindle-shaped EuO nanocrystals (average 280 nm in length and 95 nm in width) from Eu metal in liquid ammonia.[7] Here we report on the synthesis of smaller EuO nanocrystals (average diameter: 3.4 nm) by photochemical reduction of

[*] Prof. S. Yanagida, Y. Hasegawa, S. Thongchant, Y. Wada
Material and Life Science
Graduate School of Engineering
Osaka University
2-1 Yamadaoka Suita, Osaka 565-0871 (Japan)
Fax: (+81) 6-6879-7924
E-mail: yanagida@chem.eng.osaka-u.ac.jp
H. Tanaka, Prof. T. Kawai
The Institute of Scientific and Industrial Research
Osaka University
2-1 Yamadaoka Suita, Osaka 565-0871 (Japan)
T. Sakata, Prof. H. Mori
Research Center for Ultra-High Voltage Electron Microscopy
Osaka University
2-1 Yamadaoka Suita, Osaka 565-0871 (Japan)

[**] This work was supported partly by NEDO (New Energy Industrial Technology Development Organization) and Grant-in-Aid for Scientific Research No.13740397 from the ministry of Education, Science, Sports and Culture. We are grateful to Mr. S. Watase and Dr. M. Nakamoto of the Osaka City Research Center for their services in elemental analyses and ICP-AES, and Mr. Y. Yamamoto of the Institute of Scientific and Industrial Research at Osaka University for magnetic measurements. We also thank Emeritus A. Yanase at Osaka Prefecture University for helpful discussion on the magnetization of EuO, and Prof. N. Nakashima at Osaka city university for helpful discussion on the photochemical reduction of Eu^{III}.

$Eu(NO_3)_3$ in methanol. The EuO nanocrystals have two unconventional photophysical properties: their emission quantum yield in methanol is $49 \pm 5\%$ at 300 K, which is the highest efficiency reported for EuO, and their magnetization increases dramatically under UV irradiation at room temperature.

The EuO nanocrystals were prepared under an N_2 atmosphere as described in the Experimenteal Section. The TEM images revealed that the sample consisted of EuO nanocrystals (Figure 1a) with an average diameter of 3.4 nm (Figure 1b). Their size distribution is much smaller than that of the recently prepared EuO nanocrystals.[7] The electron diffraction pattern (Figure 1c) of the initial nanocrystals revealed responses at 2.95, 2.43, 1.78, and 1.51 dA, corresponding to (111), (200), (220), and (222) planes of NaCl-type EuO, in agreement with those of the spindle-shaped EuO nanocrystals.[7, 8] Magnetization measurements verified the formation of Eu^{III}-free Eu^{II} oxide (EuO). Thermogravimetric/differential thermal analysis (TGA/DTA) indicated that the EuO precipitates contain 48% of organic compounds. Elemental analyses and inductively coupled plasma atomic emission spectroscopy (ICP-AES) gave empirical formulas of precipitates prepared in the absence and presence of urea of $EuH_{6.7}C_{2.8}N_{1.2}O_{6.9}$ and $EuH_{7.7}C_{3.3}N_{2.2}O_{6.8}$, respectively. The empirical formula of the organic component was determined from the difference between these formulas to be CH_2N_2. As the removal of H_2O from NH_2CONH_2 (urea) leaves CH_2N_2, the formation of polyurea $(NHC(O)NHCH_2)_n$ on the surface of EuO was assumed, and this was confirmed by IR spectroscopy. The proposed photochemical reaction mechanism for the formation of the polyurea-modified EuO nanocrystals is shown in Figure 1d. Irradiation at the charge-transfer bands between an oxygen atom of methanol and the Eu^{III} ion of $Eu(NO_3)_3$ induces photoreduction to give an Eu^{II} ion and $HOCH_2^{\bullet}$.[9] The radical intermediate $HOCH_2^{\bullet}$ reacts with NO_3^- to give OH^- and formaldehyde. EuO is formed by the dehydrocondensation of $Eu(OH)_2$.[10] The growth of EuO nanocrystals is coupled with the polymerization of the coordinated urea with photogenerated formaldehyde on the EuO to give polyurea-modified EuO nanocrystals.

The absorption spectrum of the polyurea-modified EuO nanocrystals in methanol is shown in Figure 2a. The band at $\lambda = 280$ nm corresponds to the exciton band between the 4f and 5d orbitals of the EuO nanocrystals.[11] The larger Stokes shift of the exciton bands indicates that the electronic structure or spin state of EuO nanocrystals is significantly different from that of EuO bulk crystals. When the sample was irradiated at the exciton band, the emission spectrum exhibited a peak at around $\lambda = 357$ nm. The excitation and emission spectra in methanol are shown in Figure 2b and c. The emission quantum yield of the polyurea-modified EuO in methanol was $49 \pm 5\%$ at 300 K. Previously, the quantum efficiency of EuO single crystals was estimated to be less than 1%. Interestingly, the quantum yield of EuO nanocrystals without polyurea modification was $5 \pm 0.5\%$ at 300 K. These results suggest that the emission quantum yields of EuO nano-

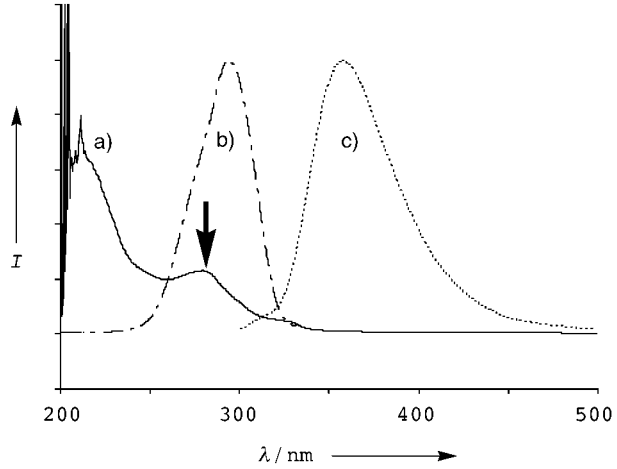


Figure 2. a) Absorption spectra of the EuO nanocrystals in methanol. The absorption below $\lambda = 250$ nm can be assigned to polyurea and methanol, and that above $\lambda = 250$ nm (arrow) to the exciton band of the EuO nanocrystals. b) Excitation spectrum of the EuO nanocrystals in methanol, monitored at $\lambda = 340$ nm. c) Emission spectrum of the EuO nanocrystals in methanol (excitation at $\lambda = 290$ nm). All spectra are corrected for detector sensitivity and lamp intensity.

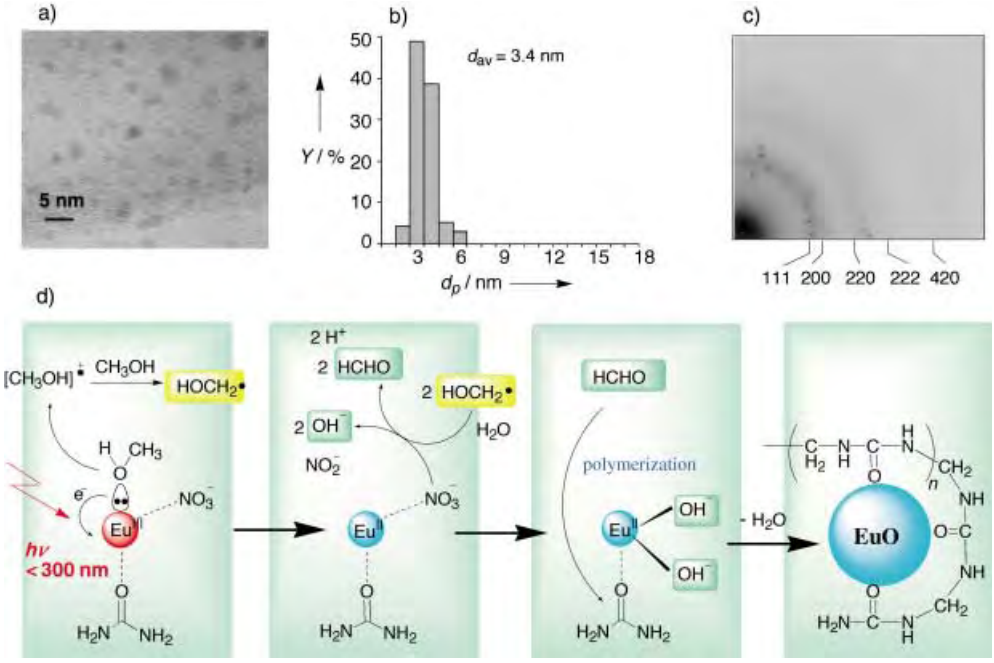


Figure 1. TEM image of the EuO nanocrystals. Images were recorded under axial illumination at approximate Scherzer focus, with a point resolution better than 0.19 mm. a) Bright-field (BF) image with weaker electron irradiation (2.4×10^{23} e m^{-2} s, beam diameter = 2 mm). b) Size distribution of a). c) Electron diffraction pattern. d) Mechanism of the photochemical reaction.

 © WILEY-VCH Verlag GmbH, 69451 Weinheim, Germany, 2002 1433-7851/02/4112-2074 $ 20.00+.50/0

crystals depend on their surface condition. We propose that the presence of polyurea on the quantum-sized EuO surface draws the quantum-confinement effect of EuO into itself.[12]

The temperature dependence of the magnetic susceptibility χ of the EuO nanocrystals is shown in Figure 3. From the slope of the T versus $1/\chi$ asymptote of the EuO nanocrystals ($3k_B/N\mu_B^2p^2$, where N = number of atoms, μ_B = Bohr constant, k_B = Boltzmann constant), the experimental effective number of Bohr magnetons p for the EuO nanocrystals was found to be

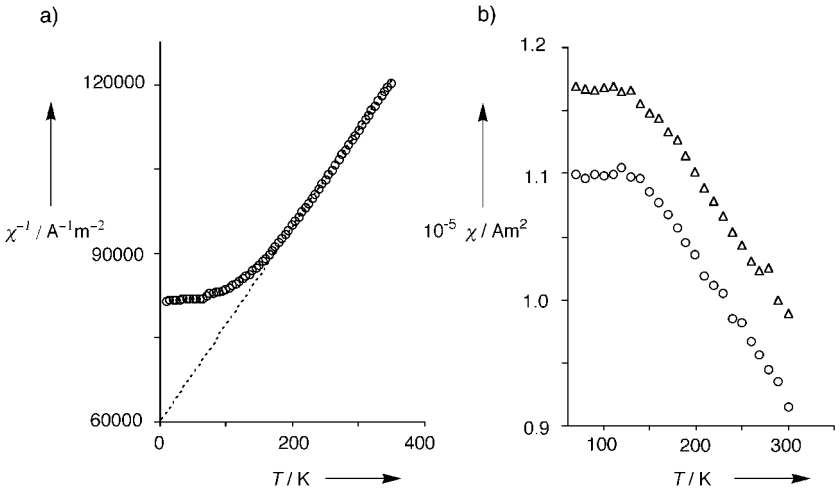


Figure 3. a) Temperature dependence of $1/\chi$ of EuO nanocrystals under field-cooled conditions at 0.1 T in the dark. b) Temperature dependence of χ under field-cooled conditions at 0.1 T in the dark (circles), and with irradiation (low-pressure mercury lamp, $\lambda = 254$ nm) via optical fibers (triangles). SQUID measurements on conventional Eu^{II} compounds (e.g., Eu_2O_3) do not reveal enhanced magnetization under irradiation.

7.98. The theoretical effective number of Bohr magnetons for Eu^{II} ($p = g[J(J+1)]^{1/2}$: total angular momentum $J = 7/2$, gyromagnetic ratio $g \approx 2$) was calculated to be 7.94. Thus, the experimental p for EuO nanocrystals agrees well with the theoretical p for the $4f^7$ configuration (Eu^{II}). We also observed a dramatic increase in the magnetization of the EuO nanocrystals under UV irradiation (254 nm) at just below room temperature (triangles in Figure 3b), and this is the first report of such behavior. The T versus χ curve of the EuO nanocrystals under irradiation paralleled that of EuO in the dark (circles in Figure 3b). This increase in magnetization under UV irradiation can be explained by a d–f exchange interaction of conducting electrons in the 5d band.[13] It is noteworthy that others recently observed photomagnetic properties of compounds only at low temperature (below 200 K).[14] The photomagnetic response of EuO nanocrystals provides experimental support for the magnetic exciton model with super-interaction between spins in the 5d band and 4f orbitals.[3]

We suggest that photo-induced increase in magnetization is attributable to the presence of an exciton band in the UV region, in accordance with the highly efficient luminescence from the polyurea-modified EuO nanocrystals. Polymers containing EuO nanocrystals are expected to be useful in applications such as plastic photo-isolators for optical fibers and photomagnetic devices.[15]

Experimental Section

Preparation of EuO nanocrystals: In a quartz vessel, $Eu(NO_3)_3$ (37.5 mM) and urea (112.5 mM) were dissolved in methanol (400 mL) under an N_2 atmosphere, and the solution was irradiated with a 500-W high-pressure mercury arc lamp at 25 °C. A yellowish powder precipitated after 30 min. After 24 h of irradiation, the powder was separated by centrifugation and washed with methanol several times. High-resolution transmission electron microscopy (TEM) images of the EuO nanocrystals were obtained with a Hitachi H-9000 TEM microscope equipped with a tilting device (±10°) and operating at 300 kV ($C_s = 0.9$ mm). Absorption and emission spectra were measured on a Hitachi U-3300 spectrophotometer and Hitachi F-4500 fluorescence spectrophotometer, respectively. Emission quantum yields were determined by standard procedures by using an integrating sphere (diameter 6 cm) and quartz cells (optical path length 1 mm).[16] The magnetic susceptibility χ of the EuO nanocrystals was measured with a superconducting quantum interface device (SQUID) magnetometer (Quantum Design, MPMS).

Received: November 7, 2001
Revised: March 15, 2002 [Z18177]

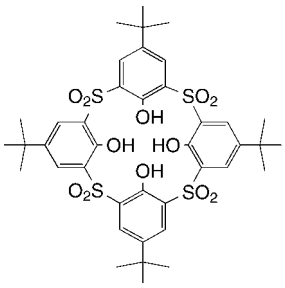
[1] D. E. Eastman, F. Holtzberg, S. Methfessel, *Phys. Rev. Lett.* **1969**, *23*, 226–229.
[2] P. Wachter, *Handbook on the Physics and Chemistry of Rare Earths*, 2nd Ed., North-Holland Publishing Company, **1979**, pp. 189–241.
[3] T. Kasuya, A. Yanase, *Rev. Mod. Phys.* **1968**, *40*, 684–696.
[4] W. Chen, X. Zhang, Y. Huang, *Appl. Phys. Lett.* **2000**, *76*, 2328–2330.
[5] P. Fumagalli, A. Schirmeisen, R. J. Gambino, *J. Appl. Phys.* **1996**, *79*, 5929–5931.
[6] M. W. Shafer, *J. Appl. Phys.* **1965**, *36*, 1145–1152.
[7] S. Thongchant, Y. Hasegawa, Y. Wada, S. Yanagida, *Chem. Lett.* **2001**, 1274–1275.
[8] The TEM image of the initial EuO was fuzzy (Figure 1a), but all TEM BF images of EuO nanocrystals agree with those of corresponding TEM centered dark-field (CDF) images, in which the incident beam is tilted such that the scattered beam remains on-axis.
[9] a) C. K. Jørgensen, J. S. Brinen, *Mol. Phys.* **1963**, *6*, 629–631; b) M. Kusaba, N. Nakashima, W. Kawamura, Y. Izawa, C. Yamanaka, *Chem. Phys. Lett.* **1992**, *197*, 136–140.
[10] M. Izaki, T. Omi, *J. Electrochem. Soc.* **1997**, *144*, L3–L5.
[11] O. Sakai, A. Yanase, T. Kasuya, *J. Phys. Soc. Jpn.* **1977**, *42*, 596–607.
[12] Wakefield, *J. Colloid Interface Sci.* **1999**, *215*, 179–182.
[13] M. Umehara, *Phys. Rev. B* **1995**, *52*, 8140–8149.
[14] a) H. Katsu, H. Tanaka, T. Kawai, *Appl. Phys. Lett.*, **2000**, *76*, 3245; b) S. Ohkoshi, K. Hashimoto, *J. Photochem. Photobiol. B* **2001**, *2*, 71–88; c) G. Rombaut, M. Verelst, S. Golhane, L. Ouahab, C. Mathoniere, O. Kahn, *Inorg. Chem.* **2001**, *40*, 1151–1159.
[15] a) K. Tanaka, K. Fujita, N. Soga, J. Qui, K. Hirao, *J. Appl. Phys.* **1997**, *82*, 840–844; b) T. Arakawa, T. Tanaka, G. Adachi, J. Shiokawa, *J. Lumin.* **1979**, *20*, 325–327.
[16] Y. Hasegawa, T. Ohkubo, K. Sogabe, Y. Kawamura, Y. Wada, N. Nakashima, S. Yanagida, *Angew. Chem.* **2000**, *112*, 365–368; *Angew. Chem. Int. Ed.* **2000**, *39*, 357–360.

 © WILEY-VCH Verlag GmbH, 69451 Weinheim, Germany, 2002 1433-7851/02/4112-2075 $ 20.00+.50/0

Zinc(II) Slides on a Ligand Surface: The X-Ray Crystal Structure and Dynamic Behavior in Solution of [Zn(H$_2$L)(tacn)]**

Takashi Kajiwara,* Shuichi Yokozawa, Tasuku Ito,* Nobuhiko Iki, Naoya Morohashi, and Sotaro Miyano*

Calix[4]arenes have been extensively investigated in supramolecular and molecular-recognition chemistry.[1–3] Substituents on the body and/or on the rims give calixarenes remarkable abilities to coordinate to metal ions, which enables the synthesis of new organic–inorganic assemblies. We have reported dinuclear nickel(II) and cobalt(II) complexes containing a *p-tert*-butylsulfonylcalix[4]arene (H_4L); $[M_2(L)(H_2O)_2(dmf)_4]$ (M = Co (**1**), Ni (**2**); dmf = dimethylformamide).[4, 5]



In complexes **1** and **2**, L^{4-} adopts the 1,2-alternate conformation, and acts as a bistridentate chelating ligand in the solid state.[4] Free H_4L in solution has shown temperature-dependent conformational dynamics.[6] Herein, we found that in [Zn(H$_2$L)(tacn)] (**3**; tacn = 1,4,7-triazacyclononane), the zinc(II) cation forces H_2L^{2-} to adopt a cone conformation in solution and that the $\{Zn(tacn)\}^{2+}$ moiety moves smoothly on the approximate plane created by eight donor oxygen atoms, from two phenol groups, two phenoxy groups, and four sulfonyl groups. We report here the synthesis and the solution and solid state structure of **3**, together with its dynamic behavior in solution.

A stoichiometric reaction of zinc(II) acetate dihydrate and H_4L in $CHCl_3$ resulted in the formation of a white precipitate. The precipitate was treated with TACN in DMF, and colorless crystals of **3**·DMF were obtained from this solution.

The solid-state structure of **3** is shown in Figure 1. In **3**, the zinc(II) cation is in an octahedral environment and is coordinated by H_2L^{2-} and TACN, both in a tridentate *fac*-fashion. The former coordinates to the Zn center in a cone conformation, through two deprotonated phenoxy oxygen atoms (O1 and O4) and one sulfonyl oxygen atom (O2), with bond lengths of 2.1229(19), 2.0729(18), and 2.1572(17) Å, respectively. The length of $O_{sulfonyl}$–Zn is slightly longer than those of the $O_{phenoxy}$–Zn bonds. However, no other complexes with $O_{sulfonyl}$–Zn bonds have been reported.[7] The same coordination mode is found in complexes **1** and **2**, and $H_{4-n}L^{n-}$ commonly acts as a tridentate facial ligand through two phenoxy oxygen atoms and one sulfonyl oxygen atom. The other sites of the Zn center are occupied by the N_3 atom donor set from the TACN ligand, with interatomic distances of 2.152(2), 2.133(3), and 2.111(2) Å. The conformation of the calix[4]arene depends strongly on several factors, such as the number of metal ions (one in **3**, two in **1** and **2**), and the size of the supporting ligand(s) (bulky TACN in **3**, relatively small DMF and H_2O molecules in **1** and **2**). When $H_{4-n}L^{n-}$ adopts a tridentate *fac*-coordination mode, the 1,3-alternate conformation is not possible, but the other three conformations, cone, partial cone,[8] and 1,2-alternate,[4] are possible. In **3**, steric hindrance between the TACN and the noncoordinating phenol groups is avoided by adoption of the cone conformation (see Figure 1, bottom). As a result, the four $O_{phenoxy}$ atoms (O1, O4, O7, and O10) and the four axial $O_{sulfonyl}$ atoms (O2, O5, O8, and O11) are arranged in a coplanar manner, with maximum deviations from the mean plane of −0.40 Å for O7 and 0.52 Å for O8. As discussed below, the zinc(II) cation moves around on the O_8 plane in solution. One *t*Bu group from a neighboring complex is included in the cavity formed by four phenyl groups (self-clathration) and thus, in the solid state, **3** is a dimer. Compound **3** has a pseudo-mirror plane, including the Zn, N3, S1, and S3, which divides the complex into two quasi-equivalent parts.

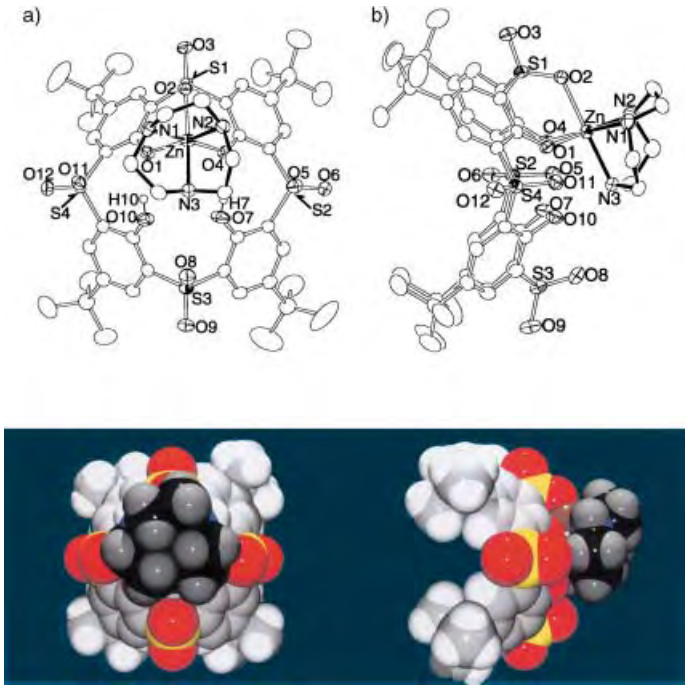


Figure 1. ORTEP drawing with thermal ellipsoids at 50% probability (top) and space-filling drawing (bottom) of the complex **3**. a) Top view and b) side view. Selected bond lengths [Å]: Zn–O1 2.1229(19), Zn–O4 2.0729(18), Zn–O2 2.1572(17), Zn–N1 2.152(2), Zn–N2 2.133(3), Zn–N3 2.111(2), S1–O2 1.4508(19). Average S–O (excluding O2) 1.437.

[*] Dr. T. Kajiwara, Prof. T. Ito, S. Yokozawa
Department of Chemistry, Graduate School of Science
Tohoku University
Aramaki Aoba-ku, Sendai 980-8578 (Japan)
Fax: (+81) 22-217-6548
E-mail: Kajiwara@agnus.chem.tohoku.ac.jp
ito@agnus.chem.tohoku.ac.jp
Prof. S. Miyano, Dr. N. Iki, Dr. N. Morohashi
Department of Biomolecular Engineering
Graduate School of Engineering, Tohoku University
Aramaki Aoba-ku, Sendai 980-8579 (Japan)
Fax: (+81) 22-217-7262
E-mail: miyano@orgsynth.che.tohoku.ac.jp

[**] H_4L = *p-tert*-Butylsulfonylcalix[4]arene (an analogue of *p-tert*-butylcalix[4]arene in which the bridging methylene groups are replaced by sulfonyl moieties) and tacn = 1,4,7-triazacyclononane. This work was supported by a Grant-in Aid for Scientific Research (Nos. 10149102 and 11740366) from the Ministry of Education, Science, Sports and Culture, Japan, as well as by JSPS Research for the Future Program.

 © WILEY-VCH Verlag GmbH, 69451 Weinheim, Germany, 2002 1433-7851/02/4112-2076 $ 20.00+.50/0

Two protons of phenol groups were found near O7 and O10 by differential-Fourier search. The O–H bonds are directed toward the $O_{phenoxy}$ atoms, which forms hydrogen bonds between O4–O7 and O10–O1, respectively. These hydrogen bonds help to stabilize the cone conformation.

In CD_2Cl_2, a 1:1 mixture of **3** and free H_4L, or TACN, the two ^{1}H NMR spectra only show superposition of the signals arising from each component up to 40 °C, which implies that neither ligand exchange nor ligand dissociation occurs in solution below room temperature. Figure 2a shows the

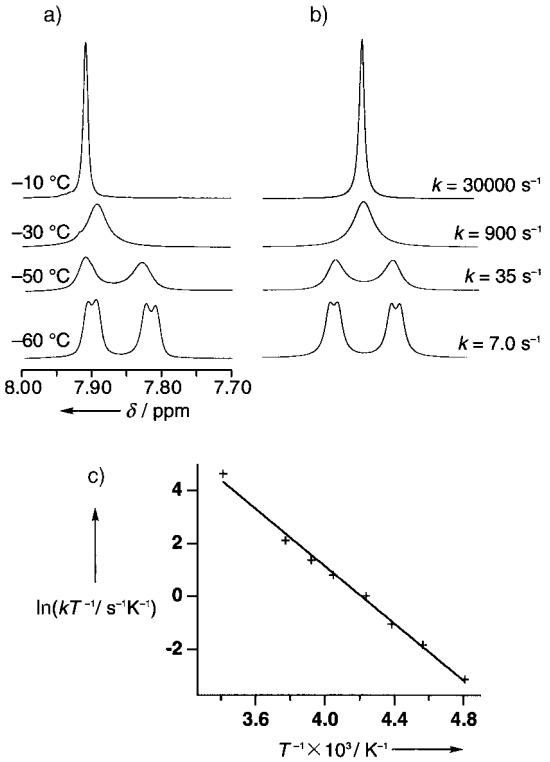


Figure 2. a) Temperature-dependent ^{1}H NMR spectra of the aromatic region of **3** in CD_2Cl_2, b) simulated spectra, and c) an Eyring plot.

temperature dependence of the ^{1}H NMR spectrum of **3** in the aromatic region. At −60 °C, the spectrum of **3** shows four singlet peaks with equal intensities at $\delta_H = 7.90$, 7.88, 7.81, and 7.80, which are assigned to the *meta* protons of the phenyl rings. This observation indicates the presence of two chemical environments for the phenyl rings, shown in Figure 3 as one ring with H_a and H_b and another ring with H_c and H_d, and also implies the presence of a mirror plane which divides the calix[4]arene into two equivalent parts. Hence, compound **3** in solution assumes a structure similar to that in the solid state. As the temperature is raised, the four peaks broaden gradually and coalesce, with a slight shift downfield. At room temperature the spectrum of **3** shows only one sharp peak, which indicates that all of the *m*-H atoms are chemically equivalent at this temperature.[9] Since ligand dissociation does not take place under these conditions, the temperature-dependent behavior is understandable only if the zinc(II) cation moves on the O_8 plane on the ^{1}H NMR spectroscopy timescale.[10] The spectra were analyzed by a conventional dynamic-NMR spectroscopic method[11], based on a model involving "the circular sliding of the zinc(II) ion over the O_8 surface" (Figure 3). The spectra simulated from this model are shown in Figure 2b, along with rate constants for the sliding process from one site to the adjoining site. Activation parameters are estimated from an Eyring plot (Figure 2c) to be $\Delta H^{\ddagger} = 45(1)$ kJ mol^{-1} and $\Delta S^{\ddagger} = -8(6)$ J mol^{-1} K^{-1}, respectively. The small negative entropy change may indicate that the sliding process occurs by an associative mechanism, which involves an additional Zn^{II}–O bond formation, or by a concerted mechanism, accompanied by fast phenol O–H bond rearrangements. In this temperature range, the methylene protons of the TACN give rise to only two quartet peaks in the ^{1}H NMR spectrum, which can be assigned to two kinds of protons, near to and far from the zinc(II) cation. This result indicates that the six methylene groups of the TACN are equivalent, even at low temperatures. Only a slight broadening of the peaks was observed at −60 °C.

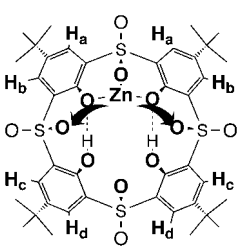


Figure 3. A schematic drawing of the Zn^{II} cation-sliding model used for the analyses. The TACN and protons (except for the *m*-H atoms of the phenyl groups, and two phenol moieties) are omitted.

Herein, we have synthesized a novel mononuclear complex of zinc(II) ion with a dianionic sulfonylcalix[4]arene, and have investigated its structure both in the solid state and in solution. In solution, **3** maintains the cone conformation and it was found that the zinc(II) ion smoothly slides on the ligand surface on the NMR spectroscopy timescale. Calixarene–metal complexes have been regarded as models for oxo-surfaces, on which chemical transformations are assisted or catalyzed.[12] Our results may provide useful information in understanding the bond-forming and bond-breaking steps in such models.

Experimental Section

3: To a chloroform solution (3 mL) of H_4L (8.49 mg, 0.01 mmol), zinc(II) acetate dihydrate (2.19 mg, 0.01 mmol) in chloroform (2 mL) was added. The colorless solution was heated under reflux for 1 h and was evaporated to dryness. The resulting white residue was then treated with TACN (0.01 mmol) in DMF (1 mL). Colorless blocks of **3**·DMF were obtained by slow evaporation at room temperature, in 54% yield.

Crystal-structure determination of [Zn(H_2L)(tacn)]·dmf (**3**·dmf): A colorless prism (ca. 0.45 × 0.18 × 0.08 mm) was analyzed with a Bruker SMART CCD-based diffractometer at 213 K with $Mo_{K\alpha}$ radiation (λ = 0.71073 Å). Monoclinic, space group $P2_1/n$, $a = 20.0157(18)$, $b = 11.4413(10)$, $c = 23.233(2)$ Å, $\beta = 102.198(2)°$, $V = 5200.3(8)$ Å^3, $Z = 4$, $\rho_{calc} = 1.424$ g cm^{-3}, $\mu(Mo_{K\alpha}) = 0.700$ mm^{-1}, $F(000) = 2352$. ω-scans, 30785 reflections measured ($2\theta_{max} = 50°$), of which 9203 were independent and 7205 were observed [$I > 2\sigma(I)$], 674 refined parameters, $R = 0.0401$, $wR2 = 0.1076$[$I > 2\sigma(I)$], residual electron density max./min. 0.703/−0.290 e Å^{-3}, max./min. transmission 0.910/0.766. Data reduction was performed with the SAINT software, which corrects for Lorentz and polarization factors. Absorption corrections were applied with SADABS, supplied by G. Sheldrick (Universität Göttingen). The structure was solved by direct methods with SHELXS-97[13] and refined by the least-squares method on F^2, SHELXL-97,[14] incorporated in SHELXTL-PC version 5.10. All non-hydrogen atoms were refined anisotropically. Hydrogens were calculated by geometrical methods and refined by using a riding model, except for the two phenol protons which were found by differential-Fourier analysis near O7 and O10, and refined isotropically. CCDC 176743 contains the

supplementary crystallographic data for this paper. These data can be obtained free of charge via www.ccdc.cam.ac.uk/conts/retrieving.html (or from the Cambridge Crystallographic Data Centre, 12, Union Road, Cambridge CB2 1EZ, UK; fax: (+44) 1223-336-033; or deposit@ccdc.cam.ac.uk).

Received: January 7, 2002 [Z18494]

[1] C. D. Gutsche, *Calixarenes, Monographs in Supramolecular Chemistry* (Ed.: J. F. Stoddart), The Royal Society of Chemistry, Cambridge, **1989**.
[2] C. D. Gutsche, *Calixarenes Revisited, Monographs in Supramolecular Chemistry* (Ed.: J. F. Stoddart), The Royal Society of Chemistry, Cambridge, **1998**.
[3] H. S. Park, Q. Lin, A. D. Hamilton, *J. Am. Chem. Soc.* **1999**, *121*, 8.
[4] T. Kajiwara, S. Yokozawa, T. Ito, N. Iki, N. Morohashi, S. Miyano, *Chem. Lett.* **2001**, 6.
[5] N. Iki, H. Kumagai, N. Morohashi, K. Ejima, M. Hasegawa, S. Miyanari, S. Miyano, *Tetrahedron Lett.* **1998**, *39*, 7559.
[6] G. Mislin, E. Graf, M. W. Hosseini, A. de Cian, J. Fischer, *Chem. Comun*. **1998**, 1345.
[7] Results of three-dimensional search and research using the Cambridge Structural Database, version 5.19.
[8] In a mononuclear complex, $[VO(H_2L)(EtOH)(MeOH)]$, H_2L^{2-} adopts the partial-cone conformation in the solid state. T. Kajiwara, S. Yokozawa, T. Ito, N. Iki, N. Morohashi, S. Miyano, unpublished results.
[9] The methyl protons of *t*Bu groups gave rise to a sharp singlet peak over the whole temperature range.
[10] A similar dynamic behavior of metal ions on a ligand surface has been reported for an octasilyl[4]radialene dianion–dilithium complex: A. Sekiguchi, T. Matsuo, H. Sakurai, *Angew. Chem.* **1998**, *110*, 1751; *Angew. Chem. Int. Ed.* **1998**, *37*, 1662.
[11] "SwaN-MR: A Complete and Expansible NMR Software for the Macintosh": G. Balacco, *J. Chem. Inf. Comput. Sci.* **1994**, *34*, 1235.
[12] a) V. Esposito, E. Solari, C. Floriani, N. Re, C. Rizzoli, A. Chiesi-Villa, *Inorg. Chem.* **2000**, *39*, 2604; b) L. Giannini, A. Caselli, E. Solari, C. Floriani, A. Chiesi-Villa, C. Rizzoli, N. Re, A. Sgamellotti, *J. Am. Chem. Soc.* **1997**, *119*, 9198.
[13] G. M. Sheldrick, SHELXS-97, Program for the Solution of Crystal Structures, University of Göttingen, Göttingen (Germany), **1997**.
[14] G. M. Sheldrick, SHELXL-97, Program for the Refinement of Crystal Structures, University of Göttingen, Göttingen (Germany), **1997**.

 © WILEY-VCH Verlag GmbH, 69451 Weinheim, Germany, 2002 1433-7851/02/4112-2078 $ 20.00+.50/0

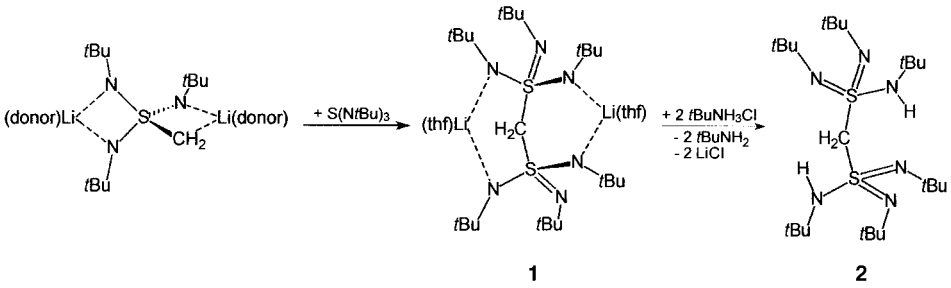
Charge-Density Study of Methane Di(triimido)sulfonic Acid $H_2C\{S(NtBu)_2(NHtBu)\}_2$—the NR Analogue of $H_2C\{S(O)_2(OH)\}_2$**

Dirk Leusser, Bernhard Walfort, and Dietmar Stalke*

Methane disulfonic acid $H_2C\{S(O)_2(OH)\}_2$ was synthesized for the first time more than 160 years ago.[1] Since then, this very strong acid[2] has been structurally studied because the hydrates form stable dihydroxonium salts $[(H_3O)_2\{(O_3S)_2CH_2\}]_\infty$ with strong hydrogen bonds.[3] The methane disulfonate dianion $H_2C(SO_3)_2^{2-}$ shows both unidentate (terminal) and bidentate (O,O chelating) coordination in many metal salts which leads to infinite solid-state structures.[4] Both features of disulfonates were recently employed in crystal engineering; $H_2C(SO_3)_2^{2-}$ ions serve as molecular pillars to separate two-dimensional galleries in tunable, hydrogen-bonded, nanoporous materials.[5] We set out to switch all six oxygen atoms in this basic compound isoelectronically to NR groups to generate molecules that would be soluble in hydrocarbons rather than exist as infinite solid-state salts.[6]

Herein we present dilithium methane di(triimido)sulfonate $[(thf)_2Li_2\{((NtBu)_3S)_2\}_2CH_2]$ (**1**), and methane di(triimido)-sulfonic acid, $H_2C\{S(NtBu)_2(NHtBu)\}_2$ (**2**), the NR analogues of $H_2C(SO_3)_2^{2-}$ and $H_2C\{S(O)_2(OH)\}_2$, respectively. Since **2** displays three different S–N bonding modes at each sulfur(VI) atom (one formal S–N(H)R single bond and two formal S=NR bonds, one of them involved in intramolecular hydrogen bonding), this is the ideal system in which to study the electron density of S–N bonds. We analyzed experimentally the charge-density distribution, $\rho(\boldsymbol{r})$, from high-resolution, low-temperature X-ray data and subsequent multipole refinement.[7]

The direct route corresponding to the established Strecker synthesis[1c] to give alkane disulfonates starting from dibromoalkanes and sodiumsulfite is precluded by the complex redox processes of the required dilithium (triimido)sulfite. However, alkylene (triimido)sulfate $[(donor)Li_2\{(CH_2)S(NtBu)_3\}]$,[8] the carba/imido analogue of the SO_4^{2-} ion, can readily be synthesized by deprotonation of $H_3CS(NtBu)_3$[9] with methyllithium. Addition of one equivalent of $S(NtBu)_3$ to the sulfur(VI)-ylide gives **1**. Subsequent protonation and salt elimination by *tert*-butylammonium chloride yields **2** (Scheme 1).



Scheme 1. Synthesis of **1** and **2**.

Unlike the known Ca^{2+}, Cd^{2+}, Ag^+, or K^+ salts of methane disulfonates,[4] **1**, forms donor-base-stabilized molecules (Figure 1, left). Both lithium cations are each coordinated, as if in pincers, by two opposing nitrogen atoms of both

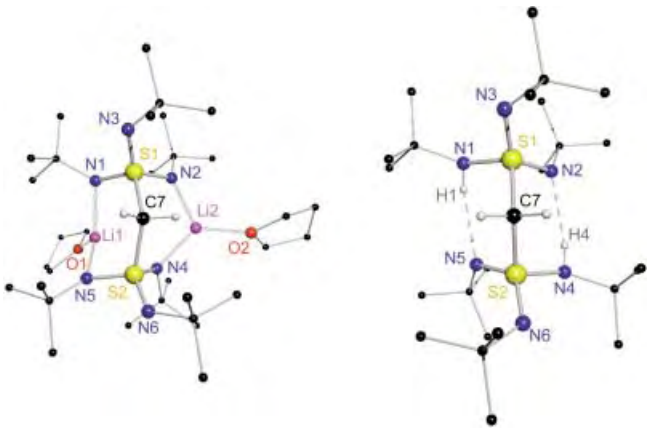


Figure 1. Left: Crystal structure of **1**. Selected bond lengths [Å] and angles [°]: S1-N1 1.572(3), S1-N2 1.568(4), S1-N3 1.527(3), S2-N4 1.519(3), S2-N5 1.558(3), S2-N6 1.579(3), S1-C7 1.847(4), C7-S2 1.845(4); S1-C7-S2 126.7(2); right: crystal structure of **2**. Selected bond lengths [Å] and angles [°] after multipole refinement: S1-N1 1.6494(2), S1-N2 1.5278(2), S1-N3 1.5179(2), S2-N4 1.6494(2), S2-N5 1.5280(3), S2-N6 1.5174(3), S1-C7 1.8161(2), C7-S2 1.8166(2); S1-C7-S2 122.20(10), N1,4-H1,4 1.032, average H1,4 ··· N5,2 2.142(13), average N-H ··· N 142.8(2).

staggered $S(NR)_3$ moieties.[10] Additional complexation of a single THF molecule leaves both metals trigonal pyramidally coordinated. On average the Li1–N1,5 bonds are considerably longer than the Li2–N2,4 bonds (2.033(11) vs. 1.939(11) Å). The longer Li–N bonds result in shorter average S–N(Li) bonds and vice versa (1.564(5) vs. 1.576(5) Å). The nitrogen atoms of the pendant imido ligands (N3,6) afford the shortest S–N bonds as there is no competition for the electron density from the metal centers (S1–N3, S2–N6: av. 1.523(5) Å). The average S1,2–C7 bond length with 1.847(4) Å is 0.08 Å longer than the S–C bond in the methyl (triimido)sulfonates.[9] The unprecedented wide S-C-S angle of 126.7(2)° reflects the considerable steric stain between the

[*] Prof. Dr. D. Stalke, Dipl.-Phys. D. Leusser, Dr. B. Walfort
Institut für Anorganische Chemie
Universität Würzburg
Am Hubland, 97074 Würzburg (Germany)
Fax: (+49) 931-888-4619
E-mail: dstalke@chemie.uni-wuerzburg.de

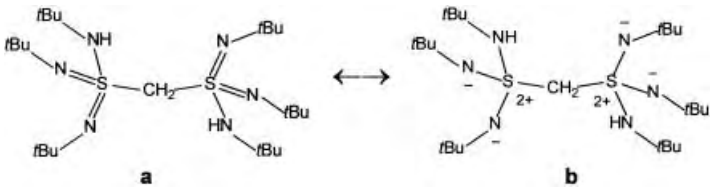
[**] This work was supported by the Deutsche Forschungsgemeinschaft and the Fonds der Chemischen Industrie. The discussions in the Würzburger Graduiertenkolleg "Elektronendichte" were very stimulating. We thank one of the referees for valuable comments.

Supporting information for this article is available on the WWW under http://www.angewandte.com or from the author.

 © WILEY-VCH Verlag GmbH, 69451 Weinheim, Germany, 2002 1433-7851/02/4112-2079 $ 20.00+.50/0

two triimidosulfonate groups which is reinforced by metal coordination.

In the crystal structure of **2**, both lithium ions in **1** are replaced by hydrogen atoms employed in intramolecular N-H···N hydrogen bonding (Figure 1, right). Three different types of S–N bonds result: two undisturbed formal S=N bonds (S1–N3, S2–N6: av. 1.5177(3) Å); two slightly elongated formal S–N double bonds involved in hydrogen bonding (S1–N2, S2–N5: av. 1.5279(3) Å) and two formal S–N(H) single bonds (S1–N1, S2–N4: av. 1.6494(2) Å). Following the Lewis notation the molecule has to be written in accord with the mesomeric structure **a** (Scheme 2) with two S=N bonds at each sulfur center to avoid formal charges in **b** (Pauling's verdict). However, that would imply valence expansion and d-orbital participation at the sulfur atom. We experimentally demonstrated that the form **b** is more appropriate to describe the bonding in the molecule.



Scheme 2. The two resonance structures of **2**.

To elucidate the charge-density distribution in **2**, especially the bonding situation of the three distinct S–N bonds, we performed a multipole refinement, with the formalism from Hansen and Coppens,[11, 12] based on 100 K high-resolution data up to $(\sin\Theta/\lambda)_{max} = 1.11$ Å^{-1} ($2\Theta_{max} = 104^\circ$ for $Mo_{K\alpha}$, $d = 0.45$ Å). The resulting topological analysis of the charge-density distribution $\rho(\boldsymbol{r})$ is presented.[13] To characterize the S–N bonds we have analyzed $\rho(\boldsymbol{r})$ and the Laplacian $\nabla^2\rho(\boldsymbol{r})$ in terms of Bader's theory of "atoms in molecules".[14] We found all anticipated $(3,-1)$ *b*ond *c*ritical *p*oints (BCPs) in the bonding regions of the molecule, including two intramolecular $(3,-1)$ BCPs between the N(H) hydrogen and the opposing formally double-bonded nitrogen atoms. All the S–N BCPs are located closer to the less-electronegative sulfur atom (see Table 1). Two $(3,+1)$ ring critical points are located in the six-membered ring made up from the two sulfur and nitrogen atoms, the bridging CH_2 carbon atom, and the N(H) hydrogen atom. A comparison of the densities $\rho(\boldsymbol{r}_{BCP})$, the algebraic sum of the eigenvalues (λ_i) of the Hessian matrix, $\nabla^2\rho(\boldsymbol{r}_{BCP})$ and the ellipticities ε_{BCP} ($\varepsilon_{BCP} = \lambda_1/\lambda_2 - 1$) at the BCPs of the S–N and S–C bonds is presented in Table 1.

Table 1. Topology of the S–N and S–C bonds in **2**.[a]

	d (A-B)	*d* (A-BCP)	*d*(BCP-B)	$\rho(\boldsymbol{r}_{BCP})$	$\nabla^2\rho(\boldsymbol{r}_{BCP})$	ε_{BCP}
S1-N1	1.650	0.780	0.870	1.89(2)	−13.41(7)	0.11
S1=N2	1.530	0.718	0.812	2.31(3)	−16.60(9)	0.10
S1=N3	1.520	0.718	0.802	2.37(3)	−16.44(9)	0.06
S1-C7	1.817	0.984	0.833	1.45(2)	−8.01(4)	0.09

[a] *d*(A-B): distance between atoms A and B along the bondpath in Å; *d*(A-BCP), *d*(BCP-B): distance between BCP and atom A and B, respectively; $\rho(\boldsymbol{r}_{BCP})$: charge density at the BCP in e Å^{-3}; $\nabla^2\rho(\boldsymbol{r}_{BCP})$: Laplacian of $\rho(\boldsymbol{r})$ at the BCP in e Å^{-5}; ε_{BCP}: ellipticity of $\rho(\boldsymbol{r})$ at the BCP.

The values of the S–C single bond are in the expected range with a bond length of 1.8161(2) Å, $\rho(\boldsymbol{r}_{BCP}) = 1.45(2)$ e Å^{-3}, $\nabla^2\rho(\boldsymbol{r}_{BCP}) = -8.01(4)$ e Å^{-5}, and $\varepsilon_{BCP} = 0.09$.[15] The two formal S1=N2,3 bond lengths of 1.5278(2) and 1.5179(2) Å, respectively, are in the range normally quoted for S=N bonds.[16] The S1–N1 bond in **2** of 1.6494(2) Å is comparable to that in S_4N_4 (1.629(1) Å), which was interpreted as a shortened S–N single bond with π contribution ($\varepsilon_{BCP} = 0.17$).[17] Bader et al. found in their pioneering theoretical study, electron-density features (two bonded and two nonbonded *v*alence *s*hell *c*harge *c*oncentrations (VSCCs), at nitrogen), which persuaded them to formulate the S–N bond in S_4N_4 as a S^+–N^- bond.[18] The marginal elongation of the S1–N1 bond in **2** can be attributed to the participation of N1 in the hydrogen bonding. Nevertheless, this bond displays the expected features of a covalent S–N single bond ($\rho(\boldsymbol{r}_{BCP}) = 1.89(2)$ e Å^{-3}, $\nabla^2\rho(\boldsymbol{r}_{BCP}) = -13.41(7)$ e Å^{-5}) and might serve as an internal standard. The charge density and the absolute value of the negative Laplacian at the BCP of the two formal double bonds S1–N2 and S1–N3 are significantly higher than for the S1–N1 bond.

The slightly lower value of $\rho(\boldsymbol{r}_{BCP})$ for S1=N2 than for the S1=N3 bond, with the first involved in the intramolecular hydrogen bonding, demonstrates the sensitivity of the method. The differences can be assigned to charge delocalization from the S1=N2 bonding region to the N2 valence-density region that points as a charge donor to the bridging hydrogen atom. All the S–N bonds show ellipticities unequal to zero ($\varepsilon_{BCP} = 0.11$ (N1), 0.10 (N2), 0.06 (N3)). At first glance this is especially confusing for the S1–N1 bond, as high bond ellipticity is commonly assigned to π contribution in nonpolar double bonds but this bond has to be regarded unequivocally a single bond. Compared to ε_{BCP} of N1 the values of the ellipticity for the formal double bonds are remarkably low. An investigation of the distribution of the negative Laplacian, $-\nabla^2\rho(\boldsymbol{r})$, uncovers an alternative explanation than the π contribution for the nonvanishing ellipticities.

Beside a critical-point search in $\rho(\boldsymbol{r})$, which leads to a characterization of bonds, we performed intensive searches for $(3,-3)$ critical points (which bear information about hybridization states) in the spatial distribution of $-\nabla^2\rho(\boldsymbol{r})$ to locate and quantify nonbonding VSCCs around the nitrogen atoms. Isosurfaces around the nitrogen atoms and contour plots which show the distribution of $-\nabla^2\rho(\boldsymbol{r})$ in planes containing the $(3,-3)$ critical points are presented in Figure 2.

The analysis of the Laplacian distribution around the nitrogen atoms indicates that they are sp^3 hybridized. As expected N1 shows one and both other, formally double-bonded nitrogen atoms, show two separated $(3,-3)$ critical points in $-\nabla^2\rho(\boldsymbol{r})$. The lone pair VSCC at N1 indicates concentration at the apical position of a trigonal-pyramidal coordinated sp^3-hybridized nitrogen atom (Figure 2, left), but it is oriented towards the bonding region of the S–N bond, as demonstrated by the small angle of 87.0° to the S1–N1 bond. This feature explains the considerable ellipticity of the S1–N1 bond. The VSCCs at N3 in the lone-pair regions affirm the

 © WILEY-VCH Verlag GmbH, 69451 Weinheim, Germany, 2002 1433-7851/02/4112-2080 $ 20.00+.50/0 *Angew. Chem. Int. Ed.* **2002**, *41*, No. 12

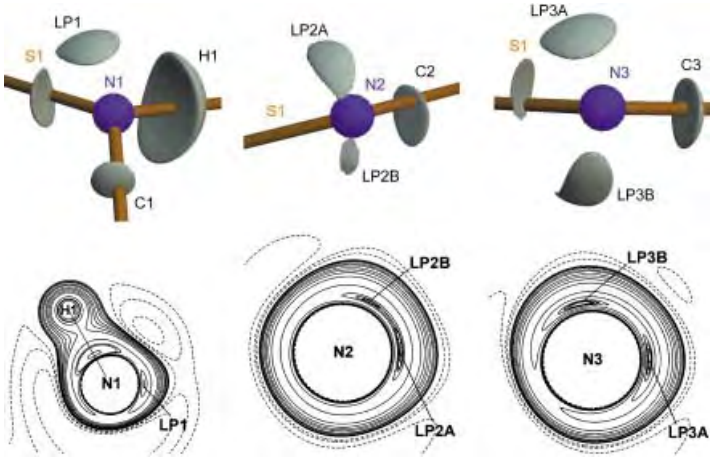


Figure 2. Isosurface map at constant $-\nabla^2\rho(\boldsymbol{r})$ values indicating bonded and nonbonded charge concentrations around N1, N2, and N3 ($-\nabla^2\rho(\boldsymbol{r}) = 47$ e Å^{-5} for N1, 48 e Å^{-5} for N2, and 46 e Å^{-5} for N3) and contour plots of charge concentrations in the H1-N1-LP1, LP2A-N2-LP2B, and LP3A-N3-LP3B plane. Maxima of the nonbonding VSCCs (lone pairs) are labeled LP. Positive values of $\nabla^2\rho(\boldsymbol{r})$ are marked by dashed lines, negative values by solid lines. Angles with lone-pair participation [°]: LP1-N1-H1 119.2, LP2A-N2-LP2B 62.8, LP3A-N3-LP3B 102.2. The angles between the normal vectors of the LP1-N1-H1 plane as well as between the LP2,3A-N2,3-LP2,3B planes and the accompanying S–N and C–N bonding vectors are 105.4° and 129.7° at N1, 99.1° and 137.9° at N2, and 107.1° and 126.8° at N3. This situation clearly indicates the orientation of the lone pairs away from the C–N towards the S–N bonding regions.

sp^3 character of N3 as the maxima in $-\nabla^2\rho(\boldsymbol{r})$ and are located above and below the S-N-C plane (Figure 2, right) with an LP3A-N3-LP3B angle of 102.2°. This angle along with the S1-N3-C3 bond angle of 126.6(1)° causes a rather distorted tetrahedral environment at N3. However, the angle between N3 and the two related BCPs is only 122.0°. This smaller angle confirms the steric strain between the *tert*-butyl group and the sulfur atom which leads to the increase of the angle from that expected for ideal tetrahedral geometry. Two maxima in $-\nabla^2\rho(\boldsymbol{r})$ are resolved in the nonbonding region at N2. The situation is similar to N3 (S1-N2-C2 123.4(1)° and BCP-N2-BCP 118.1°), although because of hydrogen bonding the maxima are less-well separated. The LP2A-N2-LP2B angle is only 62.8° because both lone-pair VSCCs at N2 interact like a bifurcated hydrogen bond (LP2A $\cdots$ H4 1.75 and LP2B $\cdots$ H4 1.91 Å) to the opposite H4 contracting the angle considerably. It is clear that all nonbonding VSCCs bend towards the associated S–N bond, as shown by the angle differences between the S–N and C–N bonds and the normal vectors of the LP-N-LP planes, which indicates the orientation of the lone pairs away from the C–N towards the S–N bonding regions (137.9°/99.1° at N2 and 126.8°/107.1° at N3). This situation causes additional an electron-density shift in the bond and leads to relatively high $\rho(\boldsymbol{r}_{BCP})$ values, a prominent negative Laplacian at the BCP, and substantial ellipticities.

Considering all the electronic features discussed above we conclude that the S–N/S=N bonding situation in **2** is much better described as a S$^+$–N$^-$ bond which is shortened by reinforcement resulting from orientation of the nitrogen lone pair towards the positively charged sulfur atom. This investigation confirms that neither valence expansion nor d-orbital contribution at the sulfur atom is required to explain the short S–N distances. This situation was predicted by computational methods more than fifteen years ago.[18, 19]

Experimental Section

All manipulations were performed under an inert-gas atmosphere of dry N_2 with Schlenk techniques or in an argon glovebox. All solvents were dried over Na/K alloy and distilled prior to use. ^{1}H, ^{7}Li, and ^{13}C NMR spectra were recorded in C_6D_6 (^{1}H: C_6HD_5: $\delta = 7.15$ ppm; ^{13}C C_6D_6: $\delta = 128.0$ ppm) using a Bruker AMX 400 spectrometer. IR spectra was recorded onto a Bruker IFS 25 FT-IR spectrometer. Elemental analyses were performed by the Microanalytisches Labor der Universität Würzburg.

1: A 1.6 M MeLi solution in diethyl ether (15.3 mL) was added dropwise to a solution of tri(*tert*-butyl)sulfurtriimide (6.00 g, 24.45 mmol) in THF (20 mL). The color of the solution changed instantaneously from yellow to colorless. After 3 h of stirring another of a 1.6 M MeLi solution in diethyl ether (15.3 mL) was added. Immediate evolution of methane gas was observed. After 1 h tri(*tert*-butyl)sulfurtriimide (6.00 g, 24.45 mmol) in THF (20 mL) was added dropwise. 50 % of the THF was removed in vacuum. After storage of the clear solution at -26 °C for 3 days colorless crystals were obtained (15.9 g, 88 %, m.p. 133 °C). ^{1}H NMR (400 MHz, C_6D_6): $\delta = 1.28$ (8 H, THF), 1.62 (s, 54 H, N*t*Bu), 3.52 (8 H, THF), 5.00 ppm (s, 2 H, SCH_2S); ^{13}C NMR (100 MHz, C_6D_6): $\delta = 25.35$, 68.40 (THF), 33.54 (C(CH_3)$_3$), 53.89 (C(CH$_3$)$_3$), 86.89 ppm (SCH_2S); ^{7}Li NMR (155.5 MHz, external reference saturated LiCl solution) $\delta = 1.15$ ppm; elemental analysis (%) calcd: C 60.45, H 10.97, N 11.44, S 8.72; found C 59.95, H 10.65, N 12.01, S 9.01.

2: **1** (15.9 g, 23.85 mmol) in THF was added to a suspension of *t*BuNH$_3$Cl (2.60 g, 23.85 mmol) in THF (15 mL). The solution was stirred for 3 h. THF was removed under vacuum and hexane (25 mL) was added. The precipitated LiCl was removed by filtration. 50 % of the solvent was removed under vacuum. After storage of the clear solution at -26 °C for 3 days colorless crystals were obtained (8.3 g, 69 %, m.p. 128 °C). ^{1}H NMR: (400 MHz, C_6D_6) $\delta = 1.41$ (s, 18 H, NHCCH_3), 1.49 (s, 36 H,=NCCH_3), 4.11 (s, 2 H, SCH_2S), 6.85 ppm (s, 2 H, N*H*CCH$_3$); ^{13}C NMR (100 MHz, C_6D_6): δ 30.95 (NHC(CH_3)$_3$), 32.31 (=NC(CH_3)$_3$), 51.82 (NHC(CH$_3$)$_3$), 53.38 (=NC(CH$_3$)$_3$), 75.90 (SCH$_2$S); IR (Nujol): 3146.7 m N(H), 3070–2860 s (Nujol), 1457.4 s, 1385.6 s, 1355.3 s, 1251.9 s, 1218.8 s, 1117.9 cm^{-1} s; elemental analysis (%) calcd: C 59.23, H 11.53, N 16.58, S 12.65; found C 59.95, H 11.65, N 16.01, S 13.01.

Received: October 15, 2001
Revised: March 15, 2002 [Z18068]

[1] a) K. Magnus, *Liebigs Ann. Chem.* **1833**, *6*, 152; b) J. von Liebig, *Liebigs Ann. Chem*. **1835**, *13*, 35; c) A. Strecker, *Liebigs Ann. Chem.* **1868**, *148*, 90; d) H. J. Backer, *Recl. Trav. Chim. Pays-Bas Belg.* **1929**, *48*, 949.
[2] T. L. Smith, J. H. Elliott, *J. Am. Chem. Soc.* **1953**, *75*, 3566.
[3] a) D. Mootz, H. Wunderlich, *Acta Crystallogr. Sect. B*, **1970**, *26*, 1820; b) P. Sartori, R. Jüschke, R. Boese, D. Bläser, *Z. Naturforsch. B*, **1994**, *49*, 1467.
[4] For example, a) F. Charbonnier, R. Faure, H. Loiseleur, *Acta Crystallogr. Sect. B*, **1979**, *35*, 1773; b) A. Karipides, *Acta Crystallogr. Sect. B*, **1981**, *37*, 2232; c) M. R. Truter, *J. Chem. Soc.* **1962**, 3393.
[5] V. A. Russell, C. C. Evans, W. Li, M. D. Ward, *Science* **1997**, *276*, 575.
[6] Review: a) R. Fleischer, D. Stalke, *Coord. Chem. Rev.* **1998**, *176*, 431; S(NR)$_3^{2-}$: b) R. Fleischer, S. Freitag, F. Pauer, D. Stalke, *Angew. Chem.* **1996**, *108*, 208; *Angew. Chem. Int. Ed. Engl.* **1996**, *35*, 204; S(NR)$_4^{2-}$: c) R. Fleischer, A. Rothenberger, D. Stalke, *Angew. Chem.* **1997**, *109*, 1140; *Angew. Chem. Int. Ed. Engl.* **1997**, *36*, 1105.
[7] T. S. Koritsanszky, P. Coppens, *Chem. Rev.* **2001**, *101*, 1583.
[8] B. Walfort, D. Stalke, *Angew. Chem.* **2001**, *113*, 3965; *Angew. Chem. Int. Ed.* **2001**, *40*, 3846.
[9] B. Walfort, A. P. Leedham, C. A. Russell, D. Stalke, *Inorg. Chem.* **2001**, *40*, 5668.

 © WILEY-VCH Verlag GmbH, 69451 Weinheim, Germany, 2002 1433-7851/02/4112-2081 $ 20.00+.50/0

[10] Crystal data for **1** and **2** (conventional/IAM refinement): The data were collected from shock-cooled crystals for **1** on an ENRAF-NONIUS CAD4 diffractometer and for **2** on an BRUKER APEX diffractometer (graphite-monochromated $Mo_{K\alpha}$ radiation, $\lambda = 0.71073$ Å) equipped with a low-temperature device at 193(2) K (**1**) and 100(2) K (**2**).[20] The structures were solved by direct methods (SHELXS-97)[20] and refined by full-matrix least-squares methods against F^2 (SHELXL-97).[22] R values defined as $R1 = \Sigma||F_o| - |F_c||/\Sigma|F_o|$, $wR2 = [\Sigma w(F_o^2 - F_c^2)^2/\Sigma w(F_o^2)^2]^{0.5}$, $w = [\sigma^2(F_o^2) + (g_1P)^2 + g_2P]^{-1}$, $P = 1/3[\max(F_o^2,0) + 2F_c^2]$. **1**: $C_{37}H_{80}Li_2N_6O_3S_2$, $M_r = 735.07$, monoclinic, space group $P2_1/c$, $a = 16.143(8)$, $b = 14.5340(18)$, $c = 19.429(8)$ Å, $\beta = 92.779(18)$, $V = 4553(3)$ Å^3, $Z = 4$, $\rho_{calcd} = 1.072$ Mg m^{-3}, $\mu = 0.155$ mm^{-1}, $F(000) = 1624$, 10144 reflections measured, 5527 unique, $R(\text{int}) = 0.0660$, $wR2$ (all data) $= 0.1768$, $R1(I > 2\sigma(I)) = 0.0639$, $g_1 = 0.0695$, $g_2 = 9.0558$ for 602 parameters and 566 restraints. **2**: $C_{25}H_{58}N_6S_2$, $M_r = 506.89$, monoclinic, space group $C2/c$, $a = 29.8239(8)$, $b = 11.4206(3)$, $c = 18.0801(4)$ Å, $\beta = 91.041(1)$, $V = 6157.2(3)$ Å^3, $Z = 8$, $\rho_{calcd} = 1.094$ Mg m^{-3}, $\mu = 0.196$ mm^{-1}, $F(000) = 2256$, 136761 reflections measured (low-angle batch, $\sin\theta/\lambda < 0.625$ Å^{-1}), 6629 unique, $R(\text{int}) = 0.0435$, 217620 reflections measured (high-angle batch, 0.625 Å$^{-1} < \sin\theta/\lambda < 1.111$ Å^{-1}), 29791 unique, $R(\text{int}) = 0.0646$, $wR2$(all data) $= 0.0932$, $R1(I > 2\sigma(I)) = 0.0315$, $g_1 = 0.0538$, $g_2 = 0.0$ for 475 parameters. All hydrogen atoms in **2** were located by difference Fourier synthesis and refined without any distance restraints. The isotropic thermal parameters of the hydrogen atoms H1 and H4 were refined independently. All other hydrogen atoms of the molecule were refined using a riding model ($U_{iso} = 1.2\,U_{eq}$ (C) for H71 and H72 and $U_{iso} = 1.5\,U_{eq}$ (C) for all other hydrogen atoms). CCDC-171900 (**1**) and CCDC-171901 (**2**) contain the supplementary crystallographic data for this paper. These data can be obtained free of charge via www.ccdc.cam.ac.uk/conts/retrieving.html (or from the Cambridge Crystallographic Data Centre, 12, Union Road, Cambridge CB2 1EZ, UK; fax: (+44) 1223-336-033; or deposit @ccdc.cam.ac.uk).

[11] N. K. Hansen, P. Coppens, *Acta Crystallogr. Sect. A* **1978**, *34*, 909.

[12] T. Koritsanszky, S. Howard, T. Richter, Z. W. Su, P. R. Mallinson, N. K. Hansen, *XD—A Computer Program Package for Multipole Refinement and Analysis of Electron Densities from Diffraction Data*, Freie Universität Berlin, **1995**

[13] Multipole refinement of **2**: data integration was performed with SAINT-NT,[23] empirical absorption correction based on Blessing's algorithm[24] with MULABS implemented in PLATON:[25] $R(\text{int}) = 0.0435$ (low-angle batch), $R(\text{int}) = 0.0646$ (high-angle batch), structure solution with SHELXS,[21] high-order refinement with SHELXL-97;[22] $wR1 = 0.0147$, $wR2 = 0.0280$, GoF $= 1.3015$, after multipole refinement. In the refinement both $S(NHtBu)(NtBu)_2$ moieties at the methylene bridge shared the same multipole parameters. In the pseudoatom model the deformation density was described by an expansion over spherical harmonics multiplied by Slater-type radial functions with energy-optimized exponents.[26] Atomic densities were expanded to hexadecapolar level for S, N, and C7, octapolar level for all other carbon atoms, for H atoms one bond-directed dipole as well as a quadrupole population were employed. The final difference Fourier syntheses after multipole refinement are virtually featureless.

[14] R. F. W. Bader, *Atoms in Molecules—A Quantum Theory*, Clarendon Press, Oxford **1990**.

[15] S. Pillet, M. Souhassou, Y. Pontillon, A. Caneschi, D. Gatteschi, C. Lecomte, *New J. Chem.* **2001**, *25*, 131.

[16] P. Rademacher, *Strukturen organischer Moleküle*, VCH, Weinheim **1987**.

[17] W. Scherer, M. Spiegler, B. Pedersen, M. Tafipolsky, W. Hieringer, B. Reinhard, A. J. Downs, G. S. McGrady, *Chem. Commun.* **2000**, 635.

[18] T.-H. Tang, R. F. W. Bader, P. J. MacDougall, *Inorg. Chem.* **1985**, *24*, 2047.

[19] a) W. Kutzelnigg, *Angew. Chem.* **1984**, *96*, 262; *Angew. Chem. Int. Ed. Engl.* **1984**, *23*, 272; b) A. E. Reed, F. Weinhold, *J. Am. Chem. Soc.* **1986**, *108*, 3586; c) D. A. Bors, A. Streitwieser, *J. Am. Chem. Soc.* **1986**, *108*, 1397; d) A. E. Reed, P. v. R. Schleyer, *J. Am. Chem. Soc.* **1990**, *112*, 1434; e) U. Salzner, P. v. R. Schleyer, *J. Am. Chem. Soc.* **1993**, *115*, 10231; f) T. Stefan, R. Janoschek, *J. Mol. Model.* **2000**, *6*, 282.

[20] D. Stalke, *Chem. Soc. Rev.* **1998**, *27*, 171.

[21] G. M. Sheldrick, *Acta Crystallogr. Sect. A* **1990**, *46*, 467.

[22] G. M. Sheldrick, SHELXL-97—Program for Crystal Structure Refinement, University of Göttingen, **1997**.

[23] Bruker Nonius Inc., *SAINT-NT*—Program for Integration of Diffraction Data from Area Detectors, Madison WI **2000**.

[24] B. Blessing, *Acta Crystallogr. Sect. A* **1995**, *51*, 33.

[25] A. L. Spek, *Acta Crystallogr. Sect. A* **1990**, *46*, C34.

[26] E. Clementi, C. Roetti, *At. Data Nucl. Data Tables*, **1974**, *14*, 177

Structural Dependence of Redox-Induced Dimerization as Studied by In Situ ESR/UV/Vis-NIR Spectroelectrochemistry: The Fluoranthenopyracylene Oligomers**

Lothar Dunsch,* Peter Rapta, Niels Schulte, and A. Dieter Schlüter

Reversible dimerization reactions of electrochemically produced organic radical ions are used as a general model for the explanation of charge injection in conducting oligomers and polymers.[1–4] Our main interest in this field is to investigate the driving force of dimerization in such structures. While detailed electrochemical and spectroscopic studies of conjugated compounds have been presented by several groups,[5–11] the number of in situ spectroelectrochemical investigations resulting in more direct information on the structural situation during dimerization is limited and the formation of σ dimers has not been demonstrated by in situ techniques. Furthermore, a variety of structures is needed to understand the dimerization as a general reaction of oligomeric systems. Thus monodisperse organic compounds with low molecular weight such as naphthalene diimides,[5] thianthrenes,[6] bipyrrols,[7] bithiophenes,[8] and extended conjugated oligomers, for example, oligothiophenes,[9] oligophenylenes,[10] and oligopyrroles[11] were used for such studies.

For structural studies of the reaction products at electrode surfaces the spectroelectrochemical techniques (including ESR/UV/Vis-NIR spectroscopy at different temperatures) were applied.[12] The existence of both π and σ dimers of oligopyrrols after a charge-transfer reaction has been dem-

[*] Priv.-Doz. Dr. L. Dunsch, Dr. P. Rapta[+]
IFW Dresden
Abteilung Elektrochemie und leitfähige Polymere
Helmholtzstrasse 20, 01069 Dresden (Germany)
Fax: (+49) 351-4659-745
E-mail: l.dunsch@ifw-dresden.de
Dr. N. Schulte, Prof. Dr. A. D. Schlüter
Institut für Chemie, Freie Universität Berlin
Takustrasse 3, 14195 Berlin (Germany)

[+] Permanent address:
Slovak University of Technology
Radlinského 9, 812 37 Bratislava (Slovakia)

[**] This work was supported by the Deutsche Forschungsgemainschaft. PR thanks Humboldt Foundation and Slovak Grant Agency for financial support. The authors thank Dr. M. Breza (STU Bratislava) for quantum-chemical calculations.

 © WILEY-VCH Verlag GmbH, 69451 Weinheim, Germany, 2002 1433-7851/02/4112-2082 $ 20.00+.50/0

onstrated.[7] We report here the oligomer-length dependence of such dimerization reactions and the stabilization of charged states in conjugated π systems.

While single-stranded oligomer chains are used to support the general scheme of redox-induced dimerization, we have used the recently synthesized unsaturated fluoranthene-type structures with ladder topologies. Such molecules have extended 2D π conjugation so can stabilize their charged state better than single-stranded oligomers and are thus a good model with which to study for the chain-length dependence of oligomer dimerization reactions following an electron-transfer step. Furthermore, they carry solubilizing chains which enable the study of single solvated molecules without the interference of ordering phenomena.

Compounds **3a**–**d** ($n = 1,2,4,6$) were prepared according to the literature (**3a**)[13] or from compounds **1** and **2** (Scheme 1). In the latter case the main steps are Diels–Alder reactions of the bisdiene **1**[14] with dienophiles **2** ($n = 1,2$), cheletropic CO elimination, and dehydrogenation of the primary adducts with 2,3-dichloro-5,6-dicyano-1,4-benzoquinone (DDQ).

The optical, redox, and magnetic properties of the oligofluoranthenes **3** (Scheme 1) were investigated by cyclic voltammetry and in situ ESR/UV/Vis-NIR spectroelectrochemistry and the structures of the products generated by the charge transfer in solution were also determined spectroscopically.

The increase in the π-conjugation length of **3a**–**3d** is reflected by the bathochromic shift of the absorption bands (Figure 1a): **3a** $\lambda = 310$, 429 nm, **3b** $\lambda = 340$, 496 nm, **3c** $\lambda = 357$, 546 nm, and **3d** $\lambda = 370$, 565 nm. The optical band gap for infinite ladder-type polymer ($n \to \infty$), $E_g = 2.05$ eV, was found by extrapolation assuming the linear dependence of the evaluated optical gap (E_g) with the inverse of the degree of polymerization (n^{-1}; see Figure 1b; even though the first

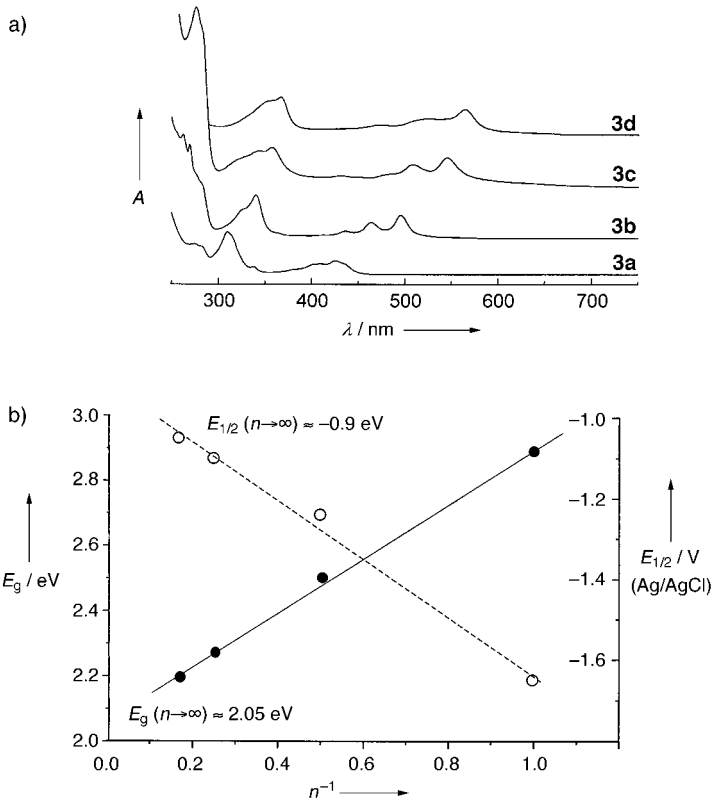
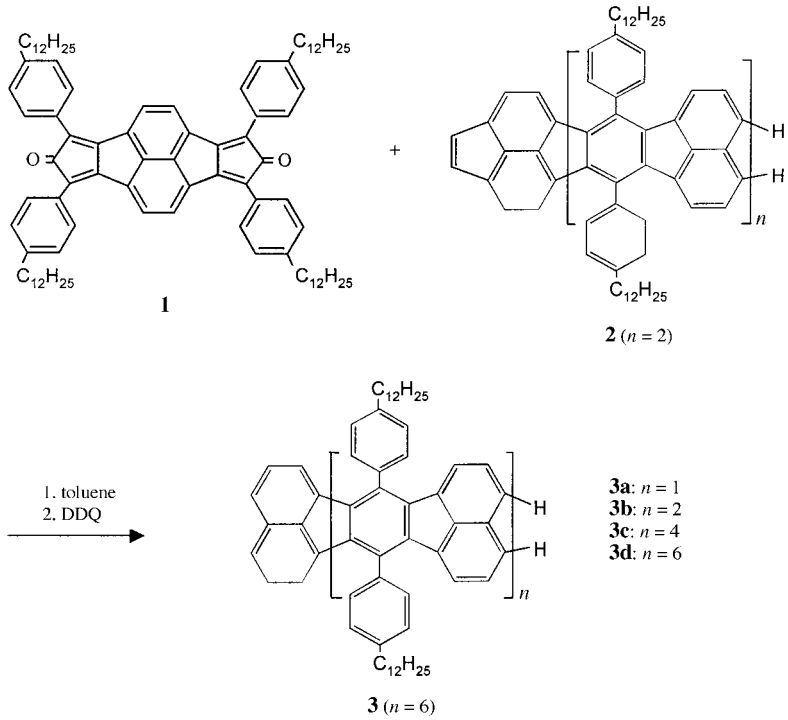


Figure 1. a) Absorption spectra of **3a**–**3d** in *o*-dichlorobenzene, b) dependence of optical band width E_g (●) and of redox potential $E_{1/2}$ (○) on the reciprocal chain length of the oligomer n^{-1}.

indications that this linearity is not generally found in conjugated systems were recently reported[15]). The electrochemical half-wave redox potentials of **3a**–**3d** (Figure 1b) for the first electron transfer ($E_{1/2}$) correlate well with the inverse of the oligomer length and the linear extrapolation to $n \to \infty$ results in $E_{1/2} = -0.9$ V (versus Ag/AgCl).

3a ($n = 1$) is electrochemically reduced in an one-electron step at $E_{1/2} = -1.65$ V (versus Ag/AgCl; Figure 2a). In the anodic back scan the appearance of a full re-oxidation peak points to a high stability of the generated anion radical. The UV/Vis-NIR and the ESR spectra of **3a** (Figure 3a) and its reduction products, measured during cyclic voltammetry, show that the one-electron reduction generates a radical anion with optical bands in the visible (555 nm) and the NIR (1390 nm) region. The intensity of the corresponding ESR signal (inset in Figure 3a) correlate well with the above-mentioned optical bands arising from transitions between the SOMO → LUMO and HOMO → SOMO orbitals. The analysis of the ESR spectrum gives the experimental splitting constants $8a_H = 0.28$ mT and $4a_H = 0.05$ mT. Semiempirical AM1 (geometry) and ab initio 6-31G* (spin distribution) calculations indicate that the $C_6H_4C_{12}H_{25}$ substituents are twisted out of plane with a twist angle of 85° and most of the spin density is



Scheme 1. Synthesis and structure of **3a**–**3d**.

 © WILEY-VCH Verlag GmbH, 69451 Weinheim, Germany, 2002 1433-7851/02/4112-2083 $ 20.00+.50/0

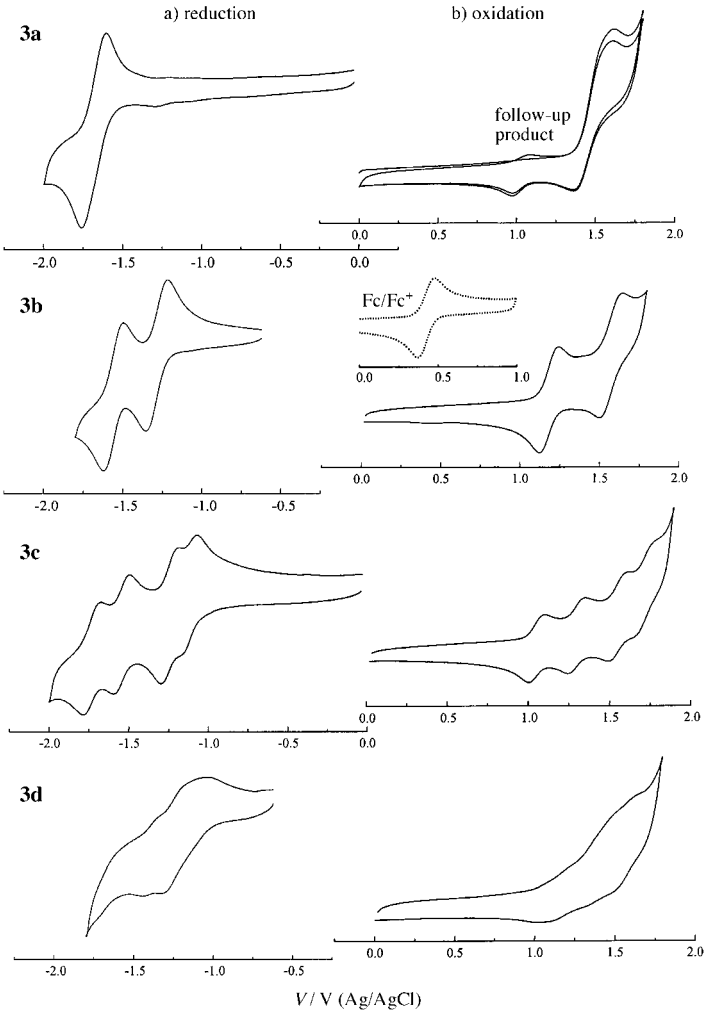


Figure 2. Cyclic voltammograms of **3a**–**3d** in 0.1 M $TBABF_4$/*o*-dichlorobenzene at a platinum electrode and a scan rate of 200 mV s^{-1}.

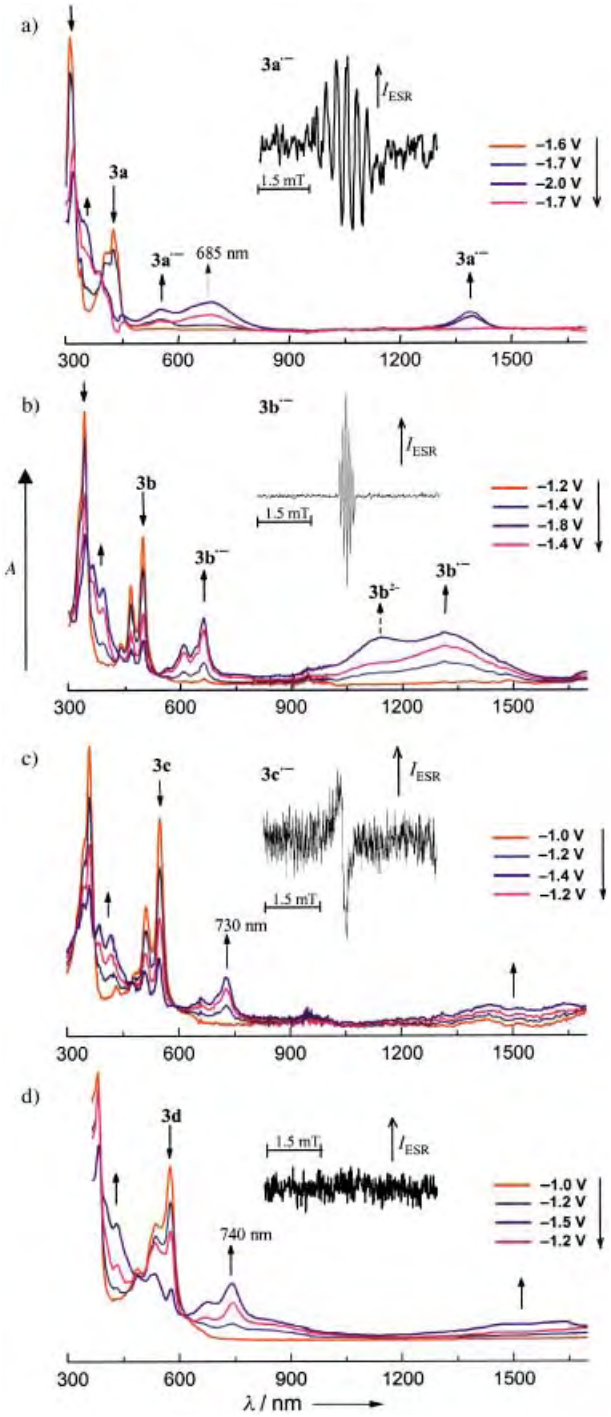


Figure 3. Vis-NIR and ESR (insets) spectroelectrochemistry of **3a**–**3d** and their reduction products, the spectra were recorded simultaneously to the voltammetric cycles (the potentials correspond to Figure 2a). a) **3a** at the first reduction peak, b) **3b** at the first two reduction peaks, c) **3c** at the first two reduction peaks, d) **3d** scan from −0.6 to −1.5 V.

delocalized over the whole planar part of the molecule. Therefore, the 12 splittings assigned to hydrogen atoms can be attributed to the protons of the two naphthalene groups on the periphery. A similar spin-density distribution was observed in the case of the radical anion of 9,10-diphenylanthracene, where the assignment of the splitting constants was determined unambiguously by using ENDOR splittings and selective deuteration.[16]

In addition to the optical spectra of radical anions we observed a new absorption band at 685 nm in the region of the first electron transfer, which increased during the reduction (Figure 3a). This can be attributed to a σ dimer $(\mathbf{3a}-\mathbf{3a})^{2-}$ formed by a chemical follow-up reaction of the radical anion $\mathbf{3a}^{\bullet-}$ as observed for short π-conjugated molecules.[7]

The oxidation of **3a** is more complex than the reduction. The cyclic voltammogram indicates the irreversible reaction of a less-stable radical cation. The presence of the follow-up products formed can be seen in the second cyclic voltammetric scan (Figure 2b; a detailed analysis of the oxidation products will be described elsewhere). According to recent results on photophysical and electrochemical properties of substituted 7,12-diphenylbenzo[*k*]fluoranthenes we can attribute these products to a singly or doubly σ-bound dimer, formed irreversibly during the oxidation under elimination of protons.[17]

In **3b** ($n=2$), the next higher homologue of **3a**, the radical anion is more stable and the cathodic formation of a stable dianion is observed (Figure 2a). The cyclic voltammogram shows two reversible one-electron reduction steps at $E_{1/2}=$

 © WILEY-VCH Verlag GmbH, 69451 Weinheim, Germany, 2002 1433-7851/02/4112-2084 $ 20.00+.50/0 *Angew. Chem. Int. Ed.* **2002**, *41*, No. 12

-1.24 V and -1.5 V. In the first reduction peak a stable radical anion (inset in Figure 3b) formed in high yield was detected by in situ ESR spectroscopy. The well resolved five-line ESR spectrum with a very small coupling constant $4a_H = 0.06$ mT indicates a similar spin distribution to that in **3a**$^{\bullet-}$. The spin is preferably localized on the planar part of the molecule which is larger than in **3a** while the twisted $C_6H_4C_{12}H_{25}$ substituents again do not conjugate effectively with the planar part. The electrochemical reduction of such structures containing the indeno[1,2,3-*cd*]fluoranthrene moiety which form stable radical anions has been reported.[18] In the UV/Vis-NIR spectrum a remarkable shift of the NIR absorption of the radical anion **3b**$^{\bullet-}$ to the lower values (1310 nm) and of the visible absorption to the higher values (660 nm) in comparison to **3a**$^{\bullet-}$ (1390 nm and 555 nm) was found. No reaction products of **3b**$^{\bullet-}$ were detected and no changes with time were observed both in its optical and ESR spectra even at 260 K. The absence of a follow-up reaction supports a stabilization of the charged **3b** and points to negligible dimer formation. In the second reduction step a new optical band at 1145 nm is found as expected for the ion **3b**$^{2-}$.

Further extension of the π-system in **3c** ($n = 4$) results in four reversible reduction steps (Figure 2a). The first cyclic voltammetric peak which is less cathodic than for **3a** and **3b** is a superposition of two one-electron transfers with close half-wave potentials (-1.1 V and -1.2 V) indicating that the two electrons are transferred successively to the tetramer. A very weak single-line ESR signal was recorded during the voltammetric scan in this potential region (inset in Figure 3c). The tetramer exists as a dianion and only a minor amount of an radical anion is formed by symproportionation of **3c** with **3c**$^{2-}$ in the diffusion layer at the electrode. A new absorption band at 730 nm and a very broad one in the NIR region (1200–1800 nm) appear during the cathodic scan (Figure 3c) which are attributed to the **3c**$^{2-}$ ion. The extended π system of the tetramer stabilizes the *dianionic* structure by minimizing the interactions between the two negative charges and dimerization is thus prevented.

The redox behavior of the hexamer **3d** with the largest π-system gives a broad cyclic voltammetric response. Several successive one-electron transfers (similar to first two one-electron transfers to the tetramer **3c**) are detected (Figure 2). No ESR signal was detected in this case (inset in Figure 3d). The optical absorption band at 740 nm and the broad one in the region 1200–1800 nm (Figure 3d) are also attributed to multicharged structures as for **3c**. The ESR-silent doubly charged structures are similar to the electronic state of a bipolaron or a dication in a ^1A_g singlet ground state carrying two individual polarons.[19]

Summarizing the influence of the oligomer length on the dimerization of the compounds **3a**–**3d** (Scheme 1) as studied by cyclic voltammetry and in situ ESR/UV/Vis-NIR spectroelectrochemistry, radical anions were found in the first reduction step for structures **3a**, **3b**, and to a very small extent for **3c**. While **3a**$^{\bullet-}$ is in equilibrium with its σ-dimer in solution, **3b**$^{\bullet-}$ is already strongly stabilized and its dimerization is negligible in the studied temperature range (260–290 K). The extended π-conjugation in structures **3c** and **3d** is found to be sufficient for stabilization of charges in the molecule without dimerization. Thus, extension of the π systems in the homologous series described here disfavors chemical dimerization. This finding is an indication that dimerization in organic conducting polymers may not necessarily be a general mechanism for the stabilization of radical ions.

Experimental Section

Synthesis of **3d** ($n = 6$): **1** (50 mg, 0.04 mM) and **2** ($n = 2$) (137 mg; 0.09 mM) were heated under reflux in toluene (20 mL) for 48 h under nitrogen. After cooling, neat DDQ (20 g, 0.09 mM) was added and the resulting solution stirred for 30 min. The solution was then filtered through a short silica-gel column and the solvent removed. The residue was purified by chromatography on silica gel (eluent: hexane/toluene = 5/1) to give **3d** ($n = 6$) as an intensely purple powder (114 mg, 67%). ^{1}H NMR ($CDCl_3$, 500 MHz): $\delta =$ 0.9, 1.4, 1.8, 2.7, 6.1, 6.6, 7.4 ppm; ^{13}C NMR ($CDCl_3$): $\delta = 14.1$, 19.7, 22.7, 24.5, 27.1, 29.4, 30.1, 31.9, 32.8, 35.7, 37.1, 37.4, 124–142 ppm (aromatic C); LD-MS: m/z 4250 [M^+].

The cyclic voltammograms were obtained using platinum wire as working and counter electrodes. An Ag/AgCl electrode served as reference, and the cyclic voltammetric measurements were carried out in a glove box (oxygen and water content below 1 ppm) with a Princeton Applied Research (PAR 270) universal electrochemical system. Ferrocene/ferricenium ion (Fc/Fc^+) ($E_{1/2}(Fc/Fc^+) = 0.44$ V vs. Ag/AgCl) was used as an internal potential marker. The scan rate was 200 mV s^{-1}.

Laminated platinum-mesh electrodes were used in all spectroelectrochemical experiments. Redox cycling of the solutions of the compounds under study in simultaneous ESR and UV/Vis-NIR measurements[12] was carried out in 0.1M tetrabutylammoniumtetrafluoroborate ($TBABF_4$; Fluka, dried under reduced pressure at 70 °C for 24 h and stored in a glove box) in *o*-dichlorbenzene (Aldrich, doubly distilled under argon over calcium hydride before use), the scan rate was 10 mV s^{-1}. A silver wire served as a pseudo reference electrode and a platinum wire as a counter electrode. ESR spectra were recorded by the 300D X-Band ESR spectrometer (Bruker, Germany), and UV/Vis-NIR spectra by the diode array UV/Vis-NIR spectrometer system TIDAS (J&M, Aalen, Germany). A PG 284 potentiostat/galvanostat (HEKA, Lambrecht, Germany) was used for these measurements.

Received: November 9, 2001
Revised: March 1, 2002 [Z18195]

[1] H. Shirakawa, *Angew. Chem.* **2001**, *113*, 2642; *Angew. Chem. Int. Ed.* **2001**, *40*, 2574.
[2] A. MacDiarmid, *Angew. Chem.* **2001**, *113*, 2649; *Angew. Chem. Int. Ed.* **2001**, *40*, 2581.
[3] A. Heeger, *Angew. Chem.* **2001**, *113*, 2660; *Angew. Chem. Int. Ed.* **2001**, *40*, 2591.
[4] *Electronic Materials: The Oligomeric Approach* (Eds.: K. Müllen, G. Wegner), Wiley-VCH, Weinheim, **1998**.
[5] J. F. Penneau, L. L. Miller, *Angew. Chem.* **1991**, *103*, 1002; *Angew. Chem. Int. Ed. Engl.* **1991**, *30*, 986.
[6] P. Hübler, J. Heinze, *Ber. Bunsen-Ges.* **1998**, *102*, 1506, and references therein.
[7] A. Merz, J. Kronberger, L. Dunsch, A. Neudeck, A. Petr, L. Parkanyi, *Angew. Chem.* **1999**, *111*, 1533; *Angew. Chem. Int. Ed.* **1999**, *38*, 1442.
[8] P. Tschuncky, J. Heinze, A. Smie, G. Engelmann, G. Koßmehl, *J. Electroanal. Chem.* **1997**, *433*, 223.
[9] a) Y. Yu, E. Gunic, B. Zinger, L. Miller, *J. Am. Chem. Soc.* **1996**, *118*, 1013; b) Y. Harima, H. Tang, L. Zhu, K. Yamashita, J. Ohsita, A. Kunai, *J. Electroanal. Chem.* **1999**, *472*, 157; c) H. Nakanishi, N. Sumi, S. Ueno, K. Takimiya, Y. Aso, T. Otsubo, K. Komaguchi, M. Shiotani, N. Ohta, *Synth. Met.* **2001**, *119*, 413.
[10] A. Smie, J. Heinze, *Angew. Chem.* **1997**, *109*, 375; *Angew. Chem. Int. Ed. Engl.* **1997**, *36*, 363.

 © WILEY-VCH Verlag GmbH, 69451 Weinheim, Germany, 2002 1433-7851/02/4112-2085 $ 20.00+.50/0

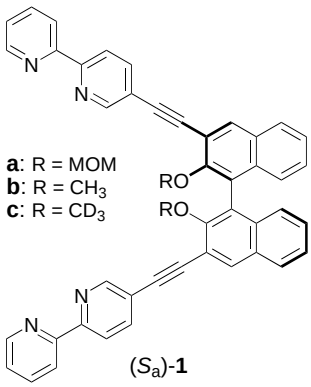
[11] J. A. E. van Haare, L. Groenendaal, E. E. Havinga, R. A. J. Janssen, E. W. Meijer, *Angew. Chem.* **1996**, *108*, 696; *Angew. Chem. Int. Ed. Engl.* **1996**, *35*, 638.
[12] a) A. Neudeck, A. Petr, L. Dunsch, *Synth. Met.* **1999**, *107*, 143; b) P. Rapta and L. Dunsch, *J. Electroanal. Chem.* **2001**, *507*, 287.
[13] B. Schlicke, J. Frahn, A. D. Schlüter, *Synth. Met.* **1996**, *83*, 173.
[14] W. D. Neudroff, N. Schulte, D. Lentz, A. D. Schlüter, *Org. Lett.* **2001**, *3*, 3115.
[15] H. Meier, U. Stalmach, H. Kolshorn, *Acta Polym.* **1991**, *48*, 379; see also: P. Bäuerle, Paper presented at 10th International Symposium on Novel Aromatic Compounds 2001, San Diego **2001**.
[16] R. Biehl, K. Hinricks, H. Kurreck, W. Lubitz, U. Mennenga, K. Roth, *J. Am. Chem. Soc.* **1977**, *99*, 4278.
[17] a) E. F. Fabrizio, A. Payne, N. E. Westlund, A. J. Bard, P. P. Magnus, *J. Phys. Chem. A* **2002**, *106*, 1516; b) J. D. Debad, J. C. Morris, V. Lynch, P. Magnus, A. J. Bard, *J. Am. Chem. Soc.* **1996**, *118*, 2374; c) J. D. Debad, J. C. Morris, P. Magnus, A. J. Bard, *J. Org. Chem.* **1997**, *62*, 530.
[18] F. Gerson, J. H. Hammons in *Nonbenzenoid Aromatics* (Ed.: J. P. Synder), New York, Academic Press, **1971**, p. 81.
[19] J. A. E. H van Haare, E. E. Havinga, J. L. J. van Dongen, R. A. J. Janssen, J. Comil, J.-L. Brédas, *Chem. Eur. J.* **1998**, *4*, 1509.

Synthesis and Stereoselective Self-Assembly of Double- and Triple-Stranded Helicates**

Arne Lützen,* Marko Hapke, Jens Griep-Raming, Detlev Haase, and Wolfgang Saak

The last decade has seen a tremendous development in the design and synthesis of self-assembled supramolecular architectures through metal-ion coordination.[1–3] Although examples have been reported in which chiral ligand units[2f,g, 4–11] were used, only a few of these units bear additional inwardly directed functional groups.[10a,c, 11] Therefore, our aim was to design and synthesize a double-branched chelating ligand, held together by a chiral core fragment bearing functional groups.

As part of our approach, the feasibility of the proposed metal–ligand complexes was explored by force-field and semiempirical calculations prior to ligand synthesis.[12] By following this approach we designed ligand **1**, which should self-assemble to form dinuclear coordination complexes with suitable metal ions (Figure 1). 5-ethynyl-2,2′-bipyridine (**4**; Scheme 1) was prepared from 2-bromopyridine (**2**). A modi-



(S_a)-**1**

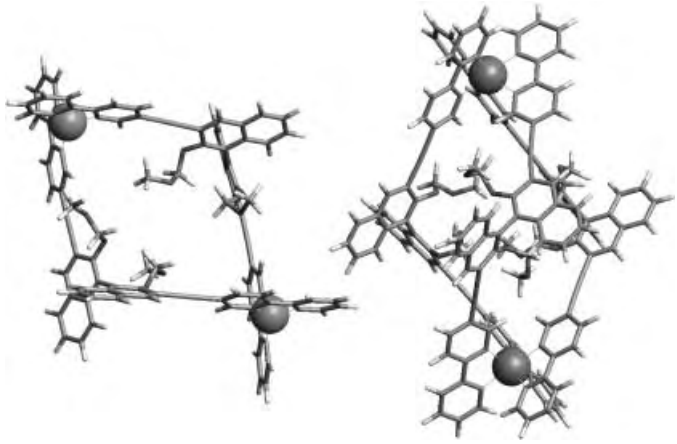
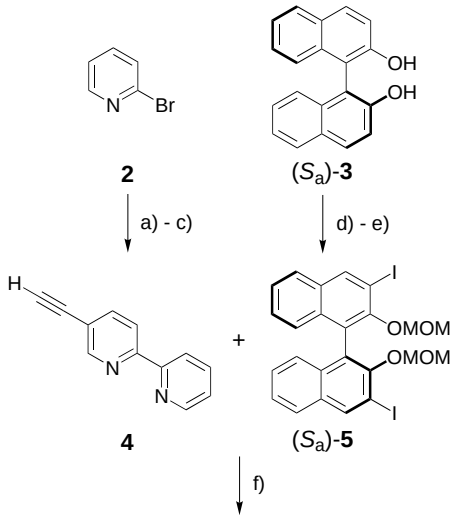


Figure 1. Energy-minimized structures (PM3-TM calculations) of the complexes $[Cu_2\{(S_a)\text{-}\mathbf{1a}\}_2]^{2+}$ (left) and $[Zn_2\{(S_a)\text{-}\mathbf{1a}\}_3]^{4+}$ (right); only one of the three possible stereoisomeric complexes is shown for each.



Scheme 1. Synthesis of (S_a)-**1a**. a) *t*BuLi, THF, −78 °C, then $ZnCl_2$, −78 °C → RT, 2 h; b) 2-chloro-5-trimethylsilylethynylpyridine, $[Pd_2(dba)_3]\cdot CHCl_3$, tBu_3P, THF, 83 %; c) KF, MeOH, 97 %; d) NaH, DMF, MOMCl, 80 %; e) *n*BuLi, TMEDA, RT, 6.5 h, I_2, −78 °C, 65 %; f) Et_3N, CuI, $[Pd_2(dba)_3]\cdot CHCl_3$, dppf, 50 °C, 78 %. dba = *trans*,*trans*-dibenzylideneacetone; TMEDA = *N*,*N*,*N*′*N*′-tetramethylethylenediamine; dppf = 1,1′-bis-(diphenylphosphanyl)ferrocene.

[*] Dr. A. Lützen, Dipl.-Chem. M. Hapke, Dr. J. Griep-Raming, Dipl.-Ing. D. Haase, Dipl.-Chem. W. Saak
University of Oldenburg
Department of Chemistry
P.O. Box 2503, 26111 Oldenburg (Germany)
Fax: (+49) 441-798-3329
E-mail: arne.luetzen@uni-oldenburg.de

[**] We thank Prof. Dr. P. Köll for providing us with excellent working conditions, and Prof. Dr. J. O. Metzger for the opportunity to perform the ESI–MS experiments. Financial support from the DFG and the Fonds der Chemischen Industrie is gratefully acknowledged. M.H. thanks the state of Lower Saxony for a graduate scholarship.

Supporting information for this article is available on the WWW under http://www.angewandte.org or from the author.

 © WILEY-VCH Verlag GmbH, 69451 Weinheim, Germany, 2002 1433-7851/02/4112-2086 $ 20.00+.50/0

fied Negishi cross-coupling reaction of **2** with 2-chloro-5-trimethylsilylethynyl-pyridine[13] furnished trimethylsilyl-protected 2,2′-bipyridine,[14] which was subsequently desilylated by use of potassium fluoride to give **4** in 81 % overall yield.[15]

Enantiomerically pure (S_a)- and (R_a)-2,2′-dihydroxy-1,1′-binaphthyl (BINOL, **3**) were obtained after clathrate formation of racemic BINOL with *N*-benzylcinchonidinium chloride.[16] Standard methoxymethyl ether (MOM) protection of the hydroxy groups afforded the 2,2′-bis-*O*-MOM protected intermediates, which were converted into *ortho*-diiodinated BINOL-derivatives **5**.[17] Finally, the Sonogashira coupling reaction of building blocks **4** and **5** using Et_3N, CuI, $[Pd_2(dba)_3]\cdot CHCl_3$, and dppf gave **1a** in a good yield of 78 %.[18]

Addition of previously prepared and thoroughly dried $[Cu(CH_3CN)_4]BF_4$, $[Ag(CH_3CN)_2]BF_4$, or $Zn(BF_4)_2$, or commercially available hydrated $Zn(ClO_4)_2\cdot 6H_2O$ or $FeSO_4\cdot 7H_2O$ to solutions of (S_a)-**1a** or (R_a)-**1a** in dichloromethane/acetonitrile resulted in instant color changes from almost colorless to intense red–brown in the case of the copper(I) and the iron(II) salts or pale yellow in the case of the silver(I) and the zinc(II) salts, which indicates the formation of metal complexes. This result was confirmed by NMR spectroscopic experiments on solutions in deuterated solvents, in which significant shifts of the signals in the ^1H and ^{13}C NMR spectra were observed.[19] The signals were very sharp, especially in the case of the silver and the zinc complexes (Figure 2), which indicates the formation of discrete, dinuclear metal complexes rather than higher oligomeric species.

Furthermore, the spectra also indicate that the zinc and iron complexes, as expected, have a different structure to the silver and copper complexes, which are very similar to each other. This structural difference is caused by the change from a tetrahedral coordination of the metal centers by two ligands in the latter cases, to an octahedral coordination of the zinc or iron cation by three ligands.

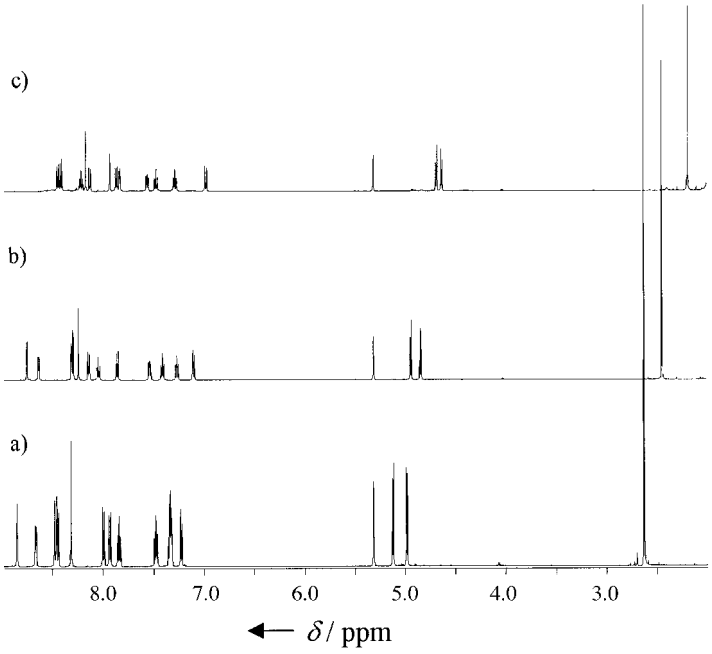


Figure 2. ^1H NMR spectra (500.1 MHz, 300 K, CD_2Cl_2/CD_3CN) of a) (S_a)-**1a**, b) (S_a)-**1a** + 1 equiv $[Ag(CH_3CN)_2]BF_4$, and c) 3 equiv (S_a)-**1a** + 2 equiv $Zn(BF_4)_2$.

In addition, the spectra, which were identical for both enantiomers (R_a)-**1a** and (S_a)-**1a**, clearly reveal that the C_2 symmetry of the ligand remained in the bis- and tris(bipyridine) complexes. Thus, the formation of dinuclear species with two differently configured metal centers can be definitely excluded because the spectra would be more complicated in this case, as the ligand would lose its symmetry.[20] Hence, on the basis of the ^1H and ^{13}C NMR spectroscopic analysis, the number of diastereomers present in solution can be narrowed down to two D_2-symmetric diastereomers with either *Λ*,*Λ*- or *Δ*,*Δ*-configured metal centers. The spectra even seem to suggest that only one of these diastereomers is present, because it is unlikely that all proton and carbon resonance signals would have the same chemical shift for both diastereomers.

The stoichiometries of the complexes could be demonstrated by ESI–MS, in which we only found signals with the expected isotope patterns for the desired dinuclear complexes and their fragmentation products, as shown in Figure 3 for the zinc complex.[21]

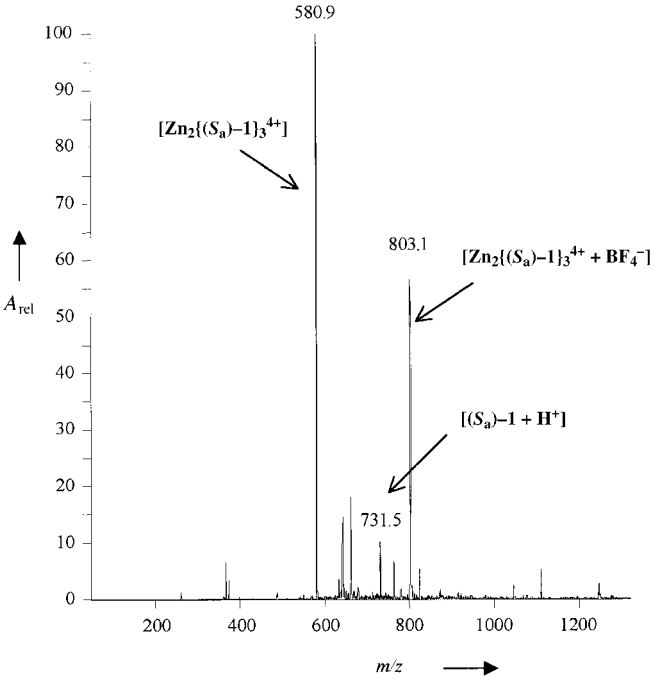


Figure 3. Positive-ion ESI mass spectrum of $[Zn_2\{(S_a)\text{-}\mathbf{1a}\}_3]^{4+}\cdot 4BF_4^-$.

As the analysis of the NMR spectroscopic experiments suggested that there should be a fast exchange of the ligands on the NMR timescale in the case of the copper(I) and the iron(II) complexes but a slow exchange in the case of the silver(I) and zinc(II) coordination compounds, further ESI–MS experiments were performed to investigate the ligand-exchange behavior. Therefore, we prepared the racemic bis(bipyridine) ligands **1b** and **1c** in which the MOM-groups of **1a** are substituted by methyl (**1b**) or deuterated methyl groups (**1c**). By mixing preformed complexes of **1b** and **1c** we corroborated our assumptions, by observing an almost immediate exchange in the case of the copper(I) complex, as

 © WILEY-VCH Verlag GmbH, 69451 Weinheim, Germany, 2002 1433-7851/02/4112-2087 $ 20.00+.50/0

demonstrated by the formation of a mixed $[Cu_2(\mathbf{1b})(\mathbf{1c})]^{2+}$ complex; no ligand exchange was observed in the case of the silver(I) or the zinc(II) complexes, even after longer mixing times.[22]

Unfortunately, CD (circular dichroism) spectroscopic measurements did not allow a definite assignment of the stereochemistry of the newly formed stereogenic metal centers because the most important region of the spectra in this respect[4, 5] (about 320–350 nm) is dominated by signals arising from the BINOL part of **1a** or its complexes. Also, sel-1D-NOESY NMR spectroscopic experiments did not help to reveal the stereochemistry, probably because the complexes are in a mass range in which no NOE contacts can be observed. We therefore performed sel-1D-ROESY NMR spectroscopic experiments on the $[Ag_2\{(S_a)\text{-}\mathbf{1a}\}_2]^{2+}$ and the $[Zn_2\{(S_a)\text{-}\mathbf{1a}\}_3]^{4+}$ complexes. These experiments gave initial indications that the stereogenic metal centers are *Δ*-configured in these cases, because ROE contacts could be observed between the bipyridine and the BINOL fragments of the ligand, which gave us the relative orientation of these two fragments and hence the stereochemistry of the newly formed tetrahedral or octahedral metal-coordination complexes.[22]

However, as ROESY measurements are more prone to misleading artifacts such as COSY or TOCSY signals, and because the ROE signals were only small—as expected from the minimum distance between these parts of about 4.5 Å—we wanted further evidence for this assignment. We finally obtained suitable crystals of the $[Zn_2\{(S_a)\text{-}\mathbf{1a}\}_3](BF_4)_4$ complex from THF/*n*-hexane/acetonitrile to perform an X-ray structural analysis[23] (Figure 4). This analysis showed unambiguously that the desired discrete dinuclear complex was formed and adopts a structure in which both octahedral metal centers are *Δ* configured, which thus gives rise to an overall D_3-symmetric *P*-configured triple-stranded helicate.

All these results lead to the conclusion that the configuration of the newly formed stereogenic metal centers is fully controlled by the configuration of the BINOL group. Further evidence for this configuration was obtained from NMR spectroscopic experiments on complexes obtained from racemic **1a**, which gave spectra that were virtually identical to those of the enantiomerically pure compounds; this similarity indicates that each ligand forms only homoleptic, diastereomerically pure complexes.[22] These complexes have well-defined chiral cavities with internal functionalities, which we are attempting to exploit in molecular-recognition studies.

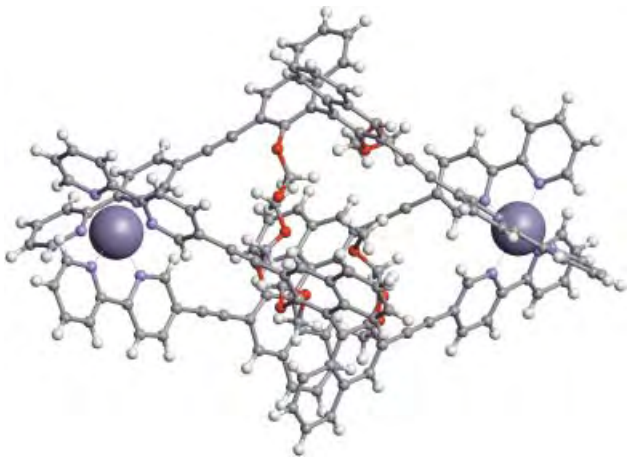


Figure 4. Crystal structure of (Δ,Δ)-$[Zn_2\{(S_a)\text{-}\mathbf{1a}\}_3]^{4+}$ (counterions and solvent molecules omitted).

Experimental Section

1a: M.p. 213 °C; (S_a)-**1a**: $[\alpha]_D^{20} = +333°$ ($c = 1.01$, THF); (R_a)-**1a**: $[\alpha]_D^{20} = -327°$ ($c = 0.99$, THF); ^1H and ^{13}C NMR spectroscopic data see Supporting Information; MS (CI, isobutane): *m/z* 731.9 (100 %); UV/Vis: $\lambda_{max}(\varepsilon) = 242$ (65 500), 332 nm (79 000); elemental analysis (%) calcd for $C_{48}H_{34}N_4O_4$: C 78.89, H 4.69, N 7.67; found: C 78.83, H 4.68, N 7.46 ((S_a)-**1a**); C 78.23, H 4.65, N 7.66 ((R_a)-**1a**).

(Δ,Δ)-$[Ag_2\{(S_a)\text{-}\mathbf{1a}\}_2](BF_4)_2$: M.p. 160–163 °C (decomp.); $[\alpha]_D^{20} = +269°$ ($c = 0.9$, CH_2Cl_2/CH_3CN 3/1); ^1H and ^{13}C NMR data see Supporting Information; MS (ESI): *m/z* (%): 839.4 ($[Ag_2(\mathbf{1a})_2]^{2+}$, $[Ag(\mathbf{1a})]^+$, 1/2 ratio, 100), 731.5 ($[\mathbf{1a}+H]^+$, 35), 1764.3 ($[Ag_2(\mathbf{1a})_2^{2+}+BF_4^-]$, 3); elemental analysis (%) calcd for $C_{96}H_{48}B_2F_8N_8O_8Ag_2$: C 62.29, H 3.70, N 6.05; found: C 62.04, H 3.96, N 6.06.

(Δ,Δ)-$[Zn_2\{(S_a)\text{-}\mathbf{1a}\}_3](BF_4)_4$: M.p. > 300 °C (decomp.); $[\alpha]_D^{20} = -1373°$ ($c = 0.70$, CH_2Cl_2/CH_3CN 3/1); ^1H and ^{13}C NMR data see Supporting Information; MS (ESI): *m/z* (%): 580.9 ($[Zn_2(\mathbf{1a})_3]^{4+}$, 100), 803.1 ($[Zn_2(\mathbf{1a})_3^{4+}+BF_4^-]$, 55), 731.5 ($[\mathbf{1a}+H]^+$, 10); elemental analysis (%; perchlorate complex $[Zn_2\{(S_a)\text{-}\mathbf{1a}\}_3](ClO_4)_4$) calcd for $C_{144}H_{102}Cl_4N_{12}O_{28}Zn_2 \cdot 4H_2O$: C 61.92, H 3.97, N 6.02; found: C 61.87, H 3.88, N 6.04.

Received: January 28, 2002 [Z 18603]

[1] a) J.-M. Lehn, *Supramolecular Chemistry*, VCH, Weinheim, **1995**, pp. 139–190; b) A. von Zelewsky, *Stereochemistry of Coordination Compounds*, Wiley, Chichester, **1995**, pp. 177–201; c) J. W. Steed, J. L. Atwood, *Supramolecular Chemistry*, Wiley, Chichester, **2000**, pp. 463–571.

[2] Reviews dealing with helicates: a) E. C. Constable, *Tetrahedron* **1992**, *48*, 10013–10059; b) C. Piguet, G. Bernardinelli, G. Hopfgartner, *Chem. Rev.* **1997**, *97*, 2005–2062; c) M. Albrecht, *Chem. Soc. Rev.* **1998**, *27*, 281–287; d) D. L. Caulder, K. N. Raymond, *J. Chem. Soc. Dalton Trans.* **1999**, 1185–1200; e) D. L. Caulder, K. N. Raymond, *Acc. Chem. Res.* **1999**, *32*, 975–982; f) A. von Zelewsky, *Coord. Chem. Rev.* **1999**, *190–192*, 811–825; g) U. Knof, A. von Zelewesky, *Angew. Chem.* **1999**, *111*, 312–333; *Angew. Chem. Int. Ed.* **1999**, *38*, 302–322; h) M. Albrecht, *Chem. Eur. J.* **2000**, *6*, 3485–3489; i) M. Albrecht, *Chem. Rev.* **2001**, *101*, 3457–3497.

[3] Reviews dealing mainly with other types of self-assembled supramolecular aggregates formed by metal-ion coordination: a) M. Fujita, K. Ogura, *Bull. Chem. Soc. Jpn.* **1996**, *69*, 1471–1482; b) M. Fujita, *Chem. Soc. Rev.* **1998**, *27*, 417–425; c) C. J. Jones, *Chem. Soc. Rev.* **1998**, *27*, 289–299; d) S. Leininger, B. Olenyuk, P. J. Stang, *Chem. Rev.* **2000**, *100*, 853–908; e) G. F. Swiegers, T. J. Malefetse, *Chem. Rev.* **2000**, *100*, 3483–3537; f) M. Fujita, K. Umemoto, M. Yoshizawa, N. Fujita, T. Kusukawa, K. Biradha, *Chem. Commun.* **2001**, 509–518; g) B. D. Holliday, C. A. Mirkin, *Angew. Chem.* **2001**, *113*, 2076–2098; *Angew. Chem.* Int. Ed. **2001**, *40*, 2022–2043.

[4] Some recent examples reported by the von Zelewsky group, which are not covered by reference [2f] or [2g]: a) O. Mamula, A. von Zelewsky, T. Bark, G. Bernardinelli, *Angew. Chem.* **1999**, *111*, 3129–3133; *Angew. Chem. Int. Ed.* **1999**, *38*, 2945–2948; b) O. Mamula, A. von Zelewsky, T. Bark, H. Stoeckli-Evans, A. Neels, G. Bernardinelli, *Chem. Eur. J.* **2000**, *6*, 3575–3585; c) O. Mamula, F. J. Monlien, A. Porquet, G. Hopfgartner, A. E. Merbach, A. von Zelewsky, *Chem. Eur. J.* **2001**, *7*, 533–539; d) T. Bark, M. Düggeli, H. Stoeckli-Evans, A. von Zelewsky, *Angew. Chem.* **2001**, *113*, 2924–2927; *Angew. Chem. Int. Ed.* **2001**, *40*, 2848–2851.

[5] a) E. C. Constable, T. Kulke, M. Neuburger, M. Zehnder, *Chem. Commun.* **1997**, 489–490; b) G. Baum, E. C. Constable, D. Fenske, T. Kulke, *Chem. Commun.* **1997**, 2043–2044; c) E. C. Constable, T. Kulke, M. Neuburger, M. Zehnder, *New J. Chem.* **1997**, *21*, 633–646; d) E. C. Constable, T. Kulke, M. Neuburger, M. Zehnder, *New J. Chem.* **1997**, *21*, 1091–1102; e) G. Baum, E. C. Constable, D. Fenske, C. E. Housecroft, T. Kulke, *Chem. Commun.* **1998**, 2659–2660; f) G.

 © WILEY-VCH Verlag GmbH, 69451 Weinheim, Germany, 2002 1433-7851/02/4112-2088 $ 20.00+.50/0

Baum, E. C. Constable, D. Fenske, C. E. Housecroft, T. Kulke, *Chem. Eur. J.* **1999**, *5*, 1862 – 1873; g) G. Baum, E. C. Constable, D. Fenske, C. E. Housecroft, T. Kulke, *Chem. Comun.* **1999**, 195 – 196; h) G. Baum, E. C. Constable, D. Fenske, C. E. Housecroft, T. Kulke, M. Neuburger, M. Zehnder, *J. Chem. Soc. Dalton Trans.* **2000**, 945 – 959.

[6] W. Zarges, J. Hall, J.-M. Lehn, C. Bolm, *Helv. Chim. Acta* **1991**, *74*, 1843 – 1852.

[7] G. C. van Stein, G. van Koten, K. Vrieze, C. Brevard, A. L. Spek, *J. Am. Chem. Soc.* **1984**, *106*, 4486 – 4492.

[8] A. L. Airey, G. F. Swiegers, A. C. Willis, S. B. Wild, *Inorg. Chem.* **1997**, *36*, 1588 – 1597.

[9] a) C. R. Woods, M. Benaglia, F. Cozzi, J. S. Siegel, *Angew. Chem.* **1996**, *108*, 1977 – 1980; *Angew. Chem. Int. Ed.* **1996**, *35*, 1830 – 1833; b) R. Annunziata, M. Benaglia, M. Cinquini, F. Cozzi, C. R. Woods, J. S. Siegel, *Eur. J. Org. Chem.* **2001**, 173 – 180.

[10] a) E. J. Enemark, T. D. P. Stack, *Angew. Chem.* **1995**, *107*, 1082 – 1084; *Angew. Chem. Int. Ed. Engl.* **1995**, *34*, 996 – 998; b) M. A. Masood, E. J. Enemark, T. D. P. Stack, *Angew. Chem.* **1998**, *110*, 973 – 977; *Angew. Chem. Int. Ed.* **1998**, *37*, 928 – 932; c) E. J. Enemark, T. D. P. Stack, *Angew. Chem.* **1998**, *110*, 977 – 981; *Angew. Chem. Int. Ed.* **1998**, *37*, 932 – 935.

[11] E. J. Corey, C. L. Cywin, M. C. Noe, *Tetrahedron Lett.* **1994**, *35*, 69 – 72.

[12] Molecular modeling was performed using the commercially available PC Spartan Pro software package from Wavefunction.

[13] 2-Chloro-5-trimethylsilylethynylpyridine was prepared according to P. N. W. Baxter, *J. Org. Chem.* **2000**, *65*, 1257 – 1272.

[14] A. Lützen, M. Hapke, *Eur. J. Org. Chem.*, in press .

[15] V. Grosshenny, F. M. Romero, R. Ziessel, *J. Org. Chem.* **1997**, *62*, 1491 – 1500.

[16] Q.-S. Hu, D. Vitharana, L. Pu, *Tetrahedron: Asymmetry* **1995**, *6*, 2123 – 2126.

[17] Bis-derivatized BINOL components have already been reported: A. Bähr, A. S. Droz, M. Püntner, U. Neidlein, S. Anderson, P. Seiler, F. Diederich, *Helv. Chim. Acta* **1998**, *81*, 1931 – 1963.

[18] Use of other phosphane ligands in the Sonogashira coupling reaction gave only unsatisfactory yields.

[19] NMR spectra were recorded on a Bruker Avance 500 at 300 K. Signals were assigned according to ^{1}H, ^{13}C, H,H-COSY, HMQC, and HMBC experiments (17 mM initial concentration of **1a**).

[20] This diastereomer can be described as a kind of *meso*-form. However, this description is not quite correct as the complex remains chiral because of the axial chirality of the BINOL. In fact, this complex is less symmetric (C_2) than the other two D_2-symmetric, helical diastereomers.

[21] ESI – MS spectra of dichloromethane/acetonitrile solutions (5×10^{-4} M concentration of **1a**, **1b**, or **1c**) were recorded on a Thermo Finnigan LCQ.

[22] See Supporting Information for further details.

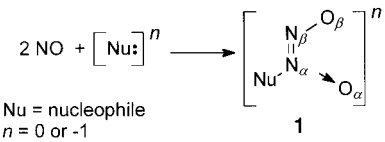
[23] Crystal structure of (Δ,Δ)-[Zn_2\{(S_a)-**1a**\}$_3$](BF$_4$)$_4 \cdot 2.5$ THF $\cdot 5$ CH$_3$CN: STOE-IPDS-diffractometer ($Mo_{K\alpha}$ radiation), $T = 193$ K. Crystal dimensions $= 0.25 \times 0.24 \times 0.17$ mm^3, $C_{164}H_{137}B_4F_{16}N_{17}O_{14.5}Zn_2$; $M_r =$ 3055.89, orthorhombic, space group $P2_12_12_1$, $a = 28.3103(10)$, $b =$ 33.0824(15), $c = 35.7949(14)$ Å, $V = 33\,525(2)$ Å^3, $Z = 8$, $\rho_{calcd} =$ 1.211 mg m^{-3}, $F(000) = 12\,640$, $\theta_{max} = 22.47°$, $-30 < h < 30$; $-35 < k < 35$; $-38 < l < 38$, 180 110 measured reflections, 43 248 independent reflections ($R_{int} = 0.2759$). All non-hydrogen atoms were anisotropically refined and the H atoms were inserted in the calculated positions. 11 548 reflections $I > 2\sigma(I)$ and 1776 refined parameters, GOF(F^2) $= 0.786$, final R indices: $R_1 = 0.1067$, $wR_2 = 0.2483$, Flack parameter $x = 0.01(2)$, max./min. residual electron density 0.980/ -0.539 e Å^{-3}. The structures were solved by the direct method (SHELXS-97)[24] and refined on F^2. CCDC-178150 ((Δ,Δ)-[Zn_2\{(S_a)-**1a**\}$_3$](BF$_4$)$_4 \cdot 2.5$ THF $\cdot 5$ CH$_3$CN) contains the supplementary crystallographic data for this paper. These data can be obtained free of charge via www.ccdc.cam.ac.uk/conts/retrieving.html (or from the Cambridge Crystallographic Data Centre, 12, Union Road, Cambridge CB2 1EZ, UK; fax: (+44) 1223-336-033; or deposit@ccdc.cam.ac.uk).

[24] G. M. Sheldrick, SHELXS-97, Program for the Solution of Crystal Structures, University of Göttingen, Göttingen (Germany), **1997**.

Traube's "Oxazomalonic Acid" is a 3-Hydroxysydnone Carboxylate with an *E*-ONNO Geometry**

Navamoney Arulsamy and D. Scott Bohle*

In his seminal early investigations of the base-mediated condensation of nitric oxide with organic acids,[1–4] Wilhelm Traube prepared an adduct of diethylmalonate, which he formulated as "$ON_2C(CO_2H)_2$" and termed an "oxazomalonic acid".[3] As written, this derivative is formally a conjugated diazotate,[5, 6] and in contrast with the low thermal stability of diazotates, Traube's disodium salt is stable to 343 °C. These observations and much of the organic chemistry of nitric oxide have received scant attention since then, but the discovery of the numerous roles of nitric oxide in biology has renewed interest in this once obscure chemistry.[7] We and others have recently extended many of Traube's original discoveries,[8–12] and one of the universal observations is that the condensation of nitric oxide with nucleophiles returns diazeniumdiolate products **1**, often in high yields and with a *Z* orientation of the two oxygen atoms that flank the newly formed N=N bond (Equation (1)).[9] We have recently reexamined Traube's reaction and his "oxazomalonic" acid product. Herein we report: 1) the product is, in fact, an unusual heterocycle with a five-membered ring and corresponds to the 3-hydroxy-2-carboxysydnone dianion; 2) the synthesis, structure, and spectroscopic analysis of its methyl ester; and 3) theoretical results, which suggest a low-lying transition state for *Z* to *E* isomerization of an initial NO condensation product. Taken together, these results allow the unambiguous characterization of a new diazeniumdiolate with an *E*-ONNO framework.[13]



(1)

Nu = nucleophile
n = 0 or -1

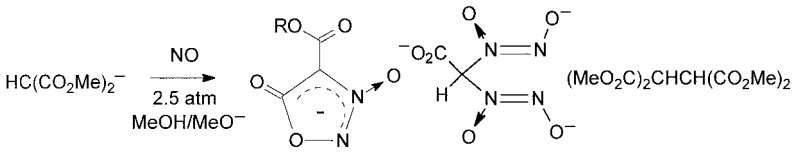
1

The condensation products of nitric oxide and dimethyl malonate depend on the temperature and on the substrate/base stoichiometry (Scheme 1). There are three predominant reactions that account for the observed products: 1) condensation of two nitric oxide molecules, followed by ring closure to give the planar heterocycle 2-carboxy-3-hydroxysydnone (**2**), which was isolated as either a monomethyl ester **2a** or as a dianionic salt **2b**,**c**; 2) condensation of four nitric oxide molecules and decarboxylation to give the bisdiazeniumdiolate **3**, which was isolated as a tripotassium salt; and 3) one-

[*] Prof. Dr. D. S. Bohle, Dr. N. Arulsamy
Department of Chemistry, University of Wyoming
Laramie, WY 82071-3838 (USA)
Fax: (+1) 307-766-2807
E-mail: Bohle@uwyo.edu

[**] This research was supported by the Airforce Office of Scientific Research and the National Institutes of Health.

Supporting information for this article is available on the WWW under http://www.angewandte.com or from the author.



2a: M = K, R = Me
b: M = K, R = K
c: M = Na, R = Na

3

4

RT	17% (as **2b**)	:	15%	:	trace
0 °C	31% (as **2a**)	:	0%	:	18%

Scheme 1. Reaction products for the nitrosylation of dimethyl malonate.

electron oxidation of the dimethyl malonate anion by nitric oxide to give the dimer $(MeO_2C)_2CHCH(CO_2Me)_2$ (**4**). The monopotassium salt **2a** was characterized by single-crystal X-ray diffraction (Figure 1) and has a coplanar array of all the heavy atoms of the anion. Based on its planarity and on the short C–C bond length, the methylcarboxylato group is conjugated with the $C_2O_3N_2$ ring. Hydrolysis of **2a** in KOH (1M) returns Traube's salt ($K_2C_3O_5N_2$, **2b**) in good yield.

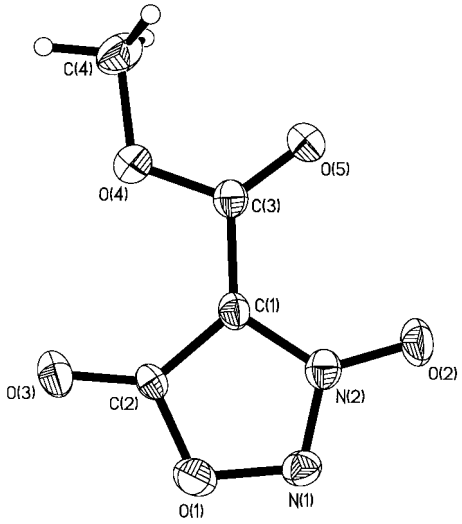
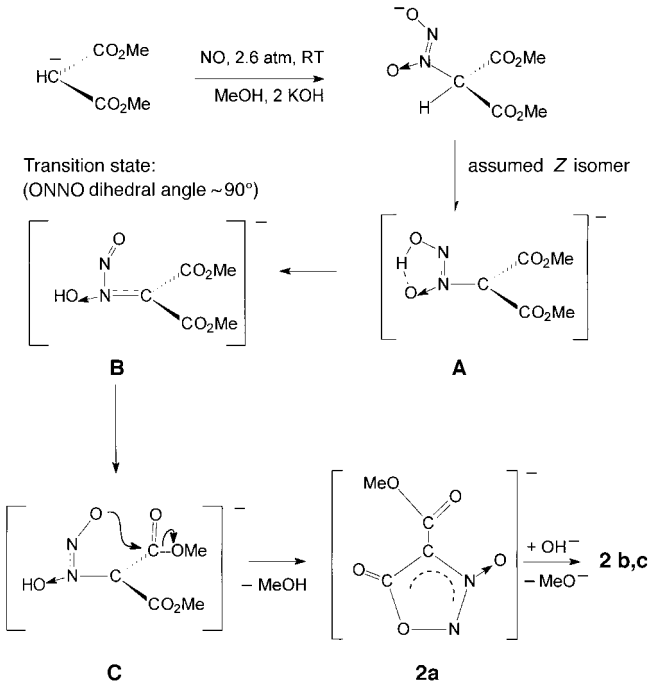


Figure 1. ORTEP view of the 1,2,3-oxadiazole-3-oxido-4-methylcarboxylate-5-hydroxylate anion in the crystals of **2a**. Important metric parameters: C(1)-N(2) 1.380(3) Å, N(2)-N(1) 1.324(3), N(2)-O(2) 1.262(3), N(1)-O(1) 1.386(3), O(1)-C(2) 1.367(3), C(2)-O(3) 1.229(3), C(2)-C(1) 1.405(3), C(1)-C(3) 1.448(3), C(3)-O(4) 1.333(3), C(3)-O(5) 1.212(3), O(4)-C(4) 1.447(3); C(1)-N(2)-O(2) 130.2(2), O(2)-N(2)-N(1) 118.3(2), N(2)-N(1)-O(1) 106.6(2), N(1)-O(1)-C(2) 109.5(2), O(1)-(2)-O(3) 119.1(2), O(1)-C(2)-C(1) 106.7(2), O(3)-C(2)-C(1) 134.1(2), C(2)-C(1)-N(2) 105.7(2), N(2)-C(1)-C(3) 125.1(2), C(2)-C(1)-C(3) 129.1(2).

The structure shown in Figure 1 is the first report of a structurally characterized diazeniumdiolate with an *E* geometry. The mechanistic origin of this geometry is in surprising contrast with the general stereospecificity observed in the products of Equation (1). We suggest that the mechanistic origins of this product are a result of a cyclizing condensation of one of the malonate esters with an *E*-ONNO group, (Scheme 2, **C**), which traps the *Z* conformer. Further, we propose that the initial diazeniumdiolate from the condensation reaction has a *Z* geometry, (Scheme 2, **A**) and that this undergoes *Z* to *E* isomerization before cyclization. The diazenium diolate moiety is recognized as a strong electron-withdrawing substituent[18] and either the α-proton will be lost or the diazeniumdiolate tautomerizes to the $N_2O_2^-$ moiety. Although our experience is that the calculated *E*/*Z* isomerization barriers are relatively high (>40 kcal mol^{-1}) for anionic diazeniumdiolates, it is possible to draw resonance structures for the first intermediate, which has a formal N–N single-bonded nitroso group in a $[(HO_2C)_2C{=}N(OH){-}N{=}O]^-$ fragment. To test more thoroughly this valence-bond prediction



Scheme 2. Proposed mechanism for the synthesis of new sydnones.

that low *Z*/*E* isomerization barriers are present when the α-nitrogen atom can form multiple bonds to its R substituent, we have examined the gas-phase isomerization potential energy surface with density functional ab initio theoretical methods (B3LYP/6-311++G**) and a quadratic synchronous transit algorithm.[14, 15] Both **A** and **C** optimize to ground-state geometries, with the *Z* conformer in **A** being 1.33 kcal mol^{-1} more stable than the *E* conformer. The lowest energy saddle point found on this surface corresponds to a species with a monoprotonated α-oxygen atom, the monoanion $[(HO_2C)_2C{=}N(OH){-}NO]^-$ (**B**), which lies 19.66 kcal mol^{-1} above the ground-state *E* and *Z* geometries. The reaction coordinate that leads from the optimized ground state of the proposed intermediate **A** to that of **C** primarily correlates with a twisting of the ONNO dihedral angle (Figure 2), and confirms that this saddle point connects the two ground states by a low-energy isomerization pathway.

As sydnones **2b** and **2c** are unique in that they are remarkably stable towards hydrolysis in base yet easily hydrolyze in acid, both trends are opposite to the stabilities of

 © WILEY-VCH Verlag GmbH, 69451 Weinheim, Germany, 2002 1433-7851/02/4112-2090 $ 20.00+.50/0 *Angew. Chem. Int. Ed.* **2002**, *41*, No. 12

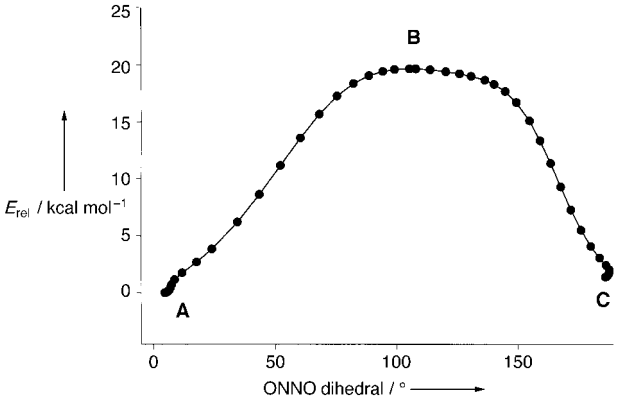


Figure 2. Ab initio calculated (B3LYP/6-311++G**) energy profile for the *Z* to *E* isomerization $(HO_2C)_2C\{N(OH)O\}^-$. The dihedral angle for the ONNO group, which dominates the internal reaction coordinate, correlates **A**, **B**, and **C** (see Scheme 2) for the proposed low-energy pathway for *Z* to *E* isomerization.

other sydnones. At neutral pH values, **2a** slowly hydrolyzes to release two equivalents of NO, and thus these new sydnones may be useful as potential NO prodrugs. A similar reactivity pattern has however been observed for methanetris(diazeniumdiolates),[12] and the products of acid hydrolysis include nitric oxide, nitrous oxide, and carbon dioxide. A closely related spectroscopically characterized heterocycle has been proposed to result from the reaction of nitrosyl chloride and 1,1,4,4-tetramethyl-1,3-butadienes.[16] This new type of compact ring structure forms dense crystals, and thus **2a,b,c** are potential energetic materials which decompose exothermally at high temperatures.

Experimental Section

2a: A solution of potassium methoxide (prepared from potassium metal (3.90 g, 0.1 mol) and absolute methanol (100 mL)), was filtered at room temperature and mixed with dimethyl malonate (13.21 g, 0.1 mol) in a glass medium-pressure reaction vessel. The vessel was cooled in an ice bath to 0 °C with rigorous exclusion of oxygen before the introduction of nitric oxide (24 kPa). Although the absorption of nitric oxide significantly subsided within 4 h, the reaction mixture was allowed to warm to room temperature and kept under an atmosphere of nitric oxide overnight. The reaction mixture was treated with water (50 mL) and filtered. Recrystallization of the resulting white solids from a chloroform/methanol solvent mixture gave bis(dimethyl malonate) (**4**) (2.4 g, 18 %).[17] The filtrate was reduced in volume (to ca. 50 mL) and the yellow solution was allowed to evaporate slowly. The colorless crystals which formed were filtered, washed with methanol, and dried to afford **2a** (6.2 g, 31 %). IR: $\tilde{\nu}$ = 2964 w, 1812 w, 1738 s, 1698 s, 1654 s, 1629 s, 1512 m, 1490 s, 1469 s, 1429 m, 1386 s, 1324 m, 1310 s, 1208 s, 1140 s, 1047 m, 1039 s, 956 s, 938 m, 806 w, 773 s, 767 s, 683 w, 678 w, 659 w, 500 cm^{-1} m; ^{1}H NMR ($CDCl_3$, 400 MHz): δ = 3.85 ppm (s); ^{13}C NMR ($CDCl_3$, 100 MHz): δ = 171.0, 163.3, 98.5, 54.4 ppm; MS (ESI): *m*/*z*: calcd for $C_4H_3N_2O_5$ [M^-] 159.078; found 159.1 [M^-], 357.1 [$M^-K^+M^-$], 119 [$M^- - NO$], 99 [$M^- - N_2O_2$]; UV/Vis (water): λ_{max} = 230 (11 540), 276 nm (8830); elemental analysis calcd for $C_4H_3N_2O_5K$ (%): C 24.24, H 1.52, N 14.14; found: C 24.16, H 1.51, N 14.08; DSC: T_{onset} = 330 °C (explodes).

2b and $\mathbf{3}\cdot H_2O$: Potassium methoxide (prepared from potassium (3.9 g) in methanol (100 mL)) under nitrogen was treated with dimethyl malonate (6.61 g, 0.05 mol), and the mixture was rigorously degassed before being pressurized with nitric oxide (24 kPa) at 20 °C with vigorous stirring. As the reaction progressed, rapid absorption of nitric oxide was observed in the first 6 h. After 2 d the reaction mixture was flushed with N_2 gas and the white precipitate (7.1 g) was filtered and dried at room temperature. The powder was dissolved in aqueous KOH (1N, 50 mL) and boiled for 30 min. The solution was filtered to remove a small amount of insoluble solids and treated with methanol (10 mL). The cloudy solution was allowed to stand at 5 °C overnight. The large colorless crystals formed were separated by filtration and dried at 120 °C for 6 h (yield: 1.9 g, 17 %). IR: $\tilde{\nu}$ = 1769 m, 1734 s, 1690 s, 1619 s, 1454 s, 1385 s, 1343 s, 1245 m, 1228 s, 1150 m, 1039 m, 1011 m, 956 m, 921 m, 823 s, 796 s, 776 m, 758 w, 728 w, 681 m, 658 m, 478 cm^{-1} w; ^{13}C NMR ($CDCl_3$, 100 MHz): δ = 172.2, 168.0, 101.7 ppm; UV/Vis (water): λ_{max} = 224 (11 130), 280 nm (8810); elemental analysis calcd for $C_3N_2O_5K_2$ (%): C 16.21, N 12.60; found C 16.24, N 12.53. The filtrate was again treated with methanol (50 mL), and the cloudy solution was allowed to stand at 5 °C for several days. Crystals of hydrated **3** formed, and were filtered and dried at room temperature under reduced pressure (yield: 2.3 g, 15 %). IR: $\tilde{\nu}$ = 3650–3260 b, 2970 m, 1670–1660 s, 1377 s, 1353 m, 1290 m, 1255 m, 1228 s, 1211 s, 1146 m, 962 s, 933 m, 862 s, 805 s, 758 s, 654 m, 585 w, 565 cm^{-1} w; ^{1}H NMR ($CDCl_3$, 400 MHz): δ = 6.40 ppm (s); ^{13}C NMR ($CDCl_3$, 100 MHz): δ = 169.70, 91.50 ppm (J = 154.1 Hz); UV/Vis (water): λ_{max} = 258 nm (15 620); elemental analysis calcd for $C_2H_3N_4O_7K_3$ (%): C 7.69, H 0.97, N 17.93; found: C 7.78, H 0.89, N 17.95; DSC: ΔH = −93.6 kcal mol^{-1}, T_{onset} = 322 °C. The sodium derivative **2c** was prepared analogously.

Crystal data for **2a:** $C_4H_3KN_2O_5$, M_r = 198.18, 298 K, monoclinic space group $P2_1/c$; a = 10.736(1), b = 4.5730(8), c = 14.874(2) Å, β = 106.23(1)°, V = 701.2(2) Å^3, Z = 4, ρ_{calcd} = 1.877 Mg m^{-3}, $F(000)$ = 400, 121 parameters; R_1 (wR_2) [$I > 2\sigma(I)$] = 0.053 (0.14), $s(GOF)$ = 1.034. Crystals of **2a** were mounted on glass fibers with epoxy, and diffraction data was collected on a Siemens P4 four-circle diffractometer equipped with a sealed molybdenum tube, which was monochromated to give λ = 0.71073 Å. The structure was solved by using direct methods and refined by using full-matrix least-squares on F^2 with SHELXTL. All non-hydrogen atoms were refined anisotropically with element assignments as described in the text. CCDC-174994 (**2a**) contains the supplementary crystallographic data for this paper. These data can be obtained free of charge via www.ccdc.cam.ac.uk/conts/retrieving.html (or from the Cambridge Crystallographic Data Centre, 12, Union Road, Cambridge CB2 1EZ, UK; fax: (+44) 1223-336-033; or deposit@ccdc.cam.ac.uk).

Theoretical calculations: Ground and transition state optimizations were performed with Gaussian98. The energies of **A**, **B**, and **C** are −677.1544, −677.1231, and −677.1522 Hartrees, respectively. Ground-state geometries and important metric parameters are collected in the Supporting Information.

Received: December 5, 2001
Revised: February 26, 2002 [Z 18330]

[1] W. Traube, *Ber. Dtsch. Chem. Ges.* **1894**, *27*, 1507.
[2] W. Traube, *Ber. Dtsch. Chem. Ges.* **1894**, *27*, 3291.
[3] W. Traube, *Ber. Dtsch. Chem. Ges.* **1895**, *28*, 1785.
[4] W. Traube, *Justus Liebigs Ann. Chem.* **1898**, *300*, 81.
[5] R. A. Moss, M. J. Landon, K. M. Luchter, A. Mamantov, *J. Am. Chem. Soc.* **1972**, *94*, 4392.
[6] A. Hantzsch, M. Lehmann, *Chem. Ber.* **1902**, *35*, 897.
[7] S. Pfeiffer, B. Mayer, B. Hemmens, *Angew. Chem.* **1999**, *111*, 1824; *Angew. Chem. Int. Ed.* **1999**, *38*, 1714.
[8] J. E. Saavedra, T. M. Dunams, J. L. Flippen-Anderson, L. K. Keefer, *J. Org. Chem.* **1992**, *57*, 6134.
[9] L. K. Keefer, J. L. Flippen-Anderson, C. George, A. P. Shanklin, T. M. Dunams, D. Christodoulou, J. E. Saavedra, E. S. Sagan, D. S. Bohle, *Nitric Oxide: Biol. Chem.* **2001**, *5*, 377.
[10] L. Grossi, S. Strazzari, *J. Org. Chem.* **1999**, *64*, 8076.
[11] D. S. Bohle, J. A. Imonigie, *J. Org. Chem.* **2000**, *65*, 5685.
[12] N. Arulsamy, D. S. Bohle, *J. Am. Chem. Soc.* **2001**, *123*, 10 860.
[13] Evidence for an *E*-ONNO geometry in a separate system has recently been found: L. K. Keffer, personal communication.
[14] C. Peng, H. B. Schlegel, *Isr. J. Chem.* **1994**, *33*, 449.
[15] C. Peng, P. Y. Ayala, H. B. Schlegel, M. J. Frisch, *J. Comp. Chem.* **1996**, *17*, 49.
[16] A. B. Nelson, *Diss. Abstr. Int. B* **1977**, *38*, 1721.
[17] F. R. Fronczek, V. K. Gupta, G. R. Newkome, *Acta Crystallogr. Sect. C* **1983**, *39*, 1113.
[18] R. B. Woodward, C. Wintner, *Tetrahedron Lett.* **1969**, 2689.

 © WILEY-VCH Verlag GmbH, 69451 Weinheim, Germany, 2002 1433-7851/02/4112-2091 $ 20.00+.50/0

Orbital Interactions in Strong and Weak Hydrogen Bonds are Essential for DNA Replication**

Célia Fonseca Guerra and F. Matthias Bickelhaupt*

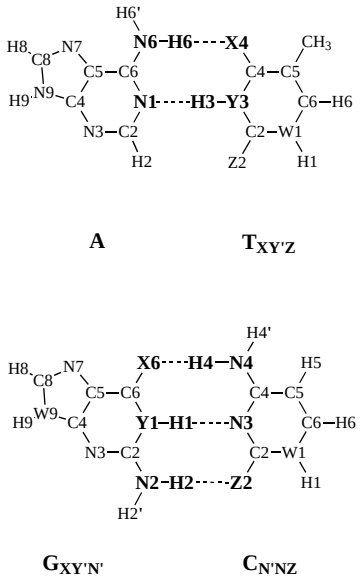
Dedicated to Professor Friedrich Bickelhaupt on the occasion of his 70th birthday

Based on a series of elegant experiments, Kool and coworkers[1] concluded that *not* Watson–Crick hydrogen bonding but steric effects, that is, the shape of DNA bases is mainly responsible for the high fidelity of DNA replication. They showed, amongst others, that 2,4-difluorotoluene (F), an isoster of thymine (T), encodes in a template strand the DNA-polymerase-catalyzed insertion of deoxyadenosine triphosphate (dATP) and that adenine (A) encodes the insertion of the deoxynucleoside triphosphate of difluorotoluene (dFTP), in spite of the supposed apolarity and the absence of hydrogen-bonding ability in F.

The above conclusion has led to a controversy in which experimental[1, 2] and theoretical[3] arguments are raised both against and in favor of the standard model[4] that reserves a key role for Watson–Crick hydrogen bonds in DNA replication. Evans and Seddon,[3a] in particular, pointed out that, according to ab initio calculations, 2,4-difluorotoluene is not apolar and thus capable of acting as a hydrogen-bond donor and acceptor. Consequently, they concluded that Kool's experiments confirm the standard model.

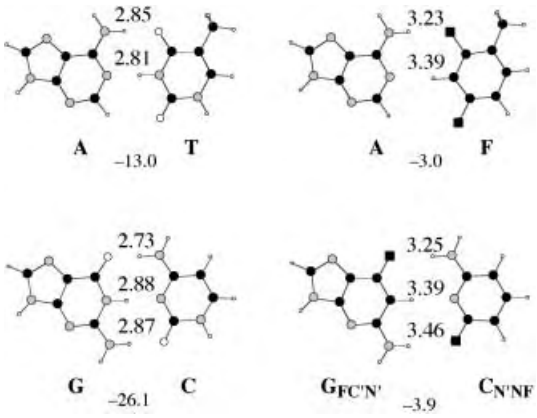
Herein, we present arguments for a third model in which steric effects and hydrogen bonding are both essential for and go hand-in-hand in high-fidelity DNA replication. An important point is that the net bond strength is insufficient for characterizing a hydrogen bond and that understanding and predicting its role and behavior requires knowledge of the different components of the bonding mechanism. In particular, it appears that covalent bonding (i.e., charge-transfer or donor–acceptor-orbital interactions) makes a significant contribution to the stability not only of the natural base pairs,[5a,b] but even to that of pairs held together by weak hydrogen bonds, such as AF.

Our evidence is based on a thorough Kohn–Sham density functional theory (DFT) investigation at BP86/TZ2P with the ADF program[6] of AT and GC (G = guanin, C = cytosin) Watson–Crick pairs and mimics thereof in which C=O and N–H bonds have been replaced by C–F and C–H (see Scheme 1). We wish to emphasize that, although seemingly a one-electron or molecular orbital (MO) model, Kohn–Sham DFT yields, in principle, exact and, in practice, with the available functionals, rather accurate energies that do take into account electron correlation and related effects, such as dispersion.[7] It is known that the BP86/TZ2P level of theory adequately describes hydrogen bonds in gas-phase and microsolvated AT and GC pairs, but also the weaker hydrogen bond between two water molecules.[5a,c]



Scheme 1. Model systems of this investigation: AT and GC Watson–Crick pairs and mimics thereof in which C=O and N–H bonds in T, G, and C have been replaced by C–F and C–H bonds (X, Z = O, F, H; W, Y = N, C).

The base-pairing energy ΔE (at 0 K) for AF (-3.0 kcal mol^{-1}) is about four-times smaller than for AT (-13.0 kcal mol^{-1}) and that the hydrogen bonds in AF are 0.4–0.6 Å longer than in AT (Scheme 2), in good agreement with other theoretical studies.[3e,g] These results raise a number of questions: 1) is F really an isoster of T if it leads to such enormous changes in the geometry relative to the Watson–Crick pair? 2) Is the A–F interaction predominantly electrostatic as one would expect for weak hydrogen bonds[8] or does it contain a sizable covalent component as has been found for the stronger hydrogen bonds in AT?[5a,b] 3) How important are hydrogen bonds for accurate DNA replication?



Scheme 2. N6–X4 and N1–Y3 distances [Å] in AT and AF and X6–N4, Y1–N3, and N2–Z2 distances in GC and $G_{FC'N'}C_{N'NF}$ obtained at the BP86/TZ2P level (see also Scheme 1).

[*] Dr. F. M. Bickelhaupt, Dr. C. Fonseca Guerra
Afdeling Theoretische Chemie
Scheikundig Laboratorium der Vrije Universiteit
De Boelelaan 1083, 1081 HV Amsterdam (The Netherlands)
Fax: (+31) 20-4447-629
E-mail: bickel@chem.vu.nl

[**] We thank the National Research School Combination—Catalysis (NRSCC) for a postdoctoral fellowship for C.F.G. and the National Computer Facilities (NCF) foundation of the Netherlands Organization for Scientific Research (NWO) for financial support.

 © WILEY-VCH Verlag GmbH, 69451 Weinheim, Germany, 2002 1433-7851/02/4112-2092 $ 20.00+.50/0

For answering the first of these questions, one must realize that steric shape or, in other words, the forces that cause steric repulsion have their origin in the quantum-mechanical effect of Pauli (and *not* electrostatic!) repulsion between the charge distributions of the two fragments.[7] Thus, making use of the conceptual framework provided by Kohn–Sham MO theory, we have decomposed the actual interaction energy (ΔE_{int}) into three physically well-defined terms: the Pauli repulsive orbital interactions between closed shells (ΔE_{Pauli}), the classical electrostatic interaction (ΔV_{elst}), and the attractive orbital interactions (ΔE_{oi}), that is, $\Delta E_{int} = \Delta E_{Pauli} + \Delta V_{elst} + \Delta E_{oi}$.[7] The results are summarized in Table 1. The orbital interactions ΔE_{oi} comprise the often distinguished attractive contributions, charge transfer, polarization (induction), and dispersion. Whether or with what precision these contributions can be quantified remains a controversial subject and we refrain from further decomposition, except by symmetry. However, we have observed that the orbital interactions in the σ-electron systems of Watson–Crick base pairs and mimics thereof are mostly of the donor–acceptor type (see below and refs. [5a,b]), and we feel it is therefore justified to denote the attractive orbital-interaction term as a covalent (or charge-transfer) contribution, as opposed to the contributions of electrostatic attraction and Pauli repulsion.

Table 1. Decomposition of base-pairing interaction energies ΔE_{int} [kcal mol^{-1}] from Kohn–Sham DFT analyses at the BP86/TZ2P level.[a]

	AF	AF*	AT	AB*
ΔE_{Pauli}	7.8	41.5	38.7	36.7
ΔV_{elst}	−7.0	−22.6	−31.8	−15.5
ΔE_{oi}	−4.0	−16.0	−22.1	−12.0
ΔE_{int}	−3.2	2.9	−15.2	9.2

[a] $\Delta E_{int} = \Delta E_{Pauli} + \Delta V_{elst} + \Delta E_{oi}$ (see text and ref. [7]). The data for AT and AF comes from equilibrium structures. In AF* and AB*, hydrogen bonds have been compressed to the equilibrium distances of AT.

The bond analyses nicely confirm that F is indeed an isoster of T. This is, however, not immediately clear if one examines only the equilibrium structure of AF. Because of the reduced bonding capabilities of F (see above), AF achieves a geometry optimum at much longer hydrogen-bond lengths than AT (Scheme 2). This situation causes all bonding components, including ΔE_{Pauli}, to be much smaller in AF: ΔE_{Pauli}, ΔV_{elst}, and ΔE_{oi} are 7.8, −7.0, and −4.0 kcal mol^{-1} in AF and 38.7, −31.8, and −22.1 kcal mol^{-1} in AT (Table 1). Kool and coworkers have provided strong evidence that the polymerase-catalyzed DNA replication involves a relatively tight active site that requires the new pair formed between template base and incoming base to conform to the Watson–Crick geometry.[1, 9] Thus, proceeding from Kool's model,[1] we have compressed AF to a geometry AF* in which the N6-H6···F4 and N1···H3-C3 hydrogen-bond distances adopt the values of the corresponding bonds in the equilibrium structure of AT, namely, 2.85 and 2.81 Å. The A–F interaction ΔE_{int} in AF* is repulsive by 2.9 kcal mol^{-1}, and ΔE_{Pauli}, ΔV_{elst}, and ΔE_{oi} are 41.5, −22.6, and −16.0 kcal mol^{-1} (Table 1). Note that the Pauli repulsion in AF* is only 2.8 kcal mol^{-1} higher than in AT and that the large difference in base-pairing energy ΔE (where $\Delta E = \Delta E_{prep} + \Delta E_{int}$; ΔE_{prep} = deformation energy) is because of a combined reduction of electrostatic and attractive orbital interactions of 15.3 kcal mol^{-1}. Thus, the forces causing the repulsive wall on the potential-energy surface are similar for AT and AF, and 2,4-difluorotoluene is a true isoster of thymine.

Next, we address the question about the nature of the A–F interaction. Unexpectedly, we find that the bonding orbital interactions in AF are of the same order of magnitude as the electrostatic attraction, that is, 36% and 64% of the total bonding interaction $\Delta E_{oi} + \Delta V_{elst}$ (Table 1). Figure 1 shows the relevant frontier-orbital interactions for AT and AF that emerge from our Kohn–Sham MO analyses. It appears that, analogous to the situation for AT,[5a,b] the ΔE_{oi} term in the A–F interaction has a significant amount of covalent character which is provided by charge transfer, that is, donor–acceptor orbital interactions in the σ-electron system between a lone pair on the fluorine atom in F and the N–H σ*-acceptor orbitals in A and between a lone pair on the nitrogen atom in A and the C–H σ*-acceptor orbitals in F. The hydrogen bonds

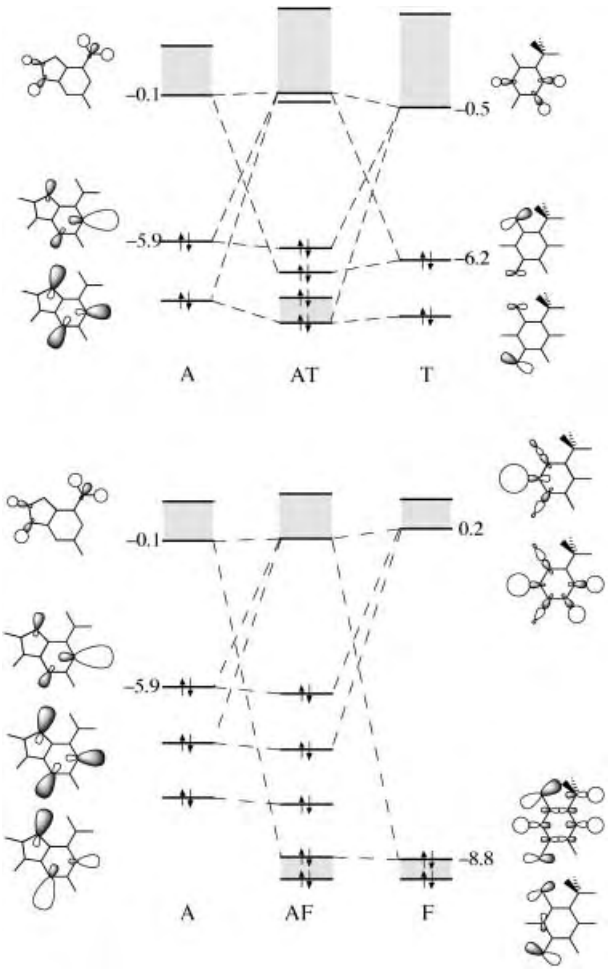


Figure 1. Frontier-orbital interactions (in the σ-electron system) between adenine and thymine in AT and between adenine and difluorotoluene in AF from Kohn–Sham DFT analyses at the BP86/TZ2P level, with HOMO and LUMO energies [eV] of the individual bases. The group of lowest unoccupied orbitals involved is represented as a gray block.

 © WILEY-VCH Verlag GmbH, 69451 Weinheim, Germany, 2002 1433-7851/02/4112-2093 $ 20.00+.50/0

in AF are weaker than in AT not only because of less electrostatic attraction ΔV_{elst} but also because of reduced orbital interactions ΔE_{oi}. The latter are weaker in AF because, compared to T, the electron-donor and -acceptor orbitals of F are lower and higher in energy, respectively, which leads to a larger orbital energy gap with the partner orbitals on A (Figure 1).

Additional support for charge transfer comes from an analysis of the redistribution of charge density caused by the interaction between two DNA bases by using the Voronoi deformation density (VDD) method.[5b, 10] In AF, the donor–acceptor interactions associated with charge transfer from A→F through the hydrogen bond N1···H-C3 are stronger than those back from F→A through the hydrogen bond N6-H···F4 leading overall to a small, negative charge of −0.004 electrons on F. All the charge transfer occurs in the σ-electron system. The π-electron systems of A and F polarize such that the accumulation of positive or negative charge around the donating or accepting atoms, caused by the charge transfer in the σ-electron system, is counteracted and partly relieved.

The base-pairing interaction in AF is not an isolated example of the importance of orbital interactions in weak hydrogen bonds, there are more cases. We have analyzed a variety of Watson–Crick base pairs, mimics, mismatches, and hydrogen-bonded molecular crystals. Figure 2, shows the

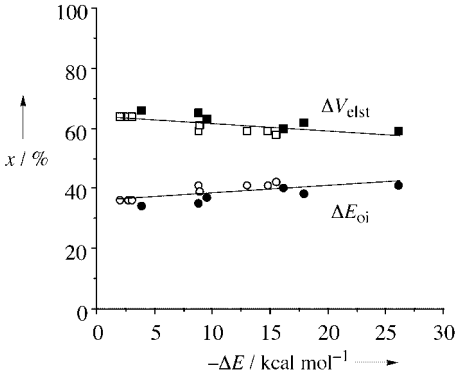


Figure 2. Relative contribution x (in % of $\Delta V_{elst} + \Delta E_{oi}$) of orbital interactions (ΔE_{oi}, circles) and electrostatic attraction (ΔV_{elst}, squares) as a function of the overall bond energy ΔE of AT (white) and GC (black) and the corresponding mimics thereof.

relative contribution of the orbital-interaction term ΔE_{oi} in the hydrogen bonds of AT, GC, and artificial mimics thereof as a function of the base-pairing energy ΔE. For the stronger hydrogen bonds ($\Delta E = -26$ kcal mol^{-1} Figure 2, right), the orbital interaction term ΔE_{oi}, which is responsible for any covalent character, contributes around 40% of the total attractive interactions ($\Delta V_{elst} + \Delta E_{oi}$). As hydrogen bonding becomes weaker (ΔE decreases from −26 to −2 kcal mol^{-1} in Figure 2), the orbital-interaction term decreases only slightly, and it is never less than one third of the total attractive interaction.

Finally, from the importance of steric factors and our analyses, it follows that hydrogen bonding also plays a key role in DNA replication. Steric factors require that the DNA bases fit into the active site of DNA polymerase, causing steric repulsion and thus a high overall activation energy for the insertion if an incoming nucleotide is too large. Base pairs of the right shape do fit into the active site without much repulsion and, therefore, with a low barrier for insertion. However, the transition state is also significantly stabilized by the Watson–Crick interaction in AT and GC, the binding energies ΔE of which are −13.0 and −26.1 kcal mol^{-1}, respectively, at 0 K (not shown in Table 1). We have shown previously[5a,c] that this intrinsic base-pairing interaction ΔE_{int} is basically affected neither by microsolvation of the major and minor grooves nor by formation of a DNA oligomer consisting of two stacked base pairs. Thus, if, for what ever reason, the bases cannot adopt the Watson–Crick geometry in the active site of the polymerase, this stabilizing interaction is lost, causing a sizable increase of the overall barrier for insertion.

But a similar argument holds true also for the formation of an AF pair: without hydrogen bonding, the barrier for this process would be restrictively high. This situation is not clear at first sight, if we just consider the *net* hydrogen-bond interaction ΔE_{int}, in AF* which is slightly repulsive (2.9 kcal mol^{-1}) and thus not stabilizing. The importance of hydrogen bonding becomes clear if one realizes that the net interaction would increase much more strongly in AF* in the absence of the underlying electrostatic attraction (−22.6 kcal mol^{-1}) and covalent orbital interactions (−16.0 kcal mol^{-1}, Table 1). Loss of the latter, for example, would raise the overall barrier for the formation of a new base pair by 16.0 kcal mol^{-1}. Note at this point that we compute the effect of the intrinsic base-pairing interaction (and its components ΔE_{oi}, ΔV_{elst}, ΔE_{Pauli}) on the barrier but not the barrier height as such. The latter depends, of course, on various other factors, such as solvent effects, stacking interactions, and the barrier associated with the nucleophilic substitution involved in the process of elongating the primer strand.[4]

In practice, it is of course difficult to switch off the orbital interactions completely, but they can be further reduced if 2,4-difluorotoluene is replaced, for example, by toluene (B). The planar, C_s-symmetric AB pair (Scheme 1, left: X, Z = H and Y, W = C) is practically unbound. To simulate again a tight DNA-polymerase active site as proposed by Kool,[1] we have compressed the AB pair to a geometry AB* in which the N6-H6···H4 and N1···H3-C3 hydrogen-bond lengths are of the same length as the corresponding bonds in the equilibrium structure of AT. The net base-pairing interaction ΔE in AB* (9.2 kcal mol^{-1}) becomes substantially more repulsive than in AF* (2.9 kcal mol^{-1}) because of a significant decrease of both the orbital interactions ΔE_{oi} and electrostatic attraction ΔV_{elst} (by a factor of 2 if compared to AT!).

Our results support aspects of both Kool's steric model of DNA replication[1] and the standard model that is based on hydrogen bonding[3a, 4] and lead to a coupling between these two models. They show that electrostatic and orbital interactions between DNA bases can also reduce the overall barrier for insertion of a nucleotide if the net hydrogen-bond strength is weak or even moderately repulsive. But our results do not rule out the possibility of this barrier being low for other reasons, for example, favorable solvent effects or

 © WILEY-VCH Verlag GmbH, 69451 Weinheim, Germany, 2002 1433-7851/02/4112-2094 $ 20.00+.50/0

stacking interactions.[11] In fact, it is plausible that one or more of these factors may be active in achieving efficient and selective replication. Full details will be published elsewhere.

Received: October 12, 2001
Revised: February 21, 2002 [Z18052]

[1] a) E. T. Kool, J. C. Morales, K. M. Guckian, *Angew. Chem.* **2000**, *112*, 1046; *Angew. Chem. Int. Ed.* **2000**, *39*, 990; b) K. M. Guckian, T. R. Krugh, E. T. Kool, *Nat. Struct. Biol.* **1998**, *5*, 954; c) J. C. Morales, E. T. Kool, *Nat. Struct. Biol.* **1998**, *5*, 950; d) K. M. Guckian, E. T. Kool, *Angew. Chem.* **1997**, *109*, 2942; *Angew. Chem. Int. Ed.* **1997**, *36*, 2825; e) S. Moran, R. X.-F. Ren, S. Rumney IV, E. T. Kool, *J. Am. Chem. Soc.* **1997**, *119*, 2056; f) B. A. Schweitzer, E. T. Kool, *J. Am. Chem. Soc.* **1995**, *117*, 1863; see also: g) U. Diederichsen, *Angew. Chem.* **1998**, *110*, 1745; *Angew. Chem. Int. Ed.* **1998**, *37*, 1655.

[2] K. S. Schmidt, R. K. O. Sigel, D. V. Filippov, G. A. van der Marel, B. Lippert, J. Reedijk, *New J. Chem.* **2000**, *24*, 195.

[3] a) T. A. Evans, K. R. Seddon, *Chem. Commun.* **1997**, 2023; b) X. Wang, K. N. Houk, *Chem. Commun.* **1999**, 2631; c) D. Barsky, E. T. Kool, M. E. Colvin, *J. Biomol. Struct. Dyn.* **1999**, *16*, 1119; d) B. D. Silverman, M. C. Pitman, D. E. Platt, *J. Biomol. Struct. Dyn.* **1999**, *16*, 1169; e) F. Ryjácek, M. Kratochvíl, P. Hobza, *Chem. Phys. Lett.* **1999**, *313*, 393; f) C. Santhosh, P. C. Mishra, *Int. J. Quantum Chem.* **1998**, *68*, 351; g) M. Meyer, J. Sühnel, *J. Biomol. Struct. Dyn.* **1997**, *15*, 619.

[4] L. Stryer, *Biochemistry*, W. H. Freeman and Company, New York, **1988**.

[5] a) C. Fonseca Guerra, F. M. Bickelhaupt, *Angew. Chem.* **1999**, *111*, 3120; *Angew. Chem. Int. Ed.* **1999**, *38*, 2942; b) C. Fonseca Guerra, F. M. Bickelhaupt, J. G. Snijders, E. J. Baerends, *Chem. Eur. J.* **1999**, *5*, 3581; c) C. Fonseca Guerra, F. M. Bickelhaupt, J. G. Snijders, E. J. Baerends, *J. Am. Chem. Soc.* **2000**, *122*, 4117.

[6] a) G. te Velde, F. M. Bickelhaupt, S. J. A. van Gisbergen, C. Fonseca Guerra, E. J. Baerends, J. G. Snijders, T. Ziegler, *J. Comput. Chem.* **2001**, *22*, 931; b) C. Fonseca Guerra, J. G. Snijders, G. te Velde, E. J. Baerends, *Theor. Chem. Acc.* **1998**, *99*, 391.

[7] F. M. Bickelhaupt, E. J. Baerends in *Reviews in Computational Chemistry Vol. 15* (Eds.: K. B. Lipkowitz, D. B. Boyd), Wiley-VCH, New York, **2000**, pp. 1–86.

[8] a) G. R. Desiraju, T. Steiner, *The Weak Hydrogen Bond*, Oxford University Press, Oxford, **1999**; b) G. A. Jeffrey, *An Introduction to Hydrogen bonding*, Oxford University Press, New York, Oxford, **1997**; c) see also T. Steiner, *Angew. Chem.* **2002**, *114*, 50–80; *Angew. Chem. Int. Ed.* **2002**, *41*, 48–76.

[9] The steric demands of the DNA-polymerase active site are less stringent for the sugar moieties, as shown by D. Summerer, A. Marx, *Angew. Chem.* **2001**, *113*, 3806; *Angew. Chem. Int. Ed.* **2001**, *40*, 3693.

[10] F. M. Bickelhaupt, N. J. R. van Eikema Hommes, C. Fonseca Guerra, E. J. Baerends, *Organometallics* **1996**, *15*, 2923.

[11] Experiments suggest indeed that hydrophobicity, for example, may also be a sufficient driving force for selective replication: a) D. L. McMinn, A. K. Ogawa, Y. Wu, J. Liu, P. G. Schultz, F. E. Romesberg, *J. Am. Chem. Soc.* **1999**, *121*, 11585; b) M. Berger, A. K. Ogawa, D. L. McMinn, Y. Wu, P. G. Schultz, F. E. Romesberg, *Angew. Chem.* **2000**, *112*, 3069; *Angew. Chem. Int. Ed.* **2000**, *39*, 2940.

$[\{Li(thf)_3\}_2Ga_2\{As(Si\mathit{i}Pr_3)\}_4]$—A Compound with Gallium–Arsenic Double Bonds**

Carsten von Hänisch* and Oliver Hampe

The synthesis of molecular compounds with multiple bonds between the heavier main-group elements is still a preparative challenge for the inorganic chemist. While various symmetric compounds with multiple bonds between two heavier atoms of Group 13 or 15 were synthesized in the last years,[1–3] most of the asymmetric compounds with multiple bonds between Group 13 and 15 elements contain one atom of the 2nd period of the periodic table.[3] Power and co-workers recently published compounds with aluminum– or gallium–nitrogen multiple bonds,[4] and compounds with boron–phosphorus and boron–arsenic double bonds $[Mes_2B{=}ER\{Li(thf)_3\}]$ (**1a**: E = P, R = $SiMe_3$; **1b**: E = As, R = Ph; Mes = mesityl) have also been described.[5] Partial multiple-bond character between the heavier elements of Group 13 and 15, however, can be observed in the ternary phases $Cs_6M_2E_4$ (M = Al, Ga; E = P, As) or in the molecular compounds $[t\mathrm{Bu}_2\mathrm{GaPMes}^*(\mathrm{SiPh}_3)]$ and $[\mathrm{MesP}\{\mathrm{Ga(Trip)}_2\}_2]$ (Trip = 2,4,6-$i\mathrm{Pr}_3\mathrm{C}_6\mathrm{H}_2$; Mes* = 2,4,6-$t\mathrm{Bu}_3\mathrm{C}_6\mathrm{H}_2$).[6, 7] In contrast, multiple bonding between the heavier Group 13 and 15 elements can be excluded in the cyclic compounds $[RMER']_n$ (M = Al, Ga; E = P, As; R, R′ = alkyl, aryl; $n = 2$, 3), because of the ring folding and the pyramidal coordination of the phosphorus and arsenic atoms.[8] Molecular compounds with double bonds between gallium and arsenic are unknown to date.

We could synthesize the compound $[\{Li(thf)_3\}_2Ga_2\{As(Si\mathit{i}Pr_3)\}_4]$ (**2**) containing two As–Ga double bonds from the reaction of $GaCl_3$ with $Li_2AsSi\mathit{i}Pr_3$ [Eq. (1)].

$$2\,GaCl_3 + 4\,Li_2AsSi\mathit{i}Pr_3 \xrightarrow{\text{THF/heptane}} [\{Li(thf)_3\}_2Ga_2\{As(Si\mathit{i}Pr_3)\}_4]\ (\mathbf{2}) + 6\,LiCl \quad (1)$$

Compound **2** crystallizes in the monoclinic space group $P2_1/n$ with two formula units per unit cell (Figure 1).[9] The central structural motive of **2** is a planar Ga_2As_2 four-membered ring with two further exocyclic As atoms bound to the Ga atoms. Each As atom is bonded to a tri(isopropyl)silyl group and each of the exocyclic As atoms is additionally bound to one $Li(thf)_3$ fragment.

The angular sum at the Ga atoms comes to 359.8(1)° thus, the coordination of these atoms is essentially trigonally planar. However, the As-Ga-As angles differ, the endocyclic As(1)-Ga-As(1′) angle is 98.36(3)°, and the As(1)-Ga-As(2) and As(1′)-Ga-As(2) angles are 121.51(4) and 139.90(4)°, respectively. The considerable difference between the exocyclic angles can be explained by the mutual repulsion of the neighboring $i\mathrm{Pr}_3\mathrm{Si}$ groups on As(1′) and As(2). The Li–As

[*] Dr. C. von Hänisch, Dr. O. Hampe
Institut für Nanotechnologie
Forschungszentrum Karlsruhe
Postfach 3640, 76021 Karlsruhe (Germany)
Fax: (+49) 7247-82-6368
E-mail: carsten.vonhaenisch@int.fzk.de

[**] This work was supported by the Strategiefond of the Helmholtz Foundation. We thank Dr. P. Kramkowski for his valuable help with the translation.

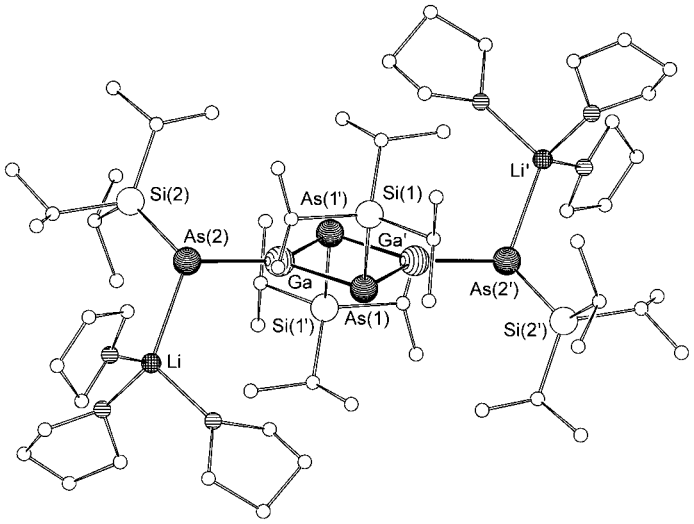


Figure 1. Molecular structure of **2**, selected bond lengths [pm] and bond angles [°]: Ga-As(1) 247.3(1), Ga-As(1′) 243.6(1), Ga-As(2): 231.8(1), As(1)-Si(1) 235.1(2), As(2)-Si(2) 231.3(2), As(2)-Li 260.6(2), Li-O 192.3(13) – 200.6(15); As(1)-Ga-As(1′) 98.36(3), As(1)-Ga-As(2) 121.51(4), As(1′)-Ga-As(2) 139.90(4), Si(1)-As(1)-Ga 103.34(6), Si(1)-As(1)-Ga′ 110.45(6), Ga-As(1)-Ga′ 81.64(3), Si(2)-As(2)-Ga 107.99(6), Si(2)-As(2)-Li 121.4(3), Ga-As(2)-Li 113.8(3).

bond length (260.6(2) pm) which is slightly shorter than in **1b** (267.0(9) pm) and similar to the Li–As distance in [{(dme)-LiAs(SiMe$_3$)$_2$}$_2$] (259(2) pm; dme = 1,2-dimethoxyethane). In the latter compound the As atoms have a coordination number of four and the Li atoms are in bridging positions.[10]

Because of the electron deficiency at the Ga atoms and the lone pair at the arsenic centers the resonance structures **A** and **B** appear plausible for **2** (Figure 2). Whereas dative (p – p) π bonds in the Ga_2As_2 ring appear impossible because of the

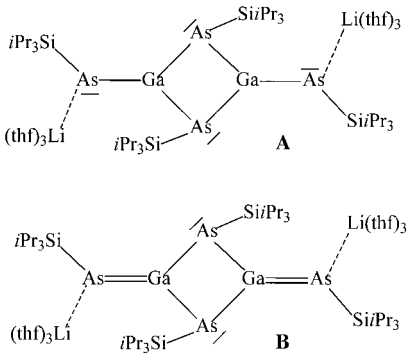


Figure 2. Resonance structures of **2**.

pyramidal coordination at As(1) and As(1′) (the angular sum at these atoms is 295.4(2)°). This situation is further reflected in the As(1)–Ga bond length of 245.5 pm (mean) which is at the lower end of the range for Ga–As single bonds (243 – 260 pm).[11] In contrast the As(2)–Ga bond is only 231.8 pm long. The angular sum at As(2) is with 343.2(1)° remarkably large and the As(1′)-Ga-As(2)-Si(2) torsion angle is only 14.6°. These values are in good agreement with the assumption of a dative (p – p) π overlap (resonance formula **B**). In **1a** the torsion angle for example is 23.15°, in **1b** the angular sum at the As atom is 341.4°.[5] The As – Li vector in **2** as well as in **1b** points out of the molecule plane; however, it has to be considered that the Li – As interaction is mainly of electrostatic nature. This ionic nature of the bond between the arsenic and the lithium atom is further confirmed by theoretical investigations of the similar boron – phosphors compound $H_2B{=}PHLi$.[12]

Ionic interactions between the negatively polarized As atom and the positively polarized gallium center have to be considered, too (resonance formula **A**). However, the observed drastic bond shortening can not be explained by these interactions alone. Overall the bonding description of **2** is closer to resonance form **B** than to form **A**. The sterically demanding and electropositive Si and Li substituents on As(2) facilitate this Ga–As π bonding by reducing the inversion barrier at the exocyclic As atoms.

Compound **2** can be formally separated into a $[Ga_2(AsSi\mathit{i}Pr_3)_4]^{2-}$ ion and two $[Li(thf)_3]^+$ ions. To support this ionic picture we performed electrospray mass spectrometry[13] and obtained the mass spectrum shown in Figure 3 upon adding a small amount of [12]crown-4 (probably acting as an Li^+-ion scavenger) to a THF solution of **2**. All the peaks

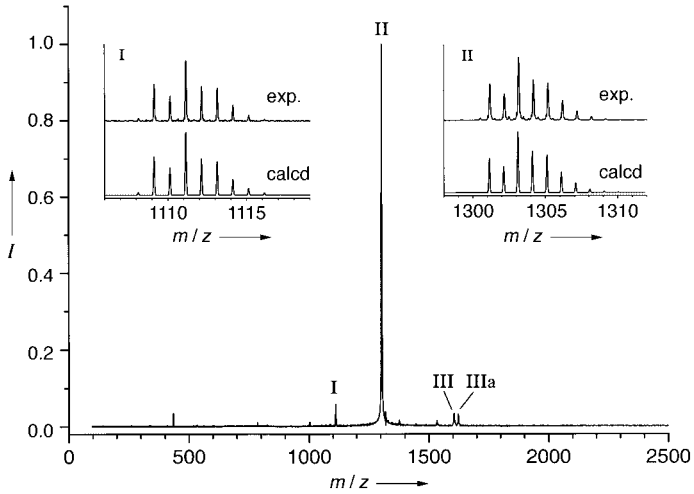


Figure 3. Negative-ion electrospray FT-mass spectrum of **2** (Insets: Comparison of experimentally observed and simulated isotope patterns).

observed in the mass spectrum were assigned as in Table 1. All the ion peaks are consistent with the picture that the ion $[Ga_2(AsSi\mathit{i}Pr_3)_4]^{2-}$ is unstable and undergoes rapid intermolecular reactions as well as partial hydrolysis with traces of water (possibly from the extremely hygroscopic crown ether). The most prominent ion peak corresponds to the singly charged $[Ga_2(AsSi\mathit{i}Pr_3)_5H_3]^-$ ion (peak II) around *m*/*z* 1303. Interestingly, the presence of peaks III and IIIa suggests the

Table 1. Assignment of negative ion mass peaks.

Peak	*m*/*z* found	*m*/*z* calcd	Ion
I	1111.14	1111.15	$[Ga_2Li(AsSi\mathit{i}Pr_3)_4H_4O_2]^-$
II	1303.18	1303.18	$[Ga_2(AsSi\mathit{i}Pr_3)_5H_3]^-$
III	1605.21	1605.16	$[Ga_3(AsSi\mathit{i}Pr_3)_6H_2]^-$
IIIa	1623.19	1623.17	$[Ga_3(AsSi\mathit{i}Pr_3)_6H_4O)]^-$

 © WILEY-VCH Verlag GmbH, 69451 Weinheim, Germany, 2002 1433-7851/02/4112-2096 $ 20.00+.50/0 *Angew. Chem. Int. Ed.* **2002**, *41*, No. 12

formation of a higher aggregate possibly with a spiro-like Ga_3As_6 unit with two four-membered rings connected by one central Ga atom.

The $[Ga_2(AsSi\mathit{i}Pr_3)_4]^{2-}$ ion shows a structural relationship with the Zintl ion $[Ga_2As_4]^{6-}$, which is contained in the ternary phase $Cs_6Ga_2As_4$.[6] This anion also has the shape of a Ga_2As_2 four-membered ring with two further exocyclic As atoms bonded to the Ga atoms. The exocyclic As–Ga bonds of the $[Ga_2As_4]^{6-}$ ions are 234.3 pm long, which is much shorter than usual for As–Ga single bonds, and suggests multiple-bond character. Because of the particular coordination numbers and conditions in this solid-state Zintl phase a comparison with the bonding situation in **2** is impossible. However, the $[Ga_2(AsSi\mathit{i}Pr_3)_4]^{2-}$ ion in **2** can be seen as a silyl derivative of the $[Ga_2As_4]^{6-}$ ion. Thus, **2** can be regarded as the first example of a silylated binary Zintl anion. So far only silylated Zintl anions of phosphorus and $[As_7(SiMe_3)_3]$ have been reported.[14]

Experimental Section

2: A butyllithium solution (1.6 M; 3.55 mL, 5.68 mmol) was added to a solution of $H_2AsSi\mathit{i}Pr_3$ (0.66 g, 2.84 mmol)[15] in THF (5 mL) of at 0 °C. After stirring for 1 h, this solution was added to a −50 °C solution of $GaCl_3$ (0.25 g, 1.42 mmol; 99.99 %) in heptane (20 mL). The reaction mixture was allowed to warm to room temperature and then stirred for additional 24 h. The resulting red solution was filtered to remove the precipitated LiCl. Subsequently this solution was reduced to about 10 mL in vacuo. After two days large orange crystals of **2** formed. Yield: 0.37 g (34 %); elemental analysis (%) calcd for $C_{60}H_{132}As_4Ga_2Li_2O_6Si_4$ (1515.0): C 47.57, H 8.78; found: C 45.77, H 8.24; ^{1}H NMR ([D$_6$]benzene): $\delta = 3.720$ (m, 12 H, $(CH_2CH_2)_2O$), 1.593 (m, 21 H, *i*Pr) 1.540 (m, 12 H, $(CH_2CH_2)_2O$), 1.449 pm (m, 21 H, *i*Pr); ^{13}C{^{1}H} NMR ([D$_6$]benzene): $\delta = 68.7$ (s, $(CH_2CH_2)_2O$), 25.7 (s, $(CH_2CH_2)_2O$), 21.3 (s, CH_3), 20.5 (s, CH_3), 16.5 (s, *C*H), 15.6 pm (s, *C*H); ^{29}Si{^{1}H} NMR ([D$_6$]benzene): $\delta = 26.7$ pm (br); UV/Vis (suspension in mineral oil): $\lambda_{max} = 410$ nm (sh), 270 nm.

ESI-FTMS: Mass spectra were taken in a Fourier-Transform Ion Cyclotron Resonance Mass Spectrometer (Bruker Daltonics, APEX II) equipped with an electrospray source (Analytica of Branford).

Received: November 30, 2001 [Z18304]

[1] Review articles: a) A. H. Cowley, *Acc. Chem. Res.* **1984**, *17*, 386–392; b) G. Trinquier, *J. Am. Chem. Soc.* **1990**, *112*, 2130–2137; c) M. Driess, H. Grützmacher, *Angew. Chem.* **1996**, *108*, 900–929; *Angew. Chem. Int. Ed. Engl.* **1996**, *35*, 828–857.

[2] a) J. Su, X.-W. Li, R. C. Robinson, *J. Am. Chem. Soc.* **1997**, *119*, 5471–5472; b) R. J. Wehmschulte, P. P. Power, *Angew. Chem.* **1998**, *110*, 3344–3346; *Angew. Chem. Int. Ed.* **1998**, *37*, 3152–3154; c) S. Loss, C. Widauer, H. Grützmacher, *Angew. Chem.* **1999**, *111*, 3546–3548; *Angew. Chem. Int. Ed.* **1999**, *38*, 3329–3331; d) B. Twamley, P. P. Power, *Angew. Chem.* **2000**, *112*, 3643–3646; *Angew. Chem. Int. Ed.* **2000**, *39*, 3500–3503.

[3] P. P. Power, *Chem. Rev.* **1999**, *99*, 3463–3503.

[4] N. J. Hardman, C. Cui, H. W. Roesky, W. H. Fink, P. P. Power, *Angew. Chem.* **2001**, *113*, 2230–2232; *Angew. Chem. Int. Ed.* **2001**, *40*, 2172–2174.

[5] a) R. A. Bartlett, H. V. R. Dias, X. Feng, P. P. Power, *J. Am. Chem. Soc.* **1989**, *111*, 1306–1311; b) M. A. Petrie, S. C. Shoner, H. V. R. Dias, P. P. Power, *Angew. Chem.* **1990**, *102*, 1061–1062; *Angew. Chem. Int. Ed. Engl.* **1990**, *29*, 1033–1034.

[6] M. Somer, D. Thiery, K. Peters, L. Walz, M. Hartweg, T. Popp, H. G. von Schnering, *Z. Naturforsch. B* **1991**, *46*, 789–794.

[7] a) M. A. Petrie, K. Ruhlandt-Senge, P. P. Power, *Inorg. Chem.* **1992**, *31*, 4038–4039; b) M. A. Petrie, P. P. Power, *Inorg. Chem.* **1993**, *32*, 1309–1312.

[8] a) D. A. Atwood, A. H. Cowley, R. A. Jones, M. A. Mardones, *J. Am. Chem. Soc*, **1991**, *113*, 7050–7052; b) H. Hope, D. C. Pestana, P. P. Power, *Angew. Chem.* **1991**, *103*, 726–727; *Angew. Chem. Int. Ed. Engl.* **1991**, *30*, 691–692; c) R. J. Wehmschulte, P. P. Power, *J. Am. Chem. Soc.* **1996**, *118*, 791–797.

[9] STOE-IPDS, Schneider-rotating anode, graphite monochromator, $Mo_{K\alpha}$ radiation, $\lambda = 0.71073$ Å; **2**: $a = 1124.8(2)$, $b = 2430.4(5)$, $c = 1487.1(3)$ pm, $\beta = 99.99(3)^\circ$, $V = 4003.8(14) \times 10^6$ pm^3; monoclinic, $P2_1/n$, $Z = 2$, $\rho_{calcd} = 1.146$ g cm^{-3}, $\mu(Mo_{K\alpha}) = 2.408$ mm^{-1}, $T = 200$ K, $2\Theta_{max} = 46^\circ$; 19418 reflections measured, 5525 independenr reflections, ($R_{int} = 0.0414$), 4787 independent reflections with $F_o > 4\sigma(F_o)$. The structure was solved by direct methods and refined by full-matrix least-squares techniques against F^2, 290 parameters (As, Ga, Si, O, Li atoms refined aniosotropically, C atoms refined isotropically with split positions, the positions of H atoms where not determind), $R1 = 0.0620$, $wR2 = 0.1942$ (all data), residual electron density: 0.575 e Å^{-3}. CCDC-174606 (**2**) contains the supplementary crystallographic data for this paper. These data can be obtained free of charge via www.ccdc.cam.ac.uk/conts/retrieving.html (or from the Cambridge Crystallographic Data Centre, 12, Union Road, Cambridge CB2 1EZ, UK; fax: (+44) 1223-336-033; or deposit@ccdc.cam.ac.uk).

[10] G. Becker, C. Witthauer, *Z. Anorg. Allg. Chem.* **1982**, *492*, 28–36.

[11] a) R. L. Wells, *Coord. Chem. Rev.* **1992**, *112*, 273–291; b) J. F. Janik, R. L. Wells, V. G. Young, A. L. Rheingold, I. A. Guzei, *J. Am. Chem. Soc.* **1998**, *120*, 532–537; c) A. Dashti-Mommertz, B. Neumüller, *Z. Anorg. Allg. Chem.* **1999**, *625*, 954–960; d) E. E. Foos, R. J. Jouet, R. L. Wells, A. L. Rheingold, L. M. Liable-Sands, *J. Organomet. Chem.* **1999**, *582*, 45–52; e) C. von Hänisch, *Z. Anorg. Allg. Chem.* **2001**, *627*, 68–72.

[12] T. L. Allen, A. C. Scheiner, H. F. Schaefer III, *Inorg. Chem.* **1990**, *29*, 1930–1936.

[13] D. Fenske, T. Langetepe, M. M. Kappes, O. Hampe, P. Weis, *Angew. Chem.* **2000**, *112*, 1925–1928; *Angew. Chem. Int. Ed.* **2000**, *39*, 1857–1860.

[14] H. G. von Schnering, D. Fenske, W. Hönle, M. Binnewies, K. Peters, *Angew. Chem.* **1979**, *91*, 755–756; *Angew. Chem. Int. Ed. Engl.* **1979**, *18*, 679–680; b) G. Fritz, P. Scheer, *Chem. Rev.* **2000**, *100*, 3341–3401.

[15] M. Westerhausen, M. Wieneke, W. Schwarz, *J. Organomet. Chem.* **1999**, *572*, 249–257.

Total Synthesis of Woodrosin I**

Alois Fürstner,* Fabien Jeanjean, and Patrick Razon

Plants belonging to the *Convovulacaeae* family are rich sources of alkaloids and resin glycosides. Although intriguingly complex in detail, the latter invariably contain (11*S*)-hydroxyhexadecanoic acid (jalapinolic acid) as a common aglycon, which is usually tied back to form a characteristic macrolide ring that spans two or more sugar units of their oligosaccharide backbones.[1] The biological functions and physiological properties of resin glycosides are far from fully understood; however, diverse and promising effects have been described for some of these compounds, for example,

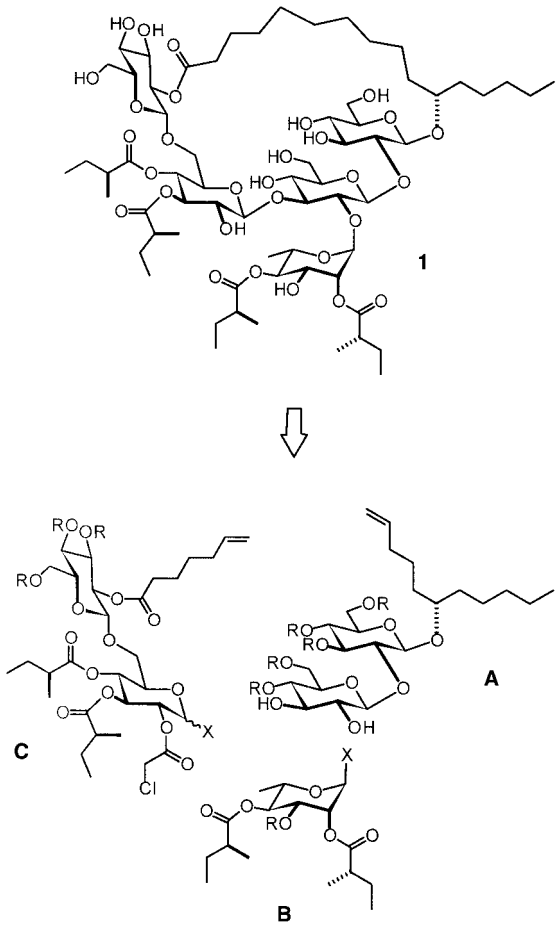
[*] Prof. A. Fürstner, Dr. F. Jeanjean, Dr. P. Razon
Max-Planck-Institut für Kohlenforschung
45470 Mülheim/Ruhr (Germany)
Fax: (+49) 208-306-2994
E-mail: fuerstner@mpi-muelheim.mpg.de

[**] Generous financial support by the Deutsche Forschungsgemeinschaft (Leibniz program) and the Fonds der Chemischen Industrie is gratefully acknowledged. We thank Prof. K. Miyahara, Osaka, Japan, for providing a sample of the closely related woodrosin II for comparison. We also thank Mrs. K. Radkowski for her valuable assistance at various stages of this project.

cytotoxicity against human cancer cell lines, hemolytic action, antibacterial activity, purgative properties, and significant plant growth regulating capacity.[1, 2] Only recently have preparative studies directed towards these challenging targets been reported in the literature which may help to map their structure – activity relationships in more detail.[2–4]

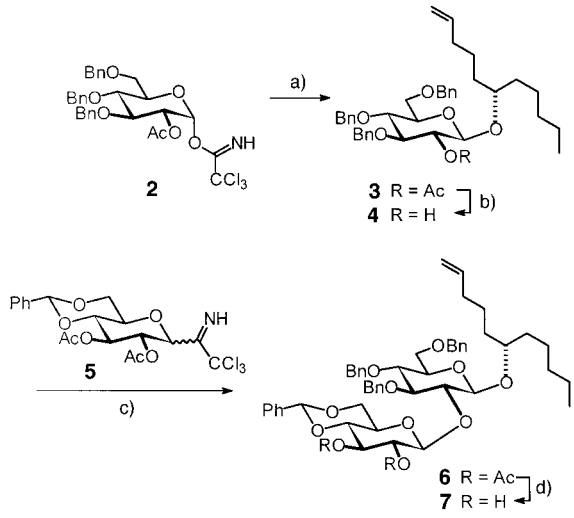
Herein, we describe the first total synthesis of woodrosin I (**1**) a glycolipid isolated from the stems of *Ipomoea tuberosa* L. (*Merremia tuberosa* (L.) Rendle). This plant is commonly called woodrose because of the shape of its dried calyx.[5] Compound **1** (Scheme 1) is one of the most complex resin glycosides known to date. Particularly challenging motifs are the lactone moiety spanning four glucose units to form a 27-membered macrocycle, the additional acylation pattern at the periphery, which seriously restricts the possible choice of temporary protecting groups, as well as the branching of the pentasaccharide perimeter at vicinal positions, which results in severe steric crowding in this region of the molecule.

Our previous experience with ring closing metathesis (RCM),[2a,b, 6, 7] encouraged us to synthesize the macrolide core of **1** by this method as well. To ensure maximum efficiency, the formation of stable chelates of the intermediate Lewis acidic metal carbene species with the polar substituents of the substrate must be avoided as such arrays seriously attenuate the activity of the catalysts used;[8, 9] this should be possible by targeting the C6–C7 bond within the aliphatic tether. Since the cycloalkene formed by RCM has to be hydrogenated anyway, benzyl ethers or benzylidene acetals are the clear choice for the residual protecting groups R, except for those positions where neighboring-group participation is needed to control the glycosylation reactions.



Scheme 1. Retrosynthetic analysis of woodrosin I (**1**).

The cyclization precursor itself can be assembled in a highly convergent manner from the disaccharide building blocks **A** and **C** and the rhamnosyl donor **B** (Scheme 1), which were obtained as described in Schemes 2 – 4. Specifically, the known trichloroacetimidate **2**[10, 11] was glycosylated with (6*S*)-undec-1-en-6-ol, which is available in excellent optical purity ($\geq$99 % *ee*) by an enantioselective addition of dipentylzinc to 5-hexenal.[2] Cleavage of the 2-O-acetyl group of **3** gave alcohol **4**, which was treated with the readily accessible trichloroacetimidate **5**[2] in the presence of catalytic amounts of $BF_3 \cdot Et_2O$ to give disaccharide **6** in 82 % yield. Subsequent deacetylation provided diol **7**, which corresponds to synthon **A** (Scheme 2).

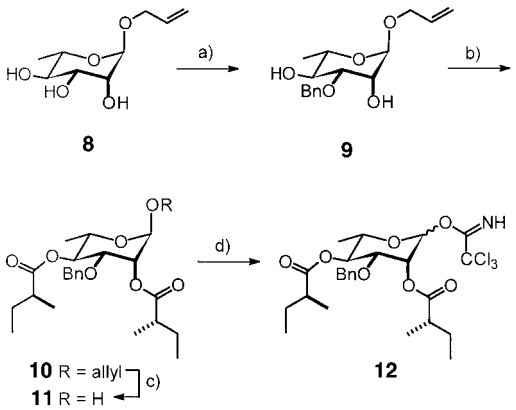


Scheme 2. Synthesis of building block **A**. a) (6*S*)-Undec-1-en-6-ol, $BF_3 \cdot Et_2O$, CH_2Cl_2/hexane, –20 °C, 68 %; b) NaOMe (cat.), MeOH, quantitative; c) **5**, $BF_3 \cdot Et_2O$, CH_2Cl_2/hexane, –20 °C, 82 %; d) NaOMe (cat.), MeOH, 88 %.

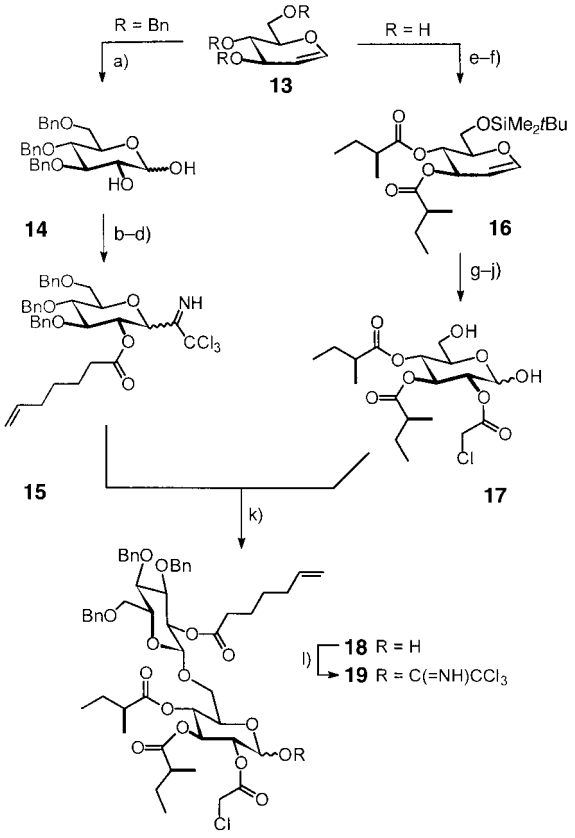
Regioselective benzylation of allyl-L-rhamnoside **8**[12] by using established stannylation methodology[13] followed by DCC-mediated esterification of the resulting product **9** with commercially available (2*S*)-methylbutyric acid provided compound **10**, which was deprotected at the anomeric position on exposure to Pd/C in acidic MeOH (Scheme 3). The resulting hemiacetal **11** was converted under standard conditions[11] into imidate **12**, which serves as rhamnosyl donor **B** in the formation of the target.

The preparation of the third fragment started with 3,4,6-tri-*O*-benzyl-D-glucose (**14**), which was derived from glucal **13** (R = Bn, Scheme 4). Substrate **14** was esterified with 6-heptenoic acid in the presence of DCC and catalytic DMAP. Deprotection of the anomeric position with hydrazine acetate followed by treatment of the resulting hemiacetal with Cl_3CCN and Cs_2CO_3 furnished glycosyl donor **15**. D-Glucal **13** (R = H) was also converted into the required glucosyl acceptor **17** by a sequence of routine manipulations. The $BF_3 \cdot Et_2O$-promoted glycosylation of imidate **15** with the 1,6-diol **17** proceeded with excellent selectivity, delivering compound **18**

 © WILEY-VCH Verlag GmbH, 69451 Weinheim, Germany, 2002 1433-7851/02/4112-2098 $ 20.00+.50/0 *Angew. Chem. Int. Ed.* **2002**, *41*, No. 12



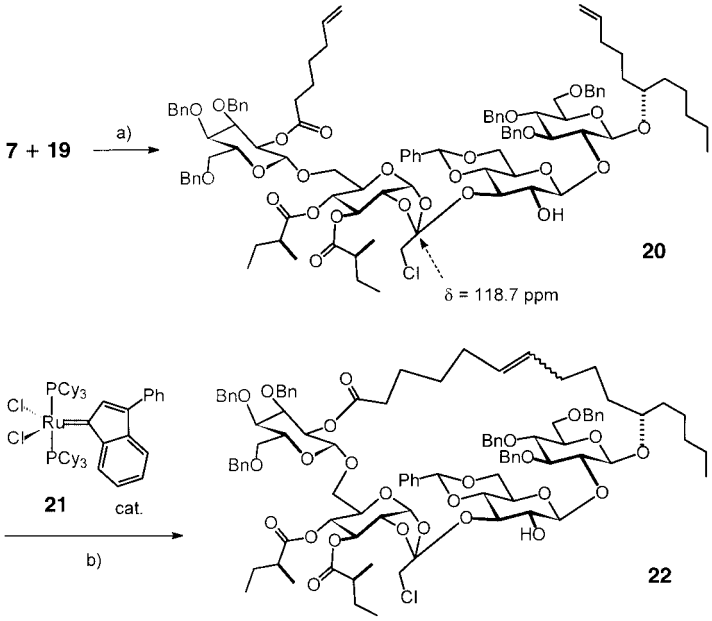
Scheme 3. Synthesis of building block **B**. a) 1) Bu_2SnO, toluene, reflux; 2) CsF, BnBr, DMF, 72%; b) (2*S*)-methylbutyric acid, DCC, DMAP, CH_2Cl_2, 89%; c) Pd/C, PPTS (cat.), MeOH, 80%; d) Cl_3CCN, Cs_2CO_3, CH_2Cl_2, 92%. DMF = *N*,*N*-dimethylformamide, DCC = *N*,*N*′-dicyclohexylcarbodiimide, DMAP = 4-dimethylaminopyridine, PPTS = pyridinum *p*-toluenesulfonate.



Scheme 4. Synthesis of building block **C**. a) OsO_4 (cat.), NMO, acetone/H_2O, 94%; b) 6-heptenoic acid, DCC, DMAP (cat.), CH_2Cl_2, 99%; c) $H_2NNH_2 \cdot HOAc$, DMF, 83%; d) Cl_3CCN, Cs_2CO_3, CH_2Cl_2, 87%; e) *t*$BuMe_2SiCl$, imidazole, DMF, 70%; f) (2*S*)-methylbutyric acid, DCC, DMAP, CH_2Cl_2, 93%; g) OsO_4 (cat.), NMO, acetone/H_2O (9:1), quantitative; h) chloroacetic acid anhydride, Et_3N, DMAP (cat.), CH_2Cl_2, $-20 \rightarrow -10\,^{\circ}C$, 83%; i) $BF_3 \cdot Et_2O$, $CHCl_3$, 81%; j) $H_2NNH_2 \cdot HOAc$, DMF, 79%; k) $BF_3 \cdot Et_2O$, CH_2Cl_2, $-20\,^{\circ}C$, 86%; l) Cl_3CCN, Cs_2CO_3, CH_2Cl_2, 54%. NMO = 4-methylmorpholine *N*-oxide.

in 86% yield. Because the anomeric position in this product was already unmasked, it was directly amenable to the preparation of the next glycosyl donor **19** (synthon **C**). This smooth reiterability of the trichloroacetimidate method is a largely unexplored feature and deserves further investigation.

The next stage of the synthesis required the efficient assembly of the individual building blocks to the pentasaccharide perimeter of woodrosin I. For steric reasons, however, this venture turned out to be far from trivial. Although it was possible to attach the rhamnose unit to the 2′-OH group of acceptor diol **7**, subsequent glycosylation of the resulting trisaccharide with donor **19** was invariably unsuccessful.[14] Therefore the alternative order for the glycosidation steps was explored. This option was facilitated by the distinctly different reactivity of the vicinal hydroxy groups in **7** which allowed consecutive glycosylation reactions without recourse to protecting groups. Thus, treatment of a mixture of **7** and **19** in CH_2Cl_2 at $-20\,^{\circ}C$ with a catalytic amount of TMSOTf afforded a single product in 84% yield. However, its NMR spectra (Bruker DMX 600) were inconsistent with the expected tetrasaccharide but corresponded to orthoester **20** formed by participation of the chloroacetyl moiety (Scheme 5). Most indicative is a singlet in the ^{13}C NMR spectrum at $\delta = 118.7$ ppm which corresponds to the newly formed orthoester junction.



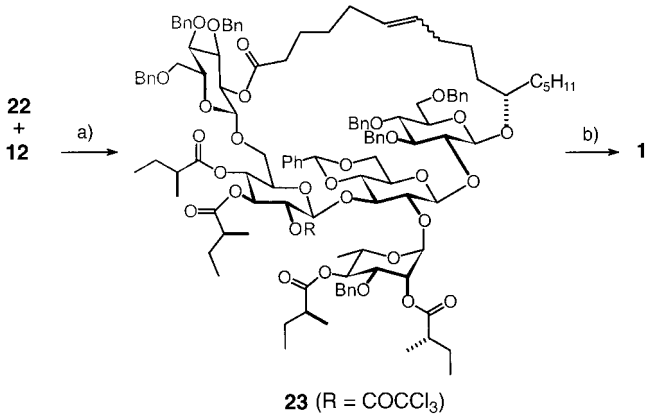
Scheme 5. Coupling of **7** and **19**, and RCM. a) TMSOTf (cat.), CH_2Cl_2, $-20\,^{\circ}C$, 84%; b) **21** (cat.), CH_2Cl_2, reflux, 94%. TMSOTf = trimethylsilyl trifluoromethanesulfonate.

The chloroacetyl group had originally been chosen because it would allow stereochemical control in the glycosidation reactions by neighboring group participation, but would still be orthogonal to the residual ester moieties in **1**. Despite some literature precedence for the engagement of chloroacetates in the formation of orthoesters, β-glycosides are usually obtained if the reactions are promoted with strong Lewis acids in the absence of a buffering base.[15, 16] Therefore the exclusive formation of **20** in the TMSOTf-catalyzed coupling of **7** and **19** was rather unexpected.

Irrespective of this outcome, the total synthesis of woodrosin I was pursued as it might be possible to rectify the connectivity pattern at a later stage. First, however, the severe steric hindrance in the vicinity of the orthoester moiety had to be overcome. Because the 2′-OH group of **20** is strongly shielded in this sector of the molecule, all attempts to attach the missing rhamnosyl unit to this innately unreactive site were in vain.[14] However, inspection of models suggested that the trajectory towards this hidden hydroxy group may be somewhat less narrow *after* forging the macrocyclic ring. Therefore the completion of the sugar backbone was postponed until after the RCM reaction.

Diene **20** cyclized in remarkably high yield to cycloalkene **22** on treatment with catalytic amounts of the indenylideneruthenium complex **21**.[17, 18] Catalyst **21** was introduced recently as a readily accessible and powerful substitute for the more popular Grubbs carbene [$(PCy_3)_2(Cl)_2Ru$=CHPh]. This favorable result highlights once more the truly remarkable utility of RCM even in complex cases.

With macrolide **22** in hand, the introduction of the missing rhamnose moiety was reinvestigated. In view of the lability of donor **12** in the presence of Lewis acids, an "inverse" glycosylation procedure was applied.[19] Thus, alcohol **22** was premixed with catalytic amounts of TMSOTf in rigorously dried Et_2O, and compound **12** was then added slowly to the resulting solution. The outcome of this key experiment surpassed our expectations (Scheme 6): not only was it



Scheme 6. Total synthesis: a) TMSOTf (cat.), Et_2O, 0 °C, slow addition of **12** (20 min), 30 min, 60 %; b) 1) $H_2NNH_2 \cdot HOAc$, DMF, $-10 \rightarrow 0$ °C, (ii) H_2 (1 atm), Pd/C, MeOH, 18 h, 84 % (over two steps).

possible to attach the missing rhamnose, but the compromising orthoester moiety of **22** was found to rearrange concomitantly to the required β-glycosidic linkage. After optimizing the premixing and addition times, product **23** was isolated in 60 % yield. In view of its selectivity, this transformation constitutes a hallmark for the power of the trichloroacetimidate method[11] and represents one of the most advanced applications of Kochetkov's orthoester protocol reported to date.[20]

Short treatment of product **23** with hydrazine acetate for the selective cleavage of the chloroacetyl group followed by extensive hydrogenation over Pd/C afforded fully deprotected woodrosin I (**1**). The spectral data (600 MHz) of this product are in excellent agreement with those reported in the literature.[5]

In summary, we have reported the first total synthesis of the complex resin glycoside woodrosin I (**1**). This venture not only showcases the relevance of RCM for natural product synthesis, but also attests to the maturity and flexibility of the trichloroacetimidate method pioneered by Schmidt et al.[11] Particularly promising yet largely unexplored aspects of the latter are the excellent selectivities observed in glycosylations of acceptors that contain more than one unprotected hydroxy group.[21]

Received: February 8, 2002 [Z 18681]

[1] For a short review, see: H. Wagner, *Nobel Symp.* **1974**, *25*, 235 – 240.

[2] For previous studies on resin glycosides from this group and for a comprehensive compilation of pertinent literature, see: a) A. Fürstner, T. Müller, *J. Am. Chem. Soc.* **1999**, *121*, 7814 – 7821; b) A. Fürstner, T. Müller, *J. Org. Chem.* **1998**, *63*, 424 – 425; c) C. W. Lehmann, A. Fürstner, T. Müller, *Z. Kristallogr.* **2000**, *215*, 114 – 117; d) see also: A. Fürstner, K. Radkowski, J. Grabowski, C. Wirtz, R. Mynott, *J. Org. Chem.* **2000**, *65*, 8758 – 8762.

[3] For a short review, see: J. Furukawa, N. Sakairi, *Trends Glycosci. Glycotechnol.* **2001**, *13*, 1 – 10.

[4] a) Z.-H. Jiang, A. Geyer, R. R. Schmidt, *Angew. Chem.* **1995**, *107*, 2730 – 2734; *Angew. Chem. Int. Ed. Engl.* **1995**, *34*, 2520 – 2524; b) D. P. Larson, C. H. Heathcock, *J. Org. Chem.* **1997**, *62*, 8406 – 8418; c) S.-F. Lu, Q. O'yang, Z.-W. Guo, B. Yu, Y.-Z. Hui, *J. Org. Chem.* **1997**, *62*, 8400 – 8405; d) J. Furukawa, S. Kobayashi, M. Nomizu, N. Nishi, N. Sakairi, *Tetrahedron Lett.* **2000**, *41*, 3453 – 3457.

[5] M. Ono, K. Nakagawa, T. Kawasaki, K. Miyahara, *Chem. Pharm. Bull.* **1993**, *41*, 1925 – 1932.

[6] Reviews: a) T. M. Trnka, R. H. Grubbs, *Acc. Chem. Res.* **2001**, *34*, 18 – 29; b) A. Fürstner, *Angew. Chem.* **2000**, *112*, 3140 – 3172; *Angew. Chem. Int. Ed.* **2000**, *39*, 3012 – 3043.

[7] For the latest examples, see: a) A. Fürstner, O. R. Thiel, N. Kindler, B. Bartkowska, *J. Org. Chem.* **2000**, *65*, 7990 – 7995; b) A. Fürstner, T. Dierkes, O. R. Thiel, G. Blanda, *Chem. Eur. J.* **2001**, *7*, 5286 – 5298; c) A. Fürstner, O. R. Thiel, L. Ackermann, *Org. Lett.* **2001**, *3*, 449 – 451, and references therein.

[8] A. Fürstner, O. R. Thiel, C. W. Lehmann, *Organometallics* **2002**, *21*, 331 – 335.

[9] A. Fürstner, K. Langemann, *Synthesis* **1997**, 792 – 803.

[10] a) A. Fürstner, I. Konetzki, *Tetrahedron Lett.* **1998**, *39*, 5721 – 5724; b) A. Fürstner, I. Konetzki, *J. Org. Chem.* **1998**, *63*, 3072 – 3080.

[11] Reviews: a) R. R. Schmidt, *Angew. Chem.* **1986**, *98*, 213 – 236; *Angew. Chem. Int. Ed. Engl.* **1986**, *25*, 212 – 235; b) R. R. Schmidt, W. Kinzy, *Adv. Carbohydr. Chem. Biochem.* **1994**, *50*, 21 – 123; c) R. R. Schmidt, K.-H. Jung in *Preparative Carbohydrate Chemistry* (Ed.: S. Hanessian), Dekker, New York, **1997**, pp. 283 – 312.

[12] J. Zhang, J. Mao, H. Chen, M. Cai, *Tetrahedron: Asymmetry* **1994**, *5*, 2283 – 2290.

[13] S. David in *Preparative Carbohydrate Chemistry* (Ed.: S. Hanessian), Dekker, New York, **1997**, pp. 69 – 86.

[14] Details will be reported separately in a full paper.

[15] For a pertinent discussion, see: T. Ziegler, *Liebigs Ann. Chem.* **1990**, 1125 – 1131 and references therein.

[16] Esters other than chloroacetates at O2 of various glycosyl donors may similarly lead to orthoesters, particularly in attempted glycosylations with sterically hindered secondary alcohols. This bias is generally increased if the reaction medium is buffered with bases. For examples and a pertinent discussion of the relevant reaction parameters, see: a) P. H. Seeberger, M. Eckhardt, C. E. Gutteridge, S. J. Danishefsky, *J. Am. Chem. Soc.* **1997**, *119*, 10064 – 10072; b) J. Banoub, D. R. Bundle, *Can. J. Chem.* **1979**, *57*, 2091 – 2097; c) H. Kunz, A. Harreus, *Liebigs Ann. Chem.* **1982**, 41 – 48; d) A. Harreus, H. Kunz, *Liebigs Ann. Chem.* **1986**, 717 – 730, and references therein.

 © WILEY-VCH Verlag GmbH, 69451 Weinheim, Germany, 2002 1433-7851/02/4112-2100 $ 20.00+.50/0

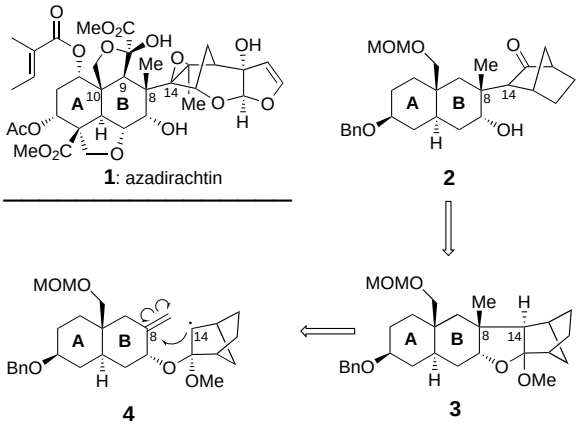
[17] A. Fürstner, O. Guth, A. Düffels, G. Seidel, M. Liebl, B. Gabor, R. Mynott, *Chem. Eur. J.* **2001**, *7*, 4811 – 4820.
[18] For previous applications of this catalyst, see: a) A. Fürstner, A. F. Hill, M. Liebl, J. D. E. T. Wilton-Ely, *Chem. Commun*. **1999**, 601 – 602; b) A. Fürstner, J. Grabowski, C. W. Lehmann, *J. Org. Chem*. **1999**, *64*, 8275 – 8280; c) A. Fürstner, O. R. Thiel, *J. Org. Chem*. **2000**, *65*, 1738 – 1742; d) A. Fürstner, J. Grabowski, C. W. Lehmann, T. Kataoka, K. Nagai, *ChemBioChem* **2001**, *2*, 60 – 68; e) A. Fürstner, K. Radkowski, *Chem. Commun*. **2001**, 671 – 672.
[19] R. R. Schmidt, A. Toepfer, *Tetrahedron Lett*. **1991**, *32*, 3353 – 3356.
[20] a) N. K. Kochetkov, A. J. Khorlin, A. F. Bochkov, *Tetrahedron Lett*. **1964**, 289 – 293; b) N. K. Kochetkov, A. J. Khorlin, A. F. Bochkov, *Tetrahedron* **1967**, *23*, 693 – 707; c) T. Ogawa, K. Beppu, S. Nakabayashi, *Carbohydr. Res.* **1981**, *93*, C6 – C9; d) D. R. Mootoo, P. Konradsson, B. Fraser-Reid, *J. Am. Chem. Soc*. **1989**, *111*, 8540 – 8542; e) T. Ogawa, T. Nukada, *Carbohydr. Res.* **1985**, *136*, 135 – 152; f) P. J. Garegg, I. Kvarnström, *Acta Chem. Scand. Ser. B* **1977**, *31*, 509 – 513; g) R. U. Lemieux, A. R. Morgan, *Can. J. Chem*. **1965**, *43*, 2199 – 2201; h) for a general discussion, see: K. Toshima, K. Tatsuta, *Chem. Rev.* **1993**, *93*, 1503 – 1531.
[21] For another application from our laboratory of trichloroacetimidates in the synthesis of complex glycolipids, see: A. Fürstner, M. Albert, J. Mlynarski, M. Matheu, *J. Am. Chem. Soc*. **2002**, *124*, 1168 – 1169.

 © WILEY-VCH Verlag GmbH, 69451 Weinheim, Germany, 2002 1433-7851/02/4112-2101 $ 20.00+.50/0

Model Studies Towards Azadirachtin: Part 1. Construction of the Crowded C8–C14 Bond by Radical Chemistry**

K. C. Nicolaou,* Markus Follmann, A. J. Roecker, and Kevin W. Hunt

Isolated from the seeds of the neem tree (*Azadirachta indica* Juss.), azadirachtin[1, 2] (**1**, Scheme 1) exhibits potent insect antifeedant activity (active against *Schistocera gregaria* at 0.04 ppm) and growth inhibitory properties across a broad

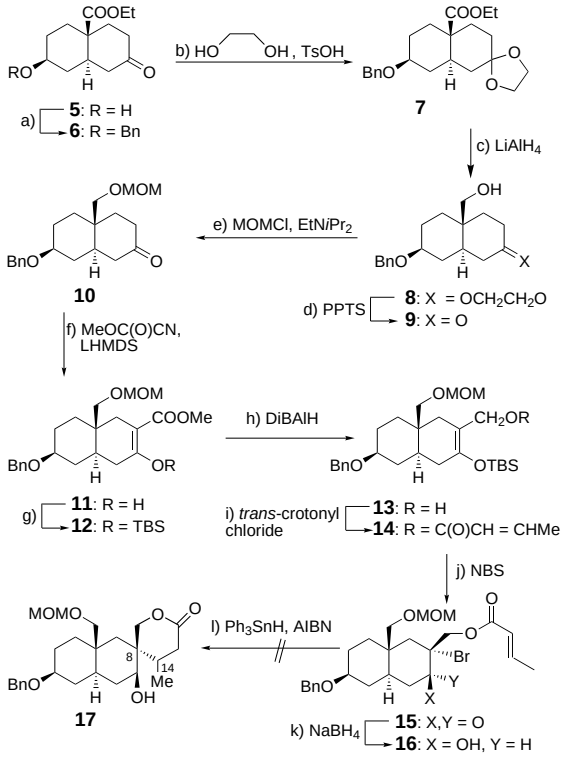


Scheme 1. Molecular structure of azadirachtin (**1**) and radical-based retrosynthesis of model system **2**.

range of insect species while having low mammalian toxicity (nontoxic to rats at doses of 8.5 g kg^{-1}).[3] Because of these important biological actions and its imposing molecular architecture, azadirachtin has elicited considerable interest from the synthetic community.[4] Despite these efforts, however, the molecule of azadirachtin still remains elusive to total synthesis, with its crowded C8–C14 bond bridging its two domains being the main obstacle. In this communication we wish to report our model studies which culminated in a potential solution to the C8–C14 problem based on a tethering strategy followed by a radical-based intramolecular coupling and dismantling of the temporary bridge.

Scheme 1 depicts the targeted model compound **2**, which contains ring systems representing the two structural domains of azadirachtin, and, in retrosynthetic format, the radical-based proposed strategy for the construction of **2**. Thus, it was reasoned that tethering the two domains through a mixed bromoketal would facilitate the intended C8–C14 coupling reaction, upon generation of the radical species **4**, by a 5-*exo*-trig cyclization to furnish **3**. Subsequent collapse of the mixed ketal bridge would then allow the generation of the targeted ring system **2** with the desired C8–C14 bond in place. The successful execution of this strategy was preceded by a number of related studies whose brief description should be instructive.

In search for a suitable *trans*-decalin system as a starting material with an angular substituent and oxygen functionalities on both rings, we found ester **5** (Scheme 2) to be an



Scheme 2. Synthesis of key building block **13** and failure of **16** to undergo 6-*endo*-trig cyclization under radical conditions. a) Benzyl 2,2,2-trichloroacetimidate (1.1 equiv), TfOH (5 mol %), cyclohexane/CH_2Cl_2 (2:1), 25 °C, 4 h, 73 %; b) ethylene glycol (3.0 equiv), TsOH (3 mol %), benzene, Dean-Stark trap, reflux, 3 h, 98 %; c) $LiAlH_4$ (1.5 equiv), THF, 0 °C, 30 min, then reflux, 4 h, 76 %; d) cat. PPTS, wet acetone, 60 °C, 18 h, 100 %; e) MOMCl (2.0 equiv), EtN*i*Pr$_2$ (2.2 equiv), CH_2Cl_2, 25 °C, 4 h, 83 %; f) MeOC(O)CN (1.4 equiv), LHMDS (2.0 equiv), HMPA (1.4 equiv), THF, −78 °C, 30 min, 68 %; g) TBSOTf (4.0 equiv), EtN*i*Pr$_2$ (5.0 equiv), CH_2Cl_2, 25 °C, 4 h, 75 %; h) DiBAlH (4.0 equiv), CH_2Cl_2, −78 °C, 1 h, 62 %; i) *trans*-crotonyl chloride (3.0 equiv), py (10.0 equiv), CH_2Cl_2, 25 °C, 1 h, 99 %; j) NBS (1.1 equiv), CH_2Cl_2, −78 °C, 2 h, 72 %; k) $NaBH_4$ (3.6 equiv), CH_2Cl_2/MeOH (1:1), −50 °C, 1 h, 78 %; l) Ph_3SnH (1.4 equiv), AIBN (0.15 equiv), toluene, 100 °C. TfOH = trifluoromethanesulfonic acid, TsOH = *p*-toluenesulfonic acid, PPTS = pyridinium *p*-toluenesulfonate, MOM = methoxymethyl, LHMDS = lithium bis(trimethylsilyl)amide, HMPA = hexamethylphosphoramide, TBS = *tert*-butyldimethylsilyl, DiBAlH = diisobutylaluminumhydride, py = pyridine, NBS = *N*-bromosuccinimide, AIBN = 2,2′-azobisisobutyronitrile.

[*] Prof. Dr. K. C. Nicolaou, Dr. M. Follmann, A. J. Roecker, Dr. K. W. Hunt
Department of Chemistry and The Skaggs Institute for Chemical Biology
The Scripps Research Institute
10550 North Torrey Pines Road, La Jolla, CA 92037 (USA)
Fax: (+1) 858-784-2469
and
Department of Chemistry and Biochemistry
University of California San Diego
9500 Gilman Drive, La Jolla, CA 92093 (USA)
E-mail: kcn@scripps.edu

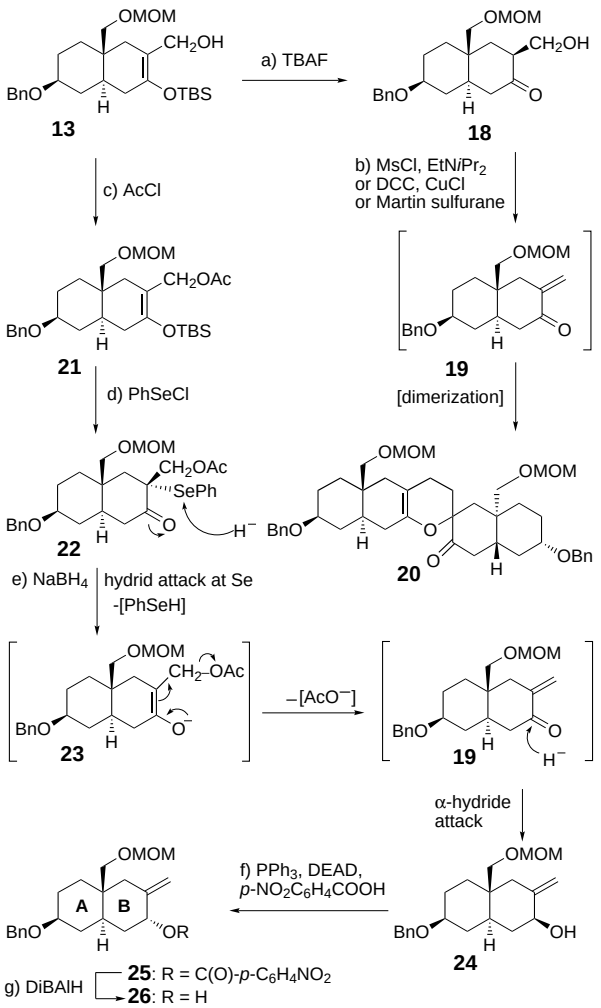
[**] We thank Drs. D. H. Huang and G. Siuzdak for NMR spectroscopic and mass spectrometric assistance, respectively. This work was financially supported by the National Institutes of Health (USA), the Skaggs Institute for Chemical Biology, postdoctoral fellowships from Bayer AG (to M.F.) and the G. E. Hewitt Foundation (to K.W.H.), a predoctoral fellowship from the Division of Organic Chemistry of the American Chemical Society sponsored by Novartis (to A.J.R.), and grants from Abbott Laboratories, ArrayBiopharma, Bayer, Boehringer Ingelheim, DuPont, Glaxo, Hoffmann-LaRoche, Merck, Novartis, Pfizer, and Schering Plough.

 © WILEY-VCH Verlag GmbH, 69451 Weinheim, Germany, 2002 1433-7851/02/4112-2103 $ 20.00+.50/0

ideal candidate for these studies. This compound is readily available in large quantities, albeit in racemic form, from commercially available starting materials by a three-step modification of a literature procedure.[5] After benzylation of the hydroxy group in **5**, the resulting ketone **6** was protected as the 1,3-dioxolane **7**. Reduction of **7** with $LiAlH_4$ followed by acid-induced hydrolysis of the ethylene ketal furnished hydroxy ketone **9** via intermediate **8** in 76% overall yield. The primary alcohol in compound **9** was then protected as a MOM acetal to produce **10**, which was regioselectively carboxymethylated with Mander's reagent[6] in the presence of LHMDS and HMPA under kinetic conditions ($-78\,^{\circ}C$) to afford enol methyl ester **11** in 68% yield. Silylation of this enol (TBSOTf/EtNiPr$_2$) then led to silyl ether ester **12** (75% yield) whose reduction with DiBAlH furnished primary alcohol **13** in 62% yield.

Our first endeavor into the C8–C14-connected model assembly required bromo acrylate **16** as a possible precursor to a spirocyclic system, **17**, through radical generation and subsequent 6-*endo*-trig cyclization. Precursor **16** was obtained from compound **13** by esterification with *trans*-crotonyl chloride (py, 99% yield), followed by bromination with NBS (72% yield) and $NaBH_4$ reduction (78% yield). However, all attempts to induce ring closure within this compound (**16**) to **17** under radical conditions (tin hydrides, AIBN) failed.[7] These failures led us to conclude that, despite its advantages, the ester bridge was not the best tether for our purposes and that a highly stabilized and congested tertiary radical on the decalin system might not be a sufficiently reactive species to form the C8–C14 bond. Hence, we opted for an alternative strategy in which a ketal linkage was to be used in conjugation with a 5-*exo*-trig cyclization to take place from the "right" domain of the molecule onto the decalin system. The latter mode of cyclization is known to be associated with higher reaction rates than the originally attempted 6-*endo*-trig ring closure[8] and its adoption was, therefore, accompanied by considerable optimism.

The new plan required allylic alcohol **26** as the decalin substrate, a compound that was synthesized from silylenol ether **13** as shown in Scheme 3. Thus, exposure of **13** to TBAF under buffered conditions resulted in the stereoselective formation of ketone **18** in quantitative yield. Attempted dehydration of **18** mediated by MsCl/EtNiPr$_2$, DCC/CuCl,[9] or Martin sulfurane[10] gave only pentacyclic compound **20** in high yield, presumably through a Diels–Alder type dimerization of the resulting enone **19**.[11] To circumvent this hurdle, it became clear that it was necessary to generate and reduce the enone **19** at low temperature. To this end, alcohol **13** was acetylated to silylenol acetate **21** which was then converted, in high yield, to **22** (PhSeCl, $-78\,^{\circ}C$). Ketoselenide **22** was treated with $NaBH_4$ in MeOH/CH_2Cl_2 at $-78\,^{\circ}C$ to furnish allylic alcohol **24** in 98% overall yield from **22**. This remarkable transformation (**22**→**24**) presumably proceeds through the cascade sequence shown in Scheme 3 via intermediates **23** and **19**. The stereochemistry of the newly generated allylic alcohol on ring **B** of compound **24** was inverted by a Mitsunobu-type reaction as modified by Martin[12] followed by DiBAlH reduction of the resulting



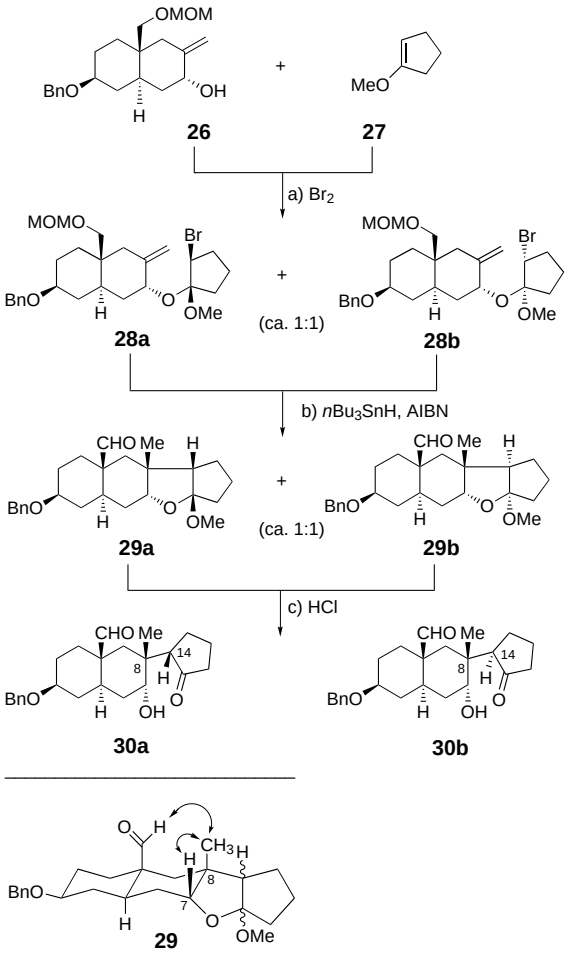
Scheme 3. Synthesis of allylic alcohol **26**. a) TBAF (1.1 equiv), THF/AcOH (100:1), 25 °C, 6 h, 100%; b) e.g., MsCl (2.5 equiv), EtNiPr$_2$ (7.5 equiv), CH_2Cl_2, 25 °C, 24 h, 83%; c) AcCl (3.0 equiv), py (10.0 equiv), CH_2Cl_2, 25 °C, 1 h, 67%; d) PhSeCl (1.1 equiv), −78 °C, 1 h, then 25 °C, 1 h; e) $NaBH_4$ (6.8 equiv), CH_2Cl_2/MeOH (1:1), −78 °C, 1 h, then 25 °C, 1 h, 98% (2 steps); f) PPh_3 (3.0 equiv), DEAD (3.0 equiv), *p*-nitrobenzoic acid (2.5 equiv), benzene, 25 °C, 14 h, 78%; g) DiBAlH (3.1 equiv), CH_2Cl_2, −78 °C, 3 h, 79%. TBAF = tetrabutylammonium fluoride, Ms = methanesulfonyl, DEAD = diethyl azodicarboxylate.

p-nitrobenzoate **25** to smoothly lead to the desired product **26** in 79% yield.

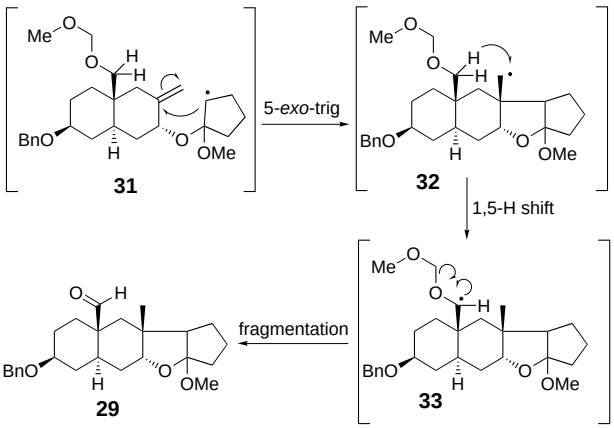
The required bromoolefin **28** was obtained as a 1:1 mixture of diastereoisomers (**28a** and **28b**) by coupling of allylic alcohol **26** with enol ether **27** in the presence of Br_2[13] as shown in Scheme 4. This shorter, mixed ketal tether, originally introduced by Stork et al.,[14] was necessary for our intentions to employ a 5-*exo*-trig radical cyclization. In the event, exposure of the diastereomeric mixture of bromoketals **28a** and **28b** to *n*Bu_3SnH/AIBN in toluene at 100 °C produced, in 79% combined yield, a diastereomeric mixture of tetracyclic compounds **29a** and **29b** through a reaction in which the expected C8–C14 bond formation was accompanied by oxidative removal of the MOM group so that the aldehyde function at the angular position was unraveled.

Scheme 5 provides a mechanistic rationale for this interesting cascade sequence that leads from the initially formed

 © WILEY-VCH Verlag GmbH, 69451 Weinheim, Germany, 2002 1433-7851/02/4112-2104 $ 20.00+.50/0 *Angew. Chem. Int. Ed.* **2002**, *41*, No. 12



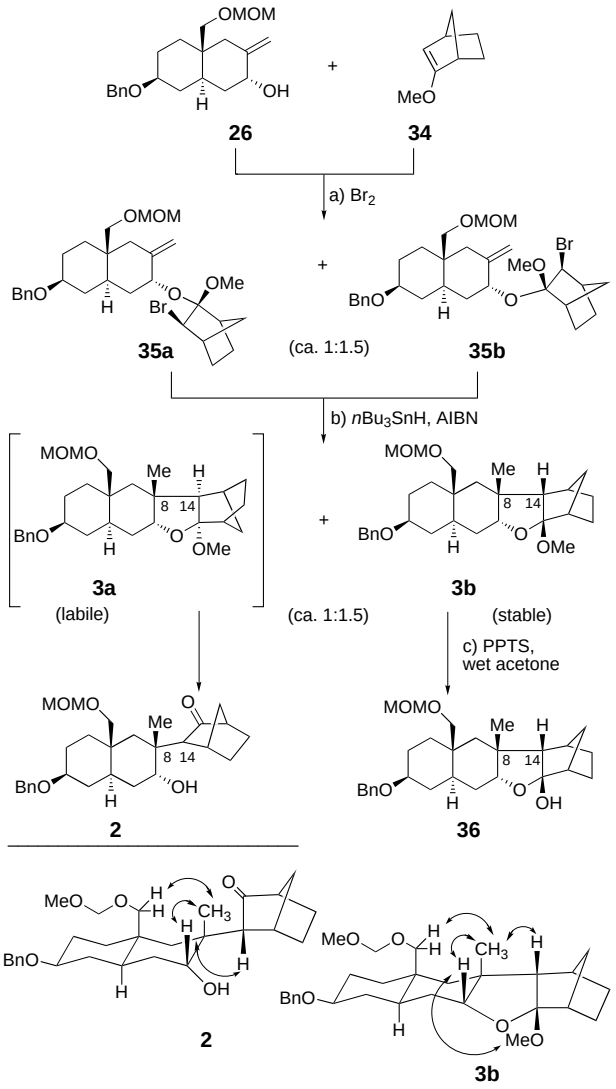
Scheme 4. Synthesis of model systems **30a** and **30b**. a) **27** (10.0 equiv), Br_2 (5.0 equiv), *N*,*N*-dimethylaniline (6.0 equiv), CH_2Cl_2, 25 °C, 12 h, 79% (mixture of diastereoisomers, ca. 1:1); b) nBu_3SnH (1.6 equiv), AIBN (0.14 equiv), 0.004 M in toluene, 12 h, 100 °C, 79%; c) 1 M aq. HCl/THF (1:3.3), 25 °C, 144 h, 70% (separated diastereoisomers, 1:1).



Scheme 5. Postulated mechanism for the radical-based cascade sequence **28** → **29**.

secondary radical **31** to the observed tetracyclic aldehyde **29** via the presumed intermediates **32** and **33** (5-*exo*-trig). The *cis*-stereochemical assignments for both obtained isomers at the newly generated decalin fusion (C7–C8) were based on NOE studies (see structures **29a** and **29b**, Scheme 4). Hydrolysis of the mixture of these two ketals under acidic conditions (aq. HCl, THF) led to the two hydroxy ketoaldehydes **30a** and **30b** (70% combined yield) which were separated by flash column chromatography (silica gel).

These encouraging results prompted us to attempt the construction of a model system closer to the structure of azadirachtin, namely compound **2** (Scheme 6). Thus, coupling of allylic alcohol **26** with racemic 1-methoxynorbornene



Scheme 6. Synthesis of azadirachtin model systems **2**, **3b** and **36**. a) **34** (5.0 equiv), Br_2 (4.3 equiv), *N*,*N*-dimethylaniline (4.65 equiv), CH_2Cl_2, 25 °C, 2 h, 71% (mixture of diastereoisomers, ca. 1.5:1); b) nBu_3SnH (1.3 equiv), AIBN (0.2 equiv), 0.003 M in toluene, 15 min, 110 °C, 70% (mixture of diastereoisomers, ca. 1.5:1); c) PPTS (0.05 equiv), acetone/H_2O (10:1), 65 °C, 72 h, 85%.

(**34**)[15] under the influence of Br_2 furnished a mixture of the two diastereomeric bromoketals **35a** and **35b** (ratio ca. 1:1.5) formed by exclusive addition of bromonium ion to the *exo* face of the norbornene framework as expected (71% total yield). On exposure to nBu_3SnH/AIBN under the above-mentioned conditions, the mixture of bromoketals **35a** and **35b** gave rise to polycyclic systems **3a** and **3b** (ca. 1:1.5 ratio, 70% combined yield) through the desired C8–C14 bond formation. Upon aqueous workup it was observed that the

minor diastereoisomer **3a** was readily converted to the opened hydroxy ketone **2** by hydrolysis. In contrast, the major component **3b** remained intact; it required acidic conditions for its hydrolysis (PPTS, H_2O/acetone, 85% yield), and then lead only to its closed hydroxy tetrahydrofuran form **36** (for selected physical properties of compounds **2** and **36**, see Table 1). This difference in reactivity for the two isomers can be rationalized considering the release of strain involved in going from the closed structure **3a** (C8 methyl group against the two-carbon bridge of the norbornene residue) to the open form **2**, whereas systems **3b** and **36** suffer from no such release of strain. The stereochemical assignments for this series of compounds were based on NOE studies on compounds **2** and **3b** as shown in Scheme 6 (arrows on structures).

Table 1. Selected physical properties of compounds **2** and **36**.

2: Colorless oil; $R_f = 0.28$ (silica, 33% EtOAc in hexanes); IR (thin film): $\tilde{\nu}_{max} = 3424, 2931, 2860, 1719, 1454, 1155, 1108, 1044\ cm^{-1}$; ^1H NMR (600 MHz, $CDCl_3$): $\delta = 7.32$ (s, 5H), 4.59 (s, 2H), 4.54 (s, 2H), 3.76 (d, $J = 9.9$ Hz, 1H), 3.51 (d, $J = 9.9$ Hz, 1H), 3.44 (m, 1H), 3.40 (d, $J = 2.5$ Hz, 1H), 3.32 (s, 3H), 2.83 (m, 1H), 2.73 (d, $J = 4.4$ Hz, 1H), 2.31 (d, $J = 4.0$ Hz, 1H), 1.84–1.36 (m, 17H), 1.19 ppm (s, 3H); ^{13}C NMR (150 MHz, $CDCl_3$): $\delta =$ 222.1, 139.3, 129.3, 128.2, 128.1, 97.4, 78.0, 76.8, 70.5, 66.1, 64.1, 55.8, 52.3, 41.3, 40.4, 38.4, 36.8, 35.8, 35.0, 34.8, 34.0, 33.7, 27.9, 25.0, 24.5, 24.1 ppm; HRMS (MALDI–FTMS), calcd for $C_{28}H_{40}O_5$ $[M+Na^+]$: 479.2768, found: 479.2776

36: Colorless oil; $R_f = 0.36$ (silica, 33% EtOAc in hexanes); IR (thin film): $\tilde{\nu}_{max} = 3412, 2931, 2872, 2343, 1448, 1114, 1031\ cm^{-1}$; ^1H NMR (600 MHz, $CDCl_3$): $\delta = 7.32$ (s, 5H), 4.59 (s, 2H), 4.55 (d, $J = 11.7$ Hz, 1H), 4.52 (d, $J =$ 11.7 Hz, 1H); 4.01 (bs, 1H), 3.71 (d, $J = 9.7$ Hz, 1H), 3.54 (d, $J = 9.7$ Hz, 1H), 3.40 (m, 1H), 3.34 (s, 3H), 2.12 (m, 3H), 1.98 (m, 1H), 1.91 (m, 1H), 1.80–1.73 (m, 3H), 1.68 (m, 1H), 1.62–1.54 (m, 8H), 1.46 (bs, 1H), 1.24 (s, 3H), 1.19–1.16 (m, 2H), 0.85 ppm (m, 1H); ^{13}C NMR (150 MHz, $CDCl_3$): $\delta = 139.3, 129.0, 128.2, 128.1, 114.1, 97.4, 81.4, 77.9, 70.4, 68.1, 65.2, 55.8,$ 44.2, 42.7, 38.0, 37.9, 37.2, 36.3, 36.0, 35.4, 34.2, 31.1, 29.9, 29.8, 27.9, 23.0 ppm; HRMS (MALDI–FTMS), calcd for $C_{28}H_{40}O_5$ $[M+Na^+]$: 479.2768, found: 479.2758

The described chemistry provides a potential solution to the construction of the difficult C8–C14 bond of azadirachtin and paves the way for a total synthesis of this formidable synthetic target. It also provides useful insights into cascade reactions and other processes involving radical cyclizations that may prove useful in other situations where fusions of sterically congested carbon–carbon bonds may be required. In the following communication we report an alternative approach for constructing azadirachtin's most challenging bond, the C8–C14 bridge.[16]

Received: March 18, 2002 [Z18924]

[1] Isolation: J. H. Butterworth, E. D. Morgan, *Chem. Commun.* **1968**, 23–24.

[2] Structure determination: a) J. N. Bilton, H. B. Broughton, P. S. Jones, S. V. Ley, Z. Lidert, E. D. Morgan, H. S. Rszepa, R. N. Sheppard, A. M. Z. Slawin, D. J. Williams, *Tetrahedron* **1987**, *43*, 2805–2815; b) W. Kraus, M. Bokel, A. Bruhn, R. Cramer, I. Klaiber, A. Klenk, G. Nagl, H. Pohnl, H. Sadlo, B. Vogler, *Tetrahedron* **1987**, *43*, 2817–2830; c) C. J. Turner, M. S. Tempesta, R. B. Taylor, M. G. Zagorski, J. S. Termini, D. R. Schroeder, K. Nakanishi, *Tetrahedron* **1987**, *43*, 2789–2804.

[3] a) A. J. Nisbet, J. A. Mordue, *An. Soc. Entomol. Bras.* **2000**, *29*, 615–632; b) M. S. Mulla, T. Su, *J. Am. Mosq. Control Assoc.* **1999**, *15*, 133–152; c) M. S. J. Simmonds, W. M. Blaney, S. V. Ley, J. C. Anderson, P. L. Toogood, *Entomol. Exp. Appl.* **1990**, *55*, 169–181; d) J. A. Immaraju, *Pestic. Sci.* **1998**, *54*, 285–289; e) J. Akudugu, G. Gade, L. Bohm, *Life Sci.* **2001**, *68*, 1153–1160.

[4] Synthetic studies: a) S. V. Ley, C. E. Gutteridge, A. R. Pape, C. D. Spilling, C. Zumbrunn, *Synlett* **1999**, 1295–1297; b) A. A. Denholm, L. Jennens, S. V. Ley, A. Wood, *Tetrahedron* **1995**, *51*, 6591–6604; c) S. V. Ley, A. A. Denholm, A. Wood, *Nat. Prod. Rep.* **1993**, 109–157; d) H. Kolb, S. V. Ley, *Tetrahedron Lett.* **1991**, *32*, 6187–6190; e) M. G. Brasca, H. B. Broughton, D. Craig, S. V. Ley, A. A. Somovilla, P. L. Toogood, *Tetrahedron Lett.* **1988**, *29*, 1853–1856; f) Y. Yamamoto, J. Ishihara, N. Kanoh, A. Murai, *Synthesis* **2000**, 1878–1893; g) H. Watanabe, T. Watanabe, K. Mori, T. Kitahara, *Tetrahedron Lett.* **1997**, *38*, 4429–4432; h) Y. Nishikimi, T. Iimori, M. Sodeoka, M. Shibasaki, *J. Org. Chem.* **1989**, *54*, 3354–3359; i) K. J. Henry, Jr., B. Fraser-Reid, *J. Org. Chem.* **1994**, *59*, 5128–5129; j) H. Scheliger, E. Winterfeldt, *Chirality* **1997**, *9*, 454–458.

[5] a) D. Nasipuri, R. Roy, G. Sarkar, M. Guha, *J. Indian Chem. Soc.* **1966**, *43*, 383–390; b) J. B. Jones, D. R. Dodds, *Can. J. Chem.* **1987**, *65*, 2397–2404.

[6] L. N. Mander, S. P. Sethi, *Tetrahedron Lett.* **1983**, *24*, 5425–5428.

[7] Nor was a 5-*exo*-trig cyclization observed in this instance as was reported for similar systems: L. Set, D. R. Cheshire, D. L. J. Clive, *J. Chem. Soc. Chem. Commun.* **1985**, 1205–1207.

[8] For excellent reviews on radical chemistry, see: a) B. Giese, *Radicals in Organic Synthesis: Formation of Carbon–Carbon Bonds*, Pergamon, Oxford, **1986**; b) D. P. Curran in *Comprehensive Organic Synthesis*, *Vol. 4* (Eds.: B. M. Trost, I. Fleming), Pergamon, Oxford, **1991**, pp. 715–831.

[9] A. K. Banerjee, M. Laya, *Monatsh. Chem.* **1997**, 1255–1260.

[10] a) R. J. Aarhart, J. C. Martin, *J. Am. Chem. Soc.* **1972**, *94*, 4997–5003; b) R. J. Aarhart, J. C. Martin, *J. Am. Chem. Soc.* **1972**, *94*, 5003–5010.

[11] For similar dimerizations, see: a) E. Romann, A. J. Frey, P. A. Stadler, A. Eschenmoser, *Helv. Chim. Acta* **1957**, *40*, 1900–1917; b) D. J. Collins, G. D. Fallon, C. E. Skene, *Aust. J. Chem.* **1992**, *45*, 71–97; c) H. Hosoyama, H. Shigemori, Y. In, T. Ishida, J. Kobayashi, *Tetrahedron Lett.* **1998**, *39*, 2159–2162.

[12] S. F. Martin, J. A. Dodge, *Tetrahedron Lett.* **1991**, *32*, 3017–3020.

[13] a) A. D. Cross, I. T. Harrison, *Steroids* **1965**, *6*, 397–407; b) J. D. White, P. Theramongkol, C. Kuroda, J. R. Engebrecht, *J. Org. Chem.* **1988**, *53*, 5909–5921.

[14] G. Stork, R. Mook, Jr., S. A. Biller, S. D. Rychnovsky, *J. Am. Chem. Soc.* **1983**, *105*, 3741–3742.

[15] P. G. Gassman, S. J. Burns, K. B. Pfister, *J. Org. Chem.* **1993**, *58*, 1449–1457.

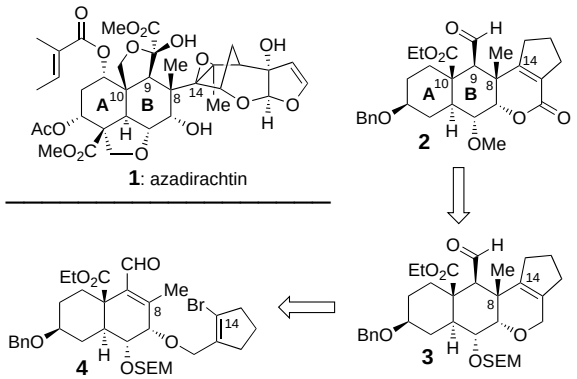
[16] K. C. Nicolaou, A. J. Roecker, M. Follmann, R. Baati, *Angew. Chem.* **2002**, *114*, 2211–2214; *Angew. Chem. Int. Ed.* **2002**, *41*, 2107–2110, following communication.

 © WILEY-VCH Verlag GmbH, 69451 Weinheim, Germany, 2002 1433-7851/02/4112-2106 $ 20.00+.50/0

Model Studies Towards Azadirachtin: Part 2. Construction of the Crowded C8–C14 Bond by Transition Metal Chemistry**

K. C. Nicolaou,* A. J. Roecker, Markus Follmann, and Rachid Baati

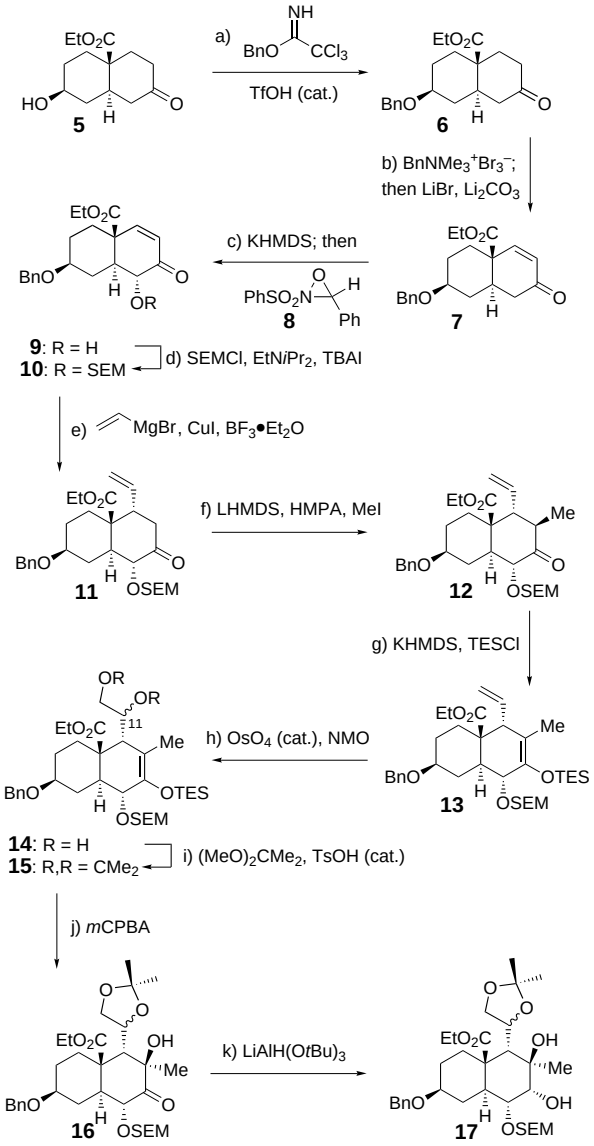
In the preceding communication,[1] we described our radical-based studies in the azadirachtin area providing a possible solution to the molecule's crowded C8–C14 bond problem. Herein, we wish to report an alternative strategy based on activated transition metal intermediates that may also offer a facile entry into the difficult C8–C14 linkage that bridges the two main domains of azadirachtin (**1**, Scheme 1).[2]



Scheme 1. Structure of azadirachtin (**1**) and model systems **2** and **3**.

To explore the application of transition-metal-based chemistry toward azadirachtin's C8–C14 bond, we defined model systems **2** and **3** as the targets of this investigation, and substrate **4** as their precursor (see Scheme 1). The latter compound includes within its structure an α,β-unsaturated aldehyde moiety as a Michael acceptor and a vinyl bromide as a progenitor to a metal species. These two functionalities are joined through a tether that could potentially be cleaved after the crucial C8–C14 bond formation. To test the above hypothesis, a suitable **AB** decalin precursor relevant to azadirachtin was sought and found in intermediate **17** (Scheme 2) as described below.

Synthesis of the required decalin fragment **17** commenced with benzylation of the known alcohol **5**[3] under acidic conditions to afford **6** in 73% yield. The resulting ketone **6**



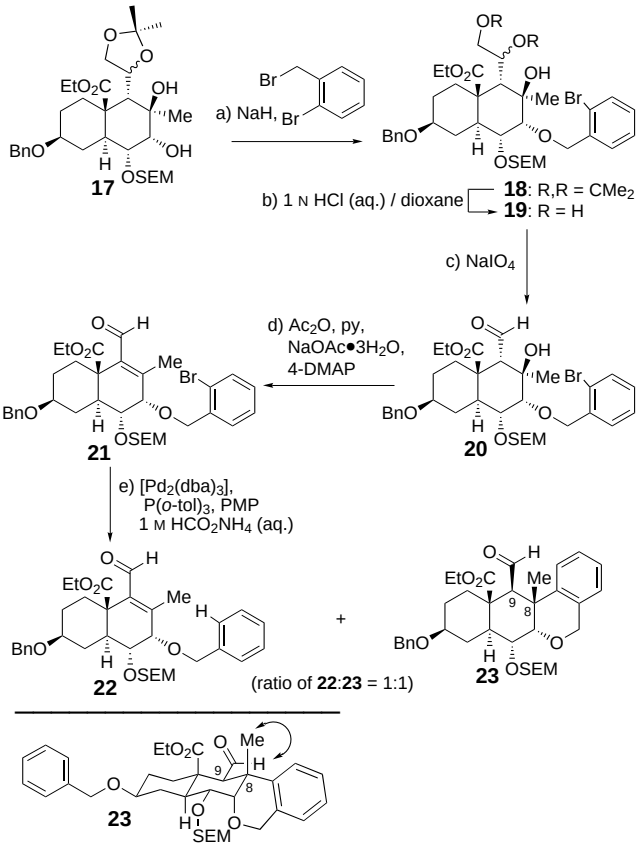
Scheme 2. Construction of key building block **17**. a) Benzyl 2,2,2-trichloroacetimidate (1.1 equiv), TfOH (0.05 equiv), 25 °C, 3 h, 73%; b) benzyltrimethylammonium tribromide (1.05 equiv), THF, 0 °C, 1 h; then LiBr (5.0 equiv), Li_2CO_3 (5.0 equiv), DMF, 110 °C, 3 h, 95%; c) KHMDS (1.2 equiv), **8** (1.1 equiv), THF, −78 °C, 1 h, 60%; d) SEMCl (2.0 equiv), EtN*i*Pr$_2$ (2.0 equiv), TBAI (1.0 equiv), CH_2Cl_2, 25 °C, 24 h, 78%; e) vinylmagnesium bromide (5.0 equiv), CuI (5.0 equiv), $BF_3 \cdot Et_2O$ (5.0 equiv), THF, −78 °C, 1 h, 97%; f) LHMDS (1.5 equiv), HMPA (2.0 equiv), MeI (10.0 equiv), THF, −40 → −5 °C, 12 h, 60%; g) KHMDS (1.5 equiv), TESCl (1.5 equiv), THF, −40 °C, 1 h, 90%; h) OsO_4 (0.05 equiv), NMO (5.0 equiv), acetone/H_2O (10:1), 25 °C, 48 h, 86%; i) TsOH (0.001 equiv), 2,2-dimethoxypropane (neat), 25 °C, 24 h, 87%; j) *m*CPBA (5.0 equiv), CH_2Cl_2, 25 °C, 24 h, 81%; k) LiAlH(O*t*Bu)$_3$ (2.5 equiv), THF, 0 °C, 1 h, 86%. Bn = benzyl, HMPA = hexamethylphosphoramide, KHMDS = potassium bis(trimethylsilyl)amide, LHMDS = lithium bis(trimethylsilyl)-amide, *m*CPBA = *meta*-chloroperbenzoic acid; NMO = 4-methylmorpholine *N*-oxide, SEM = 2-(trimethylsilyl)ethoxymethyl, TBAI = tetrabutylammonium iodide, TES = triethylsilyl, TfOH = trifluoromethanesulfonic acid, TsOH = *para*-toluenesulfonic acid.

[*] Prof. Dr. K. C. Nicolaou, A. J. Roecker, Dr. M. Follmann, Dr. R. Baati
Department of Chemistry and The Skaggs Institute
for Chemical Biology
The Scripps Research Institute
10550 North Torrey Pines Road, La Jolla, CA 92037 (USA)
Fax: (+1) 858-784-2469
and
Department of Chemistry and Biochemistry
University of California San Diego
9500 Gilman Drive, La Jolla, CA 92093 (USA)
E-mail: kcn@scripps.edu

[**] We thank Drs. D. H. Huang and G. Siuzdak for NMR spectroscopic and mass spectrometric assistance, respectively. This work was financially supported by the National Institutes of Health (USA), the Skaggs Institute for Chemical Biology, a predoctoral fellowship from the Division of Organic Chemistry of the American Chemical Society sponsored by Novartis (to A.J.R.), postdoctoral fellowships from Bayer AG (to M.F.), and Association pour la Recherche sur le Cancer (to R.B.), and grants from Abbott Laboratories, ArrayBiopharma, Bayer, Boehringer Ingelheim, DuPont, Glaxo, Hoffmann-LaRoche, Merck, Novartis, Pfizer, and Schering Plough.

was then regioselectively brominated with benzyltrimethylammonium tribromide, and the intermediate α-bromoketone was heated in DMF in the presence of LiBr and Li_2CO_3 at 110 °C to furnish enone **7** in 95% overall yield through elimination of HBr.[4] Hydroxylation of **7** was accomplished upon treatment with KHMDS followed by the addition of Davis oxaziridine[5] **8** to exclusively afford equatorial alcohol **9** in 60% yield. This α-hydroxyketone, **9**, was protected as a SEM ether, which was then efficiently engaged in a conjugate addition reaction with the cuprate derived from vinylmagnesium bromide and CuI in the presence of $BF_3 \cdot Et_2O$ to afford vinyl compound **11** as a single diastereomer in 97% yield.[6] The observed diastereoselectivity in this reaction presumably results from the bulky neighboring ester moiety which plays a decisive role in exerting stereochemical control in this and several subsequent steps as will be described below. Regioselective methylation of ketone **11** was effected upon exposure to LHMDS, HMPA, and MeI to yield compound **12** with complete selectivity for the axial methyl group (60% yield). The triethylsilyl enol ether **13** was then generated efficiently (90% yield) and regioselectively from **12** by deprotonation with KHMDS and quenching with TESCl. Chemoselective dihydroxylation of **13** then afforded diol **14** as a mixture of diastereomers (ca. 12:1, 80% combined yield). Although the stereochemical identity of the two diastereomers of **14** is presently unknown, it is of no consequence, as the newly generated stereocenter (C11) will be removed at a later stage in the synthesis. The 1,2-diol **14** was then protected as the acetonide **15** by exposure to 2,2-dimethoxypropane and catalytic amounts of TsOH (87% yield). This triethylsilyl enol ether **15** was subsequently converted to hydroxy ketone **16** by a Rubottom-type epoxidation[7] in excellent yield (81%) and with complete diastereoselectivity, presumably because of the bulky neighboring acetonide moiety. Finally, reduction of hydroxyketone **16** with $LiAlH(OtBu)_3$ proceeded through equatorial hydride attack to afford the axial secondary alcohol **17** in 86% yield.

As a first attempt to effect the desired bridging of the two azadirachtin model domains, diol **17** was converted to precursor **21** which contains the two reactive functionalities (Scheme 3). Thus, selective benzylation of the secondary hydroxy group in **17** afforded *o*-bromobenzyl ether **18** in 75% yield whose acetonide group was removed by exposure to aqueous HCl in dioxane at 40 °C to afford triol **19** (80% yield). Oxidative cleavage of the generated 1,2-diol system of **19** with $NaIO_4$ furnished aldehyde **20** in quantitative yield. Dehydration of **20** in the desired endocyclic sense required exposure to Ac_2O/pyridine in the presence of $NaOAc \cdot 3H_2O$ and 4-DMAP, and afforded the targeted intermediate **21** in 73% yield. This set the stage for the projected intramolecular coupling reaction. In the event, exposure of bromoenal **21** to catalytic amounts of $[Pd_2(dba)_3]$ in the presence of P(*o*-tol)$_3$, PMP and HCO_2NH_4 in toluene/THF at 60 °C led to the formation of equimolar amounts of the reduced product **22** (where the bromine atom was replaced by a hydrogen atom) and the bridged tetracyclic system **23** (100% combined yield).[8] The latter compound was formed as a single diastereomer and with the desired C8–C9 stereochemistry characteristic of the azadirachtin structure.

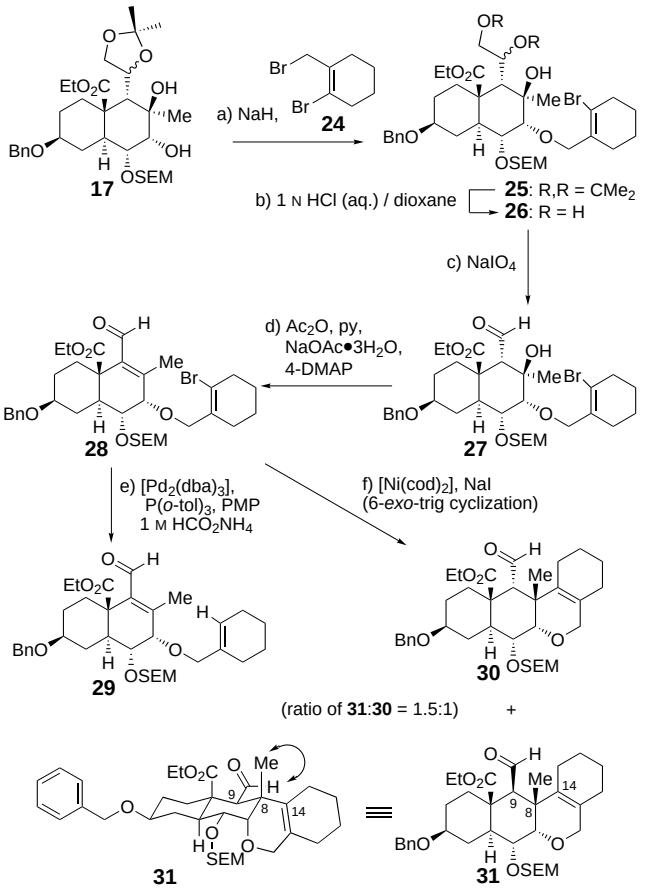


Scheme 3. Synthesis of tetracycle **23** via Pd^0-catalyzed cyclization. a) NaH (3.0 equiv), 2-bromobenzyl bromide (1.7 equiv), THF, 25 °C, 24 h, 75%; b) dioxane:1N HCl (aq.) (5:1, 0.01M), 40 °C, 1 h, 80%; c) $NaIO_4$ (1.5 equiv), THF/H_2O (2:1), 25 °C, 24 h, 100%; d) $NaOAc \cdot 3H_2O$ (15.0 equiv), 4-DMAP (3.0 equiv), Ac_2O/py (1:1), 50 °C, 24 h, 73%; e) $[Pd_2(dba)_3]$ (0.5 equiv), P(*o*-tol)$_3$ (1.0 equiv), PMP (10.0 equiv), toluene/THF/1M HCO_2NH_4 (aq.) (6:2:1), 60 °C, 11 h, 100%. dba = dibenzylideneacetone, 4-DMAP = 4-dimethylaminopyridine, PMP = 1,2,2,6,6-pentamethylpiperidine, py = pyridine.

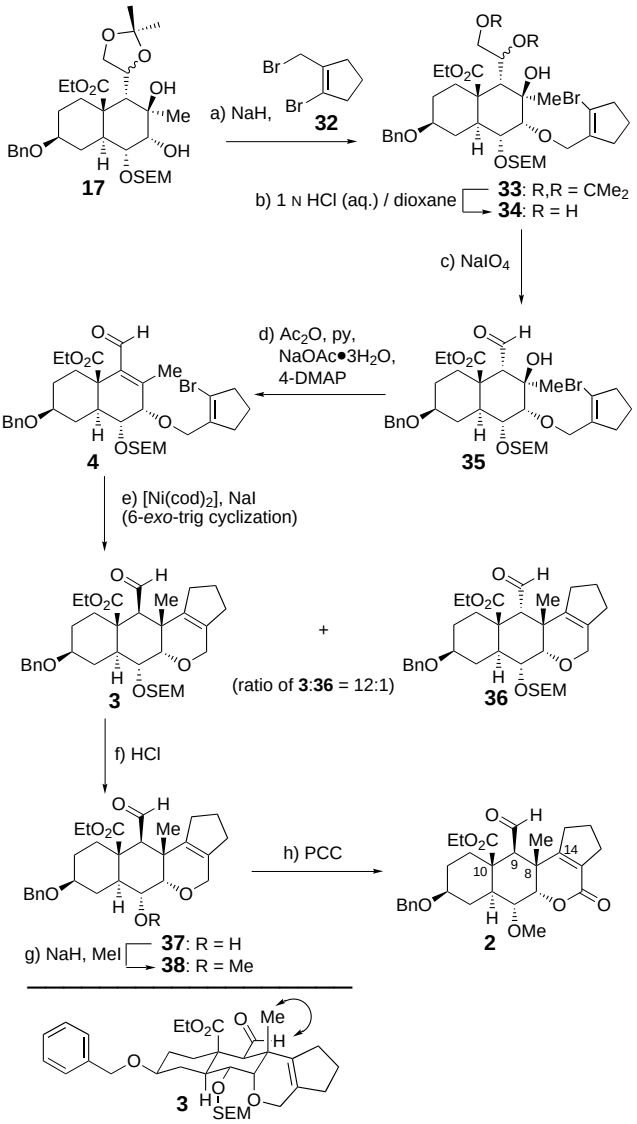
The relative stereochemistry at the C8 and C9 positions was established by nOe studies as shown in Scheme 3 (see arrows on structure **23**). This thermodynamically favored outcome implies an axial orientation for the palladium species in the transition state on C9 after the obligatory migratory insertion and release of the palladium upon donation of a formate ligand from HCO_2NH_4 followed by reductive elimination with retention of stereochemistry. This encouraging result led to the pursuit of a closer analogue to azadirachtin as described below.

The second targeted precursor in these investigations was the α,β-unsaturated aldehyde **28** equipped with a cyclohexene vinyl bromide ether moiety (Scheme 4). This intermediate was constructed in an expedient manner following similar chemistry to that utilized for the synthesis of **21** described above. On exposure of precursor **28** to palladium catalysis as mentioned above for the conversion of **21** to **23**, however, only the reduced product **29** was obtained and in quantitative yield. Failing to improve the situation in favor of the desired tetracyclic compound **31** by varying the conditions, we opted to generate the more reactive iodine counterpart of vinyl bromide **28**. To this end, we selected the method[9] that

 © WILEY-VCH Verlag GmbH, 69451 Weinheim, Germany, 2002 1433-7851/02/4112-2108 $ 20.00+.50/0



Scheme 4. Synthesis of tetracycles **30** and **31** by Ni^0-mediated cyclization. a) NaH (3.0 equiv), **24** (1.7 equiv), THF, 25 °C, 24 h, 60 %; b) dioxane:1N HCl (aq.) (5:1, 0.01M), 40 °C, 1 h 74 %; c) $NaIO_4$ (1.5 equiv), THF/H_2O (2:1), 25 °C, 24 h, 100 %; d) $NaOAc \cdot 3H_2O$ (15.0 equiv), 4-DMAP (3.0 equiv), Ac_2O/py (1:1), 50 °C, 24 h, 70 %; e) $[Pd_2(dba)_3]$ (0.5 equiv), P(*o*-tol)$_3$ (1.0 equiv), PMP (10.0 eqiuv), toluene/THF/1M HCO_2NH_4 (aq.) (6:2:1), 60 °C, 11 h, 100 %; f) $[Ni(cod)_2]$ (6.0 equiv), NaI (10.0 equiv), DMF, 80 °C, 2 h, 60 %. cod = 1,5-cyclooctadiene.



Scheme 5. Synthesis of tetracycles **3** and **36** by Ni^0-mediated cyclization and further elaboration of **3** to **2**. a) NaH (3.0 equiv), **32** (1.7 equiv), THF, 25 °C, 24 h, 63 %; b) dioxane:1N HCl (aq.) (5:1, 0.01M), 40 °C, 1 h, 74 %; c) $NaIO_4$ (1.5 equiv), THF/H_2O (2:1), 25 °C, 24 h, 100 %; d) $NaOAc \cdot 3H_2O$ (15.0 equiv), 4-DMAP (3.0 equiv), Ac_2O/py (1:1), 50 °C, 24 h, 67 %; e) $[Ni(cod)_2]$ (6.0 equiv), NaI (10.0 equiv), DMF, 80 °C, 2 h, 55 %; f) 1N HCl (aq.)/dioxane (3:1), 50 °C, 6 h, 85 %; g) NaH (10.0 equiv), MeI (10.0 equiv), THF, 50 °C, 2 h, 89 %; h) PCC (5.0 equiv), CH_2Cl_2, 50 °C, 24 h, 79 % at 56 % conversion. PCC = pyridinium chlorochromate.

requires $[Ni(cod)_2]$/NaI and proceeded to employ **28** as the substrate for the desired transformation. It was to our pleasant surprise that upon heating **28** in the presence of $[Ni(cod)_2]$ and NaI in DMF at 80 °C we observed the formation of the two diastereomers **30** and **31** in 60 % total yield (ca. 1:1.5 ratio). Although nickel-mediated Heck-type processes are known in the literature,[10] the ability of this reaction to form quaternary centers is, to the best of our knowledge, unprecedented. Also unprecedented is the use of α,β-unsaturated aldehydes in such nickel-facilitated coupling reactions. Once again, the desired *syn* stereochemistry of the two newly generated centers at C8 and C9 in the two diastereomers (**30** and **31**) was determined by NOE studies (see arrows on structure **31**, Scheme 4). The next step was to employ a cyclopentene ring on the "right wing" of the molecule as an even closer relative to azadirachtin and aimed both for the crowded C8–C14 bridge and the proper C8–C9 *syn* stereochemistry.

Scheme 5 outlines our final endeavor into the azadirachtin landscape, beginning with the coupling of diol **17** with cyclopentene dibromide **32**[11] and elaboration of the resulting product **33** to precursor **4** via intermediates **34** and **35** according to the standard sequence developed for the other two precursors (**21** and **28**) discussed above. The critical 6-*exo*-trig cyclization of **4** proceeded smoothly ($[Ni(cod)_2]$/NaI) and led to the desired stereoisomer **3** contaminated with a small amount of its C9-epimer (**36**, ca. 12:1 ratio, 55 % total yield). Again, nOe studies established the designated stereochemistry for the two compounds **3** and **36** (see arrows on structure **3**, Scheme 5). To advance the tetracyclic allylic ether **3** to its lactone counterpart **2**, it was necessary, for compatibility reasons, to exchange the SEM group for a Me substituent. PCC oxidation of the allylic ether moiety within **38** then furnished model system **2** (79 % yield based on 56 %

 © WILEY-VCH Verlag GmbH, 69451 Weinheim, Germany, 2002 1433-7851/02/4112-2109 $ 20.00+.50/0

Table 1. Selected physical properties of compounds **2** and **3**.

2: Colorless oil; $R_f = 0.56$ (silica, 50% EtOAc in hexanes); IR (thin film): $\tilde{\nu}_{max} = 2924, 2866, 1717$ (overlapping signals), 1458, 1383, 1360, 1263, 1199, 1142, 1090 cm^{-1}; ^1H NMR (500 MHz, $CDCl_3$): $\delta = 9.95$ (d, $J = 2.9$ Hz, 1H), 7.34–7.32 (m, 4H), 7.29–7.25 (m, 1H), 4.59 (d, $J = 9.9$ Hz, 1H), 4.51 (d, $J = 9.9$ Hz, 1H), 4.34 (d, $J = 2.2$ Hz, 1H), 4.26–4.20 (m, 2H), 4.02 (dd, $J =$ 9.5, 2.2 Hz, 1H), 3.46 (s, 3H), 3.42–3.37 (m, 1H), 2.66–2.60 (m, 1H), 2.54–2.48 (m, 3H), 2.30–2.23 (m, 2H), 2.03–1.98 (m, 2H), 1.95–1.88 (m, 2H), 1.43–1.39 (m, 1H), 1.32 (s, 3H), 1.30 (t, $J = 5.9$ Hz, 3H), 1.27–1.23 (m, 2H), 1.17–1.14 ppm (m, 1H); ^{13}C NMR (150 MHz, $CDCl_3$): $\delta = 200.0$, 173.4, 164.9, 162.5, 138.6, 129.7, 128.4, 127.6, 127.5, 81.0, 76.4, 75.1, 70.2, 61.5, 60.0, 57.7, 48.8, 41.7, 38.8, 35.7, 34.2, 30.1, 29.7, 28.6, 28.3, 21.2, 16.0, 14.0 ppm; HRMS (MALDI–FTMS), calcd for $C_{29}H_{36}O_7$ $[M+Na^+]$: 519.2353, found: 519.2359

3: Colorless oil; $R_f = 0.48$ (silica, 25% EtOAc in hexanes); IR (thin film): $\tilde{\nu}_{max} = 2931, 2846, 1727, 1717, 1448, 1364, 1243, 1200, 1097, 1055\ cm^{-1}$; ^1H NMR (500 MHz, $CDCl_3$): $\delta = 9.97$ (d, $J = 5.2$ Hz, 1H), 7.33–7.30 (m, 4H), 7.28–7.25 (m, 1H), 4.86 (d, $J = 7.0$ Hz, 1H), 4.79 (d, $J = 7.0$ Hz, 1H), 4.55 (d, $J = 11.8$ Hz, 1H), 4.49 (d, $J = 11.8$ Hz, 1H), 4.44 (dd, $J = 11.4$, 3.3 Hz, 1H), 4.29 (bd, $J = 15.4$ Hz, 1H), 4.25–4.17 (m, 2H), 4.09 (bd, $J =$ 15.0 Hz, 1H), 3.80–3.75 (m, 1H), 3.64–3.59 (m, 1H), 3.38 (d, $J = 3.0$ Hz, 1H), 3.37–3.32 (m, 1H), 2.39–2.34 (m, 1H), 2.35 (d, $J = 5.1$ Hz, 1H), 2.20–2.16 (m, 2H), 2.11–2.05 (m, 2H), 1.98–1.93 (m, 2H), 1.90–1.85 (m, 1H), 1.84–1.78 (m, 2H), 1.31 (t, $J = 7.3$ Hz, 3H), 1.27–1.23 (m, 2H), 1.21 (s, 3H), 1.14–1.09 (m, 1H), 1.00–0.93 (m, 2H), 0.02 ppm (s, 9H); ^{13}C NMR (125 MHz, $CDCl_3$): $\delta = 203.2$, 173.9, 139.4, 138.8, 134.9, 128.3, 127.6, 127.4, 95.1, 80.2, 74.1, 70.0, 67.4, 65.1, 61.1, 60.8, 49.1, 41.3, 38.6, 35.9, 31.9, 31.8, 29.7, 28.7, 28.5, 22.3, 18.2, 16.4, 14.1, −1.4 ppm; HRMS (MALDI–FTMS), calcd for $C_{34}H_{50}O_7Si$ $[M+Na^+]$: 621.3218, found: 621.3218

conversion) (for selected physical properties of compounds **2** and **3**, see Table 1).

The described chemistry may hold the key to a successful total synthesis of azadirachtin (**1**) by providing the basis for the construction of the C8–C14 bridge. Furthermore, this study may serve as the foundation for future developments in carbon–carbon bond forming reactions, particularly in sterically congested situations and in the construction of quaternary centers.

Received: March 18, 2002 [Z18925]

[1] K. C. Nicolaou, M. Follmann, A. J. Roecker, K. W. Hunt, *Angew. Chem.* **2002**, *114*, 2207–2210; *Angew. Chem. Int. Ed.* **2002**, *41*, 2103–2106, preceding communication.

[2] For isolation, structural elucidation, and previous synthetic studies in the area of azadirachtin (**1**), see literature cited in ref. [1].

[3] a) D. Nasipuri, R. Roy, G. Sarkar, M. Guha, *J. Indian Chem. Soc.* **1966**, *43*, 383–390; b) J. B. Jones, D. R. Dodds, *Can. J. Chem.* **1987**, *65*, 2397–2404.

[4] J. F. Templeton, L. Lin, Y. Ling, H. Majgier-Baranowska, K. Marat, *J. Chem. Soc. Perkin Trans. 1* **1997**, 2037–2044.

[5] For a general review on oxaziridines, see: F. A. Davis, B. C. Chen, *Chem. Rev.* **1992**, *92*, 919–934.

[6] a) K. Maruyama, Y. Yamamoto, *J. Am. Chem. Soc.* **1977**, *99*, 8068–8070; b) K. Maruyama, Y. Yamamoto, *J. Am. Chem. Soc.* **1978**, *100*, 3240–3241.

[7] G. M. Rubottom, J. M. Gruber, *J. Org. Chem.* **1978**, *43*, 1599–1602.

[8] R. Grigg, V. Sridharan, S. Sukirthalingam, *Tetrahedron Lett.* **1991**, *32*, 3855–3858.

[9] M. C. J. M. Hooijdonk, T. H. A. Peters, S. F. Vasilevsky, L. Brandsma, *Synth. Commun.* **1994**, *24*, 1261–1263.

[10] a) D. Sole, Y. Chancho, A. Llebaria, J. M. Moreto, A. Delgado, *J. Am. Chem. Soc.* **1994**, *116*, 12133–12134; b) D. Sole, J. Bonjoch, J. Bosch, *J. Org. Chem.* **1996**, *61*, 4194–4195.

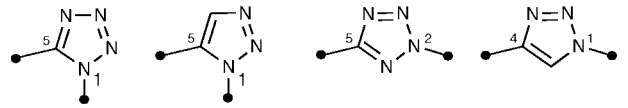
[11] T. Rajamannar, K. K. Balasubramanian, *Tetrahedron Lett.* **1988**, *29*, 5789–5792.

A Click Chemistry Approach to Tetrazoles by Huisgen 1,3-Dipolar Cycloaddition: Synthesis of 5-Sulfonyl Tetrazoles from Azides and Sulfonyl Cyanides**

Zachary P. Demko and K. Barry Sharpless*

Dedicated to Professor Rolf Huisgen

Stable in strongly acidic and basic media, as well as to oxidizing and reducing conditions, tetrazoles readily tolerate a wide range of chemical environments,[1] and new uses for this unique family of heterocycles continue to emerge in both materials science,[2] and pharmaceutical applications. They can serve as metabolically stable surrogates for a carboxylic acid group,[3] as precursors to a variety of nitrogen-containing heterocycles by Huisgen rearrangement,[4] and as simple lipophilic spacers displaying two substituents in the appropriate manner. In the latter example, the connectivity patterns of the embedded tetrazole units bear a striking resemblance to those of their 1,2,3-triazole analogues (Scheme 1).



Scheme 1. Spacial display of substituents in disubstituted tetrazoles and triazoles.

However, despite these structural similarities, the triazoles are much easier to synthesize, thanks to the direct Huisgen 1,3-dipolar cycloaddition route to triazoles ($RN_3 + RC{\equiv}CR$).[5] It has been argued that this [2+3] cycloaddition is among the rare organic reactions which approach perfection, or ideal "click-chemistry" status,[6] with many consequent applications.[7] The analogous [2+3] route to tetrazoles ($RN_3 + RC{\equiv}N$) is reliable for intramolecular cases,[8] but the existing intermolecular precedents for this process are neither general nor practical (see below).

Every chemist is familiar with the personal activation barrier to running "difficult" reactions, and it is well known that the value of a reaction increases dramatically if it is simple to perform. Therefore, uncovering a simple [2+3] fu-

[*] Prof. Dr. K. B. Sharpless, Dr. Z. P. Demko
Department of Chemistry and The Skaggs Institute for Chemical Biology
The Scripps Research Instititute, BCC-315
10550 North Torrey Pines Road, La Jolla, CA 92037 (USA)
Fax: (+1) 858-784-7562
E-mail: sharples@scripps.edu

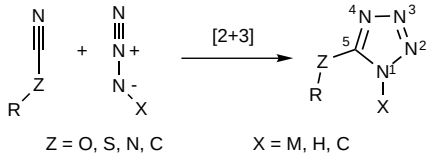
[**] We thank the National Institute of General Medical Sciences, National Institutes of Health (GM-28384), the National Science Foundation (CHE-9985553), the Skaggs Institute for Chemical Biology for a Predoctoral Fellowship (Z.D.), and the W. M. Keck Foundation for financial support. Dedicated to Professor Rolf Huisgen, the pioneer of this large and extremely useful family of reactions.

Supporting information for this article is available on the WWW under http://www.angewandte.org or from the author.

 © WILEY-VCH Verlag GmbH, 69451 Weinheim, Germany, 2002 1433-7851/02/4112-2110 $ 20.00+.50/0

sion process, a "click" reaction, to form tetrazoles would provide a rapid entry to this useful class of compounds.

A common route to 5-functionalized-1*H*-tetrazoles is by the facile addition of metal azides to nitriles, thiocyanates, cyanates, and cyanamides (Scheme 2).[9] If one could expand the scope of this reaction to include organic azides (Scheme 2; X = C), this could serve as a powerful process for fragment assembly.



Scheme 2. [2 + 3] Cycloaddition route to tetrazoles.

Unfortunately, most nitriles are not good enough dipolarophiles to engage organic azides in an intermolecular fashion, and Lewis acid catalysis has not yet been helpful. To date, only certain highly electron-deficient nitriles are known to undergo this cycloaddition intermolecularly; namely, *N*-alkylated nitriles (nitrilium salts),[10] perfluoronitriles, and trichloroacetonitrile.[11] There is also a report involving phenyl cyanate and several other electron-poor aryl nitriles, but these reactions were performed at a pressure of 10 kbar.[12]

Initial attempts to utilize unactivated nitriles gave, as expected, poor results. The only result worth mentioning was from the use of methyl thiocyanate as the solvent and β-phenethyl azide, heated in a pressure reactor at 136 °C, from which 5-methylthio-1-phenethyltetrazole (**1**) was isolated in 32 % yield. Increasing the oxidation state of the sulfur species from II → VI (i.e. R-S^{II}-CN → R-S^{VI}O$_2$-CN) was highly beneficial.

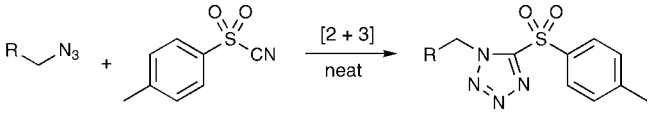
Upon simple heating of neat toluenesulfonyl cyanide with one equivalent of various unhindered azides, quantitative conversion to the 1-alkyl-5-sulfonyl tetrazole was observed; the excellent results in Table 1 establish the scope of this reaction. This procedure is the quintessence of the ideal "click-chemistry" transformation.[6] Toluenesulfonyl cyanide melts at 48 °C so, at the given reaction temperatures (80–100 °C), all the reactions performed here involved stirred, homogeneous liquids. As the reaction proceeds, the mixture solidifies as the product is formed. As the reactions are run neat and only one equivalent of each reagent is needed, there are no side products, and no workup is needed, other than chipping the stir bar away from the solid product. In addition, the reactants are not especially sensitive to air or water, so no precautions need to be taken in that respect.

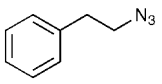
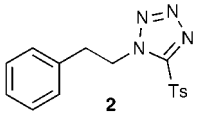
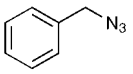
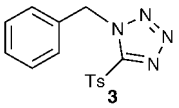
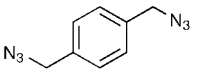
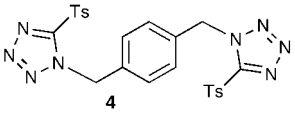
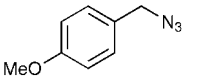
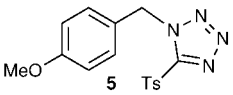
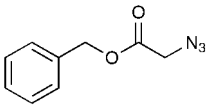
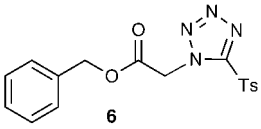
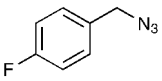
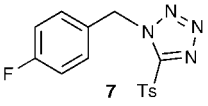
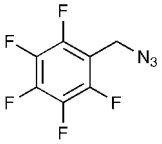
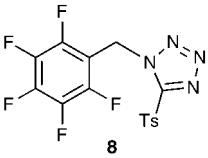
To our knowledge, these are the first examples of the direct synthesis of 1,5-substituted tetrazoles[13] by an intermolecular [2+3] cycloaddition between an organic azide and a nitrile group bound to a sulfur atom (Scheme 3). Sulfonyl cyanides were discovered in 1968,[14] and are known to be active dienophiles,[15] as well as dipolarophiles.[16]

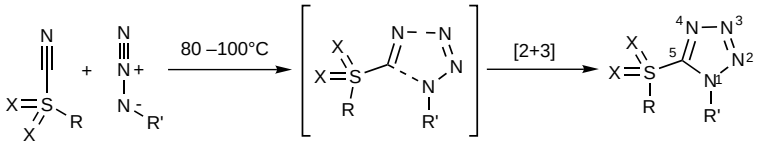
In all cases, the reaction is highly regioselective, and only one isomer is observed. Indeed, with sterically unhindered azides, the yields are virtually quantitative, and as the process is run neat, no purification is needed; truly a "click reaction"! Moreover, while the initial cycloaddition adducts **I** are stable under physiological conditions, their 5-sulfonyl substituent can be readily replaced by a variety of nucleophiles.

Sealed vials are used to ensure that the more volatile azides are not lost. In cases where the precise purity of the azide is

Table 1. [2+3] Dipolar cycloaddition of unhindered azides and toluenesulfonyl cyanide.



Reagent	Reaction conditions T [°C]	Time [h]	Product	Yield [%]
	100	16	 **2**	99
	80	16	 **3**	99
	80	16	 **4**	99
	80	16	 **5**	99
	80	16	 **6**	99
	80	16	 **7**	99
	80	40	 **8**	99



Scheme 3. Direct [2+3] cycloaddition route to 1-alkyl-5-sulfonyltetrazole.

 © WILEY-VCH Verlag GmbH, 69451 Weinheim, Germany, 2002 1433-7851/02/4112-2111 $ 20.00+.50/0

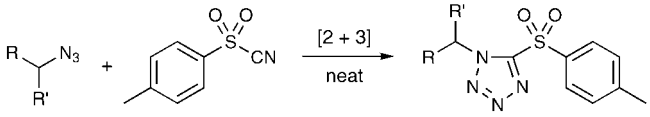
not known, a slight excess of toluenesulfonyl cyanide is added; at the end of the reaction the product is ground to a powder, and the excess TsCN reagent is simply removed by sublimation. Bulky azides and aryl azides do not react as well as unhindered azides (see Table 2 and Table 3). Yields for secondary and tertiary azides are between 46–91%, and for aryl azides, between 30–67%. Isolation of these sulfonyl tetrazoles by column chromatography is not difficult. Azides attached to electron-withdrawing groups require slightly longer reaction times or higher reaction temperatures.[11]

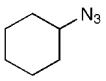
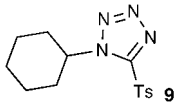
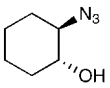
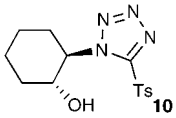
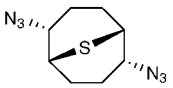
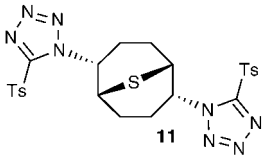
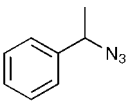
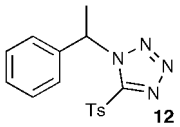
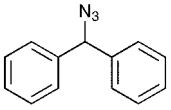
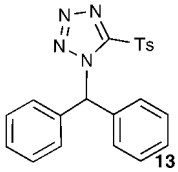
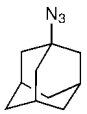
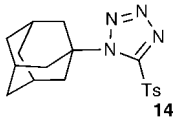
1-Substituted-5-sulfonyl tetrazoles are known to be very reactive toward nucleophilic attack by an addition–elimination pathway.[17] For example, thiophenol engages **3** at room temperature, and the corresponding adduct **19** can be isolated in 95% yield (see Scheme 4). Goltsberg and Koldobskii have demonstrated that various O, N, and C nucleophiles can add to sulfonyl tetrazoles, in yields ranging from 70–98%.[18] With this chemistry, one can functionalize sulfonyl tetrazoles with a wide range of nucleophiles. Therefore, by demonstrating a simple and expedient route to sulfonyl tetrazoles, we have provided an indirect route to a wide variety of 1,5-disubstituted tetrazoles (Scheme 5).

This chemistry enables a variety of substituents from the adjacent, or 1,5-positions of the hydrophobic tetrazole core, as shown above. This variety nicely complements the triazole cycloaddition chemistry mentioned in the introduction, as some acetylene–azide pairs are known to react to give 1,4-disubstituted triazoles with good regioselectivity[19] (Scheme 1, far right). Together, these methods provide fast access to either of the two fundamental topologies available to disubstituted azoles.

In summary, herein we extend the range of reliable dipolarophiles for intermolecular cycloadditions with organic azides, to include nitriles attached to a sulfonyl group. The examples with unhindered aliphatic azides constitute a perfect example of the ideal click-chemistry reaction—neat, thermal fusion in ≈100% yield. When sterically unhindered azides are used as the dipolar component, the reaction is virtually quantitative, and no workup procedures are necessary.

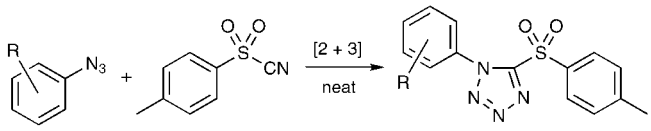
Table 2. [2+3] Dipolar cycloaddition of hindered azides and toluenesulfonyl cyanide.

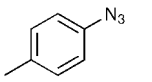
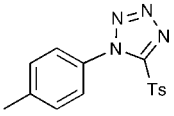
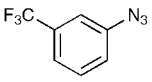
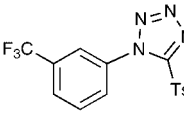
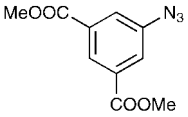
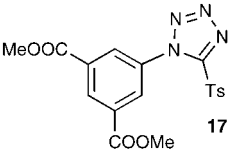
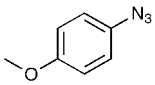
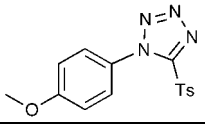


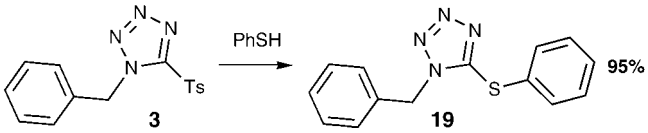
Reagent	Reaction conditions T [°C]	Time [h]	Product	Yield [%]
	80	16	 **9**	91
	80	16	 **10**	76
	80	24	 **11**	67[a]
	80	16	 **12**	59
	80	36	 **13**	48
	100	60	 **14**	46

[a] Because of the neighboring-group participation of the sulfur lone pair and the good leaving-group ability of the 5-sulfonyl tetrazole anion, a mixture of isomers is observed; see below.

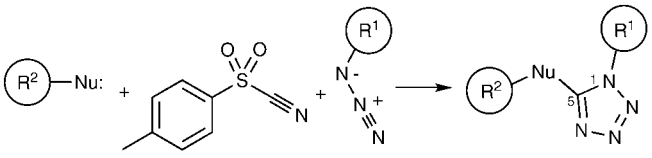
Table 3. [2+3] Dipolar cycloaddition of aryl azides and toluenesulfonyl cyanide.



Reagent	Reaction conditions T [°C]	Time [h]	Product	Yield [%]
	100	24	 **15**	62
	100	100	 **16**	67
	100	100	 **17**	43
	80	40	 **18**	30



Scheme 4. S_NAr derivatization of 5-sulfonyl tetrazoles.



Scheme 5. A general route to 1,5-disubstituted tetrazoles.

 © WILEY-VCH Verlag GmbH, 69451 Weinheim, Germany, 2002 1433-7851/02/4112-2112 $ 20.00+.50/0 *Angew. Chem. Int. Ed.* **2002**, *41*, No. 12

Together with the known substitutions of the resulting sulfonyl tetrazoles, the two-step sequence is formally equivalent to regioselective cycloadditions of azides with a wide variety of nitriles. Further studies on the scope of this chemistry will be reported.[20]

Experimental Section

Note: Many low-molecular-weight azides are known to be explosive. In this lab, no problems have been encountered, but great caution should be exercised when heating compounds of this type, especially neat. The reactions described here were run on only a few grams; an increase in the scale of these reactions will decrease the efficiency of heat dissipation and explosions may result.

A vial was charged with a stir bar, *p*-toluenesulfonyl cyanide (905 mg, 5.0 mmol), and azide (5.0 mmol), and tightly capped. The reagents were stirred neat in an oil bath set to 80 °C, for 16 h. If the reaction was not complete at this time, stirring was continued, in some cases with the temperature reset to 100 °C. In the cases of unhindered azides, the crude product, a light yellow solid, was analytically pure. To remove color, the product can be dissolved in a mixture of ethyl acetate (30 %) and hexanes (70 %), and run down a short plug of silica gel to yield a white solid. If excess toluenesulfonyl cyanide was present, the product was crushed and placed under vacuum at 80 °C for four hours. In the case of hindered azides, the product was purified by column chromatography, by eluting with ethyl acetate (10 %) and hexanes (90 %), to give the product as a white or light-tan solid. In some cases (**9**, **14**) the product was sufficiently insoluble that trituration with ethyl acetate (10 %) and hexanes (90 %) was sufficient to purify the compound.

Received: February 11, 2002 [Z 18692]

[1] R. N. Butler in *Comprehensive Heterocyclic Chemistry*, *Vol. 4* (Eds.: A. R. Katritzky, C. W. Rees, E. F. V. Scriven), Pergamon, Oxford, UK, **1996**.

[2] a) V. A. Ostrovskii, M. S. Pevzner, T. P. Kofmna, M. B. Shcherbinin, I. V. Tselinskii, *Targets Heterocycl. Syst.* **1999**, *3*, 467 – 526; b) M. Hiskey, D. E. Chavez, D. L. Naud, S. F. Son, H. L. Berghout, C. A. Bome, *Proc. Int. Pyrotech. Semin.* **2000**, *27*, 3 – 14.

[3] H. Singh, A. S. Chawla, V. K. Kapoor, D. Paul, R. K. Malhotra, *Prog. Med. Chem.* **1980**, *17*, 151 – 183.

[4] a) R. Huisgen, J. Sauer, H. J. Sturm, J. H. Markgraf, *Chem. Ber.* **1960**, *93*, 2106; b) D. Moderhack, *J. Prakt. Chem.* **1988**, *340*, 687 – 709.

[5] a) A. Michael, *J. Prakt. Chem.* **1893**, *48*, 94; b) R. Huisgen, *Proc. Chem. Soc.* **1961**, 357 – 369; c) R. Huisgen, *Angew. Chem.* **1968**, *80*, 329 – 337; *Angew. Chem. Int. Ed. Engl.* **1968**, *7*, 321 – 328.

[6] H. C. Kolb, M. G. Finn, K. B. Sharpless, *Angew. Chem.* **2001**, *113*, 2056 – 2075; *Angew. Chem. Int. Ed.* **2001**, *40*, 2004 – 2021.

[7] W. G. Lewis, L. G. Green, F. Grynszpan, Z. Radic, P. R. Carlier, P. Taylor, M. G. Finn, K. B. Sharpless, *Angew. Chem.* **2002**, *114*, 1095 – 1098; *Angew. Chem. Int. Ed.* **2002**, *41*, 1053 – 1057.

[8] a) The Chemistry of the Cyano Group (Ed.: Z. Rappaport), New York, Interscience, **1970**, p. 351; some recent examples: b) Z. P. Demko, K. B. Sharpless, *Org. Lett.* **2001**, *3*, 4091 – 4094; c) B. Davis, T. Brandstetter, C. Smith, L. Hackett, B. G. Winchester, G. Fleet, *Tetrahedron Lett.* **1995**, *36*, 7507 – 7510; d) D. Korakas, A. Kimbaris, G. Varvounis, *Tetrahedron* **1996**, *52*, 10751 – 10760; e) T. C. Porter, R. K. Smalley, M. Teguiche, B. Purwono, *Synthesis* **1997**, *7*, 773 – 777.

[9] a) W. G. Finnegan, R. A. Henry, R. Lofquist, *J. Am. Chem. Soc.* **1958**, *80*, 3908 – 3911; b) S. J. Wittenberger, *Org. Prep. Proced. Int.* **1994**, *26*, 499 – 531; c) Z. P. Demko, K. B. Sharpless, *J. Org. Chem*. **2001**, *66*, 7945 – 7950.

[10] H. Quast, L. Bieber, *Tetrahedron Lett.* **1976**, *18*, 1485 – 1486.

[11] W. R. Carpenter, *J. Org. Chem.* **1962**, *27*, 2085 – 2088.

[12] M. M. Krayushin, A. M. Beskopylnyi, S. G. Zlotin, O. A. Lukyanov, V. M. Zhulin, *Izv. Akad. Nauk. SSSR Ser. Khim.* **1980**, *11*, 2668.

[13] These 1-substituted-5-sulfonyl tetrazole systems are known, and the most common route for their synthesis is by the addition of sodium azide or trimethylsilyl azide to an isothiocyanate, to give the tetrazole thiol (see references [13a, 13b]), followed by alkylation (see reference [13c]), and oxidation to the sulfone (see reference [13d]). A less common route to such 1-substituted,5-mercaptotetrazoles is by metalation of a 1-alkylated, 5*H*-tetrazole with *n*-butyl lithium, followed by reaction with elemental sulfur (see reference [13e]). Direct alkylation of 1*H*,5-sulfidotetrazoles provides no control of regiochemistry (see references [1] and [4f]). a) E. Lieber, J. Ramachandran, *Can. J. Chem.* **1959**, *37*, 101 – 109; b) E. Lieber, R. Slutkin, *J. Org. Chem.* **1962**, *27*, 2214 – 2217; c) H. Alper, R. W. Stout, *J. Heterocycl. Chem.* **1973**, *10*, 5 – 10; d) K. Ishii, H. Hatanak, I. Ueda, *Chem. Pharm. Bull.* **1991**, *39*, 3331 – 3334; e) R. Rapp, *Can. J. Chem.* **1971**, *49*, 2139 – 2142; f) R. A. Henry, *J. Heterocycl. Chem.* **1976**, *13*, 391 – 392.

[14] a) A. M. van Leusen, A. J. W. Iedema, J. Strating, *J. Chem. Soc. Chem. Commun.* **1968**, 440 – 441; b) J. M. Cox, R. Ghosh, *Tetrahedron Lett.* **1969**, *39*, 3351 – 3352.

[15] a) R. D. Allan, B. Twitchin, *Aust. J. Chem.* **1980**, *33*, 599 – 604; b) P. Byard, F. Sainte, R. Beaudegnies, L. Ghosez, *Tetrahedron Lett.* **1988**, *29*, 3799 – 3802.

[16] a) J. Goerdeler, H. W. Linden, H, Puff, R. Hundt, *Chem. Ber.* **1985**, *118*, 3241 – 3247; b) H. Gotthardt, J. Blum, *Chem. Ber.* **1986**, *119*, 1445 – 1454.

[17] J. March, *Advanced Organic Chemistry*, Wiley, New York, **1992**, chap. 13, pp. 641 – 676.

[18] a) M. A. Goltsberg, G. I. Koldobskii, *Russ. J. Org. Chem.* **1995**, *31*, 1552 – 1553; b) M. A. Goltsberg, G. I. Koldobskii, *Russ. J. Org. Chem.* **1996**, *32*, 1194 – 1201; c) M. A. Goltsberg, G. I. Koldobskii, *Chem. Heterocycl. Comp.* **1996**, *32*, 1300 – 1304; d) A. P. Koreneva, G. I. Koldobskii, *Russ. J. Org. Chem.* **2000**, *36*(11), 1698 – 1699.

[19] Regioselectivities observed are from 3:1 to 9:1 with propiolates (references a, b). Recent work in our laboratory (V. Rostovsev et al., unpublished results) as well as in reference c has shown that copper acetylides add to azides with complete regioselectivity; a) D. Clarke, R. W. Mares, H. J. McNab, *J. Chem. Soc. Perkin Trans. 1* **1997**, 1799 – 1804; b) K. Hirota, H. Hosono, Y. Kitade, Y. Maki, C. K. Chu, R. F. Schinazi, H. Nakane, K. Ono, *Chem. Pharm. Bull.* **1990**, *39*, 2597 – 2601; c) C. W. Torne, C. Christensen, M. Meldal, *J. Org. Chem.* **2002**, *67*(9), 3057 – 3064.

[20] Note added in proof: We have recently become aware of a patent which describes the [2 + 3] cycloaddition of a number of sulfonyl cyanides and azides. Only one yield is given, and the yield and procedure are not as efficient as described here; see D. H. Klaubert, J. H. Sellstedt, US Pat. 4,526,978, July 2, **1985**.

A Click Chemistry Approach to Tetrazoles by Huisgen 1,3-Dipolar Cycloaddition: Synthesis of 5-Acyltetrazoles from Azides and Acyl Cyanides**

Zachary P. Demko and K. Barry Sharpless*

Dedicated to Professor Rolf Huisgen

The preceding communication[1] describes the facile [2+3] cycloaddition of azides and *p*-toluenesulfonyl cyanide to form 5-sulfonyl tetrazoles, interesting compounds in their

[*] Prof. Dr. K. B. Sharpless, Dr. Z. P. Demko
Department of Chemistry and The Skaggs Institute for Chemical Biology
The Scripps Research Instititute, BCC-315
10550 North Torrey Pines Road, La Jolla, CA 92037 (USA)
Fax: (+1) 858-784-7562
E-mail: sharples@scripps.edu

[**] We thank the National Institute of General Medical Sciences, National Institutes of Health (GM-28384), the National Science Foundation (CHE-9985553), the Skaggs Institute for Chemical Biology for a Predoctoral Fellowship (Z.D.), and the W. M. Keck Foundation for financial support.

Supporting information for this article is available on the WWW under http://www.angewandte.org or from the author.

 © WILEY-VCH Verlag GmbH, 69451 Weinheim, Germany, 2002 1433-7851/02/4112-2113 $ 20.00+.50/0

own right, and made all the more so by the ease of nucleophilic substitution of the 5-sulfonyl group. Just being a highly convergent route to useful tetrazoles makes this cycloaddition an interesting transformation, but its real value becomes apparent after examining the experimental details for the reaction: solvent-free fusion of the reactants at 80–100 °C affords the pure product in essentially quantitative yield.

Herein, we expand this methodology to include acyltetrazoles, which are similarly arranged for rapid functionalization. As in the preceding report, the yields are very high, and isolation is simple. In addition, as both azides and acyl cyanides are readily accessible, a modular approach to the synthesis of tetrazoles is possible—all in keeping with the tenets of "click chemistry".[2] Together with its complementary Huisgen 1,3-dipolar-cycloaddition route to triazoles ($RN_3 + RC{\equiv}CR$),[3] which, in the case of propiolates and copper acetylides, gives predominantly the 1,4-isomer,[4] these reactions provide a direct route to the various substituent patterns around an azole-ring system (Scheme 1).

It has been demonstrated that increasing the electron-withdrawing strength of the substituent bound to a nitrile tends to increase its rate of cycloaddition to azides.[5] Sulfonyl and perfluoroalkyl groups are among the most electron-withdrawing uncharged groups commonly encountered in chemistry,[6] thus it is not surprising that nitriles bound to these groups readily participate in this [2+3] cycloaddition.[1, 7] Are there other electron-poor nitriles which are activated enough to take part in the formation of synthetically useful tetrazoles?

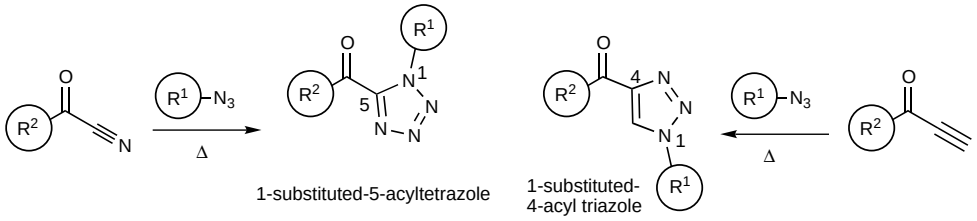
Two obvious choices, fluorinated aromatic nitriles and heteroaromatic nitriles, did not react with azides when heated, nor did some other unusual heteroatom-bound nitriles, such as dialkyl cyanophosphates. Carbonyl cyanides, while not as electron poor as sulfonyl cyanides, nor as hydrolytically stable, have the advantage of being readily available.[8] It has been demonstrated that certain acyl cyanides undergo a [2+3] cycloaddition with organic azides at a pressure of 10 kbar,[9] and also that ethyl cyanoformate undergoes a [2+3] reaction with certain organic azides upon heating,[10] both in moderate yield. We were pleased to find that a broad range of acyl cyanides,[11] cyanoformates,[12] and cyanoformamides[13] undergo a regioselective [2+3] cycloaddition with azides upon heating, neat, at 120–130 °C and ambient pressure, to give 1-substituted-5-acyl-tetrazoles in high yield (see Scheme 1, left).

To our knowledge, this report describes the first example of the direct synthesis of 1-substituted-5-acyltetrazoles[14] by an intermolecular [2+3] cycloaddition between an organic azide and an acyl cyanide at ambient pressure. Moreover, when aroyl cyanides or alkanoyl cyanides with no α proton are used in conjunction with unhindered azides as the substrate, the yields are above 90 %, and the purification is very simple, as it involves only a liquid–liquid extraction and a filtration—clearly a good "click" reaction. As dozens of acyl cyanides are commercially available, and countless more are available in one step from acyl halides, great diversity can be rapidly accessed with this cycloaddition. In addition, further important synthetic transformations are immediately available through the active aryl-ketone moiety, oxime, and hydrazone derivatives, for example.[15]

The scope of viable azide substrates is quite broad. Primary azides, when heated neat with benzoyl cyanide, provide products in 94–98 % yields (see Table 1, compounds **1**–**6**). Purification is also very simple—stirring the crude reaction mixture with aqueous potassium carbonate in a two-phase system for an hour hydrolyzes all of the unreacted acyl cyanide and, after passing the organic layer through a short plug of silica, evaporation yields the pure product. More hindered azides also react cleanly with benzoyl cyanide, although the yields are lower (**7** and **8**). When aryl azides are used as substrates, only decomposition is observed.

The scope of the reaction with various acyl cyanides is also quite broad, provided that there is not a proton in the α position (see Table 2). Aroyl cyanides react cleanly with benzyl azide to give the corresponding tetrazoles (**9**–**11**); furoyl cyanide is also a good substrate, although the reaction is not as clean (**12**). Pivaloyl cyanide is an excellent substrate (**13**), however, alkanoyl cyanides with a proton at the α position, for example pyruvoyl cyanide, show largely decomposition upon prolonged heating (**14**). This decomposition is presumably because of loss of HCN, to form the highly reactive ketene. Cyanoformamides and cyanoformates are also competent substrates (**15** and **16**). When unsaturated acyl cyanides are used as substrates, for example cinnamoyl cyanide, only decomposition is observed, even when no α proton was present, such as in α-methyl cinnamoyl cyanide.

A search for a more versatile route to acyltetrazole derivatives, one which would enable post-cycloaddition modification, lead to 4-nitrophenyl cyanoformate (**17**). When **17** is heated neat with benzyl azide at 120 °C, the corresponding activated tetrazole **18**, is produced in excellent yield. As a nitrophenolate ester of an electron-deficient heterocyclic carboxylic acid, **18** can be easily derivatized by nucleophiles (Scheme 2). As nitrophenyl esters are unstable to moisture, isolation by chromatography or crystallization gives poor yields. Fortunately, when the tetrazole formation and nucleophilic displacement reactions are run in one pot, the yields of the corresponding acyltetrazoles are generally high.

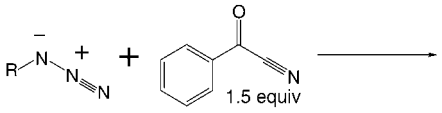


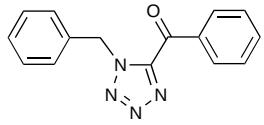
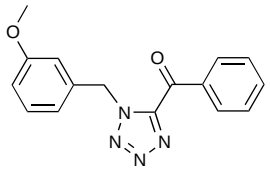
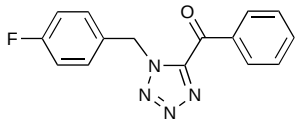
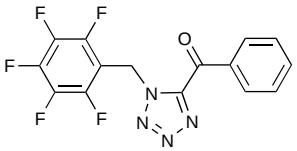
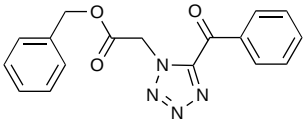
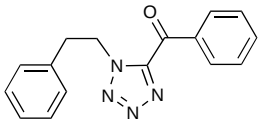
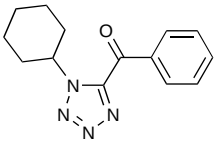
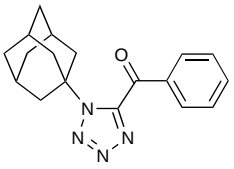
Scheme 1. Direct [2+3] cycloaddition routes to disubstituted acyltetrazoles and triazoles.

The use of **17** allows one to bring together an azide and a nucleophile in one pot to form, in high yield, a 1-substituted-5-acyltetrazole (see Scheme 3). This highly con-

 © WILEY-VCH Verlag GmbH, 69451 Weinheim, Germany, 2002 1433-7851/02/4112-2114 $ 20.00+.50/0 *Angew. Chem. Int. Ed.* **2002**, *41*, No. 12

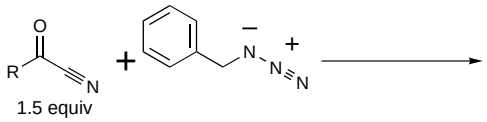
Table 1. Reaction of azides and benzoyl cyanide.[a]

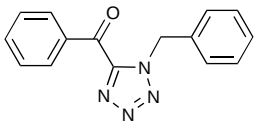
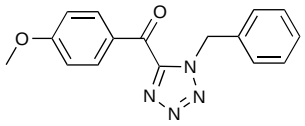
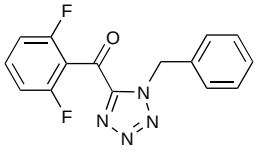
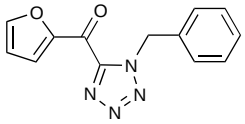
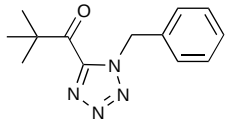
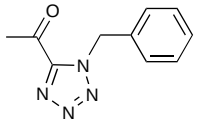
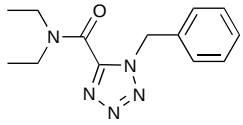
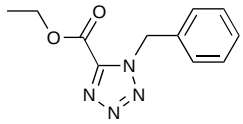


Compound	Product	Time [h]	Yield [%]
1		60	98
2		40	94
3		60	95
4		40	94
5		60	96
6		60	96
7		40	85
8[b]		80	75

[a] Reaction conditions: 1) neat, 120 °C, 2) stir with 10% Na_2CO_3, 3) filter through silica pad. [b] Product was collected by filtration and trituration.

Table 2. Reaction of acyl cyanides with benzyl azide[a].



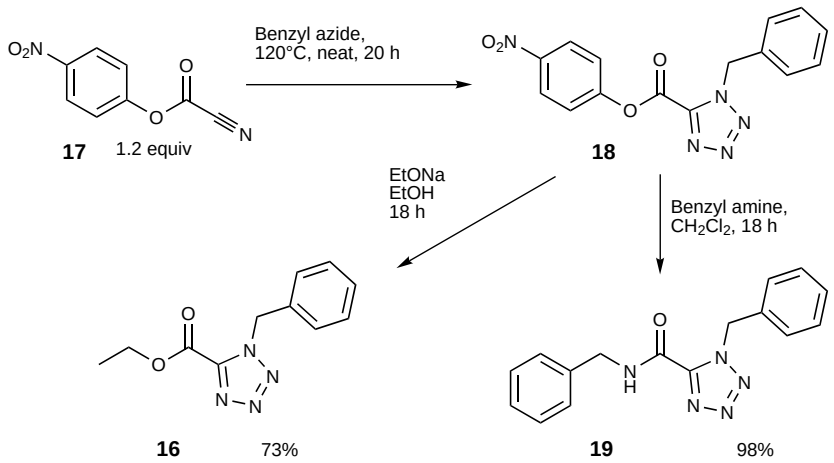
Compound	Product	Time [h]	Yield [%]
9		40	98
10		40	97
11		40	99
12[b]		20	91
13[c]		60	92
14[b,d]		24	62
15[b,c]		60	85
16[b]		40	83

[a] Reaction conditions: 1) neat, 120 °C, 2) stir with 10% Na^2CO_3, 3) filter through silica pad. [b] Purification by column chromatography was necessary. [b] Reaction run at 130 °C. [d] 10 equivalents of acyl cyanide

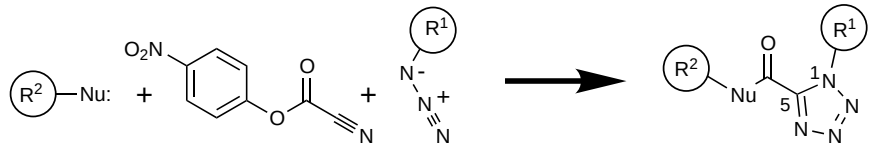
vergent route elegantly complements the triazole cycloaddition chemistry mentioned in the introduction, as carbonyl-substituted acetylene derivatives are known to react with azides to give 1,4-disubstituted triazoles with relatively good regioselectivity (see Scheme 1). These two reactions, taken together, provide a "click" route to the various geometries of disubstituted acylazoles.

In summary, outlined here is a simple route to 1-substituted-5-acyltetrazoles by a [2+3] cycloaddition of readily available acyl cyanides and aliphatic azides. The reactions are high yielding and product isolation is simple. In addition, we found that *p*-nitrophenyl cyanoformate undergoes the same cycloaddition process in high yield, and that the resulting activated esters of the 1-alkyltetrazole-5-carboxylic acid can be captured in situ by nucleophiles such as amines and alkoxides.

 © WILEY-VCH Verlag GmbH, 69451 Weinheim, Germany, 2002 1433-7851/02/4112-2115 $ 20.00+.50/0



Scheme 2. Use of *p*-nitrophenyl cyanoformate as an easily derivatizable acylnitrile source, en route to disubstituted acyltetrazoles.



Scheme 3. A general route to 1-substituted-5-acyltetrazoles.

Experimental Section

Note: Many low-molecular-weight azides, and certain tetrazoles and nitroaromatic compounds, are known to be explosive. In this lab no problems have been encountered, but great caution should be exercised when heating compounds of this type, especially neat. The reactions described here were run on only a few grams; an increase in the scale of these reactions will decrease the efficiency of heat dissipation and explosions could result.

General synthesis of acyltetrazoles: A vial was charged with a stir bar, azide (5.0 mmol), and acyl cyanide (7.5 mmol), and tightly capped. The reagents were stirred in an oil bath set to 120 °C, neat, for 40 h. If the reaction was not complete at this time, it was continued, in some cases with an increase in temperature to 130 °C, until the reaction was complete. The reaction mixture was then cooled, and dissolved in ethyl acetate (10 mL) and added to an aqueous solution of sodium carbonate (10% w/w, 50 mL) and stirred for one hour. In some cases, longer stirring times and the addition of acetone (20 mL) were necessary to effect the full hydrolysis of the acyl cyanide. The organic layer was isolated and the aqueous layer was extracted with ethyl acetate (10 mL). The combined organic layers were diluted with hexanes (60 mL) and run through a short plug of silica gel. The silica plug was washed with an equal amount and composition of solvent. The solvent was evaporated to yield the product.

Received: February 11, 2002 [Z18693]

[1] Z. P. Demko, K. B. Sharpless, *Angew. Chem. Int. Ed.* **2002**, *114*, 2214 – 2217; *Angew. Chem. Int. Ed.* **2002**, *41*, 2110 – 2113.

[2] H. C. Kolb, M. G. Finn, K. B. Sharpless, *Angew. Chem.* **2001**, *113*, 2056 – 2075; *Angew. Chem. Int. Ed.* **2001**, *40*, 2004 – 2021.

[3] a) A. Michael, *J. Prakt. Chem.* **1893**, *48*, 94; b) R. Huisgen, *Proc. Chem. Soc.* **1961**, 357 – 369; c) R. Huisgen, *Angew. Chem.* **1968**, *80*, 329 – 337; *Angew. Chem. Int. Ed. Engl.* **1968**, *7*, 321 – 328; .

[4] Regioselectivities observed are between 3:1 and 9:1. For precedents, see a) D. Clarke, R. W. Mares, H. J. McNab, *J. Chem. Soc. Perkin Trans. 1* **1997**, 1799 – 1804; b) K. Hirota, H. Hosono, Y. Kitade, Y. Maki, C. K. Chu, R. F. Schinazi, H. Nakane, K. Ono, *Chem. Pharm. Bull.* **1990**, *39*, 2597 – 2601.

[5] Z. P. Demko, K. B. Sharpless, *J. Org. Chem.* **2001**, *66*, 7945 – 7950.

[6] J. March, *Advanced Organic Chemistry*, 4th ed., Wiley, New York, **1992**, p. 18.

[7] W. R. Carpenter, *J. Org. Chem.* **1962**, *27*, 2085 – 2088.

[8] S. Hünig, R. Schaller, *Angew. Chem.* **1982**, *94*, 1; *Angew. Chem. Int. Ed. Engl.* **1982**, *21*, 36 – 49.

[9] I. V. Zavarzin, V. M. Zhulin, V. N. Yarovenko, M. M. Krayushkin, *Izv. Akad. Nauk SSSR Ser. Khim.* **1988**, *5*, 1168 – 1170.

[10] a) D. H. Klaubert, J. H. Sellstedt, C. J. Guinosso, S. C. Bell, R. J. Capetola, *Med. Chem.* **1981**, *24*, 748 – 752; b) D. H. Klaubert, S. C. Bell, T. W. Pattison, *J. Heterocycl. Chem.* **1985**, *22*, 333 – 336.

[11] a) T. S. Oakwood, C. A. Weisgerber, *Org. Synth. Coll. Vol. 3* **1955**, 112 – 114; b) N. Sperber, R. Fricano, *J. Am. Chem. Soc.* **1950**, *72*, 2792 – 2793; c) M. Tanaka, T. Kobayashi, T. Sakakura, *Angew. Chem.* **1968**, *96*, 519 – 520; *Angew. Chem. Int. Ed. Engl.* **1984**, *23*, 518 – 519; d) S. Murahashi, T. Naota, N. Nakajima, *Tetrahedron Lett.* **1985**, *26*, 925 – 928; e) S. Murahashi, T. Naota, *Synthesis* **1993**, 433 – 440; f) H. M. R. Hoffmann, K. Haase, Z. M. Ismail, S. Preftitsi, A. Weber, *Chem. Ber.* **1982**, *115*, 3880 – 3885; g) K. E. Koenig, W. P. Weber, *Tetrahedron Lett.* **1974**, *26*, 2275 – 2278.

[12] T. V. John, G. L. Larson, C. Subramaniam, US Patent 5,852,207 **1998**.

[13] H. Kobler, K.-H. Schuster, G. Simchen, *Liebigs Ann. Chem.* **1978**, 1946 – 1962.

[14] These 1-substituted-5-acyltetrazole systems are known, and a variety of routes have been described in the literature, the most common being oxidation of a hydroxymethyl tetrazole (see references [14a, 14b]) or treatment of a 5-alkylated-1-lithiotetrazole with a Weinreb amide (see references [14c, 14d]). Direct alkylation of an acyltetrazole provides poor regioselectivity (see references [14e, 14f]): a) D. Moderhack, A. Beissner, *Z. Naturforsch. B* **1996**, *51*, 1815 – 1817; b) D. L. Boger, H. Sato, A. E. Lerner, M. P. Hedrick, R. A. Fecik, H. Miyauchi, G. D. Wilkie, B. J. Austin, M. P. Patricelli, B. F. Cravatt, *Proc. Natl. Acad. Sci. USA* **2000**, *97*, 5044 – 5049; c) Y. Satoh, N. Marcopulos, *Tetrahedron Lett.* **1995**, *36*, 1759 – 1762; d) Y. Satoh, J. Moliterni, *Synlett* **1998**, *5*, 528 – 530; e) R. E. Ford, P. Knowles, E. Lunt, S. M. Marshall, A. J. Penrose, C. A. Ramsden, A. J. H. Summers, J. L. Walker, D. E. Wright, *J. Med. Chem.* **1986**, *29*, 538 – 549; f) M. Casey, C. J. Moody, C. W. Rees, R. G. Young, *J. Chem. Soc. Perkin Trans. 1* **1985**, *4*, 741 – 745.

[15] D. Moderhack, A. Beissner, *Z. Naturforsch. B* **1996**, *51*, 1815 – 1817.

 © WILEY-VCH Verlag GmbH, 69451 Weinheim, Germany, 2002 1433-7851/02/4112-2116 $ 20.00+.50/0

Controlled Hierarchical Self-Assembly and Deposition of Nanoscale Photonic Materials**

Tatjana N. Milic, Ning Chi, Dalia G. Yablon, George W. Flynn, James D. Batteas,* and Charles Michael Drain*

Nature repeatedly demonstrates exquisite control over the molecular forces that underpin the very existence of life. Inspired by nature, the synthetic introduction of specific molecular interactions to guide the association of matter is an overarching theme in current nanoscale materials and device design.[1] The technological and functional advantages of using nanoscaled or molecular components in a variety of devices has been recognized for decades.[1–5] However, the formation of functioning nanoscaled or molecular electronic devices from nonbiological components began in the 1980s.

The formation of self-organized photogated transistors from porphyrins in lipid bilayers is a key example,[6, 7] but the obvious limitation is the stability of the system. With the remarkable progress in the self-assembly of molecular components into specific arrays and polymers, there are many other recent examples of supramolecular species that are proposed as components of nanoscaled devices.[8–11]

The methodologies used to create devices on the nanometer scale can be roughly categorized as those using lithography ("top down") or self-assembly ("bottom up") approaches, with each having advantages and limitations. Certainly, self-assembly is claimed to be an important avenue toward the manufacture of the next generation of nanoscaled molecular materials, especially for use in photonic devices.[2, 7–11] But, there are several critical factors to be considered. Since the vast majority of molecular self-assembly processes are carried out in solution and utilize relatively weak intermolecular forces, can the desired products be reliably deposited onto surfaces and still retain their intended structure and function? Since the components of the self-assembled structures are organic or coordination compounds, how stable are they electrochemically, thermally, and to dioxygen? If self-assembled entities are to be used in large-scale applications, an important, yet often unacknowledged requirement is that highly pure molecular components or building blocks must be readily synthesized on large scales in high yields. Herein we report the self-assembly of porphyrinic arrays and clusters that address these issues.

Specifically, we demonstrate hierarchical solution-phase organization of self-assembled nonameric porphyrin arrays into columnar stacks that are about 6.2 nm in diameter and 0.4 nm to about 10 nm tall. These heights correspond to stacks of 1 to about 22 nonamers, and represent the self-organization of 21 to about 460 particles, respectively, of four different chemical types. The size of the aggregates is predetermined by the choice of appended alkyl group, solvent, temperature, porphyrin metalation, and an understanding of the secondary organization kinetics. Moreover, these materials can be deposited onto a variety of surfaces with high structural fidelity, with the choice of surface chemistry affording an additional modality for size selection. AFM and UV/Vis analysis shows that once deposited on surfaces these structures are stable in air for more than a year at room temperature, and retain their photophysical properties. Herein we present data for the hierarchical self-assembly of the free-base porphyrins, and note that zinc porphyrin nonameric arrays exhibit similar organizational properties. This approach provides access to a wide variety of closed arrays, and defined structures. Other approaches include liquid crystalline, and polymeric porphyrin materials on surfaces,[12–14] and other networks.[15, 16]

Earlier, we reported the self-assembly and characterization of a 21-component square-planar porphyrin nonamer.[17] The predefined geometry of either the metallo or free-base porphyrins as well as the coordination geometry of the metal-ion linker—all in the correct stoichiometry—dictates the final structure of the self-assembled arrays. In the case of the nonamer, the 180° (*trans*) coordination geometry of the 12 $PdCl_2$ species combines with four "L-shaped" porphyrins (**3**) that serve as the corners, four "T-shaped" porphyrins (**2**) that constitute the sides, and one "+-shaped" porphyrin (**1**) which resides in the center (Figure 1). We have since found that the porphyrins may be metalated in situ—during the self-assembly process—by the addition of nine equivalents of one of several acetate salts of the first-row transition metals to the mixture of nine porphyrins and 12 $[PdCl_2Bn_2]$. This process represents the self-assembly of a 30 component system. The metalloporphyrin nonamers, where all the porphyrins ligate the same transition metal (Fe^{II}, Co^{II}, Ni^{II}, or Zn^{II}) were characterized by the methods used previously.[17]

UV/Vis studies on a series of porphyrin arrays and tapes self-assembled by the same $[PdCl_2Bn_2]$ species[17, 18] reveal a remarkable similarity in the formation kinetics under the same conditions of concentration, solvent, and temperature. The rate of formation of the much more complex 21-particle nonameric array is only slightly slower than the formation of the simple 3-particle dimer or 8-particle tetramer- all occurring in less than 90 seconds (Table 1). This process is an exquisite demonstration of the cooperative formation of

[*] Prof. Dr. C. M. Drain, T. N. Milic
Department of Chemistry and Biochemistry
Hunter College and Graduate Center of
The City University of New York
695 Park Avenue, New York, NY 10021 (USA)
Fax: (+1) 212-772-5332
E-mail: cdrain@hunter.cuny.edu

Prof. Dr. J. D. Batteas, Dr. N. Chi
Department of Chemistry
The College of Staten Island and Graduate Center of
The City University of New York
2800 Victory Blvd., Staten Island, NY 10314 (USA)
Fax: (+1) 718-982-3910
E-mail: batteas@postbox.csi.cuny.edu

D. G. Yablon, Prof. Dr. G. W. Flynn
Department of Chemistry, Columbia University
3000 Broadway, MC 3167, New York, NY 10027 (USA)

[**] We gratefully acknowledge support from the National Science Foundation (CHE-0135509, CHE-0095649, and IGERT DGE-9972892), the Israel-US Binational Science Foundation (1999082), and PSC-CUNY. H. C. Chemistry department infrastructure is partially supported by NIH RCMI program GM3037. Dr. Andy Round is thanked for technical assistance.

Supporting information for this article is available on the WWW under http://www.angewandte.org or from the author.

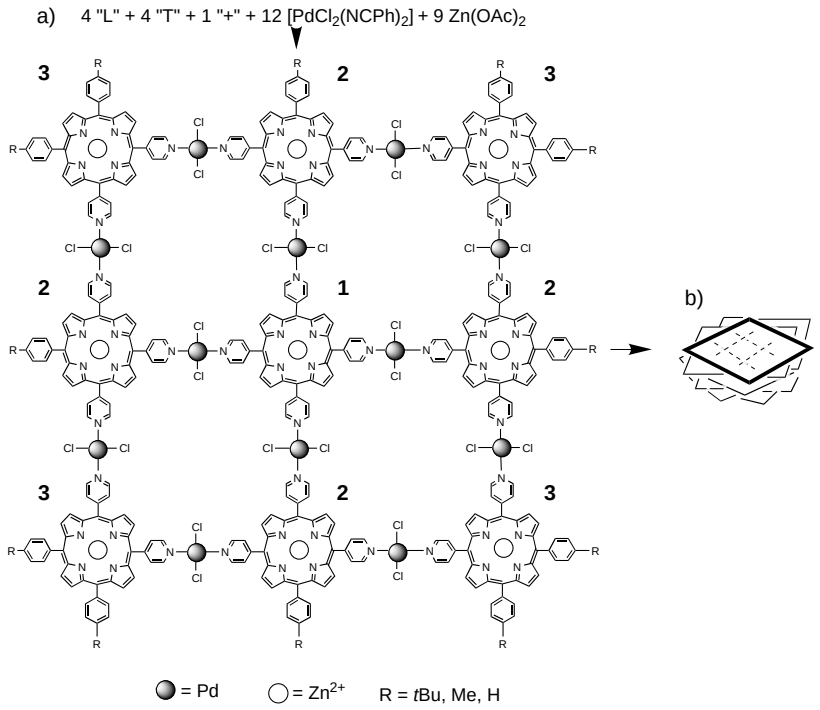


Figure 1. a) The self-assembly of a porphyrin nonameric array consisting of 30 particles is followed by b) the self-organization of these nonamers into columnar aggregates that are about 6 nm in diameter and an average of 5 nm in height. The size of these latter entities can be directed by various means (see text).

toluene in air up to about 80 °C. After cooling to 20 °C, the DLS data on these samples are identical to those before heating.

The energetics of the self-organization of the columnar stacks of porphyrin nonamers arises from the complex interplay between a variety of intermolecular forces. The π stacking of porphyrins to form face-to-face (H) or edge-to-edge (J) aggregates is a well known and understood phenomena.[19] Electronic spectra indicate both types of arrangements are present in the columnar aggregates.[17] Under the conditions described herein however, neither solutions of individual porphyrins or a mixture of them, nor the palladium complex, results in any discernible aggregation as shown by absorption and emission spectra, DLS, or AFM. Estimates of π-stacking interactions are between 3 and 5 kcal mol^{-1} per porphyrin face for meso-tetraphenylporphyrin.[19] Since the aryl groups are not coplanar with the porphyrin, these substituents also sterically prevent exact alignment of the two macrocycles. A second internonamer interaction comes from the $PdCl_2$ groups. The electrostatic and steric interactions arising from the Pd^{2+} and the

Table 1. Formation kinetics of porphyrin arrays.

	T1 [min]	T2 [min]
nonamer	1.4	26
tetramer	1.2	23
dimer	0.9	14

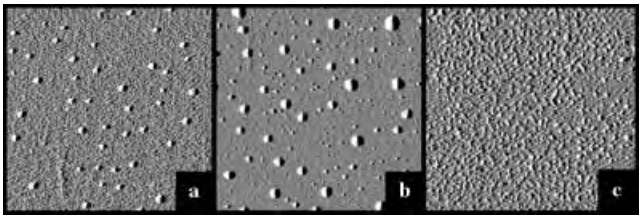


Figure 2. Aliquots of the toluene solution used in the DLS experiments were taken and deposited by syringe onto glass cover slips and the solvent evaporated. After rinsing the samples with toluene, AFM images (10 μm × 10 μm images are light shaded to enhance contrast) were taken to confirm the hypothesis that the formation of the nanoscaled aggregates of free-base porphyrin nonamers (R = Me) is dynamic. a) After 5 min, about 30-nm-high aggregates are first observed, followed by the observation b) of a bimodal distribution of these and 100s of much smaller sub-10-nm-high aggregates, and c) finally a uniform distribution of aggregates that are about 6 nm in height on average. (Since the typical size of the AFM tip was 30–50 nm, all sizes referred to by AFM are the nonamer stack heights, as the horizontal dimensions are a convolution of the tip and aggregate sizes). The AFM results correspond remarkably well with the DLS results.

thermodynamic products. The UV/Vis spectral evolution for the arrays continues, revealing a second time constant on the order of about 25 min for the nonamer. Dynamic and resonance light scattering (DLS, RLS), coupled with AFM experiments, reveal that this process is a secondary organization of these discrete self-assembled arrays into nanoscaled aggregates.

A single nonamer array when R = *t*Bu should be about 6.2 × 6.2 nm from *t*Bu to *t*Bu and about 0.4 nm in thickness. DLS of aggregates in solution and AFM of aggregates on glass show that the final aggregate is about 6 ± 1 nm in diameter and 2–10 nm tall. However, these experiments also suggest that the aggregation process is dynamic, proceeding through several intermediate stages. The initially formed kinetic products are about 30 nm tall aggregates, and these then dissociate and reorganize until the about 6 nm tall average thermodynamic products are formed. Once removed from the equilibrating solution by deposition on glass surfaces and evaporation of the solvent, the particles are trapped in the state of aggregation at the time. This procedure affords a time-based selection of the average particle size to be deposited on surfaces (Figure 2). UV/Vis and fluorescence spectra indicate the about 6 nm tall aggregates of all four types of nonamer (R = Me or *t*Bu, and M = Zn^{2+} or $2H^+$) are thermally stable in

Cl^- ions would tend to place the Cl^- ions from one nonamer over the vacant axial positions of the Pd^{2+} ions of the adjacent nonamer, over the pyrrole N–H group or in the case of the metalloporphyrins over the zinc(II) center. The nature of R (hydrogen, methyl, or *tert*-butyl), also influences the kinetics and size of the hierarchical assembly. In general, the kinetics are faster and the resultant columnar stacks are larger as one goes from R = *t*Bu, to Me, to H, with average columnar heights, determined by DLS, of 6 nm, 7 nm, 10 nm, respectively. Though the exact geometry of the nanoscaled aggregates is still under investigation, docking experiments suggest

 © WILEY-VCH Verlag GmbH, 69451 Weinheim, Germany, 2002 1433-7851/02/4112-2118 $ 20.00+.50/0

that one planar array may stack on top of another in either of two ways: a) one is rotated 30–60° relative to the next or b) one is diagonally offset by a little more than half the diameter of a single porphyrin about 0.6 nm.

The size of the hierarchical stack formed on the surface may also be explained in terms of the influence of surface energetics on π stacking (Figure 3). AFM studies reveal that

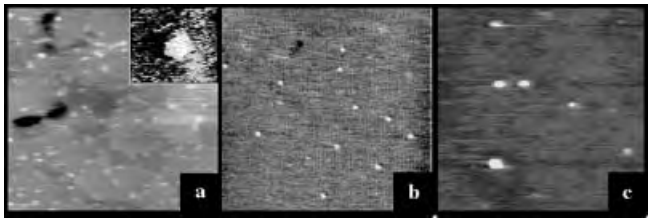


Figure 3. The size of the columnar stack of free-base porphyrin nonamers (R = *t*Bu) is also determined by the nature of the surface. a) Single nonameric arrays are typically found on Au(111) surfaces (the insert shows a single nonamer observed by STM), whereas larger aggregates are observed on b) mica (≈5–8-nonamer-high stacks) and c) glass (≈5–27-nonamer-high stacks). The images also show the expected increase in the surface density of the nonamers as the aggregates proceed from large stacks on glass to predominantly individual nonamers on Au. All images correspond to 1.15 μm × 1.15 μm, with *z* scales of 14.2 nm (a), 3 nm (b), and 11.9 nm (c). The insert in panel (a) corresponds to 16 nm × 14 nm with a *z* scale of about 5 Å, and was collected in constant current mode.

glass and mica surfaces favor absorption of nonamer aggregates, while surfaces such as gold favor dislodging the nonamer in contact with the surface from its parent nanoscaled aggregate and resulting in high surface densities of individual planar nonameric arrays on the gold surface.[20, 21] Interestingly, when nonamers are adsorbed on thin Au films, multi-supramolecular stacks (2–3 nonamers in height) preferentially decorate defects and step edges, while on the atomically flat terraces we find predominantly individual nonamers. This result is most likely due to the local dipoles formed by the Smoluchowski effect[21] at step edges, pinning the nonamers and adding an additional degree of polarization that favors stacking.[22] STM of nonamers on Au(111) clearly show the individual arrays to be about 6 × 6 × 0.4 nm in size (Figure 3a inset).

Further studies are aimed at evaluating electron conductance of stacked arrays as a function of the number of nonamers in the stacks, and as a function of light intensity. The detailed photonic properties of these aggregates are also under investigation. The controlled formation of nanocrystals and aggregates of inorganic,[23, 24] organic,[25] and hybrid materials[17, 26, 27] such as those described here, is a key step in the development of nanoscaled devices. The cooperative formation of these hierarchical structures, by using both specific and nonspecific interactions, imparts a high degree of stability and control of size not found in most supramolecular systems (Table 2).[28]

Table 2. Control of hierarchical self-assembly.

	Average height [nm]
chemistry:	
R = H	10 ± 2
R = Me	7 ± 1
R = *t*Bu	6 ± 1
surface:	
glass	6 ± 2
mica	3 ± 1
Au(111)	0.4 (single nonamer)
Au(111) edge	0.8 ± 0.3
kinetics:	
5 min (R = Me)	30 ± 5
10 min	50 ± 8
30 min	6 ± 1

Received: September 17, 2001
Revised: March 12, 2002 [Z17913]

[1] P. Ball, *Nature* **2001**, *409*, 413–416.
[2] A. P. Alivisatos, P. F. Barbara, A. W. Castleman, J. Chang, D. A. Dixon, M. L. Klein, G. L. McLendon, J. S. Miller, M. A. Ratner, P. J. Rossky, S. I. Stupp, M. E. Thompson, *Adv. Mater.* **1998**, *10*, 1297–1336.
[3] M. A. Fox, *Acc. Chem. Res.* **1999**, *32*, 201–207.
[4] *Ann. N. Y. Acad. Sci.* **1998**, *852*, 1–21 (Eds.: A. Aviram, M. Ratner).
[5] M. A. Reed, *MRS Bull.* **2001**, *26*, 113–120.
[6] C. M. Drain, D. Mauzerall, *Biophys. J.* **1992**, *63*, 1556–1563.
[7] C. M. Drain, D. Mauzerall, *Bioelectrochem. Bioenerg.* **1990**, *24*, 263–266; C. M. Drain, B. Christensen, D. Mauzerall, *Proc. Natl. Acad. Sci. USA* **1989**, *86*, 6959–6962.
[8] J.-M. Lehn, *Angew. Chem.* **1990**, *102*, 1347–1362; *Angew. Chem. Int. Ed. Engl.* **1990**, *29*, 1304–1319.
[9] J. S. Lindsey, *New J. Chem.* **1991**, *15*, 153–180.
[10] P. J. Stang, B. Olenyuk, *Acc. Chem. Res.* **1997**, *30*, 502–518.
[11] *Structure and Bonding* **2000**, *96*, 149–201 (Ed.: M. Fujita).
[12] D. M. Sarno, B. Jiang, D. Grosfeld, J. O. Afriyie, L. J. Matienzo, W. E. Jones, Jr., *Langmuir* **2000**, *16*, 6191–6199.
[13] X. Qiu, C. Wang, Q. Zeng, B. Xu, S. Yin, H. Wang, S. Xu, C. Bai, *J. Am. Chem. Soc.* **2000**, *122*, 5550–5556.
[14] C.-Y. Liu, H.-I. Pan, M. A. Fox, A. J. Bard, *Science* **1993**, *261*, 897–899.
[15] F. Wurthner, C. Thalacker, A. Sautter, *Adv. Mater.* **1999**, *11*, 754–758.
[16] D. G. Kurth, P. Lehmann, M. Schutte, *Proc. Natl. Acad. Sci. USA* **2000**, *97*, 5704–5707.
[17] C. M. Drain, F. Nifiatis, A. Vasenko, J. D. Batteas, *Angew. Chem.* **1998**, *110*, 2478–2481; *Angew. Chem. Int. Ed.* **1998**, *37*, 2344–2347.
[18] C. M. Drain, J.-M. Lehn, *Chem. Commun.* **1994**, 2314–2315.
[19] C. A. Hunter, J. K. M. Sanders, *J. Am. Chem. Soc.* **1990**, *112*, 5525–5534, and references therein.
[20] G. S. McCarty, P. S. Weiss, *Chem. Rev.* **1999**, *99*, 1983–1990.
[21] R. Smoluchowski, *Phys. Rev. Lett.* **1941**, *60*, 661–674.
[22] A. P. H. J. Schenning, F. B. G. Benneker, H. P. M. Geurts, X. Y. Liu, R. J. M. Nolte, *J. Am. Chem. Soc.* **1996**, *118*, 8549–8552.
[23] V. F. Puntes, K. M. Krishnan, A. P. Alivisatos, *Science* **2001**, *291*, 2115–2117.
[24] J. F. Banfield, S. A. Welch, H. Zhang, T. T. Ebert, R. L. Penn, *Science* **2000**, *289*, 751–754.
[25] E. R. Zubarev, M. U. Pralle, E. D. Sone, S. I. Stupp, *J. Am. Chem. Soc.* **2001**, *123*, 4105–4106.
[26] J. D. Diaz, G. D. Storrier, S. Bernhard, K. Takada, H. D. Abruña, *Langmuir* **1999**, *15*, 7351–7354.
[27] T. A. Jung, R. R. Schlitter, J. K. Gimzewski, *Nature* **1997**, *386*, 696–698.
[28] C. M. Drain, J. D. Batteas, G. W. Flynn, T. Milic, N. Chi, D. G. Yablan, H. Sommers, *Proc. Natl. Acad. Sci. USA*, DOI 10.1073/pnas.0/2521899.

 © WILEY-VCH Verlag GmbH, 69451 Weinheim, Germany, 2002 1433-7851/02/4112-2119 $ 20.00+.50/0

Identification of Jahn–Teller Effects in both Singlet and Triplet Low-Energy States of $[(\eta^6\text{-benzene})Nb(CO)_3]^+$**

Faraj Abu-Hasanayn,* Paul H.-Y. Cheong, and Matthew Oliff

Unsaturated 16e$^-$ $[CpML_n]$ intermediates play important role in the thermal and photolytic chemistry of 18e$^-$ $[CpML_{n+1}]$ complexes. A few isolated compounds and many theoretical studies have established that these intermediates have ground states with small singlet–triplet gaps, and geometries that lack the near C_{nv} symmetry characteristic of the 18e$^-$ analogues (Cp treated as a point).[1] Surprisingly, discussions of these novel electronic and structural properties have been based largely on qualitative MO concepts.[2] Studies of CH activation by d^8 [CpML] for example,[3] often refer to an extended Hückel theory (EHT) analysis[4] for an explanation of why the singlet and triplet states in this fragment are bent. An ab initio investigation of d^6 [CpRuLX][5] was superseded by an EHT study from the same group[6a] to rationalize why [CpRuLX] is planar when other d^6 $[CpML_2]$ complexes, such as $[CpMn(CO)_2]$,[7] are pyramidal. The same problem in $[CpFeL_2]^+$ was addressed by using DFT and EHT calculations.[6b] More recently, Poli and co-workers invoked EHT arguments to account for large geometric distortions in the singlet state of d^4 $[CpMoL_2X]$ calculated by using DFT,[8] but did not address deformations calculated in the triplet state of these complexes that would actually be inconsistent with the EHT arguments. Similarly, Harris and co-workers have calculated a triplet state of d^4 $[CpV(CO)_3]$ that deviated from pseudo-C_{3v},[9] but no comments were made on its origin.

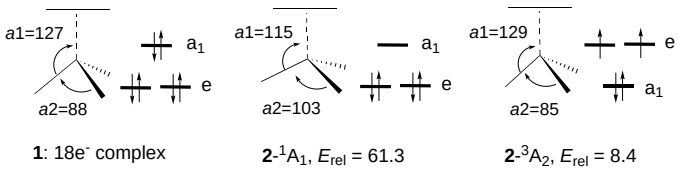
In an attempt to better understand these systems, we use DFT in the present study[10] to examine the structural and electronic properties of d^4 $[(\eta^6\text{-benzene})Nb(CO)_3]^+$. The applicability of the C_{3v} point group to this molecule allows us to demonstrate without ambiguity that both its singlet and triplet low-energy states are governed by Jahn–Teller effects[11] that have not been considered in previous studies. These effects are shown to be retained in the more chemically relevant $[\eta^5\text{-CpNb(CO)}_3]$ molecule, and to have implications for other unsaturated systems.

[*] Prof. F. Abu-Hasanayn,[+] P. H.-Y. Cheong, M. Oliff
Department of Chemistry
Bowdoin College
Brunswick, ME 04011 (USA)
Fax: (+1) 207-725-3017
E-mail: fabu@bowdoin.edu
Future address (October 2002):
Department of Chemistry
American University of Beirut
Beirut-Lebanon

[**] This research was supported by Bowdoin College during a visiting teaching position from 2000 to 2002, and by the National Computational Science Alliance under grant CHE000043N and utilized the Origin 2000 system. Prof. Jeff Nagle is thanked for useful discussions. A referee's comments on an earlier version of this study are appreciated.

Supporting information for this article is available on the WWW under http://www.angewandte.de or from the author.

It is convenient to approach the given problem starting from the 18e$^-$ $[(\eta^6\text{-benzene})Nb(CO)_3]^-$ complex (**1**; Figure 1). As found in previous studies,[12] the formally nonbonding d^6 electrons of **1** in C_{3v} occupy an a_1 MO of d_{z^2}

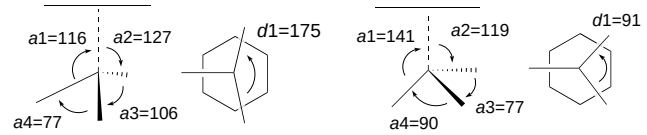


1: 18e$^-$ complex | **2**-$^1A_1$, E_{rel} = 61.3 | **2**-$^3A_2$, E_{rel} = 8.4

Figure 1. Angular parameters minimized in C_{3v} (in degrees), and partial MO diagrams for **1**, **2**-$^1A_1$ and **2**-$^3A_2$. E_{rel} (in kJ mol^{-1}) is defined relative to the energy of the ground state of **2** (**2**-$^3A'$, Figure 3).

character, and a doubly degenerate e MO that is primarily a linear combination of d_{xy} and $d_{x^2-y^2}$, with additional mixing from d_{xz} and d_{yz}. Since a_1 is higher than e in **1**, the most trivial way to obtain the 16e$^-$ $[(\eta^6\text{-benzene})Nb(CO)_3]^+$ complex (**2**) would be to remove the electron pair from the HOMO of **1**. Minimization of the resulting $^1A_1$ state affords **2**-$^1A_1$ (Figure 1), characterized as a second-order saddle point for ring slippage in either of two directions. This is a high-energy species of no interest to the present study.

Another configuration of the d^4 electrons in **2** would be $(a_1)^2(e)^2$, which would give rise to $^3A_2$, $^1A_1$, and ^1E states.[13] The triplet state leads to the true minimum **2**-$^3A_2$ (Figure 1). Unfortunately, calculation of $^1A_1$ has not been feasible with the single determinant methods employed in this study. This state is expected to be significantly higher in energy than **2**-$^3A_2$ and has not been pursued further. The ^1E state from the given configuration would be subject to a Jahn–Teller effect of the general E $\otimes$ e type,[11] meaning that the ^1E electronic state would couple with a degenerate e vibration, and the molecule would distort in two directions, one leading to a minimum and one to a transition state. In **2**, Jahn—Teller distortion lowers the point group from C_{3v} to C_s, and the symmetry of the three nonbonding d orbitals becomes a′, a′, and a″. Two $^1A'$ states can then be obtained from the $(a')^2(a'')^2$ and $(a')^2(a')^2$ configurations of the d^4 electrons. The minimized geometry of these states (**2**-$^1A'a$ and **2**-$^1A'b$ in Figure 2) can be



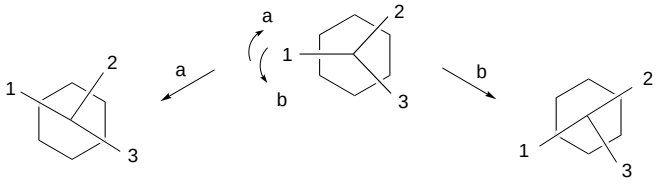
2-$^1A'a$: $(a'')^2(a')^2$ Minimum; E_{rel} = 9.1 | **2**-$^1A'b$: $(a')^2(a')^2$ Transition State; E_{rel} = 28.1

Figure 2. Angular parameters (in degrees) and occupancy of the d^4 electrons of **2**-$^1A'a$ and **2**-$^1A'b$. E_{rel} (in kJ mol^{-1}) is defined relative to the energy of the ground state of **2** (**2**-$^3A'$, Figure 3).

readily related to a parent C_{3v} structure that has undergone distortion in opposite directions. Most apparent is the dihedral between the two equivalent carbonyl ligands, *d*1,[14] which is near 180° in **2**-$^1A'a$ but is 91° in **2**-$^1A'b$. Bending of the carbonyl ligands from the benzene ring is also relevant. In **2**-$^1A'a$, for example, *a*1 is substantially smaller than *a*2 (116° versus 127°), whereas in **2**-$^1A'a$ the reverse is the case (141°

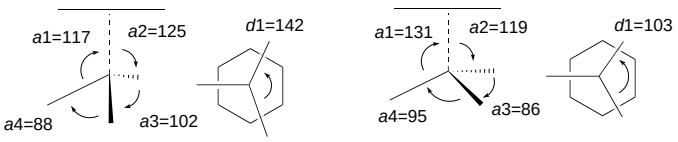
versus 119°). Not independently, the relative magnitude of the angles between the carbonyls (*a*3 and *a*4) is also reversed. The metal–carbonyl bond lengths, on the other hand, are comparable in the two geometries. From this, it may be inferred that the Jahn–Teller active vibration in this system is a linear combination of mostly two e normal modes, related to bending and inversion of the metal–carbonyl moiety.

Normal mode analysis reveals that **2**-^{1}A′a is a true minimum. **2**-^{1}A′b on the other hand is a transition state characterized by a vibration having an imaginary frequency ($\nu_i = 153i\ cm^{-1}$) with vector coordinates for a motion connecting two equivalent **2**-^{1}A′a minima as shown in Scheme 1. The activation energy for this transformation (ΔE_{act}) is 19.0 kJ mol^{-1}. **2**-^{1}A$_1$ located in C_{3v} (Figure 1) is 52.1 kJ mol^{-1} above **2**-^{1}A′a.



Scheme 1. Motion of the normal mode in **2**-^{1}A′b connecting two equivalent minima of **2**-^{1}A′a.

One last configuration of the d^4 electrons of **2** in C_{3v} would be $(a_1)^1(e)^3$, which would yield a Jahn—Teller active triplet state (^{3}E). In C_s, ^{3}A′ and ^{3}A″ states are then obtained from $(a'')^2(a')^1(a')^1$ and $(a')^2(a')^1(a'')^1$, respectively. The geometries of the states (**2**-^{3}A′ and **2**-^{3}A″, Figure 3) have exactly the same



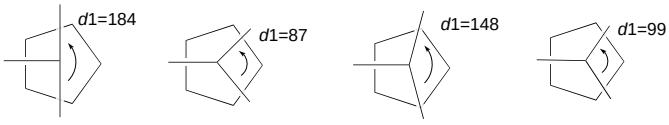
2-^{3}A': $(a'')^2(a')^1(a')^1$ Minimum; E_{rel} = 0.0

2-^{3}A'': $(a')^2(a')^1(a'')^1$ Transition State; E_{rel} = 0.3

Figure 3. Angular parameters (in degrees) and occupancy of the d^4 electrons of **2**-^{3}A′ and **2**-^{3}A″. **2**-^{3}A′ is the ground state of **2**, and is used to define E_{rel} (in kJ mol^{-1}).

distortion patterns as the singlet states, but to a substantially smaller degree. While **2**-^{3}A′ is a minimum, **2**-^{3}A″ has one imaginary frequency with coordinates similar to the loose vibration in **2**-^{1}A′b. The value of ν_i in **2**-^{3}A″ is fairly small, 24i cm^{-1} (or 70i cm^{-1} at the HF level) reflecting a rather facile intramolecular carbonyl conversion on the triplet energy surface. Consistently, **2**-^{3}A″ is only 0.3 kJ mol^{-1} above **2**-^{3}A′. The symmetric **2**-^{3}A$_2$ (Figure 1) is 8.4 kJ mol^{-1} above **2**-^{3}A′.[15] In turn, **2**-^{3}A′ is 9.1 kJ mol^{-1} below **2**-^{1}A′a, and is predicted to be the ground state of **2**.

In the Cp analogue of **2**, [CpNb(CO)$_3$] (**3**), two singlet and two triplet states can still be defined in C_s (Figure 4). The geometries of these states exhibit the same distortion patterns found in **2**, and can therefore be attributed to the same Jahn—Teller effects. In **3**, ^{1}A′a is calculated to be the ground state,



3-^{1}A'a $(a'')^2(a')^2$ Minimum E_{rel} = 0.0

3-^{1}A'b $(a')^2(a')^2$ Transition State E_{rel} = 24.0

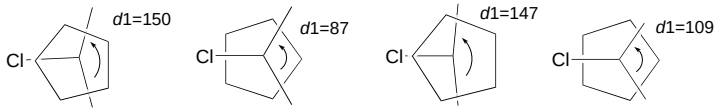
3-^{3}A' $(a'')^2(a')^1(a')^1$ Minimum E_{rel} = 7.5

3-^{3}A'' $(a')^2(a'')^1(a')^1$ Transition state E_{rel} = 8.8

Figure 4. Angular parameters (in degrees), occupancy of the d^4 electrons, and relative energy (in kJ mol^{-1}) of the low-lying singlet and triplet states of [CpNb(CO)$_3$].

and the triplet **3**-^{3}A′ is 7.9 kJ mol^{-1} higher in energy, a value unchanged at the CCSD(T) level. In turn, **3**-^{1}A′b is a transition state connecting two **3**-^{1}A′a, with $\nu_i = 180i\ cm^{-1}$, and ΔE_{act} = 24.0 kJ mol^{-1}. Similarly, **3**-^{3}A″ is a transition state with ν_i = 39i cm^{-1} and ΔE_{act} = 1.4 kJ mol^{-1}, and carries a residual frequency of 10i cm^{-1} for Cp rotation. At the CCSD(T) level, the given ΔE_{act} values become 19.4 and 3.7 kJ mol^{-1}, respectively.

To illustrate potential significance of the given Jahn—Teller effects beyond explaining the geometries of **2** and **3**, we consider d^4 [CpMo(CO)$_2$Cl] (**4**), proposed as an intermediate in reactions of [CpMo(CO)$_3$Cl].[16] As in **3**, two singlet and two triplet states can be specified for **4** in C_s (Figure 5). The geometries of theses states are close to those of **3**,[14] but they are all minima, a behavior analogous to the Jahn–Teller active d^8 ML$_3$[17a] and d^6 ML$_5$[17b] systems when substituted.



4-^{1}A'a $(a')^2(a'')^2$ E_{rel} = 80.2

4-^{1}A'b $(a')^2(a')^2$ E_{rel} = 0.0

4-^{3}A' $(a'')^2(a')^1(a')^1$ E_{rel} = 94.0

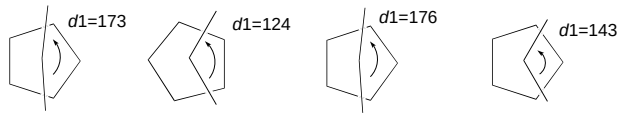
4-^{3}A'' $(a')^2(a')^1(a'')^1$ E_{rel} = 5.4

Figure 5. Angular parameters (in degrees), occupancy of the d^4 electrons, and relative energy (in kJ mol^{-1}) of the low-lying singlet and triplet states of [CpMo(CO)$_2$Cl].

Remarkably, Figure 4 and 5 reveal that the relative order of the two low singlet states is reversed in **3** and **4**. The same is true for the triplet states. For related systems there may be no reason to anticipate the correct order of these species, and it becomes essential to account explicitly for all of them. Moreover, although **4**-^{1}A′a has a much higher energy than **4**-^{1}A′b (Figure 5), **4**-^{1}A′a is actually the adiabatic product of CO dissociation from the ground state of [CpMo(CO)$_3$Cl].[18] Thus, two singlet adiabatic energy surfaces would be needed to capture the main features of the reaction. Calculated reaction coordinates for CO and N$_2$ addition to the related d^4 [CpMo(PH$_3$)$_2$Cl] complex have been recently used to interpret observed differences in the rates of these reactions,[19] but only one singlet energy surface was considered.[20]

Finally, if one ligand in the 16e$^-$ d^4 [CpML$_3$] system is substituted by an electron pair, the product would be a d^6 [CpML$_2$] complex. This suggests that the alternative planar or

pyramidal geometries known for the singlet state of d^6 [$CpML_2$] and [CpMLX] systems may actually belong to two distinct electronic states, rather than being the result of pseudo Jahn–Teller distortions in the same electronic state as previously proposed.[6, 21] Indeed, by altering the occupancy of the d^6 electrons in [$CpMn(CO)_2$] (**5**) we located a nearly planar bound stationary state (**5**-^{1}A′b, Figure 6),[22] 167 kJ mol^{-1} above the pyramidal structure (**5**-^{1}A′a). More



5-^{1}A'a	**5**-^{1}A'b	**5**-^{3}A'	**5**-^{3}A"
$(a')^2(a')^2(a')^2$	$(a')^2(a')^2(a'')^2$	$(a')^2(a'')^2(a')^1(a')^1$	$(a')^2(a')^2(a')^1(a'')^1$
E_{rel} = 198	E_{rel} = 31.4	E_{rel} = 0.0	E_{rel} = 14.5

Figure 6. Angular parameters (in degrees), occupancy of the d^6 electrons, and relative energy (in kJ mol^{-1}) of the low-lying singlet and triplet states of [$CpMn(CO)_2$].

importantly, extension of the given argument to the triplet state of **5** affords two minima (**5**-^{3}A′ and **5**-^{3}A″, Figure 6), both of which are *lower* in energy than **5**-^{1}A′a. Calculated frequencies of **5** have been invoked in the past to aid the characterization of transient intermediates observed in the photolysis of [$CpMn(CO)_3$],[7b] but only one triplet species was accounted for.

In conclusion, results from the present study reveal that both the singlet and triplet low-energy states of the unsaturated [$CpML_3$] system are subject Jahn–Teller effects. This finding can provide a basis for interpreting the geometries in other unsaturated [$CpML_n$] compounds, and suggests a need to consider more than one state in electronic structure studies of related systems.

Received: November 13, 2001
Revised: March 18, 2002 [Z18207]

[1] R. Poli, *Chem. Rev.* **1996**, *96*, 2135.
[2] A. Albright, J. K. Burdett, M. Whangbo, *Orbital Interactions in Chemistry*, Wiley, New York, **1985**.
[3] a) T. Ziegler, V. Tschinke, L. Fan, A. Becke, *J. Am. Chem. Soc.* **1989**, *111*, 9177; b) J. Song, M. Hall, *Organometallics* **1993**, *12*, 3118; c) D. G. Musaev, K. Morokuma, *J. Am. Chem. Soc.* **1995**, *117*, 799; d) M. Su, S. Chu, *J. Phys. Chem. A* **1997**, *101*, 6798.
[4] P. Hofmann, M. Padmanabhan, *Organometallics* **1983**, *2*, 1273.
[5] C. C. Bickford, T. Johnson, E. R. Davidson, K. G. Caulton, *Inorg. Chem.* **1994**, *33*, 1980.
[6] a) T. J. Johnson, K. Folting, W. E. Strib, J. D. Martin, J. C. Huffman, S. A. Jackson, O. Eisenstein, K. G. Caulton, *Inorg. Chem.* **1995**, *34*, 488; b) K. Costuas, J. Y. Saillard, *Organometallics* **1999**, *18*, 2505.
[7] a) P. Hofmann, *Angew. Chem.* **1977**, *89*, 551; *Angew. Chem. Int. Ed. Engl.* **1977**, *16*, 536; b) H. Yang, M. C. Asplund, K. T. Kotz, M. J. Wilkens, H. Frei, C. B. Harris, *J. Am. Chem. Soc.* **1998**, *120*, 10154.
[8] I. Cacelli, R. Poli, E. A. Quadrelli, A. Rizzo, K. Smith, *Inorg. Chem.* **2000**, *39*, 517.
[9] P. T. See, H. Yang, K. T. Kotz, C. K. Payne, C. B. Harris, *J. Phys. Chem. A* **1999**, *103*, 10426.
[10] Geometries were minimized at the B3LYP level by using primarily Gaussian 98. The Hay and Wadt ECPs with valence double-ξ plus d or f polarization functions were used on Cl and the metals. C, O, and H carried the 6-31g** basis set. The higher energy C_{3v} species of **2** were calculated by using Jaguar 4.1. For all the Cp complexes (**3**–**5**) CCSD(T) calculations give relative energies comparable to the DFT results. More details and a table of all calculated energies are given as supplemental material.
[11] I. Bersuker, *Chem. Rev.* **2001**, *101*, 1067.
[12] B. P. Byers, M. B. Hall, *Organometallics* **1987**, *6*, 2319.
[13] D. C. Harris, M. D. Bertolucci, *Symmetry and Spectroscopy*, Oxford University Press, New York, **1978**, chap. 5.
[14] *d*1 is defined by projection along the normal from the metal to the Cp and benzene rings, which are essentially planar in all complexes.
[15] This result was obtained using Jaguar 4.1.
[16] A. Hart-Davis, C. White, R. J. Mawby, *Inorg. Chim. Acta* **1970**, *4*, 441.
[17] a) K. Krogh Jespersen in *Computational Organometallic Chemistry* (Ed.: T. Cundari), Marcel Dekker, New York, **2001**, chap. 13; b) J. Riehl, Y. Jean, O. Eisenstein, M. Pelissier, *Organometallics* **1992**, *11*, 729.
[18] By "adiabatic" we mean a dissociation in which the symmetry of the orbitals containing the d^4 electrons in [$CpMo(CO)_3Cl$] is not changed in the course of the reaction.
[19] D. W. Keogh, R. Poli, *J. Am. Chem. Soc.* **1997**, *119*, 2516.
[20] The geometry of the singlet state of d^4 [$CpMo(PH_3)_2Cl$] reported in ref. [8] has a C_1 symmetry. Our preliminary calculations of this system show that in the C_s point group, the lower energy singlet state of d^4 [$CpMo(PH_3)_2Cl$] (matching **4**-^{1}A′b in Figure 5) is a transition state connecting two equivalent C_1 geometries, with $\Delta E_{act} = 0.4$ kJ mol^{-1}. Minimization of **4** considered in this study after distortion into the C_1 point group always converges into **4**-^{1}A′b. We thank Dr. Poli for bringing this point to our attention.
[21] T. R. Ward, O. Schaefer, C. Daul, P. Hofmann, *Organometallics* **1997**, *16*, 3207.
[22] Although normal mode analysis yields no imaginary frequencies for **5**-^{1}*A*′b, the Hessian matrix still includes one negative eigenvalue for a pyramidalization/ring slippage complex movement. At the HF level there are no imaginary frequencies or negative eigenvalues in the Hessian.

Remarkable Boosting of the Binding of Ion-Paired Organic Salts by Binary Host Systems**

Grazia Cafeo, Giuseppe Gattuso, Franz H. Kohnke, Anna Notti, Salvatore Occhipinti, Sebastiano Pappalardo, and Melchiorre F. Parisi*

The formation of host–guest complexes is normally achieved by the combined action of a number of weak noncovalent forces between the binding sites of the receptor and the target substrate.[1] However, for host–guest complex-

[*] Prof. M. F. Parisi, Dr. G. Cafeo, Dr. G. Gattuso, Prof. F. H. Kohnke, Dr. A. Notti
Dipartimento di Chimica Organica e Biologica
Università di Messina
Salita Sperone 31, 98166 Messina (Italy)
Fax: (+39) 090-393-895
E-mail: mparisi@unime.it
Prof. S. Occhipinti, Prof. S. Pappalardo
Dipartimento di Scienze Chimiche
Università di Catania
Viale A.Prof. Doria 6
95125 Catania, Italy

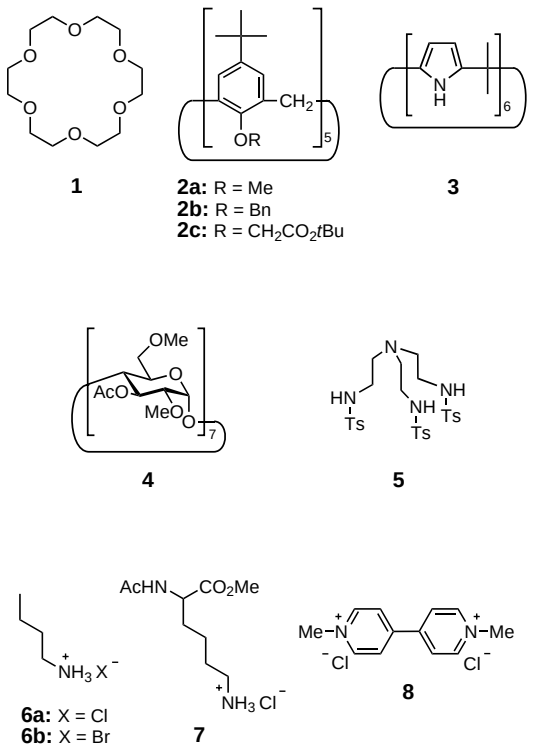
[**] The authors thank MURST (PRIN 2000 project) for financial support of this work.

 © WILEY-VCH Verlag GmbH, 69451 Weinheim, Germany, 2002 1433-7851/02/4112-2122 $ 20.00+.50/0

ation to occur, complementarity of binding sites is not the only requirement, since other factors, such as solvation, conformational changes, and in the case of charged species, the interference arising from ion-pairing effects, must concur for the process to have an overall favorable free energy.[2] Counterions also play a crucial role in the binding of charged species by neutral receptors.[3]

Ion-pair recognition, namely the simultaneous complexation of the cationic and anionic guest species, is a current challenge in host–guest and supramolecular chemistry. To this end, heterotopic receptors have been designed which take advantage of cooperative and allosteric effects.[3b, 4] Although these systems show undeniable potential for the binding of targeted ion pairs (including zwitterionic molecules),[5] an efficient assembly of cation and anion binding sites onto three-dimensional molecular platforms requires laborious multistep syntheses and careful control of the conformation. As an alternative, a combination of synthetically more-accessible anion and cation receptors (dual-host approach) has recently been used in membrane transport and extraction of inorganic salts,[6] but the mutual contributions to the overall binding process have been scarcely investigated. In the present study we demonstrate that when suitably chosen pairs of neutral receptors are used for the complexation of organic salts in apolar solvents, they exhibit a remarkable synergic effect which causes a dramatic enhancement of the binding ability of each host component towards its "complementary ion".

Scheme 1 shows the various neutral hosts employed in this study, which include [18]crown-6 (**1**), *p-tert*-butylcalix[5]-arenes with various degrees of preorganization **2a**–**c**,[7] calix[6]pyrrole (**3**),[8] per-(2,6-*O*-dimethyl-3-*O*-acetyl)-β-cyclodextrin (**4**),[9] and trisulfonamide **5**.[10] The mutual effect of appropriate pairs of cation/anion receptors in the binding of selected organic salts (*n*-butylammonium halides **6a**, **b**, N^{α}-acetyl-L-lysine methyl ester hydrochloride (**7**), methyl viologen dichloride (paraquat dichloride, **8**)) was investigated by ^{1}H NMR complexation experiments in CD_2Cl_2. The synergic effect that results in an increased binding ability of each host towards its complementary ion was evaluated by comparison with the degree of complexation observed when each host was used individually.



Scheme 1. Hosts and guests studied.

First of all we investigated the complexation of nBuNH$_3^+$Cl$^-$ (**6a**) with **1** and **3**. Calix[6]pyrrole (**3**) is known to form 1:1 complexes with halides in both the solid state and in solution, with a preference for chloride ions.[8b,c] When a solution of **3** (5×10^{-3} M) in CD_2Cl_2 is subjected to **6a** (0.5 equiv), only a weak host–guest interaction occurs, as evidenced by the small downfield shift experienced by the pyrrole NH resonance. This result is consistent with a fast complexation process of Cl$^-$ ions on the NMR timescale. However, the process becomes slow upon addition of **1** (1 equiv) to this mixture, and separate signals for the free and complexed **3** appear in the spectrum. The simultaneous complexation of nBuNH$_3^+$ ions by **1** (tripodal hydrogen bonding with the ethereal oxygen atoms, broad signal at $\delta =$ 7.21 ppm) causes a weakening of the ion pair, and greatly facilitates the uptake of chloride ions by **3**. Further addition of **6a** so as to reach a 1:1:1 ratio of the three components (**3**:**1**:**6a**), produces a single detectable species by NMR spectroscopy, that is, a supramolecular system consisting of a supercation (nBuNH$_3^+ \subset$ **1**, namely, the cation is H-bonded to the crown ether) and a superanion (Cl$^- \subset$ **3**, the anion is H-bonded to six pyrrole NH protons). This observation implies there is a nearly 100% complexation of Cl$^-$ ions by the moderate anion receptor **3** in the presence of an equimolar amount of **1**.

To further prove and quantify the synergism of appropriate binary host systems in the binding of **6a**,**b**, we next replaced the shape-unselective host **1** with three-dimensional *p-tert*-butylcalix[5]arenes **2a**–**c** as the cation receptors, which are known to selectively form 1:1 inclusion complexes with linear alkyl ammonium ions.[11] When a solution of the highly flexible **2a** in CD_2Cl_2 is exposed to **6a** (1 equiv), a doubling of the signals for the free and complexed host and guest species is observed, but less than 2% of the inclusion complex is formed. Although **2a** alone shows a very poor affinity for the nBuNH$_3^+$ ion, after the addition of the anion receptor **3** (1 equiv) the signals of the free guest disappear, while those of the included nBuNH$_3^+$ ion show up in the characteristic high-field region of the spectrum ($\delta = -0.4$ to -2.0 ppm).[11] Simultaneously, the counteranion (Cl$^-$) is completely complexed by **3**, as evidenced by the shift of the pyrrole NH resonance from $\delta = 7.74$ (free host) to $\delta = 10.91$ ppm (complex). This result confirms that the conversion into the supramolecular system (that is, the supercation (nBuNH$_3^+ \subset$ **2a**) and the superanion (Cl$^- \subset$ **3**)) is close to 100%. As in the previous case, a weak nonpreorganized receptor **2a** is transformed into a powerful one by the synergic action of a "complementary" receptor such as **3**.

The boosting of the binding affinities of the various calix[5]arene/calix[6]pyrrole pairs for *n*-butylammonium hal-

 © WILEY-VCH Verlag GmbH, 69451 Weinheim, Germany, 2002 1433-7851/02/4112-2123 $ 20.00+.50/0

ides **6** in CD_2Cl_2 and the relevant synergic factors are shown in Table 1. The complexation processes are generally slow on the NMR timescale.[12, 13] Thus, conditional association constants of the cationic (C) and anionic (A) receptors for their complementary ions ($K(C)_2$ and $K(A)_3$, respectively) and the corresponding conditional association constants observed in the presence of each other ($K(C)_{2+3}$ and $K(A)_{2+3}$) could be determined by direct analysis of the spectra. Although errors are inherent in the NMR technique for a degree of complexation outside the range 20–80%,[14] in those cases where an apparent >99% complexation was observed the K values were estimated by assuming a degree of complexation not higher than 95–98%. With this in mind, the synergic factors (computed as the ratio $K(C)_{2+3}/K(C)_2$ and $K(A)_{2+3}/K(A)_3$) are probably underestimates.

A scrutiny of Table 1 shows that, as expected, $K(C)_2$ and $K(C)_{2+3}$ for the binding of the nBuNH$_3^+$ ion depends on the degree of preorganization of the cation receptor (more preorganized hosts give higher values) and the "softness" of the counterion. The very high $K(C)_{2+3}$ values estimated for the binding of **6a**, **b** by the pair **2c** + **3** are in good agreement with the value earlier reported for the binding of the picrate salt of nBuNH$_3^+$ by **2c** ($\lg K = 6.47$, determined by UV spectroscopy in $CHCl_3$).[11a] Likewise, $K(A)_3$ values are in accord with the better size-matching of Cl^- ions for the calixpyrrole cavity. The computed synergic factors show that the binding of **6** by the binary system **2** + **3** are, in many cases, as high as 10^3–10^4 relative to **2** or **3** alone. The level of this synergic effect is similar to the increase in the cation binding affinity of the anion complexes of certain cyclic peptides.[4e] The synergic factors for the binding of **6b** are lower than those for **6a**. This observation is easily explained both by the higher $K(C)_2$ value for **6b** and by the lower affinity of **3** for Br^- ions.

This finding emphasizes the concept that pairs of receptors must be carefully chosen for optimum binding of a target ion-paired guest. Accordingly, the synergic factor in the binding of **6a**, **b** by combinations of **2a**–**c** with the C_3-symmetric anion receptor **5** (designed for tetrahedral rather than spherical anion complexation)[10] does not exceed five. Furthermore, it should be pointed out that the increased binding efficiency of these binary host systems does not in any way affect the intrinsic selectivity of each of the two host components.[15]

The latter point is of particular interest in view of possible applications in the biochemical, environmental, and analytical fields. For example, the highly preorganized calix[5]arene **2c** has recently been proposed as a potential biomimetic host for some biologically important ammonium substrates, such as N^{α}-acetyl-L-lysine methyl ester hydrochloride (**7**).[11a] One of the main problems in complexing these organic salts in nonpolar solvents is their tight ion pairing and their extremely low solubility in these media.[16] When a 1:1:1 mixture of **2c**, **3**, and **7** in CD_2Cl_2 is sonicated, the ammonium salt slowly dissolves as a result of the simultaneous complexation of the cationic and anionic components of the guest by the respective receptors. The formation of the supramolecular system is confirmed by ^{1}H NMR spectroscopic analysis, with the extent of complexation being close to 100% (Figure 1). The spectrum does not change after tenfold dilution.

The versatility and effectiveness of this approach was further confirmed by the complexation of the known herbicide paraquat dichloride (**8**) by the use of **3** in conjunction with β-cyclodextrin **4** in CD_2Cl_2. Receptor **4** is known to complex paraquat (preferably as the hexafluorophosphate salt) in polar solvents (CH_3CN, acetone).[17] However, **8**, which is sparingly soluble in a solution of CD_2Cl_2 containing one equivalent of **4**, is mostly dissolved (80%) when two equivalents of **3** are also present. The ^{1}H NMR spectrum is once again consistent with the formation of the expected supramolecular system (paraquat $\subset$ **4** supercation and $Cl^- \subset$ **3** superanion).

Since it is known that water lowers the anion binding ability of calix[6]pyrrole (**3**),[8c] we tested whether such action could be so pronounced as to produce a detectable decrease in the synergic effect. The binding of **6a** by the less effective pair of receptors (**2a** + **3**) decreased from 90 to 75% in water-saturated CD_2Cl_2. However, no significant decrease was observed with the most effective pairs of receptors.

In conclusion, we have demonstrated that effective binding of targeted ion-paired organic salts can be achieved by a suitable combination of cationic and anionic receptors. The observed synergic factors (up to 10^4) can be ascribed to the cleavage of the ion pair by the combined action of the two receptors. As a result of the negligible electrostatic interaction between the charged components of the salt when confined in the cavity of their complementary host the conditional association constants measurable by this approach may be regarded as close to those expected in an ideal case where the counterion is absent.

Received: December 14, 2001 [Z18388]

Table 1. Conditional association constants [M^{-1}] for the formation of 1:1 n-butylammonium halide complexes with receptors **2** and/or **3** (taken individually or as 1:1 pairs) and calculated synergic factors.[a,b]

Pairs	Salt	$K(C)_2$	$K(C)_{2+3}$	$K(C)_{2+3}/K(C)_2$	$K(A)_3$	$K(A)_{2+3}$	$K(A)_{2+3}/K(A)_3$
2a + **3**	nBuNH$_3^+$Cl$^-$	<5	$>7.6\times10^4$	$>1.5\times10^4$	<10	$>7.6\times10^4$	$>7.6\times10^3$
2b + **3**	nBuNH$_3^+$Cl$^-$	<10	$>2\times10^5$	$>2\times10^4$	<10	$>2\times10^5$	$>2\times10^4$
2c + **3**	nBuNH$_3^+$Cl$^-$	504[c]	$>2\times10^7$	$>2\times10^4$	<10	$>2\times10^5$	$>2\times10^4$
2a + **3**	nBuNH$_3^+$Br$^-$	24[c]	160[c]	6.7	<5	180[c]	>36
2b + **3**	nBuNH$_3^+$Br$^-$	128[c]	1750[c]	13.7	<5	1670[c]	>330
2c + **3**	nBuNH$_3^+$Br$^-$	$>1.6\times10^4$	$>2\times10^7$	$>1.2\times10^3$	<5	1.4×10^4	$>2.8\times10^3$

[a] By ^{1}H NMR complexation experiments of equimolar 5×10^{-3} M solutions of the three components in CD_2Cl_2 at 293 K. [b] See text for the definition of column headings. [c] Estimated error = 10%.

 © WILEY-VCH Verlag GmbH, 69451 Weinheim, Germany, 2002 1433-7851/02/4112-2124 $ 20.00+.50/0

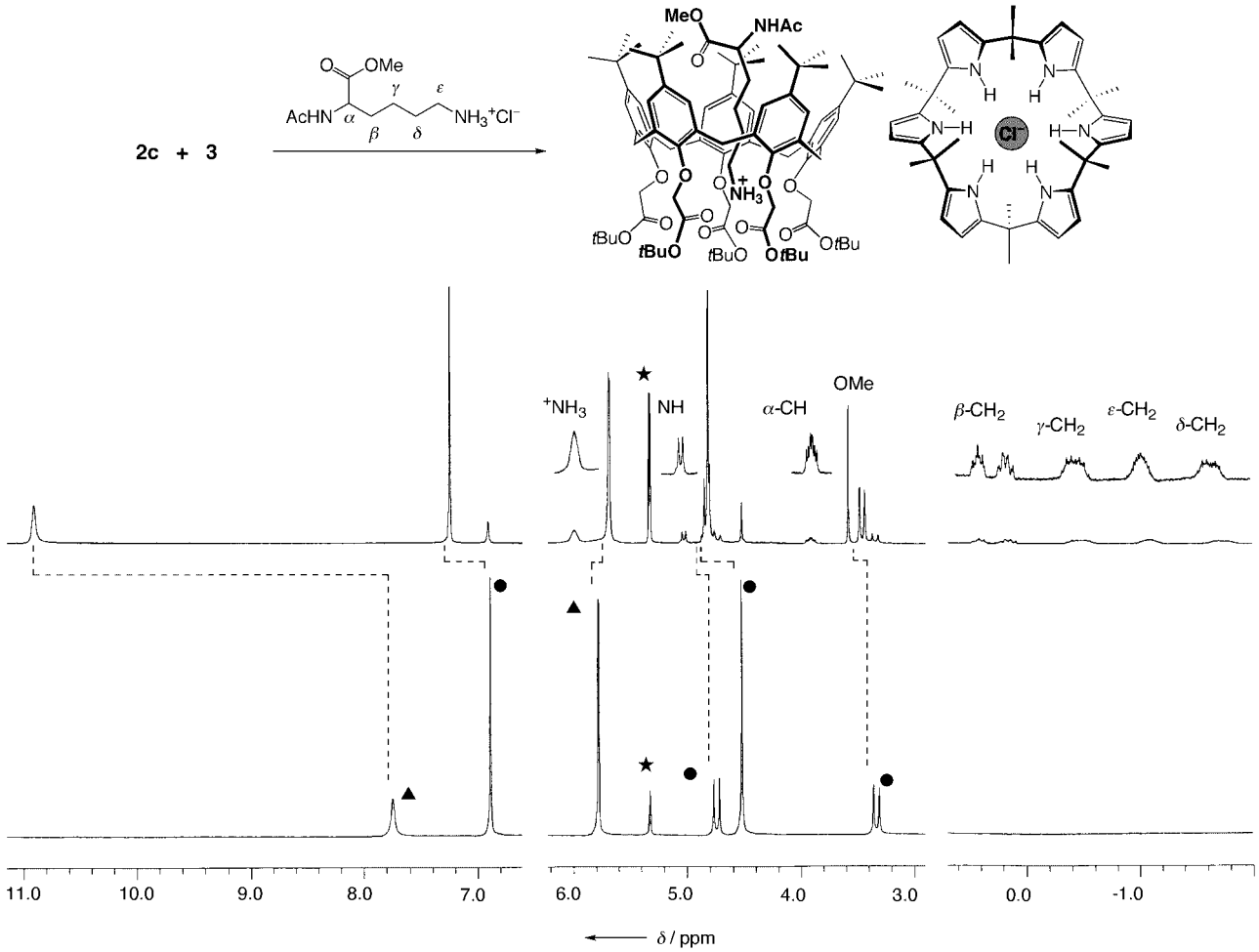


Figure 1. Selected regions of the ^{1}H NMR spectra (300 MHz, CD_2Cl_2, 293 K) of the 1:1 binary host system **2c** + **3** (bottom), and formation of the supercation N^{α}-Ac-L-Lys-OMe · H^+ ⊂ **2c** and superanion Cl^- ⊂ **3** (top) after addition of solid **7** (1 equiv). Insets (top trace) refer to the resonances of the cation included in the calix[5]arene cavity. Symbols ▲, ●, and ★ indicate the calix[6]pyrrole, calix[5]arene, and residual solvent resonances, respectively.

[1] P. D. Beer, P. A. Gale, *Angew. Chem.* **2001**, *113*, 502 – 532; *Angew. Chem. Int. Ed.* **2001**, *40*, 486 – 516; J.-M. Lehn, *Supramolecular Chemistry*, VCH, Weinheim, **1995**.

[2] A. Bianchi, E. García-España in *The Supramolecular Chemistry of Anions* (Eds.: A. Bianchi, K. Bowman-James, E. García-España), Wiley-VCH, New York, **1997**, pp. 217 – 275; R. M. Izatt, K. Pawlak, J. S. Bradshaw, *Chem. Rev.* **1995**, *95*, 2529 – 2586.

[3] a) V. Böhmer, A. Dalla Cort, L. Mandolini, *J. Org. Chem.* **2001**, *66*, 1900 – 1902; b) R. Shukla, T. Kida, B. D. Smith, *Org. Lett.* **2000**, 3099 – 3102; c) S. Bartoli, S. Roelens, *J. Am. Chem. Soc.* **1999**, *121*, 11908 – 11909.

[4] T. Tuntulani, S. Poompradub, P. Thavornyutikarn, N. Jaiboon, V. Ruangpornvisuti, N. Chaichit, Z. Asfari, J. Vicens, *Tetrahedron Lett.* **2001**, *42*, 5541 – 5544; A. Arduini, G. Giorgi, A. Pochini, A. Secchi, F. Ugozzoli, *J. Org. Chem.* **2001**, *66*, 8302 – 8308; J. B. Cooper, M. G. B. Drew, P. D. Beer, *J. Chem. Soc. Dalton Trans.* **2000**, 2721 – 2728; M. J. Deetz, M. Shang, B. D. Smith, *J. Am. Chem. Soc.* **2000**, *122*, 6201 – 6207, and references therein; S. Kubik, *J. Am. Chem. Soc.* **1999**, *121*, 5846 – 5855.

[5] A. Galán, D. Anreu, A. M. Echavarren, P. Prados, J. de Mendoza, *J. Am. Chem. Soc.* **1992**, *114*, 1511 – 1514; F. P. Schmidtchen, *J. Org. Chem.* **1986**, *51*, 5161 – 5168.

[6] K. Kavallieratos, B. A. Moyer, *Chem. Commun.* **2001**, 1620 – 1621; K. Kavallieratos, A. Danby, G. J. Van Berkel, M. A. Kelly, R. A. Sachleben, B. A. Moyer, K. Bowman-James, *Anal. Chem.* **2000**, *72*, 5258 – 5264; K. Kavallieratos, R. A. Sachleben, G. J. Van Berkel, B. A. Moyer, *Chem. Commun.* **2000**, 187 – 188; M. M. Murad, T. Hayashita, K. Shigemori, S. Nishizawa, N. Teramae, *Anal. Sci.* **1999**, *15*, 1185 – 1189; L. A. J. Chrisstoffels, F. de Jong, D. N. Reinhoudt, S. Sivelli, L. Gazzola, A. Casnati, R. Ungaro, *J. Am. Chem. Soc.* **1999**, *121*, 10142 – 10151. For membrane transport of amino acids, see M. T. Reetz, J. Huff, J. Rudolph, K. Töllner, A. Deege, R. Goddard, *J. Am. Chem. Soc.* **1994**, *116*, 11588 – 11589.

[7] D. R. Stewart, M. Krawiec, R. P. Kashyap, W. H. Watson, C. D. Gutsche, *J. Am. Chem. Soc.* **1995**, *117*, 586 – 601; G. Barret, M. A. McKervey, J. F. Malone, A. Walker, F. Arnaud-Neu, L. Guerra, M.-J. Schwing-Weill, C. D. Gutsche, D. R. Stewart, *J. Chem. Soc. Perkin Trans. 2* **1993**, 1475 – 1479.

[8] a) G. Cafeo, F. H. Kohnke, G. L. La Torre, A. J. P. White, D. J. Williams, *Angew. Chem.* **2000**, *112*, 1556 – 1558; *Angew. Chem. Int. Ed.* **2000**, *39*, 1496 – 1498; b) G. Cafeo, F. H. Kohnke, G. L. La Torre, A. J. P. White, D. J. Williams, *Chem. Commun.* **2000**, 1207 – 1208; c) G. Cafeo, F. H. Kohnke, G. L. La Torre, M. F. Parisi, R. Pistone Nascone, A. J. P. White, D. J. Williams, *Chem. Eur. J.*, in press.

[9] F. Hirayama, S. Mieda, Y. Miyamoto, H. Arima, K. Uekama *J. Pharm. Sci.* **1999**, *88*, 970 – 975.

[10] S. Valiyaveettil, J. F. J. Engbersen, W. Verboom, D. N. Reinhoudt, *Angew. Chem.* **1993**, *105*, 942 – 943; *Angew. Chem. Int. Ed. Engl.* **1993**, *32*, 900 – 901.

[11] a) F. Arnaud-Neu, S. Fuangswasdi, A. Notti, S. Pappalardo, M. F. Parisi, *Angew. Chem.* **1998**, *110*, 120 – 122; *Angew. Chem. Int. Ed.* **1998**, *37*, 112 – 114; b) G. Ferguson, A. Notti, S. Pappalardo, M. F. Parisi, A. L. Spek, *Tetrahedron Lett.* **1998**, *39*, 1965 – 1968.

[12] The only fast complexation process observed was in the binding of **6** by **3**. $K(A)_3$ values were obtained as described by Whitlock[13] using the

 © WILEY-VCH Verlag GmbH, 69451 Weinheim, Germany, 2002 1433-7851/02/4112-2125 $ 20.00+.50/0

pyrrole NH resonance as a probe to determine the molar fraction of complexed macrocycle.
[13] B. J. Whitlock, H. W. Whitlock, *J. Am. Chem. Soc.* **1990**, *112*, 3910–3915.
[14] H.-J. Schneider, R. Kramer, S. Simova, U. Schneider, *J. Am. Chem. Soc.* **1988**, *110*, 6442–6448.
[15] A control experiment has shown that iBuNH$_3^+$Cl$^-$ is complexed in CD_2Cl_2 to a low extent by **2c**, and to nearly 100% after further addition of **3** (1 equiv). However, when **6a** (1 equiv) is added to the preformed supercation iBuNH$_3^+ \subset$ **2c**, the included iBuNH$_3^+$ ion is displaced by the better fitting nBuNH$_3^+$ ion.
[16] ^{1}H NMR spectra have shown **7** to be completely insolubile in CD_2Cl_2, either alone or admixed with one equivalent of **2c** or **3**.
[17] G. Wenz, *Angew. Chem.* **1994**, *106*, 851–870; *Angew. Chem. Int. Ed.* **1994**, *33*, 803–822.

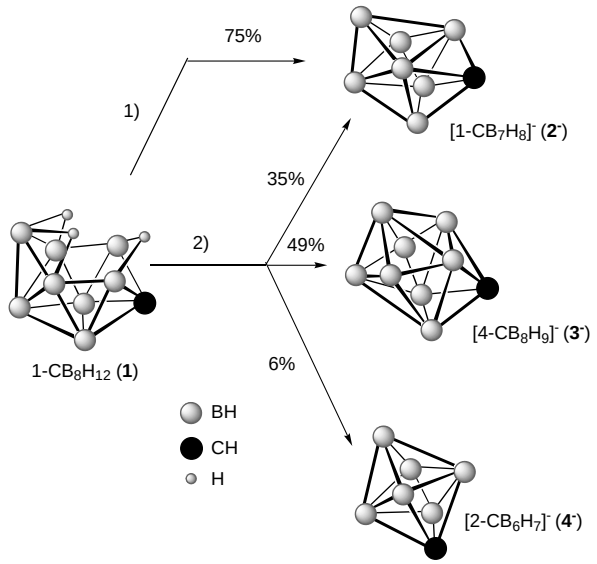
The [*closo*-2-CB_6H_7]$^-$ Ion: The First Representative of the 7-Vertex Monocarbaborane Series**

Bohumil Štíbr,* Oleg L. Tok, Wolfgang Milius, Mario Bakardjiev, Josef Holub, Drahomír Hnyk, and Bernd Wrackmeyer

In contrast to the extensively explored area of dicarbaborane chemistry,[1] that of monocarbaboranes is much less represented, and many of the fundamental cluster types, namely those of the *nido* and *arachno* series, are unreported as yet. A typical and relatively well-developed field of monocarbaborane chemistry is that of the classically *closo* monocarbaborane anions of general formula [CB_nH_{n+1}]$^-$. Of these anions, thanks also to the recent discoveries of the [CB_7H_8]$^-$ and [CB_8H_9]$^-$ ions[2, 3] a complete series from $n = 7$ to 12 has already been isolated and structurally characterized, together with the 6-vertex ion [CB_5H_6]$^-$ and its conjugated acid CB_5H_7.[4] Nevertheless, the 7-vertex ion [CB_6H_7]$^-$ has so far remained elusive. At present, most studies in the area of *closo* monocarbaboranes focus on the substitution chemistry of the [CB_9H_{10}]$^-$ and [$CB_{11}H_{12}$]$^-$ ions.[1, 5] Currently, these anions attract much attention as so-called weakly coordinating anions because of their very low Lewis basicities.[6] Moreover, *closo* monocarbaboranes are studied as starting materials for borane-based liquid crystals.[7] We now report preliminary results on the isolation and structural characterization of the [CB_6H_7]$^-$ ion, a missing member of the 7-vertex *closo* monocarbaborane series.

Under strictly anaerobic conditions (deoxygenated Ar), the reaction between *nido*-1-CB_8H_{12} (**1**)[8] and two equivalents of Et_3N in dry toluene (reflux, 24 h) resulted in the isolation of previously reported[2] anion [*closo*-1-CB_7H_8]$^-$ (**2**$^-$), yield 75% [Eq. (1); Scheme 1 (path 1)].

$$\underset{\mathbf{1}}{1\text{-}CB_8H_{12}} + 2\,Et_3N \rightarrow \underset{(\mathbf{2}^-Et_3NH^+)}{[Et_3NH]^+[1\text{-}CB_7H_8]^-} + Et_3N{\cdot}BH_3 \qquad (1)$$



Scheme 1.

In contrast, the reaction products are entirely different when the same reaction is carried out in an atmosphere containing N_2 with approximately 5% O_2 (Scheme 1, path 2)). The reaction then afforded a mixture of the known ions **2**$^-$ and [*closo*-4-CB_8H_9]$^-$ (**3**$^-$), together with a new ion [2-CB_6H_7]$^-$ (**4**$^-$; yields 35, 49, and 6%, respectively). Anion **4**$^-$ was finally isolated as a PPh_4^+ salt (**4**$^-$ PPh_4^+) by preparative TLC. The formation of **4**$^-$ seems to be in agreement with the side reaction given in Equation (2) and is consistent with the elimination of two BH vertices from structure **1**.

$$\underset{\mathbf{1}}{1\text{-}CB_8H_{12}} + 2\,Et_3N + O_2 + H_2O \rightarrow \underset{(\mathbf{4}^-Et_3NH^+)}{[Et_3NH]^+[2\text{-}CB_6H_7]^-} + Et_3N{\cdot}BH_3 + B(OH)_3 \qquad (2)$$

Iodination of **4**$^-$ PPh_4^+ with I_2 (molar ratio 1:2.1) in CH_2Cl_2 in the presence of NEt_3 (HI scavenger) at ambient temperature resulted in the isolation of the diiododerivative [4,5-I_2-*closo*-2-CB_6H_5]$^-$[PPh_4]$^+$ (4,5-I_2-**4**$^-$ PPh_4^+) in 93% yield.

[*] Prof. Dr. B. Štíbr,[+] Dr. M. Bakardjiev, Dr. J. Holub, Dr. D. Hnyk
Institute of Inorganic Chemistry
Academy of Sciences of the Czech Republic
25068 Řež (the Czech Republic)
Research Centre for New Inorganic Compounds and Advanced Materials, University of Pardubice
Fax: (+42) 0220941502
E-mail: stibr@iic.cas.cz
Dr. O. L. Tok, Dr. W. Milius, Prof. Dr. B. Wrackmeyer
Laboratorium für Anorganische Chemie der Universität Bayreuth
Postfach 101251, Bayreuth, Bayern 95440 (Germany)
[+] Laboratorium für Anorganische Chemie der Universität Bayreuth
Postfach 101251, Bayreuth, Bayern 95440 (Germany)

[**] This work was supported by the Alexander-von-Humboldt Stiftung (FRG) (B.Š.), Deutsche Forschungsgemeinschaft (B. W., O.L.T.), Fonds der Chemischen Industrie (B.W.), and the Ministry of Education of Czech Republic (Project LN00A028). We also thank the Grant Agency of the Charles University (Grant No. 203/00/B-CH/PřF) and the Supercomputing Center of the Charles University in Prague for computer time.

 © WILEY-VCH Verlag GmbH, 69451 Weinheim, Germany, 2002 1433-7851/02/4112-2126 $ 20.00+.50/0

The X-ray structure of anion $\mathbf{2}^-$ was already determined for its mono- and diiododerivatives[2] and that of the parent anion $\mathbf{3}^-$ was reported recently.[3] Although we were able to grow well-shaped crystals of $\mathbf{4}^- PPh_4^+$, the structure determination showed disorder between boron and carbon positions.

Nevertheless, as shown in Figure 1, the structure of the 7-vertex *closo* cage was determined by single-crystal X-ray diffraction analysis of 4,5-I_2-$\mathbf{4}^- PPh_4^+$.[9] The structure is

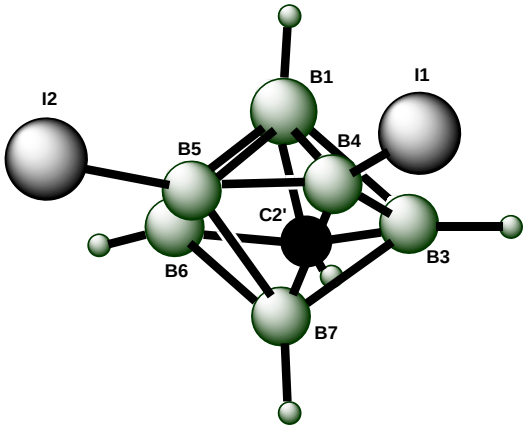


Figure 1. Representation of the crystallographically determined molecular structure of the [4,5-I_2-*closo*-2-CB_6H_5]$^-$ anion (4,5-I_2-$\mathbf{4}^-$). Selected intracluster distances [Å]: B1-C2′ 1.708(11), B1-B3 1.818(10), B1-B4 1.792(8), B1-B5 1.822(11), B1-B6 1.832(13), C2′-B3 1.539(11), B3-B4 1.617(9), B4-B5 1.639(8), B5-B6 1.624(9), C2′-B7 1.705(13), B3-B7 1.804(15), B4-B7 1.790(10), B5-B7 1.799(9), B6-B7 1.819(10), B4-I1 2.160(6), B5-I2 2.162(7).

entirely in agreement with the theoretically predicted pentagonal-bipyramidal C_s arrangement of the 7-vertex *closo* monocarbaborane cage in which the cage carbon occupies a low-coordinate cluster position.[10] This structure was found to be favored by 30.5 kcal mol^{-1} with respect to the [1-CB_6H_7]$^-$-ion minimum, with an overall symmetry of C_{5v}, as revealed from an ab initio study of the [CB_6H_7]$^-$ system performed by P. v. R. Schleyer and K. Najafian at a correlated level of theory (MP2) with the 6-31G* basis set.[11] In our work, this basis set and B3LYP/6-31G* (see Figure 2) geometries were used for GIAO calculations of the ^{11}B chemical shifts for $\mathbf{4}^-$[12] to yield an excellent agreement between calculated and experimental data (maximum deviation 1 ppm).[13, 14, 15] the NMR spectra (see Table 1) of the parent ion $\mathbf{4}^-$ are also in accord with the calculated structure. The ^{11}B NMR spectrum shows 2:2:2 patterns of doublets and that of the diiododerivative 4,5-I_2-$\mathbf{4}^-$ consists of two doublets and one singlet which integrate in the ratio 2:2:2. The ^{1}H and ^{13}C NMR spectra of both these CB_6 compounds show one CH singlet (with a triplet $^2J_{H,H}$ splitting in the ^{1}H spectrum for the diiododerivative). The ^{1}H{^{11}B(selective)} NMR spectra[16] allowed for the assignment of all BH cage positions for both compounds.

These results, allied with recent efficient routes from $B_{10}H_{14}$ to the starting monocarbaborane **1**,[3, 17, 18] mean that the 8-vertex *closo* anion $\mathbf{2}^-$ and the recently reported[3] 9-vertex *closo* species $\mathbf{3}^-$ have now become the most readily accessible highly air-stabile *closo* carboranes. The long missing repre-

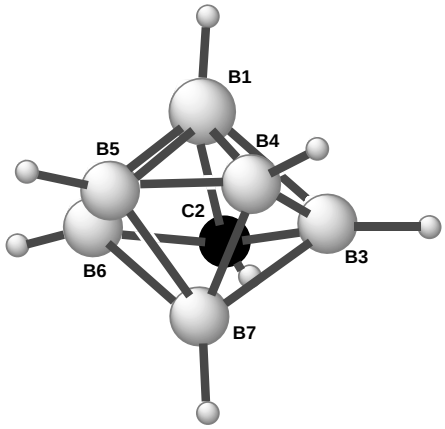


Figure 2. B3LYP/6-31G* optimized geometry of the parent [*closo*-2-CB_6H_7]$^-$ ion ($\mathbf{4}^-$). Selected calculated bond lengths [Å], and angles [°]: C2-B1 1.734, B1-B3 1.826, B1-B4 1.803, C2-B3 1.551, B3-B4 1.647, B4-B5 1.647, B3-C2-B6 117.2, C2-B3-B4 104.1.

Table 1. NMR spectroscopic data measured in CD_2Cl_2.

Compound	Nucleus	δ [ppm]
$\mathbf{4}^- PPh_4^+$	^{11}B	3.9/4.6/4.8[a] (d, $^1J_{B,H}$ = 151 Hz, B 3,6), 0.2/0.4/0.5[a] (d, $J_{B,H}$ = 138 Hz, B 4,5), −22.2/−21.4/−21.1[a] (d, $^1J_{B,H}$ = 150 Hz, B 1,7)
	^{1}H{^{11}B}	5.37 (s, H 2), 3.96 (s, H 3,6), 3.37 (s, H 4,5), −0.72 (s, H 1,7)
	^{13}C{^{1}H}	78.6/72.9/73.8[b] (m, $^1J_{C,B}$ ∼ 20 Hz, C 2)
4,5-I_2-$\mathbf{4}^- PPh_4^+$	^{11}B	3.9 (d, $^1J_{BH}$ = 158 Hz, B 3,6), −3.8 (s, B 4,5), −20.3 (d, $^1J_{BH}$ = 156 Hz, B 1,7)
	^{1}H{^{11}B}	5.16 (t, $^2J_{H,H}$ = 9.7 Hz, H 2), 3.97 (d, $^2J_{H,H}$ = 9.7 Hz, H 3,6), −0.06 (s, H 1,7)
	^{13}C{^{1}H}	78.6 (m, $^1J_{C,B}$ ∼ 20 Hz, C 2)

[a] $\delta(^{11}B)_{exp}/\delta(^{11}B)_{calcd}$ (GIAO-SCF/II//MP2/6-31G*)/$\delta(^{11}B)_{calcd}$ (GIAO-SCF/II//B3LYP/6-31G*). [b] $\delta(^{13}C)_{exp}/\delta(^{13}C)_{calcd}$ (GIAO-SCF/II//MP2/6-31G*)/$\delta(^{13}C)_{calcd}$ (GIAO- SCF/II//B3LYP/6-31G*).

sentative of the 7-vertex monocarbaborane family, the [*closo*-1-CB_6H_7]$^-$ ion $\mathbf{4}^-$, is also very stable in air and its chemistry will now contribute substantially to the development of carborane chemistry. We are currently working on the optimization of its synthesis and on the development of other chemistry of all these new 7–9-vertex monocarborane systems. For example, these anions could act as weakly coordinating ligands to complement the [CB_9H_{10}]$^-$, [$CB_{11}H_{12}$]$^-$ ions, and their derivatives,[6] and they are also likely to be amenable to extensive substitution and metallacarborane chemistries.

Experimental Section

$\mathbf{4}^- PPh_4^+$: In an N_2 atmosphere, from which the contaminant O_2 was not removed, compound **1** (827 mg, 7.8 mmol) was added to a solution of Et_3N (1616 mg, 16 mmol) in toluene (100 mL). The mixture was heated at reflux for 24 h and then evaporated in vacuum at ambient temperature. The residual semi-liquid materials were heated in vacuum (heating gun) to remove $Et_3N \cdot BH_3$ by distillation, which was collected in a trap at 0 °C (404 mg, 45 %). The residue was then extracted several times with hot water (ca. 70 °C), the combined aqueous extracts were evaporated to dryness and the residue was recrystallized twice from a minimum of hot water to give 1343 mg of a mixture of $\mathbf{2}^- [NEt_3H]^+$ and $\mathbf{3}^- [NEt_3H]^+$ (molar ratio 1:1.4, as determined from the integrated NMR spectrum) as a white crystalline material, which was not separated further. A solution of

$[PPh_4]^+Cl^-$ (300 mg, 0.8 mmol) in water (20 mL) was added to the mother liquor from this crystallization and a white precipitate was formed and collected by filtration, washed with water (2×10 mL), and dried in vacuum at RT to give 277 mg of an anionic mixture. This mixture was separated by multiple preparative TLC on silica gel, using 3% $MeCN/CH_2Cl_2$ as the mobile phase (detection UV 254 nm). The second band, $R_f = 0.5$ was collected and washed out with MeCN. Evaporation of the solvent from combined fractions gave pure $\mathbf{4}^- PPh_4^+$ (174 mg, 6%). White crystals were obtained by diffusion of Et_2O into a concentrated CH_2Cl_2 solution of $\mathbf{4}^- PPh_4^+$. M.p. 350 °C, elemental analysis calcd (%) for $C_{25}H_{27}B_6P$: B 15.33; found B 14.82.

4,5-I_2-$\mathbf{4}^- PPh_4^+$: A solution of $\mathbf{4}^- PPh_4^+$ (35 mg, 0.083 mmol) in CH_2Cl_2 (10 mL) was treated with several portions of solid I_2 (total 44 mg, 0.17 mmol) in the presence of NEt_3 (0.5 mL) under stirring at RT for 0.5 h. The mixture was extracted with 5% aqueous $Na_2S_2O_3$ (20 mL), the CH_2Cl_2 layer collected and filtered through a short column of silica gel. Evaporation of the filtrate gave pure 4,5-I_2-$\mathbf{4}^- PPh_4^+$ (52 mg, 93%). White crystals were obtained by diffusion of Et_2O vapors into a concentrated CH_2Cl_2 solution of 4,5-I_2-$\mathbf{4}^- PPh_4^+$. M.p. 210 °C; elemental analysis calcd (%) for $C_{25}H_{27}B_6PI_2$: B 9.62; found B 9.38.

Received: December 13, 2001 [Z18377]

[1] a) T. Onak in *Boron Hydride Chemistry* (Ed.: E. L. Muetterties), Academic, New York, **1973**, p. 349, and references therein; b) B. Štíbr, *Chem. Rev.* **1992**, *92*, 225, and references therein.

[2] a) J. Plešek, T. Jelínek, B. Štíbr, S. Heřmánek, *J. Chem. Soc. Chem. Commun.* **1988**, 348; b) T. Jelínek, B. Štíbr, J. Plešek, J. D. Kennedy, M. Thornton-Pett, *J. Chem. Soc. Dalton Trans.* **1995**, 431.

[3] T. Jelínek, B. Štíbr, J. Holub, M. Bakardjiev, D. Hnyk, D. L Ormsby, C. A. Kilner, M. Thornton-Pett, H.-J. Schanz, B. Wrackmeyer, J. D Kennedy, *Chem. Commun.* **2001**, 1756.

[4] a) T. Onak, R. P. Drake, G. B. Dunks, *J. Am. Chem. Soc.* **1965**, *87*, 2505; b) S. R. Prince, R. Schaeffer, *Chem. Commun.* **1968**, 451; c) T. Onak, P. Matschei, E. Groszek, *J. Chem. Soc. (A)* **1969**, 1990.

[5] a) W. H. Knoth, *J. Am. Chem. Soc.* **1967**, *89*, 1274; b) W. H. Knoth, *Inorg. Chem.* **1971**, *10*, 598; W. H. Knoth, *Inorg. Chem.* **1973**, *12*, 785.

[6] a) C. Reed, *Acc. Chem. Res.* **1998**, *31*, 133; b) S. Strauss, *Chem. Rev.* **1993**, *93*, 927.

[7] P. Kaszynski, *Collect. Czech. Chem. Commun.* **1999**, *64*, 895.

[8] a) K. Baše, S. Heřmánek, B. Štíbr, *Chem. Ind. (London)* **1977**, 951; b) K. Baše, B. Štíbr, J. Dolanský, J. Duben, *Collect. Czech. Chem. Commun.* **1981**, *46*, 2345.

[9] a) Crystal structure data for $C_{25}H_{25}B_6I_2P$: $M_r = 675.08$, white crystal, size $0.2 \times 0.18 \times 0.10$ mm^3, triclinic, space group $P\bar{1}$, $a = 7.9841(6)$, $b = 13.2428(9)$, $c = 13.5646(9)$ Å, $\alpha = 96.149(6)$, $\beta = 92.686(5)$, $\gamma = 92.994(6)°$, $V = 1422.02$ Å^3, $T = 293(2)$ K, $Z = 2$, $\rho_{calcd} = 1.577$ Mg m^{-3}, $F(000) = 652$, $\mu(Mo_{K\alpha}) = 2.28$ mm^{-1}, Data collected with a Siemens P4 four-circle diffractometer ($Mo_{K\alpha}$ radiation $\lambda = 71.073$ pm, graphite monochromator); $\theta_{max} = 25°$. A total of 6152 reflections were measured, 4986 unique ($R_{int} = 0.0277$). Absorption correction empirical (by Ψ-scans), min./max. transmission coefficients 0.2453/0.2990, GoF on F^2 was 1.125, $R1$ ($I > 2\rho(I)$) = 0.0358, $wR2 = 0.0924$. Data/restrains/parameters 4956/0/308. Largest difference Fourier peak and hole 1.511 and -1.173 e Å^{-3}. Refinement used SHELXTL V.5.1 (G. M. Sheldrick, SHELXS-97, University of Göttingen, Göttingen (Germany), **1997**). b) CCDC-175525 (4,5-I_2-$\mathbf{4}^- PPh_4^+$). contains the supplementary crystallographic data for this paper. These data can be obtained free of charge via www.ccdc.cam.ac.uk/conts/retrieving.html (or from the Cambridge Crystallographic Data Centre, 12, Union Road, Cambridge CB21EZ, UK; fax: (+44) 1223-336-033; or deposit@ccdc.cam.ac.uk).

[10] R. E. Williams, *Adv. Inorg. Chem. Radiochem.* **1976**, *18*, 67.

[11] P. v. R. Schleyer, K. Najafian, *Inorg. Chem.* **1998**, *37*, 3454.

[12] a) All calculations used the Gausian 94 program package[13] and were performed on the Power Challenge XL computer of the Supercomputing Center of the Charles University in Prague (Czech Republic). The calculations were carried out at the self-consistent field (SCF) level and employed a II Huzinaga basis set,[14] well-suited for the calculations of magnetic properties.[15] Additionally, the structure of $\mathbf{4}^-$ was optimized using a hybrid functional B3LYP with the same basis set as used in ref. [11] and analogous GIAO-calculations of the shielding tensor of $\mathbf{4}^-$ were performed. Both geometries performed almost equally well (maximum deviation from experimental $\delta(^{11}B)$ data $\pm$ 1 ppm). b) Coordinates for the B3LYP/6-31G* structure of $\mathbf{4}^-$ are available from the authors (e-mail: hnyk@iic.cas.cz).

[13] Gaussian 94 (Revision B.2), M. J. Frisch, G. W. Trucks, H. B. Schlegel, P. M. W. Gill, B. G. Johnson, M. A. Robb, J. R. Cheeseman, T. Keith, G. A. Petterson, J. A. Montgomery, K. Raghavachari, M. A. Al-Laham, V. G. Zahrzewski, J. V. Ortiz, J. B. Foresman, J. Cioslowski, B. B. Stefanov, A. Nanayakkra, M. Challacombe, C. Y. Peng, P. Y. Ayala, Y. Chen, M. W. Wong, J. L. Andres, E. S. Replogle, R. Gomprets, R. L. Martin, D. J. Fox, J. S. Binkley, D. J. Defrees, L. Baker, J. P. Stewart, M. Head-Gordon, C. Gonzales, J. A. Pople, Gaussian, Inc., Pittsburgh, PA, **1995**.

[14] S. Huzinaga, *Approximate Atomic Wave Functions*, University of Alberta, Edmonton, Canada, **1971**.

[15] W. Kutzelnigg, M. Schindler, U. Fleischer, *NMR, Basic Principles and Progress*, *Vol.* 23, Springer, Berlin, **1990**.

[16] X. L. R. Fontaine, J. D. Kennedy, *J. Chem. Soc. Dalton Trans.* **1987**, 1573.

[17] B. Brellochs in *Contemporary Boron Chemistry* (Eds.: M. G. Davidson, A. K. Hughes, T. B. Marder, K. Wade), Royal Society of Chemistry, Cambridge, **2000**, p. 212.

[18] B. Štíbr, B. Wrackmeyer, *J. Organomet. Chem.*, in press.

Conformational Locking of the Glycosyl Acceptor for Stereocontrol in the Key Step in the Synthesis of Heparin**

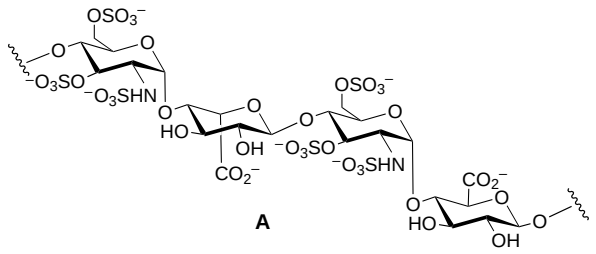
Hernan A. Orgueira, Alessandra Bartolozzi, Peter Schell, and Peter H. Seeberger*

Glycosaminoglycans (GAGs), including heparin (**A**), are linear oligosaccharides that consist of amino sugars and uronic acids.[1] Many glycosaminoglycans are involved in vital biological functions[2] but still, little is known about the molecular mechanisms responsible for their action. Much progress toward the synthesis of heparin fragments has been reported

[*] Prof. Dr. P. H. Seeberger, Dr. H. A. Orgueira, Dr. A. Bartolozzi, Dr. P. Schell
Department of Chemistry, Massachusetts Institute of Technology
Cambridge, MA 02139 (USA)
Fax: (+1) 617-253-2979
E-mail: seeberg@mit.edu

[**] Financial support from the National Institutes of Health (HL-64799 and HL-62598), The Research Corporation (Research Innovation Award to P.H.S.), CaP CURE (Research Awards to P.H.S.), FOMEC (Postdoctoral Fellowship for H.A.O.), CNRI (Italian National Research Center, Postdoctoral Fellowship for A.B.), and the DAAD (German Academic Exchange Service, Postdoctoral Fellowship for P.S.) is gratefully acknowledged. Funding for the MIT-DCIF Varian 500 MHz NMR was provided by NSF (Award CHE-9808061). Funding for the MIT-DCIF Bruker 400 MHz NMR was provided by NIH (Award 1S10RR13886-01). Funding for the MIT-DCIF Varian 300 MHz was provided by NSF (Award DBI-9729592).

Supporting information for this article is available on the WWW under http://www.angewandte.org or from the author.



A

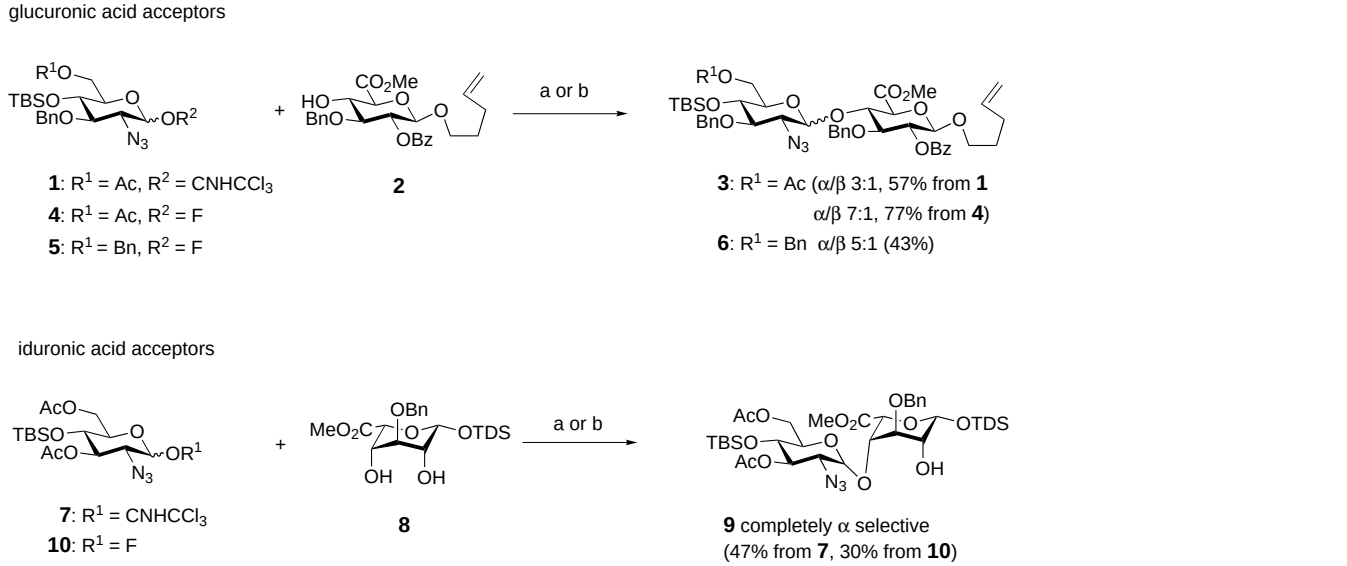
and may provide useful tools for the identification of specific recognition sequences.[3, 4] The most difficult task faced during the assembly of the heparin backbone is the selective installation of the α-glycosidic linkage by coupling glucosamine units and uronic acids. The installation of α-glucosamine linkages, ubiquitous in nature,[5] remains challenging. The C2 amino group of glucosamine is typically masked in the form of a nonparticipating azide[4d, 6] to reduce β-glucoside formation. Anomeric selectivities vary greatly and often require difficult separations. Electronic effects[7] and conformational constraint[8] of the glycosidating agent have been utilized to control the stereochemical outcome of glycosylations. Manipulation of the steric and electronic nature of the glycosyl acceptor to direct glycosylations have received less attention. Two features of the acceptor are known to influence the stereochemical course of the reaction: the intrinsic reactivity of the hydroxy group that functions as nucleophile (axial hydroxy groups are generally less reactive than equatorial hydroxy groups)[9] and steric factors, which result in matched/mismatched pairs of glycosyl donors and acceptors.[10]

Herein we discuss a new method for the stereoselective installation of α-glucosamine linkages by locking the conformation of the monosaccharide acceptor. Several key disaccharide building blocks, previously obtained as anomeric mixtures, were prepared by utilizing this approach.

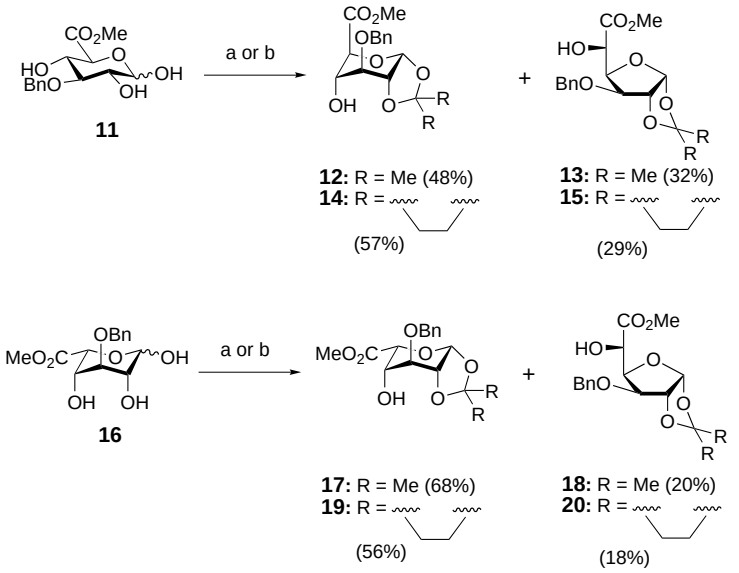
The reaction of C2-azido glucose trichloroacetimidate **1** and fluoride donors **4** and **5**[11] with glucuronic acid acceptor **2**[11] yielded anomeric mixtures of disaccharides **3** and **6** (Scheme 1). Better ratios of α-linked disaccharides were obtained with the slower reacting glycosyl fluorides. Similar results had been reported previously with other glucuronic acid acceptors.[4a,c, 12] Interestingly, glycosylations that involve iduronic acid **8**,[13] resulted exclusively in the formation of α-glucosamine linkages, in accordance with previous reports.[14] To rationalize the markedly different behavior of glucuronic and iduronic acid acceptors, we analyzed the conformational differences of the two monosaccharides. Glucuronic acids preferentially adopt a $^4C_1$ conformation with an equatorial C4 hydroxyl group. Iduronic acid in contrast adopts either a $^1C_4$ conformation with a C4 axial hydroxy group or a skewed-boat $^2S_0$ conformation in oligosaccharide sequences, depending on the substituents on the ring.[15, 16] Apparently, the stereochemical outcome of these glycosylations is related to the conformation of the acceptor.

Based on these observations we intended to use glucuronic acid acceptors in a $^1C_4$ conformation. NMR spectroscopic analysis of glucuronic acids **12** and **14** and iduronic acids **17** and **19**, which carry cyclic isopropylidene protecting groups revealed that these monosaccharides adopt a $^1C_4$ conformation, as judged by the coupling constants ($J_{4,5} \approx 3.5$ Hz ($^4C_1$: $J_{4,5} > 8$ Hz) and $J_{1,2} \approx 2.7$ Hz). Differentially protected uronic acid monomers **12**, **14**, **17**, and **19** were prepared from triols **11** and **16** by formation of isopropylidene[17] or cyclopentylidene[18] acetals upon reaction with 2-methoxypropene or methoxycyclopentene under kinetic control (Scheme 2). In addition to the desired compounds, the corresponding furanosides **13**, **15**, **18**, and **20** were obtained and were resubmitted to 1,2 acetal formation after cleavage of the acetal protective group.

With conformationally constrained glucuronic acid acceptors **12** and **14** in hand, we began to investigate the stereochemical outcome of the coupling reactions (Scheme 3).



Scheme 1. Synthesis of disaccharides by using uronic acid acceptors. a) For **1** and **7**: TBSOTf, CH_2Cl_2, $-20\,^\circ C \rightarrow$RT; b) for **4**, **5**, and **10**: $AgClO_4$, $SnCl_2$,Et_2O, molecular sieves (4 Å), $0\,^\circ C \rightarrow$RT. TBSOTf = *tert*-butyldimethylsilyl trifluoromethanesulfonate, Bz = benzoyl, TDS = dimethylthexylsilyl.



Scheme 2. Installation of 1,2-acetal protecting groups as molecular locks of uronic acid monosaccharides. a) 2-Methoxypropene, DMF, CSA; b) methoxycyclopentene, DMF, CSA. DMF = *N*,*N*-dimethylformamide, CSA = camphor sulfonic acid.

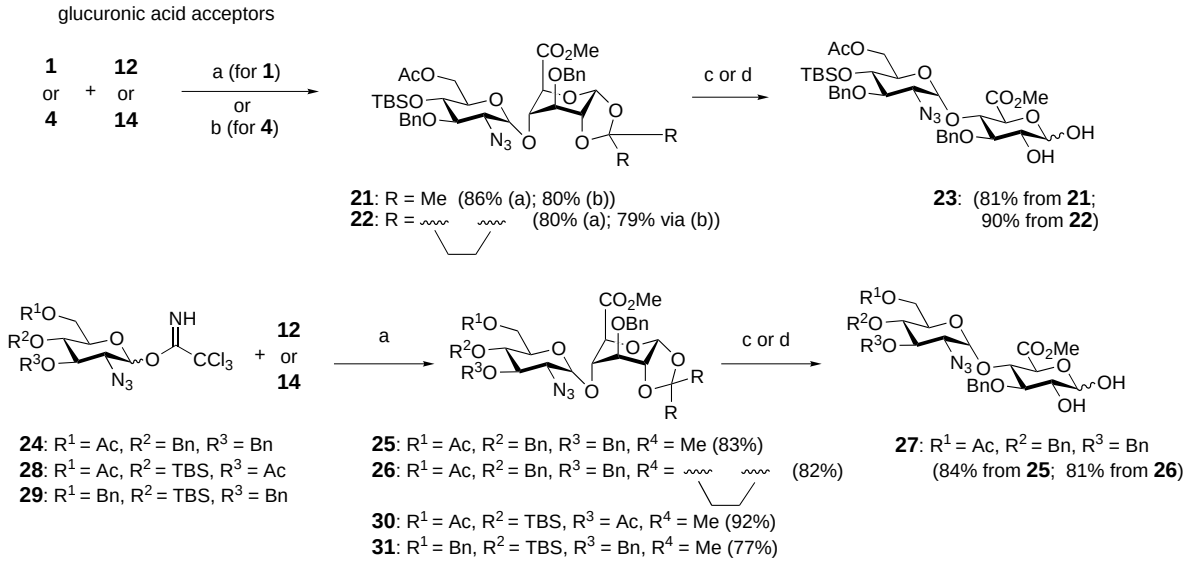
Coupling of glycosyl trichloroacetimidate **1** or glycosyl fluoride **4** with acceptors **12** and **14** resulted exclusively in the formation of α-linked disaccharides **21** (from **12**) and **22** (from **14**) in very good yields (Scheme 3). The exact nature of the cyclic protecting group (isopropylidene or cyclopentylidene) and the anomeric leaving group did not influence the selectivity of the coupling reaction. Since glycosyl trichloroacetimidates performed slightly better than glycosyl fluorides, further coupling reactions were performed with these donors. The coupling reactions of donor **24** with acceptors **12** and **14** and the coupling reactions of donors **28** and **29** with acceptor **12** were completely α-selective, as expected, and produced **25** (**24**+**12**), **26** (**24**+**14**), **30** (**28**+**12**), and **31** (**29**+**12**) as the only products (Scheme 3). Complete α-selectivity of the coupling reactions greatly simplifies access to disaccharide modules for heparin assembly and purification of the reaction products.

In addition to their use as molecular locks, 1,2-acetals are convenient for the differential protection of monosaccharides and were applied to iduronic acid acceptors. Coupling of glycosyl donors **1** and **28** with iduronic acid acceptors **17** and **19** furnished disaccharides **32** (**1**+**17**), **33** (**28**+**17**), and **34** (**28**+**19**). After the cyclic acetal protecting groups served their purpose they were readily removed to yield disaccharide diols **23** (from **21** and **22**), **27** (from **25** and **26**), **35** (from **32**), and **36** (from **33** and **34**), ready for further functionalization and incorporation as key building blocks into the modular assembly of heparin oligosaccharides (Scheme 4).

In summary, we have demonstrated a new concept for stereochemical control in the key step in the synthesis of heparin. Locking the conformation of the glucuronic acid acceptor allowed the completely selective preparation of the desired *cis* glycosides. This approach greatly simplified the preparation of disaccharide modules for the stereoselective assembly of heparin oligosaccharides. Work in this area is underway and will be reported in due course.

Experimental Section

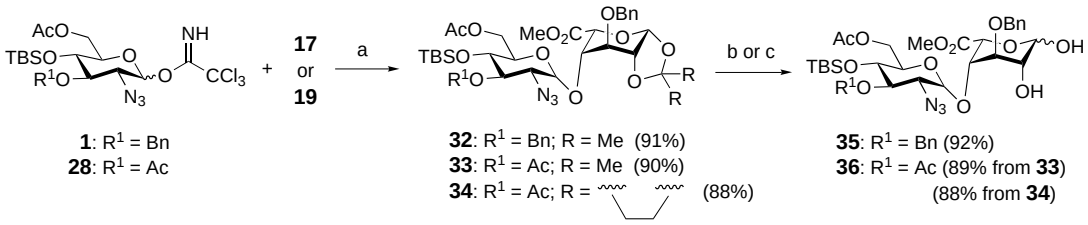
21: Glucosamine **1** (1.87 g, 3.14 mmol) and glucuronic acid **12** (850 mg, 2.51 mmol) were coevaporated with toluene and then dissolved in anhydrous CH_2Cl_2 (31 mL) before freshly activated powdered molecular sieves (4-Å, 700 mg) were added. TBSOTf (72 μL, 0.314 mmol) was added dropwise at −78 °C, and the mixture was then warmed to room temperature over 2.5 h. Triethylamine (0.5 mL) was added, the mixture was filtered through a pad of celite, and the solvent was removed under reduced pressure. Flash chromatography on silica gel (hexanes/EtOAc 85:15) afforded **21** (1.68 g, 86 %) as a colorless foam. $[\alpha]_D^{24} = +97.2$ ($c = 2.55$, CH_2Cl_2); IR (thin film on NaCl): $\tilde{\nu} = 3032$, 2953, 2930, 2858, 2106, 1746, 1455, 1250 cm^{-1}; ^1H NMR (500 MHz, $CDCl_3$): $\delta = 7.40-7.27$ (m, 10H; H_{ar}),



Scheme 3. Synthesis of disaccharides by using "locked" glucuronic acid acceptors. a) TBSOTf, molecular sieves (4 Å), CH_2Cl_2, −78 °C→RT; b) $AgClO_4$, $SnCl_2$, Et_2O, molecular sieves (4 Å), 0 °C→RT; c) for **21** and **25**: dichloroacetic acid (aqueous, 75 %); d) for **22** and **26**: dichloroacetic acid (aqueous, 50 %).

 © WILEY-VCH Verlag GmbH, 69451 Weinheim, Germany, 2002 1433-7851/02/4112-2130 $ 20.00+.50/0

iduronic acid acceptors



1: R^1 = Bn
28: R^1 = Ac

32: R^1 = Bn; R = Me (91%)
33: R^1 = Ac; R = Me (90%)
34: R^1 = Ac; R = (88%)

35: R^1 = Bn (92%)
36: R^1 = Ac (89% from **33**)
(88% from **34**)

Scheme 4. Synthesis of disaccharides by using iduronic acid acceptors. a) TBSOTf, molecular sieves (4 Å), CH_2Cl_2, $-78\,^\circ C \rightarrow RT$; b) for **32** and **33**: dichloroacetic acid (aqueous, 75 %); c) for **34**: dichloroacetic acid (aqueous, 50 %).

5.78 (d, $J = 3.7$ Hz, 1H; H1B), 5.17 (d, $J = 3.7$ Hz, 1H; H1A), 4.88 (d, $J = 11.0$ Hz, 1H; $ArCH_2$), 4.78 (d, $J = 11.0$ Hz, 1H; $ArCH_2$), 4.68 (s, 2H; $ArCH_2$), 4.59 (d, $J = 6.1$ Hz, 1H; H5B), 4.38 (dd, $J = 2.1$, 11.9 Hz, 1H; H6Aa), 4.25 – 4.21 (m, 2H; H-2B, H4B), 4.09 – 4.05 (m, 2H; H6Ab, H3B), 3.89 – 3.85 (m, 1H; H5A), 3.74 (dd, $J = 8.5$, 10.4 Hz, 1H; H3A), 3.71 (s, 3H; OCH_3), 3.63 (dd, $J = 8.5$, 9.8 Hz, 1H; H4A), 3.25 (dd, $J = 3.7$, 10.4 Hz, 1H; H2A), 2.08 (s, 3H; $COCH_3$), 1.63 (s, 3H; isopropylidene CH_3), 1.39 (s, 3H; isopropylidene CH_3), 0.89 (s, 9H; *t*Bu), 0.02 (s, 3H; CH_3), 0.00 ppm (s, 3H; CH_3); ^{13}C NMR (125 MHz, $CDCl_3$): $\delta = 170.9$, 170.1, 138.1, 137.3, 128.6, 128.4, 128.2, 128.0, 127.7, 127.5, 111.0, 98.2, 95.7, 80.0, 76.0, 75.6, 75.1, 73.9, 72.3, 71.9, 71.3, 71.2, 63.6, 62.9, 52.5, 27.6, 26.0, 25.9, 21.0, 18.1, −3.6, −4.8 ppm; MS (FAB): calcd for $C_{38}H_{53}N_3O_{12}Si$: 771.3399; found: 771.3386 $[M]^+$.

Received: September 24, 2001 [Z17964]
Revised: February 15, 2002

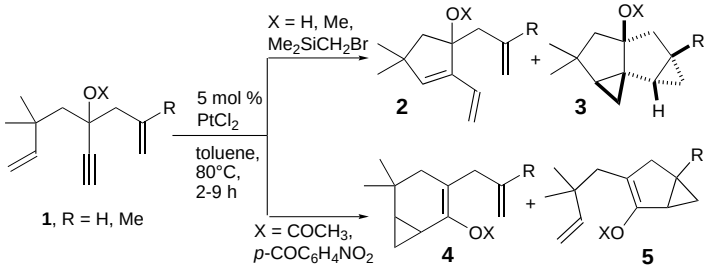
[1] A. Varky, R. Cummings, J. Esko, H. Freeze, G. Hart, J. Marth, *Essentials of Glycobiology*, CSHL Press, New York, **1999**.
[2] a) I. Capila, R. J. Linhardt, *Angew. Chem.* **2002**, *114*, 426 – 450; *Angew. Chem. Int. Ed.* **2002**, *41*, 390 – 412; b) H. E. Conrad, *Heparin Binding Proteins*, Academic Press, New York, **1998**; c) H. Engelberg, *Pharmacol. Rev.* **1984**, *36*, 91 – 110.
[3] a) S. Faham, R. E. Hileman, J. R. Fromm, R. J. Linhardt, D. C. Rees, *Science* **1996**, *271*, 1116 – 1120; b) C. Tabeur, J.-M. Mallet, F. Bono, J.-M. Herbert, M. Petitou, P. Sinaÿ, *Bioorg. Med. Chem.* **1999**, *7*, 2003 – 2012; c) J. Kovensky, P. Duchaussoy, F. Bono, M. Salmivirta, P. Sizun, J.- M. Herbert, M. Petitou, P. Sinaÿ, *Bioorg. Med. Chem.* **1999**, *7*, 1567 – 1580.
[4] a) M. Petitou, P. Duchaussoy, I. Lederman, J. Choay, P. Sinaÿ, J.-C. Jacquinet, G. Torri, C*arbohydr. Res.* **1986**, *147*, 221 – 236; b) C. A. A. van Boeckel, T. Beetz, J. N. Vos, A. J. M. de Jong, S. F. van Aelst, R. H. van den Bosch, J. M. R. Mertens, F. A. van der Vlugt, *J. Carbohydr. Chem.* **1985**, *4*, 293 – 321; c) Y. Ichikawa, R. Monden, H. Kuzuhara, *Carbohydr. Res.* **1988**, *172*, 37 – 64; d) M. Haller, G.-J. Boons, *J. Chem. Soc. Perkin Trans. 1* **2001**, 814 – 822; e) J.-L. de Paz, J. Angulo, J.-M. Lassaletta, P. M. Nieto, M. Ridondo-Horcajo, R. M. Lozano, G. Giménez-Gallego, M. Martin-Lomas, *ChemBioChem* **2001**, *2*, 673 – 685; f) C. A. A. van Boeckel, M. Petitou, *Angew. Chem.* **1993**, *105*, 1741 – 1761; *Angew. Chem. Int. Ed. Engl.* **1993**, *32*, 1671 – 1690.
[5] A. Varki, *Glycobiology* **1993**, *3*, 97 – 130.
[6] a) K. M. Koeller, M. E. B. Smith, C.-H. Wong, *Bioorg. Med. Chem. Lett.* **2000**, *8*, 1017 – 1025; b) M. Martin-Lomas, M. Flores-Mosquera, J. L. Chiara, *Eur. J. Org. Chem.* **2000**, 1547 – 1562.
[7] a) D. R. Mootoo, P. Konradsson, U. Udodong, B. Fraser-Reid, *J. Am. Chem. Soc.* **1998**, *120*, 5583 – 5584; b) X.-S. Yen, C.-H. Wong, *J. Org. Chem.* **2000**, *65*, 2410 – 2431.
[8] a) L. Green, B. Hinzen, S. J. Ince, P. Langer, S. V. Ley, S. L. Warriner, *Synlett* **1998**, 440 – 442; b) S. V. Ley, H. W. M. Priepke, *Angew. Chem.* **1994**, *106*, 2412; *Angew. Chem. Int. Ed.* **1994**, *33*, 2292 – 2294; c) D. Crich, S. Sun, *J. Am. Chem. Soc.* **1998**, *120*, 435 – 436; d) D. Crich, W. Cai, Z. Dai, *J. Org. Chem.* **2000**, *65*, 1291 – 1297; e) R. Weingart, R. R. Schmidt, *Tetrahedron Lett.* **2000**, *41*, 8753 – 8758.
[9] a) G.-J. Boons, *Carbohydrate Chemistry*, Blackie Academic and Professional, London, **1998**; b) P. Collins, R. Ferrier, *Monosaccharides*, Wiley, New York, **1995**; c) A. H. Haines, *Adv. Carbohydr. Chem. Biochem.* **1976**, *33*, 11 – 109.
[10] a) N. M. Spijker, C. A. A. van Boeckel, *Angew. Chem.* **1991**, *103*, 179 – 182; *Angew. Chem. Int. Ed.* **1991**, *30*, 180 – 183; b) N. M. Spijker, J. E. M. Basten, C. A. A. Van Boeckel, *Recl. Trav. Chim. Pays-Bas* **1993**, *112*, 611 – 617.
[11] P. Schell, H. A. Orgueira, S. Roehrig, P. H. Seeberger, *Tetrahedron Lett.* **2001**, *42*, 3811 – 3814.
[12] a) M. Petitou, P. Duchaussoy, I. Lederman, J. Choay, J.-C. Jacquinet, P. Sinaÿ, *Carbohydr. Res.* **1987**, *167*, 67 – 75; b) H. P. Wessel, L. Labler, T. B. Tschopp, *Helv. Chim. Acta* **1989**, *72*, 1268 – 1277.
[13] R. Ojeda, J. L. de Paz, M. Martín Lomas, J. M. Lassaletta, *Synlett* **1999**, *8*, 1316 – 1318.
[14] a) T. Chiba, J.-C. Jacquinet, P. Sinaÿ, C*arbohydr. Res.* **1988**, *174*, 253 – 264; b) S. Koshida, Y. Suda, M. Sobel, J. Ormsby, S. Kusumoto, *Bioorg. Med. Chem. Lett.* **1999**, *9*, 3127 – 3132; c) Y. Suda, K. Bird, T. Shiyama, S. Koshida, D. Marques, K. Fucase, M. Sobel, S. Kusumoto, *Tetrahedron Lett.* **1996**, *37*, 1053 – 1056; d) B. La Ferla, L. Lay, M. Guerrini, L. Poletti, L. Panza, G. Russo, *Tetrahedron* **1999**, *55*, 9867 – 9880; e) J. Kovensky, P. Duchaussoy, M. Petitou, P. Sinaÿ, *Tetrahedron: Asymmetry* **1996**, *7*, 3119 – 3128; f) S. Koshida, Y. Suda, Y. Fukui, J. Ormsby, M. Sobel, S. Kusumoto, *Tetrahedron Lett.* **1999**, *40*, 5725 – 5728; g) C. M. Dreef-Tromp, H. A. M. Willems, P. Westerduin, P. van Veelen, C. A. A. van Boeckel, *Bioorg. Med. Chem. Lett.* **1997**, *7*, 1175 – 1180.
[15] a) S. K. Das, J.-M. Mallet, J. Esnault, P.-A. Driguez, P. Duchaussoy, P. Sizun, J.-P. Hérault, J.-M. Herbert, M. Petitou, P. Sinaÿ, *Angew. Chem.* **2001**, *113*, 1723 – 1726; *Angew. Chem. Int. Ed.* **2001**, *40*, 1670 – 1673; b) L. Mourey, J. P. Samama, M. Delarue, M. Petitou, J. Choay, D. Moras, *J. Mol. Biol.* **1993**, *232*, 223 – 241.
[16] a) D. R. Ferro, A. Provasoli, M. Ragazzi, G. Torri, B. Casu, G. Gatti, J.-C. Jacquinet, P. Sinaÿ, M. Petitou, J. Choay, *J. Am. Chem. Soc.* **1986**, *108*, 6773 – 6778; b) M. Ragazzi, D. R. Ferro, B. Perli, P. Sinaÿ, M. Petitou, J. Choay, *Carbohydr. Res.* **1990**, *195*, 169 – 185.
[17] a) J. Celas, D. Horton, *Heterocycles*, **1981**, *16*, 1587 – 1601; b) M. L. Wolfrom, A. B. Diwadkar, J. Gelas, D. Horton, *Carbohydr. Res.* **1974**, *35*, 87 – 96.
[18] a) J. M. J. Tronchet, G. Zosimo-Landolfo, F. Villedon-Denaide, M. Balkadjian, D. Cabrini, F. Barbalat-Rey, *J. Carbohydr. Chem.* **1990**, *9*, 823 – 835; b) A. B. Smith, R. A. Rivero, K. J. Hale, H. A. Vaccaro, *J. Am. Chem. Soc.* **1991**, *113*, 2092 – 2112.

 © WILEY-VCH Verlag GmbH, 69451 Weinheim, Germany, 2002 1433-7851/02/4112-2131 $ 20.00+.50/0

The Effect of a Hydroxy Protecting Group on the $PtCl_2$-Catalyzed Cyclization of Dienynes—A Novel, Efficient, and Selective Synthesis of Carbocycles**

Emily Mainetti, Virginie Mouriès, Louis Fensterbank,* Max Malacria,* and Jose Marco-Contelles*

In the last decade, we worked on the development of highly chemo-, regio-, and stereoselective cascade processes, relying either on radical reactions[1] or on transition metal mediated processes.[2] With the perspective to reach new complex molecular architectures, we examined the possibility of running metathesis[3]–radical cyclization tandems on precursors of type **1** (Scheme 1). To the best of our knowledge, this



Scheme 1. General reaction.

functional–structural assembly has not been previously assayed in enyne metathesis reactions;[4] the most related substrates (branched dienynes) were reported by the groups of Grubbs,[5] Granja,[6] and Hanna.[7] After disappointing results with Grubbs' catalysts, we turned to platinum(II)-catalyzed cycloisomerizations as the first step because of their wide applicability with enyne systems.[8–11]

Under typical reaction conditions (5 mol% $PtCl_2$, toluene, 80 °C for 2.5 h), precursor **1a** provided a mixture of the expected formal metathesis adduct **2a**, as a minor fraction (7%), and a fairly complex structure, compound **3a**, in 48% yield (Table 1, entry 1). Its NMR spectroscopic data indicated no unsaturation and the presence of two cyclopropane rings (upfield resonances in the ^{1}H NMR spectrum between $\delta =$ 0.50 and 0.90 ppm). Finally, and more importantly, only one diastereomer was produced. Definitive structure determination was achieved by an X-ray analysis of the 4-nitrobenzoate ester derivative **3e** (Figure 1),[12] obtained by standard acylation of **3a**. Compound **3a** (Scheme 1) is a derivative of tetracyclo[4.4.0.0^{1,3}0^{8,10}]decane which has not been described before. Moreover, the formation of four C–C bonds and four new stereocontrolled centers in a synthetically simple and efficient operation (see Experimental Section) is spectacular in terms of chemo-, regio-, and stereoselectivity.[13]

Table 1. $PtCl_2$-promoted enyne cycloisomerization reaction on compounds **1** (see Scheme 1). Yields in [%].

Entry	Precursor	X	R	2	Yield	3	Yield	4	Yield
1	**1a**	H	H	**2a**	7	**3a**	48	–	
2	**1b**	$SiMe_2CH_2Br$	H	**2b**	5	**3b**	61	–	
3	**1c**	Me	H		0	**3c**	68	–	
4	**1d**	$COCH_3$	H	–		–		**4d**	88[a]
5	**1e**	p-$COC_6H_4NO_2$	H	–		–		**4e**	76[a]
6	**1f**	H	Me		0	**3f**	25	–	
7	**1g**	$SiMe_2CH_2Br$	Me		0	**3g**	16	–	
8	**1h**	Me	Me		0	**3h**	34	–	
9	**1i**	p-$COC_6H_4NO_2$	Me	–		–		**4i**	62[b]

[a] The corresponding product **5** was also formed in 5–10%. [b] The corresponding product **5** was also formed in 16%.

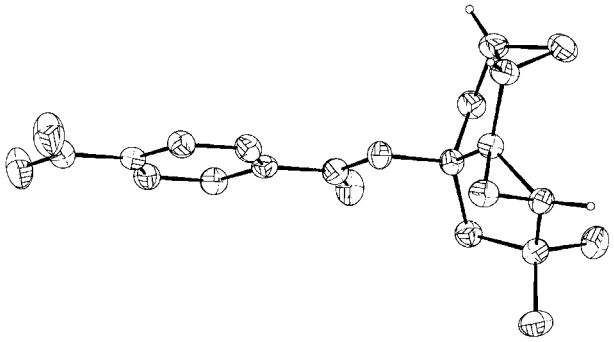


Figure 1. ORTEP presentation of the structure of compound **3e**.

This promising result prompted us to prepare other precursors for the Pt^{II}-mediated cycloisomerization and to define a mechanistic rationale. Whether the initial intermediate in these reactions is a metallacyclopentene[8c] or a carbocation[9–11], [14] has been a matter of recent debate. We felt that our system could serve as a good probe for new mechanistic insights, notably by tuning the nature of the propargylic O-protecting group X.

The bromomethyldimethylsilyl derivative **1b** gave products **2b** and **3b** in 5 and 61% yield, respectively (Table 1, entry 2). Desilylation of **3b** yielded **3a**, proving that we were dealing with the same type of reaction and that the relative configurations at all the newly formed stereocenters in compound **3b** were identical to those in product **3a**. Comparing the results for **1a** with those for **1b** we concluded that the free alcohol **1a** is slightly more fragile under our standard

[*] Dr. L. Fensterbank, Prof. Dr. M. Malacria, E. Mainetti, Dr. V. Mouriès
Université Pierre et Marie Curie
Laboratoire de Chimie Organique de Synthèse
associé au CNRS, Tour 44–54, Case 229
4, place Jussieu, 75252 Paris Cedex 05 (France)
Fax: (+33) 1-44-27-73-60
E-mail: fensterb@ccr.jussieu.fr, malacria@ccr.jussieu.fr
Dr. J. Marco-Contelles
Laboratorio de Radicales Libres, CSIC
C/Juan de la Cierva, 3, 28006 Madrid (Spain)
Fax: (+34) 91 564 48 53
E-mail: iqoc21@iqog.csic.es

[**] Acknowledgement is made to the EU for the COST D12 Action "Cascade Free Radical Reactions" and for a short-term scientific mission to Madrid (EM). We thank Nieves Arroyo (CSIC) for preliminary experiments, Dr. J. Vaissermann (UPMC) for the X-ray analysis of **3e**, Dr. M. L. Jimeno (CNQO) for NMR studies on **3a**, Dr. M.-N. Rager (ENSCP) for NMR studies on **3h**, **6**, and **11**, and Matthieu Bernard (UPMC) for performing some of the experiments. We also thank Dr. Emmanuel Lacôte and Dr. Henri Rudler (UPMC) for helpful discussions.

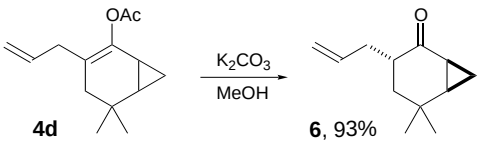
Supporting information for this article is available on the WWW under http://www.angewandte.org or from the author.

 © WILEY-VCH Verlag GmbH, 69451 Weinheim, Germany, 2002 1433-7851/02/4112-2132 $ 20.00+.50/0

reactions conditions than O-protected derivatives, which was confirmed by the fact that the methyl ether **1c** gave a diastereomerically pure material (**3c**) in 68% yield, with no detectable metathesis adduct **2** (Table 1, entry 3). The spectroscopic data for compounds **3c** and **3b** or **3a** were similar, thus confirming the same stereochemical features for all of them.

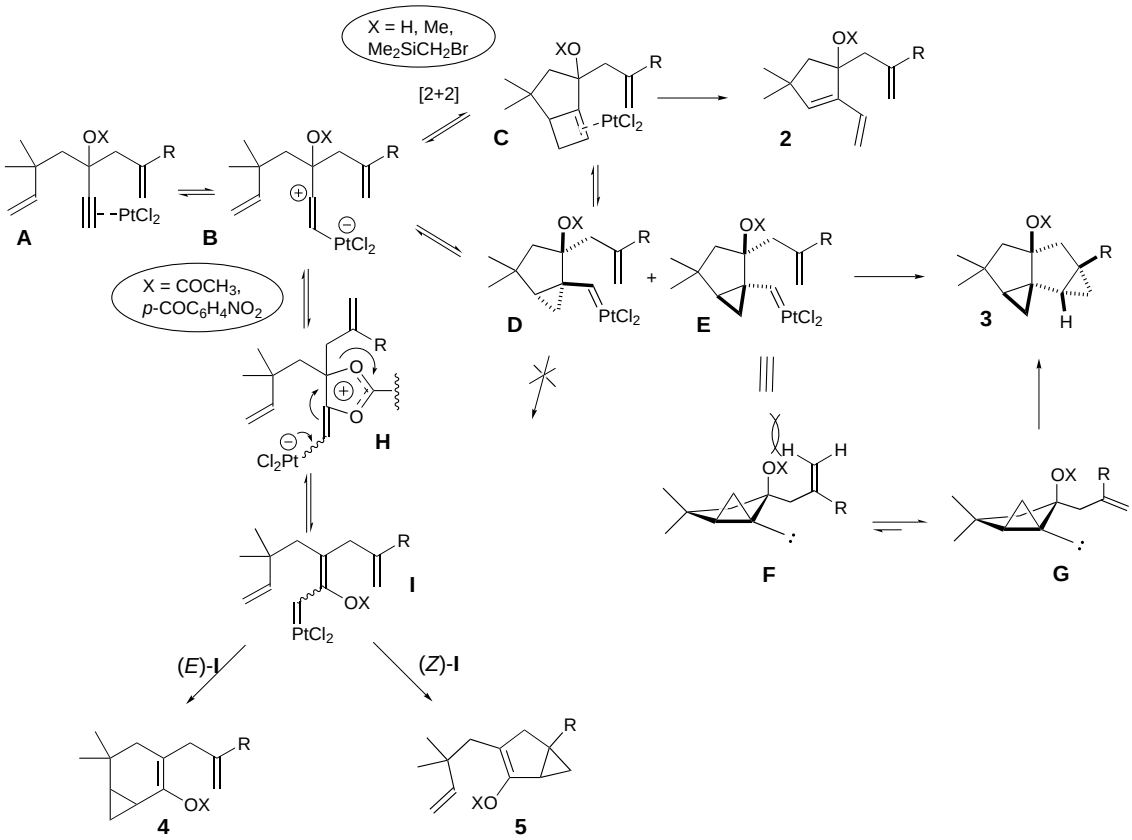
The methallyl precursors **1f**, **1g**, and **1h** showed the same pattern of reactivity: the tetracyclic derivatives **3** were still formed and isolated as single diastereomers, but in much lower yields (from 16 to 34%, Table 1, entries 6–8). No other product was identified from these reactions. The relative configurations at the newly formed stereocenters could be assigned based on NOESY studies and by comparison of the NMR data with those of the analogous compounds **3a–c**.

The behavior of the *O*-acyl derivatives **1d**, **1e**, and **1i** proved quite distinct. The reaction of **1d** was rapid and clean and afforded a compound in good yield (88%, Table 1, entry 4), whose spectroscopic and analytical data suggested a more simple, completely different adduct. NMR analysis confirmed that **4d** with a bicyclo[4.1.0] framework and an enolester conjugated with the cyclopropane ring was formed. The 4-nitrobenzoates **1e** and **1i** afforded the corresponding products **4e** and **4i** in consistent and similar high yields (Table 1, entries 5 and 9). Additional proof for the structure was obtained when compound **4d** was transformed into the *trans* ketone **6**[15] after methanolysis [Eq. (1)]. Minor adducts with structures that, based on the NMR spectra, correspond to **5** (Scheme 1) were also observed.



(1)

In Scheme 2, we propose a simple mechanistic picture for these findings. After π complexation of the alkyne moiety onto the platinum salt,[16] the intermediate **A** evolves via a slipped, polarized η^1-alkyne complex bearing a positive charge at the β position (**B**).[9], [17] For X = H, Me, and Me_2SiCH_2Br, two pathways are reasonable: 1) The identification of metathesis products **2** as minor products suggests the formation of a formal [2+2] adduct **C** through the cationic manifold proposed by Fürstner,[9d] and its reopening to provide **2**. 2) For the products **3** carbene complexes like **D** and **E** are probable intermediates. Such cyclopropyl Pt complexes have been first mentioned by Murai et al.[10] and then shown by Echavarren et al., through DFT calculations,[11b] to be key intermediates in the alkoxy cyclization of enynes. In our case, only **E**, having the *cis* disposition between the alkyl chain and the carbene entity, can evolve in a further intramolecular diastereoselective cyclopropanation (conformer **G** preferred over **F**) leading to the diquinanes **3**. This is not possible for **D**. The driving force for these reactions might be the delivery of the diene **2** or of the tetracyclic derivative **3** as the formation of **C**, **D**, and **E** is presumably reversible.

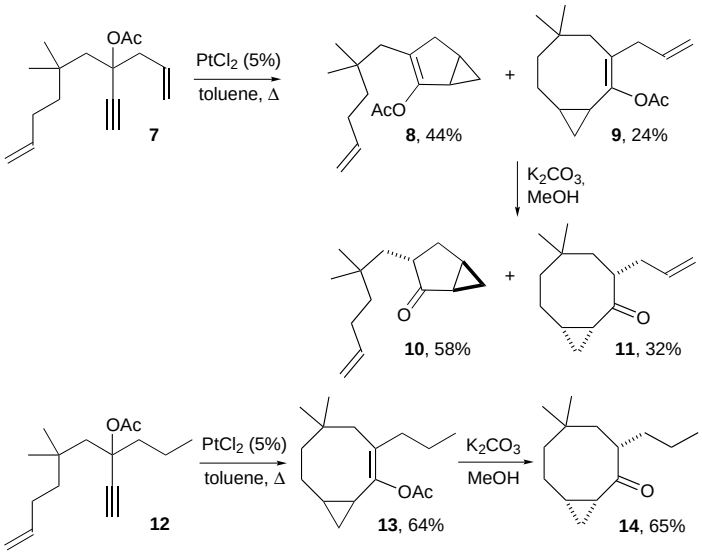


Scheme 2. Mechanistic considerations for the formation of products **2–5**.

 © WILEY-VCH Verlag GmbH, 69451 Weinheim, Germany, 2002 1433-7851/02/4112-2133 $ 20.00+.50/0

To rationalize the completely distinct behavior of the *O*-acyl precursors, we invoke further stabilization of the initial vinylcarbocation intermediate **B** through formation of the oxocarbenium species **H** (Scheme 2). Adjustment of electrons involving an *O*-acyl migration at the β carbon atom then furnishes the vinyl platinum carbene **I**, which adds, in the *E* form, to the pending double bond to give adducts **4**, whereas the minor *Z* intermediate gives adducts **5**. This whole new $PtCl_2$-catalyzed transformation was intriguing, and we next sought for a confirmation on the generality of this reactivity and versatile synthetic applications.

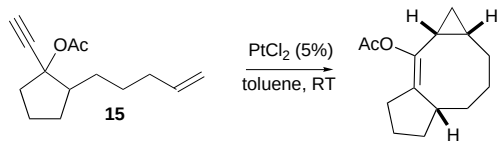
For that purpose, we examined the behavior of precursors **7** and **12** (Scheme 3). The former provided the two bicyclic derivatives **8** and **9** suggesting that the same type of



Scheme 3. Synthesis of cyclooctane derivatives.

mechanism is operating with a competition between the formation of five-membered ring **8** via a *Z* vinyl carbene species and the formation of eight-membered ring **9** involving the *E* vinyl carbene species. Presumably, these two species are in equilibrium and their relative stability and possible evolution account for the ratio. Without such a competition (compound **12**) a fair yield of the cyclooctene (64% **13**) was obtained, considering that the efficient assembly of a functionalized cyclooctane from an acyclic precursor still remains a difficult task.[18] Final methanolysis led completely diastereoselectively to the bicyclic ketones **10**, **11**, and **14**.[15]

Finally, in order to illustrate the synthetic potential of this reaction, a different type of substrate, the diastereomeric mixture **15**, was exposed to a catalytic amount of $PtCl_2$. In a completely stereoconvergent process a single diastereomer of the tricyclic adduct **16** was formed in 66% yield [Eq. (2)].[15]



(2)

In conclusion, we have shown that $PtCl_2$-catalyzed cyclizations of dienyne systems with a hydroxy group at the propargylic position can be chemo-, regio-, and stereocontrolled by tuning the nature of the protecting group at this position. With a free hydroxy group or the corresponding ethers, the previously unknown tetracyclo[4.4.0.0^{1,3}0^{8,10}]decane skeleton was obtained diastereoselectively. An *O*-acyl protecting group completely shifted the reaction towards a previously undescribed rearrangement, which afforded bicyclic enolesters with a fused cyclopropane ring in α,β position that were methanolyzed to versatile [*n*.1.0]bicylic ketones as single diastereomers. This combined two-steps protocol can be regarded as an equivalent of the well-known cycloisomerization of unsaturated α-diazocarbonyl compounds[19] with obvious advantages.

Particularly attractive is the extension of this process to efficiently produce medium-sized rings such as cyclooctanes, still a challenge in organic synthesis.[18] Because of their oxygenated functionalities and the presence of intriguing cyclopropane moieties,[20] these compounds should also be an interesting platform for further elaboration.[21] Our results provide strong support for a cationic mechanism of their formation, notably the intervention of a slipped polarized η^1-alkyne complex.

Experimental Section

To a degassed solution of 5-ethynyl-5-methoxy-3,3-dimethylocta-1,7-diene **1c** (173 mg, 0.9 mmol) in dry toluene (40 mL, 0.025 M), under argon and at room temperature (RT), $PtCl_2$ (13 mg, 0.05 mmol, 0.05 equiv) was added. The mixture was warmed to 80 °C and stirred until the reaction was complete (ca. 2.5 h). Then the mixture was cooled to RT and the solvent was evaporated under vacuum. Purification by flash chromatography on silica gel (pentane/Et_2O, 98/2) afforded the diquinane **3c** in 68% yield (118 mg) as an oil. IR (neat): $\tilde{\nu}$ = 2950, 1480, 1380 cm^{-1}; ^{1}H NMR (200 MHz, $CDCl_3$): δ = 3.28 (s, 3H), 2.36 (dd, *J* = 14.3, 7.0 Hz, 1H), 1.61 (m, 1H), 1.52 (dd, *J* = 14.3, 2.5 Hz, 1H), 1.52 (d, *J* = 14.3 Hz, 1H), 1.33 (td, *J* = 7.4, 3.4 Hz, 1H), 1.08 (d, *J* = 14.3 Hz, 1H), 1.06 (s, 3H), 0.90 (s, 3H), 0.89 (td, *J* = 8.4, 4.4 Hz, 1H), 0.82 – 0.70 (m, 3H), 0.47 ppm (q, *J* = 4.0 Hz, 1H); ^{13}C NMR (50 MHz, $CDCl_3$): δ = 104.0, 51.9, 46.2, 43.8, 39.2 (2C), 35.8, 30.7, 28.3, 22.1, 21.7, 21.2, 12.2 ppm; elemental analysis (%) calcd for $C_{13}H_{20}O$: C 81.20, H 10.48; found: C 81.07, H 10.59.

Received: January 22, 2002
Revised: April 8, 2002 [Z18566]

[1] a) P. Devin, L. Fensterbank, M. Malacria, *J. Org. Chem.* **1998**, *63*, 6764 – 6765; b) J. Marco-Contelles, *Chem. Commun.* **1996**, 2629 – 2630.

[2] a) P. Cruciani, C. Aubert, M. Malacria, *J. Org. Chem.* **1995**, *60*, 2664 – 2665; b) M. Malacria, *Chem. Rev.* **1996**, *96*, 289 – 306; c) J. Marco-Contelles, E. de Opazo, *J. Org. Chem.* **2000**, *65*, 5416 – 5419; d) J. Marco-Contelles, E. de Opazo, *Tetrahedron Lett.* **2000**, *41*, 2439 – 2441; e) J. Marco-Contelles, N. Arroyo, J. Ruiz-Caro, *Synlett* **2001**, 652 – 654.

[3] For reviews, see: a) M. Schuster, S. Blechert, *Angew. Chem.* **1997**, *109*, 2124 – 2145; *Angew. Chem. Int. Ed.* **1997**, *36*, 2036 – 2056; b) R. H. Grubbs, S. Chang, *Tetrahedron* **1998**, *54*, 4413 – 4450; c) A. Fürstner, *Angew. Chem.* **2000**, *112*, 3140 – 3172; *Angew. Chem. Int. Ed.* **2000**, *39*, 3012 – 3043.

[4] For examples of enyne metathesis, see: a) T. J. Katz, T. M. Sivavec, *J. Am. Chem. Soc.* **1985**, *107*, 737 – 738; b) A. Kinoshita, M. Mori, *Synlett* **1994**, 1020 – 1022; c) A. G. M. Barrett, S. P. D. Baugh, D. C. Braddock, K. Flack, V. C. Gibson, P. A. Procopiou, *Chem. Commun.* **1997**, 1375 – 1376; d) M. Picquet, C. Bruneau, P. H. Dixneuf, *Chem. Commun.*

 © WILEY-VCH Verlag GmbH, 69451 Weinheim, Germany, 2002 1433-7851/02/4112-2134 $ 20.00+.50/0

1998, 2249 – 2250; e) J. Renaud, C.-D. Graf, L. Oberer, *Angew. Chem.* **2000**, *112*, 3231 – 3234; *Angew. Chem. Int. Ed.* **2000**, *39*, 3101 – 3104, and references therein.
[5] S.-H. Kim, W. J. Zuercher, N. B. Bowden, R. H. Grubbs, *J. Org. Chem.* **1996**, *61*, 1073 – 1081.
[6] E. M. Codesido, L. Castedo, J. R. Granja, *Org. Lett.* **2001**, *3*, 1483 – 1486.
[7] F.-D. Boyer, I. Hanna, L. Ricard, *Org. Lett.* **2001**, *3*, 3095 – 3098.
[8] For pioneering work with platinum complexes, see: a) B. M. Trost, V. K. Chang, *Synthesis* **1993**, 824 – 832; b) J. Blum, H. Beer-Kraft, Y. Badrieh, *J. Org. Chem.* **1995**, *60*, 5567 – 5569; see also: c) B. M. Trost, G. A. Doherty, *J. Am. Chem. Soc.* **2000**, *122*, 3801 – 3810.
[9] a) N. Chatani, N. Furukawa, H. Sakurai, S. Murai, *Organometallics* **1996**, *15*, 901 – 903; b) A. Fürstner, H. Szillat, B. Gabor, R. Mynott, *J. Am. Chem. Soc.* **1998**, *120*, 8305 – 8314; c) A. Fürstner, H. Szillat, F. Stelzer, *J. Am. Chem. Soc.* **2000**, *122*, 6785 – 6786; d) A. Fürstner, F. Stelzer, H. Szillat, *J. Am. Chem. Soc.* **2001**, *123*, 11 863 – 11 869.
[10] For studies on a linear dienyne system, see: N. Chatani, K. Kataoka, S. Murai, N. Furukawa, Y. Seki, *J. Am. Chem. Soc.* **1998**, *120*, 9104 – 9105.
[11] For reactions with external trapping, see: a) M. Méndez, M. P. Muñoz, A. M. Echavarren, *J. Am. Chem. Soc.* **2000**, *122*, 11 549 – 11 550; b) M. Méndez, M. P. Muñoz, C. Nevado, D. J. Cárdenas, A. M. Echavarren, *J. Am. Chem. Soc.* **2001**, *123*, 10 511 – 10 520.
[12] CCDC-172245 contains the supplementary crystallographic data for compund **3e**. These data can be obtained free of charge via www.ccdc.cam.ac.uk/conts/retrieving.html (or from the Cambridge Crystallographic Data Centre, 12, Union Road, Cambridge CB2 1EZ, UK; fax: (+44) 1223-336-033; or deposit@ccdc.cam.ac.uk).
[13] For a related formation of a tetracyclic derivative with two cyclopropyl rings from a linear dienyne precursor, see ref. [10].
[14] For further mechanistic data, see: a) N. Chatani, H. Inoue, T. Ikeda, S. Murai, *J. Org. Chem.* **2000**, *65*, 4913 – 4918; b) S. Oi, I. Tsukamoto, S. Miyano, Y. Inoue, *Organometallics* **2001**, *20*, 3704 – 3709.
[15] The stereochemical assignment was deduced from NOESY studies.
[16] M. H. Chisholm, H. C. Clark, *Acc. Chem. Res.* **1973**, *6*, 202 – 209.
[17] For such an intermediate with Ru^{II} complexes, see: D. Pilette, S. Moreau, H. Le Bozec, P. H. Dixneuf, J. F. Corrigan, A. J. Carty, *Chem. Commun.* **1994**, 409 – 410.
[18] G. Mehta, V. Singh, *Chem. Rev.* **1999**, *99*, 881 – 930.
[19] a) A. Padwa, K. E. Krumpe, *Tetrahedron* **1992**, *48*, 5385 – 5453; b) T. Ye, A. McKervey, *Chem. Rev.* **1994**, *94*, 1091 – 1160; c) M. P. Doyle in *Comprehensive Organometallic Chemistry*, *Vol. 12* (Eds.: E. W. Abel, F. G. A. Stone, G. Wilkinson, L. Hegedus), Pergamon, Oxford, **1995**, pp. 387 – 420.
[20] a) H.-U. Reißig in *The Chemistry of the Cyclopropyl Group* (Eds.: S. Patai, Z. Rappoport), Wiley, Chichester, **1987**, pp. 375 – 443; b) J. Salaün in *The Chemistry of the Cyclopropyl Group* (Eds.: S. Patai, Z. Rappoport), Wiley, Chichester, **1987**, pp. 809 – 878.
[21] The structural – functional assembly present in adducts **3** is partially incorporated in tricyclic DNA derivatives: R. Steffens, C. J. Leumann, *J. Am. Chem. Soc.* **1999**, *121*, 3249 – 3255.

Dioxygen Activation by a Mononuclear Ir^{II} – Ethene Complex

Bas de Bruin,* Theo P. J. Peters, Simone Thewissen, Arno N. J. Blok, Jos B. M. Wilting, René de Gelder, Jan M. M. Smits, and Anton W. Gal*

In an attempt to gain a mechanistic insight into the rhodium- and iridium-catalyzed oxygenation of olefins, we have recently investigated stoichiometric oxygenation of N ligand Rh^{I}– and Ir^{I} – olefin complexes by O_2 (olefin = ethene, propene, 1,5-cyclooctadiene).[1, 2]

The reactivity of Rh^{I}– and Ir^{I} – ethene fragments towards dioxygen varied between ethene displacement (Figure 1a), formation of mixed O_2 – ethene complexes (Figure 1b), C–O bond making (giving a 3-metalla(III)-1,2-dioxolane; Figure 1c), and combined C–O bond making and O–O bond breaking (giving a 2-metalla(III)oxetane; Figure 1d) The outcome of the oxygenation reaction varies with the N ligand and the central metal.

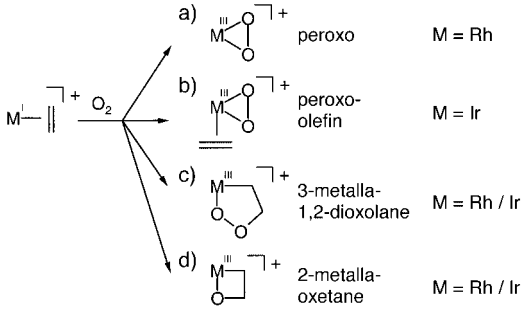


Figure 1. Oxygenation products from the reaction of $[(N\ ligand)M^{I}(olefin)]^{+}$ (M = Rh/Ir) complexes with O_2.

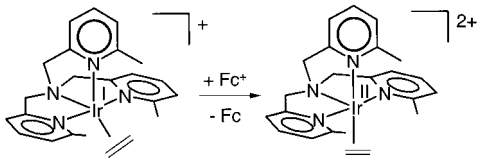
Recently, we described the oxygenation of the iridium(I) – ethene complex $[(\kappa^4\text{-}Me_3\text{-}tpa)Ir^{I}(C_2H_4)]^{+}$ (**1**; Me_3-tpa = *N*,*N*,*N*-tri((6-methyl-2-pyridyl)methyl)amine) by O_2 to the peroxo – ethene complex $[(\kappa^3\text{-}Me_3\text{-}tpa)Ir^{III}(C_2H_4)(O_2)]^{+}$ (Figure 1b) and unidentified paramagnetic species.[2] We now report the one-electron oxidation of the Ir^{I} – ethene complex **1** to the unprecedented Ir^{II} – ethene complex $[(\kappa^4\text{-}Me_3\text{-}tpa)Ir^{II}(C_2H_4)]^{2+}$ (**2**; see Scheme 1), and the reactivity of **2** towards O_2.

Treatment of **1**-PF_6 with ferrocinium hexafluorophoshate ([Fc]PF_6) in CH_2Cl_2 resulted in precipitation of **2**-$(PF_6)_2$ as a brown powder. Thus, one-electron oxidation of Ir^{I} – ethene complex **1** with Fc^{+} results in the clean formation of the stable Ir^{II} – ethene complex **2** (Scheme 1).

[*] Dr. B. de Bruin, Prof. Dr. A. W. Gal, T. P. J. Peters, S. Thewissen, A. N. J. Blok, J. B. M. Wilting, R. de Gelder, J. M. M. Smits
Department of Inorganic Chemistry
University of Nijmegen
Toernooiveld 1, 6525 ED Nijmegen (The Netherlands)
Fax: (+31) 24-355-3450
E-mail: bdebruin@sci.kun.nl, gal@sci.kun.nl

Supporting information for this article is available on the WWW under http://www.angewandte.org or from the author.

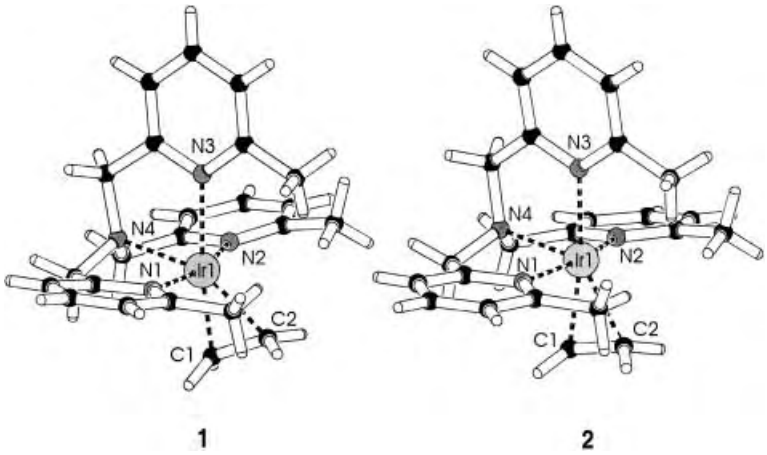
 © WILEY-VCH Verlag GmbH, 69451 Weinheim, Germany, 2002 1433-7851/02/4112-2135 $ 20.00+.50/0



1 2

Scheme 1. Oxidation of **1** with Fc^+ yielding **2**.

Dark brown crystals of **2**-$(PF_6)_2$, suitable for X-ray diffraction, were obtained from an acetone solution layered with hexane, at 10 °C. Transparent brown-red crystals of **1**-PF_6 were grown from a CH_2Cl_2 solution layered with hexane, at 4 °C. The structures of both **1** and **2** were determined by single-crystal X-ray diffraction (Figure 2 and Table 1).[3]



1 2

Figure 2. Molecular structure of **1** and **2**.

Table 1. Selected bond lengths [Å] and angles [°] for **1** and **2**.[a]

	1	**2**
N1-Ir1	2.075(7)	2.071(5)
N2-Ir1	2.043(8)	2.062(5)
N3-Ir1	2.260(7)	2.136(5)
N4-Ir1	2.154(8)	2.146(5)
C1-Ir1	2.042(9)	2.136(6)
C2-Ir1	2.143(9)	2.149(6)
C1-C2	1.451(13)	1.380(9)
N4-Ir1-C1	109.2(4)	92.4(2)
N4-Ir1-C2	149.5(3)	129.8(2)
N3-Ir1-C1	173.3(3)	172.0(2)
N3-Ir1-C2	132.8(2)	150.2(2)
N3-Ir1-N4	77.4(3)	80.03(17)

[a] For atom labeling see Figure 2.

The structure of **1** is best described as distorted trigonal bipyramidal (*tbp*), with N1 and N2 at the axial positions and N3, N4, and ethene in the equatorial plane. Remarkably, upon one-electron oxidation of **1** to **2**, the coordination geometry changes from *tbp* to distorted square pyramidal (*sqpy*), with N4 at the apical position and N1, N2, N3, and ethene in the basal plane.

Oxidation of **1** to **2** results in a stronger binding of Me_3-tpa to the Ir center; the Ir–N3 bond shortens by ~0.12 Å, whereas the N1–Ir1, N2–Ir1, and N4–Ir1 bonds do not significantly change (Table 1). The shortening of the C1–C2 bond by 0.07 Å and the elongation of the Ir–C1 bond by 0.09 Å on going from **1** to **2** indicates weakening of the Ir–ethene interaction upon oxidation of Ir^I to Ir^{II}. Since one cannot imagine a decrease in the ethene →Ir σ bonding, the weaker Ir–ethene interaction must result from decreased Ir →ethene π backbonding in **2**. In **1**, the Ir1–C2 bond is approximately 0.1 Å longer than the Ir1–C1 bond, probably because the axial Py-*Me* substituents of the Me_3-tpa ligand hinder a closer approach of C2 to the iridium center.

The EPR spectrum of **2** is shown in Figure 3 a. Simulation of the rhombic spectrum yielded: $g_{11} = 1.975$, $g_{22} = 2.265$, and $g_{33} = 2.538$. The (super)hyperfine coupling pattern for the g_{11} signal was satisfactorily simulated by assuming hyperfine coupling with the iridium center ($A_{11}^{Ir} = 129$ MHz) and superhyperfine coupling with one nitrogen atom ($A_{11}^{N} = 55$ MHz). Contributions from other N nuclei are not resolved in this direction. The g_{22} signal reveals no resolved hyperfine coupling.

The nature of the observed five-line (super)hyperfine coupling pattern of the g_{33} signal is presently not understood. It is satisfactorily simulated by assuming superhyperfine coupling with four (nearly) equivalent $I = 1/2$ nuclei, possibly the four H nuclei of the ethene fragment of **2**. However, the thus obtained superhyperfine coupling constant $A_{33}^{H} \approx 160$ MHz seems unusually large for hydrogen atoms.[4] Alternative simulations, which assume coupling with two (nearly) equivalent N nuclei or coupling with one N nucleus and two (nearly) equivalent H nuclei, yield less satisfactory results and still require unusually large superhyperfine coupling constants ($A_{33}^{N/H} \approx$ 160 MHz). We are currently investigating the origin of this fine structure.

We performed DFT calculations on both **1** and **2**.[5] The geometries of the optimized DFT structures match quite well with the X-ray structures of **1** and **2** (*tbp* geometry for **1**, *sqpy* geometry for **2**). The HOMO of **1** and the SOMO of **2** both consist mainly of an iridium d orbital, with bonding contributions of the ethene π* orbital and antibonding contributions of orbitals on N3 and N4. The oxidation of **1** to **2** removes one

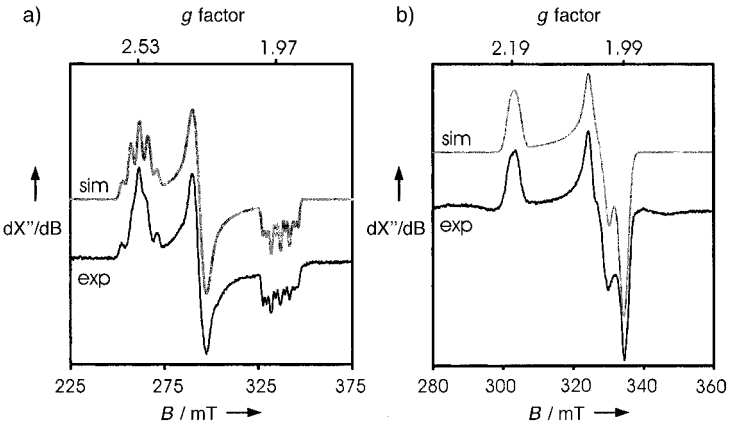


Figure 3. a) Experimental (exp) and simulated (sim) X-band EPR spectrum of **2**. b) Experimental and simulated X-band EPR spectrum of intermediate **3**. Experimental spectra in acetone:MeOH (2:3) at 40 K, 9.30 GHz. (attn. 30 dB, mod. 4 G).

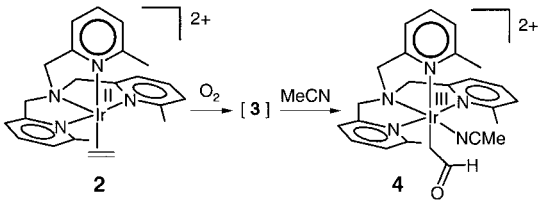
 © WILEY-VCH Verlag GmbH, 69451 Weinheim, Germany, 2002 1433-7851/02/4112-2136 $ 20.00+.50/0 *Angew. Chem. Int. Ed.* **2002**, *41*, No. 12

electron from the HOMO of **1** to give the SOMO of **2** (see Supporting Information, Figure S1). As a result, the Ir→ethene π backbonding decreases and the Ir1–N3/Ir1–N4 σ interaction increases on going from **1** to **2**. Actually, we observe that only the Ir1–C1 distance increases and only the Ir1–N3 distance decreases (Table 1), this is because Ir1–C2 in **1** is already long as a result of steric hindrance by the axial Py-*Me* substituents, whereas Ir1–N4 in **1** is already short as a result of geometrical constraints by the κ^4-Me_3-tpa ligand.

Mononuclear complexes of Rh^{II}[6] and particularly Ir^{II}[7] are rare. Most examples are stabilized by bulky dianionic porphyrinate ligands (por^{2-}). To our knowledge, only one stable mononuclear Ir^{II}–olefin complex has been reported, $[(C_6Cl_5)_2Ir^{II}(cod)]$ (cod = *Z*,*Z*-1,5-cyclooctadiene).[8] Complex **2** is the first example of a stable M^{II}–ethene (M = Rh, Ir) complex.

Recently, $[(por)M^{II}(ethene)]$ (M = Rh,[6] Ir,[9] por^{2-} = a bulky meso-tetra-arylporphyrinate dianion), formed in situ from $[(por)M^{II}]$ and ethene, have been reported to undergo bimolecular C–C radical coupling to butylene-bridged dinuclear complexes. Quite remarkably, complex **2** does *not* dimerize by radical coupling of the ethene carbon atoms. Nevertheless, the DFT calculations suggest that the coordinated ethene fragment may still have some radical character (see Supporting Information, Figure S1 and S2).

The radical character of **2** seems to be reflected in its reactivity towards O_2. Upon exposure of a solution of **2** in MeCN, acetone, or acetone:MeOH (2:3) to air or O_2 at −10 °C, the color of the solution changed from brown to purple. Upon warming these solutions to ambient temperature, the purple color vanishes, the solutions became colorless, and the ^{1}H NMR spectrum indicated the formation of *diamagnetic* products. The main product in MeCN (~70% based on ^{1}H NMR spectroscopy) was identified as formylmethyl[10] complex **4** (Scheme 2). In acetone other types of products were detected. The nature of these products and the apparent solvent dependency of their formation are currently under investigation.



Scheme 2. Oxygenation of **2** by O_2 yielding **4** via intermediate **3**.

The Ir^{II}–ethene complex **2** thus seems capable of O_2 activation and C–O bond formation. In marked contrast, oxidation of Ir^{I}–ethene complex **1** with O_2 in solution did *not* result in C–O bond formation, but yielded the peroxo–ethene complex $[(\kappa^3$-Me_3-tpa$)Ir^{III}(O_2)(C_2H_4)]^+$.[2]

The initial color change from brown to purple in the conversion of **2** into **4** at −10 °C indicates the formation of an intermediate (**3**). The EPR spectrum of **3** is shown in Figure 3b.[11] Simulation of the rhombic spectrum yields $g_{11} = 1.987$, $g_{22} = 2.030$, and $g_{33} = 2.191$. The line shape for g_{22} suggests a small iridium hyperfine coupling ($A_{22}^{Ir} \approx 38$ MHz). Thus, on going from **2** to **3** a marked decrease in anisotropy of the EPR signal is observed (Figure 3). This effect might indicate a shift in spin density from the metal center to a coordinated superoxy or superoxyethyl radical.

We have thus synthesized the unique Ir^{II}–ethene complex **2** through the one-electron oxidation of Ir^{I}–ethene complex **1**. The radical character of **2** may be responsible for the facile C–O bond formation in this complex upon contact with O_2. The observed reactivity of **2** towards O_2 points to a possible role of Ir^{II}–olefin and Rh^{II}–olefin species in rhodium- and iridium-catalyzed oxidation of olefins by O_2. This insight is of importance in the development of catalytic olefin oxygenation by Group VIII metal centers.

Experimental Section

NMR spectroscopic experiments were carried out on a Bruker DPX200 spectrometer. X-band EPR spectra were recorded on a Bruker ER220 spectrometer. Mass Spectra were recorded on a MAT 900 XL mass spectrometer. All procedures were performed under N_2 using standard Schlenk techniques unless indicated otherwise. Compound **1**-PF_6 was prepared as reported in ref. [2]

2-$(PF_6)_2$: Complex **1**-PF_6 (230 mg, 0.33 mmol) was added to a solution of $[Fc]PF_6$ (86 mg, 0.26 mmol) in CH_2Cl_2 (12 mL). The resulting green/brown mixture was stirred for 30 min at room temperature. The resulting brown precipitate was collected by filtration. Yield 186 mg (0.221 mmol, 85%; analytically pure). Deep brown/black crystals of **2**-$(PF_6)_2$, suitable for X-ray diffraction, were obtained at 10 °C from a solution of the above precipitate in acetone layered with hexane. Yield after crystallization: 72 mg (0.085 mmol, 33%). ESI$^+$-MS: *m*/*z* 276.5 $[M-(PF_6)_2]^{2+}$, 698 $[M-PF_6]^+$; elemental analysis calcd (%) for $C_{23}H_{28}N_4IrP_2F_{12}$: C 32.78, H 3.35, N 6.65; found: C 32.64, H 3.33, N 6.67.

4-$(PF_6)_2$: Exposure of a solution of **2**-$(PF_6)_2$ in MeCN to O_2 leads to a mixture of ~70% **4**-$(PF_6)_2$ and ~30% of yet unidentified products. From this mixture **4**-$(PF_6)_2$ was characterized. ^{1}H NMR (200 MHz, CD_3CN, 298 K): $\delta = 9.44$ (t, 1H, $^3J(H,H) = 4.55$ Hz, $IrCH_2C(=O)H$), 7.81 (t, 2H, Py^A-H4, $^3J(H,H) = 7.6$ Hz), 7.69 (t, 1H, Py^B-H4, $^3J(H,H) = 7.6$ Hz), 7.40–7.10 (m, 6H, $Py^{A/B}$-H3/5), 5.32 (d[AB], 2H, $^2J(H,H) = 16.4$ Hz, N-CH_2-Py^A), 4.90 (d[AB], 2H, $^2J(H,H) = 16.4$ Hz, N-CH_2-Py^A), 4.71 (s, 2H, N-CH_2-Py^B), 3.55 (d, 2H, $^3J(H,H) = 4.55$ Hz, $IrCH_2C(=O)H$), 3.18 (s, 3H, CH_3-Py^B), 2.96 (2, 3H, Ir-NC*CH3*), 2.82 ppm (s, 6H, CH_3-Py^A); $^{13}C\{^1H\}$ NMR (50 MHz, CD_3CN, 298 K): $\delta = 208.5$ ($IrCH_2C(=O)H$), {166.0,164.4, 163.4, 159.3 ($Py^{A/B}$-C2, $Py^{A/B}$-C6)}, 141.3 (Py^B-C4), 140.7 (Py^A-C4), 128.6 (Py^B-C3), 128.2 (Py^A-C3), 122.7 (Py^B-C5), 120.4 (Py^A-C5), 74.9 (N-CH_2-Py^A), 71.4 (N-CH_2-Py^B), 27.3 (Py^B-CH_3), 27.2 (Py^A-CH_3), 10.4 (Ir-CH_2C(=O)H), 5.6 ppm (Ir-NCCH_3) (Ir-NCCH_3 signal obscured by solvent signal); FT-IR (KBr): $\tilde{\nu} = 2848$, 2733 (C–H of CH=O), 1676 (C=O of CH=O), 825, 556 cm^{-1} (P–F); ESI$^+$-MS (sample prepared in CD_3CN): *m*/*z* 306 $[M-(PF_6)_2]^{2+}$, 284 $[M-(PF_6)_2-CD_3CN]^{2+}$, 757 $[M-PF_6]^+$.

Received: January 31, 2002 [Z 18624]

[1] a) B. de Bruin, J. A. Brands, J. J. J. M. Donners, M. P. J. Donners, R. de Gelder, J. M. M. Smits, A. W. Gal, A. L. Spek, *Chem. Eur. J.* **1999**, *5*, 2921–2936; b) B. de Bruin, M. J. Boerakker, J. A. W. Verhagen, R. de Gelder, J. M. M. Smits, A. W. Gal, *Chem. Eur. J.* **2000**, *6*, 298–312; c) R. J. N. A. M. Kicken, PhD thesis, University of Nijmegen (The Nederlands), **2001**; d) M. Krom, R. G. E. Coumans, J. M. M. Smits, A. W. Gal, *Angew. Chem.* **2001**, *113*, 2164–2166; *Angew. Chem. Int. Ed.* **2001**, *40*, 2106–2108.

[2] B. de Bruin, T. P. J. Peters, J. B. M. Wilting, S. Thewissen, J. M. M. Smits, A. W. Gal, *Eur. J. Inorg. Chem.*, submitted.

[3] Single crystals of **1**-PF_6 and **2**-$(PF_6)_2$ were sealed in a glass capillary under N_2. Intensity data were collected on an Enraf-Nonius CAD4 diffractometer, using graphite monochromatized $Mo_{K\alpha}$ radiation

($\lambda = 0.71073$ Å). Data were collected at room temperature ($\omega/2\theta$-scan mode). For both compounds, unit-cell dimensions were determined from the angular setting of 25 reflections. Intensity data were corrected for Lorentz and polarization effects. Semiempirical absorption correction (ψ-scan)[3a] was applied. For **1**-PF_6, this procedure by itself was not adequate enough. The difference fourier map still showed peaks up to 3.6 e Å^3 close to the Ir atom. Therefore an additional absorption correction was applied using the DIFABS procedure,[3b] resulting in final residual peaks up to 2.3 e Å^{-3}. The structures were solved by the program system DIRDIF[3c] using the program PATTY[3d] to locate the heavy atoms, and were refined with standard methods (refinement against F^2 of all reflections with SHELXL-97[3e] with anisotropic parameters for the non-hydrogen atoms. The hydrogen atoms were initially placed at calculated positions, refined isotropically in riding mode, and were subsequently refined freely. For **1**-PF_6, based on geometrical considerations alone, the unit cell could be transformed to an orthorhombic C-cell ($a =$ 9.1795(19), $b = 46.2562(78)$, $c = 11.5840(17)$ Å), but this transformation is not supported by the symmetry of the data ($R_{int} = 0.549$) nor by the unit-cell contents. From the anisotropic thermal displacement parameters for the PF_6 moieties of **2**-$(PF_6)_2$, it is clear that some atoms show a large positional disorder. Although it is possible to use several partially occupied positions for these atoms, no physically reasonable models result from these parameters, at least not any that are better than the models presented here. Summary of the crystal data for **1**-PF_6: ($C_{23}H_{28}N_4PF_6Ir$, $M_r = 697.66$): monoclinic, space group $P2_1/c$, $a =$ 9.1802(19), $b = 11.5828(18)$, $c = 23.581(4)$ Å, $\beta = 101.193(19)^\circ$, $V =$ 2459.7(7) Å^3, $Z = 4$, $\rho_{calcd} = 1.884$ g cm^{-3}. Final R indices: $R_1 = 0.0529$ (for 3815 reflections considered observed ($[I > 2\sigma(I)]$), $wR_2 = 0.1314$ (all data) for the 319 total variables. Summary of the crystal data for **2**-$(PF_6)_2$: ($C_{23}H_{28}N_4P_2F_{12}Ir$, $M_r = 842.63$): monoclinic, space group $P2_1/a$, $a = 13.072(2)$, $b = 12.454(2)$, $c = 18.860(3)$ Å, $\beta = 109.734(11)^\circ$, $V =$ 2890.0(8) Å^3, $Z = 4$, $\rho_{calcd} = 1.937$ g cm^{-3}. Final R indices: $R_1 = 0.0393$ (for 5292 reflections considered observed ($[I > 2\sigma(I)]$), $wR_2 = 0.1011$ (all data) for the 382 total variables. a) A. C. T. North, D. C. Philips, F. S. Mathews, *Acta Crystallogr. Sect. A* **1968**, *24*, 351; b) N. Walker, D. Stuart, *Acta Crystallogr. Sect. A* **1983**, *39*, 158; c) P. T. Beurskens, G. Beurskens, W. P. Bosman, R. de Gelder, S. Garcia-Granda, R. O. Gould, R. Israel, J. M. M. Smits, DIRDIF-96, A computer program system for crystal structure determination by Patterson methods and direct methods applied to difference structure factors; Crystallography Laboratory, University of Nijmegen (The Netherlands), **1996**; d) P. T. Beurskens, G. Beurskens, M. Strumpel, C. E. Nordman in *Patterson and Pattersons* (Eds.: J. P. Glusker, B. K. Patterson, M. Rossi), Clarendon, Oxford, **1987**, p. 356; e) G. M. Sheldrick, SHELXS-97, Program for the refinement of crystal structures, University of Göttingen, Göttingen (Germany), **1997**. CCDC-176107 for **1**-PF_6 and CCDC-176108 for **2**-$(PF_6)_2$ contains the supplementary crystallographic data for this paper. These data can be obtained free of charge via www.ccdc.cam.ac.uk/conts/retrieving.html (or from the Cambridge Crystallographic Data Centre, 12, Union Road, Cambridge CB2 1EZ, UK; fax: (+44) 1223-336-033; or deposit@ccdc.cam.ac.uk).

[4] Organic π radicals normally show much weaker superhyperfine coupling with H nuclei, e.g. $C_2H_4^+$ radical: 70 MHz; allyl free radical: 11–42 MHz; naphthalene anion radical: 5–13 MHz. B. H. J. Bielski, J. M. Gebicki, *Atlas of Electron Spin Resonance Spectra*, Academic Press, New York, **1967**.

[5] Geometries were optimized at the B3LYP level[12] by using the Gaussian 98 suite of programs.[13] Basis sets used include the LANL2DZ basis and pseudo potential[14] for the iridium center and STO3G[15] on all other atoms. The orbitals presented here were visualized using the Molden program (see Supporting Information).[16]

[6] D. G. DeWit, *Coord. Chem. Rev.* **1996**, *147*, 209–246, and references therein.

[7] K. K. Pandey, *Coord. Chem. Rev.* **1992**, *121*, 1–42, and references therein.

[8] M. P. Garcia, M. V. Jimenez, L. A. Oro, F. J. Lahoz, P. J. Alonso, *Angew. Chem.* **1992**, *104*, 1512–1514; *Angew. Chem. Int. Ed. Engl.* **1992**, *31*, 1527–1529.

[9] H. L. Zhai, A. Bunn, B. Wayland, *Chem. Commun.* **2001**, 1294–1295.

[10] Other formylmethyl M^{III} species (M = Rh, Ir) have been reported: a) D. Milstein, J. C. Calabrese, *J. Am. Chem. Soc.* **1982**, *104*, 3773–3774l; b) B. de Bruin, J. A. W. Verhagen, C. H. J. Schouten, A. W. Gal, D. Feichtinger, D. A. Plattner, *Chem. Eur. J.* **2001**, *7*, 416–422; c) M. Krom, R. G. E. Coumans, J. M. M. Smits, A. W. Gal, *Angew. Chem.* **2002**, *114*, 595–599; *Angew. Chem. Int. Ed.* **2002**, *41*, 576–579.

[11] During conversion of **2** into **3** at $-10\,^\circ$C in acetone:MeOH (2:3) some decomposition of **3** occurs. At approximately 50% conversion, **3** was present in about 40% of the initial spin concentration. At full conversion, **3** was present in around 30% of the initial spin concentration. Attempts to record EPR spectra of **2** and **3** in MeCN yielded very broad spectra, probably because of the poor quality of the MeCN glass and/or crystallization. However, despite the broadness of the signals, aerated samples of **2** in MeCN show EPR peaks at the same positions as those for **2** and **3** in acetone:MeOH (2:3).

[12] a) A. D. Becke, *J. Chem. Phys.* **1993**, *98*, 5648–5652; b) C. Lee, W. Yang, R. G. Parr, *Phys. Rev. B* **1988**, *37*, 785–789; c) B. Miehlich, A. Savin, H. Stoll, H. Preuss, *Chem. Phys. Lett.* **1989**, *157*, 200–206.

[13] Gaussian 98 (Revision A.7), M. J. Frisch, G. W. Trucks, H. B. Schlegel, G. E. Scuseria, M. A. Robb, J. R. Cheeseman, V. G. Zakrzewski, J. A. Montgomery, R. E. Stratmann, J. C. Burant, S. Dapprich, J. M. Millam, A. D. Daniels, K. N. Kudin, M. C. Strain, O. Farkas, J. Tomasi, V. Barone, M. Cossi, R. Cammi, B. Mennucci, C. Pomelli, C. Adamo, S. Clifford, J. Ochterski, G. A. Petersson, P. Y. Ayala, Q. Cui, K. Morokuma, D. K. Malick, A. D. Rabuck, K. Raghavachari, J. B. Foresman, J. Cioslowski, J. V. Ortiz, B. B. Stefanov, G. Liu, A. Liashenko, P. Piskorz, I. Komaromi, R. Gomperts, R. L. Martin, D. J. Fox, T. Keith, M. A. Al-Laham, C. Y. Peng, A. Nanayakkara, C. Gonzalez, M. Challacombe, P. M. W. Gill, B. G. Johnson, W. Chen, M. W. Wong, J. L. Andres, M. Head-Gordon, E. S. Replogle, J. A. Pople, Gaussian, Inc., Pittsburgh, PA, **1998**.

[14] a) W. J. Hehre, R. F. Stewart, J. A. Pople, *J. Chem. Phys.* **1969**, *51*, 2657–2664; b) J. B. Collins, P. v. R. Schleyer, J. S. Binkley and J. A. Pople, *J. Chem. Phys.* **1976**, *64*, 5142–5151.

[15] a) P. J. Hay, W. R. Wadt, *J. Chem. Phys.* **1985**, *82*, 270–283; b) W. R. Wadt, P. J. Hay, *J. Chem. Phys.* **1985**, *82*, 284–298; c) P. J. Hay, W. R. Wadt, *J. Chem. Phys.* **1985**, *82*, 299–310.

[16] G. Schaftenaar, J. H. Noordik, *J. Comput.-Aided Mol. Des.* **2000**, *14*, 123–134.

A Highly Regioselective Synthesis of Polysubstituted Naphthalene Derivatives through Gallium Trichloride Catalyzed Alkyne–Aldehyde Coupling**

Ganapathy S. Viswanathan, Mingwen Wang, and Chao-Jun Li*

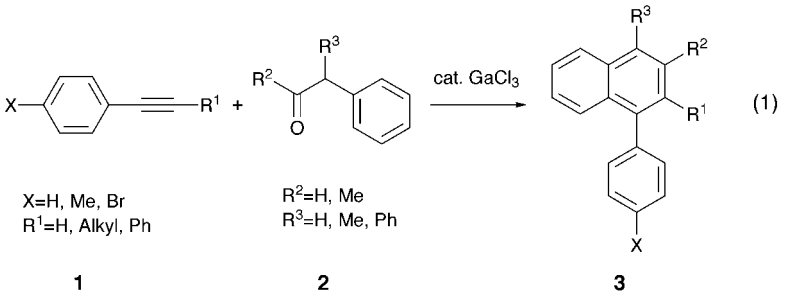
Polysubstituted aromatic compounds have played an important role in the chemical and pharmaceutical industries as well as in the fields of optical and electronic materials. Traditionally, the regioselective construction of polysubstituted aromatic compounds has been carried out by the stepwise introduction of substituents through electrophilic substitutions.[1] More modern achievements in the regioselective

[*] Prof. Dr. C.-J. Li, G. S. Viswanathan, Dr. M. Wang
Department of Chemistry, Tulane University
New Orleans, LA 70118 (USA)
Fax: (+1) 504-865-5596
E-mail: cjli@tulane.edu

[**] This work has been partially supported by the US NSF CAREER Award program and the US NSF-EPA STAR program.

Supporting information for this article is available on the WWW under http://www.angewandte.org or from the author.

construction of aromatic compounds include the direct *ortho*-metallation,[2] transition-metal-catalyzed [2+2+2] alkyne cyclizations,[3, 4] and Bergman-type[5h–i] (thermal and catalyzed) cyclization of enediynes.[5a–g, 4] Other important methods include the [4+2] cyclizations.[4] Recently, there has been considerable interest in synthesizing naphthalene derivatives and other extended aromatic systems, which are extremely useful benzenoid compounds for biological studies and material applications. The most important methods include annulation via Fischer carbenes (the Dötz reaction)[6] and palladium-catalyzed cyclization of alkynes with arylsilyl triflates via highly reactive benzynes (generated in situ).[7] Another method is based on the cyclopropane-shift type reaction,[8] which produces naphthalene derivatives only as by-products. Herein, we wish to report a hitherto unknown cyclization reaction between aromatic alkynes **1** and phenyl acetaldehydes **2** catalyzed by gallium trichloride[9] to give naphthalene derivatives **3** with complete regioselectivity of all substituents [Eq. (1)].



(1)

Recently, we reported a unique coupling reaction between aromatic alkynes and aldehydes resulting in α,β-unsaturated ketones and cyclization products. [10] In our efforts to obtain better selectivity in the formation of either of these products, we investigated the reaction between 1-phenyl-1-propyne (**1b**) and phenylacetaldehyde (**2a**) in methylene chloride in the presence of gallium trichloride (1 equiv). Surprisingly, neither expected product was obtained. Instead, a new product with a molecular weight of 218 (as shown by the GC/MS analysis of the crude reaction mixture) was obtained. Upon purification and characterization, the new product appeared to be 1-phenyl-2-methylnaphthalene (**3b**) (isolated in 41 % yield). Encouraged by this result, efforts were made to improve the yield of this novel coupling reaction (Table 1).

To begin the optimization, the effect of the amount of catalyst on the reaction was studied. When 1-phenyl-1-propyne (**1b**) was treated with phenylacetaldehyde (**2a**) in dichloromethane with gallium trichloride (1 equiv), the reaction went to completion (as was evident by the absence of the alkyne on TLC) after stirring overnight. However, the yield of the isolated product was only 41 % (Table 1, entry 1). A decrease in the amount of catalyst from 100 mol % to 5.8 mol % resulted in a better conversion (Table 1, entry 2). The same effect was also observed in the reaction of **2a** with 1-phenyl-1-pentyne (**1d**) (Table 1, entry 3). When less than 20 mol % of catalyst was used (Table 1, entries 2, 4, 6–10), although it took a relatively longer time for the alkynes to be consumed, the reactions were cleaner and yields were better

Table 1. Effect of the amount of catalyst, temperature, and solvent on the coupling reaction.

Entry	**1** (X = H)	R¹ =	**2**	R³ =	Catalyst [mol %]	Solvent	*T* [°C]	*t* [h]	**3**	Yield[a] [%]
1	**b**	Me	**a**	H	100.0	CH_2Cl_2	RT	14	**b**	41
2	**b**	Me	**a**	H	5.8	CH_2Cl_2	RT	39	**b**	55
3	**d**	Pr	**a**	H	90.7	CH_2Cl_2	RT	36	**d**	26
4	**d**	Pr	**a**	H	5.5	CH_2Cl_2	RT	42	**d**	50
5	**b**	Me	**b**	Me	115.8	CH_2Cl_2	RT	36	**i**	12
6	**a**	H	**a**	H	11.4	CH_2Cl_2	RT	38	**a**	45
7	**e**	Bu	**a**	H	5.5	CH_2Cl_2	RT	20	**e**	11
8[b]	**e**	Bu	**a**	H	5.5	CH_2Cl_2	reflux	20	**e**	52
9[b,c]	**e**	Bu	**a**	H	5.5	toluene	50	13	**e**	41
10[b]	**e**	Bu	**a**	H	5.5	CH_2Cl_2	reflux	13	**e**	39

[a] Yields of isolated compounds. [b] The reactions were monitored by TLC and stopped after the alkyne had been consumed. [c] The reaction mixture was sonicated at 50 °C.

in all cases. At room temperature, the reaction of aliphatic alkynes with **2a** and a catalytic amount of gallium trichloride gave a complicated mixture, which is still under investigation.

To see the effect of different solvents and temperature on the yield, 1-phenyl-1-hexyne (**1e**) was chosen as a standard as it is relatively non-volatile and less reactive than **1b** and **1d**. When **1e** was treated with **2a** in the presence of a catalytic amount of gallium trichloride (5.5 mol %), 1-phenyl-2-butylnaphthalene (**3e**) was obtained in 11 % yield together with unreacted **1e** after 20 h of stirring in dichloromethane at room temperature (Table 1, entry 7). However, when **1e** was heated at reflux with **2a** in dichloromethane with gallium trichloride (5.5 mol %), after 20 h of stirring, the yield of **3e** increased to 52 % (Table 1, entry 8). Chloroform and toluene were also examined as solvents. Both gave lower yields of the desired product (Table 1, entries 9 and 10).

Subsequently, several aromatic alkynes were treated with substituted and unsubstituted phenyl acetaldehydes (Table 2). The yields of the isolated products ranged from 40–70 % for

Table 2. Coupling of alkynes and carbonyl compounds to generate naphthalene derivatives.

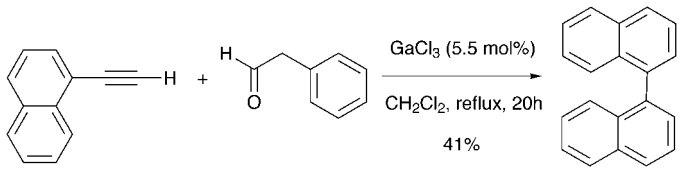
Entry	**1**	X =	R¹ =	**2**	R² =	R³ =	Catalyst [mol %]	*t* [h]	**3**	Yield[a] [%]
1	**a**	H	H	**a**	H	H	7.7	15	**a**	50
2	**b**	H	Me	**a**	H	H	7.8	16	**b**	61
3	**c**	H	Et	**a**	H	H	5.5	15	**c**	64
4	**d**	H	Pr	**a**	H	H	6.0	21	**d**	62
5	**e**	H	Bu	**a**	H	H	5.5	20	**e**	52
6	**f**	CH_3	H	**a**	H	H	5.5	20	**f**	46
7	**g**	Br	H	**a**	H	H	5.5	20	**g**	49
8	**a**	H	H	**b**	H	Me	4.9	16	**h**	51
9	**b**	H	Me	**b**	H	Me	13.0	24	**i**	70
10	**h**	H	Ph	**a**	H	H	7.7	24	**j**	25[b]
11	**a**	H	H	**c**	H	Ph	14.0	23	**k**	55[c]
12	**d**	H	Pr	**b**	H	Me	8.6	14	**l**	63
13	**c**	H	Et	**c**	H	Ph	12.4	19	**m**	68
14	**a**	H	H	**d**	Me	Ph	15.3	54	**n**	10

[a] Yields of isolated compounds. [b] The crude reaction mixture contained a large amount of unreacted diphenylacetylene, even after heating at reflux for 24 h. [c] Yield at RT.

 © WILEY-VCH Verlag GmbH, 69451 Weinheim, Germany, 2002 1433-7851/02/4112-2139 $ 20.00+.50/0

most substrates. NMR spectroscopic and GC/MS analysis of the other fractions obtained after column chromatography indicated a complicated mixture whose identity could not be determined. We believe that the rest of the starting materials could have been lost as a result of a competing polymerization reaction.

This gallium trichloride catalyzed coupling reaction produced a single regioisomer in all cases. This high regioselectivity was further confirmed by the reaction of 1-ethynylnaphthalene (**1i**) and **2a** which gave 1,1′-binaphthalene (**3o**) (a symmetric compound) as the only product [Eq. (2)].



(2)

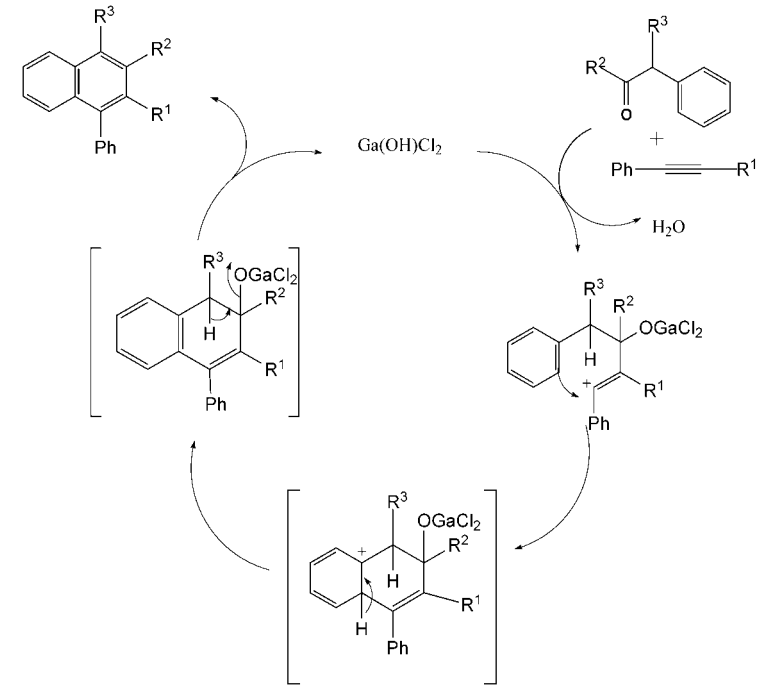
1i **2a** **3o**

Apparently, varying the amount of catalyst from 4–15 mol% did not have any major impact on the yields of the desired products. Substituents on the aromatic ring of the phenyl alkynes also had no significant effect on the yields of the isolated naphthalene derivatives (Table 2). However, the yield was 10% lower for 1-ethynylnaphthalene (**1i**) [eq. (2)] than for phenylacetylene (Table 2, entry 1). When the R^1 group of the alkyne was changed from H to methyl, ethyl, or *n*-propyl, the yield increased by about 10% (Table 2, entries 2–4), whereas when it was changed to phenyl, the yield as well as the rate of the reaction decreased (Table 2, entry 10). When the R^3 group of the aldehyde was changed from H to methyl or phenyl, the yield increased slightly (Table 2, entries 8, 9, 11–13). Phenylacetophenone (**2d**) was also effective under the reaction conditions; however, the yield was low (Table 2, entry 14) probably as a result of the increased steric effect of the ketone relative to the aldehyde. More interestingly, the reaction of 1-phenyl-1-propyne (**1b**) with **2d** generated the symmetrical tetrasubstituted naphthalene derivative **3p**, albeit in very low yield (<5%), which is still being optimized [Eq. (3)].

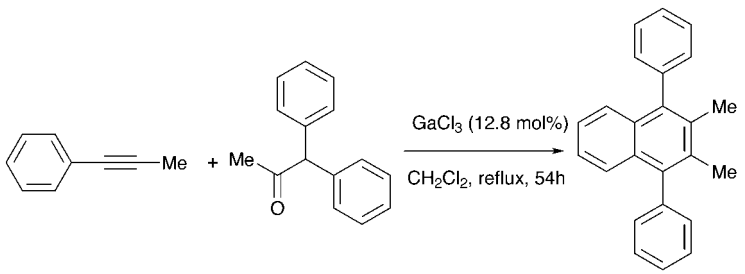
When 1-phenyl-1-butyne (**1c**) was heated at reflux with **2a** and H_2O (2 equiv) in dichloromethane in the presence of catalyst $CaCl_3$ (5 mol%), the desired product was obtained in 65% yield. When the same reaction was performed under relatively dry conditions under a nitrogen atmosphere, the yield dropped to 55%. As gallium trichloride is hydrolyzed very fast in air and the presence of water did not decrease the yield, we believe that the active catalyst could be gallium hydroxide dichloride. This is supported by our earlier work on gallium trichloride mediated coupling of alkynes and aldehydes to generate enones.[10]

Based on the results, a tentative mechanism is proposed in Scheme 1. Gallium trichloride hydrolyzes in air to generate the active catalyst gallium hydroxide dichloride, which catalyzes the regioselective electrophilic addition of the aldehyde–Lewis acid complex to C2 of the 1-phenylalkyne.[11] Intramolecular electrophilic attack of the formed alkenyl cation to the aromatic system followed by elimination of a proton generates the cyclization product, which aromatizes to form the corresponding naphthalene derivative and regenerates the active catalyst.

In summary, we have developed a new synthetic strategy to generate polysubstituted naphthalene derivatives with complete regioselectivity through the simple coupling of alkynes and phenyl acetaldehydes (and ketones) catalyzed by gallium trichloride under mild conditions.[12] The scope, mechanism, and synthetic applications of this new reaction are under investigation.



Scheme 1. Proposed mechanism for the formation of naphthalene derivatives.



(3)

1b **2d** **3p**

Experimental Section

General procedure: Gallium trichloride (7.5 mg, 0.042 mmol, 6 mol%) was added to a solution of 1-phenyl-1-pentyne (**1d**, 101.5 mg, 0.70 mmol) and phenylacetaldehyde (**2a**, 110.9 mg, 0.92 mmol) in dichloromethane (3.5 mL). The solution turned dark red instantaneously. The reaction mixture was heated at reflux for 21 h. The

 © WILEY-VCH Verlag GmbH, 69451 Weinheim, Germany, 2002 1433-7851/02/4112-2140 $ 20.00+.50/0 *Angew. Chem. Int. Ed.* **2002**, *41*, No. 12

reaction mixture was concentrated in vacuo. Subsequently, the crude mixture was purified by column chromatography with hexane as eluent to give 1-phenyl-2-propylnaphthalene (**3d**, 106 mg, 0.43 mmol, 62%).

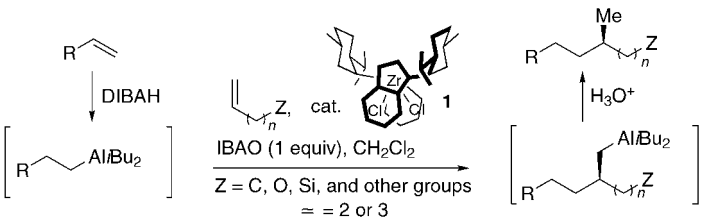
Received: January 28, 2002 [Z18598]
Revised: March 20, 2002

[1] J. March, *Advanced Organic Chemistry*, 4th ed., Wiley, New York, **1992**, chap. 11, p. 501.
[2] V. Snieckus, *Chem. Rev.* **1990**, *90*, 879.
[3] a) D. B. Grothahn in *Comprehensive Organometallic Chemistry II*, *Vol. 12* (Eds.: E. W. Abel, F. G. A. Stone, G. Wilkinson, L. S. Hegedus), Pergamon, Oxford, **1995**, p. 741; b) M. Lautens, W. Klute, W. Tam, *Chem. Rev.* **1996**, *96*, 49; c) W. Reppe, W. J. Schweckendiek, *Justus Liebigs Ann. Chem.* **1948**, *560*, 104.
[4] S. Saito, Y. Yamamoto, *Chem. Rev.* **2000**, *100*, 2901, and references therein.
[5] a) V. Gevorgyan, A. Takeda, M. Homma, N. Sadayori, U. Radhakrishnan, Y. Yamamoto, *J. Am. Chem. Soc.* **1999**, *121*, 6391; b) N. Uchiyama, Y. Yamamoto, *J. Org. Chem.* **1998**, *63*, 7022; c) V. Gevorgyan, A. Takeda, Y. Yamamoto, *J. Am. Chem. Soc.* **1997**, *119*, 11313; d) V. Gevorgyan, N. Sadayori, Y. Yamamoto, *Tetrahedron Lett.* **1997**, *38*, 8603; e) S. Saito, M. M. Salter, V. Gevorgyan, N. Tsuboya, K. Tando, Y. Yamamoto, *J. Am. Chem. Soc.* **1996**, *118*, 3970; f) R. C. Burrel, K. J. Daoust, A. Z. Bradley, K. J. DiRico, R. P. Johnson, *J. Am. Chem. Soc.* **1996**, *118*, 4218; g) R. L. Danheiser, A. E. Gould, R. F. Pradilla, A. L. Helgason, *J. Org. Chem.* **1994**, *59*, 5514; h) R. G. Bergman, *Acc. Chem. Res.* **1973**, *6*, 25; i) R. G. Bergman, R. R. Jones, *J. Am. Chem. Soc.* **1972**, *94*, 660.
[6] a) N. E. Shore, *Chem. Rev.* **1988**, *88*, 1081; b) K. H. Dötz, *Angew. Chem.* **1984**, *96*, 573; *Angew. Chem. Int. Ed. Engl.* **1984**, *23*, 587.
[7] a) E. Yoshikawa, K. V. Radhakrishnan, Y. Yamamoto, *J. Am. Chem. Soc.* **2000**, *122*, 7280; b) D. Pena, D. Perez, E. Guitian, L. Castedo, *J. Am. Chem. Soc.* **1999**, *121*, 5827; c) K. V. Radhakrishnan, E. Yoshikawa, Y. Yamamoto, *Tetrahedron Lett.* **1999**, *40*, 7533; d) R. C. Larock, Q. Tian, *J. Org. Chem.* **1998**, *63*, 2002; e) K. S. Feldman, R. E. Ruckle, Jr., S. M. Ensel, P. H. Weinreb, *Tetrahedron Lett.* **1992**, *33*, 7101.
[8] K. Wakasugi, Y. Nishii, Y. Tanabe, *Tetrahedron Lett.* **2000**, *41*, 5937.
[9] a) F. Yonehara, Y. Kido, S. Morita, M. Yamaguchi, *J. Am. Chem. Soc.* **2001**, *123*, 11310; b) Y. Kido, F. Yonehara, M. Yamaguchi, *Tetrahedron* **2001**, *57*, 827; c) J. Takaya, H. Kagoshima, T. Akiyama, *Org. Lett.* **2000**, *2*, 1577, and references therein; d) N. Asao, T. Asano, T. Ohishi, Y. Yamamoto, *J. Am. Chem. Soc.* **2000**, *122*, 4817; e) Y. Kido, S. Yoshimura, M.Yamaguchi, T. Uchimaru, *Bull. Chem. Soc. Jpn.* **1999**, *72*, 1445; f) J. Su, S. D. Goodwin, X. W. Li, G. H. Robinson, *J. Am. Chem. Soc.* **1998**, *120*, 12994; g) Y. Kido, M. Yamaguchi, *J. Org. Chem.* **1998**, *63*, 8086.
[10] G. S. Viswanathan, C. J. Li, *Tetrahedron Lett.* **2002**, *43*, 1613.
[11] a) D. J. Rodini, B. B. Snider, *Tetrahedron Lett.* **1980**, *21*, 3857; b) U. Biermann, A. Lutzen, M. S. F. L. K. Jie, J. O. Metzger, *Eur. J. Org. Chem.* **2000**, 3069.
[12] All products were characterized by ^{1}H and ^{13}C NMR and IR spectroscopy, and by MS/elemental analysis.

A New Protocol for the Enantioselective Synthesis of Methyl-Substituted Alkanols and Their Derivatives through a Hydroalumination/Zirconium-Catalyzed Alkylalumination Tandem Process**

Shouquan Huo, Ji-cheng Shi, and Ei-ichi Negishi*

We report herein a new protocol for the Zr-catalyzed enantioselective carboalumination of alkenes[1], which consists of a hydroalumination/alkylalumination tandem process (Scheme 1). The most noteworthy significance of the protocol in synthetic applications is that it permits the asymmetric synthesis of methyl-substituted alkanols and other derivatives typically in 90–93% *ee*, which represents an increase in *ee* values by roughly 15% from the previously attainable 70–80%.[1–3]



Scheme 1. Hydroalumination/Zr-catalyzed enantioselective carboalumination/hydrolysis process for the synthesis of methyl-substituted alkanols. IBAO = isobutylaluminoxane.

The development of the protocol has critically depended on the following recent findings. First, the primary alkyl groups of the RCH_2CH_2 type (R = H or alkyl group) derived from $RCH{=}CH_2$ by in situ hydroalumination[4] with iBu$_2$AlH (DIBAH) can participate selectively in the Zr-catalyzed enantioselective carboalumination; these alkyl groups compete directly with two equivalents of the *i*Bu group and the isoalkyl group generated in the desired alkylalumination. As the results summarized in Scheme 2 indicate, the reaction of *n*-decyldiisobutylalane (2 equiv[5]) with $H_2C{=}CH(CH_2)_2OTBDPS$ in the presence of (−)-bis-(neomenthylindenyl)zirconium dichloride[6] (**1**; 5 mol%, purified single isomer) in CH_2Cl_2 followed by protonolysis led to the formation of the desired product **2** in 80–84% yields with 90–91% *ee*.[7] Only traces, if any, of the isobutylaluminated product **3** were formed. Similarly, there was no indication of the formation of dimeric and oligomeric products. The main byproduct was *n*BuOTBDPS, which must have been formed

[*] Prof. E.-i. Negishi, Dr. S. Huo, Dr. J.-c. Shi
Herbert C. Brown Laboratories of Chemistry, Purdue University
West Lafayette, IN 47907-1393 (USA)
Fax: (+1) 765-494-0239
E-mail: negishi@purdue.edu

[**] We thank the National Science Foundation (CHE-0080795), the National Institutes of Health (GM36792), and Purdue University for support of this research. We also thank Albemarle and Boulder Chemical for assistance in the procurement of Al and Zr compounds, respectively.

Supporting information for this article is available on the WWW under http://www.angewandte.org or from the author.

 © WILEY-VCH Verlag GmbH, 69451 Weinheim, Germany, 2002 1433-7851/02/4112-2141 $ 20.00+.50/0

by means of H-transfer hydroalumination.[8] On the basis of a reasonable assumption that the *i*Bu group is the major hydride source, *n*Dec is about ten times as reactive as *i*Bu, after statistical correction. Similar results were observed in the reaction of *n*BuAl*i*Bu$_2$ with 1-octene and 1-decene (Scheme 2).[9] In these reactions, however, the hydroalumination products (RCH$_2$CH$_2$Al*i*Bu$_2$), must compete with *n*BuAl*i*Bu$_2$ to give dimeric by-products.[10]

Second, in contrast with the reactions of 1-octene and 1-decene, which were essentially complete within 20 h at 23 °C in the presence of only 2 mol % of **1** without the use of an aluminoxane, the corresponding reactions of 1-alkenes with proximal oxygenated substituents were rather sluggish, presumably as a result of retardation by the oxygenated substituents. The use of methylaluminoxane (MAO)[3] did accelerate these reactions significantly, but methylalumination competed up to 20 %. However, the undesirable methylalumination can be avoided by using isobutylaluminoxane (IBAO),[11] which is generated by treating *i*Bu$_3$Al with H$_2$O (1 equiv). Notably, these aluminoxanes significantly accelerate the Zr-catalyzed carboalumination but they do not significantly affect enantioselectivity under otherwise comparable conditions (Scheme 2). Thus, the improvement in *ee* from 75 ± 5 % to 90 – 93 % is almost entirely a result of the strategic shift from methylalumination to alkylalumination, rather than of the use of aluminoxanes.

Some additional examples of the use of TBS-protected ω-alkenols are shown in Table 1. The results indicate that the TBS-protected 3-butenols and longer ω-alkenols can be alkylaluminated with a variety of alkyldiisobutylalanes to produce, after hydrolysis, the corresponding methyl-substituted alkanols in good yields and 90 – 93 % *ee*. On the other hand, the same reaction of allyl alcohol derivatives ($n = 1$) was unsatisfactory, even when TBDPS-protected allyl alcohol was used as a substrate. Thus, its reaction with *n*-octyldiisobutylalane in the presence of **1** (5 mol %) produced (*R*)-2-methyldecanol only in 30 % yield and with 88 % *ee*. Deprotection of allyl alcohol occurred to a considerable extent. The difficulties and inferior results observed with allyl ethers are in sharp contrast to those observed in the Zr-catalyzed enantioselective ethylmagnesation/β-elimination tandem processes[12] and related reactions[13] of allylic hetero-substituted alkenes. In these reactions, high *ee* values were reported only with allyl ethers, allylamines, and other allylic hetero-substituted alkenes. Clearly the Zr-catalyzed enantioselective carboalumination[1–3] and these carbomagnesation reactions are fundamentally discrete and of almost totally different and complementary synthetic scopes.[14]

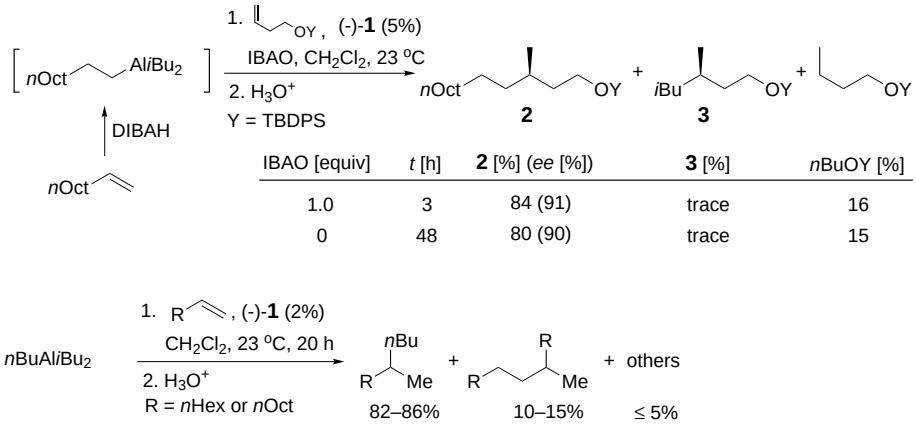
Table 1. Zr-catalyzed enantioselective alkylalumination of ω-alkenyl silyl ethers with alkyldiisobutylalanes.[a]

Entry	R–Al*i*Bu$_2$	$H_2C{=}CH(CH_2)_n$OTBS	*t* [h]	Yield[b] [%]	*ee*[c] [%]
	R	*n*			
1	*n*-pentyl	2	3	74	92[d]
2	*n*-hexyl	2	3	77	91[d]
3	2-methylpropyl	2	3	82	93[d]
4	4-methylpentyl	2	3	66	91[e]
5	cyclohexyl	2	3	81	91[e]
6	PhMe$_2$SiCH$_2$	2	3	85	90[e]
7	*n*-hexyl	3	6	83	92[f]
8	2-methylpropyl	3	3	78	91[f]
9	*n*-hexyl	4	4	76	90[g]

[a] Unless otherwise stated, the reaction was carried out at 23 °C in CH_2Cl_2 in the presence of **1** (5 mol %) and IBAO (1 equiv). RCH=CH$_2$/DIBAH/H$_2$C=CH(CH$_2$)$_n$OTBS = 1.5:1.5:1. [b] Yield based on the protected enols after protonolysis and deprotection. [c] Determined by HPLC analysis of a derivative of the alcohol (see below) on a CHIRALCEL OD-H or AD (hexane/2-propanol 95:5 or 90:10 v/v). [d] The alcohol was treated successively with $COCl_2$ and (*R*)-1-(1-naphthyl)ethylamine to give the corresponding urethane. [e] The alcohol was oxidized to the corresponding carboxylic acid and then treated with (*R*)-1-(1-naphthyl)ethylamine to give the corresponding amide. [f] As above, except that (*S*)-1-(1-naphthyl)ethylamine was used to produce the amide. [g] This *ee* determination was less accurate than in the other cases (90 ± 2 %). TBS = *tert*-butyldimethylsilyl.

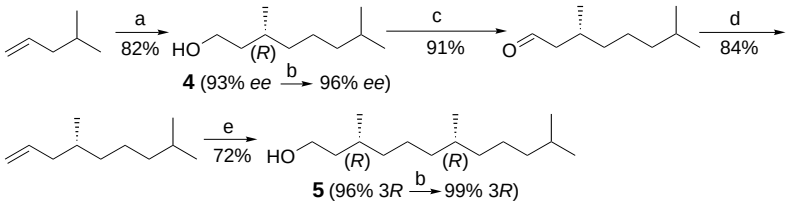
The third critical finding in this investigation is that the enantiomers of methyl-substituted alkanols ($n = 2$, 3) can be detected separately (see Table 1) as well as separated and purified by the recrystallization of their bisurethane derivatives formed in their reaction with *p*-phenylene diisocyanate.[2] Typically, (*R*)-3,7-dimethyl-1-octanol (**4**) of 93 % *ee* (Table 1, entry 3) was treated with *p*-phenylene diisocyanate (0.5 equiv) in benzene at 50 °C for 1 h in the presence of DABCO (1 mol %) to give the corresponding bisurethane (m.p. 118 – 120 °C) in 95 % yield (Scheme 3). After recrystallization from MeOH, it was purified to 96 % *ee* (70 % recovery); m.p. 122.5 – 123.5 °C; $[\alpha]_D^{23} = +3.8°$ ($c = 1.8$, $CHCl_3$).

To demonstrate the synthetic utility of this new protocol, the purified **4** was converted in three steps into **5**,[15] the C_{15} intermediate in the synthesis of vitamin E[16] (Scheme 3). For the synthesis of **4**, a twofold excess of inexpensive 4-methyl-1-pentene relative to H$_2$C=CH(CH$_2$)$_2$OTBS was employed, and the latter was used as the basis to calculate the yield. For the synthesis of **5**, however, (4*R*)-4,8-dimethyl-1-nonene must be used as the limiting reagent. Since a stoichiometric ratio of the two alkene intermediates led only to a 50 % yield of **5**, a 50 % excess of H$_2$C=CH(CH$_2$)$_2$OTBS was employed, which then required the use of *i*Bu$_3$Al



Scheme 2. Selective alkylalumination of 1-alkenes with alkyldiisobutylalanes and rate acceleration effect of IBAO. Y = TBDPS = *tert*-butyldiphenylsilyl.

 © WILEY-VCH Verlag GmbH, 69451 Weinheim, Germany, 2002 1433-7851/02/4112-2142 $ 20.00+.50/0 *Angew. Chem. Int. Ed.* **2002**, *41*, No. 12



Scheme 3. Synthesis of a C_{15} vitamin E side chain. a) 1. DIBAH, neat, 50 °C, 10 h; 2. $H_2C{=}CH(CH_2)_2OTBS$, **1** (5 mol %), IBAO (1 equiv), 23 °C, 3 h; 3. H_3O^+; 4. TBAF; b) 1. *p*-phenylene diisocyanate (0.5 equiv), DABCO (1 mol %), benzene, 50 °C, 1 h; 2. recrystallization from MeOH; 3. NaOEt/EtOH (2 M); c) DMP, CH_2Cl_2; d) $CH_2{=}PPh_3$, THF; e) 1. DIBAH (1.0 equiv), neat, 60–70 °C, 10 h; 2. $H_2C{=}CH(CH_2)_2OTBS$ (1.5 equiv), **1** (5 mol %), IBAO (1 equiv), *i*Bu_3Al (1.0 equiv), 23 °C, 24 h; 3. H_3O^+; 4. TBAF. TBAF = tetrabutylammonium fluoride, DABCO = 1,4-diazabicyclo[2.2.2]-octane.

(1.0 equiv) as well as IBAO to obtain the indicated yield of 72 %. This four-step synthesis of **5** offers a high efficiency and a respectable combination of overall yield and stereoselectivity that is significantly higher than that reported recently by us.[2]

Although hydroalumination of alkenes with DIBAH is a preferred method for the generation of RCH_2CH_2Al*i*Bu_2, they may also be generated by treating the corresponding alkyllithium compounds with $ClAl$*i*Bu_2 and using them in the Zr-catalyzed carboalumination of alkenes. It should, however, be noted that the LiCl by-product significantly retards the subsequent alkylalumination, thus leading to lower yields of product. It is therefore desirable to remove LiCl by filtration. For example, the reaction of $H_2C{=}CH(CH_2)_2OTBS$ with *n*$HexAl$*i*Bu_2 generated from *n*HexLi and DIBAH under the conditions indicated in Table 1 required 38 h to produce, after hydrolysis, (*R*)-3-methyl-1-nonanol with 89 % *ee* in 76 % yield. When the reaction was run at 0 °C for 96 h, the product was obtained in 59 % yield with 92 % *ee*. On the other hand, filtration of LiCl prior to the reaction led to the formation of the same product in 85 % yield with 89 % *ee* within 20 h. Likewise, the reaction of $H_2C{=}CH(CH_2)_3OTBS$ with *n*$HexAl$*i*Bu_2 produced (*R*)-4-methyl-1-decanol in 74 % yield with 91 % *ee*.

The Zr-catalyzed enantioselective carboalumination of alkenes has now been sufficiently well developed so that a number of its applications to the synthesis of complex natural products and related chiral compounds may be anticipated. Our own efforts along this line are in progress and will be reported in future publications.

Experimental Section

Typical procedure: *n*-Octyldiisobutylalane (prepared in situ by reacting 1-octene (337 mg, 3 mmol) and DIBAH (427 mg, 3 mmol) at 60 °C over 10 h under an argon atmosphere) was added to a solution of dichlorobis(1-neomenthylindenyl)zirconium (**1**; 67 mg, 0.1 mmol) in CH_2Cl_2 (6 mL). The mixture was stirred at 23 °C for 5 min and IBAO (1.0 M in CH_2Cl_2, 2 mL, 2 mmol; prepared by treating triisobutylalane with H_2O (1 equiv) in CH_2Cl_2 at −40 °C for 15 min and then at room temperature for 2 h) was added. After stirring at 23 °C for 5 min, the reaction mixture was cooled to 0 °C with an ice bath, and $H_2C{=}CH(CH_2)_2OTBS$ (370 mg, 2 mmol) was added dropwise to the resultant orange solution with subsequent stirring at 0 °C for 1 h and then at 23 °C for 3 h. The mixture was then treated with HCl (3 N), extracted with diethyl ether (3 × 15 mL), washed with $NaHCO_3$, water, and brine, dried over anhydrous $MgSO_4$, filtered, and concentrated. The residue was dissolved in THF (4 mL) and treated with TBAF (1.0 M in THF, 3 mL, 3 mmol) at 23 °C for 3 h. After removal of the solvent, the residue was dissolved in a minimum amount of CH_2Cl_2 and subjected to column chromatography (silica gel, hexanes/ethyl acetate 8:1). Evaporation provided (3*R*)-3-methylundecan-1-ol[17] as colorless oil (0.48 g, 78 %). $[\alpha]_D^{23} = +3.1°$ ($c = 2.1$, $CHCl_3$) [Lit. [17] $[\alpha]_D^{25} = +2.98°$ ($c = 3.23$, $CHCl_3$)]; determination of *ee*: (3*R*)-3-methylundecan-1-ol was treated successively with $COCl_2$ and (*R*)-1-(1-naphthyl)ethylamine to produce the corresponding urethane; HPLC analysis of this urethane (Chiralcel OD-H, 4.6 mm × 250 mm, hexane/2-propanol 95:5, 1 mL min^{-1}) showed two peaks ($t_R = 17.1$ and 19.4 min, 95.4:4.6), which were assigned to the *R*,*R* and *R*,*S* diastereomers, respectively (91 % *ee*).

Received: February 11, 2002 [Z 18695]

[1] a) D. Y. Kondakov, E. Negishi, *J. Am. Chem. Soc.* **1995**, *117*, 10771; b) D. Y. Kondakov, E. Negishi, *J. Am. Chem. Soc.* **1996**, *118*, 1577.

[2] S. Huo, E. Negishi, *Org. Lett.* **2001**, *3*, 3253.

[3] P. Wipf, S. Ribe, *Org. Lett.* **2000**, *2*, 1713; see also: K. H. Shaughnessy, R. M. Waymouth, *Organometallics* **1998**, *17*, 5728.

[4] K. Ziegler, H. Martin, F. Krupp, *Liebigs Ann. Chem.* **1960**, *629*, 14.

[5] Two mole equivalents of alanes were used in these experiments to ensure complete or near complete consumption of TBDPS-protected homoallyl alcohol.

[6] G. Erker, M. Aulbach, M. Knickmeier, D. Wingbermuhle, C. Kruger, M. Nolte, S. Werner, *J. Am. Chem. Soc.* **1993**, *115*, 4590.

[7] The *ee* values of the corresponding alcohols.

[8] a) E. Negishi, T. Yoshida, *Tetrahedron Lett.* **1980**, 1501; b) E. Negishi, D. Y. Kondakov, D. Choueiry, K. Kasai, T. Takahashi, *J. Am. Chem. Soc.* **1996**, *118*, 9577.

[9] As the purpose of these experiments was to investigate the relative reactivity of *n*-alkyl and *i*Bu groups, the *ee* values were not determined.

[10] The absence of the dimeric products in the reaction of $H_2C{=}CHCH_2CH_2OTBDPS$ may be a result of the stabilization of hydro- and carboalumination products through chelation.

[11] S. L. Gershkokhen, I. V. Chaplina, I. L. Poletaeva, A. V. Kisin, V. M. Nosova, N. N. Korneev, *Zh. Obsh. Khim.* **1984**, *54*, 2714; for a review on aluminoxanes, see: S. Pasynkiewicz, *Polyhedron* **1990**, *9*, 429.

[12] a) J. P. Morken, M. T. Didiuk, A. H. Hoveyda, *J. Am. Chem. Soc.* **1993**, *115*, 6697; b) J. P. Morken, M. T. Didiuk, M. S. Visser, A. H. Hoveyda, *J. Am. Chem. Soc.* **1994**, *116*, 3123; c) A. F. Houri, Z. Xu, D. A. Cogan, A. H. Hoveyda, *J. Am. Chem. Soc.* **1995**, *117*, 2943; d) M. T. Didiuk, C. W. Johannes, J. P. Moken, A. H. Hoveyda, *J. Am. Chem. Soc.* **1995**, *117*, 7097; e) M. S. Visser, A. H. Hoveyda, *Tetrahedron* **1995**, *51*, 4383; f) M. A. Visser, N. M. Heron, M. T. Didiuk, M. F. Sagal, A. H. Hoveyda, *J. Am. Chem. Soc.* **1996**, *118*, 4291; g) Z. Xu, C. W. Johannes, A. F. Houri, D. S. La, D. A. Cogan, G. E. Hofilena, A. H. Hoveyda, *J. Am. Chem. Soc.* **1997**, *119*, 10302.

[13] a) L. Bell, R. J. Whitby, R. V. H. Jones, M. C. H. Standen, *Tetrahedron Lett.* **1996**, *36*, 7139; b) G. Dawson, C. A. Durrant, G. G. Kirk, R. J. Whitby, R. V. H. Jones, M. C. H. Standen, *Tetrahedron Lett.* **1997**, *38*, 2335; c) L. Bell, D. C. Brookings, G. J. Dawson, R. J. Whitby, R. V. H. Jones, M. C. H. Standen, *Tetrahedron* **1998**, *54*, 14617; d) Y. Yamamura, M. Hyakutake, M. Mori, *J. Am. Chem. Soc.* **1997**, *119*, 7615.

[14] None of these cyclic carbozirconation-based reactions would permit methylalumination, as the presence of a β-H atom is a critical requirement in the cyclic carbozirconation of three-membered zirconacycles.

[15] For a highly enantioselective synthesis, see: a) H. Takaya, T. Ohta, N. Sayo, H. Kumobayashi, S. Akutagawa, S. Inoue, I. Kasahara, R. Noyori, *J. Am. Chem. Soc.* **1987**, *109*, 1596; b) R. Noyori, *Asymmetric Catalysis in Organic Synthesis*, Wiley, New York, **1994**, p. 42; although the enantioselectivity in each of the two asymmetric steps is ≥ 98 % *ee*, this synthesis requires 9 or 10 steps from myrcene and two *E*-selective steps for the synthesis of *E*-trisubstituted allylic hetero-substituted alkenes.

[16] J. Hübscher, R. Barner, *Helv. Chim. Acta* **1990**, *73*, 1069.

[17] V. N. Odinokov, V. R. Akhmetova, Kh. D. Khasanov, A. A. Abduvakhabov, L. M. Khalilov, B. A. Cheskis, A. M. Moiseenkov, G. A. Tolstikov, *J. Org. Chem. USSR (Engl. Transl.)* **1992**, *28*, 908.

A Synthetic Approach towards the C1 – C9 Subunit of Zincophorin

Janine Cossy,* Nicolas Blanchard, Magali Defosseux, and Christophe Meyer*

The useful anti-infectious properties displayed by many naturally occurring polyoxygenated ionophores have been explained by their capacity to form lipophilic complexes with various cations, which affects proton – cation exchange processes across biological membranes.[1, 2]

In 1984, there were two independent reports on the isolation of apparently the same antibiotic from strains of *Streptomyces griseus*.[3, 4] On the basis of its exceptional high affinity for divalent cations and especially zinc, this antibiotic was given the trivial name zincophorin (Figure 1).[3–5] Zincophorin exhibits strong in vivo activity against Gram-positive bacteria[3, 4] and its methyl ester has also been reported to possess antiviral activity.[6]

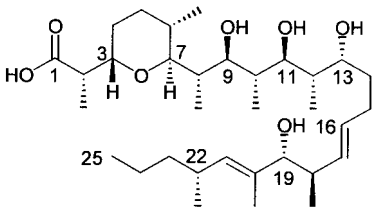
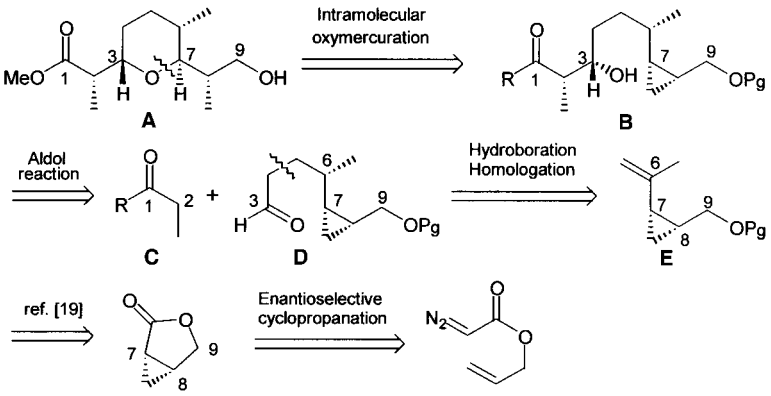


Figure 1. Structure of zincophorin.

The challenging structure of zincophorin has elicited considerable synthetic interest and syntheses of advanced elaborated fragments have been reported,[7–13] but to date a single total synthesis has been completed by the Danishefsky group.[7b] Herein, we report the results of our synthetic studies concerning a new approach towards the C1 – C9 subunit of zincophorin by using an intramolecular oxymercuration reaction of an appropriately substituted and enantiomerically enriched cyclopropylmethanol.

Whereas the intramolecular oxymercuration of alkenes has often been used to synthesize oxygenated heterocycles, and especially those encountered in naturally occurring ionophores,[14, 15] the corresponding reaction with cyclopropanes has received much less attention in the context of the total synthesis of natural products. As the intramolecular oxymercuration of cyclopropanes has been shown to proceed in some cases with high degrees of regio- and stereocontrol,[16, 17] a new approach towards the C1 – C9 subunit of zincophorin **A** was considered, to elaborate the trisubstituted tetrahydropyran (Scheme 1). This approach involved an intramolecular oxymercuration reaction, followed by reductive demercuration of the cyclopropylmethanol derivative **B**. According to the retrosynthetic analysis, the asymmetric carbon atoms C2 and C3 could be installed with the required absolute configurations by using a chiral-auxiliary-mediated aldol condensation between the enolate of ethylketone **C** and aldehyde **D**, which incorporates three contiguous stereocenters (C6 – C8). Based on previous studies,[18] the control of the relative configuration at the C6 atom could be achieved by performing a diastereoselective hydroboration of isopropenylcyclopropane **E**, followed by transformation to aldehyde **D**. Furthermore, the preparation of isopropenylcyclopropanes of type **E**, in an enantiomerically enriched form (*ee* value > 95 %) has been reported from 3-oxabicylo[3.1.0]hexan-2-one,[19] which is readily available by a rhodium-catalyzed enantioselective cyclopropanation of allyl diazoacetate (Scheme 1).[20]



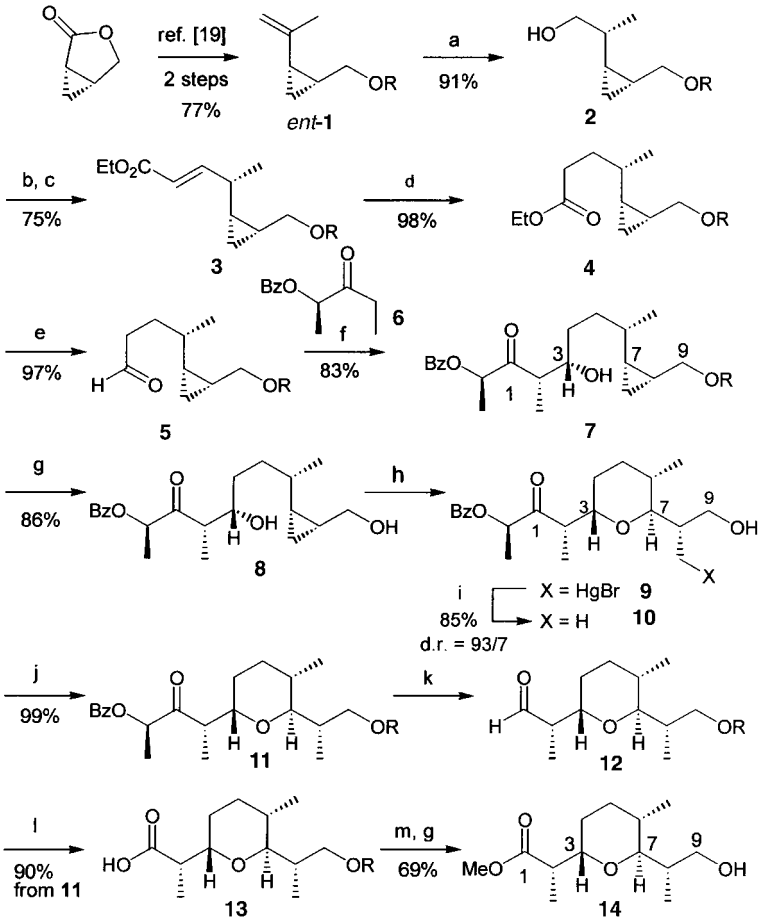
Scheme 1. Retrosynthetic analysis for the C1 – C9 subunit of zincophorin. Pg = Protecting group.

The C1 – C9 subunit of zincophorin was synthesized (Scheme 2). Hydroboration of the isopropenylcyclopropane **1** with $BH_3 \cdot THF$, followed by a standard oxidative work-up with alkaline hydrogen peroxide, afforded, with a high diastereoselectivity (d.r. > 98/2), the corresponding alcohol **2** (91 %), with a methyl group *syn* to the adjacent cyclopropane.[18] In order to transform **2** to the aldehyde **5**, compound **2** was first oxidized with pyridinium chlorochromate (PCC) to the corresponding aldehyde,[21] and subsequent Horner – Wadsworth – Emmons olefination with triethyl phosphonoacetate afforded the α,β-unsaturated ester **3** (75 %). Compound **3** was then hydrogenated over platinum oxide in ethyl acetate to give the ethyl ester **4** (98 %), which was reduced with DIBAL-H (DIBAL-H = diisobutylaluminum hydride, toluene, −78 °C) to the aldehyde **5** (97 %).

The elaboration of a suitable precursor for the oxymercuration reaction required the installation of the C2 and C3 stereocenters with an *anti* relative configuration, by using a highly diastereoselective *anti*-aldol condensation between the *E*-boron enolate derived from the ethylketone **6**[22] and the aldehyde **5**, which afforded **7** in 83 % yield (d.r. > 96/4). With aldol **7** in hand, the feasibility of the intramolecular oxymercuration could then be tested, however treatment of **7** with mercuric trifluoroacetate in CH_2Cl_2 resulted in a number of products. As the *tert*-butyldiphenylsilyl group might interfere with this reaction,[23] it was removed by treatment of **7** with $HF \cdot$ pyridine to produce cyclopropylmethanol **8** (86 %). Indeed, when **8** was subjected to the oxymercuration

[*] Prof. J. Cossy, Dr. C. Meyer, Dr. N. Blanchard, M. Defosseux
Laboratoire de Chimie Organique associé au CNRS
ESPCI, 10 rue Vauquelin, 75231 Paris Cedex 05 (France)
Fax: (+33) 1-40-79-46-60
E-mail: janine.cossy@espci.fr, christophe.meyer@espci.fr

 © WILEY-VCH Verlag GmbH, 69451 Weinheim, Germany, 2002 1433-7851/02/4112-2144 $ 20.00+.50/0



Scheme 2. Synthesis of the C1–C9 subunit of zincophorin. a) $BH_3 \cdot THF$/THF, $-30\,^{\circ}C \rightarrow$RT, then NaOH, H_2O_2; b) PCC, 4 Å molecular sieves, CH_2Cl_2, RT; c) NaH, $(EtO)_2P(O)$-CH_2-COOEt, THF; d) H_2, cat. PtO_2, EtOAc, RT; e) DIBAL-H, toluene, $-78\,^{\circ}C$; f) **6**, $EtNMe_2$, *c*Hex_2BCl, Et_2O, $0\,^{\circ}C$; add **5**, $-78\,^{\circ}C$, 2 h and $-23\,^{\circ}C$, 12 h, then MeOH, H_2O_2, pH 7 buffer; g) HF·pyridine, THF, RT; h) $Hg(OCOCF_3)_2$, CH_2Cl_2, RT then KBr/H_2O; i) *n*Bu_3SnH, toluene/THF, RT $\rightarrow 60\,^{\circ}C$ then CCl_4; j) *t*$BuPh_2SiCl$, imidazole, DMF, RT; k) $LiBH_4$, THF, $-20\,^{\circ}C \rightarrow$RT then $NaIO_4$, MeOH, RT; l) $NaClO_2$, NaH_2PO_4, 2-methylbut-2-ene, *t*BuOH/H_2O, RT; m) Me_3SiCHN_2, MeOH/C_6H_6. R = *t*$BuPh_2Si$, Bz = benzoyl.

procedure ($Hg(OCOCF_3)_2$, CH_2Cl_2, RT, aqueous KBr work-up), an extremely clean conversion to the organomercuric bromide **9** was observed. The latter was not purified but immediately subjected to reductive demercuration with tributyltin hydride;[24] this lead to tetrahydropyran **10** in 85% yield and with a high diastereoselectivity (d.r. = 93/7).[25] The relative configuration of **10** indicates that the intramolecular oxymercuration involved, as anticipated, an inversion of configuration at the C7 atom.[16, 17] The presence of the silyl protecting group interferes with the intramolecular oxymercuration of **7** (R = *t*$BuPh_2Si$), and implies additional deprotection and protection steps. The corresponding benzyl ether derivative was therefore synthesized (R = CH_2Ph), but its intramolecular oxymercuration, followed by reductive demercuration, proceeded in lower yield (46%) and diastereoselectivity (d.r. = 85/15) than for **8**. Therefore, the presence of the free alcohol at C9 was more appropriate for the intramolecular oxymercuration step, and the synthesis of the C1–C9 subunit of zincophorin was pursued from **10** (Scheme 2). The alcohol **10** was transformed to the *tert*-butyldiphenylsilyl ether **11** (99%), and reduction with lithium borohydride, followed by an oxidative cleavage with sodium periodate, afforded the aldehyde **12**,[22] which was oxidized to the corresponding acid **13** (90% from **11**). Subsequent esterification with trimethylsilyldiazomethane and deprotection of the silyl ether lead to **14** (**14** = **A**; 69%),[26] which is the C1–C9 subunit of zincophorin.

The C1–C9 subunit of zincophorin has been synthesized by an approach that involves three key steps: a diastereoselective hydroboration of an optically enriched isopropenyl-cyclopropane, an *anti*-aldol condensation, and a diastereoselective intramolecular oxymercuration of a cyclopropylmethanol.

Received: February 25, 2002 [Z18771]

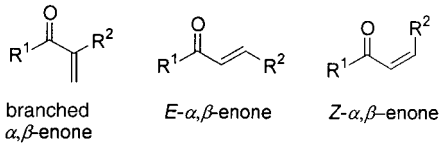
[1] *Polyether Antibiotics*, *Vol. 1* and *2* (Ed.: J. W. Westley), Marcel Dekker, New York, **1982**.
[2] M. Dobler in *Ionophores and their Structures*, Wiley, New York, **1981**.
[3] H. A. Brooks, D. Gardner, J. P. Poyser, T. J. King, *J. Antibiot.* **1984**, *37*, 1501.
[4] U. Gräfe, W. Schade, M. Roth, L. Radics, M. Incze, K. Ujszaszy, *J. Antibiot.* **1984**, *37*, 836.
[5] L. Radics, *J. Chem. Soc. Chem. Commun.* **1984**, 599.
[6] U. Gräfe (Akademie der Wissenschaften der DDR), Ger. (East) Patent, DD 231 793, **1986** [*Chem. Abstr.* **1987**, *106*, 101970].
[7] a) R. E. Zelle, M. P. DeNinno, H. G. Selnick, S. J. Danishefsky, *J. Org. Chem.* **1986**, *51*, 5032; b) S. J. Danishefsky, H. G. Selnick, R. E. Zelle, M. P. DeNinno, *J. Am. Chem. Soc.* **1988**, *110*, 4368.
[8] a) M. Balestra, M. D. Wittman, J. Kallmerten, *Tetrahedron Lett.* **1988**, *29*, 6905; b) C. L. Cywin, J. Kallmerten, *Tetrahedron Lett.* **1993**, *34*, 1103.
[9] J. A. Marshall, M. R. Palovich, *J. Org. Chem.* **1998**, *63*, 3701.
[10] S. R. Chemler, W. R. Roush, *J. Org. Chem.* **1998**, *63*, 3800.
[11] J. F. Booysen, C. W. Holzapfel, *Synth. Commun.* **1995**, *25*, 1473.
[12] S. D. Burke, R. A. Ng, J. A. Morrison, M. J. Alberti, *J. Org. Chem.* **1998**, *63*, 3160.
[13] Y. Guindon, L. Murtagh, V. Caron, S. R. Landry, G. Jung, M. Bencheqroun, A.-M. Faucher, B. Guérin, *J. Org. Chem.* **2001**, *66*, 5427.
[14] a) T. L. B. Boivin, *Tetrahedron* **1987**, *43*, 3309; b) G. Cardillo, M. Orena, *Tetrahedron* **1990**, *46*, 3321; c) J.-C. Harmange, B. Figadère, *Tetrahedron: Asymmetry* **1993**, *4*, 1711.
[15] a) D. A. Evans, S. L. Bender, J. Morris, *J. Am. Chem. Soc.* **1988**, *110*, 2506; b) K. Bratt, A. Garavelas, P. Perlmutter, G. Westman, *J. Org. Chem.* **1996**, *61*, 2109; for a related approach with allenes, see: c) R. D. Walkup, G. Park, *J. Am. Chem. Soc.* **1990**, *112*, 1597; d) R. D. Walkup, S. W. Kim, *J. Org. Chem.* **1994**, *59*, 3433.
[16] a) D. B. Collum, F. Mohamadi, J. S. Hallock, *J. Am. Chem. Soc.* **1983**, *105*, 6882; b) A. G. M. Barrett, W. Tam, *J. Org. Chem.* **1997**, *62*, 4653.
[17] For the synthesis of stereotriads involving an intramolecular oxymercuration process, see: J. Cossy, N. Blanchard, C. Meyer, *Org. Lett.* **2001**, *3*, 2567.
[18] a) J. Cossy, N. Blanchard, C. Hamel, C. Meyer, *J. Org. Chem.* **1999**, *64*, 2608; b) J. Cossy, N. Blanchard, C. Meyer, *Synthesis* **1999**, 1063.
[19] J. Cossy, N. Blanchard, C. Meyer, *Eur. J. Org. Chem.* **2001**, 339.
[20] M. P. Doyle, R. E. Austin, A. S. Bailey, M. P. Dwyer, A. B. Dyatkin, A. V. Kalinin, M. M. Y. Kwan, S. Liras, C. J. Oalmann, R. J. Pieters, M. N. Protopopova, C. E. Raab, G. H. P. Roos, Q. L. Zhou, S. F. Martin, *J. Am. Chem. Soc.* **1995**, *117*, 5763.
[21] The use of PCC or other oxidation procedures (Swern or Dess–Martin oxidations) afforded similar results and no alteration of the diastereomeric purity of the aldehyde from **2** was detected.

[22] a) I. Paterson, D. J. Wallace, S. M. Velazquez, *Tetrahedron Lett.* **1994**, *35*, 9083; b) I. Paterson, D. J. Wallace, C. J. Cowden, *Synthesis* **1998**, 639; c) C. J. Cowden, I. Paterson, *Org. React.* **1997**, *51*, 1.
[23] D. B. Collum, W. C. Still, F. Mohamadi, *J. Am. Chem. Soc.* **1986**, *108*, 2094.
[24] G. M. Whitesides, J. San Fillipo, Jr., *J. Am. Chem. Soc.* **1970**, *92*, 6611.
[25] Data for **10**: $[\alpha]_D^{20} = +44.0$ ($c = 0.04$, $CHCl_3$); IR (film): $\tilde{\nu}_{max} = 3440$, 1720, 1270, 1120, 720 cm^{-1}; ^1H NMR (300 MHz, $CDCl_3$): $\delta = 8.08$ (m, 2H), 7.59 (m, 1H), 7.48 (m, 2H), 5.60 (q, $J = 6.9$ Hz, 1H), 4.09 (m, 1H), 3.52 (m, 2H), 3.36–3.24 (m, 2H), 2.28 (br s, 1H, OH), 1.89 (m, 1H), 1.67–1.60 (m, 3H), 1.55 (d, $J = 6.9$ Hz, 3H), 1.30–1.21 (m, 2H), 1.08 (d, $J = 7.0$ Hz, 3H), 0.87 (d, $J = 7.0$ Hz, 3H), 0.84 ppm (d, $J = 6.5$ Hz, 3H); ^{13}C NMR (75 MHz, $CDCl_3$): $\delta = 210.3$ (s), 165.8 (s), 133.3 (d), 129.8 (d, 2C), 129.6 (s), 128.5 (d, 2C), 78.8 (d), 74.7 (d), 73.2 (d), 66.6 (t), 43.9 (d), 35.6 (d), 30.3 (d), 26.4 (t), 24.8 (t), 17.9 (q), 16.1 (q), 13.9 (q), 10.4 ppm (q); MS (CI^+, CH_4): m/z (%): 363 (100) $[M+H^+]$, 241 (20), 207 (22), 157 (92), 139 (61); HRMS (CI^+, CH_4): calcd for $C_{21}H_{31}O_5$ $[M+H^+]$: 363.2172, found: 363.2169. The relative configuration of compound **10** was confirmed by NMR spectroscopy, by differential NOE experiments performed on **11**.
[26] Data for **14**: $[\alpha]_D^{20} = +65.6$ ($c = 1.16$, $CHCl_3$); IR (film): $\tilde{\nu}_{max} = 3460$, 1740, 1720, 1460, 1435, 1380, 1275, 1255, 1170, 1040, 1020 cm^{-1}; ^1H NMR (300 MHz, $CDCl_3$): $\delta = 3.92$ (ddd, $J = 11.0$, 5.5, and 1.5 Hz, 1H), 3.73 (s, 3H), 3.52 (dd, $J = 9.6$ and 2.6 Hz, 1H), 3.46 (m, 2H), 3.15 (dq, $J = 11.0$ and 7.0 Hz, 1H), 3.02 (br s, 1H, OH), 1.84 (m, 1H), 1.76–1.49 (m, 4H), 1.25 (m, 1H), 1.06 (d, $J = 6.6$ Hz, 3H), 0.82 (d, $J = 7.0$ Hz, 3H), 0.81 ppm (d, $J = 6.3$ Hz, 3H), ^{13}C NMR (75 MHz, $CDCl_3$): $\delta =$ 176.3 (s), 76.7 (d), 75.1 (d), 65.7 (t), 51.9 (q), 40.0 (d), 35.7 (d), 31.8 (d), 27.2 (t), 25.1 (t), 17.4 (q), 14.2 (q), 8.8 ppm (q); MS (EI): m/z (%): 244 (3) $[M^+]$, 185 (100), 157 (38), 153 (93), 139 (26), 126 (34), 125 (43), 121 (28), 99 (28), 97 (44), 95 (41), 88 (49), 82 (28), 81 (34), 69 (43), 59 (42), 55 (65); HRMS (CI^+, CH_4): calcd for $C_{13}H_{25}O_4$ $[M+H^+]$: 245.1753, found: 245.1750.

Efficient and Selective Hydroacylation of 1-Alkynes with Aldehydes by a Chelation-Assisted Catalytic System**

Chul-Ho Jun,* Hyuk Lee, Jun-Bae Hong, and Bong-Il Kwon

Intermolecular hydroacylation is one of the most efficient methods for preparing ketones from olefins and aldehydes.[1] Recently, we developed an efficient catalytic system for the intermolecular hydroacylation of 1-alkenes by using 2-aminopyridine derivatives as a chelating auxiliary.[2] Hydroacylation of alkynes with aldehydes is also very interesting in terms of regio- and stereoselective synthesis since three possible isomers of α,β-enones can be generated from this reaction: branched as well as linear *E*- and *Z*-α,β-enones (Scheme 1).

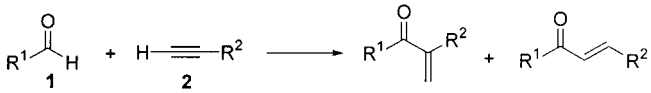


Scheme 1. Possible isomers of α,β-enones that can be generated from the hydroacylation of alkynes with aldehydes.

Although the intramolecular hydroacylation of alkynals was developed recently,[3] intermolecular hydroacylation of alkynes still remains little explored, and only a few nonselective examples have been reported with limited applications to internal alkynes[4] or benzaldehydes that bear a coordination site such as a hydroxy group at the *ortho* position.[5] Herein, we report a highly regio- and stereoselective intermolecular hydroacylation of terminal alkynes **2** with aldehydes **1** in the presence of a chelation-assisted catalytic system: $[Rh(PPh_3)_3Cl]$ (**3**), 2-amino-3-picoline (**4**), and benzoic acid (**5**). This is the most efficient catalytic system to date for the synthesis of branched or linear α,β-enones from 1-alkynes and aldehydes.

The reaction of benzaldehyde (**1a**) and 1-hexyne (**2a**) in the presence of the cocatalyst system consisting of **3** (5 mol%), **4** (40 mol%), and **5** (20 mol%) was performed in toluene at 80 °C for 12 h to afford the branched α,β-enone **6a** in 92% yield after chromatographic isolation (Table 1, entry 1). No direct selective synthetic methods for the preparation of branched α,β-enones have been reported previously, although syntheses of branched (1,1-disubstituted) vinyl compounds by hydrosilylation,[6] hydrophosphorylation,[7] and dimerization of 1-alkynes[8] have been reported. It was found that most aromatic aldehydes tested underwent smooth hydroacylation with primary alkyl alkynes to produce branched α,β-enones **6** exclusively in good to excellent yields (Table 1, entries 2–9).[9]

Table 1. Rh^I-catalyzed hydroacylation of various aldehydes and 1-alkynes.[a]



Entry	**1** (R^1)	**2** (R^2)[b]	**6**/**7**	Yield [%][c]
1	**a** (Ph)	**a** (n-C_4H_9)	100:0 (**6a**/**7a**)	92 (100)
2		**b** (n-C_6H_{13})	100:0 (**6b**/**7b**)	93 (98)
3		**c** ($PhCH_2$)	100:0 (**6c**/**7c**)	66 (71)
4	**b** (p-$CF_3C_6H_4$)	**a**	100:0 (**6d**/**7d**)	95 (100)
5	**c** (p-$MeOC_6H_4$)		100:0 (**6e**/**7e**)	76(85)
6	**d** (naphthyl)		100:0 (**6f**/**7f**)	83 (88)
7	**e** (3-thiophenyl)		100:0 (**6g**/**7g**)	96 (100)
8	**f** (4-pyridyl)		100:0 (**6h**/**7h**)	78 (100)
9	**g** (3-pyridyl)		100:0 (**6i**/**7i**)	79 (100)
10	**h** (2-pyridyl)			0
11	**i** (n-C_5H_{11})	**a**	78:22 (**6j**/**7j**)	85
12		**d** (t-C_4H_9)	0:100 (**6k**/**7k**)	74
13	**j** (cyclohexyl)	**a**	81:19 (**6l**/**7l**)	98 (100)[d]
14		**d**	0:100 (**6m**/**7m**)	63

[a] Reagents and conditions: $[Rh(PPh_3)_3Cl]$ (**3**; 5 mol%), 2-amino-3-picoline (**4**; 40 mol%), benzoic acid (**5**; 20 mol%), toluene, 80 °C, 12 h. [b] Two equivalents of **2** (based on the aldehyde) were used. [c] GC yields are given in parentheses, and <1% yields of side products were ignored. [d] Reaction time: 2 h.

[*] Prof. Dr. C.-H. Jun, Dr. H. Lee, Dr. J.-B. Hong, B.-I. Kwon
Department of Chemistry, Yonsei University
Seoul, 120-749 (Korea)
Fax: (+82) 2-364-7050
E-mail: junch@yonsei.ac.kr

[**] This work was supported by the National Research Laboratory Program (2000-N-NL-01-C-271) administered by the Ministry of Science and Technology.

Supporting information for this article is available on the WWW under http://www.angewandte.org or from the author.

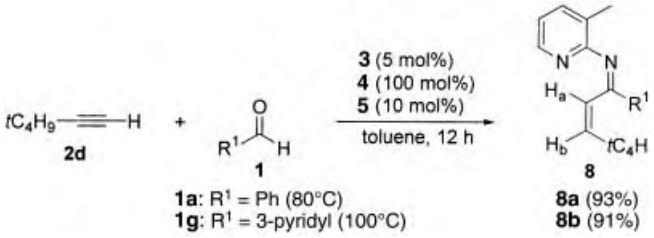
 © WILEY-VCH Verlag GmbH, 69451 Weinheim, Germany, 2002 1433-7851/02/4112-2146 $ 20.00+.50/0

No other regio- and stereoisomeric products were detected by GC and NMR spectroscopic analysis.

An electron-withdrawing substituent, for example, the trifluoromethyl group in **1b**, shows better reactivity than the electron-donating substituent in **1c** (Table 1, entries 4 and 5) owing to the facile condensation of **1b** with **4**. Interesting results were also obtained with pyridinecarboxaldehydes (Table 1, entries 8–10), since 3- and 4-pyridinecarboxaldehydes (**1g**,**f**) showed good reactivities, whereas 2-pyridinecarboxaldehyde (**1h**) did not react at all.[2c]

When the reaction was carried out with aliphatic aldehydes, a small amount of the *E* isomer as well as the branched adduct was obtained. For example, hexanal (**1i**) reacted with **2a** under the previous reaction conditions to give a 78:22 mixture of branched α,β-enone **6j** and *E*-α,β-enone **7j** in 85% yield (Table 1, entry 11). When the reaction was performed with an alkyne substituted with a sterically demanding group, *tert*-butylacetylene (**2d**), *E*-α,β-enone **7k** was isolated exclusively in 74% yield without any branched adduct **6k**. Similar results were also obtained in the reaction of cyclohexanecarboxaldehyde (**1j**) (Table 1, entries 13 and 14). These results imply that the ratio of **6**/**7** seems to be controlled by the alkyl substituent of the 1-alkyne.

When hydroacylation of **2d** with benzaldehyde **1a** was performed at 80 °C, compound **8a** ($J_{Ha,Hb} = 6.0$ Hz),[10] the ketimine of the *Z*-α,β-enone, was isolated in 93% yield without any branched or *E*-α,β-enone (Scheme 2). Since the



Scheme 2. Hydroacylation of **2d** with aromatic aldehydes to give ketimines **8**.

product was obtained as the ketimine, an equimolar amount of 2-amino-3-picoline (**4**) must be added to complete the reaction. Attempts to hydrolyze the ketimine **8a** failed.[11] The heteroaromatic aldehyde **1g** was also used in this reaction and yielded the corresponding ketimine **8b**. At the present time, it is not clear why the *Z* isomer of the α,β-unsaturated ketimine was obtained only with aromatic aldehydes.

In summary, when the hydroacylation of 1-alkynes with aldehydes was carried out in the presence of a chelation-assisted catalytic system, branched α,β-enones were isolated in high yields and with high regioselectivity. In the reaction of the sterically demanding *tert*-butylacetylene, aliphatic aldehydes gave *E*-α,β-enones exclusively, whereas aromatic aldehydes gave *Z*-α,β-unsaturated ketimines.

Experimental Section

General procedure: A mixture of **1a** (22.9 mg, 0.216 mmol) and **2a** (35.5 mg, 0.432 mmol) in a 1-mL screw-capped pressure vial was heated at 80 °C for 12 h with **3** (10 mg, 0.0108 mmol), **4** (9.4 mg, 0.0870 mmol), **5** (5.4 mg, 0.0443 mmol), and toluene (0.2 g). The resulting reaction mixture was purified by column chromatography (hexane/Et_2O 15:1) to give **6a** (37.4 mg, 92%).

Received: March 4, 2002 [Z18824]

[1] a) C. P. Lenges, P. S. White, M. Brookhart, *J. Am. Chem. Soc.* **1998**, *120*, 6965–6979; b) C. P. Lenges, M. Brookhart, *J. Am. Chem. Soc.* **1997**, *119*, 3165–3166; c) K. Kokubo, M. Murai, M. Nomura, *Organometallics* **1995**, *14*, 4521–4524; d) T. Kondo, M. Akazome, Y. Tsuji, Y. Watanabe, *J. Org. Chem.* **1990**, *55*, 1286–1291; e) T. Kondo, Y. Tsuji, Y. Watanabe, *Tetrahedron Lett.* **1987**, *28*, 6229–6230.

[2] a) C.-H. Jun, D.-Y. Lee, H. Lee, J.-B. Hong, *Angew. Chem.* **2000**, *112*, 3214–3216; *Angew. Chem. Int. Ed.* **2000**, *39*, 3070–3072; b) C.-H. Jun, J.-B. Hong, *Org. Lett.* **1999**, *1*, 887–889; c) C.-H. Jun, D.-Y. Lee, J.-B. Hong, *Tetrahedron Lett.* **1998**, *38*, 6673–6676; d) C.-H. Jun, C.-W. Huh, S.-J. Na, *Angew. Chem.* **1998**, 110, 150–152; *Angew. Chem. Int. Ed.* **1998**, *37*, 145–147; e) C.-H. Jun, H. Lee, J.-B. Hong, *J. Org. Chem.* **1997**, *62*, 1200–1201.

[3] a) K. Tanaka, G. C. Fu, *J. Am. Chem. Soc.* **2001**, *123*, 11492; b) K. Tanaka, G. C. Fu, *Org. Lett.* **2002**, *4*, *ASAP*.

[4] a) T. Tsuda, T. Kiyoi, T. Saegusa, *J. Org. Chem.* **1990**, *55*, 2554–2558; b) T. Tsuda, T. Kiyoi, T. Miyane, T. Saegusa, *J. Am. Chem. Soc.* **1988**, *110*, 8570–8572; c) C.-H Jun, H. Lee, C. W. Moon, H.-S. Hong, *J. Am. Chem. Soc.* **2001**, *123*, 8600–8601.

[5] a) K. Kokubo, K. Matsumasa, Y. Nishinaka, M. Miura, M. Nomura, *Bull. Chem. Soc. Jpn.* **1999**, *72*, 303–311; b) K. Kokubo, K. Matsumasa, M. Miura, M. Nomura, *J. Org. Chem.* **1997**, *62*, 4564–4565.

[6] a) Y. G. Young, S. B. Chang, *Org. Lett.* **2000**, *2*, 1887–1890; b) B. M. Trost, Z. T. Ball, *J. Am. Chem. Soc.* **2001**, *123*, 12726–12727.

[7] a) L.-B. Han, R. Hua, M. Tanaka, *Angew. Chem.* **1998**, *110*, 98–101; *Angew. Chem. Int. Ed.* **1998**, *37*, 94–96; b) L.-B. Han, M. Tanaka, *J. Am. Chem. Soc.* **1996**, *118*, 1571–1572; c) L.-B. Han, N. Choi, M. Tanaka, *Organometallics* **1996**, *15*, 3259–3261.

[8] a) A. Haskel, J. Q. Wang, T. Straub, T. G. Neyroud, M. S. Eisen, *J. Am. Chem. Soc.* **1999**, *121*, 3025–3034; b) A. K. Dash, J. X. Wang, J. C. Berthet, M. Ephritikhine, M. S. Eisen, *J. Organomet. Chem.* **2000**, *604*, 83–98; c) A. K. Dash, M. S. Eisen, *Org. Lett.* **2000**, *2*, 737–740.

[9] A plausible mechanism for this reaction is as follows: Formation of an aldimine from the condensation of the aldehyde **1** with **4** followed by a C–H bond activation by **3** leads to an iminoacylrhodium(III) hydride species. Hydrometalation or carbometalation of 1-alkynes with the iminoacylrhodium(III) hydride complex and reductive elimination of the resulting complex furnishes a branched α,β-unsaturaed ketimine, which is hydrolyzed by H_2O generated during the initial condensation step to give branched α,β-enone.

[10] Ketimine **8** is very stable and was characterized by COSY($^1H/^{13}C$), DEPT, and HMBC NMR spectroscopic analysis; see Supporting Information.

[11] Heating the ketimine **8** with HCl (aqueous, 1N , 100 mol%) at 130 °C for 12 h in a 1-mL screw-capped vial did not give any hydrolyzed ketone compound.

 © WILEY-VCH Verlag GmbH, 69451 Weinheim, Germany, 2002 1433-7851/02/4112-2147 $ 20.00+.50/0

A Tetranuclear Mixed-Valent $Mn^{II}_3Mn^{IV}$ Compound with a (μ_4-O)Mn_4 Core**

Tereza Afrati, Catherine Dendrinou-Samara, Catherine P. Raptopoulou, Aris Terzis, Vassilis Tangoulis,* and Dimitris P. Kessissoglou*

It has become accepted that the water-oxidation catalytic site in the oxygen-evolving complex (OEC) contains four manganese ions that are bridged together by water-derived ligands O^{2-} and OH^-. The crystal structure of OEC confirmed the presence of four manganese atoms, yet a clear image of the manganese cluster still eludes us.[1] Thus, the question whether the natural model acts as a tetranuclear or 1:3 or 2:2 cluster still remains. Working on the 1:3 model we have published some mononuclear and mixed-valent trinuclear manganese compounds.[2–4] Tetranuclear mixed-valent manganese complexes as potential models for the OEC of photosystem II (PSII) have also been reported.[5–30] Most of them also exhibit interesting magnetic behavior as a result of the ground-state spin frustration that is typical for this type of compound.[6, 7] Christou and co-workers[6, 7] and Brudvig, Crabtree, and co-workers.[12, 13] have shown that, under appropriate conditions, monofunctional carboxylato ligands support the formation of the so-called butterfly type tetranuclear clusters. However, these and other carboxylato systems are labile and tend to aggregate further. Higher-nuclearity oxo-carboxylate species with 6, 9, 10, and 12 manganese atoms have been structurally characterized.[15, 16] To date, the lowest-valence tetranuclear clusters, with an average Mn oxidation state of 2.5+ and a II,III,II,III formulation, reported are $[Mn_4O(AcO)_2(H_2O)_2(tphpn)_2]^{4+}$ (tphpn = [(*o*-py)-$CH_2]_2NCH_2CH(O^-)CH_2N[CH_2(o\text{-py})]_2$; py = pyridine) with a linear (μ-O)Mn_2 bridging moiety and $[Mn_4O_2(Ph_3$-$COO)_6)_2(OEt_2)_2]$ with a (μ_3-O)Mn bridging moiety.[18, 20] The next lowest average Mn oxidation state of 2.75+ is found in $[Mn^{II}Mn^{III}_3]$ species such as $[Mn_4O_2(X\text{-}PhCOO)_7(bpy)_2]$ (X = Cl, Br, bpy = 2,2′bipyridine)[21] with a (μ_3-O)Mn_3 bridging group and the $[Mn^{II}_2Mn^{III}Mn^{IV}]$ core of the $[Mn_4O_2(H_2O)_2(CF_3SO_3)_2(tphpn)_2]^{3+}$ ion with a (μ-O)Mn_2 bridging unit.[19] The average Mn oxidation state 3.0+ is only found in the $[Mn^{III}_4]$ formulation. Typical examples of this structure are $[Mn_4O_2(MeCOO)_6(py)_2(dbm)_2]$[22] (dbm = dibenzoylmethane) and $(NBu_4)[Mn_4O_2(X\text{-}PhCOO)_9(H_2O)]$[23] with a ($\mu$-O)$Mn_2$ bridging group. The average Mn oxidation states 3.25+ and 3.50+ are considered the most in favor of the S_1 state of the OEC and the formulations reported to date are $[Mn^{IV}Mn^{III}_3]$ and $[Mn^{III}_2Mn^{IV}_2]$. The compounds $(H_2Im)_2[Mn_4O_3Cl_6(MeCOO)_6(HIm)]$, $[Mn_4O_3Cl_4$-$(MeCOO)_3(py)_3]$, and $[Mn_4O_3Cl(MeCOO)_3(dbm)_3]$ (HIm = imidazolium) which have a distorted cubane $[Mn_4O_3Cl]$ core with a (μ_3-O)Mn_3 bridging group[22, 24, 25] represent the former formulation while the $[(Mn_2O_2)_2(tphpn)_2]^{4+}$ ion with a (μ-O)Mn_2 bridging unit[17, 26, 27] is an example of the latter. Average Mn oxidation states 3.75+ with a $[Mn^{III}Mn^{IV}_3]$ formulation, the most favorable for the S_2 state, and 4.00+ for $[Mn^{IV}_4]$ have been reported for the $[Mn_4O_6(bpy)_6]^{3+}$ and $[Mn_4O_6(bpy)_6]^{4+}$ ions, respectively.[28]

Herein the first example of a tetranuclear cluster $[Mn^{II}_3$ $Mn^{IV}(O)(pko)_4(3,4\text{-}D)_4]\cdot 2.5\,CH_3OH$ (pko = di(2-pyridyl)ketonoxime, 3,4-D = 3,4-dichlorophenoxy acetic acid) containing a (μ_4-O)Mn_4 bridging moiety is presented. The most interesting features of this compound are: 1) it is the only example of a manganese tetranuclear cluster with a $2e^-$ difference between the oxidation states of the metal ions and 2) it is the first example of a manganese tetranuclear cluster with four metal centers interacting through a μ_4-O bridging atom.

The central $[Mn_4(\mu_4\text{-}O)]^{8+}$ core is best described as a distorted Mn_4 tetrahedron with the Mn^{IV} ion Mn1 and the Mn^{II} ions Mn2, Mn3, Mn4 in octahedral environments (Figure 1). A μ_4-O atom bridges the four manganese ions. The four ketonoximato N–O groups link the Mn^{IV} ion with the three Mn^{II} ions, while each Mn^{II} ion is bridged with the other two Mn^{II} ions through carboxylato bridges. The Mn···Mn separations fall in the range of 3.185–3.607 Å with the shortest one being between Mn^{II} ions Mn2 and Mn4, which are bridged by a unidentate, double bound carboxylato ligand and a bidentate chelate carboxylato ligand, and the

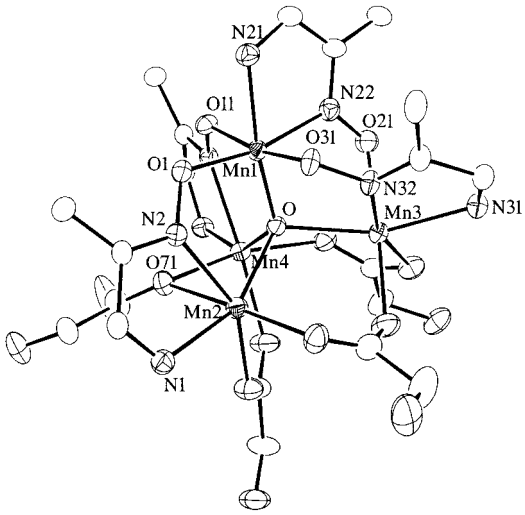


Figure 1. An ORTEP diagram of **1** with thermal ellipsoids set at 30% probability, showing the coordination environment of the tetranuclear cluster.

[*] Prof. D. P. Kessissoglou, T. Afrati, Dr. C. Dendrinou-Samara
Department of General and Inorganic Chemistry
Aristotle University of Thessaloniki
Thessaloniki 54124 (Greece)
Fax: (+30) 310997738
E-mail: kessisog@chem.auth.gr
Dr. V. Tangoulis
Department of Materials Science
University of Patras
Patras 26500 (Greece)
Fax: (+30) 610996358
E-mail: vtango@upatras.gr
Dr. C. P. Raptopoulou, Dr. A. Terzis
NCSR "Demokritos", Institute of Materials Science
15310 Aghia Paraskevi Attikis (Greece)

[**] This work was carried out in the frame of WG0010 of D21 COST action. The authors thank Prof. V. L. Pecoraro for his valuable suggestions. V.T. thanks Dr. Claudio Sangregorio and the Department of Chemistry, Florence, Italy for taking the magnetic measurements.

 © WILEY-VCH Verlag GmbH, 69451 Weinheim, Germany, 2002 1433-7851/02/4112-2148 $ 20.00+.50/0

longest one being between the Mn^{II} ions Mn2 and Mn3, which are bridged only by a bidentate chelate carboxylato ligand. For the $Mn^{IV}\cdots Mn^{II}$ separations the shortest (3.259 Å) is between Mn1 and Mn3 which are bridged by two ketonoximato moieties (Table 1). The angles around the (μ_4-O)Mn_4

Table 1. Selected interatomic distances [Å] and angles [°] for **1**.

	Distances [Å]		Distances [Å]
Mn1 ··· Mn2	3.351	Mn2 ··· Mn3	3.607
Mn1 ··· Mn3	3.259	Mn2 ··· Mn4	3.185
Mn1 ··· Mn4	3.471	Mn3 ··· Mn4	3.522
Angles [°]		Angles [°]	
Mn1-O-Mn2	115.9(2)	Mn2-O-Mn4	94.33(13)
Mn1-O-Mn3	108.1(2)	Mn3-O-Mn4	105.98(14)
Mn1-O-Mn4	120.1(2)	Mn4-O71-Mn2	88.53(13)
Mn2-O-Mn3	111.64(14)		

center vary from 94.2(1) to 120.1(2)° consistent with a distorted tetrahedral geometry and an O^{2-} ion rather than a square-pyramidal geometry which is expected for a μ_4-OH group and for which the Mn atoms should have a square-planar arrangement. All the Mn centers have distorted octahedral coordination environments. The coordination sphere of the Mn^{IV} ion (Mn1), comprises four O atoms, three of which are from the ketonoximato ligands and the fourth from the μ_4-O^{2-} ion, and two N atoms, one from the ketonoximato moiety and the second is a pyridyl nitrogen. Two of the Mn^{II} ions, (Mn2 and Mn4, have $Mn(N_{ketonoximato})$-$(N_{pyridyl})(O_{chelate\text{-}carboxylato})_2(O_{unidentate\text{-}carboxylato})(\mu_4\text{-}O)$ coordination spheres, whereas for the third Mn^{II} ion (Mn3), the unidentate carboxylato oxygen is replaced by a ketonoximato oxygen atom. Considering the oxidation states of the manganese atoms, the three of them, Mn2, Mn3, and Mn4, can be easily assigned as Mn^{II}, based on the lengths of the Mn–O bonds which fall in the range of 2.11 – 2.36 Å, while the bonds around Mn1 of 1.800(4) – 2.083(5) Å and the lack of a Jahn – Teller distortion along any of the three axes support an Mn^{IV} oxidation state. Further support for the oxidation state of the Mn1 ion is the tetrahedral coordination environment of the μ_4-O atom (with this geometry the charge balance of the cluster is only satisfied with an Mn(IV) oxidation state). To elucidate more clearly whether the oxidation state of the Mn1 ion is Mn^{IV} or Mn^{III} we have to examine closer the coordination environment of Mn1. This center has a distorted octahedral geometry with a very short Mn1–O bond 1.80 Å and the longest bond is along the same axis to the opposite apex Mn1 – N21 2.083 Å. The sum of the axial bonds O-Mn1-N21 3.883 Å, O1-Mn1-N22 3.935 Å, and O11-Mn1-O31 3.815 Å does not suggest any bond elongation or depression along any axis. The presence of the Mn–O bond of 1.8 Å could suggests an Mn=O^- moiety, but this is unlikely and is not supported by the IR data which do not show the anticipated strong bands at about 1000 and/or 750 cm^{-1} proposed by Groves and Stern.[31] To elucidate the bonding situation further we have synthesized the compound $[Zn_4(OH)_2$-$(pko)_4Cl_2]$ that has a metallacrown structure with zinc ions interacting through OH groups.[32] The IR patterns of Mn and Zn clusters in the range 1000 – 650 cm^{-1} are almost identical, not showing any additional band which could be assigned to an Mn=O bond.

Additional support to the oxidation state of Mn1 as Mn^{IV} is based on variable-temperature magnetic measurements. The temperature dependence of χT of $Mn^{IV}Mn^{II}_3$ in a field of 0.1 T is shown in Figure 2. At room temperature χT

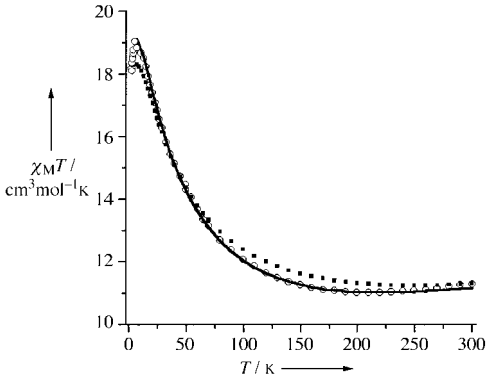


Figure 2. Temperature-dependence of the susceptibility data for $\chi_M T$ of **1** at 0.1 T. ○ is the measured data, —— is the best fit according to Equation (2), ■ is the best fit according to the $Mn^{III}Mn^{II}_3$ model [Eq (3)].

is 11.3 $cm^3 mol^{-1} K$, smaller than expected for three uncoupled $S = 5/2$ and one $S = 3/2$ spins (15 $cm^3 mol^{-1} K$) and steadily increases with decreasing temperature, reaching a maximum of $\chi T = 18.86$ $cm^3 mol^{-1} K$, at about 4.5 K. Below this point, it rapidly decreases with decreasing temperature, reaching 18 $cm^3 mol^{-1} K$ at around 2 K, possibly a result of zero-field effects. To define the exchange interactions[*] the exchange model in Equation (1) was used which is shown in Figure 3 based on crystallographic criteria.

$$\mathscr{H} = J_1 S_2 S_4 + J_2(S_1 S_3 + S_1 S_2) + J_3(S_1 S_4) \quad (1)$$

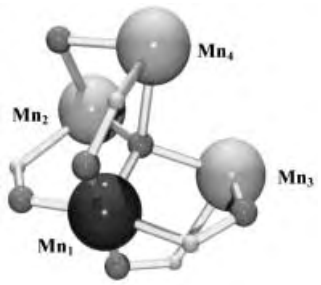


Figure 3. The graphical exchange model according to crystallographic criteria.

The $S_2 - S_4$ exchange interaction is expected to be ferromagnetic while the other two are expected to be antiferromagnetic. To define the valence of the Mn1 (two possibilities exist: Mn^{III} or Mn^{IV}) we used the same magnetic model in the

[*] Because of the valence complexity of the complex, various magnetic models were used with more exchange interactions. Even if we take into consideration the interaction $S_3 - S_4$ and $S_2 - S_3$ the fit does not improve while the energy spectrum remains the same with ground state $S = 6$.

two hypothetical cases where the $S_1 = 2$ or $S_1 = 3/2$, respectively, and in the temperature range 5–300 K [Eq. (2) and (3)].

$$Mn^{IV}Mn^{II}_3 \rightarrow J_1 = -4.15\ cm^{-1},\ J_2 = 48.4\ cm^{-1},\ J_3 = 1.33\ cm^{-1},\ g = 1.95 \quad (2)$$

$$Mn^{III}Mn^{II}_3 \rightarrow J_1 = -5.0\ cm^{-1},\ J_2 = 68.9\ cm^{-1},\ J_3 = 0.85\ cm^{-1},\ g = 2 \quad (3)$$

Both fits are superimposable in the low-temperature limit while after 100 K only the model in Equation (2) is closer to the data (Figure 2, solid line). According to the first model the ground state of the system is $S = 6$ while for the second is $S = 11/2$. To define the ground state of the system, magnetization measurements were carried out at two temperatures 2.5 and 4.5 K in the field range 0–6.5 T (Figure 4). The solid lines are

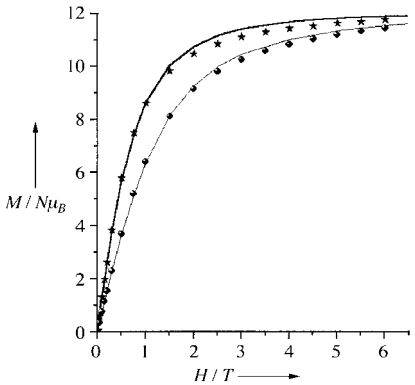


Figure 4. Magnetization measurements, in the reduced form of $M/N\mu_B$, in the field range 0–6.5 T at 2.5 K (solid stars) and 4.5 K (●). The solid lines represent the simulations according to a Brillouin function of a system with an $S = 6$ ground state and $D = 0.025\ cm^{-1}$.

the best fits using the Brillouin function for an $S = 6$ system ($g = 2$) with a small $D = 0.025\ cm^{-1}$ (where D is the zero-field splitting term) while the second case was ruled out because of unrealistic g values. Therefore, the magnetic measurements provide strong evidence that model in Equation (2), that is for an Mn^{IV} center, is the most appropriate.

Experimental Section

The compound $[Mn^{II}Mn^{II}Mn^{II}Mn^{IV}(O)(pko)_4(3,4\text{-}D)_4]\cdot 2.5\,CH_3OH$ was synthesized by adding the sodium salt of di(2-pyridyl)ketonoxime ligand (10 mmol) to a solution of $MnCl_2\cdot 4H_2O$ (10 mmol) in methanol (100 mL). The sodium salt of 3,4-D (10 mmol) dissolved in methanol (10 mL) was added. The resulting dark red-brown solution was reduced to a volume of 20 mL after 5 h of stirring. Red/black crystals suitable for X-ray diffraction studies[33] were obtained by slow evaporation. Yield 60%. Elemental analysis (%) calcd for $C_{78.50}H_{62}Cl_8Mn_4N_{12}O_{19.50}$ (1988.76): C 47.36, H 3.11, N 8.44, Mn 11.06); found: C 47.60, H 3.45, N 8.05, Mn 10.80.

Received: January 14, 2002 [Z18518]

[1] A. Zouni, H.-T. Witt, J.; Kern, P. Fromme, N. Krauß, W. Saenger, P. Orth, *Nature* **2001**, *409*, 739.
[2] D. P. Kessissoglou, M. L. Kirk, M. S. Lah, X.-h. Li, C. A. Raptopoulou, W. E. Hatfield, V. L. Pecoraro, *Inorg. Chem.* **1992**, *31*, 5424.
[3] V. Tangoulis, D. A. Malamatari, K. Soulti, V. Stergiou, C. P. Raptopoulou, A. Terzis, T. A. Kabanos, D. P. Kessissoglou, *Inorg. Chem.* **1996**, *35*, 4974.
[4] V. Tangoulis, D. A. Malamatari, G. A. Spyroulias, C. P. Raptopoulou, A. Terzis, D. P. Kessissoglou, *Inorg. Chem.* **2000**, *39*, 2621.
[5] L. Que, Jr., A. E. True, *Prog. Inorg. Chem.* **1990**, *38*, 97.
[6] G. Christou, *Acc. Chem. Res.* **1989**, *22*, 328.
[7] A. R. Schake, E. A. Schmitt, A. J. Conti, W. E. Streib, J. C. Huffman, D. N. Hendrickson, G. Christou, *Inorg. Chem.* **1991**, *30*, 3192.
[8] K. Folting, J. C. Huffman, G. Christou, D. N. Hendrickson, *J. Am. Chem. Soc.* **1987**, *109*, 5703.
[9] R. D. Guiles, A. McDermott, V. K. Yachandra, J. L. Cole, S. L. Dexheimer, R. D. Britt, K. Wieghardt, U. Bossek, K. Sauer, M. P. Klein, *Biochemistry* **1990**, *29*, 471.
[10] K. Wieghardt, *Angew. Chem.* **1989**, *101*, 1179; *Angew. Chem. Int. Ed. Engl.* **1989**, *28*, 1153.
[11] R. Hotzelmann, K. Wieghardt, U. Florke, H.-J. Haupt, D. C. Weatherburn, J. Bonvoisin, G. Blondin, J.-J. Girerd, *J. Am. Chem. Soc.* **1992**, *114*, 1681.
[12] R. Manchanda, H. H. Thorp, G. W. Brudvig, R. H. Crabtree, *Inorg. Chem.* **1991**, *30*, 494.
[13] G. W. Brudvig, R. H. Crabtree, *Prog. Inorg. Chem.* **1989**, *37*, 99.
[14] J. B. Vincent, G. Christou, *Adv. Inorg. Chem.* **1989**, *33*, 197.
[15] D. Low, D. M. Eichorn, A. Draganescu, W. H. Armstrong, *Inorg. Chem.* **1991**, *30*, 877.
[16] K. S. Hagen, W. H. Armstrong, M. M. Olmstead, *J. Am. Chem. Soc.* **1989**, *111*, 774.
[17] M. K. Chan, W. H. Armstrong, *J. Am. Chem. Soc.* **1991**, *113*, 5055.
[18] M. K. Chan, W. H. Armstrong, *J. Am. Chem. Soc.* **1989**, *111*, 9121.
[19] M. K. Chan, W. H. Armstrong, *J. Am. Chem. Soc.* **1990**, *112*, 4985.
[20] R. J. Kulawiec, R. H. Crabtree, G. W. Brudvig, G. K. Schulte, *Inorg. Chem.* **1988**, *27*, 1309.
[21] B. Albela, M. S. E. Salah, J. Ribas, K. Folting, G. Christou, D. N. Hendrickson, *Inorg. Chem.* **2001**, *40*, 1037.
[22] S. Wang, J. C. Huffman, W. E. Streib, E. A. Schmitt, J. K. McCusker, D. N. Hendrickson, G. Christou, *Angew. Chem.* **1991**, *103*, 314; *Angew. Chem. Int. Ed. Engl.* **1991**, *30*, 305.
[23] S. Wang, J. C. Huffman, K. Folting, W. E. Streib, E. B. Lobkovsky, G. Christou, *Angew. Chem.* **1991**, *103*, 1681; *Angew. Chem. Int. Ed. Engl.* **1991**, *30*, 1672.
[24] J. S. Bashkin, H.-R. Chang, W. E. Streib, J. C. Huffman, D. N. Hendrickson, G. Christou, *J. Am. Chem. Soc.* **1987**, *109*, 6502.
[25] D. N. Hendrickson, G. Christou, E. A. Schmitt, E. Libby, J. S. Bashkin, S. Wang, H.-L. Tsai, J. B. Vincent, P. D. W. Boyd, J. C. Huffman, K. Folting, Q. Li, W. E. Streib, *J. Am. Chem. Soc.* **1992**, *114*, 2455.
[26] D. W. Randall, B. E. Sturgeon, J. A. Ball, G. A. Lorigan, M. K. Chan, M. P. Klein, W. H. Armstrong, R. D. Britt, *J. Am. Chem. Soc.* **1995**, *117*, 11780.
[27] M. Zheng, G. C. Dismukes, *Inorg. Chem.* **1996**, *35*, 3307.
[28] G. Blondin, R. Davydov, C. Philouze, M.-F. Charlot, S. Styring, B. Akermark, J.-J. Girerd, A. Boussac, *J. Chem. Soc. Dalton Trans.* **1997**, 4069.
[29] W. F. Ruettinger, C. Campana and G. C. Dismukes, *J. Am Chem. Soc.* **1997**, *119*, 6670.
[30] C. Gedye, C. Harding, V. McKee, J. Nelson, J. Patterson, *J. Chem. Soc. Chem. Commun.* **1992**, 392.
[31] J. T. Groves, M. K. Stern, *J. Am. Chem. Soc.* **1988**, *110*, 8628.
[32] M. Alexiou, C. Dendrinou-Samara, C. P. Raptopoulou, A. Terzis, D. P. Kessissoglou, *Inorg. Chem.*, in press.
[33] Empirical formula: $C_{78.50}H_{62}Cl_8Mn_4N_{12}O_{19.50}$; $M_r = 1988.76$, crystal system: triclinic, space group: $P\bar{1}$, $a = 16.856(9)$, $b = 18.103(9)$, $c = 15.091(9)$ Å, $\alpha = 98.82(2)$; $\beta = 93.27(2)$, $\gamma = 107.24(2)^\circ$, $V = 4320(1)$ Å^3, $Z = 2$, $\rho_{calcd} = 1.529\ Mg\,m^{-3}$, absorption coefficient = $0.894\ mm^{-1}$, $F(000) = 2018$; crystal size = $0.10 \times 0.20 \times 0.50$ mm; θ for data collection 1.65 to 22.73°; limiting indices: $0 \le h \le 18$, $-19 \le k \le 18$, $-16 \le l \le 16$, reflections collected/unique 12095/11618 [R(int) = 0.0195], refinement method: Full-matrix-block least-squares on F^2, data/restraints/parameters:11618/0/1292; goodness-of-fit on $F^2 = 1.074$, largest differential peak and hole: 0.850 and −0.408 e Å^{-3}, final R indices: [8096 refs $I > 2\sigma(I)$]: $R1 = 0.0501$, $wR2 = 0.1312$, R indices(all data): $R1 = 0.0860$, $wR2 = 0.1560$. CCDC-177313 contains the supplementary crystallographic data for this paper. These data can be obtained free of charge via www.ccdc.cam.ac.uk/conts/retrieving.html (or from the Cambridge Crystallographic Data Centre, 12, Union Road, Cambridge CB2 1EZ, UK; fax: (+44) 1223-336-033; or deposit@ccdc.cam.ac.uk).

 © WILEY-VCH Verlag GmbH, 69451 Weinheim, Germany, 2002 1433-7851/02/4112-2150 $ 20.00+.50/0

Nucleation of MCM-41 Nanoparticles by Internal Reorganization of Disordered and Nematic-Like Silica – Surfactant Clusters**

Sajanikumari Sadasivan, Christabel E. Fowler, Deepa Khushalani, and Stephen Mann*

The synthesis of periodic mesostructures by self-assembly and cooperative organization of inorganic and organic species in aqueous media represents a significant benchmark in modern materials chemistry.[1–5] These template-directed processes generally involve charge matching interactions between inorganic oligomers and surfactant micelles,[6–8] and have been developed to produce a large number of hybrid mesophases and mesoporous replicas with surface areas of the order of 1000 $m^2 g^{-1}$. In spite of the advances in synthesis and applications of mesoporous materials, the mechanisms that give rise to periodic ordering in self-assembled hybrid systems are not well understood. Previous studies have focused on micellar structure just prior to precipitation,[9–12] or the growth of relatively large mesostructured crystals.[13–16] Details on the nucleation of the periodic mesophase have been difficult to obtain because of the relatively short timescales involved and the transient nature of the intermediates. Herein, we employ a controlled quenching process to sufficiently increase the nucleation period, such that high-resolution transmission electron microscopy (HR-TEM) can be used to reveal, for the first time to our knowledge, the structural stages associated with the nucleation of a hexagonally ordered silica – surfactant mesophase (MCM-41).

Recently, we reported the template-directed synthesis of single-domain MCM-41 nanoparticles with dimensions usually less than 150 nm by the controlled quenching of alkaline reaction mixtures containing tetraethoxysilane (TEOS) and cetyltrimethylammonium bromide (CTAB).[17] By employing a constant (40 s) dilution step, followed by variable time delays prior to arresting the reaction by instantaneous neutralization to pH 7 (see Experimental Section), we now show that it is possible to determine the structural and shape transformations of the nanoparticles during the onset and development of mesophase ordering. The earliest stage in this process was investigated by preparing samples using neutralization periods of less than 3 min. Small-angle X-ray diffraction (SAXRD) analysis showed an absence of long-range order with a broad low-angle reflection centered at 5.32 nm, consistent with swollen micelles and a low degree of silica condensation, and thermogravimetric analysis (TGA) measurements indicated that the hybrid mesophase contained 25 wt % of surfactant. Corresponding TEM images showed the presence of a homogeneous population of spherical nanoparticles with a mean size of 18 nm ($\sigma = 4$ nm). In contrast, extending the neutralization delay to 4 min produced a mixture of two types of nanoparticles, 75 % of which were spherical with increased mean diameter (35 nm, $\sigma =$ 9 nm), whereas the remaining 25 % were ellipsoidal and 67 ($\sigma = 16$) and 50 ($\sigma = 6$) nm in mean length and width, respectively.

Individual spherical nanoparticles up to about 50 nm in size were shown by high-resolution TEM imaging to consist of a loosely packed aggregate of disordered silica – surfactant micelles (Figure 1). The micelles were in the form of short rods, about 9.0 and 5.0 nm in length and width, respectively, that were "stained" by a 1 to 2 nm-thick surface layer of silica/silicate (Figure 1, arrow). Large numbers of nonaggregated spherical or slightly oblate silica-coated micelles were also imaged on the support film of the TEM grid (data not shown). Although drying artefacts cannot be ruled out, this suggests that for neutralization periods of less than 4 min the reaction mixture contained a high concentration of these discrete hybrid structures. In contrast with the disordered spherical aggregates, the ellipsoidal nanoparticles showed various degrees of internal mesostructural order. Ellipsoids that were relatively small (ca. 40 nm in length) had partially ordered interiors, which consisted of short rod-shaped silica-coated micelles preferentially aligned side-on within the nanoparticle (Figure 2 a). Although some end-on fusion of the rods parallel to the minor axis of the ellipsoids was apparent, the surfactant cylinders were in general too short to traverse the entire

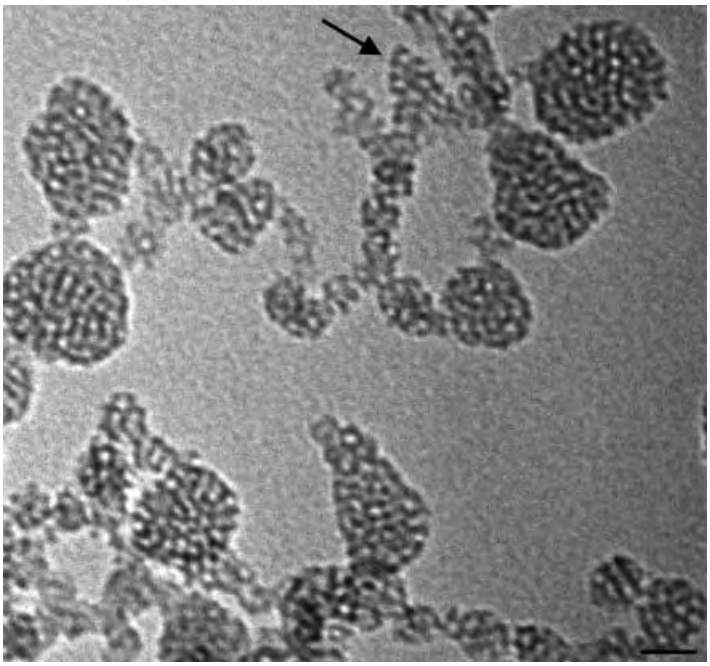


Figure 1. Initial stage in MCM-41 nucleation showing spherical clusters of disordered silica – surfactant micelles. Arrow highlights individual micelles. Scale bar = 20 nm.

[*] Prof. S. Mann, S. Sadasivan, Dr C. E. Fowler[+]
School of Chemistry
University of Bristol
Bristol BS8 1TS (UK)
Fax: (+44) 117-925-1295
E-mail: s.mann@bris.ac.uk
Dr D. Khushalani
School of Physical Sciences
University of Kent
Canterbury (UK)
[+] Current address: Forsyth Institute, 140 The Fenway, Boston MA 02115 (USA)

[**] We thank the University of Bristol for the support of an ORS award to S.S., and Dr. S. A. Davis for help with electron microscopy.

 © WILEY-VCH Verlag GmbH, 69451 Weinheim, Germany, 2002 1433-7851/02/4112-2151 $ 20.00+.50/0

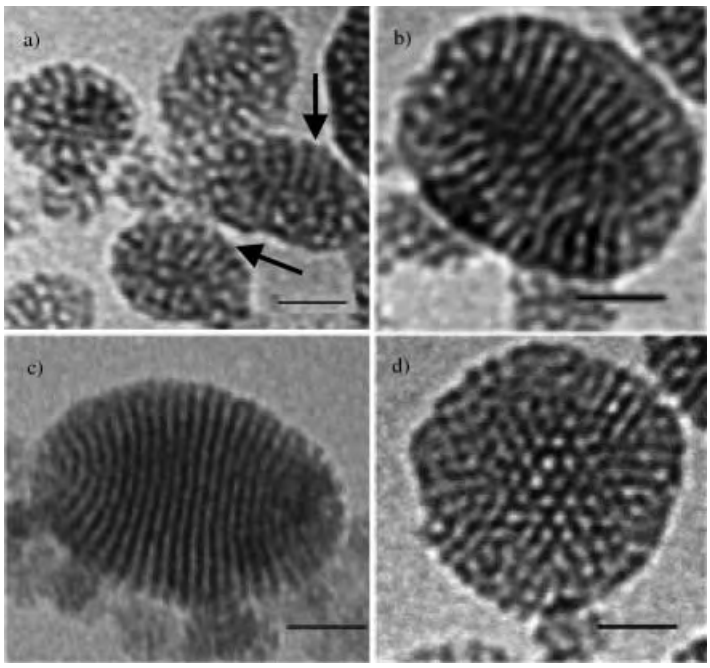


Figure 2. TEM lattice images of mesostructural ordering in oblate ellipsoidal nuclei. a) Side view of several nanoparticles, 40–50 nm in length, showing the initial stages of elongation and alignment of silica–surfactant cylinders around the periphery of the aggregated micelles (arrows). b) Side view of a 60-nm long nanoparticle showing increased levels of periodic order and central defects. c) Side view of a well-ordered single domain nanoparticle with modulated periodic mesostructure and local variations in the inter-micelle spacings. d) Top view along the radial axis showing hexagonal periodicity and 2D micelle cylinder alignment within the central regions of the nanoparticle ($d_{100} = 4.4$ nm, $a = 5.1$ nm). Scale bars = 20 nm in all micrographs.

nanoparticle. Instead, localized domains of micelle alignment and extension in length were observed predominantly in the near surface regions of the nanoparticles (Figure 2a, arrows). In contrast, larger ellipsoids that were around 60 nm in length showed a progressive increase in the internal ordering such that the silica-micelle cylinders were extended almost across the whole nanoparticle to produce a single-domain periodic mesostructure with localized defects (Figure 2b). Similar images were obtained for ellipsoids between 60 and 100 nm in length except that the lattice fringes were continuous throughout the ellipsoids (Figure 2c). Interestingly, as shown in Figure 2c, the nanoparticle interiors consisted of an unusual bilateral arrangement of parallel silica–surfactant cylinders that became progressively more curved in an outward direction with increasing displacement from the centre of the ellipsoid. As a consequence, the *d* spacings increased by about 30% from 4.2 nm in the central regions to 5.1 nm at the particle edges.

Field-emission gun scanning electron microscopy (FEG-SEM) and TEM images recorded along different projections indicated that the ellipsoidal nanoparticles were flattened spheres (oblate ellipsoids) with a diameter/thickness aspect ratio of about 1.3:1. Thus, the oval-shaped images shown in Figure 2a–c correspond to side-on projections whereas a view along the radial axis (top view) was associated with nanoparticles that appeared circular in shape. The latter only showed well-ordered 2-D hexagonal dot patterns—corresponding to the [001] channel direction—in the central regions of the nanoparticles (Figure 2d), which is consistent with the structural modulation observed in the side views. Moreover, the hexagonal lattice patterns were only observed for ellipsoids greater than about 60 nm in width, suggesting that this is the approximate critical size for the onset of long-range MCM-41 periodicity.

Extending the neutralization period to 9 min produced no internally disordered spherical nanoparticles and increased the monodispersity, as well as the mean diameter and thickness (120 ($\sigma = 19$) and 80 ($\sigma = 18$) nm, respectively), of the oblate ellipsoids, which were present in almost 100% yield. The marginal increase in aspect ratio from 1.3:1 to 1.5:1 with growth suggests that the addition of silica–surfactant micelles from the supersaturated solution occurs preferentially by side-on fusion around the radial axis of the oblate ellipsoids. This flattens the ellipsoids further, which reduces the curvature of the surface and associated internal bending of the silica–surfactant cylinders, with the consequence that disklike nanoparticles with small hexagonal faces were observed by FEGSEM. Corresponding TEM studies showed no significant changes in the internal organization of the modulated silica–surfactant mesostructure, although the lattice images were more well-defined, suggesting an increase in the degree of silica condensation. This was consistent with XRD measurements, which showed a single broad reflection with a *d* spacing centered at 4.40 nm, and TGA measurements that indicated no change in the surfactant composition (25 wt%).

The above results suggest the following model for the nucleation of MCM-41 nanoparticles under the highly specialized conditions investigated (Figure 3). Initially, the reaction mixture is at pH 13 for 40 s, which initiates TEOS hydrolysis and the formation of soluble silicate species that interact with

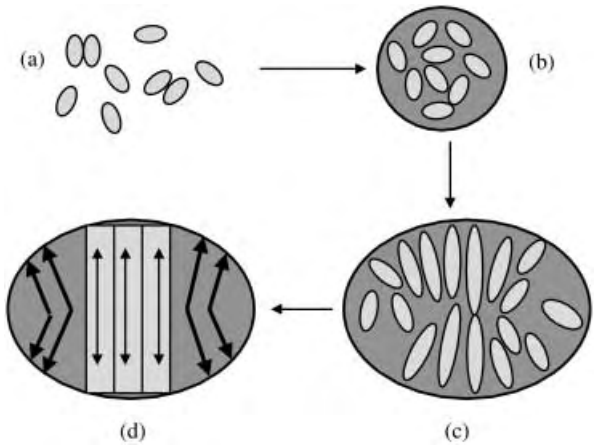


Figure 3. Schematic representation showing proposed mechanism for the nucleation of MCM-41 nanoparticles. a) Solution phase containing short rod-shaped silica-coated CTAB micelles. b) Aggregation of silica–surfactant micelles into disordered spherical nanoparticles less than 50 nm in size. c) Internal reorganization to nematic-like silica–surfactant mesostructure due to side-on ordering and cylinder elongation, and associated change in the particle morphology to an oblate ellipsoid. d) Elongation of the silica–surfactant micelles to produce single-domain nanoparticles with modulated mesostructure. Arrows indicate the local orientation of the micelle cylinders.

 © WILEY-VCH Verlag GmbH, 69451 Weinheim, Germany, 2002 1433-7851/02/4112-2152 $ 20.00+.50/0

the cationic headgroups of the CTAB micelles. Subsequent dilution reduces the pH spontaneously to around 12, which in turn decreases the rate of hydroxide-catalyzed hydrolysis, lowers the solubility of the silicate precursors, and reduces the surface charge on incipient silica–surfactant clusters present in the medium. In addition, the 85% decrease in concentration reduces the rate of cluster coalescence sufficiently that silica–surfactant micelles at various stages of aggregation can be investigated. Significantly, the individual micelles are not highly elongated as proposed in previous models of MCM-41 formation, but short rods with aspect ratios of about 1.7:1. This is consistent with recent studies using liquid-state NMR and fluorescence spectroscopy, which indicated that CTAB micelles were not significantly changed in the presence of silicate species at high pH.[18–20]

Aggregation of the individual silica-coated micelles produces spherical nanoparticles with disordered interiors and "raspberry-like" external morphology (Figure 3b). Nucleation of the periodic mesostructure occurs by internal reorganization of a disordered cluster of a few hundred loosely packed silica-coated micelles (particle diameter < 50 nm) and is associated with two stages involving the interactive coupling of structural and morphological transformations. In the first stage, side-on ordering and wall formation between the micelles produce a nematic-like silica–surfactant interior that initiates a sphere to oblate ellipsoid transformation such that the director field lies approximately parallel to the radial axis (Figure 3c). The intimate association between particle morphology and internal structure explains the preferential ordering in the near surface regions and alignment of the partially elongated micelle cylinders around the minor axis of the oblate ellipsoid. In the second stage, the shape anisotropy induced by side-on ordering of the silica–surfactant micelles becomes coupled with the subsequent structural development of the hexagonally ordered interior. As the surface to volume ratio is high, the energy required to bend the hexagonal array of silica–surfactant cylinders away from the principal director field is offset by the surface alignment of the channel directions normal to the local tangent (Figure 3d). Thus, as the cylinders increase in length and extend across the entire nanoparticle, the corresponding mesostructure becomes progressively modulated about the radial axis due to changes in the local curvature of the ellipsoids.

In conclusion, our results indicate that under our experimental conditions the nucleation of MCM-41 nanoparticles occurs heterogeneously by a disorder–order phase transition within silica–surfactant micellar aggregates less than 50 nm in size. A similar mechanism has been recently proposed for large particles of mesostructured silica although no direct structural observations were reported.[21] In our system, the onset of 2D periodicity occurs through a nematic-like intermediate that is associated with a structure-induced shape transformation. In turn, the oblate ellipsoidal morphology influences the subsequent extension and structural reorganization of the micelle cylinders to produce a modulated hexagonal silica–surfactant periodic mesophase. Further work using organo-functionalized nanoparticles is in progress to determine the generality of this nucleation mechanism.

Experimental Section

Typically, the nanoparticles were synthesized by using the following molar ratios: 0.12 CTAB:0.5 NaOH:1 SiO_2:130 H_2O. CTAB (0.8 g) was dissolved in an alkaline solution consisting of 1M NaOH (10 g) in H_2O (35.1 g) and TEOS (3.78 g) added under stirring. After 40 s (dilution delay) the reaction mixture was added to water (300 g) and left stirring for various time periods (1 to 10 min, neutralization delay) before 2M HCl was added to neutralize the solution. Stirring was stopped when the pH had decreased to 7.0, after which samples were taken directly from the reaction mixture and air-dried onto grids for TEM or field-emission gun scanning electron microscopy (FEGSEM) analysis. The dilution step reduced the reaction pH from 13 to 12.2, and subsequent neutralization delays of 1, 3, 4, 6, and 10 min corresponded to further decreases in the pH to 12.0, 10.6, 10.3, 10.25 and 10.3, respectively. The concentration of CTAB after dilution (6×10^{-3}M) remained above the critical micelle concentration.

Solid samples were obtained by evaporation of the water from the reaction mixture in air for 24 h and analyzed by small angle X-ray diffraction (SAXRD) and thermogravimetric analysis (TGA). The surfactant template was removed by calcination at 540 °C.

Received: December 18, 2001 [Z18408]

[1] C. T. Kresge, M. E. Leonowicz, W. J. Roth, J. C. Vartuli, J. S. Beck, *Nature* **1992**, *359*, 710–712.
[2] J. Y. Ying, C. P. Mehnert, M. S. Wong, *Angew. Chem. Int. Ed.* **1999**, *111*, 58–82; *Angew. Chem. Int. Ed.* **1999**, *38*, 56–77.
[3] F. Schüth, *Chem. Mater.* **2001**, *13*, 3184–3195.
[4] C. Sanchez, G. J. D. A. Soler-Illia, F. Ribot, T. Lalot, C. R. Mayer, V. Cabuil, *Chem. Mater.* **2001**, *13*, 3061–3083.
[5] A. Stein, B. J. Melde, R. C. Schroden, *Adv. Mater.* **2000**, *12*, 1403–1419.
[6] A. Firouzi, D. Kumar, L. M. Bull, T. Besier, P. Sieger, Q. Huo, S. A. Walker, J. A. Zasadzinski, C. Glinka, J. Nicol, D. Margolese, G. D. Stucky, B. F. Chmelka, *Science* **1995**, *267*, 1138.
[7] Q. S. Huo, D. I. Margolese, G. D. Stucky, *Chem. Mater.* **1996**, *8*, 1147–1160.
[8] S. H. Tolbert, C. C. Landry, G. D. Stucky, B. F. Chmelka, P. Norby, J. C. Hanson, A. Monnier, *Chem. Mater.* **2001**, *13*, 2247–2256.
[9] M. F. Ottaviani, A. Galarneau, D. Desplantier-Giscard, F. Di Renzo, F. Fajula, *Microporous Mesoporous Mater.* **2001**, *23*, 1–8.
[10] H. P. Lin, C. P. Kao, C. Y. Mou, *Microporous Mesoporous Mater.* **2001**, *23*, 135–141.
[11] F. Di Renzo, D. Desplantier, A. Galarneau, F. Fajula, *Catal. Today* **2001**, *66*, 73–77.
[12] H. Naono, M. Hakuman, T. Tsunehisa, N. Tamura, D. Nakai *J. Colloid Interface Sci.* **2000**, *224*, 358–365.
[13] S. Che, Y. Sakamoto, O. Terasaki, T. Tatsumi, *Chem. Mater.* **2001**, *13*, 2237–2239.
[14] F. Kleitz, F. Marlow, G. D. Stucky, F. Schuth, *Chem. Mater.* **2001**, *13*, 3587–3595.
[15] H. Yang, G. A. Ozin, C. T. Kresge, *Adv. Mater.* **1998**, *10*, 883–887.
[16] W. Zhou, J. Klinowski, *Chem. Phys. Lett.* **1998**, *292*, 207–212.
[17] C. E. Fowler, D. Khushalani, B. Lebeau, S. Mann, *Adv. Mater.* **2001**, *13*, 649–652.
[18] L. Sicard, J. Frasch, M. Soulard, B. Lebeau, J. Patarin, T. Davey, R. Zana, F. Kolenda, *Microporous Mesoporous Mater.* **2001**, *23*, 25–31.
[19] J. Frasch, B. Lebeau, M. Soulard, J. Patarin, R. Zana, *Langmuir* **2000**, *16*, 9049–9057.
[20] R. Zana, J. Frasch, M. Soulard, B. Lebeau, J. Patarin, *Langmuir* **1999**, *15*, 2603–2606.
[21] H. B. S. Chan, P. M. Budd, T. deV. Naylor, *J. Mater. Chem.* **2001**, *11*, 951–957.

 © WILEY-VCH Verlag GmbH, 69451 Weinheim, Germany, 2002 1433-7851/02/4112-2153 $ 20.00+.50/0

Vesicular Nanostructures Prepared by Reactive Melt Blending**

Christian Koulic, Zhihui Yin, Christophe Pagnoulle, and Robert Jérôme*

The toughening of thermoplastics with rubber is one of the most important applications in the rapidly expanding field of polymer blends. The control of the morphology of rubber-modified thermoplastics is, however, the key issue for a successful toughening process.[1] In this respect, micellar structures, such as vesicles, have been recently proposed as toughening agents. Practically, amphiphilic block copolymers are dissolved in a liquid reactive mixture which is the precursor of the matrix to be toughened. They spontaneously form nanostructures, the nature of which depends on their molecular composition and structure. In an example reported by Bates and co-workers,[2c] an epoxidized polyisoprene-*b*-polybutadiene copolymer dissolved in diglycidyl ether bisphenol A, spontaneously self assembles into spherical micelles or vesicles depending on the diblock composition. The epoxy resin is then hardened upon addition of 4,4′-methylenedianiline and the micellar structures are accordingly frozen in. This behavior is general to block copolymer/epoxy systems in which one constitutive block is miscible with the matrix and the other one is an immiscible rubbery block.[2] In the specific case of a vesicular morphology, a drastic increase in fracture toughness was observed at low copolymer content (ca. 2.5 wt %) together with a substantial decrease in modulus.[2c] Meyer and co-workers also investigated the toughening of brittle thermoplastics, such as poly(methyl methacrylate) (PMMA) and polystyrene (PS), by using the same strategy. They successfully preformed micelles of hydrogenated polybutadiene-*b*-poly(methyl acrylate) in methyl methacrylate (MMA) or styrene that were frozen in upon polymerization of the continuous monomer phase. Although the prevention of macrophase separation was confirmed by small-angle X-ray scattering (SAXS) studies, no data for the mechanical properties was made available.[3] Even though micellar nanostructures are promising toughening agents for brittle thermoplastics or thermosets, the two-step strategy based on polymerization (or cure) of the matrix after the nanophase morphology is established is not sufficiently straightforward to be viable on a large scale. Herein we report on the nanostructuration of a block copolymer by the one-step reactive melt blending with the matrix to be toughened. A core–shell morphology with a rubbery shell was targeted in the case of a polyamide matrix. For this purpose, polyamide 12 (PA12) chains, end-capped by a primary amine, were melt blended with 20 wt % of a polystyrene-*b*-polyisoprene (PS-*b*-PIP) copolymer end-capped at the PIP chain end by an anhydride. The aim was to build up a core–shell morphology with a rubbery layer between the PA12 matrix and the PS nanophase.

Previous studies[4] emphasized that the kinetics of the interfacial reaction has a decisive effect on the phase morphology in reactive blending. When all the chains are reactive and the mutually reactive groups are used in the stoichiometric molar ratio, the reaction can go to completion in the case of a high reaction rate and when the chains have a relatively low molecular weight. Since the coupling reaction of the PS-*b*-PIP diblock to PA12 must be as complete as possible, the fast reaction of the primary amine end group of PA12 with the anhydride (anh) end group of PS-*b*-PIP-anh has been considered. The diblock was synthesized by sequential anionic polymerization of styrene and isoprene initiated by *sec*-BuLi, followed by deactivation by ethylene oxide and derivatization of the ω-hydroxy end group into an anhydride.[4d] The expected end capping of the diblock by the anhydride end group was confirmed by FTIR spectroscopy (absorption at 1780 cm^{-1}) and by size-exclusion chromatography (UV detection at 366 nm) after reaction with 9-(methylaminomethyl)anthracene.[5]

Table 1. Polymers used in this study.

Code	Type	$M_n(\times 10^{-3})$ [$g\,mol^{-1}$]	M_w/M_n	Addition[b]
S1	PS-*b*-PIP	16[a]-18[b]	1.05[c]	1,4: 93 %, 3,4: 7 %
S2	PS-*b*-PIP-anh	16[a]-18[b]	1.05[c]	1,4: 93 %, 3,4: 7 %

[a] Size-exclusion chromatography using PS calibration. [b] By ^1H 400 MHz NMR spectroscopy. [c] Size-exclusion chromatographic analysis.

In this study, a symmetric diblock (Table 1) has been melt blended with PA12 at 220 °C. Observation by transmission electron microscopy (TEM) shows there is a gross phase separation in the case of nonreactive blending (Figure 1). The expected lamellar nanostructure is observed in the microdomains formed by the symmetric diblock. The thickness of the constitutive PS lamellae can be estimated to be approximately 7 nm. A drastic decrease in the particle size occurs when the blending is reactive (Figure 2 A). At higher magnification, the dispersed nanophases exhibit a core–shell structure with a three-layer substructure for the shell (Figure 2 B–

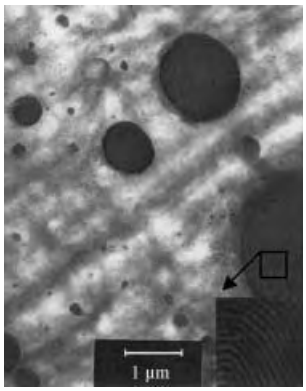


Figure 1. TEM image for the 80/20 (wt/wt) blend of PA12/**S1** (11 500 ×). The insert shows a close-up of the lamellar organization of the microphase (105 000 ×).

[*] Prof. R. Jérôme, C. Koulic, Z. Yin, Dr. C. Pagnoulle
Center for Education and Research on Macromolecules (CERM)
University of Liège
Sart-Tilman, B6a, 4000 Liège (Belgium)
Fax: (+32) 4-366-3497
E-mail: rjerome@ulg.ac.be

[**] We are grateful to the Services Fédéraux des Affaires Scientifiques, Techniques et Culturelles for general support in the frame of "PAI 4-11: Supramolecular Chemistry and Supramolecular Catalysis". We are grateful to Sunil K. Varshney (Polymer Source Inc., Canada) for training and advice in anionic polymerization and to Mrs. Martine Dejeneffe for ultramicrotomy at low temperature. Dr. Koen Janssen and Mai Quaedflieg from DSM Research (Geleen, The Netherlands) are acknowledged for making the mini-extruder available to us. C.K. is a Research Fellow of the "Fonds National de la Recherche Scienctifique" (FNRS, Belgium).

 © WILEY-VCH Verlag GmbH, 69451 Weinheim, Germany, 2002 1433-7851/02/4112-2154 $ 20.00+.50/0

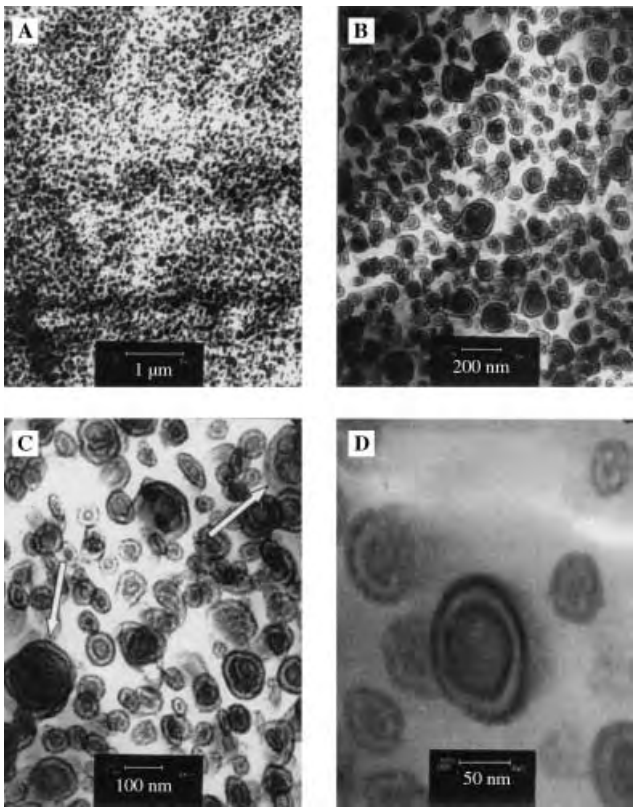


Figure 2. TEM image for the 80/20 (wt/wt) blends of: A) PA12/**S2** (11 500×), B) PA12/**S2** (39 000×), C) PA12/**S2** (73 000×), and D) PA12/**S2** (205 000×). The white arrows point out larger nanophases with a multicore substructure.

D). As a rule, the size of the nanophases is in the 40- to 80-nm range. Since the first and the third layer of the shell are the darkest domains on staining with OsO_4, they have been assigned to PIP. PS is thought to form the intermediate layer of the shell whose thickness (ca. 8 nm) is consistent with that observed for the lamellar morphology of the PS-*b*-PIP diblock. According to this picture PA12 should be the core-forming component. This hypothetical structure of a bilayer of triblock chains is reasonable because a single core–shell structure cannot be formed by a PA12-*b*-PIP-*b*-PS triblock in which the three constitutive blocks are of a comparable molecular weight ($M_{nPA12} \approx 25\,000\ g\,mol^{-1}$).[6] Indeed, dispersion in the PA12 matrix means the external brush of PA12 is wet, which triggers the curvature of the PA12/PIP and PIP/PS interfaces; the extreme situation is a PS core surrounded by a PIP shell. However, PIP and PS layers of approximately the same molecular weight cannot be accommodated in a classical core–shell structure for steric reasons. In contrast, a double triblock layer (PA12/PIP/PS/PIP/PA12) can account for the observed nanostructuration as unreacted PA12 chains can be accommodated in the core so that steric constraints are relieved, thus forming bilayered vesicular nanostructures. This morphological description also accounts for the high dispersity of the core size (10 to 65 nm), even though the shell dimension remains unchanged. Some larger nanophases (ca. 150 nm) are also observed that apparently result from partial coalescence of smaller particles, as suggested by a multicore substructure (Figure 2C). It must be noted that Thomas and co-workers accounted for the formation of single-layered vesicles in their study of binary mixtures of a diblock AB and a homopolymer A by considering the interface curvature and packing requirements of the blocks in the domain space.[7a] The same criteria were also useful to explain the nonconstant mean curvature (CMC) of the shell in the morphology of a symmetric ABC triblock.[7b]

In conclusion, the reactive dispersion of symmetric PS-*b*-PIP-anh diblock copolymer within a polyamide matrix whose chains are end-capped by a primary amine, spontaneously forms core–trilayer shell nanophases. This morphology is nothing but a dispersion of PIP-PS-PIP vesicles in the polyamide matrix, that is, the counterpart of the vesicular morphology imparted to epoxy resins by a two-step process which is responsible for their high-impact properties. This very first example of nanostructuration of a three-phase polymeric material by reactive blending paves the way for the design of new materials by classical processing techniques and to the establishment of fundamental relationships between morphology of multiphase materials and key properties such as thermoplastics toughening.

Experimental Section

Polystyrene-*b*-polyisoprene was prepared in a glass reactor previously flamed under vacuum. Polymerization of styrene in cyclohexane was initiated by *sec*-BuLi under argon at room temperature. After 4 h, freshly distilled isoprene was added and left to react at 35 °C overnight. Living chains were terminated by ethylene oxide (2 equiv with respect to the initiator) followed by the addition of a HCl/methanol/isopropanol mixture (5/70/25).[8] The PS-*b*-PIP-OH diblock was collected by precipitation in methanol, carefully dried under reduced pressure at room temperature, and treated with trimellitic anhydride chloride in dry THF as reported elsewhere.[4d] A nonreactive counterpart of the anhydride end-capped diblock was collected by picking out a sample of the reactive mixture before the addition of ethylene oxide. The living chains were deactivated by degassed methanol, precipitated in methanol, and dried under reduced pressure at room temperature.

Melt blending was carried out in a 5-cm^3 DSM microextruder at 220 °C under nitrogen for 2 min at 200 rpm. PA12 was first added followed by 20 wt % of the diblock.

The phase morphology was observed with a Philips CM100 transmission electron microscope. A Reichtert–Jung ultracryomicrotome equipped with a diamond knife was used to prepare ultrathin samples at −78 °C. The PIP phase was selectively stained with OsO_4.

Received: February 8, 2002
Revised: March 11, 2002 [Z18678]

[1] C. Koning, M. Van Duin, C. Pagnoulle, R. Jérôme, *Prog. Polym. Sci.* **1998**, *23*, 707.

[2] a) P. Lipic, F. Bates, M. Hillmyer, *J. Am. Chem. Soc.* **1998**, *120*, 8963; b) R. Grubbs, M. Broz, J. Dean, F. Bates, *Macromolecules* **2000**, *33*, 2308; c) R. Grubbs, M. Broz, J. Dean, F. Bates, *Macromolecules* **2000**, *33*, 9522; d) R. Grubbs, J. Dean, F. Bates, *Macromolecules* **2001**, *34*, 8593; e) J. Dean, P. Lipic, R. Grubbs, R. Cook, F. Bates, *J. Polym. Sci. Phys. Ed.* **2001**, *39*, 2996.

[3] I. van Casteren, H. Goosens, H. Meijer, *Polymer Processing Society (PPS) Annual Meeting*, Montreal (Canada), **2001**, Book of Abstracts.

[4] a) C. Orr, A. Adedeji, A. Hirao, F. Bates, C. Macosko, *Macromolecules* **1997**, *30*, 1243; b) C. Pagnoulle, Ph.D. Thesis, University of Liège (Belgium), **2000**; c) C. Pagnoulle, C. Koning, L. Leemans, R. Jérôme, *Macromolecules* **2000**, *33*, 6275; d) Z. Yin, C. Koulic, C. Pagnoulle, R. Jérôme, *Macromolecules* **2001**, *34*, 5132.

 © WILEY-VCH Verlag GmbH, 69451 Weinheim, Germany, 2002 1433-7851/02/4112-2155 $ 20.00+.50/0

[5] C. Koulic, Z. Yin, C. Pagnoulle, B. Gilbert, R. Jérôme, *Polymer* **2001**, *42*, 2947.
[6] a) C. Aushra, R. Stadler, *Macromolecules* **1993**, *26*, 2171; b) R. Stadler, C. Aushra, J. Beckmann, U. Krappe, I. Voigt-Martin, L. Leibler, *Macromolecules* **1995**, *28*, 3080; c) U. Breiner, U. Krappe, R. Stadler, *Macromol. Rapid Commun.* **1996**, *17*, 567; d) U. Breiner, U. Krappe, E. Thomas, R. Stadler *Macromolecules* **1998**, *31*, 135.
[7] a) D. Kinning, K. Winey, E. Thomas, *Macromolecules* **1988**, *21*, 3502; b) R. Lescannec, L. Fetters, E. Thomas, *Macromolecules* **1998**, *31*, 1680.
[8] S. Schmidt, M. Hillmyer, *Macromolecules* **1999**, *32*, 4794.

Enantioselective Photochromic Reaction of a [2.2]Metacyclophan-1-ene**

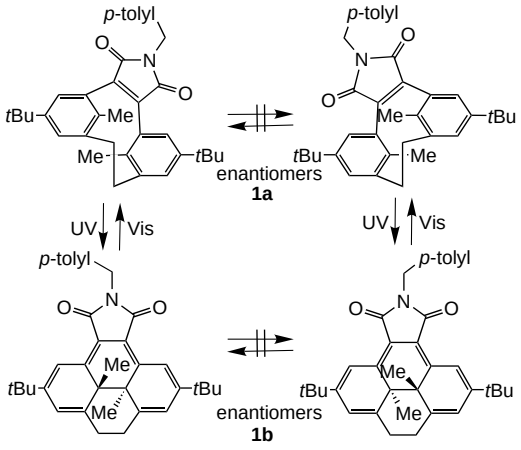
Michinori Takeshita* and Takehiko Yamato

Photochromic compounds have been extensively studied owing to their potential as photomemory and photoswitching materials.[1] Photochromic compounds reversibly change their absorption spectra (color) upon photoirradiation. However, reading the photomemory by changes in the absorption spectrum causes the destruction of the memory, since photoirradiation results in excitation of photochromic compounds.[1] Therefore, various attempts at nondestructive readout have been reported,[1] for example, by locking one of the photoisomers by the addition of chemical substances[2] or by electrooxidation (gated photochromic reaction).[3] Reading the change in chiral information originated in photochromic reactions is one of the most promising systems, since chiral information can be read without excitation of photochromic compounds.[4, 5] In photocyclization systems, for example, diarylethenes,[5a] fulgides,[5b] and spiropyrans,[5c] the enantiomers of the photochromic compounds undergo diastereoselective photocyclization. In these systems, one should be aware of the diastereoselectivity of the cyclization, since such selectivity is altered by the conditions (e.g. temperature, medium, etc). This fact encouraged us to study enantiomeric photocyclization, that is, a photochromic reaction between two enantiomers in which no racemization takes place.

We chose 1,2-disubstituted [2.2]metacyclophan-1-enes (MCP-1-enes),[6] which we recently reported,[7] as the enantiomeric photocyclization system (Scheme 1). It is well known that ring inversion of the phenyl groups in the *anti* 8,16-dimethyl[2.2]metacyclophane system is forbidden because of the steric hindrance between the inner methyl groups and the opposite phenyl groups.[8] For similar reasons, ring inversion of MCP-1-enes does not occur, and MCP-1-enes are chiral molecules because no mirror symmetry exists in the molecule.

[*] Prof. M. Takeshita, Prof. T. Yamato
Department of Applied Chemistry
Faculty of Science and Engineering, Saga University
Honjo-machi 1, Saga, 840-8502 (Japan)
Fax: (+81) 952-28-8862
E-mail: michi@ce.saga-u.ac.jp

[**] We are grateful for financial support from The Association for the Progress of New Chemistry (ASPRONC).



Scheme 1. Enantioselective photochromic reaction of [2.2]MCP-1-ene **1a** and THP **1b**.

Therefore, one can expect that racemization of the enantiomers of MCP-1-enes does not take place. MCP-1-enes show photochromism,[6, 7] and tetrahydropyrenes (THP) formed from MCP-1-enes by UV irradiation are also chiral. It is expected that no racemization occurs, even during the photochromic reaction, and that the photochromic reaction takes place with both enantiomers.

We have designed and synthesized some MCP-1-enes and found that the enantiomers of maleimide-type MCP-1-ene **1a** are easily separated.[9] MCP-1-ene **1a** was synthesized from 1,2-dicyano[2.2]MCP-1-ene[7] in three steps.[10] Figure 1 shows

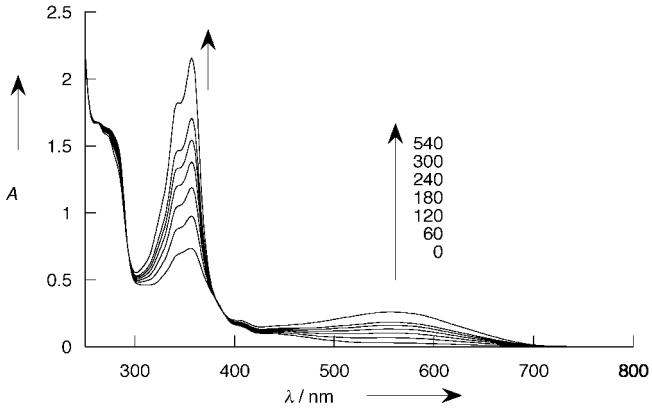


Figure 1. Changes in the absorption spectrum of **1a** (0.16 mM in hexane) upon irradiation with 313-nm light. Numbers indicate the irradiation time (s).

the changes in the absorption spectrum of a solution of **1a** in hexane upon irradiation with 313-nm light. The pale yellow solution of **1a** changed to violet upon UV irradiation, and irradiation with visible light returned the spectrum to its initial form. The violet color shows the formation of THP **1b**.[11] The photostationary state at 313 nm was analyzed with HPLC (silica gel, hexane/AcOEt 10:1, 385 nm (isosbestic point)) and contains 35 % of MCP-1-ene **1a** and 65 % of THP **1b**.

Figure 2 shows a chromatogram of the racemic mixture of **1a** (HPLC on a chiral column).[9] Three peaks were found and these peaks were assigned to one enantiomer of MCP-1-ene

 © WILEY-VCH Verlag GmbH, 69451 Weinheim, Germany, 2002 1433-7851/02/4112-2156 $ 20.00+.50/0

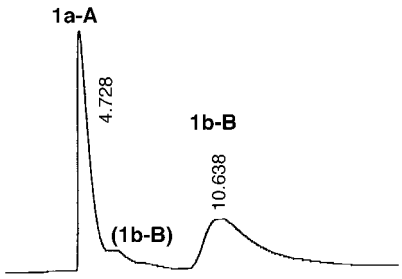


Figure 2. Chromatogram of MCP-1-ene **1a** (HPLC on chiral column).[9]

(**1a-A**), THP **1b-A**, and the other enantiomer of MCP-1-ene (**1a-B**). The enantiomers **1a-A** and **1a-B** were perfectly separated under these conditions. After separation, neither of the enantiomers racemize, even when heated at 200 °C for 1 h under Ar, and no decomposition could be detected by HPLC or by ^{1}H NMR, absorption, and circular dichroism (CD) spectroscopy either.

The CD spectra of solutions of MCP-1-enes **1a-A** and **1a-B** in hexane were measured (Figure 3, 4). The CD spectra of **1a-A** and **1a-B** were symmetrical; **1a-A** and **1a-B** are enantiomers (Figure 3). The CD spectra of the photostationary state of

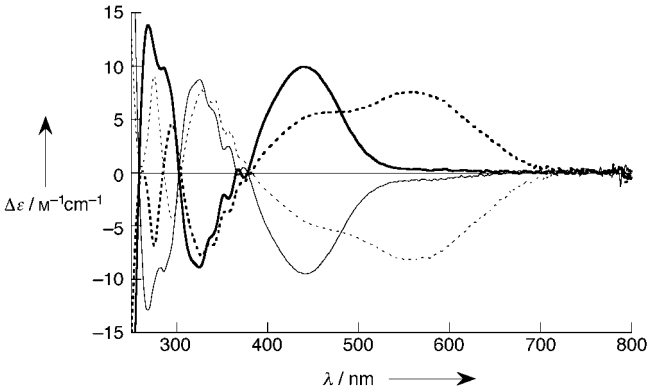


Figure 3. Changes in CD spectrum of **1** in hexane upon irradiation with 313-nm light (plain line: **1a-A**, plain dot line: PSS_{313} of **1-A**, bold line: **1a-B**, bold dot line: PSS_{313} of **1-B**).

1-A and **1-B** at 313 nm were also symmetrical. The CD spectra of **1a-A** were changed upon irradiation with 313-nm light, as shown in Figure 4. As irradiation times became longer, the concentration of **1b-A** (colored form) increased and the CD spectrum changed according to the increase in the concentration. Upon irradiation with visible light, the CD spectra were identical to the initial spectra. HPLC on a chiral column also showed that the enantiomer **1b-A** was converted back cleanly into the initial enantiomer **1a-A** after one photochromic reaction cycle (visible irradiation followed by UV irradiation). These results indicate that the photochromic reaction of the enantiomers of MCP-1-ene **1** are enantioselective and no racemization occurs.

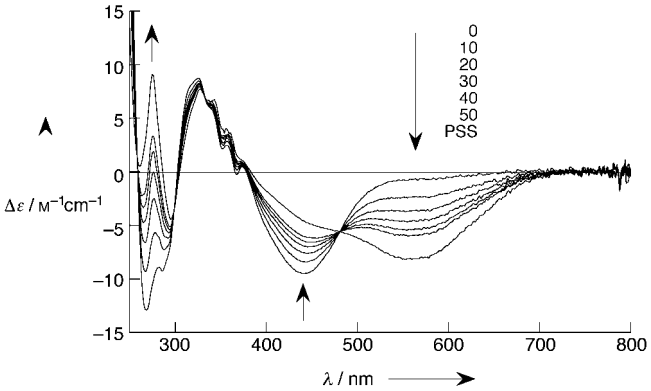


Figure 4. Changes in CD spectrum of **1a-A** in hexane upon irradiation with 313-nm light. Numbers indicate the irradiation time (s), PSS = photostationary state.

This is the first example of a photochromic reaction with two enantiomers. Thus we believe that the nondestructive read-out of photomemory will be possible by the use of this enantiomeric photochromic system.

Received: January 2, 2002
Revised: March 25, 2002 [Z 18463]

[1] M. Irie, *Chem. Rev.* **2000**, *100*, 1685.
[2] M. Irie, O. Miyatake, K. Uchida, T. Eriguchi, *J. Am. Chem. Soc.* **1994**, *116*, 9894.
[3] S.-H. Kawai, S. L. Gilet, R. Ponsinet, J.-M. Lehn, *Chem. Eur. J.* **1995**, *1*, 285.
[4] B. L. Feringa, R. A. van Delden, N. Koumura, E. M. Geertsema, *Chem. Rev.* **2000**, *100*, 1789.
[5] a) T. Yamaguchi, K. Uchida, M. Irie, *J. Am. Chem. Soc.* **1997**, *119*, 6066; b) Y. Yokoyama, Y. Shimizu, S. Uchida, Y. Yokoyama, *J. Chem. Soc. Chem. Commun.* **1995**, 785; Y. Yokoyama, S. Uchida, Y. Yokoyama, Y. Sugawara, Y. Kurita, *J. Am. Chem. Soc.* **1996**, *118*, 3100; c) L. Eggers, V. Bush, *Angew. Chem.* **1997**, *109*, 885; Angew. *Chem. Int. Ed. Engl.* **1997**, *36*, 881.
[6] C. E. Ramey, V. Boekelheide, *J. Am. Chem. Soc.* **1970**, *92*, 3681; R. Naef, E. Fischer, *Helv. Chim. Acta* **1974**, *57*, 2224; S. Murakami, T. Tsutsui, S. Saito, A. Miyazawa, T. Yamato, M. Tashiro, *Chem. Lett.* **1988**, 5; R. H. Mitchell, L.Zhang, *J. Org. Chem.* **1999**, *64*, 7140.
[7] M. Takeshita, T. Yamato, *Tetrahedron Lett.* **2001**, *42*, 4345.
[8] F. Vögtle, *Cyclophane Chemistry*, Wiley, Chichester, **1993**, p. 59.
[9] DICEL Chiralpak AD-H was used as the chiral prepacked column for HPLC separation (hexane/2-propanol (100:1), 1 mL min^{-1}).
[10] The synthesis of MCP-1-ene **1a** will be reported in the near future; **1a**, pale yellow prisms, m.p. 69.0–71.0 °C; ^{1}H NMR ($CDCl_3$, 25 °C, 300 MHz, TMS): $\delta = 0.62$ (s, 6H), 1.29 (s, 18H), 2.36 (s, 3H), 2.49–2.62 (AA′XX′ multiplet, 2H), 2.89–3.02 (AA′XX′ multiplet, 2H), 4.80 (s, 2H), 7.11 (d, 2H, $J = 2$Hz), 7.19–7.22 (d, 2H, $J = 2$Hz), 7.19–7.22 (AA′BB′ multiplet, 2H), 7.45–7.48 ppm (AA′BB′ multiplet, 2H); HRMS (EI, 70 eV): calcd for $[M^+]$ $C_{36}H_{41}NO_2$, 519.3137; found, 519.3147.
[11] The formation of tetrahydropyrene **1b** was also confirmed: ^{1}H NMR ($CDCl_3$, 25 °C, 300 MHz, TMS): $\delta = 1.11$ (s, 18H), 1.84 (s, 6H), 2.32 (s, 3H), 2.22–2.25 (AA′XX′ multiplet, 2H), 2.62–2.65 (AA′XX′ multiplet, 2H), 4.64 (s, 2H), 5.79 (d, 2H, $J = 2$Hz), 7.04 (d, 2H, $J = 2$Hz), 7.08–7.11 (AA′BB′ multiplet, 2H), 7.29–7.32 ppm (AA′BB′ multiplet, 2H).

 © WILEY-VCH Verlag GmbH, 69451 Weinheim, Germany, 2002 1433-7851/02/4112-2157 $ 20.00+.50/0

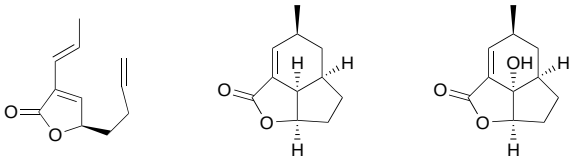
Cyclization of (−)-Pregaliellalactone in the Fungus *Galiella rufa*

Martin Johansson, Bärbel Köpcke, Heidrun Anke, and Olov Sterner*

The Diels–Alder pericyclic [4+2] cycloaddition between a diene and a dienophile is one of the most powerful carbon–carbon bond forming reactions in organic chemistry,[1] and it has been utilized in the total syntheses of many natural products.[2] However, Nature does not appear to have appreciated the reaction to the same extent as synthetic chemists: only few examples of enzyme-catalyzed Diels–Alder reactions in biosynthetic pathways have been reported.[3] Some secondary metabolites may be Diels–Alder adducts although it has been difficult to determine whether they were formed through an actual [4+2] cycloaddition or through an ionic or stepwise process.[4] In reaction pathways which comprise a Diels–Alder reaction the question whether the reaction is spontaneous or catalyzed, for example by a Diels-Alderase, still remains. The problems to demonstrate the action of a Diels-Alderase in a biosynthetic pathway are associated with the difficulties to establish such a pathway unambiguously and with the low availability of biosynthetic precursors for testing.

So far, only two enzyme-catalyzed biosynthetic Diels–Alder reactions have been reported: Oikawa et al. showed in several experiments that cell-free extracts from the fungus *Alternaria solani* catalyze the conversion of the linear triene precursor prosolanapyrone III to the bicyclic product solanapyrone A,[5] but they did not characterize the enzyme. Recently, the group of Vederas showed that isolated lovastatin nonaketide synthase, LNKS, involved in the biosynthesis of the fungal metabolite lovastatin catalyzes the *exo*-selective cyclization of a hexaketide triene.[6] The remarkable effect of the enzyme was not that it increased the reaction rate, but that it stabilized the *exo* transition state giving the opposite diastereomer compared to the spontaneous cyclization. The *exo* isomer could not be formed by chemical methods.

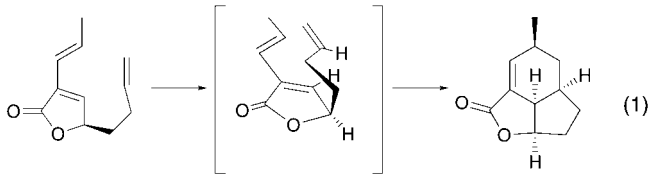
(−)-Galiellalactone (**3**) is a fungal metabolite isolated from the ascomycetes *Galiella rufa* (strains A75-86 and A111-95) as a highly selective and potent inhibitor of interleukin-6 (IL-6) signalling in HepG2 cells.[7], [8] Biosynthetic studies and the structure of the co-metabolites (−)-**1** and (+)-**2**[9] suggested that **3** is formed in vivo through an intramolecular Diels–Alder reaction.[10], [11] When (−)-pregaliellalactone (**1**) or (+)-desoxygaliellalactone (**2**) are fed to the mycelium of the fungus *Galiella rufa* they are converted to (−)-galiellalactone (**3**),[12] showing that, in vivo, the conversion of **1** to **3** takes



1 **2** **3**

place in two discrete steps. Here we wish to discuss the first step, the cyclization, which, to our knowledge, is the first example of an intramolecular Diels–Alder reaction with inverse electron demand in a polyketide biosynthetic pathway that shows a biological rate enhancement.

Initial experiments showed that the cyclization of (−)-**1** to (+)-**2** can proceed spontaneously. The reaction was found to be very sluggish in organic solvents at room temperature. When (−)-**1** was left in a chloroform solution, the cyclized product (+)-**2** could only be detected after weeks. When (−)-**1** in toluene was heated in a sealed tube at 140 °C the conversion to (+)-**2** was complete after 5 h [Eq. (1)]. As it is known that



1 **2** (1)

the rate of Diels–Alder reactions can increase in aqueous media due to the hydrophobic effect,[13] reaction (1) was also performed in water: compound **1** cyclized at room temperature cleanly to **2**, with a half-life of **1** of 65 h. When the cyclization was conducted in a 4.86 M LiCl solution the rate was further increased (approximately twice) due to the "salting-out" effect.[13] Spontaneous cyclization yielded only one isomer—natural (+)-desoxygaliellalactone (**2**) with all bridgehead hydrogen atoms on the same side of the ring system. No product from an *exo* transition state was ever observed, and the reaction is completely diastereoselective. Taken together, the absence of by-products and the rate enhancement in water as well as the effect of high concentrations of salt show that the cyclization of (−)-**1** to (+)-**2** is in fact a Diels–Alder reaction.

A series of experiments in which natural (−)-**1** was fed to the mycelium of *Galiella rufa* were conducted. The fungus was grown in a normal growth medium for 10–14 days, and when the secondary metabolism started, the mycelium was filtered off and washed thoroughly with saline to remove the growth medium. The washed mycelium was re-dispersed in saline and (−)-**1** dissolved in MeOH (0.1 %) was added, whereafter the mycelium was incubated at 24 °C. Compared with an abiotic control experiment (only **1** in saline), a rate enhancement in the production of the Diels–Alder adduct was observed in the presence of living mycelia ($k = 0.0015\ \text{min}^{-1}$), and the concentration of **1** was halved in only 9 h with the conditions used in this investigation (both experiments are summarized in Figure 1). The rate of the spontaneous abiotic reaction in

[*] Prof. Dr. O. Sterner, Dr. M. Johansson
Department of Organic and Bioorganic Chemistry
Lund University
P.O.Box 124, 221 00 Lund (Sweden)
Fax: (+46) 46-222-8209
E-mail: olov.sterner@bioorganic.lth.se
Dr. B. Köpcke, Prof. Dr. H. Anke
Institut für Biotechnologie und Wirkstoffforschung (IBWF)
Erwin-Schroedinger-Strasse 56, 67663 Kaiserslautern (Germany)

 © WILEY-VCH Verlag GmbH, 69451 Weinheim, Germany, 2002 1433-7851/02/4112-2158 $ 20.00+.50/0

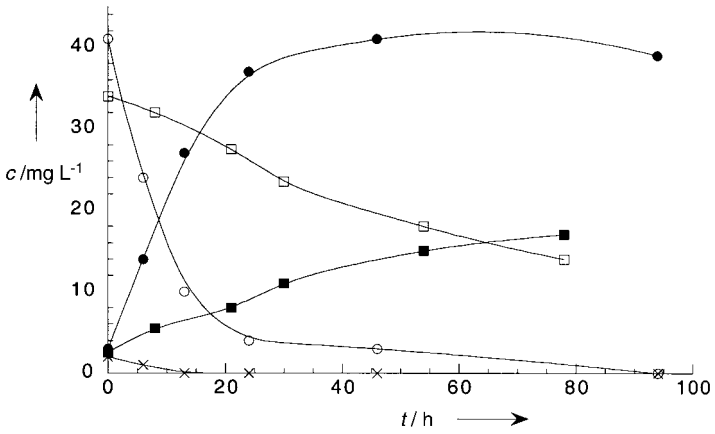
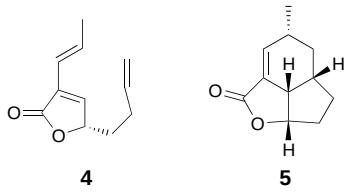


Figure 1. Comparison of the spontaneous cyclization of (−)-**1** (□) to (+)-**2** (■) in abiotic saline at 24 °C with the cyclization of (−)-**1** (○) to (+)-**2** (×) and the formation of (−)-**3** (●) at 24 °C in the presence of active mycelia from *Galiella rufa* (2 g L^{-1} mycelium dry weight) in saline.

saline ($k = 0.00018$ min^{-1}) is approximately 8 times lower. When the mycelium was autoclaved prior to the experiment the rate enhancement was lost completely, showing that no unspecific interaction of the mycelium is affecting the cyclization and thus suggesting that the cyclization is catalyzed by a macromolecule with a well-defined structure. In addition, the catalyzed cyclization is highly specific. The



4 **5**

cyclization of the nonnatural enantiomer (+)-pregaliellalactone (**4**) to **5** was not accelerated by the mycelium but proceeded at the same rate as the spontaneous reaction.

The proposed Diels–Alder reaction in the biosynthesis of (−)-galiellalactone (**3**) is different from the two earlier reported biologically catalyzed Diels–Alder reactions. In both previous cases, 1,2-dialkyldecalin systems were formed from an *E*,*E*,*E* triene, the dienophiles were activated by an electron-withdrawing group, and the enzymes catalyzed the formation of diastereomeric products which are not observed from the spontaneous chemical reaction. Clearly, these enzymes stabilize a nonfavored transition state. In the conversion of (−)-**1** to (+)-**2**, in which the dienophile is unactivated, the products of the spontaneous and biologically induced cyclizations are the same. The function of a presumed enzyme must therefore be purely rate enhancing. No attempts were yet made to isolate the factor responsible for the rate enhancement of the cyclization of (−)-**1** to (+)-**2**.

Experimental Section

General: The fungus (*Galiella rufa* A75-86) was grown in a growth medium. EIMS spectra (direct inlet, 70 eV) were recorded with a JEOL SX102 spectrometer, and the NMR spectra (in $CDCl_3$) with a Bruker DRX300 spectrometer at 300 MHz (^{1}H) and at 75 MHz (^{13}C), a Bruker DRX400 spectrometer (at 400/100 MHz) and a Bruker ARX500 spectrometer (at 500/125 MHz). All flash chromatography was performed on 60 Å 35–70 μm Matrex silica gel (Grace Amicon). HPLC separation was conducted on a HP1090 series I (column: Merck LiChroCART 125-4, LiChrospher 100, RP-18, 5 μm; linear water–acetonitrile gradient). Thin layer chromatographic analyses were made on Silica Gel 60 F_{254} (Merck) plates and visualized with anisaldehyde/sulphuric acid and heating. Natural (−)-**1**, (+)-**2**, and (−)-**3** were isolated from fermentations of *Galiella rufa* as described previously.[9]

Cyclization of (−)-**1** to (+)-**2** in toluene: Compound **1** (40 mg, 0.22 mmol) was dissolved in toluene (5 mL) in a sealable tube. The sealed tube was heated at 140 °C for 5 h and then cooled to room temperature. The solvent was removed under reduced pressure and the residue was purified with flash chromatography (hexane/ether 4:1) to afford 32 mg (80 %) of **2** as an oil. $[\alpha]_D^{20} = +69.9$ ($c = 0.98$, $CHCl_3$); ^{1}H NMR ($CDCl_3$): $\delta = 0.78$ (1, m), 1.15 (1, m), 1.19 (3, d, $J = 6.8$ Hz), 1.75 (1, m), 1.85 (2, m), 2.10 (1, m), 2.14 (1, m), 2.43 (1, m), 3.05 (1, m), 5.02 (1, m), 6.82 ppm (1, dd, $J_1 = 3.6$, $J_2 = 3.6$ Hz); ^{13}C NMR ($CDCl_3$): $\delta = 20.1$, 31.4, 31.6, 33.7, 34.5, 37.3, 44.2, 83.5, 129.9, 144.7, 170.4 ppm; HRMS (EI) calcd for $C_{11}H_{14}O_2$ 178.0994, found 178.0995.

Cyclization of (−)-**1** to (+)-**2** in water: Compound (−)-**1** (20 mg, 0.22 mmol) was dissolved in acetonitrile (0.1 mL) and the solution was added to water (110 mL). The solution was stirred at room temperature. Aliquots of 20 mL were removed at regular intervals and extracted with CH_2Cl_2. The organic phase was dried and concentrated, and the relative amounts of **1** and **2** were determined by integration of the peaks in the ^{1}H NMR spectra.

Cyclization of (−)-**1** to (+)-**2** in LiCl aqueous solution: This experiment was carried out in a 4.86 M LiCl aqueous solution instead of in water; all other parameters were identical to those given above.

Feeding experiments with (−)-**1** and mycelium of *Galiella rufa* strain A75—86: (−)-**1** (40–80 mg) was dissolved in methanol (1 mL) and added to mycelium of *G. rufa* in saline (0.9 % NaCl) in a flask as reported previously.[12] The flask was incubated on a rotary shaker at 120 rpm and 24 °C, and aliquots were removed at regular intervals and analyzed by HPLC with the natural products as reference compounds.

Preparation of (+)-**4**: The synthesis was analogous to that of (−)-**1**,[12] except for the enantioselective reduction to yield the alcohol (*S*)-4-hydroxyoct-7-en-2-ynoic acid ethyl ester which was used to prepare **4**: To a round-bottomed flask was added (*S*)-Alpine-Borane ((*S*)-*B*-isopinocampheyl-9-borabicyclo[3.3.1]nonane, O.5 M in THF; 14.43 mL, 7.21 mmol). THF was removed under reduced pressure. The remaining yellow oil was cooled with an ice bath, and 4-oxooct-7-en-2-ynoic acid ethyl ester (650 mg, 3.6 mmol) was added dropwise. The reaction mixture was stirred overnight and allowed to reach room temperature. The solution was cooled to 0 °C and acetaldehyde (2210 μL, 39.6 mmol in 5.5 mL THF) was added dropwise; then, the solution was stirred at room temperature for 1 h. The solvent was removed under reduced pressure and the remaining oil was dissolved in 5.5 mL diethyl ether and cooled to 0 °C. 1,2-diaminoethanol (435 μL, 7.21 mmol) was added dropwise, which led to the precipitation of a thick white solid. The reaction mixture was filtered and the filter washed with several portions of diethyl ether. The filtrate was concentrated. Flash chromatography (CH_2Cl_2/petroleum ether, 50 to 100 % CH_2Cl_2) afforded 391 mg (60 %) of the alcohol (*S*)-4-hydroxyoct-7-en-2-ynoic acid ethyl ester. $[\alpha]_D^{20} = +10.5$ ($c = 2.7$, $CHCl_3$), ^{1}H NMR ($CDCl_3$): $\delta = 1.31$ (3, t, $J =$ 7.1 Hz), 1.86 (2, m), 2.24 (2, m), 3.11 (1, d, $J = 4.1$ Hz), 4.23 (2, q, $J = 7.1$ Hz), 4.50 (1, q, $J = 6.0$ Hz), 5.01 (1, dq, $J_1 = 10.2$, $J_2 = 1.4$ Hz), 5.08 (1, dq, $J_1 =$ 17.3, $J_2 = 1.6$ Hz), 5.80 ppm (1, ddt, $J_1 = 6.7$, $J_2 = 10.3$, $J_3 = 16.9$ Hz); ^{13}C NMR ($CDCl_3$): $\delta = 14.4$, 29.5, 36.2, 61.7, 62.7, 77.0, 88.3, 116.1, 137.5, 154.0 ppm; HRMS (EI) calcd for $C_{10}H_{15}O_3$ (M+H) 183.1021, found 183.1014.

Received: January 2, 2002 [Z 18472]

[1] a) M. B. Smith, J. March, *March's Advanced Organic Chemistry*, 5th ed., Wiley-Interscience, New York, **2001**, pp. 1062–1075; b) M. B. Smith, *Organic Syntheses*, 1st ed., McGraw-Hill, New York, **1994**, pp. 1113–1145.

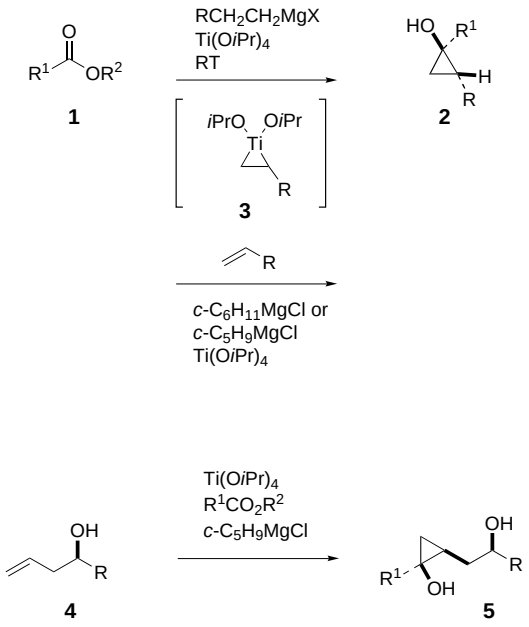
[2] a) E. Merifield, E. J. Thomas, *J. Chem. Soc. Perkin Trans. 1* **1999**, *22*, 3269–3283; b) J. M. Whitney, J. S. Parnes, K. J. Shea, *J. Org. Chem.*

1997, *62*, 8962 – 8963; S. F. Martin, H. Rueger, S. A. Williamson, S. Grzejszczak, *J. Am. Chem. Soc.* **1987**, *109*, 6124 – 6134.
[3] S. Laschat, *Angew. Chem.* **1996**, *108*, 313 – 315; *Angew. Chem. Int. Ed. Engl.* **1996**, *35*, 289 – 291.
[4] a) A. Ichihara, H. Oikawa, *Curr. Org. Chem.* **1998**, *2*, 365 – 394; b) A. Ichihara, H. Oikawa in *Comprehensive Natural Products Chemistry, Polyketides and Other Secondary Metabolites*, *Vol. 1* (Eds.: U. Sankawa, D. Barton, K. Nakanishi, O. Meth-Cohn), Elsevier, New York, **1999**, pp. 367 – 408.
[5] a) H. Oikawa, T. Kobayashi, K. Katayama, Y. Suzuki, A. Ichihara, *J. Org. Chem.* **1998**, *63*, 8748 – 8756; b) K. Katayama, T. Kobayashi, H. Oikawa, M. Honma, A. Ichihara, *Biochim. Biophys. Acta* **1998**, *1384*, 387 – 395.
[6] a) K. Auclair, A. Sutherland, J. Kennedy, D. J. Witter, J. P. Van den - Heever, C. R. Hutchinson, J. C. Vederas, *J. Am. Chem. Soc.* **2000**, *122*, 11519 – 11520; b) D. J. Witter, J. C. Vederas, *J. Org. Chem.* **1996**, *61*, 2613 – 2623.
[7] R. Hautzel, H. Anke, *Z. Naturforsch. C* **1990**, *45*, 68 – 73.
[8] M. Weidler, J. Rether, T. Anke, G. Erkel, *FEBS Lett.* **2000**, *484*, 1 – 6.
[9] M. Johansson, B. Köpcke, H. Anke, O. Sterner, *J. Antibiotics*, in print.
[10] a) H. Anke, R. Hautzel, W. S. Sheldrick, I. Casser, W. Steglich, *Abstracts of the 7th Intern. Congress of Pesticide Chemistry*, *Vol. 1*, **1990**, 1; b) W. Steglich, T. Eizenhöfer, I. Casser, B. Steffan, U. Rabe, R. Böker, H. J. Knerr, H. Anke, *DECHEMA Monogr.* **1993**, *129*, 3 – 13.
[11] M. Schneider, PhD thesis, Ludwig-Maximilians-Universität Munich (Germany), **1996**.
[12] M. Johansson, B. Köpcke, H. Anke, O. Sterner, *Tetrahedron*, in press.
[13] a) R. Breslow, *Acc. Chem. Res.* **1993**, *24*, 159 – 164; b) P. A. Grieco, *Aldrichimica Acta* **1991**, *24*, 59 – 66.

Diastereoselective Synthesis of *trans*-1,2-Dialkylcyclopropanols by the Kulinkovich Hydroxycyclopropanation of Homoallylic Alcohols**

Long Guo Quan, Se-Ho Kim, Jae Chol Lee, and Jin Kun Cha*

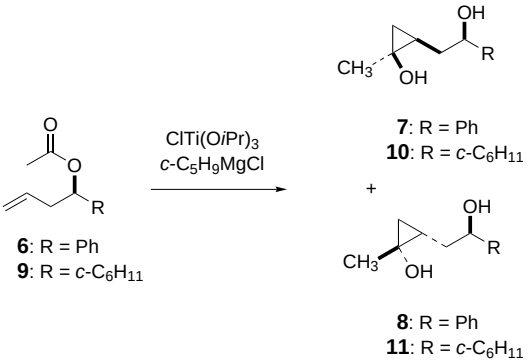
Kulinkovich and co-workers first reported an efficient preparation of cyclopropanols (**1** → **2**), by simple addition of a suitable Grignard reagent to a carboxylic ester, in the presence of titanium tetraisopropoxide (Scheme 1).[1] A key intermediate in the Kulinkovich cyclopropanation was presumed to be dialkoxytitanacyclopropane **3**.[2] An intramolecular process was developed independently by Sato's group and in our laboratories. Subsequently reported was a useful variant of the original Kulinkovich procedure, by facile olefin exchange of the initially formed titanacyclopropane with a terminal olefin, by employing a cyclohexyl or a cyclopentyl Grignard reagent.[1d, 3, 4] Other studies have included extension of the Kulinkovich cyclopropanation reaction to other



Scheme 1.

acyl derivatives and also applications of the resulting heteroatom-substituted cyclopropanes in organic synthesis.[2, 5] An enantioselective (70 – 78 % *ee*) synthesis of a *cis*-1,2-dialkylcyclopropanol was also achieved by Corey, who used a TADDOL-derived titanacyclopropane (TADDOL = (*R*,*R*)-$\alpha,\alpha,\alpha',\alpha'$-tetraaryl-1,3-dioxolane-4,5-dimethanol),[6] but its scope and generality remain untested. We report herein a diastereoselective synthesis of *trans*-1,2-dialkylcyclopropanols **5**, which starts with homoallylic alcohols **4**.[7]

Two different modes of the titanium-mediated hydroxycyclopropanation were available for homoallylic alcohols. One approach entailed an intramolecular cyclopropanation of the esters of homoallylic alcohols (Scheme 2). The related cyclopropanation reaction of but-3-enol esters was established to



Scheme 2.

give *trans*-1,2-dialkylcycloalkanols.[3a, 4a, 8] As a preliminary study with secondary homoallylic alcohols, an intramolecular cyclopropanation of acetate **6** was first examined by employing an excess of cyclopentylmagnesium chloride in the presence of $Ti(OiPr)_4$ or $ClTi(OiPr)_3$, to obtain cyclopropanols **7** and **8** as a ≈1:1 mixture in 73 % yield, along with trace

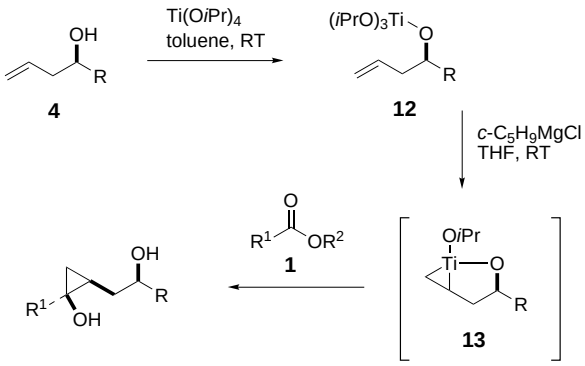
[*] Prof. J. K. Cha, Dr. L. G. Quan, S.-H. Kim, Dr. J. C. Lee
Department of Chemistry
University of Alabama
Tuscaloosa, AL 35487 (USA)
Fax: (+1) 205-348-9104
E-mail: jcha@bama.ua.edu

[**] This work was supported by the National Institutes of Health (GM35956) and National Science Foundation (CHE98-13975).

 © WILEY-VCH Verlag GmbH, 69451 Weinheim, Germany, 2002 1433-7851/02/4112-2160 $ 20.00+.50/0

amounts of the corresponding *cis*-1,2-dialkyl isomers. Similarly, no diastereocontrol was observed for cyclopropanation of **9**, which lead to cyclopropanols **10** and **11** in 61% yield.

The disappointing lack of 1,3-diastereoselectivity of the first approach prompted us to examine an alternative method involving the bicyclic titanacyclopropanes **13** via the titanate **12**, which was derived from alcohol **4** (Scheme 3).

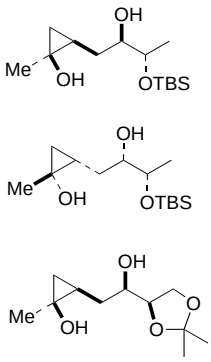


Product	R	R^1	Yield [%]	d.r.
7	Ph	Me	68	12.2:1
10	*c*-C_6H_{11}	Me	65	8.6:1
14	Ph	*n*-C_5H_{11}	62	8.0:1
15	Ph	*i*-C_5H_{11}	56	7.6:1
16	Ph	Bn	63	6.5:1
17	Ph	*i*Pr	51	3.5:1
18	Ph	*c*-C_6H_{11}	51	4.0:1
19	TMS	Me	48	6.0:1
20	*t*Bu	Me	58	8.3:1
21	2-furyl	Me	56	5.0:1
22	CH_2OTBS	Me	42	4.2:1
23	CH_2OTIPS	Me	56	7.4:1

Scheme 3. TMS = trimethylsilyl, TBS = *tert*-butyldimethylsilyl, TIPS = triisopropylsilyl, d.r. = diastereomeric ratio.

Surprisingly, the use of **13** has never been reported. For example, one-pot coupling of **12a** (R = Ph) with ethyl acetate in THF was diastereoselective and afforded a 12.2:1 diastereomeric mixture of **7** and **8** in 68–70% yield. Use of $ClTi(OiPr)_3$ in place of $Ti(OiPr)_4$ resulted in insignificant changes in diastereoselectivity and yield. Other solvents such as ether or toluene could also be employed, with comparable results (e.g., 11.4:1 diastereoselectivity in 61% yield in ether; 11:1 diastereoselectivity in 68% yield in toluene). The related cyclopropanation procedure starting with **4b** (R = *c*-C_6H_{11}) furnished **10** as the major isomer (8.6:1) in 65% yield. Also, coupling of **4a** (R = Ph) and several esters provided cyclopropanols **14**–**18** in comparable diastereoselectivity. Surprisingly, when branched esters were employed, diastereocontrol was decreased.

As can be seen from additional examples (e.g. **19**–**26**) of coupling of other respective homoallylic alcohols with ethyl acetate (Scheme 3 and 4), the hydroxycyclopropanation reaction via **13** appears to provide a general method for preparing *trans*-1,2-dialkylcyclopropanols with 1,3-diastereocontrol. As the starting alcohols are readily available in an



24: 60%, 3.3:1

25: 56%, 3.5:1

26: 32%, 5.6:1

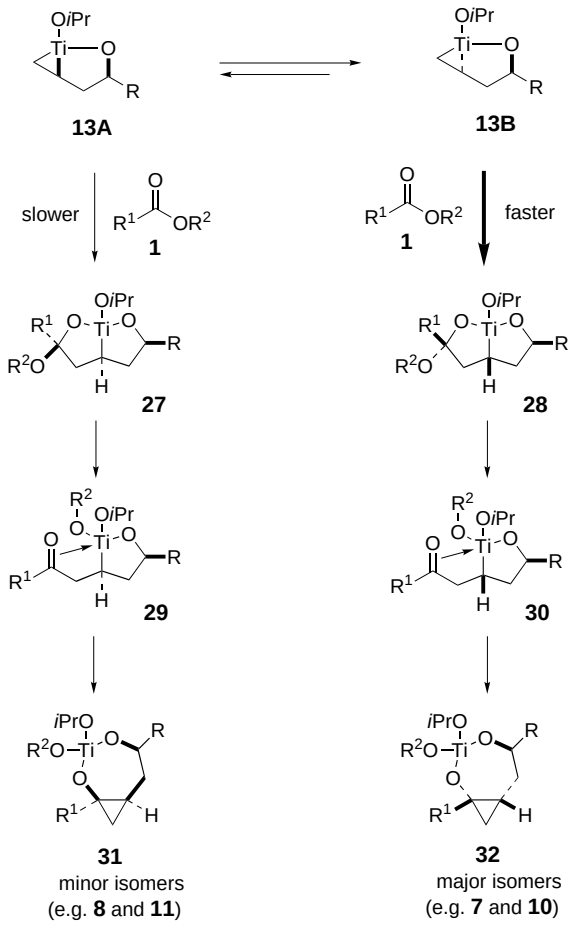
Scheme 4.

enantiomerically pure form by standard methods,[9] the present method lends itself to a convenient enantioselective synthesis (e.g., of **24**–**26**). For example, (+)-(*R*)-**4a** was easily prepared from benzaldehyde in ≈90% *ee* by the Brown asymmetric allylation,[10] and its cyclopropanation with ethyl acetate gave (+)-**7**, $\alpha_D = 91.4$ ($c = 0.87$, benzene).

The ring configuration of the cyclopropanol products (**7**, **8**, **14**–**26**) was easily ascertained by NOE measurements and comparison of chemical shifts in the ^1H NMR spectra (with those of the corresponding *E* isomers, which were prepared independently). Initially, the pivotal relative stereochemistry of the major isomers was tentatively assigned on the basis of mechanistic considerations (Scheme 5). The bicyclic titanacyclopropane intermediate would exist as the two rapidly interconverting diastereomers **13A** and **13B**, and Curtin–Hammett kinetics are thus applicable here. The subsequent competing 1,3-diastereoselectivity-controlling steps involve the insertion of the ester carbonyl group between the Ti center and the less substituted carbon of the three-membered ring; here, formation of **28** is faster than that of **27**, because of steric considerations. As shown in Scheme 5, the insertion reaction (**13B** → **28** and also **13A** → **27**) may be diastereoselective at the acetal stereogenic center, but the latter stereocenter would be inconsequential in determining the stereochemistry of the final cyclopropanol products. Migration of the alkoxy group of **28** would then generate the titanium "homoenolate" intermediate **30**.[11] Finally, because of geometrical constraints, ring closure, driven by marked oxophilicity of Ti, should afford the cyclic titanate **32**, hydrolysis of which gives the indicated *Z* ring configuration. The stereochemical assignment was unequivocally established by single-crystal X-ray diffraction analysis of **20**,[12] and the remaining cyclopropanols were assumed, by analogy, to stem from the identical sense of diastereoselectivity (i.e., **13B** → **28** in preference to **13A** → **27**).

In summary, we have developed an enantio- and diastereoselective synthesis of *trans*-1,2-dialkylcyclopropanols by use of the bicyclic titanacyclopropanes derived from homoallylic alcohols, which provides moderate to good levels of diastereocontrol. The stereoselective formation of *trans*-1,2-dialkylcyclopropanols was made possible by seven-membered cyclic titanates and nicely complements the original Kulinkovich cyclopropanation procedure, which exhibits the opposite intrinsic preference for *cis*-1,2-dialkylcyclopropanols. Exten-

 © WILEY-VCH Verlag GmbH, 69451 Weinheim, Germany, 2002 1433-7851/02/4112-2161 $ 20.00+.50/0



Scheme 5.

sion of the present strategy to an enantioselective synthesis of *cis*-1,2-dialkylcyclopropanols, as well as mechanistic studies to account for a marked divergence in levels of diastereoselectivity between the cyclopropanation reactions involving **6** and **12**, is under investigation.

Experimental Section

A solution of $Ti(OiPr)_4$ (0.16 mL, 0.55 mmol) and the alcohol (+)-**4a** (74 mg, 0.5 mmol) in toluene (1 mL) was stirred at room temperature for 1 h and then at 40 °C for 10 min. After volatile components were removed under vacuum, THF (5 mL) and ethyl acetate (44 mg, 0.5 mmol) were added at room temperature, followed by a 2 M solution of cyclopentylmagnesium chloride (1.1 mL) in tetrahydrofuran, over a period of 1 h (with a syringe pump). The reaction mixture was then stirred for an additional 10 min and quenched by addition of water (0.5 mL). The resulting mixture was stirred for 1 h, dried over anhydrous sodium sulfate, and filtered. The filter cake was washed with CH_2Cl_2 (10 mL), and the combined filtrates were concentrated under reduced pressure. Purification of the crude product by column chromatography on silica gel afforded 65 mg (68 %) of (+)-**7** as a colorless oil: $\alpha_D = 91.4$ ($c = 0.87$, benzene; ≈ 90 % *ee*); ^{1}H NMR (360 MHz, $CDCl_3$): $\delta = 0.34 - 0.43$ (m, 2H), 0.52 (m, 1H), 1.29 (s, 3H), 1.85 (ddd, J(H,H) = 5.3, 9.7, 14.8 Hz, 1H), 2.20 (apparent dt, J(H,H) = 14.8, 3.5 Hz, 1H), 3.65 (br s, 2H), 4.87 (dd, J(H,H) = 3.5, 5.3 Hz, 1H), 7.23 – 7.25 ppm (m, 5H); ^{13}C NMR (90 MHz, $CDCl_3$): $\delta = 19.8$, 20.1, 25.5, 37.3, 54.2, 73.1, 125.7, 127.0, 128.1, 144.0 ppm; HRMS [$M^+ - H_2O$] calcd for [$C_{12}H_{14}O$] 174.1044, found 174.1032.

Received: February 20, 2002 [Z18745]

[1] a) O. G. Kulinkovich, S. V. Sviridov, D. A. Vasilevskii, T. S. Prityt-skaya, *Zh. Org. Khim*. **1989**, *25*, 2244; b) O. G. Kulinkovich, S. V. Sviridov, D. A. Vasilevskii, A. I. Savchenko, T. S. Prityt-skaya, *Zh. Org. Khim*. **1991**, *27*, 294; c) O. G. Kulinkovich, S. V. Sviridov, D. A. Vasilevskii, *Synthesis* **1991**, 234; d) O. G. Kulinkovich, A. I. Savchen-ko, S. V. Sviridov, D. A. Vasilevskii, *Mendeleev Commun*. **1993**, 230; e) O. L. Epstein, A. I. Savchenko, O. G. Kulinkovich, *Tetrahedron Lett*. **1999**, *40*, 5935.

[2] For recent reviews, see: a) O. G. Kulinkovich, A. de Meijere, *Chem. Rev*. **2000**, *100*, 2789; b) F. Sato, H. Urabe, S. Okamoto, *Chem. Rev*. **2000**, *100*, 2835; For a recent theoretical study of the mechanism, see: c) Y.-D. Wu, Z.-X. Yu, *J. Am. Chem. Soc*. **2001**, *123*, 5777.

[3] a) A. Kasatkin, F. Sato, *Tetrahedron Lett*. **1995**, *36*, 6079; b) A. Kasatkin, K. Kobayashi, S. Okamoto, F. Sato, *Tetrahedron Lett*. **1996**, *37*, 1849.

[4] a) J. Lee, C. H. Kang, H. Kim, J. K. Cha, *J. Am. Chem. Soc*. **1996**, *118*, 291; b) J. Lee, H. Kim, J. K. Cha, *J. Am. Chem. Soc*. **1996**, *118*, 4198; c) J. C. Lee, M. J. Sung, J. K. Cha, *Tetrahedron Lett*. **2001**, *42*, 2059.

[5] a) V. Chaplinski, A. de Meijere, *Angew. Chem*. **1996**, *108*, 491; *Angew. Chem. Int. Ed. Engl*. **1996**, *35*, 413; b) H. B. Lee, M. J. Sung, S. C. Blackstock, J. K. Cha, *J. Am. Chem. Soc*. **2001**, *123*, 11322, and references therein.

[6] E. J. Corey, S. A. Rao, M. C. Noe, *J. Am. Chem. Soc*. **1994**, *116*, 9345.

[7] a) Presented in part at the 4th Winter Conference on Medicinal and Bioorganic Chemistry (Steamboat Springs, CO), **2001**; b) We thank Professor Amir H. Hoveyda for helpful comments.

[8] S. Racouchot, J. Ollivier, J. J. Salaün, *Synlett* **2000**, 1729.

[9] For general reviews, see: a) Y. Yamamoto, N. Asao, *Chem. Rev*. **1993**, *93*, 2207; b) A. Yanagisawa in *Comprehensive Asymmetric Catalysis*, *Vol. 2* (Eds.: E. N. Jacobsen, A. Pfaltz, H. Yamamoto), Springer, Heidelberg, **1999**, chap. 27; c) S. R. Chemler, W. R. Roush in *Modern Carbonyl Chemistry* (Ed.: J. Otera), Wiley-VCH, Weinheim, **2000**, chap. 11.

[10] a) H. C. Brown, R. S. Randad, K. S. Bhat, M. Zaidlewicz, U. S. Racherla, *J. Am. Chem. Soc*. **1990**, *112*, 2389; See also: b) W. R. Roush, L. K. Hoong, M. A. J. Palmer, J. C. Park, *J. Org. Chem*. **1990**, *55*, 4109, and references therein; c) G. E. Keck, D. Krishnamurthy, *Org. Synth*. **1998**, *75*, 12; d) S. E. Denmark, J. Fu, *J. Am. Chem. Soc*. **2001**, *123*, 9488.

[11] See a) I. Kuwajima, E. Nakamura, *Top. Curr. Chem*. **1990**, *155*, 1; b) H.-U. Reissig, H. Holzinger, G. Glomsda, *Tetrahedron* **1989**, *45*, 3139.

[12] We thank Dr. Fook Tham (University of California, Riverside) for X-ray structural analysis of **20**.

 © WILEY-VCH Verlag GmbH, 69451 Weinheim, Germany, 2002 1433-7851/02/4112-2162 $ 20.00+.50/0

Morphosynthesis of Octacalcium Phosphate Hollow Microspheres by Polyelectrolyte-Mediated Crystallization**

Adriana Bigi,* Elisa Boanini, Dominic Walsh, and Stephen Mann

Materials chemists regard the complex processes involved in the formation of biomineralized tissues with increasing interest.[1–5] Indeed, the organic/inorganic composites synthesized by living organisms often display unique and desirable morphological, structural and mechanical properties, and represent informative models for the synthesis and design of complex functional materials.[6, 7] Biomimetic approaches often involve the simulation of one or more of the different strategies used by organisms to selectively control mineral deposition for precise biological requirements.[8] A key principle in biomineralization is the involvement of biological macromolecules, such as phosphoproteins and glycoproteins containing acidic amino acid residues[9] that may be linked into structural organic matrices or secreted as soluble polyelectrolytes within the mineralization environment. When adsorbed onto a substrate, certain proteins extracted from biomineralized tissues can control the nucleation, orientation, polymorphism, and morphology of the mineral phase.[11, 12] This process has prompted a number of analogous studies on mineralization in the presence of synthetic organic templates such as Langmuir monolayers,[13, 14] self-assembled monolayers,[15] functionalized polymer substrates,[5] and supramolecular assemblies.[16] Similarly, because many biomineralization proteins in solution interact with inorganic crystal faces, and thereby inhibit growth and influence the resulting morphology,[10] a wide range of additives, such as small organic molecules,[17, 18] polymers,[19–22] and peptides,[23] have been studied to understand these processes. In the case of certain polymers, complex morphologies that bear little resemblance to the underlying crystal symmetry have been produced.[21, 22] In particular, polyanionic macromolecules such as polyaspartate (PASP) or polyacrylate (PA) have been used to produce elaborate fibrous bundles of barium sulfate,[24] and distorted spirals of calcium carbonate (vaterite).[25]

Herein we show that the crystallization of octacalcium phosphate, $Ca_8H_2(PO_4)_6 \cdot 5H_2O$ (OCP) from aqueous solutions containing PASP or PA at 60 °C and pH 5 results in the direct assembly of a complex inorganic-polymer spherical-shell architecture without the intervention of external templates. The hollow microstructures consist of a thin porous membrane of oriented OCP crystals that are highly interconnected. We show that a hierarchy of processes, involving the radial growth of dense, multilayered spheroids, secondary overgrowth of a porous thin-shell precursor, and anisotropic dissolution of the spheroidal cores, produces this remarkable structure through time-dependent changes in supersaturation and additive concentration.

Synthesis of OCP in the absence of PASP or PA yielded spherulites consisting of long blade-shaped crystals radiating from a common origin (Figure 1). The spherulite diameters

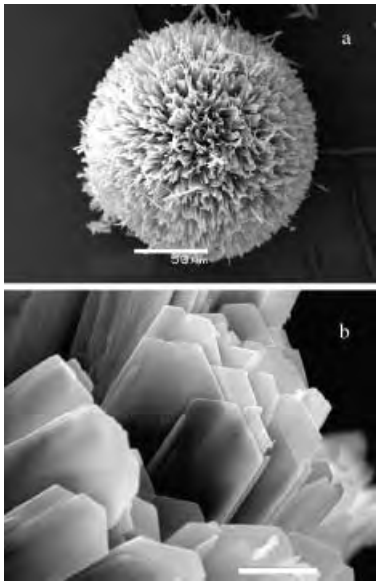


Figure 1. SEM images of a control sample of OCP isolated after 3 h of ageing in the crystallization solution. a) intact spherulite, scale bar: 50 μm, b) higher magnification image showing constituent blade-shaped OCP crystals, scale bar: 5 μm.

ranged between 150–200 μm, and the blades were 2–5 μm wide and 0.3–0.4 μm thick. The platelike morphology is commonly observed for OCP crystals and consists of large basal (100) faces of triclinic pinacoid symmetry that are elongated along the *c* axis and terminated by (011) faces. Addition of PASP or PA to phosphate solutions prior to dropwise addition of calcium acetate resulted in delayed precipitation and the formation of hollow microspheres (referred to as PASP-OCP and PA-OCP, respectively) with diameters up to 1000 μm (Figure 2a,b). The thickness of the shell wall was approximately 10 μm (PASP-OCP) and 20 μm (PA-OCP). Viewed in cross-section, broken fragments showed that the wall was highly porous and consisted of an interconnected network of short platelike OCP crystals (Figure 2c,d). The plates were oriented approximately parallel to the wall thickness such that channel-like pores of about 0.1 to 2 μm traversed the inorganic shell. Furthermore, the lamellar crystals on the surface of the hollow microspheres were slightly shorter and thinner for PASP-OCP than for PA-OCP precipitates (Figure 2e,f), with the consequence that the inorganic membrane produced by the former consisted on average of smaller pores.

X-ray diffraction data indicated that the coherence lengths of crystalline domains were significantly shorter for OCP prepared in the presence of PASP or PA compared with the

[*] Prof. A. Bigi, Dr. E. Boanini
Dipartimento di Chimica "Ciamician"
Universita' degli Studi di Bologna
via Selmi 2, 40126 Bologna (Italy)
Fax: (+39) 051-209-9456
E-mail: bigi@ciam.unibo.it
Dr. D. Walsh, Prof. S. Mann
School of Chemistry, University of Bristol
Bristol BS8 1TS (UK)

[**] This work was supported by MURST, the University of Bologna (Funds for Selected Research Topics), and the EPSRC (UK).

 © WILEY-VCH Verlag GmbH, 69451 Weinheim, Germany, 2002 1433-7851/02/4112-2163 $ 20.00+.50/0

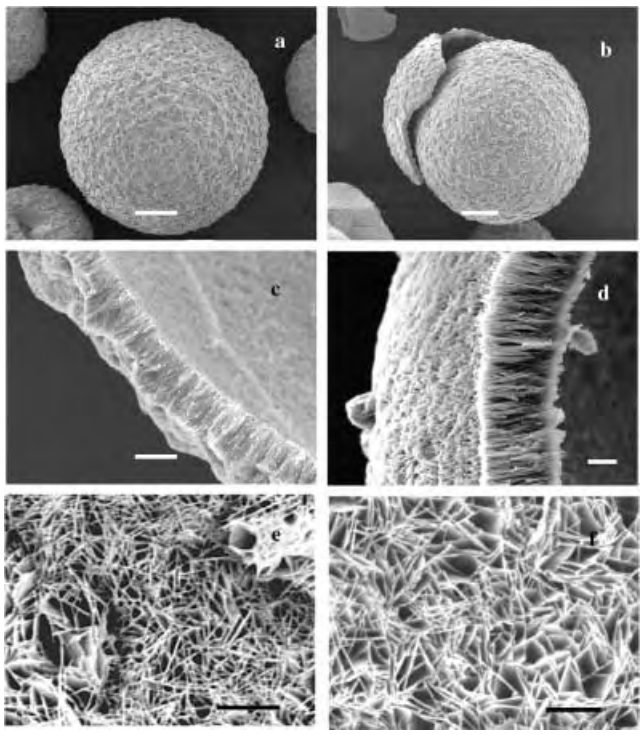


Figure 2. SEM images of OCP microstructures synthesized in the presence of PASP (a, c, e), and PA (b, d, f), and isolated after 3 h of ageing in solution. a, b) Intact hollow shell architectures, scale bars: 100 μm. In (b) a broken fragment of a shell wall is also shown. c, d) Shell-wall cross-sections showing the porous inorganic membrane consisting of an oriented network of OCP crystals, scale bars: 10 μm. e, f) Views of the external surfaces of the hollow spheres showing interconnected network of OCP bladelike crystals, scale bars: 2 μm.

control sample (Table 1). This reduction can be ascribed either to a decrease in crystal perfection because of interactions with the polyelectrolytes, or a result of phase transformation to give small amounts of hydroxyapatite, $Ca_{10}(PO_4)_6(OH)_2$ (HA), or both. Thermogravimetric data indicate that the spherulites contained <1 wt% of the adsorbed polyelectrolytes. Although the amounts were low, even small levels of organic material incorporated into biogenic minerals can greatly affect their structural and mechanical properties.[9] In addition, slight variations in the relative intensity distributions of the X-ray reflections could be attributed to a secondary HA phase, which readily forms by conversion of OCP because of close structural similarity.[26] Accordingly, the Ca:P molar ratio of the solid products increased along the sequence, control OCP, PA-OCP, PASP-OCP (Table 1).

These variations in phase composition are not sufficient however to explain the remarkable morphological differences observed between the polyelectrolyte–OCP microspheres

Table 1. Coherence lengths (τ_{hkl}) evaluated from the width at half-maximum intensity of the 100, 010, and 002 reflections of OCP, OCP-PA, and OCP-PASP materials. The Ca:P molar ratios of the solid products are also reported.

	τ_{100} [nm]	τ_{010} [nm]	τ_{002} [nm]	Ca:P molar ratio
OCP	35 ± 1	45 ± 1	62 ± 4	1.35:1
OCP-PA	22 ± 1	38 ± 1	34 ± 1	1.44:1
OCP-PASP	22 ± 1	24 ± 1	27 ± 1	1.51:1

and the control OCP spherulites. Other investigations were undertaken to determine the stages of growth and assembly of the microstructures by isolating samples from the reaction vessel at different ageing times. In the control experiments, SEM studies of the early stages of growth indicated that the spherulites develop from small, loosely packed aggregates of well-defined blade-shaped crystals that increase in number, length, and particle density as the reaction proceeds (Figure 3). The aggregated morphology of the initial crystals

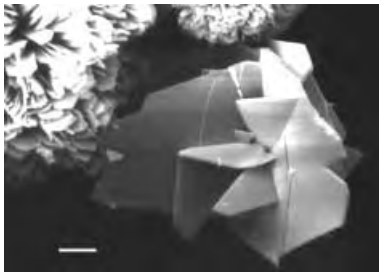


Figure 3. SEM image of early stage in the formation of OCP spherulites grown in the absence of polycarboxylates. The sample was isolated from solution after addition of approximately 50% of the calcium acetate solution to the reaction flask. Scale bar: 10 μm.

probably arises from the high tendency of OCP to undergo multiple twinning, with the wide (100) face acting as twin plane.[26, 27] In contrast, the first OCP-PASP aggregates that could be isolated from solution after complete addition of calcium acetate displayed a compact, spherical morphology (mean diameter = 300 μm), which readily fragmented to reveal cone-shaped domains with remarkable radially banded growth textures (Figure 4 a,b). On further ageing for 1 h in the reaction solution, the layered-growth mechanism was replaced by secondary overgrowth to produce a discrete thin inorganic shell on the surface of the primary spheroids that consisted of short blades oriented perpendicular to the surface

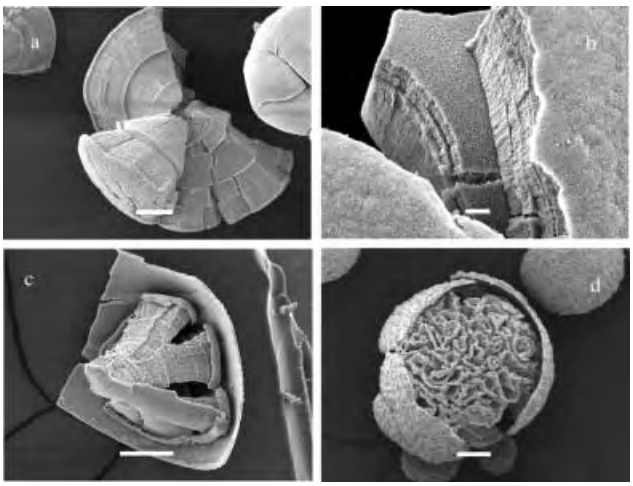


Figure 4. SEM images of OCP-polyelectrolyte architectures synthesized in the presence of PASP and isolated after different periods of ageing in solution: a, b) 45 min, scale bars: 50 μm (a) and 10 μm (b). c) 1 h 45 min, scale bar: 100 μm. d) 3 h, scale bar: 100 μm.

 © WILEY-VCH Verlag GmbH, 69451 Weinheim, Germany, 2002 1433-7851/02/4112-2164 $ 20.00+.50/0

of the core (Figure 4c). Large fragments of the shell membrane were easily detached from the central dense spheroid, indicating that the core–shell interface was discontinuous or only loosely connected. Extending the ageing time resulted in partial dissolution of the banded microstructure to produce a highly porous core with convoluted bicontinuous architecture that was enclosed by the shell wall (Figure 4d). Moreover, dissolution of the spheroids occurred inwardly from the core–shell interface without affecting the texture of the surrounding shell membrane. With time, complete dissolution of the core occurred to give the hollow microspheres shown in Figure 2. Similar results on the growth process were obtained for PA-OCP aggregates.

The spherical morphology and extensive agglomeration of OCP crystals within the layered structure shown in Figures 4a and b can be attributed in part to adsorption of polyaspartate molecules onto the crystal surfaces during growth.[28, 29] Under these conditions, the growth front has to penetrate the polyelectrolyte adsorption layer, with the consequence that the propagation of growth steps across the surface becomes severely hindered and the growth rate decreases. The multilayered banded structure indicates that growth of the spheroidal core is discontinuous with periods of relatively fast growth alternating with periods of stagnation, which presumably take place when the polyelectrolyte concentration on the crystal reaches a critical value, and the distance between the adsorbed molecules becomes smaller than the size of the critical surface nucleus.[28] One possibility is that the delayed onset of nucleation in the presence of the polymers results in the phase separation of highly supersaturated liquid droplets that subsequently undergo polyelectrolyte-mediated crystallization to produce the concentrically layered spheroids. As the process occurs within droplets of confined volume, and involves the 3D radial organization of platelike crystals, significant levels of mechanical stress can build up inside the spheroids. Indeed, the spheroids often underwent catastrophic breakage into cone-shaped fragments when air dried.

Secondary overgrowth of the porous shell on the surface of the spheroids takes place after extensive ageing when the polyelectrolyte concentration in solution is significantly reduced by prior surface adsorption and incorporation within the core microstructure. In the case of PA, which displays a slightly less inhibiting effect on OCP precipitation than PASP, shell formation should start at relatively higher polyelectrolyte concentrations, and result in a thicker shell. Furthermore, the lower levels of polyelectrolyte molecules during growth of the shell produces a more-ordered crystalline phase that is more stable than the multilayered core with respect to dissolution when the solution supersaturation is reduced to close to the solubility limit. Dissolution of the core, initially from the core–shell interface, necessitates diffusion of ions through the shell membrane. The external diameter of the structures did not change appreciably during dissolution, whereas the shell wall increased in size during ageing, as shown for example in Figures 4c and 2c, where the shell wall thickness is approximately 5 μm and 10 μm, respectively. Thus, the dissolution of the core redistributes the mineral ions and contributes to shell-wall growth such that the products isolated after 3 h of ageing consist mostly of hollow microspheres.

In conclusion, polycarboxylates, such as polyaspartate (PASP) and polyacrylate (PA) can be used to synthesize porous hollow microspheres of OCP using a straightforward solution crystallization process. OCP is employed in several technological applications,[30] and is of particular biological importance as a precursor phase in the precipitation of biological apatites.[31] We therefore envisage that the materials reported here will be useful for biomedical applications, such as drug encapsulation and controlled release. Finally, we note that the structural and morphological evolution of inorganic architectures as described here occurs in the absence of external templates through the use of intermediates capable of metamorphism. Such a strategy, involving metastable architectures with hybrid compositions, could have general importance for controlling the synthesis of complex inorganic architectures.

Experimental Section

Synthesis of OCP was carried out by dropwise addition of 0.04 M $Ca(CH_3COO)_2$ (250 mL) over a period of 50 min into a phosphate solution (750 mL) containing Na_2HPO_4 (5 mmol) and NaH_2PO_4 (5 mmol) at a starting pH of 5.[32] The reaction was undertaken at 60 °C with mechanical stirring. The precipitate was left in contact with the mother solution under gentle stirring for different periods of time, up to 3 h. Syntheses in the presence of sodium poly(aspartic acid) ($M_W = 11\,000$) or sodium polyacrylate ($M_W = 2100$) were performed by adding the polyelectrolytes to the phosphate solution. The amounts of polyelectrolytes used were equivalent to a theoretical monomeric unit concentration of 0.044 mM. The resulting OCP precipitates were characterized by scanning electron microscopy (SEM) using a JEOL JSM 5600 LV operating at 12–15 kV. X-ray-diffraction analysis was carried out using a Philips PW 1050/81 powder diffractometer equipped with a graphite monochromator and $Cu_{K\alpha}$ radiation (40 mA, 40 kV). The 2θ range was from 3 to 60° at a scanning speed of 0.5° min^{-1}. Lattice parameters were determined by least-square refinements from the well-determined positions of the most intense reflections. Silicon was used as the internal standard. Differences between the lattice parameters of OCP synthesized in the presence of the polyelectrolytes and those of a control OCP phase, $a = 19.62(5)$, $b = 9.62(9)$, $c = 6.83(6)$ Å, $\alpha = 89.4(8)$, $\beta = 92.6(8)$, $\gamma = 107.4(8)°$, were within the standard deviations. To evaluate the coherence length of the OCP crystals, additional X-ray powder diffraction data were obtained in the relevant region of 2θ by means of step scans using a fixed counting time period of 30 sec and a scan rate of 0.1° $step^{-1}$. The coherence lengths were determined from the width at half-maximum intensity of the 100, 010, and 002 reflections according to the Scherrer equation. The silicon-standard peak 111 was used to evaluate the instrumental broadening. Thermogravimetric analysis was carried out using a Perkin Elmer TGA-7. Heating was performed in a platinum crucible in air flow (20 $cm^3 min^{-1}$) at a rate of 5 °C min^{-1} up to 900 °C. The samples weights were in the range 5–10 mg. Calcium and phosphorus contents of the solid products were determined by means of a Dionex DX100 chromatography system fitted with a Dionex CD20 conductivity detector. The chromatographic data were collected and processed with a Dionex peaknet 5.1 program.

Received: February 4, 2002 [Z 18634]

[1] S. Mann, *Biomineralization. Principles and Concepts in Bioinorganic Materials Chemistry*, Oxford University Press, Oxford, UK, **2001**.
[2] A. A. Campbell, *Curr. Opin. Colloid Interface Sci.* **1999**, *4*, 40–45.
[3] A. H. Heuer, D. J. Fink, V. J. Laraia, J. L. Arias, P. D. Calvert, K. Kendal, G. L. Messing, J. Blackwell, P. C. Rieke, D. H. Thompson,

 © WILEY-VCH Verlag GmbH, 69451 Weinheim, Germany, 2002 1433-7851/02/4112-2165 $ 20.00+.50/0

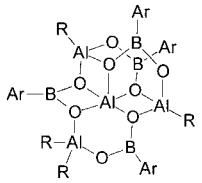
A. P. Wheeler, A. Veis, A. I. Caplan, *Science* **1992**, *255*, 1098 – 1105.
[4] P. Calvert, P. C. Rieke, *Chem. Mater.* **1996**, *8*, 1715 – 1727.
[5] B. C. Bunker, P. C. Rieke, B. J. Tarasevich, A. A. Campbell, G. E. Fryxell, G. Graff, L. Song, J. Liu, J. Virden, G. Mc Vay, *Science* **1994**, *264*, 48 – 55.
[6] S. Mann, *Angew. Chem.* **2000**, *112*, 3532 – 3548; *Angew. Chem. Int. Ed.* **2000**, *39*, 3392 – 3406.
[7] L. A. Estroff, A. D. Hamilton, *Chem. Mater.* **2001**, *13*, 3227 – 3235.
[8] S. Mann, *J. Chem. Soc. Dalton Trans.* **1997**, 3953 – 3961.
[9] S. Weiner, L., Addadi, *J. Mater. Chem.* **1997**, *7*, 689 – 702.
[10] S. Weiner, L., Addadi, *Trends Biochem. Sci.* **1991**, *16*, 252 – 256.
[11] H. Füredi-Milhofer, J. Moradian-Oldak, S. Weiner, A. Veis, K. P. Mintz, L. Addadi, *Connect. Tissue Res.* **1994**, *30*, 251 – 264.
[12] G. Hunter, *Curr. Opin. Solid State Mater. Sci.* **1996**, *1*, 430 – 434.
[13] S. Mann, B. R. Heywood, S. Rajam, J. D. Birchall, *Nature* **1988**, *334*, 692.
[14] I. Weissbuch, F. Frolow, L. Addadi, M. Lahay, L. Leiserowitz, *Science* **1991**, *253*, 637 – 645.
[15] J. Aizenberg, A. J. Black, G. M. Whitesides, *Nature* **1998**, *394*, 868 – 871.
[16] D. Walsh, J. D. Hopwood, S. Mann, *Science* **1994**, *264*, 1576 – 1578.
[17] P. V. Coveney, R. Davey, J. L. W. Griffin, Y. He, J. D. Hamlin, S. Stackhouse, A. Whiting, *J. Am. Chem. Soc.* **2000**, *122*, 11557 – 11558.
[18] K. Naka, Y. Chujo, *Chem. Mater.* **2001**, *13*, 3245 – 3259.
[19] J. N. Cha, G. D. Stucky, D. E. Morse, T. J. Deming, *Nature* **2000**, *403*, 289 – 292.
[20] S. I. Stupp, P. V. Braun, *Science* **1997**, *277*, 1242 – 1248.
[21] M. Antonietti, M. Breulmann, C. G. Göltner, H. Cölfen, K. K. W. Wong, D. Walsh, S. Mann, *Chem. Eur. J.* **1998**, *4*, 2493 – 2500.
[22] H. Colfen, L. Qi, *Chem. Eur. J.* **2001**, *7*, 106 – 116.
[23] W. Zhang, R. A. Laursen, *FEBS Lett.* **1999**, *455*, 372 – 376.
[24] L. Qi, H. Cölfen, M. Antonietti, M. Li, J. D. Hopwood, A. J. Ashley, S. Mann, *Chem. Eur. J.* **2001**, *7*, 3526 – 3532.
[25] L. A. Gower, D. A. Tirrell, *J. Cryst. Growth* **1998**, *191*, 153.
[26] J. C. Elliott, *Structure and Chemistry of the Apatites and Other Calcium Orthophosphates*, Elsevier, Amsterdam, **1994**.
[27] W. E. Brown, J. P. Smith, J. R. Lehr, A. W. Frazier, *Nature* **1962**, *196*, 1048.
[28] O. Söhnel, J. Garside, *Precipitation: basic principles and industrial applications*, Butterworth-Heinemann, Manchester, **1992**.
[29] G. H. Nancollas, S. J. Zawacki in *Industrial crystallization 84* (Eds.: S. J. Jačić, E. J. de Jong), Elsevier, Amsterdam, **1984**, p. 51.
[30] F. Caruso, *Chem. Eur. J.* **2000**, *6*, 413 – 419.
[31] D. G. A. Nelson, J. C. Barry, *Anat. Rec.* **1989**, *224*, 265 – 276.
[32] R. Z. LeGeros, R.Kijkovska, J. P. LeGeros, *Scanning Electron Microsc.* **1984**, *4*, 1771 – 1777; A. Bigi, E. Boanini, M. Borghi, G. Cojazzi, S. Panzavolta, N. Roveri, *J. Inorg. Biochem.* **1999**, *75*, 145 – 151.

Structural Characterization of a Cationic Zirconocene Olefin Polymerization Catalyst with its Methylated Boralumoxane Counterion**

Bodo Richter, Auke Meetsma, Bart Hessen,* and Jan H. Teuben

The discovery by Sinn and Kaminsky that methyl alumoxane (MAO) can act as an efficient activator for metallocene olefin polymerization catalysts[1] has triggered tremendous developments in single-site olefin polymerization catalysis.[2] Presently, more than twenty years after the initial discovery, the actual nature of MAO and its mechanism of catalyst activation are still under debate.[3] Model studies on *tert*-butyl alumoxanes led Barron et al. to formulate the hypothesis that these alumoxanes consist of oligomeric $(RAlO)_n$ clusters, containing 4-coordinate Al in strained fused 4-membered Al_2O_2 rings that can exhibit "latent Lewis acidity" by ring opening, allowing Al to abstract an alkyl anion from the transition metal dialkyl catalyst precursor.[4, 5] The direct (structural, spectroscopic) study of these processes and their products is hampered by the apparent equilibrium nature of the alkyl transfer reaction, with the equilibrium constant strongly favoring the starting materials when well-defined alumoxanes with sterically demanding alkyl groups are used. Crystal structure determinations of the products resulting from the reaction of $[t\mathrm{BuAlO}]_6$ with MeLi[5] and with RNH_2[6] gave support for the proposed activation mechanism, but as yet the products of the activation of metallocene single-site olefin polymerization catalysts by alumoxane activators have eluded full characterization.

Recently we reported the synthesis and structural characterization of a well-defined boralumoxane species, $[t\mathrm{Bu}_4\mathrm{Al}_4\mathrm{Ar}_4\mathrm{B}_4\mathrm{O}_8]$ (**1**, Ar = 2,6-diisopropylphenyl), and showed that this compound is able to activate $[\mathrm{Cp}_2\mathrm{ZrMe}_2]$ for catalytic ethene polymerization.[7] Although **1** is topologically quite



1 (R = *t*Bu, Ar = 2,6-*i*Pr$_2$C$_6$H$_3$)

different from the *t*Bu-alumoxane species isolated by Barron et al., containing 3-coordinate B and 4- and 5-coordinate Al, it shares with these compounds the presence of a strained 4-membered Al_2O_2-ring assembly (edge sharing with a $BAlO_2$

[*] Dr. B. Hessen, Dr. B. Richter, A. Meetsma, Prof. Dr. J. H. Teuben
Dutch Polymer Institute/Center for Catalytic Olefin Polymerization
Stratingh Institute for Chemistry and Chemical Engineering
University of Groningen
Nijenborgh 4, 9747 AG Groningen (The Netherlands)
Fax: (+31) 50-3634315
E-mail: hessen@chem.rug.nl

[**] Netherlands Institute for Catalysis Research (NIOK) publication RUG 02-04-01.

Supporting information for this article is available on the WWW under http://www.angewandte.org or from the author.

 © WILEY-VCH Verlag GmbH, 69451 Weinheim, Germany, 2002 1433-7851/02/4112-2166 $ 20.00+.50/0

ring) that could be instrumental in the activation process. Here we present an investigation into the latent Lewis-acidic behavior of this well-defined boralumoxane, involving studies of the reactivity of **1** with Lewis bases (pyridines) and with a zirconocene dialkyl complex. The results of this study include the first structural characterization of a salt containing a zirconocene alkyl cation and a methylated boralumoxane counterion.

The Lewis-acidic behavior of **1** was first probed by studying its reactivity with the hard Lewis bases pyridine and 2,6-dimethylpyridine. Experiments on NMR tube scale revealed a rapid reaction of **1** upon addition of one equivalent of pyridine, but with 2,6-dimethylpyridine no reaction was observed. This indicates that the reactivity of **1** with Lewis bases can be restricted by steric factors. Reaction of **1** with pyridine in pentane on a preparative scale allowed isolation of a microcrystalline product with composition $[t\mathrm{Bu}_4\mathrm{Al}_4\mathrm{Ar}_4\mathrm{B}_4\mathrm{O}_8(\mathrm{C}_5\mathrm{H}_5\mathrm{N})]$ (**2**) in 59% yield. A crystal structure determination[8] of $\mathbf{2}\cdot(\mathrm{C}_6\mathrm{H}_6)$, obtained by crystallization from benzene, showed a cluster (Figure 1) with basic structural features

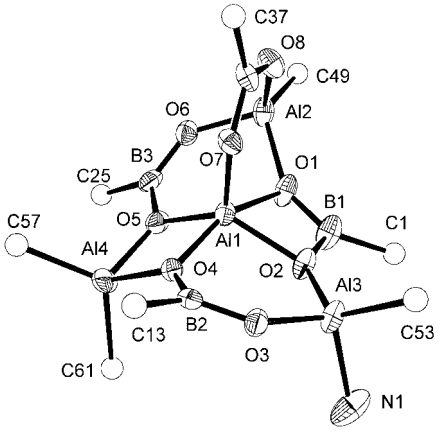
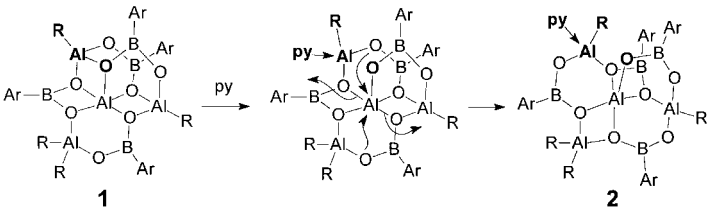


Figure 1. Molecular structure of **2**. All carbon and hydrogen atoms omitted, except for the *ipso* carbons of the groups directly bound to Al (*t*Bu) or B (2,6-$i\mathrm{Pr}_2\mathrm{C}_6\mathrm{H}_3$). Selected bond lengths [Å] and angles [°]: Al3-N1 1.961(4), Al3-C53 1.967(4), Al3-O2 1.826(3), Al3-O3 1.722(3), Al1-O1 2.004(3), Al1-O2 1.916(3), Al1-O4 1.862(3), Al1-O5 1.852(3), Al1-O7 1.709(3); O1-Al1-O2 69.53(11), O4-Al1-O5 81.93(11), O4-Al4-O5 80.95(11), O1-B1-O2 108.0(3).

similar to those of **1**, including a central 5-coordinate Al atom and interconnected 6-membered and 4-membered Al/B-O rings, but without the strained $\mathrm{Al}_2\mathrm{O}_2/\mathrm{BAlO}_2$ edge-sharing ring assembly. The pyridine molecule is coordinated to one of the two *t*BuAl moieties. It is possible that this structure arises from initial attack of pyridine on the *t*BuAl group in the strained ring, followed by a rearrangement of the oxygen atoms around the 5-coordinate Al core, as shown in Scheme 1. These intramolecular rearrangements are likely to be facile in the boralumoxane framework, as was shown by the rapid fluxionality of **1**, resulting in solution NMR spectra consistent with an average C_2 symmetry for this compound.[7] The formation of **2** from **1** and pyridine thus appears to be in line with the expected reactivity of **1** based on the concept of latent Lewis acidity. The ^{1}H NMR spectrum of **2** is complex, but



Scheme 1. Plausible mechanism for the reaction of **1** with pyridine to give **2**.

clearly shows the resonances of the coordinated pyridine, as well as four separate resonances for the Al*t*Bu groups, indicating an asymmetric structure.

Adding one equivalent of $[\mathrm{Cp}^*_2\mathrm{ZrMe}_2]$ ($\mathrm{Cp}^* = \eta^5\text{-}\mathrm{C}_5\mathrm{Me}_5$) to a solution of **1** in $\mathrm{C}_6\mathrm{D}_6$ in an NMR tube at ambient temperature results in a ^{1}H NMR spectrum that is essentially a superposition of the spectra of the starting materials. This suggests that with this zirconocene the reaction of the boralumoxane is either very sluggish, or invisible due to a highly unfavorable equilibrium constant for a possible reversible methyl transfer. In order to trap the $[\mathrm{Cp}^*_2\mathrm{ZrMe}]^+$ cation that would result from such a methyl transfer reaction, we added an excess of allyl methyl thioether to the solution containing **1** and $[\mathrm{Cp}^*_2\mathrm{ZrMe}_2]$. Allyl methyl thioether does not react with **1** itself, but is known to give stoichiometric insertion of the olefin into the Zr–Me bond of $[\mathrm{Cp}^*_2\mathrm{ZrMe}]^+$, resulting in the cationic chelate complex $[\mathrm{Cp}^*_2\mathrm{ZrCH}_2\mathrm{CH}(\mathrm{Me})\mathrm{CH}_2\mathrm{SMe}]^+$ (its OEt analogue was structurally characterized previously in our group[9]). The result of this reaction was a gradual precipitation over several hours of a red oily material and the disappearance of the NMR resonances associated with **1** and $[\mathrm{Cp}^*_2\mathrm{ZrMe}_2]$.

Performing the reaction on a preparative scale in a toluene/pentane mixture resulted in the formation of red-orange crystalline material. A crystal structure determination[8] showed this to be the salt $[\mathrm{Cp}^*_2\mathrm{ZrCH}_2\mathrm{CH}(\mathrm{Me})\mathrm{CH}_2\mathrm{SMe}][\mathrm{Me}t\mathrm{Bu}_4\mathrm{Al}_4\mathrm{Ar}_4\mathrm{B}_4\mathrm{O}_8]$ (**3**), cocrystallized with 1.5 equivalents of toluene per formula unit. The material was obtained in 89% yield. In Figure 2 top, cation and anion are shown schematically, revealing the position of the methyl group that has been transferred from the zirconocene, and in Figure 2 bottom, the core structure of the anion in **3** is shown. As with the pyridine reaction product **2**, the newly introduced group is attached to one of the *t*BuAl moieties, and again the strained $\mathrm{Al}_2\mathrm{O}_2/\mathrm{BAlO}_2$ edge-sharing ring assembly has been opened. The main difference with the structure of **2** is that the rearrangement after ring opening leads to a different arrangement around the central Al atom, but again this structure is readily derived from the presumed initial product of the ring opening (Scheme 2).

Performing the reaction in $\mathrm{C}_6\mathrm{D}_5\mathrm{Br}$ and following it with ^{1}H NMR spectroscopy showed the gradual formation of the known cation $[\mathrm{Cp}^*_2\mathrm{ZrCH}_2\mathrm{CH}(\mathrm{Me})\mathrm{CH}_2\mathrm{SMe}]^+$, and in addition a complicated set of resonances for the methylated boralumoxane anion appeared. Initially, a resonance appeared at $\delta = -0.58$ ppm, which is likely to be associated with the methyl group that is transferred to Al. In the course of time (hours) this species transformed into a product with the AlMe resonance at $\delta = -0.40$ ppm, whereas the resonances of

 © WILEY-VCH Verlag GmbH, 69451 Weinheim, Germany, 2002 1433-7851/02/4112-2167 $ 20.00+.50/0

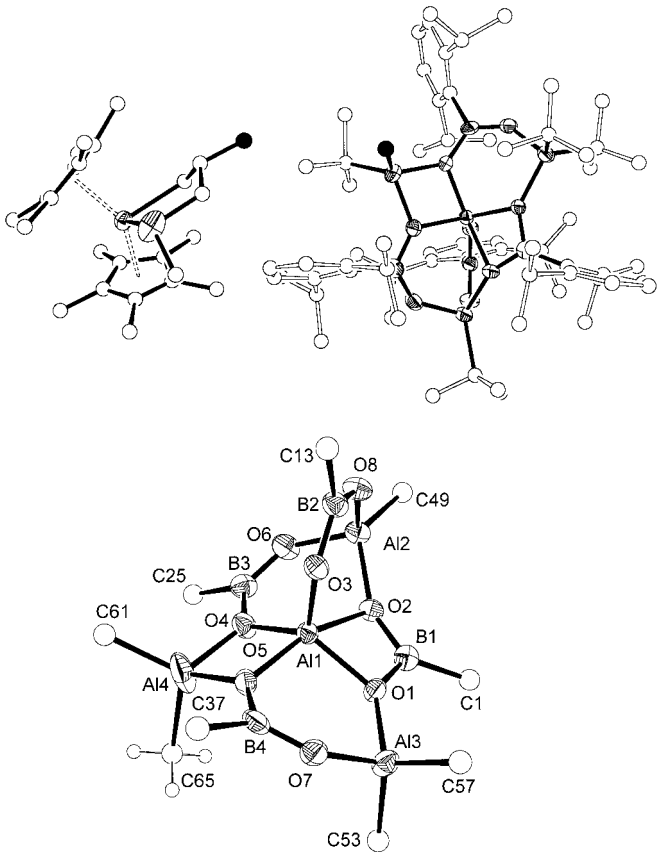
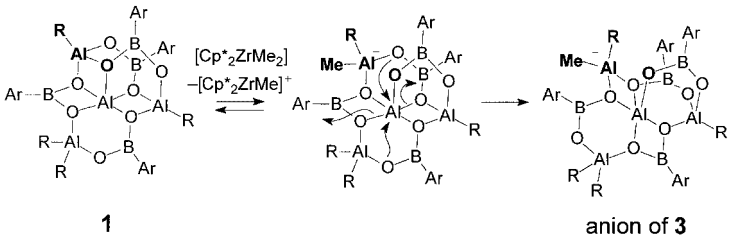


Figure 2. Molecular structure of **3**. Top left: Cation; top right: anion. Carbon atoms represented as spheres, shaded spheres representing the carbon atoms corresponding to the methyl groups that were originally bound to Zr in $[Cp^*_2ZrMe_2]$. Bottom: core of the anion. All carbon and hydrogen atoms omitted, except for the *ipso* carbons of the groups directly bound to Al (*t*Bu) or B (2,6-$iPr_2C_6H_3$), and for the methyl group transferred to Al4, for which the hydrogen atoms are also shown. Selected bond lengths [Å] and angles [°]: Al4-C65 2.091(9), Al4-C61 1.889(9), Al4-O4 1.867(4), Al4-O5 1.849(4), Al1-O1 1.883(3), Al1-O2 2.018(3), Al1-O3 1.717(3), Al1-O4 1.849(4), Al1-O5 1.856(3); O1-Al1-O2 65.52(13), O4-Al1-O5 81.37(15), O4-Al4-O5 81.08(16), O1-B1-O2 107.4(4).



Scheme 2. Plausible mechanism for the reaction of **1** with $[Cp^*_2ZrMe_2]$ and allyl methyl thioether to give **3**.

the cation remained unchanged. This suggests that the methylated boralumoxane anion is converted from a kinetically controlled to a thermodynamically controlled product. For both isomers, four separate resonances for the Al*t*Bu groups are observed, indicating asymmetric structures. Dissolving a portion of crystalline **3** (obtained from the reaction in toluene/pentane as described above) in C_6D_5Br initially showed a dominant AlMe ^{1}H NMR resonance at $\delta = -0.58$ ppm and subsequently a gradual dominance of the species with the resonance at $\delta = -0.40$ ppm. This suggests that the crystal structure of **3** most likely represents the structure of the kinetically controlled product.

The present study conclusively shows that the strained $Al_2O_2/BAlO_2$ edge-sharing ring assembly in the boralumoxane **1** is the feature responsible for the reactivity of this compound towards Lewis bases as well as zirconocene dimethyl complexes. Zirconocene dialkyl compounds are activated by alkyl transfer to the boralumoxane, and the resulting cationic species can insert olefins into the Zr– bond, as was seen by characterization of the product of the methyl allyl thioether insertion. These results give strong support for the concept of latent Lewis acidity formulated by Barron et al. for the mechanism of activation of zirconocene-based olefin polymerization catalysts by alumoxane activators. The observation of this reactivity with boralumoxane **1**, which is topologically quite different from the $[t\text{BuAlO}]_n$ alumoxanes, suggests that there may be a wider scope for metallacyclic activators for single-site olefin polymerization catalysts. It may be noted that the reaction between transition metal dialkyl compounds and alumoxane species stabilized with sterically demanding groups can be rather slow (for $[Cp^*_2ZrMe_2]$ and **1** in the order of hours at ambient temperature), making it more difficult to estimate the true activating potential of these species from polymerization experiments started by simple mixing of the metal dialkyl compound and the activator.

Experimental Section

2: Pyridine (26.5 μL, 0.328 mmol) was added to a suspension of **1** (0.378 g, 0.328 mmol) in 5 mL of *n*-pentane. Subsequently toluene (3 mL) was added, and the mixture was briefly warmed to 40 °C. After allowing the mixture to cool to ambient temperature, the supernatant was decanted and the precipitate was rinsed with 5 mL of *n*-hexane. Drying in vacuo yielded **2** (0.240 g, 59 %). Selected NMR data: ^{1}H NMR (500 MHz, [D$_6$]benzene, 25 °C): $\delta = 7.52$ (d, $J = 5.0$ Hz, 2 H, py *o*-H), 6.79 (t, $J = 7.7$ Hz, 1 H, py *p*-H), 6.40 (m, 2 H, py *m*-H), 1.26, 0.96, 0.83, 0.57 (s, 9 H each, *t*Bu) ppm. ^{11}B NMR (160 MHz, [D$_6$]benzene, 25 °C): $\delta = 30.0$ ($W_{1/2} = 2640$ Hz) ppm. ^{27}Al (130 MHz, [D$_6$]benzene, 25 °C): $\delta = 120$ (very br, $W_{1/2} > 50$ kHz), 41.9 ($W_{1/2} = 5900$ Hz) ppm. C,H,N analysis (%): calcd for $C_{69}H_{109}NO_8B_4Al_4$ (1231.8): C 67.28, H 8.92, N 1.14; found C 67.22, H 8.88, N 1.07.

3: A solution of $[Cp^*_2ZrMe_2]$ (0.134 g, 0.343 mmol) in 2 mL of toluene was added to a suspension of **1** (0.368 g, 0.319 mmol) in 3 mL of *n*-pentane. Subsequently allyl methyl thioether (0.2 mL) was added, and the mixture was allowed to stand overnight at ambient temperature. The supernatant was decanted from the red-orange crystalline material, which was rinsed with two portions of *n*-hexane (3 mL each). Drying in vacuo yielded **3**·$(C_7H_8)_{1.5}$ (0.505 g, 0.285 mmol, 89 %). Selected NMR data: ^{1}H NMR (500 MHz, [D$_5$]bromobenzene, 25 °C): cationic part: $\delta = 2.3$ (br m, 1 H, C*H*Me), 2.26 (ddd, $J = 10.8$, 4.3, 3.3 Hz, 1 H, SC*H*H), 2.14 (dd, $J = 10.7$, 12.6 Hz, 1 H, SCH*H*), 1.94 (dd, $J = 12.9$, 12.3, 1 H, ZrC*H*H), 1.67 (s, 3 H, SMe), 1.60, 1.57 (s, 15 H each, Cp*), 0.79 (d, $J = 6.3$ Hz, 3 H, CH*Me*), –1.12 (ddd, $J = 12.9$, 6.7, 3.4 Hz, 1 H, ZrCH*H*) ppm. anionic part, thermodynamic product: $\delta = 1.25$, 1.14, 1.09, 0.41 (s, 9 H each, *t*Bu), –0.40 (s, 3 H, AlMe) ppm. ^{11}B NMR (160 MHz, [D$_2$]dichloromethane, 25 °C): $\delta = 28.6$ ($W_{1/2} = 1900$ Hz) ppm. ^{27}Al NMR (130 MHz, [D$_2$]dichloromethane, 25 °C): $\delta = 124$ (very br, $W_{1/2} = 35$ kHz), 42.5 ($W_{1/2} = 3600$ Hz) ppm. C,H analysis (%): calcd for $C_{90}H_{148}O_8SB_4Al_4Zr(C_7H_8)_{1.5}$ (1770.8): C 68.49, H 9.02; found C 68.31, H 8.97.

Received: January 21, 2002 [Z 18550]

 © WILEY-VCH Verlag GmbH, 69451 Weinheim, Germany, 2002 1433-7851/02/4112-2168 $ 20.00+.50/0

[1] a) H. Sinn, W. Kaminsky, H. J. Vollmer, R. Woldt, *Angew. Chem.* **1980**, *92*, 396 – 402; *Angew. Chem. Int. Ed. Engl.* **1980**, *19*, 390 – 392; b) W. Kaminsky, *J. Chem. Soc. Dalton Trans.* **1998**, 1413 – 1418, and references therein.

[2] a) H.-H. Brintzinger, D. Fischer, R. Mülhaupt, B. Rieger, R. M. Waymouth, *Angew. Chem.* **1995**, *107*, 1255 – 1283; *Angew. Chem. Int. Ed. Engl.* **1995**, *34*, 1143 – 1170 (Erratum: H.-H. Brintzinger, D. Fischer, R. Mülhaupt, B. Rieger, R. M. Waymouth, *Angew. Chem.* **1995**, *107*, 1652; *Angew. Chem. Int. Ed. Engl.* **1995**, *34*, 1368); b) A. L. McKnight, R. M. Waymouth, *Chem. Rev.* **1998**, *98*, 2587 – 2598; c) G. J. P. Britovsek, V. C. Gibson, D. F. Wass, *Angew. Chem.* **1999**, *111*, 448 – 468; *Angew. Chem. Int. Ed.* **1999**, *38*, 428 – 447, and references therein.

[3] a) M. Ystenes, J. L. Eilertsen, J. Liu, M. Ott, E. Rytter, J. A. Støvneng, *J. Polym. Sci. A* **2000**, *38*, 3106 – 3127; b) E. Zurek, T. K. Woo, T. K. Firman, T. Ziegler, *Inorg. Chem.* **2001**, *40*, 361 – 370; c) E. Zurek, T. Ziegler, *Inorg. Chem.* **2001**, *40*, 3279 – 3292; d) E. Rytter, J. A. Støvneng, J. L. Eilertsen, M. Ystenes, *Organometallics* **2001**, *20*, 4466 – 4468.

[4] M. R. Mason, J. M. Smith, S. G. Bott, A. R. Barron, *J. Am. Chem. Soc.* **1993**, *115*, 4971 – 4984.

[5] C. J. Harlan, S. G. Bott, A. R. Barron, *J. Am. Chem. Soc.* **1995**, *117*, 6465 – 6474.

[6] Y. Koide, S. G. Bott, A. R. Barron, *Organometallics* **1996**, *15*, 5514 – 5518.

[7] B. Richter, A. Meetsma, B. Hessen, J. H. Teuben, *Chem. Commun.* **2001**, 1286 – 1287.

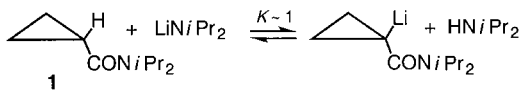
[8] Crystallographic structure determinations were performed on a Bruker SMART Apex CCD diffractometer using $Mo_{K\alpha}$ radiation ($\lambda = 0.71073$ Å). The structures were solved with Patterson methods and extended by direct methods applied to difference structure factors. Crystallographic data for **2**: $C_{69}H_{109}Al_4B_4NO_8 \cdot (C_6H_6)$, $M_r = 1309.91$, monoclinic, space group $P2_1/n$, $a = 13.8868(6)$, $b = 25.188(1)$, $c = 23.346(1)$ Å, $\beta = 106.805(1)^\circ$, $V = 7817.2(6)$ Å^3, $Z = 4$, $\rho_{calcd} = 1.113$ g cm^{-3}, $\mu = 1.1$ cm^{-1}, $T = 110$ K. A final refinement on F^2 converged at $wR(F^2) = 0.1789$ for 13782 reflections and $R(F) = 0.0733$ for 7505 reflections with $F_o \geq 4\sigma(F_o)$ and 857 parameters. Crystallographic data for **3**: $[C_{25}H_{41}SZr][C_{65}H_{107}Al_4B_4O_8] \cdot (C_7H_8)_{1.5}$, $M_r = 1770.83$, monoclinic, space group $P2_1/c$, $a = 20.6291(8)$, $b = 20.3125(8)$, $c = 26.301(1)$ Å, $\beta = 110.155(1)^\circ$, $V = 10346.0(7)$ Å^3, $Z = 4$, $\rho_{calcd} = 1.137$ g cm^{-3}, $\mu = 2.11$ cm^{-1}, $T = 110$ K. A final refinement on F^2 converged at $wR(F^2) = 0.2289$ for 18278 reflections and $R(F) = 0.0808$ for 11143 reflections with $F_o \geq 4\sigma(F_o)$ and 1145 parameters and 16 restraints. One of the toluene molecules in the lattice shows extensive orientational disorder, resulting in unrealistic displacement parameters when allowed to vary anisotropically. The other toluene molecule is disordered over an inversion center, and was described as a single molecule with 0.5 occupancy with geometrical restraints. CCDC-177577 (**2**) and CCDC-177576 (**3**) contain the supplementary crystallographic data for this paper. These data can be obtained free of charge via www.ccdc.cam.ac.uk/conts/retrieving.html (or from the Cambridge Crystallographic Data Centre, 12, Union Road, Cambridge CB2 1EZ, UK; fax: (+44) 1223-336-033; or deposit@ccdc.cam.ac.uk).

[9] E. A. Bijpost, M. A. Zuideveld, A. Meetsma, J. H. Teuben, *J. Organomet. Chem.* **1998**, *551*, 159 – 164.

BuMgN*i*Pr$_2$: A New Base for Stoichiometric, Position-Selective Deprotonation of Cyclopropane Carboxamides and Other Weak CH Acids**

Mao-Xi Zhang and Philip E. Eaton*

Organolithium (RLi) and -magnesium (R_2Mg) compounds are kinetically poor bases for proton removal from weak carbon acids. If an amine like *N*,*N*,*N*′,*N*′-tetramethylethylendiamine (TMEDA) is added, the barrier is sometimes lowered, but the nucleophility of the organometallic compound remains a problem. This can be ameliorated by using metal amides like lithium diisopropylamide (LDA) and bis(diisopropylamido)magnesium (DA_2Mg). These poor nucleophiles are still kinetically effective bases for deprotonation of weakly acidic CH groups ($pK_a \approx 30 - 35$).[1] However, as the pK_a of the liberated amine and that of the CH acid (e.g. **1**) are similar, such deprotonations are nowhere near stoichiometric (e.g. Scheme 1[2]). This is unsatisfactory.



1

Scheme 1. The equilibrium reaction of LDA with amide **1**.

We now introduce alkylmagnesium amides, here specifically BuMgN*i*Pr$_2$, denoted hereafter as BuMgDA, as an effective solution to this problem.[3] We prepare BuMgDA simply by adding 1.0 equivalent of anhydrous diisopropylamine (DAH) to commercial[4] dibutylmagnesium in heptane (ca. 1.0 M) at room temperature and then stirring the solution for five minutes at 50 °C. BuMgDA[3b] in heptane is quite reactive. Replacing heptane, all or in part, with THF (after the base has been formed) increases this usefully. Unlike Bu_2Mg and many organolithium bases, BuMgDA is stable even in refluxing THF for many hours. BuMgDA, like DA_2Mg, deprotonates/metalates amide-activated[5] cyclopropyl-CH (α, β, or beyond) and cubyl-CH (*ortho*),[6] but the BuMgDA deprotonations are driven to completion by irreversible formation of butane.

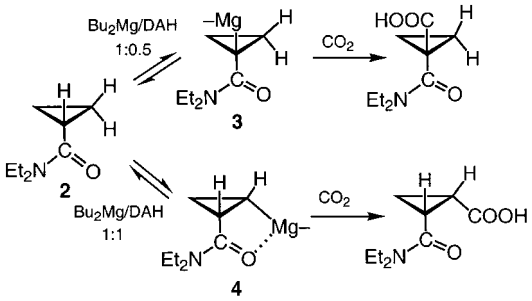
It is instructive to compare the metalation of the cyclopropylcarboxamide **2** using Bu_2Mg solutions in heptane treated first with 0, 0.5, or 1.0 equivalent of DAH. Bu_2Mg itself reacted only slowly;[7] mostly starting material was recovered. In the other two cases, when at least some BuMgDA[3b] was present, the overall deprotonation/metalation/carboxylation proceeded in high yield, but the final

[*] Prof. Dr. P. E. Eaton, Dr. M.-X. Zhang
Department of Chemistry
The University of Chicago
5735 South Ellis Avenue, Chicago, IL 60637 (USA)
Fax: (+1) 773-702-2053
E-mail: eaton@uchicago.edu

[**] This work was supported in part by Eastman Chemical. We are grateful to Z. Hantosi and C.-H. Lee for trial experiments, to I. Steele for the X-ray analyses, and to Professor S. Shuto of Hokkaido University for samples of Milnacipran precursors.

 © WILEY-VCH Verlag GmbH, 69451 Weinheim, Germany, 2002 1433-7851/02/4112-2169 $ 20.00+.50/0

outcome (Scheme 2) depended importantly on the ratio of DAH to Bu_2Mg. When this was 0.5:1.0, α metalation predominated; when it was 1:1, β metalation was favored instead. Looked at simply: when there is an excess of Bu_2Mg it scavengers the DAH generated by the initial α deprotonation;



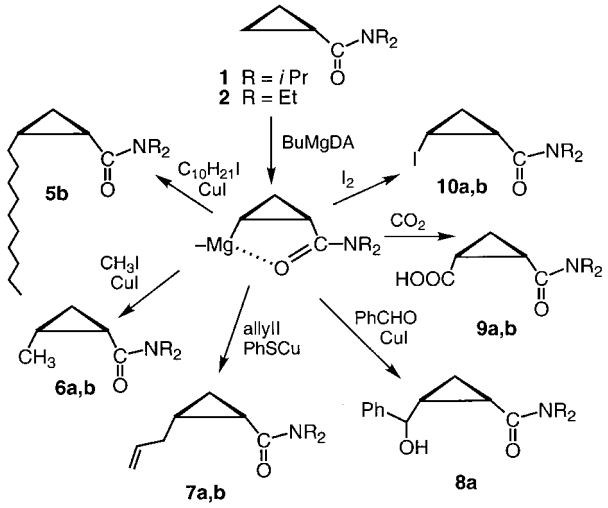
Scheme 2. Predominant position of magnesiation of **2** as a function of Bu_2Mg to DAH ratio. Standard conditions: heptane/THF (1:1); RT; two days; analysis after carboxylation at $-78 \rightarrow 0\,^{\circ}C$.

when there is no excess of Bu_2Mg, free DAH remains and equilibration can occur. Ultimately, equilibration leads mostly to the thermodynamically favored, amide-stabilized β-magnesium compound. Sooner or later, and irreversibly in both cases, butane is formed, all the DAH is consumed, and essentially stoichiometric metalation is achieved.

Whereas the α-lithiated analogues of cyclopropane carbonyl derivatives are excessively nucleophilic and often self-destruct before they can be trapped usefully,[8] the α-amido-Grignard species **3**[3b] provides a convenient and dependable route to α-substituted cyclopropane diethylcarboxamides. We made this amido-Grignard by treating **2** (ca. 0.5 M in 1:1 heptane/THF) with the mixture of bases (BuMgDA + Bu_2Mg)[3b] resulting from reaction of 0.5 equivalent of DAH with 1.05 equivalents[9] of Bu_2Mg. α-Metalation was optimum after 48 h at room temperature (longer times, higher temperature, or more THF led to some β metalation). The α-carboxy (85 % yield of isolated product), α-iodo (70 %), and α-methyl (76 %) compounds were obtained from **3** by reaction with CO_2, I_2, and CH_3I, respectively.

Treatment of the diethylamide **2** (ca. 0.5 M) with 1.05 equivalents[9] of BuMgDA in THF gave in due course mostly the β-metalated material **4**, but optimum conversion required reaction for 8 h at 60 °C. On the other hand, β metalation occurred almost immediately, even at room temperature, when the *N*,*N*-diisopropylcarboxamide **1** was used instead. Probably the larger bulk of the isopropyl group(s) favors an amide conformation with the carbonyl oxygen atom proximate to a β-site.

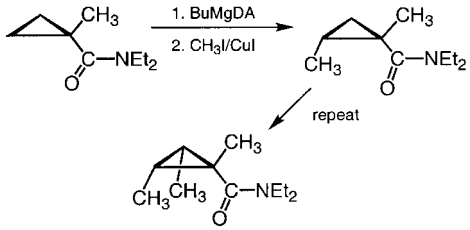
The reactions of the β-metalated compounds (ca. 0.5 M) shown in Scheme 3 were all carried out at room temperature or below, and required 1 to 24 h for completion. The addition of 20 mol % CuI or PhSCu was needed to obtain reasonable rates in the alkylations. When R was ethyl, less than 10 % of the product resulted from α substitution; when R was isopropyl, less than 5 %, often much less. No other base provides such high discrimination for β substitution on a cyclopropane carboxamide having an α proton.



Scheme 3. β Substitutions on cyclopropylamides by BuMgDA metalation. For **a**, R = ethyl; for **b**, R = isopropyl. Yields of isolated products: **5b**: 46 % (single run, 84 % based on unreacted **2**); **6a**: 76 %; **6b**: 66 %; **7a**: 76 %; **7b**: 89 %; **8a**: 43 % (single run); **9a**: 81 %; **9b**: 88 %; **10a**: 70 %; **10b**: 80 %.

These reactions produce stereospecifically the *cis*-to-the-amide isomers.[10] The more favored *trans* isomer can be obtained by purposeful epimerization with base; BuMgDA works well.[11]

Of course, β substitution can also be achieved if the α position is blocked; *cis*-β' substitution can be done as well (Scheme 4, 66 % overall yield).

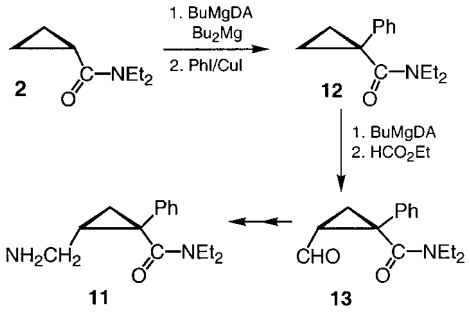


Scheme 4. The β and β' methylations of the α-methyl derivative of **2** by magnesiation with BuMgDA.

The ability to introduce numerous substituents in controlled fashion onto a readily available cyclopropane provides a new paradigm for the synthesis of complex cyclopropanes, one requiring neither carbene addition nor intramolecular cyclization.

Milnacipran (**11**), a clinically useful antidepressant, is presently prepared from reaction of epichlorohydrin with benzyl cyanide anion followed by an intramolecular displacement to close the cyclopropane ring, then functional group manipulation.[12] We present here an entirely different strategy (Scheme 5) proceeding from cyclopropane carboxylic acid, available in bulk cheaply. α Magnesiation of its diethylcarboxamide **2** with BuMgDA/Bu_2Mg followed by phenylation with iodobenzene and 5 mol % CuI gave **12** in 53 % yield (82 % based on recovered **2**). Further magnesiation, now using stoichiometric BuMgDA, occurred at the β position. The resulting amido-Grignard reacted easily with

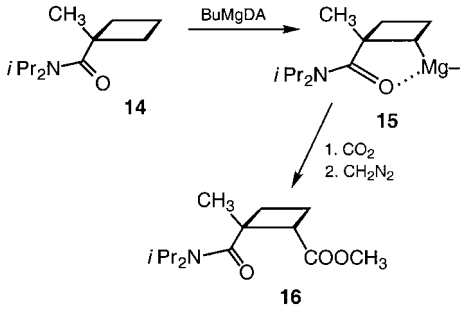
 © WILEY-VCH Verlag GmbH, 69451 Weinheim, Germany, 2002 1433-7851/02/4112-2170 $ 20.00+.50/0 *Angew. Chem. Int. Ed.* **2002**, *41*, No. 12



Scheme 5. A new approach to the synthesis of Milnacipran (**11**).

ethyl formate to give **13** (73% yield of isolated product), a known Milnacipran precursor.[12]

Aromatic and benzyl CH groups are more acidic than those of cyclopropanes and cubanes, so it is not surprising that BuMgDA stoichiometrically metalates an amide-activated CH group appropriately positioned thereupon. What if the CH group is less acidic? Cyclobutane CH is kinetically 2500 times more weakly acidic than cyclopropane CH.[13] Under conditions as harsh as most base/solvent combinations can withstand (e.g. LiTMP/THF or LiTMP + $Hg(TMP)_2$/THF at 0° C (TMP = 2,2,6,6-tetramethylpiperidine) or LDA/THF at reflux), there is no observed metalation of **14**. However, under the conditions of our preliminary trials, reaction of **14** with excess BuMgDA in THF at reflux for 5 h gave about 20% conversion[14] to the *cis*-β-metalated compound **15**, identified by formation of ester **16**[10] (17% yield of isolated product, Scheme 6). Although still to be optimized, this β deprotonation/metalation of a cyclobutane amide is extraordinary and unprecedented.



Scheme 6. Deprotonation/magnesiation of an amide-activated cyclobutane using BuMgDA.

Received: January 16, 2002
Revised: April 11, 2002 [Z18529]

[1] a) P. E. Eaton, C.-H. Lee, Y. Xiong, *J. Am. Chem. Soc.* **1989**, *111*, 8016–8018; b) P. E. Eaton, K. A. Lukin, *J. Am. Chem. Soc.* **1993**, *115*, 11370–11375; c) For a review: K. W. Henderson, W. J. Kerr, *Chem. Eur. J.* **2001**, *7*, 3430–3437, and references therein; d) Cf. Y. Kondo, M. Shilai, M. Uchiyama, T. Sakamoto, *J. Am. Chem. Soc.* **1999**, *121*, 3539–3540.
[2] Z. Hantosi, PhD Thesis, The University of Chicago, **1999**.
[3] a) As far as we can determine, amido-Grignards have not been examined elsewhere for their deprotonation/metalation abilities. b) We ignore, for the present, consideration of Schlenk equilibria and/or aggregation of magnesiated species.
[4] Aldrich Chemical sells a mixture of *n*-butyl and *s*-butyl compounds; this generates a mixture of *n*BuMgDA/*s*BuMgDA; this was what we used. The pure compounds behave similarly as bases.
[5] See: V. Snieckus, *Chem. Rev.* **1990**, *90*, 879–933.
[6] The magnesiated products have useful (but reduced) Grignard-like reactivity; cf. ref. [1].
[7] The addition of TMEDA does not improve the proton removal ability of Bu_2Mg.
[8] a) For example: H. W. Pinnick, Y.-H.Chang, S. C. Foster, M. Govindan, *J. Org. Chem.* **1980**, *45*, 4505–4507.
[] b) The α-lithio derivative of **2**, prepared by reaction of **2** with *n*BuLi at −78 °C, is stable only below 0 °C.
[9] A small excess of Bu_2Mg was used to remove adventitious water.
[10] Stereochemical assignments: aq. 30% H_2SO_4 amide hydrolysis (no isomerization; demonstrated by re-amidation) followed (e.g. for **9**) by NMR comparison to the known acid or (e.g. for **10**) by X-ray analysis; for **6** by X-ray analysis of the crystalline dicyclohexylamide analogue; for Scheme 4, ^1H and ^{13}C NMR; for **16**, X-ray single crystal analysis. CCDC-173837 (**10**), CCDC-173837 (**6**), CCDC-173571 (**16**) contain the supplementary crystallographic data for this paper. These data can be obtained free of charge via www.ccdc.cam.ac.uk/conts/retrieving.html (or from the Cambridge Crystallographic Data Centre, 12, Union Road, Cambridge CB2 1EZ, UK; fax: (+44) 1223-336-033; or deposit @ccdc.cam.ac.uk).
[11] Prolonged exposure of the products to the generating conditions also leads to isomerization.
[12] S. Shuto, S. Ono, H. Imoto, K. Yoshii, A. Matsuda, *J. Med. Chem.* **1998**, *41*, 3507–3514, and references therein.
[13] A. Streitwieser, Jr., R. A. Caldwell, W. R. Young, *J. Am. Chem. Soc.* **1969**, *91*, 529.
[14] By NMR: 20% **16**, 80% unreacted starting material.

New Methods for Proteomic Research: Preparation of Proteins with N-Terminal Cysteines for Labeling and Conjugation**

Thomas J. Tolbert and Chi-Huey Wong*

In memory of Sun Fong

Proteins with N-terminal cysteines are useful in a wide range of biotechnological applications ranging from protein semi-synthesis to site-specific N-terminal labeling. Peptides and proteins with N-terminal cysteines undergo native chemical ligation and expressed protein ligation reactions with thioesters to form native peptide bonds.[1, 2] These reactions have been used to extend the size of proteins that can be synthesized chemically and to incorporate synthetic peptides with modifications and labels into expressed proteins.[3–8] In addition, proteins with N-terminal cysteines also react chemoselectively with aldehydes to form thiazolidines, and this reaction has been utilized to label and immobilize peptides and proteins.[9–12] Here we present a novel method (Figure 1) to produce proteins with N-terminal cysteines by

[*] Prof. C.-H. Wong, Dr. T. J. Tolbert
The Department of Chemistry and Skaggs Institute for Chemical Biology
The Scripps Research Institute
10550 North Torrey Pines Road, La Jolla, CA 92037 (USA)
Fax: (+1) 858-784-2409
E-mail: wong@scripps.edu

[**] This research was supported by the NIH (R37 GM44154).
Supporting information for this article is available on the WWW under http://www.angewandte.com or from the author.

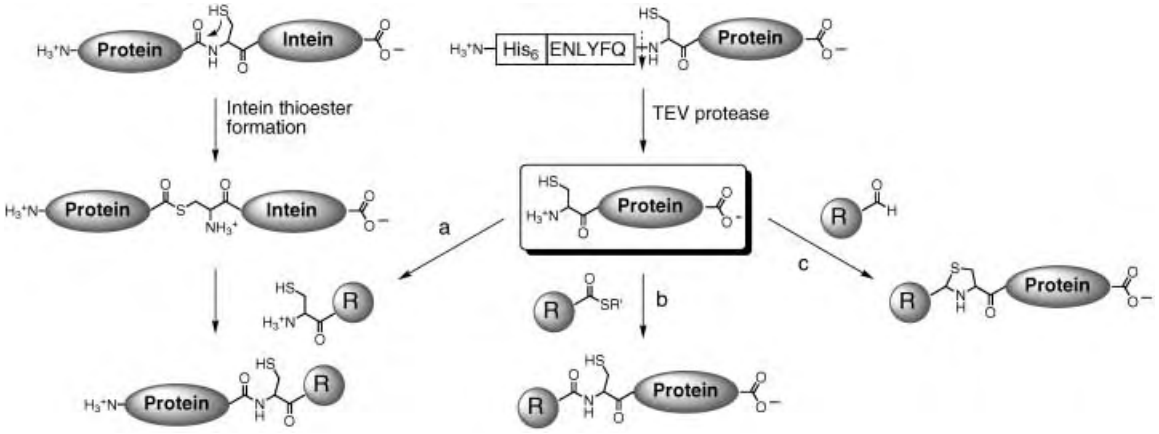


Figure 1. Generation of proteins with N-terminal cysteines using TEV protease and some examples of uses for proteins with N-terminal cysteines: a) expressed protein ligation reactions with intein generated thioesters; b) native/expressed protein ligation reactions with synthetic peptides and labels; c) chemoselective ligation with aldehydes to form thiazolidines.

using the highly selective tobacco etch virus NIa protease (TEV protease). We also demonstrate the subsequent labeling of proteins with N-terminal cysteines produced in this way using thioesters of two common protein labeling reagents. We believe that the use of TEV protease to generate N-terminal cysteines overcomes some of the limitations of existing methods, and this should make it generally useful for chemoselective ligation, proteomic labeling, and other biotechnological applications.

Current methods for producing proteins with N-terminal cysteines from affinity-tagged fusion proteins include using protein expression systems that utilize the self-cleaving activity of inteins[13] and selective proteolysis.[4, 5] Intein expression systems utilize the protein-splicing activity of inteins to catalyze the intramolecular cleavage of the intein from its fusion partner.[14] The difficulty in using the intein cleavage reaction to produce proteins from affinity-tagged intein fusion proteins is that it may cause in vivo cleavage during expression and complicate the preparation process. Many factors can affect in vivo and in vitro cleavage such as the expression conditions, structure of the desired protein, and identity of the N-terminal amino acids at the cleavage junction.[14] To obtain a construct that expresses well, screening of several expression conditions and multiple expression constructs with different amino acids at the cleavage junction is frequently required. Selective proteolysis of affinity-tagged fusion proteins to produce N-terminal cysteines generally does not suffer from expression problems since the affinity tags do not cleave themselves in vivo and can be chosen to optimize expression yield and protein folding. Unfortunately, the most common protease to be used to generate N-terminal cysteines, factor Xa,[4, 5] is not completely sequence-specific, sometimes cleaving peptide bonds after positively charged residues in the absence of its primary recognition sequence.[15, 16] This often requires careful monitoring of factor Xa cleavage reactions to prevent internal cleavage of the desired protein. For many protein applications a more selective protease than factor Xa with a lower probability of cleaving internally during affinity tag removal would be advantageous.

We decided to investigate the use of TEV protease to generate N-terminal cysteines from affinity-tagged fusion proteins because it has several advantages for labeling applications. It is a highly selective cysteine protease with a seven amino acid recognition site, recognizing six amino acids N-terminal to the scissile bond between the P1 glutamine and the P1′ serine or glycine (Figure 2a).[17, 18] Another advantage of TEV protease is that it can be expressed in active form in *E. coli* and yeast without affecting cell viability,[19] making production of TEV protease for large-scale applications inexpensive.[20] Additionally, TEV protease has already proven useful in proteomic applications, as demonstrated by a recent yeast proteomic study in which cleavage of a natural TEV recognition site, resulting in an N-terminal glycine, was used for purification of over 580 protein assemblies.[21] Finally, cleavage of the natural TEV protease recognition site can produce proteins with N-terminal serines that can be utilized in labeling through selective oxidation of the N-terminal serine to an aldehyde.[22]

Previous studies of TEV protease specificity indicated that it might be possible to use TEV protease to produce N-terminal cysteines. Genetic and biochemical analysis has shown that the P6, P3, and P1 amino acid residues are conserved in all known natural TEV cleavage sites and are major determinants of protease specificity.[17, 23] The remain-

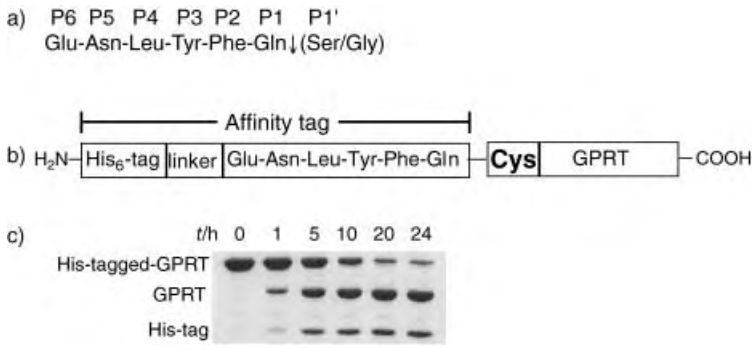


Figure 2. a) TEV protease cleavage site. b) Diagram of the histidine (His)-tagged GPRT fusion protein with mutated TEV cleavage site. c) Time course of cleavage of GPRT fusion protein (5 mg) with TEV protease (100 units; 1 unit of TEV protease will cleave 3 μg of a control substrate per hour).

 © WILEY-VCH Verlag GmbH, 69451 Weinheim, Germany, 2002 1433-7851/02/4112-2172 $ 20.00+.50/0 *Angew. Chem. Int. Ed.* **2002**, *41*, No. 12

ing residues can be mutated individually with some substitutions. Mutation of the P1′ residue to cysteine has been reported to reduce the TEV cleavage rate to 20% and only allow about 50% processing when tested in proteins produced by in vitro translation in rabbit reticulocyte lysate.[17, 18] We hypothesized that the incomplete processing and reduced cleavage rates previously observed for a P1′ cysteine mutation may be due to disulfide bond formation in the proteins produced in rabbit reticulocyte lysate. To test if mutation of the TEV site P1′ residue to cysteine would be efficiently processed, we expressed an affinity-tagged test protein, *E. coli* xanthine–guanine phosphoribosyltransferase (GPRT), with a mutated TEV cleavage site containing a cysteine replacement at P1′ (Figure 2b). A time course of the cleavage of 5 mg of the test protein with 100 units of TEV protease under reducing conditions revealed that the mutated TEV site was cleaved at approximately 70% the rate of the natural cleavage site (Figure 2c). In addition, the mutated cleavage site was processed to 95% completion in 24 h, indicating that TEV protease is synthetically useful in generating proteins with N-terminal cysteines. This procedure has also been applied to human interleukin-2 and *E. coli* sialic acid aldolase, and both proteins were cleaved to 90–95% completion at the correct sites to yield the desired N-terminal cysteines.

Next we set out to explore protein N-terminal labeling using TEV protease to generate N-terminal cysteines for chemoselective ligation. Two water-soluble thioester labeling reagents were synthesized for this purpose. Biotin and 5-carboxyfluorescein are labeling reagents commonly used to randomly label protein amines that are soluble at pH 7 and above, but will precipitate at more acidic pH because of protonation of their carboxylic acids. Reaction of biotin and 5-carboxyfluorescein with uncharged thiols produced water-insoluble thioesters that are not able to react with proteins in solution. By using *tert*-butyl mercaptoacetate to form the thioesters of biotin and 5-carboxyfluorescein, thioester labeling reagents **1** and **2** (Figure 3) were synthesized that were water soluble and able to react with proteins in aqueous solution in the absence of denaturants and organic cosolvents.

Initially simultaneous protease cleavage and thioester labeling of the affinity-tagged fusion proteins was attempted. Unfortunately the thioester labels are inhibitors of the TEV protease, possibly because the TEV protease is a cysteine protease with an active site cysteine that can be acylated by the thioesters. A two-step cleavage/labeling reaction was developed to overcome the inhibition, that is removing the affinity tag first, and then adding the thioester labels after the TEV protease cleavage was complete (Figure 3). Using this procedure it was found that 4 mM of the thioester labeling reagents were able to label 95–100% of the test protein in 12 h (Figure 4).

In summary, we have demonstrated the use of TEV protease to remove N-terminal affinity tags from fusion proteins to produce proteins with N-terminal cysteines and the subsequent use of those N-terminal cysteines for labeling. Advantages of using TEV protease to generate N-terminal cysteines include the high selectivity of the protease which makes it generally applicable to the cleavage of a wide range of fusion proteins and the ability to overexpress TEV protease for economical large scale applications. Cloning and expression of affinity-tagged fusion proteins with mutated TEV cleavage sites is straightforward and it should be simple to

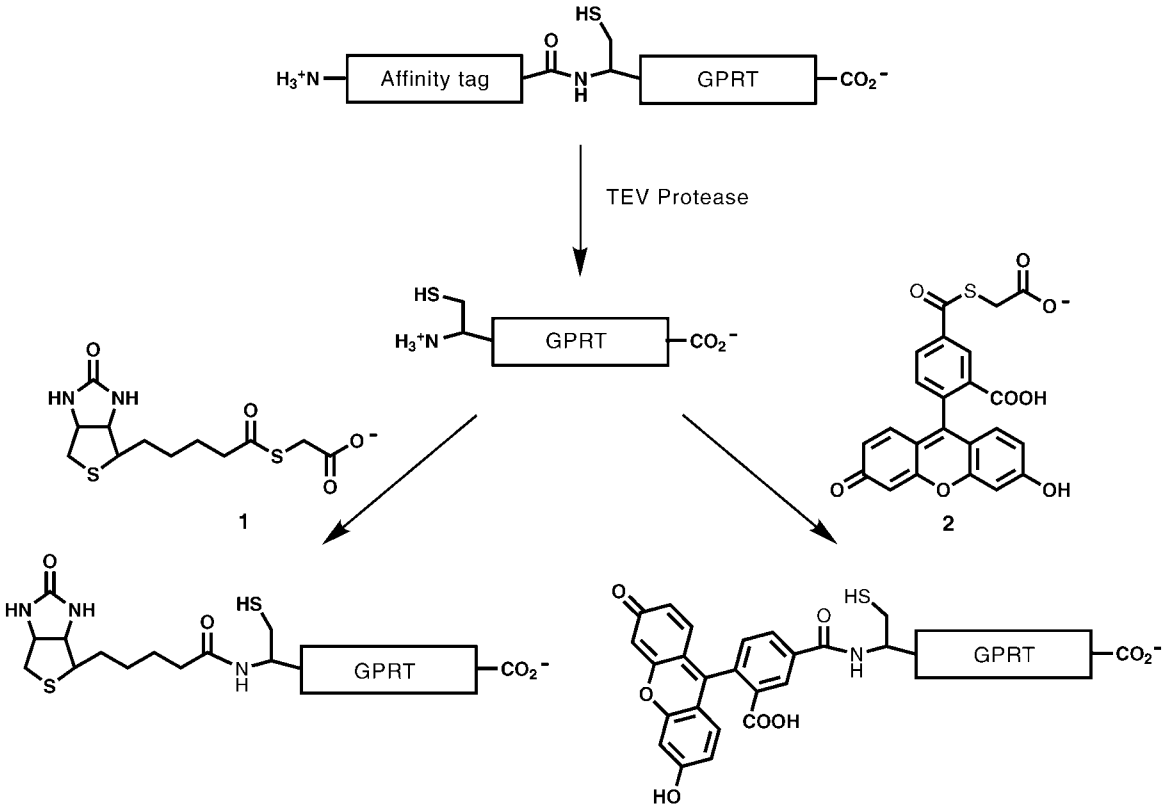


Figure 3. Two-step cleavage/labeling of GPRT using TEV protease and thioester labeling reagents **1** and **2**.

 © WILEY-VCH Verlag GmbH, 69451 Weinheim, Germany, 2002 1433-7851/02/4112-2173 $ 20.00+.50/0

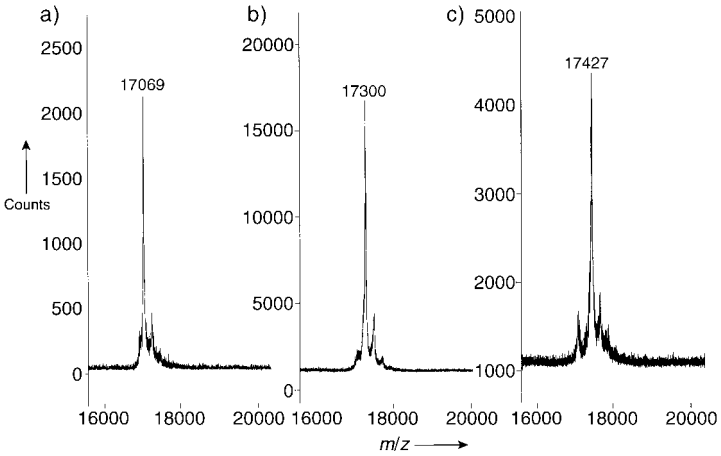


Figure 4. MALDI-TOF spectra of cleaved and labeled GPRT: a) GPRT: expected 17074, observed 17069; b) biotin-labeled GPRT: expected 17300, observed 17300; c) fluorescein-labeled GPRT: expected 17432, observed 17427.

apply to a large number of proteins. Synthesis of water-soluble thioester labels can be accomplished using *tert*-butyl mercaptoacetate, and proteins can be cleaved and labeled with these reagents in a two-step cleavage/labeling reaction under non-denaturing conditions. The affinity-tagged fusion proteins described herein are not significantly different from affinity-tagged fusion proteins produced in expression systems that have already been used to express and purify nearly all of the proteins of yeast for construction of functional protein arrays and microarrays.[24, 25] The combination of those types of expression strategies with removal of the affinity-tag and subsequent labeling with synthetic molecules should prove useful for many in vitro biochemical and proteomic applications. We hope that TEV protease generation of proteins with N-terminal cysteines will be of use in future protein labeling and semi-synthesis applications, and are currently investigating its application to a broader variety of proteins and glycoproteins, including their micro- and nano-fabrication to produce arrays with uniform orientation.

Received: March 1, 2002 [Z18809]

[1] P. E. Dawson, T. W. Muir, I. Clark-Lewis, S. B. H. Kent, *Science* **1994**, *266*, 776.
[2] T. W. Muir, D. Sondhi, P. A. Cole, *Proc. Natl. Acad. Sci. USA* **1998**, *95*, 6705.
[3] T. W. Muir, P. E. Dawson, S. B. H. Kent, *Methods Enzymol.* **1997**, *289*, 266.
[4] T. W. Muir, *Synlett* **2001**, 733.
[5] D. A. Erlanson, M. Chytil, G. L. Verdine, *Chem. Biol.* **1996**, *3*, 981.
[6] T. C. Evans, Jr., J. Benner, M.-Q. Xu, *Protein Sci.* **1998**, *7*, 2256.
[7] T. J. Tolbert, C.-H. Wong, *J. Am. Chem. Soc.* **2000**, *122*, 5421.
[8] L. A. Marcaurelle, L. S. Mizoue, J. Wilken, L. Oldham, S. B. H. Kent, T. M. Handel, C. R. Bertozzi, *Chem. Eur. J.* **2001**, *7*, 1129.
[9] L. Zhang, J. P. Tam, *Anal. Biochem.* **1996**, *233*, 87.
[10] Z. G. Zhao, J. S. Im, K. S. Lam, D. F. Lake, *Bioconjugate Chem.* **1999**, *10*, 424.
[11] M. Villain, J. Vizzavona, K. Rose, *Chem. Biol.* **2001**, *8*, 673.
[12] J. R. Falsey, M. Renil, S. Park, S. Li, K. S. Lam, *Bioconjugate Chem.* **2001**, *12*, 346.
[13] T. C. Evans, Jr., J. Benner, M.-Q. Xu, *J. Biol. Chem.* **1999**, *274*, 3923.
[14] M.-Q. Xu, T. C. Evans, Jr., *Methods (San Diego, CA, US)*, **2001**, *24*, 257.
[15] D. J. Matthews, J. A. Wells, *Science* **1993**, *260*, 1113.
[16] J. L. Harris, B. J. Backes, F. Leonetti, S. Mahrus, J. A. Ellman, C. S. Craik, *Proc. Natl. Acad. Sci. USA* **2000**, *97*, 7754.
[17] W. G. Dougherty, J. C. Carrington, S. M. Cary, T. D. Parks, *EMBO J.* **1988**, *7*, 1281.
[18] W. G. Dougherty, S. M. Cary, T. D. Parks, *Virology* **1989**, *171*, 356.
[19] T. A. Smith, B. D. Kohorn, *Proc. Natl. Acad. Sci. USA* **1991**, *88*, 5159.
[20] L. J. Lucast, R. T. Batey, J. A. Doudna, *BioTechniques* **2001**, *30*, 544.
[21] A.-C. Gavin, M. Bosche, R. Krause, P. Grandi, M. Marzloch, A. Bauer, J. Schultz, J. M. Rick, A.-M. Michon, C.-M. Cruclat, M. Remor, C. Hofert, M. Schelder, M. Brajenovlc, H. Ruffner, A. Merino, K. Klein, M. Hudak, D. Dickson, T. Rudi, V. Gnau, A. Bauch, S. Bastuck, B. Huhse, C. Leutweln, M.-A. Heurtier, R. R. Copley, A. Edelmann, E. Querfurth, V. Rybin, G. Drewes, M. Raida, T. Bouwmeester, P. Bork, B. Seraphin, B. Kuster, G. Neubauer, G. Superti-Furga, *Nature* **2002**, *415*, 141.
[22] K. F. Geoghegan, J. G. Stroh, *Bioconjugate Chem.* **1992**, *3*, 138.
[23] J. C. Carrington, W. G. Dougherty, *Proc. Natl. Acad. Sci. USA* **1988**, *85*, 3391.
[24] M. R. Martzen, S. M. McCraith, S. L. Spinelli, F. M. Torres, S. Fields, E. J. Grayhack, E. M. Phizicky, *Science* **1999**, *286*, 1153.
[25] H. Zhu, M. Bilgin, R. Bangham, D. Hall, A. Casamayor, P. Bertone, N. Lan, R. Jansen, S. Bidlingmaier, T. Houfek, T. Mitchell, P. Miller, R. A. Dean, M. Gerstein, M. Snyder, *Science* **2001**, *293*, 2101.

Icosahedral WAu_{12}: A Predicted Closed-Shell Species, Stabilized by Aurophilic Attraction and Relativity and in Accord with the 18-Electron Rule**

Pekka Pyykkö* and Nino Runeberg

Stable metal clusters are interesting for their own sake and as potential building blocks for nanostructures. This is especially true for gold due to the recently discovered catalytical properties of small or electronically tuned gold clusters.[1, 2] We here predict the existence of a series of isoelectronic clusters that may be particularly stable for three complementary reasons: 1) particularly efficient radial bonding, 2) the aurophilic attraction in the periphery, and 3) relativistic effects:

1) Consider an Au_{12} icosahedron. Its twelve 6s orbitals will span the irreducible representations of point group I_h $a_g + t_{1u} + h_g + t_{2u}$. The first three are spanned by the 6s, 6p, and 5d atomic orbitals of an atom at the center of the icosahedron, respectively. These three levels can hold 18 electrons. This is the number of valence electrons in WAu_{12} or in the isoelectronic ions $[TaAu_{12}]^-$ and $[ReAu_{12}]^+$.
2) As pointed out in ref. [3], covalent bonding and the van der Waals (vdW) bonding behind the metallophilic

[*] Prof. Dr. P. Pyykkö, Dr. N. Runeberg
Department of Chemistry
University of Helsinki
P.O. Box 55 (A.I. Virtasen aukio 1), 00014 Helsinki (Finland)
Fax: (+358) 9-191-50169
E-mail: Pekka.Pyykko@helsinki.fi

[**] This work was supported by The Academy of Finland. The computations were carried out at CSC, Espoo, Finland.

 © WILEY-VCH Verlag GmbH, 69451 Weinheim, Germany, 2002 1433-7851/02/4112-2174 $ 20.00+.50/0

attraction may be comparable in systems such as Au_4^{2+}. It turns out that the optimized peripheral Au–Au distances here are short, about 280 pm. At this distance, two Au^I centers would feel a mutual vdW attraction of roughly up to 100 kJ mol^{-1} per pair,[4] and the icosahedron has 20 such pairs.

3) Both the radial W–Au bonds and the covalent Au–Au bonds among peripheral atoms are substantially strengthened by relativistic effects.[5]

The valence-isoelectronic Au_{13}^{5+} has been discussed earlier at the Extended Hückel level by Mingos.[6] A compound containing this cluster, $[Au_{13}(PMe_2Ph)_{10}Cl_2](PF_6)_3$, was synthesized in 1981.[7] Its icosahedron is comparable with the one studied here, but distorted. Moreover there are earlier calculations on the icosahedral, neutral clusters Au_{13}[8, 9] and $Au_{12}Pd$.[8]

Sun et al. have studied the lighter homologs MCu_{12}[10] and MAg_{12}[11] (M = Sc–Ni,Y–Ag) at the density functional theory (DFT) level with emphasis on magnetic properties and did find maximum stability around M = V or Nb (Group 5). Also the calculated sizes for the systems are comparable with the ones we present here. It must be added that DFT is not reliable for describing the dispersion or vdW part of these bonds.

We have performed ab initio calculations on the neutral icosahedral WAu_{12} cluster and the isoelectronic Ta and Re ions. In order to compare the results for the WAu_{12} cluster with a gold-only case, we have also calculated the Au_{13}^{5+} cluster. It was checked using lower-level calculations (B3LYP/LANL1DZ) that the icosahedral WAu_{12} represents a local minimum; all vibrational frequencies were real and ranged from one of symmetry h at 30 cm^{-1} to one of symmetry t_{1u} at 190 cm^{-1}. This implies thermal excitation of vibrational modes at room temperature, but no danger to the chemical stability. The totally symmetrical Raman-active a_g frequencies are given in Table 2.

Our results are shown in Table 1. The trends in bond length along the isoelectronic series for the central atom M being Ta$^-$, W, Re$^+$, Au^{5+} are given in Table 2 and suggest a minimum near tungsten. The calculated radial W–Au distance of WAu_{12} is about 268 pm at the highest TZVP + P level. It is clearly shorter than the interatomic distance in metallic gold (288 pm). It is also seen that the present isoelectronic species have shorter bonds and larger force constants than the (idealized theoretical or experimental) species Au_{13}^{5+} of Mingos. This suggests that judicious use of tungsten or its neighbors would strongly fortify gold clusters.

Table 1. Calculated distances R [pm] for W–Au and the shortest Au–Au contacts in WAu_{12}.

Method	Basis set	R(W–Au)	R(Au–Au)
RIMP2	TZVP	279.8	294.2
RIMP2	TZVPP	270.2	284.2
SCF	TZVPP	286.8	301.6
RIMP2	TZVPP + f(Au)	268.0	281.7

The role of electron correlation is seen in the comparison between the SCF and RIMP2 level results in Table 2. The W–Au distance is shortened from 287 to 270 or by 17 pm. The concomitant increase of the breathing vibration is from 116 to 147 cm^{-1}. For relativistic effects on gold, see ref. [5].

Table 2. Calculated distances R [pm] for M–Au (M = central atom) and the nearest-neighbor Au–Au contacts, as well as the force constant k [atomic units] and Raman frequency ω_e [cm^{-1}] for the symmetric stretch of the isoelectronic MAu_{12} series (M = Ta$^-$, W, Re$^+$, Au^{5+}). All calculations were done using the TZVPP basis sets.

M	Method	R(M–Au)	R(Au–Au)	k	ω_e
Ta$^-$	SCF	289.1	304.0	1.10	111
W	SCF	286.8	301.5	1.21	116
Re$^+$	SCF	286.2	301.0	1.20	116
Au^{5+}	SCF	309.0	324.9	0.42	69
Ta$^-$	RIMP2	270.4	284.3	1.86	144
W	RIMP2	270.2	284.2	1.93	147
Re$^+$	RIMP2	271.2	285.2	1.69	138
Au^{5+}	RIMP2	279.1[a]	293.4	1.12	112

[a] Experimental distances in $[Au_{13}(PMe_2Ph)_{10}Cl_2](PF_6)_3$ 271.6–278.9 pm.[7]

One possible synthetic route to WAu_{12} could go through atomic vapors of W and Au. Note that W vapor is being used in organometallic synthesis. Another pathway could involve normal chemical reactions of for example WCl_6. In liquid alloys, the binary W–Au phase diagram shows no signs of solubility or stoichiometric compounds.[12] A likely reason is that the W–W bonding is even stronger than the W–Au one. Due to the difficulty of finding thermochemical reference states for W, no stability estimates are given here.

The closed-shell electronic structure and the compact geometry of WAu_{12} should help in isolating it. Its bulk stability could be improved for example by a thiolate or xenon monolayer on the surface. The isoelectronic ions $[TaAu_{12}]^-$ and $[ReAu_{12}]^+$ could form interesting Zintl-type structures including the stoichiometric salt, possibly with covered surfaces.

In the orbital energy spectrum (Figure 1) the positions of the bonding a_g, t_{1u}, and h_g orbitals are of special interest. These three orbitals have to be occupied to fulfil the 18-electron rule. The bonding a_g orbital overlaps with the gold 5d band. The HOMO–LUMO gap is 3.0 eV at the B3LYP/LANL1DZ level. This large gap was already noted for the 3d and 4d analogs by Sun et al.[10] It is interesting that both electron- and hole-type superconductors based on the icosahedral carbon fullerenes have recently been reported.[13] The degenerate h_g symmetric HOMO and LUMO apparently play a role there. The high level of degeneration raises the density of states, which in turn raises the critical temperature. This feature of C_{60} (highly degenerate frontier orbitals) is shared by WAu_{12}. Electrochemically, the h_g HOMO could be oxidized to a maximum loss of ten electrons, and the empty h_g orbital could be reduced to a maximum gain of ten electrons.

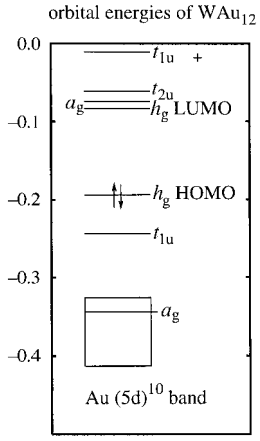


Figure 1. The B3LYP/LANL1DZ orbital energies of WAu_{12} in atomic units.

 © WILEY-VCH Verlag GmbH, 69451 Weinheim, Germany, 2002 1433-7851/02/4112-2175 $ 20.00+.50/0

Finally, just as C_{60} fullerenes yielded fullerene tubes, WAu_{12} could lead to various (now filled) extended structures. Judging from the short W–Au distances, they might have substantial mechanical strength. The mutual coupling of such structures by chemical bonds[14] or by the ionic interactions already mentioned is a further possibility.

Summarizing, if these triply stabilized, icosahedral 5d metal clusters could be made, they might provide a new structural "principle" in gold chemistry.

Computational Methods

The reported calculations have been performed at the Hartree – Fock (HF), second-order Møller – Plesset (MP2), or B3LYP DFT level. The MP2 calculations were performed within the resolution-of-identity (RI) approximation.[15, 16] The core electrons were replaced with quasirelativistic pseudopotentials[17] resulting in 14 and 19 valence electrons for W and Au, respectively. The corresponding valence basis sets are of (7s6p5d)/[6s3p3d] quality and labelled as TZVP. The TZVP was further extended by one f function for both W and Au[18] (TZVPP). The largest basis set, TZVPP + f(Au), was obtained by replacing the single f function in TZVPP by two f functions on gold.[19] All calculations have been done with the TURBOMOLE program package.[20]

Received: December 17, 2001 [Z18400]

[1] D. T. Thompson, *Gold Bull. (London)* **2001**, *34*, 56.
[2] D. A. H. Cunningham, W. Vogel, H. Kageyama, S. Tsubota, M. Haruta, *J. Catal.* **1998**, *177*, 1.
[3] P. Pyykkö, N. Runeberg, *J. Chem. Soc. Chem. Commun.* **1993**, 1812.
[4] P. Pyykkö, T. Tamm, *Organometallics* **1998**, *17*, 4842.
[5] P. Pyykkö, *Chem. Rev.* **1988**, *88*, 563. For the latest benchmarks for relativistic effects on gold atoms, molecules, and solids, see P. Pyykkö, *Angew. Chem.* **2002**, submitted.
[6] D. M. P. Mingos, *J. Chem. Soc. Dalton Trans.* **1976**, 1163. Note that only the bonding orbitals of a_g and t_{1u} symmetry were quoted. The HOMO was wrongly supposed to be t_{1u}. The present bonding h_g orbital was hidden in a 13($5d^{10}$) core band.
[7] C. E. Briant, B. R. C. Theobald, J. W. White, L. K. Bell, D. M. P. Mingos, A. J. Welch, *J. Chem. Soc. Chem. Commun.* **1981**, 201.
[8] R. Arratia-Perez, L. Hernández-Acevedo, *Chem. Phys. Lett.* **1999**, *303*, 641, and references therein.
[9] K. Michaelian, N. Rendón, I. L. Garzón, *Phys. Rev. B* **1999**, *60*, 2000.
[10] Q. Sun, X. G. Gong, Q. Q. Zheng, D. Y. Sun, G. H. Wang, *Phys. Rev. B* **1996**, *54*, 10896.
[11] Q. Sun, Q. Wang, J. Z. Yu, Z. Q. Li, J. T. Wang, Y. Kawazoe, *J. Phys. I* **1997**, *7*, 1233.
[12] A. Prince, G. V. Raynor, D. S. Evans, *Phase Diagrams of Ternary Gold Alloys*, The Institute of Metals, London, **1990**, p. 485.
[13] J. H. Schön, C. Kloc, B. Batlogg, *Nature* **2000**, *408*, 549.
[14] T. F. Fässler, *Angew. Chem.* **2001**, *113*, 4289; *Angew. Chem. Int. Ed.* **2001**, *40*, 4161.
[15] F. Weigend, M. Häser, *Theor. Chem. Acc.* **1997**, *97*, 331.
[16] F. Weigend, M. Häser, H. Patzelt, R. Ahlrichs, *Chem. Phys. Lett.* **1998**, *294*, 143.
[17] D. Andrae, U. Häussermann, M. Dolg, H. Stoll, H. Preuss, *Theor. Chim. Acta* **1990**, *77*, 123.
[18] A. W. Ehlers, M. Böhme, S. Dapprich, A. Gobbi, A. Höllwarth, V. Jonas, K. F. Köhler, R. Stegmann, A. Veldkamp, G. Frenking, *Chem. Phys. Lett.* **1993**, *208*, 111.
[19] P. Pyykkö, N. Runeberg, F. Mendizabal, *Chem. Eur. J.* **1997**, *3*, 1451.
[20] R. Ahlrichs, M. Bär, M. Häser, H. Horn, C. Kölmel, *Chem. Phys. Lett.* **1989**, *162*, 165.

Naked-Eye Sensitive Detection of Immunoglubulin G by Enlargement of Au Nanoparticles In Vitro**

Zhanfang Ma and Sen-Fang Sui*

Methods that enable the rapid, sensitive, accurate, and inexpensive detection of substances in a complex sample matrix are important tools. Immunoassays are based on the use of an antibody that reacts specifically with an antigen to be tested. The quantification of immunoassays is generally achieved by measuring the specific activity of a label, that is, its radioactivity, fluorescence, chemiluminescence, or bioluminescence. Because of its special properties which include ease of preparation, high density, large dielectric constant, and biocompatibility,[1] Au nanoparticles, as an amplification tag, have been the subject of research directed at gene analysis[2] and antibody or antigen detection.[3]

The observation of larger Au nanoparticles is beneficial. However, to increase the labeling efficiency, smaller Au nanoparticles are usually used to prepare the conjugate of the antibody or antigen and colloidal gold.[4] Particularly in histochemistry or cytochemistry, ultra-small Au nanoparticles ($\sim$1.5 nm) are essential.[5]

The sensitivity of the small immunogold particles is usually enhanced by silver staining.[6] While silver enhancement allows the signals from immunogold targeting to be seen on blots, their detecting concentration after silver staining can often reach a level of approximately a picogram per microliter ($pg\,\mu L^{-1}$).[7, 8] This is still much lower than that of fluorescent, radioactive, and enzyme-colorometric methods.[9] The lowest detecting concentration for silver staining is generally acknowledged to be 0.1 $pg\,\mu L^{-1}$.[10]

Herein we use a mixture of $HAuCl_4$ and $NH_2OH \cdot HCl$, instead of silver staining solution, to enlarge immunogold particles immobilized on the nitrocellulose strip, based on the seeding method[11] of detecting human immunoglubulin G (h-IgG) in vitro. Although silver enhancement is commonly used to visualize protein-, antibody-, and DNA-conjugated gold nanoparticles in histochemical electron microscopy studies,[4, 12] it has not been used for the enlargement of Au nanoparticles by $HAuCl_4$ and $NH_2OH \cdot HCl$ in vitro to enhance the detection of h-IgG by the naked eye. The detecting limit of the present method is significantly increased to approximately 10 $pg\,mL^{-1}$, thereby rivaling the limits of fluorescent, radioactive, and enzyme-colorometric methods.[9]

Figure 1 shows the principle behind the method used here. While NH_2OH is thermodynamically capable of reducing Au^{3+} ions to bulk metal,[13] the reaction is dramatically accelerated by Au surfaces.[14] As a result, no new particle

[*] Prof. S.-F. Sui, Dr. Z. Ma
Department of the Biological Sciences & Biotechnology
State-Key Laboratory of Biomembrane
Tsinghua University
Beijing 100084 (P. R. China)
Fax: (+86) 10-6278-4768
E-mail: suisf@mail.tsinghua.edu.cn

[**] This research was financed by grants from the National Natural Science Foundation of China (NSFC) and Tsinghua University.

 © WILEY-VCH Verlag GmbH, 69451 Weinheim, Germany, 2002 1433-7851/02/4112-2176 $ 20.00+.50/0

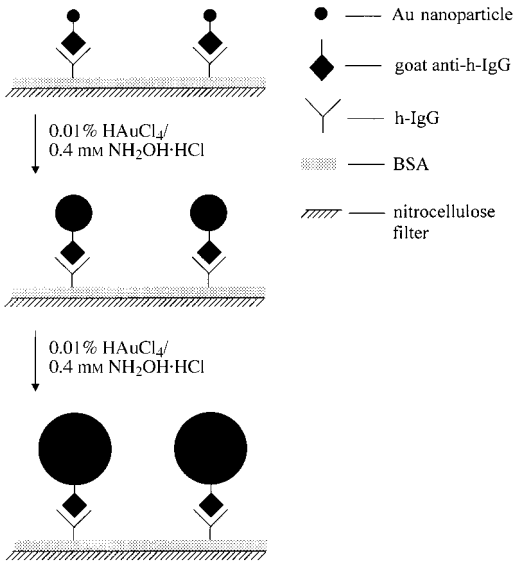


Figure 1. Schematic diagram of the immunodot assay improved by enlarging the Au nanoparticles with $HAuCl_4$ and $NH_2OH \cdot HCl$ in vitro; BSA = bovine serum albumin.

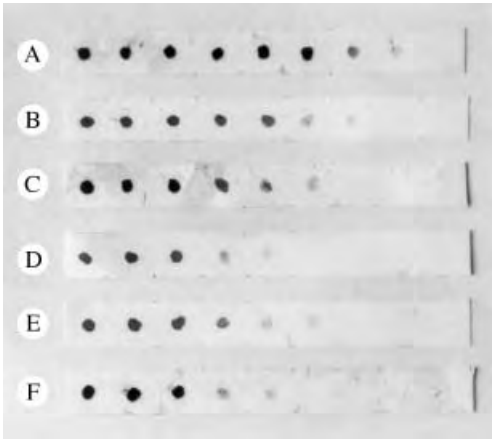


Figure 2. Immunoblot of dilutions of h-IgG detected with goat anti-h-IgG-$Au_{10\,nm}$. A 2 μL h-IgG dilution and buffer blank was applied to the nitrocellulose strips. They were then treated with 0.01 % $HAuCl_4$/0.4 mM $NH_2OH \cdot HCl$ twice (A) and once (B); with silver nitrate/hydroquinone twice (C) and once (D); and with silver acetate/hydroquinone twice (E) and once (F). The concentrations of h-IgG from left to right: 1×10^5, 4×10^4, 8×10^3, 2×10^3, 400, 300, 200, 10 pg mL^{-1}, and the buffer blank (solvent of h-IgG dilutions).

nucleation occurs in solution and all the added Au^{3+} ions go into the production of larger particles. The Au nanoparticles were immobilized on the nitrocellulose strips through the specific interaction between goat anti-h-IgG conjugated Au nanoparticles and target h-IgG preadsorbed on the nitrocellulose strips. These immobilized Au nanoparticles were enlarged by 0.01 % $HAuCl_4$ and 0.4 mM $NH_2OH \cdot HCl$. Consequently, the staining signals were considerably enhanced.

For silver staining, the detection efficiency of immunogold is closely related to the type of silver salt being used.[15] A number of silver salts, silver nitrate,[16] silver lactate,[17] and silver acetate,[18] have been used as the silver staining solution. We employed silver nitrate and silver acetate as the silver staining solution. The enlarging reaction is usually complete within 2 min,[11] therefore a time of 2 min was used for the mixture of 0.01 % $HAuCl_4$ and 0.4 mM $NH_2OH \cdot HCl$ enlargement step.

As shown in Figure 2, there is no detectable staining when the concentration of h-IgG is less than 10 and 200 pg mL^{-1}. This corresponds to the enlargement with the mixture of 0.01 % $HAuCl_4$ and 0.4 mM $NH_2OH \cdot HCl$ using double (Figure 2 A) and single staining (Figure 2 B), respectively. This result indicates that the detection limits are significantly increased to 10 and 200 pg mL^{-1}. The signals for the controls using just the solvent used for the h-IgG dilutions (20 mM Tris-HCl buffer pH 7.4, 0.15 M NaCl; Tris = tris(hydroxymethyl)-aminomethane) instead of h-IgG dilutions (Figure 2 A and B) are negative. In contrast, for silver staining with the mixture of silver nitrate and hydroquione for 30 min each in a dark room, no detectable staining can be observed when the concentration of h-IgG is less than 300 and 400 pg mL^{-1}. This concentration corresponds to the double and single staining and indicates that the detection limit is 300 pg mL^{-1} (Figure 2 C) and 400 pg mL^{-1} (Figure 2 D). Silver acetate staining gave similar results (Figure 2 E and F).

To examine the benefits of enhancing sensitivity, 10 nm Au nanoparticles (as seeds in aqueous solution) were used to study the increase of the surface area of the Au nanoparticles induced by the enlargement with 0.01 % $HAuCl_4$ and 0.4 mM $NH_2OH \cdot HCl$. The diameters of the Au nanoparticles were increased to around 60 nm and 200 nm after single and double enlargement, respectively (Figure 3). Compared with the surface areas of 10 nm Au nanoparticles without enlargement, these results mean that the surface areas of the Au nanoparticles were remarkably increased approximately 36-fold and 400-fold.

Possibly, some free Au nanoparticles exist in the conjugate of goat anti-h-IgG-$Au_{10\,nm}$. To address the nonspecific adsorption of the free Au nanoparticles on the nitrocellulose strips control experiments were performed. A 2 μL 20 mM Tris-HCl buffer (pH 7.4, 0.15 M NaCl) and a 2 μL 10 pg mL^{-1} h-IgG dilution were spotted on the nitrocellulose strips. Some of these strips were blocked with 3 % bovine serum albumin (BSA). The strips were then incubated in the free colloidal gold (10 nm) solution. The optical density $OD_{516\,nm}$ of the colloidal gold was the same as that of the conjugate of goat anti-h-IgG-$Au_{10\,nm}$. The nitrocellulose strips were treated with the mixture of 0.01 % $HAuCl_4$ and 0.4 mM $NH_2OH \cdot HCl$ for 2 min each time at 30 °C, rinsed with water, and then treated with fresh solution for another 2 min at 30 °C. Detectable staining caused by the nonspecific adsorption of free Au nanoparicles could not be observed (Figure 4). For the nitrocellulose strips without the 3 % BSA blocking, the background was very noticeable (Figure 4 B) which implies that the free Au nanoparicles were substantially adsorbed on the nitrocellulose strips. In contrast, for the nitrocellulose strips with the 3 % BSA blocking the background was fairly pale (Figure 4 A). This result suggests that 3 % BSA can effectively block the nonspecific adsorption of the free Au nanoparticles. These results demonstrate that neither nonspecific binding of gold nanoparticles nor nonspecific new gold nucleation formed onto the surface of nitrocellulose strips blocked with BSA.

 © WILEY-VCH Verlag GmbH, 69451 Weinheim, Germany, 2002 1433-7851/02/4112-2177 $ 20.00+.50/0

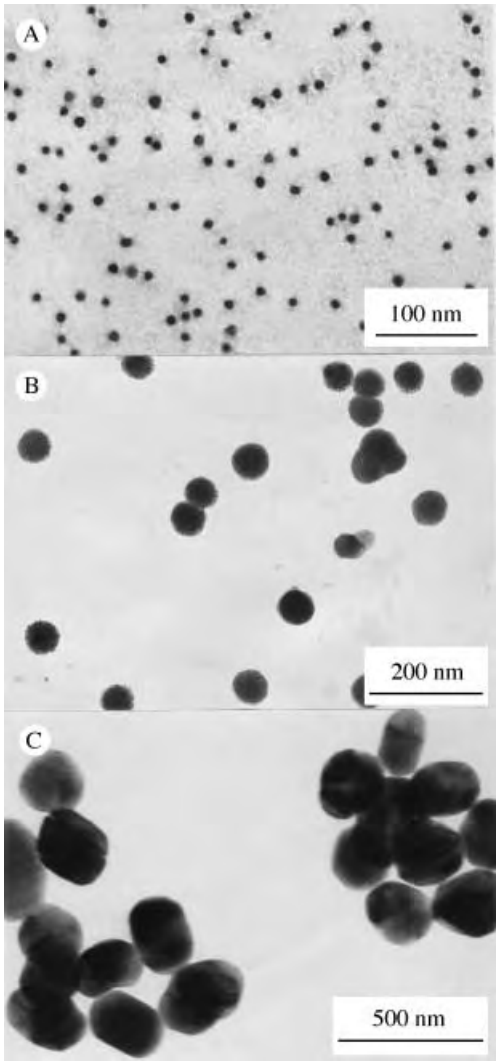


Figure 3. TEM images of Au nanoparticles enlarged by 0.01 % $HAuCl_4$ and 0.4 mM $NH_2OH \cdot HCl$ in aqueous solution. A) Seeds, B) after one treatment for 2 min, C) after two treatments each of 2 min.

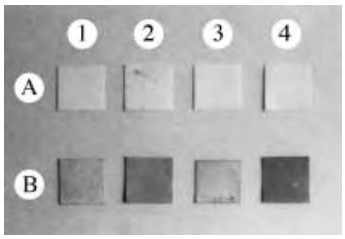


Figure 4. Effect of BSA blocking on the nonspecific adsorption of free Au nanoparticles. 2 μL 20 mM Tris-HCl buffer (pH 7.4, 0.15 M NaCl; 1 and 2) and 10 pg mL^{-1} h-IgG dilution (3 and 4) spotted onto nitrocellulose strips. These strips were incubated in a solution without Au nanoparticle and treated once (1 and 3) or twice (2 and 4) with 0.01 % $HAuCl_4$ and 0.4 mM $NH_2OH \cdot HCl$. The strips in part A were blocked while those in part B were not blocked.

In summary, enlarging Au nanoparticles immobilized on nitrocellulose strips was performed with the mixture of 0.01 % $HAuCl_4$ and 0.4 mM $NH_2OH \cdot HCl$ instead of silver staining to detect h-IgG in vitro, as a result the detection sensitivity was significantly increased to approximately 10 pg mL^{-1}. This level rivals the limits of fluorescent, radioactive, enzyme-colorometric, and chemiluminent methods. The method described is simple, rapid, economic, sensitive, specific, and is suitable for detection with the naked eye. Further experiments to understand the difference in mechanisms between the Au method and silver staining and also to compare the present method with other techniques are still underway, however, these current results suggest a new way in immunoassay.

Experimental Section

Conjugate of goat anti-h-IgG-$Au_{10\,nm}$ and h-IgG were obtained from the Xinjingke Biotechnology Company (Beijing, China). Hydrochloroauric acid ($HAuCl_4 \cdot 4H_2O$, [14-1]), hydroxylamine hydrochloride ($NH_2OH \cdot HCl$, [59-11]), silver nitrate ($AgNO_3$, [33-2]), silver acetate (AgAc, [33-61]), hydroquinone [62-4], sodium thiosulfate pentahydrate ($Na_2S_2O_3 \cdot 5H_2O$, [24-25]), aluminum potassium sulfate dodecahydrate ($KAl(SO_4)_2 \cdot 12H_2O$, [68-9]), and boric acid (H_3BO_3, [1-20]) were purchased from Beijing Chemical Reagents Company (Beijing, China, [product number]). BSA, gelatin, and Tris base were obtained from Sigma (USA). Water used in the study was Milli-Q water (18 MΩ cm^{-1}). h-IgG was diluted with 20 mM Tris-HCl buffer (pH 7.4, 0.15 M NaCl). A 2 μL of h-IgG dilutions with different concentrations were spotted on the dry nitrocellulose strips (Hybond-C, 0.45 μm; Amersham, Buckinghamshire, UK). The nitrocellulose strips were held in a dry-air thermostat at 60 °C for 1 h. The strips, after spotting, were incubated for 1 h at 37 °C in a blocking buffer (20 mM Tris-HCl, pH 7.4, 0.15 M NaCl) of 3 % BSA. The strips were then incubated in solutions of the conjugate of goat anti-h-IgG-$Au_{10\,nm}$ for 2 h at 37 °C. The strips were then fully washed with 20 mM Tris-HCl buffer (pH 7.4, 0.15 M NaCl) and Milli-Q water. Next, some strips were treated with 0.01 % $HAuCl_4$ and 0.4 mM $NH_2OH \cdot HCl$ (pH 6.0) for 2 min at 30 °C, rinsed, and then treated for two more minutes. Other strips were treated in a darkroom with silver nitrate developer (20 mM $AgNO_3$, 50 mM hydroquinone, 0.1 % gelatin, pH 3.5 citrate acid buffer), or with silver acetate developer (20 mM AgAc, 50 mM hydroquinone, 0.1 % gelatin, pH 3.5 citrate acid buffer) for 30 min at 30 °C. Some of these strips were rinsed with water and again treated with fresh silver nitrate or silver acetate developer for 30 minutes more. For the gold treatment, $NH_2OH \cdot HCl$ solution was incubated with the strips immediately after they had been incubated with 0.01 % $HAuCl_4$. For the silver treatment, hydroquinone was added to each silver developer just prior to use. A common fixer (25 % $Na_2S_2O_3$, 1.2 % $KAl(SO_4)_2$, 1.5 % Na_2SO_3, 1 % H_3BO_3, and 1 % HAc) was used for 1 min to stop the amplification prior to Milli-Q water washes. $HAuCl_4$, $NH_2OH \cdot HCl$, $AgNO_3$, and AgAc solutions were freshly prepared in a lightproof container. Only thoroughly precleaned glassware was used to prepare all of the solutions used; the removal of the dust was required from all of the materials used in the study.

Received: September 17, 2001
Revised: January 4, 2002 [Z17916]

[1] L. A. Lyon, M. D. Musick, P. C. Smith, B. D. Reiss, D. J. Pena, M. J. Natan, *Sens. Actuators*, *B* **1999**, *54*, 110 – 124.
[2] a) T. A. Taton, C. A. Mirkin, R. L. Letsinger, *Science* **2000**, *289*, 1757 – 1759; b) B. Dubertret, M. Calame, A. J. Libchaber, *Nat. Biotechnol.* **2001**, *19*, 365 – 370; c) S.-J. Park, A. A. Lazarides, C. A. Mirkin, P. W. Brazis, C. R. Kannewurf, R. L. Letsinger, *Angew. Chem.* **2000**, *112*, 4003 – 4006; *Angew. Chem. Int. Ed.* **2000**, *39*, 3845 – 3848; d) L. He, M. D. Music, S. R. Nicewarner, F. G. Salinas, S. J. Benkovic, M. J. Natan, C. D. Keating, *J. Am. Chem. Soc.* **2000**, *122*, 9071 – 9077; e) J. E. Geswicki, L. E. Strong, L. L. Kiessling, *Angew. Chem.* **2000**, *112*, 4741 – 4744; *Angew. Chem. Int. Ed.* **2000**, *39*, 4567 – 4570.
[3] K. R. Brown, A. P. Fox, M. J. Natan, *J. Am. Chem. Soc.* **1996**, *118*, 1154 – 1157.
[4] M. A. Hayat, *Colloid Gold: Principles, Methods and Applications*, *Vol. 1*, Academic Press, San Diego, **1989**.
[5] J. M. Robinson, T. Takizawa, D. D. Vandre, *J. Microsc.* **2000**, *199*, 163 – 179.

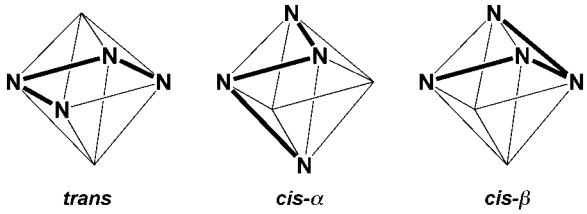
 © WILEY-VCH Verlag GmbH, 69451 Weinheim, Germany, 2002 1433-7851/02/4112-2178 $ 20.00+.50/0

[6] *Immunogold-Silver Staining: Principles, Methods and Applications* (Ed.: M. A. Hayat), Academic Press, New York, **1995**.
[7] a) P. Eliades, E. Karagouni, I. Stergiaton, K. Kiras, *J. Immunol. Methods* **1998**, *210*, 123 – 132; b) G. Mayer, R. D. Leone, J. F. Hainfeld, M. Bendayan, *J. Histochem. Cytochem.* **2000**, *48*, 464 – 469.
[8] M. G. Sumi, A. Mathai, C. Sarada, V. V. Radhakrishnan, *J. Clin. Microbiol.* **1999**, *37*, 3925 – 3927.
[9] a) V. A. J. Kempf, K. Trebesius, I. B. Autenrieth, *J. Clin. Microbiol.* **2000**, *38*, 830 – 838; b) P. Kite, B. M. Dobbins, M. H. Wilcox, M. J. McMahon, *Lancet* **1999**, *354*, 1504 – 1507; c) P. V. Coyloe, A. Desai, D. Wyatt, C. McCaughey, H. E. O'Neil, *J. Virol. Methods* **1999**, *83*, 75 – 82.
[10] J. F. Hainfeld, F. R. Furuya, *Immunogold-Silver Staining: Principles, Methods and Applications*, (Ed.: M. A. Hayat), Academic Press, New York, **1995**, p. 92.
[11] K. R. Brown, M. J. Natan, *Langmuir* **1998**, *14*, 726 – 728.
[12] R. Rufner, N. E. Carson, M. Forte, G. Danscher, J. Gu, G. W. Hacker, *Cell Vision* **1995**, *2*, 327 – 333.
[13] $E = 1$ V versus NHE(Au) and $E_{1/2} = -0.4$ V versus NHE(NH_2OH); NHE = normal hydrogen electrode. A. J. Bard, *Encyclopedia of Electrochemistry of the Elements*, *Vol. 4*, Marcel Dekker, New York, **1975**.
[14] H. Perrot, J. R. Martin, P. J. Clechet, *J. Electrochem. Soc.* **1988**, *135*, 2881 – 2885.
[15] G. W. Hacker, G. Danscher, L. Grimelius, C. Hauser-Kronberger, W. H. Muss, A. Schiechl, J. Gu, O. Dietze. *Immunogold-Silver Staining: Principles, Methods and Applications*, (Ed.: M. A. Hayat), Academic Press, New York, **1995**, p. 29.
[16] T. Krenács, E. Molnár, E. Dobó, L. Dux, *Histochem. J.* **1989**, *21*, 145.
[17] a) G. Danscher, *Histochemistry* **1981**, *71*, 1 – 16; b) G. Danscher, *Histochemistry* **1981**, *71*, 81 – 88.
[18] G. W. Hacker, L. Grimelius, G. Danscher, G. Bernatzky, W. Muss, H. Adam, J. Thurner, *J. Histotechnol.* **1988**, *11*, 213 – 221.

Ligand Topology Tuning of Iron-Catalyzed Hydrocarbon Oxidations**

Miquel Costas and Lawrence Que, Jr.*

Nature has evolved a number of nonheme iron oxygenases capable of the stereoselective oxidation of C–H and C=C bonds.[1, 2] Still far from being understood are the factors that control the ability of iron centers to catalyze a range of reactions such as alkane hydroxylation, olefin epoxidation, and olefin *cis*-dihydroxylation. In our effort to develop bio-inspired nonheme iron catalysts, we have discovered a family of iron complexes with tetradentate pyridine/amine ligands that, in combination with H_2O_2, are capable of carrying out the above transformations with high stereoselectivity.[3–7] Enantioselectivity has also been obtained with the chiral ligand *N*,*N*′-bis(2-pyridylmethyl)-*N*,*N*′-dimethyl-*trans*-1,2-diaminocyclohexane (bpmcn).[8] A priori, tetradentate ligands with this type of architecture can adopt three different topologies (Scheme 1).[9–11] While Schiff's base ligands (e.g. salen) often afford complexes with the *trans* or planar



Scheme 1. Three different topologies that can be adopted by tetradentate ligands such as *N*,*N*′-bis(2-pyridylmethyl)-*N*,*N*′-dimethyl-*trans*-1,2-diaminocyclohexane (bpmcn).

topology, ligands such as bpmcn in which the imine functionalities have been reduced give rise to complexes with *cis*-α and/or *cis*-β topologies. We have undertaken a series of systematic studies to uncover the factors that control the catalytic reactivity of the nonheme iron center in this family of complexes.[5–7] Herein we report the unexpectedly distinct oxidation behavior of two [Fe^{II}(bpmcn)] catalysts, whose structures differ only by their ligand topologies.

[Fe^{II}(bpmcn)($OTf)_2$] (**1**, OTf = trifluoromethanesulfonate) complexes in both *cis*-α and *cis*-β ligand topologies can be synthesized by independent routes, and the structures of α-**1** and the related β-[Fe^{II}(5-Me_2-bpmcn)($OTf)_2$] have recently been established by crystallography.[8, 12] The NMR spectra of the two complexes strongly suggest that they each retain their respective ligand topologies in solution (Figure 1). Complex

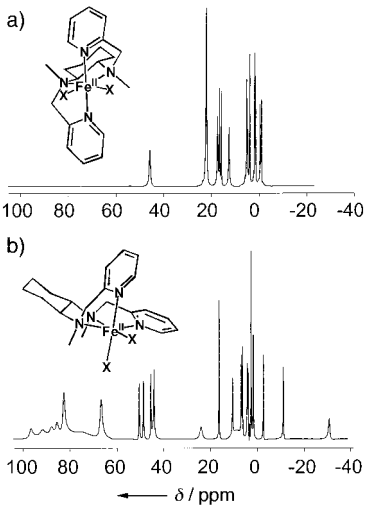


Figure 1. ^{1}H NMR spectra of α-[Fe^{II}(bpmcn)($CD_3CN)_2$]$^{2+}$ (a) and β-[Fe^{II}(bpmcn)($CD_3CN)_2$]$^{2+}$ (b) in CD_3CN solution at ambient temperature.

α-**1** exhibits 12 paramagnetically shifted signals, as expected for a C_2-symmetric high-spin Fe^{II} complex, while the β isomer shows 24 resonances. These isomers do not interconvert even after heating solutions of either isomer in acetonitrile at 50 °C for one day. The high barrier to interconversion arises from the fact that the N-methyl groups of the ligand have distinct

[*] Prof. Dr. L. Que, Jr., Dr. M. Costas
Department of Chemistry
and Center for Metals in Biocatalysis
University of Minnesota
207 Pleasant Street SE, Minneapolis, MN 55455 (USA)
Fax: (+1) 612-624-7029
E-mail: que@chem.umn.edu

[**] We thank the National Institutes of Health for financial support (GM33162 to L.Q.) and Fundacio La Caixa for a postdoctoral fellowship (M.C.).

 © WILEY-VCH Verlag GmbH, 69451 Weinheim, Germany, 2002 1433-7851/02/4112-2179 $ 20.00+.50/0

configurations in the two topologies, *anti* relative to each other in the α isomer and *syn* in the β isomer. Interconversion between the two isomers thus requires breaking of one Fe–N_{py} bond and the adjacent Fe–N_{amine} bond to allow one N-methyl group to epimerize. The inertness of the two isomers to interconversion provides us a unique opportunity to explore ligand topology effects on catalysis, and Tables 1 and 2 summarize our surprising results.

Table 1. Alkane oxidation reactivities of nonheme iron catalysts.[a]

	Fe(tpa)[b]	α-**1**	β-**1**	Fe(6-Me$_3$-tpa)[b]
cyclohexane				
A + K[c] (TN)[d]	3.2	5.9	1.9	1.4
[A]/[K]	5	9	0.9	1
KIE[e]	3.5	3.2	4.0	3.3
[$H_2{}^{18}O_2$/$H_2{}^{18}O$] (%)[f]	70/27	82/15	34/10	22/1
adamantane 3°/2°[g]	17	15	17	15
cis-DMCH[h] %RC[i]	> 99 %	> 99 %	68 %	54 %

[a] Reaction conditions: 0.7 mM catalyst, 7 mM H_2O_2, and 0.7 M substrate in CH_3CN at room temperature in air. H_2O_2 solution added by syringe pump over a 30-min period. [b] Data from references [5] and [6]. [c] A + K = alcohol + ketone. [d] TN = Turnover number. [e] KIE = Intermolecular kinetic isotope effect obtained from the competitive oxidation of *c*-C_6H_{12}/*c*-C_6D_{12} to cyclohexanol. [f] ^{18}O incorporated into cyclohexanol when $H_2{}^{18}O_2$ was used as a oxidant/when reaction was carried out in presence of 1000 equiv of $H_2{}^{18}O$. Other conditions as stated in [a]. [g] 3 × [1-adamantanol]/([2-adamantanol] + [2-adamantanone]). [h] DMCH = 1,2-dimethylcyclohexane. [i] %RC = 100 × (*cis*-*trans*)/(*cis* + *trans*).

Table 2. Olefin oxidation reactivities of nonheme iron catalysts.[a]

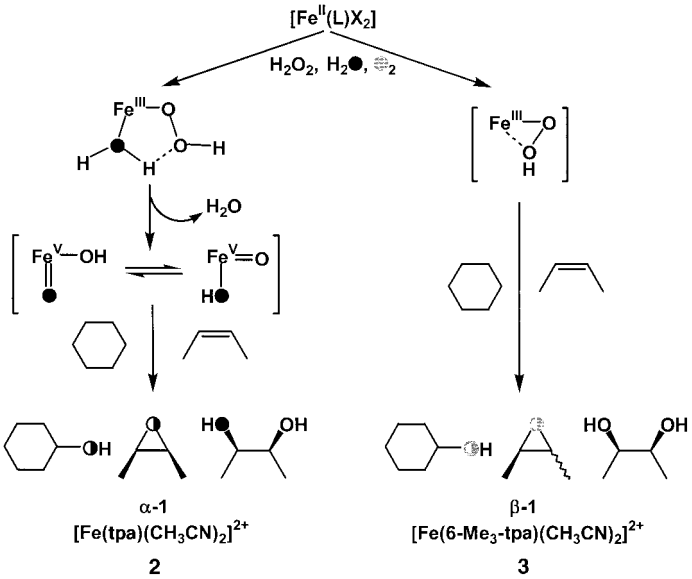
	Fe(tpa)[b]	α-**1**	β-**1**	Fe(6-Me$_3$-tpa)[b]
cyclooctene				
diol + epoxide (TN)[c]	7.4	6.5	7.7	5.6
[diol]/[epoxide]	1.2:1	0.1:1	1.8:1	7.0:1
epoxide %^{18}O [$H_2{}^{18}O_2$/$H_2{}^{18}O$](%)[d]	90/9	90/11	66/15	54/3
diol %^{18}O from $H_2{}^{18}O_2$ [noO/1O/2O](%)[e]	0/97/3	3/89/7	2/4/93	4/96
$H_2{}^{18}O$ [noO/1O/2O](%)[f]	13/86/1	11/88/1	97/3/0	99/1/0
cis-2-heptene				
diol + epoxide (TN)[c]	4.9	7.0	6.8	4.5
[diol]/[epoxide]	1.6:1	0.1:1	0.8:1	10:1
%RC[g] epoxide	80	> 99	67	35
%RC[g] diol	96	> 99	85	93
trans-2-heptene				
diol + epoxide (TN)[c]	4.8	5.7	5.6	4.1
[diol]/[epoxide]	2.2:1	0.05:1	0.6:1	13:1
%RC[g] epoxide	> 99	> 99	86	> 99
%RC[g] diol	96	> 99	81	96
1-octene				
diol + epoxide (TN)[c]	7.5	6.4	4.7	5.8
[diol]/[epoxide]	2.0:1	0.2:1	2.1:1	18:1

[a] Reaction conditions: 0.7 mM catalyst, 7 mM H_2O_2, and 0.7 M substrate in CH_3CN at room temperature in air. H_2O_2 solution added by syringe pump over a 30-min period. [b] Data from references [5] and [6]. [c] TN = Turnover number [d] ^{18}O incorporated into cyclooctene epoxide when $H_2{}^{18}O_2$ was used as a oxidant/when reaction was carried out in presence of 1000 equiv of $H_2{}^{18}O$. Other conditions as stated in [a]. [e] Percentage of *cis*-cyclooctane-1,2-diol that contains no ^{18}O/1 ^{18}O atom/2 ^{18}O atom when $H_2{}^{18}O_2$ was used as a oxidant. Other conditions as stated in [a]. [f] Percentage of *cis*-cyclooctane-1,2-diol that contains no ^{18}O/1 ^{18}O atom/2 ^{18}O atom when reaction was carried out in presence of 1000 equiv of $H_2{}^{18}O$. Other conditions as stated in [a]. [g] %RC = 100 × (*cis*-*trans*)/(*cis* + *trans*).

The data demonstrate that α-**1** is an effective catalyst for hydrocarbon oxidation, converting as much as 70% of the H_2O_2 introduced into oxidized products. Its high catalytic reactivity thus resembles that displayed by the isostructural $[Fe^{II}(bpmen)(CH_3CN)_2]^{2+}$ (bpmen = *N*,*N*′-bis(2-pyridylmethyl)-*N*,*N*′-dimethyl-1,2-diaminoethane).[13, 14] Furthermore the oxidations can be highly stereoselective. For example, the hydroxylation of *cis*-1,2-dimethylcyclohexane to the corresponding tertiary alcohol affords only the epimer with *cis*-dimethyl groups. Similarly, the oxidation of *cis*- and *trans*-2-heptene affords the corresponding epoxides and *cis*-diols with no detectable loss of stereochemistry. These stereospecific transformations, together with the high alcohol/ketone ratio obtained for cyclohexane hydroxylation, demonstrate that substrate radicals, if formed in the course of oxidation, must be quite short-lived. Thus the catalytic reactivity of α-**1** strongly parallels that of $[Fe^{II}(tpa)(CH_3CN)_2]^{2+}$ (**2**, tpa = tris(2-pyridylmethylamine)).[5–7]

Isotope-labeling experiments with $H_2{}^{18}O_2$ and $H_2{}^{18}O$ further establish the mechanistic similarity between α-**1** and **2** (Table 1 and Table 2). For cyclohexane hydroxylation and cyclooctene epoxidation carried out in the presence of H_2O, the oxygen atoms of the alcohol and epoxide products derive mainly from H_2O_2, with the balance from H_2O; little or no incorporation from O_2 is observed. Even more striking is the labeling pattern for the minor *cis*-dihydroxylation product of cyclooctene; the diol obtained from α-**1**, like that from **2**, derives one oxygen atom from H_2O_2 and the other from H_2O. These observations support the mechanism shown in Scheme 2 (left branch) invoking a low-spin Fe^{III}–OOH intermediate and a *cis*-HO–Fe^{V}=O oxidant derived therefrom; this mechanism previously proposed for **2** also accounts for all the mechanistic evidence for α-**1**.[5–7]

The oxidation behavior of β-**1** is significantly different from that of α-**1**. For this catalyst, there is strong evidence for the participation of longer lived radicals (Table 1 and Table 2): the low alcohol/ketone ratio for cyclohexane hydroxylation, the loss of stereochemistry in the oxidations of *cis*-1,2-



Scheme 2. Proposed mechanisms for the oxidations.

 © WILEY-VCH Verlag GmbH, 69451 Weinheim, Germany, 2002 1433-7851/02/4112-2180 $ 20.00+.50/0 *Angew. Chem. Int. Ed.* **2002**, *41*, No. 12

dimethylcyclohexane and *cis*-2-heptene, and the significant incorporation of O_2 into the alcohol and epoxide products. Such catalytic behavior strongly resembles that of $[Fe^{II}(6\text{-}Me_3\text{-tpa})(CH_3CN)_2]^{2+}$ (**3**).[5–7] Perhaps even more compelling is the catalysis of *cis*-dihydroxylation by β-**1**. Not only are the *cis*-diol/epoxide ratios increased by six- to tenfold relative to those observed for α-**1**, but the cyclooctene *cis*-dihydroxylation product also derives both oxygen atoms from H_2O_2, as reported for **3**.[4, 6]

Our results show that the small change in ligand topology around the metal center between α-**1** and β-**1** elicits dramatically distinct outcomes in the hydrocarbon oxidation reactions observed for these two isomers, ones that parallel the contrasting behavior of **2** and **3**. The difference between **2** and **3** is less subtle; **3** has 6-Me substituents whose steric effects affect the spin state of the Fe^{III}–OOH intermediate,[15] which in turn influences the course of the oxidations (Scheme 2, right branch).[5–7] By analogy, we propose that the distinct ligand topologies of α-**1** and β-**1** give rise to different spin states for their respective Fe^{III}–OOH intermediates. That the α-ligand topology exerts a stronger crystal field is clearly manifested in ^1H NMR experiments on the Fe^{II} catalysts in CD_3CN. While both isomers exhibit large paramagnetic shifts at 25 °C indicative of high-spin metal centers (Figure 1), the α isomer undergoes a transition to a diamagnetic low-spin form as it is cooled to -45 °C, indicated by a spectrum that spans only 12 ppm. In contrast, the β isomer remains high spin at -45 °C.

In summary, ligand effects appear to play a significant role in determining the course of hydrocarbon oxidation by nonheme iron catalysts in combination with H_2O_2. One important factor is the availability of two *cis*-labile sites as demonstrated by Chen et al.[5, 6] in a comparison of related tetradentate and pentadentate ligands and by Mekmouche et al.[16] in a comparison of $[Fe(L)X_2]$ (X = Cl or CH_3CN) catalysts. We have also shown the dramatic effect of introducing 6-methyl substituents on pyridine ligands.[5–7] Herein, we show that the catalytic chemistry can be controlled by ligand topology. This work demonstrates that exquisite tuning of the reaction mechanisms can be accomplished by subtle control of the coordination environment of the nonheme iron site. Such fine tuning may also serve as a precedent to understand the diversity on the reactions of hydrocarbon oxidation catalyzed by nonheme iron enzymes.

Experimental Section

β-$[Fe^{II}(bpmcn)(CF_3SO_3)_2]$ (β-**1**) was prepared as previously described.[8]

α-$[Fe^{II}(bpmcn)(CF_3SO_3)_2]$ (α-**1**) was prepared from α-$[Fe^{II}(bpmcn)Cl_2]$. Overnight reaction of bpmcn (1.63 g, 5 mmol) in CH_3CN (7 mL) with a vigorously stirred suspension of $FeCl_2$ (0.64 g, 5 mmol) in CH_3CN (3 mL) afforded a yellow precipitate that was filtered, washed with CH_3CN and dried under vacuum to afford the product α-$[Fe^{II}(bpmcn)Cl_2]$ (1.97 g; 87 %). Elemental analysis calcd (%) for $C_{20}H_{28}Cl_2FeN_4 \cdot H_2O$: C 51.19, H 6.44, N 11.94; found: C 51.38, H 6.20, N 12.21. A suspension of α-$[Fe^{II}(bpmcn)Cl_2]$ (800 mg, 1.78 mmol) in CH_3CN (5 mL) was then treated with a solution of $AgCF_3SO_3$ (912 mg, 3.55 mmol) in CH_3CN (4 mL), resulting in the formation of a fine precipitate of AgCl, which was filtered away after allowing the mixture to stir. The filtrate was then dried in vacuo, yielding the desired complex as a pale yellow powder. Recrystallization from CH_2Cl_2/diethyl ether afforded α-**1** as large pale yellow blocks (1.19 g, 99 %). Elemental analysis calcd (%) for $C_{22}H_{28}F_6FeN_4O_6S_2$: C 38.95, H 4.16, N 8.26, S 9.45; found: C 38.97, H 4.37, N 8.30, S 9.41.

Received: January 16, 2002
Revised: March 19, 2002 [Z18530]

[1] L. Que, Jr., R. Y. N. Ho, *Chem. Rev.* **1996**, *96*, 2607 – 2624.
[2] E. I. Solomon, T. C. Brunold, M. I. Davis, J. N. Kemsley, S.-K. Lee, N. Lehnert, F. Neese, A. J. Skulan, Y.-S. Yang, J. Zhou, *Chem. Rev.* **2000**, *100*, 235 – 349.
[3] C. Kim, K. Chen, J. Kim, L. Que, Jr., *J. Am. Chem. Soc.* **1997**, *119*, 5964 – 5965.
[4] K. Chen, L. Que, Jr., *Angew. Chem.* **1999**, *111*, 2365—2368; *Angew. Chem. Int. Ed.* **1999**, *38*, 2227 – 2229.
[5] K. Chen, L. Que, Jr., *J. Am. Chem. Soc.* **2001**, *123*, 6327 – 6337.
[6] K. Chen, M. Costas, J. Kim, A. K. Tipton, L. Que, Jr., *J. Am. Chem. Soc.* **2002**, *124*, 3026 – 3035.
[7] K. Chen, M. Costas, L. Que, Jr., *J. Chem. Soc. Dalton Trans.* **2002**, 672 – 679.
[8] M. Costas, A. K. Tipton, K. Chen, D.-H. Jo, L. Que, Jr., *J. Am. Chem. Soc.* **2001**, *123*, 6722 – 6723.
[9] J. R. Aldrich-Wright, R. S. Vagg, P. A. Williams, *Coord. Chem. Rev.* **1997**, *166*, 361 – 389.
[10] U. Knof, A. von Zelewsky, *Angew. Chem.* **1999**, *111*, 312—333; *Angew. Chem. Int. Ed.* **1999**, *38*, 302 – 322.
[11] C. Ng, M. Sabat, C. L. Fraser, *Inorg. Chem.* **1999**, *38*, 5545 – 5556.
[12] M. Costas, J.-U. Rohde, A. Stubna, R. Y. N. Ho, L. Quaroni, E. Münck, L. Que, Jr., *J. Am. Chem. Soc.* **2001**, *123*, 12931 – 12932.
[13] K. Chen, L. Que, Jr., *Chem. Commun.* **1999**, 1375 – 1376.
[14] M. C. White, A. G. Doyle, E. N. Jacobsen, *J. Am. Chem. Soc.* **2001**, *123*, 7194 – 7195.
[15] Y. Zang, J. Kim, Y. Dong, E. C. Wilkinson, E. H. Appelman, L. Que, Jr., *J. Am. Chem. Soc.* **1997**, *119*, 4197 – 4205.
[16] Y. Mekmouche, S. Ménage, C. Toia-Duboc, M. Fontecave, J.-B. Galey, C. Lebrun, J. Pecaut, *Angew. Chem.* **2001**, *113*, 975—978; *Angew. Chem. Int. Ed.* **2001**, *40*, 949 – 952.

Design of a Bilayer Structure in an Organic Inclusion Compound**

Sang-Ok Lee, Benson M. Kariuki, and Kenneth D. M. Harris*

Since their discovery over 50 years ago,[1, 2] several hundreds of urea inclusion compounds[3–11] have been prepared containing different types of guest molecules (mainly based on *n*-alkane chains, with only a limited degree of substitution allowed). The vast majority of urea inclusion compounds are based on a hexagonal host structure[3, 12] that comprises continuous, parallel tunnels constructed from a hydrogen-bonded arrangement of urea molecules. These "conventional"

[*] Prof. Dr K. D. M. Harris, Dr S.-O. Lee, Dr B. M. Kariuki
School of Chemical Sciences
University of Birmingham
Edgbaston, Birmingham B15 2TT (United Kingdom)
Fax: (+44) 121-414-7473
E-mail: K.D.M.Harris@bham.ac.uk

[**] We are grateful to the EPSRC, the University of Birmingham, and CVCP for financial support.

 © WILEY-VCH Verlag GmbH, 69451 Weinheim, Germany, 2002 1433-7851/02/4112-2181 $ 20.00+.50/0

urea inclusion compounds are characterized by a hexagonal host tunnel structure (space group $P6_122$ or $P6_522$), an incommensurate relationship[13] between the periodicities of the host and guest substructures along the tunnel axis, and substantial dynamic disorder (reorientation about the tunnel axis) of the guest molecules at ambient temperature. In a few cases,[19–23] a distorted tunnel structure is formed at ambient temperature, usually when the length of the guest molecule is close to a simple multiple of the periodic repeat distance of the urea tunnel, which allows a commensurate structure to be formed. Different host structures are also known to be formed with some polymeric guests.[24–27] However, in all of these cases, the urea host structure still comprises continuous 1D tunnels constructed from an essentially infinite 3D hydrogen-bonded network of urea molecules.

Given the similarity of the continuous-tunnel-type host structures in all of these urea inclusion compounds, it would clearly be of interest to find a fundamentally different type of urea host structure in an inclusion compound containing alkane-based guest molecules, and recently[28] we reported the first case of this type. In particular, for 1,7-diaminoheptane ($H_2N(CH_2)_7NH_2$) guest molecules, a new type of layered host–guest structure is formed. Within each layer, there are local segments of urea tunnel structure, which are structurally and topologically very similar to the conventional urea tunnel structure, and the thickness of each layer corresponds to the length of a single guest molecule. Adjacent layers are displaced relative to each other (parallel to the plane of the layers) such that the local segments of tunnel in adjacent layers do not form a continuous tunnel. Adjacent layers are held together through hydrogen bonds to methanol molecules (the solvent normally employed for crystal growth of urea inclusion compounds) that are present in the interlayer region, and the methanol molecules form hydrogen bonds both to urea molecules and to the NH_2 end groups of the 1,7-diaminoheptane guest molecules. Notably, there are no hydrogen-bonding interactions between the NH_2 end groups of the 1,7-diaminoheptane guest molecules and urea molecules. Subsequently,[29] we have shown that for other α,ω-diaminoalkane-guest molecules ($H_2N(CH_2)_nNH_2$; $n = 7-10$, 12) similar layered structures are formed, with the thickness of the layer corresponding to the length of a single guest molecule in each case. Again, there are methanol molecules in the interlayer region, and within the layer, the guest molecule is contained within a segment of tunnel that is structurally very similar to that in the conventional urea inclusion compounds.

Given the apparent robustness of this structure type for those urea inclusion compounds in which the guest molecules contain NH_2 end groups and in the presence of methanol, we now explore whether this structure type may be exploited as a design component in the formation of a more diverse range of structures for urea inclusion compounds. Herein, we recall that alkane ($CH_3(CH_2)_nCH_3$) guest molecules form urea inclusion compounds comprising continuous tunnels, whereas the end groups of α,ω-diaminoalkane ($H_2N(CH_2)_nNH_2$) guest molecules promote the formation of the new layered structure type. We therefore speculate that, for 1-aminoalkane ($H_2N(CH_2)_nCH_3$) guest molecules, the NH_2 end group may promote the formation of layers, but that the CH_3 end group will propagate a continuous tunnel. Thus, we predict that a layered structure analogous to that of the α,ω-diaminoalkane/urea/methanol systems should be formed, but in which the guest component within each layer is the "dimer" unit $H_2N(CH_2)_nCH_3\cdots H_3C(CH_2)_nNH_2$, which thus gives rise to a bilayer structure, in which the thickness of the layer is approximately double that of the corresponding α,ω-diaminoalkane/urea/methanol material.

To assess this design strategy, crystals were grown from a solution containing 1-aminooctane ($H_2N(CH_2)_7CH_3$) and urea in methanol. Powder X-ray diffraction analysis of the crystals obtained indicates a new structure type, with no detectable amounts of conventional urea inclusion compounds present in the sample.

The structure of the new material was determined from single-crystal X-ray diffraction data,[30] and is found to contain methanol, in addition to urea and 1-aminooctane, with the stoichiometry (1-aminooctane)$_2$(urea)$_{15}$(methanol)$_2$. The structure is monoclinic with space group $C2/c$ and $a = 8.08$, $b = 14.62$, $c = 59.62$ Å, $\beta = 90.61°$. For comparison, the structure of (1,7-diaminoheptane)$_1$(urea)$_7$(methanol)$_2$[28] also has space group $C2/c$, with $a = 8.32$, $b = 13.95$, $c = 29.03$ Å, $\beta = 95.03°$. Clearly the main difference between these structures is the approximate doubling of the c axis in the case of 1-aminooctane. The a and b axes are close to the orthohexagonal description of the ab plane of the host structure in the conventional urea inclusion compounds, and Figure 1 shows the tunnel segments within each layer of the 1-aminooctane/urea/methanol structure. The hydrogen-bonding topology of the urea molecules within these tunnel segments is essentially the same as that in the conventional urea tunnel structure. There are two layers within the repeat unit along the c axis, and the thickness (ca. 29 Å) of each layer is close to the length

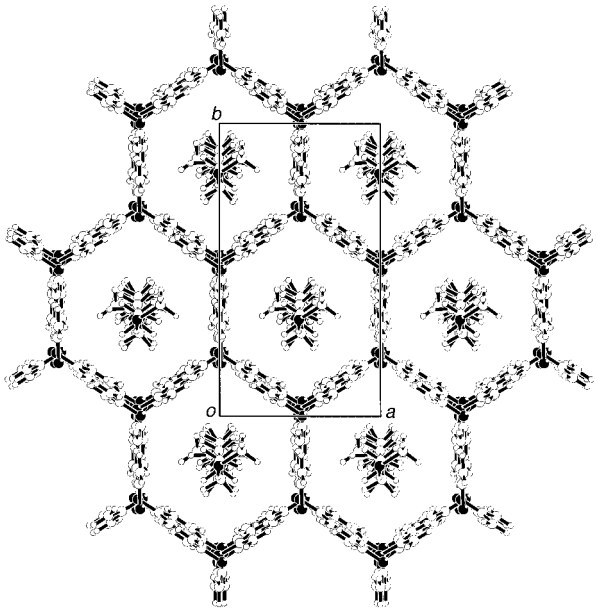


Figure 1. A single host–guest bilayer in the structure of the 1-aminooctane/urea/methanol inclusion compound, viewed along the c axis (perpendicular to the layer). The adjacent bilayer is stacked on top of this bilayer with an offset in the ab plane such that continuous tunnels along the c axis are not formed.

 © WILEY-VCH Verlag GmbH, 69451 Weinheim, Germany, 2002 1433-7851/02/4112-2182 $ 20.00+.50/0 *Angew. Chem. Int. Ed.* **2002**, *41*, No. 12

of two 1-aminooctane guest molecules. Within a given layer, all the helical tunnel segments have the same chirality, and the helical tunnel segments in adjacent layers have opposite chirality. The methanol molecules are located between adjacent layers (see Figure 2) and are engaged in hydrogen-bonding interactions with the NH_2 end groups of the 1-aminooctane guest molecules, and with urea molecules at the surface of the layers, in a direct analogy to the structure of the 1,7-diaminoheptane/urea/methanol inclusion compound; this analogy supports the view that this hydrogen-bonding motif is structurally robust, which clearly directs the structure formed in the present case. This view is further supported by the $CH_3 \cdots H_3C$ distance within the guest "dimer" in each layer. In this structure, the $C \cdots C$ distance is 4.761(8) Å, which is significantly longer than the van der Waals contact of two methyl groups (which corresponds to a $C \cdots C$ distance of approximately 4.0 Å, based on twice the van der Waals radius of the methyl group quoted by Pauling[33]). In contrast, a universal feature of conventional urea inclusion compounds is the close packing of the guest molecules along the tunnel,[6, 14] which is an important factor in promoting the incommensurate nature of these materials. For 1-aminooctane/urea/methanol, on the other hand, the main structure-directing effect is the formation of the hydrogen-bonding arrangement (which involves NH_2 end groups, urea molecules, and methanol molecules) at the surface of each layer and within the interlayer region. In the present case, this hydrogen-bonding arrangement is clearly favored at the expense of the optimal guest–guest interaction (corresponding to the van der Waals separation) between adjacent guest molecules within the layer. The formation of the region of locally empty urea tunnel, which arises from the van der Waals "gap" between the CH_3 end groups of adjacent guest molecules in this structure, is a novel feature that is not observed in conventional urea inclusion compounds. One consequence of this structural feature is that the number of urea molecules (15) associated with the $H_2N(CH_2)_7CH_3 \cdots H_3C(CH_2)_7NH_2$ "dimer" unit in the bilayer structure is greater than the number of urea molecules (14) associated with two 1,7-diaminoheptane guest molecules (i.e. in two layers) of the 1,7-diaminoheptane/urea/methanol system. Another consequence is that the density of the 1-aminooctane/urea/methanol crystal (calculated, 1.15 g cm^{-3}) is appreciably lower than that of the 1,7-diaminoheptane/urea/methanol crystal (calculated, 1.22 g cm^{-3}).

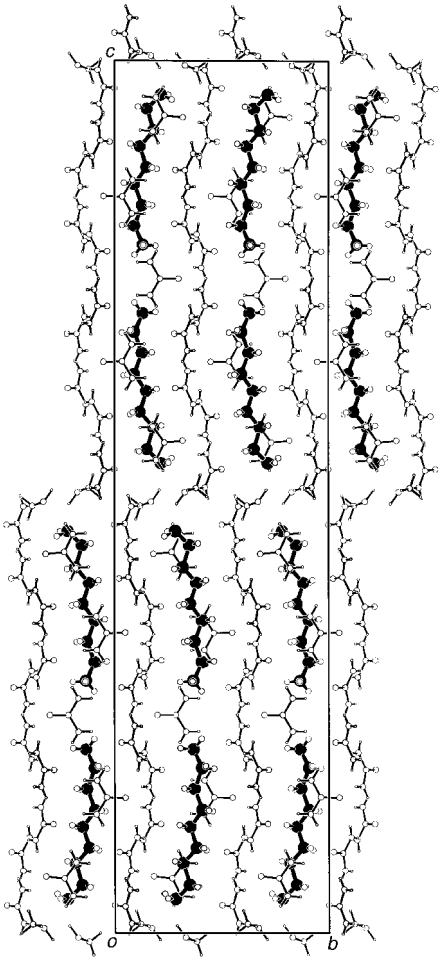


Figure 2. The complete structure of the 1-aminooctane/urea/methanol inclusion compound viewed along the *a* axis. The significant "gap" between the CH_3 end groups of adjacent guest molecules within the bilayer is evident.

The work reported herein demonstrates that the hydrogen-bonding motif formed between NH_2 end groups of aminoalkanes, urea molecules, and methanol molecules is a robust and reproducible structural motif which may be exploited in a structure-directing manner, as illustrated by the formation of the bilayer structure described here.[34] The end group separation (in this case $CH_3 \cdots H_3C$) between adjacent guest molecules within the layer is significantly greater than the van der Waals separation and may be exploited as a means of characterization of such interactions. Indeed, by forming analogous structures for a systematic series of 1-aminoalkanes $H_2N(CH_2)_nCH_3$ as a function of n, we may expect to observe a set of different, but in each case well-defined, end-group separation distances.

Received: January 4, 2002 [Z18479]

[1] M. F. Bengen, Ger. Patent 123438, **1940**.
[2] M. F. Bengen, Ger. Patent 869070, **1953** [*Chem. Abstr.* **1954**, *48*, 11479c].
[3] A. E. Smith, *Acta Crystallogr.* **1952**, *5*, 224.
[4] R. W. Schiessler, D. Flitter, *J. Am. Chem. Soc.* **1950**, *72*, 1720.
[5] L. C. Fetterly in *Non-stoichiometric Compounds* (Ed.: L. Mandelcorn), Academic Press, New York, **1964**, p. 491.
[6] F. Laves, N. Nicolaides, K. C. Peng, *Z. Kristallogr.* **1965**, *121*, 258.
[7] K. Takemoto, N. Sonoda in *Inclusion Compounds*, *Vol. 2* (Eds.: J. L. Atwood, J. E. D. Davies, D. D. MacNicol), Academic Press, New York, **1984**, p. 47.
[8] M. D. Hollingsworth, K. D. M. Harris in *Comprehensive Supramolecular Chemistry*, *Vol. 6* (Eds.: D. D. MacNicol, F. Toda, R. Bishop), Pergamon, Oxford, **1996**, p. 177.
[9] K. D. M. Harris, *Chem. Soc. Rev.* **1997**, *26*, 279.
[10] K. D. M. Harris, *J. Chin. Chem. Soc.* **1999**, *46*, 5.
[11] F. Guillaume, *J. Chim. Phys.* **1999**, *96*, 1295.
[12] K. D. M. Harris, J. M. Thomas, *J. Chem. Soc. Faraday Trans.* **1990**, *86*, 2985.
[13] The structural relationship between the periodicity of the host structure (c_h) along the tunnel and the periodicity of the guest molecules (c_g) along the tunnel is incommensurate if there are no sufficiently small integers p and q that satisfy the relationship: $p\,c_g =$

$q\,c_h$. Thus, c_g/c_h is not equal to a rational number with a sufficiently small denominator. The nature of incommensurate versus commensurate behavior in tunnel inclusion compounds is discussed elsewhere.[12, 14–18]

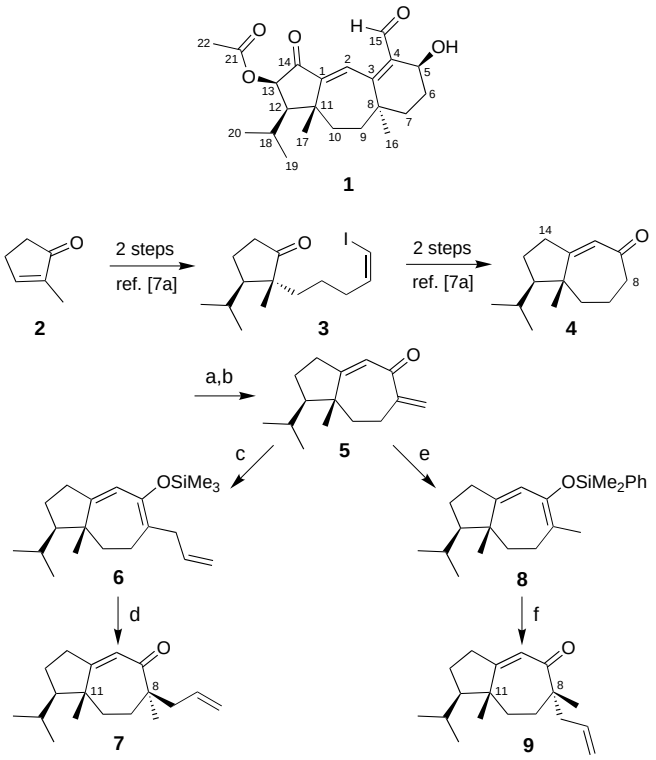
[14] A. J. O. Rennie, K. D. M. Harris, *Proc. R. Soc. London Ser. A* **1990**, *430*, 615.
[15] K. D. M. Harris, M. D. Hollingsworth, *Proc. R. Soc. London Ser. A* **1990**, *431*, 245.
[16] S. van Smaalen, K. D. M. Harris, *Proc. R. Soc. London Ser. A* **1996**, *452*, 677.
[17] R. Lefort, J. Etrillard, B. Toudic, F. Guillaume, T. Breczewski, P. Bourges, *Phys. Rev. Lett*. **1996**, *77*, 4027.
[18] T. Weber, H. Boysen, F. Frey, R. B. Neder, *Acta Crystallogr. Sect. B* **1997**, *53*, 544.
[19] S. P. Smart, Ph.D. Thesis, University of St. Andrews, **1993**.
[20] M. D. Hollingsworth, B. D. Santarsiero, K. D. M. Harris, *Angew. Chem.* **1994**, *106*, 698; *Angew. Chem. Int. Ed. Engl.* **1994**, *33*, 649.
[21] M. E. Brown, J. D. Chaney, B. D. Santarsiero, M. D. Hollingsworth, *Chem. Mater.* **1996**, *8*, 1588.
[22] M. D. Hollingsworth, M. E. Brown, A. C. Hillier, B. D. Santarsiero, J. D. Chaney, *Science* **1996**, *273*, 1355.
[23] M. D. Hollingsworth, U. Werner-Zwanziger, M. E. Brown, J. D. Chaney, J. C. Huffman, K. D. M. Harris, S. P. Smart, *J. Am. Chem. Soc.* **1999**, *121*, 9732.
[24] K. Suehiro, A. Urabe, Y. Yoshitake, Y. Nagano, *Makromol. Chem.* **1984**, *185*, 2467.
[25] A. Chenite, F. Brisse, *Macromolecules* **1991**, *24*, 2221.
[26] A. Chenite, F. Brisse, *Macromolecules* **1992**, *25*, 776.
[27] P. Eaton, N. Vasanthan, I. D. Shin, A. E. Tonelli, *Macromolecules* **1996**, *29*, 2531.
[28] S.-O.Lee, B. M. Kariuki, A. L. Richardson, K. D. M. Harris, *J. Am. Chem. Soc.* **2001**, *123*, 12684.
[29] S.-O.Lee, B. M. Kariuki, K. D. M. Harris, unpublished results.
[30] Crystal data: $2(C_8H_{19}N)\cdot 15(CH_4N_2O)\cdot 2(CH_4O)$; $M_r = 1223.50$; monoclinic; $a = 8.079(5)$, $b = 14.620(10)$, $c = 59.62(3)$ Å, $\beta = 90.612(9)$; $V = 7041(7)$ Å^3; $T = 273$ K; space group $C2/c$ (no. 15); $Z = 4$; $\mu(Mo_{K\alpha}) = 0.092$ mm^{-1}. Single-crystal X-ray diffraction data were recorded on a Rigaku R-Axis IIc diffractometer equipped with a molybdenum rotating-anode source and an image-plate detector system. The structure was solved using SHELXS-86[31] and refined using SHELXL-97.[32] The hydrogen atoms of 1-aminooctane were found in the difference Fourier map and their geometry was thereafter restrained. The other hydrogen atoms were placed in calculated positions and a riding model was used for refinement of these atoms. The highest peak (0.45 e Å^{-3}) in the final difference Fourier map was located close (0.6 Å) to one of the CH_2 carbon atoms of the 1-aminooctane guest molecule (the CH_2 group bonded to the CH_3 group)—there was no evidence for "missing" electron density within the "gap" between the CH_3 end groups of adjacent guest molecules within the bilayer. Final R indices: $R1 = 0.084$, $wR2 = 0.24$. CCDC-176977 contains the supplementary crystallographic data for this paper. These data can be obtained free of charge via www.ccdc.cam.ac.uk/conts/retrieving.html (or from the Cambridge Crystallographic Data Centre, 12, Union Road, Cambridge CB2 1EZ, UK; fax: (+44) 1223-336-033; or deposit@ccdc.cam.ac.uk).
[31] G. M. Sheldrick, SHELXS-86, Program for Crystal Structure Solution, University of Göttingen, Göttingen (Germany), **1986**.
[32] G. M. Sheldrick, SHELXS-97, Program for Crystal Structure Refinement, University of Göttingen, Göttingen (Germany), **1997**.
[33] L. Pauling, *The Nature of the Chemical Bond*, Cornell University Press, Ithaca, New York, 3rd ed., **1960**.
[34] In a general context, we note that bilayer-packing motifs have recently been cited as being of importance in solid-state reactivity.[35] Furthermore, conventional urea inclusion compounds have found applications with regard to chemical reactivity—for example, see reference [36].
[35] M. J. Vela, B. M. Foxman, *Cryst. Eng.* **2000**, *3*, 11.
[36] *Photochemistry in Organized and Constrained Media* (Ed.: V. Ramamurthy), VCH, New York, **1991**.

 © WILEY-VCH Verlag GmbH, 69451 Weinheim, Germany, 2002 1433-7851/02/4112-2184 $ 20.00+.50/0

Synthesis of the Functionalized Tricyclic Skeleton of Guanacastepene A: A Tandem Epoxide-Opening β-Elimination/Knoevenagel Cyclization**

Derek S. Tan, Gregory B. Dudley, and Samuel J. Danishefsky*

Guanacastepene A (**1**, Scheme 1) is the parent member of a family of diterpene natural products produced by an unclassified endophytic fungus from the Guanacaste Conservation Area in Costa Rica.[1] Initial interest in this compound arose from its activity against antibiotic-resistant bacteria. However, subsequent experiments in *E. coli imp* and observed hemolytic activity against human red blood cells supported nonspecific membrane lysis as its mode of action.[1b] Despite the discouraging implications for its usefulness as an antibiotic,[2] guanacastepene A remains a synthetic target of current interest owing to its novel structure and the possibility of exploring the activity of this family in other biological assays.[1c] Interestingly, the cultured fungus no longer produces guanacastepene A.[3] To date, synthetic studies have been reported by a number of other groups[4–6,28] as well as by our group.[7]



Scheme 1. Structure of guanacastepene A (**1**) and synthesis of epimeric allyl methyl hydroazulenones **7** and **9**. a) LiHMDS, THF, $-78\,^{\circ}C$, 1 h, then add to Eschenmoser's salt (Me_2NCH_2I), THF, $-78\,^{\circ}C \rightarrow RT$, 20 min; b) MCPBA, CH_2Cl_2/aqueous $NaHCO_3$ (2:1), 86% over two steps; c) $CH_2{=}CHMgBr$, CuI, HMPA, TMSCl, THF, $-78\,^{\circ}C$, 25 min; d) MeLi, THF, $0\,^{\circ}C$, 10 min, then MeI, HMPA, $-78\,^{\circ}C \rightarrow RT$, 20 min, 77% over two steps; e) $PhMe_2SiH$, Wilkinson's catalyst ($[Ph_3P]_3RhCl$; 1%), benzene, reflux, 20 min; f) MeLi, THF, $0\,^{\circ}C$, 10 min, then allyl iodide, $-78\,^{\circ}C \rightarrow RT$, 30 min, 69% over two steps. HMDS = hexamethyldisilazane, MCPBA = *m*-chloroperoxybenzoic acid, HMPA = hexamethyl phosporamide, TMS = trimethylsilyl.

[*] Prof. Dr. S. J. Danishefsky, Dr. D. S. Tan, Dr. G. B. Dudley
Laboratory for Bioorganic Chemistry
Sloan-Kettering Institute for Cancer Research
1275 York Ave., New York, NY 10021 (USA)
Fax: (+1) 212-772-8691
Department of Chemistry, Columbia University
Havemeyer Hall, 3000 Broadway, New York, NY 10027 (USA)
E-mail: s-danishefsky@ski.mskcc.org

[**] This work was supported by the National Institutes of Health (HL-25848 and CA-28824). D.S.T. is a Damon Runyon Cancer Research Foundation postdoctoral fellow (DRG-1641). G.B.D. is an NIH postdoctoral fellow (1 F32 NS11150-01). We thank Dr. George Sukenick and Sylvi Rusli (NMR Core Facility, CA-02848) for mass spectral analyses.

Supporting information for this article is available on the WWW under http://www.angewandte.org or from the author.

Our next goal was that of constructing the novel tricyclic core of guanacastepene A from the suitably configured hydroazulenone **7**. Naively, we thought this would be a straightforward matter following traditional methods of steroid and terpenoid annulation. As we show herein, the pathway from **7** to the core system was beset by several unanticipated difficulties. Fortunately, the solution devised to solve these problems carried us closer to the total synthesis goal than would have been the case through the envisioned sequence.

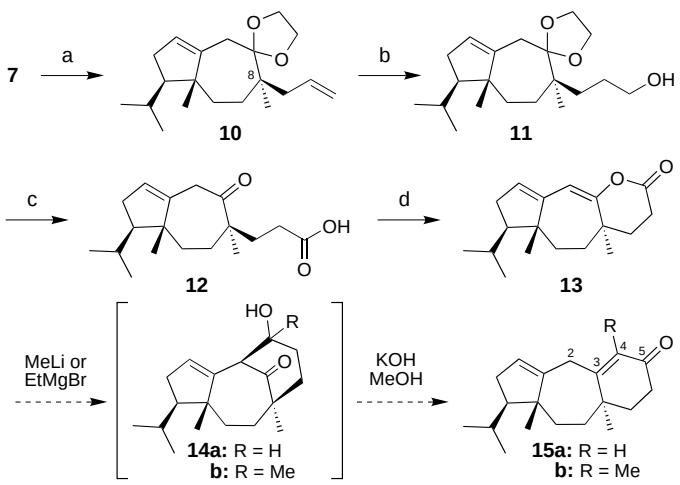
The early phase of our approach to guanacastepene A, outlined in Scheme 1, exploited successive β,α-dialkylation to fashion vinyl iodide **3**. Reductive cyclization followed by oxidative rearrangement led to **4**.[7a] Upon α-methylenation of **4** by means of the Eschenmoser salt[8a] Mannich protocol,[8b,c] compound **5** was available.[7b] As previously reported and amplified in Scheme 1, the stereochemistry at C8 (guanacastepene A numbering) can be controlled by stepwise introduction of two alkyl groups with due attention to proper sequencing. In the case of geminal allyl and methyl groups, the group introduced second enters from the face of C8 that is *anti* to the angular methyl group attached to C11 (i.e., α as shown). Correspondingly, the resident group emerges in the β configuration in **7** and **9**.

Elaboration of 8β-allyl-8α-methyl hydroazulenone **7** proceeded in analogy to literature precedent (Scheme 2).[9] Protection of the enone as a dioxolane (**10**) with concurrent double-bond migration[10] allowed efficient hydroboration and oxidation to yield alcohol **11**.[11] Jones oxidation[12] simultaneously installed the side-chain carboxylate and removed the dioxolane protecting group to generate keto acid **12**. Notably, reconjugation of the enone did not occur under these conditions. Cyclization of **12** afforded dienol lactone **13** in moderate yield.[13]

At this stage, we attempted to employ a Turner–Fujimoto protocol to generate tricycles **15a** and **15b**.[14] Unfortunately, after the addition of either methyllithium or ethylmagnesium bromide, we obtained complex mixtures of products that were not resolved by equilibration in refluxing methanolic potassium hydroxide.[15] Although the reasons for the failure of these reactions were unclear at the time, subsequent experiments suggest that complications involving C2 may thwart the desired cyclizations.

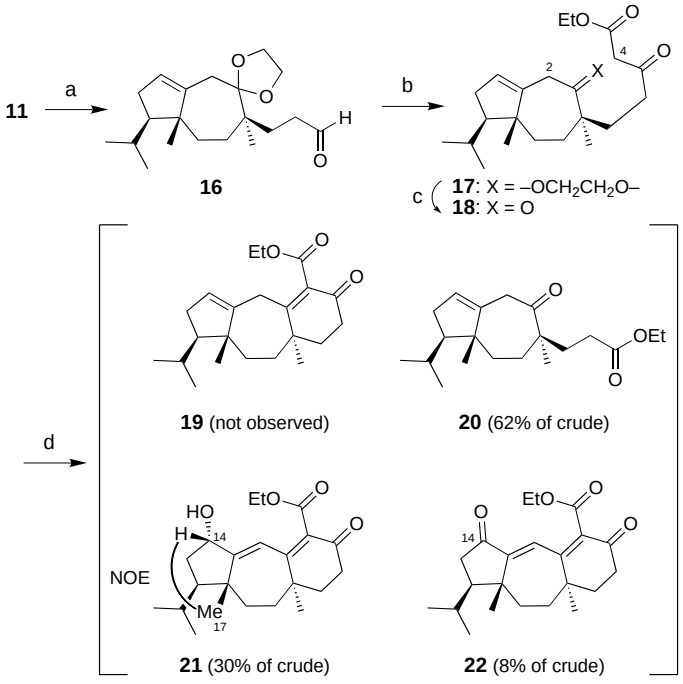
In light of the complexities of the multistep Turner–Fujimoto sequence,[15] we elected to pursue an alternative route to the tricyclic core through direct Knoevenagel cyclization of

 © WILEY-VCH Verlag GmbH, 69451 Weinheim, Germany, 2002 1433-7851/02/4112-2185 $ 20.00+.50/0



Scheme 2. Synthesis of dienol lactone **13** and attempted Turner–Fujimoto reactions. a) Ethylene glycol, TsOH, benzene, reflux, [$-H_2O$], 36 h, 89%; b) 1) 9-BBN, THF, 0 °C→RT, 3.5 h; 2) NaOH (aqueous, 3 N), H_2O_2 (aqueous, 30%), room temperature, 1.5 h, 98%; c) CrO_3, H_2SO_4, acetone, room temperature, 2 h, 62%; d) NaOAc, Ac_2O, 140 °C, 80 min, 59%. TsOH = *p*-toluene sulfonic acid, 9-BBN = 9-borabicyclo[3.3.1]nonane.

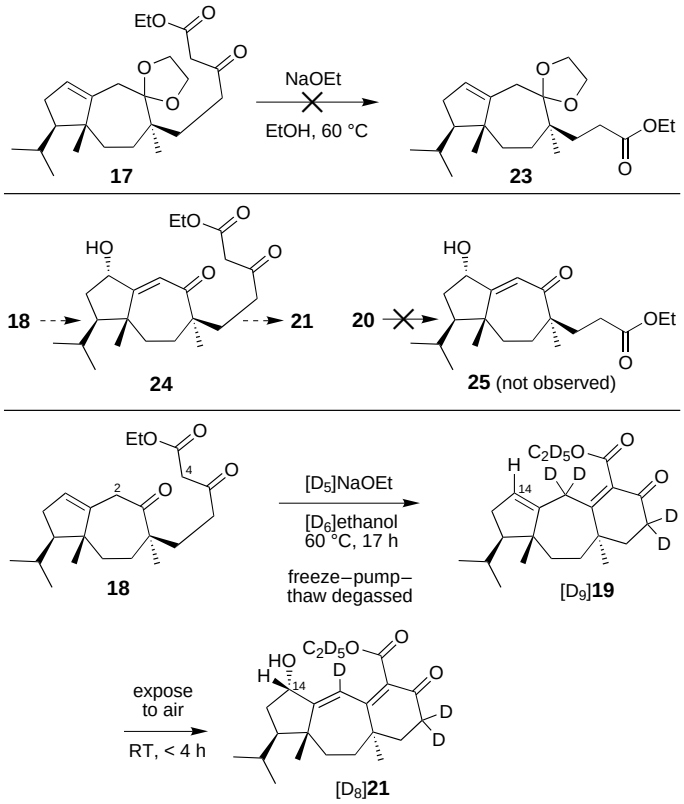
the discrete β-keto ester precursor **18** (Scheme 3). We recognized that the ethyl ester in **18** could also serve as a suitable precursor to the required C15 aldehyde in guanacastepene A (**1**). Toward this end, alcohol **11** was oxidized[16] to give aldehyde **16**, which was then converted directly into β-keto ester **17** by using ethyl diazoacetate and tin(II) chloride.[17] Deprotection of the dioxolane[18] afforded β,ζ-diketo ester **18**.[19]



Scheme 3. Conversion of alcohol **11** into β,ζ-diketo ester **18** and attempted Knoevenagel cyclization. a) Dess–Martin periodinane, CH_2Cl_2, room temperature, 2 h, 83%; b) ethyl diazoacetate ($N_2CHCOOEt$), $SnCl_2$, CH_2Cl_2, room temperature, 3.5 h; c) TsOH, H_2O in acetone (5%), 70 °C, 90 min, 80% over two steps; d) NaOEt, EtOH, 60 °C, 19 h.

With the desired substrate in hand, we were poised to attempt the key Knoevenagel cyclization.[20] Exposure of **18** to sodium ethoxide in ethanol at 60 °C resulted in slow conversion into a mixture of products.[21] Surprisingly, the expected cyclization product **19** was not observed. Instead, the major product was the "truncated" ethyl ester **20**. Additionally, two minor products were identified as tricyclic alcohol **21** and tricyclic diketone **22**. The configuration at C14 in **21** was assigned tentatively based upon NOESY correlation between 14-H and the angular C17 methyl group. Both cyclized products exist at room temperature as two slowly interconverting conformers whose NMR resonances coalesce upon heating. Similar conformational behavior has been reported for guanacastepene A.[1a]

A number of further studies were conducted to investigate the pathways leading from **18** to **20** and **21** (Scheme 4). First, exposure of the dioxolane-protected β-keto ester **17** to the Knoevenagel cyclization conditions did not result in the



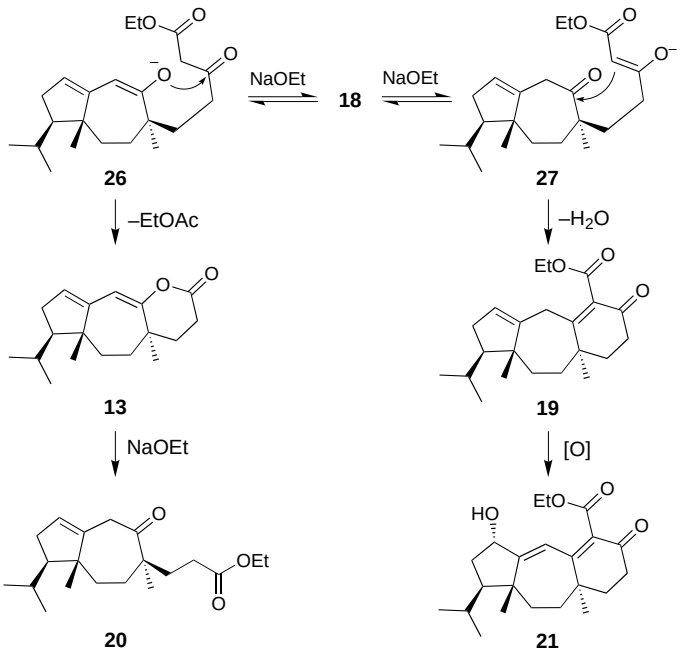
Scheme 4. Experimental probes for the mechanisms of formation of **20** and **21**.

formation of the corresponding truncated ester **23**. This clearly suggests a role of the ζ-keto group of **18** in the formation of **20**. Next, we considered the order of the oxidation and cyclization steps to form **21**. A pathway that involves initial oxidation to **24** followed by cyclization to **21** is not supported since the corresponding oxidation product **25** of the truncated ester **20** was not observed in the cyclization reaction. Finally, when the cyclization reaction was carried out with rigorous exclusion of air in deuterated solvent (gas-tight NMR tube, freeze–pump–thaw degassed five cycles), the

 © WILEY-VCH Verlag GmbH, 69451 Weinheim, Germany, 2002 1433-7851/02/4112-2186 $ 20.00+.50/0 *Angew. Chem. Int. Ed.* **2002**, *41*, No. 12

originally expected cyclization product [D_9]**19** could be detected by mass spectrometric analysis of the crude reaction mixture.[22] Furthermore, the ^{1}H NMR resonance of the C14 methine proton of [D_8]**21** ([D_6]ethanol, RT, $\delta = 4.38$ ppm, m)[23] appeared only after the reaction mixture was exposed to air.

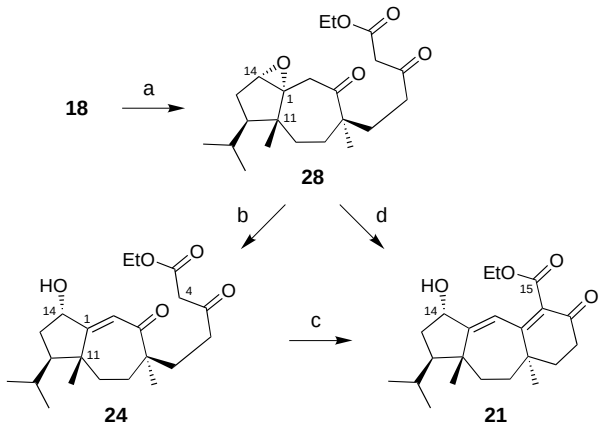
We therefore hypothesize that the truncated ester **20** and the oxidized tricycle **21** are formed from **18** by two competing reaction pathways (Scheme 5). Compound **18** is distinguished from typical Knoevenagel cyclization substrates by the



Scheme 5. Proposed mechanisms for the formation of **20** and **21** during attempted Knoevenagel cyclization of **18**. Enhanced acidity at the α-carbon of the unconjugated hydroazulenone (**18** → **26**) allows a retro-Claisen condensation to form dienol lactone **13**, which undergoes ethanolysis to give "truncated" ester **20**. This reaction competes with the desired α-deprotonation of the β-keto ester (**18** → **27**), which forms the putative unconjugated tricycle **19**. Unless oxygen is rigorously excluded from the reaction, this compound undergoes oxidation to the conjugated hydroxy tricycle **21**.

enhanced acidity of the unconjugated enone α-protons at C2. Thus, under the reaction conditions, formation of the hydroazulenone enolate **26** could set the stage for reaching dienol lactone **13** through a retrograde Claisen condensation, which would be followed by ethanolysis to **20**. The corresponding dioxolane **17**, which lacks the feature of a participating ζ-enolate, does not undergo fragmentation to **23**. Concurrently, formation of the β-keto ester enolate **27** likely does, in fact, lead to the expected unconjugated tricycle **19**. However, this compound apparently undergoes rapid oxidation (see **21** and **22**) unless oxygen is rigorously excluded from the reaction.

One cannot help but notice that tricycles **21** and **22**, although formed in low yield, possess potentially useful oxygen functionalities at C14. Accordingly, we next undertook to introduce this oxygen group *purposefully*. Thus, **18** was converted into epoxide **28** (Scheme 6). Epoxide-opening β-elimination at room temperature provided conjugated



Scheme 6. Epoxidation of unconjugated hydroazulenone **18** and stepwise or tandem epoxide-opening β-elimination/Knoevenagel cyclization to form tricycle **21**. a) MCPBA, CH_2Cl_2, 0 °C, 2 h, 89 %; b) NaOEt, EtOH, room temperature, 30 min; 82 %; c) NaOEt, EtOH, 50 °C, 6 h; 74 %; d) NaOEt, EtOH, 50 °C, 6 h, 80 %.

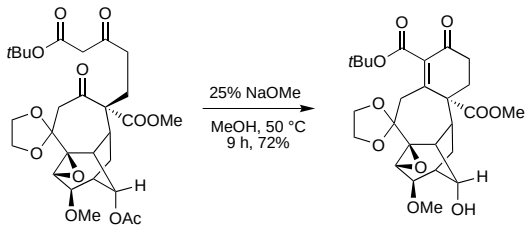
γ-hydroxy hydroazulenone **24**.[24, 25] We were gratified to find that this substrate underwent facile Knoevenagel cyclization at elevated temperature to produce tricycle **21**. Apparently, the reactivity of **24** is sufficiently altered relative to that of the unconjugated substrate **18**, that the desired cyclization reaction is favored. Notably, the corresponding truncated ester **25** was not observed in the crude product. Moreover, the yield of the reaction sequence could be further increased by converting **28** directly into **21** by means of a tandem epoxide-opening β-elimination/Knoevenagel cyclization reaction.[26]

In summary, difficulties in synthesizing the tricyclic dienone core of guanacastepene A when using the Turner–Fujimoto reaction led us to develop a novel and efficient tandem epoxide-opening β-elimination/Knoevenagel cyclization reaction. Importantly, our route has the added benefit of installing desirable oxygen functionalities at C14 and C15 of tricycle **21**. As a result, we had in hand a far more mature precursor of guanacastepene A than the initially projected target **15**. Seemingly, a clear route to **1** was in place. However, as described in the following paper, some major surprises awaited us in completing this goal.[27]

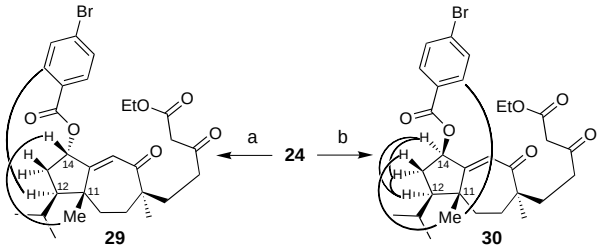
Received: March 18, 2002 [Z18910]

[1] a) S. F. Brady, M. P. Singh, J. E. Janso, J. Clardy, *J. Am. Chem. Soc.* **2000**, *122*, 2116–2117; b) M. P. Singh, J. E. Janso, S. W. Luckman, S. F. Brady, J. Clardy, M. Greenstein, W. M. Maiese, *J. Antibiot.* **2000**, *53*, 256–261; c) S. F. Brady, S. M. Bondi, J. Clardy, *J. Am. Chem. Soc.* **2001**, *123*, 9900–9901.
[2] For an explanation of the selectivity of membrane-lysing peptide antibiotics, see: M. Zasloff, *Nature* **2002**, *415*, 389–395.
[3] J. Clardy, personal communication.
[4] a) B. B. Snider, N. A. Hawryluk, *Org. Lett.* **2001**, *3*, 569–572; b) B. B. Snider, B. Shi, *Tetrahedron Lett.* **2001**, *42*, 9123–9126.
[5] P. Magnus, M. J. Waring, C. Ollivier, V. Lynch, *Tetrahedron Lett.* **2001**, *42*, 4947–4950.
[6] G. Mehta, J. D. Umarye, *Org. Lett.* **2002**, *4*, 1063–1066.
[7] a) G. B. Dudley, S. J. Danishefsky, *Org. Lett.* **2001**, *3*, 2399–2402; b) G. B. Dudley, D. S. Tan, G. Kim, J. M. Tanski, S. J. Danishefsky, *Tetrahedron Lett.* **2001**, *42*, 6789–6791.
[8] a) J. Schreiber, H. Maag, N. Hashimoto, A. Eschenmoser, *Angew. Chem.* **1971**, *83*, 355–357; *Angew. Chem. Int. Ed. Engl.* **1971**, *10*, 330–331; b) S. Danishefsky, T. Kitahara, R. McKee, P. F. Schuda, *J. Am.*

Chem. Soc. **1976**, *98*, 6715 – 6717; c) E. Piers, P. C. Marais, *J. Chem. Soc. Chem. Commun.* **1989**, 1222 – 1223.
[9] G. Stork, S. Uyeo, T. Wakamatsu, P. Grieco, J. Labovitz, *J. Am. Chem. Soc.* **1971**, *93*, 4945 – 4947.
[10] a) R. A. Daignault, E. L. Eliel, *Org. Synth., Coll. Vol. V* **1973**, 303 – 306; b) J. W. De Leeuw, E. R. De Waard, T. Beetz, H. O. Huisman, *Recl. Trav. Chim. Pays-Bas* **1973**, *92*, 1047 – 1052.
[11] H. C. Brown, J. C. Chen, *J. Org. Chem.* **1981**, *46*, 3978 – 3988.
[12] K. Bowden, I. M. Heilbron, E. R. H. Jones, B. C. L. Weedon, *J. Chem. Soc.* **1946**, 39 – 45.
[13] L. G. Barkley, W. S. Knowles, H. Raffelson, Q. E. Thompson, *J. Am. Chem. Soc.* **1956**, *78*, 4111 – 4116.
[14] a) R. B. Turner, *J. Am. Chem. Soc.* **1950**, *72*, 579 – 585; b) G. I. Fujimoto, *J. Am. Chem. Soc.* **1951**, *73*, 1856.
[15] In analogy to the Robinson annulation, initial bridged aldol products **14** (C2–C5 bond) are expected; equilibration and dehydration generates the fused products **15** (C3–C4 double bond): W. S. Johnson, J. J. Korst, R. A. Clement, J. Dutta, *J. Am. Chem. Soc.* **1960**, *82*, 614 – 622.
[16] a) D. B. Dess, J. C. Martin, *J. Org. Chem.* **1983**, *48*, 4155 – 4156; b) R. E. Ireland, L. Liu, *J. Org. Chem.* **1993**, *58*, 2899.
[17] C. R. Holmquist, E. J. Roskamp, *J. Org. Chem.* **1989**, *54*, 3258 – 3260.
[18] H. Hagiwara, H. Uda, *J. Chem. Soc. Chem. Commun.* **1987**, 1351 – 1353.
[19] Although we have not generalized this route to β-keto ester Knoevenagel cyclization substrates, it could, in principle, have advantages over methods that rely on the Nazarov reagent: a) I. N. Nazarov, S. I. Zavyalov, *Zh. Obshch. Khim.* **1953**, *23*, 1703 – 1712; b) G. Stork, R. N. Guthikonda, *Tetrahderon Lett.* **1972**, 2755 – 2758; c) B. M. Trost, R. A. Kunz, *J. Org. Chem.* **1974**, *39*, 2648 – 2650; d) R. Zibuck, J. M. Streiber, *J. Org. Chem.* **1989**, *54*, 4717 – 4719; e) R. Zibuck, J. Streiber, *Org. Synth.* **1993**, *71*, 236 – 242.
[20] We were encouraged by a literature precedent that involved the cyclization of a similar β-keto ester side chain onto a cycloheptanone system with an adjacent quaternary center: J. L. van der Baan, J. W. F. K. Barnick, G. van Beek, F. Bickelhaupt, A. L. Spek, *Tetrahedron* **1992**, *48*, 2773 – 2784.



[21] For experimental and structure determination details of **20**, **21**, and **22**, see Supporting Information.
[22] The unconjugated tricycle [D_9]**19** could not be unambiguously detected by ^{1}H NMR spectroscopic analysis because of deuterium exchange at C2 and a solvent signal that obscured the vinylic C14-H region.
[23] Assigned by analogy to C14-H for **21** in $CDCl_3$ at room temperature ($\delta = 4.34$, br d, $J = 5.31$ Hz).
[24] For early examples, see: a) W. Bergmann, F. Hirschmann, E. L. Skau, *J. Org. Chem.* **1939**, *4*, 29 – 38; b) C. Djerassi, E. Batres, M. Velasco, G. Rosenkranz, *J. Am. Chem. Soc.* **1952**, *74*, 1712 – 1715; c) H. H. Wasserman, M. J. Gorbunoff, *J. Am. Chem. Soc.* **1958**, *80*, 4568 – 4573.
[25] Confirmation of the stereochemical assignment at C14 of **24** (and indirectly at C14 of **21** and **28**) was made by multidimensional NMR spectroscopic analysis of the *p*-bromobenzoate derivative **29** and its C14 epimer **30**. Notably, whereas the angular methyl group at C11 apparently blocks the β-face at C1 to promote epoxidation on the α-face of the C1–C14 olefin of **18**, successful Mitsunobu inversion at C14 of **24** indicates that the C11 methyl group does not overridingly block the β-face at that remote site. The significance of these observations with respect to the introduction of the C13 acetoxy group will be described in the following paper.[27] a) *p*-BrBzCl, DMAP, Et_3N, CH_2Cl_2, room temperature, 1 h, 27% (not optimized); b) *p*-BrBzOH, DIAD, PPh_3, THF, 0 °C → RT, 1 h, 55% (not optimized). DMAP = 4-(dimethylamino)pyridine, DIAD = diisopropyl azodicarboxylate. NOE interactions (——).

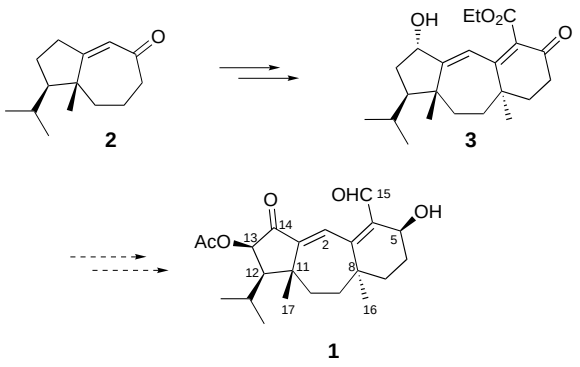


[26] Initial formation of γ-hydroxy hydroazulenone **24** was observed by TLC analysis.
[27] S. Lin, G. B. Dudley, D. S. Tan, S. J. Danishefsky, *Angew. Chem.* **2002**, *114*, 2292 – 2295; *Angew. Chem. Int. Ed.* **2002**, *41*, 2188 – 2191.
[28] Note added in proof: since the acceptance of this paper, new studies toward the synthesis of guanacastepene A have been published; see a) S. N. Gradl, J. J. Kennedy-Smith, J. Kim, D. Trauner, *Synlett* **2002**, *3*, 411 – 414; b) T. M. Nguyen, D. Lee, *Tetrahedron Lett.*, article in press, available on the WWW 1 May 2002; c) W. D. Shipe, E. J. Sorenson, *Org. Lett.*, in press, ASAP article, available on the WWW 16 May 2002.

A Stereoselective Route to Guanacastepene A through a Surprising Epoxidation**

Songnian Lin, Gregory B. Dudley, Derek S. Tan, and Samuel J. Danishefsky*

In the preceding paper we reported the preparation of compound **3** (Scheme 1),[1] which bears much of the functionality required, in principle, to reach guanacastepene A (**1**).[2, 3]



Scheme 1. Overview of the synthetic strategy towards **1**.

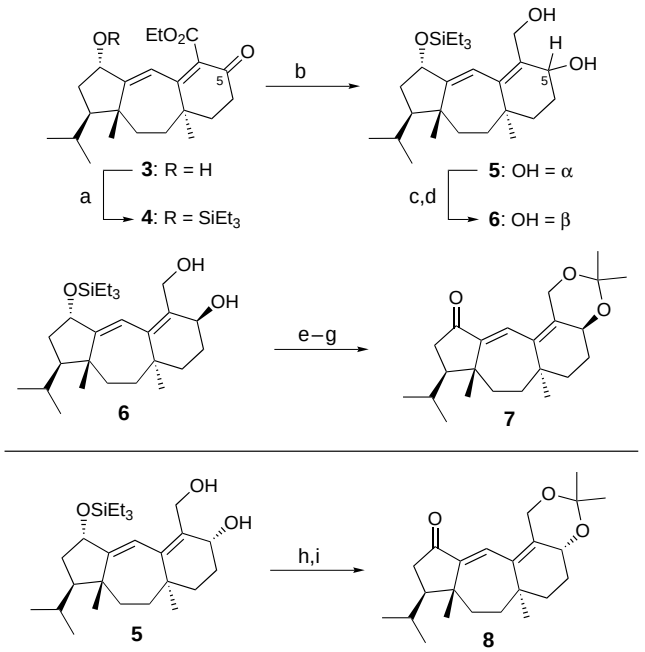
[*] Prof. Dr. S. J. Danishefsky, Dr. S. Lin, Dr. G. B. Dudley, Dr. D. S. Tan
Laboratory for Bioorganic Chemistry
Sloan-Kettering Institute for Cancer Research
1275 York Ave., New York, NY 10021 (USA)
Fax: (+1) 212-772-8691
Department of Chemistry, Columbia University
Havemeyer Hall, 3000 Broadway, New York, NY 10027 (USA)
E-mail: s-danishefsky@ski.mskcc.org

[**] This work was supported by the National Institutes of Health (CA-28824). S.L. is a US Army breast cancer research program postdoctoral fellow (DAMD-17-99-1-9373). G.B.D. is an NIH postdoctoral fellow (1 F32 NS11150-01). D.S.T. is a Damon Runyon Cancer Research Foundation postdoctoral fellow (DRG-1641). We thank Dr. George Sukenick and Sylvi Rusli (NMR Core Facility, CA-02848) for mass spectral analyses.

 © WILEY-VCH Verlag GmbH, 69451 Weinheim, Germany, 2002 1433-7851/02/4112-2188 $ 20.00+.50/0

To complete the synthesis,[4] it would be necessary to reproduce, through chemical synthesis, the densely packed and varied functionality between C13 and C5. Of particular interest were the two stereogenic centers yet to be formed. Oxidation at C13, ultimately in the form of a β-acetoxy substituent, had to be properly orchestrated with oxidation at C14 and overall two-electron reductions at C5 and C15.

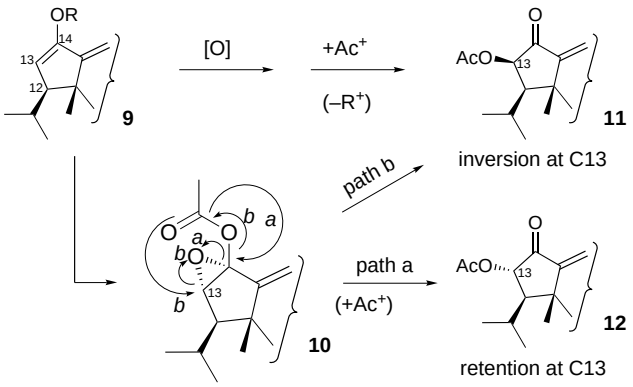
Introduction of the stereogenic center C5 is described in Scheme 2. The sequence was initiated by protection of the free hydroxy group of **3** as its triethylsilyl ether to give **4**.



Scheme 2. Preparation of the keto acetonides. a) Et_3SiOTf, pyridine, CH_2Cl_2, 0 °C, 80–85 %; b) DIBAL-H, CH_2Cl_2, −78 → 0 °C (**5**/**6** 80:20); c) Ph_3P, benzoic acid, DIAD, THF, −78 °C → RT; d) DIBAL-H, CH_2Cl_2, −78 → 0 °C; e) 2,2-dimethoxypropane, PPTS, CH_2Cl_2, 0 °C, 67 % from **4**; f) TBAF, THF, 0 °C, 91–98 %; g) Dess–Martin periodinane, pyridine, CH_2Cl_2, 90 %; h) 2,2-dimethoxypropane, PPTS, CH_2Cl_2, 0 °C, 86 %; i) HF · pyridine, pyridine, THF, then Dess–Martin periodinane, CH_2Cl_2, 77–85 %. Tf = triflate = trifluoromethanesulfonyl, DIBAL-H = diisobutylaluminum hydride, DIAD = diisopropyl azodicarboxylate, PPTS = pyridinium *p*-toluenesulfonate, TBAF = tetrabutylammonium fluoride.

Reduction of the latter with DIBAL-H in CH_2Cl_2 provided a mixture of C5 diastereomers (**5**/**6** 80:20).[5, 6] Use of various alternative reducing agents, including $LiAlH_4$, Li-(tBuO)$_3$AlH,[7] 9-BBN,[8] and $NaBH_4 \cdot CeCl_3$,[9] led to less favorable diastereomeric ratios. The diastereomers **5** and **6** can be separated by careful purification on silica gel.[10] The α epimer (**5**, major) was subjected to a Mitsunobu[11] inversion sequence via an intermediate dibenzoate. Protection of diol **6** as its acetonide, cleavage of the silyl ether, and Dess–Martin oxidation[12] in the presence of pyridine[13] provided ketone **7**. In initial experiments prior to optimization of the Mitsunobu inversion, diol **5** was advanced to ketone **8** by a sequence analogous to the transformation of **6** to **7**.

For the stereoselective installation of the C13-acetoxy substituent, we envisioned the creation of the C13–C14 enol derivative **9**, for the moment unspecified (Scheme 3). The



Scheme 3. Overview of the acetoxy installation strategy.

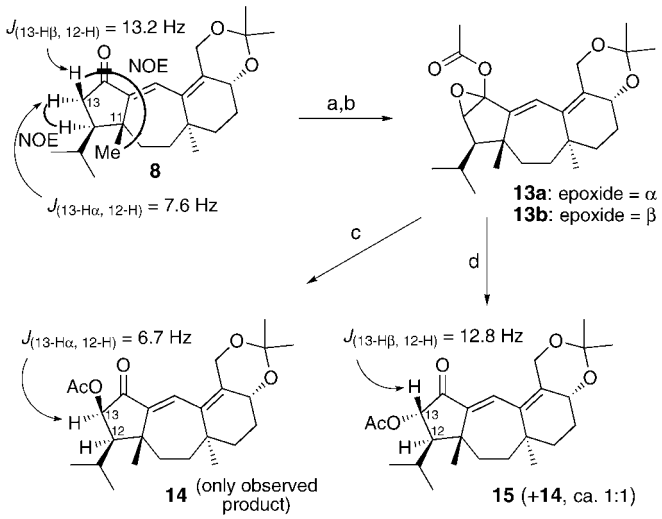
conversion **9** → **11** is intended to show, in formal terms, oxidation at C13. At this stage, the nature of the step to introduce the acetyl function is also not specified. For instance, there might be a sequential hydroxylation at C13 and acetylation. Alternatively, the delivery of the "acetyl" and "hydroxenium" components of the overall C13-acetoxy group might be coordinated. At this stage, it was expected that oxidants attacking C13 would do so from the α-face, that is, *anti* to the β C12-isopropyl and C11-methyl groups. This presumption led to a more specific proposal.

Enol acetylation of a C14-ketone would give **9** (R = Ac). Following the bias discussed above, epoxidation might well lead to **10**. Two stereochemically diverging pathways are possible in advancing from epoxide type **10** to an acetoxy ketone. In path a, we emphasize the vulnerability of the C14–O bond of the epoxide. This bond cleavage could lead to loss of $MeCO^+$ to adventitious external nucleophiles and formation of a non-acetylated C13-hydroxy function. Alternatively, but still within the confines of path a, the acylium function may be transferred internally to the emerging C13-hydroxy group. In either case, path a leads to an acetoxy ketone (see **12**) in which the stereochemistry at C13 is the same as that of the epoxide. In contrast, in path b one contemplates transfer of an intact acetoxy function from C14 to C13. Here, clearly, the stereochemistry of C13 will reflect the inversion during the migration of the acetoxy group (see **10** → **11**).[14]

Since we first obtained the keto acetonide **8** (Scheme 2), we proceeded to test our strategy in this series. Before relating our results, we should describe our method of analysis even before reaching guanacastepene A. In ketone **8**, two vicinal coupling constants (13.2 Hz and 7.6 Hz) relate the geminal protons at C13 with the α-proton at C12. Noting that $J_{(13\text{-H}\alpha,12\text{-H}\alpha)} \approx 7$ Hz in the natural product,[21] we could assign the 13.2-Hz coupling constant to 13-Hβ–12-Hα, whereas J = 7.6 Hz is a result of the coupling between α-H and 12-Hα. This assignment was substantiated by the observation of the indicated NOE interactions (Scheme 4). We hoped to assign the stereochemistry of the C13-acetoxylated product by measuring $J_{(13\text{-H},12\text{-H})}$ in the context discussed above.

In the event, ketone **8** was converted into enol acetate **13** (Scheme 4).[15] Epoxidation with DMDO led to the formation of a single observable epoxide. The stereochemistry of the oxido linkage (see **13a** or **13b**) was not known at this stage. We

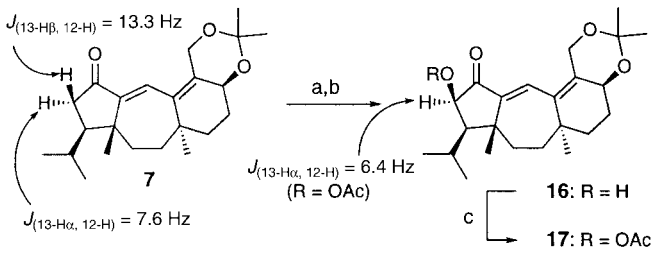
 © WILEY-VCH Verlag GmbH, 69451 Weinheim, Germany, 2002 1433-7851/02/4112-2189 $ 20.00+.50/0



Scheme 4. Investigations into the stereoselective installation of the C13-acetoxy functionality. a) Et_3N, DMAP, AcCl, Ac_2O, 100 °C, 90 %; b) DMDO/acetone, CH_2Cl_2, −78 → 0 °C; c) *p*-TsOH, $MeNO_2$, then Ac_2O, pyridine, DMAP, ≈60 % from **8**; d) 150 °C (neat), then Ac_2O, pyridine, DMAP, ≈65 % from **8** (**14**/**15** ≈ 1:1). DMAP = 4-(dimethylamino)pyridine, DMDO = dimethyldioxirane.

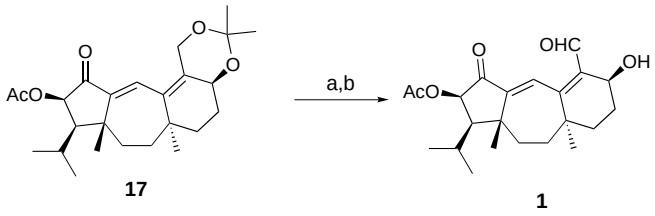
were surprised to find that when the compound was subjected to acidic conditions, which favor path a, followed by acetylation as shown, compound **14** was obtained; the coupling constant for the vicinal 13-H/12-H was similar to that of guanacastepene A. In contrast, pyrolysis of the epoxy acetate under conditions that we hoped would favor path b (inversion) ultimately led to two compounds.[16] One was the acetoxy ketone corresponding to the previously encountered **14**. The other was a new acetoxy ketone **15**, which gave a coupling constant that suggests a *trans* relationship between 12-H and 13-H. Assuming that the assignments at C13 in **14** and **15** are correct, these data can only be rationalized by the surprising conclusion that epoxidation of the enol acetate of **8** had occurred from the β-face (see **13b**).

From this newly gained insight, it was opportune to direct efforts toward the synthesis of guanacastepene A itself. For this purpose we commenced with keto acetonide **7** (Scheme 5). Since retention of the stereochemistry at C13 was desired, it was advantageous to employ a Rubottom-type protocol.[17] Conversion of **7** into its silyl enol ether was followed by exposure of the latter to DMDO, thereby providing hydroxy ketone **16** (ca. 94:6 dr, major isomer shown). Acetylation gave **17**. As before, the diagnostic



Scheme 5. Rubottom-type oxidation strategy. a) Et_3SiOTf, Et_3N, CH_2Cl_2; b) DMDO/acetone, CH_2Cl_2, −78 °C, then Me_2S, 82–90 % overall yield; c) Ac_2O, pyridine, DMAP, CH_2Cl_2, 96 %.

coupling constants demonstrated that acetoxylation had occurred *syn* to the isopropyl and methyl substituents. As the rearrangement associated with the Rubottom protocol can be safely assumed to occur by retention,[18] we must conclude that epoxidation had again occurred from the β face. The assignment of the stereochemistry of **17** was confirmed by its ultimate transformation into guanacastepene A (Scheme 6).



Scheme 6. Synthesis of **1**. a) PPTS, MeOH, 70 °C; b) $PhI(OAc)_2$, TEMPO, CH_2Cl_2, 59–65 % overall yield. TEMPO = 2,2,6,6-tetramethyl-1-piperidinyloxy, free radical.

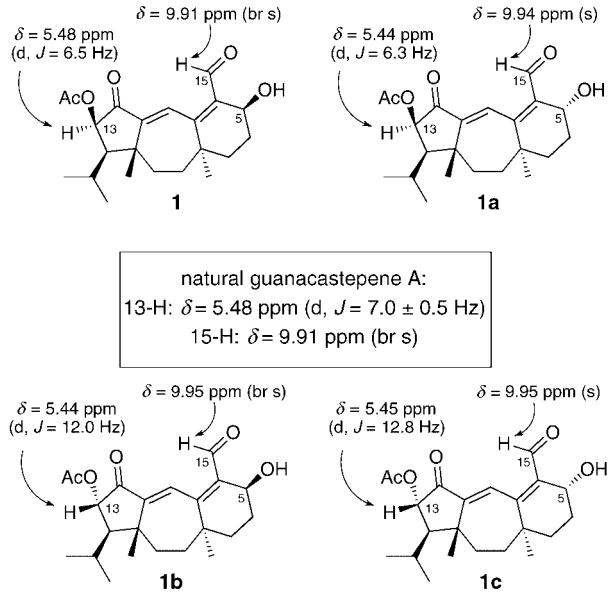
Hydrolysis of the acetonide of **17** provided an unstable diol, which was purified quickly by chromatography on silica gel and used immediately. TEMPO-catalyzed oxidation of the primary alcohol[19] to the aldehyde left the secondary alcohol undisturbed. The spectral data recorded from this product (^{1}H NMR at 25 °C and at −50 °C, ^{13}C NMR at 25 °C and at −50 °C, IR, and mass spectra) were in complete accord with those of guanacastepene A.[20, 21]

We were at this point quite confident that we had completed the total synthesis of racemic guanacastepene A. However, in the absence of an authentic sample of the natural product, we sought to demonstrate rigorously that various epimers of guanacastepene A were indeed distinguishable by NMR spectroscopy. In this spirit, we prepared the remaining three diastereomers with respect to C5 and C13 (**1a**, **1b**, and **1c**).[22] A selection of the diagnostic ^{1}H NMR data of the various diastereomers is shown in Scheme 7. In short, the C13 protons in the epimeric 13-acetoxy compounds exhibit drastically different coupling constants. Interestingly, the epimeric 5-hydroxy groups affect the peak shape of the aldehyde signal. This may reflect different, configurationally sensitive, proclivities of the C5 hydroxy groups for hydrogen bonding to the proximal formyl oxygen atom.

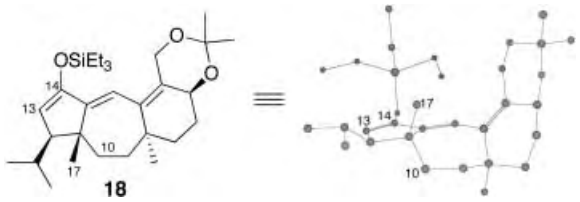
In light of the observed β-face oxidation of ketone **7**, it was appropriate to reexamine our original thinking about the steric biases of this system. Calculations with the MM2 force field[23] provided energy-minimized conformers of silyl enol ether **18** (derived from **7**), one of which is shown in Scheme 8. Based on these calculations, it appears that the pseudo-equatorial isopropyl group may not exert a dominant steric influence on facial selectivity. Furthermore, C17 and C10 are approximately equidistant from the locus of the C13–C14 double bond. By the same token, the modeling exercise did not reveal a convincing steric bias to rationalize the highly selective β-face epoxidation observed above.[24]

In summary, the total synthesis of the naturally occurring guanacastepene A has been completed. As we did not have a sample of the natural product for comparison, we could only

 © WILEY-VCH Verlag GmbH, 69451 Weinheim, Germany, 2002 1433-7851/02/4112-2190 $ 20.00+.50/0



Scheme 7. Structures and illustrative NMR data of the four guanacastepene diastereomers.



Scheme 8. Silyl enol ether **18**, and an energy-minimized representation of its three-dimensional structure.

be confident about this result after synthesizing the four guanacastepene isomers with the possible permutations of the stereogenic centers at C5 and C13. Our findings on the remarkably uniform sense of the epoxidation reactions should serve to underscore the subtlety of biases that control stereochemical outcomes. Full details of the total synthesis and a fuller consideration of this fascinating epoxidation tendency will be described shortly.

Received: March 18, 2002 [Z18911]

[1] D. S. Tan, G. B. Dudley, S. J. Danishefsky, *Angew. Chem.* **2002**, *114*, 2289 – 2292; *Angew. Chem. Int. Ed.* **2002**, *41*, 2185 – 2188.

[2] For the isolation and characterization of guanacastepene A and related natural products, see: a) S. F. Brady, M. P. Singh, J. E. Janso, J. Clardy, *J. Am. Chem. Soc.* **2000**, *122*, 2116 – 2117; b) M. P. Singh, J. E. Janso, S. W. Luckman, S. F. Brady, J. Clardy, M. Greenstein, W. M. Maiese, *J. Antibiot.* **2000**, *53*, 256 – 261; c) S. F. Brady, S. M. Bondi, J. Clardy, *J. Am. Chem. Soc.* **2001**, *123*, 9900 – 9901.

[3] For alternative approaches to the synthesis of guanacastepene A, see: a) B. B. Snider, N. A. Hawryluk, *Org. Lett.* **2001**, *3*, 569 – 572; b) B. B. Snider, B. Shi, *Tetrahedron Lett.* **2001**, *42*, 9123 – 9126; c) P. Magnus, M. J. Waring, C. Ollivier, V. Lynch, *Tetrahedron Lett.* **2001**, *42*, 4947 – 4950; d) G. Mehta, J. D. Umarye, *Org. Lett.* **2002**, *4*, 1063 – 1066; e) T. M. Nguyen, D. Lee, *Tetrahedron Lett.*, article in press, available on the WWW 1 May 2002; f) S. N. Gradl, J. J. Kennedy-Smith, J. Kim, D. Trauner, *Synlett* **2002**, *3*, 411 – 414; g) W. D. Shipe, E. J. Sorensen, *Org. Lett.*, in press, ASAP Article, available on the www 16 May 2002.

[4] For earlier accounts of our studies, see: a) G. B. Dudley, S. J. Danishefsky, *Org. Lett.* **2001**, *3*, 2399 – 2402; b) G. B. Dudley, D. S. Tan, G. Kim, J. M. Tanski, S. J. Danishefsky, *Tetrahedron Lett.* **2001**, *42*, 6789 – 6791.

[5] a) For a discussion of the general preference for axial hydride delivery to cyclohexenones, with leading references, see: A. P. Davis in *Houben-Weyl, Methods of Organic Chemistry Vol. E21: Stereoselective Synthesis, Workbench Edition*, *Vol. 7* (Eds.: G. Helmchen, R. W. Hoffmann, J. Mulzer, E. Schaumann), Thieme, Stuttgart, **1996**, pp. 4034 – 4037; b) for a closely related example, see ref. [3b].

[6] Based on extensive literature precedent (see ref. [5]), this reduction was assumed to proceed as indicated in Scheme 2; confirmation of this tentative assignment was obtained upon conversion into the natural product.

[7] For a review of reductions with lithium trialkoxyaluminum hydrides, see: J. Málek, *Org. React.* **1985**, *34*, 1 – 317.

[8] S. Krishnamurthy, H. C. Brown, *J. Org. Chem.* **1977**, *42*, 1197 – 1201. 9-BBN = 9-borabicyclo[3.3.1]nonane.

[9] A. L. Gemal, J.-L. Luche, *J. Am. Chem. Soc.* **1981**, *103*, 5454 – 5459.

[10] The minor product **6** could be used without further manipulation; thus **5** and **6** are stereoconvergent.

[11] For a review of the Mitsunobu reaction, see: D. L. Hughes, *Org. React.* **1992**, *42*, 335 – 656.

[12] a) D. B. Dess, J. C. Martin, *J. Org. Chem.* **1983**, *48*, 4155 – 4156; b) R. E. Ireland, L. Liu, *J. Org. Chem.* **1993**, *58*, 2899.

[13] The yield for this oxidation step increases from 50% to 90% in the presence of pyridine (3 equiv relative to Dess – Martin periodinane).

[14] a) Y. Zhu, L. Shu, Y. Tu, Y. Shi, *J. Org. Chem.* **2001**, *66*, 1818 – 1826; b) C. Heathcock, S. C. Smith *J. Org. Chem.* **1994**, *59*, 6828 – 6839; c) K. L. Williamson, W. S. Johnson, *J. Am. Chem. Soc.* **1961**, *83*, 4563 – 4569; d) A. H. Soloway, W. J. Considine, D. K. Fukushima, T. F. Gallagher, *J. Am. Chem. Soc.* **1954**, *76*, 2941 – 2943.

[15] J.-L. Brevet, G. Fournet, J. Gore, *Synth. Commun.* **1996**, *26*, 4185 – 4194.

[16] The product mixture comprised acetoxy and hydroxy ketones; the crude material was immediately re-acetylated prior to characterization.

[17] a) G. M. Rubottom, M. A. Vazquez, D. R. Pelegrina, *Tetrahedron Lett.* **1974**, 4319 – 4322; b) S. J. Danishefsky, J. J. Masters, W. B. Young, J. T. Link, L. B. Snyder, T. V. Magee, D. K. Jung, R. C. A. Isaacs, W. G. Bornmann, C. A. Alaimo, C. A. Coburn, M. J. DiGrandi, *J. Am. Chem. Soc.* **1996**, *118*, 2843 – 2859.

[18] G. M. Rubottom, J. M. Gruber, R. K. Boeckman, Jr., M. Ramaiah, J. B. Medwid, *Tetrahedron Lett.* **1978**, 4603 – 4606.

[19] A. De Mico, R. Margarita, L. Parlanti, A. Vescovi, G. Piancatelli, *J. Org. Chem.* **1997**, *62*, 6974 – 6977.

[20] An authentic sample is no longer available for comparison (J. Clardy, personal communication). In fact, chemical synthesis is currently the only source of this compound.

[21] Synthetic guanacastepene ([D$_6$]acetone, 400 MHz, 25 °C): $\delta = 9.91$ (br s, 1H), 7.45 (d, $J = 1.1$ Hz, 1H), 5.48 (d, $J = 6.5$ Hz, 1H), 4.62 (m, 1H), 3.97 (br s, 1H, OH), 2.08 (s, 3H), 1.99 (m), 1.90 (m), 1.79 (m), 1.63 (m), 1.40 (m), 1.27 (s, 3H), 1.12 (d, $J = 6.6$ Hz, 3H), 1.09 (s, 3H), 0.93 ppm (d, $J = 6.4$ Hz, 3H); ([D$_6$]acetone, 500 MHz, -50 °C, key signals): major isomer: $\delta = 9.96$ (s), 7.42 (s), 5.45 (d, $J = 5.6$ Hz), 4.64 (m), 4.59 (d, $J = 5.4$ Hz) (OH), 2.10 ppm (s); minor isomer: $\delta = 9.72$ (s), 7.49 (s), 5.53 (d, $J = 7.1$ Hz), 4.52 (m), 4.48 (d, $J = 4.1$ Hz, OH), 2.11 ppm (s); these data match the data obtained directly from the ^{1}H NMR spectra of the natural product. We are grateful to Prof. Jon Clardy and Dr. Sean F. Brady for providing detailed NMR spectra of natural guanacastepene A.

[22] **1a** and **1c** were prepared from **14** and **15**, respectively, by analogy to the conversion **17** → **1** (Scheme 6); **1b** was derived similarly from the minor diastereomer obtained in the Rubottom-type oxidation of **7** (Scheme 5).

[23] *MacroModel* version 5.5, Department of Chemistry, Columbia University.

[24] The possibility that the silyl group orientates itself preferentially on the α-face, thus blocking the epoxidation from below, was also considered; however, the MM2 calculations suggest little energy difference with respect to various silyl group orientations, disfavoring this hypothesis.

 © WILEY-VCH Verlag GmbH, 69451 Weinheim, Germany, 2002 1433-7851/02/4112-2191 $ 20.00+.50/0

Methyleneimine CH_2=NH as a Unidentate Ligand in Rhenium Complexes**

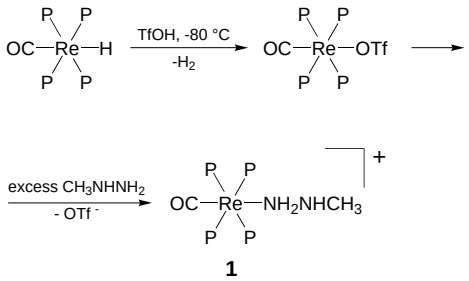
Gabriele Albertin,* Stefano Antoniutti, Alessia Bacchi, Emilio Bordignon, Maria Teresa Giorgi, and Giancarlo Pelizzi

Coordinated hydrazines $RNHNH_2$ are reported to react with oxidizing agents, such as $[Pb(OAc)_4]$ and H_2O_2, to give the corresponding diazenes RN=NH, the stabilization of which on an appropriate metal fragment allows their separation as coordinated species.[1–3] We now report a new reaction of coordinated methylhydrazine, which reacts with $[Pb(OAc)_4]$ to give a η^1-NH=CH_2 methyleneimine derivative.

The CH_2=NH molecule is a reactive species which was first obtained in 1933 from the low-temperature reaction of HCN with hydrogen.[4] It has been detected in several galactic objects[5] and proposed as a possible precursor[6] of the simplest α-amino acid, glycine. As a ligand, it is present in only one case, through π coordination[7] to an osmium center; no other report has been found on this molecule, which displays a simple constitution and structure, and has still unknown properties.

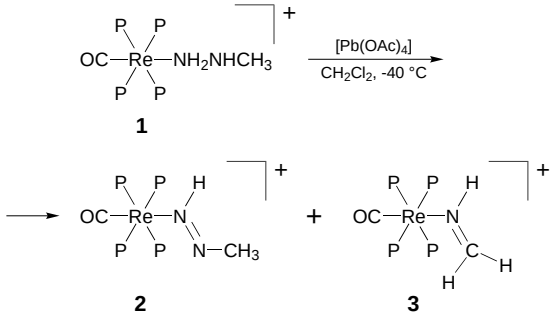
The reaction of the hydride[8] $[ReH(CO)\{P(OEt)_3\}_4]$ with triflic acid (TfOH) gives the thermally unstable $[Re(\eta^2\text{-}H_2)(CO)\{P(OEt)_3\}_4]^+(CF_3SO_3)^-$ species, which loses H_2, affording the compound $[Re(\kappa^1\text{-}OTf)(CO)\{P(OEt)_3\}_4]$. Substitution of the weakly bound triflato ligand with methylhydrazine gives *trans*-$[Re(CH_3NHNH_2)(CO)\{P(OEt)_3\}_4]^+$ (**1**), which was isolated as a BPh_4 salt (**1**-BPh_4) in about 70% yield (Scheme 1).

Complex **1**-BPh_4 was characterized by standard methods (IR, NMR, Λ_M, elemental analysis). The IR spectra show the ν_{NH} bands at 3343 and 3291 cm^{-1} of the methylhydrazine ligand, whereas the ^1H NMR spectrum exhibits resonance signals at $\delta = 4.35$ (s, br; $ReNH_2NHCH_3$), 3.93 (m, br; $ReNH_2NHCH_3$), and 2.49 ppm (d; $ReNH_2NHCH_3$) of the CH_3NHNH_2 group.



Scheme 1. P = $P(OEt)_3$.

Treatment of methylhydrazine complex **1**-BPh_4 with an equimolar amount of $[Pb(OAc)_4]$ at low temperature (−40 °C) in CH_2Cl_2 gives a mixture of methyldiazene $[Re(CH_3N{=}NH)(CO)\{P(OEt)_3\}_4]BPh_4$ (**2**-BPh_4) and methyleneimine $[Re(\eta^1\text{-}NH{=}CH_2)(CO)\{P(OEt)_3\}_4]BPh_4$ (**3**-BPh_4) derivatives (Scheme 2). These were separated by fractional crystallization in moderate yields (42% for **2**-BPh_4, 24% for **3**-BPh_4) as analytically pure white crystalline solids.



Scheme 2. P = $P(OEt)_3$.

The complexes were characterized by spectroscopy and in two X-ray diffraction studies.[9–12] Figure 1 shows the crystal structure of the cation $[Re(\eta^1\text{-}NH{=}CH_2)(CO)\{P(OEt)_3\}_4]^+$ (**3**). The most relevant feature of the complex is the presence of the methyleneimine ligand, *trans* to the carbonyl group, and coordinated with the metal in a bent mode, as required by the sp^2 character of the N atom (Re-N-C 139(1)°), with Re–N 2.32(1) and N–C 1.26(1) Å. This is, in fact, the first example of η^1 coordination of a CH_2=NH molecule to a transition metal, the only other similar case being the deprotonated CH_2=N=M fragment found in (μ^2-methyleneamido)tricarbonylbis-

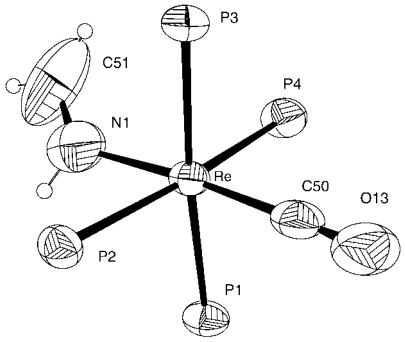


Figure 1. Structure of the core of the cation **3** (thermal ellipsoids drawn at the 30% level; ethoxy groups are omitted for clarity). Selected bond lengths [Å] and angles [°]: Re-C50 1.956(8), Re-N1 2.32(1), Re-P3 2.362(2), Re-P1 2.362(2), Re-P4 2.374(2), Re-P2 2.378(2), O13-C50 1.108(8), N1-C51 1.26(1); C50-Re-N1 175.9(3), C50-Re-P3 87.7(2), N1-Re-P3 95.9(2), C50-Re-P1 86.9(2), N1-Re-P1 89.5(2), P3-Re-P1 174.44(6), C50-Re-P4 94.4(2), N1-Re-P4 87.6(2), P3-Re-P4 90.00(7), P1-Re-P4 89.25(7), C50-Re-P2 92.9(2), N1-Re-P2 85.0(2), P3-Re-P2 91.44(6), P1-Re-P2 90.01(6), P4-Re-P2 172.56(6), O13-C50-Re 177.2(6), C51-N1-Re 134(1).

[*] Prof. G. Albertin, S. Antoniutti, E. Bordignon, Dr. M. T. Giorgi
Dipartimento di Chimica
Università Ca' Foscari di Venezia
Dorsoduro 2137, 30123 Venezia (Italy)
Fax: (+39) 041-234-8917
E-mail: albertin@unive.it
Prof. A. Bacchi, G. Pelizzi
Dipartimento di Chimica Generale ed Inorganica, Chimica Analitica
Chimica Fisica, Università di Parma
Parco Area delle Scienze 17/a, 43100 Parma (Italy)

[**] This work was supported by MIUR (Rome)—Programmi di Ricerca Scientifica di Rilevante Interesse Nazionale, Cofinanziamento 2000–2001. We thank Daniela Baldan for technical assistance.

Supporting information for this article is available on the WWW under http://www.angewandte.org or from the author.

 © WILEY-VCH Verlag GmbH, 69451 Weinheim, Germany, 2002 1433-7851/02/4112-2192 $ 20.00+.50/0

(η^5-pentamethylcyclopentadienyl)methyleneamidodimolybdenum,[13] in which the system is practically linear (M-N-C 163°). The bent geometry found for our terminal methyleneimine group fits the common structural features of alkylic and arylic $R_2C{=}NH$ ligands, which show similar M-N-C angles and generally larger N–C distances (ranging from 1.25 to 1.30 Å; the shortest ones are found in the catenabis(isopropylideneamine)gold trifluoromethanesulfonate complex at 173 K[14]). The plane of the methyleneimine ligand (Re-N1-C51) forms a dihedral angle of 38(1)° with the equatorial coordination plane containing the N donor (Re-C50-P1-P3-N1).

The ^{1}H NMR spectra of **3**–BPh_4 are diagnostic for the presence of the methyleneimine ligand, showing a broad high-frequency signal at $\delta = 13.98$ ppm, which is attributed to the =NH imine proton. Substituted imine $R_2C{=}NH$, and $RHC{=}NH$ bonded to a metal center[14, 15] are also reported to give rise to a high-frequency NH proton resonance signal. A slightly broad multiplet is also present at $\delta = 3.66$ ppm, which is coupled with the imine proton and was assigned to one of the two protons of the methylene $=CH_2$ group. The other is probably masked by the methylene signals of the $P(OCH_2CH_3)_3$ ligands. In the temperature range between +30 and −80 °C the $^{31}P\{^1H\}$ NMR spectrum displays a sharp singlet, which is assigned to a *trans* geometry like that found in the solid state.

In the crystal structure of **2**-BPh_4, the methyldiazene and carbonyl ligands in the cation are exchanged between two *trans* coordination positions, with 50% substitutional disorder, and their refinement was possible only by restraining them to conform to a plausible geometry.[16]

The ^{1}H NMR spectra of **2**-BPh_4 further support the presence of the $CH_3N{=}NH$ ligand, showing the NH resonance signal at $\delta = 15.99$ ppm and one doublet at $\delta = 4.37$ ppm, attributed to the methyl group. A mutual *trans* position of carbonyl and methyldiazene ligands is also suggested in solution by the presence of only one singlet at $\delta = 116.7$ ppm in the $^{31}P\{^1H\}$ NMR spectrum.

Other methylhydrazine complexes, such as dicarbonyls $[Re(CH_3NHNH_2)(CO)_2P_3]BPh_4$ ($P = P(OEt)_3$ or $PPh(OEt)_2$), were prepared, and their reaction with $[Pb(OAc)_4]$ led, at −40 °C, to a mixture of methyldiazene $[Re(CH_3N{=}NH)(CO)_2P_3]^+$ and methyleneimine $[Re(\eta^1\text{-}NH{=}CH_2)(CO)_2P_3]^+$ derivatives which, in the case of $P(OEt)_3$, were separated in pure form or, for $PPh(OEt)_2$, were detected by spectroscopy. The reaction affording the coordinated η^1-$NH{=}CH_2$ molecule seems to be general for the $[Re(CO)_nP_{5-n}]$ ($n = 1, 2$) fragment containing a methylhydrazine ligand, but appears to be specific for $[Pb(OAc)_4]$, as attempts to carry out the reaction with other oxidants such as MnO_2 or H_2O_2 were unsuccessful.

The formation of species **2**-BPh_4 and **3**-BPh_4 from the reaction of methylhydrazine complexes **1**-BPh_4 (Scheme 2) suggests that $[Pb(OAc)_4]$ gives rise to two parallel reactions involving selective oxidation of CH_3NHNH_2 to methyldiazene $CH_3N{=}NH$, giving **2**-BPh_4, in one case, whereas a completely new reaction involving cleavage of the N=N bond and formation of the $CH_2{=}NH$ moiety takes place in the other. Although coordinated hydrazine is known to undergo oxidation by $[Pb(OAc)_4]$ or other reagents to the corresponding diazene,[1–3] the reaction affording coordinated η^1-$NH{=}CH_2$ is new, unexpected, and interesting—not only because it allows us to prepare, and stabilize by coordination, an elusive molecule such as methyleneimine, but also because, whatever the mechanism[17] may be, cleavage of the N=N bond[18] of a coordinated hydrazine[19] takes place in the presence of an oxidizing species.

Studies are currently in progress to explore the reaction chemistry of the $M{-}NH{=}CH_2$ systems, mainly in terms of deprotonation and substitution reactions.

Experimental Section

All reactions were carried out under an inert atmosphere using dry, air-free solvents.

1-BPh_4: CF_3SO_3H (TfOH) (0.23 mmol, 20 μL) was added to a solution of $[ReH(CO)\{P(OEt)_3\}_4]$[8] (200 mg, 0.23 mmol) in CH_2Cl_2 (5 mL) cooled to −196 °C, and the reaction mixture was allowed to warm to room temperature, and stirred for 1 h. CH_3NHNH_2 (0.6 mmol, 32 μL) was added and stirring was continued for 24 h. The solvent was removed under reduced pressure to give an oil which was triturated with ethanol (3 mL) containing $NaBPh_4$ (0.6 mmol, 205 mg). A white solid slowly separated out, which was crystallized from CH_2Cl_2 and ethanol to give **1**-BPh_4 (210 mg; yield 73%). IR (KBr): $\tilde{\nu} = 3343$ (m), 3291 (m) (ν_{NH}), 1880 cm^{-1} (s) (ν_{CO}); ^{1}H NMR (200 MHz, CD_2Cl_2, 293 K, TMS): $\delta = 7.40$–6.86 (m, 20H; Ph), 4.35 (s, br, 2H; NH_2), 4.05 (m, 24H; CH_2); 3.93 (m, br, 1H; NH), 2.49 (d, $^3J_{H,H} = 6$ Hz, 3H; CH_3N), 1.29 ppm (t, 36H; CH_3); $^{31}P\{^1H\}$(200 MHz, CD_2Cl_2, 293 K, H_3PO_4 85% ext.): $\delta = 117.9$ ppm (s); elemental analysis (%) calcd for $C_{50}H_{86}BN_2O_{13}P_4Re$ (1244.14): C 48.27, H 6.97, N 2.25; found: C 48.15, H 7.01, N 2.13.

2-BPh_4, **3**-BPh_4: A sample of **1** (124 mg, 0.1 mmol) was placed in a three-necked 25-mL flask fitted with a solid-addition sidearm containing $[Pb(OAc)_4]$ (0.1 mmol, 44 mg). The system was evacuated, CH_2Cl_2 (8 mL) was added, the solution cooled to −40 °C, and $[Pb(OAc)_4]$ was added portionwise over 10–20 min to the cold stirring solution. The reaction mixture was then allowed to warm to 0 °C, stirred for 10 min, and the solvent removed under reduced pressure. The oil obtained was treated at 0 °C with ethanol (2 mL) containing $NaBPh_4$ (0.2 mmol, 68 mg). A white solid slowly separated out which was filtered and crystallized fractionally. A typical separation involved slow cooling from +20 to −25 °C of a saturated solution of the complexes prepared by adding ethanol (8 mL) to the white solid and enough CH_2Cl_2 to obtain a saturated solution at room temperature. The first crystals are of **2**-BPh_4, the second a mixture of **2**-BPh_4 and **3**-BPh_4 which was recrystallized. A total of 52 mg of **2**-BPh_4 (yield 42%) was separated. By further cooling of the solution, 29 mg of white crystals of **3**-BPh_4 (yield 24%) were obtained. Pure samples of **2**-BPh_4 and **3**-BPh_4 can also be obtained by Pasteur separation of crystals obtained by cooling a saturated solution of the reaction product in ethanol to −25 °C.

2-BPh_4: IR (KBr):$\tilde{\nu} = 1890$ cm^{-1} (s) (ν_{CO}); ^{1}H NMR (200 MHz, CD_2Cl_2, 293 K, TMS): $\delta = 15.99$ (s, br, 1H; NH), 7.40–6.70 (m, 20H; Ph), 4.37 (d, 3H; $=NCH_3$), 4.06 (m, 24H; CH_2), 1.33 ppm (t, 36H; CH_3); $^{31}P\{^1H\}$ (200 MHz, CD_2Cl_2, 293 K, H_3PO_4 ext.): $\delta = 116.7$ ppm (s); elemental analysis (%) calcd for $C_{50}H_{84}BN_2O_{13}P_4Re$ (1242.12): C 48.35, H 6.82, N 2.26; found: C 48.19, H 6.95, N 2.30;

3-BPh_4: IR (KBr): $\tilde{\nu} = 1894$ cm^{-1} (s) (ν_{CO}); ^{1}H NMR (200 MHz, CD_2Cl_2, 293 K, TMS): $\delta = 13.98$ (s, br, 1H; NH), 7.60–6.80 (m, 20H; Ph), 4.06 (m, 24H; CH_2), 3.66 (m, br, 1H; $N{=}CH_2$), 1.34 ppm (t, 36H; CH_3); $^{31}P\{^1H\}$ (200 MHz, CD_2Cl_2, 293 K, H_3PO_4 ext.): $\delta = 123.6$ ppm (s); elemental analysis (%) calcd for $C_{50}H_{83}BNO_{13}P_4Re$ (1227.11): C 48.94, H 6.82, N 1.14; found: C 49.08, H 6.96, N 1.10.

Received: March 13, 2002 [Z 18883]

[1] a) D. Sellmann, A. Brandl, R. Endell, *Angew. Chem.* **1973**, *85*, 1122; *Angew. Chem. Int. Ed. Engl.* **1973**, *12*, 1019; b) D. Sellmann, A. Brandl, R. Endell, *J. Organomet. Chem.* **1973**, *49*, C22; c) G. Huttner, W. Gartzke, K. Allinger, *Angew. Chem.* **1974**, *86*, 860; *Angew. Chem. Int. Ed. Engl.* **1974**, *13*, 822; d) D. Sellmann, K. Jödden, *Angew. Chem.* **1977**, *89*, 480; *Angew. Chem. Int. Ed. Engl.* **1977**, *16*, 464; e) D.

Sellmann, E. Böhlen, M. Waeber, G. Huttner, L. Zsolnai, *Angew. Chem.* **1985**, *97*, 984; *Angew. Chem. Int. Ed. Engl.* **1985**, *24*, 981; f) D. Sellmann, W. Soglowek, F. Knoch, M. Moll, *Angew. Chem.* **1989**, *101*, 1244; *Angew. Chem. Int. Ed. Engl.* **1989**, *28*, 1271; g) J. P. Collman, J. E. Hutchison, M. A. Lopez, R. Guilard, R. A. Reed, *J. Am. Chem. Soc.* **1991**, *113*, 2794; h) D. Sellmann, J. Käppler, M. Moll, F. Knoch, *Inorg. Chem.* **1993**, *32*, 960; i) D. Sellmann, K. Engl, F. W. Heinemann, J. Sieler, *Eur. J. Inorg. Chem.* **2000**, 1079.

[2] a) M. R. Smith III, R. L. Keys, G. L. Hillhouse, A. L. Rheingold *J. Am. Chem. Soc.* **1989**, *111*, 8312; b) M. R. Smith III, T.-Y. Cheng, G. L. Hillhouse, *J. Am. Chem. Soc.* **1993**, *115*, 8638; c) T.-Y. Cheng, A. Ponce, A. L. Rheingold, G. L. Hillhouse, *Angew. Chem.* **1994**, *106*, 703; *Angew. Chem. Int. Ed. Engl.* **1994**, *33*, 657; d) T.-Y. Cheng, J. C. Peters, G. L. Hillhouse, *J. Am. Chem. Soc.* **1994**, *116*, 204; e) D. Sutton, *Chem. Rev.* **1993**, *93*, 995.

[3] a) G. Albertin, S. Antoniutti, A. Bacchi, E. Bordignon, F. Busatto, G. Pelizzi, *Inorg. Chem.* **1997**, *36*, 1296; b) G. Albertin, S. Antoniutti, E. Bordignon, S. Pattaro, *J. Chem. Soc. Dalton Trans.* **1997**, 4445; c) G. Albertin, S. Antoniutti, A. Bacchi, M. Bergamo, E. Bordignon, G. Pelizzi, *Inorg. Chem.* **1998**, *37*, 479.

[4] a) K. H. Geib, P. Harteck, *Ber. Dtsch. Chem. Ges. B* **1933**, *66*, 1815; b) K. H. Geib, P. Harteck, *Trans. Faraday Soc.* **1934**, *30*, 131.

[5] a) J. E. Dickens, W. M. Irvine, C. H. DeVries, M. Ohishi, *Astrophys. J.* **1977**, *497*, 307; b) G. Winnewisser, C. Kramer, *Space Sci. Rev.* **1999**, *90*, 181.

[6] F. Hoyle, N. C. Wickramasinghe, *Nature* **1976**, *264*, 45.

[7] P. A. Shapley, J. M. Shusta, J. C. Hunt, *Organometallics* **1996**, *15*, 1622.

[8] G. Albertin, S. Antoniutti, S. Garcia-Fontán, R. Carballo, F. Padoan, *J. Chem. Soc. Dalton Trans.* **1998**, 2071.

[9] X-ray structural analysis: Philips PW1100 diffractometer equipped with a scintillation counter, graphite-monochromated $Mo_{K\alpha}$ radiation ($\lambda = 0.71069$ Å). Data correction for absorption effects by the ψ scan method[10] for both compounds, and intensity decay correction (40 %) for **2**-BPh_4. Structural determination: direct methods[11] and full-matrix least-squares refinement on all F^2.[12] Anisotropic displacement parameters refined in both cases for all non-hydrogen atoms; hydrogen atoms were introduced in idealized positions. Phosphite and phenyl groups were restrained to agree with typical bonding geometry from the literature. Crystal data for **2**-BPh_4: $C_{50}H_{84}BN_2O_{13}P_4Re$, $M_W = 1242.12$, crystal dimensions $0.3 \times 0.2 \times 0.2$ mm^3, space group $P2_1/c$, monoclinic, $a = 13.002(2)$, $b = 24.570(5)$, $c = 20.054(4)$ Å, $\beta = 95.49(2)^\circ$, $V = 6377(2)$ Å^3, $Z = 4$, $\rho_{calcd} = 1.308$ g cm^{-3}, $\theta_{max} = 30^\circ$, 18990 measured reflections (18537 unique), 4388 unique observed ($I > 2\sigma(I)$), $R_1 = 0.095$, $wR_2 = 0.26$ (on observed data), 176 restraints, 601 parameters, $GOF = 0.845$. Crystal data for **3**-BPh_4: $C_{50}H_{83}BNO_{13}P_4Re$, $M_W = 1227.11$, crystal dimensions $0.4 \times 0.3 \times 0.2$ mm^3, space group $P\bar{1}$, triclinic, $a = 15.393(5)$, $b = 16.977(5)$, $c = 12.916(5)$ Å, $\alpha = 100.02(5)$, $\beta = 91.63(5)$, $\gamma = 71.08(5)^\circ$, $V = 3143(2)$ Å^3, $Z = 2$, $\rho_{calcd} = 1.290$ g cm^{-3}, $\theta_{max} = 28^\circ$, 15138 measured unique reflections, 8634 unique observed ($I > 2\sigma(I)$), $R_1 = 0.048$, $wR_2 = 0.115$ (on observed data), 611 parameters, 79 restraints, $GOF = 0.912$. CCDC-181120 (**2**-BPh_4) and CCDC-181121 (**3**-BPh_4) contain the supplementary crystallographic data for this paper. These data can be obtained free of charge via www.ccdc.cam.ac.uk/conts/retrieving.html (or from the Cambridge Crystallographic Data Centre, 12, Union Road, Cambridge CB2 1EZ, UK; fax: (+44) 1223-336-033; or deposit@ccdc.cam.ac.uk).

[10] A. C. T. North, D. C. Phillips, F. S. Mathews, *Acta. Crystallogr. Sect. A* **1968**, *24*, 351.

[11] SIR97: A. Altomare, G. Cascarano, C. Giacovazzo, A. Guagliardi, M. C. Burla, G. Polidori, M. Camalli, *J. Appl. Crystallogr.* **1994**, *27*;, 435.

[12] G. M. Sheldrick, SHELXL-97, Program for structure refinement, University of Göttingen, Göttingen (Germany), **1997**.

[13] W. A. Herrmann, L. K. Bell, M. L. Ziegler, H. Pfisterer, C. Pahl, *J. Organomet. Chem.* **1983**, *247*, 39.

[14] J. Vicente, M. T. Chicote, M. D. Abrisqueta, R. Guerrero, P. G. Jones, *Angew. Chem.* **1997**, *109*, 1252; *Angew. Chem. Int. Ed. Engl.* **1997**, *36*, 1203.

[15] D. A. Knight, M. A. Dewey, G. A. Stark, B. K. Bennett, A. M. Arif, J. A. Gladysz, *Organometallics* **1993**, *12*, 4523.

[16] Coordination geometry for **2**: Re–N 2.12(1), Re–CO 2.14(1), Re–P 2.354(4), NH–N 1.251(4), N–C 1.36(2), C–O 1.12(1) Å; Re-N-N 145(2), N-N-C 123(2)°.

[17] Preliminary investigations show the presence of traces of ammonia in the final reaction mixture, but no other nitrogen-containing compound was unambiguously identified, and therefore no reaction path may be reasonably proposed.

[18] Metal-mediated N–N or N=N bond activation is a topic of current interest. For some recent examples see: A. K. Verma, S. C. Lee, *J. Am. Chem. Soc.* **1999**, *121*, 10838; R. G. Peters, B. P. Warner, C. J. Burns, *J. Am. Chem. Soc.* **1999**, *121*, 5585; M. A. Aubart, R. G. Bergman, *Organometallics* **1999**, *18*, 811; F. Maseras, M. A. Lockwood, O. Eisenstein, I. P. Rothwell, *J. Am. Chem. Soc.* **1998**, *120*, 6598.

[19] Interest in cleavage of the N–N bond of hydrazine stems from its importance to inorganic and bioinorganic reducing system(s): a) A. E. Shilov, *Metal Complexes in Biomimetic Chemical Reactions*, CRC, Boca Raton, FL, **1997**; b) R. R. Eady, *Chem. Rev.* **1996**, *96*, 3013; c) G. J. Leigh, *Science* **1995**, *268*, 827; d) R. R. Schrock, T. E. Glassman, M. G. Vale, *J. Am. Chem. Soc.* **1991**, *113*, 725; e) S. M. Malinak, K. D. Demadis, D. Coucouvanis, *J. Am. Chem. Soc.* **1995**, *117*, 3126; f) D. Sellmann, J. Sutter, *Acc. Chem. Res.* **1997**, *30*, 460.

Total Synthesis of the Amaryllidaceae Alkaloid (+)-Plicamine and Its Unnatural Enantiomer by Using Solid-Supported Reagents and Scavengers in a Multistep Sequence of Reactions**

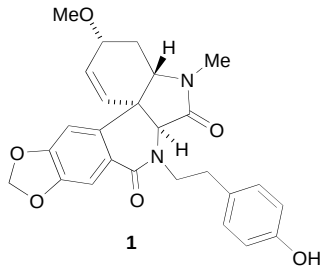
Ian R. Baxendale, Steven V. Ley,* and Claudia Piutti

Amaryllidaceae alkaloids are an important class of natural products especially as many members of the series display a wide range of potent biological activity. These properties include anticholinergic, antitumor, immunosuppresive, and analgesic activity, and they have also been shown to inhibit various cell cycle mechanisms (including HIV-1 activity), and have found recent application in the therapeutic treatment of Alzheimer's disease.[1] Thus extensive synthetic studies of this family have been carried out over a number of years.[2, 3] Furthermore, the search for new members of the series has proved to be extremely profitable.[3, 4] The recently isolated compound (+)-plicamine (**1**) is especially attractive as it exemplifies many of the structural features of these natural

[*] Prof. S. V. Ley, I. R. Baxendale
Department of Chemistry
University of Cambridge
Lensfield Road, Cambridge CB2 1EW (UK)
Fax: (+44) 1223-336-442
E-mail: svl1000@cam.ac.uk
C. Piutti
Department of Chemistry
Pharmacia S.p.A
Discovery Research Oncology
Viale Pasteur, 10, 20014 Nerviano (MI) (Italy)

[**] We gratefully acknowledge financial support from Pfizer Central Research for a Postdoctoral Fellowship (to I.R.B.), the BP endowment and the Novartis Research Fellowship (to S.V.L.), and Pharmacia & Upjohn (to C.P.).

 © WILEY-VCH Verlag GmbH, 69451 Weinheim, Germany, 2002 1433-7851/02/4112-2194 $ 20.00+.50/0



1

products and has not been previously synthesized nor have its biological properties been fully evaluated.[5]

Here, we report a conceptionally interesting approach to both enantiomers of plicamine **1** using an orchestrated multistep sequence of reactions, for which only solid-supported reagents and scavengers are used to effect the individual steps.[6] In this way, work-up of the reaction mixture is greatly facilitated, requiring only the simple operation of filtration to remove spent or excess reagents followed by evaporation to afford the product. No conventional work-up procedures such as chromatography, crystallization, or distillation are necessary. These methods not only expediate the synthesis reported here but also have relevance for chemical compound library generation. For example, we have previously shown that these approaches can be used to prepare druglike substances,[7] heterocyclic compounds,[8] and other natural products.[9]

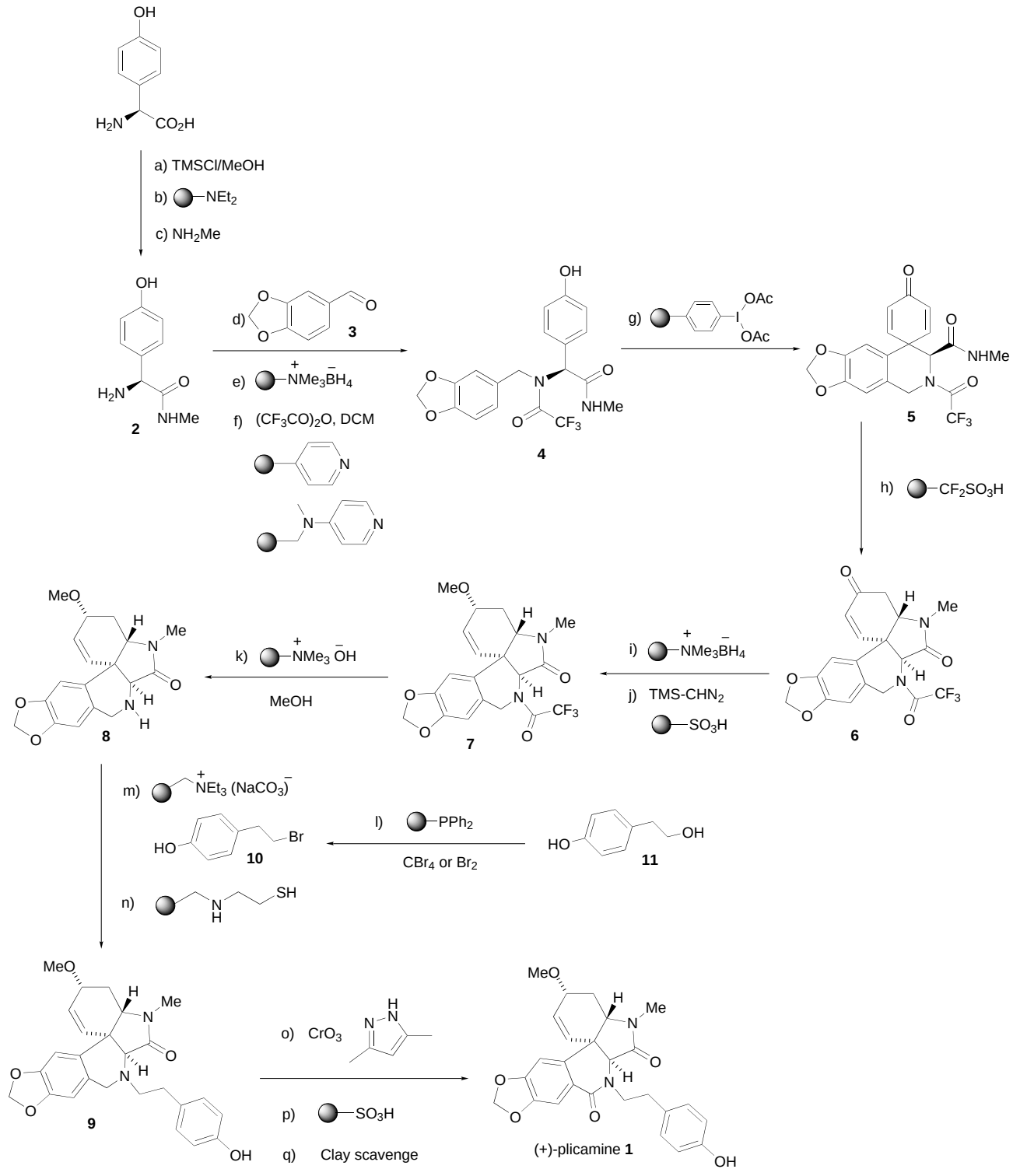
Both enantiomers of plicamine **1** have been synthesized by the appropriate selection of the commercially available optically pure form of 4-hydroxyphenylglycine. The synthesis of (+)-plicamine reported below, begins with the conversion of L-4-hydroxyphenylglycine to the amide **2** (see Scheme 1). The initial reaction with trimethylsilyl chloride (TMSCl) in methanol resulted in the formation of an intermediate methyl ester. Subsequent treatment with Amberlyst 21 resin, to act as a scavenger for hydrochloric acid, produced the free base. Addition of excess methylamine to the reaction mixture afforded the amide **2** in essentially quantitative yield. At all stages of the synthesis the product purity was evaluated by LC-MS and in all cases was found to be in excess of 95% unless stated. This level of purity was more than adequate to progress directly to the next step in the synthesis. Following procedures reported previously for the synthesis of oxomaritidine,[9c] the amino group in **2** was allowed to react with piperonal **3** and the resulting imine reduced with polymer-supported borohydride[10] in methanol and dichloromethane to give the reductively aminated product. The amine was immediately acylated with trifluoroacetic anhydride to give the protected amine **4**. Polymer-supported aminomethylpyridine (poly-DMAP) in the presence of polyvinylpyridine (PVP) was used as the catalyst in this transformation.[11] All these reactions were easily carried out on multigram scale to give the clean product **4** in 91% overall yield over the six steps (>97% purity by HPLC; Scheme 1). Phenol oxidative coupling of **4** gave the spirodieneone **5** (82% yield)[12] through the use of the solid-supported iodonium diacetate[13] in 2,2,2-trifluoroethanol as the solvent. Compound **5** was efficiently cyclized to the tetracyclic lactam **6** by using Nafion-H resin in dichloromethane (alternatively a solution of HCl in diethyl ether could be employed). Again the purity of the product at all stages of this synthesis was excellent, the product required no chromatography prior to advancing to the next step. The ketone **6** was stereoselectively reduced by using polymer-supported borohydride,[14] and the resulting alcohol was methylated by using trimethylsilyldiazomethane and a macroporous sulfonic acid exchange resin to give **7**.[15] The stereoselectivity in this reaction was confirmed by X-ray crystallographic studies and detailed NOE experiments. Next, the trifluoroacetate protecting group was removed by treatment with Ambersep 900 (OH^- form) in methanol in a sealed tube microwave reactor at 100 °C for 20 min.[16] The intermediate amino compound **8** was readily alkylated with bromide **10** in the presence of a solid-supported carbonate base[17] to give **9**. Excess bromide **10** was scavenged by using a mercaptoaminomethyl resin[18] and the product was obtained in excellent yield and purity. It should be noted that the bromide **10** is not commercially available and was prepared from the corresponding alcohol **11** by using carbon tetrabromide or bromine and an immobilized triphenylphosphane.[19] The alkylated material **9** was immediately oxidized to the amide **1** by using chromium trioxide and 3,5-dimethylpyrazole.[20] This reaction proved to be the most difficult transformation in the sequence, requiring scavenging with solid Amberlyst 15 resin to remove contaminating unoxidized amine and the pyrazole. The chromium salts could be efficiently removed by passing the reaction mixture through a mixed-bed column of Varian Chem Elut CE1005 packing material[21] and montmorillonite K 10 (1:1 wt/wt), which had been preconditioned by eluting with a 10:1 mixture of acetonitrile/water. After this process of scavenging, (+)-plicamine **1** was obtained in 70% yield and greater than 90% purity (by HPLC). To obtain analytically pure material a rapid pass through a short plug of silica gel was sufficient.[22] Following the same reaction sequence, we have also been able to prepare the unnatural enantiomer (−)-plicamine in essentially identical yields and purity starting from D-4-hydroxyphenylglycine.[23]

In summary, we have reported the first total synthesis of (+)-plicamine (**1**) and its enantiomer using only a combination of supported reagents and scavengers to effect all the synthetic steps. No less than thirteen immobilized systems were used to produce the clean product. Given the relative complexity of the molecule, the synthesis is a powerful demonstration of the ability to achieve multistep transformations without conventional chromatographic methods.

Received: February 15, 2002 [Z18719]

[1] a) C. W. Fennell, J. van Staden, *J. Ethnopharmacol.* **2001**, *78*, 15–26, and references therein; b) B. S. Min, Y. H. Kim, M. Tomiyama, N. Nakamura, H. Miyashiro, T. Otake, M. Hattori, *Phytother. Res.* **2001**, *15*, 481–486; c) S. Yui, M. Mikami, Y. Mimaki, Y. Sashida, M. Yamazaki, *Yakugaku Zasshi* **2001**, *121*, 167–171; d) E. Furusawa, S. Furusawa, J. Y. B. Lee, S. Patanavanich, *Proc. Soc. Expl. Biol. Med.* **1976**, *152*, 186–197, and references therein; e) E. Furusawa, H. Irie, D. Combs, W. C. Wildman, *Chemotherapy* **1980**, *26*, 36–41; f) E. Furusawa, S. Furusawa, J. Y. B. Lee, S. Patanavanich, *Chemotherapy* **1983**, *29*, 294–302; g) E. Furusawa, S. Furusawa, *Onocology* **1988**, *45*, 180–186; h) M. D. Antoun, N. T. Mendoza, Y. R. Rios, G. R. Proctor, D. B. M. Wickramaratne, J. M. Pezzuto, A, D. Kinghorn, *J. Nat. Prod.* **1993**, *56*, 1423–1425; i) E. Furusawa, S. Furusawa, *Chemotherapy* **1986**, *32*, 521–529; j) A. Missoum, M.-E. Sinibaldi, D. Vallée-Goyet, J.-C., Gramain, *Synth. Commun.* **1997**, *27*, 453–466.

[2] a) P. W. Jeffs in *MTP International Review of Science, Alkaloids, Organic Chemistry, Series One*, *Vol. 9* (Eds.: D. H. Hey, K. F. Wiesner), Butterworth, London, **1973**, pp. 273–318; b) S. F. Martin



Scheme 1. Total synthesis of (+)-plicamine (**1**). a) TMSCl (3 equiv), MeOH, RT, 12 h; b) Amberlyst 21 (3 equiv ~3 mmol g^{-1}); c) NH_2Me (5 equiv), MeOH, 40 °C, 24–48 h; d) piperonal **3** (1.1 equiv), EtOAc, RT, 45 min; e) PS-borohydride, MeOH/CH_2Cl_2 (2:1), 2 h; f) $(CF_3CO)_2O$, PVP (3 equiv), poly-DMAP (0.5 equiv), CH_2Cl_2, 0 °C, 1 h, (91% over six steps); g) PS-iodinium diacetae (1.5 equiv), 2,2,2-trifluoroethanol, −5 °C, 82%; h) Nafion-H, 24 h; i) PS-borohydride, MeOH/CH_2Cl_2 (1:1) 2 h, quantitative; j) TMS-CHN_2, sulfonic acid resin, MeOH/CH_2Cl_2 (3:2), 95%; k) Ambersep 900 (OH^-), MeOH, microwave, 100 °C, 20 min, 96%; l) PS-triphenylphosphane (2 equiv), CBr_4 (1.5 equiv) or Br_2 (1.5 equiv), CH_2Cl_2, 0 °C, 1 h, quantitative; m) PS-carbonate (2 equiv), bromide **10** (1.2 equiv), MeCN, microwave, 140 °C, 2 × 15 min; n) PS-mercaptoaminomethyl resin, 90% (two steps); o) CrO_3 (2.5 equiv), 3,5-dimethylpyrazole (2.5 equiv), CH_2Cl_2, −45 °C, 4 h, 82% conversion by LC-MS; p) Amberlyst 15 (10 equiv); q) (1:1 wt/wt) montmorillonite K 10/Varian Chem Elut CE1005 packing material, 70% (isolation for three steps o–q).

 © WILEY-VCH Verlag GmbH, 69451 Weinheim, Germany, 2002 1433-7851/02/4112-2196 $ 20.00+.50/0 *Angew. Chem. Int. Ed.* **2002**, *41*, No. 12

in *The Alkaloids*, *Vol. 30* (Ed.: A. Brossi), Academic Press, New York, **1987**, p. 251; c) J. R. Lewis, *Nat. Prod. Rep*. **2001**, *18*, 95 – 128.

[3] a) J. H. Rigby, A. Cavezza, M. J. Goekjian, *J. Am. Chem. Soc*. **1998**, *120*, 3613 – 3622; b) J. D. White, W. K. M. Chong, K. Thirring, *J. Org. Chem*. **1983**, *48*, 2300 – 2304; c) J. B. Hendrickson, T. L. Bogard, M. E. Fisch, S. Grossert, N. Yoshimura, *J. Am. Chem. Soc.* **1974**, *96*, 7781 – 7789; d) Y. Tsuda, A. Ukai, K. Isobe, *Tetrahedron Lett.* **1972**, 3153 – 3156; e) S. J. Danishefsky, J. Morris, G. Mullen, R. Gammill, *J. Am. Chem. Soc*. **1982**, *104*, 7591 – 7599; f) M. M. Abelman, L. E. Overman, D. V. Tran, *J. Am. Chem. Soc*. **1990**, *112*, 6959 – 6964; g) L. E. Overman, H. Wild, *Tetrahedron Lett.* **1989**, *30*, 647 – 650; h) H. Ishibashi, H. Nakatani, S. Iwami, T. Sato, N. Nakamura, M. Ikeda, *J. Chem. Soc. Chem. Commun*. **1989**, 1767 – 1769; i) T. Nishimata, M. Mori, *J. Org. Chem*. **1998**, *63*, 7586 – 7586; j) D. J. Watson, A. I. Meyers, *Tetrahedron Lett*. **2000**, *41*, 1519 – 1522.

[4] a) J. Bastida, J. M. Llabres, F. Viladomat, C. Codina, M. Rubiralta, M. Feliz, *Planta Med.* **1988**, *54*, 524 – 526; b) A. S. Chawla, T. R. Krishnan, A. H. Jackson, D. A. Scalabrin, *Planta Med.* **1988**, *54*, 526 – 528; c) A. Linden, G. Akineri, S. Noyan, T. Gozler, M. Hesse, *Acta Crystallogr. Sect. C* **1998**, *54*, 1653 – 1659; d) N. Unver, S. Noyan, T. Gozler, M. A. Onur, B. Gozler, M. Hesse, *Planta Med.* **1999**, *65*, 347 – 350; e) L. H. Pham, E. Grundemann, J. Wagner, M. Bartoszek, W. Dopke, *Phytochemistry* **1999**, *51*, 327 – 332; f) E. E. Elgorashi, S. E. Drewes, J. Van Staden, *Phytochemistry* **1999**, *52*, 533 – 536.

[5] a) N. Ünver, T. Gözler, N. Walch, B. Gözler, M. Hesse, *Phytochemistry* **1999**, *50*, 1255 – 1261; b) N. Ünver, S. Noyan, T. Gözler, M. Hesse, C. Werner, *Heterocycles* **2001**, *55*, 641 – 652.

[6] S. V. Ley, I. R. Baxendale, R. N. Bream, P. S. Jackson, A. G. Leach, D. A. Longbottom, M. Nesi, J. S. Scott, R. Ian Storer, S. J. Taylor, *J. Chem. Soc. Perkin Trans. 1* **2000**; 3815 – 4196, and references therein.

[7] a) I. R. Baxendale, S. V. Ley, *Biorg. Med. Chem. Lett*. **2000**, *10*, 1983 – 1986; b) S. V. Ley, A. Massi, *J. Comb. Chem*. **2000**, *2*, 104 – 107; c) M. Caldarelli, J. Habermann, S. V. Ley, *Biorg. Med. Chem. Lett*. **1999**, *9*, 2049 – 2052.

[8] a) S. V. Ley, L. Lumeras, M. Nesi, I. R. Baxendale, *Comb. Chem. High Throughput Screening* **2002**, *5*, 195 – 197; b) M. Caldarelli, I. R. Baxendale, S. V. Ley, *J. Green Chem*. **2000**, 43 – 45; c) M. Caldarelli, J. Habermann, S. V. Ley, *J. Chem. Soc. Perkin Trans. 1* **1999**, 107 – 110; d) J. Habermann, S. V. Ley, R. Smits, *J. Chem. Soc. Perkin Trans. 1* **1999**, 2421 – 2423; e) J. Habermann, S. V. Ley, J. J. Scicinski, J. S. Scott, R. Smits, A. W. Thomas, *J. Chem. Soc. Perkin Trans. 1* **1999**, 2425 – 2427; f) J. Habermann, S. V. Ley, J. S. Scott, *J. Chem. Soc. Perkin Trans. 1* **1998**, 3127 – 3130.

[9] a) I. R. Baxendale, G. Brusotti, M. Matsuoka, S. V. Ley, *J. Chem. Soc. Perkin Trans. 1* **2002**, *2*, 143 – 154; b) I. R. Baxendale, A.-L. Lee, S. V. Ley, *Synlett* **2001**, 1482 – 1484; c) S. V. Ley, O. Schucht, A. W. Thomas, P. J. Murray, *J. Chem. Soc. Perkin Trans. 1* **1999**, 1251 – 1252; d) J. Habermann, S. V. Ley, J. S. Scott, *J. Chem. Soc. Perkin Trans. 1* **1999**, 1253 – 1255.

[10] Borohydride, polymer-supported (borohydride on Amberlite IRA A-400, $\sim$2.5 mmol g^{-1}) available from Aldrich.

[11] Available from Aldrich, dimethylaminopyridine, polymer-bound (cat. no. 35,988-2); poly(4-vinylpyridine) 2 % cross-linked (cat. no. 22,696-3).

[12] Despite the nonquantitative yield, no other material was detectable after filtration of the resin from the solution. We speculate that, due to the radical nature of the reaction, possible coupling of the starting material to the polymer resin has occurred.

[13] a) H. Togo, M Katohgi, *Synlett* **2001**, 565 – 581; b) S. V. Ley, A. W. Thomas, H. Finch, *J. Chem. Soc. Perkin Trans. 1* **1999**, 669 – 671; c) H. Togo, G. Nogami and M. Yokoyama, *Synlett* **1998**, 534; d) for a general review on hypervalent iodine reagents see: A. Varvoglis, *Hypervalent Iodine In Organic Synthesis*, Academic Press, London, **1997**; e) see also reference [3b].

[14] Borohydride on polymer support (Amberlyst A-26 BH_4^- form, 1.5 – 4 mmol g^{-1}) available from Fluka (cat. no. 15595). The use of immobilised borohydride on Amberlite IRA 400[10] resulted in significant amounts of deprotected amino alcohol material. As an alternative, polymer-supported cyanoborohydride could be used, but in this case the reactions required more than 48 h.

[15] MP-TsOH 1.40 mmol g^{-1} available from Argonaut Technologies Inc. (cat. no. 800286; A15 was not effective in promoting this transformation).

[16] A fully automated Coherent Synthesis System microwave machine was used. This was supplied by Personal Chemistry: Hamnesplanaden 5, 753 19 Uppsala, Sweden; www.personalchemistry.com.

[17] *N*-(2-mercaptoethyl)aminomethyl polystyrene 1.2 mmol g^{-1} available from Nova Biochem. (cat. no. 01-64-0180).

[18] Carbonate on polymer support on IRA 900, $\sim$3.5 mmol g^{-1} ($NaCO_3$) available from Fluka (cat. no. 21850).

[19] Polymer-bound triphenylphosphane $\sim$3 mmol g^{-1} available from Fluka (cat. no. 93093).

[20] a) W. G. Salmond, M. A. Barta, J. L. Havens, *J. Org. Chem*. **1978**, *43*, 2057 – 2059; b) see also reference [3e].

[21] Varian Chem. Elut Column (cat. no.1219-8007).

[22] (+)-Plicamine $[\alpha]_D = +77.5$ ($c = 0.867$ in MeOH); $[\alpha]_D^{lit} = +74.4$ ($c = 0.117$ in MeOH); ^{1}H NMR (400 MHz, $CDCl_3$): $\delta = 7.59$ (s, 1H; H-9), 7.08 (d, $J = 8.3$ Hz, 2H; H-2′ and H-6′), 6.73 (d, $J = 8.3$ Hz, 2H; H-3′ and H-5′), 6.49 (s, 1H; H-12), 6.01 (s, 2H; OCH_2O), 5.81 (d, $J = 10.1$ Hz, 1H; H-2), 5.36 (d, $J = 10.1$ Hz, 1H; H-1), 4.51 (ddd, $J = 13.8$, 8.3, 4.3 Hz, 1H; H-8′a), 4.06 (m, 1H; H-4a), 3.93 (s, 1H; H-6a), 3.87 (dd, $J = 12.3$, 4.3 Hz, 1H; H-4a), 3.51 (m, 1H; H-8′b), 3.44 (s, 3H; OMe), 2.93 (m, 2H; H-7′), 2.78 (s, 3H; NMe), 2.58 (m, 1H; H-3β), 1.39 ppm (m, 1H; H-3α); IR (neat): $\tilde{\nu}_{max} = 3292.7$, 2976.2, 2983.7, 1705.8, 1668.7, 1613.3, 1514.5, 1482.7, 1442.7, 1400.7, 1386.1, 1348.3, 1233.6, 1158.4, 1102.8, 1036.2, 931.9, 929.8 cm^{-1}; HR-MS calcd for $C_{26}H_{26}N_2O_6Na$: 485.1689; found 485.1694. Numbering from original paper concerning isolation see reference [5a].

[23] (−)-Plicamine $[\alpha]_D = -76.5$ ($c = 0.678$ in MeOH).

Catalytic Enantioselective Synthesis of β^2-Amino Acids**

Huw M. L. Davies* and Chandrasekar Venkataramani

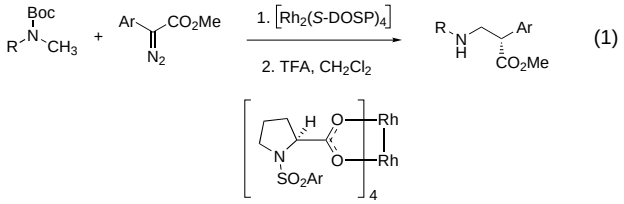
In recent years the enantioselective synthesis of β-amino acids has been of considerable interest because β-amino acids[1] are useful precursors of β-peptides[2] and β-lactams.[2b, 3] Traditionally, the asymmetric synthesis of β^2-substituted amino acids has been achieved by using chiral auxiliaries in methods such as the alkylation of chiral enolates[4] and the acylation of metalated phenylacetonitrile with a chiral carbonyl chloride.[4c] Recently, highly enantioselective, L-proline-catalyzed, asymmetric Mannich-type reactions of *N*-PMP-protected (PMP = *p*-(MeO)C_6H_5) α-iminoethyl glyoxylate with aldehydes to generate functionalized β-amino acids was reported.[5] Herein we report a catalytic asymmetric synthesis of β^2-substituted amino acids. The crucial reaction is an asymmetric C–H activation of *N*-butoxycarbonyl (Boc)-protected methylamines by means of a [Rh_2(*S*-DOSP)$_4$] (**1**) induced C–H insertion [Eq. (1); TFA = trifluoroacetic acid].

Recently, numerous applications of the rhodium – carbenoid induced intermolecular C–H activation strategy in

[*] Prof. H. M. L. Davies, C. Venkataramani
Department of Chemistry, University at Buffalo
The State University of New York
Buffalo, NY 14260-3000 (USA)
Fax: (+1) 716-645-6547

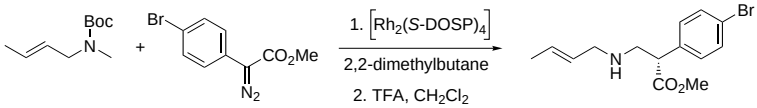
[**] This work was supported by the National Science Foundation (CHE 0092490) and the National Institutes of Health (GM57425).

Supporting information for this article is available on the WWW under http://www.angewandte.org or from the author.



1

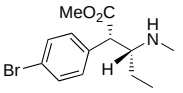
organic synthesis have been reported.[6] The results described here represent the first chemoselective C–H activations occurring at a methyl site. This reaction was discovered during studies on the development of the C–H activation of allylamines as a surrogate to the Mannich reaction.[7] Instead of the expected allylic C–H activation, the $[Rh_2(S\text{-DOSP})_4]$ (**1**)-catalyzed reaction of methyl-*p*-bromophenyldiazoacetate (**3**) with Boc-protected *N*-methylcrotylamine (**2**) formed an unexpected C–H activation product. After treatment of the crude reaction mixture with TFA to remove the Boc protecting group, the β-amino ester **4** was isolated in 58% yield and 85% *ee* [Eq. (2)]. As a selective insertion into a primary C–H



2 **3** (2 equiv) **4** 58% yield, 85% *ee*

bond is unprecedented for intermolecular carbenoid-induced C–H activations, a full study to evaluate the scope of this reaction was undertaken.

Our earlier studies have demonstrated that the rhodium carbenoid derived from aryldiazoacetates behaves as a very sterically demanding reagent.[6a, 8] Presumably, this is the cause of the selective insertion into a methyl site over the electronically much more favorable allylic site. To explore this effect further, the C–H activation of a series of *N*-Boc-protected methylamines **5** were then examined (Table 1). In every case, except for the *N*-propyl derivative **5b**, a highly regioselective C–H insertion into the *N*-methyl site occurred to form after Boc deprotection the β-amino esters **6** in 57–62% yield. With **5b** a competing insertion into the methylene site also occurred to form **7** with very high diastereoselectivity (>94% *de*) but poor enantioselectivity (24% *ee*). The second N substituent has a dramatic effect on the enantioselectivity of the C–H activation with the *N*-benzyl derivative **5e** (95% *ee*) giving the best result.



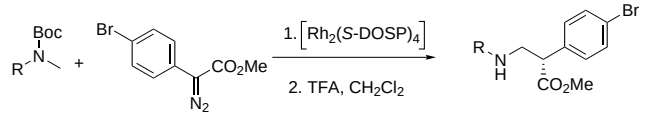
7

As all of the initial evaluations were carried out with Boc-protected amines, it was intriguing to determine if the C–H activation step was compatible with other common nitrogen protecting groups. As summarized in Table 2, the reaction was compatible with the benzyloxycarbonyl (Cbz) group but the yields were considerably lowered when the fluoren-9-ylmethoxycarbonyl (Fmoc) and 2-trimethylsilylethoxycarbonyl (Teoc) groups were used.

The intermolecular C–H insertion into **5e** is a general process for the synthesis of a range of β^2-substituted amino esters (Table 3). Various substituted phenyldiazoacetates can be used in this chemistry as well as naphthyldiazoacetate **9e**, thienyldiazoacetate **9g**, and styryldiazoacetate **9h**. The yields of the reactions are 55–67% and the enantioselectivities are 87–96% *ee*.

The discovery that the benzylamine **5e** is the optimum substrate for this chemistry is very attractive because the resulting products are readily converted to useful amino acids and

Table 1. The C–H activation of *N*-Boc-*N*-methylamines.

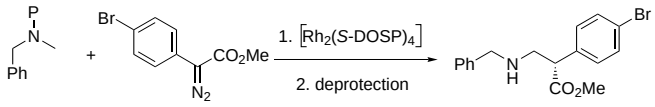


5 **3** (2 equiv) **6**

Compound	R	Yield [%][a]	*ee* [%]
5a	CH_3	61	31
5b	$CH_3CH_2CH_2$	46[b]	64
5c	$CH(CH_3)_2$	57	82
5d	$C(CH_3)_3$	58[c]	54
5e	$C_6H_5CH_2$	62	95
5f	$(CH_3)_2C{=}CHCH_2$	62	87
5g	*trans*-PhC=CHCH$_2$	60	87

[a] Yield of isolated product. [b] 8% of **7** was also formed (>94% *de*, 24% *ee*). [c] Isolated with Boc group.

Table 2. Comparison of the effects of different nitrogen protecting groups on the C–H activation step.

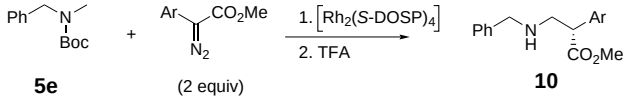


8 **3** (2 equiv) **6e**

Compound	P	Yield [%][a]	*ee* [%]
8a	Cbz	67	90
8b	Fmoc	21	69
8c	Teoc	26	94

[a] Yield of isolated product.

Table 3. The C–H activation of *N*-Boc-*N*-benzyl-*N*-methylamine.



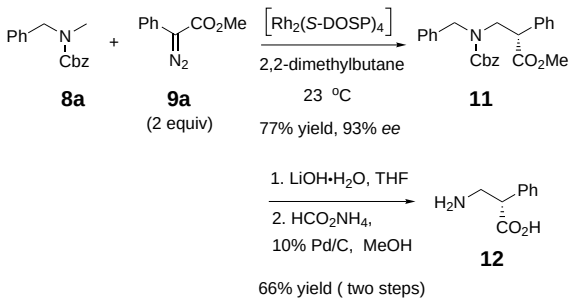
5e (2 equiv) **9** **10**

Compound	Ar	Yield [%][a]	*ee* [%]
9a	C_6H_5	67	96
9b	4-$CF_3C_6H_4$	55	92
9c	4-$OCH_3C_6H_4$	61	92
9d	4-$CH_3C_6H_4$	66	95
9e	2-naphthyl	55	87
9f	4-ClC_6H_4	62	96
9g	3-thienyl	58	90
9h	$C_6H_5CH{=}CH_2$	56[b]	96

[a] Yield of isolated product. [b] Isolated with Boc group.

 © WILEY-VCH Verlag GmbH, 69451 Weinheim, Germany, 2002 1433-7851/02/4112-2198 $ 20.00+.50/0 *Angew. Chem. Int. Ed.* **2002**, *41*, No. 12

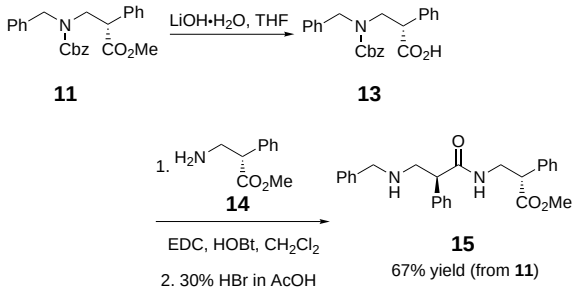
peptides. $[Rh_2(S\text{-DOSP})_4]$-catalyzed decomposition of **9a** in the presence of **8a** gave the C–H insertion product **11** in 77% yield and 93% *ee*. Cleavage of the methyl ester (**11**) using $LiOH \cdot H_2O$ in THF, followed by transfer hydrogenation provided α-phenyl-β-alanine **12** in 66% yield [Eq. (3)]. The



(3)

absolute stereochemistry was determined to be *S* by comparison of the sign of optical rotation of **12** ($[\alpha]_{25}^{D} = -87.6$, $c = 0.13$, H_2O) which was found to be opposite that of the literature value[9] ($[\alpha]_{25}^{D} = +85$, $c = 0.2$, H_2O) for the *R* isomer. Application of the predictive C–H insertion model correctly predicts the observed stereochemistry.[6d,h, 8b]

The products would also be applicable to the synthesis of β-peptides as illustrated in the synthesis of the dipeptide **15** [Eq. (4)]. Hydrolysis of **11** gave the acid **13**, which was coupled (1-(3-dimethylaminopropyl)-3-ethylcarbodiimide (EDC), 1-hydroxybenzotriazole (HOBt)) with the amine **14** (prepared from **11** by hydrogenation) to give the dipeptide **15** in 67% yield.



(4)

In summary, these preliminary studies demonstrate that the intermolecular C–H insertions of carbenoids derived from aryldiazoacetates catalyzed by $[Rh_2(S\text{-DOSP})_4]$ is an attractive method for the asymmetric synthesis of substituted β-amino acids. The reaction proceeds with good chemo- and enantioselectivity and demonstrates the remarkable steric control that is possible with these rhodium–carbenoid intermediates. Further studies to explore the full scope of this chemistry are currently underway.

Experimental Section

Representative example (**6e**): Methyl 4-bromophenyldiazoacetate (**3**) (0.23 g, 0.90 mmol) in 2,2-dimethylbutane (7 mL) was added dropwise over 3 h using a syringe pump to a solution of $[Rh_2(S\text{-DOSP})_4]$ (17 mg, 0.01mmol) and **5e** (0.100 g, 0.45 mmol) in 2,2-dimethylbutane (5 mL). After the addition, the resulting solution was stirred at 23 °C for 1 h. The solvent was removed under reduced pressure, and the residue was reconstituted in CH_2Cl_2 (10 mL) and TFA (0.2 mL, 2.26 mmol) and stirred for 16 h at 23 °C. The solution was concentrated in vacuo, and the residue was dissolved in Et_2O (20 mL) and extracted with 10% HCl (3×15 mL). The combined aqueous layers were basified ($NaHCO_3$, 1M NaOH to pH 8–9) and extracted with EtOAc (3×15 mL). The combined organic layers were washed with water (1×15 mL), brine (1×20 mL), and dried over Na_2SO_4. The product was purified by flash chromatography (SiO_2, Et_2O/pentane/NEt_3 = 25:35:2) to give the title compound **6e** (97 mg, 0.28 mmol; 62% yield). $[\alpha]_{25}^{D} = -44.7°$ ($c = 1.36$, $CHCl_3$); ^1H NMR (500 MHz, $CDCl_3$): $\delta = 7.44$ (d, $J = 7.5$ Hz, 2H), 7.32–7.22 (m, 5H), 7.16 (d, $J = 7.0$ Hz, 2H), 3.8 (s, 2H), 3.77 (m, 1H), 3.66 (s, 3H), 3.26 (m, 1H), 2.91 ppm (dd, $J = 6.5$, 11.5 Hz, 1H); ^{13}C NMR (DEPT) (125 MHz, $CDCl_3$): $\delta = 173.1$ (C), 139.8 (C), 136.1 (C), 131.8 (CH), 129.7 (CH), 128.3 (CH), 127.9 (CH), 126.9 (CH), 121.4 (CH), 53.5 (CH_2), 52.1 (CH_3), 51.7 (CH_2), 51.5 ppm (CH); IR (neat): $\tilde{\nu} = 3328$, 3024, 2948, 2844, 1730 cm^{-1}; elemental analysis calcd (%) for $C_{17}H_{18}NBrO_2$: C 58.63, H 5.21, N 4.02; found: C 58.76, H 5.25, N 4.06. To measure the enantiomeric excess of **6e**, it was converted to its trifluoroacetamide. Acylation of a small sample of the free amine from above with trifluoroacetic anhydride (TFAA) and CH_2Cl_2 followed by flash chromatography (SiO_2, Et_2O/pentane = 15:85) gave the amide in 95% *ee* (HPLC, Chiralcel-AD-RH column, 5.0% 2-propanol in hexanes, 1.0 mL min^{-1}, 1 mg mL^{-1}, $t_R = 4.62$ (major) and 8.16 (minor) min, UV 254 nm).

Received: March 13, 2002 [Z18888]

[1] a) E. Juaristi, *Enantioselective Synthesis of β-Amino Acids*, Wiley-VCH, Wiley, New York **1997**; b) G. Cardillo, C. Tomasini, *Chem. Soc. Rev.* **1996**, 117; c) D. C. Cole, *Tetrahedron* **1994**, *50*, 9517.

[2] a) S. H. Gellman, *Acc. Chem. Res.* **1998**, *31*, 173; b) T. N. Salzmann, R. W. Ratcliffe, B. G. Christensen, F. A. Bouffard, *J. Am. Chem. Soc.* **1980**, *102*, 6161; c) N. Mayachi, M. Shibasaki, *J. Org. Chem.* **1990**, *55*, 1975; d) S. Abele, D. Seebach, *Eur. J. Org. Chem.* **2000**, 1; e) D. Seebach, S. Abele, K. Gademann, G. Guichard, T. Hintermann, B. Juan, J. L. Matthews, J. V. Schreiber, L. Oberer, U. Hommel, H. Widmer, *Helv. Chim. Acta* **1998**, *81*, 932; f) D. Seebach, S. Abele, K. Gademann, G. Guichard, B. Jaun, *Angew. Chem.* **1999**, *111*, 1700; *Angew. Chem. Int. Ed.* **1999**, *38*, 1595; g) G. Guichard, S. Abele, D. Seebach, *Helv. Chim. Acta* **1998**, *81*, 187; h) G. Guichard, D. Seebach, *Chimia* **1997**, *51*, 315.

[3] E. Juaristi, D. Quintania, J. Escalante, *Aldrichimica Acta* **1994**, *27*, 3.

[4] a) N. Gangadhar, V. J. Huber, C. Lum, B. A. Goodman, *Org. Lett.* **2000**, *2*, 3527; b) D. A. Evans, F. Urpi, T. C. Sommers, J. S. Clark, M. T. Milodeau, *J. Am. Chem. Soc.* **1990**, *112*, 8215; c) R. Ponsinet, G. Chassaing, J. Vaissermann, S. Lavielle, *Eur. J. Org. Chem.* **2000**, 83; d) T. Hinternamm, D. Seebach, *Helv. Chim. Acta* **1998**, *81*, 2093; e) E. Juaristi, D. Quintana, *Tetrahedron: Asymmetry* **1992**, *3*, 723; f) D. Seebach, A. Boog, W. B. Schweizer, *Eur. J. Org. Chem.* **1999**, 335; g) E. Arvanitis, H. Ernst, A. A. Ludwig, A. J. Robinson, P. B. Wyatt, *J. Chem. Soc. Perkin Trans. 1* **1998**, 521; h) M. Calmes, F. Escale, C. Glot, M. Rolland, J. Martinez, *Eur. J. Org. Chem.* **2000**, 2459; i) M. P. Sibi, P. K. Despande, *J. Chem. Soc. Perkin Trans. 1* **2000**, 1461.

[5] A. Cordova, S. Watanabe, F. Tanaka, W. Notz, C. F. Barbas III, *J. Am. Chem. Soc.* **2002**, *124*, 1866.

[6] a) H. M. L. Davies, E. G. Antoulinakis, *J. Organomet. Chem.* **2001**, *617*, 47; b) H. M. L. Davies, T. Hansen, D. W. Hopper, S. A. Panaro, *J. Am. Chem. Soc.* **1999**, *121*, 6509; c) H. M. L. Davies, E. G. Antoulinakis, T. Hansen, *Org. Lett.* **1999**, *1*, 383; d) H. M. L. Davies, T. Hansen, M. R. Churchill, *J. Am. Chem. Soc.* **2000**, *122*, 3063; e) H. M. L. Davies, E. G. Antoulinakis, *Org. Lett.* **2000**, *2*, 4153; f) H. M. L. Davies, D. G. Stafford, T. Hansen, *Org. Lett.* **2000**, *2*, 417; g) H. M. L. Davies, P. Ren, *J. Am. Chem. Soc.* **2001**, *123*, 2070; h) H. M. L. Davies, C. Venkataramani, *Org. Lett.* **2001**, *3*, 1773; i) J. M. Axten, R. Ivy, L. Krim, J. D. Winkler, *J. Am. Chem. Soc.* **1999**, *121*, 6511; j) P. Muller, S. Tohill, *Tetrahedron* **2000**, *56*, 1725.

[7] S. E. Denmark, O. J.-C. Nicaise in *Comprehensive Asymmetric Catalysis* (Eds.: E. N. Jacobsen, A. Pfaltz, H. Yamamoto), Springer, Berlin, **1999**, pp. 954–958.

[8] a) H. M. L. Davies, *Curr. Org. Chem.* **1998**, 2, 463; b) H. M. L. Davies, *Eur. J. Org. Chem.* **1999**, 2459.

[9] E. Testa, G. Cignarella, G. Pifferi, S. Furesz, M. T. Timbal, P. Schiatti, G. Maffii, *Farmaco Ed. Sci.* **1964**, *19*, 895.